COMMUNICATIONS

Comparison of a Protein Model with Its X-ray Structure: The Ligand Binding Domain of E-Selectin

Jürgen Bajorath,*,† Ronald Stenkamp,‡ and Alejandro Aruffo†,‡

Bristol-Myers Squibb, Pharmaceutical Research Institute, 3005 First Avenue, Seattle, Washington 98121, and Department of Biological Structure, University of Washington, Seattle, Washington 98195. Received October 26, 1994®

E- and P-selectin are cell adhesion molecules implicated in the early events of inflammation. Three-dimensional models of the lectin domains have been reported by us and others prior to the availability of X-ray structural information. The models have been used to outline the ligand binding site in the selectins and to identify residues critical for function. Recently, the crystal structure of E-selectin has been reported, and thus, comparison of our E-selectin model with the X-ray data is now possible. The comparison shows that the assumptions on which the modeling was based were generally correct and provides an instructive example for the opportunities and the limitations of comparative modeling.

The selectins (E-, P-, and L-) form a family of cell adhesion molecules (*1, 2*) which are expressed on endothelial cells (E-, P-), platelets (P-), or leukocytes (L-) and play a major role in mediating the initial rolling interaction of leukocytes on activated vascular endothelium (*3*). This rolling interaction appears early in an inflammatory response and ultimately leads to leukocyte extravasation at sites of inflammation (*1, 2*). The selectins display equivalent molecular organization and show significant sequence similarity (*4*). All are transmembrane glycoproteins, having extracellular regions which consist of an amino terminal calcium-dependent (C-type) lectin domain (*5*), followed by an epidermal growth factor-like domain and a variable number of repeats with homology to complement regulatory proteins (*2, 4*). The amino terminal lectin domain is the ligand binding domain of the selectins. It specifically binds sialylated Lewis X or related carbohydrate ligands on cognate cells and is responsible for selectin-mediated adhesion (*2*). Thus, the carbohydrate recognition domain of E- and P-selectin have become a major target for the design of inhibitors to block the attachment of leukocytes to the vascular endothelium.

We and others have derived three-dimensional models of E- (*4, 6, 7*) and P-selectin (*8–10*) by comparative modeling (*11, 12*) based on the crystal structure of the C-type lectin domain of the rat mannose binding protein (MBP) at 2.5 Å resolution (*13, 14*). Briefly, this approach attempts to identify structurally conserved and variable regions in related proteins of known and unknown structure on the basis of sequence comparisons which take three-dimensional information into account. This analysis is used to build a computer model of the protein with unknown structure by complementing structurally

conserved regions (the "core") with novel structural elements (often "loops"). Selectin modeling and binding site analysis have been the subject of a review in this journal (*15*).

Recently, the X-ray structure of E-selectin, including the lectin and EGF domains, has been solved and refined at 2.0 Å resolution (*16*). This has enabled us to assess the accuracy of our model predictions. The sequences of the lectin domains in E- and P-selectin are ~65% identical. At this high level of sequence similarity, structures are generally very similar, and the rmsd (root mean square deviation) of their core regions is less than 1 Å (*17*). Therefore, the results of the comparison of the E-selectin model and crystal structure are expected to be similar for P-selectin. Here we wish to describe the assumptions on which the modeling was based, compare the predicted and experimental structures, and discuss the implications of this study for comparative protein modeling.

In contrast to the high sequence similarity of the selectins, the sequence identity between MBP and the selectins is only ~25%, a level at which the degree of structural similarity is uncertain (*12*). The alignment of the sequences of E-/P-selectin and MBP, taking the MBP crystal structure into account, suggested the conservation of some residues of the hydrophobic core regions, the disulfide bonds, and one calcium binding site, therefore suggesting greater structural similarity between the selectin and MBP lectin domains than would be predicted by the low level of sequence similarity. These initial sequence–structure correlations provided the basis for model building of the selectins, which was complicated by the unusual finding that only ~50% of the residues in MBP form regular secondary structure elements (α-helices and β-strands), whereas ~20% were found in loop regions and ~30% in extended regions of nonclassical secondary structure (*13*). Consequently, a major difficulty in modeling the selectins was assigning selectin residues in these unusual secondary structure elements and deciding which parts of these regions are

---

* To whom correspondence should be addressed. Phone/voice mail: (206) 727-3612. Fax: (206) 727-3602. Electronic mail: bajorath@protos.bms.com.
† Bristol-Myers Squibb.
‡ University of Washington.
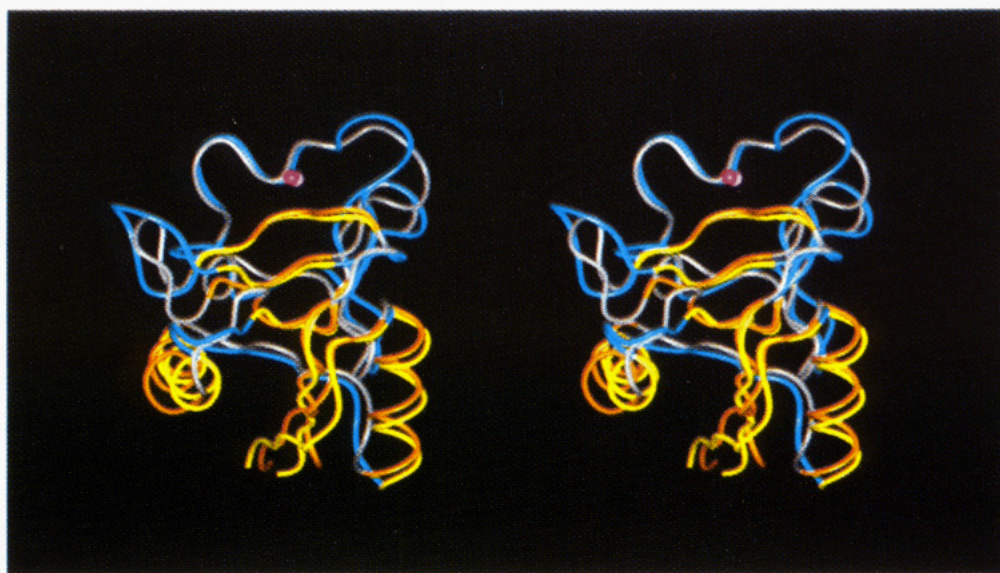
Figure 1. Comparison of the E-selectin model (blue/yellow) and crystal (gray/gold) structure. Shown is a solid ribbon representation of the lectin domains after backbone superposition. The α-helices and β-sheets in the predicted and X-ray structure are colored yellow and gold, respectively, and the extended regions of unusual secondary structure are colored blue and gray. The functional calcium in the E-selectin crystal structure is shown as a magenta sphere, and its predicted position is shown in lavender.

					β1					10									α1		20									30	
MBP_Xtal	K	F	F	V	T	N	H	E	R	M	P	F	S	K	V	K	A	L	C	S	E	L	R	G	T	V	A	I	P	R	N
ES_Xtal	W	S	Y	N	T	S	T	E	A	M	T	Y	D	E	A	S	A	Y	C	Q	Q	R	Y	T	H	L	V	A	I	Q	N
ES_model	W	S	Y	N	T	S	T	E	A	M	T	Y	D	E	A	S	A	Y	C	Q	Q	R	Y	T	H	L	V	A	I	Q	N
PS_model	W	T	Y	H	Y	S	T	K	A	Y	S	W	N	I	S	R	K	Y	C	Q	N	R	Y	T	D	L	V	A	I	Q	N

					α2				40										50	β2						L1				60	
MBP_Xtal	A	E	E	N	K	A	I	Q	E	V	A	K	T	.	.	.	S	A	F	L	G	I	T	D	E	V	T	E	G	Q	F
ES_Xtal	K	E	E	I	E	Y	L	N	S	I	L	S	Y	S	P	S	Y	Y	W	I	G	I	R	K	.	V	N	.	N	V	W
ES_model	K	E	E	I	E	Y	L	N	S	I	L	S	Y	S	P	S	Y	Y	W	I	G	I	R	K	V	.	.	N	N	V	W
PS_model	K	N	E	I	D	Y	L	N	K	V	L	P	Y	Y	S	S	Y	Y	W	I	G	I	R	K	N	.	.	N	K	T	W

	L2										70					L3				[*]		[*]	[ES]		L4		[MBP]	
MBP_Xtal	M	Y	V	.	T	G	G	R	.	.	L	T	.	.	Y	S	N	W	K	K	D	E	P	N	D	H	G	S	G	E	D
ES_Xtal	V	W	V	G	T	Q	K	P	.	.	L	T	E	E	A	K	N	W	A	P	G	E	P	N	N	R	Q	K	D	E	D
ES_model	V	W	V	.	.	G	T	Q	K	P	L	T	E	E	A	K	N	W	A	P	G	E	P	N	N	R	Q	K	D	E	D
PS_model	T	W	V	.	.	G	T	K	K	A	L	T	N	E	A	E	N	W	A	D	N	E	P	N	N	K	R	N	N	E	D

		90		β3								100					[*]		[*]	β4			110					β5			120
MBP_Xtal	C	V	T	I	V	.	(D)	(N)	.	.	D	N	G	L	W	N	D	I	S	C	Q	A	S	H	T	A	V	C	E	F	P
ES_Xtal	C	V	E	I	Y	I	K	R	E	K	D	V	G	M	W	N	D	E	R	C	S	K	K	K	L	A	L	C	Y	T	A
ES_model	C	V	E	I	Y	I	K	R	E	K	D	V	G	M	W	N	D	E	R	C	S	K	K	K	L	A	L	C	Y	T	A
PS_model	C	V	E	I	Y	I	K	S	P	S	A	P	G	K	W	N	D	E	H	C	L	K	K	K	H	A	L	C	Y	T	A

Figure 2. Structurally corresponding (topologically equivalent) residues in the crystal structures of the C-type lectin domains of the rat mannose binding protein (MBP_Xtal) and E-selectin (ES_Xtal) and the predicted topologically equivalent positions in MBP (MBP_Xtal) and E- (ES_model) and P-selectin (PS_model). The MBP_Xtal versus ES_Xtal alignment was based on comparison of the crystal structures according to ref 16. The MBP_Xtal versus ES/PS_model sequence–structure alignment was predicted after comparison of the MBP and selectin sequences on the basis of the MBP crystal structure and provided the basis for selectin modeling. Regions where the predicted and experimental topological equivalencies do not match (where the E-selectin model and crystal structures diverge) are shaded. Conserved residues in E- and P-selectin and in the selectins and MBP are shown in bold face. Secondary structure elements in MBP are overlined and taken from ref 13. The assignments are only slightly different for E-selectin according to ref 16. L1–L4 are extended regions of unusual secondary structure found in MBP. [*] indicates residues which participate in the formation of the conserved calcium binding site in both MBP and E-selectin; [MBP] and [ES] means a calcium-ligating residue only found in MBP or E-selectin, respectively.

conserved and which are variable (where residue insertions and deletions are tolerated).

Figure 1 shows the superposition of the predicted and crystallographic E-selectin lectin domain. The comparison shows that the overall fold of E-selectin and the location of its functional calcium binding site were correctly predicted. Figure 2 shows the topologically equivalent residues in MBP and E-selectin, derived from a superposition of their crystal structures, compared to the predicted (sequence–structure) alignment of E- and P-selectin relative to MBP. Details of the alignments are given in the figure legend. The comparison of the predicted and the experimental residue alignment shows that 111 of 120 residues (~93%) of the E-selectin model

were assigned to topologically corresponding positions. The predicted and experimental structures in the regions of conserved secondary structure elements are very similar, resulting in a backbone rmsd of ~1.2 Å. Deviations are larger in other parts of the structure. Three regions in E-selectin show incorrect assignments of insertions and deletions, L1 and L2 (extended regions of nonclassical secondary structure), and the loop connecting β-strands 3 and 4 (the length of one β-strand differs in MBP and E-selectin). These local misalignments lead to spatial misplacements of residues in the predicted structure. Other structural differences occur in the regions of unusual secondary structure. The conformation of E-selectin residues 83–88 in the extended region
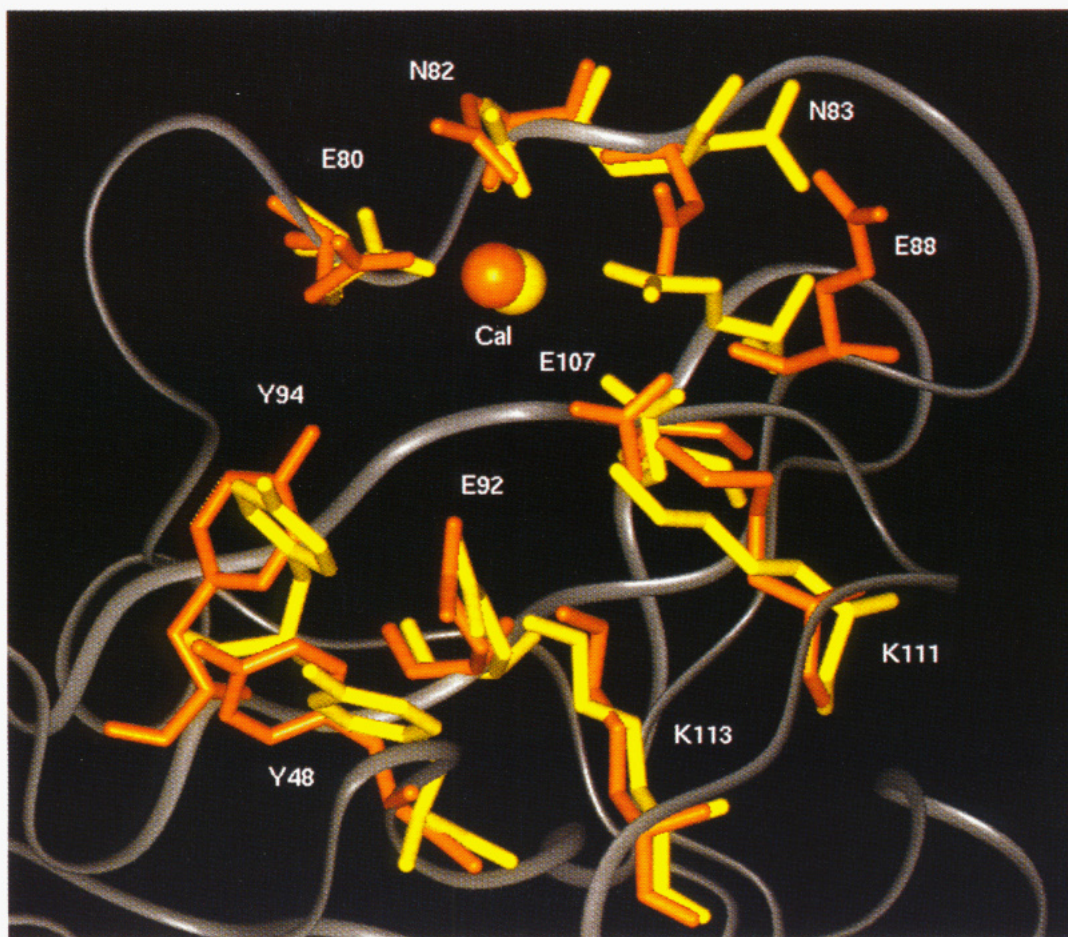
Figure 3. Close-up view of the ligand binding site in E-selectin. The residues which are critical for selectin function, including the calcium coordination sphere, are shown in their crystallographic (gold) and in their predicted (yellow) position and orientation. The orientation is according to Figure 1. For clarity, only the backbone of the E-selectin X-ray structure is shown in solid ribbon representation (gray). E88 is a calcium ligand in MBP and conserved in E- and P-selectin. Despite its conservation, E88 is replaced as a calcium ligand by N83 in the E-selectin crystal structure. This is the largest side chain deviation between the predicted and crystallographic ligand binding site in E-selectin.

L4 was assumed to be conserved in MBP and the selectins since it was close to and included one ligand of the conserved calcium binding site. However, comparison of the E-selectin model and crystal structure shows that the conformation of this region changes, giving a backbone rmsd of ~1.8 Å. Residue E88 is a calcium ligand in MBP and conserved in the selectins. However, in E-selectin E88 does not contact the calcium and is replaced as a calcium ligand by residue N83 which is not conserved in MBP (*16, 18*). Such effects where sequence conservation does not translate into structural equivalence remain unpredictable on the basis of sequence–structure comparisons. The incorporation of the non-classical secondary structure elements, including loops, in the rmsd comparison leads to a backbone rmsd of ~2.6 Å for all 120 residues of the model.

E- and P-selectin models have been used to identify the ligand binding site in the selectins with the aid of mutagenesis (*6, 8–10, 16*). A set of residues conserved in E- and P-selectin, including K111 and -113 and Y48 and -94, was found to be critical for binding of the selectins to a cellular ligand and/or immobilized glycolipid structures. The spatial prediction of the binding site was thought to be accurate since critical residues were located in a region including the central β-sheet of the selectin (*8*). The location of the binding site in E-selectin was later confirmed by mutagenesis on the basis of the E-selectin crystal structure (*16*). Figure 3 shows the comparison of the predicted and crystallographic ligand

binding site in E-selectin. As can be seen, the architecture of this site and the spatial arrangement of critical residues were accurately predicted. It follows that the model provided a meaningful basis for computer-assisted design of selectin inhibitors.

The comparison presented here has some more general implications for comparative protein modeling. The selectins and MBP share low sequence similarity, and MBP displays an unusual fold, consisting of more than 50% of unusual secondary structure. On the basis of sequence–structure comparisons, it has been difficult to decide which parts of these regions are structurally conserved in the selectins and which are variable. Consequently, the accuracy of the E-selectin model is lower in these regions than in other parts. The comparison of the MBP and the newly-available E-selectin crystal structure greatly improves the ability to assess structural conservation and variability in these regions, and variance of the C-type lectin fold will be better understood as more structures become available for comparison. The comparison also shows that the conservation of only a few key residues is sufficient to conserve the C-type lectin fold globally. This confirms the hypothesis on which modeling of the selectins was based.

LITERATURE CITED

(1) Springer, T. A. (1990) Adhesion receptors of the immune system. *Nature 346,* 425−434.

(2) Lasky, L. A. (1992) Selectins: interpreters of cell-specific carbohydrate information during inflammation. *Science 258,* 964−969.

(3) Lawrence, M. B., and Springer, T. A. (1991) Leukocytes roll on a selectin at physiologic flow rates: distinction from and prerequisite for adhesion through integrins. *Cell 65,* 859−873.

(4) Hollenbaugh, D., Bajorath, J., and Aruffo, A. (1994) Cell adhesion molecules and their cellular targets. In *Bioorganic Chemistry: Carbohydrates* (R. L. Rogers, and S. M. Hecht, Eds.) Oxford University Press, New York.

(5) Drickamer, K. (1988) Two distinct classes of carbohydrate recognition domains in animal lectins. *J. Biol. Chem. 263,* 9557−9560.

(6) Erbe, D. V., Wolitzky, B. A., Presta, L. G., Norton, C. R., Ramos, R. J., Burns, D. K., Rumberger, J. M., Narasinga Rao, B. N., Foxall, C., Brandley, B. K., and Lasky, L. A. (1992) Identification of an E-selectin region critical for carbohydrate recognition and cell adhesion. *J. Cell Biol. 119,* 215−227.

(7) Mills, A. (1994) Modelling of the carbohydrate recognition domain of human E-selectin. *FEBS Lett. 319,* 5−11.

(8) Hollenbaugh, D., Bajorath, J., Stenkamp, R., and Aruffo, A. (1993) Interaction of P-selectin (CD62) and its cellular ligand: Analysis of critical residues. *Biochemistry 32,* 2960−2966.

(9) Bajorath, J., Hollenbaugh, D., King, G., Harte, W., Jr., Eustice, D. C., Darveau, R. P., and Aruffo, A. (1994) The CD62/P-selectin binding sites for myeloid cells and sulfatides are overlapping. *Biochemistry 33,* 1332−1339.

(10) Erbe, D. V., Watson, S. R., Presta, L. G., Wolitzky, B. A., Foxall, C., Brandley, B. K., and Lasky, L. A. (1993) P- and E-selectin use common sites for carbohydrate ligand recognition and cell adhesion. *J. Cell Biol. 120* (5), 1227−1235.

(11) Greer, J. (1990) Comparative modeling methods: applications to the family of the mammalian serine proteases. *Proteins 7,* 317−334.

(12) Bajorath, J., Stenkamp, R., and Aruffo, A. (1993) Knowledge-based model building of proteins: concepts and examples. *Protein Sci. 2,* 1798−1810.

(13) Weis, W. I., Kahn, R., Fourme, R., Drickamer, K., and Hendrickson, W. A. (1991) Structure of the calcium-dependent lectin domain from a rat mannose-binding protein determined by MAD phasing. *Science 254,* 1608−1615.

(14) Weis, W. I., Drickamer, K., and Hendrickson, W. A. (1992) Structure of a C-type mannose-binding protein complexed with an oligosaccharide. *Nature 360,* 127−135.

(15) Bajorath, J., and Aruffo, A. (1994) Three-dimensional protein models. Insights into structure, function, and molecular interactions. *Bioconjugate Chem. 5,* 173−181.

(16) Graves, B. J., Crowther, R. L., Chandran, C., Rumberger, J. M., Li, S., Huang, K.-S., Presky, D. H., Familletti, P. C., Wolitzky, B. A., and Burns, D. K. (1994) Insight into E-selectin/ligand interaction from the crystal structure and mutagenesis of the lec/EGF domains. *Nature 367,* 532−538.

(17) Chothia, C., and Lesk. A. M. (1986) The relation between the divergence of sequence and structure in proteins. *EMBO J. 5,* 823−826.

(18) Weis, W. I. (1994) Lectins on a roll: the structure of E-selectin. *Structures 2,* 147−150.

REVIEWS

DNA Complexes with Polycations for the Delivery of Genetic Material into Cells

A. V. Kabanov*,† and V. A. Kabanov‡

Moscow Institute of Biotechnology, Inc. (MIB), Departments of Chemical Enzymology and Polymer Science, Faculty of Chemistry, M. V. Lomonosov Moscow State University Vorobievi Gory, Moscow V-234, Russia. Received July 22, 1994

1. INTRODUCTION

The majority of genetic engineering methods are based on delivery of foreign nucleic acids into intact cells (1). To date, a number of techniques have been developed for DNA introduction in cells, the most common of them being precipitation with calcium phosphate (2, 3), DEAE-dextran[1] (4), or polybrene (5, 6), direct introduction of DNA using cell electroporation (7, 8) or DNA microinjection (9, 10), and DNA incorporation in reconstructed virus coats (11–13).

Liposomes have been also used in some transfection protocols (14–16) in which DNA molecules are either entrapped in the internal aqueous space of liposomes or are bound on their surface. Promising results have been obtained with pH-sensitive liposomes, capable of fusing with the membranes of late endosomes and releasing DNA in the cytoplasm, which prevents DNA from accumulation and enzymatic digestion in lysosomes (15, 17). Various cationic amphiphiles, such as DOTMA (18), alkylammonium (19), cationic cholesterol derivatives (20), and gramicidin (21) have been added to liposome formulations in order to enhance their transfection efficacy. Cationic liposomes have been found to effectively bind nucleic acid molecules and fuse with cell plasma membranes, thus providing for an even more pronounced transfection than pH-sensitive vesicles (22). Particularly, the protocol using mixed DOTMA:DOPE liposomes ("lipofection") has been widely accepted as a reliable and

effective method for targeting both DNA (18) and RNA molecules (23) into cells.

However, each of the above listed methods has various specific disadvantages and limitations. Particularly, the techniques based on calcium phosphate and polycation precipitation that are probably most widespread in laboratory practice (24) are characterized by a relatively low transfection efficacy, appear ineffective for introduction of RNA molecules in cells, and cannot be used for genetic transfection in vivo. The well-known virus-transfection techniques using retrovirus or adenovirus vectors (12, 13) permit us to overcome some of these limitations. However, their application for gene therapy causes serious concerns about possible recombination with endogenous viruses, oncogenic effects, and immunologic reactions (25). To date, the lipofection protocol seems to be most promising (26), though there are some complaints about its cytotoxicity (20). Therefore, despite a great variety of already existing methods the search of new possibilities for transformation of animal, plant, and prokaryotic cells still continues.

Recently, a new approach has been developed to enhance the delivery of genetic material into cells. This method employs soluble interpolyelectrolyte complexes (IPECs)[2] of nucleic acids with linear polycations (27–29). Such complexes spontaneously assemble as a result of mixing the components due to formation of a cooperative system of interchain electrostatic bonds. The physicochemical characteristics of IPECs, in particular their solubility, dimensions, and surface charge, can be varied by altering the composition of the complex and the chemical structure of its constituents. Incorporation in IPEC results in significant changes in DNA properties, specifically in its compaction. Because it is tightly packed in the IPEC species the DNA chain is protected from the contact with the external medium, which, in particular, leads to DNA stabilization against digestion by nuclease (30). At the same time, IPECs can undergo drastic rearrangements and release polynucleotide chains during their interaction with those components of the cell membrane that are capable of competing for cooperative binding with polycations.

It has been demonstrated that incorporation in IPEC leads to an enhancement of DNA uptake into cells and an increase in its transfection activity with respect to

---

* Direct all correspondence to the present address: Department of Pharmaceutical Sciences, College of Pharmacy, University of Nebraska Medical Center, 600 South 42nd St, Box 986025, Omaha, NE 68198-6025. Phone: (402) 559-5320. Fax: (402) 559-5060.

† MIB and Department of Chemical Enzymology.

‡ Department of Polymer Science.

[1] Abbreviations: basic moles, molar expression of an amount of repeating units of a polymer; βGal, β-galactosidase; CAT, chloramphenicol acetyltransferase; DEAE-dextran, (diethylamino)ethyl dextran; CP, N-cetylpyridinium bromide; DODAC, dioctadecyldimethylammonium chloride; DOGS, (dioctadecyla-mido)glycylspermine; DOPE, dioleyl phosphatidylethanolamine; DOTMA, N-[1-(2,3-dioleyloxy)propyl]-N,N,N-trimethylammonium chloride; DPPES, dipalmitoyl phosphatidylethanolaminospermine; FITC, fluorescein isothiocyanate; IPEC, interpolyelectrolyte complex; φ, IPEC composition, i.e., the basic molar ratio [polycation]/[DNA] in the complex; MW, molecular mass, Da; LPLL and LPDL, lipopoly-L-lysine and lipopoly-D-lysine correspondingly; P_w, weight-average degree of polymerization; PANa, sodium polyacrylate; PMA, polymethacrylic acid; PMA-Na, sodium polymethacrylate; polybrene, 1,5-dimethyl-1,5-diazaundecamethylene polymethobromide; PVPE, poly(N-ethyl-4-vinylpyridinium bromide); PVPEC, random copolymer of N-ethyl-4-vinylpyridinium and N-cetyl-4-vinylpyridinium bromides.

---

[2] The term "interpolyelectrolyte complex" or "IPEC" is widely used in macromolecular science to determine the products of reaction of oppositely charged polyions (see for review refs 32–35). In this sense, the polycation–DNA complexes represent a special case of IPECs. We will use this term here in order to point out the interpenetraton of scientific disciplines and stimulate cross-interest of polymer chemists and biochemists to each others' work.

both prokaryotic (*28, 30*) and animal (*29, 31, 32*) cells. The IPEC-mediated transfection significantly differs from the methods based on DNA precipitation with polycations (*4–6*). Unlike DNA–polycation precipitates, IPECs represent a distinct class of *polymeric compounds* with strictly determined characteristics (*33–36*). These compounds can be used for targeted delivery of genetic material. By combining polycation molecules with ligands capable of specific binding with cells and uptake into them, it is possible to ensure the transport of IPECs into these cells via the receptor-mediated pathway (*27, 37–54*), as well as their *in vivo* delivery into target cells (*55–58*). Polycation conjugates with such ligands may also serve as carriers for intracellular delivery of antisense oligonucleotides (*59, 60*).

IPECs are self-assembling objects that are thermodynamically stable under a certain set of conditions, i.e., pH, ionic strength, temperature, medium composition, etc. This facilitates their preparation, storage, and application if compared, for instance, with liposomes that are usually unstable and cannot be stored for a long time. IPECs belong to a new class of self-assembling supramolecular delivery systems. Some other representatives of this class (i.e., block-copolymer micelles used as carriers for targeted delivery of low-molecular compounds and immunotoxin complexes, capable of selective activation when encounter with target cells) are described elsewhere (*61–63*). The present paper reviews the regularities of formation and behavior of DNA IPECs and discusses possibilities of their use for delivery of genetic material into cells. Other systems for DNA delivery, such as pH-sensitive and cationic liposomes, new intercalating agents, etc., were recently reviewed by other authors (*16, 64–71*). Therefore, we will not basically consider them here.

2. FORMATION AND PHYSICOCHEMICAL PROPERTIES OF DNA IPECS

Various polycations have been used so far to produce IPECs for targeted delivery of polynucleotides into cells. They include polyvinylpyridinium salts, polypeptides, and spermines (Figure 1). In many of these cases the polycation chains are covalently coupled with peptide or protein "vector" molecules (such as asialoglycoprotein, transferrin, etc.) (*37–60*), long-chain hydrophobic substituents (*28–32*), intercalating groups, and oligosaccharides (*72*). The molecular mass of polycations varies from several hundred to hundreds of thousand. Therefore, when a recombinant DNA molecule (MW from several to dozens of million) is used for IPEC formation, the polycation contour length is as a rule several times smaller than that of DNA. In this case, using the "guest–host" terminology previously introduced for IPECs of synthetic polyions (*34, 36*), the polycation can be termed "a guest" and DNA "a host". On the contrary, if a short complementary oligonucleotide is incorporated in IPECs, the polycation length usually exceeds that of the oligonucleotide. In this case, the polycation is a host and the oligonucleotide a guest.

The mechanism of formation and properties of nucleic acid IPECs are similar to those of the complexes formed by synthetic polyions (*33–36*). The mixing of nucleic acid and polycation aqueous solutions results in cooperative binding of electrostatically complimentary chains, i.e., in formation of IPEC. When the backbone of the major polycation chain is hydrophobic, the "sticking" of such a polycation to the nucleic acid, accompanied by compensation of phosphate group charges, leads to formation of a hydrophobic site (Figure 2a). The length and number of such sites is determined by the polymerization degree (length) of the guest and composition of the polycomplex

φ, i.e., the ratio of the number of polycation units and the number of nucleic acid phosphate groups in IPEC, φ = [polycation (basic moles)]/[DNA (basic moles)] (*28*), indicating that the physicochemical properties of IPECs greatly depend on their composition.

At low values of φ water-soluble nonstoichiometric complexes form in which the content of the polycation units is lower than that of the DNA units, and that contain a net negative charge. Under these conditions the polycation chains are usually evenly distributed among the DNA molecules. The complex charge elevates with an increase in the content of the polycation. Furthermore, the amount of the hydrophobic sites increases. At some point the complex reaches a critical composition φ_c (φ_c < 1), and its hydrophobicity increases to such an extent that further binding of the polycation should lead to precipitation of the complex (*30, 73*). Under these conditions uneven distribution of the polycation chains among the DNA molecules, i.e., *disproportionation*, becomes thermodynamically more favorable (*34, 36*). Two populations of complexes (nonstoichiometric and stoichiometric) that differ in composition and solubility form simultaneously. The nonstoichiometric IPEC with the critical composition ($\varphi = \varphi_c$) remains in solution. The redundant polycation molecules become incorporated in the insoluble stoichiometric IPEC ($\varphi = 1$) in which the DNA charges are completely compensated by the polycation. As the concentration of the polycation increases (φ_c < [polycation]/[DNA] < 1), the portion of the stoichiometric complex grows, while that of the nonstoichiometric one ($\varphi = \varphi_c$) falls down. When the basic molar concentrations of DNA and the polycation in the system become equal ([polycation]/[DNA] = 1) all the nucleic acid chains are involved in formation of the stoichiometric complex. Further increase in the concentration of the polycation may lead to recharging of the complex and its dissolution (*34, 36*). Under these conditions, the IPEC particles are stabilized in solution by the positively charged polycation loops bound to DNA (Figure 2a).

(1) Formation of IPECs and the Disproportionation Phenomenon. The formation of nucleic acid IPECs was studied by ultracentrifugation using complexes of phage λ and calf thymus DNA with PVPE and PVPEC as models (*28, 73, 74*). In these cases, the contour length of DNA exceeded that of the polycations by more than 1 order of magnitude. A single bound was observed on sedimentograms of the samples obtained by mixing DNA and PVPE solutions in the range of [polycation]/[DNA] ratios from 0 to 0.5 (Figure 3a). The sedimentation coefficient (S) corresponding to this bound continuously elevated from 18×10^{-13} s for free DNA to 24×10^{-13} s for IPEC (Figure 3b), implying that under these conditions (i) all the PVPE and DNA molecules in the system were incorporated in IPEC, (ii) the composition of complex coincided with the initial ratio of the polyions (0 < φ < 0.5), and (iii) the polycation chains were evenly distributed among the IPEC particles. Further increase in the polycation concentration led to disproportionation: parallel to the soluble IPEC ($S = 24 \times 10^{-13}$ s; φ = 0.5) the insoluble complex was formed with a higher content of the polycation (Figure 3a).

On the whole, the regularities of PVPEC interaction with DNA are similar to those observed for PVPE (*28, 74*). However, the range of [PVPEC]/[DNA] ratios under which the soluble IPECs form is rather narrow (from 0 to 0.25) (Figure 3b); i.e., the φ_c value in the case of PVPEC (φ_c = 0.25) is essentially lower than in the case of PVPE (φ_c = 0.5). This can be evidently explained by hydrophobic interactions of the side-chain alkyl substituents of PVPEC. The interaction between the substituents
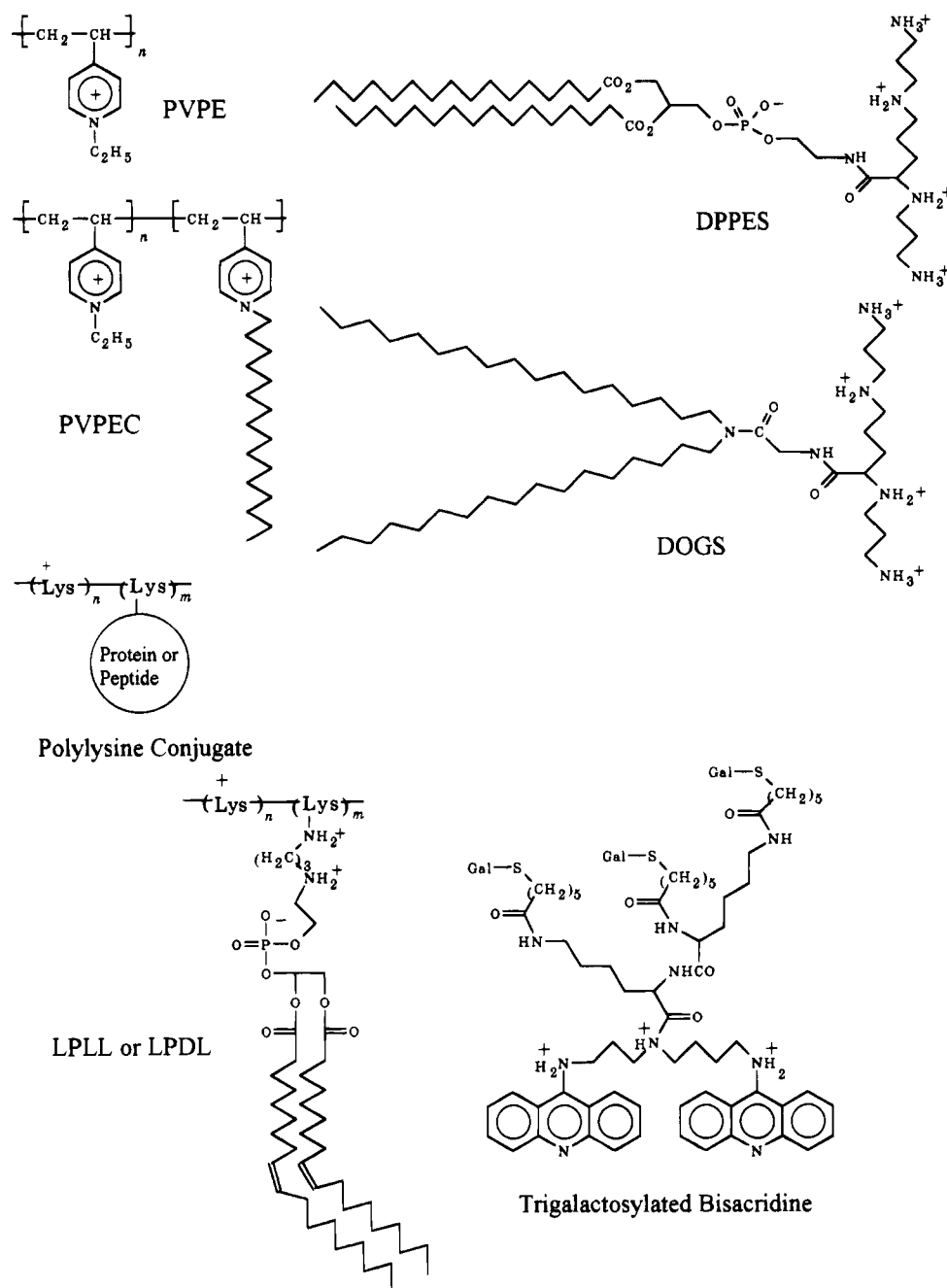
Figure 1. Polycations and oligocationic surfactants used for formation of DNA IPECs (low-molecular weight counterions are not presented): polyvinylpyridinium salts PVPE and PVPEC (*30*), lipospermines DPPES and DOGS (*29*), polylysine conjugates with proteins or peptides (*27, 48*), lipopolylysines LPLL and LPDL (*31*), and trigalactosylated spermidine—bisaccridine (*72*).

located on different polycation chains serves as a factor that stabilizes the IPEC particles containing several polycation molecules (Figure 2b). Therefore, in comparison with PVPE the PVPEC chains possess a pronounced ability for uneven distribution among the DNA molecules. A similar process is apparently characteristic of lipopolyamines that form micelles during binding with DNA that become a part of IPEC (*29, 75*).

(2) Compaction of DNA. The above-described sedimentation experiments indicate that the binding of polycations induces DNA compaction due to compensation of electrostatic charges of DNA and hydrophobic interactions of the complexed sites. For example, an almost 2-fold increase in the sedimentation coefficient of DNA observed after addition of PVPEC (Figure 3a) cannot be explained by the increase in molecular weight of the complex (it changes less than by 20%). More likely,

this phenomenon can be accounted for by DNA compaction accompanied by a decrease in the surface friction and an increase in the particle density. The compaction of DNA during its interaction with polycations (polypeptides) was registered using circular dichroism (*76, 77*), the sedimentation and light-scattering techniques (*78*), and DNA chemical modification (*79*). Direct proof of DNA compaction upon its interaction with polycations has been obtained by electron microscopy (*43, 80*). Particularly, it has been demonstrated that depending on their composition complexes of plasmids with polylysine represent either dense toroids with an average diameter of about 80—100 nm or starlike structures with dense nuclei surrounded with a shell of DNA chains. These data are in good agreement with the results of the fluorescence microscopy study of bacteriophage T4 DNA complexes with poly-L-arginine (*81*). This study reveals
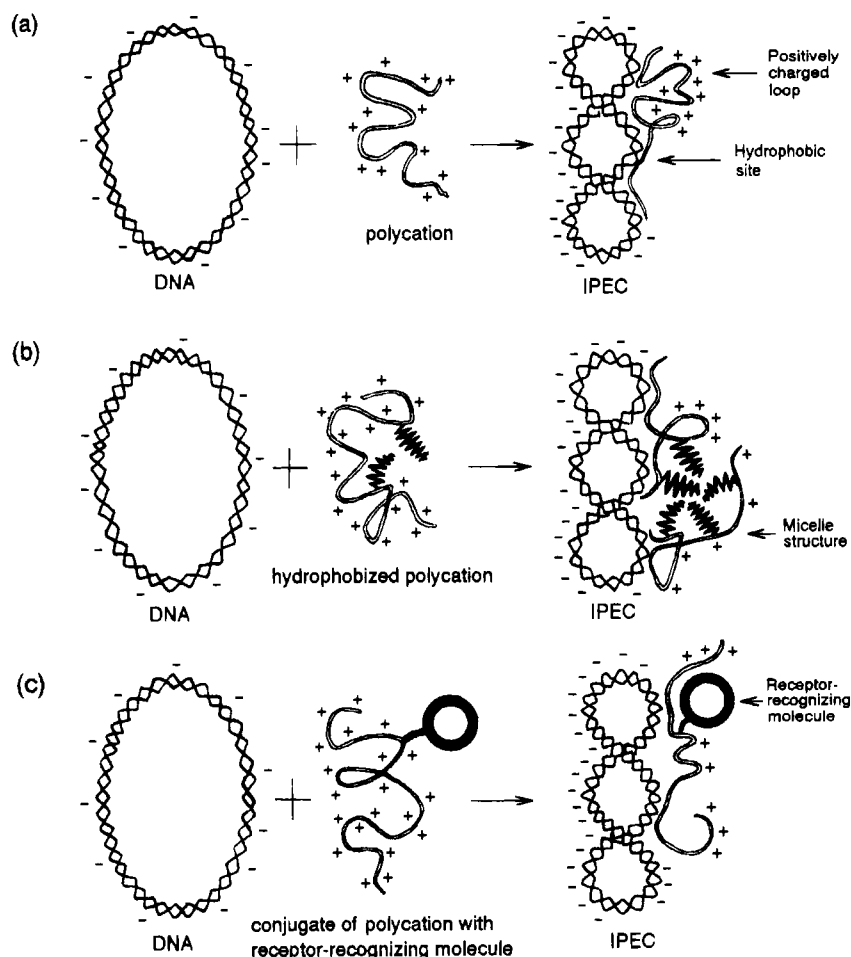
Figure 2. Formation of IPECs as a result of DNA interaction with (A) polycation, (B) polycation modified with hydrophobic substituent, and (C) polycation conjugate with receptor-recognizing molecule.
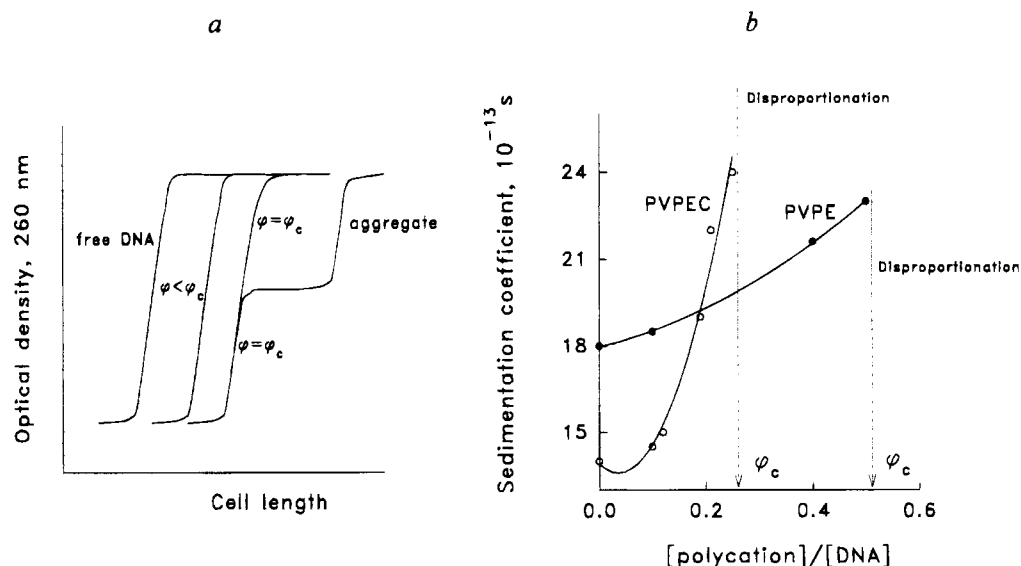

Figure 3. (a) Typical sedimentation curves and (b) dependencies of sedimentation coefficients of complexes of phage λ DNA with PVPE and PVPEC ($P_w = 400$) on the [polycation]/[DNA] ratio. Only one step is observed for free DNA and IPECs with compositions lower or equal to φ_c. Disproportionation is observed when the [polycation]/[DNA] ratio exceeds φ_c. Under these conditions, the soluble complex with $\varphi = \varphi_c$ forms in parallel to the insoluble one (aggregate). From ref *30*.

that the free DNA molecules represent elongated species with a length of the long axis equal to about 350 nm. By contrast, dense spherical particles of IPEC form when the polycation is added to free DNA. The portion of the IPEC particles increases with an increase in the [polycation]/[DNA] ratio while their dimensions decrease to

about 180 nm. A similar behavior is characteristic of DNA complexes with histones (*81*).

(3) Electrophoretic Mobility of IPECs. The formation of IPEC can be registered by electrophoresis in agarose gel (*30, 31, 37, 74*). The shift of the IPEC band during electrophoresis depends on the [polycation]/[DNA]
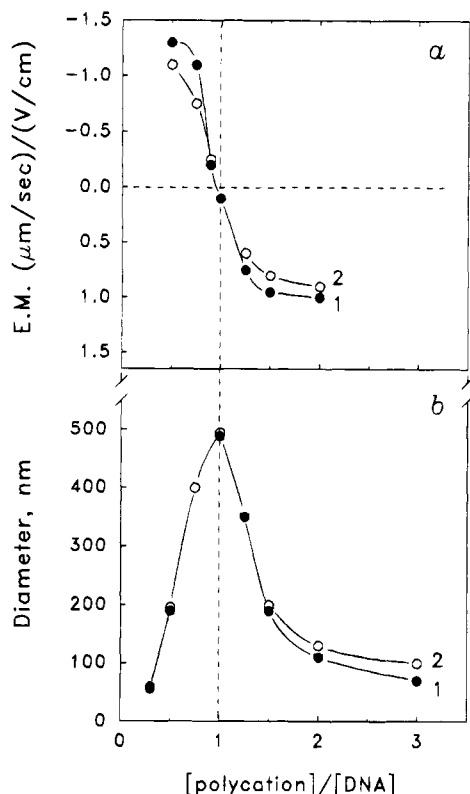
Figure 4. Dependencies (a) of electrophoretic mobility (E.M.) and (b) hydrodynamic diameter of IPECs of chicken embryo DNA with PVPE (1) and PVPEC (2) on the [polycation]/[DNA] ratio. The conditions under which the complexes are electrically neutral are marked by dotted lines. From ref *82.*

ratio that alters the IPEC net charge, as well as its size and density. At low [polycation]/[DNA] ratios the electrophoretic mobility of IPEC can be higher than that of free DNA due to the compaction effect (*74*). The IPEC species with a high content of polycation ([polycation]/[DNA] > 1) do not usually enter the gel (*31, 37*).

(4) Recharging of DNA. The effect of the polycation binding on the DNA net charge was recently studied using complexes of fragmented DNA from chicken embryo with PVPE and PVPEC (*82*) as models. In these experiments a fluorescent label was covalently linked to DNA, and IPEC formation was monitored by the fluorescence quenching. The fluorescence of DNA decreased monotonously as the concentration of polycation increased and reached a constant level (about 30% of the initial value) when the basic molar concentrations of polycation and DNA became equal. Under these conditions, the DNA chains were completely "covered" by the polycation molecules. The increase in the content of the polycation in the system was also accompanied by a decrease in the electrophoretic mobility of IPEC due to compensation of the DNA negative charges (Figure 4a). When the basic molar concentrations of the polycation and DNA were equal, the IPEC particles remained uncharged ($\varphi = 1$). Further increase in the concentration of the polycation led to a change in the charge sign of IPEC to the opposite which was indicative of incorporation of an excessive amount of the polycation molecules in the complex ($\varphi > 1$). In the composition range $0.3 < \varphi \le 1$ an aggregation of the complex was registered (Figure 4b). The size of the particles grew with an increase in the concentration of the polycation and reached the maximal value when the complex became electrically neutral ($\varphi = 1$). A further increase in the concentration of the polycation ($\varphi > 1$) results in a decrease in the size of the particles. The primary reason

for this is the electric repulsion of the positively charged polycation chains of the complex.
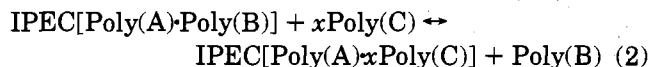
(5) DNA Stabilization in IPECs. The compaction of DNA chains in IPECs affects their accessibility to nucleases. Recently, the kinetics of digestion of IPEC-incorporated DNA by restriction enzymes was studied (*30*). Two distinctive stages of digestion were observed in the nonstoichiometric complexes containing an excess of DNA ($\varphi < 1$). The first stage involved rapid cleavage of DNA at the sites that were not covered by the polycation chains. The second stage consisted of slow restriction of remaining DNA. Meanwhile, the products of restriction were found to be the same for both native DNA and its IPECs. This suggests that the polycation bound on DNA does not hinder specific recognition of the latter by nucleases but only decelerates the process. This finding is in good agreement with the well-known dynamic properties of IPECs. The polycation chains are not rigidly fixed on the DNA chains: they migrate from one DNA region to another opening sites for restriction (see also the next section). The reaction rate is evidently limited by vacation of the restriction sites due to migration of a polycation from one DNA chain to another. In stoichiometric IPECs ($\varphi = 1$) and IPECs with an excess of polycation ($\varphi > 1$) the DNA chains are completely masked and DNA restriction does not proceed.

3. REACTIONS OF POLYELECTROLYTE EXCHANGE AND SUBSTITUTION

One of the major properties of IPECs is their ability to undergo reactions of polyelectrolyte substitution and exchange. The nature and regularities of these reactions have been analyzed in detail in reviews (*83, 84*) using complexes of synthetic polyelectrolytes as models. The reactions of substitution are processes of the following type

$$\text{IPEC}[a\text{Poly(A)}{\cdot}b\text{Poly(B)}] + c\text{Poly(C)} \leftrightarrow$$
$$\text{IPEC}[a\text{Poly(A)}{\cdot}(b - c)\text{Poly(B)}{\cdot}c\text{Poly(C)}] + c\text{Poly(B)} \quad (1)$$
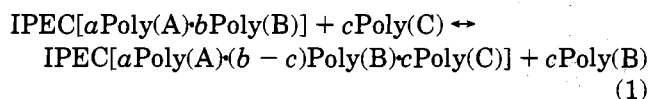
where Poly(A) is a polyion charged oppositely to polyions Poly(B) and Poly(C). When Poly(B) is identical to Poly(C), process 1 is termed "reaction of exchange". For ease of presentation we will consider below the following reaction

$$\text{IPEC}[\text{Poly(A)}{\cdot}\text{Poly(B)}] + x\text{Poly(C)} \leftrightarrow$$
$$\text{IPEC}[\text{Poly(A)}{\cdot}x\text{Poly(C)}] + \text{Poly(B)} \quad (2)$$

assuming that the degree of polymerization of Poly(A) is lower than that of Poly(B) ($P_w^A < P_w^B$) (therefore, Poly(A) and Poly(B) are termed guest and host, respectively), and the composition of IPEC does not change as a result of the reaction ($\varphi = P_w^A/P_w^B = P_w^A/xP_w^C$).

Due to cooperative character of interaction of polyions in IPEC which provides for their firm sticking to each other reaction 2 cannot proceed via the dissociation mechanism. The study of the mechanism of this reaction (*85*) has demonstrated that the first rapid stage involves migration of the free polyion Poly(C) toward the IPEC particle and formation of a triple complex IPEC[Poly-(A)·Poly(B)]·Poly(C) occurs. The bimolecular rate constant of this process amounts to approximately 10^9 M^{-1} s^{-1} which corresponds to the rate of diffuse collisions of polyion chains in aqueous solutions. The second stage consists of interchain transfer of the segments of the oppositely charged polyions which leads to substitution of Poly(B) chains by those of Poly(C). In the absence of the low molecular weight electrolyte this stage does not

proceed and the triple complex IPEC[Poly(A)·Poly(B)]·Poly(C) remains "frozen" in a nonequilibrium state. Such freezing does not occur in the presence of the low-molecular weight salt, and the reaction reaches equilibrium. Other factors that influence the kinetics of this process include the nature of low molecular weight counterions, the charge density, and the structure of polyions involved in the reaction (*85*). All these factors determine the firmness of interchain saline bonds in IPECs. The weakening of these bonds facilitates their redistribution in the complex IPEC[Poly(A)►Poly(B)]·Poly-(C) and, consequently, accelerates the interchain transfer of polyions (*85*). Finally, the rate of transfer of the Poly-(A) chains in the triple complex IPEC[Poly(A)►Poly-(B)]·Poly(C) falls down as their length decreases.

Not only the rate but the position of equilibrium in the reactions of substitution appears to be very sensitive to the structure and length of polyions as well as to the nature and concentration of low molecular weight counterions (*86*). To interpret these phenomena, it is expedient to represent the total change of free energy (ΔG_t) during reaction 2 as a sum of two components

$$\Delta G_t = \Delta G_p + \Delta G_c$$

where ΔG_p corresponds to substitution of interchain bonds A·B for A·C and ΔG_c is a difference in the energy of interaction of the low molecular weight counterion with the free chains of Poly(C) and Poly(B) involved in the reaction of substitution. As first approximation, the ΔG_p value may be represented as

$$\Delta G_p = P_w{}^A(\Delta H_{A\cdot C} - \Delta H_{A\cdot B}) - T\delta S_p$$

where $\Delta H_{A\cdot C} - \Delta H_{A\cdot B}$ is a difference in enthalpy between bonds A·C and A·B on a perunit basis, the number of the substituted links is equal to $P_w{}^A$, T is the temperature, and ΔS_p is a change in entropy of the free Poly(C) and Poly(B) chains during the reaction (not taking into account the impact of counterions). Evidently, due to cooperativity of interaction between polyions in IPEC, even slight changes in the enthalpy of the interchain links on a perunit basis should result in marked changes in net values of ΔG_p and ΔG_t. A decrease in the length of Poly(C) under conditions when the composition of IPEC remains constant leads to a growth of x (i.e., the number of the particles involved in the reaction on the left side). This, in its turn, should decrease the entropy component $T\Delta S_p$ and shift equilibrium to the left. Variations in the nature and concentrations of low molecular weight counterions do not affect the ΔG_p value. However, due to changes in ΔG_c, such variations may lead to dramatic changes in the direction of the process (ΔG_t) which is demonstrated below using reactions of DNA IPECs as models.

(1) Kinetics and Equilibrium in the Reactions of DNA IPECs. The first indication that reactions of exchange might occur in systems containing DNA IPECs was reported by Miller and Bach (*73*). The reactions of substitution of a nucleic acid by PANa and PMANa in complexes with PVPE were used to decompose IPEC-[DNA·PVPE] and IPEC[DNA·PVPEC] during the study of their restriction (*30*) and interaction with mammalian cells (*32*). Recently, the kinetic and equilibrium behavior in the reaction of substitution in complexes of DNA and PMA with PVPE were studied (*87, 88*):

IPEC[PVPE·PMA] + DNA ↔

IPEC[PVPE DNA] + PMA   (3)
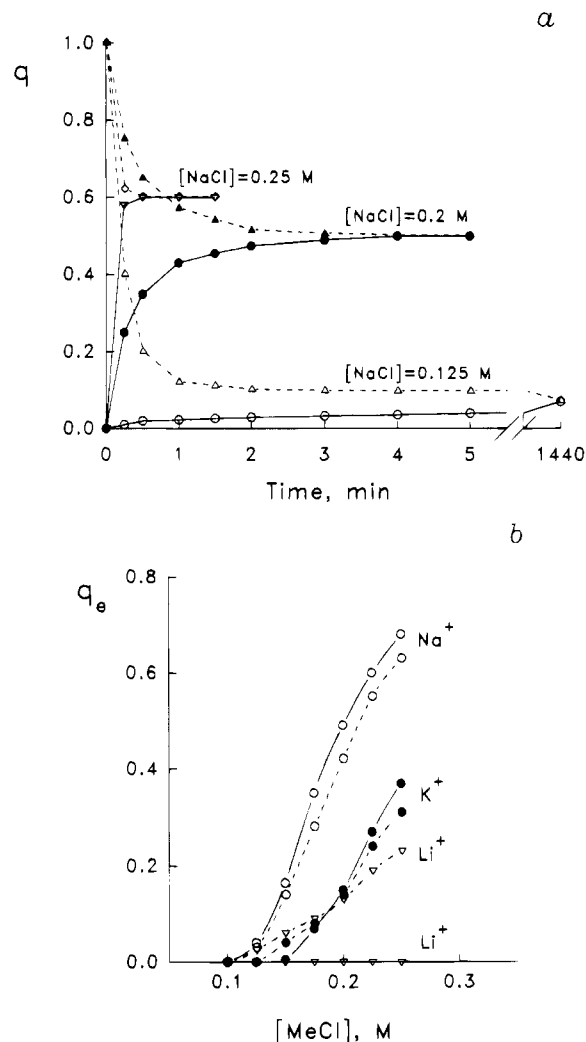
Figure 5. (a) Kinetics of transition to equilibrium in reaction 3 at various concentrations of NaCl in the system. The reagents are mixed in various orders: either free DNA is added to IPEC-[PVPE·PMA] (continuous line) or the free PMA is added to IPEC[PVPE·DNA] (dotted line). (b) Effect of elementary salt (LiCl, NaCl, and KCl) on the position of equilibrium in reaction 3 involving native (continuous line) and denatured DNA (dotted line). q: the degree of conversion of reaction 3 (q equals the ratio of the amounts of the salt bonds [PVPE·DNA]/{[PVPE·DNA] + [PVPE·PMA]}). q_e: the degree of conversion of reaction 3 under equilibrium conditions. From ref *87*.

This reaction was completely reversible: the equilibrium state was attained irrespective of the order in which the reagents were mixed (Figure 5a). However, to a great extent, the reaction rate and position of equilibrium depended on ionic strength and nature of the elementary salt present in solution. Thus, an increase in NaCl concentration from 0.125 to 0.25 M led to a practically complete shift of equilibrium to the right (from IPEC-[PVPE·PMA] to IPEC[PVPE·DNA]). At the same time, a dramatic decrease in the time of the reaction half-conversion (from dozens of minutes to several seconds) was observed. Figure 5b illustrates the effect of concentration and nature of counterions on the position of equilibrium in the reaction. After substitution of the elementary salt in the row NaCl > KCl > LiCl, the equilibrium shifted to the left (from IPEC[PVPE·DNA] to IPEC[PVPE·PMA]). It should be noted that LiCl, contrary to NaCl and KCl, influenced the direction of reactions involving native DNA and denatured DNA in different ways. Thus, the equilibrium of the reaction shifted completely toward IPEC[PVPE·PMA] in the whole

Table 1. Transfection of Mammalian Cells Using DNA IPECs with Polycations[a]

polycation(s)	cells	comparison with other methods	ref
lipospermines (DOGS and DPPES)	Porcine intermediate lobe cells, LMTK, Ras4, CHO, F9, BU4, S49, HeLa, AtT-20, 3T3, primary human keratinocytes.	More efficient than calcium phosphate precipitation and methods that use monovalent cationic surfactants (DODAC, stearylamine and phosphatidylamine). Less cytotoxic effects than in cases of DODAC and DOTMA transfection methods.	Behr *et al.* (*29, 92, 93*)
lipopolysines (LPLL and LPDL)[b]	L929, Vero, La, RDM4, CEM	Efficacy approximately equals that of lipofection. Less sensitive to serum and less cytotoxic than lipofection.	Huang *et al.* (*31*)
polyvinylpyridinium salts (PVPE and PVPEC)	3T3 NIH, MDCK,[c] Jurkat[c]	About 10-times more efficient than calcium phosphate precipitation. No essential cytotoxic effect has been observed.	Kabanov *et al.* (*32*)

[a] For the structural formula see Figure 1. [b] Under the same conditions nonmodified polylysine is not active. [c] Transfection has not studied using these cell lines; enhancement of DNA uptake after its incorporation into IPECs has been demonstrated.

range of LiCl concentrations in the case of native DNA. By contrast, a marked shift of equilibrium to the right was observed parallel to an increase in LiCl concentration when denatured DNA was used. This phenomenon can be evidently explained by a difference in the energy of Coulomb interaction of Li^+ cations with the chains of native and denatured DNA.

(2) Interaction of DNA IPECs with Lipid Membranes. The behavior of DNA complexes with polycations (PVPE, PVPEC) and a cationic surfactant (CP) in the presence of negatively charged monolamellar liposomes from the lecithin:cardiolipin (4:1) mixture was studied (*82*). The DNA complex with CP was destroyed during its interaction with the liposomes: CP incorporated in the liposome membranes changing their surface charge, while the free DNA chains remained in solution. This process closely resembled reaction 1: the DNA chains in the complex were substituted for the totality of negatively charged groups on the surface of the liposome membrane. A completely different phenomenon was observed in the case of IPEC[DNA·PVPE]. This complex did not interact with the liposomes. Moreover, after addition of free DNA to the liposomes on the surface of which PVPE had been previously adsorbed all polycation chains transferred from the surface of the liposomes to the DNA chains. In other words, the equilibrium in the reaction of substitution of DNA between IPEC[DNA·PVPE] and the liposome membrane shifted completely toward IPEC. Finally, IPEC[DNA·PVPEC] firmly bound with the surface of the liposomes forming a triple complex "DNA−PVPEC−liposome". Evidently, this happened due to incorporation in the liposome membrane of side chain cetyl substituents of PVPEC that served as "anchors". At the same time, the interchain saline links of DNA and PVPEC remained intact. It is obvious that the data obtained on comparatively simple models should be very carefully used for interpretation of processes occurring in living cells. Meanwhile, we assume that the study of behavior of DNA IPECs in such systems is important for the understanding of basic regularities of their interaction with biological structures, as well as for improving systems for nucleic acid targeting.

**4. GENE DELIVERY IN BACILLUS AND MAMMALIAN CELLS**

(1) *Bacillus Subtilis* Transformation. A possibility of enhancing genetic transformation of prokaryotic cells by incorporating plasmids in IPECs with polyvinylpyridinium salts (PVPE, PVPEC) was demonstrated using *Bacillus subtilis* cells (*28, 30*). The efficacy of transformation depended on the composition of IPEC and increased with the elevation of φ, which was accompanied by a rise in IPEC hydrophobicity (Figure 6). The transformation yield grew while the polymerization degree of
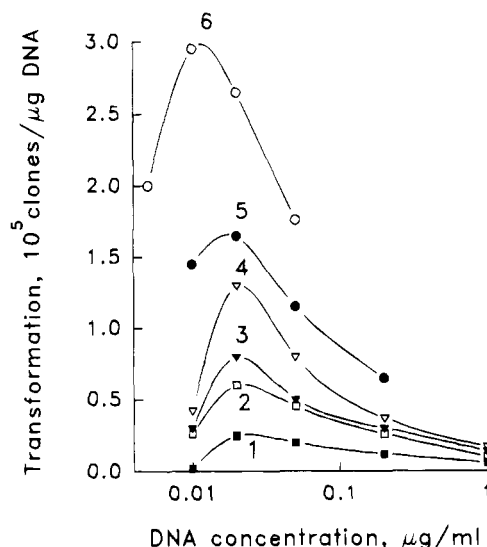
Figure 6. Transformation of *Bacillus subtilis* competent cells by free plasmid pTZ19 (1) and its IPEC with PVPE (2, 4, 5, 6) or PVPEC (3). $P_w = 400$ (2, 3, 4), or 200 (5), or 18 (6). $\varphi = 0.1$ (2), or 0.2 (3−6). From ref *30*.

PVPE decreased at a constant value of φ. The mechanism of IPEC-mediated transformation of bacillus cells is not clear. An important stage of *Bacillus subtilis* transformation consists of DNA adsorption on cell membranes (*89, 90*). DNA incorporation in IPEC enhances its adsorption on the bacillus membranes which apparently occurs due to interaction of the hydrophobic sites of IPEC with lipids (*30*). The next stage of DNA penetration into the bacillus cells is associated with DNA fragmentation and its change to a single-chain form (*89, 90*). To replicate after intracellular translocation, the DNA molecule should free itself of the polycation chains. It is probable that interaction of IPEC with negatively charged intracellular components results in migration of the polycation to these components and release of DNA in a functionally active form.

(2) Transfection of Mammalian Cells. A broad set of cell lines as well as of primary cultures has been transfected using DNA complexes with polycations (Table 1). In these works, DNA IPECs with lipospermines (*29, 91−93*), lipopolylysines (*31*), and polyvinylpyridinium salts (*32*) have been used. Hydrophobicity of the backbone of the polycation main chain (polyvinylpyridinium salts) or of the side chain substituents (lipospermines, lipopolylysines) was found to be an important prerequisite of transfection. In all these cases, the transfection efficacy depends on the [polycation]/[DNA] ratio (Figure 7). These dependencies are described by curves with saturation or by bell-shaped curves resembling those characteristic of lipofection and other mammalian cell transfection protocols that imply monovalent cationic
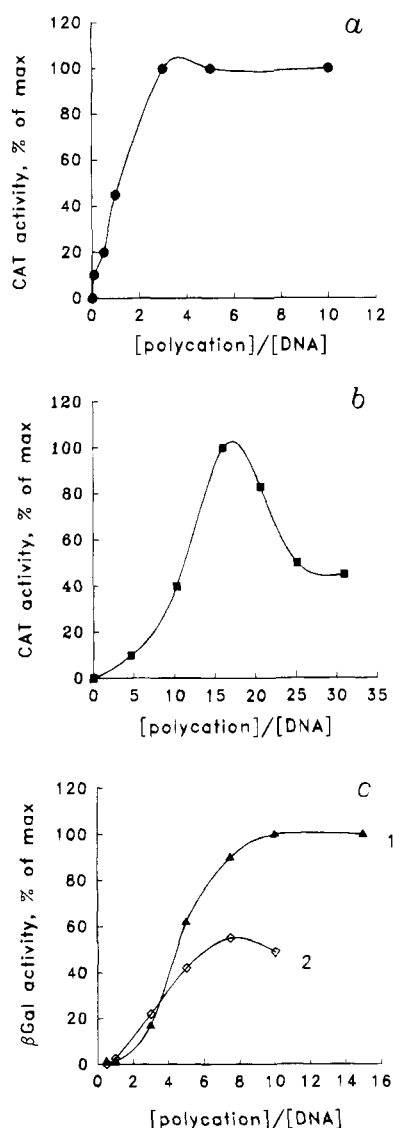
Figure 7. Effect of IPEC composition on the efficacy of mammalian cells transfection: (a) transfection of melanotrope cells using complexes of pCAT−4XB plasmid with DOGS (from ref 29); (b) transfection of L929 mouse fibroblasts using complexes of pSV2CAT plasmid with LPLL (from ref 31); (c) transfection of NIH 3T3 fibroblasts using complexes of pβGal plasmid with PVPE (1) and PVPEC (2) (from ref 32).

surfactants (26). Only the positively charged complexes (φ ≥ 1) possess a transfection activity. This is essentially different in the case of *Bacillus subtilis* transformation in which the negatively charged complexes are active. When the optimized compositions of IPECs are used, the transfection efficacy is comparable to or even surpasses that of calcium phosphate precipitation or lipofection (see Table 1). At the same time, no significant cytotoxic effects are observed[3] which is an essential advantage over some other transfection techniques.

It has been recently demonstrated that the adsorption of a plasmid on plasma membranes and its uptake in mammalian cells increase as a result of its incorporation into IPEC (32). The effect of the polycation (PVPE) on adsorbtion and uptake was revealed only for positively

charged complexes (φ ≥ 1) like in the case of cell transfection. It has been suggested that the initial stage of IPEC interaction with cells consists of binding of the positively charged segments of the polycation with the negatively charged phospholipids of the cell membrane. This accounts for enhancement of DNA binding on the cell surface. At the same time, such interaction can also dramatically affect the properties of the plasma membrane (its structure, ion permeability, etc. (96−101)), which may serve as a "signal" that induces endocytosis. Polycation-induced endocytosis has been described in the literature (102−105), and it has been hypothesized that this process may underlie the uptake of IPEC-incorporated plasmids (32). DNA compaction in the complex may also serve as a factor that facilitates DNA accommodation in endocytic vesicles, the diameter of which does not exceed 100 nm (106). Subsequent stages of cell transfection should involve release of DNA from the endocytic compartments in the cytoplasm. The low efficacy of this process impedes transfection. Therefore, further improvements of transfection systems should focus on getting them over the endosomal barrier.

The mechanisms of IPEC-mediated transfection of mammalian cells require further studies. Here are some of the most important questions which must be addressed. (i) *What accounts for bell-shaped or saturation dependencies of the efficacy of transfection on the composition of IPEC?* The amount of polycation chains that can be incorporated in a complex is evidently limited by the amount of sites on DNA that provide for cooperative electrostatic binding of the polycation. The length of such sites is sufficient for cooperative binding of polyions when it is equal to about 10 polyion units (33). Therefore, when the degree of polymerization of a polycation is equal to 100, at least 10% of the polycation units must be bound with DNA to provide for the polycation incorporation in IPEC. In other words, the maximal possible composition of such IPEC equals about 10. The excessive polycation will not incorporate in the complex, but may bind with the cell membrane preventing IPEC from adsorption and uptake which decreases the transfection efficacy. The relevance of this hypothesis to the observed dependencies should be studied. (ii) *How is DNA released from endocytic compartments into the cytoplasm?* It is probable that during endocytosis, IPEC overaccumulates in the endocytic compartments, and its concentration there substantially exceeds that in the extracellular medium. The driving force for this may probably be the free energy of endocytosis. Under these conditions, the polycation-induced fusion of the membranes (96, 97) probably occurs which results in DNA release. This problem should be analyzed in connection with the following. (iii) *How and where does DNA get rid of the polycation chains?* Negatively charged membranes and/or polynucleotides in a cell may serve as components reacting with IPEC and providing for DNA release as a result of polyelectrolyte substitution. Therefore, the fate of a polycation after its penetration in a cell should be thoroughly analyzed. (iv) *What is the role of hydrophobic interactions of polycation with cell membranes?* Hydrophobic interactions with lipids may provide for the fusogenic activity of polycations in endosomes. By optimizing the structure of the main chain of the polycation as well as the length and amount of the side chain substituents one may probably achieve higher transfection yields.

5. RECEPTOR-MEDIATED GENE TARGETING

Polycation are "building blocks" that can be easily conjugated with receptor-recognizing molecules. If such conjugate is then used for formation of IPEC, the result-

Table 2. Receptors Used for DNA Targeting into a Cell

receptors to	localization and function
asialoglycoprotein	Unique receptors of hepatocytes. Provide for binding, internalization, and lysosomal delivery of galactose terminal asialoglycoproteins (*108*). Cytoplasmic transport of constructs containing asialoglycoprotein (e.g., the conjugate of diphtheria toxin A chain with asialoglycoprotein) is also described (*109*).
insulin	Presented in various types of cells (*110*). Provide for an endocytosis of insulin and apparently its subsequent delivery to a cell nuclei (*111, 112*).
transferrin	Presented in almost all cells and mediate iron transport into cells. Provide for transferrin binding, vesicular transport in endosomes, and return to the cell surface after release of iron (*113, 114*).

Table 3. Gene and Antisense Oligonucleotide Targeting Using Polylysine Conjugates with Various Ligands

ligand	cells	major results	ref
asialoglycoprotein	human hepatoma Hep G2	receptor-mediated transfection of hepatoma cells	Wu and Wu (*27, 37*)
	hepatocytes (*in vivo*)	targeted delivery of a plasmid in liver and transfection of hepatocytes *in vivo* (rats)	Wu and Wu (*53*)
	hepatocytes (*in vivo*)	correction of genetic and analbuminemia in rats	Wu *et al.* (*56*)
	hepatocytes (*in vivo*)	improvement of hypercholesterolemia in rabbits deficient in low density lipoprotein receptors	Wilson *et al.* (*57*)
	NIH 3T3[a]	enhancement of activity of an antisense oligonucleotide	Bunnel *et al.* (*60*)
glycopeptide specific to asialoglycoprotein receptor	Hep G2, mouse hepatocytes BNL CL.2	a fusogenic peptide is incorporated into IPEC to enhance transfection	Plank *et al.* (*48*)
transferrin	avian erythroblasts (HD-3 and EGFR-*ts-myb*),REV-NPB-4 lymphoblasts, normal bone marrow, erythroleukemic K-562 cells, human epithelial cells (HBE1, KB and HeLa) etc.	receptor-mediated uptake of an IPEC-incorporated plasmid and transfection of various eukaryotic cells	Wagner *et al.* (*38, 43, 45*), Zenke *et al.* (*39*), Cotten *et al.* (*40*), Curriel *et al.* (*47*)
	Friend murine erythroleukemic (F-MEL) and J2E cells HeLa, BNL CL.2, human neuroblastoma cells GI-ME-N	stoichiometry of the conjugate and the conjugation procedure are optimized to enhance transfection	Taxman *et al.* (*107*)
		a 10-fold increase in transfection efficacy in the presence of adenovirus	Cotten *et al.* (*50*)
	K562, HeLa, BNL CL.2	a fusogenic peptide is incorporated into IPEC to enhance transfection efficacy	Wagner *et al.* (*52*)
	human leukemic cells HL-60	enhancement of uptake and activity of an antisense oligonucleotide (against c-myb gene)	Citro *et al.* (*59*)
insulin	human hepatoma cells PLC/PRF 5	transport of a plasmid to the nucleus and cell transfection	Rozenkrants *et al.* (*46*)

[a] Genetically modified cells expressing the asialoglycoprotein receptor.

ing complex (Figure 2c) will contain specific moieties capable of directing DNA into eukaryotic cells along the receptor-mediated pathway. The asialoglycoprotein, transferrin, and insulin receptors (Table 2) have been used so far for receptor-mediated transfection. Conjugates of corresponding ligands with poly-L-lysine served as carriers for plasmids. The plasmids incorporated in IPECs with such conjugates are taken up by various cells and reveal high transfection activities. Both the uptake and the efficacy of cell transfection correlate with the level of cell receptors, and are inhibited by free ligands (*37, 40, 46*). The major results obtained using this approach are summarized in Table 3 and briefly considered below.

(1) Gene Delivery into Hepatocytes Using Asialoglycoprotein Receptors. Since the asialoglycoprotein receptor is presented only on hepatocytes, the DNA targeting procedures involving this receptor are specific with respect to hepatocytes and hepatoma cells. The conjugate of asialoglycoprotein with poly-L-lysine was used for delivery of both plasmid DNA (*27, 37*) and short antisense oligonucleotides into cells (*60*). When the complex of this conjugate with a plasmid was introduced in rats about 85% of DNA accumulated in liver, and gene expression in hepatocytes was observed (*53*). This approach was successfully applied for partial correction of genetic analbuminemia in rats (*56*) and improvement of hypercholesterolemia in rabbits deficient in low density lipoprotein receptors (*57*).

An artificial glycopeptide ligand for the asialoglycoprotein receptor was recently used to design a delivery system for DNA targeting into receptor-positive cells (*48*).

The gene transfer using conjugates of this ligand with polylysine becomes significantly enhanced in the presence of amphipatic peptides derived from the *N*-terminal sequence of influenza virus hemagglutinin that possess pH-controlled membrane-disruption activity. Recently, another attempt has been made to develop synthetic cationic molecules that can deliver genes to hepatocytes (*72*). These molecules (Figure 1) contain a spermidine–bisacridine moiety capable of intercalation and electrostatic binding with DNA and thiogalactosyl groups capable of specific interaction with asialoglycoprotein receptor. Being bound with DNA, they provide for its uptake in hepatocytes. At the same time, no transfection has been observed in this case, probably because internalized DNA does not release in the cytoplasm.

(2) Transferrinfection. The transfection technique employing conjugates of transferrin with poly-L-lysine (termed "transferrinfection") can be used for gene delivery in a great variety of cells bearing the transferrin receptors. Transferrinfection is 10–100 times more effective than lipofection and methods based on DEAE-dextran or calcium phosphate precipitation (*38–40, 43–45, 47, 49–52, 107*), and it does not produce any significant cytotoxic effects. Some improvements, including optimization of synthesis, structure, and composition of a poly-L-lysine–transferrin conjugate, have been recently made to introduce this protocol more widely in laboratory practice (*107*). It has been also demonstrated that this method can be used for delivery of antisense oligonucleotides into cells (*59*).

The major limitation of transferrinfection is that IPEC-incorporated DNA is rather slowly released from intracellular vesicles into the cytoplasm (*51*). Some approaches have been recently developed to enhance this process and to decrease DNA degradation in lysosomes. Particularly, it has been demonstrated that the coupling of adenovirus to DNA complexes with poly-L-lysine results in efficient gene transfer into cells with high levels of the adenovirus receptors (*49, 51*). The inactivated adenovirus particles enhance transferrinfection up to 90% which was explained by coendocytosis of the virus and IPEC and subsequent virus-induced disruption of the endosomes (*50*). Another approach employs the fusogenic hemagglutinin peptides (*52*) similar to those used in the case of asialoglycoprotein-mediated transfection (*48*). The combination complexes consisting of plasmid DNA, poly-L-lysine conjugates with transferrin, and poly-L-lysine conjugates with peptides possess very high transfection activity which is conditioned by the peptide-induced membrane fusion and DNA release from the endosomes (*52*).

(3) Gene Delivery Using Insulin Receptor. There are only a few papers on application of insulin constructs for cell transfection (*41, 42, 46*). Although the advantages of this approach still need to be proven it may become useful for transfecting various cells containing the insulin receptor. The ability of polylysine-insulin conjugates to deliver DNA into a cell nucleus has been recently demonstrated (*46*). This suggests that this approach may be of great importance for enhancement of transfection.

6. GENE TARGETING USING ANTIBODY–POLYCATION CONJUGATES

Antibody molecules have been introduced into IPECs to develop tissue and cell-specific transfection systems. Specifically, conjugates of poly-L-lysine with monoclonal antibodies to mouse lung endothelial cells have been used for this purpose (*115*). Complexes of plasmid DNA with these conjugates are able of selective binding with cell monolayers (*58*). Meanwhile, the *in vitro* transfection activity of such IPECs is very low, apparently due to their low ability for endocytic penetration into cells (*115*). The transfection rate has been found to increase considerably after introduction of cationic liposomes into a system that apparently serve as membrane-disruptive agents. The antibody-containing IPECs have been used for *in vivo* targeted delivery of plasmid DNA into murine lung endothelial cells (*58*). However, the *in vivo* transfection of the lung cells with these complexes has not been observed.

7. CONCLUSION

More than 25 years have passed since the first studies of nucleic acid IPECs with linear polycations were initiated. Already those early investigations considered the cooperativity of interchain ionic bonds, the ability of IPECs to undergo reactions of interpolyelectrolyte exchange, and the disproportionation phenomenon (*73, 79, 80*). These works anticipated the appearance of a fascinating area of macromolecular chemistry that studies IPECs formed by synthetic linear polyions (*33–36*). For the two decades, complexes of polynucleotides with polycations have been the subject of biophysical studies which mainly dealt with structural phenomena (*76–81, 116*) and developed independently of macromolecular research of synthetic IPECs. Only recently, due to the rapid progress of works on polycation-mediated gene delivery, the scope of polymer chemists has begun to shift from synthetic polyions to polynucleotide complexes, and

dynamic properties of these complexes have been analyzed (*82, 87, 88*). One may expect that the studies of polynucleotide IPECs may generate new ideas for the research of IPECs. In contrast to linear polyions, polynucleotides are capable of forming highly organized inter- and intramolecular structures. The peculiar features of interactions of such structures with polycations (e.g., reactions of substitution in systems containing linear and circular plasmids, native and denatured DNA, etc.) are of great interest.

As far as the problem of gene targeting is concerned it must be emphasized that IPECs are probably one of the most perspective tools for its solution. Until now, significant efforts have been made aiming at development of DNA carriers on the basis of polycation conjugates with proteins, peptides, and oligosaccharides capable of highly specific interaction with target cell receptors. However, the practical significance of this approach for *in vivo* gene delivery and transfection can be limited by the problem of immunocompatibility which has not been considered yet. It is known that conjugation of natural or synthetic haptene with a linear polycation dramatically enhances the immune response of an organism with respect to that haptene (*117–130*). Therefore, using such conjugates for *in vivo* delivery of polynucleotides causes serious concern about immunological reactions and related side effects. In this respect, we believe that significant efforts must be made in order to develop IPEC-based polynucleotide delivery systems which do not contain biospecific component and are not recognized by the immune system.

LITERATURE CITED

(1) Glover, D. M., Ed. (1985) *DNA Cloning. A Practical Approach,* Vols. I, II, IRL Press, Oxford.

(2) Graham, F., and van der Eb, A. (1973) A new technique for the assay of infectivity of human adenovirus 5 DNA. *Virology. 52,* 456–462.

(3) Chen, C., and Okayama, H. (1987) High-efficiency transformation of mammalian cells by plasmid DNA. *Mol. Cell. Biol. 7,* 2745–2752.

(4) Sompayrac, L., and Danna, K. (1981) Efficient infection of monkey cells with DNA of Simian virus 40 *Proc. Natl. Acad. Sci. U.S.A. 12,* 7575–7584.

(5) Aubin, R. J., Weinfield, M., and Paterson, M. C. (1988) Factors influencing efficiency and reproducibility of polybrene-assisted gene transfer. *Somatic Cell Mol. Genet. 14,* 155–167.

(6) Helgen, J. C., and Fallon, A. M. (1990) Polybrene-mediated transfection of cultured lepidopteran cells: induction of a Drosofila heat shock promoter. *In Vitro Cell. Dev. Biol. 26,* 731–736.

(7) Neumann, E., Schaefer-Ridder, M., Wang, Y., and Hofschneider, P. H. (1982) Gene transfer into mouse myeloma cells by electroporation in high electric fields. *EMBO J. 1,* 841–845.

(8) Potter, H., Weir, L., and Leder, P. (1984) Enhancer-dependent expression of human immunoglobulin genes introduced into mouse pre-B lymphocytes by electroporation. *Proc. Natl. Acad. Sci. U.S.A. 81,* 7161–7165.

(9) Capecchi, M. R. (1980) High efficiency transformation by direct microinjection of DNA into cultured mammalian cells. *Cell 22,* 479–486.

(10) Wolf, J. A., Malone, R. W., Williams, P., Chong, W., Ascadi, G., Jani, A., and Felgner, P. L. (1990) Direct gene transfer into mouse muscle *in vivo. Science 247,* 1465–1468.

(11) Gitman, A. G., Graessmann, A., and Loyter, A. (1985) Targeting of loaded Sendai virus envelopes by covalently attached insulin molecules to virus receptor-depleted cells: fusion-mediated microinjection of ricin A and simian virus 40 DNA. *Proc. Natl. Acad. Sci. U.S.A. 82,* 7309–7313.

(12) Gilboa, E., Eglitis, M. A., Kantoff, P. W., and French Anderson, W. (1986) Transfer and expression of cloned genes using retroviral vectors. *Biotechniques 4,* 504–512.

(13) Rosenfeld, M. A., Siegfried, W., Yoshimura, K., Yoneyama, K., Fukayama, M., Stier, L. E., Paakko, P. K., Gilardi, P., Stratford-Perricaudet, L. D., Perricaudet, M., Jallat, S., Pavirani, A., Lecocq, J. P., and Crystal, R. G. (1991) Adenovirus-mediated transfer of a recombinant alpha 1-antitrypsin gene to the lung epithelium *in vivo. Science 252,* 431−434.

(14) Fraley, R., Straubinger, R. M., Rule, G., Springer, E. L., and Papahadjopoulos, D. (1981) Liposome-mediated delivery of deoxyribonucleic acid to cells: Enhanced efficiency of delivery related to lipid composition and incubation conditions. *Biochemistry 20,* 6978−6987.

(15) Wang, C. Y., and Huang, L. (1987) Plasmid DNA adsorbed to pH-sensitive liposomes efficiently transforms the target cells. *Biochem. Biophys. Res. Commun. 147,* 980−985.

(16) Felgner, P. L. (1990) Particulate systems and polymers for in vitro and in vivo delivery of polynucleotides. *Adv. Drug Deliv. Rev. 5,* 163−187.

(17) Wang, C. Y., and Huang, L. (1989) pH-sensitive immunoliposomes mediate target-cell-specific delivery and controlled expression of a foreign gene in mouse. *Biochemistry 28,* 9508−9514.

(18) Felgner, P. L., Gadek, T. R., Holm, M., Roman, R., Chan, H. W., Wenz, M., Northrop, J. P., Ringold, G. M., and Danielson, M. (1987) Lipofection: A highly efficient, lipid-mediated DNA-transfection procedure. *Proc. Natl. Acad. Sci. U.S.A. 84,* 7314−7417.

(19) Pinnaduwage, P., Schmitt, L., and Huang, L. (1989) Use of a quaternary ammonium detergent in liposome mediated DNA transfection of mouse L-cells. *Biochim. Biophys. Acta 985,* 33−37.

(20) Farhood, H., Bottega, R., Epand, R. M., and Huang, L. (1992) Effect of cationic cholesterol derivatives on gene transfer and protein kinase C activity. *Biochim. Biophys. Acta 1111,* 239−246.

(21) Legendre, J.-Y., and Szoka, Jr., F. C. (1993) Cyclic amphipatic peptide-DNA complexes mediate high-efficiency transfection of adherent mammalian cells. *Proc. Natl. Acad. Sci. U.S.A.*

(22) Legendre, J.-Y., and Szoka, Jr., F. C. (1992) Delivery of plasmid DNA into mammalian cell lines using pH-sensitive liposomes: comparison with cationic liposomes. *Pharm. Res. 9,* 1235−1242.

(23) Malone, R. W., Felgner, P. L., and Verma, I. M. (1989) Cationic liposome-mediated RNA transfection. *Proc. Natl. Acad. Sci. U.S.A. 86,* 6077−6081.

(24) ProFection Mammalian Transfection Systems. Technical Manual (1990) pp 2−9, Promega, Madison.

(25) Temin, H. M. (1990) Safety considerations in somatic gene therapy of human disease with retrovirus vectors. *Hum. Gene Ther. 1,* 111−123.

(26) Felgner, J. H., Kumar, R., Sridhar, C. N., Wheeler, C. J., Tsai, Y. J., Border, R., Ramsey, P., Martin, M., and Felgner, P. L. (1994) Enhanced gene delivery and mechanism studies with a novel series of cationic lipid formulations. *J. Biol. Chem. 28,* 2550−2561.

(27) Wu, G. Y., and Wu, C. H. (1987) Receptor-mediated *in vitro* gene transformation by a soluble DNA carrier system. *J. Biol. Chem. 262,* 4429−4432.

(28) Kabanov, A. V., Kiselev, V. I., Chikindas, M. L., Astafieva, I. V., Glukhov, A. I., Gordeev, S. A., Izumrudov, V. A., Zezin, A. B., Levashov, A. V., Severin, E. S., and Kabanov, V. A. (1989) Increasing of transforming activity of plasmid DNA by incorporating it into interpolyelectrolyte complex with a carbon chain polycation. *Dokl. Acad. Nauk SSSR* (in Russian) *306,* 226−229 (English edition: 133−136).

(29) Behr, J.-P., Demeneix, B., Loeffler, J.-P., and Perez-Mutcel, J. (1989) Efficient gene transfer into mammalian primary endocrine cells with lipopolyamine-coated DNA. *Proc. Natl. Acad. Sci. U.S.A. 86,* 6982−6986.

(30) Kabanov, A. V., Astafieva, I. V., Chikindas, M. L., Rosenblat, G. F., Kiselev, V. I., Severin, E. S. and Kabanov, V. A. (1991) DNA interpolyelectrolyte complexes as a tool for efficient cell transformation. *Biopolymers 31,* 1437−1443.

(31) Zhou, X., Klibanov, A. L., and Huang, L. (1991) Lipophilic polylysines mediate efficient DNA transfection in mammalian cells. *Biochim. Biophys. Acta 1065,* 8−14.

(32) Kabanov, A. V., Astafieva, I. V., Maksimova, I. V., Lukanidin, E. M., Georgiev, G. P., and Kabanov, V. A. (1993) Efficient transformation of mammalian cells using DNA interpolyelectrolyte complexes with carbon chain polycations. *Bioconjugate Chem. 4,* 448−454.

(33) Kabanov, V. A. (1973) The cooperative interaction of complementary synthetic macromolecules in solutions. *Pure Appl. Chem., Macromol. Chem. 8,* 121−145.

(34) Kabanov, V. A., and Zezin, A. B. (1982) Water-soluble nonstoichiometric polyelectrolyte complexes: a new class of synthetic polyelectrolytes. In *Soviet Sci. Rev. B. Chem. Rev.* (M. E. Volpin, Ed.) *4,* 207−282.

(35) Tsuchida, E., and Abe, K. (1982) Interactions between macromolecules in solution and intermacromolecular complexes. *Adv. Polym. Sci. 45,* 1−119.

(36) Kabanov, V. A., and Zezin, A. B. (1984) A new class of complex water-soluble polyelectrolytes. *Macromol. Chem., Suppl. 6,* 259−276.

(37) Wu, G. Y., and Wu, C. H. (1988) Evidence for targeted gene delivery to Hep G2 hepatoma cells *in vitro. Biochemistry 27,* 887−892.

(38) Wagner, E., Zenke, M., Cotten, M., Beug, H., and Birnstiel, M. L. (1990) Transferrin-polycation conjugates as carriers for DNA uptake into cells. *Proc. Natl. Acad. Sci. U.S.A. 87,* 3410−3414.

(39) Zenke, M., Steinlein, P., Wagner, E., Cotten, M., and Beug, H. (1990) Receptor-mediated endocytosis of transferrin-polycation conjugates: an efficient way to introduce DNA into hematopoetic cells. *Proc. Natl. Acad. Sci. U.S.A. 87,* 3655−3659.

(40) Cotten, M., Lungle-Rouault, Kirlappos, H., Wagner, E., Mechtler, K., Zenke, M., Beug, H., and Birnstiel, M. L. (1990) Transferrin-polycation-mediated introduction of DNA into human leukemic cells: stimulation by agents that affect the survival of transfected DNA or modulate transferrin receptor levels. *Proc. Natl. Acad. Sci. U.S.A. 87,* 4033−4037.

(41) Huckett, B., Ariatti, M., and Hawtrey, A. O. (1990) Evidence for targeted gene transfer by receptor-mediated endocytosis: Stable expression following insulin-directed entry of neo into HepG2 cells. *Biochem. Pharmacol. 40,* 253−263.

(42) Rozenkrants, A. A., Yachmenev, S. V., and Sobolev, A. S. (1990) The use of artificial structures for selective transfer of genetic material into human cells via receptor-mediated endocytosis. *Dokl. Acad. Nauk SSSR* (in Russian) *312,* 493−494.

(43) Wagner, E., Cotten, M., Foisner, R., and Birnsteil, M. L. (1991) Transferrin−polycation−DNA complexes: The effect of polycations on the structure of the complex and DNA delivery to cells. *Proc. Natl. Acad. Sci. U.S.A. 88,* 4255−4259.

(44) Curriel, D. T., Agarwal, S., Wagner, E., and Cotten M. (1991) Adenovirus enhancement of transferrin-polylysine-mediated gene delivery. *Proc. Natl. Acad. Sci. U.S.A. 88,* 8850−8854.

(45) Wagner, E., Cotten, M., Mechtler, M., Kirlappos, H., and Birnsteil, M. L. (1991) DNA-binding transferrin conjugates as functional gene-delivery agents: Synthesis by linkage of polylysine or ethidium homodimer to the transferrin carbohydrate moiety. *Bioconjugate Chem. 2,* 226−231.

(46) Rozenkrantz A. A., Yachmenev, S. V., Jans, D. A., Serebryakova, N. V., Murav'iev, V. I., Peters, R., and Sobolev, A. S. (1992) Receptor-mediated endocytosis and nuclear transport of a transfecting DNA construct. *Exp. Cell Res. 199,* 323−329.

(47) Curriel, D. T., Agarwal, S., Rommer, M. U., Wagner, E., Cotten, M., Birnsteil, M. L., and Boucher, R. (1992) Gene transfer to respiratory epithelial cells via the receptor-mediated endocytosis pathway. *Am. J. Respir. Cell Mol. Biol. 6,* 247−252.

(48) Plank C., Zatloukal K., Cotten, M., Mechtler, K., and Wagner, E. (1992) Gene transfer into hepatocytes using asialoglycoprotein receptor mediated endocytosis of DNA complexed with an artificial tetra-antennary galactose ligand. *Bioconjugate Chem. 3,* 533−539.

(49) Curriel, D. T., Wagner, E., Cotten, M., Birnstiel, M. L., Agarwal, S., Li, C. M., Loechel, S., and Hu, P. C. (1992) High-

efficiency gene transfer mediated by adenovirus coupled to DNA–polylysine complexes. *Hum. Gene. Ther. 3,* 147–154.

(50) Cotten, M., Wagner, E., Zatloukal, K., Phillips, S., Curriel, D. T., and Birnstiel, M. L. (1992) High efficiency receptor-mediated delivery of small and large (48Kb) gene constructs using the endosome disruption activity of defective or chemically-inactivated adenovirus particles. *Proc. Natl. Acad. Sci. U.S.A. 89,* 6094–6098.

(51) Wagner, E., Zatloukal, K., Cotten, M., Kirlappos, H., Mechtler, K., Curriel, D. T., and Birnstiel, M. (1992) Coupling of adenovirus to transferrin-polylysine/DNA complexes greatly enhances receptor-mediated gene delivery and expression of transfected genes. *Proc. Natl. Acad. Sci. U.S.A. 89,* 6099–6103.

(52) Wagner, E., Plank, C., Zatloukal, K., Cotten, M., and Birnstiel, M. (1992) Influenza virus hemagglutinin HA-2 N-terminal fusogenic peptides augment gene transfer by transferrin-polylysine-DNA complexes: Toward a synthetic virus-like gene transfer vehicle. *Proc. Natl. Acad. Sci. U.S.A. 89,* 7934–7938.

(53) Wu, G. Y., and Wu, C. H. (1988) Receptor-mediated gene delivery and expression *in vivo. J. Biol. Chem. 263,* 14621–14624.

(54) Wu, G. Y. Wilson, J. M., and Wu, C. H. (1989) Targeting genes: delivery and persistent expression of a foreign gene driven by mammalian regulatory elements *in vivo. J. Biol. Chem. 264,* 16985–16987.

(55) Wu, G. Y., and Wu, C. H. (1991) Delivery systems for gene therapy. *Biotherapy 3,* 87–95.

(56) Wu, G. Y., Wilson, J. M., Shalaby, F., Grossmann, M., Shafritz, D. A., and Wu, C. H. (1991) Receptor-mediated gene delivery *in vivo.* Partial correction of genetic analbuminemia in nagase rats. *J. Biol. Chem. 266,* 14338–14342.

(57) Wilson, J. M., Grossman, M., Wu, C. H., Roy Chowdhury, N., and Roy Chowdhury, J. (1992) Hepatocyte directed gene transfer *in vivo* leads to transient improvement of hypercholesterolemia in low density lipoprotein receptor-deficient rabbits. *J. Biol. Chem. 267,* 963–967.

(58) Trubetskoy, V. S., Torchilin, V. P., Kennel, S. J., and Huang, L. (1992) Use of N-terminal modified poly(L-lysine)-antibody conjugate as a carrier for targeted gene delivery in mouse lung endothelian cells. *Bioconjugate Chem. 3,* 323–327.

(59) Citro, G., Perrotti, D., Cucco, C., D'Agnano, I., Sacchi, A., Zupi, G., and Calabretta, B. (1992) Inhibition of leukemia cell proliferation by receptor-mediated uptake of c-myb antisense oligodeoxynucleotides. *Proc. Natl. Acad. Sci. U.S.A. 89,* 7031–7035.

(60) Bunnel, B. A., Askari, F. K., and Wilson J. M. (1992) Targeted delivery of antisense oligonucleotides by molecular conjugates. *Somat. Cell. Mol. Genet. 18,* 559–569.

(61) Kabanov, A. V., Batrakova, E. V., Melik-Nubarov, N. S., Fedoseev, N. A., Dorodnich, T. Yu., Alakhov, V. Yu., Chekhonin, V. P., Nazarova, I. R., and Kabanov, V. A. (1992) A new class of drug carriers: micelles of poly(oxyethylene)–poly(oxypropylene) block copolymers as microcontainers for drug targeting from blood in brain. *J. Contr. Release 22,* 141–158.

(62) Kabanov, A. V., Alakhov, V. Yu., and Chekhonin, V. P. (1992) Enhancement of macromolecule penetration into cells and nontraditional drug delivery systems. In *Sov. Sci. Rev. D. Physicochem. Biol.* (V. P. Skulachev Ed.) Vol. 11, Part 2, pp 1–77, Harwood Academic Publishers, Glasgow.

(63) Kabanov, A. V., and Alakhov, V. Yu. (1994) New approaches to targeting of bioactive compounds. *J. Contr. Release 28,* 15–35.

(64) McLachlin, J. R., Cornetta, K., Eglitis, M. A., and Anderson, W. F. (1990) Retroviral-mediated gene transfer. *Progr. Nucl. Acids. Res. Mol. Biol. 38,* 91–135.

(65) Karlsson, S. (1991) Treatment of genetic defects in hematopoetic cell function by gene transfer. *Blood 78,* 2481–2492.

(66) Einerhand M. P., and Valerio, D. (1992) Gene transfer into hematopoetic stem cells: prospects for human gene therapy. *Curr. Top. Microbiol. Immunol. 177,* 217–235.

(67) Makdisi, W. J., Wu, C. H., and Wu, G. Y. (1992) Methods for gene transfer into hepatocytes: progress toward gene therapy. *Prog. Liver. Dis. 10,* 1–24.

(68) Litzinger, D. C., and Huang, L. (1992) Phosphatidylethanolamine liposomes: drug delivery, gene transfer and immunodiagnostic applications. *Biochim. Biophys. Acta 1113,* 201–227.

(69) Morsy, M. A., Mitani, K., Clemens, P., and Caskey, C. T. (1993) Progress toward human gene therapy. *JAMA 270,* 2338–2345.

(70) Dorudi, S., Northover, J. M., and Vile, R. G. (1993) Gene transfer therapy in cancer. *British J. Surg.* 80, 566–572.

(71) Walsh, C. E., Liu, J. M., Miller, J. L., Nienhuis, A. W. and Samulski, R. J. (1993) Gene therapy for human hemoglobinopathies. *Proc. Soc. Exp. Biol. Med. 204,* 289–300.

(72) Haensler, J., and Szoka, Jr., F. C. (1993) Synthesis and characterization of a trigalactosylated bisacridine compound to target DNA to hepatocytes. *Bioconjugate Chem. 4,* 85–93.

(73) Miller, I. R., and Bach, D. (1968) Interaction of DNA with heavy metal ions and polybases: cooperative phenomena. *Biopolymers 6,* 169–179.

(74) Kabanov, V. A., Kabanov, A. V., and Astafieva, I. V. (1991) Complexes of DNA with synthetic polycations for cell transformation. *Polym. Prep. 32,* 592–593.

(75) Behr, J.-P. (1986) DNA strongly binds to micelles and vesicles containing lipopolyamines or liopointercalants. *Tetrahedron Lett. 27,* 5861–5864.

(76) Zama, M., and Ichimura, S. (1971) Difference between polylysine and polyarginine in changing DNA structure upon complex formation. *Biochim. Biophys. Res. Commun. 44,* 936–942.

(77) Zama, M. (1974) Structure and circular dichroism of DNA-polylysine-polyarginine complex. *Biochim. Biophys. Acta 366,* 124–134.

(78) Shapiro, J. T., Leng, M., and Felsenfeld, G. (1969) Deoxyribonucleic acid–polylysine–complexes. Structure and nucleotide specificity. *Biochemistry 7,* 3219–3132.

(79) Sklyadneva, V. B., Shie, M., and Tikhonenko, T. I. (1979) Alteration of the DNA secondary structure in the DNA-polylysine complex evidenced by sodium bisulfite modification. *FEBS Lett. 107,* 129–133.

(80) Inoue, S., and Fuke, M. (1970) An electron microscope study of deoxyribonucleoprotamines. *Biochim. Biophys. Acta 204,* 296–303.

(81) Minagawa, K., Matsuzawa, Y., Yoshikawa, K., Matsumoto, M., and Doi, M. (1991) Direct observation of the biphasic conformational change of DNA induced by cationic polymers. *FEBS Lett. 295,* 69–67.

(82) Sukhishvili, S. A., Obolskii, O. L., Astafieva, I. V., Kabanov, A. V., and Yaroslavov, A. A. (1993) DNA-containing interpolyelectrolyte complexes: interaction with liposomes. *Vysokomol. Soed.* (in Russian), *35,* 1895–1899 (English edition *Polymer Science, Ser. A 35,* 1602–1606).

(83) Izumrudov, V. A., Zezin, A. B., and Kabanov, V. A. (1991) The equilibrium of interpolyelectrolyte reactions and the phenomenon of molecular recognition in the solutions of interpolyelectrolyte complexes. *Uspekhi Khimii* (in Russian) *60,* 1510–1595.

(84) Kabanov, V. A. (1992) Template polymerization. In *Polymerization in organized media* (Paleos, C. M., Ed.) pp 369–454, Gordon and Breach Science Publishers, Philadelphia.

(85) Bakeev, K. N., Izumrudov, V. A., Kuchanov, S. I., Zezin, A. B., and Kabanov, V. A. (1992) Kinetics and mechanism of interpolyelectrolyte exchange and addition reactions. *Macromolecules 25,* 4249–4254.

(86) Izumrudov, V. A., Bronich, T. K., Saburova, O. S., Zezin, A. B., and Kabanov, V. A. (1988) The influence of chain length of a competitive polyanion and nature of monovalent counterions on the direction of the substitution reaction of polyelectrolyte complexes. *Macromol. Chem., Rapid Commun. 9,* 7–12.

(87) Kabanov, V. A., Giryakova, S. I., Kargov, S. I., Zezin, A. B., and Izumrudov, V. A. (1993) Effect of low molecular salts on the competitive binding of polyions of DNA and polymethacrylate-anions with poly-N-ethyl-4-vinylpyridinium in aqueous solutions. *Dokl. Akad. Nauk 329,* 66–70.

(88) Kabanov, V. A., Giryakova, S. I., Kargov, S. I., Zezin, A. B., and Izumrudov, V. A. (1993) Possibility of determining effect of polyion polymerization degree on the direction of competitive reaction in the solutions of nonstoichiometric interpolyelectrolyte complexes and DNA. *Dokl. Akad. Nauk 332*, 722–726.

(89) Grinus, L. P. (1986) *Transport of Macromolecules in Bacteria,* Nauka Publishers, Moscow.

(90) Prozorov, A. A. (1980) *Genetic Transformation and Transfection,* Nauka Publishers, Moscow.

(91) Behr, J.-P. (1993) Synthetic gene-transfer vectors. *Acc. Chem. Res. 26*, 274–278.

(92) Barthel, F., Remy, J.-S., Loeffler, J.-P., and Behr, J.-P. (1993) Gene-transfer optimization with lipospermine-coated DNA. *DNA Cell Biol. 12*, 553–580.

(93) Staedel, C., Remy, J.-S., Hua, Z., Broker, T. R., Chow, L. T., and Behr, J.-P. (1994) High-efficiency transfection of primary human keratinocytes with positively charged lipopolyamine:DNA complexes. *J. Invest. Dermatol. 102*, 768–772.

(94) Mayhew, E., Harlos, J. P., and Juliano R. L. (1973) The effect of polycations on cell membrane stability and transport processes. *J. Membrane Biol. 14*, 213–228.

(95) Morgan, D. M., Larvin, V. L., and Pearson, J. D. (1989) Biochemical characterization of polycation-induced cytotoxicity to human vascular endothelian cells. *J. Cell Sci. 94*, 553–559.

(96) Petrukhina, O. O., Ivanov, N. N., Feldstein, M. H., Vasilev, A. E., Plate, N. A., and Torchilin, V. P. (1986) The regulation of liposome permeability by polyelectrolyte. *J. Contr. Release 3*, 137–141.

(97) Walter, A., Steer, C. J., and Blumental, R. (1986) Polylysine induces pH-dependent fusion of acidic phospholipid vesicles: a model for polycation-induced fusion. *Biochim. Biophys. Acta 861*, 319–330.

(98) Ohki, S., and Duax, J. (1986) Effect of cations and polyamines on the aggregation and fusion of phosphatidylserine membranes. *Biochim. Biophys. Acta 861*, 177–186.

(99) Schroeder, U. K. O., and Tirrel, D. A. (1989) Structural reorganization of phosphatidylcholine vesicle membranes by poly(2-ethylacrylic acid). Influence of the molecular weight of the polymer. *Macromolecules 22*, 765–769.

(100) Takahashi, H., Matuoka, S., Kato, S., Okhi, K., and Hatta, I. (1991) Electrostatic interaction of poly(L-lysine) with dipalmitoylphosphatidic acid studied by X-ray difraction. *Biochim. Biophys. Acta 1069*, 229–234.

(101) Brashford, C. L., Alder, G. M., Menestrina, G., Miklem, K. L., Murphu, J. J., and Pasternak, C. A. (1986) Membrane damage by hemolytic viruses, toxins complement and other cytotoxic agents. *J. Biol. Chem. 261*, 9300–9308.

(102) Shen, W. G., and Ryser, H. J.-P. (1978) Conjugation of poly-L-lysine to albumin and horseradish peroxidase: A novel method for enhancing the cellular uptake of the protein. *Proc. Natl. Acad. Sci. U.S.A. 75*, 1872–1876.

(103) Ryser, H. J.-P., and Shen, W. C. (1978) Conjugation of methotrexate to poly(L-lysine) increases drug transport and overcome drug resistance in cultured cells. *Proc. Natl. Acad. Sci. U.S.A. 75*, 3867–3870.

(104) Ryser, H. J.-P., and Shen, W. C. (1986) Drug-poly(lysine) conjugates: their potential for chemiotherapy and for the study of endocytosis. In *Targeting of drugs and synthetic systems* (G. Gregoriadis, J. Senior, and G. Poste, Eds.) pp 103–121, Plenum Press, New York.

(105) Leonetti, J.-P., Degals, S., and Lebleu, B. (1990) Biological activity of oligonucleotide-poly(L-lysine) conjugates: mechanism of cell uptake. *Bioconjugate chem. 1*, 149–153.

(106) Steinman, R. M., Mollman, I. S., Muller, W. A., and Cohn, Z. A. (1983) Endocytosis and recycling of plasma membrane. *J. Cell. Biol. 96*, 1–27.

(107) Taxman, D. J., Lee, E. S., and Wojchowski, D. M. (1993) Receptor-targeted transfection using stable maleimido-transferrin/thio-poly-L-lysine conjugates. *Anal. Biochem. 213*, 97–103.

(108) Wall, D. A., Wilson, G., and Hubbard, A. L. (1980) The galactose-specific recognition system of mammalian liver: the route of ligand internalization in rat hepatocytes. *Cell 21*, 79–83.

(109) Chang, T.-M., and Kullberg, D. W. (1982) Studies of the mechanism of cell intoxication by diphteria toxin fragment A-asialoorosocomucoid hybrid toxins. Evidence for utilization of an alternative receptor-mediated transport pathway. *J. Biol. Chem. 257*, 12563–12572.

(110) Simpson, I. A., and Cushman S. W. (1986) Hormonal regulation of mammalian glucose transport. *Ann. Rev. Biochem. 55*, 1059–1089.

(111) Podlecki, D. A., Smith, R. M., Kao, M., Tsai, P., Huecksteadt, T., Brandenburg, D., Lasher, R. S., Jarett, L., and Olefsky, J. M. (1987) Nuclear translocation of the insulin receptor. A possible mediator of insulin's long term effects. *J. Biol. Chem. 262*, 3362–3368.

(112) Smith, R. M., and Jarett, L. (1988) Receptor-mediated endocytosis and intracellular processing of insulin: ultrastructural and biochemical evidence for cell-specific heterogeneity and distinction from nonhormonal ligands. *Lab. Invest. 58*, 613–629.

(113) Dautry-Varsat, A. (1986) Receptor-mediated endocytosis: the intracellular journey of transferrin and its receptor. *Biochimie 68*, 375–381.

(114) Woods J., Doriaux, M., and Farguhar, M. G. (1986) Transferrin receptors recycle to cis and middle as well as trans Golgi cisternae in Ig-secreting myeloma cells. *J. Cell. Biol. 103*, 277–286.

(115) Trubetskoy V. S., Torchilin, V. P., Kennel, S., and Huang, L. (1992) Cationic liposomes enhance targeted delivery and expression of exogenous DNA mediated by N-terminal modified poly(L-lysine)-antibody conjugate in mouse lung endothelian cells. *Biochim. Biophys. Acta 1131*, 311–313.

(116) Genderen, M. H. P., Hilbers, M. P., Koole, L. H., and Buck, H. M. (1990) Peptide-induced parallel DNA duplexes for oligopyrimidines. Stereospecificity in complexation for oligo-(L-lysine) and oligo(L-ornithine). *Biochemistry 29*, 7838–7845.

(117) Petrov, R. V., Gvozdetsky, A. N., Gorokhov, A. A., Evdakov, V. P., Kabanov, V. A., and Kabanova, E. A. (1974) Study of mechanisms of heparin and poly-4-vinylpyridine effect on immunogensis. *Jurn. Microbiol. Epidemiol. Immunol.* (in Russian) *11*, 37–40.

(118) Evdakov, V. P., Kabanov, V. A., Kojinova, E. V., Petrov, R. V., Savinova, I. V., Fedoseeva, N. A., Khaitov, R. M., and Khaustova, L. I. (1975) Effect of synthetic polyampholytes on iteraction of T and B lympholytes. *Dokl. Akad. Nauk SSSR* (in Russian) *224*, 464–467.

(119) Ivanov, A. A., Gvozdetsky, A. N., and Kabanov, V. A. (1976) Effect of poly-4-vinylpyridine, 4-vinylpyridinium-N-oxide and their copolymers on hemolytic activity of complement. *Dokl. Akad. Nauk SSSR* (in Russian) *229*, 1496–1499.

(120) Batirbekov, A. A., Evdakov, V. P., Kabanov, V. A., Kojinova, E. V., Petrov, R. V., Savinova, I. V., Fedoseeva, N. A., Khaitov, R. M., and Khaustova, L. I. (1976) Study of mechanisms of influence of synthetic polyelectrolytes and polyampholytes on the immune response. *Cytologia* (in Russian) *18*, 1259–1263

(121) Kabanov, V. A., Mustafaev, M. I., Norimov, A. Sh., Petrov, R. V., and Khaitov, R. M. (1978) Immunogenicity of the complex of bovine serum albumin with polycation containing hydrophobic side groups. *Dokl. Akad. Nauk SSSR* (in Russian) *243*, 1330–1333.

(122) Kabanov, V. A., Mustafaev, M. I., Goncharo, V. B., Petrov, R. V., Khaitov, R. M. and Norimov, A. Sh. (1980) Correlation of immunostimulating properties in the series of polymer-analogues of poly-4-vinylpyridine and immunogenicity of their mixtures with bovine serum albumin with complexation in these systems. *Dokl. Akad. Nauk SSSR* (in Russian) *250*, 1504–1507.

(123) Petrov, R. V., Kabanov, V. A., Khaitov, R. M., Mustafaev, M. I., Norimov, A. Sh. and Filatova, E. D. (1981) Modulation of immune response by an antigen bound to non-natural polyelectrolytes. *Jurn. Mikrobiol. Epidemiol. i Immunol.* (in Russian) No. 2, 57–64.

(124) Vinogradov, I. V., Kabanov, V. A., Mustafaev, M. I., Norimov, A. Sh., Petrov, R. V., and Khaitov, R. M. (1982) Complexes of proteins with non-natural polycations as thymus-independent antigens. *Dokl. Akad. Nauk SSSR* (in Russian) *263*, 228–230.

(125) Petrov, R. V, Kabanov, V. A., Khaitov, R. M, Norimov, A. Sh., Vinogradov, I. V., and Mustafaev, M. I. (1982) Complexes of proteins with carbochain linear polyampholytes as artificial antigens with decreased immunogenicity. *Immunologia* (in Russian) No. 6, 52–54.

(126) Abramenko, T. V., Vinogradov, I. V., Mustafaev, M. I., Kabanov, V. A., Khaitov, R. M., Petrov, R. V., and Filatova, E. D. (1983) Immunogenicity of the conjugate of bovin serum albumin with polyacrylic acid. *Jurn. Mikrobiol. Epidemiol. i Immunol.* (in Russian) No. 11, 86–89.

(127) Kabanov, V. A., Petrov, R. V., and Khaitov, R. M. (1984) Artificial antigens and vaccines based on non-natural polyelectrolytes. In *Sov. Sci. Rev. D. Physicochem. Biol.* (V. P. Skulachev Ed.) Vol. 5, pp 277–322, Harwood Academic Publishers, Glasgow.

(128) Kabanov, V. A., Kokorina, L. G., Suslova, T. B., Gulyaeva, J. G., Zezin, A. B., and Velichkovsky, B. T. (1985) Chemiluminiscence of peritonial macrophages activated by the nonnatural polyelectrolytes. *Dokl. Akad. Nauk SSSR* (in Russian) *282*, 206–209.

(129) Kabanov, V. A. (1986) Synthetic membrane active polyelectrolytes in design of artificial immunogens and vaccines. *Macromol. Chem. Macromol. Symp. 1*, 101–124.

(130) Kabanov, V. A., Yaroslavov, A. A., Polinsky, A. A., and Sukhishvili, S. A. (1989) The interaction between artificial antigens based on synthetic polyelectrolytes with immune system cell: physico-chemical aspects. *Makromol. Chem., Makromol. Symp. 26*, 265–280.

ARTICLES

Design, Synthesis, and Sequence Selective DNA Cleavage of Functional Models of Bleomycin. 1. Hybrids Incorporating a Simple Metal-Complexing Moiety of Bleomycin and Lexitropsin Carriers

Liren Huang, James C. Quada, Jr., and J. William Lown*

Department of Chemistry, University of Alberta, Edmonton, Alberta T6G 2G2, Canada. Received June 1, 1994[⊗]

The syntheses of functional models for bleomycin, which are composed of a simple analog of the metal-complexing moiety of bleomycin and oligo-N-methylpyrrole peptide DNA-binding moieties, are described. The extent and the relative rate of their cleavage of DNA in the presence of reductants were determined independently by an ethidium binding assay and by agarose gel electrophoresis experiments. The rate of DNA cleavage increases with the number of N-methylpyrrole units in the carrier moiety. The sequence selectivity of DNA cleavage was demonstrated by polyacrylamide sequencing gel electrophoresis of cleavage reactions on two 5'-^{32}P labeled restriction fragments: a 158 bp GC-rich fragment from pBR322 and a 241 bp AT-rich fragment fragment from SV40. Comparison of the sequence selectivity with that of bleomycin A$_2$ indicates that the poly-N-methylpyrrole moiety directs the hybrid compounds to AT-rich sequences of DNA. High-resolution denaturing gel electrophoresis of DNA cleaved by the model compounds reveals that 3' phosphate is produced exclusively, indicating that the chemistry of DNA cleavage differs from that of bleomycin.

INTRODUCTION

The bleomycins (BLM) are a family of glycopeptide antitumor antibiotics isolated from the cultures of *Streptomyces verticillus* by Umezawa and co-workers in 1966 and are clinically used in combination chemotherapy against several types of cancer (*1, 2*). Therefore, they, especially bleomycin A$_2$, which is the main constituent of the clinically used mixture of BLM, have attracted considerable interest both synthetically and biologically (Figure 1) (*3–6*). The therapeutic effect of BLM is believed to arise from its ability to cause DNA degradation (*7–14*). The process involves a redox-active metal ion such as Fe(II) and a source of oxygen and causes predominantly the cleavage of double-stranded DNA at 5'-GT-3' and 5'-GC-3' sites by abstraction of the C-4' hydrogen of the deoxyribose moiety in pyrimidine residues. Extensive investigation has shown that BLM can be structurally divided into four parts according to their functional roles. The amine–pyrimidine–imidazole metal-complexing domain coordinates with metal ions such as Fe(II) to form metallobleomycin, the combination of which with molecular oxygen can form activated bleomycin which cleaves DNA strands. Bithiazole and the C-terminal cation make up the domain responsible for DNA binding affinity and sequence selectivity *via* DNA intercalation and/or minor groove binding. Part 3 is a threonine–aminovalerate dipeptide which acts as a linker to combine each part of BLM at an appropriate distance and in a favorable organization for DNA binding. The disaccharide moiety facilitates metal–oxygen complex formation and passage across cell membranes.
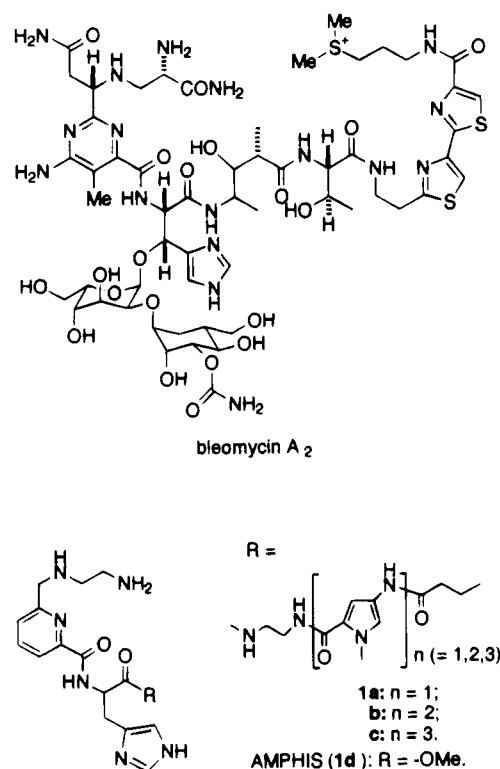
bleomycin A$_2$

Figure 1. Structures of bleomycin A$_2$ and AMPHIS derivatives.

Many studies have been performed on the synthesis of simplified analogs of bleomycin in the last decade (*15–21*). Most of them focused on modification of the DNA cleaving moiety, i.e., the metal-complexing subunit (*22–33*). However, little work has been reported on the linker–DNA binding subunit (*34–37*). Ohno et al.

reported a series of synthetic hybrids containing simplified analogs of the bleomycin metal binding moiety conjugated to distamycin (*28, 35*). Hénichart reported the synthesis of a simple subunit, methyl 2-[[2-amino-ethyl)amino]methyl]-6-carboxylpyridinehistidinate (AMPHIS, **1d**) in which only the amino groups essential to coordinate metal ion remain and its BLM analog which retains the major characteristics of the natural products (*17, 38, 39*). We report herein the first part of our studies on design, synthesis, and biological evaluation of bleomycin models, i.e., a simplified synthetic functional model of bleomycin.

Unlike other approaches that have been adopted in which attempts were made to build a model by simplifying the natural bleomycin, we have constructed a effective hybrid agent by upgrading the basic structural features of the natural product. We decided to conjugate the model AMPHIS with lexitropsin residues which are recognized as sequence-selective DNA binding moieties (*41–45*), eliminating, at first, the linker and the terminal cationic moiety of bleomycin.

EXPERIMENTAL SECTION

Chemistry. Melting points were determined with an Electrothermal apparatus and are uncorrected. ¹H NMR spectra were recorded at ambient temperature on a Bruker WH-300 spectrometer. High-resolution mass spectra (FABHRMS) were recorded on a modified Kratos MS-50 mass spectrometer using a rotating sample probe and voltage scanning, interfaced to a VG 11/250J data system. Accurate masses were calculated interactively with the data system using reference peaks such as CsI in glycerol. High-resolution EI mass spectra were recorded on a Kratos MS-50 equipped with the MSS Maspec data system. Unit resolution FAB mass spectra were recorded on a modified AEI MS9 instrument, and unit resolution EI mass spectra were recorded on a modified AEI MS12 instrument. FT-IR spectra were recorded on a Perkin-Elmer 1760 spectrophotometer interfaced to a PE 7700 microcomputer. Optical rotations were measured on Perkin-Elmer 241 polarimeter at the sodium D line (589 nm) at ambient temperature. Analytical thin-layer chromatography was performed on silica-coated plastic plates (silica gel 60 F-254, Merck) and visualized under UV light. Preparative separations were performed by flash chromatography on silica gel (Merck, 70–230 or 230–400 mesh). Tetrahydrofuran was dried by distillation from sodium benzophenone ketyl. Anhydrous dimethylformamide was purchased from Aldrich. All other solvents were used as received and were reagent grade where available.

Methyl 6-(Hydroxymethyl)pyridine-2-carboxylate (3). NaBH₄ (12.46 g, 0.328 mol) was added in portions to a stirred solution of methyl pyridine-2,6-dicarboxylate (42.40 g, 0.218 mol) in methanol (2 L) at 0 °C. After being stirred for 1 h at room temperature, the solution was acidified with concentrated hydrochloric acid to pH 3 and evaporated under diminished pressure. The residue was dissolved in water (30 mL), neutralized with saturated aqueous NaHCO₃, and extracted with dichloromethane (150 mL × 3). The organic layer was dried on Na₂SO₄, filtered, and concentrated. The title compound was obtained as a white crystalline solid (28.00 g, 77% yield) which was used in the next step without further purification. mp 84–86 °C; FT-IR (CHCl₃ cast) ν_{max} 3296 (br), 1740 (s), 1592 (m), 1448 (m), 1307 (s), 1228 (m), 1146 (m), 762 (m) cm⁻¹; ¹H-NMR (CDCl₃) δ 7.98 (d, *J* = 8.0 Hz, 1H), 7.82 (t, *J* = 8.0 Hz, 1H), 7.52 (d, *J* = 8.0 Hz, 1H), 4.82 (s, 2H), 3.92 (s, 3H), 3.64 (s, 1H, −OH); MS *m/e* 168 (M⁺ + 1), 109, 35.

Methyl 6-Formylpyridine-2-carboxylate (4). To a cooled (−78 °C) solution of oxalyl chloride (11.37 g, 128 mmol) in dry dichloromethane (230 mL) was added dropwise anhydrous dimethyl sulfoxide (19.00 mL, 268 mmol) in dichloromethane (80 mL) over 20 min. The solution was stirred for 15 min, and **3** (11.2 g, 67.1 mmol) in dichloromethane (100 mL) was added over 20 min. After being stirred at −60 to −45 °C for 2 h, the solution was treated with triethylamine (74 mL) and allowed to warm to room temperature. The mixture was washed with water, and the aqueous phase was extracted with three portions of dichloromethane. The combined organic layer was dried on Na₂SO₄ and then concentrated. The residue was purified by flash chromatography on a silica gel column eluted with 5% MeOH in dichloromethane. Recrystallization (1:1 ethyl acetate:petroleum ether) of the residue afforded the product (7.86 g, 71% yield) as a white crystalline solid: mp 100–101 °C (lit. (*46*) mp 102 °C); FT-IR (CHCl₃ cast) ν_{max} 1724 (s), 1716 (m), 1698 (m), 1360 (w), 1322 (w), 900 (m), 770 (m) cm⁻¹; ¹H-NMR (CDCl₃) δ 10.18 (s, 1H), 8.35 (dd, *J* = 8.0, 1.5 Hz, 1H), 8.15 (dd, *J* = 8.0, 1.0 Hz, 1H), 8.05 (td, *J* = 8.0, 1.0 Hz, 1H), 4.06 (s, 3H); MS *m/e* 166 (M⁺ + 1), 124, 35. Anal. Calcd for C₈H₇O₃N: C, 58.18; H, 4.27; N, 8.48. Found: C, 57.45; H, 4.16; N, 8.39.

[2-[N-(*tert*-Butoxycarbonyl)amino]ethyl]amine (5) and [2-[N-(Benzyloxycarbonyl)amino]ethyl]amine (6). To an ice-cooled solution of 1,2-diaminoethane (25.1 mL, 0.375 mol) in dichloromethane (200 mL) was added di-*tert*-butyl dicarbonate (27.27 g, 0.125 mol) in dichloromethane (50 mL) over 20 min. After being stirred at ambient temperature overnight, the suspension was filtered and the filtrate was concentrated. The residue was distilled under diminished pressure. Compound **5** (14.06 g, 70% yield) was obtained as a colorless oil: bp 85–86 °C (1 mmHg) (lit. (*4c*) bp 72 °C, 0.1 mmHg).

Compound **6** was obtained by a similar procedure with benzyl chloroformate instead of di-*tert*-butyl dicarbonate. The reaction mixture was filtered, washed with water, and dried on Na₂SO₄. Removal of the solvent gave the almost pure **6** which was used in the next step without further purification: FT-IR (CH₂Cl₂ cast) ν_{max} 3324 (br), 3111 (m), 2941 (s), 1697 (s), 1542 (s), 1454 (m), 1263 (s), 1139 (m), 747 (m), 698 (m) cm⁻¹; ¹H-NMR (CDCl₃) δ 7.34 (s, 5H), 5.18 (br, 1H, −CON*H*−), 5.08 (s, 2H), 3.25 (d, *J* = 6.0 Hz, 1H), 3.20 (d, *J* = 6.0 Hz, 1H), 2.80 (t, *J* = 6.0 Hz, 2H), 1.48 (s, 2H, −N*H₂*); HRMS *m/e* calcd for C₁₀H₁₄O₂N₂ 194.1055, found 194.1048.

Methyl 6-[[N-[2-[(*tert*-Butoxycarbonyl)amino]-ethyl]-N-(*tert*-butoxycarbonyl)amino]methyl]pyridine-2-carboxylate (9). A solution of the aldehyde 4 (7.02 g, 42.55 mmol) and amine 5 (6.81 g, 42.55 mmol) in methanol (150 mL) was stirred at room temperature for 20 min and then hydrogenated under atomspheric pressure in the presence of 10% Pd(C) (600 mg) for 30 min. The resulting solution was filtered through a glass filter covered with Celite and concentrated under reduced pressure. To the solution of the residue in dichloromethane (150 mL) containing 4-(dimethylamino)pyridine (100 mg) was added dropwise di-*tert*-butyl dicarbonate (10.22 g, 46.81 mmol) in dichloromethane (50 mL). The resulting solution was stirred at room temperature for 1 h and evaporated under diminished pressure. The residue was purified by chromatography on silica gel column eluted with 84% EtOAc in petroleum ether. The residue was dissolved in EtOAc (30 mL), diluted with petroleum ether (300 mL), and cooled on water bath. Filtration provided **9** (14.28 g, 82% yield) as a white powder: mp 97–98 °C; FT-IR (CHCl₃ cast) ν_{max} 3380 (br), 2976 (m), 1707 (s), 1509 (m), 1392 (m), 1286 (s), 1172

(s), 1138 (m), 760 (m) cm^{-1}; ^{1}H-NMR (CDCl$_3$) δ 8.20 (d, J = 8.0 Hz, 1H), 7.85 (t, J = 8.0 Hz, 1H), 7.40 (dd, J = 24, 8.0 Hz, 1H), 4.56 (s, 2H), 3.98 (s, 3H), 3.52–3.40 (m, 2H), 3.35–3.22 (m, 2H), 1.45 (s, 4.5 H, t-Bu), 1.40 (s, 9H, t-Bu), 1.28 (s, 4.5H, t-Bu); MS m/z 410 (M$^+$ + 1), 354, 310, 179, 151, 35.

6-[[N-[2-[(tert-Butoxycarbonyl)amino]ethyl]-N-(tert-butoxycarbonyl)amino]methyl]pyridine-2-carboxylic Acid (10). A solution containing the ester **9** (14.00 g, 34.23 mmol) in 0.4 N NaOH (150 mL) in 75% methanolic solution was stirred at room temperature for 1 h and then evaporated to remove MeOH. The solution was diluted with water (50 mL) and extracted with ether (100 mL × 2). The organic layer was back-extracted with saturated aqueous NaHCO$_3$ solution (100 mL). The combined aqueous layers were acidified with aqueous citric acid to pH 2 and extracted with dichloromethane (100 mL × 3). The organic layer was dried on Na$_2$SO$_4$, concentrated to 50 mL, diluted with petroleum ether (200 mL), and allowed to stand at room temperature for 30 min. The precipitate was collected and dried in vacuo. The product (12.50 g, 93% yield) was obtained as a white powder: mp 136–138 °C; FT-IR (CHCl$_3$ cast) ν_{max} 3450–2400 (br), 2978 (m), 2933 (m), 1698 (s), 1518 (m), 1461 (m), 1409 (m), 1367 (s), 1250 (s), 1171 (s), 732 (m) cm^{-1}; ^{1}H-NMR (CDCl$_3$) δ 8.10 (d, J = 8.0 Hz, 1H), 7.90 (t, J = 8.0 Hz, 1H), 7.50 (dd, J = 24, 8.0 Hz, 1H), 4.62 (s, 1H), 4.57 (s, 1H), 3.56–3.38 (m, 2H), 3.38–3.25 (m, 2H), 1.50 (s, 4.5H, t-Bu), 1.45 (s, 9H, t-Bu), 1.36 (s, 4.5H, t-Bu); MS m/e 396 (M$^+$ + 1), 296, 222, 165, 137, 119, 57. Anal. Calcd for C$_{19}$H$_{29}$O$_6$N$_3$: C, 57.70; H, 7.39; N, 10.63. Found: C, 57.73; H, 7.43; N, 10.50.

1-[(Benzyloxycarbonyl)amino]-2-[[N^α,N^{im}-bis(tert-butoxycarbonyl)-L-histidinyl]amino]ethane (12). To an ice-cooled solution of acid **11** (47) (7.25 g, 20.36 mmol) and 1-hydroxybenzotriazole hydrate (HOBT) (3.023 g, 22.40 mmol) in anhydrous THF (100 mL) was added dropwise dicyclohexylcarbodiimide (DCC) (4.614 g, 22.40 mmol) in anhydrous THF (30 mL). The mixture was stirred for 30 min before **6** (4.346 g, 22.40 mmol) in anhydrous THF (20 mL) was added at 0 °C, and stirring was continued overnight. The solvent was removed, and the residue was washed with ethyl acetate (100 mL × 3). The ethyl acetate solution was washed with saturated aqueous NaHCO$_3$ three times and dried over Na$_2$SO$_4$. Solvent removal provided a solid residue, which was washed with ether, affording the title compound **12** (7.51 g, 69% yield) as a white powder: mp 134–137 °C; [α]$^{20}_D$ +8.50° (c 1.035, MeOH); FT-IR (CHCl$_3$ cast) ν_{max} 3313 (br), 2979 (m), 2934 (m), 1757 (m), 1716 (s), 1685 (m), 1669 (m), 1540 (m), 1391 (m), 1254 (s), 1156 (s), 1012 (m), 734 (m) cm^{-1}; ^{1}H-NMR (CDCl$_3$) δ 8.10 (s, 1H), 7.31 (s, 5H), 7.24 (s, 1H), 7.08 (br, 1H, –CONH–), 5.59 (br, 2H, –CONH–), 5.05 (s, 2H), 4.36 (m, 1H), 3.48–3.22 (m, 4H), 3.02 (d, J = 6.0 Hz, 2H), 1.57 (s, 9H, t-Bu), 1.38 (s, 9H, t-Bu); FABHRMS m/e calcd for C$_{26}$H$_{37}$O$_7$N$_5$H 532.2771, found 532.2745.

1-[[N^α-[[6-[[2-[N-(tert-Butoxycarbonyl)amino]ethyl]-N-[(tert-butoxycarbonyl)amino]methyl]-2-pyridinyl]-carbonyl]histidinyl]amino]-2-[(benzyloxycarbonyl)-amino]ethane (13). An ice cooled solution of **12** (3.90 g, 7.33 mmol) in trifluoroacetic acid (20 mL) was stirred for 30 min, and the mixture was evaporated in vacuo to remove the acid. The residue was washed with ether and dried in vacuo. The amine-TFA salt was obtained as white powder, which was dissolved in dry dimethylformamide (10 mL). In another flask, a mixture of **10** (2.75 g, 6.96 mmol), 1-[3-(dimethylamino)propyl]-3-ethylcarbodiimide hydrochloride (EDCI) (1.613 g, 8.352 mmol), and HOBT (1.229 g, 9.050 mmol) in anhydrous

THF (50 mL) was stirred at room temperature for 30 min. To this solution was added dropwise triethylamine (3 mL) and subsequently the above amine–TFA salt solution. After the solution was stirred overnight, the solvent was removed in vacuo and the residue was dissolved in ethyl acetate (150 mL), washed with saturated aqueous NaHCO$_3$, and dried over Na$_2$SO$_4$. Flash chromatography on a silica gel column and elution with dichloromethane/methanol (10:1–8:1) afforded the title compound (3.380 g, 65% yield) as a white amorphous foam: R_f (CH$_2$Cl$_2$: MeOH = 8.5:1.5) 0.45; [α]$^{20}_D$ +10.45° (c 1.259, MeOH); FT-IR (CHCl$_3$ cast) ν_{max} 3328 (br), 2977 (m), 2933 (m), 1695(s), 1686 (s), 736 (m) cm^{-1}; ^{1}H-NMR (CDCl$_3$:CD$_3$OD = 5:1) δ 7.90 (d, J = 8.0 Hz, 1H), 7.72 (t, J = 8.0 Hz, 1H), 7.47 (s, 1H), 7.28 (dd, J = 24.0, 8.0 Hz, 1H), 7.25 (s, 5H), 6.78 (d, J = 8.0 Hz, 1H), 4.98 (s, 2H), 4.65 (t, J = 6.0 Hz, 1H), 4.55–4.42 (m, 2H), 3.60–3.11 (m, 8H), 3.07 (d, J = 6.0 Hz, 2H), 1.41 (s, 4.5 H, t-Bu), 1.33 (s, 9H, t-Bu), 1.29 (s, 4.5H, t-Bu); FABHRMS m/e calcd for C$_{35}$H$_{48}$O$_8$N$_8$H 709.3673, found 709.3655.

Methyl 1-Methyl-4-nitropyrrole-2-carboxylate (16). A mixture of **15** (48, 49) (9.46 g, 34.80 mmol), 4-(dimethylamino)pyridine (120 mg), and methanol (70 mL) was stirred at ambient temperature for 2 h. The resulting suspension was filtered, and the filtrate was concentrated to 20 mL, diluted with 20 mL of ether, and filtered again. The combined solid residue was washed with ether and dried in vacuo, resulting in 6.30 g (97% yield) of the title compound as a white powder: mp 112 °C (lit. (50) mp 122 °C).

Methyl 1-Methyl-4-[[(1-methyl-4-nitropyrrolyl)-2-carbonyl]amino]pyrrole-2-carboxylate (18). A suspension of **16** (4.00 g, 21.74 mmol) in methanol (40 mL) was hydrogenated under atmospheric pressure in the presence of 10% Pd(C) (1.500 g) at room temperature for 4 h. The resulting mixture was passed through Celite and concentrated under reduced pressure to completely remove methanol. The crude amine **17**, **15** (5.475 g, 20.13 mmol), and 4-(dimethylamino)pyridine (100 mg) were dissolved in chloroform (40 mL) and stirred at room temperature overnight. Filtration of the reaction mixture provided **18** (2.427 g) as a yellowish powder. The filtrate and the wash were combined, concentrated to 30 mL, and stirred for another 12 h to afford another 2.495 g of **18** (total yield 80%): mp 242–244 °C (lit. (51) mp 225 °C).

Methyl 4-[[[4-(Butyrylamino)-1-methyl-2-pyrrolyl]-carbonyl]amino]-1-methyl-2-pyrrolecarboxylate (19). A suspension of **18** (4.00 g, 13.07 mmol) and 10% Pd(C) (2.00 g) in DMF (40 mL) and methanol (30 mL) was stirred under hydrogen (H$_2$-balloon) overnight. The black mixture was passed through Celite and evaporated under reduced pressure to remove methanol. The black DMF solution was cooled on an ice–water bath and treated with triethylamine (2.18 mL, 15.68 mmol) and butyric anhydride (2.57 mL, 15.68 mmol). After being stirred for 1 h, the mixture was evaporated in vacuo to remove DMF and the residue was dissolved in dichloromethane (60 mL), washed with water, and dried on Na$_2$SO$_4$. The residue was purified by flash chromatography on silica gel eluted with ethyl acetate. The title compound was obtained as a white powder (2.710 g, 60% yield): mp 164–166 °C; FT-IR (CH$_2$Cl$_2$ cast) ν_{max} 3291 (br), 3128 (w), 2960 (m), 1707 (s), 1653 (s), 1577 (s), 1555 (s), 1439 (m), 1406 (m), 1253 (s), 1109 (m), 779 (m) cm^{-1}; ^{1}H-NMR (CDCl$_3$) δ 7.74 (s, 1H, –CONH–), 7.44 (s, 1H, –CONH–), 7.39 (d, J = 2.0 Hz, 1H), 7.06 (d, J = 1.0 Hz, 1H), 6.74 (d, J = 2.0 Hz, 1H), 6.64 (d, J = 1.0 Hz, 1H), 3.87 (s, 6H), 3.79 (s, 3H), 2.29 (t, J = 7.5 Hz, 2H), 1.73 (sex., J = 7.5 Hz, 2H), 0.98 (t, J = 7.5 Hz, 3H); MS m/e 347 (M$^+$ + 1).

4-[[[4-(Butyrylamino)-1-methyl-2-pyrrolyl]carbonyl]amino]-1-methyl-2-pyrrolecarboxylic Acid (20).
Ester **19** (2.710 g, 7.8 mmol) in 50% methanolic NaOH solution (30 mL) was stirred at room temperature overnight. The solution was evaporated to remove methanol, diluted with water (15 mL), and extracted with ether (20 mL × 2). The aqueous phase was acidified with aqueous citric acid solution to pH 4 and extracted with ethyl acetate three times. The organic layer was homogenized by adding methanol (10 mL), dried over Na_2SO_4, and concentrated. Washing the resulting residue with ether afforded **20** as a white powder (2.30 g, 89% yield): mp 156 °C dec; FT-IR (CH_2Cl_2 cast) ν_{max} 3440−2500 (br), 3100 (m), 2957 (m), 1687 (m), 1647 (s), 1623 (m), 1559 (s), 1461 (m), 1437 (m), 1358 (m), 1207 (w), 1195 (w), 784 (w) cm^{-1}; ^{1}H-NMR (CDCl$_3$:DMSO-d_6 = 5:1) δ 9.30 (s, 1H, −CONH−), 9.20 (s, 1H, −CONH−), 7.32 (d, J = 2.0 Hz, 1H), 7.10 (d, J = 2.0 Hz, 1H), 6.81 (d, J = 2.0 Hz, 1H), 6.78 (d, J = 2.0 Hz, 1H), 3.81 (s, 3H), 3.79 (s, 3H), 2.19 (t, J = 7.5 Hz, 2H), 1.61 (sex., J = 7.5 Hz, 2H), 0.87 (t, J = 7.5 Hz, 3H); HRMS *m/e* calcd for $C_{16}H_{20}O_4N_4$ − CO_2 288.1586, found 288.1584.

Methyl 4-[[[4-[[[4-(Butyrylamino)-1-methyl-2-pyrrolyl]carbonyl]amino]-1-methyl-2-pyrrolyl]carbonyl]amino]-1-methyl-2-pyrrolecarboxylate (21). To an ice-cooled solution of **20** (1.50 g, 4.52 mmol) and HOBT (0.731 g, 5.41 mmol) in dry DMF (30 mL) was added EDCI (1.038 g, 5.41 mmol) in chloroform (5 mL). The mixture was stirred for 30 min, and to this was added **17**, obtained from the hydrogenation of **16** (1.247 g, 6.78 mmol), in chloroform (5 mL). After being stirred overnight, the solvent was removed under reduced pressure and the residue was dissolved in chloroform, washed with saturated aqueous NaHCO$_3$ solution, and dried on Na$_2$SO$_4$. The residue from evaporation of the solvents was chromatographed on a silica gel column eluted with ethyl acetate, providing the title compound as a white powder (1.444 g, 68% yield): mp 215−218 °C; FT-IR (CH_2Cl_2 cast) ν_{max} 3296 (br), 3128 (w), 2958 (w), 1706 (m), 1699 (m), 1647 (s), 1579 (s), 1550 (s), 1437 (m), 1405 (m), 1252 (s), 1206 (m), 1109 (m), 778 (w); ^{1}H-NMR (CDCl$_3$) δ 9.05 (s, 1H, −CONH−), 9.03 (s, 1H, −CONH−), 8.90 (s, 1H, −CONH−), 7.08 (d, J = 2.0 Hz, 1H), 6.89 (d, J = 2.0 Hz, 1H), 6.82 (d, J = 2.0 Hz, 1H), 6.68 (d, J = 2.0 Hz, 1H), 6.59 (d, J = 2.0 Hz, 1H), 6.55 (d, J = 2.0 Hz, 1H), 3.58 (s, 6H), 3.57 (s, 3H), 3.54 (s, 3H), 1.92 (t, J = 7.5 Hz, 2H), 1.37 (sex., J = 7.5 Hz, 2H), 0.63 (t, J = 7.5 Hz, 3H); HRMS *m/e* calcd for $C_{23}H_{28}O_5H_6$ 468.2121, found 468.2129.

4-[[[4-[[[4-(Butyrylamino)-1-methyl-2-pyrrolyl]carbonyl]amino]-1-methyl-2-pyrrolyl]carbonyl]amino]-1-methyl-2-pyrrolylcarboxylic Acid (22). The ester **21** (1.444 g, 3.09 mmol) in 50% methanolic NaOH solution (30 mL) was stirred at room temperature overnight. The solution was evaporated to remove methanol, diluted with water (15 mL), and extracted with ether (20 mL × 2). The aqueous phase was acidified with aqueous citric acid to pH 4 and filtered. The solid residue was dissolved in dichloromethane/methanol (10:1) and dried over Na$_2$SO$_4$, and the solvent was removed under diminished pressure. The resulting residue was purified by chromatography on a silica gel column eluted with dichloromethane/methanol (5:1). Compound **22** was obtained as white powder (1.09 g, 71% yield): mp 218 °C dec; FT-IR (CH_2Cl_2 cast) ν_{max} 3500−2500 (br), 3090 (w), 2961 (w), 1647 (s), 1578 (s), 1466 (s), 1434 (s), 1403 (s), 1363 (m), 1263 (w), 1208 (w), 1104 (w), 797 (w) cm^{-1}; ^{1}H-NMR (CDCl$_3$:DMSO-d_6 = 5:1) δ 9.80 (s, 1H, −CONH−), 9.73 (s, 1H, −CONH−), 9.62 (s, 1H, −CONH−), 7.18 (d, J = 2.0 Hz, 1H), 7.13 (d, J = 2.0 Hz, 1H), 7.04 (d, J = 2.0 Hz, 1H), 6.97 (d, J = 2.0 Hz, 1H), 6.87 (d, J = 2.0 Hz,

1H), 6.49 (d, J = 2.0 Hz, 1H), 3.86 (s, 6H), 3.85 (s, 3H), 3.84 (s, 3H), 2.20 (t, J = 7.5 Hz, 2H), 1.60 (sex., J = 7.5 Hz, 2H), 0.90 (t, J = 7.5 Hz, 3H); FABMS *m/e* 455 (M$^+$ + 1); HRMS *m/z* calcd for $C_{22}H_{26}O_5N_6$ − CO_2 410.2066, found 410.2058.

General Procedure for Coupling of 20 and 22 with 14. Compound **13** in methanol was hydrogenated in the presence of 25% of 10% Pd(C) (w/w) at atmospheric pressure of hydrogen (H$_2$-balloon) for 1 h. The suspension was filtered and concentrated under diminished pressure. The free amine **14** was dissolved in dry dimethylformamide for the coupling reaction. In another flask, **20** or **22**, HOBT, and EDCI in DMF were stirred for 30 min and to this was added the free amine solution. The reaction mixture was stirred overnight and the solvent was then removed under diminished presure. The residue was dissolved in chloroform, washed with aqeous NaHCO$_3$, and dried over Na$_2$SO$_4$. The residue was purified on silica gel column eluted with dichloromethane/methanol (8:1−5:1). The coupling products were obtained as white powders.

N-[2-[[N^α-[[6-[[N-[2-[(tert-Butoxycarbonyl)amino]ethyl]-N-(tert-butoxycarbonyl)amino]methyl]-2-pyridinyl]carbonyl]-L-histidinyl]amino]ethyl]-4-[[4-(butyrylamino)-1-methyl-2-pyrrolyl]carbonyl]amino]-1-methyl-2-pyrrolecarboxamide (29b). Coupling of **20** (280 mg, 0.840 mmol), HOBT (140 mg, 1.037 mmol), and EDCI (190 mg, 0.99 mmol) with **14** from **13** (1.000 g, 1.410 mmol) in DMF (10 mL) afforded **29b** (485 mg, 65% yield): R_f (CH_2Cl_2:MeOH = 8.5:1.5): 0.33; [α]^{20}D +29.5° (*c* 1.000, CHCl$_3$); FT-IR (CHCl$_3$ cast) ν_{max} 3308 (br), 2974 (w), 2934 (w), 1695 (s), 1593 (m), 1575 (m), 1523 (s), 1435 (m), 1406 (m), 1251 (m), 1167 (m), 732 (m) cm^{-1}; ^{1}H-NMR (DMSO-d_6) δ 9.88 (s, 1H, −CONH−), 9.75 (s, 1H, −CONH−), 8.80 (br, 1H, −CONH−), 8.28−8.14 (m, 2H, −CONH−), 8.00−7.85 (m, 2H), 7.55 (s, 1H), 7.38 (m, 1H), 7.20 (s, 1H), 7.15 (s, 1H), 6.85 (s, 2H), 6.80 (s, 1H), 4.62 (m, 1H), 4.48 (s, 2H), 3.84 (s, 3H), 3.78 (s, 3H), 3.50−3.25 (m, 4H), 3.20 (m, 2H), 3.12 (m, 2H), 3.00 (m, 2H), 2.20 (t, J = 7.5 Hz, 2H), 1.58 (sex., J = 7.5 Hz, 2H), 1.42 (s, 4.5H, t-Bu), 1.35 (s, 9H), 1.25 (s, 4.5H, t-Bu), 0.89 (t, J = 7.5 Hz, 3H); FABHRMS *m/e* calcd for $C_{43}H_{60}N_{12}O_9H$ 889.4684, found 889.4675.

N-[2-[[N^α-[[6-[[N-[2-[(tert-Butoxycarbonyl)amino]ethyl]-N-(tert-butoxycarbonyl)amino]methyl]-2-pyridinyl]carbonyl]-L-histidinyl]amino]ethyl]-4-[[[4-[[[4-(butyrylamino)-1-methyl-2-pyrrolyl]carbonyl]amino]-1-methyl-2-pyrrolyl]carbonyl]amino]-1-methyl-2-pyrrolecarboxamide (29c). Coupling of **22** (150 mg, 0.330 mmol), HOBT (76 mg, 0.563 mmol), and EDCI (100 mg, 0.521 mmol) with **14** from **13** (468 mg, 0.660 mmol) in DMF (10 mL) afforded **29c** (219 mg, 66% yield): R_f (CH_2Cl_2:MeOH = 8.5:1.5) 0.28; [α]^{20}D +18.00° (*c* 0.667, CHCl$_3$); FT-IR (CH_2Cl_2 cast) ν_{max} 3302 (br), 2974 (m), 2934 (m), 1653 (s), 1576 (m), 1522 (s), 1435 (m), 1406 (m), 1253 (m), 1165 (m), 735 (w) cm^{-1}; ^{1}H-NMR (CDCl$_3$:DMSO-d_6:CD$_3$OD = 5:1:1) δ 7.96 (m, 1H), 7.84 (m, 1H), 7.74 (s, 1H), 7.38 (m, 1H), 7.35 (s, 2H), 7.15 (s, 1H), 6.92 (s, 1H), 6.86 (s, 1H), 6.82 (s, 1H), 6.77 (s, 1H), 4.77 (m, 1H), 4.57 (d, J = 7.0 Hz, 2H), 3.93 (s, 3H), 3.91 (s, 3H), 3.83 (s, 3H), 3.50−3.10 (m, 10H), 2.28 (t, J = 7.5 Hz, 2H), 1.70 (sex., J = 7.5 Hz, 2H), 1.50 (s, 4.5H, t-Bu), 1.42 (s, 9H), 1.35 (s, 4.5H, t-Bu), 1.00 (t, J = 7.5 Hz, 3H); FABHRMS *m/e* calcd for $C_{49}H_{66}N_{14}O_{10}H$ 1011.5164, found 1011.5145.

N-[2-[(tert-Butoxycarbonyl)amino]ethyl]-1-methyl-4-nitropyrrole-2-carboxamide (26). A solution of **15** (4.073 g, 15 mmol) and **5** (16.5 mmol) in chloroform (45 mL) was stirred at room temperature overnight. The yellow suspension was diluted with ether (50 mL) and

filtered. The solid residue was further washed with ether and dried *in vacuo*, resulting in **26** (4.150 g, 89% yield) as a white powder: mp 172–174 °C; FT-IR (CH$_2$Cl$_2$ cast) ν_{max} 3345 (br), 3140 (m), 3126 (m), 2978 (w), 2941 (w), 1683 (s), 1642 (s), 1536 (s), 1492 (s), 1417 (s), 1330 (m), 1274 (s), 1235 (m), 1160 (m), 750 (m); ^{1}H-NMR (CDCl$_3$: DMSO-d_6 = 5:1) δ 7.68 (br, 1H, −CONH−), 7.34 (d, J = 2.0 Hz, 1H), 7.06 (d, J = 2.0 Hz, 1H), 5.90 (br, 1H, −CONH−), 3.65 (s, 3H), 3.08 (m, 2H), 2.95 (m, 2H), 1.10 (s, 9H); MS m/e 313 (M$^+$ + 1), 274, 257, 213, 35.

N-[[2-[(*tert*-Butoxycarbonyl)amino]ethyl]-4-butyryl]amino]-1-methylpyrrole-2-carboxamide (27). **26** (4.760g, 15.26 mmol) and 10% Pd(C) (450 mg) in methanol was shaken under hydrogen (40–35 psi) for 1 h. The mixture was filtered through celite and concentrated under diminished pressure. To an ice-cooled solution of the residue and triethylamine (2.76 mL, 18.31 mmol) in chloroform (30 mL) was added butyric anhydride (2.90 g, 18.31 mmol) in chloroform (10 mL). After being stirred at room temperature for 3 h, the mixture was diluted with chloroform (50 mL), washed with water, dried over Na$_2$SO$_4$, and concentrated to 40 mL. The solution was allowed to stand in the refrigerator overnight. Filtration provided the product (4.440 g, 83% yield) as a white powder: mp 160–162 °C; FT-IR (CHCl$_3$ cast) ν_{max} 3307 (br), 2960 (w), 2930 (w), 1692 (s), 1641 (s), 1580 (m), 1528 (s), 1440 (m), 1366 (w), 1271 (m), 1252 (m), 1168 (m), 760 (w); ^{1}H-NMR (CD$_3$OD) δ 6.82 (d, J = 2.0 Hz, 1H), 6.40 (d, J = 2.0 Hz, 1H), 3.55 (s, 3H), 3.00 (m, 4H), 1.95 (t, J = 7.5 Hz, 2H), 1.40 (sex., J = 7.5 Hz, 2H), 1.12 (s, 9 H), 0.62 (t, J = 7.5 Hz, 3H); MS m/e 352 (M$^+$), 298, 278, 252, 208, 193, 123, 95; HRMS m/e calcd for C$_{17}$H$_{28}$N$_4$O$_4$ 352.2110, found 352.2113.

N-[[2-[[N$^\alpha$,N^{im}-Bis(*tert*-butoxycarbonyl)-L-histidinyl]amino]ethyl]-4-butyryl]amino]-1-methylpyrrole-2-carboxamide (28). To an ice cooled 4.5 M HCl/dioxane solution was added in portions **27** (2.404g, 6.83 mmol). The solution was stirred at 0 °C for 20 min. Ether was added to precipitate **25**-HCl salt, and the clear upper layer was removed by pipette. The remaining residue was dissolved in methanol and cooled in an ice–water bath. Ether (100 mL) was added, and the mixture was left to stand at 0 °C for 10 min and filtered. The amine–HCl salt was obtained as a yellowish powder. In another flask, a mixture of **11** (4.272 g, 12 mmol) and HOBT (1.782 g, 13.20 mmol) in anhydrous THF (70 mL) was treated with DCC (2.723 g, 13.20 mmol) in THF (10 mL) at 0 °C. The mixture was stirred for 30 min, and then triethylamine was added. To this was added in portions the above amine–HCl salt at 0 °C. The mixture was stirred at room temperature overnight. The solvent was removed, and the residue was dissolved in ethyl acetate (100 mL), washed with water, and dried over Na$_2$SO$_4$. The residue was purified by flash chromatography on silica gel column eluted with dichloromethane/methanol (20:1–10:1). The coupling product (2.900 g, 72% yield) was obtained as white powder: mp 126–129 °C; [α]$^{20}_D$ +3.90 (c 1.155, MeOH); FT-IR (CHCl$_3$ cast) ν_{max} 3467 (br), 2976 (w), 2934 (w), 1758 (s), 1690 (m), 1646 (s), 1580 (m), 1522 (m), 1491 (m), 1464 (s), 1391 (s), 1371 (m), 1291 (m), 1255 (s), 1157 (s), 1011 (m), 733 (w) cm^{-1}; ^{1}H-NMR (CDCl$_3$) δ 7.98 (s, 1H), 7.75 (br, 1H, −CONH−), 7.30 (d, J = 2.0 Hz, 1H), 7.17 (s, 1H), 7.12 (br, 2H, −CONH−), 6.38 (d, J = 2.0 Hz, 1H), 6.10 (br, 1H, −CONH−), 4.43 (m, 1H), 3.87 (s, 3H), 3.47–3.31 (m, 4H), 3.02 (m, 2H), 2.28 (t, J = 7.5 Hz, 2H), 1.72 (sex., J = 7.5 Hz, 2H), 1.60 (s, 9 H), 1.41 (s, 9H), 0.97 (t, J = 7.5 Hz, 3H); FABHRMS m/e calcd for C$_{28}$H$_{43}$N$_7$O$_7$H 590.3302, found 590.3291.

N-[2-[[N$^\alpha$-[[6-[[N-[2-[(*tert*-Butoxycarbonyl)amino]ethyl]-N-(*tert*-butoxycarbonyl)amino]methyl]-2-pyridinyl]carbonyl]-L-histidinyl]amino]ethyl-4-(butyrylamino)-1-methylpyrrole-2-carboxamide (29a). The procedure is similar to that of **13**. Coupling reaction of the amine–TFA salt from deprotection of **28** (2.000 g, 4.068 mmol) with **10** (1.607 g, 4.068 mmol), HOBT (0.549 g, 4.068 mmol), DCC (0.838 g, 4.068 mmol), and triethylamine (1.890 g, 13.56 mmol) in DMF (40 mL) gave the crude product. Purification on a silica gel column eluted with dichloromethane/methanol (8:1–5:1) provided **29a** (2.100 g, 81% yield) as a white foam: R_f (CH$_2$Cl$_2$/MeOH = 8.5:1.5) 0.37; [α]$^{20}_D$ +3.54° (c 1.27, CHCl3); FT-IR (CHCl$_3$ cast) ν_{max} 3315 (br), 2974 (w), 2932 (w), 1662 (s), 1594 (m), 1574 (m), 1521 (s), 1451 (m), 1406 (m), 1366 (m), 1270 (m), 1249 (w), 1167 (m), 732 (w); ^{1}H-NMR (CDCl$_3$:DMSO-d_6 = 5:1) δ 8.98 (s, 1H, −CONH−), 8.67 (br, 1H, −CONH−), 7.68 (m, 1H, −CONH−), 7.68–7.45 (m, 3H), 7.18 (s, 1H), 7.05 (dd, J = 16.0, 8.0 Hz, 1H), 6.86 (m, 1H, −CONH−), 6.50 (s, 1H), 6.35 (s, 1H), 5.55 (br, 1H, −CONH−), 4.50 (m, 1H), 4.25 (s, 1H), 4.22 (s, 1H), 3.50 (s, 3H), 3.20–2.77 (m, 10H), 1.95 (t, J = 7.5 Hz, 2H), 1.38 (sex., J = 7.5 Hz, 2H), 1.17 (s, 4.5 H, t-Bu), 1.08 (s, 9H), 1.04 (s, 4.5 H, t-Bu), 0.63 (t, J = 7.5 Hz, 3H); FABHRMS m/e calcd for C$_{37}$H$_{54}$N$_{10}$O$_8$H 767.4204, found 767.4173.

General Procedure for Deprotection of 29 to 1. A solution of **29** in TFA was stirred at 0 °C for 1 h, and the acid was removed *in vacuo*. The residue was dissolved in water, made basic with ammonium hydroxide to pH 9, and loaded on Amberlite XAD-2 resin. This was first eluted with water until the eluate was neutral and then with methanol to elute the products. Evaporation of the methanolic solution *in vacuo* provided **1a–c** as white amorphous foams.

N-[[N$^\alpha$-[[6-[[(2-Aminoethyl)amino]methyl]-2-pyridinyl]carbonyl]-L-histidinyl]ethyl]-4-(butyrylamino)-1-methylpyrrole-2-carboxamide (1a). Deprotection of **29a** (100 mg, 0.131 mmol) in TFA (3 mL) afforded **1a** (67 mg, 90% yield): R_f (n-BuOH:H$_2$O:AcOH = 1:1:1) 0.35; [α]$^{20}_D$ −8.45° (c 1.04, methanol); FT-IR (CH$_2$Cl$_2$ cast) ν_{max} 3600–2400 (br), 2966 (w), 2940 (w), 1675 (s), 1596 (m), 1576 (m), 1528 (s), 1204 (s), 1183 (m), 1134 (m) cm^{-1}; ^{1}H-NMR (DMSO-d_6) δ 9.73 (s, 1H, −CONH−), 8.94 (d, J = 8.0 Hz, 1H, −CONH−), 8.29 (br, 1H, −CONH−), 8.17 (s, 1H), 8.11 (br, 1H, −CONH−), 8.02 (t, J = 8.0 Hz, 1H), 7.83 (t, J = 8.0 Hz, 1H), 7.68 (d, J = 8.0 Hz, 1H), 7.10 (d, J = 2 Hz, 1H), 7.05 (s, 1H), 6.68 (d, J = 2.0 Hz, 1H), 4.72 (m, 1H), 4.24 (s, 2H), 3.73 (s, 3H), 3.30–2.98 (m, 10H), 2.18 (t, J = 7.5 Hz, 2H), 1.56 (sex., J = 7.5 Hz, 2H), 0.88 (t, J = 7.5 Hz, 3H); FABHRMS m/e calcd for C$_{27}$H$_{38}$N$_{10}$O$_4$H 567.3155, found 567.3156.

N-[[N$^\alpha$-[[6-[[(2-Aminoethyl)amino]methyl]-2-pyridinyl]carbonyl]-L-histidinyl]ethyl]-4-[[[4-(butyrylamino)-1-methyl-2-pyrrolyl]carbonyl]amino]-1-methyl-2-pyrrolecarboxamide (1b). Deprotection of **29b** (100 mg, 0.112 mmol) in TFA (3 mL) afforded **1b** (66 mg, 86% yield); R_f (n-BuOH:H$_2$O:AcOH = 1:1:1) 0.35; [α]$^{20}_D$ +11.72° (c 1.45, methanol); FT-IR (CH$_2$Cl$_2$ cast) ν_{max} 3600–2400 (br), 2963 (m), 2937 (m), 1674 (s), 1593 (m), 1580 (m), 1528 (s), 1437 (m), 1205 (s), 1180 (s), 1134 (m) cm^{-1}; ^{1}H-NMR (DMSO-d_6) δ 9.88 (s, 1H, −CONH−), 9.78 (s, 1H, −CONH−), 9.00 (d, J = 8.5 Hz, 1H, −CONH−), 8.23 (br, 1H, −CONH−), 8.16 (br, 1H, −CONH−), 7.95 (t, J = 7.5 Hz, 1H, −CONH−), 7.88 (d, J = 7.5 Hz, 1H), 7.63 (dd, J = 7.5, 1.0 Hz, 1H), 7.60 (s, 1H), 7.18 (d, J = 2.0 Hz, 1H), 7.13 (d, J = 2.0 Hz, 1H), 6.85 (m, 3H), 4.62 (m, 1H), 3.94 (s, 2H), 3.80 (s, 3H), 3.76 (s, 3H), 3.28–3.10 (m, 4H), 3.10–3.03 (m, 2H), 2.93 (t, J = 5.0 Hz, 2H),

Scheme 1. Synthesis of Metal-Sequestering Moiety
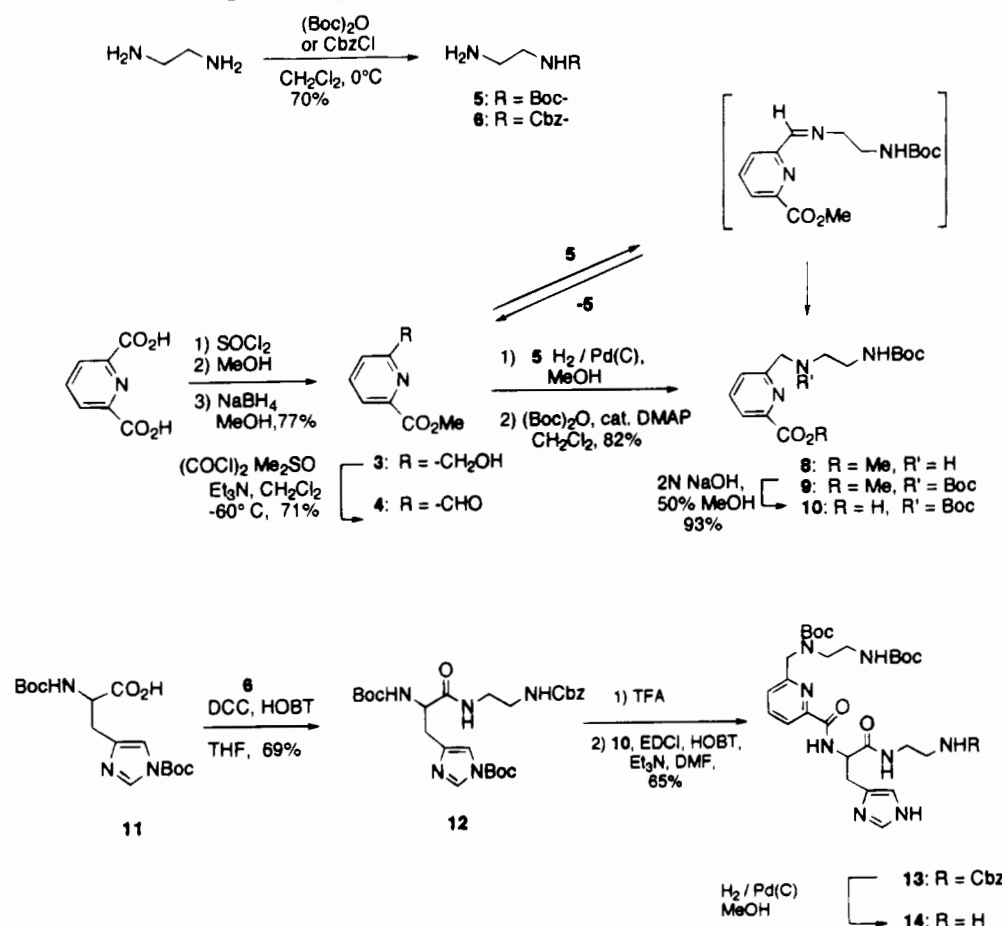
2.79 (t, J = 5.0 Hz, 2H), 2.19 (t, J = 7.5 Hz, 2H), 1.57 (sex., J = 7.5 Hz, 2H), 0.88 (t, J = 7.5 Hz, 3H); FABHRMS m/e calcd for $C_{33}H_{44}N_{12}O_5H$ 689.3602, found 689.3636.

N-[[N^α-[[6-[[(2-Aminoethyl)amino]methyl]-2-pyridinyl]carbonyl]-L-histidinyl]ethyl]-4-[[[4-[[[4-(butyrylamino)-1-methyl-2-pyrrolyl]carbonyl]amino]-1-methyl-2-pyrrolyl]carbonyl]amino]-1-methyl-2-pyrrolecarboxamide (1c). Deprotection of **29c** (50 mg, 0.49 mmol) in TFA (3 mL) afforded **1c** (36 mg, 91% yield): R_f (n-BuOH:H$_2$O:AcOH = 1:1:1) 0.33; [α]$^{20}_D$ +9.22° (c 0.683, methanol); FT-IR (CH$_2$Cl$_2$ cast) ν_{max} 3600–2400 (br), 2961 (m), 2935 (m), 1677 (s), 1594 (m), 1580 (m), 1530 (s), 1436 (m), 1206 (s), 1183 (m), 1136 (m) cm^{-1}; ^{1}H-NMR (DMSO-d_6) δ 9.90 (s, 1H, −CONH−), 9.89 (s, 1H, −CONH−), 9.78 (s, 1H,−CONH−), 9.04 (d, J = 6.0 Hz, 1H, −CONH−), 8.25 (br, 1H, −CONH−), 8.16 (br, 1H,−CONH−), 7.95 (m, 1H), 7.88 (m, 1H), 7.68 (s, 1H), 7.63 (m, 1H), 7.23 (d, J = 2.0 Hz, 1H), 7.19 (d, J = 2.0 Hz, 1H), 7.15 (d, J = 2.0 Hz, 1H), 7.03 (d, J = 2.0 Hz, 1H), 6.88 (m, 2H), 6.87 (s, 1H), 4.64 (m, 1H), 4.02 (s, 2H), 3.83 (s, 3H), 3.82 (s, 3H), 3.76 (s, 3H), 3.22 (m, 4H), 3.07 (t, J = 6.0 Hz, 2H), 2.98 (t, J = 6.0 Hz, 2H), 2.86 (d, J = 6.0 Hz, 2H), 2.20 (t, J = 7.5 Hz, 2H), 1.57 (sex., J = 2.0 Hz, 2H), 0.88 (t, J = 7.5 Hz, 3H), FABHRMS m/e calcd for $C_{39}H_{50}N_{14}O_6H$ 811.4116, found 811.4101.

Biochemistry. Buffers used and their abbreviations are as follows: TE, 10 mM Tris−HCl, 1 mM EDTA, pH 8.0; F$_{12}$ (fluorescence assay solution, pH 12), 0.02 M K$_3$-PO$_4$, 0.5 mM EDTA and 0.5 mg/mL ethidium bromide; TBE, 0.089 M Tris-borate, 0.089 M boric acid, 0.002 M EDTA, pH 8.0. Fluorescence was recorded on a Turner Model 430 spectrofluorometer; pBR322 DNA was purchased from Sigma, and was used in the experiments

without further purification (fluorescence assay showed that it contained 80% covalently closed circular form). Restriction enzymes *Hind* III and *Eco* RV were from Boehringer Mannheim, calf intestinal alkaline phosphatase, T4 polynucleotide kinase, restriction enzymes *Hpa* II and *Eco*O 109 I, SV40 viral DNA, and sonicated calf thymus DNA were from GIBCO BRL, and [γ-^{32}P]ATP was from New England Nuclear. Blenoxane was fractionated by a published procedure (10) to provide Bleomycin A$_2$ and B$_2$. Methidiumpropyl-EDTA was a gift from Professor Peter B. Dervan, California Institute of Technology. All other reagents were analytical grade and were used as received.

Kinetic Studies. The reactions of the drugs with DNA were carried out in 70 μL of TE solution which contained 1 A$_{260}$ unit of DNA, 80 μM drug−Fe(II) complexes, and 1 mM 1,4-dithiothreitol (DTT). Buffered solutions of the drug−Fe(II) complexes were freshly prepared immediately before each experiment. The reactions were run at room temperature, and 10 μL of the reaction mixture was pipetted into 2 mL of F$_{12}$ solution at 0, 10, 25, and 60 min. The fluorescence was initially recorded at room temperature. The solution was then heated at 95 °C for 5 min and cooled to room temperature before the next reading. Correction was made for the reduced stainability of form I pBR322 DNA using a factor of 1.22 (52).

Electrophoretic Mobility Shift Assays. The reactions of the drugs with DNA were carried out in 10 μL of TE solution which contained 0.93 A$_{260}$ unit of DNA and varying concentrations of drug. The reactions were run at room temperature for 90 min. The resultant reaction mixtures were examined by electrophoretic mobility shift assays through 5.6 mm thick 1% agarose slab gels with

TBE running buffer. The gels were run at room temperature at a voltage of 3.33 V/cm for 17 h. The gels were stained with ethidium bromide in water at a concentration of 0.5 μg/mL. Bands were visualized by 300 nm UV transillumination and photographed on Polaroid 667 film.

Sequencing Gel Assays. Plasmid pBR322 was cut with *Hind* III, dephosphorylated with calf intestinal alkaline phosphatase, and labeled at the 5' end using [γ-^{32}P]ATP and T4 polynucleotide kinase. The labeled DNA was then cut with *Eco* RV, and the desired 158 bp fragment was purified by nondenaturing PAGE and isolated by a crush and soak procedure (53). SV40 viral DNA was cut with *Hpa* II, dephosphorylated, and labeled as for pBR322, cut with *Eco*O 109 I, and purified and isolated as for pBR322. DNA cleavage reactions contained ~50 000 dpm of labeled DNA, 5 μM (nucleotides) sonicated calf thymus DNA, and 5 mM Na cacodylate buffer, pH 7.5, in a 10 μL reaction volume. MPE cleavage reactions contained a buffer consisting of 20 mM NaCl, 10 mM Tris−HCl, pH 7.3, and 100 μM calf thymus DNA, with the same amount of labeled DNA. Fe(II) and DTT solutions were prepared immediately before use. Concentrations of Fe(II), DNA cleaving compound, and DTT are given in the figures. Reactions were initiated by admixture of all components and were allowed to proceed at 25 °C for 30 min. Reactions were stopped by addition of a loading buffer containing 10 M urea, 1.5 mM EDTA, and 0.05% each of bromophenol blue and xylene cyanol. The reaction mixtures were then lyophilized and redissolved in 5 μL of H$_2$O, and 2.5 μL was used for PAGE analysis. Sequence lanes were produced by the method of Maxam and Gilbert (53, 54). Electrophoresis was performed in TBE buffer on 0.4 mm thick, 55 cm long, 8% polyacrylamide (the gel of Figure 6 contained 20% polyacrylamide) denaturing gels containing 7 M urea at 55 °C and 2000 V. Gels were autoradiographed at −70 °C using Kodak X-Omat AR film.

RESULTS AND DISCUSSION

Synthesis of 1a−c. Synthesis of the protected complexing portion **12** was accomplished by the reported procedure of Hénichart et al. with some modifications (17). Aldehyde **4** was synthesized in light of Ohno's procedure for the synthesis of similar compounds (22, 28). Reduction of 2,6-pyridinedicarboxylate (55) with sodium borohydride in methanol afforded 6-(hydroxymethyl)-2-pyridinecarboxymethyl ester **3** exclusively. Swern oxidation of **3** provided methyl 6-formyl-2-pyridinecarboxylate (**4**) (46) in a yield of 71% (Scheme 1). PCC also oxidizes **3** to **4** in modest yield. In the literature (17), compound **5** was obtained by Raney-Ni catalyzed hydrogenation of Boc-aminoacetonitrile which was prepared by the reaction of aminoacetonitrile with di-*tert*-butyldicarbonate. We found that condensation of 3 equiv of diaminoethane with di-*tert*-butyldicarbonate or benzyloxycarbonyl chloride in dichloromethane provided the corresponding monoprotected amines **5** or **6** in 70% yield. Reaction of **5** with aldehyde **4** in methanol results in an equilibrium between **4** and imine **7**. However, when the reaction mixture containing **4** and **7** was treated to catalytic hydrogenation, the equilibrium shifted toward **7**, resulting in a complete reaction. Thus, catalytic hydrogenation of a solution of **4** and **5** (1:1) in methanol under hydrogen (1 atmosphere pressure) in the presence of 10% of 10% Pd(C) followed by the protection of the secondary amine group by di-*tert*-butyl dicarbonate in CH$_2$Cl$_2$ provided **9** in excellent yield. Hydrolysis of **9** afforded the acid **10** in 93% yield. Coupling of diprotected histidine **11** (47)

with **6** in the presence of 1,3-dicyclohexylcarbodiimide(DCC) and 1-hydroxybenzotriazole(HOBT) in THF afforded amide **12** in 69% yield. Deprotection of **12** by trifluoroacetic acid (TFA) followed by coupling with **10** in the presence of EDCI, HOBT, and triethylamine in DMF provided the fully protected metal-complexing subunit **13**. Selective deprotection of **13** by catalytic hydrogenation afforded **14** quantitatively, which was used directly in the coupling with the lexitropsin carriers.

There are many possible routes to synthesize dipyrrole and tripyrrole peptides. In our synthesis, we selected 1-methyl-2-trichloroacetylpyrrole (**15**) (48, 49) as a key intermediate. Solvolysis of **15** in methanol in the presence of catalytic amount of 4-(dimethylamino)pyridine (DMAP) provided the methyl ester **16** (50) in 97% yield (Scheme 2). Conversion of **16** to **17** by catalytic hydrogenation followed by condensation with **15** in chloroform afforded the dipyrrole unit **18** (50) in 80% yield. Reduction of **18** by catalytic hydrogenation and acylation of the resulting amine with butyric anhydride gave rise to ester **19**, which was hydrolyzed to the netropsin moiety **20**. Coupling of **20** with **17** under the influence of EDCI and HOBT in DMF provided tripyrrole derivative **21** in modest yield, which was then hydrolyzed to the corresponding acid **22** in 71% yield. Coupling of the metal-complexing subunit **14** with the carriers **20** and **22** in the presence of EDCI and HOBT in DMF resulted in the protected hybrids **29b** and **29c** in 65% and 66% yield, respectively.

Compound **29a** was synthesized by a different strategy. Although compound **25** can be prepared by the route through **23** and **24** (Scheme 3) in good yield, the route through **26** and **27** seems to be more efficient. Condensation of **15** with **5** afforded amide **26** in 89% yield (Scheme 3). Subsequent hydrogenation and acylation with butyric anhydride provided **27** in 83% yield. Coupling of **25**, obtained from acidic deprotection of **27**, with **11** afforded **28** in a yield of 72%. Coupling of the deprotected **28** with **10** under similar conditions afforded the protected hybrid **29a** in 81% yield.

Finally, deprotection of **29a-c** in trifluoroacetic acid and purification on Amberlite XAD-2 resin provided the pure hybrids **1a-c** in excellent yields (Scheme 4).

DNA Cleavage Studies. Examination of the ability of the Fe(II) complexes of **1a−c** to cleave duplex DNA was carried out through inspection of the reaction of the complexes and thiol reductants (DTT) with pBR322 supercoiled DNA by both ethidium binding assay (56) and agarose gel electrophoresis. The ethidium bromide binding assay is convenient for studying the kinetics of reactions of supercoiled DNA with drugs. Supercoiled covalently closed circular (CC) and nicked open circular (OC) DNAs permit intercalation of ethidium to different extents which is revealed by the characteristic fluorescence intensity of bound ethidium. The difference of the fluorescence between unheated and heat denatured assay solutions can give information about DNA damage. It was observed that the ability of complexes to cleave DNA increases with the number of pyrrole units in the DNA binding subunit of the hybrids (Figure 2), especially under aerobic conditions, which is consistent with the anticipated mechanism of affinity cleavage. Agarose gel electrophoresis indicates that these complexes cleave DNA very efficiently, resulting in mainly single-strand breaks of duplex DNA (Figure 3).

It was hypothesized that the oligo(*N*-methylpyrrole) moiety of **1a−c** would provide DNA affinity and sequence selectivity, directing the metal-binding moiety to sites differing from those of bleomycin. In Figure 4, a 5'-^{32}P labeled restriction fragment corresponding to bases 30−

Scheme 2. Synthesis of AMPHIS–Lexitropsin Conjugates

29 b: n = 2 (65%);
c: n = 3 (66%).
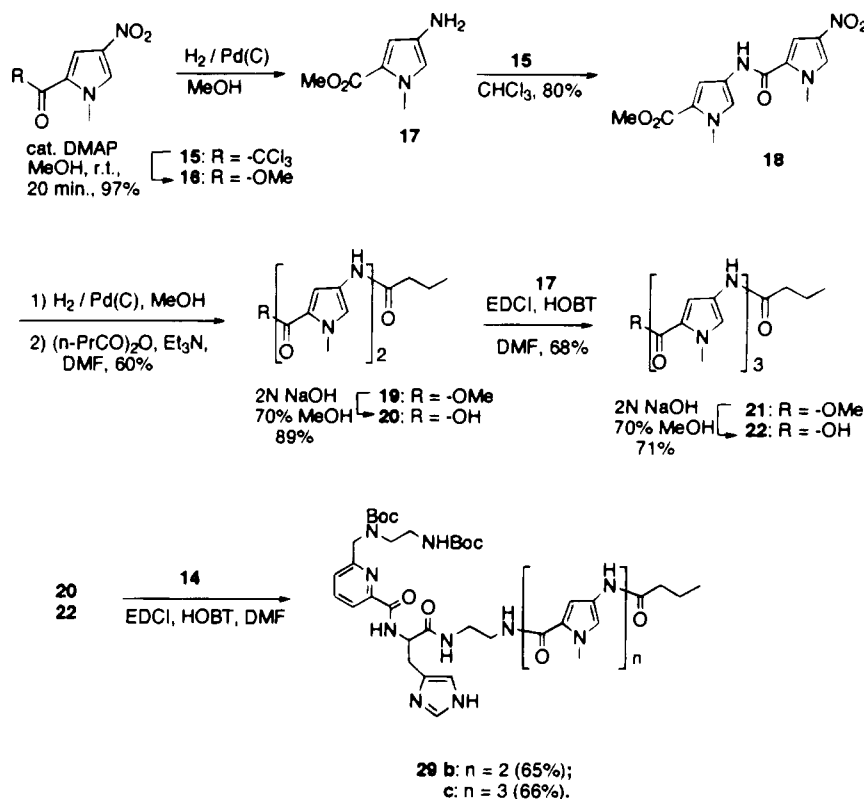
**Scheme 3. Synthesis of Lexitropsin Carriers**
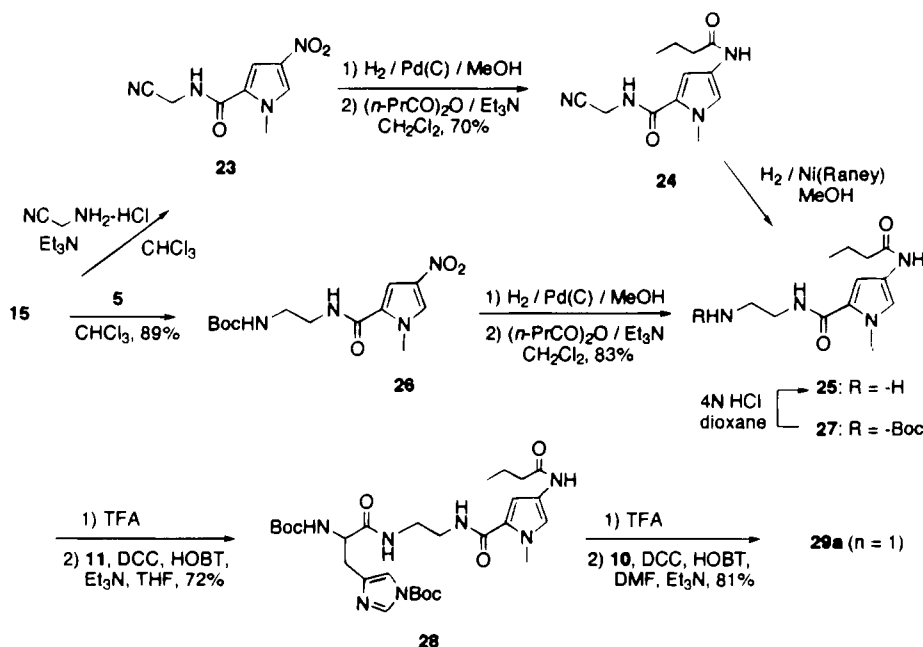
187 of pBR322 (*57*) was employed to investigate the DNA cleavage sequence selectivity of Fe(II)-**1a–c** and Fe(II)–BLM A$_2$. The hybrids were tested at 10–50 μM concentrations in order to determine the relationship between concentration and selectivity. Monopyrrole hybrid **1a** has no cleavage activity, which agrees with earlier work indicating that single *N*-methylpyrrolecarboxamides do not bind to DNA efficiently (*45*). Dipyrrole **1b** and tripyrrole **1c** demonstrate selective DNA cleavage activity in the vicinity of the two longest AT-containing tracts on the DNA. The apparent lack of activity of higher concentrations of tripyrrole **1c** was due to partial precipitation of the DNA in those lanes (data not shown).

The first cleavage site, a 5'-TTAAATT-3' (bases 56–62) sequence, is cleaved with very similar selectivity by the two hybrids, with strong cleavage at A59 in the center of the binding site and at G63 and C64 adjacent to the 3' end of the binding site. In the case of the 5'-AAATCTAA-CAAT-3' (bases 89–100) binding site, the strongest cleavage from **1b** appears at T94 in this sequence, with additional bands from **1c** at A95 and A96, as well. The position of these sites in the center of the DNA binding sequence is similar to the position of the A59 cleavage site centered within the 5'-TTAAATT-3' (bases 56–62) sequence. Weak cleavage bands also appear at C102, again adjacent to the 3' end of the binding site.

Scheme 4. Preparation of Iron Complex

1a: 90%;
1b: 85%;
1c: 91%.

Fe(II)-hybrid complexes
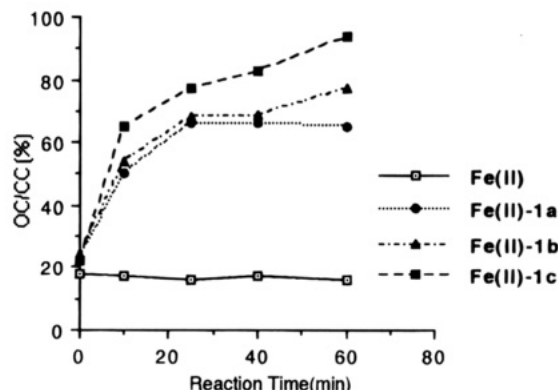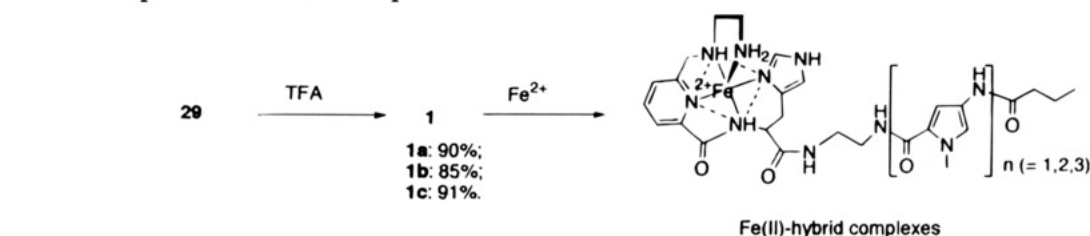
Figure 2. Plots of the percentage of the open circular (OC) DNA, (OC/CC, %) measured by ethidium fluorescence assay against reaction time. The reactions were run at 24 °C under aerobic conditions. Seventy μL of reaction mixture contained 50 μg/mL of pBR322 supercoiled covalently closed circular DNA (CCC) in 8.5 mM Tris buffer, pH 8.0, 1 mM 1,4-dithiothreitol (DTT), and, plot A, 5 μM Fe(II), plots B, C, and D, 80 μM Fe(II)−**1a,b,c** (1:1), respectively. 10 μL of reaction mixtures were used for each point.
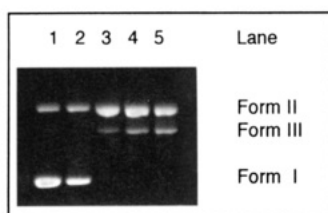
Figure 3. Supercoiled plasmid DNA cleavage by Fe(II)−**1** (1:1). The reactions were run under the same conditions as shown in Figure 2: lane 1, control DNA; lane 2, 5 μM Fe(II); lane 3, 80 μM of Fe(II)−**1a**; lane 4, 80 μM of Fe(II)−**1b**; lane 5, 80 μM of Fe(II)−**1c**. Form I: closed circular DNA. Form II: nicked circular DNA. Form III: linear DNA.

Figure 4 shows that DNA cleavage by hybrids **1a**−**c** differs from that of bleomycin and is selective for AT-rich regions of DNA. In order to further investigate the DNA cleavage activity and sequence selectivity of these compounds a DNA sequence containing several AT rich regions of varying length is needed. In Figure 5 a 5'-^{32}P labeled fragment corresponding to bases 347 to 588 of SV40(*58*) was cleaved with Fe(II)−**1(a**−**c)** and Fe(II)−BLM A$_2$. This DNA contains A$_7$, A$_6$, A$_5$, T$_5$, T$_4$, and other AT sequences, and all cleavage sites are either within or near an AT region. Monopyrrole **1a** again has no cleavage, consistent with the result shown in Figure 4. Dipyrrole **1b** and tripyrrole **1c** have nearly identical cleavage patterns. No cleavage appears at any sequence less than four bases in length; the AAA at the bottom of the figure is part of an A$_7$ sequence. Cleavage occurs consistently for two to three bases beyond the 3' end of the poly A sites; compare C405 and A406 with the CCA cleavage bands at 491−493 or 512−514. Cleavage occurs within the poly T sites, however, at the last 2 bases at the 5' end of the sequence. This is illustrated at T417 and T418, at T429 and T430, and at A448 and T449.
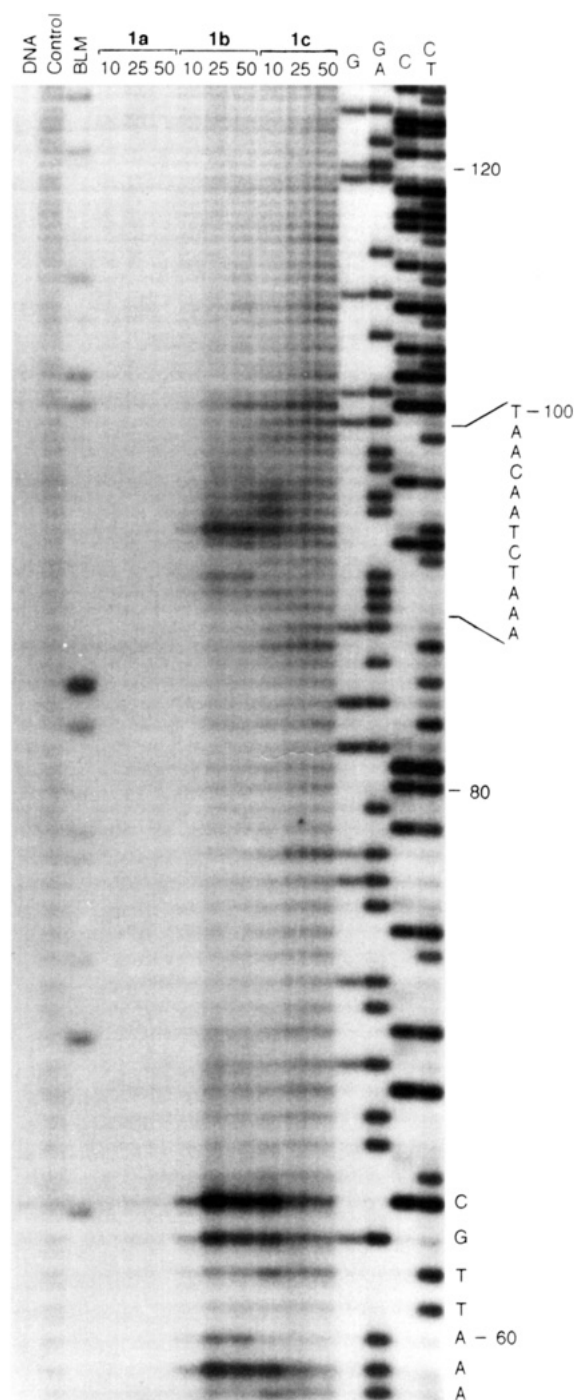
Figure 4. Sequencing gel autoradiogram of cleavage of a 5'-^{32}P labeled 158-bp restriction fragment by bleomycin and **1a**−**c**. DNA lane contains untreated DNA; control lane contains background cleavage from 50 μM Fe(II) + 250 μM DTT. BLM lane contains 1 μM Fe(II)−BLM A$_2$. Micromolar concentrations of Fe(II)−**1a**−**c** are as indicated above the central lanes; each of these lanes also contained 250 μM DTT. Lanes marked G, GA, C, and CT were treated by the Maxam−Gilbert sequence reactions for those bases.

Figure 5. Sequencing gel autoradiogram of cleavage of a 5'-^{32}P labeled 241-bp restriction fragment by bleomycin and **1a**–**c**. DNA lane contains untreated DNA; control lane contains background cleavage from 20 μM Fe(II) + 250 μM DTT. BLM lane contains 2μM Fe(II)-BLM A$_2$. Micromolar concentrations of Fe(II)-**1a**–**c** are as indicated; each of these lanes also contained 250 μM DTT. G, GA, C, and CT lanes were produced by the appropriate Maxam–Gilbert sequence reactions.

From the results in Figures 4 and 5 it can be concluded that di- and tripyrrole hybrids **1b** and **1c** cleave DNA efficiently at AT tracts and require at least a four base binding site for efficient cleavage. Further, the position of cleavage appears to be unaffected by either number of pyrroles in the DNA binding moiety of the compounds or by the size of the DNA binding site. A possible interpretation for this result is that the hybrid compounds prefer a particular end of the binding site (dependent on DNA sequence) and that the size of the binding site (beyond the 4 base minimum requirement) has no effect on the position of cleavage.

Figure 6. Portion of a high-resolution sequencing gel auto-radiogram of cleavage of a 5'-^{32}P labeled 158-bp restriction fragment by bleomycin, MPE, and **1b,c**. DNA lane contains untreated DNA; control lane contains background cleavage from 40 μM Fe(II) + 250 μM DTT. BLM lane contains 2μM Fe(II)–BLM A$_2$. MPE lanes contain 250 μM DTT and 30 or 40 μM Fe(II)–MPE, respectively. Lanes marked **1b** and **1c** contain 250 μM DTT and 20 μM Fe(II)–**1b** or 10 μM Fe(II)–**1c**. G, GA, C, and CT lanes were produced by the appropriate Maxam–Gilbert sequence reactions.

Identical nucleotide sequences which differ only in the structure of their 5' or 3' end groups can be resolved on high concentration polyacrylamide gels. This technique has been employed for the determination of cleavage products of many species, including bleomycin and analogs(*34,59*), methidiumpropyl-EDTA·Fe(II) (MPE·Fe(II)) (*60*), and ionizing radiation (*61*). In Figure 6 the DNA cleavage products from Fe(II)–BLM A$_2$, Fe(II)–MPE, and Fe(II)–**1b,c** are compared on a denaturing 20% poly-acrylamide gel. The MPE cleavage lanes have the

expected pattern of doublet bands, the lower containing a 3'-phosphoglycolate end group and the upper containing 3'-phosphate. The Maxam−Gilbert sequence lanes contain 3'-phosphate ends (54), which comigrate with the upper bands from MPE cleavage, and bleomycin produces 3'-phosphoglycolate as its major cleavage product bands at C64 and C70 (7), which comigrate with the lower MPE cleavage bands. Hybrids **1b** and **1c** produce bands which comigrate with the Maxam−Gilbert and the upper MPE cleavage bands and therefore contain 3'-phosphate end groups. Two possible interpretations for the production of 3'-phosphate by the hybrids are (1) that the simplified metal binding moiety of **1b** and **1c** is unable to form the activated species believed to cause bleomycin-type DNA cleavage or (2) that altered binding of the hybrid molecules places the activated species in an orientation favorable to abstraction of a sugar hydrogen other than the C-4' H which is abstracted by bleomycin.

Hénichart et al. (39) have shown with spin trapping ESR experiments that AMPHIS (the metal binding moiety in **1**) produces the same type and quantity of oxygen radical species as bleomycin, indicating that the same Fe(II) complex forms in both cases. Hamamichi et al. (34) showed that monothiazole bleomycin analogs containing the natural metal-binding moiety intact were capable of supporting oxidative transformations on small molecules of identical type and rate as natural bleomycin, but were unable to cleave DNA with high activity or selectivity. In addition, the monothiazole analogs formed comparable amounts of 3'-phosphate and 3'-phosphoglycolate in their DNA cleavage reactions. Research in the group of Kozarich and Stubbe (62, 63) implied that Fe−BLM cleavage products of a DNA−RNA hybrid might form via C-1' H abstraction, but were later shown to arise exclusively from C-4' H abstraction. Recently, Duff et al. (64) have shown that an altered DNA substrate containing *ara*-C (which contains a more accessible C-1' H at the cleavage site) was cleaved by bleomycin to produce products which can derive from initial C-1' H abstraction.

The minor groove of DNA contains the C-1' H, the C-4' H, and two C-5' H atoms. C-1' H abstraction in the case of neocarzinostatin (65) forms an abasic lesion containing 2-deoxyribonolactone, which when treated with base produces a strand break with 3' and 5' phosphate ends. The major pathway of DNA cleavage for both neocarzinostatin and calicheamicin (66) involves C-5' H abstraction, which results in direct strand breakage with 3' phosphate and 5' nucleoside aldehyde ends. The DNA cleaving 1,10-phenanthroline copper complex (67, 68) appears to be the only DNA cleaving agent capable of producing direct strand scission via C-1' H abstraction. The intermediate 2-deoxyribonolactone forms as with neocarzinostatin, but can decompose under the reaction conditions to 3' and 5' phosphate and 5-methylene-2(5H)-furanone. Complete conversion of the abasic lesion requires basic treatment, as with neocarzinostatin, or storage of the reaction mixture.

The reaction pathway of bleomycin−lexitropsin hybrids leading to production of 3' phosphate may resemble one of the above mechanisms or may be entirely novel. Because the 3' phosphate appears to be the only product formed from DNA cleavage by these hybrids, is formed immediately and is quite stable over time (data not shown), a C-1' mechanism similar to that of 1,10-phenanthroline−copper seems less likely than a C-5' mechanism similar to that of the enediynes. Further experiments are under way to more precisely elucidate this pathway and identify the other cleavage products.

LITERATURE CITED

(1) Umezawa, H., Maeda, K., Takeuchi, T., and Okami, Y. (1966) New antibiotics, bleomycin A and B. *J. Antibiot. Ser. A 19*, 20.

(2) Blum, R. H., Carter, S. K., and Agre, K. A. (1973) A clinical review of bleomycin—a new antineoplastic agent. *Cancer 31*, 903.

(3) Carter, S. K., Ichikawa, T., Mathe, G., and Umezawa, H. (1976) *Fundamental and Clinical Studies of Bleomycin,* University of Tokyo Press, Tokyo.

(4) Carter, S. K., Crooke, S. T., and Umezawa, H. (1978) *Bleomycin: Current Status and New Developments,* Academic Press, New York.

(5) Hecht, S. M. (1979) *Bleomycin: Chemical, Biochemical and Biological Aspects,* Springer-Verlag, New York.

(6) Sikic, B. I., Rozencweig, M., and Carter, S. K. (1985) *Bleomycin Chemotherapy,* Academic Press, Orlando, FL.

(7) Hecht, S. M. (1986) The chemistry of activated bleomycin. *Acc. Chem. Res. 19*, 383.

(8) Stubbe, J., and Kozarich, J. W. (1987) Mechanisms of bleomycin-induced DNA degradation. *Chem. Rev. 87*, 1107.

(9) Murphy, J. A., and Griffiths, J. (1993) A survey of natural products which abstract hydrogen atoms from nucleic acids. *Nat. Prod. Rep. 10*, 551.

(10) Chien, M., Grollman, A. P., and Horwitz, S. B. (1977) Bleomycin−DNA interactions: fluorescence and proton magnetic resonance studies. *Biochemistry 16*, 3641.

(11) Kross, J., Henner, D., Haseltine, W. A., Rodriguez, L., Levin, M. D., and Hecht, S. M. (1982) Structural basis for the deoxyribonucleic acid affinity of bleomycins. *Biochemistry 21*, 3711.

(12) Sugiura, Y., and Suzuki, T. (1982) Nucleotide sequence specificity of DNA cleavage by iron-bleomycin. *J. Biol. Chem. 257*, 10544.

(13) Kuwahara, J., and Sugiura, Y. (1988) Sequence-specific recognition and cleavage of DNA by metallobleomycin: minor groove binding and possible interaction mode. *Proc. Natl. Acad. Sci. U.S.A. 85*, 2459.

(14) Urata, H., Ueda, Y., Usami, Y., and Akagi, M. (1993) Enantiospecific recognition of DNA by bleomycin. *J. Am. Chem. Soc. 115*, 7135.

(15) Otsuka, M., Kittaka, A., Ohno, M., Suzuki, T., Kuwahara, J., Sugiura, Y., and Umezawa, H. (1986) Synthetic study towards man-designed bleomycins. Synthesis of a DNA cleaving molecule based on bleomycin. *Tetrahedron Lett. 27*, 3639.

(16) Kittaka, A., Sugano, Y., Otsuka, M., and Ohno, M. (1988) Man-designed bleomycins. Synthesis of dioxygen activating molecules and a DNA cleaving molecule based on bleomycin−Fe(II)−O₂ complex. *Tetrahedron 44*, 2821.

(17) Kenani, A., Lohez, M., Houssin, R., Helbecque, N., Bernier, J. L, Lemay, P., and Hénichart, J. P. (1987) Chelating, DNA-binding and DNA-cleaving properties of a synthetic model for bleomycin. *Anti-Cancer Drug Design 2*, 47.

(18) Saito, I., Morii, T., Obayashi, T., Sera, T., Sugiura, H., and Matsuura, T. (1989) Synthetic cobalt bleomycin models as a photochemical DNA cleaver. *J. Chem. Soc. Chem. Commun.* 360.

(19) Boger, D. L., Menezes, R. F., Dang, Q., and Yang, W. (1992) Deglyco GABA,Gly-desacetamidobleomycin A₂: a simplified synthetic model for Bleomycin A₂. *BioMed. Chem. Lett. 2*, 261.

(20) Owa, T., Haupt, A., Otsuka, M., Kobayashi, S., Tomioka, N., Itai, A., Ohno, M., Shiraki, T., Uesugi, M., Sugiura, Y., and Maeda, K. (1992) Man-designed bleomycins: significance of the binding sites as enzyme models and the stereochemistry of the linker moiety. *Tetrahedron 48*, 1193.

(21) Boger, D. L., Menezes, R. F., and Dang, Q. (1992) Synthesis of desacetamidopyrimidoblamic acid and deglyco desacetamidobleomycin A₂. *J. Org. Chem. 57*, 4333.

(22) Otsuka, M., Yoshida, M., Kobayashi, S., Ohno, M., Sugiura, Y., Takita, T., and Umezawa, H. (1981) Transition-metal binding site of bleomycin. A synthetic analogue capable of binding Fe(II) to yield an oxygen-sensitive complex. *J. Am. Chem. Soc. 103*, 6986.

(23) Kilkuskie, R. E., Suguna, H., Yellin, B., Murugesan, N., and Hecht, S. M. (1985) Oxygen transfer by bleomycin analogues dysfunctional in DNA cleavage. *J. Am. Chem. Soc. 107*, 260.

(24) Brown, S., and Mascharak, P. K. (1988) Characterization of a crystalline synthetic analogue of copper(II)-bleomycin. *J. Am. Chem. Soc. 110*, 1996.

(25) Lomis, T. J., Siuda, J. F., and Shepherd, R. E. (1988) Bleomycin metal site models with apical imidazole or sulphydryl donors. *J. Chem. Soc. Chem. Commun.* 290.

(26) Cristini, M., Scrimin, P., and Tonellato, U. (1989) A micellar model of bleomycin antibiotics. *Tetrahedron Lett. 30*, 2987.

(27) Aoyagi, Y., Chorgade, M. S., Padmapriya, A. A., Suguna, H., and Hecht, S. M. (1990) Synthesis of pyrimidoblamic acid and epipyrimidoblamic acid. *J. Org. Chem. 55*, 6291.

(28) Suga, A., Sugiyama, T., Otsuka, M., Ohno, M., Sugiura, Y., and Maeda, K. (1991) Oxidation of alkenes by a chiral non-porphyrinic oxidizing catalyst based on the bleomycin−Fe(II) complex. *Tetrahedron 47*, 1191.

(29) Tan, J. D., Hudson, S. E., Brown, S. J., Olmstead, M. M., and Mascharak, P. K. (1992) Syntheses, structures, and reactivities of synthetic analogues of the three forms of Co(III)-bleomycin: proposed mode of light-induced DNA damage by the Co(III) chelate of the drug. *J. Am. Chem. Soc. 114*, 3841.

(30) Guajardo, R. J., Hudson, S. E., Brown, S. J., and Mascharak, P. K. (1993) [Fe(PMA)]$^{n+}$ (n=1,2): good models of Fe-bleomycins and examples of mononuclear non-heme iron complexes with significant O_2-activation capabilities. *J. Am. Chem. Soc. 115*, 7971.

(31) Otsuka, M., Satake, H., and Sugiura, Y. (1993) Restructuring of the bleomycin metal core. Novel oxygen-activating ligands with symmetrized structure. *Tetrahedron 34*, 8497.

(32) Boger, D. L., Honda, T., Menezes, R. F., Colletti, S. L., Dang, Q., and Yang, W. (1994) Total syntheses of (+)-P-3A, epi-(−)-P-3A, and (−)-desacetamido P-3A. *J. Am. Chem. Soc. 116*, 82.

(33) Sugiyama, T., Ohno, M., Shibasaki, M., Otsuka, M., Sugiura, Y., Kobayashi, S., and Maeda, K. (1994) Transition-metal binding site of bleomycin. Significance of the β-amino-alanineamide appendage in regulating oxygen activation. *Heterocycles 37*, 275.

(34) Hamamichi, N., Natrajan, A., and Hecht, S. M. (1992) On the role of individual bleomycin thiazoles in oxygen activation and DNA cleavage. *J. Am. Chem. Soc. 114*, 6278.

(35) Otsuka, M., Masuda, T., Haupt, A., Ohno, M., Shiraki, T., Sugiura, Y., and Maeda, K. (1990) Man-designed bleomycin with altered sequence specificity in DNA cleavage. *J. Am. Chem. Soc. 112*, 838.

(36) Farinas, E., Tan, J. D., Baidya, N., and Masacharak, P. K. (1993) A designed synthetic analogue of Co(III)-bleomycin with enhanced DNA-binding and photocleaving activity. *J. Am. Chem. Soc. 115*, 2996.

(37) Zarytova, V. F., Sergeyev, D. S., and Godovikova, T. S. (1993) Synthesis of bleomycin A5 oligonucleotide derivatives and site-specific cleavage of the DNA target. *Bioconjugate Chem. 4*, 189.

(38) Hénichart, J. D., Houssin, P., Bernier, J. L., and Catteau, J. P (1982) Synthetic model of a bleomycin metal complex. *J. Chem. Soc., Chem. Commun.* 1295.

(39) Hénichart, J. P., Bernier, J. L., Houssin, R., Lohez, M., Kenani, A., and Catteau, J. P. (1985) Copper(II)- and iron(II)-complexes of methyl 2-(2-aminoethyl)-aminomethyl-pyridine-6-carboxyl-histidinate (AMPHIS), a peptide mimicking the metal-chelating moiety of bleomycin. An ESR investigation. *Biochem. Biophys. Res. Commun. 126*, 1036.

(40) Shinozuka, K., Morishita, H., Yamazaki, T., Sugiura, Y., and Sawai, H. (1991) Enantiomeric bleomycin model compounds bearing long alkyl-chain. *Tetrahedron Lett. 32*, 6869.

(41) Taylor, J. S., Schultz, P. G., and Dervan, P. B. (1984) DNA affinity cleaving. Sequence specific cleavage of DNA by

distamycin−EDTA·Fe(II) and EDTA−distamycin·Fe(II). *Tetrahedron 40*, 457.

(42) Dervan, P. B. (1986) Design of sequence-specific DNA-binding molecules. *Science 232*, 464.

(43) Lown, J. W. (1988) Lexitropsins: rational design of DNA sequence reading agents as novel anticancer agents and potential cellular probes. *Anti-Cancer Drug Design 3*, 25.

(44) Lown, J. W. (1992) Lexitropsins in antiviral drug development. *Antiviral Res. 17*, 179.

(45) Zimmer, C., and Wahnert, U. (1986) Nonintercalating DNA-binding ligands: specificity of the interaction and their use as tools in biophysical, biochemical, and biological investigations of the genetic material. *Prog. Biophys. Molec. Biol. 47*, 31.

(46) Mathes, W., Sauermilch, W., and Klein, T. (1953) Some derivatives of 2,6-lutidine. *Chem. Ber. 86*, 584.

(47) Keller, O., Keller, W. E., van Look, G., and Wersin, G. (1990) tert-Butoxycarbonylation of amino acids and their derivatives: N-tert-butoxycarbonyl-L-phenylalanine. *Organic Syntheses*; Wiley: New York, 1990; Collect. Vol. VII, p 71.

(48) Nishiwaki, E., Tanaka, S., Lee, H., and Shibuya, M. (1988) Efficient synthesis of oligo-N-methylpyrrolecarboxamides and related compounds. *Heterocycles 27*, 1945.

(49) Nishiwaki, E., Nakagawa, H., Takasaki, M., Matsumoto, T., Sakurai, H., and Shibuya, M. (1990) Synthesis of oligo-N-methylpyrrolecarboxamide derivatives and their photochemical DNA cleaving activities. *Heterocycles 31*, 1763.

(50) Bialer, M., Yagen, B., and Mechoulan, R. (1978) Total synthesis of distamycin A, an antiviral antibiotic. *Tetrahedron 34*, 2389.

(51) Lown, J. W., and Krowicki, K. (1985) Efficient total synthesis of the oligopeptide antibiotics netropsin and distamycin. *J. Org. Chem. 50*, 3774.

(52) Gravert, D. J., and Griffin, J. H. (1993) Specific DNA cleavage mediated by [salenMn(III)]$^+$. *J. Org. Chem. 58*, 820.

(53) Sambrook, J., Fritsch, E. F., and Maniatis, T. (1989) *Molecular Cloning: A Laboratory Manual*, 2nd ed., Cold Spring Harbor Laboratory Press, New York.

(54) Maxam, A. M., and Gilbert, W. (1980) Sequencing end labeled DNA with base-specific chemical cleavages. *Methods Enzymol. 65*, 499.

(55) Fife, T. H., and Przystas, T. J. (1982) Effects of divalent metal ions on hydrolysis of esters of 2-(hydroxymethyl)-picolinic acid. Metal ion catalysis of the carboxyl, hydroxide ion, and water reactions. *J. Am. Chem. Soc. 104*, 2251.

(56) Morgan, A. R., Lee, S. J., Pulleyblank, D. E., Murray, N. L., and Evans, D. H. (1979) Ethidium fluorescence assays. Part 1. Physicochemical studies. *Nucleic Acids Res. 7*, 547.

(57) Balbás, P., Soberón, X., Merino, E., Zurita, M., Lomeli, H., Valle, F., Flores, N., and Bolivar, F. (1986) Plasmid vector pBR322 and its special-purpose derivatives-a review. *Gene 50*, 3.

(58) Van Heuverswyn, H., and Fiers, W. (1979) Nucleotide sequence of the Hind-C fragment of simian virus 40 DNA. *Eur. J. Biochem. 100*, 51.

(59) Kross, J., Henner, W. D., Hecht, S. M., and Haseltine, W. A. (1982) Specificity of deoxyribonucleic acid cleavage by bleomycin, phleomycin, and tallysomycin. *Biochemistry 21*, 4310.

(60) Hertzberg, R. P., and Dervan, P. B. (1984) Cleavage of DNA with methidiumpropyl−EDTA−iron(II): reaction conditions and product analyses. *Biochemistry 23*, 3934.

(61) Henner, W. D., Rodriguez, L. O., Hecht, S. M., and Haseltine, W. A. (1983) γ Ray induced deoxyribonucleic acid strand breaks: 3' glycolate termini. *J. Biol. Chem. 258*, 711.

(62) Krishnamoorthy, C. R., Vanderwall, D. E., Kozarich, J. W., and Stubbe, J. (1988) Degradation of DNA−RNA hybrids by bleomycin: evidence for DNA strand specificity and for possible structural modification of chemical mechanism. *J. Am. Chem. Soc. 110*, 2008.

(63) Absalon, M. J., Krishnamoorthy, C. R., McGall, G., Kozarich, J. W., and Stubbe, J. (1988) Bleomycin mediated degradation of DNA-RNA hybrids does not involve C-1' chemistry. *Nucleic Acids Res. 20*, 4179.

(64) Duff, R. J., de Vroom, E., Geluk, A., and Hecht, S. M. (1993) Evidence for C-1' hydrogen abstraction from modified oligonucleotides by Fe-bleomycin. *J. Am. Chem. Soc. 115*, 3350.

(65) Goldberg, I. H. (1991) Mechanism of neocarzinostatin action: role of DNA microstructure in determination of chemistry of bistranded oxidative damage. *Acc. Chem. Res.* *24*, 191.

(66) Lee, M. D., Ellestad, G. A., and Borders, D. B. (1991) Calicheamicins: Discovery, structure, chemistry, and interaction with DNA. *Acc. Chem. Res. 24*, 235.

(67) Sigman, D. S. (1986) Nuclease activity of 1,10-phenanthroline-copper ion. *Acc. Chem. Res. 19*, 180.

(68) Goyne, T. E., and Sigman, D. S. (1987) Nuclease activity of 1,10-phenanthroline-copper ion. Chemistry of deoxyribose oxidation. *J. Am. Chem. Soc. 109*, 2846.

BC940077A

Synthesis of LHRH Antagonists Suitable for Oral Administration via the Vitamin B$_{12}$ Uptake System

G. J. Russell-Jones,*,† S. W. Westwood,† P. G. Farnworth,‡ J. K. Findlay,‡ and H. G. Burger‡

Biotech Australia Pty Ltd, P.O. Box 20, Roseville, NSW 2069, Australia, and Prince Henry's Institute of Medical Research, P.O. Box 5152, Clayton, Victoria 3168, Australia. Received April 27, 1994⊛

Conjugates have been synthesized between vitamin B$_{12}$ and two lysyl derivatives of the LHRH antagonist, ANTIDE. Lys^6-ANTIDE and Lys^8-ANTIDE were both found to have similar activities to the native analogue in the *in vitro* pituitary cell assay. The *in vitro* bioactivity of the VB$_{12}$–ANTIDE conjugates was preserved following linkage using a number of spacers; however, the *in vivo* bioactivity was lost. In order to produce conjugates which had similar *in vivo* bioactivity to the native analogue, it was necessary to link the VB$_{12}$ to the ANTIDE analogues using thiol cleavable spacers. The resultant conjugates had similar activity to ANTIDE both *in vitro* and *in vivo* and were also found to be much more water soluble than ANTIDE. These VB$_{12}$–ANTIDE conjugates show potential utility as water soluble ANTIDE analogues for parenteral use and are protease resistant LHRH antagonist analogues suitable for uptake from the intestine via the VB$_{12}$-transport system following oral administration.

INTRODUCTION

Hypothalamic gonadotrophin releasing hormone (GnRH, also known as luteinizing hormone releasing hormone, LHRH) regulates pituitary gonadotrophin synthesis and secretion (Schally et al., 1971). Over the past 23 years, numerous analogues of LHRH have been synthesized which may be classified according to their acute effects on gonadotrophin release, as either agonists (with enhancement of release) or antagonists (with inhibition of LHRH-stimulated release). The agonists often show an increase in binding affinity to pituitary LHRH receptors (Loumay et al., 1982; Perrin et al., 1980) and increased resistance to the proteolytic degradation that rapidly removes native LHRH from the circulation. The observation that these potent analogues can induce potentially reversible medical castration has provided a new approach to the treatment of various gonadotrophin dependent disorders, particularly hormone dependent prostate and breast cancer.

Two distinct phases in the induction of chemical castration with agonists occur. The agonist initially stimulates the pituitary–gonadal axis, causing a transient increase in gonadotrophin and sex steroid secretion in the first 2 weeks or so. After this period there is a down regulation of pituitary LHRH receptors, with subsequent decline in gonadotrophin and sex steroid secretion. The initial stimulation of testosterone is a substantial drawback to the use of agonists in the treatment of prostatic malignancy, as it can produce a painful flare of the disease with consequent adverse clinical effects (Eisenberger and Abrams, 1988; Crawford and Davis, 1988). By contrast, the use of LHRH antagonists should be advantageous in avoiding the initial flare. First attempts at the production of antagonists led to compounds characterized by undesirable histamine release (Karten and Rivier, 1986; Schmidt et al., 1984; Phillips et al., 1988). However, new antagonists have been developed that are characterized by improved potency and much less histamine releasing potential (e.g.,

Karten and Rivier, 1986). One of the most potent antagonists described to date is the analogue N-Ac-D-Nal-(2), D-Phe (pCl), D-Pal(3), Ser, Lys (Nic), D-Lys(Nic), Leu, Lys(iPr), Pro, D-Ala-NH$_2$, or ANTIDE, synthesized by Folkers and co-workers (Ljungstedt et al., 1987). It potently inhibits ovulation in rats (Ljungqvist et al., 1988), and single doses have profound, long lasting inhibitory effects on serum LH concentrations in castrate female cynomolgous monkeys (Leal et al., 1988). It has also been shown to be capable of inducing long term chemical castration in intact adult male rats and cynomolgous monkeys and to have an inhibitory effect on tumor growth in the Dunning R3327 prostatic carcinoma model, similar to that of castration (Habenicht et al., 1990). The new antagonist should therefore be of substantial clinical interest in all those conditions in which medical castration is desirable, particularly in the management of prostatic cancer and in various gynaecological disorders (McLachlan et al., 1986).

Current administration of ANTIDE is limited to the parenteral route. However, the dose of analogue that can be delivered by this route is limited due to the poor solubility of the antagonist. Thus, clinical trials of the long term effect of ANTIDE have been limited to doses of 2.5 mg or lower.

To date, the LHRH antagonists developed for clinical use must be given to the patient by injection or frequent nasal sprays, as they have very limited oral bioavailability. Injections are generally given daily, and patients must be educated in the use of the appropriate equipment. Clearly, the development of a technique to deliver these antagonists orally would have important advantages for both patient and doctor, and would therefore represent a significant therapeutic advance.

The oral route of administration of peptides such as LHRH and its analogues as pharmaceuticals in the treatment of systemic conditions has so far met with little success. In general, the amount of peptide required for successful oral administration has been 100–1000 times the dose required for parenteral delivery, thus making the administration of these agents via this route prohibitively expensive. There are two fundamental reasons for the lack of success. Firstly, the intestinal milieu has a high level of proteolytic activity, which rapidly degrades most peptides. Secondly, while there are well-defined

Table 1. Sequence of ANTIDE and Its Analogues

Analogue		Sequence
ANTIDE		*N*-Ac-D-Nal(2), D-Phe (*p*Cl), D-Pal(3), Ser, Lys (Nic), D-Lys(Nic), Leu, Lys(iPr), Pro, D-Ala-NH$_2$
D-Lys^{6}ANTIDE or ANTIDE-1		*N*-Ac-D-Nal(2), D-Phe (*p*Cl), D-Pal(3), Ser, Lys (Nic), D-Lys, Leu, Lys(iPr), Pro, D-Ala-NH$_2$
Lys^{5}ANTIDE or Antide-2		*N*-Ac-D-Nal(2), D-Phe (*p*Cl), D-Pal(3), Ser, Lys, D-Lys(Nic), Leu, Lys(iPr), Pro, D-Ala-NH$_2$
Lys^{8}ANTIDE or ANTIDE-3		*N*-Ac-D-Nal(2), D-Phe (*p*Cl), D-Pal(3), Ser, Lys (Nic), D-Lys(Nic), Leu, Lys, Pro, D-Ala-NH$_2$

uptake mechanisms for individual amino acids and dipeptides, there is no general mechanism for polypeptides to be transported across the membrane of the mucosal epithelium into the circulation. Rather, this membrane constitutes a general barrier to exclude the uptake of the numerous foreign proteins encountered in this environment. Thus, although a peptide may be modified to withstand the enzymatic barrage encountered in the intestine, such modification is of little value if the peptide cannot subsequently cross the mucosal barrier and enter the systemic circulation.

A delivery system suitable for the oral administration of peptides such as ANTIDE has recently been developed by Russell-Jones and co-workers (1994). This method takes advantage of the natural intrinsic factor (IF)-mediated uptake mechanism for dietary vitamin B$_{12}$ (VB$_{12}$ or cyanocobalamin) in the intestine. During the process of uptake, VB$_{12}$ first binds to IF in the upper small intestine. The VB$_{12}$−IF complex then proceeds down the small intestine and binds to an IF receptor located on the surface of the ileal epithelium. The whole VB$_{12}$−IF−receptor complex is then internalized by receptor-mediated endocytosis, and some time later the VB$_{12}$ appears in serum. Russell-Jones and co-workers (1994) have found that it is possible to modify VB$_{12}$ to provide suitable functional groups for conjugation of the derivatized VB$_{12}$ to various drugs and peptide/protein pharmaceuticals. Conjugates can be prepared which retain a high affinity for IF as well as significant bioactivity of the pharmaceutical. When the VB$_{12}$−pharmaceutical complex is administered orally the natural IF-mediated VB$_{12}$-uptake system can take up the conjugate from the intestinal lumen and thereafter deliver the pharmaceutical to the circulation.

In this paper we describe the formation of conjugates between ANTIDE derivatives and VB$_{12}$, and the bioactivity of both molecules in the conjugates, as a prelude to developing a formulation suitable for the oral administration of ANTIDE.

MATERIALS AND METHODS

Pituitary Cell Assay for Luteinizing Hormone Release. Cell cultures were prepared by trypsin/deoxyribonuclease digestion of the anterior pituitaries of 3-month-old male Sprague-Dawley rats. Cells were dispersed as a single cell suspension of 250 000 viable cells per mL in Dulbecco's modified Eagle's Medium: Ham's F12 medium (1:1) supplemented with 10% foetal bovine serum plus antibiotics. Aliquots of 0.30 mL were dispensed into 48-well tissue culture plates and maintained at 37 °C in an enclosed humidified atmosphere of 5% CO$_2$ in air. Cells were cultured for 2 days, and medium was then removed. The medium in triplicate cultures was replaced with fresh serum-free DMEM:F12 medium supplemented with 0.1% bovine serum albumin and containing a range of doses of ANTIDE, ANTIDE analogues, or VB$_{12}$−ANTIDE conjugates and was immediately supplemented with 30 nM LHRH. Concentrated stocks of all analogues were dissolved in polypropylene:water (1:1). Cells were incubated for 4 h, after which time medium was removed for the subsequent determination of its luteinizing hormone (LH) content by radioimmunoassay (RIA) (Farnworth et al., 1988). The

data from each trial were subsequently fitted to a four-parameter curve-fitting equation to determine the median inhibitory concentration (IC$_{50}$) of each analogue, which was tested in several independent experiments.

Castrate Rat Model. Adult male Sprague-Dawley rats were castrated and maintained in the animal house for 1 week prior to administration of test substances. ANTIDE and ANTIDE analogues were administered by subcutaneous injection into groups of five castrate rats. Blood samples were collected from the external jugular vein 24 h after the injection (Puénte and Catt, 1986). LH was measured by a standard radioimmunoassay.

Ethics. All animal experiments were approved by the institutional animal experimentation and ethics committee as conforming with the guidelines on animal experimentation of the National Health and Medical Research Council and the State of Victoria.

IF Assay. The affinity of the various VB$_{12}$−ANTIDE conjugates for IF was determined in a competitive binding assay (Russell-Jones, 1994). Dilutions of unlabeled VB$_{12}$ or VB$_{12}$ analogue or conjugate were mixed with 1 ng of ^{57}CoVB$_{12}$ (Amersham). One IU of IF (a unit of IF is the quantity of IF required to bind 1 ng of VB$_{12}$) was then added to the mixture, and the mixture was incubated for 20 min at room temperature (rt) before the addition of a solution of 5% activated charcoal in 0.1% BSA (IF and VB$_{12}$-free, Sigma). Samples were centrifuged, and the counts in the supernatant (IF bound) and pellet (free ^{57}Co VB$_{12}$) were used to determine the relative affinity of IF for the material tested.

Analytical Methods. Analytical RP-HPLC was carried out on a Vydac 218TP C18 column (5 μm beads, 4.6 × 250 mm) using a Waters gradient system comprised of Model 510 pumps, an automated gradient controller, and a Waters 991 photodiode array detector. The buffer system used 0.1% TFA/water as buffer A and 0.1% TFA in 70:30 acetonitrile:water as buffer B. The column was developed with a gradient of 5% to 75% buffer B over 35 min. Preparative RP-HPLC was carried out on either a Vydac semipreparative C4 column (10 μm beads, 1 × 25 cm) (column A), using a gradient of 5%−100% acetonitrile containing 0.1% TFA, or a semipreparative Vydac C18 column (10 μm beads, 1 × 25 cm) (column B), using a gradient of 5%−80% 70:30 acetonitrile:water containing 0.1% TFA. Size exclusion chromatography was carried out on a G-25 Sephadex column, eluting with 10% aqueous acetic acid. Ionspray mass spectra were obtained by Dr. Alun Jones at the Centre for Drug Design and Development, University of Queensland. UV spectra were recorded as aqueous solutions on a Shimadzu UV-160A instrument.

Synthesis of ANTIDE Analogues. Three ANTIDE analogues containing single, unmodified lysines, namely D-Lys^{6}ANTIDE (ANTIDE-1), Lys^{5}ANTIDE (ANTIDE-2), and Lys^{8}ANTIDE (ANTIDE-3), were synthesized on an Applied Biosystems Peptide Synthesizer (see Table 1). Peptides were cleaved from the resin and purified by reversed phase HPLC, using a gradient of 5−100% acetonitrile in 0.1% TFA.

Synthesis of Functionalized VB$_{12}$ Derivatives. eVB$_{12}$ Carboxylate (1b). In order to obtain a functional group suitable for conjugation of the cobalamin nucleus of VB$_{12}$ (1a) (Figure 1) to the ANTIDE analogs, cyano-
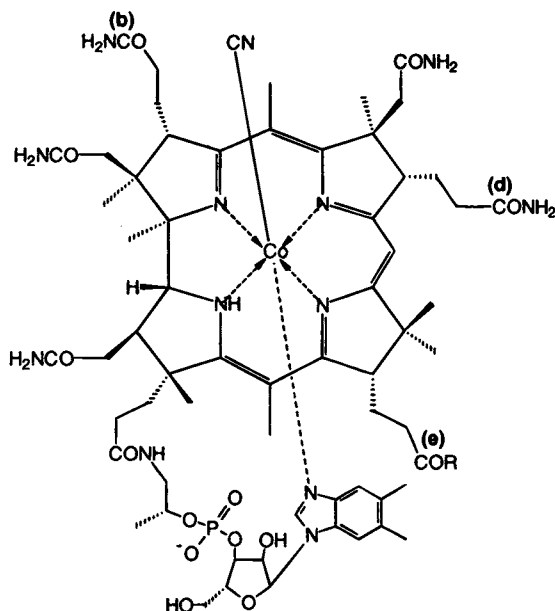
1a R = NH$_2$

1b R = OH

1c R = NH(CH$_2$)$_2$NH$_2$

1d R = NH(CH$_2$)$_6$NH$_2$

1e R = NH(CH$_2$)$_2$NHCOPhCH$_2$COOH

1f R = NH(CH$_2$)$_2$NHCO(CH$_2$)$_2$SSPy

1g R = NH(CH$_2$)$_6$NHCOPhCH(CH$_3$)SSPy

1h R = NH(CH$_2$)$_6$NHCOCH$_2$I

1i R = NH-Gly-Gly-Glu-Ala-OMe

Figure 1.

cobalamin was hydrolyzed in 0.4 M HCl for 72 h. This affords a mixture of the three isomeric monocarboxylates derived from hydrolysis at either the b, d, or e propionamide side chains. The e isomer of monocarboxy vitamin B$_{12}$ (**1b**), which has previously been shown to have the highest affinity for IF of the three isomers (Kolhouse and Allen, 1977), was separated from the b and d isomers by a combination of Dowex 1×2 chromatography and semi-preparative RP-HPLC developed with a gradient of 5–100% acetonitrile in 0.1% TFA. This procedure was an adaptation of the general protocol of Anton (Anton *et al.*, 1980).

eVB$_{12}$ 2-Aminoethylamide (1c). eVB$_{12}$ carboxylate (65 mg) was treated with 1,2-diaminoethane at pH 6.5 using a 20-fold molar excess of the diamine over e isomer and a 20-fold molar excess of 1-ethyl-3-(3-(dimethylamino)propyl)carbodiimide (EDAC; Biorad, Richmond, CA). The 2-aminoethylamide VB$_{12}$ derivative was purified by RP-HPLC (column A). Eluted material was further purified by S-Sepharose chromatography. The amino derivative was eluted with 0.1 M HCl, followed by extraction into phenol, and back-extraction into water after the addition of dichloromethane to the phenol phase. The product **1c** (42 mg) was recovered as a red powder from the water phase by lyophilization.

eVB$_{12}$ 6-Aminohexylamide (1d). eVB$_{12}$ carboxylate (100 mg) was treated with 1,6-diaminohexane at pH 6.5 using a 20-fold molar excess of the diamine over e isomer and a 20-fold molar excess of 1-ethyl-3-(3-(dimethylamino)propyl) carbodiimide (EDAC; Biorad, Richmond, CA). The VB$_{12}$ 6-aminohexylamide derivative **1d** was purified by RP-HPLC (column A). Eluted material was further purified by S-Sepharose chromatography. The amino

derivative was eluted with 0.1 M HCl, followed by extraction into phenol, and backextraction into water after the addition of dichloromethane to the phenol phase. The product **1d** (82 mg) was recovered as a red powder from the water phase by lyophilization.
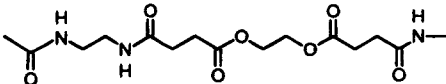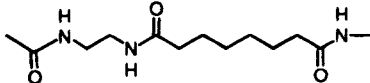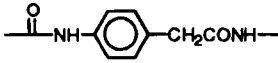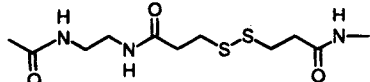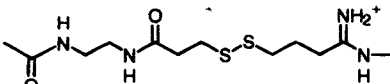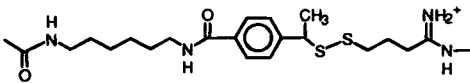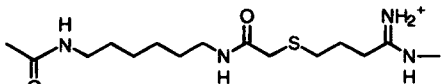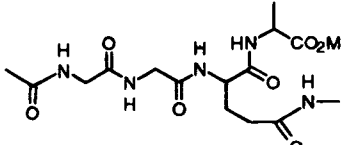
Formation of VB$_{12}$–ANTIDE Conjugates Using Direct Amide Linkage. Three ANTIDE conjugates were prepared by a direct amide linkage of the peptide to VB$_{12}$. The carboxylate **1b** was converted *in situ* to the corresponding N-hydroxysuccinimidyl ester by treatment with a 10-fold molar excess of EDAC and N-hydroxysuccinimide and added to a solution of an equivalent amount of the peptide in bicarbonate buffer (100 mM, pH 9.5). The products are B12–CONH–ANT1 (**2**); B12–CONH–ANT2 (**3**); and B12–CONH–ANT3 (**4**) depending on whether the conjugate was formed between ANTIDE-1, -2, or -3.

Formation of VB$_{12}$–ANTIDE Conjugates Using Noncleavable Bifunctional Crosslinkers. ANTIDE-1 and ANTIDE-3 were reacted with a 1.5-fold molar excess of ethylene glycol bis(succinimidyl succinate) (EGS, Pierce) for 10 min at room temperature. Aminoethyl eVB$_{12}$ **1c** was then added and the coupling allowed to proceed overnight. The conjugates formed are B12–[EGS]–ANT1 (**5**) and B12–[EGS]–ANT3 (**6**). They were purified initially by size-exclusion chromatography prior to a final cleanup by RP-HPLC (column A). This crosslinking protocol was repeated using ANTIDE-1 and disuccinimidyl suberate (DSS; Pierce, Rockford, IL). Reaction of the intermediate formed in situ with **1c** and subsequent cleanup afforded B12–[DSS]–ANT3, (**7**). Conjugates were also prepared using an anilido linkage. eVB$_{12}$ carboxylate **1b** was activated as described above with EDAC and NHS and coupled to p-aminophenylacetic acid. The resultant VB$_{12}$–anilide **1e** was in turn coupled to either ANTIDE-1 or ANTIDE-3 by activation of the VB$_{12}$ phenylacetate with EDAC/NHS and addition to a solution of the peptides in bicarbonate buffer. The product was purified by G-25 chromatography in 10% acetic acid followed by preparative RP-HPLC (column A) to give anilide-linked conjugates B12–PA–ANT1 (**8**) and B12–PA–ANT3 (**9**).

Formation of VB$_{12}$–ANTIDE Conjugates Using Thiol-Cleavable Cross-Linkers. Aminoethyl eVB$_{12}$ **1c** was reacted with N-succinimidyl 3-(2-pyridyldithio)propionate (SPDP; Pierce, Rockford, IL) using standard literature conditions (Carlsson et al., 1978). The (dithiopyridyl)ethyl eVB$_{12}$ derivative **1f** was purified by RP-HPLC (column B). A free thiol was introduced onto ANTIDE-1 by reaction with SPDP, followed by reduction of the introduced dithiopyridyl group with β-mercaptoethanol. The product (HS-ANT1) was purified by RP-HPLC (column B). Similarly, a free thiol was introduced into ANTIDE-3 by reaction with 2-iminothiolane (King et al., 1978). The thiolated product (HS-HN$^+$ANT3) was purified by RP-HPLC (column B). Formation of the disulfide linked conjugates B12–SS–ANT1 (**10**) and B12–SS–NH$^+$ANT3 (**11**) was achieved by reaction of each thiolated ANTIDE derivative with **1f** in 2.5% acetic acid for 24 h. The products were purified by Sephadex G-25 chromatography, followed by RP-HPLC (column A).

Formation of VB$_{12}$–ANTIDE Conjugates Using Cross-Linker Containing a Hindered Thiol. Aminohexyl eVB$_{12}$ **1d** was coupled with 4-[(succinimidyloxy)carbonyl]-α-methyl-α-(2-pyridyldithio)toluene (SMPT; Pierce) using standard literature conditions (Blakey et al., 1987). The product was purified by RP-HPLC (column B) to give α-methyl-α-(2-pyridyldithio)toluyl]-hexyl-eVB$_{12}$ **1g**. Iminothiolated ANTIDE-1 (HS-HN$^+$-ANT1) was prepared as outlined above for HS-HN$^+$ANT3.

Table 2. Structure of Spacer and IF Affinity of VB$_{12}$–Antide Conjugates General Structure: eVB$_{12}$–SPACER–Antide^a

Conjugate Name (Number)	Antide analogue	SPACER	IF affinity
B12-CONH-ANT (2)	Antide 1	None	N/T
(3)	Antide 2		N/T
(4)	Antide 3		N/T
B12-[EGS]-ANT (5)	Antide 1		30%
(6)	Antide 3		N/T
B12-[DSS]-ANT3 (7)	Antide 3		N/T
B12-PA-ANT (8)	Antide 1		53%
(9)	Antide 3		36%
B12-SS-ANT1 (10)	Antide 1		65%
B12-SS-NH$^+$ANT3 (11)	Antide 3		N/T
B12-TSS-ANT (12)	Antide 1		54%
(13)	Antide 3		37%
B12-SC-ANT (14)	Antide 1		82%
(15)	Antide 3		65%
B12-GGEA-ANT (16)	Antide 1		60%
(17)	Antide 3		48%

^{a} NT: not tested.

This VB$_{12}$ derivative was reacted with either the iminothiolated ANTIDE-1 or -3 derivatives as described above, and the products were purified by size-exclusion chromatography and RP-HPLC (column B) to give hindered toluyl disulfide conjugates B12–TSS–ANT1 (**12**) and B12–TSS–ANT3 (**13**).

Formation of VB$_{12}$–ANTIDE Conjugates Using A Noncleavable Thioether Linkage. Aminohexyl eVB$_{12}$ was converted to the iodoacetamido derivative by reaction with the NHS ester of iodoacetic acid. The product, **1h**, was purified by RP-HPLC (column B). A solution of (iodoacetamido)hexyl eVB$_{12}$ in diisopropylethylamide/dimethylformamide (DIEA/DMF, 1:20 v/v) was deoxygenated with argon for 10 min, and a solution of either iminothiolated ANTIDE-1 or -3 in DMF was added dropwise to the stirred reaction mixture. Each reaction mixture was stirred for 30 min at room temperature. The solution was diluted with water, and the products, the thioether linked conjugates B12–SC–ANT1 (**14**) and B12–SC–ANT3 (**15**), were isolated by preparative RP-HPLC (column B).

Formation of VB$_{12}$–ANTIDE Conjugates Using a Transglutaminase-Cleavable Linkage. eVB$_{12}$ carboxylate was activated as described previously with EDAC and NHS and added to a solution of the tetrapeptide GGEA-OMe in bicarbonate buffer (100 mM, pH 9.5). The resultant VB$_{12}$–GGEA–OMe, **1i**, was isolated from the reaction mixture by preparative RP-HPLC (column B) and was in turn conjugated to either ANTIDE-1 or ANTIDE-3 by activation of the glutamate side-chain carboxylate with EDAC/NHS and addition to a solution of the peptides in bicarbonate buffer (100 mM, pH 9.5). In each case the product was purified by RP-HPLC (column B). Each reaction mixture was stirred for 30 min at room temperature and then diluted with 2% aqueous acetic acid and filtered. The tetrapeptide linked conjugates B12–GGEA–ANT1 (**16**) and B12–GGEA–ANT3 (**17**) were isolated by RP-HPLC (column B).

Characterization of Conjugates. The structures of the VB$_{12}$–ANTIDE conjugates prepared for this study are shown in Table 2. They were characterized by analytical RP-HPLC, UV spectroscopy, amino acid analysis, and

Table 3

conjugate	HPLC retn time (min)	M+ (obsd)	M+ (calcd)
B12−CONH−ANT1 (**2**)	23.6	2825	2823
B12−CONH−ANT2 (**3**)	23.6	2824	2823
B12−CONH−ANT3 (**4**)	23.9	2889	2887
B12−[EGS]−ANT1 (**5**)	24.3	3111	3109
B12−[EGS]−ANT3 (**6**)	24.6	3174	3173
B12−[DSS]−ANT3 (**7**)	26.6	N/T^a	
B12−PA−ANT1 (**8**)	27.3	2957	2956
B12−PA−ANT3 (**9**)	27.5	3020	3020
B12−SS−ANT1 (**10**)	28.2	3057	3058
B12−SS−ANT3 (**11**)	28.5	3134	3135
B12−TSS−ANT1 (**12**)	29.0	3204	3204
B12−TSS−ANT3 (**13**)	29.5	3267	3268
B12−SC−ANT1 (**14**)	25.8	3083	3081
B12−SC−ANT3 (**15**)	26.0	3147	3145
B12−GGEA−ANT1 (**16**)	29.3	3152	3150
B12−GGEA−ANT3 (**17**)	29.2	3215	3214

^{a} NT: not tested.

ionspray mass spectrometry. Analytical RP-HPLC confirmed that the products contained no unconjugated peptide or VB$_{12}$ reagent and that the purity of the product peak was greater then 95%. UV spectra of all conjugates displayed the characteristic absorption maximum at 361 nm due to the cobalamin nucleus. Amino acid analysis confirmed the identity of the peptide component, including in the case of conjugates **16** and **17** the additional amino acids of the peptide linker. The ionspray mass spectra in all cases gave a molecular ion in agreement, within the limits of accuracy of the technique ($\pm0.1\%$), with the calculated M+ of the conjugates. The RP-HPLC retention times and ionspray MS results are compiled in Table 3.

Statistical Analysis. Bioactivity data from replicate individuals (*in vivo* trials) and from replicate experiments (*in vitro* trials) were subjected to one-way analysis of variance, and Tukey HSD post hoc tests were applied for the pairwise comparison of means, which were deemed to be significantly different at a probability level of $P < 0.05$.

RESULTS

(a) Synthesis of Analogues of ANTIDE That Are Suitable for Chemical Linkage to VB$_{12}$. *(i) Direct Conjugation of VB$_{12}$ to ANTIDE Analogues.* Three analogues of ANTIDE containing single unmodified lysine residues suitable for conjugation to eVB$_{12}$ carboxylate were synthesized: D-Lys^6-ANTIDE (ANTIDE-1), Lys^5-ANTIDE (ANTIDE-2), and Lys^8-ANTIDE (ANTIDE-3). The three ANTIDE analogues were then conjugated to a carboxylic acid derivative of VB$_{12}$ using EDAC activation, and all six substances were tested in the *in vitro* rat pituitary cell assay and *in vivo* in the castrate rat model. The data presented in Tables 4 and 5 demonstrate that ANTIDE-1 and ANTIDE-3 were as active as ANTIDE in the pituitary cell assay, whereas ANTIDE-2 was relatively inactive, and so was not used in subsequent experiments. ANTIDE-3 was found to be active when tested *in vivo*; however, ANTIDE-1 showed negligible activity when given by this route. While it was possible to produce an ANTIDE analogue which possesses similar *in vitro* and *in vivo* bioactivity to the native molecule, direct conjugation of these analogues to VB$_{12}$ greatly reduced their bioactivity (Tables 4 and 5).

(ii) Conjugation of VB$_{12}$ to ANTIDE Analogues Using Spacers. Preparation of conjugates between VB$_{12}$ and ANTIDE-1 and ANTIDE-3 with either hydrophilic cross-linking agents such as EGS (16.1 Å), hydrophobic cross-linking agents such as DSS (11.4 Å), or a shorter bulky

Table 4. In Vitro Bioassay for Blockade of LHRH-Stimulated Release of LH from Rat Pituitary Cells by ANTIDE, Its Analogues, and VB$_{12}$ Conjugates^a

analogue	IC$_{50}$	[n]
ANTIDE	$4.4 \pm 0.7^{a*}$	[20]
ANTIDE-1	2.1 ± 0.3^a	[8]
ANTIDE-2	$11.7 \pm 2.7^{a,b}$	[5]
ANTIDE-3	1.2 ± 0.2^a	[13]
B12−CONH−ANT1	88 ± 21^c	[5]
B12−CONH−ANT2	105 ± 21^c	[4]
B12−CONH−ANT3	36 ± 10	[4]

* Median inhibitory concentrations (IC50) of ANTIDE, ANTIDE analogues, and VB$_{12}$−ANTIDE conjugates for antagonizing LHRH-stimulated release of LH from rat anterior pituitary cell cultures during 4 h. Results for conjugates (mean $\pm$ SE) are given as ng of the incorporated ANTIDE analogue/mL (final concentration in culture well) from n independent trials. Results that are not significantly different from each other (i.e., $P > 0.05$) are grouped under a common superscript letter.

Table 5. Serum LH Levels in Castrate Rats Following Subcutaneous Injection of ANTIDE, ANTIDE Analogues, or Their VB$_{12}$ Conjugates

| analogue	dose (μg)	mean LH $\pm$ sd (ng/mL)
expt 1		
control		$7.35 \pm 1.90^{a*}$
ANTIDE	100	0.29 ± 0.06^b
	50	0.24 ± 0.06^b
ANTIDE-1	100	6.37 ± 1.00^a
ANTIDE-2	100	9.51 ± 3.11^a
ANTIDE-3	100	0.27 ± 0.05^b
B12−CONH−ANT3	50	10.11^a
expt 2		
Control		6.69^a
ANTIDE	50	0.44 ± 0.02^b
ANTIDE-3	16.7	0.71 ± 0.2^b
B12−CONH−ANT1	50	5.44 ± 1.4^a
B12−CONH−ANT2	50	5.56 ± 0.97^a
B12−CONH−ANT3	50	5.51 ± 0.22^a

* A common letter signifies that the mean values do not significantly differ from one another ($P > 0.05$).

anilido group, greatly increased the *in vitro* bioactivity of the conjugates, to levels comparable to that of the parent analogue (Figures 2 and 3). Thus, conjugates **5**, **6**, and **7** all had bioactivities comparable to that of native ANTIDE (Figures 2 and 3). By contrast, the *in vivo* bioactivity of these conjugates when given sc to rats was very low, as evidenced by the failure of these conjugates to cause a significant drop in serum LH levels in castrate rats, even at doses of 100 μg of analogue (Figures 4 and 5). ANTIDE and ANTIDE-3, on the other hand, were active at doses as low as 12.5 ug (Table 7). It thus appeared that some factor other than steric hindrance was affecting the *in vivo* activity of these VB$_{12}$−ANTIDE conjugates (cf. Figure 2 with 4 and Figure 3 with 5).

(iii) Conjugation of VB$_{12}$ to ANTIDE Analogues Using Biodegradable Linkers. In order to reduce the possibility of removal of the VB$_{12}$−ANTIDE conjugates from the circulation by VB$_{12}$-binding proteins following injection, VB$_{12}$−ANTIDE conjugates were prepared using a thiol-cleavable, disulfide-containing, spacer. This spacer would potentially allow the cleavage of ANTIDE from VB$_{12}$ by the low levels of reduced glutathione in serum (Letvin et al., 1986). Conjugates were therefore prepared between ANTIDE-1 and ANTIDE-3 using a thiol-cleavable spacer and a hindered thiol group. The presence of the hindered thiol in the latter spacer should mean that it would be cleaved more slowly upon exposure to serum glutathione (Thorpe et al., 1987). A conjugate containing a non-cleavable thioether linker (SC) of similar length was also prepared.
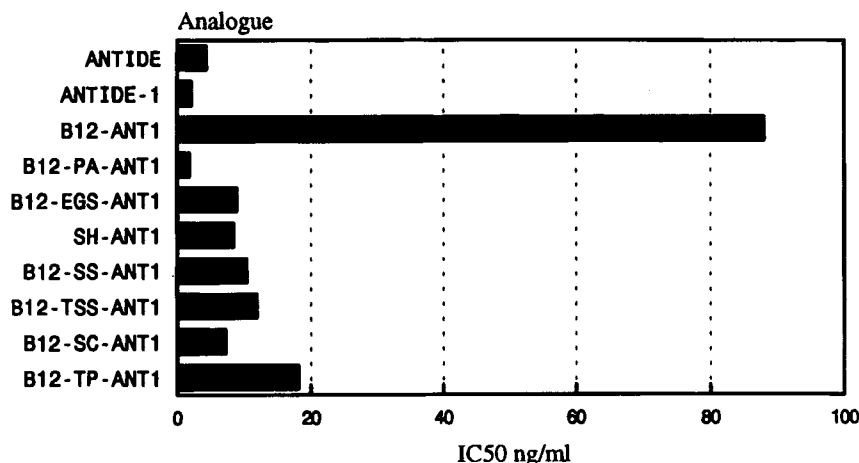
Figure 2. Median inhibitory concentrations (IC_{50}), determined by in vitro bioassay, for blockade of LHRH-stimulated release of LH from rat pituitary cells by ANTIDE, its analogues, and VB_{12} conjugates. Median inhibitory concentrations of ANTIDE, ANTIDE analogues, and VB_{12}−ANTIDE conjugates for antagonising LHRH-stimulated release of LH from rat anterior pituitary cell cultures during 4 h. Results for conjugates are given as ng of the incorporated analogue/mL (final concentration in culture well). Results that do not differ from each other (i.e., $P > 0.05$) are grouped under a common letter.
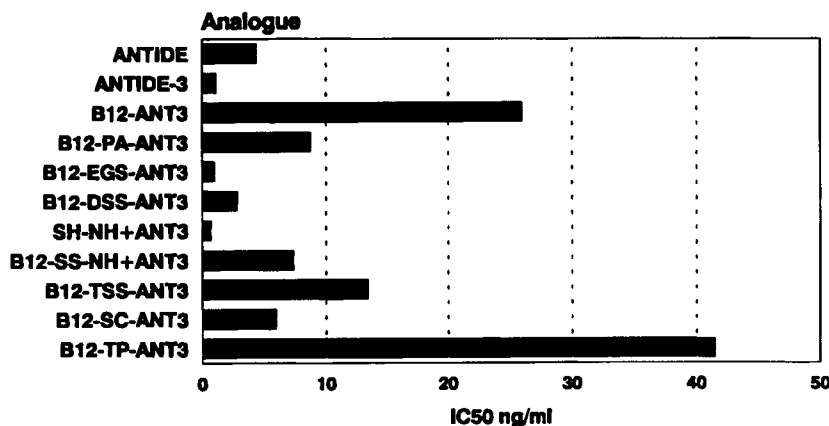
Figure 3. In vitro bioassay for blockade of LHRH-stimulated release of LH from rat pituitary cells by ANTIDE, ANTIDE-3, and its VB_{12} conjugates. See legend to Figure 2 for further details.

Table 6. In Vitro Bioassay for Blockade of LHRH-Stimulated Release of LH from Rat Pituitary Cells by ANTIDE, Its Analogues, and Disulfide-Linked VB_{12} Conjugates

analogue	IC50*	[n]
ANTIDE	4.4 ± 0.7^a	[20]
ANTIDE-1	2.1 ± 0.3^a	[8]
B12−SS−ANT1	10.4 ± 4.0^b	[3]
ANTIDE-3	1.2 ± 0.2^c	[15]
HS−NH⁺ANT3	$0.72 \pm 0.11^{a,c}$	[3]
B12−SS−NH⁺ANT3	$7.4 \pm 0.8^{a,b}$	[3]

* See legend to Table 4 for further details.

The thiol-cleavable B12−SS−ANT1 and B12−SS−NH⁺ANT3 conjugates were found to have similar *in vitro* bioactivity to the extended spacer conjugates described above (Figures 2 and 3, Tables 6 and 7). Administration of B12−SS−NH⁺ANT3 parenterally to castrate rats resulted in a similar reduction in serum LH to that seen with the unmodified ANTIDE-3, while B12-SS-ANT1 had a similar bioactivity *in vivo* to native ANTIDE (Table 7). Thus, the use of the thiol-cleavable spacer, rather than a non-cleavable spacer, in the preparation of the VB_{12}−ANTIDE conjugates, while having little effect on the IC_{50} of the VB_{12}−spacer−ANTIDE conjugates in the *in vitro* assay, greatly increased the potency of these conjugates *in vivo* to levels similar to ANTIDE (Figures 4 and 5, Tables 6 and 7). The incorporation of a tolyl group, or hindered thiol, did not significantly change the *in vitro*

Table 7. Reduction in Serum LH Level in Castrate Rats Following Subcutaneous Injection of ANTIDE, ANTIDE Analogues, or Their Disulfide-Linked VB_{12} Conjugates

analogue	dose (μg) of analogue	serum LH, % of matching control* (mean $\pm$ sd)
ANTIDE	25.0	4 ± 0.70 (1)
	12.5	15.3 ± 5.40 (3)
	6.3	80.6 ± 43.8 (3)
	3.1	100.2 ± 36.8 (3)
ANTIDE-1	100	87.6 ± 13.6 (1)
B12−SS−ANT1	25.0	19.8 ± 4.80 (5)
	12.5	34.4 ± 14.7 (5)
	6.3	73.9 ± 25.4 (6)
ANTIDE-3	100.0	3.7 ± 0.70 (1)
	25	18.0 ± 5.50 (5)
	12.5	43.0 ± 12.8 (3)
	6.3	116.1 ± 42.4 (3)
HS−NH⁺ANT3	50.0	28.2 ± 11.4 (5)
	25.0	77.3 ± 17.2 (5)
	12.5	112.8 ± 20.9 (5)
B12−SS−NH⁺ANT3	50.0	16.5 ± 5.10 (5)
	25.0	23.8 ± 9.20 (5)
	12.5	63.8 ± 16.5 (6)
	6.3	78.8 ± 24.4 (6)

* Serum LH levels (ng/mL) in the control groups were 7.35 ± 1.90 (expt 1), 5.16 ± 2.34 (expt 2), 2.73 ± 0.474 (expt 5), and 4.06 ± 0.90 (expt 6), respectively.

or *in vivo* activity of either analogue relative to the respective unhindered thiol analogue. The noncleavable conjugates formed with the thioether linkage were found to have activity similar to the thiol analogue when tested
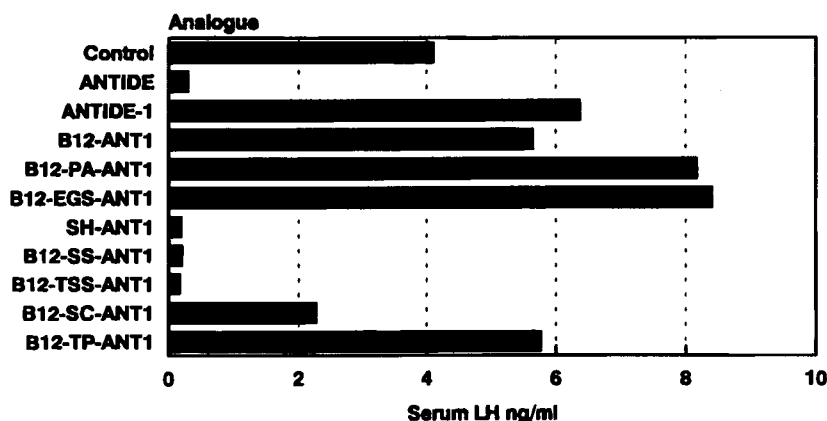
Figure 4. Reduction in serum LH level in castrate rats following injection of ANTIDE, ANTIDE-1, and its VB_{12} conjugates. The *in vivo* effect of sc injection of ANTIDE or VB12—ANTIDE conjugates was examined in 6 week old castrate rats. Twenty-four h after subcutaneous injection of a 100 μg dose of the various ANTIDE analogues, the rats were killed and trunk blood collected for analysis of serum LH levels by RIA. See Puénte and Catt (1986).
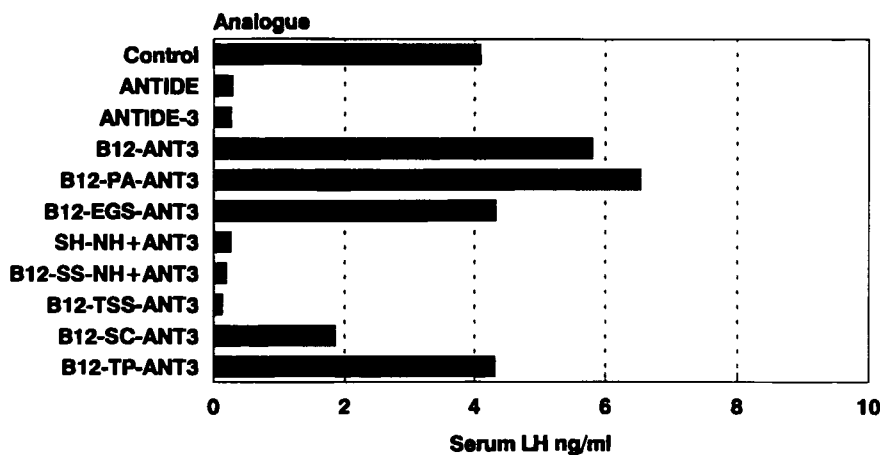
Figure 5. Reduction in serum LH level in castrate rats following sc injection of 100 μg doses of ANTIDE, ANTIDE-3, and its VB_{12} conjugates.

in vitro; however, this conjugate had a greatly reduced activity when tested *in vivo*.

(iv) Conjugation Using a Transglutaminase Cleavable Linker. Conjugates formed between VB_{12} and ANTIDE-1 and -3 using a transglutaminase cleavable γ-glutamyl-ϵ-lysine bond (B12—GGEA—ANT1, **16** and B12—GGEA—ANT3, **17**) were found to have poor activity *in vitro*, and negligible activity *in vivo* at the doses tested, suggesting that this bond was not cleaved *in vitro* or *in vivo*. The presence of the D-lysine group may have inhibited the cleavage of the ANTIDE-1 conjugates by the transglutaminase, while steric hindrance may have prevented the transglutaminase enzyme from cleaving both the ANTIDE-1 and -3 conjugates.

Affinity of VB_{12}—ANTIDE Conjugates for Intrinsic Factor. All VB_{12}—ANTIDE conjugates tested showed good affinity for intrinsic factor (Table 2). In fact, most conjugates had a relative affinity which was higher than that of the eVB_{12} isomer used to make the conjugate (normally around 35%).

DISCUSSION

The development of an LHRH antagonist suitable for use in humans for the treatment of hormone dependent mammary and prostate cancer has in the past been limited by the low potency of these molecules, their poor solubility in physiological buffers, and their poor oral bioavailability. In an attempt to resolve these problems, we have been examining the possibility of combining the relatively high bioactivity of the potent LHRH antagonist,

ANTIDE, with the high oral bioavailability of vitamin B_{12}. ANTIDE is particularly suitable for oral delivery, since it is composed of many unnatural amino acids and is resistant to the action of trypsin or chymotrypsin. ANTIDE must be modified in such a way as to provide a suitable site for conjugation to VB_{12}, as well as retaining full biological potency. ANTIDE normally possesses modified lysine residues at positions 5, 6, and 8 *viz.*: Lys-(Nic), D-Lys(Nic), and Lys(iPr), respectively. The removal of these modifications at either of the three sites provides a free amine suitable for conjugation to VB_{12}. Two derivatives of ANTIDE, D-Lys[6]-ANTIDE (ANTIDE-1), and Lys[8]-ANTIDE (ANTIDE-3), suitable for conjugation to VB_{12}, were synthesized and found to have high potency in the *in vitro* pituitary cell assay. ANTIDE-3 was also found to be highly potent when administered sc to rats, although ANTIDE-1 was found to have negligible antagonist activity, possibly due to an alteration in the rate of its clearance from serum. The *in vitro* and *in vivo* potency of either analogue was, however, greatly reduced by direct conjugation to VB_{12} (Tables 4 and 5), presumably due to steric interference with binding of the conjugate to the pituitary receptor for LHRH by the bulky VB_{12} molecule being in close proximity to the peptide.

In order to reduce the steric effect seen with direct conjugation of VB_{12} to ANTIDE-1 and ANTIDE-3, noncleavable linkers were used to produce conjugates between (2-aminoethyl)amido eVB_{12} and ANTIDE-1 and -3, thereby separating the bulky VB_{12} group from the ANTIDE analogue. VB_{12}—ANTIDE-1 conjugates formed

with either an anilido- (PA) or an EGS-derived spacer, or VB_{12}–ANTIDE-3 conjugates formed with an anilido-, EGS-, or DSS-derived spacer, all had *in vitro* activity similar to that of native ANTIDE (Figure 2), suggesting that placing the VB_{12} group at some distance from the ANTIDE restored the affinity of the ANTIDE for its receptor. These conjugates had very low activities *in vivo* (Figure 3), possibly due to the removal of the conjugates from the circulation by VB_{12}-binding proteins, such as transcobalamin I or transcobalamin II, which would greatly reduce their *in vivo* potency.

In an attempt to reduce the possibility of steric hindrance produced by the presence of the VB_{12} in the conjugates, or reduced systemic bioavailability of the conjugates as a result of clearance by VB_{12}-binding proteins, VB_{12}–ANTIDE conjugates were prepared using linkers which were potentially biodegradable *in vivo*. A disulfide linkage was initially chosen, because this linkage is most readily cleaved *in vivo,* and is found in biological conjugates such as the A–SS–B subunit toxins, tetanus toxin, and diphtheria toxin (Sandvig and Olsens, 1981; Matsuda and Yoneda, 1974). Disulfide bonds have been shown to be cleaved by the low levels of glutathione found in serum or in the cytoplasm of cells (Anderson and Meister, 1980).

The disulfide-linked VB_{12}–ANTIDE-1 and VB_{12}–ANTIDE-3 conjugates were found to have a slightly reduced *in vitro* potency in comparison to ANTIDE or the anilido- and EGS-linked VB_{12}–ANT1 and VB_{12}–ANT3 conjugates. In contrast, the disulfide linked conjugates showed a dramatic increase in their *in vivo* potencies when compared to the non-cleavable, extended spacer conjugates (Figures 4 and 5, Tables 6 and 7). For the $B12$–SS–NH^+ANT3 conjugate **11**, the *in vivo* bioactivity slightly exceeded that of the initial HS–NH^+ANT3 analogue. A conjugate containing a spacer of similar length including a noncleavable thioether bond in place of the disulfide bond showed greatly reduced *in vivo* activity, suggesting that the increased activity of the disulfide linked conjugate was due to its ability to be cleaved *in vivo*. All conjugates described above, whether they were directly linked to VB_{12} or were linked by a cleavable or noncleavable spacer, were found to be significantly more soluble in physiological buffers such as PBS or saline than the parent ANTIDE molecule (results not shown).

Conjugates between VB_{12} and ANTIDE-1 and -3 were formed with a spacer containing a γ-glutamyl-ϵ-lysine bond, which could potentially be cleaved by serum transglutaminases. Despite the high *in vitro* activity of these conjugates, their *in vivo* activity was very low, suggesting that the spacer was not cleaved *in vivo*.

The affinity of the VB_{12}–ANTIDE-1 and –ANTIDE-3 conjugates for IF was found to be equal or greater than the affinity of the eVB_{12} derivative from which the conjugates were made. A similar observation has been made for other eVB_{12} conjugates (Russell-Jones, 1994).

These studies demonstrate that it is possible to link together two molecules with disparate biological activities and to maintain substantially the biological activity of each individual component. During such conjugation, care must be taken to maintain the receptor–ligand binding activity of both molecules, as well as preserving the bioavailability of the pharmacological agent. Thus, although it was possible to make several conjugates between VB_{12} and ANTIDE analogues which show high *in vitro* activity in the pituitary cell assay, and with high relative affinity for IF, the *in vivo* bioactivity of these conjugates was greatly reduced unless a biodegradable spacer was used to join the two molecules.

It is intended that the highly active, water soluble, thiol-cleavable conjugates formed between VB_{12} and ANTIDE-1 and -3 will be used as the base compounds for a series of studies examining the potential of the VB_{12} uptake system to deliver physiologically relevant quantities of ANTIDE to the circulation following oral administration.

SUMMARY

The oral delivery of LHRH analogues would be an important advance in the treatment of various gonadotrophin dependent disorders. An oral delivery system which utilizes the normal intestinal uptake mechanism for vitamin B_{12} is currently being developed for the delivery of peptides and proteins. Research is described in which attempts have been made to link antagonists of LHRH to vitamin B_{12}. In order for such a strategy to be viable, the first requirement of the conjugation regime is that the bioactivity of each component compound is retained in the resulting conjugate. Two analogues of the potent LHRH antagonist, ANTIDE, have been synthesized that have activities similar to the native antagonist in the rat pituitary cell assay. Direct conjugation of these analogues to vitamin B_{12} was found to dramatically reduce the bioactivity of each analogue both *in vitro* and *in vivo*. Conjugation of either analogue to vitamin B_{12} *via* extended spacers regenerated their *in vitro* activity, but their *in vivo* activity was still greatly diminished. Conjugation of either analogue to VB_{12} via thiol cleavable spacers gave rise to analogues with similar *in vitro* and *in vivo* bio-activity to ANTIDE. These highly soluble analogues show potential utility both as water soluble analogues for parenteral use, and as protease resistant analogues for oral administration.

ACKNOWLEDGMENT

LITERATURE CITED

Anderson, M. E., and Meister, A. (1980) Dynamic state of glutathione in blood plasma. *J. Biol. Chem. 255,* 9530–9533.

Anton, D. L., Hogenkamp, H. P. C., Walker, T. E., and Matwiyoff, N. A. (1980) Carbon-13 Nuclear Magnetic Resonance Studies of the Monocarboxylic Acids of Cyanocobalamin. *J. Am. Chem. Soc. 102,* 2215–2219.

Blakey, D. C., Watson, G., Knowles, P., and Thorpe, P. (1987) Effect of chemical deglycosylation of Ricin A chain on the in vivo fate and cytotoxic activity of an immunotoxin composed of Ricin A chain and anti-Thy 1.1 antibody. *Cancer Res. 47,* 947–952.

Carlsson, J., Drevin, H., and Axen, R. (1978) Protein Thiolation and Reversible Protein-Protein Conjugation *Biochem. J. 173,* 723–727.

Crawford, D. D., and Davis, M. A. (1988) In *Endocrine Therapies in Breast and Prostate Cancer* (C. K. Osborne, Ed.) pp 25–38, Kluwer, Boston.

Eisenberger, M., and Abrams, J. (1988) *Drugs Today 24,* 241.

Farnworth, P. G., Robertson, D. M., de Kretser, D. M., and Burger, H. G. (1988) Effects of 31 kilodalton bovine inhibin on follicle-stimulating hormone and luteinizing hormone in rat pituitary cells *in vitro*: actions under basal conditions. *Endocrinol. 122,* 207–313.

Habenicht, U.-F., Schneider, M. R., and El Etreby, M. F. (1990) Effect of the new potent LHRH antagonist, Antide. *J. Steroid. Biochem. Molec. Biol. 37,* 397–421.

Karten, M. J., and Rivier, J. E. (1986) Gonadotropin-releasing hormone design. Structure-function studies toward the development of agonists and antagonists: rationale and perspective. *Endocrin. Rev. 7,* 44–66.

King, T. P., Li, Y., and Kochoumian, L. (1978) Preparation of protein conjugates via intermolecular disulfide bond formation. *Biochemistry 17,* 1499–1505.

Kolhouse, J. F., and Allen, R. H. (1977) Absorption, plasma transport, and cellular retention of Cobalamin analogues in the rabbit: Evidence for the existence of multiple mechanisms that prevent the absorption and tissue dissemination of naturally occurring cobalamin analogues. *J. Clin. Invest. 60,* 1381–1392.

Leal, J. A., Williams, R. F., Danforth, Gordon, K., and Hodgen, G. D. (1988) Prolonged duration of gonadotropin inhibition by a third generation GnRH antagonist. *Clin. Endocrinol. Metab. 67,* 1325–7.

Letvin, N. L., Goldmacher, V. S., Ritz, J., Yetz, J. M., Schlossman, S. F., and Lambert, J. M. (1986) In Vivo Administration of Lymphocyte-Specific Monoclonal Antibodies in Nonhuman Primates: In Vivo Stability of Disulfide-Linked Immunotoxin Conjugates. *J. Clin. Invest. 77,* 977–984.

Ljungqvist, A., Feng, D.-M., Hook, W., Shen, Z.-X., Bowers, C., and Folkers, K. (1988) Antide and related antagonists of luteinizing hormone release with long action and oral activity. *P.N.A.S. 85,* 8236–40.

Ljungstedt, A., Feng, D.-M., Tang, P.-F., Kubota, M., Okamoto, T., Zhang, Y., Bowers, C. Y., Hook, W. A., and Folkers, K. (1987) Design, synthesis and bioassays of antagonists of LHRH which have high antiovulatory activity and release negligible histamine. *Biochem. Biophys. Res. Commun. 148,* 849–856.

Loumay, E., Naor, Z., and Catt, K. J. (1982) Binding affinity and biological activity of gonadotropin releasing hormone agonists in isolated pituitary cells. *Endocrinol. 111,* 730–6.

Matsuda, M., and Yoneda, M. (1974) Dissociation of tetanus neurotoxin into two polypeptide fragments. *Biochem. Biophys. Res. Commun. 57,* 1257–1262.

McLachlan, T. R., Healy, D. L., Burger, H. G. (1986) Clinical aspects of LHRH analogues in gynaecology. *Brit. J. Obstet. Gynaec. 93,* 431–54.

Perrin, M. H., Rivier, J. E., and Vale, W. W. (1980) Radioligand assay for gonadotropin-releasing hormone: relative potencies of agonists and antagonists. *Endocrinol. 102,* 1289–96.

Phillips, A., Hahn, D. W., McGuire, J. L., Ritchie, D., Capetola, R. J., Bowers, C., and Folkers, K. (1988) Evaluation of the anaphylactoid activity of a new LHRH antagonist. *Life Sci. 43,* 883–88.

Puénte, M., and Catt, K. J. (1986) Inhibition of pituitary-gonadal function in male rats by a potent GnRH antagonist. *J. Steroid Biochem. 25,* 917–925.

Russell-Jones, G. J. (1994) Oral delivery of Therapeutic Proteins and peptides by the vitamin B_{12} uptake system. In *Peptide-based Drug Design: Controlling Transport and Metabolism* (M. Taylor, and G. Amidon, Eds.) ACS Publications, Washington, DC.

Sandvig, K., and Olsens, S. (1981) Rapid entry of nicked Diptheria toxin into cells at low pH. Characterization of the entry process and effects of low pH on the toxin molecule. *J. Biol. Chem. 256,* 9068–9076.

Schally, A. B., Arimura, A., Kastin, A. J., Matsuo, H., Baba, Y., Redding, T. W., Nair, R. M., Develjuk, L., and White, W. F. (1971) Gonadotropin-releasing hormone: one polypeptide regulates secretion of luteinizing and follicle-stimulating hormones. *Science 173,* 1036.

Schmidt, F., Sandaram, K., Thau, R. B., and Bardin, C. W. (1984) Ac-D-Nal(2)1, 4FD-Phe-2, D-Trp3, D-Arg6]-:LHRH, a potent antagonist of LHRH, produces transient edema and behavioural changes in rats. *Contraception 29,* 283.

Thorpe, P. E., Wallace, P. M., Knowles, P. P., Relf, M. G., Brown, A. N. F., Watson, G. J., Knyba, R. E., Wawrzynczak, E. J., and Blakey, D. C. (1987) New Coupling Agents for the Synthesis of Immunotoxins Containing a hindered Disulfide Bond with Improved Stability in Vivo. *Cancer Res. 47,* 5924–5931.

BC9400837

Preparation and Characterization of Antisense Oligonucleotide–Peptide Hybrids Containing Viral Fusion Peptides

Sommay Soukchareun, Geoffrey W. Tregear, and Jim Haralambidis*

Howard Florey Institute of Experimental Physiology and Medicine, University of Melbourne, Parkville, Victoria 3052, Australia. Received August 10, 1994[⊗]

We have developed a strategy for the synthesis of novel oligodeoxynucleotide (ODN)–peptide conjugates on a scale suitable for the investigation of their potential as antisense inhibitors of gene expression. These conjugates have the 3'-terminus of the antisense oligodeoxynucleotide linked covalently to the N-terminus of a peptide. This strategy allows the preparation of conjugates containing a peptide segment designed to facilitate intracellular delivery of the antisense oligodeoxynucleotide as well as providing protection against 3'-exonuclease digestion. To illustrate the synthetic approach we describe the preparation of a series of conjugates comprising antisense oligonucleotides to human immuno-deficiency virus type 1 (HIV) linked to fusion peptides derived from the HIV transmembrane glycoprotein gp41. The conjugates were prepared by the total synthesis method, in which the peptide is assembled first by the *N*-(fluorenylmethoxycarbonyl) (Fmoc) solid-phase methodology. This is followed by derivatization of the amino terminus by reaction with an α,ω-hydroxycarboxylic acid derivative which converts the terminus to a protected aliphatic hydroxy group on which standard solid phase DNA synthesis by the phosphoramidite method is performed. The purified conjugates were characterized extensively by several analytical techniques including ion spray mass spectrometry. Thermal denaturation studies showed that the interaction of the ODN–peptide conjugate with its complementary strand was similar to that of unmodified oligonucleotides. Preparation by the total synthesis method gave the purified conjugate with overall yields in the range of 6–14%.

INTRODUCTION

The use of synthetic oligodeoxynucleotides (ODNs) as inhibitors of gene expression has been the subject of intense investigation (*1, 2*). Antisense ODNs can inhibit gene expression by a number of mechanisms, including interference with mRNA processing (*3*), initiation of RNase-H mediated degradation of the target mRNA (*2*), and steric blocking (*4*). The use of exogenous antisense ODNs as tools for the elucidation of gene function has found widespread use (*5, 6*). However, as potential pharmacological agents, the efficacy of modified antisense ODNs requires the fulfillment of several criteria, including a demonstration of sequence specificity, preferably an ability to activate RNase H digestion, rapid penetration into cells, and stability to degradation by intracellular and extracellular nucleases.

Chemical modifications that increase the lipophilic properties of the ODN, such as conjugation to cholesterol (*7*) and lipids (*8, 9*), have been associated with increased activity and, in some cases, with actual increased intracellular concentration (*7*). Conjugation to polylysine, which would be expected to neutralize the negative charge on the ODN, has also been shown to result in increased activity (*10*). However, enhancement of intracellular delivery has not always been associated with sequence-specific inhibition of gene expression by antisense mechanisms (*7*). Cellular toxicity has also been observed and has been attributed to the binding of the ODNs to cellular polymerases (*11*) and ribosomes (*12*).

The addition of a fluorescently labeled ODN to cells typically results in a punctate cytoplasmic staining pattern, indicative of entrapment of oligonucleotides within endosomes (*13*). Antisense inhibition of protein expression by hybridization arrest and/or RNase H mediated degradation of target RNA require the oligonucleotides to escape the endosomal compartmentalization and bind to the intended mRNA in the cytosolic milieu. It is not known how efficiently, or by what mechanisms, ODNs penetrate endosomal membranes. For enveloped viruses that enter target cells by receptor-mediated endocytosis or direct fusion, the release of the virus from the endosomal compartment involves the fusion of the viral and cellular membranes (*14*). Although protein-mediated membrane fusion is well documented, the exact molecular mechanisms of this process remain to be clarified. In the case of the influenza virus, the process involves a series of complex, coordinated events culminating in a low-pH induced conformational change of the virally encoded protein hemagglutinin and exposure of the fusion domain prior to the membrane fusion event (*14*). The complexity of this process suggests that exogenous ODNs, acting independently, could not readily penetrate the acidic endosomal compartment by passive diffusion (*15*). The concentration of ODN added to the culture medium far exceeds the concentration needed for complete abrogation of mRNA expression, assuming that a 1:1 molar ratio of ODN to the target mRNA should be sufficient. It is not clear to what extent the low efficiency of antisense ODNs is due to their low permeation across cellular membranes or their low intracellular bioavailability. This may be due to a variety of reasons, including rapid nuclease digestion (*16*), nonspecific association with cellular proteins (*11, 12*), or selective sequestration of ODNs in intracellular sites that preclude their association with the intended mRNA target.

There are several types of peptides that have been shown to have intrinsic ability to perturb artificial membranes (*17, 18*). Fusion peptides have an important role in syncytium-mediated virus internalization and cytopathology of paramyxoviruses and retroviruses (*19*).

---

* To whom correspondence should be addressed. Tel: + 61-3-344 7285. Fax: + 61-3-348 1707.

Despite differences in the cytopathogenesis and the molecular events that precede the membrane fusion event, these viruses share the common feature of the dependency on the N-terminal fusion peptides in the virally encoded cell-surface protein to mediate several physiologically important events. These events include virus binding to target cells, followed by virus internalization by membrane fusion (*14, 19*).

The fusion peptides located in the N-terminus of the transmembrane glycoprotein gp41 of HIV have been shown to have an important role in the HIV life cycle and pathogenesis (*17–19*). Site-directed mutagenesis of residues in the conserved N-terminal fusion domain of gp41 (*20*), as well as antibodies specific to the fusion peptides of gp41, inhibited HIV infection, syncytium formation, and HIV cytopathy (*19, 21*). In addition to the demonstration of the functional importance of the fusion domain of gp41, the ability of synthetic gp41 fusion peptides to perturb and lyse artificial lipid bilayers has been documented widely. The membranotropic ability was shown to be dependent on peptide length, sequence, and temperature (*17, 22, 23*). Although a synthetic peptide comprising the first (N-terminal) 16 residues of gp41 was able to lyse liposomes, the minimum requirement for artificial planar lipid bilayer destabilization was an 11-residue peptide (residues 1–11) (*23*).

The ability of gp41 fusion peptides to destabilize model lipid bilayers and mediate liposome fusion prompted us to address the possibility that conjugates containing the gp41 N-terminal fusion peptides can facilitate ODN delivery into cells.

We have reported previously a method for the preparation of ODN–polyamide hybrid molecules as nonradioactive DNA probes by a total synthesis method (*24*). Briefly, the peptide is synthesized first by the Fmoc method, a derivatized linker attached, and the oligonucleotide assembled onto the linker by standard solid phase DNA synthesis methods. Here, we describe the application and further development of these methods to the preparation of milligram amounts of ODN–peptide hybrid molecules in which the N-terminal fusion peptides of gp41 are conjugated to the 3′-end of anti-HIV ODNs. The peptide moiety was designed to serve two important functions: to facilitate ODN delivery into cells and to protect the ODN from 3′-exonuclease degradation.

EXPERIMENTAL PROCEDURES

General. Continuous-flow solid phase peptide synthesis (SPPS) was carried out manually on the Biolynx 4175 peptide synthesizer (LKB Biochrom, Cambridge, England). Automated DNA synthesis was carried out on an Applied Biosystems 380A DNA synthesizer using standard β-cyanoethyl nucleoside phosphoramidites. Amino acid analyses were carried out on a Beckman system 6300 analyzer after hydrolysis of the samples in evacuated, sealed tubes for 24 h at 130 °C with 6 N HCl/ 0.1% phenol. Preparative and analytical reversed-phase high-performance liquid chromatography (RP-HPLC) was carried out on a Waters liquid chromatography system consisting of a Waters 600 multisolvent delivery system connected to a variable wavelength detector. The conjugates were purified with either a Synchropak preparative (Synchrom, Lafayette, IN) RP-C18 column (21.2 × 250 mm, 300 Å pore diameter, 6.5 μm particle size) or semipreparative RP-C4 column (10 × 250 mm, 300 Å pore diameter, 6.5 μm particle size), with flow rates of 10 and 3 mL/min, respectively, with 260 nm detection. Analytical RP-HPLC of the conjugate used a Phenomenex W-POREX RP-C18 column (4.6 × 250 mm, 200 Å pore diameter, 5 μm particle size) with a flow rate of 1.5 mL/

min. Capillary electrophoresis was performed on the P/ace system 2100 (Beckman, Palo Alto, CA) using the V1000P eCAP capillary cartridge (75 μm internal diameter × 50 cm).

The ODN–peptides were 5′-end labeled using γ-^{32}P-[ATP] and T4 polynucleotide kinase using established protocols (*24, 25*). The crude reaction mixture from the 5′-labeling was analyzed by polyacrylamide gel electrophoresis (PAGE). This was carried out on a 20% polyacrylamide/urea, 200 × 200 × 2 mm gel containing 0.089 M Tris, 0.089 M boric acid, 2 mM EDTA (TBE), and 7 M urea.

Materials. All reagents, unless otherwise stated, were of analytical grade. Controlled pore glass resin (CPG, 200–400 mesh, pore size of 500 Å, cat. no. 27720) was obtained from Fluka. N^α-Fmoc pentafluorophenyl (pfp) esters of amino acids, (benzotriazol-1-yloxy)trispyrrolidinophosphonium hexafluorophosphate (PyBOP), DMF (peptide synthesis grade), and trifluoroacetic acid (TFA, peptide synthesis grade) were from Auspep (Melbourne, Australia). γ-^{32}P-[ATP] was from Dupont (Melbourne, Australia) and T4 polynucleotide kinase from Promega (Melbourne, Australia).

Peptide Synthesis. Various forms of the N-terminal fusion peptides of the HIV gp41 glycoprotein were synthesized. A 17-residue peptide (gp41b, residues 1–17 of gp41 according to Starcich *et al.* (*26*)) had the sequence AVGAIGALFLGFLGAAG. A truncated version of gp41b, the 11-residue peptide ALFLGFLGAAG, was also synthesized (gp41c, residues 1–11). The gp41c peptide lacks the six amino terminal residues of gp41b.

Derivatization of Controlled Pore Glass Resin with Fmoc–ϵAhx. Continuous-flow SPPS using standard *N*-(fluoren-9-ylmethoxycarbonyl) (Fmoc) chemistry was used to assemble the gp41 peptides on a controlled pore glass (CPG) resin derivatized with aminohexanoic spacer arms and a 4-hydroxybutyrate linker (*24*). The CPG resin was initially functionalized with amino groups as previously described (*27*). A quantitative ninhydrin test (*28*) of the resin estimated the degree of derivatization to be 150 μmol/g.

To the aminopropyl CPG, two ϵAhx residues were added to act as spacers between the resin surface and the point of peptide chain assembly. This was carried out as previously described (*27*), except that the free acid was used in the coupling reactions. Briefly, to the CPG (6 g, 0.9 mmol of amino groups) was coupled Fmoc–ϵAhx (2.7 mmol, 3 equiv) *in situ* for 1.5 h with a mixture consisting of PyBOP (3 equiv, 2.7 mmol), HOBt (3 equiv, 2.7 mmol), and NMM (5 equiv, 4.5 mmol) dissolved in 4 mL of DMF. The resin was then washed (DMF, 10 min). After removal of the Fmoc group with 20% (v/v) piperidine in DMF (10 min), the resin was again coupled *in situ* with Fmoc–ϵAhx, as before. It was then washed (DMF, 10 min). To determine the amount of Fmoc–ϵAhx derivatization, an Fmoc test was performed on small samples of the resin (*27, 29*) which determined the resin loading to be 125 μmol/g. Any residual reactive amino groups were then acetylated with a mixture consisting of DMAP (50 mg, 0.4 mmol) and acetic anhydride (250 μL, 1.25 μmol) in pyridine (1 mL) for 10 min. The resin was washed thoroughly with DMF (15 min).

Derivatization with the 4-Hydroxybutyrate Linker. To incorporate a base-labile ester linkage between the conjugate and the solid support the Fmoc group of the terminal ϵAhx residue was removed by treatment with 20% piperidine in DMF (10 min) and the N-terminus converted to a protected primary aliphatic hydroxyl group by reaction with the *p*-nitrophenyl ester of the 1,4-hydroxybutyric acid derivative in which the

hydroxy group is protected as a 9-phenylxanthen-9-yl (pixyl) ether (**2**) (*24*). The CPG resin (3 g, 0.45 mmol of amino groups) was reacted with a mixture consisting of the linker **2** (0.9 mmol, 2 equiv) and HOBt (1.8 mmol, 4 equiv) dissolved in DMF (3 mL). The mixture was added to the resin and coupled for 2 h. The resin was then washed (DMF, 15 min).

To determine the degree of derivatization a pixyl assay was performed on a small amount of resin (*24, 27*) using toluenesulfonic acid. The loading was determined to be 95 μmol/g. Any free residual amino groups were then acetylated as before and the resin washed (DCM, 15 min). Removal of the pixyl protecting group just prior to peptide synthesis was afforded by treatment of the resin with 3% (v/v) dichloroacetic acid in DCM for 10 min. The resin was then washed thoroughly with DCM (10 min) and then DMF (15 min).

Synthesis of gp41b and gp41c Peptides. The synthesis of the N-terminal fusion peptide, gp41b, and gp41c was carried out manually on the LKB Biolynx peptide synthesizer, on 3 g of the derivatized CPG resin (285 μmol). The first amino acid, Fmoc-glycine, was introduced as a symmetrical anhydride. Fmoc-glycine (1.7 mmol, 6 equiv) and diisopropylcarbodiimide (DIC) (0.8 mmol, 3 equiv) were dissolved in DMF (2 mL) and stirred for 0.5 h at rt. The mixture was then added to the top of the resin. (Dimethylamino)pyridine (0.05 mmol), dissolved in DMF (0.5 mL), was added immediately to the resin. After 1 h, small amounts of the resin were removed to determine the degree of incorporation of Fmoc-glycine. An Fmoc test gave a loading of 70 μmol/g. The resin was acetylated as before, and continuous-flow SPPS using standard N^α-Fmoc chemistry employing 3 equiv (relative to the first amino acid) of the pentafluorophenyl (Pfp) esters of the N^α-Fmoc-protected amino acids (0.63 mmol) and HOBt (0.63 mmol) dissolved in 2 mL of DMF was performed. All acylations were of 30 min duration. After each acylation, completion of coupling was confirmed by carrying out a trinitrobenzenesulfonic acid (TnBSA) test on a small amount of the resin (*27, 30*). Prior to the removal of the Fmoc group of the last residue, the resin was washed with DMF (15 min).

Addition of the Linker 2 to the Peptide–Resin. After the completion of peptide assembly, the resin (1.5 g) was treated with 20% piperidine in DMF (10 min) to deprotect the terminal α-amino group of the peptide. The resin was then again reacted with the linker synthon **2** (0.1 mmol) and HOBt (0.2 mmol) in DMF (2 mL) for 2 h. The resin substitution, as estimated by the pixyl test, was 40 μmol/g. Any residual amino groups were then acetylated as before. The peptidyl resin was then extensively washed with DCM, dried, and used without any further modification in solid phase DNA synthesis.

Oligonucleotide Synthesis. Automated DNA synthesis used standard β-cyanoethyl nucleoside phosphoramidites on either a 10 or a 1 μmol scale using either DMAP/Ac$_2$O or NMI (N-methylimidazole)/Ac$_2$O for capping. It was crucial, especially in the case of the 10 μmol scale syntheses, to ensure that *all* the resin received the iodine treatment. Three different ODNs were synthesized by the "trityl on" method, in which the dimethoxytrityl (DMT) protecting group is retained on the last nucleoside. The ODNs wereas follows: a 20mer complementary to the splice donor site of the HIV envelope mRNA, d(5'-GCGTACTCACCAGTCGCCGC-3', HIV1), a 20mer complementary to the HIV *tar* mRNA, d(5'-TCCCAGGCTCAGATCTGGCT-3', TAR), and a 27mer complementary to the *rev* mRNA, d(5'-TCGTCGCTGT-GTCCGCTTCTTCCTGCC-3', REV). After the comple-

tion of ODN synthesis, the resins were transferred to a two-way sintered glass reaction vessel and thoroughly washed with DCM and dried. The ODN–peptide conjugates were simultaneously cleaved and deprotected by treatment of the resin with concentrated aqueous ammonia at 55 °C for 6 h, or 50 °C for 16 h. Rotary evaporation of the resultant solution afforded a clear residue which was dissolved in sterile water (5 mL) before being subjected to analytical HPLC.

Analysis and Purification of Conjugates by RP-HPLC. Purification of the conjugates by RP-HPLC employed buffers A (0.1 M triethylammonium acetate (TEAA), pH 7.0, freshly prepared from a 1 M stock solution and filtered prior to use) and B (acetonitrile). A linear gradient of 10%-60% B over 30 min was used. A small amount of the crude "trityl on" ODN–peptide product and the corresponding detritylated material (after treatment with acetic acid) were subjected to analytical HPLC to evaluate the efficiency of DNA synthesis. Successful syntheses were marked by the appearance of a dominant product peak in the chromatogram of the "trityl on" product with the appropriate retention time (retention time of 25.2 min, 52% CH$_3$CN for the gp41b–HIV1 conjugate). To confirm that this peak was the desired, full length product, aliquots of the "trityl on" sample (sufficient for analytical HPLC, 0.1–0.3 OD$_{260}$ units) were treated with glacial acetic acid (100 μL). After 20 min, RP-HPLC of this detritylated sample mixture gives rise to an HPLC profile in which the predominant peak has shifted to an earlier retention time (24.7 min for the gp41b–HIV1 conjugate).

Following a preparative HPLC run, analytical HPLC of the fractions collected was performed to evaluate homogeneity. The appropriate fractions were pooled (typically in 20–30 mL) and detritylated by treatment with an equal volume of acetic acid for 30 min, after which time the solvent was evaporated *in vacuo*. The residue were redissolved in water. Analytical RP-HPLC of the detritylated conjugate was then routinely used to evaluate homogeneity. Following the HPLC purification, the triethylammonium counterions are exchanged for sodium ions by dialysis against NaCl (0.1 M, at least three changes) and then against water (at least another three changes).

Thermal Denaturation Studies. Thermal denaturation experiments of an equimolar mixture of the purified gp41b–HIV1 conjugate and its complementary 20mer target ODN (2 μM in 1.5 mL of a buffer consisting of 0.7 mM MgCl$_2$ and 1 mM Tris·HCl, pH 7.5) was performed on the Cary 1 UV–vis spectrophotometer equipped with a multicell holder and a temperature controller (Varian, Melbourne, Australia). The rate of increase of the temperature was 2 °C/min, from 10 °C to 80 °C, and the temperature was sampled every 0.1 °C from a temperature probe in a cell adjacent to the sample cell. All T_m values were calculated from the first derivative of the melting curve and represent the average ($\pm$ standard deviation) of triplicate analysis.

Ion Spray Mass Spectrometry. Aliquots of the samples (5–20 μg) were lyophilized and sent for mass spectral analysis. The samples run at Fisons Instruments (Fisons plc, UK) were dissolved in water (40 μL) and aliquots (10 μL) were diluted with acetonitrile (10 μL) and 0.3% NH$_3$. The samples were analyzed on a Fisons Quattro LC MS/MS instrument running in the negative ion mode, scanning over the m/z range of 930–1430. The samples sent to Perkin-Elmer SCIEX Instruments (Toronto, Canada) were run on the PE-SCIEX instrument, using an 1 mm × 15 cm C18 HPLC column. Buffer A was 2 mM ammonium formate (adjusted to pH

Table 1. Oligonucleotide and Peptide Sequences of Conjugates Made by the Total Synthesis Method. The gp41b and gp41c Peptide Sequences Correspond to the First 17 and First 11 Residues of the gp41 Envelope Protein of HIV, Respectively

conjugate	oligonucleotide	peptide
HIV1–gp41b	GCGTACTCACCAGTCGCCGC	AVGAIGALFLGFLGAAG
REV–gp41b	TCGTCGCTGTGTCCGCTTCTTCCTGCC	AVGAIGALFLGFLGAAG
TAR–gp41b	TCCCAGGCTCAGATCTGGCT	AVGAIGALFLGFLGAAG
HIV1–gp41c	GCGTACTCACCAGTCGCCGC	ALFLGFLGAAG

Table 2. Amino Acid Analyses of gp41b Peptidyl Resin (1) and Purified Conjugates (2–5). The Expected Amino Acid Values Are in Brackets

peptide/conjugate	amino acid analyses results
(1) gp41b peptidyl resin	Gly 4.93 (5), Ala 5.05 (5), Val 0.85 (1), Ile0.99 (1), Leu 3.19 (3), Phe 2.01 (2),
(2) HIV1–gp41b	Gly 4.19 (5), Ala 4.88 (5), Val 0.92 (1), Ile0.89 (1), Leu 3.08 (3), Phe 2.02 (2)
(3) REV–gp41b	Gly 5.07 (5), Ala 4.85 (5), Val 0.95 (1), Ile 1.0(1), Leu 3.09 (3), Phe 2.03 (2)
(4) TAR–gp41b	Gly 6.04 (5), Ala 4.88 (5), Val 0.95 (1), Ile 0.95(1), Leu 3.12 (3), Phe 2.10 (2)
(5) HIV1–gp41c	Gly 3.63 (3), Ala 2.85 (3), Leu 3.07 (3), Phe 2.08 (2)

= 8 with ammonium hydroxide), buffer B acetonitrile with 2 mM ammonium formate, running a gradient of 0–100% acetonitrile over 20 min, using a flow rate of 40 μL/min.

RESULTS

ODN–peptide conjugates containing several different peptides and ODNs were prepared by the total synthesis method. Firstly, a 17-residue hydrophobic fusion peptide (AVGAIGALFLGFLGAAG, gp41b) was used. This represents residues 1–17 of the HIV gp41 protein from isolate WMJ1, after changing residue 8 from a methionine to a leucine. This amino acid change is found in the LAV-1a isolate. Slepushkin *et al.* (*23*) demonstrated that a 16 amino acid long peptide derived from isolate LAV-1a and equivalent to gp41b (the only difference being the absence of the alanine residue found in position four of the WMJ1 isolate) was capable of causing liposome lysis. The same study also showed that the minimum requirement for lipid destabilization, as determined by changes in bilayer lipid membrane conductivity, was the 11-residue peptide ALFLGFLGAAG (gp41c, LAV-1a isolate), although a minimum of 15 residues was necessary for liposome lysis, suggesting that the membranotropic activity of gp41 was length dependant. Other studies show that synthetic peptides similar to gp41b, but derived from isolate LAV-1a and containing an extra seven residues at the C-terminus, are also capable of perturbing and inducing dye leakage from artificial lipid vesicles (*17, 22*). The gp41c peptide corresponds to a truncated version of gp41b, missing the six N-terminal residues.

The target sequence for the antisense inhibition was determined by reports in the literature, which demonstrated that several target sites were effective. The oligonucleotides synthesized were complementary to three different sites in the HIV mRNA: a 20mer complementary to the splice donor site of the HIV *env* mRNA (HIV1) (*31*), a 20mer complementary to the *tar* HIV mRNA (TAR) (*32, 33*), and a 27mer complementary to the *rev* HIV mRNA (REV) (*34, 35*) (Table 1).

Peptide Synthesis. Continuous-flow solid phase peptide synthesis (SPPS) using Fmoc chemistry was used for the synthesis of the gp41 fusion peptides. Controlled pore glass (CPG) was first aminated with (3-aminopropyl)triethoxysilane (Scheme 1). Two residues of aminohexanoic acid (εAhx) were then coupled to this aminopropyl-CPG (AP-CPG) using Fmoc-εAhx-OH by *in situ* activation of the amino acid using PyBOP ((benzotriazol-1-yloxy)trispyrrolidinophosphonium hexafluorophosphate). Following deprotection of the terminal Fmoc group, the amino terminus was reacted with the *p*-nitrophenyl ester

Scheme 1. Preparation of the CPG Resin for Peptide Synthesis
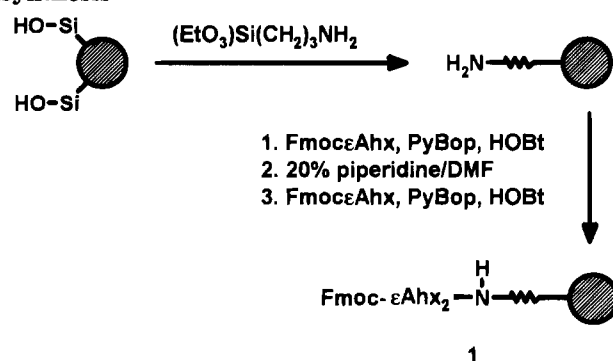
of *O*-pixyl-4-hydroxybutyric acid (**2**, Scheme 2). After removal of the pixyl protecting group, the first amino acid, Fmoc-Gly, was introduced as the symmetrical anhydride, preactivated with diisopropylcarbodiimide (DIC), with DMAP as the acylation catalyst. Standard Fmoc peptide chemistry employing a 3-fold molar excess of the pentafluorophenyl (Pfp) active esters of the amino acids was used for the remainder of the synthesis. Amino acid analysis (AAA) of the crude peptidyl resin from the synthesis of gp41b gave the expected ratios (Table 2). These results demonstrated the feasibility and efficiency of peptide synthesis on the CPG solid support derivatized with εAhx spacers.

Synthesis and Purification of Conjugates Containing the gp41b Fusion Peptide. After the completion of peptide assembly, any residual amino groups were acetylated and the terminus was converted to a protected aliphatic hydroxy group as above (Scheme 2). The derivatized peptidyl resin was then used directly in automated DNA synthesis utilizing the standard β-cyanoethyl phosphoramidite chemistry (Scheme 3). The 20mer ODN GCGTACTCACCAGTCGCCGC (HIV1) was synthesized. The cleavage of the peptide–solid phase ester bond to liberate the ODN–peptide conjugate (HIV1–gp41b), as well as removal of the protecting groups from adenine, guanine, and cytosine, was afforded by treatment of the resin with aqueous concentrated ammonia.
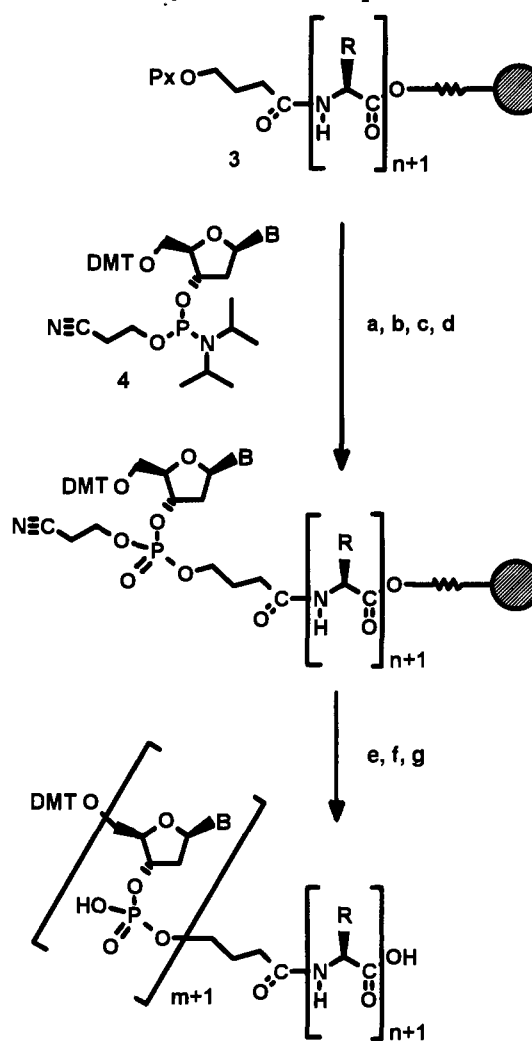
Reversed phase HPLC (RP-HPLC) analysis of the "trityl on" crude product, in which the dimethoxytrityl (DMT) protecting group is retained on the last nucleotide of the ODN, gave the chromatographic profile shown in Figure 1, in which the dominant peak (elution time of 25.20 min) contains the full length ODN–peptide hybrid. The crude products were purified by RP-HPLC. Following detritylation of the purified conjugate by acetic acid, analytical HPLC of this detritylated product showed that it consisted of highly pure ODN–peptide conjugate with

Scheme 2. Peptide Synthesis on the CPG Resin[a]

Px=9-Phenylxanthyl

Fmoc-εAhx₂—N(H)—ʍ—⬤ **1**

↓ **a**

H εAhx₂—N(H)—ʍ—⬤

O₂N—⬡—O—C(O)—CH₂CH₂CH₂—OPx **2**   HOBt

↓

PxO—CH₂—C(O)—εAhx₂—N(H)—ʍ—⬤

↓ **b, c**

Fmoc—N(H)—C(R)(H)—C(O)—O—...—C(O)—εAhx₂—N(H)—ʍ—⬤

↓ **d, e, f**

Fmoc—[N(H)—C(R)(H)—C(O)—O—]ₙ₊₁—...—C(O)—εAhx₂—N(H)—ʍ—⬤

↓ **a, g**

PxO—CH₂—C(O)—[N(H)—C(R)(H)—C(O)—O—]ₙ₊₁—C(O)—εAhx₂—N(H)—ʍ—⬤ **3**
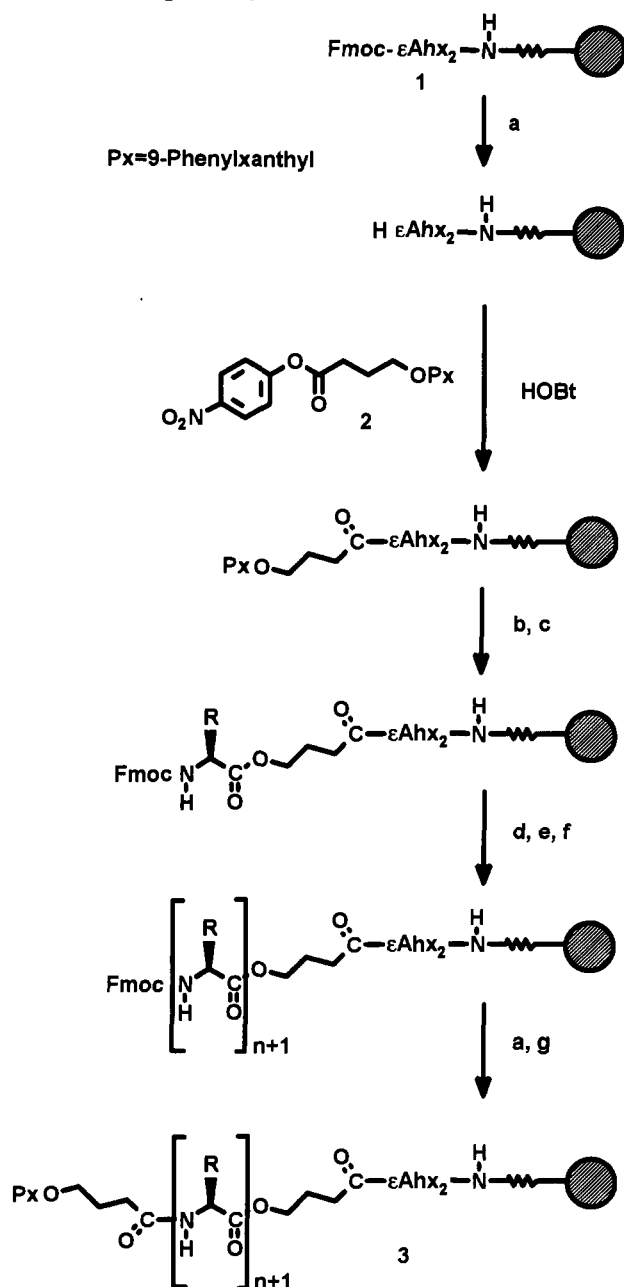
a Key: (a) 20% piperidine/DMF; (b) 3% DCA/CH₂Cl₂; (c) (Fmoc–AA)₂O, DMAP; (d) 20% piperidine/DMF; (e) Fmoc–AA–OPfp, HOBt; (f) repeat steps d and e "*n*" times; (g) **2**, HOBt.

an elution time of 24.78 min. The shift to an earlier retention time indicates removal of the lipophilic DMT group. Typical final overall yields for the purified, detritylated, and dialyzed full-length HIV1–gp41b ODN–peptide conjugate were 2.5 mg (11%, from 3 × 1 μmol scale syntheses) and 7.6 mg (10%, from a 10 μmol scale synthesis), based on the resin substitution prior to DNA synthesis.

Peptide–ODN conjugates containing the ODNs TC-CCAGGCTCAGATCTGGCT (TAR) and TCGTCGCTGT-GTCCGCTTCTTCCTGCC-3' (REV) were also synthesized and purified in the same way (Table 1). Analytical HPLC profiles of the crude trityl-on conjugates, as well as after purification and detritylation of TAR–gp41b (Figure 2a,b) and REV–gp41b (Figure 3a,b) demonstrated again a clean chromatographic profile, with the dominant peak eluting at 31.90 min for TAR–gp41b and 28.35 min for REV–gp41b. The differential retention

Scheme 3. DNA Synthesis and Deprotection[a]

PxO—CH₂—C(O)—[N(H)—C(R)(H)—C(O)—O—]ₙ₊₁—ʍ—⬤ **3**

DMTO—(sugar)—B; phosphoramidite; NC—CH₂CH₂—O—P(—O)(N(iPr)₂) **4**

↓ **a, b, c, d**

DMTO—(sugar)—B; NC—CH₂CH₂—O—P(=O)(—O)—...—C(O)—[N(H)—C(R)(H)—C(O)—O—]ₙ₊₁—⬤

↓ **e, f, g**

[DMTO—(sugar)—B; HO—P(=O)(—O)—O—]ₘ₊₁—...—C(O)—[N(H)—C(R)(H)—C(O)—OH]ₙ₊₁

a Key: (a) 3% DCA/CH₂Cl₂; (b) **4**, tetrazole; (c) Ac₂O, DMAP; (d) I₂, H₂O; (e) repeat steps a–d "m" times; (f) concd NH₃, rt, 6 h; (g) concd NH₃, 50 °C, 16 h.

characteristic of the detritylated, purified conjugates was observed (a retention time of 27.68 min and 27.47 min for the detritylated TAR–gp41b and REV–gp41b, respectively). The purified REV–gp41b conjugate, despite being eight nucleotides longer than TAR–gp41b, showed similar chromatographic retention. This suggested that the hydrophobicity of the peptide was the dominant factor in the chromatographic fractionation of the ODN–peptide conjugates. The final yield of gp41b–REV was 1.7 and 5.7 mg (6%, from 3 × 1 and 1 × 10 μmol scale syntheses, respectively) and of the gp41b–TAR 2.3 mg (10%, from 3 × 1 μmol scale syntheses).

The Synthesis and Purification of Conjugates Containing the gp41c Fusion Peptide. A conjugate containing the gp41c peptide and the HIV1 ODN was synthesized in the same manner. The HPLC elution profile of the crude HIV1–gp41c conjugate (trityl on) is shown in Figure 4, with the main peak (37.28 min) representing 60% of the total product. This main product was isolated and detritylated as before. As expected, analytical RP-HPLC of the detritylated product saw a shift in retention time to 33.87 min. The final yield after purification was 2.5 and 10.3 mg (12% and 14%, from 3 × 1 and 1 × 10 μmol scale syntheses, respectively).

Characterization of the ODN–Peptide Conjugates. Amino acid analyses (AAA) of the purified HIV1–gp41b, REV–gp41b, TAR–gp41b and HIV1–gp41c con-
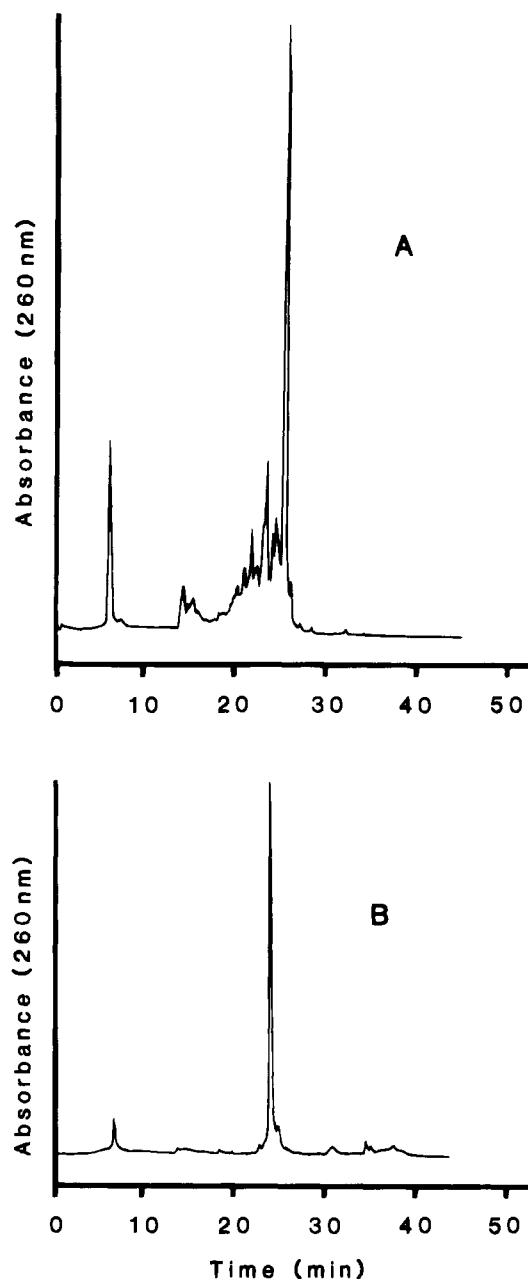
Figure 1. HPLC chromatogram of the crude HIV1–gp41b conjugate, trityl-on (A) and the purified conjugate, trityl-off (B). Chromatographic conditions: column, Synchropak RP-C4; buffer A, TEAA (0.1 M, pH 7.0); buffer B, acetonitrile; gradient, 10–60% B over 30 min.

Figure 2. HPLC chromatogram of the crude TAR–gp41b conjugate, trityl-on (A) and the purified conjugate, trityl-off (B). Chromatographic conditions: column, Synchropak RP-C4; buffer A, TEAA (0.1 M, pH 7.0); buffer B, acetonitrile; gradient, 10–60% B over 30 min.

jugates show the expected amino acid compositions (Table 2). A finding worth noting is the high glycine value observed. This appears to be associated with acid hydrolysis of samples containing ODNs. There are several observations to support this. Firstly, AAA of the peptidyl resin prior to DNA synthesis gave the expected amino acid ratio (Table 2). Secondly, AAA of peptide–ODN conjugates in which the peptides were devoid of any glycine residues also gave a high glycine value (results not shown), and AAA of normal, unmodified oligonucleotides also gave some glycine by AAA. This observation was also documented by the studies of Juby *et al.* (*36*). The molecular weights of the conjugates, determined from ion spray mass spectrometry, were as expected (see below and Table 3).

The electrophoregrams from capillary electrophoresis (CE) of the purified conjugates (Figure 5) indicate that the HPLC purified conjugates were homogeneous.

The purified conjugates were 5′-end labeled with γ-^{32}P-[ATP] and fractionated by 20% PAGE (Figure 6). The purified conjugates, HIV1–gp41b (lane B), REV–gp41b (lane C), TAR–gp41b (lane D), and HIV1–gp41c (lane E) have lower electrophoretic mobilities than the normal HIV1 ODN (lane A), and the mobility is roughly in accordance with the calculated MW of the conjugates.

Characterization of the ODN–Peptide Conjugates by Ion Spray Mass Spectrometry. The analyses of ODNs by mass spectrometric methods has, until recently, been hampered by the inability of the instrumentation to resolve the multiple sodium adducts of the molecular ions. In a recent report, Robles *et al.* used fast atom bombardment mass spectrometry (FAB-MS) to characterize a much smaller nucleopeptide (MW = 1433) (*37*). However, because the severity of the adduct forma-
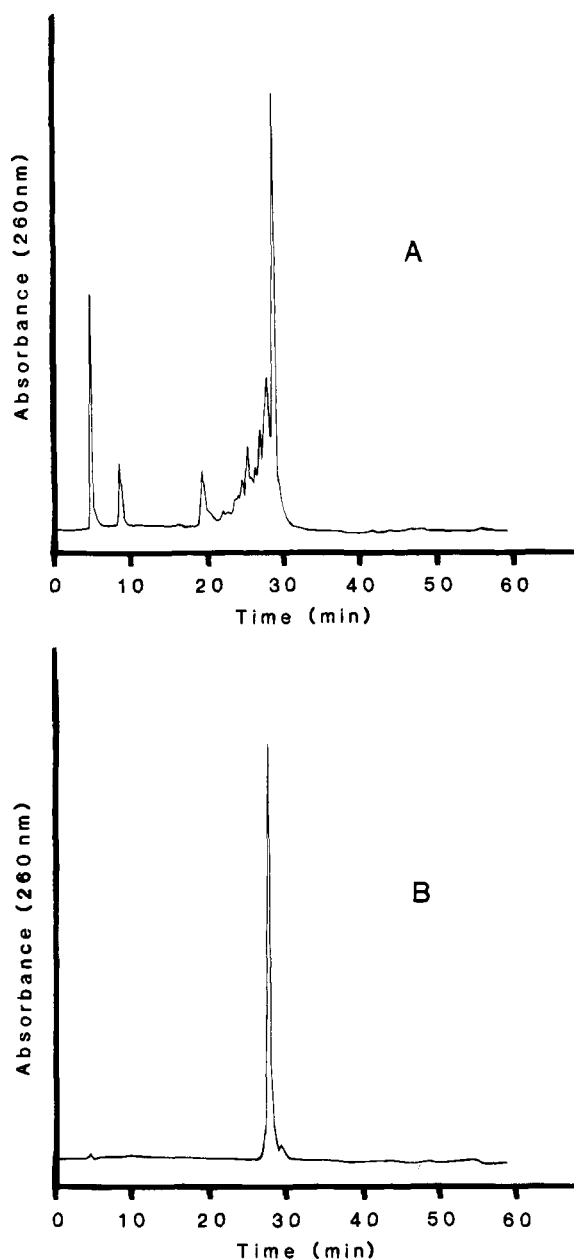
Figure 3. HPLC chromatogram of the crude REV—gp41b conjugate, trityl-on (A) and the purified conjugate, trityl-off (B). Chromatographic conditions: column, Synchropak RP-C4; buffer A, TEAA (0.1 M, pH 7.0); buffer B, acetonitrile; gradient, 10—60% B over 30 min.

tion is correlated to the length of the ODN, FAB-MS imposes limits on the quality and accuracy of the spectra of ODNs longer than 13mer (*38*). Recent developments, such as electrospray ionization and matrix-assisted laser desorption mass spectrometry, have improved the ionization procedure and have allowed the facile and routine characterization of oligonucleotides up to a 77mer (*39*). The nucleopeptide of Robles *et al.* was also analyzed by ion spray mass spectrometry (*37*). The purified ODN—peptide conjugates described in the present work are several times larger than those of Robles *et al.* Using negative ion mode detection, conjugates HIV1—gp41b, REV—gp41b, TAR—gp41b, and HIV1—gp41c gave dominant molecular ions, as summarized in Table 3. The molecular ion agrees with the calculated MW of the conjugates (Table 3). Figure 7 is a representative spectrum, obtained from the purified HIV1—gp41b conjugate, with the sodium adducts of the molecular ion clearly visible. These results point to the feasibility of
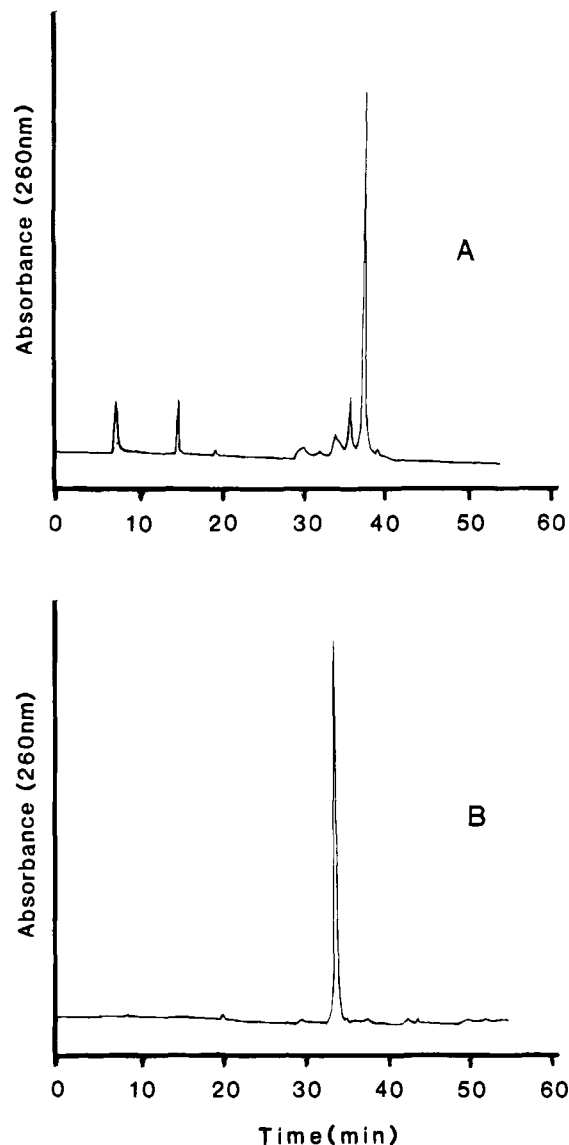
Figure 4. HPLC chromatogram of the crude HIV1—gp41c conjugate, trityl-on (A) and the purified conjugate, trityl-off (B). Chromatographic conditions: column, Synchropak RP-C4, buffer A, TEAA (0.1 M, pH 7.0); buffer B, acetonitrile; gradient, 10—50% B over 50 min.

Table 3. Dominant Molecular Ion of Purified Conjugates (±Standard Deviation) Obtained from Ion Spray Mass Spectrometry[a]

conjugate	molecular ion	calcd
HIV1—gp41b	7689.56 ± 0.77 (PE)	7691.79
	7690.4 (PE)	
	7691.5 (F)	
REV—gp41b	9787.67 ± 1.01 (PE)	9789.13
TAR—gp41b	7719.12 ± 0.95 (PE)	7721.83
HIV1—gp41c	7221.98 ± 1.21 (F)	7223.70

[a] They were run on either the Fisons (F) or PE-SCIEX (PE) instruments. Other ions, corresponding to sodium adducts, were also seen. The values for the HIV1—gp41b conjugates were obtained from the products of three different syntheses. The calculated molecular weights represent the average mass of the molecular ion.

ion spray mass spectrometry for the routine characterization of ODN—peptide conjugates of a size that would be useful in antisense or probe applications.

Overall, these results not only suggest that the peptide was stable to conditions of DNA synthesis and ODN deprotection but that DNA synthesis on the peptidyl—resin proceeded efficiently with minimal side reactions.
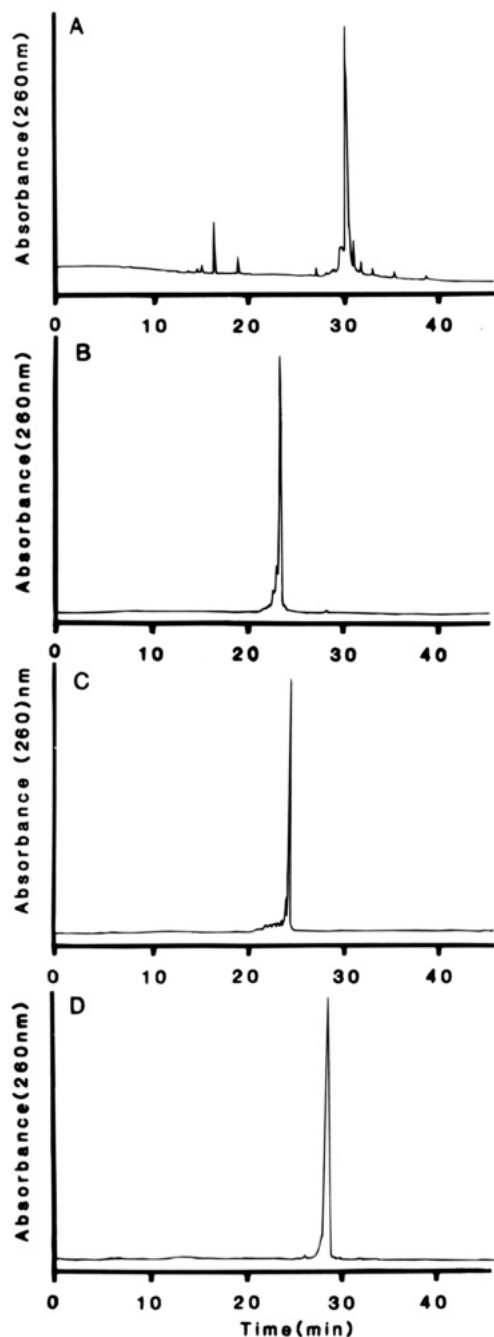
Figure 5. Capillary electrophoresis of purified and detritylated conjugates: HIV1−gp41b (A), TAR−gp41b (B), REV−gp41b, (C), HIV−gp41c (D).

Thermal Denaturation Studies of the HIV1−gp41b Conjugate. To determine whether the peptide moiety at the 3′-terminus of the 20mer HIV1 oligonucleotide has any effect on the hybridization efficiency of the antisense ODN−peptide conjugate for its complementary strand, melting temperature analysis was employed.

Melting temperature (T_m) experiments of the duplex consisting of the HIV1−gp41b conjugate and its unmodified complementary ODN of identical length show a T_m of 73.2 ± 0.1 °C. This value was not substantially different from the T_m value of a duplex consisting of the two unmodified ODNs (T_m of 72.1 ± 0.5 °C). Figure 8 shows the T_m curve of the duplex containing the conjugate (curve A) and that of the unmodified duplex (curve B). These results indicate that the 3′-linked peptide moiety does not interfere with the hybridization efficiency of the ODN.
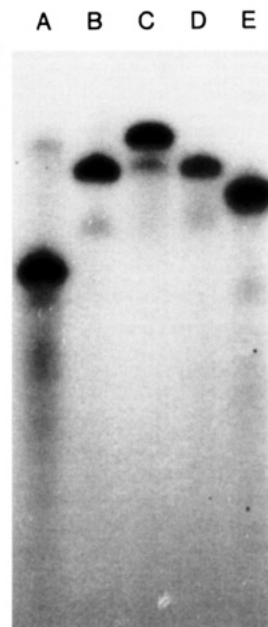
Figure 6. Polyacrylamide gel electrophoresis (20% acrylamide/urea) of 5′-end labeled purified unmodified oligonucleotide and conjugates. Normal HIV1 oligonucleotide (panel A), HIV1−gp41b (panel B), REV−gp41b (panel C), TAR−gp41b (panel D), HIV1−gp41c (panel E).
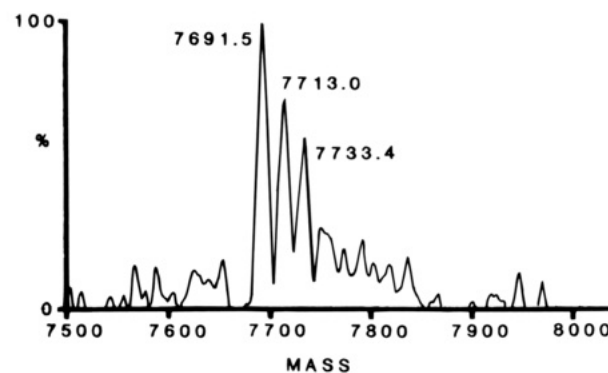
Figure 7. Mass spectrum of the purified HIV1−gp41b conjugate.
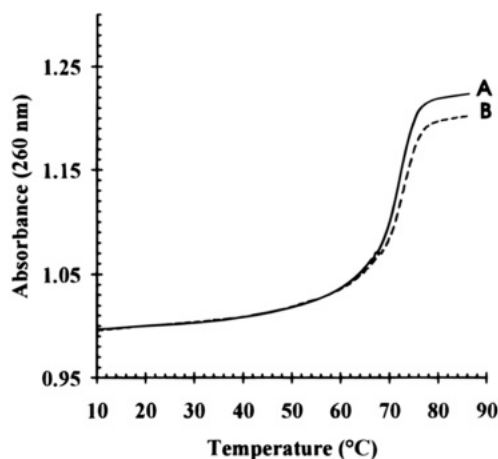
Figure 8. The melting temperature (T_m) curves of duplexes consisting of the HIV1−gp41b conjugate and its 20mer unmodified complementary oligonucleotide (curve A) and that of two unmodified complementary oligonucleotides (curve B).

DISCUSSION

The potential of antisense ODNs as a new class of therapeutic agents lies in the predictability and specificity of the complementary binding between the intracel-

lular target RNA and the exogenously applied antisense ODN by Watson–Crick interactions (1, 2). The main focus of the development of antisense ODNs as therapeutic agents for the control of various infectious diseases (2, 31–35) and for the curtailment or reversal of neoplastic growth (2, 5, 6) involves chemically modifying ODNs with the aim of enhancing nuclease stability and intracellular uptake without compromising the hybridization efficiency, binding specificity, or the ability to activate RNase H. Phosphorothioate oligonucleotides, the most studied of all modified antisense ODNs, fulfill many of these criteria. However, non-sequence-specific inhibitory effects (7, 35) as well as degradation to phosphorothioate nucleotides that subsequently act as substrates for cellular DNA polymerases (11, 12) may undermine their potential to be developed as therapeutic agents.

Modifications of antisense ODNs in which the 5'- or 3'-terminus of oligonucleotides are ligated to a peptide or protein have been the focus of considerable attention. Zuckerman and Schultz (40) described the ligation of a 3'-S-thiopyridyl modified ODN to a cysteine-derivatized staphylococcal nuclease segment to generate a hybrid construct in which the binding specificity of the ODN allowed targeted enzymic cleavage of RNA by the pendant staphylococcal nuclease. The disulfide bond between the protein and the ODN is, however, labile in the presence of reducing agents. Brunnel et al. (41) constructed an antisense ODN conjugated to asialorosomucoid (AsOR)–polylysine complex in which target cell specificity and cellular uptake were associated with receptor-mediated endocytosis of the asialoglycoprotein receptor. Specific antisense inhibition was observed by the AsOR–polylysine antisense ODN conjugates at 3 μM. The protein and the ODN are held together by an electrostatic interaction between the lysine residues and the DNA, the stability of which was not evaluated. There are a wide variety of commercially available heterobifunctional reagents that allow the chemical ligation of two protein analogues with tailored reactivities. However, in such reaction schemes, the nonspecific coupling of the multiple potential reactive sites on the proteins often means that the reaction products contain a mixture of structurally heterogenous species, and purification to obtain homogeneous products is inherently difficult.

Although the methods of solid phase peptide and DNA synthesis have advanced to the stage where both have reached a high level of automation, there are few established protocols for the chemical ligation of synthetic peptides and ODNs to produce stable, well-characterized, and structurally discrete entities. The ligation of two macromolecules in an unambiguous manner to produce a hybrid molecule has, with a few exceptions (36, 42), been limited to solution-phase block coupling procedures in which the two reactants are derivatized with mutually reactive functional groups. Eritja et al. (43) described the conjugation of a maleimide-functionalized peptide to a thiol-derivatized antisense ODN in which the SV40 large T antigen nuclear transport peptide was designed to impart intracellular targeting. The use of maleimide–thiol coupling chemistry for the synthesis of ODN–enzyme conjugate hybridization probes has also been described (44). In a slightly modified procedure, Tung et al. (45) described the coupling between a maleimide-derivatized ODN with the thiol functionality of a cysteine residue in a peptide. Most of these studies have described small scale reactions in which characterization of the products was, at best, limited to amino acid analysis and polyacrylamide gel electrophoresis. The application of the ODN–peptide conjugates in a clinical situation, however, requires more rigorous conjugate characterization procedures. Characterization of the ODN–peptide conjugates by ion spray mass spectrometry described in this paper is one such advance. The majority of studies suggest that 3'-exonuclease digestion is the predominant mechanism of ODN degradation in cell culture medium (16). Unlike the molecules reported by Eritja et al. (43) and Tung et al. (45), hybrid molecules made by the total synthesis method offer the added benefit of protecting the ODN at the 3'-end and may represent a more viable option for the development of antisense ODNs as therapeutic agents.

Thermal denaturation studies of the HIV1–gp41b conjugate indicate that the 3'-peptide moiety does not adversely affect the hybridization efficiency of the ODN. This finding is in agreement with other studies using terminally modified ODNs in which either 5'- (43) or 3'- (40) pendant moieties were not found to hinder the Watson–Crick interaction.

The preparation of hybrid conjugates by a method in which the peptide and ODN are assembled consecutively on a solid support represents an interesting problem since the conditions required to deprotect each component may not necessarily be compatible with the presence of the other component. For example, the obligatory ODN deprotection in aqueous ammonia has been implicated in the partial hydrolysis of peptide bonds (43), and the acidic conditions necessary for deprotection of the amino acid side chains are known to cause depurination of the ODN (46). We have previously reported methods for the total synthesis of oligonucleotide–peptide conjugates by a total synthesis method (24). This methodology, previously applied to the preparation of small amounts of material for use as probes and primers, has been used in this instance for the preparation of milligram amounts of conjugates for antisense studies. The purified conjugates made by this method have been extensively characterized. Collectively, the results indicate that the preformed peptide was stable to the conditions of ODN assembly and deprotection, suggesting that the chemistry of both Fmoc solid phase peptide synthesis (SPPS) and that of solid phase DNA synthesis employed in this study were sufficiently mild to support the consecutive synthesis of a peptide and an ODN and that the ODN deprotection conditions did not have an adverse effect on the peptide. Preliminary results from experiments designed to test whether the ammonia treatment results in any amino acid racemization indicate that no racemization is taking place (49). In this work, the peptides synthesized did not contain amino acids that required side chain protection. When such amino acids are present, the acidolytic treatment may degrade the ODN, the extent of this degradation being dependent on the sequence of both the ODN and the peptide (47). We are presently developing peptide synthesis methods in which amino acid side chain deprotection does not require acidic conditions, in order to develop more general methods for the preparation of ODN–peptide conjugates. A recent communication from de la Torre et al. has described some work on this subject, although the only characterization data presented was PAGE (42). These workers found the use of CPG for peptide synthesis with side chain Fmoc- and Fm-protected amino acids not to be efficient. This is in contrast to the current work, in which we achieved good yields of well-characterized material. This indicates that the efficiency of peptide synthesis on CPG may be dependent on the sequence and the nature of the side-chain protecting groups. Furthermore, these workers reported low phosphoramidite coupling yields on DNA synthesis using the standard protocols—we have not

had that problem, as indicated by the trityl tests, the HPLC profiles, and the final yield of purified product.

The solid phase preparation of conjugates by the total synthesis method offers a number of advantages over alternative solution phase block coupling methods, in which preformed peptides and ODNs are conjugated in solution. Facile conjugate preparation by the total synthesis method offers a method whereby assembly of the ODN–peptide conjugate can be achieved totally on the solid phase, without the requirement for the separate synthesis, functionalization, and purification of the reactants followed by a coupling reaction and the final subsequent purification of the conjugate. In addition to being more time-consuming, a further disadvantage of such schemes is the unavoidable loss of material in each step of the coupling procedure.

The solution phase block coupling method is also being used in our laboratory for the conjugation of the gp41 peptides to ODNs (*48*). Repeated attempts to prepare the conjugates by a block coupling procedure in which a thiol-derivatized oligonucleotide is coupled in solution to a maleimide-derivatized peptide (*43*) were fraught with difficulties, mainly due to the insolubility of the hydrophobic gp41 peptide in aqueous solvents. Attempts at solubilizing the peptide in various organic solvents prior to the conjugation were not successful (results not shown). Therefore, conjugate preparation by the total synthesis method circumvents one of the major problems associated with the classical block conjugation schemes— the limited solubility of certain peptides in solution.

In conclusion, we have developed methods for the ready synthesis of oligonucleotide–peptide hybrid molecules containing fusion peptides derived from the gp41 glycoprotein of HIV. These were characterized by a number of techniques, including ion spray mass spectrometry. The hybridization abilities of these conjugates were found to be very similar to those of the unmodified molecules. These are currently being tested as antisense inhibitors of HIV.

LITERATURE CITED

(1) Uhlman, E., and Peyman, A. (1990) Antisense oligonucleotides: A new therapeutic principle. *Chem. Rev. 90,* 543–584.

(2) Milligan, J. F., Matteucci, M. D., and Martin, J. C. (1993) Current concepts in antisense drug design. *J. Med. Chem. 36,* 1923–1937.

(3) Daum, T., Engels, J. W., Mag, M., Muth, J., Lucking, S., Schroder, H. C., Matthes, E., and Muller, W. E. G. (1992) Antisense oligodeoxynucleotide: inhibitor of splicing of mRNA of human immunodeficiency virus type 1. *Intervirology 33,* 65–75.

(4) Boiziau, C., Kurfurst, R., Cazenave, C., Roig, V., Thuong, N. T., and Toulme, J. J. (1991) Inhibition of translation initiation by antisense oligonucleotides via an RNase-H independent mechanism. *Nucleic Acid Res. 19,* 1113–1119.

(5) Heikkila, R., Schwab, G., Wickstrom, E., Loke, S. L., Pluznik, D. H., Watt, R., and Neckers, L. M. (1987) A *c-myc* antisense oligonucleotide inhibits entry into S phase by not progress from G_0 and G_1. *Nature 328,* 445–449.

(6) Murphy, P. R., Sato, Y., and Knee, R. S. (1992) Phosphorothioate antisense oligonucleotides against basic fibroblast growth factor inhibit anchorage dependent growth of a malignant glioblastoma cell line. *Mol. Endocrinol. 6,* 877–884.

(7) Krieg, A. M., Tonkinson, J., Matson, S., Zhao, Q., Saxon, M., Zhang, L., Bhanja, U., Yakubov, L., and Stein, C. A. (1993) Modification of antisense phosphodiester oligodeoxynucleotides by a 5'-cholesteryl moeity increases cellular association and improves efficacy. *Proc. Natl. Acad. Sci. U.S.A. 90,* 1048–1052.

(8) MacKellar, C., Graham, D., Will, D. W., Burgess, S., and Brown, T. (1992) Synthesis and physical properties of anti-HIV antisense oligonucleotides bearing terminal lipophilic groups. *Nucleic Acids Res. 20,* 3411–3417.

(9) Cumin, F., Asselbergs, F., Lartigot, M., and Felder, E. (1993) Modulation of human prorenin gene expression by antisense oligonucleotides in transfected CHO cells. *Eur. J. Biochem. 212,* 347–354.

(10) Degols, G., Leonetti, J., Benkirane, M., Devaux, C., and Lebleu, B. (1992) Poly-(L-Lysine)-conjugate oligonucleotides promote sequence-specific inhibition of acute HIV-1 infection. *Antisense Res. Dev. 2,* 293–301.

(11) Majumdar, C., Stein, C. A., Cohen, J. S., Broder, S., and Wilson, S. (1990). HIV reverse transcriptase stepwise mechanisms: phosphorothioate oligodeoxynucleotide as primer. *Biochemistry 28,* 1340–1346.

(12) Cazenave, C., Stein, C., Loreau, N., Thuong, N. T., Neckers, L., Subasinghe, C., Helene, C., Cohen, J., and Toulme, J. J. (1991) Comparative inhibition of rabbit globin mRNA translation by modified antisense oligodeoxynucleotides. *Nucleic Acids Res. 17,* 4255–4273.

(13) Chin, D. J., Green, G. A., Zon, G., Szoka, Jr, F. C., and Straubinger, R. M. (1990) Rapid nuclear accumulation of injected oligodeoxyribonucleotides. *New Biologist 12,* 1091–1100.

(14) White, J. M. (1992) Membrane fusion. *Science 258,* 917–924.

(15) Akhtar, S., Basu, S., Wickstrom, E., and Juliano, R. L. (1991) Interaction of antisense DNA oligonucleotide analogs with phospholipid membranes (liposomes). *Nucleic Acid Res. 19,* 5551–5559.

(16) Shaw, J. P., Kent, K., Bird, J., Fishback, J., and Froehler, B. F. (1991) Modified deoxyoligonucleotides stable to exonuclease degradation in serum. *Nucleic Acids Res. 19,* 747–750.

(17) Rafalski, M., Lear, J. D., and DeGrado, W. F. (1990) Phospholipid interactions of synthetic peptides representing the N-terminus of HIV gp41. *Biochemistry 29,* 7917–7922.

(18) Duzgunes, N., and Shavnin, S. A. (1992) Membrane destabilization by N-terminal peptides of viral envelope proteins. *J. Membrane Biol. 128,* 71–80.

(19) Bergeron, L., Sullivan, N., and Sodroski, J. (1992) Target cell-specific determinants of membrane fusion within the human immunodeficiency virus type 1 gp120 third variable region and gp41 amino terminus. *J. Virol. 66,* 2389–2397.

(20) Freed, E. O., and Myers, D. J. (1992) Identification and characterization of fusion and processing domains of the human immunodeficiency virus type 2 envelope glycoprotein. *J. Virol. 66,* 5472–5478.

(21) Chanh T. C., Dreesman, G. R., Kanda, P., Linette, G. P., Sparrow, J. T., Ho, D. D., and Kennedy, R. C. (1986) Induction of anti-HIV neutralizing antibodies by synthetic peptides. *EMBO J. 5,* 3065–3071.

(22) Gordon, L. M., Curtain, C. C., Zhong, Y. C., Kirkpatrick, A., Mobley, P. W., and Waring, A. J. (1992) The amino-terminal peptide of HIV-1 glycoprotein 41 interacts with human erythrocyte membranes: peptide conformation, orientation and aggregation. *Biochim. Biophys. Acta 1139,* 257–274.

(23) Slepushkin, V. A., Melikyan, G. B., Sidovova, M. S., Chumakov, V. M., Andreev, S. M., Manulyan, R. A., and Karamov, E. V. (1990) Interaction of human immunodeficiency virus (HIV-1) fusion peptides with artificial lipid membranes. *Biochem. Biophys. Res. Commun. 172,* 952–957.

(24) Haralambidis, J., Duncan, L., Angus, K., and Tregear, G. W. (1990). The synthesis of polyamide–oligonucleotide conjugate molecules. *Nucleic Acids Res. 18,* 493–499.

(25) Maniatis, T., Fritsch, E. F., and Sambrook, J. (1989) Molecular cloning : a laboratory manual, sections 5.61–5.65, Cold Spring Harbor Laboratory, Cold Spring Harbor, NY.

(26) Starcich, B. R., Hahn, B. H., Shaw, G. M., McNeely, P. D., Modrow, S., Wolf, H., Parks, E. S., Parks, W. P., Josephs, S. F., Gallo, R. C., and Wong-Staal, F. (1986) Identification and characterization of conserved and variable regions in the envelope gene of HTLV-III/ LAV, the retrovirus of AIDS. *Cell* 45, 637–648.

(27) Tong, G., Lawlor, J. M., Tregear, G. W., and Haralambidis, J. (1993) The synthesis of oligonucleotide–polyamide conjugate molecules suitable as PCR primers. *J. Org. Chem. 58,* 2223–2231.

(28) Sarin, V. K., Kent, B. H., Tam, J. P., and Merrifield, R. B. (1981) Quantitative monitoring of solid phase peptide synthesis by the ninhydrin reaction. *Anal. Biochem. 117,* 147–157.

(29) Milligen 9050 PepSynthesizer Technical Note 3.10, Millipore Corp., 1987.

(30) Benjamin, D. M., McCormack, J. J., and Gump, D. W. (1973) . Use of newer amino group reagents for the detection and determination of kanamycin. *Anal. Chem. 45,* 1531–1534.

(31) Agrawal, S., Goodchild, J., Civeira, M. P., Thornton, A. H., Sarin, P. S., and Zamecnik, P. C. (1988) Oligodeoxynucleotide phosphoramidates and phosphorothioates as inhibitors of human immunodefiency virus. *Proc. Natl. Acad. Sci. U.S.A. 85,* 7079–7083.

(32) Buck, H. B., Koole, L. H., van Genderen, M. H. P., Smit, L., Geelen, M. C., Jurriaans, S., and Goudsmit, J. (1990) Phosphate-methylated DNA aimed at HIV-1 RNA loops and integrated DNA inhibits viral infectivity. *Science 248,* 208–212.

(33) Bordier, B., Helene, C., Barr, P. J., Litrak, S., and Sarih-Cottin, L. (1992) *In vitro* effect of antisense oligonucleotides on human immunodeficiency virus type 1 reverse transcription. *Nucleic Acids Res. 20,* 5999–6006.

(34) Kinchington, D., Glapin, S., Jaroszewski, J. W., Ghosh, K., Subasinghe, C., and Cohen, J. S. (1992) A comparison of gag, pol and rev antisense oligodeoxynucleotides as inhibitors of HIV-1. *Antiviral Res. 17,* 53–62.

(35) Matsukura, M., Zon, G., Shinozuka, K., Robert-Guroff, M., Shimada, T., Stein, C. A., Mitsuya, H., Wong-Staal, F., Cohen, J. S., and Broder, S. (1989) Regulation of viral expression of human immunodeficiency virus *in vitro* by an antisense phosphorothioate oligodeoxynucleotide against *rev (art/trs)* in chronically infected cells. *Proc. Natl. Acad. Sci. U.S.A. 86,* 4244–4248.

(36) Juby, C. D., Richardson, C. D., and Brousseau, R. (1991).

Facile preparation of 3′- oligonucleotide–peptide conjugates. *Tetrahedron Lett. 32,* 879–882.

(37) Robles, J., Pedroso, E., and Grandas, A. (1994) Stepwise solid-phase synthesis of the nucleopeptide Phac-Phe-Val-Ser-(p$^{3′}$ACT)-Gly-OH. *J. Org. Chem. 59,* 2482–2486.

(38) Smith, R. D., Loo, J. A., Edmonds, C. G., Barinaga, C. J., and Udseth, H. R. (1990) New developments in biochemical mass spectrometry: electrospray ionization. *Anal. Chem. 62,* 882–899.

(39) Stults, J. T., and Marsters, J. C. (1991) Improved electrospray ionization of synthetic oligonucleotides. *Rapid Commun. Mass. Spectrom. 5,* 359–363.

(40) Zuckerman, R. N., and Schultz, P. G. (1989) Site-selective cleavage of structured RNA by staphylococcal nuclease–DNA hybrid. *Proc. Natl. Acad. Sci. U.S.A. 86,* 1766–1770.

(41) Bunnel, B. A., Askari, F. K., and Wilson, J. M. (1992) Targeted delivery of antisense oligonucleotides by molecular conjugates. *Somat. Cell. Mol. Genet. 12,* 599–569.

(42) de la Torre, B. G., Avino, A., Tarrason, G., Piulats, J. Albericio, F., and Eritja, R. (1994) Stepwise solid-phase synthesis of oligonucleotide–peptide hybrids. *Tetrahedron Lett. 35,* 2733–2736.

(43) Eritja, R., Pons, A., Escarceller, M., Giralt, E., and Albericio, F. (1991) Synthesis of defined peptide–oligonucleotide hybrids containing a nuclear transport signal sequence. *Tetrahedron 47,* 4113–4120.

(44) Ghosh, S. S., Kao, P. M., McCue, A. W., and Chappelle, H. L. (1990) Use of maleimide–thiol coupling chemistry for efficient synthesis of oligonucleotide–enzyme conjugate hybridization probes. *Bioconjugate Chem. 1,* 71–76.

(45) Tung, C. H., Rudolph, J. M., and Stein, S. (1991) Preparation of oligonucleotide–peptide conjugates. *Bioconjugate Chem. 2,* 464–465.

(46) Hakala, H., Oiranen, M., Saloniemi, E., Gouzaev, A., and Lonnberg, H. (1992) Acid-catalyzed depurination of di-, tri-and poly-deoxyribonucleotides: effect of molecular environment on the cleavage of adenine residue. *J. Phys. Org. Chem. 5,* 824–828.

(47) Haralambidis, J., Ede, N. J., and Soukchareun, S. Unpublished observations.

(48) Ede, N. J., Tregear, G. W., and Haralambidis, J. (1994) Routine preparation of thiol-oligonucleotides: application to the synthesis of oligonucleotide–peptide hybrids. *Bioconjugate Chem. 5,* 373–378.

(49) Haralambidis, J., and Healey, A. Unpublished observations.

Nucleosides and Nucleotides. 135. DNA Duplex and Triplex Formation and Resistance to Nucleolytic Degradation of Oligodeoxynucleotides Containing *syn*-Norspermidine at the 5-Position of 2'-Deoxyuridine[†]

Hiroshi Nara, Akira Ono,[‡] and Akira Matsuda*

Faculty of Pharmaceutical Sciences, Hokkaido University, Kita-12, Nishi-6, Kita-ku, Sapporo 060, Japan. Received June 22, 1994[⊛]

A novel 2'-deoxyuridine analogue with *syn*-norspermidine at the 5-position, 5-[4-[*N,N*-bis(3-amino-propyl)amino]butyl]-2'-deoxyuridine (**1**), has been synthesized from 5-iodo-2'-deoxyuridine. This nucleoside **1** was incorporated into heptadecadeoxynucleotides 5'-d[**1**(MT)₈]-3' and 5'-[(TM)₄**1**(MT)₄]-3' (M = 5-methyl-2'-deoxycytidine). The triamine group stabilized duplex and triplex formation of the heptadecadeoxynucleotides with a complementary strand and a target duplex, respectively. The oligonucleotides containing **1** were more resistant to nuclease P1 and snake venom phosphodiesterase than an unmodified heptadecadeoxynucleotide, 5'-d[T(MT)₈]-3'.

INTRODUCTION

Many types of oligonucleotides having amino tethers at the base, sugar, or phosphate group have been developed and used to attach additional reporter groups and other functional groups (*1–5*). One of the most interesting uses of these oligomers is to prevent nucleolytic hydrolysis by endo- and/or exo-nucleases (*6–8*). Bacteriophage φW-14 DNA, in place of thymine, contains up to 50% α-putrescinylthymine, which is known to be more resistant to nucleolytic enzymes such as DNase I and venom phosphodiesterase than unmodified DNAs (*9, 10*). This modification also causes a higher melting temperature than expected from the GC content (*11–13*). Polyamines such as putrescine, spermidine, and spermine, which are present in many types of cells, are thought to stabilize higher-ordered structures of nucleic acids (*14, 15*). Polyamines also bind strongly to DNAs (*16*) and stabilize duplex (*17, 18*) and triplex (*19–23*) DNAs, although their precise binding modes are not known. The enhanced thermal stability has been explained to be due to reduction of the anionic electrostatic repulsion between phosphate moieties by cationic polyamines. Therefore, oligodeoxynucleotides bearing polyamines would exert both properties such as stabilization of duplex and triplex formations and resistance to nucleases. However, melting temperatures of short synthetic oligodeoxynucleotides containing α-putrescinylthymine were reported to be rather lower than expected from the results in the φW-14 DNA, although they had nuclease resistance properties (*24*). In an effort to find

an oligodeoxynucleotide having both duplex/triplex stabilization and nuclease resistance properties, we report here the synthesis of 5-[4-[*N,N*-bis(3-aminopropyl)amino]-butyl]-2'-deoxyuridine (**1**) (Figure 1) and heptadecadeoxynucleotides (heptadecamers) 5'-d[**1**(MT)₈]-3' (**I**) and 5'-d[(TM)₄**1**(MT)₄]-3' (**II**) (M = 5-methyl-2'-deoxycytidine) containing **1**. Thermal stability of the duplex and triplex formations and stability of these oligomers to nucleolytic digestion were also studied.

RESULTS AND DISCUSSION

Synthesis. The modified 2'-deoxyuridine analogue carrying *syn*-norspermidine at the end of a butyl tether attached at the 5-position was synthesized starting from commercially available 5-iodo-2'-deoxyuridine. First, a 3-formylpropyl group was constructed at the 5-position of the uracil moiety, and then *syn*-norspermidine was conjugated with the formyl group (Figure 2).

A coupling reaction of 3',5'-di-*O*-benzoyl-5-iodo-2'-deoxyuridine (**2**) with 4-(*tert*-butyldimethylsiloxy)butyne in the presence of (Ph₃P)₂PdCl₂ and CuI in Et₃N (*25*) gave a 4-siloxy-1-butyn-1-yl derivative **3** in 79% yield along with a small amount of a fluorescent cyclic product **4**. When DMF was used as a solvent or when 3-butyn-1-ol was used as a terminal alkyne, undesired cyclic derivatives were obtained as the main products. Robins *et al.* (*25*) reported that the cyclic products were produced by reactions between the preformed 5-alkynyl substituent and the 4-carbonyl group with CuI. However, the reaction in the absence of CuI gave no desired coupling product. Hydrogenation of the alkynyl moiety gave 5-(4-*tert*-butyldimethylsiloxybutyl) derivative **5** quantitatively. The TBS group attached at the terminal hydroxyl group was more stable than those attached at the hydroxyl groups of the sugar moiety in nucleosides; thus, 3 equiv of TBAF and 3 days of reaction were necessary for deprotection. A newly generated hydroxyl group of **6** was oxidized by the Swern method to give the formyl derivative **7**. Attempts to deblock the benzoyl group in **7** with NaOMe before the conjugation with *syn*-norspermidine were unsuccessful due to decomposition of the product. Dimethyl acetal or 1,3-diphenylimidazolidine derivatives were prepared from **7** for protection of the formyl group but were found to be unstable during silica gel column chromatography. Therefore, we first tried conversion of
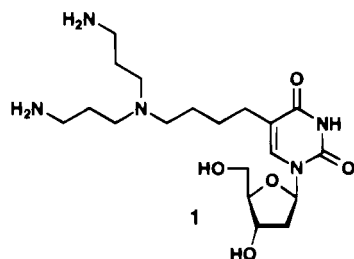

Figure 1. List of oligonucleotides synthesized. **1** = 5-[4-[*N*,*N*-bis(3-aminopropyl)amino]butyl]-2′-deoxyuridine. **M** = 5-methyl-2′-deoxycytidine.

7 to the amine derivative and then preparation of a fully protected nucleoside 3′-phosphoramidite unit.

Although an admixture of **7** with N^1,N^7-ditrityl-*syn*-norspermidine, which was readily obtained from *syn*-norspermidine with TrCl, in MeOH/THF did not give a detectable Schiff base on TLC analyses, on addition of $NaBH_3CN$ (*26*) to the mixture at pH 6–7, the reaction proceeded smoothly to give **8** in 63% yield. However, at pH 8–9, the reaction proceeded rather slowly and the alcohol derivative **6** was obtained as a main product by addition of a large excess of $NaBH_3CN$. Treatment of **8** with NaOMe followed by 80% aqueous acetic acid gave **1** as a hygroscopic foam in good yield (Figure 3). Then **1** was converted into bis(trifluoroacetamido) derivative **10**, which was purified by silica gel column chromatography. Treatment of **10** with DMTrCl in pyridine (*27*) did not give the desired product **11** but recovered **10**. However, we found that using an excess of DMTrCl in a mixture of pyridine and DMF (1:1) gave **11** in 49% yield along with 31% recovery of **10**. Although phosphitylation of **11** by the reported procedure (*27*) using 2-cyanoethyl *N*,*N*-diisopropylchlorophosphoramidite in CH_2Cl_2 in the presence of diisopropylethylamine did not give **12**, in CH_3-CN the reaction proceeded to give **12** as an oil in 53% yield, which was lyophilized from anhydrous dioxane before DNA synthesis. Thus, the 5-bulky substituent influenced the reactivities of the 5′- as well as the 3′-hydroxyls, and further improvement of the yields of **11** and **12** are under investigation in our laboratory.

The heptadecamers **I** and **II** (Figure 1) were synthesized on a DNA synthesizer using **12**. An average coupling yield of **12** was 72% using a 0.12 M solution of **12** in CH_3CN and 1800 s for the coupling time. Starting from 1 μmol of thymidine linked to controlled pore glass, 12 OD units (at 254 nm) of **I** and 6 OD units of **II**, which showed single peaks by HPLC analysis on a C-18 silica gel column (an example is shown in Figure 4a), were obtained after purification. Also, purity of the heptadecamers was examined by electrophoresis. After being labeled at the 5′-end with ^{32}P (*28*), the heptadecamers **I**, **II**, and **III** were analyzed by polyacrylamide gel electrophoresis under denaturing conditions (*28*). Although each heptadecamer showed single spots as shown in Figure 5, **I** and **II** carrying *syn*-norspermidine showed reduced mobility compared with the control heptadecamer **III**. In the modified heptadecamers, **I** carrying the triamine at the 5′-end moved more slowly than **II** carrying the triamine in its center.

To confirm the existence of **1** in the heptadecamers, **I** was completely hydrolyzed to the corresponding nucleosides by a mixture of snake venom phosphodiesterase and alkaline phosphatase, and then the nucleoside composition was analyzed by HPLC (Figure 4b). The peak corresponding to **1**, confirmed by coelution with an authentic sample, was observed and the composition of the nucleosides calculated from areas of the peaks was 1:7.8:8.3 (1:T:M), which was close to the theoretical value of 1:8:8.

Duplex and Triplex Formations by the Heptadecamers. Duplex and triplex formations of the heptadecamers with the complementary strand **IV** and the target duplex **V** were studied by thermal denaturation. One transition was observed in a melting profile of each duplex. On the other hand, two transitions were observed in a melting profile of each triplex: the transitions with higher T_ms due to the melting of the target duplex **V** (88 °C) and the transitions with lower T_ms corresponded to the dissociation of the third strands from the triplexes. T_ms are shown in Figure 6a,b. Attachment of *syn*-norspermidine to the heptadecamers stabilized duplex and triplex formation.

T_ms of **I-IV** and **II-IV** duplexes were higher than the control duplex **III-IV** in all solutions examined (Figure 6a). Addition of 3 μM *syn*-norspermidine to a solution of the control duplex in 5 mM NaCl, 10 mM Na cacodylate (pH 7.0) increased the T_m of the control duplex to 48 °C (Figure 6a, lowest bar). However, T_ms of **I-IV** (51 °C) and **II-IV** (49 °C) under the same conditions in the absence of additional *syn*-norspermidine were still higher than 48 °C. The result indicated that the attachment of the triamine to the oligodeoxynucleotides stabilized duplex formations. In the modified heptadecamers, **I** carrying the triamine at the 5′-end formed a more stable duplex than **II** carrying the triamine in its center. Probably the triamine attached at the 5′-end is in a better location for binding to the sugar−phosphate backbone of the duplex than the triamine attached in the center of **II**.

According to the expectation that the duplex-stabilization effect of the positive charges on the triamine might be more conspicuous as salt concentrations of the solutions become lower, we measured T_ms of the duplexes in buffer with several salt concentrations (Figure 6a). Actually, a difference (5°) in the T_ms of **I-IV** duplex and the control duplex **III-IV** in the solution with the lowest NaCl concentration (5 mM) was larger than the differences (3°) in T_ms of the duplexes in the solutions with higher NaCl concentrations (10 or 20 mM NaCl). However, no striking increase of the difference in T_ms of the duplexes at lower salt concentrations was observed, probably since the number of the positive charges in the oligomers was smaller than the number of the negative charges at the sugar−phosphate backbone so that remaining negative charges still repelled each other. Complete neutralization of negative charges of the phosphates by increases of the positive charges of the polyamines could efficiently stabilize duplex formation in solutions with low salt concentrations (*29*). While bacteriophage ϕW-14 DNA showed greater thermal stability than unmodified DNA, an increase in the number of α-putrescinylthymine in short synthetic oligothymidylates rather destabilized the corresponding duplexes (*24*). However, oligonucleotides bearing 5-ω-aminohexyluracil, in which the total number of atoms in the side chain is the same as that in α-putrescinylthymine, did not destabilize the duplex formation; even an increase in the number in one oligomer did not greatly destabilize it (*29*). These results showed that increases in the number of the cationic species would not stabilize the
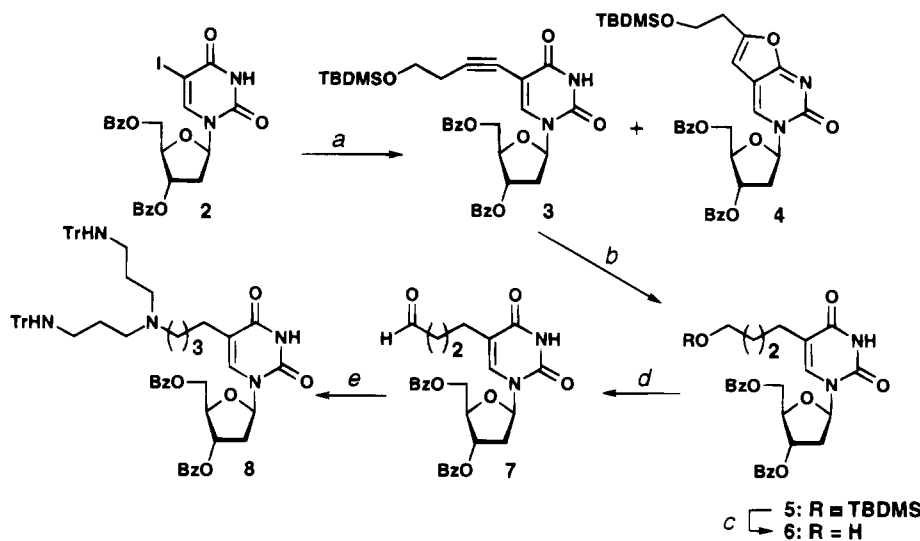
Figure 2. Key: (a) 4-(tert-butyldimethylsiloxy)butyne (1.5 equiv), (PPh₃)₂PdCl₂ (0.024 equiv), CuI (0.09 equiv), in Et₃N, 60 °C, 2 h, **3** (79%) and **4** (9%); (b) H₂, 10% Pd/C (40 psi), in EtOH, rt, 1 h quant; (c) TBAF (3 equiv), in THF, rt, 3 days, 81%; (d) oxalyl chloride (2 equiv), in DMSO (3 equiv), −30 °C, then Et₃N, 69%; (e) NaBH₃CN (1.7 equiv), N^1,N^7-ditrityl-syn-norspermidine (1.5 equiv), in THF:MeOH (4:1), rt, 1.5 h, 63%.
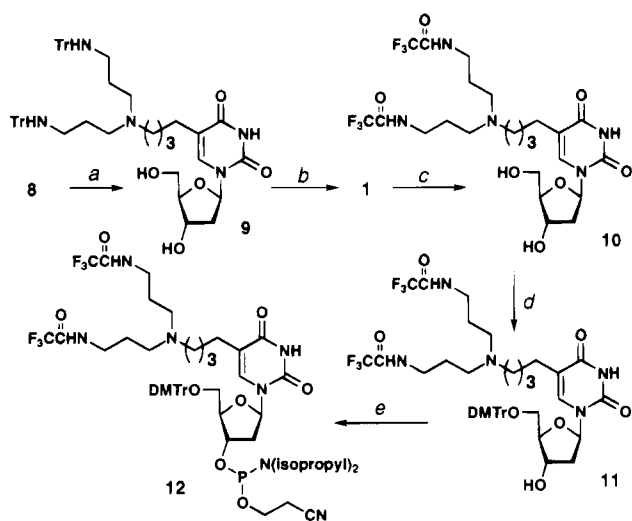

Figure 3. Key: (a) 0.2 M MeONa in MeOH (2.9 equiv) rt, 1 h, 86%; (b) 80% AcOH, 55 °C, 2 h, quant; (c) CF₃COSEt (5.1 equiv), Et₃N (5.1 equiv), in MeOH, rt, 0.5 h, 73%; (d) DMTrCl (5.5 equiv), in DMF:pyridine (1:1), rt, 2 h, **11** (49%) and **10** (31%); (e) 2-cyanoethyl N,N-diisopropylchlorophosphoramidite (1.5 equiv), N,N-diisopropylamine (2 equiv), in CH₃CN, rt, 40 min, 53%.
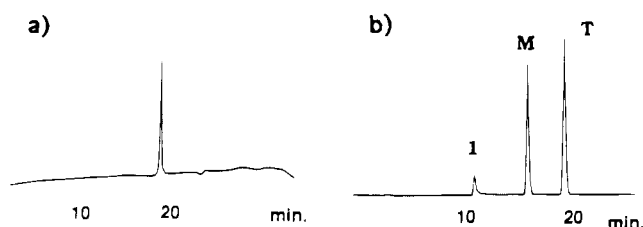
Figure 4. Key: (a) a profile for HPLC analysis of **I** with a C-18 column with a linear gradient of CH₃CN from 2.5% to 17.5% (20 min) in 0.1 M TEAA buffer (pH 6.8); (b) a profile for HPLC analysis of a nucleoside mixture obtained by complete hydrolysis of **I** with the C-18 column with a linear gradient of CH₃CN from 0% to 10% (20 min) in 0.1 M TEAA buffer (pH 6.8).

duplex formation. In contrast to these reports, our results indicated thermal stabilization effects by attachment of syn-norspermidine. Furthermore, contrary to the case of 5-ω-aminohexyluracil, incorporation of 5-ω-aminohexylcytosine in oligodeoxynucleotides stabilized the duplex formation (29). Therefore, considerations of the
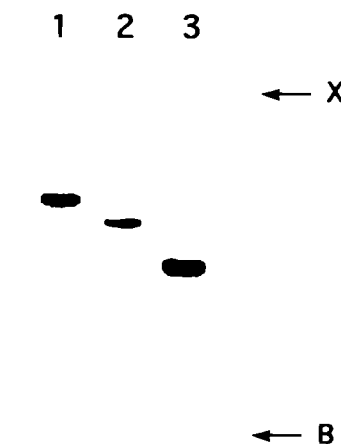
Figure 5. Profile for polyacrylamide gel electrophoresis of the heptadecamers. After they were labeled with ³²P at the 5′-end, **I** (lane 1), **II** (lane 2), and **III** (lane 3) were analyzed by electrophoresis on 20% polyacrylamide gel containing 8 M urea (26). Densities of radioactivity of the gel were read by a Bioimaging Analyzer (Bas 2000, Fuji, Co., Ltd.). **B** and **X** indicate bromophenol blue and xylene cyanole, respectively.

distal position of the cationic species and sequences would be important for designing more stable duplex formation by such amino groups.

Also, triplex formation was stabilized by this modification (Figure 6b). Addition of 3 μM syn-norspermidine to the solution containing **III-V** triplex in 50 mM NaCl, 10 mM Na phosphate increased the T_m to 32 °C (Figure 6b, lowest bar). The T_m of **I-V** triplex (34 °C) in the absence of additional syn-norspermidine was higher but the T_m of **II-V** triplex (31 °C) was slightly lower than 32 °C. It was expected that triplexes would be more efficiently stabilized by positive charges than duplexes since negative charges are more concentrated in triplexes than in duplexes. However, striking stabilization of the triplexes by positive charges of the triamine was not observed in this experiment. Our results contrast with those recently reported by Tung et al. (30). They observed that tetramines attached at the 5′-end of oligonucleotides efficiently stabilized triplex formations but did not stabilize duplex formations. Also, Thomas and Thomas (19) reported that ability for triplex stabilization by polyamines was dependent on the length of the alkyl groups between

a)

5 mM NaCl

10 mM NaCl

20 mM NaCl

5 mM NaCl +
3 µM norspermidine

45   50   55
temperature (°C)

b)

50 mM NaCl

100 mM NaCl

200 mM NaCl

50 mM NaCl +
3 µM norspermidine

25   30   35
temperature (°C)
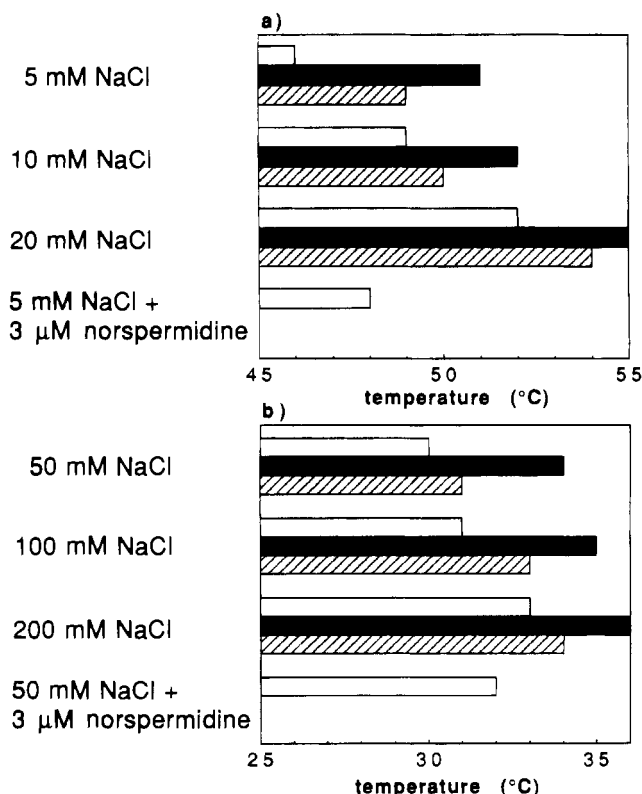
Figure 6. (a) T_{ms} of the duplexes consist of the heptadecamers and the complementary strand **IV** in solutions containing 10 mM Na phosphate and appropriate concentrations of NaCl (pH 7.0): open bars, **III-IV**; filled bars, **I-IV**; hatched bars, **II-IV**. (b) T_{ms} of the triplexes consist of the heptadecamers and the target duplex **V** in solutions containing 10 mM Na phosphate and appropriate concentrations of NaCl (pH 7.0): open bars, **III-V**; filled bars, **I-V**; hatched bars, **II-V**.

amines. Consequently, stabilization of duplex and triplex formations of nucleic acids by the polyamines is influenced by the lengths and structures of polyamines or positions at which the polyamines attached to the oligonucleotides. Another possible explanation is that the triplexes of this sequence were already stabilized by positive charges in M^+:G:C triads (*27*); thus, additional positive charges did not further stabilize them, obviously. Other types of triplexes containing no positive charge in the structures such as triplexes containing only T:A:T triads, triplexes containing neutral pseudoisocytidine:G:C triads (*31*), and triplexes containing Pu:Pu:Py type triads (*32*), which are expected to be more important for biological application of triplexes, could be efficiently stabilized by attachment of polyamines.

Partial Digestion of the Heptadecamers with Snake Venom Phosphodiesterase and Nuclease P1. As mentioned above, DNAs containing α-putrescinylthymidine are more resistant to nucleases than unmodified DNAs (*9, 10*). Therefore, stability of the heptadecamer carrying *syn*-norspermidine to nucleolitic digestion was examined. The heptadecamer **II** carrying the triamine in its center was labeled at the 5′-end with ^{32}P (*28*) and incubated with an appropriate nuclease, and then the reactions were analyzed by polyacrylamide gel electrophoresis under denaturing conditions (*28*) (Figure 7). Owing to a difference in the rates of hydrolysis between 5′-TpM-3′ linkages and 5′-MpT-3′ linkages, spots for newly generated oligomers containing an M residue at the 3′-end were faint but spots for oligomers containing a T residue at the 3′-end were bold. Although the control **III** was hydrolyzed randomly by venom phosphodiesterase, a 3′-exonuclease, after 8 h, **II** was hydrolyzed

only at the 3′-side from **1** (Figure 7a). The phosphodiester linkage at the 3′-side of **1** was resistant to the nuclease. Also, the phosphodiester linkages around **1** were more resistant to nuclease P1, an endonuclease, than the phosphodiester linkages beside thymidine (Figure 7b).

As discussed above, the duplexes and the triplexes formed by the heptadecamers carrying the triamine were more stable than the control duplex and the control triplex, respectively. Furthermore, the modified heptadecamers were more resistant to nucleases than the control heptadecamer. These properties of the oligonucleotides carrying the polyamine would be useful for biological application of oligonucleotide analogues. However, stability of duplex and triplex formation and stability of the oligonucleotide analogues to nucleases should be increased for practical uses. For completion of this goal, longer amines should be attached to the oligonucleotides or the numbers of polyamines attached to the oligonucleotides should be increased. These studies are actively under way in our laboratory and will be reported shortly.

EXPERIMENTAL PROCEDURES

General Experimental Data. TLC was done on Merck Kieselgel F254 precoated plates (Merck, Germany). The silica gel used for column chromatography was YMC gel 60A (70−230 mesh) (YMC Co., Ltd., Japan). Melting points were measured on a Yanagimoto MP-3 micromelting point apparatus (Yanagimoto, Japan) and are uncorrected. Fast atom bombardment mass spectrometry (FAB-MS) was done on a Jeol JMS-HX110 (JEOL) at an ionizing voltage of 70 eV. The ^{1}H NMR spectra were recorded on a Jeol JNM-GX 270 (270 MHz) spectrometer (JEOL) with tetramethylsilane as an internal standard. Chemical shifts are reported in parts per million (δ), and signals are expressed as s (singlet), d (doublet), t (triplet), m (multiplet), or br (broad). All exchangeable protons were detected by disappearance on the addition of D_2O. UV absorption spectra were recorded with a Shimadzu UV-240 spectrophotometer (Shimadzu Co., Japan).

4-(*tert*-Butyldimethylsiloxy)butyne. A CH_2Cl_2 solution (6 mL) containing 3-butyn-1-ol (4 mL, 52.9 mmol) was added to a CH_2Cl_2 solution (25 mL) containing TBDMSCl (9.6 g, 63.5 mmol), Et_3N (8.9 mL, 63.5 mmol), and DMAP (11 mg, 0.09 mmol) in an ice bath, and the mixture was stirred at room temperature. After 21 h, the reaction mixture was washed with water (60 mL), and then the H_2O layer was back-extracted with CH_2-Cl_2. The organic layers were combined and successively washed with H_2O and then brine, dried (Na_2SO_4), and concentrated. The residue was distilled under reduced pressure (14 mmHg, bp 69 °C) to give the desired product as an oil (8.46 g, 87%): ^{1}H-NMR ($CDCl_3$) 3.75 (t, 2 H, CH_2O, $J_{3,4}$ = 2.8 Hz), 2.40 (dt, 2 H, C≡CCH_2, $J_{1,3}$ = 7.1 Hz), 1.96 (t, 1 H, HC≡C, $J_{1,3}$ = 7.1 Hz), 0.90 [m, 9 H, SiC(CH_3)$_3$], 0.08 [m, 6 H, Si(CH_3)$_2$].

3′,5′-Di-*O*-benzoyl-5-[4-(*tert*-butyldimethylsiloxy)-butynyl]-2′-deoxyuridine (3) and 6-[2-(*tert*-Butyldimethylsiloxy)ethyl]-3-(3,5-di-*O*-benzoyl-β-D-*erythro*-pentofuranosyl)furano[2,3-d]pyrimidin-2-one (4). An Et_3N solution (700 mL) containing **1** (8.7 g, 15.5 mmol), 4-(*tert*-butyldimethylsiloxy)butyne (4.3 g, 23.3 mmol), CuI (260 mg, 1.4 mmol), and (PPh$_3$)$_2$PdCl$_2$ (260 mg, 0.37 mmol) was heated at 60 °C under an Ar atmosphere. After 2 h, the solvent was evaporated, the residue was dissolved in EtOAc, and the solution was washed with aqueous 5% EDTA (pH 4) (twice) and then H_2O, dried (Na_2SO_4), and concentrated. The residue was chromato-
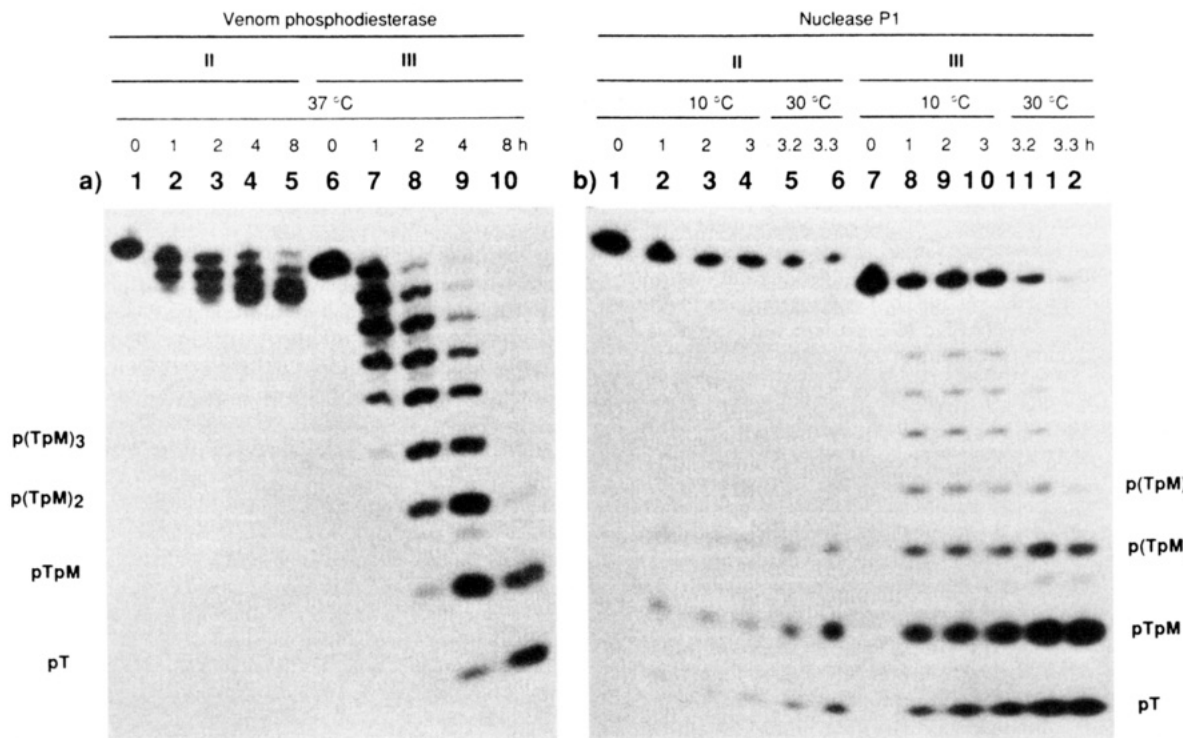
Figure 7. Polyacrylamide gel electrophoresis of oligonucleotides hydrolyzed by nucleases: (a) **II** (lanes 1–5) and **III** (lanes 6–10) were incubated with venom phosphodiesterase at 37 °C for 0 h (lanes 1 and 6), 1 h (lanes 2 and 7), 2 h (lanes 3 and 8), 4 h (lanes 4 and 9), and 8 h (lanes 5 and 10). (b) **II** (lanes 1–6) and **III** (lanes 7–12) were incubated with nuclease P1 at 10 °C for 0 h (lanes 1 and 7), 1 h (lanes 2 and 8), 2 h (lanes 3 and 9), and 3 h (lanes 4 and 10), and then at 30 °C for an additional 10 min (lanes 5 and 11), and 20 min (lanes 6 and 12). See the Experimental Procedures for conditions.

graphed on a silica gel column (5.3 × 35 cm) with 17–25% EtOAc in hexane as eluents. Concentration of the fractions gave a residue which was dissolved in a mixture of hexane and EtOAc to give **3** as white crystals (7.6 g, 79%): mp 131–132 °C; FAB-MS m/z 619 (M$^+$ + 1); UV λ_{max} (MeOH) 284 nm; ^{1}H-NMR (CDCl$_3$) 8.27 (br s, 1 H, 3-NH), 8.07–8.03 (m, 4 H, Bz), 7.78 (s, 1 H, H-6), 7.65–7.45 (m, 6 H, Bz), 6.39 (dd, 1 H, H-1′, $J_{1',2'a}$ = 5.5, $J_{1',2'b}$ = 8.8 Hz), 5.61 (m, 1 H, H-3′), 4.80 (dd, 1 H, H-5′a, J_{gem} = 12.1, $J_{4',5'a}$ = 3.8 Hz), 4.67 (dd, 1 H, H-5′b, $J_{4',5'b}$ = 3.3 Hz), 4.58 (ddd, 1 H, H-4′), 3.65 (t, 2 H, −CH_2OSi), 2.77 (ddd, 1 H, H-2′a, J_{gem} = 14.3, $J_{2'a,3'}$ = 1.7 Hz), 2.47 (m, 2 H, C≡CCH_2), 2.31 (ddd, 1 H, H-2′b, $J_{2'b,3'}$ = 6.6 Hz), 0.88 [s, 9 H, SiC(CH_3)$_3$], 0.04 [s, 6 H, Si(CH_3)$_2$]. Anal. Calcd for C$_{33}$H$_{38}$N$_2$O$_8$Si: C, 64.06; H, 6.19; N, 4.53. Found: C, 63.90; H, 6.14; N, 4.54.

Compound **4** (0.89 g, 9.3%, as a foam) was obtained as a side product: FAB-MS m/z 619 (M$^+$ + 1); ^{1}H-NMR (CDCl$_3$) 8.22 (br s, 1 H, H-4), 8.19–7.94 (m, 4 H, Bz), 7.88–7.36 (m, 6 H, Bz), 6.47 (dd, 1 H, H-1′, $J_{1',2'a}$ = 6.0, $J_{1',2'b}$ = 7.7 Hz), 5.96 (s, 1 H, H-5), 5.64 (m, 1 H, H-3′), 4.89–4.67 (m, 3 H, H-4′ and H-5′), 3.89 (t, 2 H, −CH_2-OSi), 3.21 (ddd, 1 H, H-2′a, J_{gem} = 14.6, $J_{2'a,3'}$ = 2.2 Hz), 2.82 (t, 2 H, 4-CH_2), 2.29 (ddd, 1 H, H-2′b, $J_{2'b,3'}$ = 7.7 Hz), 0.86 [s, 9 H, SiC(CH_3)$_3$], 0.02 [s, 6 H, Si(CH_3)$_2$].

3′,5′-Di-*O*-benzoyl-5-[4-(*tert*-butyldimethylsiloxy)-butyl]-2′-deoxyuridine (5). A suspension of **3** (6.6 g, 10.7 mmol) and 10% Pd/C (560 mg) in EtOH (150 mL) was shaken under an H$_2$ atmosphere (40 psi) for 1 h. The reaction mixture was filtered by a layer of Celite on a filter paper, and the Celite was washed with EtOH and then EtOAc. The organic layers were combined and concentrated to give **5** (6.6 g, 99%, as a foam): FAB-MS m/z 623 (M$^+$ + 1); UV λ_{max} (MeOH) 266 nm; ^{1}H-NMR (CDCl$_3$) 8.14 (br s, 1 H, 3-NH), 8.08–8.02 (m, 4 H, Bz), 7.66–7.58 (m, 2 H, Bz), 7.51–7.45 (m, 4 H, Bz), 7.23 (s, 1 H, H-6), 6.44 (dd, 1 H, H-1′, $J_{1',2'a}$ = 5.5, $J_{1',2'b}$ = 8.8

Hz), 5.65 (m, 1 H, H-3′), 4.78 (dd, 1 H, H-5′a, J_{gem} = 12.1 Hz), 4.67 (dd, 1 H, H-5′b, $J_{4',5'b}$ = 3.9 Hz), 4.54 (ddd, 1 H, H-4′), 3.51 (m, 2 H, −CH_2OSi), 2.72 (ddd, 1 H, H-2′a, J_{gem} = 14.3, $J_{2'a,3'}$ = 1.1 Hz), 2.35 (ddd, 1 H, H-2′b, $J_{2'b,3'}$ = 6.6 Hz), 2.06 (m, 2 H, 5-CH_2−), 1.36 (m, 4 H, −CH_2CH_2−), 0.88 [s, 9 H, SiC(CH_3)$_3$], 0.03 [s, 6 H, Si(CH_3)$_2$].

3′,5′-Di-*O*-benzoyl-5-(4-hydroxybutyl)-2′-deoxyuridine (6). A THF solution containing TBAF (1 M, 31.8 mL, 31.8 mmol) was added to a THF solution (70 mL) containing **5** (6.6 g, 10.6 mmol) in an ice bath, and the mixture was stirred at room temperature for 3 days. The solvent was concentrated, the residue was dissolved in CHCl$_3$, and then the solution was washed with H$_2$O (twice), dried (Na$_2$SO$_4$), and concentrated. The residue was chromatographed on a silica gel column (5.3 × 35 cm) with 50–86% EtOAc in hexane as eluents. Concentration of the fractions gave a residue that was dissolved in acetone to give **6** as white crystals (4.4 g, 81%): mp 132–132.5 °C; FAB-MS m/z 508 (M$^+$); UV λ_{max} (MeOH) 266 nm; ^{1}H-NMR (CDCl$_3$) 8.37 (s, 1 H, 3-NH), 8.05 (m, 4 H, Bz), 7.63 (m, 2 H, Bz), 7.49 (m, 4 H, Bz), 7.26 (s, 1 H, H-6), 6.45 (dd, 1 H, H-1′, $J_{1',2'a}$ = 5.5, $J_{1',2'b}$ = 8.8 Hz), 5.65 (m, 1 H, H-3′), 4.80 (dd, 1 H, H-5′a, J_{gem} = 12.1, $J_{4',5'a}$ = 3.3 Hz), 4.67 (dd, 1 H, H-5′b, $J_{4',5'b}$ = 4.2 Hz), 4.55 (m, 1 H, H-4′), 3.57 (m, 2 H, −CH_2OH), 2.74 (ddd, 1 H, H-2′a, J_{gem} = 14.3, $J_{2'a,3'}$ = 1.7 Hz), 2.34 (ddd, 1 H, H-2′b, $J_{2'b,3'}$ = 6.6 Hz), 2.09 (m, 2 H, 5-CH_2−), 1.40 (m, 4 H, −CH_2CH_2−). Anal. Calcd for C$_{27}$H$_{28}$N$_2$O$_8$: C, 63.77; H, 5.55; N, 5.51. Found: C, 63.65; H, 5.56; N, 5.39.

3′,5′-Di-*O*-benzoyl-5-(3-formylpropyl)-2′-deoxyuridine (7). A CH$_2$Cl$_2$ solution (12 mL) containing DMSO (2.3 mL, 32.4 mmol) was added dropwise to a CH$_2$Cl$_2$ solution (140 mL) containing oxalyl chloride (1.8 mL, 21.6 mmol) at −80 °C and the mixture was stirred for 30 min. A CH$_2$Cl$_2$ solution (37 mL) containing **6** (5.5 g, 10.8 mmol) was added dropwise to the mixture, the whole was stirred at −80 °C for 30 min, and then the temperature was

raised gradually to −30 °C over 30 min. Triethylamine (11 mL, 78.9 mmol) was added to the reaction mixture, and the whole was stirred at 0 °C for 30 min. The mixture was washed with aqueous saturated NH₄Cl and then H₂O, dried (Na₂SO₄), and concentrated. The residue was chromatographed on a silica gel column (6.2 × 15 cm) with 33−66% EtOAc in hexane as eluents. Concentration of the fractions gave **7** (3.8 g, 69%, as white crystals): mp 98−99.5 °C; FAB-MS m/z 507 (M⁺ + 1); ¹H-NMR (CDCl₃) 9.64 (t, 1 H, −CHO, J = 1.7 Hz), 8.33 (br s, 1 H, 3-NH), 8.09−7.45 (m, 10 H, Bz), 7.28 (s, 1 H, H-6), 6.45 (dd, 1 H, $J_{1',2'a}$ = 5.5, $J_{1',2'b}$ = 8.8 Hz), 5.67 (m, 1 H, H-3'), 4.82 (dd, 1 H, H-5'a, J_{gem} = 12.1, $J_{4',5'a}$ = 3.3 Hz), 4.68 (dd, 1 H, H-5'b, $J_{4',5'b}$ = 3.9 Hz), 4.56 (m, 1 H, H-4'), 2.75 (ddd, 1 H, H-2'a, J_{gem} = 14.3, $J_{2'a,3'}$ = 1.1 Hz), 2.35 (ddd, 1 H, H-2'b, $J_{2'b,3'}$ = 6.6 Hz), 2.28 (m, 2 H, −CH_2-CHO), 2.07 (m, 2 H, 5-CH_2−), 1.66 (m, 2 H, −CH₂CH_2-CH₂−). Anal. Calcd for C₂₇H₂₆N₂O₈: C, 64.03; H, 5.17; N, 5.53. Found: C, 63.95; H, 5.12; N, 5.65.

N¹,N⁷-Ditrityl-syn-norspermidine. *syn*-Norspermidine (1 mL, 7.15 mmol) and TrCl (4.4 g, 15.7 mmol) were dissolved in pyridine (20 mL), and the solution was stirred at room temperature for 3 days. The solvent was evaporated and the residue was dissolved in CHCl₃, then the solution was washed with aqueous saturated NaH-CO₃, dried (Na₂SO₄), and concentrated. The residue was chromatographed on a silica gel column (5 × 26 cm) with 0−4% MeOH in CHCl₃ as eluents. Concentration of the fractions gave a residue, which was dissolved in EtOH to give the desired product (2.6 g, 59%, as pale yellow crystals): mp 102−105 °C; FAB-MS m/z 616 (M⁺ + 1); ¹H-NMR (CDCl₃) 7.47−7.44 (m, 12 H, Tr), 7.29−7.14 (m, 18 H, Tr), 3.72 (q, 2.4 H, CH₃CH_2OH, J = 7.1 Hz), 2.66 (t, 4 H, TrNHCH_2− × 2, J = 6.6 Hz), 2.18 (t, 4 H, −CH_2-NHCH_2−, J = 6.6 Hz), 1.65 (m, 4 H, −CH₂CH_2CH₂− × 2), 1.24 (t, 3.6 H, CH_3CH₂OH). Anal. Calcd for C₄₄H₄₅-N₃·6/5EtOH: C, 83.04; H, 7.84; N, 6.26. Found: C, 82.90; H, 7.70; N, 6.28.

3',5'-Di-*O*-benzoyl-5-[*N,N*-[bis(3-tritylamino)pro-pyl]-4-aminobutyl]-2'-deoxyuridine (8). NaBH₃CN (208 mg, 3.3 mmol) was added to a mixture of THF and MeOH (4:1 ,v/v, 100 mL, containing a small amount of AcOH) containing *N¹,N⁷*-ditrityl-*syn*-norspermidine (2.0 g, 3.0 mmol) and **7** (1.0 g, 2.0 mmol), the reaction mixture was stirred at room temperature for 1.5 h, and then the solvents were evaporated. The residue was dissolved in CHCl₃, and the solution was washed with aqueous saturated NaHCO₃ and then brine, dried (Na₂SO₄), and concentrated. The residue was chromatographed on a silica gel column (6.3 × 13 cm) with 25−50% EtOAc in benzene as eluents. Concentration of the fractions gave **8** (1.4 g, 63%, as a yellow foam): FAB-MS m/z 1106 (M⁺); ¹H-NMR (CDCl₃) 8.08−8.01 (m, 4 H, Bz), 7.99−7.13 (m, 38 H, 3-NH, H-6, Bz, and Tr), 6.41 (dd, 1 H, H-1', $J_{1',2'a}$ = 5.5, $J_{1',2'b}$ = 8.8 Hz), 5.63 (m, 1 H, H-3'), 4.75 (dd, 1 H, H-5'a, J_{gem} = 12.1, $J_{4',5'a}$ = 3.3 Hz), 4.64 (dd, 1 H, H-5'b, $J_{4',5'b}$ = 3.8 Hz), 4.51 (m, 1 H, H-4'), 2.68 (m, 1 H, H-2'a), 2.39−2.08 (m, 13 H, H-2'b, 5-CH₂−, and NHCH_2− × 5), 1.98−1.22 [m, 10 H, NH, −CH₂CH_2CH₂−, and −CH₂-(CH_2)₂CH₂−]. Anal. Calcd for C₇₁H₇₁N₅O₇·1/2H₂O: C, 76.46; H, 6.51; N, 6.28. Found: C, 76.46; H, 6.49; N, 6.20.

5-[4-[*N,N*-Bis[3-(tritylamino)propyl]amino]butyl]-2'-deoxyuridine (9). Compound **8** (1.4 g, 1.3 mmol) was dissolved in 0.2 M NaOMe in MeOH (18.8 mL, 3.8 mmol), and the solution was stirred at room temperature. After 1 h, the reaction mixture was concentrated and the residue was dissolved in CHCl₃, and then the solution was washed with brine (three times), dried (Na₂SO₄), and concentrated. The residue was chromatographed on a silica gel column (2.7 × 11.5 cm) with 0−5% MeOH in

CHCl₃ as eluents. Concentration of the fractions gave **9** (0.96 g, 86%, as a white foam): FAB-MS m/z 898 (M⁺); ¹H-NMR (CDCl₃) 8.06 (br s, 1 H, 3-NH), 7.45−7.16 (m, 31 H, H-6, and Tr × 2), 6.19 (br t, 1 H, H-1'), 4.56 (m, 1 H, H-3'), 3.87−3.76 (m, 3 H, H-4', 5'), 2.74−1.11 [m, 24 H, H-2', 5-CH_2−, NCH_2− × 5, −CH₂CH_2CH₂− × 2, −CH₂(CH_2)₂CH₂− × 2, and NH × 2]. Anal. Calcd for C₅₇H₆₃N₅O₅·6/5H₂O: C, 74.43; H, 7.17; N, 7.61. Found: C, 74.34; H, 7.19; N, 7.35.

5-[4-[*N,N*-Bis(3-aminopropyl)amino]butyl]-2'-deoxy-uridine (1). Aqueous 80% acetic acid (60 mL) contain-ing **9** (960 mg, 1.1 mmol) was stirred at 55 °C for 2 h. The solution was concentrated, the residue was dissolved in H₂O, and then the white precipitates were filtered off and the filtrate was washed with Et₂O (three times). The H₂O layer was concentrated, the residue was dissolved in a small volume of MeOH, and the solution was concentrated again to give **1** (430 mg, quant. as a yellow foam): FAB exact MS calcd for C₁₉H₃₆N₅O₅ 414.2716, found 414.2708; ¹H-NMR (D₂O) 7.69 (s, 1 H, H-6), 6.29 (t, 1 H, H-1', $J_{1',2'a}$ = $J_{1',2'b}$ = 6.6 Hz), 4.46 (m, 1 H, H-3'), 4.03 (ddd, 1 H, H-4', $J_{4',5'a}$ = 3.8, $J_{4',5'b}$ = 4.4 Hz), 3.85 (dd, 1 H, H-5'a, J_{gem} = 12.4 Hz), 3.75 (dd, 1 H, H-5'b), 3.04 (m, 10 H, NCH_2 × 5), 2.36 (m, 4 H, H-2', 5-CH₂), 2.01 (m, 4 H, −CH₂CH_2CH₂−), 1.60 [m, 4 H, −CH₂(CH₂)₂-CH₂−].

5-[4-[*N,N*-Bis[3-(trifluoroacetamido)propyl]amino]-butyl]-2'-deoxyuridine (10). Triethylamine (226 μL, 1.6 mmol) and ethyl thiotrifluoroacetate (208 μL, 1.6 mmol) were added to a MeOH solution (1.5 mL) contain-ing **1** (134 mg, 0.32 mmol), and the whole was stirred at room temperature for 30 min. The reaction mixture was concentrated, and the residue was chromatographed on a silica gel column (1.8 × 5 cm) with 0−12% MeOH in CHCl₃ as eluents. Concentration of the fractions gave **10** (143 mg, 73%, as an oil): FAB exact MS calcd for C₂₃H₃₄F₆N₅O₇ 606.2362, found 606.2318; ¹H-NMR (DMSO-d_6) 11.25 (br s, 1 H, 3-NH), 9.40 (m, 2 H, −NHCOCF₃ × 2), 7.68 (s, 1 H, H-6), 6.17 (t, 1 H, H-1', $J_{1',2'a}$ = $J_{1',2'b}$ = 6.9 Hz), 5.22 (d, 1 H, 3'-OH, J = 4.4 Hz), 5.01 (m, 1 H, 5'-OH), 4.23 (m, 1 H, H-4'), 3.56 (m, 2 H, H-5'), 3.20 (m, 4 H, −CH_2NHCOCF₃ × 2), 2.52−2.05 (m, 10 H, NCH₂ × 3, 5-CH₂, and H-2'), 1.61 (m, 4 H, −CH₂CH_2CH₂- × 2), 1.38 [m, 4 H, −CH₂(CH_2)₂CH₂−].

5'-*O*-(Dimethoxytrityl)-5-[4-[*N,N*-bis[3-(trifluoro-acetamido)propyl]amino]butyl]-2'-deoxyuridine (11). After successive coevaporation with pyridine and then DMF, **10** (226 mg, 0.37 mmol) was dissolved in a mixture of pyridine and DMF (1:1 v/v, 2 mL). Triethylamine (138 μL, 0.41 mmol) and DMTrCl (138 mg, 0.41 mmol) were added to the solution, and the mixture was stirred at room temperature. After 0.5, 1, 1.5, and 2 h, further amounts of Et₃N (103 μL) and DMTrCl (138 mg) were added to the mixture. After 3 h, MeOH (1 mL) was added to the reaction mixture, the whole was concentrated, and then the residue was dissolved in EtOAc and the solution was washed with aqueous saturated NaHCO₃. The H₂O layer was back-extracted with CHCl₃ (four times), and then the organic layers were combined, dried (Na₂SO₄), and concentrated. The residue was chromatographed on a neutralized silica gel (ICN silica 60A, ICN biomedicals, Germany) column (2.8 × 13.5 cm) with 3−5% MeOH in CHCl₃ as eluents. Concentration of the fractions gave **11** (202 mg, 49%, as a foam): FAB exact MS calcd for C₄₄H₅₂F₆N₅O₉ 908.3668, found 908.3663; ¹H-NMR (DMSO-d_6) 11.31 (s, 1 H, 3-NH), 9.38 (m, 2 H, NHCOCF₃ × 2), 7.70−7.23 (m, 9 H, DMTr), 6.90−6.86 (m, 4 H, DMTr), 6.21 (t, 1 H, H-1', $J_{1',2'a}$ = $J_{1',2'b}$ = 6.9 Hz), 5.32 (d, 1 H, 3'-OH, J = 4.4 Hz), 4.32 (m, 1 H, H-3'), 3.89 (m, 1 H, H-4'), 3.73 (m, 2 H, H-5'), 3.17 (m, 4 H, CH_2NHCOCF₃ ×

2), 2.26–1.09 [m, 24 H, H-2′, NCH_2 × 3, 5-CH_2, –CH_2CH_2-CH_2– × 2, –CH_2(CH_2)$_2$CH_2-, and –OCH_3 × 2]. Unreacted **10** (70 mg, 0.11 mmol, 31%) was eluted with 8–12% MeOH in CHCl$_3$.

3′-*O*-[(2-Cyanoethyl)(*N*,*N*-diisopropylamino)phosphinyl]-5′-(dimethoxytrityl)-5-[4-[*N*,*N*-bis[3-(trifluoroacetamido)propyl]amino]butyl]-2′-deoxyuridine (12). After dehydration by coevaporation with pyridine (three times), **11** was dissolved in CH$_3$CN (4 mL), and then *N*,*N*-diisopropylethylamine (78 μL, 0.44 mmol) and 2-cyanoethyl *N*,*N*-diisopropylchlorophosphoramidite (*22*) (75 μL, 0.33 mmol) were added to the solution. The mixture was stirred at room temperature for 40 min, and then the solvent was evaporated and the residue was dissolved in EtOAc. The solution was washed with aqueous saturated NaHCO$_3$, dried (Na$_2$SO$_4$), and concentrated. The residue was chromatographed on a neutralized silica gel column (2.6 × 3 cm) with 0–20% MeOH in EtOAc as eluents. The fractions were concentrated to give **12** (131 mg, 53%, as a yellow oil): FAB exact MS calcd for C$_{53}$H$_{69}$F$_6$N$_7$O$_{10}$P 1108.4747, found 1108.4720.

Synthesis of Oligonucleotides. Oligonucleotides were synthesized on a DNA synthesizer (Applied Biosystem Model 381A, CA, U.S.A.) by the phosphoramidite method (*27*). Then fully protected oligonucleotides were deblocked and purified by the same procedure as for the purification of normal oligonucleotides. That is, each oligonucleotide linked to the resin was treated with concentrated NH$_4$OH at 55 °C for 5 h, and the released oligonucleotide protected by a DMTr group at the 5′-end was chromatographed on a C-18 silica gel column (1 × 10 cm, Waters, MA, U.S.A.) with a linear gradient of CH$_3$-CN from 0 to 30% in 0.1 M TEAA buffer (pH 7.0). The fractions were concentrated, the residue was treated with aqueous 80% AcOH at room temperature for 20 min, and then the solution was concentrated and the residue was coevaporated with water. The residue was dissolved in water, the solution was washed with Et$_2$O, and then the H$_2$O layer was concentrated to give a deprotected oligonucleotide. The sample was purified by HPLC with a C-18 silica gel column (Inertsil ODS-2, GL Science Inc., Japan) when necessary.

Complete Hydrolysis of Oligonucleotides. A solution containing alkaline phosphatase (0.4 units) (Takara Shuzo Co., Ltd., Japan) in 0.1 M Tris–HCl (pH 8.2) and 2 mM MgCl$_2$ (total 130 μL) was heated on boiling water for 10 min to inactivate adenosine deaminase activity contaminating in the enzyme solution. The solution and venom phosphodiesterase (10 μg) (Boehringer Mannheim, Germany) were added to each heptadecamer (0.2 OD units), and the whole was incubated at 37 °C for 24 h. After this was heated in boiling water for 5 min, cold EtOH (313 μL) was added to the reaction mixture and the whole was kept at −20 °C for 1 h. The cold solution was centrifuged for 20 min (12 000 rpm), and then the supernatant was separated and concentrated. The residue was analyzed by HPLC with the C-18 column.

Thermal Denaturation. Each solution contains heptadecamer (3 μM) and the complementary strand **IV** (3 μM) or the target duplex **V** (3 μM) in an appropriate buffer. Thermally induced transition of each mixture was monitored at 260 nm on a Gilford Response II.

Partial Hydrolysis of Oligonucleotide with Venom Phosphodiesterase. Each oligonucleotide labeled with ^{32}P at the 5′ end (0.01 OD units) (*28*) was incubated with venom phosphodiesterase (0.4 μg) in the presence of Torula RNA (0.3 OD units at 260 nm) in a buffer containing 37.5 mM Tris–HCl (pH 8.0) and 7.5 mM MgCl$_2$ (total 20 μL) at 37 °C. Samples of the reaction

mixture were separated and added to a solution of EDTA (5 mM, 10 μL) at appropriate times, and then the mixtures were heated at 100 °C for 3 min. The solutions were analyzed by electrophoresis on 20% polyacrylamide gel containing 8 M urea (*28*).

Partial Hydrolysis of Oligonucleotides with Nuclease P1. Each oligonucleotide labeled with ^{32}P at the 5′-end (0.01 OD units) was incubated with nuclease P1 (12 ng, Yamasa Shoyu Co., Ltd., Japan) in the presence of Torula RNA (0.3 OD units) in a buffer containing 6.8 mM ammonium acetate (pH 5.3) and 0.1 mM ZnCl$_2$ (total 22 μL) at appropriate temperatures. Samples of the reaction mixture were separated and added to a solution of EDTA (5 mM, 10 μL) at appropriate times, and then the solutions were heated at 100 °C for 5 min. The solutions were analyzed by gel electrophoresis as described above.

LITERATURE CITED

(1) Cohen, J. S., Ed. (1989) *Oligodeoxynucleotides: Antisense inhibitors of gene expression*; The Macmillan Press Ltd.: London.

(2) Uhlmann, E., and Peyman, A. (1990) Antisense oligonucleotides: A new therapeutic principle. *Chem. Rev. 90*, 544–584.

(3) Beaucage, S. L., and Iyer, R. P. (1993) The functionalization of oligonucleotides via phosphoramidite derivatives. *Tetrahedron 49*, 1925–1963.

(4) Beaucage, S. L., and Iyer, R. P. (1993) The synthesis of modified oligonucleotides by the phosphoramidite approach and their applications. *Tetrahedron 49*, 6123–6194.

(5) Crooke, S. T., and Lebleu, B., Eds. (1993) *Antisense Research and Applications*, CRC Press, Inc., Boca Raton.

(6) Ono, A., Dan, A., and Matsuda, A. (1993) Synthesis of oligonucleotides carrying linker groups at the 1′-position of sugar residues. *Bioconjugate Chem. 4*, 499–508.

(7) Ono, A., Haginoya, N., Kiyokawa, M., Minakawa, N., and Matsuda, A. (1993) A novel and convenient post-synthetic modification method for the synthesis of oligodeoxyribonucleotides carrying amino linkers at the 5-position of 2′-deoxyuridine. *BioMed. Chem. Lett. 4*, 361–366 and unpublished results.

(8) Ramasamy, K. S., Zounes, M., Gonzalez, C., Freier, S. M., Lesnik, E. A., Cummins, L. L., Griffey, R. H., Monia, B. P., and Cook, P. D. (1994) Remarkable enhancement of binding affinity of heterocycle-modified DNA to DNA and RNA. Synthesis, characterization and biophysical evaluation of N^2-imidazolylpropylguanine and N^2-imidazoyl-2-aminoadenine modified oligonucleotides. *Tetrahedron Lett. 35*, 215–218.

(9) Warren, R. A. J. (1980) Modified bases in bacteriophage DNAs. *Ann. Rev. Microbiol. 34*, 137–158.

(10) Wiberg, J. S. (1967) Amber mutants of bacteriophage T4 defective in deoxycytidine diphosphatase and deoxycytidine triphosphatase. Role of 5-hydroxymethylcytosine in bacteriophage deoxyribonucleic acid. *J. Biol. Chem. 242*, 5824–5829.

(11) Kropinski, A. M. B., Bose, R. J., and Warren, R. A. J. (1973) 5-(4-Aminobutylaminomethyl)uracil, an unusual pyrimidine from the deoxyribonucleic acid of bacteriophage ΦW-14. *Biochemistry 12*, 151–157.

(12) Cohen, S. S., and McComic, F. P. (1979) Polyamines and virus multiplication. *Adv. Virus Res. 24*, 331–387.

(13) Neuhard, J., Maltman, K. L., and Warren, R. A. J. (1980) Bacteriophage ΦW-14-infected pseudomonas acidovoraus synthesizes hydroxymethyldeoxyuridine triphosphate. *J. Virol. 34*, 347–353.

(14) Tabor, C. W., and Tabor, H. (1976) 1,4-Diaminobutane (putrescine), spermidine, and spermine. *Ann. Rev. Biochem. 45*, 285–306.

(15) Tabor, C. W., and Tabor, H. (1984) Polyamines. *Ann. Rev. Biochem. 53*, 749–790.

(16) Etter, M. C. (1990) Encoding and decoding hydrogen-bond patterns of organic compounds. *Acc. Chem. Res. 23*, 120–126.

(17) Tabor, H. (1962) Protective effect of spermine and other polyamines against heat denaturation of deoxyribonucleic acid. *Biochemistry 1*, 496–501.

(18) Thomas, T. J., and Bloomfield, V. A. (1984) Ionic and structural effects on the thermal helix-coil transition of DNA complexed with natural and synthetic polyamines. *Biopolymers 23*, 1295–1306.

(19) Thomas, T., and Thomas, T. J. (1993) Selectivity of polyamines in triplex DNA stabilization. *Biochemistry 32*, 14068–14074.

(20) Murray, N. L., and Morgan, A. R. (1973) Enzymic and physical studies on the triplex dTn·dAn·rUn. *Can. J. Biochem. 51*, 436–449.

(21) Hampel, K. J., Crosson, P., and Lee, J. S. (1991) Polyamines favor DNA triplex formation at neutral pH. *Biochemistry 30*, 4455–4459.

(22) Moser, H. E., and Dervan, P. B. (1987) Sequence-specific cleavage of double helical DNA by triple helix formation. *Science 238*, 645–650.

(23) Sun, J.-S., Francois, J.-C., Mantenay-Garestier, T., Saison-Behmoaras, T., Roig, V. Thuong, N. T., and Helene, C. (1989) Sequence-specific intercalating agents: Intercalation at specific sequences on duplex DNA via major groove recognition by oligonucleotide-intercalator conjugates. *Proc. Natl. Acad. Sci. U.S.A. 86*, 9198–9202.

(24) Takeda, T., Ikeda, K., Mizuno, Y., and Ueda, T. (1987) Synthesis and properties of deoxyoligonucleotides containing putrescinylthymine. *Chem. Pharm. Bull. 35*, 3558–3567.

(25) Robins, M. J. and Barr, P. J. (1983) Efficient conversion of 5-iodo to 5-alkynyl and derived 5-substituted uracil bases and nucleosides. *J. Org. Chem. 48*, 1854–1862.

(26) Borch, R. F., Bernstein, M. D., and Dust, H. D. (1971) Cyanohydridoborate anion as a selective reducing agent. *J. Am. Chem. Soc. 93*, 2897–2904.

(27) Atrinson, A., and Smith, M. (1984) In *Oligonucloetide Synthesis: A Practical Approach* (Gait, M. J., Ed.) IRL Press, Oxford.

(28) Maniatis, T., Fritsch, E. F., and Sambrook, J. (1982) *Molecular cloning*, Cold Spring Harbor Laboratory, New York.

(29) Hashimoto, H., Nelson, M. G., and Switzer, C. (1993) Zwitterionic DNA. *J. Am. Chem. Soc. 115*, 7128–7134.

(30) Tung, C-H., Breslauer, K. J., and Stein, S. (1993) Polyamine-linked oligonucleotides for DNA triple helix formation. *Nucleic Acids Res. 21*, 5489–5494.

(31) Ono, A., Ts'o, P. O. P., and Kan, L.-S. (1992) Triplex formation of an oligonucleotide containing 2'-O-methyl-pseudoisocytidine with a DNA duplex at neutral pH. *J. Org. Chem. 57*, 3225–3230.

(32) Beal, P. A., and Dervan, P. B. (1991) Second structural motif for recognition of DNA by oligonucleotide-directed triple-helix formation. *Science 251*, 1360–1363.

A Branched Monomethoxypoly(ethylene glycol) for Protein Modification

Cristina Monfardini, Oddone Schiavon, Paolo Caliceti, Margherita Morpurgo, J. Milton Harris,[†] and Francesco M. Veronese*

Department of Pharmaceutical Sciences, Centro di Studio di Chimica del Farmaco e dei Prodotti Biologicamente, Attivi del CNR, University of Padua, Via F. Marzolo 5, 35131 Padua, Italy, and Chemistry Department, University of Alabama in Huntsville, Huntsville, Alabama 35899. Received July 27, 1994[®]

Procedures are described for linking monomethoxypoly(ethylene glycol) (mPEG) to both ϵ and α amino groups of lysine. The lysine carboxyl group can then be activated as a succinimidyl ester to obtain a new mPEG derivative (mPEG2–COOSu) with improved properties for biotechnical applications. This branched reagent showed in some cases a lower reactivity toward protein amino groups than the linear mPEG from which it was derived. A comparison of mPEG– and mPEG2-modified enzymes (ribonuclease, catalase, asparaginase, trypsin) was carried out for activity, pH and temperature stability, K_m and K_{cat} values, and protection to proteolytic digestion. Most of the adducts from mPEG and mPEG2 modification presented similar activity and stability toward temperature change and pH change, although in a few cases mPEG2 modification was found to increase temperature stability and to widen the range of pH stability of the adducts. On the other hand, all of the enzymes modified with the branched polymer presented greater stability to proteolytic digestion relative to those modified with the linear mPEG. A further advantage of this branched mPEG lies in the possibility of a precise evaluation of the number of polymer molecules bound to the proteins; upon acid hydrolysis, each molecule of mPEG2 releases a molecule of lysine which can be detected by amino acid analysis. Finally, dimerization of mPEG by coupling to lysine provides a needed route to monofunctional PEGs of high molecular weight.

INTRODUCTION

With improved chemical and genetic methods many new peptides and proteins are now available for potential application as new drugs or specific biocatalysts. Limitations, however, still exist to more extensive use (*1–6*). As therapeutic agents, peptides and proteins are often rapidly cleared from circulation or give rise to immunological problems, sometimes when they apparently have the same structure as the homologous natural product. Also, application in biocatalysis is mostly restricted to hydrophilic substrates because of the low stability and solubility of enzymes in organic solvents.

Linking suitable hydrophilic or amphiphilic polymers to peptides and proteins presents the potential of overcoming these problems since the polymer cloud surrounding the protein increases stability toward proteolysis and reduces renal excretion and immunological complications (*1–4*). Moreover, if the polymer is soluble in organic solvents, the enzyme conjugates may acquire this same solubility, and biocatalysis may be extended to organic media (*5, 6*).

Monomethoxypoly(ethylene glycol) (mPEG)[1] has been the polymer most used for these applications thus far, with linear polymers of molecular weights (MWs) in the range of 2000–5000 being preferred, although branched

PEGs and high MW mPEGs have been used. Recent work by Somak et al. has shown the utility of high MW mPEGs for protein modification (*7*). A branched form of mPEG has been prepared by substitution of two chloride atoms of trichloro-*s*-triazine with mPEG, while using the third chloride to bind to protein; this procedure, however, presents severe limitations because of lack of specificity in protein modification, inactivation of many enzymes, and toxicity of the intermediates (*8*). In a related preparation of a branched mPEG, Yamsuki and co-workers coupled mPEG succinimidyl succinate to norleucine, activated the resulting acid, and coupled two molecules of the activated mPEG to lysine (*9*). The resulting branched acid can be activated and coupled to amines. This approach offers the advantage of providing percent modification from amino acid analysis, but disadvantages are hydrolytic instability of the succinate ester linkage, overall complexity of the synthetic procedure, and the large linker region beween mPEG and conjugated protein that may provide an antigenic site.

In view of the great utility of large or branched monofunctional PEGs for increasing the polymer cloud volume surrounding a protein while maintaining the same number of binding sites, we have prepared a new branched mPEG derivative devoid of the above disadvantages. This derivative also presents the important advantage of easy analytical characterization of the adduct. This new polymer preparation is based on direct linkage of mPEGs to the α and ϵ amino groups of lysine (to give mPEG2–COOH), followed by activation of the carboxyl group as the succinimidyl ester (to give mPEG2–COOSu), Figure 1. This paper reports also the use of this new derivative in modifying model proteins, and it reports comparison of the properties of proteins modified with linear and branched mPEGs. Furthermore, results are given on evaluation of degree of enzyme modification

---

[1] Abbreviations: MW, molecular weight; mPEG, monomethoxypoly(ethylene glycol); mPEG-Nle-OSu, mPEG carrying a norleucine spacer, activated as succinimidyl ester; mPEG2–COOH, mPEG–lysine dimer; mPEG2–COOSu, mPEG–lysine dimer activated as succinimidyl ester; TEA, triethylamine; PITC, phenyl isothiocyanate; and TAME, N_α-*p*-tosylarginine methyl ester.
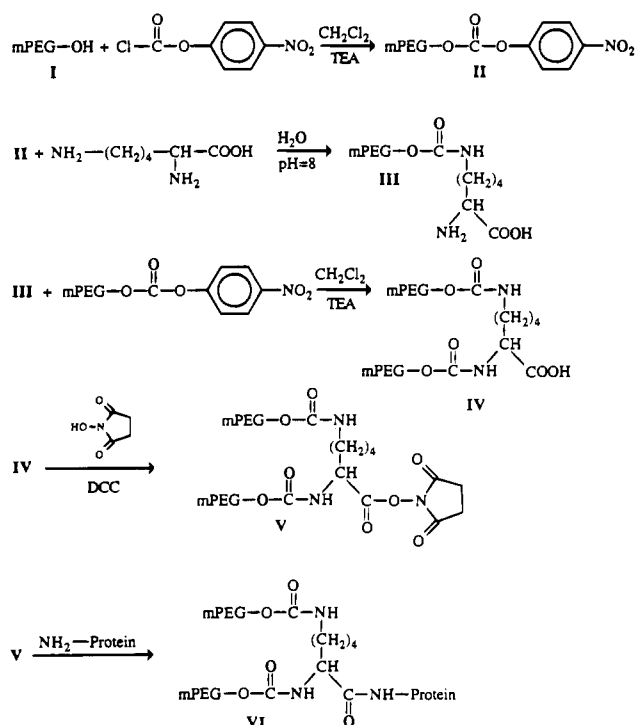
Figure 1. Scheme of synthesis of activated mPEG2−COOSu (V) through a "two-step" procedure and reaction of V with protein amino groups.

by both mPEG and the new dimer, based on amino acid analysis after acid hydrolysis.

Two procedures for preparation of mPEG2−COOH are described. The first procedure uses mPEG activated as the *p*-nitrophenyl carbonate and takes place in two steps (the first in water, the second in methylene chloride), Figure 1. The same polymer may be more easily prepared by a "single-step" procedure using more active mPEG succinimidyl carbonate (*10*). The single step procedure was used to prepare a dimer of MW 40 000.

The methodology reported here for preparing this branched mPEG dimer, carrying a single point of attachment, may be considered useful not only for PEG−enzyme chemistry but also for PEG chemistry in general since it allows doubling the amount of PEG that may be linked to the same site of drugs to obtain polymeric prodrugs (*11*), surfaces to increase their blood compatibility (*12*) and to avoid protein adsorption (*12*), bioactive components for which the two phase partitioning may be useful (*14−16*), and liposomes to obtain long-lasting preparations (*17, 18*). Also, this chemistry provides ready access to monofunctional PEGs of high molecular weight by dimerization of low-diol mPEG (note that the usual polymerization of ethylene oxide to yield mPEGs is limited to about 20 000 g/mol) (*19*).

EXPERIMENTAL SECTION

Materials. mPEG, M_n 5000, 4-nitrophenyl chloroformate, *N,N*-dicyclohexylcarbodiimide, *N*-hydroxysuccinimide, norleucine, lysine, and phosgene solution were purchased from Fluka (Buchs, Switzerland). mPEG of M_n 20 000, mPEG succinimidyl carbonate, and mPEG 5000 *p*-nitrophenyl carbonate were obtained from Shearwater Polymers (Huntsville, AL). Salts and solvents were purchased from Carlo Erba (Milan, Italy). Dimethyl sulfoxide-d_6 was from Janssen (Geel, Belgium). Ribonuclease, catalase, trypsin, pronase, elastase, subtilisin, cytidine 2′:3′ cyclic monophosphate, *N-p*-tosylarginine methyl ester, casein, and asparagine were from Sigma

Chemical Co. (St. Louis, MO). Asparaginase from *Erwinia Carativora* was from PHLS, Porton Down (Salisbury, England). α-Ketoglutaric acid, glutamic-oxalacetic transaminase, and malate dehydrogenase were from Calbiochem (San Diego, CA). For pH titration, a Radiometer autoburette ABU 80 (Copenaghen, Denmark) with titrator TTT 80 and titrigraph REA 160 was used. UV−vis analysis was performed on a Perkin-Elmer Lambda 2 spectrophotometer. ¹H-NMR spectra were performed on a 200 MHz Bruker spectrometer. Analytical gel filtration chromatography was performed with a Waters Ultrahydrogel column.

Activation of mPEG (mPEG-Nle-OSu). Linear mPEG 5000, with norleucine as an amino acid spacer arm and activated as the succinimidyl ester, was synthesized according to the method previously reported from our laboratory (*20*). Alternatively, the compound was purchased from Shearwater Polymers.

Two-Step Procedure for mPEG2−COOH. *(a) Preparation of mPEG p-Nitrophenyl Carbonate (II).* Five g (1 mmol) of mPEG−OH, M_n 5000, was dissolved in 120 mL of toluene and dried by removal of the water−toluene azeotrope. The solution was cooled to room temperature and concentrated, and 20 mL of anhydrous methylene chloride, 0.28 mL (2 mmoles) of triethylamine (TEA), and 0.4 g (2 mmoles) of *p*-nitrophenyl chloroformate were added under stirring at 0 °C; the pH was maintained at 8 with TEA (this pH measurement was made by placing a drop of solution on a piece of wet pH paper). After being allowed to stand overnight at room temperature, the reaction mixture was concentrated under vacuum to about 10 mL, filtered, and added drop by drop into 100 mL of stirred diethyl ether. The resulting precipitate was collected by filtration and crystallized twice from ethyl acetate. mPEG activation, calculated spectrophotometrically on the basis of the released 4-nitrophenol absorption at 400 nm in alkaline media, after 15 min, was 98% (ϵ of *p*-nitrophenol at 400 nm = 17 000 M⁻¹ cm⁻¹). Alternatively, this material was purchased from Shearwater Polymers.

(b) Preparation of mPEG-Monosubstituted Lysine (III). Lysine (353 mg, 2.5 mmol) was dissolved in 20 mL of water at pH 8.0−8.3, and then 5 g of mPEG *p*-nitrophenyl carbonate (1 mmol) was added in portions for 3 h, while the pH was maintained at 8.3 with 0.2 N NaOH. After being stirred overnight at room temperature, the solution was cooled to 0 °C and brought to pH 3 with 2 N HCl. Impurities were extracted with diethyl ether, the mPEG−Lys substituted at the ϵ amino group was extracted three times with chloroform, and the solution dried. After concentration, the solution was added drop by drop to diethyl ether. The precipitate was collected and then crystallized from absolute ethanol. The percentage of modified amino groups, calculated by colorimetric analysis (*21*), was 53%.

(c) Preparation of mPEG-Disubstituted Lysine (mPEG2−COOH) (IV). TEA was added to 4.5 g (0.86 mmol) of the above product, dissolved in 10 mL of anhydrous methylene chloride, to reach pH 8.0. mPEG *p*-nitrophenyl carbonate (4.9 g,1.056 mmol) was added over 3 h, while the pH was maintained at 8.0 with TEA. The reaction mixture was refluxed for 72 h, brought to room temperature, concentrated, filtered, precipitated with diethyl ether, and finally crystallized in a minimum amount of hot ethanol. The excess of activated mPEG was hydrolyzed in pH 9−10 buffer by stirring overnight at room temperature. The solution was then cooled to 0 °C and brought to pH 3 with 2 N HCl. This solution was extracted with diethyl ether to remove *p*-nitrophenol. mPEG2−COOH and the remaining traces of mPEG were

extracted from the mixture three times with chloroform, dried, concentrated, precipitated with diethyl ether, and crystallized from ethanol. No unreacted lysine amino groups remained in the polymer mixture as assessed by colorimetric analysis (*21*). mPEG2-COOH was purified from mPEG by gel filtration chromatography using a Bio Gel P100 (Bio-Rad) column (5 × 50 cm), 100–200 mesh, and water as eluent; 10 mL fractions were collected. (According to these conditions no more than 200 mg of material could be purified for each run). The fractions corresponding to mPEG2-COOH, revealed by iodine reaction (*22*), were pooled, concentrated, dissolved in ethanol, and concentrated. The product was dissolved in methylene chloride, precipitated with diethyl ether, and crystallized from ethanol.

Alternatively, the purification of the desired product from unmodified mPEG was performed by ion exchange chromatography on a QAE Sephadex A50 column (5 × 80 cm) (Pharmacia) using 8.3 mM borate buffer pH 8.9 (*23*). This procedure permitted fractionation of a greater larger of material for each run (4 g).

In both cases, purified mPEG2-COOH, titrated with NaOH, gave 100% of free carboxyl group, considering a polymer of MW 10 000. The product was also characterized by ^{1}H-NMR on a 200 MHz Bruker instrument in dimethyl sulfoxide-d_6, at a 5% W/V concentration. ^{1}H-NMR data confirmed the expected M_n of 10 000. Note that we now believe our original NMR method can give reasonable M_n values up to 20 000 g/mol (*24*).

The chemical shifts and assignments of the protons in mPEG2-COOH are as follows: 1.2–1.4 ppm (multiplet, 6H, methylenes 3,4,5 of lysine); 1.6 ppm (multiplet, 2H, methylene 6 of lysine); 3.14 ppm (s, 3H, terminal mPEG methoxy); 3.49 ppm (s, mPEG backbone methylene); 4.05 ppm (t, 2H, −CH$_2$OCO−) 7.18 ppm (t, 1H, −NH− lysine); 7.49 ppm (d, 1H, −NH−lysine).

(d) Activation of mPEG2-COOH by N-Hydroxysuccinimide (V). mPEG2-COOH (6.2 g, 0.6 mmol) was dissolved in 10 mL of anhydrous methylene chloride, cooled to 0 °C, and 0.138 g (1.2 mmol) of N-hydroxysuccinimmide and 0.48 g (1.2 mmoles) of N,N-dicyclohexylcarbodiimide were added under stirring. After the mixture was stirred overnight at room temperature, precipitated dicyclohexylurea was removed by filtration and the solution was concentrated and precipitated with diethyl ether. The final product was crystallized from ethyl acetate. The yield of esterification, calculated on the basis of N-hydroxysuccinimide absorption at 260 nm (produced by hydrolysis), was over 97% (ε of hydroxysuccinimide at 260 nm = 8000 M^{-1} cm^{-1}). The NMR spectrum was identical to that of the preceding acid except for the new succinimide singlet at 2.80 ppm (2H).

One-Step Procedure for mPEG2-COOH Preparation. *a. Preparation of mPEG-Disubstituted Lysine (mPEG2-COOH) .* A 10.8 g portion of mPEG succinimidyl carbonate 20 000 (VIII) (5.4 × 10^{-4} mol) (Shearwater Polymers, Huntsville, AL) was added to 40 mL of lysine HCl solution in borate buffer, pH 8.0, at a concentration of 0.826 mg/ml (1.76 × 10^{-4} mol). After addition of 20 mL of the same buffer, solution pH was maintained at 8.0 with aqueous NaOH solution for the following 8 h. The reaction mixture was allowed to stir at room temperature for 24 h. For dimerization of mPEG 5000 a molar excess of carbonate of only 10% is required.

After dilution with 300 mL of deionized water, the solution was adjusted to pH 3.0 by addition of oxalic acid and extracted three times with dichloromethane. The combined dichloromethane extracts were dried with anhydrous sodium sulfate. The filtrate was concentrated

to about 30 mL and the product precipitated with about 200 mL of cold ethyl ether. The yield was 90%.

Nine g of the above reaction product was dissolved in 4 L of distilled water and loaded onto DEAE Sepharose FF (500 mL of gel equilibrated with 1500 mL boric acid, sodium hydroxide buffer, 0.5%, pH 7.0 and then washed with water). Impurities of mPEG−lysine and mPEG were washed off the column with water, whereas the desired mPEG2-COOH was eluted with 10 mM NaCl. The pH of the eluate was adjusted to 3.0 with oxalic acid and the product extracted with dichloromethane, dried with sodium sulfate, concentrated, and precipitated with ethyl ether. A total of 5.1 g of the desired product was obtained. M_n was determined to be 38 000 by gel filtration chromatography and 36 700 by potentiometric titration (as described above).

(b) Preparation of mPEG2−COOSu. The procedure previously described for preparing the branched 5000 × 2 polymer was followed for activating this high-MW, branched (20 000 × 2) polymer. Yield was over 95%.

Enzyme Modification. To obtain a similar extent of amino group derivatization for each enzyme, different procedures were used for enzyme modification depending upon the type of enzyme and the polymer used (linear mPEG, activated as mPEG-Nle-OSu, or branched mPEG2−COOSu). Larger molar ratios of mPEG2−COOSu were generally required. Common conditions were 0.2 M, pH 8.5 borate buffer to dissolve proteins, and addition of polymers in small portions to facilitate dissolution (approximately 10 min required), followed by stirring for 1 h. The amount of polymer used for modification was calculated on the basis of available amino groups in the enzyme.

a. Ribonuclease (1.5 mg/ml) was modified at room temperature, and mPEG-Nle-OSu or mPEG2−COOSu was added at a molar ratio of polymer to protein amino groups of 2.5/1 and 5/1, respectively. Ribonuclease has a molecular weight of 13 700 D and 11 available amino groups.

b. Catalase (2.5 mg/ml) was modified at room temperature using mPEG/protein-NH$_2$ and mPEG2/protein-NH$_2$ molar ratios of 5/1 and 10/1, respectively. Catalase has a molecular weight of 250 000 D with 112 available amino groups.

c. Trypsin (4 mg/mL) modification was performed at 0 °C using a mPEG/protein-NH$_2$ or mPEG2/protein-NH$_2$ molar ratio of 2.5/1. Trypsin has a molecular weight of 23 000 D and 16 available amino groups.

d. Asparaginase (6 mg/ml) was modified with a mPEG/protein-NH$_2$ molar ratio of 3/1 at room temperature, while derivatization with mPEG2−COOSu (mPEG2/protein-NH$_2$ molar ratio of 3.3/1) was carried out at 37 °C. *Erwinia Carativora* asparaginase has a molecular weight of 141 000 D and 92 free amino groups.

Polymer−enzyme conjugates were purified by ultrafiltration and concentrated in an Amicon system with a PM 10 membrane (cutoff 10 000) to eliminate N-hydroxysuccinimide. The conjugates were further purified from unreacted polymer by gel filtration chromatography on a Pharmacia Superose 12 column (on an FPLC) using 10 mM phosphate buffer, pH 7.2, 0.15 M in NaCl, as eluent.

Protein concentration of the native forms of ribonuclease, catalase, and trypsin was evaluated spectrophotometrically using molar extinction coefficients of 9.45 × 10^3, 1.67 × 10^5, and 3.7 × 10^4 M^{-1} cm^{-1} at 280 nm, respectively. The concentration of asparaginase was evaluated by biuret assay. Biuret assay was also used to evaluate concentrations of modified proteins.

The extent of protein modification was evaluated colorimetrically by the method of Habeeb (*25*) or by amino acid analysis after acid hydrolysis, following the post-column procedure of Benson et al. (*26*) or precolumn derivatization by phenyl isothiocyanate (PITC) according to Bidlingmeyer et al. (*27*). For amino acid analysis, the amount of bound mPEG was evaluated from norleucine content with respect to other protein amino acids, and the amount of mPEG2 was determined from the increase in lysine content, since for each bound polymer one additional lysine is present in the hydrolysate (*28*).

Enzymatic activity of native and modified enzyme was evaluated as follows: For ribonuclease, the method of Crook et al. (*29*) was used. Catalase activity was determined by the method of Beers and Sizer (*30*). The esterolytic activity of trypsin and its derivatives was determined by the method of Laskowsky (*31*), while the proteolytic activities of the conjugates were assayed according to the method of Zwilling and Neurath (*32*). Native and modified asparaginase were assayed according to a method reported by Cooney et al. (*33*): namely, 1.1 mL containing 120 µg of α-ketoglutaric acid, 20 UI of glutamic-oxalacetic transaminase, 30 UI of malate dehydrogenase, 100 µg of NADH, 0.5 µg of asparaginase, and 10 µmol of asparagine were incubated in 0.122 M Tris buffer, pH 8.35, while the NADH absorbance decrease at 340 nm was followed.

Proteolytic Digestion of Free Enzyme and mPEG– or mPEG2-Enzyme Conjugates. Proteolytic digestion was performed in 0.05 M phosphate buffer, pH 7.0, as follows:

a. For ribonuclease and its adducts, 0.57 mg of protein was digested at room temperature with 2.85 mg of pronase or 5.7 mg of elastase or with 0.57 mg of subtilisin in a total volume of 1 mL.

b. Native and modified catalase, 0.58 mg of protein, were digested at room temperature with 0.58 mg of trypsin or 3.48 mg of pronase in a total volume of 1 mL.

c. Autolysis of trypsin and its derivatives at 37 °C was evaluated by esterolytic activity of protein solutions at 25 mg/mL of TAME.

d. For native and modified asparaginase, 2.5 µg was digested at 37 °C with 0.75 mg of trypsin in a total volume of 1 mL.

From each enzyme solution, aliquots were taken at various time intervals and enzyme activity was assayed spectrophotometrically.

Thermal Stability of Free and Conjugated Enzymes. Thermal stability of native and mPEG- or mPEG2-modified ribonuclease, catalase, and asparaginase was evaluated in 0.5 M phosphate buffer, pH 7.0, at 1, 9, and 0.2 mg/mL, respectively. The samples were incubated at the specified temperatures for 15, 10, and 15 min, respectively, cooled to room temperature and assayed spectrophotometrically for activity.

pH Stability of Free and Conjugated Enzymes. Unmodified or polymer-modified enzymes were incubated for 20 h in the following buffers: sodium acetate, 0.05 M, pH 4.0–6.0, sodium phosphate, 0.05 M, pH 7.0, and sodium borate, 0.05 M, pH 8.0–11. Enzyme concentrations were 1 mg/mL, 9 µg/mL, and 5 µg/mL for ribonuclease, catalase, and asparaginase, respectively. Stability to incubation at various pHs was evaluated on the basis of enzyme activity.

RESULTS AND DISCUSSION

Preparation of mPEG2-COOH by a Two-Step Procedure. The structure of the branched mPEG obtained by coupling two polymer chains to lysine amino groups is shown in Figure 1. This polymer was first prepared by a "two-step" procedure. In the first step of this method a single lysine amino group is modified by reaction with *p*-nitrophenyl carbonate–mPEG in aqueous buffer. Both lysine and the mPEG are soluble in aqueous medium, but the mPEG derivative undergoes hydrolysis; lysine is not soluble in organic solvents in which the activated PEG is stable. The product is readily extracted into chloroform. Modification of the second lysine amino group is achieved by reaction in dry methylene chloride, where mPEG-substituted lysine is soluble and the activated mPEG is soluble and stable. NMR analysis shows that the first mPEG chain is bound to the ε-amino group.

Although either gel filtration or ion exchange chromatography give high degrees of purification from unreacted mPEG, ion exchange is preferred because large amounts of material can be applied to the column.

The mPEG$_2$-COOH was characterized by −COOH titration and ^{1}H-NMR analysis. The NMR spectrum is consistent with the assigned structure. For example, two different carbamate NH signals are observed, with the first (at 7.18 ppm) showing a triplet for coupling with the adjacent methylene group, and the second (at 7.49 ppm) showing a doublet from coupling with the α-CH of lysine. The intensity of these signals relative to the mPEG methylene peak is consistent with the 1:1 ratio between the two carbamate groups and the expected M_n of 10,000 of the branched polymer.

For protein modification, mPEG2-COOH was activated as the succinymidyl ester according to known methods (*34*).

Preparation of mPEG2-COOH by a "One-Step" Procedure. The two-step procedure is somewhat time consuming. A more straightforward one-step method may be employed in which lysine is reacted with 2 mol of highly active mPEG succinimidyl carbonate to produce acid IV directly, Figure 1 (*10*). One particular advantage of mPEG dimerization with lysine is that monofunctional PEGs of high MW can be obtained. To demonstrate this application we applied the one-step procedure to dimerize mPEG 20 000, thus preparing a clean, monofunctional mPEG2-COOH of MW 40 000. To appreciate the importance of this application, one need only recall the great difficulty in obtaining low-MW monofunctional mPEGs by direct ethylene oxide polymerization (*19, 24*). One disadvantage of the one-step method, relative to the two-step method, is that the latter procedure allows the attachment of PEGs of two different molecular weights.

Comparison of Properties of Enzymes Modified by Linear and Branched Polymer. To evaluate the influence of linear mPEG and branched mPEG2 attachment on enzyme properties, four different model enzymes, ribonuclease, catalase, asparaginase, and trypsin, were modified with mPEG-Nle-OSu 5000 or mPEG2-COOSu (2 × 5000), and the catalytic properties of the enzymes were determined. To facilitate comparison, each enzyme was modified with the two polymers to a similar extent by a careful choice of polymer to enzyme ratios and reaction temperature (Table 1). The purpose of this comparison is to see if the larger mPEG2 will confer improved conjugate properties without increasing the number of attachment sites, as would be necessary with the smaller, linear mPEG. Recall that high MW linear mPEGs are difficult to obtain. Future studies will present more extensive comparison of various MWs of linear and branced mPEGs.

Ribonuclease. Ribonuclease with 50% and 55% of the amino groups modified with mPEG and mPEG2, respectively, presented 86% and 94% residual activity with respect to the native enzyme. In Figure 2 the stability to proteolytic digestion by pronase (a), elastase (b), and

Table 1. Properties of Enzymes Modified by mPEG and mPEG2 and Molar Ratios Used in Enzyme Modification

enzyme[a]	NH₂: polymer molar ratio	% modification	% activity	K_m (M)	K_{cat} (min⁻¹)
ribonuclease					
RN	1:0	0	100		
RP1	1:2.5	50	86		
RP2	1:5	55	94		
catalase					
CN	1:0	0	100		
CP1	1:5	43	100		
CP2	1:10	38	90		
trypsin[b]					
TN	1:0	0	100	8.2×10^{-5}	830
TP1	1:2.5	50	120	7.6×10^{-5}	1790
TP2	1:2.5	57	125	8.0×10^{-5}	2310
asparaginase					
AN	1:0	0	100	3.31×10^{-6}	523
AP1	1:3	53	110	3.33×10^{-6}	710
AP2[c]	1:3.3	40	133	3.30×10^{-6}	780

[a] N = native enzyme, P1 = enzyme modified with mPEG, P2 = enzyme modified with mPEG2. Reaction temperatures in text. [b] For trypsin, only the esterolytic activity is reported.

subtilisin (c) is reported for native and the two modified enzymes. Polymer modification greatly increases the stability to digestion by all three proteolytic enzymes, but the protection offered by branched mPEG2 is more effective than linear mPEG.

Increased thermal stability was found for the modified forms relative to the unmodified enzyme (pH 7.0, 15 min incubation), but no significant difference between mPEG and mPEG2 modification was observed (Figure 3a). Decreased stability for the branched mPEG2 derivative was found after incubation at acid and alkaline pH values (Figure 3b).

Catalase. Catalase was modified with mPEG and mPEG2 to obtain 43% and 38% modification of protein amino groups, respectively. Enzyme activity was not significantly changed after modification. However, proteolytic stability was much greater for the mPEG2 derivative than for the mPEG derivative, particularly toward pronase and trypsin where no digestion took place, Figure 4. Catalase thermal stability was not influenced by polymer modification, but the stability toward low-pH incubation of the modified forms was superior as compared to the native enzyme, Figure 5.

Asparaginase. Asparaginase with 53% and 40% modified protein amino groups was obtained by coupling with mPEG and mPEG2, respectively. Enzymatic activity was increased, relative to the free enzyme, to 110% for the mPEG conjugate and to 133% for the mPEG2 conjugate. An increase in enzyme activity following polymer derivatization has been observed for other enzymes and is also seen below for trypsin modification (*10, 35, 36*). A possibility is that polymer coupling results in conformational modification which gives either a more active form or increased affinity for substrate. In the present case it appears that a more active form is produced because the K_m values of the modified forms were not changed upon modification: 3.31×10^{-6}, 3.33×10^{-6}, and 3.3×10^{-6} M for the free, mPEG–, and mPEG2-asparaginase, respectively. The K_{cat} values for these enzyme forms are 523, 710, and 780 min⁻¹, respectively.

Modification with mPEG2 had an impressive influence on stability toward proteolytic enzymes. Increased protection was achieved at a lower extent of modification with respect to the derivative obtained with the linear polymer (Figure 6). A limited increase in thermal
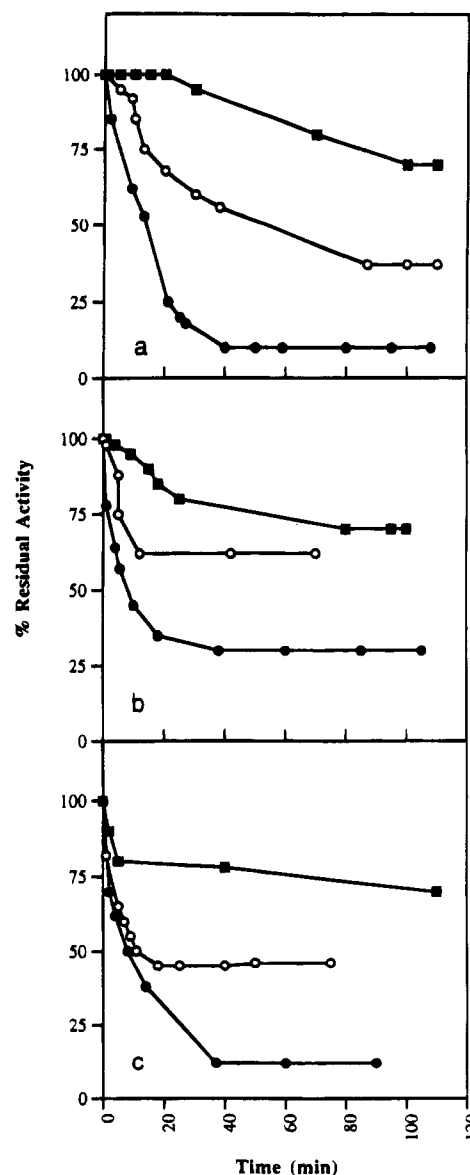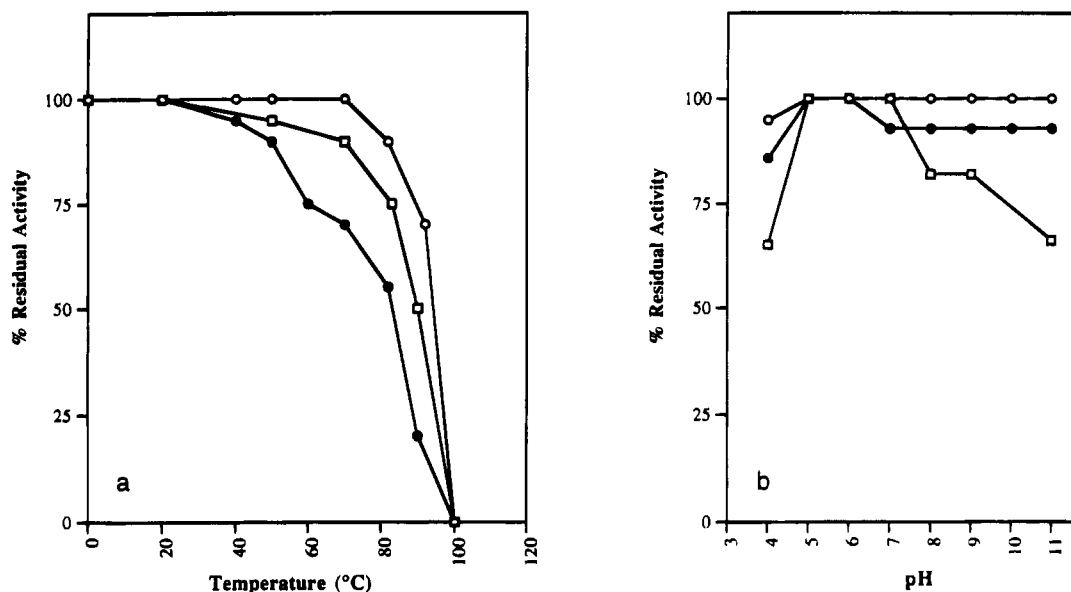

Figure 2. Time course of native ribonuclease, RN (●), mPEG ribonuclease, RP1 (○), and mPEG2 ribonuclease, RP2 (■) digestion as assessed by enzyme activity upon incubation with pronase (a), elastase (b), and subtilisin (c).

stability and stability to acid and alkaline pH values was observed for both adducts (data not shown).

Trypsin. Trypsin was modified at the level of 50% and 57% of amino groups with mPEG and mPEG2, respectively. Esterolytic activity for mPEG- and mPEG2-modified enzyme, assayed on the small substrate TAME, was 120% and 125%, respectively. Modification did not change affinity for the substrate; native and modified forms gave K_m values of 8.2×10^{-5}, 7.6×10^{-5}, and 8.0×10^{-5} M. Catalytic activity, K_{cat}, increased from 830 min⁻¹ for native trypsin to 1790 min⁻¹ for mPEG–trypsin and 2310 min⁻¹ for mPEG2–trypsin. Presumably a more active conformation is produced by polymer modification.

Modification with mPEG and mPEG2 reduced proteolytic activity of trypsin toward casein, a high molecular weight substrate: activity relative to the native enzyme was found, after 20 min incubation, to be 64% for the mPEG conjugate and only 35% for the mPEG2 adduct. In agreement with these results, the trypsin autolysis rate, evaluated by enzyme esterolytic activity, was totally prevented in mPEG2–trypsin but only reduced in mPEG–trypsin, Figure 7. To prevent autolysis with mPEG,

Figure 3. Heat (a) and pH (b) stability of native ribonuclease, RN (●), mPEG ribonuclease, RP1 (○), and mPEG2 ribonuclease, RP2 (□) following 15 min incubation at the indicated temperatures or 20 h at different pH values.
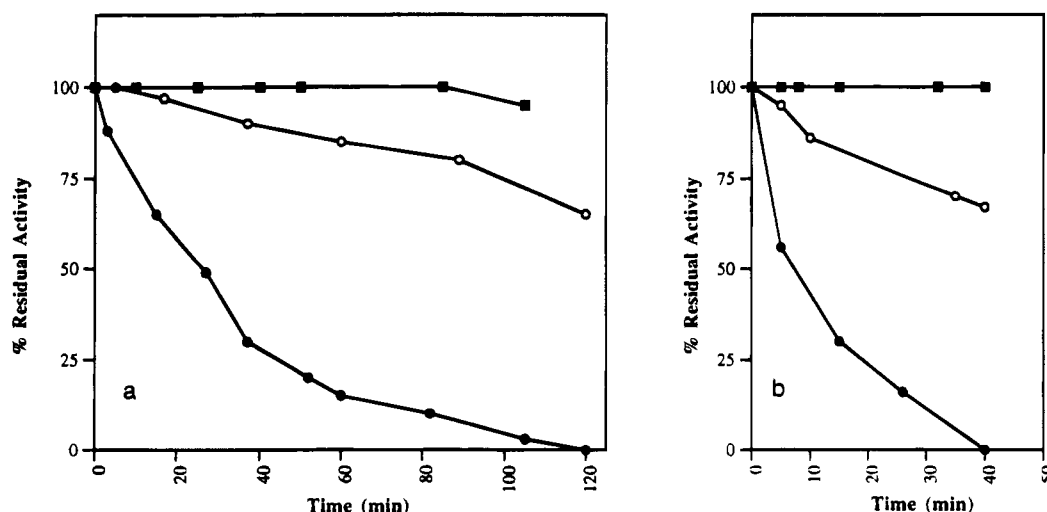
Figure 4. Time course of native catalase, CN (●), mPEG catalase, CP1 (○), and mPEG2 catalase, CP2 (■), digestion as assessed by enzyme activity upon incubation with pronase (a) and trypsin (b).

modification of 78% of the available protein amino groups was required. These data are all consistent with an increased hindrance to access to the active site by the polymer, as discussed in our previous work (*36*).

CONCLUSIONS

The results reported in this paper demonstrate that new, branched mPEG dimers may be prepared by a "two-step" procedure, using mPEG *p*-nitrophenyl carbonate, or by a "single-step" procedure, using more reactive mPEG succinimidyl carbonate. The branched polymer, activated as the succinimidyl ester (mPEG2–COOSu), reacts under mild aqueous conditions, compatible with the stability of most enzymes, to give a stable amide linkage with protein amino groups.

Here the branched mPEG2 was studied for its utility in enzyme modification, but it has a general applicability in several areas of PEG chemistry. Single-point attachment is always maintained.

Modification of four model enzymes with mPEG2 was accompanied by no appreciable loss of activity. Asparaginase, an enzyme of significant therapeutic interest, was found to undergo major loss of activity when modified

with branched chlorotriazine mPEG (*8*), but exhibited increased activity using this new mPEG2–COOSu.

Protein adducts obtained by modification with mPEG2–COOSu, having two polymer chains bound at the same reactive amino group, present increased hindrance to approaching macromolecules in comparison to the smaller, linear mPEG derivative. This is shown by the larger increase in protection to proteolysis of three proteins modified by mPEG2–COOSu compared to modification with linear mPEG-Nle-OSu. Also, the reduced hydrolytic activity of modified trypsin towards casein, and its slower autolysis rate, provides additional support for this conclusion.

Enzyme structural stability toward denaturating agents such as temperature or pH, or the substrate binding properties of the bound polymer–enzyme conjugates, do not differ significantly between mPEG– and mPEG2– enzyme adducts.

A further advantage in the use of mPEG2 in protein modification is the possibility of easy and direct evaluation of the number of bound polymer chains by amino acid analysis after acid hydrolysis. Unlike analytical methods that monitor the percentage of modified lysines,
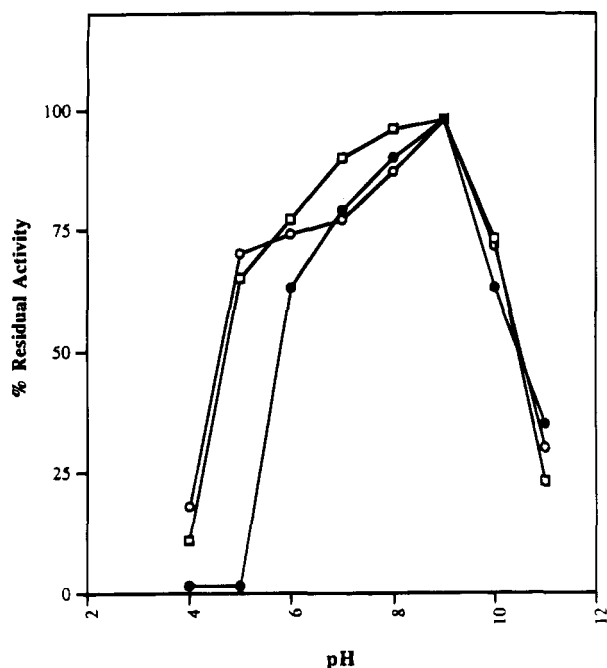
Figure 5. Native catalase, CN (●), mPEG catalase, CP1 (■), and mPEG2 catalase, CP2 (○), stability toward 20 h incubation at the indicated pH values.
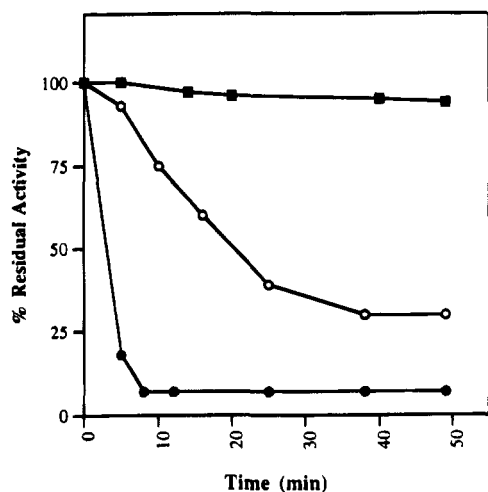

Figure 6. Time course of native asparaginase, AN (●), mPEG asparaginase, AP1 (○), and mPEG2 asparaginase, AP2 (■), digestion as assessed by enzyme activity assay upon trypsin incubation.

mPEG2 modification will release lysine when the polymer is bound to the α-amino group of a terminal amino acid or to an amino acid other than lysine (e.g., histidine or tyrosine) (*37*).

Preliminary data obtained in our laboratory suggest improved immunological properties as well as increased body residence time of mPEG2 conjugates relative to mPEG conjugates. The pharmacokinetics and immunological behavior of enzymes of potential therapeutic interest, as well as the effect on solubility and activity in organic solvents, are under active investigation and will be reported soon.

ACKNOWLEDGMENT
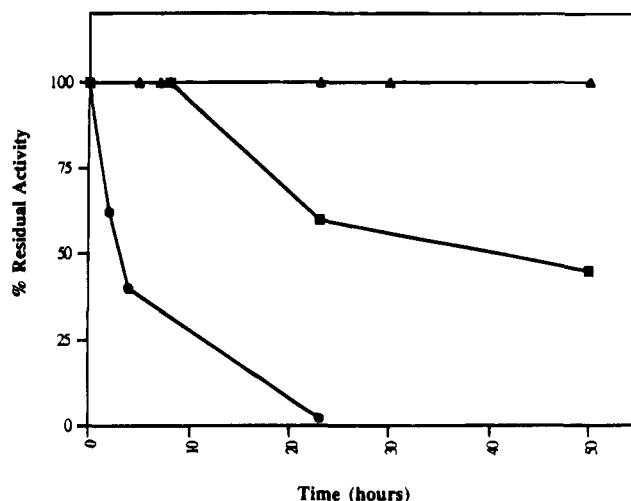
Figure 7. Time course of native trypsin, TN (●), mPEG trypsin, TP1 (■), and mPEG2 trypsin, TP2 (▲), autolysis evaluated as residual activity towards TAME.

LITERATURE CITED

(1) Nucci, M. L., Shorr, R., and Abuchoswki, A. (1991) The therapeutic value of poly(ethylene glycol)-modified proteins. *Adv. Drug Delivery Rev. 6,* 133–151.

(2) Delgado, C., Francis, G. E., and Fisher, D. (1992) The uses and properties of PEG-linked proteins. *Crit. Rev. Ther. Drug Carrier Syst. 9*(3,4), 249–304.

(3) Veronese, F. M., Caliceti, P., Schiavon, O., and Sartore, L. (1992). Preparation and properties of monomethoxypoly-(ethylene glycol)-modified enzymes for therapeutic applications. *Poly(Ethylene Glycol) Chemistry: Biotechnical and Biomedical Applications* (J. M. Harris, Ed.) pp 127–137, Plenum Publishing Corporation, New York.

(4) Katre, N. V. (1993) The conjugation of proteins with polyethylene glycol and other polymers. Altering properties of proteins to enhance their therapeutic potential. *Adv. Drug Delivery Rev. 10,* 91–114.

(5) Inada, Y., Takahashi, K., Yoshimoto, T., Ajima, A., Matsushima, A., and Saito, Y. (1986) Application of polyethylene glycol-modified enzymes in biotechnological processes: organic solvent-soluble enzymes. *TIBTECH 4,* 190–194.

(6) Ottolina, G., Carrea, G., Riva, S., Sartore, L., and Veronese, F. M. (1992) Effect of the enzyme form on the activity, stability and enantioselectivity of lipoprotein lipase in toluene. *Biotechnol. Lett. 14,* 947–952.

(7) Somak, R., Saifer, M. G. P., Williams, D. (1991) Preparation of long acting superoxide dismutase using high molecular weight polyethylene glycol (41,000–72,000 daltons) *Free Rad. Res. Commun. 12–13,* 553–562.

(8) Wada, H., Imamura, I., Sako, M., Katagiri, S., Tarui, S., Nishimura, H., and Inada, Y. (1990) Antitumor enzymes: polyethylene glycol-modified asparaginase. *Ann. N. Y. Acad. Sci. 613,* 95–108.

(9) Yamsuki, N., Matsuo, A., and Isabe, H. (1988) Novel polyethylene glycol derivatives for modification of proteins. *Agric. Biol. Chem. 52,* 2185–2196.

(10) Zalipsky, S., Selletzer, R., and Menon-Rudolf, S., (1992) Evaluation of a new reagent for covalent attachment of polyethylene glycol to protein. *Biotechnol. Appl. Biochem. 15,* 100–114.

(11) Caliceti, P., Monfardini, C., Sartore, L., Schiavon, O., Baccicchetti, F., Carlassare, F., and Veronese, F. M. (1993) Preparation and properties of monomethoxy poly(ethylene glycol) doxorubicin conjugates linked by an amino acid or a peptide as spacer. *Il Farmaco 48*(7), 919–932.

(12) Merrill, E. W. (1992) Poly(Ethylene Oxide) and Blood Contact: A Chronicle of One Laboratory. *Poly(Ethylene Glycol) Chemistry: Biotechnical and Biomedical Applications*

(J. M. Harris, Ed.) pp 199—220, Plenum Publishing Corporation, New York.

(13) Golander, C. G., Herron, J. N., Lim, K., Stenius, P., and Andrade, J. D. (1992) Properties of Immobilized PEG Film and the Interaction with Protein: Experiments and Modelling. *Poly(Ethylene Glycol) Chemistry: Biotechnical and Biomedical Applications* (J. M. Harris, Ed.) pp 221—245, Plenum Publishing Corporation, New York.

(14) Brooks, D. E., Van Alstine, J. M., Sharp, K. A., and Stocks, S. J. (1992) PEG-Derivatized Ligands with Hydrophobic and Immunological Specificity: Applications in Cell Separation. *Poly(Ethylene Glycol) Chemistry: Biotechnical and Biomedical Applications* (J. M. Harris, Ed.) pp 57—71, Plenum Publishing Corporation, New York.

(15) Johansson, G. (1992) Affinity Partitioning in PEG-Containing Two-Phase System. *Poly(Ethylene Glycol) Chemistry: Biotechnical and Biomedical Applications* (J. M. Harris, Ed.) pp 73—84, Plenum Publishing Corporation, New York.

(16) Tierneld, F. (1992) Aqueous Two-Phase Partitioning on an Industrial Scale. *Poly(Ethylene Glycol) Chemistry: Biotechnical and Biomedical Applications* (J. M. Harris, Ed.) pp 85—102, Plenum Publishing Corporation, New York.

(17) Papahadjopoulos, D., Allen, T. M., Gabizon, A., Mayhew, E., Matthay, K., Huang, S. K., Lee, K. D., Woodle, M. C., Lasic, D. D., Redemann, C., and Martin, F. J. (1991) Sterically stabilised liposomes: Improvements in pharmacokinetics and antitumor therapeutic efficacy. *Proc. Natl. Acad. Sci. U.S.A.* **88**, 11460—11464.

(18) Senior, J., Delgado, C., Fisher, D., Tilcock, C., and Gregoriadis, G. (1991) Influence of surface hydrophilicity of liposomes on their interaction with plasma protein and clearance from circulation: Studies with poly(ethylene glycol)-coated vesicles. *Biochim. Biophys. Acta* **77**, 1062.

(19) Bailey, F. E., and Koleske, J. V. (1991) *Alkylene Oxides and Their Polymers*, Marcel Dekker, New York.

(20) Sartore, L., Caliceti, P., Schiavon, O., and Veronese, F. M. (1991) Enzyme modification by MPEG with an amino acid or peptide as spacer arms. *Appl. Biochem. Biotechnol.* **27**, 45—54.

(21) Snyder, S. L., and Sobocinsky., P. Z. (1975) An improved 2,4,6-trinitrobenzenesulfonic acid method for the determination of amines. *Anal. Biochem.* **64**, 284—288.

(22) Sims, G. E. C., and Snape, Y. J. (1980) A method for the estimation of polyethylene glycol in plasma protein fraction. *Anal. Biochem.* **107**, 60—63.

(23) Zalipsky, S., Albericio, F., and Barany, G. (1985) Preparation and use of an aminoethyl polyethylene glycol-crosslinked polystyrene graft resin support for solid-phase peptide synthesis. *Peptides: Structure and Function*, (C. M. Deber, V. J. Hruby and K. D. Kopple, Eds.), pp. 257—260, Pierce Chemical Co.,

(24) Dust , J. M., Fang, Z. H., and Harris, J. M. (1990) Proton NMR characterization of poly(ethylene glycols) and derivatives. *Macromolecules* **23** 3742—3746.

(25) Habeeb, A. F. S. A. (1966) Determination of free amino groups in protein by trinitrobenzensulphonic acid. *Anal. Biochem.* **14**, 328—336.

(26) Benson, J. V., Gordon, M. J., and Patterson, J. A. (1967) Accelerated chromatographic analysis of amino acid in physiological fluids containing vitamin and asparagine. *Anal. Biol. Chem.* **18**, 288—333.

(27) Bidlingmeyer, B. A., Cohen, S. A., and Tarvin, T. L. (1984) Rapid analysis of amino acids using pre-column derivatization. *J. Chromatogr.* **336**, 93—104.

(28) Sartore, L., Caliceti, P., Schiavon, O., Monfardini, C., and Veronese, F. M. (1991) Accurate evaluation method of the polymer content in monomethoxy(polyethylene glycol) modified proteins based on amino acid analysis. *Appl. Biochem. Biotechnol.* **31**, 213—222.

(29) Crook, E. M., Mathias, A. P., and Rabin, B. R. (1960) Spectrophotometric assay of bovine pancreatic ribonuclease by the use of cytidine 2':3' phosphate. *Biochem. J.* **74**, 234—238.

(30) Beers, R. F., and Sizer, I. W. (1952) A spectrophotometric method for measuring the breakdown of hydrogen peroxide by catalase. *J. Biol. Chem.* **195**, 133—140.

(31) Laskowski, M. (1955) Trypsinogen and trypsin. *Methods Enzymol.* **2**, 26—36.

(32) Zwilling, R., and Neurath, H. (1981) Invertebrate protease. *Methods Enzymol.* **80**, 633—664.

(33) Cooney, D. A., Capizzi, R. L., and Handschumacher, R. E. (1970) Evaluation of L-asparagine metabolism in animals and man. *Cancer Res.* **30**, 929—935.

(34) Nathan, A., Zalipsky, S., Ertel, S. I., Agathos, S. N., Yarmush, M. L., and Kohn, J. (1993) Copolymers of lysine and polyethylene glycol: A new family of functionalized drug carriers. *Bioconjugate Chem.* **4**, 54—62.

(35) Munch, O., Tritsch ,D., and Biellmann, J. F., (1991) Polyethylene glycol modified trypsin kinetics in buffer and benzene: Dipeptide synthesis. *Biocatalysis* **5**, 35—47.

(36) Caliceti, P., Schiavon, O., Sartore, L., Monfardini, C., and Veronese, F. M. (1993) Active site protection of proteolytic enzymes by poly(ethylene glycol)surface modification. *J. Bioactive Compatible Polymers* **8**, 41—50.

(37) Blumberg, S., and Vallee, B. L. (1975) Superactivation of thermolysin by acylation with amino acid N-hydroxysuccinimide esters. *Biochemistry* **14**, 2410—2419.

Directed N-Terminal Elongation of Unprotected Peptides Catalyzed by Cathepsin C in Water

Carsten Gittel and Franz P. Schmidtchen*

Lehrstuhl für Organische Chemie und Biochemie, Technische Universität München, Lichtenbergstrasse 4, 85747 Garching, Germany. Received April 22, 1994[⊛]

N-terminal chain extension of unprotected amino acid amides and peptides with dipeptide amides using Cathepsin C (dipeptidyl aminopeptidase I, EC 3.4.14.1)-mediated reverse proteolysis in water was studied. Taking Pro-X-NH$_2$ as the acyl donor, the sensitivity of the kinetically controlled peptide, coupling to pH value, temperature, acetonitrile addition, and nucleophile type were investigated. Basic or hydrophobic amino acids as the α-amino-N-nucleophile proved to be much more prone to catalyzed bond formation than their neutral, hydrophilic, or negatively charged analogues. In a preparative run a pentapeptide was obtained with 83% yield by directed and regioselective coupling of ProTrpNH$_2$ with LysLeuPheNH$_2$ catalyzed by Cathepsin C in aqueous buffer.

INTRODUCTION

An abiotic method for site specific covalent attachment to form protein conjugates would enable *rational tailoring* of molecular properties of proteins with respect to the physicochemical behavior (solubility in various environments and stability toward unusual pH, ionic strength, and denaturant conditions) or to the catalytic (substrate selectivity, cofactor requirement, etc.) or biological (proteolytic degradability, targeting, etc.) features. In striving for broad applicability, methods for the derivatization of C- (Schmitter et al., 1992; Vilaseca et al., 1993) and N-termini (Jay, 1984; Jue and Doolittle, 1985; Geoghegan and Stroh, 1992; Gaertner et al., 1992) of proteins and peptides have been developed. The latter in particular appears attractive since, as most proteins undergo N-terminal processing anyway (i.e., cleavage of a signal peptide or the initial Met-residue), this end of the peptide backbone must be located at the periphery of the protein globule and thus be accessible from bulk solution. A modification at this site would in addition impose the least interference with the native protein structure and is therefore not likely to affect, for example, enzymic (constitutive) activities.

In view of the catalogue of restrictions imposed on any suitable process—(i) rapid and chemoselective formation of a stable covalent conjugate connection, (ii) reactions to be performed in aqueous buffer to retain the native, mature conformation of the protein, and (iii) unambiguous regioselectivity—we chose to investigate the N-terminal chain extension of peptides/proteins by reverse proteolysis. The formation of chemically quite stable peptide bonds between amino acids or peptides with the help of endoproteases has been intensively studied (Kasche, 1989; Schellenberger and Jakubke, 1991; Jakubke 1991, 1992) and is even used industrially, e.g., in the manufacture of insulin (Könnecke et al., 1990; Morihara et al., 1979; Breddam et al., 1981; Markussen et al. 1988). Of the two principal alternatives (thermodynamic versus kinetic control) the kinetically controlled process may give high yields of coupling products even in water provided an activated enzyme-bound covalent intermediate is formed in the course of the reaction. For

this reason serine proteases (e.g., chymotrypsin (Gaertner et al., 1991)) or thiol proteases (e.g., papain (Mitin et al., 1984; Wong et al., 1979)) have commonly been used in such conversions, the mechanism of which involves the intermediate production of an ester species. Since the use of endoproteases for N-terminal chain elongation would unavoidably lead to some adventitious degradation of the protein unless very specific "restriction proteases" are employed, we determined to exploit the regioselectivity of amino exopeptidases for recognition of the N-terminus. The exoproteolytic digestion of the protein could be circumvented by the proper choice of the peptidase and the experimental conditions.

In this context the amino dipeptidase Cathepsin C (dipeptidyl amino dipeptidase I, dipeptidyl transferase EC 3.4.14.1) (McDonald et al., 1969) was thought to be a very attractive candidate. As a lysosomal thiol protease this enzyme naturally removes dipeptide units sequentially from the N-terminus of peptides and proteins employing a thioester reactive intermediate. Due to its broad but nevertheless distinct specificity (Metrione and McGeorge, 1975; Mycek, 1970; McDonald et al., 1972), it was used for protein sequencing studies (Seifert and Caprioli, 1978).

Recently it has been reported that Cathepsin C can also act rarely as an endopeptidase (Kuribayashi et al., 1993), but clearly favors exoprotease activity. It is composed of eight subunits and has a molecular weight of 197 000 (Lynn and Labow, 1984). A cDNA for rat Cathepsin C has now been isolated and sequenced (Ishidoh et al., 1991). For full activity the enzyme requires halide ion (Gorter and Gruber, 1970) as well as sulfhydryl groups (Huang and Tappel, 1972). The latter dependence might interfere with the native tertiary structure of certain proteins. However, since Cathepsin C retains 67% of its activity with DTT concentrations as low as 0.02 mM (data not shown; this result is in accord to the findings of Huang and Tappel (1972)) and at most 25% of all proteins would be sensitive to thiol treatment (because they contain disulfide linkages), this could create only a minor limitation in applicability.

Cathepsin C is commercially available and well known for its transferase activity on dipeptide amides producing polymers in almost every case (Metrione and McGeorge, 1975; Mycek, 1970; McDonald et al., 1972). Although it is known that polymerization does not occur if Pro is the N-terminal amino acid of the dipeptide amide substrate

---

Scheme 1
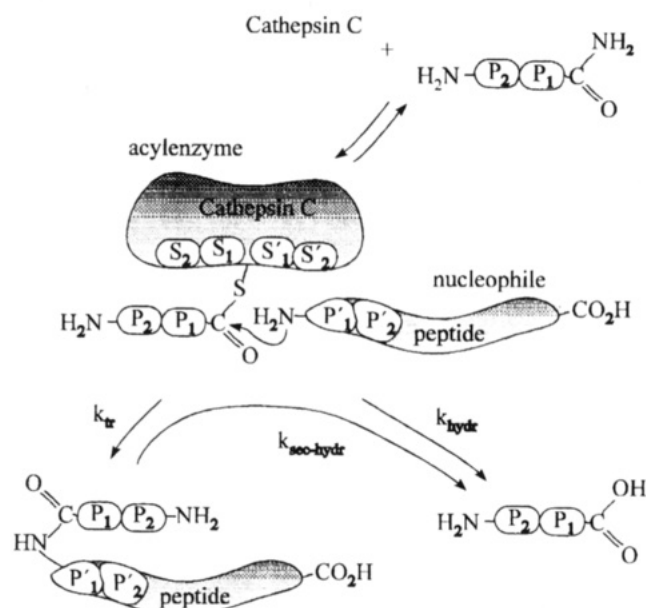
(Planta et al., 1964; Würz et al., 1962) and, therefore, leads to a defined product, this enzyme has very seldom been used as a tool for preparative protease catalyzed peptide synthesis (Johnes et al., 1952; Fruton et al., 1953; Fruton 1982).

Its subtle selectivity could well pave the way toward selective protein conjugation as depicted in Scheme 1. Here, we report on the experimental prerequisites for the use of Cathepsin C in the chain extension of unprotected amino acid derivatives and peptides in water.

MATERIALS AND METHODS

Cathepsin C from bovine spleen was obtained from Boehringer (Mannheim, Germany). The SDS−PAGE on 8−25% gel on a Phast system from Pharmacia (Laemmli, 1970) showed three bands of about 24, 14, and 12 kDa in accordance with the literature (Kuribayashi et al., 1993).

GlyPhepNA, GlyPhe-β-Na, GlyPheNH$_2$, ProPheNH$_2$, LeuPheNH$_2$, FmocLys(Boc)OH,[1] BocGlu(OtBu)OSu, Cys(Trt)NH$_2$, ZPro, MetNH$_2$, LeuNH$_2$, PheNH$_2$, TrpNH$_2$, LysNH$_2$, ArgNH$_2$, HisNH$_2$, ThrNH$_2$, GlyNH$_2$, and Asn-NH$_2$ were purchased from Bachem (Germany). GluNH$_2$ was prepared from BocGlu(OtBu)OSu and aqueous ammonia following the literature (Chen et al., 1989; Bodanszky and Williams, 1964), and CysNH$_2$ was freshly prepared by deprotection of Cys(Trt)NH$_2$ with TFA/triethylsilane as described elsewhere (Pearson et al., 1989). HBTU and FmocOSu were purchased from NOVA (Switzerland).

A Nucleosil 100-5 C 18 (250 × 4 mm i.d.) column for RP-HPLC analysis and a Toyopearl SP 650 S cation exchange resin for purification of crude peptides were used. DTT and ProPheOH were obtained from Sigma, and triethylsilane was obtained from Aldrich.

Assays. The commercial samples of Cathepsin C were checked with respect to the catalytic activity in the hydrolysis of dipeptide amides as well as in the synthesis

of hydroxamic acids from dipeptide amide starting materials (transferase activity). Though strongly favored at pH > 7, the transferase activity was always accompanied by some hydrolysis. As a quantitative measure characterizing transfer efficiency we determined the fraction of aminolysis, f_a, according to eq 1 (Mortensen

$$f_a = \frac{\text{transferase}}{\text{transferase} + \text{hydrolysis}} \quad (1)$$

et al., 1994) where "transferase" represents the molar concentration of the aminolysis product and "hydrolysis" represents the molar concentration of the hydrolysis product after 10 min of incubation. The values were obtained by peak area integration or by measurement of peak heights of the respective product peaks in HPLC chromatogramms under standard conditions.

Fluorometric Hydrolysis Assay. As described by McDonald et al. (McDonald et al., 1969), GlyPhe-β-naphthylamide was hydrolyzed (pH 6.0; 37 °C) and the fluorescence of the β-naphthylamine was recorded (E_x (313−366 Hg), E_m (>400). The Cathepsin C stock solution in glycerol contained 14 U/mL as determined by this assay.

Absorption Photometric Hydrolysis Assay. This procedure has been previously described in detail (Kuribayashi et al., 1993). Instead of mercaptoethanol we used DTT and assumed an extinction coefficient of 4-nitroaniline ($\epsilon_{405} = 10.4$ L mol^{-1} cm^{-1}). We found an activity of 17.6 U/mL.

Transferase Assay. GlyPheNH$_2$ was converted into the corresponding hydroxamic acid as described by Metrione et al. (Metrione et al., 1966) and analyzed photometrically at $\lambda = 510$ nm following conversion to the Fe(III) chelate. We obtained a specific activity of 36.4 U$_T$ (transferase units)/mL in the stock solution, consistent with the remark of Calam and Thomas (1972) who found that the transferase activity exceeded the hydrolytic activity by a factor of 3 under the conditions chosen.

Chemical Peptide Synthesis. The preparation of peptide substrates and authentic samples for comparison to the products of the enzymatic syntheses followed conventional solution phase procedures employing Fmoc (Fields and Noble, 1990; Anderson et al., 1964) or BOC protection (Jones, 1991) and HBTU (Dourtoglou and Gross, 1984) or PyBop (Hoeg-Jensen et al., 1991) coupling strategies. All peptides prepared in this way were extensively purified by ion-exchange and/or reversed phase HPLC and fully characterized by FAB-MS and ^{1}H- and ^{13}C-NMR and sometimes by amino acid sequencing.

Enzymatic Synthesis of Peptides. Unless otherwise specified all reactions were conducted at 23 °C in buffer containing 50 mM K$_2$HPO$_4$, 10 mM KCl, and 25 mM DTT. Reactions were started by addition of the enzyme (final concentration 0.36−0.72 U$_T$/mL) to the premixed and equilibrated substrates. Aliquots were withdrawn at various times and quenched by addition of TFA (pH < 1). The samples were analyzed by RP-HPLC using gradients of CH$_3$CN/0.1% TFA or CH$_3$OH/50 mM HCOOH/50 mM NaClO$_4$. The peptides were detected by absorbance at 254 nm and quantified by peak area integration or peak height.

The products were easily identified in the clean chromatograms as being the only respective increasing peaks besides those of the hydrolysis products by comparison to authentic samples and correlation to calculated t_R values (Guo et al., 1986a,b).

Preparative Example: Synthesis of ProTrpLys-LeuPheNH$_2$. To a solution (8 mL) of 20 mM ProTrpNH$_2$ and 7.9 mM LysLeuPheNH$_2$ in phosphate buffer pH 7.9

---

[1] Abbreviations: pNa, *p*- nitroanilide; β-Na, β-naphthylamide; Fmoc, fluorenylmethyloxycarbonyl; Boc, *tert*-butoxycarbonyl; tBu, *tert*-butyl; OSu, hydroxysuccinimidyl; Trt, triphenylmethyl; Z, benzyloxycarbonyl; HBTU, 2-(1*H*-benzotriazol-1-yl)-1,1,3,3-tetramethyluronium hexafluorophosphate; PyBOP, (benzotriazolyloxy)trispyrrolidinophosphonium hexafluorophosphate; TFA, trifluoracetic acid; DTT, dithiothreitol; HOHAHA, homonuclear Hartmann−Hahn technique.

containing 25 mM DTT, was added 2.9 U_T of Cathepsin C, and the mixture was incubated at 23 °C for 100 min. Finally, TFA was added until the pH reached <1 and the crude reaction mix was loaded onto a Toyopearl SP 650S cation exchange column. Elution with a gradient of ammonium formate (pH 6.5; 0.05−1.0 M) was monitored by HPLC and furnished the pentapeptide product. This was isolated by repeated lyophilization of the product-containing fractions to give 40.9 mg (83%) as the bisformate salt.

FAB-MS(glycerol): 689 $(M+H)^+$. ^{1}H-NMR (D_3COD intern = 3.35 ppm): δ in ppm = 7.65−7.03 (m, 10 H, indol- and phenyl-H's); 4.87−4.82 (t, 1H, Trp-α-CH); 4.63 (t, 1H, Phe-α-CH); 4.42, 4.34, 4.26 (3t, 3H, Lys-, Leu-, Pro-α-CH); 3.38−3.31 (m, MeOD, Pro-δ-CH_2 and 1/2 Trp-β-CH_2); 3.29−3.17 (m, 2H, 1/2 Phe- and 1/2Trp-β-CH_2); 3.05−2.99 (m, 1H, 1/2 Phe-β-CH_2); 2.86 (t, 2H, Lys-ε); 2.46−2.39 (m, 1H, 1/2 Pro-β-CH_2); 2.10−1.98 (m, 3H, 1/2 Pro-β-CH_2 and Pro-γ-CH_2); 1.85−1.76 (m, 1H, 1/2 Lys-β-CH_2); 1.75−1.30 (m, 8 H, Lys-δ-CH_2 + 1/2 Lys-β-CH_2, Leu-γ-CH, Leu-CH_2, Lys-γ-CH_2); 0.88−0.82 (dd, 6H, Leu-CH_3's). ^{13}C-NMR (D_3COD intern = 49.30 ppm): δ in ppm = 176.0 (carbonyl-C from KLF); 174.6 (carbonyl-C from KLF); 174.0 (carbonyl-C from PW); 173.9 (carbonyl-C from PW); 170.1 (Phe-carbonyl-C); 138.7 (phenyl-C1); 138.36 (indol-C3); 130.8, 129.7 (phenyl-o- and m-CH's); 128.1 (phenyl-p-CH); 125.0, 122.8, 120.2, 119.6, 112.7, 110.9 (indol-C's and CH_2's); 61.2 (Pro-α-CH); 56.4 (Phe-α-CH); 55.9 (Trp-α-CH); 54.7 (Lys-α-CH); 54.0 (Leu-α-CH); 47.8 (Pro-δ-CH_2); 42.0 (Leu-β-CH_2); 40.8 (Lys-ε-CH_2); 39.2 (Phe-β-CH_2); 32.7 (Lys-β-CH_2); 31.3 (Pro-β-CH_2); 29.1 (Trp-β-CH_2); 28.3 (Lys-δ-CH_2); 26.0 (Leu-γ-CH); 25.3 (Pro-γ-CH_2); 23.8 (Lys-γ-CH_2); 23.6, 22.3 (Leu-CH_3's).

Edman degradation using a pulse liquid protein sequencer 471 (Applied Biosystems) found the regular sequence Pro Trp Lys Leu Phe.

The identification of a cross peak in a ^{1}H-HOHAHA 2D-NMR in H_2O between the amide signal at 7.97 ppm and the lysine α-H at 4.02 ppm confirmed the presence of a conventional α-peptide bond rather than an isopeptide linking lysine to its N-terminal neighbor.

N-Terminal Elongation of Myosine Light Chain Kinase Inhibitor by Pro(pI-Phe)-NH₂.

A solution of 1.04 mM myosine light chain kinase inhibitor and 21.7 mM Pro-(pI-Phe)-NH₂ in aqueous potassium phosphate buffer 53 mM containing 21 mM KCl and 24 mM DTT was incubated at 24 °C at pH 7.9 including 0.29 U_T Cathepsin C per mL. Aliquots were withdrawn at different times, and the reaction was stopped by adding an equal volume of 5% TFA in CH_3CN which led to total solubilization of precipitated product. The samples were analyzed by RP-HPLC monitoring UV-absorption at 254 nm (data not shown) and fluorescence for Trp (Ex 280 nm, Em 350 nm). The main product was isolated and analyzed by Edman-degradation, by which the sequence was found to be P_KRRWKKNFIAV. FAB-MS yielded the molecular parent ion at m/z 1816 (intensity 12%).

RESULTS AND DISCUSSION

Kinetically controlled protease catalyzed formation of peptides holds the general virtues that it can be conducted with unprotected substrates in aqueous solution and may give high yields (>80%) of coupling products, if a number of requirements can be met. Scheme 1 illustrates the basic events with Cathepsin C as the catalyst, adopting the conventions of Schechter and Berger (1967) to designate the specificity sites in the substrate and the enzyme. In the initial step a dipeptide


mM
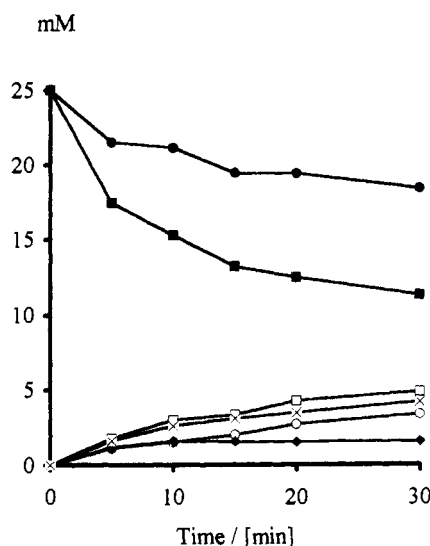
Figure 1. Time course of the transpeptidation between Pro-PheNH₂ (●) and GlyPheNH₂ (■) (25 mM each, phosphate buffer pH 7.7, 23 °C, 0.36 U_T of Cathepsin C). The concentrations of starting materials and products (GlyPheOH □, ProPheOH ○, GlyPheGlyPheNH₂ ◆, ProPheGlyPheNH₂ ×) were obtained from HPLC analysis assuming identical extinction coefficients for the hydrolysis products with regard to the parent amides. The coupling products were taken to have an ε-value twice as big as that of GlyPheNH₂.

derivative with a free α-amino group is bound to the active site of the thiol protease. This triggers an attack by the active site thiol on the carboxy end to give a thioester intermediate. The acylated enzyme may regain its nucleophilic thiol group by either of two pathways: the thioester can be cleaved by water to give the free acid (k_{hydr}) or, alternatively, a second peptide or other nucleophile (e.g., H_2NOH) may attack the intermediate resulting in the coupling of these components by a newly formed amide bond (k_{tr}). This step is reversible, so that the initially formed product will be cleaved again eventually on prolonged incubation. As is well known (Kasche, 1989; Schellenberger and Jakubke, 1991; Jakubke 1991, 1992), the ratio of the different pathways depends on experimental conditions (pH, etc.) and on the specificity pattern of the catalyst, which can be condensed into an aminolysis fraction (eq 1) characterizing the efficiency of peptide bond formation for a particular set of substrates. Transpeptidation by Cathepsin C according to this scheme has been recognized early on (Johnes et al., 1952; Fruton et al., 1953), but probably due to the wealth of competitive reactions accompanying the desired one (e.g., coupling of the acyl donor or nucleophile with itself, inverted sequence coupling, degradation of the nucleophile, etc.) has been very rarely used for peptide synthesis (Mycek, 1970; Planta et al., 1964; Würz et al., 1962). In order to exploit the potential of Cathepsin C for directed high yield preparations of unprotected peptides we incorporated some specificity restrictions already known from the literature (Metrione and McGeorge, 1975; Mycek, 1970; McDonald et al., 1972). For instance, the oligomerization of dipeptides bearing proline in the N-terminal position had been found to be extremely slow (Mycek, 1970; Planta et al., 1964; Würz et al., 1962) indicating the low nucleophilicity of the sec amino group of proline in the catalyzed process. This can also be a consequence of nonproductive or even a complete lack of complexation of the proline moiety at the S_1' subsite, since it is well established that Cathepsin C will not cleave peptides containing proline on either side of the putatively scissile bond (Metrione and McGeorge, 1975;
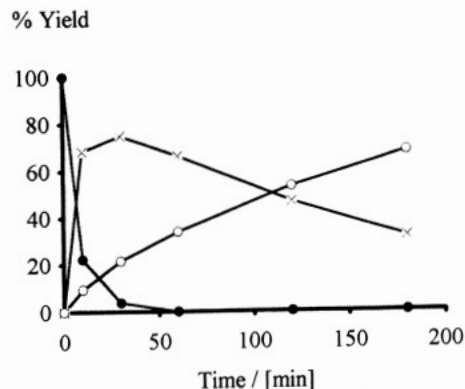
f$_a$
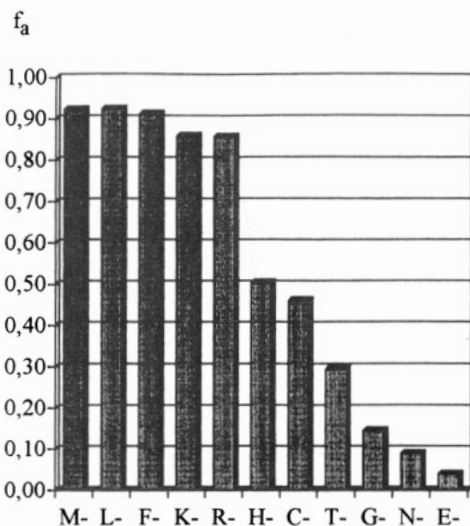
Figure 2. Dependence of the aminolysis fraction f_a (eq 1) on nucleophile type. The reaction of ProTrpNH$_2$ with a series of amino acid amides (10 mM each, 0.44 U$_T$ of Cathepsin C /mL, 23 °C) was quenched after 10 min, and the product distribution was analyzed by HPLC.
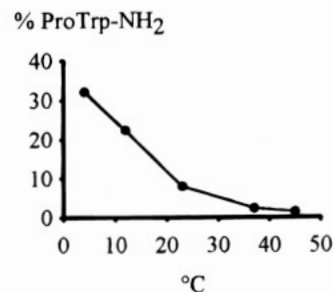
f$_a$
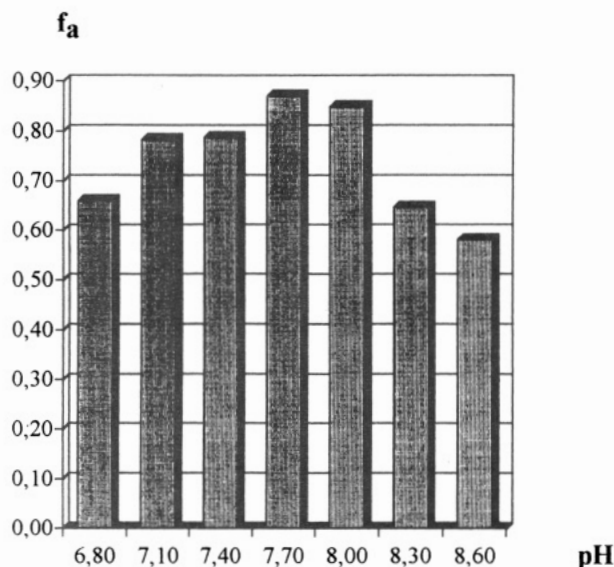
Figure 3. Dependence of the aminolysis fraction f_a (eq 1) on pH. The reaction of ProPheNH$_2$ (25 mM) and TrpNH$_2$ (12.5 mM) catalyzed by 0.72 U$_T$ of Cathepsin C /mL at 23 °C was studied in phosphate buffer.

% Yield

Figure 4. Time course of kinetically controlled reverse proteolysis of ProTrpLysNH$_2$ (×) from ProTrpNH$_2$ (●, 9.3 mM) and LysNH$_2$ (10 mM) catalyzed by 0.72 U$_T$/mL of Cathepsin C at 12 °C, pH 7.8, as analyzed by HPLC (ProTrpOH, ○).

% ProTrp-NH$_2$

Figure 5. Temperature dependence of reverse proteolysis by Cathepsin C (0.72 U$_T$/mL) at pH 7.8. The amount of ProTrpNH$_2$ starting material remaining after 10 min incubation with LysNH$_2$ (10 mM) is plotted versus the temperature.
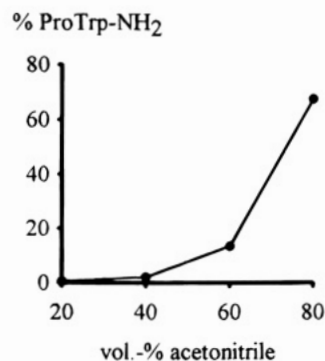
% ProTrp-NH$_2$

Figure 6. Dependence of reverse proteolysis by Cathepsin C (0.72 U$_T$/mL) on solvent composition. The amount of ProTrpNH$_2$ (●, 9.3 mM) remaining after 10 min incubation with LysNH$_2$ (10 mM) at pH 6.8 (aqueous solution) was analyzed by HPLC.

McDonald et al., 1969). As a corollary in solutions containing mixtures of a prolyl dipeptide amide and some other peptide nucleophile the former substrate can act as an acyl donor only. The initial time course of a prototypical reaction of this type is shown in Figure 1.

One observes the decrease in the concentrations of the starting dipeptide amides with GlyPheNH$_2$ disappearing about three times as fast as the prolyl dipeptide. Since the former substrate may serve as the acyl donor as well as the nucleophile, this difference is readily comprehensible. The resulting GFGFNH$_2$ tetrapeptide product, however, does not increase in concentration, because it is transformed into the hexapeptide and finally into the octapeptide, which precipitates from the solution. In addition to the expected occurrence of the dipeptide acids only one more peak accumulated which was identified as the ProPheGlyPheNH$_2$ tetrapeptide. The corresponding acid resulting from nucleophilic attack of GlyPheOH that is formed in the course of the reaction on the ProPheNH$_2$ donor could not be found. This is in agree-

ment to the results of Planta et al. (1964) and Würz et al. (1962) who characterized the acids as being much more inferior nucleophiles than their respective amides. After 30 min the reaction became very sluggish owing to coprecipitation of Cathepsin C with the peptide oligomers. Addition of fresh enzyme solution reanimated the reaction and caused further precipitation of oligomers.

In order to elucidate inherent nucleophilicities of coupling partners the aminolysis fraction of the coupling of 11 amino acid amides representing the different subgroups of side chain functions with ProTrpNH$_2$ as the acyl donor were determined (Figure 2). Figure 2 clearly demonstrates the preference of hydrophobic and positively charged amino acid nucleophiles as opposed to their hydrophilic or negatively charged counterparts in tripeptide synthesis. Since the acyl donor does not contain permanent charges it seems likely that attraction to some negative charge in the S$_1$′ enzymic site of Cathepsin C
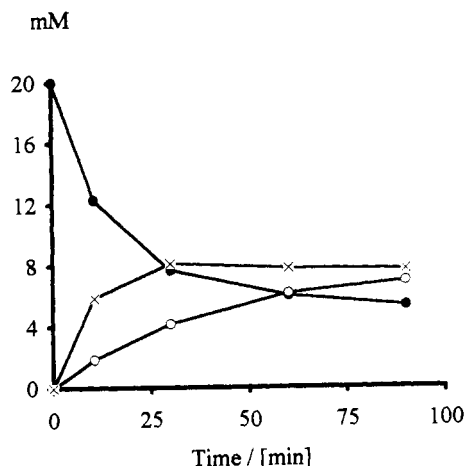
Figure 7. Time course of a preparative synthesis of the pentapeptide ProTrpLysLeuPheNH$_2$ (×) by reverse proteolysis from 20 mM ProTrpNH$_2$ (●) and 7.9 mM LysLeuPheNH$_2$ catalyzed by 0.32 U$_T$ of Cathepsin C/mL; ProTrpOH (○).

or a hydrogen bond acceptor immersed in a hydrophobic pocket causes this selectivity feature.

The ratio of hydrolysis of the acyl donor versus transfer to a nucleophile can be influenced by judicious choice of the pH conditions. More acidic values favor hydrolysis suggesting that basic pH values should be employed in order to avoid premature peptolytic degradation, if long chain peptides or proteins were used as nucleophiles. Figure 3 refers to the dependence of the aminolysis to hydrolysis fraction (f_a, eq 1) on pH taking TrpNH$_2$ as the nucleophile attacking ProPheNH$_2$ as the acyl donor. There is a distinct maximum f_a at pH 7.7 descending sharply toward higher pH values and much less pronounced toward more acidic conditions. The entire

profile, however, is rather shallow, spanning in the range from 6.8 to 8.6, but resembles that obtained when using hydroxylamine.

Surprisingly, temperature does not affect the maximum yields of coupling products in the range of 4–45 °C which points to very similar activation energies for the hydrolysis and acyl transfer processes. As can be seen from the time course of the reaction between ProTrpNH$_2$ acyl donor and LysNH$_2$ nucleophile as an example (Figure 4) the product yield reached a broad maximum (~75%) before secondary hydrolysis diminished the yield again. This typical picture, also found in other kinetically controlled reverse proteolyses (Kasche, 1989; Schellenberger and Jakubke, 1991; Jakubke 1991, 1992), underlines the importance of analytically following the reaction course in order to obtain maximum yields. Contrary to the yield the enzymic activity drastically decreased with temperature. Figure 5 gives the amount of dipeptide starting material remaining after 10 min of incubation at the temperature specified. Prolonged incubation led to complete cleavage of the tripeptide primarily formed only if the temperature was set below 23 °C. At higher temperatures the hydrolytic activity of Cathepsin C faded, so that 31% (at 37 °C) or 35% (at 45 °C) of tripeptide product remained untouched.

Many peptides exhibit higher solubility in mixed solvent systems than in the pure parent solvents alone. For this reason and because a reduction of water activity was deemed favorable for peptide coupling we tried to replace water by increasing amounts of acetonitrile. Varying the fraction of organic solvent between 0 and 80% vol we observed only a negligible influence on product yield (about 60%, pH of the aqueous buffer 6.8 before mixing) in the same reaction as used in the temperature studies. The enzymic activity appeared
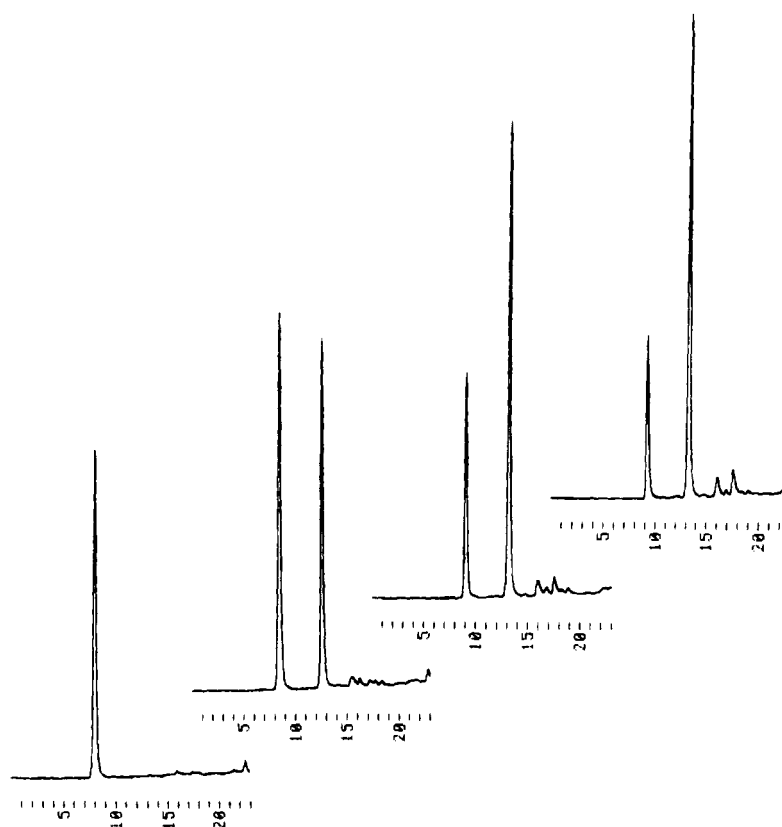
Figure 8. Trp-fluorescence monitored coupling (0.29 U$_T$ of Cathepsin C/mL) of P(p-iodo-F)-NH$_2$ (21.7 mM) with KRRWKKNFIAV-NH$_2$ (1.04 mM) at pH 7.9 and 24 °C. Samples were analyzed at 0, 10, 30, and 60 min (ascending row of chromatograms) on a Nucleosil 5C18 column using a gradient of 5%–35% (CH$_3$CN/H$_2$O with 1% TFA) in 20 min.

almost unaffected by acetonitrile concentrations up to 40% vol, but decreased dramatically in the range of 60—80% vol CH_3CN (Figure 6). Nevertheless, the progress of the reaction remained clean with no indication of product or catalyst precipitation.

To test this variant of reverse proteolysis on a preparative scale and to demonstrate the regioselectivity of Cathepsin C-catalyzed peptide formation the synthesis of a pentapeptide from a $ProTrpNH_2$ acyl donor and a tripeptide having Lys at the N-terminal position was undertaken. Though peptides with positively charged side chains at the amino terminus are only slowly digested by Cathepsin C, it was decided to apply the acyl donor in more than 100 mol % excess in order to tie up the enzyme at all times as the respective Michaelis complex (the K_M values for a number of different dipeptide amides are in the millimolar range (Huang and Tappel, 1972)). Figure 7 illustrates the time course of this preparative coupling. The maximum yield was reached after 30 min, but the reaction only finished after 100 min. Conventional treatment and purification by cation exchange gave 83% pure pentapeptide. The characterization including Edman degradation and ^{1}H-HOHAHA 2D-NMR spectra unambiguously confirmed that the newly formed connection assembled a regular α-peptide bond rather than an isopeptide involving the ε-amino function of lysine.

The value of this method to incorporate non-natural amino acids at the N-termini of medium sized peptides was shown by the attachment of an iodophenylalanine residue via the corresponding dipeptide with proline to myosine-light-chain-kinase-inhibitor. This undecapeptide in addition to a fluorophoric tryptophane (suitable for sensitive derivative detection) contains a number of side chain nucleophiles which might in principle interfere with N-terminal acylation. The preparation of specifically iodinated peptide/protein derivatives may be highly welcome for introduction of radiolabels or heavy atom analogs for X-ray examination.

As can be seen from Figure 8 myosine-light-chain-kinase-inhibitor can be transformed by Pro(p-iodo-Phe)NH_2 and Cathepsin C in aqueous buffer to a novel peptide with higher retention on a standard HPLC column. Though we cannot rigorously exclude at present the formation of multiply acylated peptides, the profoundly dominating product (>76% by peak integration) is the expected trideca peptide P(p-iodo-F)KRRWKKN-FIAV-NH_2, the structure of which was unambiguously confirmed by Edman degradation and FAB-MS after HPLC isolation.

Thus, we have demonstrated that Cathepsin C can be used with advantage for the directed N-terminal chain extension of certain unprotected peptides and amino acids in water. The substrate and regioselectivity of this kinetically controlled reverse proteolysis opens the perspective for a simple and quick route to introduce nonproteinogenic structural elements in a unique and predetermined fashion into some peptides by virtue of the well known and quite broad substrate specificity of the S_1-subsite of Cathepsin C.

ACKNOWLEDGMENT

LITERATURE CITED

Anderson, G. W., et al. (1964) The Use of Esters of N-Hydroxysuccinimide in Peptide Synthesis. *J. Am. Chem. Soc. 86*, 1839—1842.

Bodanszky, N. J., and Williams, N. J. (1964) Synthesis of Secretin. I. The protected Tetradecapeptide Corresponding to Sequence 14—27. *J. Am. Chem. Soc. 89*, 685—689.

Breddam, K., Widmer, F., and Johannsen, J. T. (1981) Carboxypeptidase Y catalyzed C-terminal Modifications of Peptides. *Carlsberg Res. Commun. 46*, 121—128.

Calam, D. H., and Thomas, H. J. (1972) Water-insoluble enzymes for peptide sequencing: Dipeptidyl aminopeptidase I (cathepsin C), an enzyme with subunit structure. *Biochim. Biophys. Acta 276*, 328—332.

Chen, T.-S., Wu, S.-H., and Wang, K. T. (1989) A Simple Method for Amide Formation from Protected Amino Acids and Peptides. *Synthesis* 37—38.

Dourtoglou,V., and Gross, B. (1984) O-Benzotriazolyl-N,N,N',N'-tetramethyluronium Hexafluorophosphate as Coupling Reagent for the Synthesis of Peptides of Biological Interest. *Synthesis* 572—574.

Fields, G. B., and Noble, R. L. (1990) Solid Phase Peptide Synthesis Utilizing 9—fluorenylmethoxycarbonyl Amino Acids. *Int. J. Peptide Protein Res. 35*, 161—214.

Fruton, J. S. (1982) Proteinase-Catalyzed Synthesis of Peptide Bonds. *Adv Enzymol. Rel. Areas Biol. 53*, 239—306.

Fruton, J. S., Hearn, W. R., Ingram, V. M., Wiggans, D. S., and Winitz, M. (1953) Synthesis of polymeric peptides in protease-catalyzed transamidation reactions. *J. Biol. Chem. 204*, 891.

Gaertner, H., Watanabe, T., Sinisterra, J. V., and Puigserver, A. J. (1991) Peptide Synthesis Catalyzed by Modified α-Chymotrypsin in Low-Water Organic Media. *J. Org. Chem. 56*, 3149—3153.

Gaertner, H. F., Rose, K., Cotton, R., Timms, D., Camble, R., and Offord, R. E. (1992) Construction of Protein Analogues by Site-Specific Condensation of Unprotected Fragments. *Bioconjugate Chem. 3*, 262—268.

Geoghegan, K. F., and Stroh, J. G. (1992) Site-Directed Conjugation of Nonpeptide Groups to Peptides and Proteins via Periodate Oxidation of a 2-Amino Alcohol. Application to Modification at N-terminal Serine. *Bioconjugate Chem. 3*, 138—146.

Gorter, J., and Gruber, M. (1970) Cathepsin C: an Allosteric Enzyme. *Biochim. Biophys. Acta 198*, 546—555.

Guo, D., Mant, C. T., Taneja, A. K., and Hodges, R. S. (1986a) Prediction of Peptide Retention Times in Reversed-Phase High-Performance Liquid Chromatography. II. Correlation of Observed and Predicted Peptide Retention Times and Factors Influencing the Retention Times of Peptides. *J. Chromatogr. 359*, 519—532.

Guo, D., Mant, C. T., Taneja, A. K., Hodges, R. S., and Parker, J. M. (1986b) Prediction of Peptide Retention Times in Reversed-Phase High-Performance Liquid Chromatography. I. Determination of Retention Coefficients of Amino Acid Residues of Model Synthetic Peptides. *J. Chromatogr. 359*, 499—517.

Hoeg-Jensen, T., Jacobson, M. H., and Holm, A. (1991) A New Method for Rapid Solution Peptide Synthesis of Shorter Peptides by use of PyBOP. *Tetrahedron Lett. 32*, 6387—6390.

Huang, F. L. , and Tappel, A. L. (1972) Properties of Cathepsin C from Rat Liver. *Biochim. Biophys. Acta 268*, 527—538.

Ishidoh, K., Muno, D., Sato, N., and Kominami, E. (1991) Molecular Cloning of cDNA for Rat Cathepsin C. *J. Biol. Chem. 266*, 16312—16317.

Jakubke, H.-D. (1991) Enzymochemische Peptidsynthese. *Kontakte (Darmstadt)* 60—72; (1992) 46—60.

Jay, D. G. (1984) A General Procedure for the End Labeling of Proteins and Positioning of Amino Acids in the Sequence. *J. Biol. Chem. 259*,15572—15578.

Johnes, M. I., Hearn, W. R, Fried, M., and Fruton, J. S. (1952) Transamidation Reactions Catalyzed by Cathepsin C. *J. Biol. Chem. 195*, 645—656.

Jones, J. (1991) *The Chemical Synthesis of Peptides*, Clarendon Press, Oxford.

Jue, R. A., and Doolittle, R. F. (1985) Determination of the Relative Position of Amino Acids by Partial Specific Cleavages of End-Labeled Proteins. *Biochemistry 24*, 162—170.

Kasche, V. (1989) *Proteases in Peptide Synthesis* in: *Proteases a Practical Approach* (R. Beynon, Ed.) pp 125−143, IRL Press, McLean, VA.

Könnecke, A., Schönfels, C., Hänsler, M., and Jakubke, H.-D. (1990) Direct Conversion of Porcine Insulin into Human Insulin Ester Catalyzed by Immobilized Trypsin. *Tetrahedron Lett. 31,* 989−990.

Kuribayashi, M., Yamada, H., Ohmori, T., Yanai, M., and Imoto, T. (1993) Endopeptidase Activity of Cathepsin C, Dipeptidyl Aminopeptidase I, from Bovine Spleen. *J. Biochem. 113,* 441−449.

Laemmli, U. K. (1970) *Nature 227,* 680−685. Phastsystem, Separation technique file no. 110, "SDS Page"; Pharmacia; Development technique file no. 210, "Sensitive silver stain".

Lynn, K. R., and Labow, R. S. (1984) A Comparison of Four Sulfhydryl Cathepsins (B, C, H and L) from Porcine Spleen. *Can. J. Biochem. Cell Biol. 62,* 1301−1308.

Markussen, J., Diers, J., Hougard, P., Langjaer, L., Norris, K., Snel, L., Soerensen, A. R., Soerensen, E., Voigt, H. O. (1988) Soluble, prolonged-acting insulin derivatives.II. Degree of protraction, crystallizability and chemical stability of insulins substituted in positions A21, B13, B23, B27 and B30. *Protein Engineering. 2,* 157−166.

McDonald, J. K., Zeitman, B. B., Reilly, T. J., and Ellis, S. (1969) New Observations on the Substructure Specificity of Cathepsin C (Dipeptidyl Aminopeptidase I). *J. Biol. Chem. 244,* 2693−2709.

McDonald, J. K., Callahan, P. X., and Ellis, S. (1972) Preparation and Specificity of Dipeptidyl Aminopeptidase I. *Methods Enzymol. 25,* 272−281.

Metrione, R. M., and MacGeorge, N. L. (1975) The Mechanism of Action of Dipeptidyl Aminopeptidase. Inhibition by Amino Acid Derivatives and Amines; Activation by Aromatic Compounds. *Biochemistry 14,* 5249−5252.

Metrione, R. M., Neves, A. G., and Fruton, J. S. (1966) Purification and Properties of Dipeptidyl Transferase (Cathepsin C). *Biochemistry 5,* 1597−1604.

Mitin, Y. V., Zapevalova, N. P., and Gorbunova, E. Y. (1984) Peptide synthesis catalyzed by papain at alkaline pH values. *Int. J. Peptide Prot. Res. 23,* 528−534.

Morihara, K., Oka, T., and Tsuzuki, H. (1979) Semi-synthesis of human insulin by trypsin catalyzed replacement of Ala-B30 by Thr in porcine insuline. *Nature 280,* 412−413.

Mortensen,U. H., Stennicke, H. R., Raaschou-Nielsen, M., Breddam,K. (1994) Mechanistic Study on Carboxypeptidase Y-Catalyzed Transacylation Reactions. Mutationally Altered Enzymes for Peptide Synthesis. *J. Am. Chem. Soc. 116,* 34−41.

Mycek, M. J. (1970) Cathepsin C. *Methods Enzymol. 19,* 285−309.

Pearson, D. A., Blanchette, M., Baker, M. L., and Guidon, C. A. (1989) Trialkylsilanes as Scavengers for the Trifluoracetic Acid Deblocking of Protecting Groups in Peptide Synthesis. *Tetrahedron Lett. 30,* 2739−2742.

Planta, R. J, Gorter, J., and Gruber, M. (1964) The Catalytic Properties of Cathepsin C. *Biochim. Biophys. Acta 89,* 511−519.

Schechter, I., and Berger, A. (1967) On the Size of the Active Site in Proteases. I. Papain. *Biochem. Biophys. Res. Commun. 27,* 157−167.

Schellenberger,V., and Jakubke, H.-D. (1991) Proteasekatalysierte kinetisch kontrollierte Peptidsynthese. *Angew. Chem. 103,* 1440−1452.

Schmitter, J.-M., Berne, P. F., and Blanquet, S. (1992) Carboxypeptidase Y-Catalyzed Transpeptidation of Esterified Oligo- and Polypeptides and its Use for the Specific Carboxy-Terminal Labeling of Proteins *J. Am. Chem. Soc. 114,* 2603−2610.

Seifert, E., and Caprioli, R. M. (1978) Hydrolysis of Proteins Using Dipeptidyl Aminopeptidases: Analysis of the N-Terminal Portion of Spinach Plastocyanin. *Biochemistry 17,* 436−441.

Vilaseca, L. A., Rose, K., Werlen, R., Meunier, A., Offord, R. E., Nichols, C. L., and Scott, W. L. (1993) Protein Conjugates of Defined Structure: Synthesis and Use of a New Carrier Molecule. *Bioconjugate Chem. 4,* 515−520.

Wong, C., Chen, S., and Wang, K., (1979) Enzymic Synthesis of Opoid Peptides. *Biochem. Biophys. Acta 576,* 247−249.

Würz, H., Tanaka, A., and Fruton, J. S. (1962) Polymerization of Dipeptide Amides by Cathepsin C. *Biochemistry 1,* 19−29.

Fluorinated *o*-Aminophenol Derivatives for Measurement of Intracellular pH

Chung K. Rhee, Louis A. Levy, and Robert E. London*

Laboratory of Molecular Biophysics, National Institute of Environmental Health Sciences, Box 12233, Research Triangle Park, North Carolina 27709. Received September 1, 1994[⊗]

The simple 2-aminophenol group which serves as a building block for many cationic indicators has been modified to yield a series of pH sensitive probes. This approach is based on the replacement of one of the *N*-acetate groups of the chelator APTRA (*o*-aminophenol *N,N,O*-triacetate) by an *N*-ethyl group. The resulting series of (*N*-ethylamino)phenol (NEAP) compounds exhibit pK values in the physiological range and negligible affinity for physiological levels of other ions. Three fluorinated analogs have been prepared: *N*-ethyl-5-fluoro-2-aminophenol *N,O*-diacetate (5F NEAP), *N*-ethyl-2-((2-fluoro-4-carboxybenzyl)oxy)-4-fluoroaniline-*N*-acetic acid (5F NEAP-2), and 1-(2-(*N*-ethylamino)-5-fluorophenoxy)-2-(2-fluoro-4-aminophenoxy)ethane-*N,N′,N′*-triacetic acid (5F NEAP-3). These derivatives exhibit total titration shifts of ∼11 ppm. NEAP-2 and NEAP-3 contain an additional fluorine to serve as an internal chemical shift reference, and NEAP-3, the most highly charged analog prepared, was designed in order to minimize leakage.

Since the pH of biological systems is an important regulator of many physiological processes considerable effort has been expended on the development of methods for its measurement (*1–3*). Intracellular pH has been determined using a variety of physical techniques, including direct measurement with microelectrodes, a variety of spectrophotometry methods, fluorescence techniques, and nuclear magnetic resonance. An important advantage of the NMR method has been the ability to carry out determinations based on the observation of endogenous phosphorylated molecules whose chemical shift is pH dependent (*1, 3–5*). This approach tends to be limited by several factors including the low concentration of inorganic phosphate, the most useful pH indicator, in many cells. Interference from extracellular phosphate if present in blood, buffers, or perfusates, as well as the overlap of the phosphate resonance with the resonances from various phosphomonoesters, can also limit the accuracy of the measurement. Finally, the absence in some cell types of a suitable metabolite to serve as a chemical shift reference also serves to limit this technique. Consequently, a number of groups have proposed and developed exogenous NMR probes of intracellular pH (*6–15*). Such probes can in principle be optimized for pH measurement by consideration of a number of criteria, including: (1) resonances should exhibit a large $\Delta\delta/\Delta$pH and a pK close to the physiological mean; (2) detection sensitivity should be high; (3) it is desirable to utilize indicators which can be loaded into cells and which will not readily leak out once they are loaded; (4) there should be minimal overlap between the resonances of the indicator and those of other endogenous metabolites; (5) if the chemical shift is the parameter of interest, the indicator should ideally contain an internal reference so that no additional referencing is required. On the basis of the above considerations, the use of fluorinated indicators is particularly attractive since criteria (2) and (4) are completely satisfied, and due to the high chemical shift sensitivity of ^{19}F, the first criterion will be fulfilled as well if the indicator is appropriately designed.

Several groups have developed fluorinated pH indicators (*9–15*). Fquene, a fluorinated analog of the fluorescent indicator quene 1, contains a fluoroquinoline

moiety and exhibits a total shift of ∼4.5 ppm (*13*). This indicator can be loaded into cells as the tetraacetoxymethyl ester (*13, 14*), and the high charge resulting after intracellular hydrolysis minimizes leakage from the cell. However, the Mg^{2+} affinity of quene 1 is relatively high (*16*), and we have found that very similar quinoline compounds have a relatively high affinity for Mg^{2+} ions. Deutsch and co-workers have evaluated a variety of fluorinated compounds to measure intracellular pH (*9–12*). The amino acid α-(difluoromethyl)alanine has a pK of 7.3 and two nonequivalent fluorine nuclei such that the chemical shift difference between the resonances can be used to determine pH without the need for an additional chemical shift standard (*10*). However, the shift is relatively small, and the compound leaks out of cells on a fairly short time scale. A series of fluorinated aniline derivatives were also evaluated as potential intracellular pH indicators (*12*). These compounds show large pH dependent shifts, in some cases sufficient to lead to slow exchange on the chemical shift time scale. However, the molecules considered had only a single carboxyl group, so that leakage is again a potential problem, and there was no additional fluorine to provide a reference shift (*12*).
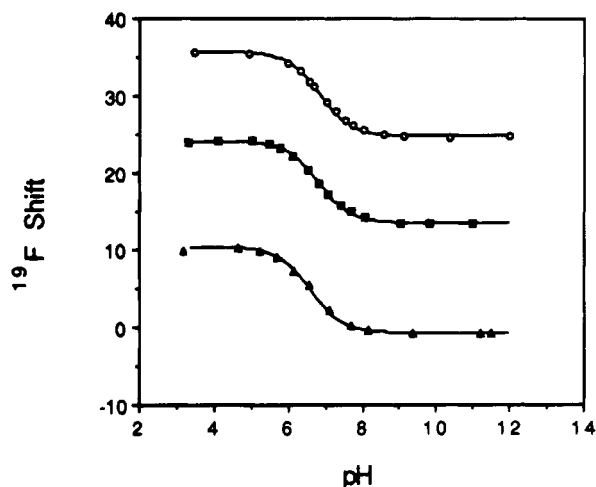
RESULTS AND DISCUSSION

Our experience with metallospecific chelators containing a fluorinated aniline unit in which the chemical shift of the para fluorine is sensitive to changes in the electronic environment of the amino group suggested the possibility of developing a useful pH sensitive indicator based on this structure. Chelators such as nF-BAPTA (*17*) and nF-APTRA (*18*) used as calcium or magnesium specific indicators and based on an aniline structure are designed to be pH insensitive in the biologically important range near 7 and, thus, have a pK of about 5.5 (for the 5F derivatives) or 4.0 (for the 4F derivatives). It was anticipated that the metal binding and pH sensitivities of these compounds could be readily altered by replacing one of the *N*-carboxymethyl groups with an alkyl group. This approach exchanges one of the chelating carboxyl functions for an electron-donating group to increase the pK of the amino group. A simple example of this strategy, *N*-ethyl-2-amino-5-fluorophenol-*N,O*-diacetic acid, 5F NEAP-1, was prepared as shown in Scheme 1. Monoethylation of 2-(benzyloxy)-4-fluoroaniline was most

---

Scheme 1[a]
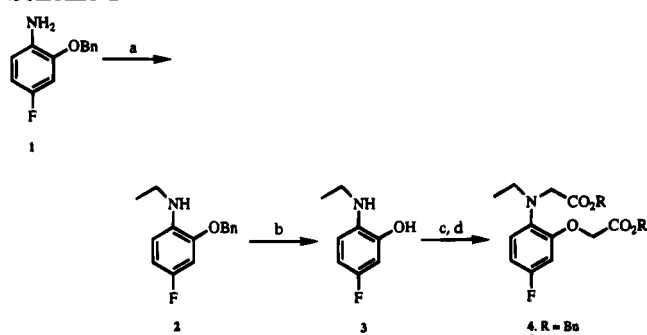
[a] Reagents: (a) NaBH$_4$/CH$_3$CO$_2$H; (b) H$_2$, Pd/C, EtOAc; (c) BrCH$_2$CO$_2$Bn, Proton Sponge, CH$_3$CN; (d) H$_2$, Pd/C, EtOAc.

Scheme 2[a]

[a] Reagents: (a) K$_2$CO$_3$, DMF; (b) H$_2$, Pd/C, EtOAc; (c) NaBH$_4$/CH$_3$CO$_2$H; (d) BrCH$_2$CO$_2$Me, Proton Sponge, CH$_3$CN; (e) NaOH, EtOH/H$_2$O.

Figure 1. Fluorine-19 shifts as a function of pH for 5F NEAP-1 (○), 5F NEAP-2 (▲), and 5F NEAP-2 (■). The shift for 5F NEAP-1 is referenced to the tetrafluorophthalate ^{19}F resonance, while the data for 5F NEAP-2 and 5F NEAP-3 correspond to the shift differences between the two fluorine resonances. The theoretical curves correspond to $\delta 1 = 35.6$ ppm, $\delta 2 = 24.7$ ppm, pK = 6.85 for 5F NEAP-1, $\delta 1 = 10.3$ ppm, $\delta 2 = -0.8$ ppm, pK = 6.6 for 5F NEAP-2, and $\delta 1 = 24.1$, $\delta 2 = 13.4$, pK = 6.8 for 5F NEAP-3. As is apparent from the data, the two ^{19}F resonances of NEAP-2 cross at lower pH, and the resonance corresponding to the fluorine on the benzoate ring shows a small additional shift perturbation at low pH due to titration of the benzoic acid.

easily effected using the alkylation reagent NaBH$_4$/CH$_3$-CO$_2$H (*19*). The removal of the benzyl protecting group and alkylation of both the amino and phenolic hydroxyl moieties yielded the benzyl ester of 5F NEAP-1 (*N*-ethyl-2-amino-5-fluorophenol *N*,*O*-diacetic acid). Hydrogenolysis of the benzyl esters then yielded the desired acid form of the indicator. Titration of the acid **5** (Figure 1), as followed by the shift of the ^{19}F resonance (tetrafluoroterphthalic acid as standard), showed our conception to be sound, yielding a pK of 6.8 and with a large, 11 ppm chemical shift.

As noted above, it is desirable that indicators for which the chemical shift serves as the parameter of interest contain an additional fluorine nucleus to serve as a chemical shift standard. In addition to the obvious advantage of convenience, this ensures that the shift reference will be in the same region of the magnetic field, so that local field variations will not affect the pH determination. Further, it is now clear that the intracellular environment can significantly perturb the shift of fluorinated compounds (*20*). We thus prepared compound **11**, 5F NEAP-2 (Scheme 2), which incorporated an additional fluorine subsitituent designed to serve as an internal reference; *i.e*, it is insensitive or nearly so to
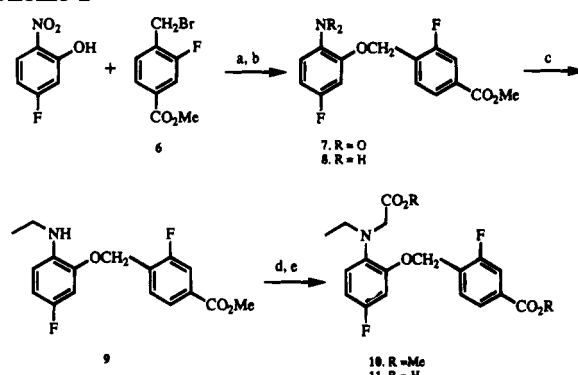
changes in pH. The synthesis of **11** (Scheme 2) makes use of the sequence development for the prototype **5**. The benzyl protecting group in **1** is now modified to contain a fluorine substituent, whose chemical shift will be pH insensitive, thereby serving as an internal standard. An additional carboxylic acid function is also present in the benzyl group in order to ensure good aqueous solubility and to retard leakage. The protecting group is therefore not removed, but remains as part of the chelator, 5F NEAP-2. Condensation of 5-fluoro-2-nitrophenol with the benzyl bromide **6** obtained from the bromination of 2-fluoro-4-carbomethoxytoluene led directly to the basic framework of the eventual indicator. Reduction of the nitro group to the aniline **8** and application of the same alkylation used in the synthesis of 5F NEAP-1 yielded the *N*-ethylaniline derivative **9**. Alkylation with methyl bromoacetate to give **10** and subsequent hydrolysis of the two ester functions produced 5F NEAP-2, **11**. Upon titration **11** showed a pH and ^{19}F chemical shift profile similar to **5** (Figure 1).

Unfortunately, the ^{19}F shift corresponding to the internal reference fluorine is fairly close to the shift of the pH sensitive resonance, such that there was overlap at high pH values. Additionally, indicator **11** is larger and more hydrophobic while having only two carboxyl groups. In order to remedy these deficiencies, we prepared compound **19**, 5F NEAP-3 (Scheme 3), which, in addition to a pH sensitive ^{19}F nucleus and pH insensitive ^{19}F to serve as an internal standard, contains three carboxyl groups to further retard the leakage of the indicator out of the cell. The synthesis of **19**, 5F NEAP-3, which contains two unequivalently substituted nitrogens, required a somewhat different strategy than the two preceding cases. The *N*-ethyl function is introduced in a masked form as an acetamide in **14**. After the coupling of **13** with 2-fluoro-4-nitrophenol to form the backbone of the indicator, the nitro group is reduced to the aniline and the acetamide moiety is reduced to the desired *N*-ethyl unit. Alkylation with benzyl bromoacetate to **18** and hydrogenolysis yields the desired indicator NEAP-3 (**19**). The reference fluorine resonance for this compound is ortho to an oxygen substituent and, hence, exhibits a large upfield chemical shift (Figure 2). As with **5** and **11** this compound also has an appropriate pK and ^{19}F chemical shift sensitivity.

The compounds described above have been loaded into several cell types and appear to function adequately in the intracellular environment. Another attractive feature of these indicators, illustrated by the derivatives discussed above, is that a wide range of analogs can be prepared by substitution at the hydroxyl oxygen without

Scheme 3[a]
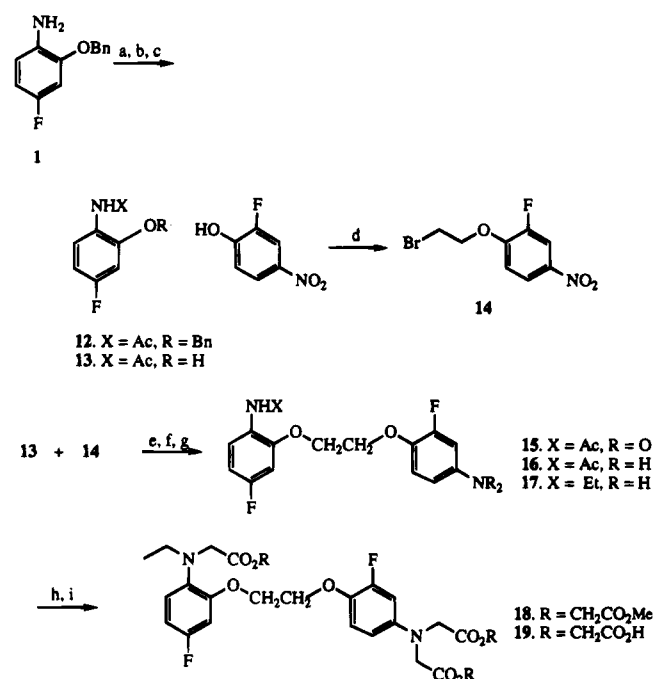
a Reagents: (a) H₂, Pt/C, EtOAc; (b) Ac₂O, Et₃N; (c) H₂, Pd/C, EtOAc; (d) BrCH₂CH₂Br, K₂CO₃, DMF; (e) K₂CO₃, DMF; (f) H₂, Pt/C, EtOAc; (g) LiAlH₄, THF; (h) BrCH₂CO₂Me, Proton Sponge, DMF; (i) KOH, MeOH.
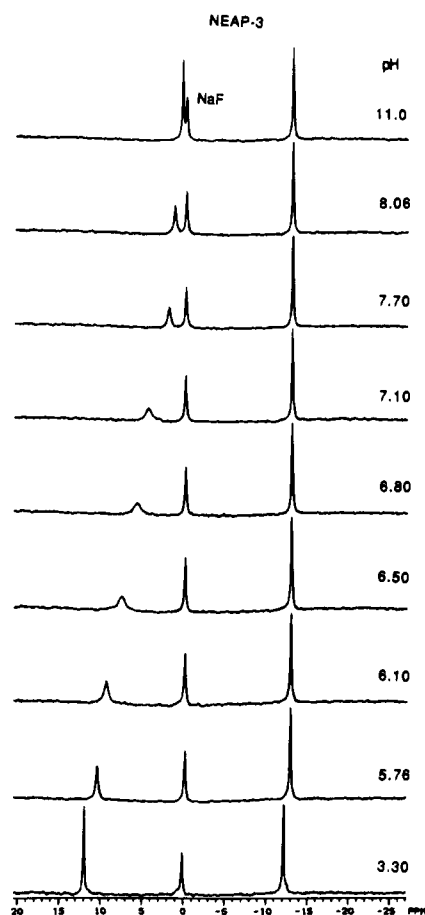
Figure 2. Fluorine-19 NMR spectra as a function of pH for 5F NEAP-3. The sample also contained NaF as an external standard.

exerting a major perturbation on the pK and fluorine shift parameters. Finally, the presence of the *o*-aminophenol

building block means that fluorescent pH indicators with structures and fluorescent properties closely analogous to existing cationic indicators can be readily prepared.

EXPERIMENTAL PROCEDURES

Fluorine-19 NMR spectra of the indicators were measured as a function of pH at 37 °C on an NT-360 spectrometer using a 5 mm probe retuned to the ¹⁹F NMR frequency of 340 MHz. Studies were carried out in a buffer containing 120 mM KCl, 20 mM NaCl, and 20 mM Tris–HEPES to model the intracellular milieu. In some studies, an external capillary with 20 mM NaF was used as a chemical shift standard.

Unless otherwise noted, commercially available reagents and dry solvents were used as received. Reactions were carried out under an atmosphere of argon, and reaction temperatures refer to the bath. Unless stated otherwise, all reported compounds were homogeneous as judged by the thin layer chromatography (TLC) analysis and their NMR spectra.

Flash column chromatography (FCC) was performed according to Still *et al.* (*21*) with Merck silica gel 60 (40–63 μm). Synthetic intermediates were characterized using ¹H nuclear magnetic resonance (¹H NMR) and ¹⁹F nuclear magnetic resonance (¹⁹F NMR) measured at 500 and 470 MHz, respectively, on a General Electric GN-500 spectrometer. Unless otherwise noted, NMR spectra were obtained in CDCl₃ solution. For ¹H NMR, the residual CHCl₃ in CDCl₃ was employed as the internal standard and assigned as 7.24 ppm downfield from tetramethylsilane (TMS). For ¹⁹F NMR, hexafluorobenzene was employed as the internal standard and assigned as 0 ppm. Melting points were determined on a Fisher-Johns melting point apparatus and are uncorrected.

***N*-Ethyl-2-(benzyloxy)-4-fluoroaniline (2).** Two pellets of NaBH₄ (311 mg) were added to a solution of 3.18 g (14.7 mmol) of 2-(benzyloxy)-4-fluoroaniline in 80 mL of glacial acetic acid. Another two pellets (320 mg) were added 0.5 h after the first addition. The reaction mixture was then stirred overnight at room temperature. The reaction mixture was neutralized with 3 N NaOH and extracted with ether, and the combined extracts were washed with H₂O and dried (MgSO₄). Removal of the solvent yielded 3.06 g of crude product. Flash chromatography (9:1 hexane/ethyl acetate) of this material yielded 1.22 g (35%) of white crystals, mp 58–59 °C. ¹H NMR: 1.24 (t, J = 7.1 Hz, 3H), 3.12 (q, J = 7.1, 2H), 5.03 (s, 2H), 6.5 (m, 1H), 6.6 (m, 2H), 7.4 (m, 5H).

***N*-Ethyl-2-hydroxy-4-fluoroaniline (3).** A solution of 847 mg (3.46 mmol) of **2** in 30 mL of ethyl acetate was hydrogenolyzed, using 109 mg of 10% Pd/C. The reaction proceeded rapidly until 1 equiv of hydrogen had been taken up. The catalyst was then filtered through a pad of Celite and the solvent removed to yield 484 mg of product (90%), mp 92–97 °C dec. This material was homogeneous by TLC, R_f = 0.2 (9:1 hexane/ethylacetate) but discolored rapidly. ¹H NMR: 1.22 (t, J = 7 Hz, 3H), 3.07 (q, J = 7 Hz, 2H), 6.5 (m, 2H), 6.7 (m, 1H).

***N*-Ethyl-2-hydroxy-4-fluoroaniline-*N,O*-diacetic Acid Dibenzyl Ester (4).** A mixture of 475 mg (3.06 mmol) of **3**, 1.60 g of Proton Sponge, 1.74 g of benzyl bromoacetate, and 20 mL of acetonitrile was heated at reflux for 48 h under an argon atmosphere. The cool solution was filtered, and ether was then added to the filtrate. The resulting precipitate was filtered off and the filtrate washed with pH 2 buffer, saturated NaCl solution, and water and dried (MgSO₄). After removal of the solvent, the resulting crude product was purified by flash chromatography (85:15 hexane/ethyl acetate) to yield 303 mg (23%) of clear colorless oil. ¹H NMR: 1.05 (t, J = 7.1

Hz, 3H), 3.27 (q, $J = 7.1$ Hz, 2H), 4.03 (s, 2H), 4.67 (s, 2H), 5.05 (s, 2H), 5.17 (s, 2H), 6.47 (dd, $J = 2.7$ and 9.8 Hz, 1H), 6.60 (ddd, $J = 8.3$, 2.4, and 2.4 Hz, 1H).

N-Ethyl-2-hydroxy-4-fluoroaniline-*N,O*-diacetic Acid (5). Hydrogenolysis of the diester **4** (54 mg, 0.1 mmol) in 15 mL of ethyl acetate with 10 mg of 10% Pd/C yielded the free acid, 27 mg, mp 54–56 °C. ¹H NMR (D₂O): 0.99 (t, $J = 7$ Hz, 3H), 3.23 (q, $J = 7$ Hz, 2H), 3.89 (br s, 2H), 4.64 (br s, 2H), 6.7 (m, 2H), 7.1 (m, 1H). ¹⁹F NMR(D₂O): 43.03 (m).

Methyl 3-fluoro-4-(bromomethyl)benzoate (6). A mixture of 7.32 g (43.6 mmol) of methyl 3-fluoro-4-methylbenzoate, 4.92 g, *N*-bromosuccinimide (NBS), and a few mg of 2,2-azobisisobutyronitrile (AIBN) in 80 mL of CCL₄ was brought to reflux and illuminated with a high intensity lamp. The reaction was rapid, and within 2 h, all of the NBS had been converted to succinimide. TLC and NMR analysis indicated a 1:1 mixture of product and starting material as judged by the appearance of a new signal at 4.49 corresponding to bromination of the methyl group. The mixture was worked up by filtering the succinimide and washing the CCl₄ solution, first with aqueous Na₂S₂O₃ and then with aqueous NaHCO₃. The product obtained after drying and removal of the solvent was recycled with additional NBS and treated as above to yield 7.46 g of yellow oil which was an 8:1 mixture of product and starting material and was used as such in the next step.

2-((2-Fluoro-4-(methoxycarbonyl)benzyl)oxy)-4-fluoronitrobenzene (7). A mixture of 7.37 g of the previously described impure **6**, 30 mL of dimethylformamide, 4.5 g of K₂CO₃, and 4.29 g (30 mmol) of 2-nitro-5-fluorophenol was heated at 70 °C in an oil bath. After 2 h, the reaction mixture was cooled and poured into ice–water and the product filtered off. The crude product was extracted with warm hexane to remove the methyl 3-fluoro-4-methylbenzoate impurity carried along from the preparation of **6**. The resulting cream colored product, 5.74 g, after recrystallization from ethyl acetate had mp 163–165 °C. ¹H NMR: 3.92 (s, 3H), 5.29 (s, 2H), 6.78 (m, 1H), 6.86 (dd, $J = 3.4$ and 9.5 Hz, xH), 7.75 (m, 2H), 7.89 (dd, $J = 1$ and 6.4 Hz, 1H), 8.00 (dd, $J = 6.9$ and 9.1 Hz, 1H).

2-((2-Fluoro-4-(methoxycarbonyl)benzyl)oxy)-4-fluoroaniline (8). A solution of 1.28 g (3.96 mmol) of **7** in 25 mL of ethyl acetate and 125 mg of 5% Pt/C was reduced with hydrogen at atmospheric pressure. After the uptake of 3 equiv of hydrogen the catalyst was filtered off and the solvent removed to yield 1.14 g (98%) of product, mp 92–95 °C. ¹H NMR: 3.92 (s, 3H), 5.16 (s, 2H), 6.54 (ddd, $J = 2.5$, 5.9 and 5.9 Hz, 1H), 6.65 (m, 2H), 7.55 (dd, $J = 7.5$ and 7.5 Hz, 1H), 7.74 (dd, $J = 1.2$ and 10.3 Hz, 1H), 7.83 (dd, $J = 1.2$ and 8 Hz, 1H).

N-Ethyl-2-((2-fluoro-4-(methoxycarbonyl)benzyl)oxy)-4-fluoroaniline (9). To a solution of 850 mg (2.90 mmol) of **8** in 17 mL of glacial acetic acid was added 4 pellets (600 mg) of NaBH₄ over a period of 2 h. TLC indicated the slow appearance of a product at $R_f = 0.8$ (7:3 hexane/ethyl acetate). Stirring at room temperature was continued for a total of 6 h. The reaction was neutralized with aqueous NaHCO₃. The product precipitated, after filtration was obtained as buff colored crystals (654 mg, 70%), and after recrystallization from hexane had mp 109–111 °C. ¹H NMR (CDCl₃): 1.25 (t, $J = 7.1$ Hz, 3H), 3.11 (q, $J = 7.1$ Hz, 2H), 3.92 (s, 3H), 5.15 (s, 2H), 6.5 (m, 1H), 6.6 (m, 2H), 7.5 (dd, $J = 7.5$ and 7.5 Hz, 1H), 7.75 (dd, $J = 1.5$ and 10.3 Hz, 1H), 7.84 (dd, $J = 1.5$ and 7.9 Hz, 1H).

N-Ethyl-2-((2-fluoro-4-(methoxycarbonyl)benzyl)oxy)-4-fluoroaniline-*N*-acetic Acid, Methyl Ester

(10). A mixture of 624 mg (1.94 mmol) of **9**, 465 mg of Proton Sponge, 360 mg of methyl bromoacetate, and 10 mL of dry acetonitrile was refluxed under argon for 54 h. After 24 h of reflux, an additional 65 mg each of methyl bromoacetate and Proton Sponge were added. The cool solution was diluted with ether and the amine salt filtered off. The filtrate was washed with pH 2 buffer and water and dried (MgSO₄). Removal of the solvent yielded 670 mg of crude product which after flash chromatography (85:15 hexane/ethyl acetate) yielded 419 mg (55%) of crystalline product, mp 61–62 °C. ¹H NMR (CDCl₃) 1.07 (t, $J = 7$ Hz, 3H), 3.26 (q, $J = 7$ Hz, 2H), 3.58 (s, 2H), 3.91 (s, 3H), 3.94 (s, 3H), 5.16 (s, 2H), 6.1 (m, 2H), 7.01 (dd, $J = 2$ and 6 Hz, 1H), 7.57 (dd, $J = 7.5$ Hz, 1H), 7.73 (dd, $J = 1$ and 10 Hz, 1H), 7.84 (dd, $J = 1$ and 7.5, Hz, 1H). ¹⁹F NMR (DMF-d_7): 43.2 (m, 1F), 45.7 (m, 1F).

N-Ethyl-2-((2-fluoro-4-carboxybenzyl)oxy)-4-fluoroaniline-*N*-acetic Acid (11). A sample of **10** (42 mg, 0.11 mm) was hydrolyzed with 1 M NaOH (3 mL) in aqueous methanol and after acidification (0.6 N HCl) yielded 33 mg (84%) of pure acid **11**, mp 73–77 °C. ¹H NMR (D₂O): 0.61 (t, $J = 7$ Hz, 3H), 2.76 (q, $J = 7$ Hz), 4.54 (s, 2H), 4.84 (s, 2H), 6.38 (ddd, $J = 7.5$, 7.5, and 2.5 Hz, 1H), 6.50 (dd, $J = 10.5$ and 2.5 Hz, 1H), 6.70 (dd, $J = 8.5$ and 6.5 Hz, 1H), 7.28 (dd, $J = 7.5$ and 7.5 Hz, 1H), 7.36 (br d, $J = 10.5$ Hz, 1H), 7.44 (br d, $J = 8.5$ Hz, 1H). ¹⁹F (DMF-d_7): 43.2 (m, 1F), 45.7 (m, 1F).

N-Acetyl-2-(benzyloxy)-4-fluoroaniline (12). Acetic anhydride (10 mL) was added to a solution of 2-(benzyloxy)-5-fluoroaniline (700 mg, 3.2 mmol) in pyridine (20 mL), and the reaction mixture was stirred for 1 h. Ice-water (10 mL) was added to the mixture, and the crude product was filtered and washed with water. Recrystallization from benzene afforded benzyl ether **12** as a white solid (801 mg, 96%), mp 136–138 °C. ¹H NMR (CDCl₃): 2.00 (s, 3H), 4.94 (br s, 2H), 6.8–6.7 (m, 2H), 7.2–7.1 (br s, 5H), 8.16 (dd, $J = 8.6$ Hz, 1H).

N-Acetyl-2-hydroxy-5-fluoroaniline (13). A mixture of benzyl ether **12** (800 mg, 3.1 mmol) in ethyl acetate (15 mL) and Pd/C (100 mg) was stirred overnight under H₂ (1 atm). The reaction mixture was filtered through Celite and concentrated under reduced pressure. The crude product was recrystallized from ethyl acetate to give phenol **13** as a white solid (512 mg, 98%), mp 185–186 °C. ¹H NMR (CDCl₃): 6.57 (dd, $J = 10.5$, 2.5 Hz, 1H), 6.75 (dd, $J = 9.5$, 2.5 Hz, 1H), 6.88 (dd, $J = 9.5$, 5.5 Hz, 1H), 7.35 (br s, 1H), 9.05 (br s, 1H).

1-Bromo-2-(2-fluoro-5-nitrophenoxy)ethane (14). Potassium carbonate (2.3 g, 16.7 mmol) was added to a solution of 2-fluoro-4-nitrophenol (1.5 g, 10 mmol) in dimethylformamide (10 mL), and the mixture was stirred for 10 min. Dibromoethane (2.5 mL, 29 mmol) was added to the reaction mixture and was heated at 90 °C overnight. The reaction mixture was diluted with ether, and the ether layer was washed with water and brine and then dried (MgSO₄). The solvent was removed under reduced pressure, and the crude product was fractionated by FCC with 2.5% ethyl acetate in hexane to yield **14** as a yellow oil (1.9 g, 75%). ¹H NMR (CDCl₃): 3.69 (t, $J = 6$ Hz, 2H), 4.44 (t, $J = 6$ Hz, 2H), 7.03 (dd, $J = 8.5$, 8.5 Hz, 1H), 8.1–7.9 (m, 2H).

1-(2-Acetamido-5-fluorophenoxy)-2-(2-fluoro-4-nitrophenoxy)ethane (15). A mixture of phenol **13** (450 mg, 2.7 mmol) and bromoethane **14** (850 mg, 3.2 mmol) in dimethylformamide (10 mL) containing K₂CO₃ (500 mg, 3.6 mmol) was heated at 70 °C overnight. The reaction mixture was quenched with ice–water, filtered, and washed with cold water. The crude product was fractionated by FCC (dry application with 50% EtOAc/

hexane) to provide **15** as a pale tan solid (1.0 g, 88%), mp 192−194 °C. ^{1}H NMR (CDCl$_3$): 2.15 (s, 3H), 4.6−4.4 (m, 2H), 7.59 (br s, 1H), 8.03 (dd, J = 10.5, 2.5 Hz, 1H), 8.08 (dd, J = 9.5, 2.5 Hz, 1H), 8.29 (dd, J = 9.5, 7 Hz, 1H).

1-(2-Acetamido-5-fluorophenoxy)-2-(2-fluoro-4-aminophenoxy)ethane (16). A mixture of nitro compound **15** (1.0 g, 3.1 mmol) in ethyl acetate (20 mL) and Pt/C (200 mg) was stirred for 2 h under H$_2$ (1 atm). The reaction mixture was filtered through Celite and concentrated under reduced pressure. The crude product was recrystallized with benzene, providing amino ethane **16** as a white solid (709 mg, 78%), mp 134−136 °C. ^{1}H NMR (CDCl$_3$): 2.12 (s, 3H), 4.29 (s, 4H), 6.4−6.3 (m, 1H), 6.46 (dd, J = 12.5, 2.5 Hz, 1H), 6.7−6.6 (m, 2H), 6.85 (dd, J = 9, 9 Hz, 1H), 8.30 (dd, J = 9, 6 Hz, 1H).

1-(2-(N-Ethylamino)-5-fluorophenoxy)-2-(2-fluoro-4-aminophenoxy)ethane (17). Lithium aluminum hydride (ca. 50 mg) was added to **16** (500 mg, 1.5 mmol) in THF (15 mL), and the reaction mixture was stirred overnight. The reaction mixture was quenched with MeOH (1 mL) and filtered through Celite. After being concentrated under reduced pressure, the crude product was fractionated by FCC with 50% EtOAc in hexane to yield **17** as a white solid (300 mg, 63%) and recovered starting material **16** (100 mg, 20%). After recrystallization from benzene, the product had mp 111−114 °C. ^{1}H NMR (CDCl$_3$): 1.23 (t, J = 7 Hz, 3H), 3.10 (q, J = 7 Hz, 2H), 4.4−4.2 (m, 2H), 6.37 (br d, J = 8.5 Hz, 1H), 6.5−6.5 (m, 2H), 6.57 (br d, J = 9 Hz, 1H), 6.6−6.5 (m, 1H), 6.85 (dd, J = 9, 9 Hz, 1H).

1-(2-(N-Ethylamino)-5-fluorophenoxy)-2-(2-fluoro-4-aminophenoxy)ethane-N,N′,N′-triacetic Acid, Trimethyl Ester (18). Methyl bromoacetate (0.34 mL, 3.6 mmol) was added to the solution of amine **17** (200 mg, 0.6 mmol) and Proton Sponge (660 mg) in CH$_3$CN (10 mL), and the reaction mixture was heated under reflux for 3 days. The cool reaction mixture was diluted with ether (40 mL) and washed with pH 2 solution (20 mL), water (20 mL), and then brine (20 mL). After being dried over MgSO$_4$, the ether solution was concentrated under reduced pressure and fractionated by FCC with 50% EtOAc in hexane yielding triacetate **18** (270 mg, 79%), mp 62−64 °C. ^{1}H NMR (CDCl$_3$): 1.87 (t, J = 7 Hz, 3H), 3.65 (s, 3H), 3.75 (s, 6H), 4.15 (s, 2H), 4.25 (x, 4H), 4.3−4.2 (m, 2H), 4.4−4.3 (q, J = 7 Hz, 2H), 4.5−4.4 (m, 2H), 6.76 (dd, J = 9, 2.5 Hz, 1H), 6.85 (dd, J = 13.5, 3 Hz, 1H), 7.2−7.1 (m, 2H), 7.46 (dd, J = 9.9 Hz, 1H), 7.83 (dd, J = 8.5, 6 Hz, 1H).

1-(2-(N-Ethylamino)-5-fluorophenoxy)-2-(2-fluoro-4-aminophenoxy)ethane-N,N′,N′-triacetic Acid (19). Potassium hydroxide (50 mg, 0.9 mmol) was added to ester **18** (100 mg, 0.2 mmol) in MeOH (3 mL) and stirred overnight. The reaction mixture was acidified with 1 M HCl, filtered, and washed with water to provide acid **19** as a white solid (73 mg, 80%), mp 110−115 °C. ^{1}H NMR (D$_2$O): 0.78 (t, J = 7 Hz, 3H), 2.92 (q, J = 7 Hz, 2H), 3.68 (br s, 4H), 4.5−4.3 (m, 2H), 4.8−4.6 (m, 2H), 6.08 (br d, J = 8.5 Hz, 1H), 6.20 (d, J = 13.5 Hz, 1H), 6.6−6.5 (m, 1H), 6.71 (d, J = 9 Hz, 1H), 7.0−6.8 (m, 2H). ^{19}F (DMSO-d_6): 42.4 (m, 1F), 30.3 (m, 1F).

LITERATURE CITED

(1) Cohen, R. D., and Iles, R. A. (1975) Intracellular pH: Measurement, Control, and Metabolic Interrelationships. In *Crit. Rev. Clin. Lab. Sci. 6*, 101−143.

(2) Nuccitelli, R. and Deamer, D. W., Eds. (1982) *Intracellular pH: Its measurement, Regulation and Utilization in Cellular Functions* Liss, New York.

(3) Jacobson, L., and Cohen, J. S. (1982) Intracellular pH Measurements by NMR Methods. In *Noninvasive Probes of Tissue Metabolism* (J. S. Cohen, Ed.) Wiley, New York.

(4) Moon, R. B., and Richards, J. H. (1973) Determination of intracellular pH by ^{31}P Magnetic Resonance. *J. Biol. Chem. 248*, 7276−7278.

(5) Roberts, J. K. M., Wade-Jardetzky, N., and Jardetzky, O. (1981) Intracellular pH Measurements by ^{31}P Nuclear Magnetic Resonance. Influence of Factors Other Than pH on ^{31}P Chemical Shifts. *Biochemistry 20*, 5389−5394.

(6) Thoma, J. W., Steiert, J. G., Crawford, R. L., and Ugurbil, K. (1986) pH Measurements by ^{31}P NMR in Bacterial Suspensions Using Phenyl Phosphonate as a Probe. *Biochem. Biophys. Res. Commun. 138*, 1106−1109.

(7) DeFronzo, M., and Gillies, R. J. (1987) Characterization of Methylphosphonate as a ^{31}P NMR pH Indicator. *J. Biol. Chem. 262*, 11032−11037.

(8) Szwergold, B. S., Brown, T. R., and Freed, J. (1989) Bicarbonate abolishes Intracellular Alkalinization in Mitogen-Stimulated 3T3 Cells. *J. Cell. Physiol. 138*, 227−235.

(9) Taylor, J. S., Deutsch, C. J., McDonald, G. G., and Wilson, D. F. (1981) Measurement of Transmembrane pH Gradients in Human Erythrocytes Using ^{19}F NMR. *Anal. Biochem. 114*, 415−418.

(10) Taylor, J. S., and Deutsch, C. J. (1983) Fluorinated α-Methylamino Acids as ^{19}F NMR Indicators of Intracellular pH. *Biophys. J. 43*, 261−267.

(11) Deutsch, C. J., and Taylor, J. S. (1987) Intracellular pH as Measured by ^{19}F NMR. *Ann. N.Y. Acad. Sci. 508*, 33−47.

(12) Deutsch, C. J., and Taylor, J. S. (1989) New class of ^{19}F pH indicators: fluoroanilines. *Biophys. J. 55*, 799−804.

(13) Metcalfe, J. C., Hesketh, T. R., and Smith, G. A. (1985) Free cytosolic Ca^{2+} Measurements with Fluorine Labeled Indicators Using ^{19}F NMR. *Cell Calcium 6*, 183−195.

(14) Beech, J. S., and Iles, R. A. (1987) ^{19}F n.m.r. indicators of hepatic intracellular pH *in vivo*. *Biochem. Soc. Trans. 15*, 871−872.

(15) Mehta, V. D., Kulkarni, P. V., Mason, R. P., and Antich, P. P. (1993) Fluorinated macromolecular probes for non-invasive assessment of pH by magnetic resonance spectroscopy. *Bioorg. Med. Chem. Lett. 3*, 187−192.

(16) Rogers, J., Hesketh, T. R., Smith, G. A., and Metcalfe, J. C. (1983) Intracellular pH of Stimulated Thymocytes Measured with a New Fluorescent Indicator. *J. Biol. Chem. 258*, 5994−5997.

(17) Smith, G. A., Hesketh, R. T., Metcalfe, J. C., Feeney, J., and Morris, P. G. (1983) Intracellular calcium measurements by ^{19}F NMR of fluorine-labeled chelators. *Proc. Natl. Acad. Sci. U.S.A. 80*, 7178−7182.

(18) Levy, L. A., Murphy, E., Raju, B., and London, R. E. (1988) Measurement of Cytosolic Free Magnesium Ion Concentration by ^{19}F NMR. *Biochemistry 27*, 4041−4048.

(19) Gribble, G. W., Lord, P. D., Skotnicki, J., Dietz, S. E., Eaton, J. T., and Johnson, J. L. (1974) Reactions of sodium borohydride in acidic media. I. Reduction of Indoles and alkylation of aromatic amines with carboxylic acids. *J. Am. Chem. Soc. 96*, 7812−7814.

(20) London, R. E., and Gabel, S. A. (1988) Determination of Membrane Potential and Cell Volume by ^{19}F NMR Using Trifluoroacetate and Trifluoroacetamide Probes. *Biochemistry 28*, 2378−2382.

(21) Still, W. C., Kahn, M., and Mitra, A. (1978) Rapid Chromatographic techniques for preparative separations with moderate resolution. *J. Org. Chem. 43*, 2923−2925.

A Novel Minor Groove Binding Reagent Designed To Serve as a "Truck" To Carry DNA Modifying Moieties into the Major Groove

Tianhan Xue, Kenneth A. Browne, and Thomas C. Bruice*

Department of Chemistry, University of California, Santa Barbara, California 93106. Received August 15, 1994[⊗]
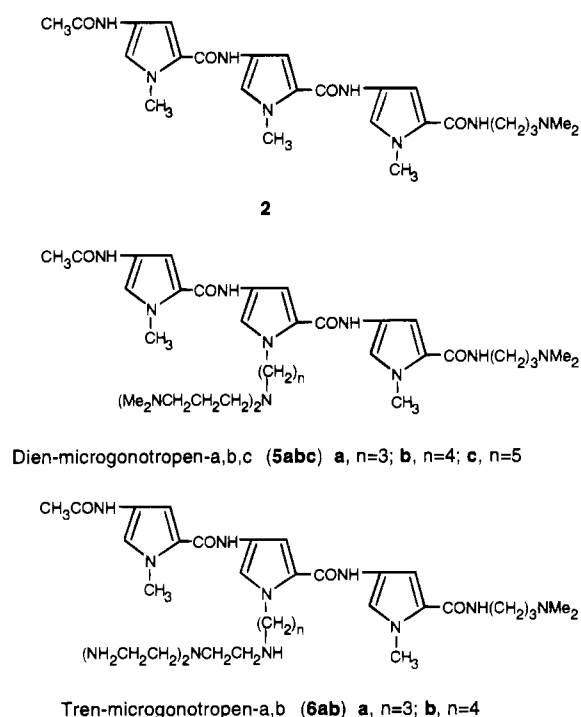
A site selective DNA minor groove binding tripyrrole peptide has been synthesized as a "truck" to place chemical functionalities into the major groove which are capable of physically modifying DNA, acting as catalysts to hydrolyze DNA, or effectively protecting DNA from various DNA modifying enzymes. The equilibrium dissociation constants for the binding of this peptide to an A_3T_3 dsDNA binding site have been determined to be nanomolar, and they are compared to the constants for other minor groove binding agents.

INTRODUCTION

There has been considerable interest in recent years in the design of reagents capable of sequence selective complexation of DNA, especially small molecules able to bind to the minor groove of B-DNA (Beerman et al., 1992; Boger and Sakya, 1992; Lown et al., 1986; Nunn et al., 1993). Microgonotropens (Chart 1; He et al., 1993, 1994) represent a novel class of reagents which bind in the minor groove of B-DNA but, in addition, extend entities up to the phosphate backbone and into the major groove. Like distamycin, the shape adapted by the microgonotropens is reflective of the peptide linkages between three 1-methyl-4-aminopyrrole-2-carboxylic acid residues (Kopka et al., 1985). To overcome the inherent instability of distamycin, the amino terminal formal group has been replaced with the more stable acetamido moiety (He et al., 1993). Our microgonotropen design is based on the concept that an ideal agent would consist of two essential parts: (i) a recognition unit (selective DNA minor groove binding molecules) which serves as a carrier and (ii) a functional moiety capable of modifying DNA [e.g., bending (He et al., 1993, 1994; Hansma et al., 1994)]. This agent may also be linked to a designed selective DNA major groove binder.

In previous syntheses (He et al., 1993, 1994), microgonotropens were prepared by synthesizing the central pyrrole units individually linked with different functional moieties (tren and dien). These different central pyrrole units were then coupled to identical carboxy and amino terminal pyrrole units. Each microgonotropen had to be constructed from simple pyrrolic starting materials through a relatively lengthy reaction sequence. From the viewpoint of synthetic economy, it would be highly desirable to construct a common tripyrrole peptide which features a suitable anchoring group. Different agents capable of modifying or cleaving DNA can then be covalently attached to the common tripyrrole carrier through coupling reactions with the anchoring group. Here we report the synthesis (Scheme 1) of one such tripyrrole peptide **1** which can be used as a common "truck" for various chemical moieties *via* a simple reductive amination or substitution reaction. In addition, this peptide's equilibrium association constants to d(GGC-GCA₃T₃GGCGG)/d(CCGCCA₃T₃GCGCC) have been evaluated and compared to the constants of other tripyrrole peptides.

Chart 1

2

Dien-microgonotropen-a,b,c **(5abc) a,** n=3; **b,** n=4; **c,** n=5

Tren-microgonotropen-a,b **(6ab) a,** n=3; **b,** n=4

EXPERIMENTAL PROCEDURES

Synthetic Materials. Reagent grade chemicals were used without purification unless otherwise stated. Dimethylformamide (DMF) was dried over $CaSO_4$ and distilled under reduced pressure. Triethylamine was dried by KOH and distilled. Methanol and DMF were stored over 4A molecular sieves. Mucobromic acid, 1-methyl-2-pyrrolecarboxylic acid, 3-(dimethylamino)-propylamine, di-*tert*-butyl dicarbonate, 3-bromopropylamine hydrochloride, and diethyl cyanophosphonate (DECP) were purchased from Aldrich. Ethyl 4-nitro-2-pyrrolecarboxylate was synthesized by condensation of equimolar quantities of sodium nitromalonic aldehyde [prepared from mucobromic acid and $NaNO_2$] and glycine ethyl ester hydrochloride (Hale and Hoyt, 1915). *N*-(*tert*-Butyloxycarbonyl)-3-bromopropylamine was prepared by treating 3-bromopropylamine with di-*tert*-butyl dicarbonate.

Synthetic Methods. Melting points were determined on a Mel-Temp device and are uncorrected. Infrared (IR) spectra were obtained on a Perkin-Elmer monochromator grating spectrometer (Model 1330) and on a Galaxy 2020

Scheme 1
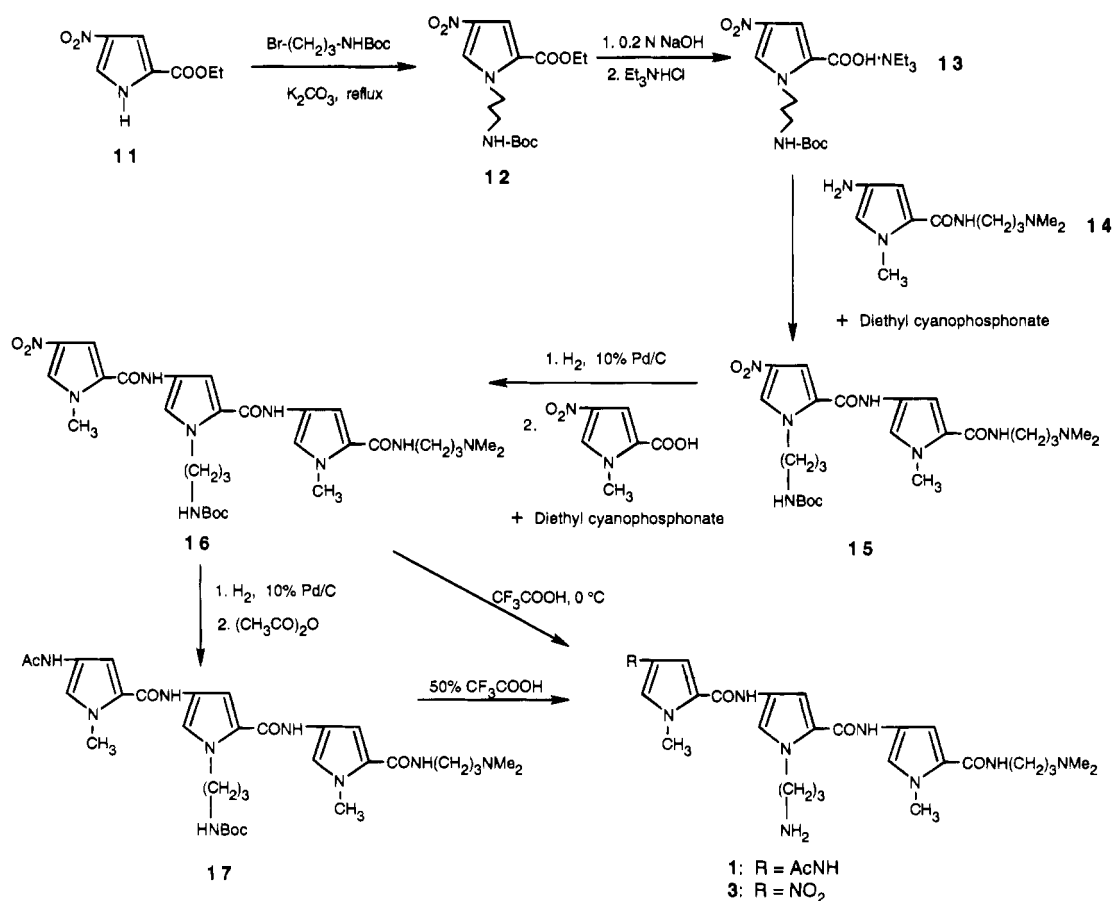
FT-IR spectrometer. Low-resolution mass spectra (LRMS) were recorded on a VG Analytical spectrometer (Model VGII-250) by electron impact (EI) or fast atom bombardment (FAB) using *m*-nitrobenzyl alcohol (NBA) or glycerol as a matrix. High-resolution mass spectrometry (HRMS) was performed at the University of California, Los Angeles. ^{1}H and ^{13}C NMR spectra were obtained in CDCl$_3$ or in DMSO-d_6 with Gemini-200 and General Electric GN-500 spectrometers. Chemical shifts are reported in δ (ppm) relative to Me$_4$Si with s, d, t, q, and m signifying singlet, doublet, triplet, quartet, and multiplet; coupling constants J are reported in hertz (Hz). Chromatographic silica gel (FisherChemical, 200−425 mesh) was used for flash chromatography, and glass-backed plates of 0.25-mm SiO$_2$ 60-F$_{254}$ (Merck) were used for thin-layer chromatography (TLC). Elemental analysis was carried out by Galbraith Laboratories, Inc. (Knoxville, TN). All nonaqueous reactions were run under argon with rigorous exclusion of water unless otherwise noted.

Ethyl 1-[3-[*N*-(*tert*-Butyloxycarbonyl)amino]propyl]-4-nitro-2-pyrrolecarboxylate (12). Potassium carbonate (5.53 g, 40 mmol) was added to a solution of ethyl 4-nitro-2-pyrrolecarboxylate (11) (3.68 g, 20 mmol) in 120 mL of acetone, and the suspension was stirred at room temperature for 1 h. A solution of *N*-(*tert*-butyloxycarbonyl)-3-bromopropylamine (9.53 g, 40 mmol) in 30 mL of acetone was added, followed by addition of 3.0 g of NaI (20 mmol). The resulting suspension was heated to reflux for 6 h. After being cooled the reaction mixture was filtered to remove inorganic salts and the filtrate was concentrated under reduced pressure. The residue was purified by a flash silica column with hexanes−EtOAc (4:1) as eluant to give 6.35 g (93%) of product 12 as a colorless solid. Mp: 72−74 °C (recrystallized from hex-

anes:EtOAc = 4:1). IR (KBr): ν_{NH} = 3310 and $\nu_{C=O}$ = 1670 cm^{-1}. ^{1}H NMR (CDCl$_3$): δ 1.37 (t, J = 7, CH$_3$, 3H), 1.45 (s, C(CH$_3$)$_3$, 9H), 2.00 (quintet, J = 7, −CCH$_2$C−, 2H), 3.16 (q, J = 7, CH$_2$NH, 2H), 4.32 (q, J = 7, OCH$_2$-Me, 2H), 4.41 (t, J = 7, pyrrole NCH$_2$−, 2H), 4.75 (br, NH, 1H), 7.45 (d, J = 2.1, pyrrole Ar-H, 1H), 7.71 (br, pyrrole Ar-H, 1H). HRMS (FAB): m/z 342.1654 (calcd for (M + H$^+$) = C$_{15}$H$_{24}$N$_3$O$_6$ 342.1665). Anal. Calcd for C$_{15}$H$_{23}$N$_3$O$_6$: C, 52.78; H, 6.79; N, 12.31. Found: C, 52.93; H, 6.97; N, 12.37.

N,N-Dimethyl-3-[1-methyl-4-[1-[3-[N-(*tert*-butyloxycarbonyl)amino]propyl]-4-nitro-2-pyrrolecarboxamido]-2-pyrrolecarboxamido]propionamine (15). Pyrrole 12 (2.3 g, 6.74 mmol) was treated with a 0.2 N NaOH solution in 70% aqueous EtOH (130 mL) at room temperature for 24 h. After the mixture was cooled, Et$_3$N·HCl (7.56 g, 54 mmol) was added. The solution was concentrated to dryness under reduced pressure, and the residue was extracted with CH$_2$Cl$_2$ (400 mL). The organic phase was washed with brine (2 × 50 mL) and dried over Na$_2$SO$_4$. Removal of the solvent gave 2.57 g (92.1%) of triethylammonium 1-[3-[N-(*tert*-butyloxycarbonyl)amino]propyl]-4-nitro-2-pyrrolecarboxylate (13) as a yellow-tinted semisolid. ^{1}H NMR (CDCl$_3$): δ 1.35 (t, J = 7, 3 × CH$_3$(Et$_3$N), 9H), 1.44 (s, CO$_2$C(CH$_3$)$_3$, 9H), 1.96 (quintet, J = 7, −CCH$_2$C−, 2H), 3.09 (q, J = 7, CH$_2$-NHBoc, 2H), 3.15 (q, J = 7, 4 × CH$_2$(Et$_3$N), 8H), 4.55 (t, J = 7, pyrrole NCH$_2$, 2H), 5.87 (br, NH, 1H), 7.32 (d, J = 2, pyrrole ArH, 1H), 7.54 (d, J = 2, pyrrole ArH, 1H).

A solution of the pyrrolic acid 13 (2.02 g, 4.88 mmol) and freshly prepared N,N-dimethyl-3-(1-methyl-4-amino-2-pyrrolecarboxamido)propylamine (14) (He et al., 1993) (1.28 g, 5.7 mmol) in 100 mL of anhydrous DMF was cooled to 0 °C. Diethyl cyanophosphonate (2.0 mL, 12.2 mmol) and Et$_3$N (2.0 mL, 14 mmol) were added dropwise

to this solution. The solution was stirred at 0 °C for 1 h and at room temperature for another 16 h. All solvent was removed *in vacuo,* and the residue was dissolved in 300 mL of CH_2Cl_2 which was washed with saturated $NaHCO_3$ solution (40 mL) and water (40 mL) and dried over K_2CO_3. The crude product was purified by a flash silica column ($EtOAc-MeOH-Et_3N = 90:9:2$) to give **15** as a yellow-tinted solid (1.84 g, 72.6%). Mp: 164–165 °C (recrystallized from EtOAc). IR(KBr): $\nu_{NH} = 3290$ and $\nu_{C=O} = 1640$ (br) cm^{-1}. ^{1}H NMR (DMSO-d_6): δ 1.33 (s, $CO_2C(CH_3)_3$, 9H), 1.58 (quintet, $J = 7$, CCH_2CNMe_2, 2H), 1.81 (quintet, $J = 7$, $CCH_2CNHBoc$, 2H), 2.10 (s, NMe_2, 6H), 2.22 (t, $J = 7$, CH_2NMe_2, 2H), 2.86 (q, $J = 7$, CH_2-NHBoc, 2H), 3.15 (q (became t when exchanged with D_2O), $J = 7$, $CONHCH_2$, 2H), 3.77 (s, pyrrole NCH_3, 3H) 4.38 (t, $J = 7$, pyrrole NCH_2, 2H), 6.78, 7.18, 7.54, and 8.24 (4d, $J = 1.8-2.0$, 4 × pyrrole ArH, 4H), 6.87 (t, $J = 5$, BocNH, 1H), 8.12 (t, exchangeable with D_2O, $J = 7$, $CONHCH_2$, 1H), 10.25 (s, exchangeable with D_2O, Pyr-CONH-Pyr, 1H). HRMS (FAB): m/z 520.2862 (calcd for $(M + H^+) = C_{24}H_{38}N_7O_6$ 520.2884. Anal. Calcd for C_{24}-$H_{37}N_7O_6$: C, 55.48; H, 7.18; N, 18.87. Found: C, 55.14; H, 7.18; N, 18.70.

N,N-Dimethyl-3-[1-methyl-4-[1-[3-[N-(*tert*-butyl-oxycarbonyl)amino]propyl]-4-(1-methyl-4-nitro-2-pyrrolecarboxamido]-2-pyrrolecarboxamido]-2-pyrrolecarboxamido]propylamine (16). A solution of the dipyrrole **15** (1.06 g, 2.04 mmol) in 60 mL of DMF was hydrogenated over 10% palladium on charcoal (500 mg) at room temperature and 50 psi of pressure using a Parr hydrogenator for 5 h (the reaction was monitored by TLC). The catalyst was removed by filtration, and the filtrate was concentrated. The residue and 1-methyl-4-nitro-2-pyrrolecarboxylic acid (0.54 g, 3.17 mmol) were dissolved in anhydrous DMF (30 mL) and cooled to 0 °C. Diethyl cyanophosphonate (1.0 mL, 6.1 mmol) and Et_3N (1.5 mL, 10.5 mmol) were added dropwise to the solution. The solution was stirred at 0 °C under argon for 2 h and at room temperature for another 12 h. Solvent was evaporated to dryness *in vacuo* and the resultant residue dissolved in 350 mL of CH_2Cl_2, washed with saturated $NaHCO_3$ solution (50 mL) and water (50 mL), and dried over K_2CO_3. The crude product was purified by a flash silica column ($EtOAc-MeOH-Et_3N = 88:12:2$) to give product **16** as a yellow-tinted solid (0.89 g, 68.0%). Mp: 218–220 °C dec. IR (KBr): $\nu_{NH} = 3325$ and $\nu_{C=O} = 1635$ (br) cm^{-1}. ^{1}H NMR (DMSO-d_6): δ 1.36 (s, $CO_2C(CH_3)_3$, 9H), 1.60 (quintet, $J = 7$, CCH_2CNMe_2, 2H), 1.77 (quintet, $CCH_2CNHBoc$, 2H), 2.13 (s, NMe_2, 6H), 2.24 (t, $J = 7$, CH_2NMe_2, 2H), 2.87 (q, $J = 7$, CH_2NHBoc, 2H), 3.17 (q (became t when exchanged with D_2O), $J = 7$, $CONHCH_2$, 2H), 3.79 and 3.96 (2s, 2 × pyrrole NCH_3, 2 × 3H) 4.31 (t, $J = 7$, pyrrole NCH_2, 2H), 6.81, 7.01, 7.19, 7.35, 7.59, and 8.19 (6d, $J = 1.5-1.9$, 6 × pyrrole ArH, 6 × 1H), 6.89 (t, $J = 5$, BocNH, 1H), 8.10 (t, exchangeable with D_2O, $J = 6$, $CONHCH_2$, 1H), 9.98 and 10.32 (2s, exchangeable with D_2O, 2 × Pyr-CONH-Pyr, 2 × 1H). HRMS (FAB): m/z 642.3361 (calcd for $(M + H^+) = C_{30}H_{44}N_9O_7$ 642.3364). Anal. Calcd for $C_{30}H_{43}N_9O_7 + 0.5$ H_2O: C, 55.37; H, 6.82; N, 19.37. Found: C, 55.54; H, 7.01; N, 18.76.

N,N-Dimethyl-3-[1-methyl-4-[1-[3-(N-(*tert*-butyl-oxyamino)amino]propyl]-4-(1-methyl-4-acetamido-2-pyrrolecarboxamido]-2-pyrrolecarboxamido]-2-pyrrolecarboxamido]propylamine (17). A solution of the nitrotripyrrole **16** (2.36 g, 3.68 mmol) in 120 mL of DMF was hydrogenated over 10% palladium on charcoal (900 mg) at room temperature and 50 psi of pressure using a Parr hydrogenator for 6 h. (The reaction was monitored by TLC, $MeOH-Et_3N = 60:2$ as eluant.

Longer hydrogenation time should be avoided since the reduced aminotripyrrole decomposes slowly.) The catalyst was removed by filtration, and the filtrate was concentrated. The residue was immediately dissolved in anhydrous DMF (30 mL) containing Et_3N (4 mL) and cooled to 0 °C. Acetic anhydride (3 mL, 31 mmol) was added dropwise to the solution. The solution was stirred at 0 °C under argon for 0.5 h and at room temperature for another 12 h. Solvents were evaporated to dryness *in vacuo,* and the residue was dissolved in 300 mL of CH_2-Cl_2, washed with saturated $NaHCO_3$ solution (50 mL) and water (50 mL), and dried over K_2CO_3. The crude product was purified by a flash silica column ($EtOAc-MeOH-Et_3N = 82:15:3$) to give product **17** as a slightly yellowish solid (1.90 g, 78%). Mp: 158–160 °C. IR (KBr): $\nu_{NH} = 3316$ and $\nu_{C=O} = 1653$ (br) cm^{-1}. ^{1}H NMR (DMSO-d_6): δ 1.35 (s, $CO_2C(CH_3)_3$, 9H), 1.59 (quintet, $J = 7.0$, CCH_2CNMe_2, 2H), 1.77 (quintet, $J = 7.0$, CCH_2-$CNHBoc$, 2H), 1.95 (s, CH_3CO, 3H), 2.12 (s, NMe_2, 6H), 2.23 (t, $J = 7$, CH_2NMe_2, 2H), 2.87 (q, $J = 7$, CH_2NHBoc, 2H), 3.17 (q, $J = 6.5$, $CONHCH_2$, 2H), 3.78 and 3.82 (2s, 2 × pyrrole NCH_3, 2 × 3H), 4.28 (t, $J = 7$, pyrrole NCH_2, 2H), 6.81, 6.85, 7.01, 7.14, 7.17, and 7.30 (6d, $J = 1.5-2.0$, 6 × pyrrole ArH, 6 × 1H), 6.88 (t, $J = 5$, BocNH, 1H), 8.08 (t, $J = 5.5$, $CONHCH_2$, 1H), 9.83 (s, 1H), and 9.92 (s, 2 × Pyr-CONH-Pyr and CH_3CONH, 2H). HRMS (FAB): m/z 654.3727 (calcd for $(M + H^+) = C_{32}H_{47}N_9O_6$ 654.3728).

N,N-Dimethyl-3-[1-methyl-4-[1-(3-aminopropyl)-4-(1-methyl-4-acetamido-2-pyrrolecarboxamido)-2-pyrrolecarboxamido]-2-pyrrolecarboxamido]propylamine (1). A solution of the tripyrrole **17** (290 mg, 0.44 mmol) in 5 mL of CH_2Cl_2 was cooled to 0 °C, and trifluoroacetic acid (5 mL) was added dropwise. The resulting clear solution was stirred under argon at 0 °C for 2 h and then at room temperature for another 1.5 h. Solvents were removed *in vacuo* at room temperature, and residual trifluoroacetic acid was removed by codistillation with toluene. The residue was dissolved in 50 mL of MeOH and stirred with 10 g of Dowex 1 × 8 100 resin (HO$^-$ form) under argon at 0 °C for 0.5 h. The resin was removed by filtration, and the filtrate was evaporated to afford **1** as a slightly yellowish solid (170 mg, 69.2%). IR (KBr): $\nu_{NH} = 3288$ and $\nu_{C=O} = 1647$ (br) cm^{-1}; ^{1}H NMR (DMSO-d_6): δ 1.60 (quintet, $J = 7.0$, CCH_2-$CNMe_2$, 2H), 1.73 (quintet, $J = 7.0$, CCH_2CNH_2, 2H), 1.96 (s, CH_3CO, 3H), 2.13 (s, NMe_2, 6H), 2.23 (t, $J = 7$, CH_2-NMe_2, 2H), 2.46 (t, $J = 7$, CH_2NH_2, 2H), 3.18 (q, $J = 6.5$, $CONHCH_2$, 2H), 3.79 and 3.82 (2s, 2 × pyrrole NCH_3, 2 × 3H), 4.33 (t, $J = 7$, pyrrole NCH_2, 2H), 6.81, 6.85, 6.99, 7.14, 7.16, and 7.28 (6d, $J = 1.5-2.0$, 6 × pyrrole ArH, 6 × 1H), 8.06 (t, $J = 5.5$, $CONHCH_2$, 1H), 9.81, 9.88 and 9.90 (3s, 2 × Pyr-CONH-Pyr and CH_3CONH, 3 × 1H). HRMS (FAB): m/z 554.3202 (calcd for $(M + H^+) = C_{27}H_{40}N_9O_4$ 554.3203).

N,N-Dimethyl-3-[1-methyl-4-[1-(3-aminopropyl)-4-(1-methyl-4-nitro-2-pyrrolecarboxamido)-2-pyrrolecarboxamido]-2-pyrrolecarboxamido]propylamine (3). A suspension of the tripyrrole **16** (60 mg) in 4 mL of CH_2Cl_2 was cooled to 0 °C, and trifluoroacetic acid (4 mL) was added dropwise. The resulting clear solution was stirred under argon at 0 °C for 2 h and then at room temperature for another 2 h. Solvents were evaporated to dryness *in vacuo* at room temperature, and residual trifluoroacetic acid was removed by codistillation with toluene. The residue was dissolved in 50 mL of MeOH and stirred with 5 g of Dowex 1 × 8 100 resin (HO$^-$ form) under argon at room temperature for 0.5 h. The resin was removed by filtration, and the filtrate was evaporated to afford **3** as a yellow-tinted solid (50 mg,

98.7%). ^{1}H NMR (DMSO-d_6): δ 1.60 (quintet, $J = 7.0$, CCH$_2$CNMe$_2$, 2H), 1.72 (quintet, $J = 7.0$, CCH$_2$CNH$_2$, 2H), 2.13 (s, NMe$_2$, 6H), 2.23 (t, $J = 7$, CH$_2$NMe$_2$, 2H), 2.46 (t, $J = 7$, CH$_2$NH$_2$, 2H), 3.17 (q, $J = 6.3$, CONHCH$_2$, 2H), 3.79 and 3.96 (2s, 2 × pyrrole NCH$_3$, 2 × 3H), 4.35 (t, $J = 7$, pyrrole NCH$_2$, 2H), 6.81, 6.98, 7.18, 7.33, 7.59 and 8.19 (6d, $J = 1.5$–1.9, 6 × pyrrole ArH, 6 × 1H), 8.06 (t, $J = 5.0$, CONHCH$_2$, 1H), 9.95 and 10.27 (2s, 2 × Pyr-CONH-Pyr, 2 × 1H). HRMS (FAB): m/z 542.2858 (calcd for (M + H$^+$) = C$_{25}$H$_{36}$N$_9$O$_5$ 542.2839).

**Reagents and Methods for DNA Binding Studies.** The complementary hexadecameric oligonucleotides d(G-GCGCAAATTTGGCGG) and d(CCGCCAAATTTGCGCC) were synthesized at UCSF's Biomolecular Resource Facility. Annealing and characterization procedures for the duplex hexadecamer have been described (Browne et al., 1993; He et al., 1994). Hoechst 33258 (Aldrich) was used without further purification. The duplex hexadecamer was maintained in a stock solution containing 0.01 M potassium phosphate buffer, pH 7.0, 0.01 M NaCl. All other stock solutions were in distilled deionized water. Stock solutions were stored on ice for the duration of a given experiment and maintained at −20 °C between experiments. In all fluorescence titrations, solutions were buffered with 0.01 M potassium phosphate buffer, pH 7.0, 0.01 M KCl ($\mu = 0.028$; filtered through a sterile 0.2 μm Nalgene disposable filter). The final concentration of duplex hexadecamer was always 5.0 × 10^{-9} M. The concentrations of 1 used were 8.93 × 10^{-9} and 1.34 × 10^{-8} M while 3 was used at 5.0 × 10^{-8}, 7.5 x 10^{-8}, and 1.0 × 10^{-7} M. Buffered solutions (2.8 mL) containing dsDNA ± 1 or 3 were titrated with a 3.5 × 10^{-6} M solution of Hoechst 33258 (Ht) until a final concentration of 1.0 × 10^{-7} M was reached. All titration volumes were measured with Gilson Pipetman microliter pipets and disposable pipet tips. The solutions were excited at 354 nm, and fluorescence emissions were measured at 450 nm using the mean value of triplicate data collections with a thermostated (35 °C) Perkin-Elmer LS-50 fluorescence spectrophotometer. The samples were continuously stirred in matched quartz cuvettes (1-cm path length) and allowed at least 2 min to equilibrate between each titrant addition and fluorescence recording. The cuvettes were washed exhaustively with 10% HNO$_3$ and rinsed $\geq$ 5 times with distilled deionized H$_2$O before drying and subsequent use. Background fluorescence intensity (buffered solution of hexadecamer before the addition of any Ht) was subtracted from each titration point to provide the corrected fluorescence intensity, F. These corrected fluorescence intensity data points were fit to theoretical curves based on eq 1 with SigmaPlot 4.1.4 (Jandel Scientific) on a Macintosh Quadra 800 computer. Since the total fluorescence ($\Sigma\Phi$) varied slightly from one experiment to the next, this value was determined for each experiment (ca. 60 fluorescence units) from a titration of the dsDNA with Ht in the absence of any added ligand.

RESULTS AND DISCUSSION

Synthesis. It was reasoned that the linker arm on the central pyrrole of the target microgonotropen, 1, would terminate in a primary amine functionality. Various DNA modifying or cleaving agents with an aldehyde or other appropriate leaving groups may then be attached to the amino group of 1 by a reductive amination or substitution reaction. Initially, phthalimide was chosen as the protective group for the primary amine group. When the pyrrole-1-sodium salt of ethyl 4-nitro-2-pyr-rolecarboxylate (pyrrole + NaH in DMF) was allowed to react with *N*-(3-bromopropyl)phthalimide, only low yields

of the desired product **7** (Chart 2) were obtained, together with impurities presumbly arising from ring opening of the phthalimide. In efforts to obviate the above problem, reductive amination (Borch et al., 1971) of pyrrolealdehyde **8** (Chart 2; Burgstahler et al., 1976; Hale and Hoyt, 1915; Muchowski and Solas, 1984; Patwardhan and Dev, 1974; Sterzychi, 1979) was carried out with ammonium acetate in hopes that the reaction could yield the primary amine **9** (Chart 2). However, only the trimeric pyrrole **10** (Chart 2) was isolated in 45% yield, as indicated by proton NMR.

Chart 2
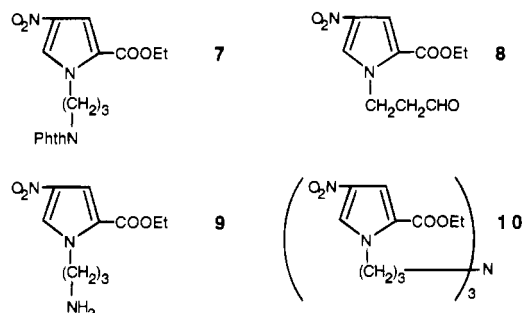
The difficulty was overcome when pyrrole **11** was condensed with *N*-(*tert*-butyloxycarbonyl)-3-bromopropy-lamine (Scheme 1) to afford a 90% yield of pyrrole **12** whose amine was protected by the *tert*-butyloxycarbonyl (Boc) group. In this reaction, potassium carbonate is preferred over the stronger bases such as sodium hydride, etc. When sodium hydride was used as a base, not only were the product yields low (54–60%), but the chromatographic separation also became difficult due to the presence of unreacted starting pyrrole which has nearly the same R_f value as that of product **12**. Alkaline hydrolysis (0.2 N NaOH) of the ethyl ester of **12** led to pyrrolecarboxylic acid **13**. Condensation of acid **13** with freshly prepared aminopyrrole **14** [synthesized in three steps (He et al., 1993) starting from commercially available materials] using diethyl cyanophosphonate (DECP; Yamada et al., 1973) as the coupling agent gave nitrodipyrrole **15** in 70–74% yields. The nitro group of **15** was reduced to the corresponding amine by catalytic hydrogenation and then acylated with 1-methyl-4-nitro-2-pyrrolecarboxylic acid in the presence of DECP to afford nitrotripyrrole **16** in 68% yield. After some initial problems, the nitropyrrole tripeptide **16** was reduced by hydrogenation to the corresponding amine with 10% palladium on charcoal at 50 psi of pressure and room temperature. The unstable aminotripyrrole was immediately converted to the acetamide tripyrrole **17** using acetic anhydride. The overall yield on going from **16** to **17** is 78%. In this case, acetic anhydride has proven to be a milder and more controllable acylating agent than acetyl chloride. Removal of the Boc protective group was achieved by dissolving the acetamide tripyrrole **17** in 50% trifluoroacetic acid to give the desired tripyrrole peptide **1**. Similarly, tripyrrole **3** was obtained by treating the nitrotripyrrole **16** with trifluoroacetic acid.

Equilibrium constants for the association of 1 and 3 with d(GGCGCAAATTTGGCGG)/d(CCGC-CAAATTTGCGCC) were determined by complexing either **1** or **3** (designated as L) to the duplex hexadecameric DNA in aqueous solutions at 35 °C (2.8 mL solutions containing 0.01 M phosphate buffer, pH 7.0, and 0.01 M KCl). The extent of complex formation was determined by titration of d(GGCGCA$_3$T$_3$GGCGG)/d(CCGCCA$_3$T$_3$GCGCC) with Hoechst 33258 (Ht; Loon-
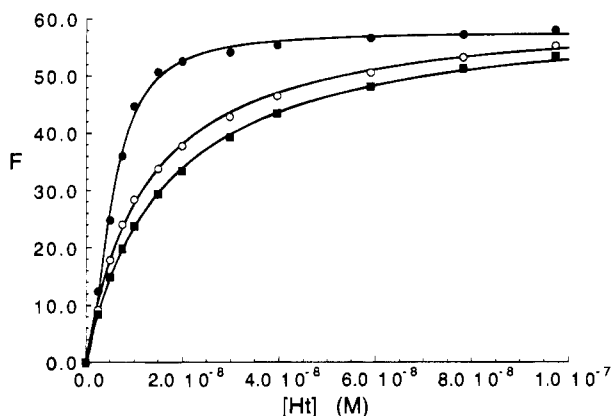
Figure 1. Plots of fluorescence (F, in arbitrary units) *vs* total Hoechst 33258 (Ht) concentration at pH 7.0 and 35 °C for **3** at 5.0×10^{-8} M (●) and **1** at 8.93×10^{-9} M (○) and 1.34×10^{-8} M (■) in the presence of 5.0×10^{-9} M d(GGCGCA$_3$T$_3$GGCGG)/ d(CCGCCA$_3$T$_3$GCGCC). The theoretical curves which fit the points were computer generated by use of eq 1.

tiens et al., 1990) and the increase in fluorescence due to formation of dsDNA:Ht complexes as Ht competes for a common A$_3$T$_3$ minor groove binding site. The concentrations of **1** and **3** were confirmed by peak integration of ^{1}H NMR resonances with resonances of an approximately equivalent but known concentration of 2,4,6-trimethyl benzoate.

Equation 1, derived from Scheme 2, relates the fluorescence (F) to each of the equilibrium binding constants, the total fluorescence ($\Sigma\Phi$), the total [L], and the total [Ht]. The rationale behind Scheme 2 and the subsequent derivation of eq 1 have been described in considerable

$$F = [\Sigma\Phi K_{\mathrm{Ht1}}[\mathrm{Ht}](0.5 + K_{\mathrm{Ht2}}[\mathrm{Ht}] + 0.5 K_{\mathrm{HtL}}[\mathrm{L}]Q')]/$$
$$[1 + K_{\mathrm{Ht1}}[\mathrm{Ht}] + K_{\mathrm{Ht1}}K_{\mathrm{Ht2}}[\mathrm{Ht}]^2 + K_{\mathrm{Ht1}}K_{\mathrm{HtL}}[\mathrm{Ht}][\mathrm{L}] +$$
$$K_{\mathrm{L1}}[\mathrm{L}] + K_{\mathrm{L1}}K_{\mathrm{L2}}[\mathrm{L}]^2] \quad (1)$$

detail (Browne et al., 1993). The values of $K_{\mathrm{Ht1}} = 3.75 \times 10^7$ M^{-1} and $K_{\mathrm{Ht2}} = 1.45 \times 10^9$ M^{-1} used in this study were determined and reported previously using 0.01 M NaCl instead of 0.01 M KCl; there is no difference in the binding constants of Ht whether one or the either of these two different salts is used. The equilibrium association constants calculated as best fits to the experimental data points for **1** and **3** with eq 1 are presented in Table 1. Representative plots of fluorescence (F) *vs* [Ht] using these constants at 5.0×10^{-8} M **3** and 8.9×10^{-9} and 1.3×10^{-8} M **1** in the presence of 5.0×10^{-9} M d(GGCGCA$_3$T$_3$-GGCGG)/d(CCGCCA$_3$T$_3$GCGCC) are shown in Figure 1.

Several conclusions concerning functional groups on this class of minor groove binding agents (tripyrrole peptides) can be made from a comparison of the equilibrium association constants found in Table 1. Substituting the amino terminal formyl group of distamycin with an acetamido and the carboxy terminal amidine with $-\mathrm{CH_2CH_2CH_2(NCH_3)_2}$ yields compound **2** along with 3 orders of magnitude decrease in binding affinity ($K_{\mathrm{L1}}K_{\mathrm{L2}}$) compared to distamycin (1.0×10^{16} M^{-2}). Changing the N-methyl group on the central pyrrole of **2** to an N-propylamino functionality (**1**) more than compensates for **2**'s decrease in binding affinity (it increases by ca. 2500-fold!). The protonated N-propylamine of the central pyrrole is able to electrostatically interact with the DNA's phosphates' oxyanions while an N-methyl group of **2** only provides van der Waals interactions with the walls of the minor groove. [A model structure of this interaction is
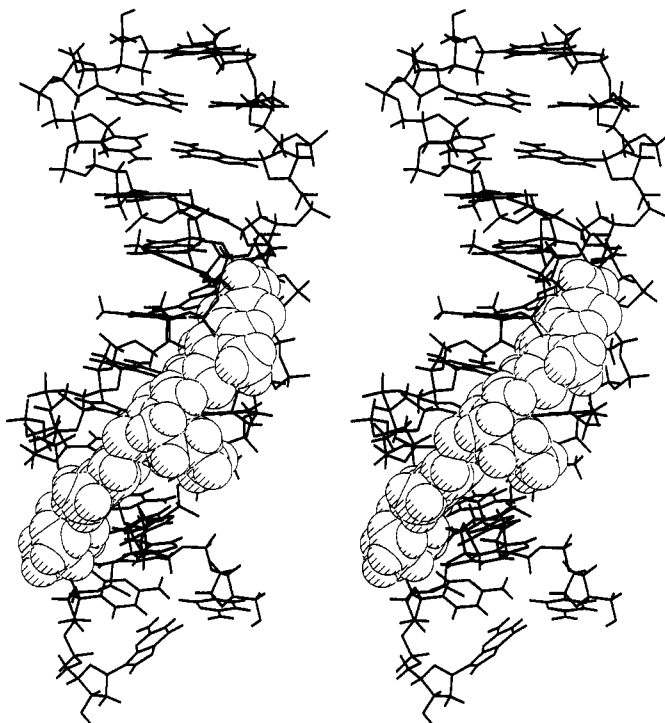
Figure 2. Stereoview of a plausible model of **1** binding to an A$_3$T$_3$ binding site of d(CGCAAATTTGCG)$_2$. The primary amine of the N-propylamine is positioned on the edge of the major groove and is acting as a salt bridge between two adjacent phosphates on the backbone of the DNA. The model was generated on a Silicon Graphics (Mountain View, CA) Iris 4D/340GTX workstation in the molecular graphics program QUANTA version 4.0 (Molecular Simulations, Inc., Waltham, MA) and is based on the ^{1}H NMR-derived solution structure of a single molecule of **6b** complexed to d(CGCAAATTTGCG)$_2$ (Blaskó et al., 1994). The extra methylene of **6b**'s butyl linker was removed along with the terminating ethylamino groups of the tris(2-aminoethyl)amino moiety. The N-propylamino moiety was CHARMm (version 21.3; Molecular Simulations) minimized for 65 steps (at which point the root mean square derivative had reached $<$ 0.5 kcal/mol·Å) using the adopted basis Newton–Raphson algorithm, while the remainder of the complex was held under harmonic constraints, to yield this model of **1** complexed to d(CGCAAATTTGCG)$_2$.

Scheme 2
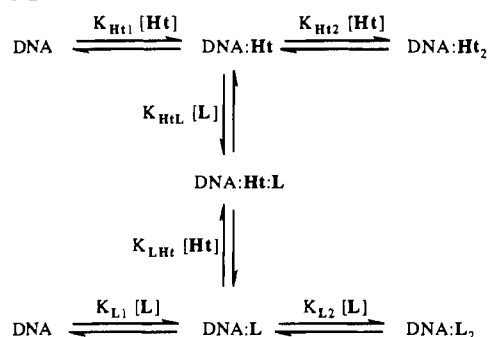
Table 1. A Comparison of the Mean Logarithmic Values of the Equilibrium Association Constants for 1, 2, 3, 6a, and Distamycin to the Hexadecameric Duplex d(GGCGCA₃T₃GGCGG)/d(CCGCCA₃T₃GCGCC).

ligand (L)	$\log K_{L1}$	$\log K_{L2}$	$\log K_{L1}K_{L2}$	$\log K_{HtL}$
2[a,b]	6.8	6.2	13.0	−1.2
3[c,d]	6.5 ± 0.34	7.4 ± 0.35	13.9	7.2 ± 0.24
1[c,e]	8.4 ± 0.15	8.0 ± 0.41	16.4	9.5 ± 0.078
6a[a,b]	9.2	9.2	18.4	10.7
distamycin[a,b]	7.6	8.4	16.0	8.8

[a] Reactions were performed in H_2O, 0.01 M phosphate buffer, pH 7.0, and 0.01 M NaCl at 35 °C. [b] Reference (He et al., 1994). [c] Reactions were performed in H_2O, 0.01 M phosphate buffer, pH 7.0, and 0.01 M KCl at 35 °C. [d] Mean values and standard deviations (σ_n) are the result of duplicate experiments at 5.0 × 10^{-8}, 7.5 × 10^{-8}, and 1.0 × 10^{-7} M in **3**. [e] Mean values and standard deviations (σ_n) are the result of triplicate experiments at 8.93 × 10^{-9} and 1.34 × 10^{-8} M in **1**.

presented in Figure 2. This view of the model shows the *N*-propylamine poised to enter the major groove.] Removing the acetamido moiety from the amino terminus of **1** and replacing it with a nitro group (**3**) leads to a 300-fold decrease in $K_{L1}K_{L2}$; this decrease is mostly manifested in K_{L1} and is due to loss of hydrogen bonding interactions of the acetamide −NH to the floor of the minor groove of the DNA [to the N3 and O2 of an adenine and a thymine, respectively (Coll et al., 1987)]. Adding three appropriate amines (that are likely protonated under neutral conditions) separated by methylene linkers to the *N*-propylamine moiety of **1** yields **6a** and an increase in $K_{L1}K_{L2}$ of 2 orders of magnitude. [Note that the tris(2-aminoethyl)amino moiety of **6a** sequesters two of the DNA's phosphodiester groups (Blaskó et al., 1994) while the *N*-propylamine of **1** can only form salt bridges (Figure 2).] The new carrier **1** is intermediate in its affinity for dsDNA in the series for $K_{L1}K_{L2}$ where **6a** ≫ **1** > distamycin ≫ **3** > **2**. Future communications from this laboratory will use **1** as the essential building block for microgonotropens with a variety of functionalities beyond those seen with **5abc** and **6ab**.

ACKNOWLEDGMENT

LITERATURE CITED

Beerman, T. A., McHugh, M. M., Sigmund, R., Lown, J. W., Rao, K. E., and Bathini, Y. (1992) Effects of Analogs of the DNA Minor Groove Binder Hoechst 33258 on Topoisomerase II and I Mediated Activities. *Biochim. Biophys. Acta 1131*, 53−61.

Blaskó, A., Browne, K. A., and Bruice, T. C. (1994) Microgono-

tropens and Their Interactions with DNA. 5. Structural Characterization of the 1:1 Complex of d(CGCAAATTT-GCG)₂and Tren-Microgonotropen-b by 2D NMR Spectroscopy and Restrained Molecular Modeling. *J. Am. Chem. Soc. 116*, 3726−3737.

Boger, D. L., and Sakya S. M., (1992) CC-1065 Partial Structures: Enhancement of Noncovalent Affinity for DNA Minor Groove Binding through Introduction of Stabilizing Electrostatic Interactions. *J. Org. Chem. 57*, 1277−1284.

Borch, R. F., Bernstein, M. D., and Durst, H. D. (1971) The Cyanohydridoborate Anion as a Selective Reducing Agent. *J. Am. Chem. Soc. 93*, 2897−2904.

Browne, K. A., He, G.-X., and Bruice, T. C. (1993) Microgonotropens and Their Interactions with DNA. 2. Quantitative Evaluation of Equilibrium Constants for 1:1 and 2:1 Binding of Dien-Microgonotropen-a, -b, and -c as Well as Distamycin and Hoechst 33258 to d(GGCGCAAATTTGGCGG)/ d(CCGC-CAAATTTGCGCC). *J. Am. Chem. Soc. 115*, 7072−7079.

Burgstahler, A. W., Weigel, L. O., and Shaefer, C. G. (1976) Improved Modification of the Rosenmund Reduction. *Synthesis 767−768.*

Coll, M., Frederick, C. A., Wang, A. H.-J., and Rich, A. (1987) A Bifurcated Hydrogen-bonded Conformation in the d(A·T) Base Pairs of the DNA Dodecamer d(CGCAAATTTGCG) and its Complex with Distamycin. *Proc. Natl. Acad. Sci. U.S.A. 84*, 8385−8389.

Hale, W. J., and Hoyt, W. V. (1915). The Constitution of the Nitro-α-Carbopyrrolic Acids. *J. Am. Chem. Soc. 37*, 2538−2552.

Hansma, H. G., Browne, K. A., Bezanilla, M., and Bruice, T. C. (1994) Bending and Straightening of DNA Induced by the Same Ligand: Characterization with the Atomic Force Microscope. *Biochemistry 33*, 8436−8441.

He, G.-X., Browne, K. A., Groppe, J. C., Blaskó, A., Mei, H.-Y., and Bruice, T. C. (1993) Microgonotropens and Their Interactions with DNA. 1. Synthesis of the Tripyrrole Peptides Dien-Microgonotropen-a, -b, and -c and Characterization of Their Interactions with dsDNA. *J. Am. Chem. Soc. 115*, 7061−7071.

He, G.-X., Browne, K. A., Blaskó, A., and Bruice, T. C. (1994) Microgonotropens and Their Interactions with DNA. 4. Synthesis of the Tripyrrole Peptides Tren-Microgonotropen-a and -b and Characterization of Their Interactions with dsDNA. *J. Am. Chem. Soc. 116*, 3716−3725.

Kopka, M. L., Yoon, C., Goodsell, D., Pjura, P., and Dickerson, R. E. (1985) The Molecular Origin of DNA-drug Specificity in Netropsin and Distamycin. *Proc. Natl. Acad. Sci. U.S.A. 82*, 1376−1380.

Loontiens, F. G., Regenfuss, P., Zechel, A., Dumortier, L., and Clegg, R. M. (1990) Binding Characteristics of Hoechst 33258 with Calf Thymus DNA, Poly[d(A-T)], and d(CCGGAA-TTCCGG): Multiple Stoichiometries and Determination of Tight Binding with a Wide Spectrum of Site Affinities. *Biochemistry 29*, 9029−9039.

Lown, J. W., Krowicki, K., Bhat, U. G., Skorobogaty, A., Ward, B., and Dabrowiak, J. C. (1986) Molecular Recognition Between Oligopeptides and Nucleic Acids: Novel Imidazole-Containing Oligopeptides Related to Netropsin That Exhibit Altered DNA Sequence Specificity. *Biochemistry 25*, 7408−7416.

Muchowski, J. M., and Solas, D. R. (1984) Protecting Groups for the Pyrrole and Indole Nitrogen Atom. The [2-(Trimethylsilyl)ethoxy]methyl Moiety. Lithiation of 1-[[2-(Trimethylsilyl)ethoxy]methyl]pyrrole. *J. Org. Chem. 49*, 203−205.

Nunn, C. M., Jenkins, T. C., and Neidle, S. (1993) Crystal Structure of d(CGCGAATTCGCG) Complexed with Propamidine, a Short-Chain Homologue of the Drug Pentamidine. *Biochemistry 32*, 13838−13843.

Patwardhan, S. A., and Dev, S. (1974) Amberlyst-15, a Superior Catalyst for the Preparation of Enol Ethers and Acetals. *Synthesis 348−349.*

Sterzychi, R. (1979) Pyridinium Tosylate, a Mild Catalyst for Formation and Cleavage of Dioxolane-type Acetals. *Synthesis 724−725.*

Yamada, S., Kasai, Y., and Shioiri, T. (1973) Diethylphosphoryl cyanide. A New Reagent for the Synthesis of Amides. *Tetrahedron Lett. 1595−1598.*

BC940089W

Intensely Luminescent Immunoreactive Conjugates of Proteins and Dipicolinate-Based Polymeric Tb(III) Chelates

Jagannath B. Lamture[†] and Theodore G. Wensel*

Verna and Marrs McLean Department of Biochemistry, Baylor College of Medicine, One Baylor Plaza, Houston, Texas 77030. Received June 27, 1994[⊗]

Partial alkylation of polylysine with 4-(iodoacetamido)-2,6-dimethylpyridine dicarboxylate (IADP), followed by exhaustive reaction with succinic anhydride, yielded polymers (PLDS, polymer of lysine, dipicolinate, and succinate) containing large numbers (50–100) of 4-substituted dipicolinic acid moieties per molecule, with the remaining lysyl side chains succinylated. Competition experiments showed that PLDS binds Tb(III) ions with much higher affinity than does EDTA and strongly enhances the visible luminescence they emit when excited with ultraviolet light. Carbodiimide-mediated coupling to proteins, including bovine serum albumin, ovalbumin, and protein A, yielded PLDS–protein conjugates whose Tb(III) chelates displayed intense green luminescence and millisecond excited state lifetimes. These conjugates retained sufficient immunoreactivity to allow their use in sensitive luminescence-based immunodetection schemes for proteins immobilized on nitrocellulose. The presence of 10 ng of ovalbumin could be easily visualized by eye when probed with rabbit anti-ovalbumin and PLDS–protein A–Tb(III). The ease of preparation of PLDS–protein–Tb(III) conjugates, and their favorable luminescence properties, make them promising reagents for use in time-resolved luminescence immunoassays and other ultrasensitive detection schemes for macromolecules.

INTRODUCTION

The use of time-gated measurements of millisecond emission from lanthanide ions to enhance background rejection and sensitivity in luminescence-based immunoassays is well established (Soini and Lovgren, 1987). The EDTA- or DTPA-based bifunctional chelating agents used to couple lanthanides such as Eu(III) to proteins, in general, do not give rise to strong sensitized emission from the bound lanthanide ions. For this reason, commercially available systems have used a multistep protocol involving dissociation of the bound ion and treatment with an enhancing reagent that does give rise to strong sensitized emission (Soini and Lovgren, 1987). In contrast to their complexes with EDTA-based chelating agents, complexes of Tb(III) or Eu(III) with chelators whose coordinating atoms are involved in conjugated π electron systems can display very strong sensitized emission. For Tb(III), one of the most efficient sensitizing chelators (Barela and Sherry, 1976) is dipicolinic acid (DPA[1]). Until recently, bifunctional reagents for coupling DPA groups to macromolecules have not been available. Recently, however, reactive 4-substituted DPA analogues have been described (Mukkala et al., 1992; Lamture and Wensel, 1993), including a 4-(iodoacetamido) derivative (IADP) that readily alkylates proteins and whose synthesis is quite simple. The main drawback to this reagent is that the stability of its Tb(III) complexes is expected to be rather low (dissociation constants in the

micromolar range), as observed for DPA itself (Grenthe, 1961), and because of the ability of each Tb(III) to coordinate three dipcolinates, protein conjugates derived from this reagent appear to be crosslinked by Tb(III).

In order to obtain a reagent with high affinity for Tb-(III) and the ability to supply sufficient ligands within a single molecule to occupy terbium's nine coordination sites, we have developed a polymeric conjugate of IADP and polylysine that can be coupled to proteins, that binds Tb(III) ions with very high affinity, and that very efficiently enhances their luminescence. It has the added advantage that multiple luminescent Tb(III)–DPA complexes are present in each labeled protein, even if only one site on the protein is modified with the polymer, so that the molar luminescence intensity is brighter than that of conventional monomeric fluorophores.

EXPERIMENTAL PROCEDURES

Materials. Reagents for preparation of IADP were as described (Lamture and Wensel, 1993). Other reagents were obtained commercially and used without further purification: EDC and Tb(NO$_3$)$_3$ atomic absorption standard solution from Aldrich, N-hydroxysulfosuccinimide from Pierce, polylysine, proteins, antisera, and Sephadex G-25 from Sigma. All reactions with polylysine and its derivatives were carried out in siliconized microfuge tubes. Buffers used were as follows: TBS, 154 mM NaCl, 10 mM Tris·HCl, pH 7.4; borate buffer, 0.1 M potassium borate, pH 9; MOPS/citrate, 0.1 M MOPS, 0.1 M sodium citrate, adjusted to pH 7 with NaOH; bicarbonate buffer, 0.1 M NaHCO$_3$, pH 9; BLOTTO, TBS with 5% (w/v) dry milk, 0.5% (v/v) Nonidet P-40 detergent, 3 mM NaN$_3$.

Instrumentation. UV spectra were measured on a Hewlett-Packard HP 8452 diode array spectrophotometer. Fluorescence measurements were made on an Aminco-Bowman spectrofluorometer modified as described (Ramdas et al., 1990). Lifetime measurements were carried out using an instrument based on a UV-optimized argon ion laser (to be described elsewhere (Lamture et al. submitted)) and similar in design to one described previously (Wensel and Meares, 1983).

* To whom correspondence should be addressed. E-mail: twensel@bcm.tmc.edu. Tel. (713) 798-6994. Fax: (713) 796-9438.

† Current address: Center for Biotechnology, Baylor College of Medicine, Woodlands, TX 77381.

[1] Abbreviations: M$_r$, average relative molecular weight for polylysine preparation; DPA, dipicolinic acid or the dipicolinate moiety within the polymers; IADP, 4-(iodoacetamido)-2,6-dimethylpyridine dicarboxylate, PLD, product of reaction between polylysine and IADP; PLDS, succinylated PLD; MOPS, 4-morpholinepropanesulfonic acid; BSA, bovine serum albumin; EDC, 1-(3-(dimethylamino)propyl)-3-ethylcarbodiimide hydrochloride.

Preparation of 4-(Iodoacetamido)-2,6-dimethyl-pyridine Dicarboxylate (IADP). IADP was synthesized as described previously (Lamture and Wensel 1993). Briefly, 4-amino 2,6-dimethylpyridine dicarboxylate (0.071 mmol) was mixed with iodoacetic anhydride (0.22 mmol) and a drop of concentrated H_2SO_4 at 60 °C for 30 min. The reaction mixture was then cooled in ice–water, and methanol (1 mL) was added to it slowly. After solvent removal, the crude reaction mixture was chromatographed over silica gel (1 × 20 cm), using hexane:ethyl acetate (1:1) as an eluant. After the faster moving impurities were removed the product was eluted and recovered after solvent removal in 67% yield as a white powder, which was characterized by TLC, ^1H and ^{13}C NMR, and GC–MS analysis as described (Lamture and Wensel, 1993).

Labeling of Polylysine with IADP (Synthesis of PLD/PLDS). A mixture of poly-L-lysine hydrobromide (Sigma, nominal average $M_r = 26\ 000$ or $10\ 000$, 2–4 mg, 9.5–19 μmol, of lysyl residues) and IADP (4–12.5 mg, 10.6–33 μmol) in 0.1 M $NaHCO_3$ (1.6 mL) was stirred at 55 °C overnight to yield dipicolinic acid-modified polylysine (PLD). Modification of amino groups was monitored by the TNBS color test (Means and Feeney, 1971). To this reaction mixture was added succinic anhydride (20 mg, 200 μmol), and the mixture was stirred at room temperature for 8 h. The pH of the reaction was constantly maintained at 8.5 by 2 N NaOH throughout the course of the reaction. The product was separated from low molecular weight reactants and side products by centrifugation through Sephadex G-25 equilibrated in bicarbonate buffer. When the product was filtered through nitrocellulose using a Slot Blot apparatus, treated with $TbCl_3$, and examined under ultraviolet light, the product, but not IADP, polylysine, or succinylated polylysine, displayed intense green emission. On the basis of the TNBS test before and after modification of polylysine, it was found that more than 90% of the original amino groups were modified to yield PLDS (succinylated PLD). SDS polyacrylamide gel electrophoresis, followed by staining with $TbCl_3$ and UV illumination, resulted in a broad band of green luminescence centered at a position corresponding to an apparent M_r of about $29\ 000$ (for reactions starting with $10\ 000$ M_r polylysine and ~0.5 DPA groups per lysyl residue). Lanes loaded with polylysine or IADP did not display this luminescent band. The concentration of dipicolinate groups was estimated from the absorbance at 254 nm, using the molar extinction coefficient of IADP of 9629 $M^{-1} \cdot cm^{-1}$ at 254 nm (determined by spectrophotometry of a highly purified sample of IADP dimethyl ester after mild alkaline hydrolysis). In general, estimated yields of DPA group incorporation into PLDS derived from UV absorbance measurements agreed well with those derived from TNBS tests, so the TNBS test was used routinely to determine the average number of DPA groups per polymer, before succinylation, and UV absorbance was used to determine the concentration of polymer and DPA groups thereafter. In four different preparations tested, succinylation yields were indistinguishable from complete modification.

Competition between EDTA and PLDS or DPA. Samples for competition experiments all contained 1 μM $Tb(NO_3)_3$ and MOPS/citrate buffer, and emission was monitored at 546 nm with 278 nm excitation. To measure the exchange of Tb(III) from PLDS or DPA to EDTA, PLDS or DPA was added first at a final concentration of 2 μM DPA groups (20 nM PLDS for the preparation used, which was prepared from M_r 26 000 polylysine) and the emission measured before and after
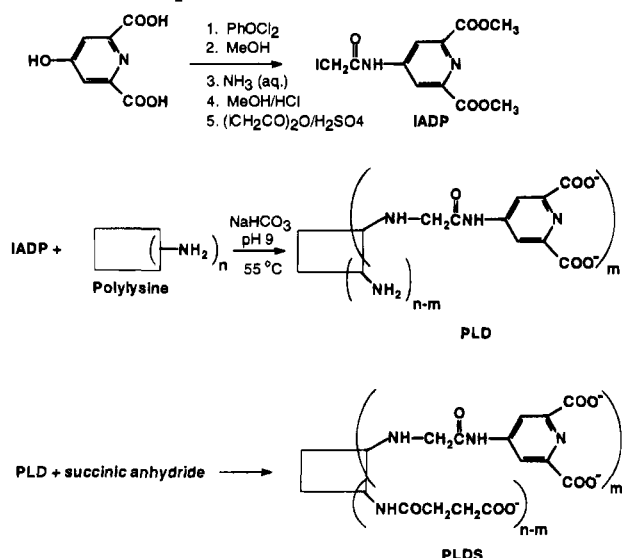
addition of 1 mM EDTA. Samples were monitored immediately after EDTA addition and several more times over a 2–3 day period, while the samples were kept at room temperature. To measure exchange of Tb(III) from EDTA to PLDS or DPA , EDTA was added first at various concentrations (10 μm to 1.0 mM) and the emission measured before and at various times after addition of PLDS or DPA to a final concentration of 2 μM DPA groups.

Conjugation of Proteins with PLDS. Typical reaction conditions are illustrated by the conditions for labeling bovine serum albumin (BSA): To an aqueous solution of PLDS (from M_r 10 000 polylysine, ~0.5 DPA/lysyl) in water (~4.9 nmol) was added EDC (500 μg) and N-hydroxysulfosuccinimide (500 μg) in a final volume of 160 μL, pH 4. After 3 min at room temperature to allow activation of PLDS, 30 μL of potassium borate buffer containing 151 μM BSA (4.5 nmol) was added and the pH was adjusted to 8.5 with NaOH. After 2 h at room temperature, the sample was analyzed by SDS polyacrylamide gel electrophoresis (Laemmli, 1970) and by immobilization on a nitrocellulose slot blot, followed by staining with $TbCl_3$. To test the stability of the Tb(III) complex, after initial visualization under UV illumination, the blots were incubated with 0.1 M EDTA, pH 8, and examined 48 h and 46 days later. Similar conditions were used to conjugate PLDS with ovalbumin, protein A, and avidin, using PLDS from M_r 26 000 polylysine, ~0.9 DPA/lysyl, and PLDS/protein molar ratios of 0.58 (ovalbumin), 1.32 (avidin), or 0.65 (protein A).

Immunodetection of proteins on blots using specific antisera and Tb–PLDS–protein conjugates. Aliquots of BSA (0.5–20 μg) were blotted onto a nitrocellulose membrane using a BioRad Bio-Dot slot-blot apparatus and blocked by a 2 h incubation in gelatin suspension. The membrane strips were washed in 2 × TBS and separately incubated overnight with rabbit BSA-specific antiserum or normal rabbit serum (both from Sigma) at a dilution of 1:80. The membranes were washed with 2 × TBS (4 × 25 mL) and incubated with a 2 × TBS solution of PLDS–BSA (350 nM, from M_r 26 000 polylysine, ~0.9 DPA/lysyl) for 1 h. Finally, the membranes were soaked in $TbCl_3$ (47 μM) for 15 min and then washed with 2 mM EDTA and visualized/photographed under UV (254 nm) light. For immunodetection of ovalbumin on blots using ovalbumin antiserum and PLDS–protein A, aliquots of ovalbumin (0.01–3 μg) were blotted onto nitrocellulose and blocked with BLOTTO (5% w/v dry milk in TBS, 0.5% NP-40, 3 mM NaN_3). They were then washed with water and 2 × TBS, followed by 4 h incubation in ovalbumin antiserum (rabbit, Sigma) at a dilution of 1:130 in 2 × TBS. The strips were washed with 2 × TBS, and incubated in a 2 × TBS solution of PLDS–protein A (380 nM, from M_r 26 000 polylysine, ~0.9 DPA/lysyl) for 30 min before addition of $TbCl_3$ (100 μM) and UV illumination.

RESULTS AND DISCUSSION

Preparation of polylysine derivatized with dipicolinate and succinate (PLDS). Reaction between IADP and polylysine (Scheme 1) was used to prepare polylysine derivatives that had multiple dipicolinic acid moieties, which were then treated with succinic anhydride to succinylate any remaining unmodified primary amine groups. The labeling yield was dependent on the molar ratios of the reactants. With a 50% molar excess of IADP over lysyl side chains, 80%–90% labeling efficiency was achieved (starting with polylysine of nominal M_r 26 000), while at a 0.5:1 ratio of IADP to lysyl side chains virtually all of the IADP reacted with the polymer

Scheme 1. Preparation of PLDS

Figure 1. Luminescence of Tb—PLDS. A. Excitation spectrum (emission at 546 nm). B. Emission spectrum (excitation at 285 nm). C. Emission decay kinetics. A solution containing 50 nM Tb—PLDS was excited with ~20 ms pulses of 275 nm light from an argon ion laser and the luminescence at 546 nm monitored as a function of time after the end of the excitation pulse. Both linear and semilogarithmic plots of the same data are shown, and the theoretical curve drawn on the semilogarithmic plot corresponds to a best-fit lifetime of 1.37 ms. The polylysine used for this PLDS preparation had a nominal M_r of 10 000 and a DPA/lysyl substitution ratio of approximately 0.4.

to give a labeling efficiency of approximately 50% (starting with polylysine of nominal M_r 26 000 or 10 000). Labeling efficiency of remaining amine groups on the polymer by succinylation was generally > 90%, regardless of the stoichiometry of the IADP labeling step. The succinylation step, which was designed to increase the number of carboxylates available for subsequent coupling to proteins, appeared to improve the solubility of the polymer and also minimized problems with formation of PLDS—PLDS crosslinks during subsequent protein coupling reactions. While our initial work has used lower molecular weight polylysines to minimize problems with solubility and surface adsorbtion, preliminary experiments (Lamture and Wensel, unpublished results) suggest that higher polymers (M_r 100 000—150 000) may also be useful for preparing derivatives with higher numbers of chelating groups per molecule.

Luminescence Properties of Tb—PLDS. Addition of TbCl$_3$ to PLDS resulted in strong sensitized Tb(III) emission, with an excitation spectrum (Figure 1A) similar to that of complexes of Tb(III) with 4-acetamidodipicolinate (Lamture et al., 1995), and a typical Tb(III) emission spectrum. The excited state lifetime of Tb—PLDS was found to be approximately 1.4 ms, somewhat longer than that observed for a 1:3 complex of Tb(III) with IADP (1.25 ms) and comparable to that of a 1:3 complex of Tb(III) with 4-acetamidodipicolinate (1.4 ms; Lamture et al., 1995), suggesting that the average number of polymer atoms coordinated to each bound ion is close to 9. Although lifetime heterogeneity is to be expected as a result of heterogeneous environments for bound metal ions, the decay curve was fit reasonably well by a single exponential function, suggesting that the various Tb(III) binding sites are not terribly dissimilar. Alternatively, some sites may have much shorter lifetimes but not be observable because of their small contribution to the total emission.

Stability of Tb-PLDS. Figure 2 shows the results of experiments comparing the stability of Tb—PLDS relative to Tb complexes with EDTA and dipicolinic acid (DPA). Because the ligand exchange reactions are quite slow, the equilibria were approached from either side. First, a solution containing 2 μM DPA groups, in monomeric (DPA) or polymeric (20 nM PLDS) form, was mixed with 1 μM Tb(NO$_3$)$_3$ to ensure quantitative complexation of Tb. Then these complexes were challenged with 1 mM EDTA. Emission intensity at 546 nm was used to follow ligand exchange because luminescence from TbEDTA is

much weaker than that from Tb—PLDS or Tb—DPA complexes; with the instrumental settings used, the Tb—EDTA signal was only a few percent above the background signal detected from buffer alone, while the Tb—PLDS and Tb—DPA signals were more than 10-fold, and more than 23-fold higher than the buffer signal, respectively (Figure 2). In the case of PLDS, the signal declined by less than 5% after 24 h (Figure 2A) or 3 days (data not shown) challenge with EDTA. In contrast, 1 mM EDTA decreased the signal from Tb—DPA to a level near background almost immediately (Figure 2B). When chelators were added to 1 μM Tb in the reverse order (i.e., EDTA before DPA or PLDS), DPA and PLDS again showed strikingly different behavior. Addition of 2 μM DPA to 10 μM EDTA and 1 μM Tb resulted in almost no increase in emission intensity (Figure 2B), even when monitored for 2 days (data not shown). When 20 nM PLDS was added to a mixture of 10 μM EDTA and 1 μM Tb, there was a slow increase in luminescence, which reached a final value nearly equal to that of the Tb—PLDS solution with no EDTA, with a half-time of about 13 min (Figure 2A). When the same experiment was carried out using 1 mM EDTA and the same final concentrations of Tb and PLDS, the luminescence increased much more slowly (half-time of 4.4 h) and reached a final value (measured 3 days later) that was 64% of that measured for Tb—PLDS without EDTA (data not shown). These results suggest that Tb—PLDS complexes are approximately 50 000 times more stable than Tb—EDTA, whose stability constant (for the fully deprotonated form of EDTA) is on the order of 10^{18} M^{-1} (Martell and Smith, 1974). In addition, the dissociation of Tb(III) from PLDS, once bound, is so slow as to be practically unmeasurable using the methods desribed here. We have observed by visual inspection under UV
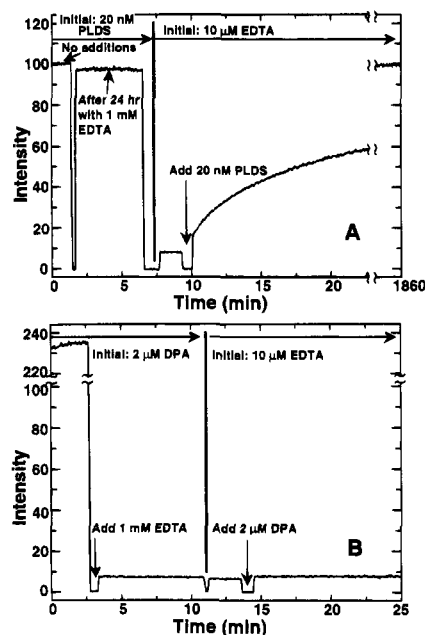
Figure 2. Competition between EDTA and PLDS or DPA. The 546 nm emission from samples excited at 278 nm was monitored continuously in samples containing 1.0 μM Tb(NO$_3$)$_3$, MOPS/citrate buffer, and one or both of the following added at the indicated concentrations: PLDS (20 nM, from M_r 26 000 polylysine, 2 μM DPA groups), DPA (2 μM), or EDTA (10 μm or 1.0 mM) added in the indicated order. Deflections of the traces to zero resulted from closing of the emission shutter as samples were changed or chelators added. A. Comparison of PLDS and EDTA. Emission first was collected from a sample containing 1 μM Tb and 20 nM PLDS and then from a sample that was identical, except that 1 mM EDTA had been added 24 h before the measurement shown, but after Tb and PLDS. The emission from this sample had not changed substantially when checked again 2 days later (not shown). Then a sample containing 10 μM EDTA and 1 μM Tb was monitored for a few minutes before addition of 20 nM PLDS. The increase in emission over the first 13 min after PLDS addition is shown, as well as the final value measured 2 days later. B. Comparison of DPA and PLDS. To a sample containing initially 2 μM DPA and t μM Tb was added EDTA to 1 mM and emission monitored before and after EDTA addition. Then a sample containing 10 μM EDTA and 1 μM Tb was monitored briefly before addition of DPA to 2 μM. When checked again 2 days later, the emission from this sample had not changed significantly (not shown).

illumination that Tb remains complexed with PLDS bound to nitrocellulose membranes after soaking for 11 days in 0.1 M EDTA.

Stoichiometry of Tb(III) Binding by PLDS. A typical result from titration of PLDS with standard Tb-(NO$_3$)$_3$ is shown in Figure 3. This titration indicates a binding stoichiometry of approximately one Tb(III) per seven DPA groups on PLDS or roughly 14 Tb(III) bound, on average, to each PLDS polymer containing, in this preparation, ~100 DPA groups per polymer. Similar titrations with different preparations of PLDS gave similar results, with the number of DPA groups per bound Tb(III) varying from 3 to 7. Lower levels of DPA substitution on polylysine tended to give higher ratios of Tb:DPA groups. These results suggest that at higher levels of DPA substitution (e.g., 80%–90%) as many as half of the DPA groups attached to PLDS may not be able to bind Tb(III), perhaps as a result of steric constraints. Although precautions were taken to minimize contamination with adventitious metal ions, we cannot rule out that some chelating sites were occupied by such contaminants. Therefore, the apparent stoichiometries observed must be considered as lower limits on the number of potential Tb(III) binding sites.
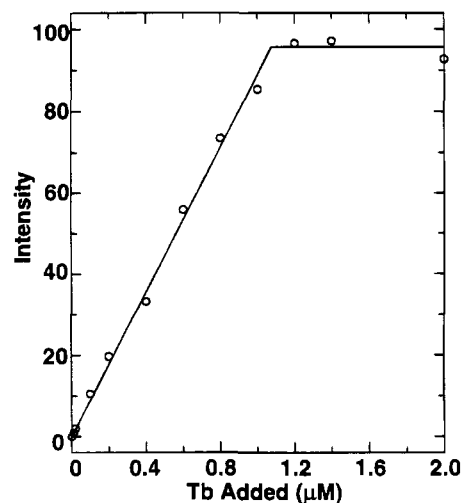
Figure 3. Titration of PLDS with Tb(NO$_3$)$_2$. Luminescence intensities were measured at 546 nm (excitation at 285 nm) for samples containing 75 nM PLDS (7.5 μM DPA groups, prepared from polylysine of nominal average M_r 26 000) and the indicated concentrations of Tb(NO$_3$)$_3$ prepared by dilution of a commercial atomic absorption standard solution.

Protein Conjugates of PLDS. Covalent coupling of PLDS to protein was achieved for bovine serum albumin (BSA), ovalbumin, protein A, avidin, and IgG. In each case, SDS–PAGE showed new bands appearing above the bands of the unlabeled proteins, and well above the PLDS bands, that showed intense green luminescence when soaked in TbCl$_3$ and illuminated with UV light. For BSA (Figure 4) and protein A, Coomassie staining showed that the majority of the protein had been converted to PLDS conjugates (and possibly some comigrating homo-oligomeric conjugates) while for avidin and ovalbumin, the yield of conjugation was relatively low (<30%). No obvious solubility problems were encountered for the BSA and protein A conjugates, but there were minor higher molecular weight species that failed to enter the stacking gel or were trapped at the top of the resolving gel. These species were positive for both sensitized Tb(III) emission and for Coomassie blue staining.

Stability of Tb(III) Complexes with PLDS–BSA. To assess the stability of Tb–PLDS–BSA, the nitrocellulose sheets with immobilized Tb–PLDS–BSA were soaked in 0.1 M EDTA. After 46 days, the luminescence from the immobilized complex was still clearly visible under UV illumination.

Immunodetection on Nitrocellulose Using Tb–PLDS–Protein Conjugates. When BSA was immobilized on nitrocellulose and probed successively with BSA antiserum, PLDS–BSA, and TbCl$_3$, bright green luminescence was observed under UV illumination (Figure 5). This detection procedure is obviously suboptimal in terms of sensitivity because of quenching by nitrocellulose, the ability of only a fraction of the bound antibodies to bind the conjugate, and the lack of time-gating. Nonetheless, this result demonstrates the feasibility of immunodetection using PLDS-labeled proteins. By using Tb–PLDS–protein A to detect antibodies in ovalbumin antiserum bound to slot-blotted ovalbumin, we were able to detect by eye as little as 10 ng of ovalbumin, a sensitivity comparable to that routinely achieved by enzyme-linked immunodetection schemes. Somewhat poorer results (~100 ng detection limit) were observed when avidin was labeled with PLDS and used in a similar assay to detect biotin-labeled goat-anti-rabbit antibodies bound to ovalbumin–antibody complexes on nitrocellulose. It will likely be possible to obtain better results
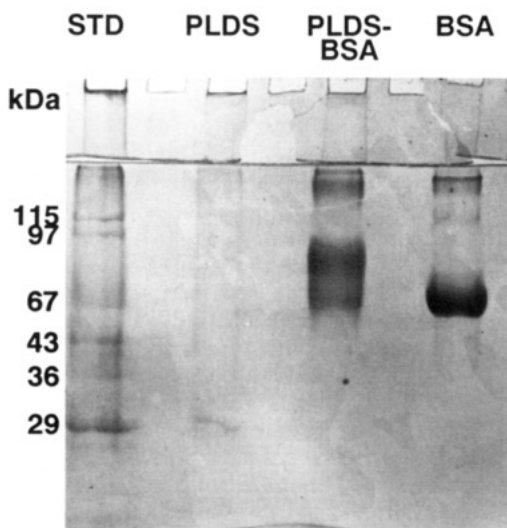
Figure 4. SDS−PAGE analysis of PLDS−BSA. Photograph of a Coomassie-Blue stained polyacrylamide (12% acrylamide) SDS gel loaded with 10 μg of BSA, before and after reaction with activated PLDS, as described in the text. Molecular weight markers are carbonic anhydrase (29 kDa), glyceraldehyde 3-phosphate dehydrogenase (36 kDa), chicken ovalbumin (43 kDa), BSA (67 kDa), glycogen phosphorylase (97 kDa), and β-galactosidase (115 kDa). Eleven μg of PLDS was loaded in the indicated lane, but the diffuse band is only faintly visualized by the stain. The PLDS was prepared from polylysine of nominal average M_r 10 000 and contained approximately 0.5 DPA/lysyl groups.
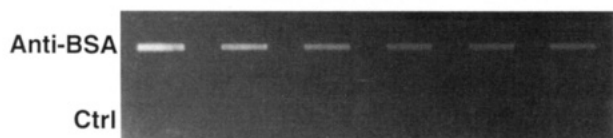
Figure 5. Detection of BSA in immunoblots using Tb−PLDS−BSA. BSA was serially diluted, and amounts ranging from 0.5 to 20 μg were blotted onto nitrocellulose under vacuum and then incubated successively with rabbit serum (either BSA antiserum, anti-BSA, or normal rabbit serum, Ctrl, as indicated), PLDS BSA (preparation of Figure 4), and TbCl$_3$ as described in the text. The nitrocellulose strips were photographed through green filters (546 nm band pass and 540 nm high pass dielectric filters) while illuminated from below by a transilluminator (305 nm).

with avidin or streptavidin by increasing reactant concentrations sufficiently to improve the labeling yield and by protecting lysines essential for biotin binding during the labeling reaction.

SUMMARY

The results reported here demonstrate that Tb(III) complexes with PLDS can be readily prepared and covalently coupled to proteins in ways that preserve binding activities essential for immunochemistry. Because these conjugates display emission intensities comparable to those of commonly used fluorophores, and offer the added advantage of background rejection through time-gating, they represent a class of reagents with great promise for ultrasensitive immunoassays and other techniques for detection of specific macromolecules.

ACKNOWLEDGMENT

LITERATURE CITED

Barela, T. D.; Sherry, A. D. (1976) A simple, one-step fluorometric method for determination of nanomolar concentrations of terbium. *Anal. Biochem. 76*, 351−357.

Grenthe, I. (1961) Stability relationships among the rare earth dipicolinates. *J. Am. Chem. Soc. 83*, 360−364.

Laemmli, U. K. (1970) Cleavage of structural proteins during the assembly of the head of bacteriophage T4. *Nature 227*, 680−685.

Lamture, J. B.; Wensel, T. G. (1993) A novel reagent for labeling macromolecules with intensely luminscent lanthanide complexes. *Tetrahedron Lett. 34*, 4141−4144.

Lamture, J. B., Zhou, Z., Suresh Kumar, A., and Wensel, T. G. (1995). Luminescence properties of Tb(III) complexes with 4-substituted dipicolinic acid analogues. *Inorg. Chem.*, in press.

Martell, A. E., and Smith, R. M. (1974) *Critical Stability Constants*, Vol. 1, p 205, Plenum Press, New York.

Means, G. E., and Feeney, R. E. (1971) *Chemical Modification of Proteins*, p 217, Holden-Day, Inc., San Francisco.

Mukkala, V.-M.; Sund, C. Kwiatkowski, N.; Pasanen, P.; Hogberg, M.; Kankare, J. (1992) New heteroaromatic complexing agents and luminescence of their Europium(III) and Terbium(III) chelates. *Helv. Chim. Acta 75*, 1621−1632.

Ramdas, L.; Disher, R. M.; Wensel, T. G. (1991) Nucleotide exchange and cGMP phosphodiesterase activation by pertussis toxin-inactivated transducin. *Biochemistry 30*, 11637−11645.

Soini, E.; Lovgren, T. (1987) Time-resolved fluorescence of lanthanide probes and applications in biotechnology. *CRC Crit. Rev. Anal. Chem. 18*, 105−154.

Wensel, T. G.; Meares, C. F. (1983) Electrostatic properties of myoglobin probed by diffusion-enhanced energy transfer. *Biochemistry 22*, 6247−6284.

BC940091N

Strand Invasion by Oligonucleotide–Nuclease Conjugates

David R. Corey,* Debbie Munoz-Medellin, and Alan Huang

Howard Hughes Medical Institute and the Department of Pharmacology, University of Texas Southwestern Medical Center at Dallas, 5323 Harry Hines Blvd., Dallas, Texas 75235. Received September 22, 1994[®]

Conjugates consisting of staphylococcal nuclease crosslinked to oligonucleotides hybridize to supercoiled duplex DNA by Watson–Crick base-pairing. Here we describe this strand invasion. Affinity cleavage by these conjugates provides a probe for the local topology of the DNA duplex and is most efficient at a target DNA sequence known to form a cruciform. Additional supercoiling of the substrate DNA increases selective cleavage at other sequences. Hybridization of the conjugate to duplex DNA is temperature dependent and is stable over time. Affinity cleavage is not substantially inhibited by a 200-fold excess of the analogous unmodified oligonucleotide, demonstrating that hybridization of the unmodified oligonucleotide must be less favored and that the nuclease is involved in substrate binding. Surprisingly, affinity cleavage is also not effectively inhibited by complementary oligonucleotides unless they contain an extended 5'-sequence capable of separate interactions with the nuclease domain of the conjugate. These results suggest that the oligonucleotide–nuclease conjugate prefers to hybridize to target sequences which will allow interactions with both the oligonucleotide and the nuclease domains. Affinity cleavage by oligonucleotide–nuclease conjugates provides general insights for the design of oligonucleotides and their conjugates for strand invasion and affords a convenient competition assay for their hybridization.

INTRODUCTION

The development of strategies for the Watson–Crick recognition of sequences within duplex DNA would allow greater control over recombination, replication, repair, and transcription. Unfortunately, target sequences within duplex DNA are already base-paired, rendering them relatively inaccessible to recognition by complementary oligonucleotides. To avoid the need to disrupt pre-existing base-pairing, triple helix formation (Moser and Dervan, 1987; Jayasena and Johnston, 1993a; Colocci et al., 1993; Francois et al., 1989) is being optimized to achieve sequence recognition through hybridization in the major groove of the DNA helix. Recent advances have extended stable hybridization into the physiological range (Koh and Dervan, 1992; Young et al., 1991), but sequence recognition by this technique is currently restricted to targets which are primarily polypurine–polypyrimidine. Other strategies attempt to avoid sequence limitations through the employment of Watson–Crick base-pairing. Peptide nucleic acids can spontaneously hybridize to duplex DNA by a combination of Watson–Crick base-pairing and triple helix formation (Neilsen et al., 1991; Peffer et al., 1993; Hanvey et al., 1992; Neilsen et al., 1993; Demidov et al., 1993) but strand invasion currently has the same sequence limitations as for triple helix formation by oligodeoxyribonucleotides. More general recognition is offered by the ability of RNA probes to form R-loops (Chen et al., 1993) and the use of RecA protein to promote strand exchange (Cheng et al., 1988; Ferrin and Camerini-Otero, 1991; Jayasena and Johnston, 1993b; Rao et al., 1993). These strategies permit sequence recognition to occur but require the use of exogenous proteins, stringent conditions, or altered base-pairing. To develop a simpler and potentially complementary approach to sequence recognition we have examined the direct incorporation of oligodeoxyribonucleotides and their conjugates into duplex DNA by strand invasion.

Single-stranded DNA will spontaneously hybridize to complementary regions within supercoiled duplex DNA to form D-loops (Beattie et al., 1977; Holloman et al., 1975). In contrast to the hybridization of complementary single strands, which is driven by the increase in enthalpy during base-pairing, D-loop formation is entropically driven by the removal of superhelical turns as the invading single strand is incorporated into the duplex. The first step is the transient denaturation of several base-pairs. The subsequent rate-limiting step is the initial nucleation in which a short helix is formed between the single-stranded DNA and the denatured region. If conditions of salt and temperature are such that base-pairing persists, more pairing will occur until either the invading strand is completely incorporated or until enough superhelical turns are removed to eliminate the driving force for incorporation. Radding and co-workers demonstrated that supercoiled DNA would spontaneously incorporate relatively long complementary single strands (Beattie et al., 1977; Holloman et al., 1975). Most recently, oligonucleotide–staphylococcal nuclease conjugates were shown to hybridize with supercoiled DNA via Watson–Crick base-pairing (Corey et al., 1989a). Here we characterize the role of the nuclease domain of an oligonucleotide–nuclease conjugate in allowing hybridization to target sites within duplex DNA to occur. We also utilize the inhibition of affinity cleavage to develop a competition assay for the hybridization of other oligonucleotide motifs.

EXPERIMENTAL METHODS

Oligonucleotide Synthesis. Underivatized controlled pore glass was purchased from CPG (Fairfield, NJ) and was derivatized with 1-*O*-(4,4'-dimethoxytrityl)-3,3'-thiopropanol (Pei et al., 1990) as described. The thiolated controlled pore glass was used to synthesize 3'-thiolated oligonucleotides on an Applied Biosystems 451 DNA synthesizer (Foster City, CA). Oligonucleotides

containing a 5'-acridine were obtained from Appligene (Pleasanton, CA). The thiolated oligonucleotides were reduced by treatment with 20 mM dithiothreitol (DTT) overnight at 37 °C in 1 mM EDTA, 10 mM Tris–HCl, pH 8.0. Most of the DTT was removed by extraction with water-saturated *n*-butanol, and the reduced oligonucleotide was desalted on a Bio-Spin 6 column (BioRad, Hercules, CA). The reduced oligonucleotide was added to an equal volume of 10 mM 2,2'-dithiodipyridine (Aldrich, Milwaukee, WI) in acetonitrile, and the mixture was incubated at room temperature for 30 min. The solution was extracted with diethyl ether (six times) to remove unreacted 2,2'-dithiodipyridine, and the 3' *S*-thiopyridyl oligonucleotide was desalted on a Bio-Spin 6 column. The presence of the thiopyridyl group was confirmed by treatment with DTT and subsequent monitoring of release of thiopyridyl anion at 342 nm (ϵ = 7060). The concentrations of oligonucleotides were determined assuming a ratio of 1 OD per 20 μg/mL for nonhairpin oligonucleotides and 1 OD per 30 μg/mL for hairpin oligonucleotides. Melting temperatures with oligonucleotide dissolved in 5 mM bis-Tris–HCl, pH 6.5, 25 mM NaCl were obtained using a Hewlett-Packard (Wilmington, DE) 8452 diode array spectrophotometer using a thermostated cell holder connected to an adjustable temperature bath.

Plasmid Preparation. Plasmid pUC19 (Yanisch-Perron et al., 1985) (New England Biolabs, Beverly MA) was prepared using strains HB101 or JM101 by the alkaline lysis method followed by chromatography using columns obtained from Qiagen (Chatsworth, CA) or by CsCl gradient centrifugation. CsCl of ultrapure grade was obtained from Gibco-BRL. The concentration of plasmid DNA was determined by UV absorbance at 260 nm assuming a ratio of 1 OD per 50 μg/mL. Topoisomerase I was either obtained from Gibco-BRL or prepared from wheat germ as described (Dynan et al., 1981). Plasmid with increased supercoiling was obtained as described (Keller, 1975) using topoisomerase I and varied concentrations of ethidium bromide. The superhelical density of pUC19 was evaluated by agarose gel electrophoresis of the topoisomers as described (Keller, 1975).

DNA Affinity Cleavage. DNA cleavage was essentially performed as described (Pei et al., 1990; Corey et al., 1989a,b) using oligonucleotide–nuclease conjugates that were synthesized via disulfide exchange between the 3' thiolated oligonucleotides and staphylococcal nuclease containing an introduced surface cysteine (K116C). Plasmid pDC1 encoding staphylococcal nuclease containing the K116C mutation was provided by Dr. Peter G. Schultz (UC Berkeley). K116C staphylococcal nuclease was expressed behind a *lac* promoter and an *ompA* signal sequence within plasmid pDC1, a pONF1 derivative (Takahara et al., 1985), and was isolated as a mixture of monomer and disulfide-linked dimer. The enzyme was completely reduced to monomer by treatment with 50 mM DTT for 8 h at 37 °C in 10 mM Tris–HCl, pH 8.0. Monomeric enzyme was separated from DTT by Mono S cation exchange chromatography (Pharmacia) in 50 mM NaHEPES, pH 7.5, 1 mM EGTA, and a gradient of 0.0–1.0 M NaCl. The reduced staphylococcal nuclease was mixed with 3'-S-(thiopyridyl)oligonucleotide, and the coupling was monitored at 342 nm. The conjugate was purified by Mono Q anion exchange chromatography (Pharmacia) in 20 mM Tris–HCl, pH 8.0, 1 mM EGTA, and a gradient of 0.0–1.0 M NaCl. The collected oligonucleotide–nuclease conjugate fractions were concentrated to 200 μL and desalted using BioSpin 6 spin columns (Biorad). Oligonucleotide–nuclease conjugates

were annealed to substrate for greater than 30 s at 25–37 °C in 25 mM NaCl, 5 mM bis Tris–HCl, pH 6.5. The mixtures were chilled on ice, and the cleavage reactions were initiated by addition of 2.5 mM CaCl$_2$ followed by termination after 1–5 s by the addition of 5 mM EGTA. The DNA was then treated with restriction enzyme to generate discrete products of identifiable size which were analyzed by 1% agarose gel electrophoresis.

Synthesis of Peptide–Oligonucleotide Conjugates. Peptides were synthesized on either a Symphony Multiplex synthesizer (Rainin, Emeryville, CA) or an Applied Biosystems Model 430A peptide synthesizer using Fmoc chemistry. The presence of predominantly one species was confirmed by reversed-phase HPLC (Rainin) using a C-18 Microsorb 5 μm 300 Å column (Rainin) and 0.1% trifluoroacetic acid in doubly distilled water (buffer A) and a gradient of 0–100% of buffer B (0.08% trifluoroacetic acid in 95:5 acetonitrile:doubly distilled water). The peptides were characterized by mass spectral analysis acquired by a VG (Altrincham, England) 30–250 quadrapole mass spectrometer using a standard VG electrospray source. The calculated and observed molecular weights were 1175.5 and 1175 for CAGAAKKACAAKK, 1135 and 1135.4 for CAAKKAAK-KAAKK, and 1172.4 and 1173 for CGGSPRKSPRK. Two to four mg of dry peptide were weighed out, dissolved in 10 mM Tris–HCl, pH 8.0 buffer, and incubated for 8–12 h at 37 °C with 10 mM DTT to reduce all material to monomeric form. The reduced peptide was purified by reversed-phase HPLC using the column and gradient described above, neutralized with 1/5 volume 100 mM Tris pH 10.2, and added to a 1 mL quartz cuvette containing the 3'-(*S*-thiopyridyl)oligonucleotide. The reaction was monitored at 342 nM utilizing a Hewlett-Packard 8452 diode array spectrophotometer. Enough peptide and oligonucleotide were used to ensure a distinct peak at 342 nm (>0.05 OD$_{342}$) upon completion of the reaction. This material was then purified by anion exchange chromatography with a Mono Q 5/5 column (Pharmacia) utilizing 20 mM Tris–HCl, pH 8.0, and a gradient of 0.0–1.0 M NaCl. The attachment of the positively charged peptides caused the conjugates to migrate significantly faster than the parent oligonucleotide. The purified conjugate was concentrated to 200 μL and was desalted using BioSpin 6 columns (BioRad). The absorbance maximum of the conjugates was at 260 nm, as would be expected of a conjugate containing DNA. Treatment of the conjugate by DTT regenerated the free peptide and free oligonucleotide as monitored by HPLC.

RESULTS

Selective Cleavage as a Probe of Plasmid Topology. Oligonucleotide–nuclease conjugates were synthesized by coupling 3'-thiolated oligonucleotides to a staphylococcal nuclease variant (K116C) (Pei et al., 1990) containing an introduced surface cysteine. The ability of the conjugates to hybridize to duplex DNA was evaluated by affinity cleavage of supercoiled plasmid DNA (Corey et al., 1989a). Plasmid DNA was prepared by cesium chloride gradient centrifugation or by chromatography and was not denatured prior to addition of the oligonucleotide–nuclease conjugate. Incubation of the oligonucleotide–nuclease conjugates with plasmid, followed by activation of the staphylococcal nuclease domain by Ca^{2+}, yielded specific cleavage. Linearized DNA was not cleaved selectively at any site by the oligonucleotide–nuclease conjugates. Selective cleavage was most efficient at target sequences which contained inverted repeats which have the potential to form cruciform structures (Lilley et al., 1980; Panayotatos and
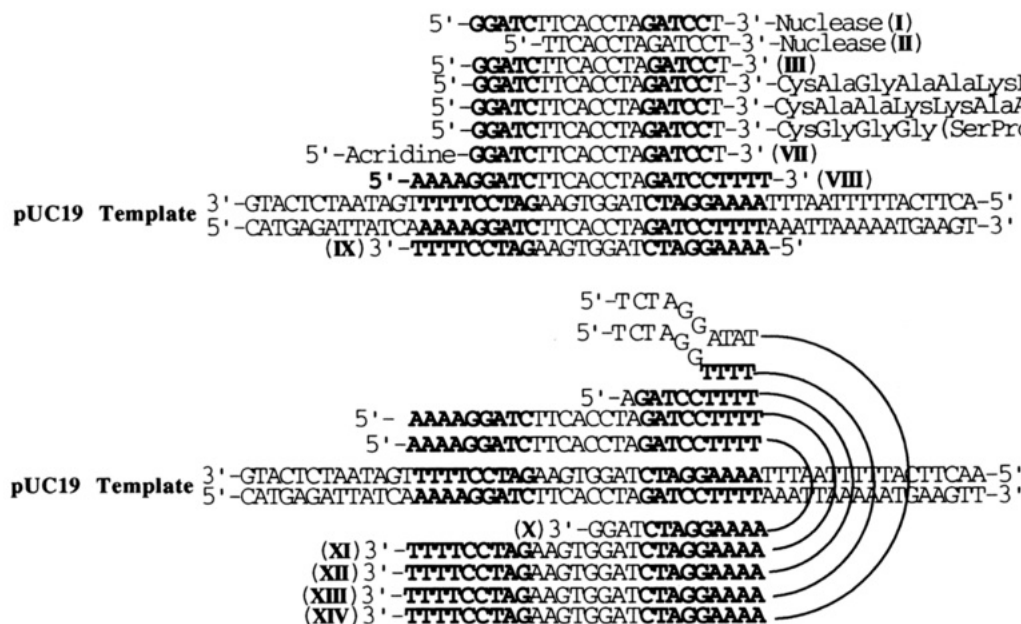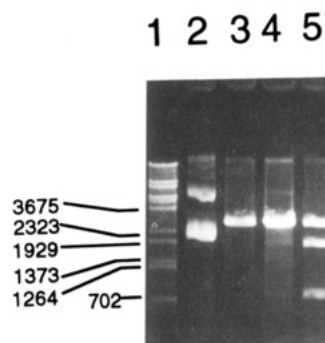
Figure 1. Oligonucleotides and oligonucleotide conjugates used in this study. The hybridization region within pUC19 was within bases 1529–1583. Self-complementary sequences within linear oligonucleotides or within the separate arms of the hairpin oligonucleotides are shown in bold. (Top) oligonucleotides and oligonucleotide conjugates. (Bottom) hairpin and related oligonucleotides. Semicircular connections represent tetracytidine linker regions.

Wells, 1981; Del Olmo and Perez-Ortin, 1993), but also occurred at sites without evident structure (Corey et al., 1989). Hydrolysis of pUC19 by the underivatized nuclease also yielded cleavage at an inverted repeat at bases 1542–1567, but in contrast to oligonucleotide-direct cleavage, hydrolysis was accompanied by substantial cleavage at other sites and required longer incubations with calcium or higher nuclease concentration (Corey et al., 1989a). Addition of free oligonucleotide in conjunction with free nuclease yielded cleavage which was similar to that produced by nuclease alone. The introduction of additional negative supercoiling into the pUC19 plasmid by treatment with topoisomerase I in conjunction with ethidium bromide (Keller, 1975) resulted in efficient cleavage at sites which were not inverted repeats (Figure 2, lane 5), suggesting that the extent of supercoiling influenced strand invasion by the oligonucleotide–nuclease conjugate.

Temperature Dependence of Selective Cleavage. The oligonucleotide–nuclease conjugates may have hybridized to substrate duplex DNA stably or they may have hybridized in a readily reversible manner. Knowledge of the stability of hybridization has important implications for the mechanism of strand invasion and its eventual experimental application. To determine whether the conjugates were stably bound we examined the effect of annealing temperature on selective cleavage. Plasmid pUC19 was mixed with oligonucleotide–nuclease conjugate **I** (Figure 1) which was directed to an inverted repeat within pUC19. Incubations to permit annealing were performed at temperatures ranging from 0 to 37 °C for 10 min, after which the mixtures were cooled to 0 °C. Affinity cleavage was then used to probe whether the incubation conditions had allowed hybridization to occur and whether it was stable over time after cooling. No affinity cleavage was observed after annealing at less than 23 °C (Figure 3 (top), lanes 3 and 4). Cleavage was observed after annealing at 24–26 °C (lanes 5–7) and reached a maximum at temperatures above 28 °C (Figure 3 (top), lanes 8 and 9). The observation of affinity cleavage after cooling to 0 °C indicated that stable hybridization of the oligonucleotide–nuclease conjugate was occurring, since reversible

Figure 2. Effect of additional supercoiling within pUC 19 on affinity cleavage by an oligonucleotide–nuclease conjugate directed to a target site which does not contain an inverted repeat. Lane 1: molecular weight markers. Lane 2: uncut pUC 19. Lanes 3–5: affinity cleavage of pUC19 treated with 0, 2.0, or 6.0 mM ethidium bromide and topoisomerase I as described in the Experimental Methods to obtain superhelical densities (σ) of -0.056 ± 0.14, -0.068 ± 0.14, and -0.12 ± 0.2. The treated pUC19 was incubated with an oligonucleotide–nuclease conjugate containing an oligonucleotide with sequence 5′-GGGGTTCCGCGCACATTTCCCCG-3′ directed to bases 2583–2605 of pUC19, and the products from affinity cleavage, if any, were digested with *Bsa*I. *Bsa*I has a single recognition site in pUC19 at 1766, and the predicted fragment sizes of *Bsa*I/oligonucleotide–nuclease cleavage were ∼840 and ∼1850.

hybridization would have yielded unbound oligonucleotide–nuclease conjugate which would not have been able to reanneal at temperatures less than 24 °C.

As noted above, the temperature dependence of selective cleavage has implications for the application of strand invasion by oligonucleotide–nuclease conjugates, and we sought to determine if intramolecular interactions within conjugate **I** might contribute to the observed temperature sensitivity. The oligonucleotide domain of the conjugate **I** is self-complementary (5′-GGATC- - -GATCC-3′, Figure 1), so the observed temperature dependence may have been partially due to intramolecular structure within the oligonucleotide domain of the conjugate. To lessen the potential for intramolecular base-pairing we synthesized oligonucleotide–nuclease conjugate **II** which was designed to possess a 14-base
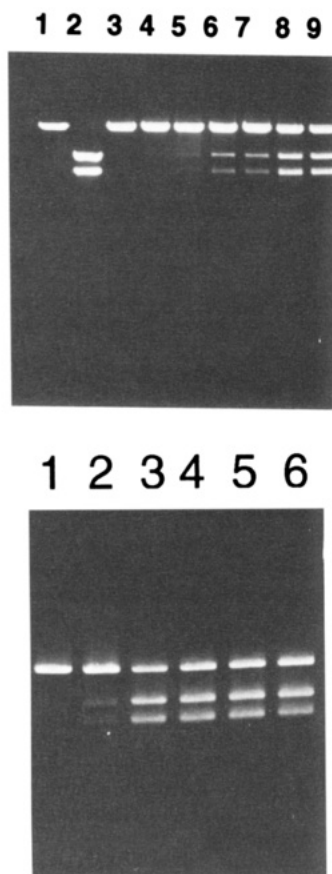
Figure 3. Effect of temperature on cleavage of pUC19 by oligonucleotide—nuclease conjugates **I** or **II**. pUC 19 (0.05 μM) was mixed with oligonucleotide—nuclease conjugates **I** or **II** (0.07 μM) at 22 °C and annealed at various temperatures for 10 min prior to cooling to 0 °C and initiation of cleavage. After cleavage the products were digested with *Bam*HI. *Bam*HI has a single recognition site within pUC 19 at 417, and the predicted fragments of cleavage by *Bam*HI and **I** or **II** were ~1140 and ~1540. (Top) Lane 1: linearized pUC19. Lane 2: pUC19 treated with *Bgl* I to yield marker fragments of 1118 and 1568 base pairs. Lanes 3–9 show the effects of annealing **I** at 22.5, 23, 24, 25, 26, 28, and, 37 °C. (Bottom) Lanes 1–6: effect of annealing **II** at 14, 16, 18, 20, 22, and 24 °C.

oligonucleotide domain which was similar to **I** but lacked five nucleotides at the 5′ terminus. Conjugate **II** exhibited maximal affinity cleavage at 18 °C (Figure 3(bottom), lane 3), 8–12 °C lower than **I** (Figure 3 (top)), suggesting that the lack of self-complementarity contributes to an altered profile of incubation temperature versus activity.

Effect on Affinity Cleavage of the Addition of the Analogous Unmodified Oligonucleotide. By design, the nuclease domain was responsible for affinity cleavage by the conjugate. Could it also effect the stability of hybridization? To determine the impact, if any, of the attached nuclease on strand invasion, we examined the effect on affinity cleavage by oligonucleotide—nuclease conjugate **I** from the addition an excess of an unmodified oligonucleotide of the same sequence **III**. Previous studies had shown that the addition of unmodified oligonucleotide efficiently inhibited the selective hydrolysis of single-stranded DNA or RNA substrates by the analogous oligonucleotide—nuclease conjugates (Corey and Schultz, 1987; Zuckermann and Schultz, 1989) by blocking the target annealing site. For duplex substrate DNA, however, we observed that up to a 200-fold excess of **III** did not substantially inhibit affinity cleavage by **I** (Figure 4, lanes 4–8). We observed this result even when **III** was preincubated with pUC19 for 8 h at 37 °C prior to the addition of oligonucleotide—nuclease conjugate **I**.
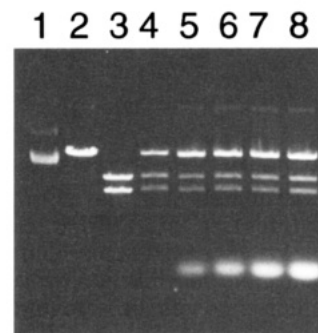
Figure 4. Effect of excess oligonucleotide on DNA cleavage by the analogous oligonucleotide—nuclease conjugate. pUC19 (0.05 μM) was mixed with varying amounts of oligonucleotide **III** for 10 min at 37 °C. Oligonucleotide—nuclease conjugate **I** (0.07 μM) was added to the mixture and annealed to plasmid for an additional 10 min at 37 °C prior to cooling to 0 °C and initiation of cleavage. The products were treated with *Bam*HI to generate discrete fragments. Lane 1: uncut pUC19. Lane 2: pUC 19 linearized by *Hin*dIII. Lane 3: *Bgl* I digest of pUC 19 to yield marker fragments of 1118 and 1568 base pairs. Lanes 4–8: digestion of pUC 19 by **I** in the presence of 0, 1.75, 3.5, 7, and 14 μM III.

One explanation for the failure of added oligonucleotide to reduce specific cleavage is that the oligonucleotide may anneal and create a D-loop structure that is readily cleaved by unbound oligonucleotide—nuclease conjugate. To account for this possibility, oligonucleotide **III** (0–200-fold excess) was added to plasmid and annealed at 37 °C prior to cooling to 0 °C and addition of oligonucleotide conjugate **I**. In spite of the opportunity for **III** to anneal and the presence of unbound **I**, no cleavage of plasmid was observed (results not shown).

Effect on Affinity Cleavage of the Addition of Oligonucleotide—Peptide Conjugates. The stabilization of stand invasion by the attachment of small molecules to oligonucleotides rather than by the attachment of staphylococcal nuclease would afford conjugates with the potential for more general utility. Staphylococcal nuclease contains 22 lysines on its surface and has a net positive charge of +12 (Loll and Lattman, 1989). To examine whether the stabilization conferred by staphylococcal nuclease could be replicated by attachment of simple positively-charged synthetic peptides we synthesized conjugates **IV** and **V**, consisting of an oligonucleotide linked via disulfide bond formation to peptides containing either four (CAGAAKKAGAAKK **IV**) or six (CAAKKAAKKAAKK,**V**) lysine residues. The dilysine repeats were chosen because they also appear on the surface of staphylococcal nuclease at residue pairs 5/6, 48/49, 63/64, 71/72, and 133/134 (Tucker et al., 1978). Similar peptides have been shown to bind in an α-helical conformation to duplex DNA (Johnson et al., 1994). The oligonucleotide—peptide conjugates did not inhibit selective cleavage by the oligonucleotide—nuclease conjugate **I** (Figure 5, lanes 6 and 7) when present at a 50-fold excess. Higher concentrations of the oligonucleotide—peptide conjugates began to inhibit selective cleavage, but inhibition was indistinguishable from that produced by similar concentrations of the free peptide (data not shown). A conjugate (**VI**) consisting of an oligonucleotide coupled to a peptide (CGGGSPKKSPKK) containing a sequence known to bind independently to DNA at A/T-rich sites (Churchill and Suzuki, 1989) also failed to inhibit the analogous oligonucleotide—nuclease conjugate **I** (Figure 5, lane 5). These results suggest that the stabilization of strand invasion may depend on structural features of staphylococcal nuclease which cannot be readily mimicked by simple cationic peptides.
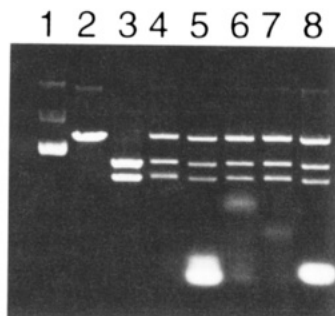
Figure 5. Effect of peptide- and acridine-linked oligonucleotides on affinity cleavage of pUC19 (0.05 mM) by oligonucleotide nuclease conjugate **I** (0.07 mM). Lane 1: uncut pUC 19. Lane 2: pUC 19 linearized with *Bam*HI. Lane 3: pUC 19 treated with *Bgl*I. Lane 4: cleavage by oligonucleotide–nuclease conjugate **I** alone. Lane 5: effect of addition of 3.5 μM oligonucleotide–peptide conjugate **VI**. Lane 6: effect of addition of 3.5 μM oligonucleotide–peptide conjugate **IV**. Lane 7: effect of addition of 3.5 μM oligonucleotide–peptide conjugate **V**. Lane 8: effect of addition of 14 μM oligonucleotide–acridine conjugate **VII**.

Effect on Affinity Cleavage of the Addition of Oligonucleotide–Acridine Conjugates. Acridine is able to intercalate between DNA bases, and its attachment to oligonucleotides had previously been shown to stabilize hybridization to single-stranded DNA (Sun et al., 1989). To assay if the linkage of acridine to an oligonucleotide could increase the stability of hybridization sufficiently to block the annealing of the oligonucleotide–nuclease conjugate we obtained oligonucleotide **VII**, which had been derivatized at the 5′ terminus with acridine. A 200-fold excess of oligonucleotide–acridine conjugate **VII** was preincubated with pUC19 prior to addition of oligonucleotide–nuclease conjugate **I**. After activation of the nuclease and subsequent analysis no inhibition of affinity cleavage was observed (Figure 5, lane 8).

Effect on Affinity Cleavage of the Addition of Hairpin and Complementary Oligonucleotides. We examined the ability of hairpin oligonucleotides to inhibit affinity cleavage. Knowledge of the cause of any inhibition would allow insight into the relative contributions to strand exchange of nuclease–DNA interactions and DNA–DNA base-pairing. Hairpin oligonucleotides are a promising motif for hybridization to duplex DNA, since they can base-pair to both strands of the target sequence and because their enhanced stability to nuclease degradation makes them better candidates for use in complex *in vitro* or *in vivo* systems (Yoshizawa et al., 1994). Hairpin oligonucleotides might inhibit affinity cleavage by directly annealing to the target site on plasmid DNA and blocking subsequent annealing of the oligonucleotide–nuclease conjugate. Alternatively, the oligonucleotide–nuclease conjugate may take advantage of nuclease–DNA interactions to stabilize annealing of the conjugate to the complementary strand of a hairpin, thus preventing it from recognizing its plasmid target.

Hairpin oligonucleotides were designed to hybridize to both strands of the target sequence (Figure 1, sequences **XI** and **XII**) and block subsequent hybridization of oligonucleotide–nuclease conjugate **I** by one of the mechanisms outlined above. Under the buffer and salt conditions used for the assay the measured melting temperature of hairpin **XI** was 72 °C. We incubated hairpin **XI** with duplex DNA at 37 °C and then added oligonucleotide–nuclease **I**. The incubation was continued for an additional 10 min at 37 °C after which the nuclease was activated. We observed that selective hydrolysis was almost completely inhibited at a 50-fold excess of (**XI**)
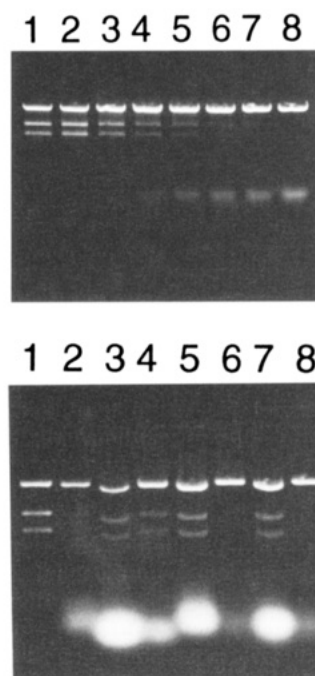
Figure 6. (Top) effect of the addition of increasing amounts of hairpin oligonucleotide XI on the affinity cleavage of pUC 19 (0.05 μM) by oligonucleotide–nuclease conjugate I (0.07 μM). Lanes 1 and 2: no hairpin added. Lanes 3–8: 0.07, 1.4, 2.1, 2.8, 3.5, and 4.9 μM hairpin oligonucleotide **XI** added. (Bottom) effect of the addition of various oligonucleotides on the affinity cleavage pUC 19 (0.05 μM) by oligonucleotide nuclease I (0.07 μM). Lane 1: no oligonucleotide added. Lane 2: 2.8 μM (40-fold excess) oligonucleotide XI added. Lane 3: 14 μM (200-fold excess) oligonucleotide VIII added. Lane 4: 14 μM (200-fold excess) oligonucleotide IX. Lane 5: 14 μM (200-fold excess) hairpin oligonucleotide complementary to bases 425–450 within pUC19. Lane 6: 2.8 μM (40-fold excess) oligonucleotide XII. Lane 7: 14 μM (200-fold excess) oligonucleotide X. Lane 8: 2.8 μM (40-fold excess) of oligonucleotide XIII.

(Figure 6 (top), lane 6, and (bottom), lane 2). Partial hairpin (**XII**) inhibited affinity cleavage similarly (Figure 6 (bottom), lane 6). No inhibition was observed if oligonucleotide–nuclease conjugate **I** was allowed to hybridize to DNA prior to addition of hairpin **XI**, indicating that the addition of the hairpin could not cause displacement of an annealed oligonucleotide–nuclease conjugate. A hairpin oligonucleotide directed to another site within pUC19 did not inhibit selective cleavage by **I** to any extent (Figure 6 (bottom), lane 5), suggesting that inhibition was due to Watson–Crick base-pairing by **XI** or **XII**.

Inhibition by the hairpin **XI** may have been due to its structure or to the sequence of its individual arms. A 200-fold excess of oligonucleotides **VIII** and **IX**, which separately make up the two arms of hairpin **XI** (Figure 1), were preincubated with plasmid either singly or in combination. Neither substantially inhibited selective cleavage by conjugate **I** (Figure 6 (bottom), lanes 3 and 4). The incomplete inhibition after preincubation with a 200-fold excess of oligonucleotide **IX** (Figure 6 (bottom), lane 4) was especially noteworthy because **IX** was complementary to the oligonucleotide–nuclease **I** and would have been expected to base-pair with it and thus directly prevent hybridization to the duplex. However, when analogous oligonucleotides with extended 5′ sequences were examined (**XIII** (Figure 6 (bottom), lane 8) (Scheme 1, iv) and **XIV** (results not shown)), we noted an inhibition of selective cleavage similar to that caused by hairpin **XI**. Hairpin **X**, which possessed a similar capacity to base-pair to pUC19 as partial hairpin **XII**,

Scheme 1. Ability of Oligonucleotide−Nuclease Conjugate I to Hybridize to pUC19 in the Presence of Oligonucleotides III, XI, IX, XIV, and X
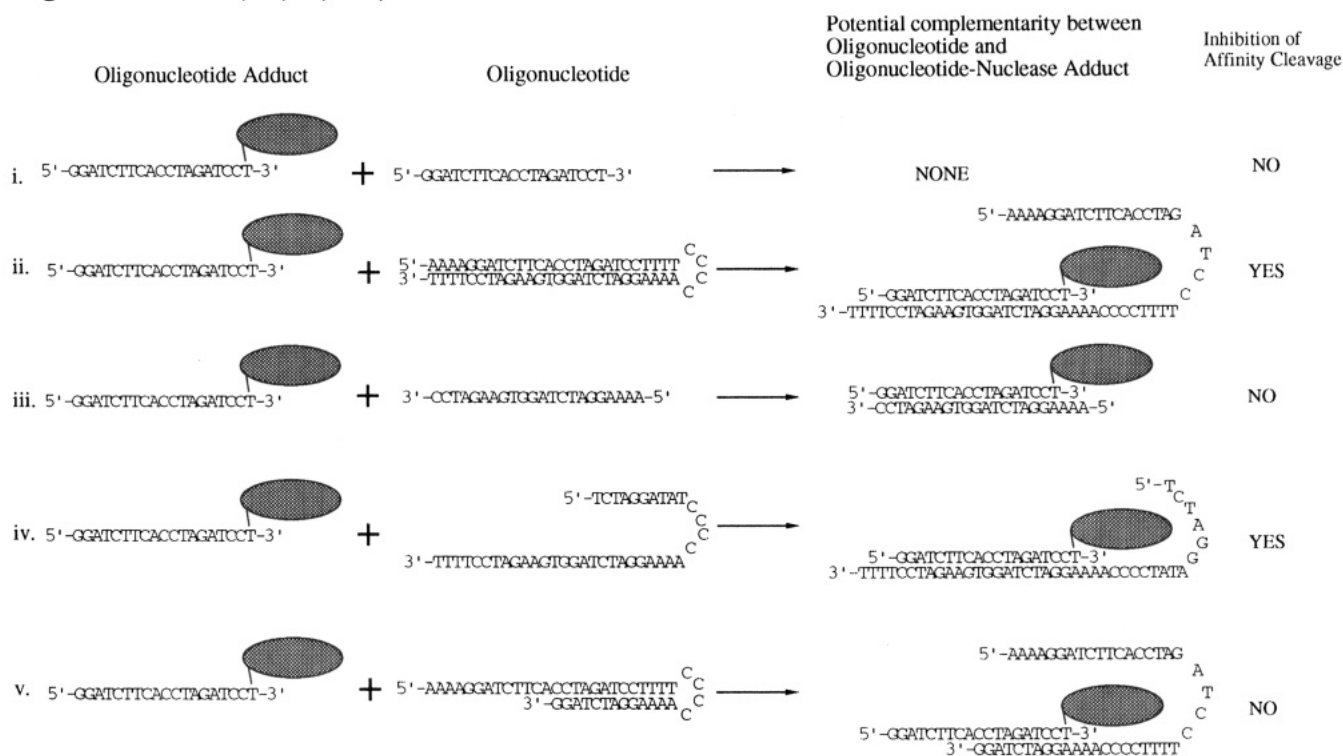
but could make fewer base-pairs with **I**, did not inhibit selective cleavage (Figure 6 (bottom), lane 7) (Scheme 1, v).

Scheme 1 summarizes the data obtained by the inhibition of affinity cleavage and our view of the base-pairing by the oligonucleotide−nuclease conjugate. (i) An oligonucleotide **III** of the analogous sequence to the oligonucleotide−nuclease conjugate does not efficiently block hybridization by the conjugate (Figure 4). (ii) Hairpin oligonucleotides containing a complementary sequence (**XI** or **XII**) can incorporate an oligonucleotide nuclease and prevent it from hybridizing to its target sequence within pUC19 (Figure 6 (top), (bottom, lanes 2 and 6)). **III** Complementary oligonucleotides (**IX**) cannot block hybridization by the oligonucleotide−nuclease (Figure 6 (bottom), lane 4) unless (iv) they contain an extended 5′-tail capable of additional interactions with the nuclease domain (Figure 6 (bottom), lane 8) (**XIII**) or (**XIV**). Finally, (v) a hairpin oligonucleotide (**X**) which is only partially complementary to conjugate **I** does not inhibit affinity cleavage (Figure 6 (bottom), lane 7) even though it contains the same potential to base-pair with pUC19 as inhibitory hairpin **XII**.

DISCUSSION

Hybridization of oligonucleotides to duplex DNA by Watson−Crick base-pairing potentially offers the most versatile route to sequence recognition. Such recognition would facilitate the control of proteins involved in recombination, replication, and transcription. This ability might have considerable implications for *in vitro* and *in vivo* functional studies. However, before functional studies can be attempted, more information is required concerning the impact on strand invasion of the topology of the target and the impact of modifications to the invading oligonucleotide. For proficient strand invasion optimized oligonucleotides will need to be targeted to optimal sequences.

Oligonucleotide−nuclease conjugates represent a valuable tool for obtaining this information because they can hybridize within duplex DNA and because their hybridization can be evaluated by affinity cleavage. Hybridization of oligonucleotide−nuclease conjugates is limited to supercoiled DNA and is most facile at sites containing inverted repeats or to template with relatively high supercoiling. The need for the target to be supercoiled is a restriction relative to recognition by triple helix formation, which allows hybridization to target sequences within relaxed DNA. However, DNA can be supercoiled *in vivo*, particularly in regions which are transcriptionally active, and certain sequence motifs are known to be particularly susceptible to strand dissociation (Benham, 1993; Huang and Kowalski, 1993). Therefore, these sequences may be the most promising targets for the extension of this strategy to the targeting of oligonucleotides and their derivatives to duplex DNA for *in vitro* or *in vivo* enzymological studies.

The oligonucleotide−nuclease conjugates appear to hybridize stably to duplex DNA since the conjugate remains hybridized and capable of affinity cleavage after cooling to 0 °C, a temperature which is too low to permit the initiation of hybridization (Figure 3 (top and bottom)). The temperature sensitivity of affinity cleavage can be altered by modulating the self-complementarity of the oligonucleotide domain of the conjugate. By contrast, unmodified oligonucleotides must not be able to hybridize as stably, since oligonucleotide **III** did not block hybridization by the analogous oligonucleotide−nuclease conjugate **I** when present in 200-fold excess. This result was also observed if the underivatized oligonucleotide was added first and allowed to incubate with the duplex target for 8 h prior to addition of the conjugate. These observations implicate the attached nuclease in the promotion of stable strand invasion. Staphylococcal nuclease, a 149 amino acid protein, possesses a net positive charge of +12, and this dense positive charge on the nuclease surface may be responsible for shifting

the equilibrium between free and DNA-associated conjugate to favor strand invasion.

How might the surface charge of staphylococcal nuclease promote the initiation and stabilization of strand invasion? At least two interrelated mechanisms may contribute. Non-sequence-specific electrostatic interactions between the positively charged surface of the nuclease and the phosphodiester backbone of the duplex could bring the attached oligonucleotide into close proximity to the duplex, increasing its local concentration near the complementary target site and facilitating strand invasion by enhancing the probability of the initiation of base-pairing. The nuclease might also stabilize local disruptions of the DNA helix at the target site, which might facilitate the initiation of base-pairing by the oligonucleotide or stabilize the base-pairing once it occurs. The promotion and stabilization of duplex unwinding would be consistent with the physiological function of staphylococcal nuclease since its active site can only accommodate nucleotides that are not base-paired (Loll and Lattman, 1989). A recent report that proteins such as bovine serum albumin and transcription factor IIIa are able to promote strand exchange between synthetic duplexes and single-stranded M13 DNA supports the notion that proteins without known roles in genetic recombination can facilitate hybridization (Kmiec and Holloman, 1994). While surface charge may play a role in hybridization, the failure of peptide–oligonucleotide conjugates (Figure 5) to stably anneal indicates that this role cannot yet be readily reproduced by unstructured collections of positively charged residues. The three-dimensional framework of the enzyme may act as a scaffold to orient positively charged residues so as to optimize interactions between the phosphate backbone and the DNA duplex. The eventual successful design of peptides or small molecules which can mimic the stabilizing function of staphylococcal nuclease may require a rigid orientation of charge and remains an attractive goal.

Additional evidence for the ability of the attached nuclease domain to affect hybridization of the conjugate stemmed from the observation that staphylococcal nuclease was able to hybridize within a 25 base-pair hairpin oligonucleotide during annealing at 37 °C (Figure 6 (top), lanes 3–8, and (bottom), lane 2). This hybridization occurs in spite of the hairpin possessing a measured melting temperature of 72 °C and in spite of the entropic favorability of intramolecular reclosure of the hairpin. Similarly, the oligonucleotide–nuclease preferred to hybridize to its plasmid target sequence rather than to preannealed complementary oligonucleotides, unless the complementary oligonucleotides possessed an extended single-stranded region at its 5′-terminus (Scheme 1). This is a particularly remarkable result since it suggests that preexisting hybridization can be broken in order to yield a final hybridized complex which allows both base-pairing and interactions between the nuclease and the target DNA. These results are significant because they reinforce the suggestion that the nuclease has a dual role involving both substrate recognition and substrate cleavage.

In conclusion, the affinity cleavage of duplex DNA by oligonucleotide–nuclease conjugates affords insights into the potential of oligonucleotides to recognize sequences within duplex DNA by strand invasion. Stable sequence recognition requires the nuclease domain of the conjugate as well as the oligonucleotide, and a detailed understanding of how the nuclease accomplishes this may lead to the design of conjugates which are more amenable to *in vitro* and *in vivo* applications. Any polynucleotide derivative able to block cleavage by the analogous oligo-

nucleotide–nuclease conjugate would have favorable hybridization properties and would merit further study. The discovery of these conjugates will be aided by the utilization of the inhibition of affinity cleavage by the oligonucleotide motifs for the rapid evaluation of novel strategies of strand invasion.

LITERATURE CITED

Beattie, K. L., Wiegand, R. C., and Radding, C. M. (1977) Uptake of homologous single-stranded fragments by superhelical DNA: Characterization of the reaction *J. Mol. Biol. 116*, 783–803.

Benham, C. J. (1993) Sites of predicted stress-induced DNA duplex destabilization occur preferentially at regulatory loci. *Proc. Natl. Acad. Sci. U.S.A. 90*, 2999–3003.

Chen, C. B., Gorin, M. B., and Sigman, D. S. (1993) Sequence-specific scission of DNA by the chemical nuclease activity of 1,10-phenanthroline-copper (I) targeted by RNA. *Proc. Natl. Acad. Sci. U.S.A. 90*, 4206–4210.

Cheng, S., Van Houton, B., Gamper, H. B., Sancar, A., and Hearst, J. E. (1988) Use of Psoralen-modified oligonucleotides to trap three stranded RecA-DNA complexes by ABC excinuclease. *J. Biol. Chem. 263*, 15110–15117.

Churchill, M. A., and Suzuki, M. (1989) SPKK motifs prefer to bind to DNA at A/T rich sites. *EMBO J. 8*, 4189–4195.

Colocci, N., Distefano, M. D., and Dervan, P. B. (1993) Cooperative Oligonucleotide-directed triple helix formation at adjacent DNA sites. *J. Am. Chem. Soc. 115*, 4468–4473.

Corey, D. R., and Schultz, P. G. (1987) Generation of a Hybrid Sequence-Specific Single-Stranded Deoxyribonuclease. *Science 238*, 1401–1403.

Corey, D. R., Pei, D., and Schultz, P. G. (1989a) The sequence-selective hydrolysis of duplex DNA by an oligonucleotide-directed nuclease. *J. Am. Chem. Soc. 111*, 8523.

Corey, D. R., Pei, D., Schultz, P. G. (1989b) The generation of a catalytic oligonucleotide-directed nuclease. *Biochemistry 28*, 8277–8286.

Del Olmo, M., and Perez-Ortin, J. E. (1993) A natural A/T-rich sequence from the yeast FBP1 gene exists as a cruciform in Escherichia coli cells. *Plasmid 29*, 222–232.

Demidov, V., Frank-Kamenetskii, M. D., Egholm, M., Buchardt, O., and Neilson, P. E. (1993) Sequence selective cleavage of double stranded DNA cleavage by peptide nucleic acid (PNA) targeting using S1 nuclease. *Nucl. Acids Res. 21*, 2103–2107

Dynan, W. S., Jendrisak, J. J., Hager, D. A., and Burgess, R. R. (1981) Purification and characterization of wheat germ DNA topoisomerase I (nicking-closing enzyme). *J. Biol. Chem. 256*, 5860–5865.

Ferrin, L. J., and Camerini-Otero, D. R. (1991) Selective cleavage of human DNA: RecA assisted restriction endonuclease (RARE) cleavage. *Science 254*, 1494–1497.

Francois, J-C., Saison-Behormas, T., Thuong, N. T., and Helene, C. (1989) Inhibition of restriction endonuclease cleavage via triple helix formation by homopyrimidine oligonucleotides. *Biochemistry 28*, 9617–9619.

Hanvey, J. C., Peffer, N. J., Bisi, J. E., Thomson, S. A., Cadilla, R., Josey, J. A., Ricca, D. J., Hassman, C F., Bonham, M. A., Au, K. G., Carter, S. G., Bruckenstein, D. A., Boyd, A. L., Noble, S. A., and Babiss, L. E. (1992) Anti-sense and anti-gene properties of peptide nucleic acids. *Science 258*, 1481–1485.

Holloman, W. K., Wiegand, R., Hoessli, C., and Radding, C. M. (1975) Uptake of homologous single-stranded fragments by superhelical DNA: A possible mechanism for initiation of genetic recombination. *Proc. Natl. Acad. Sci. U.S.A. 72*, 2394–2398.

Huang, R.-Y., and Kowalski, D. (1993) A DNA unwinding element and an ARS consensus comprise a replication origin within a yeast chromosome *EMBO J. 12*, 4521–4531.

Jayasena, S. D., and Johnston, B. H. (1993a) Sequence limitations of triple helix formation by alternate strand recognition. *Biochemistry 32*, 2800–2807.

Jayasena, V. K., and Johnston, B. H. (1993b) Complement-stabilized D-loop:RecA-catalyzed stable pairing of linear DNA molecules at Internal sites. *J. Mol. Biol. 230*, 1015–1024.

Johnson, N. P., Lindstrom, J., Baase, W. A., and von Hippel, P. H. (1994) Double-stranded DNA templates can induce a-helical conformation in peptides containing lysine and alanine: Functional implications for leucine zipper and helix-loop-helix transcription factors. *Proc. Natl. Acad. Sci. U.S.A. 91*, 4840–4844.

Keller, W. (1975) Determination of the number of superhelical turns in simian virus 40 DNA by gel electrophoresis. *Proc. Natl. Acad. Sci. U.S.A. 72*, 4876–4880.

Kmiec, E., B., and Holloman, W. K. (1994) DNA strand exchange promoted in the absence of homologous pairing. *J. Biol. Chem. 269*, 10163–10168.

Koh, J.-S., and Dervan, P. B. (1992) Design of a nonnatural deoxyribonucleoside for recognition of GC base pairs by oligonucleotide-directed triple helix formation. *J. Am. Chem. Soc. 114*, 1470–1478.

Lilley, D. M. (1980) The inverted repeat as a recognisable structural feature in supercoiled DNA molecules. *Proc. Natl. Acad. Sci. U.S.A. 77*, 6468–6472.

Loll, P. J., and Lattman, E. E. (1989) The crystal structure of the ternary complex of staphylococcal nuclease, Ca^{2+}. and the inhibitor pdTp, refined at 1.65 Å. *Prot. Struct. Func. Gen. 5*, 183–201.

Moser, H. E., and Dervan, P. B. (1987) Sequence Specific Cleavage of double strand DNA by triple helix formation. *Science 238*, 645–650.

Neilsen, P. E., Egholm, M., Berg, R. H., and Buchardt, O. (1991) Sequence-Selective Recognition by Strand Displacement with a Thymine-Substituted Polyamide. *Science 254*, 1497–254.

Neilsen, P. E., Egholm, M., Berg, P. H., and Buchardt, O. (1993) Sequence specific inhibition of DNA restriction enzyme cleavage by PNA *Nucl. Acids Res. 21*, 197–200.

Panayotatos, N., and Wells, R. D. (1981) Sequence specific inhibition of DNA restriction enzyme cleavage by PNA. Cruciform structures in supercoiled DNA. *Nature 289*, 466–470.

Pei, D., Corey, D. R., and Schultz, P. G (1990) Site specific cleavage of duplex DNA by a semisynthetic nuclease via triple helix formation. *Proc. Natl. Acad. Sci. U.S.A. 87*, 9858.

Peffer, N. J., Hanvey, J. C., Bisi, J. E., Thomson, S. A., Hassman, C. F., Noble. S. A., and Babiss, L. E. (1993) Strand invasion of duplex DNA by peptide nucleic acid oligomers. *Proc. Natl. Acad. Sci. U.S.A. 90*, 10648–10652.

Rao, B. J., Chiu, S. K., and Radding, C. M. (1993) Homologous recognition and ttriplex formation promoted by RecA protein between duplex oligonucleotides and single-stranded DNA. *J. Mol. Biol. 229*, 328–343.

Sun, J.-S., Francois, J.-C., Montenay-Garestier, T., Saison-Behmoaras, T., Roig, V., Thuong, N. T., and Helene, C. (1989) Sequence-specific intercalating agents: intercalation at specific sequences on duplex DNA via major groove recognition by oligonucleotide-intercalator conjugates. *Proc. Nat. Acad. Sci. U.S.A. 86*, 9198–9202.

Takahara, M., Hibler, D. W., Barr, P. J., Gerlt, J. A., and Inouye, M. (1985) The ompA signal peptide directed secretion of staphylococcal nuclease by Escherichia coli. *J. Biol. Chem. 260*, 2670–2674.

Tucker, P. W., Hazen, E. E., and Cotton, F. A. (1978) Staphylococcal nuclease reviewed: A prototypic study in contemporary enzymology. 1. Isolation; physical and enzymatic properties. *Mol. Cell. Biochem. 22*, 67–77.

Yanisch-Perron, C., Viera, J., and Messing, J. (1985) Improved M13 phage cloning vectors and host strains: nucleotide sequences of the M13mp18 and pUC19 vectors. *Gene 33*, 103–119.

Yoshizawa, S., Ueda, T., Ishido, Y., Miura, K., Watanabe, K., and Hirao, I. (1994) Nuclease resistance of an extraordinarily thermostable mini-hairpin DNA fragment, d(GCGAACG) and its application to in vitro protein synthesis *Nucl. Acids. Res. 22*, 2217–2221.

Young, S. L., Krawczyk, S. H., and Matteucci, M. D. (1991) Triple helix formation inhibits transcription elongation in vitro. *Proc. Natl. Acad. Sci. U.S.A.* 10023–10026.

Zuckermann, R. N., and Schultz, P. G. (1989) Site-selective cleavage of structured RNA by a staphylococcal nuclease-DNA hybrid. *Proc. Natl. Acad. Sci. U.S.A. 86*, 1766–1770.

Synthesis and Evaluation of Nuclear Targeting Peptide–Antisense Oligodeoxynucleotide Conjugates

Michael W. Reed,* Dean Fraga,[†,‡] Dennis E. Schwartz,[§] John Scholler,[⊥] and Robert D. Hinrichsen[†]

MicroProbe Corporation, 1725 220th Street SE #104, Bothell, Washington 98021, and Fred Hutchinson Cancer Research Center, 1124 Columbia Street, Seattle, Washington 98104-2092. Received May 9, 1994[⊛]

An endogenous nuclear enzyme, RNase H, is an important component in determining the efficacy of antisense oligodeoxynucleotides (ODNs). In an effort to improve the potency of antisense ODNs, conjugates with three different nuclear targeting signal peptides were prepared. These short peptide sequences have been shown to facilitate transport of macromolecules into the nucleus of cells. Efficient chemistry for the synthesis of ODN–peptide conjugates is described. Reaction of 5′-aminohexyl-modified ODNs with iodoacetic anhydride gave pure iodoacetamide ODNs (IA–ODNs) in good yield. These electrophilic intermediates were reacted with thiol-containing peptides to give ODN–peptides in excellent yield and purity. The ODN–peptides were further characterized by proteolysis with trypsin. Thermal denaturation studies with ssDNA targets showed little effect of the 5′-peptide modifications on the hybridization properties of the ODN. The effect of the nuclear signal peptides on antisense potency was evaluated in the freshwater ciliate *Paramecium*. A 3′-hexanol-modified 24-mer antisense ODN, complementary to the mRNA for calmodulin, alters regulation of membrane ion channels and swimming behavior of these cells. A 2′-*O*-methyl analog of this ODN was inactive, thus providing evidence that this activity in *Paramecium* is mediated by RNase H. Antisense ODN–nuclear signal peptide conjugates were transfected into the cells by electroporation. Surprisingly, these conjugates showed no antisense effects in comparison to a 5′-unmodified control ODN. Random peptides or amino acids conjugated to the 5′-terminus did not decrease antisense activity.

INTRODUCTION

Antisense oligodeoxynucleotides (ODNs) can hybridize to specific mRNA molecules in a cell to inhibit synthesis of the corresponding proteins (for review see (*1*)). It has been shown that an endogenous cellular nuclease, RNase H, can be an important component in determining the efficacy of this process (*2, 3*). This nuclease cleaves RNA strands present within DNA:RNA duplexes. After hybridization with an antisense ODN, the bound mRNA becomes an RNase H substrate and is inactivated by cleavage. Since the antisense ODN is not cleaved, it can presumably act catalytically to hydrolyze multiple mRNA substrates. Although antisense ODNs with modified phosphodiester backbones have improved serum stability, they often lack potency because their hybrids with mRNA are not substrates for RNase H. For example, 2′-*O*-methyl-modified antisense ODNs require a "core" of at least five deoxy nucleotides in order to retain antisense activity (*4*).

The subcellular compartment where antisense ODNs act to inhibit mRNA function is not clear, but RNAse H is known to be found in the nucleus, where it plays an important role in DNA replication (*5, 6*). Recently, it has been shown that microinjected ODNs rapidly concentrate in the nucleus of cells, apparently by diffusion through the nuclear pores and binding to nuclear proteins (*7, 8*).

Antisense ODNs, in concert with RNase H, may therefore act to degrade mRNA or pre-mRNA targets in the nucleus of cells. Although it is not understood how intracellular trafficking and nuclear binding affects antisense ODNs, we hypothesized that more efficient nuclear transport may improve the molar potency of these compounds.

It has been found that small regions (10–20 amino acids) within nuclear proteins can function as signals for transport of newly synthesized proteins to the nucleus of eukaryotic cells (for review see (*9*)). For example, the nuclear signal peptide for SV40 T antigen was chemically coupled to proteins of various molecular weights and microinjected into Vero cells (*10*). Proteins up to a molecular weight of 450 000 were transported to the nucleus. It has been shown that two nuclear membrane proteins are involved in the active transport of proteins from the cytoplasm through the nuclear pore complex (*11*).

These results suggested that a nuclear signal peptide, when conjugated to an ODN, may function similarly to enhance nuclear delivery and antisense potency. Several synthetic approaches have been used for preparation of ODN–peptide conjugates (for review see (*12*)). Relevant to the work described here was a report on conjugation of the nuclear signal peptide from SV40 T antigen to an antisense ODN (*13*). No yield data or biological effects were reported. In this paper we describe efficient chemistry for preparation of purified iodoacetamide-derivatized ODNs (IA–ODNs) from 5′-aminohexyl ODNs. These versatile ODN intermediates were conjugated to three different cysteine containing nuclear signal peptides to give ODN–peptides in good yield and purity. Several ODNs with smaller molecular weight modifications at the 5′-terminus were also prepared using this method.

We tested the effectiveness of nuclear signal peptide–antisense ODN conjugates in the freshwater ciliate

---

* Author to whom correspondence should be addressed. Tel.: (206) 485-8566. Fax: (206) 486-8336.

[†] Fred Hutchinson Cancer Research Center. Tel.: (206) 667-5000. Fax: (206) 667-6526.

[‡] Present address: Department of Biology, College of Wooster, Wooster, OH 44691.

[§] Present address: Oridigm Corporation, 6 Nickerson St., Seattle, WA 98109.

[⊥] Present address: Bristol-Myers Squibb, 3005 First Ave., Seattle, WA 98121.

[⊛] Abstract published in *Advance ACS Abstracts,* December 15, 1994.

Table 1. Structure and Properties of Modified Oligodeoxynucleotides (ODNs)

ODN[a]	5'-mod	3'-mod	MW	$A_{260} = 1$[b] (μg/mL)	HPLC[c] min	yield[d] (%)
ODN1	aminohexyl	none	4931	35.4	8.4	
ODN2	none	hexanol	7486	32.0	8.8	
ODN3	none	hexanol	7513	30.2		
AH–ODN2	aminohexyl	hexanol	7666	33.0	9.8	
IA–ODN1	iodoacetamide	none	5140	31.9	9.2	76[e]
IA–ODN2	iodoacetamide	hexanol	7834	33.7	10.7	82[f]
ODN1–PEP1	peptide 1	none	6210	38.6	9.0	30[e]
ODN1–PEP2	peptide 2	none	6435	39.9	13.0	73[e]
ODN1–PEP3	peptide 3	none	6652	41.3	15.4	67[e]
ODN2–PEP1	peptide 1	hexanol	8904	38.3	10.0	98
ODN2–PEP2	peptide 2	hexanol	9129	39.3	13.4	97
ODN2–PEP3	peptide 3	hexanol	9346	40.2	15.6	87
ODN2–PEP4	peptide 4	hexanol	8323	35.7	12.4	33
ODN2–CYS	cysteine	hexanol	7827	33.7	9.8	70
ODN2–GLUT	glutathione	hexanol	8013	34.4	9.8	69

[a] The sequences of the ODNs are described in the Experimental Procedures. Structures of the peptides are described in Table 2. [b] Calculated concentration of ODN that gives 1.00 absorbance unit at 260 nm. [c] Elution time; C-18 HPLC system described in Figure 2. [d] Percent isolated yield of ODN after purification by C-18 HPLC. [e] Purified by PRP-1 HPLC. [f] Purified by ultrafiltration.

Paramecium tetraurelia. The swimming behavior of these single-celled animals is used as a model system for the study of excitable membranes (*14*). Microinjection of a 3'-hexanol-modified 24-mer ODN complementary to calmodulin mRNA has previously been shown to alter the swimming behavior of these cells in a semiquantifiable manner (*15*). Intracellular calcium ion concentration in *Paramecium* is controlled by ion channels and pumps in the cell membrane that are regulated by calmodulin. Antisense inhibition of calmodulin levels alters the ciliary beating direction. The 3'-hexanol modification is required for potency of the ODN. It has previously been shown that this blocking group slows exonuclease degradation of phosphodiester ODNs (*16*). Microinjection or electroporation of antisense ODNs into *Paramecium* is a highly reproducible and rapid *in vivo* method that allows intracellular mechanisms to be evaluated separately from plasma membrane transport issues. Using this assay, we determined that an antisense oligonucleotide analog containing all 2'-O-methyl modifications is inactive, thus providing evidence of an RNase H mechanism. Surprisingly, we found that the nuclear signal peptide–ODN conjugates were at least 5-fold less potent than control ODNs with random peptides or amino acids conjugated to their 5'-end.

EXPERIMENTAL PROCEDURES

General Synthesis of Modified Oligodeoxynucleotides. ODNs with the sequences 5'-CTCCATCTTCGT-CACA (ODN1), 5'-TAATTATTCAGCCATTTATTAGTT (ODN2), or 5'-TACTATATCATGGATCATAATTAA (ODN3) were prepared on either a Milligen 7500 or an Applied Biosystems Model 380B synthesizer using the 1 μmol protocols supplied by the manufacturer. Protected β-cyanoethyl phosphoramidites, CPG supports, deblocking solutions, cap reagents, oxidizing solutions, and tetrazole solutions were purchased from either Milligen or Glen Research. 5'-Aminohexyl modifications were introduced into ODN1 and ODN2 using an *N*-MMT-hexanolamine phosphoramidite linker (Milligen). The 2'-O-methyl analog of ODN2 was prepared using 2'-O-methyl phosphoramidites (Glen Research). The 3'-hexanol modification was introduced into ODN2, ODN3, and the 2'-O-methyl analog of ODN2 through use of a hexanol-modified CPG solid support (*16*). Preparative HPLC purification, detritylation, and butanol precipita-
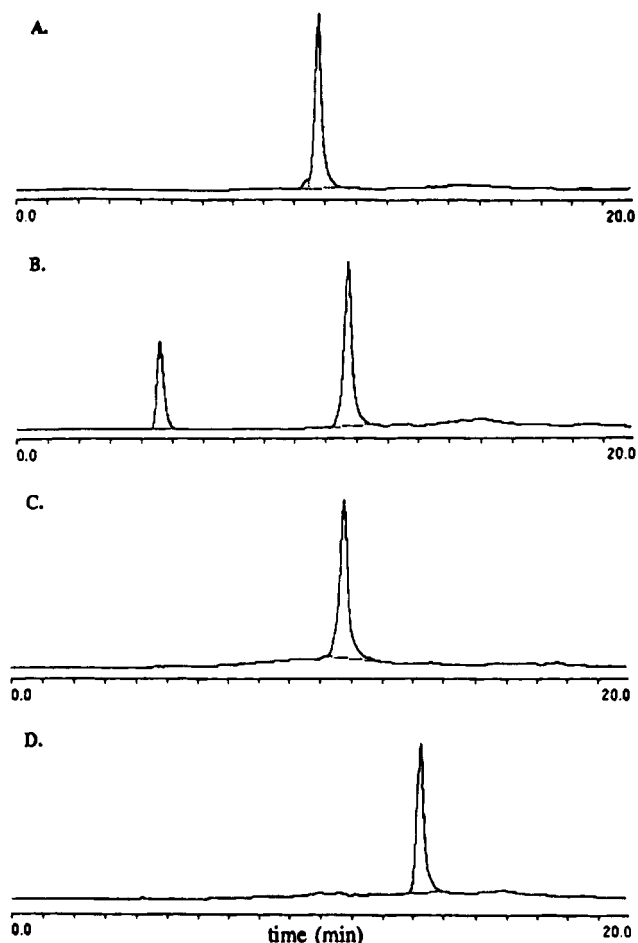
Figure 1. HPLC chromatograms describing synthesis of ODN2–PEP2. The HPLC system used a 250 × 4.6 mm C-18 column and a gradient of 5–45% solvent B over 20 min (flow rate = 1 mL/min) where solvent A = 0.1 M triethylammonium acetate (pH 7.5), solvent B = acetonitrile; detection was by UV absorbance at 260 nm. Panel A: starting aminohexyl-modified ODN (AH–ODN2). Panel B: reaction of AH–ODN2 with iodoacetic anhydride at 60 min. Panel C: iodoacetamide-modified ODN (IA–ODN2) after purification by ultrafiltration. Panel D: ODN2–PEP2 after purification by C-18 HPLC.

tion was carried out as previously described (*17*). The purified ODNs were reconstituted with 1 mL of sterile distilled water and characterized as described below.

Characterization of Modified ODNs. The concentrations of all modified ODNs were determined from the UV absorbance at 260 nm. All ODN concentrations were measured in 0.01 M Tris buffer (pH 7.1). An extinction coefficient for each ODN was determined using a nearest neighbor model (*18*), correcting for the molecular weight of appended modifications. The value for ϵ was used to calculate a theoretical ratio of A_{260} to concentration in μg/mL. The calculated concentration values (μg/mL) for $A_{260} = 1$ OD unit are listed in Table 1 for all modified ODNs. All purified ODNs were analyzed by C-18 HPLC using the method described in Figure 1. Pump control and data processing were performed using a Rainin Dynamax chromatographic software package on a Macintosh computer. ODN purity was further confirmed by polyacrylamide gel electrophoresis (PAGE). The nucleotidic bands were stained with either methylene blue or silver stain. Unless otherwise noted, modified ODNs were greater than 95% pure by C-18 HPLC and one major band by PAGE.

Synthesis of Iodoacetamide-ODNs (IA–ODN2). An aqueous solution of the 5'-aminohexyl derivative of

Table 2. Structure and Properties of 5'-Modifications

modification	MW	sequence
peptide 1[a]	1198	cys-thr-pro-pro-lys-lys-lys-arg-lys-val-CONH₂
peptide 2[b]	1423	cys-asn-ser-ala-ala-phe-glu-asp-leu-arg-val-leu-ser-CO₂H
peptide 3[c]	1640	met-asn-lys-ile-pro-ile-lys-asp-leu-leu-asn-pro-gln-cys-CONH₂
peptide 4[d]	617	cys-leu-ala-leu-ala-lys-CONH₂
glutathione	307	glutamyl-cys-gly-CO₂H
cysteine	121	cys-CO₂H

[a] Signal sequence associated with nuclear delivery of the SV40 T antigen. [b] Signal sequence associated with influenza virus nucleoprotein NP. [c] Signal sequence associated with yeast α2 protein. [d] Nontargeting peptide sequence.

ODN2 (0.50 mL, 1.41 mg, 0.184 μmols), was combined with 0.50 mL of 1.0 M sodium borate buffer (pH 8.3) in a polypropylene Eppendorf tube. Iodoacetic anhydride was added as a 50 mg/mL stock solution in acetonitrile (128 μL, 6.4 mg, 18 μmols), and the heterogeneous mixture was vortexed for 1 h. C-18 HPLC analysis indicated complete conversion of aminohexyl–ODN2 to IA–ODN2. The crude reaction mixture was transferred to a 3000 MW cutoff microconcentrator (Amicon) with 1.0 mL of 0.1 M borate buffer (pH 8.3) and centrifuged to a retentate volume of ∼0.1 mL. The retentate was reconstituted to 2 mL, and the mix was reconcentrated. This process was repeated, and the retentate was reconstituted to 1.0 mL with 0.1 M borate. C-18 HPLC analysis showed that this ultrafiltration process cleanly separated IA–ODN2 from the small molecular weight iodoacetate contaminants. The UV absorbance at 260 nm indicated a concentration of 1.18 mg/mL. This corresponds to an isolated yield of 82%. The IA–ODN solution was stored frozen at −20 °C. A sample stored at room temperature showed ∼50% decomposition after 10 days as evidenced by HPLC.

A similar procedure was used for preparation of IA–ODN1 except that the desired product was isolated by reversed-phase HPLC on a PRP-1 column (305 × 7.0 mm, 5−45% acetonitrile in TEAA over 20 min, flow rate = 2 mL/min). The product containing the fraction (11.6 min) gave an isolated yield of 76%. This solution was used directly for further reactions. The physical properties and synthetic results are shown in Table 1.

Synthesis and Characterization of Nuclear Signal Peptides. The four cysteine-containing peptides were purchased from Multiple Peptide Systems (San Diego, CA). The lyophilized solids (thiol form) were handled under argon to prevent oxidation and stored desiccated at −20 °C. The peptides were all >95% pure by C-18 HPLC. They were further characterized by time of flight mass spectral analysis (plasma desorption ionization). The structure of each of the peptides is shown in Table 2.

Synthesis of ODN–Peptide Conjugates (ODN2–PEP2). A solution of 294 μg (37.5 nmols) of iodoacetamide–ODN2 in 250 μL of 0.1 M sodium borate buffer (pH 8.3) was transferred to a 1.1 mL septum capped glass vial and degassed by sparging with argon for 10 min. A 1.0 mg/mL stock solution of the thiol-containing peptide (peptide 2) in degassed water was prepared. A 267 μL (188 nmols) portion of the peptide 2 solution was added to the solution of IA–ODN2, and the mixture was degassed and kept under an argon atmosphere for 23 h. The ODN–peptide conjugation reactions were conveniently followed by C-18 HPLC. After 20 h at room temperature, the reaction mixture was concentrated to dryness on a Speed-Vac and reconstituted with 100 μL of TEAA buffer. The mixture was purified by C-18 HPLC using the column and gradient described in Figure 1. The peak corresponding to product was collected in one fraction and dried on a Speed-Vac. The solid residue was reconstituted with 200 μL of water. Five μL of the

purified product (ODN2–PEP2) was used for analysis by C-18 HPLC. Another 5 μL of the solution was used to determine the concentration (1.54 mg/mL, 87% recovery). Triethylammonium counterion was replaced with sodium by drying with 12.6 μL (1.5 μmols) of a 1% sodium bicarbonate solution. The residue was reconstituted with 190 μL, and the homogeneous solution was used for antisense efficacy studies.

A similar procedure was used for preparation of ODN2–PEP1, ODN2–PEP3, and ODN2–PEP4. The preparation of ODN1–PEP1, ODN1–PEP2, and ODN1–PEP3 used the IA–ODN1 fraction from HPLC purification (∼25% acetonitrile in 0.1 M TEAA). PRP-1 HPLC was used for purification of the ODN1–peptide conjugates (305 × 7.0 mm, 5−45% acetonitrile in TEAA over 20 min, flow rate = 2 mL/min). The physical properties and synthetic results are shown in Table 1.

Synthesis of Other 5'-Modified ODNs. Iodoacetamide–ODN2 was also reacted with reduced cysteine and reduced glutathione to provide ODN2–CYS and ODN2–GLUT, respectively. The synthesis and purification procedure was similar to that used for preparation of the ODN–peptides except that 10 equiv of the thiol-containing compounds were used. The physical properties and synthetic results are shown in Table 1.

Thermal Denaturation Studies (ODN1–Peptides). Thermal dissociation curves were obtained by following changes in A_{260} of aqueous solutions containing equimolar amounts of the particular ODN1–peptide described above and an unmodified 20-mer ODN complement with the base sequence 5'-GTGACGAACATGGAGAACAT. The 5'-aminohexyl-modified 16-mer (ODN1) was used as a control in each run. ODNs were prepared as 2 μM solutions in pH 7.2 PBS (9.2 mM disodium phosphate, 0.8 mM monosodium phosphate, 0.131 M sodium chloride). A Gilford System 2600 UV–vis spectrophotometer equipped with a Gilford 2527 Thermo-programmer was used. The samples were heated from 15 to 85 °C with a temperature increase of 0.5 °C/min. Absorbance vs time and the first derivative data were recorded automatically. The T_m was determined using the derivative maxima. The results were as follows: ODN1, T_m = 62.8 °C; ODN1–PEP1, T_m = 61.8 °C; ODN1–PEP2, T_m = 59.0 °C; ODN1–PEP3, T_m = 60.8 °C.

Protease Degradation Studies (ODN1–Peptides). The three ODN1–peptide conjugates were further characterized by proteolytic treatment with trypsin. Solutions of 2 μg of the ODN–peptide in 7 μL of water were combined with 1 μL of 10× trypsin disruption solution (Boehringer Mannheim, 5 mg/mL trypsin), 1 μL of 100 mM Tris buffer (pH 9.0), and 1 μL of 100 mM EDTA. After digestion for 60 min, the samples were loaded on 20% denaturing polyacrylamide gel and electrophoresed using the conditions described in Figure 2.

Antisense Assay (ODN2 Analogs). Modified antisense ODNs were evaluated by electroporating the ODNs into *Paramecium* and observing their swimming behavior in a test solution. A 3'-hexanol-modified 24-mer ODN with sequence complementary to calmodulin mRNA

1   2   3   4   5   6   7   8   9
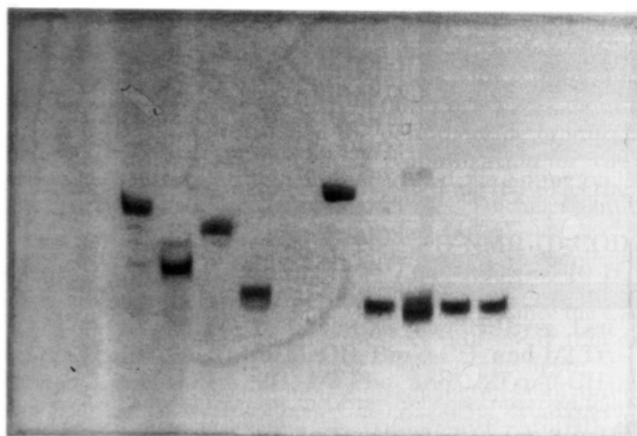
Figure 2. Polyacrylamide gel electrophoresis analysis of ODN1−peptides before and after proteolysis with trypsin. PAGE was carried out under denaturing conditions (7 M urea) using cross-linked 20% gels (bisacrylamide/acrylamide, 1:19; $0.4 \times 170 \times 390$ mm) at 45 W for 40 min. pH 8.3 TBE (100 mM tris base, 100 mM boric acid, 1 mM EDTA) was used as a running buffer. Nucleotidic bands were visualized by staining with methylene blue (0.02%). Bromophenol blue was used as a marker. Lane 1 is ODN1−PEP1. Lane 2 is ODN1−PEP1 after trypsin. Lanes 3 is ODN−PEP2. Lane 4 is ODN1−PEP2 after trypsin. Lane 5 is ODN1−PEP3. Lane 6 is ODN1−PEP3 after trypsin. Lane 7 is IA−ODN1. Lane 8 is ODN1. Lane 9 is ODN1 after trypsin.

(ODN2) was used as a positive control for evaluation of antisense efficacy, and a 3′-hexanol-modified 24-mer ODN with a random sequence (ODN3) was used as a negative control (*15*). A mutant of strain 51S (wild-type) cells designated *cam 1* was used. Cells that were in late log to early stationary phase were pelleted and resuspended in approximately 1/4 volume of 10 mM HEPES buffer (pH 7.2). Cells were washed again in 1/4 volume HEPES and finally resuspended in HEPES at a final concentration of about 10^6 cells per mL. Electroporation was with an electrocell manipulator 600 (BTX Inc., San Diego, CA). Electroporation cuvettes were used with a 0.4 cm gap between electrodes. Resistance was set at 13 Ω. Cells (250 μL) were mixed with ODN (at a final concentration of 10 μM) in the electroporation cuvette. A pulse was delivered at 200−250 V (field strength of 500−625 V/cm) for 3.9−4.2 ms using a 275 μF capacitor. All electroporations were at room temperature. Cells were then transferred into 48 volumes of a solution consisting of 1 mM Hepes (pH 7.2), 1 mM CaCl$_2$, 1 mM KCl, and 10% exhausted wheat grass solution (v/v). The cells were allowed to incubate in this solution for 10−14 h at 28 °C before testing. Cells were selected at random for testing and were individually placed in 300 μL of 1 mM Hepes (pH 7.2), 1 mM CaCl$_2$, 1 mM KCl, 10 mM NaCl, and 5 mM tetraethylammonium chloride (TEA). The time of backward swimming (defined as the time from which the cells begin to swim backward until they cease a backward movement) was measured while observing the cells under a dissecting microscope. The test solution was designed to elicit a backward swimming response of 100−150 s in untreated or control cells. Affected cells showed a 40−60% reduction in backward swimming time. Data was analyzed by the Mann−Whitney statistical test of significance. Full details of the electroporation assay will be published in a separate paper.

Concentration dependence of the antisense ODN−nuclear signal peptide conjugates was evaluated in wild-type *Paramecium* in comparison to ODN2 using the microinjection method as previously described (*15*). The

Scheme 1. Synthesis of ODN-Peptide Conjugates
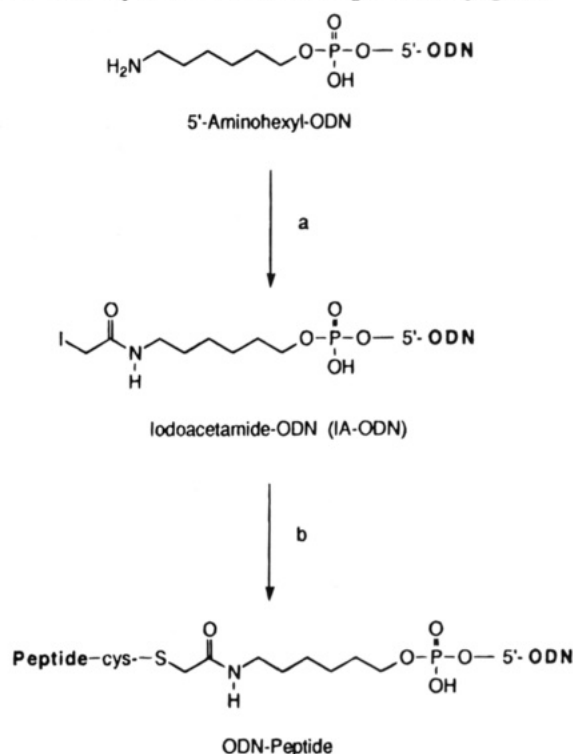
^{a} Reagents: (a) iodoacetic anhydride (100 equivs), acetonitrile, sodium borate buffer (pH 8.3); (b) HS-cys-peptide (5 equivs), sodium borate buffer (pH 8.3).

minimum effective concentration of ODN2 was 31−63 μM. The highest concentrations of ODN−peptides evaluated were as follows: ODN2−PEP1 (184 μM), ODN2−PEP2 (183 μM), ODN2−PEP3 (165 μM).

RESULTS

Scheme 1 illustrates the chemistry used to prepare ODN−peptide conjugates and other 5′-modified ODNs. The coupling step involves reaction of ODNs bearing an electrophilic iodoacetamide linking group to peptides which bear a nucleophilic thiol residue. The iodoacetamide−ODNs (IA−ODNs) were key intermediates in this synthetic approach. IA−ODNs were prepared from 5′-aminohexyl-modified ODNs in excellent yield. IA−ODNs are readily purified and stable to storage in solution as described below.

The conjugation chemistry was developed using two different ODNs. ODN1 is a 5′-aminohexyl-modified 16-mer ODN with a sequence complementary to the initiation codon region of the mRNA transcript for the Hepatitis B surface antigen in Hep3B cells. The ODN1-peptide conjugates were characterized by thermal denaturation studies and proteolysis studies. ODN2 is a 3′-hexanol-modified 24-mer ODN with a sequence complementary to the initiation codon region of the mRNA transcript for the regulatory protein calmodulin in *Paramecium tetraurelia*. The ODN2 conjugates were used for antisense efficacy assays. The aminohexyl modifications were added at the 5′-terminus of the ODNs during automated synthesis using a commercially available phosphoramidite reagent and the "trityl-on" ODNs were purified by HPLC. Acid deprotection of the monomethoxytrityl group and butanol precipitation gave the desired 5′-aminohexyl modified ODNs in >95% purity as shown by C-18 HPLC.

Treatment of the 5′-aminohexyl modified ODNs (in pH 8.3 borate buffer) with 100 equivalents of iodoacetic

anhydride (in acetonitrile) gave quantitative conversion to the desired iodoacetamide-ODN (IA–ODN). The oily reaction mixture became homogeneous after shaking for 1 h. Since ODNs have strong UV absorbance at 260 nm, the conjugation chemistry was easily monitored by reversed-phase (C-18) HPLC. As shown in Figure 1 (panels A and B) the starting aminohexyl–ODN2 (9.8 min peak) was completely converted to iodoacetamide–ODN2 (10.7 min peak) after 60 min.

Although they are reasonably stable in solution, IA–ODNs are typical of electrophilic ODNs in that they degrade if taken to dryness. Ultrafiltration techniques are well suited for purification of these reactive ODN derivatives. As shown in Figure 1 (panels B and C), the small molecular weight iodoacetyl contaminants (4.6 min) are completely separated from the purified IA–ODN2 (10.7 min peak) by ultrafiltration through a 3000 molecular weight cutoff filter. After ODN concentration was determined, the aqueous solutions of IA–ODN were stored at 5 °C for days at a time with no apparent degradation. However, a sample kept at room temperature showed ~50% degradation over a 10 day period. It is best to prepare IA–ODN solutions only as needed and to store them refrigerated or frozen.

Reversed-phase HPLC was also used for purification of IA–ODNs. In this case, the fraction containing product was used directly for conjugation reactions. HPLC was more tedious and gave less control over final IA–ODN concentration and solvent composition. Nonetheless, HPLC purification provides an advantage if large molecular weight impurities are present in the reaction mixture which cannot be separated by ultrafiltration. Further concentration or solvent exchange of HPLC-purified IA–ODN can be accomplished by ultrafiltration if so desired. If the starting aminohexyl-modified ODN was pure, the iodoacetylation reaction went to completion and ultrafiltration was the purification method of choice. The physical properties and synthetic yields for all modified ODNs are presented in Table 1. All modified ODNs were >95% pure by C-18 HPLC.

Cysteine-containing peptides of various sizes and properties were conjugated to the IA–ODNs as illustrated in Scheme 1. The sequence (N-terminal to C-terminal) and structure of the cysteine containing peptides and other 5′-modifications are shown in Table 2. In addition to the three nuclear signal peptides, a nontargeting peptide (peptide 4), glutathione, and cysteine were used as controls for antisense efficacy studies. The peptides were commercially prepared using standard solid-phase synthesis techniques and were purified by C-18 HPLC (95+ pure). The purified peptides were carefully handled under argon to prevent oxidation to the disulfides.

Treatment of the IA–ODNs with 5 equivs of the desired thiol-containing peptide gave quantitative conversion to the desired 5′-peptide modified ODN as evidenced by analytical C-18 HPLC. Lower offering ratios of peptide to IA–ODN were not investigated. Careful coinjection was required to differentiate ODN1–PEP1 from starting IA–ODN1. Different reaction kinetics were observed for the three peptides that correlated well with the cationic nature of the peptide. Reaction with peptide 1 (net charge = +5) was complete in minutes, whereas peptide 2 (net charge = 0) required 20 h, and peptide 3 (net charge = +1) required 3 h for complete reaction. Interaction of the polyanionic ODN with the more cationic peptides presumably enhances the reaction rate. The ODN–peptide conjugates were readily purified by HPLC and taken to dryness without decomposition. To ensure complete removal of the (toxic)

triethylammonium counterions, all ODNs were taken to dryness with excess sodium bicarbonate. Since the peptides are transparent at 260 nm, the fate of unreacted peptide in the purification process was unclear. Since the retention time of the conjugates was generally longer than the starting oligo, it was assumed that excess peptide eluted late in the gradient. The purified ODN–peptide conjugates all appeared as one peak by C-18 HPLC. Figure 1 (panel D) illustrates the HPLC purity and change in retention time for ODN2–PEP2.

The purity of the ODN–peptide conjugates was also evaluated by polyacrylamide gel electrophoresis (PAGE). All appeared as one major band (Figure 2, lanes 1, 3, and 5). The presence of the peptide residue in the ODN1–peptide conjugates was further confirmed by proteolytic treatment with trypsin. Trypsin catalyzes hydrolysis at the carboxyl side of lysine or arginine residues in peptides. Polyacrylamide gel electrophoresis indicated complete proteolysis of the starting ODN1–peptides (Figure 2, lanes 2, 4, and 6). Trypsin had no effect on the unmodified ODN1 controls (Figure 2, lanes 8 and 9).

The ODN–peptide conjugates prepared from ODN1 were further characterized by thermal denaturation studies. The dissociation of duplexes formed from equimolar concentrations of the ODN1-peptides and an unmodified 20-mer ODN target was examined. The 20-mer target ODN had a sequence complementary to ODN1 such that a 5-nucleotide overhang was adjacent to the 5′-modification on ODN1. The T_m curves were typical of those obtained with unmodified ODNs. The results were as follows: ODN1, T_m = 62.8 °C; ODN1–PEP1, T_m = 61.8 °C; ODN1–PEP2, T_m = 59.0 °C; ODN1–PEP3, T_m = 60.8 °C. This demonstrated that the nuclear signal peptide modifications had little adverse effect on hybridization properties of the ODN.

The effects of structural modification on antisense potency of anti-calmodulin ODN2 were evaluated in *Paramecium*. *Cam1* mutant cells were incubated in 10 μM solutions of the ODN2 analog of interest, and the ODN was introduced by electroporation. After 10–12 h in a resting solution, the cells were transferred to a testing solution and the backward swimming time was measured. The results were compared to a positive control (antisense ODN2) and a negative control (random ODN3). Cells treated with calmodulin-specific antisense ODN2 had a backward swimming response that is 40–60% reduced compared to untreated cells. Affected cells returned to normal swimming behavior after 24–48 h. In order to further explore the molecular mechanism of antisense activity, the 2′-O-methyl analog of ODN2 was prepared and tested. As shown in Figure 3 (panel A), this analog (2′-O-Me) gave no decrease in backward swimming time. Loss of antisense activity with this analog is evidence of an RNase H-mediated mechanism.

The effect of the 5′-nuclear signal peptide modifications on potency of antisense ODN2 was then evaluated. As illustrated in Figure 3 (panel A), the cells showed no significant change in swimming behavior upon treatment with ODN2-nuclear signal peptide conjugates. The antisense ODN–nuclear signal peptide conjugates were also evaluated in wild-type *Paramecium* using the microinjection method previously described (*15*). The ODN–signal peptide conjugates had no potency at concentrations up to five times the minimum effective concentration of ODN2. More concentrated solutions of the ODN–peptide conjugates were not tested.

To further elucidate the structure/activity relationships of 5′-modified ODNs, several additional conjugates of ODN2 were prepared and tested in the *Paramecium* assay. Reaction of IA–ODN2 with cysteine, glutathione,
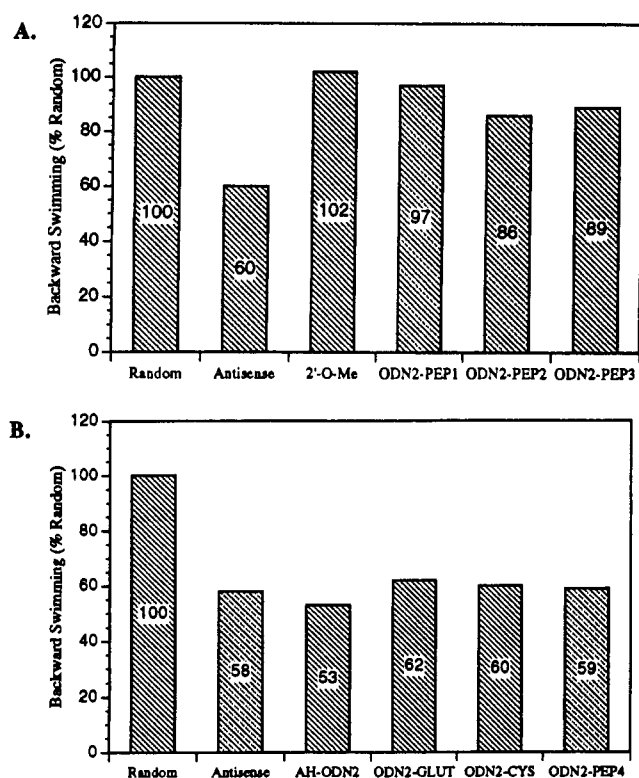
Figure 3. Effect of 5'-modifications on antisense activity in electroporated *Paramecium*. Random control (ODN3) was a 3'-hexanol-modified 24-mer with a random sequence (no 5'-modification). Antisense control (ODN2) was a 3'-hexanol modified 24-mer ODN with sequence complementary to calmodulin mRNA. All 5'-modified ODNs were derivatives of antisense ODN2 (abbreviations are described in Table 1). A 2'-O-methyl control (2'-O-Me) was a 3'-hexanol-modified analog with the same sequence as ODN2. *Cam1* cells were treated with 10 μM concentrations of each 5'-modified ODN and then tested for backward swimming behavior after 10−12 h. Test solution was 1 mM Hepes (pH 7.2), 1 mM $CaCl_2$, 1 mM KCl, 10 mM NaCl, and 5 mM TEA^+. For each ODN, 10 cells were tested by observing swimming behavior under a microscope. Data was significant by the Mann−Whitney test at $P < 0.01$. Data are presented as percent random control. Panel A: effect of nuclear targeting peptides on backward swimming time of cells. Panel B: effect of smaller molecular weight modifications on backward swimming time of cells.

or a random peptide (peptide 4) gave the desired 5'-modified ODNs in good yield. The effect of these 5'-modifications on antisense potency was tested in relation to the 5'-unmodified control (ODN2). As shown in Figure 3 (panel B), introduction of the 5'-aminohexyl modification had no adverse effect on antisense activity of ODN2. Likewise, further modification of the 5'-aminohexyl group with cysteine, glutathione, or peptide 4 did not decrease antisense activity in this assay.

DISCUSSION

ODNs modified with a nucleophilic amino or thiol group have generally been used for coupling with electrophilic conjugate groups (*19*). Although electrophilic ODN derivatives have been described, they have often been poorly characterized or showed unusual properties. For example, an electrophilic maleimide−ODN derivative used for preparation of an ODN−peptide showed multiple peaks by analytical HPLC (*12*). The fact that electrophilic ODNs can degrade rapidly if they are taken to dryness may have dissuaded other workers from pursuing this type of conjugation chemistry.

ODNs containing iodoacetamide modifications have previously been prepared and used as hybridization

triggered crosslinking agents (ref *20* and references therein). The iodoacetyl crosslinking groups were introduced into internal positions of the ODNs and reacted with guanine residues on complementary nucleic acid strands with variable reaction rates. Recently, iodoacetamide-modified ODNs were used for conjugation to poly(δ)ornithine peptides (*21*). Purification was complicated by unreacted ODN, and no yield data was provided. We report here that 5'-iodoacetamide-modified ODNs (IA−ODNs) are versatile synthetic intermediates for reaction with thiol-containing conjugate groups. Efficient chemistry was used to introduce the iodoacetamide group into 5'-aminohexyl modified antisense ODNs, and a variety of cysteine-containing peptides were coupled. Since both the peptides and ODNs were rigorously purified before use (>95% by C-18 analytical HPLC), excellent results were obtained in the coupling reactions.

The use of iodoacetic anhydride for preparation of electrophilic ODNs has not been previously reported. Conversion of 5'-aminohexyl ODNs to IA−ODNs by treatment with excess iodoacetic anhydride was rapid and quantitative and gave no detectable side reactions. Three other commercially available heterobifunctional linkers (sulfo-SIAB, SIAB, NHS-iodoacetate) were evaluated before the utility of (inexpensive) iodoacetic anhydride was discovered. As described above, IA−ODNs were readily purified by ultrafiltration and reasonably stable to refrigerated storage in solution. Ultrafiltration is particularly useful due to ease of operation, good recovery, and the ability to prepare concentrated IA−ODN solutions without drying. IA−ODNs reacted completely with thiol-containing peptides to give good yields of purified ODN−peptides. It should be noted that the chemistry was driven toward complete consumption of IA−ODN by treatment with 5 molar equiv of peptide. The fate of the unreacted peptide was not determined, but is unlikely to have the same HPLC retention time as the ODN−peptide conjugates. If valuable peptides are used, different stoichiometry (excess ODN) may be advantageous.

A list of 16 reported nuclear signal peptides was generated from a survey of the literature. The three well-documented peptide sequences shown in Table 2 were designed with either C- or N-terminal cysteine residues to provide a nucleophilic "handle" for conjugation to the electrophilic IA−ODN derivative. Peptide 1 is the signal sequence associated with nuclear delivery of the SV40 T antigen (*10, 22*). The carboxy terminus of this 10-mer was protected as the formamide to more closely resemble the conformation in the native protein. A negatively charged carboxyl residue may have interacted with the intramolecular lysine residues. Peptide 2 is the signal sequence associated with influenza virus nucleoprotein NP (*23*). The carboxy terminus of this 13-mer was left unblocked since this is the actual carboxy terminus in the native protein. This peptide was chosen since it contained no lysine residues and presumably acted via a different transport mechanism. It has been shown to act as a "retention signal" rather than an "uptake signal". Peptide 3 is the signal sequence associated with yeast α2 protein (*24*). The carboxy terminus of this 14-mer was protected as the formamide since this is a fragment from an internal portion of the protein. The N-terminal methionine was left unblocked since this residue has been shown to confer long cytoplasmic half-life to proteins (*25*). This is the first reported amino acid sequence that could target non-nuclear proteins to the nucleus.

The results from the model studies with ODN1 indicate that IA−ODNs react cleanly with the thiol group of cysteine-containing peptides without competing side

reactions with the primary amines on lysine. Especially striking were the results with the lysine rich peptide 1. Thermal denaturation studies indicate that there was no damage to the ODN during iodoacetylation (i.e., modification of the unprotected nucleotides) since this would have interfered with hybridization. There was also no evidence for unusual intramolecular or intermolecular complex formation between the cationic peptide and the ODN. The T_m studies also demonstrated that even large peptide modifications on the 5'-terminus of the ODN did not interact with the 5 nucleotide overhang of the complementary DNA strand. The proteolysis study (Figure 2) showed no degradation of the ODN, but precise hydrolytic cleavage of the peptide by trypsin. All three of the ODN—peptides were cleanly converted to a single ODN-containing product. The relative mobility of the proteolysis products from ODN1—PEP1 and ODN1—PEP2 clearly indicated the presence of residual amino acids, whereas the product from ODN1—PEP3 gave a product with the same relative mobility as ODN1.

After the properties of the ODN—peptide conjugates were tested in simple biochemical systems, the critical experiments in living cells were attempted. Since the ultimate goal of the research was to evaluate the intracellular effects of nuclear signal peptides on antisense ODN potency, it was important to avoid cellular uptake issues. The *Paramecium* antisense assay was ideal for this purpose since electroporation or microinjection introduces the ODN—peptides directly into the cytoplasm by transiently opening the plasma membrane. The previously described 24-mer ODN sequence (ODN2) was used as a positive control for the assay. In order to learn more about the importance of RNase H activity in *Paramecium*, we examined the 2'-O-methyl analog of ODN2 and found it to lack potency (Figure 3, panel A). Although 2'-O-Me oligonucleotides form more stable hybrids with complementary mRNA than the respective ODNs, the heteroduplexes are not substrates for RNase H, and therefore, they lack potency in many cell types (*4*). If antisense ODN2 was inhibiting RNA function by blocking RNA—protein or RNA—RNA interactions, then it would be expected that the 2'-O-Me analog would be more potent. We interpret the loss of antisense activity as evidence for RNase H-mediated degradation of the target calmodulin mRNA.

As shown in Figure 3 (panel A), none of the three nuclear signal peptide—antisense ODN conjugates showed significant antisense activity. Since it had already been demonstrated that the ODN—peptides had well-behaved hybridization properties, it was unclear how the 5'-peptide modifications interfered with the activity of the antisense ODNs. To answer this question, a series of four antisense ODN conjugates with nontargeting 5'-modifications of increasing molecular weight were prepared and tested. As shown in Figure 3 (panel B), 5'-modifications up to a molecular weight of 617 gave no decrease in antisense effect. Thus, the simple presence of bulky 5'-modifications did not decrease activity of the antisense ODN in this assay.

It is not clear why attachment of the nuclear signal peptides to the 5'-terminus gave a decrease in antisense potency. Since RNase H binds to DNA—RNA duplexes over a short (three—six nucleotide) region, it seems unlikely that access of the enzyme to the duplex is a problem. Since the ODN—peptides showed good hybridization properties with a ssDNA target, binding to calmodulin mRNA or pre-mRNA should not be inhibited. Although the model signal peptides have been demonstrated to localize in the nucleus of other eukaryotic cells, they may not behave similarly in the highly specialized

Paramecium. The ODN—peptides may bind to a specific nuclear transport receptor as proposed, but be unable to be released. Even if the ODN—peptide is transported through the nuclear pore complex, it may be delivered to a specific region or structure of the nucleus where it does not have access to either the mRNA transcript for calmodulin, or RNase H.

In summary, the utility of iodoacetamide-modified ODNs as versatile intermediates for synthesis of ODN conjugates was demonstrated. Although the conjugation of nuclear signal peptide sequences decreased antisense activity in the *Paramecium* assay, it was shown that other 5'-modifications are well tolerated in this system. Although the intracellular trafficking of ODNs is a difficult issue to address experimentally, it is important for the design of more potent antisense ODN conjugates. Fluorescein labeled conjugates may allow the intracellular location of antisense ODNs and nuclear targeting peptide—ODN conjugates to be determined in *Paramecium*.

LITERATURE CITED

(1) Uhlmann, E., and Peyman, A. (1990) Antisense oligonucleotides: a new therapeutic principle. *Chem. Rev. 90*, 543.

(2) Minshull, J., and Hunt, T. (1986) The use of single-stranded DNA and RNase H to promote quantitative "hybrid arrest of translation" of mRNA/DNA hybrids in reticulocyte lysate cell-free translations. *Nucleic Acids Res. 14*, 6433.

(3) Dash, P., Lotan, I., Knapp, M., Kandel, E. R., and Goelet, P. (1987) Selective elimination of mRNAs in vivo: complementary oligodeoxynucleotides promote RNA degradation by an RNase H-like activity. *Proc. Natl. Acad. Sci. U.S.A. 84*, 7896.

(4) Monia, B. P., Lesnik, E. A., Gonzalez, C., Lima, W. F., McGee, D., Guinosso, C. J., Kawasaki, A. M., Cook, P. D., and Freier, S. M. (1993) Evaluation of 2'-modified oligonucleotides containing 2'-deoxy gaps as antisense inhibitors of gene expression. *J. Biol. Chem. 268*, 14514.

(5) Crouch, R. J., and Dirksen, M.-L. (1982) Ribonucleases H. *Nucleases* (S. M. Linn and R. J. Roberts, Eds.) pp 211—241, Cold Spring Harbor Laboratory, Cold Spring Harbor, NY.

(6) Crouch, R. J. (1990) Ribonuclease H: from discovery to 3D structure. *New Biol. 2*, 771.

(7) Leonetti, J. P., Mechti, N., Degols, G., Gagnor, C, and Lebleu, B. (1991) Intracellular distribution of microinjected antisense oligonucleotides. *Proc. Natl. Acad. Sci. U.S.A. 88*, 2702.

(8) Clarenc, J.-P., Lebleu, B., and Leonetti, J.-P. (1993) Characterization of the nuclear binding sites of oligodeoxyribonucleotides and their analogs. *J. Biol. Chem. 268*, 5600.

(9) Dingwall, C., and Laskey, R. A. (1986) Protein import into the cell nucleus. *Ann. Rev. Cell Biol. 2*, 367.

(10) Lanford, R. E., Kanda, P., and Kennedy, R. C. (1986) Induction of nuclear transport with a synthetic peptide homologous to the SV40 T antigen transport signal. *Cell 46*, 575.

(11) Adam, S. A., Lobl, T. J., Mitchell, M. A., and Gerace, L. (1989) Identification of specific binding proteins for a nuclear location sequence. *Nature 337*, 276.

(12) Tung, C., Rudolph, M. J., and Stein, S. (1991). Preparation of oligonucleotide-peptide conjugates. *Bioconjugate Chem. 2*, 464.

(13) Eritja, R., Pons, A., Escarceller, M., Giralt, E., and Albericio, F. (1991) Synthesis of defined peptide—oligonucleotide hybrids containing a nuclear transport signal sequence. *Tetrahedron 47*, 4113.

(14) Hinrichsen, R., and Schultz, J. (1988) *Trends Neurosci. 11*, 27.

(15) Hinrichsen, R. D., Fraga, D., and Reed, M. W. (1992). 3′-modified antisense oligodeoxyribonucleotides complementary to calmodulin mRNA alter behavioral responses in *Paramecium. Proc. Natl. Acad. Sci. U.S.A. 89*, 8601.

(16) Gamper, H. B., Reed, M. W., Cox, T., Virosco, J. S., Adams, A. D., Gall, A., Scholler, J. K., and Meyer, R. B., Jr. (1992) Facile preparation of nuclease resistant 3′-modified oligodeoxynucleotides. *Nucleic Acids Res. 21*, 145.

(17) Reed, M. W., Adams, A. D., Nelson, J. S., and Meyer, R. B., Jr. (1991) Acridine- and cholesterol-derivatized solid supports for improved synthesis of 3′-modified oligonucleotides. *Bioconjugate Chem. 2*, 217.

(18) Cantor, C. R., Warshaw, M. M., and Shapiro, H. (1970) Oligonucleotide interactions. III. circular dichroism studies of the conformation of deoxyoligonucleotides. *Biopolymers 9*, 1059.

(19) Goodchild, J. (1990) Conjugates of oligonucleotides and modified oligonucleotides: a review of their synthesis and properties. *Bioconjugate Chem. 1*, 165.

(20) Tabone, J. C., Stamm, M. R., Gamper, H. B., and Meyer, R. B. Jr. (1994) Factors influencing the extent and regiospecifity of cross-link formation between single-stranded DNA and reactive complementary oligonucleotides. *Biochemistry 33*, 375.

(21) Zhu, T., Tung, C.-H., Breslauer, K. J., Dickerhof, W. A., and Stein, S. (1993) Preparation and physical properties of oligodeoxynucleotides with poly(δ)ornithine peptides. *Antisense Res. Dev. 3*, 349.

(22) Kalderon, D., Roberts, B. L., Richardson, W. D., and Smith, A. E. (1984) A short amino acid sequence is able to specify nuclear location. *Cell 39*, 499.

(23) Davey, J., Dimmock, N. J., and Colman, A. (1985) Identification of the sequence responsible for the nuclear accumulation of the influenza virus nucleoprotein in *Xenopus oocytes. Cell 40*, 667.

(24) Hall, M. N., Hereford, L., and Herskowitz, I. (1984) Targeting of E. coli B-galactosidase to the nucleus in yeast. *Cell 36*, 1057.

(25) Bachmair, A. Finley, D., Varshavsky, A. (1986) In vivo half-life of a protein is a function of its amino-terminal residue. *Science 234*, 179.

BC9400938

Comparative Photoaffinity Labeling Study between Azidophenyl, Difluoroazidophenyl, and Tetrafluoroazidophenyl Derivatives for the GABA-Gated Chloride Channels

Isabelle Kapfer, Patrice Jacques, Hacène Toubal, and Maurice Ph. Goeldner*

Laboratoire de Chimie Bio-organique, URA 1386 CNRS, Faculté de Pharmacie, Université Louis Pasteur Strasbourg, BP 24, 67401 Illkirch Cedex, France. Received September 1, 1994[®]

Syntheses of 2-aryl-substituted photoactivatable derivatives of 5-*tert*-butyl-1,3-dithiane and their oxidized bis-sulfone are described. The 4-azidoaryl and the 3,5-difluoro-4-azidoaryl groups were chosen as photosensitive moieties. Azidoaryl derivatives **3** and **13** were synthesized by diazotization and azidation of their corresponding arylamine precursors. The *o*-difluoroazidophenyl derivatives **2** and **9** were synthesized by transformation of the *o*-difluoro-substituted lithiophenyl into the corresponding azido derivative. The reversible binding properties of the photosensitive probes were established on bovine cortex P_2 membranes by displacement of [^{3}H]-1-phenyl-4-*tert*-butyl-2,6,7-trioxabicyclo[2.2.2]-octane ([^{3}H]TBOB), a specific ligand for the channel blocker binding site. The 2-(3′,5′-difluro-4′-azidophenyl)-5-*tert*-butyl-1,3-dithianebis-sulfone, compound **2**, exhibited the best K_i of about 11 nM, compared to K_is of 180 and 570 nM, respectively, for probes **1** (azidotetrafluorophenyl analogue) and **3** (azidophenyl analogue). On irradiation, probe **2** (0.6 μM) produced 18% irreversible loss of TBOB binding sites in brain membranes while probe **3** did not produce any photoinactivation. The loss observed with **2** was fully protectable by TBOB, demonstrating the specificity of the photochemical inactivation by compound **2** for the convulsant site of the GABA$_A$ receptor. These results, when compared to the photoaffinity labeling results obtained with the tetrafluorinated probe **1** (25% selective irreversible photochemical inactivation), establish a hierarchy between fluorinated and nonfluorinated arylazido probes and strengthen the potential of the newly described difluorinated probe **2**, combining high affinity and good labeling efficacy.

INTRODUCTION

γ-Aminobutyric acid (GABA) is the major inhibitory neurotransmitter in the brain which exerts its activity through binding to the GABA$_A$ receptor, a member of the ligand-gated ion-channel-receptor super family (*1*). Among the different ligand binding sites which modulate the function of this receptor is the convulsant site, a binding site for noncompetitive chloride channel blockers (*2*). This site can be characterized using irreversible site-directed radiolabeled probes such as photoaffinity ligands, and several candidate probes have already been described to target this convulsant binding site (*3, 4*). In particular, we recently described (*4*) compound **1** (2-(4′-azidotetrafluorophenyl)-5-*tert*-butyl-1,3-dithianebis-sulfone) as an efficient photoaffinity probe for this site. The photochemical properties of fluorinated azidophenyl derivatives were studied by Platz and co-workers (*5, 6*) and led to new developments in photoaffinity labeling technology (*7*). In particular, azidophenyl fluorinated in the ortho and/or para positions generates reactive nitrenes able to insert in inert solvents such as cyclohexane, a reaction which was not observed in the case of nonfluorinated arylazido derivatives (*6*). Therefore, fluorinated arylazido derivatives show appropriate reactivity for the labeling of a proteic environment, including reactions with nonfunctionalized amino acid side chains from hydrophobic binding sites. The proposed increase in reactivity for fluorinated arylazido derivatives could lead to improved photochemical coupling to proteins during photoaffinity labeling experiments. The only comparative labeling

* To whom correspondence should be addressed. Tel: (33) 88 67 69 91. Fax: (33) 88 67 88 91.
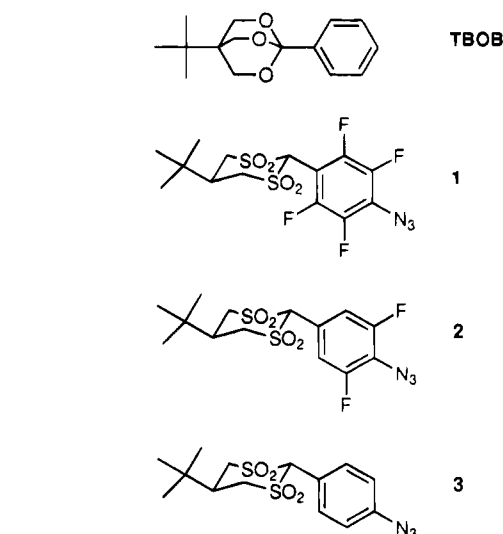
study reported failed to establish an increase in labeling of the estrogen receptor with fluorinated probes (*8*).

In the present paper, we describe the synthesis and the binding properties to the 1-phenyl-4-*tert*-butyl-2,6,7-trioxabicyclo[2.2.2]octane (TBOB) binding site on the GABA receptor, present in bovine cortex membranes of 2-substituted azidodifluorophenyl and azidophenyl derivatives of 5-*tert*-butyldithianebis-sulfone, compounds **2** and **3**, respectively. A comparative photocoupling study of these two probes as well as a formerly described tetrafluoro arylazido analogue (compound **1**) to the convulsant site of the GABA receptor is presented.

EXPERIMENTAL PROCEDURES

Materials. Melting points were obtained on a Reichert microscope or on a Mettler FP62 capillary melting

point apparatus and are uncorrected. ^{1}H NMR and ^{13}C NMR experiments were recorded on Bruker Model WP SY200 (200 and 50 MHz) spectrometers and ^{19}F NMR on Bruker Model AM400 (376.5 MHz) with proton decoupling. Chemical shifts are reported in δ (ppm), and appropriate solvent resonance spectra were consistently used as internal references (CDCl$_3$: 7.27 in proton and 77.0 in carbon NMR; acetone-d_6: 2.05 in proton and 29.8 in carbon NMR). Infrared (IR) spectra were recorded as KBr disks or in solution (CHCl$_3$) on a Perkin-Elmer 1600 series Fourier transform IR spectrophotometer with the bands reported as cm^{-1}. Mass spectra (MS) were obtained using a fast atom bombardment system (ZAB HF system, VG analytical Manchester FAB system). UV spectra were recorded on a Kontron Uvikon 860 spectrophotometer. The compounds were analyzed for C, H, and N by the Service de Microanalyse du CNRS de l'Université Louis Pasteur (Strasbourg), and the results were within 0.3% of the theoretical value. Thin-layer chromatography (TLC) was performed with Merck 5715 (F254, 0.25 mm silica gel) glass TLC plates. Spots were visualized under UV light or under visible light by spraying the TLC plate with a ninhydrin spray solution. Column chromatography utilized silica gel Merck 9385 (particle size 40−63 μm). Solvents used were dried and purified by standard methods (*9*).

p-Toluenesulfonyl azide was synthesized as described (*10*).

2-(2′,3′,5′,6′-Tetrafluoro-4′-azidophenyl)-5-*tert*-butyl-1,3-dithiane (1) was synthesized as described (*4*).

3,5-Difluorobenzyl *tert*-Butyldimethylsilyl Ether (5) (*11*). To a cooled (0 °C) solution of **4** (2.70 g, 18.75 mmol) in dry DMF (20 mL) were added imidazole (5.1 g, 37.5 mmol) and *tert*-butyldimethylsilyl chloride (5.0 g, 33 mmol) slowly. The reaction mixture was stirred for 1 h at room temperature under argon, and then water (100 mL) was added and the product extracted with ethyl acetate (3 × 50 mL). The organic layer was washed with water (2 × 20 mL) and with a saturated solution of NaCl and finally dried over MgSO$_4$. The solvent was removed to yield **5**, pure by ^{1}H NMR and by TLC (R_f (hexane) = 0.4) (colorless oil, 4.40 g, 91%): IR (CCl$_4$) 2956, 2930, 2885, 2858, 1626, 1597, 1461, 1373, 1324, 1257, 1118, 1101, 964; ^{1}H NMR δ 6.84 (dd, 2H, H$_2$ and H$_6$, $^3J_{HF}$ = 8.9, ^4J = 2.4), 6.67 (tt, 1H, H$_4$, $^3J_{HF}$ = 8.9, ^4J = 2.4), 4.71 (s, 2H, CH$_2$ benzyl), 0.96 (s, 9H, *tert*-butyl), 0.12 (s, 6H, dimethyl).

3,5-Difluoro-4-azidobenzyl *tert*-Butyldimethylsilyl Ether (6) (*12c*). To a cooled solution (−78 °C) of **5** (2 g, 7.74 mmol) in dry THF (10 mL) was added dropwise *n*-BuLi (5.32 mL of 1.6 M solution in hexane). The solution turned to a dark purple color after a few minutes and was stirred for 1 h at −78 °C under argon. A solution of tosyl azide (1.68 g, 8.51 mmol) in 10 mL of dry THF (−78 °C) was then added dropwise, and the reaction mixture was stirred for 5 h at 0 °C (the temperature was raised to 0 °C over a period of 1 h). The orange solution was hydrolyzed with Na$_4$P$_2$O$_7$·10H$_2$O (3.8 g, 8.51 mmol) in 30 mL of water, and the yellow mixture was stirred overnight at −4 °C. Fifty mL of water was added, and the product was extracted with ethyl acetate (3 × 50 mL). The organic layer was washed successively with water and with a saturated solution of NaCl and finally dried over MgSO$_4$. The solvent was removed and the product purified over silica gel column (CH$_2$Cl$_2$/hexane 10/90) to yield **6** (yellow oil, 2.08 g, 90%). The compound was 95% pure by ^{1}H NMR and pure by TLC (R_f (CH$_2$Cl$_2$/hexane 1/9) = 0.3): IR (CCl$_4$) 2956, 2930, 2858, 2126 (N$_3$), 1584, 1507, 1444, 1375, 1347, 1258, 1149; ^{1}H NMR δ 6.90 (dd,

2H, H$_2$ and H$_6$, $^3J_{HF}$ = 8.4, J = 0.7), 4.66 (s, 2H, CH$_2$ benzyl), 0.96 (s, 9H, *tert*-butyl), 0.12 (s, 6H, dimethyl).

3,5-Difluoro-4-azidobenzaldehyde (7) (*13, 14*). To a solution of **6** (2 g, 6.68 mmol) in dry THF (22 mL) was added dropwise at room temperature a solution of *n*-Bu$_4$-NF in THF (6.7 mL of a 1.1 M solution). The reaction mixture was stirred for 10 min. The product was purified over silica gel (ethyl acetate/hexane 2/8−5/5) to yield 3,5-difluoro-4-azidobenzyl alcohol (white solid, 1.04 g, 84%): IR (CCl$_4$) 2931, 2874, 2124 (N$_3$), 1582, 1508, 1445, 1347, 1295, 1105, 1038; ^{1}H NMR δ 6.92 (d, 2H, H$_2$ and H$_6$, $^3J_{HF}$ = 9.0), 4.63 (s, 2H, CH$_2$ benzyl).

To a mixture of PDC (9.0 g, 3.38 mmol) in dry CH$_2$Cl$_2$ (20 mL) was added dropwise a solution of 3,5-difluoro-4-azidobenzyl alcohol (1 g, 5.6 mmol) in dry CH$_2$Cl$_2$ (20 mL). The dark black reaction mixture was stirred overnight under argon at room temperature, and the product was purified over silica gel (ethyl ether/hexane 1/9−2/8) to yield **7** (white powder, 0.92 g, 89%). The compound was pure by TLC (R_f (ether/hexane 1/9) = 0.3). ^{1}H NMR shows a small impurity at 4 ppm: IR (CCl$_4$) 2810, 2718, 2140 (N$_3$), 1708 (CHO), 1614, 1582, 1501, 1446, 1386, 1343, 1292, 1127, 1102, 1048, 987; ^{1}H NMR δ 9.86 (t, 1H, CHO, J_{HF} = 1.8), 7.47 (d, 2H, H$_2$ and H$_6$, $^3J_{HF}$ = 8.0).

Dithianes: Compounds 9 and 11. 2-*tert*-Butylpropane-1,3-dithiol was prepared from diethyl *tert*-butylmalonate (*4*). The necessary aldehydes were either commercially available (compound **10**) or synthesized (compound **7**). 2-*tert*-Butylpropane-1,3-dithiol (1 equiv) was added to a solution of aldehyde (1.1 equiv) in dry CH$_2$Cl$_2$ containing boron trifluoride etherate (0.2 equiv). The solution was stirred at room temperature for several hours for compound **11** (reaction followed by TLC) and for 2 h for the synthesis of **9** to avoid the reduction of the azide group by thiols. After evaporation of the solvent the reaction mixtures were purified by silica gel column chromatography. The predominant "trans" isomers were eluted with ethyl ether/hexane (1/9) for **9** or CH$_2$Cl$_2$/hexane (1/1) for **11**. The crystalline derivative **11** was recrystallized from CH$_2$Cl$_2$/hexane.

2-(3′,5′-Difluoro-4′-azidophenyl)-5-*tert*-butyl-1,3-dithiane (9): yield 78%; IR (KBr) 2966, 2877, 2127 (N$_3$), 1736, 1577, 1507, 1347, 1288, 1171, 1045, 882; UV (phosphate pH 7.4 buffer) λ_{max} = 270 nm, ϵ = 11 800; ^{1}H NMR δ 7.07 (d, 2H, ^2J = 9.0 Hz, H aromatic), 5.03 (s, 1H, H$_2$), 2.97 and 2.81 (*AA′BB′X*, 4H, H$_4$, H$_6$ axial and H$_4$, H$_6$ equatorial, ^2J = 14.0 Hz, $^3J_{cis}$ = 2.7 Hz, $^3J_{trans}$ = 10.9 Hz), 1.74 (AA′BB′X, 1H, H$_5$, $^3J_{cis}$ = 2.8 Hz, $^3J_{trans}$ = 10.9 Hz), 0.96 (s, 9H, t-Bu); ^{19}F NMR (nonproton decoupling) −122.28 (d, 2F, ^2J = 8.7 Hz); ^{19}F NMR (proton decoupling) −122.28 (s, 2F); ^{13}C NMR δ 181.4, 173.4, 157.9 (d), 152.9(d), 136.0(m), 111.8 (m), 49.7 (C$_2$), 45.9 (C$_5$), 33.8 (CCH$_3$), 33.33 (C$_4$ and C$_6$), 27.2 (CH$_3$); MS-FAB$^+$ (2-nitrobenzylic alcohol, m/z) 329 (M$^+$), 301 (M$^+$ − 28), 175 (M$^+$ − difluoroazidophenyl).

2-(4′-Nitrophenyl)-5-*tert*-butyl-1,3-dithiane (11): yield: 69%; mp (°C) 158; R_f (CH$_2$Cl$_2$/hexane 1/1 = 0.45; IR (KBr) 2969, 1520, 1344, 726; ^{1}H NMR δ 8.19 (d, 2H, aromatic H$_3$ and H$_5$, ^3J = 8.8 Hz), 7.64 (d, 2H, aromatic H$_2$ and H$_6$, ^3J = 8.8), 5.20 (s, 1H, H$_2$), 3.00 and 2.85 (*AA′BB′X*, 4H, H$_4$, H$_6$ equatorial and H$_4$, H$_6$ axial, ^2J = 14.0 Hz, $^3J_{cis}$ = 2.7 Hz, $^3J_{trans}$ = 11.0 Hz), 1.77 (AA′BB′X, 1H, H$_5$, $^3J_{cis}$ = 2.7 Hz, $^3J_{trans}$ = 11.0 Hz), 0.97 (s, 9H, t-Bu); ^{13}C NMR δ 147.7 (C$_{4'}$), 145.6 (C$_{1'}$), 128.8, 123.9, 50.2 (C$_2$), 45.9 (C$_5$), 33.9 (CCH$_3$), 33.3(C$_4$ and C$_6$), 27.2 (CH$_3$). Anal. (C$_{14}$H$_{19}$NO$_2$S$_2$) C, H, N.

Oxone Oxidation: Compounds 2 and 12 (*15*). Oxone (20 equiv of potassium peroxymonosulfate) solubilized in water was added to a solution of dithiane (1

equiv) in an equal volume of acetone. This mixture was stirred, first at room temperature for 12 h and then at reflux for 3 days for **12** and 12 h for **2**, before evaporation of the solvent. For **2**, the residue was partitioned between water and ethyl acetate and extracted in ethyl acetate. The organic layers were washed with a saturated solution of NaCl and dried over MgSO$_4$, and the solvent was removed. Purification by silica gel column chromatography (ethyl acetate/hexane 3/7) gave **2** as a white powder (75%). For **12**, the residue was dried, triturated in acetone, and filtered, and the solvent of the filtrate evaporated. This operation was done two other times to afford after recrystallization in acetone **12** as a white powder (52%). No purification of **12** was possible by silica gel column chromatography because of a strong adsorption.

2-(3′,5′-Difluoro-4′-azidophenyl)-5-*tert*-butyl-1,1,3,3-tetraoxide-1,3-dithiane (2): white powder, pure by ^{1}H NMR, ^{19}F NMR, and TLC (R_f (AcOEt/hexane 4/6) = 0.35); IR (KBr) 2129 (N$_3$), 1654, 1578, 1509, 1445, 1347, 1325, 1248, 1142, 1120, 1040, 992; UV (phosphate pH 7.4 buffer) λ_{max} = 261 nm, ϵ = 8000; ^{1}H NMR δ 7.41 (d, 2H, ^2J = 9.3 Hz, H aromatic), 6.09 (s, 1H, H$_2$), 3.70 and 3.58 (AA′BB′X, 4H, H$_4$, H$_6$ equatorial and H$_4$, H$_6$ axial, ^2J = 14.3 Hz, $^3J_{cis}$ = 3.0 Hz, $^3J_{trans}$ = 11.4 Hz), 2.46 (AA′BB′X, 1H, H$_5$, $^3J_{cis}$ = 3.0 Hz, $^3J_{trans}$ = 11.4 Hz), 1.11 (s, 9H, t-Bu); ^{19}F NMR (proton decoupling) −122.26 (s, 2F); ^{13}C NMR δ 80.2 (C$_2$), 54.7 (C$_5$), 40.7 (CCH$_3$), 34.1 (C$_4$ and C$_6$), 27.3 (CH$_3$); MS-FAB$^+$ (2-nitrobenzylic alcohol, m/z) 501 (M$^+$ + nitrobenzyl), 393 (M$^+$), 366 (MH$^+$ − 28).

2-(4′-Nitrophenyl)-5-*tert*-butyl-1,1,3,3-tetraoxide-1,3-dithiane (12): pure by TLC (R_f (AcOEt/hexane 1/1) = 0.40); mp (°C) >300; IR (KBr) 2973, 1526, 1345, 1326, 1313, 1154, 1144, 881; ^{1}H NMR δ 8.38 (d, 2H, aromatic H$_3$ and H$_5$, ^3J = 8.9 Hz), 7.99 (d, 2H, aromatic H$_2$ and H$_6$, ^3J = 8.9 Hz), 6.33 (s, 1H, H$_2$), 3.72 and 3.62 (AA′BB′X, 4H, H$_4$, H$_6$ equatorial and H$_4$, H$_6$ axial, ^2J = 14.3 Hz, $^3J_{cis}$ = 3.4 Hz, $^3J_{trans}$ = 11.1 Hz), 2.51 (AA′BB′X, 1H, H$_5$, $^3J_{cis}$ = 3.4 Hz, $^3J_{trans}$ = 11.1 Hz), 1.12 (s, 9H, t-Bu).

Reduction, Diazotation, and Azidation Procedures: Compounds 13 and 3. 2-(4′-Azidophenyl)-5-*tert*-butyl-1,3-dithiane (13). A solution of **11** (178 mg, 0.6 mmol) in CH$_2$Cl$_2$ (20 mL) containing 20 mg of 10% Pd/C was hydrogenated for 6 h at atmospheric pressure. The reaction mixture was filtered through a pad of Celite, and the Celite washed with a further 10 mL of CH$_2$Cl$_2$. Evaporation of the solvent from the filtrate afforded a white powder (144 mg, 90%). Diazotation of the aminophenol was achieved in the absence of light. To a stirred solution of amine (25 mg, 0.09 mmol) in TFA (2 mL) at 0 °C was added NaNO$_2$ (20 mg, 0.3 mmol) solubilized in 0.2 mL of H$_2$O in small portions. The reaction was followed by UV. Then NaN$_3$ (60 mg, 0.9 mmol) was added directly to the diazonium salt at 0 °C, and the reaction mixture was stirred 15 min at 0 °C. The solution was neutralized with saturated Na$_2$CO$_3$ and the compound extracted with ethyl acetate (3 × 10 mL). The organic layer was dried over MgSO$_4$, and the solvent was evaporated. The crude product was purified by silica gel column chromatography. Elution with ethyl acetate/hexane (3/7 v/v) afforded **13** (6.8 mg, 25%), pure by TLC (R_f (AcOEt/hexane 2/8) = 0.50): IR (KBr) 2959, 2110 (N$_3$), 1600, 1500, 1280; UV (methanol) λ_{max} = 255 nm, ϵ = 20 000 (phosphate pH 7.4 buffer), λ_{max} = 262 nm, ϵ = 12 000; ^{1}H NMR δ 7.46 (d, 2H, H$_2$ and H$_6$ aromatic, ^3J = 8.5 Hz,), 6.99 (d, 2H, H$_3$ and H$_5$ aromatic, ^3J = 8.5 Hz), 5.12 (s, 1H, H$_2$), 2.97 and 2.84 (AA′BB′X, 4H, H$_4$, H$_6$ equatorial and H$_4$, H$_6$ axial, ^2J = 13.8 Hz, $^3J_{cis}$ = 2.6 Hz, $^3J_{trans}$ = 10.8 Hz), 1.76 (AA′BB′X, 1H, H$_5$, $^3J_{cis}$ = 2.8 Hz, $^3J_{trans}$ = 10.6 Hz), 0.97 (s, 9H, t-Bu); ^{13}C

NMR δ 140.1, 135.1, 129.2, 119.3, 50.4 (C$_2$), 46.2 (C$_5$), 33.9 (CCH$_3$), 33.6 (C$_4$ and C$_6$), 27.3 (CH$_3$); MS-FAB$^+$ (2-nitrobenzylic alcohol, m/z) 294 (MH$^+$), 265, 175.

2-(4′-Azidophenyl)-5-*tert*-butyl-1,1,3,3-tetraoxide-1,3-dithiane (3). To a solution of **12** (61 mg, 0.17 mmol) in acetone/acetic acid/H$_2$O (1/1/1 v/v/v) (3 mL) was added 3.2 mL of commercial TiCl$_3$ in HCl (2.55 mmol) in small portions (0.22 mL) followed by 5 min of stirring after each addition of TiCl$_3$ (16). When the reaction was complete (TLC), the reaction mixture was neutralized with NaOH 1 N and the product extracted with ethyl acetate (3 × 30 mL). The organic phase was washed with water (10 mL) and with saturated NaCl (20 mL) and dried over Na$_2$SO$_4$. The solvent was evaporated to afford the amine as a white powder (56 mg, 100%). Diazotation and azidation of the corresponding amino derivative (56 mg, 0.17 mmol) used the procedure described for the synthesis of **13** and afforded **3** (48 mg, yellow powder, 80%), pure by TLC (R_f (AcOEt/hexane 2/8) = 0.50): IR (KBr) 2972, 2933, 2145 (N$_3$), 1605, 1508, 1342, 1320, 1289, 1142, 1116, 859; UV (methanol) λ_{max} = 257 nm, ϵ = 19 000 (phosphate pH 7.4 buffer), λ_{max} = 260 nm, ϵ = 13 000; ^{1}H NMR δ 7.72 (d, 2H, H$_2$ and H$_6$ aromatic, ^3J = 8.7 Hz), 7.21 (d, 2H, H$_3$ and H$_5$ aromatic, ^3J = 8.7 Hz), 6.06 (s, 1H, H$_2$), 3.66−3.49 (m, 4H, H$_4$, H$_6$), 2.48 (tt, 1H, H$_5$, $^3J_{cis}$ = 3.9 Hz, $^3J_{trans}$ = 10.5 Hz), 1.11 (s, 9H, *t*-Bu); ^{13}C NMR δ 143.6, 134.8, 120.2, 118.0, 81.4 (C$_2$), 54.8 (C$_4$ and C$_6$), 40.8 (C$_5$), 34.1 (CCH$_3$), 27.3 (CH$_3$).

Receptor Assays. Binding assay and photolabeling experiment results were determined as previously described (4). For compound **2** in the photolabeling experiments, irradiated membrane suspensions (3 mL) were diluted 5.5-fold with 10 mM sodium phosphate (pH 7.4) buffer containing 0.3% of 2-methoxyethanol and incubated for 30 min at 37 °C. Samples in triplicate (3 × 5 mL) were then adsorbed under partial vacuum on GF/B (Whatman) glass-fiber filters and given nine successive rinses (3 mL of 10 mM phosphate pH 7.4 buffer containing 0.3% of methoxyethanol) to remove the unbound ligands. This dissociation procedure was followed by the [^{3}H]TBOB filter binding assay, as previously described (4).

Photolabeling Experiments. Monochromatic light was obtained from a 1000-W Xe/Hg lamp (Hanovia) connected to a grating monochromator (Jobin-Yvon). The light intensity was measured with a thermopile (Kipp and Zohnen) and adjusted through an iris diaphragm to the desired intensity.

RESULTS

Chemicals. The 2-(4′-azidotetrafluorophenyl)-5-*tert*-butyl-1,3-dithianebis-sulfone **1** was synthesized as previously described (4).

The synthetic pathway from 3,5-difluorobenzyl alcohol (**4**) to compound **2** is outlined in Scheme 1. Protection (11) of the primary alcohol of **4** as a *tert*-butyldimethylsilyl group to give **5** allows a metalation reaction in ortho position to the two fluorine atoms using *n*-butyllithium (12). Reaction of the resulting aryllithium salt with *p*-toluenesulfonyl azide provides the triazene which upon hydrolysis with an aqueous tetrasodium pyrophosphate solution gave the azido derivative **6** in 90% yield (12c). The primary alcohol of **6** was deprotected (13) and oxidized (14) to afford the 3,5-difluoro-4-azidobenzaldehyde **7**. The synthesis of the dithiane **9** was achieved by condensing the aldehyde **7** with the dithiol **8** in the presence of BF$_3$−Et$_2$O, and final oxidation (15) of the dithiane to dithianebis-sulfone with oxone yielded the product **2**.

Scheme 1. Syntheses of Difluoroarylazido Probes 9 and 2[a]
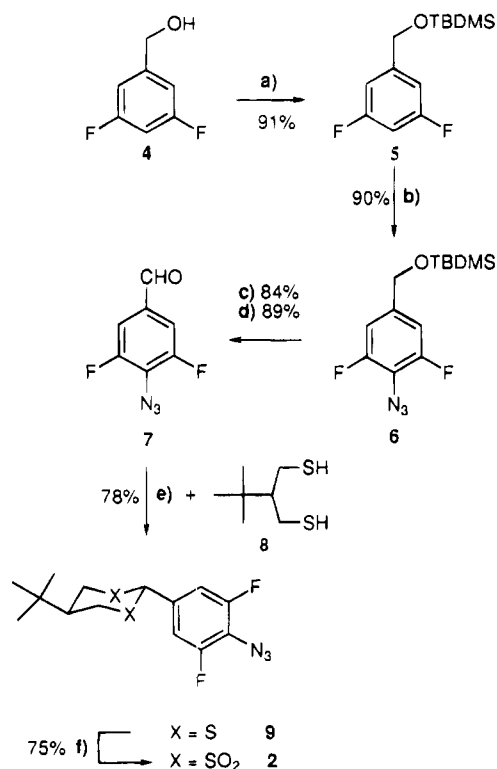
[a] Key: (a) TBDMSCl, imidazole, DMF, 0 °C to rt; (b) (1) *n*-BuLi, THF, −78 °C, (2) TosN$_3$, THF, −78 to 0 °C, (3) Na$_4$P$_2$O$_7$·10H$_2$O, H$_2$O, 4 °C; (c) *n*-Bu$_4$NF, THF, rt; (d) PDC, CH$_2$Cl$_2$, rt; (e) BF$_3$−Et$_2$O, CH$_2$Cl$_2$, rt; (f) oxone, acetone/H$_2$O, reflux then rt.

Scheme 2. Syntheses of Arylazido Probes 13 and 3[a]
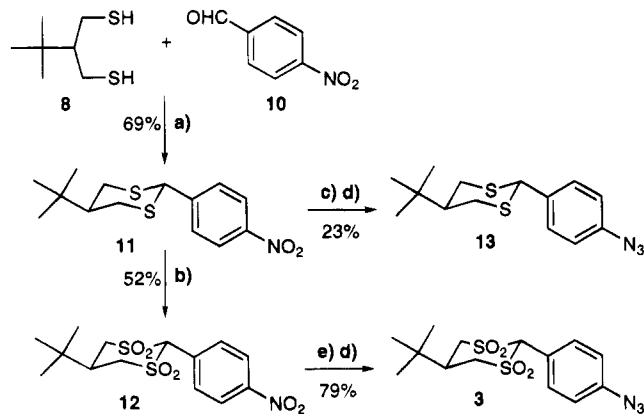
[a] Key: (a) BF$_3$−Et$_2$O, CH$_2$Cl$_2$, rt; (b) oxone, acetone/H$_2$O, reflux; (c) H$_2$, Pd/C, CH$_2$Cl$_2$, rt; (d) (1) NaNO$_2$, TFA, 0 °C, (2) NaN$_3$; (e) TiCl$_3$ in HCl, acetone/CH$_3$COOH/H$_2$O, rt.

Synthesis of 13 and 3 (Scheme 2) started with the dithiane 11, which was obtained by condensing the commercial aldehyde 10 with the dithiol 8 in the presence of BF$_3$−Et$_2$O. Catalytic hydrogenation of the nitro derivative 11 to the corresponding aniline and subsequent diazotization and azidation afforded the azido derivative 13. The moderate yield (23%) obtained in these steps can be explained by the instability of the dithiane group in trifluoroacetic acid. A diazotation and azidation procedure was tested in acetic acid, without success. Therefore, we first oxidized the nitro dithiane derivative 11 to the dithianebis-sulfone 12 with oxone (15) before reducing the nitro group to the corresponding amine in the presence of trichlorotitanium in acidic

Table 1. UV Characteristics (λ_{max} and ϵ), Stability in pH 7.4 Buffer at 25 °C (Half-life), Photodecomposition (λ = 261 nm, T = 15 °C (Half-life)), and Affinities for the Convulsant Site of the GABA$_A$ Receptor for the Three Photoactivatable Probes Tested (Compounds 1−3)[a]

		compds		
		1	2	3
UV	λ_{max}, nm	261	261	260
	ϵ, L mol^{-1} cm^{-1}	11 000	8000	13 000
chemical stability	$t_{1/2}$, h	8.8	6	>10
photodecomposition	$t_{1/2}$, min	7	5	4
affinity[b] (25 °C)	K_i, nM	180 ± 20	11 ± 1.6	570 ± 80

[a] All these experiments were done in phosphate buffer (200 mM NaCl, 10 mM NaH$_2$PO$_4$·H$_2$O) at pH 7.4. [b] The inhibition constants (K_is) were determined in bovine cortical P$_2$ membranes using [^{3}H]TBOB as described in the Experimental Procedures. Values in nanomolar are means ± SEM from three independent experiments calculated by K_i = IC$_{50}$/(1 + L/K_D), where IC$_{50}$ is the concentration producing 50% inhibition of specific binding, L is the radioligand concentration, and K_D is the radioligand dissociation constant (K_D = 6 nM, ref 19).

conditions (16). Other reduction conditions have been tested, such as catalytic hydrogenation and sodium borohydride in the presence of stannous chloride (17), but they failed in this transformation. Finally, the corresponding amino derivative was converted to the azido analogue 3 as previously described for 13. The improved yield observed for the reduction−azidation procedures can be explained by a better stability of the dithianebis-sulfone group in acidic conditions.

The UV characteristics, chemical stabilities at pH 7.4, and photochemical properties for the photoactivatable derivatives 1−3 are summarized in Table 1. Compounds 2 and 3 show both sufficient stability in the buffer to be used in photoaffinity labeling experiments. Both dithiane derivatives, compounds 9 and 13, were too unstable to be used in these conditions, i.e., for 13 $t_{1/2}$ = 8.5 min at 25 °C.

Reversible Binding of the Synthesized Molecules. Table 1 shows the binding potencies of the photoactivatable molecules 1−3 which have been synthesized and determined by displacement of [^{3}H]TBOB in the absence of light using bovine brain P$_2$ membranes. The 2-(3′,5′-difluoro-4′-azidophenyl)-5-*tert*-butyl-1,3-dithianebis-sulfone 2 is the most potent photoaffinity probe described in the dithiane series (K_i = 11 nM) (see ref 4).

Irreversible Binding at the TBOB Binding Site. The molecules 2 and 3, which are potent compounds in displacing [^{3}H]TBOB, were tested for their ability to irreversibly inactivate the TBOB binding site upon irradiation. Figure 1 shows comparative photoaffinity labeling experiments between probes 2 and 3 and includes the previously described labeling experiment for probe 1 (4). Irradiation conditions have been assessed (wavelength, energy, and time) so that the TBOB binding properties would be minimally altered (4). Each set of experiments determined the remaining [^{3}H]TBOB binding under different conditions, as indicated in the figure legends. The extent of photoinactivation is determined by comparison of the residual [^{3}H]TBOB binding sites with and without (not shown) irradiation. Selectivity for the convulsant site is determined using excess TBOB to protect against ligand-induced photoinactivation. All the binding sites could be recovered following incubation of the membranes with probes 2 and 3 in the dark (not shown). Irradiation resulted, for probe 2, in 18% additional irreversible inhibition over the control-irradiated membranes (Figure 1). This photoinactivation was completely protectable by 4 μM TBOB (Figure 1). An
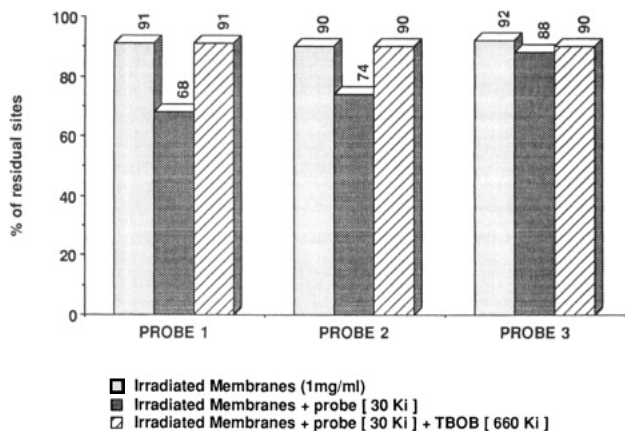
Figure 1. Comparative photoaffinity labeling experiments using probes **1**–**3**. Membranes and drugs (concentration = $30K_i$), were incubated for 1 h at 25 °C and subsequently irradiated for 15 min at 15 °C at 261 nm with a light intensity of 120 μV. Thereafter, the filter dissociation procedure and the [^{3}H]TBOB binding assay proceeded as described in the Experimental Section.

additional control experiment using the prephotolyzed probe **2** did not result in irreversible inhibition (data not shown), indicating that the probe-induced inactivation was not due to nondissociating photoproducts. In contrast, no photoinactivation was observed with probe **3** (Figure 1), even with a long irradiation time of 20 min (considering that the $t_{1/2}$ of the photodecomposition of **3** is about 4 min under the same conditions as the photolabeling experiment, see Table 1).

DISCUSSION

5-*tert*-Butyldithiane derivatives substituted in the 2-position by 4'-azidophenyl as well as 3',5'-difluoro-4'-azidophenyl groups have been synthesized as potential photoaffinity probes for the convulsant site of the GABA$_A$ receptor. Among the newly synthesized photoactivatable probes, only bis-sulfones **2** and **3** constitute new candidates since the dithianes in this series (compounds **9** and **13**) were unexpectedly unstable in neutral aqueous buffer. Considering the 3',5'-difluorinated probe **2**, a new synthetic strategy was developed using an ortho metalation methodology to aromatic fluorine (*12c*) which allowed the introduction of the azido group at the desired 4'-position (steps c and d, Scheme 1).

The two bis-sulfone derivatives have been tested for their reversible binding potency by displacement of [^{3}H]-TBOB to the convulsant site and are compared to probe **1**, a previously described tetrafluoroarylazido bis-sulfone probe (*4*). As seen in Table 1, marked differences characterize these binding potencies, varying from K_i = 570 nM to 180 nM and 11 nM for probes **3**, **1**, and **2**, respectively. Clearly, there is no direct relation between potency and the degree of fluorine substitution. Table 1 summarizes the different physicochemical characteristics of the three probes, showing their good chemical stability and similar photosensivity.

The irreversible labeling of the TBOB binding site was tested under comparable conditions for the three probes; in particular, appropriate ligand concentrations were chosen to attain identical receptor occupancy in the three irradiation experiments. The arylazido probe **3** does not induce photoirreversible receptor inactivation, while the ortho difluorophenyl azido probe, compound **2**, photoinactivated 18% of the [^{3}H]TBOB binding sites. The inactivation was totally protectable by unlabeled TBOB (4 μM). The receptor–ligand dissociation procedure has been slightly modified and used a buffer containing 0.3%

of methoxyethanol. The good binding potency and the hydrophobic character of **2** can explain the need of a buffer containing alcohol to remove unlabeled ligands. The percent of alcohol added in the buffer was determined to obtain a compromise between receptor stability and receptor–ligand dissociation (data not shown). Probe **1**, as described (*4*), led to 25% selective irreversible photochemical inactivation.

Taken together, these results indicate that both fluorinated probes **1** and **2** label the TBOB binding site of the GABA receptor after photochemical activation, in contrast to the nonfluorinated probe **3**. These observed photoaffinity labeling results corroborate the described increase in reactivity for fluorinated aryl azides over the corresponding nonsubstituted derivatives (*5*, *6*). It has been demonstrated that the singlet nitrenes, generated from fluorinated aryl azides, rearrange more slowly to the corresponding didehydroazepine, a less reactive species, thus allowing efficient CH insertion reactions. Also, the similar extent of photochemical inactivation which is observed for both fluorinated probes **2** and **3** (respectively, 18% and 25%) agrees with the predicted influence on the reactivity of fluorine distribution on the aromatic ring, i.e., ortho and/or para positions to the azido function result in a higher reactivity (*6*). The observed photoaffinity labeling results suggest that the convulsant binding site is located in a hydrophobic environment which may explain the absence of coupling for the nonfluorinated probe, assuming the three probes are similarly positioned in the binding site.

This comparative photoaffinity labeling work has led to the discovery of a new photoaffinity probe (compound **2**) for the convulsant site of the GABA$_A$ receptor, which shows excellent reversible binding properties (K_i = 11 nM) as well as satisfactory labeling efficiency. In addition, the use of difluorinated probes, when compared to the tetrafluorinated probe, make two positions available on the aromatic ring for introduction of tritium atoms. The synthesis of this radiolabeled difluoroarylazido probe is presently under investigation.

LITERATURE CITED

(1) (a) Barnard, E. A. (1992) Receptor classes and the transmitter-gated ion channels. *Trends Biochem. Sci.* 17, 368–374. (b) Betz, H. (1990) Ligand-gated ion channels in the brain: the amino acid receptor superfamily. *Neuron 5*, 383–392.

(2) Obata, T., Yamamura, H. I., Malatynska, E., Ikeda, M., Laird, H., Palmer, C. J., and Casida, J. E. (1988) Modulation of γ-aminobutyric acid-stimulated chloride influx by bicycloorthocarboxylates, bicyclophosphorus esters, polychlorocycloalkanes and other cage convulsants. *J. Pharmacol. Exp. Ther. 244*, 802–806.

(3) (a) Goeldner, M. P., Hawkinson, J. E., and Casida, J. E. (1989) Diazocyclohexadienones as photoaffinity ligands: syntheses of trioxabicyclooctane probes for the convulsant binding site of the GABA$_A$ receptor. *Tetrahedron Lett. 30*, 823–826. (b) Hawkinson, J. E., Goeldner, M. P., Palmer, C. J., and Casida, J. E. (1991) Photoaffinity ligands for the [^{3}H]TBOB binding site of the GABA$_A$ receptor. *J. Receptor Res. 11*, 391–405.

(4) Kapfer, I., Hawkinson, J. E., Casida, J. E., and Goeldner, M. P. (1994) Photoactivatable 2-(4'-azidotetrafluorophenyl)-5-*tert*-butyl-1.3-dithiane-bis-sulfone and related compounds as candidate irreversible probes for the GABA-gated chloride channels. *J. Med. Chem. 37,* 133−140.

(5) (a) Poe, R., Schnapp, K., Young, M. J. T., Grayzar, J., and Platz, M. S. (1992) Chemistry and kinetics of singlet (pentafluorophenyl)nitrene. *J. Am. Chem. Soc. 114,* 5054−5067. (b) Schuster, G. B., and Platz, M. S. (1992) Photochemistry of phenyl azide. *Adv. Photochem. 17,* 69−143.

(6) (a) Soundararajan, N., and Platz, M. S. (1990) Descriptive photochemistry of polyfluorinated azide derivatives of methylbenzoate. *J. Org. Chem. 55,* 2034−2044. (b) Schnapp, K. A., Poe, R., Leyva, E., Soundararajan, N., and Platz, M. S. (1993) Exploratory photochemistry of fluorinated aryl azides. Implications for the design of photoaffinity labeling reagents. *Bioconjugate Chem. 4,* 172−177. (c) Schnapp, K. A., and Platz, M. S. (1993) A laser flash photolysis study of di-, tri-, tetrafluorinated phenylnitrenes; implications for photoaffinity labeling. *Bioconjugate Chem. 4,* 178−183.

(7) (a) Keana, J. F. W., and Cai, S. X. (1990) New reagents for photoaffinity labelling: Synthesis and photolysis of functionalized perfluorophenyl azides. *J. Org. Chem. 55,* 3640−3647. (b) Golinski, M., Heine, M., and Watt, D. S. (1991) Prostaglandin F$_{2\alpha}$ photoaffinity probes: 18-phenoxy-19,20-bisnorprostanoids bearing perfluorinated aryl azides. *Tetrahedron Lett. 32,* 1553−1556.

(8) (a) Pinney, K. G., and Katzenellenbogen, J. A. (1991) Synthesis of a tetrafluoro-substituted arylazido and its protio analogues as photoaffinity labeling reagents for the Estrogen receptor. *J. Org. Chem. 56,* 3125−3133. (b) Pinney, K. G., Carlson, K. E., Katzenellenbogen, B. S., and Katzenellenbogen, J. A. (1991) Efficient and selective photoaffinity labeling of the Estrogen receptor using two nonstreroidal ligands that embody aryl azide or tetrafluoroaryl photoreactive functions. *Biochemistry 30,* 2421−2431.

(9) Perrin, D. D., Armarego, W. L. F., and Perrin, D. R. (1980) Purification of individual organic chemicals. *Purification of Laboratory Chemicals,* 2nd ed., Chapters 3 and 4, pp 74−548, Pergamon Press Ltd., New York.

(10) Doering, W. v. E., and DePuy, C. H. (1953) Diazocyclopentadiene. *J. Am. Chem. Soc. 75,* 5955−5957.

(11) (a) Ogilvie, K. K., and Iwacha, D. J. (1973) Use of the *tert*-butyldimethylsilyl group for protecting the hydroxyl functions of nucleosides. *Tetrahedron Lett. 4,* 317−319. (b) Ogilvie, K. K., Thompson, E. A., Quilliam, M. A., and Westmore, J. B. (1974) Selective protection of hydroxyl groups in deoxy nucleosides using alkylsilyl reagents. *Tetrahedon Lett. 33,* 2865−2868.

(12) (a) Gschwend, H. W., and Rodriguez, H. R. (1979) Heteroatom-facilitated lithiations. *Org. React. N. Y. 26,* 73 (Aryl fluorides). (b) Tamborski, C., and Soloski, E. J. (1966) Difunctional tetrafluorobenzene compounds from fluoroaromatic organolithium intermediates. *J. Org. Chem. 33,* 746−749. (c) Spagnolo, P., and Zanirato, P. (1982) General route for the facile transformation of ortho-substituted lithiobithienyls into amino derivatives. *J. Org. Chem. 47,* 3177−3180.

(13) Corey, E. J., and Venkateswarlu, A. (1972) Protection of hydroxyl groups as *tert*-butyldimethylsilyl derivatives. *J. Am. Chem. Soc. 94,* 6190−6191.

(14) Corey, E. J., and Schmidt, G. (1979) Useful procedures for the oxidation of alcohols involving pyridinium dichromate in aprotic media. *Tetrahedron Lett. 5,* 399−402.

(15) Trost, B. M., and Curran, D. P. (1981) Chemoselective oxidation of sulfides to sulfones with potassium hydrogen persulfate. *Tetrahedron Lett. 22,* 1287−1290.

(16) Somei, M., Kato, K., and Inoue, S. (1980) Titanium(III) chloride for the reduction of heteroaromatic and aromatic nitro compounds. *Chem. Pharm. Bull. 28,* 2515−2518.

(17) Satoh, T., Mitsuo, N., Nishiki, M., Inoue, Y., and Ooi, Y. (1981) Selective reduction of aromatic nitro compounds with sodium borohydride-stannous chloride. *Chem. Pharm. Bull. 29,* 1443−1445.

(18) (a) Barnard, E. A. (1992) Receptor classes and transmitter-gated ion channels. *Trends Biochem. Sci. 17,* 368−374. (b) DeLorey, T. M., and Olsen, R. W. (1992) γ-Aminobutyric Acid$_A$ receptor structure and function. *J. Biol. Chem. 267,* 16747−16750.

(19) Hawkinson, J. E., and Casida, J. E. (1992) Binding kinetics of γ-aminobutyric acid$_A$ receptor. Noncompetitive antagonists: trioxabicyclooctane, dithiane, and cyclodiene insecticide-induced slow transition to blocked chloride channel conformation. *Mol. Pharmacol. 42,* 1069−1076.

BC940097C

Evaluation of a Highly Efficient Aryl Azide Photoaffinity Labeling Reagent for the Progesterone Receptor

Philip R. Kym, Kathryn E. Carlson, and John A. Katzenellenbogen*

Department of Chemistry, University of Illinois, Urbana, Illinois 61801. Received August 10, 1994⊗

16α,17α-[(R)-1'-(4-Azidophenyl)ethylidenedioxy]pregn-4-ene-3,20-dione (**7**) was prepared in high specific activity tritium-labeled form (20 Ci/mmol) and shown to bind to the progesterone receptor with an affinity (K_d = 0.80 nM) that is 47% of that of [³H]-R 5020 (K_d = 0.38 nM). [³H]Progestin aryl azide **7** exhibits high photoattachment efficiency (60% at 1 h) compared to the commonly used progesterone receptor photoaffinity labeling reagent [³H]-R 5020 (2.2% at 1 h) and is the most efficient progesterone receptor photoaffinity labeling reagent prepared to date. The photoattachment observed with **7** proceeds in a time-dependent fashion, with most of the attachment occurring within the first 10 min of photolysis. Characterization of the photolabeled proteins by SDS-polyacrylamide gel electrophoresis shows specific labeling of two adducts of molecular weight 108 500 ± 800 and 87 000 ± 1 500 (*n* = 3), the same species as labeled by [³H]-R 5020. The ratio of progesterone receptor subunits A:B was determined to be 3.3:1 with both [³H]progestin azide **7** and [³H]-R 5020. Information on the specific amino acid(s) that attach to the ligand during photolysis awaits further analysis of the covalently bound ligand–protein adduct.

INTRODUCTION

Recent advances in our understanding of the mechanism of action of the progesterone and other steroid hormone receptors have led to renewed interest in the development of synthetic probes that can bind to and modulate their function (*1*). Despite considerable progress in this area, many aspects of the interaction of progesterone with its receptor remain only poorly understood. Most of the work in this area has focused on establishing structure–function relationships of various portions of the receptor and uncovering details of events occurring after the hormone has bound to the receptor. The cellular processes leading up to hormone binding and determination of critical hormone–receptor interactions have received only limited attention. In the absence of crystallographic data for the steroid receptors, we are left with direct chemical probe methods such as affinity labeling and indirect approaches such as mutagenesis to define critical binding interactions.

Photoaffinity labeling (*2*) (PAL) utilizes a masked reactive functionality on the molecular probe that reacts upon photolysis to reveal a reactive intermediate that can covalently attach to the receptor. Incubation of the PAL reagent with a steroid receptor in the dark, followed by photolysis of the receptor–ligand complex, increases the probability of labeling a residue within the steroid binding site. The reactive species, typically a carbene or a nitrene, can react with the receptor through nonspecific carbon–hydrogen bond insertion reactions. A variety of functional groups have been used as the photoreactive species, including azides (acyl, aroyl, aryl), diazirines, diazo ketones, conjugated enone systems, benzophenones, and nitroanisole derivatives (*3*).

The search for efficient and selective photoaffinity labeling (PAL) reagents for the progesterone receptor (PR) has relied primarily on progestins containing A,B-ring dienone systems as the photoreactive functionality (*4–6*). While some of these compounds bind with high affinity to the progesterone receptor, none of them demonstrate the required combination of high receptor
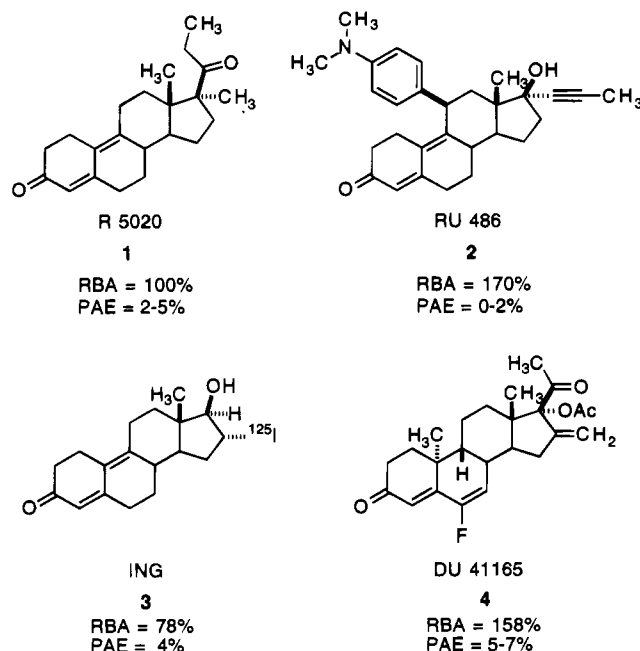
Figure 1. Photoaffinity labeling (PAL) reagents for the progesterone receptor. RBA is receptor binding affinity; PAE is photoattachment efficiency.

binding affinity (RBA), good photocovalent attachment efficiency, and low nonspecific binding necessary for efficient and selective labeling of the PR. The Roussel–Uclaf compound, promegestone (R 5020, Figure 1), is currently the most widely used PAL reagent for the PR, in spite of displaying photocovalent attachment efficiencies (PAE) of only 2–5% (*4a*). While low photoattachment efficiencies may be sufficient for identifying some sites of ligand–receptor contact, more efficient photocovalent attachment may be necessary to identify other residues in the PR hormone binding domain that are critical for ligand binding.

Protio- and tetrafluoroaryl azides incorporated into a 3-aroyl-2-arylbenzo[*b*]thiophene molecular scaffold (Figure 2) have recently been shown to have relatively high photocovalent attachment efficiencies (20–30%) in pho-
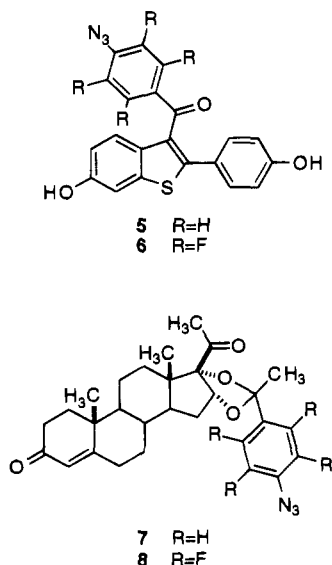
Figure 2. Aryl azide-based photoaffinity labeling (PAL) reagents for the ER and proposed aryl azide PAL reagents for the PR.

toaffinity labeling studies with the estrogen receptor (7). We have previously reported the incorporation of protio- and tetrafluoroaryl azides onto the progestin backbone through a 16α,17α-dioxolane ketal link (Figure 2) (8). These molecules were found to bind to the PR with affinity comparable to the natural ligand, progesterone (RBA of **7** = 15%, **8** = 14%, progesterone = 13%), and exhibit high photoinactivation effiencies of the PR (PIE of **7** = 80%, **8** = 80%). We now report the preparation of the protioaryl azide **7** in high specific activity tritium-labeled form and the evaluation of [³H]-**7** as a photoaffinity labeling reagent for the PR.

EXPERIMENTAL PROCEDURES

General. Reaction progress was monitored by analytical thin-layer chromatography using 0.25 mm silica gel glass-backed plates with F-254 indicator (Merck). Flash chromatography was performed with Woelm 32−63 μm silica gel packing. Visualization was accomplished by phosphomolybdic acid or ninhydrin spray reagents, iodine, or UV illumination.

Proton (¹H NMR) and carbon (¹³C NMR) magnetic resonance spectra were recorded at 500 and 125 MHz, respectively, and chemical shifts are reported as ppm downfield from an internal tetramethylsilane standard (δ scale). The data are reported in the following form: chemical shift (multiplicity, coupling constant in Hz (if applicable), number of protons). Only characteristic infrared (IR) bands are reported (as cm⁻¹). Electron ionization (EI) mass spectra data were obtained at 70 eV and are reported in the following form: *m/z* (intensity relative to base peak = 100).

4'-Azidoacetophenone and 16α,17α-[(*R*)-1'-(4-Azido-3-iodophenyl)ethylidenedioxy]pregn-4-ene-3,20-dione were prepared as previously described (8).

Chemical Synthesis. *2-(4'-Azidophenyl)-2-methyl-1,3-dioxolane (9).* Aryl azide **13** (0.510 g, 3.17 mmol) was heated at reflux in 50 mL of benzene with 5 mL of ethylene glycol and a catalytic amount of *p*-toluenesulfonic acid for 16 h; water was removed by azeotropic distillation using a Dean-Stark apparatus. Product isolation (aqueous NaHCO₃, EtOAc, brine, Na₂SO₄) afforded **9** as a brown oil. Purification by flash chromatography (8:1 hexanes:EtOAc) provided **9** as a light yellow oil (0.474 g, 73%): IR (CHCl₃) *v* 2136; ¹H NMR δ 7.46 (d,

J = 8.5 Hz, 2 H), 6.99 (d, *J* = 8.5 Hz, 2 H), 4.03−4.05 (m, 2 H), 3.75−3.78 (m, 2 H), 1.64 (s, 3 H); ¹³C NMR δ 140.16, 139.53, 126.84, 118.76, 108.50, 64.45, 27.56. MS (CI, CH₄) *m/z* 206 (M + 1), 178, 163, 151, 134, 87; HRMS calcd for $C_{10}H_{12}O_2N_3$ 206.1597, found 206.1592.

2-(2'-(Diethylamino)-3'H-azepin-5-yl)-2-methyl-1,3-dioxolane (10). Aryl azide **9** (0.210 g, 1.02 mmol) was dissolved in 2 mL of freshly distilled diethylamine in a photolysis tube and the solution degassed by three freeze−pump−thaw cycles before being flame-sealed under vacuum. The photolysis was carried out with a 450 W medium-pressure Hanovia mercury vapor arc lamp equipped with a saturated CuSO₄ filter (effective wavelength > 315 nm). The photolysis was stopped after 2 h, the photolysis tube was cracked open, and the crude reaction mixture was poured into a mixture of EtOAc (25 mL) and water (25 mL). The organic layer was extracted and dried over Na₂SO₄. Removal of solvent *in vacuo* afforded 0.187 g of a brown oil. Purification by flash chromatography (6:1 hexane:EtOAc) provided starting material (0.125 g, 59%), substituted azepine **10** (0.045 g, 18%), and two more polar products (0.005 g). The yield of **10** corrected for recovered starting material was 43%: IR (CHCl₃) *v* 1686; ¹H NMR δ 7.09 (d, *J* = 8.1 Hz, 1 H), 5.80 (d, *J* = 8.1 Hz, 1 H), 5.23 (t, *J* = 7.3 Hz, 1 H), 3.91−3.96 (m, 2 H), 3.74−3.79 (m, 2 H), 3.31−3.35 (m, 4 H), 2.2−2.8 (broad s, 2 H), 1.46 (s, 3 H), 1.05−1.10 (m, 6 H); ¹³C NMR δ 146.26, 141.69, 141.20, 108.54, 108.25, 107.52, 65.77, 64.20, 43.13, 30.43, 26.09. MS (EI, 70 eV) *m/z* 250 (M⁺, 53), 235 (37), 221 (22), 207 (26), 179 (29), 164 (22), 135 (12), 107 (25), 84 (100), 72 (31), 43 (74); HRMS calcd for $C_{14}H_{22}N_2O_2$ 250.1681, found 250.1681.

Radiochemical Synthesis and Purification. The procedure for formation of [³H]-**7** by tritiolysis of iodoaryl azide **11** was adapted from the procedure for hydrogenolysis of **11** (8). A sample of iodo azide **11** (0.010 g, 0.016 mmol) and the 5% Pd/alumina (0.015 g) was sent to Amersham Corp. (Arlington Heights, IL) to be radiolabeled with carrier-free tritium gas according to the following instructions. To a solution of iodoaryl azide **11** in 2 mL of THF add 0.015 g of 5% Pd/alumina and 7.0 μL of triethylamine. Expose the rapidly stirring solution to 10 Ci of carrier-free tritium gas for 30 min at 25 °C under atmospheric pressure. Filter the solution through a 1 cm plug of Celite to remove Pd catalyst and wash with benzene (3 × 1 mL). Remove exchangeable tritium using standard solvent exchange−evaporation cycles. Dissolve the tritium-labeled sample in 25 mL of 9:1 benzene/ethanol and store at −20 °C.

The total amount of tritium incorporated into the sample was 43 mCi (10% of theoretical). The 43 mCi sample returned from Amersham was assayed by TLC and HPLC. From coelution with unlabeled standards, the crude material was found to be a mixture of [³H]aryl azide **7** (50%), [³H]aryl amine **12** (40%), [³H]-base line material (10%), and unlabeled iodoaryl azide **11**. Flash chromatography (silica gel, 2.5:1 hexane:EtOAc) of 18 mCi of the crude mixture efficiently separated the [³H]-aryl azide **7** from the other tritium-labeled products. While some of the unlabeled iodoaryl azide (4.0 mg) was recovered, a large amount was not separated from the [³H]aryl azide **7**. Final purification of [³H]-**7** was accomplished by preparative normal phase HPLC (0.9 cm × 50 cm, Whatman Partisil M-9 SiO₂ column) eluting with 18% EtOAc in hexanes at a rate of 3 mL/min. Under these HPLC conditions, the [³H]-**7** had a retention time of 38 min and the unlabeled iodo azide **11** had a retention time of 42 min. After multiple injections, 4.3 mCi of [³H]aryl azide **7** was isolated in pure form.

Scheme 1

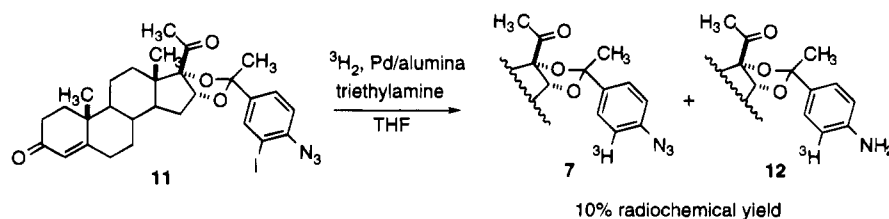10% radiochemical yield

Table 1. Comparison of Biological Data for Photoaffinity Labeling Reagents for the PR

| compd no. | compd name | receptor binding affinity (RBA)^a (%) | | photoinactivation efficiency (PIE) (%)at 60 min | photoattachment efficiency (%) |
		PR (rat)^b (R5020 = 100)	PR (human)^c (R5020 = 100)		
7	PAA 7	15	71	81	60
1	R 5020	100	100	66	2–5
2	RU 486	170	28	nd^d	<1
3	ING	78	nd	nd	4
4	DU 41165	158	178	60	5–7
	progesterone	13	8.5	nd	na^e

^{a} Relative binding affinity determined in a competitive radiometric binding assay; details are given in ref 14. Values are expressed as percentages relative to the affinity of R 5020 as tracer. The RBAs of compounds which exhibit affinities >1.0% are the average of two or more determinations, which are generally reproducible to within 30% (relative error). ^{b} Cytosol preparations were from estrogen-primed immature rat uterus, with [^{3}H]-R 5020 as tracer. ^{c} Cytosol preparations were from human T$_{47D}$ breast cancer cells, with [^{3}H]-R 5020 as tracer. ^{d} nd = not determined. ^{e} na = not applicable.

The specific activity of [^{3}H]-**7** was determined by HPLC analysis to be 20 Ci/mmol. The UV detector sensitivity was calibrated by injecting a series of known quantities of unlabeled standard and determining the peak area; simultaneous measurement of peak area and radioactivity on an injected sample of [^{3}H]-**7** enabled the specific activity to be determined. The chemical and radiochemical purity were evaluated by reinjection onto HPLC and by normal phase TLC analysis. HPLC analysis showed a single peak by UV and radiometric analysis, at the same retention time as our authentic unlabeled standard; TLC analysis (2:1 hexanes:EtOAc) indicated a single peak of radioactivity with an R_f of 0.51, identical to the R_f of an unlabeled standard run on the same plate.

Biological Procedures. Materials. Radioligands were obtained from the following sources: 16α-ethyl-21-hy-droxy-19-nor[6,7-^{3}H]pregn-4-ene-3,20-dione (ORG 2058, 58 Ci/mmol), (Amersham Corp., Arlington Heights, IL); [17α-methyl-^{3}H]promegestone (R 5020), 86 Ci/mmol, (DuPont New England Nuclear, Boston, MA). Unlabeled ligands: promegestone (DuPont New England Nuclear, Boston, MA), ORG 2058 (kindly supplied by Dr. F. Zeelen, Organon Corp., Oss, The Netherlands), and estradiol (Sigma Chemical Co., St. Louis, MO).

Preparation of Cytosol. The progesterone receptor (PR) levels in the uteri of immature rats were induced by estrogen treatment. Immature female Sprague–Dawley rats (19 days, 60 g) were given three daily subcutaneous injections of 5 μg of estradiol in 0.1 mL of sunflower seed oil–ethanol, prepared fresh daily. The cytosol was prepared 24 h after the last injection as previously reported (*9*). All cytosol for the progesterone receptor was prepared in PR buffer (0.01 M Tris–HCl:0.0015 M EDTA: 0.02% sodium azide:20 mM sodium molybdate:0.012 M mercaptoethanol:20% glycerol, pH 7.4 at 25 °C) and stored in liquid nitrogen. In all studies, glucocorticoid receptor sites in the cytosol preparations were saturated by the addition of 1 μM hydrocortisone.

Scatchard Assay. Uterine progesterone cytosol was incubated at 0 °C for 4 h with various concentrations of ^{3}H-ligand in the absence or presence of a 100-fold excess of unlabeled ORG 2058. Aliquots of the incubation solution were counted to determine the concentration of total ^{3}H-steroid. The incubation solutions were then treated with charcoal–dextran and the bound ^{3}H-steroid determined. Data were processed according to the method of Scatchard (*10*).

Photolysis. Photolysis was routinely carried out at >315 nm (450 W mercury vapor lamp, Hanovia L679A, surrounded by a solution filter of saturated aqueous copper(II) sulfate) at 2–4 °C employing Pyrex reaction vessels as previously described (*11*).

Photoattachment Assay. Rat uterine cytosol was incubated for 1 h at 0 °C with 25 nM [^{3}H]-labeled ligand in the presence or absence of a 100-fold excess of nonphotoreactive blocking agent, ORG 2058, and photolyzed at >315 nm. Covalent binding of labeled ligands was measured directly by a filter disk assay described previously for the estrogen receptor (*12*).

Electrophoresis. SDS electrophoresis samples and gels were prepared as previously reported (*13*) with standard proteins of phosphorylase B (MW 97 400), bovine serum albumin (MW 67 000), ovalbumin (MW 44 600), and carbonic anhydrase (MW 29 000).

RESULTS

Radiochemical Synthesis. The preparation of [^{3}H]-**7** was accomplished by a palladium-catalyzed hydrogenolysis of an iodoaryl precursor using carrier-free tritium gas (Scheme 1). Our preparation of iodoaryl azide **11** and development of exchange reaction conditions using hydrogen gas have been previously reported (*8*). A sample of the aryl azide iodoprogestin **11** and the palladium on alumina catalyst that we had used in the hydrogen exchange reaction were sent to Amersham Corp. to be used in the labeling experiment with carrier-free [^{3}H]H$_2$ gas. Amersham carried out the tritiolysis using the same conditions that we had used in the hydrogenolysis. Under these reaction conditions, tritium incorporation proceeded in 10% radiochemical yield.

The radiolabeled sample returned from Amersham was assayed by TLC and HPLC and found to be a mixture of [^{3}H]aryl azide **7**, [^{3}H]arylamine **12**, and unlabeled aryl azide iodoprogestin **11**. Purification of the crude mixture by flash chromatography and normal phase HPLC (see Experimental Section for details) afforded pure [^{3}H]aryl azide **7**. The specific activity of [^{3}H]-**7** was determined
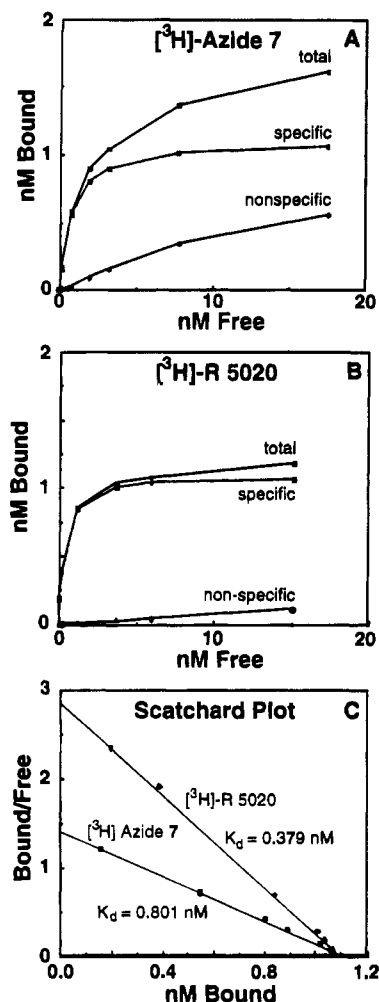
Figure 3. Direct binding curves for [^{3}H]protioaryl azide **7** and [^{3}H]-R 5020. Rat uterine cytosol was incubated at 0 °C for 4 h with various concentrations of tritium-labeled ligand in the absence and presence of 100-fold excess of unlabeled ORG 2058. Aliquots of the incubation solution were counted to determine the concentration of total tritium-labeled ligand present. The incubation solutions were then treated with charcoal—dextran, and the concentration of the bound tritium-labeled ligand was determined. Data are presented as direct (panels A and B) or Scatchard (panel C) binding plots.

by HPLC analysis to be 20 Ci/mmol, which is 70% of the theoretical maximum for incorporation of one tritium atom per molecule of azide.

Progesterone Receptor Binding Properties of Progestin Ketal 7. *Progesterone Receptor Binding Studies.* The relative binding affinity (RBA) (*14*) of the 16α,17α-(methylenedioxy)progesterones for the progesterone receptor (PR) was previously determined at 0 °C by a competitive radiometric binding assay using [^{3}H]-R 5020 as tracer (*8*). The RBA values of the progestin aryl azide **7** and several other progestins are shown in Table 1. The data are reported relative to R 5020 which is assigned a value of 100%. The RBA of progestin aryl azide **7** was found to be 15% in rat uterine cytosol, comparable to the natural hormone, progesterone, which has an RBA of 13%. In human PR, the binding affinity was somewhat higher (RBA = 71%).

Direct Binding Assay of [^{3}H]Progestin Ketal 7. The binding affinity of [^{3}H]progestin aryl azide **7** was determined in rat uterine cytosol using a charcoal adsorption assay to remove free ligand. The direct binding plots (Figure 3, panels A and B) show that the [^{3}H]progestin aryl azide **7** binds to the same number of specific PR sites

as does [^{3}H]-R 5020, but with somewhat reduced selectivity (more nonspecific binding). A comparison of the specific binding curves for **7** and [^{3}H]-R 5020 is presented as a Scatchard (*10*) plot (Figure 3, panel C). The ^{3}H-labeled aryl azide **7** has an affinity (K_d = 0.80 nM) for the PR that is 47% of the affinity of [^{3}H]-R 5020 (K_d = 0.38 nM). This is a somewhat higher affinity than measured by the RBA assay. Many progestins with high affinity for PR, like R 5020, associate slowly with the PR (*15*). The direct assay, incubated for only 4 h, may not have allowed the progestins to reach complete equilibrium, as seen after 18 h with the RBA assay.

Photoreactive Properties of Progestin Aryl Azide 7. *Photoinactivation Assay.* In our earlier study (*8*), we reported on a preliminary investigation of the photochemical behavior of nonradiolabeled **7** in the active site of the PR. Its photoinactivation efficiency (PIE) for PR was determined by photolysis of the PR complex formed by incubation of **7** with rat uterine cytosol preparations of PR for 4 h at 0 °C (*12*). Irradiation of the receptor—ligand complexes was conducted at 254 nm or >315 nm, and the loss of reversible binding capacity of the PR was measured by an exchange assay using [^{3}H]-R 5020. Control experiments in which the receptor sites were blocked with the nonphotoactive progestin ORG 2058 demonstrated high levels of PR decomposition when irradiation was carried out at 254 nm (*12*). Irradiation at >315 nm did not cause this protein damage and resulted in highly specific photoinactivation of the PR.

By this assay, progestin aryl azide **7** demonstrated the highest photoinactivation efficiency (80%) of any potential photoaffinity labeling reagent for the PR tested to date by this method (Table 1, column 5, and ref 8). Furthermore, the ability of **7** to inactivate the receptor upon photolysis was shown to be completely specific for the PR binding site. Blocking of the PR binding site with ORG 2058 prior to incubation with the photolabeling ligand **7** eliminated any photoinactivation of PR reversible binding capacity (data not shown, see ref 8).

Photolabeling of the Progesterone Receptor with [^{3}H]-Progestin Ketal 7. [^{3}H]Progestin aryl azide **7** and ^{3}[H]-R 5020 were photolyzed at >315 nm in rat uterine cytosol preparations, and the percent of specific and nonspecific attachment was examined by a filter disk—solvent extraction assay (*12*). The PR specificity of the covalent photolabeling can be determined by a simultaneous measurement of the nonspecific photolabeling done in the presence of an excess of unlabeled, nonphotoreactive blocking agent, ORG 2058. The difference between the labeling in the absence or presence of ORG 2058 is the PR specific labeling. The photoattachment efficiency is defined as the amount of PR covalently labeled as a percent of PR which was occupied reversibly by the synthetic progestin; the photoattachment selectivity is defined as the amount of specific PR labeled as a percent of the total protein labeled after photolysis.

The time course of specific photoattachment is illustrated in Figure 4. [^{3}H]Progestin aryl azide **7** exhibits high photoattachment efficiency (60% at 1 h). It is, in fact, the most efficient progesterone receptor PAL reagent prepared to date (see Table 1, column 6), being much higher than the commonly used PR PAL reagent [^{3}H]-R 5020 (2.2% at 1 h; Figure 4A). The photoattachment with **7** proceeds in a time-dependent fashion, with most of the attachment occurring within the first 10 min of photolysis. The attachment selectivity of **7** is relatively high at early time points (65% at 2 min) but falls due to increasing levels of nonspecific attachment as the photolysis experiment proceeds (30% at 1 h; Figure 4B).
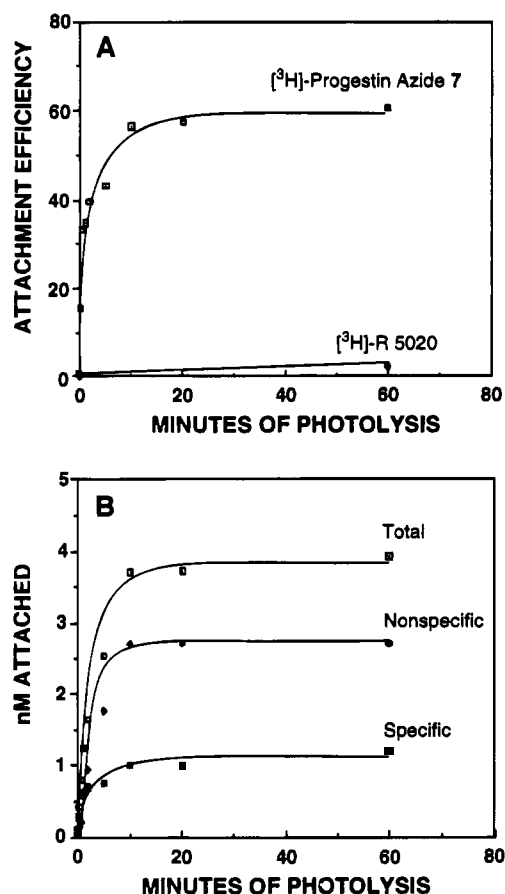
Figure 4. Time-course of photoattachment of [³H]progestin azide **7** with the PR. Rat uterine cytosol was incubated for 1 h at 0 °C with 25 nM [³H]progestin azide **7** or 25 nM [³H]-R 5020 with or without a 100-fold excess of unlabeled blocking agent ORG 2058 and then photolyzed at > 315 nm for the times indicated. Covalent attachment was measured by an ethanol disk assay (*12*). Shown in panel B are the total (no ORG 2058 blocking) and the nonspecific (ORG 2058 blocked) attachment; the specific attachment is the difference between these values. A direct comparison of the efficiency of the specific photoattachment efficiencies of [³H]progestin azide **7** and [³H]-R 5020 is shown in panel A.

Figure 5. SDS–polyacrylamide gel electrophoresis of photoattached [³H]protio azide **7** (panel A) and [³H]-R 5020 (panel B). The calibration curve of standard proteins is shown in panel C. The standard proteins are phosphorylase B (Phos B), bovine serum albumin (BSA), ovalbumin (OV), and carbonic anhydrase (CA). The coefficient of the line is 0.996 by linear regression.

At the concentration of [³H]progestin azide **7** used in the experiment shown in Figure 4B (25 nM), the selectivity of covalent attachment is lower than might be expected on the basis of the selectivity of reversible binding shown in Figure 3A. Part of this difference arises from the fact that only 60% of the reversibly bound receptor complexes undergo covalent attachment, but other proteins as well are being labeled by free or dissociated photolabel. Nevertheless, covalent labeling selectivity of 30% in an unfractionated receptor preparation (rat uterine cytosol) is quite high. The level of nonspecific attachment with [³H]progestin azide **7** is comparable to that seen with R 5020, and the nonspecific labeling is spread among many different proteins (cf. Figure 5AB below).

Control experiments were performed to demonstrate that the attachment of **7** with the PR was a chromophore-dependent, photoactivated process. First, incubation of **7** with the PR in the dark results in no covalent attachment. Prephotolysis of the [³H]progestin azide **7** for 15 min prior to incubation with the PR-rich cytosol resulted in a dramatic decrease in attachment efficiency to 4%. We also demonstrated that the blocking agent ORG 2058 (no photoactivatible chromophore) did not attach to the PR upon photolysis.

Characterization of the Progesterone Receptor Covalently Labeled with [³H]Progestin Aryl Azide 7. PR covalently labeled with [³H]progestin azide **7** in the absence and presence of an excess of unlabeled ORG 2058 was analyzed by SDS–polyacrylamide gel electrophoresis (Figure 5). For comparison, similar procedures were used to covalently label PR with [³H]-R 5020. We found that the [³H]progestin azide **7** successfully labeled two proteins with high specificity. These two proteins appear to be the same as those labeled with [³H]-R 5020 and have molecular weights similar to those reported for the two subunits of PR. Our results indicate labeling of proteins of molecular weight 108 500 ± 800 and 87 000 ± 1500 (*n* = 3). The higher molecular weight protein corresponds to literature values for subunit B of PR (109 600 ± 1200) (*4a*), and the lower molecular weight protein corresponds to literature values of subunit A of PR (85 600 ± 1200) (*4a*). The ratio of the PR subunits A:B was determined to be 3.3:1 with both [³H]progestin azide **7** and [³H]-R 5020. This is in agreement with other reports of the rat uterine A:B ratios (*4a,d*). Interestingly, the ratios of subunits A:B in human breast cells (*5*) and chick oviduct (*6*) are quite different. In addition to the intact subunits, the gels show several proteolytic fragments of PR that retain specific attachment of protioaryl azide **7**, and some free aryl azide **7** appears with the

Scheme 2

43% based on recovered SM
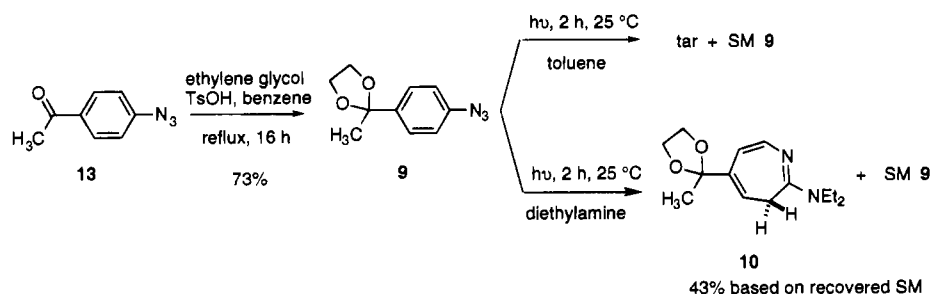
tracking dye. The molecular weight curve of the standard proteins is shown in Figure 5C.

Solution Photolysis Experiment. In an attempt to provide evidence for the type of covalent link formed upon photolysis of the ligand—receptor complex, a solution photolysis experiment was performed using a model aryl azide ketal that mimicked the protio aryl azide **7** (Scheme 2). Ketal **9** was prepared in good yield (73%) by heating aryl azide **13** under reflux in the presence of ethylene glycol and a catalytic amount of *p*-toluenesulfonic acid while removing water as a benzene azeotrope. The photochemical behavior of **9** was evaluated in two solvents: diethylamine to evaluate attachment by nucleophilic addition of the amine to the ring-expanded dehydroazepine and toluene to evaluate covalent attachment by a nonspecific C—H bond insertion mechanism. The samples were degassed by three freeze—thaw cycles prior to photolysis; the photolysis was carried out with a Hanovia mercury arc lamp equipped with a saturated $CuSO_4$ filter (effective wavelength > 315 nm).

Photolysis of aryl azide **9** in toluene resulted in an uncharacterizable tar and starting material. The major product from photolysis of **9** in diethylamine was the diethylamine adduct of the ring-expanded dehydroazepine (**10**) (43% corrected for recovered starting material). Two other products that accounted for less than 5% of the total mass recovered were not identified.

Stability of the Covalently Attached [3H]-7—PR Adduct. We examined the covalently attached [3H]-7—PR complex under a variety of conditions that are used in protein digestion and N-terminal sequencing. We found that the covalent link was stable to the protein buffer conditions that are typically used in trypsin, chymotrypsin, and V-8 protease digests (*16*). We found that it was also stable to 0.1% trifluoroacetic acid, which is commonly added to solvents used in reversed-phase HPLC of proteins. At higher concentrations of acid, however, the covalent [3H]progestin azide **7**—receptor complex was not as stable. Incubation of the complex with 70% formic acid for 1 h at room temperature (conditions used in cyanogen bromide digests) resulted in a loss of 30% of the specific attachment. Treatment of the complex with 10% trichloroacetic acid, 10% trifluoroacetic acid, or 100% trifluoroacetic acid at 0 °C or room temperature for 10 s completely destroyed the specific attachment.

DISCUSSION

The photoaffinity labeling (PAL) reagents that have been developed for the PR have, up until now, all relied on an A,B-ring dienone functionality as the photoreactive moiety, but the very inefficient attachment of these probes to the PR has been a major limitation in the uses of these PAL reagents. The [3H]progestin aryl azide **7** attaches to the PR with 60% efficiency, compared to the attachment efficiency of 5—7% for the most efficient A,B-ring dienone based PAL reagent, DU 41165 (**4**) (*4d*)

(Table 1). In addition, photoattachment of all A,B-ring dienone based PAL reagents would likely result in labeling of similar amino acid residues in primarily one area of the PR hormone binding site. The aryl azide **7** is expected to attach to amino acids in a different area of the hormone binding domain and provide new information on amino acids that are in close contact with the ligand.

The relative binding affinity (RBA) for the rat PR of the aryl azide **7** is somewhat lower than the RBAs for the A,B-ring dienone based PAL reagents, but it is still slightly higher than the natural ligand, progesterone. The binding affinity determined directly from Scatchard analysis of [3H]progestin aryl azide **7** was 47% of the affinity of [3H]-R 5020 for the PR. Its affinity for the human PR is even higher (RBA = 71%), so that it is almost comparable to that of several of the A,B-ring dienone based PAL reagents. Although the sequences of the rat and human PRs are very similar in the hormone binding domain (*17, 18*), it is not uncommon to observe significant differences in binding affinities between a probe and the same receptor from different species (*19, 20*).

Literature precedent suggests that the most likely mechanism for photoattachment for [3H]progestin azide **7** would involve attack of a nucleophilic residue on the ring-expanded dehydroazepine (*21*). This would lead to covalent attachment of the molecular probe **7** with the PR through a potentially acid-labile aminal or thioaminal linkage. The nature of the covalent link is of importance because the most commonly used N-terminal sequencing method, Edman degadation (*22*), is typically performed using trifluoroacetic acid as solvent in one step of the cycle.

The results of the photolysis experiment with the model aryl azide **9** (Scheme 2) indicated, as expected, that the preferred photochemical pathway for protioaryl azide ketals is ring expansion to the dehydroazepine, followed by covalent attachment by a nucleophilic species. These results are consistent with the extensive photochemical work that has been done on phenyl azide, which undergoes ring expansion to the complete exclusion of C—H insertion chemistry (*21*).

In our initial report on the progestin aryl azide derivatives (*8*), we also prepared a tetrafluoro azide analog **8**. Our interest in this analog was based on the reports by Platz and Keana indicating that the fluoroaryl nitrene photoproduct might have a higher likelihood of forming the more stable C—H bond insertion products (*23*), rather than the acid labile links resulting from ring expansion and nucleophilic trapping of a dehydroazepine. The tetrafluoroaryl azide **8** had comparable binding affinity and photoinactivation efficiency for PR. While it is possible that it might also form more acid-stable covalent links to PR, the full substitution of the arene ring in this analog does not make it amenable to tritium labeling by the method we have used here. An arene

analog we have not yet synthesized, having only fluorine substituents in the two critical positions *ortho* to the azide (*24*), could, in principle, be tritium-labeled at the remaining two free positions.

Although the limited stability of the covalent link between [³H]-**7** and the PR may preclude sequence analysis by Edman degradation, newly developed methods for sequencing peptides by mass spectrometry may provide an alternative method for obtaining the desired information. Our current strategy for determining the amino acids involved in covalent attachment of [³H]-**7** to PR involves initial digestion of the photoattached [³H]-**7**−PR complex with trypsin, chymotrypsin, or V-8 protease to obtain a labeled peptide, followed by analysis by electrospray ionization mass spectrometry. Our efforts at sequencing the [³H]-**7**−PR complex will be published elsewhere.

CONCLUSION

16α,17α-[(*R*)-1′-(4-Azidophenyl)ethylidenedioxy]pregn-4-ene-3,20-dione (**7**) was prepared in tritium-labeled form by a palladium-catalyzed tritiolysis of an aryl iodide precursor. The [³H]-labeled progestin aryl azide **7** was then evaluated as a photoaffinity labeling reagent for the PR. Scatchard plot analysis of the reversible binding of this compound revealed it to bind to the PR with 47% of the affinity of R 5020. Photolysis of [³H]-**7** with the PR resulted in a specific covalent attachment efficiency of 60%. The attachment efficiency of this compound far exceeds the efficiencies normally observed for A,B-ring dienone-based PAL reagents for the PR. The photoattached protein was analyzed by SDS−polyacrylamide gel electrophoresis and found to label two proteins that correspond to the two subunits of the PR. From this labeling experiment, it was determined that the two subunits of the PR were present in a 3.3:1 ratio of subunit A:subunit B. Attempts at sequencing the covalently labeled PR by protein digestion methods and electrospray ionization mass spectrometry are underway.

ACKNOWLEDGMENT

LITERATURE CITED

(1) Reviewed in: (a) McDonnell, D. P., Vegeto, E., and Gleeson, M. A. G. (1993) Nuclear hormone receptors as targets for new drug discovery. *Biotechnology 11*, 1256−1261. (b) Smith, D. F., and Toft, D. O. (1993) Steroid receptors and their associated proteins. *Mol. Endocrinol. 7*, 4−11. (c) O'Malley, B. W., and Tsai, M., J. (1992) Molecular pathways of steroid receptor action. *Biol. Reprod. 46*, 163−167.

(2) Reviewed in: Bayley, H. (1983) *Photogenerated Reagents in Biochemistry and Molecular Biology*, Elsevier, New York. (b) Singh, A., Thornton, E. R., and Westheimer, F. H. (1962) The Photolysis of Diazoacetylchymotrypsin. *J. Biol. Chem. 237*, 3006−3008. (c) Katzenellenbogen, B. S., and Katzenellenbogen, J. A. (1988) Techniques Used in Affinity Labeling Studies of Steroid and Thyroid Hormone Receptors: Estrogen Receptor. *Affinity Labelling and Cloning of Steroid and Thyroid Hormone Receptors* (H. Gronemeyer, Ed.) pp 17−27, VCH Publishers, Weinheim, Germany. (d) Katzenellenbogen, B. S.,

and Katzenellenbogen, J. A. (1988) Affinity Labeling Studies of Estrogen Receptors. *Affinity Labelling and Cloning of Steroid and Thyroid Hormone Receptors* (H. Gronemeyer, Ed.) pp 87−108, VCH Publishers, Weinheim, Germany. (e) Schuster, D. I., Probst, W. C., Ehrlich, G. K., and Singh, G. (1989) Photoaffinity Labeling. *Photochem. Photobiol. 49*, 785−804.

(3) (a) Scriven, E. F. V., Ed. (1984) *Azides and Nitrenes*, Academic Press, Inc., Orlando, FL. (b) Scriven, E. F. V., and Turnbull, K. (1988) Azides: Their Preparation and Synthetic Uses. *Chem. Rev. 88*, 298−368. (c) Patai, S., Ed. (1971) *The Chemistry of the Azido Group*, Wiley Interscience, New York. (d) Liu, M. T. H., Ed. (1987) *Chemistry of Diazirines*, CRC Press, Boca Raton, FL. (e) Dorman, G., and Prestwich, G. D. (1993) Photocovalent Modifications with the Benzophenone Photophore. *Chemtracts−Org. Chem.* 131−138. (f) Katzenellenbogen, J. A., and Katzenellenbogen, B. S. (1984) Affinity Labeling of Receptors for Steroid and Thyroid Hormones. *Vitamins and Hormones* (G. Aurbach, Ed.), Vol. 41, pp 213−274, Academic Press, New York.

(4) (a) Ilenchuk, T. T., and Walters, M. R. (1987) Rat Uterine Progesterone Receptor Analyzed by [³H]R5020 Photoaffinity Labeling: Evidence that the A and B Subunits Are Not Equimolar. *Endocrinology 120*, 1449−1456. (b) Gronemeyer, H., and Govindan, M. V. (1986) Affinity Labeling of Steroid Hormone Receptors. *Mol. Cell. Endocrinol. 46*, 1−19. (c) Clark, C. L., Fell, P. D., and Satyaswaroop, P. G. (1986) Effect of Photoaffinity Labeling on Rabbit Uterine Progesterone Receptor. *Anal. Biochem. 157*, 154−161. (d) Pinney, K. G., Carlson, K. E., and Katzenellenbogen, J. A. (1990) [³H]-DU41165: A High Affinity Ligand and Novel Photoaffinity Labeling Reagent For the Progesterone Receptor. *J. Steroid Biochem. 35*, 179−189.

(5) (a) Lessey, B. A., Alexander, P. S., and Horwitz, K. B. (1983) The Subunit Structure of Human Breast Cancer Progesterone Receptors: Characterization by Chromatography and Photoaffinity Labeling. *Endocrinology 112*, 1267−1274. (b) Horwitz, K. B. (1985) The Antiprogestin RU38486: Receptor-Mediated Progestin Versus Antiprogestin Actions Screened in Estrogen-Insensitive T47D_co Human Breast Cancer Cells. *Endocrinology 116*, 2236−2245.

(6) (a) Dure, L. S., IV, Schrader, W. T., and O'Malley, B. W. (1980) Covalent attachment of a Progestational Steroid to Chick Oviduct Progesterone Receptor by Photoaffinity Labeling. *Nature 283*, 784−786. (b) Birnbaumer, H., Schrader, W. T., and O'Malley, B. W. (1983) Photoaffinity Labeling of the Chick Progesterone Receptor Proteins. *J. Biol. Chem. 258*, 1637−1644. (c) Gronemeyer, H., Govindan, M. V., and Chambon, P. (1985) Immunological Similarity between the Chick Oviduct Progesterone Receptor Forms A and B. *J. Biol. Chem. 260*, 6916−6925.

(7) Pinney, K. G., Carlson, K. E., Katzenellenbogen, B. S., and Katzenellenbogen, J. A. (1991) Efficient and Selective Photoaffinity Labeling of the Estrogen Receptor Using Two Nonsteroidal Ligands That Embody Aryl Azide or Tetrafluoroaryl Azide Photoreactive Functions. *Biochemistry 30*, 2421−2431.

(8) Kym, P. R., Carlson, K. E., and Katzenellenbogen, J. A. (1993) Progestin 16α,17α-Dioxolane Ketals as Molecular Probes for the Progesterone Receptor: Synthesis, Binding Affinity and Biochemical Evaluation. *J. Med. Chem. 36*, 1111−1119.

(9) Laemmli, U. K. (1970) Cleavage of Structural Proteins during the Assembly of the Head of Bacteriophage T4. *Nature 227*, 680−685.

(10) Scatchard, G. (1949) The attractions of proteins for small molecules and ions. *Ann. N. Y. Acad. Sci. 51*, 660−672.

(11) For a complete description of the photolysis equipment see: Katzenellenbogen, J. A., Johnson, H. J., Carlson, K. E., and Myers, H. N. (1974) Photoreactivity of Some Light-Sensitive Estrogen Derivatives. Use of an Exchange Assay to Determine Their Photointeraction with the Rat Uterine Estrogen Binding Protein. *Biochemistry 13*, 2986−2994.

(12) Katzenellenbogen, J. A., Ruh, T. S., Carlson, K. E., Iwamoto, H. S., and Gorski, J. (1975) Ultraviolet Photosensitivity of the Estrogen Binding Protein from Rat Uterus. Wavelength

and Ligand Dependence. Photocovalent Attachment of Estrogens to Protein. *Biochemistry 14*, 2310–2316.

(13) Anker, H. S. (1970) A Solubilizable Acrylamide Gel for Electrophoresis. *FEBS Lett. 7*, 293.

(14) (a) Katzenellenbogen, J. A., Johnson, H. J., and Carlson, K. E. (1973) Studies on the Uterine, Cytoplasmic Estrogen Binding Protein. Thermal Stability and Ligand Dissociation Rate. An Assay of Empty and Filled Sites by Exchange. *Biochemistry 12*, 4092–4099. (b) Brandes, S. J., and Katzenellenbogen, J. A. (1987) Fluorinated Androgens and Progestins: Molecular Probes for Androgen and Progesterone Receptors with Potential use in Positron Emission Tomography. *Molec. Pharmacol. 32*, 391–403.

(15) (a) Aranyi, P. (1980) Kinetics of the Hormone–Receptor Interaction. Competition Experiments With Slowly Equilibrating Ligands. *Biochem. Biophys. Acta. 628*, 220–227. (b) Carlson, K. E., and Katzenellenbogen, J. A. (1993) (unpublished results).

(16) Aitken, A., Geisow, M. J., Findlay, J. B. C., Holmes, C., and Yarwood, A. (1989) Peptide Preparation and Characterization. *Protein Sequencing: A Practical Approach* (J. B. C. Findlay and M. J. Geisow, Eds.) pp 43–68, Oxford University Press, New York.

(17) Misrahi, M., Atger, M., d'Auriol, L., Loosfelt, H., Meriel, C., Fridlansky, F., Guiochon-Mantel, A., Galibert, F., and Milgrom, E. (1987) Complete Amino Acid Sequence of the Human Progesterone Receptor Deduced form Cloned DNA. *Biochem. Biophys. Res. Commun. 143*, 740–748.

(18) Park, O.-K., and Mayo, K. E. (1991) Transient Expression of Progesterone Receptor Messenger RNA in Ovarian Granulosa Cells after the Preovulatory Luteinizing Hormone Surge. *Mol. Endocrinol. 5*, 967–978.

(19) Sharoni, Y., Feldman, B., Karny, N., and Levy, J. (1986) ORG-2058 as a Ligand in the Assay of Progesterone Receptor in Breast Cancer. *Steroids 48*, 419–426.

(20) Boonkasemsanti, W., Aedo, A.-R., and Cekan, S. Z. (1989) Relative Binding Affinity of Various Progestins and Anti-

progestins to a Rabbit Myometrium Receptor. *Arzneim.-Forsch./Drug Res. 39*, 195–199.

(21) (a) Schuster, G. B., and Platz, M. S. (1992) Photochemistry of phenyl azide. *Adv. Photochem. 17*, 69–143. (b) Li, Y.-Z., Kirby, J. P., George, M. W., Poliakoff, M., and Schuster, G. B. (1988) 1,2-Didehydroazepines from the Photolysis of Substituted Aryl Azides: Analysis of their Chemical and Physical Properties by Time-Resolved Spectroscopic Methods. *J. Am. Chem. Soc. 110*, 8092–8098. (c) Leyva, E., Platz, M. S., Persy, G., and Wirz, J. (1986) Photochemistry of Phenyl Azide: The Role of Singlet and Triplet Phenylnitrene as Transient Intermediates. *J. Am. Chem. Soc. 108*, 3783–3790. (d) Schrock, A. K., and Schuster, G. B. (1984) Photochemistry of Phenyl Azide: Chemical Properties of the Transient Intermediates. *J. Am. Chem. Soc. 106*, 5228–5234.

(22) Edman, P. (1960) Phenylthiohydantoins in Protein Analysis. *Ann. N. Y. Acad. Sci. 88*, 602–610.

(23) (a) Leyva, E., Young, M. J. T., and Platz, M. S. (1986) High Yields of Formal CH Insertion Products in the Reactions of Polyfluorinated Aromatic Nitrenes. *J. Am. Chem. Soc. 108*, 8307–8309. (b) Leyva, E., Munoz, D., and Platz, M. S. (1989) Photochemistry of Fluorinated Aryl Azides in Toluene Solution and in Frozen Polycrystals. *J. Org. Chem. 54*, 5938–5945. (c) Young, M. J. T., and Platz, M. S. (1991) Mechanistic Analysis of the Reactions of (Pentafluorophenyl)nitrene in Alkanes. *J. Org. Chem. 56*, 6403.

(24) (a) Schnapp, K. A., Poe, R., Leyva, E., Soundararajan, N., and Platz, M. S. (1993) Exploratory Photochemistry of Fluorinated Aryl Azides. Implications for the Design of Photoaffinity Labeling Reagents. *Bioconjugate Chem. 4*, 172–177. (b) Schnapp, K. A., and Platz, M. S. (1993) A Laser Flash Photolysis Study of Di-, Tri- and Tetrafluorinated Phenylnitrenes; Implications for Photoaffinity Labeling. *Bioconjugate Chem. 4*, 178–183.

Mechanism of Amide Formation by Carbodiimide for Bioconjugation in Aqueous Media

Naoki Nakajima and Yoshito Ikada*

Research Center for Biomedical Engineering, Kyoto University, 53 Kawahara-cho, Shogoin, Sakyo-ku, Kyoto 606, Japan. Received June 22, 1994®

To study the mechanism of amide formation between carboxylic acid and amine in aqueous media using 1-ethyl-3-(3-(dimethylamino)propyl)carbodiimide hydrochloride (EDC), hydrogels with two different types of carboxyl group locations were employed as substrates containing the carboxylic acid, while ethylenediamine and benzylamine were used as amine. In parallel, a study was undertaken with cyclizable carboxylic acids (maleic acid and poly(acrylic acid)) and noncyclizable carboxylic acids (fumaric acid and poly(ethylene glycol) with the terminal carboxyl groups) to assess the reaction products by ^{13}C-NMR and IR. EDC rapidly lost its activity in aqueous media of low pH, producing the corresponding urea derivative, but was very stable at neutral and higher pH regions. EDC could react with carboxyl groups at a relatively narrow low pH range such as 3.5–4.5. If carboxyl groups were cyclizable, they would react quickly with EDC producing carboxylic anhydrides, which formed the corresponding amides when amine compounds were present. On the other hand, a trace of amide was formed in the case of noncyclizable carboxylic acids. In addition, an excess of EDC caused an undesired side reaction to form stable *N*-acylurea, regardless of the special location of carboxylic acids.

INTRODUCTION

Carbodiimides (RN=C=NR') are unsaturated compounds with an allene structure. Since their first synthesis from thioureas at the end of the last century, carbodiimides have been widely used in organic synthesis and biotechnology. Their synthetic methods as well as their physical and chemical properties are summarized in review articles (Kohrana, 1953; Kurzer & Douraghi-Zadeh, 1967; Williams & Ibrahim, 1981). Extensive studies have been also devoted to reactions of carbodiimides such as isomerization of themselves and addition reactions with water, alcohols, amines, phenols, and carboxylic acids. In addition, carbodiimides have been applied for peptide synthesis (Sheehan & Hlavka, 1956) and modification of polysaccharides (Danishefsky & Siskovic, 1971) and proteins (Wilchek et al., 1967; Hoare & Koshland, 1967) in aqueous systems.

Recently, attention has been paid to new synthesis and application of carbodiimides. For example, Gontar et al. synthesized perfluorodialkylcarbodiimides via the rearrangement of perfluoroazidoazomethines (Gontar et al., 1985). Synthesis of other carbodiimides was also reported (Gorbatenko et al., 1984; Matveev et al., 1988; Saito et al., 1992). Further, peptide synthesis (Kricheldorf et al., 1985; Kessler & Hutscher, 1986; Wang et al., 1987), inactivation of thrombin (Chan et al., 1988), Diels–Alder reaction (Trifonov & Orahovants, 1989), and modification of DNA (Dolinnaya et al., 1990, 1991) were investigated using carbodiimides.

Bioconjugation by carbodiimides has also been widely performed. Carbodiimides are very effective in modifying and crosslinking proteins such as lysozyme (Yamada et al. 1981), myosin (Onishi et al., 1989a,b), neurotoxin (Schmidt & Betz, 1989), actin (Takashi, 1988), F₁ adenosine triphosphatase (Bragg & Hou, 1986a,b), and cytochrome c and b₅ (Mauk & Mauk, 1989) because no

residues remain in the crosslinked protein (zero-length crosslinker).

Most of the above-mentioned studies are based on amide formation under very mild conditions between carboxylic acids and amines in aqueous and organic systems in the presence of carbodiimides. However, surprisingly few studies have focused on the elucidation of mechanism of the amide formation, particularly in aqueous systems in spite of their great importance in bioconjugation. On the contrary, reactions of carbodiimides with carboxylic acids in organic systems have been intensively studied to find that carboxylic anhydrides and the corresponding urea derivatives are produced by the reaction, as cited in the references (Kohrana, 1953; Kurzer & Douraghi-Zadeh, 1967; Williams & Ibrahim, 1981). On the other hand, Swaisgood and Natake studied the reaction of carboxyl groups in 1-glutamate dehydrogenase with glycine methyl ester in an aqueous medium in the presence of carbodiimides and found that the pH of the reaction medium strongly affected the reaction under formation of undesirable side-products if a high concentration of carbodiimide was present (Swaisgood & Natake, 1973). Frequently, an excess of carbodiimide is used in the isolation of biological membranes (Jacobson, 1977; Kalish et al., 1978) and in modification of polysaccharides (Danishefsky & Siskovic, 1971) to ensure the reaction.

In 1967 Hoare and Koshland proposed a mechanism for the amide formation by carbodiimide in aqueous media, but their mechanism is inconsistent with that proposed in text books (Solomons, 1988; Wong, 1991). Carbodiimide is thought in these text books to react with the hydroxyl groups of carboxylic acid, whereas Hoare and Koshland stressed the reaction of carbodiimide with a proton.

In the present report we investigate the effects of various factors influencing the reaction with carbodiimide in an aqueous system, such as the effect of pH and the dissociation of carboxyl and amino groups, to get deeper insight into the role of carbodiimide in amide formation. For this reason we selected hydrogel having carboxyl groups as substrates to make the separation of the

Table 1. Characteristics of Hydrogels Having Carboxyl Groups

	gel size[a] (mm)	amt of carboxyl[b] groups (nmol/piece)	water content[c] (w/w %)
Gel-A[d]	12.0 × 2.2	1,347 ± 50	95.8 ± 0.1
Gel-B[e]	9.8 × 1.7	138 ± 2	92.6 ± 0.1

[a] Diameter × thickness of swollen gel. [b] Evaluated by staining with toluidine blue and expressed as average ± S.E. ($n = 6$). [c] Expressed as average ± S.E. ($n = 3$). [d] Carboxyl groups were introduced into polyacrylamide gel by alkaline hydrolysis to 0.96 mol %. [e] Prepared by copolymerization of maleic acid and acrylamide.

products from the reaction batch easy. In addition, the difference in the location of carboxyl groups (cyclizable and noncyclizable) on amide formation was also investigated using hydrogels, water-soluble polymers, and low-molecular-weight molecules having carboxyl groups.

MATERIALS AND METHODS

1. Materials. 1-Ethyl-3-(3-(dimethylamino)propyl)-carbodiimide (EDC, MW = 191.7), a water-soluble carbodiimide (WSC), was purchased from Dohjin Kagaku Co. Ltd., Kumamoto, Japan. It was a hydrochloride salt. Toluidine blue O (MW = 305.84) and acid orange 7 (MW = 350.33) were purchased from Chroma Gessellschaft Schmidt & Co., Germany and Tokyo Kasei Kogyo Co. Ltd., Tokyo, Japan, respectively. Poly(ethylene glycol)-dioglycolic acid (PEG−COOH, $\bar{M}_w$ = 3000, free acid), poly(acrylic acid) (PAAc, $\bar{M}_w$ = 4 × 10^6, sodium salt), maleic acid (free acid), fumaric acid (free acid), ethylenediamine, ethanolamine, and deuterium oxide (D$_2$O) were obtained from Wako Pure Chem. Ind. Ltd., Osaka, Japan. Benzylamine and sodium 2,4,6-trinitrobenzenesulfonate (TNBS) were purchased from Tokyo Kasei Kogyo Co. Ltd., Tokyo, Japan. They were used without further purification. All the starting amine compounds were in free base form.

To study the effect of the location of carboxyl groups on amide formation, hydrogels were prepared by two different methods.

(A) Noncyclizable: 100 mL of aqueous solution containing 20 g of acrylamide, 100 mg of *N,N'*-methylenebis-(acrylamide), and 200 mg of ammonium peroxodisulfate as the polymerization initiator was kept at 0 °C, and then 0.05 mL of the solution was poured into a dish of 6.4 mm diameter (Corning) after an addition of 0.2 mL of *N,N,N',N'*-tetramethylethylenediamine as a coinitiator to the solution. The solution was kept at 25 °C for 60 min to set to a gel, which was taken out and hydrolyzed with 300 mL of 0.01 M NaOH at 50 °C for 30 min.

(B) Cyclizable: 1.0 g of maleic acid was added to 100 mL of acrylamide aqueous solution containing the same reagents as in A, and the pH was adjusted to 7.0. Polymerization was allowed to proceed in the same manner as the A, but without hydrolysis.

The concentration of carboxyl groups in the gels was estimated by staining with 5 × 10^{-4} M toluidine blue at 25 °C and pH 10.0 for 3 h for both the gels. After being rinsed three times with water at pH 10.0, the bound toluidine blue was extracted with 50 v/v % acetic acid. The absorbance of the dye was measured at 633 nm to determine the concentration of carboxyl groups under the assumption that the number of bound dye molecules is equal to the number of carboxyl groups in gels according to the method reported elsewhere (Uchida et al., 1993).

The hydrogels prepared by methods A and B were designated as Gel-A and Gel-B, respectively. The characteristics of these gels are summarized in Table 1.

2. Determination of EDC. The colorimetric assay reported by Jacobson and Fairman (Jacobson & Fairman, 1980) was modified to determine the carbodiimide concentration. Briefly, aqueous solution of EDC was mixed with pyridine buffer solution (2.0 M pyridine and 1.0 M ethylene diamine, pH 7.0) and the increase in the absorbance at 400 nm was measured as a function of time at 25 °C. The absorbance increased linearly with time, and the slope was determined as a function of EDC concentration. Apparently, the rate of absorbance enhancement increased quite linearly with the EDC concentration at least lower than 3.5 mg/mL (correlation coefficient = 0.9995).

3. Reaction of Carboxylic Acids with EDC. To investigate the reaction of carboxyl groups with EDC, Gel-A, PEG−COOH, and PAAc were chosen. The IR spectra of PEG−COOH and PAAc were recorded to assess the chemical structure.

Reaction of Gel-A. Three pieces of water-swollen Gel-A were put into 20 mL of 10 mg/mL of EDC aqueous solution of different pHs and kept at 25 °C for 2 h. The concentration of carboxyl groups remaining after completion of the reaction was determined by a staining method with toluidine blue.

The stability of carboxyl groups in Gel-A treated with EDC was investigated as follows. After pretreatment of the gel with 100 mL of 10 mg/mL of EDC solution (in excess) at pH 4.5 and 25 °C for 2 h, the treated gels were subjected to the reaction with 30 mL of 5.0 v/v % acetic acid at different pHs and 25 °C for 16 h. The *tert*-amino groups in gels originating from EDC residues were determined by staining with acid orange 7 as reported elsewhere (Uchida et al., 1993). Briefly, the specimen was stained with 5 × 10^{-4} M acid orange 7 at pH 3.0 and 25 °C for 3 h, and the bound acid orange was extracted with 30 v/v % ethanolamine after being rinsed three times with water at pH 3.0, and then the absorbance of the dye at 468 nm was measured to determine the concentration of the *tert*-amino groups.

Reaction of PEG−COOH. Two g of EDC (in excess) was added to 50 mL of 1.0 g/mL of PEG−COOH aqueous solution of pH 4.5 and the mixture kept at 25 °C for 60 min. The products were recovered by dialysis of the solution against water for 48 h at 25 °C, followed by freeze-drying.

Reaction of PAAc. A 0.5 g portion of EDC was added to 50 mL of 1.0 g/mL of aqueous PAAc solution of pH 4.5 and reacted at 25 °C for 5 min ([EDC] = [−COOH]/2). The products were recovered from the solution by reprecipitation with 500 mL of dried acetone and vacuum-drying at 25 °C.

The IR spectra of PEG−COOH and PAAc treated with EDC were recorded by FTIR-8100, Shimadzu Inc., Kyoto, Japan.

4. Amide Formation. *Reaction of Hydrogels.* Amide formation between a carboxyl and an amino group in the presence of EDC was investigated using Gel-A and Gel-B with two different methods. The one included two steps. Thirty pieces of gel were put into 100 mL of 0.1 M acetic acid at pH 4.5. Following an addition of 3.0 mL of 0.33 g/mL of EDC aqueous solution to the acetic acid solution ([EDC] = [−COOH]/2), the reaction was allowed to proceed for a given period of time at 0 °C. Then, these gels were taken out from the solution and immediately placed in 30 mL of aqueous amine solution (0.1 M ethylenediamine or benzylamine in 0.1 M NaH$_2$PO$_4$) at various pHs and further reacted for 30 min at 25 °C. Three pieces of gels were used for the reaction batch of each pH.

The other method was one step. Gel was put into 30 mL of a mixture of 0.1 M ethylenediamine, 0.1 M NaH$_2$-PO$_4$, and 0.01 M acetic acid at different pHs. After an addition of 0.72 mL of 40 mg/mL of aqueous EDC solution, the solution was kept at 25 °C for 30 min ([EDC] = [−COOH]/2). Three pieces of gels were used for the reaction batch of each pH.

The extent of amide formation was determined by measuring the decrease in carboxyl group in the gels with the staining method using toluidine blue. For each of the reactions with gels, the initial concentration of EDC was kept to one half of the molar concentration of total carboxyl groups involving acetic acid used to maintain the pH of solution constant.

Reaction with Small Carboxylic Molecules. Amide formation from maleic and fumaric acids was investigated as follows. A 0.5 g portion of maleic or fumaric acid and 1.0 g of ethylenediamine were dissolved in 50 mL of water. After an addition of 0.826 g of EDC ([maleic acid] = [fumaric acid] = [EDC]), the pH was adjusted to 5.0 and the reaction was allowed to proceed at 25 °C for 1 h. The reaction was stopped by an addition of 1.0 mL of 1 N HCl. A similar reaction was performed using the deactivated EDC (0.826 g of EDC was dissolved in 3.0 mL of 1 N HCl and hydrolyzed for 3 h at 25 °C). The products were recovered by freeze-drying, and ^{13}C-NMR spectra were recorded in D$_2$O (JEOL Co. Ltd., GSX-270, Tokyo, Japan).

The degree of amide formation was estimated by amine determination. Briefly, 0.25 g of maleic or fumaric acid and 0.132 g of ethanolamine were dissolved in 40 mL of water, and the pH was adjusted to 7.0. After an addition of 5.161 mL of 80 mg/mL of aqueous EDC solution, the pH was adjusted to 7.0 again and the solution was diluted exactly to 50 mL. The reaction was carried out at 25 °C under the condition of [maleic acid] = [fumaric acid] = [EDC] = [ethanolamine]. One mL of the solution was taken out at a given time, followed by hydrolysis of EDC remaining by an addition of 1.0 mL of 1 N HCl. After neutralization with 1.0 mL of 1 N NaOH, the amount of amine residue was determined with the conventional TNBS method (Habeeb, 1966). Following 100 times dilution of the solution with water, 0.5 mL of solution, 10 mL of 1.0 mg/mL of aqueous TNBS solution, and 2.0 mL of 40 mg/mL of aqueous sodium bicarbonate (pH 9.0) were mixed and incubated at 37 °C for 2 h. After the mixture was cooled to 25 °C, the absorbance before and after amide formation was measured at 335 nm. In this assay, ethanolamine was used instead of ethylenediamine because TNBS formed a water-insoluble deposit with ethylenediamine.

RESULTS

1. Stability of Carbodiimide in Aqueous Media. The stability of EDC at different pHs and 25 °C is given in Figure 1 in terms of the carbodiimide activity remaining after incubation. Apparently, EDC is quite stable at the neutral and higher pH regions, at least, for 5 h at 25 °C. This is in good agreement with the result of protein crosslinking by EDC (data not shown). On the other hand, the activity of EDC decreased at low pHs. The product formed at lower pH regions was confirmed by IR as urea derived from the EDC (data not shown).

2. Reaction of EDC with Carboxyl Groups. The pH dependence on the disappearance of carboxyl groups in Gel-A upon the reaction with EDC is given in Figure 2. The molar concentration of EDC was 260 times larger than that of carboxyl groups in order to modulate the pH of solution. The reaction markedly depended on pH, the optimal pH ranging between 3.5 and 4.5. The
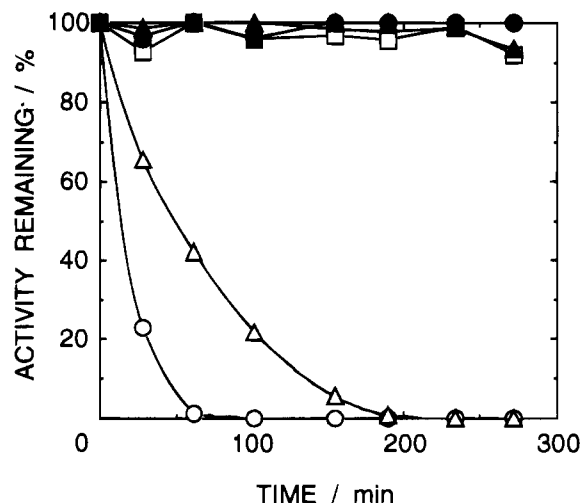
Figure 1. pH dependence of EDC stability at 25 °C. A 0.1 mL portion of 10 mg/mL of aqueous EDC solution kept at different pHs was taken out from the aliquot at given time intervals and added to 3.0 mL of pyridine buffer solution. The relative activity was evaluated from the absorbance measurement. pH: (O) = 2.52, (△) = 3.95, (□) = 6.54, (●) = 8.75, and (▲) = 9.84.
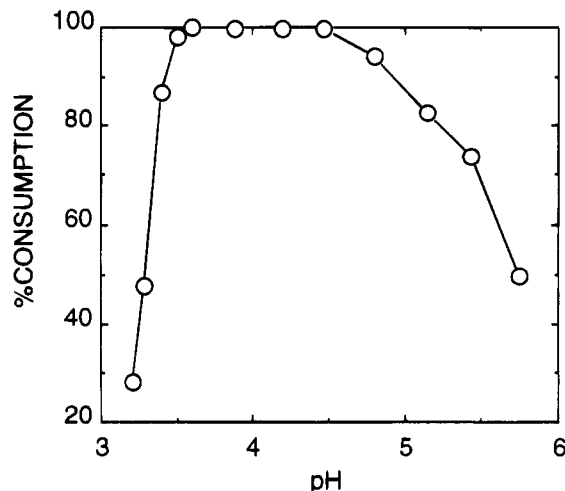
Figure 2. pH dependence of the consumption of carboxyl groups in Gel-A in the presence of EDC. Three pieces of swollen gels were placed in 20 mL of 10 mg/mL of EDC aqueous solution of different pHs without acetic acid at 25 °C for 2 h. Data are the average of three readings.

suppression of reaction at pHs lower than 3.5 should be ascribed to the decreased dissociation of carboxyl groups in Gel-A at low pHs. This suggests that proton and ionized carboxyl groups are required for the reaction with EDC. This reaction occurred only when an excess EDC was used, and no change in carboxyl groups was observed when the molar ratio of EDC to carboxyl groups was lower than 0.5.

The pH dependence of the stability of product yielded from the carboxyl groups in Gel-A and EDC is given in Figure 3. As can be seen, the reaction product was quite stable at pHs lower than 8, indicating that this product was too stable to form amide with amine.

IR spectra of PEG−COOH treated with EDC are given in Figure 4. The peak absorbance of the untreated PEG−COOH appearing at 1620 cm^{-1} is assigned to the C=O stretching vibration of −COO^{-}. Clearly, this peak became strikingly lower upon reaction with EDC and new peaks appeared at 1650 cm^{-1} and 1530 cm^{-1} assigned to C=O stretching vibration and −NH− bending vibration of amide, respectively. These results suggest that a
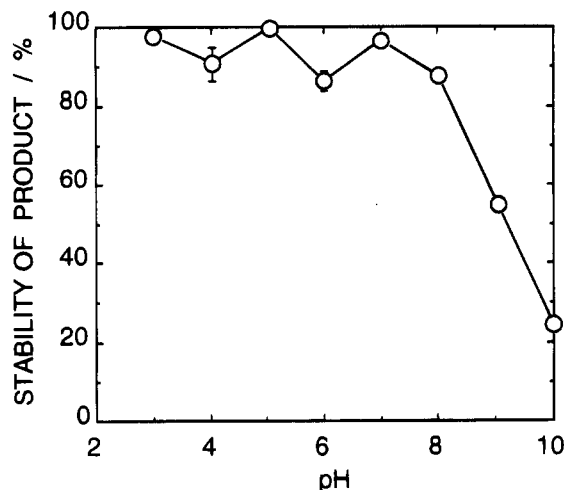
Figure 3. pH dependence of stability of the product formed between carboxyl groups in Gel-A and EDC. Thirty pieces of Gel-A were placed in 100 mL of 10 mg/mL of EDC aqueous solution of pH 4.5 at 25 °C for 2 h. Then, three pieces were taken out and treated with 30 mL of 5 v/v % acetic acid aqueous solution of various pHs at 25 °C for 16 h. Data are the average of three readings.
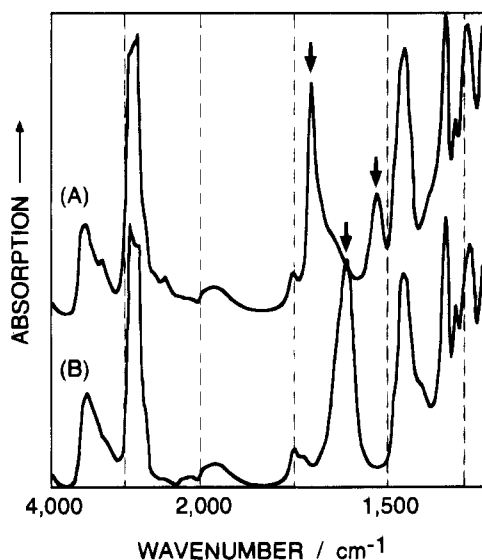
Figure 4. IR spectra of PEG—COOH treated with EDC (A) and untreated PEG—COOH (B). Both the samples were cast from the chloroform solution on a KBr plate.

stable amide such as *N*-acylurea is formed as a result of the reaction of carboxyl groups in PEG—COOH with carbodiimide. In this reaction the molar concentration of EDC was about 30 times larger than that of carboxyl groups in PEG—COOH. This stable amide was observed only when such an excess of carbodiimide was used.

IR spectra of the reaction products of PAAc with EDC are given in Figure 5. New peaks appeared at 1750, 1800, and 1050 cm^{-1} when PAAc reacted with EDC. They may be assigned to C=O and C—O—C stretching vibrations. The spectrum changed to that of the virgin PAAc when PAAc was again dissolved in water after reaction with carbodiimide (B). It is likely that the reaction of carboxyl groups in PAAc with EDC yielded carboxylic anhydride, which was highly hydrolyzable by water. In this reaction the molar concentration of EDC was about two times less than that of carboxyl groups in PAAc.

4. Amide Formation. *Reaction of Hydrogels.* Amide formation between carboxyl groups in gels and ethylene-
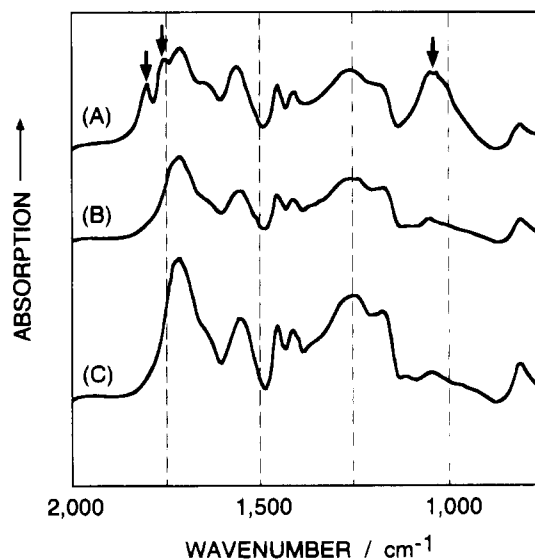
Figure 5. IR spectra of PAAc treated with EDC (A), PAAc dissolved in water after EDC treatment, followed by drying (B), and untreated PAAc (C). All the spectra were obtained by mixing the granules with KBr.

Table 2. Amide Formation between Carboxyl Groups in Gel and Ethylenediamine by Two Different Methods

| | % amide formation[a] | |
method	one step[b]	two step[c]
Gel-A	7.2 ± 1.8	0.6 ± 1.7
Gel-B	66.2 ± 0.6	46.5 ± 0.5

[a] Evaluated by staining with toluidine blue and expressed as average ± S.E. ($n = 6 \times 6$). [b] Gels were put in 100 mL of a mixture of pH 4.5 containing 0.1 M 1,2-ethylenediamine, 0.1 M acetic acid, 0.1 M NaH$_2$PO$_4$, and 1.0 g of EDC and kept at 25 °C for 30 min. [c] Gels were pretreated with EDC at pH 4.5 and 0 °C for 30 min, put in a mixture of pH 7.0 containing 0.1 M ethylenediamine and 0.1 M NaH$_2$PO$_4$, and kept at 25 °C for 30 min.

diamine was investigated using "one-step" and "two-step" methods. The results are given in Table 2. Clearly, carboxyl groups in Gel-B were more effective in formation of amide than those in Gel-A for both the methods. In addition, the extent of amide formation with the one-step method was higher than that with the two-step method, regardless of the gel type. However, it should be noted that the extent of amide formation with the one-step method was much larger than 50% in the case of Gel-B, although the molar ratio of EDC to the carboxyl group was 0.5. Therefore, the staining method by toluidine blue could only semiquantitatively evaluate the degree of amide formation.

The pH dependence of the amide formation was investigated using Gel-B with the two different methods. The results are given in Figures 6 and 7 for the two-step and the one-step method, respectively. As can be seen in Figure 6, amide formation was promoted with the increasing pH for the "two step" method, when benzylamine was employed as amine. On the other hand, such a prominent pH effect was not observed in the case of ethylene diamine, although the reaction extent was much higher than that with benzylamine throughout the pH range studied.

In the case of the one-step method the optimal pH for amide formation was observed around 5 as shown in Figure 7. This is different from the result of the "two step" method. As mentioned above, carbodiimide can react with carboxyl groups in gel only at a low pH region from 3.5 to 4.5. As amine molecules are required for amide formation to be in an unionized state, it is likely
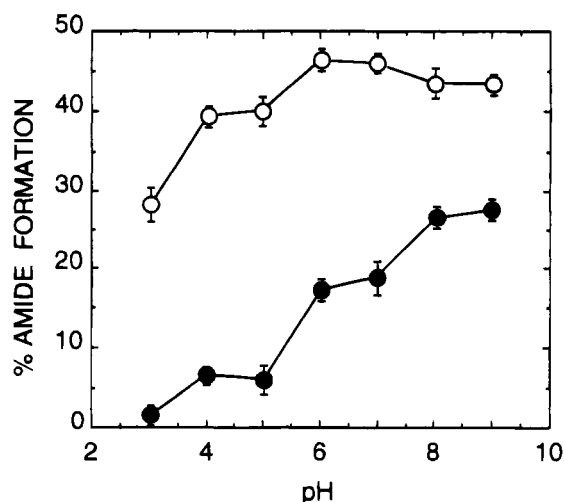
Figure 6. Amide formation from Gel-B and two different amines with the two-step method. Thirty pieces of Gel-B were placed in 100 mL of a mixture of 0.1 M acetic acid and 1.0 g of EDC at pH 4.5 and 0 °C for 30 min. Then, the gels were put in 0.1 M ethylenediamine or 0.1 M benzylamine in 0.1 M NaH_2-PO_4 at various pHs and 25 °C and allowed to react for 30 min. Data are the average of three readings: (O) ethylenediamine, (●) benzylamine.

Figure 8. Pretreatment time dependence of the amide formation from Gel-B and ethylenediamine with the two-step method. Thirty pieces of Gel-B were placed in 100 mL of a mixture of 0.1 M acetic acid and 1.0 g of EDC at 0 °C and pH 4.5 for different periods of time. Then, three pieces were taken out and immediately put in 0.1 M ethylenediamine in 0.1 M NaH_2-PO_4, followed by reaction at pH 7.0 and 25 °C for 30 min. Data are the average of three readings.

Figure 7. Amide formation from Gel-B and ethylenediamine with the one-step method. Three pieces of Gel-B were placed in 30 mL of mixture of 0.1 M ethylenediamine, 0.1 M NaH_2-PO_4, and 0.01 M acetic acid at various pHs and allowed to react at 25 °C for 30 min after an addition of 0.72 mL of 40 mg/mL of EDC aqueous solution. Data are the average of three readings.

that the two opposite requirements for amide formation may lead to the optimal reaction pH around 5.

Figure 8 shows the effect of pretreatment time on the amide formation from the carboxyl groups in Gel-B with EDC when the two-step method is employed. It is clearly seen that the reaction is strikingly rapid and decreases with time after 5 min. This suggests that the intermediate product in the gel is very unstable in aqueous media, similar to the reaction product of PAAc with EDC. Therefore, it has rapidly lost its activity by reacting with water.

Reaction of Small Carboxylic Molecules. ^{13}C-NMR spectra of maleic and fumaric acids treated with ethylene diamine in the presence of EDC are given in Figure 9. Four peaks assigned to olefinic carbons of these acids were observed around 130 ppm. The peaks for the carbon of nonreacted maleic and fumaric acid were observed at 133.5 and 135.3 ppm (arrow marks), respectively, which could be assigned by the reaction with deactivated EDC.

δ / ppm

Figure 9. ^{13}C-NMR of maleic acid (A) and fumaric acid (B) treated with ethylenediamine in the presence of EDC at 25 °C for 1 h. A 0.5 portion g of maleic or fumaric acid and 1.0 g of ethylenediamine were dissolved in 50 mL of distilled water. After an addition of 0.826 g of EDC, the pH was adjusted to 5.0 and the reaction was allowed to proceed at 25 °C for 1 h. The reaction was stopped by an addition of 1.0 mL of 1 N HCl. Products were recovered by freeze-drying and dissolved in D_2O for ^{13}C-NMR measurement.

In the case of fumaric acid, the product with the highest content was the nonreacted acid. On the other hand, the content of the nonreacted acid was relatively low in maleic acid. It is likely that maleic acid yielded a larger amount of amide than fumaric acid, though three other peaks could not be assigned. The peaks of carbonyl carbons at around 170 ppm also could not be assigned (data not shown).

Figure 10 shows the extent of amide formation between maleic or fumaric acid and ethanolamine as a function of reaction time. Maleic acid could react rapidly with
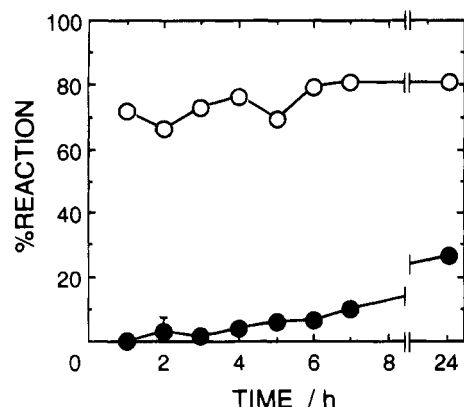
Figure 10. Amide formation between maleic or fumaric acid and ethanolamine in the presence of EDC. A 0.25 g portion of maleic or fumaric acid and 0.132 g of ethanolamine were dissolved in 40 mL of water and pH was adjusted to 7.0. After an addition of 5.161 mL of 80 mg/mL of EDC aqueous solution, the pH was adjusted to 7.0 again and the solution was exactly diluted to 50 mL. The reaction was allowed to proceed at 25 °C. The extent of amide formation was determined by the TNBS assay: (O) maleic acid, (●) fumaric acid.

ethanolamine and about 80% of amide formation was observed within 1 h, whereas the reaction of fumaric acid was very low and the yield was as low as about 30% even after 24 h. Such a considerable difference in amide formation between maleic and fumaric acids might be ascribed to the conformation of carboxyl groups in the molecules.

DISCUSSION

As shown in Figure 1, carbodiimide was hydrolyzed at low pHs such as 2.52 and 3.95, suggesting that proton is required for hydrolysis in aqueous media, though Knore et al. reported that hydrolysis of carbodiimide was catalyzed also by hydroxide ions as cited in the reference (Williams & Ibrahim, 1981). It is likely that the reaction rate constant of hydrolysis in the acidic media is much higher than in the basic media. The reaction of carbodiimide with carboxyl groups proceeds most rapidly in the pH range from 3.5 to 4.5, as shown in Figure 2. This indicates that both of protons and dissociated carboxyl groups are necessary for the reaction of carbodiimide.

As protein (Swaisgood & Natake, 1973) and polysaccharides (Danishefsky and Siskovic, 1971) possess a variety of functional groups such as $-NH_2$, $-OH$, $-SH$, and $-COOH$, which will make the passway of reaction with carbodiimide very complicated, we used hydrogels having carboxyl groups alone. One can separate the reaction products any time just by removing the gels from the reaction batch. The reaction product of the excess carbodiimide with carboxyl groups in gel and PEG–COOH may be N-acylurea, which is markedly stable in aqueous media, as shown in Figure 3, and cannot produce amide even when amine is added to this compound. Swaisgood and Natake also reported that N-acylurea was formed only when an excess of carbodiimide was used in comparison with carboxyl groups (Swaisgood & Natake, 1973). Indeed, no change in carboxyl concentration was observed for PEG–COOH, PAAc, Gel-A, and Gel-B in the absence of amine when the concentration of carbodiimide was two times lower than that of carboxyl groups.

The extent of amide formation in Gel-B was much larger than that in Gel-A as shown in Table 2. The different reaction extent may be explained in terms of location of carboxyl groups along the polymer chains in the gel. As the carboxyl groups in Gel-B were originated

from maleic acid introduced into the gel by its copolymerization with acrylamide, it probably is easy for Gel-B to form carboxylic anhydrides. On the other hand, the carboxyl groups in Gel-A were introduced by random hydrolysis with NaOH, resulting in random location of the carboxyl groups along the polymer chains because the extent of hydrolysis was as low as 0.96 mol % as shown in Table 1. Thus, it is unlikely to form carboxylic anhydrides between two neighboring carboxyl groups in Gel-A, where the carboxyl groups are present more separately from each other than in Gel-B. This result well agrees with that of the reaction of noncyclizable PEG–COOH and cyclizable PAAc.

No anhydride was formed between carboxyl groups in Gel-A and acetic acid used as a buffer molecule. This is probably because no amide formation was virtually observed for this gel when the two-step method was employed, as shown in Table 2, and generally carboxylic anhydride forms amide by an addition of amine. It follows that formation of carboxylic anhydride is essential as an intermediate for production of the corresponding amide by an addition of amine for the two-step method.

On the contrary, the one-step method yielded a small extent of amide even if Gel-A was used. It is probable that a very small fraction of carboxyl groups in Gel-A could participate in direct amide formation with amine without passing through anhydride formation because anhydride was too difficult to form in Gel-A. This may be a reason for the larger extent of amide formation for the one-step method than for the two-step method, where the intermediate carboxylic derivative is required to remain in an active state until the counterpart amine comes. This result agrees with that of the reaction of small molecules (maleic and fumaric acids) with amine in the presence of EDC. Cyclizable acid (maleic acid) formed a much larger amount of amide than noncyclizable acids (fumaric acid) as shown in Figure 10.

The above findings allow us to propose the following reaction mechanism for the amide formation in aqueous media with the use of carbodiimide in terms of carboxyl group location, although exact structural information could not be obtained because of difficulty in isolation of products. As illustrated in Figure 11, a carbodiimide molecule reacts with a proton to form a carbocation 1. This reaction mechanism well agrees with that proposed by Hoare and Koshland (Hoare & Koshland, 1967) which is based on the reaction in an organic system reported by Khorana (Khorana, 1953) though inconsistent with that by others (Solomons, 1988; Wong, 1991).

However, the reaction mechanism of carbodiimide with carboxylic acid is more complicated in aqueous media than in organic systems. Unless carboxylic acid is present, 1 will be hydrolyzed by water into the corresponding urea derivative 2. 1 can react with an ionized carboxyl group to form a compound 3 (O-acylisourea). As a result of reprotonation at the site of Schiff base, 3 will change into a carbocation 4, followed by the attack of various bases present in the aqueous system. If any nucleophile is absent, 4 will transfer into the corresponding urea derivative 2 by the reaction with water. Since an ionized carboxyl group is a very strong base, its reaction with 4 may produce carboxylic anhydride 8 in the case of cyclizable carboxyl group, which quickly forms the corresponding amide 7 when amine is present. On the other hand, in the case of noncyclizable carboxyl group, 4 will react with a water molecule or an unionized amine to yield carboxylate 6 or amide 7, respectively. The reaction with water must be prevailing, because the water concentration is much higher than that of amine and most of the amine molecules are in the ionized form
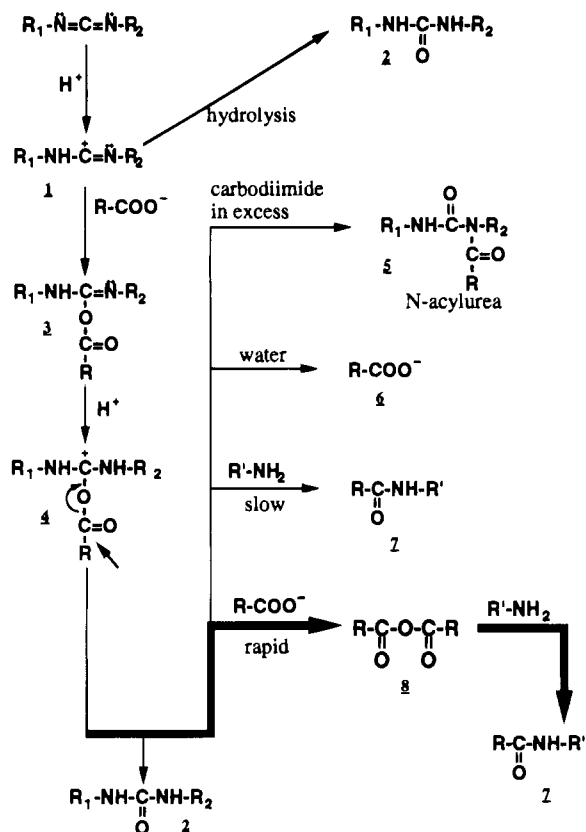
Figure 11. Proposed reaction mechanisms of the amide formation between carboxylic acid and amine in aqueous media in the presence of carbodiimide.

at the low pH region which is required for the reaction of carbodiimide with carboxyl groups. Therefore, quite a few amine molecules can react directly with **4** to form **7** without anhydride formation. In this connection, the reaction scheme of carbodiimide in aqueous systems is quite different from that in organic systems. The pathway (**4** → **8** → **7**) was not mentioned by Hoare and Koshland. In addition, carbodiimide would be able to react with compound **4** to form *N*-acylurea **5** as byproduct, if carbodiimide is present in excess. As amide was formed more readily at higher pHs, and as shown in Figure 6, it is likely that only unionized amine molecules can react with the carboxyl groups pretreated with carbodiimide. The difference in the extent of amide formation between ethylenediamine and benzylamine in Figure 6 might be ascribed to the difference in the dissociation constant. As ethylenediamine has pK_{b_1} of 6.85 and pK_{b_2} of 9.93, while benzylamine has pK_b of 9.60 at 25 °C, it is clear that the ionization of ethylenediamine is markedly suppressed even at low pHs compared with that of benzylamine.

In summary, it may be concluded that amide formation from carboxyl and amino groups in aqueous media in the presence of carbodiimide requires formation of carboxylic anhydride as intermediate. Noncyclizable carboxylic acids cannot form a larger amount of amide than cyclizable carboxylic acids. The anhydride will be formed from carboxyl groups if carbodiimide is present at less than half of the molar concentration of carboxyl groups. The pH of solution strongly affects the reaction of carbodiimide with carboxyl groups. A narrow pH range such as 3.5–4.5 is the most favorable for the formation of carboxyl anhydride, while higher pH is preferred for amide formation to suppress the ionization of amine.

Finally, it should be noted that the two-step method, in which carboxylic anhydride is first prepared from two

carboxyl groups by carbodiimide, followed by reaction with amine, may give a variety of selective reactions such as bioconjugation of enzymes to substrates having carboxyl groups without significant deactivation of enzymes, although the coupling efficiency is lower than that by the one-step method.

LITERATURE CITED

Bragg, P. D., and Hou, C. (1986a) Chemical crosslinking of α subunits in the F₁ adenosine triphosphatase of escherichia coli. *Arch. Biochem. Biophys. 244*, 361–372.

Bragg, P. D., and Hou, C. (1986b) Effect of disulfide cross-linking between α and δ subunits on the properties of the F₁ adenosine triphosphatase of escherichia coli. *Biochim. Biophys. Acta 851*, 385–394.

Chan, V. W. F., Jorgensen, A. M., and Borders, C. L., Jr. (1988) Inactivation of bovine thrombin by water-soluble carbodiimides: The essential carboxyl groups has a pKa of 5.51. *Biochem. Biophys. Res. Commun. 151*, 709–716.

Danishefsky, I., and Siskovic, E. (1971) Conversion of carboxyl groups of mucopolysaccharides into amides of amino acid esters. *Carbohydr. Res. 16*, 199–205.

Dolinnaya, N. G., Tsytovich, A. V., Sergeev, V. N., Gertsuk, M. N., and Shabarova, Z. A. (1990) Reactions in double-stranded nucleic acids. *Bioorg. Khim. 16*, 1183–1194.

Dolinnaya, N. G., Tsytocich, A. V., Sergeev, V. N., Oretskaya, T. S., and Shabarova, Z. A. (1991) Structural and kinetic aspects of chemical reactions in DNA duplex. Information on DNA local structure obtained from chemical ligation data. *Nucleic Acid Res. 19*, 3073–3080.

Gontar, A. F., Glotov, E. N., Vinogradov, A. S., Byknovskaya, E. G., and Knunyants, I. L. (1985) Synthesis of stable perfluoroazidoazomethines and their rearrangement to perfluorodialkylcarbodiimides. *Izu. Akad. Nauk SSSR, Ser. Khim. 3*, 700–703.

Gorbatenko, V. I., Matveev, Y. I., and Gertsyuk, M. N. (1984) Synthesis of α,α-dihalodialkylcarbodiimides and halo-substituted diazadienes isomeric to them. *Zh. Org. Khim. 20*, 2543–2548.

Habeeb, A. F. S. A. (1966) Determination of free amino groups in proteins by trinitrobenzenesulfonic acid. *Anal. Biochem. 14*, 328–336.

Hoare, D. G., and Koshland, D. E., Jr. (1967) A method for the quantitative modification and estimation of carboxylic acid groups in proteins. *J. Biol. Chem. 242*, 2447–2453.

Jacobson, B. S. (1977) Isolation of plasma membrane from eukaryotic cells on polylysine-coated polyacrylamide beads. *Biochim. Biophys. Acta 471*, 331–335.

Jacobson, B. S., and Fairman, K. R. (1980) A colorimetric assay for carbodiimides commonly used in peptide synthesis and carboxyl group modification. *Anal. Biochem. 106*, 114–117.

Kalish, D. H., Cohen, C. M., Jacobson, B. S., and Branton, D. Membrane isolation on polylysine-coated glass beads asymmetry of bound membrane. *Biochim. Biophys. Acta 506*, 97–110.

Kessler, H., and Kutscher, B. (1986) Synthesis of cyclic pentapeptide analogs of thymopeitin. Cyclization with carbodiimide and 4-(dimethylamino)pyridine. *Liebigs Ann. Chem. 5*, 869–892.

Khorana, H. G. (1953) The chemistry of carbodiimides. *Chem. Rev. 53*, 145–167.

Kricheldorf, H. R., Au, M., and Mang, T. (1985) Models of molecular evolution. 2. Stereospecificity of peptide syntheses by means of cyanamides and carbodiimides. *Int. J. Pept. Protein Res. 26*, 149–157.

Kurzer, F., and Douraghi-Zadeh, K. (1967) Advances in the chemistry of carbodiimides. *Chem. Rev. 2*, 107–151.

Matveev, Y. I., Gorbatenko, V. I., Samarai, L. I., Romanenko, E. A., and Turov, A. V. (1988) 1,1-Dihaloalkyl carbodiimides. IV. Synthesis and properties of perchloro-3,5-diaza-2,4-heptadiene. *Z. Org. Khim. 24*, 986–992.

Mauk, M. R., and Mauk, A. G. (1989) Crosslinking of cytochrome c and cytochrome b₅ with a water-soluble carbodiimide. Reaction conditions, product analysis and crinique of technique. *Eur. J. Biochem. 186, 186*, 473–486.

Onishi, H., Maita, T., Matsuda, G., and Fujiware, K. (1989a) Evidence of the association between two myosin heads in rigor acto-smooth muscle heavy meromyosin. *Biochemistry 28*, 1898–1904.

Onishi, H., Maita, T., Matsuda, G., and Fujiware, K. (1989b) Carbodiimide-catalyzed cross-linking sites in the heads of gizzard heavy meromyosin. *Biochemistry 28*, 1905–1912.

Saito, T., Ohmori, H., Furuno, E,. and Motoki, S. (1992) Conjugated heterocumulanes. Synthesis of conjugated carbodiimides and their facile conversion via intramolecular cycloaddition into nitrogen heterocycles, quinoline and pyrido-[2,3-*b*]-indole (α-carboline) derivatives. *J. Chem. Soc., Chem. Commun. 1*, 22–24.

Schmidt, R. R., and Betz, H. (1989) Cross-linking of *β*-bungaro-toxin to chick brain membranes. Identification of subunits of a putative voltage-gated K⁺ channel. *Biochemistry 28*, 8346–8350.

Sheehan, J. C., and Hlavka, J. J. (1956) The use of water-soluble and basic carbodiimides in peptide synthesis. *J. Org. Chem. 21*, 439–441.

Solomons, T. W. G. (1988) In *Organic Chemistry*, pp 846–847, John Wiley and Sons, Inc., New York.

Swaisgood, H., and Natake, M. (1973) Effect of carboxyl group modification of some of the enzymatic properties of 1-glutamate dehydrogenase. *J. Biochem. 74*, 77–86.

Takashi, R. (1988) A novel actin label: A fluorescent probe at glutamine 41 and its consequences. *Biochemistry 27*, 938–943.

Trifonov, L., and Orahovats, A. (1989) A nonconcerted intra-molecular diels–Alder reaction of chiral acid derivatives. *Helv. Chim. Acta 72*, 59–64.

Uchida, E., Uyama, Y., and Ikada, Y. (1993) Sorption of low-molecular-weight anions into thin polycation layers grafted onto a film. *Langmuir 9*, 1121–1124.

Wang, D., Li. L., and Zhang, P. (1987) Synthesis of some neutral, water-soluble carbodiimides and their use in the formation of peptide bonds. *Sci. Sin., Ser. B 30*, 449–459.

Wilcheck, M., Frensdorff, A., and Sela, M. (1967) Modification of ribonuclease by attachment of glycine or glanylglycine. *Biochemistry 6*, 247–252.

Williams, A., and Ibrahim, I. T. (1981) Carbodiimide chemis-try: Recent advances. *Chem. Rev. 81*, 589–636.

Wong, S. S. (1991) In *Chemistry of Protein Conjugation and Cross-Linking*, pp 195–199, CRC Press, Inc., FL.

Yamada, H., Imoto, T., Fujita, K., Okazaki, K., and Motomura, M. (1981) Selective modification of aspartic acid-101 in lysozyme by carbodiimide reaction. *Biochemistry 20*, 4836–4842.

Galactose-Containing Amphiphiles Prepared with a Lipophilic Radical Initiator[†]

Hiromi Kitano,* Katsuko Sohda, and Ayako Kosaka

Department of Chemical and Biochemical Engineering, Toyama University, Toyama 930, Japan. Received June 27, 1994[⊗]

Novel amphiphiles which contain galactose residues (degree of polymerization (DP) = 6.2, 10, and 15) were prepared by telomerization of 2-[(methacryloyloxy)ethyl]-β-D-galactopyranoside using a lipophilic radical initiator. The galactose-carrying amphiphile incorporated in a liposome was recognized by a lectin from *Ricinus communis* (RCA_{120}), which was proven by the increase in turbidity of the liposome suspension after mixing with the lectin. The recognition was largely affected by the degree of polymerization and the surface density of the amphiphile. The amphiphile would be useful as a component of the drug delivery system to hepatocytes.

INTRODUCTION

Hybrid materials, which are conjugates of a plural number of functional moieties, are very useful as intelligent materials in many research and application fields (*1*). Devices used in drug delivery systems, for example, have very often been included in a category of hybrid materials because various components (designed for targeting, encapsulation, slow release, reduction of immunogenicity, and pharmacological activity, etc.) have to be combined to prepare the systems which are practically useful (*2*).

Previously we prepared liposome-forming amphiphiles having pH- or temperature-responsiveness by polymerization of acrylic acid or N-isopropylacrylamide by using a lipophilic radical initiator (*3*) or lipophilic chain transfer reagent (*4*), respectively, or by copolymerization of polymerizable lipid with N-methacryloyl-D,L-homocysteine thiolactone (*5*). These amphiphiles would be strong candidates to be used in drug delivery systems.

Galactose residues are very important to be recognized by lectin-like proteins located on the surface of parenchymal hepatocytes (*6*). In this paper, therefore, we prepared amphiphilic compounds with several (6.2, 10, and 15) galactose residues in their hydrophilic head groups by telomerization of a galactose-containing vinyl monomer using the lipophilic radical initiator. We examined a recognition of the amphiphilic compounds by a lectin in a bilayer system. For comparison, a lipid carrying only one galactose residue was also prepared by the lactone method (*7*). The galactose-carrying lipophilic compounds examined here would be highly useful as devices for targeting to hepatocytes.

EXPERIMENTAL PROCEDURES

Materials. 2-[(Methacryloyloxy)ethyl]-β-D-galactopyranoside (MEGal,[1] Chart 1A) was prepared by the transglycosylation between *p*-nitrophenyl β-D-galactopyranoside and 2-hydroxyethyl methacrylate (HEMA) catalyzed by β-galactosidase (from *E. coli*, 340 u/mg, Sigma, St. Louis, MO) in a phosphate buffer (1/15 M, pH 6.4) (*8*) in the presence of hydroquinone. A lipophilic radical initiator (DODA-501, Chart 1B) was prepared from N,N-

Chart 1. Chemical Structures of Monomer, Initiator, and Amphiphiles
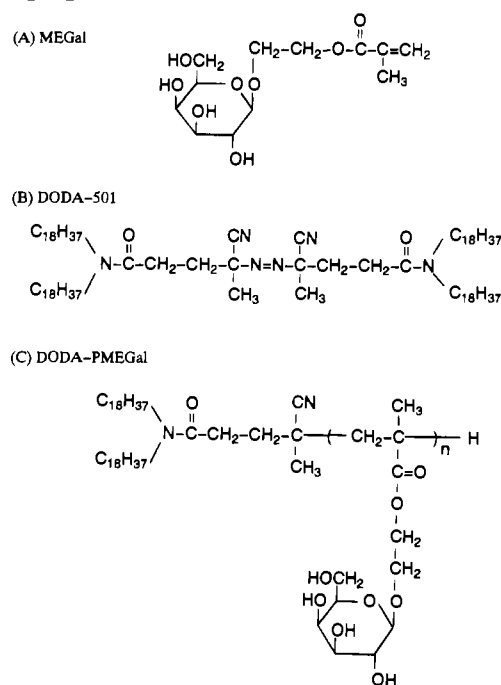
dioctadecylamine (DODA, Fluka, Switzerland) and 4,4′-azobis(cyanovaleric acid) (V-501, Wako Pure Chemicals, Osaka, Japan) as previously reported (*3*). N-Diglycyl-N,N-dioctadecylamide (GGA) was prepared by the reaction of N-benzyloxycarbonyl (Z)-diglycine *p*-nitrophenyl ester with dioctadecylamine in THF and subsequent deprotection of the Z group by the HBr—CH_3COOH method (*5*). A lectin, *Ricinus communis* agglutinin

---

[†] Presented at the Regional Meeting of the Society of Polymer Science, Japan, Toyama University, October 1994.

[⊗] Abstract published in *Advance ACS Abstracts*, January 1, 1995.

* To whom correspondence should be addressed.

---

[1] Abbreviations: DLS, dynamic light scattering; DMF, dimethylformamide; DMPC, L-α-dimyristoylphosphatidylcholine; DODA, dioctadecylamine; DODA—L-Gal, dioctadecylamine–galactose conjugate prepared by lactone method; DODA–PMEGal, dioctadecylamine–poly(2-[(methacryloyloxy)ethyl]-β-D-galactopyranoside) conjugate; DODA-501, azo radical initiator with dioctadecyl groups; DP, degree of polymerization; GGA, N-diglycyl-N,N-dioctadecylamide; HEMA, 2-hydroxyethyl methacrylate; MEGal, 2-[(methacryloyloxy)ethyl]-β-D-galactopyranoside; MeOH, methanol; RCA or RCA_{120}, *Ricinus communis* agglutinin; THF, tetrahydrofuran; V-501, 4,4′-azobis(cyanovaleric acid); Z, N-benzyloxycarbonyl.

Chart 2. Chemical Structure of DODA–L-Gal
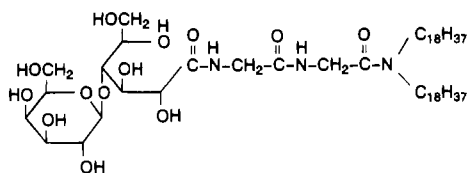
(RCA$_{120}$), and L-α-dimyristoylphosphatidylcholine (DMPC) were from Sigma. Other reagents were commercially available. A Milli-Q grade water was used for preparation of sample solutions.

Preparation of Galactose-Containing Amphiphile by Polymerization. DODA-501 (31 mg) and MEGal (112 mg) were dissolved in THF (20 mL) in a test tube. After N$_2$ gas was passed through the solution for several minutes, the reaction mixture was tightly sealed and incubated for 24 h at 70 °C. After evaporation of the solvent, the sugar-containing amphiphile was purified by washing with *n*-hexane (to remove unreacted initiator) and subsequently with cold water (to remove polymers without lipophilic end group). The amphiphile dispersed in water by a vortex mixer was further purified by passing through a GPC column (2 × 20 cm, Sephacryl S-200, mobile phase; water) and lyophilized (22 mg, DODA-PMEGal, Chart 1C) (IR, OH stretching of galactose 3350–3500 cm^{-1}, C≡N stretching 2050 cm^{-1}, C=O stretching of ester bond 1720 cm^{-1}, C=O stretching of tertiary amide 1630 cm^{-1}, CH$_2$ ν_{as} 2950 cm^{-1}, CH$_2$ ν_s 2870 cm^{-1}). The degree of polymerization (DP) of the amphiphile was determined as 6.2 by elemental analyses. Anal. Calcd for C$_{42}$H$_{82}$N$_2$O(C$_{12}$H$_{20}$O$_8$)$_{6.2}$: C, 57.20; H, 8.50; N, 1.14. Found: C, 57.23; H, 8.68; N, 1.15. By using a similar method, the amphiphiles with DP = 10 and 15 were prepared. DODA–PMEGal (DP = 10). Anal. Calcd for C$_{42}$H$_{82}$N$_2$O(C$_{12}$H$_{20}$O$_8$)$_{10}$: C, 54.75; H, 8.00; N, 0.79. Found: C, 54.53; H, 8.25; N, 0.77. DODA–PMEGal (DP = 15). Anal. Calcd for C$_{42}$H$_{82}$N$_2$O-(C$_{12}$H$_{20}$O$_8$)$_{15}$: C, 53.16; H, 7.68; N, 0.56. Found: C, 53.13; H, 7.74; N, 0.56.

Preparation of Galactose Lipid by the Lactone Method. Lactose monohydrate (12 g) was oxidized by iodine (17.1 g) in the presence of KOH (16 g) (solvent; 665 mL of MeOH and 25 mL of H$_2$O) at 40 °C. The precipitated solid was purified by recrystallization from MeOH–H$_2$O (12:5). The crystal was dissolved in H$_2$O, and the solution was passed through an ion-exchange column (2.5 × 30 cm, Amberlite IR-120 B, H$^+$ form) several times. The aqueous solution of the product was mixed with EtOH, and the solvent was evaporated at 70 °C to form a lactose–lactone (5.45 g, 48% yield) (IR, C=O stretching of lactone ring 1730 cm^{-1}). *N*-Diglycyl-*N,N*-dioctadecylamide (GGA, 0.406 g) was coupled with the lactone (0.651 g) in DMF–CHCl$_3$ (3:1, 40 mL) at 60 °C for 6 h. The galactose-carrying lipid was purified by precipitation in hexane–EtOH (2:1). The precipitate was further dissolved in CHCl$_3$ and passed through a glass filter. The filtrate was finally evaporated to give a slightly yellow powder (DODA–L-Gal (Chart 2), 21 mg, 3.4% yield). IR: OH stretching of sugar 3300–3400 cm^{-1}, C=O stretching of tertiary amide 1680 cm^{-1}, C=O stretching of secondary amide 1640 cm^{-1}, NH deformation of secondary amide 1520–1540 cm^{-1}, CH$_2$ ν_{as} 2920 cm^{-1}, CH$_2$ ν_s 2850 cm^{-1}. Anal. Calcd for C$_{52}$H$_{101}$O$_{13}$N$_3$: C, 63.97; H, 10.43; N, 4.30. Found: C, 63.76; H, 10.38; N, 4.55.

Preparation of Liposome. The galactose-containing lipid and DMPC with various molar ratios were dissolved in CHCl$_3$ (5 mL), and the solvent was evaporated. The

Table 1. Preparation of DODA–PMEGal

amphiphile	DODA-501 (g)	MEGal (g)	solvent (mL)	product (mg) [yield][b]	DP[a]
DODA–PMEGal-1	0.031	0.112	20[c]	22 [19]	6.2
DODA–PMEGal-2	0.153	0.692	20[d]	129 [11]	15
DODA–PMEGal-3	0.167	0.191	30[d]	23 [2.5]	10

[a] Degree of polymerization. [b] In regard to DODA-501 (%). [c] THF. [d] DMF.

thin lipid membrane formed was dispersed into a phosphate buffer (pH 7.2) using a vortex mixer. The dispersion was further sonicated by an ultrasonifier (Astrason W-385, Heat Systems-Ultrasonics, Inc., NY) for 3 min while N$_2$ gas was passed through the suspension. The liposome suspension was finally passed through a syringe filter (Millipore Millex-GV, pore size; 0.22 μm).

Release of Eosin Y Incorporated in Liposomes. To confirm the presence of liposomal structure in the dispersion mixture of DODA–PMEGal and DMPC, Eosin Y was dissolved in the phosphate buffer to disperse the lipids. After separation of liposomes from free Eosin Y by gel permeation chromatography (Sephacryl S-1000, 15 (i.d.) × 200 mm), the liposome suspension was sonicated for 3 min at 60 °C to disrupt the liposomes. The fluorescence intensity of the suspension at 555 nm (excitation, 305 nm) before and after the sonication was compared. Eosin Y is well known to show a significant fluorescence by dilution (*3*, *5*) due to a reduction of self-quenching phenomenon.

Dynamic Light Scattering Method. Hydrodynamic diameter of liposomes composed of various molar ratios of galactose–lipid and DMPC was determined by the dynamic light scattering (DLS) method (DLS-7000, Otsuka Electronics, Hirakata, Japan; light source, He–Ne laser 632.8 nm).

Turbidity Measurements. The lectin-induced agglutination of liposomes was followed by the increase in decadic absorbance at 450 nm by using a UV–vis spectrophotometer (Ubest-35, Japan Spectroscopic Co., Tokyo, Japan). The observation cell was thermostated by a Peltier device. The uncertainties of the rate of turbidity change were within 30%.

RESULTS AND DISCUSSION

A. Galactose-Carrying Amphiphiles. The yields of sugar-containing lipids were in general very low because of the difficulty to purify the amphiphile compounds (Table 1). The increase in fluorescence intensity of the dispersion of DODA–PMEGal and DMPC due to a release of Eosin Y from inner water pool to the bulk solution definitely proved the liposomal structure. Using the DLS method, diameter of the liposomes composed of DODA–PMEGal and DMPC was estimated to be 1400 Å on average.

B. Recognition of Galactose Residues on Liposomes by Lectin. Turbidity of galactose-carrying liposomes at 450 nm was rapidly increased by the addition of lectin, probably due to a recognition of galactose residues on the liposome surface by the lectin and subsequent aggregation of liposomes mediated by the lectin molecules.

By the addition of lactose to the liposome suspension, this aggregation of liposomes was largely inhibited (Figure 1). Furthermore, the addition of lactose or galactose to the suspension of galactose–liposome–RCA aggregates induced the reduction of turbidity: The addition of 0.45 and 18.2 mM of galactose reduced
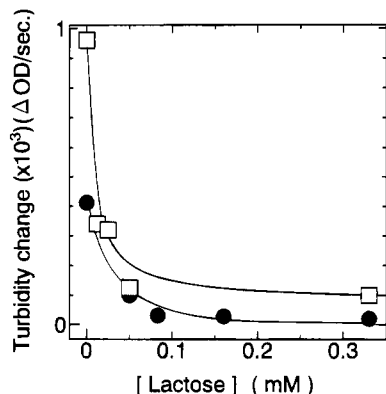
Figure 1. Inhibitory effects of lactose on the rate of turbidity change in the agglutination of galactose-containing liposomes by RCA: (●) DODA–L-Gal; (□) DODA–PMEGal (DP = 15).
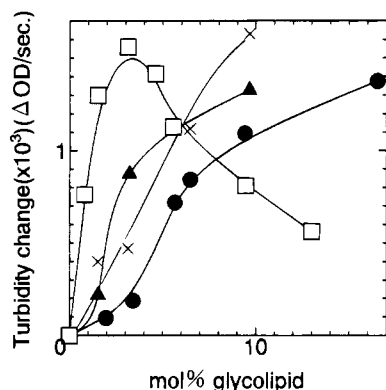
Figure 2. Effect of galactose lipid content in the liposome on the rate of turbidity change after the addition of RCA into the liposome suspension: (●) DODA–L-Gal; (▲) DODA–PMEGal (DP = 6.2); (×) DODA–PMEGal (DP = 10); (□) DODA–PMEGal (DP = 15). [RCA] = [lipid] = 0.05 mg/mL.

Figure 3. Effect of RCA concentration on the rate of turbidity change after the addition of RCA into the liposome suspension: (●) DODA–L-Gal; (▲) DODA–PMEGal (DP = 6.2); (×) DODA–PMEGal (DP = 10); (□) DODA–PMEGal (DP = 15). Galactose lipid, 9.65 mol %. [Lipid] = 0.05 mg/mL.

turbidity of the suspension of aggregated liposomes by 5% and 33% in 1 min, respectively, and that of lactose reduced the turbidity by 29% and 88%, respectively. The reduction effect of lactose was much larger than that of galactose, which was in agreement with the tendency in the aggregation of lactosylceramide-containing liposomes by RCA (*9*). These results strongly support that the turbidity change is due to the specific recognition of galactose residues on the liposomes by RCA.

The turbidity change of galactose−liposomes by the addition of RCA was dependent on the molar ratio of the galactose lipid and DMPC. Figure 2 shows that the increase in percents of galactose lipid induced the very gradual increase in the rate of turbidity change in the cases of DODA−L-Gal and DODA−PMEGal (DP = 6.2), whereas there was a relatively steeper increase in the case of DODA−PMEGal (DP = 15). The presence of threshold value in mol % of lactosylceramide in liposomes at the lectin-induced aggregation was previously reported (*9*). The tendency observed in the DODA−L-Gal liposome and DODA−PMEGal (DP = 6.2) liposome systems (very small increase in the rate of turbidity change at low glycolipid contents) is not inconsistent with that previously reported. In the case of the DODA−PMEGal (DP = 15) liposome system, however, the increase was relatively much steeper because many galactose residues are present in a polar head region of one lipid molecule, which makes it unnecessary for the lectin to bind to a plural number of sugar lipids on each liposome to realize stable aggregation and, consequently, strengthens the

agglutinability of the lectin at a low content of galactose-lipid.

Furthermore, the turbidity change by the addition of lectin was largely affected by the degree of polymerization of DODA−PMEGal incorporated in the liposome (Figure 3). As for liposomes consisting of galactose lipids with a small DP (DODA−L-Gal has only one galactose residue), the recognition of the lipids by RCA is sterically not so easy, which results in a small value of the rate of turbidity change.

With the increase in DP, the steric hindrance becomes smaller and the rate of turbidity change becomes larger (DP = 6.2). In the case of liposomes carrying galactose lipids with a large DP value (DP = 10, 15) the RCA molecule is captured in galactose-carrying long polymer chains on the liposome surface, and it is not so easy for RCA to bind to galactose residues on another liposome surface simultaneously, which reduces the rate of turbidity change. A similar tendency was previously observed in the recognition of glucose residues on the liposome surface by Concanavalin A (*10*). These results show the importance of steric hindrance for the recognition of sugar residues on the liposome surface by lectin molecules.

The galactose-carrying novel amphiphiles, DODA−PMEGal, can be easily prepared, and the degree of polymerization can be easily controlled by the ratio of the initiator (DODA-501) and monomer (MEGal) used for polymerization. Therefore, the compounds prepared here would be highly useful as a tool for drug delivery system to hepatocytes.

ACKNOWLEDGMENT

LITERATURE CITED

(1) Ikada, Y. (1984) Blood Compatible Polymers. *Adv. Polym. Sci. 57*, 103−140.

(2) (a) Ringsdorf, H. (1975) Structure and Properties of Pharmacologically Active Polymers. *J. Polym. Sci., Polym. Symp. 51*, 135−153. (b) Duncan, R., and Kopecek, J. (1984) Soluble Synthetic Polymers as Potential Drug Carriers. *Adv. Polym. Sci. 57*, 51−101.

(3) Kitano, H., Akatsuka, Y., and Ise, N. (1991) pH-Responsive Liposomes Which Contain Amphiphiles Prepared by Using Lipophilic Radical Initiator. *Macromolecules 24*, 42–46.

(4) Kitano, H., Maeda, Y., Takeuchi, S., Ieda, K., and Aizu, Y. (1994) Liposomes Containing Amphiphiles Prepared by Using a Lipophilic Chain Transfer Reagent: Responsiveness to External Stimuli. *Langmuir 10*, 403–406.

(5) Kitano, H., Wolf, H., and Ise, N. (1990) pH-Responsive Release of Fluorophore from Homocysteine-Carrying Polymerized Liposomes. *Macromolecules 23*, 1958–1961.

(6) Plank, C., Zatloukal, K., Cotten, M., Mechtler, K., and Wagner, E. (1992) Gene Transfer into Hepatocytes Using Asialoglycoprotein Receptor Mediated Endocytosis of DNA Complexed with an Artificial Tetra-Antennary Galactose Ligand. *Bioconjugate Chem. 3*, 533–539.

(7) Kobayashi, K., Sumitomo, H., and Ina, Y. (1985) Synthesis and Functions of Polystyrene Derivatives Having Pendent Oligosaccharides. *Polym. J. 17*, 567–575.

(8) Matsumura, S., Kubokawa, H., and Toshima, K. (1993) Enzymatic Synthesis of Novel Vinyl Monomers Bearing β-D-Galactopyranoside Residue. *Makromol. Chem., Rapid Commun. 14*, 55–58.

(9) Curatolo, W., Yau, A. O., Small, D. M., and Sears, B. (1978) Lectin-Induced Agglutination of Phospholipid/Glycolipid Vesicles. *Biochemistry 17*, 5740–5744.

(10) Kitano, H., and Ohno, K. (1994) Sugar-Containing Lipids Prepared by Using a Lipophilic Radical Initiator: Interfacial Recognition by Lectin as Studied by Using the Multiple Internal Reflection Fluorescence Method. *Langmuir 10*, 4131-4135.

TECHNICAL NOTES

Preparation of Oligonucleotide–Biotin Conjugates with Cleavable Linkers

Garrett A. Soukup,[†] Ronald L. Cerny,[‡] and L. James Maher, III[*,†]

The Eppley Institute for Research in Cancer and Allied Diseases and Department of Biochemistry and Molecular Biology, University of Nebraska Medical Center, 600 South 42nd Street, Omaha, Nebraska 68198-6805, and Department of Chemistry, University of Nebraska at Lincoln, Lincoln, Nebraska 68588-0362. Received September 26, 1994[⊗]

A procedure is presented for preparing an oligonucleotide–biotin conjugate that is chemically cleavable through the reduction of a disulfide bond within the linker. Conjugation involves reaction of a primary amine with an *N*-hydroxysulfosuccinimide ester linked to biotin. The oligonucleotide can be liberated from streptavidin agarose containing immobilized conjugate under mild conditions (neutral pH, 50 mM dithiothreitol). This cleavable conjugate is useful for affinity purification applications.

The conjugation of biotin and DNA is useful for the isolation, purification, and detection of nucleic acids due to the high affinity of biotin for avidin or streptavidin (*1–4*). Many strategies exist for the production of biotinylated DNA. For example, biotin may be enzymatically incorporated into DNA as a nucleoside triphosphate analog (*4*) or chemically incorporated into synthetic oligonucleotides as a phosphoramidite (*5*). Separation of biotinylated DNA from avidin is difficult because the biotin/avidin interaction is essentially irreversible. Synthesis of a linker that can be chemically cleaved has previously been shown to be useful in the recovery of DNA–protein complexes (*3*). A biotinylated thymidine analog containing a disulfide bond within the linker was used in the enzymatic production of biotinylated DNA. Nucleosomes reconstituted from histones and the biotinylated DNA were then recovered from avidin–agarose under reducing conditions.

Here, we report the synthesis of a biotinylated oligonucleotide containing a disulfide bond within the linker. The oligonucleotide displays a single biotin moiety at its 3′ terminus. Duplexes constructed using an oligonucleotide that is biotinylated in this manner provide tools for affinity purification of DNA binding proteins or other ligands. The ability to recover the DNA–ligand complex under mild conditions offers an important advantage in affinity purification applications where specific complexes with DNA are to be separated from nonspecific complexes involving the solid support. Such problems frequently arise in affinity selection from combinatorial libraries of RNA ligands (*6, 7*).

The duplex DNAs utilized in these studies are shown in Scheme 1A. Duplex **I** is nonbiotinylated (irrelevant sequence). **II** and **III** are biotinylated duplexes in which the biotin moieties are noncleavable and cleavable,

respectively. Scheme 1B outlines the synthesis of **III**, showing the chemical structure of the cleavable linkage to biotin.

Oligodeoxynucleotides were synthesized by phosphoramidite methodology using an Applied Biosystems Model 380B DNA synthesizer. The biotinylated strand of **II** was synthesized using BioTEG CPG (Glen Research, Sterling, VA). The 3′-amino oligonucleotide used in the production of the biotinylated strand of **III** was synthesized on 3′-Amino-Modifier C7-CPG (Glen Research). The synthesis of all oligodeoxynuceotides involved standard procedures using hot ammonium hydroxide for cleavage and deprotection.

3′-Amino oligonucleotide (~50 nmol) was gel purified (20% acrylamide, 7.5 M urea, 0.5× TBE), visualized by UV-shadowing, excised, and eluted overnight at 37 °C with agitation in 800 μL of water. The eluant was extracted with an equal volume of phenol:chloroform (1:1), and the oligonucleotide was precipitated by adjusting the solution to 100 mM NaCl and 10 mM MgCl₂ followed by the addition of 2.5 volumes of ethanol. Purified 3′-amino oligonucleotide and 1 μmol of sulfosuccinimidyl 2-(biotinamidoethyl)-1,3-dithiopropionate (NHS-SS-Biotin; Pierce Chemical Co., Rockford, IL) were incubated in NaHCO₃ buffer (50 mM, pH 8.5, 400 μL) for 2 h at room temperature. Oligonucleotides were precipitated from the reaction by adjusting the solution to 100 mM NaCl and 10 mM MgCl₂ followed by the addition of 2.5 volumes of ethanol. The product was again purified by gel electrophoresis. The biotin-SS-oligonucleotide exhibited lower gel mobility than the nonreacted 3′-amino oligonucleotide.

Purified 3′-amino oligonucleotide and biotin-SS-oligonucleotide were analyzed on a Bruker BenchTOF laser desorption linear time-of-flight mass spectrometer using a nitrogen laser (337 nm). Samples (10–40 pmol) were placed on the probe tip with a matrix of 2,4,6-trihydroxyacetophenone buffered with diammonium hydrogen citrate as described by Pieles et al. (*8*). Analyses were performed in the negative ion mode. The spectra shown are the summed results of 50–100 laser pulses (Figure 1). The molecular weights determined for each compound were found to be in agreement with those calculated.

* To whom correspondence should be addressed. Tel.: 402-559-8288. Fax: 402-559-4651. Internet: jmaher@unmc.edu.
† University of Nebraska Medical Center.
‡ University of Nebraska at Lincoln.
⊗ Abstract published in *Advance ACS Abstracts,* December 15, 1994.

A

mass calculated: 7392
found: 7387

B

mass calculated: 7781
found: 7776
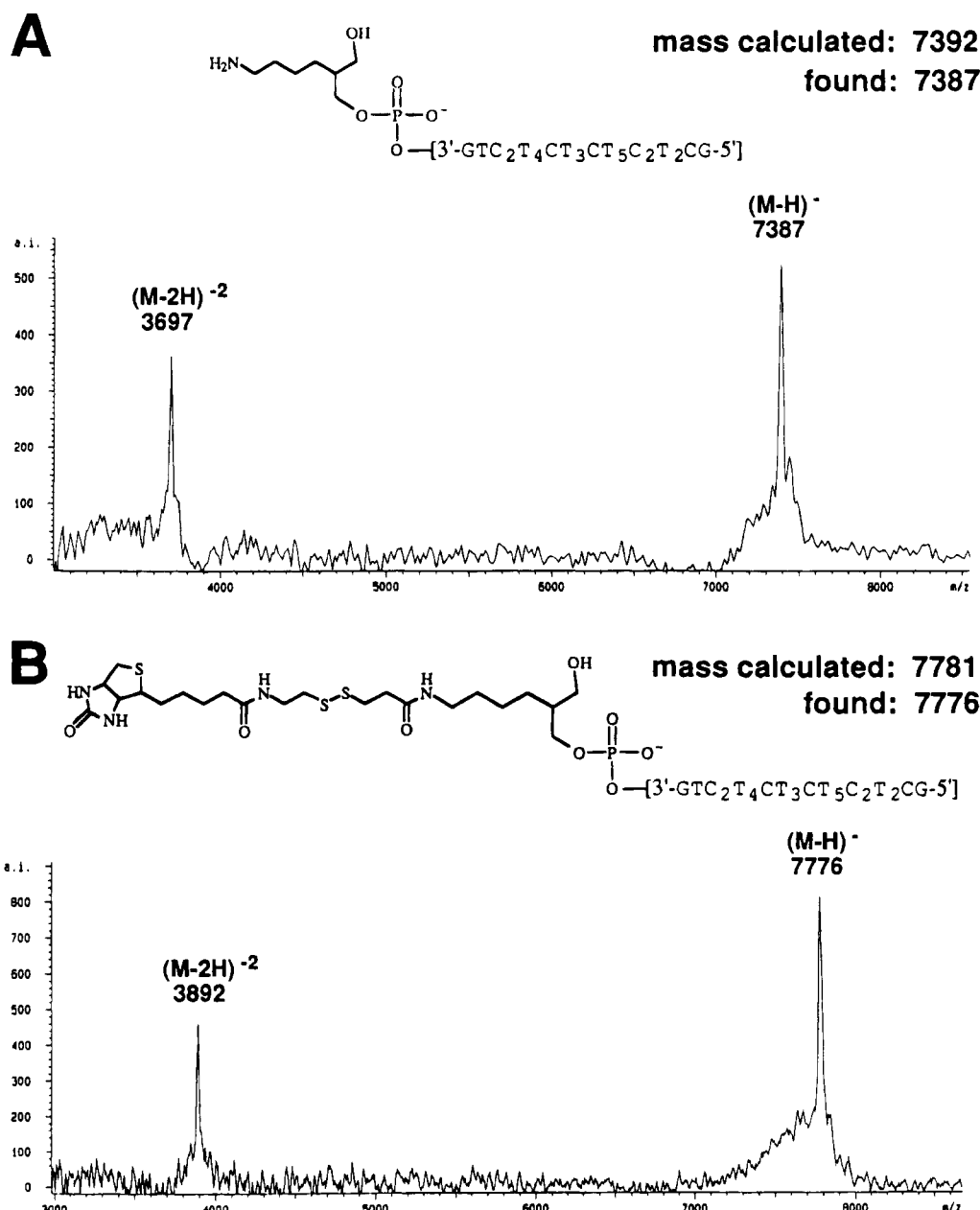
Figure 1. Mass spectra. (A) Purified 3'-amino oligonucleotide. (B) Purified biotin-SS-oligonucleotide.

Biotin-SS-oligonucleotide (3.3 nmol) was annealed to complement oligonucleotide (4.9 nmol) in a 300 μL reaction in the presence of sodium chloride (200 mM) by heating to 95 °C and cooling to room temperature to produce **III**. **III** (3.3 nmol, 5.28 μg) was immobilized on streptavidin agarose beads containing ~1.3 nmol of streptavidin (Pierce Chemical Co.) by incubation for 2 h at room temperature in phosphate buffered saline (PBS, 528 μL). Preparation of immobilized **II** from purified oligonucleotides was performed in a similar manner. Duplex **I** was prepared by annealing a 1:1 ratio of purified oligonucleotides.

The ability of dithiothreitol (DTT) to cleave immobilized **III** from streptavidin agarose was investigated under various conditions relevant to an affinity purification application. Figure 2A shows that fluorescence of ethidium bromide (EB)−DNA complexes under ultraviolet light is localized to the agarose support when the duplex is immobilized (Figure 2A, column 3, top, middle, and bottom rows). When DNA is not immobilized, the fluorescence is dispersed diffusely in the solution (Figure

2A, column 2, top, middle, and bottom rows). Figure 2A shows the pH-dependent DTT cleavage of **III** from the support. Streptavidin agarose combined with duplex **I** (0.3 μg) and streptavidin agarose linked to **III** (0.3 μg) were incubated in a 10 μL solution containing 50 mM DTT, 6 mM magnesium chloride, 2 mM spermidine trihydrochloride, and either 40 mM sodium acetate pH 5.0, 40 mM Tris acetate pH 6.5, or 40 mM Tris hydrochloride pH 7.4. Solutions were incubated at 42 °C for the indicated times (Figure 2A, columns 1−9). Streptavidin agarose (no linked duplex DNA) was incubated in PBS (Figure 2A, column 1). Reactions were transferred to ice, combined with EB (10 ng, 2 μL), and illuminated as a single droplet on a UV transilluminator. Samples containing duplex **I** demonstrate the diffuse fluorescence indicative of nonimmobilized EB-DNA complexes (Figure 2A, column 2). Efficient reduction of disulfide bonds by DTT required neutral pH conditions (Figure 2A, columns 3−9, compare top, middle, and bottom rows). Linker cleavage becomes considerably less efficient at pH 6.5

Scheme 1. (A) Structure of DNA Duplexes[a] and (B) General Scheme for Production of III[b]

[a] Duplex **I** contains no DNA modifications. **II** is modified by conjugation to a noncleavable biotin moiety. **III** incorporates biotin via a cleavable linkage. [b] Key: (a) incubation with NHS-SS-Biotin in aqueous buffer, pH 8.5; (b) incubation with oligonucleotide complementary to biotin-SS-oligonucleotide.
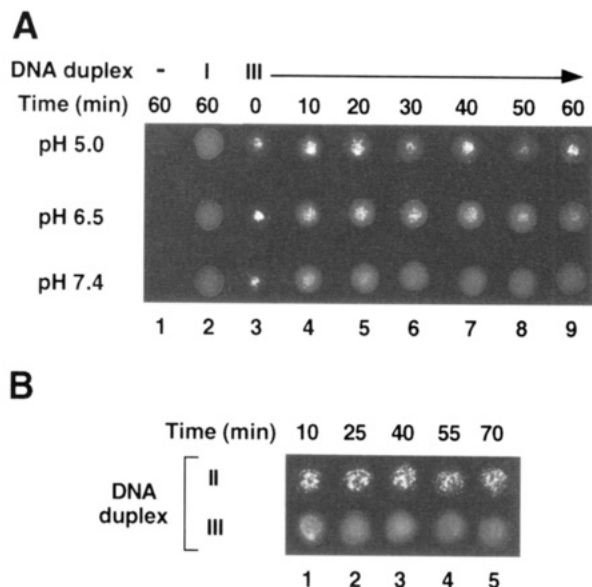
Figure 2. Linker cleavage under mild conditions. (A) pH-dependent DTT cleavage of duplex **III** from streptavidin agarose support. (B) Linker-dependent cleavage of duplex from streptavidin agarose support.

relative to pH 7.4 and is undetectable at pH 5.0 over this time course.

Figure 2B shows that DTT cleavage of **III** from the support is due to its modified linker. Streptavidin

agarose presenting 0.3 μg of noncleavable **II** (Figure 2B, columns 1–5, top row) or cleavable **III** (Figure 2B, columns 1–5, bottom row) was incubated with 50 mM DTT in PBS (10 μL) at room temperature for the indicated times. Reactions were combined with EB, and duplex DNA was visualized as described above. **II** remains bound to the support throughout DTT treatment (Figure 2B, columns 1–5, top row). In contrast, **III** is efficiently cleaved from the support (Figure 2B, columns 1–5, bottom row).

In summary, we present a simple method for producing biotinylated duplex DNA that can be immobilized on an avidin- or streptavidin-based support and liberated under mild reducing conditions. In our laboratory, this conjugate has proven to facilitate experiments requiring affinity selection and isolation of RNAs that bind to duplex DNA, using a combinatorial RNA library. Similar methods might be applied to affinity purification of DNA binding proteins if exposure to mild reducing conditions is not detrimental to the structure and function of the desired protein.

ACKNOWLEDGMENT

LITERATURE CITED

(1) Takabatake, T., Asada, K., Uchimura, Y., Ohdate, M., and Kusukawa, N. (1992) The use of purine-rich oligonucleotides in triplex-mediated DNA isolation and generation of unidirectional deletions. *Nucleic Acids Res. 20*, 5853–5854.

(2) Bock, L. C., Griffin, L. C., Latham, J. A., Vermass, E. H., and Toole, J. J. (1992) Selection of single-stranded DNA molecules that bind and inhibit human thrombin. *Nature 355*, 564–566.

(3) Shimkus, M., Levy, J., and Herman, T. (1985) A chemically cleavable biotinylated nucleotide: Usefulness in the recovery of protein-DNA complexes from avidin affinity columns. *Proc. Natl. Acad. Sci. U.S.A. 82*, 2593–2597.

(4) Klevan, L., and Gebeyehu, G. (1990) Biotinylated nucleotides for labeling and detecting DNA. *Methods Enzymol. 184*, 561–577.

(5) Misiura, K., Durrant, I., Evans, M. R., and Gait, M. J. (1990) Biotinyl and phosphotyrosinyl derivatives useful in the incorporation of multiple reporter groups on synthetic oligonucleotides. *Nucleic Acids Res. 18*, 4345–4354.

(6) Pei, D., Ulrich, H. D., and Schultz, P. G. (1991) A combinatorial approach toward DNA recognition. *Science 253*, 1408–1411.

(7) Tuerk, C., MacDougal, S., and Gold, L. (1992) RNA pseudoknots that inhibit human immunodeficiency virus type 1 reverse transcriptase. *Proc. Natl. Acad. Sci. U.S.A. 89*, 6988–6992.

(8) Pieles, U., Zurcher, W., Schar, M., and Moser, H. E. (1993) Matrix-assisted laser desorption ionization time-of-flight mass spectrometry: a powerful tool for the mass and sequence analysis of natural and modified oligonucleotides. *Nucleic Acids Res. 21*, 3191–3196.

BC940092F

Recombinant Metallothionein-Conjugated Streptavidin Labeled with ^{188}Re and ^{99m}Tc

F. Virzi, P. Winnard, Jr., M. Fogarasi, T. Sano,[†] C. L. Smith,[†] C. R. Cantor,[†] M. Rusckowski, and D. J. Hnatowich*

Department of Nuclear Medicine, University of Massachusetts Medical Center, Worcester, Massachusetts 01655, and Center for Advanced Biotechnology and Departments of Biomedical Engineering and Biochemistry, Boston University, Boston, Massachusetts 02215. Received June 27, 1994[⊛]

Consideration is now being given to the use of avidin (or streptavidin) and biotin for radiotherapy of tumor. Accordingly, the goal of this study was to radiolabel a mouse metallothionein–streptavidin fusion protein with ^{188}Re and to compare its properties to those of the same fusion protein radiolabeled with ^{99m}Tc. A recombinant metallothionein–streptavidin fusion protein was radiolabeled by transchelation with ^{99m}Tc- and ^{188}Re-glucoheptonate. Labeling efficiency, which was not optimized for either radionuclide, was approximately 60% for ^{99m}Tc and 20% for ^{188}Re. Radiochemical purity was demonstrated by size exclusion HPLC both by nearly quantitative shifts of the ^{188}Re label to higher molecular weight upon the addition of biotinylated antibody and by the absence of a shift with biotin-saturated ^{188}Re-metallothionein–streptavidin. Stability of the labels in 37 °C serum was evaluated by comparing the HPLC radiochromatograms of serum samples both before and after the addition of biotinylated antibody. The ^{188}Re label behaved like ^{99m}Tc in that the same peaks were evident, including one prominent peak due to labeled cysteine. Recoveries during HPLC analysis of serum samples showed that oxidation rates to perrhenate and pertechnetate were identical. However, instability to cysteine challenge was greater for ^{188}Re; for example, the loss of label to cysteine after 24 h under one set of conditions was 41% for ^{188}Re and 22% with ^{99m}Tc. Analysis by HPLC of liver and kidney homogenates from mice administered the labeled antibodies were qualitatively and, in large measure, quantitatively independent of label. Biodistributions at 5 h in normal mice were statistically identical between the two labels in blood and in most tissues. In conclusion, streptavidin may be radiolabeled with radiorhenium using recombinant mouse metallothionein as a bifunctional chelator, and under one set of labeling conditions at least, ^{188}Re showed similar in vitro and in vivo behavior to that of ^{99m}Tc labeled to the same fusion protein.

INTRODUCTION

Pretargeting of tumor in which unlabeled but biotinylated antitumor antibodies are administered prior to the administration of radiolabeled avidin or streptavidin has been considered as one promising approach toward improving the tumor/normal tissue ratios for diagnosis (*1–5*). Results have been generally favorable, and as such, consideration is now being given to the use of this and related pretargeting approaches for radiotherapy (*6*). Accordingly, this investigation was concerned with radiolabeling streptavidin with rhenium-188 (^{188}Re), a therapeutic radionuclide, via mouse metallothionein serving as a bifunctional chelator.

The metallothioneins are a series of single-chain proteins, each of about 6–7 kDa, found in many species and believed to function as agents of metal detoxification (*7*). Mammalian metallothioneins contain about 20 cysteine residues distributed fairly uniformly along the peptide chain (*8*). As a result, normally seven divalent metal ions (usually cadmium or zinc) are bound per metallothionein molecule (*7*). The number of cysteine residues in metallothionein and, in particular, the large number which are present as next-to-nearest neighbors, has led to investigations of this protein as a bifunctional chelating group for the labeling of antibodies with tech-

netium-99m (^{99m}Tc) (*9, 10*). Thus, metallothionein, free from cadmium and saturated with zinc to protect the free sulfhydryls, was conjugated to the B72.3 IgG antibody using a heterobifunctional crosslinking agent and effectively radiolabeled with ^{99m}Tc (*11*).

Metallothionein may therefore be an attractive chelator to label streptavidin with ^{188}Re for pretargeting applications for two reasons. Because metallothionein is itself a protein, it is possible to fuse it to other proteins through recombinant DNA technologies. Mouse and human metallothionein genes have been fused to genes coding for human growth hormone (*12*), somatostatin (*13*), and the Fab' domain of the S107 antibody (*9*). Furthermore, the chemical properties of rhenium are similar to those of technetium since both elements are members of the same family in the periodic table of the elements. Thus, it may be possible to radiolabel metallothionein-containing fusion proteins with ^{188}Re by methods which are similar to that developed for ^{99m}Tc.

Rhenium-188 is an attractive radionuclide for antibody-mediated radiation therapy (*14*). In addition to a β-ray of intermediate energy (2.12 MeV) and a suitable physical half-life (0.70 days), this radionuclide is available as a radionuclide generator product by decay of its 70-day parent, tungsten-188 (^{188}W).

Recently, an expression system for a cloned streptavidin gene was developed in which active streptavidin may be efficiently expressed in *Escherichia coli* (*15*). Thereafter, it was possible to fuse a coding sequence for mouse metallothionein to the streptavidin gene such that this target protein was expressed as a streptavidin–metallothionein chimera. The purified chimera consists

of four identical subunits; each subunit was shown to bind one biotin and approximately seven cadmium ions, thus demonstrating that both the streptavidin and metallothionein moieties are fully functional (16).

We report herein on a method for radiolabeling the recombinant streptavidin—metallothionein fusion protein with [188]Re and on the properties of the label in vitro and in vivo in mice.

EXPERIMENTAL PROCEDURES

All reagents used in this investigation, sodium citrate, acetic acid (Aldrich, Milwaukee, WI), stannous chloride dihydrate, sodium glucoheptonate, and horse kidney metallothionein (Sigma Chemical Co., St. Louis, MO), were used without purification. Technetium-99m pertechnetate was obtained from a [99]Mo—[99m]Tc generator (NEN Dupont, Billerica, MA). A 100 mCi radionuclide [188]W—[188]Re generator was kindly provided by Dr. F. F. Knapp, Jr., Oak Ridge National Laboratory. The B72.3 IgG antibody was a gift from Dr. John Rodwell (Cytogen Corp., Princeton, NJ). The recombinant metallothionein—streptavidin fusion protein was prepared as described previously (16).

Radiolabeling of Unconjugated Metallothionein. The conditions required to radiolabel metallothionein—streptavidin with [188]Re were first investigated using free, unconjugated, metallothionein. The metallothionein was of horse kidney origin and was used as obtained (i.e., without purification from its zinc and cadmium content, listed by the manufacture to be 4—7% by weight). The protein was radiolabeled by transchelation from [188]Re-labeled citrate. The [188]Re was obtained by elution of the [188]W—[188]Re generator with 5—10 mL of 0.15 M NaCl solution. The citrate complex of [188]Re was prepared by adding 50 μL (180 μCi) of [188]Re-perrhenate in saline to 50 μL of a 80 mg/mL solution of sodium citrate, pH 6.0, to which was added 20 μL of a fresh 20 mg/mL solution of stannous chloride dihydrate in 10% acetic acid. The solution was left undisturbed for 30 min at room temperature and was then adjusted to pH 4.8 by the addition of 10 μL of a 1 M solution of sodium acetate, pH 6.0. Strip chromatography with ITLC-SG (Gelman Sciences, Ann Arbor, MI) using acetone eluant, in which perrhenate migrates, and using saline eluant, in which both labeled citrate and perrhenate migrate, was used to determine the radiochemical purity of the labeled citrate complex.

Ten microliters of a fresh [188]Re-citrate solution was added to an equal volume of metallothionein in saline to give a final protein concentration in the range 0—2.5 mg/mL. Aliquots were removed at various time points over 24 h for analysis by strip chromatography.

Radiolabeling of the Metallothionein—Streptavidin Fusion Protein. Each fusion protein consisted of four identical subunits of 190 amino acids with one metallothionein bound to each subunit by a 10-amino acid tether (16). The fusion protein was saturated with zinc ions to protect the sulfhydryls from oxidation. Attempts to label the construct with [188]Re via the citrate complex were unsuccessful; therefore, the glucoheptonate complex was investigated for this purpose.

The glucoheptonate complex was prepared by dissolving 250 mg of sodium glucoheptonate in 1.0 mL of saline and adjusting the pH to 4.5 with 6 M HCl. To 25 μL of [188]Re-perrhenate generator eluant (90—160 μCi) was added 40 μL of the freshly prepared glucoheptonate solution, and the pH was adjusted to 5.0 with 10 μL of 1 M sodium bicarbonate, pH 10. To this was added 10 μL of a freshly prepared 25 mg/mL solution of stannous chloride dihydrate in 10% acetic acid. The solution was

incubated at room temperature for 1 h and analyzed by strip chromatography as for [188]Re-citrate.

Procedures for the preparation of ^{99m}Tc-labeled glucoheptonate were similar. Several vials, each containing 200 mg of sodium glucoheptonate and 0.14 mg of stannous chloride dihydrate adjusted to pH 5.5 with dilute HCl, were purged with nitrogen, sealed, and freeze dried. The vials were stored at −20 °C until needed or for up to 60 days. To one vial was added 3.0 mL of nitrogen-purged saline, and 25 μL of this solution was added to 50 μL (1.4—2.6 mCi) of ^{99m}Tc-pertechnetate generator eluant and, after 15 min at room temperature, analyzed by strip chromatography as for [188]Re-glucoheptonate.

The recombinant metallothionein—streptavidin fusion protein was concentrated by ultrafiltration to 0.45 mg/mL in 0.1 M sodium phosphate buffer, pH 6.5 (Centriprep-30, Amicon, Beverly, MA). A 25 μL aliquot of the metallothionein—streptavidin fusion protein solution was added to an equal volume of either [99m]Tc- (460—860 μCi) or [188]Re-glucoheptonate (26—47 μCi). The ^{99m}Tc preparation was purified over a 0.6 × 21 cm column of Sephadex G-50 after 1 h of incubation at room temperature, while the [188]Re preparation was purified in the same manner but after 2 h of incubation. In both cases, the radiolabeled fusion protein appeared in the column void volume.

Radiochemical purity of the labeled protein was determined by high-performance liquid chromatography (HPLC) analysis using a single 1.6 × 29 cm column of Superose-12 (Pharmacia-LKB, Piscataway, NJ) and an in-line UV and radioactivity monitors. The column was eluted at 0.5 mL/min with 0.1 M phosphate-buffered saline, pH 7 eluant. Analysis was performed on the protein with and without the addition of a large (12:1) molar excess of biotinylated B72.3 IgG antibody. Radioactivity shifting to higher molecular weight after the addition of the biotinylated antibody indicates the binding of the labeled metallothionein—streptavidin fusion protein to the biotinylated antibody. The biotinylated antibody was prepared as previously described with an average of six biotin groups per molecule as determined spectrophotometrically by measuring the displacement of 2-(4′-hydroxyazobenzene)benzoic acid (HABA) from avidin (1).

In Vitro Serum Stability Studies. Preparations of [99m]Tc- and [188]Re-labeled metallothionein—streptavidin fusion protein, after Sephadex G-50 purification, were incubated at 37 °C in fresh human serum at a concentration of 10 μg/mL. In both cases, stability was assessed by size exclusion HPLC analysis with and without the addition of biotinylated B72.3 antibody.

Mouse Studies. Each normal CD-1 mouse, 28—37 g (Charles River Laboratories, Wilmington, MA), received via a tail vein 11 μg of the fusion protein labeled with either [99m]Tc (365 μCi) or [188]Re (33 μCi). The animals were sacrificed 5 h later by spinal dislocation after metofane anesthesia. Tissues were removed, rinsed with saline, and after weighing, were counted along with blood samples in a NaI(Tl) well counter against standards of the injectates. The radioactivity counts were converted into percentage of the injected dose per gram of blood or tissue corrected to a 25 g whole body weight. Samples of urine and serum were analyzed by HPLC using the Superose-12 column in which 0.3 mL fractions were collected for counting in the well counter.

RESULTS

Radiolabeling of Unconjugated Metallothionein. Following the procedure described in the previous section, it was possible to achieve labeling efficiencies of greater than 95% in the preparation of [188]Re-citrate. Further-

more, as determined by strip chromatography, the radiochemical purity was still greater than 90% after 2 h at room temperature, with the decrease due entirely to the accumulation of perrhenate. Horse kidney metallothionein was successfully radiolabeled with [188]Re using the citrate complex. Labeling efficiencies varied from about 30% at 1 h to 60% at 24 h of incubation at metallothionein concentrations of about 1 mg/mL or greater.

Radiolabeling of Metallothionein–Streptavidin Fusion Protein. Although it was possible to radiolabel unconjugated metallothionein with [188]Re-citrate, no labeling of the metallothionein–streptavidin fusion protein was achieved using citrate as transchelator. Therefore, glucoheptonate was considered as an alternative. Radiochemical purities of both [99m]Tc- and [188]Re-labeled glucoheptonate, prepared as described, were routinely greater than 90%. The ^{99m}Tc-glucoheptonate preparations showed no change in radiochemical purity after 2 h at room temperature. In the [188]Re case, the radiochemical purity was still 90% after 2 h at room temperature with the decrease due entirely to the accumulation of perrhenate. Possibly because streptavidin does not possess cysteine residues (*16*), the "nonspecific" transfer of reduced ^{99m}Tc or [188]Re to streptavidin was not a concern; labeling studies under identical conditions showed less than 3% of [188]Re bound to unconjugated streptavidin.

Under the conditions described for the radiolabeling of the fusion protein with [99m]Tc- and [188]Re-glucoheptonate, the labeling efficiencies, determined by Sephadex G-50 chromatography, averaged 61 ± 10% (standard deviation, N = 5) and 19 ± 3% (standard deviation, *N* = 5) for ^{99m}Tc and [188]Re, respectively. The [188]Re-metallothionein–streptavidin fusion protein complex was found to be stable to storage at room temperature for at least 2 h. Figure 1 presents radiochromatographic profiles obtained by size exclusion HPLC of [99m]Tc- (Figure 1A) and [188]Re-labeled metallothionein–streptavidin (Figure 1B) with (Figure 1A2 and 1B2) and without (Figure 1A1 and 1B1) the addition of a large molar excess of biotinylated B72.3 antibody. In the case of both radiolabels, the profiles of the labeled proteins show several radiolabeled species but one prominent peak in the absence of the biotinylated antibody. Following addition of the antibody, however, a large and almost quantitative shift to the void is evident for both ^{99m}Tc and [188]Re. As such, the majority of both radiolabels must be on streptavidin, most probably via the metallothionein groups. No shift was apparent when the same study was repeated with either ^{99m}Tc-labeled metallothionein–streptavidin saturated after preparation with a 10-fold molar excess of biotin (unpublished observations) or the [188]Re-labeled fusion protein prepared in the identical fashion (Figure 1B3). Figure 2 shows the UV profile of metallothionein–streptavidin at 280 nm (Figure 2A) which has the same general shape as the radioactivity profiles (Figures 2, 1A1, 1B1, and 1B3) and that the identical shift to higher molecular weight is evident upon the addition of biotinylated antibody.

In Vitro Serum Stability Studies. Purified samples of [99m]Tc- and [188]Re-labeled metallothionein–streptavidin fusion proteins were incubated at 37 °C in fresh serum, and aliquots were removed periodically for analysis by HPLC with and without the addition of biotinylated antibody. Figure 3 presents radiochromatograms of the purified preparations themselves and of serum incubates after 1 and 24 h of incubation with and without the addition of biotinylated antibody (B-IgG). The percent
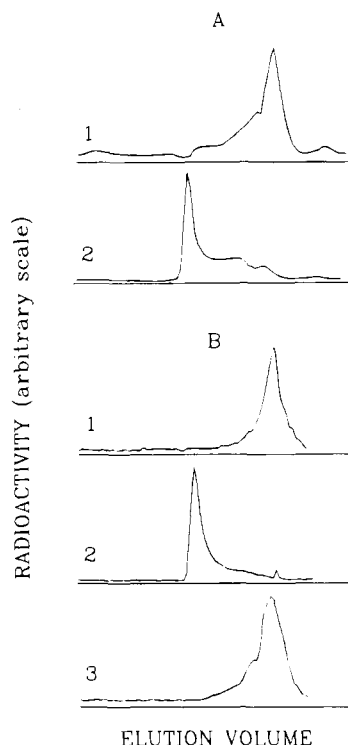
Figure 1. Radiochromatographic profiles obtained by size exclusion HPLC analysis of [99m]Tc- and [188]Re-labeled metallothionein–streptavidin fusion proteins without ([99m]Tc (A1); [188]Re (B1)) and with ([99m]Tc (A2); [188]Re (B2)) the addition of biotinylated antibody. In the case of [188]Re, the radiochromatogram obtained after adding biotinylated antibody to biotin-saturated metallothionein-streptavidin fusion protein is also presented (B3).
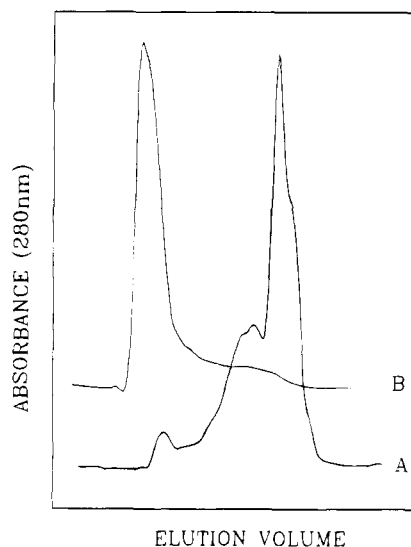
Figure 2. UV absorbance profiles obtained by size exclusion HPLC of the metallothionein–streptavidin fusion protein without (A) and with (B) the addition of biotinylated antibody.

recovery of radioactivity is listed in each chromatogram. In all chromatograms other than those of the preparation itself (i.e., injectate) in saline, a peak appears in fraction 76. In the case of ^{99m}Tc and, most probably [188]Re as well, this peak is due to radiolabeled cysteine produced by transchelation of the label from the fusion protein to this thiol (*17–19*). It may be estimated from Figure 3 that 22% of the ^{99m}Tc and 41% of [188]Re were present as labeled cysteine at 24 h. The addition of biotinylated antibody to aliquots of the serum incubates in the case of both labels resulted in a shift to higher molecular weight. The
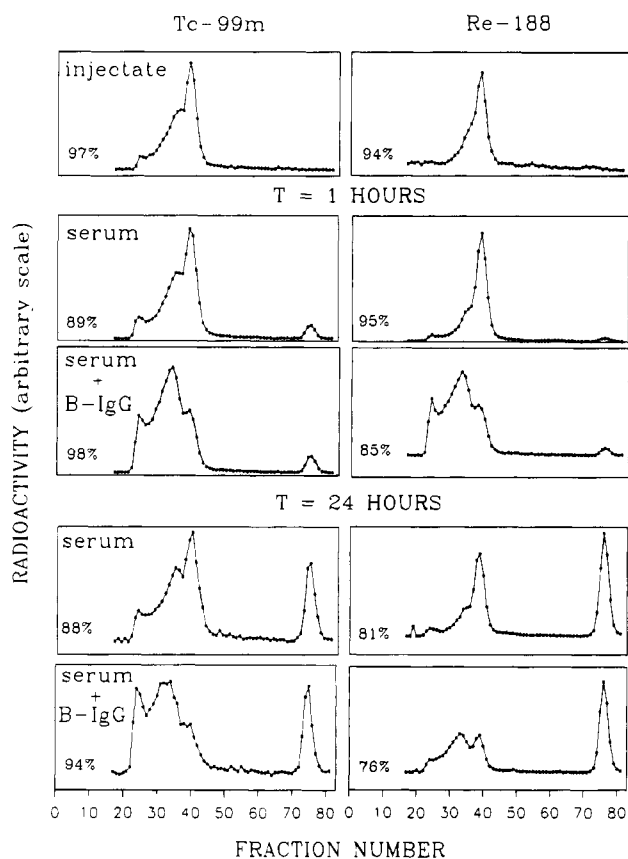
Figure 3. Radiochromatographic profiles obtained by size exclusion HPLC analysis of ^{99m}Tc- (left column) and ^{188}Re-labeled (right column) metallothionein–streptavidin. Chromatograms are presented for the preparations themselves (injectates) and serum incubates after 1 and 24 h at 37 °C. In the case of both radionuclides and both times, a chromatogram is also presented showing the change in profile following the addition of biotinylated antibody (B-IgG) to the serum incubates. The recoveries are listed for each chromatogram.

complexity of these radiochromatograms and the poor resolution do not permit an accurate estimate of the extent of these shifts.

In Vivo Mouse Studies. Samples of urine and serum obtained from mice administered ^{99m}Tc- and ^{188}Re-labeled metallothionein–streptavidin were obtained during sacrifice at 5 h post administration. The serum radiochromatograms (Figure 4) show a shift to higher molecular weight, especially in the case of ^{99m}Tc, from that of the injectates, although the profiles are generally similar. The recoveries are high indicating the absence of significant concentrations in serum of pertechnetate or perrhenate, both of which are retained by the column. A small peak centered at fraction 75 is present in both radiochromatograms and most probably is due to labeled cysteine. The urine radiochromatograms show a prominent cysteine peak in both cases and several smaller, unidentified peaks centered in fractions 51 and 58 which may be identical to peaks observed previously in similar studies of ^{99m}Tc-labeled antibodies (17). The recovery in the ^{99m}Tc case is low which indicates the presence in this urine sample of about 40% pertechnetate.

The biodistribution results at 5 h post administration of ^{99m}Tc- and ^{188}Re-labeled metallothionein-streptavidin fusion proteins are listed in Table 1. There are no significant differences (Student's T test, $p < 0.05$) between these two labels in blood and all tissues except for heart, lung and spleen ($p < 0.05$).
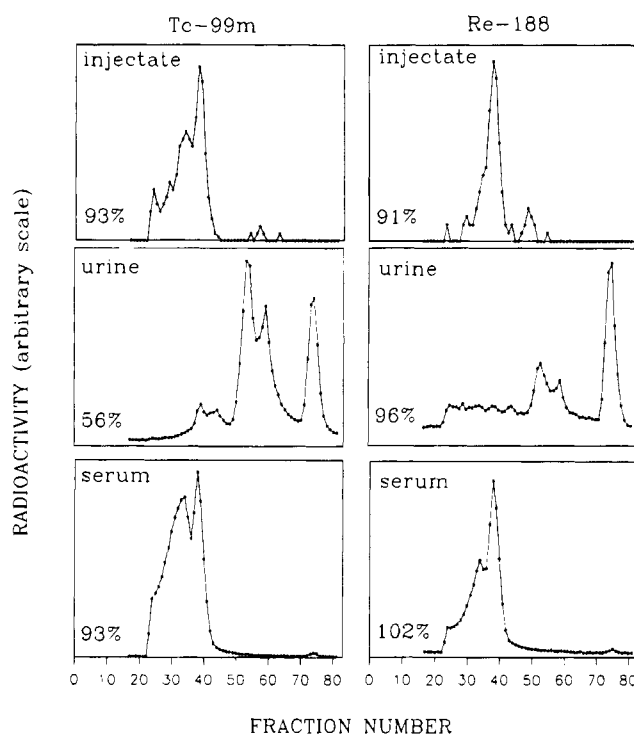
Figure 4. Radiochromatographic profiles for ^{99m}Tc (left column) and ^{188}Re (right column) obtained by size exclusion HPLC analysis of the injectates, one urine and one serum sample obtained at 5 h post administration of labeled metallothionein–streptavidin fusion protein. The recoveries are listed for each chromatogram.

Table 1. Biodistribution Results in Normal Mice at 5 h Post Administration[a]

organ	^{99m}Tc	^{188}Re	p value
liver	6.0 (0.9)	6.5 (0.7)	0.37, N.S.[b]
heart	2.8 (0.5)	1.7 (9.3)	0.006
kidneys	5.9 (1.5)	6.7 (1.1)	0.38, N.S.
lung	3.5 (0.6)	2.3 (0.2)	0.006
stomach	0.9 (0.2)	0.7 (0.1)	0.11, N.S.
spleen	12 (5)	4.8 (0.7)	0.017
muscle	0.5 (0.2)	0.3 (0.03)	0.07, N.S.
blood	13 (3)	14 (7)	0.94, N.S.
	$N = 6$	$N = 5$	

[a] Percent Injected Dose Per Gram with 1 s.d. of the mean in Parentheses [b] N.S. = not significant ($p > 0.05$, Student's T test).

DISCUSSION

The object of this investigation was to develop a suitable means of labeling a recombinant mouse metallothionein–streptavidin fusion protein with ^{188}Re, a radionuclide with attractive properties for radiotherapy of cancer. This anticipates a need for a radiolabeled streptavidin which may be used in a pretargeting approach to deliver sterilizing radiation doses to tumor. In this strategy, a biotinylated antitumor antibody would comprise the first injectate and would be followed at the proper time with the radiolabeled streptavidin (1, 3, 4). The high affinity of streptavidin for biotin immobilized at the tumor site via the antitumor antibody could offer high tumor/normal tissue ratios (5).

Like any protein, a large number of labeling methods can be considered for radiolabeling streptavidin. However, labeling streptavidin with metallothionein as a bifunctional chelator has several clear advantages. Metallothionein has been used successfully to radiolabel antibodies with ^{99m}Tc (10, 11) and thus is likely to be successful in radiolabeling with ^{188}Re as well considering the similarities in chemical properties of these two

radionuclides. Furthermore, it is now possible to use recombinant DNA techniques to fuse metallothionein to proteins. Indeed, this has already been accomplished for streptavidin (16), and a recombinant metallothionein—streptavidin fusion protein was used in this investigation.

Although glucoheptonate was used successfully to transchelate reduced ^{99m}Tc to a metallothionein-conjugated antibody (11), in this investigation, citrate was first considered as a transchelator because it has been used successfully in other thiol-based labeling procedures using radiorhenium (21, 22). Whereas it was possible to radiolabel with ^{188}Re unconjugated horse-kidney metallothionein in this manner, citrate failed to provide a label on metallothionein—streptavidin. This failure may be related to variations in properties toward radiolabeling among the different metallothioneins. In addition to the difference of horse kidney metallothionein vs streptavidin-fused murine metallothionein, we have observed greater instabilities of ^{99m}Tc when chelated to the fusion protein relative to an antibody radiolabeled with ^{99m}Tc via a rabbit metallothionein (unpublished observations). These differences may not be surprising considering the large variations in the amino acid sequences of the metallothioneins from species to species. Although each contains 20 cysteine residues, there can be as much as a 20% difference in the remaining residues. In particular, mouse metallothionein differs in amino acid composition from that of horse and rabbit metallothioneins by 10 and 2 residues, respectively (7). Furthermore, in the construct used in this investigation, the metallothionein was attached to the streptavidin core via a 10-amino acid tether (16) which may not be the optimal length to bring the metal binding sites on metallothionein into a sterically favorable position for chelation. Consequently, it may not be surprising that the coordination properties for metal binding may differ significantly among the metallothioneins.

While it was not possible to radiolabel the fusion protein with ^{188}Re via citrate, we did achieve about a 20% labeling efficiency in 2 h at room temperature with glucoheptonate. In order to maximize the labeling efficiency, the effect of such variables as time, temperature, and protein concentrations will need to be investigated. That the metallothionein—streptavidin fusion protein was radiolabeled is evident by the quantitative shift to higher molecular weight which followed the addition of biotinylated antibody (Figures 1 and 2) and the absence of a shift when the labeled metallothionein—streptavidin is saturated with biotin. The radiolabel is most probably on the metallothionein moiety since streptavidin itself cannot be radiolabeled with ^{188}Re by this approach.

The stability of the ^{188}Re in fresh human serum at 37 °C was compared to ^{99m}Tc and shown to be similar (Figure 3). Both labels were unstable toward transchelation to cysteine. From Figure 3, 22% of the ^{99m}Tc and 41% of ^{188}Re were present as labeled cysteine at 24 h. The shift of radioactivity to high molecular weight was also similar between labels both at 1 and 24 h of incubation (Figure 3).

The two labels also exhibited strong similarities when biodistributions were compared in normal mice (Table 1). Likewise, the radiochromatographic profiles obtained by size exclusion HPLC analysis of urine and serum samples obtained at sacrifice also show similarities (Figure 4). Both labels show increased levels of higher molecular weight species in serum in comparison to the injectates, and the retention times of the major low molecular weight peaks in the urine profiles were the same for both labels although the peak intensities were occasionally different. In both cases, however, a major

fraction of the label in urine was present as the cysteine complex, probably generated elsewhere and excreting through the kidneys (19).

In summary, it has been possible to radiolabel streptavidin through murine metallothionein moieties fused via recombinant DNA techniques. Relative to ^{99m}Tc labeled to the same fusion protein, the ^{188}Re label behaved in vitro and in vivo in a similar and, occasionally, identical manner.

ACKNOWLEDGMENT

LITERATURE CITED

(1) Hnatowich, D. J., Virzi, F., Rusckowski, M. (1987) Investigations of avidin and biotin for imaging applications. *J. Nucl. Med. 28*, 1294–1302.

(2) Kalofonos, H. P., Rusckowski, M., Siebecker, D. A., et al. (1990) Imaging of tumor in patients with indium-111-labeled biotin and streptavidin conjugated antibodies: preliminary communication. *J. Nucl. Med. 31*, 1791–1796.

(3) Pimm, M. V., Fells, H. F., Perkins, A. C., et al. (1988) Iodine-131 and indium-111 labeled avidin and streptavidin for pretargeted immunoscintigraphy with biotinylated anti-tumor monoclonal antibody. *Nucl. Med. Commun. 9*, 931–941.

(4) Khawli, L. A., Alauddin, M. M., Miller, G. K., et al. (1993) Improved immunotargeting of tumors with biotinylated monoclonal antibodies and radiolabeled streptavidin. *Antib. Immunoconj. Radionucl. 6*, 13–27.

(5) Sung, C., van Osdol, W. W., Saga, T., et al. (1994) Streptavidin distribution in tumors pretargeted with a biotinylated monoclonal antibody: theoretical and experimental pharmacokinetics. *Cancer Res. 54*, 2166–2175.

(6) Paganelli, G., Magnani, P., Meares, C., et al. (1993) Antibody guided therapy of CEA positive tumors using biotinylated monoclonal antibodies, avidin and ^{90}Y-DOTA-biotin: initial evaluation. *J. Nucl. Med. 34*, 94P.

(7) Kagi, J. H. R., Kojima, Y. (1987) Chemistry and biochemistry of metallothionein. *Experientia Suppl. 52*, 25–61.

(8) Nordberg, M., Kojima, Y. (1979) Metallothioinein and other low molecular weight metal-binding proteins. *Experientia Suppl. 34*, 41–116.

(9) Das, C., Kulkarni, P. V., Constantinescu, A., et al. (1992) Recombinant antibody—metallothionein: design and evaluation for radioimmunoimaging. *Proc. Natl. Acad. Sci. U.S.A. 89*, 9749–9753.

(10) Burchiel, S. W., Hadjian, R. A., Hladik, W. B., et al. (1989) Pharmacokinetic evaluation of technetium-99m-metallothionein conjugated mouse monoclonal antibody B72.3 in rhesus monkeys. *J. Nucl. Med. 30*, 1351–1357.

(11) Brown, B. A., Drozynski, C. A. Dearborn, C. B., et al. (1988) Conjugation of metallothionein to a murine monoclonal antibody. *Anal. Biochem. 172*, 22–28.

(12) Palmiter, R. D., Norstedt, G., Gelinas, R. E., et al. (1983) Metallothionein—human GH fusion genes stimulate growth of mice. *Science 222*, 809–814.

(13) Low, M. J., Hammer, R. E., Goodman, R. H., et al. (1985) Tissue-specific posttransitional processing of pre-somatostatin encoded by a metallothionein-somatostatin fusion gene in transgenic mice. *Cell 41*, 211–219.

(14) Griffiths, G. L., Goldenberg, D. M., Knapp, F. F., Jr., et al. (1991) Direct radiolabeling of monoclonal antibodies with generator-produced rhenium-188 for radioimmunotherapy: labeling and animal biodistribution studies. *Cancer Res. 51*, 4594–4602.

(15) Sano, T., Cantor, C. R. (1990) Expression of a cloned streptavidin gene in *Escherichia coli. Proc. Nat. Acad. Sci. U.S.A. 87,* 142–146.

(16) Sano, T., Glazer, A. N., Cantor, C. R. (1992) A streptavidin–metallothionein chimera that allows specific labeling of biological materials with many different heavy metal ions. *Proc. Nat. Acad. Sci. U.S.A. 89,* 1534–1538.

(17) Mardirossian, G., Wu, C., Rusckowski, M., et al. (1992) The stability of ^{99}Tcm directly labeled to an Fab′ antibody via stannous ion and mercaptoethanol reduction. *Nucl. Med. Commun. 13,* 503–512.

(18) Hnatowich, D. J., Mardirossian, G., Rusckowski, M., et al. (1993) Pharmacokinetics of the FO23C5 antibody fragment labelled with ^{99}Tcm and ^{111}In: a comparison in patients. *Nuc. Med. Commun. 14,* 52–63.

(19) Hnatowich, D. J., Mardirossian, G., Rusckowski, M., et al. (1993) Directly and indirectly technetium-99m-labeled antibodies - a comparison of in vitro and animal in vivo properties. *J. Nucl. Med. 34,* 109–119.

(20) Mardirossian, G., Bushe, H., Hnatowich, D. J. (1992) Pharmacokinetic modeling of Tc-99m labeled antibody in patients. *J. Nucl. Med. 33,* 958.

(21) Najafi, A., Alauddin, M. M., Sosa, A., et al. (1992) The evaluation of 186Re-labeled antibodies using N2S4 chelate in vitro and in vivo using tumor-bearing nude mice. *Nucl. Med. Biol. 19,* 205–212.

(22) Goldrosen, M. H., Biddle, W. C., Pancook, J., et al. (1990) Biodistribution, pharmacokinetics, and imaging studies with ^{186}Re-labeled NR-LU-10 whole antibody in LS174T colonic tumor-bearing mice. *Cancer Res. 50,* 7973–7978.

COMMUNICATIONS

Development of Rapid Mercury Assays. Synthesis of Sulfur- and Mercury-Containing Conjugates

Ferenc Szurdoki, Horacio Kido, and Bruce D. Hammock*

Departments of Entomology and Environmental Toxicology, University of California, Davis, California 95616.
Received October 3, 1994[®]

We have devised rapid analyses for mercury exploiting the high affinity of dithiocarbamate chelators for the mercuric ion. Our first assay is based on a sandwich chelate formed by a ligand supported on the well of an ELISA plate, Hg^{2+} ion of the investigated sample, and another ligand bound to a reporter enzyme. The second assay utilizes competitive binding of the analyte Hg^{2+} ions versus an organomercury conjugate to a chelating conjugate. Low ppb sensitivity and high selectivity for Hg^{2+} ions have been achieved in our pilot studies.

INTRODUCTION

Most instrumental methods for trace analysis and chemical speciation of hazardous metals (1-3) are not adaptable as low-cost, field-portable assays for monitoring a large number of environmental or biological samples. The development of immunoassays to detect metal ions has been a promising trend (4-7). However, this approach is based on highly specific monoclonal antibodies which usually are expensive to generate.

We have utilized the high affinity chelation of the mercurials by sulfur-containing ligands and the simple ELISA technique providing high signal amplification to devise sensitive and selective analyses of Hg^{2+} ion. Dithiocarbamates form stable complexes with a variety of metal ions except the alkali and alkaline earth metals (8). However, dithiocarbamates can be used to analyze Hg^{2+} selectively because Hg^{2+} replaces numerous metal ions from their dithiocarbamate chelates in fast exchange

reactions (9). Mercury–dithiocarbamate complexes have a very high thermodynamic stability (10). Dithiocarbamates seem to have similar or higher avidity only for several noble metals (1, 8, 10). In our studies, dithiocarbamates formed from secondary amine moieties of biopolymers were used because similar conjugates obtained from primary amines were reported to be unstable (11). Dithiocarbamates are difficult to prepare in pure form (12). Thus, these chelator groups were generated in the last synthetic step because of the simplified isolation of the macromolecular products.

RESULTS AND DISCUSSION

Our first approach involved a sandwich chelate of the Hg^{2+} ion with one chelator (1) immobilized on an ELISA plate and another bound to a reporter enzyme (2, format 1, Figure 1). In analogy with sandwich ELISAs (13), the acyclic dithiocarbamate (1) having presumably higher avidity for the analyte (10) was employed as immobilized ligand, and the pyrrolidine derivative (2) with lower affinity for Hg^{2+} ion was conjugated to the reporter enzyme. Secondary amino groups were formed on the biopolymers and then the resulting products were treated

* To whom correspondence should be addressed. Phone: (916) 752-7519. Fax: (916) 752-1537. E-mail: bdhammock@ucdavis.edu.
[®] Abstract published in *Advance ACS Abstracts*, February 1, 1995.
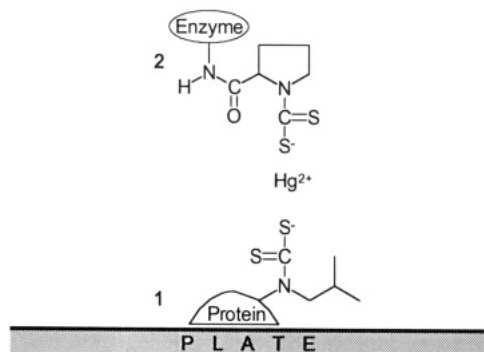
Figure 1. Chemical structures of the reagents involved in assay format 1.
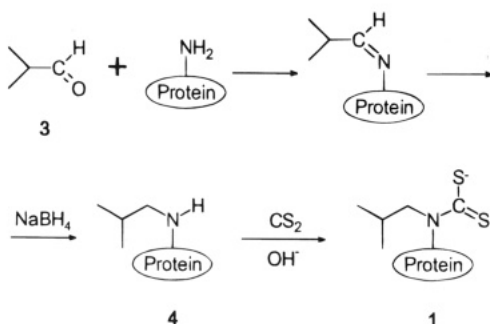
Figure 2. Synthesis of the immobilized chelator.

by carbon disulfide in alkaline solution to synthesize dithiocarbamate-bound protein and enzyme conjugates (Figures 2 and 3). Reductive alkylation (*14*) of ϵ-amino groups of lysine residues on conalbumin (CONA) with 2-methylpropionaldehyde (**3**) furnished the secondary amine intermediate (**4**−CONA) of the plate coating chelator (**1**−CONA, Figure 2). A protected secondary amino acid, *N*-(9-fluorenylmethyloxycarbonyl)-L-proline (Fmoc-Pro, **5**), served as a precursor for the preparation of the enzyme-linked chelator (**2**, Figure 3). This lipophilic acid (**5**) was efficiently conjugated to alkaline phosphatase (AP) by means of *N*-hydroxysulfosuccinimide (**6**) and a water soluble carbodiimide (**7**) (*15*). (The reagents were used in excess to ensure the completion of this coupling reaction.) The standard protocol for the cleavage of the *N*-FMOC group employs secondary amines in aprotic solvents (*16, 17*). However, deblocking of FMOC-peptides by secondary amines in solvents like formamide, 5% TFA/DMF (*17*), and 5% AcOH/CHCl$_3$ (*18*) has recently been reported. In our experiments with Fmoc-Pro (**5**), the blocking group could be removed by 4-(aminomethyl)piperidine (**10**) in alkaline aqueous solution at a slow rate (pH 11, 4 °C, 24−36 h). Under these conditions, the activity of some enzymes (AP, HRP) was preserved. In the case of biopolymers, excess reagent **10** and water soluble side products (*16*) were eliminated by dialysis in a slightly acidic buffer (Figure 3). The cleavage of the protecting group of **9**−AP resulting in **11**−AP was confirmed by UV spectroscopy.

The sandwich chelate with Hg^{2+} ion, **1**−CONA, and **2**−AP (Figure 1) was formed in slightly acidic acetate buffer containing Tween 20 with simultaneous incubation of the reagents in the wells of the ELISA plates. The quality and the concentration of the assay buffer and of the detergent as well as other assay parameters exercised profound influence on the assay performance. Contaminating heavy metal ions were removed from the buffers used in the assay by a specific ion-exchanger resin. The standard curve (Figure 4) obtained with this system has an IC$_{50}$ value of 0.54 ppb (2.7 nM) and a limit of detection
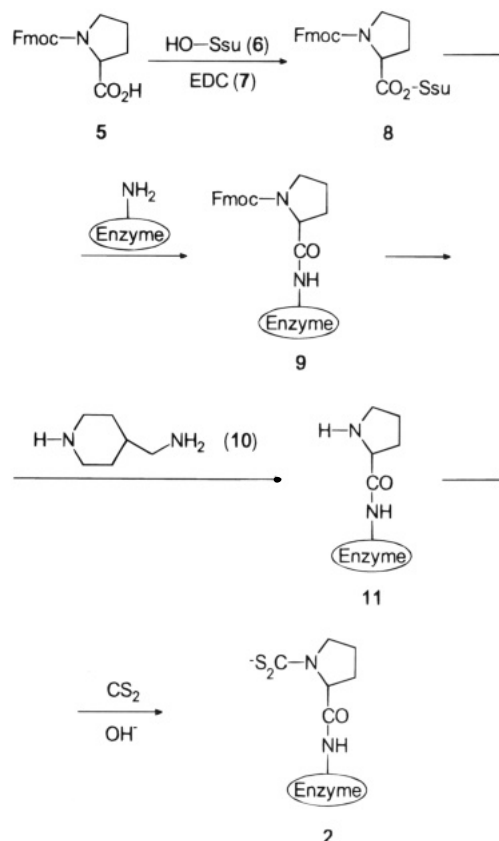
Figure 3. Synthesis of the chelator linked to the reporter enzyme.
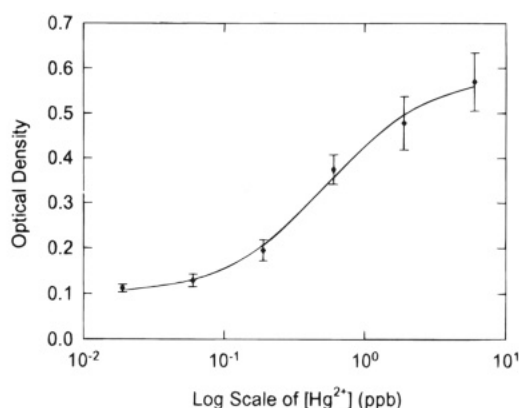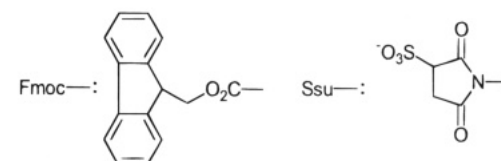
Figure 4. Standard curve of assay format 1.

(LD) of about 75 ppt (0.375 nM) of mercuric ion concentration. Most of the metal ions studied (e.g., Al^{3+}, Ca^{2+}, Cd^{2+}, Cr^{3+}, Cr^{6+}, Fe^{2+}, Mg^{2+}, Mn^{2+}, Pb^{2+}) did not significantly interfere up to about 3000 nM concentrations; however, cross-reactivities (CR = 100$^{Hg(II)}$IC$_{50}$/^{ion}IC$_{50}$) with, e.g., Ag$^+$ (7%), Au^{3+} (0.2%), Cu^{2+} (2%), Pd^{2+} (29%), and Zn^{2+} (0.3%) ions were noticed. No significant change in the IC$_{50}$ value of the Hg^{2+} standard curve was observed when the assay buffer was supplemented with 1000 nM Zn^{2+}; thus, the interference from foreign zinc ions might be reduced this way. The signal of the assay fell below background level when methylmercury was given in increased concentrations. (This unexpected downward
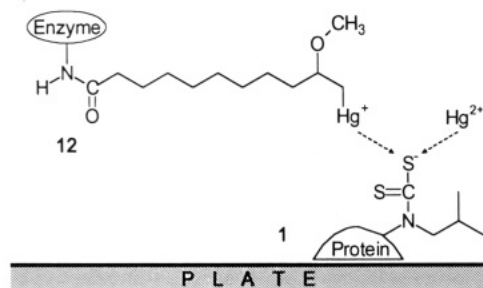
Figure 5. Chemical structures of the reagents involved in assay format 2A. Dotted lines indicate competition for the ligand bound to the plate.

trend, however, was not significant with an analogous system using different assay parameters.) Methylmercury may be competing with traces of heavy metals, remaining in the buffers and reagents, causing background signal. Total mercury content of a sample containing CH_3Hg^+ and Hg^{2+} can be determined with this assay after decomposition of the organic mercury species into mercuric ion.

Monoalkyl- and monoarylmercury salts are known to form highly stable 1:1 chelates with dithiocarbamate-ligands (*19–21*); the exact measure of the thermodynamic stability, however, is not reported to our knowledge. The second assay (format 2) is based on the competition between mercuric ions and an organomercury conjugate in binding to a chelating conjugate. The first application of this assay principle (format 2A) involved a mercury-linked reporter enzyme (**12**–AP, Figure 5) and the same immobilized chelator as used in the first assay (**1**–CONA, Figures 1 and 5). 10-Undecenoic acid (**13**) and mercuric acetate in the presence of methanol gave organomercury compound **14** (Figure 6) (*22*). This acid (**14**) was then conjugated to AP to yield mercury-containing tracer **12**–AP. The standard curve constructed with the **1**–CONA/**12**–AP assay system (format 2A, Figure 5), depicted in Figure 7, had an IC_{50} value of 40 nM (8 ppb) and a LD of 5 nM (1 ppb) of mercuric ion. This assay displayed remarkable selectivity for Hg^{2+}. No or only marginal interferences were observed with most metal ions (e.g., Al^{3+}, Ca^{2+}, Cd^{2+}, Co^{2+}, Cr^{3+}, Cr^{6+}, Fe^{2+}, Fe^{3+}, Mg^{2+}, Mn^{2+}, Ni^{2+}, Pb^{2+}) up to about 3000 nM concentrations. Significant cross-reactivity with only the following metals were detected: Ag^+ (CR: 82%), Au^{3+} (CR: <1%), and Cu^{2+} (CR: 10%). The concentration–response curves with CH_3Hg^+ and Zn^{2+} ions displayed on unexpected, slightly increasing trend. The increasing tendency with methylmercury was diminished when the slightly acidic acetate assay buffer contained trioctylmethylammonium chloride (Aliquat 336), an unusual detergent employed to reduce background signal, instead of Tween 20. The cleavage of the mercury–carbon bond in conjugate **12**–AP with sodium tetrahydroborate (*22*) without inactivating the enzyme resulted in no signal.

Another variant (format 2B) of the second assay employed a mercury-linked protein conjugate **16**–CONA and a chelate-linked tracer **2**–AP (Figure 8). Reagent **16**–CONA, used for plate coating, was produced from a mercury-containing acid, 2-[*N*-[3-(hydroxymercurio)-2-methoxypropyl]carbamoyl]phenoxyacetic acid (Aldrich's mersalyl acid) in a manner analogous to the synthesis of tracer **12**–AP. In our preliminary studies with this assay, we prepared a standard curve (IC_{50}: 25 nM) similar to that obtained with system 2A. A cross-reactivity pattern similar to that of format 2A was found, and no significant interference with a number of metal ions (e.g., Al^{3+}, Ca^{2+}, Cd^{2+}, Co^{2+}, Cr^{3+}, Fe^{2+}, Fe^{3+}, Mg^{2+}, Mn^{2+}, Ni^{2+}, and Zn^{2+}) up to 300 nM concentrations was
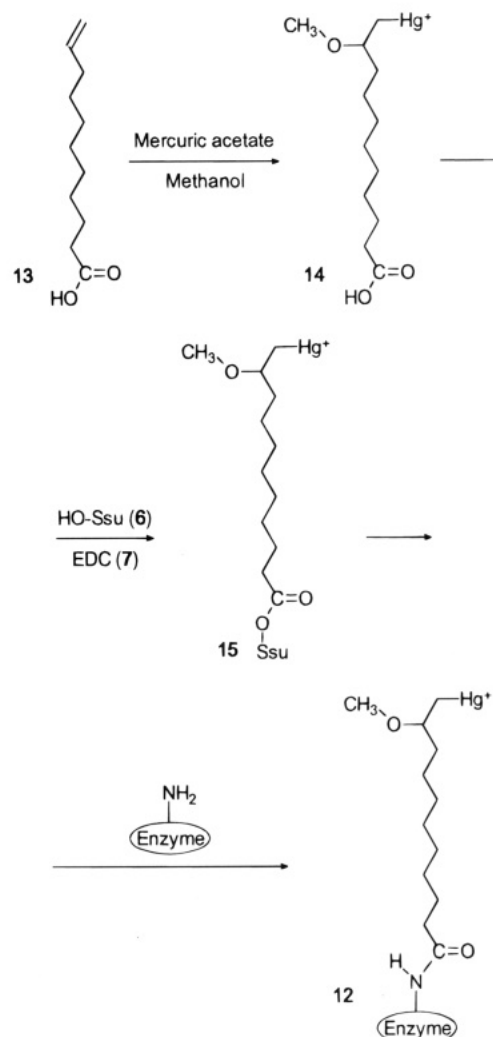
Figure 6. Synthesis of the mercury derivative linked to the reporter enzyme.
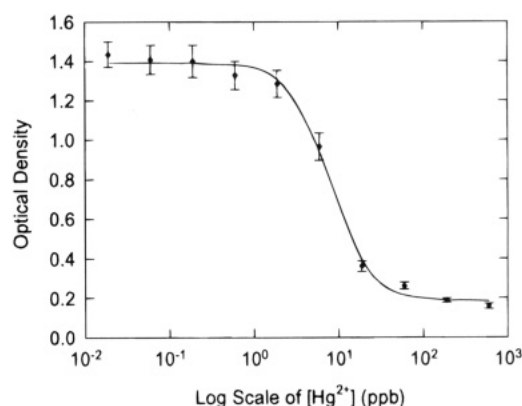
Figure 7. Standard curve of assay format 2A.

observed. Au^{3+} (CR: 11%) and CH_3Hg^+ (CR: 14%) displayed cross-reactivities.

CONA and intestinal AP were used to obtain our reagents. Intestinal AP's unpaired cysteine residues are hidden (*23*). All cysteines of CONA are blocked forming cystines (*24*). Thus, these biopolymers lack thiol groups, ligands with a very strong affinity for mercury, on their surfaces. Therefore, in experiments with CONA, AP, and intermediates instead of the corresponding reagents only low signals were observed.

Mercury is released to the environment largely in its inorganic forms. Methylmercury is produced by bacterial
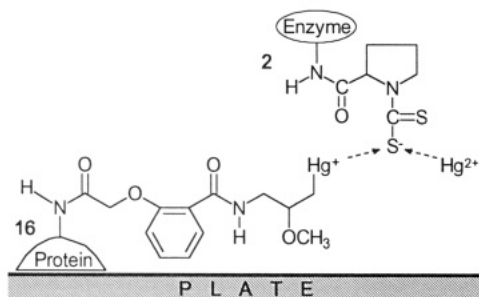
Figure 8. Chemical structures of the reagents involved in assay format 2B. Dotted lines indicate competition for the ligand bound to the reporter enzyme.

methylation of inorganic mercury in lake sediments (*25*). In natural waters, mercury is concentrated in fish, predominantly in the methylmercury form, and biomagnified through the food chain (*3, 25, 26*). Amongst the various mercury species which occur in real samples and which are reactive toward our chelators, Hg^{2+} and CH_3-Hg^+ are by far the most important. They are the most abundant mercury species in most environmental and biological matrices and have the greatest ecotoxicological significance (*25−29*). We thus focused on these two species during the preliminary characterization of our assays. The concentrations of various mercury species and of total mercury in lakes and seas far from pollution sites are usually in the low-ppt range or less (*28, 29*). However, the amount of total mercury in rivers contaminated with industrial, mining, and urban waste occasionally reaches mid-ppt to low-ppb levels (*30*). An important application of rapid mercury assays could be to monitor whether the mercury concentrations in environmental water samples complies with the regulatory limit, 1 ppb in many countries (*30, 31*). The sensitivities of some of our assays appear to be adequate for this use and are similar to those of the cold-vapor atomic absorption spectrometry and a current immunoassay method (*32*). (The amount of total mercury can be measured after decomposition of all mercury species to Hg^{2+}.) For the detection of lower concentrations of mercury, enrichment of the sample, e.g., by means of a specific ion-exchanger resin (*29*) *prior to* the analysis, is necessary. In natural waters, the concentrations of a number of ions are much higher than that of the mercury. For instance, while the large concentrations of alkali metals do not seem to cause problems, small amounts of other ions (e.g., Cu^{2+}) common in environmental samples may crossreact with some of the assays. These interferences might be eliminated by addition of specific masking agents to the assay buffer as well as by cleanup of the samples with selective ion-exchanger resins or with chelate-extraction. These remedies are currently being investigated. Studies with new ligands, tracers, assay formats, and with environmental samples are also in progress. We hope that eventually the principles of our new mercury assays will find further applications in the analysis of hazardous ions.

LITERATURE CITED

(1) Lo, J.-M., and Lee, J.-D. (1994) Dithiocarbamate extraction and Au(III) back extraction for determination of mercury in water and biological samples by anodic stripping voltammetry. *Anal. Chem. 66*, 1242−1248.

(2) Jackson, K. W., and Mahmood, T. M. (1994) Atomic absorption, atomic emission, and flame emission spectrometry. *Anal. Chem. 66*, 252R−279R.

(3) Saouter, E., and Blattmann, B. (1994) Analyses of organic and inorganic mercury by atomic fluorescence spectrometry using a semiautomatic analytical system. *Anal. Chem. 66*, 2031−2037.

(4) Reardan, D. T., Meares, C. F., Goodwin, D. A., McTigue, M., David, G. S., Stone, M. R., Leung, J. P., Bartholomew, R. M., and Frincke, J. M. (1985) Antibodies against metal chelates. *Nature 316*, 265−268.

(5) Wylie, D. E., Lu, D., Carlson, L. D., Carlson, R., Babacan, K. F., Schuster, S. M., and Wagner, F. W. (1992) Monoclonal antibodies specific for mercuric ions. *Proc. Natl. Acad. Sci. U.S.A. 89*, 4104−4108.

(6) Barbas, C. F., III, Rosenblum, J. S., and Lerner, R. A. (1993) Direct selection of antibodies that coordinate metals from semisynthetic combinatorial libraries. *Proc. Natl. Acad. Sci. U.S.A. 90*, 6385−6389.

(7) Chakrabarti, P., Hatcher, F. M., Blake, R. C., 2nd, Ladd, P. A., and Blake D. A. (1994) Enzyme immunoassay to determine heavy metals using antibodies to specific metal-EDTA complexes: optimization and validation of an immunoassay for soluble indium. *Anal. Biochem. 217*, 70−75.

(8) Sachsenberg, S., Klenke, T., Krumbein, W. E., and Zeeck, E. (1992) A back-extraction procedure for the dithiocarbamate solvent extraction method. Rapid determination of metals in seawater matrices. *Fresenius J. Anal. Chem. 342*, 163−166.

(9) Lo, J.-M., Yu, J. C., Hutchison, F. I., and Wal, C. M. (1982) Solvent extraction of dithiocarbamate complexes and back-extraction with mercury(II) for determination of trace metals in seawater by atomic absorption spectrometry. *Anal. Chem. 54*, 2536−2539.

(10) Bond, A. M., and Scholz, F. (1991) Calculation of thermodynamic data from voltammetry of solid lead and mercury dithiocarbamate complexes mechanically attached to a graphite electrode. *J. Phys. Chem. 95*, 7460−7465.

(11) Valentine, W. M., Amarnath, V., Graham, D. G., and Anthony, D. C. (1992) Covalent cross-linking of proteins by carbon disulfide. *Chem. Res. Toxicol. 5*, 254−262.

(12) Giboreau, P., and Morin, C. (1994) Procedure for the preparation of pure dithiocarbamates. *J. Org. Chem. 59*, 1205−1207.

(13) Porstmann, T., and Kiessig, S. T. (1992) Enzyme immunoassay techniques. An overview. *J. Immunol. Methods 150*, 5−21.

(14) Means, G. E., and Feeney, R. E. (1968) Reductive alkylation of amino groups in proteins. *Biochemistry 7*, 2192−2201.

(15) Bekheit, H. K. M., Lucas, A. D., Szurdoki, F., Gee, S. J., and Hammock, B. D. (1993) An enzyme immunoassay for the environmental monitoring of the herbicide bromacil. *J. Agric. Food Chem. 41*, 2220−2227.

(16) Carpino, L. A. (1987) The 9-fluorenylmethyloxycarbonyl family of base-sensitive amino-protecting groups. *Acc. Chem. Res. 20*, 401−407.

(17) Larsen, B. D., and Holm, A. (1994) Incomplete Fmoc deprotection in solid-phase synthesis of peptides. *Int. J. Peptide Protein Res. 43*, 1−9.

(18) Kates, S. A., Daniels, S. B., and Albericio, F. (1993) Automated allyl cleavage for continuous-flow synthesis of cyclic and branched peptides. *Anal. Biochem. 212*, 303−310.

(19) Parkin, J. E. (1989) High-performance liquid chromatography of mercury and phenylmercury as the N-disubstituted dithiocarbamate complexes. *J. Chromatogr. 472*, 401−405.

(20) Parkin, J. E. (1991) High-performance liquid chromatographic assay of thiomersal (thimerosal) as the ethylmercury dithiocarbamate complex. *J. Chromatogr. 542*, 137−143.

(21) Sarzanini, C., Sacchero, G., Aceto, M., Abollino, O., and Mentasti, E. (1992) Simultaneous determination of methyl-, ethyl-, phenyl-, and inorganic mercury by cold vapour atomic absorption spectrometry with on-line chromatographic separation. *J. Chromatogr. 626*, 151−157.

(22) Brown, H. C., and Rei, M.-H. (1969) The solvomercuration–demercuration of representative olefins in the presence of alcohols. Convenient procedures for the synthesis of ethers. *J. Am. Chem. Soc. 91,* 5646–5647.

(23) Fosset, M., Chappelet-Tordo, D., and Lazdunski, M. (1974) Intestinal alkaline phosphatase. Physical properties and quaternary structure. *Biochemistry 13,* 1783–1788.

(24) Williams, J., Elleman, T. C., Kingston, I. B., Wilkins, A. G., and Kuhn, K. A. (1982) The primary structure of hen ovotransferrin. *Eur. J. Biochem. 122,* 279–303.

(25) Zillioux, E. J., Porcella, D. B., and Benoit, J. M. (1993) Mercury cycling and effects in freshwater wetland ecosystems. *Environ. Toxicol. Chem. 12,* 2245–2264.

(26) Bulska, E., Emteborg, H., Baxter, D. C., Frech, W., Ellingsen, D., and Thomassen, Y. (1992) Speciation of mercury in human whole blood by capillary gas chromatography with a microwave-induced plasma emission detector system following complexometric extraction and butylation. *Analyst 117,* 657–663.

(27) Liang, L., Bloom, N. S., and Horvat, M. (1994) Simultaneous determination of mercury speciation in biological materials by GC/CVAFS after ethylation and room-temperature precollection. *Clin. Chem. 40,* 602–607.

(28) Bloom, N. S., and Effler, S. W. (1990) Seasonal variability in the mercury speciation of Onondaga Lake (New York). *Water Air Soil Pollut. 53,* 251–265.

(29) Emteborg, H., Baxter D. C., and Frech, W. (1993) Speciation of mercury in natural waters by capillary gas chromatography with a microwave-induced plasma emission detector following preconcentration using a dithiocarbamate resin microcolumn installed in a closed flow injection system. *Analyst 118,* 1007–1013.

(30) Janjic, J., and Kiurski, J. (1994) Non-flame atomic fluorescence as a method for mercury traces determination. *Water Res. 28,* 233–235.

(31) Mariscal, M. D., Galban, J., Urarte, M. L., and Aznarez, J. (1992) Study and evaluation of a fluorimetric method for the determination of inorganic mercury in water. *Fresenius J. Anal. Chem. 342,* 157–162.

(32) Wylie, D. E., Carlson, L. D., Carlson, R., Wagner, F. W., and Schuster, S. M. (1991) Detection of mercuric ions in water by ELISA with a mercury-specific antibody. *Anal. Biochem. 194,* 381–387.

REVIEWS

Functionalized Poly(ethylene glycol) for Preparation of Biologically Relevant Conjugates

Samuel Zalipsky*

Liposome Technology, Inc., 960 Hamilton Court, Menlo Park, California 94025. Received August 29, 1994

INTRODUCTION

One of the best biocompatible polymers, poly(ethylene glycol) (PEG),[1] possesses an array of useful properties (*1, 2*). Among them are a wide range of solubilities in both organic and aqueous media (*2, 3*), lack of toxicity and immunogenicity (*4*), nonbiodegradability, and ease of excretion from living organisms (*5*). During the last two decades poly(ethylene glycol) (PEG) was used extensively as a covalent modifier of a variety of substrates, producing conjugates which combine some of the properties of both the starting substrate and the polymer (*6*). Substrates modified with PEG include low molecular weight compounds, almost every class of biological macromolecules as well as particulates, and surfaces of artificial materials (see Table 1). The overwhelming majority of work in this area was prompted by a desire to alter one or more properties of a substrate of interest to make it suitable (or more suitable) for a particular biological application. This often included improvement of solubility properties, increase of molecular weight, or change of a substrate's partition properties in two-phase systems. However, as the arsenals of PEG conjugates and their applications have increased it has become apparent that many undesirable effects triggered *in vivo* by various biological recognition mechanisms can be minimized by covalent modification with PEG. For example, immunogenicity and antigenicity of proteins can be decreased (*4, 27*). Blood lifetime of liposomes, nanoparticles, and proteins can be significantly extended and their uptake by reticuloendothelial system (RES) organs, liver and spleen, diminished (*25*). Thrombogenicity, cell and protein adherence, can be reduced in the case of PEG-grafted surfaces (*26*). These beneficial properties conveyed by PEG are of enormous importance for any system requiring blood contact. Some of the properties of specific PEG conjugates and their applications have been the subject of separate reviews (*4, 12, 13, 15–19, 25, 26*).

In contrast, this review concentrates on functionalized derivatives of PEG, their synthesis, and use. While this review is reasonably comprehensive, emphasis here is given to the best PEG functionalization methods, with particular attention paid to their relevance to various bioconjugate applications. The intent here is also to summarize important recent developments in the field since the publication of previous reviews with somewhat overlapping scopes (*9, 28, 29*).

GENERAL CONSIDERATIONS OF FUNCTIONALIZATION AND CONJUGATION OF PEG

PEGs are polyether diols of general structure HO–$(CH_2CH_2O)_n$–CH_2CH_2–OH (**1**). They are commercially available in a variety of molecular weights and low dispersity ($M_w/M_n \leq 1.1$). While the polyether backbone is fairly chemically inert the primary hydroxyl groups are available for derivatization. The molecular weights of PEGs commonly used for preparation of bioconjugates vary between 1000 and 20 000 Da, although in some instances the polymers of higher and lower molecular weights than in this range were utilized. The choice of the molecular weight is usually governed by the intended use of a particular conjugate. Monomethyl ether of PEG (mPEG) is also often used for preparation of various conjugates, particularly when it is desirable to link multiple chains of the polymer to the intended substrate. The presence of only one derivatizable end group on mPEG minimizes the possibilities for crosslinking and improves homogeneity of such preparations. Therefore, some types of conjugates (e.g., derived from proteins, lipids, surfaces of biomaterials) are almost exclusively prepared using mPEGs as starting materials.

In a few cases attachment of biologically relevant molecules to PEG was achieved directly by utilizing the reactivity of terminal primary OH groups of the commercially available polymer. Examples for preparation of various conjugates containing ether (*30, 31*), ester (*7, 32–34*), or carbonate (*35*) linkages were described. Ester formation with carboxylic acid containing molecules is a particularly clean reaction, which can be driven to completion under very mild conditions (*36*). In most cases, however, suitable functionalization of the polymer is an essential first step on the way to the final conjugate. In biological literature this process is often referred to as "activation" of the polymer.

Since in many instances it is difficult to separate the desired functionalized molecules of PEG from the same polymer that underwent a side reaction or failed to react, it is important to use clean, quantitative reactions for transformation of functional groups on the polymer. In some instances when no extraneous reactive groups are introduced onto PEG and excess of the unreacted polymer can be readily separated from final conjugate, clean and quantitative transformation of the functional groups during the "activation" process is not absolutely required. This is often the case with PEG–protein conjugates which can be separated from PEG reagents on the basis of their size, charge, or hydrophobicity. Functionalization

Table 1. Summary of Various Classes of PEG Conjugates and Their Applications

conjugates of	useful properties and applications	reviews and/or leading refs
drugs	improved solubility, controlled permeability through biological barriers, longevity in bloodstream, controlled release	*7–9*
affinity ligands	used in aqueous two-phase partitioning systems for purification and analysis of biological macromolecules, cells	*10, 11*
cofactors	bioreactors with continuous regeneration and recycling of macromolecular cofactors	*12–14*
peptides	improved solubility, conformational analysis	*3, 15*
proteins	resistance to proteolysis, reduced immunogenicity and antigenicity, longevity in bloodstream. Uses: therapeutics, organic-soluble reagents, bioreactors	*4, 16–19*
saccharides	new biomaterials, drug carriers	*20, 21*
oligonucleotides and analogs	improved solubility, resistance to nucleases, cell membrane permeability	*22, 23*
lipids	used for preparation of PEG-grafted liposomes	24
liposomes and particulates	longevity in bloodstream, RES-evasion	25
biomaterials	reduced thrombogenicity, reduced protein and cell adherence	26

and conjugation strategies are often influenced by the intended use of the final product. For example, for both affinity two-phase partitioning and bioreactor applications (see Table 1), it is not critical to achieve complete substitution of the end groups with the ligand molecules. Contamination of the conjugate with unreacted PEG can usually be tolerated as well. On the other hand, the nature of the linkage between the components of a conjugate and its stability can be critically important. The most stringent requirements for purity and homogeneity apply to those conjugates intended for use as polymeric drugs. Since demonstration of biological activity and/or efficacy is a very delicate task which can be influenced by minute impurities, it is very important to avoid any type of contamination including that of unreacted or partially reacted PEG derivatives (*7, 9*).

There are two principal approaches for preparation of functional derivatives of preformed polymers that are relevant to the PEG case: (1) direct transformation of hydroxyls to the new target functionality and (2) reaction of the polymer with a bifunctional molecule so that one function forms an attachment to the polymer and the other one remains available for further chemical transformations. Both approaches are often used, and each has its merits, which should be considered when planning a specific conjugation strategy. First, the most common and versatile derivatives of PEG used in bioconjugation protocols or as intermediates for preparation of other functionalized PEGs will be discussed.

FUNCTIONALIZED DERIVATIVES OF BROAD UTILITY

Halo-Substituted Derivatives of PEG. Conversion of terminal hydroxyl groups into chloride or bromide derivatives is readily achieved by treatment with thionyl chloride (*7, 37, 38*) or bromide, respectively (*39*). These transformations are known to proceed quantitatively. Both chloro- and bromo-PEGs (**2a, 2b**) are typically used as intermediate derivatives for further transformation of functional groups (Scheme 1).

Sulfonate Esters of PEG. Reaction of primary hydroxyl groups of PEG with organic sulfonyl chlorides was used extensively as a method for placement of good leaving group residues at the polymer terminals and as an alternative to halogenation of PEG-OH (*40–45*). Sulfonate esters are usually more reactive than halides, and they are often used as convenient starting materials for the preparation of a variety of functionalized PEGs (amino (*40, 42*), thiol (*45*), phenylglyoxal (*46*), and benzaldehyde (*47*)). Tosylate-PEG (**3**) is the most commonly used sulfonate ester. Several variations on the synthesis of this derivative claimed to provide complete transformation of the functional groups (*42–45*). However, the seemingly simple reaction between tosyl chloride and hydroxyl groups of PEG is not always trouble-free. Some

Scheme 1. Commonly Used Synthetic Pathways Leading to Halo, Tosylate, and Amino Derivatives of PEG[a]
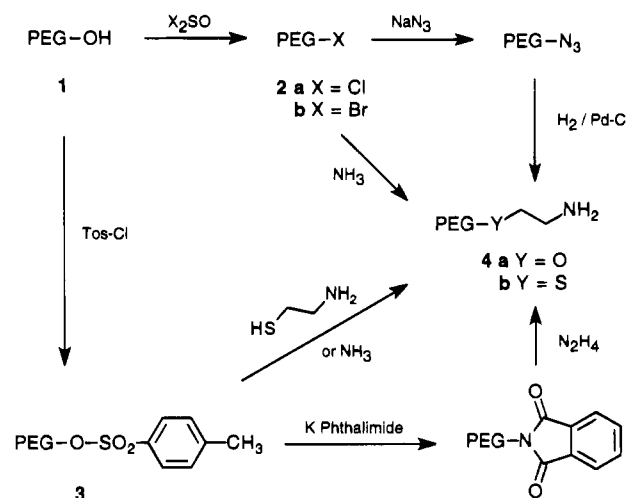
[a] The abbreviation PEG for this and the following schemes and structures refers to the residues $-(CH_2CH_2O)_n-CH_2CH_2-$ or $RO-(CH_2CH_2O)_n-CH_2CH_2-$, where R is a simple alkyl group, usually CH_3. Thus, it differs from the way this abbreviation is used in the remainder of the paper.

side reactions noticed by various authors involved PEG-chain degradation (*41*) and formation of PEG-Cl (*45*). It was also reported that in addition to being able to undergo hydrolysis, tosylates of PEG (**3**) also are susceptible to nucleophilic displacement by oxygen at position 6 from the terminal (*48*). This process can lead to formation of dioxane and PEG shortened by two ethylene oxide units. Methyl sulfonate (mesylate) esters of PEG were advocated as useful alternative derivatives to the tosylates by Harris and co-workers (*41*). Although less reactive than tosylates, they are stable upon long term storage and are easy to prepare. Biologically active mPEG–cholesterol conjugate was prepared by nucleophilic displacement of mesylate by cholesterol alkoxide (*31*).

The tresylate (2,2,2-trifluoroethanesulfonate) of PEG was introduced by Nilsson and Mosbach (*49*) as a reagent for protein modification. PEG-tresylates are approximately 2-orders of magnitude more reactive toward nucleophiles than tosylates, which react with amino groups of proteins only sluggishly. Several research groups used PEG-tresylate for modification of various proteins (*50–52*). The alkylation reaction takes place mainly on the amino groups of proteins (thiols, if present, react as well) and results in a secondary amine linkage formation between PEG and the polypeptide substrate. Tresylate-PEG was also used for linking ligands, such as ATP (*53*) and naloxone (*54*), to PEG for protein

purification by affinity partitioning. Preparation of mPEG-grafted liposomes has been also achieved using a direct mPEG-tresylate reaction with PE-containing liposomes (*55*) or alternatively by synthesizing mPEG−PE first, followed by formation of liposomes (*56*). Glass-immobilized PEG-tresylate proved useful for covalent attachment of proteins (*57*).

Amino-PEG. The higher reactivity of primary amino-PEG (**4**) compared to hydroxy-terminated PEG in nucleophilic substitution reactions makes it a widely used derivative for preparation of various bioconjugates. Low-molecular weight drugs, cofactors, and other ligands (*8, 58−61*), peptides (*62*), glycoproteins (*63*), and surfaces of biomaterials (*64, 65*) have been interlinked with amino-PEG through amide, *sec*-amine, urea, thiourea, and urethane, all stable *in vivo* linkages. Formation of an amide linkage with **4** was found to be a particularly useful reaction, which can be driven to completion under very mild conditions (*3*). For example, several useful functional groups were introduced onto PEG by treating **4** with various heterobifunctional reagents (*66−70*).

There are several published procedures for preparation of PEG with primary amino groups. All of them involve two or more synthetic steps (Scheme 1). One of the most straightforward methods for synthesis of amino-PEG (**4a**) involves conversion of hydroxyl group to halide (**2a** or **2b**) or sulfonyl ester (tosylate or mesylate) first, followed by reaction with an excess of ammonia (*37, 39, 71, 72*). This principal approach was used successfully with some variations in experimental conditions by numerous authors. This process was optimized to yield quantitative conversion of the functional groups and adapted to large scale laboratory preparation (*37*). The major drawback of this simple pathway for preparation of primary amines is in formation of secondary amine byproduct. It appears to be a minor problem in the case of high molecular weight PEG derivatives. However, the extent of this side reaction might depend on the molecular weight of the PEG, as well as on the reaction conditions. It is pertinent, therefore, to check the product by GPC for the presence of crosslinked PEG. Leonard and Dellacherie studied the conversion of mPEG-Cl of molecular weight 5000 into its amino derivative by GPC (*72*). They found that the product contained an increased amount of species of molecular weight 10 000 due to formation of mPEG$_2$NH. Under conditions used by the authors up to 28% of the Cl-end groups underwent crosslinking into mPEG$_2$NH.

The Gabriel-like synthesis of primary amine end groups on PEG was used by Mutter and co-workers (*40*). The sequence of reactions involved conversion of the originally present OH groups (**1**) into *p*-toluenesulfonate esters (**3**), followed by nuleophilic displacement of tosyl groups with potassium phthalimide and finally hydrazinolysis of the phthalimide end groups (Scheme 1). This pathway does not allow for secondary amine formation. Unfortunately, the published procedures yield only ≈80% conversion of hydroxyl groups to amines (**4a**). It was not reported what the remaining ≈20% of the end groups were.

When it is important to have quantitative conversion of the end groups to primary amines it is advisable to follow the sequence of reactions involving conversion to a halide, displacement of the halide with azide, and finally reduction of azide groups to primary amines (Scheme 1) (*73*). It is obvious that primary amines formed by this synthetic pathway cannot be contaminated by secondary amines. Each of the three steps was studied by Zalipsky *et al.* (*7*) and was shown to proceed to completion.

All three methods mentioned above led to terminal amino ethyloxy groups on PEG (**4a**) by direct transformation of hydroxyls to primary amines. Several efficient procedures were published for introduction of amino groups by endcapping the polymer with various bifunctional reagents. For example, reaction between PEG-alkoxide with 2-bromoethyl phthalimide and hydrazynolysis of the resulting phthalimido-PEG results in attachment of aminoethyl groups to the polymer. This modification of the above-mentioned Gabriel synthesis with overall ≈90% conversion of the end groups was described by Geckeler (*74*). Schacht and co-workers urethane-linked aminoethyl residues to PEG by reacting nitrophenyl carbonate derivative of the polymer with 2-(*N*-tritylamino)ethylamine, followed by acidolytic removal of the trityl protecting group (*71*). Polymeric amines of similar structure can be prepared in a one-pot procedure by reacting PEG-OH with carbonyldiimidazole followed by an excess of ethylenediamine (*75*). Conversion of the hydroxyl end groups to primary amines by both methods was essentially quantitative. Reaction between potassium aminoethanethiolate and PEG-tosylate (**3**) provides for another way for introduction of primary amino groups onto the polymer (**4b**) (*42*). The conversion of the functional groups by this route is typically higher than 90%.

Esterification of PEG-OH with amino acids provides another way for introduction of terminal NH$_2$ groups. Such α-amino acid esters are utilized as starting materials in liquid phase peptide synthesis (*3*). It was demonstrated that DMAP-catalyzed attachment of carbodiimide-activated N$^\alpha$-(*tert*-butyloxycarbonyl)-protected amino acids proceeds quantitatively under very mild conditions (*36*). Acidolytic removal of the protecting group exposes a primary amine suitable for various conjugation reactions. The basicity of α-amino esters (pK_a ≈ 7−8) is generally lower than that for the above-mentioned aminoethyl groups. This might increase the efficiency of various conjugation reactions performed in neutral or slightly acidic aqueous media. One also has to bear in mind the potential lability of the ester linkage in aqueous solutions, which might be useful for some and detrimental for other applications. The susceptibility to hydrolysis depends on the molecular weight of PEG, an amino acid residue involved, pH, and temperature. For example, it was observed that, with a few exceptions, most peptide sequences assembled by stepwise addition of amino acid residues onto PEG-amino acid esters can be split from the polymeric carrier under mild alkaline conditions (*3*). Some hydrolysis-resistant PEG-peptides were cleaved from PEG by transesterification, hydrazinolysis, or aminolysis.

Aromatic amines have even lower pK_a values (range from 3 to 6) than α-amino groups of amino acids. Such derivatives were prepared by reacting *p*-nitrobenzyl bromide with potassium alkoxide-PEG, followed by reduction of the nitro group (*76*). Alternatively, PEG was esterified with *p*-nitrobenzoyl chloride followed by reduction of the nitro group with sodium dithionate (*14*). Quantitative conversion of PEG-OH to 4-aminophenylene-PEG, although under drastic reaction conditions, was described by Weber and Stadler (*77*). The synthesis involved K$_2$CO$_3$-mediated coupling of *p*-nitrofluorobenzene to PEG-OH and reduction of the nitro group using N$_2$H$_4$/Pd/C. In addition to alkylation and acylation reactions characteristic to aliphatic amines, aromatic amines can be readily converted into diazonium salts by a treatment with nitrite and used for conjugation by diazo coupling reaction. This mode of conjugation was utilized

Scheme 2. Preparation of Hydrazide Derivatives of PEG
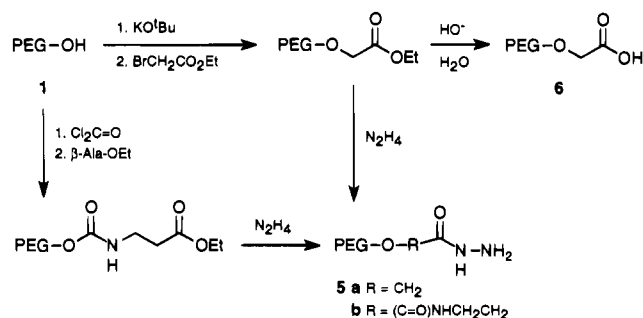
for *p*-aminobenzoate—PEG attachment to pyridoxyl 5′-phosphate producing PEG-linked cofactor for bioreactor use (*14*).

Hydrazido-PEG. One of the most versatile functionalities useful in a variety of bioconjugation protocols is the hydrazido group. The ability of hydrazides to form relatively stable hydrazones with aldehyde-containing compounds is particularly useful for site-specific modification of glycoproteins.

Andresz *et al.* described hydrazinolysis of ester groups of carboxymethyleted PEG, which is readily available by reacting alkoxide of the polymer with haloacetate ester as shown in Scheme 2 (*21*). The reaction led to PEG-hydrazides (**5a**) with an almost theoretical content of the reactive groups. The hydrazides (**5a**) were used for hydrazon formation with aldehyde groups of glucose and maltose oligomers. The conjugates obtained were utilized for enzymatic extension of the carbohydrate residues.

Reaction of PEG-tresylate with an excess of adipic acid dihydrazide was also used for introduction of hydrazido groups onto the polymer (*53*). The resulting adipoyldihydrazido-PEG was used for attachment of periodate-oxidized ATP. Functional group content of the polymeric hydrazide was not reported. However, low ATP content in the PEG conjugate (0.06 mol per mole of PEG) suggests that the hydrazide content in adipoyldihydrazido-PEG might also have been low.

Preparation of urethane-linked *β*-alanine hydrazide (**5b**) was described in patent literature (*78*). The synthesis involved, first, coupling of *β*-alanine ethyl ester to mPEG-chloroformate, followed by hydrazinolysis (Scheme 2). Conversion of the functional groups by this sequence of reactions was quantitative, as ascertained by calorimetric assay for hydrazide groups and determination of *β*-alanine content by amino acid analysis. Coupling of *tert*-butyl carbazate to carboxyl groups on PEG, followed by acidolytic removal of the *tert*-butyloxycarbonyl protecting group, is another, much milder, pathway for preparation of PEG-hydrazide (*79, 80*). Utility of hydrazido-PEG as a protein modifier was demonstrated by coupling mPEG—*β*-alanine hydrazide (**5b**) to carbodiimide-activated carboxyl groups forming diacylhydrazine linkages under acidic conditions that keep lysine residues unreactive (*78*). Site-specific modification of oligosaccharide residues of glycoproteins by periodate oxidation, followed by hydrazone formation reaction with **5b**, was also shown. In both modes of conjugation the composition of the modified proteins was determined by quantitation of *β*-alanine in their hydrolysates by amino acid analysis (*78*).

Hydrazide, which undergoes most of its reactions as a similar to primary amine nucleophile, can be easily converted into acyl azide, which is an active acyl functionality. This reaction was described in several patents as a method for *in situ* mPEG-hydrazide activation for

Scheme 3. Introduction of a Thiol Group onto PEG According to Ref 45
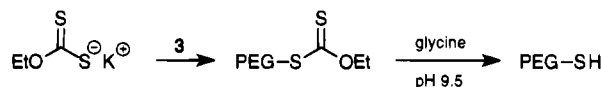
subsequent attachment of the polymer to proteins (*27, 81, 82*). The process involves two steps: treatment of PEG-hydrazide with nitrite under aqueous acidic conditions, without polymer isolation, and reaction with a protein at a basic pH. The hydrazides used in this manner were derived from carboxymethylated PEG (**5a**), and acyl azides formed from this particular functionality are more reactive than usual due to stronger electophilicity of the carboxymethyl moiety.

Mercapto-PEG. Thiol is one of the most useful functional groups in bioconjugate chemistry; however, very little attention has been given to preparation and use of thiol-PEG. A detailed procedure for preparation of PEG-SH, yielding 80—95% transformation of the functional groups, was first reported by Zalipsky *et al.* (*45*). The synthesis (Scheme 3) involved reaction of PEG-tosylate (**3**) with potassium ethyl xanthate. [Ethoxy-(thiocarbonyl)thio]-PEG isolated from this reaction was aminated with glycine to yield PEG-SH. Importance of oxygen exclusion from the reaction media and vigilant maintenance of anaerobic conditions was very important for the maximal yield of thiol groups. Several approaches to mPEG-thiol were recently discussed by Harris *et al.* (*83*). Regardless of the synthetic route chosen, the main complication in mPEG-SH preparation was formation of the disulfide, which in some cases was the only product recovered . Fortunately, (mPEG-S—)₂ can be readily detected by GPC and reduced to desirable mPEG-SH by thiolysis or using conventional reducing agents, e.g., sodium borohydride or lithium aluminum hydride. Derivatization of mPEG-NH₂ with a heterobifunctional reagent, succinimidyl 3-(2-pyridylditio)propionate, followed by reduction, was used as a method for introduction of thiol groups onto the polymer (*69*). Thus obtained, mPEG—mercaptopropionamide was used for grafting the polymer chains onto maleimide-containing liposomes.

Carboxyl-PEG and Its Active Esters. There are several convenient ways to introduce a carboxyl group onto PEG. Carboxymethylation of PEG with α-haloacetic acid or its esters offers a simple method for quantitative carboxylation of the polymer's end groups. This is best accomplished by displacement of the bromide in ethyl bromoacetate with PEG-alkoxide, followed by saponification of the ester (Scheme 2) (*39, 84, 85*). Chemical (*86, 87*) and microbial (*88*) oxidation of the primary hydroxyls can be used to place the same oxyacetate groups at the terminals of the polymer **6**. However, strong oxidizing agents, e.g., permanganate (*87*), can also cause polyether chain degradation, and one has to be very cautious with their application to PEG.

Modification of the polymer with succinic (or glutaric) anhydride is also a very straightforward way to place carboxylic acid groups at PEG terminals (Scheme 4). The reaction can be driven to completion using an excess of anhydride, under reflux, in various organic solvents (*7, 89—91*). The same product (**7**) can be readily obtained at room temperature by a (dimethylamino)pyridine/triethylamine-catalyzed process (*7*). Ester linkages connecting succinate residues to the polymer have limited stability in aqueous media, which has to be taken into account when designing a biologically relevant conjugate from PEG-succinate (*92, 93*). Succinic anhydride reaction of amino-PEG results in a more stable amide bond between the polymer and succinate residue (*39, 86*).

Scheme 4. Preparation, Use, and Side Reactions Associated with PEG-Succinate and its Succinimidyl Ester
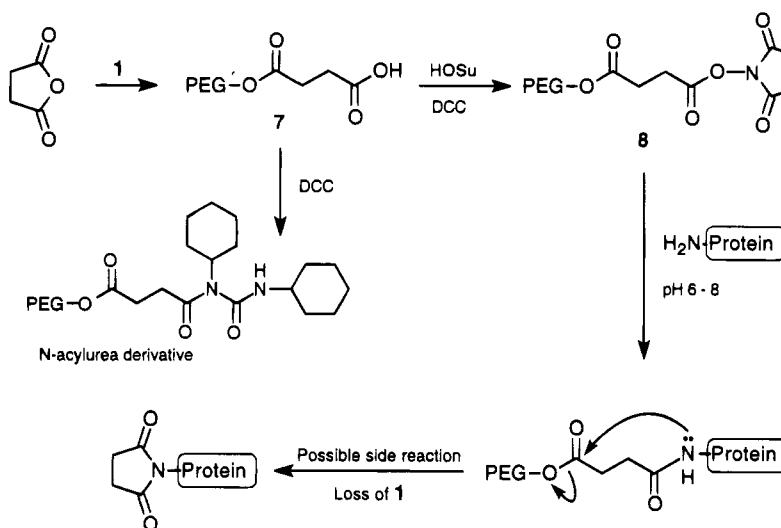
However, this approach for preparation of carboxylated PEG involves three—four synthetic steps (starting from PEG-OH).

The commercially available reagent, ethyl isocyanatoacetate, proved to be an efficient modifier of PEG's hydroxyls (*45, 73, 79, 94*). The resulting ethyl esters of the PEG-glycine carbamates can be hydrolyzed by mild aqueous alkali, exposing the free carboxyl groups (**9a**). Since urethanes under hydrolytic conditions are considerably more stable than esters, this reaction proceeds cleanly, without any loss of urethane-linked glycine residues. Alternatively, urethane-linked amino acids or peptides can be easily prepared from PEG-active carbonates (*95–97*), as described in the next section. The carboxyl groups of these derivatives (**9**) are readily available for further derivatization and conjugation reactions (*95, 98*).

Several biologically relevant ligands were covalently attached to carboxylic acid groups of PEG via ester or amide linkages (*7, 37*). Activation of carboxyls with dicyclohexylcarbodiimide (DCC) in the presence of an acyl transfer catalyst was used in most cases. It is interesting to note that while DCC facilitates esterification of PEG-OH with low molecular weight carboxylic acids, particularly in the presence of DMAP (*36*), it often fails to produce esters or even amides from **7**, yielding instead the *N*-acylurea derivative of the polymer (Scheme 4) (*7, 99*). It was found that DCC in combination with N-hydroxybenzotriazole readily converts PEG-carboxyls into amides and esters of various primary amines and alcohols (*7, 45*). On the other hand, when PEG-OH esterification with various N-protected amino acids was attempted in the presence of DCC/*N*-hydroxybenzotriazole, PEG-oxybenzotriazole ether was produced as a major product (*100*).

Active esters of various carboxylated PEGs are very widely used as reagents for modification of proteins, lipids, and other substrates (*20, 29, 86, 101, 102*). The reactions are known to proceed efficiently and selectively with primary amino groups of the substrates (*20, 86, 92*). Succinimidyl esters of carboxymethylated and succinylated PEGs (**8**) are the most popular reagents of this class (*39, 86*). Succinimidyl succinate derivatives of PEG (SS-PEG, **8**) were first introduced as reagents for protein crosslinking and preparation of PEG-peptides (*81, 90*). Due to the reagent's ease of preparation and excellent reactivity under mild aqueous conditions it was later adapted for protein modification (*103*) and still remains

one of the most popular reagents of this class (*29*). Product of the reaction between SS-PEG and a primary amino group-containing substrate yields a succinate residue linked to the substrate via amide and to PEG via ester linkages, respectively. Recently, it has been demonstrated that conjugates of this type tend to cyclize with concomitant cleavage of the hydroxyl component and formation of succinimide derivative of the amine component as the main product (Scheme 4) (*104*). By use of model compounds it has been shown that this base-catalyzed reaction takes place at physiological pH and is approximately 10 times faster than hydrolysis of a simple succinate ester. Formation of antibodies against the linking moieties, most likely to contain both succinimide and succinyl residues, left on a protein after the loss of the hydroxyl component was also reported (*105*).

Active esters of urethane-linked amino acids were recently introduced for modification of proteins, with the intent of using the amino acid-based linker for conjugate characterization (*96, 97*). For example, purified protein conjugates of mPEG–(oxycarbonyl)norleucine (**9b**) were characterized by quantitation of Nle in a hydrolyzed aliquot of the conjugate by amino acid analysis.

9 a R = H, R' = H
 b R = nC₄H₉, R' = H
 c R = nC₄H₉, R' = Su

10
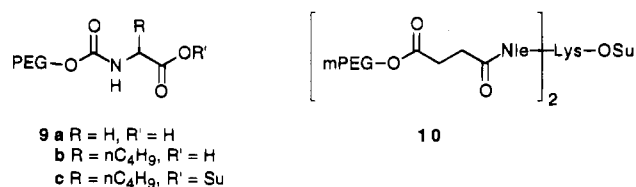
Yamasaki and co-workers used SS-PEG for reaction with Nle, and the isolated mPEG-succinate—Nle was further esterified with *N*-hydroxysuccinimide and used to modify both Nᵅ- and Nᵋ-amino groups of lysine. The carboxyl group of the lysine residue was then converted into succinimidyl ester (**10**), thus producing a new polymeric active ester containing two mPEG chains and 2 equiv of Nle (*106*). The later feature was used for characterization of the protein conjugates derived from the new reagent using amino acid analysis (*106, 107*).

Reactive Carbonate, Carbamate, and Chloroformate Derivatives of PEG. Treatment of the terminal primary hydroxyl groups of PEG with carbonyldiimidazole results in a one-step conversion of the polymer into an amino-reactive (imidazolylcarbonyl)oxy (IC) derivative (**11**). The IC-PEG was first introduced by Beauchamp

Scheme 5. Summary of Synthetic Pathways Leading to Urethane-Forming Active Carbonates, (Imidazolylcarbonyl)oxy, and Chloroformate derivatives of PEG

X = Y = Im	**11** Y = Im
X = Cl, Y = O-pNP	**12** Y = O-TCP
X = Cl, Y = O-TCP	**13** Y = O-pNP
X = Y = O-Su	HOSu ⟨ **14** Y = O-Su
X = Y = Cl	**15** Y = Cl
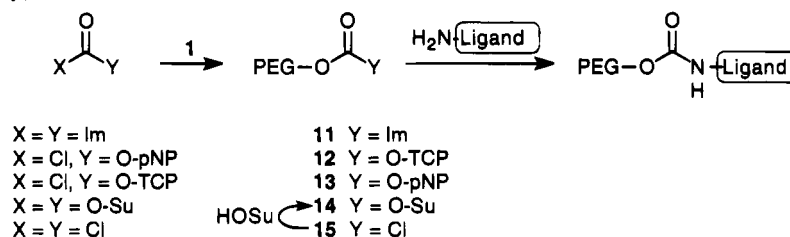
et al. as a reagent for attachment of mPEG chains to amino groups of proteins forming urethane linkages (*108*). Later on, the reagent **11** was fully characterized by NMR and UV spectroscopy and its synthesis further improved to assure complete transformation of the functional groups (*52, 109, 110*). Because of its mild reactivity, to achieve extensive protein modification with IC-PEG long reaction times at alkaline pH are required (48–72 h, pH 8.5). However, good preservation of biological activity of the conjugates was usually observed (*52, 108*). In addition to modification of polypeptide materials, the reagent was also used for preparation of mPEG–DSPE conjugates (*111, 112*) and linking various small ligands to PEG (*60, 109, 113*). It is pertinent to note that the aliphatic urethane linkage formed as a result of primary amino-containing ligand attachment to **11** is extremely stable under a variety of physiological conditions and shows very little breakdown in various buffers pH 2–11 (*60*).

Veronese and co-workers introduced mPEG-carbonate derivatives of 2,4,5-trichlorophenyl (**12**) and *p*-nitrophenyl (**13**) as protein-modifying reagents (*114*). Both derivatives were obtained by using the appropriate phenyl chloroformates in a one step "activation" process as shown in Scheme 5. As in the above-mentioned case of IC-PEG, the products of protein modification with **12** and **13** also have mPEG chains grafted onto the protein through urethane linkages. Taking advantage of the easy and quantitative conversion of the hydroxyl end groups of PEG into the *p*-nitrophenyl carbonate and its clean reaction with primary amines, **13** was used as a starting material for the introduction of new functional groups onto the polymer (amino (*71*), carboxyl (*96, 97*), aldehyde (*115*)). Conjugates of oligonucleotide analogs (*22*) and doxorubicin (*98*) prepared from **13** were also described.

The succinimidyl carbonate of PEG (SC-PEG, **14**) was recently introduced as an efficient and yet selective modifier of amino groups of proteins (*92, 95, 116, 117*). It was also successfully used for synthesis of liposome-forming mPEG–stearylamine (*118*) and PEG–DSPE conjugates (*79*). SC-PEG has higher reactivity than IC-PEG and phenyl carbonates of the polymer (derivatives **11**–**13**). It is comparable in its reactivity to the commonly used active ester derivative, SS-PEG (**8**), yet it is a urethane-forming reagent like derivatives **11**–**13** (*92*). Succinimidyl carbonate functionality was introduced onto PEG in a two-step, one-pot procedure (Scheme 5). First, PEG-OH was treated with phosgene, producing chloroformate end groups (**15**), which were then reacted with *N*-hydroxysuccinimide. This process resulted reliably in a complete conversion of the end groups to succinimidyl carbonates regardless of molecular weight of the polymer (*116*). It was impractical to use succinimidyl chloroformate, an unstable liquid for the preparation of **14**. On the other hand, disuccinimidyl carbonate in the presence of pyridine provides for a convenient alternative method for introduction of SC groups onto PEG (*79, 119*). Since the alternative approach to the introduction of SC-groups

is milder and circumvents the use of phosgene, it might be particularly useful in situations when the activation process has to be performed in the presence of another sensitive functionality (*79*).

The chloroformate derivative of PEG (**15**) by itself is a convenient intermediate for preparation of various conjugates. The advantages of **15** lie in its straightforward, side-reaction free preparation, by treatment of hydroxy-terminated PEG with phosgene (*116, 120, 121*), and its high reactivity toward various nucleophilic groups, which often results in high yields of coupling reactions. Various drugs (atropine (*122*), canabidiol (*123*), and procaine (*121*)) were linked to PEG-chloroformates through carbonate and urethane linkages under mild conditions. Recombinant N-acetylated Eglin c was modified with **15** to increase the protein's persistence *in vivo* (*124*). However, due to the higher reactivity of chloroformates as compared to the above-mentioned active carbonates, not only amino groups but various other nucleophilic residues could have been modified as well. For example, phenol groups of tyrosine readily form carbonates with mPEG-chloroformate (*92*).

Cyanuryl Chloride–PEG. Treatment of mPEG-OH with trichloro-*s*-triazine (cyanuric chloride, **16a**) was used by Davis and co-workers as a method for attachment of reactive dichlorotriazine residue to the polymer end group (**16b**) (*125*). Synthesis of the polymeric dichlorotriazine was optimized to assure reproducible and complete conversion of the terminal hydroxyls, as evidenced by chloride titration, NMR, GPC, and elemental analysis (*126, 127*). The dichlorotriazine residues can react with nucleophilic functional groups (usually amines, but also hydroxyls and sulfhydryls) (*29*), which results in displacement of one of the chlorides (**16c**). This reaction was widely utilized for attachment of mPEG chains to various proteins (*125, 127–132*), despite the fact that cyanuryl halides and derivatives are known as some of the least selective protein modifiers (*133*). This lack of selectivity resulted in marked loss of biological activity of some protein conjugates. For example, it was discovered that in the process of modification of phenylalanine–ammonia lyase **16b** reacted not only with amines, yielding attachments **16c**, but also with sulfhydryl groups (*132*), which led to substantial loss of enzymatic activity. Modification of other nucleophilic residues on proteins with mPEG–dichlorotriazine was suggested in light of the known similar reactivity of low molecular weight analogs (*29, 92*). This speculation was supported by the observation that an attempted mPEG–dichlorotriazine modification of L-asparaginase, an enzyme known to be inactivated by tyrosine-modifying reagents, produced a conjugate retaining only 7% of its original activity (*134*). Recently, during the study of silk fibrin modification with mPEG–dichlorotriazine, Gotoh *et al.* obtained convincing NMR and amino acid analysis evidence for modification of tyrosine and histidine residues of the polypeptide (*135*).

In addition to the wide use for protein modification **16b** was also applied to preparation of mPEG–lipid conju-

Scheme 6. Methods for Preparation of Various Aldehyde Derivatives of PEG
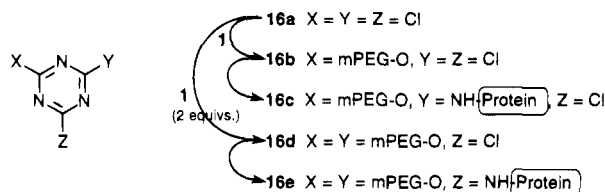
gates (*136*) and for grafting PEG chains to glass (*137*) and poly(ethylene terephthalate) (*138*) surfaces.

Reaction of **16a** with 2 mol of mPEG-OH, leading to 2,4-bis(methoxypolyethylene glycol)-6-chloro-*s*-triazine, was described by Inada and co-workers (*139–141*). Elemental analysis of the product (presumably **16d**) was consistent with substitution of two out of three chlorides of the cyanuric chloride (*139, 141*). Unfortunately, no further characterization of the product was reported until recently, when the entire procedure was reexamined and a new improved synthesis of mPEG$_2$–chlorotriazine was introduced (*142*). It was found that the old procedure yielded in addition to the desired product, **16d**, comparable amounts of **16b** and also some oligomerized mPEG–triazines. The improved procedure for synthesis of mPEG$_2$–chlorotriazine involved reflux in benzene of cyanuric chloride and mPEG-OH in a 1:2 molar ratio in the presence of zinc oxide. This process was free of the side products as was demonstrated by GPC and NMR spectroscopy (*142*). Inada and co-workers used **16d** for modification of a variety of proteins (review (*16*)). The conjugation reaction involves displacement of the remaining chloride of **16d** with an amino group of lysine residue forming a **16e** type of attachment. However, since most of the work published before 1990 used reagent preparations containing substantial amounts of mPEG–dichlorotriazine (*142*), it is difficult to judge the true value of mPEG$_2$–chlorotriazine reagent. It is clear that **16d** requires somewhat more forceful conditions than mPEG–dichlorotriazine to achieve extensive protein modification (*143*). On the other hand, the lower reactivity of a reagent usually translates into higher selectivity. Therefore, one would expect mPEG$_2$–chlorotriazine to be less susceptible to side reactions with nucleophilic residues other than amines and sulfhydryls, which in turn should lead to better preservation of protein activity. Since many of the beneficial properties of PEG–proteins (extended blood circulation time, reduced immunogenicity, etc.) are directly dependent on the PEG content of conjugates, a two-armed reagent, such as mPEG$_2$–chlorotriazine, has an intrinsic advantage over single mPEG-chain reagents in its ability to bind double the amount of the polymer for the same number of attachment sites. For example, in order to eliminate the antigenicity of BSA, approximately half the amino groups (30 out of 60 amines) have to be modified with mPEG–dichlorotriazine (*125*), while only 15 residues have to be modified with mPEG$_2$–chlorotriazine (*143*).

Aldehyde–PEG. The introduction of aldehyde groups at the PEG terminals makes the polymer suitable for conjugation via reductive amination reaction. Scheme 6 illustrates several approaches to preparation of PEG–aldehydes. Several methods for introduction of acetaldehyde residues onto PEG (**17**) were tried using oligomeric models: direct oxidation of the primary hydroxyls with various agents, periodate oxidation of the terminal 1,2-*cis*-diol, and coupling with bromoacetaldehyde diethyl acetal, followed by aldehyde deprotection (*144*). Although satisfactory synthesis of PEG-acetaldehyde (**17**) could be achieved, it was found that this functionalized polymer undergoes rather rapid decomposition in a mild aqueous base, presumably by aldol condensation. Facile inter-

and intramolecular formation of hemiacetals between hydroxyl and acetaldehyde end groups of PEG was observed by Topchieva *et al.* (*145*) during DCC/DMSO/ phosphoric acid oxidation of the bifunctional polymer (**1**). The authors demonstrated that the condensation step was faster than the oxidation, thus yielding hemiacetals as main products. This excessive reactivity and susceptibility to side reactions of **17** limits its usefulness in coupling reactions. These difficulties, however, did not preclude use of PEG–acetaldehyde by a number of research groups. It (**17**) was successfully utilized in sodium cyanoborohydrate-mediated reductive amination reactions for preparation of PEG grafts on aminopropyl glass and on saccharides (glucosamine and chitosan (*41*)), for synthesis of amino-PEG (**4a**) (*8, 41*), and for preparation of conjugates of proteins (*146, 147*). Attachment of mPEG–acetaldehyde, prepared by DMSO/acetic anhydride oxidation, to 1,3-diol groups on poly(vinyl alcohol) via acid-catalyzed cyclic acetal formation was recently described (*148*).
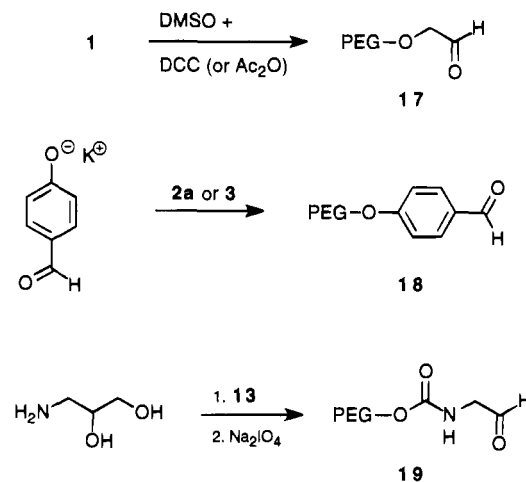
Derivatives of aromatic aldehyde **18** can readily be prepared by potassium 4-oxybenzaldehyde reaction with PEG-chloride (**2a**) (*38, 149*) or PEG-tosylate (**3**) (*47*). According to Harris *et al.* (*47*) PEG–benzaldehyde (**18**) showed low reactivity with amines, requiring heating for extended periods of time for imine formation. It was concluded that **18** is unsuitable for protein conjugation, yet it was useful for grafting the polymer onto aminated glass surfaces.

Propionaldehyde–PEG was recently described in preliminary terms as a derivative reactive enough to be useful for reductive alkylation of proteins yet resistant to side reactions in aqueous media (*47*).

A simple approach to the preparation of mPEG–aldehyde (**19**) was described by Schacht and co-workers (*115*). It involved amination of readily accessible mPEG-nitrophenyl carbonate (**13**) with 3-amino-1,2-propanediol, followed by periodate oxidation of the diol into aldehyde functionality. Conversion of the end groups was almost quantitative through the three-step synthesis. Recently this approach was utilized for introduction of aldehyde groups onto an alternating PEG–lysine copolymer, which was then reductively coupled with the primary amine-containing antibiotic, cephradine (*150*).

Epoxide-PEG. Epichlorohydrin reacts with terminal hydroxyl groups of PEG to introduce electrophilic epoxide groups onto the polymer (*64, 151, 152*) (Scheme 7). A procedure for clean and quantitative conversion of PEG-OH into PEG–epoxide, as judged by NMR and end group

Scheme 7. Preparation of Epoxide Derivative of PEG According To Refs *64* and *151*
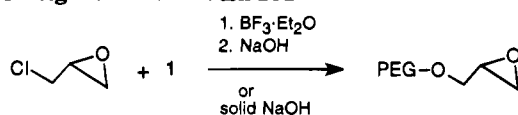
Scheme 8. Preparation and Use of Dimethylmaleic Anhydride Derivative of PEG According to Ref *155*
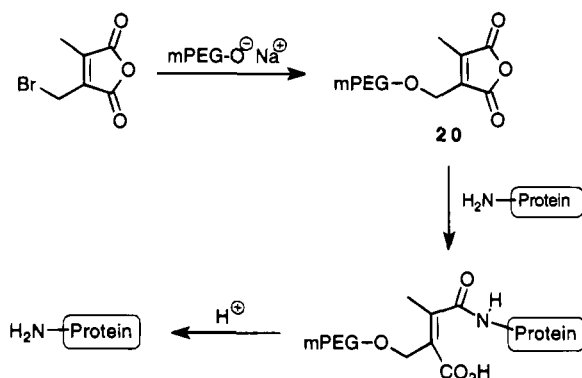
analysis, was recently published (*151*). Other versions of epoxy-terminated PEG synthesis included reactions of the PEG-OH or PEG-NH$_2$ with excess 1,4-butanediol diglycidyl ether (*153, 154*). These preparations were either inadequately characterized (*153*) or were accompanied by various complications (*154*).

PEG—epoxide is an electrophile of mild reactivity toward hydroxyl and amino groups and better reactivity toward thiols. It was utilized in several types of PEG-attachment reactions. Polysaccharides have been modified with PEG—epoxides during overnight incubation in 1 M NaOH (*152*) or via a BF$_3$-catalyzed process in dioxane (*64*). PEG—epoxides were also used for preparation of albumin— and immunoglobulin—PEG conjugates for two-phase partitioning applications (*153, 154*). These conjugation reactions required extended periods of time and/or relatively high pH media. Stark and Holmberg used α,ω-diepoxide—PEG for the immobilization of lipase on aminopropyl—glass surfaces (*57*). They observed rather slow reaction between immobilized PEG—epoxide and the enzyme at pH 9 and much faster lipase attachment to PEG—tresylate grafts. It would appear, therefore, that PEG—epoxide is a reagent of limited utility for modification of proteins, unless a low degree of conjugation is desired. On the other hand PEG—epoxide is quite suitable for grafting the polymer onto various surfaces, since they can be modified under more forceful conditions (*57, 64, 151*).

PEG DERIVATIVES FOR SPECIAL APPLICATIONS

This section describes derivatives of PEG which were prepared for a very specific end use or have not enjoyed wider use despite their potentially broader utility.

Derivatives for Modification of Specific Residues of Polypeptides. In the area of PEG—polypeptides, which is by far the most studied group of PEG conjugates, a number of PEG-based reagents were introduced with a special goal in mind or for a selective attachment of the polymer to a particular type of amino acid residue (*29*).

The dimethylmaleic anhydride analog of mPEG (**20**) was used for reversible attachment of the polymer to amino groups of plasminogen activator proteins (Scheme 8). The linkage between the conjugate components was designed so that mPEG chains were gradually cleaved under physiological conditions through an acid-catalyzed process to regenerate the original active protein (*155*). This is an elegant approach for extending bloodstream persistence of proteins acting on high molecular weight substrates, which tend to lose a significant percentage of their activity when permanently modified with PEG (*95*). The PEG reagent (**20**) was obtained by mPEG—alkoxide reaction with 2-(bromomethyl)-3-methylmaleic anhydride (Scheme 8).

A new reagent (**21**) for linking PEG to proteins was prepared by esterification of mPEG-OH with 4-fluoro-3-nitrobenzoic acid (*156*). The protein modification reaction involved the fluoride displacement by nucleophilic amino groups and was accompanied by a specific change in the reagent's chromophore (λ_{max} = 428 nm). This feature offers a convenient way for determination of the PEG/protein ratio in the conjugate products. The xanthate derivative of PEG (**22**) also reacts with amino groups of amino acids, peptides, and proteins, producing a UV-absorbing (λ_{max} = 242 nm) thiocarbamate attachment of the polymer. This was used for determination of the conjugate's composition (*45, 157*). The xanthate group is quantitatively introduced onto PEG by reacting alkoxide of the polymer with carbon disulfide, followed by chloroacetamide in a one-pot procedure. The dithiosuccinoyl (Dts) amino protecting group can be conveniently introduced onto amino-containing ligands (e.g., amino acids and short peptides) by reacting them first with **22** and then treating the purified PEG—thiocarbamate with (chlorocarbonyl)sulfenyl chloride. As shown in Scheme 9 the cleavage of the conjugate occurs with concomitant formation of Dts-heterocycle (*45*). Purification of the Dts derivatives and the thiocarbamate intermediates was greatly facilitated by the PEG properties of **22**.

Scheme 9. Preparation and Use of 4-Fluoro-3-nitrobenzoate and Xanthate Derivatives of PEG

Scheme 10. Preparation and Use of Iminoester Derivatives of PEG According to Ref 158

mPEG—alkoxide reaction / Scheme structures:

CH₂=CH—CN $\xrightarrow[\text{aq. NaOH}]{\text{mPEG-OH}}$ mPEG—O—CH₂CH₂—CN

$\downarrow$ HCl / CH₃OH

mPEG—O—CH₂CH₂—C(=$\overset{\oplus}{NH_2}$)—N(H)—[Protein] $\xleftarrow{\text{H}_2\text{N-Protein}}$ mPEG—O—CH₂CH₂—C(=$\overset{\oplus}{NH_2}$)—OCH₃ **23**

The imido ester of mPEG (**23**) was described in the patent literature (*158*). The reagent was prepared by acid-catalyzed methanolysis of mPEG—cyanoethyl ether, which is readily accessible by reacting **1** with acrylonitrile. The amino groups of proteins reacted with **23** at pH 7—9 forming positively charged amidine attachments (Scheme 10) (*158*). Thus, this coupling method causes no change in the total charge balance of the modified protein. Making use of the fact that amidine linkages survive the conditions of acidic protein hydrolysis, the extent of mPEG-amidination was determined by diminished lysine content in the conjugates.

Genetic engineering methodology allowing the selective positioning of cysteine residues in polypeptide sequences, combined with their reactivity to maleimide-terminated PEG, offered an opportunity to assemble site-specifically modified PEG—proteins (*67, 68*). The maleimide—PEGs were prepared by acylation of amino-PEG (**4a**) with common heterobifunctional reagents, succinimidyl esters of maleimido carboxylic acids. Introduction of a 3-(2-pyridyldithio)propionyl group onto mPEG-NH₂ by a reaction with SPDP was recently described in detail (*66*). The resulting reagent is useful for site-specific mPEG attachment to proteins through biodegradable disulfide linkages (*67*). Recently, a 4-pyridyldithio derivative of mPEG, having similar reactivity as its 2-pyridyl analog, was described as a modifier of the only free thiol group of papain (*159*). The content of the reactive groups in 4-pyridyldithio-PEG, which was prepared by a treatment of mPEG-SH with excess of 4,4-dithiodipyridyl, was only ≈15% of the theoretical value. No characterization of the intermediate mPEG functionalities (tosylate, thioacetate, and thiol) was furnished.

Glass and co-workers prepared the 4-phenoxy-3,5-dinitrobenzoate ester of PEG (**24**) by a direct esterification of **1**. The 4-phenoxy group was rapidly and selectively displaced at neutral pH with sulfhydryl groups of peptides to form conjugates (*160*). The linker was designed to allow chemical and/or enzymatic derivatization of the peptide sequence and thiolytic release of the modified peptide from the PEG-carrier.

Phenylglyoxal is a reagent known for selective modification of arginine residues of polypeptides (*133*). Its mPEG analog (**25**) was prepared by treatment of mPEG-tosylate (**3**) with 4-hydroxyacetophenone followed by selenium dioxide oxidation of the product (*46*). Attachment of **25** to various proteins proceeded at pH range 5.5—9.3 at room temperature and was characterized by a decrease in arginine content as determined by amino acid analysis of the conjugates. Another PEG reagent for selective modification of arginine residues (**26**) was prepared by coupling camphorquinone 10-sulfonylchloride to **4a** (*70*). The reagent **26** forms PEG—peptide conjugates in borate at pH 9, at 37 °C. The linkage between the components of the conjugates was stable to a variety of acidic and nucleophilic reagents, yet it was cleavable by a treatment with *o*-phenylenediamine. This

made **26** suitable as a carrier for enzymatic and chemical alterations of peptides, taking advantage of the properties of PEG for convenient purification of the final modified peptide and intermediate products.

Structures **24**, **25**, and **26** (chemical structures).

24 — 4-phenoxy-3,5-dinitrobenzoate ester of PEG (O₂N, O₂N, O-phenyl, O—PEG)

25 — PEG—O—C₆H₄—C(=O)—CHO

26 — camphorquinone 10-sulfonyl derivative (O₂S—N(H)—PEG)

Novel Derivatives for Modification of Surfaces. PEG is considered to be the best modifier of materials to reduce adsorption of proteins and biological cells onto their surfaces (*26*). Grafts of this type have also found uses as chromatography media (*64*) and as resin supports for synthesis of peptides (*73*). As mentioned in the previous sections, the grafts were usually prepared by coupling various activated PEGs to suitably functionalized surfaces (*64, 65, 73, 137, 138, 148, 151*). A new reagent, PEG-aryl azide (**27**), was recently described which allows attachment of the polymer onto surfaces without requiring surface functionalization first (*161*). It was synthesized by PEG-alkoxide displacement of fluoride from 4-fluoro-3-nitrophenyl azide. The grafting reaction mediated by long-wavelength (366 nm) UV light irradiation for 10 min of silanized glass preincubated with the **27** for 12 h rendered the parent surface nonplatelet adsorbing.

Synthesis of amino-reactive dithioester—PEG (**28**) was described in detail by Perlier *et al.* (*162*). It involved the following steps: mPEG—alkoxide reaction with dimethyl chloroacetamide, subsequent conversion of the amide into thioamide with Lawesson reagent, followed by S-alkylation with bromoacetic acid, and treatment with hydrogen sulfide (Scheme 11). Despite the fact that the transformation of the functional groups after the four steps was ≤68%, the products were fully characterized by IR, ^{13}C-NMR, and GPC. The reactive dithioester—PEG (**28**) was used for modification of aminopropylated silica tubes and electrophoresis cells, which resulted in lowering of the surface potential and in suppression of the electroosmosis flow (*162*).

Heterobifunctional Derivatives of PEG. Potential utility of heterobifunctional derivatives of PEG as polymeric carriers for targetable drugs (*94*) or as spacers between surfaces and various ligands has been proposed (*83*). However, synthesis of such materials is not trivial. It has been demonstrated in several laboratories that anionic polymerization of ethylene oxide onto an initiator containing a protected functional group and terminated by alkylation or aqueous workup can be used for preparation of heterobifunctional PEGs (*65, 163—165*). Several derivatives were prepared by these methods, among them α-amino-ω-hydroxy-PEG (**29**) seems to be potentially very useful for bioconjugation purposes. It was prepared by a benzaldimine ethanol-initiated polymerization reaction quenched by acidic aqueous workup (*65*), as shown in Scheme 12. Potassium bis(trimethylsilyl)amide can also initiate ethylene oxide polymerization leading to **29** via a similar process (*165*). **29** was used to graft PEG onto poly(vinylbenzyl chloride) latex particles via its amino

Scheme 11. Preparation of Aromatic Azide and Dithioester Derivatives of PEG

1 $\xrightarrow{\text{4-fluoro-3-nitrophenyl azide}}$ PEG–O–⟨aromatic ring with NO$_2$ and N$_3$⟩

27

1. ClCH$_2$CON(CH$_3$)$_2$
2. (pCH$_3$OC$_6$H$_4$PS$_2$)$_2$

PEG–O–CH$_2$–C(=S)–N(CH$_3$)$_2$ $\xrightarrow[\text{2. H}_2\text{S / DMF}]{\text{1. BrCH}_2\text{CO}_2\text{H}}$ PEG–O–CH$_2$–C(=S)–S–CH$_2$–CO$_2$H

28

Scheme 12. Summary of Various Approaches to Preparation of Heterobifunctional PEGs

H–[O–CH$_2$CH$_2$]$_n$–OH $\xrightarrow{\text{Functionalization reaction(s)}}$ X–[O]$_n$–X ; X–[O]$_n$–Y ; Y–[O]$_n$–Y

1

(benzylidene aminoethoxide Na$^+$)

or

(CH$_3$)$_3$Si–N$^-$–Si(CH$_3$)$_3$ K$^+$

1. n (ethylene oxide)
2. H$_2$O / H$^+$

→ Separation → X–[O]$_n$–Y

macrocyclic hemi-acetal $\xrightarrow{\text{KIO / H}^+}$

29 X = NH$_2$, Y = OH

30 X = OCH$_2$CO$_2$H, Y = OH

31 X = O$_2$C-Gly-OH, Y = N$_3$

32 X = O$_2$C-Gly-OH, Y = OH

33 X = O$_2$C-Gly-N$_2$H$_2$-Boc, Y = SC

group (*65*) and for preparation of cationic liposomes containing amino-PEG—lipid (*166*). There are a few examples in the literature describing the formation of PEG conjugates by ethylene oxide polymerization onto an appropriate initiator composed of a drug molecule: cholesterol (*31*) and Cinerubin A aglicon (*167*). Clearly, this method is limited in scope because very few biologically active ligands can be expected to survive the harshness of the polymerization conditions.

Although polymerization of ethylene oxide constitutes the most direct synthetic route to heterobifunctional PEGs, safe handling of this poisonous and explosive monomer presents a major limitation of this approach. To assure meticulously anhydrous polymerization conditions or to contaminate the hetrobifunctional product with α,ω-dihydroxy-PEG formed by termination and chain-transfer side reactions is another dilemma. Hence, finding alternative methods for preparation of heterobifunctional PEGs is considered desirable. Topchieva *et al.* identified one such method (*145*). The authors found conditions for preferential formation of macrocyclic hemiacetals during oxidation of hydroxyl end groups of conventional α,ω-dihydroxy-PEG (up to molecular weight 6000) to aldehydes. Mild oxidation of the macrocyclic PEG with potassium hypoiodide resulted in the formation of α-hydroxy-ω-(carboxymethyl)-PEG (**30**), which was utilized for protein modification.

A more general approach to preparation of PEGs with two different functional groups at the termini involves intentional partial functionalization of **1**, followed by separation of the heterobifunctional product from the mixture of PEG derivatives, as shown in Scheme 12. For example, ion-exchange properties of one of the functional groups may be utilized. This method was successfully used to prepare several pure heterobifunctional PEGs (**29–32**) when one of the termini contained amino or carboxyl groups (*45, 61, 84, 94*). Macromolecular ω-azido acids derived from PEG-2000 and 4000 (**31**) were prepared in this manner. They were converted into protected ω-amino acids and then attached onto aminomethyl polystyrene to be used as supports for peptide synthesis (*73*). Ion-exchange methods were also employed for purification of NAD linked to only one end of α,ω-diamino-PEG. These adducts were utilized for formation of three component conjugates by coupling the remaining amino group to an enzyme (*168*) or to another catalyst residue (*169*). Naturally, derivatives such as α-carboxyl-ω-hydroxy-PEG (**30, 32**) and α-amino-ω-hydroxy-PEG (**29**) can serve as starting materials for preparation of other heterobifunctional PEGs (*24*). For example, utilization of known protection and functionalization methods allowed for an efficient synthesis of derivative carrying succinimidyl carbonate (SC) and *tert*-butyloxycarbonyl-protected hydrazide residues as the end groups on PEG (**33**) (*79*). The SC group of **33** was used for attachment of the polymer to distearoylphosphotidylethanolamine (DSPE), followed by acydolytic exposure of the hydrazide at the other end of the polymer chain. The product of this synthesis, hydrazide—PEG—lipid, was formulated into doxorubicin-containing liposomes, which were then site-specifically linked with oligosaccharide residues of immunoglobulins (*170*). Strategy analogous to the one employed for the synthesis of hydrazide—PEG—DSPE was used in our laboratory for preparation of amino-PEG—DSPE starting from **29** (*166*). The amino group of this PEG—lipid can be conveniently utilized for further functionalization and conjugation reactions (*24*). Another end group functionalized PEG—lipid was prepared from DSPE and α,ω-bis(carboxymethyl)-PEG, followed by silica gel column chromatographic purification of HO$_2$C—PEG—DSPE (*102*). The conjugate was incorporated into liposomes to which plasminogen was attached to the carboxyl ends of the PEG chains, to be used as a targeting moiety. These proteoliposomes and the above-mentioned immunoliposomes combine target binding ability with extended circulation in the bloodstream. They constitute a practical realization of the previously proposed model for a targetable drug delivery system containing a homing device, a PEG-based carrier, and a drug compartment components (*94*).

A macromolecular analog (**34**) of a popular heterobifunctional reagent, SPDP, was recently described (*171*). It (**34**) was prepared from **29** of molecular weight 2000 by linking a 3-(2-pyridyldithio)propionate moiety to the amino group of the PEG chain and then converting the hydroxy terminal into a reactive SC group. This versatile PEG-based regent is perfectly suitable for linking ligands to biomaterials and for protein—protein crosslinking. Allen *et al.* utilized **34** for preparation of long circulating immunoliposomes (*171*).

(pyridyl)–S–S–CH$_2$CH$_2$–C(=O)–NH–CH$_2$CH$_2$–[O]$_n$–O–C(=O)–O–N(succinimidyl)

34
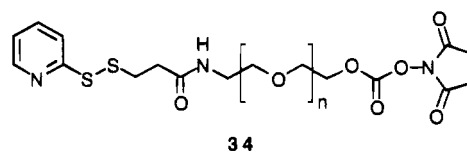
Table 2. ^{13}C-NMR (CDCl$_3$) Chemical Shifts of Functionalized PEG Derivatives^a

$-CH_2CH_3-X$	δ (ppm)
$-CH_2CH_2-OH$	72.5; 61.5
$-CH_2CH_2-OCH_3$	71.9; 58.9
$-CH_2CH_2-Cl$	71.2; 42.5
$-CH_2CH_2-Br$	71.5; 30.2
$-CH_2CH_2-I$	71.9; 2.9
$-CH_2CH_2-N_3$	69.9; 50.5
$-CH_2CH_2-NH_2$	73.1; 41.6
$-CH_2CH_2-NHCO_2C(CH_3)_3$	40.3; 155.9; 78.4; 28.4
$-CH_2CH_2-SH$	72.3; 23.7 (38.3 for disulfide)
$-CH_2CH_2-O(C=O)CH_2NHCO_2C(CH_3)_3$	68.8; 64.3; 170.4; 41.7; 155.1; 79.7; 28.4
$-CH_2CH_2-OCH_2CH(O)CH_2$ (epoxide)	72.1; 62.3; 50.8; 44.3
$-CH_2CH_2-OC_6H_4CHO$	69.4; 67.7; 163.7; 114.8; 131.7; 130.1; 190.5
$-CH_2CH_2-OSO_2C_6H_4CH_3$	68.9; 68.1; 144.2; 129.3; 127.3; 132.6; 21.1
$-CH_2CH_2-OSO_2CH_2CF_3$	69.0; 67.2; q 53.2 ($J = 32$ Hz); q 121.5 ($J = 278$ Hz)
$-CH_2CH_2-O(C=O)CH_2CH_2(C=O)OSu$	68.9; 64.1; 167.6; 26.2; 28.6; 170.9; 168.9; 25.5
$-CH_2CH_2-O(C=O)OSu$	69.0; 68.3; 151.4; 168.5; 25.4
$-CH_2CH_2-O(C=O)OC_6H_4NO_2$	68.7; 68.4; 152.5; 155.8; 121.7; 125.2; 145.7
$-CH_2CH_2-OCH_2CO_2H$	68.8; 172.4
$-CH_2CH_2-O(C=O)NHCH_2CO_2H$	68.9; 63.5; 156.0; 41.9; 170.8
$-CH_2CH_2-O(C=O)NHCH_2CO_2CH_2CH_3$	68.9; 62.6; 155.9; 42.2; 169.4; 60.4; 13.6
$-CH_2CH_2-O(C=O)NHCH_2(C=O)NHNH_2$	69.4; 64.2; 156.7; 43.4; 169.4
$-CH_2CH_2-O(C=O)NHCH_2CH_2(C=O)NHNH_2$	68.5; 63.7; 156.4; 33.9; 37.1; 171.2
$-CH_2CH_2-O(C=S)SCH_2CONH_2$	72.5; 71.3; 212.0; 38.5; 168.4
$-CH_2CH_2-OCH_2(C=S)SCH_2CO_2H$	83.3; 234.8; 36.4; 171.3

^{a} Chemical shifts from right to left represent carbons of the end group residues in the corresponding structures (left column) in the same order. The polyether backbone peak of PEG appears at 70.0 ± 0.2 ppm. The data were compiled from refs 45, 78, 79, 84, 94, 116, 162, and 175 and from unpublished results obtained in the author's laboratory.

Oligomeric heterobifunctional derivatives (two to eight ethylene oxide units) containing maleimide, iodoacetate, dithiopyridyl, and succinimidyl ester groups were recently prepared utilizing standard organic chemistry methods (172). These analogs of conventional heterobifunctional reagents were used for preparation of protein conjugates interlinked through flexible and well water solvated oligoethylene oxide spacers.

CHARACTERIZATION OF FUNCTIONALIZED PEGS

A very important aspect of PEG functionalization/conjugation methodology lies in the proper characterization of the functionalized intermediate and final products. Thus, it seems reasonable to outline here some of the useful analytical methods employed for this purpose. Molecular weights of PEG derivatives are easily determined by GPC using commercially available molecular weight standards (150). In those instances when covalent attachment of two polymeric chains is desirable for a specific product formation (see the above discussion of mPEG$_2$–chlorotriazine synthesis) (142) or is an unwanted side reaction (see the above discussions on mPEG-NH$_2$ and mPEG-SH syntheses), GPC followup of the functionalization process is prudent (72). There are several thin-layer chromatography systems useful for analysis of various PEG derivatives (61, 73). For qualitative analysis for PEG presence in aqueous solutions, e.g., chromatographic fractions, a simple test involving insoluble complex formation upon mixing with acidic solutions of polyacrylic or polymethacrylic acids is recommended (84). One can often take advantage of the optical transparence of PEG at $\lambda > 205$ nm to determine the content of UV absorbing end groups or ligands. Most of the common methods for functional group analysis are applicable to PEGs to determine degree of substitution or efficiency of a particular functionalization reaction. Since PEGs are very soluble materials they can be analyzed by a number of conventional methods used for simple organic molecules. For example, satisfactory elemental analysis of purified PEG derivatives in the several thousand Daltons range can be obtained (45, 77, 91), although occasional difficulties with this mode of

analysis were claimed (41). Both ^{1}H- and ^{13}C-NMR spectra of the PEG backbone are very simple (singlets at $\approx$3.6 and 70 ppm, respectively), which is often useful for analysis of end groups and conjugated residues. Taking advantage of this feature, composition of PEG–proteins can be determined by NMR (127, 147). Some materials, for example, insoluble peptides, are more easily analyzed by NMR in the form of their PEG adducts than in their native form (15). Several H-NMR methods were described for detection and quantitation of terminal hydroxyl groups of PEG either directly or after specific derivatization (173, 174). The power of ^{13}C-NMR as a particulary useful tool for characterization of functionalized PEGs was recognized by several laboratories (45, 162, 175). Table 2 presents a summary of ^{13}C-NMR data of various useful PEG derivatives including most of the ones discussed in this review. Note that in addition to the carbons of various end group residues, the two terminal carbons of PEG usually exhibit identifiable characteristic chemical shifts.

CONCLUDING REMARKS

Due to the unique combination of physical, chemical, and biological properties of PEG, its derivatives became some of the most useful modifiers of biologically relevant molecules. Currently, as the arsenal of interesting applications of PEG conjugates is expanding this trend seems to continue. Some of the PEG-modified substates, e.g., proteins, liposomes, blood-contact materials, already enjoy commercial use.

It is clear that many of the new therapeutic biotechnology products, be it recombinant proteins, oligosaccharides, oligonucleotides, or their analogs, can potentially benefit from protection from enzymatic degradation, extended plasma lifetime, diminished uptake by RES organs, or reduction of other unwanted manifestations of biological recognition that conjugation with PEG is almost certain to provide. In many instances a fine balance between maintenance of the biological activity and the method and the extent of covalent modification is required. The extensive experience with PEG-modified proteins that act on large size substrates shows that such

systems require a particularly great degree of fine tuning (*95*). Increasingly sophisticated PEG-reagents designed to modify selective sites of biological macromolecules certainly will emerge to address some of these challenges. Experience with functionalized PEGs gathered over the last two decades suggests that introduction of appropriate reactive groups onto the polymer can be successful provided a few simple rules are followed (see General Considerations...). In the most demanding situations, when it is essential to have no extraneous functional groups present and yet direct transformation of the hydroxyl into the target functionality is problematic, it is advisable to use a low molecular weight bifunctional reagent containing the target functionality or a protected form thereof and a reactive group that allows for a clean attachment to PEG. This approach benefits from accessibility to low molecular weight bifunctional reagents that are either commercially available or can be obtained in a pure form by conventional organic synthesis methods. Furthermore, with appropriate planning, it gives the researcher an opportunity to use the most efficient coupling chemistry for anchoring the bifunctional moiety onto the polymer.

Another important reason for the increased popularity of PEG lies in its structural simplicity. The polymer has a chemically inert backbone and only two, or in the case of mPEG one, functionalizable end groups. While this simplicity is of clear advantage in situations when it is desirable to link multiple PEG chains to a substrate intended for modification (e.g., protein, liposome), in some situations it might translate into a limitation. For example, for low molecular weight drug–PEG conjugates only a few design options exist. The number of the drug molecules that could be linked to a single PEG chain is also limited. Alternating polyurethanes, prepared by polymerization of bis-SC-PEG with lysine, were recently introduced in order to overcome these design and loading drawbacks (*80, 150*). These materials, while retaining the beneficial properties of PEG, possess high drug attachment capacity through the pendant carboxyl groups of the lysine residues. Clearly, similar systems of increased synthetic versatility could be put together from other trifunctional small molecules and suitably functionalized PEG.

ACKNOWLEDGMENT

LITERATURE CITED

(1) Bailey, J., F. E., and Koleske, J. V. (1976) *Poly(ethylene oxide)*, Academic Press, New York.

(2) Powell, G. M. (1980) Polyethylene glycol. *Handbook of Water Soluble Gums and Resins* (R. L. Davidson, Ed.) pp 18-1-18-31, McGraw-Hill, New York.

(3) Mutter, M., and Bayer, E. (1979) The Liquid-Phase Method for peptide synthesis. *The Peptides* (E. Gross, and J. Meienhofer, Eds.) pp 285–332, Academic Press, New York.

(4) Dreborg, S., and Akerblom, E. B. (1990) Immunotherapy with monomethoxypolyethylene glycol modified allergens. *Crit. Rev. Ther. Drug Carrier Syst. 6*, 315–365.

(5) Yamaoka, T., Tabata, Y., and Ikada, Y. (1994) Distribution and tissue uptake of poly(ethylene glycol) with different molecular weights after intravenous administration in mice. *J. Pharm. Sci. 83*, 601–606.

(6) Harris, J. M., Ed. (1992) *Poly(ethylene Glycol) Chemistry: Biotechnical and Biomedical Applications*, Plenum Press, New York.

(7) Zalipsky, S., Gilon, C., and Zilkha, A. (1983) Attachment of drugs to polyethylene glycols. *Eur. Polym. J. 19*, 1177–1183.

(8) Ouchi, T., Yuyama, H., and Vogl, O. (1987) Synthesis of 5-fluorouracil-terminated monomethoxypoly(ethylene glycol)s, their hydrolysis behavior, and their antitumor activities. *J. Macromol. Sci.-Chem., A24*, 1011–1032.

(9) Topchieva, I. N. (1990) Synthesis of biologically active polyethylene glycol derivatives. A review. *Polymer Sci. USSR 32*, 833–851.

(10) Walter, H., and Johansson, G. (1986) Partitioning in aqueous two-phase systems: An overview. *Anal. Biochem. 155*, 215–242.

(11) Johansson, G. (1992) Affinity partitioning in PEG-containing two-phase systems. Reference 6, pp 73–84.

(12) Okada, H., and Urabe, I. (1987) Polymerizable NAD derivative and model enzyme reactor with recycling of polyethylene glycol-bound NAD. *Methods Enzymol. 136*, 34–45.

(13) Kula, M.-R., and Wandrey, C. (1987) Continuous enzymatic transformation in an enzyme-membrane reactor with simultaneous NADH regeneration. *Methods Enzymol. 136*, 9–21.

(14) Rozzell, D. (1987) Immobilized aminotransferases for amino acid production. *Methods Enzymol. 136*, 479–497.

(15) Pillai, V. N. R., and Mutter, M. (1981) Conformational studies of poly(oxyethylene)-bound peptide and protein sequences. *Acc. Chem. Res. 14*, 122–130.

(16) Inada, Y., Matsushima, A., Kodera, Y., and Nishimura, H. (1990) Polyethylene glycol-protein conjugates: Application to biomedical and biotechnical processes. *J. Bioact. Compatible Polym. 5*, 343–364.

(17) Sehon, A. H. (1991) Suppression of antibody responses by conjugates of antigens and monomethoxypoly(ethylene glycol). *Adv. Drug Delivery Rev. 6*, 203–217.

(18) Delgado, C., Francis, G. E., and Fisher, D. (1992) The uses and properties of PEG-linked proteins. *Crit. Rev. Therap. Drug Carrier Syst. 9*, 249–304.

(19) Katre, N. V. (1993) The conjugation of proteins with polyethylene glycol and other polymers: Altering properties of proteins to enhance their therapeutic potential. *Adv. Drug Delivery Rev. 10*, 91–114.

(20) Ouchi, T., Banba, T., Masuda, H., Matsumoto, T., Suzuki, S., and Suzuki, M. (1991) Design of chitosan-5FU conjugate exhibiting antitumor activity. *J. Macromol. Sci.-Chem. A28*, 959–975.

(21) Andresz, H., Richter, G. C., and Pfannemuller, B. (1978) Chemische Synthese verzweigter Polysaccharide, 5: Kopplung von Oligosacchariden und Amilose an verschiedene Trager durch Hydrazonbindung. (Chemical synthesis of branched polysaccharides, 5. Coupling of oligosaccharides and amylose to various carriers by hydrazone linkage). *Makromol. Chem. 179*, 301–312.

(22) Stirchak, E. P., Summerton, J. E., and Weller, D. D. (1989) Uncharged stereoregular nucleic acid analogs: 2. Morpholino nucleoside oligomers with carbamate internucleotide linkages. *Nucl. Acid Res. 17*, 6129–6141.

(23) Efimov, V. A., Pashkova, I. N., Kalinkina, A. L., and Chakhmakhcheva, O. G. (1993) Synthesis of conjugates of oligonucleotides with polyethylene glycol. *Bioorgan. Khimiya 19*, 800–804.

(24) Zalipsky, S. (1995) Polyethylene glycol-lipid conjugates. *Stealth Liposomes* (D. Lasic, and F. Martin, Eds.) CRC Press, Boca Raton, FL (in press).

(25) Woodle, M. C., and Lasic, D. D. (1992) Sterically stabilized liposomes. *Biochim. Biophys. Acta 1113*, 171–199.

(26) Merrill, E. W. (1992) Poly(ethylene oxide) and blood contact: A chronicle of one laboratory. Reference 6, pp 199–220.

(27) Davis, F. F., Van Es, T., and Palczuk, N. C. (1979) Nonimmunogenic polypeptides. U.S. Patent 4,179,337.

(28) Harris, J. M. (1985) Laboratory synthesis of polyethylene glycol derivatives. *J. Macromol. Sci., Rev. Macromol. Chem. Phys. C25*, 325–373.

(29) Zalipsky, S., and Lee, C. (1992) Use of functionalized polyethylene glycols for modification of polypeptides. Reference 6, pp 347–370.

(30) Johansson, G., and Joelsson, M. (1985) Preparation of Cibacron Blue F3G-A –polyethylene glycol in large scale for use in affinity partitioning. *Biotechnol. Bioengin. 27*, 621–625.

(31) Khachadurian, A. K., Fung, C. H., Van Es, T., and Davis, F. F. (1981) Polyoxyethylated cholesterol derivatives: Organic synthesis, cellular uptake and effect on lipid metabolism in cultured skin fibroblasts. *Biochim. Biophys. Acta 665*, 434–441.

(32) Cecchi, R., Rusconi, L., Tanzi, M. C., Danusso, F., and Ferruti, P. (1981) Synthesis and pharmacological evaluation of poly(oxyethylene) derivatives of 4-isobutylphenyl-2-propionic acid (Ibuprofen). *J. Med. Chem. 24*, 622–625.

(33) Ghedini, N., Zecchi, V., Tartarini, A., Scapini, G., Andrisano, V., and Ferruti, P. (1986) Synthesis and partition profiles of nicotinic acid derivatives with oligomeric carriers. *J. Controlled Release 3*, 185–191.

(34) Dal Pozzo, A., Acquasaliente, M., Donzelli, G., Delor, F., and Ferruti, P. (1986) Synthesis and antimicrobial properties of new aroyl-acrylic esters of polyethylene glycols. *Il Farmaco 41*, 622–629.

(35) Khue, N. V., and Galin, J. C. (1985) Antiinflamatory polymer-bound steroids for topical applications I. Synthesis and characterization. *J. Appl. Polym. Sci. 30*, 2761–2778.

(36) Zalipsky, S., Gilon, C., and Zilkha, A. (1984) Esterification of polyethylene glycols. *J. Macromol. Sci., Chem. A21*, 839–845.

(37) Buckmann, A. F., Morr, M., and Kula, M.-R. (1987) Preparation of technical grade polyethylene glycol (PEG) (Mr 20,000)-N6-(2-aminoethyl)-NADH by a procedure adaptable to large-scale synthesis. *Biotechnol. Appl. Biochem. 9*, 258–268.

(38) Bayer, E., Zheng, H., and Geckeler, K. (1982) Functionalization of soluble polymers 4. Synthesis of dichloro- and di-(4-formylphenyloxyethyl) poly(oxyethylene). *Polym. Bull. 8*, 585–592.

(39) Buckmann, A., Morr, M., and Johansson, G. (1981) Functionalization of poly(ethylene glycol) and monomethoxy-poly(ethylene glycol). *Makromol. Chem. 182*, 1379–1384.

(40) Pillai, V. N. R., Mutter, M., Bayer, E., and Gatfield, I. (1980) New, easily removable poly(ethylene glycol) supports for the liquid-phase method of peptide synthesis. *J. Org. Chem. 45*, 5364–5370.

(41) Harris, J. M., Struck, E. C., Case, M. G., Paley, M. S., Yalpani, M., Van Alstine, J. M., and Brooks, D. E. (1984) Synthesis and characterization of poly(ethylene glycol) derivatives. *J. Polym. Sci.: Polym. Chem. Ed. 22*, 341–352.

(42) Ziegast, G., and Pfannemuller, B. (1984) Linear and star-shaped hybrid polymers 1. A new method for the conversion of hydroxyl end groups of poly(oxyethylene) and other polyols into amino end groups. *Makromol. Chem. Rapid Commun. 5*, 363–371.

(43) Swamikannu, A. X., and Litt, M. H. (1984) Preparation and characterization of p-toluene sulfonyl ester and amino derivatives of tri- and poly(ethylene glycol). *J. Polym. Sci. Polym. Chem. Ed. 22*, 1623–1632.

(44) De Vos, R. J., and Goethals, E. J. (1985) Convenient synthesis of α-tosyl-ω-tosyloxypoly(oxyethylene). *Makromol. Chem. Rapid Commun. 6*, 53–56.

(45) Zalipsky, S., Albericio, F., Slomczynska, U., and Barany, G. (1987) A convenient general method for synthesis of N$^\alpha$- or N$^\omega$-dithiasuccinoyl (Dts) amino acids and dipeptides: Application of polyethylene glycol as a carrier for functional purification. *Int. J. Peptide Protein Res. 30*, 740–783.

(46) Sano, A., Maeda, H., Kai, Y., and Ono, K. (1989) Polyethylene glycol derivatives, modified peptides and production thereof. *Eur. Patent Appl. 0 340 741.*

(47) Harris, J. M., Dust, J. M., McGill, A., Harris, P. A., Edgel, M. J., Herrati, R. S., Karr, L. J., and Donnelly, D. L. (1991) New polyethylene glycol for biomedical applications. *Water-Soluble Polymers* (S. W. Shalaby, C. L. McCormic, and G. B. Butler, Eds.) American Chemical Society: ACS Symposium Series, pp 418–429, American Chemical Society: Washington, DC.

(48) McManus, S. P., Karaman, R. M., Sedaghat-Herati, M. R., Shannon, T. G., Hovatter, T. W., and Harris, J. M. (1990) Chain-cleavage and hydrolysis of activated polyethylene glycol derivatives: Evidence for competitive processes. *J. Polym. Sci.: Polym. Chem. Ed. 28*, 3337–3346.

(49) Nilsson, K., and Mosbach, K. (1984) Immobilization of ligands with organic sulfonyl chlorides. *Methods Enzymol. 104*, 56–69.

(50) Delgado, C., Patel, J. N., Francis, G. E., and Fisher, D. (1990) Coupling of poly(ethylene glycol) to albumin under very mild conditions by activation with tresyl chloride: Characterization of the conjugate by partitioning in aqueous two-phase systems. *Biotechnol. Appl. Biochem. 12*, 119–128.

(51) Knusli, C., Delgado, C., Malik, F., Domine, M., Tejedor, C., Irvine, A. E., Fisher, D., and Francis, G. E. (1992) Polyethylene glycol modification of granulocyte-macrophage colony stimulating factor (GM-CSF) enhances neutrophil priming activity but not colony stimulating activity. *Brit. J. Haematol. 82*, 654–663.

(52) Yoshinga, K., and Harris, J. M. (1989) Effects of coupling chemistry on the activity of poly(ethylene glycol)-modified alkaline phosphatase. *J. Bioact. Compatible Polym. 4*, 17–24.

(53) Persson, L.-O., and Olde, B. (1988) Synthesis of ATP-polyethylene glycol and ATP-dextran and their use in the purification of phosphoglycerate kinase from spinach chloroplasts using affinity partitioning. *J. Chromatogr. 457*, 183–193.

(54) Olde, B., and Johansson, G. (1985) Affinity partitioning and centrifugal counter-current distribution of membrane-bound opiate receptors using naloxone-poly(ethylene glycol). *Neuroscience 15*, 1247–1253.

(55) Senior, J., Delgado, C., Fisher, D., Tilcock, C., and Gregoriadis, G. (1991) Influence of surface hydrophilicity of liposomes on their interaction with plasma protein and clearance from the circulation: Studies with poly(ethylene glycol)-coated vesicles. *Biochim. Biophys. Acta 1062*, 77–82.

(56) Tilcock, C., Ahkong, Q. F., and Fisher, D. (1993) Polymer-derivatized technetium 99mTc-labeled liposomal blood pool agents for nuclear medicine applications. *Biochim. Biophys. Acta 1148*, 77–84.

(57) Stark, M.-B., and Holmberg, K. (1989) Covalent immobilization of lipase in organic solvents. *Biotechnol. Bioeng. 34*, 942–950.

(58) Eidelman, O., Yanai, P., Englert, H. C., Lang, H. C., Greger, R., and Cabantchik, Z. I. (1991) Macromolecular conjugates of transport inhibitors: New tools for probing topography of anion transport proteins. *Am. J. Physiol. 260 (Cell Physiol. 29)*, C1094-C1103.

(59) Buckmann, A. F. (1987) A new synthesis of coenzymically active water-soluble macromolecular NAD and NADP derivatives. *Biocatalysis 1*, 173–186.

(60) Larwood, D. J., and Szoka, F. C. (1984) Synthesis, characterization, and in vivo disposition of iodinatable polyethylene glycol derivatives: Differences in vivo as a function of chain length. *J. Labelled Compd. Radiopharm. 21*, 603–614.

(61) Furukawa, S., Katayama, N., Iizuka, T., Urabe, I., and Okada, H. (1980) Preparation of polyethylene glycol-bound NAD and its application in a model enzyme reactor. *FEBS Lett. 121*, 239–242.

(62) Kawasaki, K., Namikawa, M., Murakami, T., Mizuta, T., Iwai, Y., Hama, T., and Mayumi, T. (1991) Amino acids and peptides XIV: Laminin related peptides and their inhibitory effect on experimental metastasis formation. *Biochem. Biophys. Res. Commun. 174*, 1159–1162.

(63) Urrutigoity, M., and Souppe, J. (1989) Biocatalysis in organic solvents with a polymer-bound horseradish peroxidase. *Biocatalysis 2*, 145–149.

(64) Mathis, R., Hubert, P., and Dellacherie, E. (1985) Polyethylene oxide: a ligand for mild hydrophobic interaction chromatography? *J. Chromatogr. 347*, 291–296.

(65) Huang, Y.-H., Li, Z.-M., and Morawetz, H. (1985) The kinetics of the attachment of polymer chains to reactive latex particles and the resulting latex stabilization. *J. Polym. Sci.: Polym. Chem. Ed. 23*, 795–799.

(66) Herman, S., Loccufier, J., and Schacht, E. (1994) End-group modification of α-hydro-ω-methoxy-poly(oxyethylene) 3: Facile methods for the introduction of a thiol-selective reactive end-group. *Macromol. Chem. Phys. 195*, 203–209.

(67) Kuan, C.-T., Wang, Q.-C., and Pastan, I. (1994) Replacement of surface exposed residues in domain II with cysteine

residues that can be modified with polyethylene glycol in a site-specific manner. *J. Biol. Chem. 269*, 7610–7616.

(68) Goodson, R. J., and Katre, N. V. (1990) Site-directed PEGylation of recombinant interlukin-2 at its glycosylation site. *Bio/Technology 8*, 343–346.

(69) Herron, J. N., Gentry, C. A., Davies, S. S., and Lin, J.-N. (1994) Antibodies as targeting moieties: Affinity measurements, conjugation chemistry, and applications in immunoliposomes. *J. Controlled Release 28*, 155–166.

(70) Glass, J. D., Miller, R., and Wesolowski, G. (1981) A stable, water soluble polymer derivative which specifically and reversibly attaches to the side chain of arginine residues. *Peptides: Structure & Function. Proceedings of the Seventh American Peptide Symposium* (D. Rich, Ed.) pp 209–212, Pierce Chemical Company, Rockford, IL.

(71) Loccufier, J., Crommen, J., Vandorpe, J., and Schacht, E. (1991) End-group modification of α-hydro-ω-methoxypoly-(oxyethylene), 2: Facile methods for the introduction of an α-amino end-group. *Makromol. Chem. Rapid Commun. 12*, 159–165.

(72) Leonard, M., and Dellacherie, E. (1988) Synthesis and characterization of a polyoxyethylene derivative for the affinity labeling of human hemoglobin. *Makromol. Chem. 189*, 1809–1817.

(73) Zalipsky, S., Chang, J. L., Albericio, F., and Barany, G. (1994) Preparation and applications of polyethylene glycol-polystyrene graft resin supports for solid-phase peptide synthesis. *Reactive Polym. 22*, 243–258.

(74) Geckeler, K. (1979) Functionalization of soluble polymers 1. Replacement of the hydroxyl groups of poly(oxyethylene) by amino groups. *Polym. Bull. 1*, 427–431.

(75) Ranucci, E., and Ferruti, P. (1990) A new synthetic method for amino-terminated poly(ethyleneglycol) derivatives. *Synth. Commun. 20*, 2951–2957.

(76) Pollak, A., and Witesides, G. M. (1976) Organic synthesis using enzymes in two-phase aqueous ternary system. *J. Am. Chem. Soc. 98*, 289–291.

(77) Weber, M., and Stadler, R. (1988) Hydrophilic–hydrophobic two-component polymer networks: 1. Synthesis of reactive poly(ethylene oxide) telechelics. *Polymer 29*, 1064–1070.

(78) Zalipsky, S., Lee, C., and Menon-Rudolph, S. (1992) Hydrazine containing conjugates of polypeptides and glycopeptides with polymers. *PCT Int. Appl. WO 92 16555*.

(79) Zalipsky, S. (1993) Synthesis of an end-group functionalized polyethylene glycol–lipid conjugate for preparation of polymer-grafted liposomes. *Bioconjugate Chem. 4*, 296–299.

(80) Nathan, A., Bolikal, D., Vyavahare, N., Zalipsky, S., and Kohn, J. (1992) Hydrogels based on water-soluble poly(ether urethane) derived from L-lysine and poly(ethylene glycol). *Macromolecules 25*, 4476–4484.

(81) Rubinstein, M., Simon, S., and Bloch, R. (1978) Process for the crosslinking of proteins. U.S. Patent 4,101,380.

(82) Shimizu, K., Nakahara, T., and Kinoshita, T. (1985) Plasminogen activator derivatives. U.S. Patent 4,495,285.

(83) Harris, J. M., Herati, M. R. S., Sather, P. J., Brooks, D. E., and Fyles, T. M. (1992) Synthesis of new poly(ethylene glycol) derivatives. Reference 6, pp 371–381.

(84) Zalipsky, S., and Barany, G. (1990) Facile synthesis of α-hydroxy-ω-carboxymethylpolyethylene oxide. *J. Bioact. Compatible Polym. 5*, 227–231.

(85) Royer, G., and Anantharmaiah, G. M. (1979) Peptide synthesis in water and the use of immobilized carboxypeptidase Y for deprotection. *J. Am. Chem. Soc. 101*, 3394–3396.

(86) Boccu, E., Largajiolli, R., and Veronese, F. M. (1983) Coupling of monomethoxypolyethylene glycols to proteins via active esters. *Z. Naturforsch. 38C*, 94–99.

(87) Johansson, G. (1986) Effects of poly(ethylene glycol)-bound alcohols and amines on the partition of albumins and thylakoid membranes in an aqueous two-phase system. *J. Chromatogr. 368*, 309–317.

(88) Matsushima, S., Yoda, N., and Yoshikawa, S. (1989) Microbial transformation of poly(ethylene glycol)s into mono- and dicarboxylic derivatives by specific oxidation of the hydroxymethyl groups. *Makromol. Chem. Rapid Commun. 10*, 63–67.

(89) Geckeler, K., and Bayer, E. (1980) Functionalization of soluble polymers 3. Preparation of carboxy-telechelic polymers. *Polym. Bull. 3*, 347–352.

(90) Joppich, M., and Luisi, P. L. (1979) Peptides flanked by two polymer chains, 1. Synthesis of glycyl-L-tryptophylglycine substituted by poly(ethylene oxide) at both the carboxy and the amino end groups. *Makromol. Chem. 180*, 1381–1384.

(91) Ferruti, P., Tanzi, M. C., Rusconi, L., and Cecchi, R. (1981) Succinic half-esters of poly(ethylene glycol)s and their benzotriazole and imidazole derivatives as oligomeric drug-binding matrices. *Makromol. Chem. 182*, 2183–2192.

(92) Zalipsky, S., Seltzer, R., and Menon-Rudolph, S. (1992) Evaluation of a new reagent for covalent attachment of polyethylene glycol to proteins. *Biotechnol. Appl. Biochem. 15*, 100–114.

(93) Ulbrich, K., Strohalm, J., and Kopecek, J. (1986) Poly-(ethylene glycol)s containing enzymatically degradable bonds. *Makromol. Chem. 187*, 1131–1144.

(94) Zalipsky, S., and Barany, G. (1986) Preparation of poly-ethylene glycol derivatives with two different functional groups at the termini. *Polym. Preprints (ACS) 27*(1), 1–2.

(95) Chiu, H.-C., Zalipsky, S., Kopeckova, P., and Kopecek, J. (1993) Enzymatic activity of chymotrypsin and its poly-(ethylene glycol) conjugates toward low and high molecular weight substrates. *Bioconjugate Chem. 4*, 290–295.

(96) Sartore, L., Caliceti, P., Schiavon, O., and Veronese, F. M. (1991) Enzyme modification by MPEG with an amino acid or peptide as spacer arms. *Appl. Biochem. Biotechnol. 27*, 45–54.

(97) Sartore, L., Caliceti, P., Schiavon, O., Monfardini, C., and Veronese, F. M. (1991) Accurate evaluation method of the polymer content in monomethoxy(polyethylene glycol) modified proteins based on amino acid analysis. *Appl. Biochem. Biotechnol. 31*, 213–222.

(98) Caliceti, P., Monfardini, C., Sartore, L., Schiavon, O., Baccichetti, F., Carlassare, F., and Veronese, F. M. (1993) Preparation and properties of monomethoxy poly(ethylene glycol) doxorubicin conjugates linked by an amino acid or a peptide as spacer. *Il Farmaco 48*(7), 919–932.

(99) Berlinova, I. V., and Panayotov, I. M. (1987) Synthesis and polymerization of poly(ethylene glycol) fumarates. *Makromol. Chem. 188*, 2141–2150.

(100) Hemmasi, B., and Bayer, E. (1977) Zur Anwendung von 1-Hydroxybenzotriazol in der Peptidsynthese. (Use of 1-hydroxybenzotriazole in peptide synthesis). *Tetrahedron Lett. 19*, 1599–1602.

(101) Klibanov, A. L., Maruyama, K., Torchilin, V. P., and Huang, L. (1990) Amphipathic polyethyleneglycols effectively prolong the circulation time of liposomes. *FEBS Lett. 268*, 235–237.

(102) Blume, G., Cevc, G., Grommelin, M. D. J. A., Bakker-Woudenberg, I. A. J. M., Kluft, C., and Storm, G. (1993) Specific targeting with poly(ethylene glycol)-modified liposomes: Coupling of homing devices to the ends of the polymeric chains combines effective target binding with long circulation times. *Biochim. Biophys. Acta 1149*, 180–184.

(103) Abuchowski, A., Kazo, G., Verhoest, C. R., Van Es, T., Kafkewitz, D., Nucci, M. L., Viau, A. T., and Davis, F. F. (1984) Cancer therapy with chemically modified enzymes I. Antitumor properties of polyethylene glycol–asparaginase conjugates. *Cancer Biochem. Biophys. 7*, 175–186.

(104) Tadayoni, B. M., Friden, P. M., Walus, L. R., and Musso, G. F. (1993) Synthesis, in vivo kinetics, and in vivo studies on protein conjugates of AZT: Evaluation as a transport system to increase brain delivery. *Bioconjugate Chem. 4*, 139–145.

(105) Carter, M. C., and Meyerhoff, M. E. (1985) Instability of succinyl ester linkages in O2'-monosuccinyl cyclic AMP–protein conjugates at neutral pH. *J. Immunol. Meth. 81*, 245–254.

(106) Yamasaki, N., Matsuo, A., and Isobe, H. (1988) Novel polyethylene glycol derivatives for modification of proteins. *Agric. Biol. Chem. 52*, 2125–2127.

(107) Yamasaki, N., Matsuo, A., Hatakeyama, T., and Funatsu, G. (1990) Some properties of ricin D modified with a methoxypolyethylene glycol derivative. *Agric. Biol. Chem. 54*, 2635–2640.

(108) Beauchamp, C. O., Gonias, S. L., Menapace, D. P., and Pizzo, S. V. (1983) A new procedure for the synthesis of polyethylene glycol–protein adducts: Effects on function, receptor recognition, and clearance of superoxide dismutase, lactoferrin and α2-macroglobulin. *Anal. Biochem. 131,* 25–33.

(109) Tondelli, L., Laus, M., Angeloni, A. S., and Ferruti, P. (1985) Poly(ethylene glycol) imidazolyl formates as oligomeric drug-binding matrices. *J. Controlled Release 1,* 251–257.

(110) Brygier, J., Gelbcke, M., Guermant, C., Nijs, M., Baeyens-Volant, D., and Looze, Y. (1993) Covalent attachment of poly-(ethylene glycol) to peptides and proteins: Reevaluation of the synthesis, properties and usefulness of carbonylimidazol-1-yl-methoxypolyethylene glycol. *Appl. Biochem. Biotechnol. 42,* 127–135.

(111) Woodle, M. C., Matthay, K. K., Newman, M. S., Hidayat, J. E., Collins, L. R., Redemann, C., Martin, F. J., and Papahadjopoulos, D. (1992) Versatility in lipid compositions showing prolonged circulation with sterically stabilized liposomes. *Biochim. Biophys. Acta 1105,* 193–200.

(112) Allen, T. M., Hansen, C., Martin, F., Redemann, C., and Yau-Young, A. (1991) Liposomes containing synthetic derivatives of poly(ethylene glycol) show prolonged circulation half-lives in vivo. *Biochim. Biophys. Acta 1066,* 29–36.

(113) Duewell, S., Wuthrich, R., von Schulthess, G. K., Jenny, H. B., Muller, R. N., Moerker, T., and Fuchs, W. A. (1991) Nonionic polyethylene glycol–ferrioxamine as a renal magnetic resonance contrast agent. *Invest. Radiol. 26,* 50–57.

(114) Veronese, F. M., Lagajolli, R., Boccu, E., Benassi, C. A., and Schiavon, O. (1985) Surface modification of proteins: Activation of monomethoxy-polyethylene glycols by phenyl-chloroformates and modification of ribonuclease and superoxide dismutase. *Appl. Biochem. Biotechnol. 11,* 141–152.

(115) Vandoorne, F., Loccufier, J., and Schacht, E. (1989) Functionalization of α-hydrogen-ω-methoxypoly(oxyethylene), 1: A new method for the conversion of hydroxyl end groups into aldehyde groups. *Makromol. Chem. Rapid Commun. 10,* 271–275.

(116) Zalipsky, S., Seltzer, R., and Nho, K. (1991) Succinimidyl carbonates of polyethylene glycol: Useful reactive polymers for preparation of protein conjugates. *Polymeric Drugs and Drug Delivery Systems* (R. L. Dunn, and R. M. Ottenbrite, Eds.) pp 91–100, American Chemical Society, Washington, DC.

(117) Sirokman, G., and Fasman, G. D. (1993) Refolding and proton pumping activity of a polyethylene glycol-bacteriorhodopsin water-soluble conjugate. *Protein Sci. 2,* 1161–1170.

(118) Poiani, J. G., Gean, K. F., Fox, J. D., Kohn, J., and Riley, D. J. (1993) Antifibrotic effect of a proline analogue delivered in liposomes to cells in culture. *Amino Acids 4,* 237–248.

(119) Miron, T., and Wilchek, M. (1993) A simplified method for preparation of succinimidyl carbonate polyethylene glycol for coupling to proteins. *Bioconjugate Chem. 4,* 568–569.

(120) Galin, J.-C., Rempp, P., Parrod, J., and Champetier, M. G. (1965) Préparation de chaînes macromoléculaires dotées d'extrémités fonctionnalles réactives (Preparation of macromolecular chains with functionally-reactive extremities). *C. R. Acad. Sc. Paris 260,* 5558–5561.

(121) Weiner, B.-Z., and Zilkha, A. (1973) Polyethylene glycol derivatives of procaine. *J. Med. Chem. 16,* 573–574.

(122) Weiner, B.-Z., Zilkha, A., Perath, G., and Grunfield, Y. (1976) Atropine attached to polyethylene glycols. *Eur. J. Med. Chem.-Chim. Therap. 11,* 525–526.

(123) Weiner, B.-Z., and Zilkha, A. (1975) Monomers and polymers of Δ1(6)-tetrahydrocannabinol and cannabidiol. *Eur. J. Med. Chem.-Chim. Therap. 10,* 79–83.

(124) Goddard, P., O'Mullaine, J., Ambler, L., Daw, A., Brookman, L., Lee, A., and Petrak, K. (1991) R-[N-Acetyl]Eglin c-poly(oxyethylene) conjugates: Preparation, plasma persistance, and urinary excreation. *J. Pharm. Sci. 80,* 1171–1176.

(125) Abuchowski, A., Van Es, T., Palczuk, N. C., and Davis, F. F. (1977) Alteration of immunological properties of bovine serum albumin by covalent attachment of polyethylene glycol. *J. Biol. Chem. 252,* 3578–3581.

(126) Shafer, S., and Harris, J. M. (1986) Preparation of cyanuric chloride-activated poly(ethylene glycol). *J. Polym. Sci.: Polym. Chem. Ed. 24,* 375–378.

(127) Jackson, C.-J. C., Charlton, J. L., Kuzminski, K., Lang, G. M., and Sehon, A. H. (1987) Synthesis, isolation, and characterization of conjugates of ovalbumin with monomethoxypolyethylene glycol using cyanuric chloride as the coupling agent. *Anal. Biochem. 165,* 114–127.

(128) Kiode, A., and Kobayashi, S. (1983) Modification of amino groups in porcine pancreatic elastase with polyethylene glycol in relation to binding activity towards anti-serum and to enzymatic activity. *Biochem. Biophys. Res. Commun. 111,* 659–667.

(129) King, T. P., Kochoumian, L., and Lichtenstein, L. M. (1977) Preparation and immunochemical properties of methoxypolyethylene glycol-coupled and N-carboxymethylated derivatives of ragweed pollen allergen, antigen E. *Arch. Biochem. Biophys. 178,* 442–450.

(130) Gaertner, H., and Puigserver, A. J. (1988) Peptide synthesis catalyzed by polyethylene glycol-modified chymotrypsin in organic solvents. *Proteins 3,* 130–137.

(131) Yoshinaga, K., Shafer, S. G., and Harris, J. M. (1987) Effects of polyethylene glycol substitution on enzyme activity. *J. Bioact. Compatible Polym. 2,* 49–56.

(132) Wieder, K. J., Palczuk, N. C., Van Es, T., and Davis, F. F. (1979) Some properties of polyethylene glycol:phenylalanine ammonia-lyase adducts. *J. Biol. Chem. 254,* 12579–12587.

(133) Atassi, M. Z. (1977) Chemical modification and cleavage of proteins and chemical strategy in immunochemical studies of proteins. *Immunochemistry of proteins* (M. Z. Atassi, Ed.) pp 1–161, Plenum Press, New York.

(134) Ashihara, Y., Kono, T., Yamazaki, S., and Inada, Y. (1978) Modification of E. coli L-asparaginase with polyethylene glycol: Disappearance of binding ability to anti-asparaginase serum. *Biochim. Biophys. Res. Commun. 83,* 385–391.

(135) Gotoh, Y., Tsukada, M., and Minoura, N. (1993) Chemical modification of Silk fibroin with cyanuric chloride-activated poly(ethylene glycol): Analysis of reaction site by 1H-NMR spectroscopy and conformation of the conjugate. *Bioconjugate Chem. 4,* 554–559.

(136) Blume, G., and Cevc, G. (1990) Liposomes for the sustained drug release in vivo. *Biochim. Biophys. Acta 1029,* 91–97.

(137) Herren, B. J., Shafer, S. G., Van Alstine, J., Harris, J. M., and Snyder, R. S. (1987) Control of electroosmosis in coated quartz capillaries. *J. Colloid Interface Sci. 115,* 46–55.

(138) Desai, N. P., and Hubbell, J. A. (1991) Biological responces to polyethylene oxide modified polyethylene terephthalate surfaces. *J. Biomed. Materials Res. 25,* 825–843.

(139) Matsushima, A., Nishimura, H., Ashihara, Y., Yokota, Y., and Inada, Y. (1980) Modification of E. coli asparaginase with 2,4-bis(O-methoxypolyethylene glycol)-6-chloro-s-triazine (activated PEG2): Disappearance of binding ability towards anti-serum and retention of enzymatic activity. *Chem. Lett.* 773–776.

(140) Takahashi, K., Ajima, A., Yoshimoto, T., Okada, M., Matsushima, Y., and Inada, Y. (1985) Chemical reactions by polyethylene glycol modified enzymes in chlorinated hydrocarbons. *J. Org. Chem. 50,* 3414–3415.

(141) Kamisaki, Y., Wada, H., Yagura, T., Matsushima, A., and Inada, Y. (1981) Reduction in immunogenicity and clearance rate of Escherichia coli L-Asparaginase by modification with monomethoxypolyethylene glycol. *J. Pharmacol. Exp. Ther. 216,* 410–414.

(142) Ono, K., Kai, Y., Maeda, H., Samizo, F., Sakurai, K., Nishimura, H., and Inada, Y. (1991) Selective synthesis of 2,4-bis(O-methoxypolyethylene glycol)-6-chloro-s-triazine as a protein modifier. *J. Biomater. Sci. Polym. Ed. 2,* 61–65.

(143) Matsushima, A., Sasaki, H., Kodera, Y., and Inada, Y. (1992) Reduction of immunoreactivity of bovine serum albumin conjugated with polyethylene glycol in relation to its esterase activity. *Biochem. Int. 26,* 485–490.

(144) Paley, M. S., and Harris, J. M. (1987) Synthesis of the aldehyde of oligomeric polyoxyethylene. *J. Polym. Sci. Part A: Polym. Chem. 25,* 2447–2454.

(145) Topchieva, I. N., Kuzaev, A. I., and Zubov, V. P. (1988) Modification of polyethylene glycol. *Eur. Polym. J. 24,* 899–904.

(146) Wirth, P., Souppe, J., Tritsch, D., and Biellmann, J.-F. (1991) Chemical modification of horsradish peroxidase with ethanal-methoxypolyethylene glycol: Solubility in organic solvents, activity, and properties. *Bioorg. Chem. 19*, 133−142.

(147) Chamow, S. M., Kogan, T. P., Venuti, M., Gadek, T., Harris, R. J., Peers, D. H., Mordenti, J., Shak, S., and Ashkenazi, A. (1994) Modification of CD4 immunoadhesin with monometoxypoly(ethylene glycol) aldehyde via reductive alkylation. *Bioconjugate Chem. 5*, 133−140.

(148) Llanos, G. R., and Sefton, M. V. (1991) Immobilization of poly(ethylene glycol) onto a poly(vinyl alcohol) hydrogel 1. Synthesis and characterization. *Macromolecules 24*, 6065−6072.

(149) Bayer, E., Zheng, H., and Geckeler, K. (1985) Functionalization of soluble polymers, 6. Preparation and kinetic aspects of linear, hydrophilic aldehydes based on poly(oxyethylene). *Polym. Bull. 13*, 431−434.

(150) Nathan, A., Zalipsky, S., Erthel, S. I., Agathos, S. N., Yarmush, M. L., and Kohn, J. (1993) Copolymers of lysine and polyethylene glycol: A new family of functionalized drug carriers. *Bioconjugate Chem. 4*, 54−62.

(151) Bergstrom, K., Holmberg, K., Safrani, A., Hoffman, A., Edgell, M. J., Kozlowski, A., Hovanes, B. A., and Harris, J. M. (1992) Reduction of fibrinogen adsorption on PEG-coated polystyrene. *J. Biomed. Mater. Res. 26*, 779−790.

(152) Pitha, J., Kociolek, K., and Caron, M. G. (1979) Detergents linked to polysaccharides: Preparation and effects on membranes and cells. *Eur. J. Biochem. 94*, 11−18.

(153) Head, D. M., Andrews, B. A., and Asenjo, J. A. (1989) Epoxyoxirane activation of PEG for protein ligand coupling. *Bitechnol. Techniq. 3*, 27−32.

(154) Elling, L., and Kula, M.-R. (1991) Immunoaffinity partitioning and use of polyethylene glycol-oxirane for coupling to bovine serum albumin and monoclonal antibodies. *Biotechnol. Appl. Biochem. 13*, 354−362.

(155) Garman, A. J., and Kalindjian, S. B. (1987) The preparation and properties of novel reversible polymer-protein conjugates. 2-ω-Methoxypolyethylene (5000) glycoxymethylene-3-methylmaleyl conjugates of plasminogen activators. *FEBS Lett. 223*, 361−365.

(156) Ladd, D. L., and Snow, R. A. (1993) Reagents for the preparation of chromophorically labeled polyethylene glycol−protein conjugates. *Analyt. Biochem. 210*, 258−261.

(157) King, T. P., and Weiner, C. (1980) Preparation of protein conjugates with alkoxypolyethylene glycols. *Int. J. Peptide Protein Res. 16*, 147−155.

(158) Ueno, H., and Fujino, M. (1987) Chemically modified protein and production thereof. Eur. Patent Appl. 0 236 987.

(159) Woghiren, C., Sharma, B., and Stein, S. (1993) Protected thiol−polyethylene glycol: A new activated polymer for reversible protein modification. *Bioconjugate Chem. 4*, 314−318.

(160) Glass, J. D., Silver, L., Sondheimer, J., Pande, C. S., and Coderre, J. (1979) 4-Phenoxy-3,5-diditrobenzoylpolyethyleneglycol: Reversible attachment of cysteine-containing polypeptides to polymers in aqueous solution. *Biopolymers 18*, 383−392.

(161) Tseng, Y.-C., and Park, K. (1992) Synthesis of photoreactive poly(ethylene glycol) and its application to the prevention of surface-induced platelet activation. *J. Biomed. Mater. Res. 26*, 373−391.

(162) Perlier, S., Levesque, G., and Depraetere, P. (1986) Synthése de poly(oxyéthyléne)s à fonction dithioester terminale. Application au traitement de cellules d'électrophorése (Synthesis of polyoxyethylene with terminal dithioester function: Application to treatment of electrophoresis cell). *Makromol. Chem. 187*, 2369−2386.

(163) Sépulchre, M., Paulus, G., and Jérôme, R. (1983) Specific functionalization of polyoxirane by amino, carboxyl, sulfo and halogeno end groups. *Makromol. Chem. 184*, 1849−1859.

(164) Ito, K., Tsuchida, H., Hayashi, A., Kitano, T., Yamada, E., and Matsumoto, T. (1985) Reactivity of poly(ethylene oxide) macromonomers in radical copolymerization. *Polym. J. 17*, 827−839.

(165) Yokoyama, M., Okano, T., Sakurai, Y., Kikuchi, A., Ohsako, N., Nagasaki, Y., and Kataoka, K. (1992) Synthesis of poly(ethylene oxide) with heterobifunctional reactive groups at its terminals by anionic initiator. *Bioconjugate Chem. 3*, 275−276.

(166) Zalipsky, S., Brandeis, E., Newman, M. S., and Woodle, M. C. (1994) Long circulating, cationic liposomes containing amino-PEG-phosphatidylethanolamine. *FEBS Lett. 353*, 71−74.

(167) Geckeler, K., and Mutter, M. (1979) Soluble polymers for substitute of biopolymers in natural compounds, I: Replacement of the oligosaccharide chain in cinerubin A by polyoxyethylene. *Z. Naturforsch. 34b*, 1024−1025.

(168) Nakamura, A., Urabe, I., and Okada, H. (1986) Anchimeric assistance in the intramolecular reaction of Glucose-dehydrogenase−polyethylene glycol NAD conjugate. *J. Biol. Chem. 261*, 16792−16794.

(169) Yomo, T., Sawai, H., Urabe, I., and Okada, H. (1989) Preparation and kinetic properties of 5-ethylphenazine−poly(ethylene glycol)-NAD⁺ conjugate, a unique catalyst having an intramolecular reaction step. *Eur. J. Biochem. 179*, 299−305.

(170) Allen, T. M., Agrawal, A. K., Ahmad, I., Hansen, C. B., and Zalipsky, S. (1994) Antibody-mediated targeting of long-circulating (Stealth) liposomes. *J. Liposome Res. 4*, 1−15.

(171) Allen, T. M., Brandeis, E., Hansen, C. B., Kao, G. Y., and Zalipsky, S. (1995) A new strategy for attachment of antibodies to sterically stabilized liposomes resulting in efficient targeting to cancer cells. *Biochim. Biophys. Acta*, in press.

(172) Akerblom, E., Dohlsten, M., Brynö, C., Mastej, M., Steringer, I., Hedlund, G., Lando, P., and Kalland, T. (1993) Preparation and characterization of conjugates of monoclonal antibodies and staphylococcal endotoxin A using a new hydrophilic crosslinker. *Bioconjugate Chem. 4*, 455−466.

(173) Dust, J. M., Fang, Z.-H., and Harris, J. M. (1990) Proton NMR characterization of poly(ethylene glycols) and derivatives. *Macromolecules 23*, 3742−3746.

(174) De Vos, R., and Goethais, E. J. (1986) End group analysis of commercial poly(ethylene glycol) monomethyl ethers. *Polym. Bull. 15*, 547−549.

(175) Bayer, E., Zheng, H., Albert, K., and Geckeler, K. (1983) Functionalization of soluble polymers 5. ¹³C-NMR studies of poly(oxyethylene) derivatives. *Polym. Bull. 10*, 231−235.

ARTICLES

Biochemical and Cytotoxic Properties of Conjugates of Transferrin with Equinatoxin II, a Cytolysin from a Sea Anemone

Cecilia Pederzolli,[†,1] Giovanna Belmonte,[†,1] Mauro Dalla Serra,[‡,1] Peter Maček,[§] and Gianfranco Menestrina[*,‡]

Dipartimento di Fisica, Universita' di Trento, 38050 Povo, Trento, Italy, CNR Centro di Fisica degli Stati Aggregati, 38050-Povo, Trento, Italy, and Department of Biology, Biotechnical Faculty, University of Ljubljana, 61000-Ljubljana, Slovenia. Received June 6, 1994[⊗]

Transferrin, a serum glycoprotein, is a major regulator of cellular growth via its cellular receptor. Because transferrin receptors are absent from the plasma membranes of most normal adult resting cells, but are present on transformed, activated, and malignant cells, it can be used to address a toxin toward these cells. The cytolysin equinatoxin II, isolated from the sea anemone *Actinia equina* L., was coupled to human apo or diferric transferrin by using a heterobifunctional cross-linking reagent, *N*-succinimidyl 3-(2-pyridyldithio)propionate (SPDP). The conjugates were separated by column chromatography, and their composition was demonstrated by electrophoresis, antibody staining, and determination of the hemolytic activity in the absence or presence of a reducing agent. The average molar ratio of equinatoxin II to transferrin for the studied conjugates was found to be ≈3.4. The activity of the conjugates against human erythrocytes and human tumor cells (Raji and Jurkat) was assessed. The conjugate is very active on tumor cells in vitro; however, the hybrid molecule maintains an unspecific hemolytic activity. This unspecific toxicity is due to the fact that transferrin-bound toxin partially retains its original ability to bind to the cell membrane directly. It could be strongly reduced (and even eliminated) by pretreating the conjugates with sphingomyelin, the natural ligand of sea anemone cytolysins. These conjugates were stable versus temperature (up to at least 40 °C), versus time (up to several weeks at 4 °C and at least 1 year at −80 °C), and versus repeated freeze–thaw cycles with liquid nitrogen (but not with −80 °C).

INTRODUCTION

Anticancer immunotoxins, built by chemically or genetically linking a toxin to an antibody directed against a transformed cell line, have been extensively studied in the last few years (*1, 2*). In most cases, toxins with an intracellular cytosolic target (so-called A−B type) have been used (*1, 2*). One reason for this is that it is possible to remove the receptor binding part from these toxins, thus strongly enhancing the specificity of the conjugate, although at the expenses of its overall cytotoxicity (*1*). In many cases, human growth factors have been used in place of antibodies of animal origin as a means to target cytotoxic agents while avoiding human anti-mouse antibody (HAMA) response (*3*).

Toxins with an intracellular target require endocytosis to become effective. In principle, other cellular compartments could be addressed with some advantage (*4*), in particular the cell membrane. One way to achieve this is by using a hemolytic toxin in place of an A−B toxin.

Immunotoxins, built by linking a hemolysin from a sea anemone to an antibody, have been described (*5, 6*). We decided to readdress this question by conjugating a hemolysin to a mitogenic molecule like human transferrin (Tfn),[2] which is often used in place of antibodies (*7*). As toxin we chose equinatoxin II, recently isolated from the sea anemone *Actinia equina* and purified to homogeneity (*8*). It is a single polypeptide chain with a molecular weight of about 19 kDa and a pI of 10.3. It shows hemolytic, cytotoxic, and cardiotoxic activity and causes platelet aggregation and lung damage at concentrations ranging from 10^{-13} to 10^{-10} M. At least in part, these effects are due to its ability to form ion channels in the membrane of the attacked cells (*9, 10*).

Tfn is a major regulator of cellular growth (*11−13*), but also a potent mitogen for a variety of tumors (*14−17*). It may induce proliferation even independently of its iron carrying properties (*12*); in fact, a regulatory role of apo-Tfn on the growth of pituitary tumor cells was

---

observed (*18*). The presence of a larger number of Tfn receptors (TR) on growing tumor cells (*12, 13*), particularly on highly metastasizing (*19*) and drug resistant (*20*) cells, as compared to the normal resting counterparts, suggests that Tfn conjugates, such as those described here, could have some use as antitumoral drugs. It is expected that upon interaction with tumor cells the toxin might be liberated at the cell surface or inside the endocytic vacuole where intracellular membranes might then become targets.

Furthermore, the presence of Tfn binding proteins on the outer membrane of pathogenic parasites (*21, 22*) and pathogenic bacteria (*23, 24*) indicates that these conjugates may also have, at least in some cases, an antimicrobial effect. Since microbial Tfn-binding proteins are genetically unrelated to the TR (*21*), conjugates employing anti-TR antibodies would be useless in this application.

EXPERIMENTAL PROCEDURES

Materials. Human iron-saturated and apo-Tfn were obtained from Miles and Sigma, respectively. Tfn has a molecular weight around 80 kDa (*11*) and a pI between 5.2 and 5.7 dependent on the microheterogeneity of its glycan chains (*25*). Bovine serum albumin (BSA), anti-human Tfn polyclonal IgG antibodies, alkaline phosphatase (AP) conjugated anti-IgG antibodies, *N*-succinimidyl 3-(2-pyridyldithio)propionate (SPDP), 3-(4,5-dimethylthiazol-2-yl)-2,5-diphenyltetrazolium bromide (MTT), and dithiothreitol (DTT) were all obtained from Sigma. SM was from Fluka and PC from Calbiochem. All other chemicals were commercial products of sequential or analytical reagent grade.

EqT II. EqT II was isolated and assayed as described elsewhere (*8*). It has a molecular weight of 19 kDa, a pI of 10.3, and a molar extinction coefficient of 3.61×10^4 M^{-1} cm^{-1} at 280 nm (*26*). Chemical modification of the lysine residues by PLP was performed according to (*27*) exactly as described earlier (*28*). The number of moles of lysine residues modified per mole of toxin was determined spectrophotometrically (*29*).

EqT II–Tfn Conjugation and Purification. The toxin was conjugated to Tfn by means of an artificial disulfide bridge introduced via the heterobifunctional cross-linking reagent *N*-succinimidyl 3-(2-pyridyldithio)-propionate (SPDP) (*30*). A three-step scheme was followed. Step 1: Tfn and toxin were separately converted into 2-pyridyl disulfide derivatives using a molar excess of SPDP of 8:1 and 2:1, respectively; after 60 min incubation at room temperature the excess of reagent was removed by gel filtration on a Sephadex G-25 column. Step 2: SPDP-modified toxin was reduced with 10 mM DTT for 1 h and the sample dialyzed to remove the excess of DTT; we found that a 2-fold molar excess of SPDP introduces an average of 1.75 of 2-pyridyldisulfide groups into the toxin, as determined by the release of pyridine-2-thione followed at 343 nm, and confirmed by ion-exchange HPLC. Step 3: freshly reduced SPDP-modified toxin was mixed with SPDP-modified Tfn (with an average of 4.1 2-pyridyldisulfide groups per molecule) in a molar ratio of 2:1 and incubated overnight at 4 °C. The extent of conjugation was again estimated by following the release of pyridine-2-thione at 343 nm, as a result of the thiol disulfide exchange reaction. Either apo or diferric Tfn was used (as specified in the text); conjugates were also made with a PLP-modified toxin prepared as described (*27*).

Conjugates were purified by liquid chromatography in two steps. First, the coupled reaction mixture was applied to a size exclusion column (10 mm i.d., 450 mm

length), loaded with Sephacryl S-200 HR from Pharmacia to remove unconjugated toxin. Fractions of 1 mL were collected at a rate of 15 mL/h. Thereafter, free Tfn was removed by passage through an ionic exchange column (10 mm i.d., 70 mm length, loaded with CM-Sepharose Fast Flow, from Pharmacia). Fractions of 1 mL were collected at a rate of 40 mL/h. The presence of the conjugate in the different fractions was estimated by the absorption at 280 nm and by titrating their hemolytic activity before and after reduction with 2.5 mM DTT.

Electrophoretic Analysis of EqT II–Tfn Conjugates. *SDS–Page.* Denaturing gel electrophoresis was performed according to Laemmli (*31*) using precast minigels (Pharmacia, Uppsala, Sweden). Density gradients ranging from 8 to 25% or 10 to 15% were both used (as it will specifically detailed in the text). A semiautomatic horizontal unit, PhastSystem by Pharmacia, was employed. Gels were stained with either Coomassie brilliant blue or silver stain, and the amount of protein was quantitated by bidimensional densitometry using a PhastImage densitometer (Pharmacia) with a band-pass filter at 613 nm, for Coomassie-stained gels, or at 546 nm, for silver-stained gels. *Western Blot.* After SDS–page the separated bands were transferred to PVDF (hydrophobic poly(vinylidene difluoride)) membrane (Immobilon-P from Millipore) with a semidry blotter (Phast-Transfer by Pharmacia) using 20 V for 20 min at 15 °C. The transfer was checked by reversible prestaining of the blotted bands with ponceau S (from Sigma) and cross-checked by Coomassie staining of the original gel. After ponceau red was removed the membranes were incubated with either antitoxin polyclonal antibodies (mice IgG raised as described (*32*)) or anti-Tfn polyclonal antibodies (goat IgG from Sigma), and the bound proteins were detected with AP conjugated to a secondary antibody (anti-IgG) (*33, 34*). The AP complex was developed using the substrates 5-bromo-4-chloro-3-indolyl phosphate (BCIP) and nitroblue tetrazolium (NBT), which form a brown insoluble precipitate (*35*).

Hemolytic Assays. Hemolytic activity of EqT II and conjugates was determined turbidimetrically at 650 nm with a microplate reader (UVmax from Molecular Devices) supported by the computer program SOFTmax. Human RBC were prepared from fresh heparinized blood by washing it three times (700 g for 10 min) and resuspending it in the saline buffer: 160 mM NaCl, 10 mM Tris·HCl, pH 7.5. Finally, the concentration of HRBC was adjusted with the buffer to an apparent absorbance of 1.0 at 650 nm in a 1 cm path length cuvette. Toxin and conjugates were 2-fold serially diluted in saline buffer (plus 0.2 mg/mL BSA, to saturate the unspecific protein binding sites of plastic which can reduce toxin activity) using flat-bottom 96-well microplates, and one volume of HRBC was added to each well. One hemolytic unit was arbitrarily defined as the reciprocal of the dilution of EqT II changing the optical density with a maximal rate of 0.01 OD/min, which in this assay corresponds to a lysis of around 50% HRBC after 30 min.

Binding of EqT II and conjugates to SUV and HRBC was determined indirectly by measuring the residual hemolytic activity after a preincubation with SUV or HRBC as follows. SUV were prepared by sonication of SM and PC mixtures, exactly as described earlier (*9*). EqT II (5×10^{-6} M) or conjugates B1 and B2 (2.6×10^{-6} M or 3.5×10^{-6} M, respectively, see Figure 2 for the sample definition) were incubated with (or without) SUV of different composition for 20 min at 30 °C or with (or without) HRBC in saline for 10 min at 30 °C. In the case of SUV, unbound toxin (or conjugate) was recovered in a filtrate obtained by centrifuging the mixtures through a
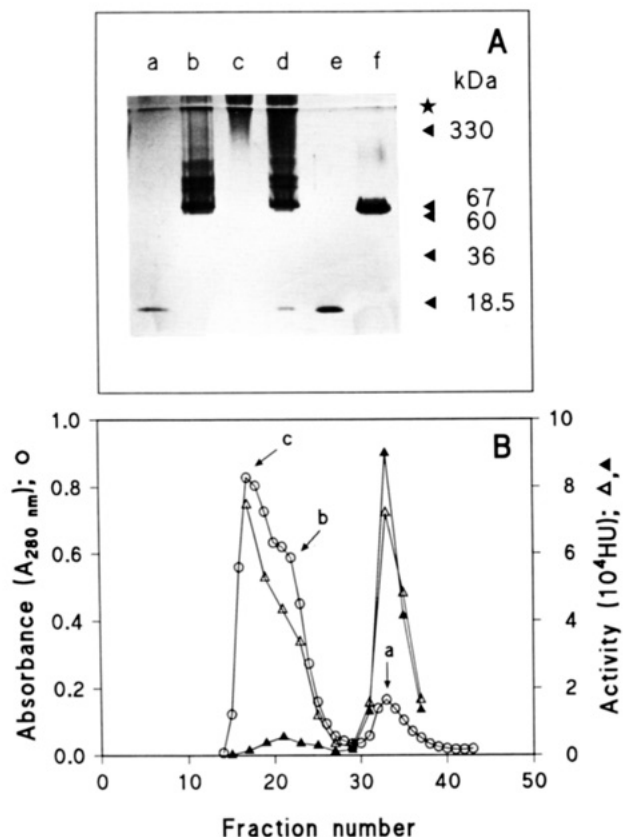
Figure 1. Separation of EqT II–Tfn conjugate from free toxin. Lower panel. Toxin and apo-Tfn were linked via an artificial disulfide bond introduced with the heterobifunctional cross-linking reagent SPDP. To remove unconjugated toxin the coupled reaction mixture was applied to a size exclusion gel filtration column (Sephacryl S-200 HR). The presence of the conjugate in the different fractions was estimated by the absorption at 280 nm (open circles) and by measuring their hemolytic activity before and after reduction with DTT (closed and open triangles respectively). Upper panel. SDS–page of the different samples: lanes a-c, fractions 33, 22, and 17 (as indicated in the lower panel); lane d, unfractionated reaction mixture; lane e, EqT II; lane f, apo-Tfn. The position of standard proteins of known molecular weight is shown on the right with full arrowheads. An asterisk marks the end of the stacking gel. Experimental conditions: polyacrylamide gradient 8–25%, SDS 1.3%, silver staining.

polysulfone filter with a MW cutoff of 300 kDa ($10000g$ for 10 min) which retained vesicles and bound toxin (or conjugate). Before usage the filters (Ultrafree-MC purchased from Millipore) were washed with a 0.2 mg/mL solution of BSA in saline to saturate unspecific protein binding sites. In the case of HRBC it was recovered in the supernatant after centrifugation at $4500g$ for 5 min. The hemolytic activity of toxin and conjugates was then tested as above.

Cytotoxicity Tetrazolium-Based Assay. Toxicity "in vitro" was measured on human Burkitt lymphoma cells (Raji cells) by the 3-(4,5-dimethylthiazol-2-yl)-2,5-diphenyltetrazolium bromide (MTT) reduction assay. Cells were maintained in RPMI-1640 medium (by Sigma) supplemented with 25 mM Hepes, 4 mM L-glutamine, 200 μg/mL of gentamicin, and 10% heat-inactivated fetal calf serum (FCS) at 37 °C in a humidified air atmosphere with 5% CO_2. MTT was dissolved in modified Dulbecco's phosphate buffered saline (PBS, purchased by Sigma) at 5 mg/mL and filtered for sterility. This solution was stored at 4 °C in a dark bottle for 1 week at most. Toxin and conjugates were serially diluted (10-fold at each step) with the RPMI-1640 medium on 96-well microtiter plates. Raji cells (4×10^4) were added to each well in a final
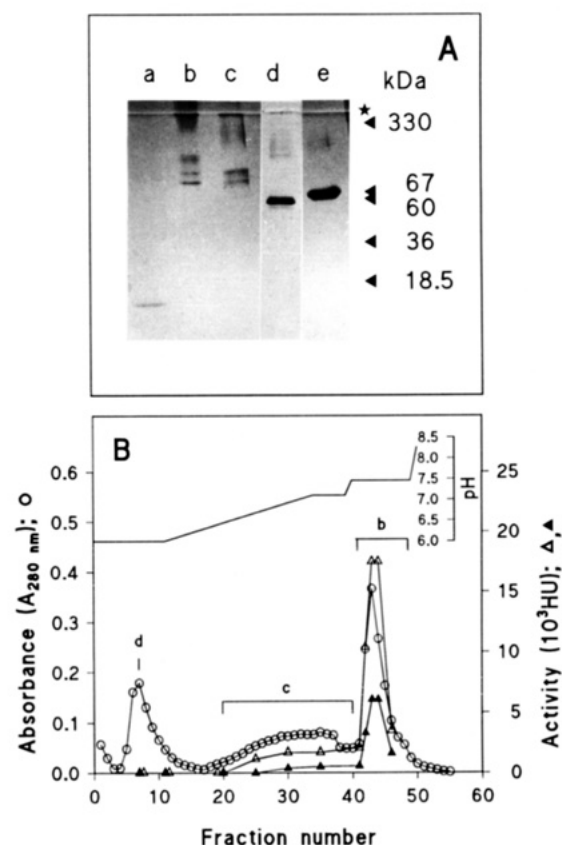
Figure 2. Separation of EqT II–Tfn conjugate from free Tfn. Lower panel. High molecular weight fractions from gel filtration were pooled and applied to a weak cation exchange column (CM-sepharose Fast Flow) to remove free apo-Tfn. The pH profile applied is reported. Fractions 20–40 and 41–48 were pooled and called conjugate B1 and B2, respectively. As in Figure 1, the presence of the conjugate was estimated by measuring the absorption at 280 nm (open circles) and the hemolytic activity before and after reduction with DTT (closed and open triangles, respectively). Upper panel. SDS–page of the different samples: lane a, EqT II; lanes b-d, fractions 41–48, 20–40, and 7 (as indicated in the lower panel); lane e, apo-Tfn. The position of standard proteins of known molecular weight is shown on the right with full arrow-heads. An asterisk marks the end of the stacking gel. Other experimental conditions as in Figure 1.

volume of 100 μL. Each well also contained 0.1 mg/mL of BSA and, if indicated, Tfn (0.4 mg/mL) or SUV of pure SM (10 μg/mL). Plates were then incubated (37 °C, 5% CO_2) for either 1 h (acute cytotoxicity test) or 24 h (long term cytotoxicity test). In the last test 5% FCS was added after the first 6 h. MTT was finally added to each well (0.2 mg/mL), and the cells were cultured for another 2 h before 100 μL of 10% SDS in 0.01 N HCl was added to dissolve the dark blue crystals. After an overnight incubation at room temperature, the optical densities at 575 nm of each well were measured with a microplate reader (UVmax from Molecular Devices).

RESULTS AND DISCUSSION

Construction and Purification of Covalent EqT II–Tfn Conjugates. EqT II and PLP-modified EqT II were conjugated to either apo or diferric Tfn by cross-linking with SPDP, as explained in the Experimental Procedures. Conjugates were purified by liquid chromatography in two steps. In the first step unreacted toxin, MW 19 kDa, was separated from Tfn, MW around 80 kDa, and higher molecular weight conjugates by high-resolution gel filtration (Figure 1). The presence of the free and conjugated toxin in the different fractions was estimated by measuring their hemolytic activity before
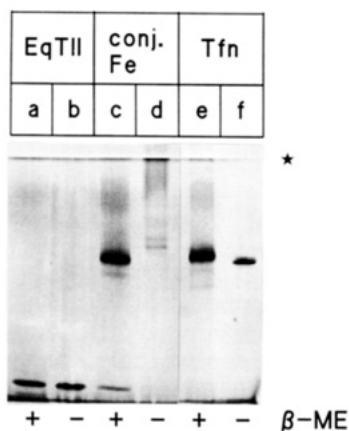
Figure 3. SDS–page of EqT II–Tfn conjugate under native and reduced conditions: lanes a, b, EqT II; lanes c, d, conjugate with diferric Tfn; lanes e, f, Tfn. Lanes a, c, and e also had 3% β-mercaptoethanol. It should be noted that in the presence of β-mercaptoethanol bands are stained heavier. The stacking gel is marked by an asterisk. Other experimental conditions: polyacrylamide gradient 10–15%, SDS 1.3%, silver staining.

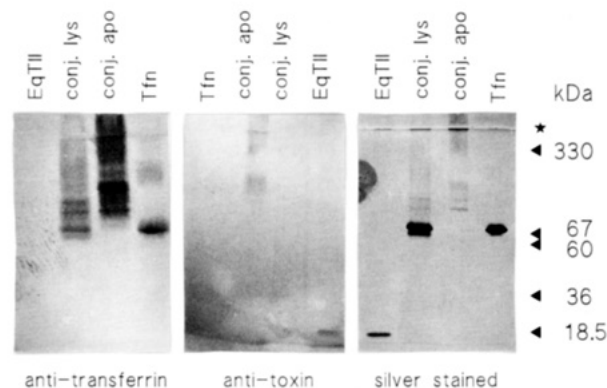**Figure 4.** Western blotting of EqT II–Tfn conjugate. Toxin, Tfn, and conjugates (as indicated) were applied in parallel to three polyacrylamide gels (gradient 10–15%) and run as in Figures 1–3. Proteins from two of the gels were then transferred to blotting membranes and stained with either anti-Tfn (left panel) or anti-toxin (middle panel) antibodies, under nonreducing condition. The third sample was silver-stained (right panel). Arrows on the right indicate the position of standard proteins of different molecular weight. "conjugate-lys" indicates a conjugate made with a lysine modified toxin (PLP modification).

and after reduction with DTT. Fractions eluting later (molecular weight around 18 kDa) had a high hemolytic activity independent of the reducing conditions, as is expected for the free toxin which lacks any disulfide bridge. On the contrary, fractions eluting at high molecular weight (between 70 and 200 kDa) displayed a relevant hemolytic activity only under the reducing conditions, which are expected to release free toxin from the conjugates.

Residual unconjugated Tfn was removed by a second step through an ionic exchange column, taking advantage of the widely different isoelectric point of Tfn and toxin, pI 5.9 and 10.3, respectively. By using a cation exchange column only the conjugates were retained at a pH lower than 7.0 (Figure 2). As expected, fractions eluting in the void volume, supposed to contain free Tfn, were devoid of any hemolytic activity, whereas fractions eluting at higher pH had a high hemolytic activity only in the presence of DTT.

Electrophoretic Characterization of EqT II–Tfn Conjugates. SDS–page analysis of EqT II–Tfn conjugates, under nonreducing conditions (Figure 3), confirmed the presence of high molecular weight compounds and the absence of polypeptides with MW corresponding to either free toxin or free Tfn. Contamination by the free components was below the resolution of the silver staining. By using reducing conditions, we confirmed that the high molecular weight compounds were actually disulfide-linked conjugates containing only one low MW component, around 17 kDa, and one high MW component, around 78 kDa.

Apparently, conjugates containing a variable number of toxin molecules were obtained (Figures 1–3). From a densitometric analysis of lane d of Figure 3, it appears that the principal conjugates had molecular weight of 110 and 125 kDa, corresponding to two and three toxin molecules bound per conjugate. The average value in different preparations was 2.4. Interestingly, the minimum number appeared in any case to be two. A possible explanation for this is that Tfn is a bilobate molecule (*36, 37*), and thus, if a highly reactive site is created with SPDP it is conceivably present in two copies per molecule. From the densities of the toxin and Tfn bands, obtained after reduction of the conjugates (lane c), and comparing to the relevant control lanes (a,e), we evaluated an average number of 3.1 EqT II molecules bound per Tfn in Figure 3. With different preparations the average

number was 3.4 ± 0.4. This number is slightly higher than that obtained under nonreducing conditions. The reason for this is that some conjugates of very high molecular weight exist, which enter the gel only under reducing conditions, otherwise remaining trapped at the end of the stacking gel (lane d). These high MW compounds concur to raise the average toxin/conjugate ratio under reducing conditions.

Immunological Characterization of the Conjugate. The nature of these compounds was made unequivocal by Western blotting experiments (Figure 4). Bands, separated by SDS–page under non reducing conditions, were transferred to a PVDF membrane and stained with either anti-toxin or anti-Tfn polyclonal antibodies. The membrane was then developed using the corresponding AP-conjugated anti-IgG antibodies. Anti-toxin antibodies stained either the free toxin or the high molecular weight bands but not free Tfn. Correspondingly, anti-Tfn antibodies stained either the free Tfn or the high molecular weight bands but not free toxin. This demonstrates that the high molecular weight bands are disulfide-linked conjugates of Tfn and toxin. Finally, PLP-modified toxin, in which the amino groups of most exposed lysine residues were modified, cross-linked only to a minor extent with Tfn (see Figure 4). This confirms that accessible amino groups are used for conjugation by SPDP.

Residual Hemolyticity of the Conjugate. A titration of the hemolytic activity of free EqT II and a purified Tfn conjugate under reducing and nonreducing conditions is shown in Figure 5. HRBC lack the TR and should be resistant to the conjugate. However, despite the removal of all free toxin, we found that, under native conditions, the conjugate was still hemolytic although 70-fold less than the toxin. Its hemolytic activity increased 9-fold when reduced, whereas that of the toxin decreased by a factor of 1.5. Although this residual, unspecific, hemolytic activity is small (less than 1.5% that of free toxin) it might be harmful and should be further investigated. It is probably due to the fact that the toxin in the conjugate, while covalently bound to Tfn, still retains, at least in part, its ability to interact with, and bind to, cell membranes. Conjugates using apo-Tfn gave results which were qualitatively similar.

To demonstrate the binding of conjugates to HRBC we titrated the amount of DTT-dependent hemolytic activity
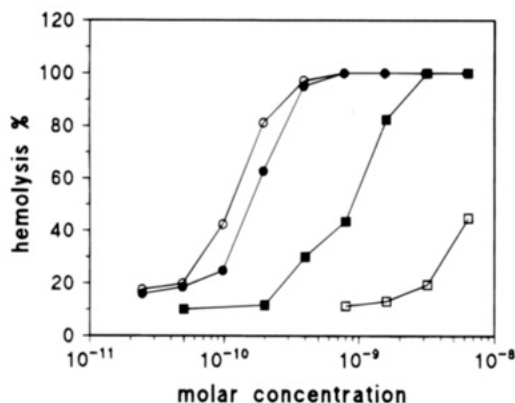
Figure 5. Hemolytic activity of the EqT II–Tfn conjugate. The hemolytic activity of free EqT II (circles) and a purified diferric Tfn conjugate (squares) were estimated under reducing (2.5 mM DTT, filled symbols) and nonreducing conditions (open symbols). The percentage of hemolysis of HRBC was determined with a microplate reader as explained in the Experimental Procedures. Molar concentrations indicated are those equivalent to the toxin content, and in the case of the conjugate, they are lower limits which were calculated assuming an average of two toxin molecules per conjugate.
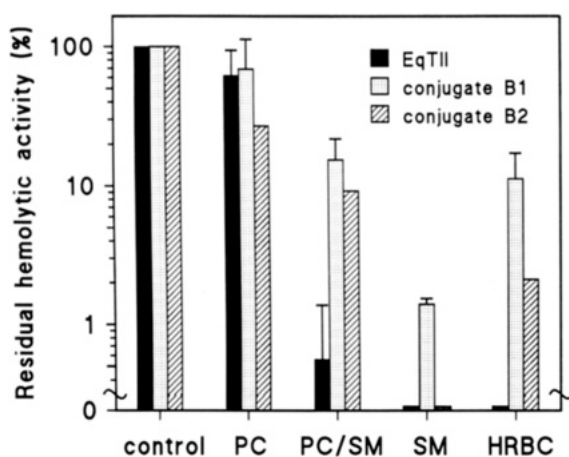
Figure 6. Binding of the EqT II–Tfn conjugate to lipid vesicles and HRBC. Binding of toxin and conjugates to SUV of different composition and to HRBC was estimated by titrating the amount of hemolytic activity remaining in solution after a preincubation with SUV or HRBC. The hemolytic activity was calculated as the reciprocal of the concentration required for 50% hemolysis in the presence of DTT and reported in percentage. One hundred percent was the activity of a pertinent sample incubated only with buffer. Incubation was with SUV for 20 min at 30 °C or with HRBC for 10 min at 30 °C. In the case of SUV, unbound toxin and conjugates were recovered in the filtrate after ultrafiltration through filters with cut off at MW 300 kDa pretreated with BSA. With HRBC they were recovered in the supernatant after centrifugation.

remaining in solution after a preincubation of the conjugate with HRBC and compared to that of the toxin (Figure 6). Assuming a linear dependence between hemolytic activity and toxin concentration, it appears that 100% of free toxin, about 90% of conjugate B1, and 98% of conjugate B2 are bound to the cells and removed from the supernatant during this step.

To demonstrate that binding is mediated by the toxin we investigated whether SM, the best known substrate for toxin action, was also able to bind the conjugate. Binding of toxin and conjugates to small unilamellar vesicles (SUV) of different composition was again determined indirectly by titrating the residual DTT-dependent hemolytic activity remaining in solution after the incubation with SUV (Figure 6). We found that indeed the free

conjugate concentration was decreased by preincubation with sphingolipids in a way qualitatively similar to free EqT II.

The nonspecific (DTT-independent) activity of the recovered conjugate is best estimated through the ratio C_-/C_+ (where C_+ and C_- are the concentration of conjugate necessary to obtain 50% hemolysis in the presence or in the absence of DTT, respectively). The larger this value the lower is the nonspecific activity. Free toxin has a value of about 1 in all cases. The B1 and B2 conjugates instead have values of 8 and 10, respectively, which then slightly increase after incubation with SM-containing SUV (to 9 and 11). This indicates that more specific complexes were recovered after the incubation with lipid, suggesting the enrichment in a population of conjugate molecules with a lower affinity for SM. Such conjugates might have improved specificity in vivo due to reduced interaction with SM.

Cytotoxicity on Tumor Cells. To test the cytotoxicity of these conjugates against cancer cells expressing the TR, a human lymphoblastoid cell line was used (Raji cells from Burkitt lymphoma). Acute toxicity (appearing within 1 h) and long-term toxicity (developed after 24 h) were determined (Figure 7). In the acute test, 50% reduction of viability by EqT II occurred at $\approx 3.5 \times 10^{-10}$ M, whereas with the diferric and apo conjugates at about 2×10^{-9} and 3×10^{-8} M, respectively (data for the apoferric conjugate are not shown). While the cytotoxic activity of EqT II was slightly enhanced by the presence of an excess of free ferric Tfn, that of the ferric conjugate was inhibited by a factor of about 3 (i.e., 66%), suggesting it was, at least in part, dependent on the expression of the TR. The slightly lower activity of the apo-Tfn conjugate, which was also inhibited by free Tfn ($\approx 70\%$), is in line with the fact that apo-Tfn has a lower affinity for the TR than diferric Tfn (*11*). However, the residual activity of the diferric conjugate, in the presence of excess Tfn, was still relatively high (50% viability at $\approx 0.6 \times 10^{-8}$ M in the acute test), confirming that the hybrid molecule could retain, at least in part, the ability to interact with cells via the toxin receptor. These considerations prompted us to examine whether pretreating the conjugate with SM, which potently inhibits free toxin, could remove its unspecific toxicity. We found that, while preincubation of free toxin with SM removes about 99% of its toxicity (and the residual activity is independent from the presence of free Tfn), the same treatment removes only about 90% of the toxicity of the diferric conjugate, and, more importantly, the residual toxicity is this time strongly reduced by free Tfn, indicating it is mediated by the TR. This can be understood on the basis of the heterogeneity of the chemical conjugates. Those conjugates in which the toxin molecules are more exposed (and hence have a higher nonspecific toxicity) would be the first to become inactivated by SM, whereas conjugates in which the SM-binding region of the toxin is less accessible (and hence have a lower nonspecific toxicity) would remain active via the Tfn part.

The long term test confirmed and extended these conclusions. As expected, the toxicities of all samples appeared at lower concentrations. Fifty percent inhibition of viability occurred at $\approx 3 \times 10^{-11}$ M with EqT II and at about 10^{-10} and 3×10^{-10} M with the diferric and the apo conjugate, respectively (data for the apo-ferric conjugate are not shown). Ferric Tfn in excess reduced the activity of the ferric and the apo conjugate (by a factor of ≈ 3), but not that of free toxin. Furthermore, in this case, preincubation of the ferric conjugate with SM produced a molecule with 50% activity around 2×10^{-9} M, which was completely inactivated by an excess of free
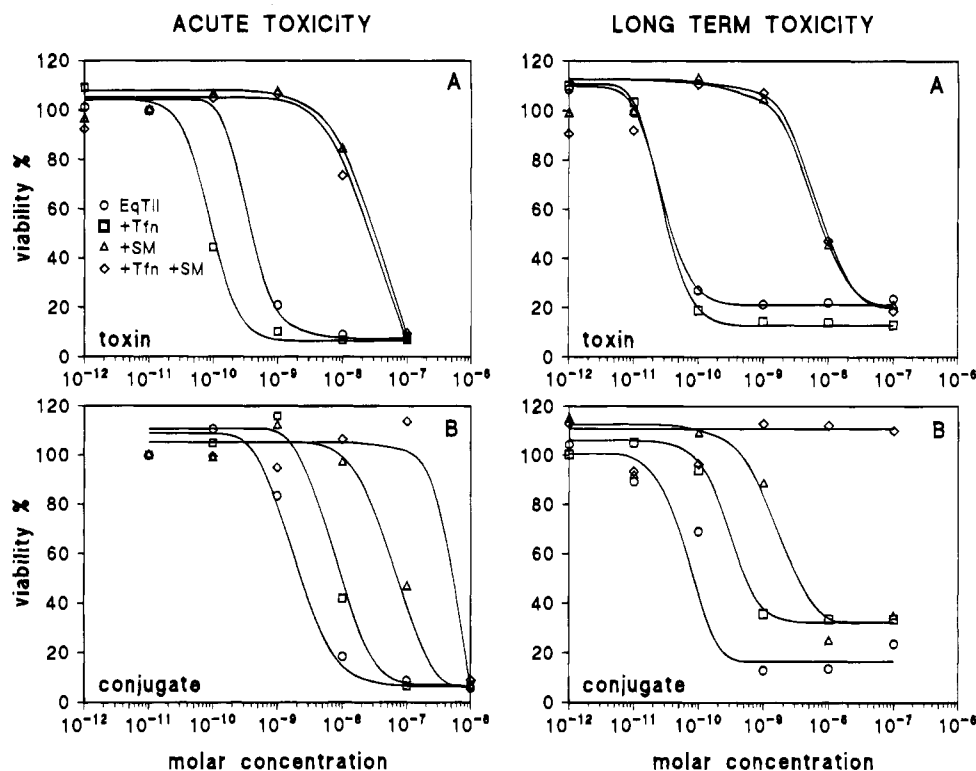
Figure 7. Cytotoxicity of EqT II and an EqT II–Tfn conjugate toward cancer cells. Left: acute cytotoxicity test. Raji cells (4×10^4) were exposed to various concentrations of toxin (A) or of conjugate (B) for 1 h at 37 °C, and thereafter their viability was determined by the MTT method. In experiments of protection of cells with SM and free ferric Tfn, the final concentrations used were 10 μg/mL and 0.4 mg/mL, respectively (but similar results were obtained with 0.1 mg/mL of Tfn). Symbols: circles, toxin or conjugate; squares, the same plus free Tfn; triangles, plus SM; diamonds, plus both Tfn and SM. Right: long term cytotoxicity test. All experimental conditions and symbols are the same as in the left panel, except that the incubation was prolonged for 24 h. Conjugate concentration was calculated as in Figure 5. Solid lines were drawn by eye. Results are from a single experiment. The tests were repeated two or three times with qualitatively similar results.

Tfn, indicating its toxicity was now absolutely dependent on the presence of the TR.

In some control experiments a different cell line expressing the TR, i.e., human lymphoblastoid (Jurkat), was used, and in this case, a protein synthesis assay, using ^{14}C-leucine, was performed as in (*38, 39*). The results were consistent and are not shown here.

Stability of the Conjugate. To measure the stability of the complex with different treatments we assayed its hemolytic activity with or without the reducing agent DTT and determined C_+, C_- and the ratio C_-/C_+ as explained above (Table 1). A decrease of C_-, and thus of the ratio C_-/C_+, is expected if the toxin dissociates from the complex, becoming free.

Stability with Temperature. To test thermal stability the conjugate was incubated for 1 h at different temperatures. It appeared to be stable, at least until 40 °C.

Stability with Storage at 4 °C. The conjugate is normally stored frozen at −80 °C and retains its properties for a period of at least 12 months (not shown). It appears that after thawing it is stable in the refrigerator at 4 °C for at least 2 weeks.

Stability with Freezing and Thawing. Cycles of freezing and thawing either with liquid nitrogen (LN$_2$) or at −80 °C were tried. We found a different response with the two protocols. Freezing and thawing the conjugate in LN$_2$ preserved all its activity, whereas freezing and thawing at −80 °C decreased its activity progressively until a maximum decrease of a factor ≈6. However, the relative ratio of activity under reducing and nonreducing conditions (C_-/C_-) was constant in both cases, indicating that the covalent bonding was stable. It appears that repeatedly freezing and thawing at −80 °C should be

Table 1. Stability of the EqT II–Tfn Conjugate with Temperature, Time, and Freezing-Thawing

		C_-,[a] nM	C_+,[a] nM	C_-/C_+
T,[b] °C	10	8.0	0.72	11.1
	20	7.0	0.98	7.1
	30	9.0	0.72	12.5
	40	8.0	0.89	9.0
time,[c] days	0	3.3	0.30	11.0
	5	5.2	0.40	13.0
	14	4.0	0.32	12.5
no. of cycles[d] LN$_2$	0	3.9	0.34	11.5
	1	4.5	0.45	10.0
	2	6.5	0.59	11.0
	3	4.9	0.50	9.8
	4	4.0	0.45	8.9
	5	4.4	0.45	9.8
no. of cycles[e] −80 °C	0	3.8	0.50	7.6
	1	4.9	0.71	6.9
	2	16.0	1.90	8.4
	3	21.0	2.70	7.8
	4	28.0	3.50	8.0
	5	25.0	3.20	7.8

[a] C_- and C_+ are the concentration of conjugate necessary to obtain 50% hemolysis in the absence and in the presence of DTT, respectively. [b] One hour incubation of the apo-Tfn conjugate (B1) at the given temperature. [c] Storage of a thawed apo-Tfn conjugate (B1) at 4 °C for the given time. [d] Freezing and thawing in LN$_2$ of the apo-Tfn conjugate (B1) for the given number of cycles. [e] As in *d* but at −80 °C with the ferric conjugate.

avoided, possibly because it might cause irreversible aggregation of the molecules.

CONCLUSIONS

The use of a cytolytic toxin from a sea anemone to build immunoconjugates was described recently (*5, 6*). We

have now used a similar approach to create a mitotoxin by linking EqT II to the mitogenic factor, Tfn. Coupling a toxin which acts upon cell membranes with an internalizing targeting ligand might seem to be a paradox. However, our experiments on human lymphoblastoid cells (Raji or Jurkat) showed that such conjugates are very active. We believe that after interaction with these cells the conjugate undergoes reduction, either on the surface of the cell or, more probably, inside the endocytic compartment, and the toxin is liberated. In this way all the internal membranes might become targets. The fact that long-term toxicity is at least 10 times higher than acute toxicity would confirm this. Furthermore, because the mode of action of EqT II is not yet completely understood, we cannot exclude the existence of other intracellular targets. The fate of the conjugate on the cell is one of our goals in the continuing of this research. The produced mitotoxins exhibit stability versus temperature (up to at least 40 °C), time (up to several weeks at 4 °C and 1 year at −80 °C), and freeze-thawing in LN_2.

One particular problem that is foreseen in the use of cytolytic toxins to create immuno- or mitotoxins is their unspecific toxicity toward innocent bystander cells. We found that indeed the hybrid Tfn−EqT II molecule maintains an unspecific hemolytic activity, and the presence of an excess of free Tfn could not completely prevent toxic effects of the conjugate on tumor cells. We demonstrated that this behavior is probably due to the ability of the toxin part of the conjugate to retain partly its ability to interact directly with cells. However, in the case of sea anemone cytolysins such unspecific toxicity can be strongly reduced (and even completely eliminated) by treating the conjugate with SM, the natural target lipid for these toxins. This suggests that, as in the case of A/B toxins, it should be possible, by chemical or genetical modification of the cytolysin, to reduce its lipid-binding properties without impairing its cytolytic activity. Such binding-incompetent toxins would be more suited for the preparation of conjugated mitotoxins with a reduced nonspecific activity.

ACKNOWLEDGMENT

LITERATURE CITED

(1) Vitetta, E. S., Fulton, R. J., May, R. D., Till, M., and Uhr, J. W. (1987) Redesigning nature's poisons to create anti-tumor reagents. *Science 238,* 1098−1104.

(2) Pastan, I., Chaudhary, V. K., and Fitzgerald, D. J. (1992) Recombinant toxins as novel therapeutic agents. *Annu. Rev. Biochem. 61,* 331−354.

(3) Pietersz, G. A., and McKenzie, I. F. C. (1992) Antibody conjugates for the treatment of cancer. *Immunol. Rev. 129,* 57−80.

(4) Tritton, T. R., and Hickman, J. A. (1990) How to kill cancer cells: membranes and calcium signaling as targets in cancer chemotherapy. *Cancer Cells 2,* 95−105.

(5) Avila, A. D., de Acosta, M. C., and Lage, A. (1988) A new immunotoxin built by linking a hemolytic toxin to a monoclonal antibody specific for immature T lymphocytes. *Int. J. Cancer 42,* 568−571.

(6) Avila, A. D., de Acosta, M. C., and Lage, A. (1989) A carcinoembryonic antigen-directed immunotoxin built by linking a monoclonal antibody to a hemolytic toxin. *Int. J. Cancer 43,* 926−929.

(7) Faulk, W. P., Harats, H., McIntyre, J. A., Berczi, A., Sun, I. L., and Crane, F. L. (1989) Recent advances in cancer research: drug targeting without the use of monoclonal antibodies. *Am. J. Reprod. Immunol. 21,* 151−154.

(8) Maček, P., and Lebez, D. (1988) Isolation and characterization of three lethal and hemolytic toxins from the sea anemone *Actinia equina* L. *Toxicon 26,* 441−451.

(9) Belmonte, G., Pederzolli, C., Maček, P., and Menestrina, G. (1993) Pore formation by the sea anemone cytolysin equinatoxin II in red blood cells and model lipid membranes. *J. Membrane Biol. 131,* 11−22.

(10) Maček, P., Belmonte, G., Pederzolli, C., and Menestrina, G. (1994) Mechanism of action of equinatoxin II, a cytolysin from the sea anemone *Actinia equina* L. belonging to the family of actinoporins. *Toxicology 87,* 205−227.

(11) Thortensen, K., and Romslo, I. (1990) The role of transferrin in the mechanism of cellular iron uptake. *Biochem. J. 271,* 1−10.

(12) May, W. S. J., and Cuatrecasas, P. (1985) Transferrin receptor: its biological significance. *J. Membrane Biol. 88,* 205−215.

(13) Gatter, K. C., Brown, G., Trowbridge, I. S., Woolston, R.-E., and Mason, D. Y. (1983) Transferrin receptors in human tissues: their distribution and possible clinical relevance. *J. Clin. Pathol. 36,* 539−545.

(14) Sutherland, R., Delia, D., Schneider, C., Newman, R., Kemshead, J., and Greaves, M. (1981) Ubiquitous cell-surface glycoprotein on tumor cells is proliferation-associated receptor for transferrin. *Proc. Natl. Acad. Sci. U.S.A. 78,* 4515−4519.

(15) Cavanaugh, P. G., and Nicolson, G. L. (1991) Lung-derived growth factor that stimulates the growth of lung-metastasizing tumor cells: identification as transferrin. *J. Cell. Biochem. 47,* 261−271.

(16) Denstman, S., Hromchak, R., Guan, X.-P., and Bloch, A. (1991) Identification of transferrin as a progression factor for ML-1 human myeloblastic leukemia cell differentiation. *J. Biol. Chem. 266,* 14873−14876.

(17) Chakal Rossi, M., and Zetter, B. R. (1992) Selective stimulation of prostatic cell proliferation by transferrin. *Proc. Natl. Acad. Sci. U.S.A. 89,* 6197−6201.

(18) Sirbasku, D. A., Pakala, R., Sato, H., and Eby, J. E. (1991) Thyroid hormone dependent pituitary tumor cell growth in serum-free chemically defined culture. A new regulatory role for apotransferrin. *Biochemistry 30,* 7466−7477.

(19) Inoue, T., Cavanaugh, P. G., Steck, P. A., Brünner, N., and Nicolson, G. L. (1993) Differences in transferrin response and number of transferrin receptors in rat and human mammary carcinoma lines of different metastatic potential. *J. Cell. Physiol. 156,* 212−217.

(20) Barabas, K., and Faulk, W. P. (1993) Transferrin receptors associates with drug resistance in cancer cells. *Biochem. Biophys. Res. Commun. 197,* 702−708.

(21) Schell, D., Evers, R., Preis, D., Ziegelbauer, K., Kiefer, H., Lottspeich, F., Cornelissen, A. W. C. A., and Overath, P. (1991) A transferrin-binding protein of *Trypanosoma brucei* is encoded by one of the genes in the variant surface glycoprotein gene expression site. *EMBO J. 10,* 1061−1066.

(22) Voyiatzaki, C. S., and Soteriadou, K. P. (1990) Evidence of transferrin binding sites on the surface of *Leishmania* promastigotes. *J. Biol. Chem. 265,* 22380−22385.

(23) Gerlach, G. F., Anderson, C., Potter, A. A., Klashinsky, S., and Willson, P. J. (1992) Cloning and expression of a transferrin-binding protein from *Actinobacillus pleuropneumoniae. Infect. Immun. 60,* 892−898.

(24) Williams, P., and Griffiths, E. (1992) Bacterial transferrin receptors− structure, function and contribution to virulence. *Med. Microb. Immunol. 181,* 301−322.

(25) de Jong, G., van Noort, W. L., and van Eijk, H. G. (1992) Carbohydrate analysis of transferrin subfractions isolated by

preparative isoelectric focusing in immobilized pH gradients. *Electrophoresis 13,* 225–228.

(26) Norton, R. S., Maček, P., Reid, G. E., and Simpson, R. J. (1992) Relationship between the cytolysin tenebrosin-C from *Actinia tenebrosa* and equinatoxin-II from *Actinia equina. Toxicon 30,* 13–23.

(27) Nishigori, H., and Toft, D. (1979) Modification of avian progesterone receptor by pyridoxal-5′-phosphate. *J. Biol. Chem. 254,* 9155–9161.

(28) Turk, T., and Maček, P. (1992) The role of lysine, histidine and carboxyl residues in biological activity of equinatoxin II, a pore forming polypeptide from the sea anemone *Actinia equina* L. *Biochim. Biophys. Acta 1119,* 5–10.

(29) Peach, C., and Tolbert, N. E. (1978) Active site studies of ribulose-1,5-bisphosphate carboxylase/oxygenase with pyridoxal-5′-phosphate. *J. Biol.Chem. 253,* 7864–7873.

(30) Carlsson, J., Drevin, H., and Axen, R. (1978) Protein thiolation and reversible protein-protein conjugation. *N*-succimidyl 3-(2-pyridyl-dithio)propionate, a new heterobifunctional reagent. *Biochem.J. 173,* 723–737.

(31) Laemmli, U. K. (1970) Cleavage of structural proteins during the assembly of the head of bacteriophage T4. *Nature 227,* 680–685.

(32) Narat, M., Maček,, P., Kotnik, V., and Sedmak, B. (1993) The humoral and cellular immune response to a lipid attenuated pore-forming toxin from the sea anemone *Actinia equina* L. *Toxicon 32,* 65–71.

(33) Bers, G., and Garfin, D. (1985) Protein and nucleic acid blotting and immunobiochemical detection. *BioTechniques 3,* 276–288.

(34) Pluskal, M. G., Przekop, M. B., Mark, R., Vecoli, C., and Hicks, D. A. (1986) Immobilon PVDF transfer membranes: a new membrane substrate for Western blotting of proteins. *BioTechniques 4,* 272–283.

(35) Towbin, H., Staehelin, T., and Gordon, J. (1979) Electrophoretic transfer of proteins from polyacrylamide gels to nitrocellulose sheets: procedure and some applications. *Proc. Natl. Acad. Sci. U.S.A. 76,* 4350–4354.

(36) Bailey, S., Evans, R. W., Garratt, R. C., Gorinsky, B., Hasnain, S., Horsburgh, C., Jhoti, H., Lindley, P. F., Mydin, A., Sarra, R., and Watson, J. L. (1988) Molecular structure of serum transferrin at 3.3-Å resolution. *Biochemistry 27,* 5804–5812.

(37) Anderson, B. F., Baker, H. M., Norris, G. E., David, W. R., and Baker, E. N. (1989) Structure of human lactoferrin: crystallographic structure analysis and refinement at 2.8 Å resolution. *J. Mol.Biol. 209,* 711–734.

(38) Colombatti, M., Dell'Arciprete, L., Chignola, R., and Tridente, G. (1990) Carrier Protein-Monensin Conjugates: Enhancement of Immunotoxin Cytotoxicity and Potential in Tumor Treatment. *Cancer Res. 50,* 1385–1391.

(39) Colombatti, M., Bisconti, M., Dell'Arciprete, L., Gerosa, M., and Tridente, G. (1988) Sensitivity of human glioma cells to cytotoxic heteroconjugates. *Int. J. Cancer 42,* 441–448.

BC9400884

Versatile Procedure of Multiple Introduction of 8-Aminomethylene Blue into Oligonucleotides

Uwe Möller,* Frank Schubert, and Dieter Cech

Humboldt-Universität zu Berlin, Institut für Chemie, Hessische Strasse 1-2, 10099 Berlin, Germany. Received August 8, 1994⊗

The coupling of 8-aminomethylene blue to oligonucleotides via poly-L-glutamic acid linker using carboxy-anchor groups will be described. The introduction of carboxy-anchor groups into oligonucleotides proceeds both during automated synthesis using 6-(ethoxycarbonyl)hexyl 1-*O*-phosphoramidite and by reaction of 5′-amino-functionalized oligonucleotides with succinic anhydride. *O*-(*N*-Succinimidyl)-1,1,3,3-tetramethyluronium tetrafluoroborate was used as activating reagent for binding of poly- L-glutamic acid to the carboxylated oligonucleotides. The successful 5′-carboxylation and poly-L-glutamic acid coupling were proven both by polyacrylamide gel electrophoreses and HPLC. 8-Aminomethylene blue in its leucoform was covalently coupled to the oligonucleotides in the presence of water soluble carbodiimide.

INTRODUCTION

Various dye conjugates with proteins, nucleic acids, and carbohydrates have been synthesized and are currently being studied for their analytical, biochemical, and medical application. The covalent attachment of dyes to biomolecules has proven to be advantageous in many approaches. Thus, different strategies of introduction of photoactive molecules onto functional groups have been developed. Dye–biomolecule conjugates now have a variety of applications from fluorescent detection of DNA fragments in semiautomated sequencing (Smith et al., 1987), to the fluorescent immuno assays (FIA), and in addition, to the investigation of the biochemical mechanism of membrane protein interaction (Garland and Moore, 1979).

More recently, however, these conjugates have developed to such an extent that they are also being used as therapeutic agents. Thus, photosensitizers which are able to generate singlet oxygen photochemically are frequently found in clinical trials of tumors (the so-called photodynamic therapy of tumors; Dougherty et al., 1987). Furthermore, site-directed DNA damaging using oligonucletides tethered to dyes stimulated by photochemical formation of singlet oxygen has been described (Buchardt et al., 1989; Fedorova et al., 1990).

It was shown in clinical trials of tumors by PDT that the specificity was increased by introduction of photosensitizers into antibodies, which are complementary to targeted surface antigenes of tumors. For that, the utility of labeled antibodies could be considerably enhanced if the label is multiply conjugated to the biopolymer. In this context, polyvinyl alcohol and polyamines served as anchor groups due to their ability to couple more than one dye molecule in a definite manner (Jiang et al., 1990).

3,7-(Dimethylamino)phenazathionium chloride (methylene blue) was shown to be a very effective singlet oxygen sensitizer in organic photochemistry. Its photochemical properties and noncovalent interactions with nucleic acids and proteins were intensivly investigated (Tuite and Kelly, 1993). Therefore, the covalent introduction of methylene blue into various biomolecules and the study of the photochemical behavior of such conjugates was of particular interest. Our recent studies of methods to incorporate different dyes into oligonucleotides for a variety of applications encouraged us to synthesize oligonucleotide–methylene blue conjugates with more than one dye molecule within the oligonucleotide (Möller et al., 1990; Schubert et al., 1990, 1994). Conceptually, poly-L-glutamic acid and methylene blue in any derivatized form served as starting compounds. Commercial available poly-L-glutamic acid has the advantage that its single N-terminal amino group favors the attachment to carboxy-alkylated oligonucleotides and was synthesized as described in the literature (Kremsky et al., 1987). The principle obstacle to the covalent coupling of methylene blue rests in the lack of any functionality within the molecule. Therefore, 8-aminomethylene blue which is easily available from methylene green seems to be a potential candidate for covalent coupling to the polylinker. The present report describes the synthesis of oligonucleotides with a poly-L-glutamic acid linker and demonstrates that the linkage to the methylene blue derivative can be stably formed.

EXPERIMENTAL PROCEDURES

All reagents used were reagent grade or better. Poly-L-glutamic acid was purchased from Sigma, TSTU from Calbiochem-Novabiochem (Bad Soden/Germany), and methylene green from Aldrich. Oligonucleotides were synthesized on a Gene Assembler Plus DNA Synthesizer (Pharmacia LKB) by an automated phosphoramidite method (commercially available phosphoramidites with benzoyl and isobutyryl as base protecting groups on G, A and C were used). 5′-Aminofunctionalization was carried out with 6-((trifluoroacetyl)amino)hexyl-2-cyanoethyl *N,N*-diisopropylphosphoramidite (Pharmacia LKB). ^{1}H- and ^{31}P-NMR and absorption spectra were recorded on a Bruker AM 300 spectrometer and on a Shimadzu UV 160 spectrophotometer, respectively.

Analytical HPLC measurements were performed on an ICI/GAT system using a LiChrosorb RP18 column (125 × 4 mm, 5 mm) and an acetonitrile containing triethylammonium acetate buffer gradient (buffer A: 50% 0.1 M TEAAC pH 6.5, 50% CH$_3$CN; buffer B: 98% 0.1 M TEAAC pH 6.5, 2% CH$_3$CN; gradient: linear from 90% buffer B to 40% buffer B in 40 min; flow rate: 1 mL/min) as eluent. Preparative HPLC was carried out on a

---

* Author to whom correspondence should be addressed.

⊗ Abstract published in *Advance ACS Abstracts,* January 1, 1995.

Hyperprep RP18 column (125 × 16 mm, 12 mm; GAT, Bremerhaven/Germany) with a flow rate of 5 mL/min using the same system and gradient.

Synthesis of 5'-Carboxy-Modified Oligonucleotides 2. *Path A.* The phosphoramidite of commercially available ethyl 6-hydroxyhexanoate was synthesized according to standard protocols (McBride and Caruthers, 1983) with 2-cyanoethyl *N,N*-diisopropylchlorophosphoramidite in 91% yield.

The phosphoramidite building block was coupled to the 5'-end of oligonucleotides during automated syntheses using standard protocols. After treatment with 0.1 M sodium hydroxide (24 h at 40 °C) and purification by HPLC on reversed-phase (Hyperprep RP 18) the carboxymodified oligonucleotides **2a** were obtained in good yields and in high purity. The coupling yield of the 6-(ethoxycarbonyl)hexyl 1-*O*-phosphoramidite (6-ECHP)[1] estimated by integration of HPLC chromatograms was approximately 90%.

Path B. For carboxylation, 100 nmol of amino-functionalized oligonucleotide was dissolved in 50 μL of water and mixed with 50 μL of an aqueous solution of SA (50 mg/mL). After the mixture was shaken for a period of 1 h further, 50 μL of the SA solution was added. After an additional hour the modified oligonucleotide was purified on Sephadex G-25 (NAP-10, Pharmacia LKB). The obtained oligonucleotide was evaporated and then treated with 500 μL of concentrated ammonia for 0.5 h at room temperature. Chromatography on Sephadex G-25 and final purification by HPLC yielded the oligonucleotide **2b** (X = −(CH₂)₆NH(CH₂)₂−).

Preparation of Poly-L-glutamic Acid Oligonucleotide Conjugates 5. The carboxy-modified oligonucleotide **2** (10 nmol) was dissolved in 2 μL of water and then diluted with 20 μL of dimethylformamide (free of amines). *O*-(*N*-Succinimidyl)-1,1,3,3-tetramethyluronium tetrafluoroborate (9 μL, 30 nmol) dissolved in dimethylformamide (10 μg/10 μL) and diisopropylethylamine (10 mL, 30 nmol) in dimethylformamide (5 × 10⁻³ μL/10 μL) were added. The mixture was stirred for 1 h, and without any further purification 50 μL (100 nmol) of an aqueous solution of p-L-Glu (19.4 mg/mL) and 8.6 μL (100 nmol) of diisopropylethylamine diluted with dimethylformamide (20 × 10⁻³ μL/10 μL) were added. After 24 h the reaction mixture was evaporated to dryness in *vacuo*. The isolation of conjugates was carried out by polyacrylamide gel electrophoreses (PAGE).

Synthesis of the Leucoform of 8-Aminomethylene Blue 7. Commercially available methylene green (**6**) was purified by silica gel chromatography using acetonitrile: water (50:50 = v:v, 0.1 M NaCl).

The purified methylene green (18 mg, 50 μmol, calculated to 1 μmol of carboxy groups) was dissolved in 2.5 mL of a mixture of dioxane:water (2:1 = v:v) and mixed with palladium/charcoal. The dye was reduced in a hydrogen atmosphere under normal pressure. After the color of methylene green disappeared, the mixture was stirred for another 0.5 h. Without any isolation of the leucoform, the obtained solution was used for coupling experiments after removal of the catalyst under exclusion of oxygen.

Conjugation of 8-Aminomethylene Blue to Poly-L-glutamic Acid Modified Oligonucleotides. Imida-

Chart 1. 8-Aminomethylene Blue p-L-Glu−Oligonucleotide Conjugate.

X = -(CH₂)₆-NH-CO-(CH₂)₂- ; -(CH₂)₅-

n = 12 - 30 ; m = ~60
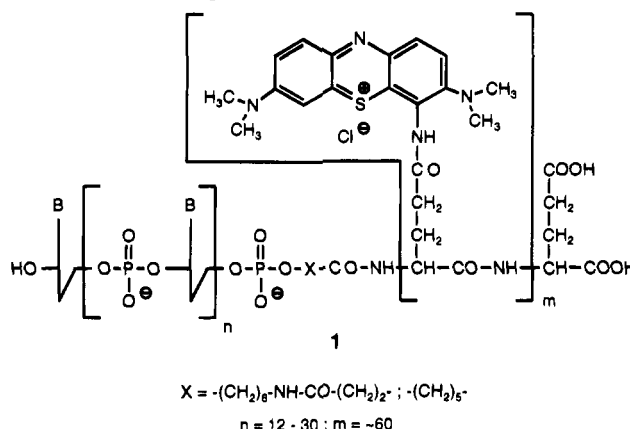
zole (68 mg, 1 mmol) was dissolved in 2.4 mL of MES buffer (0.1 M), and 100 μL of an aqueous solution of a p-L-Glu-oligonucleotide conjugate (1 μmol, compared to carboxyl groups) as well as 15 mg (75 μmol) of *N*-(3-(dimethylamino)propyl)-*N'*-ethylcarbodiimide hydrochloride were added. The solution was gassed with nitrogen for 5 min, and the leucoform of 8-AMB obtained above was added under exclusion of oxygen. The coupling mixture was stirred in the dark at room temperature for 24 h. In order to oxidize the dye, the reaction mixture was gassed with oxygen for 10 min. The dark blue solution was evaporated to dryness in *vacuo*. Conjugate **1** was isolated by dialysis against PBS.

RESULTS

Labelling of p-L-Glu−Oligonucleotide Conjugates with 8-AMB. Commercially available methylene green has served as starting material for labeling reactions because it can easily be reduced to 8-AMB. However, the commercial form contains only 60% of methylene green, and a liquid chromatographic purification on silica gel needs to be done before use. Then the purified methylene green was reduced by palladium/charcoal in a hydrogen atmosphere to the leucoform of 8-AMB. The formation of the leucoform can easily be pursued on the decolorization of the reaction mixture. Finally, after successful coupling to the oligonucleotide the leucoform was converted into the stable oxidized form by oxygen. However, the reaction of 8-AMB with poly-L-Glu−oligonucleotide conjugates did not result in the wanted conjugate **1** (Chart 1).

Since 8-AMB in its oxidized form is positively charged in the aromatic system the exocyclic amino group in position 8 does not have a sufficient nucleophilicity for a reaction with carboxyl groups. Therefore, it seems to be necessary to transform the methylene blue derivative in its leucoform. For that, the described synthesis of 8-AMB was stopped at the level of its leucoform by subsequent exclusion of oxygen. The following coupling with the carboxyl groups of p-L-Glu−oligonucleotide conjugates **5** (Scheme 1) was carried out in a mixture of buffer (MES) and dioxane under an inert atmosphere in the presence of water soluble carbodiimide. After 24 h the reaction mixture was gassed shortly with oxygen to get back 8-AMB by a complete oxidation of the leucoform. The conjugates were separated from unreacted dye by dialysis against PBS. Additional purification by chromatography on Sephadex G25 and on silica gel Si60 did not show unlabeled p-L-Glu−oligonucleotide conjugates in the dialyzed product. The isolated dye conjugates display a typical absorption maximum for oligonucleotides at 260

Scheme 1. Labeling of p-L-Glu–Oligonucleotide Conjugates with the Leuco Form of 8-AMB.

X = -(CH₂)₆-NH-CO-(CH₂)₂- ; -(CH₂)₅-

n = 12 - 30 ; m = ~60

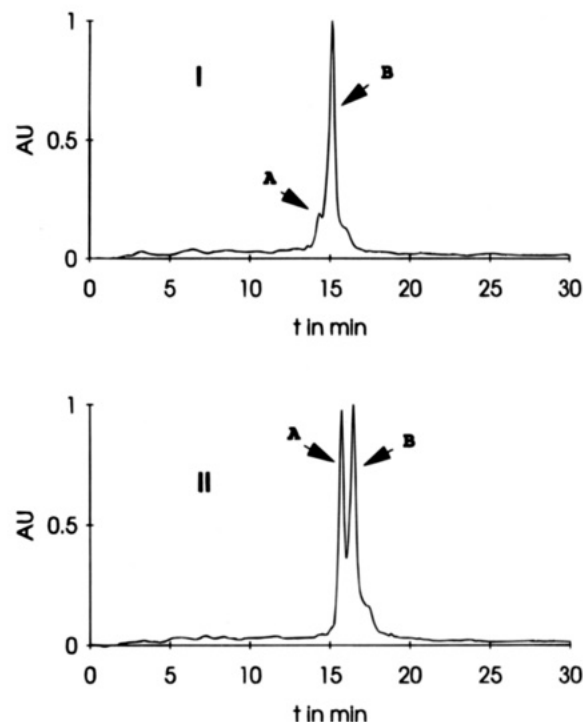**Figure 1.** HPLC chromatograms of 3'-TGA CCG GCA GCA AAA TGT TGC AGC(CH$_2$)$_6$COOH-5' (I, preparative run of the crude product) and of a 1:1-mixture of the same oligonucleotide and its unmodified analogue (II). A: unmodified oligonucleotide. B: 5'-carboxy-modified oligonucleotide. See the Experimental Procedures for detailed HPLC conditions.

Figure 2. 20% PAGE of 5'-carboxylated oligonucleotides and their starting sequences. Lanes: (1) 3'-TGA CCG GCA GCA AAA TGT TGC AGC-5', (2) 3'-TGA CCG GCA GCA AAA TGT TGC AGC(CH$_2$)$_6$COOH-5', (3) 3'-(T)$_{20}$(CH$_2$)$_3$NH$_2$-5', (4) 3'-(T)$_{20}$(CH$_2$)$_3$NHCO(CH$_2$)$_2$COOH-5'.
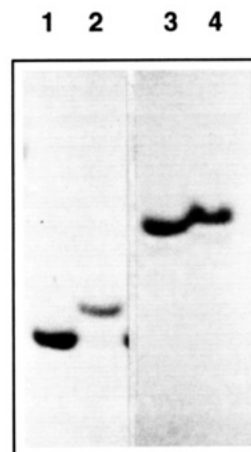
nm, and compared to free 8-AMB, the Q-band of conjugates has been shifted hypsochromically at 15 nm.

Synthesis of 5'-Carboxy-Modified Oligonucleotides. In order to incorporate numerous carboxyl anchor groups in oligonucleotides for labeling with 8-AMB it was advantageous to use p-L-Glu. Thus, 5'-carboxy prefunctionalized oligonucleotides were suitable for its introduction. In the present work two routes of introduction of a carboxy group at the 5'-end of oligonucleotides were studied. In path A 6-(ethoxycarbonyl)-hexyl 1-*O*-phosphoramidite (6-ECHP) is used as a building block in automated oligonucleotide synthesis via the phosphoramidite approach. According to standard protocols (McBride and Caruthers, 1983; Kremsky et al., 1987) the synthesis of the phosphoramidite was performed using ethyl 6-hydroxyhexanoate and 2-cyanoethyl *N,N*-diisopropylchlorophosphoramidite. 6-ECHP was obtained in 91% yield. ^{31}P- and ^{1}H-NMR indicated the high purity of the product both after distillative and aqueous isolation (data not shown). Carboxyphosphoramidite dissolved in acetonitrile was used in the last cycle of oligonucleotide synthesis under standard conditions. In contrast to the usual deblocking of protecting groups it is recommended to use 0.1 M sodium hydroxide (24 h, 40 °C) for complete deblocking of the exocyclic amino groups as well as the ethyl ester of the carboxy linker. After purification by reversed-phase HPLC 5'-carboxy-modified oligonucleotides **2** (X = −(CH₂)₅−) were obtained in a yield varying from 20% to 58% due to the reaction conditions. An enzymatical digestion has shown that no base desamination was obtained. Chromatogram I in Figure 1 shows a preparative HPLC profile of oligonucleotide **2a**.

The very simple reaction of amines with succinic anhydride (SA) is shown in path B. First, 5'-amino functionalization was performed with commercially available phosphoramidites. The fully unprotected oligonucleotide was then reacted with SA in water for 2 h. After the excess succinic anhydride was removed by Sephadex G25 chromatography the sample was treated with concentrated ammonia (30 min, rt) to cleave succinic ester at the 3'-end of oligonucleotides leaving the 5'-

terminus uneffected. A final purification on Sephadex G25 resulted in **2b** with X = −(CH₂)₆NH(CH₂)₂−. In order to estimate whether carboxyl groups are coupled at the 5'-end of oligonucleotides, polyacrylamide gel electrophoresis (PAGE) was performed. The succinylation has only caused a slight decrease in the electrophoretically mobility. Lanes 3 and 4 in Figure 2 show the small difference between a succinylated 5'-amino oligonucleotide and its unmodified sequence.

p-L-Glu–Oligonucleotide Conjugates. A fraction of the polydisperse amino acid having a molecular weight of 10 000 was chosen for coupling of p-L-Glu (**3**) with the 5'-carboxy modified oligonucleotides **2**. This implicates more than 60 anchor groups per oligonucleotide. In this case the coupling strategy of activated esters (Scheme

Scheme 2. Coupling of p-L-Glu to 5'-Carboxy-Functionalized Oligonucleotides.

a: X = -(CH$_2$)$_5$- ; b: X = -(CH$_2$)$_6$-NH-CO-(CH$_2$)$_2$-

n = 12 - 30 ; m = ~60

Figure 3. 20% PAGE of an unpurified p-L-Glu–oligonucleotide conjugate. Lanes: (1) 3'-(T)$_{20}$(CH$_2$)$_3$NHCO(CH$_2$)$_2$COOH-5', (2) 3'-(T)$_{20}$(CH$_2$)$_3$NHCO(CH$_2$)$_2$CONH-p-L-Glu-5'.
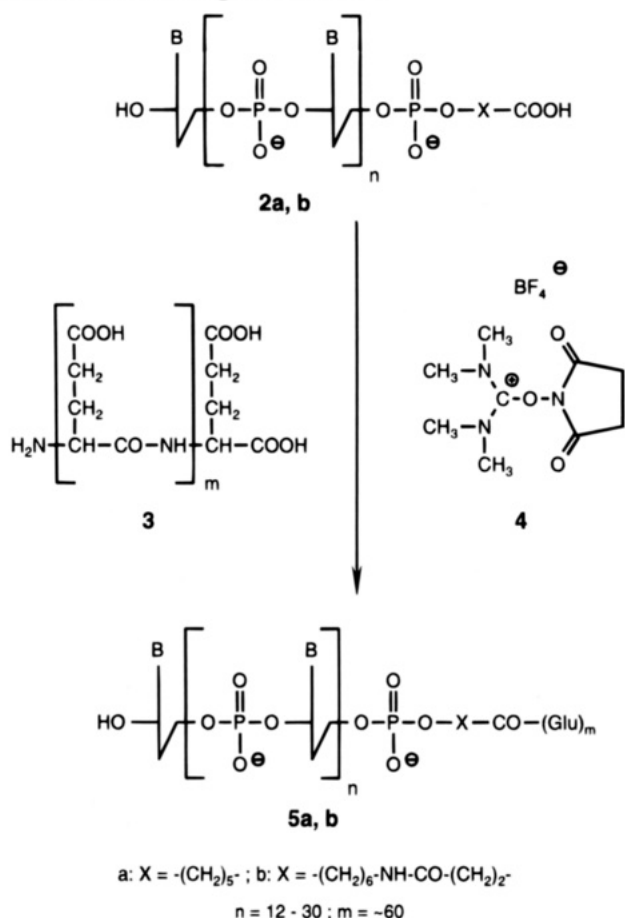
2) was used. For that, *O*-(*N*-succinimidyl)-1,1,3,3-tetramethyluronium tetrafluoroborate (TSTU) served as a coupling reagent. First, the 5'-carboxyl group of modified oligonucleotides was treated with TSTU (**4**) to form an activated ester. Without further purification the activated oligonucleotides were added to an aqueous p-L-Glu solution. Within 24 h the carboxylated oligonucleotides reacted almost quantitatively to yield **5**. In Figure 3 a 20% PAGE of the crude product of a p-L-Glu-oligonucleotide conjugate is shown. As a result of higher molecular weight the mobility of the conjugate is decreased.

DISCUSSION

For optimal generation of singlet oxygen an oligonucleotide must be labeled as best as possible by a photosensitizer. This requires attaching numerous photosensitizers like 8-AMB to each oligonucleotide. This should be achieved by a poly-L-glutamic acid polylinker which is attached to the oligonucleotide by a carboxylic amide bond. Therefore, the oligonucleotide must be carboxylated either during automated synthesis or postsynthetic after removal the oligonucleotide from the polymer support. Thus, for the synthesis of 8-AMB labeled oligonucleotides two alternative routes for 5'-carboxy modification of oligonucleotides were studied. First, we tested direct carboxylation during automated DNA-synthesis by 6-ECHP according to a described procedure by Kremsky et al. (1987). In the second method succinic acid was used in the presence of water soluble carbodiimide giving satisfactory yields of the carboxylated oligonucleotide. Although both methods worked well, 5'-carboxylation by 6-ECHP is the most elegant way. This method is preferred as 6-ECHP is easily available in good

yields. In analogy to the synthesis of nucleoside phosphoramidites 6-ECHP can be obtained in yields of about 95%. With use of 6-ECHP the oligonucleotide is modified at the end of the automated synthesis, which in contrast to the postsynthetic procedure is not time-consuming and does not need additional chromatographic purifications. Furthermore, in order to dissolve the phosphoramidite of the carboxylinker during automated oligonnucleotide synthesis, it is not necessary to add pyridine as it is essential for long chain derivatives (Kremsky et al., 1987). The coupling of the modified phopshoramidites is very efficient giving pure products as shown in the HPLC-chromatogram I in Figure 1. The HPLC profile shows a small background of side products (profile I), and a separation of the modified (B) from the unmodified sequence (A) on reversed phase HPLC is possible (profile II). The introduction of an alkyl chain into the oligonucleotide increases its hydrophobicity which causes a considerable increase in the retention time. Similarly, this effect also influences the mobility of oligonucleotide sequences in polyacrylamide gel electrophoresis (lanes 1 and 2 in Figure 2).

Yields in path B using succinic acid are similar to that obtained using 6-ECHP. Contrary to path A, polyacrylamide gel electrophoresis is recommended for isolation and characterization of carboxylated oligonucleotides (lanes 3 and 4 in Figure 2). The slight structural differences between educts and products does not permit a separation by HPLC. An advantage of the method which proceeds in aqueous solution is given by its possibility to carboxylate oligonucleotides at each position either at the 3'- or 5'-end, at any modified nucleobases, or at the phosphate backbone.

For the purpose of multiple coupling of 8-AMB to oligonucleotides, it was decided to introduce p-L-Glu, because the single amino group of p-L-Glu allows a specific introduction of the 8-AMB to the carboxylated oligonucleotides. Thus, polydisperse p-L-Glu with an average of 60 monomer units was used. Longer polypeptides were not used because there is a risk of precipitation. Although oligonucleotides are negatively charged to a certain extent, complex conjugates with aromatic substances tend to precipitate (Motsenbocker et al., 1993). The synthesis of p-L-Glu–oligonucleotide conjugates **5** has proceeded in nearly quantitative yields with all types of carboxy modified oligonucleotides. Lane 2 in Figure 3 shows a gel electrophoresis of the crude product of such a coupling reaction. The slower running slight spot is due to the differences in molecular weigth of the used p-L-Glu.

All attempts to couple 8-AMB directly to the p-L-Glu–oligonucleotide conjugates failed due to the low nucleophilicity of the primary amino group. The nucleophilicity
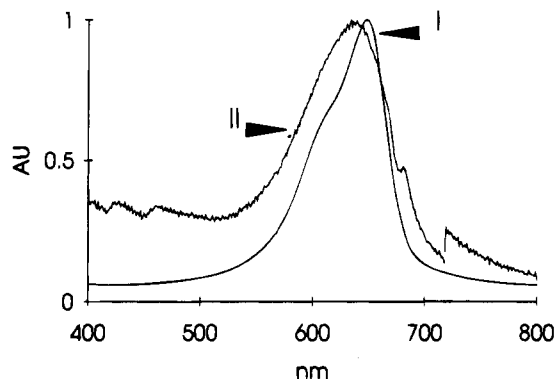
Figure 4. Absorption spectra of 8-AMB (I) and an 8-AMB-p-L-Glu—oligonucleotide conjugate (II) at pH 7.

might be increased by formation of the leucoform reducing the electron-withdrawing effect of the heteroaromatic ring system. Indeed, the direct conjugation of 8-AMB in its leucoform was possible and proceeded in high yields. The high and different molecular weights did not allow analytical characterization of the obtained dye conjugates with conventional methods, as mass spectrometry and nuclear magnetic resonance until now. However, the comparison to authentic samples of 8-AMB and non-coupled p-L-Glu—oligonucleotide conjugates by thin layer chromatogaphy demonstrates that dye conjugates are not based on any ionic or intercalating interactions. In contrast to dye conjugates a mixture of both components was separated according to their characteristic R_f values.

A further evidence for the covalent attachment of the dye is given by the UV spectra. The relatively small hypsochromic shift of the Sorret band of 8-AMB in the conjugate by 15 nm (curve II in Figure 4) does indicate formation of a covalent bond. These findings are in accordance with data found in the literature where ionic interactions of methylene blue derivatives with nucleic acids or proteins cause a blue shift of the Sorret band up to 70 nm and intercalating interaction with nucleobases a red shift of about 7 nm (Antony et al., 1993; Motsenbocker et al., 1993).

Looking at all the results together the described procedure demonstrates an opportunity to simplify the coupling of a variety of dyes being less reactive under normal coupling conditions. In principal, dyes bearing thiol or hydroxy groups can be transformed to a higher state of nucleophilicity by the represented method. These include classes of dyes such as di- and triarylmethane dyes (i.e., derivatives of malachite green), acridines, phenoxazines, phenothiazines, and phenazines.

Furthermore, the introduction of p-L-Glu as polylinker opens a way to attach numereous marker molecules to any biomolecule.

LITERATURE CITED

Antony, T., Atreyi, M., and Rao, M. V. R. (1993) Spectroscopic Studies on the Binding of Methylene Blue to Poly(riboadenylic acid). *J. Biomol. Struct. Dyn. 11,* 67–81.

Buchardt, O., Karup, G., Egholm, M., Koch, T., Henriksen, U., Meldal, M., Jeppesen, C., and Nielsen, P. E. (1989) Photonucleases. *Photochemical Probes in Biochemistry* (P. E. Nielsen, Ed.) 209–218.

Dougherty, T. J. (1987) Photosensitizers: Therapy and Detection of Malignant Tumors. *Photochem. Photobiol. 45,* 879–889.

Fedorova, O. S., Savitskii, A. P., Shoikhet, K. G., and Ponomarev, G. V. (1990) Palladium(II)-coproporphyrin I as a Photoactivable Group in Sequence Specific Modification of Nucleic Acids by Oligonucleotide Derivatives. *FEBS Lett. 259,* 335–337.

Garland, P. B., and Moore, C. H. (1979) Phosphorescence of Protein-bound Eosin and Erythrosin. A Possible Probe for Measurements of Slow Rotational Mobility. *Biochem. J. 183,* 561–572.

Jiang, F. N., Jiang, S., Liu, D., Richter, A., and Levy, J. G. (1990) Development of Technology for Linking Photosensitizers to a Model Monoclonal Antibody. *J. Immunol. Methods 134,* 139–149.

Kremsky, J. N., Wooters, J. L., Dougherty, J. P., Meyers, R. E., Collins, M., and Brown, E. L. (1987) Immobilization of DNA via Oligonucleotides Containing an Aldehyde or Carboxylic Acid Group at the 5'-Terminus. *Nucleic Acids Res. 15,* 2891–2909.

McBride, L. J., and Caruthers, M. H. (1983) An Investigation of Several Deoxynucleoside Phosphoramidites Useful for Synthesizing Oligodeoxyribonucleotides. *Tetrahedron Lett. 24,* 245–248.

Möller, U., Cech, D., and Schubert, F. (1990) P(III)-Acridine Derivatives as Building Blocks for the Solid-Phase Synthesis of Non-Radioactively Labelled Oligonucleotides. *Liebigs Ann. Chem.* 1221–1225.

Motsenbocker, M., Masuya, H., Shimazu, H., Miyawaki, T., Ichimori, Y.,and Sugawara, T. (1993) Photoactive Methylene Blue Dye Derivatives Suitable for Coupling to Protein. *Photochem. Photobiol. 58,* 648–652.

Schubert, F., Ahlert, K., Cech, D., and Rosenthal, A. (1990) One-Step Labelling of Oligo-nucleotides with Fluoresceine during Automated Synthesis. *Nucleic Acids Res. 18,* 3427.

Schubert, F., Knaf, A., Möller, U., and Cech, D. (1994) Covalent Attachment of Methylene Blue to Oligonucleotides. Manuscript in preparation.

Smith, L. M., Kaiser, R. J., Sanders, J. Z., and Hood, L. E. (1987) The Syntheses and Use of Fluorescent Oligonucleotides in DNA Sequence Analysis. *Methods Enzymol. 155,* 260–300.

Tuite, E. M., and Kelly, J. M. (1993) Photochemical Interactions of Methylene Blue and Analogues with DNA and other Biological Substrates. *J. Photochem. Photobiol. B: Biol. 21,* 103–124.

BC940100S

A Cross-Linked Monoclonal Antibody Fragment for Improved Tumor Targeting

Maria A. Stalteri and Stephen J. Mather*

Imperial Cancer Research Fund, Department of Nuclear Medicine, St. Bartholomew's Hospital, West Smithfield, London EC1A 7BE, U.K. Received May 31, 1994®

Cross-linked F(ab')$_2$ fragments derived from PR1A3, a murine monoclonal antibody used in radioimmunoscintigraphy of colorectal tumors, were produced using the bifunctional reagent bismaleimidohexane (BMH) as follows: Digestion of PR1A3 with pepsin gave F(ab')$_2$ fragments which were purified by ion-exchange chromatography. Fab' was produced by reduction of F(ab')$_2$ with cysteine. Following reaction with BMH, cross-linked F(ab')$_2$ fragments, XL-F(ab')$_2$, were isolated by preparative size-exclusion HPLC. Analysis by HPLC and SDS–PAGE demonstrated the presence of a molecule of ~100 kDa containing a nonreducible 50 000 MWt chain. Competitive and direct radioligand binding assays demonstrated that the XL-F(ab')$_2$ had a capacity to bind to antigen similar to that of unmodified F(ab')$_2$. The biodistribution of ^{125}I-labeled XL-F(ab')$_2$ and unmodified F(ab')$_2$ was compared in a nude mouse human tumor xenograft model at 4, 24, and 48 h after injection. Differences between the two preparations were most significant after 24 or 48 h. Tumor uptake of the XL-F(ab')$_2$ was greater and normal tissue retention less than with the unmodified fragment. Tumor to normal tissue ratios at 48 h ranged from 6.2 to 35.2 for XL-F(ab')$_2$ while for the normal F(ab')$_2$ they ranged from 1.5 to 14.2. These results suggest that cross-linked antibody fragments may produce better tumor targeting in clinical application.

INTRODUCTION

Antibodies labeled with various radioisotopes including iodine-123, iodine-131, indium-111, and technetium-99m have been used for radioimmunoscintigraphy and radioimmunotherapy of cancer in patients as well as tumor xenograft models (1, 2). Although monoclonal antibodies are highly specific, only a very small fraction of the injected dose, generally less than 1%, actually binds to the tumor (3). There are a number of factors responsible for this low uptake, but among the most important are (i) limited access to antigen caused by poor tumor blood flow and high interstitial pressure (4) and (ii) non-antigen-mediated mechanisms of uptake in major organs such as liver (5). Intact IgG antibodies are relatively large proteins with a molecular weight of about 150 000. They are consequently slow to clear from the circulation and localize in the tumor. The Fc portion of the molecule is also responsible for a host of interactions with systems such as the RES. It has been proposed that antibody fragments such as F(ab')$_2$, Fab', and recombinant sc-Fv[1] may improve targeting as they (a) are smaller and may therefore show better tumor penetration and (b) lack an Fc region which may reduce "nonspecific" interactions. In fact, most studies have shown that tumor uptake of radiolabeled fragments is often lower than that of intact antibodies but that a greatly enhanced rate of blood clearance does indeed result in improved tumor to background ratios (6–8).

One problem observed with the use of F(ab')$_2$ and Fab' fragments is high kidney activity. A high renal uptake of the smaller fragments can be explained by filtration at the glomerulus followed by tubular reabsorption and metabolism. However, F(ab')$_2$ fragments, which have a molecular weight of about 100 000, are generally considered to be too large to undergo glomerular filtration since they exceed the generally accepted limit of 50–60 kDa for filterable biomolecules (9, 10). Disulfide bonds which are accessible have been shown to be susceptible to reduction in-vivo (11). A likely cause of the kidney uptake of F(ab')$_2$, therefore, is in-vivo reduction of the disulfide bonds bridging the two arms of the F(ab')$_2$ which have been exposed by pepsin digestion, followed by filtration of the resultant Fab' (12). The relative merits of divalent (such as F(ab')$_2$) and monovalent (such as Fab) fragments have not been systematically independently explored. In many studies, F(ab')$_2$ normally show a higher tumor uptake than Fab, but whether this is due to the larger molecular weight or the potential for divalent binding is not clear. Elucidation of the optimum properties of the ideal fragment is further hindered by the possibility of this in-vivo reduction.

In the study described here we sought to improve the in-vivo stability of the F(ab')$_2$ fragment by replacing the labile disulfide bridge with a more stable thioether linkage.

Using a method adapted from that of Glennie (13), we have prepared a cross-linked F(ab')$_2$ fragment of the anti-CEA antibody PR1A3, XL-F(ab')$_2$, using dimaleimidohexane as a cross-linker. The ability of XL-F(ab')$_2$ to bind to MKN-45 cells, a human gastric cancer cell line, was compared to unmodified F(ab')$_2$ in both direct and indirect binding assays. The biodistribution of ^{125}I-labeled XL-F(ab')$_2$ in nude mice bearing MKN-45 human tumor xenografts was compared with that of ^{125}I-labeled unmodified F(ab')$_2$.

* To whom correspondence should be addressed. Tel: 44-71-601-7153. Fax: 44-71-796-3907. E-mail: S_MATHER@icrf.icnet.uk.

[1] Abbreviations: BMH, 1,6-dimaleimidohexane; BSA, bovine serum albumin; CEA, carcinoembryonic antigen; DEAE, (diethylamino)ethyl; DMF, dimethylformamide; DTT, dithiothreitol; EDTA, ethylenediaminetetraacetic acid; HPLC, high-pressure liquid chromatography; PAGE, polyacrylamide gel electrophoresis; PBS, phosphate-buffered saline; RES, reticuloendothelial system; RIA, radioimmunoassay; sc-Fv, single-chain Fv; SDS, sodium dodecyl sulfate; Tris, tris(hydroxymethyl)aminomethane; XL-F(ab')$_2$, cross-linked F(ab')$_2$ fragments.

MATERIALS AND METHODS

Radioisotopes. Na[^{125}I]I was obtained from ICN Radiochemicals, Irvine, CA.

Monoclonal Antibodies. PR1A3, a mouse IgG1 monoclonal antibody used in the study of colorectal cancer, was obtained from the Hybridoma Development Unit, Imperial Cancer Research Fund, London. PR1A3 is used in radioimmunoscintigraphy of patients with colorectal cancers (14). The epitope recognized by this antibody is a cell-associated form of CEA which is lost when the molecule is shed (15).

Cell Line. MKN-45 cells were obtained from the Director's Laboratory, ICRF, London. MKN-45 is a human gastric cancer cell line which expresses CEA on the surface (16). The cells were grown in vitro in Dulbecco's Modified Eagle's Medium containing 10% fetal calf serum.

HPLC. Size exclusion HPLC was performed using a Beckman 114M pump with a Beckman 160 UV detector at 254 nm connected to a Spectra-Physics SP4290 integrator or a Beckman System Gold system with a Beckman 166 UV detector at 280 nm. Analytical work was done using Du Pont Zorbax GF-250 (optimal separation range 10–250 kDa) or Beckman SEC 3000 (5–700 kDa) columns. A Du Pont Zorbax GF-250 XL column was used for preparative work. The mobile phases used were 0.2 M sodium phosphate pH 7.0, 2 mM EDTA or 0.1 M sodium phosphate pH 7.0, 2 mM EDTA. Analytical work was performed using a 20 µL injection loop and a flow rate of 0.5 mL per min. For preparative work a 2.0 mL injection loop and a flow rate of 0.5 mL per min were used.

Ion-exchange HPLC was performed using a Beckman System Gold dual pump system with a Beckman 166 UV detector at 280 nm, a 2.0 mL injection loop, and a TSK gel DEAE-5 PW column. Samples were eluted using a gradient system with 10 mM Tris–HCl pH 7.5 and 10 mM Tris–HCl pH 7.5, 0.5 M NaCl as the mobile phases at a flow rate of 1.0 mL per min.

SDS–PAGE. Antibodies and antibody fragments were analyzed by discontinuous SDS–PAGE according to the method developed by Laemmli (17), with and without reduction in 0.1 M DTT. Samples, containing 1–10 µg of protein, were run using a 5% acrylamide (w/v) stacking gel and a 12.5% running gel. Gels were stained in Coomassie brilliant blue G-250 (BDH, Poole, England) in acetic acid/methanol/water (7%/30%/63%) and then destained in acetic acid/methanol/water (7%/30%/63%). Prestained molecular weight markers were obtained from Gibco BRL, Gaithersburg, MD.

Preparation of F(ab′)₂ Fragments. Thirty mg of PR1A3 antibody was repeatedly centrifuged using Centriprep-30 microconcentrators (Amicon, Beverly, MA) in order to change the buffer to 20 mM sodium citrate, pH 3.5. The final antibody concentration was 5 mg/mL. Five hundred µL of immobilized pepsin slurry (Pierce, Rockford, IL) was added to 8 mL of 20 mM sodium citrate in a centrifuge tube, mixed well by shaking, and then centrifuged for 5 min at 2000 rpm. The supernatant was removed, and the pepsin was washed again with another 8 mL of sodium citrate. The antibody was then added to the immobilized pepsin and incubated at 37 °C with continuous rotation for 5 h. The progress of the reaction was monitored by size exclusion HPLC. When the reaction was 70–90% complete, the pepsin was pelleted by centrifuging for 5 min at 2000 rpm. The supernatant containing the F(ab′)₂ fragments and the unreacted antibody was removed and the pH was adjusted to 7.0–8.0 by addition of 0.5 mL of 1.0 M Tris–HCl pH 9.0. The digestion mixture was analyzed by SDS–PAGE.

Purification of F(ab′)₂ Fragments. The digestion mixture was centrifuged in a Centriprep 30 concentrator (Amicon, Beverly, MA) to change the buffer to 10 mM Tris–HCl, pH 7.5. The solution was then filtered through a 0.2 µm syringe filter (Sterile Acrodisc, Gelman Sciences, Ann Arbor, MI) to remove any particles before injection onto the HPLC. The fragments were purified by anion-exchange HPLC using a gradient system with 10 mM Tris–HCl pH 7.5 as buffer A and 10 mM Tris–HCl pH 7.5, 0.5 M NaCl as buffer B, at time = 0 min, 0% B; time 5–35 min, 0–30% B; time 35–40 min, 30–50% B. Using this system, PR1A3 F(ab′)₂ fragments had a retention time of 23 min, while PR1A3 antibody eluted at 33 min. The purified F(ab′)₂ fragments were analyzed by size exclusion HPLC and by SDS–PAGE.

Reduction of F(ab′)₂ Fragments Using Cysteine. Fifty-one mg of cysteine was dissolved in 1.5 mL of 0.2 M trisodium phosphate to give a 200 mM solution of cysteine. One hundred µL of the cysteine solution was added, with stirring, to 1 mL of a 3.0 mg/mL solution of PR1A3 F(ab′)₂ fragments in 0.1 M sodium phosphate pH 8.0, 0.5 mM EDTA. The reaction mixture was incubated at 37 °C with continuous rotation for 1 h 15 min. The progress of the reaction was monitored by size exclusion HPLC. When the reaction had gone to completion the solution was applied onto a 30 × 1 cm column of Sephadex G-50 and eluted with 50 mM sodium acetate pH 5.3, 0.5 mM EDTA. Three mL fractions were collected, and the presence of antibody fragments was determined by measuring the absorbance at 280 nm on a UV/vis spectrophotometer. The fractions containing antibody were pooled and analyzed by SDS–PAGE.

Cross-Linking of Reduced Fab′ Fragments. Thioether-linked PR1A3 fragments were produced using the bifunctional cross-linker BMH (Pierce, Rockford, IL), by a method similar to that of Glennie (13). All solutions were kept on ice throughout the experiment, and the sodium acetate buffer was purged with nitrogen. BMH was dissolved in anhydrous DMF (Aldrich, Milwaukee, WI) at a concentration of 4 mg/mL. The reduced Fab′ fragments were concentrated to 5 mg/mL in 50 mM sodium acetate buffer pH 5.3 containing 0.5 mM EDTA using a Centricon 30 microconcentrator. One hundred and forty µL of the BMH solution was added rapidly, with stirring, to 0.5 mL of Fab′SH fragments, and the reaction mixture was then incubated on ice for 30 min. Excess BMH was removed by passing the solution through a 30 × 1 cm column of Sephadex G-50 and eluting the sample with 50 mM sodium acetate buffer pH 5.3 containing 0.5 mM EDTA. Two mL fractions were collected and the presence of antibody fragments was determined by measuring the absorbance at 280 nm on a UV/visible spectrophotometer. The fractions (4 and 5) containing Fab′maleimide fragments (typically 80% recovery) were pooled, and 0.5 mL of Fab′SH fragments was added. The mixture was concentrated to a volume of 1 mL using a Centricon 30 microconcentrator and incubated overnight at 4 °C. The reaction mixture was analysed by size exclusion HPLC and by SDS–PAGE. The cross-linked F(ab′)₂ fragments were separated from unreacted Fab′ and from higher molecular weight species by size exclusion HPLC using a DuPont Zorbax GF-250 XL column. The purified cross-linked fragments were analyzed by SDS–PAGE.

Radiolabeling. Antibody, F(ab′)₂ fragments, and cross-linked fragments were labeled with iodine-125 using Iodogen (18). Briefly, 100 µg of antibody or antibody fragment was pipetted into a test tube containing 20 µg of dried Iodogen. A 100–200 µCi portion of iodine-125 was added, and after mixing, the vial was

incubated at room temperature for 10 min. The reaction mixture was applied to the top of a PD-10 column (Pharmacia), and the labeled antibody was eluted in 1 mL fractions of 1% BSA in PBS. The radiochemical purity of the labeled proteins was assessed by thin-layer chromatography using ITLC (Gelman Sciences, Ann Arbor, MI) developed in 85% methanol.

Measurement of Immunoreactivity. Two types of antigen binding assays were performed as follows.

Direct Binding Assay for PR1A3 Fragments Using MKN-45 Cells. The ability of the cross-linked antibody fragments to bind to MKN-45 cells was measured by RIA, using a method similar to that of Lindmo (*19*). The cells from one culture flask of MKN-45 cells were harvested by treatment with 1 mL of versene in PBS and 1 mL of 0.25% trypsin in Tris saline at 37 °C for 10 min. Eight mL of cold PBS containing 1% BSA was added, and the cells were centrifuged at 900 rpm for 10 min. The cell pellet was resuspended in 6 mL of PBS/BSA. The cell suspension was taken up several times into a syringe with a fine gauge needle in order to break up clumps. A 500 μL aliquot of the cell suspension was diluted to 10 mL with PBS/BSA, and the cells were counted using a haemocytometer slide. The assay was performed in duplicate using seven 1 mL Eppendorf tubes. Five hundred μL of PBS/BSA was added to tubes 2–5. Five hundred μL of the cell suspension was added to tubes 1, 2, and 6. Tube 2 was vortexed, and 500 μL of the cell suspension was transferred to tube 3. The process was repeated so as to give a series of double dilutions of cells in tubes 1–5. Five hundred μL of the cell suspension in tube 5 was discarded. Two μg of PR1A3 antibody was then added to tube 6. Iodine-125 labeled cross-linked antibody fragments were diluted to 50 ng/mL with PBS/BSA, and 250 μL of the labeled fragments was added to each of tubes 1–7. Tubes 1–6 were vortexed and then incubated for 2 h at room temperature with continuous rotation. The tubes were then centrifuged at 13 000 rpm for 5 min to pellet the cells. The supernatant was aspirated, taking care not to disturb the cell pellet. Five hundred μL of PBS/BSA was added, and the tubes were vortexed until the cell pellets were resuspended. The tubes were again centrifuged at 13 000 rpm for 5 min, the supernatant was removed, and the cell pellets were counted in an LKB Wallac CompuGamma CS γ counter. A measure of the immunoreactive fraction was obtained by calculating the proportion of radioactivity bound to the cells (counts in relevant tube divided by counts in tube 7) and plotting its reciprocal against the reciprocal of the cell concentration.

Indirect Binding Assay for PR1A3 Fragments Using MKN-45 Cells. The ability of the cross-linked antibody fragments to compete with labeled PR1A3 antibody in a cell-binding assay was compared with that of PR1A3 F(ab')₂ fragments and unlabeled PR1A3 antibody. The cells from one confluent 250 mL flask were obtained and counted as described for the direct binding assay and diluted with PBS/BSA to a concentration of 1.5 million cells/mL. The assay was done in duplicate, using 1 mL Eppendorf vials. Increasing amounts (0, 160, 640, 2560, 10 240, and 40 960 ng) of unlabeled PR1A3 antibody, PR1A3 F(ab')₂ fragments, or cross-linked PR1A3–PR1A3 fragments were added to rows of six Eppendorf vials. Forty ng of iodine-125 labeled PR1A3 antibody was then added to each vial, followed by PBS/BSA if necessary to give the same total volume in all the vials. The vials were vortexed, and 500 μL of the MKN-45 cell suspension was added. After vortexing, the vials were incubated at room temperature for 1 h with

continuous rotation. The vials were centrifuged for 10 min at 13 000 rpm in a microcentrifuge, and the supernatants were aspirated. The cell pellets were resuspended in 500 μL of PBS/BSA by vortexing for a few min. The vials were centrifuged for another 10 min at 13 000 rpm, the supernatants were aspirated, and the amount of radioactivity bound to the cells was determined using a γ counter.

Animal Biodistribution Studies. Three-month old nude mice were injected with transplanted MKN-45 human tumor samples (0.1 mL) subcutaneously in each flank. After 3–4 weeks, when the tumors were 0.3–0.5 cm in diameter, the animals' drinking water was supplemented with potassium iodide (10 mg/100 mL) for 3 days prior to and during the biodistribution experiments. PR1A3 F(ab')₂ fragments and PR1A3–PR1A3 cross-linked fragments were radiolabeled with iodine-125 at a specific activity of 1 mCi per microgram. The labeled antibody fragments were diluted with PBS to a final concentration of 50 μg per mL. The mice were divided into two groups of 15. Group A was injected intravenously with 100 μL of the iodine-125 labeled F(ab')₂ fragments, and group B was injected with 100 μL of the labeled cross-linked fragments. The total injected dose was calculated by accurately weighing the injection syringes before and after injecting each animal. Five animals from each group were sacrificed at 4, 24, and 48 h after injection. Samples of blood were taken, and organs and tissues of interest were resected, rinsed in saline, blotted dry, and placed into preweighed tubes. All samples were counted in an LKB Wallac 1282 Compugamma CS γ counter together with appropriate dilutions of the iodine-125 labeled F(ab')₂ and XL-F(ab')₂. Results were analyzed using Student's t-test.

RESULTS

Preparation and Characterization of XL-F(ab')₂. F(ab')₂ fragments of PR1A3, a mouse monoclonal IgG1, were produced by digestion with pepsin beads at pH 3.5. The rate of the reaction was quite sensitive to pH, becoming much slower when the pH was above 3.5. The reaction was monitored by size exclusion HPLC using a Beckman SEC 3000 column. When the digestion was allowed to go to completion lower molecular weight species, possibly due to further digestion of F(ab')₂, were also produced. We therefore decided to stop the reaction when it was 70–90% complete and to purify the F(ab')₂ from undigested antibody by ion-exchange HPLC (*20*). Figure 1 shows a chromatogram of the purification of F(ab')₂ using a DEAE HPLC column, while an analytical size exclusion HPLC chromatogram of the purified F(ab')₂ is shown in Figure 2.

Various reagents have been used for the reduction of F(ab')₂ to Fab'SH including organophosphines (*21*), DTT (*22*), mercaptoethanol (*13*), cysteamine (*23*), and cysteine (*24, 25*). We briefly investigated the use of mercaptoethanol, Reduce-Imm immobilized reducing agent (Pierce, Rockford, IL), tris(2-carboxyethyl)phosphine (*26*), and cysteine in order to determine which conditions would give complete reduction of F(ab')₂ while keeping formation of free heavy and light chains to a minimum and without affecting the immunoreactivity of the antibody. We obtained good results using 20 mM cysteine in phosphate buffer pH 8.0, 0.5 mM EDTA at 37 °C and subsequent large scale reductions were carried out using these conditions. An example of a HPLC chromatogram of this material, with a purity of 97.8% Fab', 2.2% F(ab')₂ is shown in Figure 3. Typical yields were of the order of 90%.
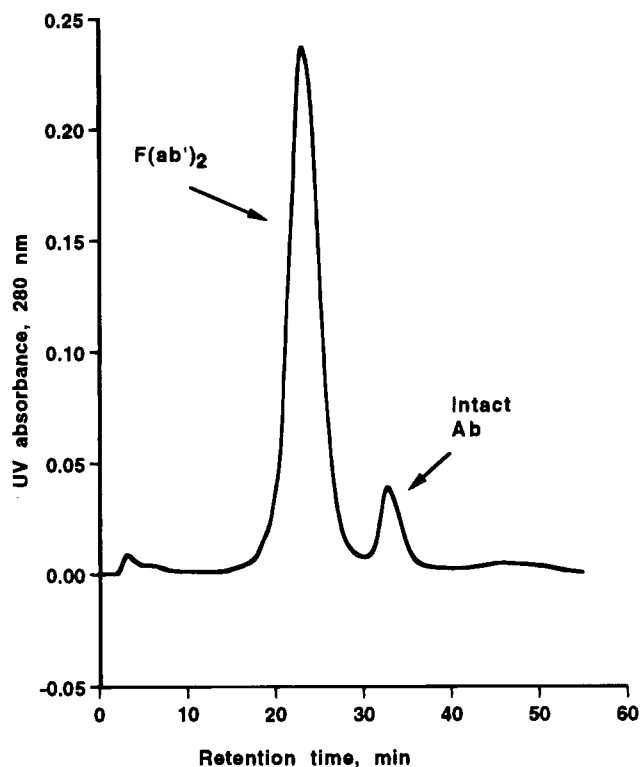
Figure 1. Purification of PR1A3 F(ab')₂ from intact antibody by ion-exchange HPLC. Separation was achieved using a DEAE-5 PW column and a gradient system with 10 mM Tris–HCl pH 7.5 as mobile phase A and 10 mM Tris–HCl pH 7.5, 0.5 M NaCl as mobile phase B, monitored at 280 nm. Key: flow rate, 1.0 mL/min; retention times, F(ab')₂ 23 min, intact antibody 33 min.

XL-F(ab')₂ were prepared using the bifunctional cross-linking agent dimaleimidohexane under conditions similar to those reported by Glennie (*13*) for the preparation of bispecific F(ab')₂. During the development of our methodology, occasional low yields of 10–20% were obtained. However, optimization of the method by using longer Sephadex columns to purify Fab'SH from the reducing agents and Fab'maleimide from excess BMH and purging the cross-linking reaction buffer with nitrogen resulted in uniformly higher yields ranging from 40 to 50% with a mean of 46.5%. In addition to XL-F(ab')₂ small amounts of higher molecular weight species, possibly aggregates, but probably F(ab')₃ as described by Glennie (*13*), were also obtained. The cross-linked fragments were purified from the reaction mixture by size exclusion HPLC using a preparative GF-250XL column and were analyzed by SDS–PAGE and analytical HPLC. Figures 4 and 5 show analytical HPLC chromatograms of the reaction mixture and the purified XL-F(ab')₂, respectively. A gel run under reducing conditions is shown in Figure 6. Lane 2 shows native PR1A3 F(ab')₂, while lanes 4–7 show different fractions from the preparative HPLC purification of the XL-F(ab')₂. Lanes 4 and 5 represent unreacted Fab' recovered from the reaction mixture, while lanes 6 and 7 are XL-F(ab')₂. The nonreducible bands of MW ~50 000 in lanes 6 and 7 demonstrate the presence of cross-linked H' chains.

Radiolabeling. Radioiodination yields typically ranged from 50 to 80%. Final purity as measured by ITLC was always greater than 95%. The specific activities of the fragment preparations used for the biodistribution study were 1.24 mCi/mg for the XL-F(ab')₂ fragment and 1.09 mCi/mg for the F(ab')₂.

Measurement of Immunoreactivity. The immunoreactivity of the cross-linked F(ab')₂ fragments was
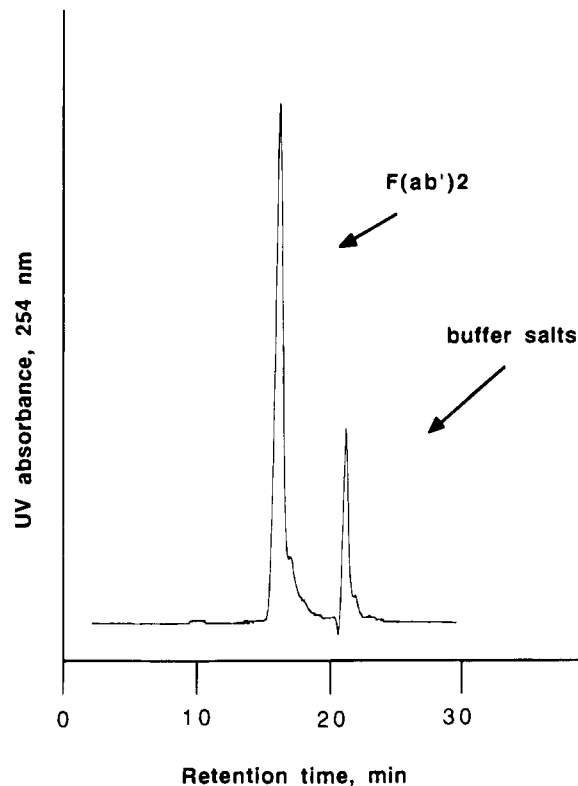
Figure 2. Analytical size exclusion HPLC profile (Beckman SEC 3000 column) of purified PR1A3 F(ab')₂, monitored at 254 nm. Key: flow rate, 0.5 mL/min; mobile phase, 0.2 M sodium phosphate pH 7.0, 2 mM EDTA; retention times, F(ab')₂ 15.94 min, buffer salts 21.22 min.
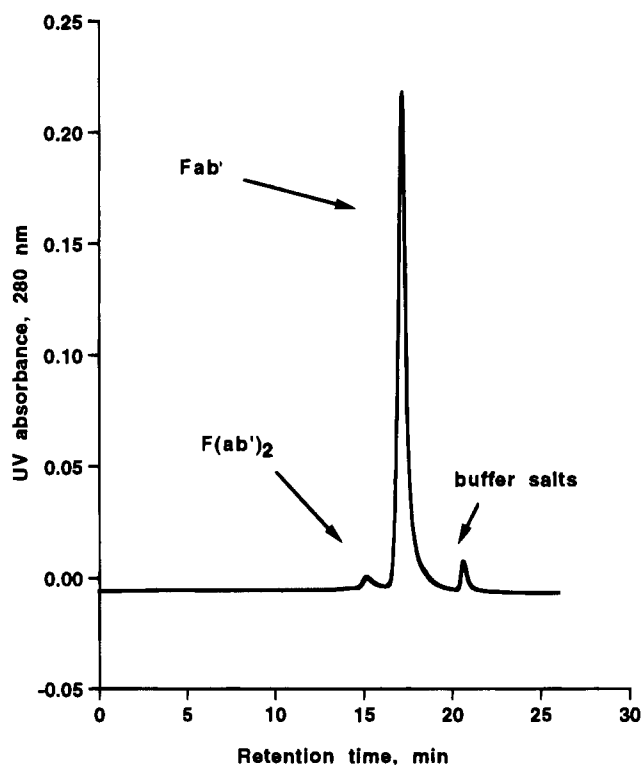
Figure 3. Analytical size exclusion HPLC profile of reduced Fab', monitored at 280 nm. Key: Beckman SEC 3000 column; flow rate, 0.5 mL/min; mobile phase, 0.2 M sodium phosphate pH 7.0, 2 mM EDTA; retention times, F(ab')₂ 15.16 min, Fab' 17.14 min, buffer salts 20.62 min.

measured by both a direct and an indirect radioimmunoassay. In the indirect RIA, increasing amounts of
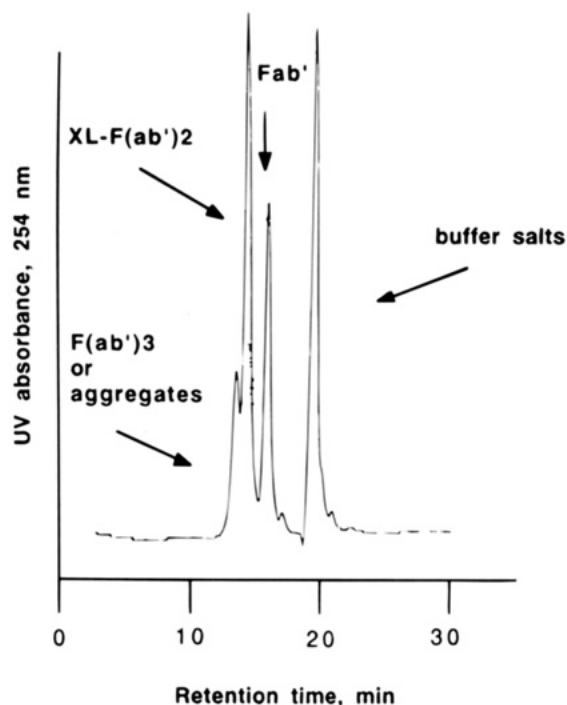
Figure 4. Analytical size exclusion HPLC profile of the cross-linked $F(ab')_2$ reaction mixture monitored at 254 nm. Key: Beckman SEC 3000 column; flow rate, 0.5 mL/min; mobile phase, 0.2 M sodium phosphate pH 7.0, 2 mM EDTA; retention times, $XL-F(ab')_3$ or aggregates 14.09 min, $XL-F(ab')_2$ 14.89 min, unreacted Fab' and Fab'maleimide 16.52 min, buffer salts 20.28 min.
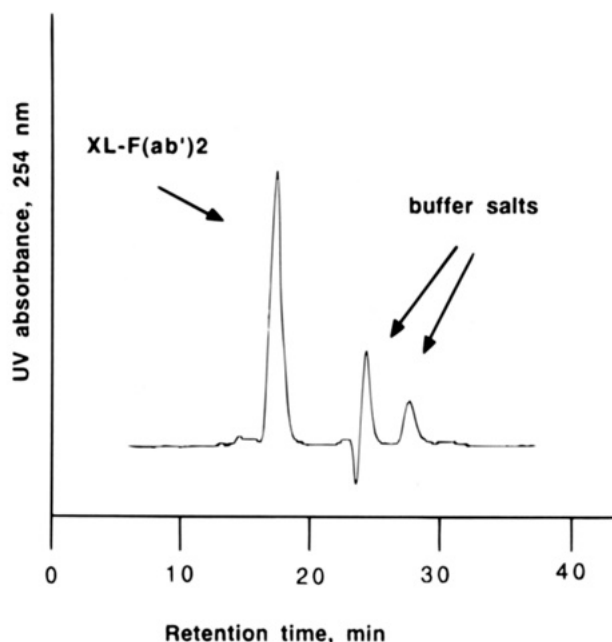
Figure 5. Analytical size exclusion HPLC profile of purified $XL-F(ab')_2$, monitored at 254 nm. Key: Du Pont Zorbax GF-250 column; flow rate, 0.5 mL/min; mobile phase, 0.1 M sodium phosphate pH 7.0, 2 mM EDTA; retention times, $XL-F(ab')_2$ 16.87 min, buffer salts 24.13 min, 27.43 min.

unlabeled antibody or fragments competed with a constant amount of iodinated intact antibody for binding to MKN-45 cells. Figure 7 shows that the $XL-F(ab')_2$ competed essentially as well as $F(ab')_2$ and intact antibody. A direct binding assay, using a method similar to that described by Lindmo (*19*), was used to determine the immunoreactive fraction of ^{125}I-labeled $XL-F(ab')_2$ and ^{125}I-labeled $F(ab')_2$. A double reciprocal plot of T/B against the reciprocal of the number of cells produces a

Figure 6. SDS−PAGE of cross-linked antibody fragments. The gel was run under reducing conditions (0.1 M DTT) using a 5% acrylamide stacking gel and a 12.5% running gel. Protein bands were visualized by staining with Coomassie blue. Lanes 1 and 8: prestained molecular weight markers, apparent molecular weights 215, 105, 70, 43, 28, 18, and 15 kDa. Lane 2: PR1A3 $F(ab')_2$. Lane 3: $F(ab')_2$ fragments from an irrelevant antibody. Lanes 4 and 5: unreacted Fab' and Fab'maleimide recovered from the preparative size exclusion HPLC purification of the cross-linked fragments. Lanes 6 and 7: purified $XL-F(ab')_2$.

Competition for binding to MKN-45 cells
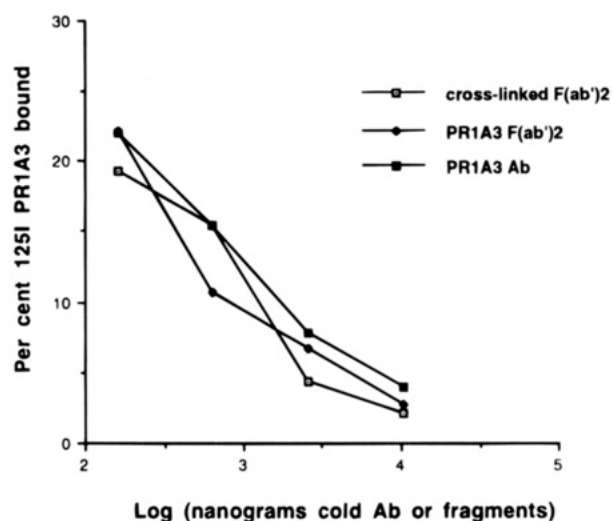
Figure 7. Competition for binding to MKN-45 cells between iodine-125 labeled PR1A3 antibody and unlabeled antibody or fragments. MKN-45 cells were incubated with 40 ng of ^{125}I-labeled intact PR1A3 antibody and 0, 160, 640, 2560, or 10240 ng of unlabeled intact PR1A3 Ab, $F(ab')_2$ or $XL-F(ab')_2$.

straight line where the reciprocal of the y-intercept gives the immunoreactive fraction. The results are shown in Figure 8. The immunoreactive fraction of ^{125}I-labeled $XL-F(ab')_2$ was 64% compared with 69% for the ^{125}I-labeled $F(ab')_2$.

Biodistribution Studies. The biodistribution of ^{125}I-labeled $XL-F(ab')_2$ was compared to that of ^{125}I-labeled $F(ab')_2$ in nude mice bearing MKN-45 human tumor xenografts. Table 1 shows the percent injected dose per gram of tissue for ^{125}I-$F(ab')_2$ and ^{125}I-$XL-F(ab')_2$ at 4, 24, and 48 h postinjection. Differences between the biodistributions of cross-linked fragments and unmodified $F(ab')_2$ were not significant at 4 h. At 24 h there was significantly less ^{125}I-$XL-F(ab')_2$ in all tissues ($p < 0.01$ except for muscle, $p < 0.05$) except tumor. At 48 h the amount of $XL-F(ab')_2$ in tumor was significantly higher ($p < 0.005$), while that in liver, spleen, and kidneys was

Direct binding to MKN-45 cells
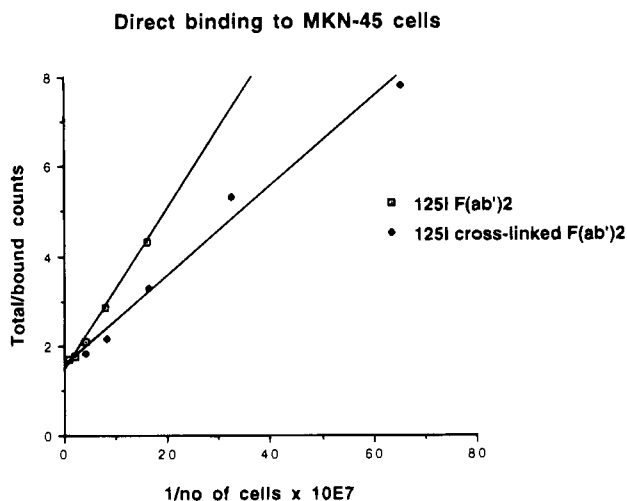
Figure 8. Comparison of direct binding of ^{125}I-labeled PR1A3 F(ab')$_2$ and ^{125}I-labeled XL-F(ab')$_2$ to MKN-45 cells. 12.5 ng of ^{125}I-F(ab')$_2$ or ^{125}I-XL-F(ab')$_2$ were incubated with a series of double dilutions of MKN-45 cells. The figure shows a Lindmo plot of total/bound counts against 1/cell number. The reciprocal of the y-intercept gives the immunoreactive fraction of the antibody fragments.

significantly lower ($p < 0.001$) than that of F(ab')$_2$. Tumor to tissue ratios for ^{125}I-XL-F(ab')$_2$ and ^{125}I-F(ab')$_2$ are given in Table 2. Tumor to tissue ratios at 48 h ranged from 1.5 to 14.2 for F(ab')$_2$ and from 6.2 to 35.2 for XL-F(ab')$_2$. Ratios for tumor to blood, liver, spleen, and kidneys were significantly higher at 24 ($p < 0.05$) and 48 h ($p < 0.005$) for XL-F(ab')$_2$.

DISCUSSION

The design of the optimum antibody-based molecule for tumor targetting is still a matter of debate. While

many antibodies have proved successful for imaging a variety of tumors, it seems likely that small molecules with rapid kinetics that mirror the short physical half lives of the best diagnostic isotopes will have advantages for imaging. For radiotherapeutic applications, the retention time of the antibody in the tumor and the degree of accretion of the radiolabel by normal tissues become increasingly important. In this arena, it seems likely that larger molecules, probably multivalent, will be preferred. The designer antibodies of the future will almost certainly be made using recombinant techniques; however, more information on the effects of changes in molecular structure needs to be acquired before the blueprints for such molecules can be finalized, and much of this data can be more easily obtained by the use of conventional protein chemistry.

We have explored the use of cross-linking agents for linking Fab' fragments of various antibodies. The first result of this approach has been the generation of a homobifunctional XL-F(ab')$_2$ fragment of the antibody PR1A3. We have characterized this molecule using conventional chromatographic techniques and shown in *in-vitro* binding assays that the extensive processing does not adversely affect the ability of the molecule to bind to its epitope. Separation techniques based on size alone are unable to distinguish between F(ab')$_2$ fragments linked by disulfide bridges or other cross-linkers. We therefore performed SDS−PAGE separation under reducing conditions to show that our XL-F(ab')$_2$ fragment contained the nonreducible 50 000 MW band of the thioether bridged chains (lanes 6 and 7) compared with the conventional F(ab')$_2$ (lane 2). This analysis does not exclude the possibility that thiol reoxidation may also occur simultaneously, resulting in the presence of a quantity of contaminating F(ab')$_2$ in our XL-F(ab')$_2$ preparation. However, we took great pains to avoid

Table 1. Biodistribution Data for ^{125}I-Labeled PR1A3 F(ab')$_2$ and Cross-Linked F(ab')$_2$ in Nude Mice Bearing MKN-45 Human Tumor Xenografts[a]

| | percent injected dose per gram | | | | | |
| tissue | PR1A3 F(ab')$_2$ | | | cross-linked PR1A3 F(ab')$_2$ | | |
	4 h	24 h	48 h	4 h[b]	24 h[b]	48 h
tumor	6.40 ± 0.85	4.02 ± 0.44	1.16 ± 0.22	6.50 ± 0.41	4.20 ± 1.52	1.95 ± 0.41
blood	13.82 ± 1.93	2.54 ± 0.38	0.38 ± 0.11	12.30 ± 1.65	1.44 ± 0.16	0.34 ± 0.12
liver	3.60 ± 0.48	0.93 ± 0.12	0.30 ± 0.05	3.32 ± 0.35	0.46 ± 0.05	0.14 ± 0.02
spleen	2.70 ± 0.39	0.92 ± 0.20	0.26 ± 0.05	2.85 ± 0.22	0.47 ± 0.12	0.14 ± 0.02
kidneys	7.26 ± 0.96	2.33 ± 0.42	0.77 ± 0.16	7.90 ± 0.34	1.00 ± 0.27	0.26 ± 0.04
lungs	5.83 ± 1.60	1.49 ± 0.18	0.30 ± 0.10	5.95 ± 0.98	0.87 ± 0.15	0.25 ± 0.07
muscle	1.00 ± 0.34	0.38 ± 0.08	0.09 ± 0.03	1.12 ± 0.10	0.24 ± 0.06	0.06 ± 0.02
femur	2.19 ± 0.80	0.61 ± 0.13	0.14 ± 0.04	1.78 ± 0.05	0.29 ± 0.08	0.09 ± 0.02
stomach	5.49 ± 1.08	3.20 ± 1.21	0.45 ± 0.38	4.53 ± 1.51	0.82 ± 0.35	0.24 ± 0.11
intestines	2.81 ± 0.42	0.58 ± 0.11	0.12 ± 0.05	1.82 ± 0.21	0.27 ± 0.06	0.07 ± 0.02
whole body clearance[c]	70.13 ± 7.04	21.28 ± 5.40	4.99 ± 1.74	63.34 ± 5.69	12.00 ± 2.36	4.11 ± 1.17

[a] Mean ± standard deviation, $n = 5$. [b] $n = 4$. [c] Percent injected dose.

Table 2. Tumor to Tissue Ratios for ^{125}I-labeled PR1A3 F(ab')$_2$ and Cross-Linked F(ab')$_2$ in Nude Mice Bearing MKN-45 Human Tumor Xenografts[a]

| | F(ab')$_2$ | | | cross-linked F(ab')$_2$ | | |
tissue	4 h	24 h	48 h	4 h	24 h	48 h
blood	0.47 ± 0.09	1.58 ± 0.15	3.09 ± 0.35	0.54 ± 0.06	2.95 ± 1.04	6.16 ± 1.47
liver	1.79 ± 0.31	4.31 ± 0.34	3.83 ± 0.32	1.99 ± 0.21	9.11 ± 2.83	14.34 ± 1.04
spleen	2.41 ± 0.50	4.44 ± 0.58	4.49 ± 0.30	2.31 ± 0.13	8.95 ± 2.11	14.54 ± 2.93
kidneys	0.88 ± 0.10	1.73 ± 0.20	1.51 ± 0.17	0.83 ± 0.04	4.50 ± 2.13	7.84 ± 1.11
lungs	1.16 ± 0.32	2.71 ± 0.47	4.01 ± 0.63	1.12 ± 0.16	4.97 ± 1.89	8.27 ± 1.25
muscle	7.32 ± 3.67	10.93 ± 2.38	14.20 ± 3.88	5.91 ± 0.65	19.46 ± 9.81	35.21 ± 10.35
femur	3.29 ± 1.37	6.65 ± 0.78	8.67 ± 1.52	3.68 ± 0.02	14.34 ± 3.93	23.22 ± 4.27
stomach	1.19 ± 0.24	1.35 ± 0.36	4.28 ± 2.79	1.59 ± 0.59	5.41 ± 1.81	10.21 ± 5.39
intestines	2.30 ± 0.40	6.96 ± 0.85	10.81 ± 2.99	3.64 ± 0.39	15.50 ± 3.91	28.55 ± 8.47

[a] Percent injected dose per gram for tumor divided by percent injected dose per gram for normal tissues.

reoxidation by the use of low pH, nitrogen-purged solvents, low temperature, and EDTA to scavenge the metal ions which catalyze the process in order to keep such contaminants to a minimum.

In biodistribution studies in tumor-bearing mice, the cross-linked and native molecules show significant differences *in-vivo*, resulting in greater retention of the radionuclide by the tumor and lower uptake by normal tissues, notably the liver and kidneys, of XL-F(ab')$_2$. There was no overall significant difference in the blood clearance of the two fragments. From an imaging perspective the end result of this comparison is that tumor to normal tissue ratios are enhanced by a factor of up to 5. From a therapeutic point of view the lower radiation burden received by normal organs would permit an escalation of the administered dose of radioactivity with a subsequent increase in tumor radiation dose. Although we have performed these studies with only one antibody the combination of these results with those in other publications (*12, 25, 27*) suggest that this could be a general phenomenon. We have also used only one radionuclide, radioiodine, in this study. The use of other radiolabels, such as radiometals, is likely to produce conjugates which show differences in biodistribution. Since the iodine–protein bond itself shows evidence of poor *in-vivo* stability (*28*), the use of more stable indium or technetium chelates may well result in a still greater differential between cross-linked and native F(ab')$_2$ fragments, but this remains to be substantiated by further experimentation.

From a technical point of view, the methodology as described above is elaborate and the multiplicity of steps results in poor yields—of the order of 10%. It is hard to imagine, therefore, that this method could be recommended for the routine preparation of cross-linked fragments for clinical application. Our aim is more to identify those important aspects of molecular design which should be incorporated into recombinant antibody molecules.

While this work was in progress two reports of biodistribution studies with maleimide-linked fragments in tumor xenograft models have appeared in the literature. Quadri et al. (*12*) prepared a series of three ^{111}In-labeled cross-linked F(ab')$_2$ and found that cross-linked F(ab')$_2$ showed significantly less kidney activity and higher tumor retention than that of unmodified F(ab')$_2$ in good agreement with our results. Bood clearance of the cross-linked fragments, however, was intermediate between that of IgG and F(ab')$_2$. The difference between this finding and our results may perhaps be related to the use of a different radiolabel. Schott *et al.* (*27*) reported the synthesis of two new maleimide reagents which they used to prepare [105]Rh-labeled F(ab')$_3$ and F(ab')$_4$ fragments. They reported that the biodistribution behavior of the F(ab')$_3$ fragments in both Balb/c and tumor-bearing nude mice was intermediate between that of IgG and unmodified F(ab')$_2$, with lower kidney uptake than unmodified F(ab')$_2$. The larger F(ab')$_4$ fragments, however, were found to accumulate in the liver in Balb/c mice.

We can, therefore, conclude that antibody fragments which are cross-linked with nonreduceable bridges have the potential to improve the current status of both immunoscintigraphy and radioimmunotherapy.

ACKNOWLEDGMENT

LITERATURE CITED

(1) Britton, K. E., Granowska, M., and Shepherd, P. Radioimmunoscintigraphy. In *Clinical Nuclear Medicine* (M. N. Maisey, K. E., Britton, and D. L. Gilday, Eds.), Chapter 20, Chapman and Hall Medical, London, 1991.

(2) Goldenberg, D. M. (1989) Future role of radiolabeled monoclonal antibodies in oncological diagnosis and therapy. *Semin. Nucl. Med. 19*, 332–339.

(3) Fazio, F., and Paganelli, G. (1993) Antibody-guided scintigraphy: targeting of the "magic bullet". *Eur. J. Nucl. Med. 20*, 1138–1140.

(4) Jain, K. R., and Baxter, L. T. (1988) Mechanisms of heterogeneous distribution of monoclonal antibodies and other macromolecules in tumors: significance of elevated interstitial pressure. *Cancer Res. 48*, 7022–7032.

(5) Boyle, C. C., Paine, A. J., and Mather, S. J. (1992) The mechanism of hepatic uptake of a radiolabeled monoclonal antibody. *Int. J. Cancer 50*, 912–917.

(6) Buraggi, G. L., Callegaro, L., Mariani, G., Turrin, A., Cascinelli, N., Attili, A., Bombardieri, E., Terno, G., and Plassio, G. (1985) Imaging with ^{131}I-labeled monoclonal antibodies to a high-molecular-weight melanoma-associated antigen in patients with melanoma: efficacy of whole immunoglobulin and its F(ab')$_2$ fragments. *Cancer Res. 45*, 3378–3387.

(7) Delaloye, B., Bischof-Delaloye, A., Buchegger, F., Fliedner, V., Grob, J. P., Volant, J. C., Pettavel, J., and Mach, J. P. (1986) Detection of colorectal carcinoma by emission-computerized tomography after injection of ^{123}I-labeled Fab or F(ab')$_2$ fragments from monoclonal anti-carcinoembryonic antigen antibodies. *J. Clin. Invest. 77*, 301–311.

(8) Yokota, T., Milenic, D. E., Whitlow, M., and Schlom, J. (1992) Rapid tumor penetrance of a single-chain Fv and comparison with other immunoglobulin forms. *Cancer Res. 52*, 3402.

(9) Taylor, A. E., Granger, N. D. (1984) In *Handbook of Physiology; The Cardiovascular System IV*. (E. M. Renkin, and C. C. Michel, Eds.), pp 467–520, Americal Physiological Society, Bethesda, MD.

(10) Takatura, Y., Fujita, T., Hashide, M., and Sezaki, H. (1990) Disposition characteristics of macromolecules in tumor-bearing mice. *Pharm. Res. 7*, 339–349.

(11) Strand, M., Scheinberg, D. A., and Gansow, O. A. (1984) Monoclonal antibody conjugates for tumor imaging and therapy. In *Cell Fusion: Gene Transfer and Transformation* (R. F. Beers, and E. G. Bassett, Eds.). Raven Press, New York pp 385–393.

(12) Quadri, S. M., Lai, J., Mohammadpour, H., Vriesendorp, H. M., and Williams, J. R. (1993) Assessment of radiolabeled stabilized F(ab')$_2$ fragments of monoclonal antiferritin in nude mouse model. *J. Nucl. Med. 34*, 2152–2159.

(13) Glennie, M. J., McBride, H. M., Worth, A. T., and Stevenson, G. T. (1987) Preparation and performance of bispecific F(ab'γ)$_2$ antibody containing thioether-linked Fab'γ fragments. *J. Immunol. 139*, 2367–2375.

(14) Granowska, M., Britton, K. E., Mather, S. J., Morris, G., Ellison, D., Soobramoney, S., Talbot, I. C., and Northover, J. M. A. (1993) Radioimmunoscintigraphy with technetium-99m labeled monoclonal antibody, 1A3, in colorectal cancer. *Eur. J. Nucl. Med. 20*, 690–698.

(15) Durbin, H., Young, S., Stewart, L. M., Wrba, F., Rowan, A. J., Snary, D., and Bodmer, W. F. (1994) A novel epitope on carcinoembryonic antigen defined by the clinically relevant antibody PR1A3. *Proc. Natl. Acad. Sci., U.S.A. 91*, 4313–4317.

(16) Hojo, H. (1977) Establishment of cultured cell lines of human stomach cancer origin and their morphological characteristics. *Niigata Igakukai Zassi 91*, 737–763.

(17) Laemmli, U. K. (1970) Cleavage of structural proteins during the assembly of the head of the bacteriophage T4. *Nature 227*, 680–681.

(18) Fraker, P. J., and Speck, J. C. (1978) Protein and cell membrane iodinations with a sparingly soluble chloroamide, 1,3,4,6-tetrachloro-3α,6α-diphenylglycoluril. *Biochem. Biophys. Res. Commun. 80*, 849–857.

(19) Lindmo, T., and Bunn, P. A. (1986) Determination of the true immunoreactive fraction of monoclonal antibodies after radiolabelling. *Methods Enz. 121,* 678–684.

(20) Parham, P., Androlewicz, M. J., Brodsky, F. M., Holmes, N. J., and Ways, J. P. (1982) Monoclonal antibodies: purification, fragmentation and application to structural and functional studies of class 1 MHC antigens. *J. Immunol. Methods 53,* 133.

(21) Levison, M. E., Josephson, A. S., and Kirschenbaum, D. M. (1969) Reduction of biological substances by water-soluble phosphines: gamma globulin (IgG). *Experientia 25,* 126–127.

(22) Cleland, W. W. (1964) Dithiothreitol, a new protective reagent for SH groups. *Biochemistry 3,* 480–482.

(23) LeDoussal, J. M., Chetanneau, A., Gruaz-Guyon, A., Martin, M., Gautherot, E., Lehur, P. A., Chatal, J. F., Delaage, M., and Barbet, J. (1993) Bispecific monoclonal antibody-mediated targeting of an indium-111-labeled DTPA dimer to primary colorectal tumors: pharmacokinetics, biodistribution, scintigraphy and immune response. *J. Nucl. Med. 34,* 1662–1671.

(24) Mezzanzanica, D., Garrido, M. A., Neblock, D. S., Daddona, P. E., Andrew, S. M., Zurawski, V. R., Jr., Segal, D. M., and Wunderlich, J. R. (1991) Human T-lymphocytes targeted against an established human ovarian carcinoma with a bispecific F(ab′)₂ antibody prolong host survival in a murine xenograft model. *Cancer Res. 51,* 5716–5721.

(25) Lamki, L. M., Yehuda, Z. P., Rosenblum, M. G., Shanken, L. J., Thompson, L. B., Schweighardt, S. A., Frincke, J. M., and Murray, J. L. (1990) Metastatic colorectal cancer: radioimmunoscintigraphy with a stabilized In-111-labeled F(ab′)₂ fragment of an anti-CEA monoclonal antibody. *Radiology 174,* 147–151.

(26) Burns, J. A., Butler, J. C., Moran, J., and Whitesides, G. M. (1991) Selective reduction of disulfides by tris(2-carboxyethyl)phosphine. *J. Org. Chem. 56,* 2648–2650.

(27) Schott, M. E., Frazier, K. A., Pollock, D. K., and Verbanac, K. M. (1993) Preparation, characterization, and in vivo biodistribution properties of synthetically cross-linked multivalent antitumor antibody fragments. *Bioconjugate Chem. 4,* 153–165.

(28) Wilbur, D. S., Hadley, S. W., Hylarides, M. D., Abrams, P. G., Beaumier, P. A., Morgan, A. C., Reno, J. M., and Fritzberg, A. R. (1989) Development of a stable radioiodinating reagent to label monoclonal antibodies for radiotherapy of cancer. *J. Nucl. Med. 30,* 216–226.

BC9400985

Poly(ethylene glycol)-Modified Phospholipids Prevent Aggregation during Covalent Conjugation of Proteins to Liposomes

Troy O. Harasym,*,† Paul Tardi,‡ Shane A. Longman,† Steven M. Ansell,‡ Marcel B. Bally,† Pieter R. Cullis,‡ and Lewis S. L. Choi‡

The University of British Columbia, Biochemistry Department, 2146 Health Sciences Mall, Vancouver, British Columbia, V6T 1Z3 Canada, and British Columbia Cancer Agency, Division of Medical Oncology, 600 West 10th Avenue, Vancouver, British Columbia, V5Z 4E6 Canada. Received October 7, 1994⊛

Liposome aggregation is a major problem associated with the covalent attachment of proteins to liposomes. This report describes a procedure for coupling proteins to liposomes that results in little or no change in liposome size. This is achieved by incorporating appropriate levels of poly(ethylene glycol)-modified lipids into the liposomes. The studies employed thiolated avidin-D coupled to liposomes containing the thio-reactive lipid N-(4-(p-maleimidophenyl)butyryl)dipalmitoyl phosphatidylethanolamine (1 mol % of total lipid) and various amounts of MePEG−S−POPE (monomethoxypoly(ethylene glycol) linked to phosphatidylethanolamine via a succinate linkage). The influence of PEG chain length and density was also assessed. The presence of PEG on the surface of liposomes is shown to provide an effective method of inhibiting aggregation and the corresponding increase in liposome size during the covalent coupling of avidin-D. A balance between the size of the PEG used and the amount of PEG−lipid incorporated into the liposome had to be achieved in order to maintain efficient coupling. Optimal coupling efficiencies in combination with minimal aggregation effects were achieved using 2 mol % MePEG$_{2000}$−S−POPE (PEG of 2000 MW) or 0.8 mol % MePEG$_{5000}$−S−POPE (PEG of 5000 MW). At these levels, the presence of PEG did not affect the biotin binding activity of the covalently attached avidin. The ability of the resulting liposomes to specifically target to biotinylated cells is demonstrated.

INTRODUCTION

Liposome-based drug carrier systems which accumulate at regions of disease are actively being developed. It is now well established that small liposomes and associated contents accumulate preferentially in sites of infection, inflammation, and cancer following iv administration *(1−10)*. The level of entrapped contents delivered to these diseased sites increases with liposome circulation longevity as well as optimized drug retention characteristics *(9−11)*. Early studies evaluating the pharmacokinetic behavior of liposomes following intravenous administration demonstrated that liposome size was a critical determinant of circulation longevity *(12, 13)*. Phosphatidylcholine−cholesterol liposomes exhibiting mean size distributions between 50 and 150 nm, for example, are retained in the circulation for extended time periods *(14, 15)*. Retention of entrapped contents is dependent on the lipid composition employed as well as the nature of the entrapped material *(11, 16, 17)*. Liposomes prepared using phospholipids with long chain saturated fatty acyl chains and cholesterol exhibit improved retention of hydrophilic compounds following iv administration.

Research has focused in three areas to develop liposomal drug carriers that have an increased propensity to accumulate in disease sites. The first concerns the use of lipids that engender extended circulation lifetime. Incorporation of the ganglioside G_{M1} or poly(ethylene glycol)-modified phospholipids in liposomes, for example, decreases uptake in the liver and increase circulating

blood levels *(18−20)*. Several studies have shown that these liposomes accumulate efficiently in sites of tumor growth *(5, 8, 9)*. The second area of interest concerns the biological elements that mediate movement of liposomes from the blood compartment to an extravascular site. Recent studies have shown that such delivery to tumors occurs through blood vessels that are hyperpermeable to circulating macromolecules *(9, 10)*. Finally, it is reasonable to assume that the extent of accumulation within disease sites, such as tumors, will be dependent on an equilibrium between circulating liposomes and liposomes in the extravascular space. Targeting liposomes to specific elements or cells within the extravascular space should shift the equilibrium in favor of further liposome accumulation at the target site.

Although approaches for attaching targeting proteins to the surface of liposomes are well established *(21−24)*, the resulting proteoliposomes often do not maintain optimal characteristics. It has been shown, for example, that protein−liposome conjugation procedures based on the use of heterobifunctional reagents lead to liposome−liposome crosslinking (i.e., increases in carrier size) which results in dramatically reduced circulation lifetimes. Further, leakage of entrapped contents is also observed *(25, 26)*. Using drug entrapment procedures based on transmembrane pH gradients, where a drug is loaded into preformed liposomes *(27)*, eliminates problems associated with drug leakage during coupling. The most significant limitation to the use of these coupling procedures is liposome aggregation.

Aggregation is generally caused by the covalent crosslinking of liposomes via a multivalent protein bridge. In addition, noncovalent protein−protein interactions can lead to further aggregation. Although aggregation can be minimized by reducing the concentration of reactants and by limiting the number of reactive groups present on both the liposomes and/or the protein, these steps

* To whom correspondence should be addressed. Fax: (604) 822-4843. Phone: (604) 822-2649.
† British Columbia Cancer Agency.
‡ The University of British Columbia.

significantly reduce coupling efficiency (28, 29). The strategy developed here is to inhibit covalent crosslinking of liposomes by incorporating poly(ethylene glycol)-modified phospholipids. It is well established that incorporation of hydrophilic polymers in liposomes provides a steric barrier inhibiting surface association of serum proteins (30). Further, studies published elsewhere suggest that vesicle size can be maintained following coupling reactions when PEG-modified lipids are incorporated into the liposomes (31, 32). It is demonstrated here that efficient conjugation of thiolated avidin to MPB–PE incorporated in liposomes containing PEG-modified phosphatidylethanolamine can be achieved with no aggregation of the liposomes. It is further demonstrated that the biotin binding activity of liposome associated avidin is maintained and that the circulation lifetime of the resulting liposome is significantly improved.

MATERIALS AND METHODS

Materials. 1,2-Distearoyl-sn-glycero-3-phosphocholine (DSPC) was purchased from Avanti Polar Lipids, and N-(4-(p-maleimidophenyl)butyryl)dipalmitoylphosphatidylethanolamine (MPB-DPPE) was synthesized as published previously (24). The synthesis and characterization of various MePEG–lipid conjugates has been described elsewhere (33), and these lipids are now commercially available through Northern Lipids, Inc. (Vancouver, B.C.). Avidin-D was obtained from Vector Laboratories and neutravidin from Pierce. Cholesterol (Chol), N-ethylmaleimide (NEM), N-succinimidyl 3-(2-pyridyldithio)propionate (SPDP), dithiothreitol (DTT), N,N'-dicyclohexylcarbodiimide (DCC), and N-hydroxysuccinimide (NHS) were obtained from Sigma. Biotinylated Thy 1.2 antibody was obtained from Cedar Lane Laboratories. Radiolabeled d-[carbonyl-^{14}C]biotin and [^{3}H]cholesteryl hexadecyl ether (^{3}H-CHE) were obtained from Amersham. Female CD1 mice were purchased from Charles River Laboratories (Ontario).

Preparation of Liposomes. Large unilamellar vesicles were prepared as described by Hope et al. (34). Lipid mixtures consisting of DSPC, cholesterol, MePEG–S–POPE, and MPB-DPPE were prepared in chloroform and subsequently concentrated to a homogeneous lipid film under a stream of nitrogen gas. The lipid film was then placed under high vacuum for at least 4 h prior to hydration at 65 °C with 300 mM citrate pH 4.0. The resulting multilamellar vesicle preparation was frozen and thawed five times (35) before the sample was extruded 10 times through stacked 100 nm polycarbonate filters (Nuclepore) employing an extrusion device (Lipex Biomembranes, Inc., Vancouver, Canada) at 65 °C. The resulting liposomes were sized by QELS using a Nicomp 270 submicron particle sizer operating at 632.8 nm.

Thiolation of Avidin-D. Avidin-D (5 mg/mL in HBS 25 mM Hepes; 150 mM NaCl, pH 7.5) was modified with the amine reactive reagent SPDP according to procedures described for streptavidin (24, 25). Briefly, SPDP (25 mM in methanol, 1–10 mol equiv) was incubated with avidin-D at room temperature for 30 min. The reaction mixture was then reduced with DTT (25 mM, 10 min), and the thiolated product was isolated by gel filtration on Sephadex G-50 equilibrated with HBS pH 7.5 and used immediately in coupling experiments. The extent of modification of avidin-D was determined by estimating the protein concentration at 280 nm (molar extinction coefficient at 280 nm of 9.52×10^4) prior to the addition of DTT and the 2-thiopyridone concentration at 343 nm (molar extinction coefficient at 343 nm of 7550) 10 min after the addition of DTT.

Coupling of Thiolated Avidin-D to Liposomes. The coupling reaction was performed by incubating thiolated avidin-D with MPB-liposomes at a ratio of 150 μg of protein per μmol of lipid (6–7 mM final lipid concentration) at pH 7.5 with stirring at room temperature. Liposomes prepared at pH 4.0 (300 mM citrate) were passed down a Sephadex G-50 column equilibrated with HBS (pH 7.5) prior to addition of the thiolated avidin-D. At selected time points coupling was stopped by the addition of β-mercaptoethanol followed by (10 min after β-mercaptoethanol addition) the addition of excess NEM. Samples were then passed down a Sepharose CL-4B column equilibrated with HBS to remove any unassociated protein. The amount of avidin coupled to the liposomes was determined by a modification of the fluorescamine assay for protein (36). Briefly, avidin–liposome conjugates were lysed by addition of 10 mM OGP before addition of 0.2 M borate buffer (pH 9.0) to raise the pH. Fluorescamine (1 mg per 5 mL of anhydrous acetone) was added with immediate vortex mixing. Standards were prepared as above using known quantities of the thiolated avidin and uncoupled liposomes. Fluorescence was then determined at an excitation wavelength of 390 nm and emission wavelength of 480 nm using a Perkin-Elmer LS50 luminescence spectrometer.

Doxorubicin Encapsulation. Doxorubicin was encapsulated in selected liposome preparations using the transmembrane pH gradient driven loading procedure as described previously (37). The liposome preparation (prepared at pH 4.0 prior to coupling avidin at pH 7.5) was heated to 60–65 °C for 10 min prior to addition to a preheated (60 °C for 10 min) solution of doxorubicin (5–6 mM in saline). A final drug-to-lipid ratio of 0.2 was typically employed. This mixture was incubated with periodic mixing for 10 min at 60 °C. Unencapsulated doxorubicin was removed by passing the sample through a Sephadex G-50 column, and the doxorubicin-to-lipid ratio was measured as described previously (16, 37).

Biotin Binding Activity. The biotin binding activity of the avidin–liposome conjugates was determined as described for streptavidin (24, 25). Briefly, avidin-liposomes (0.5 μmol of lipid in 0.5 mL) were incubated with a 10-fold excess of [^{14}C]biotin for 10 min at room temperature. Unbound biotin was removed by gel filtration on a Sepharose CL-4B column equilibrated with HBS. The extent of binding of biotin to a thiolated-avidin standard (100 μg) after gel chromatography on Sephadex G-50 was used as a reference for the calculation of coupling ratios.

Targeting to Biotin-Labeled P388 Cells. In vitro quantification of cell-associated lipid after targeting avidin-D and neutravidin-coated LUVs with 2 mol % of PEG$_{2000}$–DSPE to P388 cells was performed as follows. Avidin or neutravidin LUVs (51 and 63 μg/μmol of lipid, respectively) incorporating PEG$_{2000}$–DSPE were prepared as described above. P388 cells (10^7) were incubated with or without biotinylated anti-mouse Thy 1.2 antibody (10 μg) for 30 min at 4 °C. Cells were then washed (three 10 min centrifugations at 800g) with PBS prior to addition (2 mM final concentration) of either avidin or neutravidin LUVs. After 30 min incubation at 4 °C, the cells were further washed, and cell-associated lipid was determined via a ^{3}H-CHE lipid marker.

In Vivo Clearance Studies. Coated LUVs composed of DSPC/Chol/MePEG$_{2000}$–S–DSPE/MPB-DPPE (52:45: 2:1) containing either avidin or neutravidin were prepared as outlined previously. CD1 mice were injected iv at 30 mg of lipid/kg with one of the above protein-coated LUVs. Whole blood was collected at 1, 4, and 24 h
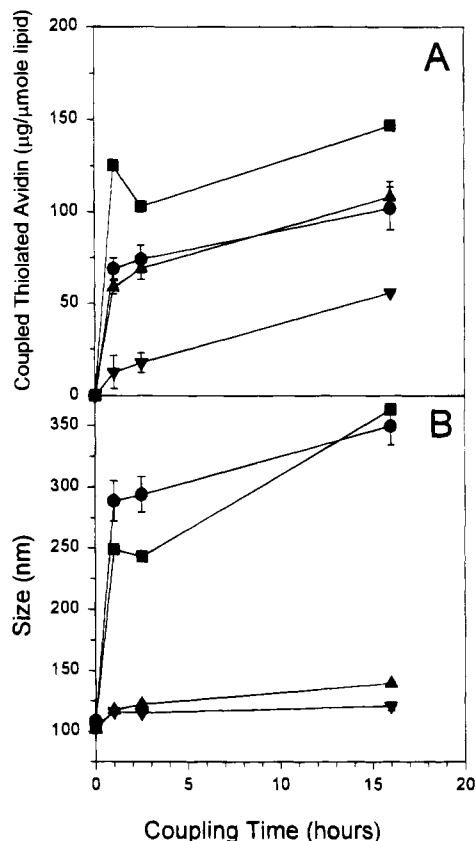
Figure 1. Effect of different MePEG−S−POPE on the coupling reaction of thiolated avidin (3.6 SH equiv, 150 μg per μmol of lipid) with MPB-liposomes (DSPC:Chol:MPB-DPPE:MePEG−S−POPE, 52:45:1:2; 6.57 mM). Panel A shows the amount of protein (expressed as μg of thiolated avidin per μmol of lipid) coupled to MPB−liposomes as a function of coupling reaction time. Panel B shows the size (nm) of the corresponding proteoliposomes as measured by QELS: control (●); MePEG$_{550}$−S−POPE (■); MePEG$_{2000}$−S−POPE (▲); and MePEG$_{5000}$−S−POPE (▼). At 16 h, LUV size for both MePEG$_{2000}$ and MePEG$_{5000}$ were significantly different from control liposomes (p < 0.001 and p < 0.005, respectively). Points: mean of three assays. Error bars: SD of at least three experiments.

intervals via cardiac puncture and collected in EDTA-coated tubes. Plasma was subsequently prepared by centrifuging at 1500g for 10 min. Lipid was then assayed via a ^{3}H-CHE lipid marker.

RESULTS

The first set of experiments was aimed at determining the influence of different sizes of PEG polymer on the coupling reaction between MPB-liposomes and thiolated avidin. Monomethoxypoly(ethylene glycol) (MePEG) of three different molecular weights (550, 2000, and 5000) was linked via a succinate bond to POPE to form the respective MePEG−lipid conjugates (MePEG$_{550}$−S−POPE, MePEG$_{2000}$−S−POPE, and MePEG$_{5000}$−S−POPE) *(33)*. These MePEG−lipid conjugates were then incorporated into MPB-containing liposomes (1 mol % MPB−DPPE/54 mol % DSPC/45 mol % Chol) at a level of 2 mol % of the total lipid. Incubation of these MePEG-coated MPB-containing liposomes with thiolated avidin resulted in the covalent attachment of protein to the liposomes (Figure 1). The rate and extent of coupling was dependent on the molecular size of the poly(ethylene glycol) incorporated. In the absence of MePEG−S−POPE substantial levels of avidin (70 μg of avidin/μmol of lipid) were conjugated to the liposomes within 1 h (Figure 1A). Subsequently, the coupling reaction occurred at a reduced
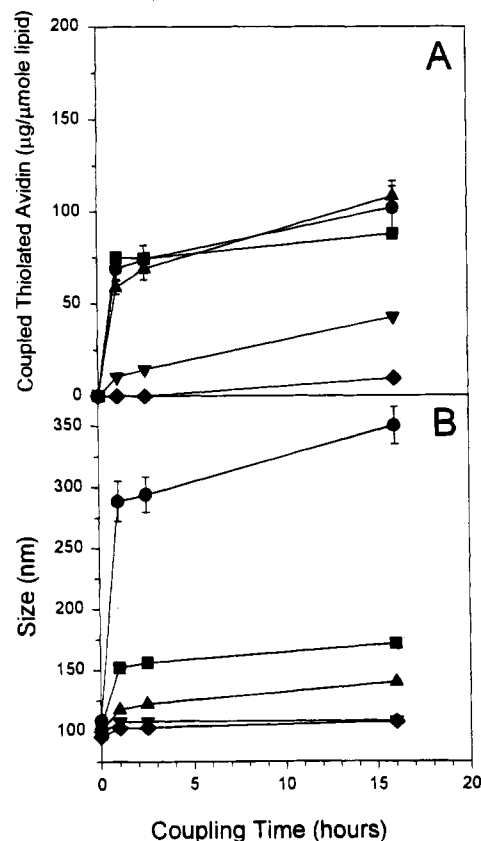
Figure 2. Effect of different levels of the polymer MePEG$_{2000}$ on the coupling reaction of the thiolated avidin (3.9 SH equiv, 150 μg per μmol of lipid) with MPB-liposomes (6.54 mM) containing various concentrations of MePEG$_{2000}$−S−POPE: 0% (●); 1% (■); 2% (▲); 5% (▼); and 8% (◆). Coordinates for panels A and B are the same as in Figure 1. At 16 h, all treatment groups were statistically significant from control (p < 0.05). Points: mean of three assays. Error bars: SD of at least three experiments.

rate ultimately leading to levels of approximately 100 μg of avidin/μmol of lipid observed at 16 h. As observed in previous studies *(25, 26)*, these liposomes exhibited a dramatic increase in size, indicative of liposome−liposome crosslinking (Figure 1B). The time course for size increase was similar to that observed for coupling. As shown in Figure 1B, incorporation of MePEG$_{2000}$− and MePEG$_{5000}$−S−POPE substantially reduced time dependent increases in liposome size. While the rate of avidin coupling to liposomes was reduced significantly when 2 mol % MePEG$_{5000}$−S−POPE was present, both the rate and extent of coupling obtained for liposomes with 2 mol % MePEG$_{550}$−S−POPE was identical to controls.

The results illustrated in Figure 1 indicated that a hydrophilic polymer coating imparted by incorporation of 2% MePEG$_{2000}$ was the most suitable for preparation of proteoliposomes in terms of protein-coupling efficiency and effectiveness in inhibiting vesicle aggregation. The next series of experiments were designed to determine whether 2 mol % MePEG$_{2000}$−S−POPE was optimal. Four different levels of MePEG$_{2000}$−S−POPE (1%, 2%, 5%, and 8%) were studied and compared with control liposomes. The different quantities of thiolated avidin that could be coupled to each type of liposome are illustrated in Figure 2A. The presence of 5 and 8 mol % MePEG$_{2000}$ significantly reduced the amount of protein that could be conjugated to the surface of the liposomes. In contrast, addition of 1 or 2 mol % MePEG$_{2000}$ did not influence the coupling reaction. For these liposomes, 70−
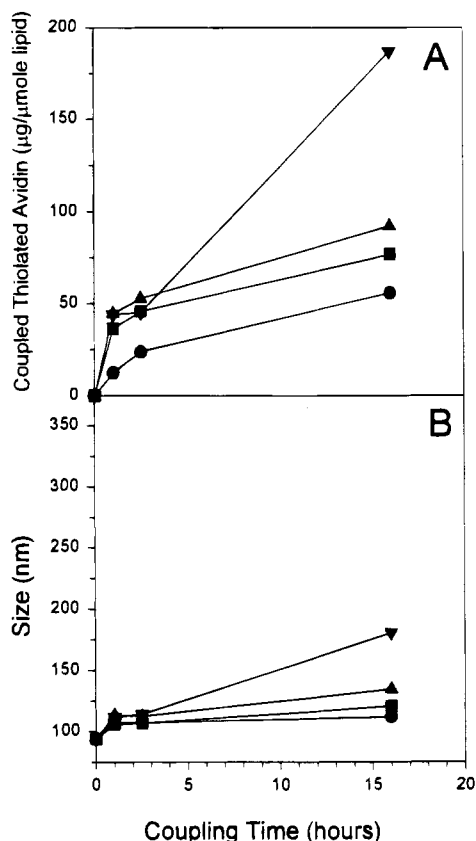
Figure 3. Effect of the degree of protein thiolation on the coupling reaction of thiolated avidin (150 μg per μmol of lipid) with pegylated liposomes (DSPC:Chol:MPB-DPPE:MePEG$_{2000}$–S–POPE, 52:45:1:2; 6.49 mM). 1.2 SH equiv (●); 1.9 SH equiv (■); 4.5 SH equiv (▲); and 5.3 SH equiv (▼). Coordinates for panels A and B are the same as in Figure 1. Points: mean of three assays. Error bars: SD of at least three experiments.

80 μg of avidin was bound to the liposomes within 1 h after addition of the thiolated protein, representing a coupling efficiency of approximately 50%. As expected, liposomes that did not efficiently couple protein showed no size increases (Figure 2B). Efficient coupling with only minimal increases in vesicle size was observed for liposomes prepared with 2% MePEG$_{2000}$.

The degree of protein thiolation is also known to have an effect on protein-coupling reactions mediated by MPB-modified lipids. In order to assess whether incorporation of 2 mol % MePEG$_{2000}$–S–POPE inhibited aggregation regardless of the extent of protein thiolation, coupling of modified avidin having approximately 1, 2, 4, and 5 thio equiv was determined (Figure 3A, B). As expected, protein association was dependent on the degree of thiolation. The presence of 2–4 thio equiv appeared optimal for efficient coupling with no associated changes in vesicle size. The amount of protein-coupling was significantly enhanced when using avidin with 5 thiol equiv; however, increases in vesicle size were observed for this system even in the presence of 2 mol % Me-PEG$_{2000}$–S–POPE.

Further investigations on the importance of the effect of molecular size of the polymer chain were conducted by comparing the coupling reaction of thiolated avidin with MPB-liposomes containing 8% MePEG$_{550}$–S–POPE or 2% MePEG$_{2000}$–S–POPE. It can be estimated that these liposomal preparations should exhibit similar numbers of PEG units on the surface of the liposomes. However, as illustrated in Figure 4A, the initial rates of protein conjugation are quite different. With 8% Me-PEG$_{550}$, the higher density of the shorter PEG$_{550}$ mol-
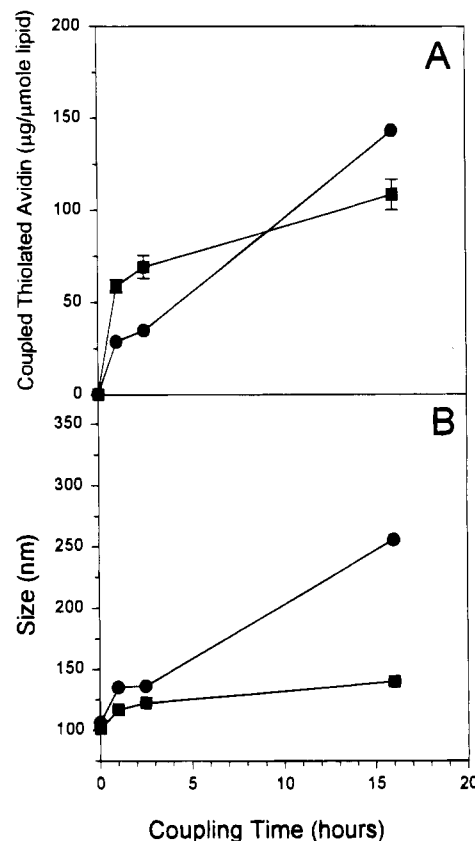
Figure 4. Effect of different polymer coatings on the coupling reaction of the thiolated avidin (4.2 SH equiv, 150 μg per μmol of lipid) with MPB-liposomes (6.15 mM) containing 8% PEG$_{550}$–S–POPE (●) or 2% MePEG$_{2000}$–S–POPE (■). Coordinates for panels A and B are as in Figure 1. Points: mean of three assays. Error bars: SD of at least three experiments.

ecules on the liposomal surface initially inhibited the coupling reaction with thiolated avidin. Alternatively, MPB-liposomes with 2% MePEG$_{2000}$–S–POPE did not exhibit any noticeable barrier to chemical coupling of thiolated avidin (Figure 4A). As indicated before, the presence of this lipid did provide a substantial barrier in terms of inhibition of intervesicular crosslinking and liposome aggregation (Figure 4B). As the coupling reaction proceeded further (16 h), the steric stabilization effect of the longer chain MePEG$_{2000}$ was apparent.

The effect of incorporating decreased quantities of the longer MePEG$_{5000}$–S–POPE on the coupling reaction between MPB-liposomes and thiolated avidin is illustrated in Figure 5. Results indicate that incorporation of 1.2, 0.8, and 0.4 mol % MePEG$_{5000}$–S–POPE effectively inhibits aggregation of the avidin–liposome conjugates (Figure 5B) without hindering the protein-coupling efficiency (Figure 5A). It should be noted that studies were initiated to determine whether G$_{M1}$, a ganglioside that is similar to PEG-modified lipids in that it can prolong the *in vivo* circulation lifetime of liposomes, prevents coupling-induced aggregation. The results (not shown) indicate that at levels of 10 mol % G$_{M1}$ the coupling reaction was not effected. Specifically, the rate and extent of coupling were identical to control liposomes, and there is a coupling dependent increase in vesicle size.

The results presented thus far demonstrate that incorporation of either MePEG$_{2000}$ or MePEG$_{5000}$ at appropriate levels inhibits vesicle–vesicle crosslinking that occurs when coupling thiolated protein to MPB-PE-containing liposomes. Optimal coupling, in terms of reaction rates and coupling efficiency, are achieved when using 2 mol % MePEG$_{2000}$–S–POPE or 0.8 mol %
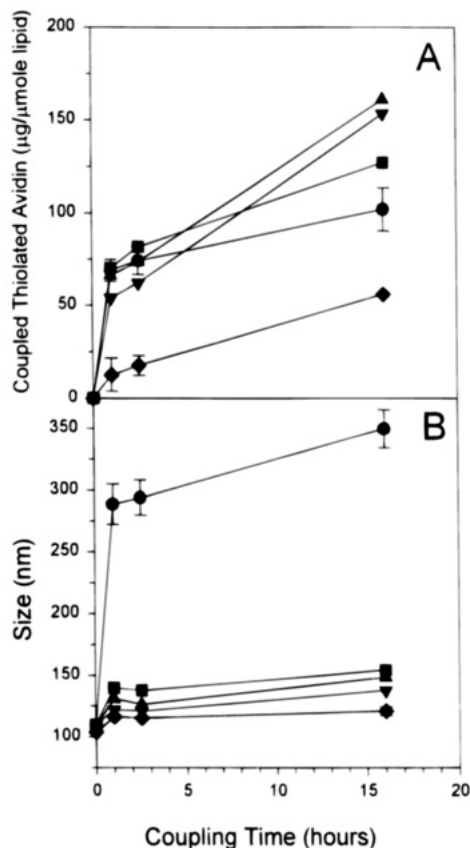
Figure 5. Effect of different levels of the polymer MePEG$_{5000}$ on the coupling reaction of thiolated avidin (3.6 SH equiv, 150 μg per μmol of lipid) with MPB-liposomes (6.2 mM) containing various concentrations of MePEG$_{5000}$−S−POPE: 0% (●); 0.4% (■); 0.8% (▲); 1.2% (▼); and 2% (◆). Coordinates for panels A and B are as in Figure 1. At 16 h, all treatment groups were statistically significant from control ($p < 0.05$). Points: mean of three assays. Error bars: SD of at least three experiments.

MePEG$_{5000}$−S−POPE. It is important to demonstrate, however, that the resulting liposomal preparations exhibit appropriate characteristics required for *in vivo* drug delivery applications. For this reason the following experiments characterized four important parameters, namely the drug loading characteristics, the biotin binding capacity, the *in vitro* cell-targeting efficiencies, and the *in vivo* plasma clearance behavior of the avidin-coated liposomes. The drug loading characteristics of avidin-D coated liposomes was assessed using the transmembrane pH gradient mediated loading procedure to encapsulate the anticancer drug doxorubicin (*10, 27*). The pH gradient was established by preparing liposomes at pH 4.0 (300 mM citrate buffer) prior to adjusting the external pH to 7.5 (as required for the protein-coupling reaction). Efficient doxorubicin loading was achieved for the avidin-D-coated liposomes prepared with different amounts of either MePEG$_{2000}$ or MePEG$_{5000}$−S−POPE (results not shown), where greater than 95% of the added doxorubicin (a drug to lipid weight ratio of 0.2) was encapsulated within 5 min at a incubation temperature of 65 °C. The resulting liposomes retain drug over storage periods (at 4 °C) in excess of 48 h.

As shown in Figure 6, the biotin binding capacity of liposomes that have bound avidin-D in the presence of incorporated MePEG$_{2000}$−S−POPE was well retained at levels below 5 mol %. At levels of 8 mol % MePEG$_{2000}$−S−POPE, a level shown to inhibit avidin-D coupling, there was a greater than 50% loss of biotin binding activity of the surface-associated avidin-D. A further indication of the biotin binding capacity of avidin-D
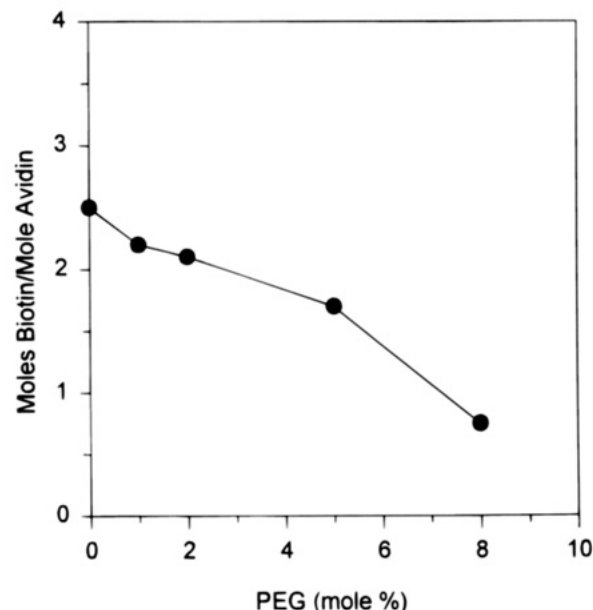
Figure 6. Biotin binding activity of proteoliposomes formed by the coupling of thiolated avidin (3.9 SH equiv, 150 μg per μmol of lipid) with various levels of MePEG$_{2000}$−S−POPE. Avidin−liposomes (1 μmol/mL) were incubated with [^{14}C]biotin (10-fold excess) for 10 min at room temperature. Unbound biotin was removed on a sepharose CL-4B column, and the extent of biotin binding was evaluated against a thiolated-avidin standard as a reference for the calculation of coupling ratios.
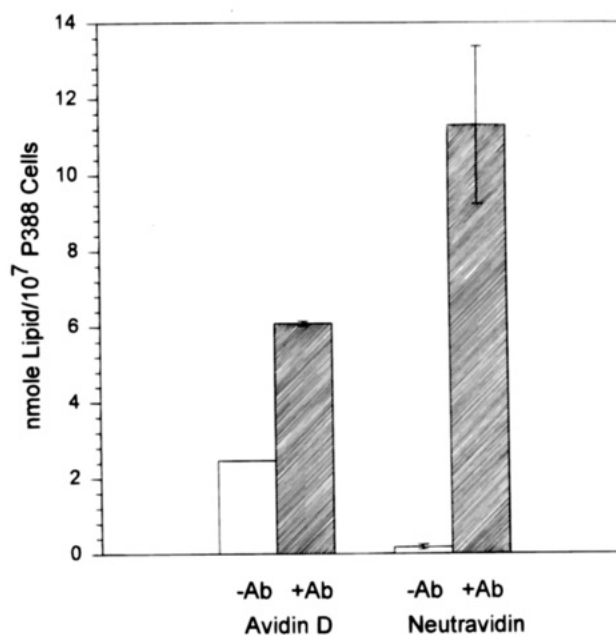
Figure 7. Quantification of cell associated lipid after targeting avidin-D and neutravidin-coated LUVs with 2 mol % PEG$_{2000}$−DSPE to P388 cells in vitro. Avidin-D or neutravidin LUVs (51 and 63 μg/μmol of lipid, respectively) incorporating PEG$_{2000}$−DSPE were prepared as described in the Materials and Methods. P388 cells (10^7) incubated with (hatched) or without (empty bars) biotinylated anti-mouse Thy 1.2 antibody (10 μg) for 30 min at 4 °C followed by a further 30 min incubation with avidin or neutravidin LUVs (2 mM final concentration). Cell-associated lipid was determined by a ^{3}H-CHE lipid marker. Neutravidin + Ab was significantly different from avidin + Ab, $p < 0.05$. Points: mean of three assays. Error bars: SD of at least three experiments.

coupled liposomes with 2 mol % MePEG$_{2000}$ is illustrated in Figure 7. Briefly, avidin-D liposomes were targeted *in vitro* to P388 cells (a murine lymphocytic leukemia cell line) prelabeled with biotinylated anti-Thy 1.2 antibody.

This convenient two-step targeting approach has been used previously by our group to assess the binding of streptavidin-coated liposomes to this cell line *(38)*. The results demonstrate that a 3-fold increase in liposome-cell association is achieved when incubating avidin-D coated liposomes with biotin-labeled P388 cells when compared with incubations with unlabeled P388. The increase in liposome targeting achieved is far less than that observed previously for liposomes with bound streptavidin *(38)*. The avidin-D coated liposomes exhibit significantly higher background (nonspecific) binding to P388 cells than streptavidin liposomes (results not shown), and this is believed to be a consequence of the carbohydrate groups present on avidin-D. The influence of the carbohydrate moiety on nonspecific cell association is illustrated in Figure 7. A deglycosylated version of avidin, referred to as neutravidin, coupled to liposomes using procedures identical to those used for avidin-D resulted in a liposome preparation with vastly improved specificity. It should be noted that the level of protein bound to these liposomes was 51 and 63 $\mu g/\mu mol$ for avidin-D and neutravidin, respectively.

It was anticipated that the carbohydrate groups on avidin-D would promote liposome clearance following iv administration of the protein-coated liposomes with 2% MePEG$_{2000}$. For this reason the deglycosylated version of avidin (neutravidin) was also selected for preliminary *in vivo* clearance studies. A further modification in the liposomes used for *in vivo* studies involved the use of MePEG$_{2000}$ linked to DSPE rather than POPE. Results from this laboratory demonstrate that, *in vivo*, the POPE-based PEG$_{2000}$ lipid conjugates rapidly exchange out of the liposomal membrane *(33)*. This study also demonstrated that DSPE-modified-PEG lipids were most appropriate for *in vivo* applications on the basis of exchangeability and stability. The DSPE−PEG lipid-containing liposomes exhibited similar protein-coupling characteristics as observed for POPE−PEG systems (results not shown). *In vivo* plasma clearance studies (in female CD1 mice), therefore, determined the circulation lifetime of protein-free, avidin-D, and neutravidin-coated liposomes with 2% MePEG$_{2000}$−S−DSPE.

The results shown in Figure 8 were obtained after iv administration of liposomes at a lipid dose of 30 mg/kg. All liposomal preparations were similar in size prior to administration, where protein-free, avidin-D, and neutravidin liposomes exhibited mean diameters (as measured by QELS) of 109, 106, 119 nm, respectively. Liposomal lipid levels were determined using [^{3}H]cholesteryl hexadecyl ether as a nonexchangeable lipid marker. Protein-free liposomes were maintained in the plasma compartment at levels greater than either of the protein-coated liposomes. The results suggest that avidin-D liposomes are removed from the circulation faster than neutravidin-coated liposomes (half-lives for avidin-coated, neutravidin-coated, and protein-free LUVs of ~2.5, 3, and 11 h, respectively). It should be noted that previous studies have already shown that in the absence of size reduction, protein-coated liposomes are rapidly cleared following iv administration *(25)*. More specifically, streptavidin liposomes prepared by the covalent coupling procedure described here, but in the absence of PEG lipids, exhibited circulation half-lives of less than 30 min *(25)*. These results suggest that the methodology developed here will be appropriate for *in vivo* targeting of liposomal carriers. Detailed characterization of the utility of MePEG$_{2000}$−S−DSPE-containing liposomes for preparation and targeting (*in vitro* and *in vivo*) of avidin-coated and IgG-coated liposomes will be provided elsewhere.
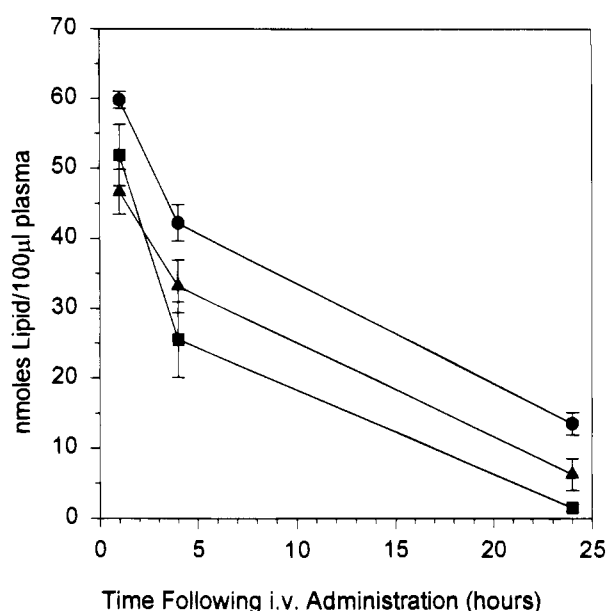
Figure 8. In vivo clearance characteristics of protein-coated LUVs composed of DSPC/Chol/MePEG$_{2000}$−S−DSPE/MPB−DPPE (52:45:2:1) containing either no protein (●), avidin (■), or neutravidin (▲) (0, 51, and 63 $\mu g/\mu mol$ of lipid, respectively). Female CD1 mice were injected via a lateral tail vein at a dose of 30 mg of lipid/kg. Whole blood was collected at the indicated time points via cardiac puncture, and plasma was prepared as outlined in the Materials and Methods. Theoretical levels of lipid at $t = 0$ are approximately 100 nmol of lipid/100 μL of plasma based on 20 g mice. At 24 h avidin and neutravidin were statistically significant from control ($p < 0.001$ and $p < 0.05$, respectively) and from each other, $p < 0.01$. Points: mean of three assays. Error bars: SD of at least three experiments.

DISCUSSION

One of the most significant problems associated with the preparation and use of protein-coated liposomes for targeting purposes concerns coupling induced liposome−liposome crosslinking. The resulting liposome aggregates release entrapped contents *(26)* and are very rapidly cleared from the circulation. The most versatile approach for attaching proteins to liposomes is based on the use of heterobifunctional reagents. The use of these coupling reagents for attaching protein to liposomes was first documented in early 1980 by the work of Leserman et al. *(21)* and Martin et al. *(22)*. However, this coupling technology has not yet resulted in a liposomal formulation that can specifically target defined cell populations *in vivo*. Research in this laboratory has focused on developing methodology that results in a protein-coated liposome preparation more appropriate for *in vivo* targeting applications. The studies described here investigate the use of PEG-modified lipids to inhibit liposome crosslinking and clearly demonstrate that efficient protein coupling to liposomes can be achieved with little or no change in liposome size when PEG-modified lipids are incorporated in the liposomes prior to coupling. The importance of providing an appropriate balance between steric inhibition of liposome−liposome crosslinking while maintaining efficient protein-coupling reactions is discussed below.

Two closely related factors are important for designing a hydrophilic-polymer coating on the surface of liposomes used for protein coupling. A balance must be reached between the polymer length of the PEG used and the density of the polymeric coating. For coupling of thiolated avidin to MPB-liposomes, either 2 mol % MePEG$_{2000}$ or 0.4−0.8 mol % MePEG$_{5000}$ on the liposomal surface is optimal for the formation of nonaggregated

avidin-D—liposome conjugates (see Figures 3 and 5). As the amount of $MePEG_{2000}$ or $MePEG_{5000}$ is increased to 5 or 2 mol %, respectively, there is a significant reduction in protein-coupling efficiencies. Lower levels are insufficient to prevent liposome crosslinking. In contrast, results with the lower molecular weight PEG ($MePEG_{550}$) suggest that this chain length is not capable of preventing liposome crosslinking at any concentration employed. Yet at levels of 8 mol % $MePEG_{550}$ there is an initial inhibition of protein coupling (Figure 4). Clearly, the higher density of the polymer coating presents a large steric barrier impeding close contact of the thiolated avidin molecule with the liposome surface. This is reflected in the initial lower amounts of protein coupled. However, once covalently conjugated, the thiolated avidin is not adequately shielded by the smaller $MePEG_{550}$ chain on the liposome surface and interliposomal crosslinking becomes more prevalent resulting in a significant increase in size of the proteoliposome.

The presence of appropriate levels of either $MePEG_{2000}$ (2%) or $MePEG_{5000}$ (0.4—0.8%) on the surface of MPB-liposomes did not impede covalent coupling of thiolated avidin; however, liposome—liposome crosslinking was inhibited. These results are consistent with studies reported by Klibanov et al. *(39)* who demonstrated that incorporation of PEG-modified lipids into liposomes prevented streptavidin-induced aggregation of biotin-labeled liposomes. It is of interest to note that the ganglioside G_{M1}, a lipid that behaves comparably to PEG-modified lipids in terms of inhibiting protein binding, reducing RES uptake and engendering long circulation lifetimes *(18)*, does not inhibit either protein-coupling reactions or protein-coupling induced liposome aggregation.

This report shows that the presence of $MePEG_{2000}$ in proteoliposomes should facilitate development of liposomes for *in vivo* targeting applications. Such liposomes must maintain an ability to efficiently encapsulate and retain drugs such as doxorubicin following covalent attachment of the selected targeting protein and still be able to bind the target antigen. As demonstrated here, the use of $MePEG_{2000}$ as a polymer coating at levels of 2 mol % did not affect binding to a target-cell population labeled with a biotinylated antibody (Figure 7). As a final consideration it is important that the proteoliposome exhibit a pharmacological behavior comparable to a liposome with no surface-associated protein. This will, in part, be dependent on the nature of the associated protein. IgG, for example, may promote liposome clearance due to Fc-mediated clearance *(38, 40)*. Alternatively, as shown here, glycoproteins attached to liposomes reduce circulation lifetime even in the presence of 2 mol % $MePEG_{2000}$. Long circulation lifetimes are particularly important when liposome targeting is attempted *in vivo* following iv administration of proteoliposomes. It has been suggested that in order to maximize liposome movement from the blood compartment to an extravascular site, the liposomes must exhibit an enhanced circulation lifetime *(9, 10)*.

Optimal levels of PEG density (required for enhanced circulation longevity) and attached targeting ligand (required for specificity) must be established for effective *in vivo* targeting to be achieved. Although it has been demonstrated that the incorporation of PEG_{2000} at 5 mol % is very effective in terms of increasing circulation lifetimes of liposome formulations *(20)*, studies presented here indicate that this level of PEG—lipid significantly reduced the quantity of protein coupled to the liposome surface (Figure 2). Further, the biotin binding capacity to covalently attached avidin—liposomes with 5 mol %

PEG_{2000} was effectively reduced. This would suggest that the ability of these liposomes to bind a biotinylated-antibody would be reduced, or alternatively, the ability of the liposomes to bind an antigen expressed on a cell may be inhibited. By incorporating PEG_{2000} at lower mole percentages greater levels of protein can be coupled to the surface of the liposome (Figure 2) and adequate target specific binding can occur (Figure 6); however, this is achieved at the risk of reduced circulation lifetimes. Thus, the appropriate balance of protein content and PEG density in *in vivo* applications is a feature of targeted liposomal systems that will have to be empirically derived through experimentation.

In summary, the presence of hydrophilic polymers such as PEG on the surface of liposomes provides a general and practical method for controlling liposome size during the covalent conjugation of proteins to liposomes. A balance between the molecular size of the MePEG chain and the concentration of the polymer on the liposomal surface has been determined to allow efficient protein coupling with little or no liposome crosslinking. The resulting liposomes exhibit characteristics suitable for development of *in vivo* targeting approaches.

LITERATURE CITED

(1) Bakker-Woudenberg, I. A., Lakerse, A. F., ten Kate, M. T., and Storm, G. (1992) Enhanced localization of liposomes with prolonged blood circulation time in infected lung tissue. *Biochim. Biophys. Acta 1138,* 318—326.

(2) Williams, B. D., O'Sullivan, N. M., Saggu, G. S., Williams, K. E., Williams, L. A., and Morgan, J. R. (1986) Imaging in rheumatoid arthritis using liposomes labeled with technetium. *Br. Med. J. 293,* 1143—1144.

(3) O'Sullivan, M. M., Powell, N., French, A. P., Williams, K. E., Morgan, J. R., and Williams, B. D. (1988) Inflammatory joint disease: a comparison of liposome scanning, bone scanning and radiography. *Ann. Rheum. Dis. 47,* 485—491.

(4) Richardson, V. J., Ryman, B. E., Jewkes, R. F., Jeyasingh, K., Tattersall, M. N., Newlands, E. S., and Kaye, S. B. (1979) Tissue distribution and tumor localization of 99m-technetium-labelled liposomes in cancer patients. *Br. J. Cancer 40,* 35—43.

(5) Gabizon, A., and Papahadjopoulos, D. (1988) Liposome formulations with prolonged circulation time in blood and enhanced uptake by tumors. *Proc. Natl. Acad. Sci. U.S.A. 85,* 6949—6953.

(6) Mayer, L. D., Bally, M. B., Cullis, P. R., Wilson, S. L., and Emerman, J. T. (1990) Comparison of free and liposomal encapsulated doxorubicin tumor drug uptake and antitumor efficacy in the SC115 murine mammary tumor. *Cancer Lett. 53,* 183—189.

(7) Forssen, E. A., Coulter, D. M., and Proffitt, R. T. (1992) Selective in vivo localization of daunorubicin small unilamellar vesicles in solid tumors. *Cancer Res. 52,* 3255—3261.

(8) Gabizon, A. (1992) Selective tumor localization and improved therapeutic index of anthracyclines encapsulated in long-circulating liposomes. *Cancer Res. 52,* 891—896.

(9) Wu, N. Z., Da, D., Rudoll, T. L., Needham, D., Whorton, A. R., and Dewhirst, M. W. (1993) Increased microvascular permeability contributes to preferential accumulation of stealth liposomes in tumor tissue. *Cancer Res. 53,* 3765—3770.

(10) Bally, M. B., Masin, D., Nayar, R., Cullis, P. R., and Mayer, L. D. (1994) Transfer of liposomal drug carriers from the blood to the peritoneal cavity of normal and ascitic tumor bearing mice. *Cancer Chemother. Pharmacol. 34,* 137—146.

(11) Boman, N. L., Masin, D., Mayer, L. D., Cullis, P. R., and Bally, M. B. (1994) Liposomal vincristine which exhibits

increased drug retention and increased circulation longevity cures mice bearing P388 tumors. *Cancer Res. 54,* 2830−2833.

(12) Senior, J., Crawley, J. C., and Gregoriadis, G. (1985) Tissue distribution of liposomes exhibiting long half-lives in the circulation after intravenous injection. *Biochim. Biophys. Acta 839,* 1−8.

(13) Hwang, K. J. (1987) Liposome Pharmacokinetics. In *Liposomes: From Biophysics to Therapeutics* (M. J. Ostro, Ed.) pp 109−156, Marcell Dekker, New York.

(14) Allen, T. M., Ryan, J. L., and Papahadjopoulos, D. (1985) Gangliosides reduce leakage of aqueous-space markers from liposomes in the presence of human plasma. *Biochim. Biophys. Acta 818,* 205−210.

(15) Chonn, A., Semple, S. C., and Cullis, P. R. (1992) Association of blood proteins with large unilamellar liposomes in vivo: relation to circulation lifetimes. *J. Biol. Chem. 267,* 18759−18765.

(16) Bally, M. B., Nayar, R., Masin, D., Hope, M. J., Cullis, P. R., and Mayer, L. D. (1990) Liposomes with entrapped doxorubicin exhibit extended blood residence times. *Biochim. Biophys. Acta 1023,* 133−141.

(17) Bally, M. B., Mayer, L. D., Hope, M. J., and Nayar, R. (1993) Pharmacodynamics of liposomal drug carriers: methodological considerations. In *Liposome Technology: Interactions of Liposomes with the Biological Mileau* (G. Gregoriadis, Ed.) pp 27−41, CRC Press, Inc., Ann Arbor.

(18) Allen, T. M., and Chonn, A. (1987) Large unilamellar liposomes with low uptake into the reticuloendothelial system. *FEBS Lett. 223,* 42−46.

(19) Gabizon, A., and Papahadjopoulos, D. (1988) Liposome formulations with prolonged circulation time in blood and enhanced uptake by tumors. *Proc. Natl. Acad. Sci. U.S.A. 85,* 6949−6953.

(20) Klibanov, A. L., Maruyama, K., Torchilin, V. P., and Huang, L. (1990) Amphipathic polyethyleneglycols effectively prolong the circulation time of liposomes. *FEBS Lett. 268,* 235−237.

(21) Leserman, L. D., Machy, P., and Barbet, J. (1981) Cell-specific drug transfer from liposomes bearing monoclonal antibodies. *Nature (London) 293,* 226−228.

(22) Martin, F. J. and Papahadjopoulos, D. (1982) Irreversible coupling of immunoglobulin fragments to preformed vesicles. *J. Biol. Chem. 257,* 286−288.

(23) Barbet, J., Machy, P., and Leserman, L. D., (1981) Monoclonal antibody covalently coupled to liposomes: specific targeting to cells. *J. Supramol. Struct. Cell Biochem. 16,* 243−258.

(24) Loughrey, H. C., Choi, L. S., Cullis, P. R., and Bally, M. B. (1990) Optimized procedures for the coupling of proteins to liposomes. *J. Immunol. Methods 132,* 25−35.

(25) Loughrey, H. C., Wong, K. F., Choi, L. S., Cullis, P. R., and Bally, M. B. (1990) Protein liposome conjugates with defined size distributions. *Biochim. Biophys. Acta 1028,* 73−81.

(26) Bredehorst, R., Ligler, F. S., Kusterback, A. W., Chang, E. L., Gaber, B. P., and Vogel, C. W. (1986) Effect of covalent attachment of immunoglobulin fragments on liposome integrity. *Biochemistry 25,* 5693−5698.

(27) Bally, M. B., Hope, M. J., Mayer, L. D., Madden, T. D., and Cullis, P. R. (1988) Novel procedures for generating and loading liposomal systems. *Liposomes as drug carriers* (G. Gregoriadis, Ed.) pp 841−853, John Wiley and Sons Ltd., Chichester.

(28) Jou, Y. H., Jarlinski, S., Mayhew, E., and Bankert, R. B. (1984) *FASEB 43,* 1971, #3218.

(29) Loughrey, H., Bally, M. B., and Cullis, P. R. (1987) A noncovalent method of attaching antibodies to liposomes. *Biochim. Biophys. Acta 901,* 157−160.

(30) Senior, J., Delgado, C., Fisher, D., Tilcock, C., and Gregoriadis, G. (1991) Influence of surface hydrophilicity of liposomes on their interaction with plasma protein and clearance from the circulation: studies with poly(ethylene glycol)-coated vesicles. *Biochim. Biophys. Acta 1062,* 77−82.

(31) Ahmad, I., Longenecker, M., Samuel, J., and Allen, T. M. (1993) Antibody-targeted delivery of doxorubicin entrapped in stearically stabilized liposomes can eradicate lung cancer in mice. *Cancer Res. 53,* 1484−1488.

(32) Allen, T. M., Agrawal, A. K., Ahmad, I., Hansen, C. B., and Zalipsky, S. (1994) Antibody-mediated targeting of long-circulating (Stealth) liposomes. *J. Liposome Res. 4,* 1−25.

(33) Parr, M. J., Ansell, S. M., Choi, L. S., and Cullis, P. R. (1994) Factors influencing the retention and chemical stability of poly(ethylene glycol)-lipid conjugates incorporated into large unilamellar vesicles. *Biochim. Biophys. Acta 1195,* 21−30.

(34) Hope, M. J., Bally, M. B., Webb, G., and Cullis, P. R. (1985) Production of large unilamellar vesicles by a rapid extrusion procedure. Characterization of size distribution, trapped volume and ability to maintain a membrane potential. *Biochim. Biophys. Acta 812,* 55−65.

(35) Mayer, L. D., Hope, M. J., Cullis, P. R., and Janoff, A. S. (1986) Solute distributions and trapping efficiencies observed in freeze-thawed multilamellar vesicles. *Biochim. Biophys. Acta 817,* 193−196.

(36) Lai, C. Y. (1977) Detection of peptides by fluorescence methods. *Methods Enzymol. 47,* 236−239.

(37) Mayer, L. D., Bally, M. B., and Cullis, P. R. (1990) Strategies for optimizing liposomal doxorubicin. *J. Liposome Res. 1,* 463−480.

(38) Longman, S. A., Cullis, P. R., Choi, L., de Jong, G., and Bally, M. B. (1994) A two-step targeting approach for delivery of doxorubicin-loaded liposomes to tumour cells in vivo. *Cancer Chemother. Pharmacol.* (in press).

(39) Klibanov, A. L., Maruyama, K., Beckerleg, A. M., Torchilin, V. P., and Huang, L. (1991) Activity of amphipathic poly(ethylene glycol) 5000 to prolong the circulation time of liposomes depends on the liposome size and is unfavorable to immunoliposome binding to target. *Biochim. Biophys. Acta 1062,* 142−148.

(40) Aragnol, D., and Leserman, L. D. (1986) Immune clearance of liposomes inhibited by an anti-Fc receptor antibody in vivo. *Proc. Natl. Acad. Sci. U.S.A. 83,* 2699−2703.

BC940105P

Conjugation of Adenine Arabinoside 5'-Monophosphate to Arabinogalactan: Synthesis, Characterization, and Antiviral Activity

Philip M. Enriquez, Chu Jung, and Lee Josephson*

Advanced Magnetics Inc., 61 Mooney Street, Cambridge, Massachusetts 02138-1038

Bud C. Tennant

Department of Clinical Sciences, College of Veterinary Medicine, Cornell University, Ithaca, New York 14850. Received July 11, 1994[⊗]

A conjugate consisting of the antiviral nucleotide analogue adenine arabinoside 5'-monophosphate (araAMP, vidarabine monophosphate) and the naturally occurring polysaccharide arabinogalactan was synthesized. The conjugate consisted of 7.9 araAMP residues per molecule of arabinogalactan. The proposed structure of the conjugate was consistent with ^{13}C NMR spectroscopic studies. Daily injections of the conjugate, at a dose of 3 mg of araAMP/kg, into woodchuck carriers of woodchuck hepatitis virus (WHV) decreased serum levels of WHV DNA. A dose of 3 mg/kg of unconjugated araAMP was ineffective, while a higher dose of araAMP (15 mg/kg, 14 days) produced a drop in WHV DNA. After cessation of dosing with the conjugate, serum viral DNA levels remained depressed for 42 days. In contrast, after cessation of dosing with araAMP, WHV DNA rapidly returned to original levels.

INTRODUCTION

Hepatitis B virus (HBV) is a major cause of acute and chronic hepatitis, cirrhosis, and hepatocellular carcinoma (*1, 2*). The nucleotide analog araAMP has been shown to be effective in reducing HBV viremia and, in 10–20% of the cases, induces extended remission (*3*). Clinically however, araAMP has unacceptable neurotoxic side effects that have prevented its use in hepatitis B therapy (*4*).

The potency of araAMP against HBV, and its extrahepatic side effects, suggest that modifying araAMP to achieve a more hepatic specific biodistribution might provide a useful drug for the treatment of HBV. Thus, araAMP has been attached to lactosylated albumin (L-HSA) for uptake by the asialoglycoprotein receptor, and this conjugate has been tested for the treatment of hepatitis B in humans (*5*). However, conjugates utilizing protein-based carriers to target drugs to receptors have deficiencies; see the Discussion and ref *6*.

Recently, we reported that a superparamagnetic iron oxide covered with arabinogalactan, a polysaccharide from the plant *Larix occidentalis*, was removed from blood by the asialoglycoprotein receptor of hepatocytes (*7, 8*). The superparamagnetic iron oxide was useful as a hepatocyte-specific magnetic resonance contrast agent. This observation suggested that arabinogalactan might serve as a carrier for targeting therapeutic agents like araAMP to the liver via the asialoglycoprotein receptor. The features of arabinogalactan that are responsible for its binding to the asialoglycoprotein receptor are (i) a highly branched structure and (ii) the presence of numerous terminal galactose residues (*9*). In its unmodified, naturally occurring form, arabinogalactan mimics the natural ligands for this receptor. In contrast, the oli-

gosaccharides of glycoproteins require sialic acid removal to attain receptor binding.

In this study we describe the synthesis, characterization, and antiviral activity against woodchuck hepatitis virus (WHV) of a conjugate consisting of the polysaccharide arabinogalactan and araAMP. Woodchucks (*Marmota monax*) infected with WHV can exhibit a viral carrier state similar to the human hepatitis B viral infection (*10*).

MATERIALS AND METHODS

Arabinogalactan was obtained from Champion Corporation (Tacoma, WA) and purified by ultrafiltration (*9*). AraAMP was provided courtesy of Parke-Davis (Ann Arbor, MI). 1-Ethyl-3-(3-(dimethylaminopropyl)carbodiimide hydrochloride was obtained from Bachem California (Torrance, CA). Dextran T-10 and dextran T-25 were obtained from American Polymer Standards (Mentor, OH). Reagent grade acetone, dimethyl sulfoxide (DMSO), and 1,4-dioxane were dried over 3 Å molecular sieves before use. D$_2$O containing 1% DSS was from Wilmad (Buena, NJ). Other reagents were obtained from Aldrich Chemical Co. (Milwaukee, WI). Elemental analyses were performed by Galbraith Laboratories (Knoxville, TN).

Synthesis of Reduced Arabinogalactan 1. The first step in the conjugation of araAMP to arabinogalactan, see Scheme 1, was the reduction of arabinogalactan with sodium borohydride.

Sodium borohydride (10 g, 250 mmol) was added to a solution of arabinogalactan (100 g, 2.5 mmol, molecular weight of 40 kDa by light scattering) in water (250 mL). After being stirred at room temperature for 18 h, the reaction mixture was neutralized with 6 M HCl and dialyzed against deionized water (Spectra/Por 3 dialysis membrane, Spectrum Medical Industries, Los Angeles, CA). The dialysate was lyophilized to give 100 g of reduced arabinogalactan 1 as a white crystalline solid.

Synthesis of Arabinogalactan Bromide 2. Bromide was introduced into reduced arabinogalactan 1 by

reaction with epibromohydrin (*11*). A solution of zinc tetrafluoroborate hydrate (40 g, 167 mmol) in water (100 mL) and epibromohydrin (500 mL, 5.8 mol) was added to an aqueous solution of **1** (100 g, 2.5 mmol) in water (250 mL). This mixture was heated to 100 °C for 1.5 h. The product was extracted with butyl acetate and purified by ultrafiltration using a 3 kDa cutoff filter (Diaflo YM3, Amicon, Beverly, MA). Lyophilization yielded a white crystalline solid **2**. Yield: 35 g (31%). Elemental analyses: 0.59 mmol of Br/g of conjugate.

Synthesis of Arabinogalactan–Amine 3. A solution of **2** (35 g, 0.8 mmol) and ethylenediamine (160 g, 755 mmol) in DMF (80 mL) was stirred at 60 °C for 4 h. Unreacted ethylenediamine was removed by vacuum distillation. The product was purified by ultrafiltration and lyophilization as described above. Yield of pale yellow crystalline solid **3**: 23 g (66%). Ninhydrin assay showed a 0.17 mmol of ethylenediamine/g of conjugate incorporation.

Synthesis of the Antiviral Conjugate, Arabinogalactan–araAMP$_8$ (4). 9-β-D-Arabinofuranosyladenine 5′-monophosphate (araAMP; 0.70 g, 2.0 mmol) was added to a solution of arabinogalactan–amine **3** (10 g, 0.25 mmol) in water (25 mL). After the solution pH was adjusted to 6.5, 1-ethyl-3-(3-(dimethylamino)propyl)-carbodiimide hydrochloride (1.8 g, 9.4 mmol) was added. The reaction mixture was stirred at room temperature for 18 h, and the product was purified by ultrafiltration and lyophilization as described above. The product was obtained in quantitative yield.

The loading was 0.18 mmol of araAMP/g as determined by UV absorbance at 260 nm using unconjugated araAMP as a reference. Anion exchange chromatography showed that 99% of the araAMP was conjugated to the arabinogalactan. On the basis of the estimate of primary amine in **3** (0.17 mmol/g), essentially all of the amines were conjugated to araAMP.

Arabinogalactan has a molecular weight of 40 kDa by light scattering, but a molecular size of 19 kDa by size exclusion chromatography, when run against dextran standards (*9*). On the basis of an approximate conjugate molecular weight of 44 kDa, there are 7.9 mol of araAMP per mole of conjugate, denoted arabinogalactan–araAMP$_8$ (**4**).

Synthesis of en-araAMP. To aid in the assignment of peaks from the ^{13}C NMR spectrum of arabinogalactan–araAMP$_8$ (**4**), ethylenediamine was attached to the phosphate of araAMP as described (*12*). The resulting compound is referred to as en-araAMP.

NMR Spectroscopy. Fourier transform NMR spectra were obtained on a Varian XL300 spectrometer (Varian Corp, Palo Alto, CA). Carbon-13 NMR (75.43 MHz) spectra were acquired with 1000–4000 transients with continuous broad band ^{1}H decoupling (decoupler offset set at ∼5 ppm). Digital resolution was 0.50 Hz (0.909 s acquisition time with 1 Hz digital line broadening). Sample temperatures were maintained within 19–22 °C (±0.3° during a single spectral acquisition). APT (attached proton test) ^{13}C NMR spectra were measured to determine C–H multiplicity. All NMR measurements were performed in D$_2$O solutions containing an internal reference standard. Carbon-13 chemical shifts were referenced to ∼1% DSS (sodium 2,2-dimethyl-2-silapentane sulfonate), DMSO (δ_{DSS} = 41.306), acetone (δ_{DSS} = 32.928), or 1,4-dioxane (δ_{DSS} = 69.174).

Molecular Size of Arabinogalactan–araAMP$_8$ (4). The size of **4** was determined by size exclusion chromatography using a Cellufine GCL-300M (30 × 0.78 cm ID) column (Amicon Corp., Beverly, MA) and a Knauer

differential refractometer. The solute was eluted with 0.1% NaN$_3$ at 0.4 mL/min (Beckman Model 110B pump).

Asialoglycoprotein Receptor Interaction. Asialoglycoprotein receptor was isolated according to the method of Hudgin (*13*). The tracer, an iodinated tyramine derivative of arabinogalactan, was prepared as described (*9*). Increasing concentrations of ligand were used to displace tracer, and the concentration inhibiting tracer binding by 50% (IC$_{50}$) was determined by the logit transformation (*40*). The IC$_{50}$ with this assay has intraassay and interassay coefficients of variation of 7.9% (n = 5) and 27% (n = 9), respectively. The IC$_{50}$'s for all ligands were obtained in a single assay. The nonspecific binding of the tracer, i.e., binding not displacable by tracer, was less than 5% of total counts.

pH Dependence of Arabinogalactan–araAMP$_8$ (4) Stability. A solution of (**4**) (120 mg/mL) was prepared in pH 7.5 water. The pH of aliquots of the stock solution was adjusted with either NaOH or HCl as appropriate to obtain solutions varying in pH from 3 to 9. The solutions were then incubated at 37 °C. Aliquots (100 μL) were withdrawn at 0, 2, 4, 6, and 20 h and added to 20 mM phosphate buffer (0.95 mL; pH 7.3, 400 mM NaCl). Samples were analyzed for (**4**), araAMP, and araA by anion exchange HPLC using a Waters 600E system (Millipore, Marlborough MA) with a Waters Model 991 photodiode array detector. The column was an anion exchange column of Synchopak Q300, 250 × 4.6 mm, (SynChrom Inc., Lafayette, IN). The mobile phase was 0.4 M NaCl, 0.1% NaN$_3$ in pH 7.3 water, and the flow rate was 1 mL/min.

Stability of Arabinogalactan–araAMP$_8$ (4) in Blood. AraAMP (50 μg/mL) and (**4**) (833 μg/mL) were each incubated in heparinized human blood at 37 °C. Samples of blood were taken at 0, 60, 90, and 120 min and centrifuged for 10 min at 1000g to recover the plasma. The plasma was then analyzed for araAMP (free and/or conjugated) by HPLC as described above.

Antiviral Activity of Arabinogalactan–araAMP$_8$ (4) in WHV-Infected Woodchucks. Woodchucks were born in captivity and infected with WHV within 1 week after birth. The carrier state was confirmed by the presence of WHV surface antigen (WHsAg) in serum over the first year of life. Woodchucks (Marmotech, Inc., Cortland, NY) were at least 1 year old, approximately 3 kg, matched for age and sex, and positive for WHsAg.

Intravenous injection and blood collection of woodchucks was accomplished through vascular access ports (Model SLA-3.5, Access Technologies, Norfolk Medical Products, Inc., Skokie, IL) placed in the test animals. The catheters were implanted in the saphenous vein of anesthetized animals and the ports positioned subcutaneously on the lateral aspect of the rear limb proximal to the catheter. Test material was administered daily through the ports, which were flushed with heparinized saline following use. Withdrawal of blood from these ports was possible only for the first week, however, and blood samples for the second week were obtained from the opposite femoral artery or vein.

Groups of three WHV carrier woodchucks in two separate experiments were treated with intravenous injections of 50 mg/kg/day of (**4**), equivalent to 3 mg/kg/day of araAMP, for 14 consecutive days. Additional animals received either 3 or 15 mg/kg/day of araAMP (Figure 4). Finally, three animals received arabinogalactan (50 mg/kg/day), data not shown. Sera for analysis of viral DNA levels were collected at predetermined time points during and following treatments.

Blood samples for serum WHV DNA were obtained at various times prior to and during treatment and moni-

Scheme 1

Figure 1. Size exclusion chromatography of arabinogalactan–araAMP$_8$ (4).
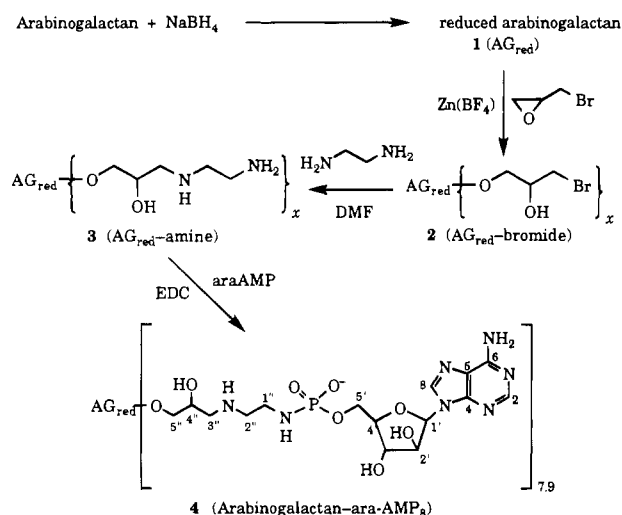
tored post-treatment for 100 days. Tests for WHsAg were performed using an ELISA assay (*16*), while assays for WHV DNA were performed as described (*17*). Standards of homologous WHV DNA were hybridized simultaneously to allow quantitation. The radioactivity of individual slots was determined using an automated β-scanner (Ambis Inc., San Diego, CA).

Single Dose Toxicity of Arabinogalactan–araAMP$_8$ (4). Mice used in this study were male CD-1 (Crl: CD-1{ICR}BR), approximately 25–30 g, obtained from Charles River Laboratories, Wilmington, MA. A limit test was conducted in male CD-1 mice according to the up-and-down method for small samples (*18*). The animals each were administered single doses of 5 g/kg arabinogalactan–araAMP$_8$ (corresponding to 300 mg araAMP/kg) by intravenous injection. In a separate study, mice were administered 5 g/kg of the conjugate but then sacrificed on day 7 for microscopic examination of the liver. The livers were evaluated for histopathological changes with hematoxylin and eosin staining.

Repeat Dose Toxicity of Arabinogalactan–araAMP$_8$ (4). Rats were male CD (Crl:CD(SD)BR), approximately 200–250 g, obtained from Charles River Laboratories (Wilmington, MA). Male rats were administered either (4) at 250 mg/kg/day (corresponding to 15 mg araAMP/kg/day), araAMP at 25 mg/kg/day, or saline in single intravenous injections per day for 30 days. Animals were observed for overt clinical signs of toxicity throughout the treatment period and then sacrificed for histological examination of the liver. Blood samples from all animals were obtained at the time of sacrifice. Serum samples were obtained for the standard profile of clinical chemistry analyses, which includes liver transaminases, on a Hitachi 747 Chemistry Analyzer. Whole blood samples were analyzed on a Baker 9000 for routine hematological profile with manually performed differential counts and spun hematocrits. These analyses were performed at the Tufts Veterinary Diagnostic Laboratory, North Grafton, MA.

RESULTS

Arabinogalactan-araAMP$_8$ (4) was synthesized according to Scheme 1.

Characterization of Arabinogalactan–araAMP$_8$ (4). Arabinogalactan–araAMP$_8$ (4) was characterized by size exclusion chromatography as shown in Figure 1. (4) eluted as a single peak with a retention time of 28.5 min, compared to T-10 dextran and T-25 dextran standards (32.1 and 23.5 min, respectively). The starting ara-
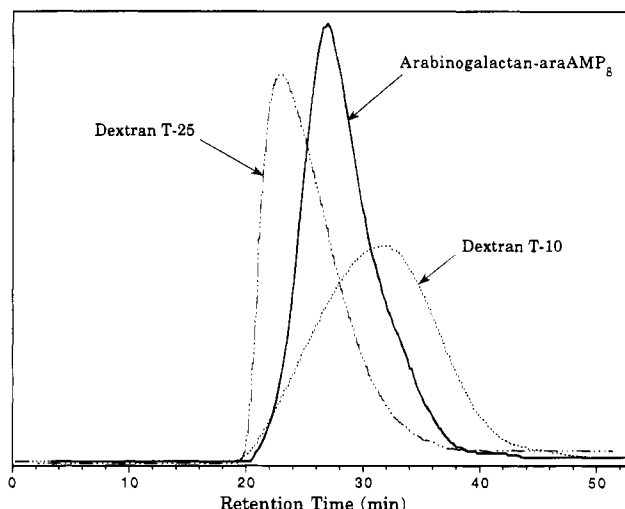
binogalactan eluted at 24.5 min and exhibited an elution profile similar to T-25 dextran. A small amount of a low molecular weight contaminant is present in (4) and may remain after the ultrafiltration, which is used to remove low molecular weight byproducts formed during the synthesis.

The ^{13}C NMR spectrum of (4) consists of resonances attributable to araAMP, arabinogalactan, and the linkage between araAMP and arabinogalactan, as shown in Figure 2 and summarized in Table 1.

The resonances of the linking group carbons, C1″–C5″, of (4) occurred in the range of 40–66 ppm. The peaks for adenine carbons, C2–C8, were observed between 140 and 160 ppm; they were assigned by its APT spectrum and comparison with the spectra of araAMP (Na$^+$ salt) (*19*) and en-araAMP. The arabinofuranose (of araAMP) resonances were in the 65–87 ppm range. The broadened line widths (14–28 Hz) of the adenine and arabinose resonances of araAMP are consistent with the conjugation of araAMP to arabinogalactan. This line broadening is attributable to the increased translational and rotation correlation times of araAMP upon conjugation to the much larger arabinogalactan (*20–24*). Under similar conditions, the line widths of the resonances of free araAMP and en-araAMP were typically 1–4 Hz. The increased line widths of (4) obscured the expected small P–C couplings (~4–9 Hz), which were observed in both en-araAMP and ara-AMP.

The arabinogalactan subspectrum of (4) is similar to the arabinogalactans from *Larix sibirica* (*25*) and *Larix dahurica* (*26*). These arabino-3,6-galactans are highly, branched structures consisting of a backbone of primarily (1→3)-β-D-galactopyranose with some (1→6)-β-D-galactopyranose groups. Branching generally occurs at C-6 of the (1→3)-Gal$p$ backbone residues. The side chains are primarily Gal$p$ or disaccharide units of Gal$p$-(1→6)-Gal-(1→6), or Ara$p$-(1→3)-Ara$f$-(1→3) (*27, 28*).

The resonances of the anomeric carbons of the arabinogalactan portion of (4) at ~106 ppm are characteristic of β-glycosidic linkages (*29*) and are assigned primarily to the backbone galactopyranosyl groups (*i.e.*, β-d-(1→6)-Gal$p$, β-d-(1→3)-Gal$p$). The anomeric carbon of the arabinose residues also occurs in this range. The major peaks at ca. 63.7, 71.4, 73.4, 75.4, and 77.8 are assigned primarily to galactopyanosyl C6 (and C5-Ara$f$), C2, C4, C3, C5, respectively. Other arabinogalactan β-arabinofuranosyl (Ara$f$) resonances were observed at 76.2 (C3) and 84.3 (C4) ppm. The former peak partially obscures
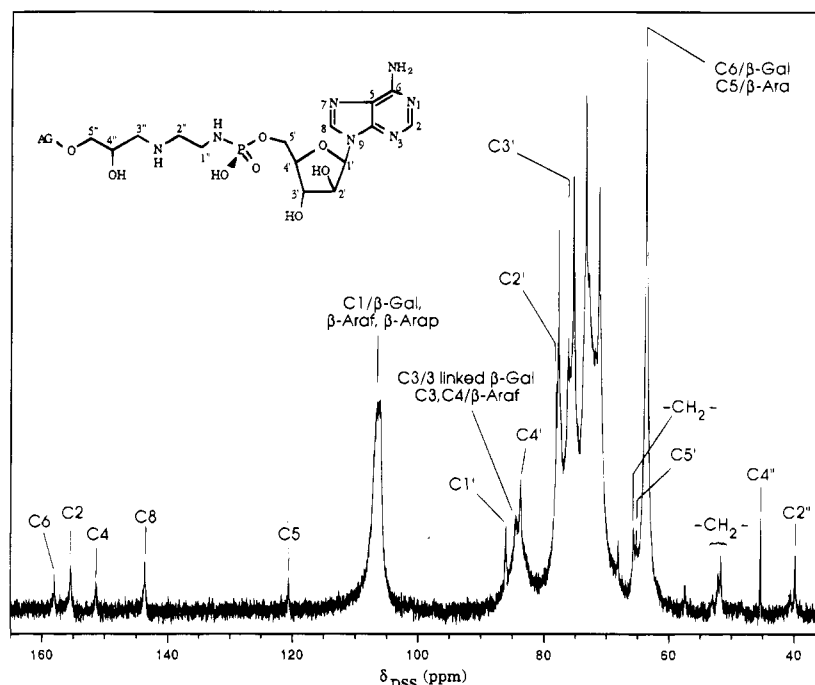
Figure 2. Carbon-13 NMR spectrum (75 MHz) of arabinogalactan−araAMP$_8$ (**4**) in D$_2$O solution.

Table 1. Carbon-13 NMR Chemical Shifts (δ_{DSS}) of Antiviral Compounds in D$_2$O^a

Na [ara-AMP]	en-ara-AMP	arabinogalactan−araAMP(**4**)	assignment
154.94	155.78	155.33	adenine C2
150.94	150.70	151.42	adenine C4
120.56	120.25	120.64	adenine C5
157.78	157.45	158.04	adenine C6
143.71	143.27	143.67	adenine C8
86.40	86.33	85.97	arabinofuranose C1'
78.24	78.19	78.15	arabinofuranose C2'
76.37	76.52	~76^b	arabinofuranose C3'
84.56 (8.6)	84.02 (8.6)	83.77	arabinofuranose C4'
65.41 (4.1)	65.80 (<4)	65.23	arabinofuranose C5'
	43.58 (5.5)		linking group methylene (C1'')
	41.18	39.93	linking group methylenes (C2''))
		51.7−52.2	linking group methylenes (C1'', C3'')
		45.45	linking group methine (C4'')
		65.72	linking group methylenes (C5'')

^{a} Chemical shifts in ppm downfield from internal DSS. Numbers in parentheses are P−C coupling constants (Hz). ^{b} Peak partially obscured by overlapping arabinogalactan resonances.

Table 2. Asialoglycoprotein Receptor Binding

ligand	IC$_{50}$ (μM)
arabinogalactan	2.0×10^{-6}
arabinogalactan−araAMP$_8$ (**4**)	1.0×10^{-6}
asialofetuin	1.3×10^{-7}
galactose	$>2 \times 10^{-2}$

the C3' peak of the conjugated araAMP. Since *O*-glycosylation generally shifts the carbon of the glycosylation site downfield by *ca.* 7−8 ppm (*29*, *30*), the resonances of glycosylated carbons of (1→6)-Gal*p* and (1→3)-Gal*p* (*31*) occur at *ca.* 71.2 and 84.3 ppm. These two peaks are coincident with the Gal*p* C2 and Ara*f* C4 peaks.

Asialoglycoprotein Receptor Interaction. The relative strength of the interactions of various ligands with the asialoglycoprotein receptor was examined by determining the IC$_{50}$ of ligands for purified receptor (Table 2). Arabinogalactan−araAMP$_8$ (**4**) bound receptor about two times less strongly than that of arabinogalactan, indicating that after modification of arabinogalactan shown in Scheme 1 receptor binding was substantially retained. Asialofetuin had a IC$_{50}$ for the receptor that

was about 7 times lower than arabinogalactan, while galactose had a high IC$_{50}$.

Stability of Arabinogalactan−araAMP$_8$ (4) as a Function of pH. The stability of (**4**) in the pH range 3−9 was determined at 37 °C; see Figure 3. At pH 7 over a 24 h period, no decomposition was discernible. At pH 5 or lower, araAMP was released as the major hydrolysis product due to hydrolysis of the phosphamide bond present in (**4**); see Scheme 1. The rate of hydrolysis of (**4**) was extremely slow at pH 7, the approximate pH of plasma, and increased rapidly at mildly acidic pH's, the approximate pH that might be encountered in the endosome.

Stability of Arabinogalactan−araAMP$_8$ (4) in Blood. The stability of (**4**) in blood was determined by incubating the conjugate or the free araAMP in whole heparinized human blood at 37 °C. After a 1 h incubation, 98% of araAMP remains conjugated in arabinogalactan−araAMP$_8$, and 69% remains after 120 min (Table 3). By comparison, 39% of unconjugated araAMP remains intact after 1 h, and less than 2% remains after a 90 min incubation.

Antiviral Activity of Arabinogalactan−araAMP$_8$
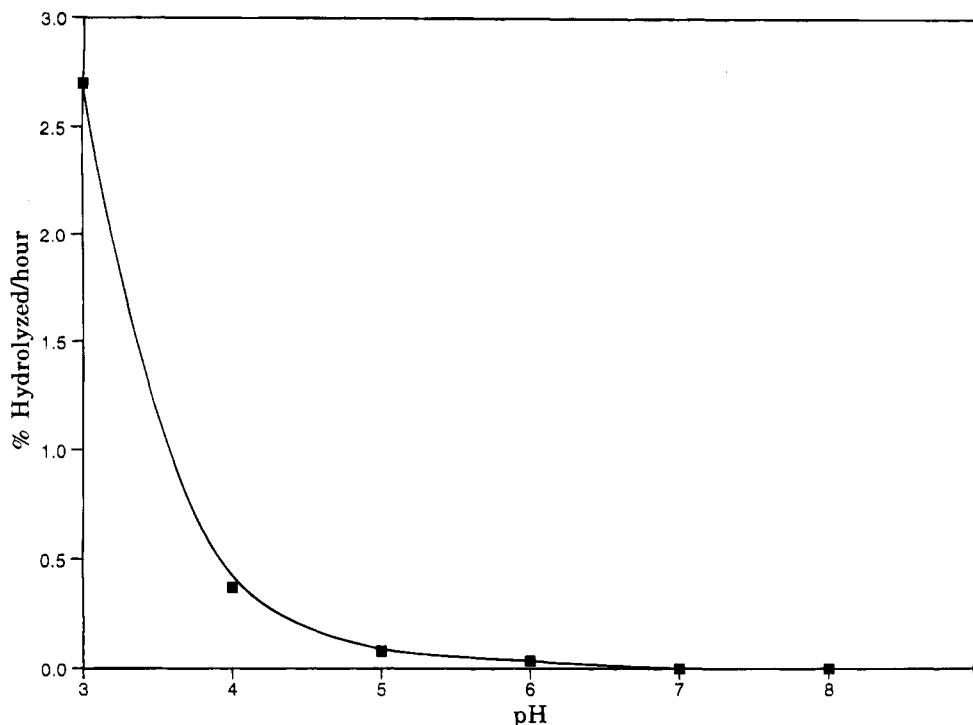
Figure 3. Hydrolysis of arabinogalactan−araAMP$_8$ (**4**) as a function of pH.
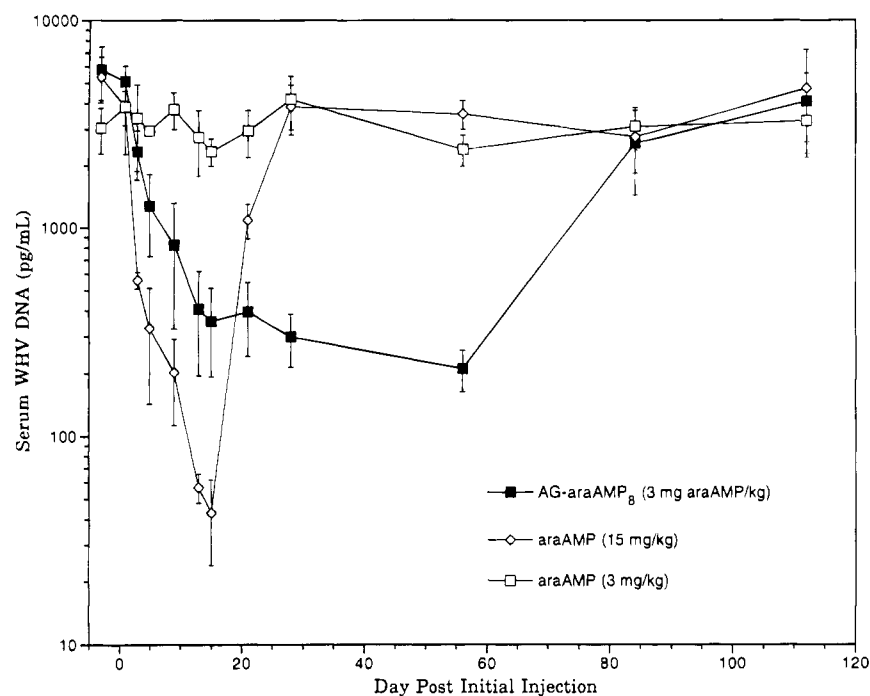
Figure 4. Serum WHV DNA in carrier woodchucks treated with arabinogalactan−araAMP$_8$ (**4**), at a dose providing 3 mg of araAMP/ kg/day, AraAMP at 3 mg/kg/day, and araAMP at 15 mg/kg/day. Animals were injected once a day for 14 days. Error bars represent one standard deviation.

Table 3. Stability Of AraAMP and Arabinogalactan−araAMP$_8$ (4) In Heparinized Blood

starting material	AraAMP in blood (% of initial concn)			
	0 h	1 h	1.5 h	2 h
AraAMP	100	39	1.2	0
arabinogalactan−araAMP$_8$ (4)	100	98	84	69

(4) in WHV-Infected Woodchucks. As shown in Figure 4, treatment of woodchucks with (**4**) resulted in a prompt decrease in WHV DNA, a decrease which persisted for at least 42 days after treatment termination

in all animals. The serum WHV DNA of four of the six animals was 71−94% below pretreatment levels 3 months after treatment ended. In contrast, woodchucks treated with 15 mg/kg/day of araAMP also responded with a prompt decrease in viral DNA, but the decrease in serum viral DNA did not persist following treatment termination. Woodchucks treated with 3 mg/kg/day of araAMP or arabinogalactan showed no decrease in viral DNA. Woodchucks treated with 50 mg/kg/day of arabinogalactan showed no change in viral DNA (data not shown).

Single Dose Toxicity of Arabinogalactan−araAMP$_8$ (4). Administration of single bolus intravenous

injections of 5 g of (4) per kg in mice resulted in no mortality. A dose of 5 g/kg is the upper limit based on solubility and volume constraints and corresponds to dose of 300 mg araAMP/kg or 100 times the dose used in woodchuck. A second group of similarly treated animals that were sacrificed on day 7 showed no evidence of liver damage or alteration, in particular vacuolization.

Repeat Dose Toxicity of Arabinogalactan–ara-AMP$_8$ (4). There were no significant differences in clinical chemistry or hematology in rats during or following 30 consecutive day treatments with (4) at 250 mg/kg/day, unconjugated araAMP at 25 mg/kg/day, or saline vehicle (2 mL/kg). Liver histopathology 24 h after the final dose revealed no hepatic vacuoles, which would have indicated compartmentalization and storage of the conjugate in liver; however, minimal multifocal necrosis of individual hepatocytes was seen in all animals receiving (4) ($n = 3$). One of three araAMP-treated animals showed a similar hepatic necrosis.

Serum samples, drawn from test and control woodchucks before and immediately following the 14 day treatment with (4), revealed no differences in serum chemistry or hematology that would suggest toxicity (data not shown).

DISCUSSION

We have synthesized and characterized a conjugate of the polysaccharide arabinogalactan with the antiviral nucleotide, araAMP.

Asialoglycoprotein Receptor Interaction of Arabinogalactan–araAMP$_8$ (4). The modification of arabinogalactan, Scheme 1, does not reduce receptor binding (Table 2). When drugs are attached to the protein portion of asialoglycoproteins or neoglycoproteins, as has often been accomplished (5, 6, 32), the receptor binding, oligosaccharide portion of the carrier is not modified. Arabinogalactan, a polysaccharide, does not offer amino acid side chains spatially removed from its receptor binding activity for the attachment of drug. Consequently, the receptor assay is needed to demonstrate that the receptor binding activity of arabinogalactan has not been destroyed by the chemistry employed.

In spite of the fact that the IC$_{50}$ of arabinogalactan is about seven times higher than that of asialofetuin (Table 2), the interaction of arabinogalactan with the receptor is sufficiently strong to permit hepatic delivery of diagnostic and therapeutic agents to the liver. Arabinogalactan has been used as a covering to deliver a magnetic resonance contrast agent, superparamagnetic iron oxide, to hepatocytes (7, 8). When a chelate of ^{57}Co was attached to arabinogalactan, and intravenously injected, 52% of the label showed hepatic uptake. Hepatic uptake dropped to 3.5% with the injections of asialofetuin (100 mg/kg) (9). Finally, the increase in antiviral activity produced by attaching araAMP to arabinogalactan (Figure 4), suggests arabinogalactan is achieving greater hepatic uptake of (4) in the woodchuck.

Stability of Arabinogalactan–araAMP$_8$ (4) in Blood. The conjugation of araAMP to arabinogalactan provides a form of araAMP that is stable in blood (Table 3). After intravenous injection of araAMP (20 mg/kg) in the woodchuck, the nucleotide was rapidly dephosphorylated and converted to ara-hypoxanthine (33). The importance of the deamination side reaction has been shown by the fact that inhibitors of adenosine deaminase, the enzyme that deaminates araA, enhance antiviral activity of araAMP (17, 34).

Stability of Arabinogalactan–araAMP$_8$ (4) in Blood and as a Function of pH. The phosphamide linkage employed between the arabinogalactan amine 3

and araAMP affords a bond that is stable at the pH of blood but unstable at lower pH. AraAMP, when bound to lactosaminated serum albumin via the same type of phosphate–amide linkage, is released largely as araAMP by lysosomal action (35).

Antiviral Activity in WHV-Infected Woodchucks Treated with Arabinogalactan–araAMP$_8$ (4). WHV carrier woodchucks treated with (4), equivalent to 3 mg of araAMP/kg/day, responded with a decrease in WHV DNA (Figure 4). Woodchucks that were treated with (4) in the two separate experiments responded in similar fashion, with prompt and similar reductions in viral DNA; the combined data for both groups ($n = 6$) is shown in Figure 4. In contrast, animals treated with 3 mg of araAMP/kg/day, i.e., the unconjugated form of araAMP, showed no change in serum WHV DNA. This demonstrates that 3 mg/kg of araAMP as (4) decreased WHV DNA, while 3 mg/kg of araAMP did not. After cessation of injection of (4) (day 14), WHV DNA was still depressed at day 56 of the study (42 days after the last injection). In contrast, treatment with araAMP produced a greater decrease in serum WHV than treatment with (4), but WHV DNA promptly returned to pretreatment levels. Such a prolonged depression in WHV DNA in response to treatment with (4) maybe due to the hepatic sequestration of (4), araA, or araATP in the liver and slow release in amounts sufficient to inhibit viral replication.

AraAMP has been conjugated to lactosaminated serum albumin (to form L-HSA–araAMP) and studied with human carriers of HBV and woodchuck carriers of WHV (33, 36). A dose of 1.5 mg/kg araAMP, as L-HSA–araAMP, lowered WHV DNA, while 5 mg/kg as araAMP was without effect. Drugs were administered by intravenous injection, once a day for 5 days. WHV DNA was determined by observers evaluating the intensity of a spot on an autoradiograph. When L-HSA–araAMP and L-HSA–acyclovir phosphate were administered together, a decrease in viral DNA was obtained that persisted after treatment was withdrawn. Comparison of the work of Ponzetto with the current study is difficult because of differing dosing schedules and the qualitative assessment of WHV DNA levels those workers employed.

Although asialoglycoproteins or neoglycoproteins have been used to deliver diagnostic and therapeutic agents to the liver, there some advantages to using arabinogalactan for this purpose.

First, arabinogalactan is cheaper than lactosylated albumins or asialoglycoproteins, often used as carriers for targeting diagnostic or therapeutic agents to the asialoglycoprotein receptor. A highly purified arabinogalactan can be purchased for less than $1 per gram, while bovine asialofetuin, the cheapest protein-based carrier for the asialoglycoprotein receptor, costs more than $100 per gram (1994 Sigma catalog prices). In some applications, notably the targeted delivery of araAMP with repeated injections, carrier costs can be a significant element in total drug cost. For example, Fiume injected humans with L-HSA–araAMP, 35 mg conjugate/kg/day for 3 days, for a total dose of about 6 g of conjugate over the 3 day dosing period (70 kg man) (5). On the basis of Figure 4, 50 mg of arabinogalactan/kg/day for 14 days, the dose for a human would be over 50 g.

Second, the chemistry shown in Scheme 1 provides a method of attaching nucleotides to a receptor-recognizing carrier molecule free of some of the problems that arise when the carrier is a protein. When carbodiimide is used to attach araAMP to L-HSA, araAMP can react with different amino acid side chains. A phosphoanhydride linkage to glutamic acid occurs at pH 5, while at pH 7.5, reaction occurs with lysine and histidine residues (36).

Another problem when carbodiimide is used to attach araAMP to L-HSA is the formation of high molecular weight aggregates, due to peptide bonds formed between two or more protein molecules. Noting these problems, Jansen and co-workers recently developed a two-step, two-pH procedure to attach araAMP and L-HSA, to minimize aggregation, and produce greater hepatocyte uptake (*35*).

In contrast in Scheme 1, araAMP is attached to the arabinogalactan amine **3**. Since the amino and hydroxyl groups differ substantially in their reactivity, the coupling of **3** with araAMP using carbodiimide proceeds exclusively with the amino group. The chemistry employed in Scheme 1 avoids the formation of high molecular weight forms of arabinogalactan by selection of the concentrations and amounts of epibromohydrin and ethylenediamine.

Finally, it should be noted that the reaction of amino groups on proteins tends to make the proteins more negatively charged. Highly negatively charged proteins are recognized by scavenger receptors (*35*), which compete with asialoglycoprotein receptors for the injected molecule. This can lead to uptake of conjugates by scavenger receptors (*37, 38*). Consisting solely of arabinose and galactose, the starting raw material, arabinogalactan, is a neutral polysaccharide (*39*). The linkage used provides a negatively charged phosphate and positively charged secondary amino group, for a net neutral charge. Therefore (**4**), consisting of neutral arabinogalactan and a neutral linkage, has a net neutral charge.

Our results are the first time a conjugate has been synthesized consisting of a polysaccharide which binds the asialoglycoprotein receptor (arabinogalactan) and an antiviral agent (araAMP). Arabinogalactan may prove to be a satisfactory carrier for the delivery of araAMP to the liver.

LITERATURE CITED

(1) Beasley, R. P., and Hwang, L. Y. (1984) Epidemiology of hepatocellular carcinoma. In *Viral Hepatitis and Liver Disease* (G. N. Vyas, J. L. Dienstag, and J. H. Hoofnagle, Eds.) pp 209–224, Grune and Stratton, New York.

(2) Kolff, R. S., and Galambos, J. T. (1987) Viral hepatitis. In *Diseases Of The Liver* (L. Schiff and E. R. Schiff, Eds.) 6th ed., pp 457–582, J. B. Lippincott, Philadelphia.

(3) Marcellin, P., Ouzan, D., Degos, F., Brechot, C., Metman, E. H., Degott, C., Chevalier, M., Berthelot, P., Trepo, C., and Benhamou, J. P. (1989) Randomized controlled trial of adenine arabinoside 5'-monophosphate in chronic active hepatitis B: comparison of the efficacy in heterosexual and homosexual patients. *Hepatology 10*, 328–31.

(4) Lok, A. S., Wilson, L. A., and Thomas, H. C. (1984) Neurotoxicity associated with adenine arabinoside monophosphate in the treatment of chronic hepatitis B virus infection. *J. Antimicrob. Chemother. 14*, 93–9.

(5) Fiume, L., Cerenzia, M. R., Bonino, F., Busi, C., Mattioli, A., Brunetto, M. R., Chiaberge, E., and Verme, G. (1988) Inhibition of hepatitis B virus replication by vidarabine monophosphate conjugated with lactosaminated serum albumin. *Lancet 2*, 13–5.

(6) Meijer, D. F. K., Jansen, R. W., and Molema, G. (1992) Drug targeting systems for antiviral agents: options and limitations. *Antiviral Res. 18*, 215–258.

(7) Josephson, L., Groman, E. V., Menz, E., Lewis, J. M., and Bengele, H. (1990) A functionalized superparamagnetic iron oxide colloid as a receptor directed MR contrast agent. *Magn. Reson. Imag. 8*, 637–46.

(8) Reimer, P., Weissleder, R., Lee, A. S., Wittenberg, J., and Brady, T. J. (1990) Receptor imaging: application to MR imaging of liver cancer. *Radiology 177*, 729–34.

(9) Groman, E. V., Enriquez, P. M., Jung, C., and Josephson, L. (1994) Arabinogalactan for hepatic drug delivery. *Bioconjugate Chem. 5*, 547–56.

(10) Raney, A. R., and McLachlan, A. (1991) The biology of hepatitis B virus. In *Molecular Biology of Hepatitis B Virus* (A. McLachlan, Eds.) pp 1–38, CRC Press, Boca Raton.

(11) Molteni, L. (1985) Dextran and inulin conjugates as drug carriers. *Methods Enzymol. 112*, 285–298.

(12) al-Deen, A. N., Cecchini, D. C., Abdel-Baky, S., Moneam, N. M., and Giese, R. W. (1990) Preparation of ethylenediaminephosphoramidates of nucleotides and derivatization with fluorescein isothiocyanate. *J. Chromatogr. 512*, 409–14.

(13) Hudgin, R. L., William E. Pricer, J., Ashwell, G., Stockert, R. J., and Morell, A. G. (1974) The isolation and properties of a rabbit liver binding protein specific for asialoglycoproteins. *J. Biol. Chem. 249*, 5536–5543.

(14) Kohn, J., and Wilchek, M. (1984) The use of cyanogen bromide and other novel cyanylating agents for the activation of polysaccharide resins. *Appl. Biochem. Biotechnol. 9*, 285–305.

(15) Hunter, W. M., and Greenwood, F. C. (1962) Preparation of iodine 131 labelled human growth hormone of high specific activity. *Nature 194*, 494.

(16) Korba, B. E., Brown, T. L., Wells, F. V., Baldwin, B., Cote, P. J., Steinberg, H., Tennant, B. C., and Gerin, J. L. (1990) Natural history of experimental woodchuck hepatitis virus infection: molecular virologic features of the pancreas, kidney, ovary, and testis. *J. Virol. 64*, 4499–506.

(17) Korba, B. E., and Gerin, J. L. (1992) Use of a standardized cell culture assay to assess activities of nucleoside analogs against hepatitis B virus replication. *Antiviral Res. 19*, 55–70.

(18) Dixson, W. J. (1965) The up and down method for small samples. *Am. Stat. Assoc. J. 60*, 969–978.

(19) Uesugi, S., Tanaka, S., and Ikehara, M. (1978) Carbon-13 nuclear magnetic resonance spectra of adenine cyclonucleosides and their phosphates. Effects of neighboring groups for elucidation of fine structure of nucleosides and nucleotides. *Eur. J. Biochem. 90*, 205–12.

(20) Benesi, A. J., and Brant, D. A. (1985) Trends in molecular motion for a series of glucose oligomers and the corresponding polymer pullulan as measured by carbon-13 NMR relaxation. *Macromolecules 18*, 1109–16.

(21) Dais, P., and Perlin, A. S. (1986) Chemical shifts of the methyl groups in di-O-isopropylidene furanoses and their relationship to molecular conformation and site of ring fusion. Spin-lattice relaxation measurements and motional characteristics. *Carbohydr. Res. 146*, 177–91.

(22) Goux, W. J., Perry, C., and James, T. L. (1982) An NMR study of carbon-13-enriched galactose attached to the single carbohydrate chain of hen ovalbumin. Motions of the carbohydrates of glycoproteins. *J. Biol. Chem. 257*, 1829–35.

(23) Matsuo, K. (1984) Carbon-13-NMR relaxation of polysaccharides: dextran and amylose in dimethyl sulfoxide and water. *Macromolecules 17*, 449–52.

(24) Vignon, M., Michon, F., Joseleau, J. P., and Bock, K. (1983) Molecular motion of branched-chain polysaccharides studied by carbon-13 NMR spin-lattice relaxation rates. *Macromolecules 16*, 835–8.

(25) Karacsonyi, S., Kovacik, V., Alfoldi, J., and Kubackova, M. (1984) Chemical and carbon-13 NMR studies of an arabinogalactan from Larix sibirica L. *Carbohydr. Res. 134*, 265–74.

(26) Odonmazig, P., Ebringerova, A., Machova, E., and Alfoldi, J. (1994) Structural and molecular properties of the arabinogalactan isolated from Mongolian larchwood (Larix dahurica L.). *Carbohydr. Res. 252,* 317–24.

(27) Churms, S. C., Merrifield, E. H., and Stephen, A. M. (1978) Regularity within the molecular structure of arabinogalactan from Western Larch (Larix occidentalis). *Carbohydr. Res. 64,* C1-C2.

(28) Clarke, A. E., Anderson, R. L., and Stone, B. A. (1979) Form and function of arabinogalactans and arabinogalactan proteins. *Phytochemistry 18,* 521–540.

(29) Sarkar, A. K., Pawar, S. M., and Matta, K. L. (1991) Synthesis of two isomeric tetrasaccharides O-α-L-fucopyranosyl-(1→3) and (1→4)-O-(2-acetamido-2-deoxy-β-D-glucopyranosyl)-(1→3)-O-(β-D- galactopyranosyl)-(1→4)-D-glucopyranose and α related tetrasaccharide O-α-L-fucopyranosyl-(1→3)-O-(2-acetamido-2-deoxy-β-D-glucopyranosyl)-(1→6)-O-(β-D-galactopyranosyl)-(1→4)-D-glucopyranose. *J. Carbohydr. Chem. 10,* 269–78.

(30) Bradbury, J. H., and Jenkins, G. A. (1984) Determination of the structures of trisaccharides by carbon-13 NMR spectroscopy. *Carbohydr. Res. 126,* 125–56.

(31) Saito, H., Miyata, E., and Sasaki, T. (1978) A carbon-13 nuclear magnetic resonance study of gel-forming (1→3)-β-D-glucans: molecular-weight dependence of helical conformation and of the presence of junction zones for association of primary molecules. *Macromolecules 11,* 1244–51.

(32) Stadalnik, R. C., Vera, D. R., Woodle, E. S., Trudeau, W. L., Porter, B. A., Ward, R. E., Krohn, K. A., and O'Grady, L. F. (1985) Technetium-99m NGA functional hepatic imaging: preliminary clinical experience. *J. Nucl. Med. 26,* 1233–42.

(33) Ponzetto, A., Fiume, L., Forzani, B., Song, S. Y., Busi, C., Mattioli, A., Spinelli, C., Marinelli, M., Smedile, A., Chiaberge, E., and et al. (1991) Adenine arabinoside mono-phosphate and acyclovir monophosphate coupled to lactosaminated albumin reduce woodchuck hepatitis virus viremia at doses lower than do the unconjugated drugs. *Hepatology 14,* 16–24.

(34) North, T. W., and Cohen, S. S. (1979) Aranucleosides and aranucleotides in viral chemotherapy. *Pharmac. Ther. 4,* 81–108.

(35) Jansen, R. W., Kruijt, J. K., van Berkel, T. J., and Meijer, D. K. (1993) Coupling of the antiviral drug ara-AMP to lactosaminated albumin leads to specific uptake in rat and human hepatocytes. *Hepatology 18,* 146–52.

(36) Fiume, L., Bassi, B., and Bongini, A. (1988) Conjugates of 9-β-D-arabinofuranosyladenine 5'-monophosphate (ara-AMP) with lactosaminated albumin. Characterization of the drug-carrier bonds. *Pharm. Acta Helv. 63,* 137–9.

(37) Fiume, L., Mattioli, A., and Spinosa, G. (1987) Distribution of a conjugate of 9-β-D-arabinofuranosyladenine 5'-monophosphate (ara-AMP) with lactosaminated albumin in parenchymal and sinusoidal cells of rat liver. *Cancer Drug Deliv. 4,* 11–6.

(38) Franssen, E. J., Jansen, R. W., Vaalburg, M., and Meijer, D. K. (1993) Hepatic and intrahepatic targeting of an anti-inflammatory agent with human serum albumin and neoglycoproteins as carrier molecules. *Biochem. Pharmacol. 45,* 1215–26.

(39) Adams, M. F., and Douglas, C. (1963) Arabinogalactan- a review of the literature. *Tech. Assoc. Pulp Paper Ind. 46,* 544–548.

(40) Chard, T. (1990) *An Introduction To Radioimmunoassay and Related Techniques,* 4th ed., pp 166–168, Elsevier, Amsterdam.

BC940106H

Preparation and *in Vitro* Evaluation of Magnetic Microsphere–Methotrexate Conjugate Drug Delivery Systems

Damayanthi Devineni,[†] Charles D. Blanton,[‡] and James M. Gallo*,[†]

Department of Medical Oncology, Fox Chase Cancer Center, Philadelphia, Pennsylvania 19111, and College of Pharmacy, University of Georgia, Athens, Georgia 30602. Received September 30, 1994[⊗]

Magnetic microsphere–methoxtrexate (MM–MTX) conjugates prepared by several different methods were analyzed for their suitability for in vivo use. MM–MTX were prepared by the following methods: (A) reaction of MTX with poly(ethylene glycol) 1500 (PEG) to form a poly(ethylene glycol)–methotrexate conjugate (PEGMTX) which was then added to a ferrous/ferric ion salt solution to give MM–MTX I; (B) reaction of ferrous/ferric ion salts with PEG to give a ferromagnetic polymer complex which was then coupled with MTX to give MM–MTX II; (C) MM–MTX IIIA were prepared by reacting MTX with amino-terminated magnetic microspheres, commercially available, in the presence of 1-ethyl-3,3-bis(methylamino)propylcarbodiimide (EDCI); (D) reaction of aminohexanol with di-*tert*-butyl dicarbonate to form an [*N*-(*tert*-butoxycarbonyl)amino]hexanol (*t*-Boc-AH), which was then coupled with MTX in the presence of 1,3-dicyclohexylcarbodiimide and 4-pyrrolidinopyridine to give a *t*-Boc-AH–MTX conjugate, which was then saturated with hydrogen chloride to give an aminohexanol-methotrexate (AH–MTX) conjugate. MM–MTX IIIB were then prepared by reacting AH–MTX with carboxyl-terminated magnetic microspheres, commercially available, in the presence of EDCI and 4-(dimethylamino)pyridine. The identity of MTX conjugates was confirmed using ultraviolet, infrared, and nuclear magnetic resonance spectroscopy. Drug content of the magnetic microsphere–methotrexate conjugates as determined by HPLC was 0.45% (w/w), 4.0% (w/w), and 6.3% (w/w) MTX for MM–MTX I, MM–MTX II, and MM–MTX IIIB, respectively. In vitro stability studies of MM–MTX in rat plasma revealed that approximately 97% (w/w) (MM–MTX I), 74% (w/w) (MM–MTX II), and 11% (w/w) (MM–MTX IIIB) of MTX was released from MM–MTX over a 24 h period. The ability to increase drug loading, compared to matrix microsphere systems, via an ester linkage offers another dimension to tumor delivery of chemotherapeutic agents.

Methotrexate, *N*-[4-[[(2,4-diamino-6-pteridinyl)methyl]methylamino]benzoyl]glutamic acid, MTX, is used for the treatment of lymphoreticular and other malignancies including metastic and recurrent primary brain tumors (*1–3*). A major drawback with MTX therapy is its poor ability to cross the blood–brain barrier (BBB) (*4*). Attempts have been made to improve transport of MTX across the BBB by (i) administering MTX directly into a brain tumor and (ii) osmotic BBB disruption techniques (*5–6*). Various macromolecules have been shown to localize in tumor cells in vivo and were suggested as possible carriers for MTX (*7–9*). A typical depot effect and prolonged plasma concentrations were demonstrated by Chu and Whiteley for MTX linked to albumin and dextran derivatives. Shen and Ryser (*10*) have reported an increased cellular uptake in vitro in MTX-resistant cells, using a poly(L-lysine)–MTX conjugate. Ghosh et al. (*11*) have reported an immunoglobin–MTX conjugate for targeting the drug to tumor-associated antigens. However, the use of drug–macromolecular conjugates as a vehicle for targeting drugs relies largely on the ability of the carrier to achieve either cell or organ specificity.

In recent years the concept of using small colloidal particles for the selective drug delivery has been explored using a variety of different physical systems, such as liposomes and polymeric microspheres or nanoparticles (*12–17*). Although the surface properties of the colloids may alter the systemic distribution, intravascular administration of such carriers results in their predominant uptake by the reticuloendothelial system.

Magnetic microspheres were therefore designed to avoid rapid reticuloendothelial clearance that is problematic for other particulate carriers (*18–19*). Magnetic microspheres are usually injected into the arterial supply of the target organ to take advantage of first-pass organ extraction. Because these spheres are 1 μm or smaller in diameter, they are able to pass through target capillaries, prior to systemic clearance. As the magnetic particles traverse the target organ capillaries, an external magnetic field can retain the particles in small arterioles and capillaries. Retained particles may undergo extravascular uptake which could ultimately lead to intracellular (i.e., tumor cell) drug uptake.

The original magnetic albumin microspheres contained approximately 1.0% (w/w) adriamycin. Widder et al. (*19*) were the first to demonstrate the utility of magnetic albumin microspheres (MM–ADR) in animal tumor models. Significantly greater responses, both in terms of tumor size and animal survival, were achieved with MM–ADR than adriamycin alone. Gupta et al. (*20*) demonstrated that the efficacy of magnetic microspheres in the targeted delivery of incorporated drug is predominantly due to the magnetic effects and not due to the particle's size or nonmagnetic holding. The ultrastructural disposition of adriamycin-associated magnetic albumin microspheres was also demonstrated in normal rats by Gupta et al. (*21*). The transmission electron micrographs showed extravascular transport of microspheres as early as 2 h after dosing and were observed and remained in the extravascular tissue for up to 72 h. Since the drug delivery device was retained in the vascular endothelium of the target tissue for up to 72 h,

---

it was suggested that the microspheres may act as a depot from which the drug is released.

The disposition of magnetic microsphere drug delivery systems with brain tumors has been a focus of our labooratory (*18*). It has been demonstrated in normal rats that a magnetic cationic polysaccharide microsphere system, containing the anticancer drug oxantrazole, significantly increased total brain oxantrazole concentration compared to a conventional administration of oxantrazole. However, in this system and other matrix microsphere devices, only a small percentage (1–2% w/w) of the drug is physically entrapped, and drug release may be fast possibly preventing significant quantities of drug from reaching tumor cells. Low drug entrapment may limit the optimal delivery of cytotoxic drugs due to the potentially large amounts of carrier required. On the contrary, if MTX is covalently attached to a magnetic carrier, then high drug loading may be achieved and drug release may be prolonged and controlled. The objectives of this investigation, therefore, were to synthesize magnetic microsphere (MM)–methotrexate (MTX) conjugated systems and analyze their suitability for in vivo use.

EXPERIMENTAL SECTION

Materials. Methotrexate was a gift from Lederle Laboratories (Pearl River, NY). 6-Amino-1-hexanol, *tert*-butyl alcohol, di-*tert*-butyl dicarbonate, 4-pyrrolidinopyridine (4-PP), dicyclohexylcarbodiimide (DCC), 4-(dimethylamino)pyridine (4-DMAP), and hydrochloric acid (anhydrous) were obtained from Aldrich Co. (Milwaukee, WI). 1-Ethyl-3-[3-(dimethylamino)propyl]carbodiimide (EDCI), ammonium hydroxide, ferrous chloride, and ferric chloride were obtained from Sigma Chemicals (St. Louis, MO). Poly(ethylene glycol) 1500 was purchased from Scientific Polymer Products, Inc. (Atlanta, GA). Spectrapor cellulose dialysis tubing (MW cutoff 1000) was obtained from Fisher Scientific (Atlanta, GA). Carboxyl-terminated biomag 4125 and amine-terminated biomag 4100 were purchased from Advanced Magnetics, Inc. (Cambridge, MA). All analytical-grade reagents and HPLC-grade solvents were obtained from J. T. Baker, Inc. (Phillipsburg, NJ).

Equipment. An electromagnet was purchased from Applied Magnetics Laboratory (Baltimore, MD). The ultrasonic water bath was a Bransonic 220 (Danbury, CT); the ultrasonic probe was a Branson sonifier (Westbury, NY). A Model 110S microfluidizer obtained from Microfluidics International Corp. (Newton, MA) was used to reduce the particle size. A Nicomp submicron particle sizer model 370 (Santa Barbara, CA) was used for particle size determinations. Ultraviolet spectra and infrared scans were obtained with a Beckman Model DU-70 spectrophotometer (Fullerton, CA) and a Nicolet 205 FT-IR spectrometer (Norwalk, CT), respectively. The HPLC system consisted of a Waters (Milford, MA) 717 pump, Lambda Max 486 variable wavelength detector, and an Alltech (Deerfield, IL) Hypersil C_{18} reversed-phase column.

Synthesis of Magnetic Microsphere–Methotrexate Conjugate (MM–MTX) Drug Delivery Systems. *Method I: Synthesis of MM–MTX I. Step I: Synthesis of Poly(ethylene glycol) 1500–Methotrexate Conjugates (PEG–MTX).* PEG–MTX conjugates were synthesized in a biphasic reaction by mixing 10 mL of poly(ethylene glycol) 1500 (50% w/w) with 8 mL of methotrexate solution (10 mg/mL) in the presence of EDCI (17.5 mg/mL) dissolved in 4 mL of PBS. The reaction mixture was stirred for 3 h at room temperature and stored overnight at 4 °C. The product was purified by dialysis using deionized distilled water (2000 mL exchanged every 12

h) for 24 h and then lyophilized and stored in a desiccator. The above procedure was repeated without adding EDCI to the reaction mixture.

Step II: Preparation of MM–MTX I Conjugates. MM–MTX I conjugates were prepared by mixing 15 mL of PEG–MTX conjugate (500 mg) with 2 mL of an aqueous solution containing 300 mg of ferric chloride and 120 mg of ferrous chloride. While stirring, the mixture was adjusted to pH 8.0–8.5 by the dropwise addition of 30% (w/v) aqueous ammonia solution. After the reaction the resulting magnetic material was kept under the electromagnet and was washed four times with 25 mL of water and then dried under nitrogen gas at room temperature. The product was then stored in a desiccator until further use.

Method II: Synthesis of MM–MTX II. Step I: Preparation of Ferromagnetic Polymer Complex. Ferromagnetic polymer complex was prepared by mixing 10 mL of 50% (w/w) poly(ethylene glycol) 1500 with 2.5 mL of an aqueous solution containing 375 mg of ferric chloride and 150 mg of ferrous chloride. This mixture was stirred at 500 rpm, the pH adjusted to 8.0–8.5 by the dropwise addition of 30% (w/v) aqueous ammonia solution, and the mixture heated to 60 °C for 10 min to remove excess ammonia. The resultant ferromagnetic polymer complex was washed four times with 50 mL of water, being separated by a magnet after each wash. The resultant ferromagnetic polymer complex was sonicated for 2 min at 200 W with an ultrasonic probe and then passed through a microfluidizer for 3 min to reduce the particle size. The ferromagnetic polymer complex was readily separated from the colloidal solution in a magnetic field of 6000 G in 2–5 min. It was washed four times with 50 mL of water, being separated by a magnet after each wash. The resultant magnetic colloid was lyophilized and then stored in a desiccator.

Step II: Chemical Modification of Methotrexate with the Ferromagnetic Polymer Complex. MM–MTX II conjugate was prepared by reacting 6 mL of a methotrexate solution (10 mg/mL) in the presence of EDCI (15 mg/mL) dissolved in 4 mL of phosphate-buffered saline, pH 7.4 (PBS), with 2 mL of ferromagnetic polymer complex (22.5 mg/mL in PBS) prepared as described in step I. The reaction mixture was sonicated in a water bath at room temperature for 10 min to yield a homogeneous system. The mixture was stirred for 3 h at room temperature and stored overnight at 4 °C and then purified by dialysis using deionized distilled water (2000 mL exchanged every 12 h) for 24 h. Following dialysis, the contents of the dialysis bag were centrifuged at 2000 rpm for 7 min, and the supernatant was decanted. The pellet, representing MM–MTX II, was washed four times with 50 mL of water and then dried under nitrogen at room temperature and stored in a desiccator. The above procedure was repeated without adding EDCI to the reaction mixture.

Method IIIA: Synthesis of MM–MTX IIIA. Amine-terminated magnetic microspheres [about 240 μmol of amine groups per gram of microsphere (MM′)] were supplied in distilled water at a concentration of 50 mg/mL. One milliliter of MM′ was transferred to a scintillation vial, 10 mL of pyridine buffer (pyridine buffer was prepared by dissolving 0.8 mL of pyridine in 1 L of water and adjusted to pH 6.0 with hydrochloric acid) was added, and the contents were shaken vigorously. The vial was kept under an electromagnet with a field of 6000 G and the contents were aspirated, leaving the microspheres as a wet cake on the container wall. This washing procedure was repeated with three more additions of coupling buffer.

MM–MTX IIIA was synthesized in a biphasic reaction by mixing 2 mL of MTX solution (8 mg/mL in PBS) in the presence of EDCI (40 mg) dissolved in 5 mL of coupling buffer with 1 mL of MM' (10 mg/mL). The reaction mixture was sonicated in a water bath at room temperature for 5 min to yield a homogeneous system and then stirred at 475 rpm for 3 h, respectively. The reaction mixture was kept under the electromagnet to separate the MM–MTX IIIA. The unreacted MTX was aspirated, and 15 mL of wash buffer (prepared by dissolving 1.21 g of Tris, 8.7 g of sodium chloride, 1 g of bovine serum albumin, 1 g of sodium azide, and 0.37 g of ethylenediaminetetraacetic acid in 1 L of water, adjusted the pH to 7.4) was added to the MM–MTX IIIA. The contents were shaken vigorously and separated magnetically, and the unreacted drug was aspirated. This washing procedure was repeated for a total of three times prior to the storage of MM–MTX IIIA as a suspension in 10 mL of wash buffer at 4 °C.

Method IIIB: Synthesis of MM–MTX IIIB. Step I: *Preparation of N-(tert-Btuoxycarbonyl)-6-amino-1-hexanol (t-Boc-AH).* In a 1 L round-bottomed flask containing sodium hydroxide (4.4 g) in 110 mL of water was added 10 g of 6-amino-1-hexanol while the mixture was stirred at ambient temperature, and the resulting mixture was then diluted with 75 mL of *tert*-butyl alcohol. To the well-stirred clear solution, 22.5 g of di-*tert*-butyl dicarbonate was added dropwise within 10 min. A white precipitate appeared during addition of the di-*tert*-butyl dicarbonate. After a short induction period, the temperature increased to 30–35 °C. The reaction was brought to completion by further stirring overnight at room temperature. At this time, the clear solution reached a pH of 7.5–8.5. The reaction mixture was extracted two times with 50 mL of ether followed by three extractions of the combined ether phases with 100 mL of saturated aqueous sodium bicarbonate solution. The combined aqueous layers were acidified to pH 1–1.5 by careful addition of a solution of 22.5 g of potassium hydrogen sulfate in 150 mL of water. The acidification was accompanied by copious evolution of carbon dioxide. The turbid reaction mixture was then extracted with two 50 mL portions of ether. The combined organic layers were washed with 25 mL of water, dried over anhydrous sodium sulfate, and filtered. The solvent was removed under reduced pressure using a rotary evaporator. The yellowish oil that remained was treated with 150 mL of hexane and placed in a freezer (−20 °C) overnight. A white precipitate was obtained from the yellow oil by collection on a Buchner funnel.

Step II: Direct Esterification of t-Boc-AH with Methotrexate. A 100 mL flask was charged with 80 mg of MTX in 5 mL of dimethylformamide (DMF), 217 mg of *t*-Boc-AH, and 50 mg of 4-pyrrolidinopyridine. The solution was stirred and cooled in an ice bath to 0 °C while 133 mg of dicyclohexylcarbodiimide was added over a 5 min period. After a further 5 min at 0 °C the ice bath was removed and the reaction mixture was stirred for 24 h at room temperature. Dicyclohexylurea which had precipitated was removed by filtration through a fritted Buchner funnel, and the filtrate was diluted with 50 mL of methylene chloride. The filtrate was then washed with two 25 mL portions of 0.5 N hydrochloric acid and two 25-mL portions of saturated sodium chloride solution. During this procedure some additional dicyclohexyl urea was precipitated, which was removed by filtration of both layers to facilitate their separation. The organic solution was dried over anhydrous sodium sulfate and concentrated with a rotary evaporator. The concentrate was distilled under reduced pressure to give *t*-Boc-AH–MTX.

Step III: Removal of t-Boc Group from t-Boc-AH–MTX.

A solution of *t*-Boc-AH–MTX (50 mg) in 10 mL of methylene chloride, cooled to 0 °C, was saturated with hydrogen chloride by passing the anhydrous gas through the solution with stirring for 20 min. The turbid reaction mixture was left for an additional 1 h at room temperature to precipitate a light-brown crystalline product, AH–MTX·HCl, that was removed by filtration.

Step IV: Free Ester. AH–MTX·HCl (30 mg) was dissolved in 5 mL of DMF at 0 °C, and 0.5 mL of anhydrous triethylamine was added in small portions. The mixture was stirred for 20 min at 0 °C and filtered to remove triethylamine·HCl. The product, AH–MTX, was precipitated with 50 mL of diethyl ether, filtered, washed extensively with water, and dried.

Step V: Synthesis of MM–MTX IIIB. Carboxyl-terminated magnetic microspheres (Biomag 4125) were supplied in distilled water at a concentration of approximately 20 mg/mL and have about 4.8 μmol of carboxyl groups per mL (240 μmol/g of biomag). One mL of the magnetic microspheres (MM) was transferred to a 20 mL scintillation vial, to which 10 mL of PBS was added, and the contents were shaken vigorously. The vial was placed between the poles of an electromagnet (6000 G) and the liquid aspirated, leaving the MM as a wet cake on the container wall. This washing procedure was repeated with three more additions of 10 mL of PBS. MM–MTX IIIB was prepared by reacting 1 mL of MM (20 mg/mL) in the presence of EDCI (40 mg) and 4-(dimethylamino)pyridine (10 mg, 4-DMAP) dissolved in 3 mL of water with 3 mL of AH–MTX solution (10 mg). The reaction mixture was sonicated in a water bath at room temperature for 5 min to yield a homogeneous system and then stirred for 3 h at ambient temperature. After 3 h, the reaction mixture was placed in the electromagnet and the MM–MTX IIIB was separated magnetically. The unreacted MTX was aspirated, and 15 mL of wash buffer was added to the MM–MTX IIIB. The contents were shaken vigorously, separated magnetically, and the unreacted drug was aspirated. This washing procedure was repeated for a total of three times. The supernatants collected from each washing step were analyzed for MTX content using HPLC. The MM–MTX IIIB was stored as a suspension in 10 mL of wash buffer at 4 °C.

Characterization of MTX Conjugates. The identity of the conjugates was confirmed using thin-layer chromatography (TLC), ultraviolet (UV), infrared (IR), and nuclear magnetic resonance (NMR) spectroscopy in combination with the control reaction, conducted in the absence of the cross-linking agent, EDCI.

Thin Layer Chromatography. Precoated silica gel plates in saturated chambers were used with the solvent system methanol/acetone/ethyl acetate (10:10:1). Absorption was observed at 254 and 366 nm. A ninhydrin spray reagent was used for the detection of free amino groups in AH–MTX conjugates.

UV Spectroscopy. UV spectra of PEG, *t*-Boc-AH, MTX, and its conjugates were recorded in PBS/methanol between 200 and 400 nm.

IR Spectroscopy. IR spectra of PEG, MTX, magnetite, ferromagnetic polymer complex, PEG–MTX, *t*-Boc-AH, *t*-Boc-AH–MTX, AH–MTX conjugates, MM–MTX (I and II) conjugates, a physical mixture of PEG and MTX, a physical mixture of ferromagnetic polymer complex and MTX, a physical mixture of PEG–MTX conjugates and magnetite, were recorded using potassium bromide (KBr) disks. KBr disks were prepared by grinding a sample (2 mg) with KBr powder (210 mg), placing the mixture between a punch and die, and applying a pressure of about 50 000 psi.

PEG (KBr): 3432, 2880, 1653, 1456, 1352, 1252, 1105, 951, 841, 581 cm^{-1}.

MTX (KBr): 3357, 1647, 1605, 1541, 1507, 1449, 1404, 1368, 1254, 1209, 1101, 941, 833, 768, 745, 581 cm^{-1}.

Ferromagnetic polymer complex (KBr): 3430, 2917, 1653, 1558, 1509, 1456, 1400, 1352, 1300, 1252, 1100, 951, 590 cm^{-1}.

PEG−MTX conjugate (KBr): 3420, 2888, 2741, 2695, 1968, 1468, 1458, 1414, 1359, 1344, 1281, 1242, 1150, 1117, 1061, 964, 947, 843, 530, 509 cm^{-1}.

MM−MTX I (KBr): 3144, 1404, 1111, 949, 843, 583 cm^{-1}.

MM−MTX II (KBr): 3436, 1636, 1559, 1507, 1457, 1208, 1090, 577 cm^{-1}.

t-Boc-AH (KBr): 3450, 3368, 3100, 2935, 2850, 1685, 1523, 1350, 1300, 1250, 1173, 1050, 1000, 600 cm^{-1}.

t-Boc-AH-MTX (KBr): 3450, 3350, 3200, 2950, 2800, 1701, 1650, 1600, 1550, 1525, 1450, 1350, 1250, 1200, 1150, 1100, 850, 800 cm^{-1}.

AH−MTX (KBr): 3400, 3150, 2950, 2850, 1729, 1649, 1600, 1550, 1500, 1400, 1200 cm^{-1}.

NMR Spectroscopy. ^{1}H NMR spectra of *t*-Boc-AH (CDCl$_3$), *t*-Boc-AH−MTX, and AH−MTX·HCl [10% (^{2}H$_6$) DMSO] were recorded with a General Electric QE 300 MHz spectrometer.

t-Boc-AH (^{1}H-NMR, CDCl$_3$): δ 1.4 ppm (s, 9H, −C(CH$_3$)$_3$), 1.2−1.6 (m, 8H, 4 CH$_2$ groups), 2.4 (s, 1H, NH), 3.1 (m, 2H, −CH$_2$*CH*$_2$NH−), 3.6 (t, 2H, −CH$_2$*CH*$_2$-OH), 4.7 (b, 1H, OH).

t-Boc-AH−MTX (^{1}H-NMR, DMSO-d_6): δ 1.3 ppm (s, 9H, −C(CH$_3$)$_3$), 1.2−1.8 (m, 8H, CH$_2$ groups at positions 2−5 of hexane moiety), 1.9−2.3 (m, 4H, −CH$_2$CH$_2$− of glutamate), 3.2 (s, 3H, N^{10}CH$_3$ of MTX), 3.9−4.0 (m, 2H, −*CH*$_2$OOC−), 3.8 (b, 1H, −CH$_2$*NH*COO−), 4.8 (s, 2H, CH$_2$ at position 9 of MTX), 6.6 (b, 2H, 2 or 4 NH$_2$ of MTX), 6.7−6.9 (m, 2H, aromatic protons of MTX), 7.4−7.5 (b, 2H, 2 or 4 NH$_2$ of MTX), 7.6−7.7 (m, 2H, aromatic protons of MTX), 8.1−8.2 (b, 1H, −CO*NH* of glutamate), 8.6 (s, 1H, CH at position 7 of MTX), 10.7 (s, −COO*H*).

AH−MTX (^{1}H-NMR, DMSO-d_6): It is essential identical to *t*-Boc-AH−MTX but without the characteristic peak at δ 1.3 ppm for the *tert*-butyl group (*t*-Boc).

Particle Size. The size distribution of the MM−MTX conjugates (I−III) were determined with a submicron particle sizer at 23 °C assuming the viscosity and refractive index to be 0.933 centipoise and 1.333, respectively. About 2 mg of the conjugate was suspended in 1 mL of PBS and sonicated in an ultrasonic water bath for 2 min to prevent the formation of aggregates and then introduced into the particle sizer with an autodiluter. Two types of particle size analyses, a Gaussian or nicomp, were conducted and expressed as the volume-weighted distribution of particle diameters. Unlike the Gaussian analysis, the proprietary (nicomp) distribution analysis does not assume any particular shape for the particle size distribution.

Drug Loading. MM−MTX conjugate (I−III, 4 mg) was suspended in 10 mL of PBS and sonicated in an ultrasonic water bath for 2 min. The contents were shaken vigorously and separated magnetically, and then the PBS was aspirated leaving the conjugate as a wet cake on the container wall. The washing procedure was repeated with two more additions of PBS. After the final wash, the conjugate was digested in 10 mL of 0.02 N NaOH for 3 h at 50 °C to release MTX and then centrifuged at 10 000 rpm for 10 min. An aliquot of the supernatant was analyzed by HPLC for MTX. Chromatographic separation was achieved using a flow rate of 1.5 mL/min on an Alltech Hypersil ODS C$_{18}$ reversed-phase column with a mobile phase consisting of 20% (v/

v) methanol in water with 40 mM dibasic potassium phosphate, pH 7.0. UV detection was made at 313 nm.

***In Vitro* Release Study.** The release of MTX from MM−MTX conjugates was monitored for 24 h in various test media (pH 7.4 buffer, pH 5.6 citrate buffer, rat plasma, and brain homogenate) at 37 °C. The conjugates (4 mg) were suspended in 2 mL of the test medium and sonicated on an ultrasonic water bath for about 2 min to yield a homogeneous system. The microspheres were placed in the test medium within dialysis tubing and dialyzed against 100 mL of PBS. Aliquots of PBS were collected periodically and analyzed for MTX using HPLC as described above.

RESULTS AND DISCUSSION

Fine ferromagnetic particles have been coated with poly(ethylene glycol) (*22*)/amino or carboxyl groups to permit the covalent attachment of proteins, glycoproteins, and other ligands with the retention of biological activity. Ferromagnetic particles have also been used for various in vivo applications such as a tracer of blood flow, in radioneuclide angiography, and for use in inducing clotting in arteriovenous malformations. Zimmermann and Pilwat (*23*) were the first ones to propose that erythrocytes or lymphocytes containing fine ferromagnetic particles could be propelled to a desired site by an external magnetic field. It was demonstrated by Freeman et al. (*24*) that iron particles could pass through capillaries when properly conditioned and later confirmed by Meyers et al. (*25*) who showed that iron particles could be magnetically controlled in the vascular system of experimental animals.

There have been no previous investigations to examine the ability of magnetic microspheres to deliver drugs to brain tumors; however, there have been two investigations in normal rats (*18, 26*). Following administration of magnetic microspheres containing oxantraxole, the brain contained 100−400 times higher oxantrazole levels than those obtained after the solution dosage form, indicating the successfulness of drug delivery via magnetic microspheres. It was evident from these studies that under the proper conditions, magnetic microspheres were capable of enhancing total brain concentrations.

Coupling MTX to a carrier must not result in permanent loss of structural features required for drug activity (e.g., an intact pteridine moiety). For this reason, logical linkage groups are the free carboxyl groups of the glutamate moiety and amino groups of the linker. The unusually high affinity of MTX for dihydrogen folate reductase (DHFR) depends upon its pteridine moiety with an amino group in position 4 (*27*). The glutamate residue at the opposite end of the molecule has been modified to some extent without seriously impairing this strong interaction (*28–31*). Przybylski et al. (*32*) described the synthesis of polymeric [poly(L-lysine), poly(iminoethylene), poly(vinyl alcohol), and carboxymethyl cellulose] derivatives of MTX and were characterized by thin layer chromatography, UV, IR, and NMR spectra. Yeshwant et al. (*33*) described the synthesis and characterization (UV, IR, and control reaction, in the absence of cross-linking agent EDCI) of an chitosan−MTX conjugate designed specifically to interact with the vascular endothelium and cross the BBB.

The simplest way of coupling MTX to a free hydroxyl/amino group of a carrier molecule would be through nonselective activation of the carboxyl groups in its glutamic acid moiety by the carbodiimide method. This method may lead to formation of two structural isomers, in which MTX is linked either through the α-carboxyl or the γ-carboxyl group of its glutamic acid moiety (*34, 35*).
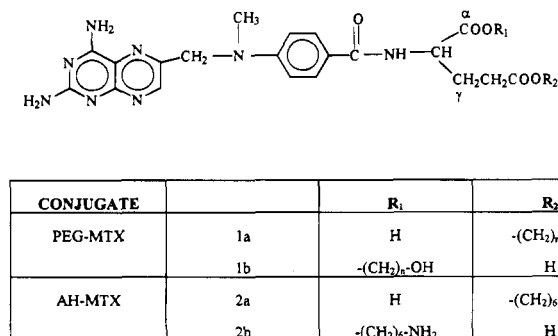
Figure 1. Structures of PEG–MTX and AH–MTX conjugates.

CONJUGATE		R₁	R₂
PEG-MTX	1a	H	-(CH₂)ₙ-OH
	1b	-(CH₂)ₙ-OH	H
AH-MTX	2a	H	-(CH₂)₆-NH₂
	2b	-(CH₂)₆-NH₂	H

Synthesis of MM–MTX I and II was attempted to obtain a small magnetic colloid that had a high drug loading and controllable release rate of drug. In both methods I and II, the reaction of ferrous (Fe^{2+}) and ferric (Fe^{3+}) ions at pH 8.0–8.5 in the presence of PEG–MTX or PEG yielded a colloidal solution of PEG–MTX or PEG-coated ferromagnetite. This adsorption may be attributed to the formation of a complex between the hydroxyl group of PEG–MTX/PEG and iron on the magnetite particles. Cross-linking between the carboxyl group (α or γ) of MTX and the hydroxyl group of PEG or PEG-coated magnetite particles using a water soluble carbodiimide could result in the formation of esters 1a or 1b (*34, 35*) (see Figure 1).

In order to simplify the synthetic procedure of producing magnetic particles, commercially available amino or carboxyl-terminated magnetic microspheres were utilized in method III (A and B). Initially, direct covalent linkage (by the EDCI method) between MTX and magnetic microspheres coated with amino groups, MM′, was attempted (MM–MTX IIIA). That this method yielded a covalent conjugate (MM–MTX IIIA) was confirmed with the control reaction, conducted in the absence of the cross-linking agent, EDCI. The MTX content of MM–MTX IIIA as determined by HPLC was found to be 4.29% (0.5 h), 5.14% (1 h), 7.19% (2 h), 8.5% (3 h), and 6.3% (17 h) depending on the reaction time. However, when MM–MTX IIIA was digested in 0.02 N NaOH for 24 h at 50 °C, only a small amount of MTX was released and suggested that the inability to cleave the amide linkage between MTX and MM′ under basic conditions would possibly lead to low drug release rates in vivo and ultimately minimal tumor cell cytotoxicity. In order to overcome this problem (viz. MM–MTX IIIB), a spacer molecule was used between MTX and carboxyl-terminated magnetic microspheres, MM, to increase the lability by formation of an accessible ester linkage. 6-Amino-1-hexanol (AH) was chosen as a spacer to link MTX and MM, since it has both amino and hydroxy groups besides having an elongated hydrocarbon chain.

Prior to the esterification of AH with MTX, the amino group was protected as a *t*-Boc derivative using di-*tert*-butyl dicarbonate (*36*) (method IIIB, step I). Di-*tert*-butyl dicarbonate is a highly reactive and safe reagent of the "ready-to-use" type which reacts under mild conditions with amino acids, peptides, hydrazine and its derivatives, amines, and CH-acidic compounds in aqueous organic solvent mixtures to form pure derivatives in very good yields (*37, 38*).

The nonspecific activation of the α- or γ-carboxyl groups in MTX by DCC may lead to formation of two structural isomers, **2a** or **2b** (see Figure 1). The reaction (method IIIB, step II) is based on both DCC and 4-pyrrolidinopyridine catalyst. This reaction was applied to a wide variety of acids and alcohols, including polyols
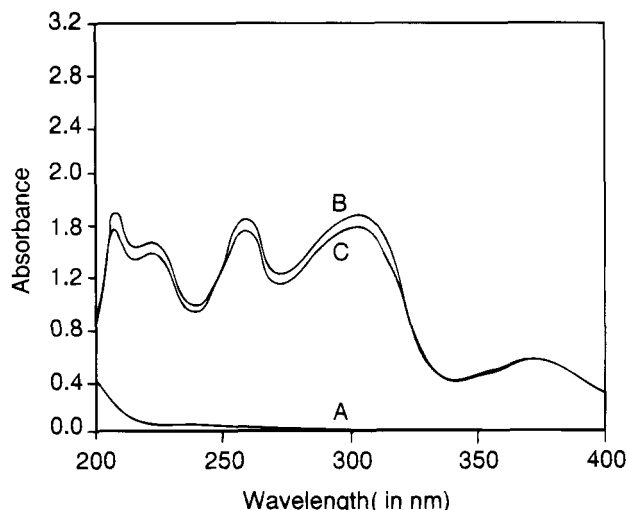
Figure 2. UV absorption spectra of (A) PEG, (B) MTX, and (C) PEG–MTX conjugate in phosphate-buffered saline (PBS).

(*39*), α-hydroxy carboxylic acid esters (*40*), and even very acid labile alcohols like vitamin A. It has also been used for the esterification of urethane-protected α-amino acids with polymeric supports carrying hydroxy groups (*41*). It was also shown by Hassner et al. (*42*) that in the absence of 4-pyrrolidinopyridine, phenyl benzoate was formed in 10% instead of 94% yield, whereas in the absence of DCC no reaction occurs.

The marked lability of *tert*-butyl esters toward anhydrous acids permits the facile cleavage of the carbo-*tert*-butoxy group in the *t*-Boc-AH–MTX (method IIIB, step II). Treatment of a methylene chloride solution of *t*-Boc-AH–MTX with anhydrous hydrogen chloride at 0 °C liberated the amino group to give AH–MTX·HCl (method IIIB, step III).

The UV spectra of PEG, MTX, and PEG–MTX in PBS are shown in Figure 2. The spectra were found to be identical, while PEG itself showed no UV absorption in this range. Since all free MTX had been previously removed by extensive dialysis, only MTX linked to PEG would lead to the identical spectra. The comparison of the UV spectra of MTX with *t*-Boc-AH–MTX and AH–MTX conjugates in methanol showed identical maxima with λ_{max} at 208, 260, and 306 nm (Figure 3). Since no free MTX could be detected on thin-layer chromatography, only MTX conjugated to *t*-Boc-AH would lead to an identical spectrum.

IR spectra were used to establish that the MM–MTX (I and II) conjugates were chemically distinct from a physical mixture of PEG and MTX and of PEG–MTX and magnetite. Computer additions of the individual spectra of PEG and MTX were found to be identical to a physical mixture of PEG and MTX but different from the PEG–MTX conjugate scan. IR spectra of a physical mixture of PEG–MTX and magnetite were found to be identical with the computer additions of the individual spectra of PEG–MTX conjugates and magnetite but different from the MM–MTX conjugate scan. Computer additions of the individual spectra of ferromagnetic polymer complex and MTX were found to be identical to a physical mixture of ferromagnetic polymer complex and MTX but different from the MM–MTX conjugate scan. The synthetic reaction conducted in the absence of EDCI did not yield a stable conjugate but rather a mixture from which MTX was rapidly dialyzed into the bulk PBS. This fact along with the spectroscopic evidence established that the conjugates were chemically different.

The bands at 1701 cm^{-1} and 1729 cm^{-1} in the IR spectra of *t*-Boc-AH–MTX and AH–MTX were attributed
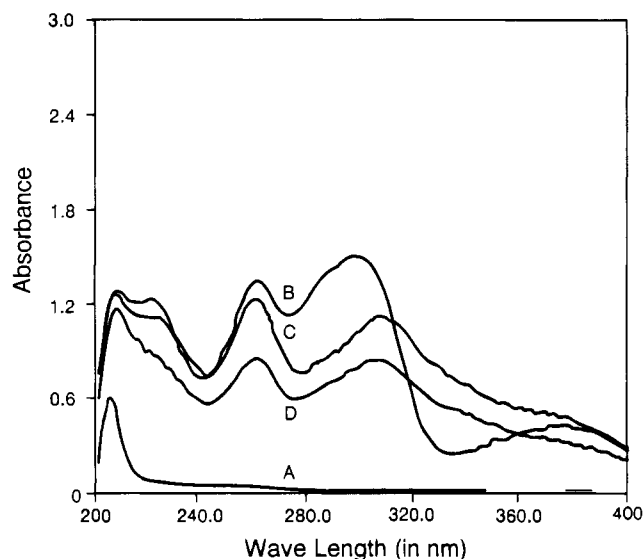
Figure 3. UV absorption spectra of (A) *t*-Boc-AH, (B) MTX, (C) *t*-Boc-AH–MTX conjugate, and (D) AH–MTX conjugate in methanol.

Figure 4. Release of methotrexate from magnetic microsphere–methotrexate delivery system (MM–MTX I) in (O) PBS, (▲) pH 5.6 citrate buffer, and (■) rat plasma.

Figure 5. Release of methotrexate from magnetic microsphere–methotrexate delivery system (MM–MTX II) in (O) PBS, (◆) pH 5.6 citrate buffer, and (●) rat plasma.

to an ester linkage formed during the reaction of the glutamic acid moiety of MTX with the hydroxyl group of *t*-Boc-AH. The proton NMR spectrum of *t*-Boc-AH, *t*-Boc-AH–MTX had a characteristic singlet at δ 1.4 ppm corresponding to the *tert*-butyl group of *t*-Boc. After the deprotection step (method IIIB, step III), this singlet was absent in the proton NMR spectrum of AH–MTX indicating the removal of *t*-Boc group from AH–MTX conjugate. The synthetic reaction (method IIIB, step V) conducted in the absence of EDCI and 4-(dimethylamino)-pyridine (4-DMAP) did not yield a stable conjugate but rather a mixture, from which MTX was rapidly washed away. Thus, the formation of a covalent linkage between magnetite–COOH and AH–MTX when reacted in the presence of EDCI and 4-DMAP was established from the control reaction.

Table 1 shows the mean diameter, MTX content of MM–MTX (I, II, and IIIB) and percent of MTX released in various test media over a 24 h p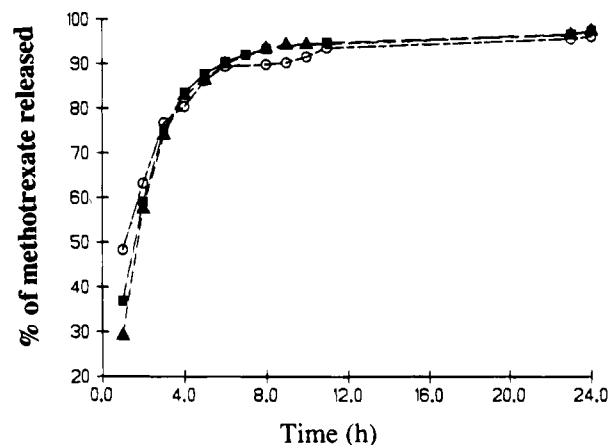eriod. Laser light-scattering particle size analyses indicated the mean diameter to be 700 ± 50 nm (MM–MTX I), 580 ± 40 nm (MM–MTX II) and 808.1 ± 39.4 nm (MM–MTX IIIB). MTX content of MM–MTX as determined by HPLC was 0.45% (w/w), 4.0% (w/w), and 6.3% (w/w) for methods I, II, and IIIB, respectively. The lower MTX content obtained in method I compared to methods II and III may be ascribed to the plausible hydrolysis of the base-sensitive ester linkage in PEG–MTX during the preparation of MM–MTX I conjugate (step II, method I).

Figures 4–6 show the percentage of MTX released as a function of time from MM–MTX suspended in various test media. Dynamic dialysis studies in PBS, pH 5.6 citrate buffer and rat plasma over a 24 h period revealed that MTX was released to an extent of about 97% (w/w) from MM–MTX I and 69% (w/w) from MM–MTX II. The

lack of significant differences in the release of MTX from MM–MTX (I and II) amongst the test media suggests that the drug may be released by hydrolysis rather than by enzymatic degradation. In vitro studies of MM–MTX IIIB in PBS, rat plasma, and brain homogenate revealed that 0% (w/w) (PBS), 11% (w/w) (rat plasma), and 3.2% (w/w) (brain homogenate) of MTX was released from MM–MTX IIIB over a 24 h period. The significant differences in release of MTX in the various test media suggest that the drug was released by enzymatic hydrolysis. The low percentage of MTX released from MM–MTX IIIB in plasma and brain homogenate may be an advantage to maintain MTX concentrations in brain tumors via the MM–MTX IIIB system. Assuming cytotoxicity is determined by free MTX, then hydrolysis of the MM–MTX IIIB conjugate in brain tumors and specifically within tumors cells is requisite for anticancer activity.

When compared to magnetic microsphere systems in which a drug is physically entrapped (*43, 44*), MM–MTX

Table 1. Characteristics of MM–MTX Conjugates Prepared by Methods I–IIIB

MM–MTX conjugate	method I	method II	method IIIB
mean diameter (nm)	700 ± 50	580 ± 40	808 ± 39
% drug loading (w/w)	0.45 ± 0.2	4.0 ± 0.9	6.3 ± 2.1
% of MTX released in PBS at 24 h	92.7	69	*a*
% of MTX released in pH 5.6 citrate buffer at 24 h	95.2	72.1	
% of MTX released in rat plasma at 24 h	97	74.2	11
% of MTX released in brain homogenate at 24 h			3.2

a Below the limit of assay sensitivity.
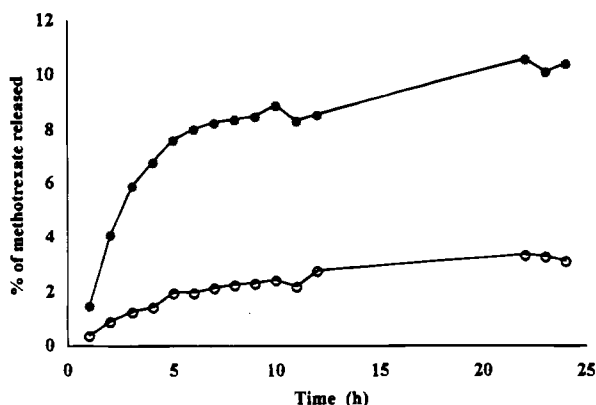
Figure 6. Release of methotrexate from magnetic microsphere—methotrexate delivery system (MM—MTX IIIB) in (●) rat plasma and (○) brain homogenate.

conjugates were found to have equal or smaller particle sizes. The drug loading of MM—MTX I conjugate was approximately the same as traditional microsphere systems, and the release of MTX was fast from the conjugates (MM—MTX I and II) and hence did not meet our initial objective. However, the MTX content of MM—MTX IIIB was approximately 50% higher than that obtained with MM—MTX II conjugate and released MTX markedly slower than typically observed with magnetic microspheres in which a drug is physically entrapped (*45, 46*). The conjugation approach may allow for greater verstality in magnetic drug delivery system design through the use of different linker molecules. On the basis of the desirable properties of MM—MTX IIIB, further investigations were recently conducted in brain tumor bearing rats (*47*).

LITERATURE CITED

(1) Allen, J. C., Walker, R., and Rosen, G. (1988) Preradiation high-dose intravenous methotrexate with leucovorin rescue for untreated primary childhood brain tumors. *J. Clin. Oncol. 6*, 649—653.

(2) Djerassi, I., Kim, J. S., Kassarov, L., et al. (1988) High dose methotrexate with citrovorum factor in astrocytoma. *Proc. Am. Soc. Clin. Oncol. 7*, 82.

(3) Martino, R. L., Benson, A. B., Merritt, J. A., et al. (1984) Transient neurologic dysfunction following moderate-dose methotrexate for undifferentiated lymphoma. *Cancer 54*, 2003—5.

(4) Gummerlock, M. K., and Neuwelt, E. A. (1987) In *Therapy of malignant brain tumors* (K. Jellinger, Ed.) pp 277—348, Springer-Verlag Wien, New York.

(5) Allen, J. C., Shapiro, W., Mehra, B., et al. (1981) Hyperosmolar intracarotid mannitol increases capillary permeability to methotrexate in brain adjacent to tumor. *Ann. Neurol. 10*, 293.

(6) Ringjob, R. (1968) Treatment of intracranial gliomas and metastatic carcinomas by local application of cytostatic agents. *Acta Neurol. Scand. 44*, 318—322.

(7) Harding, N. G. L. (1971) Amethopterin linked covalently to water-soluble macromolecules. *Ann. N. Y. Acad. Sci. 186*, 270.

(8) Chu, B., and Whiteley, J. M. (1977) High molecular weight derivatives of methotrexate as chemotherapeutic agents. *Mol. Pharmacol. 13*, 80.

(9) Slavik, K., Bures, L., Svihovcoca, P., et al. (1985) The use of protein as a carrier of methotrexate for experimental cancer chemotherapy. *Neoplasma 32*, 415.

(10) Shen, W. C., and Ryser, J.-P. H. (1979) Poly (L-lysine) and poly (D-lysine) conjugates of methotrexate: Different inhibitory effect on drug resistant cells. *Mol. Pharmacol. 16*, 614—622.

(11) Ghosh, M. K., Kilsig, D. O., and Mitra, A. K. (1989) Preparation and characterization of methotrexate—immunoglobulin conjugates. *Drug. Des. Deliv. 4*, 13—25.

(12) Fung, W. P., Przybyslki, M., and Ringsdorf, M. (1979) In vitro inhibitory effects of polymer-linked methotrexate derivatives on tetrahydrofolate dehydrogenase and murine L5178Y cells. *J. Nat. Cancer Inst. 62*, 1261—1264.

(13) Gregoriadis, G. (1977) Targeting of drugs. *Nature 265*, 407—411.

(14) Gregoriadis, G., Ed. (1979) *Drug carriers in biology and medicine*, Academic Press, London.

(15) Gregoriadis, G., Swain, C. P., Willis, E. J., et al. (1974) Drug-carrier potential of liposomes in cancer chemotherapy. *Lancet 1*, 1313—1316.

(16) Kramer, P. A. (1974) Albumin microspheres as vehicles for achieving specificity in drug delivery. *J. Pharm. Sci. 63*, 1646—1647.

(17) Hashida, M., Muranishi, S., Sezaki, H., et al. (1979) Increased lymphatic delivery of bleomycin by microspheres in oil emulsion and its effect on lymp node metastasis. *Inter. J. Pharm. 2*, 245—256.

(18) Hassan, E. E., and Gallo, J. M. (1993) Targeting anticancer drugs to the brain. I: Enhanced brain delivery of oxantrazole following administration in magnetic chitosan microspheres. *J. Drug Targeting 1*, 7—14.

(19) Widder, K. J., Senyei, A. E., and Scarpelli, D. G. (1978) Magnetic microspheres. A model system for site specific drug delivery in vivo. *Proc. Soc. Exp. Biol. Med. 58*, 141—146.

(20) Gupta, P. K., and Hung, C. T. (1990) Comparative disposition of adriamycin delivered via magnetic albumin microspheres in presence and absence of magnetic field in rats. *Life Sci. 46*, 471—479.

(21) Gupta, P. K., and Hung, C. T., and Rao, N. S. (1989) Ultrastructural disposition of adriamycin-associated magnetic albumin microspheres in rats. *J. Pharm. Sci. 78*, 290—294.

(22) Takahashi, K., Tamaura, Y., Kodera, Y., et al. (1987) Magnetic lipase active in organic solvents. *Biochem. Biophys. Res. Commun. 142*, 291—296.

(23) German patent application, KFA Julich, filed Dec 23, 1976. Inventors: Zimmermann, U., Pilwat, G., Bock, K., and Buers, H. J. German patent no. 26 56 317; British patent no. 1 560 166.

(24) Freeman, M. W., Arrott, A., and Watson, J. H. (1960) Magnetism in medicine. *J. Appl. Phys. 31*, 404S.

(25) Meyers, P. H., Cronic, F., and Nice, C. M. (1963) Experimental approach in the use and magnetic control of metallic iron particles in the lymphatic and vascular system of dogs as a contrast and isotopic agent. *Amer. J. Roentgen. 90*, 1068—1077.

(26) Ovadia, H., Paterson, P. Y., and Hale, J. R. (1983) Magnetic microspheres as drug carriers: Factors influencing localization at different anatomical sites in rats. *Isr. J. Med. Sci. 19*, 631—637.

(27) Bertino, J. R. (1963) The mechanism of action of the folate antagonists in man. *Cancer Res. 23*, 1286—1306.

(28) Whitehead, V. M. (1977) Synthesis of methotrexate polyglutamates in L1210 murine leukemia cells. *Cancer Res. 37*, 408—412.

(29) Johns, D. G., Farquhar, D., Chabner, B. A., et al. (1973) Dialkyl esters of methotrexate and 3′,5′-dichloro methotrexate: synthesis and interaction with aldehyde oxidase and dihydrofolate reductase. *Drug Metab. Dispos. 1*, 580—589.

(30) Whiteley, J. M. (1971) Some aspects of the chemistry of the folate molecule. *Ann. N. Y. Acad. Sci. 186*, 29—42.

(31) Jacobs, S. A., d'Urso-Scott, M., and Bertino, J. R. (1971) Some biochemical and pharmacologic properties of amethopterin-albumin. *Ann. N. Y. Acad. Sci. 186*, 284—286.

(32) Przybylski, M., Fell, E., Ringsdorf, H. (1976) Syntheses and characterization of polymeric derivatives of the antitumor agent methotrexate. *Makromol. Chem. 119*, 1719—1733.

(33) Sanzgiri, Y. D., Blanton, C. D., and Gallo, J. M. (1990) Synthesis, characterization, and in vitro stability of chitosan-methotrexate conjugates. *Pharm. Res. 7*, 418—421.

(34) Janaky, T., Juhasz, A., Resaki, Z., et al. (1992) Sort chain analogs of luteinizing hormone-release hormone containing cytotoxic moieties. *Proc. Natl. Acad. Sci. U.S.A. 89,* 10203–10207.

(35) Janasky, T., Juhasz, A., Bajusz, S., et al. (1992) Analogs of luteinizing hormone-releasing hormone containing cytotoxic groups. *Proc. Natl. Acad. Sci. U.S.A. 89,* 972–976.

(36) Pope, B. M., Yamamoto, Y., Tarbell, D. (1977) Di-tert-butyl dicarbonate. *Org. Synth. 57,* 45–60.

(37) Hofmann, K., Finn, F. M., and Kiso, Y. J. (1978) Avidin–Biotin affinity columns. General methods for attaching biotin to peptides and proteins. *J. Am. Chem. Soc. 100,* 3585–3590.

(38) Pirkle, W. H., Simmons, K. A., and Boeder, C. W. (1979) Dynamic NMR studies of diasteromeric carbamates: Implications toward the determination of relative configuration by NMR. *J. Org. Chem. 44,* 4891–4896.

(39) Zinic, M., Bosnic-Kasnar, B., and Kolbah, D. (1980) Chiral aminoacid containing macromolecules. *Tetrahedron Lett.* 1365.

(40) Gilon, Ch., Klausner, Y., and Hassner, A. (1979) A novel method for the facile synthesis of depsipeptides. *Tetrahedron Lett.* 3811.

(41) Wang, S. S., Yang, C., Kulesha, D., et al. (1974) Solid phase synthesis of bovine pituitary growth hormone-(123–131) nonapeptide. *Int. J. Pept. Protein Res. 6,* 103.

(42) Hassner, A., and Alexanian, V. (1978) Direct room temperature esterification of carboxylic acids. *Tetrahedron Lett.* 4475–4478.

(43) Gallo, J. M., Gupta, P. K., Hung, C. T., et al. (1989) Evaluation of drug delivery following the administration of magnetic albumin microspheres containing adriamycin to the rat. *J. Pharm. Sci. 78,* 190–194.

(44) Hassan, E., Parish, R. C., and Gallo, J. M. (1992) Optimized formulation of magnetic chitosan microspheres containing the anticancer agent, oxantrazole. *Pharm. Res. 9,* 386–393.

(45) Widder, K. J., Senjei, A. E., and Ranney, D. F. (1980) In vitro release of biologically active adriamycin by magnetically responsive albumin microspheres. *Cancer Res. 40,* 3512–3517.

(46) Ranney, D. F. (1985) Targeted modulation of acute inflammation. *Science 227,* 182–184.

(47) Devineni, D., Klein-Szanto, A., and James M. Gallo (1994) Tissue distributio nof methotrexate following administration as a solution and as a magnetic microsphere conjugate in rats bearing brain tumors. *J. Neuro-Oncol.* (in press).

BC950002M

In Vivo Cleavability of a Disulfide-Based Chimeric Opioid Peptide in Rat Brain

Ulrich Bickel, Young-Sook Kang, and William M. Pardridge*

Department of Medicine and Brain Research Institute, UCLA School of Medicine, Los Angeles, California 90024. Received October 26, 1994®

Brain delivery of systemically administered neuropeptide drugs may be achieved by the synthesis of chimeric peptides, wherein the peptide is coupled to transport vectors via avidin−biotin technology. The present study focuses on factors that optimize the linkage of drugs to transport vectors. The vector is the OX26 monoclonal antibody to the transferrin receptor, and the model peptide used in these studies is [Lys^7]dermorphin (K7DA). The K7DA is monobiotinylated at the ϵ-amino group of the Lys^7 residue with either a cleavable linker, e.g., disulfide, using NHS-SS-biotin, or a noncleavable linker, e.g., amide, using NHS-XX-biotin. Disulfide cleavage of the biotinylated derivative yields the desbiotinylated peptide, which is thiolated. Structures of the K7DA analogues were confirmed by secondary ion mass spectrometry. The biotinylated peptides were coupled to a thiol−ether conjugate of the OX26 antibody and either neutral avidin (NLA) or streptavidin. The binding constants (K_i) of the K7DA, the biotinylated K7DA (bio-XX-K7DA), the desbiotinylated K7DA, and the bio-XX- KD7A conjugated to NLA-OX26 were 0.62 ± 0.14, 1.59 ± 0.27, 1.24 ± 0.24, and >10 nM, respectively, and were determined with a μ-opioid peptide radioreceptor assay. Comparable results were obtained with in vivo tail-flick analgesia testing following intracerebroventricular (icv) injection of opioid chimeric peptides. Reversibility of pharmacologic action of thiolated peptide was demonstrated by icv naloxone administration. The cleavability of the disulfide linker in vivo in rat plasma and brain was assessed with gel filtration HPLC and internal carotid artery perfusion of labeled opioid chimeric peptides. These studies are consistent with the following conclusions: (a) opioid peptides have minimal pharmacologic activity when bound to the transport vector, indicating the need for cleavable disulfide linker; (b) the disulfide linker is stable in plasma in vivo as well as brain capillary endothelial cells, but is rapidly cleaved in rat brain in vivo, indicating that disulfide cleavage occurs beyond the endothelial cells of brain capillaries; and (c) the thiolated peptide released following disulfide cleavage is pharmacologically active at the μ-opioid peptide receptor via a naloxone reversible mechanism, indicating the thiolated peptide is not likely covalently bound to the receptor.

INTRODUCTION

The brain capillary endothelial wall, which is the anatomical basis of the blood−brain barrier (BBB) in vivo (*1*), prevents the access to brain of even relatively small peptide-based drugs. Therefore, despite the potentially high receptor-binding affinity and metabolic stability of neuropeptide analogues, centrally mediated effects are difficult to elicit after systemic administration of the peptide (*2*). In the case of opioid peptides, this could be recently quantitatively confirmed with a pharmacokinetic study using DALDA, a metabolically stable dermorphin analogue tetrapeptide (*3*). Clinically useful neuropeptide pharmaceuticals may be developed using suitable brain drug delivery strategies. One delivery approach is the use of "chimeric peptides", which consist of the nontransportable neuropeptide pharmaceutical coupled to a transport vector (*2*). A model vector is the OX26 monoclonal antibody against the rat transferrin receptor, which undergoes receptor-mediated transcytosis through the BBB in vivo (*2*). The successful practical implementation of the chimeric peptide approach requires optimization in three inter-related areas. First, vectors with high BBB transcytosis rates must be developed. Second, a linker strategy must be applied, which provides reversible high yield coupling of different peptide ligands to the vector. These goals are achieved with the use of avidin−biotin

technology and the production of avidin−vector conjugates and biotinylated peptide therapeutics (*4*). Recent studies have shown that optimal plasma pharmacokinetics of avidin−vector conjugates is obtained with the use of neutral avidin (NLA) (*5*). Another requirement with the avidin−biotin drug delivery approach is the use of a peptide ligand that is monobiotinylated. Higher degrees of biotinylation lead to the formation of aggregates owing to the multivalent binding of biotin by avidin. Third, the biotinylated peptide therapeutic must retain biologic activity following cleavage from the transport vector within the brain.

Progress toward achieving these goals has recently been demonstrated for a vasoactive intestinal peptide (VIP) analogue (*6*) and the opioid peptide, DALDA (*7*). In those studies, a cleavable biotin linker containing a disulfide bridge was used, which theoretically allows for release of the peptide moiety from the chimeric peptide following its transport into brain tissue. However, at present, at least three issues remain unresolved regarding the method of linking the peptide therapeutic to the avidin−vector conjugate. The first issue is whether a cleavable (e.g., disulfide) or noncleavable (e.g., amide) linkage should be used for attachment of the biotin moiety to the peptide. A noncleavable linker could be used if the peptide is biologically active when attached to the avidin−vector conjugate. Second, if a cleavable linkage is used, this bond must be stable in plasma in the circulation in vivo, stable during transit through the brain capillary endothelial cell, but rapidly cleaved in brain in vivo to release in biologically active form the

"desbiotinylated" peptide from the avidin–vector conjugate. Third, if the cleavable linker is a disulfide bond, then the cleaved peptide therapeutic will invariably carry an added free thiol group generated by the cleavage of the disulfide group, and it is necessary to show reversibility of pharmacologic action in brain of the peptide. It is possible that thiolated peptides may form a disulfide linkage with the receptor, which could result in irreversible activation of the peptide receptor (*8*). These three issues are addressed in the present study, which uses [Lys⁷]dermorphin, abbreviated K7DA, which has structural features similar to DALDA (*9*), but is intrinsically more potent with respect to binding to the μ-opioid peptide receptor (*10*). The K7DA peptide is conjugated with both cleavable and noncleavable biotin analogues, and the activity of the cleavable analogue, designated bio-SS-K7DA, versus the noncleavable analogue, designated bio-XX-K7DA, is investigated with opioid peptide radioreceptor assays. Second, the stability of the disulfide linker in plasma and brain in vivo and in brain capillary endothelial cells is evaluated using HPLC analysis of brain extracts. Third, the reversibility of the antinociceptive action of the thiolated K7DA in brain in vivo is shown using tail-flick analgesia assays following intracerebroventricular (icv) administration of opioid chimeric peptides or the μ-opioid antagonist, naloxone.

EXPERIMENTAL PROCEDURES

Materials. Na¹²⁵I was supplied by Amersham (Arlington Heights, IL). DAGO, [³H]DAGO (specific activity, 38.4 Ci/mmol), DPDPE, and [³H]DPDPE (specific activity, 27.38 Ci/mmol) were provided by the National Institute of Drug Abuse Research Technology Branch (Rockville, MD). [¹⁴C]Sucrose (specific activity, 632 mCi/mmol) was obtained from NEN Dupont (Wilmington, DE). Sulfosuccinimidyl 2-(biotinamidoethyl)-1,3′-dithiopropionate (NHS-SS-biotin), 2-iminothiolane (Traut's reagent), and m-maleimidobenzoyl *N*-hydroxysuccinimide ester (MBS) was supplied by Pierce Chemical (Rockford, IL). Biotin-XX-NHS was supplied by CalBiochem (San Diego, CA), where XX = bis(aminohexanoyl) spacer arm and NHS = *N*-hydroxysuccinimide. Acetonitrile was obtained from Fisher Scientific (Tustin, CA). Chloramine T was purchased from MCB Reagents (Cincinnati, OH). Neutralite avidin (NLA) was supplied by Accurate Chemicals (Westbury, NY). Recombinant streptavidin (SA) and all other reagents were obtained from Sigma (St. Louis, MO). Vydac C₄ (10 × 250 mm) reversed-phase HPLC columns were obtained from the Separations Group (Hesperia, CA), and Sephacryl S300HR was from Pharmacia (Piscataway, NJ). G-25 Quick Spin columns were obtained from Boehringer Mannheim (Indiana, IN). TSK-gel G2000 SW$_{XL}$ HPLC columns (7.8 × 300 mm) were obtained from TosoHaas (Montgomeryville, PA). The 22-gauge guide cannula, 28-gauge dummy cannula, and 28-gauge injection cannula for icv injections were supplied by Plastics One (Roanoke, VA). The Model 33 tail-flick analgesia meter was obtained from IITC Life Sciences (Woodland Hills, CA). Male Sprague–Dawley rats (220–270 g body weight) were supplied by Harlan Sprague–Dawley (Indianapolis, IN).

Synthesis and Biotinylation of the Dermorphin Analogue. Lys⁷-dermorphin analogue (K7DA) was synthesized in its α-*N*-fmoc-Tyr¹ protected form by the Peptide Synthesis Facility, Department of Biological Chemistry (University of California, Los Angeles). The solid phase peptide synthesis and subsequent HPLC purification were performed as described previously (*7*). Fmoc-K7DA was then biotinylated with either NHS-SS-biotin or NHS-XX-biotin as described (*7*). Briefly, 500

μg of the fmoc-peptide were dissolved in 400 μL of dimethyl sulfoxide, and 600 μL of 0.05 M NaHCO₃ (pH 8.3) was added. A 3- to 6-fold molar excess of the biotinylating reagent (NHS-SS-biotin or NHS-XX-biotin) in 1 mL of 0.05 M NaHCO₃ was added. After 60 min at room temperature, the reaction was stopped by the addition of 100 μL of trifluouroacetic acid (TFA) and 500 μL of ACN. After HPLC purification, the N-terminal fmoc group was removed, and the bio-SS- or bio-XX-K7DA was again HPLC purified as described (*7*). In vitro cleavage of bio-SS-K7DA to obtain desbiotinylated K7DA (desbio-K7DA) was performed with 50 mM dithiothreitol (DTT) in 50 mM phosphate buffer (pH 7.5) for 1 h at room temperature. Bio-SS-K7DA and desbio-K7DA were analyzed by secondary ion mass spectrometry (SIMS), as described (*7*). Peptide amounts after HPLC purification were quantitated with the BCA reagent (Pierce Chemical Co., Rockford, IL).

Synthesis of Avidin–OX26 Conjugates. A conjugate of the antitransferrin receptor monoclonal antibody, OX26, and either neutralite avidin (NLA) or streptavidin (SA) was prepared as described previously (*4, 5*). Briefly, OX26 was thiolated with Traut's reagent, and NLA or SA was activated with MBS. The thiolated OX26 and activated NLA or SA were then mixed, and the conjugate was purified over a Sephacryl S300 HR column (*5*). The fractions corresponding to the conjugate of NLA–OX26 or SA–OX26 were separated from unconjugated NLA or SA and from high molecular weight aggregates (*5*). The number of biotin binding sites per OX26 conjugate was determined as described previously (*5*) and was 4.2 ± 0.1 and 3.3 ± 0.3 for NLA–OX26 and SA–OX26, respectively.

In Vitro and in Vivo Testing of Opioid Receptor Affinity. Opioid radioreceptor assays (RRA) with rat brain membranes (*11*) were performed, as described in ref 7. Tail-flick analgesia measurements in rats were performed after icv injections of the following peptides: K7DA, bio-XX-K7DA, bio-XX-K7DA bound to NLA-OX26, bio-SS-K7DA bound to NLA-OX26, and desbio-K7DA. The peptides were dissolved in 5 mM Na phosphate-buffered saline containing 0.05% Tween-20. The injection volume was 20 μL. Naloxone reversibility of the analgesia was tested by an icv injection of 20 μg/20 μL naloxone in saline. The stereotaxic implantations in the lateral ventricle and the tail-flick analgesia testing was performed as described (*7*). Base-line latency was 3–4 s, and the cutoff time was set at 10 s.

Radiolabeling of bio-SS-K7DA. A 1–2 μg (0.8–1.6 nmol) portion of the peptide was labeled with 2 mCi Na¹²⁵I by the addition of 1.4–2.5 μg of chloramine T. The final reaction volume was 32 μL in 0.1 M Na phosphate buffer, pH 7.4. The reaction was stopped after 30–60 s at room temperature by the addition of 1.9–6.2 μg of sodium metabisulfite. The iodinated bio-SS-K7DA was then purified with one of two approaches. In the first approach, 0.4 nmol of the ¹²⁵I-bio-SS-K7DA was mixed with 50 μL of NLA-OX26 (1.74 mg/mL) in 5 mM PBS/ 0.05% Tween-20 followed by incubation for 15 min at room temperature. The ¹²⁵I-bio-SS-K7DA bound to the NLA-OX26 was purified from free iodine over Quick-Spin G-25 Sephadex columns (sample volume 45 μL each), which had been equilibrated with 10 mM PBS/0.05% Tween-20. The combined eluant volume from two Quick Spin columns was 120 μL. In the second purification approach, the ¹²⁵I-bio-SS-K7DA mixture was acidified by the addition of 1 mL of 1% trifluouroacetic acid (TFA), and the mixture was applied to an activated C18 SepPak cartridge. The extraction cartridge was washed with 10 mL of 0.1% TFA, and the iodinated peptide was eluted

with 5 mL of 60% acetonitrile in 0.1% TFA. The acetonitrile was removed by evaporation, and the final mixture was made 0.05 M Na_2HPO_4, pH = 7.4, 0.05% sodium azide, and was stored at 4 °C. The specific activity of the final product was 0.57 mCi/nmol with a trichloroacetic acid (TCA) precipitability of 95%.

Internal Carotid Artery Perfusion and Chromatographic Analysis. The in vivo brain uptake of the radiolabeled bio-SS-K7DA bound to the NLA-OX26 was studied with the internal carotid artery perfusion technique (6). Rats were anesthetized with ketamine (100 mg/kg) and xylazine (2 mg/kg) intraperitoneally, and the occipital, superior thyroid, and pterygopalatine arteries were closed by electrocoagulation. The external carotid artery was cannulated with PE10 tubing and before starting the perfusion of the ipsilateral brain hemisphere, the common carotid artery was completely closed by ligation. The perfusate contained ^{125}I-bio-SS-K7DA (3 μCi/mL or 10 nM) in Krebs-Henseleit buffer, 1% bovine serum albumin, and 10 nM NLA-OX26 and was oxygenated with 95% O_2 and 5% CO_2 and perfused at a rate of 1.25 mL/min for 10 min. At the end of the perfusion, the animal was decapitated, and the brain was homogenized on ice in 6 vol of homogenization buffer [0.1 M Na phosphate (pH = 7.0), 0.5 M NaCl, 0.25% bovine serum albumin (BSA), and 0.05% Tween-20] with a Polytron homogenizer for 10 s followed by sonication for 10 s. The homogenate was centrifuged at 50 000g for 60 min at 4 °C. An aliquot of the supernatant was counted for total radioactivity and a 250 μL aliquot was injected onto a TSK-gel G2000 SW$_{XL}$ gel filtration column (7.8 × 300 mm). The column was eluted at 0.5 mL/min with the same buffer used for homogenization, and 1 min fractions were collected for 40 min and the fractions were then counted for ^{125}I-radioactivity. The void and salt volumes of the columns are 6 and 14 mL, respectively. In control experiments, the same HPLC analysis was performed with tracer in buffer alone, with tracer pre-equilibrated for 60 min at room temperature with 20 mM DTT, and tracer added to fresh rat brain in ice cold homogenization buffer, which was then homogenized as described above prior to HPLC injection. In all the experiments, the tracer is ^{125}I-bio-SS-K7DA conjugated to the NLA-OX26 complex.

Brain Capillary Uptake and Chromatographic Analysis. The cleavage of the ^{125}I-bio-SS-K7DA conjugated to the NLA-OX26 complex by isolated bovine brain capillaries at 37 °C was investigated. For these experiments, brain capillaries were isolated from fresh bovine brain using the mechanical homogenization technique described previously (12). Bovine brain capillaries (equivalent to 200 μg of capillary protein) were suspended for 2 or 20 min at 37 °C in 200 μL of 10 mM Hepes/0.15 M NaCl/pH = 7.4 containing 0.1% BSA and 0.1 μCi (0.3 pmol) of ^{125}I-bio-SS-K7DA conjugated to 1 μg (5 pmol) of NLA-OX26. Control experiments included 20 min incubations of the ^{125}I-bio-SS-K7DA/NLA-OX26 without microvessels, but with 0 or 500 mM DTT. The ^{125}I-bio-SS-K7DA was purified by C18 reversed-phase HPLC prior to the experiment. After the 2 or 20 min incubation, the tubes were placed on ice and centrifuged at 10 000g for 60 s at 4 °C. The supernatant was removed for direct HPLC analysis. The capillary pellet was drained of supernatant and was suspended in 0.1 M Na phosphate (pH = 7.4), 0.5 M NaCl, 1 mM EDTA, and 0.05% Tween-20. The capillary suspension was sonicated for 20 s on ice and centrifuged at 10 000g for 10 min at 4 °C. Ten μL aliquots of the capillary supernatant were then counted for radioactivity, and the remainder was injected

onto the TSK-gel filtration HPLC column described above.

Intravenous Injection and Chromatographic Analysis. The relative stability of the disulfide linker in plasma and brain in vivo was assessed by intravenous injection of the ^{125}I-bio-SS-K7DA conjugated to the SA-OX26 complex. In these experiments, rats (270 g) were anesthetized with ketamine/xylazine as described above, and a 0.2 mL injection volume of Ringer's solution buffered with 10 mM Hepes was injected. The injection solution contained 0.1% rat serum albumin (RSA), 20 μCi of ^{125}I-bio-SS-K7DA, and 20 μg of SA-OX26. At 60 min after injection, the animals were sacrificed by decapitation, and plasma and brain were obtained. A brain hemisphere was homogenized with a Polytron homogenizer in three volumes of 0.01 M PBS, pH = 7.4, 0.05% Tween-20, followed by centrifugation at 20 000g for 30 min at 4 °C. The supernatant was then injected onto the TSK-gel filtration column as described above; 80 μL of the hemisphere supernatant was taken from each of the three rats analyzed in triplicate and pooled prior to injection onto the HPLC column. Similarly, 80 μL of the 60 min plasma was obtained from each rat, pooled, and injected onto the HPLC column, which was eluted in 0.1 M PBS, pH = 7.4, 0.05% Tween-20, as described above.

RESULTS

Fmoc-K7DA was efficiently biotinylated with NHS-SS-biotin, as more than 80% of the peptide eluted as bio-fmoc-K7DA from the HPLC column (Figure 1). Alkaline deprotection and HPLC purification of bio-SS-K7DA yielded an overall recovery of 61% of the original peptide. When the biotin-XX-NHS ester was used for biotinylation, the overall recovery of biotinylation and deprotection exceeded 90%. The bio-SS-K7DA was converted into desbio-K7DA with dithiothreitol (DTT) treatment, and this conversion was complete as shown in Figure 1. The structure of the bio-SS-K7DA and the desbio-K7DA was confirmed with secondary ion mass spectrometry (SIMS), and the experimentally determined molecular masses were within less than one mass unit of the formula weights of the compound (Figure 2).

The biologic activity of the desbio-K7DA was assessed with a μ-opioid peptide radioreceptor assay using [^{3}H]-DAGO as the μ-receptor-specific ligand. The binding isotherms for unlabeled DAGO, K7DA, and desbio-K7DA are shown in Figure 3A, and the K_i values for each of these compounds are given in Table 1. The K_i value for K7DA was 0.62 ± 0.14 nM, and this was not significantly different from the K_D of DAGO, 0.58 ± 0.08 nM (Table 1). The desbio-K7DA had an affinity for the μ-receptor approximately 50% less than that of the parent compound with a K_i of 1.24 ± 0.24 nM. The displacement of [^{3}H]DAGO from the μ-receptor by bio-XX-K7DA in either its free form or conjugated to the NLA-OX26 vector is shown in panel Figure 3B. The K_i of the bio-XX-K7DA was 1.5 ± 0.27 nM (Table 1), but the K_i of this analogue bound to the NLA-OX26 vector was immeasurably high (Figure 3, Table 1).

The high analgesic potency of K7DA is shown by the tail-flick analgesia experiments following icv injection of 0.01, 0.03, and 0.10 nmol of K7DA (Figure 4A). Similarly, bio-XX-K7DA demonstrated a strong antinociceptive response following the icv injection of 0.1 nmol (Figure 4B). In parallel with the radioreceptor assay (Figure 3B), the binding of the bio-XX-K7DA to the NLA-OX26 conjugate resulted in a more than 90% inhibition of the antinociceptive response of the biotinylated peptide (Figure 4B). Similarly, binding of the bio-SS-K7DA to the NLA-OX26 conjugate resulted in suppression of the
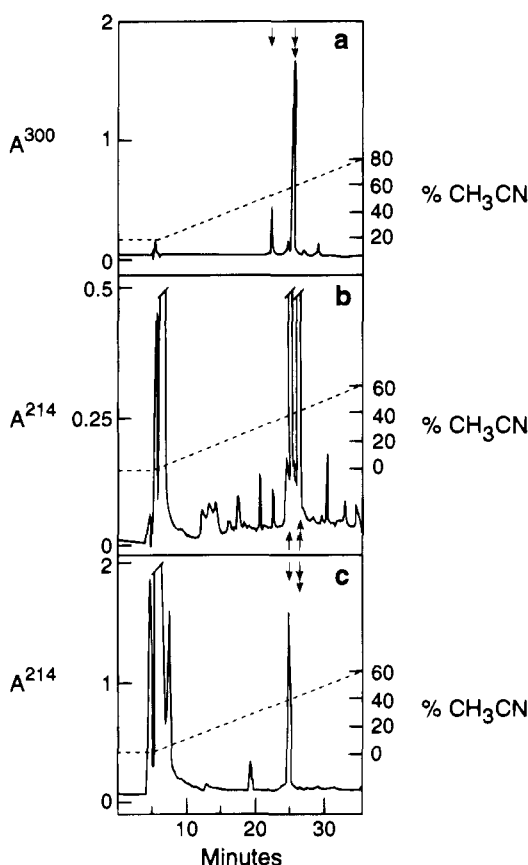
Figure 1. Reversed-phase HPLC on a Vydac C_4 column of bio-SS-fmoc-K7DA (A), bio-SS-K7DA following deprotection of the fmoc group (B), and of desbio-K7DA after cleavage by DTT (C). The elution was monitored at $\lambda = 300$ nm (A), which detects the fmoc group, or 214 nm (B, C). The broken lines indicate the gradient of acetonitrile in 0.1% trifluouroacetic acid. The single arrow in A indicates the retention time of the nonbiotinylated fmoc-K7DA. The single arrow in B denotes a reagent peak (no measurable peptide content), and the double arrows in B and C indicate the retention time of bio-SS-K7DA.

analgesic response (Figure 4C). However, when the cleavable linker was used, the analgesic potency of the vector-bound peptide was restored by cleavage under mild reducing conditions, e.g., the addition of 0.5 mM cysteine (Cys) to the icv injection solution. Doses of 0.1 and 0.3 nmol of bio-SS-K7DA bound to the NLA-OX26 conjugate showed a dose-related, yet delayed, analgesic response (Figure 4C), indicating a slow in vivo release of the desbio-K7DA from the chimeric peptide after icv injection.

The administration of 0.1 nmol of desbio-K7DA elicited a maximum analgesic response (Figure 4D). The μ-opioid nature of the analgesic effect could be demonstrated by the immediate reversibility of the analgesia by the icv injection of 25 μg of naloxone, as indicated by the arrows in panel 4D. The potency and long duration of the desbio-K7DA was evident from the gradual escape from naloxone antagonism over the next 30 min. The full naloxone effect could be restored by a repeated icv administration of an additional 25 μg dose of the antagonist. The experiments shown in Figure 4D also demonstrate that the NLA-OX26, added at a 1:1 molar ratio, did not interfere with the analgesic effect of the desbio-K7DA. In other experiments, the separate administration of 20 μL of 0.5 mM L-cysteine (equivalent to 10 nmol) had no analgesic effect following icv administration.

The selective cleavage of the disulfide linker in brain, but not in plasma, was demonstrated by intravenous injection of ^{125}I-bio-SS-K7DA bound to the NLA—OX26 conjugate. As shown in Figure 5A, the ^{125}I-bio-SS-K7Da in plasma obtained 60 min after iv administration eluted from the HPLC gel filtration column with the NLA—OX26 conjugate at 7 mL. Conversely, HPLC analysis of an extract of rat brain obtained 60 min after iv injection of the chimeric peptide demonstrated that there was nearly complete conversion of the radiolabeled chimeric peptide to the free desbio-K7DA or its metabolites (Figure 5B).

It is conceivable that the radiolabeled chimeric peptide was cleaved in the plasma compartment followed by brain uptake of low molecular weight metabolites. Therefore, the in vivo cleavage of the disulfide bond by rat brain was investigated with an internal carotid artery perfusion technique. Prior to perfusion, the ^{125}I-bio-SS-K7DA/NLA—OX26 conjugate eluted at a column volume of 7 mL (Figure 6A). No radioactivity eluted in the fractions where the free ^{125}I-bio-SS-K7DA or free iodine would be expected (Figure 6A), indicating an efficient conjugation of the biotinylated peptide to the NLA—OX26 vector. The in vitro cleavability of the chimeric peptide at the disulfide bridge was shown by pre-incubation of the labeled chimeric peptide with 20 mM DTT for 60 min at room temperature followed by gel filtration HPLC. As shown in Figure 6B, the radioactivity peak completely shifted from the elution volume (7 mL) of the NLA—OX26 to the elution volume (14 mL) corresponding to the unconjugated peptide migrating in the salt volume of the column. The ^{125}I-bio-SS-K7DA/NLA—OX26 was perfused into the internal carotid artery for 10 min, and the labeled chimeric opioid peptide reached a distribution volume of 30 $\pm$ 5 μL/g, a volume that is more than 3-fold greater than the plasma volume, 8 μL/g (5). When the brain homogenate was cleared by centrifugation and subjected to gel filtration HPLC analysis, cleavage within the 10 min brain perfusion was observed (Figure 6C). The cleavage had occurred in vivo, since a control experiment, where the tracer was added to fresh rat brain tissue prior to the same homogenization and chromatography procedure, did not reveal any cleavage of the disulfide bond, as shown in Figure 6D.

In order to determine whether brain microvessels are capable of cleaving the chimeric peptide, the ^{125}I-bio-SS-K7DA/NLA-OX26 was also incubated with isolated bovine brain capillaries at 37 °C for 2—20 min. HPLC analysis of the medium (Figure 7A) after a 20 min incubation showed minimal conversion of the ^{125}I-bio-SS-K7DA into its nonconjugated form (Figure 7A). HPLC analysis of the 20 min microvessel pellet showed that the majority of the ^{125}I-bio-SS-K7DA remained conjugated to the NLA-OX26 vector (Figure 7B). There was no difference between the chromatograms obtained at 2 or 20 min of incubation.

DISCUSSION

The results of the present studies are consistent with the following conclusions. First, a cleavable, e.g., disulfide, linker joining the opioid peptide (K7DA) to the transport vector (OX26 monoclonal antibody) is required over a noncleavable (e.g., amide) linker, because the opioid peptide has a marked reduction in biologic activity when directly conjugated to the transport vector (Figures 3 and 4). Second, a disulfide linker demonstrates optimal characteristics with stability in plasma and brain endothelial cells, but rapid cleavage in brain in vivo (Figures 5—7). Third, cleavage of the opioid peptide from the transport vector results in thiolation of the opioid peptide (Figure 2), yet the thiolated K7DA has a high degree of
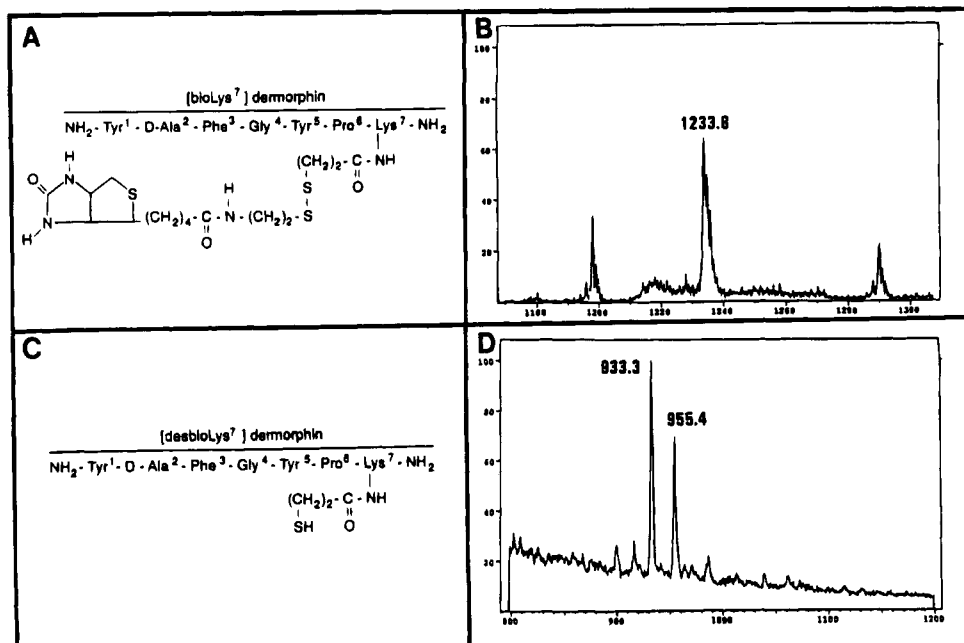
Figure 2. Structural formulas of (A) bio-SS-K7DA (also called bio-Lys[7]-dermorphin) and (C) desbio-K7DA (also called desbio-Lys[7]-dermorphin). Panels B and D show the corresponding molecular weights as measured by secondary ion mass spectrometry (SIMS). The formula weights are 1233.62 (bio-SS-K7DA) and 932.17 (bio-K7DA). The mass peak at 955.4 in D corresponds to an Na-adduct of desbio-K7DA.
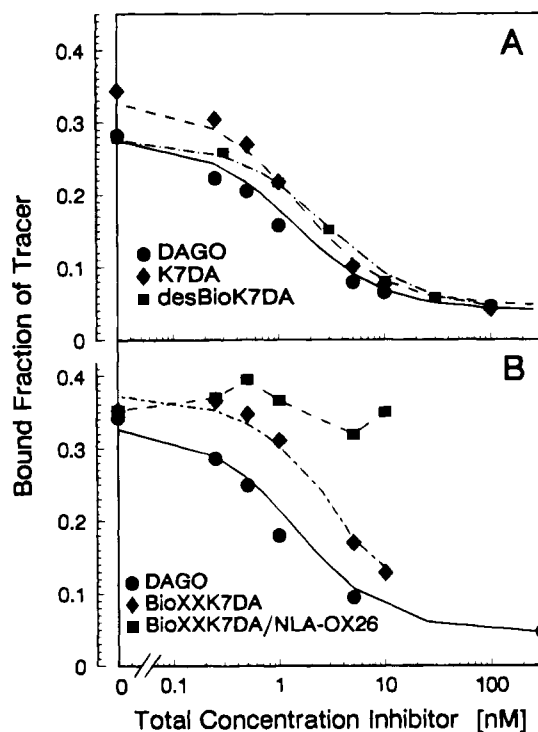
Figure 3. Competition curves of radioreceptor assays with ^{3}H-DAGO. A and B show the results of separate experiments. The data points are means of duplicates, where the coefficient of variation was less than 5%. The curves are best-fits using least-squares nonlinear regression analysis (except for bio-XX-K7DA/NLA-OX26). The corresponding inhibitor constants (K_i) are given in Table 1. The concentration of NLA−OX26 was 20 μg/mL (93 nM) and was in excess of the bio-XX-K7DA, which ranged from 0.25 to 10 nM (for the Bio-XX-K7DA/NLA−OX26 curve).

intrinsic receptor activity (Figures 3 and 4) and results in the pharmacologic activation of the μ-opioid peptide receptor that is reversible with naloxone treatment (Figure 4).

Table 1. Radioreceptor Assay with Synaptosomes from Rat Brain[a,b]

ligand	B_{max} (fmol mg_p^{-1})	K_i (nM)
DAGO	105 ● 11	0.58 ± 0.08
K7DA		0.62 ± 0.14
desbio-SS-K7DA		1.24 ± 0.24
bio-XX-K7DA		1.59 ± 0.27
bio-XX-K7DA/NLA−OX26		>10

[a] Nonspecific binding = 4.2 ± 0.5%. [b] Parameters were obtained by least-quares nonlinear regression from the competition data shown in Figure 3. [3H]DAGO was used as the labeled μ-specific ligand at a concentration of 0.5 nM.

The noncleavable biotin linker generated with the use of NHS-XX-biotin introduces a 14-atom spacer between the opioid peptide and the biotin moiety. Previous studies have shown that biotinylated β-endorphin derivatives bind the μ-opioid peptide receptor while conjugated to avidin (*13*). However, the present studies demonstrate that when the avidin is in turn conjugated through a thiol−ether linkage to a 150 000 Da monoclonal antibody, there is a marked reduction in the affinity of the opioid peptide for the μ-receptor based on either radioreceptor assays (Figure 3, Table 1) or analgesia testing following icv administration (Figure 4B). These studies indicate the necessity of choosing a cleavable linker joining the peptide therapeutic to the transport vector. Disulfide linkages are preferred because of the relative stability of this linkage in plasma (*14*) and extracellular fluids such as CSF (*15*).

The stability of the disulfide linker joining the peptide therapeutic with the NLA−OX26 transport vector in plasma and in endothelial cells is demonstrated in Figures 5 and 7, respectively. Previous studies have shown that the disulfide linker is rapidly cleaved by homogenate of rat brain in vitro at 37 °C (*16*). The present studies extend these results to the in vivo state using internal carotid artery perfusion and show that the disulfide linker is approximately 40% cleaved within 10 min of an internal carotid artery perfusion. This duration of perfusion allows the conjugate to readily access
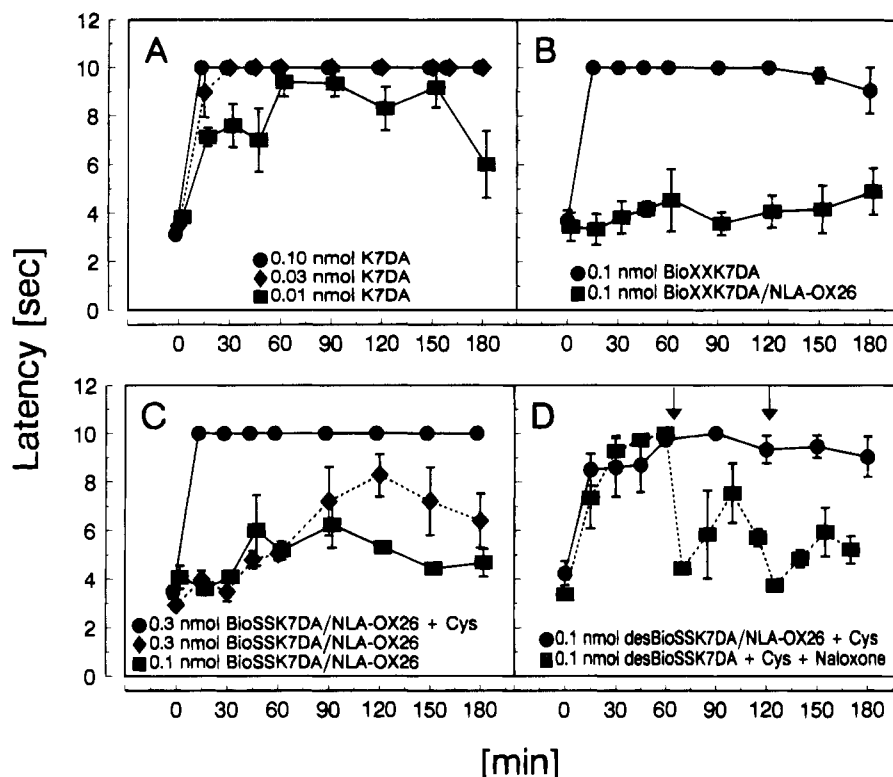
Figure 4. Tailflick analgesia measurements after icv administration of the peptide. Doses are given in the insets. A shows a dose–response curve of K7DA. B compares the analgesic effect of bio-XX-K7DA with or without binding to NLA–OX26. C shows the effect of two different doses of bio-SS-K7DA/NLA–OX26 and the effect of precleavage of the chimeric peptide with 0.5 mM cysteine (Cys). D shows the naloxone reversibility of desbio-SS-K7DA and the effect of desbio-SS-K7DA in the presence of the vector, NLA–OX26. The arrows in D indicate the time of naloxone administration. $n = 3$ for all experiments, data points are mean ± SE.
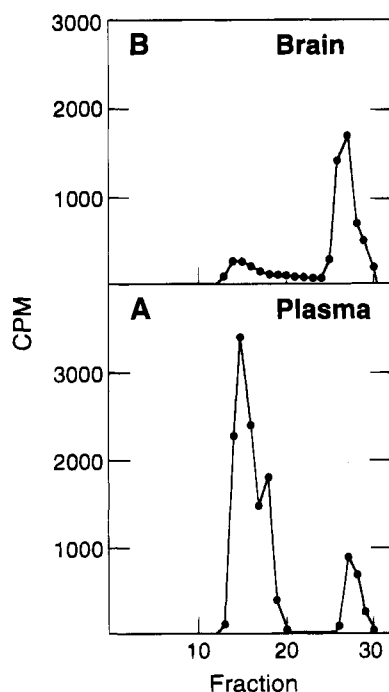
Figure 5. Gel filtration HPLC of plasma (A) and brain homogenate (B) obtained 60 min after intravenous injection of ^{125}I-bio-SS-K7DA–OX26. Aliquots of plasma or brain homogenate were pooled from three rats performed in triplicate and injected onto the TSK-gel filtration column (7.8 × 300 mm). The column was eluted at 0.5 mL/min, and 0.5 mL fractions were collected and counted for ^{125}I-radioactivity (cpm = counts per minute).

Figure 6. Gel filtration HPLC of (A) ^{125}I-bio-SS-K7DA/NLA–OX26 and (B) same tracer after treatment with 20 mM DTT. (C) Chromatogram of supernatant of brain homogenate following a 10 min brain perfusion. D is the control, where the tracer was added to fresh brain tissue in ice cold homogenization buffer before homogenization. Fractions = 0.5 mL.

brain postvascular spaces. Previous studies have shown that about 45% of the peptide/vector complex that is

taken up by the brain has distributed to the postvascular compartment (6). Longer experimental time periods lead to greater disulfide cleavage. For example, 60 min after an intravenous injection, the amount of opioid peptide bound to the transport vector within brain is minimal (Figure 6B).

The stability of the disulfide bond in brain endothelial cells (Figure 7) suggests the chimeric peptide is retained within an endosomal compartment of the microvessels and is not transferred to the endothelial cytosol, where
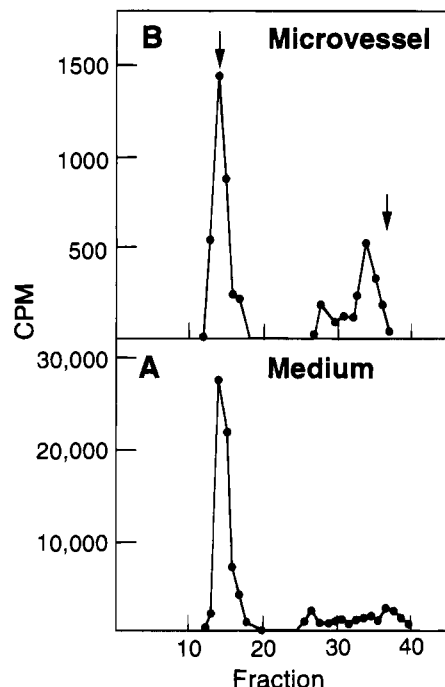
Figure 7. Gel filtration HPLC of ^{125}I-bio-SS-K7DA/NLA—OX26 incubated for 20 min with isolated bovine brain capillaries at 37 °C. A is the chromatogram of the medium obtained after centrifugation of the capillaries and B is the chromatogram of the microvessel pellet homogenate. The left-hand and right-hand arrows in panel B point to the elution volume of the ^{125}I-bio-SS-K7DA conjugated to the NLA—OX26 and after release from the NLA—OX26 with DTT treatment, respectively.

disulfide bonds are rapidly cleaved (17). These results are consistent with previous studies showing that disulfide cleavage does not occur in endosomes (18), but is primarily a concomitant of entry into the cytosolic space owing to the very high ratio of glutathione to oxidized glutathione in this compartment (19). The stability of the disulfide linkage within the endothelial compartment is believed to be an important requirement allowing efficacy of chimeric peptide pharmaceuticals in brain. If the disulfide linker was stable in plasma but was reduced in brain capillary endothelium, then peptide therapeutic may not be enabled to undergo exocytosis across the ablumenal membrane of the brain capillary endothelium and enter brain interstitial space. Previous studies with conjugates of the OX26 monoclonal antibody and 5 nm gold particles have shown that the OX26 conjugate traverses the endothelial compartment within endosomal structures and does not enter into the endothelial cytosol (20). Another possible site of disulfide cleavage is at the plasma membrane surface, and recent studies have shown that disulfide cleavage may occur at the plasma membrane owing to cell surface bound protein disulfide isomerase (PDI) (21). However, the present studies with isolated bovine brain capillaries (Figure 7) indicate there is not rapid cleavage of the disulfide linker at the surface of brain capillaries. Both luminal and abluminal membranes of the capillary endothelium are exposed in the isolated microvessel experiments. Prior work using dye-coated microspheres has shown the microvessels are patent and the luminal space is rapidly accessed by diffusion (22).

The cleavage of the opioid peptide from the transport vector via reduction of the disulfide bridge results in the release of a thiolated form of the peptide therapeutic, called desbio-K7DA. The structure for desbio-K7DA is given in Figure 2C and shows a mercaptopropionate group on the Lys[7] moiety of the opioid peptide. The high

biologic activity of the desbio-K7DA in either the radioreceptor assay or in the icv analgesia testing (Figures 3 and 4) indicates the thiol moiety on the K7DA at the Lys[7] position does not compromise interaction of the opioid peptide with the μ-receptor. The in vitro radioreceptor assays with the desbio-K7DA correspond to previous studies with desbio-DALDA showing high affinity of the thiolated or desbio-DALDA with the μ-opioid peptide receptor (7). The present studies extend the radioreceptor assays to the in vivo state and show that the cleavage of the bio-SS-K7DA from the NLA—OX26 vector with cysteine results in a marked restoration of opioid peptide-mediated analgesia, owing to release of the opioid peptide from the NLA—OX26 vector (Figure 4C). In addition to retention of biologic activity of the opioid peptide following cleavage from the transport vector, it is also desirable to maintain reversibility of biologic activity of the thiolated opioid peptide. Previous studies have shown that thiolated enkephalin derivatives covalently attach to the δ-opioid peptide receptor (8), resulting in sustained antagonism of analgesia mediated by δ-specific analogues (23). The present studies provide evidence that the thiolated or desbio-K7DA is not irreversibly attached to the μ-opioid peptide receptor, since the pharmacologic effect can be repeatedly reversed by the icv administration of naloxone (Figure 4D).

In summary, the present studies demonstrate the design features that must be incorporated in the linkage of opioid peptides to BBB transport vectors such as the OX26 monoclonal antibody. Owing to the intrinsically low efficiency of direct peptide conjugation to transport vectors using chemical coupling strategies (2), avidin—biotin technology was introduced to allow for high efficiency coupling of the peptide therapeutic to the transport vector, which consists of a stable thiol—ether conjugate of the OX26 monoclonal antibody and avidin. In forming biotinylated peptide derivatives that bind with high affinity to the NLA—OX26 conjugate, the following design features are required. First, the peptide must be monobiotinylated in order to prevent the formation of high molecular weight aggregates owing to the multivalent binding of biotin by avidin. Second, a cleavable, e.g., disulfide, linker joining the peptide therapeutic to the biotin moiety must be used owing to the lack of biologic activity of the peptide therapeutic when attached to the NLA—OX26 conjugate, which has a molecular weight of approximately 215 000 Da. Third, the cleavage of the disulfide linker must result in release of the opioid peptide in biologically active form. This requirement is achieved by selectively biotinylating the Lys[7] ϵ-amino group and maintaining a free amino terminus with the use of fmoc-protected amino terminus on the opioid peptide (Figure 2A); the free amino terminus is required for opioid peptide activity (24). Fourth, the activation of the target receptor by the thiolated or desbio-peptide therapeutic must be reversible by an antagonist such as naloxone, indicative of lack of covalent activation of the target receptor by the thiolated peptide therapeutic. Fifth, the peptide therapeutic must be metabolically stable and the stability of the K7DA is enhanced by the D-Ala[2] moiety (Figure 2), which blocks susceptibility of the peptide to aminopeptidase activity, an ecto-enzyme that is enriched in brain microvessels (25) and is naturally occurring in dermorphin peptides (26). The multiple design features that must be considered in developing an efficacious linker strategy underscore the complexities involved in the development of drug delivery paradigms and the need to achieve progress in three spheres simultaneously, namely the vector, the linker strategy, and retention of biologic activity of the therapeutic (27).

LITERATURE CITED

(1) Brightman, M. W. (1977) Morphology of blood-brain interfaces. *Exp. Eye Res. 25,* Suppl., 1−25.

(2) Pardridge, W. M. (1991) *Peptide Drug Delivery to the Brain,* pp 239−302, Raven Press, New York.

(3) Samii, A., Bickel, U., Stroth, U., and Pardridge, W. M. (1994) Blood−brain barrier transport of neuropeptides: analysis with a metabolically stable dermorphin analogue. *Am. J. Physiol. 267,* E124-E131.

(4) Yoshikawa, T., and Pardridge, W. M. (1992) Biotin delivery to brain with a covalent conjugate of avidin and a monoclonal antibody to the transferrin receptor. *J. Pharmacol. Exp. Ther. 263,* 897−903.

(5) Kang, Y.-S., and Pardridge, W. M. (1994) Use of neutral avidin improves pharmacokinetics and brain delivery of biotin bound to an avidin-monoclonal antibody conjugate. *J. Pharmacol. Exp. Ther. 269,* 344−350.

(6) Bickel, U., Yoshikawa, T., Landaw, E. M., Faull, K. F., and Pardridge, W. M. (1993) Pharmacologic effects *in vivo* in brain by vector-mediated peptide drug delivery. *Proc. Natl. Acad. Sci. U.S.A. 90,* 2618−2622.

(7) Bickel, U., Yamada, S., and Pardridge, W. M. (1994) Synthesis and bioactivity of monobiotinylated DALDA: A *mu*-specific opioid peptide designed for targeted brain delivery. *J. Pharmacol. Exp. Ther. 268,* 791−796.

(8) Bowen, W. D., Hellewell, S. B., Kelemen, M., Huey, R., and Stewart, D. (1987) Affinity labeling of δ-opiate receptors using [D-Ala^2, Leu^5, Cys^6]enkephalin: Covalent attachment via thiol-disulfide exchange. *J. Biol. Chem. 262,* 13434−13439.

(9) Schiller, P. W., Nguyen, T. M.-D., Chung, N. N., and Lemieux, C. (1989) Dermorphin analogues carrying an increased positive net charge in their "message" domain display extremely high μ-opioid receptor selectivity. *J. Med. Chem. 32,* 698−703.

(10) Negri, L., Erspamer, G. F., Severini, C., Potenza, R. L., Melchiorri, P., and Erspamer, V. (1992) Dermorphin-related peptides from the skin of *Phyllomedusa bicolor* and their amidated analogs activate two μ opioid receptor subtypes that modulate antinociception and catalepsy in the rat. *Proc. Natl. Acad. Sci. U.S.A. 89,* 7203−7207.

(11) Sharif, N. A., and Hughes, J. (1989) Discrete mapping of brain mu and delta opioid receptors using selective peptides: Quantitative autoradiography, species differences and comparison with kappa receptors. *Peptides 10,* 499−522.

(12) Pardridge, W. M., Eisenberg, J., and Yamada, T. (1985) Rapid sequestration and degradation of somatostatin analogues by isolated brain microvessels. *J. Neurochem. 44,* 1178−1184.

(13) Hochhaus, G., Gibson, B. W., and Sadée, W. (1988) Biotinylated human β-endorphins as probes for the opioid receptor. *J. Biol. Chem. 263,* 92−97.

(14) Letvin, N. L., Goldmacher, V. S., Ritz, J., Yetz, J. M., Schlossman, S. F., and Lambert, J. M. (1986) In vivo administration of lymphocyte-specific monoclonal antibodies in nonhuman primates. *J. Clin. Invest. 77,* 977−984.

(15) Muraszko, K., Sung, C., Walbridge, S., Greenfield, L., Dedrick, R., Oldfield, E. H., and Youle, R. J. (1993) Pharmacokinetics and toxicology of immunotoxins administered into the subarachnoid space in nonhuman primates and rodents. *Cancer Res. 53,* 3752−3757.

(16) Pardridge, W. M., Triguero, D., and Buciak, J. L. (1990) β-endorphin chimeric peptides: transport through the blood-brain barrier in vivo and cleavage of disulfide linkage by brain. *Endocrinology 126,* 977−984.

(17) Papini, E., Rappuoli, R., Murgia, M., and Montecucco, C. (1993) Cell penetration of diptheria toxin. *J. Biol. Chem. 268,* 1567−1574.

(18) Feener, E. P., Shen, W.-C., and Ryser, H. J. P. (1990) Cleavage of disulfide bonds in endocytosed macromolecules. *J. Biol. Chem. 265,* 18780−18785.

(19) Lodish, H. F., and Kong, N. (1993) The secretory pathway is normal in dithiothreitol-treated cells, but disulfide-bonded proteins are reduced and reversibly retained in the endoplasmic reticulum. *J. Biol. Chem. 268,* 20598−20605.

(20) Bickel, U., Kang, Y.-S., Yoshikawa, T., and Pardridge, W. M. (1994) In vivo demonstration of subcellular localization of anti-transferrin receptor monoclonal antibody-colloidal gold conjugate within brain capillary endothelium. *J. Histochem. Cytochem. 42,* 1493−1497.

(21) Ryser, H. J.-P., Levy, E. M., Mandel, R., and DiSciullo, G. J. (1994) Inhibition of human immunodeficiency virus infection by agents that interfere with thiol-disulfide interchange upon virus-receptor interaction. *Proc. Natl. Acad. Sci. U.S.A. 91,* 4559−4563.

(22) Helle, J. T., Baird-Lambert, J., Cardinale, G., Spector, S., and Udenfriend, S. (1978): Isolated microvessels: the blood-brain barrier in vitro. *Proc. Natl. Acad. Sci. U.S.A. 75,* 4544−4548

(23) Mattia, A., Farmer, S. C., Takemori, A. E., Sultana, M., Portoghese, P. S., Mosberg, H. I., Bowen, W. D., and Porreca, F. (1992) Spinal opioid delta antinociception in the mouse: Mediation by a 5'-NTII-sensitive delta receptor subtype. *J. Pharmacol. Exp. Ther. 260,* 518−525.

(24) Bewley, T. A. and Li, C. H. (1983) Evidence for tertiary structure in aqueous solutions of human β-endorphin as shown by difference absorption spectroscopy. *Biochem. 22,* 2671−2675.

(25) Kunz, J., Krause, D., Kremer, M., and Dermietzel, R. (1994) The 140-kDa protein of blood-brain barrier-associated pericytes is identical to aminopeptidase N. *J. Neurochem. 62,* 2375−2386.

(26) Charpentier, S., Sagan, S., Delfour, A., and Nicolas, P. (1991) Dermenkephalin and deltorphin I reveal similarities within ligand-binding domains of μ- and δ-opioid receptors and an additional address subsite on the δ-receptor. *Biochem. Biophys. Res. Commun. 179,* 1161−1168.

(27) Pardridge, W. M. (1994) New approaches to drug delivery through the blood-brain barrier. *Trends Biotechnol. 12,* 239−245.

BC950001U

Yttrium-90 Chelation Properties of Tetraazatetraacetic Acid Macrocycles, Diethylenetriaminepentaacetic Acid Analogues, and a Novel Terpyridine Acyclic Chelator†

Julie B. Stimmel, Marie E. Stockstill, and Frederick C. Kull, Jr.*

Division of Cell Biology, Wellcome Research Laboratories, 3030 Cornwallis Road, Research Triangle Park, North Carolina 27709. Received November 17, 1994®

Realization of the potential of yttrium-90 for the radioimmunotherapy of cancer depends on rapid and kinetically stable chelation. Conditions were evaluated that influenced the chelation efficiency of these select chelators for yttrium-90: the macrocyclic chelators 2-(ǫ-nitrobenzyl)-1,4,7,10-tetraaza-cyclododecane-*N,N′,N″,N‴*-tetraacetic acid (nitro-DOTA); α-(2-(ǫ-nitrophenyl)ethyl)-1,4,7,10-tetraaza-cyclododecane-1-acetic-4,7,10-tris(methylacetic) acid (nitro-PADOTA); 2-(ǫ-nitrobenzyl)-1,4,7,10-tetraazacyclotridecane-*N,N′,N″,N‴*-tetraacetic acid (nitro-TRITA); the acyclic chelator diethylenetri-aminepentaacetic acid (DTPA); its analogues *N*-[2-amino-3-(ǫ-nitrophenyl)propyl]-*trans*-cyclohexane-1,2-diamine-*N,N′,N″*-pentaacetic acid (nitro-CHX-A-DTPA) and 2-methyl-6-(ǫ-nitrobenzyl)-1,4,7-triazaheptane-*N,N,N′,N″,N‴*-pentaacetic acid (nitro-1B4M-DTPA or nitro-MX-DTPA); and a novel acyclic terpyridine chelator, 6,6″-bis[[*N,N,N″,N‴*-tetra(carboxymethyl)amino]methyl]-4′-(3-amino-4-methoxyphenyl)-2,2′:6′,2″-terpyridine (TMT-amine). The chelators fell into two distinct classes. The acyclic chelators, DTPA, nitro-CHX-A-DTPA, nitro-MX-DTPA, and TMT-amine, chelated instanta-neously in a concentration-independent manner. Chelation efficiency was affected minimally when the concentrations of trace metal contaminants were increased. In contrast, the macrocyclic chelators, nitro-DOTA, nitro-TRITA, and nitro-PADOTA, chelated yttrium-90 more slowly in a concentration-dependent manner where efficiency was maximal only when the chelator:metal ratio was greater than 3. Their chelation efficiency diminished in a concentration-dependent fashion as the concentra-tions of trace metal contaminants were increased. Optimum labeling efficiencies were obtained through application of these principles. Additionally, the kinetic stabilities of these chelator–yttrium-90 complexes were evaluated at low pH, where the order of stability was nitro-DOTA, nitro-PADOTA > nitro-CHX-A-DTPA, nitro-MX-DTPA > nitro-TRITA, TMT, DTPA. pH lability stratified the chelators to a conveniently measurable degree and, interestingly, correlated with their in vivo stabilities where known.

INTRODUCTION

Radioimmunotherapy utilizing yttrium-90 has shown encouraging results in hematopoietic malignancies (*1*). Yttrium-90 is a pure β-emitter and has a $T_{1/2}$ of 64.1 h and an average range in tissue of 3.9 mm. Yttrium-90 may be attached to antibodies via chelation by any of a number of chelators that are covalently conjugated to the antibodies. Like other systemic radiotherapies, *in vivo* results utilizing acyclic yttrium-90-labeled ethylenedi-aminetetraacetic acid (EDTA) or diethylenetriamine pen-taacetic acid (DTPA) conjugates demonstrated dose-limiting toxicity to bone (*2–11*). It has been speculated that some of this toxicity was due to dissociation of the chelator–metal complex (*7–11*), and it is generally believed that more stable chelation improves therapeutic value.

Recently, we have seen the introduction of a third generation of acyclic chelators. These chelators have demonstrated increased stability *in vivo* compared with DTPA. They include 2-methyl-6-[(ǫ-nitrobenzyl)diethyl-ene]-*N,N,N′,N″,N‴*-pentaacetic acid (nitro-1B4M-DTPA, or nitro-MX-DTPA, Figure 1) (*12, 13*) and *N*-[2-amino-3-(ǫ-nitrophenyl)propyl]-*trans*-cyclohexane-1,2-diamine-

N,N′,N″-pentaacetic acid (nitro-CHX-A-DTPA, Figure 1) (*14, 15, 40*). A novel terpyridine chelator, 6,6″-bis-[*N,N,N″,N‴*-tetra(carboxymethyl)amino]methyl]-4′-(3-amino-4-methoxyphenyl)-2,2′:6′,2″-terpyridine (TMT-amine, Figure 1), has demonstrated ability as a highly efficient, aqueous-stabilized fluorescent label that can chelate europium (*16*).

The acyclic chelators are not as kinetically stable as the macrocyclic chelator 1,4,7,10-tetraazacyclododecane-*N,N′,N″,N‴*-tetraacetic acid (DOTA, Figure 1) (*17, 18*). DOTA possesses unique chemistry that makes it an ideal chelator for yttrium (*19*). The kinetic stability of yt-trium–DOTA complexes has been well documented and proven to be critical for minimizing toxicity to bone (*17, 18, 20–24*).

Although yttrium-90–DOTA is kinetically stable, che-lation has proved problematic. For example, the maxi-mum efficiency of chelation that was achieved with a DOTA conjugate was < 50% (*22*). Practically, inefficient chelation is not attractive for the development of a radioimmunotherapeutic. It necessitates incorporation of another manipulation to remove unchelated yttrium-90, and this radioactivity is unrecoverable. Therefore, we sought to examine chelation conditions with the goal of improving labeling efficiency. Utilizing the macrocyclic chelators illustrated in Figure 1 (top), 2-(ǫ-nitrobenzyl)-DOTA (nitro-DOTA), α-[2-(ǫ-nitrophenyl)ethyl]-1,4,7,10-tetraazacyclododecane-1-acetic-4,7,10-tris(methylacetic)-acid (nitro-PADOTA) (*25–28*), and 1,4,7,10-tetraaza-cyclotridecane-*N,N′,N″,N‴*-tetraacetic acid (TRITA) (*29*),

---
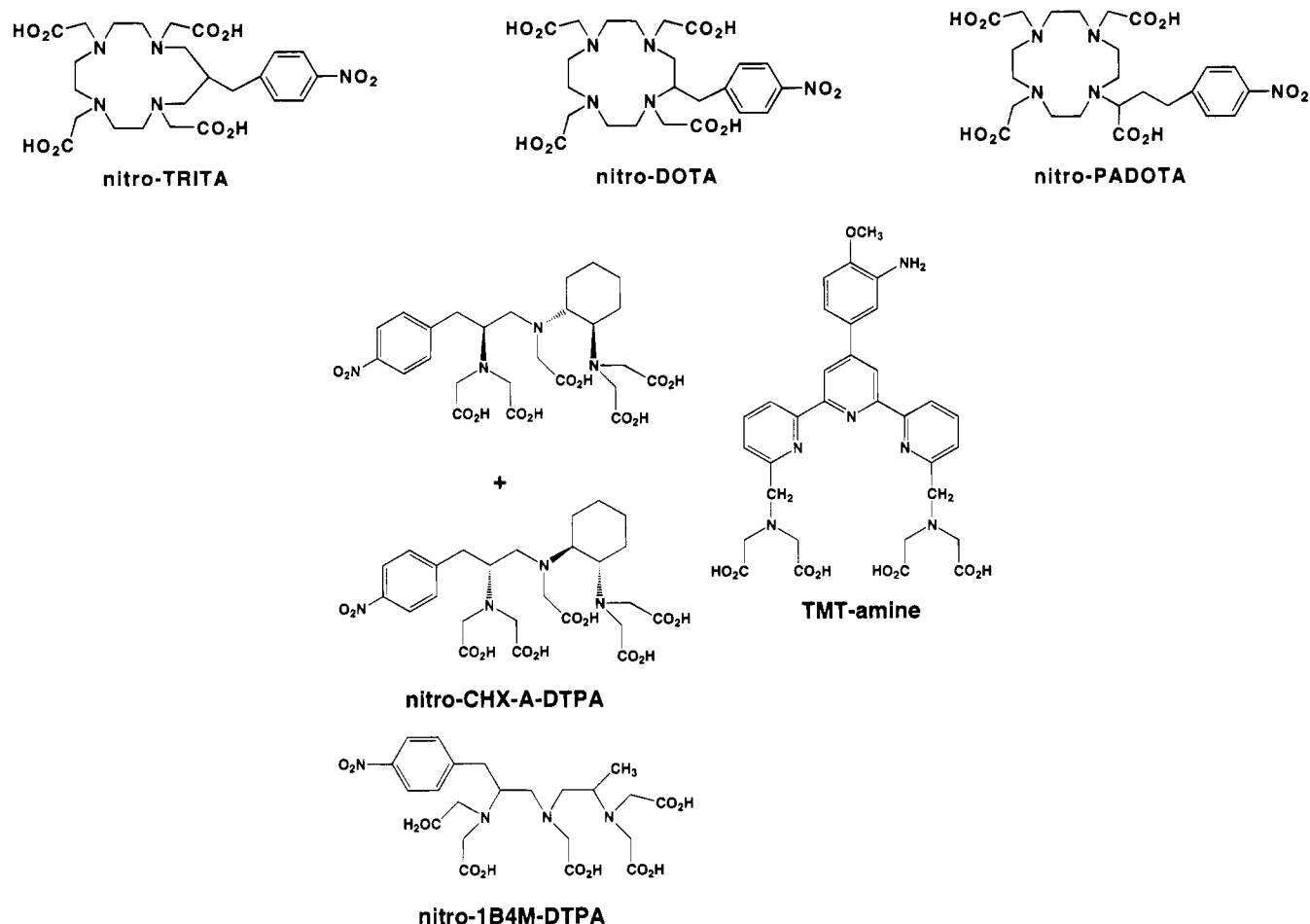
Figure 1. (Top) structures of the macrocyclic chelators compared in this study. (Bottom) structures of the acyclic chelators compared in this study.

and the acyclic chelators illustrated in Figure 1 (bottom), DTPA, nitro-CHX-A-DTPA, nitro-MX-DTPA, and an acyclic novel terpyridine derivative, TMT-amine, we evaluated the following parameters and their effect on chelation efficiency: metal and chelator concentration dependence, the minimum time interval necessary to achieve maximum labeling efficiency, and potential interference by trace metals. Our results indicate that under the appropriate conditions, efficient labeling of DOTA can be achieved in a few minutes. Having achieved efficient chelation, we also compared the kinetic stabilities of the yttrium-90−chelator complexes at low pH.

EXPERIMENTAL PROCEDURES

Materials and Reagents. Metal-free plasticware (polypropylene) or plasticware that had been soaked in 3 M HCl overnight and rinsed thoroughly with Milli-Q (18 MW) water was used throughout this work to reduce metal contamination (*30*).

All buffers and reagents were dissolved in Ultrex water (JT Baker). The reagents were analytical grade or better. All prepared buffers were treated with Chelex-100 resin (Na⁺ form, 100−200 mesh, Bio-Rad Laboratories) according to the manufacturer's instructions and passed through a 0.22 μM filter (Corning) prior to use. Diethylenetriaminepentaacetic acid (DTPA) was purchased from Sigma. Zn(II) acetate dihydrate, Ca(II) acetate hydrate, Fe(II) acetate, and yttrium-89 (cold yttrium) were purchased from Aldrich. Yttrium (^{89}YCl$_3$) was solubilized in 0.1 M ammonium acetate, pH 6.0. All chelations were per-

formed in 1.5 mL polypropylene microcentrifuge tubes that were capped.

Nitro-DOTA, nitro-PADOTA, and nitro-TRITA were synthesized in the Wellcome Research Laboratories according to literature protocols with minor modifications. Analytical evaluation confirmed the identity of the final structures. Nitro-CHX-A-DTPA and nitro-MX-DTPA were provided by Dr. Martin Brechbiel of the National Institutes of Health. TMT-amine was provided by Sterling Winthrop, Inc.

Radioactivity. Carrier-free ^{90}YCl$_3$ was purchased from Dupont/New England Nuclear (5 mCi in 10−30 μL of 0.5 N HCl, specific activity 5.6 × 10^5 Ci/g, ^{90}Sr/^{90}Y ratio < 1 × 10^{-4}%). Prior to use, the ^{90}YCl$_3$ was buffered with 6 M ammonium acetate to an approximate pH of 5.8. Stock solutions of radiolabeled yttrium were prepared by trace-labeling cold yttrium with ^{90}YoAc.

Thin-Layer Chromatography (TLC). The TLC method was used as developed by Meares *et al.* (*31*). Briefly, the TLC plate (Whatman no. 4865 821) was prepared as follows: the origin was indicated by a line drawn 2 cm from the bottom of the plate. Another line was drawn 7 cm from the bottom of the plate, and this line was scraped free of silica gel to stop the solvent front. When separation of radiolabeled metal−chelator complex from free metal was necessary, samples were added to 0.1 M sodium phosphate, pH 6.5 containing an excess of cold yttrium. A 5 μL aliquot was applied to the origin and dried with a stream of air. The samples were eluted with 10% ammonium acetate:methanol (1:1). A radioanalytical image of the plate was obtained using an

A-MK2 scanner (Automated Microbiology Systems, Inc.). Free metal remained at the origin while labeled chelator migrated to the solvent front. Data were expressed as percent metal chelated.

Radiolabeling Efficiency. Stock (200 mM) solutions of each chelator were prepared in 0.1 M ammonium acetate, pH 6.0 and two times the indicated concentrations of yttrium-90 were prepared in the same buffer. Equivolume amounts of chelator and yttrium-90 were mixed and incubated at room temperature for 2 h. The chelation was stopped by the addition of 20 μL of blocking solution, and a 5 μL aliquot was analyzed by TLC. Blocking solution was 0.1 M sodium phosphate, pH 6.5 that contained a 5-fold excess of cold yttrium over the chelator concentration and was prepared immediately before analysis to minimize precipitation of the cold yttrium. The addition of cold yttrium was necessary to prevent rechelation of yttrium-90.

Duration of Yttrium-90 Chelation. Stock solutions of chelator and yttrium-90 were prepared in 0.1 M ammonium acetate, pH 6.0. Equal volumes of 100 mM chelator and 20 mM yttrium-90 were mixed at room temperature. Five μL aliquots were removed from the mixtures immediately (time zero) and at the indicated time intervals. To terminate chelation, the samples were added directly into 10 μL of 0.1 M sodium phosphate, pH 6.5 containing an excess of cold yttrium to terminate the chelation. A 5 μL aliquot was analyzed by TLC.

Effect of Trace Metals on Yttrium-90 Chelation. Stock solutions of chelator (4 mM) and yttrium-90 (800 μM) were prepared in 0.1 M ammonium acetate, pH 6.0. In addition, the following stock concentrations of Fe(II) acetate, Ca(II) acetate hydrate, and Zn(II) acetate dihydrate were prepared in the same buffer: 20 mM, 10 mM, 2 mM, 1600, 1200, 800, 400, and 200 μM. To each polypropylene tube was added 5 μL of the indicated trace metal and 2.5 μL of the yttrium-90 stock. Finally, 2.5 μL of the chelator stock was added. The chelations were performed for 2 h at room temperature and were stopped by addition of 20 μL of sodium phosphate, pH 6.5. A 5 μL aliquot was analyzed by TLC.

Dissociation of Yttrium-90-Labeled Chelators at pH 2.0. A 2 mM stock solution of each chelator and a 400 mM stock of yttrium-90 were prepared in 0.1 M ammonium acetate, pH 6.0. Equivolumes of chelator and yttrium-90 were mixed and allowed to chelate at room temperature for 2 h. An initial time point was obtained by removing 1 μL from the chelation solution for TLC analysis. Four μL aliquots of chelation solution was diluted into 56 μL of 0.1 M glycine-HCl, pH 2.0 in triplicate and incubated at 37 °C. The final concentration of chelator was 67 μM. Five μL aliquots were removed at the indicated time and added to 10 μL of 0.1 M sodium phosphate, pH 6.5 containing a 60-fold excess of cold yttrium to stop chelation and to prevent rechelation. A 5 μL aliquot was analyzed by TLC.

RESULTS AND DISCUSSION

Preliminary work indicated that neither the tetraaza macrocyclic chelators (Figure 1 (top)) nor DTPA chelated yttrium-90 efficiently at chelator concentrations below 10 μM. Thus, this concentration appeared to be our threshold for chelation, and only chelator concentrations above 10 μM were used in the following studies. Relatedly, a minimum ligand concentration for efficient chelation of indium-111 by DTPA conjugates has been reported (21).

The effect of metal concentration on chelator labeling efficiency was examined in Table 1. In this experiment, chelator was mixed with increasing concentrations of

Table 1. Effect of Yttrium-90 Concentration on Chelator Labeling Efficiency[a]

[⁹⁰YoAc], 10⁻⁶ M	% ⁹⁰Y chelated				
	DOTA	PADOTA	TRITA	TMT	DTPA
100	49.7	38.3	53.4	97.4	97.8
50	93.3	70.0	89.6	98.4	96.3
33	97.4	92.6	95.8	97.9	94.8
25	97.8	97.0	96.3	97.9	92.9
17	97.2	97.6	94.1	97.8	79.4
10	97.2	97.4	96.2	97.3	86.4

[a] [Chelator] = 100 μM; reaction period = 2 h; pH 6.0; temperature = 22 °C; final volume of chelation = 10 μL.

Table 2. Time Interval of Yttrium-90 Chelation[a]

time (min)	% ⁹⁰Y chelated				
	DOTA	PADOTA	TRITA	TMT	DTPA
0	5.1	1.5	3.2	97.0	91.4
15	96.1	79.7	74.4	98.6	89.2
30	98.5	89.9	90.6	98.8	88.7
60	98.7	95.0	96.5	98.8	88.5
90	99.0	96.8	97.4	98.8	88.5
120	99.1	97.6	97.7	98.7	90.6

[a] [Chelator] = 50 μM; [⁹⁰YoAc] = 10 μM; temperature = 22 °C; volume of chelation = 10 μL.

yttrium-90, and the extent of chelation, expressed as a percentage, was determined. Maximum labeling efficiency with the macrocyclic chelators was achieved only when the concentration of chelator was in excess of the yttrium-90 concentration. A 3-fold chelator:metal molar ratio was sufficient to achieve labeling in excess of 90%. In contrast, the chelation of TMT-amine, nitro-CHX-A-DTPA (data not shown), nitro-MX-DTPA (data not shown), and DTPA with yttrium-90 was efficient at a metal: chelator molar ratio of 1:1. When similar experiments were performed with different concentrations of chelator (>10 μM, data not shown), maximum labeling efficiency was achieved only when the chelator:metal molar ratio >3 for the macrocyclics and >1 for the acyclics. Curiously and in contrast to yttrium-90, the macrocyclic chelators chelated divalent cobalt-57 in a chelator:metal molar ratio of 1:1 (data not shown). Thus, the chelator: metal molar ratio required for optimum efficiency may be unique for different radiometals and chelators.

In Table 2, we investigated the time course of yttrium chelation. In this experiment, yttrium-90 was incubated in the presence of a 5-fold excess of chelator, and the progress of the chelation was monitored at the time intervals indicated in Table 2. Expectedly, DTPA achieved >85% chelation instantaneously as observed previously (22). Rapid chelation was also evident with TMT-amine. We also observed this with nitro-CHX-A-DTPA and nitro-MX-DTPA (data not shown). In contrast, the macrocycles were slower to complex yttrium-90. This retardation in the progress of chelation has been documented previously with DOTA (19). Interestingly, nitro-DOTA was slightly faster than nitro-PADOTA and nitro-TRITA.

Since the final concentrations of chelator (<100 μM) and yttrium-90 (<10 μM) in a typical conjugate chelation are very low, it is not surprising that the presence of trace metals can potentially influence the efficiency of conjugate labeling (23). Therefore, we investigated the influence of divalent cations that are commonly found in commercial preparations of yttrium-90 on chelation labeling efficiency (Figure 2). Nitro-MX-DTPA was not evaluated in this study. Yttrium-90 was incubated with a 5-fold excess of chelator in the presence of increasing amounts of Zn(II) acetate (A), Fe(II) acetate (B), or Ca-(II) acetate (C). The labeling efficiency of DTPA was not affected by the presence of Ca²⁺ or Fe²⁺. However, at
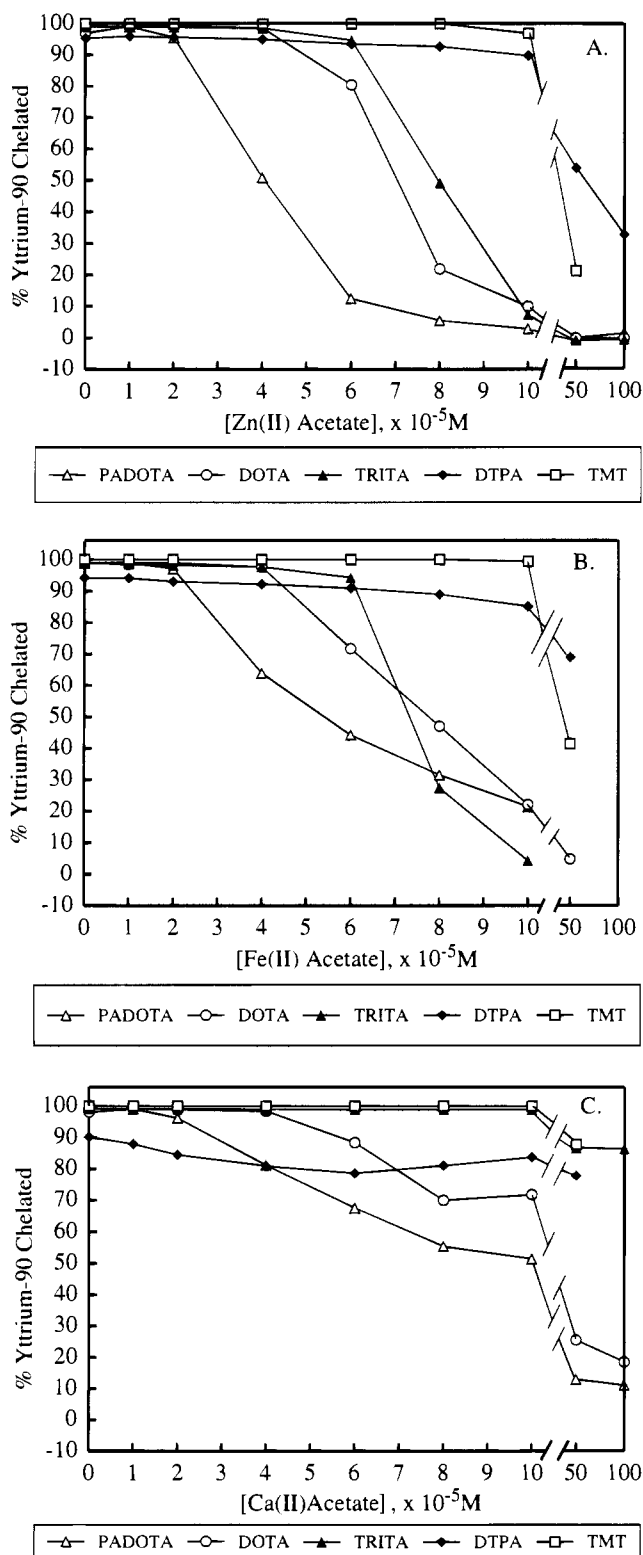
Figure 2. Effect of the presence of trace metals on chelation efficiency of macrocyclic chelators and DTPA with yttrium-90: [chelator] = 1 mM; [^{90}YoAc] = 100 mM; reaction period = 2 h; buffer = 0.1 M ammonium acetate pH 6.0; temperature = 22 °C; final volume of chelation = 10 mL; (A) Zn(II) acetate; (B) Fe(II) acetate; (C) Ca(II) acetate.

high concentrations of Zn^{2+}, there was a slight decrease in efficiency. TMT-amine and nitro-CHX-A-DTPA exhibited properties similar to those of DTPA. The labeling efficiency of TMT-amine and nitro-CHX-A-DTPA (data not shown) was not affected by the presence of increasing amounts of Ca^{2+}. In contrast, high concentrations of Zn^{2+}

and Fe^{2+} affected the labeling efficiency of TMT-amine and nitro-CHX-A-DTPA (data not shown) to a greater degree. This experiment was repeated with equimolar concentrations of DTPA, nitro-CHX-A-DTPA, TMT-amine, and yttrium-90, and the effect of Ca^{2+} on chelation efficiency was minimal. In contrast, there was a concentration dependent decrease with Fe^{2+} and Zn^{2+} (data not shown). Thus, it appeared that the contaminant-induced loss of efficiency of DTPA, nitro-CHX-A-DTPA, or TMT-amine increased as the chelator concentration decreased.

The influence of trace metals on macrocyclic chelation was more pronounced. A 1- to 3-fold contaminant concentration increase over the yttrium-90 concentration diminished labeling efficiency. In addition, yttrium-90 labeling efficiency decreased as the contaminant concentration increased in a dose-dependent manner. The extent of the influence varied with the particular chelator, but in general, nitro-PADOTA chelation demonstrated the most sensitivity followed by nitro-DOTA and nitro-TRITA. Surprisingly, nitro-TRITA labeling was not affected by the presence of Ca^{2+}. We also observed that the presence of trace metals substantially retarded the time necessary to achieve maximum efficiency (data not shown). These results clearly demonstrated the necessity of a metal contaminant-free environment to enhance chelation efficiencies. A similar conclusion has been reached relatedly in a study of the influence of Zn^{2-}, Mg^{2+}, and Ca^{2+} on the chelation efficiency of several chelators, including DOTA, for ^{67}Cu (*32*). When comparing DOTA's chelation efficiency for $^{90}Y^{3+}$ with that for $^{67}Cu^{2+}$ (*32*), the chelation efficiency for yttrium-90 was inhibited by 10-fold less contaminent; thus, the comparison underscores the fastidious requirements for chelation.

The kinetic stability of yttrium-90-labeled chelator complexes was evaluated at low pH. These studies were undertaken for two reasons. Firstly, acid-assisted dissociation is a well-documented catabolic phenomenon that contributes to in vivo physiologic stability. Secondly, pH lability (in the laboratory) was a convenient means allowing for ready discrimination among this group of chelators. We observed that the rates of dissociation increased with lowering pH and were chelator dependent. Furthermore, when comparing this group of chelators, the order of stability was maintained as pH was lowered. The degree of discrimination was most evident at pH 2–3. The results at pH 2.0 are illustrated in Figure 3. The chelators were labeled with yttrium-90 (>90%) and diluted in triplicate into a glycine—HCl buffer at pH 2.0 under conditions where reassociation was negligible. At the indicated time intervals, the yttrium-90 remaining in the chelator was quantitated. Chelator stability fell into three distinct classes. Nitro-DOTA and nitro-PADOTA exhibited exceptional stability over the course of 7 days, and then small differences between the two chelators became apparent. Nitro-CHX-A-DTPA and nitro-MX-DTPA exhibited moderate kinetic stability. Yttrium-90-labeled DTPA, TMT-amine, and nitro-TRITA were unstable at this pH. After 3 days, no radioactivity remained complexed in these latter chelators.

The kinetic stability of yttrium-90—DOTA complexes at low pHs has been demonstrated recently (*23*) but was implied in the early 1980's (*19*). Nuclear magnetic resonance analysis of lanthanide—DOTA complexes demonstrated that the steric requirements of the 12-membered tetraaza cavity resulted in unusual rigidity that retarded protonation. Even though PADOTA is in the same class of stability as DOTA, minor differences were observed. It can be inferred that functionalization at the 2-position alters the conformation enough to allow pro-
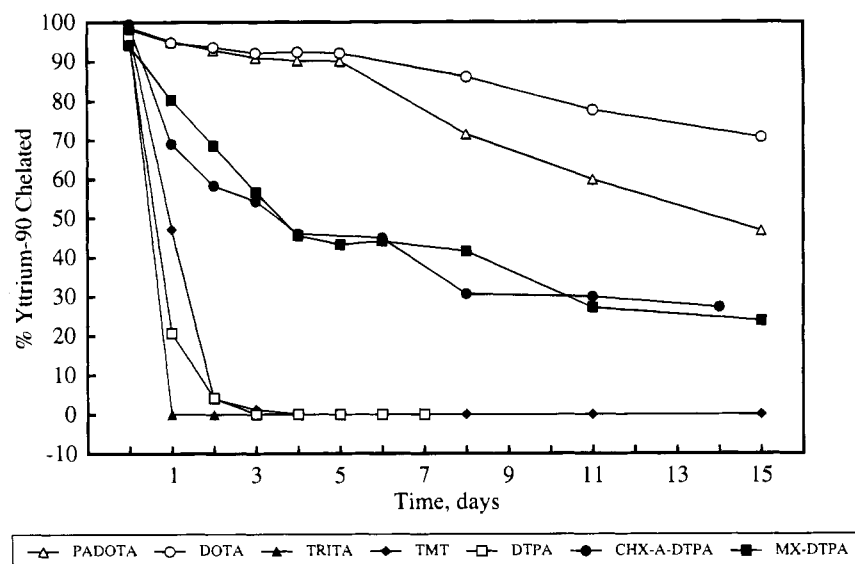
Figure 3. Stability of [90]Y—chelator complex at pH 2.0: [chelator] = 67 mM; buffer = 0.1 M glycine-HCl pH 2.0; temperature = 37 °C.

tonation to occur more easily for PADOTA than with DOTA. However, both nitro-DOTA and nitro-PADOTA complexes exhibited exceptional stability at low pH.

Nitro-MX-DTPA and nitro-CHX-A-DTPA demonstrated moderate kinetic stability at pH 2.0 that was similar to one another. Additionally, these third-generation DTPA analogues displayed biphasic stability at this pH. This could suggest the presence of diastereomeric yttrium—chelate complexes that demonstrate different kinetic stabilities. Both nitro-CHX-A-DTPA and nitro-MX-DTPA are mixtures of enantiomers (*14, 33*). Yttrium—MX-DTPA complexes have been observed to form diastereomeric mixtures that exhibited unique behavior (*33*). It is reasonable that diastereomeric mixtures also form from yttrium–CHX-A-DTPA complexes.

Recent work has demonstrated that yttrium complexes of these third generation DTPA analogues are more stable in vivo than DTPA but not as stable as DOTA (*12, 34, 35*). The kinetic stability of yttrium-90 complexes of these chelators at pH 2.0 thus appears to correlate with other analyses including in vivo stability. The kinetic instability of DTPA—metal complexes at low pH has been well established (*36—39*), and our results confirmed past experience. The novel terpyridine derivative, TMT-amine, exhibited pH stability properties similar to those of DTPA. It is interesting that the macrocycle, nitro-TRITA, also exhibited stability similar to DTPA at pH 2.0. It has been postulated that the 13-membered ring forms a metal complex conformation with metals that possess larger radii such as yttrium that is considerably more flexible and less stable than that of DOTA (*40—43*). The absence of steric constraint may have resulted in more facile protonation and resultant kinetic instability.

SUMMARY

In this study, we evaluated the relationship of metal and chelator concentration, time interval of chelation, and the presence of trace metal contaminants on the chelation efficiency of a select group of chelators for yttrium-90. We also report the kinetic stability of the chelator—yttrium-90 complexes at pH 2.0. All of these chelators have clinical utility and certain advantages for different radiometals and applications. Our principle aim was to appreciate conditions that influenced chelation so

that we could later evaluate the behavior of immunocon-jugates. We saw merit in head-to-head evaluation since the results could have been influenced by reagent purity.

Within this select group, we observed two distinct classes. The acyclic chelators, TMT-amine, nitro-MX-DTPA, nitro-CHX-A-DTPA, and DTPA, chelated yttrium instantaneously in a chelator:metal molar ratio of 1:1. Also, the labeling efficiency of these chelators was affected minimally by the presence of trace metal contaminants when the chelator concentration was 5-fold greater than the yttrium-90 concentration. However, when the contaminant concentration was equivalent to or greater than the chelator concentration, the labeling efficiency diminished in a concentration-dependent manner. Both TMT-amine— and DTPA—yttrium-90 complexes demonstrated minimal stability at pH 2.0, whereas nitro-MX-DTPA and nitro-CHX-A-DTPA demonstrated moderate kinetic stability at pH 2.0 and exhibited biphasic characteristics. These latter compounds are mixtures of enantiomers that form diastereomeric mixtures when coordinated to yttrium. The biphasic nature of the kinetic stability at pH 2.0 suggests that the diastereomers may have different kinetic stabilities.

The macrocyclic chelators, nitro-DOTA, nitro-PADO-TA, and nitro-TRITA, chelated yttrium-90 at a slower rate. Nitro-DOTA was the fastest and achieved maximum labeling efficiency in less than 30 min. Nitro-PADOTA and nitro-TRITA required less than 60 min to achieve labeling efficiencies comparable to nitro-DOTA. All three macrocycles required minimally a 3-fold excess of chelator over yttrium concentration to achieve maximum labeling efficiencies. Curiously, excess chelator was not required to chelate divalent cobalt efficiently. The labeling efficiencies of the macrocyclic chelators (5-fold excess of chelator compared to yttrium-90 concentration) were inhibited in a concentration-dependent manner by the presence of increasing amounts of trace metals (Ca^{2+}, Fe^{2+}, Zn^{2+}) that are commonly found in commercial yttrium-90 preparations. Nitro-TRITA was an exception. The labeling efficiency of the 13-membered ring chelator was not affected by increasing concentrations of Ca^{2+}. Finally, nitro-DOTA— and nitro-PADOTA—yttrium-90 complexes exhibited exceptional kinetic stability at pH 2.0. In contrast, the nitro-TRITA—yttrium-90 complex

demonstrated kinetic instability at pH 2.0 similar to TMT-amine and DTPA.

In conclusion, we demonstrate the relationship between metal and chelator concentration, time to chelation, and the necessity of maintaining a metal contaminant-free environment to achieve optimum labeling efficiencies. We also show that low pH stability stratifies these chelators. The order of stratification correlates with published observations on their physiological kinetic stabilities. We hope these observations will be especially useful for immunoconjugate chelation.

ACKNOWLEDGMENT

LITERATURE CITED

(1) Grossbard, M. L., Press, O. W., Appelbaum, F. R., Bernstein, I. D., and Nadler, L. M. (1992) Monoclonal antibody-based therapies of leukemia and lymphoma. *Blood 80,* 863–878.

(2) Hnatowich, D. J., Virzi, F., and Doherty, P. W. (1985) DTPA-coupled antibodies labeled with yttrium-90. *J. Nucl. Med. 26,* 503–509.

(3) Larson, S. M., Carrasquillo, J. A., Reynolds, J. C., Hellstrom, I., Hellstrom, K. E., Mulshine, J. C., and Mattis, L. E. (1986) Therapeutic applications of radiolabeled antibodies: current situation and prospects. *Nucl. Med. Biol. 13,* 207–213.

(4) Anderson-Berg, W. T., Squire, R. A., and Strand, M. (1987) Specific radioimmunotherapy using ^{90}Y-labeled monoclonal antibody in erythroleukemic mice. *Cancer Res. 47,* 1905–1912.

(5) Hnatowich, D. J., Chinol, M., Siebecker, D. A., Gionet, M., Griffin, T., Doherty, P. W., Hunter, R., and Kase, K. R. (1988) Patient biodistribution of intraperitoneally administered yttrium-90-labeled antibody. *J. Nucl. Med. 29,* 1428–1435.

(6) Sharkey, R. M., Kaltovich, F. A., Shih, L. B., Fand, I., Govelitz, G., and Goldenberg, D. M. (1988) Radioimmunotherapy of human colonic cancer xenografts with 90Y-labeled monoclonal antibodies to carcinoembryonic antigen. *Cancer Res. 48,* 3270–3275.

(7) Stewart, J. S. W., Hird, V., Snook, D., Sullivan, M., Myers, M. J., and Epenetos, A. A. (1988) Intraperitoneal 131I- and 90Y-labelled monoclonal antibodies for ovarian cancer: pharmacokinetics and normal tissue dosimetry. *Int. J. Cancer 42* (Suppl. 3), 71–76.

(8) Rowlinson, G., Snook, D., Stewart, S., and Epenetos, A. A. (1989) Intravenous EDTA to reduce uptake following 90Y-labelled monoclonal antibody administration. *Br. J. Cancer 59,* 322.

(9) Hird, V., Stewart, J. S., Snook, D., Dhokia, B., Coulter, C., Lambert, H. E., Mason, W. P., Soutler, W. P., and Epenetos, A. A. (1990) Intraperitoneally administered 90Y-labelled monoclonal antibodies as a third line of treatment in ovarian cancer. A phase 1–2 trial: problems encountered and possible solutions. *Br. J. Cancer Suppl. 10,* 48–51.

(10) Rosenblum, M. G., Kavanagh, J. J., Burke, T. W., Wharton, J. T., Cunningham, J. E., *et al.* (1991) Clinical pharmacology, metabolism and tissue distribution of 90Y-labeled monoclonal antibody B72.3 after intraperitoneal administration. *J. Natl. Can. Inst. 83* (22), 1629–1636.

(11) Haller, D., Cannon, L., Alavi, A., and Gulfo, J. (1992) A Phase I Trial of 90Y labeled monoclonal antibody (MoAb) B72.3 [CYT-103-90Y] administration with concurrent EDTA in refractory adenocarcinoma. *Antibody, Immunoconjugates, Radiopharm. 5,* Abstr. 100, 147.

(12) Kozak, R. W., Raubitschek, A., Mirzadeh, S., Brechbiel, M. W., Junghaus, R., Gansow, O. A., and Waldmann, T. A. (1989) Nature of the bifunctional chelating agent used for radioimmunotherapy with yttrium-90 monoclonal antibodies: critical factors in determining *in vivo* survival and organ toxicity. *Cancer Res. 49,* 2639–2644.

(13) Brechbiel, M. W., and Gansow, O. A. (1991) Backbone-substituted DTPA ligands for ^{90}Y radioimmunotherapy. *Bioconjugate Chem. 2,* 187–194.

(14) Brechbiel, M. W., and Gansow, O. A. (1992) Synthesis of C-functionalized *trans*-cyclohexyldiethylenetriaminepenta-acetic acids for labeling of monoclonal antibodies with the bismuth-212 α-particle emitter. *J. Chem. Soc., Perkin Trans. 1* 1175–1178.

(15) Camera, L., Kinuya, S., Pai, L. H., Garmestani, K., Brechbiel, M. W., Gansow, O. A., Paik, C. H., Pastan, I., and Carrasquillo, J. A. (1993) Preclinical evaluation of ^{111}In-labeled B3 monoclonal antibody: biodistribution and imaging studies in nude mice bearing human epedermoid carcinoma xenografts. *Cancer Res. 53,* 2834–2839.

(16) Toner, J. L. (1989) Terpyridine Chelating Agents. U. S. Patent No. 4,859,777.

(17) Moi, M. K., Meares, C. F., and DeNardo, S. J. (1988) The peptide way to macrocyclic bifunctional chelating agents: synthesis of 2-(ϱ-nitrobenzyl)-1,4,7,10-tetraazacyclotridecane-N,N',N'',N'''-tetraacetic acid and study of its yttrium(III) complex. *J. Am. Chem. Soc. 110,* 6267–6269.

(18) Deshpande, S. V., DeNardo, S. J., Kukis, D. L., Moi, M. K., McCall, M. J., DeNardo, G. L., and Meares, C. F. (1990) Yttrium-90-labeled monoclonal antibody for therapy: labeling by a new macrocyclic bifunctional chelating agent. *J. Nucl. Med. 31,* 473–479.

(19) Desreux, J. F. (1980) Nuclear magnetic resonance spectroscopy of lanthanide complexes with a tetraacetic tetraaza macrocycle. Unusual conformation properties. *Inorg. Chem. 19,* 1319–1324.

(20) Brechbiel, M. W., Wu, C., McMurry, T. J., Gansow, O. A., Garmestani, K., *et al.* (1993) Synthesis and evaluation of 2-(ϱ-SCN-benzyl)-trans-cyclohexyl-DTPA's for radioimmunoimaging and radioimmunotherapy with ^{111}In and ^{90}Y. *Antibody, Immunoconjugates, Radiopharm. 6,* Abstr. 47, 78.

(21) Mirzadeh, S., Brechbiel, M. W., Atcher, R. W., and Gansow, O. A. (1990) Radiometal labeling of immunoproteins: covalent linkage of 2-(4-isothiocyanatobenzyl) diethylenetriaminepentaacetic acid ligands to immunoglobulin. *Bioconjugate Chem. 1,* 59–65.

(22) Harrison, A., Walker, C. A., Parker, D., Jankowski, K. J., Cox, J. P., *et al.* (1991) The *in vivo* release of ^{90}Y from cyclic and acyclic ligand-antibody conjugates. *Nucl. Med. Biol. 18*(5), 469–476.

(23) Broan, C. J., Cox, J. P. L., Craig, A. S., *et al.* (1991) Structure and solution stability of indium and gallium complexes of 1,4,7-triazacyclononanetriacetate and of yttrium complexes of 1,4,7,10-tetraazacyclododecanetetraacetate and related ligands: kinetically stable complexes for use in imaging and radioimmunotherapy. X-Ray molecular structure of the indium and gallium complexes of 1,4,7-triazacyclononane-1,4,7-triacetic acid. *J. Chem. Soc., Perkin Trans. 2* 87–98.

(24) Kroger, L. A., DeNardo, G. L., DeNardo, S. J., Miers, L. A., and Meares, C. F. (1992) Comparative toxicity studies of a yttrium-90 labeled MX-DTPA and 2-IT-BAD conjugated monoclonal antibody (BrE-3). *Antibody, Immunoconjugates, Radiopharm. 5,* Abstr. 94, 357.

(25) Kruper, W. J., Jr. (1991) Process for preparing mono-N-alkylated polyazamacrocycles. U. S. Patent No. 5,064,956.

(26) Schlom, J., Siler, K., Milenic, D. E., Eggensperger, D., Colcher, D., *et al.* (1991) Monoclonal antibody-based therapy of a human tumor xenograft with a ^{177}lutetium-labeled immunoconjugate. *Cancer Res. 51,* 2889–2896.

(27) Schott, M. E., Milenic, D. E., Yokota, T., Whitlow, M., Wood, J. F., Fordyce, W. A., Cheng, R. C., and Schlom, J. (1992) Differential metabolic patterns of iodinated *versus* radiometal chelated anticarcinoma single-chain F_v molecules. *Cancer Res. 52,* 6413–6417.

(28) Schlom, J., Siler, K., Milenic, D. E., Eggensperger, D., Colcher, D., *et al.* (1992) Biodistribution and pre-clinical radioimmunotherapy studies using radiolanthanide-labeled immunoconjugates. *Antibodies, Immunoconjugates, Radiopharm. 5,* Abstr. 42, 340.

(29) Ruser, G., Ritter, W., and Maecke, H. R. (1990) Synthesis and evaluation of two bifunctional carboxymethylated tetraazamacrocyclic chelating agents for protein labeling with indium-111. *Bioconjugate Chem. 1,* 345–349.

(30) Thiers, R. E. (1957) Contamination in trace element analysis and its control. *Methods Biochem. Anal. 5*, 273–335.

(31) Meares, C. F., McCall, M. J., Reardan, D. T., Goodwin, D. A., Diamanti, C. I., and McTigue, M. (1984) Conjugation of antibodies with bifunctional chelating agents: isothiocyanate and bromoacetamide reagents: methods of analysis, and subsequent addition of metal ions. *Anal. Biochem. 142*, 68–78.

(32) Kukis, D. L., Li, M., and Meares, C. F. (1993) Selectively of antibody–chelate conjugates for binding copper in the presence of competing metals. *Inorg. Chem. 32*, 3981–3982.

(33) Cummins, C. H., Rutter, E. W., and Fordyce, W. A. (1991) A convenient synthesis of bifunctional chelating agents based on diethylenetriaminepentaacetic acid and their coordination chemistry with yttrium (III). *Bioconjugate Chem. 2*, 180–186.

(34) Camera, L., Kinuya, S., Garmestani, K., Wu, C., Brechbiel, M. W., *et al.* (1994) Evaluation of serum stability and in vivo biodistribution of CHX-DTPA and other ligands for yttrium labeling of monoclonal antibodies. *J. Nucl. Med. 35*, 882–889.

(35) DeNardo, G. L., Koger, L. A., DeNardo, S. J., Miers, L. A., Salako, Q., *et al.* (1994) Comparative toxicity studies of yttrium-90 MX-DTPA and 2-IT-BAD conjugated monoclonal antibody (BrE-3). *Cancer* (Suppl) *73*(3), 1012–1022.

(36) Tse, P. K., and Powell, J. E. (1985) Study of structural influence on the formation constants of lanthanide-polyamino polycarboxylate complexes. *Inorg. Chem. 24*, 2727–2730.

(37) Cacheris, W. P., Nickle, S. K., and Sherry, A. D. (1987) Thermodynamic study of lanthanide complexes of 1,4,7-triazacyclononane-N,N′,N″-triacetic acid and 1,4,7,10-tetraazacyclododecane-N,N′,N″,N‴-tetraacetic acid. *Inorg. Chem. 26*, 958–960.

(38) Nyssen, G. A., and Margerum, D. W. (1970) Multidentate ligand kinetics. XIV. Formation and dissociation kinetics of rare earth-cyclohexylenediaminetetraacetate complexes. *Inorg. Chem. 9*, 1814–1820.

(39) De Jonghe, M., and D'Olieslager, W. (1985) The dissociation kinetics of rare earths-N-methylethylenediamine-N,N′,N′-triacetate complexes. *Inorg. Chim. Acta 109*, 7–14.

(40) Ascenso, J. R., Delgado, R., and Frausto da Silva, J. J. R. (1985) Nuclear magnetic resonance studies of the protonation sequence of cyclic tetra-azatetraacetic acids. *J. Chem. Soc., Perkin Trans. 2*, 781–788.

(41) Loncin, M. F., Desreux, J. F., and Merciny, E. (1986) Coordination of lanthanides by two polyamino polycarboxylic macrocycles: formation of highly stable lanthanide complexes. *Inorg. Chem. 25*, 2646–2648.

(42) Clarke, E. T., Martell, A. E. (1991) Stabilities of the alkaline earth and divalent transition methal complexes of the tetraazamacrocyclic tetraacetic acid ligands. *Inorg. Chim. Acta 190*, 27–36.

(43) Clarke, E. T., and Martell, A. E. (1991) Stabilities of trivalent metal ion complexes of the tetraacetate derivatives of 12-, 13-, and 14-membered tetraazamacrocycles. *Inorg. Chim. Acta 190*, 37–46.

CORRECTIONS

Volume 6, Number 2, March/April 1995.

Julie B. Stimmel, Marie E. Stockstill, and Frederick C. Kull, Jr.*

YTTRIUM-90 CHELATION PROPERTIES OF TETRAAZATETRAACETIC ACID MACROCYCLES, DIETHYLENETRIAMINEPENTAACETIC ACID ANALOGUES, AND A NOVEL TERPYRIDINE ACYCLIC CHELATOR

Page 221. In the Experimental Procedures under Radiolabeling Efficiency and Duration of Yttrium-90 Chelation, the concentrations of chelator stock and yttrium-90 stock should be micromolar. Under Dissociation of Yttrium-90-labeled Chelators at pH 2.0, the concentration of yttrium-90 stock was 400 μM.

Page 222. In Figure 2, the text in the legend should state that the yttrium-90 concentration was 200 μM and the final volume of chelation was 10 μL.

Page 223. The legend for Figure 3 should state that the final concentration of chelator was 67 μM.

BC950185C

TECHNICAL NOTES

Heterobifunctional Poly(ethylene oxide): Synthesis of α-Methoxy-ω-amino and α-Hydroxy-ω-amino PEOs with the Same Molecular Weights

Sandrine Cammas,[†,‡] Yukio Nagasaki,[†] and Kazunori Kataoka*[,†,‡]

Department of Materials Science and Technology, Science University of Tokyo, Yamazaki 2641, Noda, Chiba 278, Japan, and International Center for Biomaterials Science, Science University of Tokyo, Yamazaki 2669, Noda, Chiba 278, Japan. Received July 22, 1994[®]

Well-defined α-methoxy-ω-amino and α-hydroxy-ω-amino poly(ethylene oxide)s (PEOs) were obtained after chemical modifications of α-hydroxy-ω-allyl PEO which was synthesized by anionic polymerization of ethylene oxide (EO) with allyl alcoholate as initiator; molecular weights of the prepolymer were controlled by the monomer/initiator ratio. Addition of methyl iodide on the hydroxy function of this prepolymer led to an α-methoxy-ω-allyl PEO; completion of the reaction and purity of the resulting polymer were demonstrated by ^{1}H, ^{13}C NMR and GPC studies. Addition reactions of 2-amino-ethanethiol hydrochloride on α-hydroxy-ω-allyl PEO and α-methoxy-ω-allyl PEO in the presence of azobisisobutyronitrile (AIBN) led to the expected homopolymers without any side reactions as shown by ^{1}H and ^{13}C NMR spectra.

INTRODUCTION

Owing to its nontoxicity and water solubility, poly(ethylene oxide) (PEO) has numerous applications in biochemical and biomedical fields (*1*). For example, this synthetic polymer is used as a promotor for cell fusion and hybridization (*2*) and as a chemical modification reagent for reducing or controlling the antigenicity of immunogenic proteins (*3, 4*). Nevertheless, PEO polymers present an important disadvantage: lack of reactive groups in ethylene oxide units. For this reason, synthesis of polymers having reactive end groups is of great interest.

In the last few years, numerous studies have been focused on the synthesis of well-defined homotelechelic (*5*) and heterotelechelic (*6*) PEOs (*7–9*). End groups allow us to control and adjust physicochemical properties of the resulting materials. They also permit copolymerization between PEOs oligomers and defined comonomers in order to obtain hydrophobic/hydrophilic block-copolymers, for example. Furthermore, the preparation of well-defined heterotelechelic PEOs is of great interest for bioconjugation of these polymers with molecules such as proteins (*10–13*) or with liposomes (*14–16*).

Uses of proteins or liposomes as therapeutic agents are limited because of their degradation by proteolytic enzymes, thermal instability, or immunogenicity. This problem can be reduced by the formation of a conjugate between the protein or liposome and a poly(ethylene oxide). Moreover, if heterotelechelic PEOs are used, a functional group is available at the free end of PEO

chains. This group allows the introduction of a homing device, for example. Low and co-workers had described the preparation of PEO-conjugated liposomes having folic acid bound to the free end of PEO. These liposomes can be targeted to cancer cells having a folic acid receptor (*15*). These "functionalized" liposomes have been also described by Crommelin and co-workers in their review on liposomes (*16*).

Ito and co-workers had prepared amphiphilic PEO macromonomers having their hydrophilic/hydrophobic balance influenced by the terminal alkyloxy group and/or the PEO chain length (*17, 18*). Moreover, they had shown that reactivities of such PEO macromonomers for copolymerization reactions with styrene or benzylmethacrylate depended on the nature of α and ω end groups (*17, 18*).

Recently, one of us (K.K.) and his co-workers have been studying a polymeric micelle system which can be used as high-performance vehicles for drug delivery (*19, 20*). These polymeric micelles were prepared from PEO-poly(β-benzyl-L-aspartate) block copolymer which was synthesized by ring-opening polymerization of β-benzyl-L-aspartate N-carboxyanhydride (BLA-NCA) initiated with primary amino ended PEO (*21, 22*). These polymeric micelles can entrap, chemically or physically, drugs such as adriamycin; the drug entrapped in the micelles core can be stabilized in the body and especially in the blood. Actually, a 1000-fill elevated adriamycin concentration can be maintained in the blood without any trouble as compared with adriamycin itself. Such a high concentration may be one of the reasons for the extremely high antitumor activity of this preparation (*19*).

The surface of the polymeric micelles thus prepared should be surrounded by methoxy groups. If another group, such as hydroxy, carboxyl, or thiol functions, can be introduced on the surface of the micelles, instead of methoxy groups, the resulting micelles would exhibit two interesting features: (i) characteristics of the micelle itself

---

and (ii) targeting by introduction of functional substances such as sugar or antibody on the surface of the polymeric micelles.

In this paper, we report on the synthesis of heterotelechelic PEOs having the same molecular weight and distributions. These heterotelechelic PEOs are synthesized with the aim to be used for further preparation of functional polymeric micelles as described above.

EXPERIMENTAL PROCEDURES

THF, DMF, EO, allyl alcohol, and methyl iodide were purified using conventional methods (*33*). Potassium, naphthalene, AIBN, and 2-aminoethanethiol hydrochloride were used as received.

Potassium naphthalide solution was prepared by addition of potassium over naphthalene solution in THF. The mixture was stirred for 24 h under argon (Ar) atmosphere at 15 °C, and the concentration of the solution was measured by titration with 0.1 N HCl solution.

^{1}H and ^{13}C NMR spectra were recorded in CDCl$_3$ using JEOL EX400 and EX90Q spectrometers. GPC measurements were done by using a Tosoh gel permeation chromatograph HLC-8020 equipped with a Tosoh degasser, a TSK-Gel G2000HxL precolumn, TSK-Gel G4000HxL, G3000HxL, and G2000HxL columns, an internal RI detector, and a UV-8010 detector. THF was used as solvent, and standards were poly(ethylene glycol).

Synthesis of α-hydroxy-ω-allyl PEO (1). In the polymerization flask, 160 mL of anhydrous THF, 0.54 mL (7.98 mmol) of anhydrous allyl alcohol, and 20.3 mL (7.98 mmol) of potassium naphthalide solution were added under Ar stream. This mixture was cooled into a water bath, and 50 mL (0.91 mol) of distilled EO was added via a cooled syringe under Ar stream. The solution was stirred for 48 h in the water bath under Ar atmosphere. Distilled water was added, and the polymer was extracted with chloroform. The organic phase was dried over Na$_2$SO$_4$, filtrated, and concentrated. Polymer was recovered by precipitation in a large excess of ether and freeze-dried into benzene to lead to a white powder (41.96 g, yield = 96%). GPC (THF, PEG standards): number-average molecular weight ($\bar{M}_n$) = 4900; weight-average molecular weight ($\bar{M}_w$) = 5180; polydispersity index (Ip) = 1.05. ^{1}H NMR (400 MHz, CDCl$_3$, δ in ppm): 2.92 (s, OH, 1H), 3.63 (m, CH$_2$ of PEO, 480H), 4.02 (d, CH$_2$ of allyl group, 2H), 5.17−5.30 (dd, CH$_2$ of allyl group, 2H), 5.87−5.96 (m, CH of allyl group, 1H).

Synthesis of α-Methoxy-ω-allyl PEO (2). The polymer 1 (21.06 g) was put into the reaction flask and dried under vacuum at room temperature overnight. Anhydrous THF (210 mL) was added under an Ar stream, and potassium naphthalide solution was added until a green color remained (2 equiv, 7.86 mmol). Then, 3.7 mL (15 equiv, 59 mmol) of distilled methyl iodide was added under Ar stream. The mixture was stirred for 72 h at 50 °C. Water was added, and polymer was extracted by chloroform. The organic phase was dried over Na$_2$SO$_4$. After filtration and concentration, the polymer was precipitated into ether and freeze-dried into benzene to lead to polymer 2 as a white powder (16.68 g, yield = 79%). GPC (THF, PEG standards): $\bar{M}_n$ = 4870; $\bar{M}_w$ = 5110; Ip = 1.05. ^{1}H NMR (400 MHz, CDCl$_3$, δ in ppm): 3.37 (s, CH$_3$, 3H), 3.63 (m, CH$_2$ of PEO, 568H), 4.02 (d, CH$_2$ of allyl group, 2H), 5.17−5.30 (dd, CH$_2$ of allyl group, 2H), 5.87−5.96 (m, CH of allyl group, 1H).

Synthesis of α-Hydroxy-ω-amino PEO (3). The polymer 1 (20.90 g) was put in the reaction flask and dried under vacuum at room temperature. Anhydrous DMF (150 mL) was added under an Ar stream. Sepa-

rately, 6.6 g (15 equiv, 58.4 mmol) of 2-aminoethanethiol hydrochloride and 643 mg (7.5 × 10^{-1} equiv, 2.3 mmol) of AIBN were weighed and dried under vacuum at room temperature. Thirty mL of anhydrous DMF was added under an Ar stream. This solution was transferred into the previous one under an Ar stream, and the mixture was stirred at 70 °C for 24 h under Ar atmosphere. The polymer was precipitated two times in a large excess of ether. After filtration, the white powder was dissolved into methanol, and 0.22 g (1 equiv, 3.8 mmol) of KOH dissolved in water was added. The mixture was stirred for about 30−60 min. Then, water was added and polymer was extracted by chloroform. After drying over Na$_2$SO$_4$, filtration, and concentration, the polymer was precipitated into ether and freeze-dried into benzene to lead to a white powder (17.37 g, yield = 83%). GPC (THF, PEG standards): $\bar{M}_n$ = 5190; $\bar{M}_w$ = 5560; Ip = 1.07.

Synthesis of α-Methoxy-ω-amino PEO (4). Experimentals details are the same as described above for the preparation of polymer 3 with 16.5 g of polymer 2, 120 mL of anhydrous THF, 5.2 g of 2-aminoethanethiol hydrochloride, and 378 mg of AIBN. The polymer 4 was recovered as a white powder (15 g, yield = 91%). GPC (THF, PEG standards): $\bar{M}_n$ = 4800; $\bar{M}_w$ = 5150; Ip = 1.07.

RESULTS AND DISCUSSION

The synthesis of heterotelechelic PEO, having (primary amino/hydroxy) and (primary amino/methoxy) end groups with the same molecular weight and distributions, contains the three following steps: (i) synthesis of heterotelechelic PEO with (allyl/hydroxy) end groups; (ii) methylation of hydroxy terminal group; and (iii) amination of allyl end groups.

Use of allyl alcoholate as initiator for anionic polymerization of EO allowed the introduction of an unsaturated double bond at one end and a hydroxy function at the other end of the PEO chain. These two functional groups allow several kinds of chemical modifications such as radical addition reactions (*23*) for allyl group and introduction of an active group via ether or ester bonds for the hydroxy function (*24*).

The initiator, allyl alcoholate, was prepared *in situ* by reaction between allyl alcohol and potassium naphthalide solution which was prepared by addition of potassium on naphthalene solution in THF (Scheme 1). EO was added to the allyl alcoholate solution and reacted for 2 days at room temperature (disappearence of monomer and oligomer peaks on GPC chromatogram). Hydroxy end groups were recovered by addition of an excess of acetic acid (Scheme 1). After chloroform was added to the reaction mixture, the solution was washed with water several times in order to remove impurities. The PEO thus obtained was further purified by precipitation into ethyl ether and then freeze-dried from benzene solution. The ^{1}H NMR spectrum of this α-hydroxy-ω-allyl PEO (1) showed a high degree of purity; this result was confirmed by ^{13}C NMR. Moreover, molecular weights determined by GPC (THF, PEG standards) and calculated from ^{1}H NMR were in good agreement with molecular weights obtained from the ratio monomer/initiator (Table 1). These results demonstrated that anionic polymerization of EO by allyl alcoholate led to the expected PEO with an allyl group at one end, hydroxy function at the other end, and well-defined molecular weights and narrow dispersity.

Addition of methyl iodide on hydroxy end groups of polymer was described by Kobayashi and his coworkers (*25*). However, their experimental conditions were not adapted for our case. Indeed, after 24 h at room temperature with 5 equiv of CH$_3$I, ^{1}H and ^{13}C NMR spectra

Scheme 1. Synthetic Route to α-Hydroxy-ω-amino PEO (3) and α-Methoxy-ω-amino PEO (4)
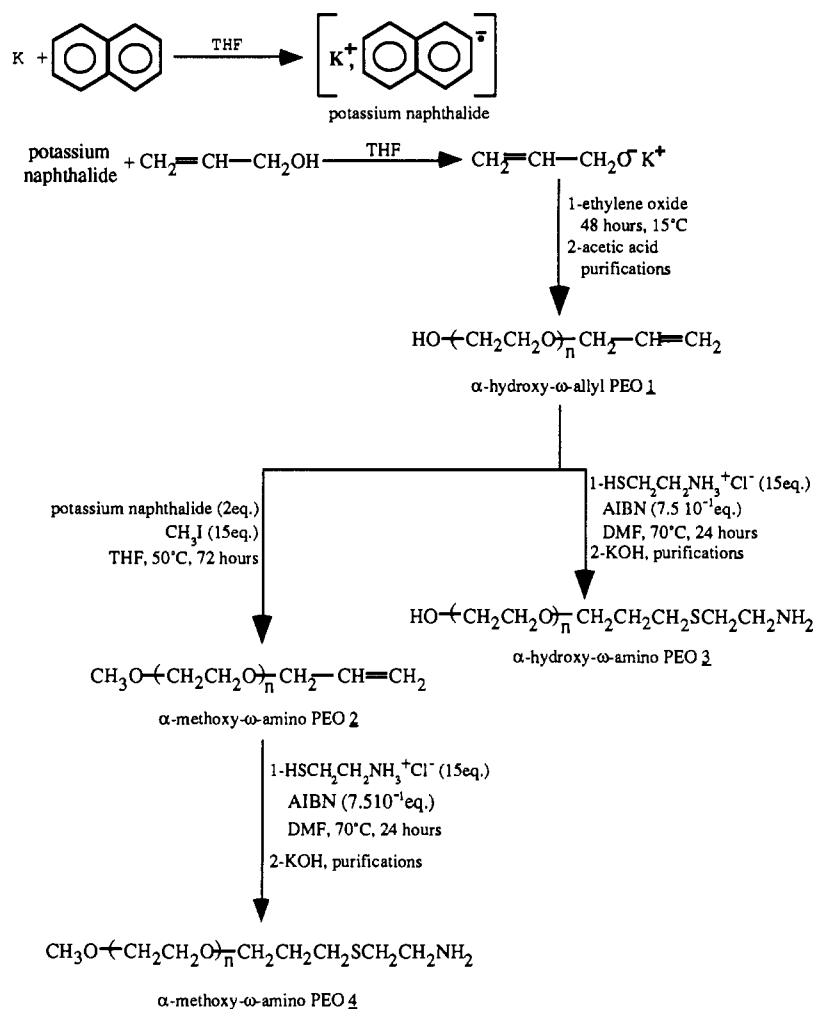
Table 1. Data for Molecular Weights of Polymers 1–4 and Their Distributions

	$\bar{M}_n{}^a$	$\bar{M}_w{}^a$	Ip	$M_s{}^a$	$M_{NMR}{}^b$	$M_{cal}{}^c$
1	4900	5180	1.05	5100	5280	5000
2	4870	5110	1.05	5100	5630	5000
3	5190	5560	1.07	5100	5060	5000
4	4800	5150	1.07	5100	5320	5000

^{a} Determined by GPC in THF with PEG standards. ^{b} Calculated from ^{1}H NMR spectra in CDCl$_3$. ^{c} Calculated from the ratio ethylene oxide/allyl alcoholate.

of the resulting polymer showed the presence of unreacted hydroxy end groups (about 30%). In order to determine if some side reactions could take place when the temperature was increased, we studied the model reaction between allyl alcohol, methyl iodide, and potassium naphthalide in THF at 50 °C. After 12 h at 50 °C, the reaction milieu was examined by GC/MS: absence of any kind of adduct on the double bond of allyl alcohol and formation of addition compound between allyl alcohol and methyl iodide via the hydroxy function were demonstrated. In view of these results, methyl iodide addition on α-hydroxy-ω-allyl PEO (1) was carried out as described in the Experimental Procedures. The ^{1}H NMR spectrum of the purified polymer demonstrated completion of this addition reaction: the peak corresponding to the hydroxy function at 2.9 ppm disappeared and a new peak appeared at 3.37 ppm, corresponding to methoxy group. These results were confirmed by the ^{13}C NMR spectrum: peaks corresponding to methylene adjacent to hydroxy function (CH$_2$CH$_2$OH: δ = 61.5 ppm, CH$_2$CH$_2$-

OH: δ = 72.33 ppm) disappeared in favor of the appearance of new peaks at 59.05 ppm (OCH$_3$) and at 72 ppm (CH$_2$CH$_2$OCH$_3$). Moreover, molecular weights determined by GPC (THF, PEG standards) and by ^{1}H NMR were very similar to those of PEO **1**; dispersity was also very narrow (Ip = 1.05, Table 1). These data demonstrated that α-hydroxy-ω-allyl PEO (1) was successfully transformed in α-methoxy-ω-allyl PEO (2) via addition of methyl iodide on hydroxy function, without any side reactions and detectable chain degradation.

Thiol compounds are known to control molecular weights of elastomers prepared by emulsion polymerization (*26*). These transfer reagents are also used to prepare specific macromonomers (*27*). Moreover, functional groups can be introduced efficiently to the end of growing polymeric chains using thiol compounds having functional groups. In addition, molecular weights of corresponding polymers can be regulated by radical telomerization via chain-transfer reactions (*23*). Takei and co-workers (*28*) have described the telomerization reaction of *N*-isopropylacrylamide using 3-mercaptopropionic acid as a chain transfer agent in the presence of AIBN at 70 °C in DMF.

On the basis of the above reports, we adopted radical addition reaction of 2-aminoethanethiol hydrochloride with an allyl end group of PEO in order to get primary amino-ended PEO at one end. The reactions were carried out under the conditions of [PEO(1 or 2)]$_0$/[HSCH$_2$CH$_2$-NH$_3^+$Cl$^-$]$_0$/[AIBN]$_0$ = 1/15/7.5 × 10^{-1} mol equiv in DMF at 70 °C. Crude polymers (**4** and **5**), thus obtained, were precipitated two times in ether in order to remove excess

$$\underset{1}{\text{HO}}\text{-}(\underset{2}{\text{CH}_2}\underset{3}{\text{CH}_2}\text{O})_n\underset{4}{\text{CH}_2}\underset{5}{\text{CH}_2}\underset{6}{\text{CH}_2}\underset{7}{\text{SCH}_2}\underset{8}{\text{CH}_2}\underset{9}{\text{NH}_2}$$
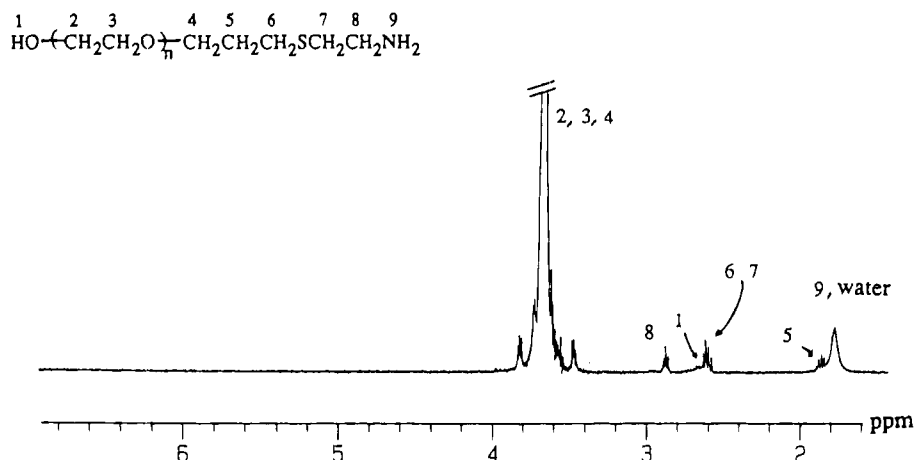
Figure 1. ^{1}H NMR (CDCl₃, 400 MHz) spectrum of α-hydroxy-ω-amino PEO (3).

$$\underset{1}{\text{CH}_3}\text{O}\text{-}(\underset{2}{\text{CH}_2}\underset{3}{\text{CH}_2}\text{O})_n\underset{4}{\text{CH}_2}\underset{5}{\text{CH}_2}\underset{6}{\text{CH}_2}\underset{7}{\text{SCH}_2}\underset{8}{\text{CH}_2}\underset{9}{\text{NH}_2}$$
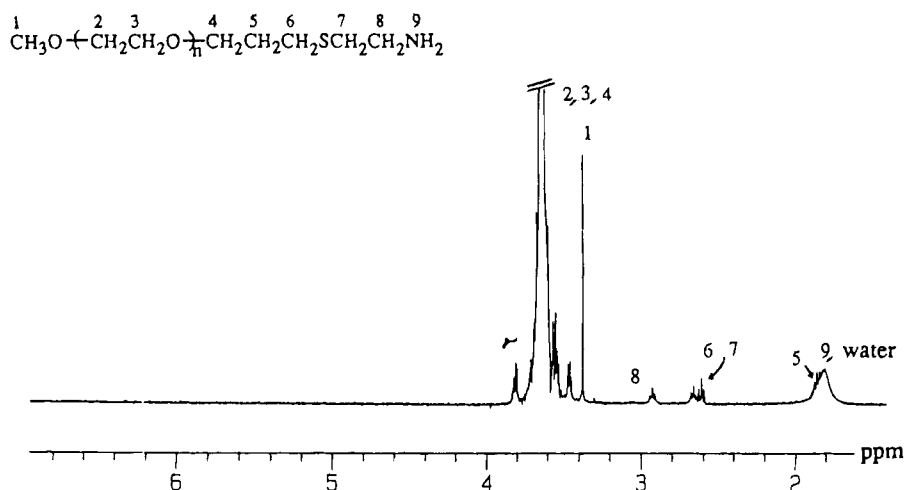
Figure 2. ^{1}H NMR (CDCl₃, 400 MHz) spectrum of α-methoxy-ω-amino PEO (4).

of reagents. Primary amine end groups were recovered by addition of potassium hydroxide solution (Scheme 1). ^{1}H NMR spectra of both α-hydroxy-ω-amino and α-methoxy-ω-amino PEOs showed completion of reaction without formation of any byproducts (Figures 1 and 2), results confirmed by ^{13}C NMR. Molecular weights determined by GPC (THF, PEG standards) were in good agreement with molecular weights calculated from ^{1}H NMR spectra and with those of starting polymer (Table 1), moreover, dispersity of both modified homopolymers stayed very narrow (Ip = 1.07). These results demonstrated that the addition reactions of 2-aminoethanethiol hydrochloride on α-hydroxy-ω-allyl and on α-methoxy-ω-allyl PEOs (1) and (2) gave access to the expected heterobifunctional PEOs without any side reactions and significant polymer alteration.

This new synthetic route is very interesting. Indeed, amino-ended PEOs are important as intermediate in the synthesis of other derivatives or in direct applications, and several routes for their preparation have been explorated (9). In 1979, Kern and co-workers have described a direct route to α,ω-diamine oligo(oxyethylene) by reaction of ditosyl esters of α,ω-dihydroxy oligo(oxyethylenes) with potassium 2-aminoethanolate: percentage of modification decreased when molecular weight of the polymers increased (29). Ziegast and co-workers brought some modifications to this synthesis route in order to modify higher molecular weight PEOs; percentage of modification is higher but not quantitative (up to 95%) (30). In 1981, Bückmann and co-workers as well as Johansson and co-workers have described two direct

syntheses for primary amino-ended PEOs. The first group used gaseous ammonium, high temperature, and high pressure (glass autoclave is required): although this method gives 100% substitution, difficulty to set up limited its use (31). The second group described a method which is easily applied but primary and secondary amine are produced (32). In comparison, addition reaction of 2-aminoethanethiol hydrochloride on α-hydroxy (or methoxy)-ω-allyl PEOs provides a simple and reproducible way to introduce primary amino end group at one end of PEO chains. Moreover, this one-step synthesis allows us to obtain 100% modification.

CONCLUSION

Heterobifunctional PEOs having a hydroxy or methoxy group at one end and primary amine function at the other end were synthesized with well-controlled molecular weights and in high yield (more than 80%). Moreover, nonmodified and modified homopolymers had a very narrow dispersity (≤1.07) probe of the efficiency of anionic polymerization of EO with allyl alcoholate and absence of any side reactions and chain degradation during chemical modifications of end-groups.

The possibility to introduce an allyl group at one end and alkyl or functional group at the other end of the PEO chain is of great interest. Indeed, physicochemical properties (solubility, copolymerization, biocompatibility) can be adjusted through the chemical modifications of these end-groups. As a result, a large family of derivatives having various applications, e.g., as surface coating

or drug delivery systems, can be synthesized. The allyl end group also allows quantitatively conversion into a primary amino moiety via radical addition reactions of amino-thiol compound.

Synthesis of poly(ethylene oxide)-*co*-poly(β-benzyl-L-aspartate), PEO/PBLA block-copolymers, with a hydroxy and/or methoxy end group with the same molecular weight and their characteristics as micelles will be published elsewhere.

ACKNOWLEDGMENT

LITERATURE CITED

(1) Suzuki, T., and Tomono, T. (1984) *J. Polym. Sci., Polym. Chem. Ed. 22,* 2829.

(2) Davidson, R. L., O'Malley, K. A., and Wheeler, T. B. (1976) *Somatic Cell Genetics 2,* 271.

(3) Abuchowski, A., Van Es, T., Plozuk, N. C., and Davis, F. F. (1977) *J. Biol. Chem. 252,* 3578.

(4) King, T. P., Kochoumian, L., and Licttenstein, L. M. (1977) *Arch. Biochem. Biophys. 178,* 442.

(5) For definition, see: Kim, Y. J., Nagasaki, Y., Kataoka, K., Kato, M., Yokoyama, M., Okano, T., and Sakurai, Y. (1994) *Polym. Bull. 33,* 1.

(6) For definition, see: Yokoyama, M., Okano, T., Sakurai, Y., Kikuchi, A., Ohsako, N., Nagasaki, Y., and Kataoka, K. (1992) *Bioconjugate Chem. 3,* 275.

(7) B. F. E. Baily, Jr., and J. V. Koleske, Eds. (1991) *Alkylene oxides and their polymers,* Marcel Dekker, New York.

(8) J. M. Harris, Ed. (1993) *Poly(ethylene glycol) chemistry,* Plenum Press, New York.

(9) Harris, J. M., and Yalpani, M. (1985) Polymer-ligands used in affinity partitioning and their synthesis. *Partitioning in aqueous two-phase systems* (H. Walter, D. E. Brooks, and D. Fisher, Eds.) Academic Press, New York.

(10) Abuchowski, A., van Es, T., Palczuk, N. C., and Davis, F. F. (1977) *J. Biol. Chem. 252*(11), 3578.

(11) Abuchowski, A., Mc. Coy, J., Palczuk, N., van Es, T., and Davis, F. (1977) *J. Cell. Chem. 252*(11), 3582.

(12) Lisli, P. J., van Es, T., Abuchowski, A., Palczuk, N. C., and Davis, F. F. (1982) *J. Appl. Biochem. 4,* 19.

(13) Woghiren, C., Sharma, B., and Stein, S. (1993) *Bioconjugate Chem. 4,* 314.

(14) Zalipsky, S. (1993) *Bioconjugate Chem. 4,* 296.

(15) Lee, R. J., and Low, P. S. (1994) *J. Biol. Chem. 269 (5),* 3198.

(16) Crommelin, D. J. A., and Schreir, H. (1994) Drugs and the Pharmaceutical Sciences (J. Swarbrick, Ed.). *Colloidal Drug Delivery System* (J. Kreuter, Ed.) Chapter 3, p 66, Marcel Dekker, Inc., New York.

(17) Ito, K., Yokoyama, S., Arakawa, F., Yukawa, Y., Iwashita, T., and Yamazaki, Y. (1986) *Polym. Bull. 16,* 337.

(18) Chao, D., Itsuno, S., and Ito, K. (1991) *Polymer J. 23 (9),* 1045.

(19) Kwon, G. S., Suwa, S., Yokoyama, M., Okano, T., Sakurai, Y., and Kataoka, K. (1994) *J. Controlled Release 29,* 17 and references cited therein.

(20) Kataoka, K., Kwon, G. S., Yokoyama, M., Okano, T., Sakurai, Y. (1993) *J. Controlled Release 24,* 119 and references cited therein.

(21) Yokoyama, M. (1989) Ph.D. Thesis, University of Tokyo, Japan.

(22) Yokoyama, M., Inoue, S., Kataoka, K., Yui, N., Okano, T., and Sakurai, Y. (1989) *Makromol. Chem. 190,* 2041.

(23) Stars, C. M. (1974) *Free Radical Telomerization,* Academic Press Inc., New York.

(24) Harris, J. M. (1985) *J. Macromol. Sci., Rev. Macromol. Chem. Phys. C25*(3), 325.

(25) Kobayashi, S., Kaku, M., Mizutani, T., and Saegusa, T. (1983) *Polym. Bull. 9,* 169.

(26) Uranek, C. A. (1976) *Rubb. Chem. Tech. 49,* 611.

(27) Rempp, P. F., and Franta, E. (1984) *Adv. Polym. Sci. 58,* 1.

(28) Takei, Y. G., Aoki, T., Sanui, K., Ogata, N., Okano, T., and Sakurai, Y. (1993) *Bioconjugate Chemistry 4,* 42.

(29) Kern, W., Iwabuchi, S., Sato, H., and Böhmer, V. (1979) *Makromol. Chem. 180,* 2539.

(30) Ziegast, G., and Pfannemüller, B. (1984) *Makromol. Chem., Rapid Commun. 5,* 363.

(31) Bückmann, A. F., Morr, M., and Johansson, G. (1981) *Makromol. Chem. 182,* 1379.

(32) Johansson, G., Gysin, R., and Flanagan, S. D. (1981) *J. Biol. Chem. 256,* 9126.

(33) Perrin, D. D., Armarego, W. L. F., and Perrin, D. R. (1980) *Purification of Laboratory Chemicals,* Pergamon Press, Oxford.

BC940101K

Formyl-Ended Heterobifunctional Poly(ethylene oxide): Synthesis of Poly(ethylene oxide) with a Formyl Group at One End and a Hydroxyl Group at the Other End

Yukio Nagasaki, Takahiko Kutsuna, Michihiro Iijima, Masao Kato, and Kazunori Kataoka*

Department of Materials Science and Technology, Science University of Tokyo, Noda 278, Japan

Shigeru Kitano and Yoshihito Kadoma

Tsukuba Research Center, Nippon Oil and Fat Company, Toko-dai, Tsukuba 300-26, Japan.
Received September 6, 1994⊗

Well-defined poly(ethylene oxide) (PEO) with a formyl group at one end and a hydroxyl group at the other terminus was synthesized by the anionic ring opening polymerization of ethylene oxide (EO) with a new organometallic initiator possessing an acetal moiety, potassium 3,3-diethoxypropyl alkoxide. Hydrolysis of the acetal moiety produced a formyl group-terminated heterobifunctional PEO with a hydroxyl group at the other end.

Poly(ethylene oxide) (PEO) chemistries have been widely studied by numerous researchers in terms of synthetic methods and mechanisms, properties, and applications (*1, 2*). In particular, the applications of PEO have become attractive in a variety of fields such as biology, biomedical science, surface chemistry, and electrochemistry, due to their unique properties such as solubility and flexibility of the chains and basicity of the ether oxygens in the main chain. Recently, end-functionalized PEOs have become very important in controlling these properties. For example, an end-functionalized PEO can be used as a surface modifier to change surface properties, *e.g.*, for biocompatible surfaces (*3*) and for capillary electrophoresis (*4*). An end-functionalized PEO is also utilized for protein modifications (*5*), conjugation (*6*), and crosslinking (*7*). For example, a protein−PEO conjugate increases the solubility and stability in water and decreases the antigenicity of the protein in general (*2*). Most of the end-functionalized PEOs, however, are semitelechelic (*8*) or homotelechelic oligomers. To expand the utility of PEO's, convenient synthesis of heterotelechelic oligomers (*9*) is needed. If such heterotelechelics are easily synthesized, these materials can be utilized as heterocrosslinkers of different substances with defined spacer lengths, surface modifiers with the remaining reactive moieties at the free end, etc. There are several reports on the synthesis of heterobifunctional PEOs using homotelechelic PEOs as the starting materials (*6, 10*). The synthetic methods, however, are complicated because they have to use several reaction steps to derivatize the PEO terminus. In addition, the efficiency for derivatizations is not very high, meaning the resulting PEO is a mixture of the starting homotelechelics and the resulting heterotelechelics to some extent.

Our strategy for heterotelechelic synthesis is to create a novel polymerization route of EO using new initiators containing defined functionalities. So far, we have synthesized heterotelechelics with a primary amino group at one end and a hydroxyl group at the other end by an anionic ring opening polymerization of EO using silyl-protected potassium amide (*11, 12*). In this paper, we
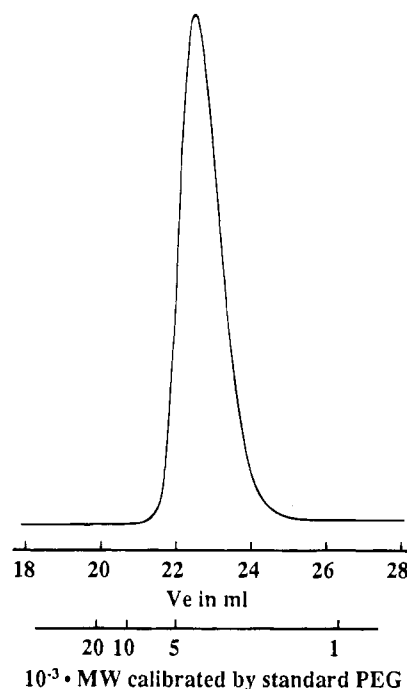
Figure 1. Gel permeation chromatogram of poly(ethylene oxide) prepared by the anionic ring opening polymerization initiated with PDA [a Shimadzu 6A liquid chromatograph was used (column: TSK-Gel G4000H8 + G3000H8 + G2500H8)].

report the synthesis of PEO with a formyl group at one end and a hydroxyl group at the other end.

A formyl group is very useful for conjugation with protein due to its stability in water and its rapid reactivity with primary amino groups. In addition, no charge variation takes place by the modification because the resulting Schiff base can be easily converted to a *sec*-amino group by reduction. The variation in charge distribution in protein sometimes induces denaturation. There are several published reports on the synthesis of formyl group-terminated PEOs. Harris and his co-workers reported the synthesis of a formyl group-ended semitelechelic PEO starting from a hydroxyl-terminated semitelechelic PEO (methoxy group at the other terminus (*13*)). A formyl group-terminated heterobifunctional PEO
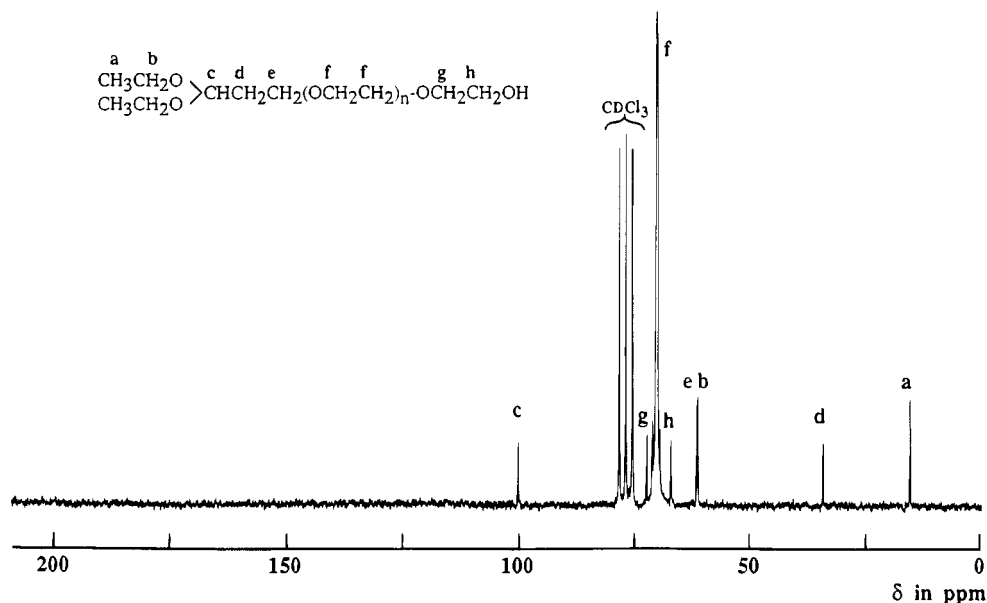
Figure 2. ^{13}C NMR spectrum of hetero-PEO prepared by the anionic ring opening polymerization initiated with PDA (the same sample as in Figure 1).
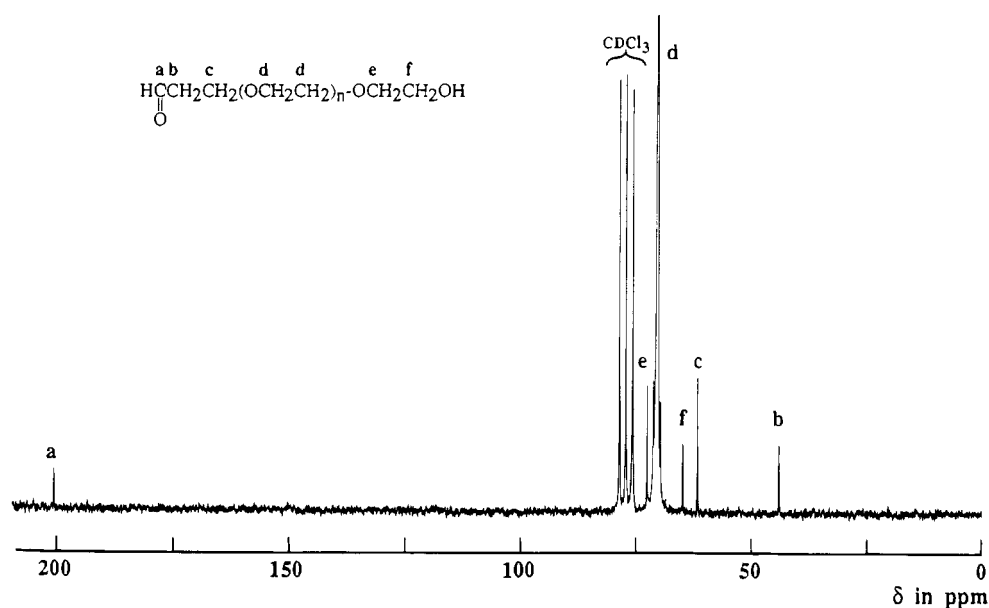
Figure 3. ^{13}C NMR spectrum of heteroPEO after acid treatment (the same polymerization conditions as in Figure 1).

was synthesized by a coupling reaction (*13, 14*) and an oxidation reaction (*15*) starting from a hydroxyl group-ended homotelechelic PEO. The PEO thus obtained still retained the above-mentioned problems such as purity and yield.

To quantitatively synthesize a formyl group-ended heterobifunctional PEO, the anionic ring opening polymerization of EO was carried out using potassium alkoxide with an acetal moiety as an initiator, *e.g.*, potassium (3,3-diethoxypropyl)alkoxide (PDA). To THF (16 mL) in a 100 mL flask with a three-way stopcock under argon atmosphere were added 3,3-diethoxypropyl alcohol (DA; 1 mmol) and potassium naphthalene (1 mmol) to form PDA. After liquid EO (70 mmol; below 0 °C) was added via a cooled syringe, the mixture was allowed to react for 2 days at room temperature. Figure 1 shows the gel permeation chromatogram (GPC) of the reaction mixture, in which it can be seen that the polymer was obtained with a narrow molecular weight distribution (M_w/M_n = 1.05; M_w and M_n denote weight average and number average molecular weights, respectively). M_n of the

Scheme 1

$$\underset{EtO}{\overset{EtO}{>}}CHCH_2CH_2OH \xrightarrow{\text{K-Naph}} \underset{EtO}{\overset{EtO}{>}}CHCH_2CH_2OK$$

$$\xrightarrow{\overset{\triangle}{O}} \underset{CH_3CH_2O}{\overset{CH_3CH_2O}{>}}CHCH_2CH_2(OCH_2CH_2)_n\text{-}OCH_2CH_2OK$$

$$\xrightarrow{\text{1N HCl}} CHOCH_2CH_2(OCH_2CH_2)_n\text{-}OCH_2CH_2OH$$
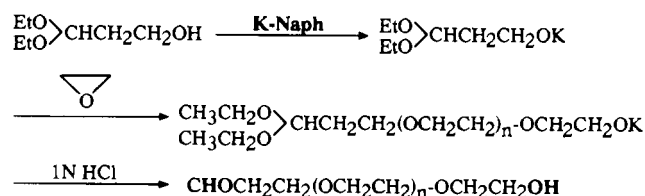
polymer determined from GPC (M_n = 3100) agreed well with that calculated using an initial monomer/initiator ratio (M_n = MW(EO)[[EO]$_0$/[PDA]$_0$] + MW(DA) = 44(70/1) + 148 = 3200), indicating that is PDA the sole initiating species for this polymerization (Scheme 1).

To obtain information on the end group of the polymer thus obtained, ^{13}C NMR analysis was carried out. Figure 2 shows the ^{13}C NMR spectrum of the polymer after purification of the polymer by precipitation in ether and freeze-drying in benzene. By referring to the literature on hydroxyl-terminated PEO (*16*) and diethoxypropyl

Table 1. ^{13}C NMR Chemical Shift Data of PEO Initiated with PDA (ppm)

carbon	a	b	c	d	e	f	g	h
obsd	15.1	61.2	100.3	33.9	61.5	70.4	72.4	67.1
calcd	14.7	57.1	118.4	39.5	60.3	70.6	72.8	63.7

$$\begin{array}{l} \overset{a}{CH_3}\overset{b}{CH_2}O \\ CH_3CH_2O \end{array}\hspace{-0.5em}\Big\rangle \overset{c}{CH}\overset{d}{CH_2}\overset{e}{CH_2}(\overset{f}{OCH_2}\overset{f}{CH_2})_n\text{-}\overset{g}{OCH_2}\overset{h}{CH_2}OH$$

Table 2. Results of Anionic Polymerizations of Ethylene Oxide (EO) with PDA as an Initiator[a]

run	$[EO]_0/[PDA]_0$	time (h)	yield (%)	$10^{-3} \times M_n{}^b$ obsd[c]	$10^{-3} \times M_n{}^b$ calcd[e]	$M_w/M_n{}^{c,d}$
1	40	50	99.3	1.8	1.8	1.08
2	70	50	97.7	3.1	3.2	1.05
3	120	50	93.5	5.3	4.6	1.09

[a] Solvent: THF. Temperature: rt. [b] M_n denotes number average molecular weight. [c] Determined from the GPC results. [d] M_w denotes weight average molecular weight. [e] Determined from the following equation: $M_n(calc) = MW(EO)[[EO]_0/[PDA]_0] + MW-(PDA) = 44[[EO]_0/[PDA]_0] + 148$.

alcohol as reference compounds, the assignments of these signals were carried out and are described in Figure 2. The assignments of these signals were in good accordance with the calculated data (17) as shown in Table 1. Further results of the anionic polymerizations under the several conditions are summarized in Table 2. The yield of the polymers was almost quantitative, and their molecular weight can be easily controlled by the monomer/initiator ratio.

Transformation of the acetal group at the polymer end to an aldehyde group was carried out by the addition of 15 mL of 1 N HCl to the reaction mixture after a 2-day polymerization. From the ^{13}C NMR spectrum of the purified polymer shown in Figure 3, it was found that the signals derived from the acetal moiety completely diminished and the three signals derived from the aldehyde moiety appeared at 43.6, 64.6, and 200.9 ppm, which are assignable to $-CH_2CH_2CHO$, $-CH_2CH_2CHO$, and $-CH_2CH_2CHO$ at the end of the polymer chain, respectively. ^1H NMR of this polymer in DMSO-d_6 shows the aldehyde proton at 9.8 ppm and the alcohol proton in 4.5 ppm, an indication of complete transformation of the acetal end group to an aldehyde group.

On the basis of the reported results, it is concluded that a heterobifunctional PEO with an aldehyde moiety at one end and a hydroxyl group at the other end was quantitatively synthesized in one pot.

LITERATURE CITED

(1) Bailey, F. E., Jr., and Koleske, J. V., Eds. (1991) *Alkylene Oxide and Their Polymers*, Vol. 35, Marcel Dekker, New York.
(2) Harris, J. M. Ed. (1993) *Poly(ethylene glycol) Chemistry, Biotechnical and Biomedical Applications*, Plenum Press, New York.
(3) Amiji, M. and Park, K. (1993) *J. Biomater. Sci., Polym. Ed. 4*, 217.
(4) Herren, B. J., Shafter, S. G., Alstine, J. V., Harris, J. M., and Snyder, R. S. (1987) *J. Colloid Int. Sci. 115*, 46.
(5) Shalaby, S. W., Hoffman, A. S., Ratner, B. D., and Horbett, T. A. (1984) *Polymers as Biomaterials*, Plenum Press, New York.
(6) Means, G. E., and Feeney, R. E. (1990) *Bioconjugate Chem. 1*, 2.
(7) Wong, S. S. (1991) *Chemistry of Protein Conjugation and Crosslinking*, CRC Press, Boca Raton.
(8) The term *telechelic oligomer* was defined as oligomer with reactive groups at the chain ends.
(9) The term *heterotelechelics* was defined in our previous paper (11), which denotes the telechelic oligomer with a functional group at one end and another functional group at the other end.
(10) Harris, J. M., and Yalpani, M., Eds. (1985) *Polymer-Ligands Used in Affinity Partitioning and Their Synthesis*, p 589, Academic Press, New York.
(11) Yokoyama, M., Okano, T., Sakurai, Y., Kikuchi, A., Ohsako, N., Nagasaki, Y., and Kataoka, K. (1992) *Bioconjugate Chem. 3*, 275.
(12) Kim, Y. J., Nagasaki, Y., Kataoka, K., Kato, M., Yokoyama, M., Okano, T., and Sakurai, Y. (1994) *Polymer Bull. 33*, 1.
(13) Harris, J. M., Dust, J. M., McGill, R. A., Harris, P. A., Edgell, M. J., Sedaghat-Herati, R. M., Karr, L. J., and Donnelly, D. L. (1991) In *Water-Soluble Polymers* (S. W. Shalaby, C. L. McCormic, and G. B. Butler, Eds.) Vol. 467, p 418, American Chemical Society, Washington, D.C.
(14) Huang, J., and Hu, Y. (1993) *J. Appl. Polym. Sci. 47*, 1503.
(15) Topchieva, I. N., Kuzaev, A. I., and Zubov, V. P. (1988) *Eur. Polym. J. 24*, 899.
(16) Kinugasa, S., Takatsu, A., Nakanishi, H., Nakahara, H., and Hattori, S. (1992) *Macromolecules 25*, 4848.
(17) Clerc, P., and Simmon, S. (1983) *Tables of Spectral Data for Structure Determination of Organic Compounds*, Springer-Verlag, Berlin.

ARTICLES

Syntheses and Properties of Luminescent Lanthanide Chelate Labels and Labeled Haptenic Antigens for Homogeneous Immunoassays

Heikki Mikola,*,†,‡ Harri Takalo,† and Ilkka Hemmilä†

Wallac Oy, P.O. Box 10, FIN-20101 Turku, Finland, and Department of Chemistry, University of Turku, FIN-20500 Turku, Finland. Received October 17, 1994®

Lanthanide chelate labels containing substituted 4-(arylethynyl)pyridine as the chromogenic moiety and iminobis(acetic acid) groups as the chelating part were synthesized. N-Succinimidyl esters of the carboxy derivatives of thyroxine and progesterone were prepared and coupled to the aliphatic amino groups of the synthesized lanthanide chelates. The luminescence properties of the chelates and labeled haptenic antigens were measured in ethanol and in an aqueous buffer containing either albumin or detergents as luminescence-modulating compounds. The energy transfer enhanced ion luminescence of the derivatives containing a para-amino-substituted phenyl ring showed particularly strong dependence on environmental changes, which makes these derivatives well suited for homogeneous time-resolved fluoroimmunoassay based on the use of external luminescence modulators.

INTRODUCTION

Time-resolved fluorometry combined with the use of luminescent long decay time emitting lanthanide chelate labels provides an excellent way to develop highly sensitive bioaffinity assays (1). The assay technology based on dissociative fluorescence enhancement (2), DELFIA (Wallac Oy), is already widely applied, particularly in the field of clinical immunodiagnostics (3), but it is also finding applications in DNA hybridization assays (4).

The use of time-resolved fluorometry is desirable for homogeneous assays because conventional fluorometry suffers from interference by the sample constituents present during the fluorometric measurement. Time-resolved fluorometry can completely eliminate the interference originating, e.g., from sample autofluorescence.

However, the DELFIA technology is not suited to homogeneous assays because the enhancement step applied requires a heterogeneous approach. To be applicable in homogeneous assays, the chelate label has to be stable and luminescent in situ, and it must in addition enable direct monitoring of the immunoreaction without any physical separation.

Two assay principles have been applied in homogeneous time-resolved fluorometric immunoassays. One of these utilizes an energy transfer between a europium cryptate and a phycobiliprotein in a concentrated fluoride solution (5). This assay principle is applicable to different types of assays but requires two separate labelings for each analyte. We have developed a straightforward system based on the use of environmentally sensitive chelate labels and the addition of luminescence-modulating compounds in the assay buffer (6). This assay principle is already employed with some steroid glucuronides (7, 8) and thyroxine (6). The weak affinity of aromatic structures to serum proteins (or detergents)—a

† Wallac Oy.
‡ University of Turku.
® Abstract published in Advance ACS Abstracts, April 15, 1995.
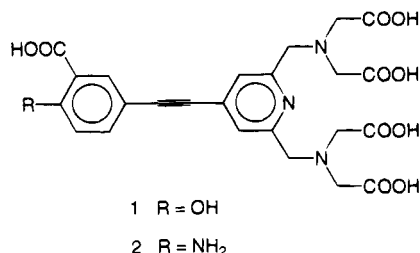
Figure 1. Structures of chelating ligands **1** and **2**.

property which generally causes problems in, e.g., polarization-based homogeneous fluoroimmunoassays (*9*)—is made use of in this system to create an alternative-binding direct homogeneous assay. The matrix effect related to sample variations is avoided by using a large excess of the luminescence-modulating compound and diluting the samples prior to assay.

Earlier investigations have shown that ligands containing 4-(arylethynyl)pyridine as the chromophoric group strongly enhance the europium ion luminescence (up to 9.5 × 10^6-fold) (*10*), and chelates incorporating this structure have been used as labels in time-resolved spectroscopy (*10–13*). The effects of ligand substituents on the luminescence of a chelated europium ion have been studied both in aqueous solution and in ethanol (*10*). An amino or a hydroxy group at the *para*-position of the phenyl ring renders the europium chelates of these ligands sensitive to environmental changes, which can be exploited in direct homogeneous assays. For further studies we chose ligands **1** and **2** (Figure 1), in which the carboxyl group at the *meta*-position makes it possible to couple them to bioaffinity reagents (*10*). In the present paper we describe the syntheses of a series of 4-(arylethynyl)pyridine derivatives bearing a short spacer arm at the *meta*-position.

To study the effects of the coupling method and ratio on the ion luminescence, we have previously coupled luminescent lanthanide chelates to proteins (*13, 14*), to be used in heterogeneous assays. In the present article we describe the conjugation of luminescent lanthanide chelates to small haptenic molecules to be applied as tracers in homogeneous assays. The coupling of the europium and terbium chelates was accomplished with *N*-hydroxysuccinimide-activated derivatives of thyroxine and progesterone. We employed here activated carboxyl derivatives to selectively use aliphatic amino groups of the synthesized chelates for couplings. The luminescence properties of the lanthanide chelates and labeled haptenic antigens are discussed, and their suitability as tracers in direct homogeneous time-resolved fluoroimmunoassays is elucidated.

EXPERIMENTAL PROCEDURES

Materials. The reagents for syntheses were purchased from Aldrich-Chemie, E. Merck, and Fluka and used as received. The solvents from E. Merck and Fluka were of p.a. grade. TLC plates and silica for flash chromatography were obtained from E. Merck. ^{1}H NMR spectra were recorded on a JEOL JNM-GX400 FT-NMR spectrometer using tetramethylsilane as internal standard. IR and UV spectra were recorded on a Perkin-Elmer 1600 FTIR and a Shimadzu UV-2100 spectrophotometer, respectively. Melting points were measured on a Gallenkamp capillary apparatus and are uncorrected. Ligands **1** and **2** (Figure 1) were prepared according to Takalo and co-workers (*10*).

The luminescence properties of the europium and terbium chelates and the labeled hapten derivatives were

Scheme 1. Synthesis of Iodobenzamides 7 and 8
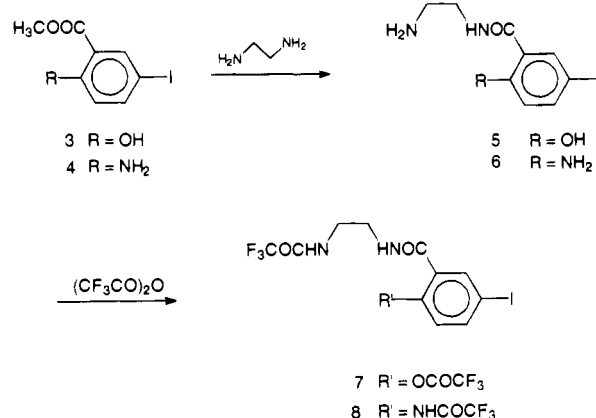
Scheme 2. Synthesis of Ligands 14–16
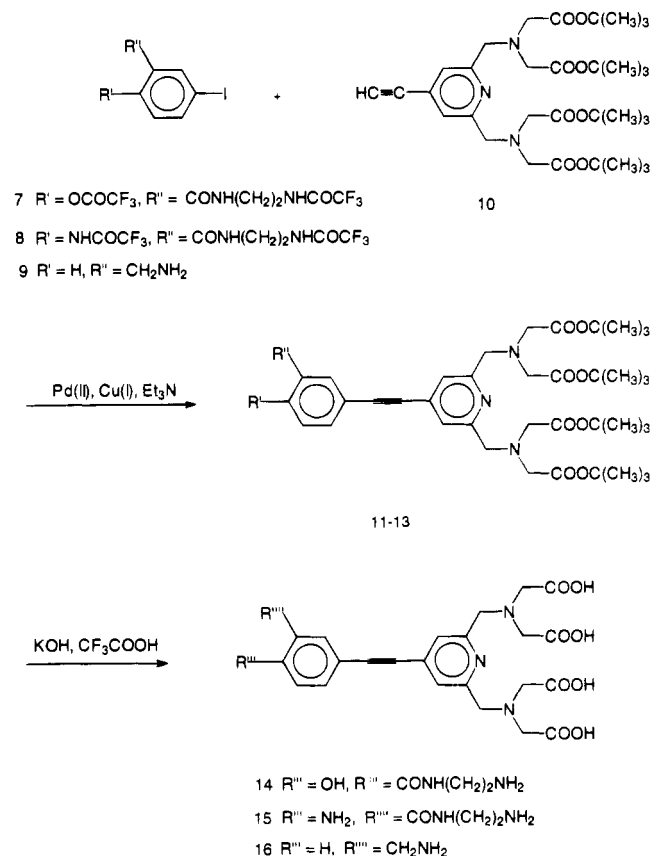
measured using a 1234 DELFIA time-resolved fluorometer (Wallac). The measurements were done in 10 nM chelate derivative concentrations both in ethanol and in Tris-HCl buffer (50 mM, pH 7.75) containing 0.9 g/L NaCl, with or without added albumin (0.5%). The measurements were standardized using 1 nM europium in the DELFIA Enhancement Solution (Wallac) as a standard, known to have a luminescence quantum yield of 0.69 and a relative fluorescence intensity ($\epsilon \times \Phi$) of 24 840 (*3*). The luminescence intensities of the studied conjugates are expressed either as counts (integrated counts within the measuring time of 1 s) or as a percentage compared to the standard.

Preparation of Chelating Ligands. The syntheses of the chelating ligands are shown in Schemes 1 and 2.

Preparation of Amides 5 and 6. A mixture of ester **3** or **4** (10 mmol) (*15*) and ethylenediamine (6.01 g, 100 mmol) was stirred at the desired temperature until the reaction was complete (0.5 h at 60 °C for **5**; 0.5 h at 75

°C for **6**). The reaction mixture was evaporated to dryness, and the product was purified by a suitable method.

N-(2-Aminoethyl)-2-hydroxy-5-iodobenzamide, **5**. The product was crystallized from acetonitrile. Yield: 89%. Mp: 163–164 °C. ^{1}H NMR: δ (d_6-DMSO) 2.82 (2 H, t, J = 6.1 Hz), 3.38 (2 H, t, J = 6.1 Hz), 4.30 (4 H, broad s), 6.45 (1 H, d, J = 8.8 Hz), 7.32 (1 H, dd, J = 2.5 and 8.8 Hz), 7.98 ppm (1 H, d, J = 2.5 Hz). IR (KBr pellet): 1620, 1575, 1540, 1450, 1295 cm^{-1} ν(CONH and NH).

2-Amino-N-(2-aminoethyl)-5-iodobenzamide, **6**. The product was purified by flash chromatography on silica gel using MeOH/CHCl$_3$ (first 0/1, then 5/3) as an eluent and finally crystallized from CH$_2$Cl$_2$ after decantation from insoluble material. Yield: 73%. Mp: 110–112 °C. ^{1}H NMR: δ (d_6-DMSO) 2.70 (2 H, t, J = 6.4 Hz), 3.23 (2 H, tt, J = 6.4 and 6.4 Hz), 3.31 (4 H, broad s), 6.55 (1 H, d, J = 9.4 Hz), 7.37 (1 H, dd, J = 2.4 and 9.4 Hz), 7.78 (1 H, d, J = 2.4 Hz), 8.34 ppm (1 H, t, J = 6.4 Hz). IR (KBr pellet): 3440, 3360, 3320, 1630, 1570, 1535, 1480, 1305 cm^{-1} ν(CONH and NH).

Preparation of Compounds 7 and 8. Benzamide **5** or **6** (3.0 mmol) was added in small portions to cold (below 5 °C) trifluoroacetic anhydride (4.6 g, 22 mmol) during 0.5 h. After being stirred for another 0.5 h below 5 °C, the reaction mixture was kept at room temperature for 2 h. Ice-cold water was added to the cooled reaction mixture. The formed solid material was filtered and washed with cold water.

N-[2-(Trifluoroacetamido)ethyl]-2-(trifluoroacetoxy)-5-iodobenzamide, **7**. Yield: 60%. Mp: 173–175 °C. ^{1}H NMR: δ(CD$_3$COCD$_3$) 3.57–3.67 (4 H, m), 6.75 (1 H, d, J = 8.8 Hz), 7.71 (1 H, dd, J = 2.4 and 8.8 Hz), 8.04 (1 H, d, J = 2.4 Hz), 8.56 (1 H, s), 8.80 ppm (1 H, s). IR (KBr pellet): 3415 and 3315 ν(NH), 1705, 1635, 1575, 1560, 1530 and 1245 ν(CONH, C=O and C−O), 1185 cm^{-1} ν(CF).

2-(Trifluoroacetamido)-N-[2-(trifluoroacetamido)ethyl]-5-iodobenzamide, **8**. The product was purified by flash chromatography on silica gel using petroleum ether (bp 40–60 °C)/ethyl acetate (5/3) as an eluent. Yield: 59%. Mp: 201–202°C (subl). ^{1}H NMR: δ(CD$_3$COCD$_3$) 3.59–3.70 (4 H, m), 7.96 (1 H, dd, J = 1.9 and 8.8 Hz), 8.18 (1 H, d, J = 1.9 Hz), 8.38 (1 H, d, J = 8.8 Hz), 8.65 ppm (3 H, broad s). IR (KBr pellet): 3305 ν(NH), 1735, 1705, 1635, 1585, 1515, 1160 cm^{-1} ν(CONH and CF).

Coupling of Compounds 7, 8, and 3-Iodobenzylamine Hydrochloride (9) to 10. Bis(triphenylphosphine)palladium(II) chloride (7 mg, 0.01 mmol) and copper(I) iodide (4 mg, 0.02 mmol) were added under nitrogen to a mixture of **7**, **8**, or 3-iodobenzylamine hydrochloride (**9**) (0.5 mmol), tetra(*tert*-butyl) 2,2′,2″,2‴-[(4-ethynylpyridine-2,6-diyl)bis(methylenenitrilo)]tetrakis(acetate) (*16*) (**10**, 0.34 g, 0.56 mmol), dry triethylamine (2mL), and tetrahydrofuran (2.5 mL). After being stirred for 2 h at room temperature, the mixture was filtered and the filtrate was evaporated to dryness. The residue was dissolved in CHCl$_3$ (15 mL), washed with water (2 × 5 mL) and dried with sodium sulfate. The product was purified by flash chromatography on silica gel.

Tetra(tert-butyl) 2,2′,2″,2‴-{{4-{{3′-[[N-(2-(trifluoroacetamido)ethyl)amino]carbonyl-4′-(trifluoroacetoxy)phenyl}ethynyl}pyridine-2,6-diyl}bis(methylenenitrilo)}tetrakis(acetate),* **11**. Eluent: petroleum ether (bp 40–60 °C)/ethyl acetate (first 10/3, then 1/1). Yield: 53%. ^{1}H NMR: δ (d_6-DMSO) 1.40 (36 H, s), 3.37–3.44 (4 H, m), 3.42 (8 H, s), 3.89 (4 H, s), 6.99 (1 H, d, J = 8.6 Hz), 7.53 (2 H, s), 7.61 (1 H, dd, J = 2.5 and 8.6 Hz), 8.12 (1 H, d, J = 2.5 Hz), 9.08 (1 H, broad, s), 9.54 ppm (1 H, broad, s).

Tetra(tert-butyl) 2,2′,2″,2‴-{{4-{{3′-[[N-(2-(trifluoroacetamido)ethyl)amino]carbonyl]-4′-(trifluoroacetamido)phenyl}ethynyl}pyridine-2,6-diyl}bis(methylenenitrilo)}tetrakis(acetate),* **12**. Eluent: petroleum ether (bp 40–60 °C)/ethyl acetate (5/3). Yield: 79%. ^{1}H NMR: δ (d_6-DMSO) 1.42 (36 H, s), 3.22–3.41 (4 H, m), 3.44 (8 H, s), 3.91 (4 H, s), 7.58 (2 H, s), 7.85 (1 H, dd, J = 2.4 and 8.1 Hz), 8.16 (1 H, d, J = 2.4 Hz), 8.42 (1 H, d, J = 8.1 Hz), 9.24 (1 H, broad s), 9.50 ppm (1 H, t, J = 5.9 Hz). IR (KBr pellet): 2220 ν(C≡C), 1735, 1650, 1590, 1545, 1225, 1155 cm^{-1} ν(CONH, C=O, C−O and CF).

Tetra(tert-butyl) 2,2′,2″,2‴-{{4-{[3′-(aminomethyl)phenyl]ethynyl}pyridine-2,6-diyl}bis(methylenenitrilo)}tetrakis(acetate),* **13**. Eluent: first petroleum ether (bp 40–60 °C)/ethyl acetate (5/3) and then MeOH. Yield: 75%. ^{1}H NMR: δ (d_6-DMSO) 1.41 (36 H, s), 3.43 (8 H, s), 3.73 (2 H, s), 3.90 (4 H, s), 7.35–7.45 (3 H, m), 7.55 (2 H, s), 7.58 (1 H, s).

Preparation of Compounds 14–16. A mixture of compound **11** or **12** (0.47 mmol), 0.5 M KOH in ethanol (16 mL), and water (13 mL) was stirred for 35 min at room temperature. The mixture was extracted with CHCl$_3$ (2 × 50 mL). The combined organic phases were washed with saturated NaCl solution (15 mL), dried with sodium sulfate, and evaporated to dryness. The residue, or **13** (0.47 mmol), was dissolved in trifluoroacetic acid (20 mL), and the mixture was kept at room temperature for 1.5 h. Trifluoroacetic acid was evaporated without heating. The residue was triturated with diethyl ether (50 mL), and the product was filtered and washed with diethyl ether. The yields were 100% for all compounds.

2,2′,2″,2‴-{{4-{{3′-[[N-(2-Aminoethyl)amino]carbonyl]-4′-hydroxyphenyl}ethynyl}pyridine-2,6-diyl}bis(methylenenitrilo)}tetrakis(acetic acid), **14**. ^{1}H NMR: δ (d_6-DMSO) 3.00–3.06 (2 H, m), 3.52 (8 H, s), 3.54–3.58 (2 H, m), 3.98 (4 H, s), 7.02 (1 H, d, J = 8.8 Hz), 7.57 (2 H, s), 7.68 (1 H, dd, J = 2.2 and 8.8 Hz), 7.84 (3 H, broad s), 8.15 (1 H, d, J = 2.2 Hz), 9.05 ppm (1 H, broad s). IR (KBr pellet): 2210 ν(C≡C), 1730, 1680, 1635, 1200 cm^{-1} ν(CONH, C=O and C−O).

2,2′,2″,2‴-{{4-{{4′-amino-3′-[[N-(2-aminoethyl)amino]carbonyl]phenyl}ethynyl}pyridine-2,6-diyl}bis(methylenenitrilo)}tetrakis(acetic acid), **15**. ^{1}H NMR: δ (d_6-DMSO) 3.01–3.03 (2 H, m), 3.40 (5 H, broad s), 3.47 (8 H, s), 3.54–3.57 (2 H, m), 3.94 (4 H, s), 7.55 (2 H, s), 7.88 (1 H, dd, J = 1.5 Hz and 8.9 Hz), 8.23 (1 H, d, J = 1.5 Hz), 8.39 ppm (1 H, d, J = 8.9 Hz). IR (KBr pellet): 2210 ν(C≡C), 1720, 1680, 1640, 1200 cm^{-1} ν(CONH, C=O and C−O).

2,2′,2″,2‴-{{4-{[3′-(Aminomethyl)phenyl]ethynyl}pyridine-2,6-diyl}bis(methylenenitrilo)}tetrakis(acetic acid), **16**. ^{1}H NMR: δ (d_6-DMSO) 3.52 (8 H, s), 3.98 (4 H, s), 4.09 (2 H, s), 7.50–7.65 (3 H, m), 7.59 (2 H, s), 7.78 (1 H, s). IR (KBr pellet): 2215 (C≡C), 1725, 1675, 1630, 1200 cm^{-1} ν(C=O and C−O).

Preparation of Europium and Terbium Chelates. The tetraacid ligands (**14–16**) were dissolved in water, and the pH was adjusted to 6–7 using solid NaHCO$_3$. An equimolar amount of aqueous solution of europium or terbium chloride hexahydrate was added during 15 min, and the pH was maintained in the range of 6–7. After 1 h of stirring at room temperature, the pH was raised to 8.5 with 1 M NaOH and the formed precipitate was removed by centrifugation. The aqueous solution was concentrated to 1–2 mL, and acetone was added to precipitate the chelates. Precipitated chelates were washed with acetone and used without additional purification.

Preparation of Octanedioic Acid Bis(*N*-succinimidyl ester). Octanedioic acid (1.0 g, 5.7 mmol),

Scheme 3. Synthesis of the Activated Thyroxine Derivative 17

Scheme 4. Synthesis of the Activated Progesterone Derivative 18
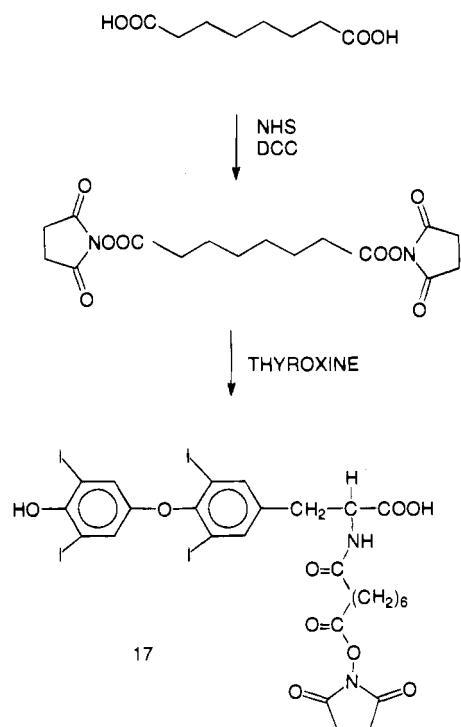
N-hydroxysuccinimide (NHS) (1.4 g, 11.7 mmol), and *N,N'*-dicyclohexylcarbodiimide (DCC) (2.4 g, 11.7 mmol) were dissolved in dry 1,4-dioxane (25 mL), and the reaction mixture was stirred at room temperature overnight (*17*). Precipitated dicyclohexylurea was removed by filtration, and the solvent was evaporated under reduced pressure. The crude product was first purified by flash chromatography using acetone/toluene (1/9) as eluent. Upon crystallization from acetone/diethyl ether a white solid (1.10 g, 52%) was obtained. Mp: 159 °C. ^{1}H NMR: δ (d_6-DMSO) 1.46–1.50 (4 H, m), 1.68–1.73 (4 H, m), 2.66 (4 H, t, J = 7.3 Hz), 2.86 (8 H, s). IR (KBr pellet): 2919, 1818, 1787, 1734, 1212, 1062, 868 cm^{-1}.

Preparation of *N*-Hydroxysuccinimide-Activated L-Thyroxine Derivative (17) (Scheme 3). A solution of octanedioic acid bis(*N*-succinimidyl ester) (100 mg, 0.27 mmol) in dry *N,N*-dimethylformamide (1.0 mL) was added to a solution of L-thyroxine (100 mg, 0.13 mmol) in dry *N,N*-dimethylformamide (1.0 mL) and dry triethylamine (40 μL). The reaction mixture was stirred overnight at room temperature. After concentration under reduced pressure, the activated thyroxine derivative 17 was purified by preparative TLC using toluene/ethanol (1/1) to develop the plates. R_f 0.5. Yield: 64%. ^{1}H NMR: δ(d_6-DMSO) 1.19–1.23 (2 H, m), 1.32–1.36 (2 H, m), 1.41–1.45 (2 H, m), 1.58–1.61 (2 H, m), 2.59 (1 H, s), 2.62 (2 H, t, J = 7.3 Hz), 2.73–2.79 (1 H, m), 2.81 (4 H, s), 3.06 (1 H, dd, J = 4.7 and 13.9), 4.22–4.25 (1 H, m), 7.05 (2 H, s), 7.74 (2 H, s). IR (KBr pellet): 2925, 1701, 1636, 1436, 1226 cm^{-1}.

Preparation of Progesterone 3-(*O*-Carboxymethyl)oxime and its *N*-Succinimidyl Ester (18) (Scheme 4). Progesterone (1.7 g, 5.4 mmol) was added to a mixture of pyrrolidine (1.2 mL, 14 mmol) and methanol (100 mL). After 15 min (aminooxy)acetic acid hemihydrochloride (1.05 g, 4.8 mmol) was added, and the mixture was stirred for 1.5 h at room temperature according to Janoski and co-workers (*18*). Methanol was evaporated, the residue was dissolved in water, and the slightly alkaline solution was extracted once with ethyl
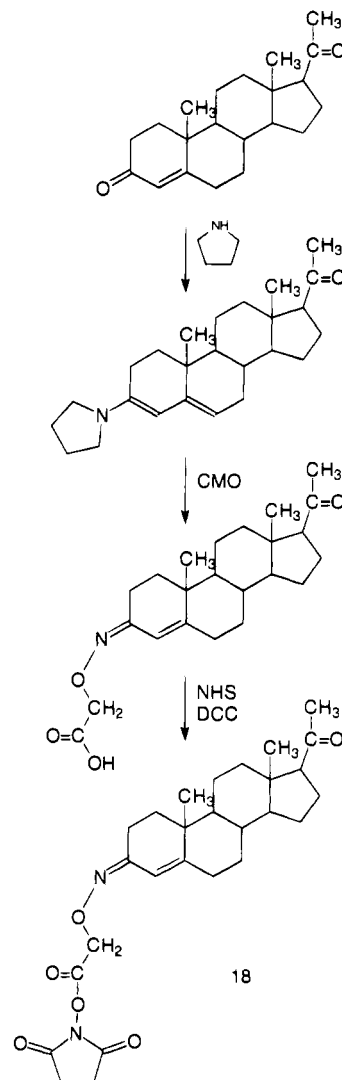
acetate to remove any unreacted steroid. The aqueous solution was acidified to pH 2 and extracted three times with ethyl acetate. The combined organic phases were evaporated to dryness to yield progesterone 3-(*O*-carboxymethyl)oxime (1.5 g, 72%), which was used without further purification. ^{1}H NMR: δ(CDCl$_3$) 0.65 (3 H, s), 1.06 and 1.09 (3 H, s, s), 2.11 (3 H, s), 4.09 (2 H, m), 5.78 and 6.43 (1 H, s, s). IR (KBr pellet): 3300–2500 (broad), 2937, 1740, 1703, 1628, 1208, 1101 cm^{-1}. UV (CH$_3$CH$_2$-OH): λ_{max} 249 nm.

Progesterone 3-(*O*-carboxymethyl)oxime (1.00 g, 2.50 mmol), *N*-hydroxysuccinimide (NHS) (317 mg, 2.75 mmol), and *N,N'*-dicyclohexylcarbodiimide (DCC) (568 mg, 2.75 mmol) were dissolved in dry 1,4-dioxane (3.0 mL), and the reaction mixture was stirred overnight at room temperature (*19, 20*). The precipitated dicyclohexylurea was removed by filtration, and the solvent was evaporated under reduced pressure. The product, *N*-succinimidyl ester of progesterone 3-(*O*-carboxymethyl)oxime, was purified on a TLC plate using acetone/toluene (1/9) or chloroform/methanol (9/1) for developing. Yield: 62%. ^{1}H NMR: δ(CDCl$_3$) 0.65 (3 H, s), 1.06 and 1.09 (3 H, s, s), 2.17 (3 H, s), 2.87 (4 H, s), 4.90 (2 H, m), 5.78 and 6.43 (1 H, s, s).

Labeling of *N*-Succinimidyl Esters of Haptens with Chelates. The *N*-succinimidyl esters of hapten derivative 17 or 18 were dissolved in 1,4-dioxane, and the europium or terbium chelate bearing an aliphatic

R = OH   A = (CH₂)₂NHCO (Ligand 14)
R = NH₂   A = (CH₂)₂NHCO (Ligand 15)
R = H   A = CH₂   (Ligand 16)
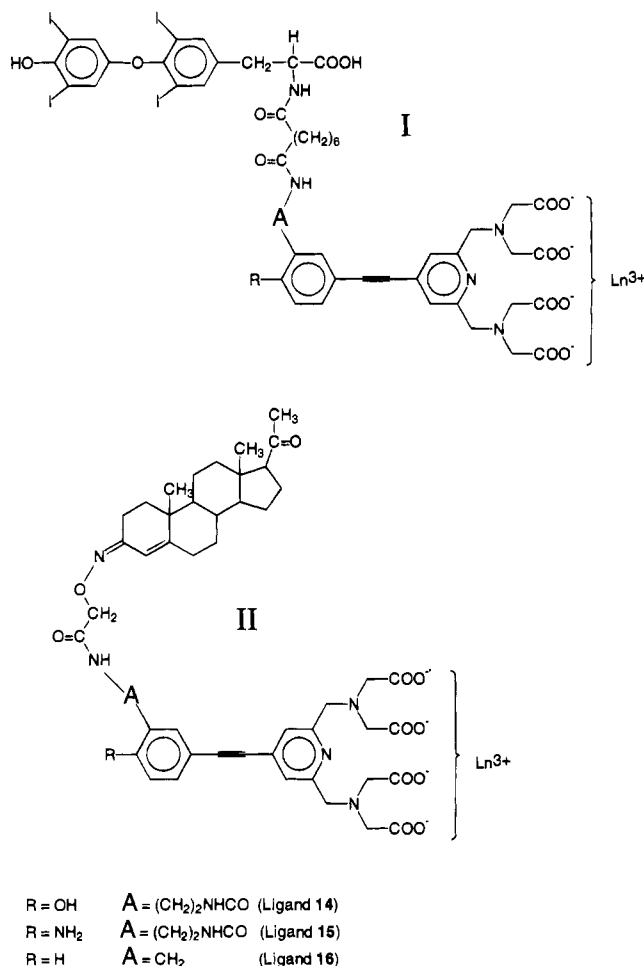
Figure 2. Structures of the lanthanide-labeled thyroxine (**I**) and progesterone (**II**) derivatives.

amino group was added as a water solution. The mixtures were stirred at room temperature for 2–3 h and concentrated under reduced pressure, acetone was added to precipitate the labeled hapten, and the solvents were removed after centrifugation. The products (Figure 2) were purified on TLC plates using acetonitrile/water (4/1) for developing. The labeled haptens obtained were used for luminescence measurements without any further purification.

RESULTS AND DISCUSSION

Syntheses of Ligands and Lanthanide Chelates. In addition to ligands **1** and **2** (Figure 1), we prepared chelates having a substituent containing an aliphatic amino group at the *meta*-position. The ester group of compounds **3** and **4** (*15*) reacted readily with ethylenediamine to produce amides **5** and **6**. Before coupling to compound **10** (*16*), the hydroxy and amino groups were protected to give trifluoroacetamides **7** and **8**. 3-Iodobenzylamine (**9**), on the other hand, did not need any protection. The iodo group of compounds **7–9** reacted with the terminal acetylene of **10** in the presence of a catalytic amount of palladium catalyst and copper(I) iodide (*16*). The protecting trifluoroacetamido, trifluoroacetoxy, and *tert*-butyl ester groups of compounds **11–13** were hydrolyzed using alkaline and acidic hydrolysis, respectively, to the tetraacetic acids **14–16**. The lanthanide chelates were synthesized using the method of Takalo and co-workers (*13*) in a slightly modified form.

Syntheses and Labeling of Hapten Derivatives. Most commonly isothiocyanato, haloacetyl, or 2,4,6-

triazinyl derivatives of europium chelates have been used to label amino groups on proteins or hapten derivatives (*13, 14, 21*). Carboxyl derivatives of steroids have also been labeled in the presence of water-soluble carbodiimide using an aromatic amino derivative of a chelate (*22–24*). However, as ligand **15** incorporates both aliphatic and aromatic amino groups, these labeling methods cannot be applied because of the presence of two reactive amino groups. Therefore, we used *N*-succinimidyl esters of carboxylic acid derivatives of the haptens, which made it possible to selectively derivatize only the aliphatic amino group of the chelating ligand.

Thyroxine is an amino acid, and for immunoassays the amino group of the molecule is usually used for derivatization. In this work we had to use a preactivated bifunctional reagent to obtain the *N*-succinimidyl ester derivative because of the carboxyl group of thyroxine. Octanedioic acid bis(*N*-succinimidyl ester) was synthesized (Scheme 3) in 1,4-dioxane using *N*-hydroxysuccinimide and carbodiimide (*17*), and the product was purified by crystallization after flash chromatography. In the ¹H NMR spectrum the characteristic singlet of eight protons of succinimidyl groups at δ 2.86 could be detected. In the IR spectrum the absence of carboxylic acid absorption (3300–2500 cm⁻¹) and the presence of new carbonyl bands near 1800 cm⁻¹, a C–N stretch band at 1212 cm⁻¹, and the band of cyclic imide at 868 cm⁻¹ were characteristic to the synthesized bifunctional reagent. *N*-succinimidyl derivative of thyroxine **17** was synthesized (Scheme 3) using a 2.1-fold molar excess of the bis-activated octanedioic acid in *N,N*-dimethylformamide, and the product was purified on TLC plates. In the ¹H NMR spectrum the characteristic chemical shift of the succinimidyl group at δ 2.81 could be detected, as could the new carbonyl band at 1701 cm⁻¹ in the IR spectrum.

Progesterone 3-(O-carboxymethyl)oxime was synthesized using the method of Janoski and co-workers (*18*) (Scheme 4), in which the 3-oxo group of the steroid dione is activated using pyrrolidine before the reaction with (aminooxy)acetic acid, whereby selective formation of 3-(O-carboxymethyl)oxime is achieved. In the UV spectra a characteristic shift of the absorption maximum from 240 to 249 nm was detected. In this reaction, cis- and trans-isomers of progesterone oxime were produced. The isomers were not separated, but they were clearly distinguishable in the ¹H NMR spectrum. The chemical shifts of the olefinic proton at carbon C-4 were 6.43 and 5.78, and those of the protons of the methyl group at carbon C-19 were 1.09 and 1.06 for the cis- and trans-isomers, respectively. According to NMR data, the ratio (cis/trans) of these isomers was 2/3. In the IR spectrum of the 3-(O-carboxymethyl)oxime derivative the characteristic carboxylic acid absorption bands, the absence of a 3-oxo band (1662 cm⁻¹), and the presence of a 20-oxo band (1703 cm⁻¹) were clearly detected. This carboxyl derivative of progesterone was then activated with *N*-hydroxysuccinimide in dioxane (Scheme 4) using carbodiimide as the condensing agent (*19, 20*). In the ¹H NMR spectrum the characteristic four-proton singlet at δ 2.87 was indicative of the produced *N*-succinimidyl ester derivative (**18**).

Labeling of N-succinimidyl ester derivatives with lanthanide chelates was carried out in 1,4-dioxane–water solution, and the produced compounds were purified only on TLC plates, which is not sufficient for immunoassays but adequate for studies of luminescence properties. On a TLC plate the unreacted chelate and hapten derivatives, as well as most of the byproducts of the labeling

Table 1. Relative Luminescence Intensities of Europium and Terbium Chelates in Ethanol and in an Aqueous Buffer with or without Albumin

	substituents			rel luminescence intensity (%)		
ligand	para	meta	lanthanide	ethanol	buffer	buffer + albumin
16	H	CH_2NH_2	Tb(III)	1.53	2.0	1.67
16	H	CH_2NH_2	Eu(III)	3.21	1.83	1.53
1	OH	COOH	Eu(III)	5.40	1.44	2.86
14	OH	$CONHCH_2CH_2NH_2$	Eu(III)	0.43	0.05	0.08
2	NH_2	COOH	Eu(III)	9.34	0.13	0.38
15	NH_2	$CONHCH_2CH_2NH_2$	Eu(III)	1.70	0.07	0.09

Table 2. Relative Luminescence Intensities of Europium- or Terbium-Labeled Progesterone and Thyroxine[a] in Ethanol and in an Aqueous Buffer with or without Albumin

			relative luminescence intensity (%)		
ligand	lanthanide	hapten	ethanol	buffer	buffer + albumin
16	Tb(III)	Progesterone	0.20	0.55	0.55
16	Tb(III)	Thyroxine	0.09	0.09	0.34
14	Eu(III)	Progesterone	5.0	0.04	0.20
14	Eu(III)	Thyroxine	4.5	0.02	0.16
15	Eu(III)	Progesterone	3.8	0.11	0.53
15	Eu(III)	Thyroxine	4.3	0.18	1.31

[a] For structures, see Figure 2.

reaction, could be removed, whereafter the only luminescent compound was the labeled hapten derivative (Figure 2).

Luminescence Properties of Chelates and Chelate-Labeled Haptenic Antigens. Table 1 shows the luminescence properties of the studied chelates in ethanol and in a Tris-HCl buffer with or without added albumin. Because of its tendency to bind aromatic structures, albumin is used as a luminescence-modulating compound to enable the construction of homogeneous assays. A high concentration of albumin also levels the inherent variations in patient sera, avoiding some of the problems derived from sample-to-sample deviations. The *para*-amino derivatives (2 and 15), in particular, demonstrate high sensitivity to environmental changes, which may occur during immunoreaction. The solvent sensitivity and the chelate affinity to the added albumin is greatly dependent on the type of substituents at the *meta*-position, and hence the final suitability of a particular chelate derivative to a homogeneous assay can only be judged after coupling of the chelate to the antigen.

In Table 2, the luminescence properties of thyroxine and progesterone derivatives labeled with three different types of chelates are compared. Chelates without *para*-substitution in the phenyl ring (16) show very little sensitivity to environmental changes. As an exception, the luminescence of the thyroxine conjugate with a terbium chelate is enhanced by albumin, probably because of strong internal quenching. In line with the results obtained with FITC-conjugated thyroxine (25), the direct quenching is diminished upon binding of the conjugate to proteins.

The effect of added albumin on the luminescence of some of the labeled antigens is demonstrated in Figure 3. The maximum luminescence enhancement was 50-fold when using thyroxine labeled with the *para*-hydroxy derivative of the europium chelate (14), whereas when using progesterone labeled with the *para*-unsubstituted derivative of the terbium chelate (16) the albumin effect was negative. To obtain the maximum enchancement, relatively high concentrations of albumin were required; i.e., the binding of the chelate to albumin is relatively weak. On the other hand, the lability of albumin binding speeds up the replacement reaction by anti-hapten antibodies in cases of low antigen concentrations in a
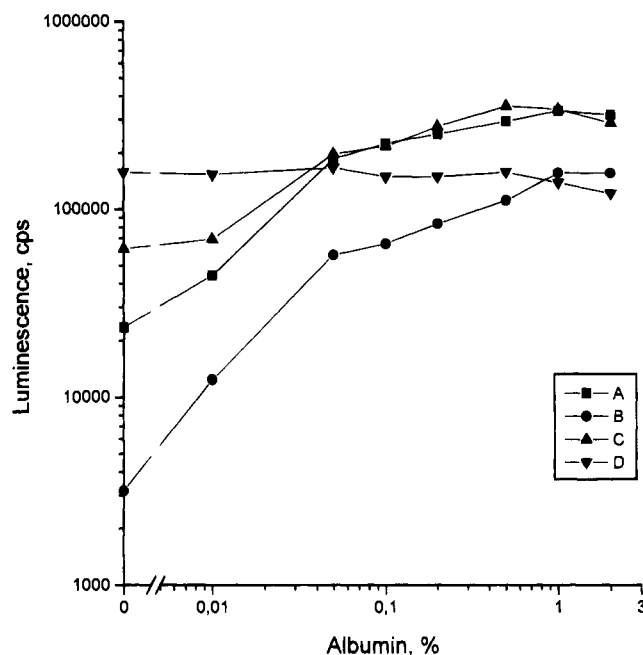
Figure 3. Effect of the albumin concentration on the luminescence of europium- or terbium-labeled haptens (for structures, see Figure 2): thyroxine labeled with the europium chelate of ligand 15 (A) and ligand 14 (B) and thyroxine and progesterone labeled with the terbium chelate of ligand 16 (C and D, respectively).

Table 3. Effect of Albumin and Various Detergents on the Luminescence Intensities of Europium (ligand 14)- and Terbium (ligand 16)-Labeled Progesterone[a]

	rel luminescence intensity (%)	
modulators in buffer	EuIII(14)	TbIII(16)
none	0.04	0.55
0.5% albumin	0.20	0.55
0.1% Triton X-100	0.20	2.74
0.1% sodium dodecyl sulfate	0.16	0.36
0.1% cetyltrimethylammonium bromide	0.05	0.10

[a] For structures, see Figure 2.

competitive assay, and thus facilitates the development of rapid homogeneous assays.

In addition to albumin, different detergents can also be used as luminescence modulating compounds. The effects of detergents depend on their charge and can be either luminescence enhancing or quenching (Table 3). Detergents can function as efficient modulators in assays in which the analyte matrix does not inherently contain high concentrations of binding proteins, such as albumin. They can be used e.g., for homogeneous analysis of urine steroids. Combining two homogeneous assays with two different lanthanide labels, europium and terbium, would even make it possible to construct simultaneous double-label homogeneous assays. The basic structure of the chelating ligand [4-(phenylethynyl)pyridine derivatives]

presented here and previously is, however, not suitable for terbium assays (*26*).

ACKNOWLEDGMENT

LITERATURE CITED

(1) Soini, E., and Hemmilä, I. (1979) Fluoroimmunoassay: Present status and key problems. *Clin. Chem. 25*, 353–361.

(2) Hemmilä, I., Dakubu, S., Mukkala, V.-M., Siitari, H., and Lövgren, T. (1984) Europium as a label in time-resolved immunofluorometric assays. *Anal. Biochem. 137*, 335–343.

(3) Hemmilä, I. (1991) *Application of fluorescence in immunoassays*, Wiley Interscience, New York.

(4) Hurskainen, P., Dahlén, P., Ylikoski, J., Kwiatkowski, M., Siitari, H., and Lövgren, T. (1991) Preparation of europium-labelled DNA probes and their properties. *Nucleic Acids Res. 19*, 1057–1061.

(5) Mathis, G. (1993) Rare earth cryptates and homogeneous fluoroimmunoassays with human sera. *Clin. Chem. 39*, 1953–1959.

(6) Hemmilä, I., Malminen, O., Mikola, H., and Lövgren, T. (1988) Homogeneous time-resolved fluoroimmunoassay of thyroxin in serum. *Clin. Chem. 34*, 2320–2322.

(7) Barnard, G., Kohen, F., Mikola, H., and Lövgren, T. (1989) Measurement of estrone-3-glucuronide in urine by rapid, homogeneous time-resolved fluoroimmunoassay. *Clin. Chem. 35*, 555–559.

(8) Barnard, G., Kohen, F., Mikola, H., and Lövgren, T. (1989) The development of non-separation time-resolved fluoroimmunoassays for the measurement of urinary metabolites. *J. Biolumin. Chemilumin. 4*, 177–184.

(9) Dandliker, W. B., Hsu, M.-L., Levin, J., and Rao, B. R. (1981) Equilibrium and kinetic inhibition assays based upon fluorescence polarization. *Methods Enzymol. 74*, 3–28.

(10) Takalo, H., Hänninen, E., and Kankare, J. (1993) Luminescence of europium(III) chelates with 4-(arylethynyl)-pyridines as ligands. *Helv. Chim. Acta 76*, 877–883.

(11) Kankare, J., Latva, M., and Takalo, H. (1991) Fluorescence intensities of Eu(III) complexes with substituted 4-phenylethynylpyridines as ligands. *Eur. J. Solid State Inorg. Chem. 28*, 183–186.

(12) Seveus, L., Väisälä, M., Syrjänen, S., Sandberg, M., Kuusisto, A., Harju, R., Salo, J., Hemmilä, I., Kojola, H., and Soini, E. (1992) Time-resolved fluorescence imaging of europium chelate label in immunohistochemistry and in situ hybridization. *Cytochemistry 13*, 329–338.

(13) Takalo, H., Mukkala, V.-M., Mikola, H., Liitti, P., and Hemmilä, I. (1994) Synthesis of europium(III) chelates suitable for labeling of bioactive molecules. *Bioconjugate Chem. 5*, 278–282.

(14) Mukkala, V.-M., Helenius, M., Hemmilä, I., Kankare, J., and Takalo, H. (1993) Development of luminescent europium-(III) chelates of 2,2′:6′,2″-terpyridine derivatives for protein labelling. *Helv. Chim. Acta 76*, 1361–1378.

(15) Takalo, H., Kankare, J., and Hänninen, E. (1988) Synthesis of some substituted dimethyl and diethyl 4-(phenylethynyl)-2,6-pyridinecarboxylates. *Acta Chem. Scand. B42*, 448–454.

(16) Hänninen, E., Takalo, H., and Kankare, J. (1988) Preparation of new complexing agents containing a highly conjugated ethynylated pyridine subunit. *Acta Chem. Scand. B42*, 614–619.

(17) Pilch, P. F. (1979) Interaction of cross-linking agents with the insulin effector system of isolated fat cells. *J. Biol. Chem. 254*, 3375–3381.

(18) Janoski, A. H., Shulman, F. C., and Wright, G. E. (1974) Selective 3-(O-carboxymethyl)oxime formation in steroidal 3,-20-diones for hapten immunospecificity. *Steroids 23*, 49–64.

(19) Anderson, G. W., Zimmerman, J. E., and Callahan F. M. (1964) The use of esters of N-hydroxysuccinimide in peptide synthesis. *J. Am. Chem. Soc. 86*, 1839–1842.

(20) Hosoda, H., Sakai, Y., Yoshida, H., Miyairi, S., Ishii, K., and Nambara, T. (1979) The preparation of steroid N-hydroxysuccinimide esters and their reactivities with bovine serum albumin. *Chem. Pharm. Bull. (Tokyo) 27*, 742–746.

(21) Mukkala, V.-M., Mikola, H., and Hemmilä, I. (1989) The synthesis and use of activated N-benzyl derivatives of diethylenetriaminetetraacetic acids: alternative reagents for labeling of antibodies with metal ions. *Anal. Biochem. 176*, 319–325.

(22) Mikola, H., and Miettinen, P. (1991) Preparation of europium labeled derivatives of cortisol for time-resolved fluoroimmunoassays. *Steroids 56*, 17–21.

(23) Mikola, H., Höglund, A.-C., and Hänninen, E. (1993) Labeling of estradiol and testosterone alkyloxime derivatives with a europium chelate for time-resolved fluoroimmunoassays. *Steroids 58*, 330–334.

(24) Mikola, H., and Hedlöf, E. (1994) Syntheses of europium-labeled digoxin derivatives and their use in time-resolved fluoroimmunoassay. *Steroids 59*, 472–478.

(25) Smith, D. S. (1977) Enhancement fluoroimmunoassay of thyroxine. *FEBS Lett. 77*, 25–27.

(26) Takalo, H., Hänninen, E., and Kankare, J. (1995) The influence of substituents on the luminescence properties of the Eu(III) and Tb(III) chelates of 4-(phenylethynyl)pyridine derivatives. *J. Alloys Compd* (in press).

Synthesis and Applications of a New Poly(ethylene glycol) Derivative for the Crosslinking of Amines with Thiols

Thomas Haselgrübler, Alexandra Amerstorfer, Hansgeorg Schindler, and Hermann J. Gruber*

Institute of Biophysics, J. Kepler University, Altenberger Str. 69, A-4040 Linz, Austria. Received July 22, 1994[®]

A heterobifunctional crosslinker was synthesized from a diamine derivative of poly(ethylene glycol) (PEG, average molecular weight 800 Da), with the functional groups 2-(pyridyldithio)propionyl (PDP) and N-hydroxysuccinimide ester (NHS). The crosslinker can be used for linkage of two different proteins for which a suitable protocol is presented, explified by crosslinking of two antibodies with 50% yield. In a second application the crosslinker is used to generate immunoliposomes. The NHS group was reacted with an aminolipid for liposome anchorage, and antibodies were bound to the PDP group via disulfide bonds. Loading of liposomes with antibodies was easily adjustable, even down to only a few per liposome. This crosslinker with its particular length appears especially suited for the flexible anchorage of biomembranes, opening new perspectives in membrane research as discussed.

INTRODUCTION

Covalent attachment of poly(ethylene glycol) (PEG[1]) to biological or biocompatible materials has become of great interest in clinical research (Merrill, 1992; Ouchi et al., 1987; Topchieva, 1990; Zalipsky et al., 1983). As a result of PEG conjugation, proteins no longer elicit strong immunogenic responses (Dreborg and Akerblom, 1990; Pool, 1990; Veronese et al., 1992; Zalipsky and Lee, 1992) and the circulation times of liposomes in blood can be sufficiently extended to be suitable for the requirements of clinical use (Blume and Cevc, 1990; Klibanov et al., 1991; Papahadjopoulos et al., 1991; Senior et al., 1991; Woodle et al., 1992). In all these cases monofunctional PEG derivatives with a nonreactive methoxy terminus and an amine-reactive group on the other end were used for PEG attachment.

Homobifunctional PEG derivatives with two amine-reactive end groups have been used to attach antibodies to liposomes via long, flexible spacers (Blume et al., 1993). Hetero-bifunctional PEG derivatives with two different reactive groups have found little application so far although several such crosslinkers and important asymmetric precursors for a larger variety have been synthesized (Yokoyama, 1992; Zalipsky and Barany, 1986; Zalipsky and Barany, 1990; Zalipsky, 1993).

The present study reports on the synthesis of a heterobifunctional PEG derivative with the coupling

functions NHS and PDP (see Scheme 1), particularly chosen for purposes of biomolecular coupling. Two examples are included in the Results, the conjugation of two soluble proteins and the preparation of immunoliposomes. Particular impact is expected from its use in methods of membrane research as outlined in the Discussion.

EXPERIMENTAL PROCEDURES

Materials. SBL (asolectin) were purified from soy bean lecithin (Sigma type II-S) by a standard method (Kagawa and Racker, 1971). EggPC was prepared chromatographically from Ovothin 200 (already 99% pure egg PC, Lucas Meyer, Hamburg, Germany) as described before (Gruber and Schindler, 1994). Anti-HSA (polyclonal sheep antibody, purified by immunsorption) was the generous gift of Dr. K. Hallermayer from Boehringer Mannheim, Penzberg, Germany. All other proteins were obtained from Sigma, and the same applies to DMPE, POPC, SATP, and to all other reagents unless specified. All solvents, aqueous buffer components, and inorganic salts were p.a. grade and purchased from Merck. DCC and ninhydrin were from the same source. NH₂-PEG-NH₂ and triethylamine were obtained from Fluka. FLUOS was obtained from Lambda Probes & Diagnostics, Graz, Austria. Argon (Linde) was 99.998% (<3 ppm O₂). SPDP was prepared as described (Ofitserov et al., 1985; Shval'e et al., 1985).

Methods. Thin Layer Chromatrography. Plastic sheets, precoated with 0.2 mm silica gel 60 without fluorescent indicator (Merck) were used. Eluents I and II contained chloroform and methanol at a ratio of 90/10 and 80/20, respectively. Eluents III and IV contained chloroform/methanol/acetic acid at volume ratios of 85/15/0.1 and 100/30/2, respectively. Eluent V was a mixture of chloroform/methanol/water (80/20/1). Amino groups were detected by spraying with 0.1% ninhydrin in 2-propanol and heating to 100 °C (Schuurmans-Stekhoven et al., 1992). Free or PEG-bound phospholipids were also visualized by spray reagents (Dittmer and Lester, 1964). By spraying with 2,6-dichlorophenolindophenol (0.1% sodium salt in ethanol; Passera et al., 1964) only the COOH of glutaric acid could be specifically detected, while all PEG derivatives with and without COOH groups gave intense dark blue spots.

Determination of PDP Group Contents of PEG Derivatives. Typically, 200 μL of an aqueous sample

---

[1] Abbreviations: AFM, atomic force microscopy; DCC, N,N'-dicyclohexylcarbodiimide; DMPE, 1,2-bis(myristoylphosphatidyl)ethanolamine; DTNB, 5,5'-dithiobis(2-nitrobenzoic acid); DTT, dithiothreitol; eggPC, egg yolk phosphatidylcholine; FLUOS, 5-(and-6)-carboxyfluorescein, succinimidyl ester; HSA, human serum albumin; NH₂-PEG-NH₂, O,O'-bis(2-aminopropyl)poly-(ethylene glycol) 800 (see Scheme 1); NHS, N-hydroxysuccinimide or N-hydroxysuccinimidyl residue (connected to NH₂-PEG-NH₂ by a glutaryl residue); PDP, 2-pyridyldithiopropionyl residue; PE, phosphatidylethanolamine; PEG, poly(ethylene glycol) (in the Experimental Procedures and Results sections the term "PEG" is used as defined in Scheme 1); POPC, 1-palmitoyl-2-oleoylphosphatidylcholine; rt, room temperature; SATP, N-succinimidyl-3-(S-acetylthio)propionate; SBL, soy bean lipids (asolectin); SPDP, N-succinimidyl-3-(2-pyridyldithio)propionate; VET₂₀₀, vesicles produced by extrusion through a double layer of 200 nm Nuclepore membranes.

Scheme 1

atmosphere. A solution of 600 mg (1.92 mmol) of SPDP in 30 mL of $CHCl_3$ was added dropwise over a period of 15 min. The solution was stirred for an additional 15 min, 1 mL of acetic acid was added, and the solvent was evaporated. Residual acetic acid was azeotroped with toluene. The residue was dissolved in 10 mL of $CHCl_3$ and subjected to chromatography on 50 g of silica gel. The product was eluted by first applying 250 mL of $CHCl_3$/MeOH/AcOH = 90/10/0.1 and then 300 mL of 70/30/5. Fractions containing the product were pooled, evaporated, and azeotroped with toluene. The residue was again dissolved in $CHCl_3$, filtered, and evaporated to yield 750 mg (0.64 mmol, 29%) of highly viscous, yellowish liquid PDP-NH-PEG-NH-NH$_3$ + acetate: R_f^{IV} (product) = 0.17−0.47, R_f^{IV} (bis(pyridyldithio)−) = 0.57−0.72, R_f^{IV} (diamine) = 0−0.1. ^{1}H-NMR (200 MHz, $CDCl_3$) δ: 1.05−1.25 (m, CH_3, 2-aminopropyl), 1.97 (CH_3COOH), 2.56 (2H, t, J = 7.1 Hz, $-COCH_2CH_2-$), 2.6 (2H, s, NH_2), 3.05 (2H, t, J = 7 Hz, $-SCH_2CH_2-$), 3.64 (broad s, PEG polymer signal), 7−8.5 (4H, 3m, pyridyl), 8.75 (1H, broad s, CH_3COOH).

Preparation of PDP-NH-PEG-NH-glu. To 700 mg (0.64 mmol) of PDP-NH-PEG-NH$_3^+$ acetate and 110 mg (0.96 mmol) of glutaric anhydride was added 7 mL of pyridine. The mixture was stirred overnight. Pyridine was evaporated and the residue azeotroped with toluene. Ten mL of water was added, and the mixture was stirred for 1 h. Water was evaporated, and the residue was again azeotroped with toluene and subjected to chromatography on silica gel. Elution with 100 mL of $CHCl_3$/MeOH 92/8 and 300 mL of $CHCl_3$/MeOH 90/10 gave 362 mg (0.296 mmol, 46%) of highly viscous liquid PDP-NH-PEG-NH-glu which was free of glutaric acid: R_f^{II} (product) = 0.35−0.5, R_f^{II} (side product) = 0.67, R_f^{II} (glutaric acid) = 0.35−0.5. ^{1}H-NMR (200 MHz, $CDCl_3$) δ: 1.1−1.3 (m, CH_3, 2-aminopropyl), 1.97 (2H, m, $-COCH_2CH_2-CH_2-$), 2.27 (2H, t, J = 7 Hz, $-COCH_2CH_2-$), 2.38 (2H, t, J = 6.8 Hz, $-CH_2CH_2COOH$), 2.58 (2H, t, J = 6.9 Hz, $-COCH_2CH_2-$), 3.06 (2H, t, J = 6.9 Hz, $-SCH_2CH_2-$), 3.63 (broad s, PEG polymer signal), 7.0−8.5 (4H, 3m, pyridyl), no proton signal was detected for the carboxylic group. IR ($CHCl_3$) ν (cm^{-1}): 3436, 3029, 1711, 1657.

Preparation of NHS-NH-PEG-NH-PDP. To a solution of 362 mg (0.296 mmol) of PDP-NH-PEG-NH-glu in ethyl acetate were added 38 mg (0.33 mmol) of NHS and 67 mg (0.33 mmol) of DCC. The reaction mixture was stirred overnight. Dicyclohexylurea was removed by filtration. The filtrate was evaporated, and the residue obtained was used without further purification. As for NMR and IR measurements, 100 mg of the residue was subjected to rapid chromatography on 10 g of silica gel (2 cm column diameter). Elution with 100 mL of $CHCl_3$/MeOH 9/1 yielded 35 mg of highly viscous liquid NHS-NH-PEG-NH-PDP: R_f^{II} (product) = 0.62, R_f^{II} (SPDP) = 0.74. ^{1}H-NMR (200 MHz, $CDCl_3$) δ: 1.05−1.25 (m, CH_3, 2-aminopropyl), 2.55 (2H, t, $-COCH_2CH_2-$), 2.84 (4H, s, $-CH_2CH_2-$, succinimidyl), 3.06 (2H, t, J = 7 Hz, $-SCH_2CH_2-$), 3.61 (broad s, PEG polymer signal), 7.0−8.5 (4H, m, pyridyl). ^{13}C-NMR (200 MHz, $CDCl_3$) δ: 70.3 (PEG); C(1) 159.7, C(2) 120.8, C(3) 137.0, C(4) 119.8, C(5) 149.6 (pyridyl). IR ($CHCl_3$) ν (cm^{-1}): 3446, 3030, 1822, 1793, 1742 , 1662. Pyridyldithio group content (without solvent correction): 0.66 mequiv/g (87% of the theoretical value).

Preparation of DMPE-NH-PEG-NH-PDP. Thirty mg (0.047 mmol) of DMPE and 10 μL of triethylamine were added to a solution of 95 mg (0.072 mmol) of NHS-NH-PEG-NH-PDP in 2 mL of $CHCl_3$, and the reaction mixture was stirred for 2 h. The solvent was evaporated, and the residue was dissolved in 5 mL of $CHCl_3$ and

containing <0.8 mM PDP groups were diluted with 1 mL of 0.1 M NaH_2PO_4, titrated to pH = 8.0 with NaOH. Insoluble compounds like DMPE-NH-PEG-NH-PDP were solubilized by inclusion of Triton X-100 (up to 1% final concentration). One mL of this mixture was pipetted into a microcuvette, and A_{343} was determined both before and after thorough mixing with 100 μL of DTT or glutathione (0.2 M in buffer A, readjusted to pH 7.5 with NaOH; see below for buffer A). The PDP group concentration for the original 200 μL sample was calculated as [PDP] = $6/\epsilon_{343}$ ($1.1A_{343}' - A_{343}$), whereby A_{343} and A_{343}' denote the absorption values before and after glutathione addition, respectively, and ϵ_{343} of the released thiopyridone is known to be 8080 cm^{-1} M^{-1} (Leserman et al., 1984). In this way background levels of absorption (e.g., from Triton) were best corrected for. Glutathione was equally effective as DTT and was much preferred in the case of large sample series to avoid the severe irritation caused by DTT.

Preparation of PDP-NH-PEG-NH$_3$ + Acetate. A solution of 2 g (2.19 mmol) of NH_2-PEG-NH_2 (see Scheme 1 for abbreviations of molecular structures) in 30 mL of $CHCl_3$ was stirred at room temperature under an argon

subjected to chromatography on 20 g of silica gel. Elution with 100 mL of $CHCl_3$/MeOH 90/10 and 150 mL of 70/30 provided 48 mg (0.026 mmol, 55%) of DMPE-NH-PEG-NH-PDP: R_f^{JI} (product) = 0.3−0.39, R_f^V (product) = 0.35−0.49; R_f^{JI} (crosslinker) = 0.62, R_f^V (crosslinker) = 0.71, R_f^{JI} (DMPE) = 0.1. ^{1}H-NMR: (200 MHz, $CDCl_3$) δ: 0.88 (6H, t, J = 6. 8 Hz, CH_3, myristoyl), 1.05−1.25 (m, CH_3, 2-aminopropyl), 1.26 (s, CH_2, myristoyl), 2.28 (4H, t, $CH_2C=O$), 3.64 (broad s, PEG polymer signal), 3.94 (m, CH_2 glycerol and $-CH_2CH_2OP-$), 4.17 (dd, J = 7, 12 Hz, $-CH_2OP-$), 4.39 (dd, J = 3, 12 Hz, $-CH_2-OC=O$), 5.2 (m, CH glycerol, 1H), 7−8.5 (4H, 3m, pyridyl). ^{13}C-NMR (200 MHz, $CDCl_3$) δ: 70.3 (PEG); pyridyl: C(1) 159.7, C(2) 120.8, C(3) 137.0, C(4) 119.8, C(5) 149.6; DMPE moiety: 14.1 (CH_3), 22.7 (CH_2CH_3), 24.9 ($CH_2CH_2C=O$), 29.6 (polyCH_2), 31.9 ($CH_2CH_2CH_3$), 34.0 and 34.2 (2 $CH_2C=O$), 45.5 ($HNCH_2CH_2$), 62.8 ($CH_2-OC=O$), 69.5 (CHOC=O), 173.1 and 173.5 (C=O of two esters). IR ($CHCl_3$) $ν$ (cm^{-1}): 3431, 2930, 2869, 1740, 1657, 1100. Pyridyldithio group content (without solvent correction): 0.47 mequiv/g (87.5% of the theoretical value).

Preparation of SATP Derivatives of Antibodies. A modification of published procedures was used (Duncan et al., 1983; Jones and Hudson, 1993). Antibodies were dissolved at 65 $μ$M protein concentration in buffer A (100 mM NaCl, 50 mM NaH_2PO_4, 1 mM EDTA, pH = 7.5 adjusted with NaOH), and proper amounts of 16−18 mM stock solutions of SATP in pure DMSO were added to achieve different initial molar ratios of reagent/protein. After 30 min incubation under argon at rt IgG was separated from the reagents by gel filtration in buffer A (PD-10 column, Sephadex G-25 M, Pharmacia). For the determination of newly-introduced, protected SH groups 1.2 mL from the PD-10 peak fraction were treated with 50 $μ$L NH_2OH reagent (500 mM NH_2OH·HCl, 25 mM EDTA, pH = 7.5 adjusted with solid Na_2CO_3) under argon for 60 min at rt, and deprotected SH groups were assayed using DTNB by the Ellman method (Ellman, 1959). A linear dose response with a constant yield (37 %) of covalent SATP incorporation into IgG was found for up to four covalently bound SATP per IgG. This simple relation allowed an adjustment of the number average of SATP groups per antibody even if direct determination was not possible, as in the presence of FLUOS labels which interfered with the Ellman test.

Double Labeling of Anti-HSA with FLUOS and SATP. As outlined in the instructions from Molecular Probes, 5 $μ$L of 16.7 mM FLUOS in DMSO was added to 500 $μ$L of 10 mg/mL anti-HSA in buffer C (100 mM NaCl, 35 mM H_3BO_3, pH = 8.6 adjusted with NaOH) and stirred for 90 min at rt in the dark. Subsequently the pH was lowered to 7.5 by the addition of 4.2 $μ$L of 1 M NaH_2PO_4, and 5 $μ$L of 33 mM SATP in DMSO were added. After 20 min of stirring at rt in the dark the mixture was loaded on a PD-10 column and eluted with buffer A. Aliquots of derivatized anti-HSA were immediately frozen and stored at −70 °C.

Crosslinking of Bovine IgG to FLUOS- and SATP-Labeled Anti-HSA. In the first step bovine IgG was derivatized with NHS-NH-PEG-NH-PDP by mixing 1450 $μ$L of buffer A containing 100 nmol of bovine IgG with 50 $μ$L of DMSO containing the 1.5- to 12-fold amount of crosslinker (determined by PDP group content) and incubating at 19 °C for 70 min in the dark. The reaction was terminated by freezing and immediately after thawing IgG with bound crosslinker was separated from free crosslinker by gel filtration on Sephadex G-100 (1 × 26 cm column, flow rate 0.25 mL/min) in buffer B (100 mM NaCl, 20 mM CH_3COOH, pH = 5.5 adjusted with NaOH).

Fractions (4 min) were assayed for protein contents by measuring A_{278} ($ε_{278}$ = 174 000 M^{-1} cm^{-1} was determined for bovine IgG) and for PDP group contents as described above. In a control run 50 $μ$L of DMSO with 300 nmol of crosslinker were first mixed with 450 $μ$L of 10 mM ethanolamine·HCl in buffer C (pH = 8.6) and incubated at 37 °C for 15 min in order to destroy all NHS ester groups before 1 mL of buffer A with 100 nmol of IgG was added and incubated for 70 min as usual.

For the second step the three peak fractions from the Sephadex G-100 column were combined which together contained 20.4 $μ$M bovine IgG with 113 $μ$M covalently bound crosslinker (determined from PDP group contents). Twenty $μ$L of this derivatized IgG was adjusted from pH = 5.5 to pH = 7.5 by the addition of 10 $μ$L of buffer D (50 mM NaCl, 100 mM NaH_2PO_4, pH = 7.66 adjusted with NaOH) and mixed with 20 $μ$L of FLUOS- and SATP-modified anti-HSA which had been thawed immediately before use and diluted to a concentration of 10 $μ$M. The tube was sealed with a rubber septum, and the gas phase was perfused with argon via hypodermic needles while vortexing for 2 min. Crosslinking was triggered by injecting 2 $μ$L of degassed NH_2OH reagent (see above) and allowed to proceed for 60 min at 25 °C in the dark. In a control experiment the newly-formed disulfide bonds were cleaved by addition of 8.2 $μ$L of 0.2 M glutathione (in buffer A, readjusted to pH = 7.5 with NaOH) and 20 min incubation at 37 °C.

Formation of Liposomes Containing DMPE-NH-PEG-NH-PDP. Lipids were mixed with the indicated amounts of DMPE-NH-PEG-NH-PDP in $CHCl_3$ and dried by evaporation and 2 h evacuation at 10^{-2} mbar. Buffer B was added to give 50 mg/ml of lipid concentration. The lipid was completely suspended by repeated vortexing, and VET$_{200}$ were prepared by freeze−thaw cycles and repeated extrusion according to established procedures (Mayer et al., 1986; Hope et al., 1985) with slight modification (Gruber and Schindler, 1994) at a final lipid concentration of 20 mg/mL. The pH 5.5 was chosen in order to extend PDP group stability (Carlsson et al., 1978).

Coupling of Bovine IgG to Liposomes via DMPE-NH-PEG-NH-PDP. Bovine IgG was derivatized with SATP to give 1.0 protected SH group per protein. A 1.2 mL portion of derivatized IgG in buffer A was deoxygenated with argon and treated with 50 $μ$L of NH_2OH reagent (see above) for 60 min at rt while maintaining an argon atmosphere. Meanwhile the vesicles (consisting of eggPC and the indicated amount of DMPE-NH-PEG-NH-PDP) were thawed from the last freeze−thaw cycle and extruded as described above. After the pH was adjusted to 7.5 with NaOH and deoxygenation with argon 1 mL of degassed vesicles was injected into the IgG solution. After 2 h of incubation under argon at rt vesicles with bound protein were separated from free protein by flotation in a sucrose gradient: Linear density gradients were formed from 6.5 mL of 15% sucrose (w/v in buffer A, the same applies to all other sucrose or trehalose solutions) and 5.5 mL of 20% sucrose, and 300 $μ$L portions of 10%, 5%, and 2% sucrose were layered on top. A 910 $μ$L portion of liposome−IgG mixture was mixed with *either* 90 $μ$L of buffer A *or* 90 $μ$L of 200 mM DTT in buffer A (control for noncovalent protein adsorption to the liposomes; compare Leserman et al., 1984) and with 330 $μ$L of 100% sucrose. The resulting dense liposome mixtures were carefully injected below the linear sucrose gradients. After centrifugation at 95000g_{max} for 3 h at 20 °C tubes were pierced from the side and 0.9 mL fractions were harvested. The remaining bottom layer (about 3.5 mL each) was mixed and termed fraction

1. All gradient fractions were analyzed for lipid (Stewart, 1980) and protein contents (Schaffner and Weissmann, 1973).

Coupling of Fluorescent Anti-HSA to Liposomes via DMPE-NH-PEG-NH-PDP. VET_{200} were prepared from a lipid mixture of POPC/SBL/DMPE-NH-PEG-NH-PDP (75/25/0.5, molar ratios) at 20 mg/mL final lipid concentration. 80 μL portions of these liposomes in buffer B were adjusted to pH = 7.5 by the addition of 40 μL buffer D (50 mM NaCl, 100 mM NaH_2PO_4, pH = 7.66 adjusted with NaOH), followed by the addition of 80 μL of freshly-thawed, double-labeled anti-HSA (17 μM, same batch as above) in buffer A. Tubes were closed with rubber septa, and through hypodermic needles the gas phase was perfused with argon for 5 min, with frequent vortexing. Coupling was initiated by injecting 5 μL of deoxgenated NH_2OH reagent (see above). Samples were incubated at rt for 2 h in the dark before vesicles with bound protein were separated from free protein by flotation in trehalose gradients, in close analogy to the sucrose gradients described above. Gradient fractions were analyzed for lipid concentration with an enzymatic method (Menagent Phospholipids from Menarini Diagnostics, Florence, Italy). Protein was determined indirectly via fluorescein labels after solubilizing liposomes with excess Triton X-100.

RESULTS

Synthesis of NHS-NH-PEG-NH-PDP. As can be seen from Scheme 1, a diamine derivative of PEG (NH_2-PEG-NH_2, MW = 800 Da) served as starting material for the heterobifunctional crosslinker. SPDP, rather than usual amine protection, was used to introduce end group asymmetry in the first step, for the following reasons: First, the resulting asymmetric product was easy to isolate from the statistical mixture of unreacted diamine and symmetric product. Second, the ever-occurring impurity PDP-OH (hydrolyzed SPDP) could be removed in this first step only when the other end group was still a NH_2 group, rather than a COOH group (i.e., it was not possible to synthesize NH_2-PEG-NH-glu first and then to react with SPDP). Third, the PDP group was sufficiently stable during all subsequent steps. These reasons dictated the synthetic route, going from PDP-NH-PEG-NH_2 via PDP-NH-PEG-NH-glu to NHS-NH-PEG-NH-PDP.

All purification steps were by silica gel chromatography. The NHS ester derivative of PEG, however, was regularly used without further purification since silica gel chromatography resulted in extensive hydrolysis. The alternative method of selective precipitation of PEG derivatives (Zalipsky, 1993) was inapplicable, as well, since precipitation only occurred if the PEG chains had a molecular weight of at least 2000 Da.

Crosslinking of Two Different Soluble Proteins via NHS-NH-PEG-NH-PDP. The crosslinking properties of NHS-NH-PEG-NH-PDP were similar to that of its short analogue SPDP (Carlsson et al., 1978) but after the first reaction step the excess of unreacted/hydrolyzed crosslinker could not be removed by simple "desalting" methods. Chromatography on Sephadex G-100, however, gave complete separation of crosslinker-modified protein (bovine IgG, Figure 1A) from free crosslinker. The control experiment in Figure 1B proved that the PEG-derived crosslinker does not adsorb to IgG in a nonspecific way. The dose dependence of IgG derivatization is summarized in Figure 1C. It is important to note that the crosslinker itself is well soluble in water but DMSO was used to prepare appropriate stock solutions because no hydrolysis of the NHS ester function occurred in this
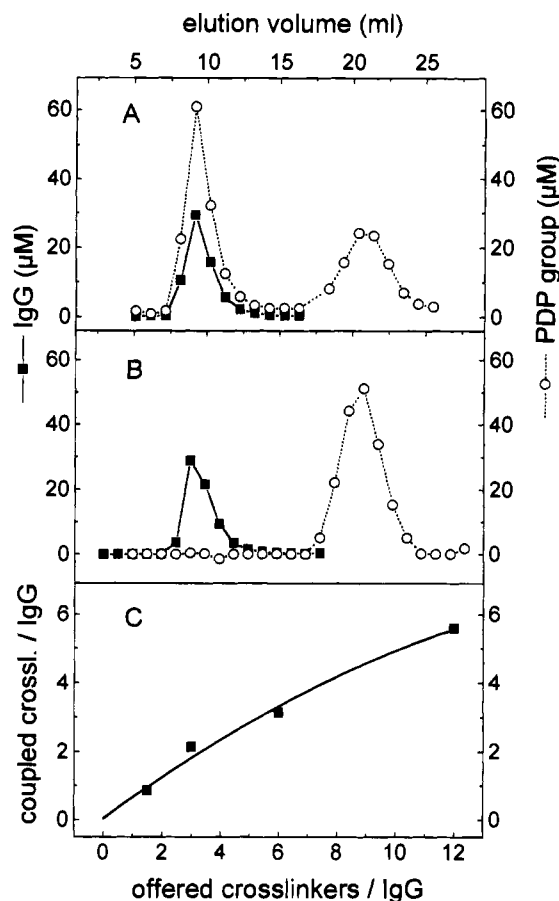
Figure 1. Derivatization of IgG with NHS-NH-PEG-NH-PDP. A: Sephadex G-100 chromatogram after reaction of bovine IgG with a 3-fold molar excess of crosslinker. B: Control experiment with conditions as in A except that the NHS ester function of the crosslinker was deactivated with excess ethanolamine·HCl before exposure to IgG. The 30% reduction of total PDP groups observed here was the only example of PDP group decay ever detected. It did not occur when the incubation with ethanolamine·HCl was carried out at room temperature instead of at 37 °C and in the absence of ethanolamine the PDP group was also completely stable at the same high pH (8.6) for days. C: Dose dependence of IgG derivatization with crosslinker. The numbers of covalently coupled crosslinkers per IgG were obtained from division of the integral of the first PDP peak by the integral of the protein peak in chromatograms like that shown in panel A.

solvent, even after several months of storage at −20 °C and repeated thawing.

In the second coupling step the PDP groups at the outer ends of the IgG-bound crosslinkers were reacted with free SH groups on another type of antibody. This second antibody (anti-HSA) was derivatized with both FLUOS (1.6 per protein) and SATP (1.8 per protein). Deprotection of bound SATP groups by NH_2OH provided the free SH groups necessary for disulfide bond formation. Figure 2 shows the HPLC gel filtration chromatogram after coupling of fluorescent anti-HSA to bovine IgG with an average number of 5.5 covalently bound crosslinkers (trace in the middle of Figure 2). Here a considerable fraction of fluorescent anti-HSA appeared in the void volume ($>10^6$ Da) and also in subsequent fractions corresponding to molecular weights larger than that of one antibody. This result meets the expectation for a high degree of crosslinking under the conditions chosen. The residual peak at 10 mL coincides with the position of unmodified IgG from the Bio-Rad standard (triangle with number 3 in Figure 2) as well as with the major fluorescence peak of FLUOS- and SATP-labeled anti-HSA
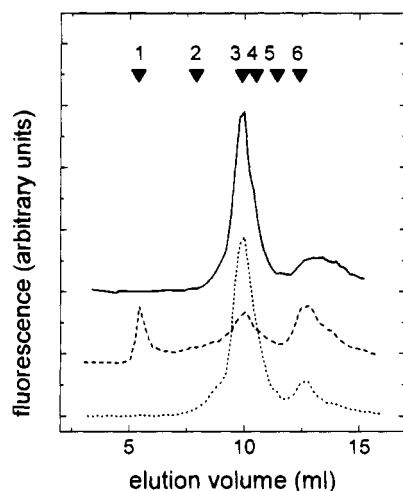
Figure 2. Crosslinking of bovine IgG with FLUOS- and SATP-labeled anti-HSA via NHS-NH-PEG-NH-PDP. Bovine IgG with 5.5 crosslinkers per protein (compare Figure 1C) was coupled to FLUOS- and SATP-modified anti-HSA by disulfide bond formation. Crosslinking was examined by HPLC gel filtration on a Bio-Sil TSK-400 column (Bio-Rad). The concentration of anti-HSA in the eluent was monitored indirectly via FLUOS label concentration. Triangles on top indicate the position of marker proteins (Bio-Rad gel filtration standard): 1 = void volume (aggregates), 2 = thyroglobulin (670 kDa), 3 = IgG (150 kDa), 4 = ovalbumin (44 kDa), 5 = myoglobin (17 kDa), and 6 = cyanocobalamine (1.35 kDa). Upper trace: control in the the absence of the crosslinker-modified bovine IgG. Middle trace: after crosslinking of bovine IgG with anti-HSA. Bottom trace: after cleavage of intermolecular disulfide bonds with glutathione.

if the crosslinking procedure was performed in the absence of crosslinker-modified bovine IgG (upper trace in Figure 2). Crosslinking was demonstrated to occur by disulfide bond formation and not by mere adsorption since 10 mM glutathione fully reversed the effect of NH_2-OH-induced crosslinking (bottom trace in Figure 2).

Heterobifunctional Coupling of Antibodies to Liposomes. The crosslinker NHS-NH-PEG-NH-PDP was first reacted with aminolipid (DMPE) in organic solvent, and the product was isolated by silica gel chromatography. Liposomes were then formed from dry films of phospholipid containing between 0.2 and 2 mol % of DMPE-NH-PEG-NH-PDP; freeze—thaw and extrusion was applied to ensure reproducible vesicle morphology and near unilamellarity.

In the second coupling step disulfide bonds were formed between the PDP groups on the liposome surface and free SH groups on antibodies. As above, coupling was triggered when IgG-bound SATP groups were deprotected with NH_2OH reagent. In a proper control experiment with liposomes prepared from highly purified eggPC this NH_2OH treatment was shown to cause absolutely no breakdown of phospholipid.

Liposomes with bound IgG were separated from free IgG by flotation in sucrose gradients (Figure 3) which does not alter vesicle morphology (H. J. Gruber et al., submitted for publication). Thirty-six percent of total IgG comigrated with the liposomes to the top of the gradient (Figure 3A), and all of it was specifically coupled by disulfide bonds, as judged from a parallel control experiment in which DTT had been included (Figure 3B). The relatively low yield of IgG coupling was certainly not due to lack of reactive PDP groups because the ratio of externally accessible PDP groups over IgG was around 16 (the external surface of this type of VET_{200} is invariably close to 40%; H. J. Gruber et al., submitted for publication). The lateral density of antibodies on the
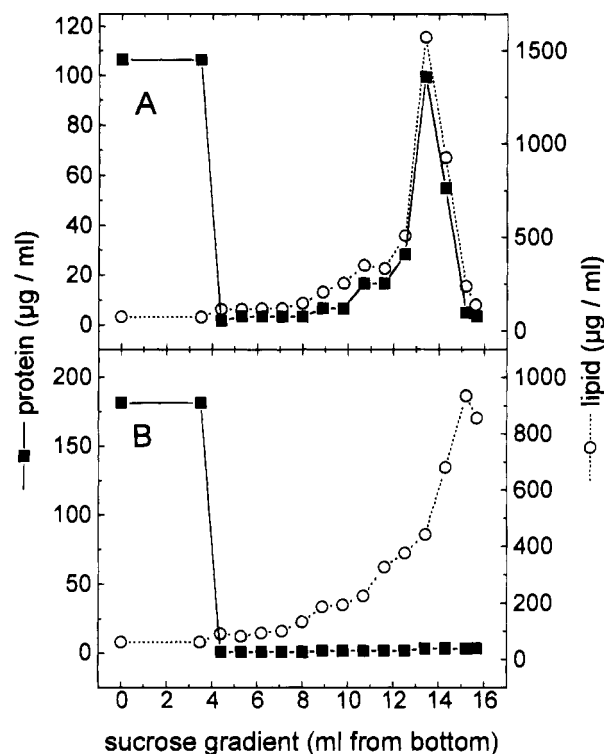
Figure 3. Flotation of liposomes after covalent coupling of SATP-derivatized bovine IgG. IgG with one SATP per protein was coupled to VET_{200} (eggPC/DMPE-NH-PEG-NH-PDP = 100/5, molar ratio) by disulfide bond formation and liposomes with bound protein were separated from free protein by flotation in a sucrose gradient (panel A). For a control, excess DTT was included in a parallel gradient (panel B).

external liposome surface in this experiment (2200 external lipids per bound IgG) was also far from maximal (86 lipids per IgG, Tamm and Bartoldus, 1988). Interestingly, the yield of IgG coupling dropped very little (from 36% to 28%) when the liposomes contained a 10-fold lower percentage of SH-reactive lipids. The incompleteness of IgG binding must, therefore, be attributed to the presence of underivatized IgG, as well as to premature deprotection and oxidation of SH groups.

Figure 4 shows that coupling of fluorescent anti-HSA to liposomes with a low percentage of SH-reactive lipids could be controlled very well by variation of the protein concentration. At infinite dilution the maximal "bindability" of the protein was extrapolated to be 65% (Figure 4, ordinate axis on the right). Coupling yield with respect to antibody dropped significantly at higher protein concentration—although the ratio of externally accessible PDP groups over anti-HSA was still 3 at the highest protein concentration. Obviously very low numbers of antibodies per vesicle (Figure 4, ordinate axis on the left) can be fine-adjusted in a reliable way by the presented method.

DISCUSSION

In this study we report on the synthesis of an SPDP-like heterobifunctional crosslinker containing a PEG spacer with a chain length of 18 ethylene glycol units (MW = 800 Da). In fact, the synthetic route was found to work also for a longer chain length of PEG (MW = 2000 Da, data not included).

Our particular interest in PEG_{800} with two different reactive groups relates to membrane research. This type of crosslinker appears to be required for application of emerging techniques of molecular microscopy allowing for resolution of single functional components in biomem-
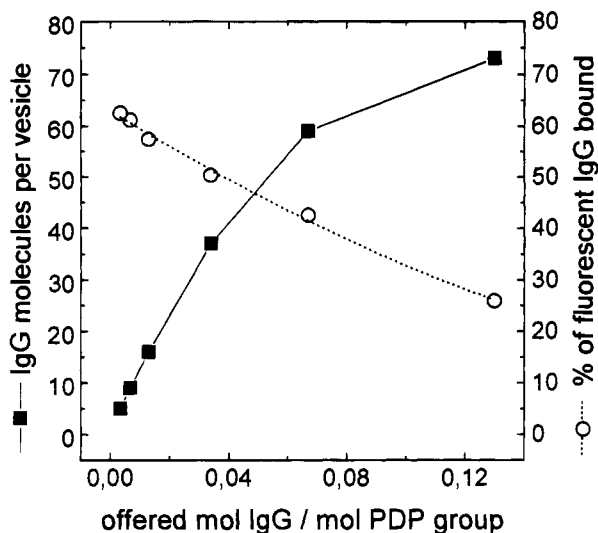
Figure 4. Coupling of low numbers of antibodies per vesicle. Anti-HSA derivatized with both FLUOS and SATP (same batch as in Figure 2) was coupled to VET$_{200}$ (containing 0.5 mol % DMPE-NH-PEG-NH-PDP) by disulfide bond formation, and vesicles with bound fluorescent anti-HSA were separated by flotation in trehalose gradients. Lipid recovery in the top part of the gradient was 95 ± 1%. Fluorescence comigrating with the liposomes was classified as "specifically bound antibody" since in the presence of DTT all fluorescence remained in the bottom of the gradient. The average vesicle was assumed to have a diameter of 200 nm and to contain 4×10^5 lipids (0.65 nm^2 area per lipid) and 2×10^3 DMPE-NH-PEG-NH-PDP.

branes. Such techniques are atomic force microscopy (AFM, for a first example see Florin et al. (1994)) and single particle tracking using fluorescence imaging (Fein et al., 1993; Ghosh and Webb, 1994). Membrane anchorage to a flat surface is indispensable in these methods. Optimally, anchorage should not perturb membrane structure, dynamics, and functions. The PEG$_{800}$ crosslinker was designed to fulfill this need: (i) It is flexible and is inert towards biomolecules. (ii) The use of lipid-conjugated PEG$_{800}$ guarantees anchorage of membranes or cells at nonadsorbing conditions and at appropriate distances. It allows for a sufficiently thick water layer (required for integrity of membranes) and for free mobility of typical membrane components, in contrast to presently applied adsorption techniques in fluorescence microscopy methods (Hinterdorfer et al., 1994). (iii) Additional selective anchorage of particular membrane proteins via PEG$_{800}$-conjugated sensor molecules (antibodies, peptide toxins, or other specific ligands) is one prerequisite to image the surface topology of intact membrane proteins by AFM techniques. (iv) Conjugation of AFM measuring tips with sensor molecules via PEG$_{800}$ allows to assign observed surface topologies to known functional components. We were able to realize this measuring principle in observing single antibody-antigen recognition events, including measurements of antibody-antigen unbinding forces (1 nN; P. Hinterdorfer et al., manuscript in preparation).

The use of PEG$_{800}$ linkage renders possible not only AFM studies but also applications of other current methods to nonperturbed, but anchored membranes. Besides these and other uses in surface science (Egger et al., 1990; Müller et al., 1993), the above-presented crosslinker may be instrumental in creating flexible protein—protein linkages or to attach homing devices to liposomes, the examples chosen in this study to evidence crosslinker functionality. In the latter application it should be noted that heterobifunctional crosslinking with an SPDP analogue provides a convenient alternative to homobifunctional coupling methods (Blume et al., 1993), and it is of particular interest for the flexible coupling of two different proteins to the same batch of liposomes (compare Vingerhoeds et al. (1993)).

LITERATURE CITED

Blume, G., and Cevc, G. (1990) Liposomes for the sustained drug release in vivo. *Biochim. Biophys. Acta 1029*, 91–97.

Blume, G., Cevc, G., Crommelin, M. D. J. A., Bakker-Woudenberg, I. A. J. M., Kluft, C., and Storm, G. (1993) Specific targeting with poly(ethylene glycol)-modified liposomes: coupling of homing devices to the ends of the polymeric chains combines effective target binding with long circulation times. *Biochim. Biophys. Acta 1149*, 180–184.

Carlsson, J., Drevin, H., and Axen, R. (1978) Protein thiolation and reversible protein-protein conjugation: N-succinimidyl 3-(2-pyridyldithio)propionate, a new heterobifunctional reagent. *Biochem. J. 173*, 723–737.

Dittmer, J. C., and Lester, R. L. (1964) A simple, specific spray for the detection of phospholipids on thin-layer chromatograms. *J. Lipid Res. 5*, 126–127.

Dreborg, S., and Akerblom, E. B. (1990) Immunotherapy with monomethoxypolyethylene glycol modified allergens. *Crit. Rev. Ther. Drug Carrier Syst. 6*, 315–365.

Duncan, R. J. S., Weston, P. D., and Wrigglesworth, R. (1983) A new reagent which may be used to introduce sulfhydryl groups into proteins, and its use in the preparation of conjugates for immunoassay. *Anal. Biochem. 132*, 68–73.

Egger, M., Heyn, S. P., and Gaub, H. E. (1990) Two-dimensional recognition pattern of lipid-anchored fab' fragments. *Biophys. J. 57*, 669–673.

Ellman, G. L. (1959) Tissue sulfhydryl groups. *Arch. Biochem. Biophys. 82*, 70–77.

Fein, M., Unkeless, J., Chuang, F. Y. S., Sassaroli, M., da Costa, R., Väänäen, H., and Eisinger, J. (1993) Lateral mobility of lipid analogues and GPI-anchored proteins in supported bilayers determined by fluorescent bead tracking. *J. Membrane Biol. 135*, 83–92.

Florin, E.-L., Moy, V. T., and Gaub, H. E. (1994) Adhesion forces between individual ligand-receptor pairs. *Science 264*, 415–417.

Ghosh, R. N., and Webb, W. W. (1994) Automated detection and tracking of individual and clustered cell surface low density lipoprotein receptor molecules. *Biophys. J. 66*, 1301–1318.

Gruber, H. J., and Schindler, H. (1994) External surface and lamellarity of lipid vesicles: a practice-oriented set of assay methods. *Biochim. Biophys. Acta 1189*, 212–224.

Hinterdorfer, P., Baber, G., and Tamm, L. K. (1994) Reconstitution of membrane fusion sites. *J. Biol. Chem. 269*, 20360–20368.

Hope, M. J., Bally, M. B., Webb, G., and Cullis, P. R. (1985) Production of large unilamellar vesicles by a rapid extrusion procedure: Characterization of size distribution, trapped volume and ability to maintain a membrane potential. *Biochim. Biophys. Acta 812*, 55–65.

Jones, M. N., and Hudson, M. J. H. (1993) The targeting of immunoliposomes to tumor cells (A431) and the effects of encapsulated methotrexate. *Biochim. Biophys. Acta 1152*, 231–242.

Kagawa, Y., and Racker, E. (1971) Partial resolution of the enzymes catalyzing oxidative phosphorylation: XXV. Reconstitution of particles catalyzing ^{32}P$_i$-adenosine triphosphate exchange. *J. Biol. Chem. 246*, 5477–5487.

Klibanov, A. L., Maruyama, K., Beckerleg, A. M., Torchilin, V. P., and Huang, L. (1991) Activity of amphipathic poly-

(ethylene glycol) 5000 to prolong the circulation time of liposomes depends on the liposome size and is unfavorable for immunoliposome binding to target. *Biochim. Biophys. Acta 1062,* 142–148.

Lesermann, L. D., Machy, P., and Barbet, J. (1984) Covalent coupling of monoclonal antibodies and protein A to liposomes: specific interaction with cells in vitro and in vivo. *Liposome Technology* (G. Gregoriadis, Ed.) Vol. III, pp 29–40.

Mayer, L. D., Bally, M. B., Hope, M. J., and Cullis, P. T. (1986) Techniques for encapsulating bioactive agents into liposomes. *Chem. Phys. Lipids 40,* 333–345.

Merrill, E. W. (1992) Poly(ethylene oxide) and blood contact: A chronicle of one laboratory. *Poly(Ethylene Glycol) Chemistry: Biotechnical and Biomedical Applications* (J. M. Harris, Ed.) pp 199–220, Plenum Press, New York.

Müller, W., Ringsdorf, H., Rump, E., Wildburg, G., Zhang, X., Angermaier, L., Knoll, W., Liley, M., and Spinke, J. (1993) Attempts to mimic docking processes of the immune system: Recognition-induced formation of protein multilayers. *Science 262,* 1706–1708.

Ofitserov, V. I., Shval'e, A. F., and Samukov, V. V. (1985) U.S.S.R. SU 1,152,953 (Cl.C07D213/71), 30 Apr 1985, Appl. 3,688,797, 9 Jan 1984.

Ouchi, T., Yuyama, H., and Vogl, O. (1987) Synthesis of 5-fluorouracil-terminated monomethoxypoly(ethylene glycol)s, their hydrolysis behavior, and their antitumor activities. *J. Macromol. Sci.-Chem., A24,* 1011–1032.

Papahadjopoulos, D., Allen, T. M., Gabizon, A., Mayhew, E., Matthay, K., Huang, S. K., Lee, K.-D., Woodle, M. C., Lasic, D. D., Redemann, C., and Martin, F. J. (1991) Sterically stabilized liposomes: Improvements in pharmacokinetics and antitumor therapeutic efficiency. *Proc. Natl. Acad. Sci. U.S.A. 88,* 11460–11464.

Passera, C., Pedrotti, A., and Ferrari, G. (1964) Thin-layer chromatography of carboxylic acids and keto acids of biological interest. *J. Chromatogr. 14,* 289–291.

Pool, R. (1990) Hairy enzymes stay in the blood. *Science 248,* 305.

Schaffner, W., and Weissmann, C. (1973) A rapid, sensitive, and specific method for the determination of protein in dilute solution. *Anal. Biochem. 56,* 502–524.

Schuurmans-Stekhoven, F. M. A. H., Tesser, G. I., Ramsteyn, G., Swarts, H. G. P., and De Pont, J. J. H. H. M. (1992) Binding of ethylenediamine to phosphatidylserine is inhibitory to Na$^+$/K$^+$-ATPase. *Biochim. Biophys. Acta 1109,* 17–32.

Senior, J., Delgado, C., Fisher, D., Tilcock, C., and Gregoriadis, G. (1991) Influence of surface hydrophilicity of liposomes on their interaction with plasma protein and clearance from the circulation: Studies with poly(ethylene glycol)-coated vesicles. *Biochim. Biophys. Acta 1062,* 77–82.

Shval'e, A. F., Ofitserov, V. I., Samurov, V. V. (1985) New synthesis of N-hydroxysuccinimide ester of 3-(2-pyridyldithio)-propionic acid. *Zh. Obshch. Khim. 55/9,* 2152.

Stewart, J. C. M (1980) Colorimetric determination of phospholipids with ammonium ferrothiocyanate. *Anal. Biochem. 104,* 10–14.

Tamm, L. K., and Bartoldus, I. (1988) Antibody binding to lipid model membranes: The large ligand effect. *Biochemistry 27,* 7453–7458.

Topchieva, I. N. (1990) Synthesis of biologically active poly-(ethylene glycol) derivatives: A review. *Polymer Sci. USSR 32,* 833–851.

Veronese, F. M., Caliceti, P., Schiavon, O., and Sartore, L. (1992) Preparation and properties of monomethoxypoly(ethylene glycol)-modified enzymes for therapeutic applications. *Poly-(Ethylene Glycol) Chemistry: Biotechnical and Biomedical Applications* (J. M. Harris, Ed.) pp 127–137, Plenum Press, New York.

Vingerhoeds, M. H., Haisma, H. J., van Muijen, M., van de Rijt, R. B. J., Crommelin, D. J. A., and Storm, G. (1993) A new application for liposomes in cancer therapy: Immunoliposomes bearing enzymes (immuno-enzymosomes) for site-specific activation of prodrugs. *FEBS Lett. 336,* 485–490.

Woodle, M. C., Matthay, K. K., Newman, M. S., Hidayat, J. E., Collins, L. R., Redemann, C., Martin, F. J., and Papahadjopoulos, D. (1992) Versatility in lipid compositions showing prolonged circulation with sterically stabilized liposomes. *Biochim. Biophys. Acta 1105,* 193–200.

Yokoyama, M., Okano, T., Sakurai, Y., Kikuchi, A., Ohsako, N., Nagasaki, Y., and Kataoka, K. (1992) Synthesis of poly-(ethylene oxide) with heterobifunctional reactive groups at its terminals by an anionic initiator. *Bioconjugate Chem. 3,* 275–276.

Zalipsky, S. (1993) Synthesis of an end-group functionalized polyethylene glycol-lipid conjugate for preparation of polymer-grafted liposomes. *Bioconjugate Chem. 4,* 296–299.

Zalipsky, S., and Barany, G. (1986) Preparation of poly(ethylene glycol) derivatives with two different groups at the termini. *Polym. Prepr. Am. Chem. Soc. Div. Polym. Chem. 27*(1), 1–2.

Zalipsky, S., and Barany, G. (1990) Facile synthesis of α-hydroxy-ω-carboxymethylpolyethylene oxide. *J. Bioact. Compatible Polym. 5,* 227–231.

Zalipsky, S., and Lee, C. (1992) Use of functionalized poly-(ethylene glycols) for modification of polypeptides. *Poly-(Ethylene Glycol) Chemistry: Biotechnical and Biomedical Applications* (J. M. Harris, Ed.) pp 347–370, Plenum Press, New York.

Zalipsky, S., Gilon, C., and Zilkha, A. (1983) Attachment of drugs to polyethylene glycols. *Eur. Polym. J. 19,* 1177–1183.

Synthesis and Characterization of Superoxide Dismutase–Deferoxamine Conjugate via Polyoxyethylene: A New Molecular Device for Removal of a Variety of Reactive Oxygen Species

Haruya Sato,* Masayo Watanabe, and Yuji Iwashita

Central Research Laboratories, Ajinomoto Company, Inc., Suzuki-cho, Kawasaki 210, Japan. Received July 27, 1994[⊗]

A conjugate of Cu,Zn-superoxide dismutase (SOD) with a strong iron chelating agent, deferoxamine (DFO), was synthesized (SOD–POE–DFO) *via* polyoxyethylene (POE) as a linking agent. N-terminal amino groups of lysine residues in SOD are modified with 1:1 binding products of polyoxyethylene and deferoxamine (POE–DFO) through a covalent amido bond. The mean number of the POE–DFO bound per one SOD molecule is calculated to be 3.3 by determining the C/N ratio after elemental analysis. The half-life of the SOD–POE–DFO is about 1.2 h in rats, whereas that of free SOD is about 5–10 min. POE plays the part not only of the linking agent but also of expanding the lifetime in the circulation. The SOD–POE–DFO possesses both the metal chelating ability (for DFO) and the ability of scavenging superoxide radicals (for SOD). Therefore, the SOD–POE–DFO of the present study can eliminate the superoxide radical and free iron simultaneously and in the same location, and thus, it would be a molecular device with multiple functions which prevents the damage to tissues by scavenging the variety of reactive oxygen species.

INTRODUCTION

The oxygen radical superoxide ($O_2^{•-}$) and the nonradical hydrogen peroxide (H_2O_2) are produced in the body and play several important roles in the self-defense system. Excessive production of $O_2^{•-}$ and H_2O_2, however, can result in tissue damage. For example, highly reactive hydroxyl radical ($OH^•$) is often generated by the Haber–Weiss reaction (eq 1), and other oxidants may be produced in the presence of catalytic iron or copper ions.

$$O_2^{•-} + H_2O_2 \rightarrow O_2 + OH^• + OH^- \qquad (1)$$
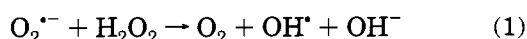
A group of enzymes such as superoxide dismutase (SOD),[1] catalase, glutathione peroxidase, ceruloplasmin, etc. work for removal of these reactive oxygen species. Another important form of antioxidant defense is the storage and transport of iron and copper ions in inert forms that cannot catalyze the formation of reactive radicals.

SOD is a typical antioxidant enzyme that scavenges $O_2^{•-}$. SOD has been investigated as a therapeutic antioxidant for the treatment of ischemia–reperfusion injury in a wide variety of organs. For example, Bernier et al. have reported that SOD is effective on arrhythmia occurred immediately after reperfusion of ischemic heart (*1*). It has been further reported that pulmonary edema

caused after occlusion and reperfusion of the pulmonary artery is prevented by SOD in the animal model (*2*).

In cases where SOD is intravenously administered, however, SOD rapidly disappears from the circulation so that a time period to exhibit its activity in blood is very short. Therefore, SOD chemically modified with polyoxyethylene was prepared by Morimoto and his collaborators (*3*), and they reported the effective prevention of arrhythmia of rat caused by reperfusion also *in vivo* by the chemically modified SOD (*4*).

On the other hand, some researchers have reported negative results on the SOD treatment of reactive hyperemia (*5*). It is also suggested that bell-shaped dose–response curves and the potential toxicity of SOD have been suggested in a number of different myocardial ischemia–reperfusion models (*6, 7*). Furthermore, SOD behaves as an enzyme that catalyzes the formation of free radicals in the presence of anionic scavengers and H_2O_2 as substrates (*8*) and also produces H_2O_2 in the superoxide dismutation reaction, which in the presence of iron results in the production of the very toxic $OH^•$ via the Fenton reaction (*9*) (eq 2).

$$Fe^{2+} + H_2O_2 \rightarrow Fe^{3+} + OH^- + OH^• \qquad (2)$$
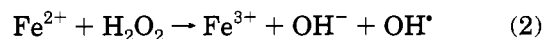
The exact mechanism of reactive oxygen damage, for example, what kind of oxygen is causing the damage, has not been clarified yet. Even in the studies up to now, neither SOD nor catalase has been enough effective to remove a variety of reactive oxygen species including singlet oxygen and hypochloride, and their pharmaceutical effects are not necessarily sufficient, either. One of the reasons must be that only one kind of reactive oxygen scavenger would not be enough to completely remove these oxygen species. Recently, the use of catalase conjugated to SOD has resulted in an inhibition of the Fenton reaction in an *in vitro* system and offered much greater protection in an isolated working heart model of ischemia–reperfusion injury (*10*).

* To whom correspondence should be addressed: Basic Research Department, Central Research Laboratories, Ajinomoto Co., Inc., 1-1, Suzuki-cho, Kawasaki-ku, Kawasaki 210, Japan. Telephone: (044)244-5813 Fax: (044)244-9617.

[1] Abbreviations: SOD, Cu,Zn-superoxide dismutase; POE, α-(carboxymethyl)-ω-(carboxymethoxy)polyoxyethylene; DFO, deferoxamine; POE–DFO, 1:1 binding product of POE and DFO; DFO–POE–DFO, 1:2 binding product of POE and DFO; activated POE–DFO, activated ester of POE–DFO with N-hydroxysuccinimide; SOD–POE–DFO, conjugate of SOD with POE–DFO.

On the basis of these observations, we have developed the hypothesis that a suitable arrangement of several antioxidants determines the physiological and pathophysiological effects of these antioxidants. A molecular device having multiple functions would be more effective for efficient prevention of damages caused by a number of reactive oxygen species. We have especially focused on the interaction and cooperation between SOD and a chelating agent.

We choose deferoxamine (DFO) as the chelating agent, which chelates iron and inhibits iron-catalyzed formation of OH· and lipid peroxidation *in vitro* (9). It is also reported to reduce reperfusion arrhythmia and reoxygenation-induced myocardial damage in isolated hearts (11). DFO has been used clinically in cases of acute iron intoxication (12). Nonetheless, acute and chronic toxicity of DFO is relatively high, and its plasma half-life is short (13). Recently, DFO has been conjugated to hydroxyethyl starch (HES), and improved toxicity of the conjugate has been reported (14, 15). The intent is to limit the distribution of DFO in the intravascular space, thereby increasing the duration of action and decreasing cellular toxicity (15).

We report here the preparation, purification, and characterization of SOD covalently modified with 1:1 binding products of polyoxyethylene (POE) and DFO. This SOD–POE–DFO conjugate possesses both the metal chelating ability (DFO) and the ability of scavenging $O_2^{·-}$ (SOD) and exhibits an increased circulatory half-life *in vivo*. These aspects of SOD–POE–DFO are expected to be especially effective for inhibition of the reactive oxygen formation and may offer much greater protection in oxygen free radical damage to tissues. The aim of our study is to create the molecular device to clarify the exact mechanism of the oxygen injury and to present a novel therapeutic means of oxygen induced damages.

EXPERIMENTAL PROCEDURES

Chemicals. Deferoxamine mesylate was purchased from Sigma (U.S.A.). Human erythrocyte-derived superoxide dismutase (SOD) was prepared by the genetic engineering method. α-(Carboxymethyl)-ω-(carboxymethoxy)polyoxyethylene (POE, mean molecular weight of about 3000 Da) was purchased from Nippon Oils & Fats Co., Ltd. (Japan). Other chemicals were of reagent grade.

General Procedures. ^{1}H-NMR spectra were measured as D_2O (POE–DFO) or DMSO-d_6 solution (activated POE-DFO) with a JNM GX-400 FT-NMR (Japan Electron Optics Laboratory, Japan). Chemical shifts were reported as parts per million (ppm) relative to tetramethylsilane or 2,2-dimethyl-2-silapentane 5-sulfoxide. Liquid secondary ion mass spectra were recorded with a JMS-DX300 spectrometer (Japan Electron Optics Laboratory, Japan) operating with a JMA3500 data system (Japan Electron Optics Laboratory, Japan). SDS–PAGE was carried out using a gradient gel (SDS–PAGE mini, 8–16%, Tefco Co., Ltd., Japan). Aliquots of reaction mixtures were mixed with a SDS-gel loading buffer containing 2% SDS, 1% 2-mercaptoethanol, 0.1% bromophenol blue, and 0.05% sodium phosphate buffer (pH7.0), heat-denatured at 95 °C for 10 min, and loaded onto the gel. The finished gel was stained with Coomassie brilliant blue.

Ion-exchange chromatography was carried out using a Hitachi HPLC system (Hitachi Ltd., Japan) for analytical work and a Biopilot (Pharmacia-LKB, Sweden) for preparative work. For analytical work, the HPLC measurement was carried out at a flow rate of 1.0 mL/min with an Asahipak ES-502N column (Asahi Chemical Industry Co., Ltd., Japan) in a 0.02 M sodium formate buffered-solution (pH 8.0). A 1 μL sample of the reaction mixture was directly loaded on the column. The detection of the POE, POE–DFO, and DFO–POE–DFO was performed by refractive index with a L3300 RI-detector and absorbance at 229 nm with a 655A UV detector. For preparative work, HPLC measurement was carried out at a flow rate of 13.0 mL/min with a Q-Sepharose high performance column (60/100, Pharmacia-LKB, Sweden). Solvent A was prepared by adding a 0.01 M diethanolamine buffered solution (pH 8.8). Solvent B was prepared by adding 0.01 M diethanolamine buffered solution (pH 8.8) containing 0.3 M NaCl. Forty milliliters of the reaction mixture was injected directly into the column. The column was equilibrated with solvent A, and products were eluted by a linear gradient of NaCl from 0 to 0.3 M for 2 h. The detection of the POE–DFO and DFO–POE–DFO was performed by the absorbance at 229 nm.

Gel-permeation chromatography of the conjugate was carried out using a Hitachi HPLC System (Hitachi Ltd., Japan). HPLC measurement was carried out at a flow rate of 1.0 mL/min with a TSK G3000SWXL column (Toyo Soda Co., Ltd., Tokyo, Japan) using a 0.1 M potassium phosphate buffered-solution (pH 6.8).

SOD activity was determined by the method of McCord et al. (16), and the SOD protein concentration was determined by absorbance at 672 nm ($E^{1\%}_{1cm} = 0.079$). The remaining activity of the conjugate was defined in term of a ratio of remaining activity to the SOD activity prior to the reaction. A mean number of POE bound per one SOD molecule was calculated by determining the weight percent ratio of carbon to nitrogen after elemental analysis according to the following equation

$$C/N = 100[12(1358 + 159n)/14(406 + 6n)]$$

where n is the number of POE–DFOs attached to one SOD molecule and C/N is the weight percent ratio of carbon to nitrogen in SOD–POE–DFO. Twelve and 14 are the atomic weights of carbon and nitrogen, respectively, and 1358 and 406 are the number of carbons and nitrogens in one SOD molecule, respectively. One hundred and fifty-nine is the number of carbons in one POE–DFO which was obtained from the average molecular weight of 3000 Da of POE, and 6 is the number of nitrogens in one DFO molecule.

Chelating ability of the immobilized DFO in SOD–POE–DFO was determined according to the method of Emery (17). The displacement of iron from ferrioxamine (DFO/Fe^{2+} complex) by gallium under reducing conditions was used to probe the change in the iron-binding characteristics of the conjugated chelator. Three milliliters of a solution including 2 mM ferrozine, 20 mM sodium ascorbate, 0.05 mM DFO, and 0.05 mM sodium acetate of pH 5.4 was pipetted into 4 mL cuvettes, and the absorbance at 562 nm (25 °C) was monitored (molar absorptivity of 29000 M^{-1} cm^{-1}). After 5 min, 158 μL of 10 mM gallium nitrate were added to the DFO, yielding a final gallium concentration of 0.5 mM. The increase in absorbance, due to formation of the ferrous iron–ferrozine complex, was followed for an additional 15 min spectrophotometrically (562 nm).

Synthesis of POE–DFO. After 1.5 mmol of DFO was dissolved in 81 mL of a 0.05 M potassium phosphate buffered solution (pH 8.0) and 0.83 mmol of activated POE, which had been obtained by converting POE into activated ester of *N*-hydroxysuccinimide with 1,3-dicyclohexylcarbodiimide (DCC). The mixture was rapidly stirred homogeneously and allowed to stand at room temperature for 1 h. Then the reaction solution was
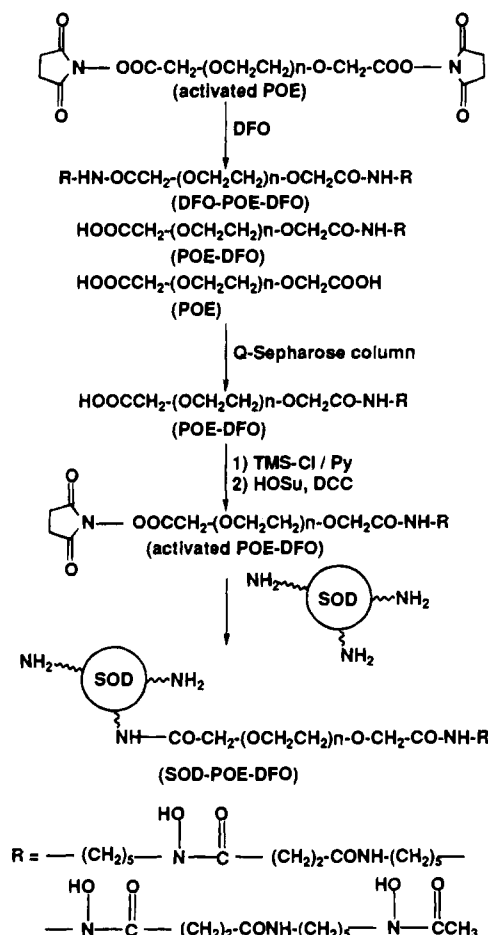
Figure 1. Synthetic scheme of SOD–POE–DFO.

Figure 2. Analytical ion-exchange HPLC analysis of a conjugation reaction with activated POE and DFO. An Asahipak ES-502N column was used with a 0.02 M sodium formate buffered solution (pH 8.0) at a flow rate of 1.0 mL/min with monitoring at 229 nm, AUFS 0.16, and refractive index, AUFS 2.0.

repeatedly subjected to ultrafiltration with a membrane YM5 (Amicon, U.S.A.) whose molecular cut is 5000 Da to remove the unreacted DFO and electrolytes. The dialyzed solution was separated using a Q-Sepharose high performance column (Pharmacia-LKB, Sweden) to isolate almost single peak of POE–DFO. After desalting and concentration using the YM5 membrane, the pH of the solution was adjusted to 2 with HCl and then freeze-dried to give the reaction product. The yield of the POE–DFO from POE was about 23%.

^{1}H-NMR(D$_2$O): δ 4.07 (2H, s), 3.93 (2H, s), 3.90–3.50 (270H, m), 3.61 (6H, t), 3.24 (2H, t), 3.16 (4H, t), 2.78 (4H, t), 2.48 (4H, t), 2.13 (3H, s), 1.67–1.47 (12H, m), 1.40–1.23 (6H, m). Mass: 3300–4300 *m/z*.

Synthesis of Activated POE-DFO. The POE–DFO (0.356 mmol) was dissolved in 4.2 mL of anhydrous pyridine, and 1.43 mmol of trimethylsilyl chloride (Tokyo Chemical Industry Co., Ltd.) was dropwise added to the solution with stirring to protect the hydroxyl group of DFO. After completion of the dropwise addition, stirring was continued for 5 h at room temperature. The solvent was distilled from the resulting reaction solution, and the viscous product adhered to the flask was dissolved in 4.2 mL of dimethylformamide. After 1.43 mmol of *N*-hydroxysuccinimide and 1.43 mmol of DCC were sequentially added to the reaction mixture, the mixture was stirred at 35 °C overnight. Precipitated urea was removed, and the filtrate was then dropwise added to 20 mL of diethyl ether to crystallize the product. The crystalline product was washed with H$_2$O and dried under high vacuum to give the activated POE–DFO. The yield of the activated POE–DFO from the crude POE–DFO was about 70%.

^{1}H-NMR (DMSO-d_6): δ 4.60 (2H, s), 3.86 (2H, s), 3.65–3.40 (270H, m), 3.45 (6H, t), 3.09 (2H, t), 3.00 (4H, t), 2.83 (4H, s), 2.58 (4H, t), 2.28 (4H, t), 1.97 (3H, s), 1.56–1.34 (12H, m), 1.30–1.17 (6H, m).

Preparation of SOD–POE–DFO. After 15.6 μmol of SOD was dissolved in 10 mL of a 0.1 M potassium phosphate buffered solution (pH 8.5), 265 μmol of the activated POE–DFO described above was added to the solution. The mixture was stirred at 4 °C for 1 h. After desalting and concentrating through ultrafiltration membrane YM30 (Amicon Co., U.S.A.), whose molecular cut is 30 000 Da, the solution was freeze-dried to give SOD–POE–DFO.

Pharmacokinetics of SOD and SOD–POE–DFO in Rats. Male CD rats weighing between 357 and 394 g were obtained from Charles River Breeding Labs (Japan). A dose of 10 mg/kg SOD was injected as a bolus into a tail vein, and samples of blood were obtained at predetermined times, up to 24 h with six groups. Then each sample was transferred to heparinized capillary tube and centrifuged to obtain plasma. Plasma volume was determined by weight and stored at −85 °C until assay. The SOD activity in plasma was determined by the method of Oyanagui et al. (*18*).

RESULTS

Synthesis of POE–DFO. The synthesis of POE–DFO is illustrated in Figure 1. The ion-exchange chromatogram of the reaction product between activated POE and DFO shown in Figure 2 indicates that the product contains three components (peaks 1–3).

Peak 3 appearing at about 7 min was assumed to be the peak of POE because there was no absorbance at 229 nm due to the hydroxamic acid group of DFO. Peaks 1 and 2 were assigned to POE–DFO and DFO–POE–DFO, respectively, because of the presence of absorbance at 229 nm. The peaks 1 and 2 were, respectively, isolated using a Q-Sepharose high performance column, and isolated samples were desalted using an ultrafiltration
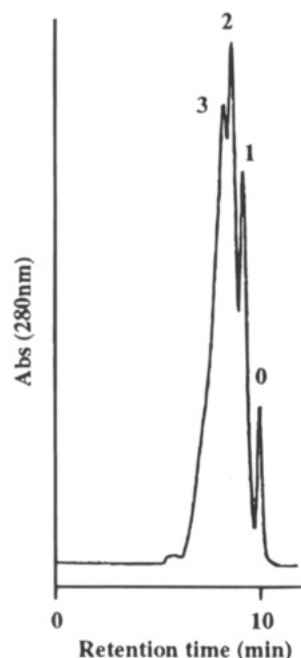
Figure 3. Gel permeation chromatography of SOD–POE–DFO on a TSK G3000SWXL column. The eluting buffer was a 0.1 M potassium phosphate buffered solution (pH 6.8) with a flow rate of 1.0 mL/min. The number 0, 1, 2, or 3 indicates the number of POE–DFO molecules attached to one SOD molecule.

Figure 4. SDS–PAGE analysis of SOD–POE–DFO using gradient gel (8–16%). Aliquots of reaction mixtures were mixed with SDS gel loading buffer, heat-denatured, and loaded onto the gel. The finished gel was stained with Coomassie brilliant blue. Five lanes were used for each compound: lane 1, low molecular weight standards; lanes 2 and 3, SOD; lanes 4 and 5, SOD–POE–DFO. The number 0, 1, 2, or 3 for SOD–POE–DFO was assumed to be the number of POE–DFO molecules attached to one SOD subunit.

membrane. Analysis by ^{1}H-NMR spectrometry demonstrated that the component of the peak 2 was assumed to be the expected 1:1 binding product of POE and DFO (POE–DFO) and that of the peak 1 was assumed to be the 1:2 binding product of POE and DFO (DFO–POE–DFO). Furthermore, analysis by liquid secondary ion mass spectrometry demonstrated that the POE–DFO showed broad signals between m/z 3300 and 4300 compared to those between m/z 2700 and 3700 for POE. The difference of molecular weight between POE and the POE–DFO was almost consistent with the molecular weight of DFO (561).

Synthesis of Activated POE–DFO. The synthesis of activated POE–DFO is shown in Figure 1. Analysis by ^{1}H-NMR spectrometry demonstrated that the degree of activation in each POE–DFO was about 100% in this reaction. On the synthesis of the activated POE–DFO, we could prevent the POE–DFO from the polymerization by protecting the hydroxyl group of DFO. The cleavage of trimethylsilyl groups was made in H_2O.

Preparation of SOD–POE–DFO. The preparation of SOD–POE–DFO is shown in Figure 1. A high performance liquid chromatogram (HPLC) using a gel permeation column of the SOD–POE–DFO is shown in Figure 3. The SOD–POE–DFO produced broader peaks on the column, and the peak of unmodified SOD almost disappeared. The yield of the SOD–POE–DFO from SOD was about 60%.

SDS–PAGE characterization of the SOD–POE–DFO sample is shown in Figure 4. SOD showed one protein band corresponding to the SOD subunit (lanes 2 and 3). On the other hand, the SOD–POE–DFO showed mainly four bands (nos. 0–3), and then the SOD–POE–DFO contained about four kinds of subunits (lanes 4 and 5). Though the SOD molecule keeps the dimeric structure in normal conditions, it dissociates to two subunits upon heating for 10 min in the presence of SDS and 2-mercaptoethanol. The number 0, 1, 2, or 3 indicates the number of POE–DFO molecules attached to one SOD subunit because the difference of the molecular weight

of the each band was almost equal (about 7000 Da). Conjugation of the POE–DFO to SOD caused a greater increase in size than predicted from its molecular weight (about 3500 Da). On the other hand, a mean number of POE–DFO bound per one SOD molecule was calculated to be about 3.3 by determining the C/N ratio after elemental analysis. This result seems to be consistent with the SDS–PAGE profile of SOD–POE–DFO.

SOD Activity. The activity of free SOD was determined about 3800 units/SOD mg by the method of McCord. The molar SOD activity of SOD–POE–DFO remained about 80% of that of free SOD after conjugation. In addition, it was found that free POE and DFO did not have a significant amount of SOD activity alone (0.03 unit/mg for POE, nil for DFO).

Chelating Ability of the Immobilized DFO. The chelating ability of the immobilized DFO in the SOD–POE–DFO was verified by the method of Emery. The displacement of iron from ferrioxamine (DFO/Fe^{2+} complex) by gallium under reducing conditions was used as a probe for alterations in the iron-binding characteristics of the conjugated chelator. The displacement curves of the free DFO and immobilized SOD–POE–DFO were very similar, and there was no detectable change of DFO in metal binding ability after conjugating of DFO to SOD (Figure 5). Furthermore, it was confirmed that free POE did not have a significant DFO mimic activity alone (data not shown).

Pharmacokinetics of SOD and SOD–POE–DFO in Rats. Figure 6 demonstrates the increased retention time of the SOD–POE–DFO in the circulation of rats. The results from six rats were averaged for each time point. SOD in its free form is cleared from the circulation in rats with a $t_{1/2}$ of 5–10 min, whereas in the conjugated form the circulation $t_{1/2}$ of SOD increased to as much as 1.2 h.

DISCUSSION

As described before, a variety of reactive oxygen species, including superoxide, hydroperoxide, hydroxide radicals, singlet oxygen, and/or hypochloride, would be produced from oxygen under pathological conditions. In
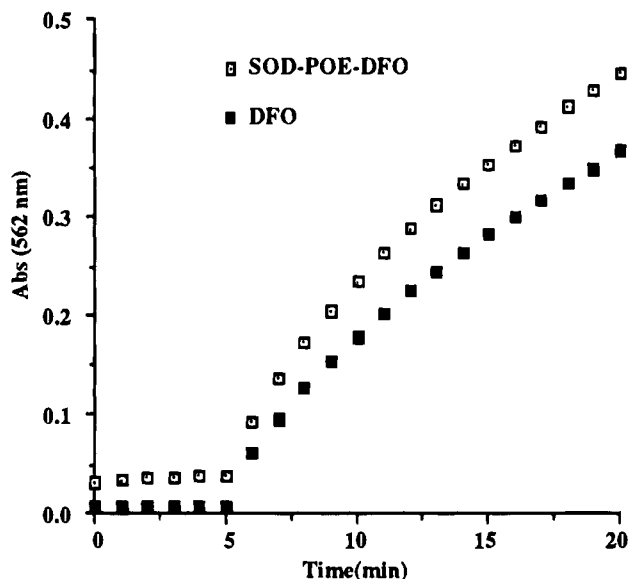
Figure 5. Reductive displacement of iron from ferrioxamine (DFO/Fe^{2+} complex) in SOD–POE–DFO and DFO by gallium. The displacement of iron from ferrioxamine was followed spectrophotometrically using ferrozine [3-(2-pyridyl)-5,6-diphenyl-1,2,4-triazine-p,p'-disulfonic acid] as the indicator. Ferrozine forms a blue complex with reduced iron, which has an absorption maximum at 562 nm and a molecular absorptivity of 29 000 M^{-1} cm^{-1}.
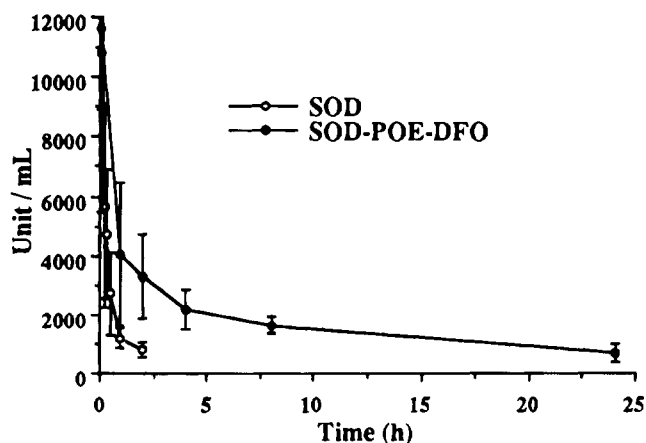
Figure 6. Plasma concentration of SOD–POE–DFO and SOD after intravenous administration to male rats. Rats were intravenously administered with a dose of 10 mg/kg of SOD into the tail vein with six groups. At indicated times after administration, blood samples were collected, and their SOD activity was determined.

living system, antioxidants including enzymes, vitamins, glutathione, etc. are arranged in three dimensions so that they can quench these oxygens effectively. On the basis of these assumptions, we have pursued the creation of a new conjugate (device) which simulates an arrangement of the antioxidants in the body.

We have prepared the conjugate of SOD that brings about the dismutation of O$_2$·$^-$, with DFO, that is the most specific chelator of iron. The preparation of the new conjugate (called SOD–POE–DFO) was designed under the assumption that SOD is easily modified with POE and that binding the terminal amino group of DFO to an anchoring molecule does not deteriorate the chelating ability *in vitro*. Then we conjugated SOD with DFO via POE as a linking agent. The intent of the conjugation is to give the potential of increasing the therapeutic ability to SOD and DFO by accumulating both activities in one molecule and to study the physiological roles and

the cooperation of SOD and DFO toward the reactive oxygen species.

SOD is an interesting enzyme since while it dismutates O$_2$·$^-$ (eq 3), it also produces a highly reactive oxidizing agent H$_2$O$_2$ which in the presence of iron results in the production of very toxic OH· via the Fenton reaction (*10*).

$$2O_2^{\cdot-} + 2H^+ \xrightarrow{\text{SOD}} O_2 + H_2O_2 \qquad (3)$$
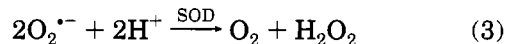
Thus, although SOD is likely an important scavenger of O$_2$·$^-$, its use as an exogenously administered antioxidant must be carefully examined. The covalent conjugation of SOD to DFO appears to ensure that if H$_2$O$_2$ is formed by a superoxide dismutation reaction, OH· will not be generated because of immediate trapping iron with DFO at the site of H$_2$O$_2$ formation. Then, this conjugate will counter the potential toxicity of SOD and offer much greater effectiveness in an antioxidative ability of SOD.

On the other hand, DFO is a high-affinity iron chelator, and a number of investigators have attempted to limit iron-dependent tissue damage in various animal models by using DFO (*19*). In fact, iron is known to catalyze the Haber–Weiss and Fenton reactions, whereby O$_2$·$^-$ and H$_2$O$_2$ give rise to the highly reactive OH· radical (*20, 21*). Recently, it has been suggested that iron is a strong catalyst for the formation of highly reactive and toxic oxygen-derived free radicals (*19, 22*). Unfortunately, DFO has two properties that diminish its usefulness for other clinical indications: (a) its considerable acute and chronic toxicity which limits the dose that can be used safely (*23*) and (b) its short plasma half-life (*15*). The conjugation of DFO to SOD increases the circulatory lifetime of DFO and limits the distribution of DFO to the extracellular space. This conjugate thereby allows an increase in the duration of action and a decrease in the cellular toxicity of DFO.

Using POE as the linking agent between SOD and DFO also alters the therapeutic potency of SOD. Upon intravenous administration, proteins are cleared via the excretion through the kidney, phagocytosis by the reticuloendothelial system, and by proteolytic degradation in the blood, lung, gastrointestinal tract, brain, muscle, etc. Filtration of proteins from the blood through the kidneys is primarily based on size and charge. In general, large, negatively charged proteins are retained longer in plasma than smaller, positively charged proteins (*24*). Unmodified SOD exhibits rapid clearance from the bloodstream as predicted for small proteins by glomerular filtration of the kidney (*25*). Attachment of POE–DFO to SOD caused the greater increase in size than predicted from its molecular mass (in SDS–PAGE), presumably due to the hydration of POE, and markedly increased its circulatory half-life in rats (1.2 h). In fact, 1 unit of polyoxyethylene is hydrated with about three H$_2$O molecules in aqueous solutions (*26*). Another explanation for the decrease in plasma clearance could be due to modification or shielding of the proteolytic sites in SOD by POE–DFO. Furthermore, POE derivatives, being nontoxic, nonimmunogenic, and amphiphilic macromolecule, were extensively used as chemical modifying reagents for the protein drugs (*27, 28*). Then, chemical modification of SOD with POE–DFO may lead to the reduction of its antigenicity and immunogenicity as well as the prolongation of its blood circulation lifetime.

On the basis of these observations, SOD–POE–DFO would be an effective antioxidant which possesses both the metal chelating ability and the ability of scavenging O$_2$·$^-$. It may preserve the efficacy of free radical scavenging during a long circulation after intravenous administration *in vivo*. This conjugated form would be advan-

tageous over the combined administration of both conjugated SOD and conjugated DFO for the following reasons.

(i) The conjugation of SOD with DFO makes the ratio of the two activities constant at any site in the body and can always help their cooperative action anywhere.

(ii) The conjugation of SOD with DFO through POE may make it possible to take the best spatial arrangement for a concerted action of the two antioxidants.

(iii) The conjugation makes the lifetimes of SOD and DFO in the body uniform and limits their escape from intravascular space.

The approach shown in this paper can also be used for the conjugation of other antioxidant enzymes with DFO or other amine-containing chelating agents. In conclusion, a molecular device having accumulated multiple antioxidative functions would be more effective than a single antioxidant molecule. Using the device, conclusions of the exact mechanism of reactive oxygen damage would be expected, including which of the reactive oxygen species is causing the damage and which of the antioxidants works for the protection.

ACKNOWLEDGMENT

LITERATURE CITED

(1) Bernier, M., Hearse, D. J., and Manning, A. S. (1986) Reperfusion-induced arrhythmias and oxygen-derived free radicals. *Circ. Res. 58*, 331–340.

(2) Horgan, M. J., Lum, H. and Malik, A. B. (1989) Pulmonary edema after pulmonary artery occlusion and reperfusion. *Am. Rev. Respir. Dis. 140*, 1421–1428.

(3) Morimoto, H., Tsuji, T., Yokoyama, M., and Iwashita, Y. (1989) Preparation of polyoxyethylene-modified superoxide dismutase from single component superoxide dismutase. *Med. Biochem. Chem. Aspects Free Radicals 615–618*.

(4) Galcia-Alves, M., Kadowaki, Y., Iwashita, Y., and Nishi, K. (1989) Pretreatment with a single bolus injection of polyoxyethylene-modified superoxide dismutase prevents reperfusion induced arrhythmias in the anesthetized rat. *Jpn. J. Pharmacol. 51*, 199–209.

(5) Helfaer, M. A., Kirsch, J. R., Haun, S. E., Moore, L. E., and Traystman, R. J. (1991) Polyethylene glycol-conjugated superoxide dismutase fails to blunt postischemic reactive hyperemia. *Am. J. Physiol. 261*, H548–H553.

(6) Bernier, M., Manning, A. S., and Hearse, D. J. (1989) Reperfusion arrhythmias: dose-related protection by anti-free radical interventions. *Am. J. Physiol. 256*, H1344–H1352.

(7) Omar, B. A., and McCord, J. M. (1990) The cardioprotective effect of Mn-superoxide dismutase is lost at high doses in the postischemic isolated rabbit heart. *Free Radic. Biol. Med. 9*, 473–478.

(8) Yim, M. B., Chock, P. B., and Stadtman, E. R. (1993) Enzyme function of copper,zinc superoxide dismutase as a free radical generator. *J. Biol. Chem. 268*, 4099–4105.

(9) Graf, E., Mahoney, J. R., Bryant, R. G., and Eaton, J. W. (1984) Iron-catalyzed hydroxyl radical formation. Stringent requirement for free iron coordination site. *J. Biol. Chem. 259*, 3620–3624.

(10) Mao, G. D., Thomas, P. D., Lopaschuk, G. D., and Poznansky, M. J. (1993) Superoxide dismutase (SOD)-catalase conjugates. Role of hydrogen peroxide and the fenton reaction in SOD toxicity. *J. Biol. Chem. 268*, 416–420.

(11) Farber N. E., Vercellotti, G. M., Jacob, H. S., Pieper, G. M., and Gross, G. J. (1988) Evidence for a role of iron-catalyzed oxidants in functional and metabolic stunning in the canine heart. *Circ. Res. 63*, 351–360.

(12) Whitten, C. F., Gibson, G. W., Good, M. H., Goodwin, J. F., and Brough, A. J. (1965) Studies in acute iron poisoning. *Pediatrics 36*, 322–335.

(13) Summers, M. R., Jacobs, A., Tudway, D., Perera, P., and Ricketts, C. (1979) Studies in desferrioxamine and ferrioxamine metabolism in normal and iron-loaded subjects. *Br. J. Haematol. 42*, 547–555.

(14) Mahoney, J. R., Halloway, P. E., Hedlund, B. E., and Eaton, J. W. (1989) Acute iron poisoning. Rescue with macromolecular chelators. *J. Clin. Invest. 84*, 1362–1366.

(15) Hallaway, P. E., Eaton, J. W., Panter, S. S., and Hedlund, B. E. (1989) Modulation of deferoxamine toxicity and clearance by covalent attachment to biocompatible polymers. *Proc. Natl. Acad. Sci. U.S.A. 86*, 10108–10112.

(16) McCord, J. M., and Fridovich I. (1969) Superoxide dismutase. An enzymic function for erythrocuprein (hemocuprein). *J. Biol. Chem. 244*, 6049–6055.

(17) Emery, T. (1986) Exchange of iron by gallium in siderophores. *Biochemistry 25*, 4629–4633.

(18) Oyanagui, Y. (1984) Reevaluation of assay methods and establishment of kit for superoxide dismutase activity. *Anal. Biochem. 142*, 290–296.

(19) Halliwell, B. (1989) Protection against tissue damage *in vivo* by desferrioxamine: What is its mechanism of action? *Free Radic. Biol. Med. 7*, 645–651.

(20) Halliwell, B., and Gutteridge, J. M. C. (1984) Oxygen toxicity, oxygen radicals, transition metals and disease. *Biochem. J. 219*, 1–14.

(21) Braughler, J. M., Duncan, L. A., and Chase, R. L. (1986) The involvement of iron in lipid peroxidation. *J. Biol. Chem. 261*, 10282–10289.

(22) Halliwell, B., and Gutteridge, J. M. C. (1992) Biologically relevant metal ion-dependent hydroxyl radical generation. *FEBS Lett. 307*, 108–112.

(23) Triantafyllou, N., Fisfis, M., Sideris, G., Triantafyllou, D., Rombos, A., Vrettou, H., Mantouvalos, V., Politi, C., Malliara, S., and Papageorgiou, C. (1991) Neurophysiological and neuro-otological study of homozygous beta-thalassemia under long-term desferrioxamine (DFO) treatment. *Acta Neurol. Scand. 83*, 306–308.

(24) Deen, W. N., Satvat, B., and Jamieson, J. M. (1980) Theoretical model for glomerular filtration of charged solutes. *Am. J. Physiol. 238*, F126–F139.

(25) Petkau, A. Chelack, W. S., Kelly. K., Barefoot, C., and Monasterski, L. (1976) Tissue distribution of bovine ^{125}I-superoxide dismutase in mice. *Res. Commun. Chem. Path. Pharmacol. 15*, 641–654.

(26) Antonsen, K. P., and Hoffman, A. S. (1992) H_2O structure of PEG solutions. In *Poly(Ethylene Glycol) Chemistry* (Harris, J. H., Ed.) pp 20–22, Plenum, New York and London.

(27) Davis, F. F., Abuchowski, A., van Es, T., Palczuk, N. C., Savoca, K., Chen, R. H.-L., and Pyatak, P. (1980) Soluble, nonantigenic polyethylene glycol-bound enzymes. *Biomedical Polymers*, pp 441–452, Academic Press, New York.

(28) Beauchamp, C. O., Gonias, S. L., Menapace, D. P., and Pizzo, S. V. (1983) A new procedure for the synthesis of polyethylene glycol-protein adducts; Effects on function, receptor recognition, and clearance of superoxide dismutase, lactoferrin, and α_2-macroglobulin. *Anal. Biochem. 131*, 25–33.

"Cleavable Trifunctional" Approach to Receptor Affinity Labeling: Chemical Regeneration of Binding to A1-Adenosine Receptors

Kenneth A. Jacobson,* Bilha Fischer, and Xiao-duo Ji

Molecular Recognition Section, Laboratory of Bioorganic Chemistry, National Institute of Diabetes, Digestive and Kidney Diseases, National Institutes of Health, Bethesda, Maryland 20892 . Received September 15, 1994[⊛]

A general approach for reversible affinity labeling of receptors has been developed. The objective is to carry out a series of chemical modifications resulting in a covalently-modified, yet functionally-regenerated, receptor protein that also may contain a reporter group. The ligand recognition site of A1-adenosine receptors in bovine brain membranes was probed to demonstrate the feasibility of this approach. Use of disulfide or ester linkages, intended for cleavage by exposure of the labeled receptor to either reducing reagents or hydroxylamine, respectively, was considered. Binding of the antagonist radioligand [³H]CPX was preserved following incubation of the native receptor with 3 M hydroxylamine, while binding was inhibited by the reducing reagent dithiothreitol (DTT) with an IC$_{50}$ of 0.29 M. Hydroxylamine displaced specific agonist ([³H]PIA) binding in a noncovalent manner. Specific affinity labels containing reactive isothiocyanate groups were synthesized from XCC (8-[4-[(carboxymethyl)-oxy]phenyl]-1,3-dipropylxanthine) and shown to bind irreversibly to A1-receptors. The ligands were structurally similar to previously reported xanthine inhibitors (e.g., DITC−XAC: (1989) J. Med. Chem. 32, 1043) except that either a disulfide linkage or an ester linkage was incorporated in the chain between the pharmacophore and the isothiocyanate-substituted ring. These groups were intended for chemical cleavage by thiols or hydroxylamine, respectively. Radioligand binding to A1-receptors was inhibited by these reactive xanthines in a manner that was not reversed by repeated washing. Hydroxylamine or DTT restored a significant fraction of the binding of [³H]CPX in A1-receptors inhibited by the appropriate cleavable xanthine isothiocyanate derivative.

INTRODUCTION

Affinity labeling is a widely used technique for the characterization of receptor proteins (1). It is particularly useful for membrane-bound proteins which are not readily characterized by other physical methods, due to the difficulty of isolation in quantities required. By the affinity labeling technique a high affinity ligand that contains a chemically reactive group, such as a bromoacetyl, methylfumaryl, or isothiocyanate (2), or a photochemically reactive group, such as azide (3), is synthesized. The electrophilic group of a chemically-reactive ligand may spontaneously combine with a nucleophilic group that may be present on the binding site of the receptor (4) or on a neighboring molecule in the membrane (5). We have utilized a variety of cross-linking reagents to covalently anchor selective, purine ligands (amine-functionalized congeners) to subtypes of adenosine receptors (2, 6, 7). Generally, receptor affinity labels have been designed without a detailed knowledge of the environment of the ligand binding site, and the identification of reactive ligands that bind covalently to the receptor protein has been empirical. A radioisotope may be incorporated into the affinity label (6, 20) for purposes of receptor detection (e.g., on electrophoretic gels) and imaging.

A deficiency of typical protein labeling is that the modified receptor, although intact in its primary structure, is functionally inactive, both in ligand binding and in activation of second messengers. It would be desirable to have a general means of regenerating the functional binding site following affinity labeling, either in its native form or in a covalently-labeled state. Thus, several groups have introduced reversible affinity labeling schemes (8, 9, 23). Patchornik et al. (8) designed a scheme for the photochemical deblocking of an affinity-labeled biopolymer to regenerate its native form. Denny and Blobel (9) reported an ¹²⁵I-labeled heterobifunctional protein cross-linking reagent (N-[4-[(p-azido-m-iodophenyl)azo]benzoyl]-3-(aminopropyl)-N'-oxysulfosuccinimide ester) that may be cleaved by the action of sodium dithionite on an azo linkage joining the two reactive moieties. The biopolymer is not regenerated in its native form; instead a radioiodine label remains with one component after cleavage. Similarly, disulfide groups are used in a variety of protein and nucleic acid cross-linkers (10), such as biotinylated probes, for subsequent cleavage under reducing conditions.

Adenosine is a neuromodulator that allows organs such as the heart, brain, and kidneys adapt to stress and maintain homeostasis, by acting at specific cell surface G-protein coupled receptors (reviewed in ref 21). As part of a detailed structural investigation of A1- and A2a-adenosine receptor subtypes, we introduced a general trifunctional approach to affinity labeling (11). By this approach a reporter group (e.g., radioactive or spectroscopic) is tethered to a receptor ligand, which delivers it to the binding site selectively, and then incorporated covalently onto the receptor protein via a chemically reactive group (an isothiocyanate) present on the same molecule. A key intermediate is a trifunctional cross-linker consisting of a 3,5-diisothiocyanatobenzene derivative (equivalent to structure 2 in Figure 1). One of the isothiocyanate groups reacts with an amine-functionalized ligand, and the other reacts with the receptor protein.

In this study we have expanded this approach conceptually to include chemically-cleavable spacer groups. An amine-functionalized ligand, 1, may be designed to contain a cleavable A−B linkage (Figure 1). Upon coupling to a trifunctional cross-linker, 2, a conjugate 3
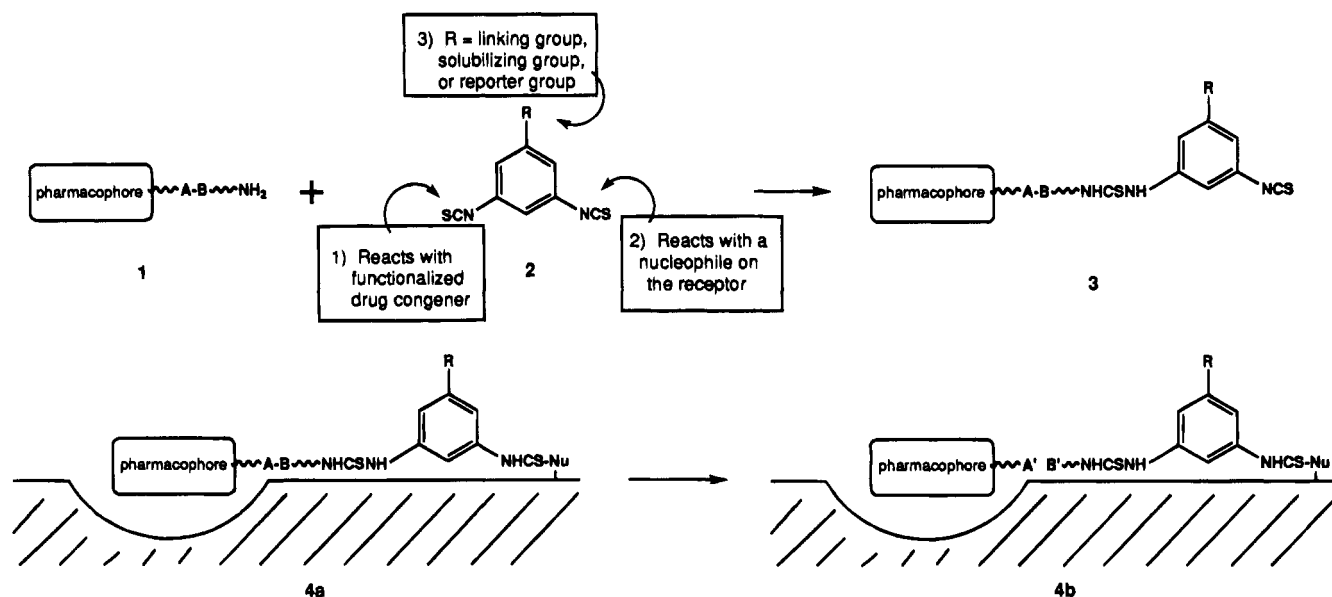
Figure 1. General scheme for reversible affinity labeling that leaves a reporter group on a receptor protein. Structure **1** is an amine-functionalized congener that contains a cleavable (A—B) linkage. A conjugate, **3**, is formed with a trifuctional cross-linking reagent (structure **2**), which may be used to affinity label a receptor (as in **4a**). The A—B linkage is then cleaved (structure **4b**), which allows the free ligand containing the pharmacophore to diffuse away from the binding site.

is obtained. In **3** the cleavage site is located between the trifunctional phenyl ring and the pharmacophore. After receptor binding and cleavage of A—B, a portion of the label remains covalently bound to the receptor protein (structure **4b**). The attached portion contains the reporter group (R) but not the pharmacophore moiety. The pharmacophore may then freely dissociate from the binding site. Thus, the receptor protein remains chemically labeled, and in principle, the receptor binding site is, at least in part, unoccupied and again able to bind radioligands.

EXPERIMENTAL PROCEDURES

Synthesis. ^{1}H NMR spectra were recorded using a Varian XL-300 FT-NMR spectrometer, and all values are reported in parts per million (ppm, δ) downfield from tetramethylsilane (TMS). Chemical ionization MS using ionized NH$_3$ gas were recorded using a Finnigan 1015D mass spectrometer modified with EXTREL electronics. Fast atom bombardment MS was carried out on a JEOL JMS-SX102 mass spectrometer. Thin-layer chromatography (TLC) analyses were carried out using EM Kieselgel 60 F254, DC-Alufolien 200 ×b5 plates and were visualized under ultraviolet light. Elemental analyses were performed by Atlantic Microlabs, Inc., Atlanta, GA. XCC,[1] *m*-DITC—XAC, and *m*-DITC—ADAC were synthesized as previously reported (*2, 16*). Cystamine dihydrochloride was obtained from Sigma (St. Louis, MO).

N-tert-Butyloxycarbonyl)cystamine, **8**. Di-*tert*-butyldicarbonate (0.48 g, 2.2 mmol) and triethylamine (0.91 mL, 3 equiv) were added to a methanolic solution (25 mL) of cystamine bis hydrochloride (0.5 g, 2.2 mmol). After 20

min the solvent was evaporated, and 1 M NaH$_2$PO$_4$ was added (10 mL, pH 4.2). The aqueous solution was extracted with ether to remove the di-*t*-Boc-cystamine (mp 106—107 °C, 0.135 g, 17.5%). The aqueous solution was basified to pH 9 by 1 M NaOH and extracted with EtOAc (5 mL × 6). The combined organic phases were dried over MgSO$_4$ and evaporated to yield the product (0.24 g, 43%). The product was isolated as the hydrochloride salt (mp. 109—110 °C). ^{1}H NMR (D$_2$O) δ: 3.40 (q, 4H, CH$_2$N, $J = 6.6$ Hz), 3.00 (q, 2H, CH$_2$S, $J = 7$ Hz), 2.87 (t, 2H, CH$_2$S, $J = 6.3$ Hz), 1.45 (s, 9H, t-BuO). MS (CI/NH$_3$) free amine: 253 (MH$^+$) 253 (MH$^+$ − *t*-Boc). Anal. Calcd. for C$_9$H$_{21}$ClN$_2$O$_2$S$_2$: C, 37.42; H, 7.33; N, 9.70. Found: C, 37.46; H, 7.34; N, 9.61.

8-[4-[[[[[1-[2-[(tert-Butyloxycarbonyl)amino]ethyl]dithio]ethyl]amino]carbonyl]methyl]oxy]phenyl]-1,3-dipropyl-xanthine, **10**. Mono-*t*-Boc-cystamine (**8**, 80 mg, 0.32 mmol), EDAC (0.165 g, 0.85 mmol), and 1-hydroxybenzotriazole (0.1 g, 0.75 mmol) were added to XCC (**9**, 0.125 g, 0.32 mmol) in dry DMF (10 mL). The reaction mixture was sonicated at room temperature for 30 min. EtOAc (10 mL) was added, and the turbid solution was extracted with water and then with 2 M Na$_2$CO$_3$ (pH 11). The combined aqueous solutions were extracted with EtOAc (10 mL × 2), dried, and evaporated under high vacuum. The solid obtained was washed with a small amount of ether and dried under high vacuum to yield a light yellowish solid (0.147 g, 75%), mp 184 °C. ^{1}H NMR (CDCl$_3$) δ: 8.23 (d, 2H, ArH, $J = 8.8$ Hz), 7.05 (d, 2H, ArH, $J = 8.8$ Hz), 4.95 (br s, 1H, NH), 4.60 (s, 2H, CH$_2$O), 4.19, 4.11 (t, 2H, CH$_2$N), 3.72, 3.43 (2H, CH$_2$NH), 2.90, 2.82 (t, 2H, CH$_2$S), 1.88, 1.77 (q, 2H, CH$_2$CH$_2$), 1.45 (s, 9H, *t*-Boc), 1.02, 0.99 (t, 3H, CH$_2$CH$_3$). MS (FAB): 621 (M$^+$). Anal. Calcd. for C$_{28}$H$_{40}$N$_6$O$_6$S$_2$: C, 54.18, H, 6.49; N, 13.54. Found: C, 54.28; H, 6.54; N, 13.47.

8-[4-[[[[[1-[(2-Aminoethyl)dithio]ethyl]amino]carbonyl]-methyl]oxy]phenyl]-1,3-dipropylxanthine Trifluoroacetate, **11**. Compound **10** (0.047 g, 0.756 mmol) was dissolved in trifluoroacetic acid (1.5 mL), and the solution was stirred at room temperature under nitrogen. After 10 min, the flow rate of nitrogen was increased, and trifluoroacetic acid was evaporated. Ether (5 mL) was added to the glassy residue to form a white solid, which

^{1} Abbreviations: ADAC, N^6-[4-[[[[4-[[[(2-aminoethyl)amino]-carbonyl]methyl]anilino]carbonyl]methyl]phenyl]adenosine; Boc, *tert*-butyloxycarbonyl; Cbz, benzyloxycarbonyl; CPX, 8-cyclo-pentyl-1,3-dipropylxanthine; DITC, phenylene diisothiocyanate; DTT, dithiothreitol; EDAC, *N*-ethyl-*N* '-(3-diaminopropyl)car-bodiimide hydrochloride; EtOAc, ethyl acetate; IBMX, 3-isobu-tyl-1-methylxanthine; PIA, N^6-phenylisopropyladenosine; TFA, trifluoroacetic acid; Tris, tris(hydroxymethyl)aminomethane; XAC, 8-[4-[[[(2-aminoethyl)amino]carbonyl]methyl]oxy]phenyl]-1,3-dipropylxanthine; XCC, 8-[4-[[(carboxymethyl)oxy]phenyl]-1,3-dipropylxanthine.

was dried under high vacuum for 48 h (0.044 g, 92%), mp > 230 °C. ^{1}H NMR (CD₃OD) δ: 8.02 (d, 2H, ArH, J = 8.7 Hz), 7.13 (d, 2H, ArH, J = 8.7 Hz), 4.83 (s, 2H, OCH₂CO), 4.13, 3.97 (t, 2H, CH₂N, J = 7 Hz), 3.63 (t, 2H, CH₂NH₂), 3.50 (q, 2H, CH₂NH, J = 7 Hz), 2.98, 2.91 (t, 2H, CH₂S), 1.75, 1.64 (q, 2H, CH₂CH₂), 0.99, 0.95 (t, 3H, CH₂CH₃). Anal. Calcd. for C₂₅H₃₃N₆O₆S₂F₃ (hydrotrifluoroacetate of 11)·1/2H₂O: C, 46.65; H, 5.32; N, 13.06. Found: C, 46.67; H, 5.26; N, 12.77.

8-[4-[[[[[1-[[2-[[[(3-Isothiocyanatophenyl)amino]thiocarbonyl]amino]ethyl]dithio]ethyl]amino]carbonyl]methyl]oxy]phenyl]-1,3-dipropylxanthine, 12. A dry DMF solution (5 mL) of product 11 (0.032 g, 0.053 mmol), triethylamine (0.1 mL, 2 equiv), and *m*-phenylene diisothiocyanate (ref 6, 30 mg, 3 equiv) was stirred at room temperature for 0.5 h. The solvent was removed under high vacuum (bath temperature 36 °C) to leave a semisolid residue, which was purified on a micro silica column (EtOAc + 1% Et₃N), followed by treatment of the product with dry ether and drying under high vacuum (30 mg, 84%), dec 185 °C. The product was homogeneous by TLC (R_f = 0.82, silica, using chloroform:methanol: acetic acid 85:10:5, by vol) and reacted with ethylenediamine to form cleanly a new compound of R_f 0.30 in the same system. ^{1}H NMR (CDCl₃) δ: 8.93 (s, 1H, ArH-2), 8.16 (d, 2H, ArH, J = 8.7 Hz), 7.34 (m, 1H, ArH), 7.04 (d, 2H, ArH, J = 8.7 Hz), 6.96 ('t', 2H, ArH, J = 5.2 Hz), 4.60 (s, 2H, CH₂O), 4.17 (t, 2H, CH₂N), 3.73 (q, 2H, CH₂NH), 3.14, 3.12 (q, 2H, CH₂N), 3.02, 2.87 (t, 2H, CH₂S), 1.86, 1.71 (q, 2H, CH₂CH₂), 1.01, 0.96 (t, 3H, CH₂CH₃). Anal. Calcd. for C₃₁H₃₆N₈O₄S₄: C, 52.23; H, 5.09; N, 15.72. Found: C, 51.80; H, 5.26; N, 15.13.

2-[(Benzyloxycarbonyl)amino]ethanol, 13. 2-Aminoethanol (0.91 g, 15 mmol) was dissolved in ethyl acetate (30 mL), and sodium carbonate (3 g) was added. The mixture was treated with a solution of benzyl chloroformate (3.3 g, 19 mmol) dissolved in 30 mL of ethyl acetate, added in aliquots with stirring. The mixture was filtered, and the filtrate was treated with water and ethyl acetate. After separation of the layers, the organic layer was extracted with pH 7 phosphate buffer and then with 0.1 M HCl. The organic layer was evaporated to dryness leaving a residue which was triturated with petroleum ether. The resulting solid was collected and recrystallized fron ethyl acetate/petroleum ether to provide the product as white crystals (mp 58–59 °C, 36% yield). MS: 214, 196 (M + 1). The NMR spectrum was consistent with the assigned structure.

(tert-Butyloxycarbonyl)-β-alanine 2-[(Benzyloxycarbonyl)amino]ethyl Ester, 15. A solution of (*tert*-butyloxycarbonyl)-β-alanine (14, 0.98 g, 5.2 mmol) and compound 13 (0.81 g, 4.15 mmol) in DMF (40 mL) was treated with EDAC (1.3 g, 6.8 mmol) and DMAP (0.8 g, 6.6 mmol) with stirring. After 2 h, half-saturated sodium chloride was added. The product was extracted into ethyl acetate, which was washed with 0.1 M HCl and then 0.1 M Na₂CO₃, dried (Na₂SO₄), and evaporated, leaving an oil (0.96 g, 63% yield). MS: 384, 367 (M + 1), 328, 311, 267. The NMR spectrum was consistent with the assigned structure.

β-Alanine 2-[(Benzyloxycarbonyl)amino]ethyl Ester Trifluoroacetate, 16. Compound 15 (0.51 g, 1.4 mmol) was dissolved in a minimum volume of trifluoroacetic acid, and the solution was stirred at room temperature under nitrogen. After 30 min, the trifluoroacetic acid was evaporated, and the glassy residue was dried under high vacuum (0.33 g, 63% yield). MS: 267 (M + 1), 240, 212. The NMR spectrum was consistent with the assigned structure.

8-[4-[[[[[1-[[[2-[(Benzyloxycarbonyl)amino]ethyl]oxy]carbonyl]ethyl]amino]carbonyl]methyl]oxy]phenyl]-1,3-dipropylxanthine, 17. Compound 16 (0.15 g, 0.39 mmol), EDAC (0.4 g, 1.8 mmol), and 1-hydroxybenzotriazole (0.05 g, 0.37 mmol) were added to XCC (9, 0.12 g, 0.31 mmol) in dry DMF (20 mL). The reaction mixture was sonicated at room temperature for 30 min. Water was added, and a precipitate formed. The solid obtained was washed with water and dried under high vacuum (0.111 g, 56%), mp 204–205 °C (heated slowly). The product 17 was homogeneous by TLC.

Anal. Calcd. for C₃₂H₃₈N₆O₈·1/2H₂O: C, 59.71, H, 6.11; N, 13.06. Found: C, 59.72; H, 5.98; N, 13.15.

8-[4-[[[[[1-[[(2-Aminoethyl)oxy]carbonyl]ethyl]amino]carbonyl]methyl]oxy]phenyl]-1,3-dipropylxanthine Hydrobromide, 18. Compound 17 (26.6 mg, 42 ×b5mol) was dissolved with vortexing in 30% HBr/acetic acid (1 mL), and the solution was stirred at room temperature under nitrogen for 30 min. The flow rate of nitrogen was increased leaving an oil, and the product was precipitated as a microcrystalline solid from methanol/ether. The supernatant was removed with a Pasteur pipette, and the remaining white solid was washed (ether, 3×) and dried under high vacuum (25 mg, 100%),mp 273 °C dec. The product was homogeneous by TLC (R_f = 0.78, silica, using chloroform:methanol:acetic acid 10:10:1, by vol). MS: 501 (M + 1), 483, 329. ^{1}H NMR (DMSO-d_6) δ: 8.29 (t, H, CONH), 8.08 (d, 2H, J = 8.8 Hz, 8-ArH, ortho), 7.83 (br s, 2H, NH₂), 7.09 (d, 2H, J = 8.8 Hz, 8-ArH, meta), 4.57 (s, 2H, CH₂O), 4.20 (t, 2H, CH₂), 4.02, 3.87 (each, t, 2H, J = 7 Hz, Pr, CH₂), 3.40, 3.09 (each: m, 2H, CH₂), 2.57 (t, 2H, J = 6.9 Hz, CH₂), 1.74, 1.58 (each: q, 2H, Pr, CH₂), 0.89 (m, 2 × 3H, Pr, CH₃) ppm.

8-[4-[[[[[1-[[2-[[[(3-Isothiocyanatophenyl)amino]thio]carbonyl]amino]ethyl]oxy]carbonyl]ethyl]amino]carbonyl]methyl]oxy]phenyl]-1,3-dipropylxanthine, 19. Compound 19 was synthesized in 91% yield from compound 18 and *m*-phenylene diisothiocyanate by the general method given for compound 12. The product was recrystallized from DMF/ether, was homogeneous by TLC (R_f = 0.84, silica, using chloroform:methanol:acetic acid 85:10:5, by vol), and reacted with ethylenediamine to form cleanly a new compound of lower R_f. ^{1}H NMR (DMSO-d_6) δ: 9.80 (s, 1H, ArNH), 8.23 (m, 2H, carbonyl-NH), 8.08 (d, 2H, 8-ArH, ortho), ArNCS: 7.60 (1H, H₆), 7.34 (2H, H₂,₄), 7.15 (1H, H₃), 7.06 (d, 2H, 8-ArH, meta), 4.55 (s, 2H, CH₂O), 4.19 (m, 2H, CH₂), 4.01 (t, 2H, Pr, CH₂), 3.87 (t, 2H, Pr, CH₂), 3.73, 3.62, 3.15 (each: 2H, CH₂), 3.02, 2.87 (each: t, 2H, CH₂), 1.74, 1.58 (each: q, 2H, Pr, CH₂), 0.88 (m, 2 × 3H, Pr, CH₃) ppm.

8-[4-[[[[[1-[[2-[[[[3-Isothiocyanato-5-[[2-[[3-(4-hydroxyphenyl)propionyl]amino]ethyl]amino]carbonyl]phenyl]amino]thiocarbonyl]amino]ethyl]oxy]carbonyl]ethyl]amino]carbonyl]methyl]oxy]phenyl]-1,3-dipropylxanthine, 20. Compound 18 (8 mg, 14 μmol) and 1-[[3-(4-hydroxyphenyl)propionyl]amino]-3,5-diisothiocyanatobenzene (ref 11, 19 mg, 45 μmol) were dissolved in 1 mL of DMF, and diisopropylethylamine (5 μL) was added with stirring. After 1 h, all of the amine (R_f = 0.08) had been consumed, as judged by TLC (silica, using chloroform:methanol: acetic acid 85:10:5, by vol). Ether was added, causing an oil to separate. The supernatant was removed, and the residue was crystallized from MeOH/ether. The solid was washed with ether and dried under vacuum to provide 8.6 mg of product (66% yield), which was homogeneous by TLC (R_f = 0.51, same system as above). ^{1}H NMR (DMSO-d_6) δ: 10.0 (s, 1H, ArNH), 8.7 (br s, 1H, OH), 8.59, 8.25 (each: t, 1H, NH), 8.08 (d, 2H, J = 8.8 Hz, 8-ArH, ortho), 7.94, 7.81 (each: m, 1H, NH), 7.76, 7.59 (each s, 1H, ArNCS), 7.07 (d, 2H, J = 8.8 Hz,

8-ArH, meta), 6.96, 6.64 (each, d, 2H, J = 8.3 Hz, ArOH), 4.55 (s, 2H, CH$_2$O), 4.19 (t, 2H, J = 5.3 Hz, CH$_2$), 4.01 (t, 2H, J = 6.9 Hz, Pr, CH$_2$), 3.86 (t, 2H, J = 7.3 Hz, Pr, CH$_2$), 3.74, 3.40, 3.25, 3.20 (each: m, 2H, CH$_2$), 2.68, 2.55, 2.29 (each: t, 2H, CH$_2$), 1.74, 1.58 (each: q, 2H, Pr, CH$_2$), 0.89 (m, 2 × 3H, Pr, CH$_3$) ppm.

Binding Assays. Bovine cerebral cortical membranes were prepared as described previously (*12*), from frozen brains obtained from Pel-Freeze Biologicals Co. (Rogers, Arkansas). Membranes were treated with adenosine deaminase (0.5 U/mL) for 20 min at 37 °C prior to radioligand binding studies or incorporation studies.

Inhibition of binding of 1 nM [^{3}H]-N^6-phenylisopropyladenosine or 0.2 nM [^{3}H]-8-cyclopentyl-1,3-dipropylxanthine (Dupont NEN, Boston, MA) to A$_1$-adenosine receptors in bovine cerebral cortex membranes was assayed as described (*13, 14*). Membranes (40 μg, 150 μL) were incubated for 1 h at 25 °C in a total volume of 1 mL, containing 100 μL of radioligand of the indicated concentration and 25 μL of the competing ligand (dissolved as a stock solution in DMSO). Samples of the drugs were dissolved freshly from solid and stored at −80 °C. The DMSO solutions were diluted to a concentration of less than 0.1 mM prior to adding to aqueous medium. Bound and free radioligand were separated by addition of 4 mL of a solution containing 50 mM Tris hydrochloride, at pH 7.4 at 5 °C, followed by vacuum filtration on glass filters with additional washes totaling 12 mL of buffer. Nonspecific binding was determined with 10 μM 2-chloroadenosine or 100 μM N^6-cyclopentyladenosine. Protein was determined using the BCA protein assay reagents (Pierce Chemical Co., Rockford, IL).

All competition binding data was analyzed by nonlinear regression using the InPlot computer program (GraphPAD, San Diego, CA), and IC$_{50}$ values were converted to K_i values using the Cheng−Prusoff equation (*15*). The K_d values, used in these calculations for [^{3}H]PIA and [^{3}H]-CPX binding to bovine brain A$_1$-receptors were 130 ± 4 pM and 74 ± 3 pM, respectively (*13*).

To assay for irreversible inhibition, an incubation at 37 °C for 1 h in 50 mM Tris pH 7.4 with an isothiocyanate derivative was carried out and optionally followed by a second incubation in 50 mM Tris pH 7.4 with DTT or hydroxylamine to test for chemical reversibility. The incubation with DTT was always carried out at room temperature, and the incubation with hydroxylamine was either at rt or 37 °C (latter preferrable). Washing cycles for inhibition experiments between incubations involved three cycles of centrifugation and resuspending the membrane pellet by stirring or homogenization using the Polytron. At the final step, prior to radioligand binding, the membranes were homogenized using a glass tissue grinder.

RESULTS

In order to demonstrate the conceptual approach of Figure 1, it was necessary to identify linkages (A−B in amine congener 1) that may be cleaved chemically using reagents that are not detrimental to adenosine receptors and that would be compatible with an aqueous medium. Two likely possibilities were the reduction of disulfide bonds by thiols and the aminolysis of ester bonds by hydroxylamine. Receptors and other proteins, even those containing structurally important disulfide bridges, may be exposed to either thiol reagents or hydroxylamine below determined concentration limits and remain active (*7*).

The stability of adenosine receptors to potential cleavage conditions at room temperature was examined. The effects of chemical reagents on radioligand binding were

Table 1. Stability of Bovine A$_1$-Adenosine Receptors to Reagents for Use in Cleavage Reaction: (A) at Fixed Concentration with Intervening Wash^a and (B) Concentration Dependence of Inactivation of Receptor Binding by Reagents for Potential Regeneration, with and without Intervening Wash^b

(A) reagent	specific binding remaining (% of control)	
	[^{3}H]CPX	[^{3}H]PIA
none	100	100
DTT (5 mM)	98 ± 3	97 ± 19
DTT (50 mM)	98 ± 2	98 ± 2
H$_2$NOH (250 mM)	96 ± 5	70 ± 8

(B) reagent	IC$_{50}$ (mM) or % inhibition (at concn indicated)			
	[^{3}H]CPX		[^{3}H]PIA	
wash:	+	−	+	−
DTT	290 ± 37	158 ± 42	308 ± 17	85 ± 8
H$_2$NOH	0% (2 M)	0% (3 M)	15% (2 M)	385 ± 144

^{a} Data are means ± SE of three to four experiments. Dithiothreitol or hydroxylamine was added during a 1 h preincubation with membranes at room temperature prior to radioligand binding. The concentrations of radioligand used were 0.2 and 1.0 nM for [^{3}H]CPX and [^{3}H]PIA, respectively. ^{b} Data are means ± s.e.m. of four to five experiments. Dithiothreitol or hydroxylamine was added either (1) during a 1 h preincubation with membranes at room temperature and removed by washing or (2) during the radioligand binding. The concentrations of radioligand used were 0.2 and 1.0 nM for [^{3}H]CPX and [^{3}H]PIA, respectively.

measured in two different ways (Table 1): (1) as a preincubation with membranes followed by a washing step prior to radioligand binding and (2) addition of the reagent to the binding assay medium in the presence of the radioligand. Any difference between the two results might represent reversible competition by the highly concentrated chemical reagent for the radioligand binding site.

The stability of A$_1$ receptors to potential chemical cleavage conditions has not been reported. By analogy with a closely related protein sequence, our previous study of rabbit A$_{2a}$ receptors demonstrated moderate stability of the receptor to 5 mM dithiothreitol (DTT) or 250 mM hydroxylamine (*7*). However, A$_{2a}$ receptors potentially have more disulfide bridges (four have been proposed (*24*)) than do A$_1$ receptors; thus, it was necessary to test the stability of A$_1$ receptors to these reagents. Bovine brain membranes containing A$_1$ adenosine receptors were exposed for 60 min to either a thiol or hydroxylamine and then washed and subjected to radioligand binding. It was observed that at a 5 mM concentration of DTT, the binding of [^{3}H]CPX, an A$_1$-selective antagonist, and [^{3}H]PIA, an A$_1$-selective agonist, was maintained near control levels (Table 1A). The stability of the receptor to hydroxylamine was even more striking, with a concentration of 250 mM tolerated.

The limits of stability at yet higher concentrations were probed (Table 1B). At room temperature, concentrations of hydroxylamine up to 3 M (maximum allowed by solubility) were well tolerated by the receptor, especially when [^{3}H]CPX was used in the subsequent binding assay. Without an intervening wash, the IC$_{50}$ values for DTT inhibition of radioligand binding were 158 mM for [^{3}H]-CPX and 85 mM for [^{3}H]PIA binding. When DTT was removed prior to the binding assay, IC$_{50}$ values increased to 290 mM for [^{3}H]CPX and 308 mM for [^{3}H]PIA binding. The latter values more closely reflect the effects of DTT on the receptor protein, which likely contains disulfide linkages. When the hydroxylamine remained in the medium concurrently with the radioligand, agonist binding alone was adversely affected. The IC$_{50}$ value for hydroxylamine inhibition of [^{3}H]PIA binding was 385

Chart 1

5

6
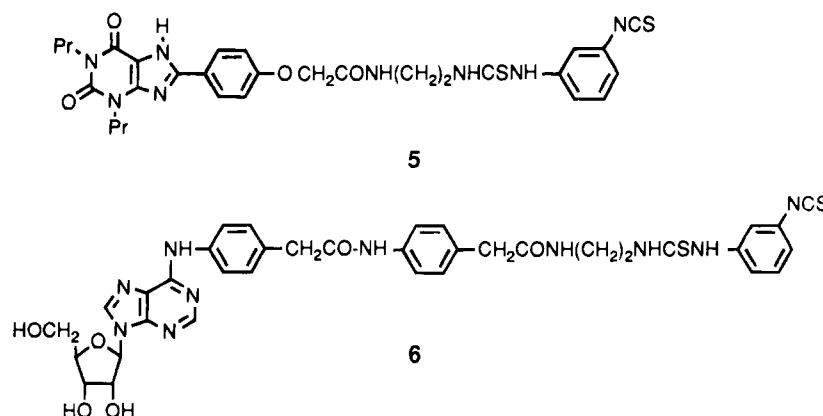
Table 2. Inhibition of Bovine A₁-Adenosine Receptors by Purine Isothiocyanate Derivatives (without Cleavable Chains) and the Stability of this Inhibition to Reagents for Later Use in Cleavage Reaction[a]

| | | inhibition (% of control) | | | |
| | | m-DITC–XAC, 5 | | m-DITC–ADAC, 6 | |
reagent	concn (mM)	[³H]CPX	[³H]PIA	[³H]CPX	[³H]PIA
none		80 ± 4 (7)	55 ± 7 (3)	48 ± 8 (6)	51 ± 4 (4)
DTT	5	82 ± 4 (8)	55 ± 4 (4)	50 ± 4 (8)	52 ± 11 (4)
DTT	50	78, 81	nd	52, 58	nd
H₂NOH	250	78 ± 3 (9)	61 ± 8 (9)	47 ± 6 (6)	50 ± 12 (6)

[a] Data are means ± s.e.m. of three to nine experiments (n given in parentheses). After incubation with the isothiocyante derivative (5 or 6) at 37 °C, membranes were washed three times, incubated overnight with IBMX (200 μM) in the presence of the indicated reagent, and again washed three times with IBMX and twice for DTT or hydroxylamine treatment. Radioligand binding was carried out with 0.2 nM [³H]CPX (14) or 1 nM [³H]PIA (13). nd: not determined.

mM. Curiously, with an intervening wash, even a concentration of hydroxylamine of 2 M resulted in only 15% inhibition of [³H]PIA binding. This suggests that high concentrations of hydroxylamine interact noncovalently with a site on the receptor or on the radioligand that interferes with agonist binding alone. This complication notwithstanding, the use of hydroxylamine is acceptable in the scheme proposed in this study, because a washing step may be included and because an antagonist radioligand alone may suffice to demonstrate the feasibility of the cleavage scheme.

The next step was to identify purine derivatives that may be employed in this scheme. The previous trifunctional study (11) utilized a series of functionalized xanthine derivatives, based on the A₁ antagonist XAC (8-[4-[[[(2-aminoethyl)amino]carbonyl]methyl]oxy]phenyl]-1,3-dipropylxanthine), that acted as irreversible A₁-inhibitors at concentrations in the range of 10⁻⁷–10⁻⁶ M. We have also shown that several isothiocyanate derivatives of ADAC, an agonist with selectivity and subnanomolar affinity for A₁ adenosine receptors, acted as irreversible inhibitors of the receptor at concentrations in the range of 10⁻⁸ M. We reexamined the compounds m-DITC–XAC, 5, and m-DITC–ADAC, 6, as irreversible A₁-inhibitors in bovine brain membranes (Chart 1, Table 2). It is to be noted that these ligands are analogous to structure 3 in Figure 1 in which R = H, except that they are lacking the cleavable group A–B. A 1 h incubation with 100 nM m-DITC–XAC or with 10 nM m-DITC–ADAC resulted in inhibition of 80 or 48% of the [³H]CPX binding, respectively. This inhibition was not reversible upon repeated washing of the membranes.

It was necessary to demonstrate that the receptor inhibition was not reversible under the conditions intended to be employed for the cleavage step (i.e., exposure to DTT or hydroxylamine). If binding ability of the receptor were restored, as was found in a study of affinity labels for A₂ₐ-adenosine receptors (7), it would indicate that the site of reaction between the isothiocyanate group and the receptor protein would be sensitive to these chemical reagents. The inhibition was stable, as summarized in Table 2. Neither DTT (50 mM) nor hydroxylamine (250 mM), present during a second incubation after removal of the affinity label, reversed this inhibition.

In the previous study of irreversible inhibitors of A₁-adenosine receptors (2) based on XAC and ADAC, it was observed that the chain length separating the pharmacophore and the reactive electrophilic group (an isothiocyanate) could be varied somewhat without loss of the irreversible binding feature of the ligand. Thus, it was reasonable that a chain extension to include a cleavable linkage (A–B) would not preclude covalent binding to the A₁-receptor. The antagonist series, rather than the agonist series, was developed in the subsequent compounds to avoid ambiguity, since agonist binding is subject to modulation by the state of coupling between the receptor and G-protein. Also, the binding of the antagonist [³H]CPX is less sensitive than [³H]PIA binding to the presence of hydroxylamine. Thus, we designed several new amine congeners related to XAC, in which the terminal ethylenediamine moiety of the chain was extended by the CH₂ABCH₂ group placed in the middle. AB consisted of either SS (thiol cleavable), 11 (Figure 2), or COO (hydroxylamine cleavable), 18 (Figure 3). These amine congeners corresponded to structure 1 in the general scheme (Figure 1). Each amine congener was to be coupled to a bifunctional or trifunctional cross-linking reagent to form a potentially cleavable affinity label (structure 3).

The amine congeners were synthesized from a xanthine carboxylic congener, 9 (XCC, 8-[4-[(carboxymethyl)oxy]phenyl]-1,3-dipropylxanthine), which also served as an intermediate in the synthesis of XAC (16). The cysteamine (HS(CH₂)₂NH₂) conjugate of XCC, a thiol derivative, was prepared previously and found to be a potent adenosine antagonist (17). The Kᵢ value of the cysteamine conjugate of XCC (17) was determined to be 16 nM vs [³H]PIA at rat A₁ receptors. That conjugate was also shown to be biologically active in a functional assay, in the inhibition of adenosine agonist-induced stimulation of adenylate cyclase via A₂ₐ-receptors, with a K_B value was 76 nM (17). Cystamine (compound 7) is a disulfide dimer of cysteamine. The conjugate of XCC and cystamine (compound 11, Figure 2), an amine congener, was
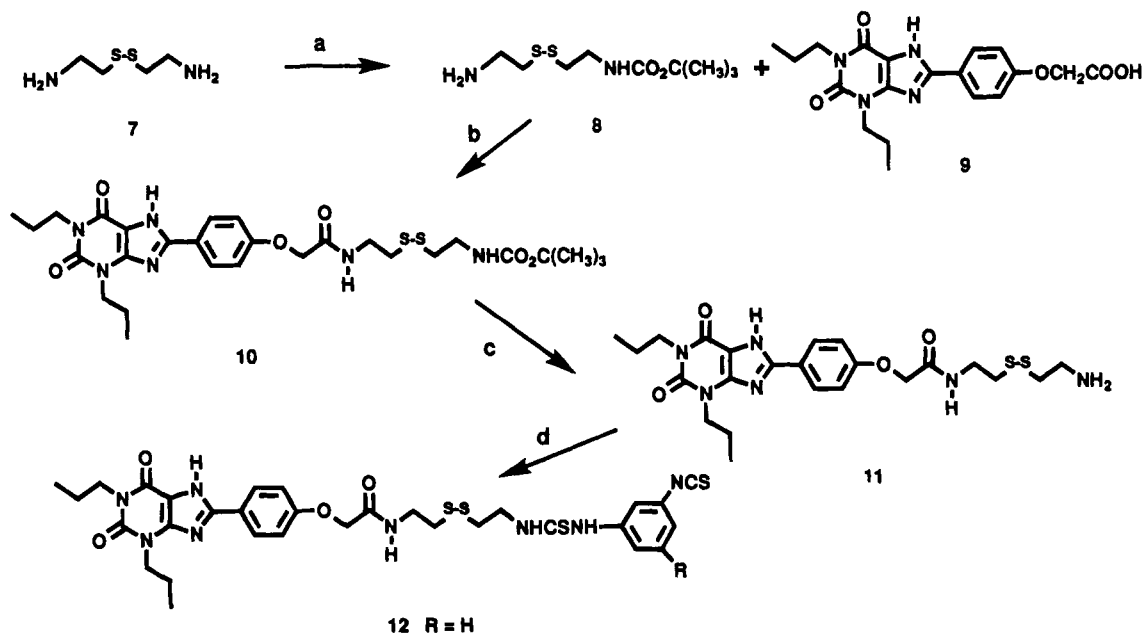
Figure 2. Synthesis of a thiol-cleavable xanthine amine congener, 11, containing a disulfide linkage. The final step consisted of reaction with *m*-phenylene isothiocyanate to form 12. Reagents: (a) di-*tert*-butyl dicarbonate; (b) EDAC/1-hydroxybenzotriazole, DMF; (c) TFA; (d) *m*-phenylene diisothiocyanate (R = H) or derivative thereof.
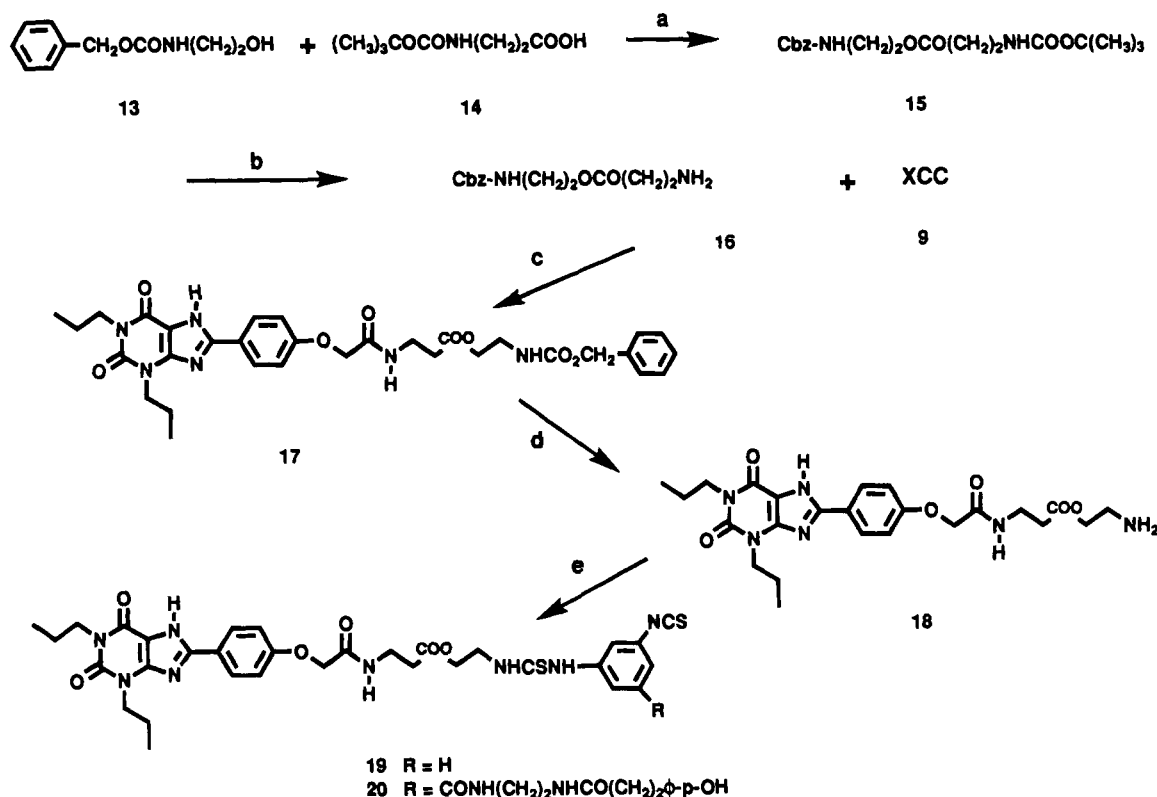
Figure 3. Synthesis of a hydroxylamine-cleavable xanthine amine congener, 18, containing an ester linkage. The final step consisted of reaction with *m*-phenylene isothiocyanate to form 19 or with 4-[2-[[[2-[[3,5-diisothiocyanatobenzoyl]amino]ethyl]amino]carbonyl]-ethyl]-2-iodophenol to form 20. Reagents: (a) EDAC/DMAP, DMF; (b) TFA; (c) EDAC/1-hydroxybenzotriazole, DMF; (d) HBr/acetic acid; (e) *m*-phenylene diisothiocyanate (R = H) or derivative thereof.

isolated previously as a byproduct in the synthesis of the cysteamine derivative. In this study compound 11 was synthesized by condensing XCC, 9, with Boc-cystamine, 8, followed by deprotection using TFA (Figure 2). The K_i value of the disulfide compound 11 was found to be 10 nM vs [^{3}H]PIA at rat A$_1$ receptors, indicating that chain extension was not detrimental to binding affinity.

The ester-containing amine congener (compound 18, Figure 3) was synthesized by condensing XCC with the

β-(Cbz-amino)ethyl ester of β-alanine, 16, followed by deprotection using HBr/acetic acid.

The next step was to couple compounds 11 and 18 to diisothiocyanate derivatives and to show that the conjugates would irreversibly bind to bovine A$_1$ receptors. The amine derivatives reacted with *m*-phenylene diisothiocyanate to form compounds 12 and 19, respectively. The K_i values for 12 and 19 in the displacement of [^{3}H]CPX in a "competitive" assay were found to be 2.1

Table 3. Irreversible Inhibition of Radioligand Binding by Compound 12 and Reversal of the Inhibition by DTT^a

concn of DTT (mM)	[^{3}H]CPX		[^{3}H]PIA	
	% inhibn	% reversal	% inhibn	% reversal
0	63 ± 5		69 ± 5	
5	57 ± 5	6	52 ± 1	17
50	48 ± 4	15	44 ± 7	25
100	38 ± 4	25	40 ± 3	29

^{a} Data are means ± s.e.m. of three to 11 experiments, expressed as percent of control binding. After incubation with the isothiocyante derivative 12 (500 nM) for 1 h at 37 °C, membranes were washed three times, incubated with DTT for 60 min at room temperature, washed twice, and then incubated with 0.2 nM [^{3}H]CPX (*14*) or 1 nM [^{3}H]PIA (*13*).

Table 4. Relationship between Concentration of Compound 19 and the Ability of Hydroxylamine to Restore Binding of [^{3}H]CPX

concn of 19 (nm)	inhibition of [^{3}H]CPX binding (% control)		reversal of inhibition (% control)
	(−H$_2$NOH)	(+H$_2$NOH)	
100	54.4	34.5	20
250	63.3 ± 1.2	43.6 ± 4.9	20
500	76.0 ± 3.0	54.0 ± 4.0	22

^{a} Data are means ± s.e.m. of three experiments or a single experiment. After incubation with the isothiocyanate derivative at 37 °C for 1 h, membranes were washed three times, incubated with hydroxylamine (500 mM, 37 °C for 1 h), washed twice, and then incubated with 0.2 nM [^{3}H]CPX (*14*). When the hydroxylamine incubation was carried out at 25 °C for 1 h, the degree of reversal was 8% (100 nM 19), 9% (250 nM 19), or 15% (500 nM 19).

± 0.26 and 9.7 ± 3.5 nM, respectively. Thus, receptor affinity has been preserved. In an assay of irreversible binding, both **12** and **19** were shown to be effective inhibitors (Tables 3 and 4), comparable in effectiveness to *m*-DITC−XAC, **5**.

The ability of DTT or hydroxylamine, present during a second incubation, to reverse this inhibition by compound **12** or **19**, respectively, was examined. Compound **12** at a concentration of 500 nM caused a loss of 63−69% of the radioligand binding (Table 3). This binding was partially restored (recovered 15−25% relative to control level) upon exposure to DTT. At 100 mM DTT the reversal of inhibition of the antagonist binding site was more effective than at 50 mM.

In Table 2 and in our previous study (*2*), 3-isobutyl-1-methylxanthine (IBMX) was added to the washing medium as a precaution for the removal of noncovalently bound xanthine. In the present study it was not necessary to wash the membranes overnight with IBMX. A comparison of the reversal of inhibition by compound **12** (preincubation at 500 nM) using DTT (10, 50 or 100 mM) overnight at room temperature, either in the presence or absence of IBMX (200 μM), gave identical results (data not shown).

Preincubation of bovine brain membranes with compound **19** (250 nM) caused a loss of 63% of the [^{3}H]CPX binding (Table 4). This binding was partially restored upon exposure to hydroxylamine (100−500 mM). At 37 °C, 20% of the radioligand binding relative to control level was recovered, while at room temperature the recovery was less effective (Table 5). Varying the concentration of the isothiocyanate derivative did not improve the percent of subsequent recovery of binding.

Compound **20** was prepared from the amine congener, **18**, and a diisothiocyanate containing a (*p*-hydroxyphenyl)propionyl group for radioiodination (*18*). This diisothiocyanate, corresponding to structure **2** (Figure 1)

Table 5. Relationship between Temperature and the Regeneration by Hydroxylamine of [^{3}H]CPX Binding Following Inhibition by Compound 19

concn of 19 (mM)	reversal of inhibition (% control)	
	37 °C	rt
250	24 ± 3	9 ± 5
500	23 ± 2	15, 15 (*n* = 2)

^{a} Data are means ± s.e.m. of three experiments, unless noted. After incubation with the isothiocyanate derivative **19** at 37 °C for 1 h, membranes were washed three times, incubated with hydroxylamine (500 mM) at 37 °C for 1 h, washed three times, and then incubated with 0.2 nM [^{3}H]CPX (*14*). Regeneration following overnight incubation with hydroxylamine at room temperature resulted in regeneration comparable to 1 h at 37 °C (data not shown).
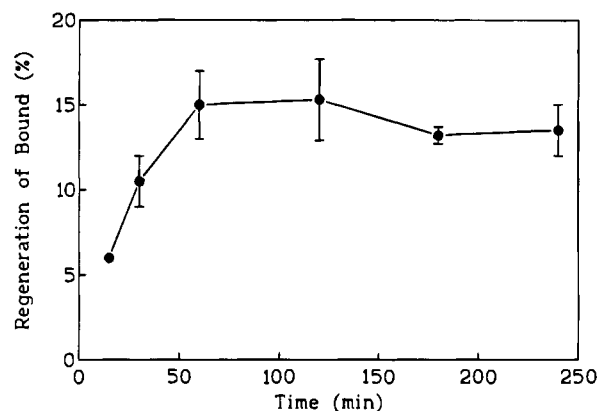
Figure 4. Time course for the regeneration by hydroxylamine of the specific binding of [^{3}H]CPX to A$_1$ receptors (percent of initial control binding) following exposure of bovine brain membranes to compound **20**. The preincubation with **20** (500 nM) was carried out for 1 h at 37 °C. Following the standard washing procedure (3×), the membranes were treated with hydroxylamine (250 mM) for 1 h at 37 °C, and aliquots were removed at the times indicated and immediatedly diluted and washed 3× in preparation for radioligand binding using 0.2 nM [^{3}H]CPX. The curve is from a single regeneration experiment, in which the binding at each time point was determined three times (mean ± s.e.m. shown).

in which R = CONH(CH$_2$)$_2$NHCO(CH$_2$)$_2$PhOH, was reported previously as a trifunctional cross-linker (*11*). The K_i value for **20** in the displacement of [^{3}H]CPX in a "competitive" assay was found to be 9.3 ± 2.0 nM. Preincubation of membranes with compound **20** at a concentration of 500 nM followed by washing caused a loss of 86 ± 2% (*n* = 6) of the [^{3}H]CPX binding. This binding was partially restored (19 ± 3% of the fraction that was lost, *n* = 5) upon exposure to hydroxylamine (250 mM at 37 °C), reaching maximal regeration after 1 h (Figure 4).

Temperature of incubation and pH were varied in an effort to improve the degree of recovery of binding following inhibition by compound **20**. The hydroxylamine incubation was compared at 37 °C for 1 h or at 25 °C overnight. The resulting regeneration of [^{3}H]CPX binding was comparable in both cases. An overnight incubation of membranes at 37 °C increased the recovery (to 45%) but the binding in control membranes was diminished by 50% by 400 mM hydroxylamine. At 37 °C, an incubation with hydroxylamine for 1−2 h gave the highest degree of recovery of [^{3}H]CPX binding. Incubations longer than 2 h resulted in the loss of binding in control membranes. The pH of the hydroxylamine medium (37 °C for 1 h) was varied from 6 to 10.5 (Table 6). Within the pH range of 7.4−9.5 the differences in recovery of [^{3}H]CPX binding were minor, while outside of that range less binding was recovered.

Table 6. Relationship between pH and the Regeneration by Hydroxylamine of [³H]CPX Binding Following Inhibition by Compound 20

pH	reversal of inhibition (% control)
6.0	6
6.5	8
7.4	14 ± 3
8.5	13 ± 1
9.5	15 ± 3
10.5	9 ± 3

a Data are means ± s.e.m. of three experiments or the mean for two experiments. After incubation with the isothiocyante derivative **20** at 37 °C for 1 h, membranes were washed three times, incubated with hydroxylamine (300 mM) for 1 h at 37 °C, washed three times, and then incubated with 0.2 nM [³H]CPX (*14*).

DISCUSSION

A general approach for the reversible affinity labeling of receptors has been demonstrated for A₁-adenosine receptors. Two sequential steps of chemical modifications of the receptor protein, *i.e.*, affinity labeling and cleavage, result in a functionally-regenerated receptor protein (structure **4b**, Figure 1) that also contains a site for a reporter group (R). Such a reporter group may consist of a radioactive or spectroscopic label, and numerous possibilities have been explored in our previous studies of trifunctional reagents (*11*, *20*). The chain cleavage used in this study was chemically-induced, but as an alternative method photosensitive groups such as *o*-nitrobenzyl (*8*) may be included in protein-affinity labeling reagents.

The effects on the pharmacology of a portion of the cleaved ligand being left on the receptor following restoration of the radioligand binding is the subject of ongoing studies. Thus, the regerated receptor may not be identical in binding properties to the native receptor.

The cleavable portion of the ligand consists of a xanthine amine congener, in which the pharmacophore and an amino group are separated by a cleavable, *i.e.*, disulfide or ester, linkage (compounds **11** and **18**, respectively). Cystamine, **7**, was previously incorporated into thiol-cleavable cross-linking reagents for oligonucleotides (*19*) and in biotin avidin probes (*10*). In those studies the disulfide bond was easily reduced in the presence of DTT. Similarly, hydroxylamine readily cleaves ester groups, and its ability to remove an affinity label from a fragment of the *β*-adrenergic receptor fragment was interpreted to indicate an ester linkage (*22*).

Use of these linkages in cleavable affinity labels assumes that the receptor itself is stable to the conditions needed for the cleavage reaction. In control experiments (Table 1) the native bovine A₁-receptor was not denatured by moderate concentrations of DTT or high concentrations of hydroxylamine. Millimolar concentrations of DTT denatured the A₁-receptor, presumably through reduction of protein disulfide bridges, as have been proposed in a receptor model (*21*). Nevertheless, somewhat selective reduction of the disulfide bond of the receptor-bound affinity label appears to have been accomplished in the concentration range of 0.05–0.1 M DTT. Hydroxylamine alone displaced agonist ([³H]PIA) binding from bovine A₁-receptors in a noncovalent manner. Perhaps hydroxylamine in its protonated form binds to the putative Na⁻ binding site on the second transmembrane helix of the A₁-receptor, identified by a consensus sequence (*21*). Binding at this site would be expected to affect agonist binding adversely, but not antagonist binding, consistent with the present findings.

Since the A₁-receptor was more stable to hydroxylamine than to DTT, it was the ester linkage that was

selected for inclusion in a ligand, **20**, containing the iodinatable (*18*) (*p*-hydroxyphenyl)propionyl group. This group has been used to incorporate an ¹²⁵I label in a xanthine that readily cross-links to purified A₁-receptors (*20*).

Isothiocyanate derivatives **12**, **19**, and **20** inhibited radioligand binding to A₁-receptors in bovine brain membranes in a manner that was not reversed by repeated washing. Similar behavior was observed for the binding of *m*-DITC–XAC, **5**, to bovine brain receptors, in which case covalent cross-linking was demonstrated by Western blot analysis (*6*). Hydroxylamine or DTT successfully restored binding of [³H]CPX in A₁-receptors inhibited by the appropriate cleavable xanthine isothiocyanate derivative. Binding was not fully restored, but the partial reversal is sufficient to illustrate the feasibility of this approach. It may be possible to purify the cleaved and functional receptor by affinity chromatography.

The A₁-receptor itself was stable to a wide pH range. Within this range, hydroxylamine reversed labeling by **20** by approximately 20% of the control value. Cleavage of an ester by hydroxylamine requires the free amine. At low pH, hydroxylamine is primarily protonated, which may explain why below pH 6.5 it was not effective.

The development of this approach for adenosine receptors may serve as a model for extending the method to derivatizing other G-protein coupled receptors, which have the same overall architecture, and conceivably to other biopolymers. A site-specifically labeled receptor that still binds ligand is potentially of use in the screening of drug analogs for affinity. A spectroscopic reporter group, such as a fluorescent label, present in a functional ligand binding site, may show sensitivity to ligand-bound and free states of the receptor. Thus, such a group may give a detectable signal that would report drug-receptor interactions in real time. Also, incorporation of a reactive handle, such as a thiol group, that likely results after DTT treatment of the A₁ receptor labeled by compound **12**, offers new possibilities for derivatizing receptors.

It may be possible to bind a functionalized receptor (e.g., bearing a free thiol group) to an affinity column. Binding of the receptor to an affinity support column may also be accomplished by immobilizing group R in a derivative similar to compound **20**, followed by the solubilized receptor and subsequently hydroxylamine. Such an immobilized receptor would have many envisioned uses, such as the determination of affinity of soluble ligands by retention on a flow through column. The biospecific elution of an adsorbed radioligand would indicate the presence of a high affinity competing ligand in solution. This scheme could potentially be used for screening libraries for active congeners (*23*).

LITERATURE CITED

(1) Newman, A. H. (1990) Irreversible ligands for drug characterization. *Ann. Rep. Med. Chem. 25*, 271–280.

(2) Jacobson, K. A., Barone, S., Kammula, U., and Stiles, G. L. (1989) Electrophilic derivatives of purines as irreversible inhibitors of A₁-adenosine receptors. *J. Med. Chem. 32*, 1043–1051.

(3) Barrington, W. W., Jacobson, K. A., and Stiles, G. L. (1989) Demonstration of distinct agonist and antagonist conformations of the A₁ adenosine receptor. *J. Biol. Chem. 264*, 13157–13164.

(4) Curtis, C. A., Wheatley, M., Bansal, S., Birdsall, N. J., Eveleigh, P., Pedder, E. K., Poyner, D., and Hulme, E. C. (1989) Propylbenzylcholine mustard labels an acidic residue in transmembrane helix 3 of the muscarinic receptor. *J. Biol. Chem. 264*, 489–495.

(5) Chorev, M., Feigenbaum, A., Keenan, A. K., Gilon, C., and Levitski, A. (1985) *Eur. J. Biochem. 146*, 9–14.

(6) Stiles, G. A., and Jacobson, K. A. (1987). A new high affinity iodinated adenosine receptor antagonist as a radioligand/ photoaffinity crosslinking probe. *Mol. Pharmacol. 32*, 184– 188.

(7) Jacobson, K. A., Stiles, G. L., and Ji, X.-D. Chemical modification and irreversible inhibition of striatal A₂-adenosine receptors. *Mol. Pharmacol. 42*, 123–133.

(8) Patchornik, A., Jacobson, K. A., and Strub, M. P. (1986) Photo-reversible affinity labeling. In *Design and Synthesis of Organic Molecules Based on Molecular Recognition*, Proceedings of the XVIIIth Solvay Conference on Chemistry (van Binst, G., Ed.) pp 235–241, Brussels, Springer .

(9) Denny, J. B., and Blobel, G. (1984) ¹²⁵I-labeled crosslinking reagent that is hydrophilic, photoactivatable, and cleavable through an azo linkage. *Proc. Natl. Acad. Sci. U.S.A. 81*, 5286–5290.

(10) Haeussling, L., Ringsdorf, H., Schmitt, F. J., and Knoll, W. (1991) Biotin-functionalized self-assembled monolayers on gold: surface plasmon optical studies of specific recognition reactions. *Langmuir 7*, 1837–1840.

(11) Boring, D. L., Ji, X.-D., Zimmet, J., Taylor, K. E., Stiles, G. L., and Jacobson, K. A., (1991) Trifunctional agents as a design strategy for tailoring ligand properties: Irreversible inhibitors of A₁ adenosine receptors. *Bioconjugate Chem. 2*, 77–88.

(12) Chong, P. C. S., and Hodges, R. S. (1981) A new heterobifunctional cross-linking reagent for the study of biological interactions between proteins. *J. Biol. Chem. 256*, 5064–5070.

(13) Garritsen, A. (1990) Molecular pharmacology of the adenosine A₁ receptor. Ph.D. Thesis, Center for Bio-pharmaceutical Research, Leiden, Netherlands, 58.

(14) Bruns, R. F., Fergus, J. H., Badger, E. W., Bristol, J. A., Santay, L. A., Hartman, J. D., Hays, S. J., and Huang, C. C. (1987) Binding of the A₁-selective adenosine antagonist 8-cyclopentyl-1,3-dipropylxanthine to rat brain membranes. *Naunyn Schmiedebergs Arch. Pharmacol. 335*, 59–63.

(15) Cheng, Y.-C., and Prusoff, W. H. (1973) Relationship between the inhibition constant (K_i) and the concentration of inhibitor which causes 50 percent inhibition (IC₅₀) of an enzyme reaction. *Biochem. Pharmacol. 22*, 3099–3108.

(16) Jacobson, K. A., Kirk, K. L., Padgett, W. L., and Daly, J. W. (1985) Functionalized congeners of 1,3-dialkylxanthines: preparation of analogues with high affinity for adenosine receptors. *J. Med. Chem. 28*, 1334–1340.

(17) Jacobson, K. A., de la Cruz, R., Schulick, R., L. Kiriasis, Padgett, W., Pfleiderer, W., Kirk, K. L., Neumeyer, J. L., and Daly, J. W. (1988) 8-Substituted xanthines as antagonists as A₁ and A₂-adenosine receptors. *Biochem. Pharmacol. 37*, 3653–3661.

(18) Bolton, A. E., and Hunter, W. M. (1973) The labelling of proteins to high specific radioactivities by conjugation to a ¹²⁵I-containing acylating agent. *Biochem. J. 133*, 529–539.

(19) Ferenz, A. E., and Verdine, G. L. (1991) Disulfide crosslinked oligonucleotides. *J. Am. Chem. Soc. 113*, 4000–4002.

(20) Jacobson, K. A., Olah, M. E., and Stiles, G. L. (1992) Trifunctional ligands: A radioiodinated high affinity acylating antagonist for the A₁ adenosine receptor. *Pharmacol. Commun., 1*, 145–154.

(21) van Galen, P. J. M., Stiles, G. L., Michaels, G., and Jacobson, K. A. (1992) Adenosine A₁ and A₂ receptors: Structure-function relationships. *Med. Res. Rev. 5*, 423–471.

(22) Eshdat, Y., Chapot, M.-P., and Strosberg, A. D. (1989) Chemical characterization of ligand binding site fragments from turkey β-adrenergic receptor. *FEBS Lett. 246*, 166–170.

(23) Zuckermann, R. N., Kerr, J. M., Siani, M. A., Banville, S. C., and Santi, D. V. (1992) Identification of highest-affinity ligands by affinity selection from equimolar peptide mixtures generated by robotic synthesis. *Proc. Nat. Acad. Sci. U.S.A. 89*, 4505–4509.

(24) Jacobson, K. A., van Galen, P. J. M., Ji, X.-d., Ramkumar, V., Olah, M., and Stiles, G. L. (1993) Molecular Characterization of A₁ and A₂ₐ adenosine receptors. *Drug Devel. Res. 28*, 226–231.

BC950003E

Calcium Responsive Two-Dimensional Molecular Assembling of Lipid-Conjugated Calmodulin

Nares Damrongchai, Eiry Kobatake, Tetsuya Haruyama, Yoshihito Ikariyama,[†] and Masuo Aizawa*

Department of Bioengineering, Faculty of Bioscience and Biotechnology, Tokyo Institute of Technology, 4259 Nagatsuta, Midori-ku, Yokohama 226, Japan. Received September 19, 1994[⊗]

Calmodulin (CaM), a calcium ion sensitive protein, was conjugated with dioctadecyldimethylammonium bromide and subsequently assembled into a monolayer at the air–water interface using the LB method. The lipid-conjugated calmodulin (LCC) retains its calcium sensitivity, determined from the changes in the area–pressure isotherm of the monolayer obtained at the air–water interface. The functionality of this protein assembly was characterized by the activation of phosphodiesterase (PDE), a CaM responsive enzyme. The enzyme activity of PDE coupled with LCC at the air–water interface was measured by using the enzymatic method. It was found that LCC retained its enzyme activity modulating function of calmodulin, which is triggered by calcium ions. This characteristic plays an important role in fabricating molecular assembly of proteins which have a cooperative interaction at the molecular level.

INTRODUCTION

Results of studies using molecular biology techniques indicate that biosystems form complex functional networks, interacting in a purpose-oriented manner, like the parts in a machine. Thus, it is challenging to invent methods to fabricate artificial supramolecular machines by arranging appropriate molecules in a planned manner. Especially in constructing molecular-sensing and information-processing devices, complex arrays composed of many functional elements can be achieved by molecular assembly design. Such molecular devices have great potential in the development of microelectronics, integrated optics, sensors and actuators, memories with high storage capacity, information-processing devices, and energy conversion devices.

Proteins can play an important role in composing these functional elements, since they possess all the above-mentioned functions. Many proteins and enzymes act like sensors, signal transducers, switches, and amplifiers. There have been many recent studies centering on the use of the specific recognition and binding sites of proteins as environmentally responsive components in fabricating the superstructures that can be used as molecular sensing and transducing devices [1]. The Langmuir–Blodgett (LB)[1] monolayer production and deposition technique has offered an approach to that purpose [2–7]. Using the LB technique, simple supramolecular devices can be obtained by constructing sets of different kinds of molecules that when properly arranged interact in an intended manner.

There have been many attempts in using the LB technique to fabricate biomolecular devices such as biosensors. Sriyudthsak *et al.* (8) have prepared a lipid–protein monolayer for biosensors using the LB technique and enzyme glucose oxidase as the protein. Other molecular protein assembly work has been done by Aizawa *et al.* (9, 10) who fabricated biosensors by means of bioaffinity combined with electrochemical techniques. Another recent work by Samuelson *et al.* (11) has shown the feasibility of integrating conductive polymers into molecular assemblies to enhance optical signal transduction.

Calmodulin (CaM), a water-soluble protein, is the material that we chose for our molecular assembling experiment because of its calcium ion responsive characteristics (12, 13). Upon binding to calcium ions, calmodulin dynamically alters its conformation and thus activates a group of enzymes and proteins. For this reason, calcium ion sensitivity of calmodulin and its modulating function was used to demonstrate its possibility as an environmentally responsive molecular assembly. In past studies, there have been many efforts to utilize CaM in a molecular device, such as by covalently conjugating CaM with PDE (14) or by using the coordinated function of CaM and melittin monolayer formed at the air–water interface (15) to fabricate a new environment-responsive material. However, although some molecules can be stably formed at the air–water interface due to their polar/non polar nature, there are still some difficulties in making monolayers of proteins, including the entering of molecules into the aqueous subphase due to water solubility and surface denaturation problems (16).

Like most other proteins, CaM cannot form a stable monolayer at the air–water interface because of its water solubility. However, in this study we overcame this problem by conjugating CaM with lipid molecules to make CaM hydrophobic.

Our method will give a promising opportunity for fabricating an environmentally responsive material made of a protein assembly, which has the functions of sensing and transduction.

EXPERIMENTAL PROCEDURES

Reagents. Phosphodiesterase 3':5'- cyclic nucleotide activator (calmodulin) from bovine brain (>98% by SDS gel electrophoresis), phosphodiesterase (PDE; from bo-
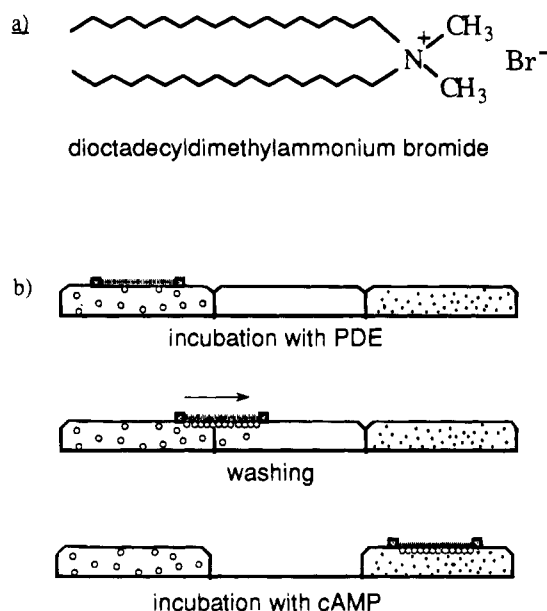
Figure 1. (a) DC-1-18 lipid. (b) Procedure in measuring PDE enzyme activity using the LB trough.

vine brain), as well as its substrate, adenosine 3':5'-cyclic monophosphate (cyclic AMP), were purchased from Sigma (MO). The lipid, dioctadecyldimethylammonium bromide (DC-1-18) was purchased from Sogo Pharmaceutical Co., Ltd. (Tokyo, Japan) (Figure 1a) *(17)*.

Thin layer chromatography plates with 250 μm-thick silica gel are products of Analtech, Inc. (DE). Sepharose CL-6B is a product of Pharmacia LKB (Uppsala, Sweden). Protein Assay Kit is the product of Bio-Rad Laboratories (CA).

Alkaline phosphatase (AP; from calf intestine) and adenosinedeaminase (ADA; from calf intestine) were purchased from Böeringer Mannheim (Postfach, Germany). All other reagents used were of the highest purity grade.

Preparation of Lipid-Conjugated Calmodulin. Calmodulin was conjugated with the positively charged lipid. Twenty milligrams of lipid were suspended in 5 mL of acetate buffer (pH 5.6). Sonication was carried out until the suspension became transparent. Subsequently, 5 mL of 1.0 mg/mL of calmodulin solution was added, and the mixed solution was stirred overnight at 4 °C. The solution was then centrifuged at 8000 rpm for 5 min. After the supernatant was discarded, the sediment was collected and freeze dried before being stored at −20 °C.

Characterization of Lipid-Conjugated Calmodulin. This lipid-conjugated calmodulin (LCC) was tested with various methods to define the molecular weight along with the conjugate ratio between protein and lipid. The spectra of 0.1 mg/mL of LCC in chloroform were examined in comparison with that of native calmodulin of the same concentration using a JASCO UVIDEC-610C double beam spectrophotometer. The absorbance peak appeared between 250 and 300 nm. Consequently, we tested LCC with thin layer chromatography (TLC). TLC was performed with a mixture of the following solutions as the mobile phase: chloroform/acetone/acetic acid/formic acid/water 70/30/12/4/2, respectively.

To determine the conjugate ratio between protein and lipid, we applied LCC to gel filtration chromatography using the organic solvent *N,N*-dimethylformamide (DMF). Organic solvent-resistant Sepharose CL-6B was chosen because of the need to use DMF as a running buffer. The

conjugate was subjected to both spectrophotometry and colorimetric analysis as is explained below to determine the protein and lipid composition.

Protein concentration was determined by the method of Bradford, using Bio-Rad's protein assay kit. After the sample was mixed with diluted dye, the absorption of the solution at 595 nm was measured.

The concentration of lipid portion in LCC was determined using colorimetric method. Six mL of chloroform and 1.0 mL of phosphate buffer (pH 7.0) were added to the sample. The mixture was left for over 15 min, and then 2.0 mL of copper solution (1 M triethanolamine/1 M acetic acid/6.45% copper sulfate (9 + 1 + 10, v/v) was added. After vigorous shaking, the mixture was centrifuged at 2500 rpm and the colored copper supernatant was drawn out using a vacuum. Three mL of chloroform layer from the sample was taken and added with 1.0 mL of the colorizing solution (100 mg of bathocuproine dissolved in 9 mL of chloroform, mixed with 200 mg of hydroquinone dissolved in 5 mL of ethanol). Finally, the absorption at 480 nm was measured and concentration of the sample was calculated from the following equation

$$\text{sample concentration} = {}^{E_{A'}}\!/_{E_{B'}} 0.5 \ (\text{mequiv L}^{-1})$$

where $E_{A'}$ = absorption of the sample at 480 nm and $E_{B'}$ = absorption of the standard solution (2.0 mM palmitoic acid) at 480 nm.

Assembling of LCC Monolayer at Air−Water Interface. The characteristics of LCC assembled at the air−water interface were examined by means of the LB method. We used a Fromherz circular type multicompartment LB trough combined with a double-barrier driving assembly and an electronic control unit, the Monofilmmeter *(18)*. Twenty μL of a 0.2 mg/mL of LCC sample was applied at the air−water interface. The temperature was kept at 14 °C when forming LCC at the air−water interface. Calcium response was examined using ultrapure water containing 0, 0.01, 0.1, 1, and 10 mM CaCl$_2$.

Calmodulin Monolayer Coupled with Phosphodiesterase. To functionalize the LCC monolayer, we coupled LCC with PDE, a target enzyme modulated by calmodulin. Here we utilized the fact that calmodulin increases PDE's hydrolysis rate of its substrate, cAMP, to AMP in the presence of calcium. Activity of PDE at the air−water interface was determined by means of an enzymatic method using alkaline phosphatase (AP) and adenosinedeaminase (ADA) and a spectrophotometric method *(19)* (Scheme 1).

Scheme 1. Reaction of Enzymes

$$\text{cAMP} + \text{H}_2\text{O} \xrightarrow{\text{PDE/calmodulin}} \text{AMP}$$

$$\text{AMP} + \text{H}_2\text{O} \xrightarrow{\text{AP}} \text{adenosine} + \text{Pi}$$

$$\text{adenosine} + \text{H}_2\text{O} \xrightarrow{\text{ADA}} \text{inosine} + \text{NH}_3$$
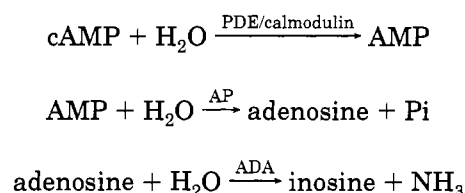
Twenty mL of 1 mg/mL of LCC (dissolved in DMF solution) was spread on the 0.1 M glycyl glycine buffer (GG buffer; pH 7.5) subphase with and without calcium ion (0 or 10 mM). After the surface pressure was slowly compressed to 45 mN/m, the monolayer was shifted, while surface pressure was kept constant, to the adjacent trough compartment which contained 0.06 units of PDE solution (Figure 1b). The LCC monolayer was left in this compartment for incubation with the PDE subphase
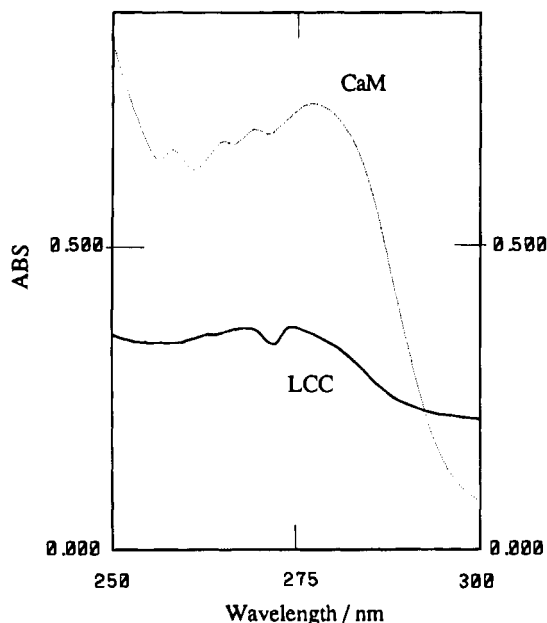
Figure 2. Spectrum of LCC, compared to that of calmodulin.

solution for 3 h. After washing, the PDE-coupled LCC monolayer was moved to another compartment containing 50 μM cAMP, the substrate for PDE. The coupled monolayer was incubated for another 3 h for the enzyme reaction. After the reaction was terminated, the subphase was assayed for AMP, the product of PDE activity. The temperature was kept at 37 °C throughout the enzyme reaction experiment.

RESULTS

Characteristics of Lipid-Conjugated Calmodulin. The quantity of LCC obtained after freeze drying was 11.0 mg, equivalent to 44% product yield. After dissolution in chloroform, a spectrum of LCC was measured (Figure 2).

From Figure 2, it is apparent that though the spectra of CaM and LCC differed in magnitude, both patterns were similar, obviously due to the contribution from the calmodulin portion while DC-1-18 alone does not have any absorbance peak in this region.

Results from thin layer chromatography (Figure 3) showed that the lipid portion of LCC segregated from the conjugate and traveled with the mobile phase. The R_f value for lipid detached from LCC is 0.70, very close to the R_f value of pure lipid which is 0.72. Both chromatograms of LCC and calmodulin showed that the protein remained at the starting point in the gel.

The calmodulin and lipid portions of LCC were determined separately by spectrophotometric analysis after being eluted from Sepharose CL-6B (Figure 4). Calculating the lipid and protein portions in the fraction, we found that the protein to lipid molar ratio was 1:88 on average.

Calcium-Responsive Pressure—Area Isotherm at Air—Water Interface. The monolayer of lipid-conjugated calmodulin is highly stable at the air—water interface compared to the calmodulin monolayer under the same conditions (Figure 5). For comparison, the surface pressure—area isotherm of calmodulin at the air—water interface is shown (Figure 6). The unusually small limiting area (molecular area) obtained by extrapolation of the linear portion of the curve and also the small maximum surface pressure indicate that calmodulin barely forms a monolayer at the air—water interface. The validity of this interpretation is obvious when compared

Figure 3. Thin layer chromatography. Five mg/mL of samples in chloroform solution were applied. Spots are as follows: (1) lipid, (2) calmodulin, (3) lipid and calmodulin mixture, (4) lipid-conjugated calmodulin.
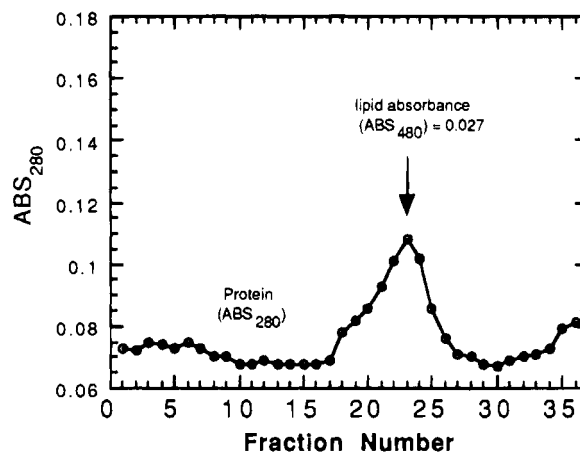
Figure 4. Fraction pattern of LCC measured at 280 nm absorption. The sample was subjected to Sepharose CL-6B gel filtration chromatography using N,N-dimethylformamide (DMF) as the solvent. Lipid was measured in fractions that contain substantial peak absorbance of protein and not all the fractions. The column volume was 26.5 mL, and the fraction volume was 1 mL per one fraction.

to melittin (Figure 7). Melittin is an amphiphilic molecule found in honey bee toxin and is also a calmodulin inhibitor. The fact that approximately the same area per molecule was seen in the pressure—area isotherm of melittin, a peptide with a molecular weight only 1/6 that of calmodulin, indicates that melittin has greater preferability for forming a monolayer at the air—water interface, apparently due to the molecule's amphiphilicity.

The stability can also be seen by repeatedly decompressing and recompressing the LCC monolayer. From our results, the LCC monolayer at the air—water interface can be decompressed and recompressed more than
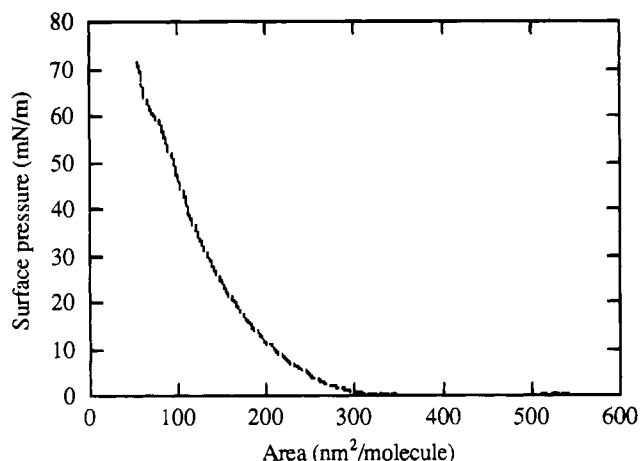
Figure 5. Pressure—area isotherm of lipid-conjugated calmodulin measured at the air—water interface. The sample concentration was 0.2 mg/mL and 20 μL volume applied.
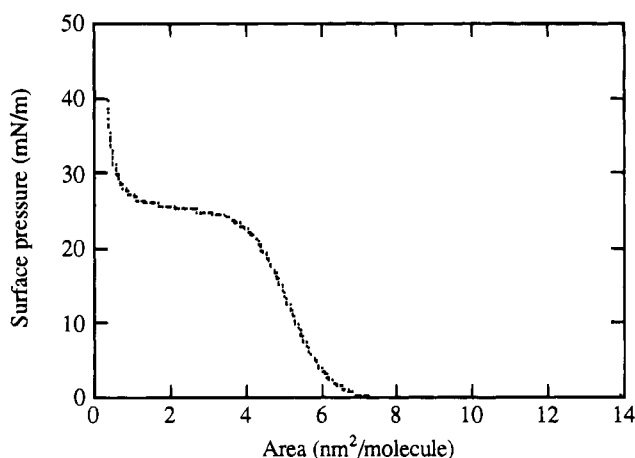
Figure 6. Pressure—area isotherm of CaM. The protein sample concentration was 7.5 mg/mL while 20 μL of sample solution was applied on the aqueous subphase.
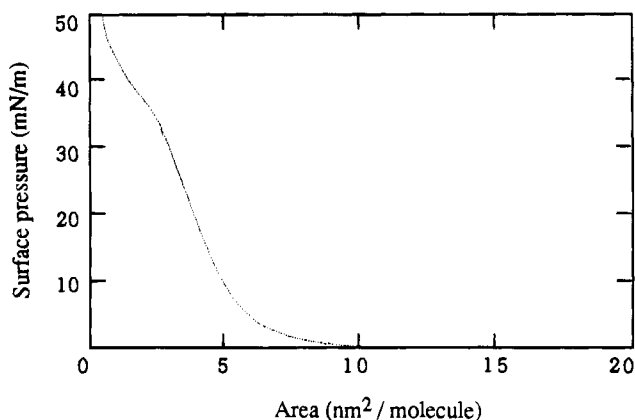
Figure 7. Pressure—area isotherm of melittin. One hundred μM, 20 μL of sample solution was applied on the aqueous subphase.

six times while generating almost the same area—pressure isotherm (data not shown).

Calcium responsive characteristics of LCC at the air—water interface were investigated. As shown in Figure 8, the surface pressure-area isotherm of LCC, after being tested with various concentrations of calcium ion, shifted to higher surface pressure when exposed to 10 mM calcium ion. The cause of this phenomena may be due to structural changes in the calmodulin molecule upon binding to calcium ions. The effect of calcium ions was not detected for the monolayer when contained only DC-1-
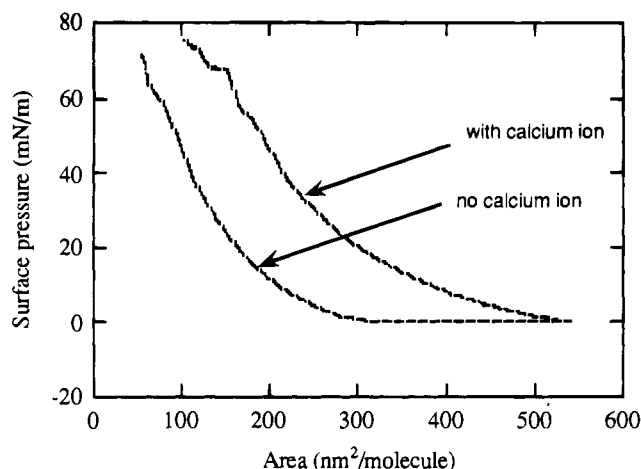
Figure 8. Effect of calcium ions on the pressure—area isotherm of LCC. The upper curve represents the pressure—area isotherm of LCC with no calcium ion in the subphase, while the lower curve represents the result of a condition with 10 mM of calcium ion in the subphase.

18 because we observed no major shift in pressure—area isotherm of the DC-1-18 monolayer (data not shown).

Calcium-Responsive Enzyme Activity of PDE Coupled with the Calmodulin Monolayer. The enzyme activity modulating function of the LCC monolayer was investigated by using the enzyme activity modulating characteristics of calmodulin. By coupling LCC with phosphodiesterase (PDE), a target enzyme modulated by calmodulin, it was possible to trace the enzyme activity at the air—water interface with and without calcium ions.

This enzymatic assay is based on the fact that calmodulin increases the rate of hydrolysis of cAMP to AMP catalyzed by PDE in the presence of calcium ion. The AMP formed in this reaction is dephosphorylated to adenosine in the presence of AP. Subsequently, adenosine is hydrolyzed to inosine in the presence of ADA. Generally, the rate of adenosine consumption, measured by the decrease in absorbance at 265 nm, is used to estimate the amount of calmodulin present in the monolayer. Our results showed that the decrease in ABS_{265} is observed only after depriving the monolayer-forming molecule of lipid. Therefore, in each experiment lipid was washed from the LCC monolayer by moving the monolayer to an anion-containing subphase before starting each enzyme reaction. Our results indicated that activity of the calmodulin-coupled PDE monolayer depends on the presence or absence of calcium ions. In the absence of calcium ion (control experiment), the absorbance at 265 nm increased 0.046 after injection of enzymes. On the contrary, in the presence of calcium ions the absorbance decreased for 0.155 after the injection. The results are reproducible. They showed that the large decrease in absorbance at 265 nm was due to consumption of cAMP, while the PDE enzyme activity was calculated as follows.

The difference in the linear molar absorption coefficients of cAMP and inosine *(19)* is $\Delta\epsilon = 8.2 \times 10^2$ L mol^{-1} min^{-1}, therefore the catalytic concentration in the sample is,

$$b = \frac{\Delta A \times 10^3}{\epsilon d \delta t \varphi} = \frac{10^3}{(8.2 \times 10^2) \times \frac{1}{10^3} \times 10 \times 1} \frac{\Delta A}{\Delta t} =$$

$$(12.2 \times 10^3)\frac{\Delta A}{\Delta t} \text{ U L}^{-1}$$

While ΔA is the difference in absorption at 265 nm, Δt is the reaction time (min), φ is the ratio between the volume of sample used in assay and the assay volume, and d represents the length of the light path (cm).
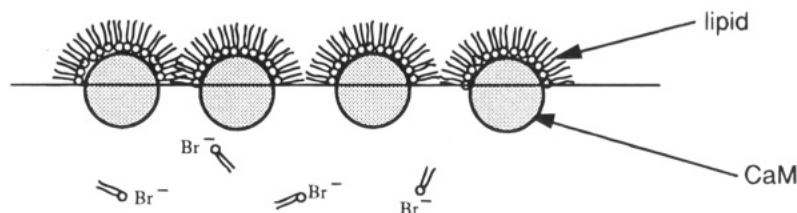
Figure 9. Diagrammatic drawing of LCC at the air–water interface after the lipid was washed out. The remaining lipid faces the air and the washed side of LCC molecule faces the water, which consequently creates a "virtual amphipathic molecule".

From our results

$$\Delta A = 0.200$$

$$\Delta t = 180 \text{ min.}$$

Then the catalytic activity concentration of PDE is,

$$b = (12.2 \times 10^3)\frac{0.20}{180} = 13.6 \text{ U L}^{-1}$$

DISCUSSION

In the presence of calcium ions, calmodulin binds 4 mol of calcium ion and undergoes conformational changes (20). The calcium-bound form of calmodulin then binds to PDE and activates the enzyme, which consequently catalyzes the cAMP hydrolysis reaction. This resulted in a prominent decrease in absorbance at 265 nm, due to the consumption of AMP.

The initial aim was to build a protein assembly that retains the ability to form a monolayer at the air–water interface. However, since the LCC monolayer coupled with PDE did not show enzyme activity, we removed lipid from the monolayer-forming molecule. To our surprise, even after lipid was removed the monolayer was still stable, and moreover, it has the ability to catalyze the reaction of cAMP hydrolysis.

Our assumption is that all the lipid may not have been removed by anion in the subphase. If this is true, the monolayer forming molecule may have turned into a form of "virtual amphipathic molecule", with the remaining lipid on the air side and the washed calmodulin facing the water side (Figure 9).

One problem in assembling a monolayer at the air–water interface is that the molecule has to be amphiphilic (21). This means that the hydrophobic part always faces the air while the hydrophilic part always faces the water. In the case of calmodulin, the target molecule binding site is considered to be dominantly hydrophobic (sometimes referred to as the hydrophobic pocket) (22), thus preventing the protein monolayer from effectively binding with its target enzyme in the subphase. With this method, the protein does not have to be amphiphilic yet still has the ability to form a monolayer with its recognition site randomly facing water.

Conjugating protein with lipid has proven to be one way to help fabricate water-soluble protein assemblies at the air–water interface. The manner in which protein molecules arrange in the monolayer at the air–water interface has yet to be investigated by using more powerful tools such as atomic force microscopy (AFM). However, our experiments have shown the possibility of using this two-dimensional assembly in fabricating an environmentally responsive material.

LITERATURE CITED

(1) Kuhn, H. (1994) Organized Monolayer Assemblies: Their role in constructing supramolecular devices and in modeling evolution of early life. *IEEE Eng. Med. Biol. 13*(1), 33–44.

(2) Verger, R., and Pattus, F. (1976) Spreading of membranes at the air/water interface. *Chem. Phys. Lipids. 16*, 285–291.

(3) Heckl, W. M., Thompson, M., and Mohwald, H. (1989) Fluorescence and electron microscopic study of lectin-polysaccharide and immunochemical aggregation at phospholipid Langmuir–Blodgett Monolayers. *Langmuir 5*, 390–394.

(4) Turko, I. V., Yurkevich, I. S., and Chashchin, V. L. (1991) Langmuir–Blodgett films of immunoglobulin G for immunosensors. *Thin Solid Films 205*, 113–116.

(5) Tachibana, H., Azumi, R., Nakamura, T., Matsumoto, M., and Kawabata, Y. (1992) New types of Photochemical switching Phenomena in Langmuir–Blodgett films. *Chem. Lett.* (1), 173–176.

(6) Tang, F. Q., Li, J. R., Zhang, L., and Jiang, L. (1992) Improvement of enzymatic activity and lifetime of Langmuir–Blodgett films using submicron SiO₂ particles. *Biosensors Bioelectron. 7*, 503–507.

(7) Barraud, A., Perrot, H., Billard, V., Martelet, C., and Therasse, J. (1993) Study of immunoglobulin G thin layers obtained by the Langmuir–Blodgett method: application to immunosensors. *Biosensors Bioelectron. 8*, 39–48.

(8) Sriyudthsak, M., Yamagishi, H., and Moriizumi, T. (1988) Enzyme-immobilized Langmuir–Blodgett film for a biosensor. *Thin Solid Films 160*, 463–469.

(9) Aizawa, M., Owaku, K., Matsuzawa, M., Shinohara, H., and Ikariyama, Y. (1989) Molecular film technology for biosensors. *Thin Solid Films 180*, 227–233.

(10) Aizawa, M., Matsuzawa, M., and Shinohara, H. (1988) An optical chemical sensor using a fluorophor-embedded Langmuir–Blodgett film. *Thin Solid Films 160*, 477–481.

(11) Samuelson, L. A., Wiley, B., and Kaplan, D. L. (1994) Intelligent systems based on ordered arrays of biological molecules using the LB technique. *J. Intell. Mater. Syst. Struct. 5*, 305–310.

(12) VanBerkum, M. F. A., George, S. E., and Means, A. R. (1990) Calmodulin activation of target enzymes. *J. Biol. Chem. 265*, 3750–3756.

(13) Hahn, K. M., Waggoner, A. S., and Taylor, D. L. (1990) Calcium-sensitive fluorescent analog of Calmodulin based on a novel calmodulin-binding fluorophore. *J. Biol. Chem. 265*(33), 20335–20345.

(14) Miwa, T., Damrongchai, N., Shinohara, H., Ikariyama, Y., and Aizawa, M. (1991) Activity self-controllable enzyme-calmodulin hybrid by Ca²⁺ information—an approach towards the regulation of a molecular device which breaks chemical structure. *J. Biotechnol. 20*, 141–150.

(15) Aizawa, M., Damrongchai, N., Kobatake, E., and Ikariyama, Y. (1992) Coordinated function of different proteins in surface membrane. *Membr. Symp. 4*, 89–92.

(16) MacRitchie, F. (1986) Spread monolayers of proteins. *Ad. Colloid Interface Sci. 25*, 341.

(17) Okahata, Y., and Ijiro, K. (1988) A lipid-coated lipase as a new catalyst for triglyceride synthesis in organic solvents. *J. Chem. Soc., Chem. Commun.* 1392–1394.

(18) Fromherz, P. (1971) A new technique for investigating lipid protein films. *Biochim. Biophys. Acta 225*, 382–387.

(19) Schiefer, S. (1985). Structural and regulatory protein-Calmodulin. *Methods of Enzymatic Analysis* Vol. 9, pp 317–331, Weinheim, W. Germany-Deerfield Beach.

(20) Klee, C. B., and Vanaman, T. C. (1982) Calmodulin. *Adv. Protein Chem. 35*, 213–321.

(21) Langmuir, I., and J. Schaefer, V. (1939) Properties and structure of protein monolayers. *Chem. Rev. 24*, 181–202.

(22) Strynadka, N. C. J., and James, M. N. G. (1990) Model for the interaction of amphiphilic helices with Troponin C and Calmodulin. *Proteins 7*, 234–248.

Synthesis and Use of a New Bromoacetyl-Derivatized Heterotrifunctional Amino Acid for Conjugation of Cyclic RGD-Containing Peptides Derived from Human Bone Sialoprotein

Boris Ivanov,*,† Wojciech Grzesik,‡ and Frank A. Robey†

Peptide and Immunochemistry Unit, Laboratory of Cell Development and Oncology, and Bone Research Branch, The National Institute of Dental Research, National Institutes of Health, Bethesda, Maryland 20892. Received October 31, 1994⊗

A new amino acid derivative, N^α-(*tert*-butyloxycarbonyl)-N^β-(bromoacetyl)diaminopropionic acid (BBDap), has been synthesized as a reagent for introducing side-chain bromoacetyl groups into any position of a peptide sequence during solid-phase peptide synthesis. By using minor modifications to the protocol of the automated peptide synthesizer and a two-step *in situ* neutralization procedure, the syntheses of (bromoacetyl)diaminopropionic acid (BDap) in Arg-Gly-Asp-containing peptides from human bone sialoprotein were optimized and completed. Following HPLC purification, the BDap-derivatized peptides were cyclized or/and conjugated to carrier protein or to glass cover slips. In addition, a new procedure for site-specific conjugation of cyclic peptides to protein carriers or to glass was developed. The cell attachment activity of the peptide derivatives and conjugates was tested in cell adhesion assays with human osteoblasts, and the specificity of the binding was confirmed by competition with linear and/or cyclic forms of GRGDS. The results show that conjugates containing the linear and cyclic derivatives of the peptide EPRGDNYR supported cell attachment and spreading in a dose-dependent manner when the peptides were immobilized as described. Cell attachment to the intact bone sialoprotein and to conjugates containing the linear peptides was abolished by competition with linear and cyclic RGD-containing peptides, whereas the attachment to conjugates containing the cyclic peptide was inhibited only partially, and the cell spreading was preserved even in the presence of RGD-peptides.

INTRODUCTION

Conformationally constrained analogs of biologically active peptides have proved to be useful starting points for the rational design of biomaterials containing peptides that possess unique biological activities. It has been shown in a number of reports that cyclizing or polymerizing peptides can influence their receptor selectivity (*1*), metabolic stability (*2*), and antigenic/immunogenic properties (*3*, *4*). However, despite all the progress that has been made in the field of peptide chemistry, there still is a paucity of reliable synthetic techniques for making conjugates and polymeric forms of these conformationally constrained peptides.

Recently, N-terminal chloroacetylation and bromoacetylation were shown to be very efficient tools for the conjugation of synthetic peptides to proteins and for cyclizing or polymerizing peptides (*5–7*). Subsequently, the synthesis of N^α-(*tert*-butyloxycarbonyl)-N^ϵ-(N-(bromoacetyl)-β-alanyl)lysine (BBAL),[1] a heterotrifunctional spacer which could be placed at any desirable position in a peptide chain, was reported (*8*).

Although BBAL is quite versatile, there are certain limitations to its use in syntheses of constrained and especially cyclic analogues. These limitations are due to the length (12 carbon bonds) of the side chain bearing the bromoacetyl moiety. Now, we report on the design, preparation, and use of a new reagent, N^α-(*tert*-butyloxycarbonyl)-N^β-(bromoacetyl)diaminopropionic acid (BBDap),

which is suitable for automated peptide synthesis and has a much shorter (5 bonds) side chain than BBAL.

In this report, we demonstrate the use of BBDap to construct several conformationally constrained peptide analogues designed to mimic the cell attachment site of human bone sialoprotein (BSP), which is a member of a family of RGD-containing proteins that resemble vitronectin, a cell attachment protein in which RGD may be found in quasicyclic conformation (*10*). Since cyclic RGD peptides are 100-fold more active toward binding to the vitronectin receptor than binding to the fibronectin receptor (*1*), it was of interest to us to extend the previous vitronectin findings and study the effect of conformationally constrained RGD-peptides from BSP on osteoblast RGD receptors. The information obtained from such a study, together with novel methods to conjugate the conformationally constrained peptides, could be useful in developing osteoblast-specific therapeutics.

EXPERIMENTAL PROCEDURES

Materials and Methods. GRGDS was purchased from Calbiochem Corp. (San Diego, CA), and ITS⁺ (insulin, transferrin, and selenium + BSA) was obtained from Collaborative Research, Inc. (Bedford, MA). Boc-

---

* Author to whom correspondence should be addressed. Tel: (301) 496-2616. Fax: (301) 402-0823.
† Peptide and Immunochemistry Unit.
‡ Bone Research Branch.
⊗ Abstract published in *Advance ACS Abstracts,* April 15, 1995.

[1] Abbreviations: AcOH, acetic acid; BBDap, N^α-(*tert*-butyloxycarbonyl)-N^β-(bromoacetyl)diaminopropionic acid; BDap, N^β-(bromoacetyl)diaminopropionic acid; BBAL, N^α-(*tert*-butyloxycarbonyl)-N^ϵ-(N-(bromoacetyl)-β-alanyl)lysine; BSA, bovine serum albumin; BSP, bone sialoprotein; CEC, S-(1-carboxyethyl)-cysteine; CMC, S-(carboxymethyl)cysteine; Dap, diaminopropionic acid; DCC, dicyclohexylcarbodiimide; DCM, dichloromethane; DIEA, diisopropylethylamine; DIC, diisopropylcarbodiimide; NMP, 1-methylpyrrolidone; TCEP, tris(carboxyethyl)phosphine; TEA, triethylamine; TFA, trifluoroacetic acid; chl, chloroform; MeOH, methanol.
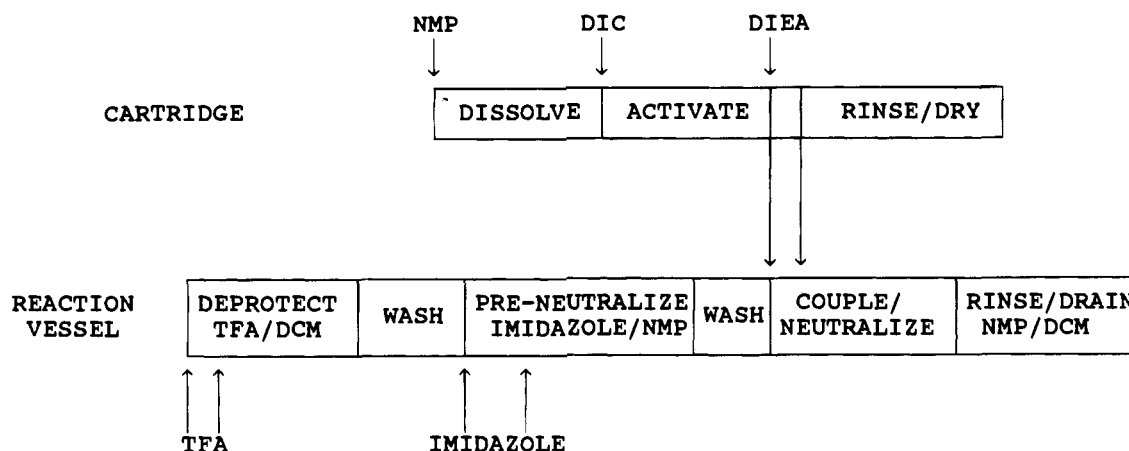
Figure 1. Structure of the the ABI 430A synthetic cycle for Boc/DIC chemistry using two-step *in situ* neutralization. The activator and reaction vessel cycle procedures are aligned. The time scale is not presented.

L-α,β-diaminopropionic acid (Boc-Dap) and Boc-β-alanine were obtained from Bachem Bioscience Inc. (Philadelphia, PA). Bromoacetic acid, 2-bromopropionic acid, 2-(bromomethyl)propionic acid, 3-bromopropionic acid, *m*-cresole, TEA, DIC, and imidazole were from Aldrich Chemical Co. (Milwaukee, WI). Radioactive [C1-^{14}C] bromoacetic acid (58.0 mCi/mmol) was from DuPont (Boston, MA). Tris-(2-carboxyethyl)phosphine hydrochloride (TCEP) was supplied by Molecular Probes, Inc. (Eugene, OR). BSA and *S*-(carboxymethyl)cysteine were purchased from Sigma (St. Louis, MO). All chemicals for peptide synthesis with the exception of BDap, DIC, and imidazole were purchased from Applied Biosystems, Inc. (Foster City, CA). Reagent grade methanol, ethyl acetate, diethyl ether, chloroform, and pentane were ordered from Mallinckrodt (Paris, KN). HPLC grade water and acetonitrile were from J. T. Baker Inc. (Phillipsburg, NJ). Analytical and preparative HPLC were performed on a Vydac C18 (4.6 × 250 mm) reversed-phase column (Separation Group, Hesperia, CA) using a Waters 840 HPLC system (Millipore Corp., Millford, MA) or on a Vydac C18 (25 × 250 mm) column with a Waters 600E system, correspondingly. Silica Gel 60 F254 plates (EM Science, Gibbstown, NJ) were used for TLC. Picotag amino acid analysis developed by Waters Associates was performed as described by the manufacturers but with the use of an HP 1090 LC module (Hewlett-Packard, Inc., Gaithersburg, MD). Melting points were determined on a Kofler apparatus and are uncorrected. Elemental analyses of the samples were performed by Galbraith Laboratories, Inc. (Knoxville, TN).

Normal human bone cells were obtained as described (*11*). Briefly, cells were obtained by outgrowth from small (<1 mm in diameter) collagenase-treated fragments of human trabecular bone. Cells were grown in low (0.2 mM) Ca^{2+} medium (DMEM/Ham's F12, Biofluids Inc., Rockville, MD) supplemented with 2 mM glutamine and 100 units/mL penicillin/streptomycin (Biofluids Inc.), 50 mg/mL ascorbate, and 10% fetal bovine serum (Gibco BRL, Gaithersburg, MD) until confluent (usually 4–7 weeks).

Synthesis of BBDap. A precooled 0.5 M solution of DCC in DCM (120 mL, 60 mmol) was added to a stirred solution of bromoacetic acid (16.56 g, 120 mmol) in DCM (50 mL) at 0 °C. The reaction mixture was stirred for 30 min at 0 °C and filtered to remove the dicyclohexylurea that had formed, and the filtrate was evaporated on a Buchi rotary evaporator at 20 °C. The residue was dissolved in 20 mL of acetonitrile, and the solution was immediately added to a solution of Boc-L-Dap (8.32 g, 40 mmol) and TEA (5.6 mL, 40 mmol) in 40 mL of 50% aq.

acetonitrile. The reaction mixture was stirred at 0 °C for 10 min, an additional 5.6 mL of TEA (40 mMol) was added, and stirring was continued for 60 min more at room temperature. The acetonitrile was evaporated, and EtOAc (300 mL) was added to the residual solution. The mixture was successively washed with 0.1 N sulfuric acid (200 mL × 3) and saturated sodium chloride (200 mL × 2), dried over sodium sulfate, and evaporated. The residual oil was dissolved in dry ether (50 mL), and petroleum ether (200 mL) was added. A gum-like precipitate appeared after the mixture stood at 4 °C for 24 h, and white crystals (9.98 g, 30.7 mmol, 77% yield) were later obtained, which were washed with dry ether (50 mL ×2) and pentane (100 mL), filtered, and air-dried. Recrystallization of the product from warm chloroform (15 mL) was performed by adding dry diethyl ether (50 mL). Six and one-half grams (20 mmol, 50%) of the final product that was pure by TLC (chl:MeOH:AcOH (80:18: 2), chlorine/toluidine staining, R_f 0.5) were obtained: mp 138 °C (decomp). Anal. Calcd for C$_{10}$H$_{17}$N$_2$O$_5$Br: C, 36.92; H, 5.27; O, 24.61; N, 8.62; Br, 24.58. Found: C, 36.80; H, 5.11; O, 24.88; N, 8.60; Br, 24.61; Cl, < 0.5.

Synthesis of BDap-Containing Peptides. A two-step neutralization procedure for the ABI 430A peptide synthesizer using a *t*-Boc synthesis protocol is briefly outlined in Figure 1. Typically the peptides were synthesized on a 0.4–0.45 mmol scale. The peptide synthesis program was created by modifying the standard NMP/ HOBt "rboc11" program of the instrument (version 1.41, ABI). The additions of DMSO and DIEA to the end of the synthesis cycle as well as the "end capping" procedure were omitted from the reaction vessel cycle. DIEA in reagent bottle 1 was replaced with a 1 M solution of imidazole in NMP which provided mild preneutralization of the peptidyl resins after the removal of the *t*-Boc group. Because of the high viscosity of NMP, the delivery time of the solution of DIEA in the original rboc 11 program was increased to 11 s, providing delivery of 1 mL of the solution.

DIC (1 M solution in NMP) was used for activation of the amino acids and placed in reagent bottle 8. Reagent bottle 7 was used for delivery of a precise volume of a DIEA solution to the reaction vessel, and programs were written for the activator and concentrator programs to allow delivery from reagent bottle 7 (0.5 M DIEA). Two millimoles of Boc-amino acids, bromocarboxylic acids or BBDap was dissolved in the cartridges in 3 mL of NMP as a part of the "opt11" routine (except for Boc-Asn which was dissolved in 2 mL of 1 M HOBt/NMP before synthesis). Two milliliters of 1 M DIC/NMP was transferred to the cartridges from bottle 8 with the assistance of a

user-defined function, and the activations were allowed to proceed in the cartridges for 30 min with periodic agitation. Then the activated reagents were directly transferred from the cartridges to the reaction vessel, bypassing the activator and concentrator vessels. Then 1 mL of 0.5 M DIEA/NMP solution was transferred to the reaction vessel *via* the cartridge. All of the Boc-amino acids and the bromo-containing reagents were coupled using the same synthetic cycle.

Reagent bottles 4 and 5 were not used in the syntheses.

Deprotection and Purification. The peptides were cleaved from the resin by treatment with HF/*m*-cresol (9:1, v/v, −4 °C, 1 h). HF was evaporated under reduced pressure, and the crude peptides were precipitated and washed twice with dry ether. The crude peptides were extracted in ice-cold 10% acetic acid (200 mL per gram of the peptidyl resin), purified by preparative HPLC using a gradient of acetonitrile in 0.1% TFA, and lyophilized.

Peptide Cyclization. Typical reaction conditions were the following: the peptide to be cyclized (50 μMol) was dissolved in 25−50 mL of 0.1% TFA, and the pH of the solution was brought to 8−9 by the dropwise addition of TEA. Usually, after 5 min at room temperature, the Ellman test for the presence of free thiols (*12*) in the reaction mixture was negative. Monitoring the reaction by HPLC typically showed complete conversion of the starting peptide to the cyclic form; the cyclic form elutes 1−3 min earlier on a reversed-phase column than the linear peptide. The yields after HPLC purification ranged from 70 to 85%.

Conjugation to BSA. TCEP (28 mg, 100 μmol) was dissolved in PBS (0.5 mL), neutralized with 4 M sodium hydroxide (100 μL, 400 μmol), and immediately mixed with a solution of BSA (34 mg, 0.5 μmol) in PBS (2 mL). After being stirred at room temperature for 30 min, the reaction mixture was loaded onto a column of Toyopearl HW-40f (25 × 500 mm) in degassed PBS. The fractions containing the high molecular weight components were collected, and the BSA concentration was determined by absorbance at 280 nm. The Ellman test showed 20−22 μmol of free SH groups per 1 μmol of the reduced protein. Two to 20 μmol of bromoacetylated (LBP, CBA) or 2-bromopropionylated peptide (CBP, <u>CCP</u>) was dissolved in the solution of the reduced BSA, and the pH of the reaction mixture was adjusted to 8−9 with 4 M NaOH solution. Monitoring of the reaction by HPLC and the Ellman test showed that the reaction was completed within 2 h at room temperature where bromoacetylated peptides were conjugated and overnight when 2-bromopropionylated peptides were conjugated. Dialysis of the reaction mixture against water (3 × 5000 mL × 12 h) followed by lyophylization yielded peptide−protein conjugates which contained 10−25% (w/w) peptide as was determined by PicoTag amino acid analysis (see Table 2).

Peptide Conjugation to Glass. Microscope cover glasses (22 × 22 mm, No. 1) were soaked in 0.2 M sodium hydroxide solution overnight and rinsed in water until neutral; the glasses then were refluxed in 50% aq. NMP containing 1% (3-mercaptopropyl)trimethoxysilane (Aldrich) for 2 h and successively washed with 50% aq. methanol (3×) and 0.1% acetic acid. Then the glasses were immediately immersed in coupling buffer (degased 0.05 M phosphate, pH 8) containing 50 nmol/mL bromoacetylated peptide and incubated overnight at room temperature. The glasses were transferred to coupling buffer containing 5 mg/mL iodoacetamide, incubated for 2 h, extensively washed with water, and air-dried. For cell attachment assays the glasses next were placed in Petri dishes and washed with serum-free medium.

To estimate the number of free SH groups that (3-mercaptopropyl)trimethoxysilane coupled to the glass surface, the thiolated glasses were incubated overnight in coupling buffer containing 10−50 pmol/mL [C1-^{14}C]-bromoacetic acid and washed with water (5×). The glasses were placed in scintillation vials with 10 mL of CytoScint (ICN Biomedicals, Inc., Irvine, CA), and the retained radioactivity was counted with a Beckman LS1801 counter. All mesurements were done in triplicates.

Cell Attachment Assay. Bacteriological Petri dishes were coated with 10 mL of substrate solution in PBS containing 1 mM $CaCl_2$, resulting in a sample-coated ("dot") area of approximately 0.12 cm^2. After 16 h of incubation at 4 °C, the fluid was aspirated and 10 μL of ice-cold 60% aq. methanol was added to each dot followed by 2 h of incubation at 4 °C. Methanol was then aspirated, and the plates or prepared glasses were washed for 30 min at 4 °C with washing buffer (50 mM Tris-HCl, pH 7.8, 110 mM NaCl, 5 mM $CaCl_2$, 0.1 mM PMSF, 1% BSA, and 0.001% sodium azide). This was followed by washing three times with serum-free DMEM/Ham's F12 (1:1) medium supplemented with 2 mM glutamine, 100 units /mL penicillin/streptomycin, 0.5% ITS$^+$, and 50 mg/mL ascorbate. Bone cells obtained as described above were trypsinized, centrifuged, resuspended in serum-free medium, and incubated for 30 min at 37 °C in order to allow recovery after trypsinization. Next, cells were seeded at a density of 10 000/cm^2 onto prepared dishes, and simultaneously with plating, several studied compounds (GRGDS, CBA, LBP) were added to the medium. After 24 h of incubation at 37 °C, the plates were washed twice in serum-free medium to remove nonadherent cells and fixed with 80% aq. methanol at −20 °C for 20 min. Next, cells were stained with 0.1% Amido Black, and the attached cells were counted using the Optomax HV image analyzer. The results were expressed as percent of the number of the cells attached to plastic coated with a 0.2 μM solution of BSP.

RESULTS

N^α-(*tert*-Butyloxycarbonyl)-N^β-(bromoacetyl)-L-diaminopropionic acid (BBDap) was synthesized from commercial N^α-(*tert*-butyloxycarbonyl)-L-diaminopropionic acid (Boc-Dap) and the symmetric anhydride of bromoacetic acid as shown in Scheme 1. The product was judged to be approximately 95% pure as determined by TLC and HPLC after crystallization from ethyl acetate/ether and recrystallization from chloroform/ether. Although some exchange of Br with Cl in the bromoacetyl moiety has been reported when Cl-containing reagents have been used for treatment of BBAL (*8*), in this study we did not observe the phenomenon widely using a saturated solution of NaCl for extractions and chloroform for crystallization. BBDap was obtained in crystalline form and was stable after being allowed to stand as a powder at room temperature for at least 6 months.

Studies that we have performed on the stability of bromoacetyl moieties in solid-phase peptide synthesis revealed that the bromoacetyl moiety appears to be stable under acidic conditions but unstable in the presence of repeat exposure to a base like TEA or DIEA (data not shown). We found that two or three standard NMP/HOBt cycles completely destroyed the bromoacetyl moiety introduced in the peptide chain. To minimize the exposure of BDap to an excess of base during the neutralization step, an *in situ* neutralization procedure (*13*) was slightly modified and programmed into the ABI 430A synthesizer.

Scheme 1

Scheme 2

R₁=Me
R₂=H, Me
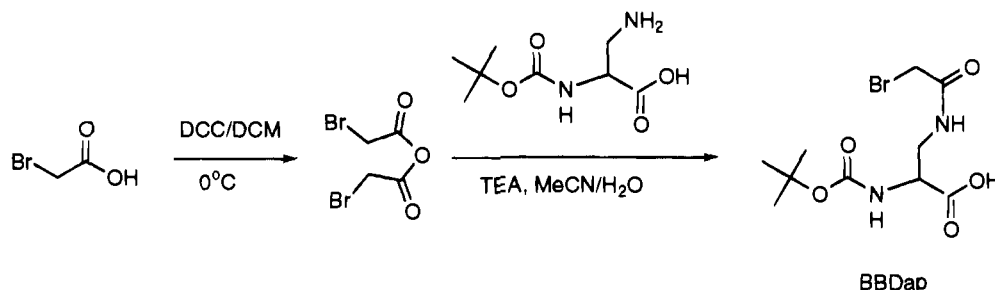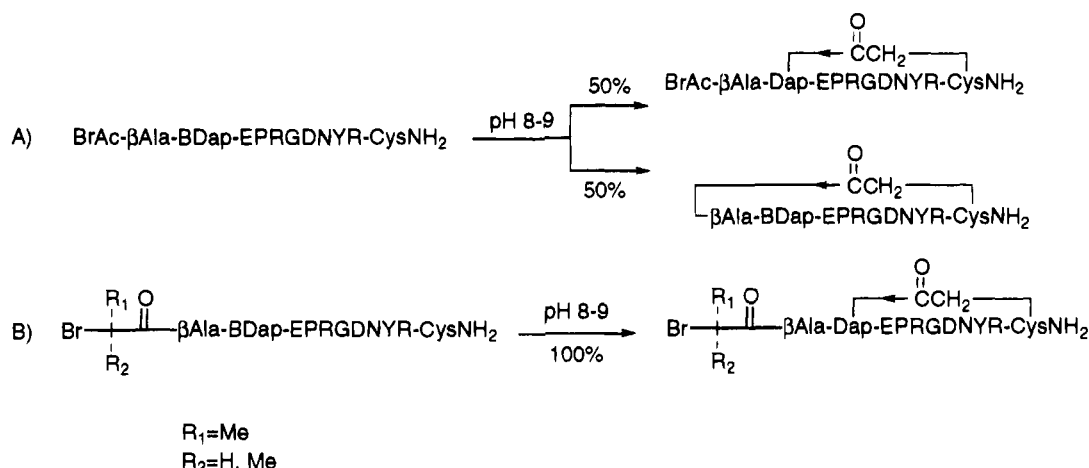
The primary feature of the modification is an initial step of preneutralization of resin with a mild base. Briefly, after the TFA deprotection of the *t*-Boc group, peptidyl resins were preneutralized by a wash solution of imidazole in NMP to remove excess TFA absorbed on the resin (see Figure 1). Transfer of the activated amino acids to the preneutralized resin was followed by the addition of a stoichiometric amount of DIEA to the reaction vessel for completion of the neutralization and coupling steps. The preneutralization step, which neutralized the TFA bound to the resin without deprotonating the N^α-amine on the resin, increased the coupling efficiency by allowing the use of a minimal amount of DIEA for neutralization of the resin.

Activations of all amino acids except of Boc-Asn were performed without HOBt to eliminate its possible reaction with the bromoacetyl moiety. Activations of Boc-amino acids were carried out with DIC in NMP for 30 min using a 4-fold excess of Boc-amino acids over the amount of the amino groups of the resin. Activated amino acids were then added to the preneutralized resins, and after that, a precise amount of DIEA was added to the reaction vessel to complete the neutralization *in situ*. A ninhydrin test (*14*) showed that the coupling yields were usually higher than 99.5% after 15 min at room temperature. This method yielded peptides containing BDap at the C-terminus or in a central position of the peptide chain in high yield and with good quality (data not shown).

After the crude linear peptides were purified by reversed-phase HPLC, cyclizing the peptides was carried out by raising the pH of 0.1−5 mg/ml peptide solution in 0.1% TFA (see Scheme 2). The absence of free thiols was noted to be complete after 5 min of the reaction at room temperature. HPLC analysis of the reaction mixtures revealed quantitative conversion of the starting material to the cyclic analogue with an elution time on reversed-phased HPLC that was earlier than that obtained for the

linear peptide (Figure 2). Picotag amino acid analysis of the cyclic peptides showed the presence of stoichiometric amounts of CMC in the cyclized peptide's hydrolysate, thereby proving that a thioether bond had formed between Cys and BDap (Figure 3a).

Peptides with Two Bromoacetyl Moieties for Conjugating Cyclic Peptides. The designations and structures of the peptides used in this study are presented in Table 1. The introduction of a second bromoacetyl moiety into peptides (CBA, cyclic *b*romoacetylated RGD peptide; see Table 1) led to the formation of two cyclic products during the cyclization due to alternative attack of the sulfhydryl group by equally reactive bromoacetyl moieties (Scheme 2a). HPLC analysis of the reaction mixture showed the formation of two products with close retention times, and the two products had identical amino acid contents (data not shown).

In an attempt to increase the selectivity of the cyclization, we tested the activity of various other bromoacetyl derivatives toward thiols using the described conditions. Model studies showed that α-bromoisobutyryl and β-bromopropionyl moieties of CBB and βCBP (cyclic α-*b*romoisobutirylated and cyclic β-*b*romopropionylated RGD peptides) peptides did not react with *N*-acetyl cysteine or cysteine-containing peptides under the conditions applied, while an α-bromopropionyl moiety reacted with thiols at a rate that was much slower than the rate at which the bromoacetyl moiety would react (data not shown). The difference in the reactivity between bromoacetyl and α-bromopropionyl moieties allows for the selective formation of a thioether bond between Cys and the bromoacetyl group, thereby leaving the slower reacting α-bromopropionyl moiety intact and available for further reaction with other thiol-containing materials under more rigorous reaction conditions (Scheme 2).

Peptides CBP and CCP (cyclic α-bromopropionylated RGD peptide and *c*yclic control α-bromopropionylated non-RGD peptide) bearing Cys at their C-termini, BDap
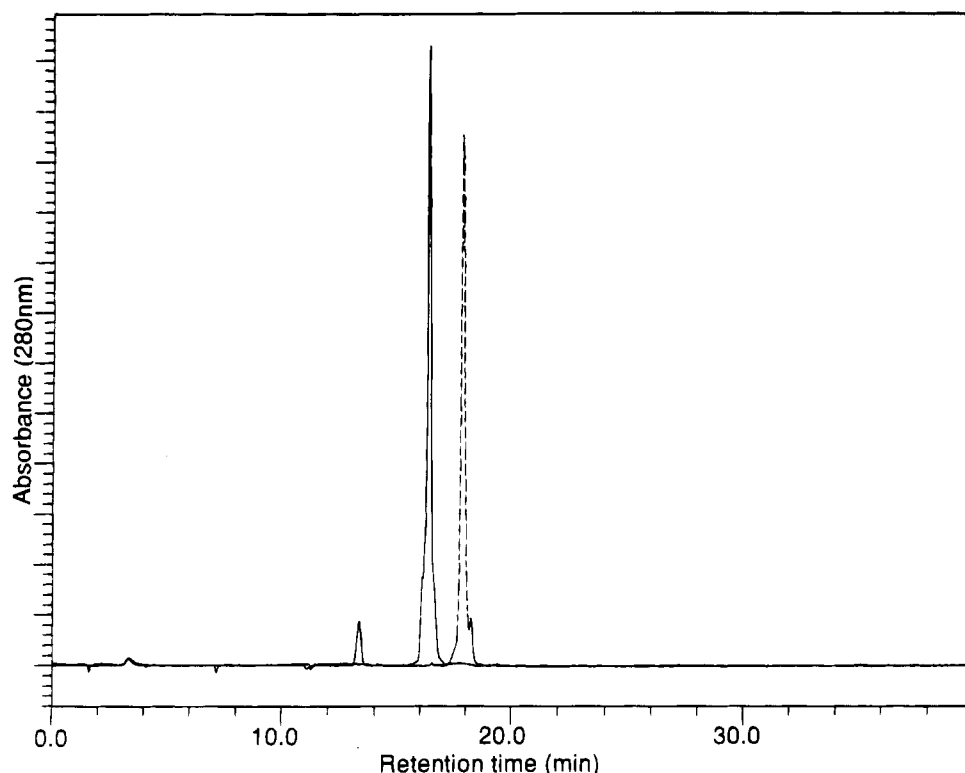
Figure 2. Overlaid HPLC profiles of linear precursors of CBP (dashed line) and the product resulting from cyclizing the peptide using the chemistry described herein (solid line). The peptides were eluted from a Vydac C18 (4.6 × 250 mm) column with an elution gradient of 0 to 70% acetonitrile in 0.1% TFA and a flow rate of 1 mL/min.
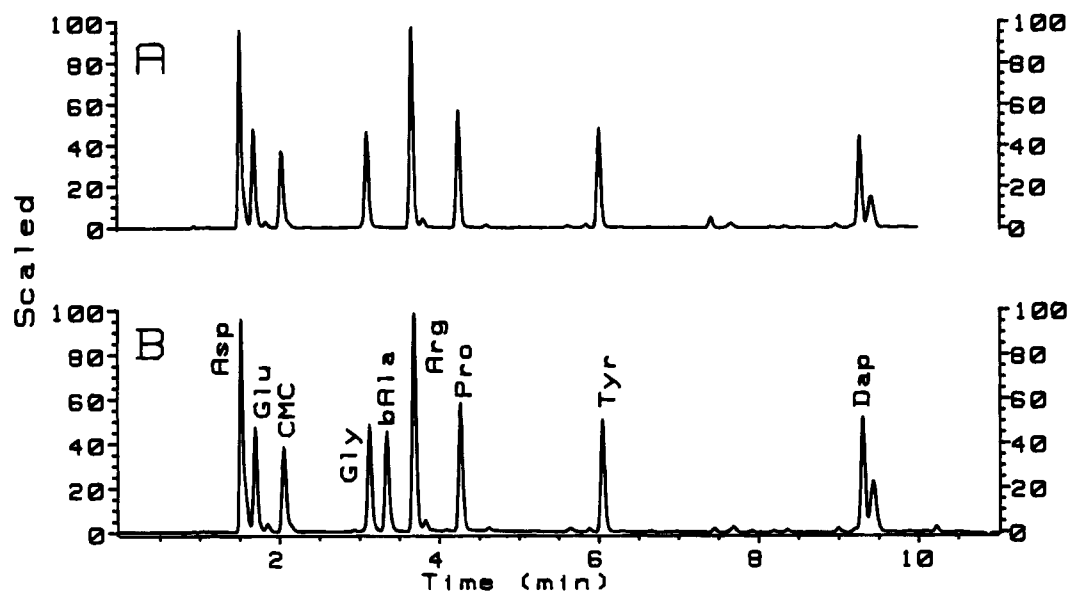
Figure 3. Picotag amino acid analyses of the acid hydrolysate of 1 mg of the cyclic peptides: (A) CNB; (B) CBP. The peptides were obtained from the linear analogues by cyclizing *via* the bromoacetyl moiety of BDap and Cys, producing CMC (RT 2.06 min), which is stable in the conditions of the acid hydrolysis and clearly resolved in the Picotag system.

in a central position, and α-bromopropionyl moiety at their N-termini were synthesized. Cyclizing the peptides resulted in the rapid (*ca.* 5 min) formation of the thioether bond between Cys and BDap. No products formed by cyclizing *via* the N-terminally branched bromoacetyl moieties were detected by HPLC or amino acid analysis (Figure 3b).

Peptides containing bromoacetyl moieties can be conjugated easily to carriers bearing available sulfhydryl groups (*6*). Two different strategies of peptide anchoring were employed either *via* the C-terminal bromoacetyl moiety of the linear peptide LBP or *via* an additional

N-terminal α-bromopropionic moiety of cyclic peptides CBP and CCP.

The linear and cyclic peptides were coupled to thiol-containing carriers as shown in Scheme 3. In this study, we used thiol-derivatized glass or BSA which had been reduced with the water-soluble phosphine TCEP (*15*). The peptide–protein conjugates were analyzed by amino acid analysis after acidic hydrolysis of the conjugates. The hydrolyses liberate thioalkylated cysteine derivatives which are formed during the conjugation step (Scheme 3) and can be easily quantitated with amino acid analysis (*7*). The presence of the cysteine derivatives in the

Table 1. Designated Abbreviations and Structures of Linear and Cyclic Peptides Used in the Study

peptide designation	peptide structure[a]
LBP	EPRGDNYR-BDap-NH$_2$
LCP[b]	EPRGENYR-BDap-NH$_2$
CNB	Dap-EPRGDNYR-CysNH$_2$ └────COCH$_2$────┘
CBA	BrCH$_2$CO-βAla-Dap-EPRGDNYR-CysNH$_2$ └────COCH$_2$────┘
CBP	BrCH(CH$_3$)CO-βAla-Dap-EPRGDNYR-CysNH$_2$ └────COCH$_2$────┘
βCBP	BrCH$_2$CH$_2$CO-βAla-Dap-EPRGDNYR-CysNH$_2$ └────COCH$_2$────┘
CCP[b]	BrCH(CH$_3$)CO-βAla-Dap-EPRGENYR-CysNH$_2$ └────COCH$_2$────┘
CBB	BrC(CH$_3$)$_2$CO-βAla-Dap-EPRGDNYR-CysNH$_2$ └────COCH$_2$────┘

[a] BDap, β-bromoacetyl-α,β-diaminopropionic acid, single letter codes were used for all amino acids except cisteinamide, β-alanine, and α,β-diaminopropionic acid. [b] The designations of the control RGE-containing peptides are underlined.

Table 2. Composition[a] of the Conjugates

conjugates	CMC[b]/ Val ratio	peptide/ protein ratio (mol/mol)	peptide content in conjugates (pmol/mg)
BSA-LBP	0.36	13	80
BSA-LCP	0.62	22	210
BSA-CBA	1.03	18	220
BSA-CBP	0.09	3	30
BSA-CCP	0.16	6	50

[a] Data were obtained by Picotag amino acid analysis. [b] CEC in the case of BSA-CBP and BSA-CCP.

analysis confirms the covalent bond between peptide and BSA and allows calculation of the peptide/protein ratio in the conjugates under study (Table 2). The conjugation of peptides LBP, LCP (*l*inear *b*romoacetylated RGD peptide and linear control bromoacetylated non-RGD peptide), and CBA *via* a bromoacetyl moiety resulted in S-carboxymethylcysteine (CMC) formation, while the conjugation via racemic 2-bromopropionyl moiety (CBP, CCP peptides) formed a pair of diastereomeric S-(1-carboxyethyl)cysteines (CEC) which were clearly resolved in the analysis as well (Figure 4). During the course of this study we learned that there is no benefit to using optically pure 2-(+)-bromopropionic acid, which also forms a pair of diastereomeric products because of racemization occurring in the reaction with thiols.

A three-step chemical procedure was employed for the conjugation of bromoacetylated peptides to glass. In the first step, glass was silanized by a thiol- containing reagent, (3-mercaptopropyl)trimethoxysilane, to present free thiols as components of the glass surface. Next, the modified glass was treated with bromoacetylated or 2-bromopropionylated peptides under conditions favoring

the thioether bond formation and finally, unreacted thiols, which would remain on the glass after the peptide conjugation, were blocked with an excess of iodoacetamide.

The number of bromoacetyl-reactive sites on the glass surface was estimated with the use of radioactive bromoacetic acid [C1-^{14}C]. Treatment of the thiolylated glass with 10 and 50 nmol/mL bromoacetic acid solutions resulted in the same amount of radioactivity retained by the glass surface, 11 ± 3 pmol/cm^2. This finding indicates that the number of coupling sites on the modified glass surface is limited by the amount of free thiol groups available. Our data correlate with the value of the saturated surface concentration of peptides grafted to tresyl-activated glass, which was 12 pmol/cm^2 as reported by Massia and Hubbel (*16*). Since the amount of peptide in the coupling buffer greatly exceeded the amount sufficient to reach saturation of the glass surface, the peptide-grafted glasses were assumed to have the maximum surface concentration of the peptides.

Osteoblast Cell Attachment. Finally, the cell attachment activity of the peptides conjugated to BSA (Table 2) or glass was tested in the cell attachment assay (*17*). All synthetic peptides conjugated to BSA mediated cell attachment and spreading in a dose-dependent manner.

Osteoblast attachment to immobilized intact BSP and linear peptide—BSA conjugates was abolished by the addition of linear and cyclic RGD-containing peptides into the medium. Bone cell attachment to the conjugate containing the cyclic RGD peptide was inhibited only slightly by the addition of a single conformation of competing peptide (either linear or cyclic) and full blocking of the attachment was observed only when both linear and cyclic peptides were simultaneously added into the medium (Figure 5).

To examine whether the short peptides would support the attachment of the bone cells to an artificial surface without a large proteinaceous carrier, we tested the activity of the peptides covalently bound to the glass microscopic slides. The number of cells attached to the peptides covalently linked to the glass proved difficult to estimate due to the high nonspecific background attachment of the cells to the underivatized glass. However, inclusion of cycloheximide (a protein synthesis inhibitor) to the cell growth medium resulted in differences in the cell spreading. Cells that were plated on the glass—CBA (cyclic RGD peptide) surface displayed spreading, while those plated on glass alone, glass—CCP (cyclic non-RGD peptide), or glass—LBP (linear RGD-peptide) did not spread upon attachment (Figure 6).

DISCUSSION

The coupling of BBDap to any position in a synthetic peptide was most successful when the peptide synthesizer

Scheme 3
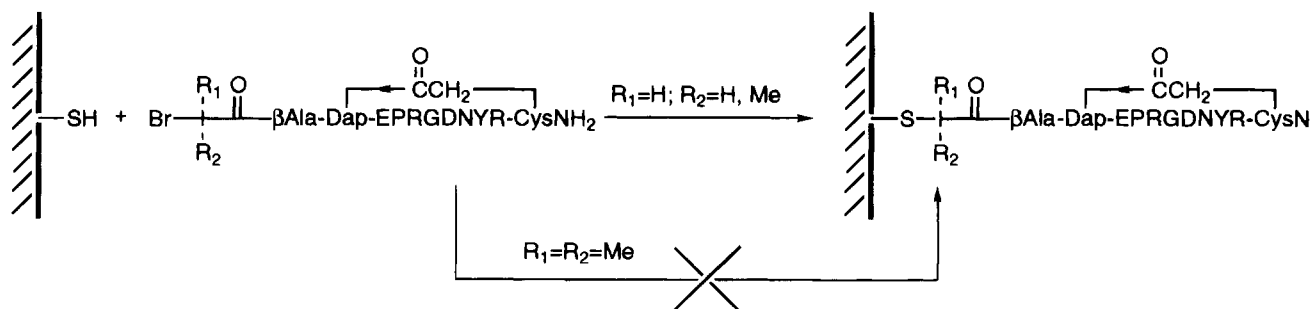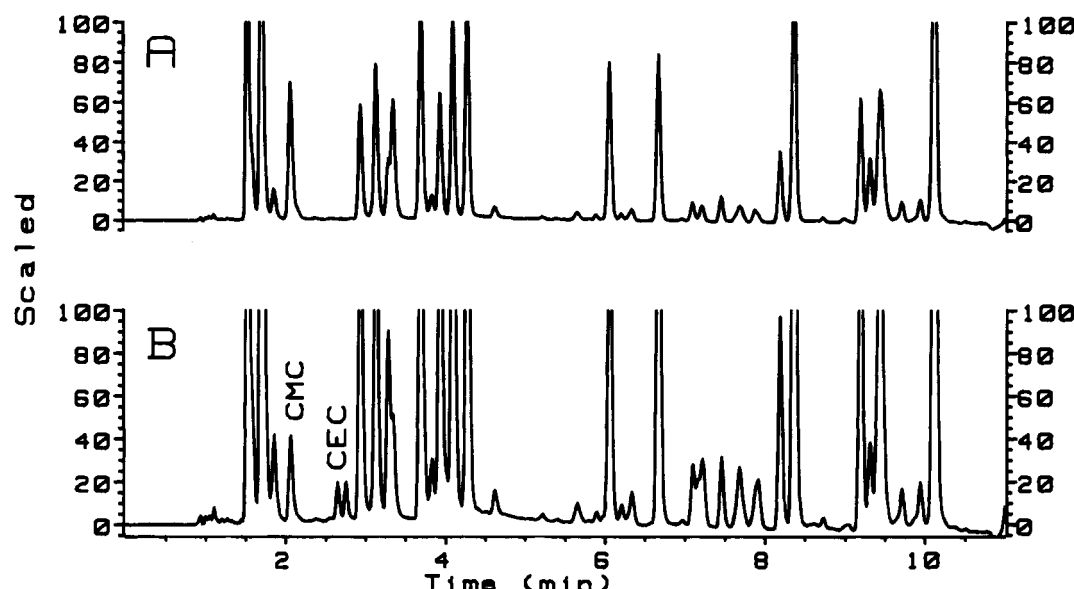
Figure 4. Picotag amino acid analyses of the acid hydrolysate of 1 mg of the conjugates of the cyclic peptides with BSA: (A) BSA–CBA conjugate; (B) BSA–CBP conjugate. These conjugates release S-(carboxymethyl)cysteine or/and S-(1-carboxyethyl)cysteine during the hydrolysis.

was modified to minimize undesirable side reactions between the bromoacetyl moiety on BBDap and the N^α-amine of the peptide, HOBt, and/or the carboxylate on residual TFA. In developing the optimized conditions for the syntheses of BDap-containing peptides, we followed the procedure of *in situ* neutralization established by Schnölzer et al. (*13*). However, we found it necessary to modify that procedure even further; side reactions involving the bromoacetyl moieties were most noticeable when an excess of DIEA was present during the reaction with the N^α-amine on the resin. To circumvent these side reactions, we minimized the amount of time the bromoacetyl moiety was exposed to the free N^α-amine on the resin. In this "preneutralization" step, we used imidazole to neutralize the free TFA that was adsorbed, presumably hydrophobically, to the resin and to the walls of the reaction vessel. Imidazole is basic enough to neutralize free TFA but, as we have learned, not to dissociate the TFA from the N^α-amine.

Second, following the preneutralization step, we added the bromoacetyl-containing amino acid in its activated form together with an amount of DIEA that would be needed to deprotonate the N^α-amine on the resin.

In developing this method, we learned that 2,6-lutidine could substitute for imidazole in the preneutralization step; however, because of the offensive odor of lutidine, we prefer to use imidazole, which is odorless.

Conjugates of synthetic peptides are being employed increasingly in biomedical research and biotechnology. Applications of peptide conjugates include implant materials, protein antigens, and immunogens. Recent uses of haloacetyl peptide chemistry generally have been limited to N^α-amine derivatization, and past uses of this technology have included the syntheses of cyclic RGD peptides as antithrombotics (*18*), the preparation of a well-defined sugar–peptide conjugate vaccine candidate against *Neisseria meningitidis* (*19*) and the synthesis of a backbone-engineered HIV protease constructed by dovetailing unprotected synthetic peptides (*20*). This report adds to the growing list of uses for haloacetyl peptide chemistry with the introduction of RGD protein and glass conjugates used as osteoblast adhesion support matrices. A review of RGD peptides has been published (*21*).

BBDap, as well as its predecessor, BBAL (*8*), were designed and synthesized for the purpose of providing additional chemical tools for the growing repertoire of cross-linking agents used to perform controlled inter- and/or intramolecular peptide conjugation reactions *via* haloacetyl-derivatized peptide chemistry. In conjunction with the well-known carbodiimide coupling chemistry routinely used to link amino acids, due to the stability of bromoacetyl and chloroacetyl groups in HF, we now are able to place reactive leaving groups at any position in a peptide, and the applications will include countless new discoveries of conformationally constrained peptide-based derivatives having controlled and specific biological activities.

The cyclization reaction of the peptide described in this paper went to completion in under 5 min (see Experimental Procedures). Although peptide cyclization *via* the formation of disulfide bonds appears to be the preferred method for cyclizing peptides, we have found that, for the amino acid sequences described here, the sulfhydryl oxidation is slow, often taking several days, and often the reaction does not proceed to completion (unpublished data). Products formed using sulfhydryl oxidation also are susceptible to being covalently coupled to thiol-containing materials *via* disulfide-exchange reactions. Such potentially permanent modifications of proteins *in vivo* could lead to autoimmune concerns should the newly modified conjugates be immunogenic *in vivo*.

In addition, cyclizing peptides by using the reaction of a thiol with a haloacetyl moiety present in the peptide provides a very strong thioether linkage in the cyclic peptide that can be oxidized further to add rigidity to the degrees of freedom of the peptide (*18*).

As an alternative approach to incorporating haloacetyl groups into a peptide prior to HF deprotection, Wetzel et al. (*22*) developed a method for incorporating an iodoacetyl moiety at the amino terminus of a peptide after HF deprotection. The iodoacetic acid anhydride reacts preferentially with the N^α-amine of a peptide at a pH of 6.0, and this allows for the specific tagging of the α-amine with a good leaving group.

Template-assembled synthetic proteins (TASPs) have been produced over the last decade for creatively constructing new proteins and enzymes (*23*, *24*). The

B

□ control

▨ CBA (cyclic) [1 mM]

◩ GRGDS (linear) [1mM]

■ CBA (cyclic) [0.5 mM] + GRGDS (linear) [0.5 mM]
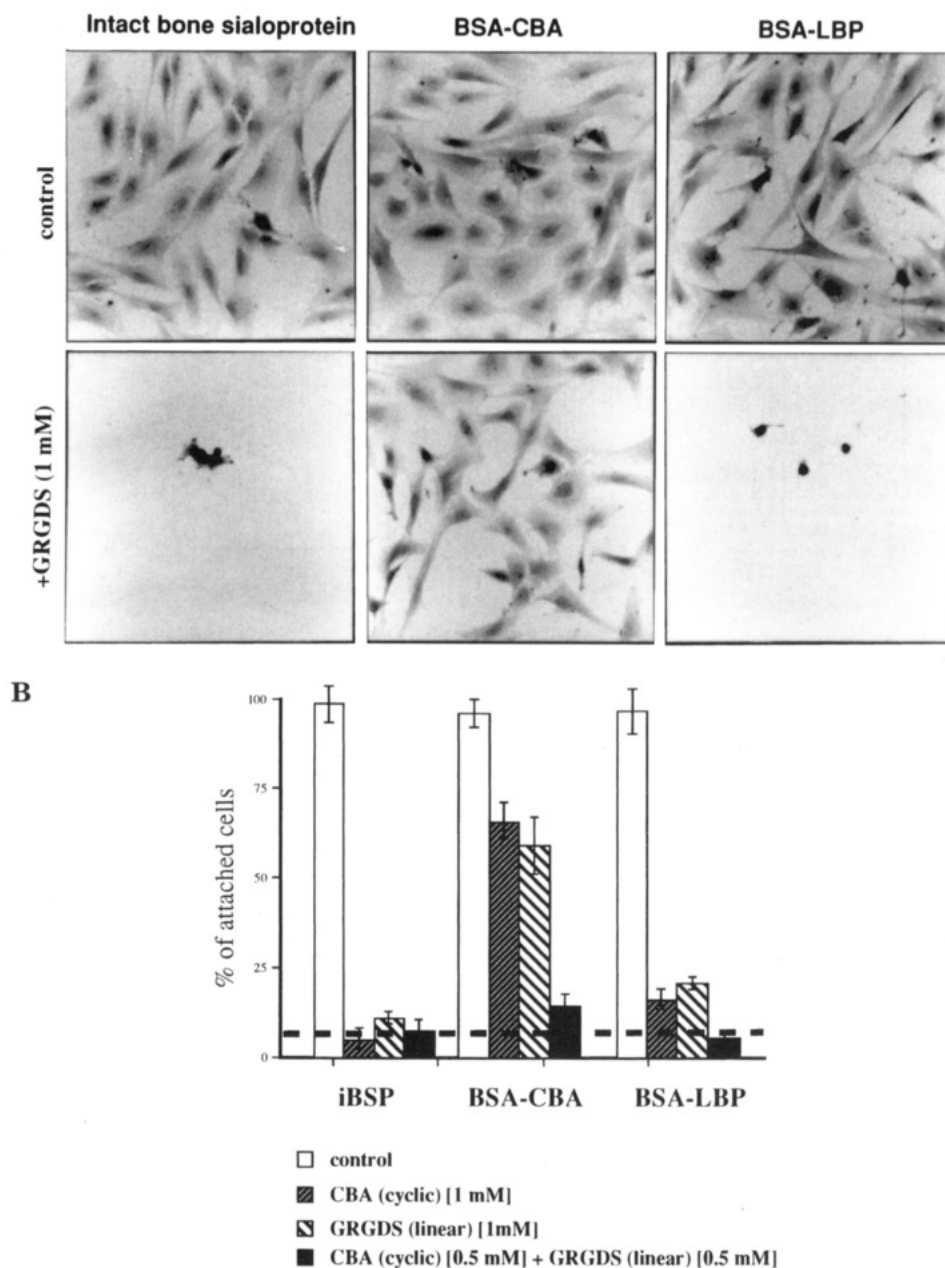
Figure 5. (A) Normal human osteoblastic cells on intact BSP, BSA−CBA, and BSA−LBP conjugates after 24 h of incubation in the absence (control) and presence of linear GRGDS peptide in the medium. Original magnification, 200×. (B) Effect of various blocking peptides on osteoblastic cell attachment to intact BSP, BSA−CBA, and BSA−LBP peptide conjugates. Data present means of triplicates; the dashed line shows the background attachment to BSA.
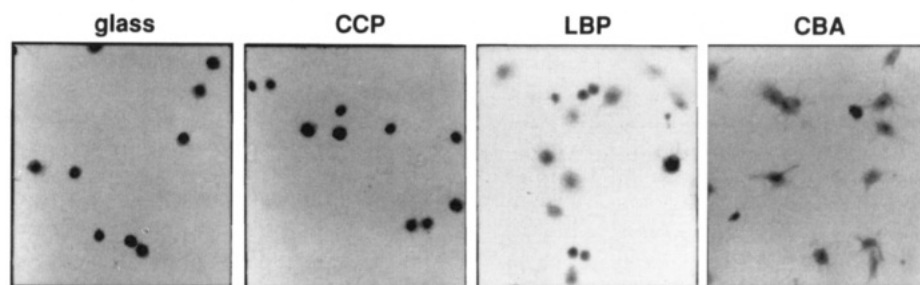
Figure 6. Normal human osteoblastic cells on glass and *CCP*, LBP, and CBA peptides conjugated to glass: 24 h of incubation in the presence of cycloheximide; original magnification, 200×.

approach provided here can complement the TASPs, especially as interest in the syntheses of conformationally constrained α-helices increases. Dawson and Kent (*23*) recently reported using bromoacetyl-modified peptides in the synthesis of a 4-helix TASP product, and more applications using haloacetyl peptide chemistry to make

conformationally constrained synthetic peptides will be forthcoming from this laboratory.

Immobilization of bioactive molecules, *e.g.*, cell adhesion molecules, to control cellular interactions is a well-established way to enhance biocompatibility of artificial materials. Covalent attachment of chemically defined

peptide ligands is preferred to surface adsorption of proteins or protein conjugates. A method to covalently modify glass has been reported in which the surface hydroxyl groups were activated with a sulfonyl chloride, thus forming a surface-coupled sulfonyl ester (*16, 25*). This group is then displaced by primary amine and/or thiol groups. It appears that the only obvious limitation to this process would be the possible inability of the procedure to protect N^ϵ-amines of lysines from reacting with the glass surface. For many proteins and peptides, the most reactive N^ϵ-amines could be needed to play critical roles in the biological function of the protein or peptide.

The methods described here for synthesis, cyclization, and conjugation of peptides appear to be useful tools for studying biological functions of specific sequences within proteins. All BSP-derived peptides analyzed here showed expected biological activity (evaluated by cell attachment assay), and in addition, we were able to detect differences in their action depending on the spatial conformation of the peptide (cyclic vs linear).

LITERATURE CITED

(1) Pierschbacher, M. D., and Ruoslahti, E. (1987) Influence of stereochemistry of the sequence Arg-Gly-Asp-Xaa on binding specificity in cell adhesion. *J. Biol. Chem. 262*, 17294–17298.

(2) Szewczuk, Z., Gibbs, B. F., Yue, S. Y., Purisima, E. O., and Konishi, Y. (1992) Conformationally restricted thrombin inhibitors resistant to proteolytic digestion. *Biochemistry 31*, 9132–9140.

(3) Christodoulides, M., McGunness, B. T., and Heckels, J. E. (1993) Immunization with synthetic peptides containing epitopes of the class I outer-membrane protein of *Neisseria meningitidis*: production of bactericidal antibodies on immunization with a cyclic peptide. *J. Gen. Virol. 139*, 1729–1738.

(4) Dorow, D. S., Shi, P.-t., Carbone, F. R., Minasian, R., Todd, P. E. E., and Leach, S. J. (1985) Two large immunogenic and antigenic myoglobin peptides and the effect of cyclization. *Mol. Immunol. 22*, 1255–1264.

(5) Lindner, W., and Robey, F. A. (1987) Automated synthesis and use of N-chloroacetyl-modified peptides for the preparation of synthetic peptide polymers and peptide–protein immunogens. *Int. J. Pept. Protein Res. 30*, 794–800.

(6) Robey, F. A., and Fields, R. L. (1989) Automated synthesis of N-bromoacetyl-modified peptides for the preparation of synthetic peptide polymers, peptide–protein conjugates, and cyclic peptides. *Anal. Biochem. 177*, 373–377.

(7) Kolodny, N., and Robey, F. A. (1990) Conjugation of synthetic peptides to proteins: quantitation from S-carboxymethylcysteine released upon acid hydrolysis. *Anal. Biochem. 187*, 136–140.

(8) Inman, J. K., Highet, P. F., Kolodny, N., and Robey, F. A. (1991) Synthesis of N^α-(*tert*-butoxycarbonyl)-N^ϵ-[N-(bromoacetyl)-β-alanyl]-L-lysine: its use in peptide synthesis for placing a bromoacetyl cross-linking function at any desired sequence position. *Bioconjugate Chem. 2*, 458–463.

(9) Fisher, L. W., McBride, O. W., Termine, J. D., and Young, M. F. (1990) Human bone sialoprotein: deduced protein sequence and chromosomal localization. *J. Biol. Chem. 265*, 2347–2351.

(10) Oldberg, A., Franzen, A., and Heinegard, D. (1988) The primary structure of a cell-binding bone sialoprotein. *J. Biol. Chem. 263*, 19430–19432.

(11) Gehron Robey, P., and Termine, J. D. (1985) Human bone cell in vitro. *Calcif. Tissue Int. 37*, 453–460.

(12) Riddles, P. W., Blakeley, R. L., and Zerner, B. (1983) Reassessment of Ellman's reagent. *Methods Enzymol. 91*, 49–60.

(13) Schnölzer, M., Alewood, P., Jones, A., Alewood, D., and Kent, S. B. H. (1992) *In situ* neutralization in Boc-chemistry solid phase peptide synthesis. Rapid, high yield assembly of difficult sequences. *Int. J. Pept. Protein Res. 40*, 180–193.

(14) Sarin, V. K., Kent, S. B., Tam, J. P., and Merrifield, R. B. (1981) Quantitative monitoring of solid-phase peptide synthesis by the ninhydrin reaction. *Anal. Biochem. 117*, 147–157.

(15) Burns, J. A., Butler, J. C., Moran, J., and Whitesides, G. M (1991) Selective reduction of disulfides by tris(2-carboxyethyl)phosphine. *J. Org. Chem. 56*, 2648–2650.

(16) Massia, S. P., and Hubbel, J. A. (1990) Covalent surface immoblization of Arg-Gly-Asp- and Tyr-Ile-Gly-Ser-Arg-containing peptides to obtain well-defined cell-adhesive substrates. *Anal. Biochem. 187*, 292–301.

(17) Grzesik, W. J., and Robey, P. G. (1994) Bone matrix RGD glycoproteins: immunolocalization and interaction with human primary osteoblastic bone cells in vitro. *J. Bone Miner. Res. 9*, 487–496.

(18) Barker, P. L., Bullens, S., Bunting, S., Burdick, D. J., Chan, K. S., Deisher, T., Eigenbrot, C., Gadek, T. R., Gantzos, R., Lipari, M. T., Muir, C. D., Napier, M. A., Pitti, R. M., Padua, A., Quan, C., Stanley, M., Struble, M., Tom, J. Y. K., and Brunier, J. P. (1992) Cyclic RGD peptide analogues as antiplatelet antithrombotics. *J. Med. Chem. 35*, 2040–2048.

(19) Boons, G. J., Hoozerhout, P., Poolman, J. T., van der Marel, G. A. and van Boom, J. H. (1991) Preparation of a well-defined sugar–peptide conjugate: A possible approach to a synthetic vaccine against *Neisseria meningitidis*. *Bioorg. Med. Chem. Lett. 1*, 303–308.

(20) Schnölzer, M., and Kent, S. B. (1992) Constructing proteins by dovetailing unprotected synthetic peptides: backbone-engineered HIV protease. *Science 256*, 221–225.

(21) Robey, F. A. (1993) Biology and chemistry of extracellular matrix cell attachment proteins, in *Biologically Active Peptides: Design, Syntheses and Utilization*, (W. V. Williams, and D. B. Weiner, Eds.) Vol. 1, pp 307–324, Technomic Publishing Co., Lancaster, PA.

(22) Wetzel, R., Halualani, R., Stults, J. T., and Quan, C. (1990) A general method for highly selective cross-linking of unprotected polypeptides via pH-controlled modification of N-terminal α-amino groups. *Bioconjugate Chem. 1*, 114–122.

(23) Dawson, P. E., and Kent, S. B. H. (1993) Convenient total synthesis of a 4-helix TASP molecule by chemoselective ligation. *J. Am. Chem. Soc. 115*, 7263–7266.

(24) Mutter, M. (1980) In *Peptides–Chemistry and Biology, Proceedings of the 10th American Peptide Symposium* (G. R. Marshall, Ed.) pp 349–535, Escom, Leiden.

(25) Massia, S. P., and Hubbell, J. A. (1991) Human endothelial cell interactions with surface-coupled adhesion peptides on a nonadhesive glass substrate and two polymeric biomaterials. *J. Biomed. Mater. Res. 25*, 223–242.

Selective Binding of Pyrido[2,3-*d*]pyrimidine 2'-Deoxyribonucleoside to AT Base Pairs in Antiparallel Triple Helices

Ross H. Durland,† T. Sudhakar Rao, Krishna Jayaraman, and Ganapathi R. Revankar*

Triplex Pharmaceutical Corporation, 9391 Grogans Mill Road, The Woodlands, Texas 77380. Received November 15, 1994⊛

Triple helix-forming oligonucleotides (TFOs) offer the potential to specifically modulate expression of gene in a sequence dependent manner. TFOs containing G and T residues that bind to duplex DNA, forming a series of GGC and TAT base triplets, have been well studied. It has been observed that T is relatively nonspecific in that it binds with similar affinity to AT, GC, and CG base pairs. This may significantly reduce the specificity of a given TFO, leading to undesired effects on the expression of genes unrelated to the intended target. We have now prepared 3-(2-deoxy-β-D-*erythro*-pentofuranosyl)-pyrido[2,3-*d*]pyrimidine-2,7(8*H*)-dione (P) and incorporated it into TFOs using the solid-support, phosphoramidite chemistry. It has been demonstrated that a limited substitution of P for T in a G-rich 26-mer TFO can improve binding specificity for AT base pairs in antiparallel motif under certain conditions. The specificity exhibited by P is suggestive of base pair specific interactions that influence the binding strength and consequently enhance the potential therapeutic application of TFOs. However, the effect of substitution of P for T is dependent on the binding conditions, as well as the number and position of substitutions.

INTRODUCTION

Triple helix formation by oligonucleotides has been an area of intense investigation since it was first demonstrated in 1987 (*1*). A number of investigators have shown that under suitable conditions, triplex-forming oligonucleotides (TFOs)[1] can bind in the major groove of duplex DNA to form a triple helix (*2* and references cited therein). Since TFOs bind to duplex DNA in the major groove, they have the potential to interfere with the binding of various proteins. Formation of triplex at such a site would block access of the protein to the DNA, thus preventing binding (*3–5*). Binding of TFOs to specific sites in a variety of eukaryotic genes can also inhibit transcription of these genes, either *in vitro* or in cell culture (*5–9*), thus acting as synthetic, site-selective transcriptional repressors. Gene expression is known to be regulated by the actions of a variety of proteins, many of which act by binding to DNA sequences. It has been documented that expression of certain genes is critical for the progression of many diseases, especially viral and malignant diseases. The ability to design a TFO that would bind to a specific sequence and shut off (or turn on) a particular gene could have enormous benefits for the treatment of such diseases.

Two factors that are critical for developing TFOs as therapeutics are stability and specificity of triplex formation. Stability relates to the strength of the three-stranded complex. Obviously, TFOs that bind with high affinity to their target sequences will be more effective than those that bind weakly. Specificity refers to the relative affinity of the TFO for sequences other than the intended target and determines (at least in part) whether a TFO will have unexpected effects on expression of unrelated genes. We have previously shown that G in

the third strand is highly specific for GC base pairs in the target duplex (*10*). However, binding of T to a target duplex to form a antiparallel triplex is relatively nonspecific. Although binding of T to AT base pairs to form a canonical T·AT triplet is favored, binding to GC and CG base pairs is significant (*10*). As a result, discrimination between related duplex targets is poor.

As part of a program to improve triplex formation through selective chemical modification of TFOs, we have explored various alternatives to T that may provide increased affinity or selectivity in binding to AT base pairs in a target duplex. One base analog that has been examined in this regard is pyridopyrimidine [3-(2-deoxy-β-D-*erythro*-pentofuranosyl)pyrido[2,3-*d*]pyrimidine-2,7-(8*H*)-dione, **1**, P] (*11*). It has been shown by Ohtsuka et al. (*11*) that P forms a stable Watson–Crick base pair with G and a less stable wobble base pair with A within double-helical DNA. Our preliminary modeling studies indicated that P can form Hoogsteen hydrogen bonding with AT base pair in the antiparallel triplex motif. The presence of multiple hydrogen-bonding groups on P and its extended ring system may afford increased stacking interactions with neighboring bases in the third strand of the triplex. Thus, we have prepared TFOs containing P and studied their affinity and specificity for AT base pairs. During the preparation of this paper, a paper appeared in which the sequence specificity of P in parallel triplex motif is described (*12*). The results are strikingly similar to the results reported in this paper.

EXPERIMENTAL PROCEDURES

General. The ^{1}H NMR spectrum was recorded at 400 MHz on a Brüker AM400 spectrometer. The ^{31}P NMR spectrum was recorded at 161.98 MHz on the same spectrometer. Chemical shifts are reported in parts per million downfield from tetramethylsilane (^{1}H, internal) or 85% phosphoric acid (^{31}P, external). Elemental analysis was performed by Quantitative Technologies, Inc., White House, NJ. Reagent grade chemicals were used without further purification unless noted.

Scheme 1. Preparation of Pyrido[2,3-*d*]pyrimidine Nucleoside DMT phosphoramidite (3)
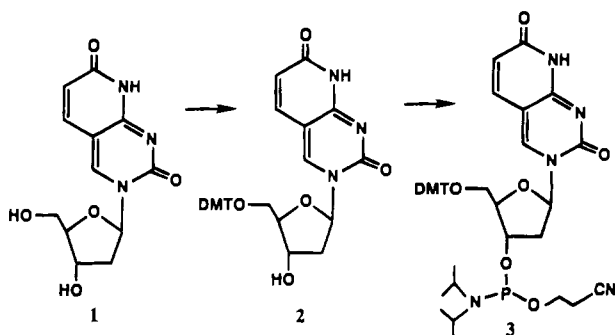
Synthesis of 3-[5-*O*-(4,4'-Dimethoxytrityl)-2-deoxy-β-D-*erythro*-pentofuranosyl]pyrido[2,3-*d*]pyrimidine-2,7(8*H*)-dione 3'-*O*-(2-cyanoethyl)-*N*,*N*-diisopropylphosphoramidite (3). The precursor 3-[5-*O*-(4,4'-dimethoxytrityl)-2-deoxy-β-D-*erythro*-pentofuranosyl]pyrido[2,3-*d*]pyrimidine-2,7(8*H*)-dione (**2**) was prepared as reported by Inoue et al. (*11*) by tritylation of **1** (Scheme 1). Conversion of **2** to the corresponding phosphoramidite (**3**) proceeded as follows: Compound **2** (0.58 g, 1 mmol) and *N*,*N*-diisopropylethylamine (0.70 mL, 4 mmol) were dissolved in anhydrous CH$_2$Cl$_2$ (8 mL). 2-Cyanoethyl *N*,*N*-diisopropylchlorophosphoramidite (0.28 mL, 1.3 mmol) was added under an argon atmosphere and stirred for 30 min at room temperature. The reaction mixture was diluted with EtOAc (100 mL), and the organic layer was washed with saturated NaHCO$_3$ solution (30 mL). The organic layer was separated, dried (Na$_2$SO$_4$), and evaporated under reduced pressure. The residue was purified by silica gel column chromatography using CH$_2$Cl$_2$:EtOAc:NEt$_3$ (45:45:10, v/v) as the eluent. The fractions containing the pure product were pooled, concentrated under reduced pressure, and precipitated into pentane at -30 °C to yield a colorless powder. The powder was collected by filtration and dried under vacuum to yield 0.60 g (77%) of **3**. ^{31}P NMR (CD$_3$CN): δ 149.68, 149.81. ^{1}H NMR (CD$_3$CN): δ 1.00-1.25 (m, 12 H, isopropyl), 1.93 (m, 2 H, C*H* of isopropyl), 2.43-2.76 (m, 6 H, 2'*H*$_2$ and OC*H*$_2$C*H*$_2$CN), 3.59 (m, 2 H, 5'*H*$_2$), 3.74 (s, 3 H, OC*H*$_3$), 3.75 (s, 3 H, OC*H*$_3$), 4.18 (m, 1 H, 4'*H*), 4.67 (m, 1 H, 3'*H*), 5.90 (d, 1 H, vinylic proton), 6.14 (m, 1 H, 1'*H*), 6.45, 6.48 (2d, 1 H, vinylic proton), 6.85 (m, 4 H, DMT), 7.23-7.45 (m, 9 H, DMT), 8.68 and 8.70 (2s, 1 H, N$_8$*H*). Anal. Calcd for C$_{42}$H$_{48}$N$_5$O$_8$P·0.75 H$_2$O: C, 63.42; H, 6.27; N, 8.81. Found: C, 63.19; H, 6.75; N, 8.78.

Oligonucleotide Synthesis and Characterization. All oligonucleotides used in this study were synthesized employing standard solid-support, phosphoramidite chemistry on an Applied Biosystems Model 380B or 394 automated DNA synthesizer. In order to minimize potential degradation of the novel nucleoside under standard deprotection conditions (30% NH$_4$OH, 56 °C, 16 h), TFOs containing P were prepared using the 2-*N*-(dimethylformamidine 5'-*O*-DMT-3'-phosphoramidite of dG (Applied Biosystems) in place of standard dG phosphoramidite. All other oligonucleotides were prepared using standard β-cyanoethyl phosphoramidites from Milligen. Deprotection was carried out in 30% NH$_4$OH at room temperature for 16 h. Under these conditions, no detectable degradation of the oligomers was observed. Crude deblocked oligonucleotides were purified by anion exchange chromatography on a Q Sepharose column equilibrated with 10 mM NaOH, using a gradient of 0.5-1.5 M NaCl, and desalted by passage through a C18 Sep-Pack (Waters) column. Aliquots of purified oligonucle-

otides were analyzed by gel electrophoresis to confirm the purity and expected lengths of the oligomers.

For nucleoside composition analysis (*13*), 0.2-0.3 OD260 units of oligomer was incubated with 2 units of P1 nuclease and 1.5 units of bacterial alkaline phosphatase (Boehringer Mannheim) in 100 μL of 30 mM NaOAc (pH 5.3), 1 mM ZnSO$_4$ at 37 °C for 12 h. The pH of the mixture was adjusted to 8.5 by the addition of 20 μL of 0.5 M Tris, and the samples were incubated for an additional 2 h at 37 °C. Twenty-five to 75 μL of the digested sample was injected onto a C18 reversed-phase HPLC column, and the components were separated using a gradient of acetonitrile in 50 mM KH$_2$PO$_4$. Peak retention times and UV spectra were compared to those of known standards (corresponding to the nucleosides expected for a given oligomer). The calculated relative ratios of the nucleosides were in good agreement with the experimental ratios indicating that P was successfully incorporated using conventional phosphoramidite chemistry.

Analysis of Triplex Formation. *In vitro* triplex formation was assayed using the gel mobility shift method, essentially as described previously (*14, 15*). Briefly, trace concentrations of radiolabeled (^{32}P) synthetic duplex (0.1 × 10^{-10} M) were mixed with increasing concentrations of TFO (10^{-10} to 10^{-6} M). The standard binding buffer was 20 mM Tris-HCl, pH 7.6, 10 mM MgCl$_2$, and 10% sucrose. Samples were incubated at 37 °C for 18-24 h (except as noted) and electrophoresed on 12% polyacrylamide gels buffered with 89 mM Tris, 89 mM boric acid, 10 mM MgCl$_2$ (final pH ≈ 8.3). Electrophoresis was performed at room temperature at 3-5 V/cm. The gels were dried and autoradiographed. Apparent dissociation constants for a given TFO·duplex interaction were estimated to be equal to the TFO concentration required to bind 50% of the labeled duplex (*15*).

RESULTS

Comparison of P·AT and T·AT Triplets in Antiparallel Triplexes. Table 1 presents the initial binding data (acquired at 20 °C) for pyridopyrimidine (P) in antiparallel triplexes. As shown, P binds to AT base pairs with substantial affinity, but shows little or no binding to TA, GC, or CG base pairs. In comparison, T binds with substantial affinity to AT, but also binds well to CG and GC pairs, resulting in a relative lack of specificity. It should be noted, however, that binding of T to AT appears to be slightly better than binding of P to AT. Figure 1 shows a schematic of a possible P·AT base triplet. P can exist in two tautomeric forms, Figure 2 (*12*). Both tautomers (P1 and P2) are capable of binding to AT base pairs. It appears that tautomer P1 that carries a proton at N-8 may bind in antiparallel orientation and the tautomer P2 that carries a proton at N-1 may bind in parallel orientation. It is not known whether both tautomers are present or one is predominant over the other. It may also be possible that the duplex base pair may have an influence on one tautomer over the other.

When binding studies were repeated at 37 °C, a different profile was obtained (Table 2). Under these conditions, the oligomer containing T (Z102-56) binds to the duplex containing AT base pairs (ZRY102-7) with about 10-fold higher affinity than the oligomer containing P (Z102-79). Furthermore, the specificity of the interaction between P and AT was reduced at 37 °C. Discrimination by Z102-79 between the intended target, ZRY102-7, and the mismatched target ZRY100-0 was about 100-fold at 20 °C, but only about 20-fold at 37 °C. Although

Table 1. Comparison of T and P in Antiparallel Triplexes at 20 °C[a]

duplex	TFO	sequence	apparent K_d(M)
ZRY102-7		5'-ccccttccctccttcctccttctccc-3' 3'-ggggaagggaggaaggaggaagaggg-5'	
	Z102-56	5'-ggggttgggtggttggtggttgtggg-3'	1×10^{-8}
	Z102-79	5'-ggggttgggpggttggpggttgpggg-3'	2×10^{-8}
ZRY102-8		5'-ccccttcccaccttccaccttcaccc-3' 3'-ggggaagggtggaaggtggaagtggg-5'	
	Z102-56	5'-ggggttgggtggttggtggttgtggg-3'	»1×10^{-6}
	Z102-79	5'-ggggttgggpggttggpggttgpggg-3'	»1×10^{-6}
ZRY100-0		5'-ccccttcccccccttcccccttccccc-3' 3'-ggggaaggggggaaggggggaaggggg-5'	
	Z102-56	5'-ggggttgggtggttggtggttgtggg-3'	2×10^{-8}
	Z102-79	5'-ggggttgggpggttggpggttgpggg-3'	>1×10^{-6}
ZRY102-0		5'-ccccttcccgccttccgccttcgccc-3' 3'-ggggaagggcggaaggcggaagcggg-5'	
	Z102-56	5'-ggggttgggtggttggtggttgtggg-3'	1×10^{-8}
	Z102-79	5'-ggggttgggpggttggpggttgpggg-3'	»1×10^{-6}

[a] Triplex incubations were in 20 mM Tris—HCl, pH 7.6, 10 mM MgCl₂, 10% sucrose. Samples were incubated at ~20 °C for 3—5 h prior to electrophoresis.
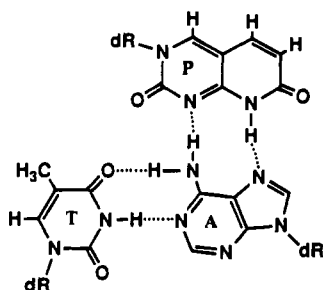
Figure 1. Hypothetical hydrogen bonding interaction between pyridopyrimidine (P) and a standard duplex AT base pair.
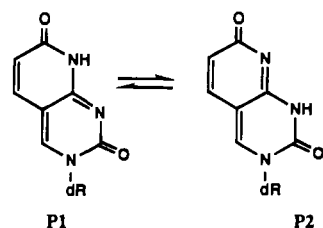
Figure 2. Tautomeric forms of P.

subtle changes in binding conditions are expected to alter the absolute affinity of any given complex, we observe changes in relative affinities of P and T as well. At present, we do not know what factors account for the differences in relative binding. One factor may be that G-rich oligonucleotides are known to have substantial secondary and tertiary structure under certain ionic conditions (*16—18*). It is possible that the observed interaction between oligomer and duplex is complicated by temperature dependent conformation transitions in the free oligomers. Although most of the studies on G-tetrad formation employ medium containing alkaline cations (Na⁺ or K⁺), examples of higher order structure of G-rich oligonucleotides in the presence of Mg²⁺ are also known (*19, 20*).

Further Evaluation of P·AT Triplets. Binding of the oligonucleotides containing P was assessed by the gel mobility shift method as outlined in the Experimental Procedures. The results of these analyses are presented in Table 3. We first examined the binding of oligomer Z102-103, in which all of the T residues in Z102-56 are replaced with P. As shown in Table 3, binding of this oligomer to the ideal target, ZRY102-7, did not result in

Table 2. Comparison of T and P in Antiparallel Triplexes at 37 °C[a]

duplex	TFO	sequence	apparent K_d(M)
ZRY102-7		5'-ccccttccctccttcctccttctccc-3' 3'-ggggaagggaggaaggaggaagaggg-5'	
	Z102-56	5'-ggggttgggtggttggtggttgtggg-3'	5×10^{-10}
	Z102-79	5'-ggggttgggpggttggpggttgpggg-3'	5×10^{-9}
ZRY102-8		5'-ccccttcccaccttccaccttcaccc-3' 3'-ggggaagggtggaaggtggaagtggg-5'	
	Z102-56	5'-ggggttgggtggttggtggttgtggg-3'	»1×10^{-6}
	Z102-79	5'-ggggttgggpggttggpggttgpggg-3'	»1×10^{-6}
ZRY100-0		5'-ccccttcccccccttcccccttccccc-3' 3'-ggggaaggggggaaggggggaagggggg-5'	
	Z102-56	5'-ggggttgggtggttggtggttgtggg-3'	1×10^{-8}
	Z102-79	5'-ggggttgggpggttggpggttgpggg-3'	1×10^{-7}
ZRY102-0		5'-ccccttcccgccttccgccttcgccc-3' 3'-ggggaagggcggaaggcggaagcggg-5'	
	Z102-56	5'-ggggttgggtggttggtggttgtggg-3'	2×10^{-9}
	Z102-79	5'-ggggttgggpggttggpggttgpggg-3'	1×10^{-6}

[a] Conditions were identical to those used in Table 1, except that incubations were at 37 °C for 18—24 h.

Table 3. Binding Studies of Pyridopyrimidine in the Z100/Z102 System at 37 °C[a]

duplex	TFO	sequence	apparent K_d(M)
ZRY102-7		5'-ccccttccctccttcctccttctccc-3' 3'-ggggaagggaggaaggaggaagaggg-5'	
	Z102-56	5'-ggggttgggtggttggtggttgtggg-3'	5 × 10⁻¹⁰
	Z102-79	5'-ggggttgggPggttggPggttgPggg-3'	5 × 10⁻⁹
	Z102-103	5'-ggggPPgggPggPPgggPggPPgPggg-3'	>3 × 10⁻⁶
ZRY100-0		5'-ccccttccccccttcccccttccccc-3' 3'-ggggaaggggggaaggggggaaggggg-5'	
	Z100-50	5'-ggggttgggggggttgggggttggggg-3'	2 × 10⁻¹⁰
	Z102-78	5'-ggggPtggggggPtggggggPtggggg-3'	2 × 10⁻⁹
	Z102-80	5'-gPggttgPggPgttgPgPgttgPgPg-3'	»1 × 10⁻⁶
ZRY101-0		5'-ccccatcccccatcccccatccccc-3' 3'-ggggtagggggtagggggtaggggg-5'	
	Z100-50	5'-ggggttgggggggttgggggttggggg-3'	2 × 10⁻¹⁰
	Z102-78	5'-ggggPtggggggPtggggggPtggggg-3'	3 × 10⁻⁹
ZRY101-1		5'-ccccctccccccctcccccctccccc-3' 3'-gggggagggggggagggggagggggg-5'	
	Z100-50	5'-ggggttgggggggttgggggttggggg-3'	2 × 10⁻¹⁰
	Z102-78	5'-ggggPtggggggPtggggggPtggggg-3'	3 × 10⁻⁹
ZRY101-2		5'-ccccgtcccccgtcccccgtccccc-3' 3'-ggggcagggggcagggggcaggggg-5'	
	Z100-50	5'-ggggttgggggggttgggggttggggg-3'	1 × 10⁻⁹
	Z102-78	5'-ggggPtggggggPtggggggPtggggg-3'	3 × 10⁻⁷

[a] Conditions were identical to those used in Table 2.

any apparent triplex formation at TFO concentrations up to 3×10^{-6} M. These data demonstrated that substituting all nine Ts in Z102-56 with Ps (Z102-103) reduced the binding affinity significantly. On the basis of our observation that the binding affinity is considerably reduced at 37 °C, it was not surprising that substitution with nine Ps resulted in significant reduction in binding affinity. Staubli and Dervan (*12*) have reported that PP stacking had the least favorable energy of base stacking. Z-102-103 contains three PP stackings. P could also promote the secondary structure of G-rich TFO resulting in reduced triplex formation. We prepared several additional TFOs with P substituted at varying positions. Comparison of the binding of Z100-50, Z102-78, and Z102-80 indicated that the affinity of P for different base pairs can be strongly influenced by the sequence context (Table 3). In all cases, however, P·AT triplets appeared to be substantially weaker than T·AT triplets (e.g., compare binding of Z102-78 and Z100-50 to ZRY100-0).

DISCUSSION

The data obtained in this study are of considerable interest in the field of triple helical DNA. Our group is one of several that is currently studying triplex-forming oligonucleotides (TFOs) as potential human therapeutics (*21*). TFOs have been shown to bind in a sequence-specific manner to targets in eukaryotic promoters (*14, 22*). Under ideal conditions, binding occurs with high affinity and, in the case of antiparallel triplexes, at physiological pH (*14, 15*). Several reports have claimed that TFOs are capable of modulating gene expression in cultured cells (*7, 8*). However, much remains to be done to develop this technology to its full potential.

One question that has largely been ignored is that of specificity. Although several groups have demonstrated that TFOs can bind to their intended targets with high affinity, few systematic studies on binding specificity have been described. Recently, we found that under certain conditions, antiparallel triplex formation can be less specific than is desirable (*10*). In particular, we found that in some sequences, T in the third strand is unable to effectively discriminate between AT, GC, and CG base pairs in a duplex target. This leads to a situation where a single TFO may bind with comparable affinity to several related target sequences. One major attraction of triplex technology is the potential ability to alter gene expression in a highly sequence dependent manner. Thus, the potential loss of specificity when using T in the third strand is a significant drawback.

We hoped that substituting pyridopyrimidine (P) for T in antiparallel TFOs would improve binding specificity with little effect on affinity for the intended target. The present data suggest that such an observation appears to be valid only at lower temperature with limited P substitution at selected positions. At high incubation temperatures, it becomes apparent that P·AT triplets are clearly weaker than T·AT triplets. This effect becomes more pronounced when a larger percentage of T residues are replaced with P. Our results are in agreement with that of Staubli and Dervan (*12*).

P may be the only example of a nonnatural nucleoside studied so far that has shown similar results in both parallel and antiparallel triplex formation. The sequence specificity toward AT base pairs and the effect of base stacking on triplex stability are striking in both cases. The ease with which P can participate in parallel as well as antiparallel triplex formation suggests that both tautomers (Figure 2) may be involved in triplex formation with equal efficiency.

Aside from the binding properties of P, it is an attractive base because of its strong fluorescent properties (*11*). TFOs containing P may be useful for measuring triplex formation by the quenching of fluorescence. It will also be worthwhile to study the effect of P on the secondary structure of G-rich TFOs to understand the loss in binding affinity when P is substituted.

LITERATURE CITED

(1) Moser, H. E., and Dervan, P. B. (1987) Sequence-specific cleavage of double helical DNA by triple helix formation. *Science 238,* 645–650.

(2) Thuong, N. T., and Hélène, C. (1993) Sequence-specific recognition and modification of double-helical DNA by oligonucleotides. *Angew. Chem., Int. Ed. Engl. 32,* 666–690.

(3) Maher, L. J., III, Wold, B., and Dervan, P. B. (1989) Inhibition of DNA binding proteins by oligonucleotide-directed triple helix formation. *Science 245,* 725–730.

(4) Blume, S. W., Gee, J. E., Shrestha, K., and Miller, D. M. (1992) Triple helix formation by purine-rich oligonucleotides targeted to the human dihydrofolate reductase promoter. *Nucleic Acids Res. 20,* 1777–1784.

(5) Duval-Valentin, G., Thuong, N. T., and Hélène, C. (1992) Specific inhibition of transcription by triple helix forming oligonucleotides. *Proc. Natl. Acad. Sci. U.S.A. 89,* 504–508.

(6) Le Doan, T., Perrouault, L., Praseuth, D., Habhoub, N., Decout, J.-L., Thuong, N. T., Lhomme, J., and Hélène, C. (1987) Sequence-specific recognition, photocrosslinking and cleavage of DNA double helix by an oligo-[α]-thymidylate covalently linked to an azidoproflavine derivative. *Nucleic Acids Res. 15,* 7749–7760.

(7) Postel, E. H., Flint, S. J., Kessler, D. J., and Hogan, M. E. (1991) Evidence that a triplex-forming oligodeoxyribonucleotide binds to the *c-myc* promoter in HeLa cells, thereby reducing *c-myc* mRNA levels. *Proc. Natl. Acad. Sci. U.S.A. 88,* 8227–8231.

(8) Orson, F. M., Thomas, D. W., McShan, W. M., Kessler, D. J., and Hogan, M. E. (1991) Oligonucleotide inhibition of IL2Rα mRNA transcription by promoter region collinear triplex formation in lymphocytes. *Nucleic Acids Res. 19,* 3435–3441.

(9) Maher, L. J., III, Dervan, P. B., and Wold, B. (1992) Analysis of promoter-specific repression by triple-helical DNA complexes in a Eukaryotic cell-free transcription system. *Biochemistry 31,* 70–81.

(10) Durland, R. H., Rao, T. S., Revankar, G. R., Tinsley, J. H., Myrick, M. A., Seth, D. M., Rayford, J., Singh, P., and Jayaraman, K. (1994) Binding of T and T analogs to CG base pairs in antiparallel triplexes. *Nucleic Acids Res. 22,* 3233–3240.

(11) Inoue, H., Imura, A., and Ohtsuka, E., (1985) Synthesis and hybridization of dodecadeoxyribonucleotides containing a fluorescent pyridopyrimidine deoxynucleoside. *Nucleic Acids Res. 13,* 7119–7128.

(12) Staubli, A. B., and Dervan, P. B. (1994) Sequence specificity of the non-natural pyrido[2,3-*d*]pyrimidine nucleoside in triple helix formation. *Nucleic Acids Res. 22,* 2637–2642.

(13) Gehrke, C. W., McCune, R. A., Gama-Sosa, M. A., Ehrlich, M., and Kuo, K. C. (1984) Quantitative reversed-phase high-performance liquid chromatography of major and modified nucleosides in DNA. *J. Chromatogr. 301,* 199–219.

(14) Cooney, M., Czernuszewicz, G., Postel, E. H., Flint, S. J., and Hogan, M. E. (1988) Site-specific oligonucleotide binding represses transcription of the human *c-myc* gene *in vitro. Science 241,* 456–459.

(15) Durland, R. H., Kessler, D. J., Gunnell, S., Duvic, M., Pettitt, B. M., and Hogan, M. E. (1991) Binding of triple helix forming oligonucleotides to sites in gene promoters. *Biochemistry 30,* 9246–9255.

(16) Dugaiczyk, A., Robberson, D. L., and Ullrich, A. (1980) Single-stranded poly(deoxyguanylic acid) associates into double- and triple-stranded structures. *Biochemistry 19,* 5869–5873.

(17) Henderson, E., Hardin, C. C., Walk, S. K., Tinoco, I., Jr., and Blackburn, E. H. (1987) Telomeric DNA oligonucleotides form novel intramolecular structures containing guanine-guanine base pairs. *Cell 51,* 899–908.

(18) Sen, D., and Gilbert, W. (1988) Formation of parallel four-stranded complexes by guanine-rich motifs in DNA and its implications for meiosis. *Nature 334,* 364–366.

(19) Lee, J. S. (1990) The stability of polypurine tetraplexes in the presence of mono- and divalent cations. *Nucleic Acids Res. 18,* 6057–6060.

(20) Hardin, C. C., Watson, T., Corregan, M., and Bailey C. (1992) Cation-dependent transition between the quadruplex and Watson-Crick hairpin forms of d(CGCG3GCG). *Biochemistry 31,* 833–841.

(21) Chubb, J. M., and Hogan, M. E. (1992) Human therapeutics based on triple helix technology. *Trends Biotech. 10,* 132–136.

(22) Milligan, J. F., Krawczyk, S. H., Wadwani, S., and Matteucci, M. D. (1993) An antiparallel triple helix motif with oligodeoxynucleotides containing 2'-deoxyguanosine and 7-deaza-2'-deoxyxanthosine. *Nucleic Acids Res. 21,* 327–333.

BC950006R

Targeted Gene Delivery with a Low Molecular Weight Glycopeptide Carrier

Manpreet S. Wadhwa,[†] Daren L. Knoell, Anthony P. Young, and Kevin G. Rice[*,†]

College of Pharmacy, The Ohio State University, Columbus, Ohio 43210. Received November 28, 1994[⊗]

A low molecular weight glycopeptide carrier was prepared by coupling a tyrosinamide–triantennary oligosaccharide to dp19 poly-L-lysine resulting in a 1:1 conjugate. The glycopeptide carrier complexed with plasmid DNA as evidenced by displacement of intercalated dye, light scattering by condensed DNA, and immobility of complexed DNA upon agarose gel electrophoresis. DNA–carrier complexes were endocytosed into HepG2 cells via the asialoglycoprotein receptor due to recognition of terminal galactose residues on the oligosaccharide. The resulting luciferase reporter gene expression was dramatically influenced by the solubility of complexes, the extent of complexation, and the presence of the lysosomotropic agent chloroquine. The results suggest that low molecular weight glycopeptides may be suitable for further development as well-defined DNA carriers for receptor-mediated gene delivery in vivo.

INTRODUCTION

Genes are attractive candidates for use in a variety of disease states due to the ability to produce therapeutic biomolecules using the biosynthetic machinery provided by host cells (1–4). Established protocols for transfecting genes into cells include calcium phosphate or DEAE[1] dextran coprecipitation, electroporation, particle bombardment, scrape loading, sonication, liposomal delivery, gene transfer by viral vectors, and receptor-mediated gene delivery (5–8). Although all of these methods can be applied to mammalian cells in culture, transfection of cells in vivo for gene therapy or for probing biological function poses special problems, thus restricting the use of most of these methods to ex vivo protocols.

Viral vectors, cationic liposomes, receptor-mediated gene delivery, and direct injection of DNA have emerged as promising noninvasive approaches for the introduction of DNA into cells in vivo (5–8). Of these, receptor-mediated gene delivery has the greatest potential for targeting specific tissue or cell types based on the specific recognition of ligands by unique receptors on these cells. DNA carriers have been designed to transfect hepatocytes via the asialoglycoprotein receptor (ASGP-R) (9–15) or the insulin receptor (16, 17). Mouse lung endothelial cells have been targeted for gene delivery via thrombomodulin (18) and leukaemic T cells targeted by means of a mucin antigen (19). Alternatively, diverse cell types derived

from both normal and tumor tissues have been transfected by means of the transferrin receptor (20–22).

Carriers for receptor-mediated gene delivery typically employ a receptor ligand covalently attached to a polycationic anchor that binds DNA by ionic interaction (9). Selective transfection of hepatocytes via the ASGP-R has been accomplished with ligands possessing terminal galactose residues such as asialoorosomucoid (9, 10, 12), galactosylated proteins or polymers (13, 14, 16), and galactosylated synthetic ligands (11, 15). The anchor utilized most often is poly-L-lysine in the molecular weight range of 20–60 kDa. An important property of polylysine is its ability to condense DNA into compact structures which may be small enough for internalization into cells by endocytosis (23, 24). Carriers may also include effector molecules like fusogenic peptides (25) to allow efficient lysosomal escape of internalized DNA (13, 26–28).

A further consideration is the use of well-characterized components to produce carriers of defined structure. This may be essential to carefully control the preparation of DNA–carrier complexes in order to achieve highly reliable gene delivery. We have taken a step toward this objective by selecting a triantennary oligosaccharide as a low molecular weight, high affinity ligand for the ASGP-R (29, 30), which was coupled to 2.5 kDa poly-L-lysine to produce a low molecular weight glycopeptide carrier. The carrier allowed formulation of soluble DNA complexes which were monitored and optimized by spectroscopic methods. Carrier-complexed plasmid was endocytosed into hepatoma cells possessing the ASGP-R and resulted in reporter gene expression, indicating the potential of low molecular weight carriers for efficient DNA delivery in vivo.

EXPERIMENTAL PROCEDURES

Materials. Poly-L-lysine hydrobromide, of average dp 19 (PL), succinic anhydride, 1-ethyl-3-[3-(dimethylamino)propyl]carbodiimide methiodide (EDC), and chloroquine were obtained from Sigma Chemical Co., St. Louis, MO. D-Luciferin, luciferase from *Photinus pyralis* (EC 1.13.12.7), and β-galactosidase (EC 3.2.1.23) from bovine testes were obtained from Boehringer Mannheim, Indianapolis, IN. HepG2 cells were from American Type Culture Collection, Rockville, MD. Bradford reagent was

---

[1] Abbreviations: ASGP-R, asialoglycoprotein receptor; AUFS, absorbance units full scale; Boc, *tert*-butyloxycarbonyl; DEAE dextran, [(diethylamino)ethyl]dextran; DMF, dimethylformamide; DTT, dithiothreitol; EDC, 1-ethyl-3-[3-(dimethylamino)-propyl]carbodiimide methiodide; dp, degree of polymerization; EDTA, ethylenediaminetetraacetic acid; FAB-MS, fast atom bombardment-mass spectroscopy; FCS, fetal calf serum; HBS, hepes-buffered saline; HPAEC, high pH anion exchange chromatography; MEM, minimum essential media; PL, poly-L-lysine (of average dp 19); RLU, relative light units; RP-HPLC, reversed phase HPLC; TFA, triflouroacetic acid; Tri, galactose-terminated triantennary oligosaccharide; TriPL, Tri–polylysine (average dp19) conjugate; Agal–TriPL, TriPL devoid of terminal galactose residues.

purchased from BioRad, Hercules, CA, and thiazole orange was a gift from Beckton Dickinson Immunocytometry Systems, San Jose, CA. Gel filtration HPLC column (G2000 SWXL) was purchased from Tosohaas, Montgomeryville, PA; C8 reversed phase columns (MV Microsorb, with 5 μm packing) were from Rainin, Emeryville, CA, and analytical and semipreparative reversed phase polymer columns (PRP-1, with 10 μm packing) were from Hamilton Co., Reno, NV. HPLC was performed using equipment from ISCO (Lincoln, NE), consisting of computer-interfaced pumps, variable wavelength UV detector, and automated fraction collector. High pH anion exchange chromatography (HPAEC) was performed on a carbohydrate analyzer from Dionex Corp., Sunnyvale, CA, with a CarboPac PA1 column. Fluorescence and light scattering measurements were performed using a computer-interfaced fluorimeter (LS50B) from Perkin-Elmer, U.K. UV spectroscopy was conducted on a Beckman DU640 spectrophotometer, and luciferase light units were recorded on a luminometer (Lumat LB 9501) from Berthold Systems, Pittsburgh, PA.

Preparation of Oligosaccharide—Polylysine (TriPL) Conjugate. *Succinylation of Triantennary Oligosaccharide.* Boc-protected tyrosinamide triantennary oligosaccharide (Boc-Tri) was prepared from bovine fetuin as previously described (*29*). Boc-Tri (1 μmol) was freeze dried and reacted with 200 μL of TFA for 10 min at room temperature. The Boc-deprotected oligosaccharide (Tri) was then freeze dried three times to obtain a neutral pH.

Tri (500 nmol, prepared in 450 μL of 0.2 M sodium bicarbonate buffer, pH 8.0) was reacted with succinic anhydride (12.5 mg in 50 μL DMF) for 15 min at room temperature, along with the addition of 150 μL of 1 M sodium hydroxide to maintain the pH between 7.5—8. The reaction was terminated by adjusting the pH to 12 by the addition of 150 μL of 1 M sodium hydroxide and incubated at 37 °C for 10 min, followed by acidification to pH 3 by adding 100 μL of 4 M TFA prior to HPLC purification.

Succinyl-Tri was purified from a semipreparative polymeric RP-HPLC column (305 × 7 mm) equilibrated at 3 mL/min with 0.1% TFA and 4% acetonitrile. Following injection of 500 nmol of succinyl-Tri (900 μL) into a 1 mL loop, an acetonitrile gradient of 4% to 15% was developed over 13 min while Abs$_{274nm}$ 0.2 AUFS was monitored. The peak eluting at 9 min was collected and freeze dried and the yield estimated by Abs$_{274nm}$ (ϵ = 1450 M^{-1} cm^{-1}).

Boc-Tri, Tri, and succinyl-Tri were prepared for proton NMR spectroscopy by freeze drying 1 μmol twice in 99.98% deuterium oxide containing 0.01% acetone as an internal standard and analyzed on a Bruker 500 MHz NMR spectrometer operating at 23 °C. The acquired spectra were processed utilizing resolution enhancement parameters supplied with Felix software (Hare Research, Eugene, OR). Samples were prepared for FAB-MS by dissolving 20 nmol in 10 μL of water and 1 μL of α-monothioglycerol. The water was removed by speed vacuum, and the 1 μL sample was applied to the probe of a Finnigan Matt 900 FAB-MS operated in the positive ion mode.

Conjugation of Succinyl-Tri with Polylysine. Succinyl-Tri (400 nmol in 400 μL water) was added to PL (2.5 μmol in 400 μL of water), and the coupling reaction was initiated by adding 800 μL of EDC (500 mM in 20 mM borax/hydrochloride buffer, pH 7.5). After incubation at room temperature for 2 h, the reaction was quenched by the addition of 16 μL of 2 M hydrochloric acid.

The glycopeptide conjugate (TriPL) was purified in 200 nmol (800 μL) portions on an analytical (250 × 4.1 mm) polymeric RP-HPLC column (50 °C) equilibrated at 1 mL/min with 0.1% TFA and 1% acetonitrile. The acetonitrile concentration was held at 1% for 20 min followed by a step to 15% acetonitrile over 1 min and elution continued for 10 min while monitoring Abs$_{274nm}$ 0.1 AUFS. The peak eluting at 23 min was collected and freeze dried and the yield determined by Abs$_{274nm}$.

Preparation of Agalatco—Triantennary—Polylysine Conjugate. Agal—TriPL was prepared by incubating 100 nmol of TriPL (in 200 μL of 50 mM sodium phosphate citrate buffer, pH 4.3) with 40 mU of β-galactosidase for 24 h at 37 °C. The product was purified on an analytical polymer reversed phase column as described for TriPL and characterized by monosaccharide compositional analysis as described below.

Compositional Analysis of TriPL. The amine content of TriPL (determined by Abs$_{274}$) was obtained by fluorescamine assay as described (*31*), using a PL standard, with the fluorescence being measured at excitation and emission wavelengths of 390 and 475 nm (5 nm slit widths). Amino acid analysis of the conjugates was performed by Picotag analysis (*32*), and monosaccharide composition analysis was performed by HPAEC following TFA and hydrochloric acid hydrolysis (*33*).

Gene Delivery and Expression. *Complexation of Plasmid DNA with Carrier.* A 5.6 kbp plasmid pCMVL encoding the gene for luciferase (*34*) under the control of cytomegalovirus promoter was prepared by the alkaline lysis method and purified on a cesium chloride gradient to obtain the supercoiled form (*35*). Quantitation was based on absorbance of DNA at 260 nm (1 μg = 0.02 o.d. units).

TriPL—pCMVL complexes were prepared with DNA concentrations ranging from 0.2 to 40 μg/mL and TriPL—pCMVL ratios (nmol carrier/μg DNA) varying from 0.1 to 1.2. The optimized complex was prepared at a DNA concentration of 20 μg/mL and a carrier—DNA ratio of 0.8 by adding TriPL (16 nmol, in 500 μL of solvent) to pCMVL (20 μg, in 500 μL of solvent) while vortexing and allowing the mixture to incubate at room temperature for 30 min. The amounts and volumes of carrier and DNA were linearly scaled for preparing different amounts of complex. Solvents used were 0.15 M sodium chloride (saline), 20 mM Hepes (pH 7.4) with 0.15 M sodium chloride (HBS), and 0.72 M mannitol. For control experiments, TriPL was substituted with PL or Agal—TriPL.

Assays for Monitoring DNA—Carrier Complexes. TriPL—pCMVL solubility was determined by analyzing an aliquot (1 μg of DNA) of the complex before and after centrifugation at 13000g for 4 min at room temperature. The aliquots were diluted to 1 mL in the appropriate solvent (saline, HBS, or mannitol), and the DNA remaining in solution was measured by Abs$_{260}$.

Complexation was monitored by a fluorescence assay based on displacement of intercalating dye from DNA by TriPL or PL. An aliquot of TriPL—pCMVL (1 μg of DNA, in 25—500 μL) was diluted to 0.5 mL in solvent and then diluted with 3 mL of solvent containing 0.117 μM thiazole orange (from a 0.1 mg/mL stock in 1% methanol, ϵ_{476} = 30 000 M^{-1} cm^{-1}). Fluorescence of the intercalated dye was measured using excitation at 500 nm and emission at 530 nm, with the slits set at 15 and 20 nm, respectively, to maximize sensitivity.

Complexes were also measured by light scattering in order to monitor DNA condensation. Traces of dust were removed from sample tubes by means of 0.1 μm filtered pressurized air, and solvents were filtered through 0.2 μm surfactant free cellulose acetate filters. TriPL—
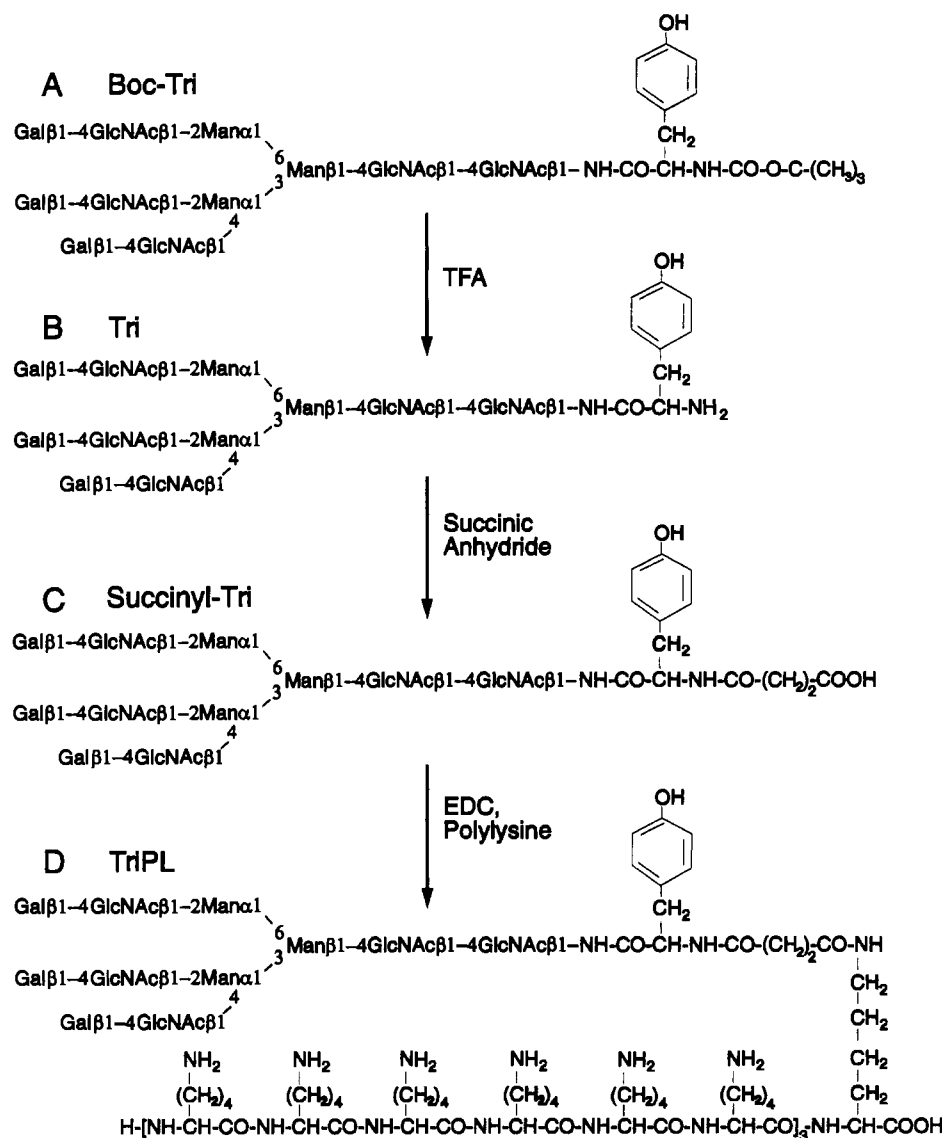
Figure 1. Reaction scheme for conjugation of triantennary oligosaccharide with polylysine. Boc-protected tyrosinamide triantennary oligosaccharide (Boc-Tri, A) was converted into Tri by treatment with TFA which exposed the N-terminus of tyrosine by removal of Boc (B). The amine was reacted with succinic anhydride to introduce a carboxylic group in succinyl-Tri (C). The carboxylic group was activated by EDC and coupled with an amine on polylysine to produce TriPL conjugate (D). TriPL was a prepared as 1:1 conjugate by controlling stoichiometry of reactants; however, the structure shown is only meant for illustration since the oligosaccharide was randomly coupled to one of the amines on polylysine of average dp 19.

pCMVL (1 μg of DNA) was diluted to 3.5 mL in solvent, and scattered light intensity at 90° was measured by keeping both monochromaters at 350 nm (2.5 nm slits). Light scattering synchronous scans were obtained by simultaneous scanning of emission and excitation monochromaters paired at the same wavelength.

Additionally, band retardation assay was used to monitor complexation (9). TriPL–pCMVL (200 ng of DNA) was mixed with gel loading buffer and electrophoresed on a 1% agarose gel at 70 V, and DNA was visualized postrun by ethidium bromide staining and UV detection.

Transfection and Gene Expression. HepG2 cells were plated on 6 × 35 mm wells ((0.5–1) × 10^6 cells per well) and grown to 40–70% confluency in minimum essential media (MEM) with 10% fetal calf serum (FCS) supplemented with penicillin and streptomycin. Transfections were performed in MEM (2 mL per 35 mm well) with 2% FCS, with or without 100 μM chloroquine. pCMVL–TriPL (0.1–20 μg of DNA, in 0.5 mL) was added dropwise

to triplicate wells. After 5 h incubation at 37 °C, the media was replaced with MEM supplemented with 10% FCS.

Luciferase expression was determined at 24 h (19 h post transfection). Cells were washed twice with ice-cold phosphate-buffered saline (calcium, magnesium free) and then treated with 0.5 mL of ice-cold lysis buffer (25 mM tris chloride pH 7.8, 1 mM EDTA, 8 mM magnesium chloride, 1% Triton X-100, with 1 mM DTT added fresh) for 10 min. The cell lysate mixture was scraped, transferred to 1.5 mL microcentrifuge tubes, and centrifuged for 7 min at 13000g at 4 °C to pellet debris.

Lysis buffer (350 μL), sodium-ATP (4 μL of a 180 mM solution, pH 7, 4 °C), and cell lysate (100 μL, 4 °C) were combined in a test tube, briefly mixed, and immediately placed in the luminometer. Luciferase light units were recorded with 10 s integration after automatic injection of 100 μL of 0.5 mM D-luciferin (prepared fresh in lysis buffer without DTT). Relative light units (RLU) of luciferase activity were converted to femtomoles of luciferase (after subtraction of background counts, typically

150–200 RLU) based on a standard curve obtained with known triplicate concentrations of firefly luciferase in lysis buffer in the presence of untransfected HepG2 cell lysate. The standard curve was linear between 200 and 10^6 RLU, and each femtomole was equivalent to 740 000 RLU.

Protein concentration in the cell lysate was measured by Bradford assay (*36*) using bovine serum albumin as a standard (the sample size of the cell lysate was 50 μL or less, and no interference from triton X-100 was observed). The femtomoles of luciferase in each sample were normalized to mg of protein and the mean and standard deviation obtained from each triplicate.

RESULTS

Preparation of Oligosaccharide–Polylysine (TriPL) Conjugate. A hepatocyte-targeted gene delivery carrier was prepared by conjugating a natural triantennary oligosaccharide to an amine side chain of dp 19 polylysine. The conjugation results in an amide linkage between the oligosaccharide and polylysine such that the three galactose-terminated antennae are accessible for binding with the ASGP-R.

The reaction scheme is outlined in Figure 1. Triantennary oligosaccharide was purified from fetuin after reducing end modification as previously described (*29*) and obtained as a Boc-protected tyrosinamide oligosaccharide (Boc-Tri, Figure 1A). Treatment of Boc-Tri with TFA removed the Boc group and exposed the N-terminal amine on tyrosine for further modification (Figure 1B). Deprotection was carried out for 10 min in the absence of water and the product freeze dried immediately to avoid hydrolysis of glycosidic linkages of the oligosaccharide. Under these conditions, the conversion to deprotected oligosaccharide was quantitative, as evidenced by elution on RP-HPLC.

A carboxylic group was introduced into the oligosaccharide by succinylation of the exposed amine (Figure 1C). The reaction proceeded quickly when the pH was maintained between 7.5 and 8 in order to deprotonate the amine terminus on Tri. In addition to succinylation of the amine, esterification of hydroxyl groups of the oligosaccharide also occurred but was reversed at an elevated pH while the succinimide linkage was maintained. Succinyl-Tri was isolated from a polymeric reversed phase column at >90% yield.

The elution of Boc-Tri, Tri, and succinyl-Tri on RP-HPLC is shown in Figure 2A–C. Tri was much less hydrophobic than Boc-Tri and eluted earlier, while succinyl-Tri had intermediate hydrophobicity under identical conditions. These differences in properties on RP-HPLC allowed the monitoring of Boc-Tri, Tri, and succinyl-Tri for optimizing reaction conditions and evaluating purity.

Proton NMR analysis of the purified Boc-Tri, Tri, and succinyl-Tri showed characteristic signals from anomeric protons on the oligosaccharide (*37, 29*). In addition, proton signals at 1.35 ppm from methyl groups on Boc-Tri were absent from Tri and succinyl-Tri, and the latter showed the presence of methylene protons on the succinyl group between 2.30 and 2.45 ppm. FAB-MS analysis provided molecular ions corresponding to M + Na for Boc-Tri and Tri (*29*) and a M + 2Na ion for succinyl-Tri (2313.3) which was within 0.5 amu of the calculated molecular weight.

Succinyl-Tri was converted to TriPL by coupling its carboxylic group to an amine side chain of PL after activation with EDC (Figure 1D). The reaction was monitored by gel filtration HPLC. The appearance of an early eluting product peak having absorbance at 274 nm was dependent upon the pH, time of reaction, and the
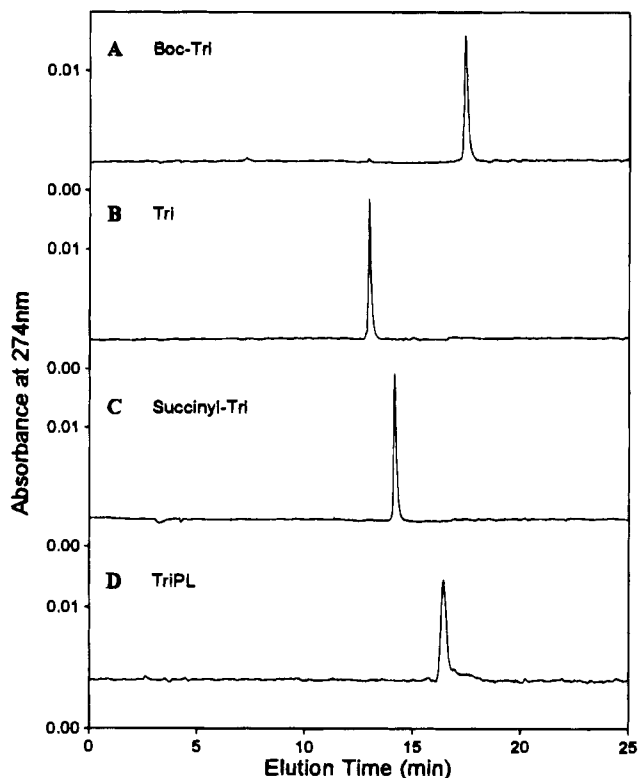
Figure 2. Analytical RP-HPLC characterization of oligosaccharide conjugates. Purified Boc-Tri (A), Tri (B), and succinyl-Tri (C) (4 nmol each) were injected into a C8 silica column (50 °C) equilibrated at 1 mL/min with 0.1% TFA and 1% acetonitrile. Acetonitrile concentration was held at 1% for 5 min, ramped to 20% over 5 min, and kept constant at 20% for 15 min while Abs$_{274}$ was monitored at AUFS 0.02. TriPL (D) was chromatographed on the same column using similar conditions, however, with a step gradient: acetonitrile concentration was held constant at 1% for 9 min, stepped upto 25% over 1 min, and kept constant at 25% for another 15 min. Analytical RP-HPLC allowed monitoring of reactions shown in Figure 1 and established the purity of each intermediate.

molar concentrations of succinyl-Tri, PL, and EDC. The reaction was optimized and a succinyl-Tri to PL stoichiometry of 1:6 chosen to allow the reproducible isolation of a 1:1 conjugate as determined by amino acid analysis. Increasing the molar ratio (succinyl-Tri to PL) progressively to 4:3 resulted in higher molecular weight conjugates which were resolved on gel filtration HPLC. Amino acid analysis of the isolated products indicated that these contained multiple oligosaccharide units conjugated to each polylysine. Alternatively, decreasing the molar ratio to 1:12 inhibited the reaction.

TriPL was isolated with an overall 60% yield (starting from Boc-Tri) on a polymer RP-HPLC column. The purification removed free polylysine and excess EDC which eluted earlier. RP-HPLC of TriPL on a C-8 column is shown in Figure 2D, while gel filtration chromatography is shown in Figure 3. TriPL eluted earlier compared to succinylated oligosaccharide on gel-filtration HPLC due to its increased molecular weight. The monosaccharide composition of TriPL was identical to that of Boc-Tri, and fluorescamine analysis of TriPL using a PL standard indicated 1.03 nmol of polylysine dp 19 for every nmol of tyrosine absorbance. Furthermore, amino acid analysis resulted in a lysine to tyrosine ratio of 20:1, establishing an approximate 1:1 conjugate between polylysine and oligosaccharide.

A control carrier molecule was prepared by trimming terminal galactose residues from TriPL with β-galactosidase. Agal-TriPL was purified in a manner similar to
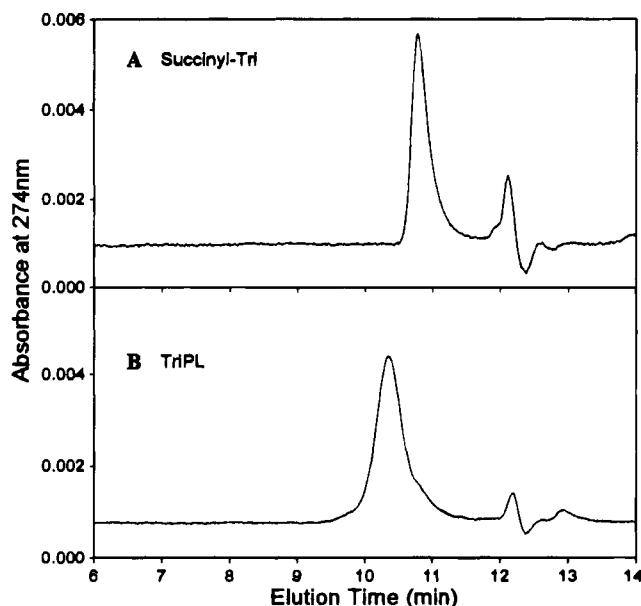
Figure 3. Analytical gel filtration HPLC characterization of TriPL. Succinyl-Tri (A) and TriPL (B) were chromatographed on a gel filtration HPLC column eluted at 1 mL/min with 50 mM sodium phosphate (pH 4.5) and 300 mM sodium chloride. TriPL (MW: ~4700) eluted 40 s earlier than succinyl-Tri (MW: 2269) due to its higher molecular weight. Analytical gel filtration HPLC was used to monitor reaction progress of TriPL formation.

TriPL and was found to be devoid of galactose residues upon monosaccharide analysis.

DNA Complexation and Transfection. TriPL–pCMVL complexes were defined as soluble if centrifugation under the conditions selected failed to remove DNA from the supernatant. This assay established that the solvent used to prepare complexes dramatically influenced solubility. Complexation in saline or HBS at a final DNA concentration of 20 μg/mL led to the formation of a fine precipitate which sedimented upon centrifugation. Alternatively, DNA–carrier complexes prepared in a mannitol solution were more soluble. This effect was unrelated to viscosity. Subsequently, it was found that complexes prepared in low or nonionic conditions did not sediment upon centrifugation, and under these conditions, the presence of mannitol was not necessary for solubility, but its presence avoided hypotonicity.

The formation of TriPL–pCMVL precipitates correlated with greatly diminished transfection efficiencies. Complexes prepared in saline or HBS were 5–12% soluble and resulted in gene expression levels 2 orders of magnitude lower than complexes prepared in mannitol which were typically 90% soluble (Figure 4).

The complexation of DNA with TriPL was initially evaluated by a band retardation assay (9). A fixed amount of pCMVL was titrated with increasing amounts of TriPL resulting in complexes which showed complete retardation on a 1% agarose gel when the carrier to DNA ratio was 0.2 nmol/μg, which approximates the calculated ratio for neutralization of assumed unit charges on DNA by unit charges on TriPL (Figure 5, inset).

Similar titrations were monitored by fluorescence and light scattering assays. The addition of PL or TriPL was found to displace intercalated probe from DNA resulting in a decrease of fluorescence (Figure 5). This assay indicated 45% fluorescence quench at a carrier–DNA ratio of 0.2 and a 95% quench at a ratio of 0.8.

Alternatively, complexes were monitored by light scattering at 90°. Synchronous scans showed that the light scattering spectra were dependent upon the energy
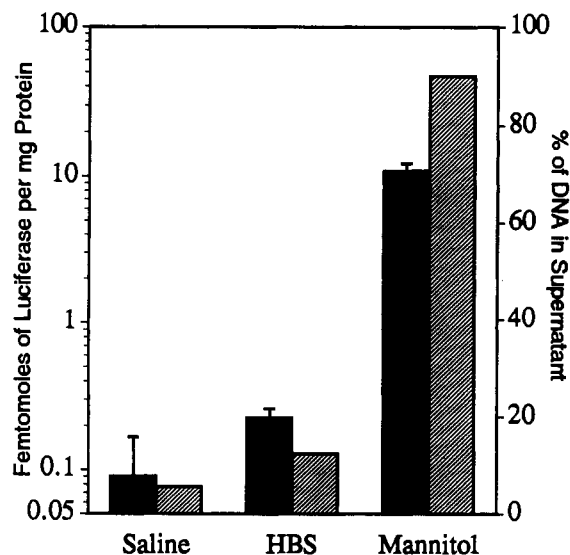
Figure 4. Effect of solvent on solubility and gene transfection. TriPL–pCMVL complexes were prepared (pCMVL 20 μg/mL and TriPL 16 nmol/mL) in saline, HBS, or mannitol solution and were analyzed for solubility and transfection competency in HepG2 cells in the presence of chloroquine as described in the Experimental Procedures. The shaded bars represent percent of DNA remaining in solution after centrifugation, while the solid bars represent luciferase expression obtained at 24 h.

profile of the source lamp which provided the highest intensity of scattered light at 350 nm. Complexes prepared with increasing ratios of TriPL to pCMVL resulted in increased light scattering at 350 nm until an asymptote was reached. Light scattering was nearly at solvent background at a carrier–DNA ratio of 0.2 and at 95% of the asymptote at a ratio of 0.8 (Figure 5). Light scattering and fluorescence intensity could be measured for the same sample by adjusting slit widths and monochromators since the presence of thiazole orange did not produce any significant difference in the scattered light intensity.

HepG2 cells were transfected with complexes containing different ratios of TriPL to pCMVL or PL to pCMVL in either the presence or absence of chloroquine. The level of reporter gene expression was amplified by more than 2 orders of magnitude when the carrier–DNA ratio was increased from 0.2 to 0.8 nmol/μg. Further increase in the carrier–DNA ratio to 1.2 caused only a modest 2-fold increase in reporter gene expression (Figure 6). Gene expression was also observed when TriPL was substituted with PL; however, this was 2 orders of magnitude lower than that observed with TriPL. In either case, an enhancement of gene expression (1–2 orders of magnitude) was obtained when the transfection was carried out in the presence of chloroquine (Figure 7). On the basis of these results, an optimized ratio of 0.8 nmol of TriPL carrier per μg of DNA (approximate molar ratio of 3000; approximate positive:negative charge ratio of 5) was selected for further experiments.

To confirm that the enhancement of gene expression was due to specific recognition of terminal galactose residues on TriPL by the ASGP-R, TriPL was substituted with Agal–TriPL. The resulting gene expression was approximately equivalent to that seen with PL (Figure 7). In addition, TriPL–pCMVL complexes provided the same background gene expression as PL–pCMVL when incubated with HeLa cells, a human cell line lacking the ASGP-R (data not shown).

The influence of fetal calf serum (FCS) concentration on transfection in the presence of chloroquine was investigated. Transfections in the presence of serum free
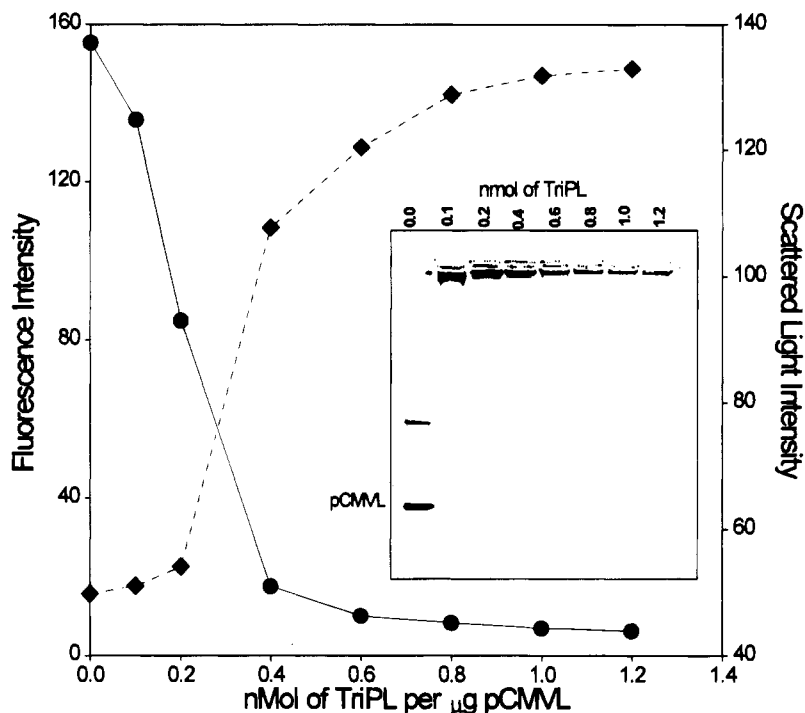
Figure 5. Assays for monitoring DNA complexation. TriPL—pCMVL complexation in mannitol solution was evaluated at different ratios of carrier to DNA by a band retardation assay on 1% agarose gel (inset), by fluorescence quench of intercalated dye (solid line, circles), and by light scattering of complexes (dashed line, diamonds). The band retardation assay showed complete complexation at a TriPL—pCMVL ratio (nmol/μg) of 0.2 or more. However, fluorescence quench and light scattering reached 95% of their asymptotic values at a ratio of 0.8 or higher.
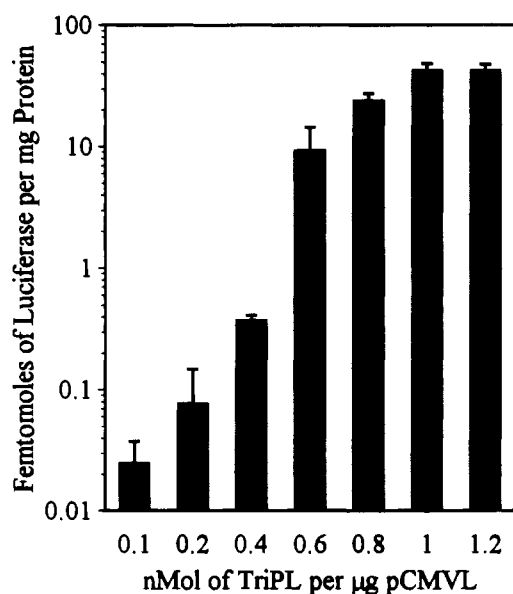
Figure 6. Influence of carrier—DNA ratios upon gene transfection. Complexes were prepared in mannitol solution at increasing ratios of TriPL to pCMVL (10 μg of DNA), and their transfection competency was analyzed in HepG2 cells in the presence of chloroquine. The bars show luciferase expression at 24 h. A good correlation was observed between complexation level indicated by spectroscopic assays and transfection competency.

media or in 10% FCS resulted in similar luciferase levels (not shown). However incubation in the presence of 2% FCS was chosen since gene expression was 2-fold higher compared to transfection in 10% FCS or serum free media. Although peak level of expression was at 3 days (not shown), luciferase activity was routinely assayed at 24 h for rapidity.

Dose—response experiments established a nonlinear increase in reporter gene expression with increasing dose
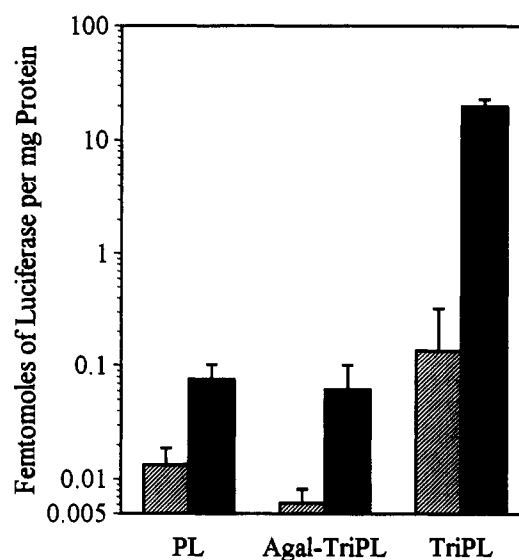
Figure 7. Influence of carrier type on receptor-mediated gene delivery to hepatoma cells. Carrier—pCMVL complexes were prepared with 10 μg of pCMVL and 8 nmol of PL, Agal—TriPL, or TriPL in mannitol solution and transfected into HepG2 cells in the absence (shaded bars) and presence (solid bars) of 80 μM chloroquine. Complexes prepared with TriPL showed luciferase expression 2 orders of magnitude above those made with PL (polylysine dp19). However, this enhancement was dependent only on the presence of terminal galactose residues on TriPL which were recognized by the asialoglycoprotein receptor on hepatocytes since Agal—TriPL—pCMVL showed expression similar to PL—pCMVL.

of TriPL—pCMVL up to the maximum of 20 μg of DNA dose tested (Figure 8). In the presence of chloroquine, luciferase expression was observed even with 0.1 μg of pCMVL. Increasing the dose from 1 to 10 μg resulted in a 1000-fold increase in luciferase expression, while further increasing the dose to 20 μg led to a 2.5-fold increase in luciferase levels. The highest level of expres-
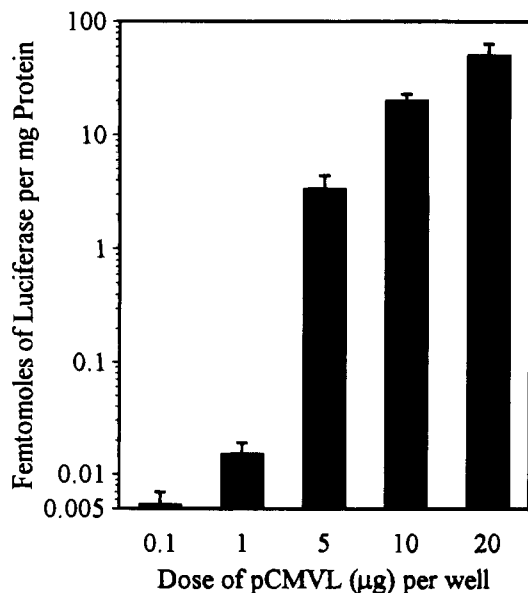
Figure 8. Effect of TriPL—pCMVL dose on reporter gene expression. TriPL—pCMVL (0.1–20 μg of DNA) complexes prepared in mannitol solution were transfected into HepG2 cells at a carrier—DNA ratio 0.8 nmol/μg in the presence of chloroquine and the transfection competency analyzed at 24 h. Increasing levels of expression were obtained with increasing dose of DNA.

sion seen with 20 μg of DNA in the presence of chloroquine corresponds to an average of 7×10^6 light units from the entire 35 mm well (37×10^6 light units per mg protein).

DISCUSSION

One of the major limiting factors for the widespread application of gene therapy is the development of safe, efficient, and well characterized DNA delivery methods for routine transfection *in vivo* (*4–7*). Receptor-mediated gene delivery may potentially provide such a method.

We have constructed a well-characterized, low molecular weight carrier for receptor-mediated gene delivery. The carrier (TriPL) consists of a galactose terminated triantennary oligosaccharide covalently coupled to low molecular weight polylysine (dp 19). This oligosaccharide was chosen since it can be prepared from bovine fetuin in high yield (*29*), and it targets hepatocytes *in vivo* (*30*) due to its high affinity ($K_d = 4$ nM) for the ASGP-R.

The use of a low molecular weight ligand and anchor creates a distinct advantage in preparation and characterization of carrier conjugates. Purification procedures employed RP-HPLC separations, which gave reproducible and scalable isolation of desired products. In contrast, carriers made with proteinaceous ligands and high molecular weight polylysine pose many difficulties in characterization and purification (*22, 38*). This is in part due to the presence of several reactive groups on both ligand and anchor which makes the conjugation chemistry difficult to control and results in considerable heterogeneity in products. In the case of TriPL, the triantennary oligosaccharide has only one reactive carboxylic group, but it is attached randomly to one of the amines of polylysine. An additional source of heterogeneity is the polydispersity of commercially available polylysine, and the potential to form crosslinks, which is compounded in the case of higher molecular weight polylysines.

Complexation between DNA and carrier is a critical parameter for receptor-mediated gene delivery. Unfortunately, complexation also frequently results in precipi-

tation of DNA, limiting the concentration of DNA that can be used (*21, 38*). Complexation of pCMVL with TriPL in saline or HBS resulted in precipitates at 20 μg/mL of DNA, even though TriPL is nearly 50% carbohydrate by weight. These precipitates resulted in transfection levels that were 2 orders of magnitude lower than those observed when soluble complexes were prepared in a solution of mannitol, a nontoxic carbohydrate which can be used *in vivo* (Figure 4). Further experimentation has demonstrated that DNA—carrier complexes remain soluble in a variety of solutions of very low ionic strength, making possible the use of isotonic vehicles prepared with nonionic excipients like mannitol (unpublished data).

The process of complexation between DNA and carrier is usually monitored by an electrophoretic band retardation assay on an agarose gel. In order to further characterize DNA complexes, we have used two spectroscopic assays (Figure 5).

Dye displacement assays utilize dyes that show increased quantum yield of fluorescence when intercalated within nucleic acids and are usually utilized to monitor binding of intercalating molecules. However, our results demonstrate that this type of assay may also be used to monitor ionic binding of polycations to DNA, even though the modes of binding of dye and polycation are different. Thiazole orange (*39*) was selected due to its almost nonfluorescent nature when unbound and moderate affinity for DNA which allowed facile displacement of the dye. However, other dyes fulfilling these criteria may also be used, especially in situations where buffer components interfere with the wavelength being monitored.

An important consequence of complexation between polycations and DNA is condensation of DNA into compact structures (*23, 24*). Band retardation assay cannot be used to evaluate DNA condensation. However, total intensity laser light scattering may be used to evaluate extent of condensation while quasielastic laser light scattering may be used for size analysis of condensates (*40–41*). At the DNA concentrations used in our study, light scattering may result from DNA condensation as well as aggregation. Nevertheless, the results with light scattering intensity measurements complement those obtained with the dye displacement assay.

Band retardation on an agarose gel indicated complete complexation at a TriPL—pCMVL ratio (nmol/μg) of 0.2 or more. Fluorescence quench and light scattering assays indicated 95% complexation or condensation at a carrier—DNA ratio of 0.8. At the same time, luciferase expression levels were 2 orders of magnitude higher at a carrier—DNA ratio of 0.8 compared to 0.2 (Figure 6). Thus, spectroscopic assays were more predictive of transfection competency compared to band retardation assay. Further, these can be performed in the same buffer or solvent that the complex is prepared in and may allow complexation to be studied under varying conditions.

We investigated the specificity of gene delivery based on the ligand recognition characteristics of the ASGP-R (*42, 43*). The results established that the transfection seen was dependent upon the presence of terminal galactose residues on TriPL (Figure 7). Millimolar concentrations of galactose can inhibit binding of galactose terminated triantennary to the ASGP-R (*42*); however, expression levels were not inhibited by transfection in the presence of 100 mM free galactose (not shown). This may be due to the very high affinity of complexes for the ASGP-R when multiple oligosaccharide residues are clustered on condensed DNA. Reporter gene expression was enhanced 1–2 orders of magnitude when transfection was conducted in the presence of the lyso-

somotropic agent chloroquine, consistent with a receptor-mediated endocytosis process.

From a standpoint of *in vivo* gene delivery, it is significant that transfection levels with 10% FCS were the same as with serum free media. At the same time, dose response results emphasize the importance of achieving high solubility of plasmid complexes in order to maximize expression levels.

The triantennary galactose-terminated oligosaccharide used in this study is a good ligand for the ASGP-R. However, it is possible to create even higher affinity oligosaccharide ligands by enzymatic remodeling (*30*) which may lead to more efficient gene delivery, especially in an *in vivo* situation. There is also potential for substitution with oligosaccharides that are ligands for other cell surface receptors.

We have used dp19 (2.5 kDa) polylysine as the DNA anchor for reasons discussed earlier. Most previous studies on receptor mediated gene delivery have used high molecular weight polylysine, and one report cites low transfections levels with transferrin conjugates when polylysines of 30 kDa or lower were used (*22*). This may be due to the large size of ligand used, requiring comparable size polylysine for stable binding to DNA. Although strict comparisons cannot be made, levels of luciferase expression obtained in this study are similar to those observed in previous studies where high molecular weight carriers were used for chloroquine-enhanced, ASGP-R-mediated gene delivery to HepG2 cells (*11, 13*).

The results obtained from this study lead us to conclude that it is possible to achieve reliable receptor-mediated gene delivery with low molecular weight DNA carriers. Oligosaccharide ligands or synthetic analogs designed to bind with high affinity to target receptors may be linked to polycationic oligopeptides of known sequence to obtain completely defined carrier structures. The use of highly characterized carriers will lead to greater reproducibility in gene delivery and expression. Furthermore, it will allow rational manipulation of carrier design for stability and solubility, modulation of DNA and receptor binding characteristics, and incorporation of additional effector molecules like fusogenic and nuclear targeting peptides.

LITERATURE CITED

(1) Morgan, R. A., and Anderson, W. F. (1993) Human gene therapy. *Annu. Rev. Biochem. 62,* 191–217.
(2) Roemer, K., and Friedmann, T. (1992) Concepts and strategies for human gene therapy. *Eur. J. Biochem. 208,* 211–225.
(3) Miller, A. D. (1992) Human gene therapy comes of age. *Nature 357,* 455–460.
(4) Mulligan, R. C. (1993) The basic science of gene therapy. *Science 260,* 926–932.
(5) Schreier, H. (1994) The new frontier: gene and oligonucleotide therapy. *Pharm. Acta Helv. 68,* 145–159.

(6) Lyerly, H. K., and DiMaio, J. M. (1993) Gene delivery systems in surgery. *Arch. Surg. 128,* 1197–1206.
(7) Ledley, F. D. (1993) Hepatic gene therapy: present and future. *Hepatology 18,* 1263–1273.
(8) Chang, A. G. Y., and Wu, G. Y. (1994) Gene therapy: Applications to the treatment of gastrointestinal and liver diseases. *Gastroenterology 106,* 1076–1084.
(9) Wu, G. Y., and Wu, C. H. (1988) Evidence for targeted gene delivery to HepG2 hepatoma cells in vitro. *Biochemistry 27,* 887–892.
(10) Wu, G. Y., and Wu, C. H. (1988) Receptor-mediated gene delivery and expression *in vivo. J. Biol. Chem. 263,* 14621–14624.
(11) Plank, C., Zatloukal, K., Cotten, M., Mechtler, K., and Wagner, E. (1992) Gene transfer into hepatocytes using asialoglycoprotein receptor mediated endocytosis of DNA complexed with an artificial tetra-antennary galactose ligand. *Bioconjugate Chem. 3,* 533–539.
(12) Cristiano, R. J., Smith, L. C., and Woo, S. L. C. (1993) Hepatic gene therapy: Adenovirus enhancement of receptor-mediated gene delivery and expression in primary hepatocytes. *Proc. Natl. Acad. Sci. U.S.A. 90,* 2122–2126.
(13) Midoux, P., Mendes, C., Legrand, A., Raimond, J., Mayer, R., Monsigny, M., and Roche, A. C. (1993) Specific gene transfer mediated by lactosylated poly-L-lysine into hepatoma cells. *Nucleic Acids Res. 21,* 871–878.
(14) Ferkol, T., Lindberg, G. L., Chen, J., Perales, J. C., Crawford, D. R., Ratnoff, O. D., and Hanson, R. W. (1993) Regulation of the phosphoenolpyruvate carboxykinase/human factor IX gene introduced into the livers of adult rats by receptor-mediated gene transfer. *Faseb J. 7,* 1081–1091.
(15) Haensler, J., and Szoka, F. C., Jr. (1993) Synthesis and characterization of a trigalactosylated bisacridine compound to target DNA to hepatocytes. *Bioconjugate Chem. 4,* 85–93.
(16) Huckett, B., Ariatti, M., and Hawtrey, A. O. (1990) Evidence for targeted gene transfer by receptor-mediated endocytosis. Stable expression following insulin-directed entry of *neo* into HepG2 cells. *Biochem. Pharmacol. 40,* 253–263.
(17) Rosenkranz, A. A., Yachmenev, S. V., Jans, D. A., Serebryakova, N. V., Murav'ev, V. I., Peters, R., and Sobolev, A. S. (1992) Receptor-mediated endocytosis and nuclear transport of a transfecting DNA construct. *Exp. Cell Res. 199,* 323–329.
(18) Trubetskoy, V. S., Torchilin, V. P., Kennel, S. J., and Huang, L. (1992) Use of N-terminal modified poly(L-lysine)–antibody conjugate as a carrier for targeted gene delivery in mouse lung endothelial cells. *Bioconjugate Chem. 3,* 323–327.
(19) Thurnher, M., Wagner, E., Clausen, H., Mechtler, K., Rusconi, S., Dinter, A., Birnstiel, M. L., Berger, E. G., and Cotten, M. (1994) Carbohydrate receptor-mediated gene transfer to human T leukaemic cells. *Glycobiology 4,* 429–435.
(20) Wagner, E., Zenke, M., Cotten, M., Beug, H., and Birnstiel, M. L. (1990) Transferrin–polycation conjugates as carriers for DNA uptake into cells. *Proc. Natl. Acad. Sci. 87,* 3410–3414.
(21) Cotten, M., Wagner, W., and Birnstiel, M. L. (1993) Receptor-mediated transport of DNA into eukaryotic cells. *Meth. Enzymol. 217,* 618–644.
(22) Taxman, D. J., Lee, E. S., and Wojchowski, D. M. (1993) Receptor-targeted transfection using stable maleimido-transferrin/thio-poly-L-lysine conjugates. *Anal. Biochem. 213,* 97–103.
(23) Laemmli, U. K. (1975) Characterization of DNA condensates induced by poly(ethylene oxide) and polylysine. *Proc. Natl. Acad. Sci. U.S.A. 72,* 4288–4292.
(24) Wagner, E., Cotten, M., Foisner, R., and Birnstiel, M. L. (1991) Transferrin–polycation–DNA complexes: The effect of polycations on the structure of the complex and DNA delivery to cells. *Proc. Natl. Acad. Sci. U.S.A. 88,* 4255–4259.
(25) Lear, J. D., and DeGrado, W. F. (1987) Membrane binding and conformational properties of peptides representing the NH$_2$ terminus of influenza HA-2. *J. Biol. Chem. 262,* 6500–6505.
(26) Wagner, E., Plank, C., Zatloukal, K., Cotten, M., and Birnstiel, M. L. (1992) Influenza virus hemagglutinin HA-2 terminal fusogenic peptides augment gene transfer by trans-

ferrin-polylysine-DNA complexes: Toward a synthetic virus-like gene-transfer vehicle. *Proc. Natl. Acad. Sci. U.S.A. 89*, 7934–7938.

(27) Plank, C., Oberhauser, B., Mechtler, K., Koch, C., and Wagner, E. (1994) The influence of endosome-disruptive peptides on gene transfer using synthetic virus-like gene transfer systems. *J. Biol. Chem. 269*, 12918–12924.

(28) Haensler, J., and Szoka, F. C., Jr. (1993) Polyamidoamine cascade polymers mediate efficient transfection of cells in culture. *Bioconjugate Chem. 4*, 372–379.

(29) Tamura, T., Wadhwa, M. S., and Rice, K. G. (1994) Reducing-end modification of N-linked oligosaccharides with tyrosine. *Anal. Biochem. 216*, 335–344.

(30) Chiu, M. H., Tamura, T., Wadhwa, M. S., and Rice, K. G. (1994) In vivo targeting function of N-linked oligosaccharides with terminating galactose and N-acetylgalactosamine residues. *J. Biol. Chem. 269*, 16195–16202.

(31) Naoi, M., and Lee, Y. C. (1974) A fluorometric measurement of ligands incorporated into BrCn-activated polysaccharides. *Anal. Biochem. 57*, 640–644.

(32) Bidlingmeyer, B. A., Cohen, S. A., and Tarvin, T. L. (1984) Rapid analysis of amino acids using pre-column derivatization. *J. Chromatogr. 336*, 93–104.

(33) Hardy, M. R. (1989) Monosaccharide analysis of glycoconjugates by high-performance anion-exchange chromatography with pulsed amperometric detection. *Methods Enzymol. 179*, 76–82.

(34) de Wet, J. R., Wood, K. V., DeLuca, M., Helsinki, D. R., and Subramani, S. (1987) Firefly luciferase gene: Structure and expression in mammalian cells. *Mol. Cell. Biol. 7*, 725–737.

(35) Sambrook, J., Fritsch, E. F., and Maniatis, T. (1989) *Molecular Cloning: A Laboratory Manual*; Cold Spring Harbor Laboratory Press: Plainview, NY.

(36) Bradford, M. M. (1976) A rapid and sensitive method for the quantitation of microgram quantities of protein utilizing the principle of protein-dye binding. *Anal. Biochem. 72*, 248–254.

(37) Vliegenthart, J. F. G., Lambertus, D., and van Halbeek, H. (1983) High-resolution, ^{1}H-nuclear magnetic resonance spectroscopy as a tool in the structural analysis of carbohydrates related to glycoproteins. *Adv. Carbohydr. Chem. Biochem. 41*, 209–374.

(38) McKee, T. D., DeRome, M. E., Wu, G. Y., and Findeis, M. A. (1994) Preparation of asialoorosomucoid-polylysine conjugates. *Bioconjugate Chem. 5*, 306–311.

(39) Lee, L. G., Chen, C. H., and Chiu, L. A. (1986) Thiazole orange: A new dye for reticulocyte analysis. *Cytometry 7*, 508–517.

(40) Wilson, R. W., and Bloomfield, V. A. (1979) Counterion-induced condensation of deoxyribonucleic acid. A light scattering study. *Biochemistry 18*, 2192–2196.

(41) Bloomfield, V. A., He, S., Li, A. Z., and Arscott, P. B. (1991) Light scattering studies on DNA condensation. *Biochem. Soc. Trans. 19*, 496.

(42) Lee, Y. C., Townsend, R. R., Hardy, M. R., Lonngren, J., Arnarp, J., Haraldsson, M., and Lonn, H. (1983) Binding of synthetic oligosaccharides to the hepatic gal/galNAc lectin. Dependence on fine structural features. *J. Biol. Chem. 258*, 199–202.

(43) Rice, K. G., Weisz, O. A., Barthel, T., Lee, R. T., and Lee, Y. C. (1990) Defined geometry of binding between triantennary glycopeptide and the asialoglycoprotein receptor on rat hepatocytes. *J. Biol. Chem. 265*, 18429–18434.

Dual-Specificity Interaction of HIV-1 TAR RNA with Tat Peptide–Oligonucleotide Conjugates

Ching-Hsuan Tung,†,‡ Jihong Wang,†,§ Michael J. Leibowitz,‖ and Stanley Stein*,†,§,‖

Center for Advanced Biotechnology and Medicine, 679 Hoes Lane, Piscataway, New Jersey 08854, Department of Chemistry, Rutgers University, Piscataway, New Jersey 08855, and Department of Molecular Genetics and Microbiology, UMDNJ-Robert Wood Johnson Medical School, 675 Hoes Lane, Piscataway, New Jersey 08854. Received December 16, 1994⊗

An oligonucleotide–peptide conjugate, having dual binding capability for a designated RNA, was designed. The peptide portion of the conjugate interacts with a folded domain in the RNA, whereas the oligonucleotide portion hybridizes with a nearby single-stranded region in the RNA. The dual specificity was proven in a model HIV-1 TAR RNA system using an RNase H cleavage assay to assess antisense binding to this RNA. The peptide portion of the conjugate was shown to confer increased specificity on the oligonucleotide.

INTRODUCTION

There are numerous examples on the use of antisense oligonucleotides to inhibit expression of a variety of genes in cell culture (*1*) or in live animals (*2, 3*), with the prospective application of this technology to human diseases, such as AIDS (*4*). Specificity for the selected target is an important property to achieve in an antisense therapeutic agent in order to avoid possible deleterious effects from inhibition of nontarget genes. Unfortunately, sequences only several nucleotides in length are sufficient for DNA/RNA hybridization, and the same short sequences can be repeated numerous times within the cellular population of mRNAs (*5*). Even partial complementarity with longer antisense DNA molecules can lead to hybridization with mismatched nontarget RNAs. Furthermore, the affinity of an antisense oligonucleotide is not only dependent on the number and type of base pairs formed with its target but also strongly dependent on whether the complementary sequence is present in the target RNA in single-stranded or double-stranded form (*6*).

We now report a new strategy to increase the specificity for recognition of the desired RNA target. In this strategy, the antisense agent has two components: one interacts with a single-stranded sequence, whereas the other interacts with a folded domain in the target RNA. TAR RNA of HIV-1 has been chosen as the model target for our dual-recognition peptide–oligonucleotide conjugates, since it has a Tat peptide binding domain adjacent to a six-nucleotide single-stranded loop (*7, 8*).

EXPERIMENTAL PROCEDURES

Oligonucleotides were synthesized on an Applied Biosystems (Foster City, CA) 380B instrument using phosphoramidite chemistry. Primary amino groups were introduced at either the 5′- or 3′-terminus using amino-

link reagents (Clontech, Palo Alto, CA). The Tat peptide, H-Arg-Lys-Lys-Arg-Arg-Gln-Arg-Arg-Arg-Cys-NH₂, representing the TAR-binding domain of the Tat protein with an additional residue of cysteine for coupling to the oligonucleotide, was purchased from Genosys (The Woodlands, TX) and used directly without further purification. H-(Arg)₃-NH₂ was synthesized on an Excell peptide synthesizer (Milligen/Biosearch, Burlington, MA) and purified by reverse-phase chromatography. The aliphatic primary amine on the oligonucleotide was activated by reaction with *N*-hydroxysuccinimide–iodoacetic acid, purified by ion-exchange HPLC, and then coupled to the cysteinyl thiol group on the peptide (*9*). The product was purified by reverse-phase HPLC, dried *in vacuo*, and dissolved in water. Concentration was determined by absorbance at 260 nm using nearest neighbor extinction coefficients.

The RNase H assay was performed in buffer containing 20 mM KCl, 10 mM MgCl₂, 20 mM Tris•HCl, pH 7.5, 0.1 mM EDTA, 0.1 mM DTT, and 5′-³²P-labeled ΔTAR (15 nM). An antisense oligonucleotide or peptide–oligonucleotide conjugate (2 μM) was added to the reaction buffer, and the mixture was incubated at 37 °C for 10 min. Digestion was started by addition of RNase H (50 units/mL, USB), and incubation was at 37 °C for 2 h. Cleavage of the ΔTAR was monitored on a 15% 8 M urea-denaturing polyacrylamide gel.

RESULTS AND DISCUSSION

Peptides and oligonucleotides were synthesized separately and then covalently linked using a modification of a previously developed procedure (*9*). The technique of RNase H footprinting has been adopted to assess interaction of the peptide–oligonucleotide conjugates with TAR RNA. A 27-mer model TAR RNA (ΔTAR) (Figure 1A), prepared by transcription from chemically synthesized template DNA using T7 polymerase and 5′-labeled with ³²P using T4 polynucleotide kinase, was resistant to degradation by RNase H (*Escherichia coli*) in the absence of antisense DNA (Figure 2, lane 6). A series of antisense compounds, consisting of an oligodeoxynucleotide moiety (Figure 1B) linked to a peptide moiety (Figure 1C), were prepared. The 6-mer with an appended C₆-amino-link group at its 3′-terminus (**6b**), complementary to the six-base loop, could effectively form a substrate for RNase H (Figure 2, lane 1). Covalent attachment of the 6-mer via a 3′-C₆-amino-link spacer to

* Address correspondence to this author at CABM, 679 Hoes Lane, Piscataway, NJ 08054 [telephone, (908) 235-5319; FAX, (908) 235-4850].
† Center for Advanced Biotechnology and Medicine.
‡ Present address: GeneMedicine, Inc., 8080 North Stadium Drive, Suite 2100, Houston, TX 77054-1823.
§ Rutgers University.
‖ UMDNJ-Robert Wood Johnson Medical School.
⊗ Abstract published in *Advance ACS Abstracts,* April 15, 1995.

(A)

(B)

4	5'	TCCC	3'
4 a	5'	NH$_2$-(CH$_2$)$_{12}$-TCCC	3'
5	5'	TCCCA	3'
5 a	5'	NH$_2$-(CH$_2$)$_{12}$-TCCCA	3'
6	5'	TCCCAG	3'
6 a	5'	NH$_2$-(CH$_2$)$_{12}$-TCCCAG	3'
6 b	5'	TCCCAG-(CH$_2$)$_6$-NH$_2$	3'
6 c	5'	NH$_2$-(CH$_2$)$_6$-TCCCAG	3'

(C)

t a t	Arg-Lys-Lys-Arg-Arg-Gln-Arg-Arg-Arg-Cys-NH$_2$
R$_3$	Arg-Arg-Arg-Cys-NH$_2$
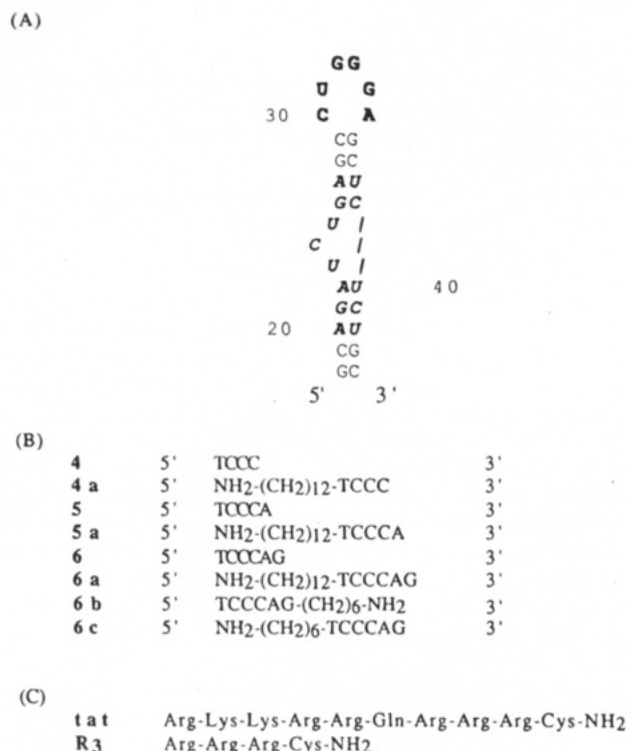
Figure 1. (A) Sequence and predicted secondary structure of ΔTAR (nucleotides 18–44 of HIV-1 TAR). The loop region (shown in boldface) is predicted to be the antisense oligonucleotide binding region. The bulge region (shown in boldface italic) is the Tat peptide binding site. (B) Sequences and abbreviations are listed for antisense oligonucleotides complementary to the loop region of TAR. (C) Primary sequences and abbreviations of peptides used in this study. In each peptide, the C-terminus is amidated. The Tat peptide corresponds to amino acids 49–57 of Tat protein. The C-terminal cysteine was added for use in conjugation to the oligonucleotide.

the Tat peptide (**6b-tat**) resulted in decreased activation of RNase H cleavage (Figure 2, lane 2). The most effective stimulator of RNase H was a conjugate in which the 6-mer was appended via a 5'-C$_{12}$-amino-link group to the Tat peptide (**tat-6a**; Figure 2, lane 4). Attachment of the Tat peptide to the 6-mer via a 5'-C$_6$-amino-link group (**tat-6c**) showed decreased stimulation of RNase H activity (Figure 2, lane 5). A 6-mer conjugate of a triarginine peptide (**6b-R$_3$**) was also an effective RNase H stimulator (Figure 2, lane 3). On the basis of the T1 and Phy M nuclease cleavage ladders, RNase H cleavage was predominantly between nucleotides 33–34 and 34–35 of the HIV-1 transcript, although the ratio of cleavage products varied with the conjugate tested. It may be concluded that both the position and length of the linker to the peptide can affect the site and extent of RNase H cleavage directed by the oligonucleotide (cf. lanes 2, 4, and 5, Figure 2). No cleavage of ΔTAR was evident after incubation with any of the conjugates in the absence of RNase H (data not shown).

Conjugates were prepared in which a 5-mer and a 4-mer were appended via a 5'-C$_{12}$-amino-link group to the Tat peptide (Figure 1), and they were compared with the unconjugated 5-mer and 4-mer (both without an amino-link moiety) for RNase H activation. Cleavage was now predominantly between nucleotides 35 and 36 for both conjugates (Figure 3). Whereas the (unconjugated) 5-mer could form a substrate for RNase H degradation, the 4-mer could not (Figure 3). Thus, the 4-mer–Tat peptide conjugate might have the desired target specificity, since the oligonucleotide should only bind to its complementary
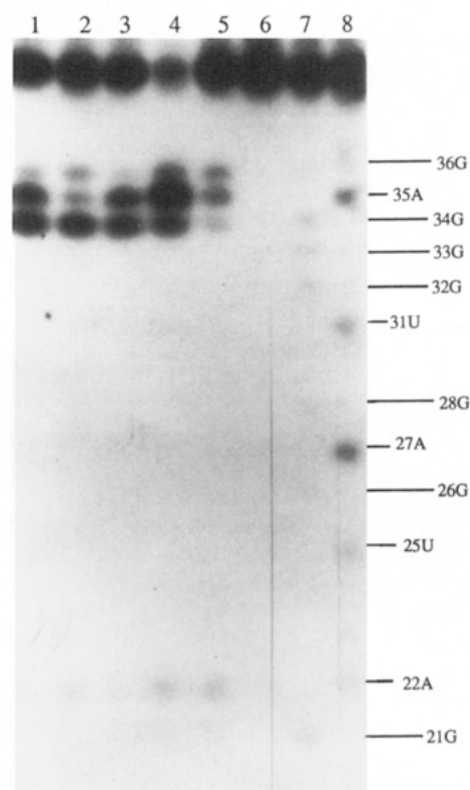
Figure 2. RNase H cleavage assay of ΔTAR with different peptide–oligonucleotide conjugates: lane 1, **6b**; lane 2, **6b-tat**; lane 3, **R$_3$-6b**; lane 4, **tat-6a**; lane 5, **tat-6c**; lane 6, ΔTAR with RNase H control; lane 7, T1 ladder; lane 8, Phy M ladder.

	1	2	3	4	5	6
ΔTAR	+	+	+	+	+	+
5	+	-	-	-	-	-
tat-5a	-	+	-	-	-	-
4	-	-	+	-	-	-
tat-4a	-	-	-	+	-	-
RNase H	+	+	+	+	-	-
RNase T1	-	-	-	-	+	-
RNase Phy M	-	-	-	-	-	+
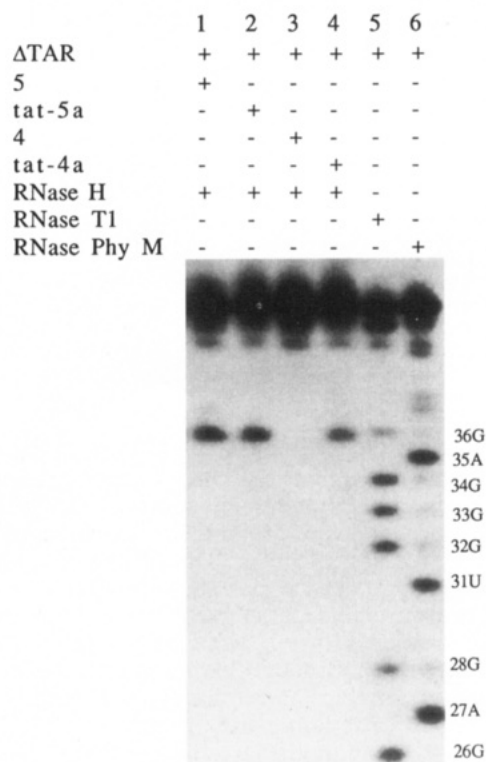
Figure 3. RNase H cleavage assay of ΔTAR with short oligonucleotide–Tat peptide conjugates.

target sequence in the presence of the nearby peptide-binding element of TAR.

Quantitatively, the order of cleavage-stimulating activity for the series of either unconjugated or peptide-linked oligodeoxynucleotides was found to be 6-mer > 5-mer >

Table 1. Percent RNase H-Stimulated Cleavage of ΔTAR and Modified ΔTAR Transcripts by Oligonucleotides and Their Tat Peptide Conjugates

	ΔTAR[a]	SE[b]	ΔTAR(G33C)	SE	ΔTAR(U23A)	SE
4	0.0	0.1	0.0	0.1	0.0	0.1
tat-4a	2.8	0.5	0.0	0.1	0.5	0.2
5	9.4	1.3	0.5	0.5	6.5	1.4
tat-5a	10.1	1.5	0.3	0.4	2.0	0.8
6	49.3	1.2				
6a	53.7	2.3	1.1	0.9	54.1	5.3
tat-6a	65.7	1.9	0.8	0.6	53.3	5.0

[a] The cleavage percentage is from at least triplicate determinations done in separate experiments. A blank reading of 0.2 has been subtracted from each value. The quantitative value was obtained from the phosphor imaging system (GS-250, Bio-Rad). [b] SE, standard error.

	1	2	3	4	5	6
ΔTAR	+	+	+	-	-	+
ΔTAR(U23A)	-	-	-	+	-	-
ΔTAR(G33C)	-	-	-	-	+	-
tat-4a	-	-	+	+	+	-
RNase H	-	-	+	+	+	+
RNase T1	+	-	-	-	-	-
RNase Phy M	-	+	-	-	-	-
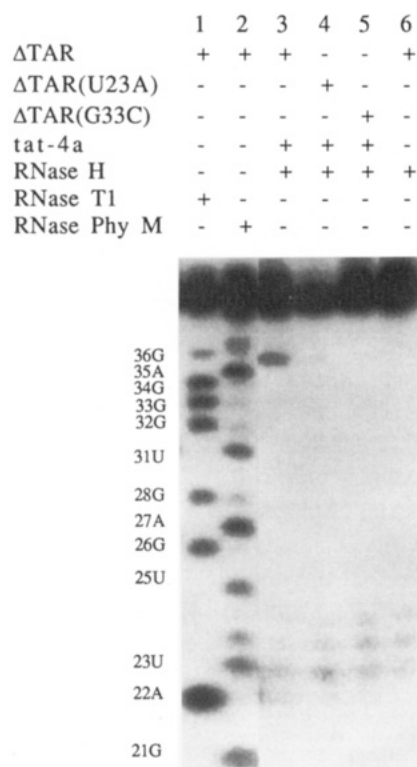
Figure 4. RNase H cleavage assay of ΔTAR and modified forms of ΔTAR with 4-mer–Tat peptide conjugates.

4-mer (Table 1). Approximately two-thirds of the ΔTAR was cleaved by the 6-mer conjugate, demonstrating that the TAR loop is readily accessible to RNase H. To further evaluate specificity, two RNA transcripts with single base changes (U to A at nucleotide 23 and G to C at nucleotide 33) were prepared. Disruption of oligonucleotide complementarity at nucleotide 33, ΔTAR(G33C), eliminated the ability to form an RNase H substrate for the 4-mer and 5-mer compounds, although barely detectable cleavage was observed for the 6-mer compounds (Table 1). Disruption of the Tat-binding site at nucleotide 23, ΔTAR-(U23A), resulted in appreciable loss of RNase H-stimulating ability for all Tat peptide conjugates (Figure 4; Table 1), confirming the high degree of specificity of these bifunctional antisense compounds. A trace amount of cleavage product (0.5%) was still detected for the 4-mer–Tat conjugate (Figure 4). The dissociation constant for Tat peptide and ΔTAR has been reported to decrease about 10-fold when U23 is mutated to A (10). Hence, the trace cleavage may be due to this low level of residual binding to the mutant RNA. In comparison to the

peptide used in this study, a longer Tat peptide (10) and the Tat protein (11) have better specificity for recognition of ΔTAR. Through additional structural modifications, the development of an antisense compound having unique specificity for TAR RNA and strong RNase H-stimulating activity should be achievable.

The concept of highly specific ligand-binding domains in RNA is well established. A prominent example is the guanine cofactor site in group 1 introns (12), which also binds the amino acid arginine (13). There are two examples in HIV-1 of specific RNA–peptide interactions, namely, TAR–Tat and RRE–Rev (14). RNA structural specificity can be selected using solid support-bound ligands (15–17), and we suggest that it may be possible to select for ligand-specific binding sites in any chosen RNA using peptide or other polymer library techniques.

The RNase H footprinting technique has significance with respect to an antisense therapeutic agent. Degradation of mRNA by RNase H, rather than translation arrest, has been suggested to be the predominant mode of inhibition of gene expression by antisense oligonucleotides *in vivo* (18, 19). Indeed, the ability to stimulate RNase H cleavage at the complementary site in the target RNA may be crucial to the efficacy of an antisense agent in mammalian cells (6). The issue of target specificity has been studied in *Xenopus* oocytes (20, 21), and it has been concluded that misdirected RNase H cleavage of nontarget RNAs can be problematic. Our results demonstrate that the desired target specificity may be achievable with the dual-site recognition strategy. The 4-mer oligonucleotide, by itself, was found to be insufficient to stimulate measurable RNase H degradation of the TAR loop, whereas significant degradation occurred when the peptide portion of the 4-mer conjugate bound to its corresponding Tat-binding domain. Considering the importance to HIV-1 replication of a functional TAR–Tat protein transactivation mechanism (22–24) and of a conserved sequence in the six-base loop (25), this 4-mer–oligonucleotide–peptide conjugate may be a lead compound toward the development of an antisense agent for AIDS.

ACKNOWLEDGMENT

LITERATURE CITED

(1) Crooke, S. T. (1992) Therapeutic applications of oligonucleotides. *Bio/Technology 10*, 882–886.

(2) Skutella, T., Probst, J. C., Jirikowski, G. F., Holsboer, F., and Spanagel, R. (1994) Ventral tegmental area (VTA) injection of tyrosine hydroxylase phosphorothioate antisense oligonucleotide suppress operant behavior in rats. *Neurosci. Lett. 167*, 55–58.

(3) Zhou, L.-W., Zhang, S.-P., Qin, Z.-H., and Weiss, B. (1994) *In vivo* administration of an oligodeoxynucleotide antisense to the D$_2$ dopamine receptor messenger RNA inhibits D$_2$ dopamine receptor-mediated behavior and the expression of D$_2$ receptors in mouse striatum. *J. Pharmacol. Exp. Ther. 268*, 1015–1023.

(4) Agrawal, S., and Tang, J. Y. (1992) GEM91—An antisense oligonucleotide phosphorothioate as a therapeutic agent for AIDS. *Antisense Res. Dev. 2*, 261–266.

(5) Fakler, B., Herlitze, S., Amthor, B., Zenner, H.-P., and Ruppersberg, J.-P. (1994) Short oligonucleotide-mediated inhibition is strongly dependent on oligo length and concen-

tration but almost independent of location of the target sequences. *J. Biol. Chem. 269*, 16187–16194.

(6) Monia, B. P., Lesnik, E. A., Gonzalez, C., Lima, W. F., McGee, D., Guinosso, C. J., Kawasaki, A. M., Cook, P. D., and Freier, S. M. (1993) Evaluation of 2′-modified oligonucleotides containing 2′-deoxy gaps as antisense inhibitors of gene expression. *J. Biol. Chem. 268*, 14514–14522.

(7) Feng, S., and Holland, E. C. (1988) HIV-1 *tat trans*-activation requires the loop sequence within *tar*. *Nature 334*, 165–167.

(8) Frankel, A. D. (1992) Peptide models of the Tat-TAR protein-RNA interaction. *Protein Sci. 1*, 1539–1542.

(9) Zhu, T., Wei, Z., Tung, C.-H., Dickerhof, W., Breslauer, K., Georgopoulos, D., Leibowitz, M. J., and Stein, S. (1993) Oligonucleotide-poly-L-ornithine conjugates: Binding to complementary DNA and RNA. *Antisense Res. Dev. 3*, 265–275.

(10) Weeks, K. M., and Crothers, D. M. (1992) RNA binding assays for Tat-derived peptides. Implications for specificity. *Biochemistry 31*, 10281–10287.

(11) Pearson, L., Chen, C.-H. B., Gaynor, R. P., and Sigman, D. S. (1994) Footprinting RNA-protein complexes following gel retardation assays: application to the R-17-procoat-RNA and tat-TAR interactions. *Nucleic Acids Res. 22*, 2255–2263.

(12) Cech, T. R., Herschlag, D., Piccirilli, J. A., and Pyle, A. M. (1992) RNA catalysis by a Group I ribozyme. *J. Biol. Chem. 267*, 17479–17482.

(13) Yarus, M. (1988) A specific amino acid binding site composed of RNA. *Science 240*, 1751–1758.

(14) Battiste, J. L.,Tan, R., Frankel, A. D., and Williamson, J. R. (1994) Binding of an HIV Rev peptide to Rev responsive element RNA induces formation of purine-purine base pairs. *Biochemistry 33*, 2741–2747.

(15) Burgstaller, P., and Famulok, M. (1994) Isolation of RNA aptamers for biological cofactors by in vitro selection. *Angew. Chem. 33*, 1084–1086.

(16) Jenison, R. D., Gill, S. C., Pardi, A., and Polisky, B. (1994) High-resolution molecular discrimination by RNA. *Science 263*, 1425–1429.

(17) Connell, G. J., and Yarus, M. (1994) RNAs with dual specificity and dual RNAs with similar specificity. *Science 264*, 1137–1141.

(18) Dash, P., Lotan, I., Knapp, M., Kandel, E. R., and Goelet, P. (1987) Selective elimination of mRNAs in vivo: Complementary oligodeoxynucleotides promote RNA degradation by an RNase H-like activity. *Proc. Natl. Acad. Sci. U.S.A. 84*, 7896–7900.

(19) Walder, R. Y., and Walder, J. A. (1988) Role of RNase H in hybrid-arrested translation by antisense oligonucleotides. *Proc. Natl. Acad. Sci. U.S.A. 85*, 5011–5015.

(20) Woolf, T. M., Melton, D. A., and Jennings, C. G. B. (1992) Specificity of antisense oligonucleotides *in vivo*. *Proc. Natl. Acad. Sci. U.S.A. 89*, 7305–7309.

(21) Morgan, R., Edge, M., and Colman, A. (1993) A more efficient and specific strategy in the ablation of mRNA in *Xenopus laevis* using mixtures of antisense oligos. *Nucleic Acids Res. 21*, 4615–4620.

(22) Sodrowski, J., Rosen, C., Wong-Staal, F., Salahuddin, S. Z., Popovic, M., Arya, S., Gallo, R. C., and Haseltine, W. A. (1985) Trans-acting transcriptional regulation of human T-cell leukemia virus type III long terminal repeat. *Science 227*, 171–173.

(23) Fisher, A. G., Feinberg, M. B., Josephs, S. F., Harper, M. E., Marselle, L. M., Reyes, G., Gonda, M. A., Aldovini, A., Debouk, C., Gallo, R. C., and Wong-Staal, F. (1986) The trans-activator gene of HTLV III is essential for virus replication. *Nature 320*, 367–371.

(24) Dayton, A. I., Sodroski, J. G., Rosen, C. A., Goh, W. C., and Haseltine, W. A. (1986) The trans-activator gene of the human T cell lymphotropic virus type III is required for replication. *Cell 44*, 941–947.

(25) Harrich, D., Hsu, C., Race, E., and Gaynor, R. B. (1994) Differential growth kinetics are exhibited by human immunodeficiency virus type I TAR mutants. *J. Virol. 68*, 5899–5910.

BC9500195

Improved Synthesis of 6-[*p*-(Bromoacetamido)benzyl]-1,4,8,11-tetraazacyclotetradecane-*N,N',N'',N'''*-tetraacetic Acid and Development of a Thin-Layer Assay for Thiol-Reactive Bifunctional Chelating Agents

Justin K. Moran, Douglas P. Greiner, and Claude F. Meares*

Department of Chemistry, University of California, Davis, California 95616-0935. Received January 11, 1995[®]

Monoclonal antibodies labeled with radiometals such as copper-67 have applications in radioimmunodiagnosis and radioimmunotherapy. Moi et al. [(1985) *Anal. Biochem. 148*, 249–253] showed that 6-[*p*-(bromoacetamido)benzyl]-1,4,8,11-tetraazacyclotetradecane-*N,N',N'',N'''*-tetraacetic acid (BAT) is an effective reagent for linking copper to proteins, and antibodies labeled with copper radionuclides are currently undergoing clinical trials. Here we describe improvements in the original synthesis that increase the overall yield of BAT to 23%. We also describe a new assay useful to determine the activity of bifunctional chelating agents with thiol-reactive functional groups.

INTRODUCTION

In recent years radiolabeled monoclonal antibodies have seen extensive use in radioimmunodiagnosis and radioimmunotherapy (*1–4*). This has been due in part to the increased use of antibodies labeled with radiometals. For example, copper-67 has been used to label antibody conjugates because it emits high energy electrons (β particles) for use in radioimmunotherapy and γ-rays for tumor imaging (*5–7*).

In order to efficiently label antibodies with radiometals, a variety of bifunctional chelating agents (BCA's[1]) have been developed (*8, 9*). BCA's are compounds that contain a strong chelating group at one end and a reactive functional group at the other. BAT, a BCA developed in our laboratory, has been shown to be an effective chelator for copper and is currently undergoing clinical trials (*10–12*). The synthesis of BAT, the first macrocyclic bifunctional chelating agent, was first reported in 1985 (*13*). This was followed by an improved synthesis in 1990, affording an overall yield ≤0.9% starting from nitrobenzyl bromide and diethyl malonate (*14*). Since the publication of the original synthesis, several other groups have reported the synthesis of similar bifunctional chelating agents (*15–17a*). Here we describe improvements in our original synthesis that increase the overall yield of BAT to 23%. Due to the reactivity of the bromoacetamido group, it is important to determine the activity prior to conjugation. We also describe a new assay useful to determine the activity of bifunctional chelating agents with thiol-reactive functional groups.

MATERIALS AND METHODS

Diethyl malonate, *p*-nitrobenzyl bromide, 1 M BH₃·THF, palladium on carbon, bromoacetic acid, and bromoacetyl bromide were purchased from Aldrich Chemical Co. *N,N'*-Bis(2-aminoethyl)-1,3-propanediamine was purchased from Eastman Kodak Chemical Co. Lithium diisopropylamide was purchased from Fluka Chemical Co. 2-Iminothiolane was purchased from Sigma Chemical Co. Plastic-backed silica gel TLC plates (Kieselgel 60 F₂₅₄, EM Science) and glass-backed aminopropyl silica gel plates (HPTLC Fertigplatten NH₂ F₂₅₄ₛ, EM Science) were purchased from Alltech. All other reagents were obtained from commercial sources and used without further purification. Pure water (18 MΩ cm⁻¹) was used throughout. When metal-free conditions were needed all glassware was washed with a mixed acid solution (concentrated sulfuric and nitric 1:1) and thoroughly rinsed with deionized distilled water. THF was distilled over sodium benzophenone ketyl prior to use.

High-Performance Liquid Chromatography. HPLC was carried out on a Rainin HPXL system with titanium piston washing pump heads. UV absorbance was monitored at 254 nm. Reversed-phase HPLC was performed at room temperature with a Dynamax 21.4 × 250 mm C₁₈ column, using the one of the following gradients: (1) solvent A, 0.1 M ammonium acetate pH 6.0; solvent B, methanol; 15–65% B, 0–25 min; 65–100% B, 25–30 min; (2) solvent A, 0.1 M sodium acetate pH 6.0; solvent B, methanol; 15–30% B, 0–20 min; 30–100% B, 20–25 min.

NMR Spectroscopy. ¹H and ¹³C NMR spectra were obtained on a GE QE 300 spectrometer at 300 and 75.47 MHz, respectively. Chemical shifts are reported relative to either HDO (4.80 ppm) or CHCl₃ (7.24 ppm).

Mass Spectroscopy. FAB mass spectra were obtained on a ZAB-HS-2F mass spectrometer.

Diethyl (*p*-Nitrobenzyl)malonate (1). This compound was synthesized from nitrobenzyl bromide and diethyl malonate by a previously published procedure (*17a,b*).

6-(*p*-Nitrobenzyl)-1,4,8,11-tetraazacyclotetradecane-5,7-dione (2). To a solution of 7.05 g (44 mmol) of *N,N'*-bis(2-aminoethyl)-1,3-propanediamine in 500 mL of methanol was added 13.01 g (44 mmol) of diethyl (*p*-nitrobenzyl)malonate (1) in 500 mL of methanol. The solution was refluxed for 21 days. The solvent was removed under reduced pressure until a precipitate began to form, and the mixture was cooled to 4 °C overnight before the precipitate was collected. The volume of the filtrate was again reduced until a precipitate formed and the resulting solid was filtered after cooling. Additional product could be precipitated by the addition of acetonitrile. Yield: 12.51 g (78%) as a tan

[1] Abbreviations: BAT, 6-[*p*-(bromoacetamido)benzyl]-1,4,8,11-tetraazacyclotetradecane-*N,N',N'',N'''*-tetraacetic acid; BCA, bifunctional chelating agent; NO₂Bn-TETA, 6-(*p*-nitrobenzyl)-1,4,8,11-tetraazacyclotetradecane-*N,N',N'',N'''*-tetraacetic acid.

Scheme 1. Synthesis of BAT
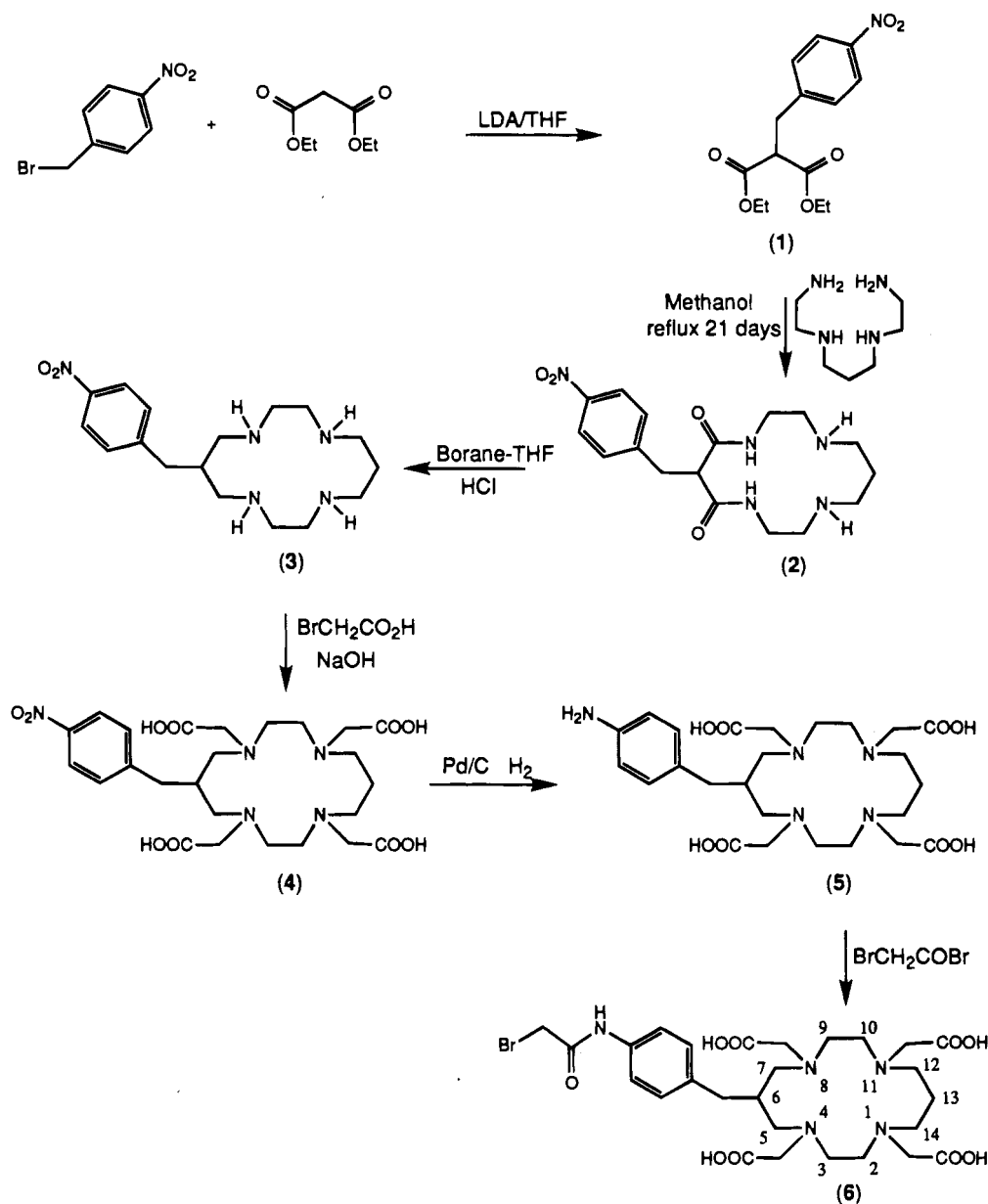
solid. Reversed-phase HPLC: using gradient 1, the product peak is at 23.5 min. FAB-MS *m/e*: 364 (M + H⁺). ¹H NMR (D₂O) δ: 1.90 (m, 2H), 2.98–3.20 (m, 12H), 3.5–3.6 (m, 3H), 7.25 (d, 2H), 7.96 (d, 2H). ¹³C NMR (D₂O) δ: 20.9 (*CH₂*), 33.7 (*CH₂*Ar), 36.7 (*CH₂*), 43.6 (*CH₂*), 45.7 (*CH₂*), 54.5 (*CH*),123.6 (*Ar*), 129.7 (*Ar*), 145.6 (*Ar*), 146.2 (*Ar*), 172.2 (*C*=O).

6-(*p*-Nitrobenzyl)-1,4,8,11-tetraazacyclotetrade-cane (3). To a three-necked flask equipped with a dropping funnel and condenser was added 5.01 g (13.8 mmol) of 6-(*p*-nitrobenzyl)-1,4,8,11-tetraazacyclotetrade-cane-5,7-dione (2). The flask was flushed with N₂, and 30 mL of dry tetrahydrofuran was added. The solid was dissolved by stirring at 0 °C for 30 min. To this solution was added dropwise 125 mL of 1.0 M BH₃·THF at 0 °C. The solution was stirred for 30 min at 0 °C and then warmed to reflux and refluxed for 24 h. The solution was cooled and the excess borane destroyed by the slow addition of water until the evolution of gas ceased. The solvent was removed under reduced pressure and the residue taken up in 120 mL of 6 M HCl. The resulting solution was refluxed for 3 h followed by stirring at room temperature for 24 h. The solvent was removed, and the

residue was taken up in 30 mL of water. The pH was adjusted to 11.5 using concentrated aqueous NH₃. The solution was extracted five times with 100 mL of chloroform. The combined chloroform extracts were dried over sodium sulfate, and the solvent was removed under reduced pressure to yield a yellowish solid. Yield: 4.49 g (97%). HPLC shows only the desired product. Reversed-phase HPLC: when gradient 1 is used the product peak is at 19.0 min. FAB-MS *m/e*: 336 (M + H⁻). ¹H NMR (CDCl₃) δ: 1.60 (m, 2H), 1.96 (m, 1H), 2.3–2.8 (m, 18H), 7.20 (d, 2H), 8.12 (d, 2H). ¹³C NMR (CDCl₃) δ: 29.6 (*CH₂*), 39.1 (*CH₂*Ar), 41.1 (*CH₂*), 49.6 (*CH₂*), 49.7 (*CH₂*), 51.1 (*CH₂*), 55.5 (*CH*),123.9 (*Ar*), 130.2 (*Ar*), 146.8 (*Ar*), 149.0 (*Ar*).

6-(*p*-Nitrobenzyl)-1,4,8,11-tetraazacyclotetrade-cane-*N,N′,N″,N‴*-tetraacetic Acid (4). The pH of a solution of 1.34 g (4 mmol) of 6-(*p*-nitrobenzyl)-1,4,8,11-tetraazacyclotetradecane (3) in 20 mL of water was adjusted to 10 using 10 M NaOH. The solution was warmed to 60 °C, and a solution of 4.2 g (30 mmol) of bromoacetic acid in 5 mL of water was added over a 5 h period. The pH was maintained at 10 by the addition of 10 M NaOH with a Radiometer autoburette. The reac-

Table 1. Yields from Each Step of the Synthesis of 6-[p-(Bromoacetamido)benzyl]-1,4,8,11-tetraazacyclotetradecane-N,N',N",N'''-tetraacetic Acid

compd	previous yield (%)	new yield (%)
diethyl p-nitrobenzylmalonate	63[13]	60[17b]
6-(p-nitrobenzyl)-1,4,8,11-tetraazacyclotetradecane-5,7-dione	21[13]	78
6-(p-nitrobenzyl)-1,4,8,11-tetraazacyclotetradecane	58[13]	97
6-(p-nitrobenzyl)-1,4,8,11-tetraazacyclotetradecane-N,N',N",N'''-tetraacetic acid	12[13]	57
6-(p-aminobenzyl)-1,4,8,11tetraazacyclotetradecane-N,N',N",N'''-tetraacetic acid	95[14]	95
6-[p-(bromoacetamido)benzyl]-1,4,8,11-tetraazacyclotetradecane-N,N',N",N'''-tetraacetic acid	not reported	95
overall	0.9[a]	23

[a] Overall yield assumes quantitative yield from the final step.

Scheme 2

Scheme 3

X = Unreactive functional group
Br = Thiol reactive functional group
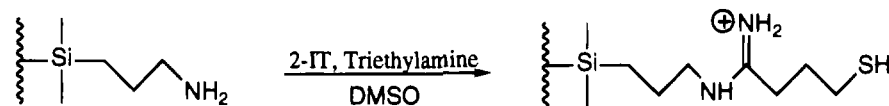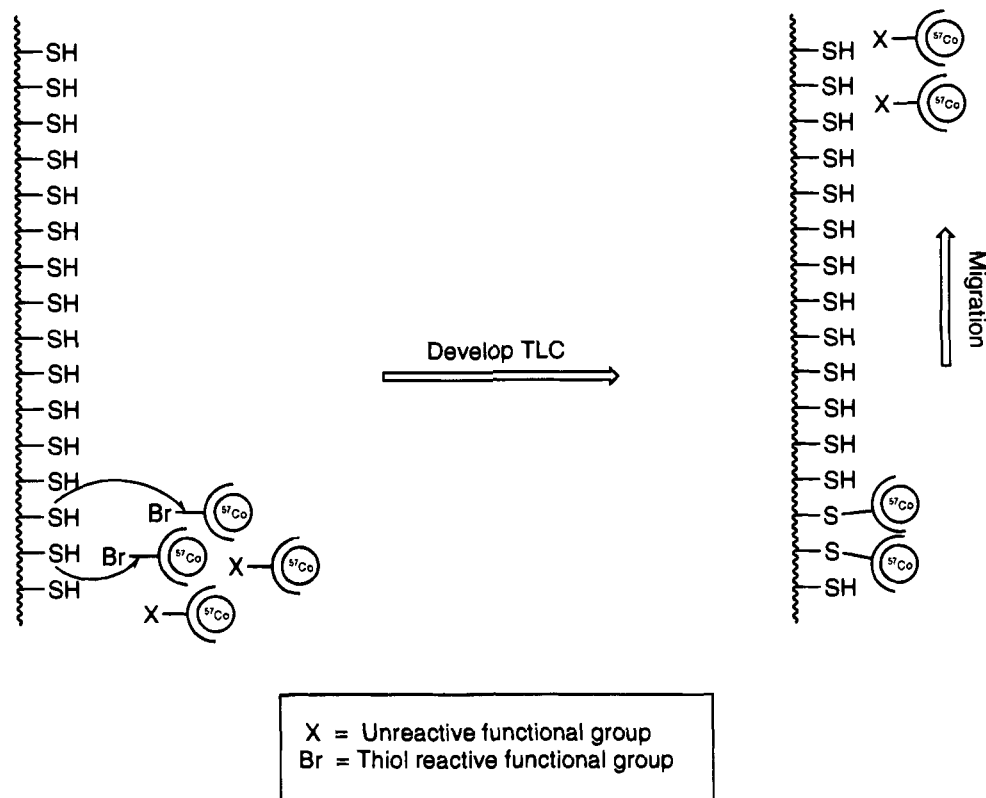
tion was monitored by HPLC, watching for the disappearance of the starting material peak and the appearance of the product peak. When the desired product was present in good yield, the reaction was quenched by lowering the pH to 6.5 with 6 M HCl. The product was purified by HPLC. Yield: 1.30 g (57%). Reversed-phase HPLC: when gradient 1 is used the product peak is at 12.5 min. FAB-MS m/e: 568 (M + H$^+$). ^{1}H NMR (D$_2$O) δ: 1.5–4.6 (m, 29H), 7.31 (d, 2H), 7.98 (d, 2H). ^{13}C NMR (D$_2$O) δ: 20.4 (CH$_2$), 36.1 (CH$_2$Ar), 49.9 (CH$_2$), 50.9 (CH$_2$), 51.2 (CH$_2$), 56.9 (CH$_2$CO), 60.8 (CH), 123.7 (Ar), 129.9 (Ar), 146.2 (Ar), 146.9 (Ar), 174.4 (C=O).

6-(p-Aminobenzyl)-1,4,8,11-tetraazacyclotetradecane-N,N',N",N'''-tetraacetic Acid (5). Nitrobenzyl-TETA (4) 0.500 g (0.88 mmol) was dissolved in 150 mL of water. The pH of the solution was adjusted to 11.5 using 5 M NaOH. The solution was cooled to 0 °C, and 0.114 g of Pd/C was added. The flask was evacuated and then filled with N$_2$ for four cycles and with H$_2$ for three cycles. The solution was stirred under 1 atm of hydrogen

overnight. The solution was filtered through a 0.2 μm nylon filter, and the pH was adjusted to 6.5 using 6 M HCl. The solvent was removed under reduced pressure and the solid was lyophilized. Yield: 0.449 g (95%). Reversed-phase HPLC: when gradient 1 is used the product peak is at 6.0 min. FAB-MS m/e: 538 (M + H$^-$). ^{1}H NMR (D$_2$O) δ: 1.75–3.5 (m, 29H), 6.8 (d, 2H), 7.2 (d, 2H).

6-[p-(Bromoacetamido)benzyl]-1,4,8,11-tetraazacyclotetradecane-N,N',N",N'''-tetraacetic Acid (6). (Aminobenzyl)-TETA (5) 0.245 g (0.46 mmol) was dissolved in 7 mL of water. The pH was adjusted to 7–8 using diisopropylethylamine. This solution was added dropwise to a stirring solution of 0.190 mL of bromoacetyl bromide in 7 mL of chloroform. The pH of the resulting solution was adjusted to 7.0 with diisopropylethylamine and stirred vigorously for 5 min. HPLC analysis of a small aliquot revealed that the reaction had gone to completion by the disappearance of the starting material peak and the appearance of a new peak. The layers were separated, and the aqueous phase was extracted with

chloroform. The pH of the aqueous phase was adjusted to 7−8 with diisopropylethylamine and extracted with chloroform. This was repeated four more times. The pH of the aqueous phase was adjusted to 1.5−1.8 with 3 M HCl and extracted twice with equal volumes ethyl ether. The pH was readjusted with 3 M HCl and the aqueous phase extracted twice with ethyl ether. This was continued until the pH remained constant. Residual ether was removed from the aqueous solution under reduced pressure. The pH of the solution was adjusted to 4.5 with 3 M NaOH, and the solution was divided into aliquots, frozen in liquid nitrogen, and stored at −70 °C. The concentration of the solution was determined by cobalt metal binding assay (*18*). Reversed-phase HPLC: when gradient 2 is used the product peak is at 15.5 min, the same as that of an authentic sample prepared by the previous method. FAB-MS m/e: 658 (M + H$^+$). No NMR data were collected due to decomposition of the material during data collection.

Preparation of Thiol Plate. A 10 cm × 10 cm glass NH$_2$ silica gel plate was placed in a 150 mm × 75 mm crystallizing dish, and 0.100 g (0.727 mmol) of 2-iminothiolane dissolved in 40 mL of anhydrous dimethyl sulfoxide was added to cover the plate. Because 2-IT hydrolyzes easily, a fresh bottle was always used. To deprotonate the amine groups on the plate, triethylamine (0.507 mL, 2.91 mmol) was added to the solution. The dish was tightly covered with a glass plate and gently agitated for 1 h on an orbital shaker table at room temperature. The reaction solution was decanted, and the plate was washed once with 200 mL of anhydrous dimethyl sulfoxide and three times with 200 mL methanol for 5 min each with gentle agitation. After washing, the plate was dried in air at room temperature. To assure that an adequate degree of conjugation has occurred, a small corner of the plate can be tested with 5,5′-dithiobis(2-nitrobenzoic acid) (*19*). This should yield a bright yellow color.

Before use, the plate was developed five times using methanol as the solvent and drying in air between developments. The same orientation of the plate was maintained to allow any reactants or side-products to migrate to the top of the plate. Afterwards, the plate was marked with a light horizontal pencil line 3 cm from the bottom and horizontally scored 2 cm from the top; 9 mm lanes were scored perpendicular from the top score to the bottom edge of the plate. The plate was wrapped in plastic until needed and used within 3 days of preparation.

Calibration of Thiol Plate Using Mixtures of BAT and NO$_2$Bn-TETA. A standard solution of 26.8 mM CoCl$_2$ trace radiolabeled with ^{57}Co was prepared. Standard aqueous solutions of 22.5 mM NO$_2$Bn-TETA and 25.7 mM BAT were prepared and assayed. Analyte samples were prepared by adding 5 μL (0.132 μmol) of radiolabeled ^{57}Co solution to 45 μL of buffer, 0.2 M tetramethylammonium phosphate, pH 8.0. After the solution was incubated at room temperature for 1 h, 2 equiv (0.264 μmol) of chelate solution was added, along with enough buffer to bring the total volume up to 70 μL. The reaction mixture was allowed to stand at room temperature for 1 h; 4 μL of the radiolabeled chelate solution was applied to a TLC plate by spotting 2 μL at a time. After drying, the plate was developed in a solution containing equal volumes of 10% (w/v) aqueous sodium acetate and methanol. Following development, the TLC plate was visualized by an AMBIS radioimaging system, cut at R_f 0.2, and counted in a γ counter.

Determination of Half-Life of BAT. To 20 μL of BAT (31.5 mM) in a 500 μL tube was added 20 μL of
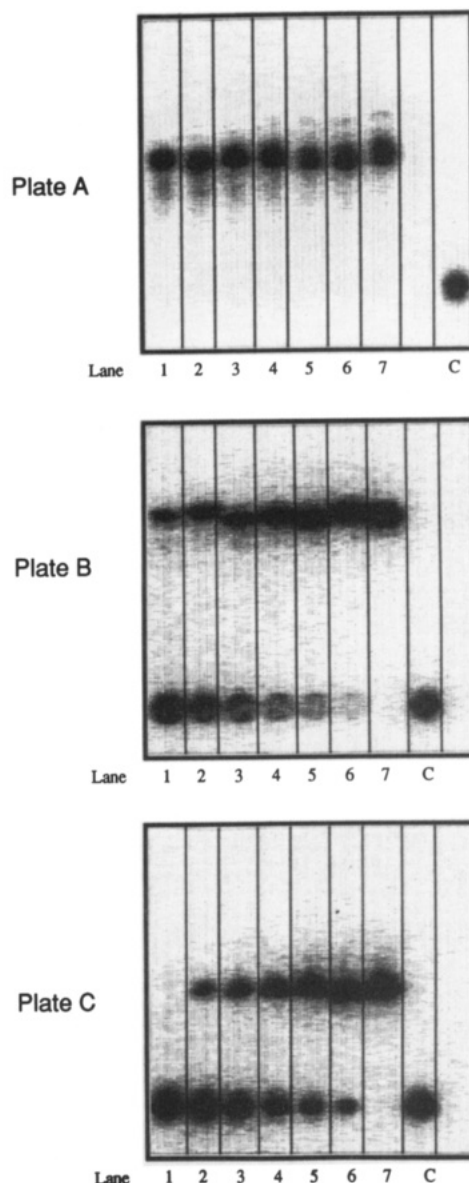
Figure 1. Radioimages of silica plate (A), amine plate (B), and thiol plate (C). Key: Lane 1, pure BAT; lanes 2−6, BAT:NO$_2$-Bn-TETA, 4:1, 2:1, 1:1, 1:2, and 1:4, respectively; lane 7, pure NO$_2$Bn-TETA; lane C, ^{57}Co control (no chelate).

CoCl$_2$ (15.75 mM spiked with ^{57}Co). To this solution was added 80 μL of 0.1 M tetramethylammonium phosphate, pH 8.0. The pH of the solution was adjusted to 9.5 using triethylamine. The solution was placed in a 37 °C bath, and 4 μL aliquots were removed after 0, 5, 10, 20, 30, 60, 120, and 240 min and frozen in liquid nitrogen. The 4 μL aliquots were applied to a thiol TLC plate by spotting 2 μL at a time. After drying, the plate was developed in a solution containing equal volumes of 10% (w/v) aqueous sodium acetate and methanol. The TLC plate was visualized and counted as above.

RESULTS AND DISCUSSION

BAT was synthesized in six steps from nitrobenzyl bromide and diethyl malonate with an overall yield of 23% (Scheme 1). With the exception of the synthesis of diethyl (nitrobenzyl)malonate, the yield of each of the steps was increased with respect to previously reported results (*13, 14*).

The first major improvement occurred in the cyclization reaction. By running the reaction under very dilute
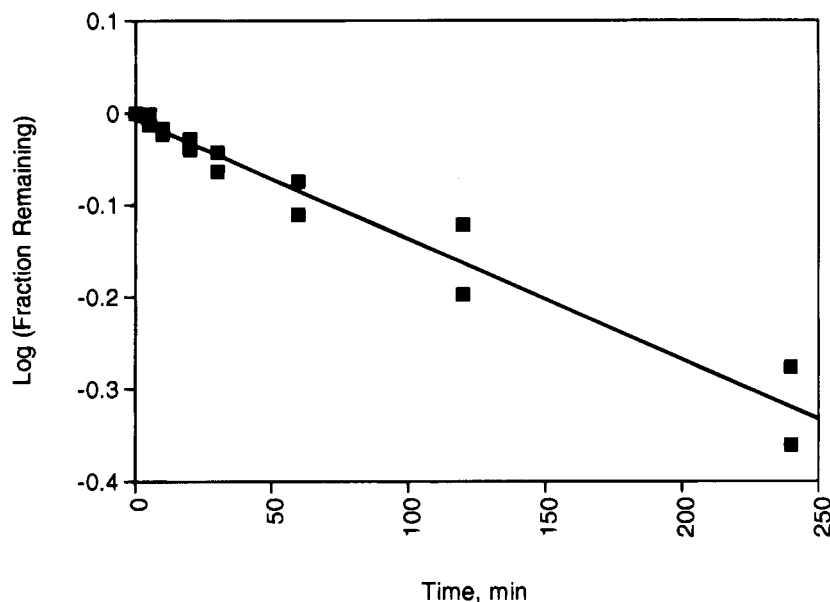
Figure 2. Fraction of 6-[*p*-(bromoacetamido)benzyl]-1,4,8,11-tetraazacyclotetradecane-N,N',N'',N'''-tetraacetic acid remaining versus time for hydrolysis at 37 °C and pH 9.5.

conditions (0.09 M versus the original 4 M) and for an extended time (21 days) due to the decrease in concentration, the yield of **2** was increased from 21% to 78%. The dilution helps to minimize polymer formation, which accounted for the previous lower yield. In addition, the solvent was also changed from ethanol to methanol; the lower boiling solvent may reduce the production of polymer. One important benefit of the new synthesis is that with fewer side products, the need for column chromatography to purify the product is eliminated.

The second major improvement in the synthesis occurred during the reduction of the carbonyl groups of **2**, increasing the yield of tetraamine **3** to 97% from 58%. The original 10:1 mole ratio of borane to carbonyl with a 5 h reaction time has been replaced with a 4:1 mole ratio of borane to carbonyl group and a 24 h reaction time. Significant improvement in this reaction yield also results from changes in the subsequent workup of the borate esters. Previously, methanol was added to the reaction mixture and the solution saturated with HCl gas to cleave the borate esters. This has been replaced by destruction of excess borane with water, followed by solvent removal. The improved purity of **3** resulting from these changes has eliminated the need for HPLC purification.

The alkylation of **3** with bromoacetate was accomplished as previously reported, except 7−8 mol of bromoacetic acid per mole of **3** was used instead of 4. By increasing the number of equivalents of bromoacetic acid, the amount of the desired tetrasubstituted product **4** is increased from 12% to 57%.

Compound **5** is synthesized as previously reported, using palladium on carbon and hydrogen to reduce the nitro group to an amino group. The reduction is nearly quantitative with yields of 95−97%.

The final step in the synthesis of BAT, the bromoacetylation of **5**, is similar to that previously reported (*14*), with the following exceptions: (1) fewer equivalents of bromoacetyl bromide are used (5 versus 8), and (2) after chloroform extraction, the pH of the aqueous solution is adjusted to 1.5−1.8 and extracted with diethyl ether. This final step ensures that all of the bromoacetyl bromide and bromoacetic acid are removed.

Starting from nitrobenzyl bromide and diethyl malonate, the overall yield of 6-[*p*-(bromoacetamido)benzyl]-

1,4,8,11-tetraazacyclotetradecane-N,N',N'',N'''-tetraacetic acid has been improved to 23% from below 0.9%. The major improvements of the synthesis are in the cyclization and carbonyl reduction steps (see Table 1), in which the yields are more than doubled. The improvements in the synthesis of **6** are particularly significant in light of a recent report comparing the *in vivo* stability of two different isomers of benzyl-TETA (*7*). It was shown that benzyl-TETA with the side chain in the 6-position (**6**) decomposes approximately 4-fold more slowly under physiological conditions than the isomer with the side chain in the 2-position. Other research groups have reported the synthesis of similar tetraaza macrocycle chelates (*15−17a*). The nine-step synthesis of 2-(*p*-nitrobenzyl)-TETA from ethylenediamine-N,N'-dipropionic acid and (nitrobenzyl)ethylenediamine has been reported with an overall yield of 4.3% (*16*). Direct comparison of the synthesis and of our improved synthesis of 6-(nitrobenzyl)-TETA is not possible because different synthetic schemes were used. However, both syntheses have two steps in common: (1) the reduction of the amide carbonyls and (2) the alkylation of the tetraamines. In both cases the methods reported here gave higher yields. The (nitrobenzyl)tetraazacyclotridecane−tetraacetic acid analog has been reported, with an overall yield of 12.1% (*17a*). The main difference in the two syntheses is that the cyclization yield of the tridecane analog was 28%, whereas the cyclization yield of the tetradecane described here is 78%.

Typically, the reactive group in a bifunctional chelating agent is an electrophile that can react with amines or sulfhydryls (thiols) on biological molecules. The bromoacetamide group reacts quickly with sulfhydryls and more slowly with amines. Electrophilic reagents are subject to hydrolysis, so that preparations of BCA's may contain varying portions of hydrolyzed products (e.g., glycolamide groups) that will not react with the biological molecule of interest.

The degree of hydrolysis depends not only on the initial purity of the reagent, but also on the time it has remained in aqueous solution at ambient temperature (and the conditions, including pH). For example, repeated freezing and thawing of a solution results in increasing amounts of hydrolyzed products. We have devised a simple method to test for the presence of such products

and have found that it provides useful information for quality control and for comparison of different samples of these reagents.

Scheme 2 shows how the silica-linked propylamine is modified with 2-IT (20) to generate a free thiol. The free thiol can be alkylated by a radiolabeled BCA that is specific for thiols (Scheme 3). After the thiol reactive TLC plate is developed, BCA's are immobilized quantitatively at the origin while chelates that are incapable of alkylation have migrated. By comparing the ^{57}Co counts in each case, bifunctional chelates can be quantified.

To determine the validity of this assay technique, we used known mixtures of BAT and NO$_2$Bn-TETA (developed plates are shown in Figure 1). The total concentration of chelate was kept constant and the total amount of chelate present was twice that of ^{57}Co. A 2-fold molar excess of chelating agent was used to ensure that all of the ^{57}Co was complexed. Lane 1 contains pure BAT and lane 7 contains NO$_2$Bn-TETA. Lanes 2 through 6 contain mixtures with 4:1, 2:1, 1:1, 1:2, and 1:4 ratios of BAT: NO$_2$Bn-TETA. Lane C contains ^{57}Co without any chelate. Equal volumes of each reaction mixture were spotted on an ordinary silica gel plate (A), an amine plate (B), and a thiol plate (C). Plate A demonstrates that BAT is unreactive to silica and that both BAT and NO$_2$Bn-TETA comigrate while the unchelated ^{57}Co remains at the origin. Plate B shows that BAT has some reactivity toward the free amine but is not quantitatively immobilized at the origin (lane 1). Finally, the thiol plate, C, shows quantitative immobilization of BAT (lane 1). In agreement with Figure 2, the quantitative results of γ counting confirmed that the ratio of immobilized BAT to mobile NO$_2$Bn-TETA was identical, within experimental error, to the known ratio (data not shown). The activity of BAT synthesized using the improved method has been compared to previous batches of BAT using the thiol plate assay. Both new and old BAT samples show the same activity, indicating that the new synthetic method produces BAT of similar quality. This procedure has been used successfully to determine the purity of bromoacetamido derivatives of EDTA, DOTA, and NOTA.

In addition to determining the activity of thiol reactive chelates, the thiol TLC plate has also been used to determine the rate of hydrolysis of BAT under conditions used during conjugation reactions (i.e., 37 °C and pH 9.5). The fraction of BAT remaining was plotted versus time (Figure 2). The slope of this semilogarithmic plot gives the pseudo-first-order rate constant for hydrolysis, which was calculated to be 0.003 min^{-1} (half-life $\approx$230 min, with upper and lower 95% confidence limits of 266 and 204).

ACKNOWLEDGMENT

LITERATURE CITED

(1) DeNardo, S. J., DeNardo, G. L., Peng, J.-S., and Colcher, D. (1983) Monoclonal Antibody Radiopharmaceuticals of Cancer Radioimmunotherapy. *Radioimmunoimaging and Radioimmunotherapy* (S. Burchiel, and B. Rhodes, Eds.) pp 409–417, Elsevier, New York.

(2) Bloomer, W. D., Lipsztein, R., and Dalton, J. F. (1985) Antibody Mediated Radiotherapy. *Cancer 55*, 2229–2233.

(3) Meares, C. F., Moi, M. K., Diril, H., Kukis, D. L., McCall, M. J., Deshpande, S. V., DeNardo, S. J., Snook, D., and Epenetos, A. A. (1990) Macrocyclic Chelates of Radiometals for Diagnosis and Therapy. *Br. J. Cancer, Suppl. 10*, 21–26.

(4) Yuanfang, L., and Chuanchu, W. (1990) Radiolabeling of Monoclonal Antibodies with Metal Chelates. *Pure Appl. Chem. 3*, 427–463.

(5) Deshpande, S. V., DeNardo, S. J., Meares, C. F., McCall, M. J., Adams, G. P., and DeNardo, G. L. (1988) Copper-67-Labeled Monoclonal Antibody Lym-1, A Potential Radiopharmaceutical for Cancer Therapy: Labeling and Biodistribution in RAJI Tumored Mice. *J. Nucl. Med. 29*, 217–225.

(6) Morphy, J. R., Parker, D., Kataky, R., Harrison, A., Eaton, M. A. W., Millican, A., Phipps, A., and Walker, C. (1989) Towards Tumour Targeting with Copper-Radiolabeled Macrocycle-Antibody Conjugates. *J. Chem. Soc., Chem. Commun.* 792–794.

(7) Kukis, D. L., Diril, H., Greiner, D. P., DeNardo, S. J., DeNardo, G. L., Salako, Q. A., and Meares, C. F. (1994) Comparative Study of Copper-67 Radiolabeling and Kinetic Stabilities of Antibody-Macrocyclic Chelate Conjugates. *Cancer 73*, 779–786.

(8) Sundberg, M. W., Meares, C. F., Goodwin, D. A., and Diamanti, C. I. (1974) Chelating Agents for the Binding of Metal Ions to Macromolecules. *Nature 250*, 587–588.

(9) Meares, C. F., and Wensel, T. G. (1984) Metal Chelates as Probes of Biological Systems. *Acc. Chem. Res. 17*, 202–209.

(10) DeNardo, G. L., DeNardo, S. J., Meares, C. F., Kukis, D., Diril, H., McCall, M. J., Adams, G. P., Mausner, L. F., Moody, D. C., and Deshpande, S. V. (1991) Pharmacokinetics of Copper-67 Conjugated Lym-1, a Potential Therapeutic Radioimmunoconjugate, in Mice and in Patients with Lymphoma. *Antibody, Immunoconjugates, Radiopharm. 4*, 777–785.

(11) Mathias, C. J., Welch, M. J., Green, M. A., Diril, H., Meares, C. F., Gropler, R. J., and Gergmann, S. R. (1991) In Vivo Comparison of Copper Blood Pool Agents: Potential Radiopharmaceuticals for Use with Copper-62. *J. Nucl. Med. 32*, 475–480.

(12) Anderson, C. J., Connett, J. M., Schwarz, S. W., Rocque, P. A., Guo, L. W., Philpott, G. W., Zinn, K. R., Meares, C. F., and Welch, M. J. (1992) Copper-64-Labeled Antibodies for PET Imaging. *J. Nucl. Med. 33*, 2006–2013.

(13) Moi, M. K. Meares, C. F., McCall M. J., Cole, W. C., and DeNardo, S. J. (1985) Copper Chelates as Probes of Biological Systems: Stable Copper Complexes with a Macrocyclic Bifunctional Chelating Agent. *Anal. Biochem. 148*, 249–253.

(14) McCall, M. J., Diril, H., and Meares, C. F. (1990) Simplified Method for Conjugating Macrocyclic Bifunctional Chelating Agents to Antibodies via 2-Iminothiolane. *Bioconjugate Chem. 1*, 222–226.

(15) Morphy, J. R., Parker, D., Alexander, R., Bains, A., Carne, A. F., Eaton, M. A. W., Harrison, A., Millican, A., Phipps, A., Rhind, S. K., Titmas, R., and Weatherby, D. (1988) Antibody Labelling with Functionalized Cyclam Macrocycles. *J. Chem. Soc., Chem. Commun.* 156–158.

(16) McMurry, T. J., Brechbiel, M., Kumar, K., and Gansow, O. A. (1992) Convenient Synthesis of Bifunctional Tetraaza Macrocyles. *Bioconjugate Chem. 3*, 106–117.

(17) (a) Ruser, G., Ritter, W., and Maecke, H. R. (1990) Synthesis and Evaluation of Two New Bifunctional Carboxymethylated Tetraazamacrocyclic Chelating Agents for Protein Labeling with Indium-111. *Bioconjugate Chem. 1*, 345–349. (b) The reported yield for diethyl (nitrobenzyl)-malonate is 75%; however, the best yield we were able to achieve was 60%.

(18) Goodwin, D. A., Meares, C. F., Watanabe, N., McTigue, M., Chaovapong, W., Ransone, C. M., Renn, O., Greiner, D. P., Kukis, D. L., and Kronenberger, S. I. (1994) Pharmacokinetics of Pretargeted Monoclonal Antibody 2D12.5 and Y-88-Janus-2-(p-nitrobenzyl)-1,4,7,10-Tetraazacyclododecanetetraacetic Acid (DOTA) in BALB/C Mice with KHJJ Mouse Adenocarcinoma-A Model For Y-90 Radioimmunotherapy. *Cancer Res. 54*, 5937–5946.

(19) Ellman, G. L. (1959) Tissue Sulfhydryl Groups. *Arch. Biochem. Biophys. 82*, 70–77.

(20) Jue, R., Lambert, J. M., Pierce, L. R., and Traut, R. R. (1978) Addition of Sulfhydryl Groups to *Escherichia coli* Ribosomes by Protein Modification with 2-Iminothiolane (Methyl 4-Mercaptobutyrimidate). *Biochemistry 17*, 5399–5406.

BC950013F

Construction of Coordinatively Saturated Rhodium Complexes Containing Appended Peptides

Niranjan Y. Sardesai, Susanne C. Lin, Kaspar Zimmermann, and Jacqueline K. Barton*

Division of Chemistry and Chemical Engineering, California Institute of Technology, Pasadena, California 91125. Received January 31, 1995[®]

Phenanthrenequinone diimine (phi) complexes of rhodium(III) bearing appended peptides have been prepared using two complementary solid phase synthetic strategies. The first method involves the direct coupling of the coordinatively saturated rhodium complex containing a pendant carboxylate to the N-terminus of a resin-bound peptide, in a manner analogous to the chain-elongation step in solid phase peptide synthesis. The second involves coupling a bidentate chelator containing the pendant carboxylate to the resin-bound peptide, followed by coordination of $[Rh(phi)_2]^{3+}$ to the bidentate chelator attached to the peptide. Peptides of length 5–30 residues have been covalently attached to rhodium complexes in 5–18% yield using both methods. Despite the low overall yields, the regioselective modification of the peptide chain afforded by these strategies is a distinct advantage over solution phase methods. With coordination complexes which are stable to peptide deprotection and cleavage conditions from the resin, the solid phase synthetic strategies are convenient to apply. Amino acid analysis, electronic spectroscopy, and circular dichroism confirm the presence of the two components in the metal–peptide chimeras; the metal–peptide complexes exhibit the combined spectral properties of the parent metal complex and the appended peptide. Significantly, plasma desorption mass spectrometry reveals a novel pattern of peptide fragmentation for the metal–peptide chimeras that is not observed in the absence of the tethered metal complex; this fragmentation facilitates the sequence analysis of the appended peptide. Thus, metal–peptide chimeras may be conveniently prepared using solid phase methodologies, and features of coordination chemistry may be exploited for new peptide design and analysis.

INTRODUCTION

There has been increased attention focused on the assembly of peptides containing coordinated transition metal complexes (*1–24*). The coordination geometry about a metal ion provides a rigid, well-defined center from which to append peptides for a specific function. As with larger metalloproteins, the metal ion may serve a structural role in bringing together discrete elements of peptide secondary structure (*1–18*) or it may serve a functional role in catalysis (*19–24*). Furthermore, as is also found with larger protein systems, the presence of the transition metal center provides a convenient spectroscopic handle to assay function. Examples of the incorporation of coordination chemistry in peptide design include the application of metal ion coordination to stabilize peptide α-helices (*1–8*) and β-turns (*9*), the *de novo* design of three and four helix bundle proteins through crosslinking peptide helices by metal ions (*1–6, 10–12*), and the construction of donor–acceptor assemblies in studies of photoinduced electron transfer across peptides (*14–17*).

Our laboratory has focused on the design of transition metal complexes to explore site-specific recognition of nucleic acids (*25–28*). As a part of this effort to construct smaller functional mimics of DNA-binding proteins, we became interested in incorporating appended peptides in our design. We recently reported the site-selective recognition of double helical DNA by metal–peptide constructs, in which the recognition characteristics of the complex are governed by the appended peptide (*29*). In these studies, peptides (13 residues) were appended to a sequence-neutral (*28*) metallointercalator, [Rh(phi)₂-(phen)]³⁺ (phi = 9,10-phenanthrenequinone diimine; phen

= 1,10-phenanthroline) so as to produce a sequence-specific DNA-binding molecule (*29*). Using this strategy, an array of metal–peptide complexes with different recognition characteristics may be constructed.

Here we describe the syntheses and characterization of metal complexes containing different tethered peptides, and we explore the advantages and limitations of the methodology. Figure 1 illustrates a representative metal–peptide chimera. Our strategy involves the assembly of the metal–peptide complexes on a solid support. Peptides of length 5–30 amino acids have been synthesized by standard solid phase synthesis (*30–32*). Thereafter, metal complexes are appended onto the resin through two distinct coupling methodologies: (i) by direct coupling of $[Rh(phi)_2L]^{3+}$ (L = a bidentate chelator containing a pendant carboxylate) to the peptide on the resin or (ii) by first coupling L to the resin-bound peptide, followed by coordination of $[Rh(phi)_2]^{3+}$ to L. Meyer and co-workers have used a similar strategy of direct coupling to synthesize a tripeptide containing $[Ru(bpy)_3]^{2+}$ (*14*). These syntheses complement solution phase coordination methodologies (*1–24*). The solution method relies, however, on the selective coordination of the metal center to the desired side chain functionalities on the peptide. Regioselective ligation in solution may be limited if the desired peptide sequence contains, for example, several cysteine or histidine residues. Instead, coordination directly on the resin offers control through the selective deprotection of side-chain functionalities for ligation.

We also describe the characterization of these metal–peptide constructs using mass spectrometric analysis in addition to the more conventional spectrophotometric methods. Here too, the metal ion yields distinct advantages. In the presence of the appended coordination complex, a novel pattern of peptide fragmentation is
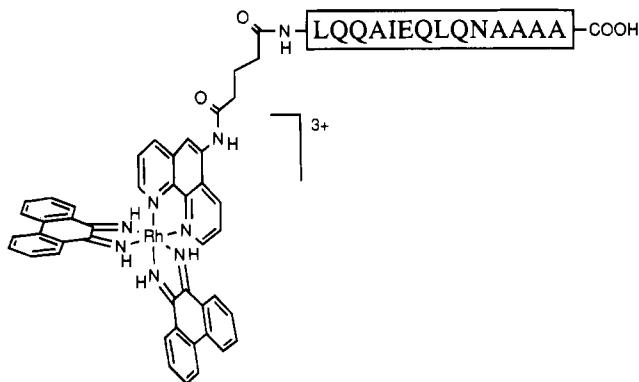
Figure 1. Representative metal–peptide chimera showing a 14-residue peptide tethered to [Rh(phi)₂(phen)]³⁺ via a glutaryl linker on the 1,10-phenanthroline.

found which is not observed in the absence of the pendant metal complex, and this fragmentation greatly facilitates the sequence analysis of the appended peptide.

EXPERIMENTAL SECTION

Materials. RhCl₃·6H₂O was purchased from Aesar Johnson-Matthey, and 5-amino-1,10-phenanthroline was purchased from Polysciences, Inc. All other chemicals were purchased from Aldrich. Anhydrous solvents were purchased from Fluka. 4-(4-Carboxybutyl)-4'-methyl-2,2'-bipyridine (bpy') was prepared by the method of Della Ciana, Hamachi, and Meyer (*33*). [Rh(phi)₂Cl₂]Cl was synthesized following published protocols (*34*). 9,10-Diaminophenanthrene was recrystallized from ethanol–water prior to use. For manual FMOC[1] synthesis, PEG resin, BOP, and the amino acids were purchased from Milligen. HMP resin for automated FMOC synthesis and MBHA and PAM resins for *t*-Boc synthesis and their respective amino acids were purchased from Applied Biosystems, Inc.

Instrumentation. ¹H-NMR spectra were recorded on a 300 MHz GE QE Plus spectrometer. *J* values are given in Hz. Ultraviolet–visible spectra were recorded on a Hewlett-Packard 8452A diode array or Cary 219 spectrophotometer. Circular dichroism studies were performed on a JASCO J-500 or J-600 spectrometer using 1 cm path length cells. The peptide concentrations were determined by quantitative amino acid analysis as the average of three runs on an ABI420 amino acid analyzer. The concentrations of metal–peptide complexes were determined by UV–vis spectroscopy using ϵ_{350} (isosbestic)

---

[1] Abbreviations: Bom, benzyloxymethyl; BOP, (benzotriazole-*N*-oxy)tris(dimethylamino)phosphonium hexafluorophosphate; Br-Z, 2-bromobenzyloxycarbonyl; Bzl, benzyl; CID, collision-induced dissociation; Cl-Z, 2-chlorobenzyloxycarbonyl; DBU, 1,8-diazabicyclo[5.4.0]undec-7-ene; DCC, *N,N*-dicyclohexylcarbodiimide; DIEA, *N,N*-diisopropylethylamine; DMAP, 4-(dimethylamino)pyridine; DMF, *N,N*-dimethylformamide; DSC, *N,N*-disuccinimidyl carbonate; DTT, dithiothreitol; FAB-MS, fast atom bombardment mass spectroscopy; FMOC, 9-fluorenylmethoxycarbonyl; HMP, 4-(hydroxymethyl)phenoxy; HOBt, 1-hydroxybenzotriazole; MBHA, 4-methylbenzhydrylamine; MeOBzl, 4-methoxybenzyl; Mts, mesitylene-2-sulfonyl; NMP, 4-methylpyrrolidone; OBzl, benzyl; ODhbt, 3,4-dihydro-4-oxo-1,2,3-benzotriazin-3-yl; OPfp, pentafluorophenyl; PAM, (phenylacetamido)methyl; PDMS, plasma desorption mass spectrometry; PEG, poly(ethylene glycol); PMC, 2,2,5,7,8-pentamethylchroman-6-sulfonyl; *t*-Boc, *tert*-butyloxycarbonyl; tBu, *tert*-butyl; TBTU, *O*-(1*H*-benzotriazol-1-yl)-*N,N,N'*-tetramethyluronium tetrafluoroborate; TSTU, *O*-(*N*-succinimidyl)-*N,N,N'*-tetramethyluronium tetrafluoroborate; TFA, trifluoroacetic acid; TFMSA, trifluoromethanesulfonic acid; Trt, triphenylmethyl.

= 23 600 M⁻¹ cm⁻¹. ²⁵²Cf plasma desorption mass spectrometry (PDMS) was recorded on a time-of-flight spectrometer (Bio-Ion/Applied Biosystems 20 K, Uppsala, Sweden). The mass scale was calibrated on the hydrogen and nitrate ions, and the experimental error is <1 u per 2000 u. Automated FMOC and *t*-Boc syntheses were done on ABI433 and ABI430 peptide synthesizers, respectively. High-performance liquid chromatography (HPLC) was carried out on a Waters 600E system equipped with a Waters 484 tunable detector.

Synthesis of Metal Complexes and Ligands. *5-(Amidoglutaryl)-1,10-phenanthroline, phen'.* A suspension of 5-amino-1,10-phenanthroline (1.0 g, 5.1 mmol) in 50 mL of anhydrous pyridine was heated to 70 °C. Then, glutaric anhydride (1.17 g, 10.2 mmol) was added. The solution was stirred at 100 °C, and another 585 mg (5.1 mmol) and 1.17 g (10.2 mmol) of anhydride were added after 1 and 2 h, respectively. After 3 h, the pyridine was reduced in vacuo to 5 mL, and 250 mL of acetonitrile was added. The solution was stirred at room temperature for 1 h to precipitate the desired product. The precipitate was collected by filtration and washed with acetonitrile (2 × 20 mL) to yield phen' as an off-white powder (785 mg, 49.6%). TLC [silica gel, without fluorescent indicator; CH₂Cl₂–MeOH (1:1); stained with (NH₄)₂Fe(SO₄)₂]: $R_f = 0.41$. ¹H NMR (*d₆*-DMSO) δ: 1.88 (quint, *J* = 7.3, 2H, CH₂*CH₂*CH₂); 2.33 (t, *J* = 7.3, 2H, CH₂COO); 2.56 (t, *J* = 7.3, CH₂CON); 7.70 (dd, *J* = 8.1, 4.3, 1H, H-C(8)); 7.78 (dd, *J* = 8.4, 4.3, 1H, H-C(3)); 8.15 (s, 1H, H-C(6)); 8.41 (dd, *J* = 8.1, 1.7, 1H, H-C(7)); 8.60 (dd, *J* = 8.4, 1.6, 1H, H-C(4)); 8.99 (dd, *J* = 4.3, 1.7, 1H, H-C(9)); 9.09 (dd, *J* = 4.3, 1.6, 1H, H-C(2)); 10.11 (s br, 1H, NH); 12.12 (s br, 1H, OH).

A substantial byproduct observed in the synthesis is the corresponding glutarimide that results from cyclization of phen'. The yield of this cyclized product accounts for the remainder of the starting material, 5-amino-1,10-phenanthroline.

[Rh(phi)₂(DMF)₂](OTf)₃. [Rh(phi)₂Cl₂]Cl (187.6 mg, 301.7 μmol), prepared as described earlier (*34*), and silver triflate (233.2 mg, 907.6 μmol) were suspended in 10 mL of dry DMF and heated at 65 °C for 24 h in the dark. The solution was filtered through a medium fritted funnel and used immediately in coordination reactions.

Bis(phenanthrenequinone diimine)((5-amidoglutaryl)-1,10-phenanthroline)rhodium(III) trichloride, [Rh(phi)₂(phen')]Cl₃. [Rh(phi)₂(DMF)₂](OTf)₃ (300 μmol) was filtered directly into a flask containing phen' (113.0 mg, 365.3 μmol) and heated at 65 °C for 18 h. The reaction mixture was diluted with 50 mL of 1:1 H₂O/CH₃CN and adsorbed on a Sephadex SP C-50 40–120 μm (H⁺-form) cation exchange column. The column was washed with 300 mL of H₂O/CH₃CN. The product mixture was then chromatographed with a HCl gradient (100 mL of 0.1 N and 100 mL of 0.2 N HCl in H₂O/CH₃CN). The main fraction was eluted at ca. 0.15 N HCl. The solvents were removed in vacuo, and the residue was dissolved in 30 mL of H₂O. After lyophilization, [Rh(phi)₂(phen')]Cl₃ (246.0 mg, 87.6%) was obtained as an orange fluffy powder. ¹H-NMR (*d₆*-DMSO, 300 MHz) δ: 1.86–1.96 (m, 2H, CH₂*CH₂*CH₂); 2.36 (t, *J* = 7.3, 2H, CH₂COO); 2.71 (t, *J* = 7.3, 2H, CH₂CON); 7.52 (t, *J* = 7.6, 1H); 7.63 (t, *J* = 7.6, 1H); 7.78 (t, *J* = 7.7, 1H); 7.84 (t, *J* = 7.8, 1H); 8.09 (dd, *J* = 8.3, 5.4, 1H); 8.18 (dd, *J* = 8.6, 5.3, 1H); 8.43–8.54 (m, 8H); 8.61–8.64 (m, 1H); 8.66 (s, 1H); 8.75 (d, *J* = 7.8, 1H); 8.86 (d(br), *J* = 7.9, 1H); 8.90 (d, *J* = 5.4, 1H); 8.984 (d, *J* = 7.7, 1H); 8.985 (d, *J* = 8.3, 1H); 9.03 (d, *J* = 5.3, 1H); 9.28 (d, *J* = 8.6, 1H); 10.94 (s, 1H, HN (amide)); 14.09, 14.12 (2s, 1H each); 14.26, 14.29 (2s, 1H each). UV–vis (H₂O, pH 5) λ_{max} (ϵ M⁻¹ cm⁻¹): 251

(69 800); 270 (83 300); 380 (32 900). PDMS: [Rh(phi)$_2$-(phen′)]$^{3+}$ − 2H$^+$]$^+$ obsd m/z 823.9, calcd m/z 822.7; [Rh-(phi)(phen′)]$^{3+}$ − 2H$^+$]$^+$ obsd m/z 618.9, calcd m/z 616.5; [Rh(phi)$_2$$^{3+}$ − 2H$^+$]$^-$ obsd m/z 515.4, calcd m/z 513.4; [Rh(phen′)]$^{3+}$ − 2H$^+$]$^+$ obsd m/z 412.3, calcd m/z 410.2; [Rh(phi)$^{3+}$ − 2H$^+$]$^+$ obsd m/z 309.6, calcd m/z 307.1; [phi]$^+$ obsd m/z 206.5, calcd m/z 206.3.

Bis(phenanthrenequinone diimine)(4-(4-carboxybutyl)-4′-methyl-2,2′-bipyridine)rhodium(III) Trichloride, [Rh-(phi)$_2$(bpy′)]Cl$_3$. [Rh(phi)$_2$(DMF)$_2$](OTf)$_3$ (189 μmol) was filtered directly into a flask containing bpy′ (56.5 mg, 220.3 μmol), heated at 65 °C for 16 h, and then rotavapped to dryness. Purification was carried out by cation exchange chromatography on Sephadex-SP C-50, 40−120 μm (H$^+$-form), in 1:1 H$_2$O/CH$_3$CN, and eluted with a gradient of 0−0.2 N HCl. The major fraction was collected and lyophilized to yield 118.6 mg (135.1 μmol, 71.5%) of [Rh(phi)$_2$(bpy′)]Cl$_3$ as an orange powder. TLC: (silica gel, without FI; n-BuOH−H$_2$O−AcOH = 5:3:2; R_f = 0.17−0.21 (orange, double spot). ^{1}H-NMR (D$_2$O, water suppression 300 MHz) δ: 2.06 (m (quint), 2H, C^{2}H$_2$); 2.46 (t, J = 7.2, 2H, C^{3}H$_2$); 2.64 (s, 3H, H$_3$C(C(4′))); 2.98 (t, J = 7.5, 2H, C^{1}H$_2$); 7.54−7.65 (m (quint, 6H), 7.80−7.88 (m (q), 4H), 8.25−8.42 (m, 10H), 8.52 (s br, 2H) signals of aromatic protons of bpy and phi. UV−vis (H$_2$O, pH 5) λ_{max} (ϵ M^{-1} cm^{-1}): 270 (66 700); 295 (48 200); 385 (32 300). PDMS: [Rh(phi)$_2$(bpy′)$^{3+}$ − 2H$^+$]$^+$ obsd m/z 769.8, calcd m/z 769.7; [Rh(phi)(bpy′)$^{3+}$ − 2H$^+$]$^+$ obsd m/z 564.8, calcd m/z 563.5; [Rh(phi)$_2$$^{3+}$ − 2H$^+$]$^+$ obsd m/z 515.2, calcd m/z 513.4; [Rh(bpy′)$^{3+}$ − 2H$^+$]$^-$ obsd m/z 357.2, calcd m/z 357.2; [Rh(phi)$^{3+}$ − 2H$^+$]$^+$ obsd m/z 309.0, calcd m/z 307.3; [bpy′]$^+$ obsd m/z 256.1, calcd m/z 256.3; [phi]$^+$ obsd m/z 206.1, calcd m/z 206.3.

Resolution of Enantiomers of [Rh(phi)$_2$(phen′)]Cl$_3$. The eluent potassium (+)-tris[l-cysteinesulfinato(2-)-S,N]cobaltate(III), K$_3$[Co(l-cysu)$_3$], was synthesized according to literature protocols (*35, 36*). A 115 × 2.5 cm column was filled with Sephadex-SP C-25 cation exchange resin that had been swelled in water. The resin was washed with 0.1 M KCl and then with copious amounts of water. [Rh-(phi)$_2$(phen′)]Cl$_3$ (100 mg) was dissolved in water and loaded on a minimum of resin. A 0.1 M [Co(l-cysu)$_3$]$^{3-}$ solution was recirculated at a flow rate of about 1 mL/min. After 12 h, two distinct orange bands could be seen. Each band was separated and eluted off the resin using 0.2 M HCl in 1:1 H$_2$O/CH$_3$CN. The bands were dried in vacuo, dissolved in water, and lyophilized to yield Δ- and Λ-[Rh(phi)$_2$(phen′)]Cl$_3$ (20 mg each). For the Δ- isomer, Δϵ_{280} = −26 M^{-1} cm^{-1}; Δϵ_{450} = −10 M^{-1} cm^{-1}.

Peptide Synthesis. Manual t-Boc peptide synthesis was performed according to standard procedures (*30, 31*) N-α-t-Boc-L-amino acids were used with the following side chain protecting groups: Arg(Mts), Asp(OBzl), Cys(4-MeOBzl), Glu(OBzl), His(Bom), Lys(Cl-Z), Ser(Bzl), Thr-(Bzl), Trp(CHO), Tyr(Br-Z). The amino acids were coupled by using t-Boc amino acid (4 equiv) and DCC (4 equiv) except for Arg and Glu which were HOBt esters (4 equiv of amino acid, 4 equiv of DCC, and 4 equiv of HOBt) and Gln and Asn which were symmetric anhydrides (4 equiv of amino acid and 2 equiv of DCC). All couplings were monitored by ninhydrin (*37*), and the cycle was repeated until >99% coupling efficiency was achieved.

The manual FMOC synthesis was performed according to standard procedures (*32*). The N-α-FMOC-L-amino acids were OPfp esters, except for serine and threonine, which were ODhbt esters, and arginine, which was the free acid. The following protected side chain amino acids were used: Arg(PMC), Asn(Trt), Asp(OtBu), Cys(Trt), Gln(Trt), Glu(OtBu), His(Trt) or His(t-Boc), Lys(t-Boc), Ser(tBu), Thr(tBu), Tyr(tBu). The FMOC protecting

group was removed using 2% (v/v) DBU in DMF (*38*). The amino acid OPfp esters and ODhbt esters (4 equiv) were activated with HOBt (4 equiv). The free acids (4 equiv) were activated with BOP (4 equiv) and NMM (4 equiv). All couplings were monitored by ninhydrin (*37*), and the cycle was repeated until >99% coupling efficiency was achieved. The resin was capped with 0.3 M acetic anhydride/HOBt in 9:1 DMF/CH$_2$Cl$_2$.

A portion of each resin (50−200 mg) was cleaved and deprotected for characterization by HPLC, amino acid analysis, and PDMS. The peptide resins were stored dry at −20 °C.

Synthesis of Metal−Peptide Chimeras. Two strategies for coupling [Rh(phi)$_2$(phen′)]$^{3+}$ have been successfully employed with both t-Boc and FMOC peptides and are described below. The rhodium complex is stable to HF, TFMSA, and TFA peptide cleavage and deprotection conditions, allowing it to be coupled to the peptide on the resin. The analogous reactions have also been accomplished using [Rh(phi)$_2$(bpy′)]Cl$_3$.

Removal of Amino-Terminal Protecting Group. (a) t-Boc. Resin containing the required peptide (40 μmol) was washed with CH$_2$Cl$_2$ (3 × 10 mL). The resin was treated with the TFA solution (25% (v/v) and 0.1% anisole in CH$_2$Cl$_2$) for 1.5 and 30 min. After the resin was washed with CH$_2$Cl$_2$ (6 × 10 mL), it was treated with 4 mL of 10% (v/v) DIEA in CH$_2$Cl$_2$ for 1.5 min (2×) and washed again with CH$_2$Cl$_2$ (6 × 10 mL). The resin was dried on the aspirator and then under vacuum. *(b) FMOC.* The peptide resin was swollen in DMF and washed once. Then, the resin was treated with 2% (v/v) DBU in DMF for 1 min and then 5 min. The resin was washed with DMF (6 × 10 mL), CH$_2$Cl$_2$, 1:1 CH$_2$Cl$_2$/MeOH, and absolute EtOH. Then the resin was dried on the aspirator and then under vacuum.

Removal of Base Labile Protecting Groups. Since phi complexes of rhodium are unstable to aqueous bases,[2] the base labile protecting groups like formyl-Trp in t-Boc synthesis must be removed prior to coupling the rhodium complex. To deprotect the Trp side chain, the resin was treated with 10 mL of 2-aminoethanol (6% in 5:95 water/DMF) for 30 min. The solution was drained and the resin washed with DMF (3 × 4 mL). The 2-aminoethanol treatment and washing were repeated. Finally, the resin was washed with CH$_2$Cl$_2$, 1:1 CH$_2$Cl$_2$/MeOH and absolute EtOH and dried under vacuum.

Coordination Strategy. (a) Activation of Phen′. Phen′ (24.6 mg, 80 μmol), TBTU (32 mg, 100 μmol), DMAP (ca. 1 mg, 4 μmol), and NMM (22 μL, 200 μmol) were taken in a 25 mL round bottom flask with 2 mL of NMP and stirred at room temperature for 15 min.

(b) Coupling of Phen′ to the N-Terminus of Peptide. The N-terminus-deprotected peptide−resin (40 μmol) was transferred to a 25 mL round bottom flask and stirred with 5 mL of CH$_2$Cl$_2$ for 15 min. The phen′ solution was added to the slurry, and the reaction was stirred at ambient temperature for 36 h. The reaction was followed by ninhydrin assay (*37*). Double coupling of phen′ may be required to ensure >95% coupling efficiency. The resin was filtered to remove excess reagents and washed with CH$_2$Cl$_2$, 1:1 CH$_2$Cl$_2$/MeOH, and absolute EtOH and dried under vacuum.

(c) Coordination of Resin−Peptide−Phen′ to [Rh-(phi)$_2$(DMF)$_2$](OTf)$_3$. The phen′−peptide resin was placed in a 25 mL round bottom flask in 5 mL of CH$_2$Cl$_2$ and stirred for 15 min to swell the resin. The [Rh(phi)$_2$-

---

[2] After treatment of [Rh(phi)$_2$(phen′)]Cl$_3$ with 2-aminoethanol at 0 °C at pH 10 for 5 min, about 10% of the metal complex is degraded.

$(DMF)_2](OTf)_3$ solution (40 µmol, in 5 mL of DMF) was added and the resulting mixture stirred in the dark at 70 °C for 36 h. The solution was removed by filtration, and the dark red resin was washed several times with DMF and 1:1 CH_2Cl_2/DMF over 30 min with agitation. Finally, the resin was washed with CH_2Cl_2, 1:1 CH_2Cl_2/MeOH, and absolute EtOH and dried under vacuum.

Direct Coupling Strategy. (a) Activation of [Rh-(phi)$_2$(phen')]Cl$_3$. [Rh(phi)$_2$(phen')]Cl$_3$ (13 mg, 14 µmol), HOBt (2.0 mg, 14 µmol), DCC (3.1 mg, 14 µmol), and DMAP (ca. 1 mg, 4 µmol) were taken in a 5 mL round bottom flask. Anhydrous NMP (0.5 mL) was added, and the solution was stirred at room temperature for 15 min. The activation can also be done using DSC (1 equiv) and DMAP (ca. 0.3 equiv).

(b) Coupling of [Rh(phi)$_2$(phen')]Cl$_3$ to the N-Terminus of the Peptide. The N-terminus deprotected peptide–resin (7 µmol) was placed into a 5 mL round bottom flask. The rhodium solution was added to the resin. The whole mixture was stirred under argon in the dark for 24 h. The resin was washed with NMP until the filtrate was clear and further washed with CH_2Cl_2, 1:1 CH_2Cl_2/MeOH, and absolute EtOH. The resin was dried in vacuo for several hours, and the coupling was repeated. The resin turns from orange to dark red in conjunction with the coupling of the metal complex. Ninhydrin analysis indicated *ca.* 70% coupling efficiency (*37*).

Deprotection and Cleavage of Metal–Peptide Complexes. Cleavage and deprotection of the *t*-Boc peptides were accomplished according to either the two-step TFMSA (*39*) or HF cleavage procedures. The HF cleavage was done in the presence of *p*-cresol and *p*-thiocresol for 60 min at 0 °C (*30*). The cleavage and deprotection of the FMOC peptides were done using 82.5% TFA, 5% H_2O, 5% phenol, 5% thioanisole, and 2.5% ethanedithiol for 2–5 h (*40*). The cleavage solutions were filtered into chilled (−20 °C) *tert*-butyl methyl ether (50 mL). After the solution was stored at −70 °C for at least 30 min, the solution was centrifuged for 10 min at 5 000 rpm. The ether was decanted off, and the orange precipitate was washed with cold ether twice. Alternatively, the peptide was isolated by filtration through a fine sintered glass funnel. The precipitate was then taken up in 5% acetic acid and lyophilized to dryness or directly purified by HPLC. The residual resin should be pale orange, but some of the metal–peptide chimera may remain associated with the resin giving it a darker color. Soaking the resin with DMF/CH_2Cl_2 should recover additional cleaved chimera.

HPLC Purification of Metal–Peptide Complexes. The metal–peptide complexes were purified on a Vydac semipreparative C_{18} reversed phase column using a water (0.1% TFA)/acetonitrile (0.1% TFA) gradient (15%–40% acetonitrile over 19 min) with a flow rate of 4.5 mL/min. The free peptides eluted first followed by phen'–peptides and finally the metal–peptide complexes (35–40% acetonitrile). The elution profiles were monitored at 220 and 370 nm with peaks containing the intact metal–peptide complexes showing the strongest absorbance at 370 nm. The HPLC fractions corresponding to the metal–peptide complexes were lyophilized and stored dry at −20 °C.

Rhodium–peptide complexes containing a disulfide bond can be reduced by reacting the complex with 1 equiv of DTT in 10 mM Tris·HCl, pH 8 for 1 h. The DTT should be removed since phi complexes of rhodium are unstable to thiols over time.[3]

Mass Spectroscopic Characterization. Molecular weight determinations of the tethered peptide complexes were carried out using ^{252}Cf PDMS at an accelerating voltage of 15 kV. The samples were adsorbed on nitrocellulose surfaces by applying solutions (200 pmol) of the tethered peptide complexes in 25% acetonitrile (0.1%TFA)–75% water and allowed to dry. Excess salt, if present, was removed from the adsorbed samples by rinsing with 1:1 EtOH/water prior to data accumulation.

Representative Metal–Peptide Complexes. *[Rh-(phi)$_2$(bpy')]$^{3+}$–AANVAISQWERAA-CONH$_2$.* The peptide was synthesized on the MBHA resin using manual *t*-Boc techniques and the rhodium complex coupled using the direct coupling strategy. After cleavage and deprotection with TFMSA, the chimera was isolated as an orange powder. Amino acid analysis observed (calculated) ratio: Asx 0.7 (1), Glx 1.8 (2), Ser 0.9 (1), Arg 1.0 (1), Ala 5.0 (5), Val 1.1 (1), Ile 1.1 (1). PDMS: [M^{3+} − 2H$^+$]$^+$ obsd *m/z* 2138.6, calcd *m/z* 2138.3.

[Rh(phi)$_2$(phen')]$^{3−}$–GGFAE-CO$_2$H. The peptide was synthesized on the PEG resin using manual FMOC techniques and the rhodium complex added using the direct coupling technique. After cleavage and deprotection for 2 h, the chimera was isolated as an orange powder. Amino acid analysis observed (calculated) ratio: Glx 1.0 (1), Gly 2.0 (2), Ala 1.1 (1), Phe 1.0 (1). PDMS: [M^{3+} − 2H$^−$]$^+$ obsd *m/z* 1283.3, calcd *m/z* 1284.2.

[Rh(phi)$_2$(phen')]$^{3+}$–LQQAIEQLQNAAAA-COOH. The peptide was synthesized on the PAM resin using automated *t*-Boc techniques and the rhodium complex coupled using the coordination method. After cleavage and deprotection by TFMSA, the chimera was isolated as an orange powder. Amino acid analysis observed (calculated) ratio: Asx 1.1 (1), Glx 5.0 (5), Ala 5.0 (5), Ile 1.2 (1), Leu 2.2 (2). PDMS: [M^{3+} − 2H$^+$]$^+$ obsd *m/z* 2274.7, calcd *m/z* 2273.3.

[Rh(phi)$_2$(phen')]$^{3−}$–TQQSKKQLQNKAAA-CONH$_2$. The peptide was synthesized on the MBHA resin using automated *t*-Boc techniques and the rhodium complex coupled using the coordination method. After cleavage and deprotection by TFMSA, the chimera was isolated as an orange powder. Amino acid analysis observed (calculated) ratio: Asx 0.7 (1), Glx 3.2 (4), Ser 1.0 (1), Thr 1.0 (1), Ala 3.0 (3), Leu 1.2 (1), Lys 2.5 (3). PDMS: [M$^{3−}$ − 2H$^−$]$^+$ obsd *m/z* 2348.2, calcd *m/z* 2347.5.

[Rh(phi)$_2$(phen')]$^{3−}$–AANVAIAAWERAA-CONH$_2$. The peptide was synthesized using automated *t*-Boc techniques and the rhodium complex added using both the direct coupling and the coordination technique. After cleavage and deprotection by TFMSA, the chimera was isolated as an orange powder. Amino acid analysis observed (calculated) ratio: Asx 1.0 (1), Glx 1.1 (1), Arg 1.1 (1), Ala 7.0 (7), Val 1.1 (1), Ile 0.9 (1). PDMS: [M^{3+} − 2H$^−$]$^+$ direct coupling obsd *m/z* 2118.5, coordination obsd *m/z* 2118.0, calcd *m/z* 2118.2.

[Rh(phi)$_2$(phen')]$^{3+}$–GGFACTVSYCGKRFTRSDEL-QRHKRTHTGE-CO$_2$H. The peptide was synthesized on the PAM resin using automated *t*-Boc techniques and the rhodium complex added using the coordination strategy. After cleavage and deprotection by HF, the chimera was isolated as an orange powder. Amino acid analysis observed (calculated) ratio: Asx 0.9 (1) Glx 2.6 (3), Ser 2.0 (2), Gly 4.1 (4), His 1.7 (2), Arg 4.2 (4), Thr 3.8 (4), Val 1.2 (1), Ala 1.1 (1), Tyr 0.8 (1), Val 1.2 (1), Cys 2.9 (2.0), Ile 1.0 (1), Lys 1.9 (2). PDMS: [M$^{3−}$ − 2H$^+$]$^+$ obsd *m/z* 4234.2, calcd *m/z* 4233.6.

RESULTS

Synthesis of Functionalized Ligands and Rhodium Complexes. Both bpy' and phen' may be readily

Scheme 1. Synthesis of [Rh(phi)₂(phen′)]Cl₃.
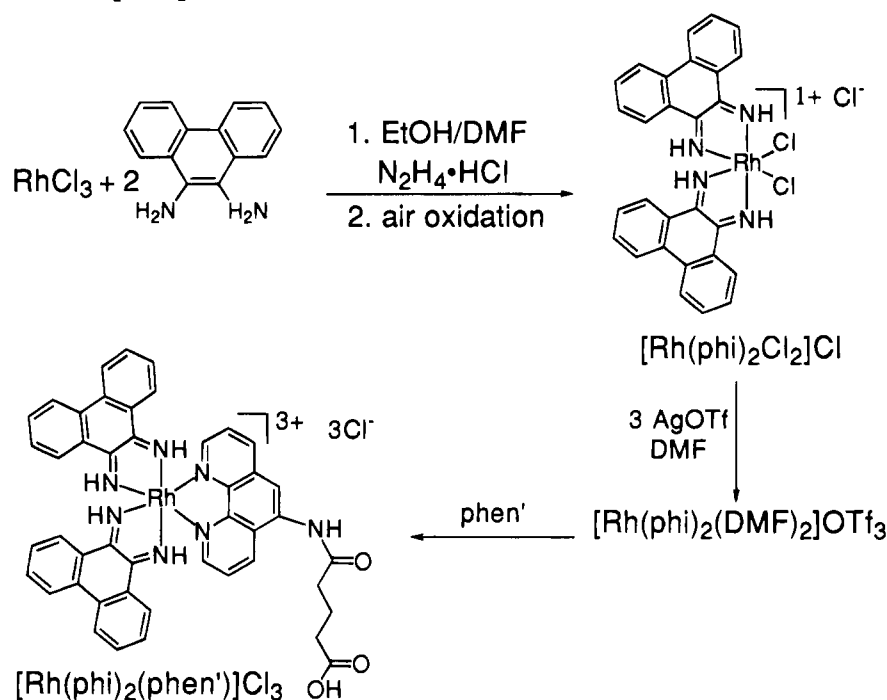
prepared. Bpy′ is synthesized as described by others (*33*) in 30% yield. Phen′ is achieved in one step by reaction of 5-amino-1,10-phenanthroline with glutaric anhydride in dry pyridine in 50% yield.
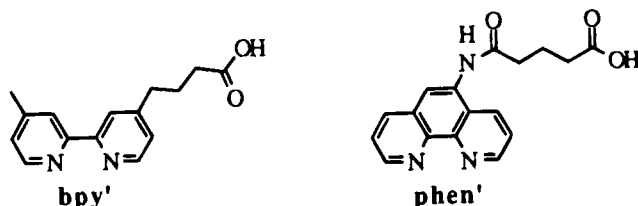
Scheme 1 illustrates the assembly of [Rh(phi)₂(phen′)]³⁺, which contains a pendant carboxylate for attachment to a peptide. To produce [Rh(phi)₂(phen′)]Cl₃, [Rh(phi)₂Cl₂]-Cl is first reacted with silver triflate to exchange the chloride ligands. After complete removal of silver ions, the substitutionally facile [Rh(phi)₂(DMF)₂](OTf)₃ complex is then heated with phen′ to promote coordination of the third chelating ligand. No coordination to the rhodium center by the ancillary carboxylate has been observed. [Rh(phi)₂(bpy′)]Cl₃ is synthesized in an analogous fashion.

Coupling of the Rhodium Complex to the Peptide. The metal–peptide chimera is synthesized using one of two strategies: (i) the coordination method or (ii) direct coupling. In the coordination strategy (Scheme 2), the chelating ligand containing a pendant carboxylate, bpy′ or phen′, is first coupled onto the amino terminus of the peptide on the resin. Then, the resin-bound peptide containing the chelating ligand is reacted with [Rh(phi)₂(DMF)₂](OTf)₃, in a manner similar to the synthesis of the parent rhodium complex. In the direct coupling strategy (Scheme 3), the coordinatively saturated metal complex containing the pendant carboxylate is first assembled. Then the functionalized metal complex and the terminal amine of the peptide bound to the resin are condensed in one step, in a manner that is analogous to the addition of another residue onto the growing peptide chain. For both strategies, the metal–

peptide complex is deprotected and cleaved from the resin in the same manner as for the free peptide.

A variety of conditions for synthesis have been examined. Peptides have been constructed using both FMOC and *t*-Boc methodologies and using manual as well as automated solid phase techniques (*30–32*). Prior to coupling of the ligand or metal complex onto the resin, a small portion of the resin is cleaved and the free peptide analyzed by HPLC to check the fidelity and efficiency of the synthesis. Yields of the final metal–peptide chimera (*vide infra*) are limited by the efficiency of the peptide synthesis.

A range of coupling agents have been examined using both strategies. In the case of the coordination method, several different coupling reagents have been used with similar success. These reagents include DCC/HOBt, DSC, TBTU, and TSTU. With the direct coupling method, we observe that the presence of the metal center makes the coupling reaction less efficient. The explanation for this poorer reactivity may be a function of either electronic deactivation or steric accessibility on the resin, or likely both. Because of the lower reactivity, more potent coupling agents should be favored. However, we also observe in the case of phen′ that intramolecular cyclization can be competitive with very potent activating agents. Given these factors, only DCC/HOBt and DSC have been found to promote reaction by the direct coupling strategy.

The metal–peptide complexes are observed to be more difficult to cleave off the resin than the peptide alone. Longer reaction times and harsher conditions (HF versus TFMSA) may be needed. For example, for the 30 residue metal–peptide complex, HF cleavage was required. However, neither the peptide nor the metal complex are stable to extended exposure to the cleavage and deprotection conditions. Several linkages to the resins such as MBHA, PAM, and PEG–PAM were also examined, but the variation in linker does not appear to affect the yield of cleaved product.

The metal–peptide complexes are purified by HPLC. In all cases observed so far, the retention time of the

Scheme 2. Coordination method for the synthesis of metal–peptide chimeras.
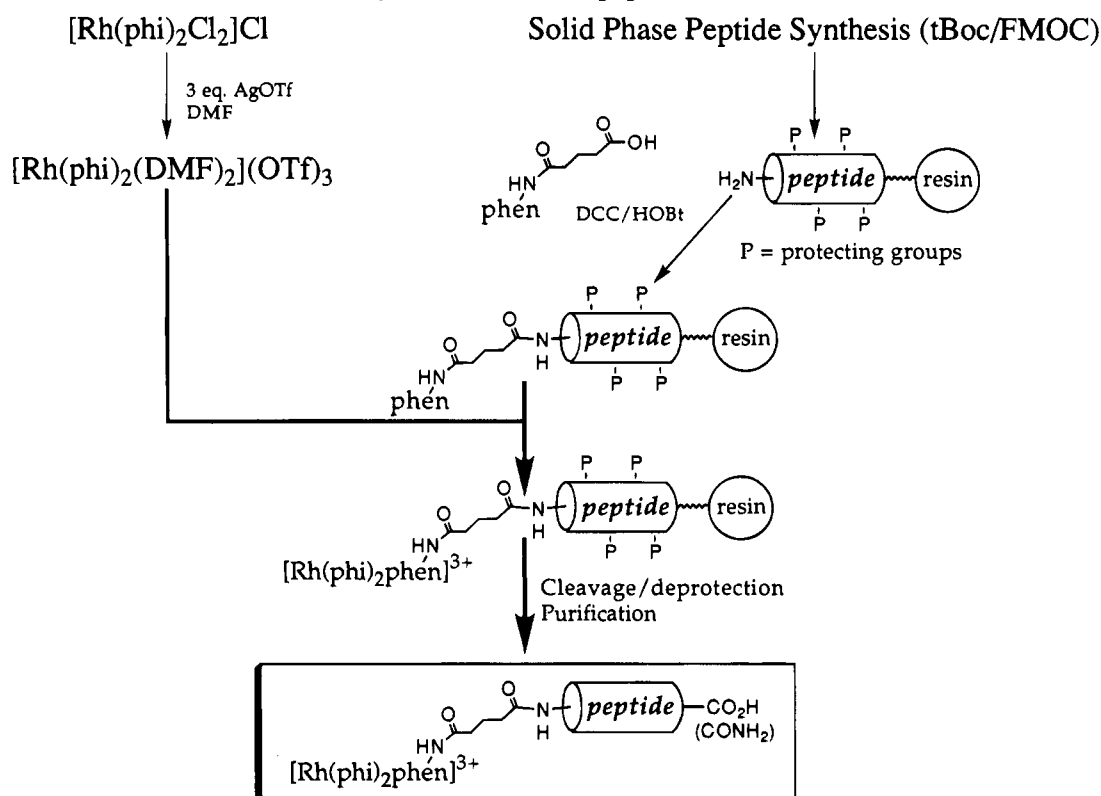
Scheme 3. Direct coupling method for the synthesis of metal–peptide chimeras.
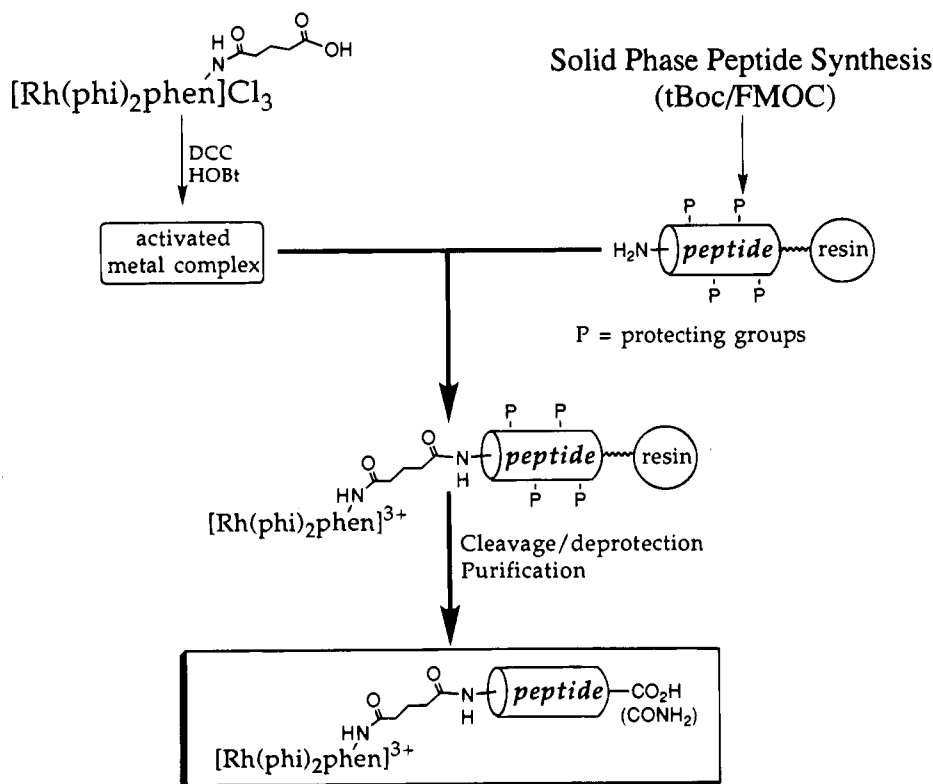
metal–peptide complexes is found to be longer than that of the corresponding free peptide.

Overall Yields. Theoretical yields of metal–peptide complexes may be determined based upon the initial substitution of the resin. Actual recovered yields of pure chimera (after two rounds of HPLC purification) are found to be in the range of 5–18%. Not surprisingly, the major determinant of the yield for the reaction is the

initial synthesis of the peptide. Yields of metal–peptide chimeras correlate closely with the recovered yields for the individual peptides before metal–complex attachment. For small peptides (<16 residues), the number of failure sequences tend to be small, and thus the overall yield of the desired chimera is found to be higher than for yields of chimeras with longer appended peptides. The presence of the metal complex, does, however, signifi-

cantly decrease the overall yield. If one compares the recovered yields of a 30-residue peptide to its corresponding [Rh(phi)₂(phen′)]³⁺ chimera, we find the yield to be 37% for the peptide and 5% for the metal−peptide.

Yields do not differ substantially between the coordination and direct coupling strategies. The presence of the metal center is observed to inhibit the coupling reaction both in solution and on the resin, and the presence of the solid support may somewhat interfere with coordination. The coordination of [Rh(phi)₂(DMF)₂]-(OTf)₃ and phen′ in solution is accomplished in 90% yield. No significant differences in yield for the metal−peptide complex are found using bpy′ versus phen′, an indication that the competing intramolecular cyclization, which is available for phen′ but not bpy′, is not limiting. A chief difficulty in the synthesis is recovery of metal−peptide chimera from the resin. The presence of the covalently bound metal complex certainly inhibits cleavage of the chimera from the resin, whether electronic or steric factors are dominating is not known.

Characterization of the Chimeras. *Electronic Spectroscopy.* As shown in Figure 2, the UV−visible spectra of the metal−peptide complexes are observed to be a composite of the spectrum of the parent rhodium complex and that of the peptides independently. Since the peptides do not absorb significant light at wavelengths ≥ 300 nm, the concentration of chimera may be quantitated based upon the extinction coefficient of the rhodium complex at 350 nm. It is noteworthy that at ≤300 nm some reduction in the absorption intensity for the metal−peptide complex is observed compared to the metal complex. As with the parent metal complexes, there are pH dependent changes observed in the spectrum which depend upon the protonation state of the coordinated phi ligands (*34, 41*). The peptide content of the chimera is ascertained by standard amino acid analysis. Comparison of the quantitation by UV−vis spectroscopy and amino acid analysis reveals a 1:1 ratio of rhodium complex to peptide in all cases.

Considerations of Chirality. So as to isolate diastereomerically pure metal−peptide chimeras, pure enantiomers of the functionalized metal complex may be used in the direct coupling strategy or metal−peptide chimeras may be synthesized without regard to isomeric purity at the metal center and diastereomers separated by chiral chromatography following coupling. The enantiomers of [Rh(phi)₂(phen′)]³⁻ are resolved on a cation exchange column using a chiral eluent (+)-tris[*l*-cysteinesulfinato-(2−)-*S,N*]cobaltate(III) (*35, 36*). As may be seen in Figure 3, the isomers separate into two bands which show characteristic CD spectra. The assignment of enantiomeric configuration is made based upon comparison to spectra of [Rh(phen)₂(phi)]³⁺ and [Rh(en)₂(phi)]³⁺ (en = ethylenediamine) (*42, 43*). Pure diastereomers may then be obtained by direct coupling of the enantiomers of the rhodium complex to the peptide. Conditions for coupling, deprotection, and cleavage from the resin do not lead to racemization at the metal center.

Optically pure metal−peptide diastereomers may also be isolated from chimeras which are racemic about the metal center using a protocol of chiral elution on Sephadex CM-C25 analogously to that used for the parent metal complex. The CD spectrum of the diastereomerically pure metal−peptide complex (Figure 3) isolated by chiral elution is observed to be the composite of the spectrum of the corresponding enantiomer of the rhodium complex and that of the peptide.

We also considered the possibility of chiral induction about the metal center either in the direct coupling or coordination of metal complexes to the diastereomerically
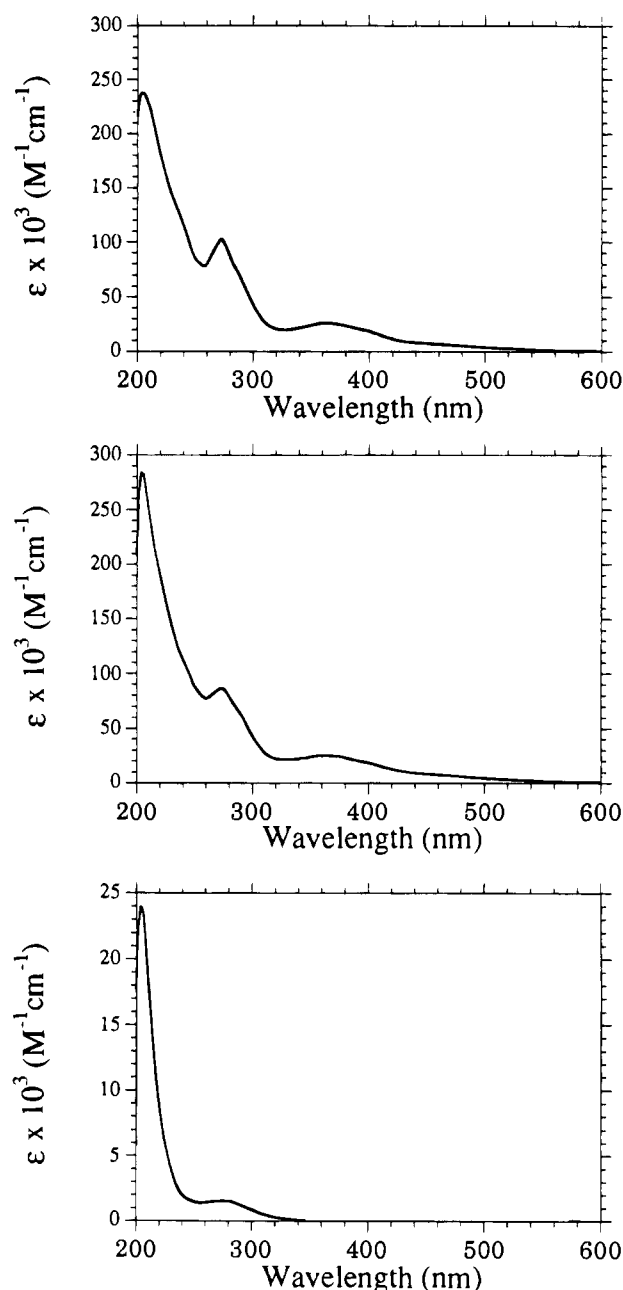
Figure 2. UV−vis spectra in 10 mM Tris·HCl, pH 7.0 of [Rh-(phi)₂(phen′)]Cl₃ (top), [Rh(phi)₂(phen′)]³⁺−GGFACTVSYCGK-RFTRSDELQRHKRTHTG-CO₂H (middle), and NH₂-GGFAC-TVSYCGKRFTRSDELQRHKRTHTG-CO₂H (bottom).

pure peptides on the resin. However, the synthesis of the metal−peptide complexes is found to proceed without diastereoselectivity using either strategy. Figure 3 also shows the CD spectrum of a metal−peptide chimera produced by coordination of racemic [Rh(phi)₂]³⁺ onto a 14-residue peptide containing coupled phen′. The circular dichroism shows negative ellipticity below 240 nm which is characteristic of the peptide, but no features above 250 nm are evident, which is indicative of a racemate at the rhodium center. This result is to be contrasted to the results of crosslinking peptide α-helical bundles in solution by [Fe(bpy)₃]²⁺ (*5*) or [Ni(bpy)₃]²⁺ (*2*) where isomeric induction was observed.

Mass Spectrometry. The mass spectrometry of the chimera establishes that the metal complex and peptide are covalently bound. As is evident in Figure 4, the PDMS spectrum of [Rh(phi)₂(phen′)]³⁺−LQQAIEQLQN-AAAA-COOH shows the expected molecular ion peak
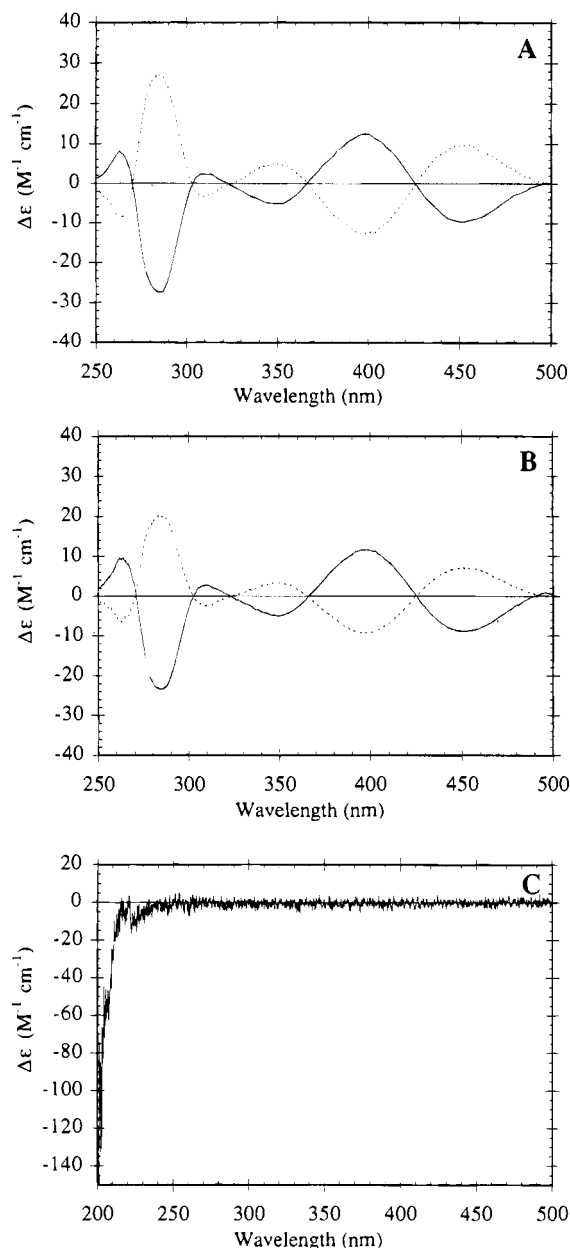
Figure 3. Circular dichroism of: (A) the Δ- (—) and Λ- (- - -) enantiomers of [Rh(phi)₂(phen′)]Cl₃ in 10 mM Tris·HCl, pH 7.0; (B) the Δ- (—) and Λ-(- - -) diastereomers of [Rh(phi)₂(phen′)]³⁺–TQQSKKQLQNKAAA-CONH₂ in 10 mM Tris·HCl, pH 7.0; and (C) racemic [Rh(phi)₂(phen′)]³⁺–TQQSKKQLQNKAAA-CONH₂ in 20 mM Tris·HCl, pH 7.0.

$[M^{3-} - 2H^+]^+$ at obsd m/z 2274.7, calcd m/z 2273.3, [Rh(phi)₂ $- 2H^+]^+$ at obsd m/z 515, calcd m/z 513, and [Rh(phi) $- 2H^+]^+$ at obsd m/z 309, calcd m/z 307.

Importantly, the presence of the covalently attached metal complex promotes fragmentation of the attached peptide. As shown in Figure 4, we observe a series of A_n fragments which reflect cleavage of the C_α–CO bond in the metal–peptide chimera. In contrast, no fragmentation is evident for the peptide lacking the metal complex. In addition, for each A_n fragment we observe a corresponding fragment of 206 u lower. These pairs of fragments correspond to A_n fragments with the intact rhodium complex attached and A_n fragments containing metal complexes in which one of the phi ligands has been lost. For metal–peptide chimeras containing ≤14 residues, the complete series of A_n fragments is observed. For longer metal–peptide chimeras, only the first few N-terminal fragments are found with the larger molec-

ular weight fragments not detected; presumably folding of the longer peptide inhibits fragmentation.

It is also noteworthy that all the peaks observed for the metal–peptide complexes correspond to the singly charged species. It is unlikely that these fragments correspond to Rh(I) complexes, but to [Rh(III) − 2H⁺]⁺. This feature is observed even with highly positive charged metal–peptide complexes. The doubly or triply charged ion peaks are small or not observable. Therefore, all molecular ion and fragment peaks are calculated as [M³⁺ − 2H⁺]⁻.

DISCUSSION

Scope of the Synthesis. We have developed a general method for the covalent attachment of inert coordinatively saturated rhodium complexes to a specific site on synthetic peptides. The peptides may be of any length synthetically accessible, contain any desired amino acid residues, and be coupled to rhodium complexes with different chelating ligands. Other coordinatively saturated metal complexes which are stable to the conditions required may also be utilized (*14, 15, 44*). In this study, all the natural amino acids except methionine have been used in the synthesis, and peptides ranging in length from 5 to 30 amino acids have been successfully coupled to the rhodium complex. Since the peptides are made using solid phase methodology, this strategy also allows for selective deprotection of one functional group on the peptide to serve as or to attach to a specific ligand for the metal complex, and this selectivity represents a clear advantage over solution phase strategies. In our case, the amino terminus has been used as the attachment point for a chelator. Allowing the synthesis to proceed on a solid support also ensures the separation of unreacted reagents by filtration, making the subsequent chromatographic purification easier. Indeed, the chromatograms accurately reflect the efficiency of the initial peptide synthesis.

Two strategies for coupling together the metal center and the peptide have been described, the coordination method and direct coupling, and each offers certain advantages. No substantial differences in yield are observed. The presence of the metal center tends to inhibit the coupling reaction, but coordination on the resin is of lower efficiency than the coordination of the metal complex alone in solution. The direct coupling method also preserves the integrity of the metal center and may be preferable under conditions where diastereomerically pure samples are needed. The conditions for synthesis do not lead to racemization about the metal center, if enantiomerically pure metal complexes are used in the coupling. Nonetheless, we have also found that pure metal–peptide chimeras may be resolved by chromatography with chiral eluents from samples which are racemic about the metal center. Furthermore, UV–visible spectroscopy offers a sensitive gauge of the coordination about the metal center.

The presence of these two strategies therefore provides versatility, and the preferred strategy should depend upon the application required. Both strategies offer distinct advantages over solution phase methods, in that functionalization of side chains is precluded. Thus, selective attachment of the metal center to a specific residue or to the N-terminus can be reliably accomplished.

Limitations of the Method. The obvious limitation of such an approach is that only metal complexes that are stable to the deprotection and cleavage conditions from the resin support can be used. The overall yields of the rhodium–peptide complex are modest and are

A

A_2
-phi

A_1

A_3
-phi

A_2/A_5
-phi

A_3 A_4

A_6
-phi

A_6
-phi

A_5

A_7
-phi

A_6

A_8
-phi

A_7

A_9
-phi

A_8

A_{10}
-phi

A_9

A_{10}

900 1000 1100 1200 1400 1600 1800 m/z

$[Rh(phi)_2]^+$
515.3

$[Rh(phi)]^+$
309.5

M^+
2274.7

M^+
- phi
2071.1

300 400 600 1000 1400 1800 2200 m/z

M^+
1467.8

300 400 600 1000 1400 m/z

B

A_1 A_3 A_5 A_7 A_9
890.9 1147.1 1331.4 1588.6 1829.9 2015.1 2157.2 2273.3

Ala-Ala-Ala-Ala-CO$_2$H

513.4

1039.0 1218.2 1457.4 1701.8 1944.0 2086.2 2228.3
A_2 A_4 A_6 A_8 A_{10}

L Q Q A I E Q L Q N

Figure 4. ^{252}Cf PDMS spectra and fragmentation pattern of a representative metal–peptide complex, [Rh(phi)$_2$(phen')]$^{3+}$–LQQAIEQLQNAAAA-COOH. (A) PDMS spectrum of the metal–peptide complex (top) showing the molecular ion (M$^+$) peak, fragments characteristic of cleavage at the metal center, and A$_n$ fragments arising from cleavage of the peptide C$_\alpha$–CO bond. The top inset in A above shows an enlarged view of the 800–1950 region with A$_1$–A$_{10}$ fragments labeled. Shown at the bottom of panel A is the PDMS spectrum of free peptide, H$_2$N-LQQAIEQLQNAAAA-COOH, showing the M$^+$ peak and no other significant fragmentation. (B) Schematic representation of the A$_n$ fragments for the metal peptide complex and their calculated mass. Since only singly charged species are observed, all calculated masses are given for the [M^{3+} − 2H$^+$]$^+$ ion.

dependent primarily on the yield of the initial peptide synthesis. The presence of the metal center does, however, further limit the yield, and in particular we observe that the presence of covalently bound metal complex tends to inhibit recovery of the product from the solid support.

Features of the Metal–Peptide Chimeras. The spectroscopic characteristics of the metal–peptide complexes are seen to be the sum of those of the isolated metal complex and the appended peptide. The electronic spectra for the chimeras are very similar to those of the parent [Rh(phi)$_2$L]$^{3+}$ (L = phen' or bpy') complexes. The coordination sphere of the rhodium is not perturbed by

coupling to the peptide; any ligand exchange with side chain coordination would be sensitively detected spectroscopically. Besides providing a measure of concentration (because of higher extinction coefficients at longer wavelengths for the chimera than for the peptide alone), the electronic spectrum also is diagnostic of the integrity of the metal–peptide complex.

Significantly, we do not observe any induced CD signals above 300 nm despite having a chiral peptide attached to a diastereotopic metal complex. The chirality of the individual peptides is not strong enough to favor formation of one enantiomer about the metal center. Likewise, the CD spectra of the pure diastereomers of

the metal—peptide complex are equal and opposite above 250 nm. However, below 250 nm the CD spectrum is the sum of the contribution of the peptide (negative ellipticity) and the enantiomerically pure metal complex making up each diastereomer.

Another important benefit of metal attachment to the peptide is evident in the mass spectral analysis. The PDMS spectra of the metal—peptide complexes show, in addition to the parent molecular ion peaks, two families of fragments that reflect the sequential analysis of the metal—peptides. Under conditions used in our experiments, no fragmentation of the peptide is evident without the metal being attached. Thus, the covalently bound metal complex enhances the intensity of the A_n fragments substantially, probably because of the nascent positive charge on the rhodium center causes charge remote fragmentation of the peptide (45). In other studies, derivatization of both the N- and C-terminus by organic molecule that place a fixed positive (46) or negative (47) charge on the peptide has caused an increase in fragmentation as seen by FAB-MS-MS or FAB/CID, respectively. With these methods, many different series of fragments are seen which makes complete sequence analysis possible but difficult. With PDMS, derivatization of the N-terminus of ribonuclease A via an (ethyl)-triphenylphosphonium produced only a weak incomplete series of A_n fragments. It was postulated that the labile nature of the phosphonium group inhibited the fragmentation. Guanidination of the amino terminal lysine residue produced better fragmentation (48). However, the attachment of our rhodium complex is not dependent on the presence of any amino acid, and derivatization of other positions is precluded while it produces a clean and complete series of sequence-specific fragments.

This sequential fragmentation may be powerfully exploited in the analysis of the metal—peptide chimera. Using PDMS as a diagnostic technique, we have been able to characterize mutant chimeras containing deleted amino acids and we have been able to establish sites where side chain protecting groups were still bound. Since our chimeras are blocked at the amino terminus with the rhodium complex, common sequencing techniques are not viable.

Implications. Metal—peptide chimeras may therefore be readily constructed using solid-phase synthesis. The spectroscopic characteristics of the coordination complexes provide a convenient handle to monitor the structure and reactivity, and the mass spectral characteristics provide a unique handle to analyze the peptide sequence. In these metal—peptide chimeras, therefore, as with metalloproteins, features of coordination chemistry may be incorporated in new designs and exploited.

ACKNOWLEDGMENT

LITERATURE CITED

(1) Ghadiri, M. R., and Fernholz, A. K. (1990) Peptide Architecture. Design of Stable α-Helical Metallopeptides via a Novel Exchange-Inert Ru^{III} Complex. *J. Am. Chem. Soc. 112*, 9633.

(2) Ghadiri, M. R., Soares, C., and Choi, C. (1992) A Convergent Approach to Protein Design. Metal Ion-Assisted Spontaneous Self-Assembly of a Polypeptide into a Triple-Helix Bundle Protein. *J. Am. Chem. Soc. 114*, 825.

(3) Ghadiri, M. R., Soares, C., and Choi, C. (1992) Design of an Artificial Four-Helix Bundle Metalloprotein via a Novel Ruthenium(II)-Assisted Self-Assembly Process. *J. Am. Chem. Soc. 114*, 4000.

(4) Ghadiri, M. R., and Choi, C. (1990) Secondary Structure Nucleation in Peptides. Transition Metal Ion Stabilized α-Helices. *J. Am. Chem. Soc. 112*, 1630.

(5) Lieberman, M., and Sasaki, T. (1991) Iron(II) Organizes a Synthetic Peptide into Three-Helix Bundles. *J. Am. Chem. Soc. 113*, 1470.

(6) Lieberman, M., Tabet, M., and Sasaki, T. (1994) Dynamic Structure and Potential-Energy Surface of a 3-Helix Bundle Protein. *J. Am. Chem. Soc. 116*, 5035.

(7) Ruan, F. Q., Chen, Y. Q., and Hopkins, P. B. (1990) Metal Ion Enhanced Helicity in Synthetic Peptides. *J. Am. Chem. Soc. 112*, 9403.

(8) Ruan, F. Q., Chen, Y. Q., Itoh, K., Sasaki, T., and Hopkins, P. B. (1991) Synthesis of Peptides Containing Unnatural, Metal-Ligating Residues- Aminodiacetic Acid as a Peptide Side-Chain. *J. Org. Chem. 56*, 4347.

(9) Imperiali, B., and Kapoor, T. M. (1993) The Reverse Turn as a Template for Metal Coordination. *Tetrahedron 49*, 3501.

(10) Robertson, D. E., Farid, R. S., Moser, C. C., Urbauer, J. L., Mulholland, S. E., Pidikiti, R., Lear, J. D., Wand, A. J., DeGrado, W. F., and Dutton, P. L. (1994) Design and Synthesis of Multi-Heme Proteins. *Nature 368*, 425.

(11) Choma, C. T., Lear, J. D., Nelson, M. J., Dutton, P. L., Robertson, D. E., and DeGrado, W. F. (1994) Design of a Heme-Binding Four-Helix Bundle. *J. Am. Chem. Soc. 116*, 856.

(12) Handel, T. M., Williams, S. A., and DeGrado, W. F. (1993) Metal Ion-Dependent Modulation of the Dynamics of a Designed Protein. *Science 261*, 879.

(13) Handel, T., and DeGrado, W. F. (1990) De Novo Design of a Zn^{2+}-Binding Protein. *J. Am. Chem. Soc. 112*, 6710.

(14) Peek, B. M., Ross, G. T., Edwards, S. W., Meyer, G. J., Meyer, T. J., and Erickson, B. W. (1991) Synthesis of Redox Derivatives of Lysine and Related Peptides Containing Phenothiazine or *tris*(2,2'-Bipyridine)ruthenium(II). *Int. J. Peptide Protein Res. 38*, 114.

(15) Mecklenburg, S. L., Peek, B. M., Schoonover, J. R., McCafferty, D. G., Wall, C. G., Erickson, B. W., and Meyer, T. J. (1993) Photoinduced Electron Transfer in Amino-Acid Assemblies. *J. Am. Chem. Soc. 115*, 5479.

(16) Imperiali, B., and Fisher, S. L. (1991) (S)-α-Amino-2,2'-bipyridine-6-propanoic acid—A Versatile Amino Acid for *de novo* Metalloprotein Design. *J. Am. Chem. Soc. 113*, 8527.

(17) Wuttke, D. S., Gray, H. B., Fisher, S. L., and Imperiali, B. (1993) Semisynthesis of Bipyridyl-Alanine Cytochrome *c* Mutants: Novel Proteins with Enhanced Electron-Transfer Properties. *J. Am. Chem. Soc. 115*, 8455.

(18) Pessi, A., Bianchi, E., Crameri, A., Venturini, S., Tramontano, A., and Sollazzo, M. (1993) A Designed Metal-Binding Protein with a Novel Fold. *Nature 362*, 367.

(19) Merkle, D. L., Schmidt, M. H., and Berg, J. M. (1991) Design and Characterization of a Ligand-Binding Metallopeptide. *J. Am. Chem. Soc. 113*, 5450.

(20) Krizek, B. A., Merkle, D. L., and Berg, J. M. (1993) Ligand Variation and Metal Binding Specificity in Zinc Finger Peptides. *Inorg. Chem. 32*, 937.

(21) Wade, W. S., Koh, J. S., Han, N., Hoekstra, D. M., and Lerner, R. A. (1993) Engineering Metal Coordination Sites into an Antibody Light Chain. *J. Am. Chem. Soc. 115*, 4449.

(22) Barbas, C. F., III., Rosenblum, J. S., and Lerner, R. A. (1993) Direct Selection of Antibodies that Coordinate Metals from Semisynthetic Combinatorial Libraries. *Proc. Natl. Acad. Sci. U.S.A. 90*, 6385.

(23) Wade, W. S., Ashley, J. A., Jahangiri, G. K., McElhaney, G., Janda, K. D., and Lerner, R. A. (1993) A Highly Specific Metal-Activated Catalytic Antibody. *J. Am. Chem. Soc. 115*, 4906.

(24) Shullenberger, D. F., Eason, P. D., and Long, E. C. (1993) Design and Synthesis of a Versatile DNA-Cleaving Metallopeptide Structural Domain. *J. Am. Chem. Soc. 115*, 11038.

(25) Pyle, A. M., and Barton, J. K. (1990) Probing Nucleic Acids with Transition Metal Complexes. *Prog. Inorg. Chem. 38*, 413–465.

(26) Chow, C. S., and Barton, J. K. (1992) Transition-Metal Complexes as Probes of Nucleic Acids. *Methods Enzymol. 212,* 219.

(27) Dupureur, C. M, and Barton, J. K. The Assembly of Transition Metal Complexes for Site-Specific Recognition of Nucleic Acids. *Comprehensive Supramolecular Chemistry,* Pergamon Press, New York (in press).

(28) Sitlani, A., Long, E. C., Pyle, A. M., and Barton, J. K. (1992) DNA Photocleavage by Phenanthrenequinone Diimine Complexes of Rhodium(III): Shape-Selective Recognition and Reaction. *J. Am. Chem. Soc. 114,* 2303.

(29) Sardesai, N. Y., Zimmermann, K., and Barton, J. K. (1994) DNA Recognition by Peptide Complexes of Rhodium(III): Example of a Glutamate Switch. *J. Am. Chem. Soc. 116,* 7502.

(30) Stewart, J. M., and Young, J. D. (1984) *Solid Phase Peptide Synthesis,* 2nd ed., Pierce Chemical Co., Rockford, IL.

(31) Edmondson, J. M., Klebe, R. J., Zardeneta, G., Weintraub, S. T., and Kanda, P. (1988) Methods for Solid-Phase Peptide-Synthesis Which Employ a Minimum of Instrumentation. *BioTechniques 6,* 866.

(32) Atherton, E., and Sheppard, R. C. (1989) *Solid Phase Peptide Synthesis: A Practical Approach,* IRL Press, Oxford.

(33) Della Ciana, L., Hamachi, I., and Meyer,T. J. (1989) Synthesis of Side-Chain Derivatives of 2,2′-Bipyridine. *J. Org. Chem. 54,* 1731.

(34) Pyle, A. M., Chiang, M. Y., and Barton, J. K. (1990) Synthesis and Characterization of Physical, Electronic, and Photochemical Aspects of 9,10-Phenanthrenequinone Diimine Complexes of Ruthenium(II) and Rhodium(III). *Inorg. Chem. 29,* 4487.

(35) Dollimore, L. S., and Gillard, R. D. (1973) Optically Active Co-ordination Compounds. Part XXXII. Potassium (+) Tris-[L-cysteinesulphinato(2-)-SN]cobaltate(III): A Versatile Agent for Resolution of 3+ Species. *J. Chem. Soc., Dalton Trans.* 933.

(36) Cartwright, P. S., Gillard, R. D., and Sillanpaa, E. R. J. (1987) Optically Active Coordination Compounds-XLVI. Resolution of Tris-di-imine Compounds of Chromium(III) Using *fac*-(+)Tris(L-cysteinesulphinato(2-)-SN]cobaltate(III). *Polyhedron 6,* 105.

(37) Sarin, V. K., Kent, S. B. H., Tam, J. P., and Merrifield, R. B. (1981) Quantitative Monitoring of Solid-Phase Peptide Synthesis by the Ninhydrin Reaction. *Anal. Biochem. 117,* 147.

(38) Wade, J. D., Bedford, J., Sheppard, R. C., and Tregear, G. W. (1991) DBU as an N^α-Deprotecting Reagent for the Fluorenylmethoxycarbonyl Group in Continuous Flow Solid-Phase Peptide Synthesis. *Pept. Res. 4,* 194.

(39) Swedloff, M. D., Anderson, S. B., Sedgwick, R. D., Gabriel, M. K., Brambilla, R. J., Hindenlang, D. M., and Williams, J. T. (1989) Solid Phase Synthesis of Bioadhesive Peptide with Trifluoromethanesulfonic Acid Cleavage from PAM Resin. *Int. J. Pept. Prot. Res. 33,* 318.

(40) King, D. S., Fields, C. G., and Fields, G. B. (1990) A Cleavage Methods which Minimizes Side Reactions Following Fmoc Solid Phase Peptide Synthesis. *Int. J. Pept. Prot. Res. 36,* 255.

(41) Krotz, A. H., Kuo, L. Y., and Barton, J. K (1993) Metallointercalators: Syntheses, Structures, and Photochemical Characterizations of Phenanthrenequinone Diimine Complexes of Rhodium(III). *Inorg. Chem. 32,* 5963.

(42) David, S. S., and Barton, J. K. (1993) NMR Evidence for Specific Intercalation of Δ-Rh(phen)$_2$phi^{3+} in [d(GTCGAC)$_2$]. *J. Am. Chem. Soc. 115,* 2984.

(43) Krotz, A. H., Kuo, L. Y., Shields, T. P., and Barton, J. K. (1993) DNA Recognition by Rhodium(III) Polyamine Intercalators: Considerations of Hydrogen Bonding and van der Waals Interactions. *J. Am. Chem. Soc. 115,* 3877.

(44) Jenkins, Y., and Barton, J. K. (1992) A Sequence-Specific Molecular Light Switch—Tethering of an Oligonucleotide to a Dipyridophenazine Complex of Ruthenium(II). *J. Am. Chem. Soc. 114,* 8736.

(45) Gross, M. L. (1992) Charge-Remote Fragmentations: Method, Mechanism and Applications. *Int. J. Mass Spectrom. Ion Processes 118/119,* 137.

(46) Watson, J. T., Wagner, D. S., Chang, Y., Strahler, J. R., Hanash, S. M., Gage, D. A. (1991) Characterization of the Ethyl-triphenylphosphonium Derivative of Model Peptides by Fast Atom Bombardment Collisionally-activated Dissociation Tandem Mass Spectrometry using B/E linked Scans. *Int. J. Mass Spectrom. Ion Processes 111,* 191.

(47) Lindh, I., Griffiths, W. J., Bergman, T. and Sjovall, J. (1994) Charge-Remote Fragmentation of Peptide Derivatized with 4-Aminonaphthalenesulphonic Acid. *Rapid Commun. Mass Spectrom. 8,* 797.

(48) Bunk, D. M., and Macfarlane, R. D. (1993) Derivatization to Enhance Sequence-Specific Fragmentation of Peptide and Proteins. *Int. J. Mass Spectrom. Ion Processes 126,* 123.

BC950007J

TECHNICAL NOTES

Electrophoretic Method for the Quantitative Determination of a Benzyl-DTPA Ligand in DTPA Monoclonal Antibody Conjugates

Diep T. Pham, Frans M. Kaspersen, and Ebo S. Bos*

N.V. Organon, P.O. Box 20, 5340 BH OSS, The Netherlands. Received December 12, 1994[⊗]

A simple electrophoretic IEF procedure was developed for the quantitation of bifunctional DTPA ligand molecules in DTPA–protein conjugates. From a calibration plot of pI versus substitution ratios of reference conjugates, the concentrations of DTPA conjugated to protein were determined. Molar ratios of DTPA to protein agreed satisfactorily with the ratios obtained by a spectrophotometric technique using a colored yttrium(III) complex of arsenazo III. The IEF method was successfully applied on preparations of benzyl-DTPA to mAbs MOPC-21, SC-20 (aCEA), and human serum albumin.

INTRODUCTION

For over a decade, radiolabeled monoclonal antibodies have been studied as a tool in the diagnosis and therapy of cancer (1–3). The most interesting isotopes employed in radioimmunodiagnosis and -therapy, e.g., ^{111}In and ^{90}Y, are metal ions, which can be bound to the targeting moiety only when captured in a chelation structure either directly to the antibody or via carrier molecules like serum albumin or polylysine. Determination of the number of ligands introduced is an essential part in the quality control of chelator–conjugate preparations for preclinical purposes and clinical use.

The number of metal binding sites in ligand mAb conjugates can be quantitated by several analytical methods, e.g., ^{111}In or [57]Co binding assays (4, 5) or the spectrophotometric titration with a yttrium–arsenazo III complex (6). A drawback of the two former procedures is that radioactive isotopes are employed as analytical reagents and the procedure has to be carried out in restricted areas, whereas in the latter method the use of the suspectedly carcinogenic arsenazo III compound requires special precautions. Moreover, the reproducibility of the isotope binding assays is poor at least in our hands in contrast to that of the spectrophotometric assay.

The introduction of metal-binding ligands from the amino polycarboxylate class (e.g., DTPA, DOTA, LILO[1]) will add to the total negative charge of a protein causing an acidic shift in pI of the conjugate compared to the unmodified protein. As a consequence, these ligand–mAb conjugates will show an anodal shift in IEF dependent on the number of ligands introduced.

The objective of this study was to develop a qualitative and quantitative determination of the chelator content

of DTPA–protein conjugates by IEF and to compare this electrophoretic method with the spectrophotometric procedure using the yttrium–arsenazo complex.

EXPERIMENTAL PROCEDURES

Materials. MOPC-21 and SC-20 were a kind gift of Dr. B. Butman (PerImmune Inc., Rockville MD). HSA was purchased from the Central Blood Bank, Amsterdam, the Netherlands. Arsenazo III complex was obtained from Sigma, St. Louis, MO. All chemicals used were of analytical grade from Baker Deventer, The Netherlands, or Merck, Darmstadt, FRG.

Preparation of (p-Isothiocyanatobenzyl)–DTPA. (p-Isothiocyanatobenzyl)–DTPA was synthesized according to the procedure of Brechbiel et al. (7) except that tert-butyl groups were used for protection of the carboxylic acid groups.

(p-Nitrobenzyl)diethylenetriamine was reacted with excess (15 equiv) tert-butyl bromoactate in refluxing ethanol in the presence of triethylamine (15 equiv) for 20 h. After removal of the salts by extraction, the product was purified by chromatography on Al_2O_3 (n-hexane/ethyl acetate, 85/15 v/v), yielding pure tert-butyl (p-nitrobenzyl)diethylenetriaminepentaacetate as an oil in 45% yield; FAB-MS m/z = 809 ((M + H)+).

Subsequently, tert-butyl (p-nitrodibenzyl)ethylenetriaminepentaacetate was reduced for 4 h in ethanol using H_2 (3 atm of pressure) with Pd/C (10%) as catalyst. After removal of the catalyst, the product was purified by chromatography on Al_2O_3 (n-hexane/ethyl acetate; 8:2 v/v), yielding pure tert-butyl p-aminobenzyldiethylenetriamine pentaacetate as an oil in 45% yield.

This was further reacted in dichloromethane with thiophosgene for 4 h at room temperature. The product, tert-butyl (p-isothiocyanatobenzyl)diethylenetriaminepentaacetate, was isolated as an oil in 50% yield by chromatography on Al_2O_3 (n-hexane/ethyl acetate, 85/15 v/v). IR (liquid): 2090 cm^{-1} (N=C=S); 1744 cm^{-1} (COO-tBu). ^{1}H-NMR (CDCl$_3$): 1.40 ppm (tBu); 7.08 and 7.25 ppm (phenyl). FAB-MS: m/z = 821 ((M + H)−) and m/z = 843 ((M + Na)+).

Preparation of Benzyl-DTPA Conjugates. The proteins to be conjugated were transferred to PBS by chromatography on PD10. The PBS used in this proce-

[1]Abbreviations: CBB, Coomassie brilliant blue; CEA, carcinoembryonic antigen; DOTA, 1,4,7,10-tetraazacyclododecane N,N′,N″,N‴-tetraacetic acid; DTPA, diethylenetriaminepentaacetic acid; HSA, human serum albumin; IEF, isoelectric focusing; LILO, 1,3-bis[N-[N-(2-aminoethyl)-2-aminoethyl]-2-aminoacetamido]-2-(4-isothiocyanatobenzyl)propane-N,N,N′,N″,N‴,N⁗,N⁗′,N⁗″-octaacetic acid; PBS, phosphate-buffered saline; TFA, trifluoroacetic acid.
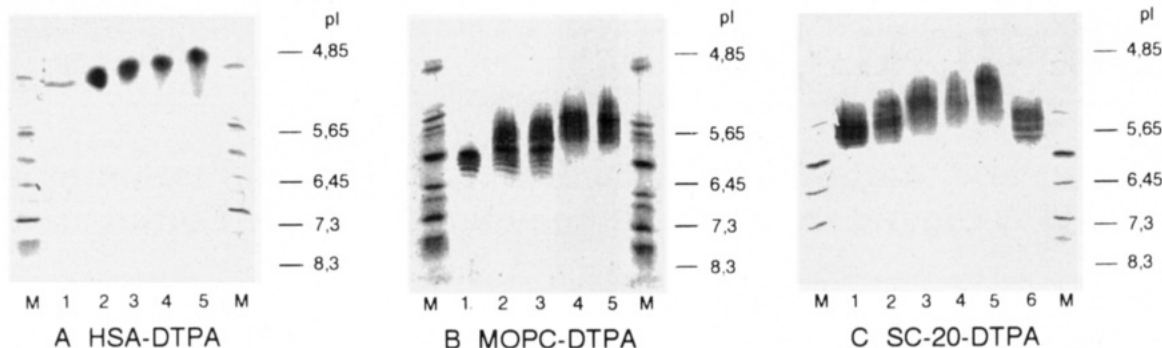
Figure 1. IEF analysis of antibody— and HSA—DTPA conjugates. (A) HSA—DTPA: M, p*I*-markers; (1) HSA; (2) HSA—DTPA (0.4 mol/mol); (3) HSA—DTPA (1.0 mol/mol); (4) HSA—DTPA (1.7 mol/mol); (5) HSA—DTPA (3.3 mol/mol). (B) MOPC—DTPA: M, p*I*-markers; (1) MOPC; (2) MOPC—DTPA (2.0 mol/mol); (3) MOPC—DTPA (2.2 mol/mol); (4) MOPC—DTPA (4.4 mol/mol); (5) MOPC—DTPA (7.3 mol/mol). (C) SC-20—DTPA: M, p*I*-markers; (1) SC-20—DTPA (1.8 mol/mol); (2) SC-20—DTPA (2.2 mol/mol); (3) SC-20—DTPA (3.1 mol/mol); (4) SC-20—DTPA (3.8 mol/mol); (5) SC-20—DTPA (5.0 mol/mol); (6) SC-20.
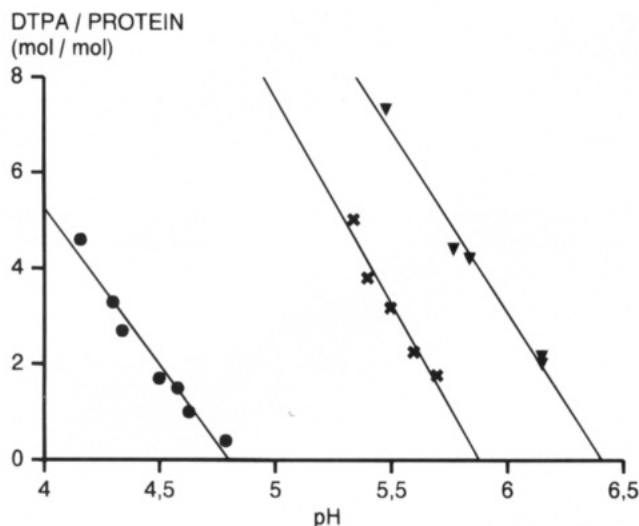
Figure 2. Calibration curves of HSA—, MOPC—, and SC-20—DTPA derived from the IEF analyses of Figure 1. ●: HSA—DTPA. ×: SC-20—DTPA. ▼: MOPC—DTPA.

Table 1. Determination of Chelator Content of DTPA Conjugates with IEF and Spectrophotometric Method

		IEF	yttrium—arsenazo
MOPC—DTPA	1	3.1	3.0
	2	6.4	6.8
	3	5.3	5.4
	4	2.8	2.6
HSA—DTPA	1	3.0	3.1
	2	2.7	2.8
SC-20—DTPA	1	2.82 ± 0.48	2.22 ± 0.45
	2	4.56 ± 0.50	4.51 ± 0.62
	3	5.55 ± 0.27	5.21 ± 2.1

dure was chromatographed on Chelex-100 in order to remove unwanted metal ion contaminants. (*tert*-Butyl-benzyl)-DTPA was deprotected by incubation for 4 h in TFA (1 g/L) at ambient temperature. TFA was removed by a gentle stream of nitrogen. The residue was dissolved in 1 mL of dichloromethane and again evaporated to dryness; this procedure was repeated three times leaving the unprotected chelator as a white powder. FAB-MS: $m/z = 539$ ((M − H)⁻) and $m/z = 577$ ((M + K − 2H)⁻).

The unprotected chelator was dissolved in PBS to a final concentration of approximately 5 g/L. Usually, deprotected (*p*-isothiocyanatobenzyl)-DTPA was added to the protein solutions in PBS at a molar protein/chelator ratio of 1:10. The pH of the reaction mixture was adjusted to 8.9 with 0.1 mol/L of triethylamine. Incubation was performed for 2 h at 37 °C. Excess reagent was removed by gel filtration on PD10 equilibrated in Chelex-
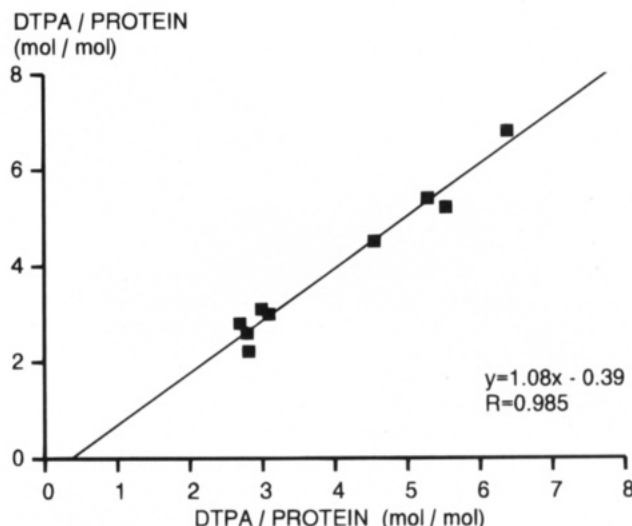
Figure 3. Correlation curve between IEF and spectrophotometric analysis. Abscissa: electrophoretic method. Ordinate: spectrophotometric method.

treated PBS. The substitution efficiency was approximately 30%.

Determination of Chelator Content of DTPA Conjugates. *Spectrophotometric Method.* This method was carried out according to Pippin et al. (*6*). To 500 µL of yttrium—arsenazo solution was added 10 µL of conjugate solution in PBS, and after mixing the absorbance at 652 nm was measured in a Pye-Unicam 8700 spectrophotometer. A calibration curve was prepared using 10 µL of DTPA solutions in a concentration range of 20—100 nmol/L.

Electrophoretic Method. IEF of DTPA conjugates was carried out in pH 3—9 gels in a Phast Electrophoresis System (Pharmacia) essentially according to the manufacturers' instructions. Gels were stained with CBB G250 as described by Neuhoff (*8*) and scanned in a computing densitometer 300 A of Molecular Dynamics using Imagequant 3.3. The median p*I* values of the protein and conjugate peaks were estimated using the prestained Electran p*I* calibration kit pH 4.7—10.6 (BDH) as a reference.

RESULTS AND DISCUSSION

In Figure 1, the IEF analysis of MOPC—DTPA, SC-20—DTPA, and HSA—DTPA conjugates of different, known substitution ratios (determined by the spectrophotometric method) is presented. The antibody— and albumin—DTPA conjugates showed the predicted anodal
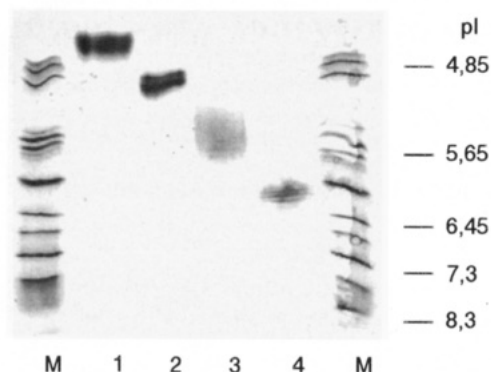
Figure 4. Qualitative IEF analysis of MOPC− and HSA−chelator conjugates: M, p*I*-marker; (1) HSA−chelator; (2) HSA; (3) MOPC−chelator; (4) MOPC. The chelator was a carboxylic acid-containing chelator, analogous to DOTA.

shift compared to the unmodified proteins. Measurement of pI changes by computer imaging resulted in the calibration curves presented in Figure 2. From these curves, the chelator substitution ratio of various antibody and HSA−conjugates was derived and compared with the values obtained by the spectrophotometric analysis. As can be concluded from Table 1, a good correlation was found between the chelator content determined by the electrophoretic and spectrophotometric method, the correlation coefficient being 0.985 (Figure 3). Except at high substitution ratios, the interassay variation of both methods (as determined in three consecutive experiments) was comparable and in the same order as published by Pippin et al. (*6*). The reason we found a high variation at elevated DTPA contents may be the inaccuracy at low absorbance values of the spectrophotometer used. Since the electrophoretic method is only dependent on the number of carboxylic acid groups introduced at conjugation of the chelator, no corrections have to be made for the intrinsic metal-binding capacity of the protein itself, thus providing a direct value for the total chelator content of the conjugates rather than the total available binding sites for metal ions. In particular, the intrinsic metal binding capacity of HSA is substantial, i.e., 3 mol/mol protein, whereas for mAbs usually a

value under 0.2 mol/mol was found. Moreover, IEF allows a convenient and an at least qualitative control on the attachment of carboxylic acid-containing chelators that can bind the (radioactive) metal ions only at elevated temperatures as is shown in Figure 4. For the DOTA-like structure used in this experiment (trans)chelation occurred only above 70 °C. Thus, at temperatures compatible with the protein carrier, no reaction of the mAb−chelator conjugate with the yttrium−arsenazo complex was observed, whereas a substantial anodal shift was found with IEF.

In conclusion, IEF offers an easy, qualitative and quantitative method for the determination of the chelator content of conjugates between proteins and DTPA or probably other amino polycarboxylate chelators.

LITERATURE CITED

(1) Waldman, T. A. (1991). Monoclonal Antibodies in diagnosis and therapy. *Science 252*, 1657−1662.

(2) Goldenberg, D. M. (1993). Monoclonal Antibodies in cancer detection and therapy. *Am. J. Med. 94*, 297−312.

(3) Fritzberg, A. R., Beaumier, P. L., Bottino, B. J., and Reno, J. M. (1994). Approaches to improved antibody- and peptide-mediated targeting for imaging and therapy of cancer. *J. Controlled. Rel. 28*, 167−173.

(4) Paik, C. H., Murphy, P. R., Eckelman, W. A., Volkert, W. A., and Reba, R. C. (1983). Optimization of the DTPA mixed anhydride reaction with antibodies at low concentrations. *J. Nucl. Med. 24*, 932−936.

(5) Meares, C. F., McCall, M. J., Reardon, D. T., Goodwin, D. A., Diamanti, C. I., and McTigue, M. (1984). Conjugation of antibodies with bifunctional chelating agents: Isothiocyanate and bromoacetamide reagents, Methods of analysis and subsequent addition of metal ions.

(6) Pippin, C. G., Parker, T. A., McMurry, T. J., and Brechbiel, M. W. (1992). Spectrophotometric method for the determination of a bifunctional DTPA ligand in DTPA-monoclonal antibody conjugates. *Bioconjugate Chem. 3*, 342−345.

(7) Brechbiel, M. W., Gansow, O. A., Atcher, R. W., Schlom, J., Esteban, J., Simpson, D. E., and Colcher, D. (1986). Synthesis of 1-(p-isothiocyanatobenzyl) derivatives of DTPA and EDTA. Antibody labeling and tumor imaging studies. *Inorg. Chem. 25*, 2772−2781.

(8) Neuhoff, V., Stamm, R., and Eibl, H. (1985). Clear background and highly sensitive protein staining with Coomassie Blue dyes in polyacrylamide gels: a systematic analysis. *Electrophoresis 6*, 427−448.

Strategies for the Synthesis and Screening of Glycoconjugates. 1. A Library of Glycosylamines

Dirk Vetter and Mark A. Gallop*

Affymax Research Institute, 4001 Miranda Avenue, Palo Alto, California 94304. Received September 28, 1994[⊗]

A simple one-step procedure is found to be highly effective for the "functionalization" of glycodiversity. This study encompasses 50 unprotected mono- and oligosaccharides, which are subjected to Kochetkov aminations in saturated aqueous ammonium carbonate. The reaction allows for the stereo- and regioselective introduction of an amino group into all oligosaccharides tested, as well as into a great variety of monosaccharides including charged species. The resulting unprotected glycosylamines are stable compounds, and the inherent amino group provides a convenient site for chemoselective conjugation and modification as described in the following paper in this issue.

INTRODUCTION

Carbohydrates have recently attracted significant attention from the pharmaceutical industry (*1*). Natural sources provide a great wealth of structurally diverse and biologically relevant carbohydrates, many of which are available as commercial products. Rare native structures may be routinely obtained by polysaccharide and glycosaminoglycan hydrofluorolysis or automated hydrazinolysis of glycoproteins. Nevertheless, a systematic screening of the carbohydrate pool for drug discovery purposes is complicated by synthetic difficulties associated with the chemical modification of sugars.

More widespread utilization of glycodiversity in ligand discovery would be facilitated by general strategies for straightforward functional group manipulation. Reductive amination is one such versatile reaction, though this transformation results in disruption of the pyranose or furanose ring structures of monosaccharides or the reducing termini of oligosaccharides.

This paper describes the one-step conversion of a variety of unprotected mono- and oligosaccharides to their corresponding glycosylamines. Subsequent acylation with spacer molecules carrying a biotin moiety or succinimidyl ester for immobilization to streptavidin-coated microtiter wells or amino-functionalized resin, respectively, will be described in future papers.

EXPERIMENTAL SECTION

General. Saccharides were from Sigma, Boehringer Mannheim, or Oxford Glycosystems, lyxosylamine was from Toronto Research Chemicals. Ammonium carbonate was purchased from Fluka.

Glycosylamine Preparations. A solution of the saccharide (1%, w/v, 5–50 mg, up to 1 g for less expensive saccharides) in saturated aqueous ammonium carbonate was stirred at room temperature for 5 days. Solid $(NH_4)_2CO_3$ (ca. 40 mg/mg saccharide) was added in fractions during the course of the reaction to ensure saturation. Kinetics were followed by TLC (K 60, 1-propanol/ethyl acetate/water, 6:1:3, detection with orcinol and ninhydrin reagents, respectively). After the conversion, samples were frozen and lyophilized for 3 days. Gravimetrically determined yields were typically in the order of 100–110%. Samples showing yields >120% were repeatedly lyophilized. Excess solid $(NH_4)_2CO_3$ was most effectively removed by dissolving the crude glycosylamine in warm methanol (ca. 70 °C). After termination of CO_2 evolution, the methanol was slowly evaporated and the residual material dried *in vacuo*.

Batches where gravimetry indicated large amounts of residual ammonium carbonate (yields ≫ 150%) were discarded. This was the case for reactions with 3-methylglucose and 6-methylgalactose. The reason for the persistance of ammonium carbonate with these sugars is unclear.

^{1}H-NMRs of glycosylamines were run in D_2O, and conversions were found in the range 50–90%. However, by comparing D_2O spectra with d_6-DMSO spectra for identical samples it became apparent that the hydrolytic stability of different glycosylamines varied significantly. In D_2O the half-life of some glycosylamines fell within the time frame of a ^{1}H-NMR experiment (5 min), making the lower conversions artifactual. A striking example is the difference between the 1-amines of lactose and 2'-methyl-lactose. Both reactions afforded over 95% conversions when monitored in d_6-DMSO. In D_2O the lactosylamine gave the same result, but its 2'-methyl derivative showed 50% hydrolysis.

Diagnostic analytical data as well as yields for 54 glycosylamines are summarized in Table 1.

RESULTS AND DISCUSSION

Recently, a simple derivatization procedure (Kochetkov reaction) for unprotected mono- and oligosaccharides was disclosed and subsequently employed in a number of representative reactions (*2*). The anomeric hydroxyl group of a reducing sugar is converted to an amino group upon treatment with aqueous ammonium carbonate. The literature describes the successful amination of 25 different carbohydrates (*3–7*). Realizing that the Kochetkov amination should be applicable to a much broader range of saccharide structures, we decided to subject a large number of commercially available carbohydrates to these reaction conditions.

We confirm the findings of other groups and extend the range of substrates for this reaction to oligosaccharides with the reducing termini Gal, Man, Ara, GalA, and GalNAc (*8*). We add AllNAc, All3NAc, Glc6NAc, Glc3NAc, and Xyl to the list of neutral monosaccharides. Also, we describe for the first time the glycosylamine derivatives

---

Table 1. Analytical Data for 1-Amino-1-deoxy Sugars Prepared in This Study (Glycosylamines Are Characterized by FAB-MS and 300 MHz ¹H-NMR in D₂O. If Glycosylamines Were Obtained from a Commercial Source or Attempted Conversions Failed, This Is Indicated)

saccharide	glycosylamine: m/z (calcd/found for low or high resolution MS), ¹H-NMR (δ and J) for the anomeric proton of the hemiaminal, yield^a (%)
neutral monosaccharides	
1. Lyx	glycosylamine obtained from Toronto Research, nd, 4.019 ppm (d, 1.2 Hz)
2. Ara	failed
3. Glc	glycosylamine obtained from Sigma, nd, 4.093 ppm (8.7 Hz)
4. Gal	glycosylamine obtained from Sigma, nd, 4.035 ppm (8.7 Hz)
5. Fuc	glycosylamine obtained from Sigma, nd, 4.023 ppm (8.7 Hz)
6. Man	nd, 4.343 (s), 80
7. Rib	failed
8. Xyl	150.0766/150.0761 (M + H⁺), 4.169 ppm (d, 9.1 Hz), 50
9. GlcNAc	glycosylamine obtained from Sigma, nd, 4.156 ppm (d, 9.0 Hz)
10. GalNAc	221.1138/221.1142 (M + H⁺), 4.081 ppm (d, 9.4 Hz), 90
11. ManNAc	221.1137/221.1135 (M + H⁺), 4.153 ppm (d, 4.4 Hz), 90
12. Glc6NAc	221.1138/221.1133 (M + H⁺), 4.074 ppm (d, 8.8 Hz), 50
13. Glc3NAc	221.1138/221.1135 (M + H⁺), 4.177 ppm (d, 8.7 Hz), 70
14. Gal6Me	failed
15. Glc3Me	failed
16. AllNAc	221.1137/221.1139 (M + H⁺), 4.385 ppm (d, 9.6 Hz), 70
17. All3NAc	220/221.0 (M + H⁺), 4.294 ppm (d, 9.4 Hz), 50
charged monosaccharides	
18. GlcA	215/238.0 (M$_{sodium\ salt}$ + Na⁺), 4.111 ppm (d, 8.8 Hz), 60
19. GalA	nd, 4.032 ppm (d, 8.8 Hz), 50
20. GlcNAc3SO₃⁻	nd, 4.281 ppm (d, 9.4 Hz), 50
21. GlcNAc6SO₃⁻	322/345.1 (M$_{sodium\ salt}$ + Na⁺), 4.192 ppm (d, 8.8 Hz), 90
22. GlcNAc6PO₃²⁻	344/345.1 (M$_{disodium\ salt}$ + H⁺), 4.169 ppm (d, 8.8 Hz), 90
23. GlcN2,3(SO₃⁻)₂	382/405.1 (M$_{disodium\ salt}$ + Na⁺), 4.226 ppm (d, 8.8), 50
24. GlcN2,6(SO₃⁻)₂	382/405.1 (M$_{disodium\ salt}$ + Na⁺), 4.221 ppm (d, 8.4 Hz), 70
25. Man6PO₃²⁻	nd, 4.361 (s), 70
26. Gal6PO₃²⁻	nd, 4.066 ppm (d, 8.8 Hz), 90
27. Gal6SO₃⁻	282.0260/282.0255 (M$_{sodium\ salt}$ + H⁺), 4.068 ppm (d, 8.6 Hz), 70
28. Rib5PO₃²⁻	failed
neutral disaccharides	
29. Glc(α1−4)Glc	342.1400/342.1391 (M + H⁺), 4.117 ppm (d, 8.7 Hz), 90
30. Gal2Me(β1−4)Glc	356.1557/356.1563 (M + H⁺), 4.136 ppm (d, 8.3 Hz), 50
31. Glc(β1−4)Glc	342.1400/342.1407 (M + H⁺), 4.125 ppm (d, 8.7 Hz), 40
32. Gal(β1−4)Glc	341/342.1 (M + H⁺), 4.129 ppm (d, 8.9 Hz), 90
33. GlcNAc(β1−4)GlcNAc	424.1931/424.1930 (M + H⁺), 4.157 ppm (d, 8.7 Hz), 90
34. Gal(β1−4)GlcNAc	383.1666/383.1661 (M + H⁺), 4.189 ppm (d, 8.7 Hz), 90
35. GlcNAc(β1−6)GlcNAc	424.1931/424.1930 (M + H⁺), 4.148 ppm (d, 9.4 Hz), 90
36. Gal(β1−3)GlcNAc	383.1666/383.1669 (M + H⁺), 4.042 ppm (d, 8.7 Hz), 70
37. Gal(β1−6)GlcNAc	383.1666/383.1665 (M + H⁺), 4.183 ppm (d, 9.4 Hz), 90
38. GlcNAc(β1−6)Gal	383.1666/383.1665 (M + H⁺), 4.024 ppm (d, 8.7 Hz), 90
39. Gal(α1−4)Gal	nd, 4.104 ppm (d, 8.6 Hz), 50
40. Gal(β1−6)Gal	342.1400/342.1404 (M + H⁺), 4.065 ppm (d, 8.9 Hz), 50
41. Gal(β1−3)GalNAc	382/383 (M + H⁺), 4.137 ppm (d, 9.0 Hz), 90
42. Gal(β1−4)Man	342.1400/342.1404 (M + H⁺), 4.374 (s), 50
43. Gal(β1−3)Ara	312.1295/312.1300 (M + H⁺), 4.165 (s), 50
44. Man(α1−3)Man	342.1400/342.1407 (M + H⁺), 4.361 ppm (s), 50
45. Fuc(α1−2)Gal(β1−4)Glc	488.1979/488.1975 (M + H⁺), 4.103 ppm (d, 8.8 Hz), 90
46. Galβ1−4(Fucα1−3)Glc	488.1979/488.1975 (M + H⁺), 4.134 ppm (d, 8.8 Hz), 90
47. Glc(α1−4)Glc(α1−4)Glc	503/504.2 (M + H⁺), 4.121 ppm (d, 8.8 Hz), 90
48. Fucα1−4Galβ1−4(Fucα1−3)Glc	634.2558/634.2551 (M + H⁺), 4.092 ppm (d, 8.9 Hz), 90
49. Galβ1−3(Fucα1−4)-GlcNAcβ1−3Galβ1−4Glc	853.3301/853.3283 (M + H⁺), 4.123 ppm (d, 8.7 Hz), 90
charged oligosaccharides	
50. GalA(α1−4)GalA	369/370 (M$_{diacid}$ + H⁺), 4.189 ppm (d, 8.8 Hz), 90
51. Neu5Ac(α2−3)Gal(β1−4)Glc	633.2354/633.2350 (M$_{sodium\ salt}$ + H⁺), 4.064 ppm (d, 9.1 Hz), 90
52. Neu5Ac(α2−6)Gal(β1−4)Glc	655.2174/655.2170 (M$_{sodium\ salt}$ + H⁺), 4.023 ppm (d, 9.0 Hz), 90
53. Neu5Ac(α2−3)Gal(β1−4)GlcNAc	696.2439/696.2391 (Msodium salt + H⁺), nd
54. Neu5Ac(α2−6)Gal(β1−4)GlcNAc(β1−3)Gal(β1−4)Glc	nd, 4.120 ppm (d, 8.7 Hz), 90

^{a} Yields were determined from ¹H-NMR spectra in D₂O and are based on the integral ratio for the anomeric proton of the glycosylamine and underivatized saccharide, respectively. It should be borne in mind that the yields determined in D₂O may be artificially low due to hydrolysis of the glycosylamines, and more likely are a measure of hydrolytic susceptibility (see Experimental Section). n.d.: not determined.

of a variety of charged monosaccharides, comprising GalA, GlcA, Gal-6PO₃²⁻, GlcNAc6PO₃²⁻, Man6PO₃²⁻, GlcNAc6SO₃⁻, GlcN2,3(SO₃⁻)₂, GlcN2,6(SO₃⁻)₂, and Gal6SO₃⁻.

In all cases, products are white, fluffy solids and are stable for months under anhydrous conditions. Compounds encompassed in this study are listed in Table 1.

We failed to obtain glycosylamines from some furanosidic or pentopyranosidic monosaccharides (Rib, Rib5PO₃²⁻, Ara). Substantial browning and side-product formation in these reactions is attributed to Amadori rearrangements and Maillard reactions, due to enhanced reactivity of the immonium ion intermediate (*9*). On the other hand, glycosylamine derivatives of Gal(β1−4)Ara and Xyl could be prepared without any problems. This suggests that only a few furanosidic or pentopyranosidic 1-amino-1-deoxy sugars are either not accessible *via* this route or might require optimization of the amination protocol.

NMR investigation of the obtained glycosylamines reveals that the Kochetkov amination yields stereochemically well-defined products, with >95% β-anomer obtained in all cases (*10*).

The extent of conversions of the saccharides to the glycosylamines are typically 80–95%. One typical side reaction during the amination procedure is condensation of the product glycosylamine with the initial saccharide. The resulting diglycosylamines can make up to 10% of the mass fraction of product. They cannot be separated by size exclusion chromatography in aqueous media as many of the glycosylamines are highly susceptible to hydrolysis. However, since neither the diglycosylamines nor the parent saccharides are substrates for subsequent chemoselective acylation reactions, conjugates of the desired monoglycosylamines are readily isolated and purified.

Another constituent of the products from the amination procedure is residual ammonium carbonate which can usually not be completely removed by lyophilization without lowering the yield of glycosylamine. Ammonia can be detrimental to subsequent acylation reactions by scavenging the activated acid of the conjugation reagent. If the active ester is present in stoichiometric or substoichiometric ratios, measures must be taken to remove all traces of ammonium salts. This is achieved by warming the glycosylamine in methanol until termination of gas evolution and subsequent evaporation *in vacuo.*

LITERATURE CITED

(1) Alper, J. (1993) Carbohydrates surge through clinical trials. BIO/TECHNOLOGY *11*, 1093.

(2) Likhosherstov, L. M., Novikova, O. S., Derevitskaja, V. A., and Kochetkov, N. K. (1986) A new simple synthesis of amino sugar β-D-glycosylamines. *Carbohydr. Res. 146*, C1–C5.

(3) Kallin, E., Lonn, H., Norberg, T., and Elofsson, M. (1989) Derivatization procedures for reducing oligosaccharides, Part 3: Preparation of oligosaccharide glycosylamines, and their conversion into oligosaccharide-acrylamide copolymers. *J. Carbohydr. Chem. 8*, 597–611.

(4) Urge, L., Kollat, E., Hollosi, M., Laczko, I., Wroblewski, K., Thurin, J., and Otvos, L., Jr. (1991) Solid-phase synthesis of glycopeptides: synthesis of N^α-fluorenylmethoxycarbonyl L-asparagine N^β-glycosides. *Tetrahedron Lett. 32*, 3445–3448.

(5) Urge, L., Otvos, L., Jr., Lang, E., Wroblewski, K., Laczko, I., and Hollosi, M. (1992) Fmoc-protected, glycosylated asparagines potentially useful as reagents in the solid-phase synthesis of N-glycopeptides. *Carbohydr. Res. 235*, 83–93.

(6) Manger, I. D., Rademacher, T. W., and Dwek, R. A. (1992) 1-N-Glycyl β-oligosaccharide derivatives as stable intermediates for the formation of glycoconjugate probes. *Biochemistry 31*, 10724–10732.

(7) Cohen-Anisfeld, S. T., Lansbury, P. T., Jr. (1993) A practical, convergent method for glycopeptide synthesis. *J. Am. Chem. Soc. 115*, 10531–10537.

(8) We use the condensed system of the abbreviated terminology of oligosaccharide chains according to IUPAC recommendations (1982) *J. Biol. Chem. 257*, 3347–3351. The only trivial name employed is lactose (Lac) for Gal(β1–4)Glc.

(9) Isbell, H. S., and Frush, H. L. (1958) Mutarotation, hydrolysis, and rearrangement reactions of glycosylamines. *J. Org. Chem. 23*, 1309–1319.

(10) Certain 1-β-glycosylamines, e.g., β-mannosylamine, having axial substituents at C-2 are particularly susceptible to mutarotation; see ref 9. However, other workers report exclusive predominance of the β-anomer for mannosylamine in solution: Linek, K., Alfoldi, J., and Defaye, J. (1993) Structure of glycosylamines and diglycosylamines in the arabinose, mannose, and rhamnose series. *Carbohydr. Res. 247*, 329–335. See also ref 5.

Strategies for the Synthesis and Screening of Glycoconjugates. 2. Covalent Immobilization for Flow Cytometry

Dirk Vetter, Emily M. Tate, and Mark A. Gallop*

Affymax Research Institute, 4001 Miranda Avenue, Palo Alto, California 94304.   Received September 28, 1994[⊗]

Glycosylamines are readily available carbohydrate derivatives that undergo acylation reactions with homobifunctional *N*-hydroxysuccinimidyl esters. The product glycosylamides carry a spacer group equipped with one active ester functionality. This route provides well-defined glycoconjugates, which may be cross-linked to various amino-functionalized resins. Carbohydrate recognition of the resulting sugar–bead conjugates is probed by lectin immunostaining or flow cytometry using a fluorescently labeled lectin.

INTRODUCTION

Carbohydrates play various physiological roles and have drawn attention as potential constituents of pharmacophores (*1*). The systematic screening of the carbohydrate pool would greatly facilitate the drug discovery process in this area. In one development, the use of flow cytometry has been introduced for the assessment of carbohydrate–protein specificities and affinities (*2–4*). Instead of cells, carbohydrate-functionalized latex or polystyrene beads are subjected to fluorescence-activated particle scanning and sorting techniques.

We are currently interested in generating combinatorial libraries of sugar–bead conjugates that may be screened for receptor binding using flow cytometry methods. Our group has been using a similar approach to screen large libraries of peptides synthesized on spherical microbeads, wherein the structure of the ligand on any bead is encoded by the parallel synthesis of a single-stranded DNA molecule (*5*). Individual beads with appropriate receptor binding characteristics can be sorted from the population, and the DNA tag can be amplified and sequenced to reveal the structure of the cognate ligand.

As a prerequisite to the synthesis of encoded carbohydrate libraries, this paper describes a simple two-step method for the immobilization of a variety of glycosylamines on amino-functionalized resin, using mild amide bond-forming chemistry. Sugar–bead conjugates are subjected to lectin binding assays, and flow cytometry is employed to select binding populations from pools of immobilized carbohydrates.

EXPERIMENTAL SECTION

Mono(succinimidyl) Mono(sialyllactosylamido)-suberate. A 304 mg portion of disuccinimidyl suberate (0.83 mmol, Pierce) and 107 mg of 1-hydroxybenzotriazole were dissolved in DMSO (1.25 mL, heat). After the mixture was cooled to room temperature, 50 mg of sialyllactosylamine (79 μmol) was added and the resulting mixture stirred for 2 h. The reaction was followed by TLC (1-propanol/ethyl acetate/water, 6:1:3, R_f educt 0.40, R_f product 0.67). After complete conversion, product was precipitated with acetone/ether (1:2, 10 mL). Following centrifugation, the residue was washed with acetone/

* To whom correspondence should be addressed. Phone: (415) 812-8706. Fax: (415) 424-9860.

ether (1:1, 10 mL) and dried in vacuo. Yield: 60 mg (86%). For analytical data see Table 2.

Other active ester–sugar conjugates were prepared accordingly.

A similar strategy was applied to the biotinylation of a library of 50 glycosylamines (unpublished results), and some influence of carbohydrate structure on the yields of conjugate obtained was observed. Most critical was the conjugate precipitation step: with monosaccharides of decreased hydrophilicity (for instance, Xyl or Glc3NAc), addition of acetone/ether either did not precipitate the glycoconjugate or only very low yields were obtained. However, all oligosaccharide–conjugates prepared here were efficiently precipated, due to their high polarity.

Lactose–TentaGel. A 102 mg portion of mono-(succinimidyl) mono(lactosylamido)suberate (171 μmol) was dissolved in 1 mL of DMF and mixed with 156 mg of TentaGel S NH$_2$ (Rapp Polymere, 0.25 mmol/g, 39 μmol of amino groups). After sonication for 1 h and vortexing for 20 more hours, beads were recovered by centrifugation, washed with DMF and water, and lyophilized.

Conjugates of maltose, sialyllactose, chitobiose, Lac-NAc, GlcNAc6SO$_3$$^-$, and GlcNAc6PO$_3$$^{2-}$ with TentaGel were prepared analogously.

Lactose–Microresin. A 1.5 mg portion of mono-(succinimidyl) mono(lactosylamido)suberate (2.5 μmol) was dissolved in 50 μL of DMF with 0.3 mg of HOBt and 5 μL of DIEA and vortexed with 1 mg (0.1 μmol of amino groups) of 10 μm dodecylamine-grafted polystyrene resin (*5*) for one hour. Beads were washed thoroughly with DMF.

Conjugates of maltose, sialyllactose, chitobiose, Lac-NAc, GlcNAc6SO$_3$$^-$, and GlcNAc6PO$_3$$^{2-}$ with this resin were prepared analogously.

Solid Phase Assays. Carbohydrates were detected on beads using adapted digoxigenin immunoassays (Glycan Detection Kit, Glycan Differentiation Kit, Boehringer Mannheim, see product sheets for detailed information) or direct fluorescent lectin staining.

(A) Ca. 5 mg of TentaGel beads were treated as follows: 1 mL of periodate solution (14 mmol/L) for 1 h, 10 μL of digoxigenin hydrazide (5 mmol/L in DMF) plus 0.2 mL of acetate buffer for 1 h, 1 mL of casein solution (2% w/v in Tris-buffered saline (TBS)) for 1 h, 1 mL of antidigoxigenin–alkaline peroxidase conjugate (1 ng/mL) for 1 h, 1 mL of nitro-blue tetrazolium staining solution, overnight.

(B) Ca. 2.5 mg of TentaGel-beads was incubated in the following order: 1 mL of casein (2% w/v) in TBS for 1 h, 0.1 mL of digoxigenin–lectin conjugate (RCA 120 at 1

Table 1. Literature Studies Describing the Solution-Phase Acylation of Unprotected 1-Amino, 1-deoxy Sugars

acylating agent	condns	ref
acryloyl chloride	THF/MeOH/Na$_2$CO$_3$	Kallin et al., 1989 (8)
Fmoc-Asp(OPfp)-OtBu	DMF/water	Otvos et al., 1989 (9)
Asp-containing peptide	BOP or HBTU in DMSO or DMF in presence of DIEA	Anisfeld and Lansbury, 1990 (10)
Fmoc chloride	aqueous Na$_2$CO$_3$/dioxane	Kallin et al., 1991 (11)
Asp-containing peptide	HBTU, HOBt or HBTU, DIEA	Cohen-Anisfeld and Lansbury, 1993 (14)
dansyl chloride	aqueous Na$_2$CO$_3$/acetone	Manger et al., 1992 (15)
fluorescein-OSu	aqueous Na$_2$CO$_3$/DMF	
chloroacetic anhydride	aqueous Na$_2$CO$_3$	

Table 2. Diagnostic Analytical FAB-MS and 300 MHz (D$_2$O) ^{1}H-NMR Data for Glycosylamide-Active Ester Conjugates

product	m/z (calcd/found for FAB-MS), δ and J for the N-linked anomeric proton
ethylene glycol mono(succinimidyl succinate) mono(maltosylamidosuccinate)	682/683.2 (M + H$^+$), 4.894 ppm (d, 8.3 Hz)
ethylene glycol mono(succinimidyl succinate) mono(lactosylamidosuccinate)	nd,^{a} 4.916 ppm (d, 8.6 Hz)
mono(succinimidyl) mono(lactosylamido)suberate	594/595.3 (M + H$^+$), 4.906 ppm (d, 8.6 Hz)
mono(succinimidyl) mono(sialyllactosylamido)suberate	nd, 4.988 ppm (d, 8.7 Hz)
mono(succinimidyl) mono(lactosyl-N-acetylamido)suberate	635/561.2 (M − Su + Na$^+$),^{b} 5.062 ppm (d, 9.1 Hz)
mono(succinimidyl) mono(chitobiosylamido)suberate	676/602.3 (M − Su + Na$^+$),^{b} 5.091 ppm (d,8.9 Hz)
mono(succinimidyl) mono(GlcNAc6PO$_3$$^{2-}$ amido)suberate	597/501.1 (M$_{disodium\ salt}$ − Su + H$^+$),^{b} 5.091 ppm (d, 8.9 Hz)
mono(succinimidyl) mono(GlcNAc6SO$_3$$^-$-amido)suberate	575/501.1 (M$_{sodium\ salt}$ − Su + Na$^+$),^{b} 5.091 ppm (d, 8.9 Hz)

^{a} nd: not determined. ^{b} M − Su is product without the succinimidyl (Su) group. The corresponding free acid appears to be a FAB-MS-induced artifact as the intact succinimidyl ester is detected in the ^{1}H-NMR: 2.878 (4 H, s, N-succinimidylate); free N-hydroxysuccinimide resonates at higher field (2.173 ppm, 4 H, s). Also indicative is the shift of the methylene protons of suberic acid moiety: the methylene groups neighboring the glycosylamide linkage resonate at 2.663 ppm (2 H, t, α-CH2) and 1.665 ppm (2 H, m, β-CH2), the methylene groups next to the succinimidyl ester resonate at 2.264 ppm (2 H, t, α'-CH2) and 1.569 ppm (2 H, m, β'-CH2).
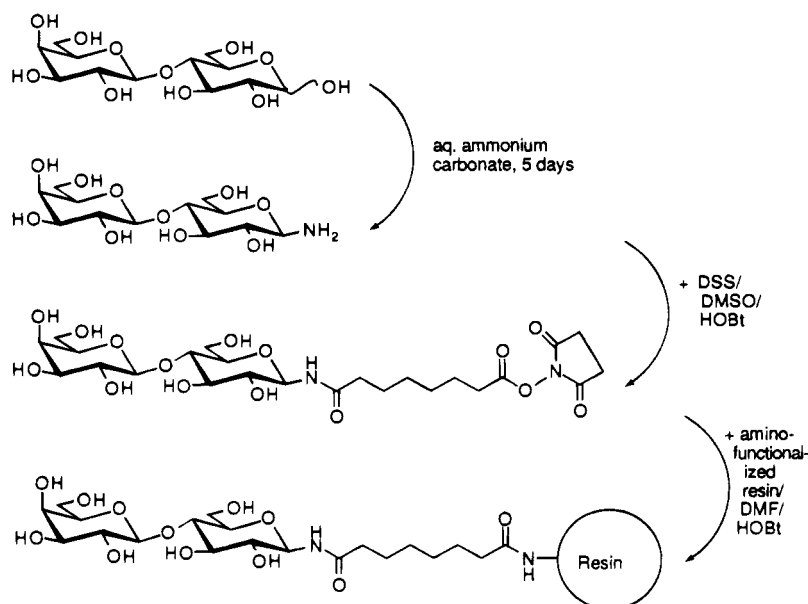
Figure 1. Structures of lactose, lactosylamine, mono(lactosylamido) mono(succinimidyl)suberate, and lactosyl resin, illustrating the reaction sequence for the covalent immobilization of carbohydrates on polystyrene beads.

mg/mL, MAA at 0.2 mg/mL) for 1 h, 1 mL of antidigoxigenin−alkaline peroxidase conjugate (1 ng/mL) for 30 min, 1 mL of nitro-blue staining solution for 5 min (RCA 120), or overnight (MAA).

(C) Ca. 0.2 mg of 10 μm diameter polystyrene resin was incubated in the following order: 0.35 mL of 2% BSA/TBS for 30 min, 0.3 mL of WGA−fluorescein (Molecular Probes) or RCA 120−fluorescein (Sigma) in TBS (each at 0.5 mg/mL) for 30 min. Bead suspensions were then subjected to fluorescence activated particle analysis on a FACScan instrument (Becton-Dickinson). For each histogram, 10 000 events were acquired.

RESULTS AND DISCUSSION

In the preceding paper we described a glycosylamine library consisting of 50 mono- and oligosaccharides (6).

Forty-five 1-amino-1-deoxy sugars were generated from the unprotected parent saccharides in a simple one-step conversion (7). Five glycosylamines from commercial sources were added to this group.

Glycosylamines are very attractive precursors for glycoconjugate chemistry.

A primary amino function is introduced into the reducing terminus of a carbohydrate without affecting ring structure and conformation, allowing for the selective derivatization with a variety of reagents.

When we started this study, glycosylamines had been used as substrates for various conjugation reactions (8–14). See Table 1 for a survey of preceding work on the acylation of 1-amino-1-deoxy sugars. Recently, however, concerns were raised in the literature that the acylation of glycosylamines might be an unreliable reaction. Ex-
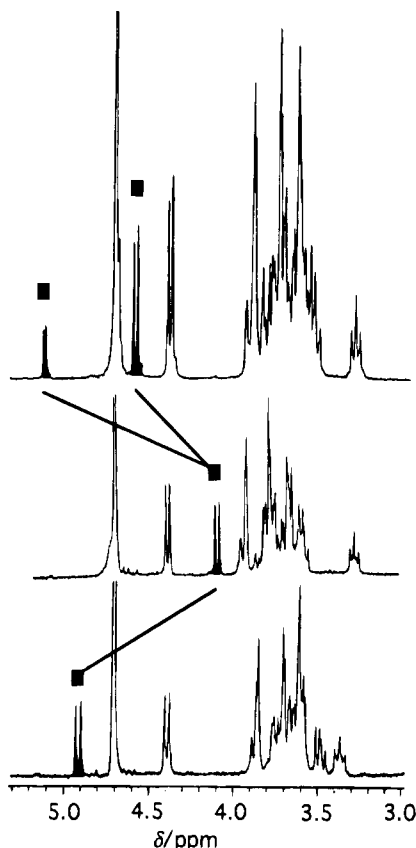
Figure 2. Typical shift displacement of the anomeric proton of the reducing terminus of an oligosaccharide (lactose) upon amination and acylation. Top: lactose, the free reducing terminus displays α/β stereoisomerism. Center: lactosylamine, amination shifts H-1 ca. -0.6 ppm upfield, yielding the β anomer exclusively. Bottom: lactosylamide, the anomeric proton is shifted ca. 0.9 ppm downfield, fully retaining its β configuration upon acylation.

plicitly, Manger et al. stated "that direct modification of the 1-amino function of a glycosylamine is both inefficient and difficult to control" (*15*). This led Manger et al. to suggest 1-*N*-glycyl oligosaccharides as superior intermediates for the formation of glycoconjugate probes.

Using 1-amino-1-deoxy-β-lactose, we set out to investigate the glycosylamine reactivity toward common hetero- or homobifunctional conjugation reagents, such as *N*-succinimidyl *S*-acetylthioacetate, 2-iminothiolane, *N*-succinimidyl bromoacetate, disuccinimidyl suberate (DSS), and ethylene glycol bis(succinimidyl succinate) (EGS). Although unprotected glycosylamines contain both primary and secondary hydroxyl groups, we anticipated that the primary amino group of these sugars should undergo

mild, chemoselective acylation by the *N*-hydroxysuccinimidyl esters of these conjugating reagents. Conversions are followed by ^{1}H-NMR as exemplified in Figure 2.

Water was found to be detrimental to the amidation reactions of glycosylamines. As mentioned in our previous communication (*6*), glycosylamines exhibit various stabilities toward water, with half-lives of minutes in aqueous media being quite common. This may explain the problems encountered by Manger et al. in attempting glycosyl amidations in aqueous carbonate buffer.

Of the reagents employed in our study, DSS clearly gave the best reaction profile. With conjugation reagents other than DSS or EGS, typical side products included glycosylamine dimers and epimeric glycosylamides.

The condensation reactions with DSS were carried out in the presence of a large excess of the homobifunctional reagent and yielded the unsymmetrical amido ester exclusively (Figure 1). The resulting products are versatile glycosylamide conjugation reagents because one *N*-hydroxysuccinimidyl ester is left intact, allowing for further derivatization.

To demonstrate the scope of this approach, seven glycosylamide-active ester conjugates were prepared from the glycosylamines of maltose, chitobiose, lactose, sialyllactose, LacNAc, GlcNAc6SO$_3^-$, and GlcNAc6PO$_3^{2-}$ (*16*). Subsequently, the glycosylamides were immobilized on amino-functionalized ethyleneglycol-grafted polystyrene resin (TentaGel). The extent of conjugate immobilization was probed by periodate oxidation of the carbohydrate resins: the aldehydes generated from the oxidation were labeled with digoxigenin hydrazide and detected immunochemically by means of an antidigoxigenin–alkaline phosphatase antibody conjugate and a precipitative stain (*17*) (data not shown).

In order to probe these sugar–bead conjugates in lectin binding assays, populations of each of the seven sugar–beads were treated with maackia amurensis agglutinin (MAA) separately. The assay involved incubation with digoxigenin-labeled lectin and detection with antidigoxigenin–alkaline phosphatase and a precipitative stain (*18*). The lectin is specific for Neu5Ac($\alpha2$–3)Gal and unambiguously recognized the epitope in the ligand sialyllactose (see Figure 3).

For flow cytometry studies, the seven glycosylamide *N*-hydroxysuccinimidyl ester derivatives were separately conjugated to a 10 μm diameter, monodisperse polystyrene resin (*5*). The beads were then mixed and incubated with fluorescently labeled lectin (wheat germ agglutinin (WGA)–fluorescein or ricinus communis agglutinin (RCA 120)–fluorescein). Fluorescence-activated particle scanning (Figure 4) showed that the different lectins selectively bound fractions of the pool. These subpopulations were identified as chitobiosylamide or
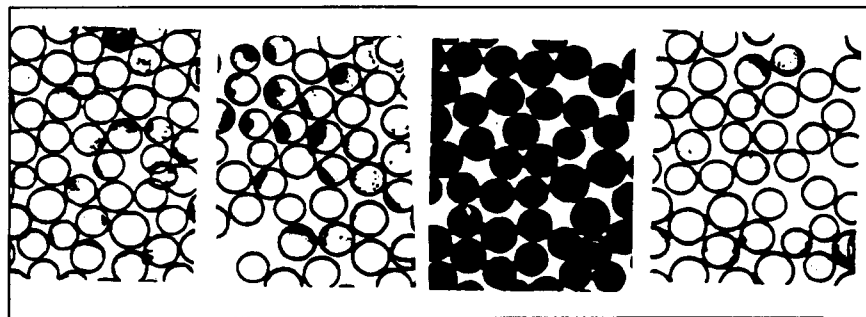
Figure 3. Solid phase lectin binding assay. Beads were treated with digoxigenin-labeled maackia amurensis agglutinin (sialic acid specific lectin). Bound lectin was detected by means of an antidigoxigenin/peroxidase conjugate and precipitative stain formation. The lectin selectively recognized its corresponding ligand Neu5Acα(2–3)Gal from a pool of several different sugar–bead conjugates. From left to right: TentaGel, maltosyl-TentaGel, sialyllactosyl-TentaGel, lactosyl-TentaGel.
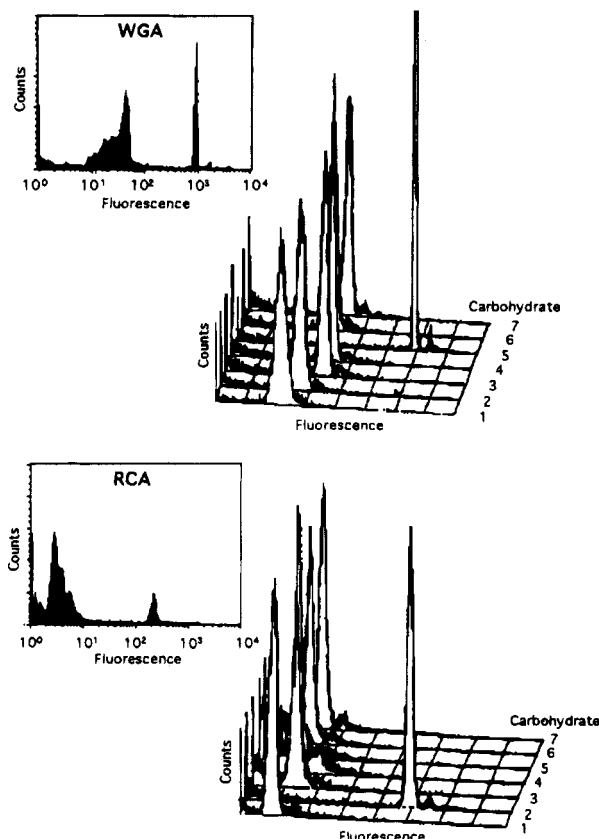
Figure 4. Flow cytometry histograms of sugar—bead conjugates incubated with fluorescently labeled lectin: wheat germ agglutinin (WGA, top histogram) and ricinus communis agglutinin (RCA 120, bottom histogram) each one selected out of a mixture of seven different bead-bound carbohydrates. The seven saccharide structures presented were as follows: maltose, 1; lactose, 2; sialyllactose, 3; LacNAc, 4; chitobiose, 5; GlcNAc6-PO_3^{2-}, 6; GlcNAc6SO$_3^-$, 7. WGA recognizes its ligand chitobiose (no. 5) and RCA 120 selects lactose (no. 2) as inferred from assaying each sugar—bead conjugate individually (3D histogram arrays).

lactosylamide beads, respectively, as inferred from assaying the seven sugar—bead conjugates individually. These disaccharides are known ligands for WGA or RCA.

These results indicate that fluorescence-activated particle sorting can be employed for the detection and isolation of bioactive members from a library of immobilized synthetic carbohydrate epitopes. We have subsequently extended this work to the generation of encoded glycopeptide libraries in which various glycosylamines are used to amidate the γ-carboxyl of a glutamate residue embedded in a randomly synthesised pentapeptide (*19*). The amino acid sequence of the peptide is recorded by the parallel synthesis of a PCR-amplifiable oligonucleotide tag, as previously described (*5*). As our method requires the use of milligram quantities of saccharide, the constituents of such a carbohydrate library would generally be based on various mono- to pentasaccharides rather than on less abundant complex multiantennary carbohydrates.

LITERATURE CITED

(1) Alper, J. (1993) Carbohydrates surge through clinical trials. *BIO/TECHNOLOGY 11*, 1093.

(2) Yednock, T. A., Stoolman, L. M., and Rosen, S. D. (1987) Phosphomannosyl-derivatized beads detect a receptor involved in lymphocyte homing. *J. Cell Biology 104*, 713—723.

(3) Handa, K., Nudelman, E. D., Stroud, M. R., Shiozawa, T., and Hakomori, S. (1991) Selectin GMP-140 (CD62; PADGEM) binds to sialosyl-Lea and sialosyl-Lex, and sulfated glycans modulate this binding. *Biochem. Biophys. Res. Commun. 181*, 1223—1230.

(4) de Bruijne-Admiraal, L. G., Modderman, P. W., Von dem Borne, A. E. G. K., and Sonnenberg, A. (1992) P-Selectin mediates Ca^{2+}-dependent adhesion of activated platelets to many different types of leukocytes: Detection by flow cytometry. *Blood 80*, 134—142.

(5) Needels, M. C., Jones, D. S., Tate, E. M., Heinkel, G. L., Kochersperger, L. M., Dower, W. J., Barrett, R. W., and Gallop, M. A. (1993) Generation and screening of an oligonucleotide-encoded synthetic peptide library. *Proc. Natl. Acad. Sci. U.S.A. 90*, 10700—10704.

(6) Vetter, D., and Gallop, M. A. (1995) Strategies for the synthesis and screening of glycoconjugates. 1. A library of glycosylamines. *Bioconjugate Chem. 6*, 316—318.

(7) Likhosherstov, L. M., Novikova, O. S., Derevitskaja, V. A., and Kochetkov, N. K. (1986) A new simple synthesis of amino sugar β-D-glycosylamines. *Carbohydrate Res. 146*, C1—C5.

(8) Kallin, E., Lönn, H., Norberg, and T., Elofsson, M. (1989) Derivatization procedures for reducing oligosaccharides, Part 3: Preparation of oligosaccharide glycosylamines, and their conversion into oligosaccharide—acrylamide copolymers. *J. Carbohydr. Chem. 8*, 597—611.

(9) Otvos, L., Jr., Wroblewski, K., Kollat, E., Perczel, A., Hollosi, M., Fasman, G. D., Ertl, H. C. J., and Thurin, J. (1989) Coupling strategies in solid-phase synthesis of glycopeptides. *Pept. Res. 2*, 362—366.

(10) Anisfeld, S. T., and Lansbury, P. T., Jr. (1990) A convergent approach to the chemical synthesis of asparagine-linked glycopeptides. *J. Org. Chem. 55*, 5560—5562.

(11) Kallin, E., Lönn, H., Norberg, T., Sund, T., and Lundqvist, M. (1991) Derivatization procedures for reducing oligosaccharides, Part 4: Use of glycosylamines in a reversible derivatization of oligosaccharides with the 9-fluorenylmethoxycarbonyl group, and HPLC separations of the derivatives. *J. Carbohydr. Chem. 10*, 377—386.

(12) Urge, L., Kollat, E., Hollosi, M., Laczko, I., Wroblewski, K., Thurin, J., and Otvos, L, Jr. (1991) Solid-phase synthesis of glycopeptides: synthesis of Nα-fluorenylmethoxycarbonyl L-asparagine Nβ-glycosides. *Tetrahedron Lett. 32*, 3445—3448.

(13) Urge, L., Otvos, L., Jr., Lang, E., Wroblewski, K., Laczko, I., and Hollosi, M. (1992) Fmoc-protected, glycosylated asparagines potentially useful as reagents in the solid-phase synthesis of N-glycopeptides. *Carbohydr. Res. 235*, 83—93.

(14) Cohen-Anisfeld, S. T., and Lansbury, P. T., Jr. (1993) A practical, convergent method for glycopeptide synthesis. *J. Am. Chem. Soc. 115*, 10531—10537.

(15) Manger, I. D., Rademacher, T. W., and Dwek, R. A. (1992) 1-N-Glycyl β-oligosaccharide derivatives as stable intermediates for the formation of glycoconjugate probes. *Biochemistry 31*, 10724—10732.

(16) Trivial names or abbreviations represent Glc(α1—4)Glc (maltose), GlcNAc(β1—4)GlcNAc (chitobiose), Gal(β1—4)Glc (lactose), Neu5Ac(α2—3)Gal(β1—4)Glc (sialyllactose), and Gal-(β1—4)GlcNAc (LacNAc).

(17) Haselbeck, A., and Hösel, W. (1990) Description and application of an immunological detection system for analyzing glycoproteins on blots. *Glycoconjugate J. 7*, 63—74.

(18) Haselbeck, A., Schickaneder, E., von der Eltz, H., and Hösel, W. (1990) Structural characterization of glycoprotein carbohydrate chains by using digoxigenin-labeled lectins on blots. *Anal. Biochem. 191*, 25—30.

(19) Vetter, D., Heinkel, G., Raab, R., Cheng, G., Schunk, C., Sugarman, J., and Gallop, M. A. (manuscript in preparation).

A Convenient Route to Thiol Terminated Peptides for Conjugation and Surface Functionalization Strategies

T. M. Winger,[†] P. J. Ludovice,[†] and E. L. Chaikof*,[†,‡]

School of Chemical Engineering, Georgia Institute of Technology, Atlanta, Georgia 30332, and Department of Surgery, Emory University School of Medicine, Atlanta, Georgia 30322. Received December 12, 1994[®]

The derivatization of poly(*p*-(chloromethyl)styrene-*co*-divinylbenzene) (Merrifield resin) with *N*-(*tert*-butoxycarbonyl)-2-aminoethanethiol is presented as a convenient route for the generation of thiol terminated peptides using a solid phase methodology. Maximum resin substitution reached 92% (773 μmol/g) after 24 h. However, at 30 min, yields exceeded 400 μmol/g, above which the resin is suitable for solid phase peptide synthesis. Thiol terminated peptides are well-suited for subsequent chemical conjugation reactions or for the formation of organic monolayers on metal substrates.

INTRODUCTION

Self-assembled organic monolayers of various functionality have been formed on solid substrates on the basis of the coordination of thiol or disulfide groups with gold, silver, and platinum (*1*). In this regard, most strategies directed at the creation of a peptide monolayer have used the presence of cysteine residues in synthesized or genetically engineered peptides or proteins to mediate surface binding (*2*). An alternative method has been recently reported by Whitesell and Chang. Following the amination of a gold surface with an aminotrithiol, a peptide monolayer was produced by in situ polymerization (*3*). The inability to precisely control peptide chain growth led to significant variability in ellipsometric measurements and appears to be a limitation of this approach.

Although thiol groups act as an effective binding residue to gold and other metal substrates, the chemical structure of the entire molecule will affect both packing density and chain orientation of any self-assembled monolayer (*4*). As noted above, most peptide monolayers have been bound to gold substrates by a β-carboxylate-bearing thiol, like cysteine. Since the supramolecular structure of a thin film may significantly alter its physical and chemical properties, we began to explore the synthesis of less hindered thiol-terminated peptides. We present an effective solid phase procedure for the creation of ω-thiol oligopeptides. This approach is based on the modification and extension of earlier studies which examined the derivatization of chloromethylated polystyrene resins through a nucleophilic substitution reaction in the presence of a thiol (*5*). The advantages of terminal thiols produced in this fashion for the formation of peptide conjugates were not evaluated. Nonetheless, we believe that peptides produced by this technique may be effectively used in chemical conjugation schemes, if so desired.

* Author to whom correspondence should be addressed: Elliot L. Chaikof, M.D., Ph.D., Department of Surgery, Emory University Hospital, Box M-11, 1364 Clifton Rd, N.E., Atlanta, GA 30322. (404) 727-8413 phone, (404) 727-3660 fax, echaiko@eagle. cc.emory.edu.
† Georgia Institute of Technology.
‡ Emory University School of Medicine.
® Abstract published in *Advance ACS Abstracts*, May 1, 1995.

EXPERIMENTAL PROCEDURES

Materials. The Merrifield resin (0.84 mequiv/g, 1% cross-linked with divinylbenzene, Fluka) was washed with methanol before use, and fine floating beads were discarded. 1,4-Dioxane (Aldrich) was treated with basic alumina to remove peroxides. Trifluoroacetic acid, tetrabutylammonium hydroxide (TBAH; 1 M in MeOH), cystamine dihydrochloride, and methylamine (MeNH$_2$; 2 M in MeOH) were purchased from Aldrich. All other chemicals used for resin derivatization were reagent or spectrophotometric grade.

Peptides were prepared on a fully automated Applied Biosystems Model 430A peptide synthesizer (0.5-mmol scale). The apparatus used for hydrogen fluoride cleavage was from Peninsula Laboratories. All solvents were of synthetic grade and were supplied by Burdick and Jackson. Highest grade (*tert*-butyloxy)carbonyl (Boc)-protected amino acids were purchased from commercial sources (Applied Biosystems, Inc. (Foster City, CA), Bachem Biosciences (King of Prussia, PA), and Advanced Chemtech (Louisville, KY)). The side-chain protecting groups were [(2-bromobenzyl)oxy]carbonyl (2-BrZ) for tyrosine and mesitylenesulfonyl (Mts) for arginine (Bachem Biosciences).

Analytic Methods. Thin layer chromatography (TLC) analysis was performed with iodine vapor for nonspecific detection of all compounds, and the ninhydrin spray test was used for the detection of free amines. The reagents (monitors 1, 2, and 3) used in the ninhydrin assay (*6*) were obtained from Applied Biosystems. The 250-μm layer thickness silica plates used for TLC were purchased from Whatman.

^{1}H nuclear magnetic resonance (NMR) was performed on a General Electric QE 300 Plus spectrometer at 300 MHz in deuterated chloroform (CDCl$_3$). Chemical shifts (δ) were measured with respect to tetramethylsilane (TMS), which was used as the 0 ppm internal reference. Fast atom bombardment (FAB) mass spectrometry was measured on a VG Instruments 70SE mass spectrometer.

Synthesis of *N,N'*-Bis(*tert*-butoxycarbonyl)cystamine (2). The synthetic approach for **2** and its subsequent reduction to **3**, as described below, is similar to those in the literature (*5, 7–9*). An aqueous/organic biphasic mixture of 2 g (225.20 g/mol, 8.88 mmol) of cystamine dihydrochloride (**1**), 40 mL of *p*-dioxane, 10 mL of water, 7.8 mL (6.3 equiv) of triethylamine, and 4.3 g (218.25 g/mol, 2.2 equiv) of di-*tert*-butoxycarbonate was stirred for 18 h in an open 100-mL round-bottom flask

at room temperature. The reaction mixture was then concentrated to a final volume of 10 mL and poured into 280 mL of water, upon which the bis-protected disulfide **2** precipitated. Precipitation was complete after continuous overnight stirring at room temperature, followed by a 30-min sojourn at 0 °C. Filtration and high vacuum drying in a desiccator over NaOH yielded 3 g (96%) of crude (BocNHCH$_2$CH$_2$S)$_2$, which was subsequently allowed to crystallize from toluene/hexane (1/3 v/v) for 2 days in the refrigerator. Vacuum drying afforded 2.9 g (8.23 mmol, 93%) of product in the form of white needles. Purity was checked by TLC in CHCl$_3$/MeOH (80/20 v/v). The R_f values for the starting material **1** and the bis-Boc-protected product **2** were 0.00 and 0.76, respectively.

Synthesis of *N*-(*tert*-Butoxycarbonyl)-2-aminoethanethiol (3). A mixture of 2.9 g (8.23 mmol) of **2**, 1.1 mL of *N,N*-diethylethanolamine, 1.28 g of dithiothreitol (DTT), and 80 mL of dichloromethane was stirred at room temperature for 24 h in a 250-mL round-bottom flask. The reaction mixture was then washed twice with 80 mL of a 0.1 N HCl solution. The organic phase was separated and washed four times with 80 mL of water, dried over MgSO$_4$, filtered, and evaporated to dryness. The resulting oily residue was subsequently dissolved in 20 mL of hexane and left at room temperature for 2 days in order to allow the remaining starting material to crystallize. Subsequent filtration and evaporation to dryness under nitrogen afforded 2.5 g (85%) of **3** (95+% pure). Purity was confirmed by TLC in hexane/ethyl acetate (EtOAc) (80/20 v/v). The R_f values for the starting material **2** and the product **3** were 0.40 and 0.62, respectively. ^{1}H NMR (CDCl$_3$) data were as follows: δ 1.36 (t, 1H, -SH), δ 1.45 (s, 9H, 3 × CH$_3$), δ 2.64 (q, 2H, -NHC*H*$_2$$^-$), δ 3.32 (q, 2H, $-$CH$_2$C*H*$_2$SH), δ 4.98 (broad s, 1H, -CON*H*-).

Derivatization of the Merrifield Resin. A screw-cap glass flask (100-mL capacity, Gibco) was loaded with 5.14 g of Merrifield resin **4** (4.11 mmol of active sites), 22 mL of *p*-dioxane, 15 mL of MeOH, 1.17 g (1.6 equiv) of **3**, and 5.75 mL of a 1 M solution of TBAH in MeOH. The reactor was sparged with nitrogen for 5 min, capped and sealed with Teflon, and vigorously shaken for 20 h at 65 °C. The supernatant was then discarded, and the resin was washed twice with 100 mL *p*-dioxane/MeOH (1/1) (polarity index (p.i.) ≈ 17), twice with 100 mL of iPrOH/water (1/1) (p.i. ≈ 50), and again twice with 100 mL of *p*-dioxane/MeOH (1/1) (p.i. ≈ 17). All solvent compositions given are volumetric (v/v). Low polarity index washes caused the resin to swell. At high p.i., the polystyrene beads shrank. Cyclic low p.i./high p.i. washes therefore improved the rinsing of the resin. End-capping was performed in the presence of a 25-fold molar excess of methylamine by continuous shaking of the resin in 50 mL of a 2 M solution of methylamine in methanol at 65 °C for 6 h. The liquid was subsequently discarded and the resin washed twice with 100 mL of *p*-dioxane/MeOH (1/1), twice with 100 mL of iPrOH/water (1/1), and twice with 100 mL of chlorobutane (BuCl) (p.i. ≈ 14).

The resin was deprotected by reaction with 100 mL of BuCl/trifluoroacetic acid (TFA) (2/1 v/v) added in portions of 10 mL at 0 °C for 5.5 h at room temperature. The resin was then washed twice with 100 mL of BuCl, twice with 100 mL of *p*-dioxane, twice with 100 mL of iPrOH/water (6/1), and twice with 100 mL of MeOH. It was then predried on a rotary evaporator at 50 °C. Drying was completed in high vacuum (0.1 mmHg) for 4 h at room temperature. This afforded 4.89 g of amine-functionalized resin **6**. The substitution of the functionalized Merrifield resin was determined by a ninhydrin test adapted from the method developed by Sarin (6). In

order to determine the optimal period for maximal substitution, the resin substitution reaction was evaluated after reaction times of 0.5, 1.5, and 24 h. At the indicated time, the resin was end-capped, deprotected, and worked up as previously stated. The ninhydrin test was performed in triplicate for each reactor.

Solid Phase Peptide Synthesis and Purification. The synthesis of a decapeptide (SFLLRN(βA)$_3$Y(CH$_2$)$_2$-SH) was performed in routine fashion. The first amino acid to be attached to the previously thiolamino-derivatized Merrifield resin was activated with dicyclohexylcarbodiimide (DCC) and reacted with 1-hydroxybenzotriazole (HOBt) to form the HOBt ester. Mixing at basic pH readily yielded the protected amino acid-functionalized resin through nucleophilic inactivation of the ester. Acidic deblocking in the presence of trifluoroacetic acid yielded the free amino terminus. The subsequent three cycles consisted of similar coupling/deprotection sequences using DCC-activated β-alanine as the electrophile. The remaining six amino acids were coupled in routine fashion. The peptide was cleaved from the resin and the side-chain protecting groups removed by treatment with 1.3 mL of anisole and 26 mL of liquid hydrogen fluoride (HF) for 90 min at 0 °C. After removal of the HF at 0 °C with a stream of nitrogen, the excess anisole was removed by four washes, each with 30 mL of anhydrous ether. The peptide was subsequently extracted using an aqueous acetic acid solution (50% v/v), and the resulting mixture was freeze-dried in water.

Purification of the peptide was achieved by reverse-phase high performance liquid chromatography (RP-HPLC) using a Waters Delta Prep 3000 preparative system and a Waters 3000 systems controller equipped with a Waters 740 data module. The column used was an Aquapore RP-300 C$_{18}$ silica column (1 × 10 cm, Applied Biosystems). Elution was performed with a gradient of acetonitrile in water using two buffers: a 0.1% aqueous TFA solution for the first (buffer A) and a mixture of CH$_3$CN/water (80/20 v/v) containing 0.1% TFA for the second (buffer B). The fractions of interest were combined, concentrated on SpeedVac at room temperature, lyophilized, and stored under nitrogen at -20 °C. Purity of the fractions was checked by microbore RP-HPLC on a reverse-phase C$_{18}$ silica column (1 × 250 mm, Applied Biosystems). The final sample was analyzed by mass spectrometry for molecular weight confirmation.

RESULTS AND DISCUSSION

Synthetic Scheme. The route taken for the synthesis of thiol terminated peptides is summarized in Scheme 1. Precursor synthesis involves the nucleophilic attack of the free amines of neutralized cystamine **1** onto either one of the two carbonyl groups of di-*tert*-butoxycarbonate (Boc$_2$O). The Boc-protected cystamine **2** thereby obtained is subsequently cleaved into its two *N*-(*tert*-butoxycarbonyl)-2-aminoethanethiol monomers **3** through a disulfide reduction reaction in the presence of DTT (5). The derivatization of poly(*p*-(chloromethyl)styrene-*co*-divinylbenzene) (Merrifield resin) involves a simple nucleophilic substitution (S$_N$2) of a resin-borne chlorine atom **4** by a thiol. Since the nucleophile is a negatively charged thiolate, resin functionalization requires the presence of an organic base. By working in basic conditions, one also prevents undesirable acidolysis of the Boc group. Such a reaction would deprotect the amino group of compound **3**, allowing potential substitution of the chlorine atom leading to a misoriented product. The reactivity of a thiolate (pK_a ≈8.3) is 1000 times greater than that of a primary amine (pK_a ≈ 9.5). Thus, the above-mentioned side reaction would only occur to a limited extent,

Table 1. Ninhydrin Test Results for the Determination of the Degree of Substitution of the Merrifield Resin vs Reaction Time

	reaction time (h)			
	0.5	1	5	24
resin wt (mg)	5.45 ± 0.05	5.54 ± 0.05	5.41 ± 0.05	5.42 ± 0.05
av absorbance at 570 nm	0.139 ± 0.002	0.193 ± 0.002	0.199 ± 0.002	0.201 ± 0.002
substitution[a] (μmol of NH_2/g)	532 ± 156	726 ± 210	767 ± 222	773 ± 223

[a] $\epsilon' = 0.012 \pm 0.003$ based on the actual weight of pure peptide recovered from a given solid phase synthesis.

Scheme 1. Preparation of Precursors and Derivatization of the Merrifield Resin

$(HCl.H_2NCH_2CH_2S)_2$ **1**

↓ Boc_2O

$(BocNHCH_2CH_2S)_2$ **2**

↓ DTT

$BocNHCH_2CH_2SH$ **3** $ClCH_2$—⟨◯⟩⟩ **4**

└─────────────┬─────────────┘

↓ Et_3N, Δ

$BocNHCH_2CH_2SCH_2$—⟨◯⟩⟩ **5**

↓ TFA

$H_2NCH_2CH_2SCH_2$—⟨◯⟩⟩ **6**
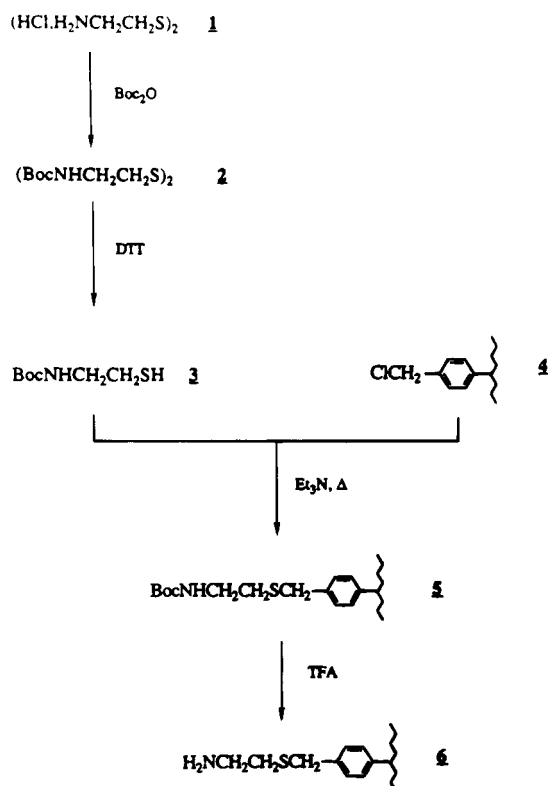
provided the pH is kept between 8 and 10. Unreacted chloromethyl functions were end-capped by a similar S_N2-type reaction with methylamine. Acidolysis of the Boc groups at the surface of the derivatized resin yields the amine-functionalized resin suited for solid phase peptide synthesis. Following peptide synthesis, para-substituted benzyl thioethers generate a free thiol upon cleavage with hydrogen fluoride (*10*).

Chemical and Physical Characterization of Resin Substitution.

Resins that exhibit optimal characteristics for solid phase peptide synthesis have a typical substitution of $400-800$ μmol/g. In our case, approximately 20 min of reaction time was required for a small scale batch (150 mg of resin) to reach the 400 μmol/g threshold, above which the resin becomes well-suited for solid phase peptide synthesis (Table 1). Maximum resin substitution reached 92% (773 μmol/g) after 24 h. For scaled-up batches of 5 g of resin, a longer reaction time of 20 h was used to ensure maximal conversion. Subsequent analysis with a ninhydrin assay indicated a substitution of 354 ± 170 μmol/g.

Incidentally, we noted a simple correlation between bead density and its degree of substitution. Indeed, preliminary resin substitution experiments yielded a binodal bead distribution. A small fraction of the resin was substituted at 200 μmol/g, while the remainder represented a high-substitution population starting at 400 μmol/g. The low-substitution beads floated on BuCl/

TFA (2/1 v/v) (which has a density of approximately 1.08 g/mL) but settled in BuCl (0.89 g/mL). Hence, the density of the 200 μmol/g beads lay between 0.89 and 1.08 g/mL. The high-substitution beads, on the contrary, settled in BuCl/TFA (2/1) (1.08 g/mL) but stayed afloat on CH_2Cl_2 (1.32 g/mL), indicating that their density lay between those two values.

Thiol Terminated Peptide Synthesis.

The peptide synthesized for the purpose of the present study was a human thrombin receptor activating sequence, Ser-Phe-Leu-Leu-Arg-Asn-(βAla)$_3$-Tyr-NHCH$_2$CH$_2$SH. Initially, 554 mg (88%) of crude peptide was obtained. After HPLC purification, the overall yield was approximately 60% (97% purity). The peptide was characterized by TLC in hexane/chloroform/2-propanol/glacial acetic acid/water (15/5/60/3/17 v/v). The TLC spot (R_f 0.51) turned bright yellow upon application of a few drops of a 1 mg/mL aqueous solution of Ellman's reagent (5,5'-dithiobis(2-nitrobenzoic acid)) (*11*). As expected, ninhydrin testing confirmed the presence of free amino groups. The respective disulfide had an R_f of 0.35 and stained positive with ninhydrin but not with Ellman's reagent. FAB mass spectrometry confirmed the expected molecular weight (1184.4 g/mol).

Solid phase methodology was introduced by Merrifield in 1963 (*12*) and has since become an invaluable tool for routine peptide synthesis. In this method, a growing polypeptide chain is covalently anchored, usually by its C-terminus, to an insoluble solid support such as beads of polystyrene resin, and the appropriately blocked amino acids and reagents are added in the proper sequence. Our results demonstrate the successful preparation of a thiol-terminated oligopeptide through the use of a (chlorobenzyl)polystyrene resin. Derivatization with an aminoethanethiol anchor yielded the thiol terminated peptide directly, without the addition of a cysteine residue or the use of other postsynthesis derivatization steps.

LITERATURE CITED

(1) Bain, C. D., Troughton, E. B., Tao, Y.-T., Evall, J., Whitesides, G. M., and Nuzzo, R. G. (1989) Formation of monolayer films by the spontaneous assembly of organic thiols from solution onto gold. *J. Am. Chem. Soc. 111*, 321–335.

(2) Amador, S. M., Pachence, J. M., Fischetti, R., and McCauley, J. P., Jr. (1993) Use of self-assembled monolayers to covalently tether protein monolayers to the surface of solid substrates. *Langmuir 9*, 812–817.

(3) Whitesell, J. K., and Chang, H. K. (1993) Directionally aligned helical peptides on surfaces. *Science 261*, 73–76.

(4) Ulman, A. (1991) *An Introduction to Ultrathin Organic Films. From Langmuir-Blodgett to Self-Assembly*, pp 237–301, Academic Press, San Diego.

(5) Inman, J. K., Dubois, G. C., and Appella, E. (1977) Synthesis of macroporous polystyrene derivatives for supports in sequential degradation of peptides. *Solid Phase Methods in*

Protein Sequence Analysis, INSERM Symposium, pp 81–94, Elsevier/North-Holland Biomedical Press, New York.

(6) Sarin, V. K., Kent, S. B. H., Tam, J. P. and Merrifield, R. B. (1981) Quantitative monitoring of solid-phase peptide synthesis by the ninhydrin reaction. *Anal. Biochem. 117,* 147–157.

(7) Moroder, L., Hallet, A., Wünsch, E., Keller, O. and Wersin, G. (1976) Di-tert-butyl-dicarbonate, a useful tert-butyloxy-carbonylating reagent. *Hoppe-Seylers Z. Physiol. Chem. 357,* 1651–1653.

(8) Van den Broek, L. A. G. M., Fennis, P. J., Arevalo, M. A., Lazaro, E., Ballesta, J. P. G., Lelieveld, P., and Ottenheijm, H. C. J. (1989) The role of hydroxymethyl function on the biological activity of the antitumor antibiotic sparsomycin. *Eur. J. Med. Chem. 24,* 503–510.

(9) Stindl, A., and Keller, U. (1993) The initiation of peptide formation in the biosynthesis of actinomycin. *J. Biol. Chem. 268,* 10612–10620.

(10) Greene, T. W. (1981) *Protective Groups in Organic Syntheses,* pp 193–217, Wiley-Interscience Press, New York.

(11) Ellman, G. L. (1959) Tissue sulfhydryl groups. *Arch. Biochem. Biophys. 82,* 70–77.

(12) Merrifield, R. B. (1963) Solid phase peptide synthesis. I. The synthesis of a tetrapeptide. *J. Am. Chem. Soc. 85,* 2149–2154.

COMMUNICATIONS

Synthesis, Hybridization Properties, Nuclease Stability, and Cellular Uptake of the Oligonucleotide–Amino-β-cyclodextrins and Adamantane Conjugates

Ivan Habus, Qiuyan Zhao, and Sudhir Agrawal*

Hybridon, Inc., One Innovation Drive, Worcester, Massachusetts 01605. Received March 29, 1995[®]

Synthesis of the oligonucleotides conjugated with amino derivatives of β-cyclodextrin and adamantane, at the 3′-end of host oligonucleotide, has been described. The oligonucleotide conjugates were examined for their nuclease stability, hybridization properties, and cellular uptake. The oligonucleotide conjugates had increased nuclease resistance compared to their parent oligonucleotides. Conjugation of adamantane to the oligonucleotides did not adversely affect the ability of the oligonucleotides to hybridize with their complementary RNA. Conjugation with amino derivatives of β-cyclodextrin, however, significantly destabilized the duplex formation. In the cellular uptake studies, we found that amino derivatives of β-cyclodextrin attached at 3′-end of the oligonucleotides did not help to increase the uptake by cells. Cellular uptake of oligonucleotide–adamantane conjugates in association with 2-(hydroxypropyl)-β-cyclodextrin (HPCD) as a "carrier" was significantly higher than that of control oligonucleotides.

Oligonucleotides are widely used as research tools for inhibiting specific gene expression and are under investigation for possible use as therapeutic agents (1–4). Cellular uptake and internalization of such oligonucleotides are important factors in determining their effectiveness as potential therapeutics. Oligonucleotide uptake is a sequence-independent saturable process and is dependent on temperature and energy (5, 6). To improve cellular uptake, several groups of oligonucleotide conjugates have been synthesized and studied (3, 7, 8). Although some of these conjugates showed increases in cellular uptake and stability against nucleases, cytotoxicity or/and non-sequence-specific activities increased.

In our earlier studies (9, 10) we have explored the possibility of using β-cyclodextrin and its analogues as "carriers" to increase the cellular uptake of oligonucleotides. Cyclodextrins are cyclic oligosaccharides known for their ability to form inclusion complexes with many lipophilic drugs, changing the physicopharmaceutical properties of the drugs such as aqueous solubility, thereby changing their bioavailability and improving

stability and effectiveness (11, 12). We demonstrated that cellular uptake of phosphorothioate oligonucleotide was 2–3-fold increased in the presence of cyclodextrin analogues in H9, CEM, and Molt-3 cell lines. The uptake of the oligonucleotide mediated by cyclodextrins was a cyclodextrin concentration and time dependent process, and the intracellular presence of the oligonucleotide was confirmed by confocal microscopy. In this study, we have further explored the possibility of using β-cyclodextrin and its analogues as "carriers" to increase the cellular uptake of oligonucleotides. Because the adamantane molecule can enter into the β-cyclodextrin cavity and form a stable inclusion complex (13, 14), and because cyclodextrin derivatives can act as a selective hosts with several binding sites for nucleotides (15, 16), we decided to link a molecule of adamantane or a molecule of the amino derivatives of β-cyclodextrin at the 3′-end of a synthetic oligonucleotide.

A molecule of adamantane was attached to an oligonucleotide via an amino linker. 3-Aminopropyl solketal 1 was synthesized as described (17) and further reacted with 1-adamantanecarbonyl chloride (Scheme 1) to give N-adamantoyl-3-(aminopropyl)solketal (2) with a yield of 97%. Adamantoyl derivative 2 was treated with a

* To whom correspondence should be addressed. Phone: 508-752-7000. Fax: 508-751-7692.

Scheme 1
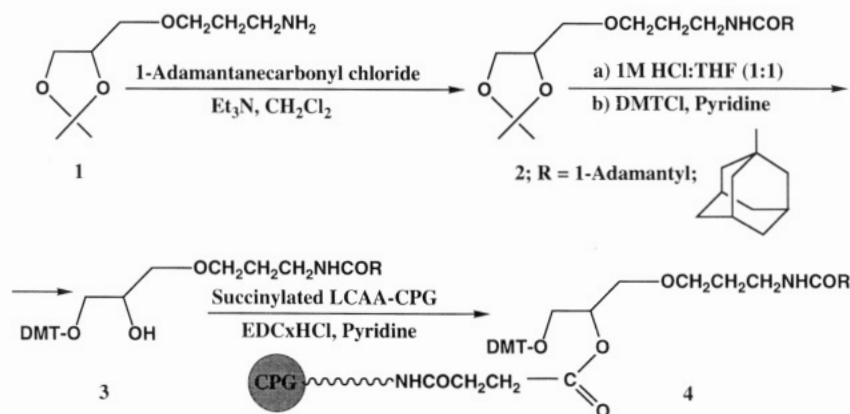
mixture of 1 M hydrochloric acid and tetrahydrofuran (1:1) to remove the isopropylidene group and *in situ* reacted with 4,4'-dimethoxytrityl chloride in anhydrous pyridine to give 1-*O*-(4,4'-dimethoxytrityl)-3-*O*-(*N*-adamantoyl-3-aminopropyl)glycerol (**3**) with a yield of 61% (Scheme 1). The DMT derivative **3** was further attached (*18*) onto long chain (alkylamido)propanoic acid controlled pore glass (LCAA-CPG) beads to give **4** and was as such used for oligonucleotide synthesis. The loading efficiency was 22.1 µmol/g of CPG.

Synthesis of the oligonucleotides **5** and **6**, containing either phosphodiester (PO) or phosphorothioate (PS) internucleoside linkages, respectively, was carried out on 10 µmol scales using **4** and β-cyanoethyl 3'-phosphoramidites on an automated DNA synthesizer (Milligen/Bioresearch 8700 series). The oxidation reagents used

5 Seq.#1; X=O; PO; R = 1-Adamantyl
6 Seq.#2; X=S; PS; R = 1-Adamantyl
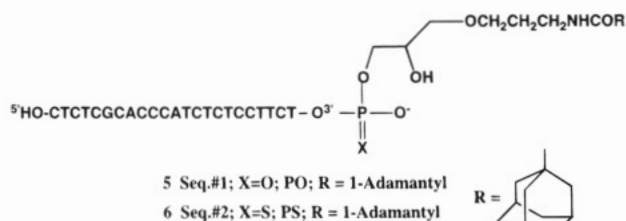
for the synthesis were a standard solution of iodine for PO linkage formation and a 1% solution of 3*H*-1,2-benzodithiol-3-one 1,1-dioxide in acetonitrile for PS linkage formation. Oligonucleotides **5** and **6** were released from the support by treatment with ammonia for 6 h at 55 °C and purified by reversed-phase HPLC at pre- and post-DMT removal stages (Figure 1).

Amino derivatives of β-cyclodextrin (**7** and **8**) were prepared as previously described (*19*, *20*) and attached at the 3'-end of the oligonucleotides via carbamate (−OCONH−) linkage (*21−23*) (Scheme 2). Synthesis of oligonucleotides **9** and **10** was carried out on 1 µmol scale using β-cyanoethyl 5'-phosphoramidites on an automated DNA synthesizer with the last DMT removed. The 3'-OH group was further activated with bis(*p*-nitrophenyl)-carbonate in anhydrous 1,4-dioxane with triethylamine as the catalyst (3 drops) for 2 h to give the active

7 R'=NH₂

8 R'=NHCH₂CH₂NH₂
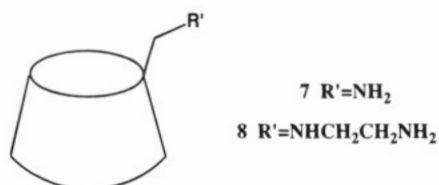
carbonates **11** and **12** (Scheme 2). The active oligonucle-
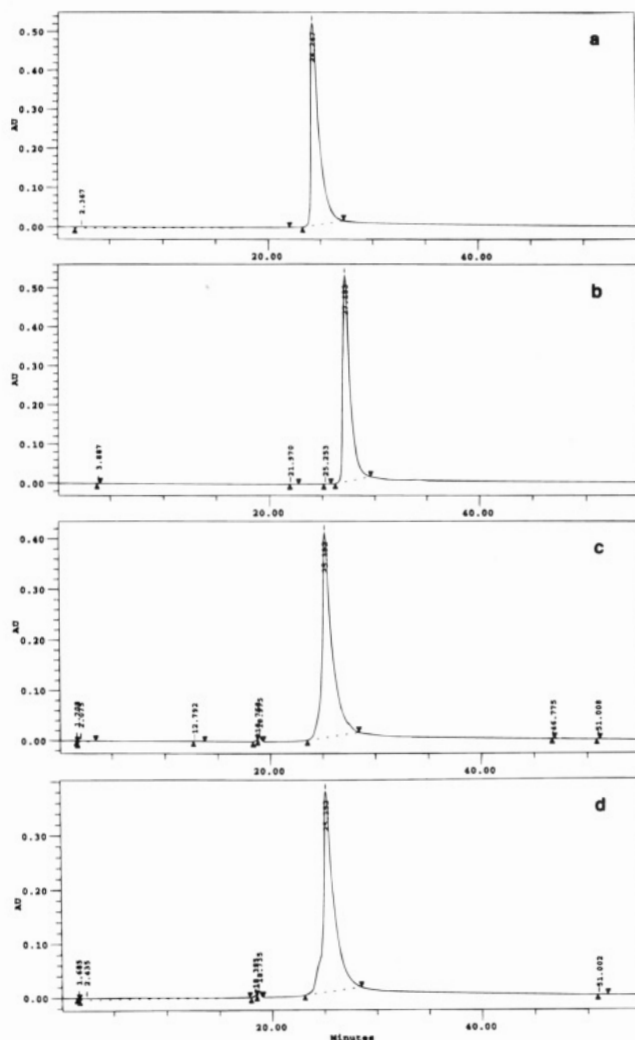
Figure 1. Reversed-phase HPLC profile of oligonucleotides. (a) Standard PO oligonucleotide with the same chain length and base composition as **5**, **17**, and **18** and with no modification at 3'-end; (b) oligonucleotide **5**; (c) **17**; (d) **18**. HPLC was carried out using Waters 600E system controller, 996 Photodiode array detector, NEC PowerMate 486/33i, and Millenium 2010 chromatography manager. For reversed-phase HPLC, the column used was Radial-Pak Cartridge (Waters), buffers (A) 0.1 M ammonium acetate and (B) buffer A containing 80% acetonitrile; gradient 0% buffer B for 2 min, 0−20% buffer B for 30 min, flow 1.5 mL/min, detector 254 nM.

otide carbonates were then successively washed with anhydrous 1,4-dioxane and acetonitrile, dried by purging with argon, and reacted with **7** or **8** in anhydrous pyridine for 6 h to give **13−16**. After successive washings with pyridine and acetonitrile, oligonucleotides were released

Scheme 2
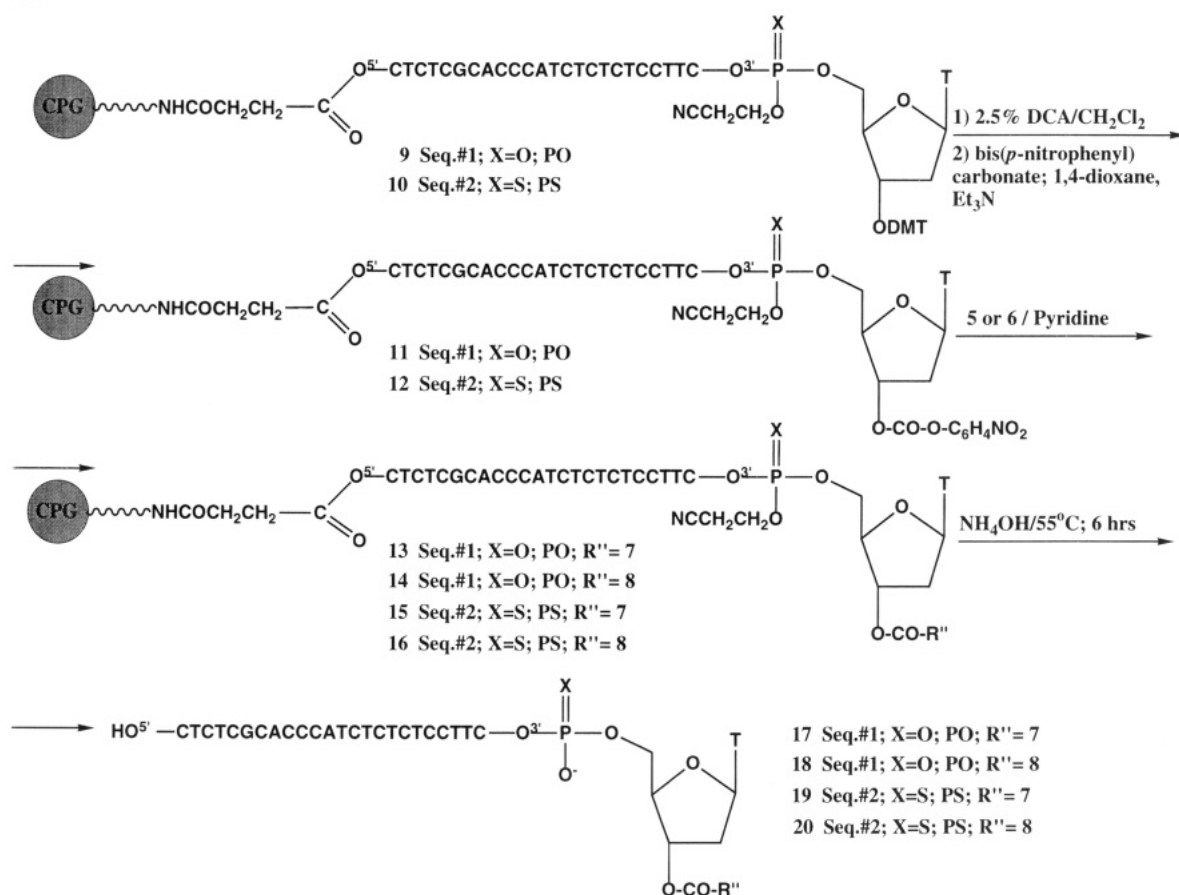
Table 1. Hybridization Data of Oligonucleotides[a]

Entry	Oligonucleotide	Tm[b], (°C)	Tm[c], (°C)	ΔTm, (°C)
1	5; PO;	70.6	70.0	-
2	6; PS	62.5	62.3	-
3	17; PO;	42.9	70.0	-27.1
4	19; PS	36.0	62.3	-26.3
5	18; PO;	42.3	70.0	-27.7
6	20; PS	35.8	62.3	-26.5

[a]Oligonucleotides were hybridized with complementary RNA; [b]Absorbance vs temperature profiles were measured at 0.2 A_{260} Units of each strand in 1 mL of buffer (100 mM Na^{+}, 10 mM phosphate, pH 7.0); [c]Standard PO and PS oligonucleotides with the same chain length and sequence as the oligonucleotides 5, 6, 17-20, and with no modification at the 3'-end.
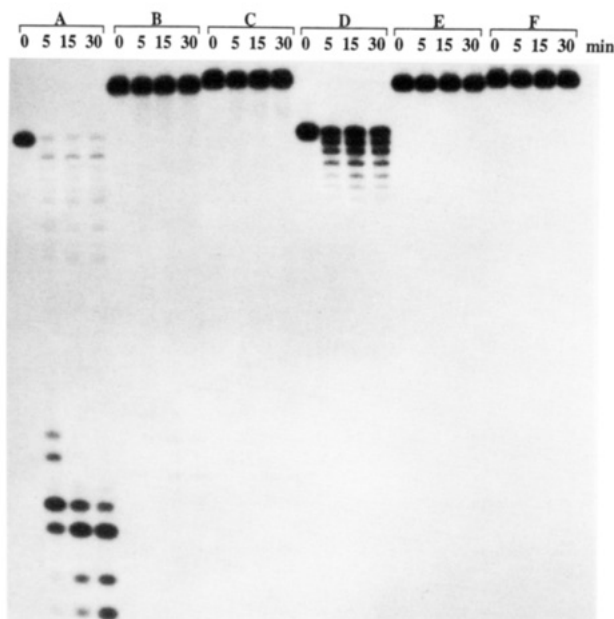
Figure 2. PAGE of enzymatically digested oligonucleotides with the amino β-cyclodextrins covalently linked at the 3'-end. The standard oligonucleotides (25-mers), with the same sequence as oligonucleotides **17–20**, containing all PO linkages (A) and all PS linkages, (D); oligonucleotides **17** (B), **18** (C), **19** (E), and **20** (F) were labeled (*25*) with [γ-³²P]ATP. T4 DNA polymerase resistance was studied by incubating 30 pmol of each oligonucleotide with 5 units (≥5 units/mg) of the enzyme at 37 °C in 20 μL of buffer (50 mM Tris, pH 8.0, 5 mM Mg²⁺, 5 mM DTT, 0.05% bovine serum albumin). At the indicated time, an aliquot (5 μL) was removed, and to each aliquot stop solution (6 μL; 95% formamide, 10 mM EDTA, 0.05% bromophenol blue, 0.05% xylene cyanol) was added. The samples were then analyzed by electrophoresis on 20% polyacrylamide gel containing 8 M urea.

from the support, deprotected by treatment with ammonia for 6 h at 55 °C, and purified by polyacrylamide gel electrophoresis to give oligonucleotides **17–20** (Figure 1).

Hybridization studies indicated that attachment of a molecule of adamantane via an amino linker at the 3'-end of oligonucleotides, **5** and **6**, does not affect the stability of the duplexes formed between oligonucleotides and their complementary RNA (Table 1, entries 1 and 2). The same behavior in the hybridization was previously observed with an oligonucleotide with a molecule of adamantane attached at 3'-end via a phosphorothioate linkage (*24*). The attachment of amino derivatives of β-cyclodextrin, **7** or **8**, via a carbamate linkage at the 3'-end of oligonucleotides **17–20** caused a significant reduction in binding (Table 1, entries 3–6). This poor binding could be related to complexation properties (*15, 16*) of nucleotidic units of an oligonucleotide and an amino derivative of β-cyclodextrin that is attached to the host oligonucleotide. In addition, β-cyclodextrin is a sterically crowded molecule. A combination of these factors resulted in only partial duplex formation of oligonucleotides **17–20** with the complementary RNA (Table 1, entries 3–6).

We determined the nuclease resistance of oligonucleotides **17–20** to a 3'-exonuclease, such as T4 DNA polymerase (Figure 2). The kinetic study showed complete degradation of PO oligonucleotide (25-mer, with the same sequence as **18** and **19**) in less than 5 min, while the great majority of PO oligonucleotides **18** and **19**, which had amino derivatives of β-cyclodextrin **7** and **8** attached at their 3'-ends, remained intact even after 30 min. The PS oligonucleotide exhibited better stability
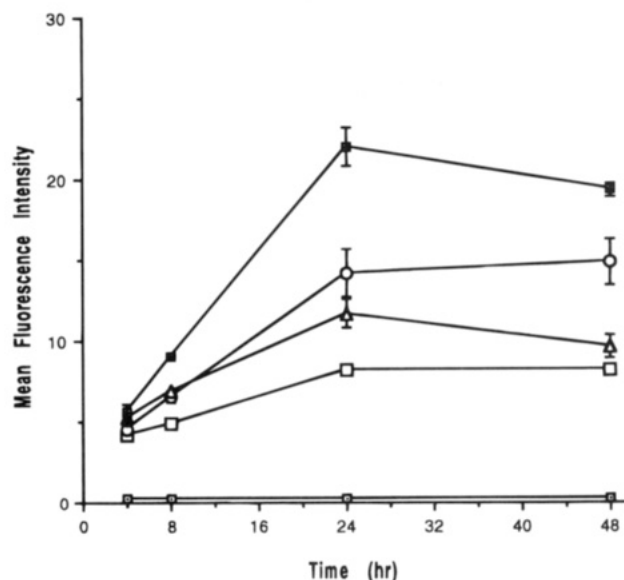
Figure 3. Cellular uptake profiles of oligonucleotides mediated by 2-(hydroxypropyl)-β-cyclodextrin (HPCD). Oligonucleotide **6** and HPCD (−■−); oligonucleotide **6** (−△−); PS oligonucleotide (25-mer, the same sequence as **6**) (−□−); PS oligonucleotide & HPCD (−○−); and media without oligonucleotide (−⊡−). Each oligonucleotide was mixed with 1.25% solution of HPCD (sterilized prior to use by passing through 0.2 μm filter) in plain RPMI media to give a concentration of 10 μg of oligonucleotide *per* mL of media, sonicated at 4 °C for 2 h, and followed by complexation at 4 °C overnight. H9 cells were cultured in RPMI media supplemented with 10% heat inactivated (56 °C for 30 min) fetal bovine serum (FBS), 2 mM glutamine, 10 μg/mL of streptomycin, 100 units/mL of penicillin, and 50 μM mercaptoethanol at 37 °C in a humidified air incubator (5% CO₂–95% O₂). Each fluorescein-labeled oligonucleotide alone or as HPCD complex was separately mixed with H9 cells (10⁶ cells/mL) in the 1:1 (v/v) ratio and incubated at 37 °C in incubator. At various time points, ranging from 2 to 48 h, the aliquots were removed from each mixture, washed, and resuspended in Hank's balanced salt solution (HBSS) supplemented with 0.1% bovine serum albumin (BSA) and 0.1% sodium azide. Propidium iodide staining was used to distinguish viable cells from dead cells. Flow cytometric data on 5,000 viable cells was acquired in listmode on Epics XL flow cytometer and data were analyzed by Epics XL version 1.5 software after gating on living cells by forward scatter vs side scater and propidium iodide staining.

under the same conditions than the PO oligonucleotide, which is expected, and the PS oligonucleotides **19** and **20** showed no sign of degradation even after 30 min (Figure 2).

To determine the usefulness of cyclodextrins as "carriers" for oligonucleotides which were labeled (*26*) with fluorescein at the 5'-end, we screened a series of cyclodextrins and their analogues (*9, 10*). In the studies involving oligonucleotide–adamantane conjugate **6**, 2-(hydroxypropyl)-β-cyclodextrin (HPCD) was the most efficient carrier (Figure 3). In these experiments the same oligonucleotide **6** as a non-HPCD complex, PS oligonucleotide (25-mer, the same sequence as **6** but without adamantane) as an HPCD complex, or alone were used as the controls (Figure 3). We observed the highest level of oligonucleotide uptake with oligonucleotide **6** as HPCD complex. The lowest cellular uptake was exhibited by the control PS oligonucleotide alone and was improved by HPCD complexation (Figure 3). More significant changes in uptake between oligonucleotides were observed after 8 h of incubation reaching the maximum at 24 h, with no significant changes in the following 24 h.

We also studied PS oligonucleotides **18** and **20** fluorescein-labeled (*26*) at the 5'-end, with the amino derivatives of β-cyclodextrin attached at 3'-end, using the same

conditions as described for the above oligonucleotides. They exhibited no higher cellular uptake than did the standard PS oligonucleotide. Previous studies suggest that cellular uptake of the oligonucleotides mediated by cyclodextrins is dependent on the concentration of the cyclodextrin (*9*, *10*). To observe changes in uptake it is necessary to have $7-(7 \times 10)^3$-fold excess in molar ratio of cyclodextrin to that of oligonucleotide. There is no parallel between uptake of the oligonucleotides conjugated with and the oligonucleotides associated with cyclodextrins; however, the results presented here show that one molecule of cyclodextrin attached to an oligonucleotide does not make a difference in cellular uptake.

We have successfully synthesized oligonucleotide–amino-β-cyclodextrins and oligonucleotide–adamantane conjugates. Although oligonucleotides with amino derivatives of β-cyclodextrin attached at the 3'-end exhibited a significant increase in stability against 3'-exonucleases, duplex formation with complementary RNA was destabilized, and we observed no increase in cellular uptake compared to standard oligonucleotide. Oligonucleotide–adamantane conjugates associated in complex with 2-(hydroxypropyl)-β-cyclodextrin (HPCD) also showed higher stability against 3'-exonucleases than standard PS oligonucleotides and increased cellular uptake and had no negative effects on duplex stability. This latter treatment is therefore attractive for use in studies of gene-expression. Oligonucleotide–adamantane conjugates might also better cross the blood–brain barrier (BBB), as was demonstrated with an AZT–adamantane prodrug complex (*27*). The oligonucleotide–adamantane conjugates are presently being studied for their gene-regulation activity.

ACKNOWLEDGMENT

Supporting Information Available: Listings of synthetic procedures and spectral data for all new compounds (10 pages). Ordering information is given on any current masthead page.

LITERATURE CITED

(1) Agrawal, S., and Iyer, R. P. (1995) Modified Oligonucleotides as Therapeutic and Diagnostic Agents. *Curr. Opin. Biotechnol. 6*, 12–19.

(2) Stein, C. A., and Cheng, Y.-C. (1993) Antisense Oligonucleotides as Therapeutic Agents—Is the Bullet Really Magical? *Science 261*, 1004–1012.

(3) *Antisense Research and Applications* (1993) In (Crooke, S. T., and Lebleu, B., Eds.) CRC Press, Boca Raton, and references cited therein.

(4) Agrawal, S. (1991) Antisense Oligonucleotides: A Possible Approach for Chemotherapy of AIDS. In *Prospects for Antisense Nucleic Acid Therapy of Cancer and AIDS* (Wickstrom, E., Ed.) pp 143–158, Wiley-Liss, Inc., New York.

(5) Bennett, R. M. (1993) As Nature Intended? The Uptake of DNA and Oligonucleotides by Eukaryotic Cells. *Antisense Res. Dev. 3*, 235–241.

(6) Zamecnik, P., Aghajanian, J., Zamecnik, M., Goodchild, J., and Witman, G. (1994) Electron Micrographic Studies of Transport of Oligodeoxynucleotides Across Eukaryotic Cell Membranes. *Proc. Natl. Acad. Sci. U.S.A. 91*, 3156–3160.

(7) Temsamani, J., Kubert, M., Tang, J.-Y., Padmapriya, A., and Agrawal, S. (1994) Cellular Uptake of Oligodeoxynucleotide Phosphorothioates and Their Analogs. *Antisense Res. Dev. 4*, 35–42.

(8) Uhlmann, E., and Peyman, A. (1990) Antisense Oligonucleotides: A New Therapeutic Principle. *Chem. Rev. 90*, 543–584 and references cited therein.

(9) Zhao, Q., Temsamani, J., and Agrawal, S. (1995) Use of Cyclodextrin and its Derivatives as Carriers for Oligonucleotide Delivery. *Antisense Res. Dev.* (in press).

(10) Zhao, Q., Habus, I., and Agrawal, S. (1995) Use of Cyclodextrin as Carrier for Oligonucleotides. *J. Cellular Biochemistry. Keystone Symposia on Molecular & Cellular Biology. Supplement 19A*, Jan 5–26, 1995, A4–210, pp 176, Wiley-Liss, Inc., New York.

(11) Brewster, M. E., Simpkins, J. W., Singh Hara, M., Stern, W. C., and Bodor, N. (1989) The Potential Use of Cyclodextrins in Parenteral Formulations. *J. Parenteral Sci. Technol. 43*, 231–240 and references cited therein.

(12) Duchene, D., Glomot, F., and Vaution, C. (1987) Pharmaceutical Applications of Cyclodextrins. In *Cyclodextrins and Their Industrial Uses* (Duchene, D., Ed.) pp 211–257, Editions de Sante, Paris, and references cited therein.

(13) Brinker, U. H., Buchkremer, R., Kolodziejczyk, M., Kupfer, R., Rosenberg, M., Poliks, M. D., Orlando, M., and Gross, M. L. (1993) Carbenes in Constrained Systems I: 1,3 C–H Insertion Reaction of Adamantylidene within the β-Cyclodextrin Cavity. *Angew. Chem., Int. Ed. Engl. 32*, 1344–1345.

(14) Ueno, M., Murakami, A., Makino, K., and Morii, T. (1993) Arranging Quaternary Structure of Peptides by Cyclodextrin-Guest Inclusion Complex: Sequence-Specific DNA Binding by a Peptide Dimer with Artificial Dimerization Module. *J. Am. Chem. Soc. 115*, 12575–12576.

(15) Eliseev, A. V., and Schneider, H.-J. (1993) Aminocyclodextrins as Selective Hosts with Several Binding Sites for Nucleotides. *Angew. Chem., Int. Ed. Engl. 32*, 1331–1333.

(16) Eliseev, A. V., and Schneider, H.-J. (1994) Molecular Recognition of Nucleotides, Nucleosides, and Sugars by Aminocyclodextrins. *J. Am. Chem. Soc. 116*, 6081–6088.

(17) Misiura, K., Durrant, I., Evans, M. R., and Gait, M. J. (1990) Biotinyl and Phosphotyrosinyl Phosphoramidite Derivatives Useful in the Incorporation of Multiple Reporter Groups on Synthetic Oligonucleotides. *Nucleic Acids Res. 18*, 4345–4354.

(18) Damha, M. J., Giannaris, P. A., and Zabarylo, S. V. (1990) An Improved Procedure for Derivatization of Controlled-Pore Glass Beads for Solid-Phase Oligonucleotide Synthesis. *Nucleic Acids Res. 18*, 3813–3821.

(19) Melton, L. D., and Slessor, K. N. (1971) Synthesis of Monosubstituted Cyclohexaamyloses. *Carbohydr. Res. 18*, 29–37.

(20) Beeson, J. C., and Czarnik, A. W. (1994) Synthesis and Transacylating Reactivity of β-Cyclodextrin Ethylenediamines. *BioMed. Chem. 2*, 297–303.

(21) Mungall, W. S., and Kaiser, J. K. (1977) Carbamate Analogues of Oligonucleotides. *J. Org. Chem. 42*, 703–706.

(22) Wang, H., and Weller, D. D. (1991) Solid Phase Synthesis of Neutral Oligonucleotide Analogues. *Tetrahedron Lett. 32*, 7385–7388.

(23) Habus, I., Temsamani, J., Agrawal, S. (1994) Synthesis of Di-, Tri-, and Tetrameric Building Blocks with Novel Carbamate Internucleoside Linkages and their Incorporation into Oligonucleotides. *BioMed. Chem. Lett. 4*, 1065–1070.

(24) MacKellar, C., Graham, D., Will, D. W., Burgess, S., and Brown, T. (1992) Synthesis and Physical Properties of Anti-HIV Antisense Oligonucleotides Bearing Terminal Lipophilic Groups. *Nucleic Acids Res. 20*, 3411–3417.

(25) Sambrook, J., Fritsch, E. P., Maniatis, T. (1989) *Molecular Cloning: A Laboratory Manual*, Cold Spring Harbor Laboratory Press, Cold Spring Harbor.

(26) Product Protocols for Fluorescein-ON Phosphoramidite and 3'-Fluorescein-ON CPG. Clontech Laboratories, Inc., 4030 Fabian Way, Palo Alto, CA 94303–4607.

(27) Tsuzuki, N., Hama, T., Kawada, M., Hasui, A., Konishi, R., Shiwa, S., Ochi, Y., Futaki, S., and Kitigawa, K. (1994) Adamantane as a Brain-Directed Drug Carrier for Poorly Absorbed Drug. 2. AZT Derivatives Conjugated with the 1-Adamantane Moiety. *J. Pharm. Sci. 83*, 481–484.

REVIEWS

Biodegradable Polymers for Protein and Peptide Drug Delivery

Wayne R. Gombotz* and Dean K. Pettit

Department of Drug Delivery and Formulation, Immunex Corporation, 51 University Street, Seattle, Washington 98101. Received December 7, 1994

TABLE OF CONTENTS

I. INTRODUCTION

Over the past decade developments in the field of biotechnology have led to the cloning, characterization, and commercial availability of many clinically useful proteins and peptides. While the technology exists for the discovery and development of these molecules, several challenges need to be solved with regard to their delivery in convenient, controlled release, and targeted formulations. In contrast to conventional synthetic pharmaceuticals, proteins are large molecular weight polypeptides which are susceptible to proteolysis, chemical modification, and denaturation during storage and administration (*1, 2*). Significant efforts have gone into the investigation of formulations which stabilize proteins over sufficiently long storage times. Key problems which continue to be addressed in this area include protein aggregation, proteolytic degradation, and chemical modification. Additional research has focused on the development of dosage forms which either prolong the activity of the protein *in vivo* or assist in targeting the protein to specific tissues.

The most convenient route for the systemic delivery of pharmaceuticals is oral; however, attempts to deliver large molecular weight proteins and peptides orally have not been widely successful. Bioavailability via this route is poor for molecules of molecular mass greater than several hundred daltons. In addition, proteins are susceptible to hydrolysis and modification at gastric pH levels and can be degraded by proteolytic enzymes in the small intestine (*3*). Parenteral delivery of proteins and peptides has been the method of choice for systemic delivery due to ease of administration, the avoidance of biological barriers through which it is difficult for proteins to pass, and the ability to achieve pharmacologic levels of circulating protein over a relatively short period of time. In addition to parenteral administration, interest has increased in the area of local delivery of proteins to mucosal tissues of the gut, sinus, and lungs by both oral and inhalation delivery systems (*4–6*). In these applications, proteins must be administered in formulations which protect against proteolysis and target the mucosal tissues. Recently, there has been interest in the use of degradable polymer systems for controlled release of protein vaccines to be administered, either via the parenteral route or targeted to mucosal tissues (*7–11*).

* Author to whom correspondence should be addressed. E-mail: wgombotz@Immunex.com; tel: (206) 389-4085; FAX: (206) 624-7496.

Table 1. Natural Derived and Synthetic Biodegradable Polymers Utilized in Protein Drug Delivery

polymer	protein delivered and reference
Naturally Derived	
albumin	insulin (*161*), urokinase (*162*), YIGSR (*201*), gp120 peptide (*202*), IIF-2 (*203*), growth hormone (*204*), SOD (*205*), CD4 (*206*)
alginate	albumin (*35*), TGF-β_1 (*145*), bFGF (*146, 150*), TNF receptor (*147*), angiogenesis factor (*148*), EGF (*148*), urogastrone (*148*), NGF (*149*)
cellulose derivatives	TGF-β_1 (*135–137*), aFGF (*138*)
collagen	IL-2 (*151, 152*), NGF (*153*), insulin (*154*), EGF (*155*), TGF-β_1 (*156*)
fibrin	(*227, 228*)
gelatin	IFNα (*157, 207*), insulin (*158, 168, 170*), albumin (*159*), IFNγ (*159*), GM-CSF (*159*), vasopressin (*168, 169*), SOD (*208*), IL-1α (*209*), TNF (*210*)
hyaluronic acid	insulin (*142*), NGF (*143*)
polysaccharides	IFNα (*163*), albumin (*164*), lysozyme (*164*), immunoglobulin G (*164*), carbonic anhydrase (*164*)
Synthetic	
maleic anhydride–alkyl vinyl ether copolymers	IFNα (*134*), HSA (*134*)
pluronic polyols	BSA (*85*), IL-2 (*124, 125*), urease (*126*), natriuretic factor (*127*), TGF-β_1 (*128*)
poly(acrylic acid)	EGF (*51*)
poly(cyanoacrylates)	insulin (*98*), growth hormone-releasing factor (*99, 100*), calcitonin (*101*)
poly(amino acids)	antibody (*192*)
poly(anhydrides)	insulin (*109–111*), myoglobin (*109, 110*), lysozyme (*112*), trypsin (*112*), heparinase (*112*), ovalbumin (*112*), albumin (*112*), immunoglobulin (*112*)
poly(depsipeptide)	(*229*)
poly(esters):	
poly(lactic acid) (PLA)	HSA (*38*), insulin (*66*), LHRH (*71*), albumin (*81*), BSA (*85, 91*), bone morphogenetic protein (*92*)
poly(lactic-co-glycolic acid) (PLGA)	carbonic anhydrase (*39*), IL-2 (*46*), G-CSF (*47*), insulin (*65*), LHRH (*67–70*), LHRH analogs (*21, 52, 72–75*), BSA (*76–78, 84, 91*), diphtheria toxoid (*80*), calcitonin (*82*), cytochrome c (*87*), myoglobin (*87*), somatrotropin (*87*), albumin (*87*), TGF-β_1 (*166*)
poly(β-hydroxybutyrate)	(*230*)
poly(caprolactone)	(*231*)
poly(dioxanone)	(*234*)
poly(ethylene glycol)	IL-2 (*46, 178, 179, 181, 188*), G-CSF (*47*), BSA (*91, 133*), bone morphogenetic protein (*92*), immunoglobulin (*182*), pseudomonas exotoxin A mutants (*189*)
poly((hydroxypropyl)methacrylamide)	transferrin (*175*), antibodies (*172, 173, 175*)
poly[(organo)phosphazene]	(*232, 233*)
poly(ortho esters)	LHRH analog (*116*), insulin (*117, 118*), lysozyme (*119*)
poly(vinyl alcohol)	cytochrome c (*87*), myoglobin (*87*), somatrotropin (*87*), albumin (*87*), BSA (*129–131*)
poly(vinylpyrrolidone)	chymotrypsin (*132*), BSA (*133*)

The use of degradable microspheres that contain protein vaccines can potentially reduce the number of inoculations, reduce the total antigen dose required to achieve immune protection, and enhance the immune response (*12, 13*). Site-specific delivery of proteins to topical wounds and bony defects through the use of degradable polymer delivery sysytems has also been reported.

The primary interest for degradable polymers in drug delivery has been in controlled release systems (*14–16*). In these applications protein drugs are embedded in polymer matrices which undergo hydrolysis or enzymatic digestion, resulting in controlled release of the protein upon administration. Polymers have also been widely investigated for use in protein–polymer conjugates. These systems have generally been utilized for prolonging the circulation half-lives of proteins or for delivering targeted payloads of protein pharmaceuticals to specific tissues.

Degradable polymeric drug delivery systems have several advantages compared to conventional drug therapies. These include improved patient compliance, avoidance of the peaks and valleys of drug plasma levels associated with conventional injections, localized delivery of the drug to a particular body compartment or cell type, thereby lowering the systemic drug level, protection of drugs that are rapidly degraded in the body, and improved drug efficacy. The obvious advantage of biodegradable polymers for drug delivery over nondegradable systems is that they do not have to be removed from the patient.

This review will describe the various types of degradable polymers that have been used for the delivery of proteins and peptides. The discussion will emphasize some of the practical issues, problems, and unique challenges that are associated with the development of degradable delivery systems for protein pharmaceuticals. Next, an overview of polymer matrix systems will be given that describes the different degradable polymers available, their degradation mechanisms, and the types of protein release kinetics that can be expected from these systems. Specific examples from the literature will be described. The paper will conclude with a discussion of the conjugation of degradable polymers to proteins along with specific examples.

II. PRACTICAL ISSUES FOR PROTEIN AND PEPTIDE DELIVERY

A. Biodegradable Polymers. There is often confusion related to the term biodegradation because the word has been defined in many different ways (*17–19*). The degradable polymer delivery systems described in this review will encompass materials that degrade by hydrolysis or solubilization. These systems include non-water-soluble polymers that are degraded by surface or bulk erosion in addition to water-soluble gels that dissolve and are cleared from the body without undergoing a decrease in molecular weight.

There are many different types of biodegradable polymers that can potentially be used in the preparation of protein delivery systems. They include both naturally

derived and synthetic materials (Table 1). The development of biodegradable polymers for drug delivery has been largely empirical; that is, few polymers have been developed specifically for the purpose of drug delivery. A case in point is the widespread use of poly(lactic-co-glycolic acid) (PLGA) homo- and copolymers for the preparation of degradable microspheres. These polymers were first used in the production of biodegradable sutures and later found to have properties desirable for controlled release devices. The degradation characteristics of PLGA and the elimination of the breakdown products are well documented (*20–22*). It is not surprising that these materials are by far the most widely studied class of biodegradable polymers. Other commonly used drug delivery polymers have long histories of biocompatibility or are derived from biological materials and modified for drug delivery applications.

As we have mentioned, biodegradable polymers may break down either hydrolytically (e.g., PLGA) or through solubilization (e.g., pluronics). The modes of polymer degradation may be either bulk erosion, surface erosion, hydration and solubilization, or cleavage of specific linkages designed into protein–polymer conjugates. There are several types of labile bonds that are used to form biodegradable polymers. These bonds may be categorized by their relative rates of hydrolysis under physiological conditions based on the known hydrolysis rates of low molecular weight analogs (*23*).

polycarbonates > polyesters > polyurethanes > polyorthoesters > polyamides
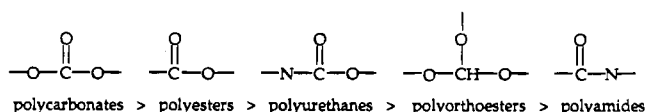
Since polymer morphology and the presence of substituent groups can influence the rates of hydrolysis significantly, the above comparison is only an approximate guide.

B. Biocompatibility of Polymeric Systems. Polymers used as drug delivery systems for protein pharmaceuticals need to exhibit "biocompatible" characteristics in terms of both the polymer's effect on the organism receiving the drug delivery system and the polymer's effect on the protein to be delivered. Several aspects of a polymeric delivery system ultimately contribute to its overall biocompatibility, or lack thereof. The polymer itself, which consists of a repeating monomeric species, may potentially be antigenic (*24, 25*), carcinogenic (*26, 27*), or toxic (*28, 29*) or have some inherent incompatibility with organisms. The shape of an implanted material has been implicated in its biocompatibility as well, smooth surfaces being less irritating and more biocompatible than rough surfaces (*30*). A key factor which influences the biocompatibility of an implanted polymer is the presence of low molecular weight extractables, or unreacted residual monomers and polymerization initiators (*31*). These residual materials are usually extracted by organic solvents prior to the manufacture or preparation of a drug delivery system. However, residual solvents also may have adverse biological effects and must be removed prior to administration of a degradable drug delivery system. In some cases, soluble polymers or breakdown products are sequestered within organs, resulting in long term adverse effects. The accumulation of high molecular weight poly(vinylpyrrolidone) in the liver following prolonged exposure is one such example (*32, 33*).

Generally, those polymers described for use in drug delivery systems have had long histories as implants or as excipients used in the pharmaceutical industry such as PLGA copolymers or poly(ethylene glycol) (PEG). Other polymers such as those listed in Table 1 have also been known to exhibit good biocompatibility when injected as a component of a biodegradable drug delivery system.

C. Protein Pharmaceuticals and Protein Stability Issues. Many low molecular weight drugs have been successfully incorporated into degradable polymeric delivery systems and released in an active form. Larger molecular weight proteins, however, behave quite differently in such systems. Serum albumin is among the most well studied of proteins in the development of drug delivery systems (*34, 35*). However, the properties of serum albumin do not in general mimic those of specific protein pharmaceuticals. Therefore, the extension of the results achieved with low molecular weight drugs or serum albumin to other types of high molecular weight protein pharmaceuticals is limited at best.

Interactions between proteins and polymeric materials appear to be protein and polymer specific. At issue are the following: (i) the protein molecular weight, which is an important parameter with regard to diffusion characteristics, (ii) the isoelectric point (pI) of the protein (and polymer as well in some cases), which governs charge–charge interactions (protein–polymer and protein–protein), (iii) the presence of cysteines on the protein which may participate in the formation of intermolecular (i.e., protein–polymer) disulfide bonds, (iv) the primary amino acid sequence of the protein which may be rendered susceptible to chemical modification in association with a polymeric material (e.g., β-elimination, or other modification), (v) the presence or absence of carbohydrates on the protein, which may enhance or prevent interaction with polymeric materials and affect the protein's hydrodynamic volume, (vi) the relative hydrophobicity of a protein which could interact with hydrophobic sites on a polymer, and (vii) the heterogeneity of protein pharmaceuticals, which often exists for proteins produced by recombinant methods. While a certain degree of pre-evaluation is feasible, each type of delivery system needs to be tested independently with each protein of interest in order to evaluate the specific protein–polymer interactions involved with each particular protein–polymer pair. These interactions, as well as the rates of biodegradation of the polymeric system, will ultimately influence the protein release rate and the overall condition of the released protein.

There are several challenges in the development of drug delivery systems with regard to maintaining the integrity and activity of incorporated proteins. First, in the process of preparing drug delivery systems, proteins may be exposed to extreme stresses. Necessary manufacturing steps may include excessive exposure of the protein to heat, shear forces, pH extremes, organic solvents, freezing, and drying, to name a few. Following manufacture or preparation, the drug delivery systems must be stored for some extended period of time prior to administration. While many studies have described the storage stability of lyophilized or liquid formulations of proteins, relatively little information is available on the subject of long term stability of proteins within biodegradable drug delivery systems. Next, when biodegradable polymer drug delivery systems are administered, the incorporated proteins may become hydrated at relatively high concentrations for prolonged periods of time. Proteins in this type of environment are susceptible to denaturation and aggregation (*36*). Also, when a polymer begins to degrade following administration, a highly concentrated microenvironment is created from the released protein and polymer breakdown byproducts in and

around the microspheres (such as acidic monomers). Proteins may be susceptible to aggregation, hydrolytic degradation, and/or chemical modification in such an environment. Finally, proteins may undergo reversible or irreversible adsorption to the polymers used to fabricate degradable delivery systems, which can affect the drug delivery rate and ultimately lead to denaturation, aggregation, and inactivation of the protein. Protein adsorption to polymeric materials has been widely studied in the area of polymeric implants (*37*); however, the deleterious effects of protein adsorption are no less significant for protein drug delivery applications. In a specific example, human serum albumin was shown to undergo a multilayer adsorption to PLA nanospheres (*38*). Furthermore, some of the albumin was found to be irreversibly adsorbed to this material.

Several approaches have been taken to stabilize proteins and reduce denaturation in polymeric delivery systems. These include the following: (i) the addition of stabilizing additives to prevent protein aggregation or adsorption to the polymer's surface (*36, 39, 40*), (ii) the addition of excipients to increase hydration of the system and enhance both protein diffusion and polymer degradation (*41, 42*), and (iii) the modification of the protein or the polymer with water-soluble polymers to prevent protein aggregation (*43*) and/or adsorption (*44, 45*).

Protein modification with PEG has been demonstrated with two proteins in PLGA delivery systems: interleukin-2 (IL-2) (*46*) and granulocyte colony-stimulating factor (G-CSF) (*47*). In both cases, the unmodified protein exhibited a poor release profile, and much of the protein remained trapped within the polymer after several weeks of incubation in solution. The poor release was attributed to difficulty in resolubilization of the encapsulated protein. The PEG-modified proteins, however, were released much more readily form the systems, probably due to increased protein solubility, decreased aggregation, and decreased protein adsorption to the polymeric surfaces.

D. Sterilization. Although issues of sterilization of drug delivery systems are rarely discussed in the literature, many challenging problems in this area need to be solved. Several approaches which are routinely applied to the sterilization of polymers or implantable polymeric devices are ethylene oxide gas, steam, sub-micron filtration in organic solvents, or γ-irradiation. These methods, however, are not generally applicable to proteins. Proteins can be denatured by ethylene oxide gas, by exposure to organic solvents, and by temperatures required for steam sterilization (121 °C). In addition, proteins may undergo severe aggregation and degradation following exposure to γ-irradiation. Conversely, typical sterilization methods for protein pharmaceuticals such as filtration through sub-micron filters in aqueous solution would not be applicable to polymeric drug delivery systems which may be greater than 100 μm in diameter, be water insoluble, or undergo hydrolysis on exposure to water.

Therefore, methods of sterilization of polymeric drug delivery systems must be tailored to each individual product. For parenteral systems, all components must be sterile filtered in solution prior to formation of the delivery system. This involves filtration of both an aqueous protein solution and often an organic polymer solution. Once the individual components are filtered, an aseptic process must be employed during fabrication of the delivery system. The use of clean rooms and validation of an aseptic manufacturing process can add considerable cost to a parenteral controlled release product. The existing marketed peptide delivery products, Lupron Depot (Takada Abbott) and Zoladex (ICI),

are manufactured under aseptic conditions. Both of these products release peptide analogs of luteinizing hormone-releasing hormone (LHRH) for 1 month. Decapeptyl (Ipsen Biotech), another LHRH delivery system, is terminally sterilized by γ-irradiation since the incorporated peptide was found to be resistant to degradation by this treatment.

E. *In Vitro* **vs** *in Vivo* **Analysis Comparisons.** Many excellent studies have been published which describe the *in vitro* release of proteins from degradable delivery systems. These *in vitro* studies are essential for determining the reproducibility of a system's release kinetics and the integrity of the released protein. *In vitro* release kinetics, however, often do not mimic *in vivo* performance of the system. Many polymers, for example, may degrade faster in the body than in a test tube due to the presence of proteolytic enzymes. Makino et al. have reported that the degradation rate of PLA microcapsules in aqueous solution was accelerated by the addition of albumin, γ-globulins, and fibrinogen (*48*). They showed that these proteins adsorbed to the polymer surface and also increased the polymer solubility. On the other hand, certain polymers can become encapsulated with fibrotic tissue and adsorb proteins from serum or interstitial fluid *in vivo*, which results in a slower release. *In vitro* hydration of a polymer may occur more rapidly than *in vivo*, particularly in hydrogel systems, resulting in a faster *in vitro* release. In an attempt to more closely mimic *in vivo* release conditions, *in vitro* release studies have been performed in more physiological solutions such as serum or fetal calf serum (38); however, *in vivo* data must always be included in a complete characterization of a new degradable drug delivery system.

III. POLYMERS FOR CONTROLLED RELEASE

A. Theory vs Practice of Controlled Release. 1. Polymer Degradation Mechanisms. The different mechanisms of biodegradation have been categorized into discrete mechanisms by several investigators (*16, 49, 50*). Understanding these mechanisms is important to the design of a particular drug delivery system and can have a profound effect on the release kinetics. Figure 1 is a schematic representation of the different types of polymer degradation mechanisms. In the first example, an unstable (biodegradable) bond is incorporated into the polymer backbone. Cleavage of the bond converts a water-insoluble polymer into water-soluble, low molecular weight polymer fragments. Hydrolysis of the labile bond can be both chemically or enzymatically induced. Polymers that undergo this type of erosion include poly(esters), poly(anhydrides), poly(amides), poly(ortho esters), and poly(cyanoacrylates). In the second example, the polymer exists as a covalently or ionically cross-linked network, and cleavage of unstable linkages in the cross-links releases soluble polymer fragments. The size of these fragments depends on the density of the hydrolyzable bonds in the cross-linked network. Covalently cross-linked hydrogels and ionically cross-linked polymers such as calcium alginate degrade by this mechanism. The third example shown is polymer solubilization. With this mechanism the polymer itself does not disintegrate and its molecular weight remains essentially unchanged. In the simplest type of solubilization, water diffuses into the polymers, leading to the formation of a swollen system which ultimately dissolves. Polymer gels made of poly(ethylene oxide), poly(vinyl alcohol) (PVA), dextrans, or (carboxymethyl)cellulose degrade by this mechanism. A more complex solubilization mechanism involves the hydration of water-insoluble polymers with side groups
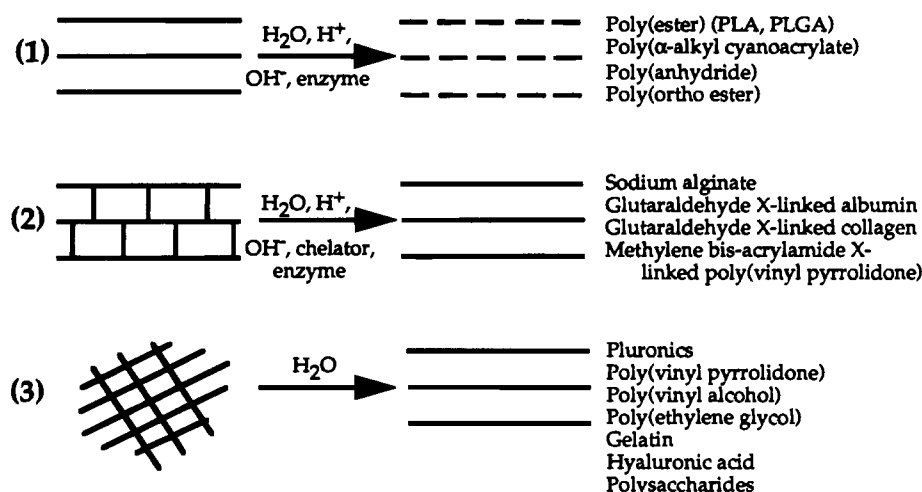
Figure 1. Schematic representation of different polymer degradation mechanisms: (1) Hydrolysis of the polymer backbone may occur via acid, base, or enzymatic mechanisims. The degradation byproducts are of low molecular weight and are generally water soluble, which allows the embedded protein or peptide to be released. (2) Hydrolysis of a cross-linked polymer network is catalyzed via acid, base, or metal ion chelator, or enzymatically. Cross-links may be made with divalent cations (sodium alginate), or with a divalent activated chain such as glutaraldehyde or methylenebis(acrylamide). Broken cross-links allow protein or peptide release. (3) Hydration of a polymer matrix allows for diffusion of proteins or peptides. In some examples (e.g., esterified hyaluronic acid), solubilization occurs through hydrolysis of a hydrophobic side chain, resulting in a main-chain molecule which is hydrophilic and will solubilize in water.

that are converted to water-soluble polymers as a result of ionization, protonation, or hydrolysis of the groups. Some materials that exhibit this type of degradation mechanism include partially esterified hyaluronic acid, partially esterified copolymers of maleic anhydride, or derivatives of cellulose acetate.

Polymer degradation may also be described in physical terms and may be either homogeneous or heterogeneous. In the more commonly observed homogeneous degradation, hydrolysis of an implant occurs at an even rate throughout the polymer matrix. In heterogeneous degradation or surface erosion, the delivery system degrades only at its surface. The drug release kinetics from this type of system are more predictable. In reality, most systems rarely fall into these two discrete categories, and as a result release kinetics can be difficult to predict. Protein—polymer interactions, polymer crystallinity, polymer hydrophobicity/hydrophilicity, and device morphology can all influence the degradation rate and ultimately the release rate of the protein.

2. Delivery System Morphologies and Release Mechanisms. Biodegradable protein and peptide delivery systems can be fabricated in a variety of morphologies. These systems can be classified as reservoir or monolithic matrix devices (*16, 50*). In a biodegradable reservoir system a core of drug is surrounded by a polymer coating. In a monolithic matrix system, the drug is uniformly distributed throughout the solid polymer. The majority of systems discussed below are of the monolithic matrix system type.

Microspheres and nanospheres are one of the most desirable types of parenteral delivery systems since they can be administered by a routine injection with a narrow gauge needle. Larger systems such as cylindrical implants have also been fabricated which require injection through a trochar or surgical implantation. Polymeric gels are another type of system that can be administered by injection but can suffer drawbacks related to local inflammation if organic solvents are used to solubilize the polymer. Gels have also been studied extensively for the topical administration of proteins for applications such as wound healing, in particular, the administration of epidermal growth factor (EGF) for dermal wounds (*51*).

The release of a protein from a degradable delivery system can be governed by several mechanisms: (i) pure drug diffusion through the polymer matrix (diffusion controlled), (ii) degradation of the polymer (erosion controlled), or (iii) countercurrent diffusion of aqueous medium into the polymer (swelling controlled). These classifications are useful for understanding a given delivery system and in the development of mathematical models to describe *in vitro* drug release. However, many biodegradable polymer—protein delivery systems are very complex, and the release of the drug is often due to a combination of mechanisms. For example, in a degradable PLGA microsphere system, release of a protein is often initially controlled by desorption of protein from the surface of the PLGA microsphere, followed by diffusion of the protein through porous channels in the polymer matrix which in turn is influenced by the swelling rate of the system. At later times, the polymer begins to degrade, and a combined erosion/diffusion-controlled release mechanism occurs. In addition, the physical state of a polymer can change as it degrades, which can further complicate the release kinetics. Park has reported that water hydration in PLGA microspheres allowed the polymer morphology to change from a glassy to a rubbery state by lowering the glass transition temperature (*52*). This in turn led to a faster degradation rate.

Rather than describe detailed mathematical models depicting the release of proteins from degradable systems, we felt it would be instructive to show some of the more commonly observed release profiles. Figure 2 demonstrates the cumulative percent release of a drug from four different delivery systems over time. The zero-order release profile depicts the constant release of drug from a device over time. The first-order release profile is typical of a diffusion-controlled system and is characterized by a decreasing release rate with time.

The burst profile can be attributed to release of the drug from the surface of a device or represents drug that was not incorporated into the system. A small burst of 10−20% is often seen preceding the other release profiles shown in the graph. The biphasic release profile has been shown to occur in many biodegradable PLGA microsphere systems (*53*). The initial release is the result of diffusion of protein from the surface and through the porous network of the device. Once this drug is depleted,
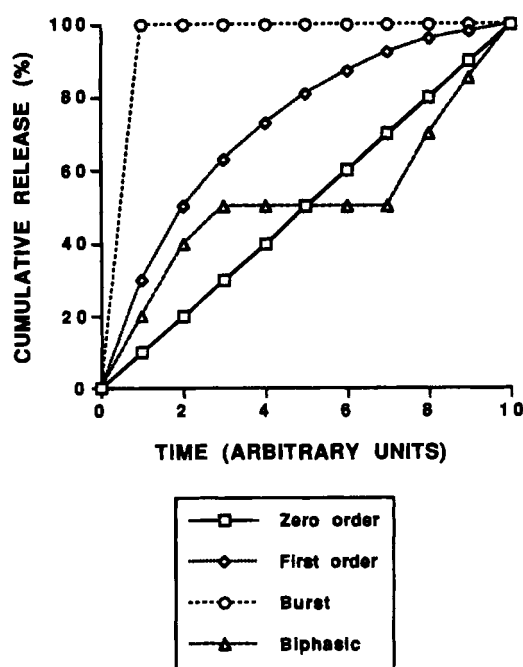
Figure 2. Different cumulative percent release profiles commonly observed in biodegradable protein delivery systems as a function of time.

Figure 3. Chemical formula for poly(lactic-co-glycolic acid) (PLGA). The hydrolysis of PLGA is catalyzed by water and is accelerated by the presence of acid or base. The degradation byproducts of PLGA are lactic and glycolic acid.

the release stops and a plateau is observed in the release profile. As the polymer begins to degrade, drug that was completely surrounded by the polymer matrix is liberated, and a second phase of release is observed.

B. Examples from the Literature. It would be difficult to describe all of the degradable polymeric protein and peptide delivery systems that have been reported over the past decade. This review will focus on some of the more significant reports in the published literature in an attempt to provide a more broad overview of the different types of systems that have been developed.

1. **Bulk Erosion Polymers.** *i. Poly(lactic-co-glycolic acid) (PLGA) Copolymers.* The use of PLGA copolymers for the controlled release of proteins and peptides is widely described in the literature (*54–57*). These polymers have been used successfully for several decades in biodegradable sutures and more recently as drug delivery microcarriers, and as a result much is known about their biocompatibility (*58–60*) and physicochemical characteristics. PLGA copolymers are well suited for use in delivery systems since they can be fabricated into a variety of morphologies including films, rods, microspheres, and nanospheres by solvent casting, compression molding, or solvent evaporation techniques. PLGA copolymers are prepared by polycondensation reactions with lactic and glycolic acids (*61*). On exposure to water, PLGA undergoes random chain scission by simple hydrolysis of the ester bond linkage (Figure 3). Devices made from PLGA copolymers undergo bulk erosion as compared to surface erosion.

The chemical composition and ratio of monomers used in the polycondensation reaction strongly influence the degradation characteristics of the copolymer, and thus drug release kinetics as well. The degradation rates for PLGA (which range from weeks to months under physiologic conditions) have been shown to be influenced by factors which affect polymer chain packing (i.e., crystallinity) and hydrophilicity. Since PLGA degradation is catalyzed by hydrolysis, a crystalline or hydrophobic polymer composition disfavors dissolution and degradation and slows drug release kinetics. The specific factors
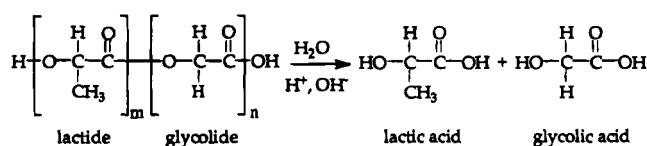
affecting copolymer crystallinity and hydrophilicity include the following: (i) the ratio of lactide to glycolide monomer in the copolymer (copolymers with approximately 20–70% glycolide content are amorphous whereas copolymers rich in either lactide or glycolide are crystalline) (*61, 62*), (ii) the stereoregularity of the monomer units in the polymer affects polymer chain packing (e.g., D,L-poly(lactic acid) exists as a more amouphous solid than L-poly(lactic acid)) (*63*), (iii) randomness of lactide and glycolide repeat units in the copolymer backbone decreases the ability of chains to crystallize, and (iv) low molecular weight polymers tend to be more hydrophilic and degrade faster than high molecular weight polymers (*64*), especially when the end groups are free acid rather than end capped with ester or other groups.

One of the first studies describing the delivery of a protein from PLGA microcapsules was reported by Chang in 1976 (*65*). Insulin was incorporated into the delivery system, and its release rate was varied from 50% in 5 h to 2.5% in 24 h. A more detailed study was reported 10 years later in which both *in vitro* and *in vivo* release of insulin was demonstrated from pellets and microspheres made from poly(lactic acid) (PLA) (*66*). The microspheres were prepared by a solvent evaporation technique while the pellets were made by solvent casting. The duration of action of the microbeads *in vivo* could be varied from a few hours to several days, while the pellets lowered the glucose levels of chemically induced diabetic rats for more than 2 weeks. A pore-release model was used to describe the mechanism of insulin release from both microbeads and pellets.

Three peptide drug delivery systems made from PLGA copolymers have successfully met regulatory approval and are available as marketed products. They are Lupron Depot, Zoladex, and Decapeptyl, and each of these release peptide analogs of LHRH. The success of these products is due to several factors which are related to both the drug and polymers used in the delivery systems. Chronic administration of LHRH analogs has been shown to cause a reversible chemical shutdown of the pituitary gland, resulting in regression of hormone-responsive tumors including prostate and breast carcinomas. The desired clinical effect is therefore one of downregulation, and a well-defined delivery pattern is not necessary as long as a sufficient quantity of drug is provided. Since these drugs were originally administered by injection one or more times daily, the development of a once monthly delivery system was desirable from a patient compliance point of view. An initial burst effect of these peptides was not a problem due to their low toxicity. The peptides are also relatively stable compounds that can be incorporated into polymeric devices with minimal loss of bioactivity. Finally, the PLGA polymers used in the devices required minimal toxicological testing.

Zoladex is a cylindrical implant approximately 1 mm in diameter and 3–6 mm in length (*67*). The device is made from a 50:50 PLGA copolymer and contains 3.6 mg of drug which is homogeneously dispersed throughout the matrix. After subdermal injection in the abdominal wall,

the drug is released over 28 days. Release of the peptide is initially controlled by a dissolution/diffusion mechanism from polypeptide domains at or near the surface of the device. At later times, the degradation of the polymer leads to the generation of microporosity and enhanced water uptake by the system, which ultimately results in further release of the drug.

Lupron Depot is a biodegradable PLGA microsphere delivery system also designed to release the LHRH analog, leuprolide acetate, over 1 month (68–70). The microspheres were prepared by a water/oil/water emulsion technique using a PLGA (75:25) copolymer with a molecular weight of approximately 14 000. Gelatin was added to the inner water phase of the system together with the peptide in order to increase the viscosity in the inner phase of the emulsion. This increased viscosity resulted in complete incorporation of the drug in the microspheres, and loadings of 10–20% by weight were obtained. The release of peptide from this system was described as biphasic. After a small initial burst, a diffusion-controlled release occurred followed by polymer degradation and further erosion-controlled release. This product is administered by subcutaneous or intramuscular injection.

A second generation product designed to continuously deliver LHRH for 3 months has recently been described (71). After screening several PLA and PLGA polymers, it was determined that microspheres prepared from PLA with a molecular weight of 15 000 that contained 12% LHRH by weight gave the most desirable release profile. The absence of water-soluble oligomers (less than 0.1%) in the polymer was important for reducing the initial burst of drug. The system was proven to be pharmacologically active in rats and provided linear sustained release and persistent serum levels of LHRH for over 3 months.

There are a number of additional reports that describe the use of PLGA microcapsules for the delivery of LHRH analogs (21, 53, 72–74). Microspheres containing the analog nafarelin were prepared by a coacervation technique, and the release of peptide was described as triphasic. In the first phase the drug was released by diffusion from the surface of the spheres. The second phase exhibited a slow or negligible release rate. The third phase was characterized by a more significant release of the drug and was attributed to degradation of the PLGA matrix. By selection of the appropriate polymer molecular weight and copolymer composition, the second phase of low peptide release could be minimized.

Another PLGA delivery system for a LHRH analog was prepared by a hot-press technique (75). The powdered drug and polymer were mixed at 70 °C and then compressed within a Teflon tube into a rod 1 cm in length and 2 mm in diameter. When the rods were subcutaneously implanted in rats, it was found that the rates of polymer erosion and peptide release decreased with time over 15 weeks, after which time the polymer was completely degraded.

A water/oil/water emulsion preparation technique that was similar to the process used to manufacture Lupron Depot has been used to incorporate the model proteins bovine serum albumin (BSA) and horseradish peroxidase into PLGA microspheres (76). More than 90% incorporation efficiency was achieved, and different *in vitro* release rates were obtained by modifying factors in the preparation procedure such as mixing rate and the volume of inner water and organic phases. A more recent report by Sah et al. describes the modification of BSA release kinetics from PLGA microspheres by the blending of different molecular weight polymers prior to preparation of the delivery system (77). Zero- or first-order release kinetics could be achieved by using a combination of a high molecular weight PLGA (75:25) and a low molecular weight PLA 2000. The porosity, degree of water uptake, and degradation rate of the microspheres could also be varied by changing the polymer composition. Another study describes a detailed characterization of BSA loaded PLPG microspheres that were prepared by a water/oil/water emulsion technique (78). Confocal laser scanning microscopy analysis and *in vitro* studies indicated that heterogeneous microparticles in which the BSA was not evenly distributed throughout the microsphere provided a fast release profile with a large protein burst (62%), while homogeneous microparticles release the BSA more slowly with only a 7% burst.

The incorporation of several protein antigens in PLGA microspheres for vaccine delivery has also been reported for tetanus (79) and diphtheria toxoid (80). These systems were capable of inducing an immune response in mice that was comparable to conventional multidose injections.

Cylindrical monolithic matrix release devices were made by extruding an albumin suspension in a PLA acetone solution, to form rods (81). The rods were then coated with pure poly(D,L-lactide) and cut into different lengths. Release of the albumin from the short cylinders (0.5–1 cm) was primarily diffusion controlled. Release of the protein from longer devices (2–4 cm) was controlled by a combination of diffusion and osmotic pressure. The duration of release could range from 200 to 800 h depending of the loading and length of the device.

The tendency for some proteins to adsorb to PLGA polymers has been used in the development of a microsphere delivery system for salmon calcitonin (82). In this system, preformed PLGA microspheres were prepared by a solvent extraction process and then exposed to an aqueous calcitonin solution. This process resulted in multiple layers of adsorbed peptide on the polymer surface, which exhibited a 3–4 day release after subcutaneous injection in a rat model. When the model macromolecule dextran was adsorbed into preformed PLA microspheres, its release could be increased by exposing the spheres to low ultrasonic energy (83).

PLGA copolymers will spontaneously form solid depots when a solution of the copolymer in either dimethyl sulfoxide (DMSO) or *N*-methyl-2-pyrrolidone (NMP) is injected into water (84). Fluorescently-labeled BSA was incorporated as a dry powder (1% w/w) in this type of system, and the *in vitro* protein release was studied as a function of polymer molecular weight and solvent type. When the polymer solution that contained the suspended BSA was dropped into release media, spherical matrices (0.3 cm in diameter) were formed as the polymer solidified. For high molecular weight PLGA in NMP, an initial burst of BSA was followed by a zero-order release for up to 2 weeks. With low molecular weight PLGA in DMSO or NMP, it was possible to eliminate the initial burst and obtain zero-order delivery for at least 1 week. The toxicity profile from the *in vivo* injection of the solvents DMSO or NMP with these delivery systems has not yet been reported.

ii. PLGA Polymer blends. One approach that has been used to modify the release of proteins from PLGA and PLA delivery systems is to blend together several different types of polymers. In one study, films containing bovine serum albumin were prepared from blends of pluronic polyols (85) (Figure 4) and poly (L-lactic acid). The addition of the nonionic pluronics to the system resulted in films with different phase-separated mor-

Pluronic Polyol
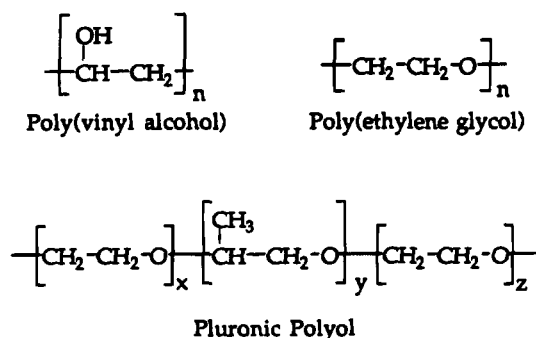
Figure 4. Chemical structures of three common hydrophilic polymers used in degradable drug delivery systems. These polymers have been utilized in several ways in degradable drug delivery systems including: (i) as stabilizers which minimize undesirable contact between proteins and hydrophobic polymers, (ii) as additives which enhance water uptake and the dissolution of hydrophobic drug delivery systems, (iii) as gel matrices for the incorporation and slow release of proteins and peptides, and (iv) as covalent carriers for protein pharmaceuticals.

phologies and different degrees of hydration. When used as drug releasing matrices, these blends extended protein release and minimized the initial protein burst compared to the pure polymer. To further reduce the burst effect, these polymer films were coated with poly(ethylenimine) (PEI) (*86*). The authors suggested that the PEI diffused into the polymer matrices and cross-linked the protein molecules by ionic interactions. The PEI–protein network near the surface region of the matrix acted as a diffusional barrier for further release of the protein.

Films based on blends of poly(vinyl alcohol) (PVA) (Figure 4) with PLGA have been prepared with incorporated cytochrome *c*, myoglobin, somatotropin, or albumin (*87*). Chemical hydrolysis, as determined by a decrease in molecular weight, was shown to increase with an increase in PVA content of the system, and release of both myoglobin and cytochrome *c* followed first-order kinetics.

   iii. Block Copolymers of PEG, and Lactic and Glycolic Acid. Copolymers of PEG (Figure 4) and PLA have been synthesized for use in delivery systems (*88, 89*). The net result is a biodegradable polymer with a reduced amount of hydrophobicity that is an inherent property of PLA systems. These copolymer systems can be composed of (i) random blocks of the two polymers, (ii) two blocks in which case the molecules are amphiphilic, or (iii) triblocks (*90*) in which hydrophilic microphases are present. Proteins which are incorporated into devices made from these copolymers are less likely to adsorb to the delivery system through hydrophobic interactions. A recent paper by Youxin describes the release of BSA from ABA triblock copolymers consisting of PLA or PLGA A-blocks attached to central PEG B-blocks (*91*). The polymers were shown to swell very rapidly due to microphase separation, and degradation occurred over 2–3 weeks. Microspheres containing BSA were prepared from the copolymers. Continuous release was attained when the A-blocks were made from PLPG, while pulsatile release was observed with A-blocks made from PLA. In another study, PLA–PEG block copolymers were used as a delivery system for bone morphogenetic protein (BMP) (*92*). The copolymer consisted of a PLA segment with a molecular weight of 650 and a PEG segment with a molecular weight of 200. The copolymer containing the BMP was an injectable viscous semiliquid. When implanted under the fasciae of the dorsal muscles of mice, the composites were completely absorbed and replaced by newly induced bone with hematopoietic marrow. The composites induced twice as much bone as composites of BMP and a 650 dalton homopolymer. The same system was shown to

induce bone formation in large segmental bone defects in the tibiae of rabbits (*93*). The amphiphilic nature of the PLA–PEG two block copolymer system has also been used to create nanoparticulate carriers using a two-phase oil-in-water emulsion system (*94*).

Block copolymers of PLA–PEG were used to surface coat PLGA nanospheres (*95*). The result was an increase in surface hydrophilicity and decrease in surface charge of the nanospheres. A PEG chain length of 2000 daltons was shown to provide an effective repulsive barrier to albumin adsorption. *In vivo* clearance studies in a rat model showed that the PLA–PEG-coated PLGA nanospheres had a dramatically increased blood circulation time and decreased hepatic uptake as compared to uncoated PLGA nanospheres.

   iv. Poly(cyanoacrylates). Poly(cyanoacrylates) have received attention as delivery systems for proteins and peptides. They undergo spontaneous polymerization at room temperature in the presence of water, and their erosion has been shown to be controlled by the length of the monomer chain and the pH (*96*). Once formed, the polymer is slowly hydrolyzed, leading to a chain scission and liberation of formaldehyde (Figure 5). While the polymers are not toxic, the formaldehyde released as the degradation byproduct does create a toxicity concern (*97*).

A nanocapsule delivery system for insulin was prepared by the interfacial emulsion polymerization of alkyl cyanoacrylate (*98*). The nanospheres had an average diameter of 220 nm and were capable of sustaining the release of insulin when administered either subcutaneously or orally. Nanospheres made from poly(isohexyl cyanoacrylate) were shown to deliver growth hormone-releasing factor in a rat model for 24 h after subcutaneous injection (*99, 100*). This was a significant improvement compared to the injection of free drug which was undetectable after 100 min. Release of the protein from the nanoparticles resulted from degradation of the polymeric matrix and was not due to passive diffusion of peptide through the polymer. Detailed autoradiography studies and transmission electron microscopy analysis showed that the particles containing radiolabeled polymer remained intact at the site of injection for at least 24 h. Poly(isobutyl cyanoacrylate) nanoparticles have also been used as a sustained release system for calcitonin (*101*). The peptide was loaded into the particles either before or after polymerization of the isobutyl cyanoacrylate. For both formulations, the incorporation efficiency of calcitonin was more than 95%, suggesting a strong interaction between the polymer and the peptide. *In vitro* studies showed that calcitonin was released from the surface-loaded nanoparticles but not from the particles that contained peptide which was added during polymerization. In an *in vivo* rat model, both systems were capable of inducing a more prolonged hypocalcemic effect than free calcitonin.

2. Surface Erosion Polymers. *i. Poly(anhydrides).* The systems described in the previous section are comprised of polymers that are hydrolytically cleaved throughout the bulk of the matrix. Poly(anhydrides) (Figure 6), which were developed for drug delivery applications by Langer and collaborators, represent a class of surface-eroding polymers (*102–104*). A recent publication reviews the different types of polyanhydrides with a detailed description of their erosion kinetics (*105*). Hydrolysis of the anhydride bond is suppressed by acid, which results in an inhibition of bulk erosion by the acidity of the carboxylic acid products of the polymer hydrolysis process (*106*). By varying the ratio of the hydrophobic component 1,3-bis(*p*-carboxyphenoxy)pro-
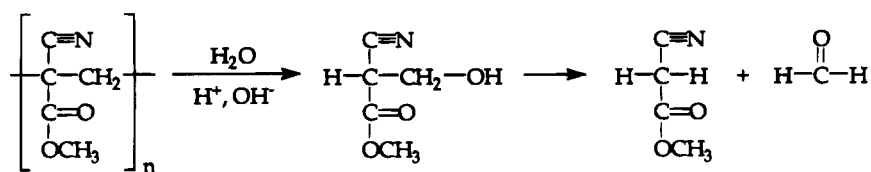
Figure 5. The hydrolytic degradation of poly(cyanoacrylate) is a two-step process. Formaldehyde is a byproduct of the second step.
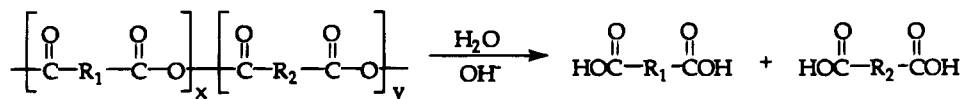
Figure 6. The hydrolytic degradation of poly(anhydrides) is catalyzed by base. The specific R groups used in the monomeric subunits (diacids) strongly influence the rates of degradation and drug release.

pane and sebacic acid, degradation rates ranging from days to years can be achieved (*107*).

Poly(anhydrides) can be fabricated into delivery systems by injection molding or compression molding. Injection molding requires higher than ambient temperatures and can result in a reaction of the amine groups on a drug with the anhydride linkage, thus making this technique difficult to implement with easily denatured proteins (*108*). Nevertheless, several proteins have been successfully incorporated into, and released, from poly(anhydride) delivery systems. The incorporation of insulin and myoglobin has successfully been achieved in poly(anhydride) microspheres using both a hot-melt microencapsulation technique (*109*) or microencapsulation by solvent removal (*110*). The incorporation of the drug affected the surface erosion rate of the polymer. *In vivo* studies showed that the poly(anhydride) insulin delivery system could reduce glucose levels in diabetic rats for several days. Exposure of the microspheres to ultrasound resulted in increased drug release and polymer degradation rates (*111*). A recent report describes the incorporation of several proteins into poly(anhydride) microspheres including lysozyme, trypsin, heparinase, ovalbumin, albumin, and immunoglobulin (*112*). The microspheres were prepared by a solvent evaporation technique method using a double emulsion. All proteins were released at a near-constant rate for more than 25 days without any large initial burst, irrespective of the polymer molecular weight and protein loading.

ii. Poly(ortho esters). Poly(ortho esters) are another example of surface-eroding polymers that have been developed for drug delivery systems (*113*). Hydrolysis of the ortho ester group is acid-catalyzed (*114*). One particular type of poly(ortho ester) is made of 2,2-dialkoxytetrahydrofuran, 1,6-hexanediol, and 1,4-cyclohexanedimethanol. Upon hydrolysis, the acidic byproduct hydroxybutyric acid is released which causes an increasing erosion rate of the system over time. Basic additives such as $Mg(OH)_2$ can be included in the delivery system to suppress bulk hydrolysis and enhance surface erosion. Conversely, the inclusion of an acidic species such as 9,10-dihydroxystearic acid can be used to increase the rate of surface erosion (*115*). The rate of the poly(ortho ester) surface erosion can also be controlled by the hydrophobicity of the polymer and the cross-link density. An increase in the cross-linking can also reduce the diffusional release of drug.

Several proteins and peptides have been incorporated into poly(ortho ester) delivery systems including the LHRH analog nafarelin (*116*), insulin (*117, 118*), and lysozyme (*119*). In the latter system the polymer was prepared by a transesterification reaction between a triol and an alkyl orthoacetate to produce a viscous ointment at room temperature. Protein incorporation into this system was accomplished by simple mixing at room temperature without solvents.

3. Hydrogel Systems. The use of biodegradable hydrogels as delivery systems for proteins is of particular interest due to their biocompatability and their relative inertness toward protein drugs (*120, 121*). Hydrogels are the only class of polymer that can enable a protein to permeate through the continuum of the carrier. The initial release rate of proteins from biodegradable hydrogels is therefore generally diffusion controlled through the aqueous channels of the gel and is inversely proportional to the molecular weight of the protein. Once polymer degradation occurs, and if protein still remains in the hydrogel, erosion-controlled release may contribute to the system. Several disadvantages must be considered when using a biodegradable hydrogel system for the release of proteins. Their ability to rapidly swell with water can lead to very fast release rates and polymer degradation rates. In addition, hydrogels can rapidly decrease in mechanical strength upon swelling with water.

Biodegradable hydrogels have been prepared from natural or synthetic polymers (*122*). Three examples of polymers commonly used to prepare hydrogels are shown in Figure 4. Formation of the hydrogels can be achieved by both chemical or physical means. Chemically cross-linked gels are prepared by polymerization of monomers by chemical cross-linking of water-soluble polymers. Upon hydrolysis of the cross-links, the polymer becomes water soluble and is eliminated from the body. Hydrogels formed by physical means contain polymers that are associated through extended junction zones. These associations can be created by a simple entanglement of polymer chains or by interactions between hydrophobic or crystalline regions of the polymer or may be ionic in nature. Many water-soluble polymers form hydrogels by simple entanglement, particularly, naturally occurring polymers such as hyaluronic acid. The synthesis of block copolymers or the blending of two different polymers has been used to create physical hydrogels with a wide variation in physical and mechanical properties. Several polysaccharide systems such as alginates and pectin will form hydrogels upon the introduction of counterions.

i. Pluronic Polyols. Pluronic polyols or polyoxamers are block copolymers of poly(ethylene oxide) and poly(propylene oxide) (Figure 4). One particular polymer, pluronic F127, has been used extensively as a gel forming polymer matrix to deliver proteins. Pluronic F127 consists by weight of approximately 70% ethylene oxide and 30% propylene oxide, with an average molecular weight of 11 500. The polymer exhibits a reversible thermal gelation in aqueous solution at concentrations of 20% or more (*123*). Thus, a solution of this polymer is liquid at room temperature, but rapidly gels in the body. Although
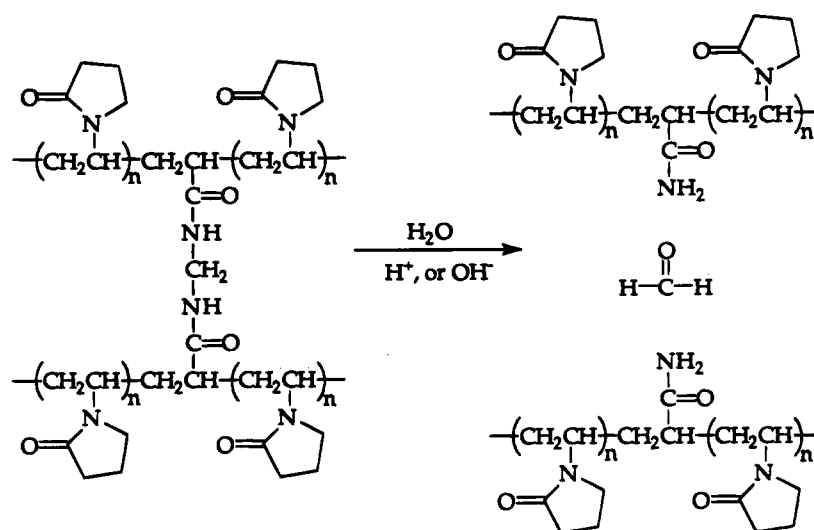
Figure 7. Cross-linked poly(vinylpyrrolidone) is hydrolytically degraded into chains of water-soluble poly(vinylpyrrolidone). Formaldehyde is released as a degradation byproduct. Proteins embedded in this type of drug carrier are released by a combination of degradation and diffusional mechanisms.

this polymer is not metabolized by the body, the gels do slowly dissolve over time and the polymer is eventually cleared. As a result of its good biocomaptibility and nondenaturing effects on proteins, pluronic F127 gels have been used as delivery systems for several proteins including IL-2 (*124, 125*), urease (*126*), rat intestinal natriuretic factor (*127*), and TGF-β_1 (*128*). These systems are easily administered by subcutaneous injection and generally release the protein over a period of 1–2 days.

ii. Poly(vinyl alcohol). Poly(vinyl alcohol) (PVA) is another polymer that can be made into a hydrogel that degrades by solubilization (Figure 4). Bovine serum albumin was incorporated into PVA discs, and release of the drug was studied *in vitro* (*129*). The initial release of the drug was attributed to diffusion of drug through water-filled pores near the surface of the polymer matrix. As the polymer swelled, structural changes occurred in the polymer and diffusion of the protein occurred through both the hydrated polymer matrix and the water-filled pores.

Physically cross-linked PVA gels have been prepared by a freeze–thawing process which causes structural densification of the hydrogel due to the formation of semicrystalline structures (*130, 131*). When BSA was incorporated into these gels, the release was essentially complete within 50 h and was controlled by a pure diffusional mechanism.

iii. Poly(vinylpyrrolidone). One of the earliest studies reporting on the use of a chemically cross-linked biodegradable hydrogel as a protein delivery system was done with the incorporation of chymotrypsin in poly(vinylpyrrolidone) (PVP) gels (*132*). The PVP was cross-linked with N,N'-methylenebis(acrylamide). Hydrolysis of the cross-linking agent resulted in the production of formaldehyde and degradation of the hydrogel (Figure 7). Degradation of this type of hydrogel was very sensitive to the concentration of cross-linking agent. More than 1–2% cross-linking agent produced an essentailly noneroding hydrogel. Once the cross-link density fell below a critical value of 1%, the hydrogel began to dissolve and the enzyme was released by diffusion from the gel. The cross-link density therefore controlled both the rate of hydrogel solubilization and the release rate of the chymotrypsin. Gels with too high a cross-link density remained insoluble, and only a fraction of the chymotrypsin was released. Gels with too low of a cross-link density, on the other hand, completely dissolved. Be-

cause of their high porosity, however, the protein underwent a rapid diffusional release within a time of 2–3 days, and kinetics were difficult to control.

Heller et al. were able to fabricate a degradable hydrogel system by first preparing a prepolymer of PEG and either fumaric acid, ketomaionic acid, ketoglutaric acid, or diglycolic acid. The prepolymers were then cross-linked to PVP by copolymerization (*133*). When BSA was entrapped in microspheres of these gels, the duration of *in vitro* zero-order release could be varied between 10 days up to 7 weeks by the choice of ester structure and the amount of vinylpyrrolidone cross-links.

iv. Maleic Anhydride–Alkyl Vinyl Ether Copolymers. Maleic anhydride–alkyl vinyl ether copolymers have been used to fabricate polymeric films containing α-interferon (IFNα) (*134*). These devices were designed as ophthalmic implants. The IFNα was coincorporated with human serum albumin as a suspension into to gels. Albumin was used both as a diluent for the IFNα and as an intermolecular binder for the polymer matrix. The kinetic release data indicate that the erosion of the polymer matrix plays an important role in the release process. It was also hypothesized that the depletion of protein from the device by a diffusion process was inhibited by hydrophilic interactions of the protein with the polymer.

v. Cellulose. Methylcellulose gels which degrade by solubilization have been effectively used for the site-specific delivery of several proteins. Beck et al. used 3% methylcellulose gels to deliver transforming growth factor-β_1 (TGF-β_1) both to topical skin wounds (*135, 136*) and to bone defects (*137*). In both cases, the protein in the gel showed a significant enhancement in the healing of skin wounds or bone defects when compared to protein that was applied to the site in a saline buffer solution.

A 1% (hydroxyethyl)cellulose gel was used to incorporate acidic fibroblast growth factor (aFGF) for a wound healing formulation (*138*). The addition of heparin to the gel in a 3:1 ratio with aFGF was found to be necessary for maintaining full biological activity and conformational stability of the growth factor. *In vitro*, aFGF was release from the gel over 24 h. Application of the gel to full-thickness wounds in diabetic mice was found to accelerate healing when compared to a phosphate buffer control.

vi. Hyaluronic Acid Derivatives. Hyaluronic acid derivatives are a good example of naturally occurring polymers that have been modified to control the degrada-
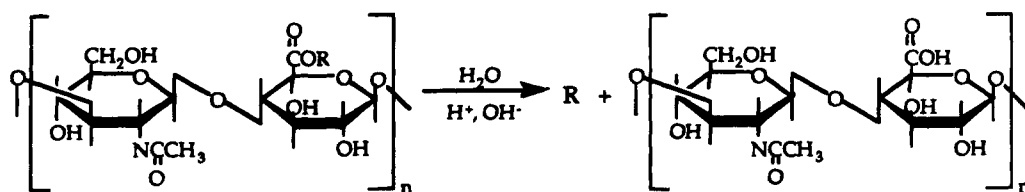
Figure 8. Esterified hyaluronic acid and primary degradation products following hydrolysis. The R group is generally hydrophobic (ethyl or benzyl esters) such that the esterified hyaluronic acid is hydrophobic, and hydrolysis results in solubilization of the hyaluronic acid and release of the entrapped protein.
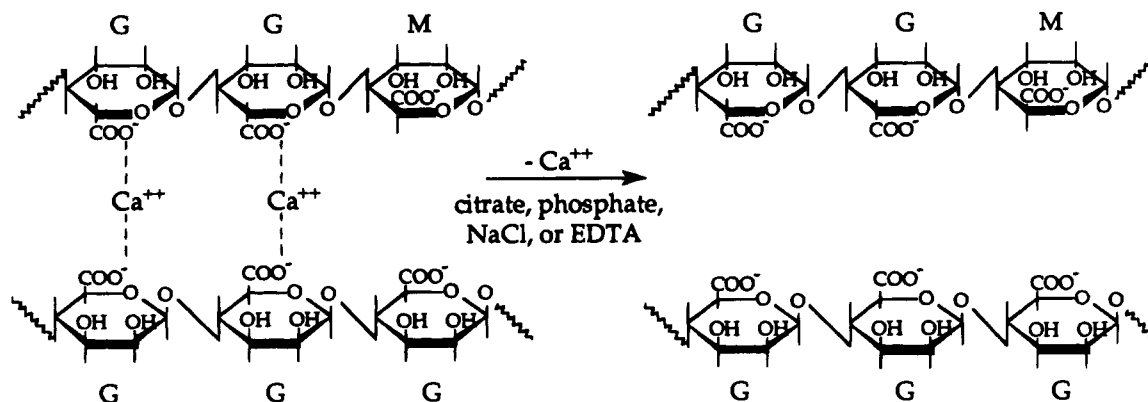
Figure 9. Alginate exists as a copolymer consisting of $1-4$-linked α-L-guluronic acid (G) and β-D-mannuronic acid (M). Alginate is cross-linked by divalent cation (e.g., Ca^{2+}, Sr^{2+}) associations between guluronic acid-rich regions of the alginate chains. The alginate hydrogel solubilizes on exposure to agents which chelate or exchange with the divalent cations.

tion and release rates. Hyaluronic acid is a naturally occurring mucopolysaccharide consisting of residues of D-glucuronic acid and *N*-acetyl-D-glucosamine in an unbranched chain (Figure 8). The polymer has an average molecular weight of $(5-6) \times 10^6$ and exhibits excellent biocompatibility. Both chemical cross-linking and derivatization of hyaluronic acid have been used to enhance the rheological properties or increase the degradation time (*139—141*). In one study, microspheres prepared from hyaluronic acid esters were used for the nasal delivery of insulin (*142*). Blank spheres were prepared by an emulsification/solvent evaporation technique and then exposed to an insulin solution for an hour and lyophilized. When administered to sheep, the mean bioavailability was found to be 11% when compared with insulin administered by the subcutaneous route. This system has also been used as a delivery device for nerve growth factor (NGF) (*143*). Permeability and partition coefficients were measured for a series of peptides and proteins in membranes formed from ethyl or benzyl esters of hyaluronic acid (*144*). The diffusion coefficients were correlated to the size of the solute molecule, and the slopes of the correlations varied with the type of ester used. In general, for a given protein or peptide, diffusion was more rapid in the ethyl ester membrane. These results suggest that the hyaluronate ester matrix can be tailored to give a desired release rate for a polypeptide of interest.

vii. Alginate. Alginate is a linear polysaccharide that is extracted from red-brown seaweed. It contains the repeating units of 1,4-linked α-L-guluronic acid and β-D-mannuronic acid (Figure 9). In the presence of divalent cations such as calcium, sodium alginate spontaneously forms a hydrogel matrix. Cross-linking occurs through the guluronic acid residues. Ionically cross-linked alginate gels have been used to incorporate several different proteins for controlled release applications including TGF-β_1 (*145*), basic fibroblast growth factor (bFGF) (*146*), tumor necrosis factor receptor (TNFR) (*147*), and angiogenic molecules such as angiogenesis factor, epidermal growth factor (EGF), and urogastrone (*148*). Because
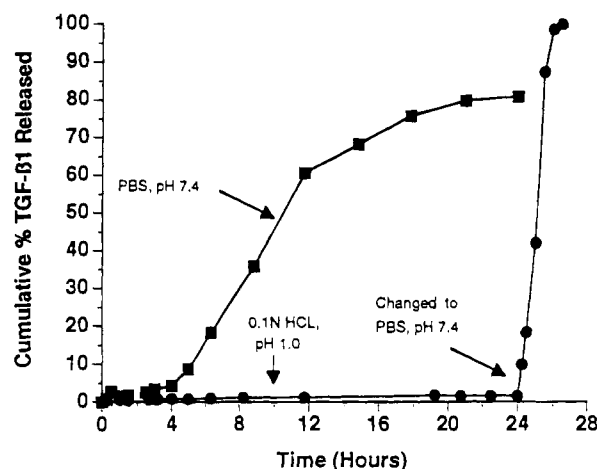
Figure 10. The cumulative percent *in vitro* release of ^{125}I-TGF-β_1 at 37 °C in phosphate-buffered saline (PBS), pH 7.4 (squares), or 0.1 N HCl, pH 1.0, transferred to PBS after 24 h (circles). Reprinted with permission from Mumper et al. (*145*).

alginate is an anionic polymer at pH 7.4, proteins with a net positive charge can ionically bond to the polymer and thus exhibit reduced bioactivity upon incorporation into an alginate delivery system. TGF-β_1, with a p*I* of 9.8, is one example of a protein with a net positive charge at physiologic pH. When incorporated into alginate beads, ^{125}I-labeled TGF-β_1 was not released when the beads were incubated in 0.1 N HCl (*145*). The protein did release when the beads were incubated in phosphate-buffered saline, pH 7.4 (Figure 10). Furthermore, when the released TGF-β_1 was assayed by ELISA, little binding of the monoclonal antibody to the protein occurred. The addition of poly(acrylic acid) to the alginate bead was shown to prevent the inactivation of TGF-β_1 by the alginate. In another study, bFGF was first adsorbed to heparin—Sepharose beads and then incorporated into the alginate matrix (*148*). This preadsorption to the heparin resulted in the retention of significant bioactivity in the bFGF. Proteins have been successfully delivered from

alginate beads in several *in vivo* models. NGF was incorporated into poly(L-lysine)-coated alginate microspheres. When implanted in the cerebral cortex of rats that had received a cortical lesion, the neural degeneration in these animals was decreased when compared to the controls (*149*). The bFGF system described above was implanted in the perivascular space, and the distribution of protein was compared to that with a conventional intravenous injection of the protein (*150*). The alginate system was found to be much more efficient than intravenous delivery at depositing bFGF within the arterial wall.

viii. Collagen. The majority of collagen-based systems are in the form of either implantable devices or injectable gels. Several groups have demonstrated the release of proteins from collagen matrices. One concern with collagen is its potential for causing a immunogenic response in the patient. Atelocollagen has been used in order to decrease the potential immunogenicity of collagen (*151*). This material is collagen that has been subjected to protease treatment to remove the telopeptides. In studies by Fujiwara et al., IL-2 was incorporated into a collagen pellet that was prepared by homogeneously mixing an aqueous solution of atelocollagen with the protein to obtain a uniform gel mixture (*151, 152*). The gel mixture was then subjected to molding and then drying to produce cylindrical pellets 1 mm in diameter and 10 cm long. The pellets were implanted subcutaneously in mice containing solid tumors and were found to have a significant effect in the inhibition of tumor growth. No *in vitro* release kinetics were shown in this study. A similar collagen system was used to continuously deliver NGF to the hippocampus of gerbils (*153*). The NGF was colyophilized with human serum albumin prior to mixing with the collagen. The delivery of NGF was able to prevent neuronal cell damage, and NGF concentrations in the hippocampus were shown to remain high in for 5 days as determined by an enzyme immunoassay.

Collagen monolithic devices varying in cross-link density, collagen structure, and type of cross-linking agent were fabricated for the controlled release of the model macromolecule inulin (*154*). *In vitro* release rates were linear with the square root of time, indicating a diffusion-controlled system.

Collagen gels have been reported to effectively deliver epidermal growth factor (EGF) (*155*) and TGF-β_1 (*156*) to experimentally induced wounds in a mouse model. In both cases, the growth factors were shown to accelerate wound healing.

ix. Gelatin. A gelatin-based microsphere delivery system containing IFNα was prepared by sonication of an aqueous solution of the drug and gelatin in toluene and chloroform that contained the surfactant span 80 (*157*). The gelatin was then cross-linked with glutaraldehyde. *In vitro* degradation of this system was observed with the addition of collagenase and was inversely proportional to the cross-linking density. A potential problem with this system is the use of glutaraldehyde as a nonspecific cross-linking agent which can potentially bond to both the collagen and the interferon, thus inactivating some of the drug.

Gelatin-based films originally designed as a wound dressing material have been used to deliver ^{125}I-labeled insulin (*158*). The film adhered to open wounds but was permeable to body fluids. Insulin was released *in vitro* for 4 days. Incorporation of collagen into the release solution resulted in a significant increase in the insulin release rate.

Investigators have utilized the process of complex coacervation to prepare microspheres containing albumin, γ-interferon, and granulocyte macrophage colony-stimulating factor (GM-CSF) (*159*). The system relies on the spontaneous phase separation process that occurs when oppositely charged polyelectrolytes are mixed in an aqueous medium. The system described by Shao and Leong (*160*) utilized gelatin and chondroitin sulfate, which were coacervated in the presence of the drug and then cross-linked with glutaraldehyde. Spherical microspheres ranging from 5 to 30 μm in diameter were obtained and were shown to degrade *in vitro* in the presence of collagenase. *In vivo* the microspheres containing GM-CSF were shown to elicit a systemic antitumor immune response in mice. As with the gelatin system described above, the glutaraldehyde cross-linking poses a potential problem when used with protein pharmaceuticals.

x. Albumin. Albumin microspheres were developed as an injectable degradable system for the delivery of insulin (*161*). Insulin crystals were suspended in a phosphate buffer solution that contained bovine serum albumin. While the suspension was stirred rapidly in a mixture of petroleum ether and corn oil to form a water-in-oil emulsion, cross-linking of the spheres was initiated by the addition of 2.5% or 5% glutaraldehyde. Microspheres ranging in diameter from 50 to 1000 μm were obtained. A sustained release of bioactive insulin in rats was obtained over for more than 60 days. Albumin microspheres have also been prepared that contained covalently immobilized urokinase using glutaraldehyde chemistry (*162*).

xi. Starches and Dextrans. Cross-linked polysaccharide microparticles have been used by several groups as protein delivery systems. In one study, recombinant mouse IFNα was covalently coupled to polyacryl starch microspheres using carbonyldiimidazole chemistry (*163*). The bound IFNα was found to activate cultured macrophages for nitrite production and had an anti-leishmanial effect in mice. Low doses of IFNα, which had no effect in the free form, when bound to microparticles significantly reduced the load of *Leishmania donovani* in infected mice. Other biodegradable polysaccharides have been used to delivery the model proteins, albumin, lysozyme, immunoglobulin G, and carbonic anhydrase (*164*). The polysaccharides maltodextrin or hydroxyethyl starch were derivatized with acrylic acid glycidyl ester. The protein polymer solution was then polymerized in a water-in-oil emulsion. Proteins were released from the microspheres over a 12 week period. Polyacryldextran microspheres containing several different proteins were prepared using a similar polysaccharide derivatization system (*165*). The heat stability of carbonic anhydrase was improved when incorporated into the microspheres, and degradation was enhanced in the presence of dextranase.

4. Composite Systems. The combination of synthetic polymers with natural materials is another approach that has been taken in the development of protein delivery systems. In these systems the polymer can afford mechanical strength while the natural material affords protein stability. As mentioned above, the Lupron Depot microspheres contain PLGA, gelatin, and the drug LHRH. In another study, the protein, TGF-β_1, was first absorbed onto demineralized bone matrix (DBM) (*166*). This material is a bone derivative that is prepared by demineralizing cadaver bone with HCl and is comprised of more than 90% collagen along with small amounts of lipids, proteins, and proteoglycans. A colyophilized preparation of the protein and the DBM was

$$R-C_6H_4-N=N-C_6H_4-R \xrightarrow{\text{Bacterial Reductase}} R-C_6H_4-NH_2 + H_2N-C_6H_4-R$$

azoaromatic group   aromatic amines
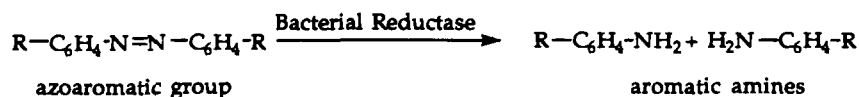
Figure 11. The azoaromatic group is insensitive to acid-catalyzed hydrolysis in the stomach; however, bacteria residing in the gut are able to reduce the azo bond to amines with reductases. This compound has been investigated as an enteric coating for the oral delivery of insulin and vasopressin.
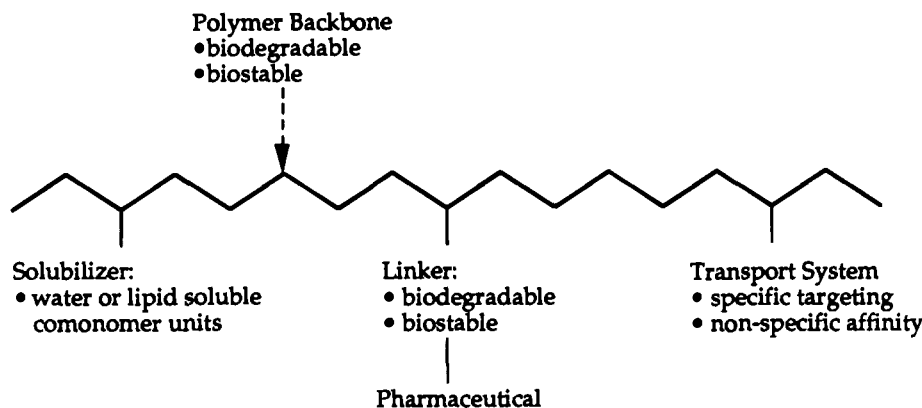
Figure 12. Model for a pharmacologically active polymer.

then incorporated into a PLGA matrix and fabricated into 2 mm thick discs which were designed to stimulate bone growth. *In vitro* release studies demonstrated that the released TGF-β_1 retained between 80% and 90% of its bioactivity.

Duncan and Kopecek have described a unique composite hydrophilic gel comprised of hydroxypropyl methacrylamide copolymers which are cross-linked via a degradable oligopeptide (*167*). Fluorescent labeled dextrans of different molecular weights were incorporated into the gels. The rate of release was found to depend mainly on the equilibrium degree of swelling and not on the structure of the cross-links. However, the degradation of the gels by a mixture of lysosomal enzymes or chymotrypsin was dependent on both swelling and cross-link structure (length of the oligopeptide and type of amino acid residues).

In another example of composite systems Saffran and co-workers have described a novel system for oral delivery of insulin and vasopressin to the colon. Their work takes advantage of the fact that certain azopolymers are resistant to degradation by proteolytic enzymes in the stomach; however, on passage to the colon these polymers may be cleaved by bacterial reductases (Figure 11). Saffran and co-workers describe a system where crystalline insulin or vasopressin is loaded into a gelatin capsule which is further coated with an azoaromatic cross-linked polymer (*168–170*). Oral administration of vasopressin and insulin in this form to anesthetized rats or dogs produced biological responses, antidiruresis, and hypoglycemia, respectively, characteristic of the peptide hormones.

IV. PROTEIN–POLYMER CONJUGATES

A. Potential Applications and Challenges with Conjugates. In the preceding sections biodegradable protein drug delivery systems were described where proteins were noncovalently embedded or contained within degradable matrices. Proteins may also be delivered in the form of covalent conjugates with water-soluble, biodegradable polymers. Modifications of proteins via conjugation with polymers have been envisioned and investigated for a variety of purposes. Ringsdorf first described protein–polymer conjugates as a means to create "pharmacologically active polymers" (*171*). In his

model (schematically represented in Figure 12) a biodegradable or biostable polymer chain serves as a backbone carrier for at least three different species. First, the pharmaceutical agent (or protein) is linked to the polymer via stable or degradable linkages. Also conjugated onto the polymer or designed into the monomer repeat units of the polymer itself may be a solubilizer to enhance the water or lipid solubility of the conjugate. Finally, a homing device such as an antibody (*172, 173*), a carbohydrate (*174*), a receptor binding ligand (*175*), or simply an electrically charged species (*176*) may be conjugated onto the polymer backbone to assist in targeting specific tissues or regions of the body.

There are many potential advantages to forming protein–polymer conjugates as drug delivery systems. Among these are the ability to alter the circulation pharmacokinetics of the protein–polymer conjugate. The kidney glomerular membrane serves to clear small circulating molecules (less than 70 kDa) by filtration. Conjugation of low molecular weight proteins with water-soluble polymers effectively increases their hydrodynamic radius, thereby reducing renal clearance. Systematic studies investigating proteins conjugated with noncationic polymers of various molecular weights have clearly demonstrated that circulation half-lives are increasingly prolonged when larger molecular weight polymer chains are conjugated onto these proteins (*177, 178*). Similarly, the influence of multiple polymer conjugates on individual protein molecules has also been demonstrated to prolong circulation half-lives (*178*). Other potential advantages of forming protein–polymer conjugates include the reduction of antigenicity of the protein (*179, 180*), improvement of protein solubility (*181*), and a reduction in the susceptibility of a protein to proteolysis (*182*) (also see refs 183–185 for reviews). Several protein–polymer conjugates are now entering the clinic for treatment of a variety of disorders (*186*).

Problems associated with conjugating polymers and proteins often involve inactivation or alteration of protein activity. While convenient conjugation chemistries take advantage of the ϵ-amino group of lysine or carboxylic acid side chains, proteins which are conjugated with polymers at these positions often suffer from inactivation or alteration of bioactivity. The extent of inactivation or alteration is protein specific, depending on the position

of the conjugation sites relative to the active region of the protein molecule. For many protein–polymer conjugation schemes, a balance between the desirable effects of conjugation and the loss of bioactivity must be established. Recently, investigators have attempted to avoid the problem of inactivation by the use of site-specific conjugation strategies. A popular technique with antibody conjugation is to utilize the carbohydrate in the hinge region, a site distant from the antigen binding domain, to safely form conjugates (*187*). Also, through methods of protein engineering, a specific amino acid residue such as cysteine may be designed into a protein molecule to provide a specific site for conjugation which will maintain the desired bioactivity of the protein (*188, 189*). Other site-specific methods have been described which utilize N- or C-terminal amino acid site-specific chemistry (*190*).

B. Examples from the Literature. For the purposes of this review we will consider a protein–polymer conjugate to be biodegradable if either (i) the polymer carrier is hydrolytically or enzymatically degradable or (ii) the chemical linkage between the protein and polymer carrier is hydrolytically or enzymatically degradable. Each of these possibilities is discussed below.

1. Conjugates Where the Carrier Is Biodegradable. A clear advantage for biodegradable polymeric carriers of proteins is that the carrier can be metabolized or hydrolyzed and will eventually be eliminated from the body. The importance of this attribute is underscored by the undesirable effects of the accumulation of high molecular weight poly(vinylpyrrolidone), a non-biodegradable polymer, following administration as a plasma expander (*32, 33*). Biodegradable polymers to be used as carriers for conjugates must be soluble in aqueous solutions. This suggests that either the polymer is inherently hydrophilic or it is of low molecular weight.

One family of polymers which has been widely reported as biodegradable carriers for synthetic pharmaceuticals are polyamino acids: poly(L-lysine) (*191*), poly(L-glutamic acid) (*192*), and poly(L-aspartic acid) (*193*). Numerous reports of conjugating peptides to poly(amino acids) suggest that these carriers could also be useful in protein drug delivery applications; however, few reports exist in the literature. In order to be biodegradable, the monomers used in the preparation of these polymers must be of the L configuration, the D configuration being non-biodegradable. Poly(amino acids) offer chemical versatility with regard to protein or peptide conjugation (*194, 195*) and control of the backbone degradation rate (*196, 197*). Unlike poly(ethylene glycol), poly(amino acids) are negatively charged at physiological pH, and this charge influences their biological behavior. For example, circulation half-lives of poly(amino acids) have been demonstrated to depend on electrical charging as well as molecular weight (*198*). Another biological feature of poly(amino acids) which is most likely related to electrical charging is their propensity to serve as adjuvants for conjugated peptides and elicit an immune response (*199, 200*). This would clearly be an undesirable feature in many protein drug delivery applications.

Pharmacologically inactive proteins have also been utilized as carriers for other pharmacologically active proteins. In this scheme the carrier protein is chemically linked to a protein pharmaceutical. The conjugation of the two proteins together acts to increase circulation half-life and shield the protein pharmaceutical from proteolytic digestion and immunologic detection. Often such a conjugate may simply provide a spatial architecture necessary for function of active polypeptides. Albumin has been used as a pharmaceutical carrier to enhance

circulation half-lives of peptides such as the laminin cell binding peptide YIGSR (*201*) and SP68—a 21 amino acid peptide from gp120 of the human immunodeficiency virus type HIV-1 (*202*). Albumin conjugated with tumor invasion-inhibiting factor-2 (IIF-2) demonstrated a 40–60-fold reduction in the amount of peptide required to inhibit cancer cell invasion (*203*), and albumin conjugated with human growth factor led to a 20–40-fold increase in stability as compared to uncoupled growth hormone (*204*). A significant increase in circulation half-life, from 4 min to 6 h following intravenous administration, was achieved when albumin was conjugated with superoxide dismutase (*205*). Undesirable heterogeneities which resulted from chemical conjugation techniques have led to the development of a recombinant fusion protein of albumin and CD-4 (*206*). In this system a fusion protein may be produced in yeast at large scale without the heterogeneities observed with chemical coupling. Gelatin and succinyl-gelatin have also been investigated as biodegradable protein carriers for the delivery of α-interferon (*207*) superoxide dismutase (*208*), IL-1α (*209*), and TNF (*210*). In the case of cytokine delivery (γ-interferon, IL-1α, and TNF) gelatin appears to enhance the performance of the conjugated proteins by binding to cells of the immune system and eliciting a mild immune reaction.

Other synthetic polymers not generally regarded as biodegradable may be synthesized from low molecular weight polymers connected with biodegradable cross-linkers. For example, copolymers of (hydroxypropyl)-methacrylamide have been prepared with bifunctional pentapeptide sequences to deliver macromolecules (*211, 212*). In this system the "backbone" of the drug carrier is degraded by enzymatic cleavage of protease-labile linkages, releasing low molecular weight polymer units and a bound drug.

In addition to those biodegradable carriers mentioned above, investigators have conjugated proteins with molecules of DNA for use as amplification probes or reporter systems (*213*). While these reports have not suggested the use of DNA as a biodegradable protein carrier, the versatile chemical properties and desirable pharmacokinetic properties of DNA (*214*) suggest that poly(nucleic acids) may be investigated for this purpose in the future.

2. Conjugates Where the Protein–Polymer Linkage Is Biodegradable. Polymers may be conjugated to proteins with either stable or biodegradable linkers. The purpose of biodegradable linkages may be to release a protein from a polymer in a time controlled fashion, or to release a protein in response to certain physiological conditions. In certain situations a degradable linkage may be necessary to regain the activity of a linked protein. One class of biodegradable linkages are those in which the chemical bond between the protein and polymer degrades hydrolytically. Some of the more common chemical linkages between proteins and polymers include reactions with amino acid side chains: (1) the ε-amino group of lysine and the α-amino groups of proteins (amide, thiourea, alkylamine, and urethane linkages), (2) the thiol group of free cysteine residues (thioether linkage), and (3) carboxylic acid groups of aspartic and glutamic acid (amide and alkylamine) (*215–217*). Amide linkages generated with succinate esters such as *N*-hydroxysuccinimide (NHS) have been widely utilized in conjugation chemistries and are well characterized with regard to their hydrolytic instability (*218*). Protein–polymer conjugates formed with succinate esters such as succinimidyl succinate have been demonstrated to degrade under physiological conditions, i.e., PBS, pH 7.4, at 37 °C (*219, 220*). Thiol conjugation chemistries

are also degradable under physiological reducing conditions and have also been investigated as reversible protein—polymer linkages (*221*).

Another class of biodegradable linkages are those which are susceptible to enzymatic degradation. Several examples in the literature describe proteins or pharmaceuticals which are linked to polymeric carriers via short polypeptide sequences. The specific sequence and length of the peptide strongly influence the ability of specific enzymes to degrade the linkages (*222—226*). However, it should be emphasized that proteins themselves are clearly susceptible to enzymatic cleavage as well. Therefore, protein—polymer conjugates designed with enzymatically degradable linkages should be designed for specific protease action within specific compartments of the body.

V. SUMMARY

We have reviewed a large cross-section of degradable polymeric delivery systems for protein and peptide pharmaceuticals. These systems include monolithic type devices in which the drug is dispersed throughout the polymer and protein—polymer conjugates where the drug is covalently bound to the polymer. These delivery systems have unique challenges associated with their development that are related to both protein stability and protein release kinetics. Despite numerous reports in the scientific literature which include many encouraging results in preclinical models, very few of these systems have been developed into viable products. The products that have made it to market, however, have proven to be very successful and demonstrate the significant advantages that these systems can provide. The continuous advances in biotechnology will produce more proteins and peptides that will be difficult to administer by conventional means, and an increased demand for controlled or site-specific delivery systems is anticipated.

LITERATURE CITED

(1) Manning, M. C., Patel, K., and Borchardt, T. (1989) Stability of protein pharmaceuticals. *Pharm. Res. 6*, 903–918.

(2) Wang, Y. J., and Hanson, A. (1988) Parenteral formulations of proteins and peptides: stability and stabilizers. *J. Parenter. Sci. Technol. Suppl. 42*, S3–S26.

(3) Bai, J. P., and Chang, L. L. (1993) Comparison of site-dependent degradation of peptide drugs within the gut of rats and rabbits. *J. Pharm. Pharmacol. 45*, 1085–1087.

(4) Banga, A. K., and Chien, Y. W. (1988) Systemic delivery of therapeutic peptides and proteins. *Int. J. Pharm. 48*, 15–50.

(5) Davis, S. S. (1992) Delivery systems for biopharmaceuticals. *J. Pharm. Pharmacol. 44*, 186–190.

(6) Wearley, L. L. (1991) Recent progress in protein and peptide delivery by non invasive routes. *Crit. Rev. Ther. Drug Carrier Syst. 8*, 331–394.

(7) Wise, D. L., Trantolo, D. J., Marino, R. T., and Kitchell, J. P. (1987) Opportunities and challenges in the design of implantable biodegradable polymeric systems for the delivery of antimicrobial agents and vaccines. *Adv. Drug Delivery Rev. 1*, 19–39.

(8) Eldridge, J. H., Hammond, C. J., Meulbroek, J. A., Staas, J. K., Gilley, R. M., and Tice, T. R. (1990) Controlled vaccine release in the gut-associated lymphoid tissues. I. Orally administered biodegradable microspheres target the Peyer's Patches. *J. Controlled Release 11*, 205–214.

(9) Walker, R. I. (1994) New strategies for using mucosal vaccination to achieve more effective immunization. *Vaccine 12*, 387–400.

(10) Rabinovich, N. R., McInnes, P., Klein, D. L., and Hall, B. (1994) Vaccine technologies: View to the future. *Science 265*, 1401–1404.

(11) Cohen, S., Alonso, M. J., and Langer, R. (1994) Novel approaches to controlled-release antigen delivery. *Int. J. Tech. Assoc. Health Care 10*, 121–130.

(12) Morris, W., Steinhoff, M. C., and Russell, P. K. (1994) Potential of polymer microencaspsulation technology for vaccine innovation. *Vaccine 12*, 5–11.

(13) McGee, J. P., Davis, S. S., and O'Hagan, D. T., (1994) The immunogenicity of a model protein entrapped in poly(lactide-co-glycolide) microparticles prepared by a novel phase separation technique. *J. Controlled Release 31*, 55–60.

(14) Pitt, C. G. (1990) The controlled parenteral delivery of polypeptides and proteins. *Int. J. Pharm. 59*, 173–196.

(15) Lee, V. H. (1991) *Peptide and Protein Drug Delivery*, Marcel Dekker, New York.

(16) Langer, R. (1990) New methods of drug delivery. *Science 249*, 1527–1532.

(17) Robey, M. J., Field, G., and Styzinski, M. (1989) Degradable plastics. *Materials Forum 13*, 1–10.

(18) Wood, D. A. (1980) Biodegradable drug delivery systems. *Int. J. Pharm. 7*, 1–18.

(19) Kamath, K. R., and Park, K., (1993) Biodegradable hydrogels in drug delivery. *Adv. Drug Delivery Rev. 11*, 59–84.

(20) Lewis, D. D. (1990) Controlled release of bioactive agents from lactide/glycolide polymers. *Biodegradable Polymers as Drug Delivery Systems* (M. Chasin and R. Langer, Eds.) pp 1–41, Marcel Dekker, New York.

(21) Sanders, L. M., Kell, B. A., McRae, G. I., and Whitehead, G. W. (1986) Prolonged controlled release of Nafarelin, a lutenizing hormone-releasing hormone analog, from biodegradable polymeric implants: influence of composition and molecular weight of polymer. *J. Pharm. Sci. 75*, 356–360.

(22) Pitt, C. G., and Shindler, A. (1983) Biodegradation of polymers. *Controlled Drug Delivery* (S. D. Bruck, Ed.) pp 53–80, CRC Press, New York.

(23) Baker, R. (1987) *Controlled Release of Biologically Active Agents*, John Wiley & Sons, New York.

(24) De Lustro, F., Dasch, J., Keefe, J., and Ellingsworth, L. (1990) Immune responses to allogeneic and xenogeneic implants of collagen and collagen derivatives. *Clin. Orthop. 260*, 263–279.

(25) De Lustro, F., Condell, R. A., Nguyen, M. A., and McPherson, J. M. (1986) A comparative study of the biologic and immunologic response to medical devices derived from dermal collagen. *J. Biomed. Mater. Res. 20*, 109–120.

(26) Nakamura, T., Shimizu, Y., Okumura, N., Matsui, T., Hyon, S. H., and Shimamoto, T. (1994) Tumorigenicity of poly-L-lactide (PLLA) plates compared with medical-grade polyethylene. *J. Biomed. Mater. Res. 28*, 17–25.

(27) Weiss, W. M., Riles, T. S., Gouge, T. H., and Mizrachi, H. H. (1991) Angiosarcoma at the site of a Dacron vascular prosthesis: a case report and literature review. *J. Vasc. Surg. 14*, 87–91.

(28) Yoshida, S. H., Chang, C. C., Teuber, S. S., and Gershwin, M. E. (1993) Silicon and silicone: theoretical and clinical implications of breast implants. *Regul. Toxicol. Pharmacol. 17*, 3–18.

(29) Busch, H. (1994) Silicone toxicology. *Semin. Arthritis Rheum. 24*, 11–17.

(30) Matlaga, B. F., Yasenchak, L. P., and Salhouse, T. N. (1976) Tissue response to implanted polymers: the significance of shape. *J. Biomed. Mater. Res. 10*, 391–397.

(31) King, D. J., and Noss, R. R. (1989) Toxicity of polyacrylamide and acrylamide monomer. *Rev. Environ. Health 8*, 3–16.

(32) Roske-Nielsen, E., Bojsen-Moller, M., Vetner, M., and Hansen, J. C. (1976) Polyvinylpyrrolidone-storage disease. *Acta Pathol. Microbiol. Scand., Sect. A. 84*, 397–401.

(33) Meijer, A. E. F. H., and Willighagen, R. G. J. (1963) The activity of glucose-6-phosphate, adenosine triphosphatase, succinic dehydrogenase and acid phosphates after dextran or polyvinylpyrrolidone uptake by liver in vivo, *Biochem. Pharmacol. 12*, 973–979.

(34) Otsuka, M., Matsuda, Y., Suwa, Y., Fox, J. L., and Higuchi, W. I. (1994) A novel skeletal drug-delivery system using self-setting calcium phosphate cement. 3. Physicochemical properties and drug-release rate of bovine insulin and bovine albumin. *J. Pharm. Sci. 83*, 255–258.

(35) Polk, A., Amsden, B., De Yao, K., Peng, T., and Goosen, M. F. (1994) Controlled release of albumin from chitosan-alginate microcapsules. *J. Pharm. Sci. 83,* 178–185.

(36) Liu, W. R., Langer, R., and Klibanov, A. M. (1991) Moisture-induced aggregation of lyophilized proteins in the solid state. *Biotech. Bioeng. 37,* 177–184.

(37) Horbett, T. A., and Brash, J. L. (1987) Proteins at interfaces: current issues and future prospects. *Proteins at Interfaces: Physiochemical and Biochemical Studies* (T. A. Horbett and J. L. Brash, Eds.) ACS Symposium Series 343, pp 1–33, American Chemical Society, Washington, DC.

(38) Verrecchia, T., Huve, P., Bazile, D., Veillard, M., Spenlenhauer, G., and Couvreur, P. (1993) Adsorption/desorption of human serum albumin at the surface of poly(lactic acid) nanoparticles prepared by a solvent evaporation process, *J. Biomed. Mater. Res. 27,* 1019–1028.

(39) Lu, W., and Park, T. G. (1995) Protein release from poly-(lactic-co-glycolic acid) microspheres: Protein stability problems. *PDA J. Pharm. Sci. Technol. 49,* 13–19.

(40) Costantino, H. R., Langer, R., and Klibanov, A. M. (1994) Moisture-induced aggregation of lyophilized insulin. *Pharm. Res. 11,* 21–29.

(41) Ogawa, Y., Yamamoto, M., Takada, S., Okada, J., and Shimamoto, T. (1988) Controlled-release of Leuprolide Acetate from polylactic acid or copoly(lactic/glycolic) acid microcapsules: influence of molecular weight and copolymer ratio of polymer. *Chem. Pharm. Bull. 36,* 1502–1507.

(42) Okada, H., Heya, T., Ogawa, Y., Toguchi, H., and Shimamoto, T. (1991) Sustained pharmacological activities in rats following single and repeated administration of once-a-month injectable microspheres of leuprolide acetate. *Pharm. Res. 8,* 787–791.

(43) Delgado, C., Francis, G. E., and Fisher, D. (1992) The uses and properties of PEG linked proteins. *Crit. Rev. Ther. Drug Carrier Syst. 9,* 249–304.

(44) Cohn, D., and Younes, H. (1988) Biodegradable PEO/PLA block copolymers. *J. Biomed. Mater. Res. 22,* 993–1009.

(45) Sawhney, A. S., Pathak, C. P., van Rensburg, J. J., Dunn, R. C., and Hubbell, J. A. (1994) Optimization of photopolymerized bioerodible hydrogel properties for adhesion prevention. *J. Biomed. Mater. Res. 28,* 831–838.

(46) Hora, M. S., Rana, R. K., Nunberg, J. H., Tice, T. H., Gilley, R. M., and Hudson, M. E. (1990) Controlled release of interleukin-2 from biodegradable microspheres. *Bio/Technology 8,* 755–758.

(47) Camble, R., Timms, D., and Wilkinson, A. J. (1994) Continuous release pharmaceutical compositions. U.S. Patent 5,320,840.

(48) Makino, K., Ohshima, H., and Kondo, T. (1987) Effects of plasma proteins on degradation properties of poly(L-lactide) microcapsules. *Pharm. Res. 4,* 62–65.

(49) Heller, J. (1980) Controlled release of biologically active compounds from bioerodible polymers. *Biomaterials 1,* 51–58.

(50) Langer, R. S., and Peppas, N. A. (1981) Present and future applications of biomaterials in controlled drug delivery systems. *Biomaterials 2,* 201–214.

(51) Celebi, N., Erden, N., Gonul, B., and Koz, M. (1994) Effects of epidermal growth factor dosage forms on dermal wound strength in mice. *J. Pharm. Pharmacol. 46,* 386–387.

(52) Park, T. G. (1994) Degradation of poly(D,L-lactic acid) microspheres: effect of molecular weight. *J. Controlled Release 30,* 161–173.

(53) Sanders, L. M., McRae, G. I., Vitale, K. M., and Kell, B. A. (1985) Controlled delivery of an LHRH analogue from biodegradable injectable microspheres. *J. Controlled Release 2,* 187–195.

(54) Bodmer, D., Kissel, T., and Traechslin, E. (1992) Factors influencing the release of peptides and proteins from biodegradable parenteral depot systems. *J. Controlled Release 21,* 129–138.

(55) Watts, P. J., Davies, M. C., and Melia, C. D. (1990) Microencapsulation using emulsification/solvent evaporation: An overview of techniques and applications. *CRC Crit. Rev. Ther. Drug Carrier Sys. 7,* 235–259.

(56) Marcotte, N., Polk, A., and Goosen, M. F. A. (1990) Kinetics of protein diffusion from poly(D,L-lactide) reservoir systems. *J. Pharm. Sci. 79,* 407–410.

(57) Camarata, P. J., Suryanarayanan, R., Turner, D. A., Parker, R. G., and Ebner, T. J. (1992) Sustained release of nerve growth factor from biodegradable polymer microspheres. *Neurosurgery 30,* 313–319.

(58) Yamaguchi, K., and Anderson, J. M. (1993) In vivo biocompatibility studies of Medisorb 65/35 D,L-lactide/glycolide copolymer microspheres. *J. Controlled Release 24,* 81–93.

(59) Visscher, G. E., Robinson, R. L., Maulding, H. V., Fong, J. W., Pearson, J. E., and Argentieri, G. J. (1985) Biodegradation of and tissue reaction to 50:50 poly (DL-lactide-co-glycolide) microcapsules. *J. Biomed. Mater. Res. 19,* 349–357.

(60) Visscher, G. E., Robinson, R. L., and Argentieri, G. J. (1987) Tissue response to biodegradable injectable microcapsules. *J. Biomater. Appl. 2,* 118–131.

(61) Gilding, D. K., and Reed, A. M. (1981) Biodegradable polymers for use in surgery—poly(glycolic)/poly(lactic acid) homo and copolymers: 1. *Polymer 20,* 1459–1464.

(62) Reed, A. M., and Gilding, D. K. (1981) Biodegradable polymers for use in surgery—poly(glycolic)/poly(lactic acid) homo and copolymers: 2. In vitro degradation. *Polymer 22,* 494–498.

(63) Migliaresi, C., Fambri, L., and Cohn, D. (1994) A study on the in vitro degradation of poly(lactic acid). *J. Biomater. Sci., Polym. Ed. 5,* 591–606.

(64) Chawla, A. S., and Chang, T. M. S. (1985) In-vivo degradation of poly(lactic acid) of different molecular weights. *Biomater. Med. Devices, Artif. Organs 13,* 153–162.

(65) Chang, T. M. S. (1976) Biodegradable semipermeable microcapsules containing enzymes, hormones and vaccines, and other biologicals. *J. Bioeng. 1,* 25.

(66) Kwong, A. K., Chou, S., Sun, A. M., Sefton, M. V., and Goosen, M. F. A. (1986) In vitro and in vivo release of insulin from poly(lactic acid) microbeads and pellets. *J. Controlled Release 4,* 47–62.

(67) Hutchinson, F. G., and Furr, B. J. A. (1985) Biodegradable polymers for the sustained release of peptides. *Biochem. Soc. Trans. 13,* 520–523.

(68) Ogawa, Y., Okada, H., Yamamoto, M., and Shimamoto, T. (1988) In vivo profiles of leuprolide acetate from microcapsules prepared with polylactic acids or copoly(lactic/glycolic) acids and in vivo degradation of these polymers. *Chem. Pharm. Bull. 36,* 2576–2581.

(69) Ogawa, Y., Yamamoto, M., Okada, H., Yashiki, T and Shimamoto, T. (1988) A new technique to efficiently entrap leuprolide acetate into microcapsules of polylactic acid or copoly(lactic/glycolic) acid. *Chem. Pharm. Bull. 36,* 1095–1103.

(70) Okada, H., Inoue, Y., Heya, T., Ueno, H., Ogawa, Y., and Toguchi, H. (1991) Pharmacokinetics of once-a-month injectable microspheres of leuprolide acetate. *Pharm. Res. 8,* 787–791.

(71) Okada, H., Doken, Y., Ogawa, Y., and Toguchi, H. (1994) Preparation of three-month depot injectable microspheres of leuprorelin acetate using biodegradable polymers. *Pharm. Res. 11,* 1143–1147.

(72) Ruiz, J. M., Tissier, B., and Benoit, J. P., (1989) Microencapsulation of peptide: a study of the phase separation of poly(D,L-lactic acid-co-glycolic acid) copolymers 50/50 by silicone oil. *Int. J. Pharm. 49,* 69–77.

(73) Sanders, L. M., Kent, J. S., McRae, G. I., Vickery, B. H., Tice, T. R., and Lewis, D. H. (1984) Controlled release of luteinizing hormone-releasing hormone analogue from poly-(D,L-lactide-co-glycolide) microspheres. *J. Pharm. Sci. 73,* 1294.

(74) Niwa, T., Takeuchi, H., Hino, T., Kunou, N., and Kawashima, Y. (1994) In vitro drug release behavior of D,L-lactide/glycolide copolymer (PLGA) nanospheres with nafarelin acetate prepared by a novel spontaneous emulsification solvent diffusion method. *J. Pharm. Sci. 83,* 727–732.

(75) Asano, M., Yoshida, M., Kaetsu, I., Imai, K., Mashimo, T., Yuasa, H., Yamanaka, H., Suzuki, K., and Yamazaki, I. (1985) Biodegradability of hot-pressed poly(lactic acid) formulation with controlled release of LHRH agonist and its pharmaco-

logical influence on rat prostate. *Makromol. Chem., Rapid Commun. 6,* 509–513.

(76) Cohen, S., Yoshioka, T., Lucarelli, M., Hwang, L. H., and Langer, R. (1991) Controlled delivery of systems for proteins based on poly(lactic/glycolic acid) microspheres. *Pharm. Res. 8,* 713–720.

(77) Sah, H., Toddywala, R., and Chien, Y. W. (1994) The influence of 0biodegradable microcapsule formulations on the controlled release of a protein. *J. Controlled Release 30,* 201–211.

(78) Yan, C., Resau, J. H., Hewetson, J., West, M., Rill, W. L. and Kende, M. (1994) Characterization and morphological analysis of protein-loaded poly(lactide-co-glycolide) microparticles prepared by water-in-oil-in-water emulsion technique. *J. Controlled Release 32,* 231–241.

(79) Alonso, M., Cohen, S., Park, T. G., Gupta, R. K., Siber, G. R., and Langer, R. (1993) Determinants of release of tetanus vaccine from polyester microspheres. *Pharm. Res. 10,* 945–953.

(80) Singh, M., Singh, A., and Talwar, G. P. (1991) Controlled delivery of diphtheria toxoid using biodegradable poly(D,L-lactide) microcapsules. *Pharm. Res. 8,* 958–961.

(81) Zhang, X., Wyss, U. P., Pichora, D., Amsden, B., and Goosen, M. F. A. (1993) Controlled release of albumin from biodegradable poly(DL-lactide) cylinders. *J. Controlled Release 25,* 61–69.

(82) Mehta, R., Jeyanthi, R., Calis, S., Thanoo, B. C., Burton, K. W., and DeLuca, P. P. (1994) Biodegradable microspheres as depot system for parenteral delivery of peptide drugs. *J. Controlled Release 29,* 375–384.

(83) Sopersaxo, A., Kou, J. H., Teitelbaum, P., and Maskiewicz, R. (1993) Preformed porous microspheres for controlled and pulsed release of macromolecules. *J. Controlled Release 23,* 157–164.

(84) Lambert, W., and Peck, K. D. (1995) Development of an in situ forming biodegradable poly-lactide-co-glycolide system for the controlled release of proteins. *J. Controlled Release 33,* 189–195.

(85) Park, T. G., Cohen, S., and Langer, R. (1992) Poly(L-lactic acid)/pluronic blends: Characterization of phase separation behavior, degradation, and morphology and use as protein-releasing matrices. *Macromolecules 25,* 116–122.

(86) Park, T. G., Cohen, S., and Langer, R. (1992) Controlled protein release from polyethyleneimine-coated poly(L-lactic acid)/pluronic blend matrices. *Pharm. Res. 9,* 37–39.

(87) Pitt, C. G., Cha, Y., Shah, S. S., and Zhu, K. J. (1992) Blends of PVA and PGLA: control of permeability and degradability of hydrogels by blending. *J. Controlled Release 19,* 189–200.

(88) Cohn, D., and Younes, H. (1988) Biodegradable PEO/PLA block copolymers. *J. Biomed. Mater. Res. 22,* 993–1009.

(89) Zhu, K. J., Bihai, S., and Shilin, Y., (1989) Super microcapsules (SMC). I. Preparation and characterization of star polyethylene oxide (PEO)–polylactide (PLA) copolymers. *J. Polym. Sci., Part A: Polym. Chem. 27,* 2151–2159.

(90) Youxin, L., and Kissel, T. (1993) Synthesis and properties of biodegradable ABA triblock copolymers consisting of poly-(L-lactic acid) or poly(L-lactic-co-glycolic acid) A-blocks attached to central poly(oxyethylene). *J. Controlled Release 27,* 247–257.

(91) Youxin, L., Volland, C., and Kissel, T. (1994) In vitro degradation and bovine serum albumin release of the ABA triblock copolymers consisting of poly (L(+) lactic acid), or poly (L+) lactic acid-co-glycolic acid) A-blocks attached to central polyoxyethelene B-blocks. *J. Controlled Release 32,* 121–128.

(92) Miyamoto, S., Takaoka, K., Okada, T., Yoshikawa, H., Hashimoto, J., Suzuki, S., and Ono, K. (1993) Polylactic acid–polyethylene glycol block copolymer. A new biodegradable synthetic carrier for bone morphogenetic protein. *Clin. Orthop. 294,* 333–343.

(93) Miyamoto, S., and Takaoka, K. (1993) Bone induction and bone repair by composites of bone morphogenetic protein and biodegradable synthetic polymers. *Ann. Chir. Gynaecol., Suppl. 207,* 69–75.

(94) Gref, R., Minamitake, Y., Peracchia, M., Trubetskoy, V., Torchilin, V., and Langer, R. (1994) Biodegradable long-circulating polymeric nanospheres. *Science 263,* 1600–1603.

(95) Stolnik, S., Dunn, S. E., Garnett, M. C., Davies, M. C., Coombes, A. G., Taylor, D. C., Irving, M. P., Purkiss, S. C., Tadros, T. F., Davis, S. S., and Illum, L. (1994) Surface modification of poly(lactide-co-glycolide) nanospheres by biodegradable poly(lactide)–poly(ethylene glycol) copolymers. *Pharm. Res. 11,* 1800–1808.

(96) Leonard, F., Kulkarni, R. K., Brandes, G., Nelson, J., and Cameron, J. J. (1966) Synthesis and degradation of poly(alkyl) α-cyanoacrylates. *J. Appl. Polym. Sci. 10,* 259.

(97) Collins, J. A., Pani, J. C., Lehman, R. A., and Leonard, F. (1966) Biological substrates and cure rates of cyanoacrylate tissue adhesives. *Arch. Surg. 93,* 428–432.

(98) Damge, C., Michel, C., Aprahamian, M., and Couvreur, P. (1988) New approach for oral administration of insulin with polyalkylcyanoacrylate nanocapsules as drug carrier. *Diabetes 7,* 246–251.

(99) Grainger, J. L., Puygrenier, M., Gautier, J. C., and Couvreur, P. (1991) Nanoparticles as carriers for growth hormone releasing factor. *J. Controlled Release 15,* 3–13.

(100) Gautier, J. C., Grainger, J. L., Barbier, A., Dupont, P., Dussossoy, D., Pastor, G., and Couvreur, P. (1992) Biodegradable nanoparticles for subcutaneous administration of growth hormone releasing factor (hGRF). *J. Controlled Release 20,* 67–78.

(101) Tasset, C., Barette, N., Thysman, S., Ketelslegers, J. M., Lemoine, D., and Preat, V. (1995) Polyisobutylcyanoacrylate nanoparticles as sustained release system for calcitonin. *J. Controlled Release 33,* 23–30.

(102) Linhardt, R., Rosen, H., and Langer, R. (1983) Bioerodable polyanhydrides for controlled drug delivery. *Polym. Prepr. 24,* 47–48.

(103) Rosen, H., Chang, J., Wnek, G., Linhardt, R., and Langer, R. (1983) Bioerodible polyanhydrides for controlled drug delivery. *Biomaterials 4,* 131–133.

(104) Ron, E., Turek, T., Mathiowitz, E., Chasin, M., Hageman, M., and Langer, R. (1993) Controlled release of polypeptides from polyanhydrides. *Proc. Natl. Acad. Sci. U.S.A. 90,* 4176–4180.

(105) Tamada, J. A., and Langer, R. (1993) Erosion kinetics of hydrolytically degradable polymers. *Proc. Natl. Acad. Sci. U.S.A. 90,* 552–556.

(106) Domb, A. J., and Langer, R. (1987) Polyanhydrides. I. Preparation of high molecular weight polyanhydrides. *J. Polym. Sci., Part A: Polym. Chem. 25,* 3373–3386.

(107) Leong, K., Brott, B., and Langer, R. (1985) Bioerodible polyanhydrides as drug carrier matrices. I. Characterization, degradation and release characteristics. *J. Biomed. Mater. Res. 19,* 941–955.

(108) Leong, K., D'Amore, P., Marletta, M., and Langer, R. (1986) Bioerodible polyanhydrides as drug carrier matrices. I. Biocompatability and chemical reactivity. *J. Biomed. Mater. Res. 20,* 51–64.

(109) Mathiowitz, E., and Langer, R. (1987) Polyanhydride microspheres as drug carriers. I. Hot-melt microencapsulation. *J. Controlled Release 5,* 13–22.

(110) Mathiowitz, E., Saltzman, W. M., Domb, A., Dor, P., and Langer, R. (1988) Polyanhydride microspheres as drug carriers. II. Microencapsulation by solvent removal. *J. Appl. Polym. Sci. 35,* 755–774.

(111) Leong, K., Kost, J., Mathiowitz, E., and Langer, R. (1986) Polyanhydrides for controlled release of bioactive agents. *Biomaterials 7,* 364–371.

(112) Tabata, Y., Gutta, S., and Langer, R. (1993) Controlled delivery systems for proteins using polyanhydride microspheres. *Pharm. Res. 10,* 487–496.

(113) Heller, J. (1985) Controlled drug release from poly(ortho esters)—a surfaced eroding polymer. *J. Controlled Release 2,* 167–177.

(114) Heller, J., Penhale, D. W. H., Helwing, R. F., and Fritzinger, B. K. (1981) Release of norethindrone from poly-(ortho esters). *Polym. Eng. Sci. 21,* 727–731.

(115) Heller, J. (1989) Chemically self-regulated drug delivery systems. *J. Controlled Release 8,* 111–125.

(116) Heller, J., Ng, S. Y., Penhale, D. W., Fritzinger, B. K., Sanders, L. M., Bruns, R. A., Gaynon, M. G., and Bhosale, S. S. (1987) Use of poly(ortho esters) for the controlled release of 5-fluorouracil and an LHRH analog. *J. Controlled Release 6,* 217–224.

(117) Heller, J., Penhale, D. W., and Fritzinger, B. K. (1985) A bioerodible self-regulated insulin delivery device. *Proc. Int. Symp. Controlled Release Bioact. Mater. 13,* 37–38.

(118) Heller, J., Chang, A. C., Rodd, G., and Grodsky, G. M. (1989) Release of insulin from a pH-sensitive poly(orthoester). *Proc. Int. Symp. Controlled Release Bioact. Mater. 15,* 155–156.

(119) Heller, J., Roskos, K. V., Ng, S. Y., Wuthrich, P., Duncan, R., and Seymour, L. W. (1992) The use of poly(orthoesters) in the treatment of cancer and in the pulsed release of proteins. *Proc. Int. Symp. Controlled Release Bioact. Mater. 19,* 128–129.

(120) Park, K., Shalaby, W. S., and Park, H. (1993) *Biodegradable Hydrogels for Drug Delivery,* Technomic Publishing Co., Lancaster.

(121) Domb, A., Davidson, G. W., and Sanders, L. M. (1990) Diffusion of peptides t0hrough hydrogel membranes. *J. Controlled Release 14,* 133–144.

(122) Heller, J. (1987) Bioerodible Hydrogels. *Hydrogels in Medicine and Pharmacy, Volume III: Properties and Applications* (N. A. Peppas, Ed.) pp 137–149, CRC Press, Boca Raton.

(123) Schmolka, I. R. (1972) Artificial skin. I. Preparation and properties of pluronic F-127 gels for treatment of burns. *J. Biomed. Mater. Res. 6,* 571–582.

(124) Morikawa, K., Okada, O., Hosokawa, M., and Kobayashi, H. (1987) Enhancement of therapeutic effects of recombinant interleukin-2 on a transplantable rat fibrosarcoma by the use of a sustained release vehicle, pluronic gel. *Cancer 47,* 37–41.

(125) Johnston, T. P., Punjabi, M. A., and Froelich, C. J. (1992) Sustained delivery of interleukine-2 from a polyoxamer 407 gel matrix following intraperitoneal injection in mice. *Pharm. Res. 9,* 425–434.

(126) Fults, K. A., and Johnston, T. P. (1990) Sustained-release of urease from a polyoxamer gel matrix. *J. Parenter. Sci. Technol. 44,* 58–65.

(127) Juhasz, J., Lenaerts, V., Raymond, P., and Ong, H. (1989) Diffusion of rat atrial natriuretic factor in thermoreversible polyoxamer gels. *Biomaterials 10,* 265–268.

(128) Puolakkainen, P. A., Twardzick, D. R., Ranchalis, J. E., Pankey, S. C., Reed, M. J., and Gombotz, W. R. *Ann. Surg.* (in press).

(129) Korsmeyer, R. W., Gurny, R., Doelker, E., Biru, P., and Peppas, N. A. (1983) Mechanisms of solute release from porous hydrophilic polymers. *Int. J. Pharm. 15,* 25–35.

(130) Peppas, N. A., and Scott, J. E., (1992) Controlled release from poly(vinyl alcohol) gels prepared by freezing-thawing processes. *J. Controlled Release 18,* 95–100.

(131) Ficek, B. J., and Peppas, N. A. (1993) Novel preparation of poly(vinyl alcohol) microparticles without crosslinking agent for controlled drug delivery of proteins. *J. Controlled Release 27,* 259–264.

(132) Torchillin, V. P., Tischenko, E. G., Smirnov, V. V., and Chazoc, E. I. (1977) Immobilization of enzymes on slowly soluble carriers. *J. Biomed. Mater. Res. 11,* 223–235.

(133) Heller, J., Helwing, R. F., Baker, R. W., and Tuttle, M. E. (1983) Controlled release of water-soluble macromolecules from bioerodible hydrogels. *Biomaterials 4,* 22–23.

(134) Chiellini, E., Solaro, R., Leonardi, G., Giannasi, D., Lisciani, R., and Mazzanti, G. (1992) New polymeric hydrogel formulations for the controlled release of α-interferon. *J. Controlled Release 22,* 273–282.

(135) Beck, S. L., Chen, T. L., Mikalauski, P., and Amman, A. J. (1990) Recombinant human transforming growth factor-beta 1 (rhTGF-β1) enhances healing and strength of granulation skin wounds. *Growth Factors 3,* 267–275.

(136) Beck, S. L., Deguzman, L., Lee, W. P., Xu, Y., McFatridge, L. A., and Amento, E. P. (1991) TGF-β1 accelerates wound healing: reversal of steroid-impaired healing ion tars and rabbits. *Growth Factors 5,* 295–304.

(137) Beck, L. S., Deguzman, L., Lee, W. P., Xu, Y., McFatridge, C. A., Gillet, N. A., and Amento, E. P. (1991) TGF-β1 induces bone closure in skull defects. *J. Bone Miner. Res. 6,* 1257–1265.

(138) Matuszewska, B., Keogan, M., Fisher, D. M., Soper, K. A., Hoe, C., Huber, A. C., and Bondi, J. V. (1994) Acidic fibroblast growth factor: Evaluation of topical formulations in a diabetic mouse wound healing model. *Pharm. Res. 11,* 65–71.

(139) Cortivo, R., Brun, P., Rastrelli, A., and Abatangelo, G. (1991) In vitro studies on biocompatibility of hyaluronic acid esters. *Biomaterials 2,* 727–730.

(140) Benedetti, L. M., Topp, E. M., and Stella, V. J. (1990) Microspheres of hyaluronic acid esters—fabrication methods and in vitro hydrocortisone release. *J. Controlled Release 13,* 33–41.

(141) Hunt, J. A., Joshi, H. N., Stella, V. J., and Topp, E. M. (1990) Diffusion and drug release in polymer films prepared from ester derivatives of hyaluronic acid. *J. Controlled Release 12,* 159–169.

(142) Illum, L., Farraj, N. F., Fisher, A. N., Gill, I., Miglietta, M., and Bendetti, L. M. (1994) Hyaluronic acid microspheres as a nasal delivery system for insulin. *J. Controlled Release 29,* 133–141.

(143) Ghezzo, E., Benedetti, L. M., Rochira, M., Biviano, F., and Callegaro, L. (1992) Hyaluronic acid derivative microspheres as NGF delivery devices: preparation methods and in vitro release characterization. *Int. J. Pharm. 87,* 21–29.

(144) Papini, D., Stella, V. J., and Topp, E. M. (1993) Diffusion of macromolecules in membranes of hyaluronic acid esters. *J. Controlled Release 27,* 47–57.

(145) Mumper, R. J., Hoffman, A. S., Puolakkainen, P. A., Bouchard, L. S., and Gombotz, W. R. (1994) Calcium-alginate beads for the oral delivery of transforming growth factor-β1 (TGF-β1): stabilization of TGF-β1 by the addition of poly-acrylic acid within acid-treated beads. *J. Controlled Release 30,* 241–245.

(146) Edelman, E. R., Mathiowitz, E., Langer, R., and Klagsbrun. M. (1991) Controlled and modulated release of basic fibroblast growth factor. *Biomaterials 12,* 619–625.

(147) Wee, S., and Gombotz, W. R. (1994) Controlled release of recombinant human tumor necrosis factor receptor from alginate beads. *Proc. Int. Symp. Controlled Release Bioact. Mater. 1,* 730–731.

(148) Downs, E. C., Robertson, N. E., Riss, T. L., and Plunkett, M. L. (1992) Calcium alginate beads as a slow-release system for delivering angiogenic molecules in vivo and in vitro. *J. Cell. Physiol. 152,* 422–429.

(149) Maysinger, D., Jalsenjak, I., and Cuello, A. C. (1992) Microencapsulated nerve growth factor: effects on the forebrain neurons following devascularizing cortical lesions. *Neurosci. Lett. 140,* 71–74.

(150) Edelman, E. R., Nugent, M. A., and Karnovsky, M. J. (1993) Perivascular and intravenous administration of basic fibroblast growth factor: vascular and solid organ deposition. *Proc. Natl. Acad. Sci. U.S.A. 90,* 1513–1517.

(151) Fujiwara, T., Sakagami, K., Matsuoka, J., Shiozaki, S., Fujioka, K., Takada, Y., Uchida, S., Onoda, T., and Orita, K. (1991) Augmentation of antitumor effect on syngeneic murine solid tumors by an interleukine 2 slow delivery system, the IL-2 mini-pellet. *Biotherapy 3,* 203–209.

(152) Fujiwara, T., Sakagami, K., Matsuoka, J., Shiozaki, Y., Uchida, S., Fujioka, K., Takada, S., Onoda, T., and Orita, K. (1990) Application of an interleukine 2 slow delivery system to the immunotherapy of established murine colon 26 adenocarcinoma liver metastases. *Cancer Res. 50,* 7003–7007.

(153) Yamamoto, S., Yoshimine, T., Fujita, T., Kuroda, R., Irie, T., Fujioka, K., and Hayakawa, T. (1992) Protective effect of NGF atelocollagen mini-pellet on the hipocampal delayed neuronal death in gerbils. *Neurosci. Lett. 141,* 161–165.

(154) Gilbert, D. L., and Kim, S. W. (1990) Macromolecular release from collagen monolithic devices. *J. Biomed. Mater. Res. 24,* 1221–1239.

(155) Brown, G. L., Curtsinger, L. J., White, M., Mitchell, R. O., Pietsch, J., 0Nordquist, R., vonFraunhofeer, A., and Schultz, G. S. (1988) Acceleration of tensile strength incisions treated with EGF and TGF-β. *Ann. Surg. 208,* 788–794.

(156) Mustoe, T. A., Pierce, G. F., Thomason, A., Gramates, P., Sporn, M. B., and Deuel, T. F. (1987) Accelerated healing of incisional wounds in rats induced by transforming growth factor-β. Science 237, 1333–1336.

(157) Tabata, Y., and Ikada, Y. (1989) Synthesis of gelatin microspheres containing interferon. Pharm. Res. 6, 422–427.

(158) Shinde, B. G., and Erhan, S., (1992) Flexibilized gelatin film-based artificial skin model: II. Release kinetics of incorporated bioactive molecules. Bio-Med. Mater. Eng. 2, 127–131.

(159) Golumbek, P. T., Azhari, R., Jaffee, E. M., Levitsky, H. I., Lazenby, A., Leong, K., and Pardoll, D. (1993) Controlled release, biodegradable cytokine depots: a new approach in cancer vaccine design. Cancer Res. 53, 5841–5844.

(160) Shao, W., and Leong, K. W. (1995) Microcapsules obtained from complex coacervation of collagen and chondroitin sulfate. J. Biomed. Mater. Res. (in press).

(161) Goosen, M. F. A., O'Shea, G. M., Gherapetian, H. M., Chow, S., and Sun, A. M. (1985) Optimization of microencapsulation parameters: semipermeable microcapsules as an artificial pancreas. Biotechnol. Bioeng. 27, 146–150.

(162) Bhargave, K., and Ando, H. Y. (1992) Immobilization of active urokinase on albumin microspheres: Use of a chemical dehydrant and process monitoring. Pharm. Res. 9, 776–781.

(163) Degling, L., Stjarnkvist, P., and Sjoholm, I. (1993) Interferon-alpha in starch microparticles: Nitric oxide-generating activity in vitro and antileishmanial effect in mice. Pharm. Res. 6, 783–790.

(164) Artursson, P., Edman, P., Laakso, T., and Sjoholm, I. (1984) Characterization of polyacryl starch microparticles as carriers for protein drugs. J. Pharm. Sci. 73, 1507–1513.

(165) Edman, P., Ekman, B., and Sjoholm, I. (1980) Immobilization of proteins in microspheres of biodegradable polyacryldextran, J. Pharm. Sci. 69, 838–842.

(166) Gombotz, W. R., Pankey, S. C., Bouchard, L. S., Ranchalis, J., and Puolakkainen, P. (1993) Controlled release of TGF-β1 from a biodegradable matrix for bone regeneration. J. Biomater. Sci., Polym. Ed. 5, 46–63.

(167) Duncan, R., and Kopecek, J. (1990) Release of macromolecules and daunomycin from hydrophilic gels containing enzymatically degradable bonds. J. Biomater. Sci., Polym. Ed. 1, 261–278.

(168) Saffran, M., Kumar, G. S., Savariar, C., Burnham, J. C., Williams, F., and Neckers, D. C. (1986) A new approach to the oral administration of insulin and other peptide drugs. Science 233, 1081–1084.

(169) Saffran, M., Bedra, C., Kumar, G. S., and Neckers, D. C. (1990) Vasopressin: a model for the study of effects of additives on the oral and rectal administration of peptide drugs. J. Pharm. Sci. 77, 33–38.

(170) Saffran, M., Field, J. B., Pena, J., Jones, R. H., and Okuda, Y. (1991) Oral insulin in diabetic dogs. J. Endocrinol. 131, 267–278.

(171) Ringsdorf, H. (1975) Structure and properties of pharmacologically active polymers. J. Polym. Sci. 51, 135–153.

(172) Rihova, B., and Kopecek, J. (1985) Biological properties of targetable poly[N-(2-hydroxypropyl)-methacrylamide]–antibody conjugates. J. Controlled Release 2, 289–310.

(173) Seymour, L. W., Flanagan, P. A., Al-Shamkhani, A., Subr, V., Ulbrich, K., Cassidy, J., and Duncan, R. (1991) Synthetic polymers conjugated to monoclonal antibodies: Vehicles for tumour-targeted drug delivery. Sel. Cancer Ther. 7, 59–73.

(174) Wedge, S. R., Duncan, R., and Kopeckova, P. (1991) Comparison of the liver subcellular distribution of free daunomycin and that bound to galactosamine targeted N-(2-hydroxypropyl)methacrylamide copolymers, following intravenous administration in the rat. Br. J. Cancer 63, 546–549.

(175) Flanagan, P. A., Kopeckova, P., Kopecek, J., and Duncan, R. (1989) Evaluation of protein–N-(2-hydroxypropyl)methacrylamide copolymer conjugates as targetable drug carriers. 1. Binding, pinocytic uptake and intracellular distribution of transferrin and anti-transferrin receptor antibody conjugates. Biochim. Biophys. Acta 993, 83–91.

(176) Clegg, J. A., Hudecz, F., Mezo, G., Pimm, M. V., Szerkerke, M., and Baldwin, R. W. (1990) Carrier design: biodistribution of branched polypeptides with a poly(L-lysine) backbone. Bioconjugate Chem. 1, 425–430.

(177) Seymour, L. W., Duncan, R., Strohalm, J., and Kopecek, J. (1987) Effect of molecular weight (Mw) of N-(2-hydroxypropyl)methacrylamide copolymers on body distribution and rate of excretion after subcutaneous, intraperitoneal and intravenous administration to rats. J. Biomed. Mater. Res. 21, 1341–1358.

(178) Knauf, M. J., Bell, D. P., Hirtzer, P., Luo, Z. P., Young, J. D., and Katre, N. V. (1988) Relationship of effective molecular size to systemic clearance in rats of recombinant interleukin-2 chemically modified with water-soluble polymers. J. Biol. Chem. 263, 15064–15070.

(179) Katre, N. V. (1990) Immunogenicity of recombinant IL-2 modified by covalent attachment of polyethylene glycol. J. Immunol. 144, 209–213.

(180) Dintzis, R. Z., Okajima, M., Middleton, M. H., Greene, G., and Dintzis, H. M. (1989) The immunogenicity of soluble haptenated polymers is determined by molecular mass and hapten valence. J. Immunol. 143, 1239–1244.

(181) Katre, N. V., Knauf, M. J., and Laird, W. J. (1987) Chemical modification of recombinant interleukin 2 by polyethylene glycol increases its potency in the murine Meth A sarcoma model. Proc. Natl. Acad. Sci. U.S.A. 84, 1487–1491.

(182) Cunningham-Rundles, C., Zhuo, Z., Griffith, B., and Keenan, J. (1992) Biological activities of polyethylene-glycol immunoglobulin conjugates. Resistance to enzymatic degradation. J. Immunol. Methods 152, 177–190.

(183) Delgado, C., Francis, G. E., and Fisher, D. (1992) The uses and properties of PEG-linked proteins. Crit. Rev. Ther. Drug Carrier Sys. 9, 249–304.

(184) Duncan, R. (1985) Biological effects of soluble synthetic polymers as drug carriers. CRC Crit. Rev. Ther. Drug Carrier Sys. 1, 281–310.

(185) Maeda, H., Seymour, L. W., and Miyamoto, Y. (1992) Conjugates of anticancer agents and polymers: advantages of macromolecular therapeutics in vivo. Bioconjugate Chem. 3, 351–362.

(186) Burnham, N. L. (1994) Polymers for delivering peptides and proteins. Am. J. Hosp. Pharm. 51, 210–218.

(187) O'Shannessy, D. J., and Kent, S. B. H. (1987) Labeling of the oligosaccharide moieties of immunoglobulins. J. Immunol. Methods 99, 89–95.

(188) Goodson, R. J., and Katre, N. V. (1990) Site-directed pegylation of recombinant interleukin-2 at its glycosylation site. Biotechnology 8, 343–346.

(189) Benhar, I., Wang, Q. C., FitzGerald, D., and Pastan, I. (1994) Pseudomonas Exotoxin A Mutants. Replacement of surface-exposed residues in domain III with cysteine residues that can be modified with polyethylene glycol in a site-specific manner. J. Biol. Chem. 269, 13398–13404.

(190) Vilaseca, L. A., Rose, K., Werlen, R., Meunier, A., Offord, R. E., Nichols, C. L., and Scott, W. L. (1993) Protein conjugates of defined structure: synthesis and use of a new carrier molecule. Bioconjugate Chem. 4, 515–520.

(191) Hudecz, F., Clegg, J. A., Kajtar, J., Embleton, M. J., Szederke, M., and Baldwin, R. W. (1992) Synthesis, conformation, biodistribution, and in vitro cytotoxicity of daunomycin-branched polypeptide conjugates. Bioconjugate Chem. 3, 49–57.

(192) Tsukada, Y., Kato, Y., Umemoto, N., Takeda, Y., Hara, T., and Hirai, H. (1984). An anti-α-fetoprotein antibody–daunorubicin conjugate with a novel poly-l-glutamic acid derivative as intermediate drug carrier. J. Natl. Cancer Inst. 73, 721–729.

(193) Pratesi, G., Savi, G., Pezzoni, G., Bellini, O., Penco, S., Tinelli, S., and Zumino, F. (1985) Poly-L-aspartic acid as a carrier for doxorubicin: a comparative in vivo study of free and polymer-bound drug. Br. J. Cancer 52, 841–848.

(194) Gegg, C. V., and Etzler, M. E. (1993) Directional coupling of synthetic peptides to poly-l-lysine and applications to the ELISA. Anal. Biochem. 210, 309–313.

(195) Drijfhout, J. W., Bloemhoff, W., Poolman, J. T., and Hoogerhout, P. (1990) Solid-phase synthesis and applications of N-(S-acetylmercaptoacetyl) peptides. Anal. Biochem. 187, 349–354.

(196) Hayashi, T., and Iwatsuki, M. (1990) Biodegradation of copoly(L-aspartic acid/L-glutamic acid) in vitro. Biopolymers 29, 549–557.

(197) Pramanick, D., and Ray, T. T. (1987) Synthesis and biodegradation of polymers derived from aspartic acid. *Biomaterials 8*, 407–410.

(198) Nathan, A., Zalipsky, S., Ertel, S. I., Agathos, S. N., Yarmush, M. L., and Kohn, J. (1993) Copolymers of lysine and polyethylene glycol: a new family of functionalized drug carriers. *Bioconjugate Chem. 4*, 54–62.

(199) Palfreyman, J. W., Aitcheson, T. C., and Taylor, P. J. (1984) Guidelines for the production of polypeptide specific anti-sera using small synthetic oligopeptides as immunogens. *J. Immunol. Methods 75*, 383–393.

(200) Rajnavolgyi, E., Hudcez, F., Mezo, G., Szekerke, M., and Gergely, J. (1986) Isotype distribution and fine specificity of the antibody response on inbred mouse strains to four compounds belonging to a new group of synthetic branched polypeptides. *Mol. Immunol. 23*, 27–37.

(201) Kolodny, N., and Robey, F. A. (1990) Conjugation of synthetic peptides to proteins: quantitation from S-carboxymethylcysteine released upon acid hydrolysis. *Anal. Biochem. 187*, 136–140.

(202) Zegers, N., Gerritse, K., Deen, C., Boersma, W., and Claassen, E. (1990) An improved conjugation method for controlled covalent coupling of synthetic peptides to proteins using glutaraldehyde in a dialysis method. *J. Immunol. Methods 130*, 195–200.

(203) Isoai, A., Goto-Tsukamoto, H., Murakami, K., Akedo, H., and Kumagai, H. (1993) A potent anti-metastatic activity of tumor invasion-inhibiting factor-2 and albumin conjugate. *Biochem. Biophys. Res. Commun. 192*, 7–14.

(204) Poznansky, M. J., Halford, J., and Taylor, D. (1988) Growth hormone–albumin conjugates. Reduced renal toxicity and altered plasma clearance. *FEBS Lett. 239*, 18–22.

(205) Mao, G. D., and Poznansky, M. J. (1989) Superoxide dismutase: improving its pharmacological properties by conjugation with human serum albumin. *Biomater., Artif. Cells, Artif. Organs 17*, 229–244.

(206) Yeh, P., Landais, D., Lemaitre, M., Maury, I., Crenne, J. Y., Becquart, J., Murry-Brelier, A., Boucher, F., Montay, G., Fleer, R., Hirel, P. H., Mayaux, J. F., and Klatzmann, D. (1992) Design of yeast-secreted albumin derivatives for human therapy: biological and antiviral properties of a serum albumin–CD4 genetic conjugate. *Proc. Natl. Acad. Sci. U.S.A. 89*, 1904–1908.

(207) Tabata, Y., Uno, K., Yamaoka, T., Ikada, Y., and Muramatsu, S. (1991) Effects of recombinant α-interferon–gelatin conjugate on in vivo murine tumor cell growth. *Cancer Res. 51*, 5532–5538.

(208) Kojima, Y., Haruta, A., Imai, T., Otagiri, M., and Maeda, H. (1993) 0Conjugation of Cu, Zn-superoxide dismutase with succinylated gelatin: pharmacological activity and cell-lubricating function. *Bioconjugate Chem. 4*, 490–498.

(209) Tabata, Y., Uno, K., Ikada, Y., Kishida, T., and Muramatsu, S. (1993) Potentiation of in vivo anti tumor effects of recombinant interleukin-1 alpha by gelatin conjugation. *Jpn. J. Cancer Res. 84*, 681–688.

(210) Tabata, Y., Uno, K., Ikada, Y., and Muramatsu, S. (1993) Suppressive effect of recombinant TNF–gelatin conjugate on murine tumour growth in vivo. *J. Pharm. Pharmacol. 45*, 303–308.

(211) Ulbrich, K., Zacharieva, E. I., Obereigner, B., and Kopecek, J. (1980) Polymers containing enzymatically degradable bonds. V. Hydrophilic polymers degradable by papain. *Biomaterials 1*, 199–204.

(212) Kopecek, J. (1984) Controlled biodegradability of polymers—a key to drug delivery systems. *Biomaterials 5*, 19–25.

(213) Goodchild, J. (1990) Conjugates of oligonucleotides and modified oligonucleotides: a review of their synthesis and properties. *Bioconjugate Chem. 1*, 165–187.

(214) Goodchild, J., Kim, B., and Zamecnik, P. C. (1991) The clearance and degradation of oligodeoxynucleotides following intravenous injection into rabbits. *Antisense Res. Dev. 1*, 153–160.

(215) Duncan, R., and Kopecek, J. (1984) Soluble synthetic polymers as potential drug carriers. *Adv. Polym. Sci. 57*, 53–101.

(216) Brinkley, M. (1992) A brief survey of methods for preparing protein conjugates with dyes, haptens, and cross-linking reagents. *Bioconjugate Chem. 3*, 2–13.

(217) Means, G. E., and Feeney, R. E. (1990) Chemical modifications of proteins: history and applications. *Bioconjugate Chem. 1*, 2–12.

(218) Lomants, A. J., and Fairbanks, G. (1976) Chemical probes of extended biological structures: synthesis and properties of the cleavable protein cross-linking reagent [35S] dithiobis-(succinimidyl propionate). *J. Mol. Biol. 104*, 243–248.

(219) Dreborg, S., and Akerblom, E. B. (1990) Immunotherapy with monomethoxypolyethylene glycol modified allergens. *Crit. Rev. Ther. Drug Carrier Syst. 6*, 315–365.

(220) Zalipsky, S., Seltzer, R., and Menon-Rudolph, S. (1992) Evaluation of a new reagent for covalent attachment of polyethylene glycol to proteins. *Biotechnol. Appl. Biochem. 15*, 100–114.

(221) Woghiren, C., Sharma, B., and Stein, S. (1993) Protected thiol–polyethylene glycol: a new activated polymer for reversible protein modification. *Bioconjugate Chem. 4*, 314–318.

(222) Kopecek, J., Refjanova, P., and Chytry, V. (1981) Polymers containing enzymatically degradable bonds. I. Chymotrypsin catalyzed hydrolysis of p-nitroanilides of phenylalanine and tyrosine attached to side-chains of copolymers of *N*-(2-hydroxypropyl)methacrylamide. *Makromol. Chem. 182*, 799–807.

(223) Kopecek, J. (1984) Controlled biodegradability of polymers—a key to drug delivery systems. *Biomaterials 5*, 19–25.

(224) Krinick, N. L., Sun, Y., Joyner, D., Spikes, J. D., Straight, R. C., and Kopecek, J. (1994) A polymeric drug delivery system for the simultaneous delivery of drugs activatable by enzymes and/or light. *J. Biomater. Sci., Polym. Ed. 5*, 303–324.

(225) Duncan, R., Lloyd, J. B., and Kopecek, J. (1980) Degradation of side chains of N-(2-hydroxypropyl)methacrylamide copolymers by lysosomal enzymes. *Biochem. Biophys. Res. Commun. 94*, 284–290.

(226) Franssen, E. J. F., Koiter, J., Kuipers, C. A. M., Bruins, D. P., Moolenaar, F., deZeeuw, D., Kruizinga, W. H., Kellogg, R. M., and Meijer, D. K. F. (1992) Low molecular weight proteins as carriers for renal drug targeting. Preparation of drug–protein conjugates and drug-spacer derivatives and their catabolism in renal cortex homogenates and lysosomal lysates. *J. Med. Chem. 35*, 1246–1259.

(227) Senderoff, R. I., Sheu, M. T., and Sokoloski, T. D. (1991) Fibrin based drug delivery systems. *J. Parenter. Sci. Technol. 45*, 2–6.

(228) Miyazaki, S., and Tanekazu, N. (1980) Use of fibrin film as a carrier for drug delivery: In vitro drug permeabilities of fibrin film. *Chem. Pharm. Bull. 28*, 2261–2264.

(229) Yoshida, M., Asano, M., Kumakura, M., Katakai, R., Mashimo, T., Yuasa, Y., Imai, K., and Yamanaka, H. (1990) Sequential polydepsipeptides as biodegradable carriers for drug delivery systems. *J. Biomed. Mater. Res. 24*, 1173–1184.

(230) Dave, P., Gross, R. A., Brucato, C., Wong, S., and McCarthy, S. P. (1991) Biodegradation of blends containing poly(3-hydroxybutyrate-co-valerate). *Biotechnology and Polymers* (C. G. Gebelein, Ed.) pp 53–61, Plenum Press, New York.

(231) Pitt, C. G., Marks, T. A., and Schindler, A. (1980) Biodegradable drug delivery systems based on aliphatic polyesters: Applications to contraceptives and narcotic antagonists. *Controlled Release of Bioactive Materials* (R. Baker, Ed) pp 19–44, Academic Press, London.

(232) Crommen, J. H. L., Schacht, E. H., and Mense, E. H. G. (1992) Biodegradable polymers. II. Degradation characteristics of hydrolysis-sensitive poly[(organo)phosphazenes]. *Biomaterials 13*, 601–611.

(233) Crommen, J., Vandorpe, J., and Schacht, E. (1993) Degradable polyphosphazenes for biomedical applications. *J. Controlled Release 24*, 167–180.

(234) Ray, J. A., Doddi, N., Regula, D., Williams, J. A., and Melveger, A. (1981) Polydioxanone (PDS), a novel monofilament synthetic absorbable suture. *Surgery 153*, 497–507.

ARTICLES

Synthesis and Characterization of (d)NTP[1] Derivatives Substituted with Residues of Different Photoreagents

Wjatschesslaw A. Wlassoff,*,† Michael I. Dobrikov,§ Igor V. Safronov,§ Roman Y. Dudko,§
Victor S. Bogachev,§ Vera V. Kandaurova,‡ Gennadiy V. Shishkin,§ Grigory M. Dymshits,† and
Olga I. Lavrik§

Institute of Cytology and Genetics, Siberian Division, Russian Academy of Sciences,
Lavrentieva 10, 630090, Novosibirsk, Russia, Novosibirsk Institute of Organic Chemistry,
Siberian Division, Russian Academy of Sciences, Lavrentieva 9, 630090, Novosibirsk, Russia, and
Novosibirsk Institute of Bioorganic Chemistry, Siberian Division, Russian Academy of Sciences,
Lavrentieva 8, 630090, Novosibirsk, Russia. Received September 13, 1994®

Chemical cross-linking agents having a photoactivable azido group are promising for the study of the spatial organization of biopolymers. We describe here a variety of (d)NTPs derivatives (**6a, 6b, 7, 11, 12, 14,** and **16**) bearing the residues of three different photoreagents containing an aromatic azido group (**1a, 2a,** and **3a**). These conjugates provide a wide choice of instruments to investigate nucleic acid−nucleic acid and nucleic acid−protein interaction. The synthesis of new photoreagent **2a** has been also fulfilled. This compound is the most attractive for affinity modification of the nucleic acids.

INTRODUCTION

Detailed molecular understanding of cellular processes including replication, transcription, RNA processing, and translation requires tools to study a structural topography of nucleic acid−protein and nucleic acid−nucleic acid interactions. Cross-linking provides a very promising tool for structure function study. The use of the photochemical cross-linking reagents can yield detailed information about which parts of each interacting molecules are in close proximity and therefore have become increasingly popular over the years. The main advantage of these reagents compared with chemical cross-linkers is the independence of their reactivity from the majority of outer factors such as pH, ionic strength, presence of some other reactive compounds, temperature (if not too high), and their inertness under very severe conditions in the absence of the light, *i.e.,* they combine both high reactivity and stability in solution.

A great number of examples can demonstrate the utility of photoactivable reagents in molecular biology and biochemistry. *p*-Azidophenacyl residue attached to the anticodon loop of tRNA^Arg1 has been used for the photochemical cross-linking of this tRNA to the 30S

ribosomal subunit (Chen et al., 1985). The same reagent was applied for mapping the active site of ribonuclease P RNA (Burgin and Pace, 1990). Azidopurine nucleosides have frequently been used for the study of nucleotide binding sites on proteins (Haley, 1983). Polynucleotides containing 8-azidoadenosine and 8-azidoinosine residues were employed as photoaffinity probes to explore the subunit topography of RNA polymerase from *E. coli* (Cartwright and Hutchinson, 1980). The use of 5-azido-2′-deoxyuridine-substituted nucleic acids was adopted to study *lac* operator−repressor complexes (Evans et al., 1986). 5-[(4-Azidophenacyl)thio]cytidine 5′-triphosphate was used in the photoaffinity labeling of *E. coli* and T7 RNA polymerases (Hanna et al., 1993). Oligonucleotide reagents carrying *p*-azidotetrafluorobenzoyl, 2-nitro-5-azidobenzoyl, and *p*-azidobenzoyl groups were used for the complementary addressed photoaffinity modification of DNA (Dobrikov et al., 1992b). Different photoreagent residues were shown to react preferably with certain nucleotides in the sequence. The same photoreactive derivatives of oligonucleotides were applied to affinity labeling of the human immunodeficiency virus reverse transcriptase (Mitina et al., 1992). *exo-N*-[2-[(4-Azido-2,3,5,6-tetrafluorobenzoyl)amino]ethyl]deoxycytidine 5′-triphosphate (**14**) has been previously used as a substrate for DNA polymerase α (Doronin et al., 1992) and to determine the molecular mass of the transcription factor interacting with FBS-2 site in c-fos promoter (Svinarchuk et al., 1993). The compound **14** was found to be very useful in the investigation of nucleic acid−protein interactions, but the synthetic procedures leading to **14** have not been documented carefully. In addition, the presence of four fluorine substituents in the aromatic ring of **1a** caused an undesirable hypsochromic shift in the UV spectra (Dobrikov et al., 1992a). Though the photoactivable (d)NTP appears to be useful for the study of the systems of template biocatalysis, the variety of (d)NTP derivatives bearing an azido group is limited: commonly used ones are azidonucleotides [for a review, see Sylvers

and Wower (1993)]. These are short-range cross-linkers and reflect only the most immediate environment of the base. Besides, azidonucleotides undergo a pH-dependent tautomeric rearrangement to tetrazoles which are considered to be nonphotoreactive (MacFarlane et al., 1982). The chemical synthesis of the derivatives of nucleoside 5′-triphosphates containing long-range cross-linkers, with the rare exception (Hanna et al., 1993), is not described. We describe here the synthesis of various conjugates of (d)NTPs (**6a, 6b, 7, 11, 12, 14,** and **16**), which fill up this gap. They contain three different photoreagents including a newly elaborated reagent **2a** that has improved characteristics compared with the previously described reagents **1a** and **3a**.

EXPERIMENTAL PROCEDURES

Except as noted, reagents were obtained commercially and used without further purification. DCC and *N*-hydroxysuccinimide was from Merck (Germany). *O*-(Carboxymethyl)hydroxylamine hemihydrochloride was obtained from Fluka (Switzerland). Adenosine 5′-monophosphate, 2′-deoxyadenosine 5′-monophosphate, and dCTP were from Reanal (Hungary). 4-Azido-2,3,5,6-tetrafluorobenzaldehyde was from Novosibirsk Institute of Organic Chemistry (Russia). DEAE−cellulose DE-32 was purchased from Whatman (England). Sephadex G-10 and A-25 was from Pharmacia (Sweden). DMF was distilled under reduced pressure from CaH_2 and stored over 4 Å molecular sieves. Pyridine was distilled four times from P_2O_5, *p*-toluenesulfonyl chloride, NaOH, and P_2O_5 and stored over 4 Å molecular sieves. Acetonitrile was distilled from P_2O_5 and stored over CaH_2. Triethylamine was purified as described for pyridine. Absolute ethanol was obtained by distillation from CaO. MeIm was dried over 4 Å molecular sieves. dUMP was synthesized from 2′-deoxyuridine (Fluka, Switzerland) in accordance with the method described earlier (Kohler et al., 1980). 5-(*trans*-3-Aminopropenyl-1)uridine 5′-triphosphate (**5b**) was prepared according to the procedure has been reported (Langer et al., 1981). 5-(*trans*-3-Aminopropenyl-1)deoxycytidine 5′-triphosphate (**15**) was synthesized as described earlier (Strobel et al., 1989). *N*-Hydroxysuccinimide esters of photoreagents **1b** and **3b** were synthesized as described by Dobrikov et al. (1992a).

The ^1H, ^{31}P, and ^{13}C NMR spectra (200.132 MHz, 81.015 MHz, and 50.323 MHz, respectively) were recorded with a Bruker AC 200 spectrometer and ^{19}F spectra with a Bruker WP 200 SY spectrometer (188.282 MHz). The signals in the ^{13}C NMR spectra of (d)NTP derivatives were assigned based on earlier published chemical shifts for nucleoside ^{13}C atoms (Kalinowski et al., 1988). Absorption spectra were taken on a Karl Zeiss instrument Specord UV−vis. Analytical TLC were carried out (if not indicated specially) on silica gel plates (Merck, Kieselgel 60 F_{254}) in dioxane/NH_4OH/water, 6:1:4, v/v. The compounds containing an amino group were visualized by ninhydrin reaction (0.3% ninhydrin, 3% acetic acid in butanol-1). HPLC purifications were performed using a Waters 600E controller equipped with a multisolvent delivery system and a Model 484 tunable absorbance detector. Polisil SA-500 (15 μm, Vector, Russia), Lichrosorb RP-18 (10 μm, Merck, Germany), and Nucleosil 100-7C_{18} (7 μm, Macherey-Nagel, Germany) were used as a sorbent for HPLC. The kinetics of photolysis were studied by the irradiation of samples in a 1 cm cell during certain periods of time at 303−313 nm by filtered light of a high-pressure mercury lamp (energy 1×10^{-4} J·cm^{-2}·s^{-1}) following the UV spectra recording of irradiated solutions.

4-Azido-2,3,5,6-tetrafluorobenzaldehyde *O*-(Car-

boxymethyl)oxime (2a). *O*-(Carboxymethyl)hydroxylamine hemihydrochloride (545 mg, 5 mmol) was dissolved in 50% aqueous methanol (10 mL). A solution of 4-azido-2,3,5,6-tetrafluorobenzaldehyde (1.1 g, 5 mmol) in methanol (3 mL) was added dropwise with stirring at room temperature. After 1 h of standing at 4 °C, the white precipitate was filtered, washed with 50% aqueous methanol (3 × 1 mL) and water (2 × 1 mL), and dried under reduced pressure in the dark to give 1.315 g (90% yield) of **2a** as a white powder: mp 148−149 °C dec; R_f 0.65−0.70 (ethanol/$CHCl_3$, 1:10, v/v); UV (ethanol) λ_{max} = 212 nm (ϵ = 12 000), 289 nm (ϵ = 31 000); IR (KBr) cm^{-1} 3040 (CF), 2930 (CH_2), 2200 and 2130 (−N_3), 1730 (HOC=O), 1650 (C=NO), 1495 and 1470 (FC=CF arom), 1250 (OCH$_2$), 1120 and 990 (CF); ^1H NMR (DMF-d_7) δ 5.11 (s, 2H, OCH$_2$COO), 8.70 (s, 1H, ArCH=NO), 10.47 (s, bs, 1H, COOH). Anal. Calcd for $C_9H_4N_4O_3F_4$: C, 36.9; H, 1.56, N, 19.3. Found: C, 36.9; H, 1.64; N, 19.1.

***N*-4-Azido-2,3,5,6-tetrafluorobenzaldehyde *O*-[[(Succinimidooxy)carbonyl]methyl]oxime (2b).** To a solution of DCC (403 mg, 2 mmol) in dried DMF (5 mL) was added **2a** (365 mg, 1.25 mmol) and *N*-hydroxysuccinimide (145 mg, 1.27 mmol). The mixture was stirred at room temperature for 1 h and then left at 4 °C overnight. The white precipitate of *N,N*′-dicyclohexylurea was filtered off, and the filtrate was evaporated to the solid residue which was recrystallized from hexane: $CHCl_3$ = 2:1 (12 mL). The white precipitate was filtered and dried under reduced pressure in the dark: yield 312 mg (64%); mp 93−95 °C; R_f 0.65−0.75 (dioxane/benzene, 1:9, v/v); UV (ethanol) λ_{max} = 208 nm (ϵ = 11 000), 287 nm (ϵ = 24 000); IR (KBr) cm^{-1} 2925 (CH_2), 2175 and 2125 (−N_3), 1825 (NOC=O), 1735 (−NC(R)=O), 1650 (C=NO), 1480 and 1495 (FC=CF arom), 1240 (OCH$_2$), 1195 and 995 (CF); ^1H NMR (CDCl$_3$) δ 2.84 (m, COCH$_2$-CH$_2$CO, 4H), 5.09 (s, OCH$_2$COO, 2H), 8.28 (s, ArCH=NO−, 1H). Anal. Calcd for $C_{13}H_7N_5O_5F_4$: C, 40.1; H, 1.81; N, 18.0. Found: C, 39.6; H, 1.72; N, 18.2.

5-[*N*-(2-Nitro-5-azidobenzoyl)-*trans*-3-aminopropenyl-1]uridine 5′-Triphosphate (Lithium Salt) (6b). Fifteen mg (49.2 μmol) of **3b** was dissolved in 200 μL of DMF. **5b** (9.7 μmol) was dissolved in 150 μL of a H_2O/DMF mixture (1/2, v/v), and 10 μL of MeIm was added. The solution of **3b** (100 μL) was added to the solution of **5b**. After reaction proceeded for 30 min, 50 μL of the solution of **3b** was added once more, and the final 50 μL of this solution was added after 60 min of reaction. After 1 h of incubation the reaction mixture was diluted with 5 volumes of water and applied on a DEAE−cellulose DE-32 column (0.9 × 24 cm). The column was washed with 0−0.3 M linear gradient of TEAB, pH 7.5 (0.5 L). The fractions containing the product were pooled, evaporated to dryness, redissolved in water, and applied on a Lichroprep RP-18 column (1 × 25 cm). The product **6b** was purified using a linear gradient 0−30% acetonitrile in 0.05 M TEAB, pH 7.5. The solvent was removed on a rotary evaporator, and the residue was evaporated three times with absolute ethanol, redissolved in the minimum volume of water, and precipitated by 10 volumes of 2% $LiClO_4$ in acetone. The product was dried *in vacuo*. All procedures were carried out in a minimum of light: yield 90%; R_f 0.3; UV (H_2O) λ_{max} = 301 (ϵ = 13 900), λ_{min} = 269 (ϵ = 11 100); ^1H NMR (D$_2$O) δ 4.1 (d, *J* = 4.5 Hz, H9, 2H), 4.15−4.5 (m, bs, H2′, H3′, H4′, H5′, 5H), 6.05 (d, *J* = 4.5 Hz, H1′, 1H), 6.45 (t, *J* = 4.5 Hz, H8, 1H), 6.5 (s, H7, 1H), 7.3 (d, *J* = 2.5 Hz, H16, 1H), 7.35 (dd, *J* = 8.5 and 2.5 Hz, H14, 1H), 7.9 (s, H6, 1H), 8.24 (d, *J* = 8.5 Hz, H13, 1H). ^{13}C NMR (D$_2$O) δ 42.3 (C9), 65.5 (C5′), 69.5 (C2′), 73.8 (C3′), 83.3 (C4′), 88.8 (C1′), 113.3 (C5), 119.2 (C16), 121.4 (C13), 124.6 (C8), 126.0 (C7), 127.3 (C14),

132.9 (C11), 137.6 (C6), 141.4 (C12), 147.3 (C15), 150.1 (C2), 165.0 (C4), 168.9 (C10).

5-(*trans*-3-Aminopropenyl-1)-2′-deoxyuridine 5′-Monophosphate (Triethylammonium Salt) (4). dUMP was converted into **4** as described for the corresponding triphosphate (Langer et al., 1981): yield 89% (13% of *cis*-isomer); R_f 0.46; UV (H$_2$O) λ_{max} = 240 nm (ϵ = 10 500), 289 nm (ϵ = 7100), λ_{min} = 262 nm (ϵ = 4200); ^{1}H NMR (D$_2$O) δ 1.21 (t, J = 7.5 Hz, CH$_3$ of (C$_2$H$_5$)$_3$NH$^+$, 18H), 2.19 (m, bs, H2′, 2H), 3.10 (q, J = 7.5 Hz, CH$_2$ of (C$_2$H$_5$)$_3$NH$^-$, 12H), 3.48 (d, J = 6 Hz, H9, 2H), 3.80 (m, H5′, 2H), 3.97 (m, H4′, 1H), 4.40 (m, H3′, 1H), 6.12 (t, J = 6 Hz, H1′, 1H), 6.29 (t, J = 6 Hz, H8, 1H), 6.33 (s, H7, 1H), 8.13 (s, H6, 1H).

5-(*trans*-3-Aminopropenyl-1)-2′-deoxyuridine 5′-Triphosphate (Triethylammonium Salt) (5a). A 0.83 mmol portion of **4** was dried by three evaporations of its solution in anhydrous pyridine, and the residue was suspended in 4 mL of absolute acetonitrile. A 0.84 mL (6 mmol) portion of trifluoroacetic anhydride and 0.51 mL (4 mmol) of dry *N*,*N*-dimethylaniline were added to this suspension. After the dissolution of **4** a clear solution was evaporated *in vacuo* and the mixture of 0.32 mL (4 mmol) MeIm and 0.6 mL (4.1 mmol) of triethylamine in 1 mL of acetonitrile was added to the residue. When the activation was complete (about 2 min), 3 mL (3 mmol) of 1 M bis(tri-*n*-butylammonium) pyrophosphate in dry acetonitrile was added. After 5 min the reaction mixture was treated with 25% aqueous ammonia (1.5 mL) and 70% methanol (6 mL), and the precipitate of ammonium pyrophosphate was filtered off and washed by 70% methanol (3 × 10 mL). The filtrate was evaporated, dissolved in 20 mL of water, and extracted two times with chloroform (2 × 20 mL), and the product **5a** with the *N*-trifluoroacetic protecting group was isolated by the ion exchange chromatography on DEAE−Sephadex A-25 (50 mL) using a gradient of ammonium bicarbonate (0−0.6 M, pH 8.5). The fractions corresponding to triphosphate were pooled and evaporated. The solid residue was treated with concentrated aqueous ammonia during 3 h to remove the trifluoroacetic protecting group. The solution was evaporated, the solid residue was dissolved in the minimum volume of water, and the product **5a** was precipitated by 2% LiClO$_4$ in acetone and dried *in vacuo*: yield 60%; R_f 0.1; UV (H$_2$O) λ_{max} = 242 nm (ϵ = 10 700), 290 nm (ϵ = 7100), λ_{min} = 266 nm (ϵ = 4300); ^{1}H NMR (D$_2$O) δ 2.14 (m, bs, H2′, 2H), 3.77 (d, J = 5 Hz, H9, 2H), 3.95 (m, bs, H4′, H5′, 3H), 4.37 (m, bs, H3′, 1H), 6.01 (t, J = 6 Hz, H1′, 1H), 6.10 (s, H7, 1H), 6.16 (t, J = 5 Hz, H8, 1H), 7.63 (s, H6, 1H); ^{31}P NMR (D$_2$O) δ −22.55 (t, J = 20 Hz, P$_\beta$, 1P), −11.58 (d, J = 20 Hz, P$_\alpha$, 1P), −8.89 (d, J = 20 Hz, P$_\gamma$, 1P).

5-[*N*-(2-Nitro-5-azidobenzoyl)-*trans*-3-amino-propenyl-1]-2′-deoxyuridine 5′-triphosphate (lithium salt) (6a) was synthesized from **5a** and **3b** according to the method described above for the synthesis of compound **6b**: yield 88%; R_f 0.26; UV (H$_2$O) λ_{max} = 299 (ϵ = 13 900), λ_{min} = 266 nm (ϵ = 11 100); ^{1}H NMR (D$_2$O) δ 2.23 (m, H2′, 2H), 3.95 (d, J = 5.5 Hz, H9, 2H), 4.03 (m, bs, H3′, H4′, H5′, 4H), 6.16 (t, J = 7 Hz, H1′, 1H), 6.31 (s, H7, 1H), 6.36 (t, J = 5.5 Hz, H8, 1H), 7.10 (d, J = 2.3 Hz, H16, 1H), 7.16 (dd, J = 2.3 Hz and 8.9 Hz, H14, 1H), 7.78 (s, H6, 1H), 8.07 (d, J = 8.9 Hz, H13, 1H); ^{13}C NMR (D$_2$O) δ 43.50 (C2′), 46.67 (C9), 70.06 (C5′), 75.43 (C3′), 90.15 (C1′), 90.36 (C4′), 116.97 (C5), 123.80 (C16), 125.55 (C13), 127.51 (C8), 131.37 (C7), 131.92 (C14), 138.18 (C11), 142.91 (C6), 145.84 (C12), 151.94 (C15), 155.61 (C2), 169.09 (C4), 173.48 (C10).

5-[3-[[[[(4-Azido-2,3,5,6-tetrafluorobenzylidene]-amino]oxy]methyl]carbonyl]-*trans*-3-aminopro-

penyl-1]-2′-deoxyuridine 5′-triphosphate (lithium salt) (7) was synthesized from **5a** and **2b** according to the method described above for the synthesis of the compound **6b** except that triethylamine was used instead of MeIm: yield 91%; R_f 0.46; UV (H$_2$O) λ_{max} = 285 nm (ϵ = 35 000); ^{1}H NMR (D$_2$O) δ 2.44 (m, H2′, 2H), 4.04 (d, J = 5 Hz, H9, 2H), 4.1−4.5 (m, bs, H3′, H4′, H5′, H11, 6H), 6.30 (t, J = 5.5 Hz, H1′, 1H), 6.34 (s, H7, 1H), 6.36 (t, J = 5 Hz, H8, 1H), 7.88 (s, H6, 1H), 8.50 (s, H12, 1H); ^{13}C NMR (D$_2$O) δ 38.90 (C2′), 40.78 (C9), 65.53 (C5′), 70.79 (C3′), 72.99 (C11), 85.46 (C1′), 85.71 (C4′), 106.22 (m, C13), 112.47 (C5), 121.5 (m, C16), 122.27 (C8), 127.70 (C7), 137.76 (C6), 138.5 and 142.5 (m, J = 250 Hz, C14 and C18, ^{19}F−^{13}C coupling), 142.81 (C12), 143.5 and 147.5 (m, J = 250 Hz, C15 and C17, ^{19}F−^{13}C coupling), 150.87 (C2), 164.06 (C4), 171.70 (C10); ^{19}F NMR (D$_2$O) δ 11.18 (m, F14, F18, 2F), 23.08 (m, F15, F17, 2F).

8-Bromoadenosine 5′-monophosphate (triethyl-ammonium salt) (8b) was synthesized using a previously described method (Ikehara and Kaneko, 1970) for 8-bromoadenosine synthesis. Adenosine 5′-monophosphate disodium salt hexahydrate (0.865 g, 1.8 mmol) was dissolved in 18 mL of 0.5 M NaOAc, pH 4.2, and the solution of Br$_2$ (0.34 mL (6.57 mmol) (first dissolved in 36 mL of the same buffer) was added. After 1 h at room temperature the concentrated aqueous solution of Na$_2$SO$_3$ was added dropwise until the solution became yellowish. The pH of the solution obtained was adjusted to neutral, the solution was applied to a Nucleosil 7C$_{18}$ column (2 × 25 cm), and the product was eluted using a linear gradient ranging from 0 to 30% acetonitrile against 0.05 M TEAB, pH 7.5. The solvent was removed on a rotary evaporator, and the residue was evaporated three times with absolute ethanol: yield 85%; R_f 0.54; UV (H$_2$O) λ_{max} = 212 nm (ϵ = 20 800), 269 nm (ϵ = 15 500), λ_{min} = 236 nm (ϵ = 4200); ^{1}H NMR (D$_2$O) δ 1.38 (t, J = 7.5 Hz, CH$_3$ of (C$_2$H$_5$)$_3$NH$^-$, 18H), 3.29 (q, J = 7.5 Hz, CH$_2$ of (C$_2$H$_5$)$_3$NH$^+$, 12H), 3.9−4.5 (m, bs, H2′, H3′, H4′, H5′, 5H), 6.19 (d, J = 7.5 Hz, H1′, 1H), 8.25 (s, H2, 1H): ^{13}C NMR (D$_2$O) δ 7.81 (CH$_3$ of (C$_2$H$_5$)$_3$NH$^+$), 45.73 (CH$_2$ of (C$_2$H$_5$)$_3$NH$^-$), 64.32 (C5′), 69.66 (C3′), 70.64 (C2′), 83.23 (C4′), 89.42 (C1′), 118.33 (C5), 127.46 (C8), 149.54 (C6), 152.58 (C2), 153.24 (C4). 8-Bromo-2′-deoxyadenosine 5′-monophosphate (8a) was synthesized by the same manner.

8-[(4-Aminobutyl)amino]-2′-deoxyadenosine 5′-Monophosphate (Triethylammonium Salt) (9a). Compound **8a** (1.53 mmol) was dissolved in water (1.5 mL), and freshly distilled diaminobutane (1 mL) was added. The reaction mixture was heated overnight at 75 °C and then cooled at room temperature. Water (25 mL) was added, and the solution was applied to a DEAE−cellulose DE-32 column (0.9 × 24 cm). The product **9a** was eluted using a 0−0.2 M gradient of TEAB, pH 7.5 (0.3 L). The solvent was removed on a rotary evaporator, and the residue was evaporated twice with absolute ethanol: yield 92%; R_f 0.36; UV (H$_2$O) λ_{max} = 278 nm (ϵ = 21 500), λ_{min} = 239 nm (ϵ = 2400); ^{1}H NMR (D$_2$O, 0.5% CF$_3$COOD) δ 1.24 (t, J = 7.5 Hz, CH$_3$ of (C$_2$H$_5$)$_3$NH$^-$, 18H), 1.71 (m, H11, H12, 4H), 2.25 (m, H2′, 2H), 3.01 (t, bs, H13, 2H), 3.16 (q, J = 7.5 Hz, CH$_2$ of (C$_2$H$_5$)$_3$NH$^+$, 12H), 3.45 (t, bs, H10, 2H), 4.15−4.5 (m, bs, H3′, H4′, H5′, 4H), 5.99 (d, J = 7.5 Hz, H1′, 1H), 7.98 (s, H2, 1H); ^{13}C NMR (D$_2$O, lithium salt of **9a**) δ 25.71 and 25.90 (C11 and C12), 37.05 (C2′), 39.34 (C13), 42.09 (C10), 65.40 (C5′), 70.64 (C3′), 83.55 (C1′), 85.63 (C4′), 116.53 (C5), 149.34 (C8 and C6, double signal), 151.61 (C2), 152.48 (C4). The product **9b** was synthesized by the same manner.

8-[(4-Aminobutyl)amino]adenosine 5′-triphosphate (triethylammonium salt) (10b) was synthesized as

described above for the synthesis of compound **5a**. After the ammonium pyrophosphate precipitate was removed and the filtrate was evaporated, the residue was treated with concentrated aqueous ammonia during 3 h. Ammonia was removed under reduced pressure, and the residue was separated on DEAE−cellulose DE-32 (0.9 × 18 cm) using a 0−0.3 M linear gradient of TEAB, pH 7.5. The fractions corresponding to the product were pooled, the solvent was removed on a rotary evaporator, and the residue was evaporated three times with absolute ethanol: yield 40%; R_f 0.1; UV (H$_2$O) λ_{max} = 279 nm (ϵ = 21 500), λ_{min} = 241 (ϵ = 2300); ^{1}H NMR (D$_2$O) δ 1.24 (t, J = 7.5 Hz, CH$_3$ of (C$_2$H$_5$)$_3$NH$^+$, 27H), 1.76 (m, H11, H12, 4H), 3.08 (s, bs, H13, 2H), 3.15 (q, J = 7.5 Hz, CH$_2$ of (C$_2$H$_5$)$_3$NH$^+$, 18H), 3.50 (s, bs, H10, 2H), 4.15−4.6 (m, bs, H2′, H3′, H4′, H5′, 5H), 5.98 (d, J = 7.5 Hz, H1′, 1H), 8.02 (s, H2, 1H); ^{31}P NMR (D$_2$O) δ −22.75 (t, J = 23 Hz, P$_\beta$, 1P), −11.63 (d, J = 23 Hz, P$_\alpha$, 1P), −10.02 (d, J = 23 Hz, P$_\gamma$, 1P). The product **10a** was synthesized in the same manner.

8-[*N*-[(2-Nitro-5-azidobenzoyl)-4-aminobutyl]amino]adenosine 5′-triphosphate (lithium salt) (11) was synthesized from **10b** and **3b** according to the method described above for the synthesis of compound **6b**: yield 92%; R_f 0.3; UV (H$_2$O) λ_{max} = 282 nm (ϵ = 28 500), λ_{min} = 244 nm (ϵ = 12 500); ^{1}H NMR (D$_2$O) δ 1.91 (m, H11, H12, 4H), 3.59 (m, bs, H10, H13, 4H), 4.3−4.75 (m, bs, H2′, H3′, H4′, H5′, 5H), 6.11 (d, J = 7.8 Hz, H1′, 1H), 7.14 (d, J = 2.5 Hz, H20, 1H), 7.38 (dd, J = 2.5 Hz and 9 Hz, H18, 1H), 8.17 (s, H2, 1H), 8.23 (d, J = 9 Hz, H17, 1H); ^{13}C NMR (D$_2$O) δ 26.70 (C13)*, 27.01 (C12)*, 41.15 (C13), 43.37 (C10), 67.14 (C5′), 71.46 (C3′), 72.04 (C2′), 85.74 (C4′), 87.62 (C1′), 117.76 (C5), 120.28 (C20), 122.07 (C17), 128.44 (C18), 134.95 (C15), 142.41 (C16), 148.41 (C19), 150.17 (C6), 150.95 (C8), 152.61 (C2), 153.44 (C4), 170.06 (C14) (*tentative assignment).

8-[*N*-[(4-Azido-2,3,5,6-tetrafluorobenzoyl)-4-aminobutyl]amino]-2′-deoxyadenosine 5′-triphosphate (lithium salt) (12) was synthesized from **10a** and **1b** according to the method described above for the synthesis of compound **6b**: yield 64%; R_f 0.42; UV (H$_2$O) λ_{max} = 263 nm (ϵ = 37 000), λ_{min} = 234 nm (ϵ = 12 500); ^{1}H NMR (D$_2$O) δ 1.62 (m, H11, H12, 4H), 2.57 (m, H2′, 2H), 3.31 (m, H10, 2H), 3.39 (m, H13, 2H), 4.0−4.1 (m, H4′, H5′, 3H), 4.26 (m, H3′, 1H), 6.24 (dd, J = 9 Hz and 6.5 Hz, H1′, 1H), 7.88 (s, H2, 1H); ^{13}C NMR (D$_2$O) δ 29.84 and 30.13 (C11 and C12), 41.79 (C2′), 44.53 (C13), 46.37 (C10), 70.09 (C5′), 75.27 (C3′), 88.14 (C1′), 90.25 (C4′), 114.60 (m, C15), 120.99 (C5), 126.83 (m, C18), 143.62 and 146.88 (m, J = 250 Hz, C16 and C20, ^{19}F−^{13}C coupling), 146.12 and 149.24 (m, J = 250 Hz, C17 and C19, ^{19}F−^{13}C coupling), 153.70 (C8), 153.81 (C6), 156.13 (C2), 156.75 (C4), 164.90 (C14).

5-[*N*-[(4-Azido-2,3,5,6-tetrafluorobenzoyl)-*trans*-3-amino]propenyl-1]-2′-deoxycytidine 5′-triphosphate (lithium salt) (16) was synthesized from **15** and **1b** according to the method described above the synthesis of the compound **6b** except that isolation of **16** from the reaction mixture was performed by HPLC on a Polisil SA-500 column (1 × 25 cm, linear gradient of 0−0.5 M TEAB, pH 7.5, against 10% acetonitrile) without further purification by the reversed phase chromatography: yield 82%; R_f 0.5; UV (H$_2$O) λ_{max} = 256 nm (ϵ = 28 000), λ_{min} = 229 nm (ϵ = 17 200); ^{1}H NMR (D$_2$O) δ 2.39 (m, H2′, 2H), 4.1 (d, J = 5.5 Hz, H9, 2H), 4.15−4.4 (m, bs, H3′, H4′, H5′, 4H), 6.10 (t, J = 7 Hz, H1′, 1H), 6.30 (s, H7, 1H), 6.32 (t, J = 5.5 Hz, H8, 1H), 7.97 (s, H6, 1H); ^{19}F NMR (D$_2$O) δ 15.34 (m, F12, F16, 2F), 23.54 (m, F13, F15, 2F).

4-(*β*-Aminoethyl)-2′-deoxycytidine 5′-Triphosphate (Sodium Salt) (13). A 6.4 g portion of ethylenediamine,

Scheme 1
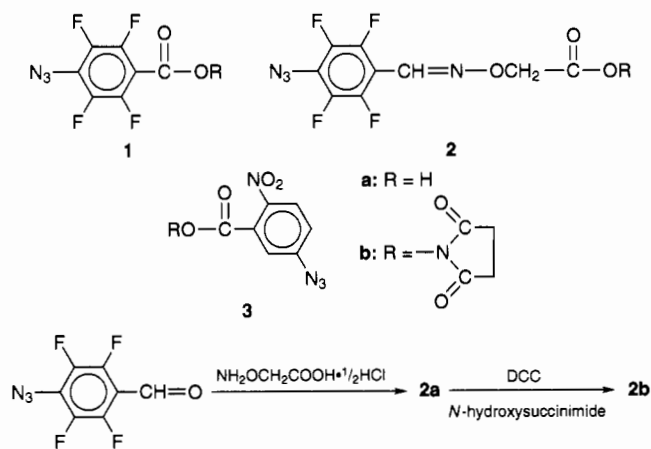
750 mg of Na$_2$S$_2$O$_5$ or 1 g of Na$_2$SO$_3$, 600 mg of morpholinoethanesulfonic acid, and 16 mg of hydroquinone were dissolved in 6 mL of H$_2$O, and the pH of the solution was then adjusted to neutral by addition of 10 N NaOH. Then an aqueous solution of the Na$_4$ salt of deoxycytidine 5′-triphosphate (1.37 g, 2.4 mmol in 8 mL of H$_2$O) was added, and the pH of final solution was adjusted to 6.2. After 24 h the pH of the solution was adjusted to 9 for 1 h to stop the reaction. The final reaction mixture containing 86% of **13**, 11% of deoxycytidine 5′-triphosphate and 3% of 4-(*β*-aminoethyl)deoxycytidine 5′-diphosphate was desalted on a Sephadex G-10 column (2.5 × 100 cm) in H$_2$O. Fractions, containing nucleotide material, were pooled and applied on a Sephadex A-25 column (2.5 × 40 cm) in the Cl$^-$ form and eluted by the linear gradient of 0−0.3 M LiCl. The fractions containing **13** were pooled and lyophilized. The obtained powder was dissolved in 10 mL of H$_2$O and desalted on Sephadex G-10 in H$_2$O. The solution of **13** was neutralized by 10 M NaOH and lyophilized: yield 1.19 g (78%); UV (H$_2$O) λ_{max} = 274 nm (ϵ = 10 500); ^{1}H NMR (D$_2$O) δ 2.48−2.68 (m, H2′, 2H), 3.79 (s, H7, H8, 4H), 4.41 (m, H4′, H5′, 3H), 4.8 (s, H3′, 1H), 6.28 (d, J = 7.5 Hz, H5, 1H), 6.53 (t, J = 6.5 Hz, H1′, 1H), 7.96 (d, J = 7.5 Hz, H6, 1H); ^{1}H NMR (D$_2$O, 1% CF$_3$COOD) δ 3.63 (t, J = 5.5 Hz, H7, 2H), 4.11 (t, J = 5.5 Hz, H8, 2H).

***exo-N*-[2-(4-Azido-2,3,5,6-tetrafluorobenzamido)-ethyl]-2′-deoxycytidine 5′-triphosphate (sodium salt) (14)** was synthesized from **13** to **1b** according to the method described above for the synthesis of compound **6b**: yield 85%; UV (H$_2$O) λ_{max} = 260 nm (ϵ = 23 000); ^{1}H NMR (D$_2$O) δ 2.3−2.6 (m, H2′, 2H), 3.69 (m, H7, H8, 4H), 4.2−4.3 (m, H4′, H5′, 3H), 4.6−4.7 (m, H3′, 1H), 6.15 (d, J = 7.5 Hz, H5, 1H), 6.38 (t, J = 6.5 Hz, H1′, 1H), 7.90 (d, J = 7.5 Hz, H6, 1H); ^{13}C NMR (D$_2$O) δ 39.27 (C2′), 39.28 and 39.68 (C7 and C8), 65.32 (C5′), 70.54 (C3′), 85.33 (C4′), 85.84 (C1′), 97.78 (C5), 110.30 (m, C10), 122.50 (m, C14), 137.85 and 141.01 (m, J = 250 Hz, C11 and C15, ^{19}F−^{13}C coupling), 140.09 (C6), 142.77 and 146.02 (m, J = 250 Hz, C12 and C14, ^{19}F−^{13}C coupling), 157.92 (C2), 160.91 (C4), 164.87 (C9); ^{31}P NMR (D$_2$O) δ −20.96 (t, J = 22 Hz, P$_\beta$, 1P), −10.70 (d, J = 22 Hz, P$_\alpha$, 1P), −5.85 (d, J = 22 Hz, P$_\gamma$, 1P); ^{19}F NMR (D$_2$O) δ 15.66 (m, F11, F15, 2F), 23.36 (m, F12, F14, 2F).

RESULTS

The synthesis of the new photoactive heterobifunctional cross-linking reagent 4-azido-2,3,5,6-tetrafluorobenzaldehyde *O*-[[(succinimidooxy)carbonyl]methyl]oxime (**2b**) was accomplished as shown in Scheme 1. Treatment of 4-azido-2,3,5,6-tetrafluorobenzaldehyde with

Scheme 2
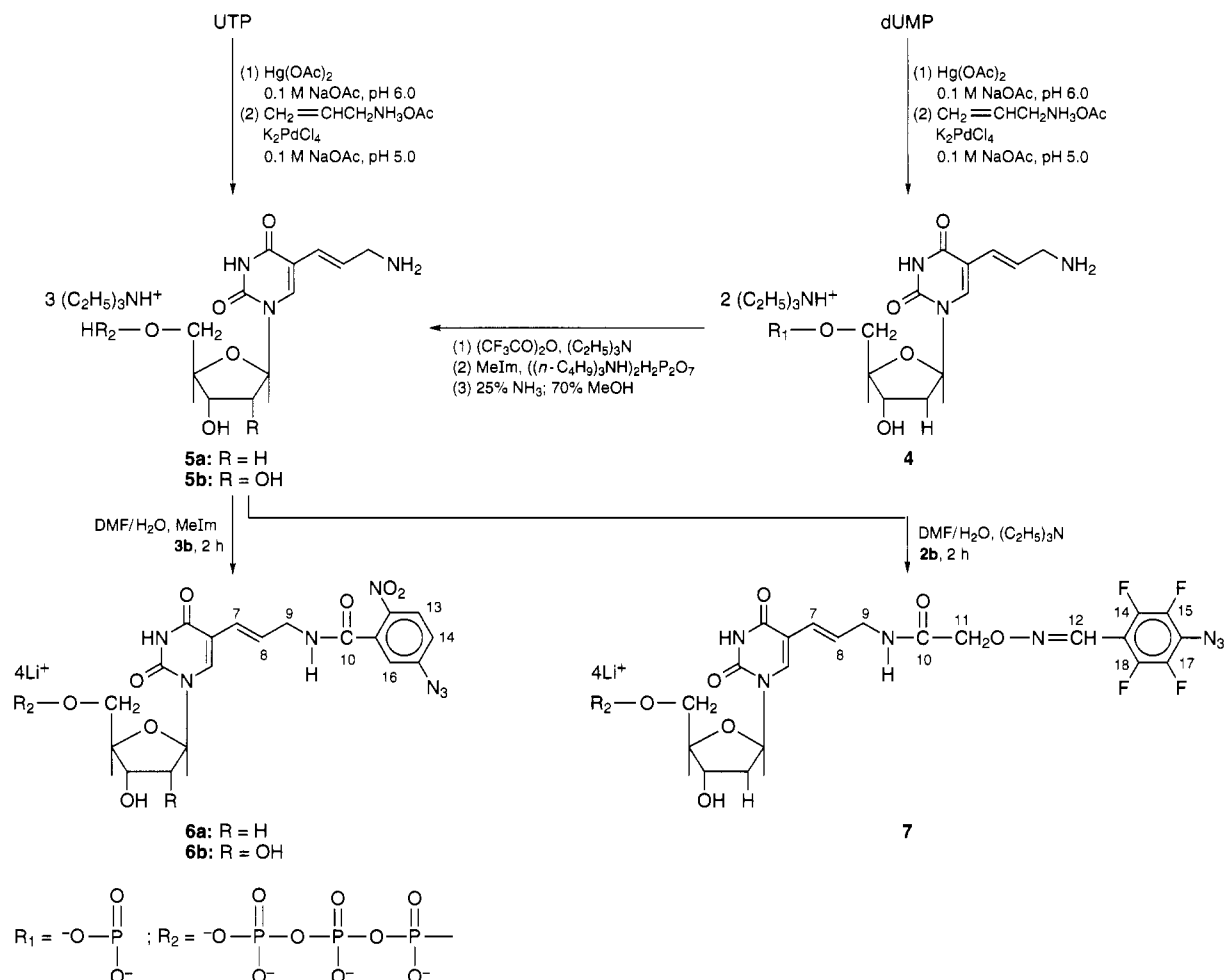
O-(carboxymethyl)hydroxylamine hemihydrochloride gave **2a** with 90% yield. Reaction of 4-azido-2,3,5,6-tetrafluo-robenzaldehyde *O*-(carboxymethyl)oxime (**2a**) and *N*-hydroxysuccinimide with DCC as a coupling reagent gave after recrystallization **2b** with 64% yield. The synthesis of **1b** and **3b** was described earlier (Dobrikov et al., 1992a).

Compound **5b** (Scheme 2) was obtained using the previously described method (Langer et al., 1981) with a yield 50%. Langer et al. have not found the *cis*-isomer; however, we observed in our samples nearly 11% of it. An analogous derivative of dUTP **5a** was synthesized from dUMP. dUMP was converted to 4 by mercuration following the treatment of mercurated nucleotide by K_2PdCl_4 and allylammonium acetate in the sodium acetate buffer pH 5.0 (Langer et al., 1981): the use of dUMP instead of dUTP permitted an increase in the yield of up to 89% (including 13% of the *cis*-isomer). Compound 4 was transformed to the corresponding triphosphate **5a** according to the method described earlier (Bogachev, 1995). The reaction of the triethylammonium salt of 4 with trifluoroacetic anhydride in dry acetonitrile leads to the formation of trifluoroacetic deoxynucleoside 5′-phosphoric mixed anhydride. In the presence of MeIm this mixed anhydride produced nucleoside 5′-triphosphate **5a** when it was allowed to react with bis(tri-*n*-butylammonium) pyrophosphate. The main advantages of this method consist of high reaction rates (several minutes when compared with 3−4 days for the commonly used method of Moffatt (Moffatt, 1964)) and the absence of preliminary protection of the aliphatic amino group—the trifluoroacetic protecting group forms simultaneously

with the mixed anhydride formation. The treatment of reaction mixture with concentrated aqueous ammonia permits the elimination of the protecting group quantitatively when the reaction is completed. The synthesis of photoreactive derivatives of (d)UTP was carried out from *N*-hydroxysuccinimide esters of photoreagents **2b** and **3b** and triethylammonium salts of the modified nucleotides **5a** and **5b** bearing aliphatic amino groups. The reactions were performed in a DMF−water mixture in the presence of MeIm or triethylamine in the dark at room temperature for 2−3 h. The products were separated from the reaction mixture by ion exchange and reversed phase chromatography. The yield was usually 80−90%.

8-[(4-Aminobutyl)amino]-(d)AMP (**9**) (Scheme 3) was prepared from (d)AMP by the method suggested for the synthesis of the corresponding derivative of deoxyadenosine (Sarfati et al., 1987). (d)AMP was brominated at the C8 position (Ikehara and Kaneko, 1970), and the product **8** was separated by reversed phase chromatography and treated with an excess of diaminobutane in water at 75 °C for 12 h. Compound **9** was purified by ion exchange chromatography. Conversion of **9** in the respective triphosphate **10** was carried out by the method of Bogachev (Bogachev, 1995), as described above. The use of (d)AMP as a starting material instead of 2′-deoxyadenosine allows the synthetic procedures toward **10** to be shortened sufficiently compared with the previously described method and consequently the yield of the product to be increased. The photoactivable derivatives of (d)ATP **11** and **12** were synthesized *via* a coupling

Scheme 3
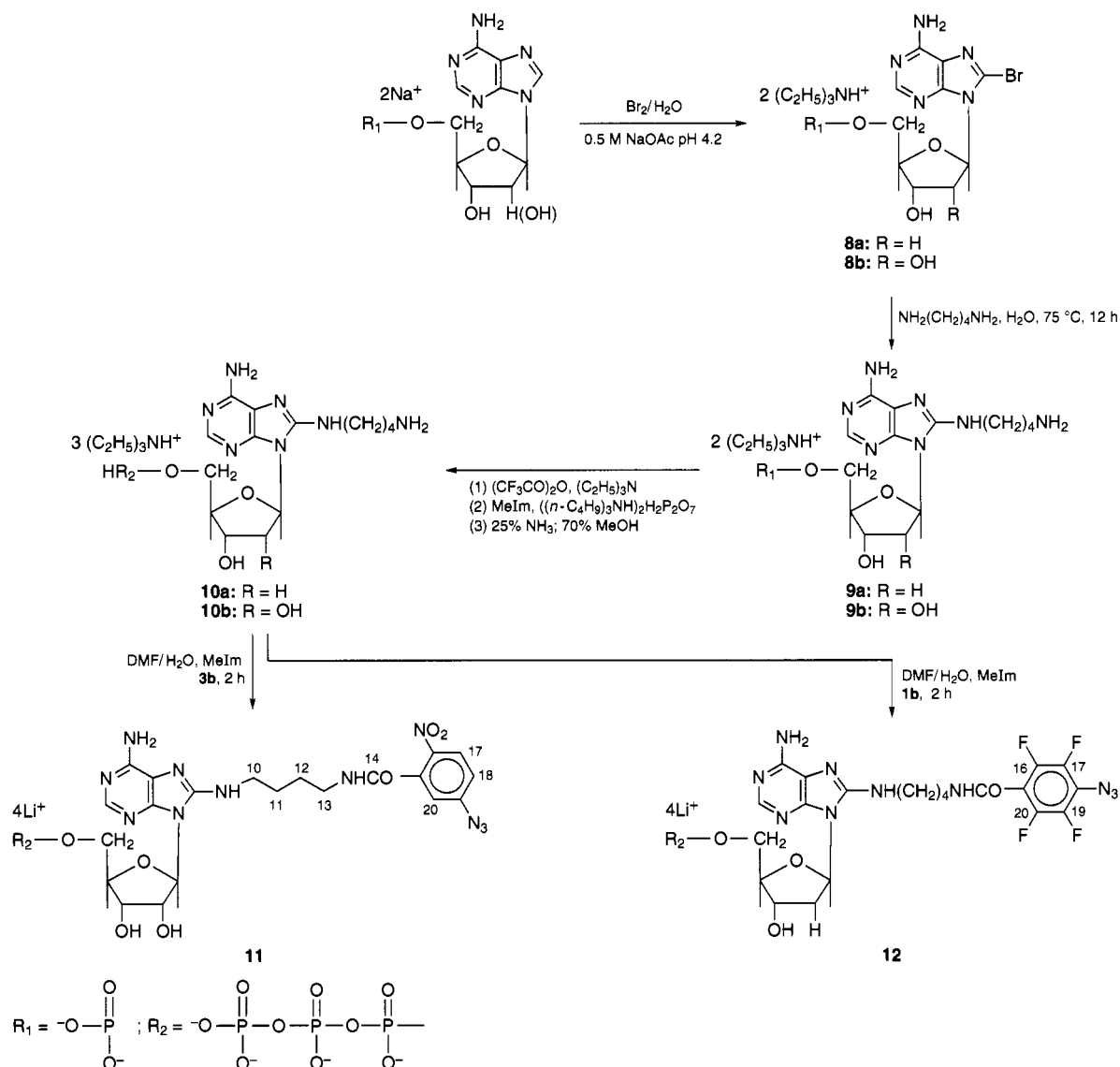
reaction of **10b** with **3b** and **10a** with **1b** correspondingly, as is described above in the explanation of Scheme 2.

4-(β-Aminoethyl)deoxycytidine 5′-triphosphate (**13**) (Scheme 4) was synthesized through bisulfate-catalyzed transamination of deoxycytidine 5′-triphosphate by ethylenediamine. Several changes to known procedures (Gebeyehu et al., 1987; Doronin et al., 1992) were made to increase yield of the target product to 78%. 5-(trans-3-Aminopropenyl-1)deoxycytidine 5′-triphosphate (**15**) was obtained using the previously described procedure (Strobel et al., 1989). The authors do not mention the yield of **15**, but we found this procedure to be unefficient: the yield of product is only 10−12%, and a small quantity of cis-isomer is observed (nearly 10%). dCTP derivatives **14** and **16** substituted with the photoreagent residues were obtained by the reactions of **13** and **15** with **1b**, as it is described above for the synthesis of the photoreactivable (d)UTP.

The products were characterized by UV and NMR (^{1}H, ^{13}C, ^{19}F, ^{31}P) spectra, and the kinetics of their photolysis under UV irradiation were studied. Compounds **6a**, **6b**, **7**, **11**, **12**, **14**, and **16** have characteristic adsorption spectra (Figures 1−3) representing superposition of the spectra of the corresponding modified nucleotides **5a**, **5b**, **10a**, **10b**, **13**, and **15** and amides of photoreagents **1a**, **2a**, and **3a**. Under UV irradiation the spectral compo-
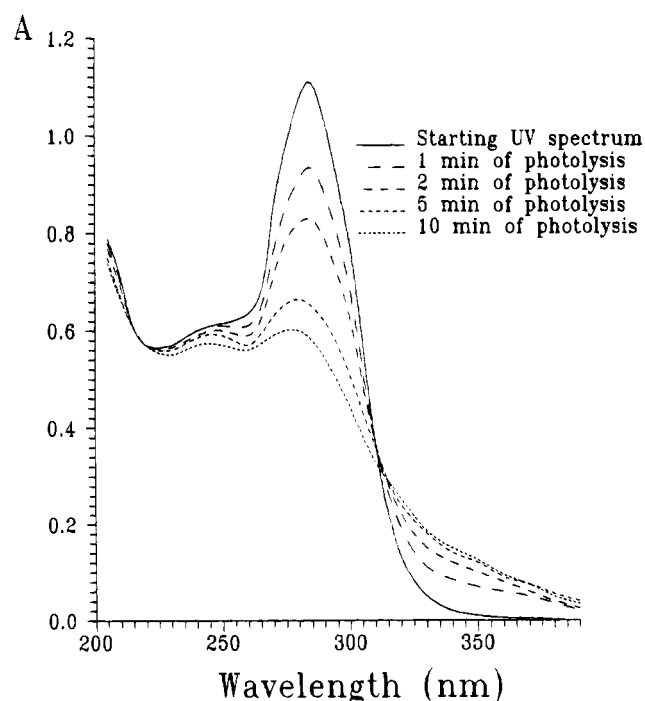
Figure 1. Absorption spectra of **7** and the products of its photolysis.

Scheme 4
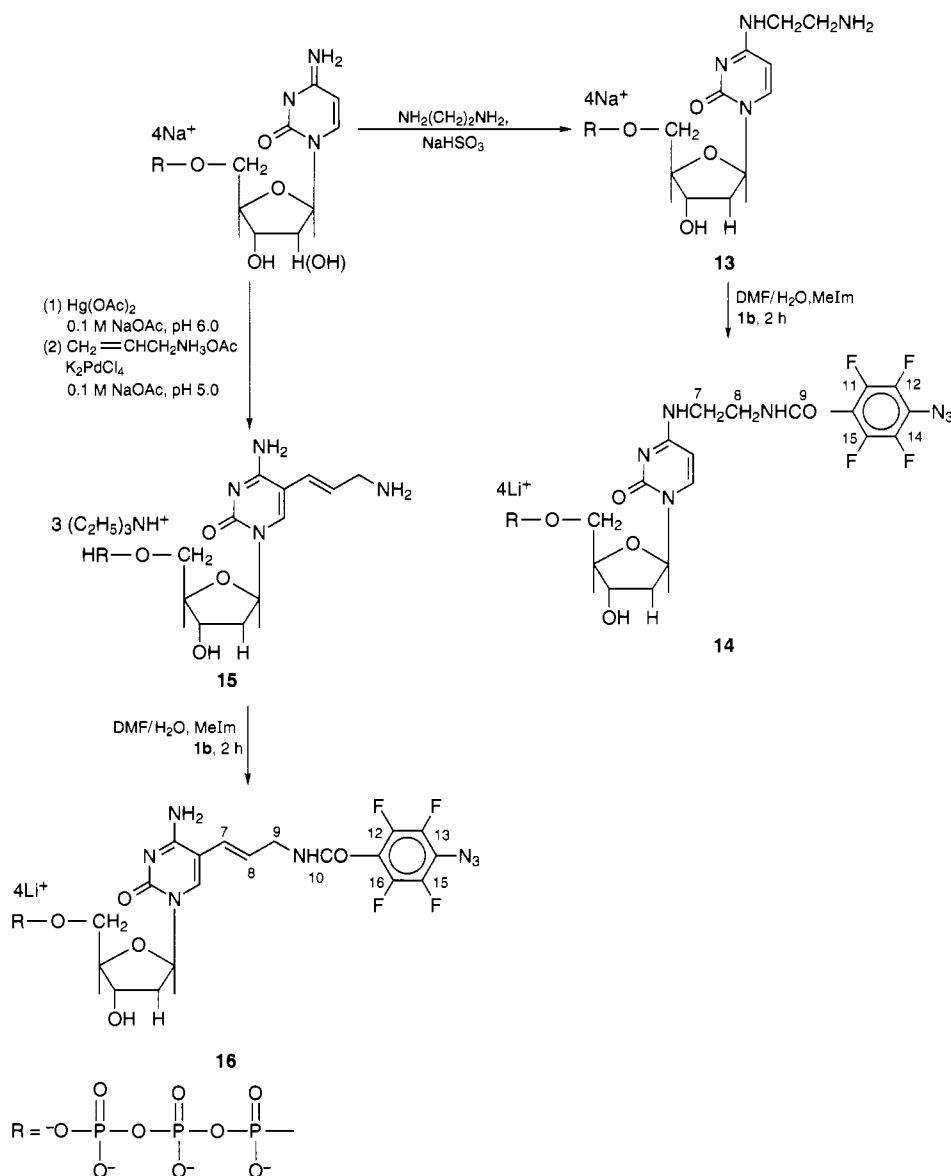
nent corresponding to a photoreagent residue gradually disappears. The rate of photolysis of **6a**, **6b**, **7**, **11**, **12**, **14**, and **16** in water is in accordance with the one of the corresponding photoreagents. Analysis of the data performed in the Figures 1–3 allowed us to conclude that the bathochromic and bathofloric shifts in **7** caused the increase of the photoreactivity in 15 times as compared with **12** and in two times as compared with **11** at the equal conditions of UV irradiation.

DISCUSSION

Far UV light (nearly 254 nm) irradiation structurally damages both nucleic acids and proteins and may lead to the lack of their biological relevance. For this reason, it is preferable to use photoreagents having λ_{max} in the near-UV region (300–360 nm). Amides of compound **3a** have λ_{max} = 318 nm, but amides of more photoreactive **1a** have λ_{max} = 258 nm, *i.e.*, in the far-UV region (Levina et al., 1993), and the photochemical properties of the latter reagent cannot be used effectively. To overcome this difficulty, photoreagent **2a** has been prepared. This reagent has an oxime group conjugated with a perfluorinated aromatic ring. An additional conjugation causes a bathochromic shift of λ_{max} of the *p*-azidotetrafluorophenyl group spectrum to 288 nm, which leads to the

increase of the photolysis rate in the conditions described in the Experimental Procedures and, consequently, to the less damaging influence on the investigated object by near-UV light, so **2b** is likely to be more useful for photoaffinity labeling.

Base-substituted analogs of dNTPs (NTPs) containing azido groups open new possibilities of the photoaffinity labeling of the template dependent enzymes such as DNA and RNA polymerases. The introduction of the reactive group into the 3'-end base of the growing chain by the catalytic activity of the enzymes permits the modification under UV-irradiation of both template and the protein near the catalytic site of DNA (RNA) polymerase. This approach looks promising for the fast kinetic analysis of the different stage of DNA (RNA) polymerization. (d)NTP derivatives containing long-range cross-linkers could be involved in the specific interactions with the active site pocket or even to be catalytically active after covalent binding to the enzyme. Therefore, these compounds can be used for catalytically competent labeling of the enzymes as was described recently (Doronin et al., 1994).

The use of photoreagents derived from *p*-azidotetrafluorobenzoic, 2-nitro-5-azidobenzoic, and 4-azidobenzoic acids shows that the degree of modification directed to proteins and nucleic acids considerably differs. In this
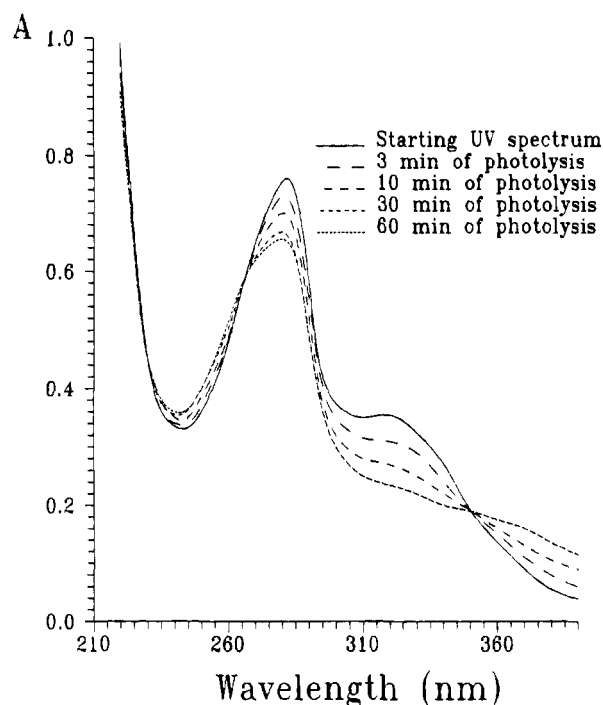
Figure 2. Absorption spectra of **11** and the products of its photolysis.
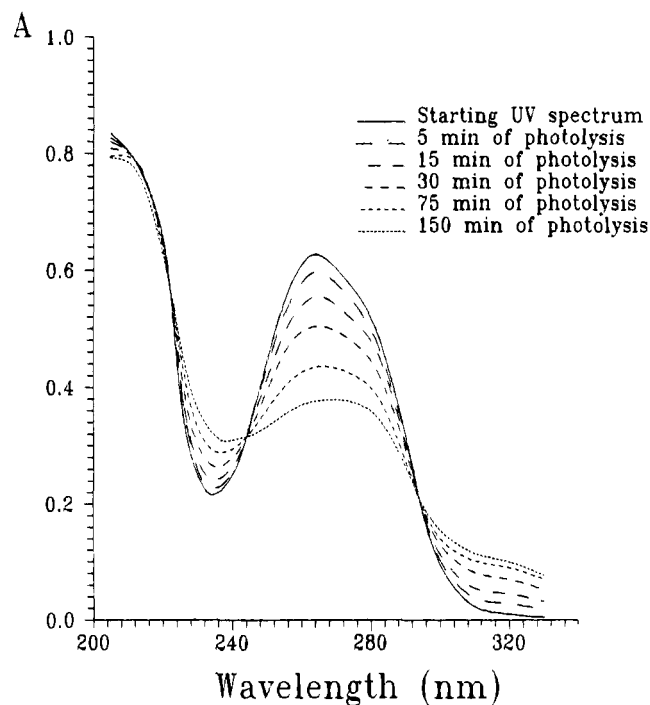
Figure 3. Absorption spectra of **12** and the products of its photolysis.

row, the degree of nucleic acid modification decreases, but the degree of protein modification increases. The reactivity of photoreagents depends on the type of particles generated under UV-light irradiation. The aromatic azides generate triplet nitrene, singlet nitrene, and 1,2-azacycloheptatetrene (Leyva et al., 1989; Keana and Cai, 1990), the singlet nitrene being the most reactive among them. The yield of singlet nitrene among the photolysis products is the largest in the case of the *p*-azidotetrafluorobenzoyl group, so the level of nucleic acid modification by this group is the highest. These remarkable properties provide the unique opportunity of the selective action both on the proteins and on the

nucleic acids using the derivatives of (d)NTPs conjugated with different photoreagents when protein–nucleic acid interactions are investigated.

LITERATURE CITED

Bogachev, V. S. (1995) Trifluoroacetic anhydride – a versatile reagent for preparation of wide range nucleotide derivatives. *Bioorg. Khim.* (in press).

Burgin, A. B., and Pace, N. R. (1990) Mapping the active site of ribonuclease P RNA using a substrate containing a photo-affinity agent. *EMBO J. 9*, 4111–4118.

Cartwright, I. L., and Hutchinson, D. W. (1980) Azidopolynucle-otides as photoaffinity reagents. *Nucleic Acids Res. 8*, 1675–1691.

Chen, J.-K., Franke, L. A., Hixson, S. S., and Zimmermann, R. A. (1985) Photochemical cross-linking of tRNA^Arg1 to the 30S ribosomal subunit using aryl azide reagents attached to the anticodon loop. *Biochemistry 24*, 4777–4784.

Dobrikov, M. I., Prichodjko, T. A., Safronov, I. V., and Shishkin, G. V. (1992a) Synthesis of photosensitive kapron membranes. Photoimmobilization of DNA. *Sib. Khim. J. 2*, 18–23.

Dobrikov, M. I., Zarytova, V. F., Komarova, N. I., Levina, A. S., Lokhov, S. A., Prikhodjko, T. A., Shishkin, G. V., Tabatadze, D. R., and Zaalishvilli, M. M. (1992b) Effective sequence-specific photomodification of nucleic acids by oligonucleotide derivatives bearing aromatic azido groups. *Bioorg. Khim. 18*, 540–549.

Doronin, S. V., Dobrikov, M. I., and Lavrik, O. I. (1992) Photoaffinity labeling of DNA polymerase α DNA primase complex based on the catalytic competence of a dNTP reactive analog. *FEBS Lett. 313*, 31–33.

Doronin, S. V., Dobrikov, M. I., Buckle, M., Roux, D., Buc, H., and Lavrik, O. I. (1994) Affinity modification of human immunodeficiency virus reverse transcriptase and DNA template by photoreactive dCTP analogs. *FEBS Lett. 354*, 200–202.

Evans, R. K., Johnson, J. D., and Haley, B. E. (1986) 5-Azido-2'-deoxyuridine 5'-triphosphate: a photoaffinity labeling reagent and tool for the enzymatic synthesis of photoactive DNA. *Proc. Natl. Acad. Sci. U.S.A. 83*, 5382–5386.

Gebeyehu, G., Rao, P. I., SooChan, P., Simms, D. A., and Klevan, L. (1987) Novel biotinylated nucleotide – analogs for labeling and colorimetric detection of DNA. *Nucleic Acids Res. 15*, 4513–4534.

Haley, B. E. (1983) Development and utilization of 8-azidopurine nucleotide photoaffinity probes. *Fed. Proc. 42*, 2831–2836.

Hanna, M. M., Zhang, Y., Reidling, J. C., Thomas, M. J., and Jou, J. (1993) Synthesis and characterization of a new photocrosslinking CTP analog and its use in photoaffinity labeling *E. coli* and T7 RNA polymerases. *Nucleic Acids Res. 21*, 2073–2079.

Ikehara, M., and Kaneko, M. (1970) Studies of nucleosides and nucleotides—XLI. Purine cyclonucleosides-8: Selective sulfonylation of 8-bromoadenosine derivatives and an alternate synthesis of 8,2'- and 8,3'-S-cyclonucleosides. *Tetrahedron 26*, 4251–4259.

Kalinowski, H.-O., Berger, S., Braun, S. (1988) *Carbon-13 NMR spectroscopy*, pp 399–400, John Wiley & Sons, Chichester, New York, Brisbane, Toronto, Singapore.

Keana, J. F. W., and Cai, S. X. (1990) New reagent for photoaffinity labeling: synthesis and photolysis of function-alized perfluorophenyl azides. *J. Org. Chem. 55*, 3640–3647.

Kohler, P., Wachtl, M., and Tamm, C. (1980) Nucleoside und Nucleotide. Teil 15. Synthese von Desoxyribonucleosid-monophosphaten und triphosphaten mit 2(1H)-Pyrimidinon,

2(1H)-Pyridinon und 4-Amino-2(1H)-pyridinon als Basen. (Nucleosides and nucleotides. Part 15. Synthesis of deoxyribonucleoside monophosphates and triphosphates with 2(1H)-pyrimidinone, 2(1H)-pyridinone and 4-amino-2(1H)-pyridinone as bases.) *Helv. Chim. Acta 63,* 2488−2494.

Langer, P. R., Waldrop, A. A., and Ward, D. C. (1981) Enzymatic synthesis of biotin-labeled polynucleotides: novel nucleic acid affinity probes. *Proc. Natl. Acad. Sci. U.S.A. 78,* 6633−6637.

Levina, A. S., Tabatadse, D. R., Khalimskaya, L. M., Prichodko, T. A., Shishkin, G. V., Alexandrova, L. A., and Zarytova, V. P. (1993) Oligonucleotide derivatives bearing reactive and stabilizing groups attached to C5 of deoxyuridine. *Bioconjugate Chem. 4,* 319−325.

Leyva, E., Munoz, M. S., and Platz, J. (1989) Photochemistry of fluorinated aryl azides in toluene solutions and in frozen polycrystals. *J. Org., Chem. 54,* 5938−5945.

MacFarlane, D. E., Mills, D. C. B., and Srivastava, P. C. (1982) Photoaffinity labeling of red blood cell platelets with 2-azidoadenosine triphosphate. *Biochemistry 21,* 544−549.

Mitina, R. L., Doronin, S. V., Dobrikov, M. I., Tabatadze, D. R., Levina, A. S., and Lavrik, O. I. (1992) Human immunodefi-ciency virus type I reverse transcriptase: Affinity labeling of the primer binding site. *FEBS Lett. 312,* 249−251.

Moffatt, J. G. (1964) A general synthesis of nucleoside-5'-triphosphates. *Can. J. Chem. 42,* 599−604.

Sarfati, S. R., Pochet, S., Guerreiro, C., Namane, A., Huynh-Dinh, T., and Igolen, J. (1987) Synthesis of fluorescent or biotinylated nucleoside compounds. *Tetrahedron 43,* 3491−3497.

Svinarchuk, F., Mastyugin, V., Dobrikov, M., and Doronin, S. (1993) Determination of the molecular mass of the transcription factor interacting with FBS2 in c-fos promoter. *Nucleic Acids Res. 21,* 2535−2536.

Strobel, O. K., Bobst, E. V., and Bobst, A. M. (1989) Nick translation of λ phage DNA with a deoxycytidine analog spin labeled in the 5 position. *Arch. Biochem. Biophys. 273,* 597−601.

Sylvers, L. A., and Wower, J. (1993) Nucleic acid-incorporated azidonucleotides: probes for studying the interaction of RNA or DNA with protein and other nucleic acids. *Bioconjugate Chem. 4,* 411−418.

Galactose-Containing Amphiphiles Prepared with a Lipophilic Radical Initiator: Association Processes between Liposomes Triggered by Enzymatic Reaction[†]

Kohji Ohno, Katsuko Sohda, Ayako Kosaka, and Hiromi Kitano*

Department of Chemical and Biochemical Engineering, Toyama University, Toyama 930, Japan. Received December 14, 1994[⊗]

A galactose-containing monomer (2-(methacryloyloxy)ethyl β-D-galactopyranoside, MEGal) was polymerized by using a lipophilic radical initiator. The amphiphile obtained formed a liposome by mixing with bis(*trans,trans*-2,4-dioctadecadienoyl)phosphatidylcholine (DDPC), and the liposome obtained was physically stabilized by the polymerization of DDPC by UV irradiation. The enzymatic treatment of the galactose-containing liposomes with galactose oxidase resulted in the formation of aldehyde groups on the liposome surface. By the subsequent mixing of the liposome suspension with the amino group-containing liposome suspension, a rapid increase in turbidity was observed due to the formation of Schiff bases between the aldehyde groups and the amino groups at the interface of the liposomes. The rate of turbidity change strongly depended on the degree of polymerization of MEGal, the surface densities of galactose and amino groups on the liposome, the distance from the liposome surface to amino end groups, and the flexibility and deformability of the liposomes.

INTRODUCTION

Mutual recognition of cells *in vivo* is an essential factor for the organization of tissues and organs and the immunological protection system (*1*). In recent years, some potential techniques have been developed using the specific binding of ligand to receptor at the lipid–lipid interface (so-called cross-linked liposomes) (*2–5*). We have been studying the mutual recognition between liposomes whose surfaces are modified with complementary compounds (enzyme–enzyme inhibitor, biotin–avidin, for example) (*4, 5*). Previously, Novogrodsky reported that lymphocyte cytotoxicity could be induced by treatment with neuraminidase and galactose oxidase or with the periodate of either the effector cells or the target cells, which initiated cross-linkage between the effector and target cells via a Schiff base (*6*). In this study, as a model system of this phenomenon, we examined the recognition of amino group-containing liposomes by galactose-containing liposomes that had been treated with galactose oxidase beforehand.

Previously we prepared liposome-forming amphiphiles having pH or temperature responsiveness by the polymerization of acrylic acid or *N*-isopropylacrylamide by using a lipophilic radical initiator (*7*) or lipophilic chain transfer reagent (*8*), respectively. Using the lipophilic radical initiator (DODA-501[1] (Figure 1a)) and a galactose-containing vinyl monomer (2-(methacryloyloxy)ethyl β-D-galactopyranoside, MEGal (Figure 1b)), we prepared galactose-containing amphiphiles with various degrees of polymerization (Figure 1c). A lipid carrying only one galactose residue (Figure 1d) was also prepared by the lactone method for comparison (*9*). By incorporating the galactose-containing amphiphile in liposomes, we could study the association processes of liposomes mediated by the Schiff bases, which were triggered by the enzymatic reaction.

EXPERIMENTAL PROCEDURES

Materials. A lipophilic radical initiator (DODA-501) was synthesized from *N*,*N*-dioctadecylamine (DODA, Fluka, Switzerland) and 4,4'-azobis(cyanovaleric acid) (V-501, Wako Pure Chemicals, Osaka, Japan) as described previously (*7*). A galactose-containing monomer, 2-(methacryloyloxy)ethyl β-D-galactopyranoside (MEGal), was prepared by trans-glycosylation between *o*-nitrophenyl β-D-galactopyranoside and 2-hydroxyethyl methacrylate (HEMA) catalyzed by β-galactosidase (from *Escherichia coli*, 340 units/mg, Sigma, St. Louis, MO) in a phosphate buffer (1/15 M, pH 6.4) (*10*) in the presence of hydroquinone. Anal. Calcd for $C_{12}H_{20}O_8 \cdot 1/2H_2O$: C, 47.84; H, 7.02; O, 45.14. Found: C, 47.65; H, 6.88; O, 45.47. ^{1}H NMR (D$_2$O): δ 6.15 (s, 1H, CH_2=C<, Z form H), 5.65 (s, 1H, CH_2=C<, E form H), 4.37 (m, 2H, COOCH_2CH$_2$), 3.68 (m, 2H, COOCH$_2$CH_2), 1.85 (s, 3H, CH_3), 4.80–3.40 (m, 11H, others), 4.77 (water of crystallization). *N*-Diglycyl-*N*,*N*-dioctadecylamide (GGA) was prepared by the reaction of *N*-benzyloxycarbonyl(Z)diglycine *p*-nitrophenyl ester with dioctadecylamine in THF and subsequent deprotection of the Z group by the HBr/CH$_3$COOH method (*11*). *N*-Glycyl-*N*,*N*-dioctadecylamide (GA) was also prepared from *N*-benzyloxycarbonyl(Z)glycine *p*-nitrophenyl ester in a similar way. A polymerizable lipid,

[1] Abbreviations: DDPC, bis(*trans,trans*-2,4-dioctadecadienoyl)-phosphatidylcholine; DLS, dynamic light scattering; DMF, dimethylformamide; DMPC, L-α-dimyristoylphosphatidylcholine; DODA, dioctadecylamine; DODA-L-Gal, dioctadecylamine–galactose conjugate prepared by the lactone method; DODA-PMEGal, dioctadecylamine–poly(2-(methacryloyloxy)ethyl β-D-galactopyranoside) conjugate; DODA-501, azo radical initiator with dioctadecyl groups; DP, degree of polymerization; DPPC, L-α-dipalmitoylphosphatidylcholine; EtOH, ethanol; GA, *N*-glycyl-*N*,*N*-dioctadecylamide; GGA, *N*-diglycyl-*N*,*N*-dioctadecylamide; HEMA, 2-hydroxyethyl methacrylate; HEPES, *N*-(2-hydroxyethyl)piperazine-*N*'-2-ethanesulfonic acid; MEGal, 2-(methacryloyloxy)ethyl β-D-galactopyranoside; MeOH, methanol; THF, tetrahydrofuran; T_m, the temperature of the midpoint of transition; V-501, 4,4'-azobis(cyanovaleric acid); WSC, 1-ethyl-3-[3-(dimethylamino)propyl]carbodiimide hydrochloride; Z, *N*-benzyloxycarbonyl.

(a) DODA-501

(b) MEGal

(c) DODA-PMEGal
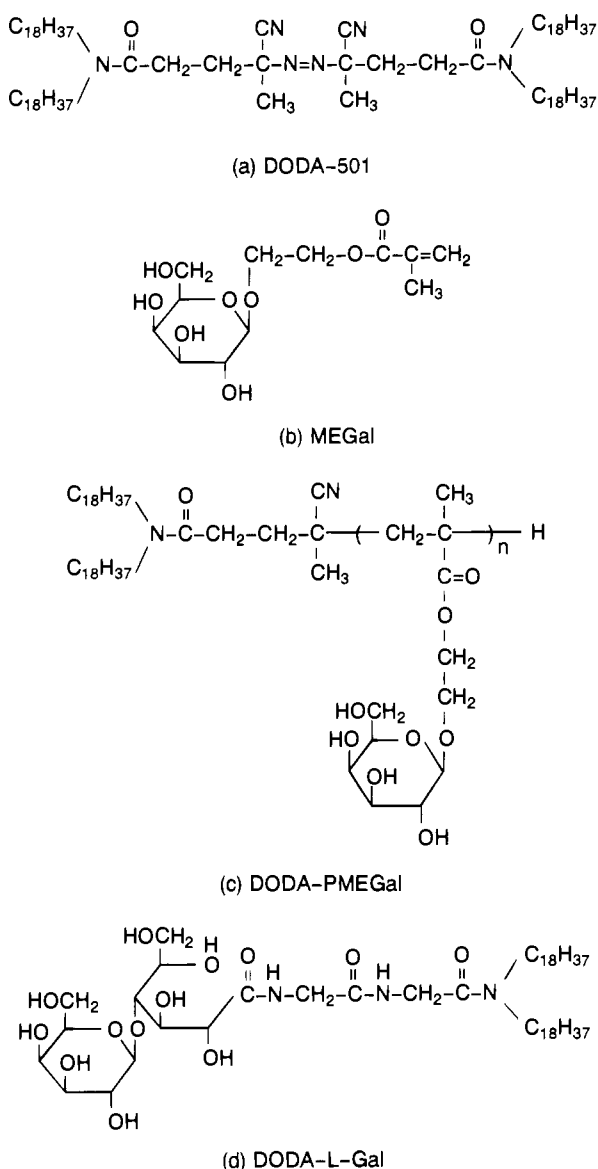
(d) DODA-L-Gal

Figure 1. Chemical structures of DODA-501 (a), MEGal (b), DODA-PMEGal (c), and DODA-L-Gal (d).

bis(*trans,trans*-2,4-dioctadecadienoyl)phosphatidylcholine (DDPC), was kindly donated by the Japan Fat and Oil Co. (Tokyo, Japan). L-α-Dipalmitoylphosphatidylcholine (DPPC), L-α-dimyristoylphosphatidylcholine (DMPC), and galactose oxidase (from *Dactylium dendroides*) were from Sigma. 1-Ethyl-3-[3-(dimethylamino)propyl]carbodiimide hydrochloride (WSC) and ammonium chloride were from Wako Pure Chemicals. Other reagents were commercially available. Deionized water was distilled before use.

Preparation of Galactose-Containing Amphiphile by Polymerization. The MEGal monomer (200 mg) and DODA-501 (176 mg) were dissolved in THF (20 mL), and after N_2 was bubbled for several minutes, the solution mixture was incubated in a tightly sealed test tube at 70 °C for 24 h. After evaporation of the solvent *in vacuo*, the viscous oil was washed with *n*-hexane to remove unreacted initiator by centrifugation at 10000g and 20 °C for 15 min. After decantation, the precipitate was dried *in vacuo* and dispersed in water (6 mL). Polymers without lipophilic end groups were removed by centrifugation at 10000g and 4 °C for 15 min. The lipid precipitate was collected and dried *in vacuo* to give white powder (8 mg, DODA-PMEGal, DP = 3.1). Further, the

products with a higher degree of polymerization in the supernatant solution were purified by passage through a GPC column (Sephacryl S-200, 2 cm i.d. × 18 cm, mobile phase, water) and lyophilized (69 mg, DODA-PMEGal, DP = 8.4). IR: O—H stretching of galactose, 3350–3500 cm^{-1}; C≡N stretching, 2050 cm^{-1}; C=O stretching of the ester bond, 1720 cm^{-1}; C=O stretching of tertiary amide, 1630 cm^{-1}; CH_2 ν_{as}, 2950 cm^{-1}; CH_2 ν_s, 2870 cm^{-1}. The degree of polymerization (DP) of the amphiphile was determined by elemental analysis. DODA-PMEGal (DP = 3.1) Anal. Calcd for $C_{42}H_{82}N_2O(C_{12}H_{20}O_8)_{3.1}$: C, 61.78; H, 9.56; N, 1.82. Found: C, 61.71; H, 9.46; N, 1.81. DODA-PMEGal (DP = 8.4) Anal. Calcd for $C_{42}H_{82}N_2O(C_{12}H_{20}O_8)_{8.4}$: C, 55.43; H, 8.36; N, 0.91. Found: C, 55.44; H, 8.42; N, 0.91. DODA-PMEGal (DP = 15) was also prepared in a similar way (129 mg). DODA-PMEGal (DP = 15) Anal. Calcd for $C_{42}H_{82}N_2O(C_{12}H_{20}O_8)_{15}$: C, 53.16; H, 7.68; N, 0.56. Found: C, 53.13; H, 7.74; N, 0.56.

Preparation of Galactose Lipid by the Lactone Method. Details of the preparation are described elsewhere (*12*). Briefly, lactose monohydrate was oxidized by iodine in the presence of KOH at 40 °C. The precipitated solid was purified by recrystallization from MeOH–H_2O (12:5). The crystal was dissolved in H_2O, and the solution was passed through an ion-exchange column (Amberlite IR-120 B, H$^+$ form) several times. The aqueous solution of the product was mixed with EtOH, and the solvent was evaporated at 70 °C to form a lactose–lactone. *N*-Diglycyl-*N,N*-dioctadecylamide (GGA) was coupled with the lactone in DMF–CHCl$_3$ (3:1) at 60 °C for 6 h. The galactose-carrying lipid was purified by precipitation in *n*-hexane–EtOH (2:1). The precipitate was further dissolved in CHCl$_3$ and passed through a glass filter. The filtrate was finally evaporated to give a slightly yellow powder (DODA-L-Gal).

Preparation of Liposomes. *Galactose-Containing Liposomes.* DDPC was dissolved in chloroform in a small, round-bottomed flask. After evaporation of the solvent, the thin lipid membrane was dispersed in an *N*-(2-hydroxyethyl)piperazine-*N'*-2-ethanesulfonic acid (HEPES) buffer (pH 6.0, 10 mM) in which DODA-PMEGal had been dispersed beforehand. The dispersion was sonicated by an ultrasonifier (Astrason W-385, Heat System-Ultrasonics, Inc., New York) for 3 min while N_2 gas was passed through the suspension. To remove large aggregates, the liposome suspension obtained was passed through a membrane filter (SLGV025LS, Millipore, pore size 0.22 μm). The liposome passed through the filter was irradiated in a quartz cell by a UV lamp (HB-251A, Ushio, Tokyo, Japan) at room temperature for 4 h to enhance the physical stability of the liposome by polymerization. The progress of polymerization was followed by the decrease in absorbance at 258 nm by using a UV–visible spectrophotometer (Ubest-35, Japan Spectroscopic Co., Tokyo, Japan). To block a very small amount of carboxyl groups, corresponding to methacrylic acid residues that had been generated by cleavage of the ester bond in the galactose-containing amphiphile, the polymerized liposome suspension was incubated with WSC and ammonium chloride in HEPES buffer (pH 6.0, 10 mM) at room temperature for 12 h. The liposome suspension was separated from unreacted reagents by the GPC column (Sephadex G-10, 2 cm i.d. × 15 cm, eluting solution HEPES buffer (pH 6.0, 10 mM)). The turbid fraction was collected, and the ζ potential of the liposome was confirmed to be approximately 0 mV by using a laser zee meter (Model 501, Pen Kem, Inc., Bedford Hills, NY).

Amino Group-Containing Liposome. A phospholipid (DMPC or DPPC) and the amino group-containing lipid

(GGA or GA) were dissolved in chloroform in a small, round-bottomed flask. After evaporation of the solvent, the thin lipid membrane was dispersed in HEPES buffer (pH 6.0, 10 mM) by using a vortex mixer. The dispersion was further sonicated by the ultrasonifier for 3 min, while N_2 gas was passed through the suspension. The liposome suspension was finally passed through the membrane filter.

Characterization of Liposomes. Formation of liposomal structure was confirmed by the fluorescence dye incorporation technique using Eosin Y as a probe (7, 11) (excitation at 305 nm, emission at 571 nm, FP-777, Japan Spectroscopic Co.).

Dynamic Light Scattering Method. Hydrodynamic diameter of the liposomes was estimated by the dynamic light scattering (DLS) technique (DLS-7000, Otsuka Electronics, Hirakata, Japan, light source He−Ne laser, 632.8 nm).

Turbidity Measurement. The aggregation of liposomes mediated by Schiff bases was followed by the increase in turbidity at 350 nm by using the UV−visible spectrophotometer. The observation cell was thermostated at 37 °C by a Peltier device (EHC-363, Japan Spectroscopic Co.). The uncertainties of the rate of turbidity change were within 10%. The data in the figures represent the mean values of three measurements.

Enzyme Activity Measurement. The oxidation reaction of galactose residues catalyzed by galactose oxidase was followed using a spectrophotometric method (13, 14): Hydrogen peroxide formed by the oxidation of galactose was reduced by reaction with 4-aminoantipyrine and phenol catalyzed by peroxidase, and the increase in optical density due to the production of quinoneimine dye was measured at 500 nm for 5 min by the spectrophotometer thermostated at 25 °C. The initial increase in optical density per minute was calculated from the initial linear portion of the curve. One unit of galactose oxidase causes the formation of one micromole of hydrogen peroxide per minute at 25 °C. The stock solution of galactose oxidase was diluted to the appropriate concentrations, and the catalytic activity of the enzyme was checked just before use.

Distribution of Galactose-Containing Amphiphiles in Liposome. Galactose-containing DMPC liposomes were incubated with galactose oxidase, and the amount of quinoneimine dye produced was measured simultaneously by using the spectrophotometric method described earlier. After the mixture was sonicated to completely disrupt the liposome structure by the ultrasonifier for 10 min at 60 °C, the production of quinoneimine dye due to oxidation of galactose residues on the reorganized liposomes was measured.

Determinations of Aldehyde Groups and Amino Groups on the Liposome Surfaces. The determination of aldehyde groups was carried out with 3-methyl-2-benzothiazolinone hydrazone (15): 1 mL of 0.4 wt % aqueous solution of 3-methyl-2-benzothiazolinone hydrazone hydrochloride was added to 1 mL of sample solution. After 20 min, 1 mL of aqueous solution containing 1 wt % ferric chloride hexahydrate and 1.6 wt % sulfamic acid was added to the mixture. Ten minutes later, 2 mL of water was added to the mixture. Subsequently the absorbance at 610 nm of the final mixture was read.

The determination of amino groups was carried out with 2,4,6-trinitrobenzenesulfonic acid (16): 0.5 mL of 0.1 M $Na_2B_4O_7$ in 0.1 N NaOH was added to 0.5 mL of sample solution at 30 °C. Five minutes later, 20 μL of 1.1 M 2,4,6-trinitrobenzenesulfonic acid solution was added to the mixture. After 5 min, 2 mL of the solution
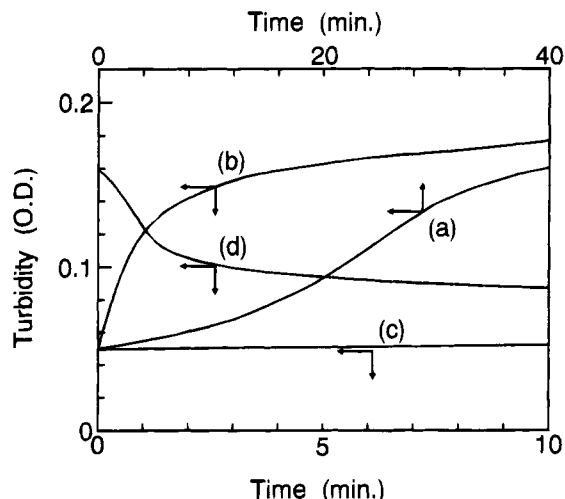
Figure 2. Typical profiles of a turbidity change. (a) Galactose oxidase solution was injected into the mixture of galactose-containing liposome suspension and amino group-containing liposome suspension incubated at 37 °C. (b) Amino group-containing liposome suspension was injected into galactose-containing liposome suspension that had been incubated with galactose oxidase solution for 30 min at 37 °C beforehand. (c) Amino group-containing liposome suspension was injected into galactose-containing liposome suspension that had been incubated with a buffer for 30 min at 37 °C beforehand. (d) 1/10 N NaOH solution (0.5 mL) was injected into the mixture (3 mL) after experiment b was complete. The final pH of experiment d was 10.5. In all experiments, the contents of galactose-containing lipid (DP = 8.4) and amino group-containing lipid (GGA) were 4.5 and 10 mol %, respectively. The concentrations of both liposomes were 100 μg of lipid/mL, and the concentration of enzyme was 0.1 unit/mL (HEPES (10 mM, pH 6.0) buffer; wavelength = 350 nm).

(the mixture of 0.3 mL of 0.1 M Na_2SO_3 and 19.7 mL of 0.1 M KH_2PO_4) was added to the mixture to stop the reaction. Subsequently, the absorbance at 420 nm of the final mixture was read.

RESULTS AND DISCUSSION

Association of Amino Group-Containing Liposome with Aldehyde Group-Carrying Liposome. By using a dynamic light scattering technique, the average diameters of the galactose-containing liposomes and the amino group-containing liposomes were estimated to be 900 and 1400 Å, respectively. After the incubation of galactose-containing liposome with a solution of galactose oxidase, the production of H_2O_2 was confirmed by the spectrophotometric method. When the concentrations of galactose-containing DMPC liposome (DODA-PMEGal (DP = 8.4), 4.5 mol %) and galactose oxidase were 46 μg of lipid/mL and 0.09 unit/mL, respectively, galactose residues on the outer liposome surfaces were completely oxidized by the enzyme in 30 min, which showed that the enzyme could effectively oxidize galactose residues on the liposome surface (17). We could determine that the affinity of galactose oxidase for the galactose residues on the liposome surface (K_m = 2.2 mM) was larger than that for free galactose (K_m = 17.3 mM) and that V_{max} values were comparable each other. Further investigations of the catalytic behavior of enzymes at membrane interfaces are now in progress and will be reported shortly.

By injecting the solution of galactose oxidase into the mixture of the galactose-containing liposome suspension and the amino group-containing liposome suspension, the turbidity increased gradually and then increased steeply (Figure 2a), whereas after the amino group-containing liposome suspension was mixed with the suspension of

the galactose-containing liposomes that had been incubated with a galactose oxidase solution for 30 min at 37 °C, the turbidity increased quickly (Figure 2b). On the contrary, when the suspension of the galactose-containing liposomes incubated only with a buffer solution in place of the enzyme solution was used, there was no increase in the turbidity (Figure 2c), which shows that the enzymatic reaction triggers the turbidity change. The apparent liposome diameter after the turbidity increased and leveled off was estimated to be around 8300 Å by using the dynamic light scattering technique.

To verify that the liposomes were aggregated and not fused, we examined the leakage of fluorescence dye after mixing the amino group-containing liposomes (Eosin Y had been incorporated) with the galactose-containing liposomes that had been incubated with the galactose oxidase solution for 30 min at 37 °C beforehand. The increase in fluorescence intensity observed was only comparable to that in the control experiment in which the galactose-containing liposome *without* oxidation by galactose oxidase was used. This result suggests that both liposomes were *not* fusing.

Furthermore, when a 0.1 N NaOH solution was injected into the mixture after experiment b was complete, the turbidity gradually decreased (Figure 2d) probably due to the disruption of aggregates. These results show that the increase in turbidity is due to the specific recognition of aldehyde groups on the liposome surfaces by the amino group-containing liposomes, which results in the aggregation of both liposomes mediated by the Schiff bases. The Schiff base is well-known to be easily cleaved by acids and bases (*18*). To confirm whether a number of other things could have happened to affect the turbidity measurement under the strong alkaline conditions (after the injection of 0.1 N NaOH), the amounts of aldehyde groups and amino groups in the mixed liposome suspension after the injection of 0.1 N NaOH were compared with those before aggregation. The amounts of aldehyde groups and amino groups were approximately equivalent in each case. Furthermore, the average diameter of liposome mixtures after the injection of 0.1 N NaOH was estimated to be 1150 Å by using the dynamic light scattering method (the average diameters of the galactose-containing liposomes and the amino group-containing liposomes were 900 and 1400 Å, respectively). These results support the turbidity decreasing gradually because of the disruption of aggregates. To simplify the reaction system hereafter, the enzymatic treatment of galactose-containing liposomes was carried out for 30 min prior to mixing with the amino group-containing liposomes.

Effect of DP on the Association Processes. The rate of turbidity change was largely affected by the degree of polymerization of DODA-PMEGal in the liposomes (Figure 3). As for liposomes containing DODA-L-Gal, which has only one galactose residue, there was no increase in turbidity. When the reactivity of the enzyme with galactose-containing amphiphiles on the liposome surface was examined, the increment of optical density in 30 min due to the production of quinoneimine dye for the DODA-L-Gal liposome was only 14% of that for the DODA-PMEGal (DP = 8.4) liposome. Furthermore, when the amino group-containing liposome suspension was injected into the suspension of the DODA-L-Gal-containing liposomes that had been incubated with the solution of galactose oxidase for 24 h at 37 °C beforehand, the increase in turbidity was not observed at all. These results show that the reactivity of the enzyme with DODA-L-Gal on the liposome surface was very low.
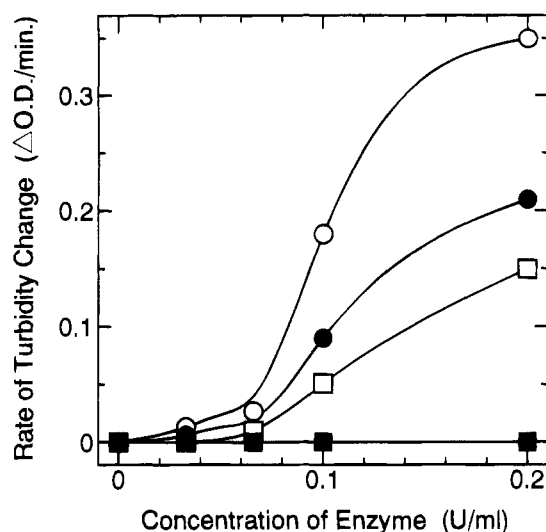
Figure 3. Effect of concentration of enzyme on the rate of turbidity change after injection of the amino group-containing liposome suspension into the galactose-containing liposome suspension that had been incubated with galactose oxidase for 30 min at 37 °C beforehand: (○) DODA-PMEGal (DP = 15); (●) DODA-PMEGal (DP = 8.4); (□) DODA-PMEGal (DP = 3.1); (■) DODA-L-Gal. The contents of galactose-containing lipid and GGA were 4.5 and 10 mol %, respectively. The concentrations of both liposomes were 100 μg of lipid/mL (HEPES (10 mM, pH 6.0) buffer; wavelength = 350 nm).

By increasing the degree of polymerization, the rate of turbidity change became larger probably because of the decrease in the steric hindrance. Previously the lectin-induced aggregation of sugar-containing liposomes was examined (*12, 19*). The lectin was captured in sugar-carrying long polymer chains on the liposome surface, and it was not so easy for the lectin to bind to sugar residues on the other liposome surface simultaneously, which reduced the rate of turbidity change at high degree of polymerization. In the liposome—liposome system examined here, such complete capture of the amino group-containing liposome by the liposome carrying long polymer (PMEGal) chains might not occur because the liposomes are gigantic. Consequently, the increase in the rate of turbidity change with the degree of polymerization of DODA-PMEGal observed here is understandable.

Effect of Surface Concentration of Aldehyde Group on the Association Processes. The distribution of the galactose-containing amphiphiles in the liposome was determined by the method described in the Experimental Procedures section. The amount of quinoneimine dye produced after sonication was 8.6% of that before sonication, which shows that the galactose-containing amphiphiles were preferentially (85.3%) distributed in the outer layer of the liposome. Consequently, the number of galactose residues on the outer layer of the liposome was estimated to be about 4300 times as many as that of enzyme molecules when the concentrations of galactose-containing liposome (DODA-PMEGal (DP = 15), 4.5 mol %) and enzyme were 100 μg of lipid/mL and 0.1 unit/mL, respectively.

By varying the concentration of galactose oxidase to be incubated with galactose-containing liposomes, we tried to examine the effect of the concentration of aldehyde groups on the liposome surface on the rate of turbidity change (Figure 3). Since the production of aldehyde groups is directly proportional to the concentration of enzyme, the increase in the rate of turbidity change with concentration of enzyme could be expected. The rate of turbidity change, however, did not increase significantly at low concentrations of the enzyme and

Figure 4. Effect of mixing ratio of DDPC and DODA-PMEGal (DP = 15) in the liposome on the rate of turbidity change after injection of the amino group-containing liposome suspension into the galactose-containing liposome that had been incubated with galactose oxidase for 30 min at 37 °C beforehand: (○) DMPC/GGA liposome; (●) DMPC/GA liposome; (□) DPPC/GGA liposome; (■) DPPC/GA liposome. The content of amino group-containing lipid was 10 mol %. The concentrations of both liposomes were 100 μg of lipid/mL. The concentration of enzyme was 0.1 unit/mL (HEPES (10 mM, pH 6.0) buffer; wavelength = 350 nm).

then increased steeply with the concentration, which suggests the presence of a threshold value in the recognition of aldehyde groups by amino group-containing liposomes. This result is in accordance with the steep increase in the turbidity 15 min after the onset of the reaction observed in Figure 2a. To realize the stable binding between two kinds of liposomes, the multiple formation of Schiff bases between many aldehyde groups and amino groups might be necessary, thus bringing about a threshold phenomenon.

To examine the effect of the surface concentration of galactose residues on the rate of turbidity change, liposomes with various molar ratios of DODA-PMEGal (DP = 15) and DDPC were prepared. Figure 4 shows that the rate of turbidity change increased with the content of DODA-PMEGal (DP = 15), in contrast to the results of Figure 3. This is probably because the catalytic behavior of the enzyme at interfaces is more complicated compared to that with the free substrate in solution. Further findings about this will be reported in the near future.

We also investigated the role of lipid composition on membrane—membrane dissociation reactions: The suspension of the galactose-containing liposome with various molar ratios of DODA-PMEGal (DP = 8.4) and DDPC was incubated with galactose oxidase for 60 min at 37 °C. After the liposome suspension was mixed with the amino group-containing liposome suspension, the turbidity increased and leveled off. Subsequently, 0.05 N NaOH was injected into the turbid mixture. The rates of decrease in turbidity had *no* obvious differences in the range of concentration ratios in which these experiments were carried out (DODA-MEGal, 1.7—6.6 mol %; GGA, 10 mol %) (data not shown). The number of galactose residues on the liposome surface even at the lowest molar ratio (DODA-PMEGal (DP = 8.4), 1.7 mol %) was about 1.4 times as many as that of the amino groups on the liposome surface. Since the growth of the multiple formation of Schiff bases would be restricted due to the steric hindrance, the number of Schiff bases formed until

the turbidity leveled off might be approximately similar in each case. Therefore, the surface concentration of aldehyde groups on the liposome might affect the initial association processes between liposomes, but probably not the dissociation processes at lipid—lipid interfaces.

Effects of Membrane Flexibility and Deformability on the Association Processes. The rate of turbidity change due to the association of aldehyde group-containing liposome with the amino group-containing liposome composed of DMPC and GGA was larger than that with the liposome composed of DPPC and GGA. A similar result was obtained when GA was used instead of GGA (Figure 4). Since the experiment was carried out at 37 °C, DMPC (T_m = 24 °C) and DPPC (T_m = 42 °C) were in the liquid crystal phase and the gel phase, respectively. The membrane flexibility and deformability of the liposome prepared with DMPC would be, therefore, higher than those of DPPC liposomes, which makes it easier for amino groups to form Schiff bases with aldehyde groups.

Previously we examined the effect of temperature on the inhibition of trypsin by soybean trypsin inhibitor at the lipid—lipid interface (*4*). The K_i value was strongly dependent on the gel—liquid crystal phase transition temperature of the liposome, which supports the importance of deformability of liposomes in the recognition at the lipid—lipid interface.

As shown in Figure 4, the rate of turbidity change for the GGA liposome was slightly larger than that for the GA system (the length between a primary amino group and a tertiary amide group of GGA was longer than that of GA by one glycine residue (about 4 Å)). These results show the importance of steric hindrance for the recognition of amino groups by the aldehyde groups.

Effect of Surface Concentration of Amino Group on the Association Processes. To examine the effect of pH in the solution on the rate of turbidity change, a suspension of the amino group-containing liposome with various pH values was injected into the galactose-containing liposome suspension that had been incubated with the galactose oxidase solution for 30 min at pH 6 beforehand (Figure 5). The rate of turbidity change decreased largely with the increase in pH of the solution after mixing, and at pH > 8.5 we could observe no change in turbidity (no aggregation of liposomes in other words), which shows the large pH sensitivity of association processes between the liposomes.

By using amino group-containing liposomes with various ratios of GGA and DMPC, we could examine the effect of the surface concentration of amino groups on the rate of turbidity change. As shown in Figure 6, the rate of turbidity change increased with the surface concentration below about 9 mol % of GGA in the liposome and then decreased significantly. The rate of the condensation reaction to produce the Schiff base is known to be the largest in the pH range 3—5 (*20*). As a possibility, the pH in the vicinity of the liposome surface with a high content of GGA might become higher than that in bulk solution, which makes it more difficult to form Schiff bases between two kinds of liposomes. Therefore, the surface concentration of amino groups strongly affects the rate of turbidity change. This result is consistent with the pH sensitivity of association processes described earlier.

In conclusion, primary hydroxyl groups of galactose residues bound to the polymer chains existing on the liposome surface could be oxidized by galactose oxidase and converted into aldehyde groups. The Schiff bases formed between aldehyde groups and amino groups on the other liposome surfaces resulted in aggregation of the
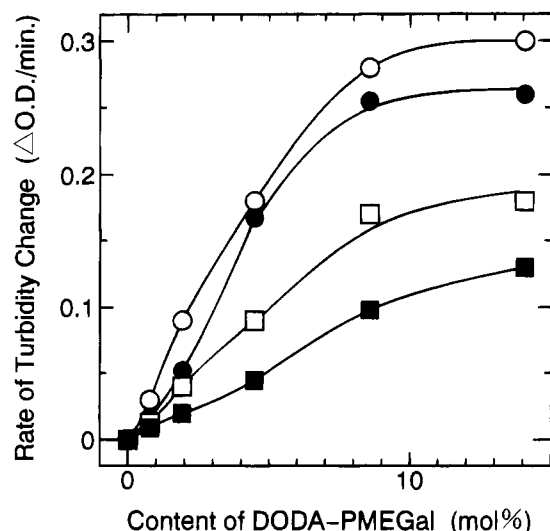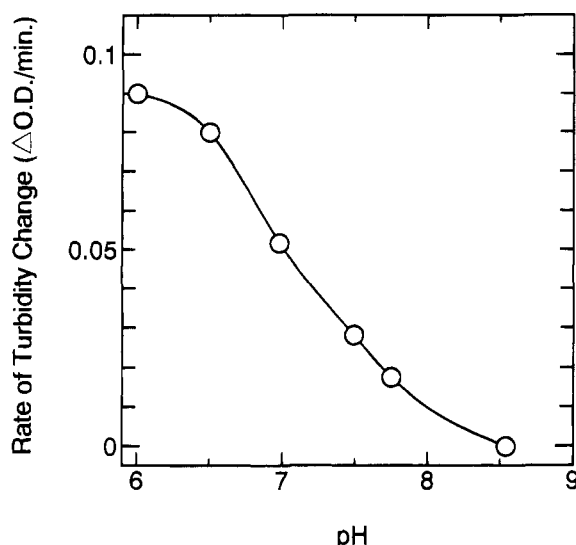
Figure 5. Effect of pH in the solution on the rate of turbidity change after injection of the amino group-containing liposome suspension with various pH values into the galactose-containing liposome that had been incubated with galactose oxidase for 30 min at 37 °C beforehand. The contents of DODA-PMEGal (DP = 8.4) and GGA were 4.5 and 10 mol %, respectively. The concentrations of both liposomes were 100 μg of lipid/mL. The concentration of enzyme was 0.1 unit/mL. The galactose-containing liposome was incubated with the enzyme in HEPES (10 mM, pH 6.0) buffer (wavelength = 350 nm).
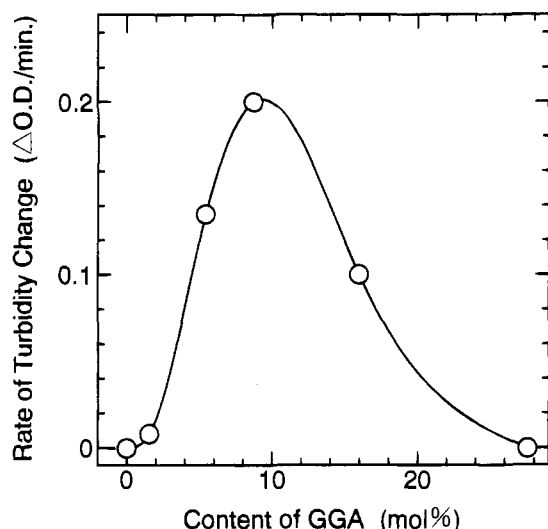
Figure 6. Effect of the mixing ratio of DMPC and GGA in the liposome on the rate of turbidity change after injection of the amino group-containing liposome into the galactose-containing liposome that had been incubated with galactose oxidase for 30 min at 37 °C beforehand. The content of DODA-PMEGal (DP = 15) was 4.5 mol %. The concentrations of both liposomes were 100 μg of lipid/mL. The concentration of enzyme was 0.1 unit/ mL (HEPES (10 mM, pH 6.0) buffer; wavelength = 350 nm).

liposomes. The rate of turbidity change depended on the densities of galactose and amino groups on the liposome surfaces, the distance from the liposome surface to the galactose residue and amino end groups, and the membrane flexibility and deformability. The results obtained also suggest the importance of morphology of the cell surface in cell—cell recognition phenomena such as lymphocyte cytotoxicity.

ACKNOWLEDGMENT

LITERATURE CITED

(1) Stevenson, B. R., Gallin, W. J., and Paul, D. L. (1992) *Cell-Cell Interactions,* Oxford University Press, New York.

(2) Müller, W., Ringsdorf, H., Rump, E., Wildburg, G., Zhang, X., Angermaier, L., Knoll, W., Liley, M., and Spinke, J. (1993) Attempts to Mimic Docking Processes of the Immune System: Recognition-Induced Formation of Protein Multilayers. *Science 262,* 1706–1708.

(3) Chiruvolu, S., Walker, S., Israelachvili, J., Schmitt, F.-J., Leckband, D., and Zasadzinski, J. A. (1994) Higher Order Self-Assembly of Vesicles by Site-Specific Binding. *Science 264,* 1753–1756.

(4) Kitano, H., Kato, N., Tanaka, N., and Ise, N. (1988) Mutual Recognition between Polymerized Liposomes: Enzyme and Enzyme Inhibitor System. *Biochim. Biophys. Acta 942,* 131–138.

(5) Kitano, H., Kato, N., and Ise, N. (1989) Mutual Recognition between Polymerized Liposomes: Macrophage Model System by Polymerized Liposomes. *J. Am. Chem. Soc. 111,* 6809–6813.

(6) Novogrodsky, A. (1975) Induction of Lymphocyte Cytotoxicity by Modification of the Effector or Target Cells with Periodate or with Neuraminidase and Galactose Oxidase. *J. Immunol. 114,* 1089–1093.

(7) Kitano, H., Akatsuka, Y., and Ise, N. (1991) pH-Responsive Liposomes Which Contain Amphiphiles Prepared by Using Lipophilic Radical Initiator. *Macromolecules 24,* 42–46.

(8) Kitano, H., Maeda, Y., Takeuchi, S., Ieda, K., and Aizu, Y. (1994) Liposomes Containing Amphiphiles Prepared by Using a Lipophilic Chain Transfer Reagent: Responsiveness to External Stimuli. *Langmuir 10,* 403–406.

(9) Kobayashi, K., Sumitomo, H., and Ina, Y. (1985) Synthesis and Functions of Polystyrene Derivatives Having Pendant Oligosaccharides. *Polym. J. 17,* 567–575.

(10) Matsumura, S., Kubokawa, H., and Toshima, K. (1993) Enzymatic Synthesis of Novel Vinyl Monomers Bearing β-D-Galactopyranoside Residue. *Makromol. Chem., Rapid Commun. 14,* 55–58.

(11) Kitano, H., Wolf, H., and Ise, N. (1990) pH-Responsive Release of Fluorophore from Homocysteine-Carrying Polymerized Liposomes. *Macromolecules 23,* 1958–1961.

(12) Kitano, H., Sohda, K., and Kosaka, A. (1995) Galactose-Containing Amphiphiles Prepared with a Lipophilic Radical Initiator. *Bioconjugate Chem. 6,* 131–134.

(13) Cooper, J. A. D., Smith, W., Bacila, M., and Medina, H. (1959) Galactose Oxidase from *Polyporus circinatus,* Fr. *J. Biol. Chem. 234,* 445–448.

(14) Avigad, G., Amaral, D., Asensio, C., and Horecker, B. L. (1962) The *D*-Galactose Oxidase of *Polyporus circinatus. J. Biol. Chem. 237,* 2736–2743.

(15) Pesez, M., and Bartos, J. (1974) *Calorimetric and Fluorimeter Analysis of Organic Compounds and Drugs,* pp 264–266, Marcel Dekker, New York.

(16) Fields, R. (1971) Measurement of Amino Groups in Proteins and Peptides. *Biochem. J. 124,* 581–590.

(17) Sharon, N. (1975) *Complex Carbohydrates: Their Chemistry, Biosynthesis, and Functions,* Addison-Wesley, Reading, MA.

(18) March, J. (1977) *Advanced Organic Chemistry: Reactions, Mechanisms, and Structure,* 2nd ed., p 806, McGraw-Hill, New York.

(19) Kitano, H., and Ohno, K. (1994) Sugar-Containing Lipids Prepared by Using a Lipophilic Radical Initiator: Interfacial Recognition by Lectin as Studied by Using the Multiple Internal Reflection Fluorescence Method. *Langmuir 10,* 4131–4135.

(20) Pine, S. H. (1987) *Organic Chemistry,* 5th ed., p 248, McGraw-Hill, New York.

Cobra Venom Factor Immunoconjugates: Effects of Carbohydrate-Directed versus Amino Group-Directed Conjugation[†]

Jane Zara,[‡,§] Nicholas Pomato,[∥] Richard P. McCabe,[∥,⊥] Reinhard Bredehorst,[‡,▽] and Carl-Wilhelm Vogel*,[‡,▽]

Departments of Biochemistry and Molecular Biology and Medicine, Georgetown University, Washington, D.C. 20007, and Organon Teknika Corporation/Biotechnology Research Institute, Rockville, Maryland 20850. Received November 29, 1994[⊛]

Human IgM monoclonal antibody 16-88, derived from patients immunized with autologous colon carcinoma cells, was derivatized with two different cross-linkers, S-(2-thiopyridyl)-L-cysteine hydrazide (TPCH), which is carbohydrate-directed, and N-succinimidyl-3-(2-pyridyldithio)propionate (SPDP), which is amino group-directed. Two antibody functions, antigen binding and complement activation, were assayed upon derivatization with TPCH and SPDP. TPCH allowed for extensive modification (up to 17 TPCH molecules per antibody) without impairment of antigen binding activity, while this function was significantly compromised upon derivatization with SPDP. Antibody molecules derivatized with 16 SPDP residues showed almost complete loss of their antigen binding function. The complement activating ability of antibody 16-88 was significantly decreased after derivatization with TPCH or SPDP. In the case of SPDP derivatization, this decrease of the complement activating ability is predominantly a consequence of the impaired binding function. Upon conjugation of cobra venom factor (CVF), a nontoxic 137-kDa glycoprotein which is capable of activating the alternative pathway of complement, the antigen binding activity of SPDP-derivatized antibody was further compromised, whereas that of TPCH-derivatized antibody remained unaffected even after attachment of three or four CVF molecules per antibody. In both conjugates CVF retained good functional activity. CVF was slightly more active when attached to SPDP-derivatized antibody, suggesting a better accessibility of amino group-coupled CVF for its interaction with other complement proteins. These results indicate that carbohydrate-directed conjugation compromises the antibody function of complement activation, but allows for the generation of immunoconjugates with unimpaired antigen binding capability. Accordingly, carbohydrate-directed cross-linkers may contribute to improve the efficacy of immunoconjugates in cancer therapy.

The vast majority of immunoconjugates consisting of two proteins are synthesized by chemical methods with heterobifunctional cross-linking reagents consisting of two differently reactive groups (for reviews, see *1–4*). The ε-amino groups of lysine residues, present on the surface of most proteins including antibodies, are especially suitable for the attachment of cross-linkers in that they react with a number of reagents under conditions that leave other groups in the protein unmodified. As a result, heterobifunctional cross-linking reagents containing a primary amine-reactive group have gained wide popularity. Lysine residues, however, are randomly distributed on the surface of proteins, and therefore, derivatization of their ε-amino groups with heterobifunctional cross-

linking reagents may lead to impairment of protein function, e.g., antigen binding function in the case of antibodies. For a variety of antitumor monoclonal antibodies significant compromises in antigen binding activity have been observed upon derivatization with amine-reactive heterobifunctional cross-linking reagents such as N-succinimidyl-3-(2-pyridyldithio)propionate (SPDP)[1] *(5–7)*. In addition, the impairment of the antigen binding function is further increased for steric reasons when another protein is coupled to amine-attached cross-linker molecules at or in proximity to the antigen binding site.

Recently, we developed a novel heterobifunctional cross-linking reagent, S-(2-thiopyridyl)-L-cysteine hydrazide (TPCH), which contains a hydrazide moiety for coupling to aldehyde groups generated in the carbohydrate residues of antibodies by mild periodate oxidation, and a pyridyl disulfide group for coupling of effector molecules with a free sulfhydryl group *(8)*. Since the carbohydrate moieties are distal to the antigen binding region of antibodies *(9)*, derivatization with this cross-linker and subsequent coupling of effector molecules can be expected to minimize impairment of the antigen binding function. In the present study, we evaluated the effects of carbohydrate-directed and amino group-directed conjugation procedures using the human monoclonal IgM antibody 16-88 raised against human colon carcinoma

* To whom correspondence should be addressed: University of Hamburg, Department of Biochemistry and Molecular Biology, Martin-Luther-King-Pl. 6, 20146 Hamburg, Germany.

[‡] Georgetown University.

[§] Current address: Department of Pharmacology, University of Texas Southwestern Medical Center, Dallas, TX 75235.

[∥] Organon Teknika Corporation/Biotechnology Research Institute.

[⊥] Current address: Centocor Corporation, Malvern, PA 19355.

[▽] Current address: Department of Biochemistry and Molecular Biology, University of Hamburg, Martin-Luther-King-Pl. 6, 20146 Hamburg, Germany.

[1] Abbreviations: CVF, cobra venom factor; TPCH, S-(2-thiopyridyl)-L-cysteine hydrazide; SPDP, N-succinimidyl-3-(2-pyridyldithio)propionate; DTT, dithiothreitol; PBS, 10 mM Na-phosphate and 100 mM NaCl, pH 7.2; GPBS²⁺, PBS containing 0.1% (w/v) gelatin, 0.5 mM $MgCl_2$, and 0.9 mM $CaCl_2$.

cells (*10*) and cobra venom factor (CVF), a nontoxic 137-kDa glycoprotein which is capable of activating the alternative pathway of complement (for a review, see *11*), as a model system. The results of this comparative analysis demonstrate that IgM–CVF conjugates synthesized with SPDP are severely impaired in their antigen binding activities. In contrast, the novel carbohydrate-directed cross-linker TPCH allowed for the synthesis of IgM–CVF conjugates with no measurable impairment of the antigen binding function even when the antibody was derivatized with up to 17 TPCH molecules and three or four CVF molecules. Therefore, coupling of effector molecules to the carbohydrate region of antibodies may provide immunoconjugates with improved efficacy for the treatment of cancer.

MATERIALS AND METHODS

Antibody Derivatization with TPCH. Human monoclonal IgM antibody 16-88 was obtained from hollow fiber culture and purified by gel filtration and ion exchange chromatography as described previously (*10, 12*). The antibody (2 mg, 2.2 nmol) in 1.0 mL of 0.1 M sodium acetate, pH 5.5, was oxidized at 0 °C with 1 mM sodium metaperiodate for 15 min in the presence of 15 mM TPCH. The reaction mixture was subjected to size-exclusion chromatography on Sephadex G-25 (Pharmacia, Piscataway, NJ) equilibrated in 10 mM sodium phosphate and 100 mM sodium chloride (PBS), pH 7.2, and the derivatized antibody was stored at 4 °C. The extent of TPCH incorporation was determined by the release of pyridine-2-thione at 343 nm upon reduction with dithiothreitol (DTT) (*13*).

Antibody Derivatization with SPDP. The 16-88 antibody (2 mg, 2.2 nmol) was incubated with either 7, 13, or 26 nmol of SPDP (Sigma, St. Louis, MO) in a total volume of 1.0 mL of PBS, pH 7.2. After 30 min at 25 °C the pyridyldithio-derivatized antibody was purified by gel filtration on a G-25 Sephadex column in PBS, pH 7.2. The extent of cross-linker incorporation was determined as described above for TPCH.

Conjugation of CVF to Cross-Linker-Derivatized Antibody. CVF was purified from lyophilized cobra venom (*Naja naja kaouthia,* Serpentarium Laboratories, Salt Lake City, UT) and derivatized with SPDP as described previously (*14*). The SPDP-derivatized CVF (2.8 mol of SPDP/mol of CVF) was incubated in the presence of 50 mM DTT for 20 min at 25 °C to reduce the pyridyl disulfide residues, subjected to gel filtration chromatography on Sephadex G-25 equilibrated with deaerated PBS, pH 7.2, and then used immediately for conjugation to either TPCH-modified or SPDP-modified antibody. The reaction mixture containing cross-linker-derivatized antibody (1.3 mg) and sulfhydryl-modified CVF (1.5 molar excess over the number of antibody-attached cross-linker molecules) in a total volume of 1.0 mL of PBS, pH 7.2, was flushed with nitrogen and incubated for 15 h at 25 °C and then for 24 h at 4 °C. After purification of the antibody conjugates by size-exclusion chromatography using a Fractogel HW 65F column (1.5 × 115 cm) (EM Reagents, Gibbstown, NJ) equilibrated in PBS, pH 7.2, the fractions were pooled, concentrated by ultrafiltration (Amicon, Danvers, MA) and stored at 4 °C. To determine the ratio of CVF per antibody molecule, ^{125}I-labeled CVF (1.5 × 10⁶ cpm/mg) was used for conjugation. Stoichiometries were determined from the difference in specific radioactivity before and after conjugation.

Determination of Antigen Binding Activity. The antigen, obtained from human WIDR colon carcinoma cells by ammonium sulfate precipitation as described

previously (*15*), was coated onto Immulon-2 removable wells (Dynatech, Alexandria, VA) at a concentration of 10 μg/mL protein in PBS, pH 7.2, for 1 h at 37 °C. The wells were then blocked with 3% (v/v) fish gelatin (Norland Products, Inc., New Brunswick, NJ) in PBS, pH 7.2, for 1 h at 25 °C and washed three times with an aqueous solution containing 5% (v/v) glycerol and 0.05% (v/v) Tween-20. Varying amounts (8–2000 ng) of unmodified antibody 16-88, cross-linker-derivatized antibody, and conjugates (amounts are based on the antibody moiety) in 50 μL of PBS, pH 7.2, were mixed with 30 ng of ^{125}I-labeled antibody 16-88 (specific radioactivity: 2 × 10⁶ cpm/μg) in 50 μL of PBS, pH 7.2, added to the antigen-coated wells, and incubated for 15 h at 4 °C. After three washes with PBS, pH 7.2, containing 1% (w/v) bovine serum albumin, the wells were counted for radioactivity. The percent inhibition of [125I]antibody binding was calculated from the formula [1 − (bound cpm in the presence of non-iodinated antibody/bound cpm in the absence of non-iodinated antibody)] × 100.

Determination of the Hemolytic Activity of CVF. The complement activating ability of CVF was determined in a bystander lysis assay as described previously (*14*). Briefly, 9 × 10⁶ guinea pig erythrocytes were incubated with 20 μL of guinea pig serum (diluted 1:2 with PBS) at 37 °C for 30 min in the presence of varying concentrations of SPDP-derivatized or antibody-conjugated CVF in a total volume of 60 μL. Hemolysis was determined by measuring the release of hemoglobin from the lysed erythrocytes spectrophotometrically at 412 nm.

Determination of the Complement Activating Ability of Antibody 16-88. The ability of unmodified and cross-linker-derivatized antibody 16-88 to activate complement in the presence of antigen immobilized onto microtiter plates was measured in a complement depletion assay. The assay was based on a protocol described for a similar method using soluble antigen (*16*). Briefly, Costar 48-well polystyrene plates (Costar, Cambridge, MA) were coated with 500 μL of a crude antigen extract (5 μg) obtained from WIDR cells (*15*) for 15 h at 4 °C. After the wells were washed three times with GPBS²⁺, 250 μL of antibody (at either 5, 2.5, or 0.5 μg/mL) in GPBS²⁺ and 125 μL of diluted human serum as complement source were added. The serum used was diluted in GPBS²⁻ to a concentration which caused 90% hemolysis of sheep erythrocytes sensitized with hemolysin as described (*16*). After overnight incubation of the plates at 4 °C, the reaction mixtures were transferred to glass tubes and 125 μL of sensitized sheep erythrocytes (6.3 × 10⁶ cells) was added. The solutions were incubated for 30 min at 37 °C, diluted with 0.5 mL of cold GPBS²⁻, and centrifuged for 10 min at 4 °C (800*g*). Released hemoglobin was measured spectrophotometrically at 412 nm. Percent consumption of complement hemolytic activity was calculated from these data.

Other Methods. CVF was labeled with Na¹²⁵I using immobilized chloramine-T (Iodo-Beads, Pierce, Rockford, IL) (*17*). Protein concentrations were determined by the Lowry method (*18*).

RESULTS

Effect of Cross-Linker Derivatization on Antibody Binding. Human monoclonal IgM antibody 16-88, directed against a cytoplasmic antigen from human colon carcinoma cells, was derivatized with the carbohydrate-directed cross-linker TPCH or the amino group-directed cross-linker SPDP. The effect of cross-linker attachment on two antibody functions, antigen binding and complement activation, was evaluated. Figure 1 shows that the antigen binding ability decreased with
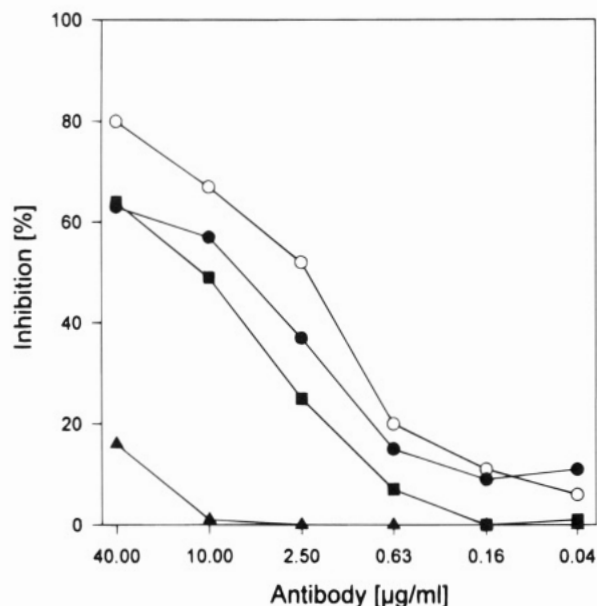
Figure 1. Effect of SPDP derivatization on the antigen binding activity of antibody 16-88. Shown is the ability of unmodified and modified antibody to bind antigen in a competition assay with ^{125}I-labeled antibody 16-88. Unmodified antibody (○) and SPDP-modified antibody at 2.0:1 (●), 8.6:1 (■), and 16.0:1 (▲) mol of SPDP/mol of antibody.

Figure 3. Effect of SPDP (left panel) and TPCH derivatization (right panel) on the complement activating ability of antibody 16-88. The complement activating ability was determined using a complement depletion assay as described in Materials and Methods.

Figure 2. Effect of TPCH derivatization on the antigen binding activity of antibody 16-88. Shown is the ability of unmodified and modified antibody to bind antigen in a competition assay with ^{125}I-labeled antibody 16-88. Unmodified antibody (○) and TPCH-modified antibody at 1.8:1 (●), 9.2:1 (■), and 16.6:1 (▲) mol of TPCH/mol of antibody.

increasing SPDP modification. Antibodies derivatized with 16 SPDP residues exhibited almost complete loss of antigen binding function. In contrast, modification of antibody 16-88 with TPCH led to no measurable change in the antigen binding capability, even when 16 or 17 TPCH residues were attached per antibody molecule (Figure 2).

Effect of Cross-Linker Derivatization on the Complement-Activating Ability of the Antibody. Figure 3 shows that derivatization of the 16-88 antibody with TPCH or SPDP caused a similar decrease in complement consumption. Since the assay requires first the binding of the antibody to its antigen, the observed

Figure 4. Effect of cross-linker attachment site on CVF coupling efficiency. The conjugation was performed with a 1.5-fold molar excess of sulfhydryl-derivatized CVF (2.8 mol of SH groups/mol of CVF) over the number of antibody-attached cross-linker molecules. SPDP-derivatized antibody, open bars; TPCH-derivatized antibody, hatched bars.

decrease in complement consumption with SPDP-derivatized antibody appears to be a consequence of the compromised antigen binding rather than impairment of the complement activating ability (compare Figure 1). In contrast, the observed decrease in complement consumption with TPCH-derivatized antibody demonstrates that this cross-linker impairs the complement activating ability of the antibody since the antigen binding ability of TPCH-derivatized antibody is indistinguishable from that of unmodified antibody (compare Figure 2).

Effect of Cross-Linker Attachment Site on CVF Coupling Efficiency. Figure 4 shows the coupling efficiency of sulfhydryl-derivatized CVF to either SPDP- or TPCH-derivatized antibody 16-88. Two antibody preparations containing approximately 5 or 8 mol of
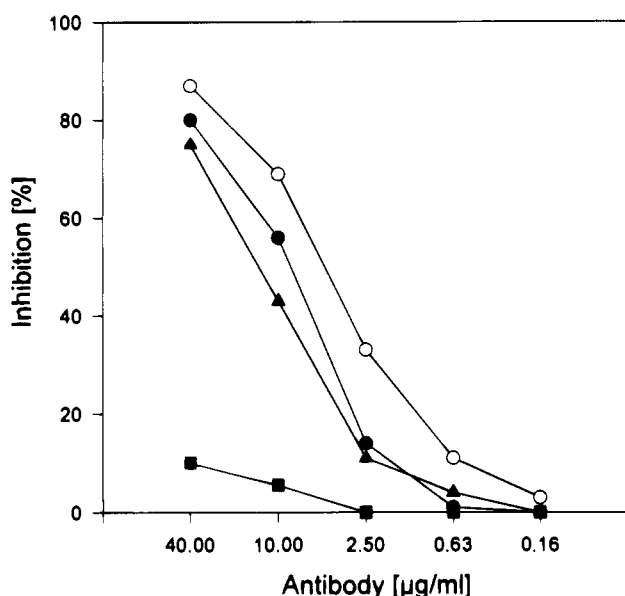
Figure 5. Effect of CVF conjugation to SPDP-derivatized antibody 16-88 on its antigen binding ability. Shown is the ability of unmodified antibody (O) and antibody–CVF conjugates [●, 1.2 mol of CVF/mol of antibody (derivatized with 2.4 mol of SPDP/mol of antibody); ▲, 3.0 mol of CVF/mol of antibody (derivatized with 5.0 mol of SPDP/mol of antibody); ■, 5.6 mol of CVF/mol of antibody (derivatized with 8.6 mol of SPDP/mol of antibody)] to bind antigen in a competition assay with ^{125}I-labeled antibody 16-88.

Figure 6. Effect of CVF conjugation to TPCH-derivatized antibody 16-88 on its antigen binding ability. Shown is the ability of unmodified antibody (O) and antibody–CVF conjugates containing, per mole of antibody (derivatized with 8.0 mol of TPCH/mol of antibody) 0.5 (●), 2.0 (■) or 3.2 mol of CVF (▲) to bind antigen in a competition assay with ^{125}I-labeled antibody 16-88.

either cross-linker per mole of antibody were tested in these experiments. With SPDP-derivatized antibody 65–70% of the available pyridyl disulfide groups were used for coupling of CVF, compared to only 15–40% with TPCH-derivatized antibody. These data suggest that the carbohydrate-bound pyridyl disulfide groups introduced by TPCH are less accessible for coupling of CVF than the amino-bound pyridyl disulfide groups introduced by SPDP.

Effect of CVF Attachment Site on the Antigen Binding Activity. As shown in Figure 5, CVF conjugates prepared from SPDP-derivatized antibody were significantly compromised in their antigen binding capability. The compromise in binding activity increased with higher coupling ratios of CVF per antibody. On the basis of the data in Figures 1 and 5, both SPDP derivatization and CVF coupling contributed to the compromise in antigen binding ability. At a low coupling ratio (1–3 CVF molecules/antibody) the additional compromise due to CVF coupling was moderate, but it increased to more than 80% at a coupling ratio of 5 or 6 CVF molecules per antibody (Figure 5). In contrast, virtually no compromise in antigen binding ability was observed when CVF was coupled to TPCH-derivatized antibody (Figure 6). Even those conjugates containing 3 or 4 CVF molecules per antibody were almost indistinguishable in their antigen binding ability from unmodified antibody. These data demonstrate that the carbohydrate moieties can serve as attachment sites for large effector molecules such as CVF without impairment of antigen binding function.

Effect of Attachment Site on the CVF Hemolytic Activity. Figure 7 shows the effect of conjugation on the hemolytic activity of CVF. Compared to SPDP-derivatized CVF, antibody-conjugated CVF exhibited a decreased hemolytic activity whether coupled to SPDP- or TPCH-derivatized antibody. The compromise in activity was greater for carbohydrate-attached CVF than for amino-attached CVF, suggesting a lower accessibility of
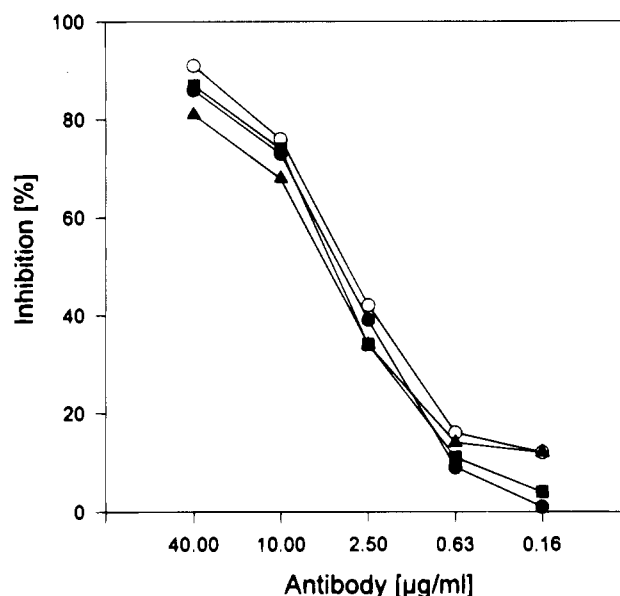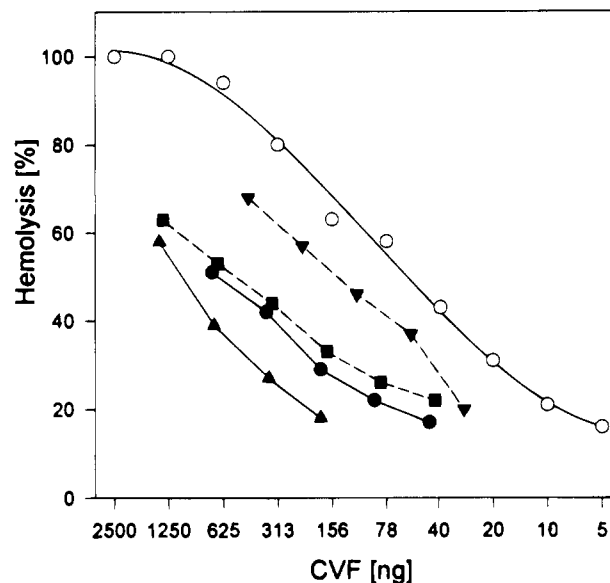
Figure 7. Effect of attachment site on the hemolytic activity of conjugated CVF. The hemolytic activity of CVF (derivatized with 2.8 mol of SPDP/mol of CVF) before and after conjugation to SPDP-derivatized (- -) or TPCH-derivatized (—) antibody 16-88 was measured in a bystander lysis assay as described in Materials and Methods; O, SPDP-derivatized CVF; ▼, antibody-conjugated CVF (2.0 mol of CVF/mol of antibody); ■, antibody-conjugated CVF (0.4 mol of CVF/mol of antibody); ●, antibody-conjugated CVF (3.2 mol of CVF/mol of antibody); ▲, antibody-conjugated CVF (0.5 mol of CVF/mol of antibody). Due to the comparatively low derivatization of CVF with 2.8 mol of SPDP/mol of CVF, the hemolytic activity of the derivatized CVF was virtually indistinguishable from that of unmodified CVF (not shown) (6).

the carbohydrate-attached CVF molecules for factor B (92 kDa) and/or complement component C5 (191 kDa) required for its hemolytic activity.

DISCUSSION

The results of this study demonstrate that amino group-directed and carbohydrate-directed attachment of

cross-linker molecules have different effects on two antibody functions, complement activation and antigen binding. Derivatization of the carbohydrate moieties of human monoclonal IgM 16-88 with as many as 16 or 17 TPCH molecules did not affect its binding activity, whereas attachment of the same number of molecules of the amino group-directed crosslinker SPDP caused virtually complete loss of the antibody's binding function. These data show that carbohydrate-attached TPCH molecules are located distal to the antigen binding region, whereas at least some of the amine-attached SPDP molecules are located within the antigen binding region. When SPDP-modified antibodies were used for the conjugation of CVF, the antigen binding function was further compromised. In contrast, coupling of CVF to TPCH-modified antibodies did not cause any significant impairment of antigen binding function. Even those conjugates carrying 3 or 4 CVF molecules were indistinguishable in their antigen binding ability from unmodified antibody molecules.

The ability to activate complement was also tested, since the carbohydrate moieties are proposed to be involved in complement activation and, in particular, C1q binding. Several lines of evidence for this have been reported: The complement activating ability of a murine monoclonal IgG$_{2b}$ antibody was abolished in the corresponding aglycosyl derivative (*19*); deglycosylation of rabbit IgG by β-aspartyl-N-acetylglycosamido hydrolase eliminated the antibody's ability to bind C1q (*20*); human IgG treated with β-galactosidase showed a significant reduction in C1q binding (*21*). The carbohydrates, which are proposed to act as a bridge between constant domains of an immunoglobulin molecule (*22*), are thought to provide a higher order structure which is necessary for the constant region of the antibody to participate in C1q binding and to function as a specific ligand for receptor recognition and binding. The results of our study support the view that carbohydrates are involved in complement activation. It remains to be determined, however, whether the observed compromise in the complement activating ability upon TPCH derivatization is due to a direct alteration of the carbohydrates or to subsequent structural alteration(s) of the protein as a result of cross-linker attachment.

When TPCH- and SPDP-modified antibodies were used to couple CVF, different coupling efficiencies were observed. The amine-attached SPDP residues were more accessible to coupling of CVF than the carbohydrate-attached TPCH residues. This may be due to the localization of the carbohydrates in a sterically hindered region of the antibody, between the constant domains of the immunoglobulin. In addition, the discrete area in which the carbohydrates are localized may limit the number of CVF molecules that can be attached. The limited accessibility of the carbohydrate region is also suggested by the greater compromise observed in the hemolytic activity of CVF coupled to TPCH-derivatized antibody compared to SPDP-derivatized antibody. Factor B, which must bind to CVF in order to activate complement through the alternative pathway, has a molecular mass of 92 kDa and may for sterical reasons have impaired access to CVF when it is coupled to the carbohydrate region. The same applies to complement component C5 (191 kDa), the binding of which is also required for the hemolytic activity of CVF. CVF coupled to the antibody through the more exposed amines via the cross-linker SPDP appears to have increased accessibility for interaction with factor B and C5, providing for immunoconjugates with better retention of CVF hemolytic activity.

The contention that the somewhat compromised activity of CVF when coupled via TPCH to the carbohydrate moieties in the hinge region of the antibody is due to steric hindrance because of the comparatively large molecular weight of CVF and its requirement to interact with two rather large proteins to exert activity is further supported by the observation that the activity of barley toxin, a significantly smaller effector molecule, when coupled via TPCH to the same antibody was indistinguishable from the activity of the derivatized but noncoupled barley toxin (*8*).

Although a rather large number of heterobifunctional cross-linking reagents have been developed over the last 15 years, only very few reactive groups are employed and, consequently, very few conceptionally different cross-linking reagents exist (for a review, see *23*). Although the successful derivatization of the carbohydrate moieties of antibody molecules without impairment of the binding function was demonstrated some time ago (*24*), carbohydrate-directed heterobifunctional cross-linking reagents such as TPCH have only been described more recently (*8, 25*).

In conclusion, immunoconjugates synthesized with the carbohydrate-directed cross-linker TPCH appear to be superior compared to those synthesized with amino group-directed cross-linker molecules. Although the use of TPCH causes a slight decrease in the coupling efficiency, even large effector molecules such as CVF can be coupled to TPCH-derivatized antibodies without impairment of the antigen binding function.

LITERATURE CITED

(1) Wawrzynczak, E. J., and Thorpe, P. E. (1987) Methods for preparing immunotoxins: effect of the linkage on activity and stability. In *Immunoconjugates, Antibody Conjugates in Radioimaging and Therapy of Cancer* (C.-W. Vogel, Ed.) pp 28–55, Oxford University Press, Oxford, New York.

(2) Vogel, C.-W. (1987) Antibody conjugates without inherent toxicity: the targeting of cobra venom factor and other biological response modifiers. In *Immunoconjugates, Antibody Conjugates in Radioimaging and Therapy of Cancer* (C.-W. Vogel, Ed.) pp 170–188, Oxford University Press, Oxford, New York.

(3) FitzGerald, D. J. P. (1987) Construction of immunotoxins using *Pseudomonas* exotoxin A. *Methods Enzymol. 151*, 139–145.

(4) Frankel, A. E., Welsh, P. C., Withers, D. I., and Schlossman, D. M. (1988) Immunotoxin preparation and testing *in vitro*. In *Antibody-Mediated Delivery Systems* (J. D. Rodwell, Ed.) pp 225–244, Marcel Dekker, Inc., New York, Basel.

(5) Vogel, C.-W. (1988) Synthesis of antibody conjugates with cobra venom factor using heterobifunctional cross-linking ragents. In *Antibody-Mediated Delivery Systems* (J. D. Rodwell, Ed.) pp 191–224, Marcel Dekker, Inc., New York, Basel.

(6) Petrella, E. C., Wilkie, S. D., Smith, C. A., Morgan, A. C., Jr., and Vogel, C.-W. (1987) Antibody conjugates with cobra venom factor. Synthesis and biochemical characterization. *J. Immunol. Methods 104*, 159–172.

(7) Juhl, H., Petrella, E. C., Cheung, N.-K. V., Bredehorst, R., and Vogel, C.-W. (1990) Complement killing of human neuroblastoma cells: A cytotoxic monoclonal antibody and its F(ab)'$_2$-cobra venom factor conjugate are equally cytotoxic. *Mol. Immunol. 27*, 957–964.

(8) Zara, J., Wood, R., Boon, P., Kim, C.-H., Pomato, N., Bredehorst, R., and Vogel, C.-W. (1991) A carbohydrate-directed heterobifunctional cross-linking reagent for the synthesis of immunoconjugates. *Anal. Biochem. 194*, 156–162.

(9) Silverton, E. W., Navia, M. A., and Davies, D. R. (1977) Three-dimensional structure of an intact human immunoglobulin. *Proc. Natl. Acad. Sci. U.S.A. 74*, 5140–5144.

(10) Haspel, M. V., McCabe, R. P., Pomato, N., Janesch, J. J., Knowlton, J. V., Peters, L. C., Hoover, H. C., Jr., and Hanna,

M. G., Jr., (1985) Generation of tumor cell-reactive human monoclonal antibodies using peripheral blood lymphocytes from actively immunized colorectal cancer patients. *Cancer Res. 45,* 3951−3960.

(11) Vogel, C.-W. (1990) Cobra venom factor, the complement-activating protein of cobra venom. In *Handbook of Natural Toxins, Vol. 5, Reptile and Amphibian Venoms* (A. T. Tu, Ed.) pp 147−188, Marcel Dekker, Inc., New York, Basel.

(12) McCabe, R. P., Peters, L. C., Haspel, M. V., Pomato, N., Carrasquillo, J. A., and Hanna, M. G., Jr., (1988) Preclinical studies on the pharmacokinetic properties of human mono-clonal antibodies to colorectal cancer and their use for detection of tumors. *Cancer Res. 48,* 4348−4353.

(13) Carlsson, J., Drevin, H., and Axen, R. (1978) Protein thiolation and reversible protein−protein conjugation. *N*-succinimidyl 3-(2-pyridyldithio) propionate, a new heterobi-functional reagent. *Biochem. J. 173,* 723−737.

(14) Vogel, C.-W., and Müller-Eberhard, H. J. (1984) Cobra venom factor: Improved method for purification and bio-chemical characterization. *J. Immunol. Methods 73,* 203−220.

(15) Hanna, M. G., Jr., (1989) Human tumor antigens and specific tumor therapy. In *U.C.L.A. Symposia on Molecular and Cellular Biology* (R. S. Metzgar and M. S. Mitchell, Eds.), Vol. 99, pp 127−136, Alan R. Liss, Inc., New York.

(16) Mayer, M. M. (1961) Complement and complement fixation. In *Experimental Immunochemistry* (E. A. Kabat and M. M. Mayer, Eds.) pp 133−240, Charles C. Thomas, Springfield, IL.

(17) Lee, D. S. C., and Griffiths, B. W. (1984) Comparative studies on Iodo-bead and Chloramine-T methods for radio-iodination of human α-fetoprotein. *J. Immunol. Methods 74,* 181−189.

(18) Lowry, O. H., Rosebrough, N. J., Farr, A..L., and Randall, R. J. (1951) Protein measurement with the folin phenol reagent. *J. Biol. Chem. 193,* 265−275.

(19) Nose, M., and Wigzell, H. (1983) Biological significance of carbohydrate chains on monoclonal antibodies. *Proc. Natl. Acad. Sci. U.S.A. 80,* 6632−6636.

(20) Winkelhake, J. L., Kunicki, T. J., Elcombe, B. M., and Aster, R. H. (1980) Effects of pH treatment and deglycosy-lation of rabbit IgG on the binding of C1q. *J. Biol. Chem. 255,* 2822−2828.

(21) Tsuchiya, N., Eneo, T., Matsuta, K., Yoshinoya, S., Aikawa, T., Kosuge, E., Takeuchi, F., Miyamoto, T., and Kobata, A. (1989) Effects of galactose depletion from oligosaccharide chains on immunological activities of human IgG. *J. Rheu-matol. 16,* 285−290.

(22) Parekh, R. B., Dwek, R. A., Sutton, B. J., Fernandes, d. L., Leung, A., Stanworth, D., Rademacher, T. W., Mizuochi, T., Taniguchi, T., Matsuta, K., Takeuchi, F., Nagano, Y., Miyamoto, T., and Kobata, A. (1985) Association of rheuma-toid arthritis and primary osteoarthritis with changes in the glycosylation pattern of total serum IgG. *Nature 316,* 452−457.

(23) Mattson, G., Conklin, E., Desai, S., Nielander, G., Savage, M. D., and Morgensen, S. (1993) A practical approach to crosslinking. *Mol. Biol. Rep. 17,* 167−183.

(24) Rodwell, J. D., Alvarez, V. L., Lee, C., Lopes, A. D., Goers, J. W. F., King, H. D., Powsner, H. J., and McKearn, T. J. (1986) Site-specific covalent modification of monoclonal anti-bodies: In vitro and in vivo evaluations. *Proc. Natl. Acad. Sci. U.S.A. 83,* 2632−2636.

(25) Chamow, S. M., Kogan, T. P., Peers, D. H., Hastings, R. C., Byrn, R A., and Ashkenazi, A. (1992) Conjugation of soluble CD4 without loss of biological activity via a novel carbohydrate-directed cross-linking reagent. *J. Biol. Chem. 267,* 15916−15922.

BC950021W

Preliminary Study of the Metal Binding Site of an Anti-DTPA-Indium Antibody by Equilibrium Binding Immunoassays and Immobilized Metal Ion Affinity Chromatography

Valérie Boden,[†] Carole Colin,[†] Jacques Barbet,[‡] Jean Marc Le Doussal,[‡] and Mookambeswaran Vijayalakshmi*,[†]

Limtech S, Centre de Recherches de Royallieu, Université de Technologie de Compiègne, BP 649, 60206 Compiegne Cedex, France, and Immunotech SA, 130 avenue de Tassigny, BP 177, 13276 Marseille Cedex 9, France. Received February 22, 1995[⊗]

Creating metal coordination sites by modifying an existing enzyme or by eliciting antibodies against metal chelate haptens is of great interest in biotechnology to create enzyme catalysts with novel specificities. Here, we investigate the metal binding potential of a monoclonal antibody raised against a DTPA-In(III) hapten (mAb 734). We study its relative binding efficiency to metals of biological relevance by equilibrium binding immunoassays and immobilized metal ion affinity chromatography, two approaches which can give complementary information regarding composition and/or structure of the metal binding site(s). Fe(III), Fe(II), Cu(II), Mg(II), Ca(II), and Zn(II) binding was compared to In(III). All of them were shown to displace indium, but their affinity for mAb 734 decreased by 100-fold compared to indium. Competitive metal binding immunoassays between Zn(II) and In(III) revealed an unusual behavior by Zn(II) which remains to be explained. Moreover, IMAC allowed us to predict the metal binding amino acids involved in the antibody paratope. The antibody metal binding site was shown to contain at least two histidine residues in a cluster, and the presence of aspartic and glutamic acid as well as cysteine residues could not be excluded. Thus, simple competition studies allows us to obtain some partial information on the metal binding structural features of this anti-metal chelate antibody and to guide our screening of its catalytic potential.

INTRODUCTION

Metallobiomolecules are involved in many fundamental biological processes. They are highly elaborate coordination complexes whose metal containing sites, comprising one or more metal ions and their ligands, are usually the loci of electron transfer (cytochromes, photosystem II), dioxygen binding (myoglobin, hemoglobin), and catalysis (e.g., carboxypeptidase, superoxide dismutase, carbonic anhydrase, hydrolases). Systematic studies on the composition of these metal coordination sites have provided valuable information concerning the metals and amino acid residues involved in these features. Mg, Mn, Fe, Co, Cu, Zn, and Mo were identified for their role in substrate activation and catalysis. Histidine and cysteine residues were shown to be systematically involved in the binding of the catalytically important metal ion (*1, 2*).

Creating metal coordination sites by modifying an existing protein (*3*) or by eliciting antibodies against metal chelate haptens (*4*) is a challenging aim in abzyme biotechnology. If the created metal binding site matches the reaction requirements [appropriate ligand geometry and affinity >10^5 M^{-1} (*5*)], enzyme catalysts with novel specificities can be expected from a small subset of amino acid residues and first row transition metals (e.g., Fe, Cu, Zn).

Recently, two studies have shown that antibodies to metal ligand complexes can bind metals productively and perform redox (*6*) and hydrolytic (*7*) reactions.

In this report, on the basis of the knowledge accumulated on recognition of proteins by metal chelates

n=1 ---> IDA
n=2 ---> EDTA
n=2.5 ---> DTPA

X= His or other amino acid

hapten: metal chelate

predicted amino acids of the anti-metal chelate antibody paratope
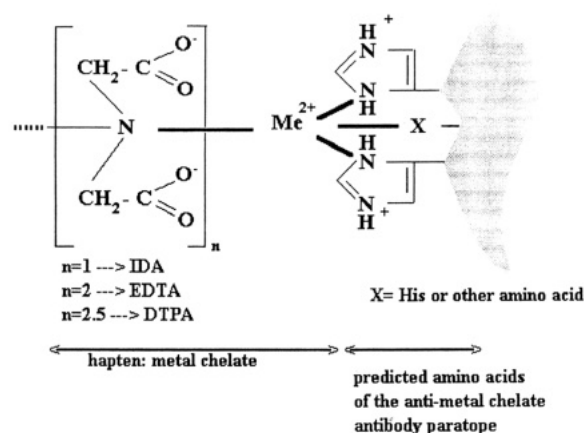
Figure 1. Schematic diagram representing the complementarity between the metal chelate hapten and the hapten binding site in the anti-metal chelate antibody based on the IMAC recognition theory.

and more specifically by iminodiacetate (IDA)[1] complexes (*8*), we attempt to predict the metal binding feature of an anti-metal chelate antibody in order to guide the screening of its eventual catalytic properties. As presented in Figure 1, IDA could be assimilated to the basic motif of chelating agents wherein EDTA or DTPA can be schematically represented as 2 times IDA and 2.5 times IDA, respectively. We expect that when complexed to metals and used as hapten, this basic motif will

---

[1] Abbreviations: BSA, bovine serum albumin; DNP, dinitrophenol; DTPA, diethylenetriaminepentaacetic acid; EDTA, ethylenediaminetetraacetic acid; IDA, iminodiacetic acid; IgG, immunoglobulin; IMAC, immobilized metal ion affinity chromatography; mAb, monoclonal antibody; PBS, phosphate-buffered saline.

Table 1. Experimental Details on the Equilibrium Binding Assays to Immobilized Fab' 734: Competition between DTPA-In(III) and Free or Chelated Zn(II)^a

	I Fab 734	II Fab 734	III Fab 734	IV Fab 734 preincubated with ZnCl$_2$	V Fab 734 preincubated with DTPA-Zn(II)	VI Fab 134 (nonspecific mAb)
				experiment no.		
(a)	DTPA*-In	DTPA*-In	DTPA*-In	DTPA*-In	DTPA*-In	DTPA*-In
(b)	DTPA-In	DTPA-In	DTPA-Zn	DTPA-In	DTPA-In	DTPA-In
(c)	Hepes	Hepes + ZnCl$_2$	Hepes	Hepes	Hepes	Hepes + ZnCl$_2$

^{a} The same procedure as the one explained for experiment III was repeated from experiment I to VI.

present a corresponding paratope structure close to the catalytic sites of metalloenzymes (*1*).

We intend to verify our hypothesis by investigating the metal binding potential of an anti-diethylenetriamine-pentaacetate (DTPA)-In(III) monoclonal antibody originally used for radioimaging purposes (*9*). We study its relative binding efficiency to metals other than indium and of biological relevance by equilibrium binding immunoassays and immobilized metal ion affinity chromatography (IMAC), two approaches which can give complementary information regarding composition and/or structure of the metal binding site(s). These data can, in turn, enable the screening of eventual catalytic potential.

MATERIALS AND METHODS

Monoclonal Antibodies and Fragments. Monoclonal anti-DTPA-In(III) antibody 734 (*9*) and anti-dinitrophenol (DNP) monoclonal antibody (mAb 134) were from Immunotech SA (Marseille, France). Fab fragments were prepared by papain digestion (*10*).

Preincubation of Fab 734 with DTPA-In(III), DTPA-Zn(II), or ZnCl$_2$. Biotinylated Fab 734 (solid-phase immunoassays) or Fab 734 (chromatographic experiments) was incubated with ZnCl$_2$, DTPA-Zn(II) (30 mM), or DTPA-In(III) (3 mM) in 100 mM acetate, 20 mM citrate buffer, and 0.15 M NaCl adjusted at pH 4.5 with 0.5 M NaOH. Excess zinc, DTPA-Zn(II), or DTPA-In-(III) was eliminated by passing the solution through the Chelex 100 resin (Bio-Rad, Ivry/Seine, France) (solid-phase assays) or a PD 10 (Pharmacia, Uppsala, Sweden) (chromatographic experiments). Protein concentration was then determined by measuring the absorbance at 280 nm using an absorbance of 1.48 for a 1 mg/mL solution.

Solid-Phase Immunoassays. *Equilibrium Binding to Immobilized 734 IgG: Competition between DTPA-In-(III) and Different DTPA-M(II or III).* Anti-DTPA-In(III) mAb (50 ng/mL) was coated on plastic tubes using the Immunotech proprietary technique (*11*). Constant tracer amounts (40 000 cpm) of radioactive ^{111}In-DTPA were incubated in duplicate overnight at 37 °C with increasing concentrations of competitors [DTPA-Fe(III), DTPA-Fe-(II), DTPA-Cu(II), DTPA-Mg(II), DTPA-Ca(II), and DTPA-

Zn(II)] in a final volume of 1 mL of phosphate-buffered saline (PBS)−0.1% bovine serum albumine (BSA). Tubes were then emptied and washed once with PBS, 9% NaCl, and 0.05% Tween 20, and radioactivity was counted.

Equilibrium Binding to Immobilized Fab 734: Competition between DTPA-In(III) and Free or Chelated Zn(II). Anti-DTPA-In(III) Fab 734 [preincubated or not with Zn-(II) or DTPA-Zn(II)] or anti-DNP Fab (1 µg/mL) was coated on plastic tubes (*11*). Six different experiments were run. Experimental details are given in Table 1. Ten different concentrations of nonradioactive DTPA complexes per experiment were run (in duplicate). After 12 h of incubation at 4 °C with the biotinylated Fab 734, the tubes were incubated for 12 h at 4 °C with the following solutions added together: (a) radioactive DT-PA* previously iodinated (*8*) and chelated to In(III) (25 000 cpm corresponding to 1.32 × 10^{-11} M final concentration); (b) in tubes 1−10 (in duplicate), addition of increasing concentrations of nonradioactive DTPA-In-(III) or DTPA-Zn(II) for final concentrations from 0 to 10^{-6} M; (c) 20 mM Hepes buffer and 0.15 M NaCl, pH 6, with or without 30 mM ZnCl$_2$. The tubes were then emptied and washed once with PBS, 9% NaCl, and 0.05% Tween 20, and radioactivity was counted.

Immobilized Metal Ion Affinity Chromatography (IMAC) Experiments. *Chromatography on Affi-Gel-DTPA-In(III).* For IMAC, Affi-Gel (Bio-Rad, Ivry/Seine, France) was coupled with DTPA cyclic anhydride (Sigma Chemical Co., St. Louis, MO) and packed into a column (1 cm × 10 cm) providing a 1.1−mL bed volume. The chelating gel was loaded with a solution of 1 mM InCl$_3$/100 mM acetate/10 mM citrate, pH 4.5. After the unbound indium was removed, the column was equilibrated with the starting buffer (20 mM Hepes, 0.3 M NaCl, pH 7). Then, 220 µg of Fab 734 preincubated or not with DTPA-In(III) or ZnCl$_2$ was applied to the column at a flow rate of 20 mL/h. For elution of the protein, either a discontinuous gradient of DTPA-In(III) or a pH step gradient was used. To perform the gradient with DTPA-In(III) as competitor, increasing concentrations of DTPA-In(III) from 1 µM to 100 mM were incorporated into the starting buffer. The pH step gradient was run by applying to the column buffers containing 50 mM
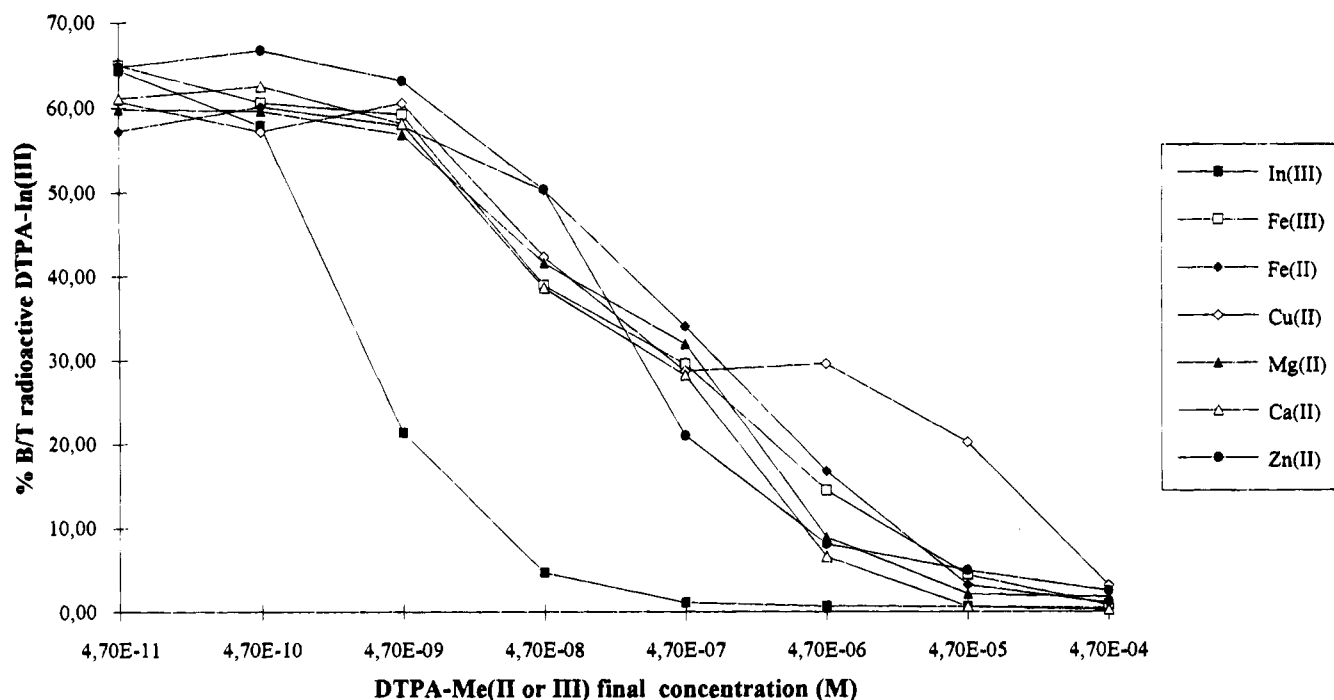
Figure 2. Equilibrium binding assays to immobilized mAb 734: competition between DTPA-In(III) and different DTPA-M(II or III). mAb 734 (50 ng/mL) was coated on plastic tubes through a biotin—avidin link. Radioactive DTPA-^{111}In(III) (40 000 cpm) and increasing concentrations of nonradioactive DTPA-M(II or III) were simultaneously incubated in duplicate for 12 h at 37 °C. Tubes were emptied and washed, and radioactivity was counted.

phosphate at pH 6 and 100 mM acetate and 10 mM citrate at pH 5 and pH 4, respectively; all these buffers contained 0.3 M NaCl. Metal and remaining proteins were eluted with 50 mM EDTA.

Chromatography on Sepharose-IDA-Zn(II). Sepharose 6B (Pharmacia, Uppsala, Sweden) was coupled to iminodiacetate (IDA) as described earlier (*12*) and packed into a column (1 cm × 10 cm) providing a 1.1-mL bed volume. The chelating gel was loaded with a solution of 50 mM ZnSO$_4$ in water. After the unbound Zn was removed, the column was equilibrated with the starting buffer (20 mM phosphate buffer + 1 M NaCl, pH 7). Then, 500 μg of Fab 134 (anti-dinitrophenol) or 734 preincubated or not with DTPA-In(III) or ZnCl$_2$ was applied to the column at a flow rate of 20 mL/h. A classical pH step gradient was run by applying to the column buffers containing 20 mM phosphate + 1 M NaCl at pH 6.5 and pH 6 and 0.1 M acetate + 1 M NaCl at pH 5.5, pH 5, pH 4.5, and pH 4, respectively.

RESULTS AND DISCUSSION

Equilibrium Binding Assays to Immobilized mAb 734: Competition between DTPA-In(III) and Different DTPA-M(II or III). DTPA chelates Zn and few other metals as well as In (*13*). Based on this, the competitive binding of DTPA complexes of selected trivalent [Fe(III)] and divalent metals [Fe(II), Cu(II), Mg(II), Ca(II), and Zn(II)] to the anti-DTPA-In(III) Fab was studied as described in Materials and Methods.

Figure 2 shows the data obtained for the competitive binding of nonradioactive DTPA-In(III) and the other DTPA complexes in the presence of labeled DTPA-^{111}In-(III). About 50% of the labeled DTPA-^{111}In(III) was displaced by 4 × 10^{-9} M nonradioactive DTPA-In(III) or by 4 × 10^{-7} M for the other nonradioactive DTPA-metal complexes. The antibody binding affinity was 2 orders of magnitude less for DTPA-Fe(III), -Fe(II), -Cu(II), -Mg-(II), -Ca(II), or -Zn(II) than for DTPA-In(III). The affinity

also reduced by 100-fold when DTPA was replaced by EDTA (*8*). Indium has a *Z* number of 49. It belongs to the fifth period (*Z* > 37) and group IIIA (one electron in the p orbital level). Alternatively, all the other selected metals belong to the fourth period known as the first series of transition (except Ca and Mg). They possess an incomplete d orbital level (except Zn). Thus, the affinity decrease observed for metals other than indium could be the result of their differences in electronic and shape complementarity. It would be interesting to test metal ions which are electronically similar to In(III) such as Ga(III) or Al(III) (group IIIA) to check if they would present a higher affinity.

Nevertheless, even if the affinity of mAb 734 for metals from the first series of transition (except Mg, Ca) is lower, metal coordination complexes with useful affinities (K_a superior to 10^6 M^{-1}) can still be readily achieved in the antibody—antigen cleft. In addition, the ability to use both Cu(II) and Zn(II) as cofactors allows considerations of redox as well as hydrolytic reactions.

Moreover, according to the "hardness—softness" concept based on the polarizability of the interacting ions (*14*), these competitive equilibrium binding immunoassays allow us to predict the metal ligands on the Fab 734. Hard metals such as Ca(II) or Mg(II) or semihard metals such as Fe(III) or In(III) as well as intermediary metals such as Fe(II), Zn(II), or Cu(II) will exhibit a high affinity for ligands containing oxygen, nitrogen, or sulfur atoms. In general, Ca(II) and Mg(II) will associate more strongly with oxygen as ligand than softer metal ions which will preferentially bind nitrogen or sulfur ligands.

If we go further and detail all the amino acid residues involved in the metal binding sites of metalloproteins, we will see that they are constituted of histidine for nitrogen ligands, glutamic acid or water for oxygen ligands, and cysteine (sometimes methionine) for sulfur ligands (*2*). The fact that no particular selectivity was observed for metals other than indium suggests that we could expect oxygen ligands (glutamic or aspartic acid)
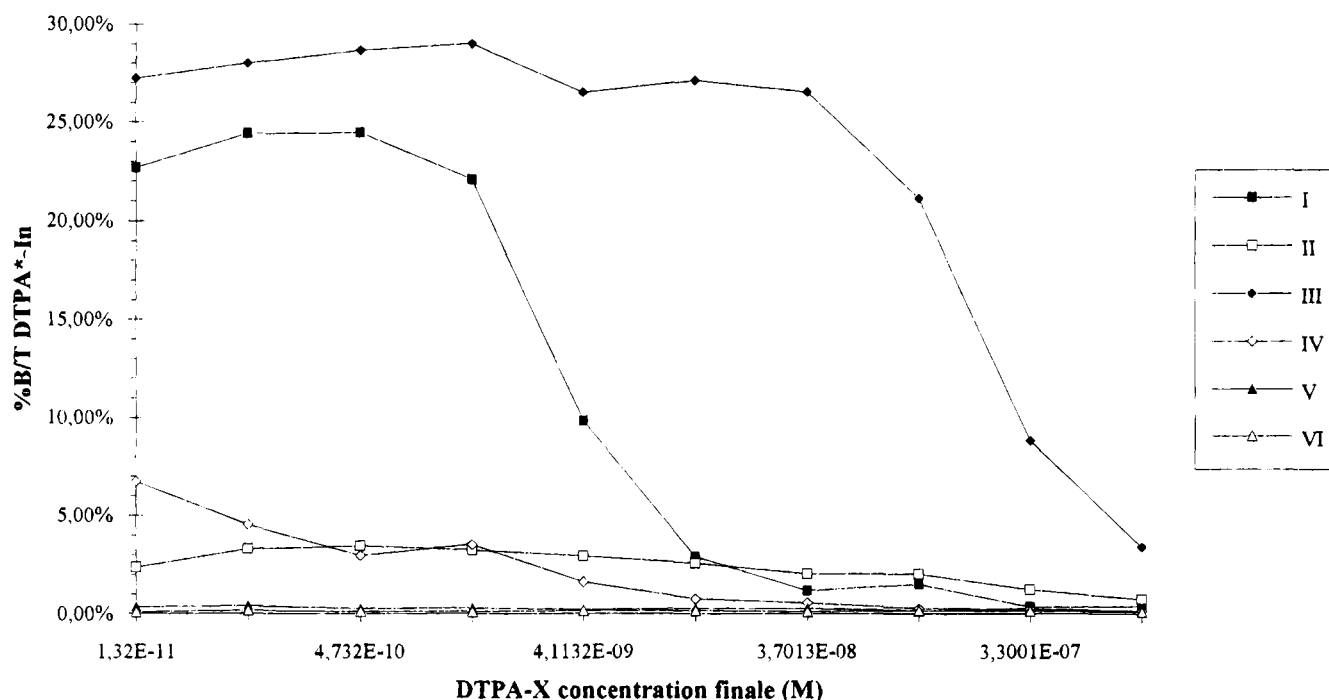
Figure 3. Equilibrium binding assays to immobilized Fab 734: competition between DTPA-In(III) and free or chelated Zn(II). Fab 734 (1 μg/mL) or anti-DNP Fab preincubated or not with ZnCl$_2$ (see Table 1) was coated on plastic tubes through a biotin–avidin link. Radioactive DTPA*-In(III) (25 000 cpm) and increasing concentrations of nonradioactive DTPA-In(III) or DTPA-Zn(II) with or without ZnCl$_2$ (see Table 1) were incubated in duplicate 12 h at 37 °C. Tubes were emptied and washed, and radioactivity was counted.

as well as nitrogen or sulfur ligands (histidine and cysteine) in the metal binding site of our anti-DTPA-In-(III) mAb.

Equilibrium Binding Assays to Immobilized Fab 734: Competition between DTPA-In(III) and Free or Chelated Zn(II) to Fab 734. Among the biologically significant metal ions, Zn(II) plays a predominant role in enzyme catalysis. So, in the following series of equilibrium binding assays, we investigated more specifically the binding potential of the anti-DTPA-In(III) Fab to Zn(II).

Six different experiments were run to study the competition between free Zn(II), chelated Zn(II), and DTPA-In(III) to Fab 734 by equilibrium binding experiments. Experimental details are given in Table 1 and displacement curves in Figure 3. The maximum binding corresponds to the amount of bound radioactive DTPA*-In(III) after the different washings divided by the initial radioactive DTPA-In(III) concentration (1.32 × 10^{-11} M) with no competitor.

Experiment I (Table 1), which served as reference, shows the competitive binding of radioactive DTPA*-In-(III) with increasing concentrations of nonradioactive DTPA-In(III). Under these experimental conditions, the maximum binding of radioactive DTPA*-In(III) was only 25%. In accordance with Figure 2, as much as 4 × 10^{-9} M nonradioactive DTPA-In(III) was required to displace 50% of the initially bound radioactive DTPA*-In(III).

Experiment II (Table 1) was run in presence of 30 mM ZnCl$_2$. The maximum binding fell to 3.6%. This low binding indicates that a 30 mM concentration of free Zn-(II) inhibits the binding of radioactive DTPA*-In(III) to Fab 734. In these conditions, the Fab 734 metal binding site was predominantly occupied by zinc ions.

For experiment III (Table 1), nonradioactive DTPA-In(III) from experiment I was replaced by nonradioactive DTPA-Zn(II). As already observed in Figure 2, about 50% of the initially bound radioactive DTPA*-In(III) was displaced by 4 × 10^{-7} M DTPA-Zn(II) against 4 × 10^{-9}

M DTPA-In(III). This confirms the previous data of 100-fold reduction in the affinity of Zn to the anti-DTPA-In-(III) antibody.

Experiment IV (Table 1) shows the competitive binding of radioactive DTPA-In(III) with increasing concentrations of nonradioactive DTPA-In(III) when Fab 734 was preincubated with ZnCl$_2$.

If we suppose that Fab 734 was loaded with an equimolar quantity of Zn(II) ions, the Zn(II) concentration was only 2 × 10^{-11} M (1 μg/tube of Fab with 50 000 molecular weight equivalent to 2 × 10^{-11} M). The maximum binding for 1.32 × 10^{-11} M radioactive DTPA-In(III) was only 7.26%.

Moreover, when Fab is preincubated with DTPA-Zn-(II) [experiment V (Table 1)] instead of ZnCl$_2$, the maximum binding fell to 0.34%.

Preincubation of Fab 734 with zinc ions or DTPA-Zn-(II) inhibited partially (experiment IV) or quasitotally (experiment V) the binding of radioactive DTPA*-In(III).

This result indicates that when free Zn(II) or DTPA-Zn(II) occupies the metal binding site prior to contact with the hapten, even an equivalent concentration of radioactive DTPA*-In(III) [which was previously shown to be 100 times more affine than DTPA-Zn(II)] was not sufficient to displace the zinc. This peculiar Zn(II) behavior is difficult to explain. The Zn dissociation kinetics could be extremely slow. Moreover, on the basis of the data of Iverson et al. (*15*) and Wade et al. (*16*), who engineered metal coordination sites with three histidine residues in an anti-fluorescein mAb and observed comparable behavior toward Zn(II), it could be possible that Zn(II) induces a tight conformation where any Zn ion previously bound is difficult to be displaced.

Further, the specific nature of metal binding to anti-DTPA-In(III) antibody was checked with an irrelevant antibody (anti-DNP mAb) and showed that the binding of radioactive DTPA*-In(III) never exceeded 0.17% [experiment VI (Table 1)].
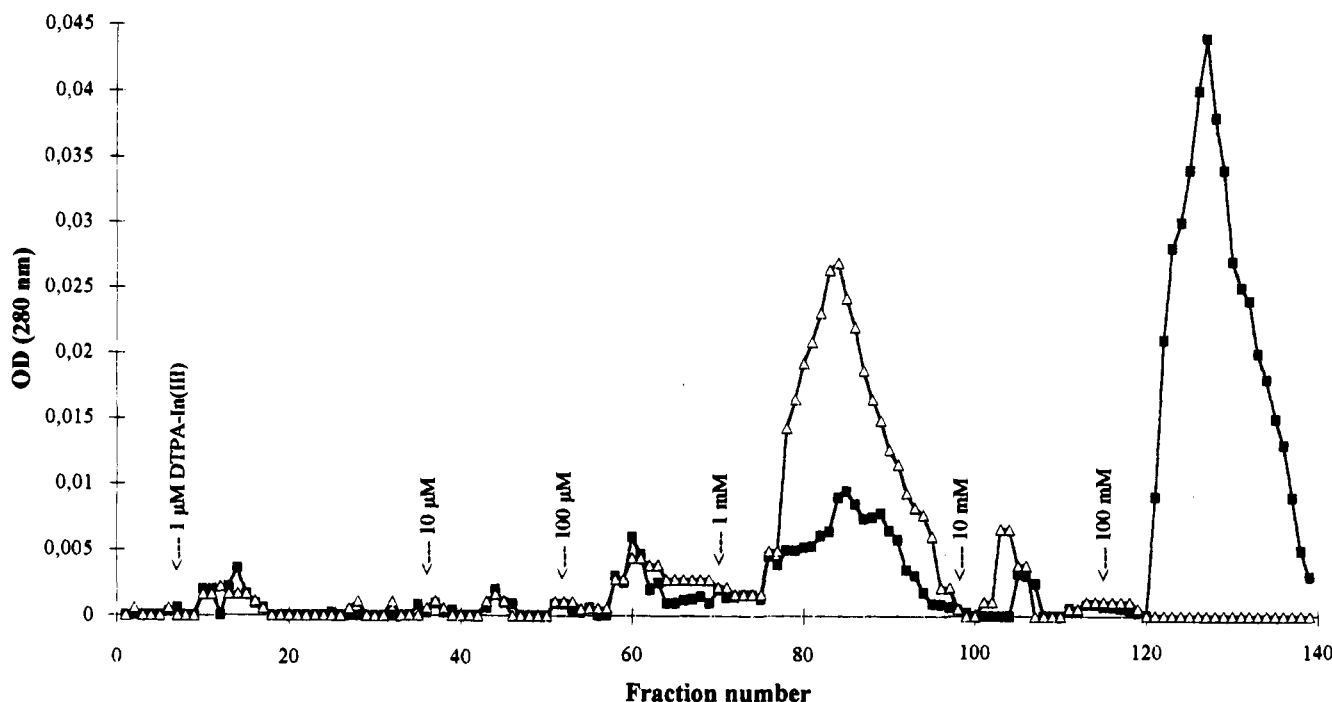
Figure 4. Chromatography on Affi-Gel-DTPA-In(III) using a discontinuous DTPA-In(III) gradient of the Fab 734 preincubated (△) or not (■) with ZnCl₂. Elution conditions: increasing concentrations of DTPA-In(III) from 1 μM to 100 mM were incorporated into the starting buffer, 20 mM Hepes, pH 7, + 0.3 M NaCl. Protein injected: 220 μg of Fab. Bed volume: 1.1 mL. Flow rate: 20 mL/h. Fraction volume: 1 mL.

Competitive Binding Studies between DTPA-In-(III) and Free or Chelated Zn(II) by the Chromatographic Approach.

Immobilized metal ion affinity chromatography (IMAC) was used in addition to the equilibrium binding assays to predict the metal binding amino acids of the Fab fragment of the anti-DTPA-In-(III) mAb, which indicated the presence of histidines in its paratope (*17*). Indeed, IMAC introduced by Porath (*12*) may serve as a simple probe of the surface topography of potential electron donor residues ("Porath triad"): cysteine, histidine, and tryptophan (*8*).

Two chromatographic supports were used to study the interaction of Fab734 with different immobilized ligands: Affi-Gel-DTPA-In(III), which represents the immobilized hapten of mAb734 (Figures 4 and 5), and Sepharose 6B-IDA-Zn(II), which was shown to be a useful tool to study the topography of the accessible histidine residues on proteins (*18, 19*) (Figure 6).

Figure 4 shows that chromatography of the Fab 734 (non-preincubated with metal) on Affi-Gel-DTPA-In(III) gave two populations: 85% were eluted with 100 mM DTPA-In(III) and the remaining 15% with 1 mM DTPA-In(III). This may imply the presence of two different paratopes.

Fab 734 preincubated with ZnCl₂ showed a major peak eluted with 1 mM DTPA-In(III). Two other minor peaks were eluted at 100 μM and 10 mM DTPA-In(III), respectively.

The fact that the Zn(II) preincubated Fab 734 presents a decrease (but no suppression) of the retention compared to the free Fab 734 indicates that a zinc ion is able to occupy at least partially the strong affinity binding site of DTPA-In(III). Some of the zinc binding ligands are presumably identical to the indium binding ligands, but there are still accessible ligands for interaction with Affi-Gel-DTPA-In(III).

Moreover, as shown in Figure 5, only 10% of the Fab 734 preincubated with zinc was eluted on Affi-Gel-DTPA-In(III) with a pH step gradient protocol. Elution of the

remaining protein was possible only with 50 mM EDTA. As previously shown in Figure 4, preincubation of Fab 734 with Zn(II) does not abolish the paratope/epitope recognition. Alternatively, when Fab 734 is complexed with its hapten DTPA-In(III), 78% of injected protein is not retained on Affi-Gel-DTPA-In(III) whereas the remaining protein (presumably corresponding to unloaded Fab) was eluted with 50 mM EDTA. As expected, the Fab/Affi-Gel-DTPA-In(III) affinity is specific and due to the paratope/epitope recognition phenomenon.

In Figure 6, we can see that the Fab 734 (not incubated with metal) presents an extremely strong retention on Sepharose 6B-IDA-Zn(II). No elution was possible up to pH 4. As much as 50 mM EDTA was required to elute the same. Sulkowski (*8*) has provided some ground rules regarding the number and position of histidine residues required for recognition by different metal-IDA chelates. A cluster of histidines [His-(X)ₙ-His with $n = 2$ or 3] is necessary for adsorption on Sepharose-IDA-Zn(II). On this basis, there are at least two accessible histidine residues in a cluster in the metal binding site of Fab 734. Nevertheless, the presence of cysteine residues in the binding site could not be excluded, but the direct participation of cysteine residues in IMA retention has never been demonstrated in an unequivocal manner. Adsorption of the Fab 734 in the presence of high salt concentration (1 M NaCl) abolishes the hypothesis of an exclusive contribution from aspartic or glutamic acids in IMAC retention (*20*), but they could be present in the metal binding site, in addition to histidine or cysteine residues. On the other hand, the Fab 734 preincubated with its hapten [DTPA-In(III)] is mainly eluted in the injection buffer (60%) whereas the remaining protein (presumably corresponding to unloaded Fab) was eluted with 50 mM EDTA (31%). This clearly indicates that the retention of the Fab 734 on Sepharose-IDA-Zn(II) is due to the presence of a histidine cluster located in the anti-DTPA-In(III) Fab paratope and not to a histidine cluster outside of the Fab 734 paratope.
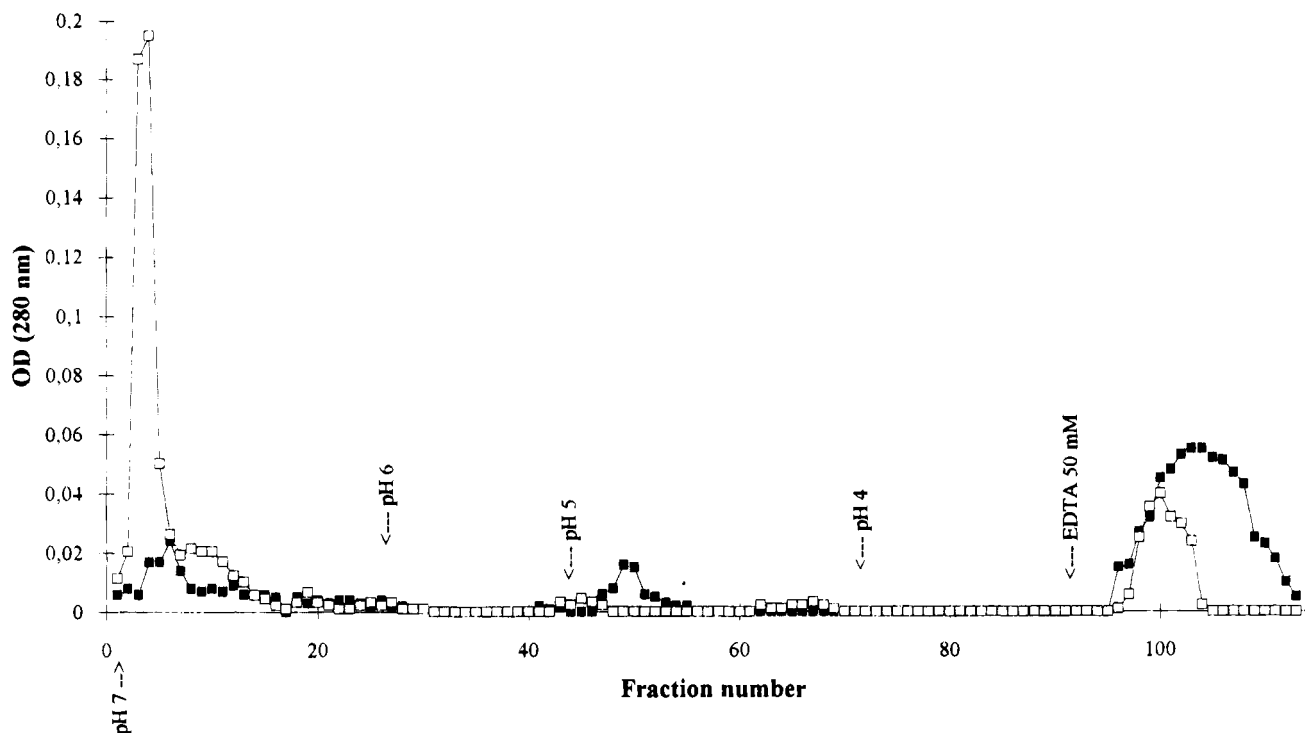
Figure 5. Chromatography on Affi-Gel-DTPA-In(III) using a pH step gradient of the Fab 734 preincubated with DTPA-In(III) (□) or ZnCl₂ (■). Elution conditions: (pH 7, pH 6) 20 mM phosphate + 0.3 M NaCl; (pH 5, pH 4) 100 mM acetate, 10 mM citrate + 0.3 M NaCl, and 50 mM EDTA. Protein injected: 220 μg of Fab. Bed volume: 1.1 mL. Flow rate: 20 mL/h. Fraction volume: 1 mL.
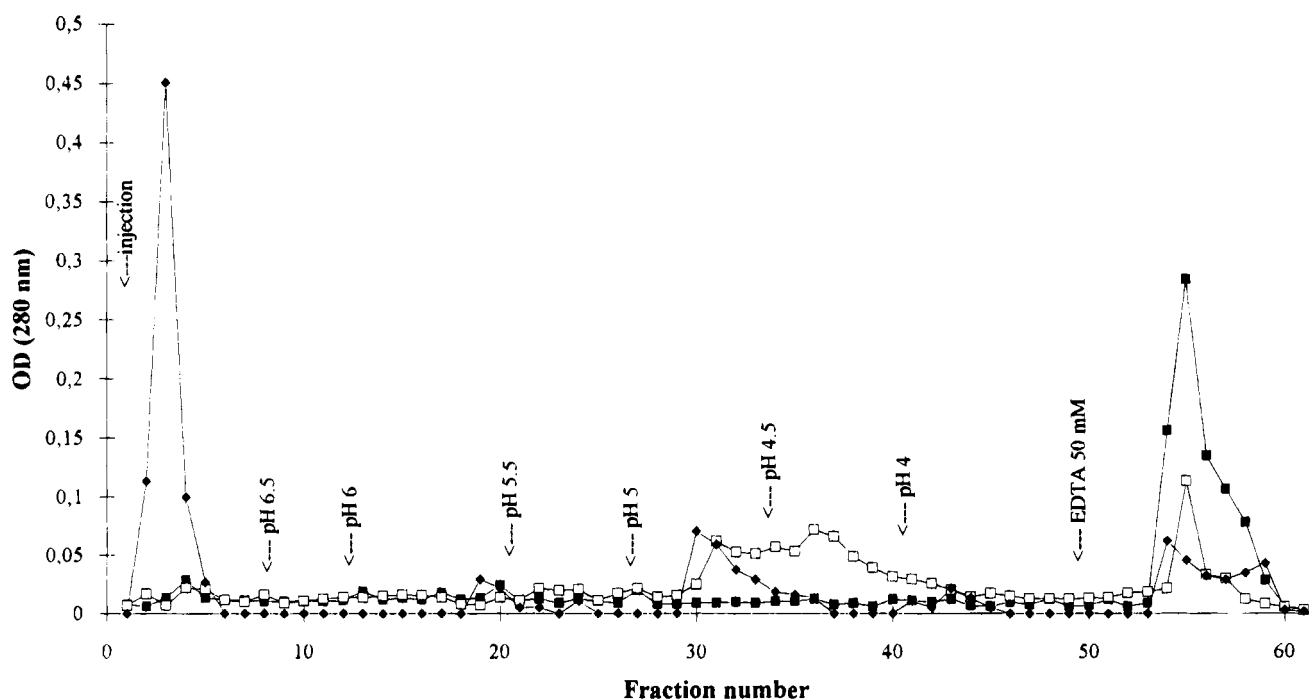
Figure 6. Chromatography on Sepharose 6B-IDA-Zn(II) using a pH step gradient of Fab 734 (■) and Fab 734 preincubated with DTPA-In(III) (◆) or ZnCl₂ (□). Elution conditions: (pH 7, pH 6.5, pH 6) 20 mM phosphate + 1 M NaCl; (pH 5.5, pH 5, pH 4.5, pH 4) 100 mM acetate + 1 M NaCl and 50 mM EDTA. Protein injected: 500 μg of Fab. Bed Volume: 1.1 mL. Flow rate: 20 mL/h. Fraction volume: 1 mL.

Further, Fab 734 preincubated with Zn(II) presented a reduced affinity, but the retention was not totally abolished (Figure 6), indicating that there is still an accessible cluster of histidine residues on the Fab 734 preincubated with zinc. Thus, on both supports, the Zn-(II) binding site is not superimposable to the DTPA-In-(III) paratope: there are still accessible ligands (at least two histidine residues in a cluster) for IMA retention after preincubation with Zn(II). Control chromatography

with a non-anti-metal chelate Fab (anti-DNP Fab) showed no retention on Sepharose IDA-Zn(II) (data not shown). This is in accord with the data obtained with the equilibrium binding studies (Figure 3 and Table 1).

CONCLUSION

In this study, competitive metal binding assays and immobilized metal ion affinity chromatography have been used as complementary approaches to investigate the
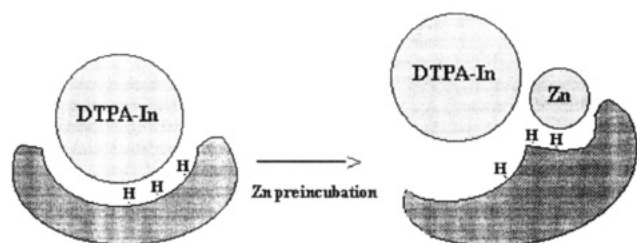
Figure 7. Schematic representation of the presumed action of Zn(II) binding to the paratope of the anti-DTPA-In(III) Fab 734.

metal specificity and the metal binding amino acid ligands in an anti-DTPA-In(III) monoclonal antibody (mAb 734). As already shown in a previous study (8), mAb 734 recognized DTPA-In(III) with specificity for the chelated metal. Its affinity for all the other selected metals chelated with DTPA was reduced by 100-fold compared to indium. Equilibrium binding immunoassays also revealed a peculiar Fab 734 behavior toward Zn(II) which remains to be clearly elucidated. When complexed to Zn(II), the DTPA-In(III) binding site presumably undergoes a slight modification of its initial conformation. Effectively, immobilized metal ion affinity chromatography studies clearly indicate that part of the DTPA-In-(III) binding amino acid ligands are identical to the Zn(II) binding ligands. IMAC approach also points out that the binding of the Fab 734 occurs via its paratope which contains a histidine cluster (apparently more than two histidine residues) favorable to an eventual catalytic activity. Therefore, as proposed in Figure 7, we can suppose that the Zn(II) binding reduces the DTPA-In-(III) binding to amino acid ligands which remain available, by partially saturating the site involving histidines. Thus, these simple experiments allowed us to obtain some partial information on the structure of the Fab 734 paratope and to guide our screening of its catalytic potential. Further studies of sequence determination and molecular modeling of the Fab 734 are under way to confirm this preliminary result.

ACKNOWLEDGMENT

LITERATURE CITED

(1) Vallee, B. L., and Auld, D. S. (1990) Zinc coordination, function, and structure of zinc enzymes and other proteins. *Biochemistry 29*, 5647−5659.

(2) Ibers, J. A., and Holm, R. H. (1980) Modeling coordination sites in metallobiomolecules. *Science 209*, 223−235.

(3) Regan, L., and Clarke, N. D. (1990) A tetrahedral Zn(II)-binding site introduced into a designed protein. *Biochemistry 29*, 10878−10883.

(4) Reardan, D. T., Meares, C. F., Goodwin, D. A., Mc Tigue, M., David, G. S., Stone, M. R., Leung, J. P., Bartholomew, R.

M., and Frincke, J. M. (1985) Antibodies against metal chelates. *Nature 316*, 265−267.

(5) Ghadiri, M. R., and Choi, C. J. (1990) Secondary structure nucleation in peptides. Transition metal ion stabilized α-helices. *J. Am. Chem. Soc. 112*, 1630−1632.

(6) Cochran, G., and Shultz, A. G. (1990) Peroxidase activity of an antibody-heme complex. *J. Am. Chem. Soc. 112*, 9414−9415.

(7) Iverson, L. I., and Lerner, R. A. (1989) Sequence-specific peptide cleavage catalyzed by an antibody. *Science 243*, 1184−1188.

(8) Sulkowski, E. (1987) Immobilized metal ion affinity chromatography of proteins. In *Protein purification: Micro to Macro* (R. Burgess, Ed.) pp 149−162, Alan R. Liss Inc., New York.

(9) Le Doussal, J. M., Gruaz Guyon, A., Martin, M., Gautherot, E., Delaage, M., and Barbet, J. (1990) Targeting of indium 111-labeled bivalent hapten to human melanoma mediated by bispecific monoclonal antibody conjugates: imaging of tumors hosted in nude mice. *Cancer Res. 50*, 3445−3452.

(10) Le Doussal, J. M., Chetanneau, A., Gruaz-Guyon, A., Martin, M., Gautherot, E., Lehur, P. A., Chatal, J. F., Delaage, M., and Barbet, J. (1993) Bispecific monoclonal antibody-mediated targeting of an indium-111-labeled DTPA dimer to primary colorectal tumors: pharmacokinetics, biodistribution, scintigraphy and immune response. *J. Nucl. Med. 34*, 1662−1671.

(11) Delaage, M., Drocourt, J. L., and Prince, P. (1984) Procédé de fixation de macromolécules biologiques sur des supports. Eur. Pat. Appl. 122209.

(12) Porath, J., Carlsson, J., Olsson, I., and Belfrage, G. (1975) Metal chelate affinity chromatography, a new approach to protein fractionation. *Nature 258*, 598−599.

(13) Lloyd, R. D., Mays, C. W., Jones, C. W., Lloyd, C. R., Taylor, G. N., and Wrenn, M. E. (1985) Effect of age on the efficacy of Zn-diethylene triamine-pentaacetic acid therapy for removal of Am and Pu from beagles. *Radiat. Res. 101*, 451.

(14) Pearson, R. G. (1968) Hard and Soft Acids, HSAB, Part I: Fundamental principles. *J. Chem. Educ. 45*, 581−592.

(15) Iverson, B. I., Iverson, S. A., Roberts, V. A., Getzoff, E. D., Tainer, J. A., Benkovic, S. J., and Lerner, R. A. (1990) Metalloantibodies. *Science 249*, 659−662.

(16) Wade, W. S., Koh, J. S., Han, N., Hoekstra, D. M., and Lerner, R. A. (1993) Engineering metal coordination sites into the antibody light chain. *J. Am. Chem. Soc. 115*, 4449−4456.

(17) Boden, V., Colin, C., Barbet, J., Le Doussal, J. M., and Vijayalakshmi, M. A. (1995) Complementary approach for the determination of histidine in the metal binding site of an anti-DTPA-Indium monoclonal antibody. *Ann. N.Y. Acad. Sci.* (in press).

(18) Hemdan, E. S., Zhao, Y. J., Sulkowski, E., and Porath, J. (1989) Surface topography of histidine residues: a facile probe by immobilized metal ion affinity chromatography. *Proc. Natl. Acad. Sci. U.S.A. 86*, 1811−1815.

(19) Berna, P., Moraes, J. J., Barbotin, J. N., Thomas, D., and Vijayalakshmi, M. A. (1993) One step affinity purification of a recombinant cyclodextrin glycosyl transferase by (Cu(II), Zn(II) tandem column) immobilized metal ion affinity chromatography. *Advances in molecular and cell biology* (Klaus Mosbach Symposium) JAI Press Inc. (in press).

(20) Belew, M., and Porath, J. (1990) Effect of solute structure, ligand density and salt concentration on the retention of peptides. *J. Chromatogr. 516*, 333−354.

BC950026T

Synthesis and Physicochemical Properties of Protein Conjugates with Water-Soluble Poly(alkylene oxides)

Irina N. Topchieva,* Nadezhda V. Efremova,† Nikolai V. Khvorov,‡ and Natalya N. Magretova‡

Department of Chemistry, Moscow State University, Lenin Hills, Moscow 119899, Russia, A. N. Bach Institute of Biochemistry, Russian Academy of Science, Leninsky Prospect 33, Moscow 117071, Russia, and A. N. Belozersky Institute of Physico-Chemical Biology, M. V. Lomonosov Moscow State University, 119899 Moscow, Russia. Received August 8, 1994⊛

Conjugates of proteins (bovine serum albumin (BSA) and α-chymotrypsin (CHT)) with poly(ethylene glycol) and amphiphilic block copolymers of ethylene oxide and propylene oxide (proxanols) were synthesized, using monoaldehyde polymer derivatives as the amino group modifying reagents. Four types of conjugates varying in the placement of hydrophobic block and type of polymer chain distribution were obtained. Methods of purification and characterization of proteins conjugated with proxanols were developed. It was shown that conjugates based on CHT retain high enzymatic activity toward both substrates investigated—N-benzoyl-L-tyrosine and casein—up to high degrees of modification (11 polymer chains per protein molecule). At the same time, CHT—proxanol conjugates were characterized by higher thermostability, the stabilizing effect increasing in parallel with the degree of modification. It was shown that the alteration of sedimentation coefficients of proteins caused by modification was negligible. On the basis of data obtained by the methods of hydrophobic chromatography, sedimentation, and differential scanning calorimetry, conformational models of protein—proxanol conjugates were suggested. It was supposed that conjugates form compact structures in aqueous solutions, which resemble intramolecular micelles, stabilized by hydrophobic interactions between poly(propylene oxide) blocks of proxanols.

INTRODUCTION

Covalent attachment of nonionic water-soluble polymers to proteins is a progressive way of imparting new useful properties to a protein molecule. Among the polymers so far studied for this purpose, poly(vinylpyrrolidones) (1), dextrans (2), and poly(ethylene glycols) (PEG)[1] (3, 4) are most often employed. PEG, with a history of being a plasma expander and of being nonimmumogenic, amphiphatic, and nontoxic, has been applied to various enzymes as a superior agent for modification (5). The products of the reaction—polymer—protein conjugates—are characterized by reduced immunogenicity, protracted retention in circulation, and in some cases, by enhanced stability (6). These features are due to the effect of "steric stabilization" of protein globule caused by the attachment of polymer chains.

The next stage in the construction of new polymer—protein conjugates is the modification of polymer chain by the insertion of foreign fragments (blocks) in the macromolecule due to copolymerization process. Using this approach, PEG was changed by well-known and commercially available copolymers, namely, block co-

polymers of ethylene oxide and propylene oxide (proxanols) (7). These polymers are nonionic surfactants in which poly(ethylene oxide) and poly(propylene oxide) are the hydrophilic and hydrophobic parts of the compounds, respectively. In contrast to PEG—protein conjugates, conjugates based on proxanols are characterized by the diversity of polymer—protein structures. The amphiphilic character of proxanol—protein conjugates provides new functions of modified proteins, such as the capability of translocation across biological membrane (8, 9), maintenance of effective solubilization and transport of insoluble biologically active compounds (10, 11), and the ability to form molecular assemblies due to interaction with various amphiphilic compounds (12, 13). In this work, we report various methods of synthesis, purification, and characterization of proxanol—protein conjugates, as well as some of their functional properties.

EXPERIMENTAL PROCEDURES

Chemicals. CHT, double crystallized, with an activity of 40–60 IU/mg, was purchased from Sigma; crystalline delipidized BSA, monomethyl ether of PEG MW 1900, and N-benzoyl-L-tyrosine (BT) and its ethyl ester (BTEE) were purchased from Serva; azocasein (casein, containing covalently bound p-sulfodiazobenzene) was a generous gift of Prof. V. V. Mozhaev (M. V. Lomonosov Moscow State University, chair of chemical enzymology); monobutyl ethers of block copolymers of ethylene oxide (E) and propylene oxide (P) (proxanols), differing in the type of blocks arrangement, RPE or REP, MW 2000, both containing 40 mol % of propylene oxide, were purchased from the factory NPO "NIOPIK" (Russia) and purified as described earlier (12). All other reagents were analytical grade and were purchased from Reakhim (Russia).

Synthesis of Polymeric Monoaldehydes. The polymeric monoaldehyde derivatives were synthesized by

* Address correspondence to this author at the Department of Chemistry, Moscow State University. Tel: (007-095) 939-31-27; Fax: (007-095) 939-01-74.
† A. N. Bach Institute of Biochemistry, Russian Academy of Science.
‡ A. N. Belozersky Institute of Physico-Chemical Biology, M. V. Lomonosov Moscow State University.
[1] Abbreviations used: BBI, soybean Bauman-Birk proteinase inhibitor; BSA, bovine serum albumin; BT, N-benzoyl-L-tyrosine; BTEE, N-benzoyl-L-tyrosine ethyl ester; CHT, α-chymotrypsin; PEG, poly(ethylene glycol); TNBS, 2,4,6-trinitrobenzenesulfonic acid; RPE, REP–proxanols, block copolymers of ethylene oxide and propylene oxide.

Table 1. Characteristics of Conjugates of CHT with PEG and Proxanols

N	polymer	molar ratio of polymeric reagent to CHT	type of conjugate	degree of modification	wt % of CHT	no. of unmodified surface NH_2 groups (m)	designation of conjugate
1	PEG	20	I[a]	3	81.0 (80.5)[b]	12	$(PEG)_3$-CHT
2	PEG	30	I	9	58.1 (58.8)	5	$(PEG)_9$-CHT
3	RPE	17	IIa	2	86.2 (86.1)	13	$(RPE)_2$-CHT-a
4	RPE	20	IIa	3	82.1 (79.8)	12	$(RPE)_3$-CHT-a
5	RPE	30	IIa	6	67.5 (66.7)	8	$(RPE)_6$-CHT-a
6	RPE	35	IIa	7	64.0 (64.1)	7	$(RPE)_7$-CHT-a
7	RPE	45	IIa	10	55.6	4	$(RPE)_{10}$-CHT-a
8	RPE	20	IIb	3	80.6	11	$(RPE)_3$-CHT-b
9	RPE	25	IIb	5	71.5 (71.0)	9	$(RPE)_5$-CHT-b
10	RPE	30	IIb	6	67.4 (67.5)		$(RPE)_6$-CHT-b
11	RPE	45	IIb	11	45.5 (46.0)		$(RPE)_{11}$-CHT-b
12	REP	20	III	3	80.6 (80.7)	12	$(REP)_3$-CHT
13	REP	30	III	7	64.2 (64.0)		$(REP)_7$-CHT

[a] I, IIa, IIb, and III are conjugates having the structures shown in Figure 1. [b] The amount of CHT present in each conjugate was determined by UV spectroscopy and by the biuret procedure (values in parentheses).

Table 2. Characteristics of Conjugates of BSA with PEG and Proxanols

N	polymer	molar ratio of polymeric reagent to BSA	type of conjugate	degree of modification	content of BSA, wt % biuret method	content of BSA, wt % 280 nm	content of BSA, wt % ^{13}C NMR	designation of conjugate
1	PEG	30	I	5	87	87		$(PEG)_5$-BSA
2	PEG	50	I	14	70	71		$(PEG)_{14}$-BSA
3	RPE	30	IIa	5	87	87		$(RPE)_5$-BSA-a
4	RPE	40	IIa	8	81	80	78	$(RPE)_8$-BSA-a
5	RPE	50	IIb	15	70	69	70	$(RPE)_{15}$-BSA-b
6	REP	30	III	6	85	84		$(REP)_6$-BSA
7	REP	45	III	11	75	75		$(REP)_{11}$-BSA

oxidation of poly(alkylene oxides) in dry chloroform in the presence of MnO_2 (*14*). Though the block copolymer REP contains mostly secondary alcohol end groups, there are always about 8–12% of primary alcohol end groups present (*15*), which were subsequently oxidized to aldehydes. Aldehydes were quantitated with (2,4-dinitrophenyl)hydrazine (*16*). The content of aldehyde groups was 66% for PEG, 80% for RPE copolymer, and 12% for REP copolymer. These reagents were used for modifying proteins without purification.

Synthesis of Conjugates. Conjugates of proteins with poly(alkylene oxides) were synthesized by the interaction of protein ϵ-NH_2 groups with monoaldehyde derivatives of poly(alkylene oxides) by reductive amination. Synthesis of conjugates with various degrees of NH_2 group modification n, corresponding to the average number of polymer chains coupled per protein molecule, was carried out using molar ratios of polymeric monoaldehyde/protein ranging from 17:1 to 50:1 (see Tables 1 and 2).

Synthesis of Conjugates of CHT with Poly(alkylene oxides). Method A. A 2.5 mL aliquot of the polymeric monoaldehyde solution in 0.1 M borate buffer, pH 8.0, was added to the solution of CHT (50 mg) in 2.5 mL of the same buffer, containing 71 mg of BT. The reaction mixture was incubated for 2 h at 20 °C, then 100-fold molar excess of sodium cyanoborohydride over amino groups was added, and the mixture was stirred for 30 min.

Method B. The polymeric monoaldehyde was dissolved in the mixture of 60 vol % buffer and 40 vol % ethanol. The solution was added slowly under stirring to the CHT, dissolved in borate buffer. The other procedures were carried out as in method A.

Syntheses of BSA—Poly(alkylene oxide) Conjugates. Method A. A 2 mL aliquot of the polymeric monoaldehyde solution in 0.04 M borate buffer, pH 8.5, was added

to the solution of BSA (50 mg) in 2 mL of the same buffer. The reaction mixture was incubated at 20 °C for 1.5 h, and then sodium borohydride was added in 3 portions at intervals of 15 min (the molar ratio of the whole quantity of sodium borohydride to protein amino groups was 100:1). The mixture was stirred for 15 min.

Method B. The polymeric monoaldehyde was dissolved in the mixture containing 60 vol % of borate buffer and 40 vol % of ethanol. The solution was added slowly under stirring to the solution of BSA in borate buffer. The rest procedures were the same as in method A.

Purification of Conjugates. In order to remove the excess of polymeric monoaldehyde and low-molecular-weight contaminations from conjugate, two methods were used.

I. Precipitation by Acetone. The low-molecular-weight compounds were removed from the reaction mixture by dialysis for 24 h against distilled water. After that, the solution was concentrated to the volume of 3 mL and poured into 12 mL of acetone, in order to precipitate the conjugate, which was then separated by centrifugation and dried in vacuo.

II. Gel-permeation chromatography. The reaction mixture was passed through a 2 × 60 cm column packed with gel Toyopearl HW-50 (TOYO SODA, Japan), using a mixture of 20 vol % of ethanol and 80 vol % of 0.02 M phosphate buffer as eluent. The effluent was assayed by spectrophotometric reading at 280 nm, and fractions containing protein were collected. The ethanol and sodium phosphate were removed by dialysis, and the conjugate was freeze-dried.

Thin-Layer Chromatography. The control for the presence of polymer contaminations was performed using thin-layer chromatography on Silufol plates (Czechoslovakia) in the system chloroform—ethanol—water (36:12:1). The polymer migrated with the solvent front (R_f = 1), while the conjugate remained at the starting point

$(R_f = 0)$. Iodine vapor was used to visualize the spots. In cases where the conjugate contained polymeric contaminations, the purification procedure was repeated.

Characterization of Conjugates. *Analysis for Conjugate Composition.* Protein content in the conjugates was determined either spectroscopically at 280 nm or using the biuret reaction (*17*) (native proteins were used as standards). The composition of the conjugates was analyzed also by ^{13}C NMR spectroscopy, which allowed determination of both protein and polymer content.

^{13}C NMR spectra of the samples dissolved in D_2O were recorded on a spectrometer FT-80A (Varian, USA), in pulse regime with signal accumulation. Experimental parameters: spectrum width 5000 Hz, time of signal accumulation 1.0 s, high frequency impulse duration 8 μs, time delay to the next impulse 0.8 s, the number of accumulated impulses 32 000–36 000. Time of experiment 16–18 h.

The analysis procedure consisted of several stages. First, ^{13}C NMR spectra of the individual components of the conjugates—the polymer and protein—were registered in order to choose regions where their signals do not interfere. For BSA, it was the region of 172–180 ppm, corresponding to a signal from the carbon atoms of carboxyl groups; for RPE copolymer, it was the region of 70–77 ppm, corresponding to a signal from the carbon atoms of methylene groups of the backbone chain. Then, the ^{13}C NMR spectra of the conjugates were registered; samples of BSA and RPE mixtures in various weight ratios served as standards. The integrated signals characteristic for BSA and RPE were recorded for all samples, and by reference to the "standards", the weight composition of the conjugates was computed.

Enzymatic Assay. Enzymatic activity of CHT–polymer conjugates toward low-molecular-weight substrate was assayed by determining the initial rate of hydrolysis of BTEE, which was registered spectroscopically at $\lambda = 257$ nm ($\epsilon = 990$ M^{-1} cm^{-1}). The initial concentration of the substrate was $(1-5) \times 10^{-4}$ M, and the enzyme concentration 1×10^{-7} M. Tris (0.05 M)–CaCl$_2$ (0.2 M) buffer, pH 7.8, was used as the reaction medium.

The method of measuring enzymatic activity toward the protein substrate, azocasein, was based on the enzymatic hydrolysis of substrate by CHT–protein conjugates, stopping the reaction by the addition of trichloracetic acid, and spectrophotometric assay of unprecipitated colored tyrosine–histidine-containing peptides ($\lambda = 400$ nm) (*18*).

The concentration of active sites in CHT and CHT–polymer conjugates was determined as described in ref 19.

Titration of Amino Groups in Conjugates. Titration with 2,4,6-trinitrobensenesulfonic acid (TNBS) was carried out as described in ref 20. Titration with *o*-phthalic aldehyde and mercaptosuccinic acid was fulfilled according to ref 21.

Sedimentation Analysis. Sedimentation of the conjugates was studied using an analytical ultracentrifuge, Beckman Model E, equipped with absorption optical system, monochromator, and photoelectric scanning system. Assays were carried out at 280 nm, and rotor speed was 48 000 rpm at 20 °C. The samples were investigated in the concentration range 1–10 mg/mL, using 0.1 M Tris-HCl buffer, pH 8.0, as a solvent.

Calorimetric Study. Calorimetric measurements were carried out using the differential adiabatic scanning microcalorimeter DASM-4 (Biopribor, Russia), whose construction and principles have been described elsewhere (*22*). Capillary construction of the 0.47 mL platinum measuring cell prevented to a great extent the

artifacts caused by thermally induced protein aggregation. The heating rate was 1 K/min. Sample concentration varied over 0.5–2 mg/mL. Sodium phosphate buffer (20 mM), pH 7.0, was used as a solvent.

RESULTS AND DISCUSSION

Synthesis of Conjugates. Conjugates of proteins with poly(alkylene oxides) were synthesized by the interaction of protein ϵ-amino groups with monoaldehyde derivatives of poly(alkylene oxides), leading to the formation of labile iminium groups, which were subsequently reduced by sodium borohydride or sodium cyanoborohydride. As a result, polymer chains became grafted to the polypeptide through a very stable secondary amine bond. The total charge of the protein did not change in the process of modification. An analogous reaction was used in ref 23 for the synthesis of horseradish peroxidase conjugates with PEG.

The reactions of CHT–poly(alkylene oxide) conjugation were performed in the presence of reversible inhibitors of the active site of the enzyme. Sodium cyanoborohydride is a preferable reducing agent in this case, for its use leads to better preservation of the protein's native structure, while NaBH$_4$ is able to reduce S–S bonds between polypeptide chains of CHT.

The following monoaldehyde derivatives of poly(alkylene oxides) were used for protein modification:

(1) Monomethoxy–PEG monoaldehyde (PEG–CHO):

   CH$_3$(OCH$_2$CH$_2$)$_{44}$OCH$_2$CHO

(2) RPE block copolymer monoaldehyde (RPE–CHO):

   C$_4$H$_9$(OCHCH$_2$)$_{14}$(OCH$_2$CH$_2$)$_{20}$OCH$_2$CHO
               |
              CH$_3$

(3) REP block copolymer monoaldehyde (REP–CHO):

   C$_4$H$_9$(OCH$_2$CH$_2$)$_{20}$(OCHCH$_2$)$_{14}$OCH$_2$CHO
                          |
                         CH$_3$

It is seen that the only difference between block copolymers 2 and 3 is in the position of poly(ethylene oxide) and poly(propylene oxide) blocks toward the aldehyde group. Using these polymer reagents, two main types of conjugates with hydrophobic blocks at the periphery or inside conjugate structure were synthesized.

Molecular models of the conjugates studied in this work are presented in Figure 1. It is seen that the conjugates have a star-shaped structure in which the protein occupies the central place, with polymer chains growing from it as branches. The length of polymer chains is of the same order as or even bigger than the diameter of protein molecule. That is why the protein in the conjugate should be sterically stabilized toward the action of macromolecular substrates, antibodies, and proteolytic enzymes. It is evident that this property depends on the number of polymer chains and the type of their distribution on the surface of protein.

It was necessary to find methods sensitive to different types of polymer distribution. One of the approaches to the investigation of the steric arrangement of the polymer chains consists of the study of the ability of bound polymers to interact with the bulky cyclic reagent β-cyclodextrin, which was shown to form inclusion-type complexes with proxanols (*24*, *25*). It was shown that conjugates of type II which were synthesized in aqueous buffer media do not form complexes with β-cyclodextrin, whereas conjugates of the same type obtained in water–alcohol media do form crystalline complexes (*13*). This is obviously due to the fact that in the first case polymer
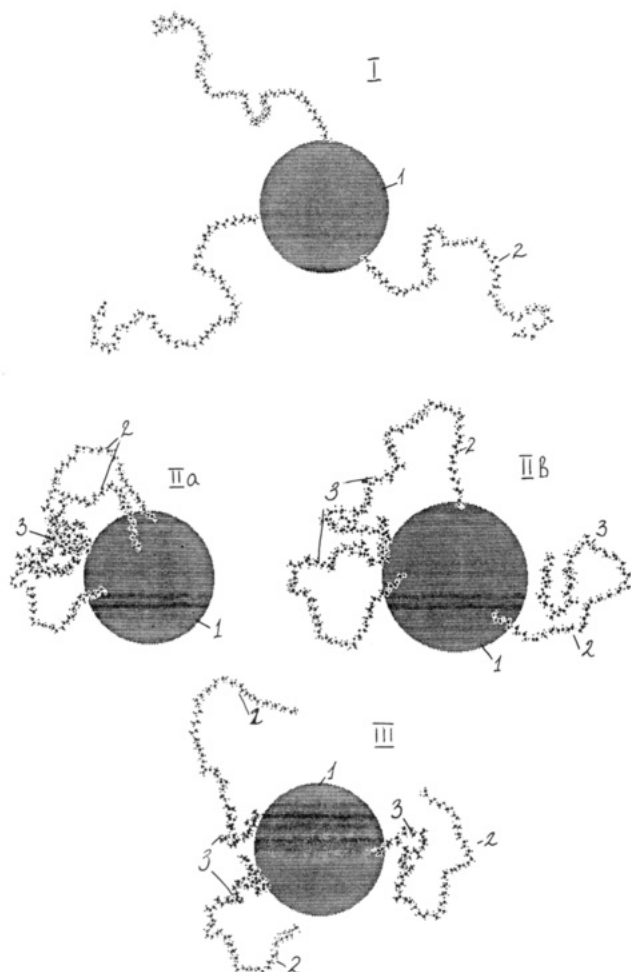
Figure 1. Molecular models of protein conjugates with PEG (I) and proxanols of various types: IIa, conjugates with clustered distribution of polymer chains; IIb, with statistical distribution of polymer chains; III, with hydrophilic blocks at the periphery of the structure. 1, protein globule; 2, poly(ethylene oxide) block; 3, poly(propylene oxide) block. The models were designed on computer with the help of the program "Atom". The radius of central globule was chosen to correspond to the average radius of CHT molecule: 25 Å (38).

chains form cluster structures at the surface of the protein (type IIa), thus making the reaction with β-cyclodextrin highly improbable; in the second case polymers are randomly distributed on the protein surface (type IIb). It should be noted that the ethanol concentration in the reaction media was enough to destroy polymer micelles but much lower than denaturing concentrations for the proteins under investigation (26).

Purification of Conjugates. The separation of conjugates from excess proxanols offers more difficulties than the purification procedure in the case of PEG–protein conjugates. This is accounted for by the amphiphilic properties of proxanols, which lead to association between unreacted reagent and polymer chains in the conjugate. This explains the low efficiency of commonly used methods of purification, such as dialysis and ultrafiltration in aqueous media. The effective purification can be achieved only by using aqueous organic media, which leads to the dissociation of these complexes. Taking into account all these considerations, two methods of purification were proposed: precipitation of conjugate by acetone and gel-permeation chromatography using 20% ethanol as eluent. Thin-layer chromatography was used to evidence the absence of polymer contamination in the conjugate.

Analysis of Conjugates. In Tables 1 and 2 characteristics of the obtained conjugates of proteins with PEG and proxanols are presented. Protein content in the conjugates was determined either spectroscopically at 280 nm or by using biuret reaction. It was shown that neither PEG nor proxanol interferes with the protein assay using the spectrophotometric method (A_{280}) and the biuret reaction. The results of both methods were in good agreement (see Tables 1 and 2).

¹³C NMR Spectroscopy. ¹³C NMR spectroscopy presents a direct method for determination of both protein and polymer content in conjugates, because there exist regions where signals from polymer and protein do not interfere. Two conjugates of BSA with RPE copolymer (preparations 4 and 5 in Table 2) were analyzed by this method. The results turned out to be in good agreement with data obtained by UV spectroscopy, and the biuret method (see Table 2). One may see that each of the used methods is available for the analysis of conjugates composition.

The degree of modification n, which denotes the average number of polymer chains coupled with protein molecule, was calculated from the data on conjugates composition using the following formula:

$$n = \frac{(\text{wt \% of polymer})/(M \text{ of polymer})}{100 - (\text{wt \% of polymer})/(M \text{ of protein})} \quad (1)$$

where M is molecular mass.

Titration of Surface Amino Groups in Conjugates. Titration of NH_2 groups with TNBS is most commonly used for the determination of the degree of modification of the protein in conjugates. The degree of modification n is given by the formula:

$$n = a - m \quad (2)$$

where a stands for the total number of surface NH_2 groups in native protein and m for the number of unmodified NH_2 groups in conjugate. In our case, however, not only unmodified NH_2 groups but also resulting secondary amino groups of conjugate interacted with TNBS, giving the same number of surface amino groups as in native protein. These results are in good agreement with those described in the review (27) for PEG–tresylate-modified proteins. Thus, it was necessary to use a reagent for primary amino groups only. We have chosen o-phthalic aldehyde and titrated NH_2 groups by the method of Roth (21). This method was applied to a number of conjugates based on CHT. The degrees of modification calculated by formula 2 assuming $a = 15$ for CHT (28) were in good agreement with the results obtained on the basis of protein content determination by UV spectroscopy and the biuret method by formula 1 (column 5 in Table 1).

Enzymatic Properties of Conjugates. Kinetic characteristics of the reactions of enzymatic hydrolysis of conjugates on the basis of CHT are presented in Table 3. These data show the following:

(1) Conjugates retain high enzymatic activity toward both investigated substrates—low-molecular-weight substrate BTEE and azocasein. It should be noted that the attempts to modify CHT in the absence of the inhibitor (N-acetyl-L-tyrosine or N-benzoyl-L-tyrosine) led to the considerable loss of enzymatic activity (30%, in relation to native enzyme (12)). Thus, the preservation of enzymatic properties is obviously due to sterical screening of active site by the inhibitor during the conjugation reaction.

Topchieva et al.

Table 3. Enzymatic Properties of CHT Conjugates with PEG and Proxanols

N	enzyme, conjugate	enzymatic hydrolysis of casein	enzymatic hydrolysis of BTEE			content of active sites, %
		act., %	act., %	k_{cat}, s^{-1}	K_m, M × 10^5	
1	CHT	100	100	31.2 ± 0.5	6.27 ± 0.94	80
2	(RPE)$_5$-CHT-a	102	97	42.4 ± 2.8	13.0 ± 2.0	61
3	(RPE)$_3$-CHT-b	103	115			80
4	(RPE)$_6$-CHT-b	96	98	32.5 ± 1.2	6.18 ± 0.82	67
5	(RPE)$_{11}$-CHT-b	50	57	37.0 ± 0.4	21.7 ± 3.5	40
6	(PEG)$_6$-CHT	97	98	40.4 ± 0.8	9.3 ± 1.5	80
7	(REP)$_3$-CHT	98	100			80

(2) There are insignificant changes in the values of K_m and the catalytic constant for hydrolysis of the low-molecular-weight substrate BTEE by conjugates with degrees of modification of from 3 to 6, comparing to parent enzyme. Analogous results were obtained for hydrolysis of the high-molecular-weight substrate azocasein (data not shown).

(3) Noticeable decrease of the enzymatic activity was observed only for conjugate with a high degree of modification ($n = 11$). The same tendency was described earlier for PEG–CHT conjugates with degrees of modification from 10 to 14 (*29*). It is seen from Table 3 that the loss of activity is accounted for by two factors: the decrease in content of active sites in conjugates, and the increase in K_m (which is obviously due to the steric hindrance). The fact that values of k_{cat} for this conjugate and CHT are practically the same should mean that the reductive alkylation of CHT with copolymers had not changed the microenvironment of the active site of CHT.

Thermal Stability of Conjugates. It is well-known that chemical modification of proteins is one of the effective approaches to the change of their thermal stability. In the case of PEG–protein conjugates it was shown that the attachment of polymer chains either increases or does not change thermal stability of protein (*3, 6*). The peculiarity of conjugates based on proxanols consists in the possibility to regulate thermal stability of modified protein by the variation of a number of parameters, such as the degree of modification, the number and type of blocks arrangement, hydrophilic-lipophilic balance, and the type of polymer distribution on the surface of protein globule. For these reasons we studied the thermal inactivation of all types of conjugates on the basis of CHT. The thermal stabilities of PEG–CHT conjugate and of native CHT were studied for comparison. Kinetic curves of thermoinactivation of CHT and its conjugates with polymers are presented in Figure 2. The thermostability of conjugates of CHT decreases in the following order: (PEG)$_9$-CHT > (RPE)$_5$-CHT-b > (RPE)$_6$-CHT-a > (RPE)$_3$-CHT-a > CHT-(REP)$_3$-a > CHT. It should be noted that all CHT–proxanol conjugates with the exception of (RPE)$_5$-CHT-b are of the IIa type.

It is seen that the rate of thermal inactivation of the enzyme decreases significantly as a result of the attachment of three polymer chains. The stabilizing effect becomes even more pronounced with increasing the degree of modification of CHT. The maximal stabilizing effect is achieved for the CHT–PEG conjugate with nine polymer chains. It is remarkable that conjugate (RPE)$_5$-CHT-b with a random mode of distribution of polymer chains possesses higher thermostability than conjugate (RPE)$_6$-CHT-a with clustered distribution. At the same time, the difference in the placement of the hydrophobic block in conjugates with an equal number of copolymer chains leads to a change in their thermostability: conjugate of type IIa is more stable than conjugate of reversed type (III).
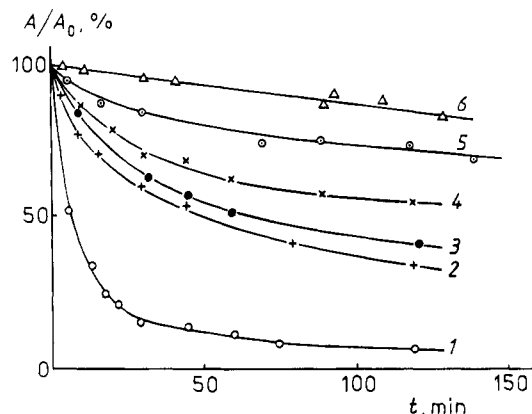
Figure 2. Kinetics of thermal inactivation of CHT and its conjugates with poly(alkylene oxides): 1, CHT; 2 (REP)$_3$-CHT; 3, (RPE)$_3$-CHT-a; 4, (RPE)$_6$-CHT-a; 5, (RPE)$_5$-CHT-b; 6, (PEG)$_9$-CHT. Conditions of thermal inactivation: 0.2 M Tris-HCl, pH 8.05; 45 °C. The concentration of protein in the probe is 0.1 μM. The solution of CHT or its conjugate was incubated in a thermostated cell at 45.0 ± 0.05 °C. After selected time intervals, the residual activities of aliquots were assayed by determining the initial rate of hydrolysis of BTEE. The enzymatic activity is expressed in percent relative to the initial activity of corresponding preparations.
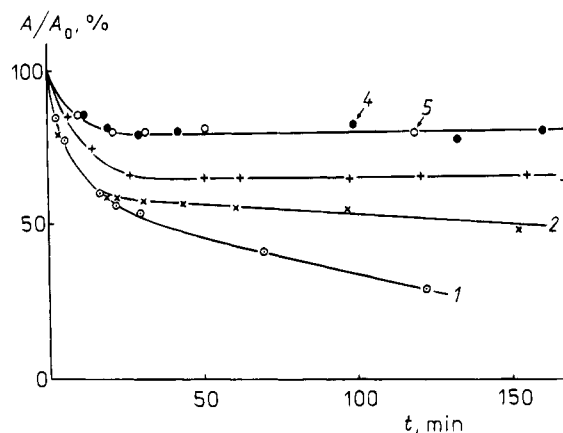
Figure 3. Kinetics of thermal inactivation of conjugate (RPE)$_4$-CHT-a alone (1) and in the presence of added free RPE copolymer in a molar excess (with respect to CHT) of 50 (2), 100 (3), 500 (4), and 750 (5). Thermal inactivation conditions as in Figure 2.

One of the unique properties of protein conjugates with proxanols is their ability to interact with both synthetic (surfactants) and natural (lipids) amphiphilic compounds (*12, 31*). The functional aspect of these interactions was demonstrated in the study of thermoinactivation. Thermal stability of conjugates may be enhanced by the addition of free proxanol into the incubation system. This phenomenon is illustrated in Figure 3, which demonstrates thermal inactivation of conjugate (RPE)$_4$-CHT-a (type IIa) in the presence of added free proxanol in molar excess over the conjugate ranging from 50 to 750. The
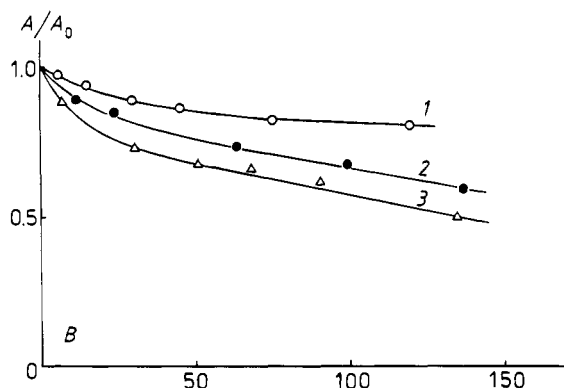
Figure 4. Kinetics of thermal inactivation of CHT–proxanol conjugate (RPE)$_3$-CHT-b (1), the same conjugate in the presence of β-cyclodextrin (2), and egg yold lecithin (3). Molar ratio conjugate:additive 1:50. Thermal inactivation conditions as in Figure 2.

kinetic curves in Figure 3 show that addition of free proxanol to the solution up to a 500-fold molar excess increases the stability of enzyme in the conjugate. Further increase in the proxanol concentration does not significantly influence the thermal inactivation kinetics, perhaps due to saturation of the conjugate by associated copolymer.

One can assume that an increase in the stability of CHT–proxanol conjugates comparing to the parent protein is due to the ability of polymer chains to screen hydrophobic domains at the surface of the protein (*32, 33*). An additional increase in the stability of CHT–proxanol conjugate in the presence of free proxanols may be accounted for by interaction between free and bound proxanols, leading to a formation of a thick polymer coat surrounding the protein globule.

Addition of egg yolk lecithin and β-cyclodextrin produces an opposite effect on the stability of protein in conjugate (Figure 4). All additives themselves do not affect the behavior of the native enzyme. Probably in the latter case these additives are stronger competitors for hydrophobic bond formation with proxanols than the corresponding domains of the protein globule. As a result, the steric arrangement of polymer chains is changed in such a way that the hydrophobic domains of protein become exposed again and destabilization of the enzyme structure as compared with conjugate takes place.

The data presented above give the examples of changes in thermal stability of conjugates due to their interaction with amphiphilic molecules. As a matter of fact, study of thermal stability may be successfully used for detection of the interactions between conjugates and different partners. On the other hand, noncovalent supramolecular structures based on conjugates and additives initiate new approaches to elucidation of the mechanisms of transport and functioning of proteins as drugs.

Differential Scanning Calorimetry (DSC). Taking into consideration the results on thermal stability of conjugates, gained through the investigation of their enzymatic properties, it was interesting to study thermally induced transitions in proteins modified with proxanols and PEG by the direct method of DSC. Figure 5 shows DSC data for CHT and its conjugates with polymers in aqueous buffering media. The heat sorption peak for CHT is slightly asymmetric and possesses one maximum with $T_{max} = 49.6$ °C, which is in good agreement with the results presented in ref 22.

Considerable changes in the form of heat sorption peaks are observed for CHT conjugates with polymers
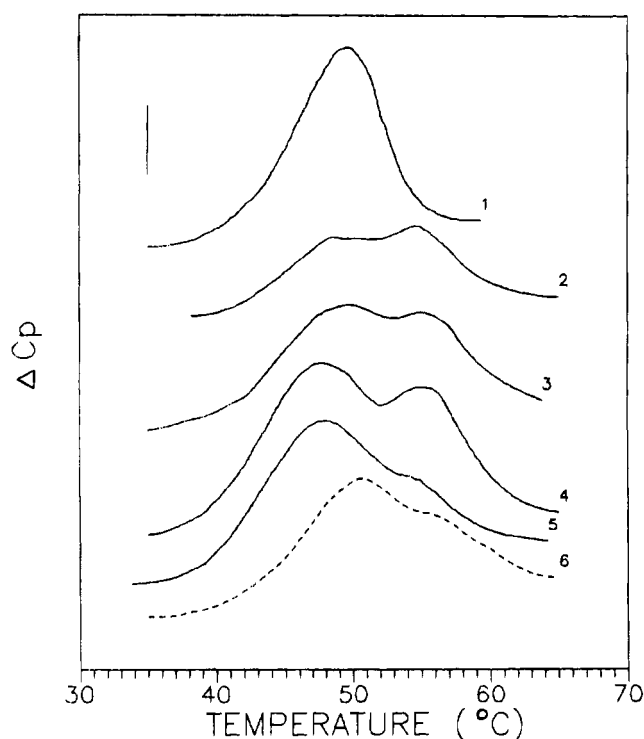
Figure 5. Temperature dependences of excess heat capacity (ΔC_p) for CHT (1) and its conjugates (PEG)$_3$-CHT (2), (RPE)$_3$-CHT-b (3), (RPE)$_3$-CHT-a (4), (REP)$_3$-CHT (5), and (RPE)$_7$-CHT-b (6). The concentration was 1.0 mg/mL; buffer: 20 mM phosphate, pH 7.0. The vertical bar corresponds to 1.0 kJ K^{-1} kg^{-1}.

(curves 3–6 in Figure 5). Besides the first maximum, located in the temperature limits 47.6–49.6 °C, there arises the second maximum on heat sorption curves of conjugates (RPE)$_3$-CHT-a, (RPE)$_3$-CHT-b, and (PEG)$_3$-CHT, which is located at 54.5–55.5 °C. In the heat sorption curve of (REP)$_3$-CHT there arises a shoulder in the same temperature region. Trivial explanation of this phenomenon is that the existence of two maxima on heat sorption curves is due to the heterogeneity of conjugates, namely, that the conjugate's fraction with low degree of modification gives rise to the first maximum and the fraction with higher degree of modification gives rise to the second. This suggestion is not confirmed by the DSC data on the conjugate with a high degree of modification (curve 6), which revealed only one maximum ($T_{max} = 51.2$ °C) and a shoulder in the region 54.5–55.5 °C.

One may suppose that in the course of protein globule denaturation hydrophobic parts of the protein molecule became accessible for the interaction with hydrophobic blocks of copolymer, coupled to protein. The emergence of the second maximum on heat sorption curves of conjugates may be due to the melting of such a polymer–protein complex.

In order to support this suggestion, we conducted some additional experiments, using mixtures of CHT with PEG and proxanol. The following was shown:

(1) Heating of a solution of CHT, containing proxanol (1:20), from 20 to 60 °C, does not lead to aggregation and precipitation of protein.

(2) Analogous heating of solutions containing pure CHT or a mixture of CHT and PEG (1:20) leads to aggregation of protein followed by precipitation.

(3) Protein-containing product, obtained from a CHT–proxanol mixture after heating and purification from excess of proxanol, contained only 50% of protein. The rest, according to the data of ^{1}H NMR (data not shown), is a bound proxanol.

(4) The heat sorption curve of a solution containing a mixture of CHT and proxanol has only one peak with T_{max} = 54.5 °C, which coincides with the position of the second maximum on DSC curves of conjugates.

These facts demonstrate the ability of proxanols to interact with CHT in aqueous solutions under heating.

It should be noted that the heat sorption curve corresponding to the (REP)$_3$-CHT conjugate is similar to the thermogramm of CHT and contains only a little shoulder in the high temperature region. Probably this is due to the fact that the poly(propylene oxide) block directly attached to the protein possesses rather poor ability for complexation.

We should focus our attention on the fact that on the curve of heat sorption of (PEG)$_5$-CHT conjugate two peaks of melting are observed. This effect may be explained using the concept of poly(alkylene oxide) solubility in water. According to the theory of Kjellander and Florin (*34*), the solubility of PEG is due to its ability to fit into the crystal structure of water. The coupling of hydrophobic groups or complex fragments containing both hydrophobic and polar groups to the end groups of PEG leads to a sufficient change in the conformational state of the polymer chains in a conjugate. One may suppose that fragments of PEG chains, located in the vicinity of the protein globule, lose their ability to fit into the structure of water and hence became hydrophobic. Another explanation of this effect is based on the analogy of the structure of conjugate and micelle. According to the star model proposed by Halperin (*35*), PEG chains located in the corona of micelle structure are in a semidiluted condition with a decreased concentration (or increased hydration) profile along the radius.

Thus, DSC study of CHT conjugates with PEG and proxanols shows the following: (a) Conjugates are more stable than parent proteins. (b) The thermal stability of proxanol—CHT conjugates is comparable with the thermal stability of PEG—CHT conjugates. (c) The emergence of the second maximum on DSC curves of conjugates is very likely due to the formation of intramolecular polymer—protein complexes.

Sedimentation of Conjugates. Hydrodynamic properties of conjugates were investigated using the sedimentation analysis method. Sedimentation coefficients obtained for the conjugates and for the initial proteins are summarized in Table 4. Ony may see that alteration of the sedimentation coefficients of proteins caused by the modification is negligible. Thus, sedimentation data show that solutions of conjugates do not contain products of intermolecular interaction under the investigated conditions.

Even in the absence of intermolecular interactions the attachment of polymer chains might have influence on the value of sedimentation coefficients. The fact that no considerable alteration of sedimentation coefficients of proteins after modification is observed should mean that the effect of growth of molecular mass is compensated by the flotating action of polymer chains (*36*).

Conformational Models of Conjugates Based on Proteins and Proxanols. In the previous work (*37*) the relative hydrophobicity of proxanol conjugates with BBI was evaluated using reverse-phase hydrophobic HPLC. Figure 6 shows the results of hydrophobic HPLC for native BBI and (RPE)$_5$-BBI conjugate. One may see that the retention volume of the conjugate is less than that of the native protein, thus indicating its lesser affinity for the hydrophobic sorbent. The same tendency was observed for CHT and its conjugate with proxanol. At first glance, this result would seem surprising since the polymer chains entering the conjugate contain hydro-

Table 4. Sedimentation Coefficients for Proteins and Their Conjugates with PEG and Proxanols[a]

N	protein conjugate	concn, mg/mL	$\bar{S}_{20}$, S
1	BSA	1	4.3 ± 0.2
2	(PEG)$_{15}$-BSA	1	4.2 ± 0.2
3	(RPE)$_8$-BSA-a	1	4.5 ± 0.3
		2	4.0 ± 0.2
		4	4.0 ± 0.2
		6	4.2 ± 0.2
		10	4.6 ± 0.2
4	(REP)$_6$-BSA	1	4.1 ± 0.2
5	CHT	1	2.0 ± 0.15
		4	2.02 ± 0.15
		8	2.2 ± 0.17
		10	2.45 ± 0.12
6	(RPE)$_3$-CHT-a	1	2.3 ± 0.1
		3	2.42 ± 0.15
		5	2.51 ± 0.16
		6	2.61 ± 0.21
		7	2.60 ± 0.18
7	(RPE)$_3$-CHT-b	1	1.91 ± 0.13
		3	1.99 ± 0.15
		5	2.11 ± 0.08
		10	2.25 ± 0.13

[a] T = 20 °C, 48 000 min^{-1}, 0.02 M phosphate buffer, pH 7.0.
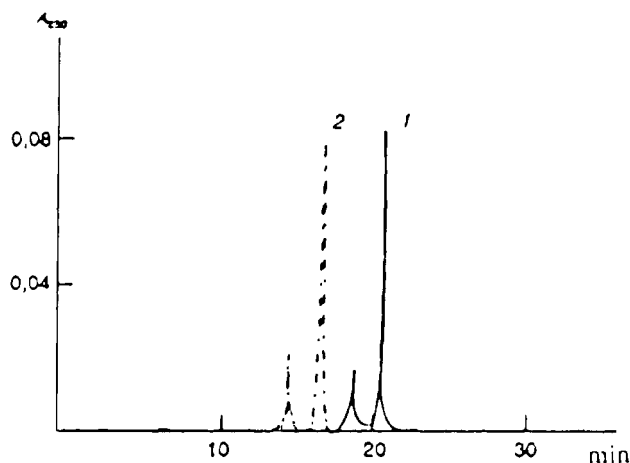
Figure 6. High-performance liquid chromatography on a Zorbax C-8 column. The eluent was acetonitrile—water (70:30, vol %). (1) Native BBI; (2) (RPE)$_5$-BBI-a conjugate.

phobic blocks. However, this may be accounted for by the fact that the surface of the protein globules of the conjugate is covered mainly with the hydrophilic blocks of the polymer due to the intramolecular interactions of the hydrophobic blocks of proxanol and the hydrophobic regions of the protein molecule.

The whole complex of data received on the basis of methods of hydrophobic chromatography, sedimentation, and DSC indicate the presence of general regularities in structure formation of conjugates synthesized by coupling of proxanols to proteins. These properties have been demonstrated most clearly in the case of conjugates with hydrophobic blocks at the periphery of conjugate structure (type II). For these conjugates, an excess of hydrophobicity may be compensated by formation of either intermolecular associates or intramolecular structures. As associates in diluted water buffering solution of these conjugates were not detected, it is natural to suppose the formation of structures stabilized by intramolecular interactions. The increase in hydrophilicity of conjugates as compared to the native protein, shown by the method of hydrophobic chromatography, allows us to suggest the formation of structures similar to intramolecular micelles in which poly(propylene oxide) blocks "adhere" to the surface of protein.

It may be suggested that formation of compact structures of a similar type presents a prerequisite for complexation between polymer chains of proxanols and protein occurring at elevated temperatures.

It should be particularly emphasized that these structures possess certain conformational lability. This property is revealed in the presence of hydrophobic or amphiphilic "partners", such as lipids (*31*), proxanols (*12*), and cyclodextrins (*13*), and is realized in the formation of mixed associates or complexes.

ACKNOWLEDGMENT

LITERATURE CITED

(1) Von Specht, B. U., and Brendel, W. (1977) Preparation and properties of trypsin and chymotrypsin coupled covalently to poly(N-vinylpirrolidone). *Biochim. Biophys. Acta 484*, 109–114.

(2) Marshall, J. J., and Rabinowitz, M. L. (1975) Modification of amino groups of α-amylase with dextran. *Arch. Biochem. Biophys. 117*, 777–779.

(3) Abuchowski, A., McCoy, I. R., Palczuk, N. C., and Davis, F. F. (1977) Effect of covalent attachment of polyethylene glycol on immunogenicity and circulating life of bovine liver catalase. *J. Biol. Chem. 252*, 3582–3586.

(4) Abuchowski, A., Van Es, T., Palczuk, N. C., and Davis, F. F. (1977) Alteration of immunological properties of bovine serum albumin by covalent attachment of polyethylene glycol. *J. Biol. Chem. 252*, 3578–3581.

(5) Kurganov, B. I., and Topchieva, I. N. (1991) Conjugates of proteins with poly(ethylene glycol) (review). *Usp. Biol. Khim. 32*, 63–86 (in Russian).

(6) Veronese, F. M., Caliceti, P., Pastorino, A., Schiavon, O., and Sartore, L. (1989) Preparation, physico-chemical and pharmacokinetic characterization of monomethoxypoly(ethylene glycol)-derivatized superoxide dismutase. *J. Controlled Release 10*, 145–154.

(7) Lundsted, L. G., and Schmolka, I. R. (1976) Synthesis and properties of block copolymer surfactants. *Block and Graft Copolymerization* (R. J. Ceresa, Ed.) pp 174–205, John Wiley, New York.

(8) Kirillova, G. P., Mochova, E. N., Deduchova, V. L., Tarakanova, A. N., Ivanova, V. P., Efremova, N. V., and Topchieva, I. N. (1993) The influence of pluronics and their conjugates with proteins on the rate of oxygen consumption by liver mitochondria and thymys lymphocytes. *Biotechnol. Appl. Biochem. 18*, 329–339.

(9) Topchieva, I. N., Mokhova, E. N., Kirillova, G. P., and Efremova, N. V. (1994) Membranotropic properties of protein conjugates with block copolymers of ethylene oxide and propylene oxide. *Biokhimiya 59*, 11–15 (in Russian).

(10) Gorskaya, I. A., Bushueva, M. V., Kurganov, B. I., Topchieva, I. N., Ivanova, V. P., Panova, I. G., and Rudakova, I. P. (1991) Conjugates of bovine serum albumin with poly(alkylene oxide)s as a new type of carriers: transport of riboflavin esters to mitochondria. *Dokl. Akad. Nauk SSSR 319*, 1008–1011 (in Russian).

(11) Topchieva, I. N., Kurganov, B. I., Teplova, M. V.; Gorskaya, I. N., and Rudakova, I. P. (1993) Use of conjugates of bovine serum albumin with poly(alkylene oxide)s for solubilization of riboflavin ester. *Biotechnol. Appl. Biochem. 17*, 337–348.

(12) Efremova, N. V., Mozhaev, V. V., and Topchieva, I. N. (1992) Thermal stability of conjugates of α-chymotrypsin with water-soluble poly(alkylene oxide)s. *Biokhimiya 57*, 342–346 (in Russian).

(13) Efremova, N. V., and Topchieva, N. V. (1993) Supramolecular structures based on protein conjugates with polyalky-lene oxides: β-cyclodextrin complexes. *Biokhimiya 58*, 753–757 (in Russian).

(14) Boccu, E., Largajolli, R., and Veronese, F. M. (1983) Coupling of monomethoxy PEG to proteins via active esters. *Z. Naturforsch. C. 38*, 94–99.

(15) Furukawa, J., & Saegusa, T. (1963) *Polymerization of aldehydes and oxides*, p 201, Interscience Publishers, Division of John Wiley & Sons, New York, London, and Sydney.

(16) Korenman, I. M. (1975) *Methods of analysis of organic compounds*, p 126, Khimia, Moscow (in Russian).

(17) Kochetov, G. A. (1980) *Prakticheskoye rukovodstvo po enzymologii*, p 222, High School, Moscow (in Russian).

(18) Danilevitchus, M. V., and Ionushkene, Z. Yu. (1988) Standardization of coloured substrate OKA-Ac. In *Production and Use of Biopreparates*, pp 96–105, Transactions of VNI-IGPE, Vilnus (in Russian).

(19) Kezdy, F. J., and Kaiser, E. T. (1970) Principles of active site titration of proteoiytic enzymes. *Methods Enzymol. 19*, 3–20.

(20) Habeeb, A. F. S. A. (1966) Determination of free amino groups in proteins by trinitrobenzenesulfonic acid. *Anal. Biochem. 14*, 328–336.

(21) Roth, M. (1971) Fluorescence reaction for amino acids. *Anal. Chem. 43*, 880–882.

(22) Tischenko, V. M., Tiktopulo, E. L., and Privalov, P. L. (1974) Calorimetrical study of conformational transitions in α-chymotrypsin. *Molekulyarnaya Biophyzika 19*, 400–404 (in Russian).

(23) Wirth, P., Souppe, J., Tritsch, D., and Biellmann, J.-F. (1991) Chemical modification of horseradish peroxidase with ethanal-methoxypolyethylene glycol: solubility in organic solvents, activity, and properties. *Bioorg. Chem. 19*, 133–142.

(24) Topchieva, I. N., Kolomnikova, E. L., Banatzkaya, M. I., and Kabanov, V. A. (1993) Complexation between β-cyclodextrins and poly(ethylene oxide)-poly(propylene oxide) block copolymers. *Polymer Sci. 4*, 464–466.

(25) Topchieva, I. N., Blumenfeld, A. L., Klyamkin, A. A., Polyacov, V. A., and Kabanov, V. A. (1994) Supramolecular structures based on poly(ethylene oxide)-poly(propylene oxide) block copolymers and cyclodextrins. *Polymer Sci. 36*, 221–227.

(26) Khmelnitsky, Yu. L., Belova, A. B., Levashov, A. V., and Mozhaev, V. V. (1991) Relationship between surface hydrophilicity of a protein and its stability against denaturation by organic solvents. *FEBS Lett. 284*, 267–269.

(27) Zalipsky, S., and Lee, C. (1992) Use of functionalized polyethylene glycols for modification of polypeptides. *Poly(ethylene glycol) Chemistry: Biotechnical and Biomedical Applications* (J. M. Harris, Ed.) pp 347–379, Plenum Press, New York.

(28) Birktoft, J. J., and Blow, D. M. (1972) Structure of crystalline α-chymotrypsin. V. Atomic structure of tosyl α-chymotrypsin at 2 Å resolution. *J. Mol. Biol. 68*, 187–240.

(29) Chiu, H.-C., Zalipsky, S., Kopeckova, P., and Kopecek, J. (1993) Enzymatic activity of chymotrypsin and its polyethylene glycol conjugates toward low and high molecular weight substrates. *Bioconjugate Chem. 4*, 290–295.

(30) Bloss, P., Hergeth, W.-D., Wohlfarth, C., and Wartewig, S. (1992) Viscometric characterization of poly(oxyethylene)-block-poly(oxypropylene)-block-poly(oxyethylene) in aqueous solution. *Makromol. Chem. 193*, 957–973.

(31) Topchieva, I. N., Osipova, S. V., Banatskaya, M. I., and Valkova, I. A. (1989) Membranotropic properties of ethylene and propylene oxide. *Dokl. Akad. Nauk SSSR 308*, 910–913 (in Russian).

(32) Mozhaev, V. V., and Martinek, K. (1984) Structure-stability relationship in proteins: new approaches to stabilizing enzymes. *Enzyme Microb. Technol. 6*, 50–59.

(33) Mozhaev, V. V., Martinek, K., and Berezin, I. V. (1988) Structure-stability relationship in proteins: fundamental tasks and strategy for the development of stabilized enzyme catalysts for biotechnology. *CRC Crit. Rev. Biochem. 23*, 235–275.

(34) Kjellander, R., and Florin, E. (1981) Water structure and changes in thermal stability of the system poly(ethylene oxide)-water. *J. Chem. Soc., Faraday Trans. 77*, 2053–2077.

(35) Halperin, A. (1987) Polymeric micelles: a star model. *Macromolecules 20,* 2943–2946.

(36) Bailey, F. E., Jr., and Koleske, J. V. (1966) Configuration and hydrodynamic properties of the polyoxyethylene chain in solution. In *Nonionic Surfactants* (M. J. Schick, Ed.) pp 794–821, Marcel Dekker, New York.

(37) Larionova, N. I., Glagysheva, I. P., Topchieva, I. N., and Kazanskaya, N. F. (1993) Conjugation of the classical soybean Bauman-Birk inhibitor with a copolymer of ethylene oxide and propylene oxide. *Biokhimiya 58,* 1658–1664 (in Russian).

(38) Krigbaum, W. R., and Godwin, R. W. (1968) Molecular conformation of chymotrypsinogen and chymotrypsin by low-angle X-ray diffraction. *Biochemistry 7,* 3126–3140.

Poly(ethylene glycol)–Doxorubicin Conjugates Containing β-Lactamase-Sensitive Linkers

Peter D. Senter,* Håkan P. Svensson, George J. Schreiber, Jennifer L. Rodriguez, and Vivekananda M. Vrudhula

Bristol-Myers Squibb Pharmaceutical Research Institute, 3005 First Avenue, Seattle, Washington 98121. Received January 13, 1995[®]

7-Aminocephalosporin doxorubicin (AC-Dox) was condensed with monomethoxypoly(ethylene glycol)-propionic acid *N*-hydroxysuccinimide ester (5 kDa) or with a branched form of poly(ethylene glycol)-propionic acid *N*-hydroxysuccinimide ester (10 kDa), forming M-PEG-AC-Dox and B-PEG-AC-Dox, respectively. These polymer drug derivatives were designed such that doxorubicin would be released upon *Enterobacter cloacae* β-lactamase (bL)-catalyzed hydrolysis. Both M-PEG-AC-Dox (IC_{50} = 80 μM) and B-PEG-AC-Dox (IC_{50} = 8 μM) were less toxic to H2981 human lung adenocarcinoma cells than doxorubicin (IC_{50} = 0.1–0.2 μM) and could be activated in an immunologically specific manner by L6-bL, a monoclonal antibody–bL conjugate that bound to H2981 cell surface antigens. In addition, the polymers were relatively stable in mouse plasma (<26% hydrolysis after 24 h at 37 °C) and were less toxic to mice (maximum tolerated dose > 52 μmol/kg) than doxorubicin (maximum tolerated dose = 13.8 μmol/kg). Pharmacokinetic studies were performed in mice bearing subcutaneous 3677 melanoma tumors. B-PEG-AC-Dox cleared from the blood more slowly than M-PEG-AC-Dox and was retained to a 2.1-fold greater extent in human 3677 melanoma tumor xenografts over a 4 h period. The intratumoral concentrations of both polymers far exceeded that of doxorubicin. Thus, the PEG-AC-Dox polymers offer the possibility of generating large intratumoral doxorubicin concentrations owing to their reduced toxicities, the amounts that accumulate in tumors, and the fact that doxorubicin is released upon β-lactam ring hydrolysis.

INTRODUCTION

There has been a great deal of investigation concerning the use of polymers as carriers of anticancer drugs (reviewed in *1*, *2*). The basis for much of this work is that attachment of toxic drugs to high molecular weight carriers can lead to reductions in systemic toxicity, longer retention time in the body, alterations in biological distribution, and improvements in therapeutic efficacy. Poly(ethylene glycol) (PEG,[1] *3–6*), PEG copolymers (*7*), dextran (*8*), (hydroxypropyl)methacrylamide (*9*), and poly(styrene-*co*-maleic acid) (*10*) are but a few examples of polymers that have been used to deliver anticancer drugs and other biologically active molecules to target tissues.

In most cases, release of active anticancer drugs from the polymer support is mediated by simple aqueous hydrolysis or by proteolytic or esterase enzymes (*1*, *2*). Since the conditions for these reactions are not necessarily confined to tumor tissues, some nonspecific drug release is inevitable. Consequently, there may be advantages in developing strategies for drug release that exploit some of the physiological and biochemical differences between neoplastic and normal tissues. Such differences may be either inherent or established by targeting enzymes to tumor cell surfaces in the form of mAb–enzyme conjugates that recognize tumor-associated antigens. This targeting strategy, which has been suc-
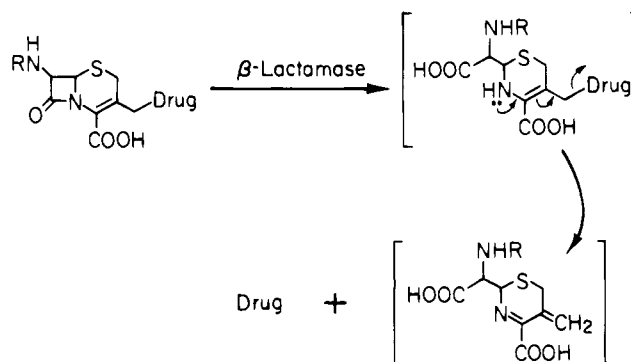
Figure 1. Mechanism of drug release catalyzed by β-lactamase.

cessfully applied to the activation of a number of low molecular weight anticancer prodrugs (*11–13*), should also be applicable to the release of active drugs that are covalently bound to polymer supports.

Many of the enzymes utilized for prodrug activation carry out reactions not normally occurring in mammalian systems. For example, cephalosporin-containing prodrugs undergo drug elimination according to the mechanism shown in Figure 1 when hydrolyzed by *Enterobacter cloacae* β-lactamases (bL, *14*, *15*). Because of the broad substrate specificity of bL (*14*, *15*), it was expected that the enzyme would also release active anticancer drugs from polymeric drug carriers. Prodrugs containing polymeric substituents should have vastly different pharmacological properties compared to the active drugs that they release (*1*, *2*).

Here we report the syntheses of two PEG–cephalosporin–Dox derivatives from which doxorubicin is released upon bL-catalyzed hydrolysis. These polymers can be activated in vitro in an immunologically specific manner. In vivo studies are presented indicating that

---

these polymers are relatively nontoxic to mice, remain in the circulation for hours, and are retained in tumors to a greater extent than is doxorubicin.

EXPERIMENTAL PROCEDURES

Materials. M-PEG-propionic acid (5 kDa, linear polymer capped on one end with a methoxy group) and B-PEG-propionic acid (10 kDa, branched polymer with eight arms projecting from a polyalcohol core) were obtained from Shearwater Polymers, Inc., Huntsville, AL. Aminocephalosporin doxorubicin (AC-Dox) was prepared from cephalosporin doxorubicin (C-Dox, *16*) and purified as previously described (*17*). The L6 and P1.17 mAbs (both are mouse IgG$_{2a}$) and bL from *Enterobacter cloacae* were obtained as previously described (*14*). L6 binds to antigens present on the H2981 human lung adenocarcinoma cell line (*18*). The mAb-bL conjugates used were dimeric, and consisted of two mAb F(ab)' fragments attached to bL. These were prepared by reacting a free thiol group on the mAb F(ab)' fragments with maleimide groups appended to bL (*19*). The 3677 cell line was established at Bristol-Myers Squibb, Seattle, WA, from a human metastatic melanoma. Female athymic nu/nu mice (Harlan−Sprague−Dawley, Indianapolis, IN) were injected with 10^7 cells subcutaneously, and growing tumors were excised and used for subsequent in vivo experiments. Tumor pieces (approximately 2 × 2 mm) were implanted subcutaneously. All in vivo experiments were performed using tumors that had undergone 1−3 in vivo passages. Phosphate-buffered saline consists of 10 mM sodium phosphate and 150 mM sodium chloride at pH 7.2.

Preparation of M-PEG-AC-Dox. To a stirred solution of M-PEG propionic acid (10 g, 2 mmol) in 50 mL of CH$_2$Cl$_2$ was added 516 mg (2.5 mmol) of dicyclohexylcarbodiimide and 288 mg (2.5 mmol) of *N*-hydroxysuccinimide. After approximately 12 h, the solids were filtered off, and the filtrate was added dropwise to rapidly stirred ether (approximately 250 mL) at 4 °C. The resulting solid (M-PEG-NHS ester) was collected, dried under high vacuum, and stored at 4 °C until use. The yield of the fine white powder was 9.9 g.

AC-Dox (0.107 mmol) was added to a freshly prepared solution of M-PEG-NHS ester (1.62 g, 0.32 mmol) in 5 mL of 50 mM borate, pH 8.0. After 3.75 h at 37 °C, HPLC analysis indicated that >90% of the AC-Dox was consumed. The reaction mixture was partitioned between saturated aqueous NaCl containing 1% acetic acid, and CHCl$_3$ containing 20% ethanol. After several such extractions, the combined organic layers were dried (MgSO$_4$), filtered, and concentrated to dryness. The residue was dissolved in H$_2$O and stirred with approximately 25 g of Amberlite XAD-7 resin (Sigma Chemical Co., prewashed with CH$_3$OH followed by H$_2$O) until the supernatant was almost colorless. The resin was poured onto a 5 × 10 cm bed of prewashed XAD-7 resin, and the resulting column was washed with H$_2$O (0.5 L), followed by H$_2$O containing 10% (0.5 L), 20% (0.5 L), 25% (0.2 L), and 80% CH$_3$OH (0.4 L). The solvent was evaporated from the 80% CH$_3$OH fraction, and traces of H$_2$O were azeotropically removed from the residue with toluene. A fine red solid (1.24 g) was obtained by slowly adding a solution of the product in CH$_2$Cl$_2$ to rapidly stirred ice-cold ether. λ_{max} (phosphate buffered saline) 495 nm. ^{1}H NMR (300 MHz, DMSO-d_6, with suppression of the singlet for OCH$_2$CH$_2$O at δ 3.40) δ 8.81 (d, 1H, NH, $J_{NH,7}$ = 8.2 Hz), 7.92 (d, 1H, ArH, J = 4.8 Hz), 7.65 (m, 2H, ArH), 6.93 (d, 1H, H-6, $J_{6,7}$ = 8.0 Hz), 5.65 (m, 1H, H-7), 5.46 (d, 1H, OH, J = 3.6 Hz), 5.20 (br s, 1H, H-1″), 5.03 (d, 1H, H-4″, J = 4.8 Hz), 4.88 (s, 1H), 4.60−

4.50 (m, 2H, H-14′), 4.13 (m, 1H, H-5″), 3.98 (s, 3H, ArOCH$_3$), 3.03−2.79 (m, 2H), 2.67 (t, 2H, PEG-COCH_2-CH$_2$, J = 6.0 Hz) 2.20−2.05 (m, 2H, H-8′), 1.90−1.75 (m, 1H, H-2″A), 1.50−1.40 (m, 1H, H-2″B), 1.11 (d, 3H, H-6″, $J_{5″,6″}$ = 6.4 Hz).

Preparation of B-PEG-AC-Dox. A solution of B-PEG-propionic acid (1 g, 0.1 mmol) in 10 mL of CH$_2$Cl$_2$ containing dicyclohexylcarbodiimide (206 mg, 1 mmol) and *N*-hydroxysuccinimide (92 mg, 0.8 mmol) was stirred at 23 °C for 4.5 h. The precipitate was filtered and washed with CH$_2$Cl$_2$. The filtrate was concentrated to dryness, and the residue was placed under high vacuum and then stored at 4 °C until use. The yield of B-PEG-NHS ester (semisolid oil) was 1 g.

To a 37 °C solution of AC-Dox (0.122 mmol) in 10 mL of 0.25 M borate, pH 8.0, was added 243 mg (24 μmol) of B-PEG-NHS ester. Additional aliquots (350 and 250 mg) of B-PEG-NHS ester were added 3 and 6 h later, respectively. After a total of 10 h at 37 °C, aminoethanol was added (120 mM final concentration) to quench any remaining active esters, and the material was bound to XAD-7 resin as previously described. The resulting XAD-7 column was washed with H$_2$O (1 L) and then with H$_2$O containing 25% (0.5 L), 37% (0.5 L), 50% (0.25 L), and 75% (0.5 L) CH$_3$OH. Polymer-bound drug was mainly contained in the 75% CH$_3$OH fraction. This fraction was concentrated to dryness, dissolved in CH$_2$-Cl$_2$ containing 5% CH$_3$OH, and extracted with saturated aqueous NaCl containing 1% acetic acid. After several back extractions of both layers, the combined organic phases were dried (MgSO$_4$), filtered, and concentrated to dryness. The red residue was lyophilized from H$_2$O to give 439 mg of B-PEG-AC-Dox as a dark red powder. λ_{max} (phosphate-buffered saline) 485 nm. ^{1}H NMR (300 MHz, DMSO-d_6, with suppression of the singlet for OCH$_2$-CH$_2$O at δ 3.40) δ 8.90−8.80 (m, 1H, NH), 8.27 (d, 1H, ArH, J = 7.8 Hz), 7.97−7.89 (m, 2H, ArH), 6.92 (d, 1H, H-6, J = 5.7 Hz), 6.02−5.58 (m, 1H), 5.45 (d, 1H, OH, J = 4.5 Hz), 5.21 (br s, 1H, H-1″), 4.92 (br s, 1H), 4.62−4.50 (m, 2H, H-14′), 4.20−4.04 (m, 1H, H-5″), 3.98 (s, 3H, ArOCH$_3$), 2.90−2.82 (m, 2H, PEG-COCH_2CH$_2$).

Kinetic Studies. The kinetic parameters for the hydrolyses of 5−100 μM solutions of either M-PEG-AC-Dox or B-PEG-AC-Dox (in phosphate-buffered saline containing 12.5 μg/mL bovine serum albumin) with bL (0.2 μg/mL for M-PEG-AC-Dox, 1.0 μg/mL for B-PEG-AC-Dox) were determined spectrophotometrically by determination of the initial velocities of the reactions as a function of substrate concentration. Lineweaver−Burk plots of the data were used to estimate the K_m and V_{max} values. Cleavage of the β-lactam ring resulted in a loss of absorbance at 260 nm for both M-PEG-AC-Dox ($\Delta\epsilon_{260nm}$ = −7.9 × 10^{-3} M^{-1} cm^{-1}) and B-PEG-AC-Dox ($\Delta\epsilon_{260nm}$ = −3.8 × 10^{-3} M^{-1} cm^{-1}).

In Vitro Cytotoxicity Assays. H2981 cells were grown in monolayer cultures in Iscove's modified Dulbecco's medium supplemented with 10% (v/v) fetal bovine serum, 0.1 mg/mL streptomycin, and 0.06 mg/ml penicillin G, plated out into 96-well plates (10 000 cells/well for M-PEG-AC-Dox, 5000 cells/well for B-PEG-AC-Dox), and allowed to adhere for 18 h at 37 °C. The plates were washed with Roswell Park Memorial Institute 1640 medium RPMI, antibiotic free, mAb-bL conjugates were added (3.16 μg of mAb component/mL for M-PEG-AC-Dox, 1 μg/mL mAb component for B-PEG-AC-Dox), and incubation was continued for 30 min at 4 °C. The cells were washed three times with RPMI, treated with prodrug (1 h for M-PEG-AC-Dox, 2 h for B-PEG-AC-Dox) at 37 °C, washed, and incubated for 18 h at 37 °C. [^{3}H]-Thymidine (1 μCi) was added to each well, and the cells

were harvested and counted after 5 h (for M-PEG-AC-Dox) or 4 h (for B-PEG-AC-Dox). The results were compared to untreated cells, cells that were saturated with L6 (1 mg/mL) prior to conjugate exposure, and to non-conjugate-treated cells that were treated with doxorubicin instead of PEG-AC-Dox.

Pharmacokinetics. All experiments were performed in athymic female nu/nu mice (Harlan–Sprague–Dawley, Indianapolis, IN) and were initiated when the animals reached an age of 6–10 weeks. 3677 human tumor xenografts from in vivo passaging were implanted subcutaneously and allowed to grow to approximately 200 mm^3. B- and M-PEG-AC-Dox (freshly prepared at 5.2 mM in phosphate-buffered saline) were injected (intraveneously) so that each mouse received 52 μmol of PEG-AC-Dox/kg of body weight. Doxorubicin (1.55 mM in saline) was injected so that each mouse received 15.5 μmol of doxorubicin/kg (9 mg/kg). At various time points, the mice (3 animals/group) were anesthetized, bled via the retro-orbital plexus, and then euthanized. Tumors were rapidly excised, frozen in liquid N_2, and stored at -70 °C. Heparinized blood samples were centrifuged, and the plasma was frozen at -70 °C.

Methanol (0.5 mL) was added to 50-μL aliquots of freshly thawed plasma samples. The samples were sonicated and centrifuged at 10 000g for 3 min. The supernatants were evaporated to dryness under reduced pressure, and the residues were dissolved in 50 μL of 20% acetonitrile in 50 mM triethylammonium formate, pH 2.8, for HPLC analyses. Tumor samples (approximately 200 mg/sample) were rapidly thawed, weighed, and homogenized in 0.5 mL of methanol. Solids were removed by centrifugation (10 000g for 3 min), and the supernatants were evaporated to dryness under reduced pressure. The residues were dissolved in 50 μL of 20% acetonitrile in 50 mM triethylammonium formate, pH 2.8, for HPLC analyses. Standard curves were obtained by extracting tumor and plasma samples containing known amounts of doxorubicin or the PEG-AC-Dox polymers.

HPLC Analysis. Two different HPLC analytical systems were used for the PEG-AC-Dox preparations. A Beckman HPLC system was used to characterize the different preparations, to confirm that doxorubicin was released upon addition of bL, and to measure the stability of the polymer preparations in phosphate-buffered saline and mouse plasma. Analyses were performed using a Phenomenex 4 × 150 mm C-18 reversed-phase column, detection at 495 nm, and a flow rate of 1 mL/min. A linear gradient of 20–80% CH_3CN in 50 mM triethylammonium formate buffer at pH 2.8 was employed as the eluting solvent. A Hewlett Packard 1090 HPLC system with a refrigerated autosampler and a diode array detector was used to determine plasma and intratumoral PEG-AC-Dox and doxorubicin concentrations. Separation of samples was achieved using a 2.1 × 250 mm Spheri-5 RP-18 column (Applied Biosystems/Brownlee) equipped with a matching guard column. Samples were eluted and detected as described above, but at a flow rate of 0.2 mL/min. Concentrations were determined by integration of the absorbance peaks and comparision to standard curves obtained from tumor and blood samples having known amounts of added doxorubicin, M-PEG-AC-Dox, or B-PEG-AC-Dox.

Stability Studies. Solutions of the PEG-AC-Dox samples at 0.5 mM were prepared in phosphate-buffered saline or mouse plasma and incubated at 37 °C. At periodic intervals, samples were subjected to HPLC analysis as described above. The mouse plasma samples were diluted with 1 vol of methanol, and the precipitated

Chart 1
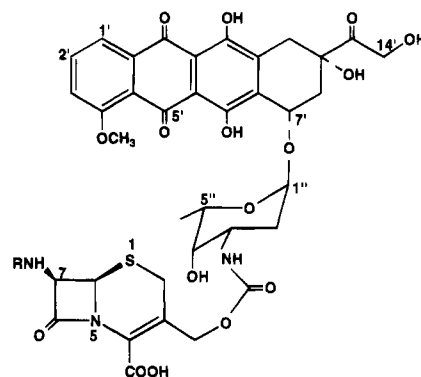
R	Compound
$C_6H_5CH_2CO$	C-Dox
H	AC-Dox
M-PEG-OCH$_2$CH$_2$CO	M-PEG-AC-Dox
B-PEG-OCH$_2$CH$_2$CO	B-PEG-AC-Dox

proteins were separated by centrifugation. The resulting supernatants were analyzed by HPLC.

RESULTS

Preparation and Characterization of PEG-AC-Dox Derivatives. 7-Aminocephalosporin doxorubicin (AC-Dox, Chart 1) was prepared by enzymatic hydrolysis of 7-phenylacetylcephalosporin doxorubicin (C-Dox, 16) with penicillin-G amidase as previously described (*17*). Purification was achieved using reversed-phase chromatography. Condensation of AC-Dox with the *N*-hydroxysuccinimide esters of monomethoxy-PEG-propionic acid (MW 5 kDa) or branched-PEG-propionic acid (MW 10 kDa) led to the formation of M-PEG-AC-Dox and B-PEG-AC-Dox, respectively. Branched-PEG-propionic acid is an octomeric form of PEG that is prepared by ethoxylation of a polyalcohol. A two-step purification procedure was used to separate the desired product from unconjugated doxorubicin, doxorubicin derivatives, and PEG. Unmodified polymer was removed chromatographically on a column of polyacrylic ester resin (Amberlite XAD-7) using a stepwise gradient of methanol for compound elution. Under these conditions, free polymer eluted off the column before PEG-AC-Dox. Further purification was achieved by extracting the polymer solution with weak acid to remove amine-containing impurities.

The ^{1}H-NMR spectra (300 MHz) for the PEG-AC-Dox derivatives revealed the expected protons for PEG, cephalosporin, and doxorubicin and were therefore consistent with the structures shown in Chart 1. Integration of the peaks indicated that the PEG to doxorubicin molar ratios for both polymers were approximately 1. The polymers were further characterized by reversed-phase HPLC, in which M-PEG-AC-Dox (Figure 2A) and B-PEG-AC-Dox (Figure 2B) eluted primarily as single peaks. The HPLC profile for the B-PEG-AC-Dox used in the studies reported here (Figure 2B) indicates the presence of some free doxorubicin (1.2% of the total integrated value). More recent preparations of B-PEG-AC-Dox were free of any detectable unbound doxorubicin (data not shown). Reaction of the polymers with bL led to the formation of doxorubicin, on the basis of a comparison with an authentic sample (Figure 2C,D). These studies provide evidence for the structural assignments and indicate that
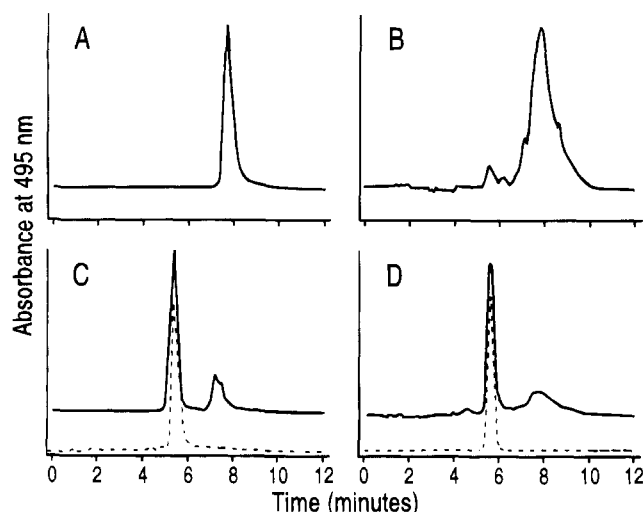
Figure 2. HPLC analyses of PEG-AC-Dox samples. (A) M-PEG-AC-Dox. (B) B-PEG-AC-Dox. (C) M-PEG-AC-Dox + bL (solid line) and doxorubicin (dotted line). (D) B-PEG-AC-Dox + bL (solid line) and doxorubicin (dotted line).

Table 1. Kinetic Constants for bL[a]

substrate	V_{max} (μmol/min/mg)	k_{cat} (s^{-1})	K_m (μM)
M-PEG-AC-Dox	46 ± 11	33 ± 8	34 ± 13
B-PEG-AC-Dox	37 ± 10	28 ± 6	43 ± 12
C-Dox	400 ± 96	280 ± 67	46 ± 6

[a] The values were obtained from 3 or 4 independently run experiments.

free doxorubicin can be released from the PEG-AC-Dox polymers upon bL-catalyzed hydrolysis.

A spectophotometric method was used to quantify the rate of β-lactam-catalyzed hydrolysis for each of the polymers. The kinetic constants, derived from Lineweaver–Burk plots, were compared to those obtained for the hydrolysis of C-Dox (Table 1). The turnover rates with M-PEG-AC-Dox and B-PEG-AC-Dox as substrates for bL were 8–13 times slower than with C-Dox as substrate (*17*). In contrast, the K_m values for the three substrates were similar. Thus, the polymers and C-Dox apparently bind equally well to bL, but undergo hydrolysis at differing rates.

An HPLC assay was used to determine the stabilities of M-PEG-AC-Dox and B-PEG-AC-Dox in phosphate-buffered saline and mouse plasma. After 24 h in phosphate-buffered saline at 37 °C, both polymers underwent a small amount of hydrolysis resulting in the release of approximately 10% of the bound doxorubicin. Incubation of M-PEG-AC-Dox and B-PEG-AC-Dox in mouse plasma at 37 °C led to the release of 26% and 7% of doxorubicin, respectively. Thus, under the test conditions, most of the doxorubicin remains covalently attached to the polymer support.

In Vitro Cytotoxic Activities. The cytotoxic effects of M-PEG-AC-Dox, B-PEG-AC-Dox, doxorubicin, and combinations of the mAb-bL conjugates with the polymer preparations were determined on the H2981 human lung adenocarcinoma cell line. Several experiments were performed, and the conditions described represent those that led to the highest degrees of immunologically specific prodrug activation and cytotoxic differentials between prodrug and drug. The bivalent [F(ab)′]₂-bL conjugates used were prepared by combining maleimide substituted bL with L6 F(ab′)-SH as previously described (*19*). This conjugation procedure does not alter mAb binding or the enzymatic activity of bL (*19*).
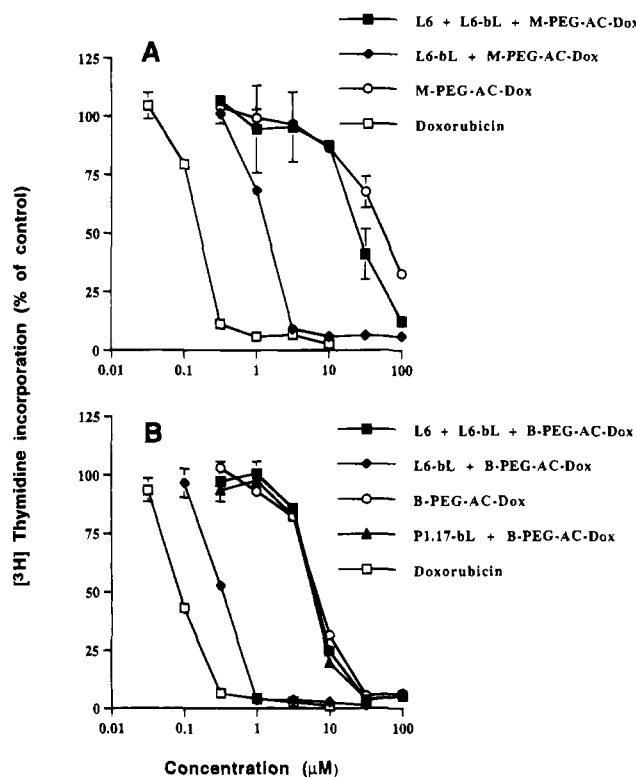
Figure 3. effects of PEG-AC-Dox samples ± mAb-bL conjugates on H2981 lung adenocarcinoma cells as determined by the incorporation of [³H]thymidine into DNA compared to untreated control cells. (A) Cells were exposed to L6-bL, washed, and then treated with M-PEG-AC-Dox for 1 h. (B) Cells were exposed to conjugates, washed, and then treated with B-PEG-AC-Dox for 2 h.

H2981 cells were exposed to the polymers (1 h for M-PEG-AC-Dox, 2 h for B-PEG-AC-Dox) and washed. After further incubation, toxicity was determined by measuring the incorporation of [³H]thymidine into DNA. The cytotoxic activities of M-PEG-AC-Dox (IC₅₀ = 80 μM) and B-PEG-AC-Dox (IC₅₀ = 8 μM) were much lower than that of doxorubicin (IC₅₀ = 0.1–0.2 μM, Figure 3). There is probably no significance in the 10-fold difference in IC₅₀ values between the two polymers, since they were tested under different conditions and since B-PEG-AC-Dox contained a small amount of free doxorubicin (1.2%) at the beginning of the assay (Figure 2B). A significant increase in cytotoxicity was obtained on cells that were pretreated with L6-bL. It is noteworthy that the L6-bL + PEG-AC-Dox combinations did not yield the same level of cytotoxic activity as doxorubicin. This is most likely due to incomplete drug release under the conditions of the assay, since higher degrees of activation were obtained by not washing off unbound conjugate or by adding high concentrations of free bL to the polymer samples (data not shown).

Activation of the polymers took place in an immunologically specific manner as evidenced by the fact that the cytotoxic activities of the polymers were not increased on H2981 cells that were saturated with unmodified L6 mAb prior to exposure to L6-bL. In addition, P1.17-bL did not effect the activation of B-PEG-AC-Dox on H2981 cells (P1.17 antigen negative). Taken together, these studies show that both M-PEG-AC-Dox and B-PEG-AC-Dox are relatively noncytotoxic doxorubicin prodrugs that can be activated by L6-bL on cells that are L6 antigen positive.

In Vivo Studies. The toxicities of the polymer preparations in nude mice were compared to that of

doxorubicin. The maximum tolerated dose (defined as the drug dose that gave <20% weight loss and no deaths and was within 30% of the dose where >20% weight loss and/or deaths occurred) of doxorubicin after a single intravenous injection was 13.8 μmol/kg body of weight (8 mg/kg). Although the maximum tolerated doses for the polymers have not yet been determined, it was possible to safely administer 52 μmol/kg of M-PEG-AC-Dox and B-PEG-AC-Dox with no weight loss or long-term toxicities. Some animals experienced considerable discomfort immediately after treatment with the polymers. This was most likely due to the non-isotonic nature of the injected solutions, since equivalent doses of free PEG elicited the same immediate response. Intraperitoneal injection of the polymers circumvented this problem, but subsequent studies were performed using the intravenous route, since this is the usual mode of administration for doxorubicin.

Tumor uptake and blood clearance studies were undertaken in nude mice bearing subcutaneous 3677 human melanoma tumors. At a point when the tumors were approximately 200 mm^3 in volume, the animals were given intravenous injections of doxorubicin (15.5 μmol/kg), M-PEG-AC-Dox (52 μmol/kg), or B-PEG-AC-Dox (52 μmol/kg). Blood and tumors were removed at various time points, and an HPLC assay was used to determine the concentrations of the injected materials in the extracted samples. Calibration curves were obtained from several tumors and blood samples that were spiked with varying concentrations of free doxorubicin, M-PEG-AC-Dox, or B-PEG-AC-Dox. None of the extracted samples contained detectable levels of AC-Dox, indicating that the amide bond between the cephalosporin 7-amino group and the terminal carboxyl group on PEG is stable.

The blood levels of B-PEG-AC-Dox were higher than those of M-PEG-AC-Dox for all of the time points tested (Figure 4A). This is due most likely to slower blood clearance of B-PEG-AC-Dox compared to M-PEG-AC-Dox. The highest level of plasma doxorubicin measured, 0.64 nmol/g at 15 min, was substantially lower than the polymer levels. The doxorubicin levels in Figure 4A are consistant with a previously reported pharmacokinetic study which showed that doxorubicin had an initial half-life of 2 min in mice (*20*). Thus, it was not surprising that no free doxorubicin was detected in plasma obtained from mice that were treated with the PEG-AC-Dox polymers. In addition to having a longer plasma half-life, B-PEG-AC-Dox was retained in 3677 tumors to a greater extent than was M-PEG-AC-Dox (Figure 4B). The highest intratumoral level of B-PEG-AC-Dox was obtained 30 min after injection, and substantial levels were still present 4 h postinjection. Over the 4-h measurement period, the area under the curve for B-PEG-AC-Dox was 2.1-fold greater than that for M-PEG-AC-Dox. It is noteworthy that the intratumoral doxorubicin levels were quite low in mice that received doxorubicin. The maximum doxorubicin level, 1.41 nmol/g at 30 min postinjection, was much lower than the polymer concentrations at all time points tested. Thus, both polymers deliver substantially greater amounts of intratumoral doxorubicin equivalents over an extended period of time compared to systemic doxorubicin treatment.

DISCUSSION

Doxorubicin was attached to two different forms of PEG such that drug release took place upon addition of bL. It was found that the polymeric prodrugs and C-Dox had similar K_m values with bL, but were hydrolyzed at substantially different rates. On the basis of a math-
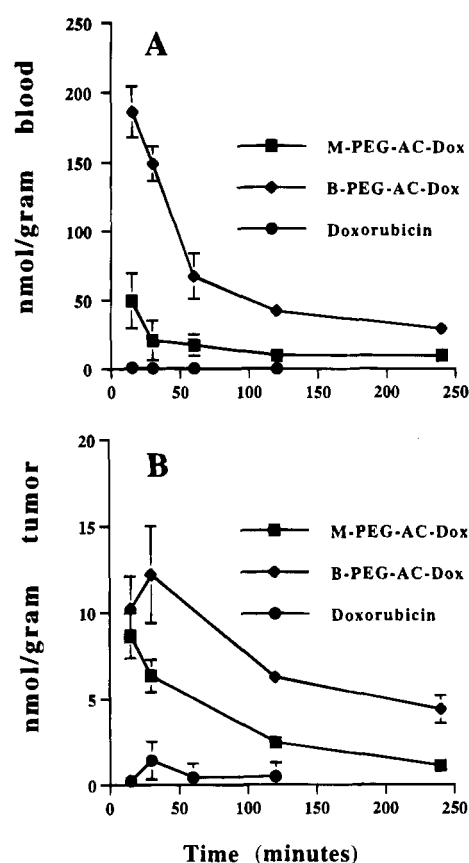
Figure 4. of PEG-AC-Dox samples and doxorubicin in nude mice bearing subcutaneous 3677 human tumor xenografts. Tumor and blood samples were extracted, and the amount of prodrug and drug was quantified by HPLC. (A) Blood levels of M-PEG-AC-Dox and B-PEG-AC-Dox after intravenous prodrug injection (52 μmol/kg). The results are compared with doxorubicin levels in animals receiving 15.5 μmol/kg doxorubicin. (B) Tumor levels of M-PEG-AC-Dox, B-PEG-AC-Dox, and doxorubicin after intravenous injection (52 μmol of polymer/kg, 15.5 μmol of free doxorubicin/kg).

ematical model that predicts higher tumor to blood drug concentration ratios for enzymes that have lower k_{cat} values (*21*), the slower release of doxorubicin from M-PEG-AC-Dox and B-PEG-AC-Dox compared to C-Dox may actually be advantageous for the targeting strategy described here.

M-PEG-AC-Dox and B-PEG-AC-Dox were significantly less cytotoxic than doxorubicin and could be activated in vitro by a mAb-bL conjugate in an immunologically specific manner. These results provided the basis for in vivo pharmacokinetic studies that demonstrated that the serum levels of both polymeric prodrugs were significantly greater than doxorubicin over an extended period of time. In addition, the intratumoral concentrations of M-PEG-AC-Dox and B-PEG-AC-Dox were greater than those of doxorubicin. Thus, these prodrugs may lead to substantially higher doxorubicin levels compared to systemic doxorubicin administration, providing that the tumor-associated mAb-bL conjugate effects efficient drug release. The fact that the intratumoral concentration of B-PEG-AC-Dox was higher than that of M-PEG-AC-Dox may result from both differences in molecular weight and structural differences in the polymers themselves. From the data presented here, it appears that B-PEG-AC-Dox may be more promising than M-PEG-AC-Dox for in vivo applications.

The pharmacokinetic and toxicity data suggest that there may be significant advantages in using PEG-AC-Dox polymers in combination with mAb-bL conjugates

compared to systemic doxorubicin therapy, since an opportunity exists to generate higher concentrations of intratumoral drug. It will probably be of particular importance to achieve high tumor to blood mAb-bL ratios when these polymers are used therapeutically, since they have long blood residence times. Future studies will involve the antitumor activities and the amount of drug that can be generated intratumorally by mAb-bL in combination with PEG-AC-Dox polymers.

ACKNOWLEDGMENT

LITERATURE CITED

(1) Maeda, H., Seymore, L. W., and Miyamoto, Y. (1992) Conjugates of anticancer agents and polymers: Advantages of macromolecular therapeutics in vivo. *Bioconj. Chem. 3,* 351–362.

(2) Takakura, Y., and Hashida, M. (1995) Macromolecular drug carrier systems in cancer chemotherapy: macromolecular prodrugs. *Crit. Rev. Oncol. Hematol. 18,* 207–231.

(3) Zalipsky, S., Gilon, C., and Zilkha, A. (1983) Attachment of drugs to polyethylene glycols. *Eur. Polym. J. 12,* 1177–1183.

(4) Ouchi, T., Hagihara, Y., Takahashi, K., Takano, Y., and Igarashi, I. (1992) Synthesis and antitumor activity of poly-(ethylene glycol)s linked to 5-fluorouracil via a urethane or urea bond. *Drug Des. Discovery 9,* 93–105.

(5) Caliceti, P., Monfardini, C., Sartore, L., Schiavon, O., Baccichetti, F., Carlassare, F., and Veronese, F. M. (1993) Preparation and properties of monomethoxy poly(ethylene glycol) doxorubicin conjugates linked by an amino acid or peptide as spacer. *Farmaco 48,* 919–932.

(6) Panarin, E. F., and Solovskij, M. V. (1989) Polymer derivatives of β-lactam antibiotics of the penicillin series. *J. Controlled Release 10,* 119–129.

(7) Poiani, G. J., Riley, D. J., Fox, J. D., Kemnitzer, J. E., Gean, K. F., and Kohn, J. (1994) Conjugates of cis-4-hydroxy-L-proline and poly(PEG-lys), a water soluble poly(ether urethane): Synthesis and evaluation of antifibrotic effects *in vitro* and *in vivo. Bioconj. Chem. 5,* 621–630.

(8) Munechika, K., Sogame, Y., Kishi, N., Kawabata, Y., Ueda, Y., Yamanouchi, K., and Yokoyama, K. (1994) Tissue distribution of macromolecular conjugate, adriamycin linked to oxidized dextran in rat and mouse bearing tumor cells. *Biol. Pharm. Bull. 17,* 1193–1198.

(9) Seymore, L. W., Ulbrich, K., Steyger, P. S., Brereton, M., Subr, V., Strohalm, J., and Duncan, R. (1994) Tumor tropism and anti-cancer efficacy of polymer-based doxorubicin prodrugs in the treatment of subcutaneous murine B16F10 melanoma. *Br. J. Cancer 70,* 636–641.

(10) Maeda, H. (1992) The tumor blood vessel as an ideal target for macromolecular anticancer agents. *J. Controlled Release 19,* 315–324.

(11) Bagshawe, K. D. (1994) Antibody-directed enzyme prodrug therapy. *Clin. Pharmacokinet. 27,* 368–376.

(12) Deonarain, M. P., and Epenetos, A. A. (1994) Targeting enzymes for cancer therapy: Old enzymes in new roles. *Br. J. Cancer 70,* 786–794.

(13) Senter, P. D., Wallace, P. M., Svensson, H. P., Vrudhula, V., Kerr, D. E., Hellström, I., and Hellström, K. E. (1993) Generation of cytotoxic agents by targeted enzymes. *Bioconj. Chem. 4,* 3–9.

(14) Vrudhula, V. M., Svensson, H. P., Kennedy, K. A., Senter, P. D., and Wallace, P. M. (1993) Antitumor activities of a cephalosporin prodrug in combination with monoclonal antibody-β-lactamase conjugates. *Bioconj. Chem. 4,* 334–340.

(15) Meyer, D. L., Jungheim, L. N., Law, K. L., Mikolajczyk, S. D., Shepherd, T. A., Mackensen, D. G., Briggs, S. L., and Starling, J. J. (1993) Site-specific prodrug activation by antibody-β-lactamase conjugates: regression and long-term growth inhibition of human colon carcinoma xenograft models. *Cancer Res. 53,* 3956–3963.

(16) Hudyma, T. W., Bush, K., Colson, K. L., Firestone, R. A., and King, H. D. (1993) Synthesis and release of doxorubicin from a cephalosporin based prodrug by a β-lactamase-immunoconjugate. *Bioorg. Med. Chem. Lett. 3,* 323–328.

(17) Vrudhula, V. M., Svensson, H. P., and Senter, P. D. (1995) Cephalosporin derivatives of doxorubicin as prodrugs for activation by monoclonal antibody β-lactamase conjugates. *J. Med. Chem. 38,* 1380–1385.

(18) Hellström, I., Horn, D., Linsley, P. S., Brown, J. P., Brankovan, V., and Hellström, K. E. (1986) Monoclonal antibodies raised against human lung carcinoma. *Cancer Res. 46,* 3917–3923.

(19) Svensson, H. P., Wallace, P. M., and Senter, P. D. (1994) Synthesis and characterization of monoclonal antibody-β-lactamase conjugates. *Bioconj. Chem. 5,* 262–267.

(20) Bosslet, K., Czech, J., and Hoffman, D. (1994) Tumor-selective prodrug activation by fusion protein-mediated catalysis. *Cancer Res. 54,* 2151–2159.

(21) Yuan, F., Baxter, L. T., and Jain, R. K. (1991) Pharmacokinetic Analysis of two-step approaches using bifunctional and enzyme-conjugated antibodies. *Cancer Res. 51,* 3119–3130.

Tethered Benzophenone Reagents for the Synthesis of Photoactivatable Ligands

John D. Olszewski,† György Dormán,† John T. Elliott,† Yang Hong,‡ David G. Ahern,‡ and Glenn D. Prestwich*,†

Department of Chemistry, University at Stony Brook, Stony Brook, New York 11794-3400, and E. I. DuPont de Nemours & Co. (Inc.), Biomedical Products Division, 549 Albany Street, Boston, Massachusetts 02118. Received January 17, 1995®

A new radiolabeled, bifunctional photoaffinity cross-linking reagent, *N*-succinimidyl *p*-benzoyl-[2,3-$^3H_2$]dihydrocinnamate, has been synthesized in high yield and with high specific activity. This reagent can be used to append the benzophenone photophore to amino groups of small molecules, such as *O*-aminoalkylinositol polyphosphates and polypeptides. The resulting tritiated photoaffinity labels can be purified and manipulated in ambient light and can be activated at 360 nm.

INTRODUCTION

Although many mono- and bifunctional reagents incorporating photoactivatable groups have been described, only arylazide and diazoester photophores have been commercially available. Moreover, few existing photophore-containing heterobifunctional reagents have been available in a radioactively labeled form. In connection with our efforts in mapping binding sites for peptide hormones and for inositol polyphosphates, we required a versatile, high specific activity, tritium-labeled reagent that was chemically robust and stable in ambient light. The benzophenone (BP) photophore appeared well-suited to this task, and BP-containing photoaffinity labels have been employed to circumvent many of the problems associated with the use of nitrene- and carbene-producing photoaffinity labels (Dormán & Prestwich, 1994). In particular, (i) BPs can be activated at wavelengths (>320 nm) that are not associated with protein damage, (ii) BPs are reported to give highly efficient covalent labeling via insertion into unreactive C−H bonds, (iii) BP photolabeling shows no interference from water or bulk nucleophiles, and (iv) no special lighting conditions are necessary during synthesis and biochemical manipulations. Recently, the BP moiety has been used in polypeptides as 4-benzoylphenylalanine (O'Neil & DeGrado, 1989; O'Neil et al., 1989; Boyd et al., 1991; McNicoll et al., 1992; Shoelson et al., 1993; Williams & Shoelson, 1993) and as 4-benzoylbenzoyl esters and amides in nucleotides (Mahmood et al., 1989; Boyer et al., 1990; Chavan et al., 1990; Gonzalez et al., 1990; Pal & Coleman, 1990; Aloise et al., 1991; Bar-Zvi et al., 1992; Pal et al., 1992; Rajagopalan et al., 1993; Salvucci et al., 1993; Zarka & Shoshan-Barmatz, 1993), in sugars (Holman et al., 1988), in phospholipids (Ishidate et al., 1992), and in proteins (Leszyk et al., 1988; Agarwal et al., 1991; Rajasekharan et al., 1991; Combeau et al., 1992; Thiele & Fahrenholz, 1993). Interactions within lipid bilayers have also been probed using BP−lipid analogs (Yamamoto et al., 1993).

We report herein the development of a versatile BP-based heterobifunctional cross-linking reagent that may be used to modify small molecules or peptides for photoaffinity labeling studies. Figure 1 shows this new reagent, 4-benzoyldihydrocinnamic acid *N*-hydroxysuccinimidate (BZDC-NHS) (**1a**), which is readily prepared
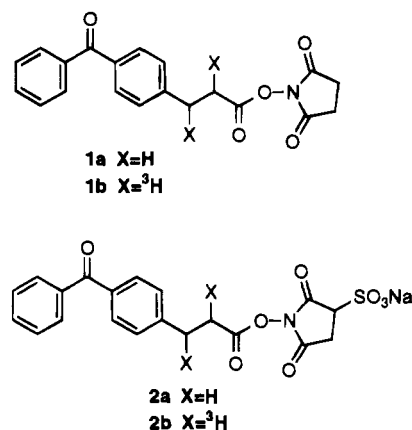
Figure 1.

in tritiated form, specific activity > 30 Ci/mmol, with the label in non-solvent-exchangeable positions (**1b**). A second reagent, 4-benzoyldihydrocinnamic acid sulfo-*N*-hydroxysuccinimidate (BZDC-sulfo-NHS, **2a,b**) was prepared for modification of proteins in aqueous solutions. The amide linkage between reagent and polypeptide (or other ligand) is stable under standard conditions for HPLC purification of peptides, Edman degradation, CNBr digestion, and proteolysis, thus facilitating mapping of the covalently modified binding site.

EXPERIMENTAL PROCEDURES

Materials and Methods. All NMR spectral data were obtained on either QE-300 or AC-250 instruments. Melting points are uncorrected. Elemental analyses were performed by M-H-W Laboratories (Phoenix, AZ). All reagents were obtained from Aldrich Chemical Co. (Milwaukee, WI), except sulfo-NHS, which was obtained from Pierce Chemical Co. (Rockford, IL). All solvents used were reagent grade or HPLC grade. CH_2Cl_2 was distilled from CaH_2, and DMF was dried by storage over molecular sieves. The normal workup procedure involved extraction three times with the appropriate solvent, washing the combined organic extracts once with brine, drying over anhydrous $MgSO_4$, filtration, and concentration. Chromatographic purification was performed over "flash" grade SiO_2. HPLC retention times are denoted as t_R.

***p*-Benzoylcinnamic Acid (4) (Mourey et al., 1993).** The following detailed description contains modifications

LSDDMPATPADQEMYRQDPEQIDSRT–N–C–C–YFSPRL-NH₂
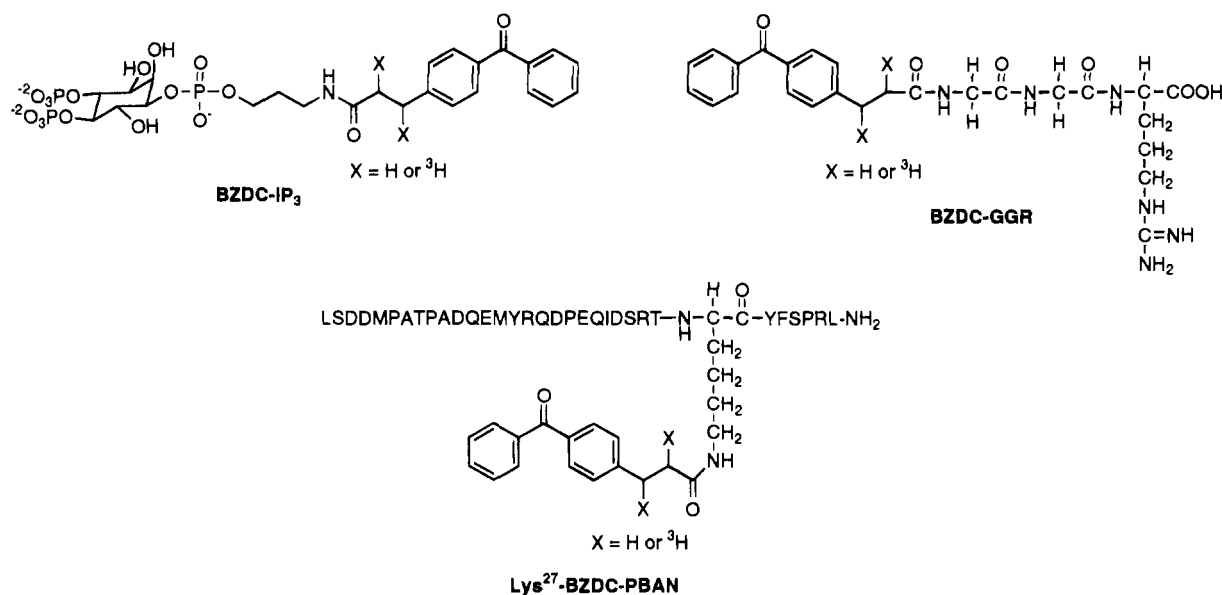
Figure 2.

to the original procedure to ensure optimal yield. To a three-necked round-bottomed flask was added p-aminobenzophenone (3) (800 mg, 4.06 mmol), 15 equiv of 48% HBr (3.2 mL, 58.86 mmol), and 8–10 mL of acetone. The mixture was stirred at 0 °C in an ice/salt bath while 5 M aqueous sodium nitrite was added dropwise until a dark brown color was achieved. After the mixture was stirred an additional 5 min at 0 °C, 30 equiv of acrylic acid (8.34 mL, 121.8 mmol) was added while the temperature was maintained at 0–5 °C, and the mixture was immediately placed under a steady stream of nitrogen and stirred at 0 °C for 15 min. Cuprous bromide (2 mol %, 12 mg, 0.08 mmol) was added, the flow of nitrogen was removed, and the mixture was stirred at 0 °C (10 min) and at ambient temperature (30 min, or until gas evolution had ceased). The mixture was then poured into 5 vol of water and allowed to sit overnight. A yellow-orange oil that separated out was extracted with CH_2Cl_2, the normal workup procedure was followed, and the product was eluted from SiO_2 with $CHCl_3$, followed by 50% MeOH in $CHCl_3$. The product (ca. 94%) containing traces of acrylic acid was used without further purification.

Crude α-bromoacid (1.2 g, 3.60 mmol) was dissolved in 40 mL of MeOH, powdered NaOH (2.25 g, 56.3 mmol) was added, and the mixture was stirred for 40 min at ambient temperature as a white precipitate formed. The reaction mixture was concentrated *in vacuo*, the resulting solid was dissolved in water, and the mixture was slowly acidified with concentrated hydrobromic acid while it was stirred. The cinnamate 4 precipitated as an off-white solid after being stored overnight at 4 °C (88% yield). Sometimes a slightly yellow product was obtained, which could be purified by suspending it in hot acetone and collecting the insoluble material after cooling to give 4: mp = 229–230 °C. Anal. Calcd for $C_{16}H_{12}O_3$: C, 76.18; H, 4.79. Found: C, 75.93; H, 5.00.

p-Benzoyldihydrocinnamic Acid (5, *x* = 1). Cinnamate 4 (200 mg, 0.793 mmol) was suspended in 20 mL of 95% ethanol, and 5% palladium on carbon (14 mg, 7% by weight) was added. The flask was evacuated and filled with hydrogen to atmospheric pressure. The mixture was stirred vigorously for 110 min, filtered over a bed of Celite, and washed several times with MeOH. The filtrate was concentrated, and the product was eluted from SiO_2 with 3:1:1 Hex/EtOAc/CH_2Cl_2 containing 1% acetic acid to give a white solid in 82.5% yield of 5: mp

= 99–100 °C. ¹H-NMR ($CDCl_3$, 300 MHz) δ 2.74 (t, 2H, J = 7.5 Hz), 3.05 (t, 2H, J = 7.5 Hz), 7.33 (d, 2H, J = 8.1 Hz), 7.47 (t, 2H, J = 7.2 Hz), 7.58 (t, 1H, J = 7.2 Hz), 7.77 (t, 4H, J = 8.4, 8.7 Hz), 11.45 (br s, COOH). ¹³C-NMR ($CDCl_3$, 63 MHz) δ 30.49, 35.09, 128.28, 130.00, 130.56, 132.37, 135.91, 137.73, 145.23, 178.64, 196.59. Anal. Calcd for $C_{16}H_{14}O_3$: C, 75.57; H, 5.55. Found: C, 75.34; H, 5.69.

N-Succinimidyl p-Benzoylcinnamate (6) was prepared according to known procedures. The product could be recrystallized from Et_2O/Hex to result in fine white needles in 84.5% yield: mp = 176–177 °C. Anal. Calcd for $C_{20}H_{15}NO_5$: C, 68.76; H, 4.33; N, 4.01. Found: C, 68.92; H, 4.17; N, 4.14.

N-Succinimidyl p-Benzoyldihydrocinnamate (1a) was prepared as described (Estevez, 1991). The product was crystallized from Et_2O/Hex and isolated as fine white needles in 84% yield: mp = 100–102 °C. ¹H-NMR ($CDCl_3$, 300 MHz) δ 2.85 (s, 4H), 2.98 (t, 2H, J = 7.8 Hz), 3.16 (t, 2H, J = 7.8 Hz), 7.36 (d, 2H, J = 8.1 Hz), 7.48 (t, 2H, J = 7.2 Hz), 7.59 (t, 1H, J = 7.2 Hz), 7.79 (m, 4H). ¹³C-NMR ($CDCl_3$, 63 MHz) δ 169.04, 167.70, 143.92, 137.65, 136.13, 132.35, 130.62, 129.98, 128.28, 32.16, 30.37, 25.59. Anal. Calcd for $C_{20}H_{18}NO_{5.5}$ (partially hydrated): C, 66.66; H, 5.03; N, 3.89. Found: C, 67.02; H, 5.28; N, 4.05.

N-Sulfosuccinimidyl p-Benzoyldihydrocinnamate (2a). Acid 5 (69 mg, 0.272 mmol) was dissolved in DMF (6 mL). Sulfo-*N*-hydroxysuccinimide (65 mg, 0.299 mmol) was added, followed by a solution of DCC (61.6 mg, 0.299 mmol) in 3 mL of DMF, and the mixture was stirred for 24 h at ambient temperature. An additional 0.5 equiv of both sulfo-NHS and DCC were added, and stirring was continued for another 24 h. The flask was stored at −4 °C overnight, and the cyclohexylurea byproduct was removed by filtration. After being washed with 5 mL of cold DMF, the filtrate was concentrated under reduced pressure to give a light yellow solid. The solid was suspended in CH_2Cl_2, filtered, and washed repeatedly with CH_2Cl_2 and EtOAc. The filtrate, which had become cloudy with voluminous precipitate, was filtered and washed with a small amount of cold EtOAc to give the product as an off-white solid in 79% yield: mp = 254-255 °C (dec). ¹H-NMR (DMSO-d_6, 250 MHz) δ 2.83 (s, 1H), 2.90 (s, 1H), 3.07 (s, 4H), 3.96 (br d, 1H), 7.47–7.71 (m, 9H). ¹³C-NMR (DMSO-d_6, 63 MHz) δ

168.75, 165.39, 144.65, 135.19, 132.54, 129.85, 129.51, 128.64, 128.55, 56.25, 31.14, 30.85, 29.68. FAB-MS Calcd for $C_{20}H_{17}NO_8S$ (sulfonic acid form): 431.42. Found: 431.0.

p-[³H]Benzoyldihydrocinnamic Acid (5, x = 3). Hydrogenation using carrier-free tritium gas was performed at DuPont-New England Nuclear (Boston, MA). A mixture of **5** (15 mg, 0.06 mmol) and 5% palladium on carbon (1.2 mg, 8% by weight), suspended in 2 mL of EtOH, was stirred under an atmosphere of carrier-free tritium gas for 90 min. Labile tritium was removed, and the mixture was filtered through a 5 × 25 mm bed of Celite and washed with 10 mL of MeOH. After concentration, the product was purified by preparative TLC; first with Hex/EtOAc/CH_2Cl_2 (3:1:1) on a Whatman PLK_5 silica plate and then with MeOH/H_2O/HOAc (70:30:0.1) on a Whatman PKC_{18} plate. The product was isolated in 30% yield (800 mCi) with specific activity = 44.8 Ci/mmol as determined by MS.

N-[³H]Succinimidyl p-Benzoyldihydrocinnamate (1b). Hydrogenation using carrier-free tritium gas was performed at DuPont-New England Nuclear. Unsaturated ester **6** (18 mg, 0.05 mmol) and 5 mg of 5% palladium on carbon were suspended in 2 mL of EtOAc, placed under an atmosphere of carrier-free tritium gas, and stirred at atmospheric pressure and ambient temperature for 4 h. The catalyst was removed by filtration and washed twice with 2 mL of EtOAc. The filtrate was concentrated, and labile tritium was removed by rotary evaporation twice using MeOH as a carrier. The product was purified by preparative HPLC using a Zorbax silica column with detection at 280 nm. For analytical scale separations, the elution solvent was 97.5:2.5 CH_2Cl_2/EtOAc, and the flow rate was 1 mL/min; t_R = 29.45 min for the starting material and 48.52 min for the product. The product may be stored in Hex/EtOAc at or below −20 °C (≤5 mCi/mL) for several months without chemical or radiochemical decomposition. Specific activity of different lots of [³H]BZDC-NHS ranged from 30 to 60 Ci/mmol.

[³H]-N-Sulfosuccinimidyl p-Benzoyldihydrocinnamate (2b). From a stock solution of p-[³H]benzoyldihydrocinnamic acid in methanol, an aliquot containing 2 mCi was placed in a 5-mL reaction vessel and evaporated to dryness under a stream of argon. Dry DMF (20 μL) and solutions of sulfo-NHS (3 μL of a 5 mg/mL stock) and DCC (3 μL of a 5 mg/mL stock) in DMF were added, and the mixture was stirred at ambient temperature for 48 h. Due to slow progression of the reaction (analysis by TLC and autoradiography), additional sulfo-NHS (3 μL of stock) and DCC (3 μL of stock) were added and stirring was continued for an additional 48 h. These additions were repeated and stirring was continued for another 48 h. The crude reaction mixture was applied to a SiO_2 column (0.8 × 8 cm), and the product was eluted with 4:1 $CHCl_3$/MeOH in 8% radiochemical yield. Analysis by TLC and autoradiography showed that the product R_f matched that of the cold standard and had a purity > 95%.

General Procedure for p-[2,3-³H₂]Benzoyldihydrocinnamyl Derivatives of P-1-(O-Aminoalkyl) Tethered Inositol Polyphosphates. An example for the Ins(1,4,5)P_3 derivative is described (Mourey et al., 1993). The [³H]BZDC-NHS ester (0.5 mL of stock solution containing 2 mCi/mL in ethyl acetate/hexane, 1:1) was carefully concentrated under nitrogen. The residue was redissolved in 50 μL of DMF and added to 50 μL of a stirred solution (0.42 mM in 0.25 M triethylammonium bicarbonate, TEAB) of the P-1-(O-aminopropyl)-Ins(1,4,5)-P_3 (Prestwich et al., 1991). The reaction mixture was stirred for 48 h at ambient temperature and then

concentrated *in vacuo.* The residue was taken up in 50 μL of water and concentrated to dryness again to remove any remaining TEAB and DMF. The residue was taken up in 0.5 mL of water and applied to a 4 × 0.5 cm column of DEAE-cellulose (HCO_3^- form). The column was washed with 1 mL of water and eluted sequentially with 1-mL volumes of 0.1 M TEAB, 0.2 M TEAB, 0.3 M TEAB, and 0.4 M TEAB followed by 2-mL volumes of 0.5 M TEAB, 0.6 M TEAB, and 0.8 M TEAB. A 1-μL aliquot of each fraction was monitored by liquid scintillation counting.

The high-activity fractions (generally 0.4 and 0.5 M TEAB) were analyzed by reversed-phase HPLC (RP-HPLC, Aquapore RP-300) (15% CH_3CN in 0.05 M KH_2-PO_4 buffer, pH = 4.4) using UV 220, 254, and 280 nm and BetaRam radiochemical detectors; the pure fractions were pooled to obtain a 30−40% radiochemical yield.

General Procedure for Unlabeled and p-[2,3-³H₂]-Benzoyldihydrocinnamyl Derivatives of Peptides. Probes synthesized include derivatives of Gly-Gly-Arg and pheromone biosynthesis activating neuropeptide (PBAN, amino acid sequence LSDDMPATPADQEMYR-QDPEQIDSRTKYFSPRL-amide derivatized at Lys²⁷). The synthesis and purification of the radiolabeled peptides were carried out in the same manner as for the cold peptides. Representative protocols for N-terminal or Lys modification are illustrated.

BZDC-GGR. To a solution of 1.2 mg (3.5 mmol) of Gly-Gly-Arg acetate in 0.1 mL of water was added 175 μL of 0.05 M BZDC-NHS ester in DMF (8.75 mmol) and 160 μL of 0.5 M triethylamine (70 mmol) in DMF/water (1:1). The reaction mixture was left for 48 h at ambient temperature in darkness. A blank reaction, containing all the reagents except for the peptide, was performed in parallel. Both reactions were quenched with 0.35 mL of 0.1 M ethanolamine in MeOH, concentrated *in vacuo,* redissolved in 0.5 mL of phosphate buffer (0.2 M, pH 7.2) and purified by HPLC (Aquapore RP-300): mobile phase, A = 0.1% TFA in water, and B = 80% CH_3CN, 19.9% water, and 0.1% TFA; gradient 0−80% B (40 min), 80% B (15 min); t_R = 25.4 min for BZDC-Gly-Gly-Arg and 32.5 min for BZDC-ethanolamide.

Alternatively, rapid purification could be achieved using a NENSORB-20 cartridge. Thus, an aliquot (10 μL from the phosphate-buffered solution) was diluted to 200 μL in a Tris buffer (reagent A) and applied to the cartridge. A solvent consisting of 20% propanol in water was used for elution, and the first 200-μL fraction showed the majority of the pure peptide as determined by HPLC (see above). ¹H-NMR (D_2O, 600 MHz) δ 7.63−7.72 (m, 5H), 7.50 (t, 2H), 7.36 (d, 2H), 4.23 (m, 1H), 3.59 (m, 4H), 3.05 (t, 2H), 2.97 (t, 2H), 2.27 (t, 2H), 1.78 (m, 2H), 1.64 (m, 2H), 1.48 (m, 2H).

Lys²⁷-BZDC-PBAN. Synthetic PBAN (3 mg, 0.75 μmol) was dissolved in 100 μL of DMF, and 12 μL of 0.05 M BZDC-NHS ester in DMF was added, followed by 9 μL of 0.7 M triethylamine in DMF. The reaction mixture was stored for 16 h at ambient temperature, and the products were first analyzed and then purified by RP-HPLC using the system as described above for BZDC-GGR; t_R = 28 min for Lys²⁷-BZDC-PBAN, 30 min for N-terminal-BZDC-PBAN, 33 min for doubly-labeled BZDC-PBAN, and 36 min for BZDC-NHS ester.

Verification of Lys²⁷ Modification. PBAN (10 nmol) or Lys²⁷-BZDC-PBAN was mixed with 0.1 nmol of Lys-C in 20 μL of 50 mM Tris-HCl, pH 9.0, and incubated for 6 h at 30 °C. Cleavage of unmodified PBAN occurred at Lys²⁷ as detected by the shift of the peak corresponding to PBAN (1−33) in the HPLC spectrum profile to a shorter t_R peak assigned as PBAN(1−27). In contrast, Lys²⁷-BZDC-PBAN was insensitive to the Lys-C protease,

Scheme 1
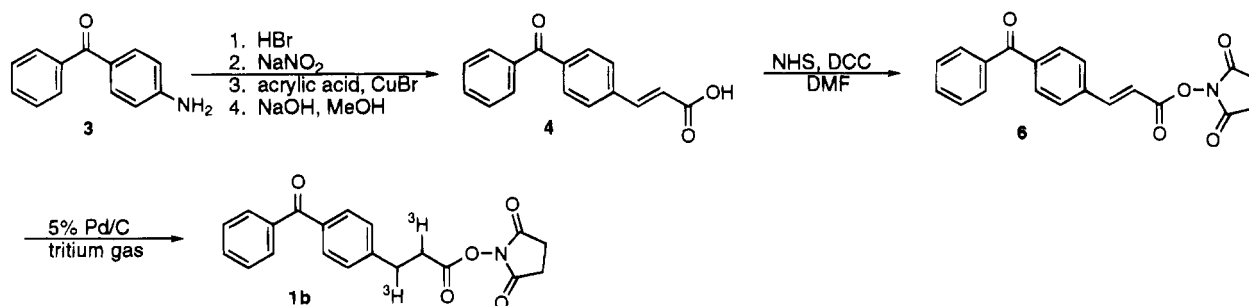
Scheme 2
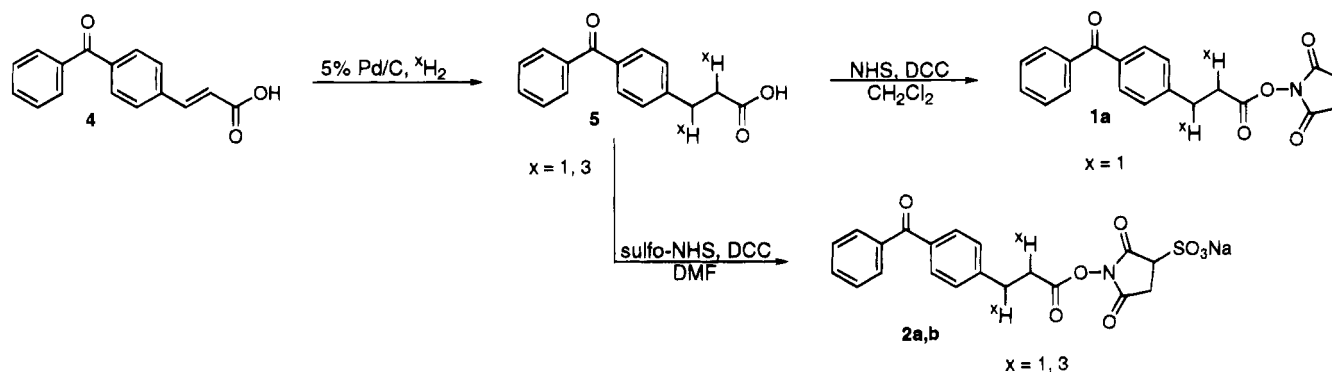
showing no peak shift as monitored by HPLC and supporting the modification at the lysine residue.

RESULTS AND DISCUSSION

The BZDC photophore was first employed in mapping the inositol 1,4,5-trisphosphate binding site of the IP_3 receptor (Mourey et al., 1993). However, in this study the unsaturated cinnamyl NHS ester **6** was attached to a pendant amino group *prior* to tritium gas reduction to the [2,3-$^3H_2$]BZDC amide. Relatively low specific activity materials (≤ 4 Ci/mmol) were obtained by this route, since the reductive tritiation was carried out in aqueous solution. We have improved this process by preparing [^{3}H]BZDC-NHS, a heterobifunctional cross-linking reagent of general utility, which allows removal of reduction byproducts *prior* to coupling to the ligand of interest.

Scheme 1 shows the preparation of the reagent. Aminobenzophenone (**3**) was diazotized, and acrylic acid and cuprous bromide were added to achieve a Meerwein arylation (Cleland, 1961, 1971; Rondestvedt, 1976; Doyle et al., 1977). The resulting (α-bromobenzoyl)hydrocinnamic acid was isolated and then dehydrobrominated. Acidification resulted in precipitation of 4-benzoylcinnamic acid (BZC, **4**), which was converted to active ester, BZC-NHS (**6**). Hydrogenation at atmospheric pressure afforded BZDC-NHS ester (**1a**). Tritium gas reduction of BZC-NHS (**6**) with 5% Pd/C under carrier-free tritium gas gave [^{3}H]BZDC-NHS (**1b**), which was purified by preparative HPLC (flash chromatography failed to separate **6** and **1b**). A small amount of the benzhydrol byproduct was occasionally produced in different lots.

To prepare the sulfo-NHS derivative, 4-benzoylcinnamic acid (**4**) was hydrogenated or tritiated using 5% palladium on carbon. The purified dihydro acid (**5**) was coupled to sulfo-*N*-hydroxysuccinimide using DCC. The product (**2a**) was crystallized from the reaction mixture (Scheme 2).

Derivatization of four different *O*-aminoalkyl tethered inositol polyphosphates [P-1 tethered Ins(1,4,5)P$_3$ and Ins(1,3,4,5)P$_4$, P-5 tethered Ins(1,2,5,6)P$_4$, (Chaudhary et

al., 1994) and P-2-*O*-aminohexyl tethered Ins(1,2,3,4,5,6)-P$_6$] with **1b** has been accomplished (A. A. Profit, G. Dormán, J. D. Olszewski, and G. D. Prestwich, unpublished results). This reaction may be performed in organic or mixed organic–aqueous solvent systems. For these derivatives, **1b** in DMF was added to a solution of the P-1-*O*-aminoalkyl polyphosphate in triethylammonium bicarbonate and allowed to react for 48 h. After removal of all solvents and buffer, purification was achieved via a DEAE-cellulose column (HCO$_3^-$ form). Fractions were analyzed by RP-HPLC using UV and radiochemical detection. The new reagent provides specific activities in the range of 30–60 Ci/mmol, improving sensitivity of detection by an order of magnitude over the previous method (Mourey et al., 1993).

We have also modified the N-terminal amino group and internal Lys amino groups of polypeptides to prepare peptide photoaffinity labels (Figure 2). The derivatization can be performed in either a mixed aqueous–organic system (DMF/water) or in an entirely organic system (DMF) at room temperature. Reaction times ranged from 6 to 48 h with purification and analysis performed by RP-HPLC using UV and radiochemical detection. In one example, the simple tripeptide Gly-Gly-Arg (GGR) was modified on the N-terminal glycine amino group using **1b** in 1:1 DMF/water with excess triethylamine added. Purification was achieved via RP-HPLC or by using step gradient elution from a NENSORB 20 cartridge. In the next example, selection of reaction conditions allowed differentiation between an N-terminus and an internal amine (Myers et al., 1991). The unique internal Lys[27] of PBAN, a 33 amino acid polypeptide important in activating insect pheromone biosynthesis (Raina & Menn, 1993), was selectively modified in the presence of the unblocked N-terminal amino group. The site of modification was verified by digestion of both modified and unmodified peptides with endoproteinase Lys-C.

CONCLUSION

In summary, we prepared a new heterobifunctional tritium-labeled reagent for conversion of a variety of

biological ligands to photoaffinity labels. The selectivity and ease of use of both unlabeled BZDC-NHS **1a** and the high specific activity tritium-labeled reagent **1b** are discussed. The development of **1b** now allows access by biochemical laboratories to a wide range of new photoprobes for receptor site characterization. The successful use (Mourey et al., 1993) of [³H]BZDC-IP₃ can now be extended to identification of peptide carrier proteins, other inositol polyphosphate receptors, targets for anticancer agents, odorant receptors, and other systems.

ACKNOWLEDGMENT

LITERATURE CITED

Agarwal, R., Rajasekharan, K. N., and Burke, M. (1991) Identification of the Site of Photocross-linking Formed in the Absence of Magnesium Nucleotide from SH2 (Cys-697) in Myosin Subfragment 1 Labeled with 4'-Maleimidylbenzophenone. *J. Biol. Chem. 266,* 2272–2275.

Aloise, P., Kagawa, Y., and Coleman, P. S. (1991) Comparative Mg²⁺-dependent Sequential Covalent Binding Stoichiometries of 3'-*O*-(4-Benzoyl)benzoyl Adenosine 5'-Diphosphate of MF1, TF1, and the α₃β₃ Core Complex of TF1. *J. Biol. Chem. 266,* 10368–10376.

Bar-Zvi, D., Bar, I., Yoshida, M., and Shavit, M. (1992) Covalent Binding of 3'-*O*-(4-Benzoyl)benzoyl Adenosine 5'-Triphosphate (BzATP) to the Isolated α and β subunits and the α3β3 Core Complex of TF1. *J. Biol. Chem. 267,* 11029–11033.

Boyd, N. D., White, C. F., Cerpa, R., Kaiser, E. T., and Leeman, S. E. (1991) Photoaffinity Labeling the Substance P Receptor Using a Derivative of Substance P Containing *p*-Benzoylphenylalanine. *Biochemistry 30,* 336–342.

Boyer, J. L., Cooper, C. L., and Harden, T. K. (1990) [³²P]3'-*O*-(4-Benzoyl)benzoyl ATP as a Photoaffinity Label for a Phospholipase C-coupled P2Y-Purinergic Receptor. *J. Biol. Chem. 265,* 13515–13520.

Chaudhary, A., Dormán, G., and Prestwich, G. D. (1994) Synthesis of P-5 Tethered Inositol-1,2,6-Trisphosphate, an Affinity Reagent for α-Trinositol Receptors. *Tetrahedron Lett. 35,* 7521–7524.

Cremo, C. R., and Yount, R. G. (1987) 2'-Deoxy-3'-*O*-(4-benzoylbenzoyl)- and 3'(2')-*O*-(4-Benzoylbenzoyl)-1,N₆-ethenoadenosine 5'-Diphosphate, Fluorescent Photoaffinity Analogues of Adenosine 5'-Diphosphate. Synthesis, Characterization, and Interaction with Myosin Subfragment 1. *Biochemistry 26,* 7524–7534.

Chavan, A., Rychlik, W., Blaas, D., Kuechler, E. D., Watt, S., and Rhoads, R. E. (1990) Phenyl Azide-Substituted and Benzophenone-Substituted Phosphonamides of 7-Methylguanosine 5'-Triphosphate as Photoaffinity Probes for Protein Synthesis Initiation Factor eIF-4E and a Proteolytic Fragment Containing the Cap-Binding Site. *Biochemistry 29,* 5521–5529.

Cleland, G. H. (1961) The Meerwein Reaction in Amino Acid Synthesis. I. α-Bromo-*o*-, *m*-, and *p*-Chlorohydrocinnamic Acids and the Corresponding Chlorophenylalanines; α-Bromo- and α-Chlorohydrocinnamide. *J. Org. Chem. 26,* 3362–3364.

Cleland, G. H. (1971) *p*-Acetyl-α-bromohydrocinnamic Acid. *Org. Synth. 51,* 1–4.

Combeau, C., Didry, D., and Carlier, M.-F. (1992) Interaction between G-actin and Myosin Subfragment-1 Probed by Covalent Cross-linking. *J. Biol. Chem. 267,* 14038–14046.

Dormán, G., and Prestwich, G. D. (1994) Benzophenone Photophores in Biochemistry. *Biochemistry 33,* 5661–5673.

Doyle, M. P., Siegfried, B. and Dellaria, J. F., Jr. (1977) Alkyl Nitrite-Metal Halide Deamination Reactions. 2. Substitutive Deamination of Arylamines by Alkyl Nitrites and Copper (II) Halides. A Direct and Remarkably Efficient Conversion of Arylamines to Aryl Halides. *J. Org. Chem. 42,* 2426–2436.

Estevez, V. A. (1991) Synthesis and Biochemical Applications of Affinity Labels for Inositol Polyphosphate Receptors, Ph.D. Dissertation, State University of New York at Stony Brook.

Gonzalez, F. A., Wand, D.-J., Huang, N.-N., and Heppel, L. A. (1990) Activation of Early Events of the Mitogenic Response by a P2Y Purinoceptor with Covalently-Bound 3'-*O*-(4-Benzoyl)-benzoyladenosine 5'-Triphosphate. *Proc. Natl. Acad. Sci. U.S.A. 87,* 9717–9721.

Holman, G. D., Karim, A. R., and Karim, B. (1988) Photolabeling of Erythrocyte and Adipocyte Hexose Transporters Using a Benzophenone Derivative of bis(D-Mannose) *Biochim. Biophys. Acta 946,* 75–84.

Ishidate, K., Matsuo, R., and Nakazawa, Y. (1992) CDP-Choline: 1,2-Diacyglycerol Cholinephosphotransferase from Rat Liver Microsomes. II. Photoaffinity Labeling by Radioactive CDP-Choline Analogs. *Biochim. Biophys. Acta 1124,* 36–44.

Kuechler, E., Steiner, G., and Barta, A. (1988) Photoaffinity Labeling of Peptidyltransferase. *Methods in Enzymology* (Noller, H. F., Jr., & Moldave, K., Eds.) Academic Press, New York, *164,* 361–372.

Leszyk, J., Collins, J. H., Leavis, P. C., and Tao, T. (1987) Cross-Linking of Rabbit Skeletal Muscle Troponin with the Photoactive Reagent 4-Maleimidobenzophenone: Identification of Residues in Troponin I That Are Close to Cysteine-98 of Troponin C. *Biochemistry 26,* 7042–7047.

Mahmood, R., Elzinga, M., and Yount, R. G. (1989) Serine-324 of Myosin's Heavy Chain Is Photoaffinity-Labeled by 3'(2')-*O*-(4-Benzoylbenzoyl)adenosine Triphosphate. *Biochemistry 28,* 3989–3995.

McNicoll, N., Escher, E., Wilkes, B. C., Schiller, P. W., Ong, H., and De Lean, A. (1992) Highly Efficient Photoaffinity Labeling of the Hormone Binding Domain of Atrial Natriuretic Factor Receptor. *Biochemistry 31,* 4487–4493.

Mourey, R. J., Estevez, V. A., Marecek, J. F., Barrow, R. K., Prestwich, G. D., and Snyder, S. H. (1993) Inositol 1,4,5-Trisphosphate Receptors: Labeling the Inositol 1,4,5-Trisphosphate Binding Site With Photoaffinity Ligands. *Biochemistry 32,* 1719-1726.

Myers, R. A., Zafaralla, G. C., Gray, W. R., Abbott, J., Cruz, L. J., and Olivera, B. M. (1991) α-Conotoxins, Small Peptide Probes of Nicotinic Acetylcholine Receptors. *Biochemistry 30,* 9370–9377.

O'Neil, K. T., and DeGrado, W. F. (1989) The Interaction of Calmodulin With Fluorescent and Photoreactive Model Peptides: Evidence for a Short Interdomain Separation. *Proteins: Struct., Funct., Genet. 6,* 284–293.

O'Neil, K. T., Erickson-Viitanen, S., and DeGrado, W. F. (1989) Photolabeling of Calmodulin with Basic, Amphiphilic α-Helical Peptides Containing *p*-Benzoylphenylalanine. *J. Biol. Chem. 264,* 14571–14578.

Pal, P. K., and Coleman, P. S. (1990) Detecting Precatalytic Conformational Changes in F1-ATPase with 4-Benzoyl(benzoyl)-1-amidofluorescein, a Novel Fluorescent Nucleotide Site-Specific Photoaffinity Label. *J. Biol. Chem. 265,* 14996–15002.

Pal, P. K., Ma, Z., and Coleman, P. S. (1992) The AMP-binding Domain on Adenylate Kinase. *J. Biol. Chem. 267,* 25003–25009.

Prestwich, G. D., Marecek, J. F., Mourey, R. J., Theibert, A. B., Ferris, C. D., Danoff, S. K., and Snyder, S. H. (1991) Tethered IP₃. Synthesis and Biochemical Applications of the 1-*O*-(3-Aminopropyl) Ester of Inositol 1,4,5-Trisphosphate. *J. Am. Chem. Soc. 113,* 1822-1825.

Raina, A. K., and Menn, J. J. (1993) Pheromone Biosynthesis Activating Neuropeptide—from Discovery to Current Status. *Arch. Insect Biochem. Physiol. 22,* 141–151.

Rajagopalan, K., Chavan, A. J., Haley, B. E., and Watt, D. S. (1993) Synthesis and Application of Bidentate Photoaffinity Cross-linking Reagents. *J. Biol. Chem. 268,* 14230–14238.

Rajasekharan, K. N., Morita, J.-I., Mayadevi, M., Ikebe, M., and Burke, M. (1991) Formation and Properties of Smooth Muscle

Myosin 20-kDa Light Chain-Skeletal Muscle Myosin Hybrids and Photocrosslinking from the Maleimidylbenzophenone-Labeled Light Chain to the Heavy Chain. *Arch. Biochem. Biophys. 288,* 584–590.

Rondestvedt, J., and Christian, S. (1976) Arylation of Unsaturated Compounds by Diazonium Salts (The Meerwein Arylation Reaction). *Org. React. 24,* 225–259.

Salvucci, M. E., Rajagopalan, K., Sievert, G., Haley, B. E., and Watt, D. S. (1993) Photoaffinity Labeling of Ribulose-1,5-bisphosphate Carboxylase/Oxygenase Activase with ATP γ-Benzophenone. *J. Biol. Chem. 268,* 14239–14244.

Shoelson, S. E., Lee, J., Lynch, C. S., Backer, J. M., and Pilch, P. F. (1993) BpaB25 Insulins. *J. Biol. Chem. 268,* 4085–4091.

Thiele, C., and Fahrenholz, F. (1993) Photoaffinity Labeling of Central Cholecystokinin Receptors with High Efficiency. *Biochemistry 32,* 2741–2746.

Williams, K. P., and Shoelson, S. E. (1993) A Photoaffinity Scan Maps Regions of the p85 SH2 Domain Involved in Phosphoprotein Binding. *J. Biol. Chem. 268,* 5361–5364.

Yamamoto, M., Warnock, W. A., Milon, A., Nakatani, Y., and Ourisson, G. (1993) Selective Photolabeling near the Middle of Bilayers with a Photosensitive Transmembrane Probe. *Angew. Chem., Int. Ed. Engl. 32,* 259–263.

Zarka, A., and Shoshan-Barmatz, V. (1993) Characterization and Photoaffinity Labeling of the ATP Binding Site of the Ryanodine Receptor from Skeletal Muscle. *Eur. J. Biochem. 213,* 147–154.

Glycosylated Polylysine/DNA Complexes: Gene Transfer Efficiency in Relation with the Size and the Sugar Substitution Level of Glycosylated Polylysines and with the Plasmid Size

Patrick Erbacher, Annie Claude Roche, Michel Monsigny, and Patrick Midoux*

Glycobiologie, Centre de Biophysique Moléculaire BatB, CNRS et Université d'Orléans, rue Charles Sadron F-45071, Orléans Cedex 02, France. Received October 10, 1994[®]

A DNA delivery system based on the use of polylysine substituted with small recognition signals, such as carbohydrate moieties specifically recognized by membrane lectins present in a given cell line, has been developed [Midoux *et al.* (1993) *Nucleic Acids Res. 21*, 871–878]. Human hepatoma (HepG2) cells which express a galactose-specific membrane lectin are efficiently transfected in the presence of chloroquine with pSV2Luc plasmid complexed with a lactosylated polylysine. The optimization of the parameters involved in the formation of DNA/glycosylated polylysine complexes leads to the following conclusions: a high gene transfer efficiency is reached when (i) DNA/glycosylated polylysine complexes are completely retarded when subjected to electrophoresis and when (ii) 31 ± 4% or 40 ± 8% of the amino groups of a polylysine having a degree of polymerization (DP) of 190 are substituted with lactosyl or β-D-galactosyl residues, respectively. In addition, carbohydrate residues bound to polylysine decrease the electrostatic strength between plasmid DNA and glycosylated polylysine, suggesting that the strength of the electrostatic interactions between the plasmid and the glycosylated polylysine plays an important role in the efficiency of the gene expression. The optimal lactosylated polylysine conjugate (polylysine DP 190 substituted with 60 lactosyl residues) transfers a 5 kb and a 12 kb plasmid with a similar efficiency.

INTRODUCTION

The introduction of a foreign gene into a mammalian cell is of great interest both for academic purposes and for gene therapy. A new attractive approach is a DNA plasmid complexed with soluble macromolecules such as polylysine substituted with a protein acting as a recognition signal such as asialoorosomucoid (for reviews, see refs 1 and 2), transferrin (for a review, see ref 3), insulin *(4)*, antibodies *(5, 6)*, or polylysine substituted with small ligands also acting as recognition signals such as carbohydrate moieties recognized by membrane lectins (or sugar receptors) (for a review, see ref 7). Moreover, the transfection efficiency obtained by using such DNA delivery methods is greatly improved when cells are incubated in the presence of chloroquine *(8, 9)* or in the presence of either a defective adenovirus *(10)* or a fusogenic peptide *(8, 11–13)* which help the DNA to reach the cytosol by crossing an intracellular membrane. The preparation of protein–polylysine conjugates must be conducted in a high ionic strength medium to avoid the formation of insoluble aggregates; the conjugates themselves are weakly soluble in serum or in phosphate-balanced saline. To circumvent these pitfalls, we chose to develop a DNA delivery system based on the use of polylysine substituted with small recognition signals such as carbohydrate moieties specifically recognized by membrane lectins which are present at the surface of numerous normal and tumor cells *(14)*. We previously described a specific gene transfer method mediated by poly(L-lysine) partially substituted with lactosyl residues, as recognition signals specific for the cell surface lectin of liver parenchymal cells and hepatoma cells such as HepG2 cells *(8)*. Glycosylated polylysines *(7, 8)* offer the advantage of being fully synthetic, rapidly prepared, easy to purify, and highly soluble at neutral pH in a physiological ionic strength buffer as well as in serum.

In order to reach a very high gene transfer efficiency, we undertook a study on the influence of the average number and of the nature (lactose or β-D-galactose) of the sugar residues bound per polylysine molecule, the size of the polylysine, and that of the plasmid.

The highest gene transfer efficiency into HepG2 cells was obtained in the presence of chloroquine with polylysine [average degree of polymerization (DP)[1] = 190] having 31 ± 4% of the amino groups substituted with lactosyl or 40 ± 8% with β-D-galactosyl residues and with DNA/glycosylated polylysine complexes prepared with a plasmid to glycosylated polylysine ratio leading to a complete retardation of the electrophoretic migration of the DNA. These results suggest that the partial neutralization of the charges of the polycation induces a decrease in the strength of the electrostatic interactions between the plasmid and the polylysine conjugates and plays an important role in the efficiency of the gene expression.

MATERIALS AND METHODS

Chemicals. Luciferin, chloroquine, Triton X-100, and bicinchoninic acid were from Sigma (St. Louis, MO); L-glutamine, dimethyl sulfoxide, ATP, glycerol, and $MgCl_2$ were from Merck (Darmstadt, Germany); dithiothreitol was from Serva (Heidelberg, Germany); diisopropylethylamine, *p*-toluenesulfonic acid, and EDTA were from Aldrich (Strasbourg, France); Dowex 2 × 8, 20–50 mesh, was from Bio-Rad (Richmond, CA). 4-Isothiocyanatophen-

---

* To whom correspondence should be addressed. Phone number: 33.38.51.55.95; FAX number: 33.38.69.00.94.

---

[1] Abbreviations: BSA, bovine serum albumin; DP, degree of polymerization; EDTA, ethylenediaminetetraacetate; FBS, fetal bovine serum; Gal, galactosyl residue; Glc, glucosyl residue; Lact, lactosyl residue; PBS, phosphate-buffered saline, pH 7.4; pLK, poly(L-lysine).

yl β-D-lactoside, 4-isothiocyanatophenyl β-D-galactopyra-noside, and 4-isothiocyanatophenyl α-D-glucopyranoside were prepared as previously described *(15)*; poly(L-lysine), HBr 70 000–150 000, pLK$_{633}$ (average molecular weight = 131 000; DP 633) was from Sigma; poly(L-lysine), HBr 30 000–50 000, pLK$_{190}$ (average molecular weight = 40 000; DP 190), poly(L-lysine), HBr 10 000–20 000, pLK$_{72}$ (average molecular weight = 15 000; DP 72), and poly(L-lysine), HBr 5000–10 000, pLK$_{36}$ (average molecular weight = 7500; DP 36) were from Bachem Feinchemikalien (Bubendorf, Switzerland). Poly(L-lysine), HBr (1 g in 200 mL of H$_2$O), was passed through an anion exchange column (Dowex 2 × 8, OH$^-$ form, 20–50 mesh, 35 × 2.5 cm) in order to remove bromide ions *(16)*, which are highly toxic for cells *(17)*. The effluent solution was neutralized with 10% p-toluenesulfonic acid in water (a nontoxic compound) and freeze-dried.

Preparation of Glycosylated Poly(L-lysine) Conjugates. Poly(L-lysine) (pLK$_{190}$) was partially substituted with different numbers of either lactosyl or galactosyl residues as previously described *(8)*. 4-Isothiocyanatophenyl β-D-lactoside (20–80 equiv; 15–61 μmol) or 4-isothiocyanatophenyl β-D-galactopyranoside (45–100 equiv; 34–76 μmol) was added to p-toluenesulfonate poly-(L-lysine) (40 mg; 0.76 μmol) in 2 mL of dimethyl sulfoxide in the presence of diisopropylethylamine (36 μL; 0.25 mmol) and reacted for 24 h at 20 °C. The glycosylated polylysine was precipitated by adding 10 volumes of 2-propanol and spun down by centrifugation (1800g for 15 min). The pellets were washed in 2-propanol, collected by centrifugation (1800g for 15 min), solubilized in distilled water, and freeze-dried. The polylysine conjugate concentration was determined with a trypan blue assay *(18)*. In order to take into account the polylysine substitution level, standard curves were made on the basis of the precise weighted amount of each polylysine conjugate. These curves were used to determine the polymer concentrations. The average number of remaining free amino groups on polylysine conjugates was assessed using TNBS *(19)*. The average number of lactosyl or galactosyl residues bound per poly(L-lysine) molecule was calculated from the sugar content determined by using the resorcinol sulfuric acid micromethod *(20)*. Polylysines were substituted, in a high yield (>95%), with various numbers of either lactosyl residues [Lact$_x$pLK$_{190}$ (with x = 20, 30, 40, 52, 60, 66, 70, or 80); Lact$_x$pLK$_{72}$ (with x = 10, 20, 25, or 30); Lact$_x$pLK$_{36}$ (with x = 4, 8, 10, or 16); Lact$_x$pLK$_{633}$ (with x = 79, 110, 169, 209, or 332)] or galactosyl residues [Gal$_x$pLK$_{190}$ (with x = 45, 62, 68, 76, or 93)]. Glc$_{90}$pLK$_{190}$ was prepared as described above by reaction of pLK$_{190}$ with 4-isothiocyanatophenyl α-D-glucoside. Fluoresceinylated and glycosylated polylysine was prepared as previously described *(8)*.

Cells and Cell Culture. HepG2 cells (a human hepatoma cell line) possess a membrane lectin recognizing glycoproteins terminated by β-D-galactose residues *(21)* (ATCC 8065 HB, ATCC, Rockville, MD). HepG2 cells were cultured at 37 °C in humidified atmosphere (95% air, 5% CO$_2$) in complete DMEM medium: DMEM (GIBCO, Renfrewshire, U.K.) supplemented with 10% heat inactivated fetal bovine serum, (FBS) (GIBCO), 2 mM L-glutamine (Merck), and antibiotics (100 units/mL penicillin and 100 μg/mL streptomycin) (Eurobio, Paris, France).

Plasmids. pSV2Luc (5.0 kb) plasmid was kindly given by Dr. A. B. Brasier (Massachusetts General Hospital, Boston, MA) *(22)*; pNAF (4.75 kb) plasmid *(23)* by Dr. S. Saragosti (Hôpital Cochin, Paris, France); pLTR$_{HIV}$XLuc (6.4 kb) plasmid by Dr. O. Schwartz (Institut Pasteur,

Paris, France) *(24)*; pAR6 (7 kb) plasmid by Dr. G. Sczakiel (EMBL, Heidelberg, Germany), *(25)*; pSVβGal (6.75 kb), pSVHI-28 (9.5 kb), pCOS90–1 (10.9 kb), pROF27 (12 kb), and pROF23 (12.9 kb) plasmids by Dr. A. Legrand and Dr. J. Raimond (CBM, Orléans, France); HDYS (17.6 kb) plasmid by Dr. H. Gilgenkrantz (Hôpital Cochin, Paris, France).

Gene Transfer. DNA/polymer complexes were prepared by adding, dropwise and with constant mixing, a glycosylated poly(L-lysine) in 0.6 mL of DMEM to 20 μg (6 pmol) of pSV2Luc plasmid in 1.4 mL of DMEM. The solution was kept for 30 min at 20 °C. HepG2 cells (4 × 10^5 cells per well) were plated (day 0) into 12-well tissue culture plates. On day 1, the medium was removed, and then 1 mL of solution containing a plasmid/glycosylated polylysine complex, supplemented with 1% heat inactivated FBS and made 100 μM in chloroquine, was added into each well. After a 4 h incubation at 37 °C, the supernatant was removed and 2 mL of fresh complete DMEM medium containing 10% FBS was added; cells were further incubated for 48 h at 37 °C.

Luciferase Assay. Luciferase gene expression was measured by luminescence according to De Wet *et al.* *(26)*. The culture medium was discarded, and cells were harvested upon incubation at 37 °C in PBS containing 0.2 mg/mL EDTA and 2.5 μg/mL trypsin (GIBCO) and then washed three times in PBS. The homogenization buffer (200 μL; 8 mM MgCl$_2$, 1 mM dithiothreitol, 1 mM EDTA, 1% Triton X-100, and 15% glycerol, 25 mM Tris–phosphate buffer, pH 7.8) was added onto the pellet. The suspension was mixed with a vortex and kept for 10 min at 20 °C. The solution was spun down (5 min, 800g). ATP (95 μL of a 2 mM solution in the homogenization buffer without Triton X-100) was added to 60 μL of supernatant, and then luciferin (167 μM, 150 μL) was added. The luminescence was recorded for 4 s by using a luminometer (Lumat LB 9501, Berthold, Wildbach, Germany); measurements were done in triplicate.

Protein Assay. Protein assay was performed for each sample by using the bicinchoninic acid (BCA) colorimetric method *(27)* modified according to Hill and Straka *(28)* to overcome the interference due to the presence of dithiothreitol in the homogenization buffer. In this assay, 1.2 × 10^6 HepG2 cells give the absorbance of 1 mg of BSA (crystallized and purified fatty acid-free albumin, A 7511, Sigma). RLU is the luciferase activity from 1.2 × 10^6 HepG2 cells expressed as relative light units per milligram of BSA.

Binding and Uptake of DNA/Lactosylated Polylysine Complexes. pSV2Luc (25 ng) was radiolabeled with ^{32}P by random priming protocol by using the Megaprime DNA labeling system (Amersham, Buckinghamshire, U.K.) and [α-^{32}P]dCTP (9.25 MBq, Amersham). DNA/polymer complexes were prepared by adding, dropwise with constant mixing, glycosylated polylysine in 0.6 mL of DMEM to 1.4 mL of DMEM containing 20 μg of unlabeled pSV2Luc plasmid and 12.5 ng of [^{32}P]pSV2Luc plasmid (specific activity = 2 × 10^9 cpm/μg). The solution was kept for 30 min at 20 °C. HepG2 cells (1 × 10^5 cells per well) were plated into 48-well tissue culture plates and incubated for 2 h at either 4 or 37 °C with 250 μL of various concentrations of DNA/polymer complexes in the presence of 1% heat inactivated fetal bovine serum. Then, cells were washed twice in cold serum-free DMEM, harvested by incubation for 3 min at 37 °C in PBS containing 0.2 mg/mL EDTA, and radioactivity was counted by using a Beckman scintillation spectrometer.

Measurement of the Stability of DNA/Lactosylated Polylysine Complexes. DNA/polymer complexes were prepared by adding, dropwise with constant mixing,

either pLK_{190} (2.5 μg), $Lact_{20}pLK_{190}$ (5 μg), $Lact_{40}pLK_{190}$ (10 μg), $Lact_{60}pLK_{190}$ (12.5 μg), $Lact_{70}pLK_{190}$ (15 μg), or $Lact_{80}pLK_{190}$ (20 μg) in 0.3 mL of 0.15 M NaCl to 5 μg of pSV2Luc plasmid in 0.7 mL of 0.15 M NaCl. The solution was kept for 30 min at 20 °C. To study the effect of the ionic strength on the stability of the complexes, NaCl concentration was increased up to 2 M by addition of aliquots of a 4 M NaCl solution. After 15 min at 20 °C, solutions were passed through nitrocellulose filters (0.45 μm) presoaked and rinsed with a solution at the same NaCl concentration. DNA/polymer complexes were retained on the filter while free DNA was not. The amount of free DNA in filtrates was determined by using 4′,6-diamidino-2-phenylindole dihydrochloride (DAPI) *(29)*. The filtrates containing free DNA were made 2.8 μM in DAPI, and the fluorescence intensities were measured (excitation wavelength = 360 nm; emission wavelength = 450 nm). The percentage of DNA/polymer complex was calculated according to:

$$[(I_0 - I)/I_0] \times 100$$

where I_0 is the fluorescence intensity of the total amount of DNA minus the fluorescence intensity of DAPI in the absence of DNA at the same NaCl concentration and I is the fluorescence intensity of the filtrate containing free DNA minus the fluorescence intensity of DAPI in the absence of DNA at the same NaCl concentration.

RESULTS

Formation of DNA/Lactosylated Polylysine Complexes. HepG2 cells possess a membrane lectin which recognizes glycoproteins containing β-D-galactosyl residues in a nonreducing terminal position and can accommodate polymers substituted with either lactosyl or β-D-galactosyl residues. An expression plasmid, pSV2Luc, encoding the firefly luciferase gene under the control of the SV40 T large antigen promoter was used as a reporter gene to monitor the efficiency of the gene transfer and of the luciferase expression depending on the lactosylated polylysine used as plasmid carrier. As previously reported *(8)*, the transfection efficiency of HepG2 cells by $DNA/Lact_{60}pLK$ (DP 190; Lact/pLK molar ratio = 60) depends on the LactpLK/DNA molar ratio: the transfection of HepG2 cells with 3 pmol of pSV2Luc plasmid (10 μg/mL), mixed in 1 mL of DMEM with 650 pmol (50 μg/mL) of $Lact_{60}pLK$ (LactpLK/DNA molar ratio = 220), gave the highest luciferase activity; increasing the LactpLK molar ratio decreased the luciferase activity. The luciferase activity was 2-fold lower when the plasmid (3 pmol) was mixed with 325 pmol (25 μg/mL) of $Lact_{60}pLK$ (LactpLK/DNA molar ratio = 110), but the luciferase activity was much lower when the same amount of plasmid was complexed with 162 pmol (12.5 μg/mL) (LactpLK/DNA molar ratio = 54) or 81 pmol (6.25 μg/mL) (LactpLK/DNA molar ratio = 27) of $Lact_{60}pLK$. Therefore, great transfections were obtained when DNA/$Lact_{60}pLK$ complexes were made with a LactpLK/DNA molar ratio of 110 or 220. Electrophoresis through a 0.6% agarose gel shows that, in DNA/$Lact_{60}pLK$ complexes with a LactpLK/DNA molar ratio of 110 or 220, the DNA did not migrate due to the condensation of the DNA in the presence of lactosylated polylysine (Figure 1A); the DNA was not completely retarded when the LactpLK/DNA molar ratio was lower than 110 (Figure 1A). Therefore, efficient transfections of HepG2 cells were obtained with DNA/LactpLK complexes, leading to a complete retardation of all the DNA in electrophoresis. As shown in Figure 1B, the solutions containing DNA/
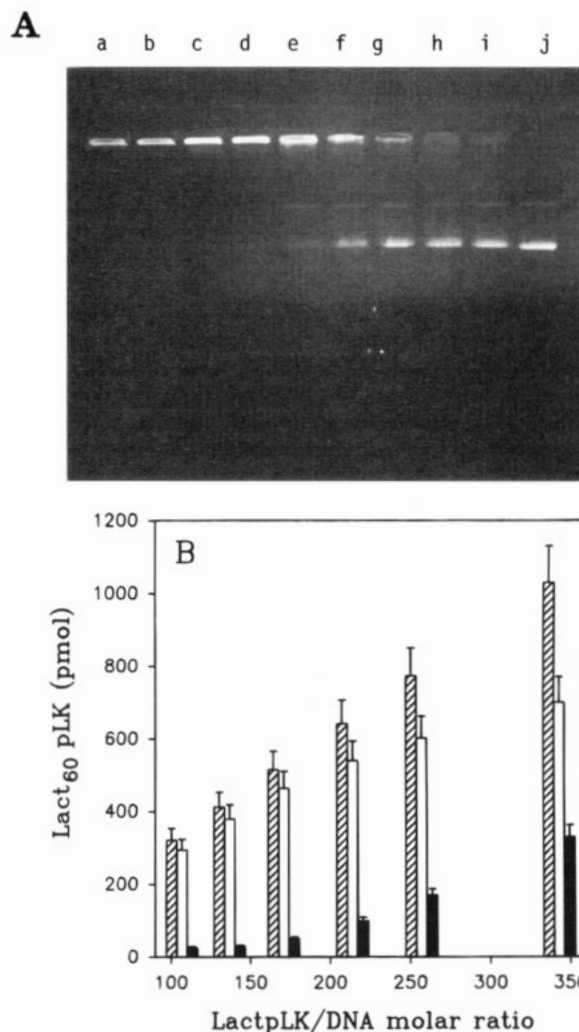
Figure 1. (A) Electrophoretic migration of pSV2Luc plasmid related to the plasmid/lactosylated polylysine molar ratio. Plasmid/LactpLK complexes were prepared by adding, dropwise with constant mixing, 133 (a), 107 (b), 80 (c), 66 (d), 53 (e), 40 (f), 27 (g), 13 (h), 2.7 (i), and 0 (j) pmol of $Lact_{60}pLK_{190}$ in 60 μL of DMEM to 2 μg (0.6 pmol) of pSV2Luc plasmid in 140 μL of DMEM. After incubation for 30 min at 20 °C, 20 μL of each sample was analyzed by electrophoresis for 2 h under 80 V/cm, through a 0.6% agarose gel containing ethidium bromide (1 μg/mL of gel) to visualize DNA in a Tris−borate−EDTA buffer (95 mM Tris, 89 mM boric acid, and 2.5 mM EDTA), pH 8.6. (B) pSV2Luc plasmid (3 pmol) was mixed in 1 mL of phosphate-buffered saline, pH 7.4, with fluoresceinylated $Lact_{60}pLK_{190}$ in the range of 330−1050 pmol. After incubation for 30 min at 20 °C, DNA/LactpLK complexes were spun down in a microfuge and the amount of free fluoresceinylated $Lact_{60}pLK_{190}$ (filled bars) was determined from the absorbance at 495 nm of the supernatant. The amount of DNA-associated $Lact_{60}pLK_{190}$ (open bars) was the total amount of $Lact_{60}pLK_{190}$ (hatched bars) minus the amount of free $Lact_{60}pLK_{190}$ (filled bars).

$Lact_{60}pLK_{190}$ complexes made with a LactpLK/DNA molar ratio of 110 or 132 contain 8% of free $Lact_{60}pLK_{190}$, indicating that all the polymer was complexed with the DNA. The amount of free $Lact_{60}pLK_{190}$ increases when the LactpLK/DNA molar ratio increases and reaches 32% at a molar ratio of 340. Complexes made with LactpLK/DNA molar ratio greater than 110 were slighly more efficient in transfecting HepG2 cells, but those complexes should be purified to remove excess of free $Lact_{60}pLK_{190}$. Moreover, those complexes which are highly cationic due to excess of LactpLK could induce unspecific binding to the negatively charged cell surface *via* charge interactions. Therefore, LactpLK/DNA complexes made with the lowest LactpLK/DNA molar ratio leading to a com-

plete retardation of all the DNA in electrophoresis (called optimal retard complex) were subsequently used because their preparation did not require further purification steps.

Poly(L-lysine) (pLK_{190}) was substituted with various numbers of lactosyl residues (from 20 to 80) in order to test the influence of the number of sugar residues bound per polylysine molecule on the gene transfer efficiency. The pSV2Luc plasmid was complexed with pLK_{190} substituted with either 20, 30, 40, 52, 60, 66, 70, or 80 lactosyl residues, and the lowest LactpLK/DNA molar ratio leading to a complete retardation of all the DNA in electrophoresis was determined. Optimal retard DNA/$Lact_xpLK_{190}$ complexes determined as described above had a LactpLK/DNA molar ratio of 28, 39, 49, 71, 89, 110, 207, and 260 when polylysine was substituted with 0, 20, 30, 40, 52, 60, 70, and 80 lactosyl residues, respectively. The formation of pSV2Luc/LactpLK complexes was not possible when polylysine was substituted with more than 80 lactosyl residues per polylysine (pLK_{190}) molecule. The LactpLK/DNA molar ratio in optimal retard complexes increases nonlinearly when the number of lactosyl residues bound per polylysine molecule increases (Figure 2A, insert). The number of positive charges (ϵ-amino group of a lysine residue) per negative charge (the phosphate group of a nucleotide residue), i.e., the NH_3^+/nucleotide ratio, in the complexes (number of free amino groups per LactpLK molecule × LactpLK/DNA molar ratio/number of phosphate groups of DNA) unexpectedly increases with the substitution level of pLK (Figure 2A). Furthermore, this increase is not linear: the NH_3^-/nucleotide ratio increases from 0.5 to 2.8 when polylysine was substituted with lactosyl residues from 0 to 80, respectively (Figure 2A). This result shows that the formation of the complex between the plasmid and a lactosylated polylysine does not depend directly on just a neutralization of phosphate groups by the amino groups of free lysine.

Optimal Gene Transfer Depends on the Number of Lactosyl Residues Bound per Polylysine (pLK_{190}) Molecule. HepG2 cells were incubated for 4 h at 37 °C in the presence of 100 μM chloroquine with optimal retard complexes made between pSV2Luc plasmid and lactosylated polylysine containing different numbers of lactosyl residues. The efficiency of the gene transfer into HepG2 cells was evaluated 48 h after transfection by measuring the luciferase activity in cell lysates (Figure 2B). The luciferase activity was greater when cells were incubated with complexes made with polylysine containing 52—66 lactosyl residues corresponding to 31 ± 4% substitution of its amino groups. When cells were incubated with polylysine containing a lower number of lactosyl residues (40 and below) or with a higher number of lactosyl residues (above 70), the luciferase activity was 10-fold or more lower.

Influence of the Size of Poly(L-lysine). Poly(L-lysines) with various degrees of polymerization were substituted with different numbers of lactosyl residues, and their efficiency in transfecting HepG2 cells was compared to that obtained with lactosylated pLK_{190}. The pSV2Luc plasmid was complexed with either pLK_{36} (DP 36), pLK_{72} (DP 72), or pLK_{633} (DP 633) substituted with various numbers of lactosyl residues, and the optimal retard complexes were determined upon electrophoresis as described above. Those complexes had a LactpLK/DNA molar ratio of 75, 93, 111, 141, and 331 when pLK_{72} was substituted with 0, 10, 20, 25, and 30 lactosyl residues, respectively, and 153, 206, 248, 297, and 366 when pLK_{36} was substituted with 0, 4, 8, 10, and 16 lactosyl residues, respectively. The LactpLK/DNA molar
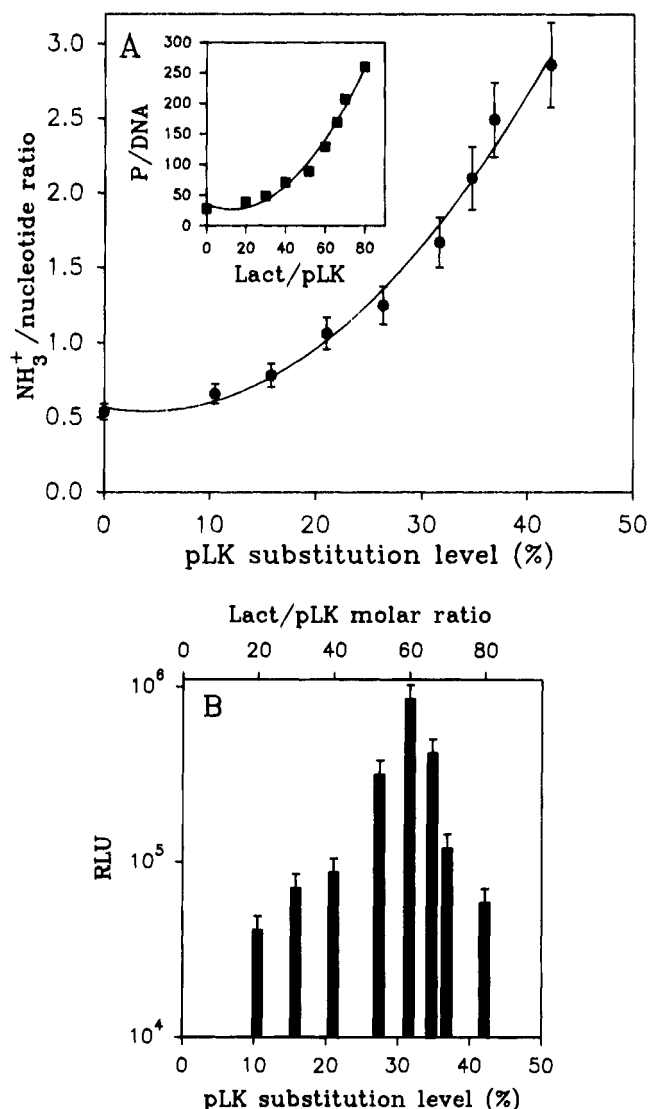
Figure 2. Importance of the number of lactosyl residues bound onto one polylysine molecule. (A) Formation of DNA/lactosylated polylysine complexes: dependence of the NH_3^+/nucleotide ratio. pSV2Luc plasmid (0.6 pmol) was mixed in 0.2 mL of DMEM with $Lact_xpLK_{190}$ containing up to 80 lactosyl residues. The NH_3^+/nucleotide ratio shown on the graph was the number of free amino groups per LactpLK molecule × LactpLK/DNA molar ratio/the number of phosphate groups of DNA in optimal retard complexes. Insert: Formation of DNA/lactosylated polylysine complexes: dependence of LactpLK/DNA molar ratio. LactpLK/DNA was the lowest lactosylated polylysine to plasmid molar ratio of complexes giving a complete retardation of all the DNA in electrophoresis; Lact/pLK was the average number of lactosyl residues bound per polylysine molecule. (B) Influence on the gene transfer efficiency. Optimal retard complexes were formed between pSV2Luc plasmid and $Lact_xpLK_{190}$ containing different numbers of lactosyl residues. HepG2 cells (4 × 10^5 cells) were incubated at 37 °C for 4 h in 1 mL of culture medium containing 1% FBS and in the presence of 100 μM chloroquine with 0.375 nM pSV2Luc complexed with lactosylated polylysines. Then, the medium was removed and cells were further incubated in 2 mL of culture medium containing 10% FBS in the absence of any other additive. Gene expression was determined 48 h later by assaying the luciferase activity of cell lysates. RLU, the number of relative light units, represented the luciferase activity of 1 mg of protein. Lact/pLK was the average number of lactosyl residues bound per polylysine molecule.

ratio of the complexes increases nonlinearly when the sugar substitution level of pLK_{72} increases as in the case of pLK_{190} (Figure 3A, insert); the NH_3^-/nucleotide ratio equal to 0.5 with the sugar-free polylysine remained constant until pLK_{72} was substituted with 25 lactosyl
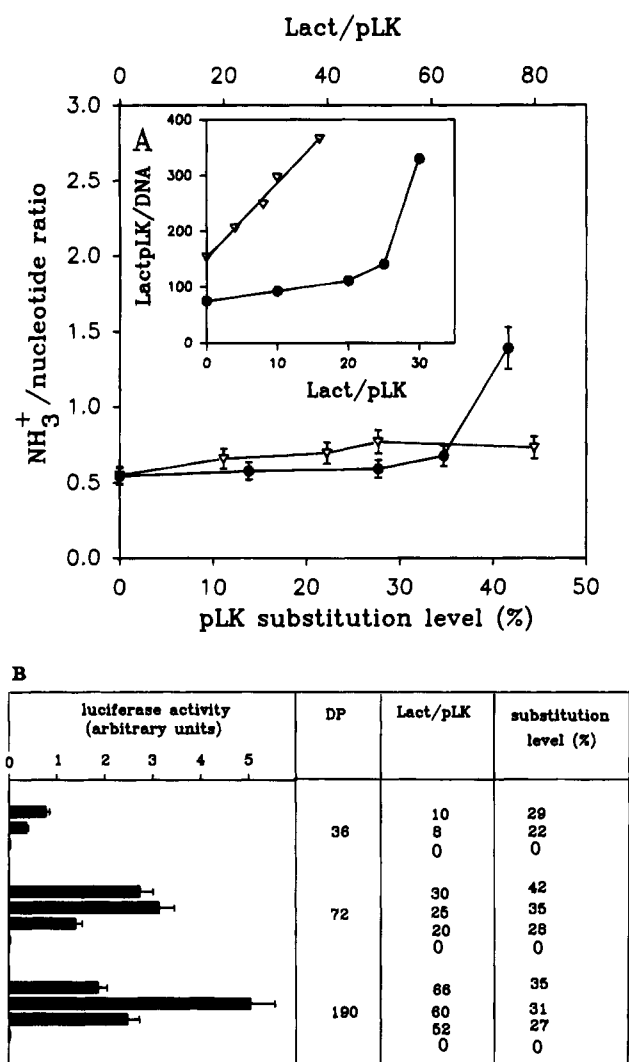
Figure 3. Transfection efficiency in relation with the size of polylysine. (A) Influence of the size of polylysine on the formation of DNA/lactosylated polylysine complexes. pSV2Luc plasmid (0.6 pmol) was mixed in 0.2 mL of DMEM with either pLK_{72} (●) or pLK_{36} (▽) containing various numbers of lactosyl residues. The NH_3^+/nucleotide ratio shown on the graph was the number of free amino groups per LactpLK molecule × the LactpLK/DNA molar ratio/the number of phosphate groups of DNA in optimal retard complexes. Insert: Formation of DNA/lactosylated polylysine complexes: dependence of the LactpLK/DNA molar ratio. LactpLK/DNA was the lowest lactosylated polylysine to plasmid molar ratio of complexes giving a complete retardation of all the DNA in electrophoresis; Lact/pLK was the average number of lactosyl residues bound per polylysine molecule. (B) Influence of the size of lactosylated polylysine on the gene transfer efficiency. Optimal retard complexes were formed between pSV2Luc plasmid and either $Lact_xpLK_{190}$ or $Lact_xpLK_{36}$ or $Lact_x$-pLK_{72} containing various numbers of lactosyl residues. HepG2 cells (4 × 10⁵ cells) were incubated at 37 °C for 4 h in 1 mL of culture medium containing 1% FBS and in the presence of 100 μM chloroquine with 1.5 nM pSV2Luc complexed with lactosylated polylysines. Then, the medium was removed and the cells were further incubated in 2 mL of culture medium containing 10% FBS in the absence of any other additive. Gene expression was determined 48 h later by assaying the luciferase activity of cell lysates. Lact/pLK was the average number of lactosyl residues bound per polylysine molecule. DP was the degree of polymerization of polylysine.

residues corresponding to 35% substitution of the amino groups of pLK_{72}; when polylysine was more heavily substituted ($Lact_{30}pLK_{72}$), the NH_3^+/nucleotide ratio reached 1.5 (Figure 3A). In the case of the smallest polylysine (pLK_{36}), the LactpLK/DNA molar ratio increased linearly when the sugar substitution level of

pLK_{36} increased (Figure 3A, insert) and the NH_3^+/nucleotide ratio remained constant (Figure 3A): it was 0.5 with sugar-free polylysine as well as with any glycosylated polylysine containing up to 44% of the amino groups of pLK_{36} substituted with lactosyl residues.

The transfection of HepG2 cells was low when pSV2Luc was complexed with pLK_{36} as well as with any of the lactosylated pLK_{36} (Figure 3B). This low efficiency was not due to cytotoxicity of pLK_{36}: no toxic effect on HepG2 cells was observed in the presence of those complexes which did not contain free pLK_{36}. Conversely, transfection with pSV2Luc complexed with either $Lact_{25}pLK_{72}$ or $Lact_{30}pLK_{72}$ (35% or 42% sugar substitution level) was close to that obtained with $Lact_{52}pLK_{190}$ or with $Lact_{66}$-pLK_{190} (27–35% sugar substitution level). Transfection of HepG2 cells with pSV2Luc plasmid complexed with pLK_{633}, having 33% of the amino groups of lysine residues substituted with lactosyl residues, was as efficient as a pSV2Luc plasmid/$Lact_{60}pLK_{190}$ complex (data not shown). Therefore, similar efficient transfections were obtained when polylysine DP 72, DP 190, and DP 633 have 31 ± 4% of their lysine residues substituted with lactosyl residues.

Galactosylated Polylysine. Polylysine (pLK_{190}) was substituted with different numbers of β-D-galactosyl residues (from 45 to 93), and their gene transfer efficiency into HepG2 cells was tested. The pSV2Luc plasmid was complexed with galactosylated polylysine containing various numbers of galactosyl residues, and the optimal retard complexes were determined upon electrophoresis as described above. Those complexes had a GalpLK/DNA molar ratio of 28, 52, 100, 123, 146, and 235 when polylysine (DP 190) was substituted with 0, 45, 62, 68, 76, and 93 galactosyl residues, respectively, and as in the case of LactpLK contained less than 10% of free GalpLK. The GalpLK/DNA molar ratio of those complexes increased nonlinearly when the number of galactosyl residues bound per polylysine molecule increased (Figure 4A insert). The corresponding NH_3^+/nucleotide ratio also increased nonlinearly with the substitution level of polylysine as in the case of polylysine substituted with lactosyl residues (Figure 4A). However, this ratio was smaller than that obtained in the case of LactpLK: the NH_3^+/nucleotide ratio was 1.2 (Figure 4A) and 1.5 (Figure 2A) when pLK was 30% substituted with galactosyl and with lactosyl residues, respectively.

The transfection was more efficient when polylysine was substituted with 75 ± 15 galactosyl residues (40 ± 8% sugar substitution level) as DNA carrier (Figure 4B). The luciferase activity obtained by using the DNA/Gal_{76}-pLK_{190} complex (RLU = 1.6 × 10⁶/mg of protein) was close to that obtained with a DNA/$Lact_{60}pLK_{190}$ complex (RLU = 1.9 × 10⁶/mg of protein). The uptake of pSV2Luc plasmid/$Gal_{76}pLK_{190}$ complexes by HepG2 cells shows that the amount of DNA associated with cells was as great as that obtained with the plasmid complexed with $Lact_{60}pLK_{190}$ (Figure 5B): 158 ng of DNA was found per 10⁵ cells when HepG2 cells were incubated at 37 °C for 2 h in the presence of 1.5 nM pSV2Luc plasmid complexed with $Gal_{76}pLK_{190}$.

Cell Binding and Uptake of DNA/Lactosylated Polylysine Complexes. The amount of DNA associated with HepG2 cells upon incubation at 4 °C with pSV2Luc plasmid complexed with lactosylated polylysine (DP 190) substituted with 20–60 lactosyl residues was higher than that of cells incubated with a complex formed with sugar-free polylysine (Figure 5A). The binding of the DNA/$Lact_{60}pLK_{190}$ complex at 3 nM was greater than that of the DNA/$Lact_{20}pLK_{190}$ complex due to the excess of cationic charges in the DNA/$Lact_{60}pLK_{190}$ complex and

Gal/pLK

Gal/pLK
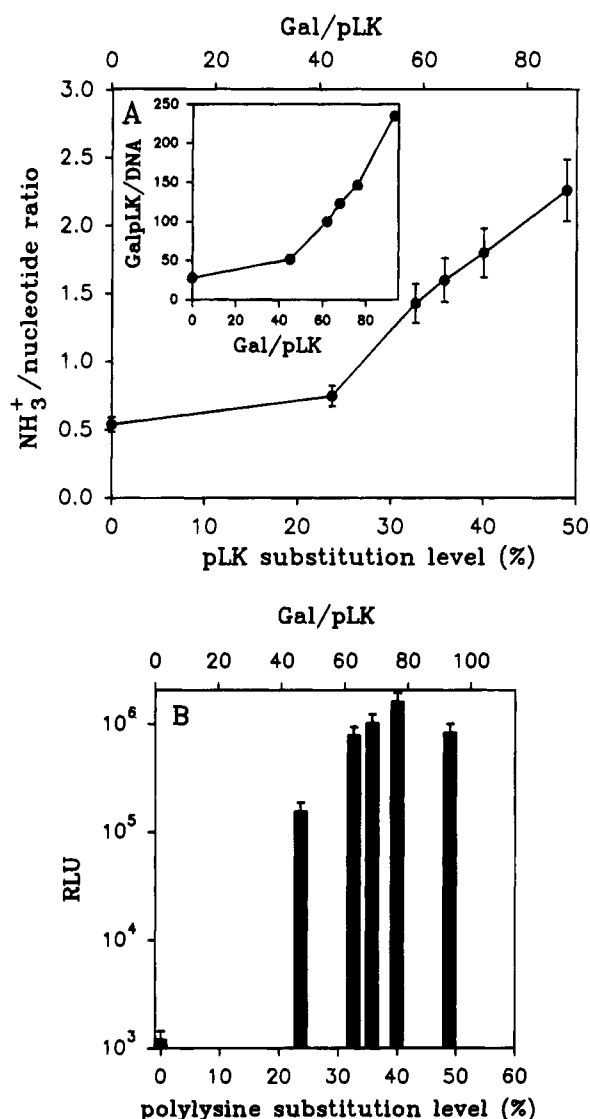
Figure 4. Importance of the number of galactosyl residues bound onto one polylysine molecule. (A) Formation of DNA/galactosylated polylysine complexes: dependence of the NH_3^+/nucleotide ratio. pSV2Luc plasmid (0.6 pmol) was mixed in 0.2 mL of DMEM with galactosylated polylysines (pLK_{190}) containing up to 93 galactosyl residues. The NH_3^+/nucleotide ratio shown on the graph was the number of free amino groups per GalpLK molecule × the GalpLK/DNA molar ratio/the number of phosphate groups of DNA in optimal retard complexes. Insert: Formation of DNA/galactosylated polylysine complexes: dependence of the GalpLK/DNA molar ratio. GalpLK/DNA was the lowest galactosylated polylysine to plasmid molar ratio of complexes giving a complete retardation of all the DNA in electrophoresis; Gal/pLK was the average number of galactosyl residues bound per polylysine molecule. (B) Influence on the gene transfer efficiency. Optimal retard complexes were formed between pSV2Luc plasmid and Gal_xpLK_{190} containing various numbers of galactosyl residues. HepG2 cells (4 × 10⁵ cells) were incubated at 37 °C for 4 h in 1 mL of culture medium containing 1% FBS and in the presence of 100 μM chloroquine with 1.5 nM pSV2Luc complexed with galactosylated polylysines. Then, the medium was removed and the cells were further incubated in 2 mL of culture medium containing 10% FBS in the absence of any other additive. Gene expression was determined 48 h later by assaying the luciferase activity of cell lysates. RLU, the number of relative light units, represented the luciferase activity of 1 mg of protein. Gal/pLK was the average number of β-galactosyl residues bound per polylysine molecule.

a decrease of its solubility (Figure 2A). The nonspecific binding was assessed using the DNA/$Glc_{90}pLK_{190}$ complex because as in the case of $Gal_{90}pLK_{190}$ (Figure 4A) it was
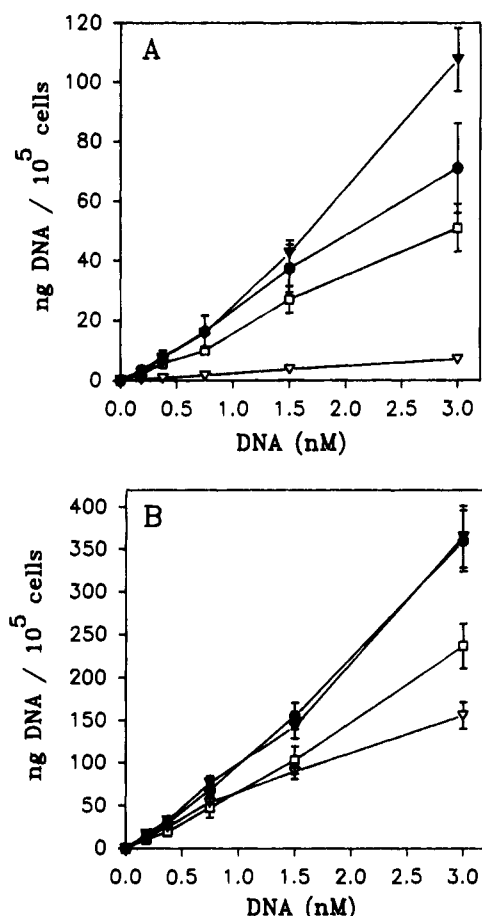
Figure 5. Cell binding and uptake of DNA/$LactpLK_{190}$ complexes. HepG2 cells (10⁵ cells) were incubated in 48-well culture plates in 250 μL of DMEM for 2 h at either (A) 4 °C (binding) or (B) 37 °C (binding and uptake) in the presence of various concentrations of either ($\triangledown$) ³²P-labeled pSV2Luc/pLK_{190}, ($\bullet$) ³²P-labeled pSV2Luc/$Lact_{20}pLK_{190}$, ($\blacktriangledown$) ³²P-labeled pSV2Luc/$Lact_{60}$-pLK_{190}, or ($\square$) ³²P-labeled pSV2Luc/$Glc_{90}pLK_{190}$ complexes. The cells were washed twice with cold serum-free DMEM and harvested by incubation for 3 min at 37 °C with PBS containing 0.2 mg/mL EDTA, and the radioactivity was counted. Experiments were done in triplicate.

as cationic as the DNA/$Lact_{60}pLK_{190}$ complex. The binding of the DNA/$Glc_{90}pLK_{190}$ complex was lower than that of the DNA/$Lact_{60}pLK_{190}$ or DNA/$Lact_{20}pLK_{190}$ complexes in relation to the specific recognition of DNA/LactpLK complexes by HepG2 galactose-specific membrane lectins (Figure 5A). The amount of DNA associated with HepG2 cells upon incubation at 37 °C with either DNA/$Lact_{20}$-pLK_{190}, DNA/$Lact_{60}pLK_{190}$ (Figure 5B), or DNA/Gal_{76}-pLK_{190} (data not shown) complexes was similar and 4-fold greater than that obtained upon incubation at 4 °C due to uptake of complexes as previously shown by confocal microscopy *(8)* and flow cytometry *(7)*. Therefore, the 50-fold lower luciferase activity obtained with the DNA/$Lact_{20}pLK_{190}$ complex in comparison with the DNA/$Lact_{60}pLK_{190}$ complex cannot be explained by a lower uptake of the DNA/$Lact_{20}pLK_{190}$. The amount of DNA associated with HepG2 cells upon incubation at 37 °C with pSV2Luc/pLK_{190} or pSV2Luc/$Glc_{90}pLK_{190}$ complexes was only 2-fold lower than that obtained with pSV2Luc/LactpLK (Figure 5B) and pSV2Luc/$Gal_{76}pLK_{190}$ (data not shown). Under the same conditions, the luciferase activity was 850- and 42- (2 × 10⁴ RLU/mg of protein; data not shown) fold lower with pSV2Luc/pLK_{190} and pSV2Luc/$Glc_{90}pLK_{190}$, respectively, than with pSV2Luc/$Lact_{60}$-pLK_{190} (Figure 2B). These results suggest that the

transfection efficiency is not directly related to the extent of uptake of the complexes.

Influence of the Plasmid Size. Plasmids of various sizes (from 4.7 to 17.6 kb) were complexed with various amounts of $Lact_{60}pLK_{190}$, and the optimal retard complexes were analyzed by gel electrophoresis. The lowest LactpLK/DNA molar ratio which gives the complete retardation of all the DNA in electrophoresis increased as expected when the plasmid size increased, while the corresponding NH_3^+/nucleotide ratio unexpectively decreased from 1.5 with a 5 kb plasmid to 0.5 with a 17.6 kb plasmid (Figure 6A).

HepG2 cells were transfected in the presence of chloroquine with the optimal retard complexes formed with a plasmid of 12 kb encoding for the gene of luciferase (pROF27) under the control of the large SV40 T antigen promoter and with $Lact_xpLK_{190}$ (x = 30, 40, 52, 60, 66, or 70). The transfection efficiency of the pROF27 gene was evaluated by measuring the luciferase acitivity in cell lysates as in the case of the pSV2Luc plasmid (Figure 6B). The luciferase activity in HepG2 cells transfected with pPROF27 is close to that obtained with pSV2Luc (Figure 2B), and the highest activity was obtained when pROF27 plasmid was complexed with polylysine substituted with 59 ± 7 lactosyl residues as in the case of pSV2Luc plasmid.

DNA/Polycation Complex Stability. Optimal retard complexes were formed in 0.15 M NaCl between pSV2Luc plasmid and either sugar-free polylysine (pLK_{190}) or polylysine substituted with 20–80 lactosyl residues. The strength of the electrostatic interactions between DNA and LactpLK was assessed by increasing the ionic strength of the solution with NaCl and by measuring the amount of dissociated DNA upon filtration through a nitrocellulose filter (0.45 μm in diameter) (Figure 7). Indeed, free DNA passed through the nitrocellulose filter while DNA/LactpLK complexes were retained on the nitrocellulose filter due to interactions of polylysine with the filter. The stability of complexes depends upon the number of positive charges on the polycation and decreases when the number of lactosyl residues bound per polylysine molecule increases (Figure 7). The dissociation between the plasmid and lactosylated polylysine required about the same ionic strength (about 1.4 M) when polylysine was sugar-free or substituted with less than 60 lactosyl residues: the $DNA/Lact_{60}pLK_{190}$ complex was dissociated at a lower NaCl concentration, and heavily substituted polylysines were still less stable.

DISCUSSION

We have previously shown that HepG2 cells which express a galactose-specific membrane lectin were efficiently and selectively transfected with complexes formed between pSV2Luc plasmid and lactosylated polylysine *(8)*. HepG2 cells which do not express membrane lectin specific for mannose were poorly transfected with pSV2Luc/mannosylated polylysine complexes, and HeLa cells which do not express membrane lectin specific for galactose were poorly transfected with pSV2Luc/lactosylated polylysine complexes *(8)*. The transfection was very efficient when it was conducted in the presence of either chloroquine or a fusogenic peptide *(8)*; the transfection was not efficient in the absence of either chloroquine or a fusogenic peptide.

The transfection efficiency was found to depend on both the lactosylated polylysine to plasmid (LactpLK/DNA) molar ratio and the polylysine sugar substitution level (Lact/pLK molar ratio). High luciferase activity was obtained when the cells were transfected with complexes formed with a LactpLK/DNA molar ratio giving a com-
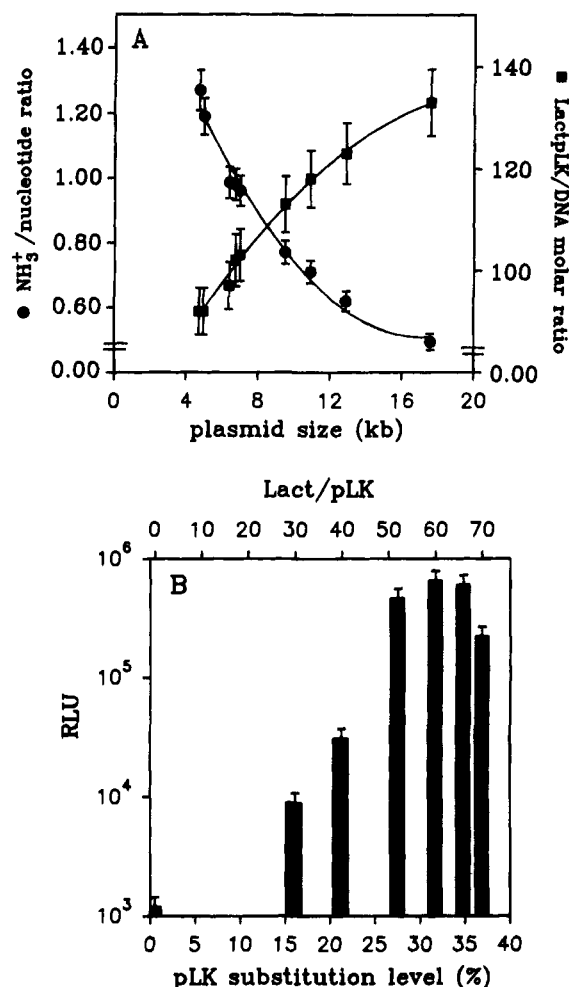
Figure 6. Transfection efficiency in relation with the size of plasmid. (A) Influence of the plasmid size on the formation of plasmid/$Lact_{60}pLK_{190}$ complexes. Complexes were prepared by adding dropwise, with constant mixing, 2.7–133 pmol of $Lact_{60}$-pLK_{190} in 60 μL of DMEM to 2 μg of each plasmid in 140 μL of DMEM. The NH_3^+/nucleotide ratio shown on the graph was the number of free amino groups per LactpLK molecule × the LactpLK/DNA molar ratio/the number of phosphate groups of DNA in optimal retard complexes. LactpLK/DNA was the lowest lactosylated polylysine to plasmid molar ratio of complexes giving a complete retardation of all the DNA in electrophoresis. (B) Influence of the number of lactosyl residues bound per polylysine (pLK_{190}) molecule on the gene transfer efficiency of a plasmid of 12 kb. Optimal retard complexes were formed between 1.44 pmol of pPROF27 plasmid and $Lact_xpLK_{190}$ containing various numbers of lactosyl residues. HepG2 cells (4×10^5 cells) were incubated at 37 °C for 4 h in 1 mL of culture medium containing 1% FBS and in the presence of 100 μM chloroquine with 0.625 nM pPROF27 complexed with lactosylated polylysines. Then, the medium was removed and the cells were further incubated in 2 mL of culture medium containing 10% FBS in the absence of any other additive. Gene expression was determined 48 h later by assaying the luciferase activity of cell lysates. RLU, the number of relative light units, represented the luciferase activity of 1 mg of protein. Lact/pLK was the average number of lactosyl residues bound per polylysine molecule.

plete retardation of the DNA migration in electrophoresis. Among them, a complex which has the lowest LactpLK/DNA molar ratio was called optimal retard complex because, under these conditions, the totality of lactosylated polylysine was complexed with the DNA (the amount of free lactosylated polylysine was 8%) and no purification of the complexes was required. The formation of DNA/glycosylated polylysine complexes depends on the number of remaining ϵ-amino groups after substitution of polylysine with sugar residues and is not
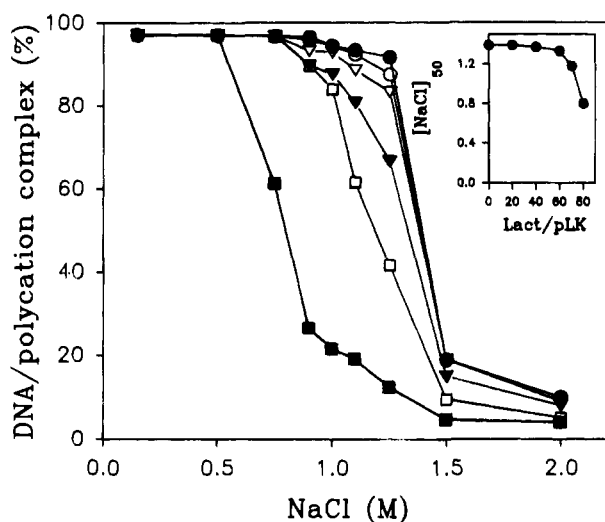
Figure 7. Effect of the ionic strength on the stability of optimal DNA/lactosylated polylysine complexes. Optimal retard complexes were formed between pSV2Luc plasmid (5 μg in 0.7 mL of 0.15 M NaCl) and either (●) pLK_{190}, (○) $Lact_{20}pLK_{190}$, (▽) $Lact_{40}pLK_{190}$, (▼) $Lact_{60}pLK_{190}$, (□) $Lact_{70}pLK_{190}$, or (■) $Lact_{80^-}pLK_{190}$ in 0.3 mL of 0.15 M NaCl. The solution was kept for 30 min at 20 °C. Then, the NaCl concentration was increased up to 2 M by addition of aliquots of a 4 M NaCl solution. After 15 min at 20 °C, the solutions were passed through nitrocellulose filters (0.45 μm in diameter) presoaked in and rinsed with a solution at the same NaCl concentration. The amount of free DNA in filtrates was determined by adding DAPI up to 2.8 μM (final concentration), and the fluorescence intensities were measured (excitation wavelength = 360 nm; emission wavelength = 450 nm) with a spectrofluorometer. The percentage of DNA/polymer complex was calculated as described in the Materials and Methods. Insert: Stability of DNA/LactpLK complexes versus Lact/pLK molar ratio. $[NaCl]_{50}$ was the NaCl concentration required for half-dissociation of a DNA/polycation complex; Lact/pLK was the average number of lactosyl residues bound per polylysine molecule.

explained by a simple neutralization of the phosphate groups of DNA by the amino groups of free lysine: the NH_3^+/nucleotide ratio in complexes having the lowest polymer/DNA molar ratio, and leading to a complete retardation of all the DNA, increased when the sugar substitution level increased, suggesting a contribution of the sugar moiety in the formation of complexes. Very efficient transfections were obtained with complexes formed with polylysine (DP 190) substituted with 59 ± 7 lactosyl residues corresponding to a polylysine substitution level of 31 ± 4%. Complexes formed with polylysine substituted with more than 35% lactosyl residues or with less than 30% lactosyl residues were less efficient. Polylysine substituted with more than 42% lactosyl residues did not form complexes with the plasmid. Efficient transfections were also obtained with DNA complexed with galactosylated polylysine (DP 190), but in this case 40 ± 8% of the amino groups of polylysine have to be substituted with galactosyl residues. Plank et al. (30) found that complexes formed between a plasmid and a polylysine (DP 200) substituted under reducing conditions (sodium cyanoborohydride which kept up the positive charge of the ε-amino groups of polylysine) with 150–160 lactityl units were not efficient in transfecting HepG2 cells. Conversely, when galactoside clusters known to be much better ligands for the asialoglycoprotein receptor (31) than lactose or lactitol were used, they showed that polylysine (DP 200) substituted with only 8 galactoside clusters (each cluster comprises 4 β-galactosyl residues in a terminal nonreducing position) was highly efficient in transfecting HepG2 cells (30). In the latter case, the few galactoside

clusters ensure an efficient binding because of their individual affinity for the galactose-specific membrane lectin, and the low substitution of the polylysine does not impair the formation of stable complexes with the plasmid.

The transfection efficiency was found to be quite similar by using DNA/LactpLK complexes formed with polylysines having an average degree of polymerization of either 72, 190, or 633 and having 31 ± 4% of their amino groups substituted with lactosyl residues. Transfections were not efficient with lactosylated polylysine having an average degree of polymerization of 36 which is in agreement with the fact that DNA condensation is not induced in the presence of polylysines containing less than 60 lysine residues (32). Recently, it was reported that DNA/transferrin–polylysine complexes made with a polylysine DP 320 (average molecular weight: 66 000) gave higher transfection efficiency in erythroleukemic cells than complexes made with a polylysine DP 145 (average molecular weight: 30 000) or with a polylysine DP 72 (average molecular weight: 15 000) (33). The authors mentioned also that the preparation of transferrin–polylysine conjugates was difficult when a longer polylysine (DP 720; average molecular weight: 150 000) was used.

The formation of a complex between a plasmid and a glycosylated polylysine depends also on the size of the plasmid: the NH_3^+/nucleotide ratio of complexes which have the lowest LactpLK/DNA molar ratio, and which give a complete retardation of all the DNA in electrophoresis, decreased when the size of the plasmid increased, suggesting a contribution of the structure of the plasmid in the formation of the complex. Polylysine (pLK_{190}) substituted with 52–66 lactosyl residues was found to be a good carrier to transfer, with a similar efficiency, a 5 kb and a 12 kb plasmid. Therefore, glycosylated polylysine, such as pLK_{190} substituted with 59 ± 7 lactosyl residues, is efficient in the presence of chloroquine in transfering plasmids of various sizes as in the case of transferrin–polylysine (34).

DNA complexes formed with polylysine (DP 190) substituted with 59 ± 7 lactosyl residues contain an excess of cationic charges and give a great luciferase activity; those formed with $Lact_{40}pLK_{190}$ are neutral and give 10-fold lower luciferase activity; those formed with $Lact_{20}pLK_{190}$ or with sugar-free pLK contain an excess of anionic charges and poorly transfect the cells. That might suggest a possible role of this difference in charge in cellular uptake and in transfection efficiency. Nevertheless, when HepG2 cells were incubated with a $pSV2Luc/Lact_{20}pLK_{190}$ complex (globally anionic), the amount of DNA associated to the cells was as great as when the cells were incubated with a $pSV2Luc/Lact_{60^-}pLK_{190}$ complex (globally cationic). In the meantime, the luciferase activity was 50-fold lower than with a pSV2Luc/$Lact_{60}pLK_{190}$ complex. The amount of DNA associated to the cells was similar upon incubation with nonspecific complexes, i.e., a $pSV2Luc/Glc_{90}pLK_{190}$ complex (globally as cationic as a $pSV2Luc/Lact_{60}pLK_{190}$ complex) and a $pSV2Luc/pLK_{190}$ complex (globally anionic). Even if the uptake of a nonspecific cationic complex (containing an optimal number of sugar residues, i.e., 90 glucosyl residues) was 2-fold lower than with specific cationic complexes (containing an optimal number of sugar residues, i.e., 60 lactosyl or 76 galactosyl residues), great transfections were obtained when polylysine was substituted with the relevant sugar residues in relation to the recognition by the HepG2 galactose-specific membrane lectin. Moreover, DNA/$Lact_{60}pLK_{190}$ complexes are either cationic when the plasmid has a size below 7 kb, neutral

when the plasmid has a size of 7 kb, or anionic when the plasmid has a size above 7 kb (Figure 6A). Nevertheless, the luciferase activity obtained with complexes made with a plasmid of 12 kb (anionic) was as great as that made with a plasmid of 5 kb (cationic). Consequently, these results suggest that there is no direct correlation between the global charge of the optimal DNA/LactpLK complexes and either the extent of the binding or the uptake of the complexes or the efficiency of the transfection.

Upon the uptake of DNA/glycosylated polylysine complexes, the delivery of the plasmid into the cytosol and/or the nucleus is a critical step for the expession of the gene. Chloroquine, a cell-permeant base, is used to enhance the transfection efficiency *(35)*. In the absence of chloroquine very low transfections are obtained with any polylysine formulations. Chloroquine is known to induce a partial neutralization of acidic cell compartments, to reduce the fusion between endosomes and lysosomes, to decrease intracellular degradation of the internalized plasmid by lysosomal enzymes, and to cause an increase in the volume of endocytotic vesicles; moreover, chloroquine which binds to DNA might also protect DNA molecules from nuclease degradation *(35)*. Glycerol (unpublished results) and fusogenic peptides have also been used to enhance gene transfer efficiency *(8, 11–13)*.

In addition, to be expressed, the gene should be made available to the cytosol or nucleus machinery, and therefore the plasmid should dissociate from glycosylated polylysine. The electrostatic interactions between the charges of the DNA and of the amino groups of polylysine induce a condensation of the DNA and stabilize a tertiary structure of the complex *(32)*. Given the molecular mass of a 5 kb plasmid and of a glycosylated polylysine such as pLK_{190} substituted with 59 ± 7 lactosyl residues, and taking into account that about 130 ± 10 lactosylated polylysine molecules are required to form a high transfection efficiency complex, it can be calculated that the complex has a molecular mass of about 10 000 000 corresponding to a volume of 10^4 nm^3 and equivalent to a sphere with a diameter of about 28 nm. If the complex has a toroid structure as was shown in the case of a DNA/transferrin polylysine complex *(36)*, it is expected to have a diameter slightly higher than 28 nm, but much lower than that (80–150 nm) estimated in the case of DNA/transferrin polylysine *(36)* and DNA/surfactant protein A polylysine *(37)* complexes and significantly higher than that (12 nm) estimated in the case of DNA/α-galactosylated polylysine complexes *(38)*.

The strength of the electrostatic interactions in plasmid/lactosylated polylysine complexes which depends on the level of the polylysine substitution could play an important role in the release of the DNA to the complex and therefore in the transfection efficiency. The dissociation of plasmid from lactosylated polylysine is highly facilitated when 30–42% of the amino groups of polylysine are substituted with lactosyl residues. On the opposite, when 27% or less amino groups of polylysine are substituted, the dissociation requires an ionic strength (close to 1.5 M NaCl) as high as with nonsubstituted polylysine. Perales *et al.* *(38)* described the formation of DNA/galactosylated polylysine complexes at 1.03 M NaCl. In this case, 0.8–1% of the amino groups of the polylysine (DP 100) were substituted with α-galactosyl residues. That agrees with our results showing that sugar-free polylysine and weakly substituted lactosylated polylysine are not dissociated in 1.03 M NaCl.

In conclusion, the substitution of polylysine with sugar residues has three main consequences: one is that, as a recognition signal, the sugar increases the targeting of the plasmid transfer into cells expressing the corresponding cell surface lectin; the second is that, by substitution of a portion of the amino groups, the sugar moiety decreases the stability of the plasmid/glycosylated polylysine complex; the third is that the glycosylation of polylysine leads to a very large increase in the expression efficiency which may come, in addition to the first two consequences, from a modulation of the intracellular traffic of the plasmid/glycosylated polylysine complexes.

LITERATURE CITED

(1) Wu, G. Y., and Wu, C. H. (1991) Delivery systems for gene therapy. *Biotherapy 3*, 87–95.

(2) Frese, J., Jr., Wu, C. H., and Wu, G. Y. (1994) Targeting of genes to the liver with glycoprotein carriers. *Adv. Drug Delivery Rev. 14*, 137–153.

(3) Wagner, E., Curiel, D., and Cotten, M. (1994) Delivery of drugs, proteins and genes into cells using transferrin as a ligand for receptor-mediated endocytosis. *Adv. Drug Delivery Rev. 14*, 113–136.

(4) Rosenkranz, A. A., Yachmenev, S. V., Jans, D. A., Serebryakova, N. V., Murav'ev, V. I., Peters, R., and Sobolev, A. S. (1992) Receptor-mediated endocytosis and nuclear transport of a transfecting DNA construct. *Exp. Cell Res. 199*, 323–329.

(5) Trubetskoy, V. S., Torchilin, V. P., Kennel, S. J., and Huang, L. (1992) Use of N-terminal modified poly(L-lysine)–antibody conjugate as a carrier for targeted gene delivery in mouse lung endothelial cells. *Bioconjugate Chem. 3*, 323–327.

(6) Ferkol, T., Kaetzel, C. S., and Davis, P. B. (1993) Gene transfer into respiratory epithelial cells by targeting the polymeric immunoglobulin receptor. *J. Clin. Invest. 92*, 2394–2400.

(7) Monsigny, M., Roche, A. C., Midoux, P., and Mayer, R. (1994) Glycoconjugates as carriers for specific delivery of therapeutic drugs and genes. *Adv. Drug Delivery Rev. 14*, 1–24.

(8) Midoux, P., Mendes, C., Legrand, A., Raimond, J., Mayer, R., Monsigny, M., and Roche, A. C. (1993) Specific gene transfer mediated by lactosylated poly(L-lysine) into hepatoma cells. *Nucleic Acids Res. 21*, 871–878.

(9) Zenke, M., Steinlein, P., Wagner, E., Cotten, M., Beug, H., and Birnstiel, M. L. (1990) Receptor-mediated endocytosis of transferrin–polycation conjugates: an efficient way to introduce DNA into hematopoietic cells. *Proc. Natl. Acad. Sci. U.S.A. 87*, 3655–3659.

(10) Curiel, D. T., Agarwal, S., Wagner, E., and Cotten, M. (1991) Adenovirus enhancement of transferrin-polylysine-mediated gene delivery. *Proc. Natl. Acad. Sci. U.S.A. 88*, 8850–8854.

(11) Wagner, E., Plank, C., Zatloukal, K., Cotten, M., and Birnstiel, M. L. (1992) Influenza virus hemagglutinin HA-2 N-terminal fusogenic peptides augment gene transfer by transferrin–polylysine–DNA complexes: Toward a synthetic virus-like gene-transfer vehicle. *Proc. Natl. Acad. Sci. U.S.A. 89*, 7934–7338.

(12) Haensler, J., and Szoka, F. C. (1993) Polyamidoamine cascade polymers mediated efficient transfection of cells in culture. *Bioconjugate Chem. 4*, 372–379.

(13) Plank, C., Oberhauser, B., Mechtler, K., Koch, C., and Wagner, E. (1994) The influence of endosome-disruptive peptides on gene transfer using synthetic virus-like gene transfer systems. *J. Biol. Chem. 269*, 12918–12924.

(14) Monsigny, M., Roche, A. C., Kieda, C., Midoux, P., and Obrenovith, A. (1988) Characterization and biological implications of membrane lectins in tumor, lymphoid and myeloid cells. *Biochimie 70,* 1633−1649.

(15) Monsigny, M., Roche, A. C., and Midoux, P. (1984) Uptake of neoglycoproteins via membrane lectin (s) of L 1210 cells evidenced by quantitative flow cytofluorometry and drug targeting. *Biol. Cell 51,* 187−196.

(16) Derrien, D., Midoux, P., Petit, C., Nègre, E., Mayer, R., Monsigny, M., and Roche, A. C. (1989) Muramyl dipeptide bound to poly(L-lysine) substituted with mannose and gluconoyl residues as macrophage activators. *Glycoconjugate J. 6,* 241−255.

(17) Weiss, S. J., Test, S. T., Eckmann, C. M., Roos, D., and Regiani, S. (1986) Brominating oxidants generated by human eosinophils. *Science 234,* 200−202.

(18) Shen, W.-C., Yang, D., and Ryser, H. J. P. (1984) Colorimetric determination of microgram quantities of polylysine by Trypan Blue precipitation. *Anal. Biochem. 142,* 521−524.

(19) Fields, R. (1971) The measurement of amino groups in proteins and peptides. *Biochem. J. 124,* 581−590.

(20) Monsigny, M., Petit, C., and Roche, A. C. (1988) Colorimetric determination of neutral sugars by a resorcinol sulfuric acid micromethod. *Anal. Biochem. 175,* 525−530.

(21) Schwartz, A. L., Fridovich, S. E., Knowles, B. B., and Lodish, H. F. (1981) Characterization of the asialoglycoprotein receptor in a continuous hepatoma line. *J. Biol. Chem. 256,* 8878−8881.

(22) Brasier, A. R., Tate, J. E., and Habener, J. F.(1989) Optimized use of the firefly luciferase assay as a reporter gene in mammalian cell lines. *Biotechniques 7,* 1116−1123.

(23) Ventura, M., Wang, P., Franck, N., and Saragosti, S. (1994) Ribozyme targeting of HIV-1 LTR. *Biochem. Biophys. Res. Commun. 203,* 889−898.

(24) Schwartz, O., Virelizier, J. L., Montagnier, L., and Hazan, U. (1990) A microtransfection method using the luciferase-encoding reporter gene for the assay of human immunodeficiency virus LTR promoter activity. *Gene 88,* 197−205.

(25) Rittner, K., and Sczakiel, G. (1991) Identification and analysis of antisense RNA target regions of the human immunodeficiency virus type 1. *Nucleic Acids Res. 19,* 1421−1426.

(26) De Wet, J. R., Wood, K. V., De Luca, M., Helinski, D. R., and Subramani, S. (1987) Firefly luciferase gene: Structure and expression in mammalian cells. *Mol. Cell. Biol. 7,* 725−737.

(27) Smith, P. K., Krohn, R. I., Hermanson, G. T., Mallia, A. K., Gartner, F. H., Provenzano, M. D., Fujimoto, E. K., Goeke, N. M., Olson, B. J., and Klenk, D. C. (1985) Measurement of protein using bicinchoninic acid. *Anal. Biochem. 150,* 76−85.

(28) Hill, H. D., and Straka, J. G. (1988) Protein determination using bicinchoninic acid in the presence of sulfhydryl reagents. *Anal. Biochem. 170,* 203−208.

(29) Brunk, C. F., Jones, K. C., and James, T. W. (1979) Assay for nanogram quantities of DNA in cellular homogenates. *Anal. Biochem. 92,* 497−500.

(30) Plank, C., Zatloukal, K., Cotten, M., Mechtler, K., and Wagner, E. (1992) Gene transfer into hepatocytes using asialoglycoprotein receptor mediated endocytosis of DNA complexed with an artificial tetra-antennary galactose ligand. *Bioconjugate Chem. 3,* 533−539.

(31) Lee, Y. C., Townsend, R. R., Hardy, M. R., Lonngren, J., Arnarp, J., Haraldsson, M., and Lonn, H. (1983) Binding of synthetic oligosaccharides to hepatic Gal/GalNac lectin. Dependence on fine structural features. *J. Biol. Chem. 258,* 199−202.

(32) Reich, Z., Ittah, Y., Weinberger, S., and Minsky, A. (1990) Chiral and structural discrimination in binding of polypeptides with condensed nucleic acid structures. *J. Biol. Chem. 265,* 5590−5594.

(33) Taxman, D. J., Lee, E. S., and Don Wojchowski, M. (1993) Receptor-targeted transfection using stable maleimido-transferrin/thio-poly(L-lysine) conjugates. *Anal. Biochem. 213,* 97−103.

(34) Cotten, M., Wagner, E., Zatloukal, K., Phillips, S., Curiel, D. T., and Birnstiel, M. L. (1992) High-efficiency receptor-mediated delivery of small and large (48 kilobase) gene constructs using the endosome-disruption activity of defective or chemically inactivated adenovirus particles. *Proc. Natl. Acad. Sci. U.S.A. 89,* 6094−6098.

(35) Luthman, H., and Magnusson, G. (1983) High efficiency polyoma DNA transfection of chloroquine treated cells. *Nucleic Acids Res. 11,* 1295−1308.

(36) Wagner, E., Cotten, M., Foisner, R., and Birnstiel, M. L. (1991) Transferrin-polylysine-DNA complexes: The effect of polycations on the structure of the complex and DNA delivery to cells. *Proc. Natl. Acad. Sci. U.S.A. 88,* 4255−4259.

(37) Ross, G. F., Morris, R. E., Ciraolo, G., Huelsman, K., Bruno, M., Whitsett, J. A., Baatz, J. E., and Korfhagen, T. R. (1995) Surfactant protein A−polylysine conjugate for delivery of DNA to airway cells in culture. *Hum. Gene Ther. 6,* 31−40.

(38) Perales, J. C., Ferkol, T., Beegen, H., Ratnoff, O. D., and Hanson, R. W. (1994) Gene transfer in vivo: sustained expression and regulation of genes introduced into the liver by receptor-targeted uptake. *Proc. Natl. Acad. Sci. U.S.A. 91,* 4086−4090.

Photoimmobilization of a Bioactive Laminin Fragment and Pattern-Guided Selective Neuronal Cell Attachment

Jean-François Clémence,[†] John P. Ranieri,[‡] Patrick Aebischer,[‡] and Hans Sigrist[*,†]

Institute of Biochemistry, University of Bern, Freiestrasse 3, CH-3012 Berne, Switzerland, and Division of Surgical Research, Centre Hospitalier Universitaire Vaudois, CH-1011 Lausanne, Switzerland. Received December 29, 1994[®]

To attain light-dependent functionalization of biocompatible materials, a photolabel-derivatized, bioactive laminin fragment has been synthesized, chemically characterized, and photoimmobilized. Covalent high-resolution patterning of the laminin fragment CDPGYIGSR to hydroxylated fluorinated ethylene propylene (FEP-OH), poly(vinyl alcohol), and glycophase glass has been achieved. The synthetic peptide CDPGYIGSR was thermochemically coupled to either *N*-[*m*-[3-(trifluoromethyl)-diazirin-3-yl]phenyl]-4-maleimidobutyramide or 4-maleimidobenzophenone. Photolabel-derivatized peptides were radiolabeled, and 20 and 300 μm-sized patterns were visualized by autoradiography. The biospecific interaction of photoimmobilized laminin fragments with cells was investigated by analyzing the selective attachment of NG 108-15 neuroblastoma × glioma cells which bear CDPGYIGSR-specific cell surface receptors. On photopatterned FEP-OH membranes NG 108-15 cells differentiated in serum-supplemented media within 1 day. Specific attachment to the immobilized oligopeptide CDPGYIGSR was assessed in serum-free media with competitive binding studies, showing an 82% decrease in cell adherence after the cell receptors were blocked with soluble CDPGYIGSR.

INTRODUCTION

Tissue-engineered material systems require the molecular design of biomaterials to elicit a desired, receptor-specific cellular response (Aebischer et al., 1992; Peppas and Langer, 1994; Ratner, 1993; Bellamkonda and Aebischer, 1994). Two-dimensional patterned substrates have been developed to control neural cell attachment and differentiation. Information derived from these investigations is expected to promote (i) modeling of neuronal development (Baier and Bonhoeffer, 1994), (ii) the design of protocols for nerve regeneration, and (iii) the selection of components for biosensors and bioelectronic devices (Connolly, 1994). To date, several routes have been taken to pattern cell lines or primary cells on material surfaces.

In conjunction with masking techniques, selective surface functionalization has been achieved with thiosilanes on glass substrates (Bhatia et al., 1993), with methyl- and aminosilanes on silicon and silicon dioxide (Kleinfeld et al., 1988; Sundarababu et al., 1995), with glass or fused silica (Britland et al., 1992; Lom et al., 1993), and with aminosilanes on FEP-OH[1] (Ranieri et

al., 1993). Topically selective cell attachment has been reported to occur with physically adsorbed extracellular matrix proteins (e.g., laminin, fibronectin) and glycosaminoglycans such as keratan sulfate and chondroitin sulfate (Snow et al., 1990). Fromherz et al. (1991) have accomplished the same goal by irradiating physically adsorbed laminin through a mask using UV radiation <300 nm. This treatment denaturated the exposed laminin regions and was inhibitory toward neural cell attachment and neurite outgrowth. Neuronal cell attachment has also been achieved by covalent immobilization or adsorption of the minimum cell recognition sequences of fibronectin (RGD) and laminin (YIGSR, IKVAV) onto Sepharose, modified glass, or culture dishes (Pierschbacher and Ruoslahti, 1984; Massia and Hubbell, 1990; Jucker et al., 1991; Ranieri et al., 1995). Graf et al. (1987) provided evidence that the synthetic peptide CDPGYIGSR mediates cell adhesion and migration via a receptor-specific interaction.

Investigations presented in this work aim at the light-induced immobilization of this peptide using photoactivatable reagents and photopatterning procedures. Aryl azides, aryldiazirines, and benzophenones have been previously introduced as light-sensitive photolabels and heterobifunctional cross-linkers (Bayley, 1983; Sigrist and Zahler, 1985; Brunner, 1993). More recently, these types of substances were successfully used for biomolecule immobilization to material surfaces (Sigrist et al., 1992; Guire, 1993; Sundarababu and Sigrist, 1994). Upon irradiation with nondestructive UV light (≥320 nm), heterobifunctional diazirines and benzophenones were covalently linked to biomolecules (peptides, proteins, enzymes, antibodies, nucleic acids) and solid supports such as glass, titanium dioxide, and organic polymers (Sänger et al., 1992; Gao et al., 1994; Tao et al., 1986; Rozsnyai et al., 1992; Collioud et al., 1993) (Figure 1). In contrast to thermochemical coupling reactions, light-dependent immobilization procedures are addressable, noninvasive, and experimentally facile. Biological activities of photoimmobilized biomolecules are, in gen-

---

[1] Abbreviations: Bp-Mal, 4-maleimidobenzophenone; Bp-Mal-[³⁵S]Cys, [³⁵S]cysteinyl-4-maleimidobenzophenone; CDPGYIGSR, Cys-Asp-Pro-Gly-Tyr-Ile-Gly-Ser-Arg-NH₂; DMF, dimethylformamide; EDTA, (ethylenedinitrilo)tetraacetic acid; FEP, fluorinated ethylene propylene; FEP-OH, hydroxylated fluorinated ethylene propylene; GPTMS, 3-(glycidyloxy)propyltrimethoxysilane; HEPES, 4-(2-hydroxyethyl)piperazine-1-ethanesulfonic acid; HPLC, high-performance liquid chromatography; MAD, *N*-[*m*-[3-(trifluoromethyl)diazirin-3-yl]phenyl]-4-maleimidobutyramide; MAD-[³⁵S]Cys, [³⁵S]cysteinyl-*N*-[*m*-[3-(trifluoromethyl)diazirin-3-yl]phenyl]-4-maleimidobutyramide; NaCNBH₃, sodium cyanoborohydride; PBS, phosphate-buffered saline (150 mM NaCl, 5 mM sodium phosphate buffer, pH 7.4); PVA, poly(vinyl alcohol); SIMS, secondary ion mass spectroscopy; TEA, triethylamine; TFA, trifluoroacetic acid.
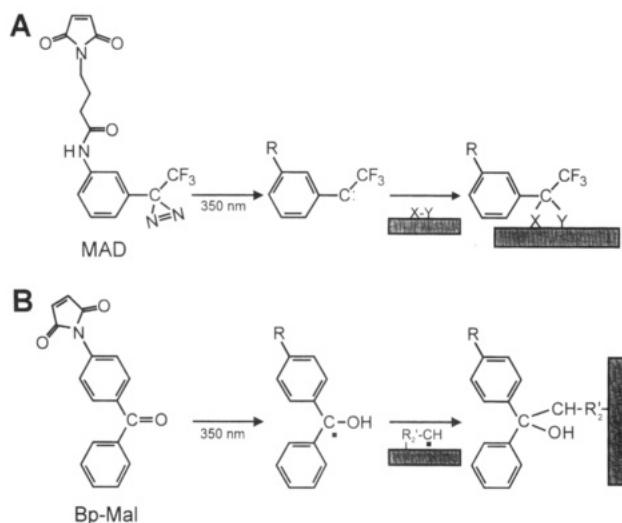
Figure 1. Light-dependent immobilization of photoactivatable reagents onto solid substrates. (A) Upon irradiation at 350 nm, aryldiazirines form highly reactive carbenes, which lead to covalent substrate modification. (B) Light-activated benzophenones form triplet-state radicals. Protons are abstracted from C−H groups of the substrate. Generated radicals combine and form a stable covalent bond.

eral, not affected by the conditions used for light activation (Sigrist et al., 1995).

This study describes the synthesis of photosensitive oligopeptide derivatives and their light-dependent immobilization on FEP-OH, PVA, and glycophase glass. The molecular interaction of neuroblastoma × glioma cells NG 108-15 with the derivatized surfaces is assessed for their ability to control topically cell attachment.

EXPERIMENTAL PROCEDURES

Materials. Photolabel irradiation was performed with an Osram HBO 350 high-pressure mercury lamp (filtered with a Schott WG 320 filter and a 1 cm layer of saturated copper sulfate in H_2O; transmission bandwidth 320−550 nm), in combination with a timer (MU 4, Müller Electronics, Noosinning, Germany) and a SVH 200 power supply providing a constant power output of 200 W. Light intensities were measured with a Suss UV intensity meter, model 1000 (Hilpert AG, Neuenhof, Switzerland). HPLC was carried out using a Hewlett-Packard HP 1090 liquid chromatograph equipped with a Perkin-Elmer LC75 detector, a HP 3396A integrator, and a Bakerbond Standard Wide-Pore Butyl (C_4) column (particle size 5 μm, column dimensions 4.6 × 250 and 10 × 250 mm). Absorption spectra were recorded on a Uvicon 810 spectrophotometer, and radioactive disintegrations were measured in 5 mL of scintillation fluid [1080 mL of toluene, 5.4 g of 2,5-diphenyloxazole, 0.2 g of 2,2′-*p*-phenylenebis(5-phenyloxazole), 920 mL of Triton X-100, and 40 mL of acetic acid] on a Kontron Betamatic V liquid scintillation counter. SIMS was performed with a VG Auto Spec Q. Dialysis was carried out with a Dianorm-4 system (Dianormgeräte, Munich, Germany) including Macro-2-Teflon cells covered with dialysis membranes (molecular weight cutoff 10 000, Diachema, Dianorm). Sonication was performed in a bath-type sonicator (W. Scherrer, Wil, Switzerland). Fully hydroxylated FEP-OH and 20 and 300 μm of pattern-hydroxylated FEP-OH membranes (diameter 3 cm) were prepared by radio-frequency glow discharge and provided by Dr. J. A. Gardella, SUNY, Buffalo, NY. Briefly, FEP membranes were exposed in a vacuum chamber to methanol and hydrogen gases at a combined pressure of 133 mbar. For the preparation of the pattern-hydroxylated FEP-OH the

same procedure was carried out in the presence of 20 and 300 μm photo masks (Ranieri et al., 1993). PVA membranes were obtained from Aicello Chemical Co., Alsdorf, Germany. Glass coverslips (diameter 3 cm, thickness 1) were purchased from Assistent, Sondheim, Germany. Nickel photo masks with 300 μm × 15 mm slits separated by 500 μm spacings (Figure 4A) and 20 μm × 15 mm slits separated by 180 μm spacings were purchased from Towne Laboratories Inc., Somerville, NJ. MAD was synthesized according to Collioud et al. (1993). [35S]-Cysteine, [14C]formaldehyde, and X-ray films (Hyperfilm MP and Hyperfilm β-max) were purchased from Amersham. CDPGYIGSR and Bp-Mal were obtained from Sigma. All other chemicals were reagent grade. The NG 108-15 cell line was a generous gift from Dr. M. Nirenberg, National Institutes of Health. Cell attachment was monitored by microscopy using a Zeiss Axiovert 100TV with 200× Hoffman optics.

Methods. (A) Synthesis. *Synthesis of MAD-[35S]-cysteine.* MAD (0.16 mg, 0.42 μmol) was dissolved in 400 μL of 20 mM citrate, 35 mM disodium hydrogen phosphate, 108 mM sodium chloride, and 1 mM EDTA, pH 6.5/methanol (1:1 by volume). [35S]Cysteine (0.4 μmol, 60.6 μCi) was added, and the mixture was stirred for 15 min. The products were isolated immediately after the reaction by reversed-phase chromatography. HPLC separation conditions were flow rate 1.3 mL/min, detection 280 nm, fraction size 1.3 mL, and gradient elution 0−100% (30 min) solvent B in solvent A [solvent A, 0.1% TFA in water; solvent B, 0.1% TFA in acetonitrile/water (4:1 by volume)]. Elution of radioactive material was recorded by analyzing aliquot samples (10 μL) from each fraction. The purified product was quantitated by the diazirine absorption coefficient ($\epsilon_{348nm} = 446$ M^{-1} cm^{-1}). MAD-[35S]Cys had a specific radioactivity of 150 μCi/μmol, and the chemical yield was 90%.

Synthesis of [35S]Cysteinyl-4-maleimidobenzophenone (Bp-Mal-[35S]Cys). [35S]Cysteine (10 μL, 1.2 μmol, 151.6 μCi) was incubated with Bp-Mal (0.55 mg, 2 μmol) in 360 μL of anhydrous DMF. The mixture was stirred at room temperature. Product formation was completed after 15 min, and Bp-Mal-[35S]Cys was purified by reversed-phase HPLC. Separation conditions were flow rate 1 mL/min, detection 280 nm, fraction size 0.50 mL, and gradient elution 0−100% (30 min) solvent B in solvent A [solvent A, 0.1% TFA in water; solvent B, 0.1% TFA in acetonitrile/water (4:1 by volume)]. Radioactivity was measured in the individual fractions as detailed above.

Synthesis of MAD-CDPGYIGSR. CDPGYIGSR (1 mg, 0.78 μmol) was dissolved in 800 μL of 5 mM sodium phosphate buffer, pH 6.5, containing 1 mM EDTA. The solution was stirred with MAD (0.63 mg, 1.72 μmol, in 100 μL of ethanol) for 15 min. After completion, MAD-CDPGYIGSR was separated by reversed-phase HPLC on Bakerbond (C_4): flow rate, 1.3 mL/min; detection, 280 nm; fraction size, 0.43 mL. Gradient elution (0 min, 0% B; 5 min, 0% B; 20 min, 30% B; 30 min, 100% B) was carried out by adding solvent B to solvent A [solvent A, 0.1% TFA in water; solvent B, 0.1% TFA in acetonitrile/water (4:1 by volume)]. The product was chemically characterized by UV spectroscopy, amino acid analysis, and secondary ion mass spectroscopy (SIMS). At 348 nm, the diazirine showed a characteristic absorption maximum ($\epsilon = 446$ M^{-1} cm^{-1}) which disappeared upon irradiation (Collioud et al., 1993). The observed and calculated (in parentheses) values for the amino acid composition of HPLC-purified MAD-CDPGYIGSR were Asp 0.97 (1.00), Ser 0.83 (1.00), Gly 2.13 (2.00), Arg 1.02 (1.00), Pro 1.05 (1.00), Tyr 0.96 (1.00), Cys derivatized (not detectable as Cys), and Ile 1.04 (1.00). SIMS

analysis of the MAD-CDPGYIGSR complex showed a major peak at m/z 1331 Da (calculated, 1331 Da) and a minor peak at m/z 1303 (-28 Da, N_2). For Bp-Mal-CDPGYIGSR a value of 1243 Da (calculated, 1243 Da) was measured.

Reductive [^{14}C]-Methylation of MAD-CDPGYIGSR. Reductive methylation was carried out according to Jentoft and Dearborn (1979). MAD-CDPGYIGSR was synthesized (but not purified) as described above. The reaction mixture (MAD-CDPGYIGSR, 740 µL, 0.32 µmol) was combined with 100 µL of NaCNBH$_3$ (240 mM), 100 µL of HEPES (1 M, pH 7.5), and 64 µL of [^{14}C]formaldehyde (2 µmol, 100 µCi) and stirred during 4 h at ambient temperature. The radiolabeled peptide was purified by reversed-phase HPLC, and characterization was carried out as described for MAD-CDPGYIGSR.

Synthesis of Bp-Mal-[^{14}C]CDPGYIGSR. CDPGYIGSR (1 mg, 0.72 µmol) and Bp-Mal (0.3 mg, 1.07 µmol) were dissolved in 300 µL and 120 µL of DMF, respectively. The reagents were combined and stirred for 15 min at ambient temperature. NaCNBH$_3$ (60 µL, 240 mM), HEPES (60 µL, 1 M, pH 7.5), and [^{14}C]formaldehyde (64 µL, 2 µmol, 100 µCi) were added and stirred during 4 h at 37 °C. Purification of the radiolabeled peptide was carried out by reversed-phase HPLC as described for the purification of Bp-Mal-[^{35}S]Cys.

Preparation of Glycophase Glass. According to Massia and Hubbell (1990), glass coverslips that are surface-rich in organic hydroxyls are referred to as glycophase glass. Coverslips (diameter 3 cm) were placed in round-bottom glass vials and incubated for 5 min in a boiling solution (30 mL) of ammonia (25%)/hydrogen peroxide (35%)/water, 1:1:5 by volume. After this treatment, the glass disks were washed with doubly distilled water (3 × 30 mL) and incubated for 5 min in a boiling solution of hydrochloric acid (37%)/hydrogen peroxide (35%)/water, 1:1:5 by volume. The coverslips were washed with doubly distilled water (3 × 30 mL) and acetone (3 × 30 mL). Residual acetone was removed by a stream of nitrogen. The dry disks were placed in a custom-made holder and refluxed under argon for 3 h in a 750 mL Schmitzo reaction vessel containing a solution of 3 mL of GPTMS and 3 mL of TEA in 300 mL of dry toluene. The coverslips were successively washed in chloroform (3 × 30 mL), acetone (3 × 30 mL), and methanol (3 × 30 mL) and dried in vacuum (Kallury et al., 1988). Finally, the coverslips were rinsed with 1 mM HCl, incubated for 60 min at 90 °C in 1 mM HCl, and washed with doubly distilled water (3 × 30 mL), yielding glycophase glass.

(B) Photopatterning. *Photocoupling of MAD-[^{35}S]-Cys onto FEP and FEP-OH Using a Photo Mask.* Prior to use, FEP and FEP-OH films were cleaned by sonication first in hexane and then in methanol. The membranes were placed in custom-made vessels and covered with 500 µL of MAD-[^{35}S]Cys (50 nmol, 7.6 µCi) in water/acetonitrile (1:1 by volume). The solvents were evaporated by incubation at 37 °C and 20 mbar for 3 h. Irradiation through the photo mask was carried out with the high-pressure mercury lamp for 5 min at 10 mW cm^{-2}. The irradiated membranes were successively sonicated for 1 min each in 40 mL of ethanol, methanol, methanol/water (1:1 by volume), water, and methanol. Patterns were visualized by autoradiography.

Photopatterning of MAD-[^{14}C]CDPGYIGSR onto FEP and FEP-OH. MAD-[^{14}C]CDPGYIGSR (600 µL, 3.6 µCi) was applied onto FEP, fully hydroxylated FEP-OH, and pattern-hydroxylated FEP-OH (20 and 300 µm) membranes and dried at 37 °C under reduced pressure (20 mbar) overnight. FEP and fully hydroxylated FEP-OH membranes were irradiated through the photo mask,

whereas the pattern-hydroxylated FEP-OH disks were exposed to light without the mask (irradiation time, 5 min at 10 mW cm^{-2}). Membranes were then washed by sonication (30 s) in 40 mL of ethanol, followed by methanol, methanol/water (1:1 by volume), water, and methanol. Radioactivity patterns were visualized by autoradiography after 5 days of exposure.

Photoimmobilization of Bp-Mal-[^{35}S]Cys and Bp-Mal-[^{14}C]CDPGYIGSR to PVA Membranes. Prior to use, PVA membranes (diameter 2.4 cm) were washed in methanol and water. Glycerol entrapped in commercially available PVA membranes was removed by Soxhlet extraction in methanol for 24 h (Kobayashi et al., 1991). The membranes were dried overnight at 37 °C and 20 mbar and stored over KOH in a desiccator until used. The photo mask was placed between a glass coverslip and the PVA membrane, and the layer set was clamped to the bottom of a vessel, which was filled with 1 mL of Bp-Mal-[^{35}S]-Cys (1.42 µCi) or Bp-Mal-[^{14}C]CDPGYIGSR (1.74 µCi) dissolved in water. Samples were irradiated from below with mirror-deflected light through photo masks with 20 or 300 µm spacings. Following irradiation, PVA films were rinsed with doubly distilled water, transferred to dialysis cells, and dialyzed against 1 L of doubly distilled water overnight. Radioactivity retained on the PVA membranes was visualized by autoradiography. Photolabeled [^{35}S]Cys binding to PVA was measured by liquid scintillation procedures.

Photoimmobilization of Bp-Mal-[^{14}C]CDPGYIGSR to Glycophase Glass. The same protocol as for PVA was followed to pattern Bp-Mal-[^{14}C]CDPGYIGSR onto glycophase glass. After the photoimmobilization step, the coverslips were washed in 40 mL of ethanol, followed by methanol, methanol/water (1:1 by volume), water, and methanol. Radioactivity patterns were visualized by autoradiography after 6 days of exposure.

(C) Neuronal Cells. *Cell Culture.* NG 108−15 cells were cultured in Dulbecco's-modified Eagle's medium (DMEM) and supplemented with 0.1 mM hypoxanthine, 0.4 mM aminopterin, 16 mM thymidine, and 10% fetal calf serum. The cells were maintained in tissue culture flasks within an incubator at 37 °C in a humidified atmosphere of 94% air and 6% CO$_2$. The cells were mechanically removed from their tissue culture flasks, centrifuged at 250g, and then resuspended in the desired cell plating medium.

Cell Attachment to Pattern-Modified FEP-OH Membranes. Five thousand NG 108-15 cells were plated on the 20 µm and 75 000 cells on the 300 µm CDPGYIGSR-derivatized membranes in 2 mL of serum-containing medium. The wells were kept in the incubator, and selective attachment response and neurite outgrowth were assessed at 8 h and at 1 day intervals for a maximum of 7 days.

Competitive Binding Assays on Fully Hydroxylated FEP-OH Films. Cell attachment assays were carried out in triplicate with fully hydroxylated, oligopeptide-derivatized FEP-OH membranes. The membranes were first pretreated with 2 mL of a 0.1% bovine serum albumin solution in phosphate-buffered saline (PBS) at 37 °C for 2 h to block nonspecific cell attachment. The albumin solution was removed, and the membranes were washed 3 times with PBS. Ten thousand NG 108-15 cells were suspended either in 2 mL of serum-free medium or in 2 mL of serum-free medium containing 1 mg/mL CDPGYIGSR. After 30 min of preincubation, the cells were plated onto the membranes and placed in an incubator set at 37 °C for 1 h. Cell attachment was monitored by microscopy. A minimum of 300 cells per well were

A

MAD-CDPGYIGSR

B
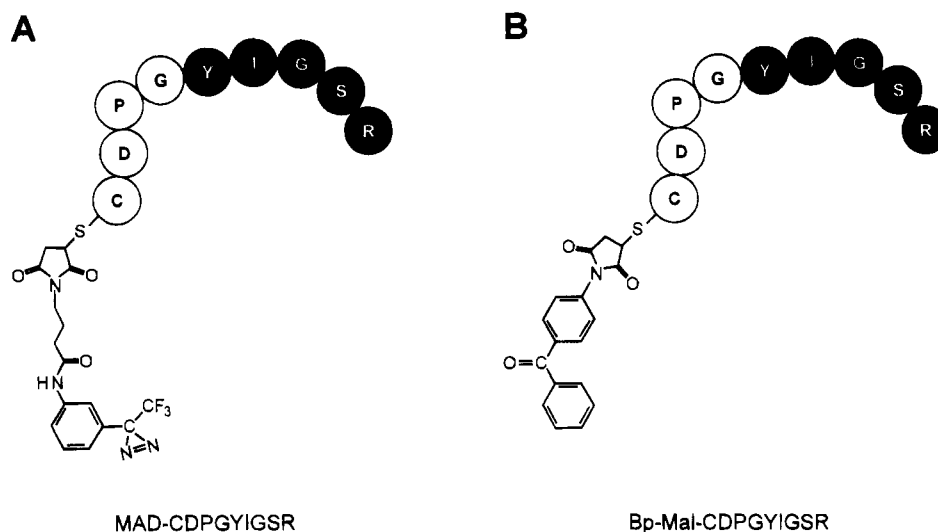
Bp-Mal-CDPGYIGSR

Figure 2. Structures of photolabel-derivatized synthetic peptides: (A) MAD-CDPGYIGSR; (B) Bp-Mal-CDPGYIGSR. The minimal active sequence YIGSR (black) protrudes in the medium and thus facilitates receptor interaction.

counted. The Student t-test was used to assess statistical significance ($P < 0.05$) for all attachment assays.

RESULTS

Thermochemical Functionalization of Cysteine and CDPGYIGSR with MAD and Bp-Mal. *Modification of [^{35}S]Cysteine with MAD and Bp-Mal.* The reaction of MAD and Bp-Mal with cysteine was completed within 15 min. Product formation was analyzed by HPLC. Eluted products were identified by reference analysis (cysteine, MAD, Bp-Mal) and on the basis of the radioactivity elution pattern ([^{35}S]Cys, MAD-[^{35}S]Cys, and Bp-Mal-[^{35}S]Cys). Pool fractions of MAD-Cys were further characterized by UV spectroscopy. MAD-Cys in water/acetonitrile (1:1 by volume) showed a characteristic diazirine absorption band at 357 nm that disappeared after photoactivation. Typical specific radioactivity values obtained for MAD-[^{35}S]Cys and Bp-Mal-[^{35}S]Cys were in the range of 100–150 μCi/μmol.

Modification of [^{14}C]CDPGYIGSR and CDPGYIGSR with MAD and Bp-Mal. Commercially available CD-PGYIGSR, stabilized with salts and 2-mercaptoethanol, was modified with a 3-fold molar excess of MAD or Bp-Mal, which was sufficient to react with the peptide and the included stabilizer, 2-mercaptoethanol (Figure 2). Peptides, modified with either MAD or Bp-Mal were then radiolabeled without prior purification. MAD-[^{14}C]CD-PGYIGSR or Bp-Mal-[^{14}C]CDPGYIGSR was separated by HPLC (Figure 3). Similar elution patterns were obtained for either of the photolabeled peptides. The retention times for MAD-CDPGYIGSR and Bp-Mal-CDPGYIGSR were 27.2 and 15.9 min, respectively. Pool fractions of MAD-CDPGYIGSR or Bp-Mal-CDPGYIGSR and MAD-[^{14}C]CDPGYIGSR or Bp-Mal-[^{14}C]CDPGYIGSR were characterized by amino acid analysis, UV spectroscopy, radioactivity, and SIMS. A typical specific radioactivity value obtained for MAD-[^{14}C]CDPGYIGSR (or Bp-Mal-[^{14}C]CDPGYIGSR) was 90 μCi/μmol.

Photopatterning of MAD-[^{35}S]Cys to FEP and FEP-OH. MAD was derivatized with [^{35}S]cysteine to yield the radiolabeled reagent MAD-[^{35}S]Cys. Surface coating and topical photolabel activation on fully hydroxylated FEP-OH through a 300 μm nickel grid showed preferential covalent attachment of MAD-[^{35}S]Cys. Some areas of the film showed good contrasts between irradiated and nonirradiated regions. It was noted, however, that some membranes were not uniformly modified with
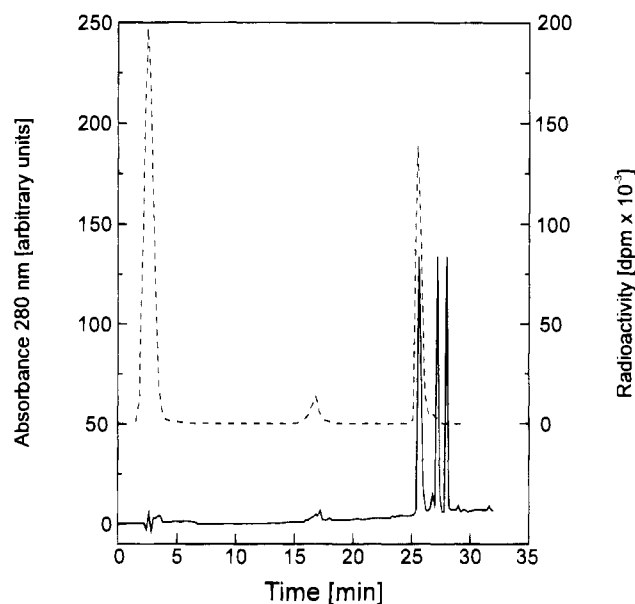
Figure 3. Purification of MAD-[^{14}C]CDPGYIGSR by HPLC on Bakerbond Butyl C$_4$. Elution was recorded by 280 nm absorption (—) and radioactivity counting (- - -). Under the conditions used for product separation, the retention times were 2.5 min for Cys, 16.5 min for CDPGYIGSR, 25.7 min for MAD-[^{14}C]-CDPGYIGSR, 27.2 min for MAD-mercaptoethanol, and 28.1 min for MAD.

MAD-[^{35}S]Cys, a result that may be due to uneven hydroxylation of the FEP membrnae by the radiofrequency glow discharge process. Photopatterns obtained with FEP-OH membranes showed approximate 10 μm transition zones between the irradiated and nonirradiated sections (data not shown). MAD-[^{35}S]Cys binding to unmodified FEP was not observed, indicating that carbene insertion into C–F bonds did not occur.

Photocoupling of MAD-[^{14}C]CDPGYIGSR onto FEP and FEP-OH. In accordance with the results obtained with MAD-[^{35}S]Cys, there was no binding to FEP with photoactivated MAD-[^{14}C]CDPGYIGSR. Covalent attachment of MAD-[^{14}C]CDPGYIGSR and patterning were obtained on both fully hydroxylated FEP-OH and 20 and 300 μm pattern-hydroxylated FEP-OH surfaces. High-contrast patterns were attained with pattern-hydroxylated FEP-OH membranes. Photolabel insertions occurred only in the hydroxylated regions of
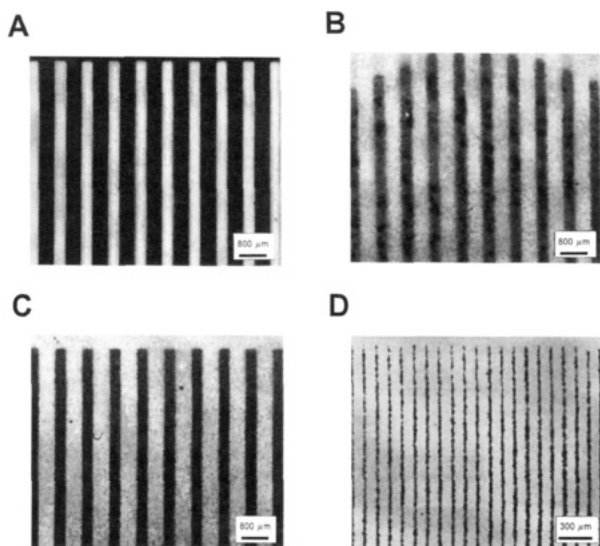
Figure 4. Photopatterning on FEP-OH, glycophase glass, and PVA. (A) Photo mask. The 300 μm patterning experiments were performed with a nickel grid (38 μm thick), with rectangular openings (white) of 300 μm × 15 mm and a land spacing (black) of 500 μm. (B) Autoradiography of topically immobilized MAD-[^{14}C]CDPGYIGSR on pattern-hydroxylated FEP-OH membranes. MAD-[^{14}C]CDPGYIGSR was spread on the surface and dried. The coated membrane was irradiated for 10 min and with 10 mW cm^{-2}. Physically adsorbed MAD-[^{14}C]CDPGYIGSR was removed by washing as described in the Methods section, and residual photoimmobilized label distribution was detected by autoradiography. Black (radioactive) areas correspond to the slit openings (300 μm × 15 mm) of the mask. (C) Autoradiography of topically immobilized Bp-Mal-[^{14}C]CDPGYIGSR on glycophase glass disks. The glycophase glass disk was underlayered with a photo mask (slit width 300 μm, spacings 500 μm) and mounted in a vessel. The Bp-Mal-[^{14}C]CDPGYIGSR solution was added on top of the glycophase glass into the vessel and irradiated from below with a deflected beam (30 min, 10 mW cm^{-2}). Physically adsorbed Bp-Mal-[^{14}C]CDPGYIGSR was removed by washing as described in the Methods section. Detection of photoimmobilized peptides was carried out as mentioned above. (D) Autoradiography of 20 μm pattern-modified Bp-Mal-[^{14}C]CDPGYIGSR on PVA membranes. Bp-Mal-[^{14}C]CDPGYIGSR on PVA was treated as described above for glycophase glass. Peptide-modified PVA membranes were dialyzed to remove nonspecifically adsorbed oligopeptide.

the membrane, and this resulted in a good contrast between modified FEP-OH and unmodified FEP areas (Figure 4B).

Photoimmobilization of Bp-Mal-[^{35}S]Cys and Bp-Mal-[^{14}C]CDPGYIGSR onto PVA Membranes and Glycophase Glass. After HPLC purification, Bp-Mal-[^{35}S]Cys was obtained with a specific radioactivity of 41 μCi/μmol. Photocoupling on PVA and glycophase glass was highly specific. A value of 30.2 nCi was measured on the illuminated PVA membranes, whereas only 0.05 nCi was recorded on nonilluminated control samples. Assuming a flat surface, the density was 53 pmol of Bp-Mal-[^{35}S]Cys/cm^2 with 0.08 pmol/cm^2 of the cysteine being nonspecifically adsorbed.

Immobilization experiments with 300 and 20 μm masks that were visualized by autoradiography yielded patterns of high contrast. Nonspecific peptide adsorption on PVA and glycophase glass was considerably reduced by the fact that Bp-Mal-[^{35}S]Cys did not require drying prior to illumination. Photopatterns of comparable high quality were obtained with Bp-Mal-[^{14}C]CDPGYIGSR on glycophase glass (Figure 4C) and PVA (Figure 4D).

Neuronal Cell Attachment. In order to assess cell attachment on the patterned bioactive substrates, NG 108-15 cells were plated in medium containing fetal calf serum onto MAD-CDPGYIGSR-modified FEP-OH mem-

branes (fully and pattern hydroxylated), Bp-Mal-CD-PGYIGSR-modified PVA, and glycophase glass. On pattern-hydroxylated FEP-OH, the cells selectively attached within 6 h to the peptide-patterned areas. After removal of nonattached cells, the substrates were inspected by inverted microscopy. The cells adhered almost exclusively on the photoimmobilized peptide areas with low attachment to unmodified FEP (Figure 5A,B). Non-irradiated substrates showed no pattern-guided cell attachment after 8 h (Figure 5C). On 20 μm patterned surfaces, cells selectively aligned on the CDPGYIGSR-modified regions. Differentiation was indicated by the spreading of the cells and the extension of neurites (Figure 5D). The NG 108-15 cells were found viable for more than 7 days on CDPGYIGSR-modified pattern-hydroxylated FEP-OH surfaces in serum-containing medium. Only a few cells adhered randomly on fully hydroxylated FEP-OH films that were derivatized with oligopeptides through a 300 μm photo mask (data not shown).

On peptide-modified glycophase glass, cell patterning was not as evident as on pattern-hydroxylated FEP-OH substrates derivatized with MAD-CDPGYIGSR. Cell adherence was close to random, suggesting that unmodified glycophase glass is an adhesive substrate for NG 108-15 cells, both in serum-containing medium and in serum-free medium. On the contrary, peptide-modified PVA was nonadhesive for the NG 108-15 cells. There was no significant selective attachment on pattern-modified PVA substrates either in serum-free or in serum-containing medium (data not shown).

Competitive Binding. To determine if the selective NG 108-15 cell attachment response was receptor specific, competitive binding assays were performed on fully hydroxylated FEP-CDPGYIGSR membranes. In serum-free medium, 33 ± 7 cells/0.28 mm^2 attached to the membrane. When soluble CDPGYIGSR was present in the plating medium, only 6 ± 5 cells/0.28 mm^2 adhered to the surface, corresponding to an 82% reduction in cell attachment (Figure 6).

DISCUSSION

The development of bioactive material systems that specifically recognize cell membrane receptors will play a crucial role in tissue engineering and for implant coating. As presented in this study, oriented and light-dependent functionalization of biocompatible surfaces has been accomplished with the synthetic peptide CDPGYIG-SR. The immobilized oligopeptide is capable of presenting its bioactive sequence YIGSR for specific interaction with cell surface receptors as determined by competitive binding assays. This is in agreement with observations of Massia and collaborators showing that covalently immobilized YIGSR promotes cell spreading on a glycophase surface (Massia et al., 1993).

The requirements of orientation, covalency, and selective light-induced reactivity were fulfilled by modifying the biocompatible substrates FEP-OH, PVA, and glycophase glass with aryldiazirine- and benzophenone-based photoactivatable reagents. Either maleimide-containing diazirine or benzophenone photo-cross-linkers were chosen; the selection criteria were the stability of the biomolecule to drying and/or the substrate properties. The maleimido function, which is common to both cross-linkers, reacts specifically with accessible sulfhydryl groups of biomolecules (Collioud et al., 1993). Both MAD and Bp-Mal are distinctly beneficial photo-cross-linkers. On the one hand, MAD-mediated linking does not impose major restrictions to the surface chemistry. Solvent removal significantly increased diazirine-based coupling
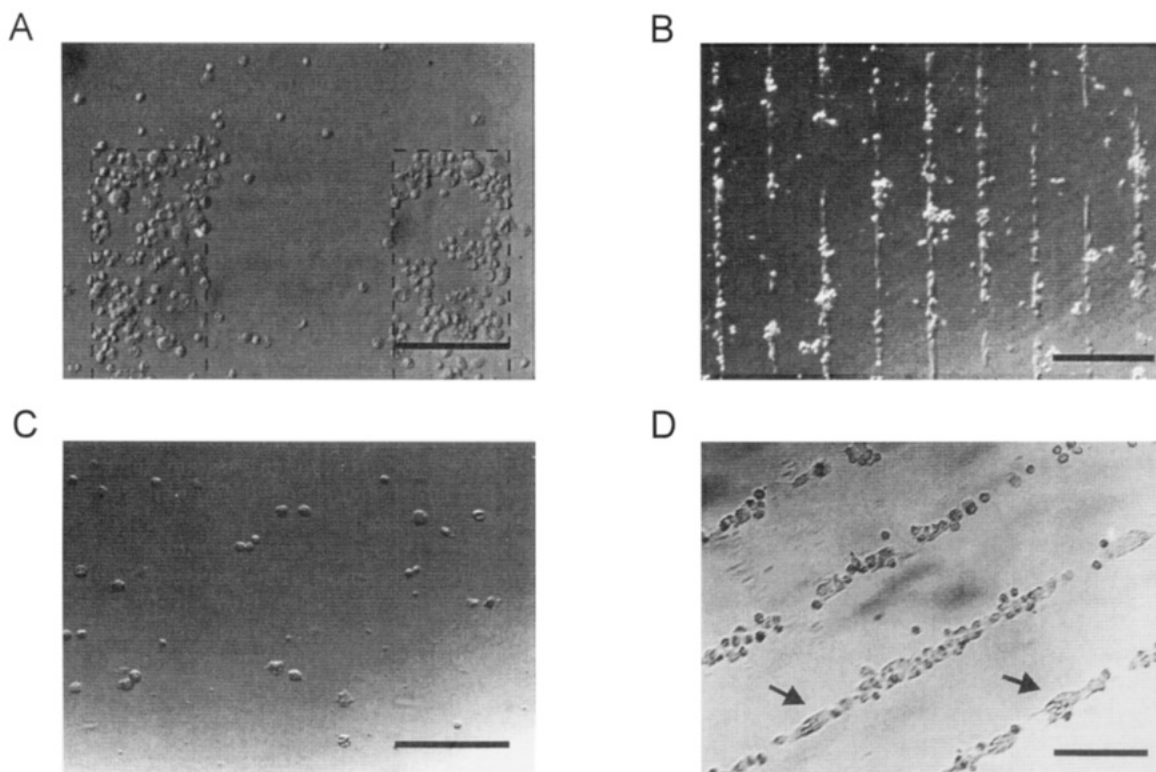
Figure 5. NG 108-15 cell attachment to pattern-hydroxylated and CDPGYIGSR-modified FEP-OH membranes. (A) Magnified section of two pathways at the top end of the 300 µm photo mask (outlined by dashed lines). Cell attachment was analyzed 8 h after plating. Scale bar = 300 µm. (B) NG 108-15 cell adherence to 20 µm CDPGYIGSR-derivatized tracks (low magnification, scale bar = 400 µm). (C) Cell attachment to 300 µm pattern-hydroxylated but not light-exposed FEP-OH membranes (plating time 8 h, scale bar = 300 µm). (D) NG 108-15 cell binding to 20 µm patterned and CDPGYIGSR-modified tracks. After 4 days in culture the cells remained within the peptide-derivatized pathways and showed neurite outgrowth (indicated by arrows, scale bar = 180 µm).
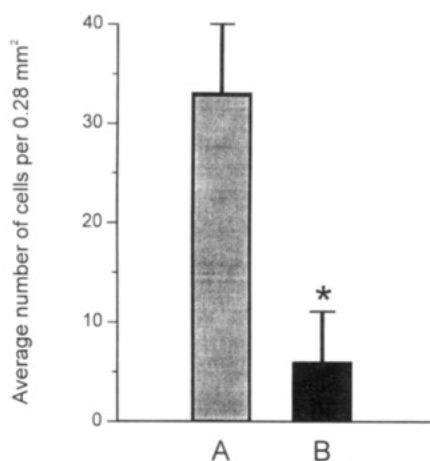
Figure 6. Competitive cell attachment to CDPGYIGSR-modified surfaces. (A) NG 108-15 cell attachment in serum-free medium to fully hydroxylated and MAD-CDPGYIGSR-derivatized FEP-OH membranes. (B) Cell binding in the presence of 5 mM soluble CDPGYIGSR to surfaces prepared as in (A) (*, $P < 0.05$).

yields but also nonspecific adsorption. On the other hand, benzophenone-based photoimmobilization is feasible in aqueous media. However, this procedure necessitates substrate-borne C−H bonds for proton abstraction and reagent binding (Figure 1). MAD- and Bp-Mal-mediated peptide immobilization was controlled by topically selective irradiation. Visualization of high-resolution and light-addressed surface patterning has been achieved with ^{35}S- and ^{14}C-labeled reagents.

PVA, glycophase glass, and FEP-OH were investigated with respect to nonspecific adsorption of the cross-linking agents and the oligopeptides. Generally, it was found that nonspecific adsorption was low on hydrophilic substrates and with benzophenone-based procedures in aqueous media. Two material/photo-cross-linker systems were successful in terms of peptide binding: pattern-hydroxylated FEP-OH functionalized with MAD-CDPGYIGSR, and PVA or glycophase glass modified with Bp-Mal-CDPGYIGSR. Prior to photoimmobilization, FEP was fully or pattern hydroxylated by radio-frequency glow discharge. This process rendered the substrate chemically reactive by inserting hydroxyl functions on inert FEP (Vargo et al., 1991). In contrast, PVA did not demand any modification prior to use. Both PVA and glycophase glass bear C−H bonds at the surface and are therefore suited to react with benzophenone derivatives.

In general, unmodified FEP-OH and PVA were nonadhesive toward neuronal cells in serum-containing media. Glycophase glass was previously reported to prevent endothelial cell adhesion (Hubbell et al., 1991). This observation was not confirmed with NG 108-15 cells. They attached nonspecifically within 1 h to glycophase glass in serum-free media, but in serum-containing media, few cells adhered. Although the 300 and 20 µm photopatterning of CDPGYIGSR showed excellent contrasts on either of the substrates, the extent of cell attachment differed significantly. On pattern-hydroxylated FEP-OH surfaces, NG 108-15 cells attached and differentiated almost exclusively on the peptide-modified areas with low adhesion to adjacent FEP. Recognition specificity for the YIGSR sequence was demonstrated by competitive binding studies, which showed an 82% decrease in cell attachment when the plating medium contained soluble CDPGYIGSR.

In summary, the results suggest that permissive pathways alone are not sufficient to control the spatial alignment of neuronal cells and the direct neurite outgrowth. It is expected that the experimentally facile, light-dependent immobilization procedures will facilitate the screening of factors that control cell attachment and differentiation (Baier and Bonhoeffer, 1994). Light-induced patterning of bioactive peptides provides means for the fabrication of two-dimensional substrates *in vitro* and the prerequisites for future structuring of three-dimensional biomimetic material systems.

ACKNOWLEDGMENT

LITERATURE CITED

Aebischer, P., Goddard, M., and Galletti, P. M. (1992) Biomaterials and artificial organs in materials science and technology, a comprehensive treatment (R. W. Cahn, P. Haasen, and E. J. Kramer, Eds.) *Medical and Dental Materials* (D. F. Williams, Vol. Ed.) Vol. 14, pp 133–176, VCH Publishers, Cambridge.

Baier, H., and Bonhoeffer, F. (1994) Attractive axon guidance molecules. *Science 265*, 1541–1542.

Bayley, H. (1983) *Photogenerated reagents in biochemistry and molecular biology*, Elsevier Science Publishers, Amsterdam.

Bellamkonda, R., and Aebischer, P. (1994) Tissue engineering in the nervous system. *Biotechnol. Bioeng. 43*, 543–554.

Bhatia, S. K., Teixeira, J. L., Anderson, M., Shriver-Lake, L. C., Calvert, J. M., Georger, J. H., Hickman, J. J., Dulcey, C. S., and Ligler, F. S. (1993) Fabrication of surfaces resistant to protein adsorption and application to two-dimensional protein patterning. *Anal. Biochem. 208*, 197–205.

Britland, S., Clark, P., Connolly, P., and Moores, G. (1992) Micropatterned substratum adhesiveness: A model for morphogenetic cues controlling cell behavior. *Exp. Cell Res. 198*, 124–129.

Brunner, J. (1993) New photolabeling and crosslinking methods. *Annu. Rev. Biochem. 62*, 483–514.

Collioud, A., Clémence, J.-F., Sänger, M., and Sigrist, H. (1993) Oriented and covalent immobilization of target molecules to solid supports: Synthesis and application of a light-activatable and thiol reactive cross linking reagent. *Bioconjugate Chem. 4*, 528–536.

Connolly, P. (1994) Bioelectronic interfacing: micro- and nanofabrication techniques for generating predetermined molecular arrays. *TIBTECH 12*, 123–127.

Fodor, S. P. A., Read, J. L., Pirrung, M. C., Stryer, L., Lu, A. T., and Solas, D. (1991) Light-directed, spatially addressable parallel chemical synthesis. *Science 251*, 767–773.

Fromherz, P., Schaden, H., and Vetter, T. (1991) Guided outgrowth of leech neurons in culture. *Neurosci. Lett. 129*, 77–80.

Gao, H., Kislig, E., Oranth, N., and Sigrist, H. (1994) Photolinker-polymer-mediated immobilization of monoclonal antibodies, f(ab')₂ and f(ab') fragments. *Biotechnol. Appl. Biochem. 20*, 251–263.

Graf, J., Ogle, R. C., Robey, F. A., Sasaki, M., Martin, G. R., Yamada, Y., and Kleinman, H. K. (1987) A pentapeptide from the laminin B1 chain mediates cell adhesion and binds the 67000 laminin receptor. *Biochemistry 26*, 6896–6900.

Guire, P. E., and Dunkirk, G. (1993) Method of biomolecule attachment to hydrophobic surfaces. U.S. Patent 5 258 041.

Hubbell, J. A., Massia, S. P., Desai, N. P., and Drumheller, P. D. (1991) Endothelial cell-selective materials for tissue engineering in the vascular graft via a new receptor. *Bio/Technology 9*, 568–572.

Jentoft, N., and Dearborn, D. G. (1979) Labeling of proteins by reductive methylation using sodium cyanoborohydride. *J. Biol. Chem. 254*, 4359–4365.

Jucker, M., Kleinman, H. K., and Ingram, D. K. (1991) Fetal rat septal cells adhere to and extend processes on basement membrane, laminin, and a synthetic peptide from the laminin A chain sequence. *J. Neurosci. Res. 28*, 507–517.

Kallury, K. M. R., Krull, U. J., and Thompson, M. (1988) X-ray photoelectron spectroscopy of silica surfaces treated with polyfunctional silanes. *Anal. Chem. 60*, 169–172.

Kleinfeld, Kahler, K. H., and Hockberger, P. E. (1988) Controlled outgrowth of dissiciated neurons on patterned substrates, *J. Neurosci. 8*, 4098–4120.

Kobayashi, H., and Ikada, Y. (1991) Covalent immobilization of proteins on to the surface of poly(vinyl alcohol) hydrogel. *Biomaterials 12*, 747–751.

Lom, B., Healy, K. E., and Hockberger, P. E. (1993) A versatile technique for patterning biomolecules onto glass coverslips. *J. Neurosci. Methods 50*, 385–397.

Massia, S. P., and Hubbell, J. A. (1990) Covalent surface immobilization of arg-gly-asp- and tyr-ile-gly-ser-arg-containing peptides to obtain well-defined cell-adhesive substrates. *Anal. Biochem. 187*, 292–301.

Massia, S. P., Rao, S. S., and Hubbell, J. A. (1993) Covalently immobilized laminin peptide tyr-ile-gly-ser-arg (YIGSR) supports cell spreading and co-localization of the 67-kilodalton laminin receptor with a α-actinin and vinculin. *J. Biol. Chem. 268*, 8053–8059.

Peppas, N. A., and Langer, R. (1994) New challenges in biomaterials. *Science 263*, 1715–1720.

Pierschbacher, M. D., and Ruoslahti, E. (1984) Cell attachment activity of fibronectin can be duplicated by small synthetic fragments of the molecule. *Nature 309*, 30–33.

Ranieri, J. P., Bellamkonda, R., Jacobs, J., Vargo, T. G., Gardella, J. A., and Aebischer, P. (1993). Selective neuronal cell attachment to a covalently patterned monoamine on fluorinated ethylene propylene films. *J. Biomed. Mater. Res. 27*, 917–925.

Ranieri, J. P., Bellamkonda, R., Bekos, E. J., Vargo, T. G., Gardella, J. A., and Aebischer, P. (1995) Neuronal cell attachment to fluorinated ethylene propylene films with covalently immobilized laminin oligopeptides YIGSR and IKVAV. *J. Biomed. Mater. Res.* (in press).

Ratner, B. D. (1993) New ideas in biomaterial science—a path to engineered biomaterials. *J. Biomed. Mater. Res. 27*, 837–850.

Rozsnyai, L. F., Benson, D. R., Fodor, S. P. A., and Schultz, P. G. (1992) Photolithographische Immobilisierung von Biopolymeren auf festen Trägern. *Angew. Chem. 104*, 801–802.

Sänger, M., Borle, F., Heller, M., and Sigrist, H. (1992) Light-inducing coupling of aqueous soluble protein to liposomes formed from carbene-generating phospholipids. *Bioconjugate Chem. 3*, 308–314.

Sigrist, H., and Zahler, P. (1985) Selective covalent modification of membrane components. The enzymes of biological membranes. (A. N. Martonosi, Ed.) Vol. 1, pp 333–370, Plenum Press, New York and London.

Sigrist, H., Gao, H., and Wegmüller, B. (1992) Light-dependent, covalent immobilization of biomolecules on 'inert' surfaces. *Bio/Technology 10*, 1026–1028.

Sigrist, H., Collioud, A., Clémence, J.-F., Gao, H., Luginbühl, R., Sänger, M., and Sundarababu, G. (1955) Immobilization of biomolecules by light. *Opt. Eng.* (in press).

Snow, D. M., Lemmon, V., Carrino, D. A., Caplan, A. I., and Silver, J. (1990) Sulfated proteoglycans inhibit neurite outgrowth in vitro. *Exp. Neurol. 109*, 111–130.

Sundarababu, G., and Sigrist, H. (1994) Photoinduced surface immobilization of biomolecules. *Trends in Photochemistry and Photobiology*, Vol. 3, pp 229–241, Research Trends, India.

Sundarababu, G., Gao, H., and Sigrist, H. (1995) Photochemical linkage of antibodies to silicon chips. *J. Photochem. Photobiol.* (in press).

Tao, T., Scheiner, C. J., and Lamkin, M. (1986) Site-specific photo-cross-linking studies on interactions between troponin and tropomyosin and between subunits of troponin. *Biochemistry 25*, 7633–7639.

Vargo, T. J., Gardella, J. A., Meyer, A. E., and Baier, R. E. (1991) Hydrogen/liquid vapor radio frequency glow discharge plasma oxidation/hydrolysis of expanded poly(tetrafluoroethylene) (ePTFE) and poly(vinylidene fluoride) (PVDF) surfaces. *J. Polym. Sci., Part A-1: Polym. Chem. 29*, 555–570.

Oligodeoxyribonucleotides with Conjugated Dihydropyrroloindole Oligopeptides: Preparation and Hybridization Properties

Eugeny A. Lukhtanov, Igor V. Kutyavin,* Howard B. Gamper, and Rich B. Meyer, Jr.

MicroProbe Corporation, 1725 220th Street SE, Bothell, Washington 98021. Received February 24, 1995[®]

Synthesis of a new class of conjugates between oligodeoxyribonucleotides (ODNs) and minor groove binders (MGBs) is described. The MGBs are analogs of the potent antibiotic CC-1065 and consist of repeating 1,2-dihydro-3H-pyrrolo[3,2-e]indole-7-carboxylate (DPI) subunits with N-3 carbamoyl or *tert*-butyloxycarbonyl groups (CDPI or BocDPI subunits, respectively). The ODN–MGB conjugates were obtained by postsynthetic modification of 5'- or 3'-amino-tailed ODNs with the 2,3,5,6-tetrafluorophenyl (TFP) esters of $CDPI_{1-3}$ or $BocDPI_{1-2}$ or by ODN synthesis using a $CDPI_3$-modified controlled pore glass (CPG) support. The hybridization properties of MGB-tailed octathymidylates were determined; they varied with respect to the site of conjugation (3' or 5'), the nature of the linker, the length of the DPI oligopeptide, and the type of N-3 substitution. Optical melting studies showed that the linkage of $CDPI_{1-3}$ residues to $(dTp)_8$ significantly increased the stability of hybrids formed by the latter with poly(dA). The extent of stabilization increased with the length of the peptide. When $CDPI_3$ was conjugated to either end of $(dTp)_8$, the melting temperature (T_m) of the hybrid formed with poly(dA) was increased by 43–44 °C. Free $CDPI_3$ stabilized the $(dTp)_8$–poly(dA) hybrid by only 2 °C, thus demonstrating the importance of conjugation. $(dTp)_8$–$CDPI_{1-3}$ conjugates also formed stabilized duplexes with poly(rA). The extent of stabilization was half that observed with poly(dA).

INTRODUCTION

We recently described the formation of very stable hybrids between two A-T rich ODNs,[1] one of which was conjugated to an *N*-methylpyrrolecarboxamide (MPC) peptide 2–5 subunits long *(1)*. When covalently liked to one strand of a duplex, these analogs of netropsin and distamycin A (see Figure 1) are postulated to reside in the minor groove and therefore provide significant stabilization. Free MPC antibiotics selectively interact with the minor groove of A-T rich DNA through van der Waals contacts, hydrophobic and electrostatic interactions, and highly oriented hydrogen bonds *(2)*. The minor groove of G-C containing DNA or any DNA·RNA duplex does not accommodate free MPC oligopeptides. As might be predicted, these hybrids are not stabilized by conjugated MPC peptides.

CC-1065 is another minor groove binding agent *(3)*. This antitumor antibiotic is composed of three repeating dihydropyrroloindole (DPI) subunits (Figure 1). The left-hand or A subunit contains a reactive cyclopropyl function which alkylates the N-3 of adenine *(4)*. The right-hand B and C subunits confer a high binding affinity for the narrow minor groove of A-T rich DNA. A simplified, nonreactive analog of CC-1065 composed of three 1,2-dihydro-3H-pyrrolo[3,2-e]indole-7-carboxylate subunits (CDPI$_3$) possesses similar DNA binding properties *(5)*. The isohelical fit of these molecules with the minor groove

of DNA is driven by hydrophobic interactions, since they lack the ionic character and the hydrogen-bonding capabilities of netropsin and distamycin A. CDPI peptides conjugated to ODNs might stabilize a wider spectrum of nucleic acid hybrids.

CDPI$_3$ has been synthesized by coupling suitably protected DPI subunits in the presence of activating agents *(6)*. We describe an improved coupling procedure which uses the 2,3,5,6-tetrafluorophenyl (TFP) ester of CDPI or BocDPI as active intermediates. We also describe the synthesis of 3'- and 5'-MGB-tailed ODNs by two alternative procedures. In the first procedure amino-tailed ODNs were postsynthetically modified with various TFP–CDPI$_{1-3}$ and TFP–BocDPI$_{1-2}$ esters. In the second approach, a special CPG support was prepared. CDPI$_3$ was bound to the solid support through a specially designed amino diol linker which provided attachment points for (a) the desired conjugate molecule, (b) the solid support, and (c) the initial 3'-nucleic acid residue. By using this CPG, 3'-CDPI$_3$-tailed ODNs could be isolated directly after synthesis, thus saving time and improving yield. The physical properties of the MGB–octathymidylate conjugates including their ability to form very stable hybrids with complementary poly(rA) and poly(dA) is also presented.

EXPERIMENTAL PROCEDURES

Reagents. All air and water sensitive reactions were carried out under a slight positive pressure of argon. Anhydrous solvents were obtained from Aldrich (Milwaukee, WI). Flash chromatography was performed on 230–400 mesh silica gel. Elemental analysis was performed by Quantitative Technologies Inc. (Boundbrook, NJ). UV–visible absorption spectra were recorded in the 200–400 nm range on a Lambda 2 (Perkin-Elmer) spectrophotometer. ^{1}H NMR spectra were run at 20 °C on a Varian Gemini FT-200 or on a Varian Gemini-300 spectrophotometer; chemical shifts are reported in ppm downfield from TMS.

ODN Synthesis. All ODNs were prepared from 1 μmol of the appropriate CPG support on an ABI 394

---

[1] Abbreviations used: ODN, oligodeoxyribonucleotide; MPC, 1-methylpyrrole-2-carboxamide; DPI, 1,2-dihydro-3H-pyrrolo[3,2-e]indole-7-carboxylate; CDPI and BocDPI, 3-carbamoyl and 3-(*tert*-butyloxycarbonyl)-1,2-dihydro-3H-pyrrolo[3,2-e]indole-7-carboxylate, respectively; TFA, trifluoroacetate; TFP, 2,3,5,6-tetrafluorophenyl; CPG, controlled pore glass; T_m, melting temperature; MGB, minor groove binder; DMF, *N,N*-dimethylformamide; DMSO, dimethyl sulfoxide; Fmoc, fluorenylmethoxycarbonyl; placement of the MGB to the left or right of the ODN denotes 5'- or 3'-conjugation, respectively.

Netropsin

N-Methylpyrrole carboxamide (MPC) peptides

$H_2N(CH_2)_5C$ ... $NH(CH_2)_5CO(CH_2)_2SCH_2PhNNPh$ n= 2 - 5

CC-1065

CDPI₃ methyl ester
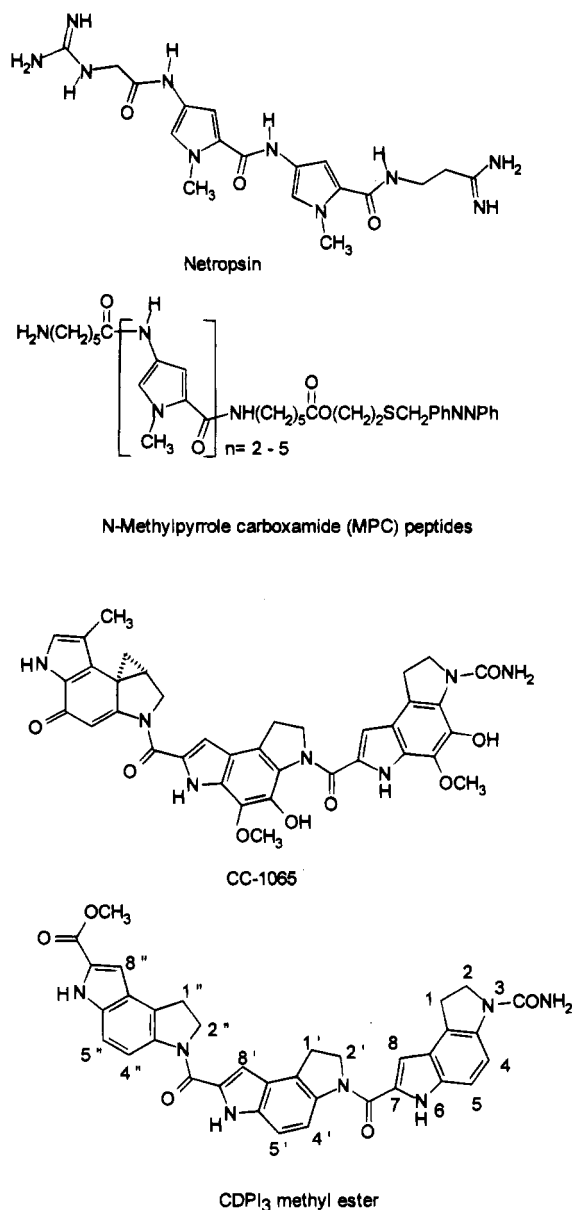
Figure 1. Structures of the minor groove binding antibiotics netropsin and CC-1065 and their respective synthetic analogs MPC₂₋₅ and CDPI₃.

using the protocol supplied by the manufacturer. Standard reagents for the β-cyanoethyl phosphoramidite coupling chemistry were purchased from Glen Research. 5'-Aminohexyl modifications were introduced using an N-(4-monomethoxytrityl)-6-amino-1-hexanol phosphoramidite linker (Glen Research). 3'-Aminohexyl modifications were introduced using the CPG prepared as previously described *(7)*. For direct synthesis of 3'-MGB-tailed ODNs, a long-chain alkylamine CPG (500 Å, Sigma) was chemically modified as described below.

Molar Extinction Coefficients of Polynucleotides, ODNs, and Their Derivatives. The molar extinction coefficient (ϵ_{260}) of (dTp)₈ was determined to be 65.8 mM^{-1} cm^{-1} by measuring the absorption of the ODN before and after complete hydrolysis by venom nuclease *(8)*. With this value in hand, ^{32}P-labeled (dTp)₈–CDPI₁₋₃ conjugates with known specific activities were prepared and their ϵ_{260}s determined to be 103.0, 102.8, and 110.1 mM^{-1} cm^{-1}, respectively *(9)*. These extinction coefficients were used to determine the concentration of all the synthesized MGB-tailed octathymidylates, including the analogous CDPI₁₋₃–(pdT)₈, BocDPI₁₋₂–(pdT)₈ and (dTp)₈–BocDPI₁₋₂

conjugates. For poly(dA) and poly(rA), ϵ_{260}s of 8.4 and 10.3 mM^{-1} cm^{-1} were used *(10)*.

UV Mixing Curves. Mixing curves for the interactions of octathymidylates and polyadenylates were determined by using the method of continuous variations *(11)*. Equimolar solutions (3.2 × 10^{-5} M in nucleotide residues) of (dTp)₈, (dTp)₈–CDPI₁₋₃, poly(dA), and poly-(rA) were prepared in 140 mM KCl, 10 mM MgCl₂, 20 mM HEPES-HCl (pH 7.2). For each hybrid the two respective solutions (starting volume 500 µL) were progressively diluted with each other until the two mixtures contained equimolar amounts of TMP and AMP residues. After every dilution the A_{260} was determined at a temperature 10 °C below the T_m of the respective hybrid (for T_ms, see Table 1). Each dilution was designed to alter the nucleotide composition of the mixture by approximately 5%.

Thermal Denaturation Studies. Hybrids formed between MGB-tailed (dTp)₈ conjugates and complementary polyadenylates were melted at a rate of 0.5 °C/min in 140 mM KCl, 10 mM MgCl₂, and 20 mM HEPES-HCl (pH 7.2) on a Lambda 2 (Perkin-Elmer) spectrophotometer with a PTP-6 automatic multicell temperature programmer. Each ODN (2 × 10^{-6} M) was mixed with sufficient polymer to give a T:A ratio of 1:1. The melting temperatures (T_m's) of the hybrids were determined from the derivative maxima and are collected in Table 1. Prior to melting, samples were denatured at 100 °C and then cooled to the starting temperature over a 10 min period.

2,3,5,6-Tetrafluorophenyl 3-Carbamoyl-1,2-dihydro-3*H*-pyrrolo[3,2-*e*]indole-7-carboxylate (1a) (Scheme 1). 2,3,5,6-Tetrafluorophenyl trifluoroacetate *(12)* (2.6 g, 10 mmol) was added dropwise to a solution of 3-carbamoyl-1,2-dihydro-3*H*-pyrrolo[3,2-*e*]indole-7-carboxylic acid *(6)* (1.4 g, 6.1 mmol) and triethylamine (1.4 mL, 10 mmol) in 15 mL of anhydrous DMF. After 1 h, the reaction mixture was concentrated under vacuum (0.2 mm) using a rotary evaporator. The residue was triturated with 2 mL of dry dichloromethane. Ethyl ether (50 mL) was added, and the mixture was left at 0 °C overnight. The precipitate was collected by filtration on a sintered-glass funnel, washed first with 50% ether/CH₂-Cl₂ (10 mL) and then with ether (50 mL), and dried *in vacuo*. The product was obtained as a yellow solid (1.8 g, 75%): ^{1}H NMR (Me₂SO-d_6, 200 MHz) δ 12.32 (s, 1H, NH), 8.13 (d, 1H, J = 9 Hz, C4-H), 8.01 (m, 1H, C₆F₄H), 7.41 (s, 1H, C8-H), 7.26 (d, 1H, J = 9 Hz, C5-H), 6.17 (s, 2H, CONH₂), 3.99 (t, 2H, J = 9 Hz, NCH₂CH₂), 3.30 (t, 2H, J = 9 Hz, NCH₂CH₂ partially obscured by water). Anal. Calcd for C₁₈H₁₁N₃O₃F₄·2H₂O: C, 50.36; H, 3.52; N, 9.79. Found: C, 50.81; H, 3.60; N, 9.95.

2,3,5,6-Tetrafluorophenyl 3-(*tert*-Butyloxycarbonyl)-1,2-dihydro-3*H*-pyrrolo[3,2-*e*]indole-7-carboxylate (1b). 2,3,5,6-Tetrafluorophenyl trifluoroacetate (2.6 g, 10 mmol) was added dropwise to a solution of 3-(*tert*-butyloxycarbonyl)-1,2-dihydro-3*H*-pyrrolo[3,2-*e*]indole-7-carboxylic acid *(6)* (1.0 g, 3.7 mmol) and triethylamine (1.5 mL, 10 mmol) in 10 mL of anhydrous CH₂Cl₂. After 4 h, CH₂Cl₂ was removed by evaporation at reduced pressure using a rotary evaporator. Flash chromatography (silica gel, column 4 × 20 cm, hexane/ethyl acetate, 1:2) afforded **1b** as a yellow crystalline solid (1.25 g, 75%): ^{1}H NMR (Me₂SO-d_6, 200 MHz) δ 12.39 (d, 1H, J = 1.4 Hz, NH), 8.02 (m, 1H, C₆F₄H), 7.9 (br s, 1H, C4-H), 7.45 (d, 1H, J = 1.4 Hz, C8-H), 7.33 (d, 1H, J = 9 Hz, C5-H), 4.02 (t, 2H, J = 9 Hz, NCH₂CH₂), 3.26 (t, 2H, J = 9 Hz, NCH₂CH₂), 1.51 (s, 9H, C(CH₃)₃). Anal. Calcd for C₂₂H₁₈N₂O₄F₄: C, 58.67; H, 4.03; N, 6.22. Found: C, 58.45; H, 4.09; N, 6.13.

3-Carbamoyl-1,2-dihydro-3*H*-pyrrolo[3,2-*e*]indole-7-carboxylate Dimer Methyl Ester (2a). A solution of DPI methyl ester (0.6 g, 1.5 mmol), **1a** (0.45 g, 2.25 mmol), and triethylamine (0.2 mL, 1.4 mmol) in 10 mL of anhydrous DMF was incubated at room temperature for 24 h and then at 0 °C for 12 h. The resulting insoluble solid was collected by filtration and washed with DMF (10 mL) and ether (20 mL). Drying *in vacuo* afforded **2a** (0.61 g, 91%) as a pale yellow solid: ^{1}H NMR (Me$_2$SO-d_6, 200 MHz) δ 12.00 (s, 1H, NH'), 11.54 (s, 1H, NH), 8.28 (d, 1H, J = 9 Hz, C4'-H), 7.97 (d, 1H, J = 9 Hz, C4-H), 7.33 (d, 1H, J = 9 Hz, C5'-H), 7.22 (d, 1H, J = 9 Hz, C5-H), 7.13 (d, 1H, J = 1.4 Hz, C8'-H), 6.94 (d, 1H, J = 1.1 Hz, C8-H), 6.10 (s, 2H, CONH$_2$), 4.62 (t, 2H, J = 8 Hz, (NH$_2$CH$_2$)'), 3.98 (t, 2H, J = 8 Hz, NCH$_2$CH$_2$), 3.88 (s, 3H, CH$_3$), 3.41 (t, 2H, J = 8 Hz, (NCH$_2$CH$_2$)'), 3.29 (t, 2H, NCH$_2$CH$_2$, partially obscured by water).

3-(*tert*-Butyloxycarbonyl)-1,2-dihydro-3*H*-pyrrolo-[3,2-*e*]indole-7-carboxylate Dimer Methyl Ester (2c). A solution of DPI methyl ester (0.5 g, 2.5 mmol), **1b** (1.0 g, 2.2 mmol), and triethylamine (0.1 mL, 0.7 mmol) in 10 mL of anhydrous DMF was incubated at room temperature for 10 h and at 0 °C for 12 h. The resulting insoluble solid was collected by filtration and washed with DMF (5 mL) and ether (40 mL). Drying *in vacuo* afforded **2c** (0.81 g, 74%) as an off-white solid: ^{1}H NMR (Me$_2$SO-d_6, 200 MHz) δ 12.01 (s, 1H, NH'), 11.64 (s, 1H, NH), 8.28 (d, 1H, J = 9 Hz, C4'-H), 7.8 (br s, 1H, C4-H), 7.32 (apparent t, 2H, C5'-H + C5-H), 7.13 (d, 1H, J = 1.1 Hz, C8'-H), 6.98 (d, 1H, J = 1.1 Hz, C8-H), 4.62 (t, 2H, J = 8 Hz, (NH$_2$CH$_2$)'), 4.02 (t, 2H, J = 8 Hz, NCH$_2$-CH$_2$), 3.88 (s, 3H, CH$_3$), 3.41 (t, 2H, J = 8 Hz, (NCH$_2$-CH$_2$)'), 3.25 (t, 2H, NCH$_2$CH$_2$), 1.52 (s, 9H, C(CH$_3$)).

2,3,5,6-Tetrafluorophenyl 3-carbamoyl-1,2-dihy-dro-3*H*-pyrrolo[3,2-*e*]indole-7-carboxylate dimer (2e). 2,3,5,6-Tetrafluorophenyl trifluoroacetate (2.6 g, 10 mmol) was added dropwise to a suspension of **2b** (prepared by deprotection of **2a** as previously described *(6)*) (1.2 g, 2.8 mmol) in 15 mL of anhydrous DMF. Triethylamine (1.4 mL, 10 mmol) was added, and the mixture was stirred for 3 h. The mixture was concentrated *in vacuo* (0.2 mm) using a rotary evaporator. The residue was triturated with 20 mL of dry dichloromethane. The product was filtered, washed with dichloromethane (10 mL) and ether (20 mL), and dried down to give **2e** as a yellow solid (1.5 g, 93%): ^{1}H NMR (Me$_2$SO-d_6, 200 MHz) δ 12.51 (d, 1H, J = 1.8 Hz, NH'), 11.58 (s, 1H, NH), 8.39 (d, 1H, J = 8.9 Hz, C4'-H), 8.04 (m, 1H, C$_6$F$_4$H), 7.98 (d, 1H, J = 8.8 Hz, C4-H), 7.58 (s, 1H, C8'), 7.42 (d, 1H, J = 9 Hz, C5'-H), 7.22 (d, 1H, J = 9 Hz, C5-H), 6.98 (s, 1H, C8-H), 6.11 (s, 2H, CONH$_2$), 4.66 (t, 2H, J = 7.8 Hz, (NCH$_2$CH$_2$)'), 3.98 (t, 2H, J = 9.1 Hz, NCH$_2$CH$_2$), 3.47 (t, 2H, J = 8 Hz, (NCH$_2$CH$_2$)'), 3.29 (t, 2H, NCH$_2$CH$_2$ partially obscured by water). Anal. Calcd for C$_{29}$H$_{19}$N$_5$O$_4$F$_4$·1.5H$_2$O: C, 57.62; H, 3.67; N, 11.59. Found: C, 57.18; H, 3.31; N, 11.54.

2,3,5,6-Tetrafluorophenyl 3-(*tert*-Butyloxycarbon-yl)-1,2-dihydro-3*H*-pyrrolo[3,2-*e*]indole-7-carboxy-late Dimer (2f). 2,3,5,6-Tetrafluorophenyl trifluoroac-etate (0.75 g, 2.9 mmol) was added dropwise to a suspension of **2d** (prepared by deprotection of **2c** as previously described *(6)*) (0.25 g, 0.5 mmol) and triethylamine (0.5 mL, 3.5 mmol) in a mixture of anhydrous CH$_2$Cl$_2$ (8 mL) and DMF (2 mL). The mixture was stirred for 20 h. The resultant clear solution was concentrated *in vacuo* and added dropwise to 40 mL of 1 M sodium acetate (pH 7.5). The precipitate was centrifuged and washed with water (2 × 40 mL), with 10% MeOH in ether (2 × 40 mL), with ether (40 mL), and with hexane (40

mL). Finally, it was dried *in vacuo* to give **2f** as a pale yellow solid (0.29 g, 91%): ^{1}H NMR (Me$_2$SO-d_6, 200 MHz) δ 12.51 (s, 1H, NH'), 11.66 (s, 1H, NH), 8.39 (d, 1H, J = 8.8 Hz, C4'-H), 8.03 (m, 1H, C$_6$F$_4$H), 7.8 (br s, 1H, C4-H), 7.57 (s, 1H, C8'-H), 7.41 (d, 1H, J = 9.1 Hz, C5'-H), 7.29 (d, 1H, J = 8.6 Hz, C5-H), 7.01 (s, 1H, C8-H), 4.65 (t, 2H, J = 8 Hz, (NCH$_2$CH$_2$)'), 4.02 (t, 2H, J = 9 Hz, NCH$_2$CH$_2$)'), 3.46 (t, 2H, J = 8 Hz, (NCH$_2$CH$_2$)'), 3.25 (t, 2H, J = 8.9 Hz, NCH$_2$CH$_2$), 1.51 (s, 9H, C(CH$_3$)$_3$). Anal. Calcd for C$_{33}$H$_{26}$N$_4$O$_5$F$_4$·0.5H$_2$O: C, 61.59; N, 8.71. Found: C, 61.73; H, 4.12; N, 8.61.

3-Carbamoyl-1,2-dihydro-3*H*-pyrrolo[3,2-*e*]indole-7-carboxylate Trimer Methyl Ester (3a). A solution of methyl 1,2-dihydro-3*H*-pyrroloindole-7-carboxylate (1.0 g, 5 mmol), **2e** (1.2 g, 2.1 mmol), and triethylamine (0.1 mL, 0.7 mmol) in 15 mL of anhydrous DMF was incu-bated at room temperature for 24 h and at 0 °C for 12 h. The resulting insoluble solid was collected by filtration and washed with DMF (10 mL), CH$_2$Cl$_2$ (20 mL), and ether (20 mL). Drying *in vacuo* afforded **3a** (1.1 g, 83%) as a pale yellow solid: ^{1}H NMR (Me$_2$SO-d_6, 200 MHz) δ 12.02 (s, 1H, NH''), 11.75 (s, 1H, NH'), 11.56 (s, 1H, NH), 8.28 (apparent t, 2H, J = 8.3 Hz, C4-H'' + C4'-H), 7.98 (d, 1H, J = 9 Hz, C4-H), 7.39–7.33 (2 d, 2H, C5''-H + C5'-H), 7.23 (d, 1H, J = 8.7 Hz, C5-H), 7.14 (d, 1H, J = 1.6 Hz, C8''-H), 7.10 (d, 1H, J = 1 Hz, C8'-H), 6.97 (s, 1H, C8-H), 6.11 (br s, 2H, CONH$_2$), 4.65 (apparent t, 4H, (NCH$_2$CH$_2$)'' + (NCH$_2$CH$_2$)'), 3.98 (t, 2H, J = 8.7 Hz, NCH$_2$CH$_2$), 3.88 (s, 3H, CH$_3$), 3.48–3.25 (m, 6H, (NCH$_2$-CH$_2$)'' + (NCH$_2$CH$_2$)' + NCH$_2$CH$_2$ partially obscured by water).

2,3,5,6-Tetrafluorophenyl 3-carbamoyl-1,2-dihy-dro-3*H*-pyrrolo[3,2-*e*]indole-7-carboxylate Trimer (3c). 2,3,5,6-Tetrafluorophenyl trifluoroacetate (2.6 g, 10 mmol) was added dropwise to a suspension of **3b** (pre-pared from **3a** as previously described *(6)*) (1.1 g, 1.8 mmol) in 15 mL of anhydrous DMF and triethylamine (1.4 mL, 10 mmol). The mixture was stirred for 3 h and then concentrated *in vacuo* (0.2 mm) using a rotary evaporator. The residue was triturated with a mixture of dry dichloromethane (20 mL) and methanol (2 mL). The product was filtered off, washed with dichlo-romethane (20 mL) and ether (20 mL), and dried down to give **3c** (1.3 g, 95%) as a yellow-green solid: ^{1}H NMR (Me$_2$SO-d_6, 200 MHz) δ 12.54 (d, 1H, J = 1 Hz, NH''), 11.79 (s, 1H, NH'), 11.56 (s, 1H, NH), 8.41 (d, 1H, J = 9.3 Hz, C4''-H), 8.27 (d, 1H, J = 9.4 Hz, C4'-H), 8.03 (m, 1H, C$_6$F$_4$H), 7.98 (d, 1H, J = 9 Hz, C4-H), 7.59 (s, 1H, C8''-H), 7.45–7.35 (m, 2H, C5''-H + C5'-H), 7.23 (d, 1H, J = 9.2 Hz, C5-H), 7.13 (s, 1H, C8'-H), 6.97 (s, 1H, C8-H), 6.11 (br s, 2H, CONH$_2$), 4.65 (m, 4H, (NCH$_2$CH$_2$)'' + (NCH$_2$CH$_2$)'), 3.98 (t, 2H, J = 8.7 Hz, NCH$_2$CH$_2$), 3.8–3.6 (m, 6H, (NCH$_2$CH$_2$)'' + (NCH$_2$CH$_2$)' + NCH$_2$CH$_2$ partially obscured by water). Anal. Calcd for C$_{40}$H$_{27}$N$_7$-O$_5$F$_4$·2H$_2$O: C, 60.23; H, 3.92; N, 12.29. Found: C, 60.98; H, 3.96; N, 11.93.

(3-Carbamoyl-1,2-dihydro-3*H*-pyrrolo[3,2-*e*]indole-7-(*N*-3-hydroxypropyl)carboxamide Trimer (3d). A solution of 3-amino-1-propanol (70 μL, 1.4 mmol), **3c** (75 mg, 0.1 mmol) and triethylamine (0.1 mL, 0.7 mmol) in 2.5 mL of anhydrous DMF was stirred at room temper-ature for 10 h. The resulting insoluble solid was collected by filtration and washed with DMF (2 mL), CH$_2$Cl$_2$ (10 mL) and ether (20 mL). Drying *in vacuo* afforded **3d** (55 mg, 89%) as a pale yellow solid: ^{1}H NMR (Me$_2$SO-d_6, 200 MHz) δ 11.76 (s, 1H, NH''), 11.65 (s, 1H, NH'), 11.57 (s, 1H, NH), 8.47 (m, 1H, NH), 8.24 (m, 2H, C4''-H + C4'-H), 7.99 (d, 1H, J = 8.4 Hz, C4–H), 7.40–7.32 (2d, 2H, C5''-H + C5'-H), 7.24 (d, 1H, J = 8.9 Hz, C5-H), 7.12 (s, 1H, C8''-H), 7.10 (s, 1H, C8'-H), 6.99 (s, 1H, C8-H), 6.12

(s, 2H, CONH$_2$), 4.66 (apparent t, 4H, (NCH$_2$CH$_2$)″ + (NCH$_2$CH$_2$)′), 3.98 (t, 2H, J = 8.7 Hz, NCH$_2$CH$_2$), 3.51–3.25 (m, 10H, (NCH$_2$CH$_2$)″ + (NCH$_2$CH$_2$)′ + NCH$_2$CH$_2$ + NHCH$_2$ + CH$_2$OH partially obscured by water), 1.70 (m, 2H, CH$_2$CH$_2$CH$_2$).

2,3,5,6-Tetrafluorophenyl 3-[N-(9-Fluorenylmeth-oxycarbonyl)amino]propanoate (4). 2,3,5,6-Tetraflu-orophenyl trifluoroacetate (1.7 g, 6.5 mmol) was added dropwise to a solution of Fmoc-β-alanine (2.0 g, 6.4 mmol) and triethylamine (1.0 mL, 7 mmol) in 20 mL of anhy-drous CH$_2$Cl$_2$. After 1 h, CH$_2$Cl$_2$ was removed at reduced pressure by rotary evaporation, and the residue was redissolved in 30 mL of ethyl acetate/hexane (1:1). Flash chromatography (silica gel, column 4 × 20 cm, hexane/ethyl acetate, 3:1) afforded **4** as a white solid. It was recrystallized from hexane/ethyl acetate to give the desired product as a white crystalline solid (2.3 g, 78%): ^{1}H NMR (CDCl$_3$, 200 MHz) δ 7.73 (d, 2H, J = 7.1 Hz, aromatic protons), 7.75 (d, 2H, J = 7.7 Hz, aromatic protons), 7.24–7.42 (m, 4H, aromatic protons), 7.01 (m, 1H, C$_6$F$_4$H), 5.21 (br s, 1H, CONH), 4.40 (d, 2H, J = 7.1 Hz, CH$_2$OCO), 4.22 (m, 1H, benzyl proton), 3.58 (m, 2H, NCH$_2$), 2.93 (t, 2H, J = 5.4 Hz, CH$_2$CO). Anal. Calcd for C$_{24}$H$_{17}$NO$_4$F$_4$: C, 62.75; H, 3.73; N, 3.05. Found: C, 62.52; H, 3.59; N, 3.01.

3-[[3-[(9-Fluorenylmethoxycarbonyl)amino]-propanoyl]amino]-(R,S)-1,2-propanediol (5). A solu-tion of **4** (2.0 g, 4.35 mmol) in 20 mL of anhydrous CH$_2$-Cl$_2$ was added to a stirred solution of 3-amino-1,2-propanediol (0.6 g, 6.6 mmol) in 10 mL of MeOH. After 10 min, acetic acid (3 mL) was added, and the mixture was evaporated to dryness. The residue was triturated with 100 mL of water. The resultant solid was filtered off, washed with water, and dried by coevaporation with toluene (2 × 50 mL) at reduced pressure. Washing with 50 mL of ethyl acetate followed by drying *in vacuo* overnight yielded **5** as a white crystalline solid (1.65 g, 99%): ^{1}H NMR (CDCl$_3$ + MeOD-d_4, 200 MHz) δ 7.79 (d, 2H, J = 7.7 Hz, aromatic protons), 7.63 (d, 2H, J = 7.3 Hz, aromatic protons), 7.45–7.29 (m, 4H, aromatic protons), 4.35 (d, 2H, J = 7.1 Hz, CH$_2$OCO), 4.21 (m, 1H, benzyl proton), 3.72 (m, 1H, NHCH$_2$CHOHCH$_2$OH), 3.52–3.27 (m, 6H, OCONHCH_2 + NHCH$_2$CHOHCH_2-OH), 2.44 (t, 2H, J = 6.6 Hz, CH$_2$CO). Anal. Calcd for C$_{21}$H$_{24}$N$_2$O$_5$: C, 65.61; H, 6.29; N, 7.29. Found: C, 65.43; H, 6.28; N, 7.21.

3-[[3-[(9-Fluorenylmethoxycarbonyl)amino]-propanoyl]amino]-2-O-(dimethoxytrityl)-(R,S)-1,2-propanediol (6). To a stirred solution of **5** (1.6 g, 4.2 mmol) in 30 mL of anhydrous pyridine was added 4,4′-dimethoxytrityl chloride (1.6 g, 4.7 mmol). After stirring for 3 h under argon, the mixture was evaporated to dryness. Residual pyridine was removed by coevapora-tion with toluene. The residue was dissolved in 100 mL of CH$_2$Cl$_2$, washed with 2 × 100 mL of water, dried over sodium sulfate, and evaporated to dryness. The residue was purified by flash chromatography (silica gel, 4 × 20 cm column) using ethyl acetate as an eluent. The fractions containing pure product were combined and evaporated to dryness to give 1.9 g (66%) of **6** as a colorless foam: ^{1}H NMR (CDCl$_3$, 200 MHz) δ 7.72 (d, 2H, J = 7.2 Hz, aromatic protons), 7.56 (d, 2H, J = 7 Hz, aromatic protons), 7.40–7.20 (m, 13H, aromatic protons), 6.80 (d, 4H, J = 9 Hz, DMTr protons), 5.76 (br s, 1H, NH), 5.42 (br s, 1H, NH), 4.35 (d, 2H, J = 6.6 Hz, CH$_2$-OCO), 4.17 (m, 1H, benzyl proton), 3.83 (m, 1H, NHCH$_2$-CHOHCH$_2$OH), 3.75 (s, 6H, OCH$_3$), 3.6–3.4 (m, 3H, OCONHCH_2 + CH_2CHOHCH$_2$O), 3.3–3.15 (m, 1H, OCONHCH_2) 3.13 (d, 2H, J = 5.4 Hz, CH$_2$ODMTr), 2.30

(t, 2H, J = 5.4 Hz, CH$_2$CO). Anal. Calcd for C$_{42}$H$_{42}$N$_2$-O$_7$: C, 73.45; H, 6.16; N, 4.08. Found: C, 73.30; H, 6.51; N, 4.26.

2,3,5,6-Tetrafluorophenyl 3-[[3-[(9-Fluorenylmeth-oxycarbonyl)amino]propanoyl]amino]-(R,S)-2-[(di-methoxytrityl)oxy]prop-1-yl Butanedioate (7). To a solution of **6** (1.2 g, 1.75 mmol), triethylamine (0.2 g, 2 mmol), and 1-methylimidazole (20 μL) in 10 mL of anhydrous CH$_2$Cl$_2$ was added 0.2 g (2 mmol) of succinic anhydride. This solution was stirred for 20 h. Trieth-ylamine (60 μL) was added to the solution followed by 0.6 g (2.2 mmol) of 2,3,5,6-tetrafluorophenyl trifluoroac-etate. After 1 h, CH$_2$Cl$_2$ was removed by evaporation at reduced pressure, and the residue was redissolved in 15 mL of ethyl acetate/hexane (1:2). Flash chromatography (silica gel, column 4 × 20 cm, hexane/ethyl acetate, 2:1) afforded **7** as a pale yellow foam (1.2 g, 73%): ^{1}H NMR (CDCl$_3$, 300 MHz) δ 7.74 (d, 2H, J = 7.2 Hz, aromatic protons), 7.56 (d, 2H, J = 7 Hz, aromatic protons), 7.45–7.20 (m, 13H, aromatic protons), 7.00 (m, 1H, C$_6$F$_4$H), 6.81 (d, 4H, J = 7 Hz, DMTr protons), 5.83 (br s, 1H, NH), 5.51 (br s, 1H, NH), 5.19 (m, 1H, NHCH$_2$CH(O)-CH$_2$O), 4.35 (d, 2H, J = 6.2 Hz, CH$_2$OCO), 4.19 (t, 5.5 Hz, 1H, benzyl proton), 3.77 (s, 6H, OCH$_3$), 3.68 (m, 1H, OCONHCH_2), 3.39 (m, 3H, OCONHCH_2 + NHCH_2CH-(O)CH$_2$O), 3.23 (d, 2H, 2.5 Hz, CH$_2$O-DMTr), 3.00 (m, 2H, COCH$_2$CH$_2$CO), 2.75 (t, 2H, 6.3 Hz, COCH_2CH$_2$CO), 2.24 (t, 2H, 5.2 Hz, CH$_2$CO). Anal. Calcd for C$_{52}$H$_{46}$N$_2$O$_{10}$F$_4$: C, 66.80; H, 4.96; N, 3.00. Found: C, 66.18; H, 4.98; N, 2.86.

Preparation of CDPI$_3$-Modified CPG (10) for the Automated Synthesis of ODN–CDPI$_3$ Conjugates (Scheme 3). A mixture of 5.0 g of long chain alkyl-amine–CPG, 0.5 mL of 1-methylimidazole, and 0.45 g (0.5 mmol) of **7** in 20 mL of anhydrous pyridine was swirled in a 100 mL flask (orbital mixer, 150 rpm). After 3 h, the CPG was filtered on a sintered-glass funnel and washed with 100 mL portions of DMF, acetone, and diethyl ether. The CPG was dried *in vacuo* and treated with a mixture of pyridine (20 mL), acetic anhydride (2 mL), and 1-methylimidazole (2 mL). After the mixture was swirled for 30 min, the CPG was washed with pyridine, methanol, and diethyl ether and then dried *in vacuo*. The product (**8**) was analyzed for dimethoxytrityl content according to the literature method *(13)* and found to have a loading of 28 μmol/g. The modified CPG (**8**) (3.0 g) was treated twice with 20 mL of 20% piperidine in dry DMF for 5 min each time. The product **9** was washed with 100 mL portions of DMF, methanol, and diethyl ether and then dried. A mixture of 2.5 g of **9**, 7.5 mL of triethylamine, and 0.38 g (0.5 mmol) of **3c** (Scheme 1) in 7.5 mL of anhydrous DMSO was swirled in a 50 mL flask (orbital mixer, 150 rpm). After 2 days, the CPG was filtered on a sintered-glass funnel and washed with 100 mL portions of DMSO, acetone, and diethyl ether. The CPG was dried and treated with a mixture of pyridine (10 mL), acetic anhydride (1 mL), and 1-meth-ylimidazole (1 mL). After the mixture was swirled for 30 min, the final product **10** was washed with DMSO, pyridine, methanol, and diethyl ether and then dried *in vacuo*.

Preparation of MGB-Tailed ODNs (Scheme 2). *Method A.* To a solution of the cetyltrimethylammonium salt *(14)* of an aminohexyl-tailed ODN (30–50 nmol) and 1.5 μL of *N,N*-diisopropylethylamine in 40 μL of dry DMSO was added 40 μL of a 4 mM solution of one of the MGB TFP esters (**1a**, **1b**, **2e**, **2f**, or **3c**). The reaction mixture was kept for 12 h at room temperature. The ODN-related material was precipitated by addition of 1.5 mL of 2% LiClO$_4$ in acetone. The pellet was redissolved
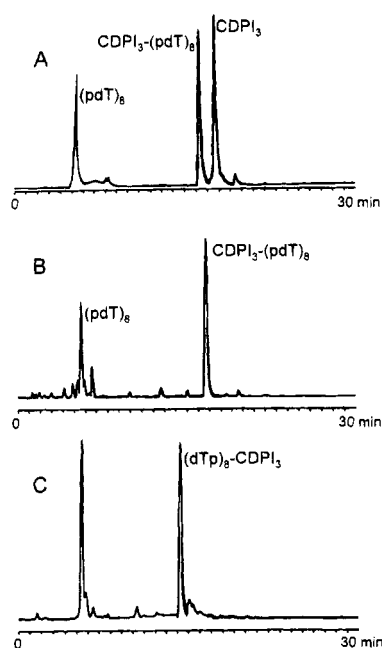
Figure 2. Elution profiles on a Dynamax-300A analytical column (C-18, 4.6 × 250 mm, Rainin) of reaction mixtures for the synthesis CDPI₃–(pdT)₈ by method A (A) and method B (B) and (dTp)₈–CDPI₃ by method C (C). For panels A, B, and C the gradient of acetonitrile was from 10 to 50% (30 min) at a flow rate of 1 mL/min. Detection is at 260 nm.

in 60 μL of water and reprecipitated twice with 2% LiClO₄ in acetone. Finally, the conjugates were purified by HPLC (4.6 × 250 mm, C-18, Dynamax-300A, Rainin). A typical HPLC trace is shown in Figure 2 (panel A). The fraction containing pure product was dried in a speedvac. The residue was dissolved in 60–80 μL of H₂O and precipitated with 1.5 mL of 2% LiClO₄ in acetone. After washing with acetone (1.5 mL) and drying *in vacuo*, the pellet was dissolved in 100 μL of water. The yield of the conjugates was 20–50%.

Method B. CPG containing 5′-aminohexyl-derivatized ODN (~1 μmol) was treated with 2% dichloroacetic acid in CH₂Cl₂ to remove the monomethoxytrityl residue from the amino group followed by washing with acetonitrile and drying by flushing with argon. The CPG was transferred into a 1.5 mL plastic tube. Triethylamine (10 μL) and a 50 mM solution of the desired MGB–TFP ester in anhydrous DMSO (100 μL) was added. The tube was shaken for 24 h at room temperature, then washed with 3 × 1.5 mL DMSO and 2 × 1.5 mL acetone, and dried *in vacuo*. The CPG was treated with concentrated ammonia to deprotect the ODN using standard conditions. The reaction products were separated using reverse phase HPLC (see Figure 2, panel B). Typical yield was 50–80%.

Method C. 3′-Modified conjugates were synthesized on a 1 μmol scale using the previously described CPG (10) (see Scheme 3). The trityl-OFF product was isolated by HPLC. Typical profile is shown on Figure 2 (panel C).

RESULTS AND DISCUSSION

Synthesis of TFP–CDPI₁₋₃ (1a, 2e, and 3c) and TFP–BocDPI₁₋₂ (1b and 2f). 2,3,5,6-Tetrafluorophenyl (TFP) esters were chosen as active intermediates for the synthesis of DPI-oligopeptides as well as for the conjugation of these derivatives to ODNs. TFP esters are usually stable enough to be purified by flash chromatography, crystallized, and stored for several months. They react with aliphatic and aromatic amino groups. Moreover, the

hydrophobic TFP residue improves the solubility of DPI derivatives in organic solvents, thus eliminating an obstacle for the synthesis of long DPI peptides (6).

Starting CDPI and BocDPI-carboxylic acids were prepared according to the literature method (6). Treatment of these compounds with 2,3,5,6-tetrafluorophenyl trifluoroacetate provided the TFP esters **1a** and **1b**. As illustrated in Scheme 1, reaction of the TFP esters with the methyl ester of DPI afforded methyl esters of CDPI₂ (**2a**) and BocDPI₂ (**2c**). After selective saponification of the methyl esters (water/organic LiOH), the resultant acids **2b** and **2d** were converted into the corresponding TFP esters **2e** and **2f** using reaction conditions identical to those used to produce monomers **1a** and **1b**. The condensation of TFP–CDPI₂ (**2e**) with methyl ester of DPI was carried out in DMF. While all starting reagents were soluble, the resulting product **3a** crystallized out. In the previously reported method (6), both starting materials and product were insoluble. The use of soluble TFP esters simplified the synthesis and isolation of DPI oligomers in this work. Compounds **2a**, **2c**, and **3a** prepared using this procedure were identical to those described in the literature (6). TFP–CDPI₃ (**3c**) was obtained from **3b** and TFP trifluoroacetate in a 95% yield of >90% pure material, suitable for conjugation to oligonucleotides.

Preparation of CDPI- and BocDPI-Tailed ODN Conjugates. *Method A.* We have investigated several different approaches for the preparation of MGB-tailed ODN conjugates. Initially, we used postsynthetic modification of ODNs in solution phase (Scheme 2, method A). The general procedure involved introduction of an aminohexyl residue at the 5′- or 3′-end of the ODN using a commercially available N-(monomethoxytrityl)-6-aminohexan-1-ol phosphoramidite for the 5′-modification or a specially modified CPG (7) for the 3′-modification. The ODNs were converted into organic-soluble cetyltrimethylammonium salts (14) and treated with one of the TFP esters (**1a**, **1b**, **2e**, **2f**, or **3c**) in DMSO. The desired conjugate as well as any unreacted ODN were precipitated with 2% LiClO₄ in acetone a few times, washed with acetone, and finally purified by reverse-phase HPLC. Despite the high conjugation efficiency (60–90% as judged by analytical HPLC), this multistep procedure provided only moderate yields (15–50%) of purified CDPI₁₋₃- and BocDPI₁₋₂-tailed ODN conjugates. Furthermore, this method was complicated by the coprecipitation of free CDPI₃ carboxylic acid along with the CDPI₃-tailed ODN in acetone. Multiple precipitations did not completely remove the CDPI contamination, and HPLC purification was required (Figure 2, panel A).

Method B. This on-column method (Scheme 2, method B) was developed as an improved version of the preceding protocol. First, a detritylated 5′-amino-tailed ODN was synthesized on a 1 μmol scale and left attached to the CPG support. The support was washed, dried, and treated with a solution of **3c** and triethylamine in dry DMSO. After 10–30 h of incubation at room temperature, the CPG was washed with DMSO and CH₂Cl₂, dried, and treated with ammonia at 43–45 °C over night. The CDPI peptides turned to be quite stable in the aqueous ammonia, as shown by the chromatogram of crude CDPI₃–(pdT)₈ in Figure 2 (panel B). Deblocked conjugates were isolated by reverse-phase HPLC in 50–80% yield. With this method, the loss of ODN caused by multiple precipitations in acetone was eliminated and the synthesis was simplified. This synthetic route is limited to 5′-MGB-tailed ODN conjugates. As expected, conjugates prepared by methods A and B were identical by

Scheme 1.^a **Synthesis of CDPI and BocDPI Peptides**

R= CH₃, R'= H (DPI methyl ester)
1a R= TFP, R'= CONH₂ (TFP-CDPI)
1b R= TFP, R'= ᵗBoc (TFP-Boc-DPI)

2a R= CH₃, R'= CONH₂ (CDPI₂ methyl ester)
2b R= H, R'= CONH₂ (CDPI₂)
2c R= CH₃, R'= ᵗBoc (Boc-DPI₂ methyl ester)
2d R= H, R'= ᵗBoc (Boc-DPI₂)
2e R= TFP, R'= CONH₂ (TFP-CDPI₂)
2f R= TFP, R'= ᵗBoc (TFP-Boc-DPI₂)

3a R= OCH₃ (CDPI₃ methyl ester)
3b R= OH (CDPI₃)
3c R= O-TFP (TFP-CDPI₃)
3d R=NH(CH₂)₃OH (CDPI₃ 3-hydroxypropylamid)
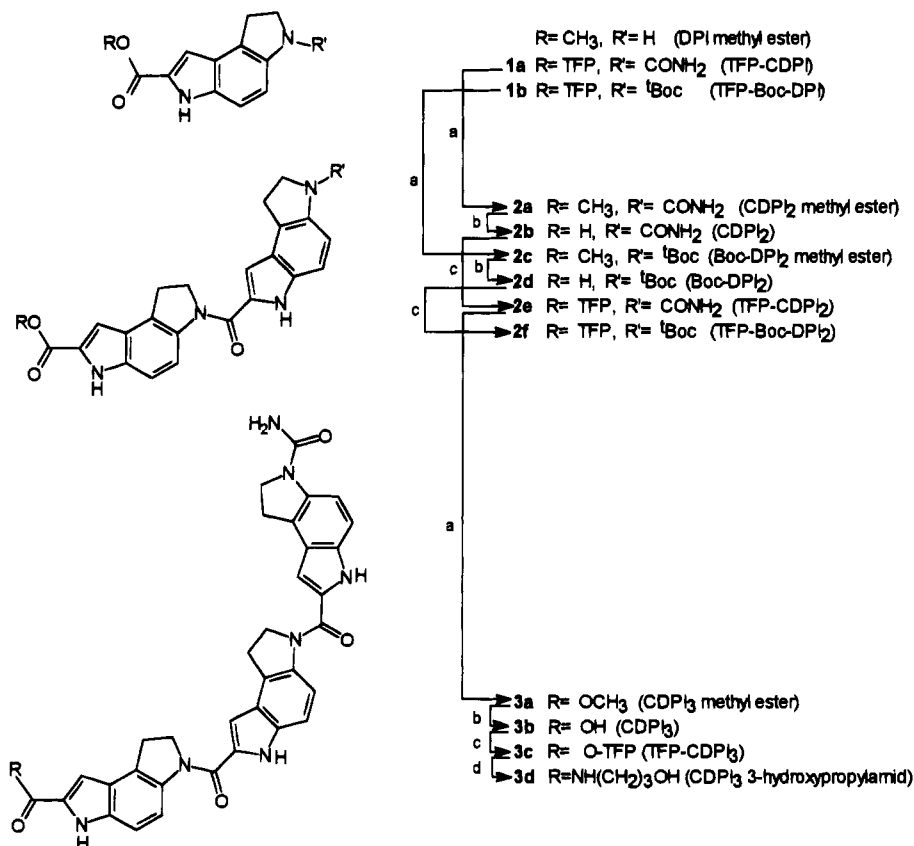
ᵃ Reagents: (a) DPI methyl ester, Et₃N, DMF; (b) LiOH, MeOH, THF; (c) TFP–TFA, Et₃N, DMF; (d) 3-aminopropanol, Et₃N, DMF.

reverse-phase HPLC, gel electrophoresis, and UV–visible spectroscopy.

In order to prove structure of the isolated MGB-tailed ODN conjugates, CDPI₃–(pdT)₈ (∼1 × 10⁻⁵ mmol) was treated with snake venom phosphodiesterase I (2.5 units) and alkaline phosphatase (4 units) from calf intestine in 10 mM MgCl₂, 50 mM Tris-HCl, pH 8.5. After 5 h of incubation at 37 °C, two major low-mobility products, along with thymidine, were detected by analytical reverse-phase HPLC. Based on the UV absorbance, one of them was thymidine 5'-phosphate conjugated to CDPI₃-residue. Addition of more phosphodiesterase and longer incubation did not change significantly the cleavage profile. The second, most hydrophobic, product had a spectrum and retention time identical to 3-carbamoyl-1,2-dihydro-3H-pyrrolo[3,2-e]indole-7-(N-(6-hydroxyhexyl)carboxamide) trimer (analog of **3d**, see Scheme 1), which was prepared by reaction of 6-amino-1-hexanol with **3c** in DMSO as a marker.

Method C. The need for a more versatile and reliable synthesis of 3'-MGB-tailed ODN conjugates prompted us to develop a CPG support prederivatized with the desired CDPI₃ tail. A custom linker was prepared by reacting the TFP ester of N-(Fmoc)-protected β-alanine (**4**) with 1-amino-2,3-propanediol (Scheme 3). The resulting compound **5** was converted into the 4,4'-dimethoxytrityl derivative (**6**), and, after reaction with succinic anhydride, was treated with trifluoroacetate TFP-ester to give **7**. Reaction of **7** with aminoalkyl CPG gave N-Fmoc-amine-modified CPG support **8** with a loading of 28 μmol/g. The CPG was treated with 20% piperidine in DMF to remove the Fmoc-amino protecting group. Treatment with excess TFP–CDPI₃ (**3c**) gave the desired CPG (**9**). Residual amino groups were capped with a mixture of 10% acetic anhydride and 10% 1-methylimidazole in pyridine.

ODN–CDPI₃ conjugates were prepared from this CPG support on a 1 μmol scale using β-cyanoethyl phosphoramidite coupling chemistry (Scheme 2, method C). The ODN–CDPI₃ was deblocked and cleaved from the CPG by ammonia treatment and isolated in good yield by a single HPLC purification. The desired conjugate was well-resolved from the most of side products due to the presence of the hydrophobic CDPI₃ group. Some of the side products have retention times longer than ODN–CDPI₃, caused by repeated iodine treatment during ODN synthesis. These side products are identified by a UV absorption in a region over 300 nm different from the CDPI₃. They do not reduce the yield of the desired product, nor do then complicate the purification of 8–16-mers. In general, the retention times for MGB-tailed ODN conjugates on a C-18 column were sensitive to the length of the peptide and the type of N-3 substituent (data not shown). Prior to further characterization, all MGB-tailed ODN conjugates were repurified by C-18 HPLC.

Spectral Properties of ODN–CDPI₁₋₃ Conjugates. CDPI containing ODNs exhibited absorption peaks at both 260 and 340 nm (see Figure 3). The absorption at 340 nm is due solely to the CDPI group while the absorption at 260 nm is attributable to both the ODN and the MGB. In the case of (dTp)₈–CDPI₃, the absorption spectrum of the conjugate was very close to the sum of the spectra for the unmodified ODN and free MGB (Figure 3). Interestingly, the absorption peak of free CDPI₃ occurred at 380 nm in water and at 330 nm in organic solvents. This suggests that in the conjugate CDPI₃ associates with the bases of the ODN to create a more hydrophobic environment.

Thermal Stability of Duplexes Formed by CDPI₁₋₃- and BocDPI₁₋₂-Tailed (dTp)₈ with Polyadenylates.

Scheme 2. Synthesis and Structure of CDPI$_{1-3}$- and BocDPI$_{1-2}$-Tailed ODNs

Method A:

R = CONH$_2$ or t-Boc

Method B:

N* - protected nucleoside
p* - β-cyanoethyl phosphate residue
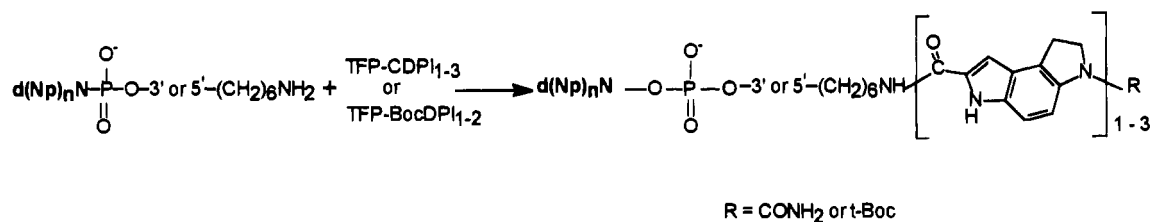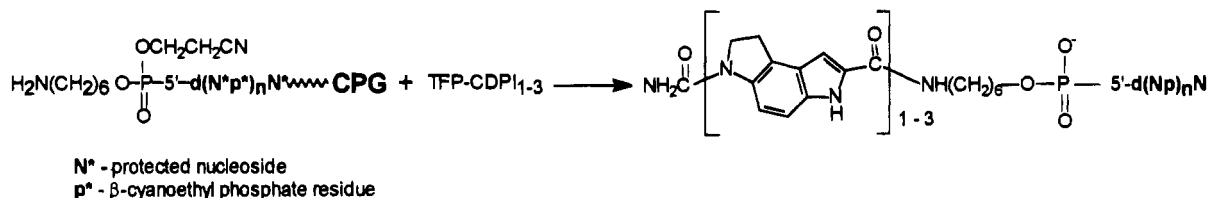
Method C:
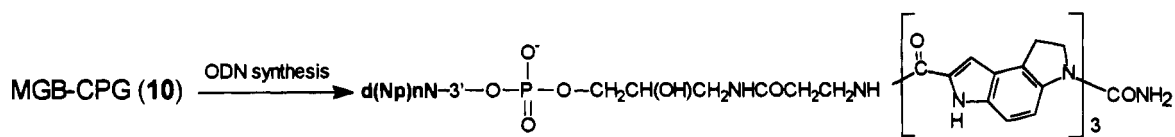
The hybridization properties of octadeoxythymidylates conjugated to CDPI$_{1-3}$ or BocDPI$_{1-2}$ were evaluated spectrophotometrically using complementary single-stranded polyribo- and polydeoxyriboadenylate in a buffer which contained physiologically relevant concentrations of K$^+$ and Mg^{2+}. Spermine was omitted due to precipitation of the nucleic acid in its presence. The results are summarized in Table 1. Relative to (dTp)$_8$, the same ODN conjugated to CDPI$_{1-3}$ formed more stable hybrids with poly(dA). The extent of stabilization was the same for 5'- and 3'-conjugates. One, two and three subunits of CDPI linked to octathymidylate increased the T_m of duplexes formed with poly(dA) by 7−9, 25, and 43−44 °C, respectively. As the length of the appended peptide was increased, the duplex melted with increasing hyperchromicity but constant cooperativity (see Figure 4). No significant increase in T_m was observed when an equivalent concentration of free CDPI$_3$ 3-hydroxypropylamide (**3d**, see Scheme 1) and unmodified (dTp)$_8$ were incubated together with poly(dA). The T_m was increased by only 2 °C, thus underscoring the importance of covalent linkage of MGB to ODN.

The strength of the (dTp)$_8$·poly(rA) hybrid was also affected by the presence of terminally conjugated CDPI$_{1-3}$ subunits. Surprisingly, 5'- and 3'-CDPI$_2$-tailed octathymidylates did not form detectable hybrids with poly-(rA). This may reflect a propensity of these conjugates to self-associate since they undergo a hyperchromic transition between 40 and 80 °C (see Figure 4). By contrast, conjugated CDPI$_1$ and CDPI$_3$ groups increased the T_m of duplexes with poly(rA) by 2−5 °C and 18−23 °C, respectively. The reduced stabilization of poly(rA) hybrids relative to poly(dA) hybrids by octathymidylate-conjugated CDPI$_{1-3}$ groups mirrors the lower affinity of most minor groove binders for DNA·RNA duplexes.
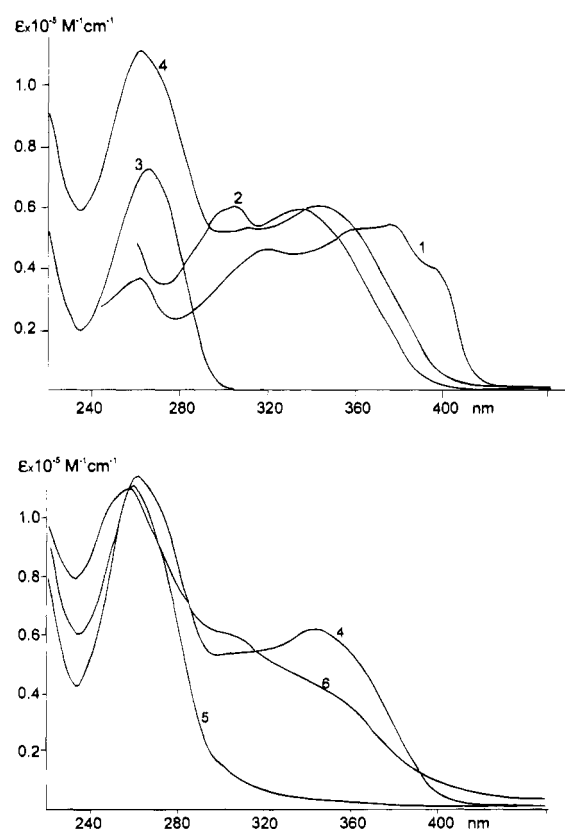
Figure 3. UV−visible spectra of (2) free CDPI$_3$ (compound **3d**, see Scheme 1) in DMSO and (1) free CDPI$_3$ (**3d**), (3) (dTp)$_8$, (4) (dTp)$_8$−CDPI$_3$, (5) (dTp)$_8$−CDPI$_1$, and (6) (dT)$_8$−CDPI$_2$, all in water.

Scheme 3.[a] **Preparation of CDPI₃–CPG (10)**
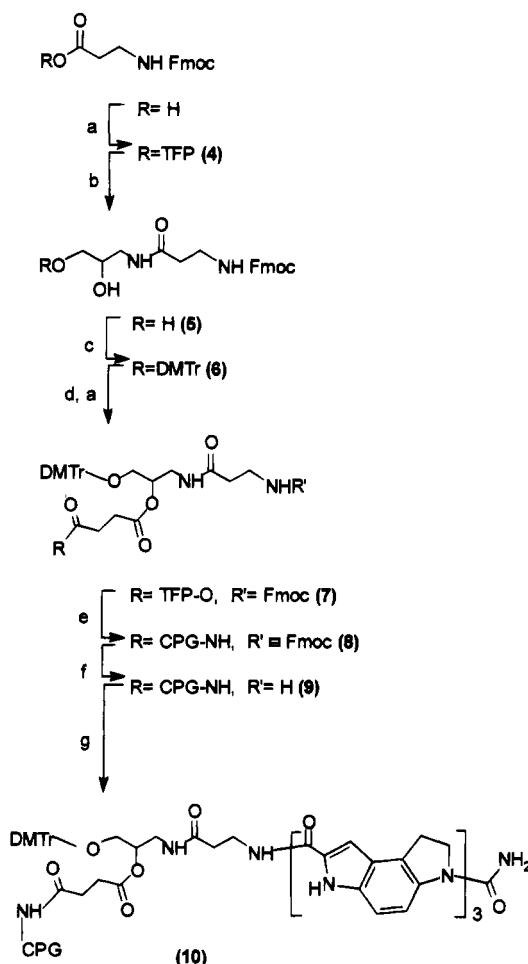
[a] Reagents: (a) TFP–TFA, Et₃N, CH₂Cl₂; (b) 3-amino-1,2-propanediol, CH₂Cl₂; (c) DMTrCl, pyridine; (d) succinic anhydride, *N*-methylimidazole, CH₂Cl₂; (e) alkylamine CPG, pyridine; (f) piperidine, DMF; (g) TFP–CDPI₃, DMF.

Table 1. Melting temperatures (°C) of Duplexes Formed by Poly(dA) and Poly(rA) with Octathymidylate Strands Terminally Linked to CDPI₁₋₃ and BocDPI₁₋₂ Ligands[a]

octathymidylate derivative	poly(dA)		poly(rA)	
	T_m	ΔT_m[c]	T_m	ΔT_m[c]
(dTp)₈–O(CH₂)₆NH₂	25		13	
(dTp)₈–O(CH₂)₆NH₂ + 3d (1:1 ratio)	27	2		
(dTp)₈–CDPI₁	34	9	18	5
(dTp)₈–CDPI₂	50	25	_[b]	
(dTp)₈–CDPI₃	68(65)	43(40)	32(31)	19(18)
(dTp)₈–BocDPI₁	26	1	12	−1
(dTp)₈–BocDPI₂	43	18	17	4
NH₂(CH₂)₆O–(pdT)₈	24		12	
CDPI₁–(pdT)₈	31	7	14	2
CDPI₂–(pdT)₈	49	25	_[b]	
CDPI₃–(pdT)₈	68	44	35	23
BocDPI₁–(pdT)₈	23	−1	9	−3
BocDPI₂–(pdT)₈	41	17	19	7

[a] The (dTp)₈–MGB conjugates were prepared by method A. For comparison, data obtained with (dTp)₈–MGB conjugates synthesized by method C are presented in parentheses. [b] No melting transition was observed. [c] Difference between ODNs with and without conjugated MGBs.

The limited melting data obtained with duplexes formed using the 5′- and 3′-BocDPI₁₋₂-tailed octathymidylates showed that relative to the carbamoyl substituent the presence of the bulky *tert*-butyloxycarbonyl substituent usually reduced hybrid stability. With the poly(dA)-
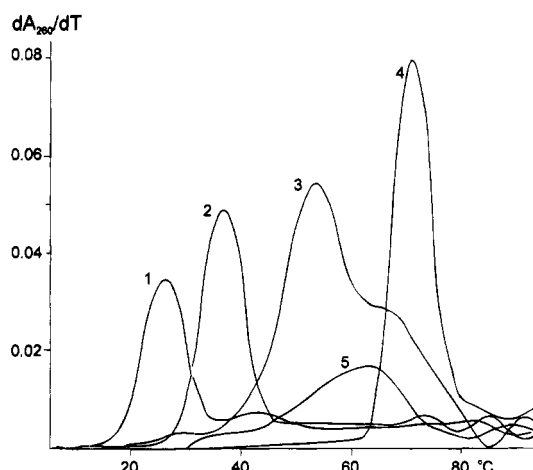
Figure 4. Differential melting curves for the complexes formed by (1) (dTp)₈, (2) (dTp)₈–CDPI₁, (3) (dTp)₈–CDPI₂, and (4) (dTp)₈–CDPI₃ with poly(dA) in 140 mM KCl, 10 mM MgCl₂, and 20 mM HEPES-HCl (pH 7.2). The concentration of each ODN was 2 × 10⁻⁶ M and the A:T ratio was 1:1. Curve 5 is for the melt of the (dTp)₈–CDPI₂ conjugate alone in the same buffer.
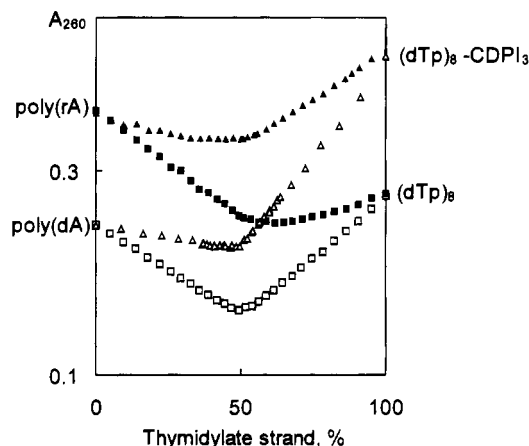
Figure 5. Mixing curves for complexation of (dTp)₈ and (dTp)₈–CDPI₃ with poly(dA) and poly(rA).

containing hybrids, this destabilization amounted to 8 °C and was independent of length or placement of the MGB. Hybrids formed between BocDPI₂-carrying octathymidylates and poly(rA), which were 5–7 °C more stable than control hybrids, were notable exceptions. As mentioned previously, the corresponding CDPI₂ conjugates did not hybridize to poly(rA).

For complexes of oligothymidylate with polyadenylate, triple strand formation is a possibility even at the A:T base ratio of 1:1 used in these experiments. To prove that the melting data in Table 1 is due to duplex formation, we carried out UV mixing experiments with four pairs of Watson/Crick strands. The results are presented in Figure 5. With all four mixing curves, straight lines fitted to the data points on either side of the A₂₆₀ minimum intersected with each other at or near an A:T ratio of 1:1, thus providing direct evidence for double-strand formation. Optical melting experiments conducted at A:T ratios of 1:2 or 2:1 (data not shown) also failed to detect hyperchromic transitions attributable to triplex formation by any of the Watson/Crick pairs studied here.

The hybridization properties of (dTp)₈–CDPI₁₋₃ conjugates differ in some respects from those reported by us for (dTp)₈–MPC₁₋₅ conjugates (1). Most notable is the ability of the CDPI but not the MPC conjugates to form

stabilized hybrids with complementary polyriboadenylate. A 3'-conjugated CDPI$_3$ group provided 19 °C of stabilization whereas a similarly conjugated MPC$_5$ group had no affect on hybrid stability. By contrast, when 5'- and 3'-CDPI$_3$-tailed octathymidylate conjugates are compared to a (dTp)$_8$–MPC$_5$ conjugate, both provided the same degree of hybrid stabilization with a DNA complement. Although both of these minor groove binders probably occupy the same length of duplex, they clearly differ in their mode of interaction. Whereas free MPC$_5$ can form up to six hydrogen bonds with the host DNA, free CDPI$_3$ may form more van der Waals contacts and enter into stronger hydrophobic interactions with the host duplex.

In this article we have limited our biochemical study to octathymidylate conjugates. We have found the chemistry is equally applicable to mixed sequences, varying lengths, and differing backbone modifications, as will be described later.

CONCLUSIONS

Straightforward methods are described for the synthesis of CDPI and BocDPI peptides and their conjugation to amino-tailed ODNs. The direct synthesis of ODN–CDPI$_3$ conjugates is also described using a custom prepared CPG support. The CDPI$_3$ derivatives of octathymidylate form unusually stable complexes with complementary poly(dA) and poly(rA). The T_m of these hybrids is increased by up to 44 °C and 23 °C, respectively, when compared to control duplexes which lack an MGB. These results justify the further investigation of CDPI$_3$-tailed ODN conjugates for use as diagnostic probes or antisense agents.

LITERATURE CITED

(1) Sinyakov, A. N., Lokhov, S. G., Kutyavin, I. V., Gamper, H. B., and Meyer, R. B. (1995) Exceptional and selective stabilization of A-T rich DNA-DNA duplexes by *N*-methylpyrrole carboxamide peptides conjugated to oligodeoxynucleotides. *J. Am. Chem. Soc. 117*, 4995.

(2) Zimmer, C., and Wahnert, U. (1986) Nonintercalating DNA-binding ligands: specificity of the interaction and their use as tools in biophysical, biochemical and biological investigations of the genetic material. *Prog. Biophys. Mol. Biol. 47*, 31.

(3) Hanka, L. J., Dietz, A., Gerpheide, S. A., Kuentzel, S. L., and Martin, D. G. (1978) CC-1065 (NSC-298223), a new antitumor antibiotic. Production, *in vitro* biological activity, microbiological assays and taxonomy of the producing microorganism. *J. Antibiot. 31*, 1211.

(4) Hurley, L. H., Reynolds, V. L., Swenson, D. H., Petzold, G. L., and Scahill, T. A. (1984) Reaction of the antitumor antibiotic CC-1065 with DNA: structure of a DNA adduct with DNA sequence specificity. *Science 226*, 843.

(5) Boger, D. L., and Sakya, S. M. (1992) CC-1065 partial structures: enhancement of noncovalent affinity for DNA minor groove binding through introduction of stabilizing electrostatic interactions. *J. Org. Chem. 57*, 1277.

(6) Boger, D. L., Coleman, R. S., and Invergo, B. J. (1987) Studies on the total synthesis of CC-1065: preparation of a synthetic, simplified 3-carbamoyl-1,2-dihydro-3*H*-pyrrolo[3,2-*e*]indole dimer/ trimer/ tetramer (CDPI dimer/ trimer/ tetramer) and development of methodology for PDE-I dimer methyl ester formation. *J. Org. Chem. 52*, 1521.

(7) Petrie, C. R., Reed, M. W., Adams, A. D., and Meyer, R. B., Jr. (1992) An improved CPG support for the synthesis of 3'-amine-tailed oligonucleotides. *Bioconjugate Chem. 3*, 85.

(8) Shabarova, Z. A., Dolinnaya, N. G., Drutsa, V. L., Melnikova, N. P., and Purmal, A. A. (1981) DNA-like duplexes with repetitions. III. Efficient template guided chemical polymerization of d(TGGGCCAAGCTp). *Nucleic Acids Res. 9*, 5747.

(9) Lokhov, S. G., Podyminogin, M. A., Sergeev, D. S., Silnikov, V. N., Kutyavin, I. V., Shishkin, G. V., and Zarytova, V. P. (1992) Synthesis and high stability of complementary complexes of *N*-(2-hydroxyethyl)phenazinium derivatives of oligonucleotides. *Bioconjugate Chem. 3*, 414.

(10) Riley, M., Maling, B., and Chamberlin, M. J. (1966) Physical and chemical characterization of two- and three-stranded adenine-thymidine and adenine-uracil homopolymer complexes. *J. Mol. Biol. 20*, 359.

(11) Job, P. (1928) *Anal. Chim. Acta 9*, 113.

(12) Gamper, H. B., Reed, M. W., Cox, T., Virosco, J. S., Adams, A. D., Gall, A. A., Scholler, J. K., and Meyer, R. B., Jr. (1993) Facile preparation of nuclease resistant 3' modified oligodeoxynucleotides. *Nucleic Acids Res. 21*, 145.

(13) Atkinson, T., and Smith, M. (1984) Solid-Phase Synthesis of Oligodeoxyribonucleo-tides by Phosphite-Triester Method. *Oligonucleotide Synthesis, A Practical Approach*. (M. Gait, Ed.) pp 35–81, IRL Press, Washington, DC.

(14) Jost, J.-P., Jiricny, J., and Saluz, H. (1989) Quantitative precipitation of short oligonucleotides with low concentrations of cetyltrimethylammonium bromide. *Nucleic Acids Res. 17*, 2143.

Improved Cytotoxicity of Antitumor Compounds Deliverable by the LDL Pathway[1,2]

Gene M. Dubowchik* and Raymond A. Firestone

Bristol-Myers Squibb Pharmaceutical Research Institute, P.O. Box 5100, Wallingford, Connecticut 06492-7660. Received September 19, 1994[⊗]

The concept of LDL-based chemotherapy of cancer is based on the fact that many tumors have high LDL requirements. A series of compounds has been synthesized, some of which meet all criteria for such therapy, i.e., they can be reconstituted with LDL, they do not leak out of the reconstituted LDL (rLDL), and they are potent enough to kill cells exclusively via the LDL receptor pathway. Two of these compounds are significantly superior to the best one from our earlier study [Firestone et al. (1984) *J. Med. Chem. 27*, 1037–1043], being cytotoxic in rLDL at concentrations reasonably attainable *in vivo*.

INTRODUCTION

There is growing interest in targeting cytotoxic compounds to tumors via low density lipoprotein (LDL) (3). The rationale is that many types of cancer take up large amounts of LDL, presumably because dividing cells require an increased amount of cholesterol to assemble membrane, and LDL is the body's principal vehicle for delivering LDL to tissues. Cells ingest LDL by receptor-mediated endocytosis into lysosomes, where degradation releases its core of about 1500 molecules of cholesterol ester per particle. The core is surrounded by a polar coat of phospholipid, unesterified cholesterol, and apoprotein B (Apo B) that is recognized by LDL receptors (4–6). High LDL requirements have been documented for these malignancies: AML (7), monocytic (FAB-M5) and myelomonocytic (FAB-M4) leukemias, chronic myeloid leukemia in blast crisis (8), epidermoid cervical cancer EC-50, endometrial adenocarcinoma AC-258 (9) and four other gynecological cancers (10), gastric carcinoma, parotid adenoma (11), medulloblastoma, oligodendroma, malignant meningioma (12), glioma V-251MG (13), G2 hepatoma (14, 15), squamous lung tumor (16), and choriocarcinoma (17). The LDL uptake of most tumors has not yet been measured. Some parasitic infections are also potential targets for LDL-based therapy (3).

Drugs have been associated with LDL by simple mixing (18), by reconstituting LDL particles with the result that all or part of the core is replaced by drug (19), and by creating new drug-loaded particles (microemulsions), each bearing an Apo B molecule (20). In the earliest procedure, LDL is lyophilized onto potato starch, delipidated with heptane, and then reconstituted with drug replacing cholesterol ester in the core (21). The method fails unless the drug is compatible with the phospholipid coat, whose lipid chains are arrayed on its inside surface. LDL anchors such as oleoyl, retinyl, and cholesteryl facilitate reconstitution (22). Once inside the LDL particle, the drug must remain there for a reasonable time (days) without leaking out. To ascertain that drug enters target cells only via LDL receptors, a variety of controls are possible: receptor-negative cells should be spared; there should be no cytotoxicity with rLDL made from methylated, acetylated, or oxidized LDL, which recognizes scavenger but not normal LDL receptors; and excess native LDL should compete with rLDL

for uptake. Once inside the target cells, the drug must be released from its LDL anchor. Finally, the quantity of drug that can be carried in rLDL, combined with its intrinsic cytotoxicity, must be sufficient to kill cells. This is important because the LDL uptake mechanism is saturable.

We reported in 1984 the synthesis and reconstitution with LDL of 20 new cytotoxic compounds (23). Some of them failed to reconstitute; others reconstituted but leaked out of the rLDL; still others reconstituted successfully, but the rLDL killed cells poorly or not at all; and one, "Compound 25" (1, Figure 1), reconstituted using the core replacement technique, met all criteria in that it afforded stable rLDL that killed all of the target cells at a reasonable concentration. This compound behaved equally well in other hands using the microemulsion technique (24), but was insufficiently cytotoxic (25) by a modified reconstitution method (19) which removes only part of the core, presumably replacing it with too few molecules of antitumor drug.

Structure–activity relationships within this group of compounds led us to the following conclusions: (1) A single LDL anchor, oleoyl, was sufficient to enable successful reconstitution, but not to prevent leakage. Two anchors, oleoyl and cholesteryl, were needed to provide fully stable rLDL. (2) A single nitrogen mustard (NM) warhead per prodrug molecule conferred enough cytotoxicity to kill cells. (3) However, since LDL receptor occupancy is saturable, if a substance such as "Compound 19" (2) lacked sufficient potency, no increase in concentration of rLDL could overcome this defect. Even at the highest concentration, rLDL bearing 2 killed only about half the target cells, inhibiting, but not killing, the remainder. (4) A carbamate linkage, but not some others, was susceptible to intracellular cleavage, sometimes with satisfactory ease. (5) Efficiency of cleavage was highly dependent on placement of the drug–anchor linkage within the oleoyl steroid, presumably because of steric factors which might limit access of lysosomal esterases or proteases.

EXPERIMENTAL SECTION

General. Steroidal starting materials were purchased from Steraloids Inc. (Wilton, NH), oleoyl chloride was from Sigma Chemical Co., and diphosgene was from Fluka Chemical Co. All other reagents were purchased from Aldrich Chemical Co. and were used as received. Butyllithium concentration was determined by titration
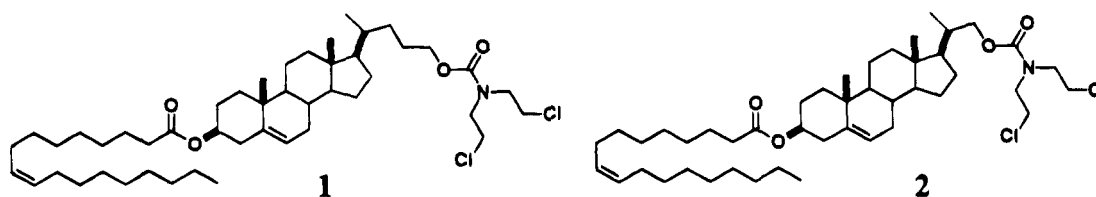
Figure 1.

with diphenylacetic acid. Tetrahydrofuran was distilled from benzophenone ketyl, and methylene chloride was distilled from calcium hydride. All other solvents were reagent grade and used as received. NMR spectra were run on a Varian Gemini 300 spectrometer in CDCl₃, unless otherwise indicated. Microanalyses were carried out at Oneida Research Services. Reactions were run at room temperature unless otherwise indicated.

3β-Hydroxy-5-cholenic Acid N-Hydroxysuccinimide Ester (4). 3β-Hydroxy-5-cholenic acid (3) (4.646 g, 12.40 mmol) and NHS (2.000 g, 1.4 equiv) in THF (175 mL) at 0 °C were treated with DCC (3.583 g, 1.4 equiv). The mixture was stored at 4 °C for 48 h. DCU was removed by filtration and washed with THF. The filtrate was evaporated, and the residue was dissolved in refluxing toluene (200 mL). As the mixture cooled, DCU and NHS precipitated out of solution. These were filtered off, and the toluene was evaporated. The resulting solid was crystallized from CH₂Cl₂/hexane to give **4** as a white solid (6.807 g, 97%): ¹H NMR δ 0.71 and 1.03 (each 3H, s, C-18 and C-19 CH₃), 0.98 (3H, d, C-21 CH₃, J = 5.2 Hz), 0.80–1.77 (17H, m, steroid CH₂ and CH), 1.92 (4H, m, C-7 and C-2 CH₂), 2.31 (2H, m, C-4 CH₂), 2.62 (2H, m, C-23 CH₂), 2.85 (4H, s, NHS CH₂), 3.54 (1H, m, C-3 CH), 5.37 (1H, m, C-6 CH); ¹³C NMR δ 71.7 (C-3), 121.5 and 140.7 (C-5 and C-6), 169.0 and 169.1 (C-24 and NHS CO); MS (DCI) 472 (M)⁺. Anal. Calcd for C₂₈H₄₁NO₅: C, 71.31, H, 8.76, N, 2.97. Found: C, 70.99, H, 8.79, N, 3.27.

Similarly Prepared: 3β-Hydroxy-25,26-bishomo-5-cholenic Acid Oleate N-Hydroxysuccinimide Ester (11). (4.976 g, 100%): ¹H NMR δ 0.87 (3H, t, oleoyl CH₃, J = 6.4 Hz), 2.25 (4H, m, COCH₂ and C-4 CH₂), 2.53 (2H, m, C-23 CH₂), 2.81 (4H, brs, NHS CH₂), 4.55 (1H, m, C-3 CH), 5.31 (3H, m, vinyl CH).

3β-Hydroxy-22,23-bisnor-5-cholenic Acid N-Hydroxysuccinimide Ester (19). (19.37 g, 94%): ¹H NMR δ 2.67 (1H, m, COCH), 2.77 (4H, brs, NHS CH₂), 3.46 (1H, m, C-3 CH), 5.29 (1H, d, vinyl CH, J = 4.6 Hz); MS (DCI) 443 (MH⁺), 426 (M-H₂O)⁺, 329 (M-C₄H₄NO₃)⁺. Anal. Calcd for C₂₆H₃₇NO₅: C, 70.40, H, 8.41, N, 3.16. Found: C, 69.15, H, 7.91, N, 2.88.

4-[3β-[(tert-Butyldimethylsilyl)oxy]androst-5-en-17β-yl]-2-(hydroxymethyl)pentanol Bis[hemiglutarate] Bis-N-hydroxysuccinimide Ester (41). The compoud was chromatographed on silica, eluting with 4% CH₃OH/CH₂Cl₂ (0.039 g, 51%). ¹H NMR δ 0.01 (6H, s, SiCH₃), 0.85 (9H, s, t-Bu), 2.42 and 2.66 (each 4H, t, COCH₂, J = 7.5 and 7.3 Hz), 2.88 (8H, brs, NHS CH₂), 3.42 (1H, m, C-3 CH), 4.01 (4H, m, OCH₂), 5.27 (1H, brs, vinyl CH); MS (FAB) 928 (MH)⁺.

3β-(Oleoyloxy)-5-cholenic Acid N-Hydroxysuccinimide Ester (5). A stirred solution of alcohol **4** (2.850 g, 6.043 mmol) in CH₂Cl₂ (50 mL) under argon at 0 °C was treated with oleoyl chloride (2.000 g, 1.1 equiv) and pyridine (0.54 mL). The cooling bath was removed after 30 min, and stirring was continued for 16 h. More CH₂-Cl₂ was added, and the mixture was washed with biphthalate buffer (pH 5) and water, dried, and evaporated to give **5** as a waxy solid (4.273 g, 96%): ¹H NMR δ 0.63 and 1.02 (each 3H, s, C-18 and C-19 CH₃), 0.89

(3H, t, oleoyl CH₃, J = 6.6 Hz), 0.99 (3H, d, C-21 CH₃, J = 6.5 Hz), 1.20 and 1.23 (20H, brs, oleoyl CH₂), 0.70–1.60 (19H, steroid CH₂ and CH and oleoyl CH₂), 1.70–1.95 (10H, m, C-2 and C-7 CH₂), 2.21 (4H, m, oleoyl COCH₂ and C-4 CH₂), 2.53 (2H, m, C-23 CH₂), 2.77 (4H, brs, NHS CH₂), 4.53 (1H, m, C-3 CH), 5.27 (3H, m, vinyl CH); ¹³C NMR δ 73.6 (C-3), 122.5 and 139.7 (C-5 and C-6), 129.7 and 129.9 (oleoyl vinyl), 169.1 and 169.1 (C-24 and NHS CO), 173.2 (oleoyl CO); MS (DCI) 734 (MH)⁺, 454 (M-C₁₈H₃₃O₂)⁺. Anal. Calcd for C₄₆H₇₃NO₆: C, 75.06, H, 10.00, N, 1.90. Found: C, 75.09, H, 9.78, N, 2.43.

Similarly Prepared: 3β-(Oleoyloxy)-22,23-bisnor-5-cholenic Acid N-Hydroxysuccinimide Ester (20). (10.45 g, 89%): ¹H NMR δ 0.87 (3H, t, oleoyl CH₃, J = 6.6 Hz), 2.27 (4H, m, COCH₂ and C-4 CH₂), 2.80 (4H, brs, NHS CH₂), 4.58 (1H, m, C-3 CH), 5.31 (3H, m, vinyl CH); MS (FAB) 709 (MH)⁺, 429 (M-C₁₈H₃₃O₂)⁺. Anal. Calcd for C₄₄H₆₉NO₆: C, 74.64, H, 9.82, N, 1.98. Found: C, 74.34, H, 9.57, N, 2.34.

4-[3β-(Oleoyloxy)androst-5-en-17β-yl]-2-(hydroxymethyl)pentanol Bis[bis(2-chloroethyl)amine carbamate] (39). The compoud was chromatographed on silica, eluting with 25% EtOAc/hexane (0.131 g, 86%): ¹H NMR δ 2.24 (4H, m, COCH₂ and C-4 CH₂), 3.62 (16H, m, NCH₂ and ClCH₂), 4.09 (4H, m, OCH₂), 4.56 (1H, m, C-3 CH), 5.31 (3H, m, vinyl CH); ¹³C NMR δ 42.0 and 42.1 (ClCH₂), 51.0 and 51.3 (NCH₂), 64.8 and 67.5 (OCH₂), 74.1 (C-3), 123.3 (C-6), 130.3 and 130.5 (oleoyl vinyl), 140.2 (C-5), 156.4 (NCO), 174.4 (CO); MS (FAB) 1013 (M+Na)⁻, 804 (M-C₅H₈NO₂Cl₂)⁺; HRMS calcd for C₅₃H₈₉N₂O₆Cl₄: 989.5475. Found: 989.5453.

4-[3β-(Oleoyloxy)androst-5-en-17β-yl]-2-(hydroxymethyl)pentanol Bis(5-hydroxypentanoate) Bis[bis-(2-chloroethyl)amine carbamate] (45). The compound was chromatographed on silica, eluting with 1% CH₃OH/CH₂Cl₂ (0.103 g, 84%): ¹H NMR δ 0.87 (3H, t, oleoyl CH₃, J = 6.5 Hz), 2.25 (4H, m, COCH₂ and C-4 CH₂), 2.30 (4H, brt, COCH₂), 3.59 (16H, m, NCH₂ and ClCH₂), 3.96 and 4.09 (8H, m, OCH₂), 4.57 (1H, m, C-3 CH), 5.30 (3H, m, vinyl CH); MS (FAB) 1192 (MH)⁺, 1007 (M-C₅H₈NO₂Cl₂)⁺. HRMS calcd for C₆₃H₁₀₅N₂O₁₀Cl₄: 1189.6523. Found: 1189.6538.

2-(2-[3β-(Oleoyloxy)androst-5-en-17β-yl]propyl)-4-(hydroxymethyl)-5-hydroxypentanol Tris[bis(2-chloroethyl)amine carbamate] (72). The compound was chromatographed on silica, eluting with 20–25% EtOAc/hexane (0.721 g, 94%): ¹H NMR δ 0.86 (3H, t, oleoyl CH₃, J = 6.5 Hz), 2.23 (4H, m, COCH₂ and C-4 CH₂), 3.61 (24H, m, NCH₂ and ClCH₂), 3.94–4.15 (6H, m, OCH₂), 4.57 (1H, m, C-3 CH), 5.31 (3H, m, vinyl CH); MS (FAB) 1217 (MH)⁺, 1239 (M+Na)⁻, 1032 (M-C₅H₈NO₂Cl₂)⁺. HRMS calcd for C₆₁H₁₀₁N₃O₈Cl₆: 1214.5798. Found: 1214.5770.

2-(4-[3β-(Oleoyloxy)androst-5-en-17β-yl]pentyl)-4-(hydroxymethyl)-5-hydroxypentanol Tris[bis(2-chloroethyl)amine carbamate] (73). The compound was chromatographed on silica, eluting with 20–25% EtOAc/hexane (0.299 g, 98%): ¹H NMR δ 0.87 (3H, t, oleoyl CH₃, J = 6.7 Hz), 2.26 (4H, m, COCH₂ and C-4 CH₂), 3.60 (24H, m, NCH₂ and ClCH₂), 3.98–4.15 (6H, m, OCH₂),

4.58 (1H, m, C-3 CH), 5.31 (3H, m, vinyl CH); MS (FAB) 1247 (MH)+, 1269 (M+Na)+, 1062 (M-C5H8NO2Cl2)+. HRMS calcd for C63H105N3O8Cl6: 1241.6111. Found: 1242.6081.

3β-(Oleoyloxy)-5-cholenic Acid (p-Bromobenzoyl)-methyl Ester (78). The compound was crystallized from ethanol (2.760 g, 99%): 1H NMR δ 0.82 (3H, t, oleoyl CH3, J = 6.9 Hz), 2.20 (4H, m, COCH2 and C-4 CH2), 4.53 (1H, m, C-3 CH), 5.20 (2H, s, COCH2O), 5.28 (3H, m, vinyl CH), 7.65 (4H, AXq, Ph); MS (FAB) 836 (MH)+.

4-[3β-(Oleoyloxy)androst-5-en-17β-yl]pentanol (6). Active ester 5 (11.50 g, 15.6 mmol) in THF (50 mL) under argon at 0 °C was treated with a cold solution of 0.5 M NaBH4 in diglyme (100 mL, 3.2 equiv). The mixture was stirred for 24 h and then carefully poured into a mixture of crushed ice and 10% citric acid (300 mL). The resulting suspension was stirred vigorously for 1 h, and the white solid was collected by filtration, washed with water and dissolved in CH2Cl2. The solution was washed with water, and brine, dried, and evaporated. The residue was chromatographed on basic alumina (grade II–III, 70–230 mesh), eluting with CH2Cl2, to give 6 as a waxy solid (6.54 g, 67%): 1H NMR δ 0.83 (3H, t, oleoyl CH3, J = 6.7 Hz), 2.23 (4H, m, COCH2 and C-4 CH2), 3.54 (2H, m, OCH2), 4.53 (1H, m, C-3 CH), 5.26 (3H, m, vinyl CH); 13C NMR δ 63.6 (OCH2), 73.7 (C-3), 122.5 and 139.7 (C-5 and C-6), 129.7 and 130.0 (oleoyl vinyl), 173.2 (CO); MS (DCI): 625 (M)+, 343 (M-C18H33O2). Anal. Calcd for C42H72O3: C, 80.71, H, 11.61. Found: C, 80.77, H, 11.59.

Similarly Prepared: 6-[3β-(Oleoyloxy)androst-5-en-17β-yl]heptanol (12). (3.023 g, 71%) 1H NMR δ 3.62 (2H, q, OCH2, J = 5.7 Hz), 4.57 (1H, m, C-3 CH), 5.32 (3H, m, vinyl CH); 13C NMR δ 63.1 (OCH2), 73.7 (C-3), 122.5 and 139.7 (C-5 and C-6), 129.7 and 130.0 (oleoyl vinyl), 173.3 (CO); MS, (DCI) 653 (M)+, 371 (M-C18H33O2)+. Anal. Calcd for C44H76O3·0.5H2O: C, 79.82, H, 11.72. Found: C, 79.98, H, 11.86.

4-[3β-(Oleoyloxy)androst-5-en-17β-yl]pentyl 5-Hydroxypentanoate (16). The compound was chromatographed on silica, eluting with 1% CH3OH/CH2Cl2 (0.178 g, 75%). 1H NMR δ 2.24 (6H, m, COCH2 and C-4 CH2), 3.61 (2H, m, OCH2), 3.97 (2H, m, CO2CH2), 4.57 (1H, m, C-3 CH), 5.32 (3H, m, vinyl CH); MS (FAB) 726 (MH)+.

2-[3β-[(tert-Butyldimethylsilyl)oxy]androst-5-en-17β-yl]propanol (33). (6.834 g, 65%) 1H NMR δ 0.02 (6H, s, SiCH3), 0.84 (9H, s, t-Bu), 3.32 and 3.59 (each 1H, m, OCH2), 3.42 (1H, m, C-3 CH), 5.27 (1H, m, vinyl CH); MS (DCI) 447 (MH)+, 429 (MH-H2O)+, 315 (M-C6H15-OSi)+. Anal. Calcd for C28H50O2Si: C, 75.27, H, 11.28. Found: C, 74.69, H, 11.14.

4-[3β-[(tert-Butyldimethylsilyl)oxy]androst-5-en-17β-yl]-2-(hydroxymethyl)pentanol Bis(5-hydroxypentanoate) (42). The compound was chromatographed on silica, eluting with 4% CH3OH/CH2Cl2 (0.389 g, 42%): 1H NMR δ 0.01 (6H, s, SiCH3), 0.82 (9H, s, t-Bu), 2.30 (4H, t, COCH2, J = 9.2 Hz), 3.42 (1H, m, C-3 CH), 3.59 (4H, m, OCH2), 4.00 (4H, m, CO2CH2), 4.72 (2H, brs, HO), 5.25 (1H, d, vinyl CH, J = 5.5 Hz); MS (FAB) 727.4 (M+Na)+, 743.6 (M+K)+. Anal. Calcd for C41H72O7Si·0.5H2O: C, 68.96, H, 10.30. Found: C, 69.22, H, 10.11.

4-[3β-(Oleoyloxy)androst-5-en-17β-yl]pentyl Mesylate (7). The alcohol 6 (5.063 g, 8.10 mmol) in CH2Cl2 (15 mL) at 0 °C under argon was treated with methanesulfonyl chloride (1.03 mL, 1.6 equiv) and Et3N (1.84 mL, 1.6 equiv). The mixture was stirred for 16 h. Hexane (80 mL) was added, and the mixture was washed with 10% H2SO4, water, saturated NaHCO3, and brine, dried, and evaporated. The residue was chromato-

graphed on silica, eluting with CH2Cl2, to give 7 as a waxy solid (5.200 g, 91%): 1H NMR δ 0.83 (3H, t, oleoyl CH3, J = 6.9 Hz), 2.23 (4H, m, COCH2 and C-4 CH2), 3.54 (2H, m, OCH2), 4.53 (1H, m, C-3 CH), 5.26 (3H, m, vinyl CH); 13C NMR δ 36.6 (SCH3), 70.6 (OCH2), 73.6 (C-3), 122.4 and 139.7 (C-5 and C-6), 129.7 and 129.9 (oleoyl vinyl), 173.2 (CO); MS (FAB) 725.3 (M+Na)+, 741.4 (M+K)+. HRMS calcd for C43H74SO5: 702.5257. Found: 702.5266.

Similarly Prepared: 2-[3β-[(tert-Butyldimethylsilyl)oxy]androst-5-en-17β-yl]propyl Mesylate (34). (1.561 g, 95%) 1H NMR δ 0.02 (6H, s, SiCH3), 0.83 (9H, s, t-Bu), 2.97 (3H, s, SCH3), 3.44 (1H, m, C-3 CH), 3.96 and 4.15 (each 1H, m, OCH2), 5.29 (1H, m, vinyl CH); MS (DCI) 526 (MH)+, 394 (M-C6H15OSi)+.

N-(tert-Butoxycarbonyl)-3-aminopropyl Mesylate (51). The compound was chromatographed on silica, eluting with 2% CH3OH/CH2Cl2; it was unstable (5.800 g, 61%): 1H NMR δ 1.34 (9H, s, t-bu), 1.86 (2H, q, CH2, J = 7.2 Hz), 2.95 (3H, s, CH3), 3.19 (2H, m, NCH2), 4.12 (2H, t, OCH2, J = 8.0 Hz), 4.79 (1H, br, NH).

4-[3β-[(tert-Butyldimethylsilyl)oxy]androst-5-en-17β-yl]pentyl Mesylate (61). The compound was chromatographed on silica, eluting with 15% EtOAc/hexane (1.948 g, 68%): 1H NMR δ 0.03 (6H, s, SiCH3), 0.86 (9H, s, t-Bu), 2.98 (3H, s, SCH3), 3.43 (1H, m, C-3 CH), 4.18 (2H, m, OCH2), 5.29 (1H, d, vinyl CH, J = 5.2 Hz); MS (DCI) 553 (MH)+, 421 (M-C6H15OSi)−.

Di-tert-butyl 2-(4-[3β-(Oleoyloxy)androst-5-en-17β-yl]pentyl)malonate (8). Di-t-butyl malonate (1.96 mL, 8.74 mmol) in THF (15 mL) under argon was cooled to −78 °C and treated with NaH (60% in mineral oil, 0.320 g, 0.92 equiv). The mixture was allowed to warm to RT (carefully, to avoid foaming). After 30 min the solution was homogeneous, and the steroid mesylate 7 (5.120 g, 0.83 equiv) in THF (15 mL) was added all at once. The reaction mixture was heated at reflux for 16 h, diluted with hexane, and washed with 10% citric acid, water, and brine. The organic phase was dried and evaporated to give a yellow oil, which was chromatographed on silica, eluting with 6% EtOAc/hexane, to give 8 as a colorless oil (5.630 g, 94%): 1H NMR δ 1.42 (9H, s, t-Bu), 2.22 (4H, m, COCH2 and C-4 CH2), 3.07 (1H, t, mal CH, J = 7.5 Hz), 4.57 (1H, m, C-3 CH), 5.30 (3H, m, vinyl CH); 13C NMR δ 28.0 (t-Bu CH3), 73.7 (C-3), 81.2 (OCMe3), 122.6 and 139.7 (C-5 and C-6), 129.8 and 129.9 (oleoyl vinyl), 169.0 and 173.3 (CO); MS (FAB) 823.4 (MH)−, 845.6 (M+Na)+. Anal. Calcd for C53H89O6: C, 77.42, H, 10.91. Found: C, 77.03, H, 10.92.

2-(4-[3β-(Oleoyloxy)androst-5-en-17β-yl]pentyl)-malonic Acid (9). The di-tert-butyl ester 8 (5.630 g, 6.84 mmol) was dissolved in TFA (15 mL), and the mixture was stirred for 5 h. EtOAc (150 mL) and water (200 mL) were added. The organic phase was washed with water (2×) and brine, dried, and evaporated to give a thick, yellow oil, which was flushed with CH2Cl2 to remove traces of TFA. The crude product was carried on without further purification (5.160 g, 98%): 1H NMR δ 2.23 (4H, m, COCH2 and C-4 CH2), 3.39 (1H, m, mal CH), 4.57 (1H, m, C-3 CH), 5.32 (3H, m, vinyl CH); 13C NMR δ 74.2 (C-3), 122.6 and 139.7 (C-5 and C-6), 129.8 and 130.0 (oleoyl vinyl), 173.7 and 175.5 (CO); MS (FAB) 733 (M+Na)+. Anal. Calcd for C45H74O6: C, 76.01, H, 10.49. Found: C, 75.80, H, 10.53.

3β-Hydroxy-25,26-bishomo-5-cholenic Acid Oleate (10). The steroid malonic acid 9 (5.160 g, 7.26 mmol) in DMSO (10 mL) under argon was heated to between 160 and 180 °C for 30 min. Upon cooling. 3:1 hexane/EtOAc (150 mL) and water (200 mL) were added. The organic phase was washed with water (3×) and brine, dried, and

evaporated to give **10** as a waxy solid (4.351 g, 90%): ^{1}H NMR δ 2.02 (4H, m, C-7 CH_2 and $COCH_2$), 2.30 (4H, m, $COCH_2$ and C-4 CH_2), 4.59 (1H, m, C-3 CH), 5.31 (3H, m, vinyl CH); ^{13}C NMR δ 73.7 (C-3), 122.5 and 139.7 (C-5 and C-6), 129.7 and 130.0 (oleoyl vinyl), 173.3 and 179.3 (CO); MS (DCI) 667 (M)$^-$, 385 (M-$C_{18}H_{33}O_2$)$^-$. HRMS calcd for $C_{44}H_{74}O_4$: 666.5587. Found: 666.5600.

6-[3β-(Oleoyloxy)androst-5-en-17β-yl]heptanol Bis-(2-chloroethyl)amine Carbamate (13). A solution of alcohol **12** (0.123 g, 0.188 mmol) and pyridine (0.015 mL, 1 equiv) in CH_2Cl_2 (3 mL) was added to diphosgene (0.017 mL, 0.75 equiv) in CH_2Cl_2 (1 mL) under argon at 0 °C. After 45 min the mixture had warmed to 20 °C and a solution of bis(chloroethyl)amine-HCl (0.067 g, 2 equiv) and Et_3N (0.16 mL) in CH_2Cl_2 (2 mL) was added. The mixture was stirred for 45 min, and then water (25 mL) was added. The organic phase was washed with 10% citric acid and water, dried, and evaporated. The residue was chromatographed on silica, eluting with CH_2Cl_2, to give **13** as a colorless oil (0.138 g, 90%): ^{1}H NMR δ 2.24 (4H, m, $COCH_2$ and C-4 CH_2), 3.63 (8H, m, NCH_2 and $ClCH_2$), 4.08 (2H, t, OCH_2, J = 6.7 Hz), 4.57 (1H, m, C-3 CH), 5.32 (3H, m, vinyl CH); ^{13}C NMR δ 42.0 and 42.3 (ClCH$_2$), 50.7 and 51.1 (NCH$_2$), 66.0 (OCH$_2$), 73.7 (C-3), 122.5 and 139.7 (C-5 and C-6), 129.7 and 129.9 (oleoyl vinyl), 155.9 (N-CO), 173.2 (CO); IR (film) 1707 (carbamate CO str), 1737 (ester CO str); MS (FAB) 819 (MH)$^-$, 841 (M+Na)$^-$, 634 (M-$C_5H_8NO_2Cl_2$)$^+$. HRMS calcd for $C_{49}H_{81}NO_4Cl_2$: 817.5542. Found: 817.5563.

Similarly Prepared: 4-[3β-(Oleoyloxy)androst-5-en-17β-yl]pentyl 5-Hydroxypentanoate Bis[(2-chloroethyl)amine Carbamate] (17). (0.125 g, 43%): ^{1}H NMR δ 2.26 (6H, m, $COCH_2$ and C-4 CH_2), 3.62 (8H, m, NCH_2 and $ClCH_2$), 3.98 and 4.06 (each 2H, m, OCH_2), 4.55 (1H, m, C-3 CH), 5.30 (3H, m, vinyl CH); ^{13}C NMR δ 41.8 and 42.2 (ClCH$_2$), 50.6 and 51.0 (NCH$_2$), 64.9 and 65.3 (OCH$_2$), 73.5 (C-3), 122.4 (C-6), 139.6 (C-5), 129.7 and 129.9 (oleoyl vinyl), 155.7 (N-CO), 173.1 (CO); MS (FAB) 894 (MH)$^+$, 916 (M+Na)$^+$, 709 (M-$C_5H_8NO_2Cl_2$)$^-$. HRMS calcd for $C_{52}H_{88}NO_6Cl_2$: 892.5988. Found: 892.5972.

4-[3β-(Oleoyloxy)androst-5-en-17β-yl]pentyl Hemiglutaric Acid (14). Alcohol **6** (1.569 g, 2.51 mmol) in CH_2Cl_2 (10 mL) was treated with glutaric anhydride (0.573 g, 2 equiv) and pyridine (0.5 mL, 2 equiv). The mixture was stirred for 4 days and then diluted with EtOAc and 0.1 M HCl. The organic phase was washed with 0.1 M HCl, water, and brine, dried, and evaporated. The residue was chromatographed on silica, eluting with (1) CH_2Cl_2 and (2) 3% CH_3OH/CH_2Cl_2, to give **14** as a waxy solid (1.758 g, 95%): ^{1}H NMR δ 2.24 and 2.39 (6H, m, $COCH_2$ and C-4 CH_2), 4.02 (2H, m, OCH_2), 4.56 (1H, m, C-3 CH), 5.30 (3H, m, vinyl CH); ^{13}C NMR δ 65.1 (OCH$_2$), 73.7 (C-3), 122.5 and 139.7 (C-5 and C-6), 129.7 and 130.0 (oleoyl vinyl), 172.9, 173.4 and 178.5 (CO). Anal. Calcd for $C_{47}H_{78}O_6$: C, 76.38, H, 10.64. Found: C, 76.23, H, 10.54.

3β-(Oleoyloxy)-22,23-bisnor-5-cholenic Acid 3-Hydroxypropanamide (21). Active ester **20** (0.255 g, 0.36 mmol) and 3-aminopropanol (0.055 mL, 2 equiv) in THF (2 mL) were stirred overnight. The mixture was partitioned between EtOAc and 10% citric acid, and the organic phase was washed with water and brine, dried, and evaporated. The residue was chromatographed on silica, eluting with 80% EtOAc/hexane, to give **21** as a waxy solid (0.202 g, 84%): ^{1}H NMR δ 0.81 (3H, t, oleoyl CH_3, J = 6.8 Hz), 2.07 (2H, m, CH_2), 2.22 (4H, m, $COCH_2$ and C-4 CH_2), 3.32 (2H, m, NCH_2), 3.55 (2H, t, OCH_2, J = 7.5 Hz), 4.54 (1H, m, C-3 CH), 5.29 (3H, m, vinyl CH), 5.99 (1H, t, NH); MS (FAB) 668 (M)$^-$.

Similarly Prepared: 3β-(Oleoyloxy)-22,23-bisnor-5-cholenic Acid 4-Hydroxybutanamide (22). (0.134 g, 81%): ^{1}H NMR δ 0.83 (3H, t, oleoyl CH_3, J = 6.6 Hz), 2.22 (4H, m, $COCH_2$ and C-4 CH_2), 3.21 (2H, m, NCH_2), 3.63 (2H, t, OCH_2, J = 7.8 Hz), 4.57 (1H, m, C-3 CH), 5.31 (3H, m, vinyl CH), 5.62 (1H, t, NH); MS (FAB) 682 (M)$^+$.

3β-(Oleoyloxy)-22,23-bisnor-5-cholenic Acid 5-Hydroxypentanamide (23). (0.220 g, 86%) ^{1}H NMR δ 0.81 (3H, t, oleoyl CH_3, J = 6.7 Hz), 2.22 (4H, m, $COCH_2$ and C-4 CH_2), 3.18 (2H, m, NCH_2), 3.59 (2H, t, OCH_2, J = 7.8 Hz), 4.53 (1H, m, C-3 CH), 5.29 (3H, m, vinyl CH), 5.61 (1H, t, NH); MS (FAB) 696 (M)$^-$.

3β-(Oleoyloxy)-22,23-bisnor-5-cholenic Acid 4-(Hydroxymethyl)-5-hydroxypentanamide (55). (0.293 g, 65%): ^{1}H NMR δ 0.82 (3H, t, oleoyl CH_3, J = 7.0 Hz), 2.24 (4H, m, $COCH_2$ and C-4 CH_2), 3.18 (2H, m, NCH_2), 3.38 (2H, br, OH), 3.78 (4H, m, OCH_2), 4.55 (1H, m, C-3 CH), 5.31 (3H, m, vinyl CH), 5.82 (1H, t, NH); MS (FAB) 726 (MH)$^-$. HRMS calcd for $C_{46}H_{80}NO_5$: 726.6037. Found: 726.6013.

6-[3β-(Oleoyloxy)androst-5-en-17β-yl]-2-(hydroxymethyl)heptanol (29). The malonic acid **9** (3.057 g, 4.30 mmol) in THF (10 mL) at 0 °C was treated with NHS (1.24 g, 2.5 equiv) and DCC (2.22 g, 2.5 equiv). The mixture was stirred overnight, filtered to remove DCU, and evaporated. The oily residue was dissolved in THF (20 mL), cooled to 0 °C, and then treated with 0.5 M $NaBH_4$ in diglyme (52 mL). After being stirred overnight, the reaction was poured onto a mixture of 10% citric acid/crushed ice. The suspension was extracted with CH_2Cl_2, and the organic phase was evaporated. NMR of the crude solid showed it to be mainly the monoreduced 3-hydroxypropanoic acid **28**. The solid was treated as above with NHS (0.60 g) and DCC (1.10 g). Filtration, treatment with 0.5 M $NaBH_4$ in diglyme (25 mL), and workup as above gave a white solid, which was chromatographed on silica, eluting with 4% CH_3OH/CH_2Cl_2, to give **29** as a waxy, white solid (1.030 g, 35%): ^{1}H NMR δ 2.25 (4H, m, $COCH_2$ and C-4 CH_2), 3.71 (4H, ABX, OCH_2), 4.58 (1H, m, C-3 CH), 5.33 (3H, m, vinyl CH); ^{13}C NMR δ 66.4 and 66.6 (OCH$_2$), 73.6 (C-3), 122.4 (C-6), 139.6 (C-5), 130.1 and 130.3 (oleoyl vinyl), 173.2 (CO); MS (FAB) 684.1 (MH)$^+$, 705.8 (M+Na)$^+$, 725.9 (M+K)$^+$. Anal. Calcd for $C_{45}H_{78}O_4\cdot0.5H_2O$: C, 78.09, H, 11.50. Found: C, 77.97, H, 11.45.

N,N-Bis(2-chloroethyl)amine Chloroformate (30). Bis(chloroethyl)amine hydrochloride (20.00 g, 112.05 mmol) in water (20 mL) at 0 °C was treated with a cold solution of KOH (87%, 7.22 g, 1 equiv) in water (50 mL). The mixture was vigorously stirred for 1 min, and then ether was added. The organic phase was separated and dried, and the solvent was removed on the rotovap with the water bath at 15 °C. The resulting viscous liquid was >95% pure by NMR. A portion of the crude amine (10.00 g, 70.4 mmol) in ether (100 mL), cooled to −78 °C in a jacketed addition funnel, was added to diphosgene (2.74 mL, 22.2 mmol) in CH_2Cl_2 (20 mL) at 0 °C, over several minutes with stirring. After 4 h the mixture was filtered, the filtrate was evaporated, and the residue was distilled in vacuo to give **30** as a colorless oil (14.21 g, 62%): bp 80−85 °C/0.01 mmHg [lit. bp 92−96 °C/0.1 mmHg (*26*)].

2-(Hydroxymethyl)-6-[3β-(oleoyloxy)androst-5-en-17β-yl]heptanol Bis[bis(2-chloroethyl)amine carbamate] (31). The steroid diol **29** (0.144 g, 0.210 mmol) in CH_2Cl_2 (5 mL) at 0 °C was treated with N,N-bis(2-chloroethyl)amine chloroformate **30** (0.172 g, 4 equiv), DMAP (0.051 g, 2 equiv), and DBU (0.1 mL, 3 equiv). The reaction mixture was stirred overnight and then diluted with 10% citric acid and EtOAc. The organic

phase was washed with water and brine, dried, and evaporated. The oily residue was chromatographed on silica, eluting with 15% EtOAc/hexane, to give **31** as a glass (0.146 g, 68%): ^{1}H NMR δ 2.22 (4H, m, COCH$_2$ and C-4 CH$_2$), 3.60 (16H, m, NCH$_2$ and ClCH$_2$), 4.06 (4H, m, OCH$_2$), 4.53 (1H, m, C-3 CH), 5.31 (3H, m, vinyl CH); ^{13}C NMR δ 42.1 and 42.2 (ClCH$_2$), 50.9 and 51.3 (NCH$_2$), 65.8 and 65.9 (OCH$_2$), 74.0 (C-3), 123.1 (C-6), 130.8 and 131.0 (oleoyl vinyl), 140.3 (C-5), 156.3 (NCO), 174.0 (CO); MS (FAB) 1039 (M+Na)$^+$, 1055 (M+K)$^+$. HRMS calcd for C$_{55}$H$_{93}$N$_2$O$_6$Cl$_4$: 1017.5788. Found: 1017.5754.

Similarly Prepared: 3β-(Oleoyloxy)-22,23-bisnor-5-cholenic Acid 3-[[Bis(2-chloroethyl)amino]carbamoyl]propanamide (24). (0.144 g, 82%): ^{1}H NMR δ 0.84 (3H, t, oleoyl CH$_3$, J = 6.8 Hz), 2.22 (4H, m, COCH$_2$ and C-4 CH$_2$), 3.23 (2H, m, NCH$_2$), 3.62 (8H, m, ClCH$_2$ and NCH$_2$), 4.14 (2H, m, OCH$_2$), 4.57 (1H, m, C-3 CH), 5.31 (3H, m, vinyl CH), 5.82 (1H, brt, NH); ^{13}C NMR δ 42.3 and 42.7 (ClCH$_2$), 51.4 and 51.6 (NCH$_2$), 63.5 (OCH$_2$), 74.2 (C-3), 122.8 (C-6), 130.6 and 130.7 (oleoyl vinyl), 140.5 (C-5), 156.8 (NCO), 174.4 and 177.8 (CO); MS (FAB) 835 (MH)$^+$, 650 (M-C$_5$H$_8$NO$_2$Cl$_2$)$^-$. HRMS calcd for C$_{48}$H$_{81}$N$_2$O$_5$Cl$_2$: 835.5522. Found: 835.5538.

3β-(Oleoyloxy)-22,23-bisnor-5-cholenic Acid 4-[[Bis(2-chloroethyl)amino]carbamoyl]butanamide (25). (0.053 g, 87%) ^{1}H NMR δ 0.82 (3H, t, oleoyl CH$_3$, J = 6.6 Hz), 2.21 (4H, m, COCH$_2$ and C-4 CH$_2$), 3.21 (2H, m, NCH$_2$), 3.59 (8H, m, ClCH$_2$ and NCH$_2$), 4.07 (2H, t, OCH$_2$, J = 7.9 Hz), 4.55 (1H, m, C-3 CH), 5.29 (3H, m, vinyl CH), 5.48 (1H, brt, NH); ^{13}C NMR δ 42.4 and 42.7 (ClCH$_2$), 51.0 and 51.7 (NCH$_2$), 65.7 (OCH$_2$), 74.0 (C-3), 123.3 (C-6), 130.4 and 130.7 (oleoyl vinyl), 140.6 (C-5), 156.5 (OCN), 174.2 and 177.7 (CO); MS (FAB) 849 (MH)$^+$, 664 (M-C$_5$H$_8$NO$_2$Cl$_2$)$^+$. HRMS calcd for C$_{49}$H$_{83}$N$_2$O$_5$Cl$_2$: 849.5679. Found: 849.5695.

3β-(Oleoyloxy)-22,23-bisnor-5-cholenic Acid 5-[[Bis(2-chloroethyl)amino]carbamoyl]pentanamide (26). (0.130 g, 91%): ^{1}H NMR δ 0.82 (3H, t, oleoyl CH$_3$, J = 6.5 Hz), 2.23 (4H, m, COCH$_2$ and C-4 CH$_2$), 3.18 (2H, m, NCH$_2$), 3.60 (8H, m, ClCH$_2$ and NCH$_2$), 4.05 (2H, t, OCH$_2$, J = 7.7 Hz), 4.54 (1H, m, C-3 CH), 5.29 (3H, m, vinyl CH), 5.48 (1H, brt, NH); ^{13}C NMR δ 42.5 and 43.0 (ClCH$_2$), 51.0 and 51.8 (NCH$_2$), 66.0 (OCH$_2$), 74.1 (C-3), 123.5 (C-6), 130.5 and 130.7 (oleoyl vinyl), 140.3 (C-5), 156.6 (OCN), 173.9 and 177.5 (CO); MS (FAB) 863 (MH)$^-$, 678 (M-C$_5$H$_8$NO$_2$Cl$_2$)$^+$. HRMS calcd for C$_{50}$H$_{85}$N$_2$O$_5$Cl$_2$: 863.5835. Found: 863.5859.

4-[3β-[(*tert*-Butyldimethylsilyl)oxy]androst-5-en-17β-yl]-2-(hydroxymethyl)pentanol Bis[bis(2-chloroethyl)amine carbamate] (37). (0.163 g, 91%): ^{1}H NMR δ 0.01 (6H, s, SiCH$_3$), 0.84 (9H, s, *t*-Bu), 3.42 (C-3 CH), 3.60 (16H, m, NCH$_2$ and ClCH$_2$), 4.09 (4H, m, OCH$_2$), 5.27 (1H, m, vinyl CH); ^{13}C NMR δ 42.5 and 42.6 (ClCH$_2$), 51.1 and 51.5 (NCH$_2$), 66.0 and 66.2 (OCH$_2$), 73.2 (C-3), 121.9 (C-6), 142.3 (C-5), 156.3 (CO); MS (DCI) 842 (MH)$^+$. HRMS calcd for C$_{41}$H$_{71}$N$_2$O$_5$Cl$_4$Si: 839.3886. Found: 838.3898.

4-[3β-[(*tert*-Butyldimethylsilyl)oxy]androst-5-en-17β-yl]-2-(hydroxymethyl)pentanol Bis(5-hydroxypentanoate) Bis[bis(2-chloroethyl)amine carbamate] (43). (0.945 g, 72%): ^{1}H NMR δ 0.01 (6H, s, SiCH$_3$), 0.84 (9H, s, *t*-Bu), 2.32 (4H, m, COCH$_2$), 3.42 (1H, m, C-3 CH), 3.60 (16H, m, NCH$_2$ and ClCH$_2$), 4.01 and 4.07 (8H, m, OCH$_2$), 5.26 (1H, m, vinyl CH); ^{13}C NMR δ 0.0 (SiCH$_3$), 41.4, 41.7, and 42.2 (ClCH$_2$), 51.2, 51.3, and 51.5 (NCH$_2$), 63.5, 65.6, and 65.9 (OCH$_2$), 72.9 (C-3), 121.6 (C-6), 142.1 (C-5), 156.5 (NCO), 173.9 (CO); MS (FAB) 1042 (MH)$^-$, 857 (M-C$_5$H$_8$NO$_2$Cl$_2$)$^+$.

3β-(Oleoyloxy)-22,23-bisnor-5-cholenic Acid Bis[bis(2-chloroethyl)amino]carbamoyl]ethan-

amide (49). The compound was chromatographed on silica, eluting with 35% EtOAc/hexane (0.105 g, 75%): ^{1}H NMR δ 0.82 (3H, t, oleoyl CH$_3$, J = 6.9 Hz), 2.26 (4H, m, COCH$_2$ and C-4 CH$_2$), 3.61 (20H, m, ClCH$_2$ and NCH$_2$), 4.21 (4H, 2t, OCH$_2$), 4.58 (1H, m, C-3 CH), 5.32 (3H, m, vinyl CH); ^{13}C NMR δ 42.5 (ClCH$_2$), 51.6 (NCH$_2$), 63.6 and 64.0 (OCH$_2$), 74.1 (C-3), 123.3 (C-6), 130.6 and 130.7 (oleoyl vinyl), 140.6 (C-5), 156.2 and 156.6 (OCN), 174.3 and 178.1 (CO); MS (FAB) 1032 (MH)$^+$, 847 (M-C$_5$H$_8$NO$_2$-Cl$_2$)$^+$. HRMS calcd for C$_{54}$H$_{90}$N$_3$O$_7$Cl$_4$: 1032.5532. Found: 1032.5514.

3β-(Oleoyloxy)-22,23-bisnor-5-cholenic Acid 4-[[[Bis(2-chloroethyl)amino]carbamoyl]methyl]-5-[[bis(2-chloroethyl)amino]carbamoyl]pentanamide (56). (0.077 g, 83%): ^{1}H NMR δ 0.83 (3H, t, oleoyl CH$_3$, J = 6.7 Hz), 2.27 (4H, m, COCH$_2$ and C-4 CH$_2$), 3.21 (2H, m, NCH$_2$), 3.62 (16H, m, ClCH$_2$ and NCH$_2$), 4.09 (4H, d, OCH$_2$, J = 7.2 Hz), 4.59 (1H, m, C-3 CH), 5.31 (3H, m, vinyl CH), 5.45 (1H, s, NH); ^{13}C NMR δ 42.2 (ClCH$_2$), 51.0 (NCH$_2$), 65.8 (OCH$_2$), 74.1 (C-3), 123.3 (C-6), 130.6 and 130.7 (oleoyl vinyl), 140.5 (C-5), 156.4 (OCN), 174.1 and 177.5 (CO); MS (FAB) 1062 (MH)$^+$, 877 (M-C$_5$H$_8$NO$_2$Cl$_2$)$^+$. HRMS calcd for C$_{56}$H$_{94}$N$_3$O$_7$Cl$_4$: 1060.5845. Found: 1060.5818.

2-(2-[3β-[(*tert*-Butyldimethylsilyl)oxy]androst-5-en-17β-yl]propyl)-4-(hydroxymethyl)-5-hydroxypentanol Tris[bis(2-chloroethyl)amine carbamate] (68). The compound was chromatographed on silica, eluting with 25% EtOAc/hexane (0.807 g, 87%): ^{1}H NMR δ 0.01 (6H, s, SiCH$_3$), 0.83 (9H, s, *t*-Bu), 3.41 (1H, m, C-3 CH), 3.60 (24H, m, ClCH$_2$ and NCH$_2$), 3.90−4.13 (6H, m, OCH$_2$), 5.27 (1H, d, vinyl CH); MS (FAB) 1064 (MH)$^+$, 882 (M-C$_5$H$_8$NO$_2$Cl$_2$)$^-$.

2-(4-[3β-[(*tert*-Butyldimethylsilyl)oxy]androst-5-en-17β-yl]pentyl)-4-(hydroxymethyl)-5-hydroxypentanol Tris[bis(2-chloroethyl)amine carbamate] (69). (0.433 g, 83%): ^{1}H NMR δ 0.01 (6H, s, SiCH$_3$), 0.84 (9H, s, *t*-Bu), 3.43 (1H, m, C-3 CH), 3.62 (24H, m, ClCH$_2$ and NCH$_2$), 3.97−4.13 (6H, m, OCH$_2$), 5.28 (1H, d, vinyl CH, J = 5.4 Hz); MS (FAB) 1095 (MH)$^+$, 910 (M-C$_5$H$_8$-NO$_2$Cl$_2$)$^+$.

3β-(Oleoyloxy)-22,23-bisnor-5-cholenic Acid Tris[[[bis(2-chloroethyl)amino]carbamoyl]methyl]methanamide (75). (0.025 g, 72%): ^{1}H NMR δ 0.84 (3H, t, oleoyl CH$_3$, J = 6.8 Hz), 2.25 (4H, m, COCH$_2$ and C-4 CH$_2$), 3.63 (24H, m, ClCH$_2$ and NCH$_2$), 4.48 (6H, s, OCH$_2$), 4.57 (1H, m, C-3 CH), 5.32 (3H, m, vinyl CH), 6.59 (1H, s, NH); ^{13}C NMR δ 42.3 (ClCH$_2$), 51.2 (NCH$_2$), 64.8 (OCH$_2$), 74.0 (C-3), 123.5 (C-6), 130.6 and 130.8 (oleoyl vinyl), 140.4 (C-5), 156.2 (OCN), 174.1 and 175.1 (CO); MS (FAB) 1245 (MH)$^+$, 1061 (M-C$_5$H$_8$NO$_2$Cl$_2$)$^+$. HRMS calcd for C$_{61}$H$_{101}$N$_4$O$_9$Cl$_6$: 1243.5700. Found: 1243.5674.

3β-[(*tert*-Butyldimethylsilyl)oxy]-22,23-bisnor-5-cholenic Acid *N*-Hydroxysuccinimide Ester (32). A solution of the alcohol **19** (5.01 g, 11.29 mmol) in CH$_2$Cl$_2$ (25 mL) at 0 °C was treated with *tert*-butyldimethylsilyl chloride (2.04 g, 1.2 equiv), Et$_3$N (1.6 mL, 1.2 equiv), and DMAP (0.50 g). The mixture was stirred for 16 h and then diluted with CH$_2$Cl$_2$ (250 mL) and 5% citric acid (300 mL). The organic phase was washed with water and brine, dried, and evaporated. The residue was precipitated from CH$_2$Cl$_2$/hexane to give **32** as a white solid (4.28 g, 70%); more product could be chromatographed from the mother liquors: ^{1}H NMR δ 0.03 (6H, s, SiCH$_3$), 0.87 (9H, s, *t*-Bu), 2.69 (1H, m, COCH), 2.79 (4H, brs, NHS CH$_2$), 3.43 (1H, m, C-3 CH), 5.28 (1H, m, vinyl CH); MS (DCI) 556 (MH)$^+$, 542 (M-CH$_3$)$^+$, 500 (M-C$_4$H$_9$)$^+$, 443 (M-C$_4$H$_4$NO$_3$)$^+$, 426 (M-C$_6$H$_{15}$SiO)$^+$. Anal. Calcd for

$C_{32}H_{51}NO_5Si$: C, 68.90, H, 9.21, N, 2.51. Found: C, 68.81, H, 9.47, N, 2.90.

Similarly Prepared: 3β-[(*tert*-Butyldimethylsilyl)oxy]-5-cholenic Acid Methyl Ester (59). The compound was crystallized from CH_3OH (2.63 g, 96%): ^{1}H NMR δ 0.03 (6H, s, $SiCH_3$), 0.87 (9H, s, *t*-Bu), 3.43 (1H, m, C-3 CH), 3.62 (3H, s, OCH_3), 5.28 (1H, d, vinyl CH, *J* = 5.2 Hz); MS (DCI) 503 (MH)+, 371 (M-$C_6H_{15}OSi$)−.

23-(Ethoxycarbonyl)-3β-hydroxy-5-cholenoyl *tert*-Butyldimethylsilyl Ether Ethyl Ester (35). Sodium hydride (60% in mineral oil, 0.476 g, 11.9 mmol) suspended in THF (5 mL) at −78 °C under argon was treated with diethyl malonate (1.91 mL, 1.06 equiv), and the mixture was allowed to warm to room temperature. When it became homogeneous, the steroid mesylate **34** (1.249 g, 0.2 equiv) in THF (8 mL) was added all at once. The mixture was heated at reflux overnight, diluted with hexane, and washed with saturated NH_4Cl. The organic phase was washed with water and brine, dried, and evaporated. The residue was chromatographed on silica, eluting with 5% EtOAc/hexane, to give **35** as a white solid (1.122 g, 81%): ^{1}H NMR δ 0.02 (6H, s, $SiCH_3$), 0.84 (9H, s, *t*-Bu), 1.22 (6H, 2t, Et CH_3, *J* = 7.3 Hz), 3.41 (2H, m, mal CH and C-3 CH), 4.17 (4H, m, Et CH_2), 5.28 (1H, m, vinyl CH); MS (DCI) 589 (MH)+, 573 (M-CH_3)−, 531 (M-C_4H_9)−, 457 (M-$C_6H_{15}OSi$)−.

Similarly Prepared: Diethyl 2-[(*N*-(*tert*-Butoxycarbonyl)amino)propyl]malonate (52). The compound was chromatographed on silica, eluting with 25−35% EtOAc/hexane (5.751 g, 79%): ^{1}H NMR δ 1.18 (6H, t, Et CH_3, *J* = 7.9 Hz), 1.35 (9H, s, *t*-Bu), 1.81 (2H, m, CH_2), 3.04 (2H, q, NCH_2, *J* = 7.4 Hz), 3.24 (1H, t, CH, *J* = 6.2 Hz), 4.10 (4H, q, Et CH_2, *J* = 7.9 Hz), 4.62 (1H, br, NH); MS (FAB) 318 (MH)−, 262 (M-C_4H_9), 218 (M-$C_5H_9O_2$). Anal. Calcd for $C_{15}H_{27}NO_6$: C, 56.77, H, 8.57, N, 4.41. Found: C, 56.65, H, 8.45, N, 4.42.

4-[3β-(*tert*-Butyldimethylsilyloxy)androst-5-en-17β-yl]-2-(hydroxymethyl)pentanol (36). The steroid malonate **35** (1.122 g, 1.90 mmol) in THF (10 mL) at 0 °C was treated with 1 M $LiAlH_4$ in THF (9.5 mL), dropwise over 5 min. The mixture was allowed to warm to room temperature and was stirred overnight. After being recooled to 0 °C, the mixture was quenched with EtOAc and then diluted with more EtOAc and 15% citric acid. The organic phase was washed with water and brine, dried, and evaporated. The residue was chromatographed on silica, eluting with 9% CH_3OH/CH_2Cl_2, to give **36** as a white solid (0.806 g, 89%): ^{1}H NMR δ 0.02 (6H, s, $SiCH_3$), 0.87 (9H, s, t-Bu), 3.45 (C-3 CH), 3.68 (4H, m, OCH_2), 5.30 (1H, m, vinyl CH); MS (DCI) 505 (MH)+, 487 (M-H_2O)−, 373 (M-$C_6H_{15}OSi$)−. Anal. Calcd for $C_{31}H_{56}O_3Si$: C, 73.75, H, 11.18. Found: C, 73.52, H, 11.19.

Similarly Prepared: 4-[3β-[(*tert*-Butyldimethylsilyl)oxy]androst-5-en-17β-yl]pentanol (60). (2.462 g, 100%): ^{1}H NMR δ 0.03 (6H, s, $SiCH_3$), 0.87 (9H, s, *t*-Bu), 3.46 (1H, m, C-3 CH), 3.59 (2H, m, OCH_2), 5.29 (1H, d, vinyl CH, *J* = 5.4 Hz); ^{13}C NMR δ 63.5 (OCH_2), 72.6 (C-3), 121.0 (C-6), 141.6 (C-5); MS (DCI) 475 (MH)+. HRMS calcd for $C_{30}H_{55}O_2Si$: 475.3971. Found: 475.3953.

2-(2-[3β-(*tert*-Butyldimethylsilyl)oxy]androst-5-en-17β-yl]propyl)-4-(hydroxymethyl)-5-hydroxypentanol (66). (0.579 g, 94%): ^{1}H NMR δ -0.06 (6H, s, $SiCH_3$), 0.79 (9H, s, *t*-Bu), 3.10−3.62 (7H, m, OCH_2 and OCH), 5.22 (1H, d, vinyl CH, *J* = 5.6 Hz); MS (DCI) 563 (MH)−, 545 (M-H_2O)+. HRMS calcd for $C_{34}H_{63}O_4Si$: 653.4496. Found: 563.4490.

2-(4-[3β-[(*tert*-Butyldimethylsilyl)oxy]androst-5-en-17β-yl]pentyl)-4-(hydroxymethyl)-5-hydroxypentanol (67). (0.291 g, 96%): ^{1}H NMR δ -0.02 (6H, s,

$SiCH_3$), 0.83 (9H, s, *t*-Bu), 3.28−3.72 (7H, m, OCH_2 and OCH), 5.27 (1H, d, vinyl CH, *J* = 4.8 Hz); ^{13}C NMR δ 65.0, 65.8 and 66.1 (OCH_2), 73.4 (C-3), 121.9 (C-6), 142.1 (C-5); MS (FAB) 591 (MH)+, 613 (M+Na)+, 629 (M+K)+.

4-[3β-(3β-Hydroxyandrost-5-en-17β-yl)]-2-(hydroxymethyl)pentanol Bis[bis(2-chloroethyl)amine carbamate] (38). The TBDMS-protected steroid **37** (0.161 g, 0.191 mmol) in THF (2 mL) was treated with 1 M TBAF in THF (0.38 mL, 2 equiv). The mixture was stirred overnight and then evaporated to dryness. The residue was dissolved in EtOAc, and the solution was washed with water and brine, dried, and evaporated. The residue was chromatographed on silica, eluting with 35% EtOAc/hexane, to give **38** as a colorless glass (0.131 g, 94%): ^{1}H NMR δ 3.48 (1H, m, C-3 CH), 3.62 (16H, m, NCH_2 and $ClCH_2$), 4.09 (4H, m, OCH_2), 5.30 (1H, m, vinyl CH); ^{13}C NMR δ 42.3 and 42.4 ($ClCH_2$), 51.3 and 51.7 (NCH_2), 65.4 and 67.2 (OCH_2), 73.1 (C-3), 122.1 (C-6), 141.4 (C-5), 156.4 (CO); MS (FAB) 725 (MH)−, 708 (M-H_2O)−, 539 (M-$C_5H_8NO_2Cl_2$)−.

Similarly Prepared: 4-[3β-(3β-Hycroxyandrost-5-en-17β-yl]-2-(hydroxymethyl)pentanol Bis(5-hydroxypentanoate) Bis[bis(2-chloroethyl)amine carbamate] (44). The compound was chromatographed on silica, eluting with 2% CH_3OH/CH_2Cl_2 (0.171 g, 96%): ^{1}H NMR δ 2.28 (2H, t, $COCH_2$), 3.43 (1H, m, C-3 CH), 3.58 (16H, m, NCH_2 and $ClCH_2$), 3.92 and 4.03 (8H, m, OCH_2), 5.26 (1H, d, vinyl CH); MS (FAB) 928 (MH)−, 950 (M+Na)−, 743 (M-$C_5H_8NO_2Cl_2$)−.

2-[2-(3β-Hydroxyandrost-5-en-17β-yl)propyl]-4-(hydroxymethyl)-5-hydroxypentanol Tris[bis(2-chloroethyl)amine carbamate] (70). (0.607 g, 88%): ^{1}H NMR δ 3.46 (1H, m, C-3 CH), 3.59 (24H, m, $ClCH_2$ and NCH_2), 3.90−4.18 (6H, m, OCH_2), 5.28 (1H, d, vinyl CH, *J* = 5.2 Hz); MS (FAB) 954 (MH)+, 976 (M+Na)+.

2-[4-(3β-Hydroxyandrost-5-en-17β-yl)pentyl]-4-(hydroxymethyl)-5-hydroxypentanol Tris[bis(2-chloroethyl)amine carbamate] (71). (0.250 g, 83%): ^{1}H NMR δ 3.46 (1H, m, C-3 CH), 3.60 (24H, m, $ClCH_2$ and NCH_2), 3.95−4.27 (6H, m, OCH_2), 5.29 (1H, d, vinyl CH, *J* = 5.5 Hz); MS (FAB) 980 (MH)+, 1002 (M+Na)+.

4-[3β-[(*tert*-Butyldimethylsilyl)oxy]androst-5-en-17β-yl]-2-(hydroxymethyl)pentanol Bis(hemiglutarate) (40). Steroid diol **36** (0.072 g, 0.151 mmol) in pyridine (4 mL) under argon was treated with glutaric anhydride (0.344 g, 20 equiv) and DMAP (0.040 g, 2.2 equiv). The mixture was heated at 84 °C for 16 h and then diluted with EtOAc. The solution was washed with 10% citric acid (3×), water, and brine, dried, and evaporated to give a waxy solid, which was carried on without purification (0.078 g, 70%): ^{1}H NMR δ 0.01 (6H, s, $SiCH_3$), 0.84 (9H, s, *t*-Bu), 2.36 (8H, 2t, $COCH_2$, *J* = 8.2 Hz), 3.42 (1H, m, C-3 CH), 4.02 (4H, m, OCH_2), 5.27 (1H, m, vinyl CH).

3β-(Oleoyloxy)-22,23-bisnor-5-cholenic Acid (46). 22,23-Bisnor-5-cholenoyl-3β-ol **18** (2.303 g, 6.646 mmol) in pyridine (25 mL) was treated with DMAP (1.624 g, 2 equiv) and oleoyl chloride (2.000 g, 1 equiv), dropwise over 5 min. After 1 h the mixture was heated to 80 °C for 30 min and then allowed to stir overnight. The mixture was partitioned between CH_2Cl_2 and 10% HCl, and the organic phase was washed with water (2×), dried, and evaporated to give **46** as a waxy solid (3.045 g, 75%): ^{1}H NMR δ 0.83 (3H, t, oleoyl CH_3, *J* = 7.0 Hz), 2.23 (4H, m, $COCH_2$ and C-4 CH_2), 4.58 (1H, m, C-3 CH), 5.32 (3H, m, vinyl CH); MS (DCI) 612 (MH)+.

3β-(Oleoyloxy)-22,23-bisnor-5-cholenic Acid Pentafluorophenyl Ester (47). Carboxylic acid **46** (0.336 g, 0.550 mmol) and pentafluorophenol (0.111 g, 1.1 equiv) in CH_2Cl_2 (5 mL) at 0 °C were treated with DCC (0.125

g, 1.1 equiv). After 2 h the mixture was filtered, and the solid was washed with CH_2Cl_2. The filtrate was evaporated, and the resulting thick oil was carried on without further purification.

3β-(Oleoyloxy)-22,23-bisnor-5-cholenic Acid Bis-(2-hydroxyethyl)amide (48). A mixture of the crude active ester **47** (ca 0.55 mmol) and bis(2-hydroxyethyl)-amine (0.087 g, 1.5 equiv) in THF (5 mL) under argon was heated at 50 °C overnight. The mixture was partitioned between EtOAc and 10% citric acid, and the organic phase was washed with water and brine, dried, and evaporated. The residue was chromatographed on silica, eluting with 6% CH_3OH/CH_2Cl_2, to give **48** as a white solid (0.180 g, 47%): ^1H NMR δ 0.83 (3H, t, oleoyl CH_3, $J = 6.8$ Hz), 2.24 (4H, m, $COCH_2$ and C-4 CH_2), 2.71 (2H, brt, OH), 3.49 (4H, m, NCH_2), 3.74 (4H, m, OCH_2), 4.56 (1H, m, C-3 CH), 5.31 (3H, m, vinyl CH); MS (FAB) 699 (MH)$^+$, 681 (M-H_2O)$^+$. Anal. Calcd for $C_{44}H_{75}NO_5$·$2H_2O$: C, 71.99, H, 10.85, N, 1.91. Found: C, 72.43, H, 10.78, N, 1.97.

N-(tert-Butoxycarbonyl)-3-aminopropanol (50). A solution of 3-aminopropanol (15 mL, 0.20 mol) in CH_2Cl_2 (50 mL) was treated with tert-butylpyrocarbonate (42.02 g, 1 equiv) in CH_2Cl_2 (25 mL), dropwise over 2 h. After being stirred overnight, the mixture was evaporated, flushed with heptane (3×), and dried in vacuo to give **50** as a thick oil (34.31 g, 100%): ^1H NMR δ 1.48 (9H, s, t-Bu), 3.12 (1H, br, OH), 3.22 (2H, q, NCH_2, $J = 7.5$ Hz), 3.60 (2H, q, OCH_2, $J = 7.8$ Hz), 4.81 (1H, br, NH); MS (DCI) 176 (MH)$^-$. Anal. Calcd for $C_8H_{17}NO_3$: C, 54.84, H, 9.78, N, 7.99. Found: C, 54.80, H, 9.82, N, 7.97.

N-(tert-Butoxycarbonyl)-5-amino-2-(hydroxymethyl)pentanol (53). The diester **52** (4.957 g, 15.62 mmol) in ether (100 mL) under argon at 0 °C was treated with $LiBH_4$ (2 M in THF, 24 mL, 3 equiv) and then with CH_3OH (1.9 mL, 3 equiv). The mixture was heated at reflux for 2.5 h and then carefully quenched with CH_3-OH (25 mL) followed by acetic acid (2.7 mL, 3 equiv) upon cooling to room temperature. The mixture was evaporated and flushed with CH_2Cl_2 (2×). The residue was dissolved in CH_3OH (100 mL), and the mixture was heated at reflux overnight and then evaporated. The resulting oil was dissolved as far as possible in $CHCl_3$ (100 mL) with sonication, and the solid inorganics were removed by filtration. The filtrate was evaporated, and the residue was chromatographed on silica, eluting with 9% CH_3OH/CH_2Cl_2, to give **53** as a thick oil (2.770 g, 76%): ^1H NMR δ 1.21 and 1.41 (each 2H, m, CH_2), 1.37 (9H, s, t-Bu), 1.60 (1H, m, CH), 2.98 (2H, q, NCH_2, $J = 7.4$ Hz), 3.68 (4H, m, OCH_2), 3.96 (1H, br, OH), 4.97 (1H, brt, NH); MS (DCI) 234 (MH)$^+$, 178 (M-C_4H_9)$^+$, 134 (M-$C_5H_9O_2$)$^+$. Anal. Calcd for $C_{11}H_{23}NO_4$: C, 56.63, H, 9.94, N, 6.00. Found: C, 56.16, H, 9.83, N, 5.94.

5-Amino-2-(hydroxymethyl)pentanol-TFA (54). A solution of 5% water in 50% TFA/CH_2Cl_2 (4 mL) was added to diol **53** (0.145 g, 0.621 mmol), and the mixture was stirred for 1 h. The solvents were evaporated, and the residue was flushed with CH_2Cl_2 (2×) (0.153 g, 100%): ^1H NMR δ 1.22 and 1.50 (each 2H, m, CH_2), 1.69 (1H, m, CH), 2.82 (2H, br, NCH_2), 3.51 (4H, d, OCH_2, $J = 6.9$ Hz), 7.78 (3H, br, NH_3^+); MS (DCI) 134 (MH)$^+$.

Diethyl 2-[(tert-Butoxycarbonyl)ethyl]malonate (57). To a suspension of NaH (60% in mineral oil, 2.63 g, 65.8 mmol) in THF (25 mL) under argon at 0 °C was added diethyl malonate (10 mL, 1 equiv), carefully, to avoid foaming. The mixture was allowed to warm to room temperature for 30 min and then was cooled to −78 °C. To this was added tert-butyl acrylate (8.9 mL, 0.91 equiv), and the reaction mixture was warmed to room

temperature overnight. The mixture was partitioned between 50% EtOAc/hexane and saturated NH_4Cl, and the organic phase was washed with water and brine, dried, and evaporated. The residue was distilled under reduced pressure to give **57** as an oil (6.83 g, 39%): bp 100−110 °C/0.01 mmHg; ^1H NMR δ 1.21 (6H, t, Et CH_3, $J = 7.9$ Hz), 2.12 (2H, q, CH_2), 2.26 (2H, t, $COCH_2$, $J = 7.1$ Hz), 3.38 (1H, t, CH, $J = 8.2$ Hz), 4.17 (4H, q, Et CH_2, $J = 7.9$ Hz); MS (DCI) 401 (MH)$^+$, 345 (M-C_4H_9)$^+$, 328 (M-C_4H_9O)$^+$. HRMS calcd for $C_{14}H_{25}O_6$: 289.1651. Found: 289.1641.

3β-Hydroxy-5-cholenic Acid Methyl Ester (58). A solution of 5-cholenoyl-3β-ol **3** (2.059 g, 5.497 mmol) in CH_3OH (6 mL) was treated with 1 M NaOH (5.5 mL, 1 equiv). The solvents were evaporated, and the solid was flushed with CH_2Cl_2 (3×), suspended in DMF (40 mL), and treated with methyl iodide (0.685 mL, 2 equiv). The mixture was stirred overnight and then poured into ice water (500 mL). The resulting solid was collected by filtration, washed with water, and dried in vacuo to give **58** as a white solid (2.133 g, 99%): ^1H NMR δ 3.48 (1H, m, C-3 CH), 3.64 (3H, s, OCH_3), 5.31 (1H, d, vinyl CH, $J = 5.3$ Hz); MS (DCI) 389 (MH)$^+$.

2-[3β-[(tert-Butyldimethylsilyl)oxy]androst-5-en-17β-yl]propyl Iodide (62). A mixture of mesylate **34** (0.189 g, 0.360 mmol) and NaI (0.270 g, 5 equiv) in acetone (6 mL) was heated at reflux overnight. The mixture was partitioned between ether and water, and the organic phase was washed with water and brine, dried, and evaporated. The residue was chromatographed on silica, eluting with 5% EtOAc/hexane, to give **62** as a white solid (0.166 g, 83%): ^1H NMR δ 0.01 (6H, s, $SiCH_3$), 0.84 (9H, s, t-Bu), 3.22 (2H, m, ICH_2), 3.44 (1H, m, C-3 CH), 5.28 (1H, d, vinyl CH, $J = 4.9$ Hz); MS (DCI) 557 (MH)$^+$, 425 (M-$C_6H_{15}Si$)$^+$. Anal. Calcd for $C_{28}H_{49}$-OSiI: C, 60.41, H, 8.87. Found: C, 60.35, H, 8.91.

Similarly Prepared: 4-[3β-[(tert-Butyldimethylsilyl)oxy]androst-5-en-17β-yl]pentyl Iodide (63). (0.424 g, 99%): ^1H NMR δ 0.02 (6H, s, $SiCH_3$), 0.87 (9H, s, t-Bu), 3.12 (2H, m, ICH_2), 3.44 (1H, m, C-3 CH), 5.29 (1H, d, vinyl CH, $J = 5.3$ Hz); MS (DCI) 583 (MH)$^-$, 453 (M-$C_6H_{15}OSi$)$^+$. Anal. Calcd for $C_{30}H_{53}OSiI$: C, 61.62, H, 9.14. Found: C, 62.07, H, 9.23.

23-[(Diethylmalonyl)methyl]-3β-hydroxy-5-cholenic Acid tert-Butyldimethylsilyl Ether tert-Butyl Ester (64). The triester **57** (0.518 g, 1.797 mmol) in THF (4 mL) at −78 °C under argon was treated with freshly prepared LDA (2.2 equiv), and the mixture was allowed to stir for 20 min. To this was added the steroid iodide **62** (0.625 g, 0.6 equiv) in THF (8 mL) over several minutes. The cooling bath was removed, and the reaction mixture was stirred at room temperature overnight. The mixture was partitioned between 30% EtOAc/hexane and saturated NH_4Cl, and the organic phase was washed with water and brine, dried, and evaporated. The residue was chromatographed on silica, eluting with 6% EtOAc/hexane, to give **64** as a glass (0.788 g, 98%): ^1H NMR δ 0.00 (6H, s, $SiCH_3$), 0.82 (9H, s, Si-t-Bu), 1.21 (6H, 2t, Et CH_3, $J = 7.5$ Hz), 1.40 (9H, s, O-t-Bu), 3.42 (1H, 2ABq, mal CH), 3.41 (1H, m, C-3 CH), 4.15 (4H, m, Et CH_2), 5.27 (1H, d, vinyl CH, $J = 5.2$ Hz); MS (FAB) 755 (M+K)$^+$, 717 (MH)$^+$, 659 (M-C_4H_9)$^+$, 643 (M-C_4H_9O)$^-$. HRMS calcd for $C_{42}H_{71}O_7Si$: 715.4969. Found: 715.4973.

Similarly Prepared: tert-Butyl 2-[(Diethylmalonyl)methyl]-6-[3β-[(tert-butyldimethylsilyl)oxy]-androst-5-en-17β-yl]heptanoate (65). (0.387 g, 78%): ^1H NMR δ 0.01 (6H, s, $SiCH_3$), 0.87 (9H, s, Si-t-Bu), 1.22 (6H, 2t, Et CH_3, $J = 7.3$ Hz), 1.43 (9H, s, O-t-Bu), 3.33 (1H, ABq, mal CH), 3.42 (1H, m, C-3 CH), 4.18 (4H, m, Et CH_2), 5.29 (1H, d, vinyl CH, $J = 4.8$ Hz); MS

(FAB) 746 (MH)⁺, 689 (M-C₄H₉)⁺. Anal. Calcd for C₄₄H₇₆O₇Si·H₂O: C, 69.24, H, 10.30. Found: C, 68.91, H, 10.06.

3β-(Oleoyloxy)-22,23-bisnor-5-cholenic Acid Tris-(hydroxymethyl)methanamide (74). A mixture of active ester **20** (1.084 g, 1.47 mmol) and tris(hydroxymethyl)aminomethane (3.602 g, 20 equiv) in 80% CH₃OH/CH₂Cl₂ (25 mL) was sonicated for 1 h and then stirred for 2 days. The solvents were evaporated, and the residue was chromatographed on silica, eluting with EtOAc, to give **74** as a colorless glass (0.284 g, 26%): ¹H NMR δ 0.81 (3H, t, oleoyl CH₃, *J* = 6.8 Hz), 2.22 (4H, m, COCH₂ and C-4 CH₂), 3.57 (6H, brs, OCH₂), 4.56 (1H, m, C-3 CH), 4.71 (3H, br, OH), 5.32 (3H, m, vinyl CH), 6.47 (1H, s, NH); MS (DCI) 742 (MH)⁺, 724 (M-H₂O)⁺. Anal. Calcd for C₄₆H₇₉NO₆: C, 74.45, H, 10.73, N, 1.89. Found: C, 74.01, H, 10.88, N, 1.87.

***N,N′*-Bis(Hydroxymethyl)-5-fluorouracil (76).** A suspension of 5-fluorouracil (1.152 g, 8.855 mmol) in formalin (37.3%, 1.45 mL, 2.2 equiv) was heated at 60 °C. After 10 min the mixture became homogeneous. With continued heating the mixture was put under vacuum (0.01 mmHg) to remove water. After 1 h a colorless glass remained, which was dissolved in acetonitrile to a concentration of 1 M. This solution was stored at 0 °C and used in subsequent steps.

5-Cholenoyl-3β-ol (*p*-Bromobenzoyl)methyl Ester (77). A solution of 5-cholenoyl-3β-ol **1** (2.010 g, 5.54 mmol) in THF (60 mL) and DMSO (8.5 mL) was treated with 2,4′-dibromoacetophenone (2.46 g, 1.6 equiv) and Et₃N (31 mL). The reaction mixture was stirred for 24 h and then filtered. The filtrate was diluted with EtOAc (100 mL), and this was washed with water (2×) and brine, dried, and evaporated. The residue was chromatographed on silica, eluting with 1% CH₃OH/CH₂Cl₂, to give **77** as a white solid (2.174 g, 69%): ¹H NMR δ 3.49 (1H, m, C-3 CH), 5.25 (2H, s, COCH₂O), 5.32 (1H, d, vinyl CH, *J* = 5.4 Hz), 7.60 and 7.75 (each 2H, AXq, Ph); MS (DCI) 571 (MH)⁺, 373 (M-C₈H₆OBr)⁺, 357 (M-C₈H₆O₂Br). Anal. Calcd for C₃₂H₄₃O₄BrH₂O: C, 65.19, H, 7.69. Found: C, 65.35, H, 7.77.

3β-(Oleoyloxy)-5-cholenic Acid (79). Diester **78** (2.900 g, 3.47 mmol) in THF (40 mL) was treated with glacial acetic acid (25 mL) and zinc dust (3.51 g). The mixture was stirred for 24 h and filtered to remove inorganics. The filtrate was diluted with EtOAc (100 mL), and this was washed with water (5×), dried, and evaporated. The residue was crystallized from ethanol to give **79** as a white solid (1.885 g, 85%): ¹H NMR δ 0.91 (3H, t, oleoyl CH₃, *J* = 6.9 Hz), 2.25 (4H, m, COCH₂ and C-4 CH₂), 4.61 (1H, m, C-3 CH), 5.36 (3H, m, vinyl CH); MS (FAB) 689 (M+Na)⁺, 705 (M+K)⁺.

3β-(Oleoyloxy)-25,26-bishomo-5-cholenic Acid *N*¹-(Hydroxymethyl)-5-fluorouracil Ester (82). A solution of the acid **10** (0.145 g, 0.217 mmol) and **76** (1 M in acetonitrile, 0.26 mL, 1.2 equiv) in THF (2 mL) was treated with DCC (0.049 g, 1.1 equiv) and DMAP (0.029 g, 1.1 equiv), and the mixture was stirred overnight. DCU was removed by filtration, and the filtrate was evaporated. The residue was carried on as described for **81** above (0.103 g, 59%): ¹H NMR δ 0.88 (3H, t, oleoyl CH₃, *J* = 6.7 Hz), 2.25 (4H, m, COCH₂ and C-4 CH₂), 4.58 (1H, m, C-3 CH), 5.32 (3H, m, vinyl CH), 5.63 (2H, s, OCH₂O), 7.61 (1H, d, 5-FU CH, *J* = 5.5 Hz), 9.45 (1H, br, NH). Anal. Calcd for C₄₉H₇₇N₂O₆F·0.5H₂O: C, 71.93, H, 9.61, N, 3.42. Found: C, 72.14, H, 9.86, N, 3.42.

Similarly Prepared: 3β-(Oleoyloxy)-22,23-bisnor-5-cholenic Acid *N*¹-(Hydroxymethyl)-5-fluorouracil Ester (80). (0.085 g, 32%): ¹H NMR δ 0.88 (3H, t, oleoyl CH₃), 2.23 (4H, m, COCH₂ and C-4 CH₂), 4.59 (1H, m,

C-3 CH), 5.30 (3H, m, vinyl CH), 5.62 (2H, s, OCH₂O), 7.61 (1H, d, 5-FU CH, *J* = 5.2 Hz). Anal. Calcd for C₄₅H₆₉N₂O₆F: C, 71.77, H, 9.24, N, 3.72. Found: C, 71.61, H, 9.39, N, 3.64.

3β-(Oleoyloxy)-5-cholenic Acid *N*¹-(Hydroxymethyl)-5-fluorouracil Ester (81). (0.238 g, 78%): ¹H NMR δ 0.80 (3H, t, oleoyl CH₃), 2.20 (4H, m, COCH₂ and C-4 CH₂), 4.49 (1H, m, C-3 CH), 5.25 (3H, m, vinyl CH), 5.51 (2H, s, OCH₂O), 7.49 (1H, d, 5-FU CH, *J* = 5.5 Hz), 9.42 (1H, br, NH). Anal. Calcd for C₄₇H₇₃N₂O₆F·0.5H₂O: C, 71.45, H, 9.44, N, 3.55. Found: C, 71.46, H, 9.74, N, 3.68.

4-[3β-(Oleoyloxy)androst-5-en-17β-yl]pentyl Hemiglutaric Acid *N*¹-(hydroxymethyl)-5-fluorouracil Ester (83). (0.162 g, 52%): ¹H NMR δ 0.85 (3H, t, oleoyl CH₃), 2.23 (4H, m, COCH₂ and C-4 CH₂), 2.35 and 2.44 (each 2H, t, COCH₂), 4.00 (2H, m, OCH₂), 4.58 (1H, m, C-3 CH), 5.30 (3H, m, vinyl CH), 5.61 (2H, s, OCH₂O), 7.58 (1H, d, 5-FU CH, *J* = 5.4 Hz), 9.36 (1H, br, NH). Anal. Calcd for C₅₀H₇₇N₂O₈F·0.5H₂O: C, 69.65, H, 9.12, N, 3.25; found: C, 69.56, H, 8.81, N, 3.58.

RECONSTITUTION AND CYTOTOXICITY ASSAYS

LDL reconstitutions and biological assays were carried out as described previously (*23*). Briefly, purified human LDL was lyophilized in the presence of potato starch, and the immobilized LDL was delipidated by extraction with heptane at −10 °C, removing the neutral core lipids. The remnants were treated with the oleoyl steroid prodrug of interest in heptane for 1 h at −10 °C. The heptane was evaporated, and the rLDL was solubilized in Tricine buffer (pH 8.4, 4 °C) and purified by centrifugation.

Chinese hamster ovary (CHO) cells were grown and then plated in 24-well plates and incubated for 4 h at 37 °C. The rLDL was added, and incubation continued for 3 days. The medium was removed, and the wells were washed with PBS to remove dead cells. The remaining cells were fixed with formalin, stained with crystal violet, and evaluated visually. The results appear as a series of wells either with or without a mat of stained cells. In all assays, the concentration of rLDL was varied in the series 10, 5, 2, 1, 0.1, and 0 μg of rLDL/mL. In almost all cases, the endpoint well was clear and the next one was overgrown. The data points are reported as the highest concentration that was clear. Thus a reported endpoint of 1 μg of rLDL/mL really means <1 but > 0.1. Sometimes there was a visibly transitional well, and in these cases both the transitional concentration and the lowest clear one (e.g., 2−5) are reported. In this survey, most compounds were assayed once. Compounds **25**, **26**, and **39** were evaluated twice, with the same result, and **1** was duplicated in that the present endpoint (2−5) is very close to that reported by us in 1984 (3−10) (*23*).

There is yet another check on the reliability of our data for **1**, **31**, and **39**. All three compounds were also evaluated against T-47D breast cancer cells by Lundberg using his own reconstitution procedure, which consists of incorporating delipidated Apo B into a drug−triolein−EPC−polysorbate 80 microemulsion. The advantage is higher reconstituted drug yields, and possibly ease of preparation. His results duplicate ours in that his IC₅₀s have ratios of **1:39** = 1.81 and **1:31** = 2.24 (*29*).

RESULTS AND DISCUSSION

As a point of reference for the design of new compounds we used **1** and **2** from the earlier study. Since the greater potency of **1** over **2** apparently resided in facilitated access of hydrolytic enzymes to the site of cleavage, we thought that moving the carbamate a greater distance

Scheme 1[a]

i $\begin{cases} \textbf{3 R, R'=H} \\ \textbf{4 R=Suc, R'=H} \end{cases}$
ii $\begin{cases} \textbf{5 R=Suc, R'=oleoyl} \end{cases}$

iv $\begin{cases} \textbf{6 R=H} \\ \textbf{7 R=SO}_2\textbf{CH}_3 \end{cases}$

vi $\begin{cases} \textbf{8 R=t-Bu} \\ \textbf{9 R=H} \end{cases}$

i
iii
viii $\begin{cases} \textbf{10 R=H, X=O} \\ \textbf{11 R=Suc, X=O} \\ \textbf{12 R=H, X=H}_2 \\ \textbf{13 R=CONM, X=H}_2 \end{cases}$

6 $\xrightarrow{\text{ix}}$

i
iii
viii $\begin{cases} \textbf{14 R=H, X=O} \\ \textbf{15 R=Suc, X=O} \\ \textbf{16 R=H, X=H}_2 \\ \textbf{17 R=CONM, X=H}_2 \end{cases}$

i $\begin{cases} \textbf{18 R, R'=H} \\ \textbf{19 R=Suc, R'=H} \end{cases}$
ii $\begin{cases} \textbf{20 R=Suc, R'=oleoyl} \end{cases}$

$\xrightarrow{\text{x}}$ NH(CH₂)ₙOR

21 n=3, R=H
22 n=4, R=H
23 n=5, R=H

xi
24 n=3, R=CONM
25 n=4, R=CONM
26 n=5, R=CONM
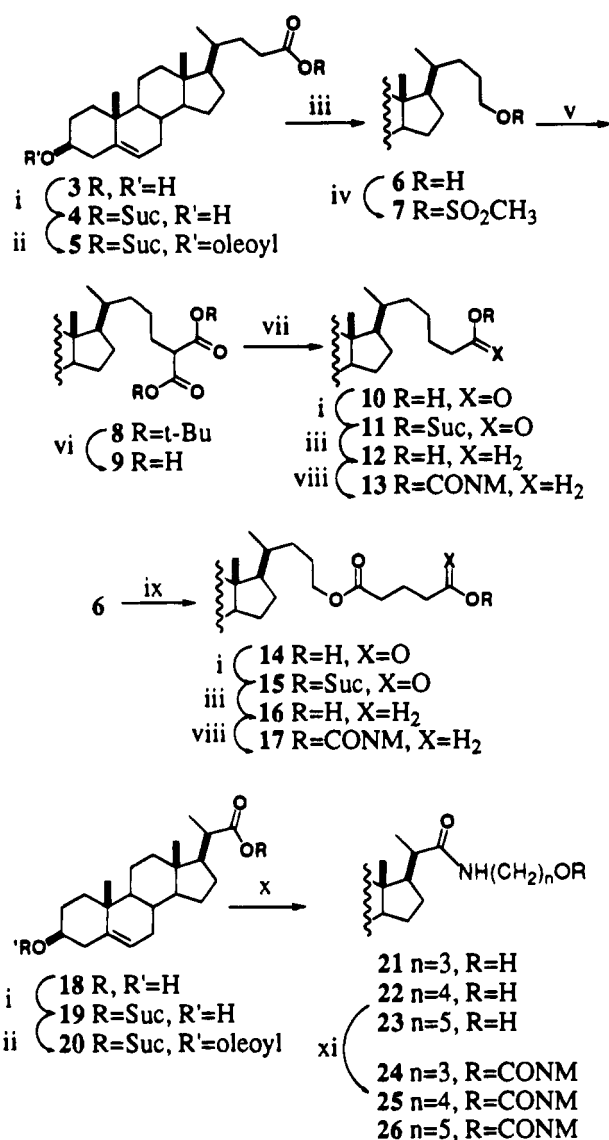
[a] Reagents: (i) NHS, DCC, THF; (ii) oleoyl chloride, pyridine; (iii) NaBH₄, diglyme; (iv) CH₃SO₂Cl, TEA; (v) t-butyl malonate, NaH, THF, D; (vi) TFA, CH₂Cl₂; (vii) DMSO, Δ; (viii) Cl₃COCOCl, pyridine, then bis-2-chloroethylamine; (ix) glutaric anhydride, DMAP; (x) H₂N(CH₂)ₙOH, THF; (xi) **30**, DBU, DMAP.

from the bulky steroid might further improve potency by increasing the rate of drug release. Therefore, compounds with a variety of longer arms at the steroid's 17-β-position were made (Scheme 1).

Two carbon homologation of **1** was carried out by formation of the NHS active ester (**4**) of commercially available 3β-hydroxy-5-cholenic acid (**3**), oleoylation of the A-ring hydroxyl, and reduction of the active ester with sodium borohydride (**27**). Mesylate **7** was formed from alcohol **6** and was displaced by the sodium salt of di-*tert*-butyl malonate. After acidic deprotection and decarboxylation the NHS activation and borohydride reduction steps were repeated, giving bis-homologated alcohol **12**. This was treated with diphosgene, and the chloroformate formed *in situ* was condensed with nitrogen mustard to give carbamate **13**. The highly extended ester **17** was prepared by treating alcohol **6** with glutaric anhydride and carrying on the resulting carboxylic acid **14** in a manner similar to that for **10** above. Compounds **24**–**26** were chosen because they were especially easy to prepare from steroid active ester **20** and a series of linear hydroxylamines.

Table 1. Activity of rLDL Reconstituted with Steroidal Prodrugs Containing a Single Nitrogen Mustard against Wild-Type CHO Cells and Receptor-Deficient Mutants (LDLA-7)

compound	CHO, μg of rLDL/mL[a]	LDLA-7, μg of rLDL/mL[a]	yield rLDL, mg/mL
1	2–5	>10	1.26
13	5–10	>10	1.05
17	>10	>10	0.85
24	>10	>10	1.05
25	5–10	>10	1.49
26	10	>10	1.47
cholest. oleate			0.98–1.31
heptane			0.21–0.27

[a] See the description of the cytotoxicity assay above.

A
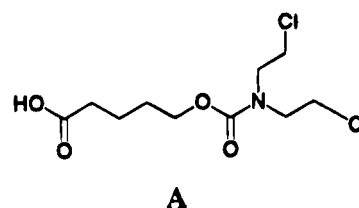
Figure 2.

Cytotoxicities of rLDL made from these target compounds are shown in Table 1. In accord with our previous finding (*23*), all of these double-anchored compounds reconstituted well. This is demonstrated in Table 1 by the protein yields in comparison with reconstitution using cholesterol oleate, the primary natural constituent of the LDL core, and with the heptane solvent alone. Stability of the rLDLs toward leakage, and thus exclusivity of uptake via LDL receptors, was assured by finding that receptor-negative LDLA-7 cells were spared.

Contrary to our expectations, simple extension of the D-ring side chain of **1** by two methylene groups reduced the activity of **13**, perhaps owing to association of the hydrophobic pentamethylene chain with the steroid in the aqueous environment of the lysosome. Substituting an amide for two of the methylene groups while retaining overall chain length (**24**), however, led to complete loss of activity, within the limits of the assay. Further extension by one and then two methylene groups gave rise to an increase (**25**) and then a decrease (**26**) in cytotoxicity. The activity of **25** is almost equal to that of **1**. These variations are puzzling and may reflect complex specificities of the hydrolytic enzyme(s) involved in drug release. Valeryl ester **17**, containing the longest chain, similarly possessed no activity, perhaps because rapid cleavage of the ester gives the acid **A** (Figure 2), a lysosomophobic substance that might quickly exit the lysosome before the carbamate can be hydrolyzed.

Another way to increase cytotoxicity is to increase the number of warheads in the prodrug. Provided that access to the hydrolytic enzyme is maintained, activity should be proportional to the number of NM moieties. Indeed, activity might be more than proportional if there were subsets of LDL receptors of unequal binding and internalizing strength, since then a multiarmed compound might be able to dispense with the least efficient subset and still carry in enough NM to kill cells.

The synthesis of multiarmed prodrugs is illustrated in Schemes 2–4. Steroid malonic acid **9** was activated and reduced to 1,3-diol **29**, which was treated with the chloroformate of nitrogen mustard (**30**) to give bis-(carbamate) **31**. To be efficient, this reaction requires both strong base (DBU) and transacylation catalyst (DMAP). The shorter, doubly armed prodrug **39** was similarly prepared except that silyl protection of the

Scheme 2*a*
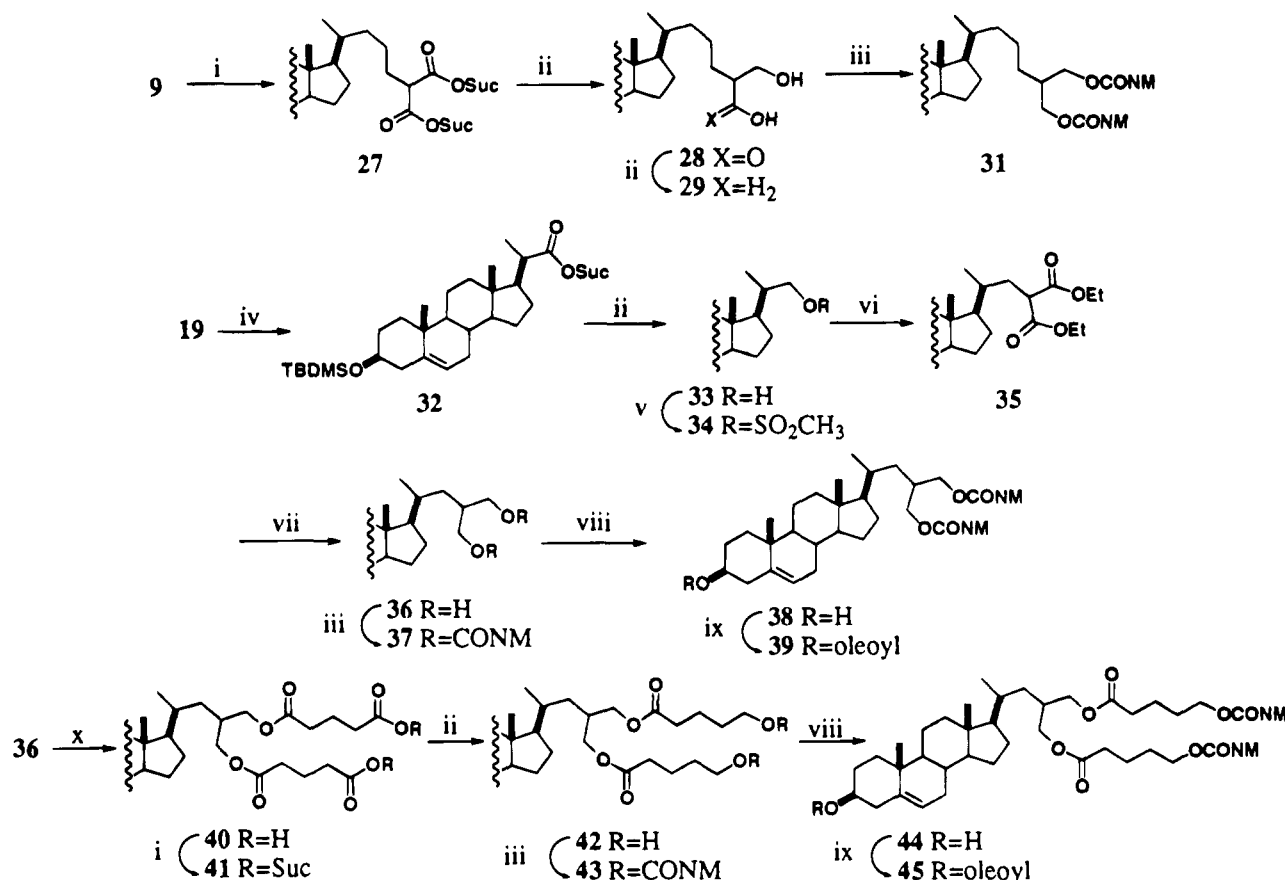
a Reagents: (i) NHS, DCC; (ii) NaBH₄, diglyme; (iii) ClCONM (**30**), DBU, DMAP; (iv) TBDMSCl, TEA; (v) CH₃SO₂Cl, TEA; (vi) diethyl malonate, NaH, THF, Δ; (vii) LiAlH₄, THF; (viii) TBAF, THF; (ix) oleoyl chloride, pyridine; (x) glutaric anhydride, DMAP.

Scheme 3*a*
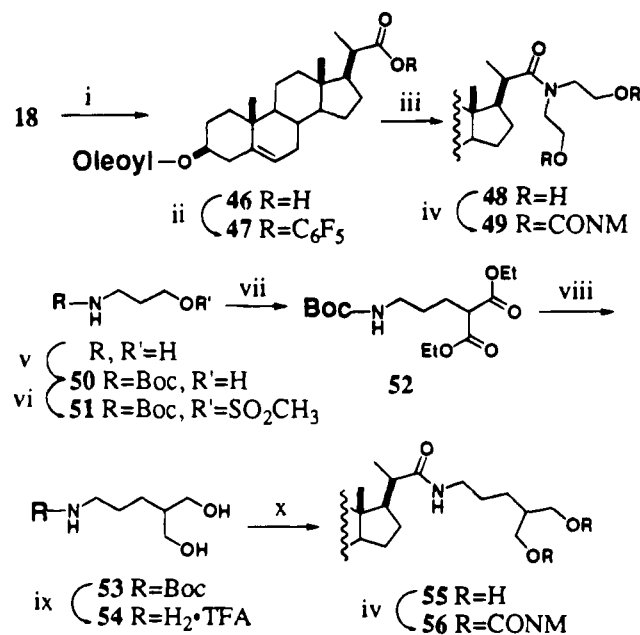
a Reagents: (i) oleoyl chloride, pyridine; (ii) C₆F₅OH, DCC; (iii) bis-2-hydroxyethylamine,THF, Δ; (iv) **30**, DBU, DMAP; (v) Boc₂O, CH₂Cl₂; (vi) CH₃SO₂Cl, TEA; (vii) diethyl malonate, NaH, THF, Δ; (viii) LiAlH₄, THF; (ix) TFA, CH₂Cl₂; (x) **20**, THF.

A-ring hydroxyl allowed direct LiAlH₄ reduction of the diethyl malonate ester **35** with silyl removal and oleoylation as the last step in a shorter overall process (*28*). The bis(hydroxyvaleryl carbamate) **45** was prepared in an analogous manner to that of **17** from diol **36**.

Two doubly armed prodrugs (**49** and **56**, Scheme 3) were made by coupling bisnorcholenic acid **18** with two aminodiols (dihydroxyethylamine and **54**), followed by reaction with chloroformate **30**.

Scheme 4 shows the preparation of three triply armed prodrugs (**72**, **73**, and **75**). The all-carbon frameworks of **72** and **73** were constructed by alkylation of triester **57** with steroid iodides **62** and **63**, which occurs exclusively at the most reactive carbon (*28*). The amide-linked tris(carbamate) **75** is derived from tris(hydroxymethyl)-aminomethane and active ester **20**.

A potential problem with these multiarmed compounds is that an excess of molecular scaffolding, making the prodrug less and less like the normal cholesterol ester contents of the particle core, might eventually overpower the LDL anchors, causing leakage from the rLDL. However, all of the target prodrugs in Schemes 2–4 reconstituted well. Their cytotoxic activities are shown in Table 2.

LDL reconstituted with the doubly armed compounds **31** and **39** was at least 2-fold more potent than rLDL containing **1**, and thus we have achieved our goal of moving significantly beyond the cell-killing power of **1**. Compounds **31** and **39** are the most powerful ones we have made to date that can be reconstituted into stable rLDL and that are able to kill 100% of the test cells while sparing receptor-negative cells, at concentrations easily attainable *in vivo*. Considering the difference in cytotoxicity between **1** and **2**, presumably due to steric crowding, it is perhaps surprising that **31** and **39** have essentially equal activities. The 2-fold higher potencies of **31** and **39** in comparison with **1** have been confirmed by Lundberg (see above) (*29*).

Scheme 4[a]
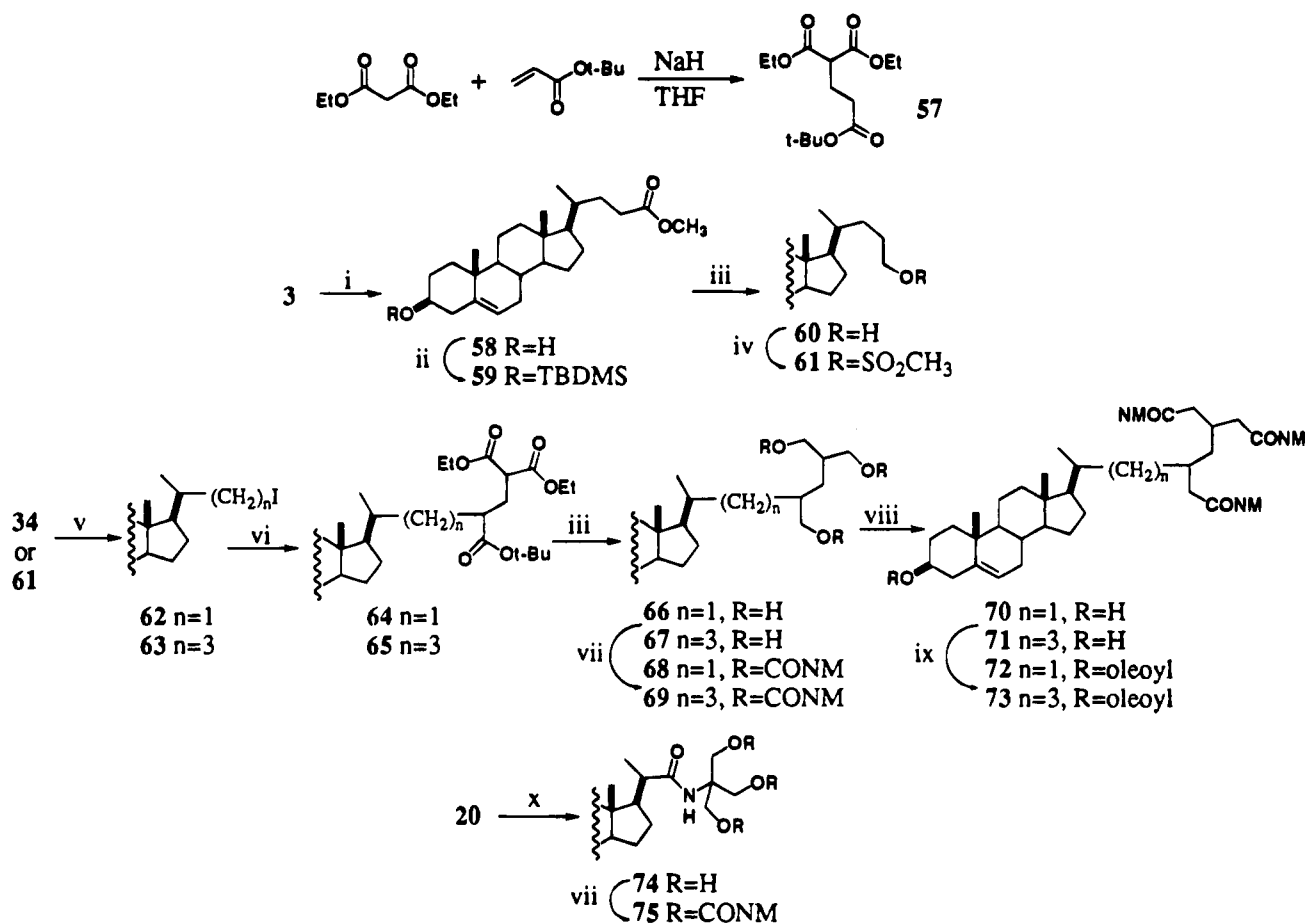
[a] Reagents: (i) 1 eq NaOH, then CH$_3$I, DMF; (ii) TBDMSCl, TEA; (iii) LiAlH$_4$, THF; (iv) CH$_3$SO$_2$Cl, TEA; (v) NaI, acetone; (vi) **57**, 2.2 eq LDA; (vii) **30**, DBU, DMAP; (viii) TBAF, THF; (ix) oleoyl chloride, pyridine; (x) tris-hydroxymethylaminomethane, CH$_2$Cl$_2$/CH$_3$OH.

Table 2. Activity of rLDL Reconstituted with Steroidal Prodrugs Containing Two or Three Nitrogen Mustard Moieties against Wild-Type CHO Cells and Receptor-Deficient Mutants (LDLA-7)

compound	CHO, µg of rLDL/mL[a]	LDLA-7, µg of rLDL/mL[a]	yield rLDL, mg/mL
31	1	>10	1.36
39	1	>10	1.56
45	>10	>10	1.09
49	>10	>10	1.41
56	>10	>10	1.58
72	>10	>10	1.37
73	>10	>10	1.35
75	>10	>10	1.03

[a] See the description of the cytotoxicity assay above.

All of the other doubly armed prodrugs (**45**, **49**, and **56**) showed no activity as rLDL conjugates. In the case of bisvaleryl ester **45** the reason may be the same as suggested above for the analogous single-armed compound **17**. We were disappointed that none of the triply armed prodrugs, especially **72** and **73**, which are structurally related to our potent bis mustards **31** and **39**, demonstrated any utility. Knowing little about the active sites of the hydrolytic enzymes involved, we can only speculate that these compounds are simply too bulky for active drug to be efficiently released.

We have also attempted to target drugs other than NM through rLDL. Four 5-fluorouracil (5-FU) derivatives (**80–83**) were synthesized, with varied linkers to the steroid LDL anchor using established methods to make lipophilic 5-FU prodrugs (Scheme 5) (*30*). However, none

of them could be reconstituted with LDL, probably owing to the polarity of 5-FU. A differentiating agent, retinoic acid (*31*), was coupled to cholesterol with the expectation that reconstitution of this lipophilic conjugate **84** (Figure 3) would be facile. To our surprise reconstitution of **84** failed. Other LDL compounds that are soluble in heptane containing more potent antitumor drugs such as doxorubicin have been prepared but have not yet been reconstituted and tested *in vitro*.

CONCLUSIONS

The following impediments to *in vivo* treatment with **31** or **39** in rLDL remain: (1) Delipidating patients to reduce competition of rLDL with native LDL for receptors on tumor cells, since excess LDL abolishes the cytotoxicity of 1-LDL (*32*). This will also upregulate LDL receptor activity on both tumor and normal cells to an unknown relative extent. However, since LDL-derived cholesterol downregulates hepatocyte LDL receptors only weakly (*33*), delipidation-induced uptake in the liver might also be weak. LDL uptake in liver and adrenals in comparison with tumor can be diminished (*34*), (2) Removing aggregate from rLDL, which is always formed in the Krieger process (*32*), and which does not behave normally *in vivo* as monomeric rLDL does. Aggregation is not a problem with rLDL made by the Masquelier process, but its reduced drug load makes it unsuitable for targeting **31** and **39**.

However, delipidation of patients has now been reduced to a routine procedure (*3*), and aggregate can be removed from rLDL (*32*). Therefore, *in vivo* trials are

Scheme 5[a]

[a] Reagents: (i) 2, 4'-dibromoacetophenone, TEA; (ii) oleoyl chloride, pyridine; (iii) Zn, AcOH; (iv) **76**, DCC, DMAP.

84
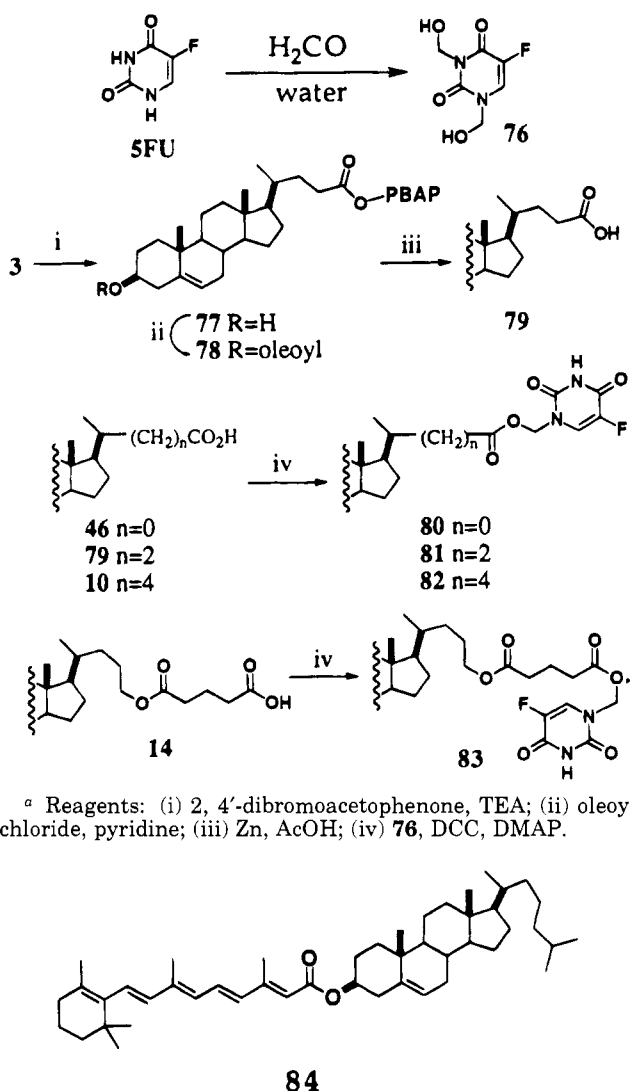
Figure 3.

now feasible. Although there are numerous potential tumor targets, a good first choice might be acute myeloid leukemia because it has exceptionally high LDL requirements (**7**), is particularly difficult to cure, and is a disseminated tumor with good access of rLDL to the cells.

ACKNOWLEDGMENT

LITERATURE CITED

(1) Paper no. 9 in the series Lysosomotropic Agents.

(2) Paper no. 8: Cabantchik, Z. I., Silfen, J., Firestone, R. A., Krugliak, M., Nissani, E., and Ginsburg, H. (1990) Effects of Lysosomotropic Detergents on the Human Malarial Parasite *Plasmodium falciparum* in In Vitro Culture. *Biochem. Pharmacol. 38*, 1271–1277.

(3) Firestone, R. A. (1994) Low Density Lipoprotein as a Vehicle for Targeting Antitumor Compounds to Cancer Cells. *Bioconj. Chem. 5*, 105–113.

(4) Goldstein, J. L., Anderson, R. G. W., and Brown, M. S. (1979) Coated Pits, Coated Vesicles and Receptor-Mediated Endocytosis. *Nature 279*, 679–684.

(5) Brown, M. S., Kovanen, P. T., and Goldstein, J. L. (1980) Evolution of the LDL Receptor Concept—From Cultured Cells to Intact Animals. *Ann. N.Y. Acad. Sci. 348*, 48–68.

(6) Brown, M. S., Kovanen, P. T., and Goldstein, J. L. (1981) Regulation of Plasma Cholesterol by Lipoprotein Receptors. *Science 212*, 628–635.

(7) Ho, Y. K., Smith, R. G., Brown, M. S., and Goldstein, J. L. (1978) Low-Density Lipoprotein (LDL) Receptor Activity in Human Acute Myelogenous Leukemia Cells. *Blood 52*, 1099–1114.

(8) Vitols, S., Gahrton, G., Ost, A., and Peterson, C. (1984) Elevated Low Density Lipoprotein Receptor Activity in Leukemic Cells with Monocytic Differentiation. *Blood 63*, 1186–1193.

(9) Gal, D., Ohashi, M., MacDonald, P. C., Buchsbaum, H. J., and Simpson, E. R. (1981) Low-Density Lipoprotein as a Potential Vehicle for Chemotherapeutic Agents and Radionucleotides in the Management of Gynecologic Neoplasms. *Am. J. Obstet. Gynecol. 139*, 877–885.

(10) Gal, D., MacDonald, P. C., Porter, J. C., and Simpson, E. R. (1981) Cholesterol Metabolism in Cancer Cells in Monolayer Culture. III. Low-Density Lipoprotein Metabolism. *Int. J. Cancer 28*, 315–319.

(11) Rudling, M. J., Reihner, E., Einarsson, K., Ewerth, S., and Angelin, B. (1990) Low Density Lipoprotein Receptor-Binding Activity in Human Tissues: Quantitative Importance of Hepatic Receptors and Evidence for Regulation of Their Expression In Vivo. *Proc. Natl. Acad. Sci. U.S.A. 87*, 3469–3473.

(12) Rudling, M. J., Angelin, B., Peterson, C. O., and Collins, V. P. (1990) Low Density Lipoprotein Receptor Activity in Human Intracranial Tumors and its Relation to the Cholesterol Requirement. *Cancer Res. 50*, 483–487.

(13) Rudling, M. J., Collins, V. P., and Peterson, C. O. (1983) Delivery of Aclacinomycin A to Human Glioma Cells In Vitro by the Low-Density Lipoprotein Pathway. *Cancer Res. 43*, 4600–4605.

(14) Havekes, L., van Hinsbergh, V., Kempen, H. J., and Emeis, J. (1983) The Metabolism In Vitro of Human Low-Density Lipoprotein by the Human Hepatoma Cell Line Hep G2. *Biochem. J. 214*, 951–958.

(15) Dashti, N., Wolfbauer, G., Koren, E., Knowles, B., and Alaupovic, P. (1984) Catabolism of Human Low-Density Lipoproteins by Human Hepatoma Cell Line Hep G2. *Biochim. Biophys. Acta 794*, 373–384.

(16) Kerr, D. J., Hynds, S. A., Shepherd, J., Packard, C. J., and Kaye, S. B. (1988) Comparative Cellular Uptake and Cytotoxicity of a Complex of Daunomycin-Low Density Lipoprotein in Human Squamous Lung Tumor Cell Monolayers. *Pharmacology 37*, 3981–3986.

(17) Simpson, E. R., Bilheimer, D. W., MacDonald, P. C., and Porter, J. C. (1979) Uptake and Degradation of Plasma Lipoproteins by Human Choriocarcinoma Cells in Culture. *Endocrinology 104*, 8–16.

(18) Iwanik, M., Shaw, K. V., Ledwith, B., Yanovich, S., and Shaw, J. M. (1984) Preparation and Interaction of a Low-Density Lipoprotein-Daunomycin Complex with P388 Leukemia Cells. *Cancer Res. 44*, 1206–1213.

(19) Masquelier, M., Vitols, S., and Peterson, C. (1986) Low-Density Lipoprotein as a Carrier of Antitumoral Drugs: In Vivo Fate of Drug-Human Low-Density Lipoprotein Complexes in Mice. *Cancer Res. 46*, 3842–3847.

(20) Walsh, M. T., Ginsburg, G. S., Small, D. M., and Atkinson, D. (1982) Apo B-Lecithin-Cholesterol Ester Complexes: Reassembly of Low Density Lipoprotein. *Arteriosclerosis 2*, 445a.

(21) Krieger, M., Brown, M. S., Faust, J. R., and Goldstein, J. L. (1978) Replacement of Endogenous Cholesteryl esters of Low Density Lipoprotein with Exogenous Cholesteryl Linoleate. *J. Biol. Chem. 253*, 4093–4101.

(22) Krieger, M., McPhaul, M. J., Goldstein, J. L., and Brown, M. S. (1979) Replacement of Neutral Lipids of Low Density Lipoprotein with Esters of Long Chain Unsaturated Fatty Acids. *J. Biol. Chem. 254*, 3845–3853.

(23) Firestone, R. A., Pisano, J. M., Falck, J. R., McPhaul, M. M., and Krieger, M. (1984) Selective Delivery of Cytotoxic Compounds to Cells by the LDL Pathway. *J. Med. Chem. 27*, 1037–1043.

(24) Lundberg, B. (1987) Preparation of Drug-Low Density Lipoprotein Complexes for Delivery of Antitumoral Drugs via the Low Density Lipoprotein Pathway. *Cancer Res. 47,* 4105–4108.

(25) Communication from Dr. S. Vitols.

(26) Childs, A. F., Goldsworthy, L. J., Harding, G. F., King, F. E., Nineham, A. W., Norris, W. L., Plant, S. G. P., Selton, B., and Tempsett, A. L. L. (1948) Amines Containing 2-Halogenethyl Groups. *J. Chem. Soc.* 2174–2179.

(27) Nikawa, J.-i., and Shiba, T. (1979) Reduction of Carboxylic Acids to Alcohols Through 1-Succinimidyl Esters with NaBH$_4$. *Chem. Lett. 1979,* 981–982.

(28) Dubowchik, G. M., and Firestone, R. A. (1994) The Synthesis of Branched Steroidal Prodrugs of Nitrogen Mustard for Antitumor Targeting via Reconstituted LDL. *Tetrahedron Lett. 35,* 4523–4526.

(29) Lundberg, B. (1994) Cytotoxic Activity of Two New Lipophilic Steroid Nitrogen Mustard Carbamates Incorporated into Low-Density Lipoprotein. *Anti-Cancer Drug Des. 9,* 471–476.

(30) Ahmad, S., Ozaki, S., Nagase, T., Iigo, M., Tokuzen, R., and Hoshi, A. A (1987) Facile Method for Synthesis of N-Acyloxymethyl-5-fluorouracils as a Class of Antitumor Agents. *Chem. Pharm. Bull. 35,* 4137–4143.

(31) Castaigne, S., Chomienne, C., Daniel, T., Ballerini, P., Berger, R., Fenaux, P., and Degos, L. (1990) All-Trans Retinoic Acid as a Differentiation Therapy for Acute Promyelocytic Leukemia. *Blood 76,* 1704–1709.

(32) Unpublished observations from Dr. M. Krieger.

(33) Havekes, L. M., De Wit, E. C. M., and Princen, H. M. G. (1987) Cellular Free Cholesterol in Hep G2 Cells is Only Partially Available for Down-Regulation of Low-Density Lipoprotein Receptor Activity. *Biochem. J. 247,* 739–746.

(34) Hynds, S. A., Welsh, J., Stewart, J. M., Jack, A., Soukop, M., McArdle, C. S., Calman, K. C., Packard, C. J., and Shepherd, J. (1984) Low-Density Lipoprotein Metabolism in Mice with Soft Tissue Tumors. *Biochim. Biophys. Acta 795,* 589–595.

BC950031X

Site-Specific Prodrug Activation by Antibody–β-Lactamase Conjugates: Preclinical Investigation of the Efficacy and Toxicity of Doxorubicin Delivered by Antibody Directed Catalysis

Damon L. Meyer,[*,†] Kevin L. Law,[‡] Janice Kindle Payne,[†] Stephen D. Mikolajczyk,[†] Hamideh Zarrinmayeh,[‡] Louis N. Jungheim,[‡] James K. Kling,[‡] Timothy A. Shepherd,[‡] and James J. Starling[‡]

Hybritech Incorporated, P.O. Box 269006, San Diego, California 92196, and Lilly Research Laboratories, Eli Lilly and Company, Lilly Corporate Center, Indianapolis, Indiana 46285. Received October 31, 1994[⊗]

Antibody directed catalysis (ADC), the catalytic conversion of prodrugs to drugs by enzymes localized at disease targets by appropriate monoclonal antibodies, has shown promise in the treatment of cancer in nude mouse xenograft models. We investigated this concept using antibody enzyme conjugates constructed from β-lactamase and Fab's reactive with carcinoembryonic antigen, CEA, and tumor associated glycoprotein, TAG-72, to convert prodrugs that are cephalosporin sulfoxide derivatives into oncolytic drugs. Previous work focused on ADC delivery of the potent vinca alkaloid derivative desacetylvinblastine carboxhydrazide (DAVLBHYD). In the current study the ability of the system to deliver doxorubicin was tested in MCF7 breast carcinoma xenografts and OVCAR3 ovarian carcinoma xenografts, and in T380 and LS174T colon tumor xenografts for comparison with previous DAVLBHYD results. ADC enhanced the delivery of doxorubicin in the model systems investigated. Tumor growth suppression was equivalent to or greater than that observed with free doxorubicin at its maximum tolerated dose (MTD). In contrast to the DAVLBHYD results, ADC delivery of doxorubicin did not regress tumors, but did result in a substantial increase in the MTD.

INTRODUCTION

Antibody directed catalysis (ADC)[1] is a therapeutic method in which a relatively nontoxic prodrug is catalytically converted to its active cytotoxic form at the tumor site by a prelocalized antibody–enzyme conjugate (*1*). ADC may offer several advantages over antibody–drug conjugates as an approach to the site-specific delivery of oncolytic agents to tumors. One potential advantage is that a single antibody–enzyme conjugate can be used to deliver a number of different drugs so long as they are each designed to be a substrate for the same enzyme. This obviates the need to prepare multiple antibody–drug conjugates for combination therapy procedures. Another putative advantage of the ADC system is that the stoichiometric constraints of covalent chemoimmunoconjugates (i.e., a defined maximum number of drug molecules can be conjugated to an antibody molecule) can be circumvented by the ability of a single targeted enzyme molecule to rapidly convert a large number of prodrug molecules to the cytotoxic form of the drug.

Previous studies from our laboratory (*2*) demonstrated that the site-specific conversion of a cephalosporin–vinca (ceph-vinca) prodrug to the toxic vinca alkaloid DAVLBHYD by Fab'–β-lactamase conjugates caused significant antigen-mediated antitumor effects in two different human colon carcinoma xenografts. These studies also demonstrated that the antitumor activity achieved with the ADC system was superior to that accomplished with covalent antibody–vinca immunoconjugates. Other researchers have also noted the suitability of the β-lactamase/cephalosporin combination for site-specific prodrug activation (*3–7*).

As an extension of this previous work, we now report on the utilization of a cephalosporin–doxorubicin (ceph-dox) prodrug as a component in the ADC-based therapy of four different human tumor xenografts. These studies demonstrate that ADC is applicable to a variety of antigen targets and prodrug species.

MATERIALS AND METHODS

Prodrug Synthesis. Synthesis of the prodrug LY300663, "ceph-dox", reported in detail elsewhere (*8*), took advantage of the methodology for forming carbamate linkages at the cephalosporin 3' position originally developed for the ceph-vinca prodrug, LY266070. (Synthesis of a closely related compound has also been reported by other authors (*9*).) The starting material was the commercially available cephalosporin, cephalothin, which was converted to the 3-(hydroxymethyl)-2-cephem derivative in two steps and then protected as the allyl ester. Oxidation of the sulfide, with concomitant olefin isomerization, provided the 1-(β-sulfoxy)-3-cephem.

The carbamate linkage between cephalosporin and oncolytic agent was formed by selective nucleophilic attack on the carbonate ester with doxorubicin hydrochloride. Deprotection was accomplished by palladium-(0)-catalyzed hydrolysis, and the resulting prodrug was purified by reverse phase HPLC. Preferred purification conditions utilized a preparative Hypersil phenyl column, 22 × 250 mm (Phenomenex Corp.). Buffer A was 0.1% TFA in water; buffer B was 0.1% TFA in acetonitrile. The ceph-dox reaction mixture was dissolved in dimethyl

[1] Abbreviations: ADC, antibody directed catalysis; CEA, carcinoembryonic antigen; TAG-72, tumor-associated glycoprotein; DAVLBHYD, desacetylvinblastine carboxhydrazide; MTD, maximum tolerated dose; ceph-vinca, cephalosporin–DAVLBHYD adduct (see ref 2); ceph-dox, cephalosporin–doxorubicin adduct (see Figure 1), BL, β-lactamase; IgG, nonspecific murine monoclonal antibody.
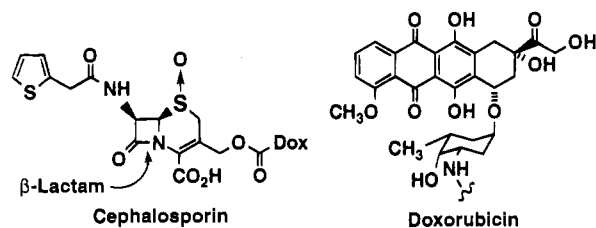
Figure 1. Structure of the ceph-dox prodrug LY300663 and the oncolytic agent doxorubicin. Hydrolysis of the β-lactam ring results in expulsion of the carbamate.

Figure 2. Schematic representation of the 3/wk × 3 wk dose schedule used in the experiments of Figues 3–7. Time between tumor implantation and treatment varied.

sulfoxide at 25–50 mg/mL with 50–80 mg applied to the column at 40% buffer B. The column was eluted with 40% buffer B for 30 min at a flow rate of 5 mL/min, followed by a gradient from 40% to 60% buffer B in 10 min and a 30 min isocratic elution at 60% B. The column was then re-equilibrated at 40% buffer B. Elution was monitored by absorbance at 494 nm and the desired prodrug eluted after approximately 32 min.

Construction of Fab′–β-Lactamase Conjugates.
Antibody–enzyme conjugates were constructed from Fab′ fragments of antibodies recognizing the tumor-associated antigens carcinoembryonic antigen, CEA, and tumor-associated glycoprotein, TAG-72 (antibodies CEM231 (*10*) and CC-49 (*11*), respectively). A conjugate was also prepared from an irrelevant antibody Fab′ fragment that recognizes no antigen in the mouse or tumor line, to show the effect of "nonspecific" conjugate. The conjugation methodology involved linkage of lysine ϵ-amino groups on the surface of P99 β-lactamase to hinge region sulfhydryls of the Fab′ fragments using sulfosuccinimidyl 4-(*N*-maleimidomethyl)cyclohexane-1-carboxylate (Pierce) as described previously (*12*).

Kinetics of Drug Release by P99 β-Lactamase.
The hydrolysis of the ceph-dox prodrug by β-lactamase was monitored spectrophotometrically at 266 nm. It was determined by HPLC that the decrease in absorbance at 266 nm was linear and proportional to the hydrolysis of the cephalosporin ring and release of free doxorubicin. HPLC analysis also showed that a decrease of 31% of the initial 266 nm absorbance corresponded to 100% hydrolysis. The analytical HPLC procedure was similar to the preparative procedure used to purify the prodrug: ceph-dox containing samples were isocraticallyl eluted through a 4.6 × 250 mm Hypersil phenyl column with 50% aqueous acetonitrile containing 0.1% TFA and monitored at 494 nm. Under these conditions, doxorubicin eluted at 4.9 min and prodrug at 7.6 min.

The kinetics of prodrug hydrolysis catalyzed by β-lactamase was studied at 37 °C in 0.1 M Tris, pH 7.4, in stirred cells with a Hewlett Packard Model 8452 diode array spectrophotometer. Immediately prior to addition of the enzyme, the substrate (prodrug) concentration was determined by reading the absorbance at 494 nm (ϵ = 7890). The absorbance at 266 nm of 2 mL reaction mixtures containing prodrug and 5 ng of β-lactamase (based on a measured extinction coefficient $A^{1\%}_{280} = 22$) was monitored for 70 s. Lineweaver–Burk plots were constructed from three different sets of epxeriments. The reported values of k_{cat} and K_M are the average of the three determinations.

In Vitro Cytotoxicity Studies. LS174T cells were resuspended in 75% leucine-deficient media containing 10% dialyzed fetal calf serum to a concentration of 1 × 10^5 cells/mL. Aliquots containing 0.2 mL were seeded into individual wells of a 96 well microtiter plate and incubated overnight at 37 °C in a 95% air/5% CO_2
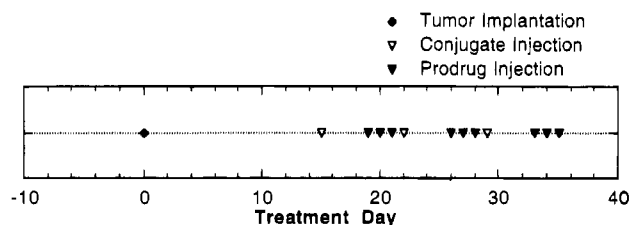
incubator. The medium was removed, and cells were incubated in the presence or absence of 10 μg/mL conjugate for 1 h at 37 °C. The cells were washed, and free doxorubicin or ceph-dox prodrug was added at various concentrations (log dilutions starting at 1 μg/mL for doxorubicin or the molar equivalent 1.67 μg/mL ceph-dox). After 5 h at 37 °C the cells were washed and fresh medium was added for 48 h at 37 °C. The medium was removed, and 4 μCi of [^{3}H]leucine in 0.2 mL of media was added per well. The cells were incubated for an additional 18 h at 37 °C. The medium was removed, and the amount of ^{3}H incorporation was determined. All samples were run in quadruplicate.

Tumor Therapy Studies. Tumor studies were performed with MCF7 (*13*) breast carcinoma cells, LS174T (*14*) and T380 (*15*) colon carcinoma cells, and OVCAR3 (*16*) ovarian carcinoma cells. Previous studies indicated that the α-CEA antibody used to construct the conjugate binds to T380 and LS174T colon tumor xenografts and that the α-TAG-72 antibody binds to LS174T tumors (*2*) and OVCAR3 tumors (*17, 18*). The behavior of these antigens on antibody binding has been shown to be suitable for ADC delivery. Data from our laboratories demonstrated that the α-CEA antibody also binds to MCF7 breast carcinoma xenografts in nude mice.

MCF7 cells were initially grown in nude mice by sc injection of 1.5 × 10^6 cells in 1:2 Matrigel (Collaborative Biomedical Products). Tumors to be transferred into mice for passage or experimentation were minced, and a 0.2 mL slurry without Matrigel was injected into the flank of female athymic nude mice (Harlan Sprague Dawley, Indianapolis, IN; 8 mice per group). A 0.36 mg 17β-estradiol pellet (Innovative Research of America, Toledo, OH) was implanted sc with a 10 gauge trochar needle 24 h prior to tumor implantation. LS174T tumors were implanted by sc inoculation of 1 × 10^7 cells in the flank of female athymic nude mice (Charles River Breeding Laboratories, Wilmington, MA; 7 mice per group) for both the ADC study and the MTD study. T380 tumors were implanted by sc inoculation of a 0.1 mL tumor slurry, prepared by suspending 1 g of fresh tumor from a "passage" mouse in 1 mL of buffer, in the flank of female athymic nude mice. OVCAR3 tumors were implanted by ip inoculation of 0.5 mL of ascites fluid taken from a mouse into which the tumor had been serially transplanted (10 mice per group).

The "3/wk × 3 wk" dose schedule used in all studies is depicted in Figure 2. Tumors were implanted on day 0; conjugate (α-CEA, α-TAG-72, IgG, or saline) was administered when the tumors were the appropriate size, beginning 1–2 weeks later, except for OVCAR3, in which conjugate was administered a few hours after tumor implantation. A 96 h prelocalization time was allowed between conjugate and prodrug administration, which was fractionated over 3 days (hence, "3/wk"). Doxorubicin or saline was substituted for prodrug in experiment control arms. Treatments were administered for 3 consecutive weeks. Exact timing of doses is included in
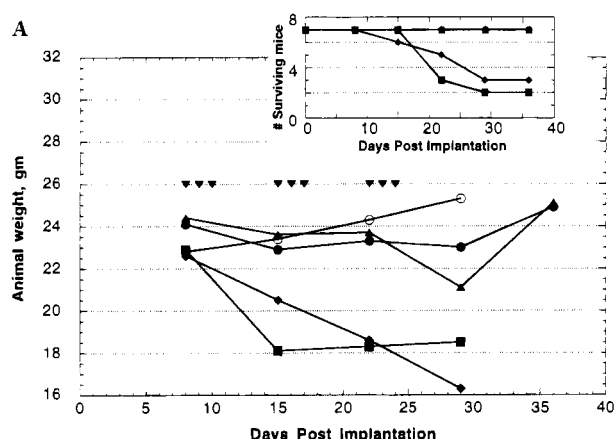
Figure 3. (A) Weight and survival (inset) of mice treated with saline or doxorubicin on the days denoted by the inverted filled triangles, ▼. Curve symbols are defined in panel 3B. (B) LS174T growth curves following treatment with various doses of doxorubicin on the 3/wk × 3 wk schedule. Daily doses are indicated in the figure.
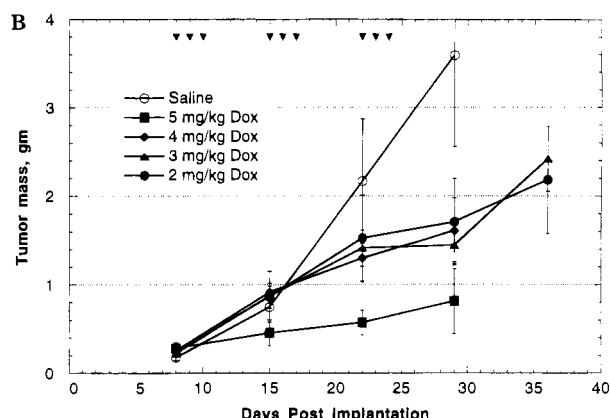
Figures 3−7. All injections were made in the tail vein, and all injections were well tolerated.

Conjugate doses were a constant 35 μg/injection in all studies except the OVCAR3 study, in which 100 μg of conjugate was used. Prodrug doses were either 12 or 14.4 mg/kg doxorubicin equivalents, compared to 3 or 4 mg/kg free doxorubicin in the control arms, as described in the Results. In the MTD experiment of Figure 3 saline was administered as a surrogate for conjugate 96 h before the first prodrug injection in all experiment arms, and the doxorubicin was administered at 2, 3, 4, or 5 mg/kg.

Tumor masses were calculated from tumor volume (assuming a tissue density of 1 g/cm^3), which was determined by caliper measurements, using the formula mass = (1 g/cm^3) × 0.5 × L × W^2, where L and W are the longest dimension and its perpendicular in cm, respectively. Tumor dimensions and animal weights were measured once or twice weekly. Growth curves were considered to be significantly different when error bars did not overlap. In the LS174T studies, mice were weighed together.

RESULTS

The cephalosporin−doxorubicin prodrug (Figure 1) was shown to be a substrate for 265A β-lactamase with k_{cat} = 480 ± 130 s^{-1} and K_M = 28 ± 8 μM. Hence, the ratio k_{cat}/K_M that dictates the rate of release of drug in the low substrate concentration range expected *in vivo* is comparable to that for the ceph-vinca prodrug studied previously (*2, 12*). Treatment of LS174T cells *in vitro* showed that the ceph-dox prodrug was less toxic than free doxorubicin, but was activated by conjugate specifically bound to tumor cells. The ID$_{50}$ values and k_{cat}/K_M ratios are compared with those of the ceph-vinca prodrug in Table 1.

Previous studies have indicated that the conjugates bound the target cell lines as described in Materials and Methods and that 72 or 96 h was a sufficient interval to allow clearance of conjugate from the blood before administering prodrug (*2*). A 96 h interval was adopted to minimize prodrug activation by residual circulating conjugate.

Preliminary dose ranging studies (up to 19 mg/kg doxorubicin equivalent in each of three doses on weekly intervals) indicated that ceph-dox following antibody−enzyme conjugate could be given at much higher doses than free doxorubicin (MTD = 9 mg/kg/wk). To exceed the maximum single injection dose, a fractionated protocol was adopted, due to the limitations of injection

Table 1. *In vitro* Parameters for the Ceph-Dox Prodrug Compared with the Ceph-Vinca Prodrug[a]

prodrug	k_{cat}/K_M (μM·s)$^{-1}$	ID$_{50}$, parent drug (μM)	ID$_{50}$, prodrug (μM)	ID$_{50}$, prodrug + conjugate (μM)
Ceph-dox (LY300663)	16	0.2	1.5	0.2
Ceph-vinca (LY266070)	11	0.1	0.3	0.05

[a] The k_{cat} and K_M values were determined from Lineweaver−Burk plots of prodrug degradation on treatment with β-lactamase. Reaction velocities were determined by either spectrophotometric or chromatographic methods as described. ID$_{50}$ values were determined with LS174T cells with or without conjugate using a 5 h incubation of cells with drug or prodrug as described.

volume and solubility, in which prodrug was administered on three consecutive days beginning 96 h after conjugate administration. This nonoptimized schedule, i.e., "3/wk × 3 wk" (Figure 2), was administered in all the experiments described in this paper. The antibody−enzyme conjugate dose was based on results from previous studies, and the prodrug doses were based on dose ranging studies with the 3/wk × 3 wk schedule (up to 57 mg/kg/wk), suggesting that higher doses increased toxicity but did not increase activity.

Experiments were performed in nude mice bearing tumor xenografts to establish the MTD of doxorubicin on the 3/wk × 3 wk schedule. In the LS174T study the MTD was 3 mg/kg/day (Figure 3A) as indicated by weight loss and survival (inset). All deaths at higher doses occurred during or soon after the treatment period. Fractionation did not reduce the toxicity of the free drug since this value gives the same cumulative dose as the MTD for nonfractionated treatment (9 mg/kg/wk). Some tumor growth inhibition was observed at the MTD, and higher doses did appear to increase activity (Figure 3B), suggesting that efficacy is limited by toxicity. Comparable results were observed in T380 tumors.

ADC treatment of MCF7 tumor bearing nude mice with α-CEA−β-lactamase conjugate followed by 14.4 mg/kg doxorubicin equivalents of ceph-dox resulted in growth inhibition (Figure 4A). Tumor growth essentially stopped at about 1.2 gm from day 32 to 62 after implantation as a result of treatment. Equivalent growth inhibition was observed in animals treated with 4 mg/kg of doxorubicin, but significant treatment-related toxicity was observed in this group as measured by both weight loss (Figure 4B, solid lines) and survival (Figure 4B, inset). The toxicity in the free drug group confirmed that 4 mg/kg is above the MTD for doxorubicin on this schedule. Treat-
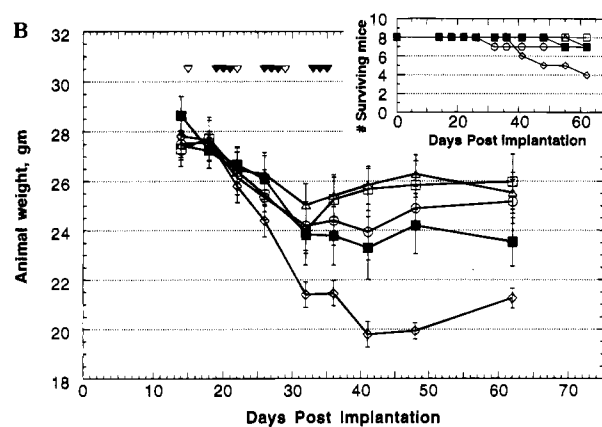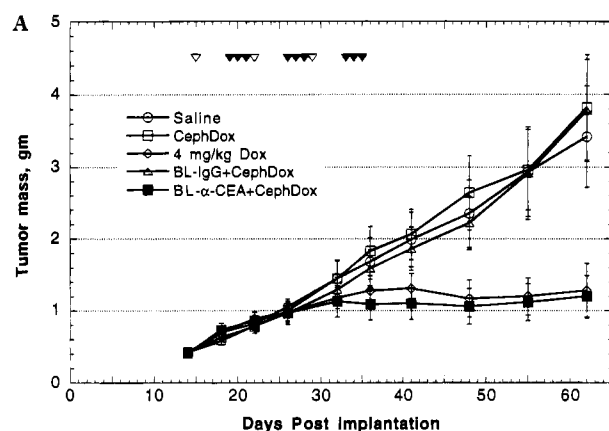
Figure 4. (A) MCF7 growth curves following ADC treatment. Administration of 35 μg of conjugate or saline, ∇, was followed after 96 h by ceph-dox at a dose equivalent to 14.4 mg/kg/day doxorubicin, by 4 mg/kg/day doxorubicin, or by saline, ▼. Treatment groups are identified in the graph. (B) Weight and survival (inset) curves for the animals of panel A.
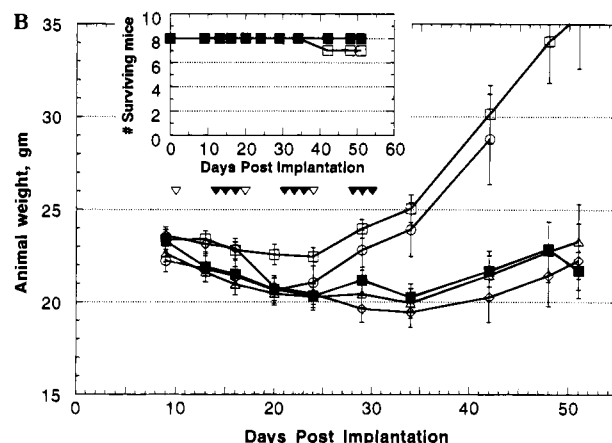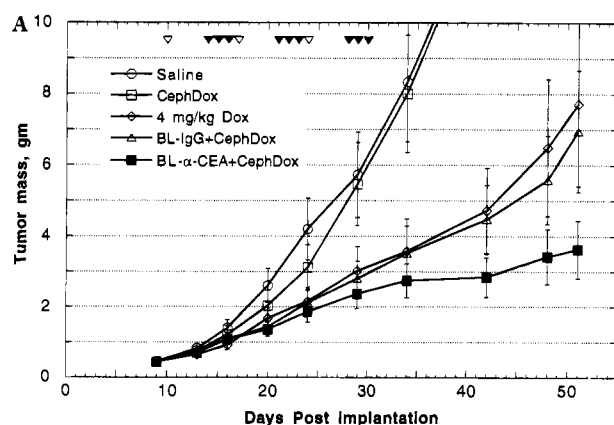
Figure 5. (A) T380 growth curves following ADC treatment. Administration of 35 μg of conjugate or saline, ∇, was followed after 96 h by ceph-dox equivalent to 14.4 mg/kg/day doxorubicin, by 4 mg/kg/day doxorubicin, or by saline, ▼. Treatment groups are identified in the graph. (B) Weight and survival curves (inset) for the animals of panel A.

ment with irrelevant conjugate followed by prodrug, or with prodrug alone at the same dose, had no effect on MCF7 tumor growth (Figure 4A).

In order to compare activity of doxorubicin with DAV-LBHYD when delivered by ADC, efficacy was tested in LS174T and T380 colon carcinoma lines. In T380 tumors (Figure 5A) ADC delivery of 14.4 mg/kg doxorubicin equivalents as prodrug was significantly more effective than either free drug treatment (4 mg/kg) or irrelevant conjugate followed by prodrug. The efficacy enhancement occurred when the tumors were large, e.g., 2.5+ g, and the effects continued well after treatment was concluded. In this experiment one animal death occurred in the group of mice receiving prodrug only (Figure 5B, inset); it was not believed to be treatment related. All animals showed some weight loss, but the animals receiving drug, irrelevant conjugate/prodrug, and α-CEA conjugate/prodrug (that is, all animals receiving drug or enzyme + prodrug) showed weight loss that was more severe and more prolonged than those treated with saline or prodrug alone.

In LS174T tumors (Figure 6A) ADC delivery of 12 mg/kg doxorubicin equivalents of prodrug resulted in growth inhibition comparable to that of free doxorubicin at 3 mg/kg. Efficacy was statistically equivalent whether the conjugate targeted the TAG-72 or the CEA antigen. While free drug and ADC treatment were equally effective in this experiment, even 3 mg/kg doxorubicin caused some toxicity as indicated by weight loss and survival (Figure 6B) in this experiment. Irrelevant conjugate was

less effective than α-TAG-72 or α-CEA targeted ADC treatment, and less effective than free drug.

Finally, the ability of ADC treatment to increase the lifespan of nude mice bearing intraperitoneal OVCAR3 tumors was evaluated (Figure 7). In this experiment α-TAG-72 conjugate dose was increased to 100 μg in order to compensate for the relatively inefficient targeting of iv injected antibodies to ip grown tumors (*19*). Saline-treated animals died between 15 and 28 days post-implantation with a median survival of 20.5 days. Prodrug alone had no significant effect on survival (median survival 25.5 days). Free drug, irrelevant conjugate/prodrug, and ADC treatment all increased lifespan measurably, with median survival times of 37.0, 38.0, and 45.0 days, respectively. ADC treatment, with 14.4 mg/kg doxorubicin equivalents as prodrug, was more effective than free drug at its MTD (log rank $p \leq 0.0065$), and more effective than irrelevant conjugate/prodrug (log rank $p \leq 0.007$), demonstrating the importance of antibody specificity to activity.

DISCUSSION

Doxorubicin is frequently prescribed to treat advanced breast cancer, yet its utility is limited by both acute and cumulative toxicity. Facilitating the use of this agent at elevated dose levels or with reduced toxicity was the aim for our ADC program, given the availability of α-CEA and α-TAG-72 antibodies that bind to many advanced breast carcinomas (*20, 21*). Further, comparison of the
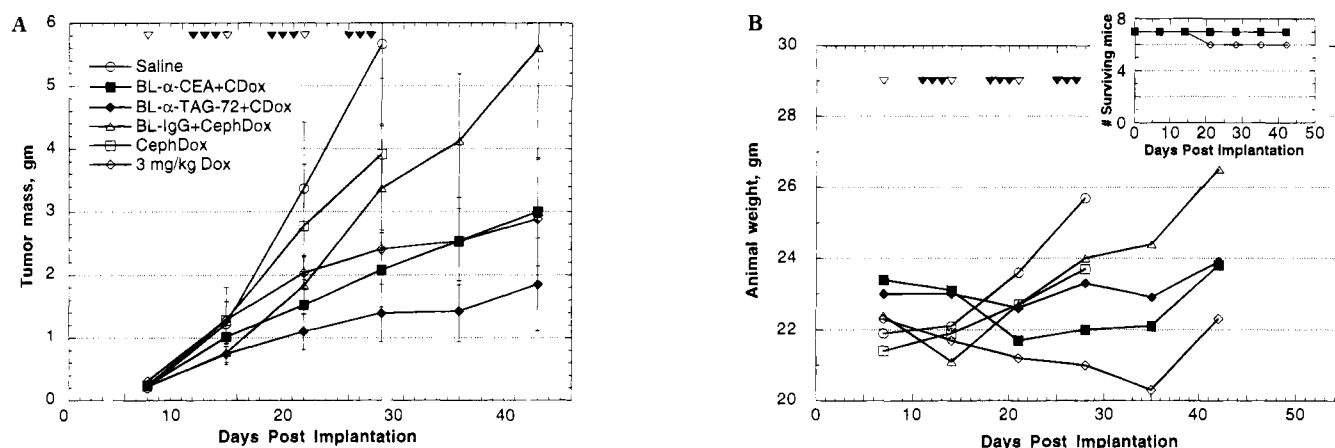
Figure 6. (A) LS174T growth curves following ADC treatment. Administration of 35 μg of conjugate or saline, ▽, was followed after 96 h by ceph-dox prodrug ("CDox") at a dose equivalent to 12 mg/kg/day doxorubicin, by 3 mg/kg/day doxorubicin, or by saline, ▼. Treatment groups are identified in the graph. (B) Weight and survival (inset) curves for the animals of panel A.
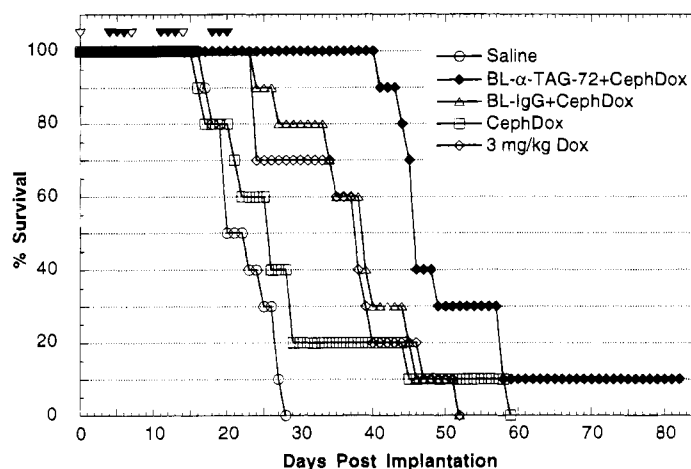
Figure 7. Survival curves of mice bearing OVCAR3 carcinoma tumors following ADC treatment. Administration of 100 μg of conjugate or saline, ▽, was followed after 96 h by ceph-dox equivalent to 12 mg/kg/day doxorubicin, by 3 mg/kg/day doxorubicin, or by saline, ▼. Treatment groups are identified in the graph.

effect of ADC delivery of doxorubicin with previous results from ADC delivery of DAVLBHYD in colon carcinoma xenografts advances the understanding of the delivery system by showing how efficacy enhancements from two different agents can vary, and by showing that an individual enzyme—antibody conjugate is capable of activating different prodrugs. Other researchers have also seen doxorubicin as a good candidate for delivery in a targeted prodrug activation format (*22–24*).

The synthesis of the ceph-dox prodrug, LY300663 (Figure 1), used in this study has been described previously (*8*). The *in vitro* properties reported here suggest that it is a good candidate for use with ADC delivery. Specifically, the k_{cat}/K_M ratio indicates that as a substrate for P99 β-lactamase it is comparable or superior to the ceph-vinca studied previously. Furthermore, cellular cytotoxicity experiments on colon carcinoma cells indicate that the ceph-dox prodrug is less toxic than doxorubicin and that it is activated by conjugate bound to target cells. The data in Table 1 suggest that *in vitro* the ceph-dox and ceph-vinca prodrugs behave similarly.

Preliminary experiments indicated that only marginal efficacy was observed with the ADC delivery of doxorubicin at a dose equivalent to the MTD of free doxorubicin. Hence, subsequent experiments were designed to compare optimal ADC delivery of ceph-dox with free doxorubicin at or near its MTD. To do so, the efficacy and toxicity of doxorubicin on the 3 dose/wk × 3 wk schedule were examined in LS174T nude mouse models. The

MTD was found to be 3 mg/kg/day (9 mg/kg/week), as evidenced by both survival and weight loss. Tumor growth inhibition in these experiments was limited by toxicity, since a 5 mg/kg dose was clearly superior to 3 mg/kg (Figure 3). The MTD of DAVLBHYD was between 2 and 3 mg/kg/wk (*2*). Thus, although the IC_{50}'s of doxorubicin and DAVLBHYD are similar *in vitro*, DAVLBHYD appears to be somewhat more potent and more toxic *in vivo*.

Growth of the breast cancer line MCF7 was inhibited both by ADC treatment and by treatment with free doxorubicin (Figure 4). Since irrelevant conjugate followed by prodrug had no effect, the ADC treatment was clearly antigen mediated. Free doxorubicin was administered at 4 mg/kg in this experiment, slightly above the MTD, to show the maximum possible treatment efficacy of drug alone. As expected, mice treated with 4 mg/kg doxorubicin showed weight loss and death resulting from treatment. Since efficacious levels of drug could be administered without toxicity, ADC delivery was clearly advantageous in this model of its intended use: treatment of CEA positive breast carcinoma.

Studies of the efficacy of ADC delivery of doxorubicin were undertaken in the LS174T (Figure 5) and T380 (Figure 6) colon carcinoma lines to allow comparison with previous studies with the DAVLBHYD-derived ceph-vinca (*2*). In T380 tumors α-CEA conjugate/ceph-dox (ADC) treatment showed superiority to free drug and irrelevant conjugate/ceph-dox treatment. However, in

contrast to the ADC delivery of DAVLBHYD, doxorubicin enhancement required doses substantially above 1 molar equivalent of free drug, and tumor regressions were not observed. Likewise, in LS174T tumors, ADC delivery of doxorubicin appeared to be equivalent or superior to free drug treatment and showed reduced toxicity, but did not result in regressions. In this case also, ceph-dox doses required to achieve these effects were 4-fold higher than free drug on a molar basis.

Availability of the OVCAR3 cell line allowed us to test ADC delivery in a model of ovarian cancer, another disease for which doxorubicin is clinically useful. In this model system where tumor was in the intraperitoneal cavity but treatment was administered iv, ADC delivery targeting TAG-72 was significantly more effective in slowing tumor growth than any other treatment arm, although free drug alone at 3 mg/kg, and irrelevant conjugate followed by prodrug, also increased animal survival significantly over saline (Figure 7).

Hence, ADC enhanced the efficacy of doxorubicin in T380 and OVCAR3 models, as it had increased the efficacy of DAVLBHYD in LS174T and T380 models. Toxicity appeared to be reduced by ADC delivery, but it was not clear whether the reduced toxicity was advantageous, because the increased dose required to obtain equivalent efficacy could offset the reduction in toxicity. In ADC delivery of DAVLBHYD, similar results were obtained targeting three different antigens. Similarly, ADC delivery of doxorubicin targeting CEA and TAG-72 antigens also gave statistically equivalent results in the LS174T model in which they were compared. The ADC-mediated efficacy enhancement for either antigen was much greater with DAVLBHYD than with doxorubicin: both regressions and long-term tumor suppression were observed in the DAVLBHYD system and not the doxorubicin system. On the other hand, the toxicity reduction was greater for doxorubicin, for which the MTD increased by a factor of at least 4. There is no obvious difference in substrate activity or *in vitro* potency of the two prodrugs and drugs (Table 1) to explain this difference. As further verification of the theory behind the ADC delivery system, previous studies in our laboratory demonstrated that prodrug activation was not accomplished when unconjugated (i.e., no β-lactamase) α-CEA or α-KS1/4 antibodies were targeted to LS174T tumor cells prior to prodrug exposure *in vitro* (data not shown).

It is possible that the efficacy level that we have observed with doxorubicin represents a maximal response of these cell lines *in vivo* to this agent, so that higher concentrations at the tumor simply have no additional therapeutic effect, and that there is no comparable limitation in the response to DAVLBHYD. Additional experiments were performed increasing the total prodrug dose to 19.2 mg/kg doxorubicin equivalents/day 3 days/week for 3 weeks; and the dose intensity: up to 29 mg/kg doxorubicin equivalents 3 times/day for 3 days. In both cases, we observed increased toxicity but no increased efficacy, which could support the hypothesis that a maximal efficacy had been reached. However, a hypothetical maximum response of the target cell lines to doxorubicin does not explain the fact that ADC delivery of doxorubicin substantially increased its MTD, while ADC delivery of DAVLBHYD did not.

The response to ADC treatment seen in these data is comparable to that observed by other researchers with analogous systems (*25, 26*). Also, Bosslet *et al.* recently reported preclinical results using an antibody enzyme fusion protein recognizing the CEA antigen to release doxorubicin (*22*). Efficacy was measured in LoVo colon carcinoma xenografts similar to the T380 and LS174T

lines reported here. The activity observed in that study is also very similar to the activity seen in Figures 5A and 6A. The most frequent observation in all of these preclinical studies is reduced toxicity for the ADC system, which enables the use of higher doses of therapeutic agent, thereby generating some increase in response. The consistency of this finding makes the increased activity at an equivalent dose with the ceph-vinca prodrug the more exceptional.

Hence, there is a qualitative difference in performance between the ceph-vinca and the ceph-dox prodrugs that is not related to substrate propensity or to drug potency. It seems likely that pharmacological behavior of the prodrugs could explain these differences. In particular, more rapid clearance of ceph-dox from the circulation would lead to decreased toxicity and decreased efficacy relative to doxorubicin, as has been observed in these studies. If so, manipulation of prodrug pharmacology by modification of its chemical properties could further improve the efficacy of ADC delivery. It should be mentioned that while we feel that the tumor xenograft studies described in this paper represent a rigorous preclinical test of the ADC concept, we have not yet extended our experiments to include nude mouse models of human tumor metastasis.

Determination of how advantageous ADC delivery can be in animals or humans will clearly require the optimization of several parameters: conjugate dose, conjugate level in plasma at the time of prodrug administration (and methods of reducing this level), prodrug pharmacological properties, optimization of dose schedule, conjugate design, etc. We have undertaken a quantitative investigation of the pharmacokinetics of the ceph-dox prodrug in hopes of better understanding optimum delivery parameters.

LITERATURE CITED

(1) Shepherd, T. A., Jungheim, L. N., Meyer, D. L., and Starling, J. J. (1991) A Novel Targeted Delivery System Utilizing a Cephalosporin-Oncolytic Prodrug Activated by an Antibody β-Lactamase Conjugate for the Treatment of Cancer. *BioMed. Chem. Lett. 1*, 21–6.

(2) Meyer, D. L., Jungheim, L. N., Law, K. L., Mikolajczyk, S. D., Shepherd, T. A., Mackensen, D. G., Briggs, S. L., and Starling, J. J. (1993) Site-Specific Prodrug Activation by Antibody-β-Lactamase Conjugates: Regression and Long-Term Growth Inhibition of Human Colon Carcinoma Xenograft Models. *Cancer Res. 53*, 3956–63.

(3) Alexander, R. P., Beeley, N. R. A., Driscoll, M., O'Neill, F. P., Millican, T. A., Pratt, A. J., and Willenbrock, F. W. (1991) Cephalosporin Nitrogen Mustard Carbamate Prodrugs for "ADEPT". *Tetrahedron Lett. 32*, 3269–72.

(4) Vrudhula, V. M., Svensson, H. P., Kennedy, K. A., Senter, P. D., and Wallace, P. M. (1993) Antitumor Activities of a Cephalosporin Prodrug in Combination with Monoclonal Antibody-β-Lactamase Conjugates. *Bioconjugate Chem. 4*, 334–40.

(5) Goshorn, S. C., Svensson, H. P., Kerr, D. E., Somerville, J. E., Senter, P. D., and Fell, H. P. (1993) Genetic Construction, Expression, and Characterization of a Single Chain Anti-Carcinoma Antibody fused to β-Lactamase. *Cancer Res. 53*, 2123–7.

(6) Hanessian, S., and Wang, J. (1993) Design and Synthesis of a Cephalosporin-Carboplatinum Prodrug Activatable by a β-Lactamase. *Can. J. Chem. 71*, 896–906.

(7) Svensson, H. P., Kadow, J. F., Vrudhula, V. M., Wallace, P. M., and Senter, P. D. (1992) Monoclonal Antibody-β-Lactamase Conjugates for the Activation of a Cephalosporin Mustard Prodrug. *Bioconjugate Chem. 3*, 176–81.

(8) Jungheim, L. N., Shepherd, T. A., and Kling, J. K. (1993) Synthesis of a Cephalosporin–Doxorubicin Antitumor Prodrug: A Substrate for an Antibody Targeted Enzyme. *Heterocycles 35*, 339–48.

(9) Hudyma, T. W., Bush, K., Colson, K. L., Firestone, R. A., and King, H. D. (1993) Synthesis and Release of Doxorubicin from a Cephalosporin Based Prodrug by a β-Lactamase-Immunoconjugate. *Bioorg. Med. Chem. Lett. 3,* 323–8.

(10) Beidler, C. B., Ludwig, J. R., Cardenas, J., Phelps, J., Papworth, C. G., Melcher, E., Sierzega, M., Myers, L. J., Unger, B. W., Fisher, M., David, G. S., and Johnson, M. J. (1988) Cloning and High Level Expression of a Chimeric Antibody with Specificity for Human Carcinoembryonic Antigen. *J. Immunol. 141,* 4053–60.

(11) Muraro, R., Kuroki, M., Wunderlich, D., Poole, D. J., Colcher, D., Thor, A., Greiner, J. W., Simpson, J. F., Molinolo, A., Noguchi, P., and Schlom, J. (1988) Generation and Characterization of B72.3 Second Generation Monoclonal Antibodies Reactive with the Tumor-associated Glycoprotein 72 Antigen. *Cancer Res. 48,* 4588–96.

(12) Meyer, D. L., Jungheim, L. N., Mikolajczyk, S. D., Shepherd, T. A., Starling, J. J., and Ahlem, C. N. (1992) Preparation and Characterization of β-Lactamase–Fab' Conjugates for the Site Specific Activation of Oncolytic Agents. *Bioconjugate Chem. 3,* 42–8.

(13) Soule, H. D., Vazquez, J., Long, A., Albert, S., and Brennan, M. (1973) A Human Cell Line from a Pleural Effusion Derived from a Breast Carcinoma. *J. Natl. Cancer Inst. 51,* 1409–13.

(14) Tom, B. H., Rutzky, L. P., Jakstys, M. M., Oyasu, R., and Kaye, C. I. (1976) Human Colonic Adenocarcinoma Cells. I. Establishment and Description of a New Cell Line. *In Vitro 12,* 180–90.

(15) Halpern, S. E., Hagan, P. L., Garver, P. R., Koziol, J. A., Chen, A. W. N., Frincke, J. M., Bartholomew, R. M., David, G. S., and Adams, T. H. (1983) Stability, Characterization, and Kinetics of ^{111}In-labeled Monoclonal Antitumor Antibodies in Normal Animals and Nude Mouse-Human Tumor Models. *Cancer Res. 43,* 5347–55.

(16) Hamilton, T. C., Young, R. C., McCoy, W. M., Grotzinger, K. R., Green, J. A., Chu, E. W., Whang-Peng, J., Rogan, A. M., Green, W. R., and Ozols, R. F. (1983) Characterization of an Ovarian Carcinoma Cell Line (NIH:OVCAR-3) with Androgen and Estrogen Receptors. *Cancer Res. 43,* 5379–89.

(17) Thor, A., Gorstein, F., Ohuchi, N., Szpak, C. A., Johnston, W. W., and Shlom, J. (1986) Tumor-Associated Glycoprotein (TAG-72) in Ovarian Carcinomas Defined by Monoclonal Antibody B72.3. *J. Natl. Cancer Inst. 76,* 995–1006.

(18) Starling, J. J., Maciak, R. S., Law, K. L., Hinson, N. A., Briggs, S. L., Laguzza, B. C., and Johnson, D. A. (1991) *In Vivo* Antitumor Activity of a Monoclonal Antibody-Vinca Alkaloid Immunoconjugate Directed Against a Solid Tumor Membrane Antigen Characterized by Heterogeneous Expression and Noninternalization of Antibody–Antigen Complexes. *Cancer Res. 51,* 2965–72.

(19) Moseley, K. R., Battaile, A., Knapp, R. C., and Haisma, H. J. (1988) Localization of Radiolabelled F(ab')₂ Fragments of Monoclonal Antibodies in Nude Mice Bearing Intraperitoneally Growing Human Ovarian Cancer Xenografts. *Int. J. Cancer 42,* 368–72.

(20) Hand, P. H., Nuti, M., Colcher, D., and Schlom, J. (1983) Definition of Antigenic Heterogeneity and Modulation among Human Mammary Carcinoma Cell Populations Using Monoclonal Antibodies to Tumor-Associated Antigens. *Cancer Res. 43,* 728–35.

(21) Lamki, L. M., Buzdar, A. U., Singletary, S. E., Rosenblum, M. G., Bhadkamkar, V., Esparza, L., Podoloff, D. A., Zukiwski, A., Hortobagyi, G. N., and Murray, J. L. (1991) Indium-111-Labeled B72.3 Monoclonal Antibody in the Detection and Staging of Breast Cancer: A Phase I Study. *J. Nucl. Med. 32,* 1326–32.

(22) Bosslet, K., Caech, J., and Hoffmann, D. (1994) Tumor-selective Prodrug Activation by Fusion Protein-mediated Catalysis. *Cancer Res. 54,* 2151–9.

(23) Kerr, D. E., Senter, P. D., Burnett, W. V., Hirschberg, D. L., Hellström, I., and Hellström, K. E. (1990) Antibody-Penicillin-V-Amidase Conjugates Kill Antigen Positive Tumor Cells When Combined with Doxorubicin phenoxyacetamide. *Cancer Immunol. Immunother. 31,* 202–6.

(24) Rodrigues, M. L., Presta, L. G., Kotts, C. E., Wirth, C., Mordenti, J., Osaka, G., Wong, W. L. T., Nuijens, A., Blackburn, B., and Carter, P. (1995) Development of a Humanized Disulfide-stabilized Anti-p185HER2 Fv-b-Lactamase Fusion Protein for Activation of a Cephalosporin Doxorubicin Prodrug. *Cancer Res. 55,* 63–70.

(25) Senter, P. D. (1990) Activation of Prodrugs by Antibody-Enzyme Conjugates: A New Approach to Cancer Therapy. *FASEB J. 4,* 188–93.

(26) Bagshawe, K. D. (1989) Towards Generating Cytotoxic Agents at Cancer Sites. *Br. J. Cancer 60,* 275–81.

BC950032P

Comparison of Three Common Amine Reactive Fluorescent Probes Used for Conjugation to Biomolecules by Capillary Zone Electrophoresis

Peter R. Banks* and Donald M. Paquette

Department of Chemistry and Biochemistry, Concordia University, 1455 de Maisonneuve Boulevard West, Montreal, Quebec H3G 1M8, Canada. Received March 9, 1995®

The conjugation of three amine reactive fluorescent probes, each containing the fluorophore fluorescein but different reactive moieties, was compared using the protein myoglobin and the amino acid L-lysine as reagents. The three different reactive moieties were an isothiocyanate group (FITC), a succinimidyl ester group (CFSE), and a dichlorotriazine group (DTAF). The relative performance was based on the degree of conjugation to myoglobin, the rate of reaction, freedom from hydrolysis, and the stability of a conjugate with lysine. Performance was evaluated by separating the conjugation reaction reagents and products on-line, using capillary zone electrophoresis, and assessing relative amounts by absorbance detection. Each of the reactive probes demonstrated the ability to achieve a similar degree of conjugation, which depended mostly on allowed conjugated reaction time, and a rate of conjugation that rendered hydrolysis of the reactive moiety insignificant. For the relative rate of conjugation between probes and stability of the resulting conjugate, CFSE demonstrated superior performance, followed by DTAF and then FITC, for both the protein myoglobin and the amino acid L-lysine. The FITC conjugation reaction was much easier to control, however, which may be significant for applications that require a precise degree of conjugation. With regard to conjugate-bond stability, the FITC conjugate demonstrated inferior performance when subjected to incubation at 37 °C.

INTRODUCTION

Fluorescent methods can dramatically increase both the sensitivity and selectivity of analysis relative to absorbance-based methods *(1)*. In immunoassays, for example, analyte concentrations as small as 10^{-15} M can be detected using time-resolved immunofluorometric assays *(2)*. Although many important biomolecules (amino acids, peptides, and proteins) are nonfluorescent or weakly fluorescent in the UV, the use of fluorescent probes can provide the means for their sensitive fluorometric detection. A host of fluorescent probes are commercially available which can be attached through covalent or noncovalent interactions *(3)*. Recently, a survey has been published which documents a number of popular methods used for preparing protein conjugates with fluorescent probes *(4)*.

Perhaps the most widely used fluorophore in protein conjugation is the amine reactive probe fluorescein isothiocyanate (FITC) *(5)*. FITC's popularity stems from the fact that its fluorophore, fluorescein, possesses a high molar absorptivity (ϵ = 90 000 cm^{-1} M^{-1} at 490 nm, pH 9) *(3)* and a fluorescence quantum yield which approaches unity, qualities that are largely incorporated into the biomolecule conjugate, allowing low sample detection limits in serum *(6)*. The isothiocyanate moiety is quite stable in aqueous solution and reacts with protein amine groups to form thiourea bonds. However, it has been reported that both the reactive moiety *(7)* and antibody conjugates *(3)* prepared from fluorescent isothiocyanates can deteriorate over time. These findings have led to the investigation and use of other reactive probes.

For example, carboxyfluorescein succinimidyl ester (CFSE) has spectroscopic properties almost identical to its isothiocyanate cousin but conjugates with amine groups to produce an amide bond, known for its stability *(4)*. For this reason, one commercial company prefers the

use of succinimidyl esters over isothiocyanates for the synthesis of protein conjugates *(3)*. The succinimidyl ester is susceptible to hydrolysis, however, and can significantly compete with the biomolecule conjugation, especially at the alkaline conditions suitable for reaction with amine groups *(8)*.

Another amine reactive fluorescein derivative which competes with FITC and CSFE as a fluorescent probe is fluorescein dichlorotriazine (DTAF). Relative to FITC, this molecule is inexpensive, simple to prepare without the need for toxic reagents, and stable once made *(9)*. Furthermore, antibody conjugates with DTAF demonstrate qualities similar to those prepared with FITC with regard to preparation and immunofluorescence, leading some to promote its use *(10)*.

The isothiocyanate, succinimidyl ester, and dichlorotriazine moieties are similar in that all react with nucleophiles and thus are conjugated to biomolecules almost exclusively through the ϵ-amino group of lysine residues and the N-terminal α-amino group *(10)*. Since conjugation predominantly occurs through the same functional group on the target molecule, discrimination between the reactive probes can be straightforward and may be based on (1) the degree of conjugation (i.e., for peptides and proteins, the number of fluorochromes incorporated per biomolecule), (2) the rate of reaction, (3) the freedom from competing reactions such as hydrolysis, and (4) the stability of conjugation. This evaluation may be done by monitoring the conjugation reaction with time: specifically, the consumption of biomolecule and reactive probe and the production of biomolecule conjugate(s) or hydrolysis product(s). Without the ability to discriminate between different reactants and products, it is necessary to separate the participants. This may be done by periodically sampling the reaction mixture with a sufficiently small volume sample such that the reaction is not influenced by the process. Furthermore, the separa-

---

tion must be rapid to achieve a suitable time resolution for the reaction.

A method which can be used for this analysis is capillary zone electrophoresis (CZE) with UV absorbance detection. Sample sizes for CZE are typically much smaller than microliters in volume such that the proper unit for describing sample size using 50 μm i.d. capillaries is the nanoliter. Thus the sampling size can be at least 5 orders of magnitude smaller that the total volume of the reaction mixture. Analyses are rapid and can typically be completed in minutes. Furthermore, it has been demonstrated that the flat flow profile inherent to CZE separations can yield separation efficiencies approaching half a million theoretical plates for conjugated amino acids *(11)*, which should be more than sufficient to separate the reaction participants if the biomolecule of interest is an amino acid.

Achieving such large separation efficiencies for proteins and large peptides using CZE with fused silica capillaries is more difficult, however. Ionic and hydrophobic interactions between the capillary walls and proteins can lead to zone broadening, producing tailing peaks and even irreversible adsorption to the capillary *(12)*. Various methods have been reported that address this problem, although perhaps the simplest is to use a run buffer with a pH that is significantly higher that the isoelectric point (pI) of the biomolecule of interest. Since adsorption to the capillary walls for many large biomolecules is primarily due to an electrostatic interaction with the negatively charged, deprotonated silanol groups, a biomolecule which is similarly negatively charged will be electrostatically repulsed from the walls and experience little adsorption and therefore higher separation efficiencies. Lauer and McManigill used this method to achieve theoretical plate counts of over 500 000 and 800 000 for carbonic anhydrase B *(13)*, which provides a similar separation efficiency for that experienced analyzing amino acids.

This paper is a continuation of a previous study which analyzed the conjugation reaction between myoglobin and FITC *(14)*. In this previous work, FITC conjugations of 5:1 and 10:1 molar ratios relative to myoglobin were monitored with time. Kinetic analysis of the data indicated that the myoglobin participated in the reaction according to first-order kinetics, but FITC did not. In this paper, our aim is not to characterize a specific conjugation reaction but to compare the fluorescent amine reactive probes, FITC, CFSE and DTAF, on the bases described above, using CZE techniques. This analysis will aid in determining which amine reactive probe functions best for the fluorescent labeling of biomolecules.

EXPERIMENTAL PROCEDURES

Apparatus. Instrumentation for capillary electrophoresis separations has been previously described *(14)* except for the following. Detection was provided using a Unicam (Mississauga, Ontario) 4225 UV absorbance D$_2$ lamp-based detector operating at 200 nm and with a W lamp-based detector operating at either 412 or 495 nm, depending on the purpose of use.

Conjugation to Myoglobin. Myoglobin conjugations with FITC, DTAF, and CSFE were achieved using molar ratios of 10:1 and 5:1 fluorescent probe to protein. Typically, 5 mg/mL solutions of myoglobin in run buffer (0.1 M borate, pH 9.28, for FITC and DTAF; 0.1 M borate, pH 8.5, for CSFE) were used. Conjugation was initiated by addition of an aliquot, which was one-tenth the volume of the myoglobin solution, of amine reactive probe in DMF. Regardless of which conjugation/run buffer was

used, its pH was always at least one pH unit greater than the pI of myoglobin [pI 6.8, 7.3 *(15)*] such that little or no protein adsorption was evident in the separation.

Separations. All separations were performed as previously described *(14)* except those with CFSE as a conjugation reactant which were made using a positive potential of 22 kV (current approximately 45 μA).

Degree of Conjugation. Degrees of conjugation were estimated from electropherograms using the same techniques previously reported *(14)*. Briefly, separated peaks in the electropherograms of the myoglobin-reactive probe mixtures were attributable to successive numbers of reactive probe conjugated to myoglobin (M): i.e., M + nF where n varied from 0 [no FITC (F) incorporated into myoglobin] to 8 (eight molecules of FITC incorporated into myoglobin). The number and migration times of separated peaks determined the degree of conjugation.

Since peak assigments in the electropherograms are critical for the evaluation of conjugation degree, verification of the assignments made in the previous work *(14)* was performed using absorbance detection at 412 nm. At this wavelength, absorbance of the conjugate is only significantly attributable to the Fe(III) of the heme group in myoglobin. This allows evaluation of the molar ratios of conjugated reactive probe to protein (F/P) using peak areas without the need for the correction procedure used in the previous work *(14)*. The evaluated F/P ratios from the electropherograms were then compared to the F/P ratios calculated by spectrophotometric means as previously outlined. The reactive probe–protein solutions used in this verification study were obtained by the following procedures.

Three separate conjugation reactions between myoglobin and FITC (1:10 molar ratio) were stopped at 30, 60, and 160 min by the addition of a 50 molar excess of hydroxylamine relative to FITC. The resulting solutions were then individually passed through separate Sephadex G-25 columns equilibrated with borate run buffer. The first 0.75 mL of colored fraction was collected in each case, attributable to conjugated myoglobin free of hydroxylamine–FITC conjugate. A 0.5 mL portion of the fraction was concentrated 10-fold using Amicon (Beverely, MA) Microcon microconcentrators (MWCO 10 kDa) to obtain electropherogram-based F/P ratios. Spectrophotometric-based F/P ratios were obtained for each conjugation reaction by diluting the remaining 0.25 mL of the fractions obtained from the G-25 columns 20-fold and measuring absorbance at 412 and 495 nm using a Hewlett-Packard (Palo Alto, CA) Model 8451A diode array spectrophotometer.

F/P ratios evaluated from the individual integrated peak areas of the electropherograms were calculated using the equation:

$$\text{av F/P} = \frac{\sum_{n=0}^{8} nM_n}{\sum M_n}$$

where n refers to the number of FITC molecules incorporated into myoglobin and M_n to the area of each peak attributable to a separated M + nF component.

Spectrophotometrically determined F/P ratios were calculated according to the same method outlined in the previous work *(14)*.

Hydrolysis of Reactive Probes. Twenty microliter aliquots of 0.03 M reactive probe standards in DMF were diluted 10 times in the appropriate run buffer and their electropherograms recorded periodically over a 3 day time
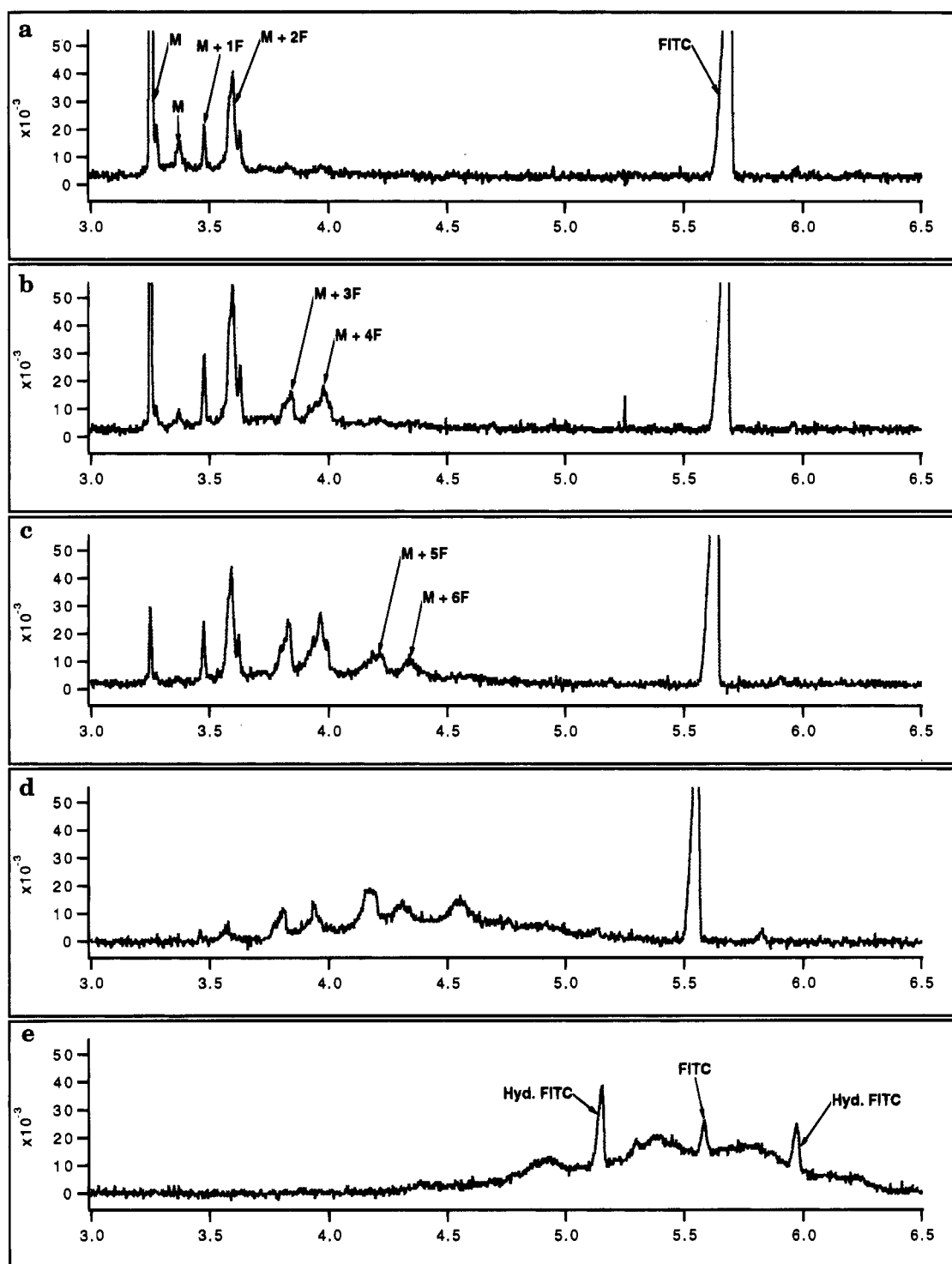
Figure 1. Electropherograms for a 10:1 molar ratio conjugation of FITC to myoglobin at various times after the initiation of the conjugation reaction: (a) 2 min; (b) 12 min; (c) 33 min; (d) 112 min; (e) 22 h. Peaks labeled with M are attributable to myoglobin; M + 1F, to myoglobin with one FITC molecule conjugated; M + 2F, to myoglobin with two FITC molecules conjugated; ...; M + 7F, to myoglobin with seven FITC molecules conjugated; Hyd. FITC, to hydrolyzed FITC.

period. This amount of reactive probe equals the same amount used in 10:1 conjugations of reactive probe to myoglobin. The electropherograms were recorded at 20 ± 1 °C, although hydrolysis was allowed to progress at room temperature. Detection was accomplished using the W lamp operating at 495 nm to overlap with the absorbance maximum of the fluorochrome. Fluorescence spectra were obtained using a Shimadzu (Kyoto, Japan) Model RF5000U spectrofluorophotometer.

Conjugation to Lysine. Lysine conjugations were performed at a molar ratio of 5:1 with respect to the

amine reactive probe. Typically, 5 mM solutions of L-lysine in run buffer (0.1 M borate, pH 9.28, for FITC and DTAF; 0.1 M borate, pH 8.5, for CSFE) were used. Aliquots of reactive probe were added in a fashion similar to that described for the myoglobin conjugation. Peak assignments were verified by conjugating both N^{α}-t-BOC-L-lysine and N^{ϵ}-t-BOC-L-lysine under the same conditions, followed by removal of the t-BOC protecting group by the procedure outlined by Stahl *et al.* *(16)*.

Stability Studies. Two procedures were used to evaluate the stability of the conjugation between lysine
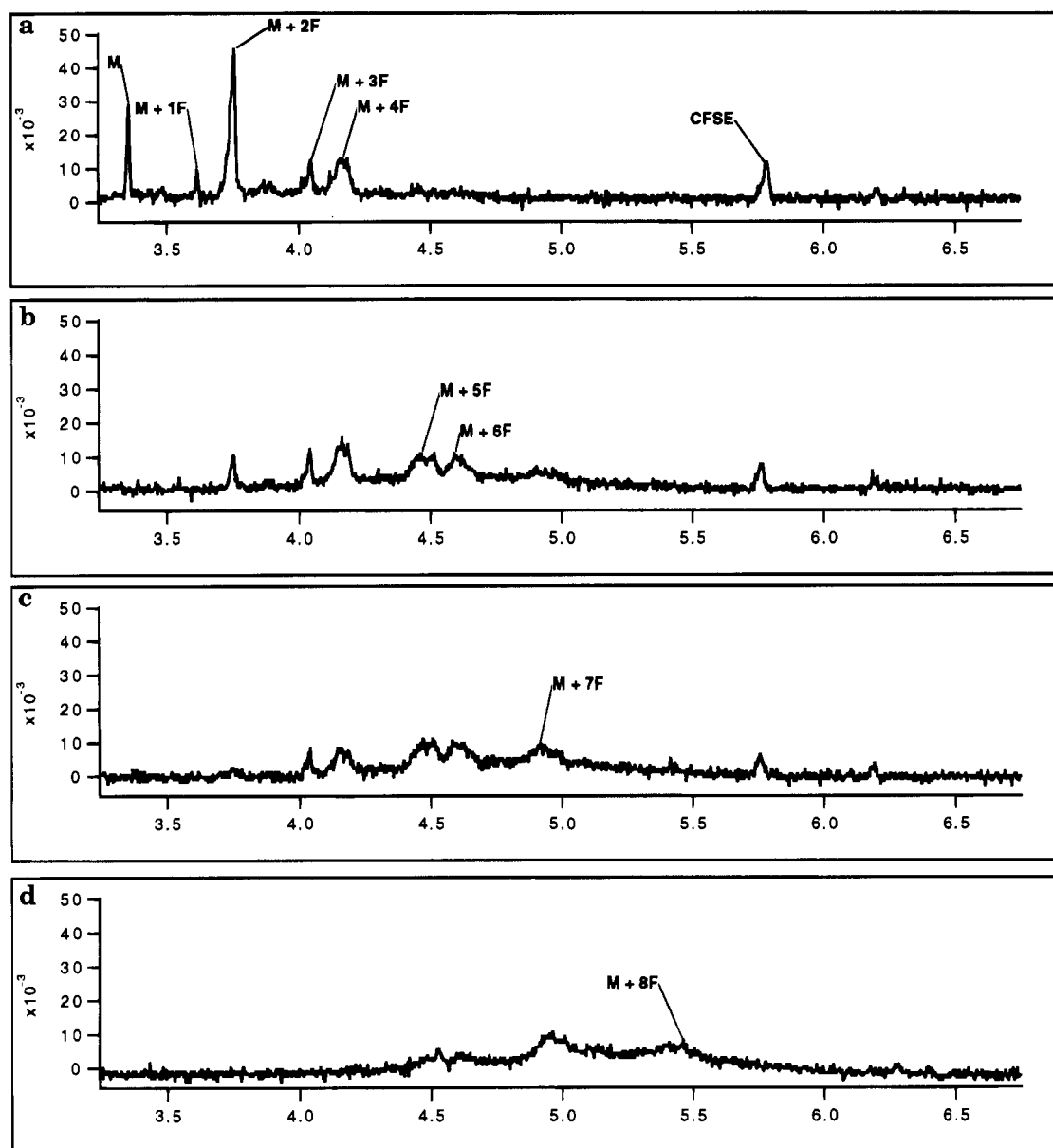
Figure 2. Electropherograms for a 10:1 molar ratio conjugation of CFSE to myoglobin at various times after the initiation of the conjugation reaction: (a) 2 min; (b) 12 min; (c) 33 min; (d) 112 min. Peaks labeled with M are attributable to myoglobin; M + 1F, to myoglobin with one CFSE molecule conjugated; M + 2F, to myoglobin with two CFSE molecules conjugated; ...; M + 8F, to myoglobin with eight CFSE molecules conjugated.

and reactive probe. In the initial procedure, the respective conjugation solution was kept in the dark at room temperature; then the electropherogram of the solution was recorded periodically. As this stability study produced only minor changes in the electropherograms, a separate procedure was developed where the conjugate solutions were incubated at 37 °C for a period of 10 days; then their electropherograms recorded.

Chemicals. L-Lysine (>99% purity) was obtained from ICN Biochemicals Inc. (St. Laurent, PQ). N^α-t-BOC-L-lysine, N^ϵ-t-BOC-L-lysine, myoglobin from horse heart (95–100%), Sigma grade borax (approximately 99%), Sephadex G-10–120, and Sephadex G-25–80 were purchased from Sigma Chemical Co. (St. Louis, MO). HPLC grade N,N-dimethylformamide (DMF) was purchased from Aldrich Chemical Co. (Milwaukee, WI). Fluorescein-5-isothiocyanate, isomer I (FITC), 5-carboxyfluorescein succinimidyl ester (CSFE), and 5-(4,6-dichlorotriazinyl)-aminofluorescein (DTAF) were purchased from Molecular Probes (Eugene, OR).

RESULTS

Conjugation of Reactive Probes to Myoglobin: Degree of Conjugation. The conjugation of FITC to myoglobin has been previously studied *(14)*. The reaction demonstrated a semistepwise incorporation of FITC molecules into the myoglobin, through lysine residues. FITC was found to participate in the conjugation with a 1.3:1 stoichiometry relative to myoglobin. Since lysine residues are positively charged and the fluorescein molecule in FITC is negatively charged at the pH used for the conjugation/run buffer, conjugation resulted in a significant change in pI for myoglobin. Due to the fact that Lauer and McManigill's technique for CZE protein separation relies on pI differences to separate different proteins, the technique was able to resolve peaks attributable to $n = 1$–7 FITC molecules conjugated to myoglobin (see Figure 1). Although the peak assignments have been shown to agree acceptably with conventional spectroscopic techniques based on average degrees of conjugation *(14)*, further verification of peak
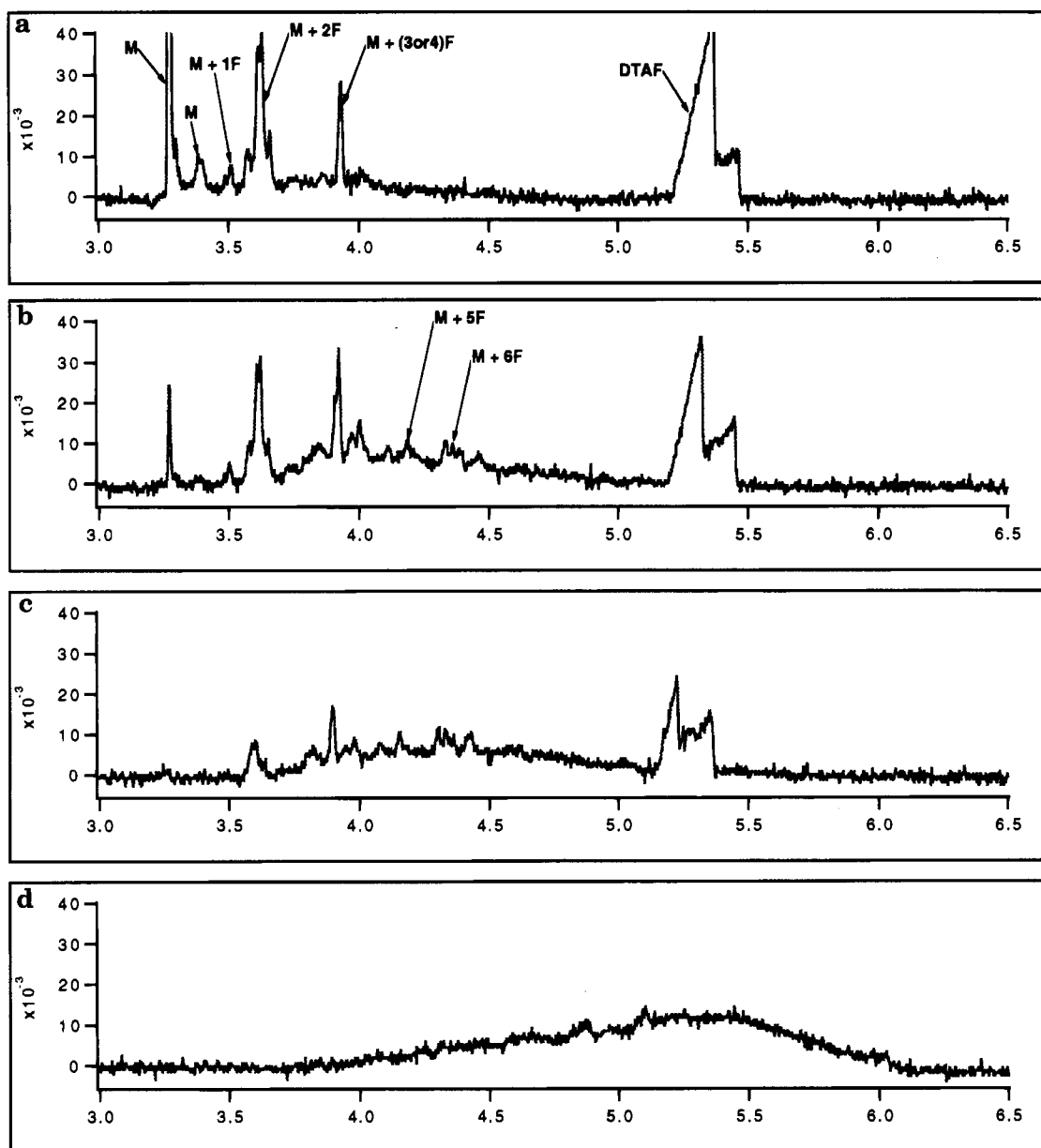
Figure 3. Electropherograms for a 10:1 molar ratio conjugation of DTAF to myoglobin at various times after the initiation of the conjugation reaction: (a) 2 min; (b) 12 min; (c) 31 min; (d) 5 h. Peaks labeled with M are attributable to myoglobin; M + 1F, to myoglobin with one DTAF molecule conjugated; M + 2F, to myoglobin with two DTAF molecules conjugated; ...; M + 6F, to myoglobin with six DTAF molecules conjugated.

Table 1. Comparison of F/P Ratios Determined by Peak Areas from Electropherograms and by Spectrophotometric Means

reaction time (min)	peak area F/P	spectrophotometric F/P
30	2.9	3.2
60	4.3	4.4
160	5.9	6.2

assignments in the electropherograms was performed. Comparison results of FITC to myoglobin conjugation ratios obtained from electropherograms and conventional spectrophotometric techniques appear in Table 1 for three separate reactions which have been stopped at 30, 60, and 160 min. The agreement between these two methods is acceptable, which indicates that peak assignments are valid.

In general, from the analysis of the electropherograms contained in Figure 1 and previous results *(14)*, it is evident that the higher conjugated myoglobin peaks grow

as the conjugation reaction proceeds at the expense of the lower conjugated myoglobin peaks. After 112 min of reaction in the 10:1 molar ratio, no peak attributable to myoglobin is evident and little M + 1F or M + 2F. Even the peak heights of M + 3F and M + 4F have begun to diminish. Another interesting aspect in the electropherograms is that lower conjugated protein peaks display sharper zones. Numerous peaks appear to be underlayed by the M + nF envelopes. This indicates that separation is based not only on pI changes induced by the degree of conjugation but also to the relative position of the fluorescent probe labels in the protein conformation, albeit to a lesser extent. Also evident in the electropherograms is the development of a broad background with time, on which the peaks are superimposed. If the reaction is allowed to continue for 22 h, the broad background increases further and shifts to longer migration times indicative of multiconjugation of the protein.

Figure 2 contains electropherograms for a conjugation reaction between CFSE and myoglobin at a molar ratio
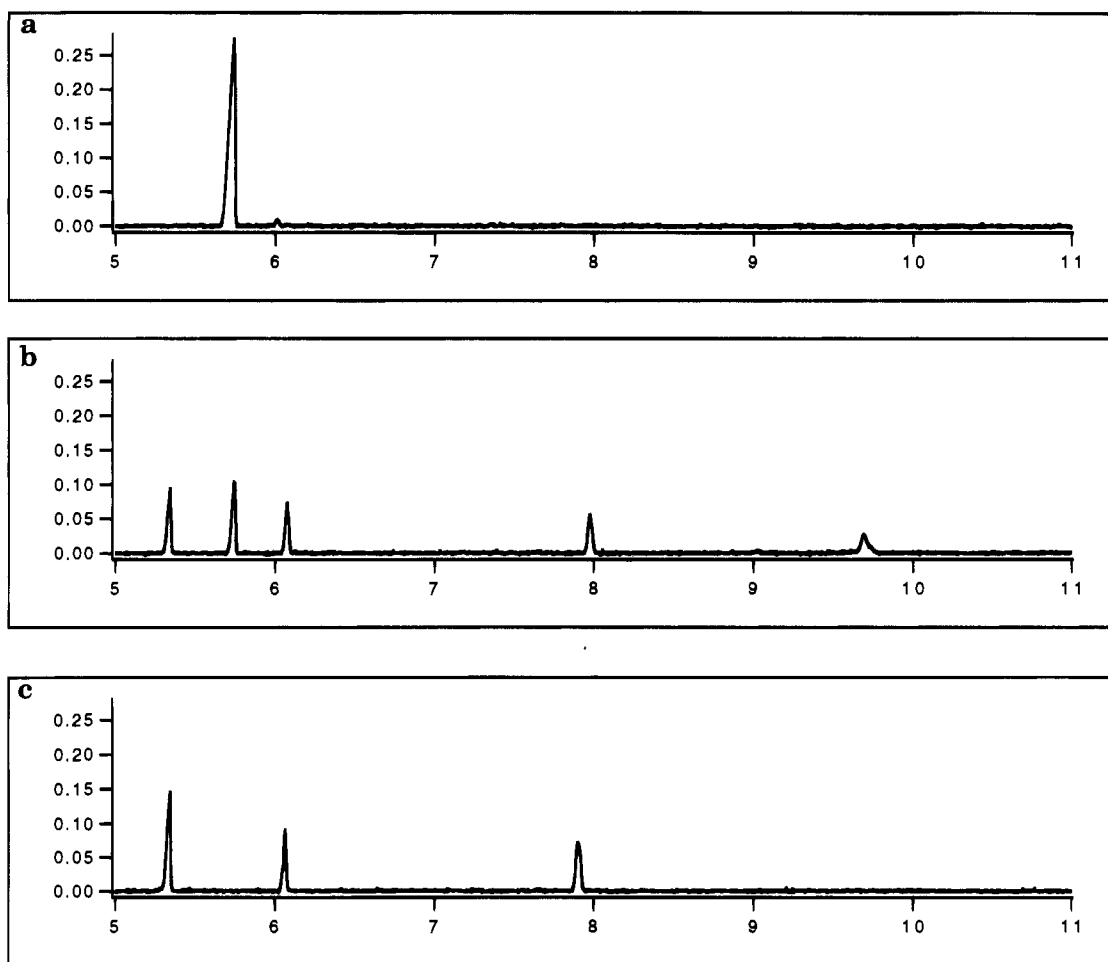
Figure 4. Electropherograms for the hydrolysis of a 0.0027 M FITC solution in DMF/run buffer (1:10 v/v) at various times after the 10× dilution of a FITC/DMF solution with run buffer: (a) 2 min; (b) 24 h; (c) 75 h.

of 10:1 fluorescent probe to protein. The development of similar peaks in the early electropherograms to the FITC conjugation is apparent, suggestive of a similar conjugation reaction mechanism. However, it is apparent that the rate of reaction for CFSE far exceeds that for FITC. The myoglobin peak has disappeared after only 10 min of reaction time, as opposed to 112 min for a similar molar ratio for FITC. If the molar ratio of reactive probe to myoglobin is lowered to 5:1, the conjugation reaction appears to proceed in a similar fashion as compared to the 10:1 molar ratio, albeit at a diminished rate.

Figure 3 contains electropherograms for a conjugation reaction between DTAF and myoglobin at a molar ratio of 10:1 reactive probe to protein. It is immediately apparent that the electropherograms are different to those for both FITC and CFSE conjugations in that there appears to be only two dominant peaks other than myoglobin. The migration time for the first eluting peak matches that for M + 2F evident in the FITC and CFSE conjugations, but the second eluting peak splits the migration times for M + 3F and M + 4F. It appears that the DTAF molecule is more selective than either FITC or CFSE in which lysine residues it reacts with in the myoglobin molecule. The rate of reaction is again much faster than that for FITC, judging from the rate of disappearance of the myoglobin peak, but slower than that for CFSE. Similarly to CFSE, lowering the molar ratio of fluorescent probe to protein to 5:1 has no effect on the conjugation other than lowering its relative rate.

Reaction Rates for the Conjugation to Myoglobin. Since the myoglobin peak shape is Gaussian, peak

height is directly proportional to concentration according to Beer's law, and kinetic analysis of the data can be made. Myoglobin peak height time profiles for a 10:1 fluorescent probe to protein conjugation follow an exponential decline described by pseudo-first-order kinetics due to the excess concentrations of reactive probe. It is evident that the rate of conjugation reaction is fastest for CFSE, followed by DTAF and then FITC. Effective rate constants (k_{eff}) can be obtained from the slope of plots of the natural logarithm of the myoglobin peak height versus conjugation reaction time. It should be noted, however, that since the myoglobin time profiles for CFSE consist of only two points, and the second point represents only baseline noise, k_{eff} was calculated using a myoglobin peak height from a standard which contained the appropriate amount of DMF but no CFSE. This peak height was taken to represent the initial myoglobin concentration. Therefore, the effective rate constant for CFSE conjugations has a larger degree of uncertainty than that for both DTAF and FITC. The effective rate constants for each of the reactive probes for 5:1 and 10:1 conjugations (reactive probe to myoglobin) are contained in Table 2 along with the straight line correlation coefficients (FITC and DTAF) for each of the plots from which the effective rate constant was obtained.

It is apparent from the Table that the conjugation reaction using CFSE is about 15 times faster than that for FITC, if an average between the 10:1 or 5:1 conjugation ratios to myoglobin is used. CFSE is also 6 times faster than DTAF, which in turn is about 2.5 times faster than FITC.
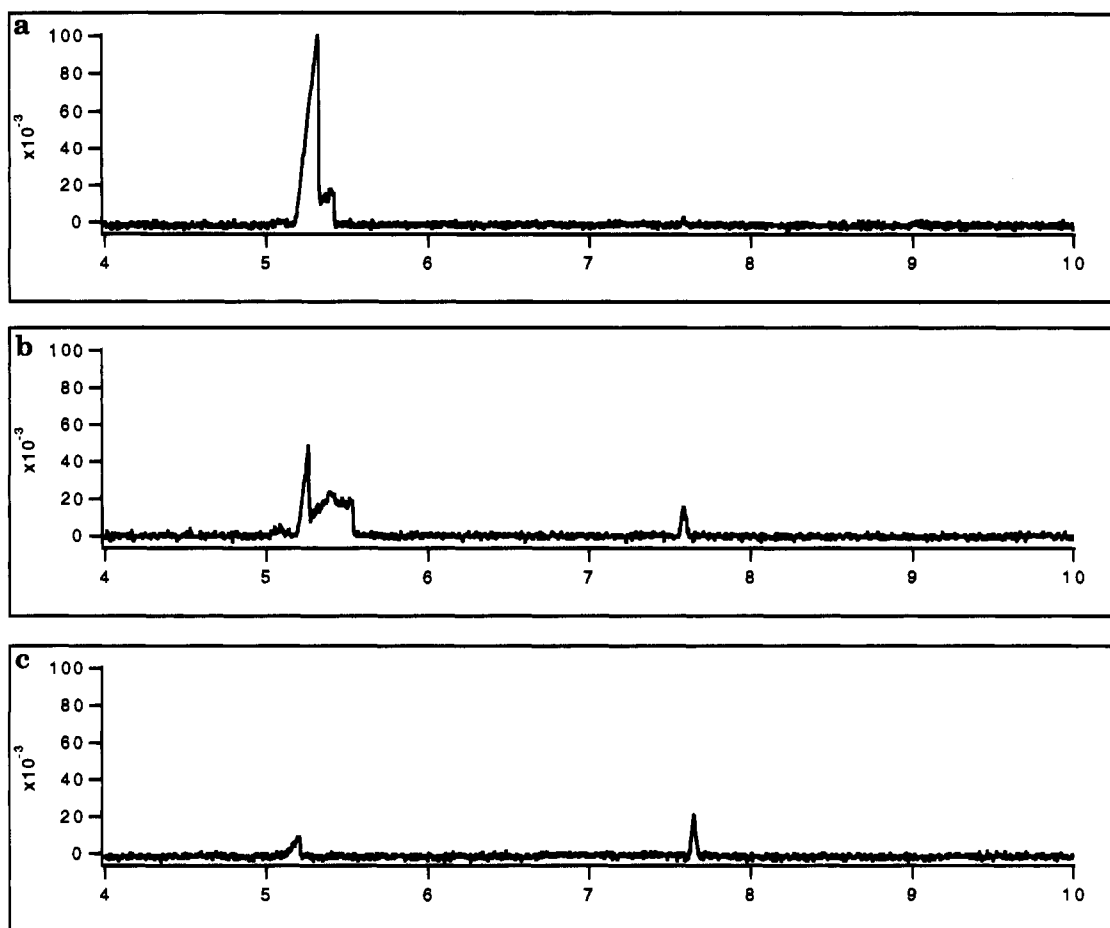
Figure 5. Electropherograms for the hydrolysis of a 0.0027 M DTAF solution in DMF/run buffer (1:10 v/v) at various times after the 10× dilution of a DTAF/DMF solution with run buffer: (a) 2 min; (b) 104 min; (c) 77 h.

Table 2. Effective Rate Constants for the Conjugation between the Reactive Probes FITC, DTAF, and CFSE with Myoglobin

	FITC		DTAF		
conjugation ratio	k_{eff} (min^{-1})	r	k_{eff} (min^{-1})	r	CFSE k_{eff} (min^{-1})
10:1	0.060	0.998	0.17	0.994	0.78
5:1	0.023	0.996	0.049	0.993	0.40

Hydrolysis of the Reactive Probes. Figures 4, 5, and 6 contain electropherograms of 0.0027 M solutions of reactive probe standards in the appropriate conjugation/run buffer over a 3 day period. In the FITC electropherograms (Figure 4), a small hydrolysis peak appears immediately after dilution with a longer migration time than the FITC peak. It has grown only marginally after 4 h; the typical duration of reaction for conjugation, and has been joined by a number of other, rather insignificantly sized peaks. It should be noted that the original height of the FITC peak is largely retained after 4 h in the conjugation buffer, indicating that hydrolysis is an insignificant competing reaction in the conjugation. Of interest is that none of these hydrolyzed FITC peaks corresponds to that for fluorescein, indicating that the hydrolysis of FITC involves more complex chemistry than the simple loss of the isothiocyanate moiety. After 24 h, hydrolysis of FITC has become significant and has almost totally consumed the FITC peak 24 h later. Hydrolysis is complete by 75 h, and the electropherogram is unchanged after a further 24 h period.

Hydrolysis of DTAF is also apparent immediately upon dilution (Figure 5). After 30 min, the peak area of DTAF has been reduced by 30%, and after 2 h, a typical

conjugation reaction time, the area has been reduced by 75%. Therefore, hydrolysis may have a significant effect on the conjugation of DTAF to biomolecules. An effective rate constant of 0.014 min^{-1} was determined from the slope of a plot of the natural logarithm of DTAF peak area and conjugation reaction time; therefore, hydrolysis is not a serious competitor for DTAF in relation to myoglobin as the respective effective rate constant for the 10:1 conjugation is more than an order of magnitude larger. Complete hydrolysis of the DTAF is evident after 1 day as subsequent electropherograms remain unchanged.

Hydrolysis of CFSE is extremely complex as demonstrated by the electropherograms contained in Figure 6. In fact, it is difficult, if not impossible, to decipher which peak is attributable to CFSE. There are three peaks, one sharp at 5.7 min and two broad between 9 and 10 min, which begin to be reduced appreciably after 30 min of conjugation, but each is very small in peak height or area relative to the peaks displayed for both FITC and DTAF. The combined peak area for these three peaks in Figure 6a is less than one-third that for DTAF and one-fifth that for FITC at similar times in the hydrolysis experiment. These peaks are replaced by two broad, tailing peaks between 10 and 11 min in the electropherograms. It was originally believed that these peaks were attributable to hydrolyzed CFSE, yet the conjugation reaction is still efficient if CFSE is exposed to buffer (CFSE solvent: 1:1 water/DMF v/v) for 2 h and then used in both 5:1 and 10:1 conjugations with myoglobin.

The complexity of the CFSE blanks may be explained by solvent effects generated by the gradual replacement
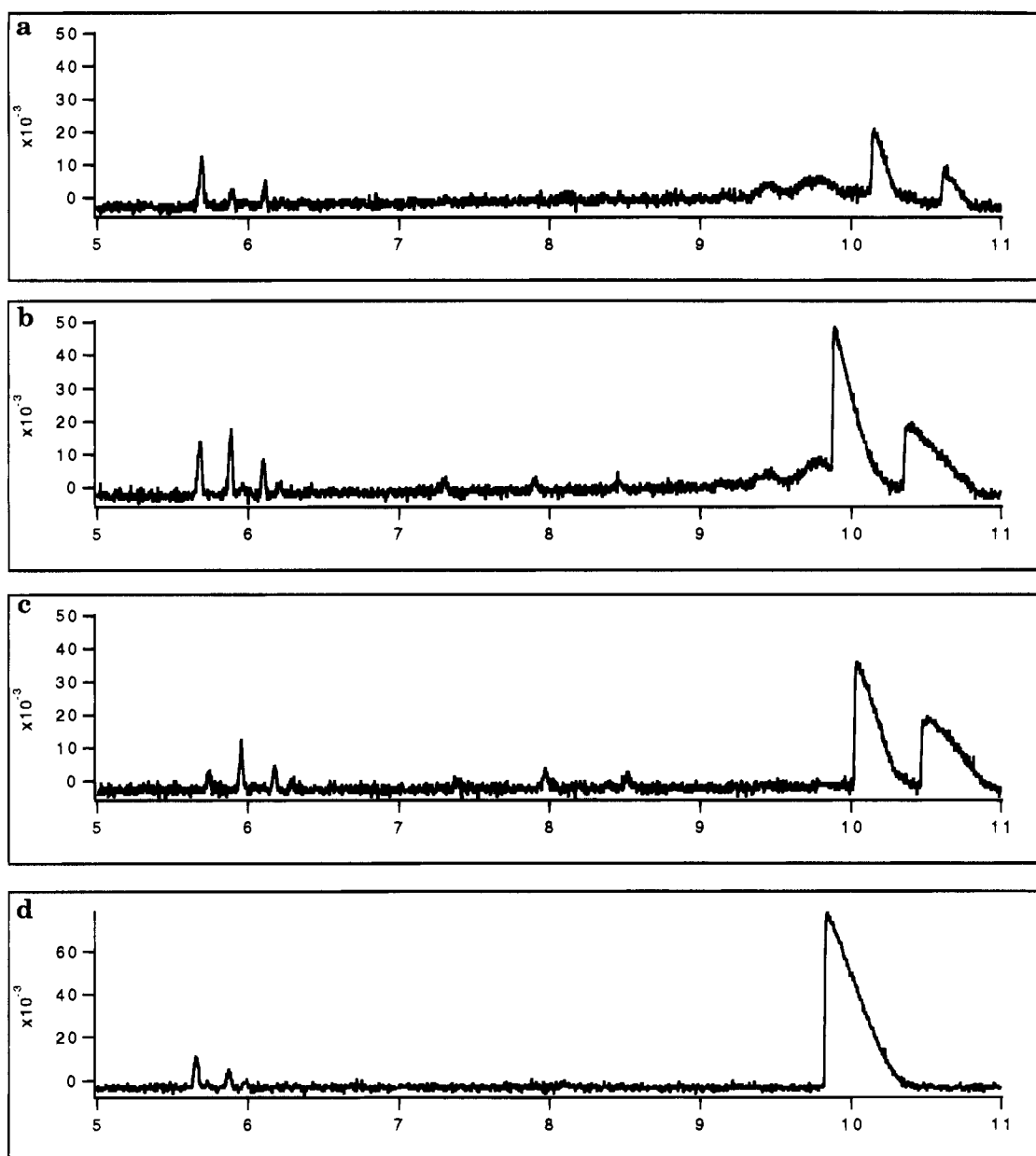
Figure 6. Electropherograms for the hydrolysis of a 0.0027 M CFSE solution in DMF/run buffer (1:10 v/v) at various times after the 10× dilution of a CFSE/DMF solution with run buffer: (a) 2 min; (b) 16 min; (c) 60 min; (d) 72 h.

of the solvent cage around the fluorophore. Solute–solvent interactions can change the chemical or electrostatic environment around the fluorophore and thus its absorptivity *(17)*. It is known that the succinimidyl ester moiety is hydrophobic *(8)*, and thus, there may be a tendency for CFSE to only slowly exchange its solvation sphere from DMF to water. This is supported by the visual appearance of the reactive probe when it is first mixed with run buffer. Initially, the color of a 0.0027 M solution of CFSE in 10:1 water/DMF v/v is yellow-orange, which is followed by a change to yellow after about 2 min and then to yellow-green after about 10 min.

Fluorescence spectroscopy is a good indicator of solvent effects on the physical characteristics of a fluorophore. Generally, fluorescence emission requires solvent relaxation, which is a reorganization of the solvent cage surrounding the fluorophore due to the increase in dipole moment of the fluorophore caused by the absorption of a photon *(18)*. This reorganization of the solvent cage is dependent on the physical characteristics of the solvent, so one would expect a difference in solvent relaxation for

DMF and water. The change in the fluorescence spectra of a 3×10^{-5} M CFSE solution in water with time is pronounced. The fluorescence maximum is blue shifted, by about 4 nm, and the fluorescence intensity increases by over an order of magnitude, 1 h from a 500× dilution of a 0.015 M CFSE/DMF solution with run buffer. The increase in fluorescence intensity is essentially completed after 1 h, which corresponds to the time taken for the stabilization of the electropherograms in Figure 6, and thus supports the premise of a slow solvent exchange around the fluorophore. The large increase in fluorescence intensity with time could possibly be the result of intermolecular CFSE/H$_2$O hydrogen bonding which has stabilized the fluorophore and increased its fluorescence quantum yield.

Stability of the Conjugation. Electropherograms recording the progress of a 5:1 conjugation of lysine to FITC and its subsequent stability in run buffer appear in Figure 7. The conjugation reaction is over in 2 h, with the FITC peak at about 5.8 min being almost totally consumed and replaced by three separate peaks. The
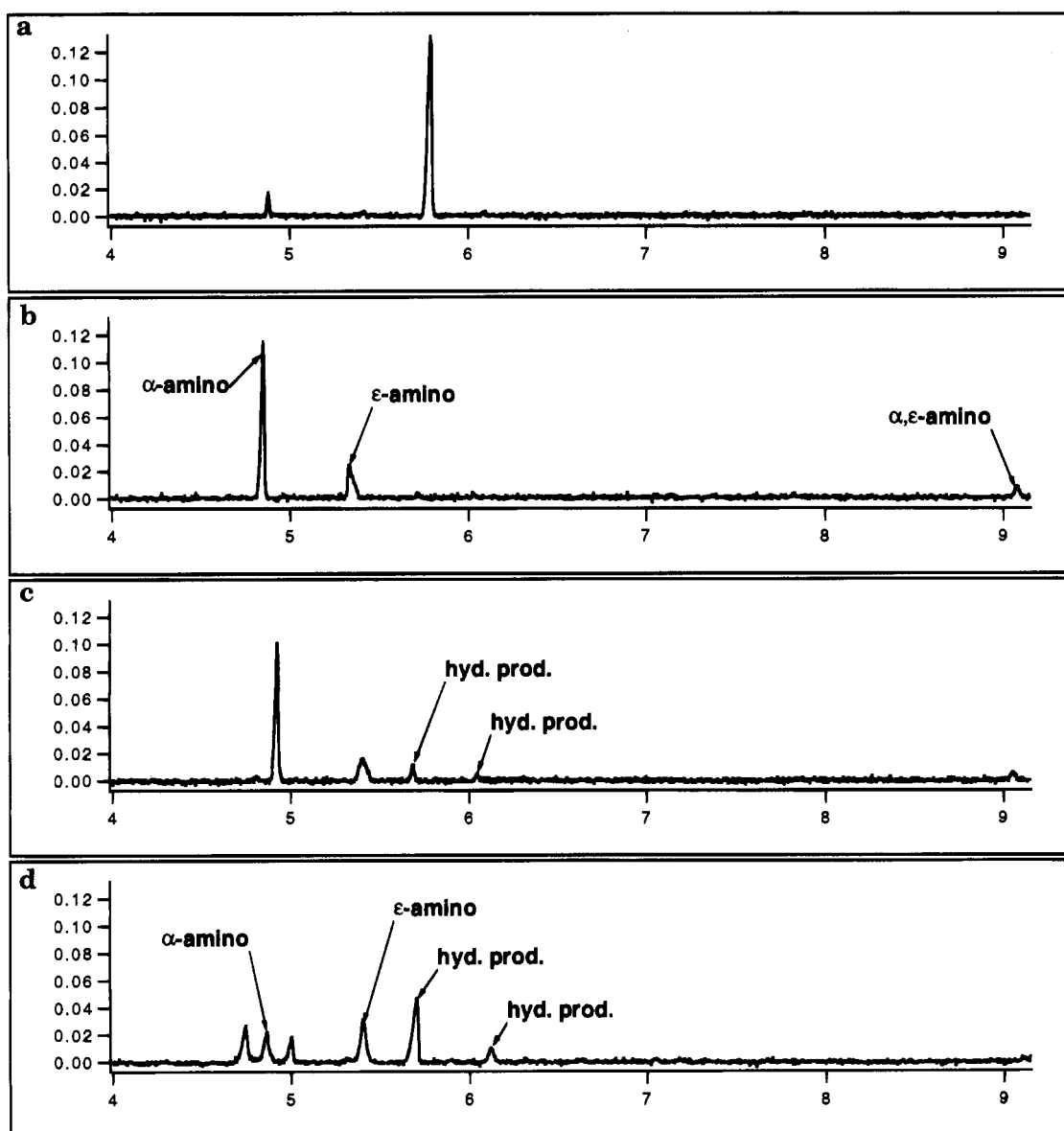
Figure 7. Electropherograms for the conjugation and stability of the resulting conjugate of a 5:1 molar ratio between lysine and FITC. Electropherograms were recorded at various times after the addition of FITC to a lysine solution in run buffer: (a) 2 min at 20 °C; (b) 30 min at 20 °C; (c) 1 week at 20 °C; (d) 10 days at 37 °C.

three peaks are attributable to FITC being conjugated to the α-amino group of the side chain (4.9 min) and the ε-amino group (5.4 min) and FITC being conjugated to both (9.1 min). Since the conjugation of two FITC molecules will make lysine a doubly charged anion, it is expected that this peak will elute last. Increasing the fluorescent probe to amino acid molar ratio to equimolar levels leads to the substantial increase of this peak, which supports this assignment. Differentiation between α- and ε-amino conjugation is based on spiking conjugation solutions with singly conjugated L-lysine in run buffer produced by the conjugation of N^{α}-t-BOC-L-lysine and N^{ϵ}-t-BOC-L-lysine, followed by the removal of the t-BOC group.

After 24 h, no significant change is seen in the peaks; however, after 2 days of elapsed time, a peak appears to grow with a migration time at about 5.7 min, which is close to the original FITC peak. It reaches and maintains a signal to noise ratio (S/N) of 10 after 75 h. In addition to this, another peak at about 6.1 min also grows, although its S/N never exceeds 5. The changes seen in the electropherograms suggest that some form of hy-

drolysis of the conjugate is occurring, although the effects are rather insignificant.

A greater change in the electropherograms is seen if the conjugate is incubated at 37 °C for 10 days. The two peaks attributable to α- and ε-amino conjugation, evident after the conjugation is complete, have been replaced by six peaks. The α- and ε-peaks were identified by spiking the solution with freshly conjugated lysine to ensure proper identification. It appears that the majority of the peak area attributable to α-amino conjugation has been lost, whereas that for the ε-amino conjugation has been retained, if not added to. In addition to these findings, the doubly conjugated lysine peak has disappeared. These two circumstances suggest that the α-amino conjugated FITC molecule has been removed from the doubly conjugated lysine to produce a singly conjugated lysine through the ε-amino group.

Also evident in the 37 °C incubation study is that the peaks seen in the room temperature incubation at 5.7 and 6.1 min have been enlarged such that the peak at 5.7 min dominates the electropherogram. In addition to these two, a further two peaks have materialized with
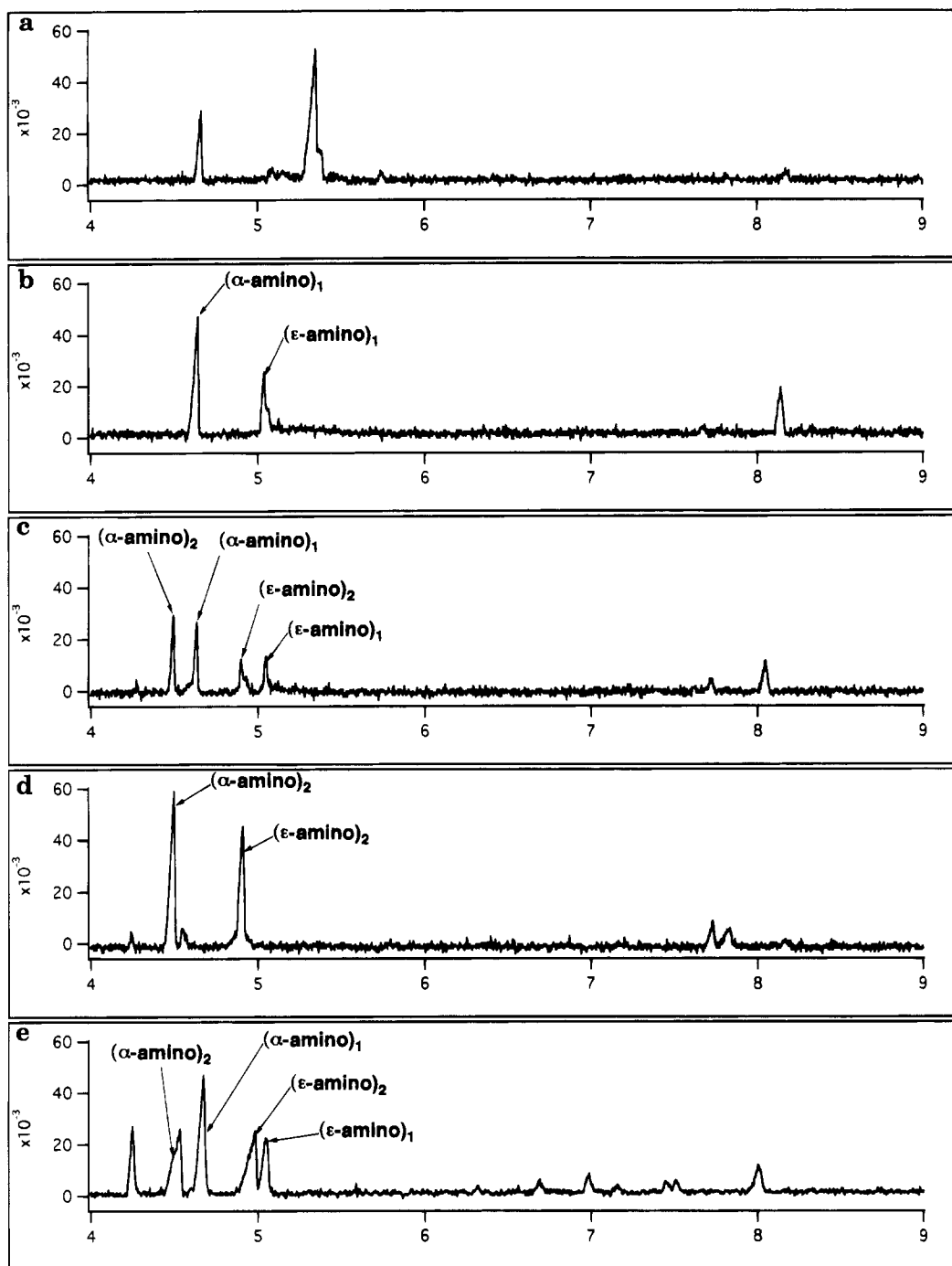
Figure 8. Electropherograms for the conjugation and stability of the resulting conjugate of a 5:1 molar ratio between lysine and DTAF. Electropherograms were recorded at various times after the addition of DTAF to a lysine solution in run buffer: (a) 2 min at 20 °C; (b) 46 min at 20 °C; (c) 47 h at 20 °C; (d) 1 week at 20 °C; (e) 10 days at 37 °C.

migration times of 4.7 and 5.0 min. It is uncertain what these peaks are attributable to. Altogether, this electropherogram is suggestive that significant hydrolysis has occurred.

To obtain a definitive impression of whether the thioether bond formed from the conjugation of the α-amino group of lysine and FITC is being ruptured in the incubation studies, size-exclusion chromatography can be used to separate which peaks are attributable to fluorescent probe removed from the conjugate and which peaks are attributable to fluorescent probe associated with lysine. A Sephadex G-10 column was used which can separate globular proteins with molecular masses up to 700 Da. Fluorescein has a molecular mass of 332 Da whereas singly conjugated lysine has a molecular mass

of about 478 Da, so some degree of separation should occur. Approximately 0.5 mL of the incubated solution was applied to the G-10 column, and 0.2 mL fractions were collected. The electropherogram for fraction 1 was almost totally devoid of the peaks that eluted at 5.7 and 6.1 min, but they reappeared in the electropherogram for fraction 5. It is evident that these peaks are attributable to fluorescent probe removed from the conjugate and that the thioether bond, preferentially between the α-amino group of lysine and FITC, was significantly broken in the 37 °C incubation study, presumably from hydrolysis.

The conjugation of DTAF to lysine, apparent in the electropherograms of Figure 8, is more rapid than that of FITC, as expected from the myoglobin conjugation data, and is essentially complete after 46 min. As with
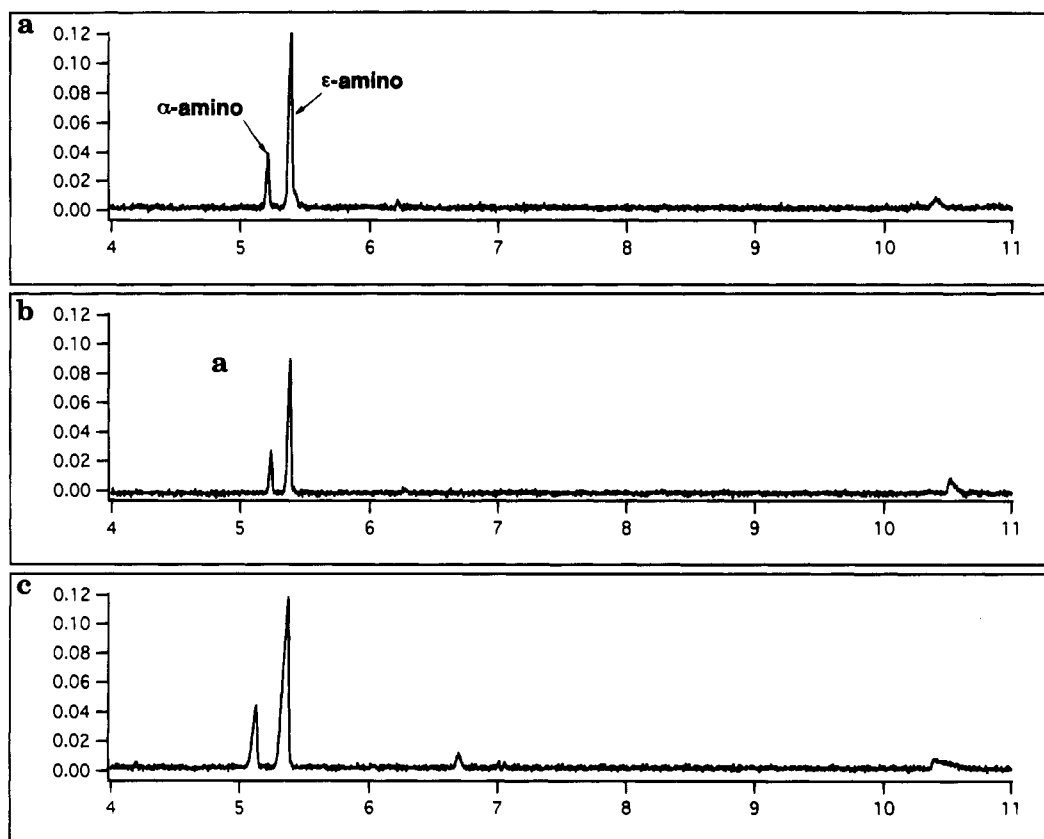
Figure 9. Electropherograms for the conjugation and stability of the resulting conjugate of a 5:1 molar ratio between lysine and CFSE. Electropherograms were recorded at various times after the addition of FITC to a lysine solution in run buffer: (a) 2 min at 20 °C; (b) 1 week at 20 °C; (c) 10 days at 37 °C.

FITC, the first eluting peak is the largest and is due to α-amino conjugation. After 24 h has elapsed from the start of the conjugation, however, the peak heights have been reduced significantly, and the formation of new peaks in the electropherogram becomes apparent. After 47 h, each of the original peaks attributable to conjugated lysine has been split into two equal peaks. After 72 h, the newly formed peaks are obviously growing at the expense of the initial conjugation peaks, which is further confirmed at 94 h. The replacement of the original peaks by the new peaks is essentially complete 1 week after the conjugation was initiated. This splitting of the peaks suggests that DTAF remains conjugated to lysine at both ε- and α-amino groups, but the way in which it was initially conjugated has been altered.

The structure of DTAF contains a dichlorotriazinyl group through which fluorescein can be conjugated to biomolecules. Only one of the chloro groups participates in the conjugation, however, and it is supposed that the remaining, relatively inert, chloro group hydrolyzes slowly *(10)*. This phenomenon is likely to be what is causing the splitting of the peaks evident in the electropherograms.

While the splitting of the peaks does not confer an instability of the conjugation, this poses a problem for researchers who wish to use DTAF as a fluorescent probe for fluorescence detection using capillary electrophoresis as a separation tool. The multiple peaks would lead to an extremely confused electropherogram if a large number of solutes were to be separated.

If the conjugate is incubated at 37 °C for 10 days, the two peaks attributable to α- and ε-amino conjugation have again been split and are joined by a significant peak with a migration time at 4.2 min. This peak also appeared in the stability study conducted at room tem-

perature, although with a S/N of only 3, and may therefore be indicative of instability in the linkage of DTAF to lysine. It is unclear why the peaks attributable to α- and ε-amino conjugation are split after incubation at 37 °C for 10 days when at 20 °C the splitting process seems to have been completed after 1 week. These results suggest that a reversible equilibrium is operating here rather than an irreversible hydrolysis of the remaining chloro group. Further experiments would have to be performed to test this hypothesis, however.

To determine whether the peak at 4.2 min, or either of the split peaks, is due to free reactive probe caused by conjugate—bond rupture, the same size-exclusion chromatography experiment was conducted using a G-10 column. No significant difference was seen in the electropherograms obtained from any of the fractions collected: the relative peak height of each of the peaks was maintained. This indicates that the peak at 4.2 min and also the split peaks correspond to conjugated lysine, rather than to hydrolyzed fluorescent probe.

Figure 9 contains electropherograms taken during and after a 5:1 conjugation of lysine to CFSE. Of note is the fact that the reaction was completed before the first electropherogram could be recorded and the switching of relative peak heights for the first two eluting peaks relative to both FITC and DTAF. With CFSE, the height of the second peak, again attributable to ε-amino conjugation, is about three times that for the first, indicating that the ε-amino group is being conjugated preferentially at the expense of the α-amino group of the side chain. This is not due to the small drop in buffer pH used for CFSE conjugations relative to FITC and DTAF conjugations. The conjugation reaction of FITC to lysine showed no significant variation when performed at pH 8.5 as opposed to pH 9.28: α-amino conjugation was signifi-

cantly favored by a large ratio. Rather, the selectivity for the ε-amino group demonstrated by CFSE seems to be attributable to the succinimidyl ester reactive moiety itself.

Of more significance to our stability study, however, is that the electropherograms remain essentially unchanged after 1 week in the run buffer, suggesting a very stable conjugation. Furthermore, when incubated at 37 °C for 10 days, the electropherograms remain unchanged, indicative of more stable conjugation relative to the other two fluorescent probes.

DISCUSSION

From the above mentioned studies, some conclusions can be drawn about the relative usefulness of the three amine reactive fluorescent probes, FITC, CFSE, and DTAF. Each provides suitable degrees of conjugation depending on the time allowed for conjugation; however, the time required to achieve a standard degree of conjugation differs considerably between the three fluorescent probes. The rate of reaction for CFSE is significantly faster than that for DTAF, which, in turn, is faster than FITC for both the protein myoglobin and the amino acid lysine. However, the degree of conjugation with FITC may be easily controlled by manipulating the duration of exposure to the reactive probe. The conjugation can be easily stopped by adding an excess of hydroxylamine or any small, inert molecule with a primary amine group (Tris buffer).

It was anticipated that the hydrolysis of CFSE may significantly compete with conjugation at the basic conditions suitable for lysine conjugation, but this proved to be groundless. While each of the fluorescent probes demonstrated characteristics indicative of hydrolysis in the electropherograms, hydrolysis was not a significant competitor to amine conjugation for any of the fluorescent probes with the conditions used.

In terms of the stability of the bond formed through the conjugation of the fluorescent probe to the amino acid lysine, it was apparent that each fluorescent probe provided a satisfactory stability in solution over the period of 1 week at room temperature, although DTAF-conjugated lysine demonstrated troubling extra peaks in electropherograms caused presumably by the hydrolysis of the remaining, relatively inert, chloro group. If the conjugates were incubated at 37 °C for 10 days, however, the FITC-conjugated lysine demonstrated significant hydrolysis of the thioether bond linking the fluorescent probe with the lysine. Although DTAF-conjugated lysine showed no evidence of actual fluorescent probe–lysine bond rupture in the 37 °C incubation study, an additional peak appears in the electropherogram indicative of a change occurring in the conjugate. CFSE-conjugated lysine, on the other hand, demonstrated no further change in its electropherograms.

For most applications, it appears that the succinimidyl ester would be the reactive moiety of choice on the basis of the rate of reaction and stability of the conjugation bond.

LITERATURE CITED

(1) Bright, F. V. (1988) Bioanalytical Applications of Fluorescence Spectroscopy. *Anal. Chem. 60*, 1031A–1039A.

(2) Christopoulos, T. K., and Diamandis, E. P. (1992) Enzymatically Amplified Time-Resolved Fluorescence Immunoassay with Terbium Chelates. *Anal. Chem. 64*, 342–246.

(3) Haugland, R. P. (1992–1994) *Handbook of Fluorescent Probes and Research Chemicals* (K. D. Larison, Ed.) 5th ed., Molecular Probes Inc., Eugene, OR.

(4) Brinkley, M. (1992) A Brief Survey of Methods for Preparing Protein Conjugates with Dyes, Haptens, and Cross-Linking Reagents. *Bioconjugate Chem. 3*, 2–13.

(5) Nakamura, R. M., Tucker, E. S., and Carlson, I. H. (1991) Immunoassays in the Clinical Laboratory. In *Clinical Diagnosis and Management by Laboratory Methods* (J. B. Henry, Ed.) 18th ed., p 870, W. B. Saunders Co., Philadelphia, PA.

(6) Castillo, B. D., Alvarez-Builla, J., and Lerner, D. A. (1991) Fluorogenic Reagents and Fluorescent Probes. In *Luminescence Techniques in Chemical and Biochemical Analysis* (W. R. G. Bayeens, D. De Keukeleleire, and K. Korkidis, Eds.) p 79, Marcel Dekker Inc., New York.

(7) The, T. H., and Feltkamp, T. E. W. (1970) Conjugation of Fluorescein Isothiocyanate to Antibodies; II. A Reproducible Method. *Immunology 18*, 875–881.

(8) Lomants, A. J., and Fairbanks, G. (1976) Chemical Probes of Extended Biological Structures: Synthesis and Properties of the Cleavable Protein Cross-linking Reagent [^{35}S]Dithiobis-(succinimidyl propionate). *J. Mol. Biol. 104*, 243.

(9) Blakeslee, D. (1977) Immunofluorescence using Dichlorotriazinylaminofluorescein (DTAF); II. Preparation, Purity, and Stability of the Compound. *J. Immunol. Methods 17*, 361–364.

(10) Blakeslee, D., and Baines, M. G. (1976) Immunofluorescence using Dichlorotriazinylaminofluorescein (DTAF); I. Preparation and Fractionation of Labelled IgG. *J. Immunol. Methods 13*, 305–320.

(11) Cheng, Y. F., and Dovichi, N. J. (1988) Subattomole Amino Acid Analysis by Capillary Zone Electrophoresis and Laser-Induced Fluorescence. *Science 242*, 562–564.

(12) Jorgenson, J. W., and Lukacs, K. D. (1983) Capillary Zone Electrophoresis. *Science 222*, 266–272.

(13) Lauer, H. H., and McManigill, D. (1986) Capillary Zone Electrophoresis of Proteins in Untreated Fused Silica Tubing. *Anal. Chem. 58*, 166–170.

(14) Banks, P. R., and Paquette, D. M. (1995) Monitoring of a Conjugation Reaction between Fluorescein Isothiocyanate and Myoglobin by Capillary Zone Electrophoresis. *J. Chromatogr.* (in press).

(15) Radola, B. J. (1973) Isoelectric Focusing in Layers of Granulated Gels. I. Thin Layer Isoelectric Focusing of Proteins. *Biochim. Biophys. Acta 295*, 412–428.

(16) Stahl, G. L., Walter, R., and Smith, C. W. (1978) General Procedure for the Synthesis of Mono-N-acylated 1,6-Diaminohexanes. *J. Org. Chem. 43*, 2285–2286.

(17) Rao, C. N. R. (1975) Solvent Effects. In *Ultra-Violet and Visible Spectroscopy*, 3rd ed., pp 206–209, Butterworths, Boston.

(18) Lakowicz, J. R. (1983) Effects of Solvents on Fluorescence Emission Spectra. In *Principles of Fluorescence Spectroscopy*, pp 189–215, Plenum Press, New York.

BC950034+

Vitamin B₁₂ Mediated Oral Delivery Systems for Granulocyte-Colony Stimulating Factor and Erythropoietin

G. J. Russell-Jones,*,‡ S. W. Westwood,‡ and A. D. Habberfield§

Biotech Australia Pty Ltd., P.O. Box 20, Roseville, NSW 2069, Australia, and Amgen Inc., Amgen Center, Thousand Oaks, California 91320. Received March 17, 1995⊛

As a prelude to the development of orally active erythropoietin (EPO) and granulocyte-colony stimulating factor (G-CSF), conjugates have been formed between these molecules and vitamin B12. During the formation of these conjugates intramolecular cross-linking of the proteins was avoided by the use of hydrazidyl derivatives of vitamin B12. A potentially biodegradable linkage was formed between vitamin B12 and G-CSF by reaction of the buried thiol in G-CSF with a long chain dithiopyridyl derivative of vitamin B12. In vitro and in vivo testing of the conjugates showed that their bioactivity was substantially maintained and that they were actively transported in an intrinsic factor dependent fashion across CaCo-2 cells and from the intestine to the circulation in a biologically active form.

INTRODUCTION

G-CSF (granulocyte-colony stimulating factor) and EPO (erythropoietin) represent two of the most exciting molecules to emerge out of the recent developments in recombinant DNA technology. G-CSF has been shown to be a powerful stimulator of neutrophil production in humans and has found application in the stimulation of neutrophils in cancer patients, thereby reducing the period of neutropenia after conventional chemotherapy (Bronchud et al., 1987; Golde & Gasson, 1988; Morstyn & Burgess, 1988). It also has application in the treatment of chronic neutropenia. EPO, on the other hand, stimulates the maturation of erythroid progenitor cells into mature erythocytes, and is used for the treament of anemia in kidney dialysis patients (Krantz & Goldwasser, 1984).

Despite the enormous therapeutic potential of these two proteins, their use is limited by the fact that they must be administered parenterally to patients, as the proteins are not active following oral administration. The inability of these molecules to be efficacious orally stems primarily from their inability to pass through the villous epithelium of the gastrointestinal tract (GIT). Therefore, even if methods could be found to protect these proteins from proteolysis within the GIT, they would be excluded from entering the circulation by the cell membrane of the intestinal enterocyte, which forms an almost impenetrable barrier to the uptake of all but the smallest of molecules. Thus, in common with virtually all proteins, peptides, and other large bioactive molecules, there is currently no method for the oral delivery of either G-CSF or EPO.

Recently, a delivery technology has been described which overcomes the impenetrable barrier that the small intestinal ileocytes present and which could potentially enable orally administered compounds, such as G-CSF and EPO, to pass from the intestinal lumen, across the ileocyte, and into the circulation. This technology is based upon the natural uptake system for vitaminB₁₂ (VB₁₂), or cyanocobalamin (Cbl). VB₁₂ itself is an unusually large vitamin (MW 1356), which is too big to be taken up from the intestine by means of simple diffusion. Instead VB₁₂ is taken up from the intestinal lumen by receptor-mediated endocytosis. In this process VB₁₂ must first be bound by intrinsic factor (IF) produced in the stomach. The [IF−VB₁₂] complex then binds to an IF receptor located on the lumenal surface of the ileocyte, which stimulates internalization of the VB₁₂ and subsequent transcytosis of the vitamin across the ileocyte (Robertson & Gallagher, 1985; Gallagher & Foley, 1971; Baillant et al., 1990; Simpson et al., 1993).Russell-Jones and co-workers (Russell-Jones & Aizpurua, 1988; Russell-Jones, 1994) have found that it is possible to covalently link peptides and proteins to VB₁₂ and have demonstrated that these molecules are cotransported from the intestinal lumen to the circulation with VB₁₂ following oral administration. In order for the transport system to be effective it is important that during the conjugation of VB₁₂ to the peptides/proteins care is taken to preserve the bioactivity of both the peptide and the VB₁₂ to which it is coupled. In this paper we describe methods for the conjugation of VB₁₂ to the two protein therapeutics, G-CSF and EPO, in such a manner as to preserve the binding affinity of VB₁₂ for IF while preserving the biological activity of these two protein therapeutics.

MATERIALS AND METHODS

VB₁₂ was obtained from Rousell-Uclaf (Paris, France). G-CSF and EPO were obtained from Amgen Inc. Manufacturing. 1-Ethyl-3-[(dimethylamino)propyl]carbodiimide·HCl (EDAC·HCl) was obtained from Bio-Rad (Richmond, CA). Succinimidyl 3-(2-pyridyldithio)propionate (SPDP) and succinimidyl 6-[3-(2-pyridyldithio)propionamido]hexanoate (LC-SPDP) were obtained from Pierce Chemical Co. (Rockford, IL). All other reagents were obtained from Fluka (Buchs, Switzerland).

Synthesis of VB₁₂ Reagents and General Conjugation/Characterization Protocols. (A) Production

---

1a R = NH₂
1b R = OH
1c R = NH(CH₂)₂NH₂
1d R = NH(CH₂)₆NH₂
1e R = NH(CH₂)₁₂NH₂
1f R = NHCH₂CH(OH)CH₂NH₂
1g R = NH(CH₂)₂SS(CH₂)₂NH₂
1h R = NH(CH₂)₂NHCO(CH₂)₂SSPy
1i R = NH(CH₂)₆NHCO(CH₂)₂SSPy
1j R = NH(CH₂)₆NHCO(CH₂)₂SSPy
1k R = NH(CH₂)₆NHCO(CH₂)₆CONH(CH₂)₁₂NH₂
1l R = NH(CH₂)₆NHCO(CH₂)₆CONH(CH₂)₁₂NHCO(CH₂)₂SSPy
1m R = NHNH₂
1n R = NH(CH₂)₂SS(CH₂)₂NHCO(CH₂)₂NHNH₂
1o R = NHNHCO(CH₂)₄CONHNH₂

Figure 1.

and purification of the *e* isomer of monocarboxy-VB₁₂ (*e*VB₁₂). Native VB₁₂ (1a) (Figure 1) contains no suitable site for conjugation to either EPO or G-CSF. For conjugation, a carboxylic acid group can be introduced into the molecule by mild acid hydrolysis of one of the three propionimide side chains of the corrin ring. Following hydrolysis (0.4 M HCl, 72 h, RT), the *e* isomer of monocarboxy vitamin B₁₂ (1b) (*e*VB₁₂, *e* isomer; Anton and co-workers, 1980), was separated from the *b* and *d* isomers, also formed during acid hydrolysis, by a combination of Dowex AG 1−X2 (Bio-Rad) chromatography and semipreparative C-18 RP-HPLC (using a gradient of 5−100% acetonitrile in 0.1% TFA).

(B) Production of Amino Derivatives of *e*VB₁₂. Five amino derivatives of *e*VB₁₂ were prepared by reacting the *e* isomer with 1,2-diaminoethane, 1,6-diaminohexane, 1,12-diaminododecane, 1,3-diamino-2-hydroxypropane, and 1,6-diamino-3,4-dithiahexane (a.k.a. cystamine) to give amino VB₁₂ derivatives 1c, 1d, 1e, 1f, and 1g, respectively. All reactions were performed at pH 6.5 using a 20-fold molar excess of the diamine over *e* isomer and a 20-fold molar excess of EDAC. In a typical reaction 135 mg of *e*VB₁₂ was dissolved in distilled water (6 mL) to which was added 1.2 mL of 1.0 M diamine, pH 6.5. Dry EDAC (270 mg) was then added, and the reaction mixture was left overnight at room temperature. All amino derivatives were purified by reverse-phase chromatography on a semiparative C-4 column using a gradient of 5−100% acetonitrile in 0.1% TFA. Eluted material was further purified by S-Sepharose chromatography. Non-amino VB₁₂ derivatives were removed by washing the column with water, and the amino derivatives were subsequently eluted with 0.1 M HCl, followed by extraction into phenol, and back-extraction into water after the addition of dichloromethane to the phenol phase. The amino *e*VB₁₂ derivatives were then recovered from the water phase by lyophilization. The derivatives were

Scheme 1
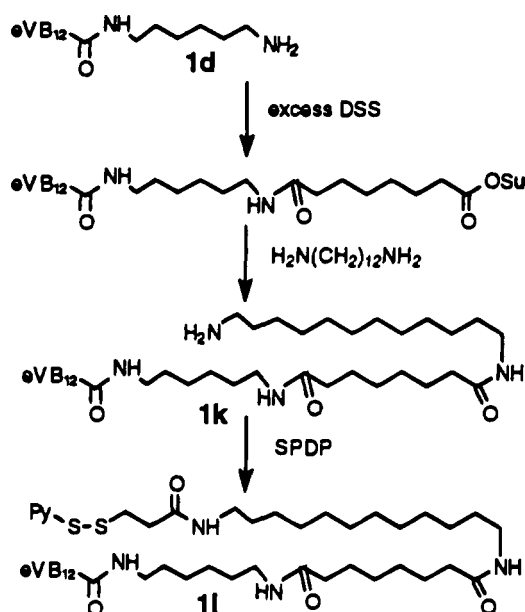
pure (>98%) by analytical RP-HPLC analysis. Ion spray MS characterization data: (1c) obsd M⁺ 1398, calcd M⁺ 1398; (1d) obsd M⁺ 1454, calcd M⁺ 1454; (1e) obsd M⁺ 1598, calcd M⁺ 1598; (1f) obsd M⁺ 1428, calcd M⁺ 1428; (1g) obsd M⁺ 1490, calcd M⁺ 1491.

(C) Preparation of 3-(2-Pyridyldithio)propionamido Derivatives of Amino-*e*VB₁₂. Three dithiopyridyl (DTP) amino-*e*VB₁₂ derivatives were prepared by reacting SPDP with 2-aminoethyl-*e*VB₁₂ (1c), 6-aminohexyl-*e*VB₁₂ (1d), and 12-aminododecyl-*e*VB₁₂ (1e) to give the respective derivatives (1h), (1i) and (1j). In a typical reaction the terminal amino-*e*VB₁₂ was dissolved at 50 mg/mL in 0.1 M PO₄ buffer, pH 7.5, containing 0.1 M NaCl. SPDP was dissolved at 50 mg/mL in acetone, and 800 μL of the solution was added to the amino-*e*VB₁₂. After reaction overnight at room temperature the DTP-amino-*e*VB₁₂ product was purified by RP-HPLC on a semiprep C-4 column and then lyophilized. Ionspray ms characterization data: (1h) obsd M⁺ 1595, calcd M⁺ 1596; (1i) obsd M⁺ 1652, calcd M⁺ 1652; (1j) obsd M⁺ 1736, calcd M⁺ 1736.

(D) Preparation of a Long-Chain Analogue of the DTP-aminododecyl-*e*VB₁₂ Reagent. This spacer was prepared from 6-aminohexyl-*e*VB₁₂ (1d) by sequential reaction with disuccinimidyl suberate (DSS) (to give [[(monosuccinimidyl)suberyl]hexyl]-*e*VB₁₂) and 1,12-diaminododecane to give [[(12-aminododecyl)suberyl]hexyl]-*e*VB₁₂ (1k). The resultant spacer, which is more than twice the length of 1e, was derivatized at the terminal amino group with SPDP, purified on RP-HPLC, and lyophilized to give derivative 1l. The synthesis is outlined in Scheme 1. Ionspray ms characterization data: (1k) obsd M⁺ 1793, calcd M⁺ 1793; (1l) obsd M⁺ 1990, calcd M⁺ 1990.

(E) Production of Hydrazide Derivatives of *e*VB₁₂ Carboxylate. Three hydrazide derivatives of *e*VB₁₂ carboxylate were prepared for conjugation to carboxyl groups of G-CSF by reaction with EDAC. The hydrazide derivatives used, and their (shorthand) chemical structures, were hydrazido-*e*VB₁₂ (*e*VB₁₂-CONHNH₂) (1m), Cys-hydrazido-*e*VB₁₂ (*e*VB₁₂-CONH(CH₂)₂SS-(CH₂)₂NHCO-(CH₂)₂CONHNH₂) (1n), and (adipyl hydrazido)-*e*VB₁₂ (*e*VB₁₂-CONHNHCO(CH₂)₄CONHNH₂) (1o). Hydrazido-*e*VB₁₂ (1m) was prepared by a two-step synthesis involving the coupling of *tert*-butyl carbazate to *e*VB₁₂ carbox-

Scheme 2
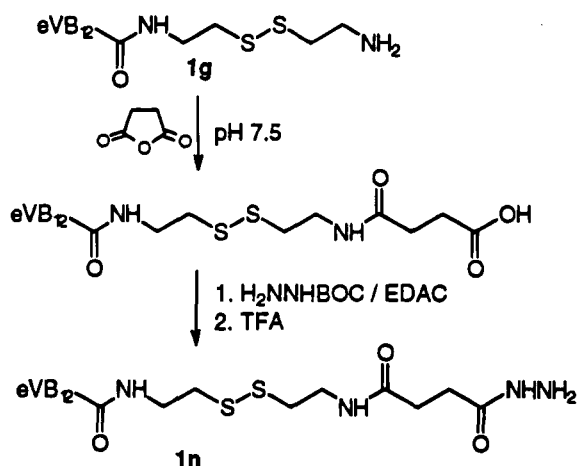
ylate and subsequent removal of the *t*-Boc group to generate the free hydrazide. Cys-hydrazido-*e*VB$_{12}$ was synthesized from *e*VB$_{12}$ cystamine (**1g**). The conversion of this material to *e*VB$_{12}$ Cys-hydrazide (**1n**) proceeded by succinylation of the *e*VB$_{12}$ cystamine and subsequent conversion of the resultant terminal carboxyl group to a hydrazide by the procedure outlined above for *e*VB12 hydrazide. This synthesis is outlined in Scheme 2. The (adipylhydrazido)-*e*VB$_{12}$ reagent (**1o**) was readily prepared in one step from *e*VB$_{12}$ carboxylate and a 20-fold excess of adipylhydrazide by the addition of EDAC. Ionspray MS characterization data: (**1m**) obsd M$^+$ 1370, calcd M$^+$ 1370; (**1n**) obsd M$^+$ 1604, calcd M$^+$ 1604; (**1o**) obsd M$^+$ 1512, calcd M$^+$ 1512.

(F) Determination of VB$_{12}$−Protein Substitution Ratios. The UV absorbance of an aqueous conjugate solution was measured at 361 and 278 nm. Absorbance at 361 nm is only due to VB$_{12}$. The concentration of cobalamin in solution was calculated from the literature value for its 361-nm absorbance, assuming that the cobalamin conjugated to protein has the same absorbance as native VB$_{12}$. Protein concentrations were subsequently calculated from the 278-nm absorption after subtraction of the contribution to the 278-nm absorption due to cobalamin. Amino acid analysis of all VB$_{12}$ conjugates was performed on an Applied Biosystems amino acid analyzer. Protein concentrations measured from UV absorbance agreed (±10%) with the concentrations determined by amino acid analysis.

(G) Analysis of VB$_{12}$ Conjugates via SDS−PAGE and Western Blotting. Both EPO and G-CSF conjugates were analyzed by SDS−PAGE according to the method of Laemmli (1970) using 12.5% and 17−20% SDS−PAGE minigels, respectively (ISS Daiichi minigels). A method was developed at Amgen for the detection of VB$_{12}$ in western blots using a modification of the method of Russell-Jones and co-workers (Russell-Jones & Gotschlich, 1984; Blake et al., 1984). Briefly, proteins were transferred from gels to Millipore Immobilon-P membranes (Millipore, Bedford, MA). After blocking with 10% goat serum in PBS, the VB$_{12}$-containing bands were developed using a primary monoclonal antibody of mouse anti-VB$_{12}$ (Sigma, St. Louis, MO), followed by a goat anti-mouse biotinylated second antibody (Sigma). An Extravidin alkaline phosphatase conjugate (Sigma) was then added, after which the VB$_{12}$-containing bands were visualized using 5-bromo-4-chloroindolyl phospate and nitroblue tetrazolium.

Formation of VB$_{12}$−G-CSF Complexes: General Protocol for Purification of [VB$_{12}$−G-CSF] conjugates. [VB$_{12}$−G-CSF] conjugates were separated from

unreacted VB$_{12}$ and other reagents by size-exclusion chromatography on Sephadex G-50 in 2.5% acetic acid. Fractions containing [VB$_{12}$−G-CSF] were pooled, concentrated by membrane filtration (Amicon YM10 membrane), and dialyzed (4 °C) for at least 20 h against sterile distilled water. Aliquots were removed for amino acid analysis, IF assay, and spectroscopic and HPLC analysis. The structures of the various conjugates are shown in Table 1.

Synthesis of disulfide-linked G-CSF conjugates. (A) Conjugation of DTP-amino-*e*VB$_{12}$ Derivatives to G-CSF. In preliminary experiments with G-CSF it was found that it was not possible to modify the free cysteine (Cys-17) in G-CSF with standard thiol-modifying agents. Initial experiments with DTP-ethyl-*e*VB$_{12}$, however, showed that it was possible to achieve some 20% substitution of G-CSF with the VB$_{12}$ in the absence of guanidine and that this level rose to >80% in the presence of 4 M guanidine. It was therefore decided that it might be possible to access the free thiol with DTP-amino-*e*VB$_{12}$ in the absence of guanidine if a longer spacer was used for the conjugation. In a second series of experiments G-CSF was reacted with DTP-aminoethyl-, DTP-aminohexyl- and DTP-aminododecyl-*e*VB$_{12}$ in the presence or absence of 4 M guanidine in 0.1 M sodium acetate buffer, pH 4.0. The degree of substitution of G-CSF by various DTP-amino-*e*VB$_{12}$ analogues is shown in Table 3. As it was possible to conjugate to G-CSF using DTP-dodecyl-*e*VB$_{12}$ in the absence of guanidine, the reaction was scaled up as follows: To 2.5 mL of G-CSF (6 mg/mL; 15 mg) was added 1.6 mL of DTP-dodecyl-*e*VB$_{12}$ (10 mg/mL in 2.5% acetic acid). The reaction was allowed to proceed for 48 h at 4 °C, after which the unreacted VB$_{12}$ was separated from the conjugate by the standard purification protocol. The resultant conjugate, GBC-1, was stored at 4 °C prior to analysis in bioactivity studies.

Another disulfide-linked *e*VB$_{12}$−G-CSF conjugate containing a long-chain hydrocarbon spacer (Table 1) between VB$_{12}$ and G-CSF was formed by the reaction of G-CSF with DTP-[(12-dodecylsuberyl)hexyl]-*e*VB$_{12}$ (prepared as described above) using the method described. The resultant conjugate, LC-GBC1, was purified in the usual fashion.

(B) Synthesis of Amide-Linked G-CSF Conjugates. In order to prepare conjugates between amino-*e*VB$_{12}$ derivatives and G-CSF, it was necessary to perform the conjugation reaction at an acid pH, as G-CSF was found to aggregate quickly as the pH of the reaction mixture was raised above pH 7.0. Two amide-linked VB$_{12}$−G-CSF conjugates were prepared: GBC-2, by reaction of cystaminyl-*e*VB$_{12}$ with G-CSF; and GBC-3, by reaction of 3-amino-2-hydroxypropyl-*e*VB$_{12}$ with G-CSF. Typically a solution of amino-*e*VB12 (26.5 mg, 18 μmol) in 2 mL of G-CSF (6 mg/mL, 0.63 μmol) was cooled to 4 °C. An aliquot of freshly prepared EDAC solution (100 mg/mL, 120 μl, 63 μmol) was added. After 24 h at 4 °C a second aliquot of freshly prepared EDAC solution was added. The reaction was allowed to proceed for a total of 48 h at 4 °C, after which the unconjugated amino-*e*VB$_{12}$ derivative was separated from the conjugate and aggregate by chromatography on Sephadex G50 in 2.5% acetic acid.

(C) Synthesis of Acyl Hydrazide-Linked G-CSF Conjugates. In order to reduce the level of aggregation of the G-CSF found when amino-*e*VB$_{12}$ derivatives were coupled to G-CSF using EDAC, it was decided to use the more reactive hydrazidyl derivatives of VB$_{12}$, which would enable the reaction to be carried out at a lower pH and with lower quantities of the carbodiimide. Three VB$_{12}$−hydrazido-G-CSF conjugates were synthesized:

Table 1. Structures of VB₁₂-G-CSF and VB₁₂—EPO Conjugates

GBC-4, by reaction of hydrazido-VB₁₂ with G-CSF; GBC-5, by reaction of (cystaminylhydrazido)-VB₁₂ with G-CSF; and GBC-6, by reaction of (adipylhydrazido)-eVB₁₂ with G-CSF.

In a typical synthesis a solution of the VB₁₂ hydrazide (10 mg) in 4 mL of G-CSF solution (4 mg/mL, 0.84 μmol) was cooled to 4 °C and an aliquot of EDAC solution (50 mg/mL, 40 mL, 10 μmol) was added. After 5 h an identical aliquot of fresh EDAC solution was added, and the reaction mixture was left overnight at 4 °C. Conjugate was removed from unreacted VB₁₂ and other reagents by chromatography on Sephadex G-50 in 2.5% acetic acid.

Preparation of VB₁₂—EPO Complexes. VB₁₂—EPO complexes were prepared by conjugation via an amide linkage, formed by EDAC-mediated coupling of an amino-eVB₁₂ derivative to carboxyl groups on EPO such as the C-terminus of EPO, the carboxylate side chains of the Asp/Glu residues, or the sialic acid residues of the carbohydrate portion of EPO. Second, conjugates were formed via an acyl hydrazide linkage, between hydrazido-eVB₁₂ and the carboxylate side chains of the Asp/Glu residues of EPO or the carboxylate groups of the sialic acid residues of the carbohydrate portion of EPO. Finally an attempt was made to form a hydrazone linkage between a hydrazido-eVB₁₂ derivative and an aldehyde group generated by periodate oxidation of the carbohydrate residues of EPO.

(A) Synthesis of Amide-Linked VB₁₂—EPO Conjugates. Two amide-linked conjugates between amino-eVB₁₂ were formed: EBC-1, by reaction of 2-aminoethyl-

VB₁₂ with EPO; and EBC-2, by reaction of (6-amino-dithiahexyl)-eVB₁₂ with EPO. In a typical reaction, a mixture of amino-eVB₁₂ (8 mg, 5.7 μmol) and EPO (27 mg/mL, 200 μL, 0.18 μmol) was cooled to 4 °C and an aliquot of EDAC solution (10 mg/mL, 100 μL, 5 μmol) was added. The reaction mixture was left for 64 h at 4 °C and finally purified by size-exclusion chromatography on a Superdex-75 column. Elution with a buffer consisting of Tris (pH 7.5, 10 mM)/NaCl (100 mM) afforded the purified VB₁₂—EPO complex.

(B) EDAC-Mediated Conjugation of eVB₁₂-hydrazides to EPO. Two VB₁₂ -hydrazido—EPO conjugates were synthesized; EBC-3 by reaction of hydrazido-eVB₁₂ with EPO; and EBC-4, by reaction of (adipyl-hydrazido)-eVB₁₂ with EPO. Briefly, a solution of the eVB₁₂ hydrazide (10 mg, 7.3 μmol) in 7 mL of EPO solution (2.6 mg/mL, 0.6 μmol) was cooled to 4 °C and an aliquot of EDAC solution (20 mg/mL, 50 μL, 5 μmol) was added. After 5 h a second aliquot of fresh EDAC solution (10 mg/mL, 25 μL, 1.3 μmol) was added, and the reaction mixture was left overnight at 4 °C. The conjugate was purified by size-exclusion chromatography on a Sephadex G50 column. Elution with a buffer consisting of Tris (pH 7.5, 10 mM)/NaCl (100 mM) afforded the purified EPO—VB₁₂ complex.

RESULTS AND DISCUSSION

The most desirable linkage between VB₁₂ and G-CSF would be a linkage that could be cleaved in serum to produce native G-CSF once it had been transported from the intestine into the circulation. Such a linkage could

Table 2. Structures of EPO Conjugates

Conjugate Name	SPACER
EBC-1	
EBC2	
EBC3	
EBC4	

Table 3. Substitution of G-CSF with DTP-eVB$_{12}$ Derivatives[a]

spacer	−guanidine (%)	+guanidine (%)
DTP-aminoethyl	37.5	89.3
DTP-aminohexyl	45.5	95.2
DTP-aminododecyl	100.0	100.0

[a] G-CSF was reacted with DTP-aminoethyl-, DTP-aminohexyl- and DTP-dodecyl-eVB$_{12}$ in the presence or absence of 4 M guanidine in 0.1 M sodium acetate buffer, pH 4.0. After 24 h the degree of substitution of G-CSF by various DTP-amino-eVB$_{12}$ analogues was determined following RP-HPLC of the conjugates.

Table 4. IF Affinity and VB$_{12}$-Substution of VB$_{12}$-G-CSF Conjugates

conjugate	VB$_{12}$:G-CSF ratio	IF affinity (%)	*In vitro* bioactivity[a] (%)	*in vivo* bioactivity[b] (%)
GBC-1	0.97:1	2.6	11.2	61
LC-GBC-1	1:1	23	8.5	66
GBC-2	0.8:1	2.8	31	85
GBC-3	0.8:1	ND[c]	ND	29
GBC-4	3.4:1	4	18	85
GBC-5	ND	15	78	100
GBC-6	1.6:1	4	24	ND

[a] The *in vitro* bioactivity was assessed using the stimulation of mitogenesis, as assayed by the incorporation of [³H]thymidine into primary cell cultures of mouse bone marrow cells (Jensen-Pippo, 1995). [b] The *in vivo* bioactivity of the VB$_{12}$−G-CSF conjugates was assessed in Syrian hamsters. Briefly, vehicle and two doses of G-CSF or VB$_{12}$−G-CSF conjugate (20 and 100 µg/kg) were administered as single s.c. injections. Blood samples were take at 12, 24, 48, and 72 h, and the total white blood cell count was determined at each point. The percent activity of the conjugates was calculated from the 48-h median area under the curve analysis. The affinity of IF for the various [VB$_{12}$−protein] conjugates compared to the affinity of IF for VB$_{12}$ was determined in a competitive binding assay. Dilutions of the conjugate were mixed with 1 ng of ⁵⁷Co VB$_{12}$ (Amersham). One IU of IF was then added and the mixture was incubated for 20 min. at room temperature before the addition of a suspension of 5% activated charcoal in 0.1% BSA (IF and VB$_{12}$-free, Sigma). Samples were centrifugated and the relative number of counts in the supernatant (IF bound) and pellet (free ⁵⁷Co-VB$_{12}$) were used to determine the relative affinity of the material tested for IF. [c] ND Not determined.

be achieved by the formation of a disulfide bond with the free (but buried) thiol of Cys-17 in G-CSF. The disulfide bond would potentially be cleaved in serum to regenerate the native G-CSF and free thiolated VB$_{12}$ through the reducing action of serum glutathione. Initial attempts to modify the Cys-17 thiol using standard thiol-modifying agents such as Ellman's reagent proved unsuccessful. Subsequent experiments, using various DTP derivatives of VB$_{12}$ in the presence or absence of guanidine, showed that it was in fact possible to achieve significant levels of modification of this thiol even in the absence of guanidine when a suitably long hydrophobic spacer was attached to the VB$_{12}$ (Table 3). It can be seen that the initial attempts to conjugate to the free thiol group in G-CSF using the DTP-aminoethyl derivative of eVB$_{12}$ resulted in a small degree of conjugation, around 20−40% in the absence of guanidine. The addition of 4 M guanidine (final concentration) raised the conjugation efficiency to over 80% (Table 3). Preparation of a longer, more hydrophobic derivative of VB$_{12}$, DTP-dodecyl-eVB$_{12}$, resulted in 100% substitution of G-CSF after 24 h at 4 °C, without the need for the addition of guanidine. The use of the thiol interchange chemistry in this reaction proved advantageous, as the VB$_{12}$ conjugation was surprisingly successful at the pHs required to minimize the extent to which G-CSF undergoes spontaneous aggregation. The recent publication of Arakawa and co-workers (1993) has subsequently shown that Cys-17 is partially solvent-exposed and shows differential reactivity with sulfhydryl-modifying reagents. One of the most elegant aspects of this chemistry was the observation that the thiol insertion reaction which was required to form the disulfide-linked conjugate between G-CSF and VB$_{12}$ (to form GBC-1) could be performed at high efficiencies at

very low pH (pH 2−3) thereby enabling the G-CSF to remain fully soluble during conjugation and workup. The resultant conjugate (GBC-1) had good *in vivo* bioactivity but low IF binding ability (2−3% of native) (Table 4). The loss in IF affinity of the VB$_{12}$−G-CSF conjugate was presumably due to the close proximity of the VB$_{12}$ molecule to G-CSF, thus sterically interfering with the ability of IF to bind to VB$_{12}$ (Table 4). In order to increase the IF affinity of the disulfide-linked conjugate, a conjugate with increased IF affinity was prepared by synthesizing a longer chain analogue of the DTP-(dodecyl-amino)-eVB$_{12}$. The synthesis of this analogue, LC-GBC 1, used the same SPDP chemistry to conjugate through the cysteine of G-CSF; however a longer spacer arm was attached to the VB$_{12}$. By increasing the length of the cross-linker still further, another thiol-linked conjugate,

Table 5. IF Affinity and VB$_{12}$ Substution of VB$_{12}$–EPO Conjugates

conjugate	VB$_{12:ECSF}$ ratio	IF affinity (%)	*in vivo* bioactivity[a] (%)
EBC-1	1.14:1	3.2	3.4
EBC-2	0.7:1	ND[b]	ND
EBC-3	1.6:1	5.9	22
EBC-4	1.8:1	11.4	17

[a] The *in vivo* bioactivity of the VB$_{12}$–EPO conjugates was assessed in the exhypoxic polycythemic mouse model of Cotes and Bangham (1961). Briefly, female BDF1 mice were maintained under hypobaric conditions of 0.4 atm for 18–24 h/day for a total of 14 days. Following the hypobaric exposure the mice were brought up ro ambient pressure for 72 h prior to testing with the VB$_{12}$–EPO conjugates. EPO or VB$_{12}$–EPO conjugates were injected i.p. at 0 and 24 h. At 48 h the mice were injected via the tail vein with 200 μL of 0.9% NaCl, 0.3% trisodium citrate, and 0.5–1.0 μCi of ^{59}FeCl$_3$. After a further 48 h the mice were sacrificed with CO_2 and weighed. Blood was collected to determine haematocrit volume and percent incorporation of ^{59}FeCl$_3$ into erythrocytes. [b] ND, not determined.

LC-GBC1, was formed which showed a 10-fold increase in IF affinity (Table 4). Thus, increasing the length of the spacer joining the VB$_{12}$ to the G-CSF from 6.8 to 15.6 Å produced a conjugate in which the *in vivo* bioactivity (65%) of the G-CSF was preserved, but with a higher affinity for IF (23%) (*e*VB$_{12}$, 25%) than GBC-1 (2.3%). The functional group most commonly used for formation of protein–protein conjugates is the amino group. Studies at Amgen (unpublished observations) had previously shown that modification of amino groups on G-CSF quickly leads to inactivation of the molecule. Thus, cross-linking with traditional amino-reactive spacer molecules was not attempted. Initially amide-linked conjugates were prepared between G-CSF and VB$_{12}$ by activating carboxyl groups on G-CSF using the carbodiimide, EDAC, and reacting the activated ester with cystamido- and [(hydroxypropyl)amido]-*e*VB$_{12}$ derivatives. The two conjugates so formed (GBC-2 and GBC-3, respectively) showed variable *in vivo* bioactivity (85 and 29.5%, respectively); however, the yields of the conjugates were low due to unacceptably high levels of aggregation of the G-CSF during the conjugation. Conjugates were therefore prepared using hydrazido-*e*VB$_{12}$ derivatives. Three conjugates were prepared between G-CSF and hydrazido-*e*VB$_{12}$ derivatives. EDAC-mediated coupling of hydrazido-*e*VB$_{12}$ analogues to the carboxylate side-chains of G-CSF proceeded more readily, and required significantly lower amounts of VB$_{12}$ derivative and EDAC, than conjugations of the corresponding amino VB$_{12}$ derivatives to G-CSF. This is readily explainable in terms of the relative basicity of hydrazides (pK_a ~ 2.6) in comparison with amines (pK_a ~ 8–9). Thus at the pH at which the G-CSF coupling takes place (~4–5) a hydrazido VB$_{12}$ derivative would be primarily in the reactive, non-protonated form, while an amino VB$_{12}$ derivative will be primarily in the nonreactive, protonated form. The hydrazido derivatives (GBC-4, hydrazido-; GBC-5, Cys-hydrazido and GBC-6; adipyl-hydrazido-) proved to be much more reactive at the low pHs required for the maintenance of G-CSF solubility; therefore much less EDAC could be used during conjugate formation, thereby reducing the level of dimer and trimer formation during conjugation. GBC-4 and GBC-5 were both found to have good *in vivo* bioactivity with moderate affinity for intrinsic factor (4% and 15% respectively; Table 3). The slight increase in spacer length from GBC-4 to GBC-6 did not result in any significant improvement in IF affinity (4%), although it did increase the *in vitro* bioactivity of the conjugate slightly (from 18% to 24%; not significant in this assay). GBC-1, GBC-2, and GBC-4 were incubated with IF and

tested in transport studies in CaCo-2 cell cultures. All three were transported in an IF-dependent fashion. Several of the VB$_{12}$–G-CSF conjugates, namely, GBC-1, LC-GBC-1, and GBC-4, were also tested in rat duodenal uptake studies and found to be actively transported from the duodenum to the circulation. (Habberfield et al., 1995). Two classes of VB$_{12}$–EPO conjugates were prepared by the reaction of the carbodiimide, EDAC, with the carboxyl groups of the C-terminus of EPO, the Asp/Glu residues, or the sialic acid residues of the carbohydrate portion of EPO. Two amide-linked conjugates, EBC-1 and EBC-2 were prepared using 2-aminoethyl-*e*VB$_{12}$ and (6-amino-3,4-dithiahexyl)-*e*VB$_{12}$, respectively. The use of the amino derivatives during this conjugation strategy required high levels of EDAC for efficient conjugation and thus resulted in considerable dimer formation. Although the mono and di forms of EBC-1 and EBC-2 were separable by SEC, it was decided to prepare similar conjugates using hydrazido derivatives of VB$_{12}$ rather than the amine derivatives. Two conjugates, EBC-3 and EBC-4, were prepared using hydrazido and adipylhydrazido derivatives of VB$_{12}$. Conjugates formed in this fashion were vastly superior to those formed with the amino derivatives of VB$_{12}$, as they had low levels of dimer formation and good bioactivity in the hypoxic mouse model and maintained good IF binding activity (Table 4). EBC-4 has subsequently been found to be actively transported into serum following intraduodenal infusion in rats (Habberfield et al., 1995). Deglyocosylation of the VB$_{12}$–EPO conjugates showed that in all cases the VB$_{12}$ was linked to Asp/Glu residues and not to the sialic acid groups.

SUMMARY

For the successful formation of bioconjugates between two molecules of disparate functional activities, care must be taken to maintain the bioactivities of each of the molecules within the complex. Procedures are described for the formation of stable conjugates between VB$_{12}$ either and G-CSF or EPO which have the potential to be taken up from the intestine following oral administration by the normal VB$_{12}$-uptake mechanism. Through the choice of appropriate chemistries and spacers it was found that it was possible to form conjugates which maintained significant affinity for intrinsic factor, while maintaining substantial bioactivity of G-CSF and EPO when tested *in vivo*. Successful conjugation was achieved between VB$_{12}$ and a buried thiol within G-CSF. The linkage so formed had the potential to regenerate the intact, unaltered protein in serum. Other studies have shown that several of the conjugates were transported in an intrinsic factor dependent fashion across CaCo-2 cells, and also from the intestine to the circulation in rats in a biologically active form. EPO and G-CSF which were not conjugated to VB$_{12}$ were not transported in these systems.

LITERATURE CITED

Anton, D. L., Hogenkamp, H. P. C., Walker, T. E., and Matwiyoff, N. A. (1980) Carbon-13 nuclear magnetic studies of the

monocarboxylic acids of cyanocobalamin. Assignments of the b-, d-, and e-Monocarboxylic acids. *J. Am. Chem. Soc. 102*, 2215−2219.

Arakawa, T., Prestrelski, S. J., Narhi, L. O., Boone, T. C., and Kenney, W. C. (1993) Cysteine 17 of recombinant human granulocyte-colony stimulating factor is partially solvent exposed. *J. Protein Chem. 12*, 525−531.

Blake, M. S., Johnston, K. H., Russell-Jones, G. J., and Gotschlich, E. C. (1984) A rapid, sensitive method for the detection of alkaline phophatase conjugated anti-antibodies on Western blots. *Anal. Biochem., 136*, 175−179.

Bronchud, M. H., Scarffe, J. H., Thatche, N., Crowther, D., Souza, L. M., Alton, N. K., Testa, N. G., and Dexter, T. M. (1987) Phase I/II study of recombinant human granulocyte colony-stimulating factor in patients receiving intensive chemotherapy for small cell lung cancer. *Br. J. Cancer 56*, 806−813.

Cotes and Bangham (1961) Bio-assay of erythropoietin in mice made polycythaemic by exposure to air at a reduced pressure. *Nature 191*, 1065−1067.

Gallagher, and K. Foley (1971) Intrinsic factor-independent transport of vitamin B₁₂ across the gut of the neonatal rat. *Gastroenterology 61*, 332−338.

Golde, D. W., & Gasson, J. C. (1988) Hormones that stimulate the growth of blood cells. *Sci. Am.*, 34−42.

Habberfield, A., K. Jensen-Pippo, L. Ralph, S. W. Westwood, and G. Russell-Jones (1995) Vitamin B12-mediated uptake of recombinant therapeutic proteins from the gut. *Nature* (submitted).

Jensen-Pippo, K. E., K. L. Whitcomb, R. B. DePrince, L. Ralph, and A. D. Habberfield (1995) Enteral Bioavailability of Human Granulocyte Colony Stimulating Factor Conjugated to Poly(ethylene glycol). *Pharm. Res.* (submitted).

Krantz, S. B., and E. Goldwasser (1984) Specific binding of erythropoietin to spleen cells infected with the anemia strain of Friend virus. *Proc. Natl. Acad. Sci. U.S.A. 81*, 7574−7584.

Laemmli, U. K. (1970) Cleavage of structural proteins during the assembly of the head of bacteriophage T4. *Nature (London), 227*, 680−685.

Morstyn, G. and A. W. Burgess (1988) Hemopoietic growth factors: A review. *Cancer Res. 48*, 5624−5637.

Roberton, J. A., and N. D. Gallagher. (1985) In vivo evidence that cobalamin is absorbed by receptor-mediated endocytosis in the mouse. *Gastroenterol., 88*, 908−912.

Russell-Jones, G. J. (1994) Oral delivery of Therapeutic Proteins and peptides by the vitamin B12 uptake system. in *Peptide-based Drug Design: Controlling Transport and Metabolism* (Taylor, M., and Amidon, G., Eds.) pp 182−198, ACS Publications, Washington, DC.

Russell-Jones, G. J., and E. C. Gotschlich (1984) Identification of protein antigens of group B streptococci, with special reference to the Ibc antigens. *J. Exp. Med. 160*, 1476−1484.

Russell-Jones, G. J. and H. J. de Aizpurua (1988) Vitamin B12: A novel carrier for orally presented antigens. *Proc. Int. Symp. Control. Rel. Bioact. Mater. 15*, 142−143.

Russell-Jones, G. J., S. W. Westwood, P. G. Farnworth, J. K. Findlay, and H. G. Burger (1995) Synthesis of LHRH antagonists suitable for oral administration via the vitamin B₁₂ uptake system. *Bioconj. Chem. 6*, 34−42.

Simpson, K. W., D. H. Alpers, J. de Wilde, P. Swanson, S. Farmer, and R. G. Sherding (1993) Cellular localization and hormonal regulation of pancreatic intrinsic factor secretion in the dog. *Am. J. Physiol. 265*, G179-G188.

Tsai, C. M., and Frasch, C. E., (1982) A sensitive silver stain for detecting lipopolysaccharide in polyacrylamide gels. *Anal. Biochem. 119*, 115−119.

Vaillant, C., Horadagoda, N. U., and Batt, R. M. (1990) Cellular localization of intrinsic factor in pancreas and stomach of the dog. *Cell Tissue Res. 260*, 117−122.

Preparation and Nuclease Activity of Hybrid "Metallotris(methylpyridinium)porphyrin Oligonucleotide" Molecules Having a 3'-Loop for Protection against 3'-Exonucleases

Béatrice Mestre, Geneviève Pratviel, and Bernard Meunier*

Laboratoire de Chimie de Coordination du CNRS, 205 route de Narbonne, 31077 Toulouse Cedex, France. Received November 22, 1994[⊛]

A 5'-GCGAAAGC minihairpin structure was added to the 3'-end of an oligonucleotide substituted at the 5'-end by a manganese cationic porphyrin in order to enhance the 3'-exonuclease resistance of these cleaver-antisense molecules. The influence of this minihairpin on the 3'-exonuclease resistance, the binding affinity to a target ssDNA, and the cleaving efficiency of Mn-cationic porphyrin oligonucleotide conjugates was compared to that of the parent molecule without the 3'-hairpin. The results showed that the 3'-hairpin slightly decreased the binding affinity and consequently the cleaving efficiency of the conjugated molecule toward a target sequence, but the much higher nuclease resistance makes 3'-minihairpin-protected metalloporphyrin oligonucleotides good candidates as reactive antisense oligonucleotides for studies on cells.

INTRODUCTION

The inhibition of gene expression by modified oligonucleotides is currently a possible approach in the chemotherapy of cancers or viral diseases (1−6). One way to enhance the antisense activity of an oligonucleotide is to mediate irreversible damage on its target nucleic acid (RNA or DNA) sequence. Different transition metal complexes have been used as oxidative DNA and RNA cleavers and linked to oligonucleotide vectors: Fe-EDTA[1] (7, 8), Cu-oP (4), and metalloporphyrins (9−12). A hybrid "nucleic acid cleaver-oligonucleotide" suitable for possible development as a therapeutic agent must be able to cleave DNA or RNA with a high chemical yield (8), inside of selected cells (for recent articles on different methods to improve cell penetration by modified oligonucleotides, see 13−15).

We focused our attention on cationic manganese porphyrin complexes as nucleic acid cleavers to be linked to oligonucleotides for the following reasons: (i) cationic metalloporphyrins have an affinity for dsDNA ranging from 10^4 to 10^6 M^{-1} (16, 17), (ii) the parent manganese-(III) meso-tetrakis(4-N-methylpyridiniumyl)porphyrin, Mn-TMPyP, is a very efficient DNA cleaver able to hydroxylate carbon−hydrogen bonds of deoxyriboses accessible from the minor groove of B DNA (18, 19); (iii) these cationic metalloporphyrins provided good bleomycin models when attached to an intercalating agent (20, 21), and these latter hybrid molecules also have an anti-HIV activity (22); and (iv) the tris(4-N-methylpyridiniumyl)-porphyrinatomanganese(III) motif (Mn-trisMPyP) is able

to cleave DNA and RNA of HIV-1 at low concentrations (5−100 nM) (11, 12, 23) when tethered to the 5'-end of a 19-mer oligonucleotide complementary to the initiation region of tat. For in vitro experiments, the metalloporphyrin moiety is activated by potassium monopersulfate, KHSO₅, a water-soluble peroxide able to generate metal-oxo species in water solutions (24). We expect the in vivo activation mode of these DNA cleavers to be similar to that of bleomycin; i.e., molecular oxygen and a reducing agent will be used inside of cells (25). So we intend to address the DNA/RNA cleaving activity of the cationic metalloporphyrin moiety (Mn-trisMPyP) for a selected RNA/DNA sequence in vivo by the means of its covalent attachment to an antisense oligonucleotide. The Mn−porphyrin cleaver is here positioned at the 5'-end of the oligonucleotide.

The metabolic stability of oligonucleotides is low due to the action of nucleases (mainly 3'-exonucleases) in extracellular fluids and intracellular compartments. Chemical modifications of oligonucleotides have been described to improve their stability (1−6), but the sugar−phosphate backbone chemical modification did not always improve the antisense activity, and little is known about the toxicity and the mutagenicity of the metabolites arising from oligomer analogues.

One simple way to make an oligonucleotide resistant to 3'-exonucleases without any associated chemistry is to add at the 3'-end of the antisense a defined short sequence in order to form a remarkable stable minihairpin structure (26−29) (see Chart 1).

In the present work we compared the DNA cleavage efficiency of Mn-trisMPyP−oligonucleotide that carried a highly stable minihairpin at the 3'-end of the oligonucleotide vector (Chart 1, conjugate 2) with the "3'-unprotected" corresponding antisense (Chart 1, conjugate 1). We prepared the Mn-trisMPyP conjugates with some modifications of published procedures (12, 30). The two antisense oligonucleotides shared the same 19-mer sequence. The 19-mer sequence is complementary to the initiation codon of the tat gene of HIV-1. The longer 27-mer is 3'-protected by a previously described stable minihairpin structure (26, 27) consisting of eight nucleotides added on its 3'-end (5'-GCGAAAGC). The DNA cleavage activity was assayed on a ss-35-mer oligonucleo-

Chart 1. Structures of Mn-trisMPyP-19mer (1) and Mn-trisMPyP-27mer (2)[a]

Conjugate **1**, Mn-trisMPyP-19-mer oligonucleotide = GGCTCCATTTCTTGCTCTC-$\overset{3'}{OH}$

Conjugate **2**, Mn-trisMPyP-27-mer oligonucleotide = GGCTCCATTTCTTGCTCTCGCG$_A$

35-mer target = 3'-HO-ATCCTAGATGACCGAGGTAAAGAACGAGAGGAGAC-OH

[a] The manganese(III) axial ligand is a water at pH < 7 and a hydroxyl at basic pH values on one side and a water molecule on the other side.

tide corresponding to nucleotides 5360–5394 of the HIV-1 genome (*11, 31*).

We found that the 3'-minihairpin-protected oligonucleotide (27-mer) was stable toward 3'-exonucleases. The cleavage efficiency of the 3'-looped conjugate was slightly below that of the standard 19-mer conjugate, probably because of a lower affinity for the target.

EXPERIMENTAL PROCEDURES

Synthesis, Purification, and Labeling of Oligonucleotides. The oligonucleotides were synthetized by standard solid-phase β-cyanoethyl phosphoramidite chemistry on a Cyclone Plus DNA synthesizer from Milligen/Biosearch. Functionalization at the 5'-end of both 5'-OH-19-mer and −27-mer oligonucleotides by 1,6-hexanediamine was performed as previously described (*32*). Hexanediamine 5'-substituted oligonucleotides are referred to as 5'-NH₂-19(or 27)-mer.

The oligonucleotides were purified either on 20% polyacrylamide denaturing gels, in the case of the 35-mer target, or by HPLC using a reverse-phase C18 column (Nucleosil C18, 10 μm from Interchrom; eluents, A = 0.1 M TEAA (pH 6.5), B = CH₃CN; linear gradient, 10 to 30% B over 45 min; flow rate, 1 mL/min; λ = 260 nm), in the case of 5'-OH-19(or 27)-mer or 5'-NH₂-19(or 27)-mer oligonucleotides. The 5'-end of the 35-mer was labeled by ³²P using a standard procedure with T₄ polynucleotide kinase and [γ-³²P]ATP purchased from Biolabs and Dupont, respectively. Concentrations of single-stranded oligonucleotides were determined at 260 nm (*33*).

Synthesis of the Manganese(III) Tris(methylpyridiniumyl)porphyrin Conjugates Mn-trisMPyP-19mer (1) and Mn-trisMPyP-27mer (2). To 60 μL of a 5 mM solution of manganese(III) tris(methylpyridiniumyl)porphyrin precursor (0.3 μmol) (Y = OH; see Chart 1 for structure and references 12 and 29 for preparation) in dry DMF (DMF was dried over BaO, distilled, and kept

over 4-Å molecular sieves) was added 10 μL of a 370 mM solution of CDI (3.7 μmol) in dry DMF. Formation of the imidazolide derivative was allowed to take place over 90 min at room temperature. Then 10 μL of a 350 mM HOAt solution (3.5 μmol) in dry DMF was added. After 1 h at room temperature the excess CDI was hydrolyzed by addition of 62.5 μL of 20 mM MOPS buffer (pH 7.5). After 15 min, the solution of the activated ester was added to the 5'-NH₂-oligonucleotide (62.5 nmol, *i.e.*, 10 OD₂₆₀ units of 5'-NH₂-19-mer or 14.5 OD₂₆₀ units of 5'-NH₂-27-mer) in 62.5 μL of 20 mM MOPS buffer (pH 7.5). The solution was incubated at 37 °C for 2 h. Five hundred microliters of methanol was added, and the medium was centrifuged. After removal of the supernatant, the pellet was washed with methanol (2 × 500 μL). The crude product was dissolved in 500 μL of 200 mM HEPES buffer (pH 8) and purified by HPLC using an anion-exchange column (Protein Pak DEAE 8 HR from Waters; A = 25 mM Tris/HCl (pH 8.5), B = A + 1 M NaCl; linear gradient, 20 to 50% B over 45 min; flow rate, 0.7 mL/min. HPLC profiles were monitored by a two-channel diode array detector 440 from Kontron). The conjugate was desalted on a column of Bio-Gel P-2(F) from Bio-Rad equilibrated with water. Yields (measured by UV absorbance at 260 nm) after purification and desalting were approximatively 30% for the two hybrid molecules with respect to the 5'-NH₂-oligonucleotides (this yield include the coupling reaction itself and the purification steps).

Spectrophotometric data of oligonucleotides and conjugates were as follows: (i) Oligonucleotides, ϵ_{260} (5'-OH or (5'-NH₂)-19-mer) = 16 × 10⁴ M⁻¹ cm⁻¹, ϵ_{260} (5'-OH or (5'-NH₂)-27-mer) = 23 × 10⁴ M⁻¹ cm⁻¹. (ii) Manganese(III) tris(methylpyridiniumyl)porphyrin (Y = OH), ϵ_{468} = 10 × 10⁴ M⁻¹ cm⁻¹. (iii) Hybrid molecules, observed visible/UV ratios monitored by the diode-array detector spectra of the conjugate peak: A_{468}/A_{260} for **1** = 0.65, A_{468}/A_{260} for **2** = 0.32. The HPLC retention times were 19.7 and 25.6 min for **1** and **2**, respectively, compared to 21

and 28 min for the corresponding 5′-NH₂-oligonucleotides. Concentrations of conjugate solutions were determined by using UV–vis data at 260 nm as for single-stranded oligonucleotides.

Resistance to 3′-Exonucleases. Comparative resistances of oligonucleotides (5′-OH-19-mer and 5′-OH-27-mer) toward 3′-exonucleases were assayed with *Crotalus adamanteus* venom phosphodiesterase purchased from Sigma and with RPMI 1640 culture medium purchased from Polylabo containing 10% (v/v) heat-inactivated (56 °C, 30 min) fetal calf serum. The fate of conjugate **2** in the presence of venom phosphodiesterase was also monitored (detailed studies on the resistance of oligonucleotides having the 3′-miniloop were performed with the 5′-OH-27-mer in order to save the metalloporphyrin conjugate **2**).

Oligonucleotides and conjugate **2** (6.25 μM final concentration, *i.e.*, 1, 1.4, and 1.6 OD$_{260}$ units/mL for 5′-OH-19-mer, 5′-OH-27-mer, and conjugate **2**, respectively) were incubated in the presence of 5 × 10^{-4} unit/mL venom phosphodiesterase in 0.01 M MgCl₂ and 0.1 M Tris/HCl buffer (pH 9.4) at 37 °C. Aliquots of reaction medium (100 μL) were analyzed by HPLC after a phenol extraction step onto an anion-exchange column (Protein Pak DEAE 8 HR from Waters; A = 25 mM Tris/HCl (pH 8.5), B = A + 1 M NaCl; linear gradient, 10 to 90% B over 45 min; flow rate, 0.7 mL/min). In the case of conjugate **2**, the inactivation of the enzyme was performed by heating the aliquots for 10 min at 70 °C before HPLC analyses. In these conditions, HPLC retention times were 27, 29, and 26 min for 5′-OH-19-mer, 5′-OH-27-mer, and conjugate **2**, respectively. The degradation of oligonucleotides and conjugate **2** was monitored by following the decay of the parent HPLC peak as a function of time. The same procedure was applied for studies of respective stabilities of oligonucleotides in culture medium, except that they were directly dissolved in commercial RPMI 1640 + 10% heat-inactivated fetal calf serum.

Single-Stranded DNA Cleavage. Each DNA cleavage reaction (total reaction volume, 16 μL) was performed with the 5′-labeled 35-mer target (13 nM; 10 000–20 000 cpm), in the presence of 1–100 nM conjugate (DNA cleavers: **1** and **2**; target/conjugate compound ratio from 0.1 to 10) and 0.4 mM in nucleotides of double-stranded herring testes DNA (880 equiv with respect to the target) in 100 mM NaCl and 50 mM Tris/HCl buffer (pH 8). Annealing of the conjugates with the 35-mer was achieved by heating at 90 °C for 1 min followed by slow cooling to 25 °C and overnight storage at 4 °C. For reactions without conjugate, the free 5′-OH-19-mer was hybridized with the 35-mer and then preincubated with 100 nM or 1 μM parent DNA cleaver Mn-TMPyP (pentaacetate of *meso*-tetrakis(4-*N*-methylpyridiniumyl)porphyrinato-manganese(III); see reference 34 for preparation). DNA cleavage reactions were initiated by adding a freshly prepared solution of KHSO₅ (final concentration, 1 mM). After 1 h at 4 °C, 1 μL of 1 M Hepes (pH 8) was added to stop the reaction. Piperidine and heating treatments, performed on DNA cleaved by conjugate **1**, consisted of a thermal step at 90 °C during 1 h in the presence or absence of 1 M piperidine. All samples were then diluted with 100 μL of 0.3 M sodium acetate buffer (pH 5.2) containing yeast tRNA at 0.1 mg/mL and precipitated with 300 μL of cold ethanol overnight at −20 °C. After centrifugation, the DNA pellet was washed with cold 70% ethanol, dried under vacuum (Speed Vac), and dissolved in formamide with marker dyes. DNA fragments were subjected to electrophoresis on denaturing (7 M urea) 20% polyacrylamide gel (3 h at 2300 V).
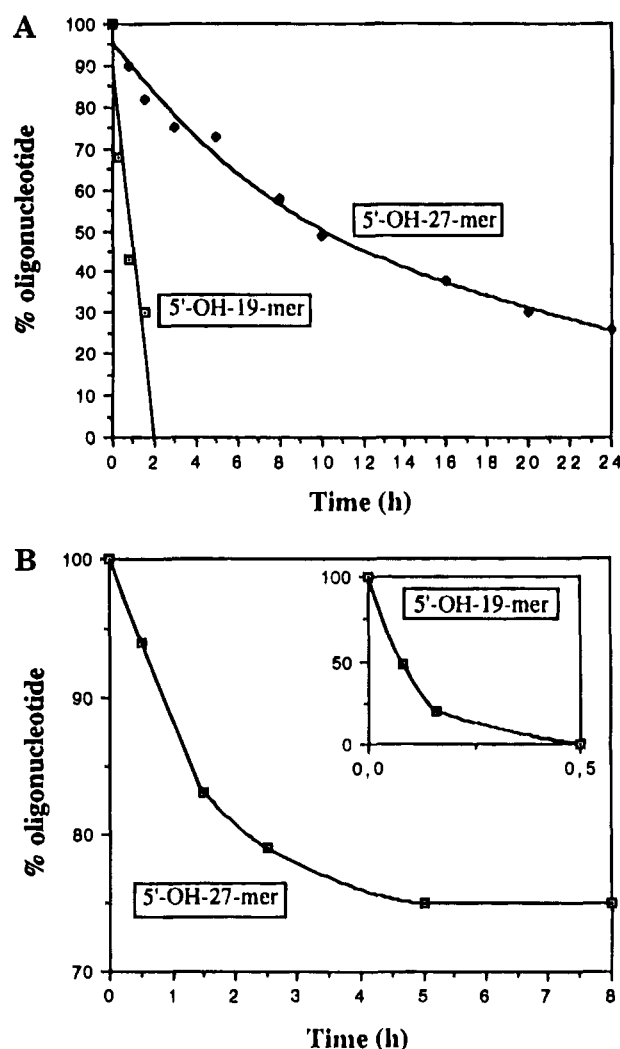
Figure 1. (A) Degradation profiles of 19-mer and 27-mer oligonucleotides in RPMI 1640 + 10% heat-inactivated calf serum. (B) 3′-Exonuclease degradation profiles of 19-mer and 27-mer oligonucleotides.

Thermal Melting Experiments. Optical measurements were performed on a diode-array spectrophotometer (HP8452 from Hewlett Packard) equipped with a temperature programmer (Peltier HP-89090A). Cuvettes were 1 cm path length quartz cells. Solutions contained the conjugate or the antisense (various concentrations between 1.5 and 4 μM) and the 35-mer oligonucleotide target (1 equiv with respect to conjugate or oligonucleotide) in 100 mM NaCl and 40 mM sodium phosphate buffer (pH 8.5). The melting profiles were obtained at 260 nm between 10 and 90 °C at heating increments of 4 °C from 10 to 60 °C and 2 °C from 60 to 90 °C, every 6 min.

RESULTS AND DISCUSSION

Resistance to 3′-Exonucleases. We studied the comparative degradation of oligonucleotide either with purified 3′-exonuclease or with 10% FCS heat-denatured RPMI 1640 cell culture medium. Analysis of the reaction mixture by injection onto an anion-exchange HPLC column allowed separation of DNA fragments at 1-base resolution. The results presented in Figure 1 correspond to the decrease of the peak corresponding to the full-length starting material. Without question, the 3′-minihairpin structure was very efficient toward 3′-exonuclease degradation. While the 5′-OH-19-mer

Chart 2. Cleavage sites of the ($n - 2$) 25-mer oligo-nucleotide by the Mn-TMPyP/KHSO$_5$ system: evidence for the formation of a large loop after removal of the last two nucleotides of the minihairpin structure of the 27-mer.

5'-OH-27-mer-3'-(n-2)

A

B

Absorbance

Scale 1   Temperature (°C)   Scale 2

Figure 2. Melting temperature profiles of oligonucleotides and conjugates with complementary 35-mer target in a 40 mM sodium phosphate and 100 mM NaCl buffer (pH 8): (A) 19-mer and 27-mer oligonucleotides; (B) conjugates 1 and 2.
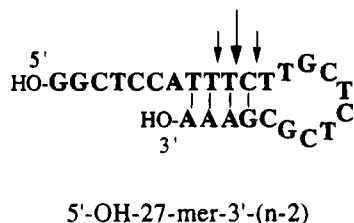
substrate was totally degraded within 2 h in RPMI medium or within 30 min in the 3'-exonuclease test, the 5'-OH-27-mer could still be observed (30% of initial full-length 27-mer) after 24 h in RPMI and (75% *idem*) in venom phosphodiesterase medium after 8 h. We checked that the metalloporphyrin conjugate **2** having the same minihairpin GCGAAAGC-3' as 5'-OH-27-mer is also very slowly degraded by the 3'-exonuclease: 95% and 75% of intact conjugate is still observed after 1- and 5-h incubation times, respectively, with venom phosphodiesterase in the same conditions as for 5'-OH-27-mer. It must be noted that these two percentages remaining are identical to the values found for the oligonucleotide vector with the minihairpin without the metalloporphyrin entity (see Figure 1B).

In the RPMI medium or with the 3'-exonuclease the 5'-OH-19-mer was progressively transformed to mononucleotides, but the 5'-OH-27-mer substrate led to only one degradation product having the same retention time as the corresponding ($n - 1$) fragment (26-mer) (data not shown). The unexpected further resistance of the 26-mer ($n - 1$ fragment) toward 3'-exonuclease degradation is due, in this particular case, to the folding capacity of the 5'-GAAA loop sequence onto the 5'-TTTC sequence near the middle of the antisense oligonucleotide. This secondary folding could take place after the elimination of the C or C and G nucleotides at the 3'-end of the minihairpin. This particular folding was confirmed by studying the cleavage of the ($n - 2$) 25-mer by the "free" Mn-TMPyP activated by potassium monopersulfate (for details on the specificity of this cleaver for three consecutive AT base pairs, see references 18 and 19). The 5'-labeled 25-mer was actually cleaved by Mn-TMPyP/KHSO$_5$ at the expected 3'-side of the three ATs on the upper strand (C$_{11}$ being the major cleavage site; see Chart 2). We found that the 3'-truncated ($n - 1$) 26-mer and the ($n - 2$) 25-mer were totally stable toward the venom phosphodiesterase degradation after a 4-h incubation. These data indicate that even after the degradation of the last two nucleotides of the minihairpin the remaining oligonucleotide can be protected from 3'-exonuclease digestion if the presence of three Ts on the oligonucleotide allows the formation of a larger hairpin. But the possibility of the secondary folding makes this loop with the AAA sequence not perfectly suitable for the 3'-protection of the presently used antisense **2** containing a TTT sequence not very far from its 3'-end. This observation should be extended to any antisense sequence containing three consecutive T bases near the 3'-end. However, this problem can be overcome by changing the minihairpin for another one without three consecutive A bases (*e.g.*, 5'-GCGAAGC; see reference 27).

Melting Temperature (T_m). Although it was shown that the 3'-hairpin structure did not affect the T_m values of a modified oligonucleotide compared to the standard (*28*) when annealed to the complementary RNA sequence,
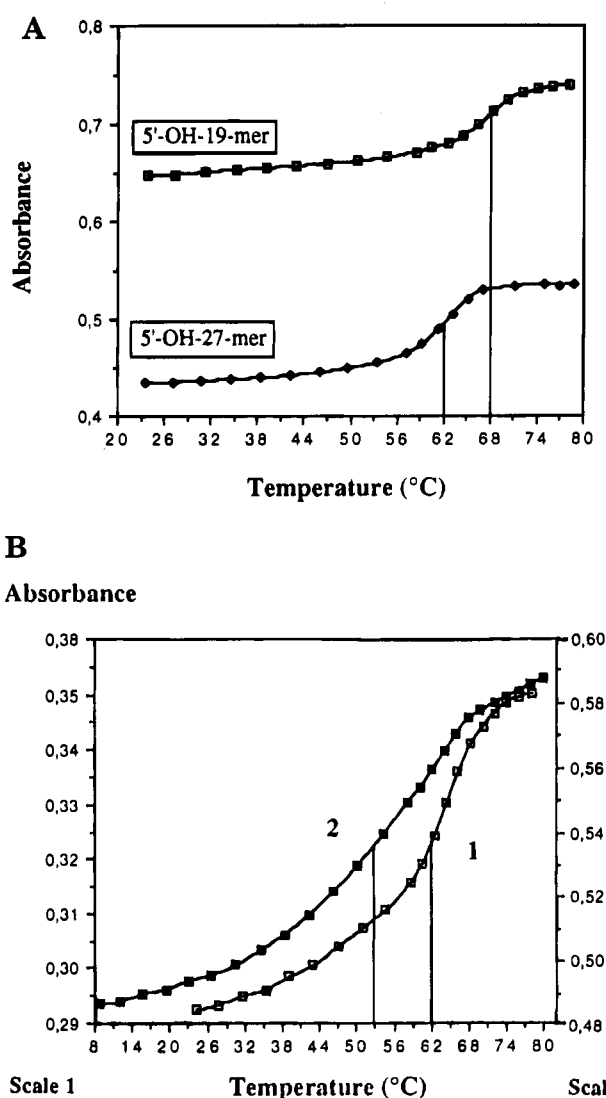
we observed that the 3'-hairpin in the 27-mer decreased the overall affinity of the oligonucleotide with the complementary 35-mer ssDNA target (see Figure 2). The T_m values of duplexes between the 5'-OH-19-mer and the 5'-OH-27-mer with the 35-mer single-stranded DNA were 68 and 62 °C, respectively. The T_m values of duplexes of conjugates 1 and 2 with the same 35-mer sequence were 62 and 53 °C, respectively. These data indicate that the presence of the cationic metalloporphyrin entity at the 5'-end of an oligonucleotide slightly decreased the stability of the modified antisense with its target.

Single-Stranded DNA Cleavage by the Mn-TrisMP-yP-Substituted Oligonucleotides. The parent cationic metalloporphyrin compound is known to be a very efficient DNA cleaving agent (*18, 19*). When the Mn-trisMPyP moiety was covalently attached to the 19-mer oligonucleotide (conjugate 1 of this work), the DNA cleaving reactivity of the cationic metalloporphyrin was directed specifically to the single-stranded RNA/DNA sequence recognized by hybridization of the oligonucleotide vector of the conjugate (*11, 12, 23*). The cleavage of the target nucleic acid occurred in the vicinity of the location of the DNA cleaver conjugates. Because the 3'-hairpin might be able to modify the binding affinity of an oligonucleotide with its complementary sequence, we
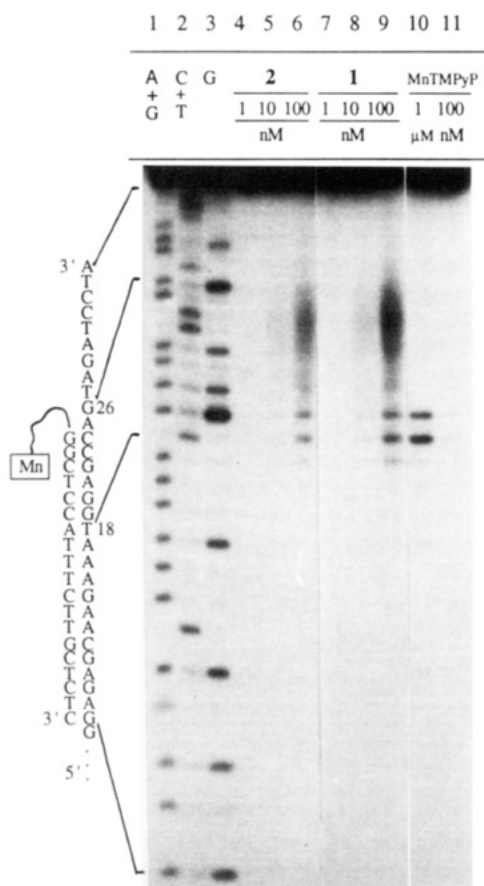
Figure 3. Analysis by electrophoresis of the cleavage of the 5′-labeled 35-mer target by conjugates **1** and **2**. Lane 1, Maxam–Gilbert A+G; lane 2, C+T; lane 3, G; lanes 4–6, 1, 10, and 100 nM conjugate **1**; lanes 7–9: 1, 10, and 100 nM **2**; lanes 10 and 11, 1 μM and 100 nM, respectively, Mn-TMPyP (1 mM KHSO$_5$).

Figure 4. Piperidine treatment of cleavage products of the 5′-labeled 35-mer target by conjugate **1**. Lanes 1–3, 100, 10, and 1 nM conjugate **1** in conditions similar to those in Figure 3; lanes 4–6, the same material as in lanes 1–3 after 1 h at 90 °C in the presence of 1 M piperidine; lanes 7–9, controls, the same material as in lanes 1–3 in the absence of KHSO$_5$ but followed by piperidine treatment; lanes 10–12, lanes 1–3 after 1 h at 90 °C. The experiments represented by lanes 13–15 were performed on a duplex DNA consisting of the 5′-labeled 35-mer target annealed with the complementary free 5′-OH-19-mer: lane 13, KHSO$_5$ alone followed by piperidine treatment; lanes 14 and 15, Mn-TMPyP, 1 μM and 100 nM, respectively. The positions of corresponding Maxam and Gilbert standards are shown (due to a salt effect on the left side of the gel during migration, bands in lanes 4–15 have been slightly retarded).

compared the antisense cleaving reactivity of conjugates **1** and **2**. The target sequence was a 5′-labeled 35-mer oligonucleotide (see Chart 1) at a final concentration of 13 nM, which was incubated in the presence of various concentrations of conjugates and an excess of random dsDNA, in order to evidence the efficiency of the targeting of nuclease activity of the metalloporphyrin by the oligonucleotide vector. Nonspecific interactions between a cationic metalloporphyrin and a random double-stranded DNA would lead to target cleavage at higher concentrations. We have previously shown that this is the case for nonvectorized cationic metalloporphyrins, which have a strong affinity for AT-rich regions (*11*). The assayed concentrations of conjugates ranged from 1 to 100 nM. The oxidative cleavage of DNA was initiated by the addition of a freshly prepared KHSO$_5$ solution. Typically, the cleavage of the target nucleic acid can be observed at 10 nM conjugate concentration (Figure 3, lanes 5 and 8) corresponding to a 1/1 ratio of cleaving antisense/target. At 100 nM the pattern of cleavage products consisted of a smear from G20 to G26 and of two main individual bands at G19 and T18. The two latter bands correspond to the two known cleaving sites of the "free" Mn-TMPyP reagent (*18, 19*). Well-defined DNA breaks are only observed with nonvectorized metalloporphyrins for which the high-valent metal-oxo species is allowed to freely move within the minor groove to reach a C–H bond at 5′ positions of deoxyribose units (*18, 24b*). The smear was probably due to multiple modes of oxidative cleavage events. Because of the presence of an excess dsDNA, Mn-TMPyP cleavage of the 5′-labeled

35-mer was only observable at 1 μM concentration of reagent (Figure 3, lane 10).

In order to investigate the origin of the smear in DNA cleavage by these metalloporphyrin–oligonucleotide conjugates, we decided to further analyze the DNA cleavage pattern by conjugate **1** by a piperidine treatment of samples. After 1 h of oxidative degradation at 4 °C, the reaction samples were heated at 90 °C during 1 h in the presence of 1 M piperidine. The results are shown in Figure 4 with lanes 1–3 corresponding to lanes 7–9 of Figure 3. The two discrete bands at T$_{18}$ and G$_{19}$ observed by direct cleavage resisted piperidine treatment in lanes 4 and 5. But the smear of cleavage products was transformed to discrete bands corresponding mainly to G$_{19}$ and to some lower extent to G$_{20}$, G$_{22}$, or even G$_{26}$. The intensity of the G cleavage products revealed by piperidine decreased with the distance from the location of the metalloporphyrin moiety. One can also notice that a major part of the full-length material left after the cleavage reaction at 4 °C (lanes 1–3) was also piperidine sensitive (lanes 4–6) and transformed into cleavage products at G residues. The piperidine degradation increased with the oxidative damage mediated at 4 °C

(compare lanes 1 and 4 or 2 and 5). After piperidine treatment, damage on the target 35-mer can be estimated to 50% for a conjugate/target ratio of 1 (10 nM/10 nM) (lane 5) and to 90% for a ratio of 10 (100 nM/10 nM) (lane 4). The cleavage fragments obtained after piperidine treatment comigrate with Maxam and Gilbert sequencing bands and thus corresponded to fragments bearing 3′-phosphate termini. The piperidine treatment revealed the real amount and location of oxidative lesions mediated by the metalloporphyrin conjugate on the DNA target contrarily to a direct analysis after the oxidative reaction. The exact nature of the damages still remains to be elucidated, but it is clear that guanine damage revealed by the piperidine treatment strongly suggests that the active manganese-oxo species is not acting only as a deoxyribose cleaver as observed when the cationic manganese porphyrin is not tethered to an oligonucleotide (*24b* and references therein).

From densitometric measurements on an underexposed autoradiography film, Mn-TMPyP in lane 10 of Figure 3 cleaved the 35-mer substrate to a 6% extent at 1 μM concentration. In contrast, 40 or 20% of the target was directly cleaved at 100 nM concentration of conjugate **1** or **2**, respectively. Both of them showed the same cleavage behavior: the smear accounted for 80% of the cleavage products, and the two discrete bands accounted for only 20% (lanes 6 and 9, Figure 3). The lower binding affinity of conjugate **2** toward the complementary sequence is probably responsible for its weaker reactivity. But the key point is the higher cleavage efficiency of the manganese porphyrin when linked to an oligonucleotide. These data confirmed that oligonucleotides modified by metalloporphyrins are able to recognize and to cut a selected ssDNA sequence at remarkably low concentration.

GENERAL CONCLUSIONS

In view of cell culture or *in vivo* assays, an easy way to increase the metabolic stability of an antisense oligonucleotide is to add a 3′-minihairpin structure at the 3′-end of its sequence. We performed the synthesis and checked the reactivity of antisense oligonucleotides that are carrying a cationic metalloporphyrin as nucleic acid cleaver at their 5′-end. We addressed the question of the interference of the 3′-loop on the DNA cleaving efficiency of these modified oligonucleotides. We found that the presence of the 3′-loop slightly decreased the binding affinity of the conjugated oligonucleotide (the T_m of conjugate **2** is inferior by 6 °C compared to conjugate **1**). The cleaving efficiency was slightly reduced by the presence of the 3′-minihairpin. But this decrease of reactivity may be compensated by the higher metabolic stability of these modified antisenses for experiments in cell culture medium or *in vivo*. Addition of this 3′-minihairpin having three consecutive A bases should be restricted to antisense oligonucleotides that do not contain three Ts near the 3′-end in order to avoid the formation of a larger loop as described in Chart 2 after losing the two last nucleotides.

ACKNOWLEDGMENT

LITERATURE CITED

(1) Agrawal, S. (1991) Antisense oligonucleotides: A possible approach for chemiotherapy of AIDS. *Prospects for Antisense Nucleic Acid Therapy of Cancer and AIDS* (Wickstrom, E., Ed.) pp 143−158, Wiley-Liss, New York.

(2) Goodchild, J. (1990) Conjugates of oligonucleotides and modified oligonucleotides: A review of their synthesis and properties. *Bioconj. Chem. 1*, 165−187.

(3) Uhlmann, E., and Peyman, A. (1990) Antisense oligonucleotides: a new therapeutic principle. *Chem. Rev. 90*, 543−584.

(4) Hélène, C., and Toulmé, J. J. (1990) Specific regulation of gene expression by antisense, sense and antigene nucleic acids. *Biochem. Biophys. Acta 1049*, 99−125.

(5) Englisch, U., and Gauss, D. H. (1991) Chemically modified oligonucleotides as probes and inhibitors. *Angew. Chem., Int. Ed. Engl. 30*, 613−722.

(6) Sigman, D. S., Bruice, T. W., Mazumder, A., and Sutton, C. L. (1993) Targeted chemical nucleases. *Acc. Chem. Res. 26*, 98−104.

(7) Oakley, M. G., Turnbull, K. D., and Dervan, P. B. (1994) Synthesis of a hybrid protein containing the iron-binding ligand of bleomycin and the DNA-binding domain of Hin. *Bioconj. Chem. 5*, 242−247 and references therein.

(8) Dervan, P. B. (1992) Reagents for the specific cleavage of megabase DNA. *Nature 359*, 87−88.

(9) Frolova, E. I., Ivanova, E. M., Zarytova, V. F., Abramova, T. V., and Vlassov, V. V. (1990) Porphyrin-linked oligonucleotides. Synthesis and sequence-specific modification of ss-DNA. *FEBS Lett. 269*, 101−104.

(10) Le Doan, T., Praseuth, D., Perrouault, L., Chassignol, M., Thuong, N. T., and Hélène, C. (1990) Sequence-targeted photochemical modifications of nucleic acids by complementary oligonucleotides covalently linked to porphyrins. *Bioconj. Chem. 1*, 108−113.

(11) Pitié, M., Casas, C., Lacey, J., Pratviel, G., Bernadou, J., and Meunier, B. (1993) Efficient cleavage of a 35-mer single-stranded DNA containing the initiation codon of the TAT gene of HIV-1 by a targeted cationic manganese porphyrin. *Angew. Chem., Int. Ed. Engl. 32*, 557−559.

(12) Casas, C., Lacey, C. J., and Meunier, B. (1993) Preparation of hybrid "DNA cleaver-oligonucleotide" molecules based on a metallotris(methylpyridiniumyl)porphyrin motif. *Bioconj. Chem. 4*, 366−371.

(13) Clarenc, J. P., Degols, G., Leonetti, J. P., Milhaud, P., and Lebleu, B. (1993) Delivery of antisense oligonucleotides by poly(L-lysine) conjugation and liposome encapsulation. *Anti-Cancer Drug Des. 8*, 81−94.

(14) Truffert, J. C., Lorthioir, O., Asseline, U., Thuong, N. T., and Brack, A. (1994) One-line phase synthesis of oligonucleotide−peptide hybrids using silica supports. *Tetrahedron Lett. 35*, 2353−2356.

(15) De La Torre, B. G., Avino, A., Tarrason, G., Piulats, J., Albericio, F., and Erijta, R. (1994) Stepwise solid-phase synthesis of oligonucleotide−peptide hybrids. *Tetrahedron Lett. 35*, 2733−2736.

(16) Marzilli, L. G. (1990) Medical aspects of DNA−porphyrin interactions. *New J. Chem. 14*, 409−420.

(17) Ding, L., Bernadou, J., and Meunier, B. (1991) Oxidative degradation of cationic metalloporphyrins in the presence of nucleic acids: A way to binding constants? *Bioconj. Chem. 2*, 201−206.

(18) Pitié, M., Pratviel, G., Bernadou, J., and Meunier, B. (1992) Preferential hydroxylation by the chemical nuclease *meso*-tetrakis-(4-*N*-methylpyridiniumyl)porphyrinato-manganese[III] pentaacetate/KHSO$_5$ at the 5′ carbon of deoxyriboses on both 3′ sides of three contiguous A·T base pairs in short double-stranded oligonucleotides. *Proc. Natl. Acad. Sci. U.S.A. 89*, 3967−3971.

(19) Pratviel, G., Duarte, V., Bernadou, J., and Meunier, B. (1993) Nonenzymatic cleavage and ligation of DNA at a three AT base pair site. A two-step "pseudohydrolysis" of DNA. *J. Am. Chem. Soc. 115,* 7939–7943.

(20) Ding, L., Etemad-Moghadam, G., and Meunier, B. (1990) Oxidative cleavage of DNA mediated by hybrid "metalloporphyrin-ellipticine" molecules and functionalized metalloporphyrin precursors. *Biochemistry 29,* 7868–7875.

(21) Ding, L., Etemad-Moghadam, G., Cros, S., Auclair, C., and Meunier, B. (1991) Water-soluble cytotoxic hybrid molecules "cationic metalloporphyrin-ellipticine" having a high affinity for DNA. *J. Med. Chem. 34,* 900–906.

(22) Ding, L., Balzarini, J., Schols, D., Meunier, B., and De Clercq, E. (1992) Anti-human immunodeficiency virus effects of cationic metalloporphyrin-ellipticine complexes. *Biochem. Pharmacol. 44,* 1675–1679.

(23) Pitié, M., Blumenfeld, M., Pratviel, G., Vasseur, M., and Meunier, B., unpublished data.

(24) (a) Bernadou, J., Fabiano, A. S., Robert, A., and Meunier, B. (1994) "Redox tautomerism" in high-valent metal-oxo-aquo complexes. Origin of the oxygen atom in epoxidation reactions catalyzed by water-soluble metalloporphyrins. *J. Am. Chem. Soc. 116,* 9375–9376. (b) Pitié, M., Bernadou, J., and Meunier, B. (1995) Oxidation at carbon-1' of DNA deoxyriboses by the Mn-TMPyP/KHSO$_5$ system results from a cytochrome P-450-type hydroxylation reaction. *J. Am. Chem. Soc. 117,* 2935–2936.

(25) Pratviel, G., Bernadou, J., and Meunier, B. (1989) Evidence for high-valent iron-oxo species in the DNA breaks mediated by iron-bleomycin. *Biochem. Pharmacol. 38,* 133–140.

(26) Hirao, I., Nishimura, Y., Tagawa, Y.-i., Watanabe, K., and Miura K.-i. (1992) Extraordinarily stable mini-hairpins: electrophoretical and thermal properties of the various sequence variants of d(GCGAAAGC) and their effect on DNA sequencing. *Nucleic Acids Res. 20,* 3891–3896.

(27) Hirao, I., Kawai, G., Yoshizawa, S., Nishimura, Y., Ishido, Y., Watanabe, K., and Miura, K.-i. (1994) Most compact hairpin-turn structure exerted by a short DNA fragment, d(GCGAAGC) in solution: an extraordinarily stable structure resistant to nucleases and heat. *Nucleic Acids Res. 22,* 576–582.

(28) Khan, I. M., and Coulson J. M. (1993) A novel method to stabilize antisense oligonucleotides against exonuclease degradation. *Nucleic Acids Res. 21,* 2957–2958.

(29) Vasseur, M., Blumenfeld, M., and Poddevin, B., personnal communication.

(30) Casas, C., Saint-Jalmes, B., Loup, C., Lacey, C. J., and Meunier, B. (1993) Synthesis of cationic metalloporphyrin precursors related to the design of DNA cleavers. *J. Org. Chem. 58,* 2913–2917.

(31) Wain-Hobson, S., Sonigo, P., Danos, O., Cole, S., and Alizon, M. (1985) Nucleotide sequence of the AIDS virus, LAV. *Cell 40,* 9–17.

(32) Wachter, L., Jablonski, J. A., and Ramachandran, K. L. (1986) A simple and efficient procedure for the synthesis of 5'-aminoalkyl oligodeoxynucleotides. *Nucleic Acids Res. 14,* 7985–7994.

(33) Fasman, G., Ed. (1975) *Handbook of Biochemistry and Molecular Biology—Nucleic Acids,* 3rd ed., p 175. CRC Press, Boca Raton, FL.

(34) Bernadou, J., Pratviel, G., Bennis, F., Girardet, M., and Meunier, B. (1989) Potassium monopersulfate and a water-soluble manganese porphyrin complex [Mn(TMPyP)](OAc)$_5$, as an efficient reagent for the oxidative cleavage of DNA. *Biochemistry 28,* 7268–7275.

BC950037M

Synthesis of Novel Phosphoramidite Reagents for the Attachment of Antisense Oligonucleotides to Various Regions of the Benzophenanthridine Ring System

Jer-kang Chen,[†] H. Lee Weith,[‡] Rupinder S. Grewal,[†] Guangyi Wang,[†] and Mark Cushman*,[†]

Departments of Medicinal Chemistry and Pharmacognosy and Biochemistry, Purdue University, West Lafayette, Indiana 47907. Received March 28, 1995[⊛]

Four benzophenanthridine phosphoramidite reagents have been prepared in which the linker chain between the benzophenanthridine and the phosphoramidite moiety is attached to C-2, C-6, C-9, and C-12 of the benzophenanthridine ring system. These benzophenanthridine phosphoramidites should prove to be useful in the syntheses of antisense oligonucleotide–intercalator conjugates in which the linker chain is attached to various regions of the benzophenanthridine intercalator. One of the new benzophenanthridine phosphoramidite reagents was used to prepare an antisense oligonucleotide–intercalator conjugate in which the oligonucleotide TCAGTGGTp was connected at its 5′-hydroxyl group through a linker chain to the C-2 hydroxyl group of a benzophenanthridine.

INTRODUCTION

The control of gene expression by antisense oligonucleotides offers an exciting as well as rational strategy for the treatment of viral diseases, cancer, and genetic diseases. Antisense oligonucleotides bind specifically to complementary sequences in DNA or RNA and interfere with either transcription or translation. The field has been surveyed repeatedly and several recent reviews are available (*1−18*). Despite many promising results in *in vitro* systems, however, the potential application of antisense oligonucleotides themselves as therapeutic agents is severely limited by their instability to nucleases and their poor membrane penetration. Additional problems relate to their binding site selectivity and affinity for the target sequence. In view of these considerations, various chemical modifications of oligonucleotides have been made in order to improve their properties as potential therapeutic agents. These have included the replacement of the phosphodiester linkages with methyl phosphonates, phosphorothioates, and phosphorodithioates.

One of the possible structural modifications of antisense oligonucleotides which may improve their therapeutic potential is the attachment of intercalating agents to the 3′ and/or 5′ ends through linker chains. This may stabilize the ends of the oligonucleotide toward hydrolysis by exonucleases (*19−23*). The increase in lipophilicity provided by the intercalator may also facilitate cell membrane penetration (*19*). The intercalation and/or stacking interactions of the intercalators with the base pairs of the miniduplex also increases its affinity for the target nucleic acid and (*22−27*), if chosen correctly, could also add to the binding site selectivity. Acridine (*20, 22, 23, 26, 28−37*) intercalators have most often been linked to oligonucleotides, although oxazolopyridocarbazole (*38, 39*), anthraquinone (*25*), phenanthridine (*40*), phenazine (*41*), and ellipticine (*27*) conjugates have also been prepared. In certain cases, it has been demonstrated that oligonucleotide–acridine conjugates were effective in inhibiting gene expression, whereas the corresponding oligonucleotides themselves were inactive (*19, 21, 42–44*).

There are many variables which must be considered in the design of oligonucleotide–intercalator conjugates, including the sequence of the oligonucleotide, the point of attachment of the linker chain to the oligonucleotide, the length and type of linker chain, the point of attachment of the linker chain to the intercalating agent, and the choice of the intercalator. For potential use in the control of HIV gene expression, we felt that an ideal intercalator should (1) be a potent inhibitor of viral gene expression on its own, without any attached oligonucleotide, by binding to the template primers; (2) possess selectivity for binding to viral DNA polymerases as opposed to other DNA and RNA polymerases; (3) be nonmutagenic; and (4) have established binding site selectivity that could be taken advantage of in targeting the conjugate to specific sequences of viral RNA. Both nitidine chloride (**1**) and fagaronine chloride (**2**), as well as some structurally related benzophenanthridine alkaloids, inhibit RNA-directed DNA polymerase activity from avian myeloblastosis virus, Raucher murine leukemia virus, and simian sarcoma virus by binding to the template primers (*45−50*). They also inhibit viral DNA polymerase to a greater extent than mouse embryo RNA polymerase, DNA polymerase, and poly(A) polymerase (*49*). In a study of the activities of 15 benzophenanthridine alkaloids against avian myeloblastosis virus, fagaronine chloride (**2**) was found to be the most active, followed closely by *O*-methylfagaronine sulfate and nitidine chloride (**1**) (*50*). Viral DNA polymerase activity was greatly diminished when A:T template primers were used; however, no inhibition occurred with G:C template primers (*45, 47−49*). It has also been demonstrated that nitidine chloride is not mutagenic (*51*).

1
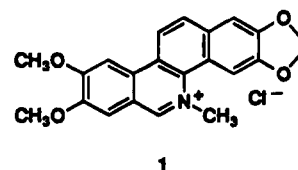
The goal of the present study was to synthesize a series reactive phosphoramidites attached through linker chains to multiple regions of the benzophenanthridine intercalator system. These molecules were designed to allow

---

[†] Department of Medicinal Chemistry and Pharmacognosy.
[‡] Department of Biochemistry.
[⊛] Abstract published in *Advance ACS Abstracts,* July 1, 1995.

the eventual preparation of a series of benzophenanthridine—oligonucleotide conjugates in which the point of attachment of the linker chain to the benzophenanthridine intercalator is varied. In more specific terms, methodology was sought which would allow the attachment of the linker chain to the "top", "bottom", "right-hand side", and "left-hand side" of the intercalator. The effect of the point of attachment of the linker chain to the intercalator on affinity for the target sequence has not previously been investigated systematically with any oligonucleotide—intercalator conjugates.

EXPERIMENTAL PROCEDURES

Melting points were determined in capillary tubes and are uncorrected. ^{1}H NMR spectra were recorded at 200 or 500 MHz using $CDCl_3$ as the solvent, except where noted otherwise. Low-resolution chemical ionization mass spectra (CIMS) were determined using 2-methylpropane as the reagent gas. Various other types of mass spectra are abbreviated as follows: FABMS (fast atom bombardment mass spectrum), HRFABMS (high-resolution fast atom bombardment mass spectrum), HRCIMS (high-resolution chemical ionization mass spectrum), HREIMS (high-resolution electron impact mass spectrum). Microanalyses were performed by the Purdue Microanalytical Laboratory. Column chromatography was carried out on silica gel (Merck, grade 60, 230–400 mesh).

2-[[5'-(Ethoxycarbonyl)-n-pentyl]oxy]-3,8,9-trimethoxy-N-methylbenzo[c]phenanthridinium Chloride (3). Potassium *tert*-butoxide (1 M THF solution, 308.6 µL) was added dropwise to the solution of fagaronine chloride (**2**, 80 mg, 0.208 mmol) in dry dimethyl sulfoxide (2.1 mL), and the mixture was stirred at room temperature for 30 min. Ethyl 6-(tosyloxy)hexanoate (328.8 mg, 1.047 mmol) was then added, and the reaction mixture was stirred at room temperature for 24 h. The solvent was evaporated at room temperature under reduced pressure. The residue was redissolved in MeOH and subjected to preparative, centrifugally accelerated, radial, thin layer chromatography on silica gel, eluting with chloroform—MeOH (9:1) (52–55). Recrystallization from chloroform—petroleum ether furnished the pure product **3** (100 mg, 91%): mp 221–223 °C dec; IR (KBr) 3060–3000, 2920, 1730, 1615, 1510, 1280, 1010 cm^{-1}; NMR δ 10.57 (s, 1 H), 8.39 (d, J = 9.9 Hz, 1 H), 8.03 (br d, 2 H), 7.92 (s, 1 H), 7.88 (s, 1 H), 7.34 (s, 1 H), 5.13 (s, 3 H), 4.26 (s, 3 H), 4.22 (t, J = 6.6 Hz, 2 H), 4.13 (q, J = 7.2 Hz, 2 H), 4.08 (s, 3 H), 4.07 (s, 3 H), 2.36 (t, J = 7.5 Hz, 2 H), 1.99 (m, 2 H), 1.75 (m, 2 H), 1.59 (m, 2 H), 1.25 (t, J = 7.5 Hz, 3 H); FABMS, m/z (relative intensity) 492 (M$^-$ − Cl, 100); HRFABMS calcd for $C_{29}H_{34}NO_6$ (M$^+$ − Cl) 492.2385, found 492.2372.

5,6-Dihydro-2-[(6'-hydroxy-n-hexyl)oxy]-3,8,9-trimethoxy-N-methylbenzo[c]phenanthridine (4). Lithium aluminum hydride (95%, 27.74 mg, 0.69 mmol) was added to a solution of compound **3** (61 mg, 0.12 mmol) in THF (6 mL). The reaction mixture was stirred at room temperature for 4 h. The reaction mixture was cooled to 0 °C and decomposed by addition of water (0.1 mL), 15% aqueous NaOH (0.1 mL), and finally water (0.3 mL). The mixture was stirred for 15 min and filtered. The aluminate was washed with chloroform. The combined organic layers were dried (Na$_2$SO$_4$) and evaporated. The residue was dissolved in chloroform and subjected to preparative, centrifugally accelerated, radial, thin-layer chromatography on silica gel, eluting with EtOAc—hexane (8:2) to afford pure product **4** (40 mg, 77%): mp 162–164 °C dec; IR (KBr) 3540, 3040, 2920, 2850, 1600, 1500, 1455, 1240, 1000 cm^{-1}; NMR δ 7.69 (d, J = 8.7 Hz,

1 H), 7.61 (s, 1 H), 7.49 (d, J = 8.4 Hz, 1 H), 7.30 (s, 1 H), 7.11 (s, 1 H), 6.79 (s 1 H), 4.14 (s, 2 H), 4.13 (t, J = 6.8 Hz, 2 H), 4.03 (s, 3 H), 3.98 (s, 3 H), 3.93 (s, 3 H), 3.66 (t, J = 6.5 Hz, 2 H), 2.61 (s, 3 H) 1.94 (m, 2 H), 1.61 (m, 2 H), 1.56 (m, 2 H), 1.47 (m, 2 H); CIMS, m/z (relative intensity) 452 (MH$^+$, 100); HREIMS calcd for $C_{27}H_{33}O_5N$ (M$^+$) 451.2359, found 451.2359.

2-[(6'-Hydroxy-n-hexyl)oxy]-5,6-dihydro-3,8,9-trimethoxy-N-methylbenzo[c]phenanthridine 6'-O-(2-Cyanoethyl N,N-diisopropylphosphoramidite) (5). N,N-Diisopropylethylamine (0.11 mL) was added to the solution of compound **4** (28 mg, 0.06 mmol) in THF (2 mL). The solution was stirred for 10 min. 2-Cyanoethyl N,N-diisopropylchlorophosphoramidite (69 µL, 0.31 mmol) was added to the solution, and the reaction mixture was stirred at room temperature for 1.5 h. The reaction mixture was then subjected to preparative, centrifugally accelerated, radial, thin-layer chromatography on silica gel, eluting with EtOAc—hexane—triethylamine (5:4:1), to yield the phosphoramidite **5** (36.3 mg, 90%) as an oil: ^{1}H NMR δ 7.69 (d, J = 8.6 Hz, 1 H), 7.61 (s, 1 H), 7.49 (d, J = 8.5 Hz, 1 H), 7.30 (s, 1 H), 7.11 (s, 1 H), 6.79 (s, 1 H), 4.14 (s, 2 H), 4.13 (t, J = 6.9 Hz, 2 H), 4.03 (s, 3 H), 3.98 (s, 3 H), 3.93 (s, 3 H), 3.83 (m, 1 H), 3.77 (m, 1 H), 3.67 (m, 1 H), 3.58 (m, 3 H), 2.61 (s, 3 H), 2.61 (t, J = 6.5 Hz, 2 H), 1.93 (m, 2 H), 1.65 (m, 2 H), 1.53 (m, 2 H), 1.47 (m, 2 H), 1.17 (d, J = 3.0 Hz, 6 H), 1.16 (d, J = 3.0 Hz, 6 H); ^{31}P NMR (202 MHz) δ 147.99.

12-Acetoxy-5,6-dihydro-8,9-dimethoxy-N-methyl-2,3-(methylenedioxy)-6-oxobenzo[c]phenanthridine (7). A solution of trans-N-methyl-8,9-dimethoxy-2,3-(methylenedioxy)-6,12-dioxo-4b,5,6,10b,11,12-hexahydrobenzo[c]phenanthridine (**6**) (3.81 g, 10 mmol) and p-toluenesulfonic acid monohydrate (0.95 g, 5 mmol) in isopropenyl acetate (150 mL) was heated at reflux under air for 24 h and then heated at 85 °C for another 24 h. The reaction mixture was diluted with ether, and the precipitate (2.52 g) was filtered and washed with ether. The filtrate was concentrated and dissolved in chloroform (100 mL). The resulting solution was washed with 2 N Na$_2$CO$_3$ (3 × 50 mL), dried (Na$_2$SO$_4$), and concentrated. The residue was chromatographed on silica gel using 25% ethyl acetate in methylene chloride to give an additional crop of **7** (1.40 g). The total yield was 3.92 g (93%). Recrystallization from methylene chloride/ethyl acetate gave an analytically pure sample: mp 275–277 °C; IR (KBr) 2915, 2820, 1757, 1641, 1608, 1502, 1469, 1387, 1362, 1305, 1253, 1205, 1033 cm^{-1}; NMR δ 7.92 (s, 1 H), 7.76 (s, 1 H), 7.66 (s, 1 H), 7.45 (s, 1 H), 7.19 (s, 1 H), 6.13 (s, 2 H), 4.10 (s, 3 H), 4.06 (s, 3 H), 3.97 (s, 3 H), 2.52 (s, 3 H); CIMS m/z (relative intensity) 422 (MH$^-$, 100), 381 (11), 380 (17), 379 (9); HRCIMS calcd for $C_{23}H_{20}$NO$_7$ 422.1240, found 422.1230.

5,6-Dihydro-8,9-dimethoxy-12-[[4'-(ethoxycarbonyl)-n-pentyl]oxy]-N-methyl-2,3-(methylenedioxy)-benzo[c]phenanthridine (8). A mixture of 12-acetoxy-5,6-dihydro-8,9-dimethoxy-N-methyl-2,3-(methylenedioxy)-6-oxobenzo[c]phenanthridine (**7**) (632 mg, 1.5 mmol) and sodium hydroxide (600 mg) in ethanol (30 mL) and water (15 mL) was stirred at room temperature for 2 h. The solvent was evaporated in vacuo, and the residue was thoroughly dried under vacuum. Dry DMSO (15 mL) was added and the resulting mixture stirred for 20 min. Ethyl 5-bromovalerate (2.0 g, 9.5 mmol) was added and the mixture stirred for 18 h. The resulting clear solution was acidified with 2 N HCl under cooling with ice and diluted with chloroform (100 mL). The mixture was washed with water (3 × 60 mL), dried (Na$_2$SO$_4$), and concentrated. Most of the excess ethyl 5-bromovalerate was removed under vacuum. The residue was chromato-

graphed on silica gel using 25% ethyl acetate in methylene chloride to give a white solid (710 mg, 91%): IR (KBr) 2924, 1734, 1629, 1506, 1474, 1424, 1390, 1315, 1272, 1254, 1185, 1144, 1037 cm^{-1}; CIMS m/z (relative intensity) 522 (MH$^+$, 100); HRCIMS calcd for C$_{29}$H$_{32}$NO$_8$ 522.2128, found 522.2139.

5,6-Dihydro-12-[(6'-hydroxy-n-hexyl)oxy]-8,9-dimethoxy-5-N-methyl-2,3-(methylenedioxy)benzo[c]phenanthridine (9). A suspension of the ester **8** (0.71 g, 1.36 mmol) and lithium aluminum hydride (0.5 g, 13.6 mmol) in dry THF (70 mL) was heated at reflux under nitrogen for 18 h. The reaction was quenched with 15% NaOH under cooling with ice. The organic layer was separated and the residue extracted with THF (3 × 10 mL). The combined extracts were dried (Na$_2$SO$_4$) and the solvent evaporated. The residue was chromatographed on silica gel using 20% ethyl acetate in methylene chloride to give **9** (0.38 g, 60%) as a white solid. Recrystallization from ethyl acetate–hexane gave an analytically pure sample: mp 125 °C; IR (KBr) 3509, 1939, 1869, 1607, 1526, 1501, 1460, 1399, 1345, 1316, 1279, 1236, 1201, 1118, 1037 cm^{-1}; NMR δ 7.63 (s, 1 H), 7.58 (s, 1 H), 7.24 (s, 1 H), 7.01 (s, 1 H), 6.81 (s, 1 H), 6.06 (s, 2 H), 4.20 (t, J = 6.0 Hz, 2 H), 4.11 (s, 2 H), 4.01 (s, 3 H), 3.96 (s, 3 H), 3.69 (t, J = 6.5 Hz, 2 H), 2.53 (s, 3 H), 1.96 (m, 2 H), 1.69–1.47 (m, 6 H); CIMS m/z (relative intensity) 466 (MH$^+$, 100), 465 (M$^+$, 48); HRCIMS calcd for C$_{27}$H$_{32}$NO$_6$ 466.2230, found 466.2221.

12-[(6'-Hydroxy-n-hexyl)oxy]-5,6-dihydro-8,9-dimethoxy-N-methyl-2,3-(methylenedioxy)benzo[c]phenanthridine 6'-O-(2-Cyanoethyl-N,N-diisopropylphosphoramidite) (10). A solution of the alcohol **9** (186 mg, 0.4 mmol) and N,N-diisopropylethylamine (309 mg, 2.4 mmol) in dry methylene chloride (2 mL) was added dropwise to a solution of 2-cyanoethyl N,N-diisopropylchlorophosphoramidite (188 mg, 0.8 mmol) in dry methylene chloride (1 mL) at 0 °C under nitrogen. The solution was stirred at room temperature for 50 min and diluted with methylene chloride at 0 °C. The resulting solution was washed with cold 2N Na$_2$CO$_3$ (10 mL) and then water (3 × 10 mL), dried (Na$_2$SO$_4$), and concentrated. The residue was chromatographed on silica gel (chromatotron) using 30% ethyl acetate in methylene chloride to afford **10** (163 mg, 61%) as a semisolid material: IR (neat) 2964, 2936, 2869, 2251, 1608, 1527, 1501, 1460, 1238, 1221, 1202, 1121, 1036 cm^{-1}; NMR δ 7.63 (s, 1 H), 7.57 (s, 1 H), 7.25 (s, 1 H), 7.01 (s, 1 H), 6.81 (s, 1 H), 6.06 (s, 1 H), 4.20 (t, J = 6.0 Hz, 1 H), 4.11 (s, 2 H), 4.02 (s, 3 H), 3.96 (s, 3 H), 3.89–3.56 (m, 6 H), 2.62 (t, J = 6.5 Hz, 2 H), 2.53 (s, 3 H), 1.99–1.92 (m, 2 H), 1.73–1.47 (m, 6 H), 1.18 (q, J = 6.5, 1.5 Hz, 12 H); FABMS m/z (relative intensity) 666 (MH$^+$, 44), 665 (M$^+$, 68), 664 (76), 364 (100).

3-Isopropoxy-4-methoxybenzaldehyde (12). A mixture containing anhydrous potassium carbonate (15.0 g), isovanillin (**11**, 5.00 g, 0.0329 mol), 2-bromopropane (15.0 mL, 0.160 mol), and DMF (10 mL) was stirred at room temperature for 15 min and then heated under reflux for 2.5 h, cooled, and poured into water (20 mL). The mixture was extracted with chloroform (4 × 20 mL). The combined chloroform extracts were washed with water (5 × 10 mL), dried (Na$_2$SO$_4$), and concentrated to give **12** (6.29 g, 98%) as a liquid: bp 101–105 °C (0.6 mm) [lit. (56) bp 110–113 °C (1 mm)]; IR (thin film) 2970, 2920, 1680, 1575, 1500, 1425, 1260, 1120 cm^{-1}; ^{1}H NMR δ 9.84 (s, 1 H), 7.45 (d, J = 7.9 Hz, 1 H), 7.42 (s, 1 H), 6.98 (d, J = 7.9 Hz, 1 H), 4.65 (sept, J = 6.2 Hz, 1 H), 3.95 (s, 3 H), 1.41 (d, J = 6.2 Hz, 6 H); CIMS (isobutane) m/z (relative intensity) 195 (MH$^+$, 100).

3-Isopropoxy-3',4,4'-trimethoxychalcone (14). A

solution of 3-isopropoxy-4-methoxybenzaldehyde (**12**, 6.28 g, 0.0323 mol) and 3,4-dimethoxyacetophenone (**13**, 5.83 g, 0.0323 mol) in ethanol (60 mL) was treated with 10% aqueous sodium hydroxide (6.0 mL, 0.015 mol). The mixture was stirred at room temperature for 20 h. Some of the ethanol was removed on the rotary evaporator at room temperature. Water (100 mL) was added to the residue, and the mixture was extracted with chloroform (3 × 50 mL). The combined organic layer was washed with water (25 mL), dried (Na$_2$SO$_4$), and concentrated to give **14** (11.40 g, 99%) as an oil: bp 245–250 °C (1.2 mm); IR (thin film) 2960, 2930, 2825, 1650, 1595, 1580, 1510, 1440, 1255, 1130, 1015 cm^{-1}; ^{1}H NMR δ 7.75 (d, J = 15.6 Hz, 1 H), 7.70 (d, J = 9.0 Hz, 1 H), 7.62 (s, 1 H), 7.41 (d, J = 15.6 Hz, 1 H), 7.28 (d, J = 9.0 Hz, 1 H), 7.21 (s, 1 H), 6.92 (d, J = 8.1 Hz, 1 H), 6.90 (d, J = 8.1 Hz, 1 H), 4.60 (sept, J = 5.8 Hz, 1 H), 3.95 (s, 6 H), 3.89 (s, 3 H), 1.40 (d, J = 5.8 Hz, 6 H); CIMS (isobutane) m/z (relative intensity) 357 (MH$^+$, 100), 356 (M$^+$, 8).

2-(3-Isopropoxy-4-methoxyphenyl)-4-(3,4-dimethoxyphenyl)-4-oxobutyronitrile (15). Acetic acid (2.3 mL) was added to a solution of enone **14** (10.40 g, 0.0292 mol) in 2-ethoxyethanol (53 mL) at 100 °C. An aqueous solution of potassium cyanide (5.1 g, 0.078 mol) in water (9.4 mL) was then added to the solution at 118 °C, and the mixture was stirred at 118 °C for 7 min. The reaction mixture was cooled to room temperature and poured into ice water (150 mL). Recrystallization of the crude material from methanol gave nitrile **15** (10.47 g, 93%): mp 104–105 °C; IR (KBr) 2955, 2920, 2825, 1668, 1585, 1507, 1455, 1337, 1305, 1250, 1237, 1150, 1135, 1100, 1010 cm^{-1}; ^{1}H NMR δ 7.51 (d, J = 5.9 Hz, 1 H), 7.50 (s, 1 H), 6.95–6.98 (m, 4 H), 4.46–4.58 (m, 2 H), 3.94 (s, 3 H), 3.92 (s, 3 H), 3.84 (s, 3 H), 3.64 (dd, J = 17.7, 7.8 Hz, 1 H), 3.44 (dd, J = 17.7, 6.5 Hz, 1 H), 1.38 (d, J = 6.2 Hz, 3 H), 1.36 (d, J = 6.2 Hz, 3 H); CIMS (isobutane) m/z (relative intensity) 384 (MH$^+$, 100); HRCIMS calcd for C$_{22}$H$_{26}$NO$_5$ 384.1811, found 384.1815. Anal. Calcd for C$_{22}$H$_{25}$NO$_5$: C, H.

2-(3-Isopropoxy-4-methoxyphenyl)-4-(3,4-dimethoxyphenyl)-4-oxobutyric Acid (16). A mixture containing nitrile **15** (4.50 g, 0.0117 mol), water (50 mL), ethanol (21.6 mL), and sodium hydroxide (4.77 g, 0.119 mol) was heated under nitrogen at reflux for 8 h. The mixture was cooled, and water (25 mL) was added. The resulting mixture was washed with ether (35 mL). The aqueous layer was acidified with 10% HCl and extracted with chloroform (3 × 30 mL). The combined chloroform extracts were dried (Na$_2$SO$_4$) and concentrated to give acid **16** (3.75 g, 79%), which was recrystallized from benzene–hexanes: mp 162–163 °C; IR (KBr) 3700–2400, 1705, 1674, 1590, 1510, 1448, 1420, 1325, 1255, 1135, 1015 cm^{-1}; ^{1}H NMR δ 10.70 (br s, 1 H), 7.59 (d, J = 8.5 Hz, 1 H), 7.51 (s, 1 H), 6.92–6.81 (m, 4 H), 4.53 (sept, J = 5.8 Hz, 1 H), 4.21 (dd, J = 10.0, 3.9 Hz, 1 H), 3.94 (s, 3 H), 3.91 (s, 3 H), 3.86 (m, 1 H), 3.83 (s, 3 H), 3.26 (dd, J = 17.8, 3.9 Hz, 1 H), 1.36 (d, J = 5.8 Hz, 3 H), 1.35 (d, J = 5.8 Hz, 3 H); CIMS (isobutane) m/z (relative intensity) 403 (MH$^+$, 100); HRCIMS calcd for C$_{22}$H$_{27}$O$_7$ 403.1756, found 403.1750. Anal. Calcd for C$_{22}$H$_{26}$O$_7$: C, H.

2-(3-Isopropoxy-4-methoxyphenyl)-4-(3,4-dimethoxyphenyl)butyric Acid (17). A mixture of intermediate **16** (3.50 g, 0.00870 mol) and 10% Pd/C (1.00 g) in acetic acid (112 mL) was hydrogenated at atmospheric pressure at room temperature for 3 days. The catalyst was filtered off. The solvent was removed under high vacuum at room temperature, and the residue was taken up in chloroform, dried (Na$_2$SO$_4$), and concentrated to give acid **17** (3.32 g, 98%), which was crystallized from ethyl

acetate−hexanes: mp 79−82 °C; IR (KBr) 3650−2400, 1705, 1590, 1515, 1450, 1415, 1260, 1230, 1135, 1100, 1020 cm^{-1}; ^{1}H NMR δ 11.63 (br s, 1 H), 6.97−6.61 (m, 6 H), 4.52 (sept, J = 6.1 Hz, 1 H), 3.85 (s, 6 H), 3.84 (s, 3 H), 3.48 (t, J = 7.6 Hz, 1 H), 2.54 (t, J = 7.0 Hz, 2 H), 1.97−1.88 (m, 2 H), 1.36 (d, J = 6.1 Hz, 6 H); CIMS (isobutane) m/z (relative intensity) 389 (MH^{+}, 16), 347 (MH^{+} − C$_3$H$_6$, 100); HREIMS calcd for C$_{22}$H$_{28}$O$_6$ 388.1886, found 388.1878.

2-(3-Isopropoxy-4-methoxyphenyl)-6,7-dimethoxy-1-tetralone (18). A mixture containing acid **17** (3.00 g, 0.00772 mol), potassium carbonate (14.0 g, 0.101 mol), and dry chloroform (18 mL) was stirred at room temperature for 0.5 h under nitrogen. Phosphorus oxychloride (6.6 mL, 0.0708 mol) was added, and the mixture was heated at 80 °C for 75 min. The reaction mixture was poured into ice water (100 mL), made alkaline with 5% NaOH (50 mL), and extracted with chloroform (3 × 40 mL). The combined extracts were dried (Na$_2$SO$_4$) and concentrated. The residue was chromatographed on a silica gel column using 25% ethyl acetate−hexanes to afford pure **18** (1.56 g, 55%): mp 115−116 °C; IR (KBr) 2970, 2930, 2830, 1672, 1603, 1518, 1450, 1370, 1338, 1270, 1195, 1135, 1020 cm^{-1}; ^{1}H NMR δ 7.58 (s, 1 H), 6.95−6.66 (m, 4 H), 4.49 (sept, J = 6.0 Hz, 1 H), 3.95 (s, 3 H), 3.92 (s, 3 H), 3.84 (s, 3 H), 3.69 (t, J = 7.6 Hz, 1 H), 3.19−2.83 (m, 2 H), 2.58−2.25 (m, 2 H), 1.34 (d, J = 6.0 Hz, 3 H), 1.33 (d, J = 6.0 Hz, 3 H); CIMS m/z (relative intensity) 371 (MH^{+}, 100); HRCIMS calcd for C$_{22}$H$_{27}$O$_5$ 371.1858, found 371.1862. Anal. Calcd for C$_{22}$H$_{26}$O$_5$: C, H.

1,2,3,4-Tetrahydro-2-(3′-isopropoxy-4′-methoxyphenyl)-6,7-dimethoxy-1-(methylimino)naphthalene (19). Methylamine (5.0 g) was bubbled through a chloroform solution (10 mL) containing **18** (0.60 g, 0.00162 mol) at 0 °C for 10 min. The solution was added to a solution of titanium(IV) chloride (0.40 mL, 0.00364 mol) in chloroform (5 mL) at 0 °C under nitrogen. The reaction mixture was stirred at room temperature for 18 h under nitrogen. The precipitate was filtered off, and the filtrate was concentrated to give **19** (0.62 g, 100%) as an oil. This material was used immediately in the next step without any further purification: ^{1}H NMR δ 7.90 (s, 1 H), 6.79−6.59 (m, 4 H), 4.41 (sept, J = 6.0 Hz, 1 H), 4.28 (m, 1 H), 4.01 (s, 3 H), 3.91 (s, 3 H), 3.82 (s, 3 H), 3.24 (s, 3 H), 2.95−2.00 (m, 4 H), 1.32 (d, J = 6.0 Hz, 3 H), 1.30 (d, J = 6.0 Hz, 3 H); CIMS (isobutane) m/z (relative intensity) 384 (MH^{+}, 100).

***cis*-1,2,3,4-Tetrahydro-2-(3′-isopropoxy-4′-methoxyphenyl)-6,7-dimethoxy-1-(methylamino)naphthalene (20).** Sodium borohydride (0.35 g, 0.00925 mol) was added to a solution of imine **19** (0.62 g, 0.00162 mol) in methanol (30 mL). The reaction mixture was stirred at room temperature for 1.5 h. Methanol was removed on the rotary evaporator, and water (20 mL) was added to the residue. The mixture was extracted with chloroform (3 × 25 mL). The combined chloroform extracts were dried (Na$_2$SO$_4$) and concentrated to give **20** (0.58 g, 93%) as an oil, which was used in the next step without any further purification: IR (thin film) 3310, 2980, 2940, 2840, 2780, 1610, 1520, 1470, 1460, 1445, 1335, 1265, 1140, 1125, 1030 cm^{-1}; ^{1}H NMR δ 6.87−6.81 (m, 4 H), 6.66 (s, 1 H), 4.48 (sept, J = 6.0 Hz, 1 H), 3.88 (s, 3 H), 3.87 (s, 3 H), 3.85 (s, 3 H), 3.62 (d, J = 3.6 Hz, 1 H), 3.16 (dt, J = 11.7, 3.6 Hz, 1 H), 3.00−2.64 (m, 2 H), 2.54−2.25 (m, 1 H), 2.22 (s, 3 H), 2.10−1.86 (m, 1 H), 1.36 (br s, 1 H), 1.35 (d, J = 6.0 Hz, 6 H); CIMS (isobutane) m/z (relative intensity) 386 (MH^{+}, 23), 355 (MH^{+} − CH$_3$NH$_2$, 100); HRCIMS calcd for C$_{23}$H$_{32}$NO$_4$ 386.2331, found 386.2335.

***cis*-1,2,3,4-Tetrahydro-2-(3-isopropoxy-4-methoxyphenyl)-6,7-dimethoxy-1-(N-methylformamido)naphthalene (21).** A mixture containing amine **20** (570.2 mg, 1.479 mmol), chloral (0.40 mL, freshly prepared by mixing chloral hydrate with an equal amount of concentrated sulfuric acid and then distilling it), and dry chloroform (10 mL) was heated at reflux for 3 h under nitrogen. Water (20 mL) was added, and the mixture was extracted with chloroform (3 × 30 mL). The chloroform extracts were dried (Na$_2$SO$_4$) and concentrated. The residue was chromatographed on two silica gel plates (2 mm thickness) using 60% ethyl acetate−hexanes to give **21** (480.6 mg, 79%), which was recrystallized from benzene−hexanes: mp 140−141 °C; IR (KBr) 2930, 2825, 1670, 1605, 1515, 1440, 1425, 1245, 1110, 1010 cm^{-1}; ^{1}H NMR δ 7.80 (s, $^{1}/_5$ H), 7.63 (s, $^{4}/_5$ H), 6.97−6.56 (m, 4 H), 6.52 (s, 1 H), 4.63 (d, J = 5.0 Hz, 1 H), 4.50 (sept, J = 6.1 Hz, 1 H), 3.90 (s, 3 H), 3.84 (s, 3 H), 3.81 (s, 3 H), 3.27−2.78 (m, 3 H), 2.56 (s, $^{3}/_5$ H), 2.52 (s, $^{12}/_5$ H), 2.36−1.93 (m, 2 H), 1.36 (d, J = 6.1 Hz, 6 H); CIMS (isobutane) m/z (relative intensity) 414 (MH^{+}, 9), 355 (MH^{+} − C$_2$H$_5$NO, 100); HRCIMS calcd for C$_{24}$H$_{32}$NO$_5$ 414.2280, found 414.2238. Anal. Calcd for C$_{24}$H$_{31}$NO$_5$: C, H.

2-(3-Isopropoxy-4-methoxyphenyl)-6,7-dimethoxy-1-(N-methylformamido)naphthalene (22). DDQ (767.7 mg, 3.382 mmol) was added to a solution of formamide **21** (463.7 mg, 1.121 mmol) in dry benzene (25 mL) at room temperature under nitrogen. The mixture was heated at reflux for 2 h. The resulting precipitate was filtered, and the filtrate was concentrated. The residue was taken in chloroform (25 mL) and washed with 5% NaOH solution (20 mL). The aqueous layer was extracted again with chloroform (4 × 25 mL). The combined chloroform extracts were dried (Na$_2$SO$_4$) and concentrated to give **22** (419 mg, 91%), which was recrystallized from benzene−hexanes: mp 147−148 °C; IR (KBr) 2970, 2930, 2830, 1685, 1510, 1465, 1420, 1335, 1320, 1260, 1240, 1220, 1160, 1135, 1105, 1020, 995 cm^{-1}; ^{1}H NMR δ 8.42 (s, $^{1}/_5$ H), 8.19 (s, $^{4}/_5$ H), 7.76 (d, J = 8.3 H, 1 H), 7.38 (d, J = 8.3 Hz, 1 H), 7.21 (s, 1 H), 7.05−6.80 (m, 4 H), 4.53 (sept, J = 5.8 Hz, 1 H), 4.04 (s, 3 H), 3.99 (s, 3 H), 3.89 (s, 3 H), 3.09 (s, $^{12}/_5$ H), 2.96 (s, $^{3}/_5$ H) 1.38 (d, J = 5.8 Hz, 6 H); CIMS (isobutane) m/z (relative intensity) 410 (MH^{+}, 65), 152 (100); HRCIMS calcd for C$_{24}$H$_{28}$NO$_5$ 410.1967; found 410.1925. Anal. Calcd for C$_{24}$H$_{27}$NO$_5$: C, H.

9-Isopropoxy-2,3,8-trimethoxy-5-methylbenzo[c]-phenanthridinium Chloride (23). Phosphorus oxychloride (0.40 mL) was added to a solution of formamide **22** (200.2 mg, 0.489 mmol) in acetonitrile (10 mL) at room temperature under nitrogen. The mixture was heated at reflux for 0.5 h. The mixture was cooled and poured into ice water (10 mL). The resulting precipitate was filtered and washed with cold water (3 mL) and benzene (10 mL). The precipitate was recrystallized from methanol−chloroform to give **23** (187.1 mg, 89%): mp 276−279 °C; IR (KBr) 3400, 2860, 1610, 1505, 1455, 1425, 1380, 1267, 1210, 1090, 1000 cm^{-1}; ^{1}H NMR (CF$_3$COOD) δ 9.39 (s, 1 H), 8.58 (d, J = 8.8 Hz, 1 H), 8.29 (d, J = 8.8 Hz, 1 H), 8.26 (s, 1 H), 8.18 (s, 1 H), 7.81 (s, 1 H), 7.69 (s, 1 H), 5.30 (sept, J = 5.8 Hz, 1 H), 5.10 (s, 3 H), 4.28 (s, 3 H), 4.25 (s, 3 H), 4.24 (s, 3 H), 1.68 (d, J = 5.8 Hz, 6 H); CIMS (isobutane) m/z (relative intensity) 378 (MH^{+} − CH$_3$Cl, 100); HRCIMS calcd for C$_{23}$H$_{24}$NO$_4$ 378.1705, found 378.1654.

9-Hydroxy-2,3,8-trimethoxy-5-methylbenzo[c]-phenanthridinium Chloride (24). A mixture containing **23** (60.4 mg, 0.141 mmol) and methanesulfonic acid (2.5 mL) was heated at 57 °C for 2 h. The mixture was cooled and poured into diethyl ether (25 mL). The

resulting precipitate was filtered and stirred with 10% NaCl solution (8 mL) at room temperature for 1 h. The resulting solid was filtered, washed with cold water (1 mL), and dried. This solid was recrystallized from methanol to give **24** (35.1 mg, 64%): mp 250–252 °C (lit. (57) mp 261–263 °C); IR (KBr) 3600–2200, 1612, 1540, 1450, 1410, 1320, 1302, 1275, 1210, 1172, 1125, 1010 cm^{-1}; ^{1}H NMR δ 9.39 (s, 1 H), 8.56 (d, J = 9.0 Hz, 1 H), 8.35 (s, 1 H), 8.27 (d, J = 9.0 Hz, 1 H), 8.17 (s, 1 H), 7.75 (s, 1 H), 7.67 (s, 1 H), 5.09 (s, 3 H), 4.27 (s, 3 H), 4.25 (s, 6 H); CIMS (isobutane) m/z (relative intensity) 350 (M$^+$ − Cl$^-$, 41), 336 (MH$^+$ − CH$_3$Cl, 100).

9-[5-(Ethoxycarbonyl)-*n*-pentoxy]-5,6-dihydro-2,3,8-trimethoxy-5-methylbenzo[*c*]phenanthridine (25). NaH (60% in mineral oil, 200 mg, 5 mmol) was added in portions to a mixture of 9-hydroxy-5-methyl-2,3,8-trimethoxybenzo[*c*]phenanthridinium chloride (**24**, 385 mg, 1 mmol) and dry DMSO (30 mL). The reaction mixture was stirred for 30 min and ethyl 6-bromohexanoate added. The reaction mixture was stirred overnight, and a clear solution was obtained. Sodium borohydride (76 mg, 2 mmol) was added and the resulting mixture stirred for 1 h and diluted with methylene chloride (70 mL). The solution was washed with 2 N sodium carbonate (5 × 40 mL), dried (Na$_2$SO$_4$), and concentrated. The residue was chromatographed through a short column (silica gel) using methylene chloride and ethyl acetate to give **25** (388 mg, 79%). Recrystallization from ethyl acetate–hexane gave an analytically pure sample: mp 133 °C; IR (KBr) 2942, 2868, 1733, 1605, 1504, 1463, 1364, 1301, 1251, 1012 cm^{-1}; NMR δ 7.93 (s, 1 H), 7.91 (d, J = 8.0 Hz, 1 H), 7.61 (d, J = 8.6 Hz, 1 H), 7.16 (s, 1 H), 7.03 (s, 1 H), 6.56 (s, 1 H), 4.13 (s, 2 H), 3.99 (q, J = 7.0 Hz, 2 H), 3.86 (t, J = 6.2 Hz, 2 H), 3.64 (s, 3 H), 3.53 (s, 6 H), 2.66 (s, 3 H), 2.14 (t, J = 7.1 Hz, 2 H), 1.78–1.35 (m, 6 H), 0.99 (t, J = 7.1 Hz, 3 H); CIMS m/z (relative intensity) 494 (MH$^-$, 100); HRCIMS calcd for C$_{29}$H$_{36}$NO$_6$ 494.2543, found 494.2523. Anal. Calcd for C$_{29}$H$_{35}$NO$_6$: C, H, N.

5,6-Dihydro-9-[(6'-hydroxy-*n*-hexyl)oxy]-2,3,8-trimethoxybenzo[*c*]phenanthridine (26). Lithium aluminum hydride (50 mg, 1.34 mmol) was added to a solution of the ester **25** (329 mg, 0.66 mmol) in dry ether (40 mL), and the resulting mixture was stirred at room temperature for 1 h. The reaction mixture was quenched with 2 N sodium carbonate solution (3 mL) at 0 °C. The organic layer was separated, and the residue was diluted with 2 N sodium carbonate solution (30 mL) and extracted with methylene chloride (4 × 30 mL). The combined organic layer was dried (Na$_2$SO$_4$) and concentrated to give **26** (242 mg, 80%). Chromatography on silica gel with 30% ethyl acetate in methylene chloride and recrystallization from ethyl acetate–hexane afforded an analytically pure sample: mp 150 °C; IR (KBr) 3529, 2935, 2860, 1605, 1561, 1503, 1463, 1350, 1300, 1247, 1206, 1153, 1012 cm^{-1}; ^{1}H NMR δ 7.92 (s, 1 H), 7.90 (d, J = 7.8 Hz, 1 H), 7.53 (s, 1 H), 7.02 (s, 1 H), 6.55 (s, 1 H), 6.04 (d, J = 8.4 Hz, 1 H), 4.12 (s, 2 H), 3.92 (m, 2 H), 3.63 (s, 3 H), 3.52 (s, 6 H), 3.43–3.22 (m, 2 H), 2.65 (s, 3 H), 1.86–1–63 (m, 2 H), 1.60–1.12 (m, 6 H); CIMS m/z (relative intensity) 452 (MH$^+$, 100); HRCIMS calcd for C$_{27}$H$_{34}$NO$_5$ 452.2437, found 452.2418. Anal. Calcd for C$_{27}$H$_{33}$NO$_5$: C, H, N.

9-[(6'-Hydroxy-*n*-hexyl)oxy]-5,6-dihydro-2,3,8-trimethoxy-5-methylbenzo[*c*]phenanthridine 6'-*O*-(2-Cyanoethyl *N,N*-diisopropylphosphoramidite) (27). A solution of 2-cyanoethyl *N,N*-diisopropylchlorophosphoramidite (107 mg, 0.45 mmol) was added dropwise to a solution of the alcohol **26** (102 mg, 0.22 mmol) and *N,N*-diisopropylethylamine (174 mg, 1.35 mmol) at 0 °C in dry methylene chloride (2 mL) under nitrogen. The

resulting solution was stirred for 40 min, diluted with methylene chloride (20 mL), and washed with cold 2 N Na$_2$CO$_3$ (4 × 10 mL). The organic layer was dried (Na$_2$SO$_4$) and concentrated. The residue was chromatographed on silica gel (chromatotron) with 30% ethyl acetate in methylene chloride to give **27** (106 mg, 79%) as a semisolid: IR (neat) 2935, 2251, 1606, 1503, 1477, 1463, 1355, 1348, 1300, 1246, 1220, 1205, 1154, 1012 cm^{-1}; ^{1}H NMR (CDCl$_3$) δ 7.70 (d, J = 8.5 Hz, 1 H), 7.66 (s, 1 H), 7.54 (d, J = 8.5 Hz, 1 H), 7.33 (s, 1 H), 7.14 (s, 1 H), 6.81 (s, 1 H), 4.16 (s, 2 H), 4.14 (t, J = 7.0 Hz, 2 H), 4.08 (s, 3 H), 4.02 (s, 3 H), 3.94 (s, 3 H), 3.90–3.56 (m, 6 H), 2.63 (m, 5 H), 1.95–1.88 (m, 2 H), 1.71–1.44 (m, 6 H), 1.19–1.17 (m, 12 H); FABMS m/z (relative intensity) 652 (MH+, 37), 651 (M+, 67), 650 (86), 350 (100).

6-Hex-5'-enyl-5,6-dihydro-8,9-dimethoxy-5-methyl-2,3-(methylenedioxy)benzo[*c*]phenanthridine (28). Magnesium (250 mg, 10.28 mmol) was added to a solution of 6-bromo-1-hexene (1.31 g, 8.03 mmol) in dry THF (10 mL) and the mixture stirred at room temperature for 30 min. The reaction mixture was then heated at reflux for 1 h. Nitidine chloride (**1**, 300 mg, 0.78 mmol) was added. The reaction mixture was heated at reflux for 1 h, the reaction was quenched with 1 N HCl (30 mL), and the resulting mixture was extracted with chloroform (3 × 40 mL). The combined chloroform extracts were washed with water (25 mL), dried (Na$_2$SO$_4$), and concentrated. The residue was chromatographed on a silica gel plate (1 mm thickness) using 25% ethyl acetate in hexane to give **28** (248 mg, 74%) as an oil: IR (neat) 2935, 2845, 1635, 1603, 1522, 1500, 1470, 1397, 1350, 1250, 1175, 1145, 1035 cm^{-1}; ^{1}H NMR δ 7.70 (s, 1 H), 7.67 (d, J = 8.4 Hz, 1 H), 7.47 (d, J = 8.4 Hz, 1 H), 7.32 (s, 1 H), 7.11 (s, 1 H), 6.72 (s, 1 H), 6.04 (s, 2 H), 5.74 (m, 1 H), 4.90 (m, 2 H), 3.98 (s, 3 H), 3.95 (s, 3 H), 3.84 (m, 1 H), 2.62 (s, 3 H), 1.97 (m, 2 H), 1.71–1.10 (m, 6 H); CIMS m/z (relative intensity) 432 (MH$^+$, 100), 431 (M$^+$, 25); HREIMS calcd for C$_{27}$H$_{29}$NO$_4$ 431.2097, found 431.2101.

6-(6-Hydroxyhexyl)-8,9-dimethoxy-5-methyl-2,3-(methylenedioxy)benzo[*c*]phenanthridine (29). 9-BBN (6.4 mL, 0.5 M in THF, 3.2 mmol) was added to a solution of **28** (230 mg, 0.53 mmol) in dry THF (15 mL) under nitrogen, and the mixture was stirred at room temperature for 3 days. NaOH (1.5 N, 4.0 mL) and 30% hydrogen peroxide (2.0 mL) were added, and the mixture was heated at 50 °C for 1 h. Water (20 mL) was added, and the mixture was extracted with chloroform (3 × 25 mL). The combined chloroform extracts were dried (Na$_2$SO$_4$) and concentrated. The residue was chromatographed on a silica gel plate (2 mm thickness) using 60% ethyl acetate in hexane to give **29** (185 mg, 77%) as an oil: IR (neat) 3350, 2905, 2840, 1595, 1515, 1490, 1450, 1390, 1340, 1235, 1160, 1135, 1015 cm^{-1}; ^{1}H NMR δ 7.70 (s, 1 H), 7.69 (d, J = 8.3 Hz, 1 H), 7.48 (d, J = 8.3 Hz, 1 H), 7.32 (s, 1 H), 7.11 (s, 1 H), 6.73 (s, 1 H), 6.05 (s, 2 H), 3.99 (s, 3 H), 3.95 (s, 3 H), 3.84 (t, J = 6.0 Hz, 1 H), 3.56 (t, J = 6.0 Hz, 2 H), 2.62 (s, 3 H), 2.00–1.00 (m, 11 H); CIMS m/z (relative intensity) 450 (MH$^+$, 100); HRCIMS calcd for C$_{27}$H$_{32}$NO$_5$ 450.2280, found 450.2234.

6-[(6'-Hydroxy-*n*-hexyl)oxy]-5,6-dihydro-8,9-dimethoxy-5-methyl-2,3-(methylenedioxy)benzo[*c*]phenanthridine 6'-*O*-(2-Cyanoethyl *N,N*-diisopropylphosphoramidite) (30). A solution of 2-cyanoethyl *N,N*-diisopropylchlorophosphoramidite (123 mg, 0.52 mmol) in dry methylene chloride (2 mL) was added dropwise to a stirred solution of the alcohol **29** (120 mg, 0.26 mmol) and *N,N*-diisopropylethylamine (134 mg, 1.04 mmol) in dry methylene chloride (3 mL) at 0 °C under nitrogen. The reaction mixture was stirred at room

temperature for 50 min, diluted with methylene chloride, and washed with cold 10% NaHCO$_3$ (15 mL) and with cold water (3 × 15 mL). The organic layer was dried (Na$_2$-SO$_4$) and concentrated *in vacuo* at room temperature. The residue was chromatographed on silica gel (chromatotron) using 30% ethyl acetate in methylene chloride to give **30** (148 mg, 89%) as a semisolid: IR (neat) 2965, 2930, 2868, 1607, 1526, 1499, 1396, 1363, 1350, 1312, 1243, 1200, 1183, 1147, 1079, 1039 cm^{-1}; NMR δ 7.70 (d, J = 8.5 Hz, 1 H), 7.70 (s, 1 H), 7.48 (d, J = 9.0 Hz, 1 H), 7.32 (s, 1 H), 7.12 (s, 1 H), 6.73 (s, 1 H), 6.08–6.05 (m, 2 H), 3.99 (s, 3 H), 3.96 (s, 3 H), 3.83–3.41 (m, 7 H), 2.65–2.58 (m, 5 H), 1.60–1.23 (m, 1 H), 1.22–1.12 (m, 12 H); ^{31}P NMR (202 MHz) 146.29; FABMS 650 (MH$^+$, 5), 649 (M$^+$, 15), 648 (M$^+$ − 1, 21), 432 (12), 349 (49), 348 (100); HRFABMS calcd for C$_{36}$H$_{49}$N$_3$O$_6$P 650.3356, found 650.3231.

Benzophenanthridine−Oligonucleotide Conjugate 34. Automated solid phase oligonucleotide synthesis was performed on a modified Milligen 7500 DNA Synthesizer. A three-way valve was placed between the synthesis column and the synthesizer to permit manual introduction of small volumes of phosphoramidite solutions without removing the synthesis column from the machine. The synthesis reagents and deoxyribonucleoside phosphoramidites were obtained from Milligen. The solid support was (dimethoxytrityl)uridine CPG (30 μmol/g, Milligen). Oligonucleotide synthesis was conducted using a standard 1 μmol scale synthesis protocol. After the final 5′-dimethoxytrityl group was removed, and the support washed extensively with acetonitrile, the synthesizer was halted to permit manual addition of the dihydrofagaronine phosphoramidite. Phosphoramidite **5** (20 μmol) was dissolved in 1*H*-tetrazole−acetonitrile solution (0.35 M, 540 μL) in a syringe and introduced to the system and allowed to react with the support-bound oligonucleotide for 5 min. The synthesizer was then allowed to continue a normal coupling cycle. The final phosphite triester linkage and the fagaronine moiety were oxidized by the synthesizer using standard aqueous I$_2$ solution (0.05 M I$_2$ in THF, water, pyridine (7:2:1), 1 min exposure). After the synthesis was completed by the machine, the support containing the fagaronine oligonucleotide conjugate was placed in a pressure vial and treated with 2 mL of concentrated ammonium hydroxide solution at 55 °C for 12−14 h. The supernatant solution was then filtered to remove the controlled pore glass and concentrated to dryness *in vacuo*. The fagaronine−oligonucleotide conjugate **33** was isolated by reverse phase HPLC. Conjugate **33** was loaded on the column (30 × 0.4 cm column MCG-10/MicroPack, Varian) in H$_2$O and eluted with a linear gradient from 100% solvent A (0.1 M triethylammonium acetate, pH 6.5) to 40% solvent B (95% aqueous acetonitrile) over 40 min at a flow rate of 1 mL/min. The purified product was characterized by FAB mass spectrometry in the positive ion mode (dithiothreitol−dithioerythritol, 3:1 v/v, calcd for C$_{115}$H$_{142}$N$_{32}$O$_{63}$P$_9$ M$^+$ *m/z* 3257, found *m/z* 3257). The 3′ ribonucleoside residue was then removed by periodate oxidation and β-elimination (0.04 M NaIO$_4$, 0 °C, 1 h in the dark; excess periodate removed by incubation with 0.05 M methionine, 0 °C, 30 min; β-elimination 0.04 M cyclohexylamine, 0.1 M HEPES, pH 8.0, 45 °C, 90 min) to give conjugate **34**. The final product was then purified by anion exchange HPLC (58).

RESULTS AND DISCUSSION

A. Attachment of the Linker Chain to the "Right-Hand" Side. Fagaronine (**2**) was reacted with the tosylate of ethyl 6-hydroxyhexanoate in the presence of

Scheme 1
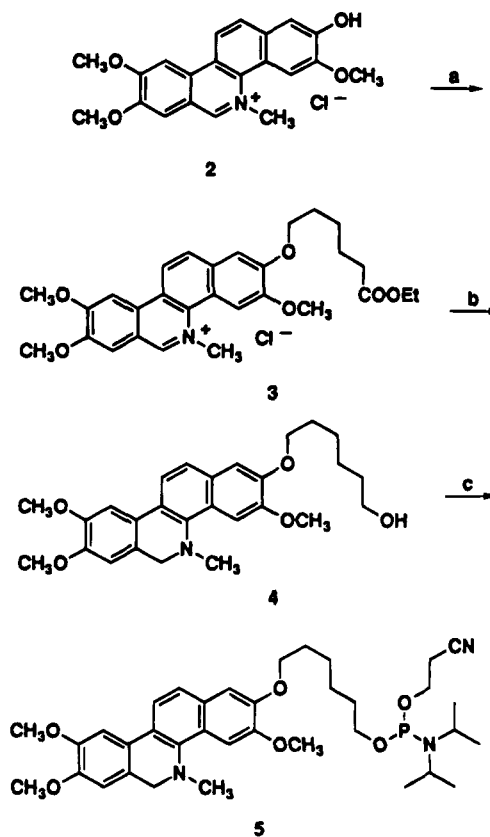
^{a} Reagents: (a) (1) KO-*t*-Bu, DMSO, room temperature (30 min), (2) TsO(CH$_2$)$_5$COOEt, room temperature (24 h); (b) LiAlH$_4$, THF, room temperature (4 h); (c) (1) EtN(*i*-Pr)$_2$, THF, room temperature (10 min), (2) 2-cyanoethyl *N*,*N*-diisopropylchlorophosphoroamidite, room temperature (1.5 h).

potassium *tert*-butoxide in dry DMSO at room temperature to afford the alkylated product **3** (Scheme 1) (*59*). Initially, the 5,6-didehydro derivative of **4**, having a charged *N*-methylisoquinolinium ring system, was prepared by a separate approach from that presented in Scheme 1 and was found to be practically insoluble in various organic solvents, causing the preparation of the corresponding phosphoramidite to proceed poorly. Furthermore, this phosphoramidite failed to react with the 5′-hydroxyl group of synthetic oligonucleotides. In view of these difficulties, both the ester and iminium group of intermediate **3** were reduced with lithium aluminum hydride in tetrahydrofuran to give intermediate **4**, which was readily converted to the phosphoramidite **5** in quantitative yield. It was anticipated that the dihydroisoquinoline ring system present in **5** would be oxidized to the desired aromatic, *N*-methylisoquinolinium moiety during the iodine oxidation of the phosphite linkage during the synthesis of the oligonucleotide−intercalator conjugates (Scheme 5). This approach involving dihydroisoquinolines was also taken in the subsequent syntheses of additional phosphoramidites in which the linker chain was attached to various other regions of the benzophenanthridine alkaloid ring system.

B. Attachment of the Linker Chain to the "Top". The starting material **6** was obtained as previously described in our total synthesis of nitidine chloride (*60*). Treatment of **6** with isopropenyl acetate in the presence of *p*-toluenesulfonic acid and air afforded the aryl acetate **7** (Scheme 2) (*61*). Hydrolysis of the acetate **7** with sodium hydroxide in aqueous ethanol and alkylation of the resulting anion with ethyl 6-bromoacetate gave intermediate **8**, which was reduced to **9** with lithium

Scheme 2
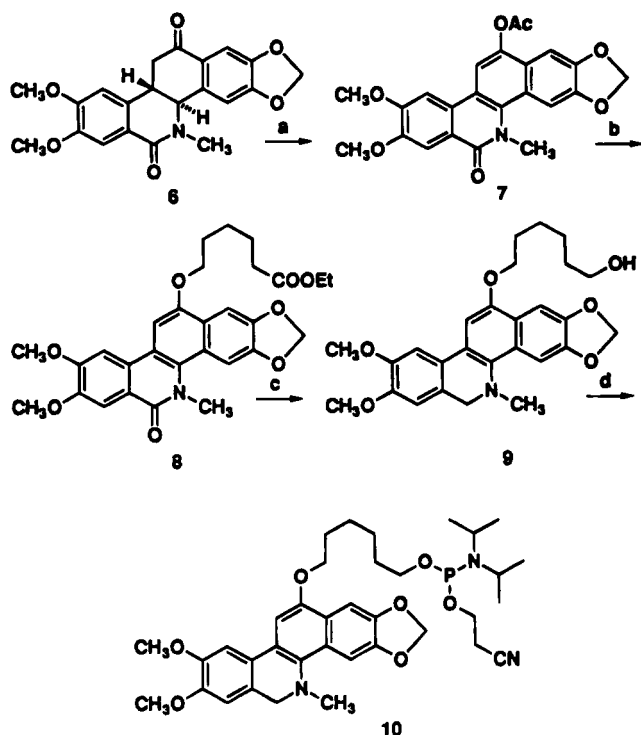
^{a} Reagents: (a) p-TsOH, isopropenyl acetate, air, reflux (24 h), 85 °C (24 h); (b) (1) NaOH, EtOH, H_2O, room temperature (2 h), (2) DMSO, ethyl 6-bromohexanoate, room temperature (18 h), (c) LiAlH$_4$, THF, reflux (18 h); (d) EtN(i-Pr)$_2$, 2-cyanoethyl N,N-diisopropylchlorophosphoramidite, CH_2Cl_2, 0 °C to room temperature (50 min).

aluminum hydride in refluxing THF. The primary alcohol **9** was converted to the corresponding phosphoramidite **10** with 2-cyanoethyl N,N-diisopropylchlorophosphoramidite in the presence of N,N-diisopropylethylamine in dry methylene chloride.

C. Attachment of the Linker Chain to the "Left-Hand" Side. A benzophenanthridine system having a phenolic hydroxyl group on the "left-hand" side was required in order to attach a linker chain using our approach. Since no suitable naturally occurring benzophenanthridines were available, the phenolic benzophenanthridine intermediate **24** was synthesized using an approach established by Ishii et al. (Scheme 3) (*56, 62, 63*). This approach utilizes an isopropyl protecting group for the phenol, which can be removed under acidic conditions.

Alkylation of the potassium phenoxide anion derived from the phenol **11** with 2-bromopropane in refluxing DMF afforded the isopropyl ether **12** (*56*). Condensation of the aldehyde **12** with 3,4-dimethoxyacetophenone (**13**) under basic conditions gave the chalcone **14**, which was converted to the nitrile **15** in the presence of potassium cyanide. Hydrolysis of the nitrile **15** with sodium hydroxide in refluxing aqueous ethanol gave the corresponding acid **16**. The ketone group of **16** was converted to a methylene by prolonged hydrogenolysis over palladium on charcoal to yield **17**, which underwent an intramolecular Friedel—Crafts reaction on treatment with phosphorus oxychloride to yield the substituted tetralone **18**. The imine intermediate **19** was obtained from treatment of the tetralone **18** with methylamine in the presence of titanium tetrachloride. Reduction of the imine **19** with sodium borohydride in methanol yielded the amine intermediate **20**, which was assigned the cis stereochemistry on the basis of the observed 3.5 Hz

Scheme 3
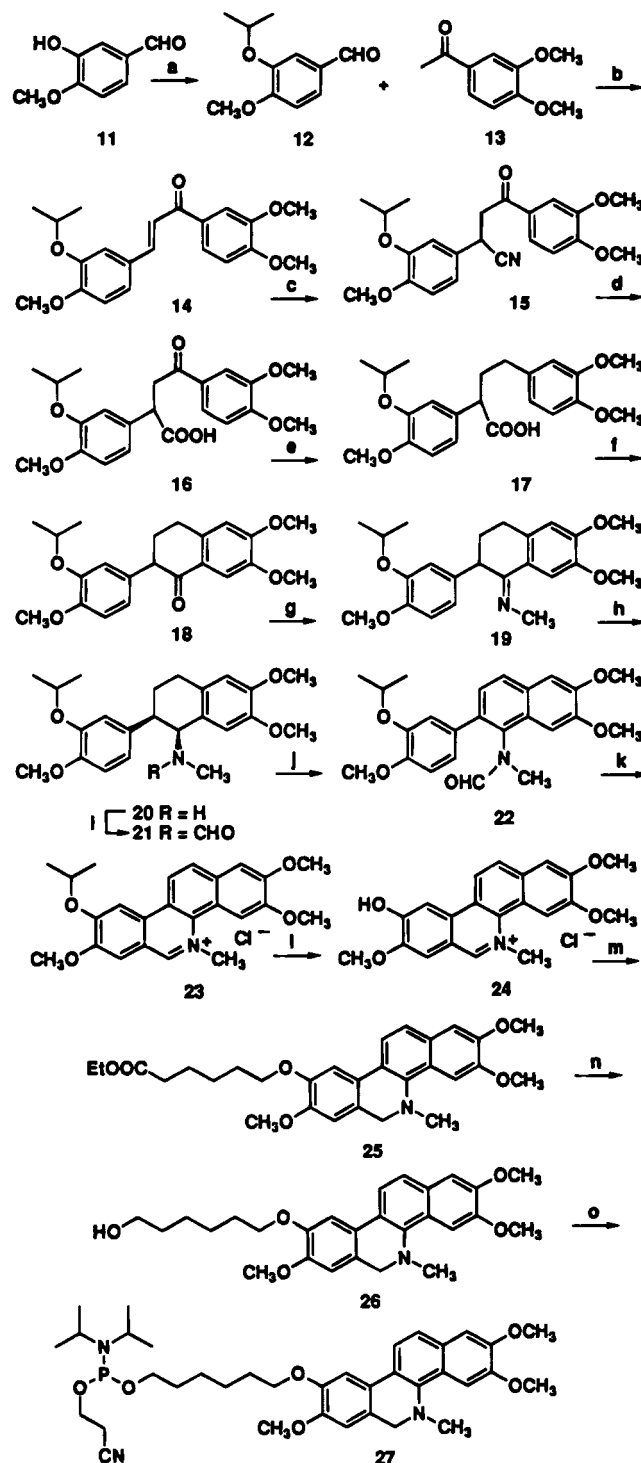
^{a} Reagents: (a) $CH_3CHBrCH_3$, K_2CO_3, DMF, reflux (2.5 h); (b) NaOH, EtOH, room temperature (20 h); (c) KCN, $CH_3CH_2OCH_2CH_2OH$, AcOH, H_2O, 118 °C (7 min); (d) NaOH, aqueous EtOH, reflux (8 h); (e) H_2, Pd/C, aqueous AcOH, room temperature (3 days); (f) (1) K_2CO_3, $CHCl_3$ (30 min), (2) $POCl_3$, 80 °C (75 min); (g) CH_3NH_2, $TiCl_4$, $CHCl_3$, room temperature (18 h); (h) NaBH$_4$, MeOH, room temperature (1.5 h); (i) CCl_3CHO, $CHCl_3$, reflux (3 h); (j) DDQ, C_6H_6, reflux (2 h); (k) $POCl_3$, CH_3CN, reflux (30 min); (l) CH_3SO_3H, 57 °C (2 h); (m) (1) NaH, DMSO, room temperature (30 min), (2) ethyl 6-bromohexanoate, room temperature (12 h), (3) NaBH$_4$, room temperature (1 h); (n) LiAlH$_4$, Et_2O, room temperature (1 h); (o) EtN(i-Pr)$_2$, 2-cyanoethyl N,N-diisopropylphosphoramidite, CH_2Cl_2, 0 °C to room temperature (40 min).

coupling constant between the methine protons in the ^{1}H NMR spectrum, in contrast to the 10 Hz coupling

Scheme 4
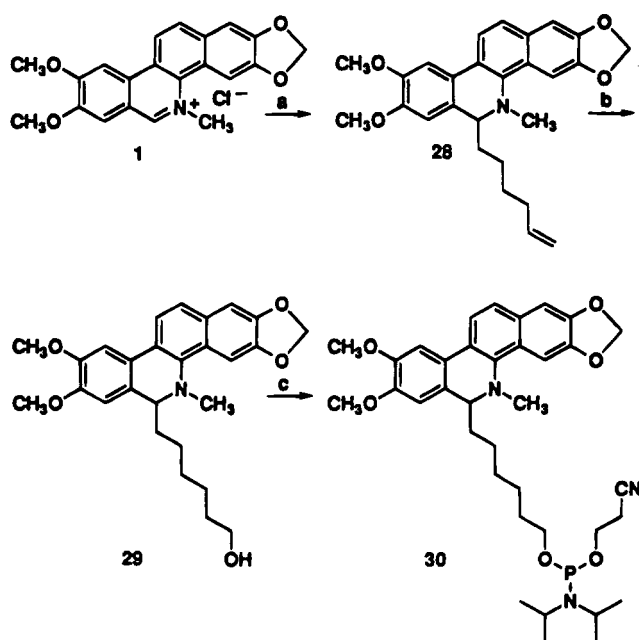
^{a} Reagents: (a) HC=CH(CH$_2$)$_4$MgBr, THF, reflux (1 h); (b) (1) 9-BBn, THF, room temperature (3 days), (2) H$_2$O$_2$, NaOH, THF, 50 °C (1 h); (c) EtN(i-Pr)$_2$, 2-cyanoethyl N,N-diisopropylphosphoramidite, CH$_2$Cl$_2$, 0 °C to room temperature (50 min).

constant expected for the corresponding *trans* isomer (*56, 62, 63*). Formylation of the amine **20** with chloral in refluxing chloroform provided the desired formamide **21**, which, in the presence of phosphorus oxychloride, underwent Bischler–Napieralski cyclization to the benzophenanthridine system **23**. The isopropyl protecting group was removed when **23** was heated at 57 °C in methanesulfonic acid for 2 h (*64*). Alkylation of the sodium phenoxide anion derived from the phenol **24** with ethyl 6-bromohexanoate in DMSO, followed by reduction of the iminium functionality with sodium borohydride, afforded compound **25**. The ester **25** was reduced to the primary alcohol **26** with lithium aluminum hydride. Treatment of the primary alcohol **26** with 2-cyanoethyl N,N-diisopropylchlorophosphoramidite in the presence of N,N-diisopropylethylamine in dry methylene chloride gave the phosphoramidite **27**.

D. Attachment of the Linker Chain to the "Bottom". The naturally occurring benzophenanthridine alkaloid nitidine chloride (**1**) was used as the starting material for the attachment of the linker chain to the "bottom" region. Addition of 5-hexenylmagnesium bromide to the iminium ion **1** afforded the alkene **28**, which underwent smooth hydroboration–oxidation to the primary alcohol **29** (Scheme 4). Treatment of the alcohol **29** with 2-cyanoethyl N,N-diisopropylphosphoramidite in the presence of N,N-diisopropylethylamine gave the phosphoramidite **30**.

E. Utilization of the Phosphoramidite 5 in the Synthesis of an Antisense Oligonucleotide–Intercalator Conjugate. In order to demonstrate the synthetic utility of these new benzophenanthridine phosphoramidite reagents, phosphoramidite **5** was used to prepare an oligonucleotide–fagaronine conjugate by semiautomated solid phase synthesis. The oligonucleotide containing a free 5'-hydroxyl group was constructed on an automated synthesizer using standard DNA synthesis procedures. After removal of the 5'-hydroxyl protecting group, the synthesizer was halted to permit manual addition of the fagaronine phosphoramidite. The phosphoramidite **5** was mixed with tetrazole in acetonitrile

Scheme 5
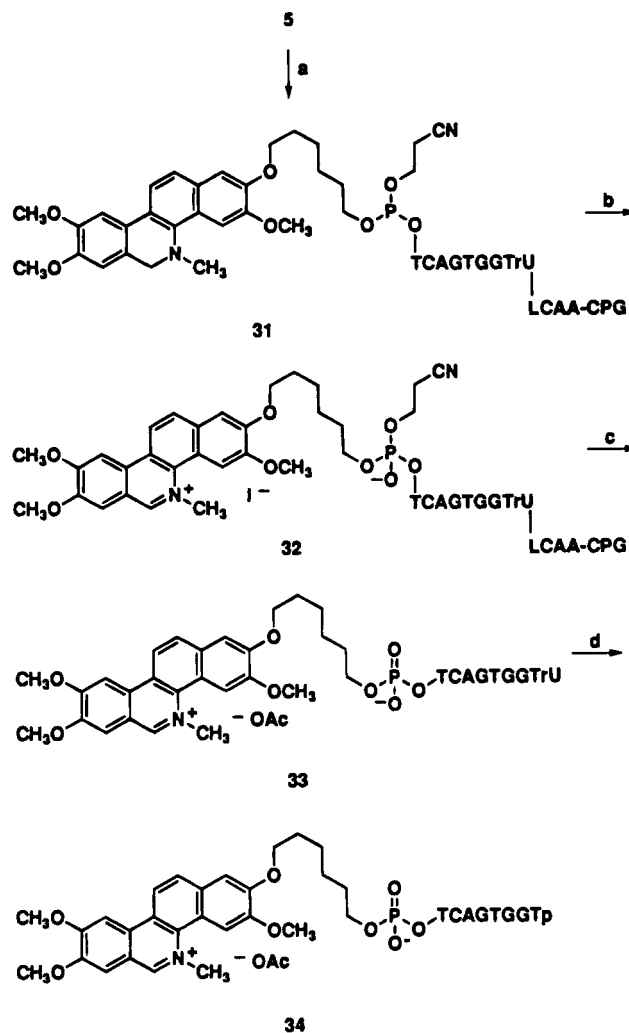
^{a} Reagents: (a) HO-5'-TCAGTGGTrU-LCAA-CPG, 1H-tetrazole in CH$_3$CN, 20 °C (5 min); (b) I$_2$ in THF, pyridine, H$_2$O, 20 °C (1 min); (c) concentrated NH$_4$OH, 55 °C (12–14 h); (d) NaIO$_4$, 0 °C (dark, 1 h); cyclohexylamine, HEPES, pH 8, 45 °C (90 min).

solution and reacted with the oligonucleotide on the solid support for 5 min to yield intermediate **31** (Scheme 5). The final phosphite linkage as well as the dihydrofagaronine residue were then oxidized by treatment with standard aqueous I$_2$ solution on the DNA synthesizer to provide **32**. The oligonucleotide–fagaronine conjugate was then released from the glass support and deprotected with concentrated ammonium hydroxide to yield the product **33**, which was isolated by reverse phase chromatography. FABMS in the positive ion mode displayed a peak at m/z 3257, consistent with structure **33**. Periodate oxidation and β-elimination afforded the final product **34**, bearing a 3'-terminal phosphate, which was purified by anion exchange HPLC (Figure 1). As judged from the HPLC trace in Figure 1, the iodine-mediated dehydrogenation of the dihydropyridine ring of **31** during its conversion to **32** occurs in high yield. The major component isolated from HPLC showed a significant absorbance in the UV/VIS spectrum at 390 nm, which is a characteristic absorbance of fagaronine chloride. The oligonucleotide sequence TCAGTGGT was designed to be complementary to residues 490–497 of rabbit β-globin mRNA, and the 3' terminal phosphate residue was included to prevent priming cDNA synthesis when the conjugates are tested as inhibitors of HIV-1 reverse transcriptase (*65*).
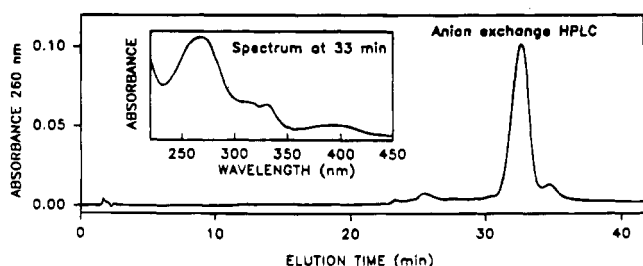
Figure 1. HPLC elution profile and UV/VIS spectrum obtained during the purification of **34**.

The binding of the conjugate **34** and the parent oligonucleotide TCAGTGGTp to a complementary RNA oligonucleotide were investigated by analysis of UV absorbance vs temperature melting curves. The T_m of the oligonucleotide TCAGTGGTp was 37 ± 1 °C, while the T_m of the conjugate **34** was 50 ± 1 °C (*66*). The IC_{50} values vs HIV-1 reverse transcriptase (globin mRNA assay) of 23 and 7 μM for TCAGTGGTp and the conjugate **34**, respectively, correlate with the T_m values (*65, 66*). However, the IC_{50} value of fagaronine chloride (**2**) itself was 2.2 μM.

The new benzophenanthridine phosphoramidite reagents described here should prove useful in the preparation of an array of antisense oligonucleotide—benzophenanthridine conjugates in which the linker chain is connected to various regions of the intercalator. This may in turn help to define the optimal orientation of the intercalating moiety in the double helix for inhibition of gene expression by the antisense oligonucleotide—intercalator conjugates.

ACKNOWLEDGMENT

LITERATURE CITED

(1) Whitton, J. L. (1994) Antisense Treatment of Viral Infection. *Adv. Virus Res. 44,* 267–303.

(2) Milligan, J. F., Matteucci, M. D., and Martin, J. C. (1993) Current Concepts in Antisense Drug Design. *J. Med. Chem. 36,* 1923–1937.

(3) Tonkinson, J. L., and Stein, C. A. (1993) Antisense Nucleic Acids - Prospects for Antiviral Intervention. *Antiviral Chem. Chemother. 4,* 193–400.

(4) Stein, C. A., and Cheng, Y.-C. (1993) Antisense Oligonucleotides as Therapeutic Agents - Is the Bullet Really Magic? *Science 261,* 1004–1012.

(5) To, R. Y.-L., and Neiman, P. E. (1992) *The Potential for Effective Antisense Inhibition of Retroviral Replication Mediated by Retroviral Vectors,* pp 261–271, Raven Press, Ltd., New York.

(6) Stein, C. A. (1992) Anti-sense Oligodeoxynucleotides - Promises and Pitfalls. *Leukemia 6,* 967–974.

(7) Degols, G., Leonetti, J.-P., Milhaud, P., Mechti, N., and Lebleu, B. (1992) Antisense Inhibitors of HIV: Problems and Perspectives. *Antiviral Res. 17,* 279–287.

(8) Agrawal, S., and Sarin, P. S. (1991) Antisense Oligonucleotides: Gene Regulation and Chemotherapy of AIDS. *Adv. Drug Del. Rev. 6,* 251–270.

(9) Mirabelli, C. K., Bennett, C. F., Anderson, K., and Crooke, S. T. (1991) *In vitro* and *In vivo* Pharmacologic Activities of Antisense Oligonucleotides. *Anti-Cancer Drug Des. 6,* 647–661.

(10) Cook, P. D. (1991) Medicinal Chemistry of Antisense Oligonucleotides - Future Opportunities. *Anti-Cancer Drug Des. 6,* 585–607.

(11) Cohen, J. S. (1991) Antisense Oligodeoxynucleotides as Antiviral Agents. *Antiviral Res. 16,* 121–133.

(12) Cohen, J. S. (1991) Oligonucleotides as Therapeutic Agents. *Pharm. Ther. 52,* 211–225.

(13) Calabretta, B. (1991) Inhibition of Protooncogene Expression by Antisense Oligodeoxynucleotides: Biological and Therapeutic Implications. *Cancer Res. 51,* 4505–4510.

(14) Hélène, C. (1991) Rational Design of Sequence-specific Oncogene Inhibitors Based on Antisense and Antigene Oligonucleotides. *Eur. J. Cancer 27,* 1466–1471.

(15) Uhlmann, E., and Peyman, A. (1990) Antisense Oligonucleotides: A New Therapeutic Principle. *Chem. Rev. 90,* 543–584.

(16) Tidd, D. M. (1990) A Potential Role for Antisense Oligonucleotide Analogues in the Development of Oncogene Targeted Cancer Chemotherapy. *Anticancer Res. 10,* 1169–1182.

(17) Toulmé, J.-J., and Hélène, C. (1988) Antimessenger Oligodeoxyribonucleotides: An Alternative to Antisense RNA for Artificial Regulation of Gene Expression. *Gene 72,* 51–58.

(18) Zon, G. (1988) Oligonucleotide Analogues as Potential Chemotherapeutic Agents. *Pharm. Res. 5,* 539–549.

(19) Verspieren, P. (1987) An Acridine-linked Oligodeoxynucleotide Targeted to the Common 5' End of Trypanosome mRNA Kills Cultured Parasites. *Gene 61,* 307–315.

(20) Stein, C. A., Mori, K., Loke, S. L., Subasinghe, C., Shinozuka, K., Cohen, J. S., and Neckers, L. M. (1988) Phosphorothioate and Normal Oligodeoxyribonucleotides with 5'-Linked Acridine: Characterization and Preliminary Kinetics of Cellular Uptake. *Gene 72,* 333–341.

(21) Cazenave, C., Chevrier, M., Thuong, N. T., and Hélène, C. (1987) Rate of Degradation of Alpha- and Beta-oligodeoxynucleotides in *Xenopus* Oocytes. Implications for Antimessenger Strategies. *Nucleic Acids Res. 15,* 10507–10521.

(22) Thuong, N. T., Asseline, U., Roig, V., Takasugi, M., and Hélène, C. (1987) Oligo(α-deoxynucleotide)s Covalently Linked to Intercalating Agents: Differential Binding to Ribo- and Deoxyribopolynucleotides and Stability Towards Nuclease Digestion. *Proc. Natl. Acad. Sci. U.S.A. 84,* 5129–5133.

(23) Asseline, U., Thuong, N. T., and Hélène, C. (1985) Oligonucleotides Covalently Linked to Intercalating Dyes. *J. Biol. Chem. 260,* 8936–8941.

(24) Hélène, C., Montenay-Garestier, T., Saison, T., Takasugi, M., Toulmè, J. J., Asseline, U., Lancelot, G., Maurizot, J. C., Toulmè, F., and Thuong, N. T. (1985) Oligodeoxynucleotides Covalently Linked to Intercalating Agents: A New Class of Gene Regulatory Substances. *Biochemie 67,* 777–783.

(25) Mori, K., Subasinghe, C., and Cohen, J. (1989) Oligodeoxynucleotide Analogs with 5'-linked Anthraquinone. *FEBS Lett. 249,* 213–218.

(26) Asseline, U., Delarue, M., Lancelot, G., Toulmè, F., Thuong, N. T., Montenay-Garestier, T., and Hélène, C. (1984) Nucleic Acid-binidng Molecules with High Affinity and Base Sequence Specificity: Intercalating Agents Covalently Linked to Oligodeoxynucleotides. *Proc. Natl. Acad. Sci. U.S.A. 81,* 3297–3301.

(27) Vasseur, J.-J., Gauthier, C., Rayner, B., Paoletti, J., and Imbach, J.-L. (1988) Efficient and Easy Synthesis of Octathymidylate Covalently Linked to Intercalating 9-Aminoellipticine. *Biochem. Biophys. Res. Commun. 152,* 56–61.

(28) Durand, M., Maurizot, J. C., Asseline, U., Barbier, C., Thuong, N. T., and Hélène, C. (1989) Oligothymidylates Covalently Linked to an Acridine Derivative and with Modified Phosphodiester Backbone: Circular Dichroism Studies of Their Interactions with Complementary Sequences. *Nucleic Acids Res. 17,* 1823–1837.

(29) Lancelot, G., Guesnet, J.-L., Asseline, U., and Thuong, N. T. (1988) NMR Studies of Complex Formation Between the Modified Oligonucleotide d(T*TCTGT) Covalently Linked to an Acridine Derivative and Its Complementary Sequence d(GCACAGAA). *Biochemistry 27,* 1265–1273.

(30) Thuong, N. T., and Chassignol, M. (1987) Synthesis and Reactivity of Oligothymidylates Substituted with an Intercalating Agent and a Thiophosphate Group. *Tetrahedron Lett. 28,* 4157–4160.

(31) Asseline, U., and Thuong, N. T. (1988) Oligothymidylates Substituted with an Acridine Derivative at the 5' Position, at Both the 5' and 3' Positions, or on an Internucleotide Phosphate. *Nucleosides Nucleotides 7,* 431–455.

(32) Asseline, U., Thuong, N. T., and Hélène, C. (1986) Oligonucleotides Substituted on the 5' Position with an Acridine Derivative. *Nucleosides Nucleotides 5,* 45–63.

(33) Asseline, U., Toulme, F., Thuong, N. T., and Hélène, C. (1984) Oligodeoxynucleotides Covalently Linked to Intercalating Dyes as Base Sequence-specific Ligands. Influence of Dye Attachment Site. *EMBO J. 3,* 795–800.

(34) Praseuth, D., Chassignol, M., Takasugi, M., Le Doan, T., Thuong, N. T., and Hélène, C. (1987) Double Helices with Parallel Strands Are Formed by Nuclease-resistant oligo-[α]-deoxynucleotides and Oligo-[α]deoxynucleotides Covalently Linked to an Intercalating Agent with Complementary Oligo-[β]-deoxynucleotides. *J. Mol. Biol. 196,* 939–942.

(35) Sun, J., Asseline, U., Rouzaud, D., Montenay-Garestier, T., Thuong, N. T., and Hélène, C. (1987) Oligo-[α]-deoxynucleotides Covalently Linked to an Intercalating Agent. Double Heleces with Parallel Strands Are Formed with Complementary oligo-[β]-deoxynucleotides. *Nucleic Acids Res. 15,* 6149–6158.

(36) Boidot-Forget, M., Chassignol, M., Takasugi, M., Thuong, N. T., and Hélène, C. (1988) Site-specific Cleavage of Single-stranded and Double-stranded DNA Sequences by Oligodeoxyribonucleotides Covalently Linked to an Intercalating Agent and an EDTA-Fe Chelate. *Gene 72,* 361–371.

(37) Asseline, U., Thuong, N. T., and Hélène, C. (1983) New Substances with High and Specific Affinity Toward Nucleic Acid Sequences. *C. R. Acad. Sci. Paris 297,* 369–372.

(38) Gautier, C., Morvan, F., Rayner, B., Huynh-Ding, T., Igolen, J., Imbach, J.-L., Paoletti, C., and Paoletti, J. (1987) α-DNA IV: α-Anomeric and β-Anomeric Tetrathymidylates Covalently Linked to Intercalating Oxazolopyridocarbazole. Synthesis, Physicochemical Properties and Poly(rA) Binding. *Nucleic Acids Res. 15,* 6625–6641.

(39) Bazile, D., Gautier, C., Rayner, B., Imbach, J.-L., Paoletti, C., and Paoletti, J. (1989) α-DNA X: α and β Tetrathymidylates Covalently Linked to Oxazolopyridocarbazolium (OPC): Comparative Stabilization of Oligo β-[dT]:Oligo and β-[dA] and Oligo α[dT]:Oligo β-[dA] Duplexes by the Intercalating Agent. *Nucleic Acids Res. 17,* 7749–7759.

(40) Letsinger, R. L., and Schott, M. E. (1981) Selectivity in Binding a Phenanthridinium-Dinucleotide Derivative to Homopolynucleotides. *J. Am. Chem. Soc. 103,* 7394–7396.

(41) Kutyaven, I. V., Podyminogin, M. A., Bazhina, Y. N., Fedorova, O. S., Knorre, D. G., Levina, A. S., Mamayev, S. V., and Zartova, V. F. (1988) N-(2-Hydroxyethyl)phenazinium Derivatives of Oligonucleotides as Effectors of the Sequence-specific Modification of Nucleic Acids with Reactive Oligonucleotide Derivatives. *FEBS Lett. 238,* 35–38.

(42) Cazenave, C., Loreau, N., Thuong, N. T., Toulmé, J.-J., and Hélène, C. (1987) Enzymatic Amplification of Translation Inhibition of Rabbit β-Globin mRNA Mediated by Antimessenger Oligodeoxynucleotides Linked to Intercalating Agents. *Nucleic Acids Res. 15,* 4717–4736.

(43) Zerial, A., Thuong, N. T., and Hélène, C. (1987) Selective Inhibition of the Cytopathic Effect of Type A Influenze Viruses by Oligonucleotides Covalently Linked to an Intercalating Agent. *Nucleic Acids Res. 15,* 9909–9919.

(44) Toulmé, J. J., Krisch, H. M., Loreau, N., Thuong, N. T., and Hélène, C. (1986) Specific Inhibition of mRNA Translation by Complementary Oligonucleotides Covalently Linked to Intercalating Agents. *Proc. Natl. Acad. Sci. U.S.A. 83,* 1227–1231.

(45) Sethi, V. S., and Sethi, M. L. (1975) Inhibition of Reverse Transcriptase Activity of RNA-Tumor Viruses by Fagaronine. *Biochem. Biophys. Res. Commun. 63,* 1070–1076.

(46) Sethi, M. L. (1985) Comparison of Inhibition of Reverse Transcriptase and Antileukemic Activities Exhibited by Protoberberine and Benzophenanthridine Alkaloids and Structure-activity Relationships. *Phytochemitry 24,* 447–454.

(47) Sethi, M. L. (1985) Enzyme Inhibition VIII: Mode of Inhibition of Reverse Transcriptase Activity by Analogues, Isomers, and Related Alkaloids of Coralyne. *J. Pharm. Sci. 74,* 889–891.

(48) Sethi, M. (1979) Inhibition of Reverse Transcriptase Activity by Benzophenanthridine Alkaloids. *J. Nat. Prod. 42,* 187–196.

(49) Sethi, V. S. (1976) Inhibition of Mammalian and Oncornavirus Nucleic Acid Polymerase Activities by Alkoxybenzophenanthridine Alkaloids. *Cancer Res. 36,* 2390–1295.

(50) Sethi, M. L. (1981) Screening of Benzophenanthridine Alkaloids for Their Inhibition of Reverse Transcriptase Activity and Preliminary Report on the Structure-activity Relationships. *Can. J. Pharm. Sci. 16,* 29–34.

(51) Cheng, C. C., Engle, R. R., Hodgson, J. R., Ing, R. B., Wood, H. B., Jr., Yan, S.-J., and Zee-Cheng, R. K. Y. (1977) Absence of Mutagenicity of Coralyne and Related Antileukemic Agents: Structural Comparison with the Potent Carcinogen 7,12-Dimethylbenz[a]anthracene. *J. Pharm. Sci. 66,* 1781–1783.

(52) Harrison, I. T. (1990) *Model 7924 Chromatotron Instruction Manual,* Harrison Research, 840 Moana Court, Palo Alto, CA.

(53) Heimbel, A., and Bosold, F. (1990) The Chromatotron. *Angew. Chem. 102,* A298.

(54) Hostettman, K., Hostettman, M., and Marston, A. (1988) *Preparative Chromatography Techniques. Applications in Natural Products Isolation,* Springer-Varlag, New York.

(55) Pelletier, S. W. (1985) Advances in Medicinal Plant Reserch. In *Advances in Medicinal Plant Research* (A. J. Vlietinck and R. A. Domisse, Eds.) pp 153–195, Wissenschaftliche Verlagsgesellschaft mbH, Stuttgart.

(56) Ishii, H., Chen, I.-S., and Ishikawa, T. (1987) Basic Intramolecular Acylation. Synthesis of 2-Aryl-1-tetralones Bearing Isopropoxy or Benzyloxy Groups, Synthetic Intermediates for Phenolic Antileukemic Benzo[c]phenanthridine Alkaloids, from 2,4-Diarylbutyric Acid Derivatives. *J. Chem. Soc., Perkin Trans. 1* 2415–2420.

(57) Stermitz, F. R., Gillespie, J. P., Amoros, L. G., Romero, R., Stermitz, T. A., Larson, K. A., Earl, S., and Ogg, J. E. (1975) Synthesis and Biological Activity of Some Antitumor Benzophenanthridinium Salts. *J. Med. Chem. 18,* 708–713.

(58) Lawson, T. G., Regnier, F. E., and Weith, H. L. (1983) Separation of Synthetic Oligonucleotides on Columns of Microparticulate Silica Coated with Crosslinked Polyethylene Imine. *Anal. Biochem. 133,* 85–93.

(59) Fieser, M., and Fieser, L. (1967) *Reagents for Organic Synthesis,* Vol. 1, pp 914, John Wiley and Sons, Inc., New York.

(60) Cushman, M., and Cheng, L. (1978) Total Synthesis of Nitidine Chloride. *J. Org. Chem. 43,* 286–288.

(61) Wang, G., and Cushman, M. (1991) A Convenient Method fo the Conversion of α-Tetralones to Aryl Acetates. *Synth. Commun. 21,* 989–996.

(62) Ishii, H., Chen, I.-S., Ueki, S., Akaike, M., and Ishikawa, T. (1987) Studies on the Chemical Constituents of Rutaceous Plants. LXIV. Structural Establishment of Oxyterihanine, a Phenolic Benzo[c]phenanthridine Alkaloid. Syntheses of Phenolic Benzo[c]phenenthridine Alkaloids, Terihanine and Isoterihanine, and Related Compounds. *Chem. Pharm. Bull. 35,* 2717–2725.

(63) Ishii, H., Chen, I.-S., and Ishikawa, T. (1987) Studies on the Chemical Constituents of Rutaceous Plants. Part 62. Efficient Synthesis of Fagaronine, and Phenolic Benzo[c]phenanthridine Alkaloid with Antileukemic Activity. *J. Chem. Soc., Parkin Trans. 1* 671–676.

(64) Cheng, R. K. Y., and Cheng, C. C. (1973) Synthesis of 5,6-Dihydro-6-methoxynitidine and a Practical Preparation of Nitidine Chloride. *J. Heterocycl. Chem. 10,* 85–88.

(65) Byrn, S. R., Carlson, D. V., Chen, J. K., Cushman, M. S., Goldman, M. E., Ma, W. P., Pidgeon, C. L., Ray, K. A., Stowell, J. G., and Weith, H. L. (1991) Drug-oligonucleotide Conjugates. *Adv. Drug. Delivery Rev. 6,* 287–308.

(66) Chen, J.-k., Carlson, D. V., Weith, H. L., O'Brien, J. A., Goldman, M. E., and Cushman, M. (1992) Synthesis of an Oligonucleotide-Intercalator Conjugate in Which the Linker Chain is Attached Via the Phenolic Hydroxyl Group of Fagaronine. *Tetrahedron Lett. 33,* 2275–2278.

BC9500397

Enantioselective Release of 5-Fluorouracil from N-(2-Hydroxypropyl)methacrylamide-Based Copolymers via Lysosomal Enzymes

David Putnam and Jindřich Kopeček*

Departments of Pharmaceutics and Pharmaceutical Chemistry/CCCD and of Bioengineering, University of Utah, Salt Lake City, Utah 84112. Received March 30, 1995®

Water soluble copolymers based on N-(2-hydroxypropyl)methacrylamide (HPMA) containing oligopeptide side chains terminated in an α-substituted glycine derivative of the anticancer compound 5-fluorouracil (5-FU) were synthesized by a new facilitated synthetic route and studied for their ability to release free 5-FU in the presence of lysosomal enzyme preparations. In addition, the properties of the low molecular weight α-substituted glycine derivatives were studied in the presence of lysosomal enzyme preparations and leucine aminopeptidase. The results revealed that (1) the stereochemistry (L vs D) of the α-substituted glycine derivative, (2) the hydrophobicity (Ala vs Leu) of the penultimate amino acid residue relative to the α-substituted glycine derivative, and (3) the total length of the oligopeptide sequence spacer (tetrapeptide vs hexapeptide) terminated in the α-substituted glycine derivative and the polymer carrier all directly influence the enzymatically catalyzed release of free 5-FU.

INTRODUCTION

Numerous polymeric carriers of anticancer compounds have been synthesized and used for targeted drug delivery (for review see ref 1). Ringsdorf (2) first reported a clear representation of the potential of polymers as targetable lysosomotropic drug carriers. This landmark paper describes the necessity of site-specific liberation of the active compound from the polymer carrier in order to maximize the efficacy of the conjugate.

In recent years polymer drug conjugates were created for the delivery of the anticancer compound, 5-fluorouracil (5-FU)[1] (3–7). However, these conjugates permitted hydrolysis of the drug from the polymer carrier in the blood circulation and, therefore, reduced the site-specific release of the drug *in vivo*. The attachment of drug molecules to polymer carriers limits the cellular entry of the drug to the process of endocytosis, and the endocytosed polymer–drug conjugate ultimately resides within the lysosomal compartment of the cell. Therefore, stabilization of the connection between the drug and polymer while in the bloodstream with a spacer that is hydrolyzed by lysosomal enzymes would greatly improve the targeting potential of polymer conjugates containing 5-FU. To this end, we have synthesized copolymers based on N-(2-hydroxypropyl)methacrylamide (HPMA) that contain oligopeptide side chains terminated with an α-substituted glycine derivative of 5-FU. The oligopeptide sequences are tailor-made to be stable in the

bloodstream (8), susceptible to enzymes within the lysosomal compartment of the cell (9), and able to produce free 5-FU and not amino acid derivatives thereof.

The release mechanism of 5-FU from the glycine α-carbon stems from the inherent instability of α-substituted glycines. Substitution at the α-carbon of glycine with a good leaving group, such as the secondary amine of 5-FU, results in an intrinsically unstable glycine derivative that spontaneously decomposes into the α-substituent and a glyoxylate according to Scheme 1 (10). However, acylation of the glycyl amino group, for example, through formation of a peptide bond, stabilizes the α-substituted glycine derivative. Therefore, addition of a stabilizing amino acid results in a stable α-substituted glycine drug derivative. Removal of the stabilizing amino acid, for example, through enzymatically catalyzed hydrolysis by aminopeptidases within the lysosomal compartment of the target cell, will create the unstable glycine drug derivative and subsequently result in the formation of the free drug.

α-Substituted glycine derivatives of 5-fluorouracil were first synthesized to study the potential of glycine derivatives for antimicrobial agent delivery (10). More recently, α-substituted glycine derivatives of 5-fluorouracil were synthesized to study their potential as anticancer agent prodrugs (11). The purposes of this work were as follows: (1) to describe a new facilitated synthetic route for these α-substituted glycine derivatives of 5-fluorouracil, (2) to study the effects of the stereochemistry of the α-substituted glycine derivatives upon the enzymatically catalyzed release of 5-FU, (3) to study the effects of the hydrophobicity of the stabilizing amino acid upon the enzymatically catalyzed release of 5-FU from low molecular weight α-substituted glycine derivatives, and (4) to study the effect of side chain length and composition upon lysosomal enzyme catalyzed release of 5-FU from HPMA-based copolymers containing oligopeptide side chains terminated in the α-substituted glycine derivative of 5-FU.

* Corresponding author. E-mail: jindrich.kopecek@m.cc. utah.edu; telephone: (801) 581-7211; fax: (801) 581-7848.

[1] Abbreviations: Amino acid abbreviations are those recommended by IUPAC-IUB; cf. (1972) *J. Biol. Chem.* 247, 977. Bz, benzoyl; DMSO, dimethyl sulfoxide; EDTA, ethylenediaminetetraacetic acid; 5-FU, 5-fluorouracil; GSH, glutathione; HPMA, N-(2-hydroxypropyl)methacrylamide; MA, methacryloyl; NAp, p-nitroanilide; ONp, p-nitrophenoxy; P, HPMA copolymer backbone; P-Gly-Phe-ONp, copolymer of HPMA and N-methacryloylglycylphenylalanine p-nitrophenyl ester; P-Gly-Phe-Leu-Gly-ONp, copolymer of HPMA and N-methacryloylglycylphenylalanylleucylglycine p-nitrophenyl ester; PQ, primaquine; TMS, tetramethylsilane.

Scheme 1. The Stabilization of a Glycine Derivatized with 5-FU[a]

Unstable glycine derivative

Stable glycine derivative
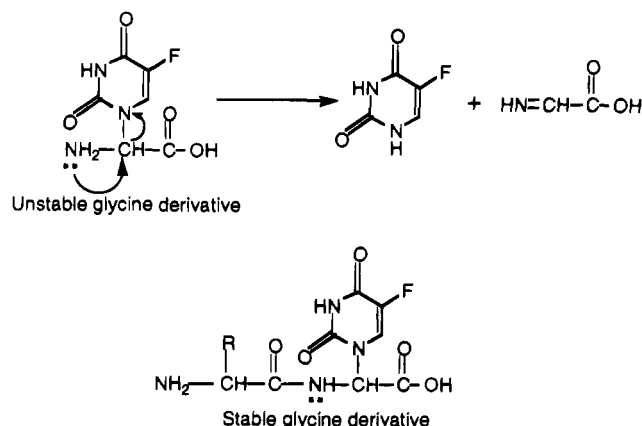
[a] Acylation of the glycyl α-amino group occupies the free amino electrons and stabilizes the bond between the glycine α-carbon and the N1 of the 5-FU (modified from ref 10).

EXPERIMENTAL PROCEDURES

Chemicals and General Methods. Melting points (uncorrected) were determined on an Electrothermal digital melting point apparatus. ¹H NMR spectra were recorded on a Bruker instrument (200 or 500 MHz) using 1.0% v/v TMS as an internal standard. UV spectra were obtained either from a Perkin Elmer Lambda 19 spectrophotometer or a Perkin Elmer 7 spectrophotometer. TLC was performed using an aluminum backed silica gel 250 μm layer from Whatman (Kent, England). HPLC was performed using a Dionex pumping system equipped with either an analytical Zorbax C_{18} (4.6 × 150 mm) or a preparative C_{18} Whatman Partisil 10 ODS-3 column with a UV Linear UVIS 204 detector and Axxiom data processing software. Polarimetry measurements were made on a Jasco DIP-370 digital polarimeter. General elemental analysis was performed by Atlantic Microlabs (Norcross, GA). Fluorine trace analysis was performed by Galbraith Laboratories (Knoxville, TN). CBZ-Ala-Ser-OMe, porcine microsomal leucine aminopeptidase (EC 3.4.11.2), Leu-NAp, Bz-Phe-Val-Arg-NAp, reduced glutathione (GSH), and Triton X-100 were purchased from Sigma (St. Louis, MO, USA). CBZ-Leu-Ser-OMe was purchased from Bachem Bioscience Inc. (Philadelphia, PA, USA). Palladium/charcoal, cyclohexene, lead tetraacetate, and 5-fluorouracil were purchased from Aldrich (Milwaukee, WI, USA). Dialysis tubing (Spectrapor, molecular weight cutoff: 6000−8000) and Gelman Acrodisc LC 13 PVDF filters were purchased from Baxter Scientific Products (Mcgaw Park, IL) All other chemicals were of reagent grade or better.

N-(2-Hydroxypropyl)methacrylamide (HPMA) (*12*), MA-Gly-Phe-ONp (*13*), P-Gly-Phe-ONp (*14*), and P-Gly-Phe-Leu-Gly-ONp (*15*) were synthesized as previously reported. Lysosomal enzymes were isolated in the form of tritosomes according to the method of Trouet (*16*). The term tritosomes is used to signify the use of Triton WR-1339 to alter the density of the lysosomal compartment and facilitate their isolation by centrifugation. The program SCIENTIST was purchased from Micromath, Salt Lake City, UT.

N-(Carbobenzyloxy)-L-alanyl-L,D-2-acetoxyglycine Methyl Ester (1). Compound 1 was prepared according to the procedure described by Steglich (*17*). Dry ethyl acetate (100 mL) was added to a dried 250 mL three-neck round bottom flask through a rubber septum using a glass syringe and needle under dry N_2. CBZ-Ala-Ser-OMe (3.24 g, 10 mmol), Pb(OAc)₄ (6.65 g, 15

mmol), and 4 Å molecular sieves (8 g) were added with stirring. The mixture was allowed to reflux until the reaction was complete (approximately 2 h) as determined by TLC (mobile phase, ethyl acetate). The reaction apparatus was cooled to room temperature with stirring and filtered through Celite and the filtrate stirred with 20% aqueous citric acid (100 mL) for 10 min. The mixture was separated, and the organic layer was washed twice with 10% aqueous NaCl (75 mL each), dried over MgSO₄, and reduced to a yellowish residue *in vacuo*. Pure product was obtained by recrystalization from ethyl acetate/hexane. Yield: 1.91 g (54.3%); mp 127−129 °C; TLC (silica gel; ethyl acetate) showed one spot, $R_f = 0.5$. ¹H NMR (200 MHz, CDCl₃, ppm); 1.4 (overlapping d, 3H, diastereomeric alanyl CH₃); 2.1 (s, 3H, acetyl CH₃); 3.8 (s, 3H, methyl ester CH₃); 4.3 (br m, 1H, alanyl CH); 5.1 (s, 1H, benzylic CH₂); 6.4 (d, 1H, glycyl CH); 7.35 (s, 5H, aromatic H). Anal. Calcd for $C_{16}H_{20}N_2O_7$: C, 54.54; H, 5.68; N, 7.95. Found: C, 54.72; H, 5.77; N, 7.93.

N-(Carbobenzyloxy)-L-alanyl-2-(5-fluorouracil-1-yl)-L,D-glycine Methyl Ester (2). According to the method reported by Kingsbury (*10*), acetate 1 (337.9 mg, 0.96 mmol), 5-fluorouracil (119.7 mg, 0.92 mmol), and triethylamine (128.2 μL, 0.92 mmol) were stirred in dry DMF (2 mL) for 20 h. The DMF was removed by rotoevaporation *in vacuo* to a thick yellowish residue. The residue was dissolved in ethyl acetate (20 mL) and extracted once with water (20 mL). The organic layer was isolated and the water layer extracted with ethyl acetate (2 × 20 mL). The ethyl acetate extracts were combined and washed with water (2 × 20 mL), dried over MgSO₄, and evaporated *in vacuo*. The product was isolated by silica gel chromatography (60−200 mesh) with a mobile phase of dichloromethane/methanol (98:2). Yield: 160 mg (40%); mp 113.5−114.5 °C (viscous liquid); TLC (silica gel; dichloromethane/methanol/formic acid, 95:5:1) showed one spot, $R_f = 0.25$. ¹H NMR (200 MHz, CDCl₃, ppm): 1.4 (overlapping d, 3H, diastereomeric alanyl CH₃); 3.75 (s, 3H, methyl ester CH₃); 4.5 (q, 1H, alanyl CH); 5.1 (s, 2H, benzyl CH₂); 5.95 (m, 1H, glycyl CH); 7.3 (s, 5H, aromatic H); 7.7 (overlapping d, 1H, pyrimidine CH). Anal. Calcd for $C_{18}H_{19}N_4O_7F_1$: C, 51.18; H, 4.50; N, 13.27. Found: C, 51.00; H, 4.57; N, 13.21.

N-(Carbobenzyloxy)-L-alanyl-2-(5-fluorouracil-1-yl)-L,D-glycine (3). The methyl ester of 2 was removed by treatment with sodium hydroxide. Compound 2 (54.2 mg, 0.128 mmol) was dissolved in the smallest amount of methanol, to which 0.5 M NaOH (2.71 mL) was added, stirred for 1 min, cooled in an ice bath, and then acidified with stirring to pH = 2.0 with 2 N HCl. The methanol was removed by rotoevaporation *in vacuo*, the aqueous solution was extracted with ethyl acetate (3 × 5 mL), the ethyl acetate extracts were combined and dried with sodium sulfate, and the ethyl acetate was removed by rotoevaporation *in vacuo*. Yield: 40 mg (76%); mp 170 °C (viscous liquid); TLC (silica gel; chloroform/methanol, 1:1) one spot, $R_f = 0.5$. ¹H NMR (200 MHz, DMSO-d_6, ppm): 1.3 (overlapping d, 3H, diastereomeric alanyl CH₃); 4.3 (br m, 1H, alanyl CH); 5.1 (s, 2H, benzyl CH₂); 6.1 (d, 1H, glycyl CH); 7.3 (s, 5H, aromatic H); 7.8 (overlapping d, 1H, pyrimidine CH).

Separation of L,L and L,D Diastereomers of 3 (3a and 3b). The diastereomers of 3 were separated by preparative reverse phase high pressure liquid chromatography using a C_{18} Whatman Partisil 10 ODS-3 column eluted with isocratic 0.1% acetic acid (pH 3.2)/methanol (75:25) at a rate of 2 mL/min and detected at 254 nm. Fractions of 3 (30 mg each) were dissolved in water containing the least amount of methanol (less than 2%)

and injected into the HPLC system, and the peaks located between 90–105 min and 106–140 min were collected. The acetic acid and methanol were removed *in vacuo*, and the products were obtained by lyophilization.

First peak (**3a**): Anal. Calcd for $C_{17}H_{17}N_4O_7F \cdot H_2O$: C, 47.88; H, 4.46; N, 13.14. Found: C, 48.07; H, 4.32; N, 13.08. Second peak (**3b**): Anal. Calcd for $C_{17}H_{17}N_4$-$O_7F \cdot H_2O$: C, 47.88; H, 4.46; N, 13.14. Found: C, 47.62; H, 4.13; N, 12.95. All other analysis correlated to compound **3**.

L-Alanyl-2-(5-fluorouracil-1-yl)-L-glycine (4a) and L-Alanyl-2-(5-fluorouracil-1-yl)-D-glycine (4b). The CBZ deprotection of **3a** and **3b** to produce **4a** and **4b** was conducted according to the procedure described by Kingsbury (*10*). Compounds **3a** or **3b** (71.4 mg, 0.175 mmol), palladium/charcoal 10% (75 mg), and cyclohexene (0.125 mL) were combined in anhydrous methanol (8.75 mL) and refluxed with stirring for 20 min. The reaction mixture was filtered while hot through Celite, the filtrate solvent removed by rotoevaporation, and the product dried *in vacuo*. Yields: (**3a**) 42 mg (88%); (**3b**) 44 mg (92%). To ensure purity, the products were isolated using preparative reverse phase HPLC. The samples were dissolved in distilled water (0.75 mL) and isolated from a C_{18} Whatman Partisil 10 ODS-3 column eluted with distilled water at a rate of 2 mL/min with detection at 254 nm, followed by lyophilization.

(**4a**) $[\alpha]^{25}_D = +136.18°$ ($c = 0.073$, H_2O); UV (H_2O) λ_{max} = 268 nm, $\epsilon = 7450$. ^{1}H NMR (200 MHz, DMSO-d_6, ppm): 1.25 (d, 3H, alanyl CH_3); 3.95 (q, 1H, alanyl CH); 5.9 (s, 1H, glycyl CH); 7.8 (d, 1H, pyrimidine CH). Anal. Calcd for $C_9H_{11}N_4O_5F \cdot H_2O$: C, 36.98; H, 4.45; N, 19.17. Found: C, 37.07; H, 4.48; N, 19.07.

(**4b**) $[\alpha]^{25}_D = -117.68°$ ($c = 0.064$, H_2O); UV (H_2O) λ_{max} = 268 nm, $\epsilon = 7450$. ^{1}H NMR (200 MHz, DMSO-d_6, ppm): 1.3 (d, 3H, alanyl CH_3); 4.0 (q, 1H, alanyl CH); 5.9 (s, 1H, glycyl CH); 7.85 (d, 1H, pyrimidine CH). Anal. Calcd for $C_9H_{11}N_4O_5F \cdot H_2O$: C, 36.98; H, 4.45; N, 19.17. Found: C, 37.04; H, 4.51; N, 19.07.

N-(Carbobenzyloxy)-L-leucyl-L,D-2-acetoxygly-cine Methyl Ester (5). Compound **5** was synthesized according to the procedure described by Steglich (*17*). The procedure and chemical concentrations used were identical to that described for compound (**1**). Yield: 2.888 g (73%); mp 99.5–101.5 °C. TLC (silica gel; ethyl acetate) showed one spot, $R_f = 0.6$. ^{1}NMR (200 MHz, CDCl$_3$, ppm): 0.95 (m, 6H, leucyl CH_3); 1.6 (br m, 2H, leucyl CH_2); 1.7 (br m, 1H, leucyl CH); 2.1 (s, 3H, acetyl CH_3); 3.8 (s, 3H, methyl ester CH_3); 4.2 (br, 1H, leucyl α-CH); 5.1 (s, 2H, benzylic CH_2); 6.4 (overlapping d, 1H, glycyl CH); 7.35 (s, 5H, aromatic H). Anal. Calcd: C, 57.87; H, 6.59; N, 7.11. Found: C, 57.97; H, 6.64; N, 7.11.

N-(Carbobenzyloxy)-L-leucyl-2-(5-fluorouracil-1-yl)-L,D-glycine Methyl Ester (6). According to the method reported by Kingsbury (*10*), acetate **5** (1.514 g, 3.84 mmol), 5-FU (0.478 g, 3.68 mmol), and triethylamine (512.9 μL, 3.68 mmol) were stirred in dry DMF (8 mL) for 20 h. The DMF was removed by rotoevaporation *in vacuo* to a thick yellowish residue. The residue was dissolved in ethyl acetate (80 mL) and extracted once with water (80 mL). The organic layer was isolated and the water layer extracted with ethyl acetate (2 × 80 mL). The ethyl acetate extracts were combined and washed with water (2 × 40 mL), dried over MgSO$_4$, and evaporated *in vacuo*. The pure product was isolated by silica gel chromatography (60–200 mesh) with a mobile phase of dichloromethane/methanol (98:2). Yield: 550 mg (30.8%); mp 103.5–105.5 °C (viscous liquid); TLC (silica gel; dichloromethane/methanol/formic acid, 95:5:1) showed one spot, $R_f = 0.4$. ^{1}H NMR (200 MHz, DMSO-d_6, ppm):

0.9 (m, 6H, leucyl CH_3); 1.4 (br m, 2H, leucyl CH_2); 1.6 (br m, 1H, leucyl CH); 3.7 (s, 3H, methyl ester CH_3); 4.15 (q, 1H, leucyl α-CH); 5.0 (s, 2H, benzylic CH_2); 6.4 (d, 1H, glycyl CH); 7.3 (s, 5H, aromatic H); 8.0 (overlapping d, 1H, pyrimidine CH). Anal. Calcd: C, 54.31; H, 5.38; N, 12.06. Found: C, 54.08; H, 5.48; N, 11.94.

N-(Carbobenzyloxy)-L-leucyl-2-(5-fluorouracil-1-yl)-L,D-glycine (7). The synthetic intermediate, **7**, was formed by the removal of the methyl ester of **6** by treatment with NaOH. The compound **6** (550 mg, 1.18 mmol) was dissolved in the smallest amount of methanol (0.75 mL), to which 0.4 N NaOH (25.2 mL) was slowly added with stirring. The solution was stirred for 1 min, cooled in an ice bath, and brought to pH 2.0 with 5 N HCl and the methanol removed by rotoevaporation. The cloudy reaction mixture was extracted with ethyl acetate (3 × 25 mL), whereupon the aqueous solution turned clear. The ethyl acetate extracts were combined and dried with anhydrous sodium sulfate, the solvent was removed by rotoevaporation, and the product was dried *in vacuo*. Yield: 360 mg (67.8%). ^{1}N NMR (200 MHz, DMSO-d_6, ppm): 0.85 (m, 6H, leucyl CH_3); 1.4 (m, 2H, leucyl CH_2); 1.6 (m, 1H, leucyl CH); 4.1 (br q, 1H, leucyl α-CH); 5.0 (s, 2H, benzyl CH_2); 6.25 (d, 1H, glycyl CH); 7.25 (s, 5H, aromatic H); 8.0 (d, 1H, pyrimidine CH). The intermediate was used directly for the synthesis of **8**.

L-Leucyl-2-(5-fluorouracil-1-yl)-L,D-glycine (8). The CBZ deprotection of **7** to produce **8** was conducted according to the procedure described by Kingsbury (*10*). Compound **7** (360 mg, 0.8 mmol), palladium/charcoal 10% (343 mg), and cyclohexene (0.57 mL) were combined in anhydrous methanol (40 mL) and refluxed with stirring for 20 min. The reaction mixture was filtered while hot through Celite, the filtrate solvent removed by rotoevaporation, and the product dried *in vacuo*. Yield: 220 mg (87%). The diastereomers were purified directly from the product and then analyzed.

Separation of L,L and L,D Diastereomers of 8 (8a and 8b). The diastereomers of compound **8** were separated by preparative reverse phase chromatography. Compound **8** (50 mg) was dissolved in distilled water (1 mL) and eluted from a preparative C_{18} Whatman Partisil 10 ODS-3 column with a 0.1% acetic acid (pH = 3.2) mobile phase with detection at 254 nm. The peaks eluting from 80 to 100 min and from 150 to 180 min were collected.

(**8a**) The first peak collection weighed 10 mg following lyophilization: $[\alpha]^{25}_D = +94.4°$ ($c = 0.036$, H_2O); UV (H_2O) λ_{max} = 270 nm, $\epsilon = 7340$. ^{1}H NMR (500 MHz, DMSO-d_6, ppm): 0.95 (m, 6H, leucyl CH_3); 1.5 (m, 2H, leucyl CH_2); 1.65 (m, 1H, leucyl CH); 3.6 (m, 1H, leucyl α-CH); 5.8 (s, 1H, glycyl CH); 7.8 (d, 1H, pyrimidine CH), $m/z = 316$.

(**8b**) The second peak collection weighed 25 mg following lyophilization: $[\alpha]^{25}_D = -70.6°$ ($c = 0.034$, H_2O); UV (H_2O) λ_{max} = 270 nm, $\epsilon = 7560$. ^{1}H NMR (500 MHz, DMSO-d_6, ppm): 0.95 (m, 6H, leucyl CH_3); 1.4 (m, 2H, leucyl CH_2); 1.6 (m, 1H, leucyl CH); 3.6 (m, 1H, leucyl α-CH); 5.8 (s, 1H, glycyl CH); 7.8 (d, 1H, pyrimidine CH), $m/z = 316$.

Synthesis of P-Gly-Phe-Ala-Gly-α(5-FU) (9). Copolymer **9** was synthesized from the polymer precursor P-Gly-Phe-ONp (4.1 mol % ONp, 0.27 mmol of ONp/g of polymer) and the diastereomeric mixture of **4**. The polymer precursor (210 mg, 0.0567 mmol ONp), 19.43 mg of **4** (0.079 mmol), and 9.02 μL of ethylmorpholine (0.079 mmol) were combined in 0.8 mL of anhydrous DMSO and stirred for 24 h. Aminopropanol (25 μL) was added to hydrolyze any unreacted ONp groups and the polymer immediately precipitated into an excess of acetone. The

polymer was isolated by filtration, thoroughly dried, dissolved in distilled water, and dialyzed (Spectrapor, molecular weight cutoff: 6000−8000) against distilled water for 3 days. The 5-FU-containing polymer was isolated by lyophilization and the 5-FU content quantitated by UV spectroscopy and elemental analysis. UV: 1.97 mol % of 5-FU containing comonomer (using $\epsilon = 7450$) which corresponds to 7642 g of polymer/mol of 5-FU. Anal. Calcd: F, 0.248. Found: F, 0.27.

Synthesis of P-Gly-Phe-Leu-Gly-Ala-Gly-α(5-FU) (10). Copolymer **10** was synthesized from the polymer precursor P-Gly-Phe-Leu-Gly-ONp (4.8 mol % ONp, 0.29 mmol of ONp/g of polymer, $\bar{M}_w = 20\,000$, $\bar{M}_w/\bar{M}_n = 1.3$) and the diastereomeric mixture of **4**. The polymer precursor (121 mg, 0.0351 mmol of ONp), 14.4 mg of **4** (0.0526 mmol), and 6.7 μL of ethylmorpholine (0.0526 mmol) were combined in 0.6 mL of anhydrous DMF and stirred for 24 h. Aminopropanol (25 μL) was added to hydrolyze any unreacted ONp groups and the polymer immediately precipitated into an excess of acetone. The polymer was isolated by filtration, thoroughly dried, dissolved in distilled water, and dialyzed (Spectrapor, molecular weight cutoff: 6000−8000) against distilled water for 3 days. The 5-FU-containing polymer was isolated by lyophilization, and the 5-FU content was quantitated by UV spectroscopy and elemental analysis. UV: 2.95 mol % of 5-FU containing comonomer (using $\epsilon = 7450$) which corresponds to 5417 g of polymer/mol of 5-FU. Anal. Calcd: F, 0.35. Found: F, 0.32.

Synthesis of P-Gly-Phe-Leu-Gly-α(5-FU) (11). Copolymer **11** was synthesized from the polymer precursor P-Gly-Phe-ONp (4.1 mol % ONp, 0.27 mmol of ONp/g of polymer) and a diastereomeric mixture of **8**. The polymer precursor (200 mg, 0.0532 mmol of ONp), 21.01 mg of **8** (0.0665 mmol), and 8.5 μL of ethylmorpholine (0.0665 mmol) were combined in 0.6 mL of anhydrous DMSO and stirred for 24 h. Aminopropanol (25 μL) was added to hydrolyze any unreacted ONp groups and the polymer immediately precipitated into an excess of acetone. The polymer was isolated by filtration, thoroughly dried, dissolved in distilled water, and dialyzed (Spectrapor, molecular weight cutoff: 6000−8000) against distilled water for 3 days. The 5-FU-containing polymer was isolated by lyophilization and the 5-FU content quantitated by UV spectroscopy and elemental analysis. UV: 1.59 mol % of 5-FU-containing comonomer (using $\epsilon =$ average of L,L and L,D diastereomer $= 7450$) which corresponds to 9432 g of polymer/mol of 5-FU. Anal. Calcd: F, 0.20. Found: F, 0.27.

Synthesis of P-Gly-Phe-Leu-Gly-Leu-Gly-α(5-FU) (12). Copolymer **12** was synthesized from the polymer precursor P-Gly-Phe-Leu-Gly-ONp (4.8 mol % ONp, 0.29 mmol of ONp/g of polymer, $\bar{M}_w = 20\,000$, $\bar{M}_w/\bar{M}_n = 1.3$) and a diastereomeric mixture of **8**. The polymer precursor (171 mg, 0.0496 mmol of ONp), 20.37 mg of **8** (0.0645 mmol), and 8.2 μL of ethylmorpholine (0.0645 mmol) were combined in 0.5 mL of anhydrous DMSO and stirred for 24 h. Aminopropanol (25 μL) was added to hydrolyze any unreacted ONp groups and the polymer immediately precipitated into an excess of acetone. The polymer was isolated by filtration, thoroughly dried, dissolved in distilled water, and dialyzed (Spectrapor, molecular weight cutoff: 6000−8000) against distilled water for 3 days. The 5-FU-containing polymer was isolated by lyophilization and the 5-FU content quantitated by UV spectroscopy and elemental analysis. UV: 2.74 mol % of 5-FU containing comonomer (using $\epsilon =$ average of L,L and L,D diastereomer $= 7450$) which corresponds to 5841 g of polymer/mol of 5-FU. Anal. Calcd: F, 0.325. Found: F, 0.32.

Synthesis of P-Gly-Phe-Leu-Gly-Leu-Gly-α(L,L)-(5-FU) (12a). Copolymer **12a** was synthesized from the polymer precursor P-Gly-Phe-Leu-Gly-ONp (5.7 mol % ONp, 0.34 mmol of ONp/g of polymer, $\bar{M}_w = 16\,800$, $\bar{M}_w/\bar{M}_n = 1.51$) and **8a**. The polymer precursor (126 mg, 0.043 mmol of ONp), 20 mg of **8a** (0.0532 mmol), and 13.52 μL of ethylmorpholine (0.106 mmol, note: 2 equiv due to salt form of **8a**) were combined in 0.4 mL of anhydrous DMSO and stirred for 24 h. Aminopropanol (25 μL) was added to hydrolyze unreacted ONp groups and the polymer immediately precipitated into an excess of acetone. The polymer was isolated by filtration, dissolved in distilled water, and dialyzed (Spectrapor, molecular weight cutoff: 6000−8000) against distilled water for 3 days. The 5-FU-containing polymer was isolated by lyophilization and the 5-FU content quantitated by UV spectroscopy and elemental analysis. UV: 1.25 mol % of 5-FU containing comonomer ($\epsilon = 7340$) which corresponds to 11 841 g of polymer/mol of 5-FU. Anal. Calcd: F, 0.16. Found: F, 0.18.

Enzyme Activity Assay. Enzyme activities were determined spectrophotometrically and are expressed in terms of units. One unit of enzyme will hydrolyze 1 μmol of NAp/min from its substrate (either Leu-NAp for aminopeptidase activity, or Bz-Phe-Val-Arg-NAp for endopeptidase activity).

The endopeptidase activity of tritosome preparations was determined by following the liberation of NAp spectrophotometrically at 410 nm ($\epsilon = 8600$ M^{-1}) (19) from the substrate Bz-Phe-Val-Arg-NAp in a 1 mL sample containing 0.84 mL of citrate/phosphate buffer (citric acid 21.6 mM, Na$_2$HPO$_4$ 56.8 mM, EDTA 0.784 mM, pH 5.5), 0.020 mL of Triton X-100 solution (10% in buffer), 0.020 mL of glutathione solution (0.25 M in buffer), 0.020 mL of Bz-Phe-Val-Arg-NAp solution (11.2 mM in DMSO), and 0.1 mL of tritosome preparation.

The aminopeptidase activity of tritosome preparations was determined by following the liberation of NAp spectrophotometrically at 410 nm from the substrate Leu-NAp in a 1 mL sample containing 0.827 mL of citrate/phosphate buffer, 0.020 mL of Triton X-100 solution (10% in buffer), 0.020 mL of glutathione solution (0.25 M in buffer), 0.033 mL of Leu-NAp (24 mM in DMSO), and 0.1 mL of tritosome preparation.

The aminopeptidase activity of leucine aminopeptidase was determined by following the liberation of NAp spectrophotometrically at 405 nm ($\epsilon = 9800$ M^{-1}) (19) from the substrate Leu-NAp in a 1 mL sample containing 0.867 mL of phosphate buffer (KH$_2$PO$_4$ 50 mM, pH 7.2), 0.033 mL of Leu-NAp (24 mM in DMSO), and 0.1 mL of leucine aminopeptidase stock solution in buffer.

HPLC Analysis. 5-FU, **4a**, **4b**, **8a**, and **8b** were analyzed by HPLC using a Zorbax C$_{18}$ (4.6 × 150 mm) analytical column with mobile phase: 0.1% acetic acid, flow rate: 0.5 mL/min, UV detection: 254 nm, and injection volume: 25 μL. All samples were filtered through a 0.2-μm filter (Gelman Acrodisc LC 13 PVDF) prior to HPLC analysis. Quantitation was conducted according to standard curves of the compounds.

Enzymatically Catalyzed Release of 5-FU from 4a and 8a. *Enzymatically Catalyzed Release by Leucine Aminopeptidase.* Enzymatic hydrolysis of **4a** and **8a** for the determination of Michaelis−Menten parameters was conducted in 1 mL volumes with phosphate buffer (KH$_2$-PO$_4$ 50 mM, pH = 7.2) at 37 °C. Stock solutions of **4a** (2.68 × 10^{-3} M) and **8a** (2.79 × 10^{-3} M) were prepared in the buffer, aliquots of which were used to produce concentrations ranging from 1 × 10^{-5} to 1 × 10^{-3} M. Leucine aminopeptidase (6.02 × 10^{-3} unit) was added from a stock solution. The reaction was halted by the

addition of concentrated HCl. 5-FU formation was determined by HPLC. In all samples the percent of cleavage of the starting material was limited to below 10%. All samples were run in triplicate, and Michaelis–Menten parameters (V_{max} and K_M) were determined using Lineweaver–Burk plot analysis.

Enzymatically Catalyzed Release by Tritosomes. Enzymatic hydrolysis of **8a** for the determination of Michaelis–Menten parameters was conducted in 1 mL volumes with citrate/sodium phosphate buffer (citric acid 21.6 mM, Na_2HPO_4 56.8 mM, EDTA 0.784 mM, pH 5.5) containing 0.020 mL of Triton X-100 solution (10% in buffer) and 0.02 mL of glutathione solution (0.25 M in buffer) at 37 °C. A stock solution of **8a** (2.02×10^{-3} M) was prepared in the buffer, aliquots of which were used to produce the concentrations ranging from 5.05×10^{-5} to 1.01×10^{-3} M. Tritosomes (0.1 mL), corresponding to 1.28×10^{-3} unit of tritosome aminopeptidase activity, were added. The reaction was halted by immediate sample freezing. Samples were thawed immediately prior to analysis of 5-FU formation as determined by HPLC. In all samples the percent of cleavage of the starting material was limited to below 10%. All samples were run in triplicate and Michaelis–Menten parameters (V_{max} and K_M) were determined using Lineweaver–Burk plot analysis.

The lysosomal enzyme catalyzed release of 5-FU from **8a** over 24 h was determined by incubating 1 mL samples containing 0.8 μmol of **8a** (0.16 mL of a 5×10^{-3} M stock solution), 0.7 mL of citrate/sodium phosphate buffer (citric acid 21.6 mM, Na_2HPO_4 56.8 mM, EDTA 0.784 mM, pH 5.5), 0.02 mL of Triton X-100 (10% in buffer), 0.02 mL of glutathione (0.25 M in buffer), and 0.1 mL of tritosome preparation (2.53×10^{-3} unit of aminopeptidase activity). Triplicate samples were taken at 1, 6, 12, and 24 h, frozen immediately, and then thawed immediately prior to analysis by HPLC.

Enzymatically Catalyzed Release of 5-FU from Polymers. *Percent Release Profiles.* The percentage of 5-FU and 5-FU derivatives released from polymers **9–12** after 24 h was determined by incubating the quantity of each polymer to equal 1 μmol of 5-FU in each sample, i.e., polymers **9**, 7.6 mg; **10**, 5.4 mg; **11**, 9.4 mg; **12**, 5.8 mg, in 1 mL volumes containing citrate/sodium phosphate buffer (citric acid 21.6 mM, Na_2HPO_4 56.8 mM, EDTA 0.784 mM, pH 5.5), 0.02 mL of Triton X-100 (10% in buffer), 0.02 mL of glutathione (0.25 M in buffer), and 0.1 mL of tritosome preparation (1.28×10^{-3} unit of aminopeptidase activity, 1.53×10^{-3} unit of endopeptidase activity). The samples were incubated in a shaking water bath at 37 °C. Following 24 h, each sample was eluted with 1 mL fractions of water through a PD-10 column to separate the high and low molecular weight components. Fractions 7–15 containing the low molecular weight compounds were isolated, lyophilized, and reconstituted to a volume of 2 mL with distilled water. The reconstituted fractions were analyzed by HPLC.

Time Release Profiles. The time release profiles of 5-FU and **8a** and **8b** from polymers **12** and **12a** were determined by incubating the quantity of each polymer to equal 0.35 and 0.3 μmol of 5-FU respectively, i.e., polymer **12**, 2.04 mg, and polymer **12a**, 3.55 mg, in 0.25 mL volumes containing citrate/sodium phosphate buffer (citric acid 21.6 mM, Na_2HPO_4 56.8 mM, EDTA 0.784 mM, pH 5.5), 0.08 mL of Triton X-100 (2.5% in buffer), 0.08 mL of glutathione (0.0625 M in buffer), and 0.025 mL of tritosome preparation (6.33×10^{-4} unit of aminopeptidase activity, 1.44×10^{-3} unit of endopeptidase activity). Samples were taken at 1, 6, 12, and 24 h and immediately frozen. Each sample was thawed immedi-

Table 1. Quick Reference for Compound Abbreviation Identification

compd no.	compound name
1	*N*-(carbobenzyloxy)-L-alanyl-L,D-2-acetoxyglycine methyl ester
2	*N*-(carbobenzyloxy)-L-alanyl-2-(5-fluorouracil-1-yl)-L,D-glycine methyl ester
3a	*N*-(carbobenzyloxy)-L-alanyl-2-(5-fluorouracil-1-yl)-L-glycine
3b	*N*-(carbobenzyloxy)-L-alanyl-2-(5-fluorouracil-1-yl)-D-glycine
4a	L-alanyl-2-(5-fluorouracil-1-yl)-L-glycine
4b	L-alanyl-2-(5-fluorouracil-1-yl)-D-glycine
5	*N*-(carbobenzyloxy)-L-leucyl-L,D-2-acetoxyglycine methyl ester
6	*N*-(carbobenzyloxy)-L-leucyl-2-(5-fluorouracil-1-yl)-L,D-glycine methyl ester
7	*N*-(carbobenzyloxy)-L-leucyl-2-(5-fluorouracil-1-yl)-L,D-glycine
8a	L-leucyl-2-(5-fluorouracil-1-yl)-L-glycine
8b	L-leucyl-2-(5-fluorouracil-1-yl)-D-glycine
9	P-Gly-Phe-Ala-Gly-α(5-FU)
10	P-Gly-Phe-Leu-Gly-Ala-Gly-α(5-FU)
11	P-Gly-Phe-Leu-Gly-α(5-FU)
12	P-Gly-Phe-Leu-Gly-Leu-Gly-α(5-FU)
12a	P-Gly-Phe-Leu-Gly-Leu-Gly-α(L,L)(5-FU)

ately prior to elution with 1 mL water fractions from a PD-10 column. Fractions 7–15 which contained the low molecular weight components were collected for each sample, lyophilized, reconstituted to a volume of 2 mL, and analyzed by HPLC. All samples were run in triplicate.

Kinetic Mathematical Modeling. The data resulting from the degradation of polymer **12a** in the presence of lysosomal enzymes were modeled to estimate the kinetic rate constants associated with the formation of **8a** and 5-FU. The release process can be modeled according to an irreversible degradation pattern of A goes to B goes to C assuming pseudo first order kinetics. This mathematical model can be described by the following set of differential equations:

$$A \xrightarrow{k_1} B \xrightarrow{k_2} C$$
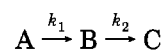
$$\frac{d[A]}{dt} = -k_1[A]$$

$$\frac{d[B]}{dt} = k_1[A] - k_2[B]$$

$$\frac{d[C]}{dt} = k_2[B]$$

The data obtained for the enzymatically catalyzed release of **8a** and 5-FU from polymer **12a** (Figure 4) were used to estimate the values of k_1 and k_2. The analytical solutions to the differential equations were used in the program SCIENTIST, and the data were fit by the method of least squares.

RESULTS AND DISCUSSION

Synthesis. A quick reference for the compound abbreviations used in this text is given in Table 1.

Previous investigators of α-substituted glycine derivatives of 5-FU have utilized the formation of a hydroxyglycine amino acid derivative as a precursor to acylated glycine intermediates such as **1** and **5**. The new synthetic route described herein bypasses this intermediate through the direct conversion of serine residues to the acylated glycine intermediate. Comparison of the two synthetic routes is shown in Scheme 2.

Scheme 2. Comparison of Old (A) and New (B) Methods of Synthesizing α-Substituted Glycine Derivatives[a]

[a] The new method provides a much faster synthetic pathway.

An excellent discussion of the pitfalls associated with the earlier synthetic route is given in ref 11. The principle drawbacks of the earlier synthetic route are long reaction times, modification of the 5-FU chemical structure, and the formation of diketopiperazines by internal cyclization during CBZ deprotection using cyclohexene as a hydrogen-transfer agent. To minimize the formation of these side products, the authors used 1,4-cyclohexadiene as the hydrogen-transfer agent during CBZ deprotection and also formed a salt at the α-amine through the addition of methanolic acetic acid.

However, using the new synthetic route, none of the described side products were detected even though cyclohexene was used as the hydrogen-transfer agent. This may be due to the removal of the methyl ester carboxyl protecting group prior to CBZ deprotection. Dipeptides containing amino groups and esterified carboxyl groups are known to undergo diketopiperazine formation (28); therefore, removal of the carboxyl group prior to CBZ deprotection dramatically decreases the potential of diketopiperazine formation.

The fast removal of the methyl ester protecting group by 0.4 N NaOH at room temperature was unexpected. Methyl ester removal from amino acids using a similar NaOH concentration usually requires 2 h of reaction time (20). The removal of the methyl ester from the 5-FU-containing dipeptides may be due to an intramolecular catalysis mechanism induced by the 5-FU (21). This short time of contact with NaOH is fortuitous since 5-FU may be degraded following prolonged exposure to basic medium (22). Removal of the methyl ester also increased the aqueous stability of the 5-FU-containing dipeptides (data not shown). The formation of free 5-FU due to chemical hydrolysis was greatly increased in the methyl ester-containing compound relative to the free carboxyl compound.

The synthetic route used for the α-substituted glycine derivatives of 5-FU produced an asymmetric carbon at the 5-FU attachment carbon, resulting in diastereomers of compounds 4 and 8 designated as 4a (L,L), 4b (L,D), 8a (L,L), and 8b (L,D) as assigned by their optical rotations and susceptibility to enzymatic hydrolysis. The isolation

Figure 1. Release of 5-FU from **8a** by the aminopeptidase activity of tritosomes. Open triangle: 5-FU; closed triangle: **4a, 4b, 8b**, and controls.

Table 2. Michaelis–Menten Kinetic Parameters for the Cleavage of 4a and 8a with Tritosome Preparations and Leucine Aminopeptidase

compd	V_{max} (mM/min)	K_m (mM)	k_{cat} (min^{-1})
	Tritosomes[a]		
8a	$3.08 \times 10^{-4} \pm 8.75 \times 10^{-5}$	$1.05 \pm 3.45 \times 10^{-1}$	0.000294
	Leucine Aminopeptidase[b]		
4a	$9.66 \times 10^{-2} \pm 4.2 \times 10^{-2}$	3.63 ± 1.66	0.026
8a	$4.61 \times 10^{-2} \pm 2.0 \times 10^{-2}$	3.64 ± 1.81	0.013

[a] Substrates **4a, 4b,** and **8b** were not cleaved. [b] Substrates **4b** and **8b** were not cleaved.
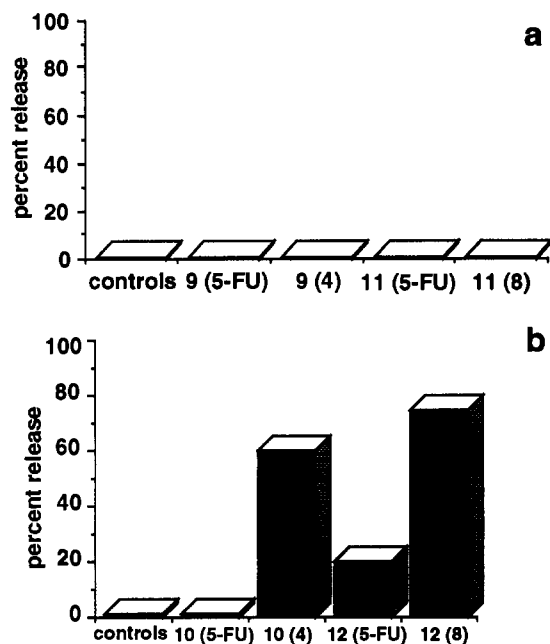
Figure 2. (a) Incubation of polymers **9** and **11** with tritosomes for 24 h. This graph shows the inability of the tritosomes to cleave the tetrapeptide side chain sequence. In parentheses are the released components from the polymers. (b) Incubation of polymers **10** and **12** with tritosomes for 24 h. This bar graph shows the ability of tritosomes to cleave the hexapeptide side chain sequence, and also the inability of tritosomes to remove the Ala stabilizing amino acid. In parentheses are the released components from the polymers.

of **4a** and **4b** was accomplished by separation using preparative HPLC of compound **3** into **3a** and **3b** followed by CBZ deprotection. The separation of **8** into **8a** and **8b** was performed by direct preparative HPLC of compound **8**.

Enzymatically Catalyzed Release of 5-FU from Low Molecular Weight α-Substituted Glycine Derivatives. The enzymatically catalyzed release of 5-FU from compounds **4a, 4b, 8a,** and **8b** was studied using two enzyme preparations: (1) leucine aminopeptidase,
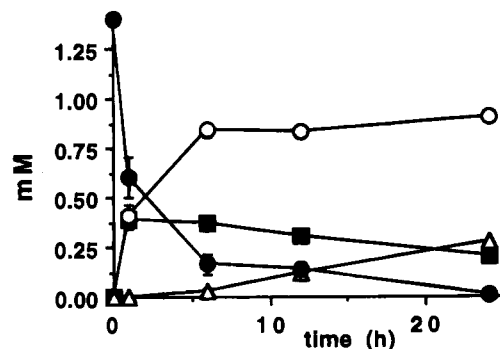
Figure 3. Incubation of polymer **12** with tritosomes over 24 h. Open circle: **8b**; closed square: **8a**; open triangle: 5-FU; closed circle: amount of 5-FU left on polymer (as calculated from released components).
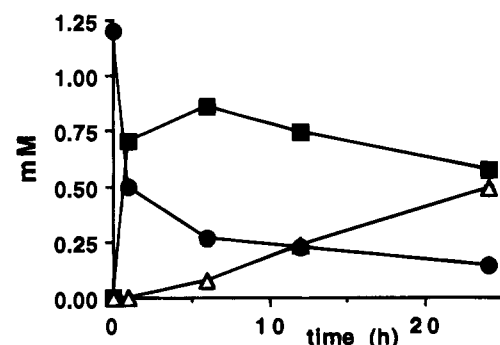
Figure 4. Incubation of polymer **12a** with tritosomes over 24 h. Closed square: **8a**; open triangle: 5-FU; closed circle: amount of 5-FU left on polymer (as calculated from released components).

isolated from porcine kidney microsomes; and (2) lysosomal enzymes isolated in the form of tritosomes from rat liver. Leucine aminopeptidase, an enzyme that the polymer-bound 5-FU should not encounter *in vivo,* was used in order to study the feasibility of α-substituted glycine derivatives of 5-FU as potential prodrug compounds. Tritosomes, which contain a variety of hydrolytic enzymes, were used to mimic the enzyme population that the polymer-bound 5-FU glycine derivatives would encounter *in vivo.*

Initial experiments using diastereomeric mixtures of **4** and **8** showed that leucine aminopeptidase was able to catalyze the production of 5-FU from both **4** and **8**. However, subsequent experiments with diastereomeric mixtures of **4** and **8** with tritosome preparations showed that only **8** was enzymatically converted to free 5-FU. The active site of leucine aminopeptidase preferentially binds compounds with hydrophobic residues in the S_1' position, which may account for these results (*23*).

The tritosome preparation results also correspond well with recently published data in this field (*24*). In this reference the kinetic rate constants for the cleavage of Ala and Leu from peptide derivatives of the antileishmanial drug, primaquine (PQ), by lysosomal aminopeptidases were calculated. Their results indicate that lysosomal aminopeptidases have higher specificity for Leu-containing compounds than for Ala-containing compounds. However, in their experiments the Ala-containing compound was cleaved by the lysosomal aminopeptidase activity, whereas in our experiments, the Ala was not cleaved. These results can be explained in that the active site of the lysosomal aminopeptidase must accommodate the drug compound (*25*). In the case of the experiments outlined in ref 24, Ala was the second amino acid from PQ and Leu was directly attached to the drug,

Scheme 3. Illustration of the Stages of Release for Glycine Derivatives of 5-FU and the Chemical Structure of the Illustrated Copolymer

Gly-Phe-Leu-Gly-Leu-Gly-(5-FU)

(endopeptidase)

Gly-Phe-Leu-Gly   +   Leu-Gly-(5-FU)

(aminopeptidase)

Leu + [Gly-(5-FU)]

Where ⟩ is the HPMA copolymer backbone.
The copolymer structure is shown below.

$$\left(CH_2-C\right)_x \left(CH_2-C\right)_y$$

CH₃ / C=O / NH / CH₂ / CH—OH / CH₃

CH₃ / C=O / NH / CH₂ / C=O / NH / CH—CH₂—(phenyl) / C=O / NH / CH—CH₂—CH(CH₃)₂ / C=O / NH / CH₂ / C=O / NH / CH—CH₂—CH(CH₃)₂ / C=O / NH / CH—(5-FU ring) / C=O / OH

whereas in our experiments, the Ala and Leu are both attached directly to the glycine 5-FU derivative. Therefore, it is feasible that in our case, 5-FU negatively influences the interactions between the aminopeptidase and the dipeptide that only the Leu-containing dipeptide can overcome. Literature regarding the S_1-P_1 subsite interactions of the principle lysosomal aminopeptidase, cathepsin H, supports this explanation. The S_1 subsite of cathepsin H is a large hydrophobic pocket that requires a large amino acid side chain residue to achieve optimal interaction (*26*). Comparison of the K_M values for cathepsin H toward amino acyl-β-naphthylamide substrates shows a 10-fold increase in K_M for the alanine-containing substrate (1.0 mM) compared to the leucine-containing substrate (0.093 mM) (*27*). This substantial increase in K_M demonstrates the influence of the hydrophobicity and/ or amino acid side chain size of the P_1 residue occupying the S_1 subsite. In addition, the cleavage of kemptide, Leu-Arg-Arg-Ala-Ser-Leu-Gly, by cathepsin H proceeds through the first three amino acids and ceases at the Ala residue, further exemplifying the poor aminopeptidase activity of cathepsin H toward the Ala residue (*27*).

A salient point regarding the effect of stereochemistry upon the enzymatically catalyzed release of 5-FU is that only for the L,L configuration can the stabilizing amino acid be cleaved. This is not a suprising result considering that L is the configuration of amino acids in the body and that enzymes can be very stereoselective within their active sites. For this reason, the enzymatically catalyzed release of 5-FU from these α-substituted glycine derivatives is termed enantioselective since only one stereochemical configuration is able to undergo catalysis.

These 5-FU derivatives provide an excellent example for the importance of stereochemically pure compounds for use in biological systems. Although each configuration contains the same chemical species, the spatial arrangement of those species is vitally important to the bioactivity of the compounds.

The liberation of 5-FU via tritosomes from **8a** over 24 h compared to that from **4a**, **4b**, and **8b** is shown in Figure 1. The kinetic constants derived for compounds **4a** and **8a** are summarized in Table 2.

Enzymatically Catalyzed Release of 5-FU from HPMA-Based Copolymers Containing α-Substituted Glycine Derivatives of 5-FU. The percent release of 5-FU and 5-FU derivatives over 24 h from polymers **9-12** was conducted to screen for those polymers that warranted more intensive investigation. The results shown in Figure 2 show that both of the tetrapeptide side chain-containing polymers, **9** and **11**, did not release 5-FU or 5-FU derivatives in the presence of tritosomes whereas both the hexapeptide side chain-containing polymers, **10** and **12**, released 5-FU and/or 5-FU derivatives.

Previous work by our group and collaborators (for example, ref 29) focused on the use of tetrapeptide spacers for the release of the anticancer compound, adriamycin. The HPMA-based copolymers in those studies contained side chains consisting of Gly-Phe-Leu-Gly with the adriamycin attached via an amide bond to the carboxyl end of the glycine. The side chains of these copolymers were designed to optimally interact with the subsites of the lysosomal enzyme, cathepsin B. At the time these copolymers were created, the X-ray structure of cathepsin B was not known, and the specificity of the enzyme was determined by traditional mapping of the enzyme's active site (*9, 30*). One of the results of these studies was that the P_2 residue on the copolymer side chain should be hydrophobic. Leu in this position adequately fulfills this requirement. The X-ray structure of cathepsin B suggests that the P_2 side chain interacts with Ala200 and Ala173 of the active site cleft floor (*31*). In addition, the side chain of the P_1 residue must project out of the active site cleft and electrostatically interact with Glu 122. This requirement is avoided with the use of Gly in this position since the synthesis of copolymers containing ionizable side chains is difficult. These copolymers freely released adriamycin in the presence of tritosomes. However, the copolymers **9** and **11** containing tetrapeptide side chains did not release 5-FU. These results can be explained with respect to the interactions of the copolymer side chain residues with the active site subsites in cathepsin B. The 5-FU-containing tetrapeptides in copolymers **9** and **11** are terminated in an α-substituted glycine 5-FU derivative and not with a glycyl derivative containing the drug bound via an amide bond at the carboxyl end. In order to accommodate this substitution into the enzyme active site, the enzyme subsites must align closer to the polymer backbone which is energetically unfavorable.

Additionally, comparing the release products from polymers **10** and **12**, polymer **10** produced only 5-FU derivatives, corresponding to compound **4**, while polymer

12 produced 5-FU derivatives, corresponding to compound **8**, along with free 5-FU. The formation of free 5-FU from polymer **12** and not from polymer **10** corresponds well to the low molecular weight results discussed previously. The hexapeptide sequences of these polymers optimize the cathepsin B catalyzed release of the dipeptide derivatives **4** and **8** by providing additional substrate binding sites. If subsite S_2 is occupied by the Leu residue closest to the polymer backbone, then the S_1' position is occupied by a readily accepted Ala (**4**) or Leu (**8**) residue. The S_2' subsite contains two binding functionalities. The side chains of His199, Ala176, Phe180, and Leu 181 and the benzene part of Trp221 form a shallow hydrophobic pocket for the P_2' residue side chain. In addition, the P_2' residue carboxylate group would be electrostatically attracted to the exposed imidazole ring of His111 to help fixate the substrate in the active site (*31*).

Since the N1 position of 5-FU must be free in order for the 5-FU to be activated *in vivo* (*32*), from these results it was concluded that polymer **12** was the best candidate for detailed investigation. The time release profile of the enzymatically catalyzed release of 5-FU and **8a** and **8b** from polymer **12** via tritosomes is shown in Figure 3. The results show the formation of **8b** increasing over time while the formation of **8a** increases over the first hour and then decreases upon conversion to 5-FU presumably via the tritosome aminopeptidase activity. The conversion of **8a** to 5-FU corresponds well to the results obtained from the incubation of **8a** alone with tritosomes (Figure 1) if one considers a nonproductive association of **8b** with the aminopeptidases in the tritosomes.

The logical extension of the results obtained from polymer **12** was to synthesize polymer **12a** containing only the (L,L) configuration of the 5-FU glycine derivative. The time release profile results are shown in Figure 4. Again, the conversion of **8a** to 5-FU correlates well to the results obtained with tritosomes with **8a** alone.

Since the formation of 5-FU from **12a** requires two stages resulting from tritosome endopeptidase activity (rate constant, k_1) followed by tritosome aminopeptidase (rate constant, k_2) activity as shown in Scheme 3, a rate limiting step may be functional. Modeling the data shown in Figure 4 resulted in a good estimate of the rate constants for each step. The modeling gave values for $k_1 = 1.24$ h^{-1} and $k_2 = 0.025$ h^{-1}. Therefore, the rate limiting step for the release of 5-FU from polymer **12a** can be expected to be the aminopeptidase catalyzed conversion of **8a** to 5-FU.

In conclusion, a new synthetic route to α-substituted glycine derivatives of the anticancer compound 5-FU was described. The degradation of the low molecular weight derivatives by lysosomal enzyme preparations is dependent upon the hydrophobicity and/or amino acid side chain size of the stabilizing amino acid, and upon the stereochemistry of the α-carbon of the derivatized glycine. Covalent attachment of these 5-FU derivatives to water soluble polymers containing oligopeptide side chains of varying lengths results in high molecular weight polymer conjugates stable to chemical hydrolysis. The degradation of these conjugates by lysosomal enzyme preparations directly depends upon the length and composition of the oligopeptide side chains.

ACKNOWLEDGMENT

LITERATURE CITED

(1) Putnam, D., and Kopeček, J. (1995) Polymer conjugates with anticancer activity. *Adv. Polym. Sci. 122*, 55–123.

(2) Ringsdorf, H. (1975) Structure and properties of pharmacologically active polymers. *J. Polym. Sci.: Polym. Symp. 51*, 135–153.

(3) Ozaki, S., Ohnishi, J., Watanabe, Y., Nohda, T., Nagase, T., Akiyama, T., Uehara, N., and Hoshi, A. (1989) Preparation of potentially antitumor-active vinyl polymers having 5-fluorouracil unit as a component. *Polym. J. 21*, 955–958.

(4) Ouchi, T., Hagita, K., Kwashima, M., Inoi, T., and Tahiro, T. (1988) Synthesis and anti-tumor activity of vinyl polymers containing 5-fluorouracils attached via carbamoyl bonds to organosilicon groups. *J. Controlled Release 8*, 141–150.

(5) Ohya, Y., Inosaka, K., and Ouchi, T. (1992) Synthesis and antitumor activity of 6-O-carboxymethyl chitin fixing 5-fluorouracils through pentamethylene, monomethylene spacer groups via amide, ester bonds. *Chem. Pharm. Bull. 40*, 559–561.

(6) Yang, F., and Zhuo, R. (1990) Synthesis and antitumor activity of poly(L-cysteine) bonded covalently 5-fluorouracil. *Polym. J. 22*, 572–577.

(7) Ohya, Y., Huang, T. Z., Ouchi, T., Hasegawa, K., Tamura, J., Kadowaki, K., Matumoto, T., Suzuki, S., and Suzuki, M. (1991) Synthesis and antitumor activity of α-1,4-polygalactosamine and N-acetyl-α-1,4-polygalactosamine immobilized 5-fluorouracils through hexamethylene spacer groups via urea, urea bonds. *J. Controlled Release 17*, 259–266.

(8) Rejmanová, P., Kopeček, J., Duncan, R., and Lloyd, J. B. (1985) Stability in rat plasma and serum of lysosomally degradable oligopeptide sequences in N-(2-hydroxypropyl)-methacrylamide copolymers. *Biomaterials 6*, 45–48.

(9) Rejmanová, P., Kopeček, J., Pohl, J., Baudyš, M., and Kostka, V. (1983) Polymers containing enzymatically degradable bonds, 8. Degradation of oligopeptide sequences in N-(2-hydroxypropyl)methacrylamide copolymers by bovine spleen cathepsin B. *Makromol. Chem. 184*, 2009–2020.

(10) Kingsbury, W. D., Boehm, J. C., Mehta, R. J., Grappel, S. F., and Gilvarg, C. (1984) A novel peptide delivery system involving peptidase activated prodrugs as antimicrobial agents. Synthesis and biological activity of peptidyl derivatives of 5-fluorouracil. *J. Med. Chem. 27*, 1447–1451.

(11) Nichifor, M., and Schacht, E. H. (1994) Synthesis of peptide derivatives of 5-fluorouracil. *Tetrahedron 50*, 3747–3760.

(12) Strohalm, J., and Kopeček, J. (1978) Poly[N-(2-hydroxypropyl) methacrylamide] IV. Heterogeneous Polymerization. *Angew. Makromol. Chem. 70*, 109–118.

(13) Kopeček, J. (1977) Reactive copolymers of N-(2-hydroxypropyl)methacrylamide with N-methacryloylated derivatives of L-leucine and L-phenylalanine I. Preparation, characterization and reaction with diamines. *Makromol. Chem. 178*, 2169–2183.

(14) Rejmanová, P., Obereigner, B., and Kopeček, J. (1981) Polymers containing enzymatically degradable bonds 2. Poly[N-(2-hydroxypropyl)methacrylamide] chains connected by oligopeptide sequences cleavable by chymotrypsin. *Makromol. Chem. 182*, 1899–1915.

(15) Říhová, B., Bilej, M., Vetvička, V., Ulbrich, K., Strohalm, J., Kopeček, J., and Duncan, R. (1989) Biocompatibility of N-(2-hydroxypropyl)methacrylamide copolymers containing adriamycin. *Biomaterials 10*, 335–342.

(16) Trouet, A. (1974) Isolation of modified liver lysosomes. *Methods Enzymol. 31*, 323–329.

(17) Apitz, G., and Steglich, W. (1991) Conversion of serine and threonine residues into α-acyloxy-, α-alkylthio-, and α-halogenoglycine moieties: a new strategy for the modification of peptides. *Tetrahedron Lett. 32*, 3163–3166.

(18) Schwartz, W. N., and Barrett, A. J. (1980) Human Cathepsin H. *Biochem. J. 191*, 487–497.

(19) Friberger, P. (1982) Chromogenic peptide substrates: their use for the assay of factors in the fibrinolytic and the plasma kallikrein-kinin systems. *Scand. J. Clin. Lab. Invest. 42*, 1–98.

(20) Bodanszky, and Bodanszky, A. (1984) Hydrolysis: Base catalyzed hydrolysis of alkyl esters (saponification with alkali). *The Practice of Peptide Synthesis*, pp 177–178, Springer-Verlag, Berlin.

(21) Nollet, A. J., and Pandit, U. K. (1969) Michael addition of 4-O-ethyluracil: a method for specific N_1-alkylation of hydroxypyrimidines. *Tetrahedron Lett. 53*, 4605–4606.

(22) Garrett, E. R., Nestler, H. J., and Somodi A. (1968) Kinetics and mechanism of hydrolysis of 5-halouracils. *J. Org. Chem. 33*, 3460–3468.

(23) Rich, D. H., Moon, B. J., and Harbeson, S. (1984) Inhibition of aminopeptidases by amastatin and bestatin derivatives. Effect of inhibitor structure on slow binding processes. *J. Med. Chem. 27*, 417–422.

(24) Borissova, R., Stjarnkvist, P., Karlsson, M., and Sjöholm, I. (1995) Biodegradable microspheres. 17. Lysosomal degradation of primaquine–peptide spacer arms. *J. Pharm. Sci. 84*, 256–262.

(25) Krinick, N. L., and Kopeček, J. (1991) Soluble Polymers as Targetable Drug Carriers. *Handbook of Experimental Pharmacology, Vol. 100, Targeted Drug Delivery* (R. L. Juliano, Ed.) pp 130–131, Springer-Verlag, Berlin.

(26) Rothe, M., Zichner, A., Auerswald, E. A., and Dodt, J. (1994) Structure/function implications for the aminopeptidase specificity of aleurain. *Eur. J. Biochem. 224*, 559–565.

(27) Takahashi, T., Dehdarani, A. H., and Tang, J. (1988) Porcine spleen cathepsin H hydrolyzes oligopeptides solely by aminopeptidase activity. *J. Biol. Chem. 263*, 10952–10957.

(28) Greenstein, J. P., and Winitz, M. (1961) *Chemistry of the Amino Acids*, Vol. 2, p 1514, John Wiley and Sons, New York.

(29) Duncan, R., Hume, I., Kopečková, P., Ulbrich, K., Strohalm, J., and Kopeček, J. (1989) Anticancer agents coupled to N-[2-hydroxypropyl]methacrylamide copolymers. 3. Evaluation of adriamycin conjugates against mouse leukaemia L1210 *in vivo. J. Controlled. Release 10*, 51–63.

(30) Kopeček, J. (1984) Controlled biodegradability of polymers—a key to drug delivery systems. *Biomaterials 5*, 19–25.

(31) Musil, D., Zucic, D., Turk, D., Engh, R. A., Mayr, I., Huber, R., Popovic, T., Turk, V., Towatari, T., Katunuma, N., and Bode, W. (1991) The refined 2.15 Å X-ray crystal structure of human liver cathepsin B: the structural basis for its specificity. *EMBO J. 10*, 2321–2330.

(32) Calabresi, P., and Parks, R. E. (1985) Antiproliferative Agents and Drugs Used for Immunosuppression. *Goodman and Gillman's: The Pharmacological Basis of Therapeutics* (A. G. Gilman, L. S. Goodman, T. W. Rall, and F. Murak, Eds.) pp 1268–1271, MacMillan Publishing Co., New York.

Catabolism of Radioiodinated Murine Monoclonal Antibody F(ab')₂ Fragment Labeled Using *N*-Succinimidyl 3-Iodobenzoate and Iodogen Methods

Pradeep K. Garg, Kevin L. Alston, and Michael R. Zalutsky*

Department of Radiology, Duke University Medical Center, Durham, North Carolina 27710. Received February 7, 1995⊛

The F(ab')₂ fragment of monoclonal antibody (MAb) Me1−14 was labeled with ^{125}I using the Iodogen method and by reaction with *N*-succinimidyl 3-[^{125}I]iodobenzoate (SIB). The labeled catabolites generated after exposure to tissue homogenates *in vitro* and following administration of labeled F(ab')₂ into normal mice were investigated by size-exclusion HPLC, gel electrophoresis, and reverse-phase HPLC. Rapid conversion of F(ab')₂ to Fab was observed with both labeling methods. With F(ab')₂ labeled using the Iodogen method, the primary low molecular weight catabolites appeared to be [^{125}I]iodide and, to a lesser extent, mono[^{125}I]iodotyrosine. With SIB, [^{125}I]iodide and [^{125}I]iodobenzoic acid (IBA) as well as the glycine and lysine conjugates of IBA were all observed. Differences in low molecular weight catabolic products could explain the more rapid normal tissue clearance with MAbs and MAb fragments labeled with SIB compared with those labeled using iodogen.

INTRODUCTION

The impact of radiolabeled monoclonal antibodies (MAbs) on the clinical management of cancer remains limited. This has led to numerous strategies for optimization of this approach for tumor diagnosis and therapy including the development of improved radiolabeling methodology. A key criterion for evaluating the suitability of a protein labeling method for *in vivo* applications is the extent to which normal tissue uptake can be avoided. While tissue distribution measurements can provide valuable information pertinent to this problem, an understanding of the nature of the labeled species created in the catabolism of labeled MAbs may be even more instructive, particularly in facilitating the design of next generation acylation agents.

The catabolism of labeled MAbs has been investigated directly in only a few publications, and these have dealt with intact IgG and F(ab')₂ fragments labeled with ^{111}In, ^{90}Y, and ^{99m}Tc. These studies have utilized a variety of analytical techniques including HPLC, SDS−PAGE, and thin layer chromatography to characterize the labeled species created following *in vitro* exposure to liver homogenates (*1*) and *in vivo* administration in mice (*2−5*). These studies have documented the existence of multiple labeled catabolites of both high and low molecular weight and differences in stability between different labeling methods (*3, 5*) and radionuclides (*1*) and attempted to explain the mechanisms responsible for increased retention of radiometals compared with radioiodine in normal tissues.

The more rapid normal tissue clearance of radioiodinated MAbs and fragments compared with radiometals is one factor that has led to the continued use of ^{131}I for MAb labeling in spite of its less than ideal nuclear decay properties. Iodine-131 remains the most commonly used radionuclide in clinical radioimmunotherapy trials, and encouraging responses have been observed in certain

patient populations (*6−9*). Clinical investigations have utilized MAbs labeled by direct methods which result predominantly in the formation of an iodinated tyrosine residue on the protein (*10*), and indirect evidence, such as thyroid uptake, has suggested that MAbs labeled using these methods undergo dehalogenation *in vivo* (*11, 12*). To circumvent this problem, alternative radioiodination strategies have been developed, the most successful of which involves the synthesis of *N*-succinimidyl 3- or 4-[^{131}I]iodobenzoate (SIB) by iododestannylation, followed by reaction of SIB with the MAb (*13−17*). Significant reduction in thyroid uptake compared with MAbs labeled using direct methods generally has been observed, and in one report, radioiodination of a MAb using SIB increased its effectiveness for the treatment of human tumor xenografts in athymic mice (*18*).

The nature of the catabolites generated from radioiodinated MAbs has not been investigated extensively. With conventionally labeled MAbs, loss of label generally is assumed to occur via deiodination. However, the production of free iodide has only been inferred indirectly, through the accumulation of activity in the thyroid and stomach (*13*). A better understanding the nature of the labeled species generated from the catabolism of radioiodinated MAbs is clearly needed. In this investigation, we report our preliminary observations on the catabolic products generated from a radioiodinated F(ab')₂ fragment labeled using the iodogen and SIB methods.

EXPERIMENTAL PROCEDURES

Materials. Sodium [^{125}I]iodide in pH 7−11 NaOH was obtained from DuPont−New England Nuclear. Iodogen was purchased from Pierce Chemical Co. Mel−14 F(ab')₂ was obtained as a gift from Dr. Darell Bigner of Department of Pathology, Duke University Medical Center. This MAb reacts with the chondroitin sulfate proteoglycan present on human gliomas and melanomas (*19*). Tumor targeting of Mel−14 F(ab')₂ radioiodinated using the iodogen (*20*) and SIB methods (*21, 22*) has been documented in athymic mouse xenograft models, and ^{131}I-labeled Mel−14 F(ab')₂ is currently being evaluated in clinical radioimmunotherapy trials (*9*). The purifica-

* Correspondence should be addressed to this author at the Department of Radiology, Box 3808, Duke University Medical Center, Durham, NC 27710. Phone: (919) 684-7708; FAX: (919) 684-7121.

tion and fragmentation of this murine IgG$_{2a}$ F(ab')$_2$ fragment have been described in a previous publication (20). All other reagents were purchased from Aldrich Chemical Co.

General. NMR spectra were recorded on a General Electric Midfield GN-300 spectrometer. Chemical shifts for protons are reported in ppm downfield from an internal tetramethylsilane standard (0.00 ppm). Mass spectral data and elemental analyses were provided by Oneida Research Services (Whitesboro, NY). Melting points were taken on a Haake-Buchler variable heat apparatus and are uncorrected.

Radioiodination of Me1−14 F(ab')$_2$ Using Iodogen. Me1−14 F(ab')$_2$ (2.5 mg/mL in 100 μL of PBS) and ^{125}I (350 μCi) were added to a glass tube coated with 10 μg of iodogen and allowed to incubate at room temperature for 10 min. The labeled MAb fragment was isolated in 80% yield by performing gel-filtration chromatography using a Sephadex G-25 column eluted with 100 mM PBS. Protein-associated activity, determined by trichloroacetic acid precipitation, was 97%.

Radioiodination of Me1−14 F(ab')$_2$ Using SIB. Synthesis of N-succinimidyl 3-(tri-n-butylstannyl)benzoate and its subsequent reaction with radioiodine to produce SIB has been described (13, 23). Briefly, SIB was prepared by adding 10 μL of 5% acetic acid, 20 μmol of tert-butyl hydroperoxide, and 5 μmol of N-succinimidyl 3-(tri-n-butylstannyl)benzoate to the sodium [^{125}I]iodide solution. After a 10 min reaction at room temperature, SIB was isolated by HPLC using a silica column (Alltech, Adsorbosphere-10, 10 μm, 250 × 4.6 mm) eluted with ethyl acetate/hexane/acetic acid (30:70:0.2). After solvent evaporation, Me1−14 F(ab')$_2$ (250 μg; 5 mg/mL) was added to the SIB residue and incubated for 15 min at room temperature. After termination of the reaction by addition of 200 μL of 0.2 M glycine in borate buffer (pH 8.5), the ^{125}I-labeled MAb fragment was isolated using a Sephadex G-25 gel filtration column eluted with 100 mM PBS. Protein-associated activity, determined by trichloroacetic acid precipitation, was 99%.

Preparation of Standards for HPLC Analysis. To facilitate interpretation of the reverse-phase HPLC analyses of lower molecular weight catabolites, the glycine and lysine conjugates of 3-iodobenzoic acid (IBA) were synthesized. SIB (unlabeled) was first prepared by dissolving IBA (2.0 g, 0.01 M) in 100 mL of THF followed by the addition of 2.06 g of dicyclohexylcarbodiimide and 1.15 g of N-hydroxysuccinimide. After stirring for 6 h at room temperature, the precipitated dicyclohexylurea was filtered off and the solvent was evaporated on a rotary evaporator. The desired compound was obtained as a white crystalline compound, mp 154−155 °C, by purifying the residue on a silica column eluted with hexane, with 10% ethyl acetate in hexane, and finally, with 30% ethyl acetate in hexane.

To produce 2-[N-(3-iodobenzamido)]acetic acid, the glycine conjugate of IBA (IBA-Gly), glycine (25 mg), was dissolved in 100 μL of a (50:50) DMF/borate buffer, pH 8.5, mixture and added to a solution of SIB (115 mg) in 200 μL of THF. The mixture was stirred for 2 h at room temperature, and the required compound was separated as a white crystalline compound (mp 140−141°C) from the reaction mixture using a silica column. Mass spectra, m/z (EI mode) 306, 288, 261, 231, 225. Anal. Calcd for C$_9$H$_8$NO$_3$I: C, 35.43; H, 2.64; N, 4.59. Found: C, 35.90; H, 2.74; N, 4.90. The lysine conjugate of IBA (IBA-Lys), 6-[N-(3-iodobenzamido)]-2-aminocaproic acid, was prepared by first reacting a solution of SIB (345 mg) in anhydrous THF with N α-t-Boc-lysine (246 mg) dissolved in the borate buffer (200 μL; pH 8.5). After stirring at

room temperature for 4 h, the t-Boc derivative was isolated in 65% yield by employing silica gel flash column chromatography. Anal. Calcd for C$_{18}$H$_{25}$N$_2$O$_5$I: C, 45.38; H, 5.25; N, 5.88. Found: C, 45.14; H, 5.56; N, 5.45. The t-Boc protective group was then removed by treating with trifluoroacetic acid in methylene chloride at 60 °C for 30 min. The solvent was evaporated off, and the desired compound was isolated in 55% radiochemical yield as a white compound (mp 261−263 °C). Mass spectra, m/z (EI mode) 377, 333, 314, 265, 225. Anal. Calcd for C$_{13}$H$_{17}$N$_2$O$_3$I: C, 41.49; H, 4.52; N, 7.45. Found: C, 41.81; H, 4.62; N, 7.29.

HPLC Analysis. Radiolabeled catabolite analyses by HPLC were performed on a Beckman System Gold package which included a Model 126 programmable solvent module, a Model 168 diode array detector, and a Model 170 radioisotope detector. Data analysis was accomplished using Beckman Gold software V 7.11 on an IBM computer. Size-exclusion chromatography was performed using a Bio-Sil SEC 250 gel filtration column (Bio-Rad, 600 × 7.5 mm) eluted with PBS at a flow rate of 1 mL/min. Fractions of 0.5 mL were collected and counted using an automated γ counter. Molecular weight assignments were made based on comparison with gel filtration molecular weight standards (Bio-Rad) which were run under identical conditions.

Compounds with molecular masses of less than 10 kDa (LMW) were separated from the tissue homogenate supernatants using Centricon-10 filtering cartridges (Amicon) and were analyzed by HPLC using a reverse-phase column (Alltech, Adsorbosphere C-18 10 μm, 250 × 4.6 mm) eluted in isocratic mode with MeOH/H$_2$O/AcOH (45:55:0.2) at a flow rate of 1 mL/min. One milliliter fractions were collected and counted for ^{125}I activity using an automated γ counter. Cold compounds, including IBA, IBA-Gly, and IBA-Lys, were analyzed by HPLC to determine the retention time for these potential catabolic products. Because of the potential for variability in retention time with column age and minor change in buffer preparation for the reverse-phase column, these HPLC standards were run before each series of tissue analyses.

SDS−PAGE. Iodine-125-labeled Me1−14 F(ab')$_2$ and aliquots of tissue supernatants were analyzed by SDS−PAGE using 4−20% gradient gels (Bio-Rad) under non-reducing conditions. Dried gels were exposed to X-ray film (Ektascan MEM-1, Kodak, Rochester, NY), and the distribution of radioactivity among the different bands was analyzed using a Bio-Rad GS-670 imaging densitometer.

***Ex Vivo* Studies.** Urine and blood were collected from 2−3 normal Balb/c mice. Additional groups of 2−3 mice were killed by halothane overdose, and the liver, spleen, and kidneys were excised, washed with saline, chopped coarsely with scissors, and homogenized in a hand-held glass tissue homogenizer. Depending on organ weight, between 0.2 and 1.0 g of each tissue homogenate, as well as 0.2−0.5 mL of urine and blood, was incubated at 37 °C with 5−10 μCi of ^{125}I-labeled Me1−14 F(ab')$_2$. The generalized scheme for sample analysis is summarized in Figure 1. After 3 and 24 h, homogenates and biological fluids were centrifuged at 1300g for 15 min, and the pellet was washed twice with 300 μL of PBS, pH 7.4. Aliquots of both the combined supernatants and pellets were assayed for ^{125}I to determine the fraction of the activity remaining in the pellet. The supernatant was passed through a 0.45 μm filter and analyzed using size-exclusion HPLC as well as SDS−PAGE. A portion of the supernatant was centrifuged through a Centricon-10 cartridge (Millipore, Bedford, MA) to isolate catabolites
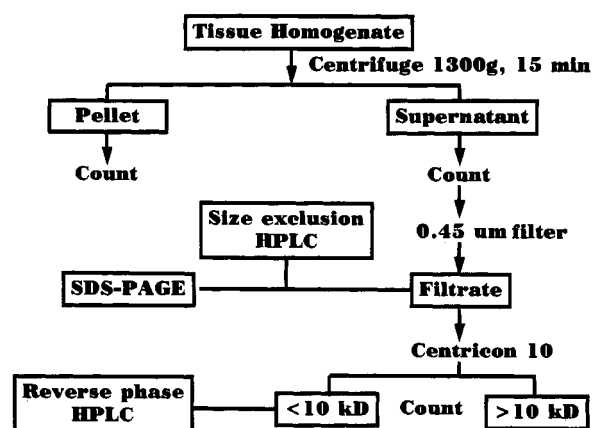
Figure 1. Scheme used for sample preparation and analysis of catabolites from radioiodinated Mel−14 F(ab')₂.

Table 1. Tissue Distribution of Radioiodine Following Injection of ¹²⁵I-Labeled Mel−14 F(ab')₂ in Normal Mice Prepared Using Iodogen and SIB Methods

	% injected dose per organ[a]			
	3 h postinjection		24 h postinjection	
tissue	SIB	iodogen	SIB	iodogen
liver	5.37 ± 0.66	7.63 ± 0.43	0.51 ± 0.05	1.12 ± 0.13
spleen	0.34 ± 0.03	0.46 ± 0.05	0.04 ± 0.01	0.08 ± 0.01
lungs	1.79 ± 0.11	2.87 ± 0.50	0.14 ± 0.01	0.19 ± 0.01
kidneys	10.60 ± 0.10	14.30 ± 0.50	0.52 ± 0.03	1.22 ± 0.41
blood	21.90 ± 2.40	29.60 ± 1.80	1.21 ± 0.07	2.53 ± 0.20

[a] Mean ± standard deviation.

with molecular weights less than 10 kDa. These were analyzed by reverse-phase HPLC.

Analysis of Labeled Catabolites Generated *in Vivo*. Experiments were performed using ¹²⁵I-labeled Mel−14 F(ab')₂ prepared by both the iodogen and SIB methods. Balb/c mice were injected intravenously with 10 μCi (5−7 μg) of radioiodinated Mel−14 F(ab')₂, and groups of 3 animals were killed by halothane overdose after 3 and 24 h. Urine was collected before killing the mice. Liver, spleen, lung, kidneys, and blood were removed and washed with saline. After counting the tissues for ¹²⁵I activity, analysis of labeled catabolites was performed using the same procedures described for the *in vitro* studies.

RESULTS

The tissue distribution of ¹²⁵I activity was measured to ensure that differences in normal tissue uptake observed in prior studies existed in the animals used in the catabolism experiments. As summarized in Table 1, accumulation of ¹²⁵I activity in normal tissues following injection of ¹²⁵I-labeled Mel−14 F(ab')₂ was higher when the iodogen method was used for radioiodination. Even at 3 h, significantly lower normal tissue levels were seen with F(ab')₂ labeled using SIB ($P < 0.05$).

Prior to initiation of the catabolism experiments, each preparation of ¹²⁵I-labeled Mel−14 F(ab')₂ was analyzed by size-exclusion HPLC. The HPLC profiles illustrated in Figure 2 indicate that 96% and 98% of the ¹²⁵I activity for F(ab')₂ labeled using iodogen and SIB, respectively, was associated with a 100 kDa species. In both cases, less than 1% of the total radioactivity was observed as <10 kDa impurities. In this HPLC system, comparison to the molecular weight standards indicated that F(ab')₂ eluted approximately in fractions 35−36, aggregates and other high molecular weight complexes earlier (fractions 22−26), 50 kDa molecular weight species (presumed to
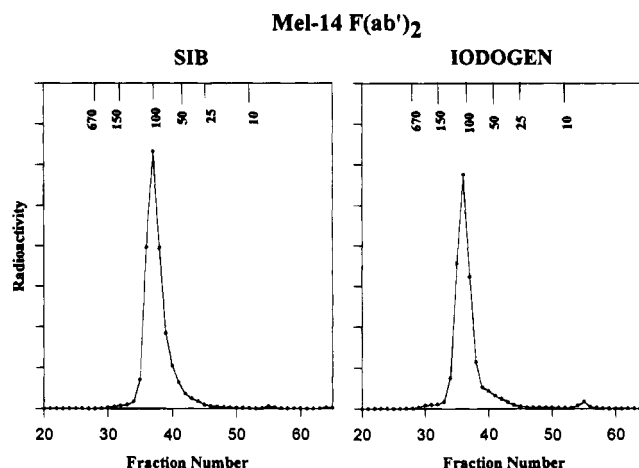
Figure 2. Size-exclusion radiochromatogram of radioiodinated Mel−14 F(ab')₂ obtained prior to exposure to tissue samples. Numbers on the top of the graphs indicate the elution positions for the molecular weight standards (kDa). Left panel, SIB labeling method; right panel, iodogen labeling method.

Table 2. Distribution of Radioiodine in Tissue Samples following 24 h Exposure to Radioiodinated Mel−14 F(ab')₂ Presented as the Percentage Activity Isolated in the Pellet and Supernatant

	labeled using iodogen			labeled using SIB		
sample	pellet[a]	>10 kDa[b]	<10 kDa[c]	pellet[a]	>10 kDa[b]	<10 kDa[c]
in vivo[d]						
liver	19	75	6	18	80	2
spleen	21	70	9	25	69	6
kidneys	52	38	10	45	41	14
serum	<1	91	9	<1	99	1
urine	<0.5	17	83	0	15	85
in vitro[e]						
liver	14	76	10	18	74	8
spleen	5	87	8	7	87	6
kidneys	11	84	5	12	83	5
serum	1	97	2	2	97	1
urine	2	91	7	2	94	4

[a] Percentage of activity isolated in the pellet. [b] Percentage of activity retained on 10 kDa filter. [c] Percentage of activity passed through 10 kDa filter. [d] Tissue samples obtained 24 h after injection in mice. [e] Incubation of tissue homogenate or fluid for 24 h at 37 °C.

be Fab) in fraction 41, and <5 kDa compounds in fraction 54. To simplify data presentation, the elution profile was divided into four molecular weight categories: >150 kDa, ~100 kDa F(ab')₂, ~30−70 kDa, and <30 kDa. Generally, about 20% of the radioactivity added to the tissue homogenates was retained in the tissue pellet following centrifugation. An exception was the kidneys, where 40−50% of the radioactivity was retained in the homogenate pellet *in vivo*, but not *ex vivo*. No major differences between the two radioiodination methods were observed. When the supernatants were further processed using the 10 kDa molecular weight cutoff cartridge, 3−20% of the total supernatant radioactivity was isolated as <10 kDa species for most tissues (Table 2). Greater than 80% of the radioactivity in urine samples obtained from mice injected with ¹²⁵I-labeled Mel−14 F(ab')₂ was present as LMW species. Again, no major differences in the degree of <10 kDa catabolites were observed between F(ab')₂ labeled using iodogen and SIB.

Size-exclusion HPLC profiles were analyzed to determine the distribution of supernatant radioactivity into the four molecular weight groups noted above. Similar trends were observed following 3 and 24 h *ex vivo* and *in vivo* exposures. The results for the 3 h time point are summarized in Table 3. No major differences in labeled

Table 3. Size-Exclusion HPLC Analysis of Radioiodine Activity in Tissue Samples Obtained 3 h after Injection and 3 h after Incubation at 37 °C

sample	% of activity			
	>150 kDa	~100 kDa	~50 kDa	<30 kDa
in vivo				
liver				
SIB	10	13	63	10
iodogen	9	9	57	20
spleen				
SIB	6	31	29	13
iodogen	5	31	32	16
lungs				
SIB	2	70	19	1
iodogen	3	65	12	13
kidneys				
SIB	7	15	65	3
iodogen	11	11	54	21
serum				
SIB	7	87	4	1
iodogen	8	33	31	20
in vitro				
liver				
SIB	4	7	71	11
iodogen	6	11	75	9
serum				
SIB	3	88	7	1
iodogen	13	76	6	3

product distribution between the two methods were seen after *ex vivo* incubation of ^{125}I-labeled Me1−14 F(ab′)$_2$ with liver homogenate and serum. Unlike serum, the majority of the ^{125}I activity in the liver had a molecular weight corresponding to an Fab fragment (Figure 3).

More striking differences between the labeling methods were observed in the tissue samples harvested from the mice injected with ^{125}I-labeled Me1−14 F(ab′)$_2$. For example, the fraction of LMW species present in liver (Figure 4) and kidney supernatants in the iodogen groups was 2- and 7-fold higher, respectively, compared with animals receiving F(ab′)$_2$ labeled using SIB. Even larger differences in the contribution of LMW catabolites were measured in both the lungs and serum. The serum sample from the SIB group showed 87% of the supernatant activity present as a 100 kDa species, while for the iodogen group, only 33% was present as 100 kDa with 31% present as a ~50 kDa species (Figure 3). In addition, 20% of the serum activity was present as <30 kDa species in the iodogen group compared with 1% for animals receiving Me1−14 F(ab′)$_2$ radioiodinated using SIB. Similarly, 21% of the radioactivity in the supernatant from 3 h kidney samples of iodogen group was associated with LMW component compared with only 3% for the SIB group (Figure 3). A similar profile was seen for the 3 h *ex vivo* liver samples from the two groups on size-exclusion HPLC.

Analysis of tissue supernatants by reverse-phase HPLC revealed that the majority of the radioactivity could be accounted for by [^{125}I]iodide, IBA, IBA-Gly, and IBA-Lys. Different tissue homogenate surpernatants and biological fluids exhibited varied distribution patterns of these catabolites. Incubation of ^{125}I-labeled Me1−14 F(ab′)$_2$ labeled using SIB with urine for 3 h (Figure 5) and 24 h (Figure 6) yielded two primary peaks corresponding to [^{125}I]iodide and IBA, with the latter predominating at 24 h. In contrast, *in vivo* urine samples were characterized by two main peaks. The larger corresponded to IBA-Lys, and the smaller, to IBA-Gly, with <3% of radioactivity present as [^{125}I]iodine. *Ex vivo* urine samples from the iodogen group at 3 h showed >75% of the activity as [^{125}I]-iodine and <10% of the activity as the mono[^{125}I]-iodotyrosine (Figure 5). At 24 h, mono[^{125}I]iodotyrosine
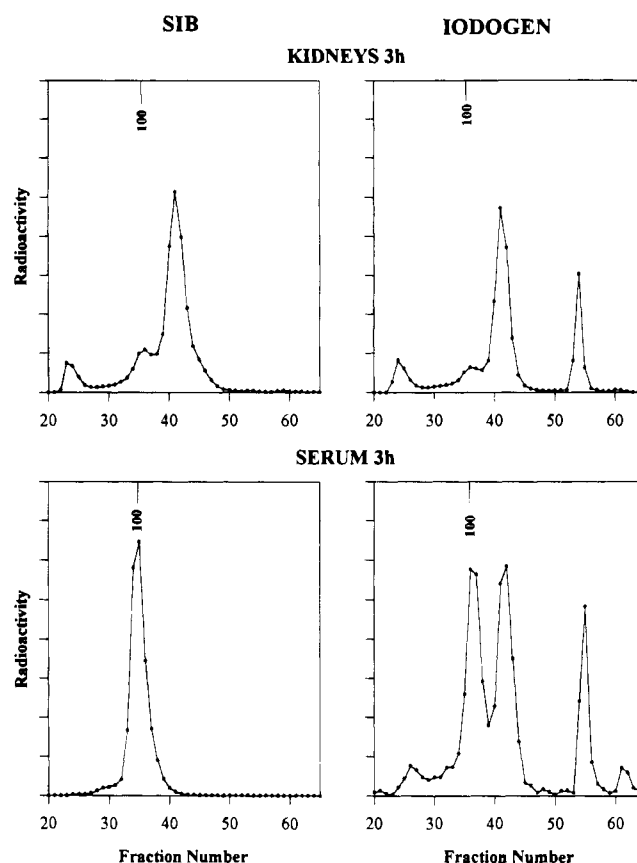
Figure 3. Size-exclusion radiochromatogram of radioactivity obtained 3 h after injection of radioiodinated Me1−14 F(ab′)$_2$ in normal mice. Kidney supernatant (top panels) and serum (bottom panels) for F(ab′)$_2$ labeled using SIB (left panels) and iodogen methods (right panels). The elution position corresponding to a 100 kDa F(ab′)$_2$ fragment is indicated for comparison.

levels had increased to ~15−20%. In contrast, >95% of the radioactivity was present as [^{125}I]iodide in both the 3 and 24 h *in vivo* groups (Figures 5 and 6).

Reverse-phase HPLC chromatograms of liver and kidney supernatant samples from the *in vivo* experiments are illustrated in Figure 7. Radioactivity in the liver supernatant from the SIB group was distributed primarily among IBA (30%), IBA-Lys (55%), and IBA-Gly (5%). In the 3 h kidney supernatant samples from the SIB group, 92% of the LMW catabolites were present as IBA and <2% as IBA-Gly. Kidney and liver samples from the iodogen group showed [^{125}I]iodide as major catabolite with < 20% of the radioactivity present as mono[^{125}I]iodotyrosine (Figure 7).

SDS−polyacrylamide gel electrophoresis was performed on selected *ex vivo* and *in vivo* tissue homogenate supernatants obtained after injection of ^{125}I-labeled Me1−14 F(ab′)$_2$. The distribution of catabolites observed on SDS−PAGE was in general agreement with that seen on size-exclusion HPLC. Figure 8 is an autoradiograph comparing the band distribution of samples from the spleen, lung, kidney, and liver from the 3 h SIB group along with molecular weight standards. In lungs and spleen, the major bands seen were at 100 kDa (spleen 50%; lungs 69%) and 50 kDa (spleen 30%; lung 10%). In the liver, ^{125}I was distributed among multiple bands with 35% at 100 kDa, 32% at 50 kDa, and 22% in two bands at ~25 kDa, and the remainder was associated with species of <14 kDa. In the kidney supernatant samples, <2% of the activity was found as intact F(ab′)$_2$. The predominant species seen on SDS−PAGE were bands approximating 50 kDa (25%) and three bands at about
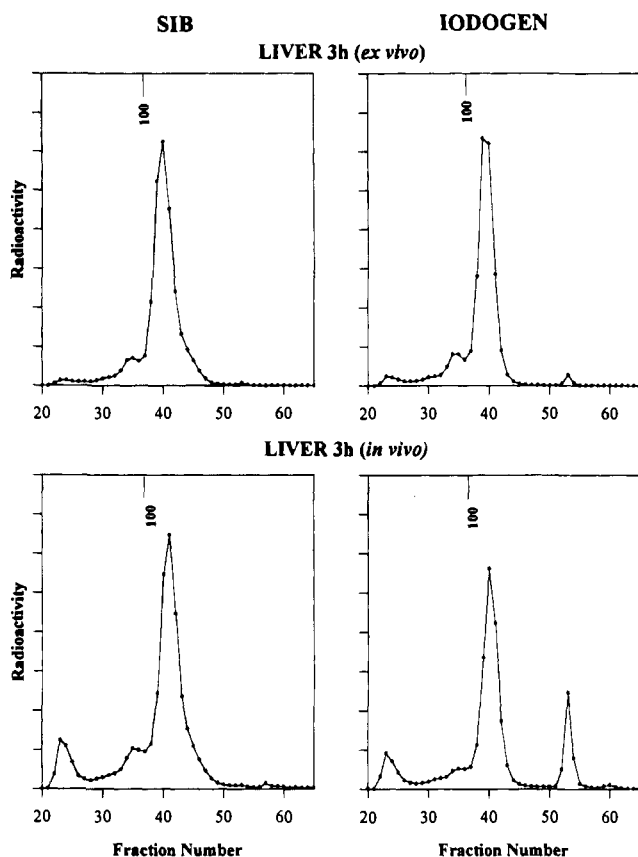
Figure 4. Size-exclusion radiochromatogram from analysis of liver homogenate supernatant obtained 3 h after injection of radioiodinated Me1−14 F(ab′)₂ in normal mice (bottom panels) or after 3 h incubation *ex vivo* (top panels). F(ab′)₂ was labeled using SIB (left panels) and iodogen methods (right panels). The elution position corresponding to a 100 kDa F(ab′)₂ fragment is indicated for comparison.

Figure 5. Reverse-phase HPLC chromatogram from analysis of urine obtained 3 h after injection of radioiodinated Me1−14 F(ab′)₂ in normal mice (bottom panels) or after 3 h incubation *ex vivo* (top panels). F(ab′)₂ was labeled using SIB (left panels) and iodogen methods (right panels). The elution position corresponding to anticipated low molecular weight catabolites are indicated for comparison.

25 kDa (45%), with the remainder present as <20 kDa species. SDS−PAGE analyses of spleen and kidney samples obtained 3 h after injection of F(ab′)₂ labeled using iodogen also were performed. In spleen, the distribution of activity was 100 kDa (6%) 50 kDa (28%), 25 kDa (40%), and <20 kDa (18%). As observed with the SIB group, only a small fraction (<5%) of the supernatant activity was found as intact F(ab′)₂, and the predominant species were bands of approximately 50 kDa (18%) and 25 kDa (45%), with the remainder present as <20 kDa species.

DISCUSSION

Normal tissue uptake of radiolabeled MAbs can confound detection of occult tumor sites and, for therapeutic applications, limit doses to below curative levels. In attempting to limit normal tissue uptake from labeled MAbs, two parameters which should be considered are the radionuclide and the radiolabeling method. Clearly, a better understanding of the nature of the labeled species which are present following administration of labeled MAbs should facilitate the development of approaches for altering normal tissue accumulation.

This investigation considered the catabolites generated in normal mice in order to avoid products which might be generated as a consequence of the interaction of MAb with tumor. These species would be expected to be different for various types of antigens. For example, *in vitro* investigations have shown that MAbs which become internalized can undergo proteolysis in lysosomes, resulting in the generation of monoiodotyrosine (*24, 25*).

Alternatively, if antigen is present in the circulation, antigen−antibody complexes can be generated (*26, 27*), and their catabolism is likely to be different from that of free MAb. An F(ab′)₂ fragment was studied instead of an intact IgG because of the more rapid catabolism of the smaller molecule (*2*). This accelerated catabolism presumably contributes to the superior tumor-to-normal tissue ratios for F(ab′)₂ compared with IgG, albeit at the expense of more rapid clearance of radioactivity from tumor (*20*).

Understanding the catabolites generated from MAbs labeled using direct radioiodination techniques such as the iodogen method is important because this labeling approach is utilized most frequently in clinical radioimmunotherapeutic investigations. These include an evaluation of Me1−14 F(ab′)₂, utilized in the current work, labeled with ¹³¹I, for the treatment of neoplastic meningitis (*9*). Direct iodination approaches result predominantly in the creation of iodinated tyrosine residues (*10*), and in the absence of intracellular tumor processing, loss of label is generally believed to occur by dehalogenation rather than proteolytic release of monoiodotyrosine. This supposition is based on the observation of high levels of activity in stomach and thyroid (*11*), tissues known to accumulate free radioiodide (*28*); however, little direct evidence has been available concerning the chemical nature of the normal tissue catabolites which have been generated.

Minimizing dehalogenation was one of the motivations for the development of other radioiodination approaches such as SIB. Indeed, MAbs labeled using SIB exhibit
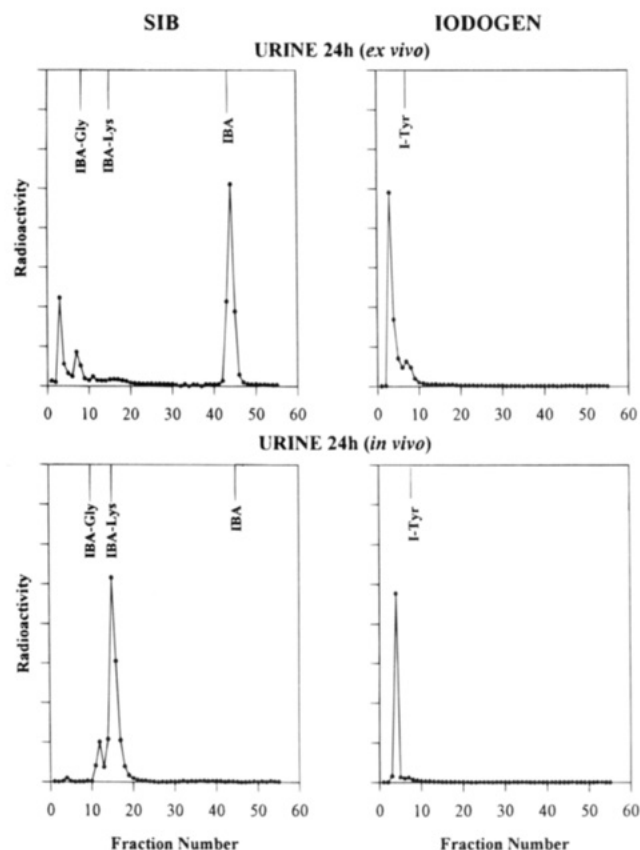
Figure 6. Reverse-phase HPLC chromatogram from analysis of urine obtained 24 h after injection of radioiodinated Me1−14 F(ab')$_2$ in normal mice (bottom panels) or after 24 h incubation *ex vivo* (top panels). F(ab')$_2$ was labeled using SIB (left panels) and iodogen methods (right panels). The elution position corresponding to anticipated low molecular weight catabolites are indicated for comparison.

Figure 7. Reverse-phase HPLC chromatogram from analysis of supernatants from liver (top panels) and kidneys (bottom panels). Tissues obtained 3 h after injection of radioiodinated Me1−14 F(ab')$_2$ labeled using SIB (left panels) and iodogen methods (right panels). The elution position corresponding to anticipated low molecular weight catabolites are indicated for comparison.

considerably lower levels of radioiodine in the thyroid (*13, 14, 29*) and, in some cases, increased tumor uptake (*30*), compared with coadministered MAbs labeled using direct methods. Two other criteria considered in the designing SIB are relevant to the current study. First, SIB avoids exposure of the MAb to oxidizing agents which can have an effect on protein structure (*31*). And second, with SIB, IBA is a potential catabolite and, if generated, would be expected to be excreted rapidly via the urine as a glycine conjugate (*32*). Indeed, paired-label studies in mice have demonstrated that IBA is cleared from normal tissues even more rapidly than iodide. In addition, normal tissue levels for F(ab')$_2$ labeled using SIB are significantly lower than those using iodogen (*29*), an observation that was confirmed in the present study.

With both radioiodination methods, >95% of the product eluted on size-exclusion HPLC with a retention time characteristic of a F(ab')$_2$ fragment. In contrast to serum, where *in vitro* incubation had only a modest effect, exposure to liver homogenates for only 3 h resulted in extensive conversion to Fab and the production of about 10% <10 kDa species. Characterization of the catabolites created during *in vitro* incubation of radioiodinated MAbs with liver homogenates has not been reported previously. Although it would be difficult to make direct comparisons with our results using an F(ab')$_2$, it should be noted that the effect of liver homogenates on intact MAbs labeled with radiometals has been investigated. In one study evaluating ^{111}In-labeled MAbs,, use of 1B4M, CHX-B, and cDTPA conjugates yielded a single peak corresponding to intact IgG (*3*). In another report, *in vitro* incubation with liver homogenates demonstrated significant differ-
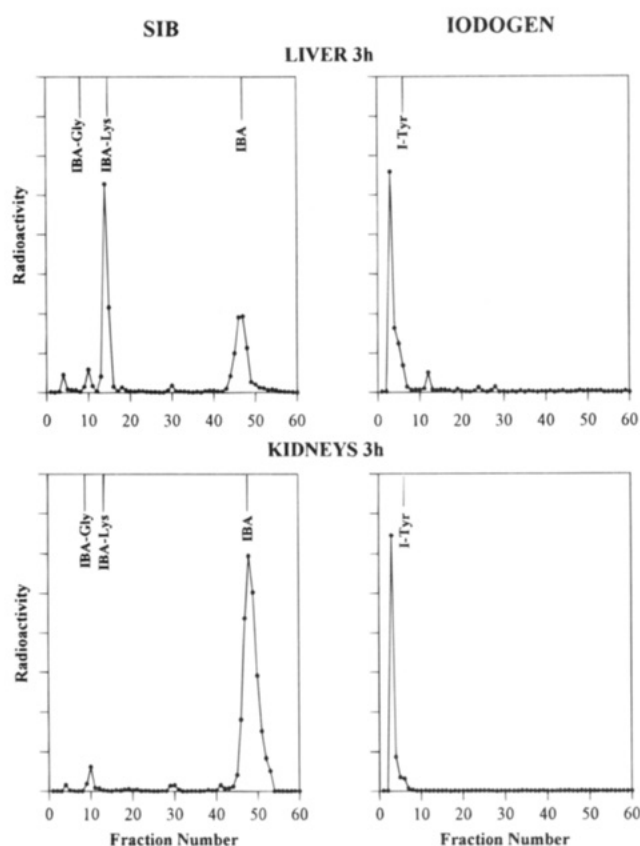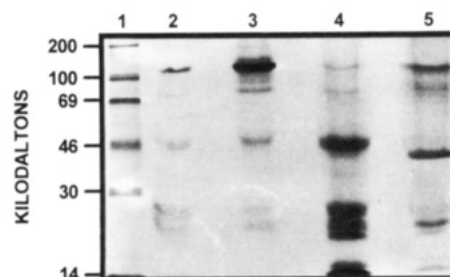
Figure 8. Autoradiograph of SDS−PAGE run under nonreducing conditions of labeled catabolites. Iodine-125-labeled Me1−14 F(ab')$_2$ prepared using SIB method injected into normal mice and tissues obtained 3 h later. Molecular weight standards (lane 1), spleen (lane 2), lung (lane 3), kidney (lane 4), and liver (lane 5).

ences in stability of ^{111}In- and ^{90}Y-labeled C110 MAb prepared using either cDTPA or SCN-Bz-DTPA (*1*).

Our results suggest that *in vitro* incubation with liver homogenates may be a more useful preliminary indicator of stability test for radioiodinated MAbs than incubation with serum. However, because of the possibility of transchelation to transferrin, serum incubation remains an important criteria for evaluating MAbs labeled with radiometals. An additional implication of this study is that, at least for F(ab')$_2$, use of liver as a negative control homogenate in immunoreactivity assays (*23, 30*) may not be advisable. Rapid conversion of divalent F(ab')$_2$ to monovalent Fab in liver homogenates at 37 °C could alter the binding properties of the labeled species, confounding the interpretation of nonspecific binding levels.

Size-exclusion HPLC and SDS–PAGE analyses suggest that a catabolite with a molecular weight similar to Fab accounted for a significant amount of the radioactivity present *in vivo*. This was particularly apparent in metabolically active organs such as the liver and kidneys; even at 3 h, more than half of the radioiodine was identified as Fab. This behavior is contrary to that reported for an ^{111}In-labeled SCN-Bz-DTPA conjugate of NP-4 F(ab')₂, which was rapidly catabolized *in vivo* to low molecular weight components with only a low level of Fab detected (*2*).

The most obvious explanation for the difference in catabolites observed in the current study is the nature of the radionuclide and labeling method; however, there may be other contributory factors such as the different murine isotypes of Mel−14 (IgG$_{2a}$) and NP-4 (IgG₁ (*33*)). Degradation of chimeric F(ab')₂ has been reported to vary with the human subclass of the parental MAb (*34*). For example, 12 h after injection, the percentage free iodide in serum was more than twice as high for F(ab')₂ derived from human IgG₁ compared with IgG₂. Thus, extrapolation of the catabolic patterns observed in the current study to F(ab')₂ fragments generated from other MAbs would not be recommended.

The most substantive difference in catabolites between the two labeling methods observed *in vivo* was the contribution of LMW species. When labeling was performed using iodogen, a 2-fold higher percentage of the liver supernatant activity was present as <10 kDa species and 7- to 20-fold differences were observed in other tissues (Table 3). This could be explained by the more rapid loss of label and the generation of slower clearing catabolites from MAb labeled using iodogen. The later factor could account for the particularly large differences observed in serum and kidneys. A potential catabolite of MAbs labeled using SIB is IBA, a compound which forms a glycine conjugate that is cleared from normal tissues and excreted much more rapidly than iodide (*29*). For example, blood levels of IBA were more than 4 times lower than those observed for iodide at 4 h.

Differences between the two radioiodination methods were most apparent in the reverse-phase HPLC analyses. Our results are consistent with past speculations, generally based on indirect evidence, that deiodination is a major event in the catabolism of MAbs labeled via electrophilic iodination of tyrosine residues on the protein. With F(ab')₂ labeled using iodogen, >80% and >95% of the LMW activity isolated from the liver and the kidneys, respectively, was present as [^{125}I]iodide, with the remainder eluting with a retention time corresponding to mono[^{125}I]iodotyrosine. The presence of both species suggests that deiodination and proteolysis both may contribute to the catabolism of F(ab')₂ labeled using this method. Unfortunately, monoiodotyrosine itself can be rapidly deiodinated in liver and kidney (*35*), confounding quantification of the relative magnitude of MAb dehalogenation and proteolysis.

The LMW catabolites generated from F(ab')₂ radioiodinated using SIB were different from those observed for the iodogen method. In general, proteolysis appeared to be more important than deiodination (either direct action on the F(ab')₂ or secondary action on a precursor catabolite). Reverse-phase HPLC analyses of LMW catabolites suggested the presence of IBA as well as its glycine and lysine conjugate, with little evidence of [^{125}I]iodide. These results confirm previous studies which inferred, based on low thyroid uptake levels, that MAbs labeled using SIB were inert to dehalogenation *in vivo* (*13, 14*).

With the exception of the kidneys, IBA-Lys was the predominant LMW compound generated *in vivo* from F(ab')₂ radioiodinated using SIB. The SIB method is presumed to involve conjugation with the ε-amino group on lysine residues. The observation of IBA-Lys is consistent with this assumption and suggests catabolism of the F(ab')₂ fragment via hydrolysis of the peptide bond between the conjugated lysine residues and the adjacent amino acid. The generation of IBA-Lys would be anticipated from the results reported for other proteins where a small molecule was coupled to lysine ε-amino groups. Following lysosomal degradation of ^{111}In-labeled glycoproteins, ^{111}In-DTPA−lysine has been reported (*36*). Likewise, stable lysine−drug conjugates have been observed after the catabolism of low molecular weight protein−drug conjugates in lysosomal lysates (*37*).

In kidney, nearly all of the LMW catabolites eluted on reverse-phase HPLC with a retention time corresponding to IBA. The kidney is known to play a significant role in the metabolism of proteins and peptides, particularly those of lower molecular weight (*38*). SDS–PAGE analysis of kidney supernatant indicates the presence of multiple bands representing labeled catabolites in the 15−25 kDa range. Since these species are small enough to undergo processing by renal cells, we hypothesize that the amide bond between IBA and lysine in these labeled intermediates could have become hydrolyzed in the kidney, thus producing IBA.

IBA also was found to a lesser extent in other normal tissues such as the liver. Whether this represents recirculation of IBA produced in the kidney or generation within these tissues cannot be ascertained. The former explanation is supported by the fact that IBA was not found in the urine obtained from these animals. In most tissues, IBA-Gly also was observed, accounting for about 5% of the LMW catabolites. This is consistent with the results of previous studies, which have shown that IBA can form glycine conjugates *in vivo* (*39*).

With both labeling methods, the catabolites generated by exposure to urine were considerably different from those excreted into the urine. When Mel−14 F(ab')₂ was labeled using iodogen, incubation with urine *ex vivo* yielded [^{125}I]iodide and mono[^{125}I]iodotyrosine while the *in vivo* studies indicated that all of the activity was excreted as [^{125}I]iodide. With SIB, IBA and [^{125}I]iodide were the primary catabolites generated *ex vivo*, while IBA-Gly and IBA-Lys were the species excreted into the urine. The presence of IBA-Gly in the urine is consistent with a previous report which identified IBA-Gly in the urine of mice injected with an intact MAb labeled using SIB (*40*). The differences between *in vivo* and *ex vivo* urinary catabolites suggests that the urine itself is capable of hydrolytic degradation of F(ab')₂ fragments.

In summary, the catabolism of this radioiodinated F(ab')₂ fragment resulted in the production of multiple species in the low and high molecular weight range. Lower molecular weight catabolites accounted for a small fraction of the total activity in most tissues; however, as would be expected, differences between the radioiodination methods were most apparent in this molecular weight region. These differences are in concert with the more rapid normal tissue clearance observed for MAbs and MAb fragments labeled using SIB. Experiments are in progress to investigate the tumor-mediated catabolism of radioiodinated F(ab')₂ and to compare the catabolism of MAb fragments labeled with SIB and its analog acylation agents *N*-succinimidyl [^{211}At]astatobenzoate and *N*-succinimidyl [^{18}F]fluorobenzoate.

LITERATURE CITED

(1) Mardirossian, G., Wu, C., and Hnatowich, D. J. (1993) The stability in liver homogenates of indium-111 and yttrium-90 attached to antibody via two popular chelators. *Nucl. Med. Biol. 20,* 65−74.

(2) Motta-Hennessy, C., Sharkey, R. M., and Goldenberg, D. M. (1990) Metabolism of indium-111-labeled murine monoclonal antibody in tumor and normal tissue of the athymic mice. *J. Nucl. Med. 31,* 1510−1519.

(3) Kinuya, S., Jeong, J. M., Garmestani, K., Saga, T., Camera, L., Brechbiel, M. W., Gansow, O. A., Carrasquillo, J. A., Neumann, R. D., and Paik, C. H. (1994) Effect of metabolism on retention of indium-111-labeled monoclonal antibody in liver and blood. *J. Nucl. Med. 35,* 1851−1857.

(4) Sakahara, H., Saga, T., Endo, K., Hattori, N., Hosono, M., Kobayashi, H., Shirato, M., Yamamuro, T., Toyama, S., Arano, Y., Yokoyama, A., and Konishi, J. (1993) *In Vivo* instability of reduction-mediated ^{99m}Tc-labeled monoclonal antibody. *Nucl. Med. Biol. 20,* 617−623.

(5) Hnatowich, D. J., Mardirossian, G., Rusckowski, M., Fogarasi, M., Virzi, F., and Winnard, Jr., P. (1993) Directly and indirectly technetium-99m-labeled antibodies: a comparison of in vitro and animal in vivo properties. *J. Nucl. Med. 34,* 109−119.

(6) Lashford, L. S., Davies, A. G., Richardson, R. B., Bourne, S. P., Bullimore, J. A., Eckert, H., Kemshead, J. T., and Coakham, H. B. (1988) A pilot study of ^{131}I monoclonal antibodies in the therapy of leptomeningeal tumors. *Cancer 61,* 857−868.

(7) Press, O. W., Eary, J. F., Appelbaum, F. R., Martin, P. J., Badger, C. C., Nelp, W. B., Glenn, S., Butchko, G., Fisher, D., Porter, B., Matthews, D. C., Fisher, L. D., and Berstein, I. D. (1993) Radiolabeled-antibody therapy of B-cell lymphoma with autologous bone marrow support. *N. Eng. J. Med. 329,* 1219−1224.

(8) Kaminski, M. S., Zasadny, K. R., Francis, I. R., Milik, A. W., Ross, C. W., Moon, S. D., Crawford, S. M., Burgess, J. M., Petry, N. A., Butchko, G. M., Glenn, S. D., and Wahl, R. L. (1993) Radioimmunotherapy of B-cell lymphoma with [^{131}I]-anti-B1 (anti-CD20) antibody. *N. Engl. J. Med. 329,* 459−465.

(9) Bigner, D. D., Brown, M., Coleman, R. E., Friedman, A. H., Friedman, H. S., McLendon, R. E., Bigner, S. H., Wikstrand, C. J., Pegram, C. N., Kerby, T., and Zalutsky, M. R. (1995) Phase I studies of treatment of malignant gliomas and neoplastic meningitis with ^{131}I-radiolabeled monoclonal antibodies anti-tenascin 81C6 and anti-chondroitin proteoglycan sulfate Me1−14 F(ab')$_2$ - a preliminary report. *J. Neuro-Oncol.,* Submitted.

(10) Eary, J. F., Krohn, K. A., Kishore, R., and Nelp, W. B. (1989) Radiochemistry of halogenated antibodies. *Antibodies in Radiodiagnosis and Therapy* (M. R. Zalutsky, Ed.) pp 83−102, CRC Press, Boca Raton, FL.

(11) Hayes, D. F., Zalutsky, M. R., Kaplan, W., Noska, M., Thor., A., Colcher, D., and Kufe, D. (1986) Pharmacokinetics of radiolabeled monoclonal antibody B6.2 in patients with metastatic breast cancer. *Cancer Res. 46,* 3157−3163.

(12) Carrasquillo, J. A. (1989) Radioimmunoscintigraphy with polyclonal and monoclonal antibodies. *Antibodies in Radiodiagnosis and Therapy* (M. R. Zalutsky, Ed.) pp 169−198, CRC Press, Boca Raton, Fl.

(13) Zalutsky, M. R., and Narula, A. S. (1987) A method for the radiohalogenation of proteins resulting in decreased thyroid uptake of radioiodine. *Int. J. Radiat Appl. Instrum. [Part A] 38,* 1051−1055.

(14) Wilbur, D. S., Hadley, S. W., Hylarides, M. D., Abrams, P. G., Beaumier, P. A., Morgan, A. C., Reno, J. M., and Fritzberg, A. R. (1989) Development of a stable radioiodinating reagent to label monoclonal antibodies for radiotherapy of cancer. *J. Nucl. Med. 30,* 216−226.

(15) Khawli, L. A., and Kassis, A. I. (1989) Synthesis of ^{125}I labeled N-succinimidyl p-iodobenzoate for use in radiolabeling antibodies. *Nucl. Med. Biol. 16,* 727−733.

(16) Badger, C. C., Wilbur, D. S., Hadley, S. W., Fritzberg, A. R., and Bernstein, I. D. (1990) Biodistribution of p-iodobenzoyl (PIP) labeled antibodies in a murine lymphoma model. *Nucl. Med. Biol. 17,* 381−387.

(17) Quadri, S. M., Zhang, Y. Z., and Williams, J. R. (1991) Improvements in radioiodination of monoclonal antibodies for diagnosis and treatment of cancer. *Antibody Immunoconjugates Radiopharm. 4,* 283−296.

(18) Schuster, J. M., Garg, P. K., Bigner, D. D., and Zalutsky, M. R. (1991) Improved therapeutic efficacy of a monoclonal antibody radioiodinated using N-succinimidyl-3-(tri-n-butyl-stannyl)benzoate. *Cancer Res. 51,* 4164−4169.

(19) Carrel, S., Accolla, R. S., Carmagnola, A. L., and Mach, J. P. (1980) Common human melanoma-associated antigen(s) detected by monoclonal antibodies. *Cancer Res. 40,* 2523−2528.

(20) Colapinto, E. V., Humphrey, P. A., Zalutsky, M. R. (1988) Comparative localization of murine monoclonal antibody Me1−14 F(ab')$_2$ fragment and whole IgG$_{2a}$ in human glioma xenografts. *Cancer Res. 48,* 5701−5707.

(21) Zalutsky, M. R., Garg, P. K., Friedman, H. S., and Bigner, D. D. (1989) Labeling monoclonal antibodies and F(ab')$_2$ fragments with the alpha particle emitting nuclide astatine-211: Preservation of immunoreactivity and *in vivo* localizing capacity. *Proc. Natl. Acad. Sci. U.S.A. 86,* 7149−7153.

(22) Garg, P. K., Bigner, D. D., and Zalutsky, M. R. (1991) Tumor dose enhancement via improved antibody radiohalogenation. *Monoclonal Antibodies - Applications in Clinical Oncology* (A. A. Epenetos, Ed.) pp 103−114, Chapman and Hall.

(23) Garg, P. K., Archer, G. E., Jr., Bigner, D. D., and Zalutsky, M. R. (1989) Synthesis of radioiodinated N-succinimidyl Iodobenzoate: optimization for use in antibody labeling. *Int. J. Rad. Appl. Instrum. [Part A] 40,* 485−490.

(24) Geissler, F., Anderson, S. K., and Press, O. (1991) Intracellular catabolism of radiolabeled anti-CD3 antibodies by leukemic T-cells. *Cell. Immunol. 137,* 96−110.

(25) Geissler, F., Anderson, S. K., Venkatesan, P., and Press, O. (1992) Intracellular catabolism of radiolabeled anti-μ antibodies by malignant B-cells. *Cancer Res. 52,* 2907−2915.

(26) Primus, F. J., Bennett, S. J., Kim, E. E., DeLand, F. H., Zahn, M. C., and Goldenberg, D. M. (1980) Circulating immune complexes in cancer patients receiving goat radiolocalizing antibodies to carcinoembryonic antigen. *Cancer Res. 40,* 497−501.

(27) Zalutsky, M. R., Bast, R. C., Jr., and Knapp, R. C. (1989) Pharmacokinetics of a radioiodinated monoclonal antibody F(ab')$_2$ fragment in a xenograft model with circulating antigen. *Nucl. Med. Biol. 16,* 405−411.

(28) Garg, P. K., Harrison, C. L., and Zalutsky, M. R. (1990) Comparative tissue distribution in mice of the α-Emitter ^{211}-At and ^{131}I as labels of a monoclonal antibody and F(ab')$_2$ fragment. *Cancer Res. 50,* 3514−3520.

(29) Zalutsky, M. R., and Narula, A. S. (1988) Radiohalogenation of a monoclonal antibody using an N-succinimidyl 3-(tri-n-butylstannyl)benzoate intermediate. *Cancer Res. 48,* 1446−1450.

(30) Zalutsky, M. R., Noska, M. A., Colapinto, E. V., Garg, P. K., and Bigner, D. D. (1989) Enhanced tumor localization and *in vivo* stability of a monoclonal antibody radioiodinated using N-succinimidyl-3-(tri-n-butylstannyl)benzoate. *Cancer Res. 49,* 5543−5549.

(31) Zalutsky, M. R. (1988) Radiohalogenation of antibodies: chemical aspects. *Radiolabeled Monoclonal Antibodies for Imaging and Therapy* (S. C. Srivastava, Ed.) pp 195−214, Plenum Press, New York.

(32) Gatley, J. S., and Sherratt, H. S. A. (1977) The synthesis of hippurate from benzoate and glycine by rat liver mitochondria. *Biochem. J. 166,* 39−47.

(33) Primus, J. F., Newell, K., Blue, A., and Goldenberg, D. M. (1983) Immunological heterogeneity of carcinoembryonic

antigen: antigenic determinants of carcinoembryonic antigen distinguished by monoclonal antibodies. *Cancer Res. 43*, 688–692.

(34) Buchegger, F., Pèlegrin, A., Hardman, N., Heusser, C., Lukas, J., Dolci, W., and Mach, J.-P. (1992) Different behaviour of mouse-human chimeric antibody F(ab')₂ fragments of IgG₁, IgG₂, and IgG₄ sub-class *in vivo*. *Int. J. Cancer 50*, 416–422.

(35) Dumas, P. (1979) Deshalogenation de divers deries iodes phenoliques chez le rat normal et thyroidectomise. *Biochem. Pharmacol. 22*, 1599–1605.

(36) Duncan, J. R., and Welch, M. J. (1993) Intracellular metabolism of indium-111-DTPA-labeled receptor targeted proteins. *J. Nucl. Med. 34*, 1728–1738.

(37) Franssen, E. J. F., Koiter, J., Kuipers, C. A. M., Bruins, A. P., Moolenaar, F., de Zeeuw, D., Kruizinga, W. H., Kellogg, R. M., and Meijer, D. K. F. (1992) Low molecular weight

proteins as carriers for renal drug targeting. Preparation of drug-protein conjugates and drug-spacer derivatives and their catabolism in renal cortex homogenates and lysosomal lysates. *J. Med. Chem. 35*, 1246–1259.

(38) Maack, T., Park, C. H., and Camargo, M. J. (1992) Filtration, transport, and metabolism of proteins. In *The Kidney: Physiology and Pathophysiology* (D. W. Seldin, G. Giebisch, Eds.) pp 3005–3038, Raven Press, New York.

(39) Vaidyanathan, G., and Zalutsky, M. R. (1993) Radioiodination of proteins using N-succinimidyl 4-hydroxy-3-iodobenzoate. *Bioconjugate Chem. 4*, 78–84.

(40) Garg, P. K., Slade, S. K., Harrison, C. L., and Zalutsky, M. R. (1989) Labeling proteins using aryl iodide acylation agents: influence of *meta vs para* substitution on *in vivo* stability. *Nucl. Med. Biol. 16*, 669–674.

TECHNICAL NOTES

Quantitation of Triple-Helix Formation Using a Photo-Cross-Linkable Aryl Azide/Biotin/Oligonucleotide Conjugate

Daniel A. Geselowitz* and Ronald D. Neumann

Department of Nuclear Medicine, Clinical Center, National Institutes of Health, Building 10/1C401, 10 Center Drive MSC 1180, Bethesda, Maryland 20892-1180. Received February 7, 1995®

DNA triple-helix formation has potential applications in gene mapping and as the basis of "antigene" pharmaceuticals; however, the methods for quantitation of triple-helix formation are limited, especially for purine(purine-pyrimidine)-based triplexes. We present a novel method for detection and quantitation of triple-helix formation by triple-helix-forming oligonucleotides. The oligonucleotide is conjugated to a photoactivatable cross-linker, sulfosuccinimidyl 3-[[2-[6-(biotinamido)-2-(p-azidobenzamido)hexanamido]ethyl]dithio]propionate. After incubation with the target DNA, exposure to light labels the target with biotin. The labeled target can be quantified by a chemiluminescent assay. A 26-mer oligonucleotide previously reported to form a purine(purine-pyrimidine) triplex with the upstream region of the c-*myc* gene was studied and found to bind to its target with K_d of approximately 100 nM at 37 °C, 10 mM MgCl$_2$, pH 7.5, consistent with previous reports. This new technique can be used under a variety of conditions and in kinetic experiments and may be extendible to use in living cells.

INTRODUCTION

Triple-helix-forming oligonucleotides are receiving considerable attention due to their potential applications in DNA mapping (*1–3*) and as "antigene" agents and potential pharmaceuticals (*4–7*). Unfortunately, the methods used to detect triple-helix formation in solution—spectrophotometry (melting curves), affinity cleavage of target DNA by conjugated agents, and gel-shift assays—all have some limitations, and none can currently be used inside a living cell. For example, melting curves are useful for studying Py(Pu·Py) triplexes, but the results do not translate easily into dissociation constants (*8*). Moreover, Pu(Pu·Py) triplex melting curves tend to be difficult to interpret (*9, 10*). Affinity-cleavage reactions generally depend on hydroxyl radical production by a pendant group and use DNA footprinting to detect partial cleavage of the target DNA, but these cleavage reactions tend to be inefficient. Gel-shift assays are limited to electrophoretic conditions and are not amenable to kinetic studies. A general method giving dissociation constants and kinetic data for triplex formation and which could be used inside a living cell would greatly enhance research in this area.

Affinity photo-cross-linking technology offers a functional approach to the solution studies of the association of molecules, but has been used rarely in triplex research. Praseuth and co-workers (*11*) were able to cross-link a triple-helix-forming oligonucleotide conjugated to proflavin to its target, allowing a footprinting assay of the binding site. An efficient cross-linker would allow the possibility of quantitative detection of the triple-helix interaction and the possibility for use inside cells. One of us has previously reported, for example, using an oligonucleotide conjugated to the ¹²⁵I-labeled Denny-Jaffe photo-cross-linker to detect cellular membrane and cytoplasmic proteins associated with the conjugate after addition to the medium (*12*).

We now report a novel technique to study the association in solution of a triple-helix-forming oligonucleotide with a duplex target using the recently developed SBED [sulfosuccinimidyl 3-[[2-[6-(biotinamido)-2-(p-azidobenzamido)hexanamido]ethyl]dithio]propionate] trifunctional reagent. The aryl azides, upon photolysis, yield aryl nitrenes, relatively long-lived species (10^{−4} s) which can react in a number of ways with a variety of chemical species (*13–15*). The oligonucleotide conjugate undergoes a photo-cross-linking reaction tagging its target with biotin, which is easily detectable and quantifiable using a chemiluminescent assay.

EXPERIMENTAL PROCEDURES

Oligonucleotide Synthesis. Oligodeoxynucleotides were prepared using the phosphoramidite methodology with commercially available reagents and synthesizer (Applied Biosystems Model 394). The *n*-hexylamine phosphate group at the 5′-end of the molecule was added using a commercial phosphoramidite reagent (Aminolink 2, Applied Biosystems). The oligonucleotides were precipitated twice with ethanol from 0.3 M sodium acetate and were assayed specrophotometrically.

The sequences of the target DNA and the triple-helix-forming and control oligonucleotides are shown in Figure 1. The target site is found in the human c-*myc* gene about 120 bp upstream of the P1 transcription start site. Sequence 1, which is the sequence designated as "PUGT26ap" by Durland and co-workers (*16*), is based on G(G·C) and T(A·T) triplets with the oligonucleotide running antiparallel to the purine-rich target strand. Sequence 2 differs from sequence 1 at four bases and is designed to serve as a poorly binding control. A third oligonucleotide, 3, of unrelated sequence was also prepared for use as a scavenger. The oligonucleotides

```
            2180        2190        2200        2210
             •           •           •           •

5'   CTCCTCCCCACCTTCCCCACCCTCCCCACCCTCCCCATAGCG...(+)strand
3'   GAGGAGGGGTGGAAGGGGTGGGAGGGGTGGGAGGGGTATTCC...(-)strand

        5' GGTTGGGGTGGGTGGGGTGGGTGGGG        sequence 1

        5' GGTTGAGGTGGGTGGCGTGTGTGAGG        sequence 2
```
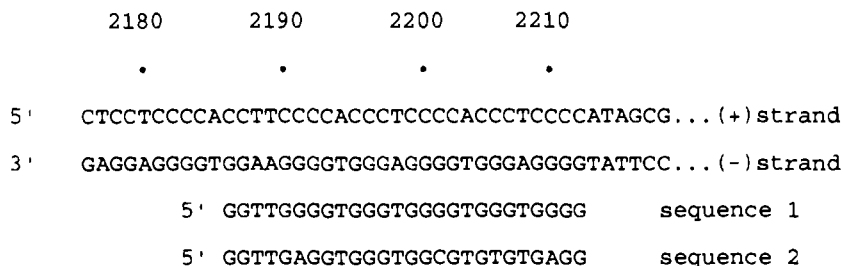
Figure 1. Sequences of target region of c-myc and targeting oligonucleotides used in this study. Sequence numbers shown refer to the numbering scheme in Genbank sequence HSMYCC.
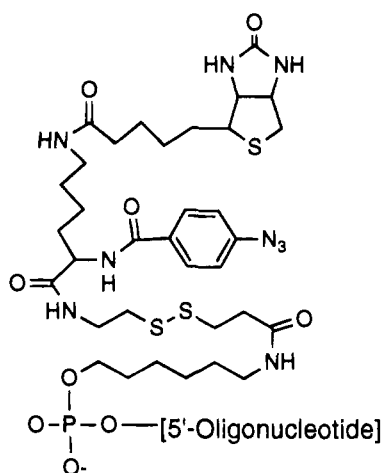
Figure 2. Schematic structure of the oligonucleotide–BED conjugates.

prepared are shown below, with L referring to the 5'-hexylamine group:

(L)GGTTGGGGTGGGTGGGGTGGGTGGGG   **(1-L)**

(L)GGTTGAGGTGGGTGGCGTGTGTGAGG   **(2-L)**

AGCTTATGCTCTGATTTGAAATCAGCTG   **(3)**

Preparation of SBED Conjugate. Work with sulfosuccinimidyl 3-[[2-[6-(biotinamido)-2-(p-azidobenzamido)hexanamido]ethyl]dithio]propionate (SBED; Pierce Chemical Co.) was performed under a red safelight. The reagent was dissolved in dimethyl sulfoxide in the dark to give a 50 mM solution. To 45 μL of a 0.50 mM solution of **1-L** or **2-L** in a sodium borate buffer (pH 8.5, 100 mM) was added 5.0 μL of the SBED stock solution. After 30 min, 250 μL of 0.3 M NaCl solution and 900 μL of ethanol were added, and the tube was centrifuged. The pellet was washed with 70% ethanol, air-dried and then resuspended in 100 μL of water. The conjugates of the oligonucleotides **1-L** and **2-L** will be designated **1-BED** and **2-BED,** respectively. The chemical structure of the oligonucleotide–BED conjugate is shown in Figure 2.

c-myc Plasmid. A plasmid containing the 862-bp *Pvu*II fragment (corresponding to bases 1979–2840 of Genbank sequence HSMYCC) of the human c-myc gene (MC-41) cloned into pGEM3 was obtained from Dr. Maria Zajac-Kaye. When this 6.7-kb concatameric plasmid is cut with *Pvu*II, it yields the 2.9-kb parent and a 3.8-kb fragment consisting of the parent plasmid plus the insert. Plasmid digested with *Pvu*II was deproteinized using a filter (Probind, Millipore), precipitated with ethanol, redissolved in water, and assayed spectrophotometrically.

Photo-Cross-Linking to Triple-Helix Target. A stock solution was prepared containing 5.0 × 10⁻³ μg/μL of the cut plasmid in 100 mM Tris·HCl, pH 7.5, with 10

mM MgCl₂. Additionally, 10.0 mM cytidine or 10.0 μM oligonucleotide **3** was present in some experiments. Under safelight, the oligonucleotide conjugate **1-BED** or **2-BED** was serially diluted into the stock solution to give five 21.6-μL samples at 1000, 320, 100, 32, and 10 nM. In separate tubes, a sample of each conjugate which had been exposed to light was also diluted to give 1000 nM or a lower concentration. The tubes were incubated in the dark at 37 °C for 1 h; they were then exposed to white light from a light box for 5 min. The samples were treated with 2 μL of 50 mM DTT and 0.5 μL of 0.5 M EDTA for 5 min at 60 °C and then with loading buffer, and half of the sample was loaded onto a 1.2% agarose/Tris–acetate–EDTA/ethidium gel (11 × 14 cm) and electrophoresed. After determination of the band positions by UV transillumination, the gel was treated with denaturing buffer (0.5 M NaOH, 1.5 M NaCl), neutralizing buffer (0.5 M Tris, 1.5 M NaCl, pH 7.0), and 20× SSC for 30 min each and then capillary-blotted onto a nylon (Maximum Strength Nytran, Schleicher and Schuell) membrane. Standards prepared by dilution of the stock conjugate solution were dotted onto the lower portion of the blot, and the blot was treated with UV light (0.12 J/cm²) (Stratagene Stratalinker). The blot was then developed using a kit (New England Biolabs Phototope) involving treatment with streptavidin, a biotin–alkaline phosphatase conjugate, and AMPPD chemiluminescent substrate and then exposed to X-ray film.

Densitometry. The developed films were transilluminated with a white-light box and photographed using a black-and-white video camera with a 55-mm lens. The data were digitized and analyzed on a personal computer (Macintosh IIfx) with a video capture board and image analysis software (NIH Image (*17*)).

The spots or bands of interest were quantified by calculating the mean density of an area around the band, subtracting the mean density of an appropriate background region, and multiplying by the area. For a given exposure, a standard curve was prepared for integrated density versus quantity of conjugate in the spot. These plots were found to give smooth curves, easily interpolable from about 1 to 50 fmol. Precision was not thoroughly analyzed, but reproducibility seemed to be better than 10%. It was difficult to assess the effect on accuracy of a high background signal in the lane, but background was quite low in most of the lanes. Analyses were also done using the intensity data subjected to a log transform, and these were found to yield similar results.

RESULTS

When the c-myc plasmid fragments are treated with **1-BED** or **2-BED** at pH 7.5, 10 mM MgCl₂, for 1 h at 37 °C and then photolyzed, both fragments are labeled with biotin in the photo-cross-linking reaction. In Figure 3, the results of the study with 10 mM of cytidine present are shown. The results of the reaction in the absence of
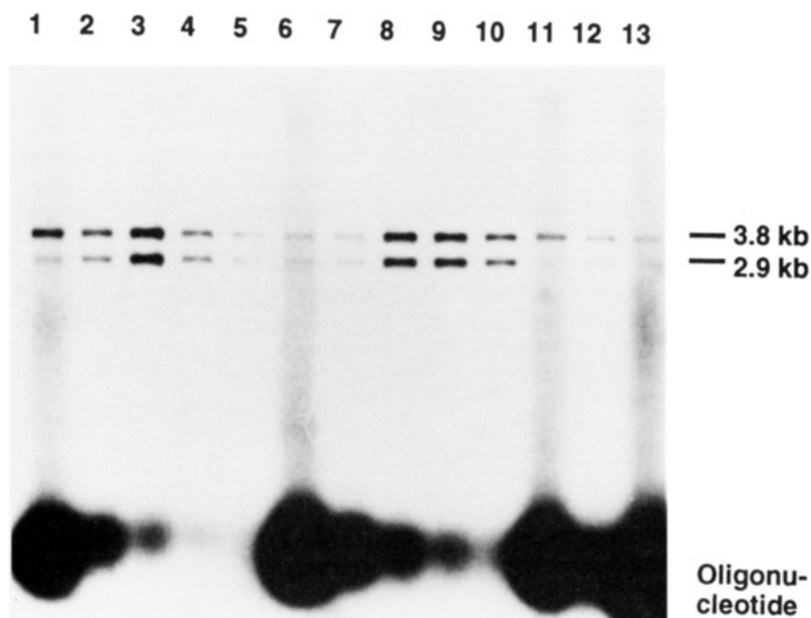
Figure 3. Photo-cross-linking of oligonucleotide conjugates to plasmid fragments in the absence of scavenger. Conjugate oligonucleotide **1-BED** at 1000, 316, 100, 31.6, or 10 nM (lanes 1−5) or **2-BED** at 1000, 316, 100, 31.6, or 10 nM (lanes 6−10) was incubated with 5.0×10^{-3} μg/μL of the digested c-*myc* plasmid in 100 mM Tris, 10 mM $MgCl_2$, and 10 mM cytidine, pH 7.5, for 1 h at 37 °C, then photolyzed, and treated and electrophoresed as described. Lanes 11−13 are controls using photo-deactivated **1-BED** at 1000 and 100 nM, and **2-BED** at 1000 nM, respectively. The 3.8-kb fragment contains the target site; the 2.9-kb fragment does not.
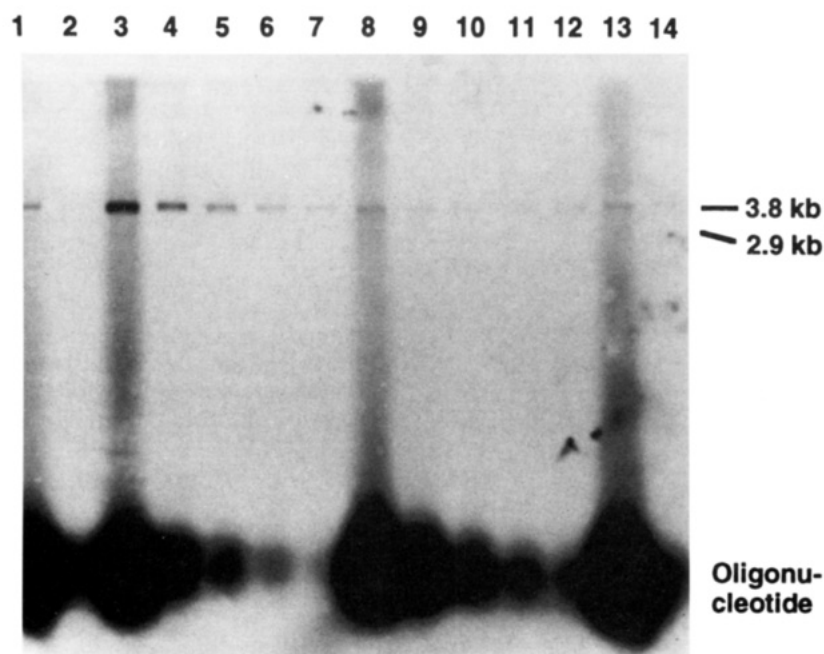
Figure 4. Photo-cross-linking of oligonucleotide conjugates to plasmid fragments in the presence of scavenger. Conjugate oligonucleotide **1-BED** at 1000, 316, 100, 31.6, or 10 nM (lanes 3−7) or **2-BED** at 1000, 316, 100, 31.6, or 10 nM (lanes 8−11) was incubated with 5.0×10^{-3} μg/μL of the digested c-*myc* plasmid in 100 mM Tris, 10 mM $MgCl_2$, and 10 μM of oligonucleotide **3**, pH 7.5, for 1 h at 37 °C, then photolyzed, and treated and electrophoresed as described. Lanes 1, 2, 13, and 14 are controls using photo-deactivated **1-BED** at 1500 and 70 nM, and **2-BED** at 1500 and 70 nM, respectively.

cytidine (not shown) are almost identical to these. Note that, in lanes 1 and 2, with **1-BED** at 1000 or 316 nM, the 3.8-kb plasmid fragment, which contains the target sequence, is preferentially labeled over the 2.9-kb fragment. Quantitation suggests that the 3.8-kb plasmid band has approximately 10 fmol of biotin (there is about 8.4 fmol of plasmid in the band). However, as the concentration of **1-BED** is lowered, the relative amount of labeling of the 2.9-kb fragments increases; this is a nonspecific labeling. At 100 or 32 nM (lanes 3 and 4), the amount of nonspecific labeling actually increases over

that at 1000 or 316 nM, and targeted labeling of the 3.8-kb band is obscured. The control conjugate **2-BED** shows no preferential labeling of the 3.8-kb fragment at 1000 nM, but shows a similar nonspecific labeling of both fragments as its concentration is lowered. The ratio of label in the oligonucleotide band to that in the plasmid fragments plainly decreases dramatically as the concentration of conjugate is lowered.

When the experiment is performed in the presence of 10 μM of the scavenger oligonucleotide **3**, the results are quite different (Figure 4). When the restriction-digested
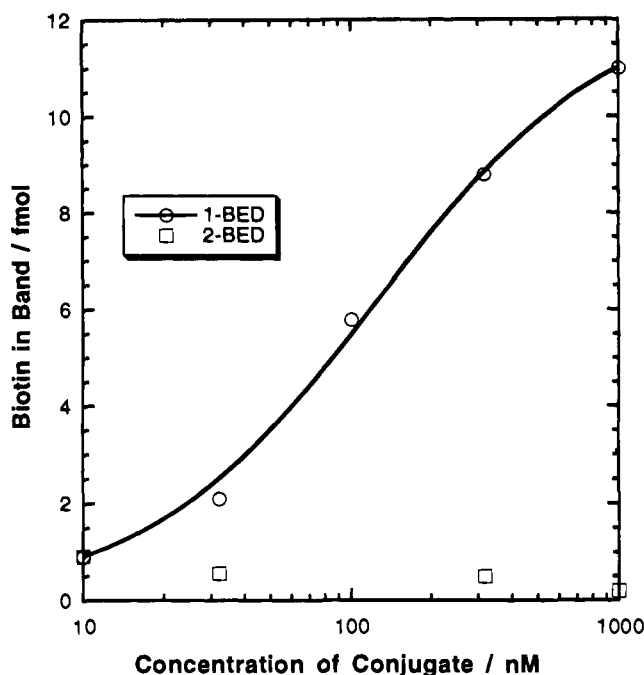
Figure 5. Amount of biotin in 3.8-kb fragment bands from Figure 4 plotted versus concentration of conjugate. The bands were quantified densitometrically from photographic film as described. The five data for 1-BED were fitted to a simple dissociation equilibrium equation, yielding values of 12.4 fmol at 100% binding and $K_d = 126$ nM.

c-*myc* plasmid is treated with **1-BED** or **2-BED** and then photolyzed, virtually no labeling of the 2.9-kb fragment is seen at any of the concentrations used (lanes 3−12). However, the 3.8-kb target fragment is plainly labeled by **1-BED**, with the amount of label decreasing with decreasing concentration of the conjugate (lanes 3−7). Only a low level of labeling of the 3.8-kb target is seen at all concentrations of the control conjugate, **2-BED** (lanes 8−12). As before, a tendency of the deactivated conjugate to comigrate with the 3.8-kb band is observed at 1000 nM (lanes 1 and 13).

Assuming the binding has reached equilibrium in 1 h (*16*), the data can be used to estimate the triplex dissociation constant, K_d. The densitometrically quantified values of biotin in the 3.8-kb bands for the five concentrations studied are shown in Figure 5. When the five data for **1-BED** are fitted to a simple dissociation equation, the 100% binding value is calculated to be 12.4 fmol and the K_d is found to be 126 nM. Each lane contains 8.4 fmol of plasmid, and it is likely that the discrepancy in the calculated 100% binding value is due to the value of 11 fmol at 1000 nM being an overestimate due to the background signal in the lane; the value at 316 nM, where there is little background signal, is 8.8 fmol. The concentration of conjugate yielding one-half of this latter value is about 70 nM. The correction for backgound signal needs to be further considered to improve precision, but the value of K_d almost certainly lies in the range 70−130 nM, and we will take the value to be approximately 100 nM.

DISCUSSION

Our results suggest that photo-cross-linking affinity studies using the BED conjugates will be a useful technique for solution studies of triple-helix association. The technique is reasonably fast and sensitive and requires no radioactivity. Detection of the photo-cross-linked products requires blotting of an electrophoretic gel followed by about an hour of workup, and 1 fmol of product is detectable within 30 min of film exposure. The data are reasonably quantitative and allow the determination of binding isotherms.

We find that these experiments must be done in the presence of a scavenger of the aryl nitrenes. Nonspecific labeling is a common problem with aryl azide cross-linkers, due to the relatively long lifetime and selective reactivity of the nitrene intermediates (*13*). Tris, which is recommended as a scavenger, plainly was ineffective at 100 mM, as was cytidine added at 10 mM. It is obvious that polynucleotides are preferred targets for the aryl nitrene, and oligonucleotide **3** made an excellent scavenger. It is crucial that any scavenger used not bind to the oligonucleotide−BED conjugate, as this would lower the effective concentration of the conjugate in solution. Duplex formation between scavenger **3** and **1-BED** or **2-BED** is not expected under these conditions, and the binding to the target does not appear to be affected, based on a comparison of Figures 3 and 4.

The nonspecific labeling seen in the absence of scavenger (Figure 3) follows an interesting pattern, increasing roughly 10-fold to almost 1 biotin per 3.8-kb fragment as the conjugate concentration is lowered from 1000 to 100 nM, then decreasing as the concentration is further lowered. The relative amount of labeling of plasmid fragments and the conjugate itself increases as the conjugate concentration is lowered over the entire range. At the conjugate concentration of 316 nM, where a similar amount of labeling of plasmid and conjugate is seen, the plasmid represents 15 μM total nucleotide and the oligonucleotide about 8 μM total nucleotide. This suggests a bimolecular mechanism, where the conjugate reacts primarily with either another conjugate molecule or a plasmid molecule in amounts depending on the relative concentrations of target nucleotide. This is interesting as it suggests that the intramolecular reaction of the conjugate with itself is relatively insignificant under these conditions.

Our results indicate that **1-BED** binds to the c-*myc* 862-bp *Pvu*II fragment (presumably at the target site) while **2-BED**, differing in sequence at four bases, does not. This demonstrates the base selectivity of triplex binding. Our data indicate a value of approximately 100 nM for the dissociation constant of the **1-BED**−target complex. This is consistent with that seen in an affinity-cleavage study (*16*) using an oligonucleotide of sequence 1 conjugated to eosin. Those results, under similar conditions to those used here (10 mM Tris, pH 7.4, 20 mM MgCl$_2$, 37 °C), suggest that K_d is approximately 50 nM. Of course, the two experiments are not exactly comparable as the conjugate portion of the molecule may influence the binding constant.

The technique described here should allow the determination of dissociation constants of triple-helix-forming oligonucleotides under a wide variety of conditions. The use of scavengers and possibly of smaller target fragments should control the nonspecific labeling. With a bright light source, the aryl azide should be depleted within seconds (*13*), and kinetic experiments should require only the photolysis of samples at the desired times. Moreover, these conjugates should be useful in protein binding studies as well. We have found that these oligonucleotide−BED conjugates will readily label associated proteins, both in solution and in living cells (data not shown). We hope to develop this photo-cross-linking technique into a screening method of general utility in antisense and antigene work to study oligonucleotide−target interactions inside cultured cells.

LITERATURE CITED

(1) Ferrin, L. J., and Camerini-Otero, R. D. (1994) Long-range mapping of gaps and telomeres with RecA-assisted restriction endonuclease (RARE) cleavage. *Nat. Genet. 6,* 379–83.

(2) Moser, H. E., and Dervan, P. B. (1987) Sequence-specific cleavage of double helical DNA by triple helix formation. *Science (Washington, D.C.) 238,* 645–50.

(3) Perrouault, L., Asseline, U., Rivalle, C., Thuong, N. T., Bisagni, E., Giovannangeli, C., Le Doan, T., and Helene, C. (1990) Sequence-specific artificial photo-induced endonucleases based on triple helix-forming oligonucleotides. *Nature (London) 344,* 358–60.

(4) Birg, F., Praseuth, D., Zerial, A., Thuong, N. T., Asseline, U., Le Doan, T., and Helene, C. (1990) Inhibition of simian virus 40 DNA replication in CV-1 cells by an oligodeoxynucleotide covalently linked to an intercalating agent. *Nucleic Acids Res. 18,* 2901–8.

(5) Postel, E. H., Flint, S. J., Kessler, D. J., and Hogan, M. E. (1991) Evidence that a triplex-forming oligodeoxyribonucleotide binds to the c-*myc* promoter in HeLa cells, thereby reducing c-myc mRNA levels. *Proc. Natl. Acad. Sci. U.S.A. 88,* 8227–31.

(6) Postel, E. H. (1992) Modulation of c-myc transcription by triple helix formation. *Ann. N.Y. Acad. Sci. 660,* 57–63.

(7) Uhlmann, E., and Peyman, A. (1990) Antisense oligonucleotides: A new therapeutic principle. *Chem. Rev. 90,* 544–84.

(8) Roberts, R. W., and Crothers, D. M. (1991) Specificity and stringency in DNA triplex formation. *Proc. Natl. Acad. Sci. U.S.A. 88,* 9397–401.

(9) Xodo, L. E., Alunni-Fabbroni, M., Manzini, G., and Quadrifoglio, F. (1993) Sequence-specific DNA-triplex formation at imperfect homopurine-homopyrimidine sequences within a DNA plasmid. *Eur. J. Biochem. 212,* 395–401.

(10) Pilch, D. S., Levenson, C., and Shafer, R. H. (1991) Structure, stability, and thermodynamics of a short intermolecular purine-purine-pyrimidine triple helix. *Biochemistry 30,* 6081–8.

(11) Praseuth, D., Le Doan, T., Chassignol, M., Decout, J. L., Habhoub, N., Lhomme, J., Thuong, N. T., and Helene, C. (1988) Sequence-targeted photosensitized reactions in nucleic acids by oligo-α-deoxynucleotides and oligo-β-deoxynucleotides covalently linked to proflavin. *Biochemistry 27,* 3031–8.

(12) Geselowitz, D. A., and Neckers, L. M. (1992) Analysis of oligonucleotide binding, internalization, and intracellular trafficking utilizing a novel radiolabeled cross-linker. *Antisense Res. Dev. 2,* 17–25.

(13) Das, M., and Fox, C. F. (1979) Chemical cross-linking in biology. *Annu. Rev. Biophys. Bioeng. 8,* 165–93.

(14) Peters, K., and Richard, F. M. (1977) Chemical cross-linking reagents and problems in studies of membrane structure. *Annu. Rev. Biochem. 46,* 523–51.

(15) Knowles, J. R. (1972) Photogenerated reagents for biological receptor-site labeling. *Acc. Chem. Res. 5,* 155–60.

(16) Durland, R. H., Kessler, D. J., Gunnell, S., Duvic, M., Pettitt, B. M., and Hogan, M. E. (1991) Binding of triple helix forming oligonucleotides to sites in gene promoters. *Biochemistry 30,* 9246–55.

(17) Rasband, W., NIH Image 1.55, National Institutes of Health, Bethesda, MD.

BC9500204

CORRECTIONS

Volume 6, Number 2, March/April 1995.

Julie B. Stimmel, Marie E. Stockstill, and Frederick C. Kull, Jr.*

YTTRIUM-90 CHELATION PROPERTIES OF TETRAAZATETRAACETIC ACID MACROCYCLES, DIETHYLENETRIAMINEPENTAACETIC ACID ANALOGUES, AND A NOVEL TERPYRIDINE ACYCLIC CHELATOR

Page 221. In the Experimental Procedures under Radiolabeling Efficiency and Duration of Yttrium-90 Chelation, the concentrations of chelator stock and yttrium-90 stock should be micromolar. Under Dissociation of Yttrium-90-labeled Chelators at pH 2.0, the concentration of yttrium-90 stock was 400 μM.

Page 222. In Figure 2, the text in the legend should state that the yttrium-90 concentration was 200 μM and the final volume of chelation was 10 μL.

Page 223. The legend for Figure 3 should state that the final concentration of chelator was 67 μM.

BC950185C

COMMUNICATIONS

Surface-Modified Diamond Nanoparticles as Antigen Delivery Vehicles

Nir Kossovsky,*,† Andrew Gelman,† H. James Hnatyszyn,† Samir Rajguru,† Robin L. Garrell,*,‡ Shabnam Torbati,‡ Siobhán S. F. Freitas,‡ and Gan-Moog Chow§

Biomaterials Bioreactivity Characterization Laboratory, University of California, Los Angeles School of Medicine, Los Angeles, California 90024-1732, Department of Chemistry & Biochemistry, University of California, Los Angeles, California 90024-1569, and Laboratory for Molecular Interfacial Interactions, Center for Bio/Molecular Science and Engineering, Code 6930, Naval Research Laboratory, Washington, DC 20375. Received June 26, 1995®

Recognition of antigens by immunocompetent cells involves interactions that are specific to the chemical sequence and conformation of the epitope (antigenic determinant). Adjuvants that are currently used to enhance immunity to antigens tend to either alter the antigen conformation through surface adsorption or shield potentially critical determinants, e.g., functional groups. It is demonstrated here that surface-modified diamond nanoparticles (5–300 nm) provide conformational stabilization, as well as a high degree of surface exposure to protein antigens. By enhancing the availability and activity of the antigen *in vivo*, a strong, specific immune response can be elicited. Results are demonstrated for mussel adhesive protein (MAP), a substance for which conventional adjuvants have proven only marginally successful in evoking an immune response. Surface-modified diamond nanoparticles as antigen delivery vehicles are a novel example of the exciting marriage of materials science, chemistry, and biology.

The ability to generate antigen-specific antibodies has led to significant advances in molecular localization (*1*), molecular recognition and catalysis (*2*), biosensors and immunoassays (*3*), vaccine development, and the characterization of conformational changes induced by molecular interactions (*4*). Nevertheless, certain fields of research have been hampered or misguided by the inability to evoke reactive antibodies in a mammalian

host. For example, when Freund's adjuvant is used, mussel adhesive protein (MAP) elicits only a weak immune response in New Zealand white rabbits (*5*). This has hindered the development of a simple, antibody-based purification for MAP, which is potentially useful as a corrosion inhibitor and surgical adhesive (*6*). The apparently weak immunogenicity of MAP has also led to the inference that MAP is likely to be a safe material for use *in vivo* (*5*), which in turn has led to tests of MAP-based adhesives in animal models (*7*). We show here that surface-modified diamond nanoparticles can be used as very effective antigen delivery vehicles. The coated particles, which consist of a diamond substrate, a glassy carbohydrate film, and an immunologically active surface

* Authors to whom correspondence should be addressed.
† University of California, Los Angeles School of Medicine.
‡ University of California, Los Angeles.
§ Naval Research Laboratory.

molecule in an aqueous dispersion, represent a novel marriage of materials science, surface chemistry, and immunology. It will be shown that these antigen delivery vehicles evoke a strong immune response to antigens such as MAP. These results indicate the need to re-evaluate the apparent biocompatibility of MAP-based materials. More generally, they suggest that modified diamond nanoparticles have great potential as alternatives to conventional adjuvants. Our results demonstrate the feasibility of optimizing antigen–substrate interactions to enhance antigen presentation and immunogenicity.

Antigen carriers and adjuvants are selected ostensibly to enhance the immunogenicity of protein antigens; they play a major role in controlling the conformation of the antigen by virtue of their close physical association with it (8). Although B-cells usually recognize protein antigens in their native conformational state (9), conventional methods for raising antibodies tend to either alter the antigen through surface adsorption or shield potentially critical determinants (8). Several years ago, we developed a solid-phase, high surface-area nanocrystalline antigen carrier that restricts antigen penetration into the surface of the carrier, thereby preventing determinant shielding (10). *In vivo* experiments with surface-modified tin oxide yielded antibodies that exhibited *in vitro* viral neutralization. Because of the desirability of using a high surface energy ceramic, but concerned over the potential toxicity of tin, we subsequently began experiments with carbon ceramic (diamond) nanoparticles.

Figure 1 is a transmission electron micrograph showing acid- and water-washed nanocrystalline diamond particles (General Electric, Worthington, OH) that were dried and suspended on a carbon-coated TEM grid. The morphology of the particles was assessed by bright field imaging, which showed that the particles are multifaceted with varying aspect ratios. Dark field imaging revealed a mixture of crystallite sizes ranging from 5 to 10 nm, with rare 100–300 nm polygons. The crystalline nature of the particles is seen extending to the surface.

The actual antigen carrier consisted of the diamond particles coated with cellobiose, a disaccharide.[1] Because diamond is a high-surface energy material, it was anticipated that thermodynamics would favor adsorption and adhesion of cellobiose onto the diamond particles. This would create a colloid surface capable of hydrogen-bonding to the proteinaceous antigen that would subsequently be adsorbed. Furthermore, the disaccharide could act as a dehydroprotectant and help minimize surface-induced denaturation of the subsequently adsorbed antigen (11). Figure 2 is a HRTEM image of the diamond particles modified with cellobiose. The glassy (amorphous) cellobiose coating was visible only by HR-TEM and was between 4 and 6 nm thick. The coating was generally not uniform and focally seemed to consist of two layers. The nonuniformity may be related to the aspect ratio of the particles, since the shape of the
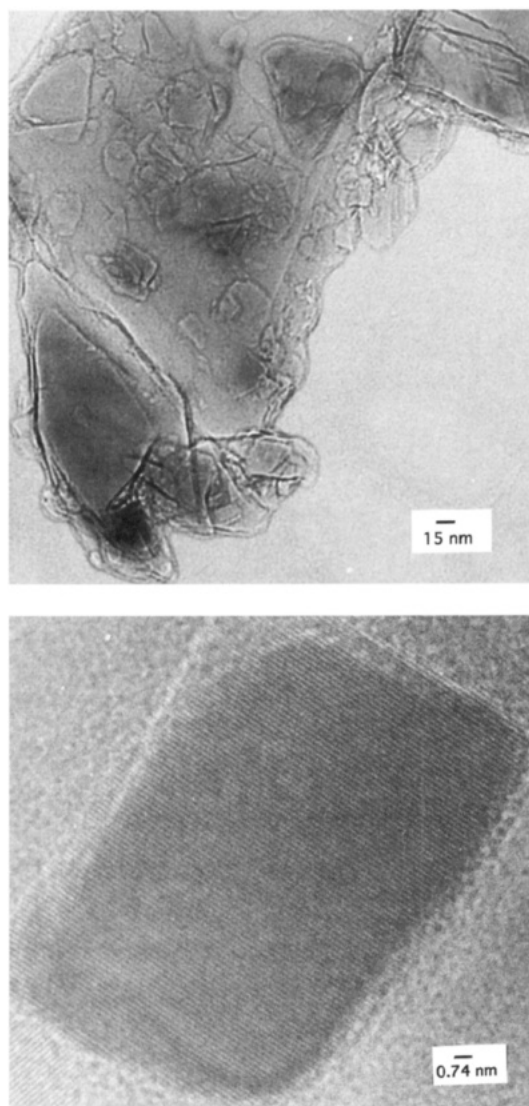
Figure 1. Transmission electron micrograph of acid- and water-washed and sonicated nanocrystalline diamond particles. Images obtained by (top) conventional microscopy with a JEOL JEM 200CX electron microscope operated at 200 keV and (bottom) high-resolution transmission electron microscopy (HR-TEM) with a Hitachi H-9000UHR microscope at 300 keV. The lattice fringes for the two particles in this field correspond to the (111) planes.

diamond crystals may affect the adsorption onto their their surfaces. The equilibrium shape of a crystal is such that the total surface free energy is a minimum, and it can be geometrically constructed by Wulff's theorem (12). For a crystal with a polyhedral shape, the surface energy is different for different faces, and adsorption onto the facets will therefore also differ, leading to nonuniform coverage and thickness of adsorbed layers. For diamond, the surface energy for the (111) plane is much smaller than that of the (100) plane (i.e., 5400 ergs/cm^2 and 9400 ergs/cm^2, respectively) (Harkins, ref 12).

The antigen used in these studies was MAP. It is an unusual protein, consisting largely of a repeating (con-

---

[1] One g of diamond powder (General Electric, Worthington OH) was cleaned by 400 W sonication at 4 °C in 12 N HCl for 16 h and subsequently washed with ultrafiltered water until the pH was near 7. The resulting opaque dispersion was layered over glass plates and baked in a vacuum oven for 2 days at 185 °C. The dried diamond was then rehydrated and acid washed as described above. The clean, activated diamond dispersions in ultrafiltered deionized water were diluted to 1.0 mg/mL and then added to 250 mM cellobiose [Sigma, St. Louis, MO] and lyophilized for 24 h. Unadsorbed cellobiose was removed by ultrafiltration dialysis against sterile water in a 100 kD nominal molecular-weight-cutoff stir cell [Filtron, Northborough, MA] at room temperature.

[2] MAP was purified according to the procedure developed by Waite (15). The final purification step was by gel filtration on a Sephadex G-150 column. Fractions were analyzed by UV–vis spectroscopy to find the fraction with maximum absorbance (usually the first fraction after the void volume). Identity and purity were assessed by PAGE (slab gels, Coomassie Blue and NitroBlue Tetrazolium (NBT) stain, which is Dopa-specific) and HPLC against an authentic sample (courtesy of J. H. Waite).
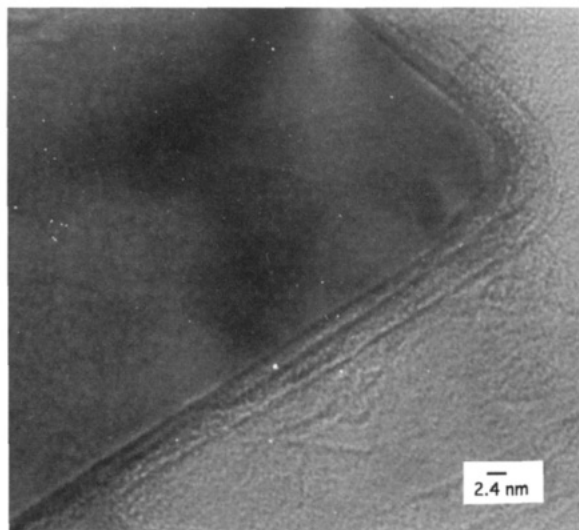
Figure 2. HRTEM image of cellobiose-modified diamond nanoparticles.

a) ELISA of Rabbit anti-MAP Antibody Activity (PS plate)

b) ELISA of Rabbit anti-MAP Antibody Activity on PS and PDMS-coated PS

Figure 4. Rabbit serum antibody avidity to surface immobilized MAP as measured by ELISA. (a) Binding of immunized serum and naive (nonimmunized) serum to MAP (specific binding) and BSA (nonspecific binding) immobilized on standard polystyrene ELISA plates. Each error bar represents the standard deviation in five measurements. (b) Comparison of antibody binding (specific and nonspecific) to proteins immobilized on polystyrene and poly(dimethylsiloxane)-coated ELISA plates (PDMS = poly(dimethylsiloxane)).

Figure 3. MAP from *Mytilus edulis*, MW ~130 kD, consists primarily of repeating deca- and hexapeptide sequences, in which the •'s indicate sites of additional hydroxyl groups on some of the repeats. Figure based on ref *13*.

sensus) decapeptide in which hydroxyl or amine groups are present on virtually every residue (Figure 3) (*13*). Previous reports indicated only poor or marginal success in generating antibodies to MAP using Freund's adjuvant (*5*), which is mineral-oil based. The lack of success may be partly attributable to the hydrophilicity of the protein. MAP may be sequestered in aqueous microdroplets within the adjuvant bolus, denatured at the oil-intercellular fluid interface, or complexed with trehalose–dimycolate moieties (*14*) at the surface of the bolus in a way that diminishes MAP's immunogenicity.

To prepare the MAP–diamond nanoparticle couple, highly purified MAP[2] was mixed with ca. 4–20 nm-diameter cellobiose-modified diamond particles and dialyzed.[3] Adsorption of MAP onto the cellobiose-coated particles was assessed by electrophoretic light scattering, which revealed colloidally dispersed solid aggregates with a mean diameter of 300 nm.[4] The product, an aqueous

---

[3] To adsorb MAP onto the modified diamond particles, 1.0 mg of MAP was first solubilized in 2.5 mL of 0.10 M acetic acid (pH 4.7) by gentle agitation. This was added to 1.0 mL of 1.0 mg/mL cellobiose-coated diamond in water in a 100 kD stir cell at 4 °C and then dialyzed against 150 mL of 20 mM phosphate buffer (pH 7.4). Under these conditions, MAP precipitates irreversibly (*6*).

[4] MAP adsorption onto the cellobiose-modified diamond was assayed by measuring changes in the nanoparticle electrophoretic mobility (DELSA 440, Coulter Electronics Inc., Hialeah, FL) as described previously (*16*). Prior to measurement, all samples were diluted 1:50 in one of several pH buffer solutions prepared from monobasic and dibasic sodium phosphates spanning the range from pH 5.8 to 9.4. Samples were positioned so that mobility readings were taken at the solvent's stagnant point. Light scattering was used to assess the particles' terminal velocity (mobility) under the influence of an electric field, which is proportional to the ζ potential or surface charge. The electrophoretic mobility of the cellobiose-coated diamond particles did not change significantly over a period of 8 weeks in cold storage or at room temperature. As a further test of the stability of the cellobiose coating, a suspension of 1.0 mg/mL cellobiose-coated diamond that was aged at least 2 weeks at room temperature and centrifuged at 60000g to precipitate the particles. The supernatant was analyzed by HPLC with a Waters SC-1011 column and refractive index detection. The concentration of dissolved cellobiose was only 6.3 μM, which corresponds to a loss of only 0.2% of the original mass of the suspended coated particles. Together, the electrophoretic mobility and HPLC results indicate that the sugar coating does not redissolve appreciably. The MAP-modified particles are stable in cold storage for at least 1 month, although aggregation and other changes occur within a few days at room temperature.

[5] Five 2-month-old female New Zealand white rabbits were injected intramuscularly in the right hind leg with approximately 500 μg of the MAP–diamond conjugate carried in 1.0 mL of 20 mM phosphate buffer (pH 7.4). After 2 weeks, the rabbits were boosted with an additional 100 μg of suspended MAP conjugate. The animal was exsanguinated by intracardial puncture 2 weeks after the boost, and anti-MAP antibodies were quantified by enzyme-linked immunoassay (ELISA).

colloid comprised of a three-layered solid phase (diamond/cellobiose/MAP), was fluid and readily injectable. Antibodies were raised against the surface-immobilized MAP in New Zealand white rabbits,[5] and their specificity against MAP and its various conformational epitopes was measured by ELISA.[6]

In contrast to earlier efforts in which anti-MAP antibodies were raised only with difficulty (5), the presentation of antigen on surface-modified diamond nanocrystalline particulates yielded a strong and specific antibody response (Figure 4). Figure 4a shows the actual ELISA data for immunized serum and naive serum, binding to MAP (specific binding) and BSA (nonspecific binding) immobilized on standard polystyrene (PS) ELISA plates. Each error bar represents the standard deviation in five measurements. The binding avidity of rabbit anti-MAP antibodies to the immobilized MAP is substantially greater than for immobilized bovine serum albumin (BSA). The latter response (nonspecific binding activity) is comparable to that measured for naive serum. The standard deviation in the antibody activity of serum from four different animals was 0.014 absorbance units, less than the standard deviation in three successive activity measurements on the same serum (0.040). This demonstrates that the effectiveness of cellobiose-coated diamond particles as antigen delivery vehicles is reproducible in different animals.

Figure 4b shows the same data as Figure 4a, along with data for plates that were coated with PDMS prior to protein adsorption. The absorbances have been normalized relative to the value measured for immunized serum binding to MAP. Antibodies raised against the aqueous conformation of MAP bind avidly to MAP immobilized on the more hydrophilic surface (standard

---

[6] The binding avidity of rabbit IgG to MAP was assayed by conventional ELISA protocol using purified MAP as the test antigen, bovine serum albumin (BSA) as the negative antigen control, and naive rabbit serum as a negative serum control. The conformational specificity of the antibody binding avidity was measured against MAP immobilized on polystyrene surface and MAP immobilized on a siliconized surface. Briefly, standard polystyrene 96-well microtiter plates (Falcon 3913 microtest III, Becton Dickinson, Franklin, NJ) were cleaned with 1.2 N HCl for 1 h to remove all surface contaminants. The plates were neutralized by washing three times with water and then were either left untreated (noncoated) or were filled with 300 μL per well poly(dimethylsiloxane) (PDMS) oil (Dow Corning 200 fluid, 100 cSt) and then emptied gravitometrically upside down at 1000 rpm for 10 min. MAP (1 mg in 3 mL 100 mM acetic acid, pH 4.7) or BSA (1 mg in 3 mL 20 mM potassium phosphate buffer, pH 7.3) was then added to completely fill each well and allowed to bind overnight at 4 °C, after which the wells were emptied. A blocking solution of 250 μL of 2% BSA in PBS was added to each well and incubated for 3 h at room temperature. The plates were washed with three successive 250 μL aliquots of wash buffer (1.91 mM KH_2PO_4/8.08 mM Na_2HPO_4/150 mM NaCl/0.5% v/v Tween-20, at pH 7.4). Two hundred fifty μL of sera from the rabbits were added in triplicate (diluted 1:100 in phosphate-buffered saline per well per plate) and incubated overnight at 4 °C. The following morning, the plates were washed three times with wash buffer, after which 125 μL of secondary goat anti-rabbit Ig alkaline phosphate conjugate (Sigma, St. Louis, MO), diluted 1:1000 in 50 mM pH 7.4 Tris, was added to each well and incubated 45 min at 25 °C. Following three additional washes with wash buffer, 125 μL of freshly prepared pNPP substrate (*p*-nitrophenol phosphate tablets, Sigma, St. Louis, MO) (5 mg tablets dissolved in 1.0 M diethanolamine/0.5 mM $MgCl_2$/0.02% NaN_3 to a concentration of 1 mg/mL, pH 9.8) was added to each well and allowed to incubate at 25 °C in the dark for 10 min. The colorimetric reaction was quantified by visible absorption 405 nm (BioRad Model 3550 Microplate Reader, Hercules, CA).

Figure 5. Schematic representation of the structure of the ~300 nm diamond−cellobiose−MAP antigen delivery system, consisting of 5−10 nm diamond particles coated with adsorbed layers of cellobiose and MAP. The construct is held together by van der Waals interactions and hydrogen bonds.

treated polystyrene) but substantially less avidly to MAP immobilized on the very hydrophobic (PDMS-treated) surface. The latter is known to alter protein conformations (9, 17). These data provide evidence for the conformational specificity of the elicited antibodies.

The diamond−cellobiose−MAP antigen delivery system is illustrated conceptually in Figure 5. We believe that the effectiveness of using saccharide-coated diamond particles as antigen delivery vehicles is attributable to the nature of the cellobiose matrix and the protein−cellobiose interactions at the surface of the particles. Because cellobiose binds water (18), the sugar is in a hydrated glassy state that, when dried onto the diamond particles, lacks long range order (19). This macroscopic thermodynamic description is supported by the HRTEM images (Figure 2). The sugar bonds to the diamond surface because the high interfacial energy of diamond is reduced by the adsorbed film, thus lowering the free energy of the system (12). Hydrogen bonding within the glassy sugar matrix confers three-dimensional stability and retards dissolution. The driving forces for protein adsorption are the formation of protein−cellobiose hydrogen bonds and the enthalpically-favorable release of water from the surfaces of the cellobiose and protein to the bulk aqueous phase (20). Because the protein is adsorbed, rather than embedded in the matrix (as with conventional adjuvants), most of the protein surface can probably retain its mobility, remaining hydrated and accessible to antibodies. These are essential aspects for strong immunological reactivity; the most potent antigenic regions of proteins are characterized by high mobility and low packing density, which allow localized conformational rearrangements and induced fit to the antibody (21).

Because of our success in raising antibodies to MAP using modified diamond as the antigen carrier, we have been able to develop a new, antibody-based purification method for MAP (22). More generally, the immunogenicity of MAP demonstrated here suggests the need for further immunological studies of the utility of MAP as a potential surgical adhesive.

Through a combination of materials science, surface chemistry, and biology, we have demonstrated the efficacy of a new organically-modified ceramic antigen delivery vehicle. The coated nanoparticulate carrier concept is not limited to proteinaceous antigens and is, therefore, likely to prove widely applicable to problems in antigen delivery, molecular immobilization, and mo-

lecular recognition. The same design principles are currently being applied in our laboratories to the development of new antiviral drug delivery systems and acoustic sensor-based assays.

LITERATURE CITED

(1) Burnens, A., Demotz, S., Corradin, G., Binz, H., and Bosshard, H. R. (1987) Epitope mapping by chemical modification of free and antibody-bound protein antigen. *Science 235*, 780. Jemmerson, R., and Paterson, Y. (1986) Mapping epitopes on a protein antigen by the proteolysis of antigen-antibody complexes. *Science 232*, 1001.

(2) Schultz, P. G., and Lerner, R. A. (1993) Antibody catalysis of difficult chemical transformations. *Acc. Chem. Res. 26*, 391. Burton, D. R. (1993) Monoclonal antibodies from combinatorial libraries. *Acc. Chem. Res. 26*, 405. Lerner, R. A., Benkovic, S. J., and Schultz, P. G. (1991) At the crossroads of chemistry and immunology: catalytic antibodies. *Science 252*, 659. Berzofsky, J. (1985) Intrinsic and extrinsic factors in protein antigenic structure. *Science 229*, 932 .

(3) Wise, D. L., Ed. (1989) *Applied Biosensors* Butterworths, Boston, MA. Scheller, F., and Schubert, F. (1989) *Biosensoren*, Akademie-Verlag, Berlin. Vanderlaan, M., Stanker, L. H., Watkins, B. E., and Roberts, D. W., Eds. (1991) *Immunoassays for Trace Chemical Analysis*, ACS Symposium Series 451, American Chemical Society, Washington, DC.

(4) Rini, J. M., Schelze-Gahmen, U., and Wilson, I. A. (1992) Structural evidence for induced fit as a mechanism for antibody—antigen recognition. *Science 255*, 959. Darst, S. A., Robertson, C. R., and Berzofsky, J. A. (1988) Adsorption of the protein antigen myoglobin affects the binding of conformation-specific monoclonal antibodies. *Biophys. J. 5*, 533.

(5) Benedict, C., Waite, J. H. (1986) Location and analysis of byssal structural proteins of *Mytilus edulis*. *J. Morphol. 189*, 171. Sáez, C., Pardo, J., Gutierrez, E., Brito, M., and Burzio, L. O. (1991) Immunological studies of the polyphenolic proteins of mussels. *Comp. Biochem. Physiol. 98B*, 569.

(6) Waite, J. H. (1991) Mussel beards: A coming of age. *Chem. Ind.* 607. Waite, J. H. (1990) Marine adhesive proteins: Natural composite thermosets. *Int. J. Biol. Macrom. 2*, 139. Waite, J. H. (1987) Nature's underwater adhesive specialist. *Int. J. Adhes. Adhes. 7*, 9.

(7) Fulkerson J. P., Norton, L. A., Gronowicz, G., Picciano, P., Massicotte, J. M., and Nissen, C. W. (1990) Attachment of epiphyseal cartilage cells and 17/28 rat osteosarcoma osteoblasts using mussel adhesive protein. *J. Orthop. Res. 8*, 793. Pitman, M. I., Menche, D., Song, E. K., Ben-Yishay, A., Gilbert, D., and Grande, D. A. (1989) The use of adhesives in chondrocyte transplantation surgery: In-vivo studies. *Bull. Hosp. Joint Dis. Orthop. Inst. 49*, 213. Robin, J. B., Picciano, P., Kusleika, R. S., Salazar, J., and Benedict, C. (1988) Preliminary evaluation of the use of mussel adhesive protein in experimental epikeratoplasty. *Arch. Opthalmol. 106*, 973.

(8) Unanue, E. R. (1992) Antigen Processing. *Encyclopedia of Immunology* (I. M. Roitt, and P. J. Delves, Eds.) pp 116–118, Academic Press, New York. Goodlick, L., and Braun, J. (1994) Revenge of the microbes: superantigens of the T and B cell lineage. *Am. J. Path. 144*, 623. Harding, C. V., and Unanue, E. R. (1990) Cellular mechanisms of antigen processing and the function of class I and II major histocompatibility complex molecules. *Cell Regulat. 1*, 499. Brodsky, F. (1991) The cell biology of antigen processing and presentation. *Ann. Rev. Immunol. 9*, 707.

(9) Sela, M. (1992) Antigens. *Encyclopedia of Immunology* (I. M. Roitt, and P. J. Delves, Eds.) pp 128–133, Academic Press, New York: Sela, M. (1989) Antigenicity: Some molecular aspects. *Science 166*, 1365. Kossovsky, N., and Freiman, C. (1994) Silicone breast implant pathology: Clinical data and immunological consequences. *Arch. Path. Lab. Med. 118*, 686. Chedid, L. (1987) *Synthetic Vaccines* (R. Arnon, Ed.) Vol. 1, pp 93–103, CRC Press, Boca Raton, FL.

(10) Kossovsky, N., Gelman, A., Sponsler, E., and Millett, D. (1991) Nanocrystalline Epstein-Barr virus decoys. *J. Appl. Biomat. 2*, 251. Kossovsky, N., and Bunshah, R. F. U.S. Pat. 5,178,882.

(11) Kossovsky, N., Nguyen A., Sukiassians, K., Festekjian, A., Gelman, A., and Sponsler E. (1994) Secondary structure of albumin acquired rapidly by modified conventional ATR-FTIR is comparable to CD spectral data. *J. Colloid Interface Sci. 166*, 350. Kossovsky, N., and Bunshah, R. F. U.S. Pat. 5,219,477.

(12) Herring, C. (1951) Some theorems on the free energies of crystal surfaces. *Phys. Rev. 82*, 87. Harkins,W. D. (1942) Energy relations of the surface of solids: I. Surface energy of the diamond *J. Chem. Phys. 10*, 268.

(13) Waite, J. H., Housley, T. J., and Tanzer, M. L. (1985) Peptide repeats in a mussel glue protein: Theme and variations. *Biochemistry 24*, 5010.

(14) Retzinger, G. S., Meredith, S. C., Takayam, K., Hunter, R. L., and Kezdy, F. J. (1981) The role of surface in the biological activities of trehalose 6,6'-dimycolate. *J. Biol. Chem. 256*, 8208.

(15) Waite, J. H. Redox-Active Amino Acids in Biology. *Methods in Enzymology* (J. P. Klinman, Ed.) Academic Press, New York (in press).

(16) Woodle, M. C., Collins, L. R., Sponsler, E., Kossovsky, N., Papahadjopoulos, D., and Martin, F. J. (1992) Sterically stabilized liposomes—reduction in electrophoretic mobility but not electrostatic surface potential. *Biophys. J. 61*, 902. Tatsumi, N., Tsuda, I., Masaoka, M., and Imai, K. (1992) Measurement of the zeta potential of human platelets by the used of laser-light scattering. *Thromb. Res. 65*, 585.

(17) Kossovsky, N., Zeidler, M., Chun, G., Nugyen, A., Rajguru, S., Papasian, N., Gelman, A., and Sponsler E. (1993) Surface dependent antigens identified by high binding avidity of serum antibodies in a subpopulation of patients with breast prostheses. *J. Appl. Biomat. 4*, 281.

(18) Hardy, B. J., and Sarko, A. (1993) Molecular dynamics simulation of cellobiose in water. *J. Comput. Chem. 14*, 848.

(19) Green, J. L., and Angell, C. A. (1989) Phase relations and vitrification in saccharide-water solutions and the trehalose anomaly. *J. Phys. Chem. 93*, 2880.

(20) Lemieux, R. U. (1993) How proteins recognize and bind oligosaccharides. *Carbohydrate Antigens* ACS Symposium Series 519, (P. J. Garegg, A. A. Lindberg, Eds.), Chapter 2, p 5, American Chemical Society, Washington, DC.

(21) Geysen, H. M., Tainer, J. A., Rodda, S. J., Mason, T. J., Alexander, H., Getzoff E. D., and Lerner, R. A. (1987) Chemistry of antibody binding to a protein. *Science 235*, 1184.

(22) Garrell, R. L. et al. Unpublished results.

BC9500608

Transfection of Folate–Polylysine DNA Complexes: Evidence for Lysosomal Delivery

Kimberly A. Mislick,[†] John D. Baldeschwieler,[*,†] Jon F. Kayyem,[‡] and Thomas J. Meade[*,‡]

Division of Chemistry and Chemical Engineering, and Division of Biology and the Beckman Institute, California Institute of Technology, Pasadena, California 91125. Received June 15, 1995[®]

We are utilizing the folate receptor for the intracellular delivery of DNA. In this study, a folate–poly-L-lysine (FPLL) conjugate was synthesized and equilibrated with plasmid DNA encoding the firefly luciferase gene. The FPLL–DNA complexes were added to KB cells treated with chloroquine. Luciferase activity of cells incubated with FPLL–DNA was 6-fold higher than of cells exposed to poly-L-lysine (PLL)–DNA. The addition of free folic acid competitively inhibited the enhancement of gene expression. Removal of chloroquine from the media significantly inhibited transfection efficiency of FPLL–DNA complexes. We conclude that FPLL–DNA complexes are delivered into KB cells via folate receptor-mediated endocytosis and likely follow a lysosomal pathway into the cytoplasm.

INTRODUCTION

Although gene therapy has progressed significantly in the past five years, problems associated with transferring foreign genetic material into cells remain. The delivery of genes across the cell membrane and into the nucleus is nontrivial since DNA is not readily endocytosed. Thus, DNA must be packaged into a vehicle capable of efficient entry into cells. Ideally, this vehicle possesses a mechanism to avoid lysosomal degradation and can be targeted to particular tissues as well as receptors that are expressed on specific cell types.

Nonspecific methods for delivering genes include the use of positively charged macromolecules such as polyamidoamines (1), polylysine (2, 3), and lipid-based amphiphiles (4) to bind and electrically neutralize DNA. The DNA complexes attach to the cell surface and are internalized by nonspecific endocytosis or by destabilization of the plasma membrane. As a cell-specific alternative to these methods, receptor-mediated polylysine constructs have been developed. A fraction of the ε-amino moieties of polylysine are covalently linked to a receptor ligand, and the modified polylysine is incubated with the DNA. The resulting complex promotes uptake of the DNA via receptor-mediated endocytosis. Using this technique, polylysine–DNA complexes have been transfected via the endocytosis of a variety of receptors including asialoorosomucoid (5), transferrin (6), and insulin (7). In addition, fusion peptides linked to the polylysine backbone have significantly enhanced expression by allowing complexes to escape lysosomal degradation (8).

We are exploring the delivery of polylysine–DNA based on the cell–surface receptor for folic acid. The folate receptor is a glycophospholipid-linked membrane protein (9) responsible for internalizing folic acid and folate analogs (10) and is expressed at high levels on specific tissue types including ovarian carcinomas (11). When the folate receptor binds a ligand it localizes in nonclathrin-coated caveolae, and the receptor/ligand complex undergoes potocytosis. The ligand dissociates from the folate receptor and passes through an anion channel into the cytoplasm (12).

In previous studies, the folate receptor has been used to target antisense oligonucleotides (13) as well as liposomes *in vitro* (14–16). In addition, a cytotoxin, momordin, conjugated to folic acid has been shown to enter the cytoplasm as a functionally intact compound (17) suggesting that lysosomal degradation can be avoided using the folate receptor for delivery. The mechanism whereby folate-conjugated proteins enter the cytoplasm is still undefined (18).

Recently, it has been shown that cytoplasmic entry of toxins and genes delivered via folate receptor endocytosis can be enhanced by the presence of translocation peptides (19) and viral components (20), respectively. It is possible that translocation domains provide a mechanism for folate conjugates to avoid deposition into lysosomes. Since the intracellular destinations of folate conjugates are still uncharacterized, we have investigated the involvement of the lysosomal compartment in the intracellular trafficking of folate–polylysine DNA complexes.

In this paper, we describe the synthesis of a folate–poly-L-lysine (FPLL) conjugate and the formation of complexes with DNA encoding firefly luciferase as a reporter gene (Figure 1). The FPLL–DNA complexes were delivered to cells via folate receptor specific endocytosis. This resulted in significant gene expression in the presence of chloroquine, an agent shown to inhibit routing of endocytosed macromolecules to lysosomes (21). Chloroquine was removed from the medium to test whether DNA uptake was via a nonlysosomal pathway as suggested for toxin delivery (17). In the absence of chloroquine, however, gene expression was dramatically reduced, suggesting that the conjugates enter the cytoplasm via a lysosomal pathway similarly employed by other receptor systems.

MATERIALS AND METHODS

Cell Culture. KB cells derived from a human nasopharyngeal carcinoma were generously donated by Professor Philip S. Low (Purdue University) and maintained at 37 °C in a 5% CO_2 humidified atmosphere. Cultures were propagated in folate-free Dulbecco's Modified Eagle's Media (ffDMEM) (17), supplemented with
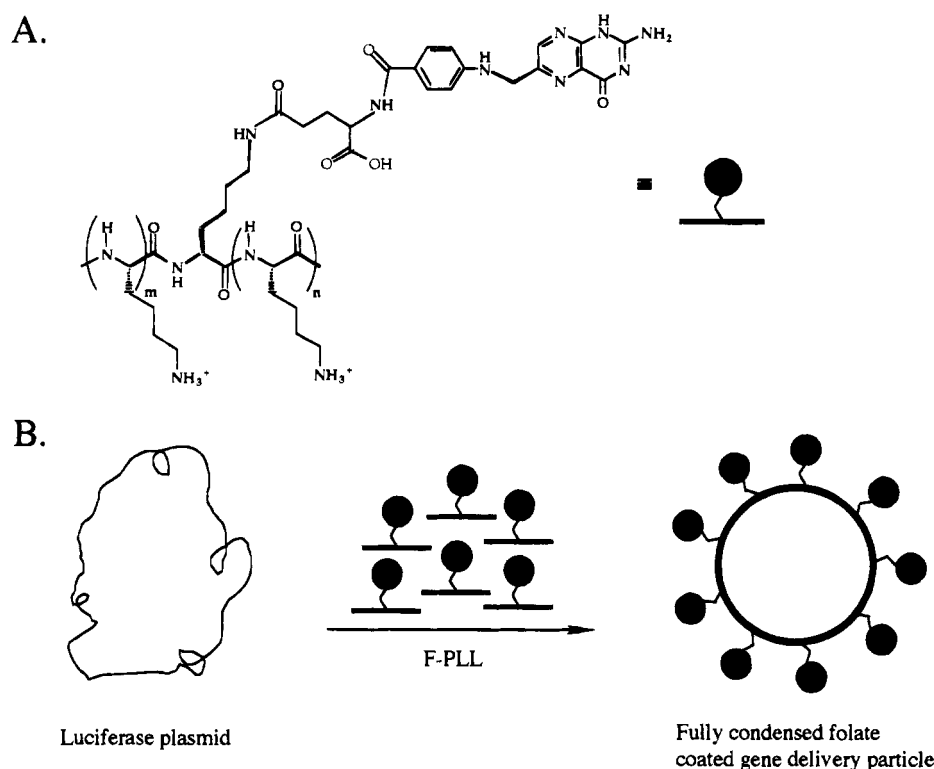
Figure 1. (Top) structure of the modified folate—polylysine conjugate. Polylysine (95k) is modified with folate ($m + n \approx 600$). No effort was made to isolate the isomers. (Bottom) the formation of the FPLL—DNA complex. The modified polylysine is condensed with the luciferase plasmid to form a gene delivery particle (*21*).

10% fetal bovine serum (FBS, Gibco) and 40 mg/L of gentamicin (Gibco). Monolayers were grown to confluency and subcultured once every 7 days.

For transfection experiments, 2 mL of cell suspension was seeded at a density of 1×10^5 cells/mL into a 35 × 10 mm Falcon petri dish. After 24 h, the media was decanted, and cells were rinsed twice in 2 mL of Dulbecco's phosphate-buffered saline (DPBS, Gibco). Immediately prior to the addition of DNA complexes, ffDMEM supplemented with 10% dialyzed fetal bovine serum (dFBS, Gibco) and 100 μM chloroquine (Sigma) was added to the cells. Folic acid (1×10^{-5} M) was added to the media of the control samples.

Plasmids. The PGL2 vector (6046 base pairs; Promega) encoding the genes for firefly luciferase and ampicillin resistance was amplified in competent JM109 *Escherichia coli* (Promega). The plasmid was purified using a Maxi DNA Prep Kit (Qiagen) according to the manufacturer's instructions.

Preparation of Folate—Polylysine Conjugates. All materials and reagents were purchased from Aldrich and used as received. One hundred milligrams (0.23 mmol) of folic acid (pteroyl glutamic acid) was dissolved in anhydrous dimethyl sulfoxide (5 mL) containing pyridine (18 μL). One equivalent each of *N*-hydroxysuccinimide and dicyclohexylcarbodiimide were added to the dissolved folate. The reaction mixture was stirred continuously in the dark at 10 °C for 14 h, and the insoluble byproduct dicyclohexylurea was removed by filtration.

A 4-fold excess of NHS—folate (2.1×10^{-4} mmol) was added to poly-L-lysine (5.3×10^{-5} mmol) dissolved in 1 mL of 50 mM NaHCO₃, pH 8.0. After 3 h, the mixture was passed down a PD-10 G-25M column (Pharmacia) equilibrated in DPBS. The sample was dialyzed against deionized water to remove unreacted NHS—folate and salts and lyophilized. The sample was redissolved to 100 μg/mL in sterile water and purified by size exclusion FPLC on a Superdex-75 column (Pharmacia). The mobile

phase was 150 mmol of NaPi, pH 7.5 (peak retention times: FPLL, 11 min; unreacted folate, 19 min) monitored at 214 and 280 nm ($\sim$50% yield). No effort was made to separate the isomers of the modified derivative. Polylysine content in purified samples was quantitated by the fluoraldehyde assay (Pierce) and compared to folate content ($\epsilon_{363} = 6200$; (*22*)). In these experiments, 0.5 molar equiv of folate was conjugated to each equivalent of polylysine. UV—vis analysis revealed three absorption maxima, $\lambda_{max} = 220$, 283, and 368 nm.

Preparation of DNA Complexes and Transfection. Polylysine—DNA complexes were prepared with minor modifications to published procedures (*6*). Three μg of plasmid DNA (100 μg/mL) was added to 150 μL of Hepes-buffered saline (HBS; 150 mM NaCl/10mM Hepes, pH 7.4). To the buffered plasmid was added varying amounts (1.5, 2.0, 2.5, or 3.0 μg of 100 μg/mL in sterile water) of poly-L-lysine (PLL) or folate—poly-L-lysine (FPLL). Samples were mixed and left to equilibrate for approximately 40 min at room temperature, and the complexes were added to cells. After a 4 h incubation, transfection media was removed and replaced with 2 mL of fresh ffDMEM, 10% FBS. Cells were lysed and assayed for luciferase activity after 22 h.

To harvest the cells, the monolayers were rinsed three times in DPBS (calcium and magnesium free) and scraped with a rubber policeman into 1.5 mL eppendorf tubes. Cells were resuspended in DPBS and counted in a hemocytometer. Cell pellets were mixed with 120 μL of luciferase assay lysis buffer (Analytical Luminescence Laboratories) and kept at 4 °C for 15 min. The lysate was combined with the assay substrates according to the manufacturer's protocol. Light units were integrated over a 10 s interval in a Monolight 2010 Luminometer (Analytical Luminescence Laboratories). A second group of cells was transfected and assayed for overall protein synthesis as described elsewhere (*17*).
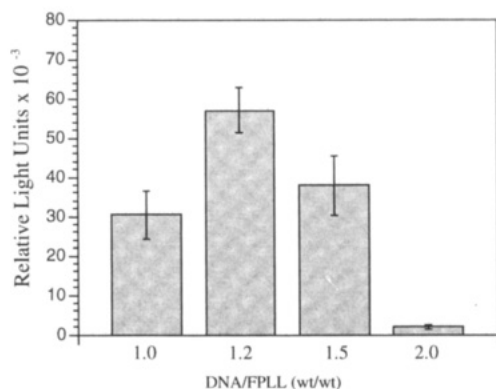
Figure 2. Determination of optimum DNA to FPLL ratio. To prepare the DNA complexes, varying amounts of FPLL were added to 3 µg of DNA (100 µg/mL H_2O) in 150 µL of HBS, pH 7.4. Complexes were mixed gently, incubated at room temperature for 40 min, and added to 2×10^5 KB cells growing in 2 mL of ffDMEM 10% dFBS containing 100 µM chloroquine. After 4 h, media was removed and replaced with fresh ffDMEM, 10% FBS. Twenty-two hours later cellular lysates were assayed for luciferase activity. Luminescence was integrated over 10.0 s in an Analytical Luminescence Laboratories Monolight 2010 luminometer. The data represent the mean of duplicate samples normalized per 10^6 cells, and error bars represent the range of the observed experimental values.
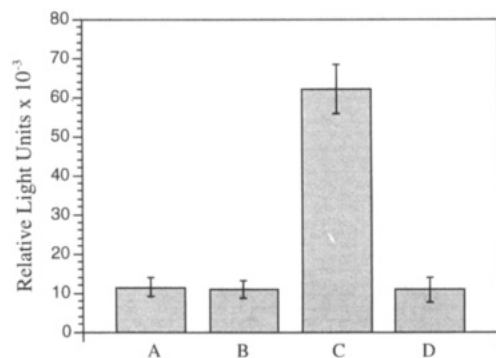
Figure 3. Demonstration of folate receptor specific gene delivery. Cells were transfected with an optimized amount of PLL or FPLL as described in Figure 2. Free folate was added $(1 \times 10^{-5}$ M) to the appropriate cells to demonstrate folate receptor specific transfection: (A) PLL−DNA; (B) folate + PLL−DNA; (C) FPLL−DNA; (D) folate + FPLL−DNA. Results are the average of duplicate samples normalized per 10^6 cells.

RESULTS AND DISCUSSION

To determine the optimum ratio of DNA to FPLL, increasing quantities of FPLL were combined with 3 µg of DNA and added to cells in the presence of chloroquine. Figure 2 shows that transfection is optimized at a DNA to FPLL weight ratio of 1.2 (*23*). The addition of DNA to FPLL at this ratio resulted in complete retardation of the DNA on a 1% agarose gel. Addition of excess FPLL decreased the transfection efficiency, presumably due to the presence of unassociated folate−polylysine in the media able to compete for receptor binding.

The results shown in Figure 3 demonstrate that FPLL−DNA complexes were transfected via folate receptor-mediated endocytosis. Transfection with PLL−DNA at the optimum predicted ratio resulted in a 6-fold lower level of luciferase activity than with FPLL−DNA. Addition of free folate to cells incubated with PLL−DNA had virtually no effect on expression levels. Thus, a covalent linkage between folate and polylysine was essential for the enhanced expression of luciferase. Free folate, added to cells exposed to FPLL−DNA, competed effectively in transfection and reduced luciferase activity to levels obtained by PLL−DNA.
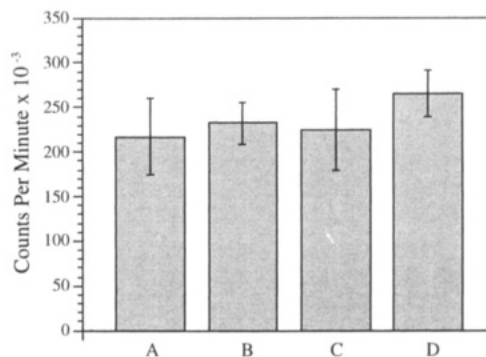
Figure 4. Effect of transfection conditions on protein synthesis. A separate group of cells were transfected using the optimum DNA to FPLL or PLL ratio as described in Figure 2: (A) PLL−DNA; (B) folate + PLL−DNA; (C) FPLL−DNA; (D) folate + FPLL−DNA. Twenty-four hours after the addition of complexes to cells, media was removed and replaced with 2 mL of leucine-free DMEM supplemented with 1 µCi of [^{3}H] leucine. Two hours later, cells were rinsed three times in 2 mL of DPBS and dissolved in 1 mL of 0.1 N KOH. Cellular proteins were precipitated in trichloroacetic acid (1mL, 30%) and collected onto Whatman glass fiber filters. Dried filters were added to 5 mL of Safety Solve scintillation cocktail, and radioactivity (counts per minute) was quantitated in a Beckman model LS 5000 TD scintillation counter. Results are normalized per 10^6 cells.
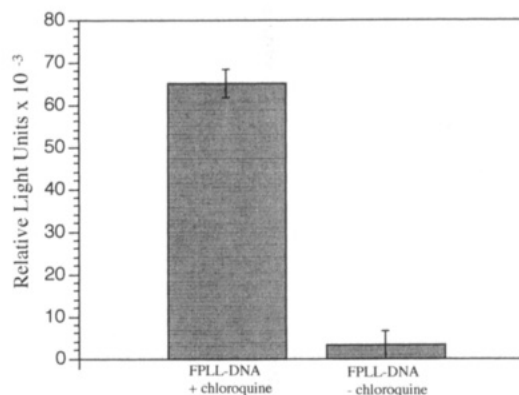
Figure 5. Effect of chloroquine on expression of firefly luciferase. Using the optimum DNA to FPLL ratio, a group of cells were transfected in the absence or presence of chloroquine (50 µM). Cells were treated as described in Figure 2. Results are the average of duplicate samples normalized per 10^6 cells.

To ensure that expression levels were not due to differences in overall protein synthesis, the extent of [^{3}H]-leucine incorporation into cellular proteins was measured in cells exposed to each of the transfection combinations in Figure 3. No significant differences in protein synthesis were observed (Figure 4).

Folate receptor-mediated endocytosis has been described as a general way to achieve nondestructive delivery of macromolecules (*16, 17, 22*). This was based largely on the observation that a folate-conjugated cytotoxin, momordin, could effectively inhibit protein synthesis in a time and concentration-dependent manner, although the effects of chloroquine were not investigated (*17*). To test the role of lysosomes in the cytoplasmic delivery of the DNA complexes, cells were transfected both in the presence and absence of chloroquine (Figure 5). Expression levels were approximately 20 times lower when chloroquine was eliminated from the transfection media. Thus, FPLL−DNA complexes entered the cytoplasm by a chloroquine-sensitive pathway.

This chloroquine sensitivity suggests a lysosomal delivery as is seen in clathrin associated receptor systems. However, the size, chemical composition, and multivalency of the FPLL−DNA could influence its

intracellular fate. Therefore, it is possible that the intracellular destination of FPLL—DNA is different from that of other folate conjugates.

In summary, this work has demonstrated the use of folate receptor mediated endocytosis for the delivery of genes into cells. Although uptake appears to be via a lysosomal pathway, the folate receptor remains a highly attractive target for gene therapy due to its variable expression on tissues *in vivo.*

ACKNOWLEDGMENT

LITERATURE CITED

(1) Haensler, J., and Szoka, F. C., Jr. (1993) Polyamidoamine cascade polymers mediate efficient transfection of cells in culture. *Bioconjugate Chem. 4,* 372—379.

(2) Felgner, P. L. (1990) Particulate systems and polymers for in vitro and in vivo delivery of polynucleotides. *Adv. Drug Delivery Rev. 5,* 163—187.

(3) Kabanov, A. V., and Kabanov, V. A. (1995) DNA complexes with polycations for the delivery of genetic material into cells. *Bioconjugate Chem. 6,* 7—20.

(4) Behr, J. P. (1994) Gene transfer with synthetic cationic amphiphiles: Prospect for gene therapy. *Bioconjugate Chem. 5,* 382—389.

(5) Wu, G. Y., and Wu, C. H. (1988) Evidence for targeted gene delivery to HepG2 hepatoma cells in vitro. *Biochemistry 27,* 887—892.

(6) Zenke, M., Steinlein, P., Wagner, E., Cotten, M., Beug, H., and Birnstiel, M. L. (1990) Receptor-mediated endocytosis of transferrin-polycation conjugates: An efficient way to introduce DNA into hematopoietic cells. *Proc. Natl. Acad. Sci. U.S.A. 87,* 3655—3659.

(7) Huckett, B., Ariatti, M., and Hawtrey, A. O. (1990) Evidence for targeted gene transfer by receptor-mediated endocytosis: Stable expression following insulin-directed entry of neo into HepG2 cells. *Biochem. Pharmacol. 40,* 253—263.

(8) Wagner, E., Plank, C., Zatloukal, K., Cotten, M., and Birnstiel, M. L. (1992) Influenza-virus hemagglutinin-HA-2 N-terminal fusogenic peptides augment gene-transfer by transferrin polylysine DNA complexes—toward a synthetic virus-like gene-transfer vehicle. *Proc. Natl. Acad. Sci. U.S.A. 89,* 7934—7938.

(9) Rothberg, K. G., Ying, Y., Kolhouse, J. F., Kamen, B. A., and Anderson, R. G. W. (1990) The glycophospholipid-linked folate receptor internalizes folate without entering the clathrin-coated pit endocytic pathway. *J. Cell Biol. 110,* 637—649.

(10) Antony, A. C., Kane, M. A., Portillo, R. M., Elwood, P. C., and Kolhouse, J. F. (1985) Studies of the role of a particulate folate binding protein in the uptake of 5-methyltetrahydrofolate by cultured human KB cells. *J. Biol. Chem. 260,* 4911—4917.

(11) Mantovani, L. T., Miotti, S., Menard, S., Canevari, S., Raspagliesi, F., Bottini, C., Bottero, F., and Colnaghi, M. I. (1994) Folate binding-protein distribution in normal-tissues and biological-fluids from ovarian-carcinoma patients as detected by the monoclonal antibodies MOV18 and MOV19. *Eur. J. Cancer. 30A,* 363—369.

(12) Anderson, R. G. W., Kamen, B. A., Rothberg, K. G., and Lacey, S. W. (1992) Potocytosis—sequestration and transport of small molecules by caveolae. *Science 255,* 410—411.

(13) Citro, G., Szczulik, C., Ginobbi, P., Zupi, G., and Calabretta, B. (1994) Inhibition of leukemia-cell proliferation by folic-acid polylysine-mediated introduction of c-myb antisense oligodeoxynucleotides into HL-60 Cells. *Br. J. Cancer 69,* 463—467.

(14) Lee, R. J., and Low, P. S. (1994) Delivery of liposomes into cultured KB cells via folate receptor mediated endocytosis. *J. Biol. Chem. 269,* 3198—3204.

(15) Lee, R. J., and Low, P. S. (1995) Folate-mediated tumor cell targeting of liposome-entrapped doxorubicin in vitro. *Biochim. Biophys. Acta 1233,* 134—144.

(16) Wang, S., Lee, R. J., Cauchon, G., Gorenstein, D. G., and Low, P. S. (1995) Delivery of antisense oligodeoxyribonucleotides against the human epidermal growth factor receptor into cultured KB cells with liposomes conjugated to folate via polyethylene glycol. *Proc. Natl. Acad. Sci. U.S.A. 92,* 3318—3322.

(17) Leamon, C. P., and Low, P. S. (1992) Cytotoxicity of momordin-folate conjugates in cultured human cells. *J. Biol. Chem. 267,* 24966—24971.

(18) Turek, J. J., Leamon, C. P., and Low, P. S. (1993) Endocytosis of folate—protein conjugates—ultrastructural-localization in KB cells. *J. Cell Sci. 106,* 423—430.

(19) Leamon, C. P., Pastan, I., and Low, P. S. (1993) Cytotoxicity of folate—Pseudomonas Exotoxin conjugates toward tumor tells. *J. Biol. Chem. 268,* 24847—24854.

(20) Gottschalk, S., Cristiano, R. J., Smith, L. C., and Woo, S. L. C. (1994) Folate receptor mediated DNA delivery into tumor cells: potosomal disruption results in enhanced gene expression. *Gene Therap. 1,* 185—191.

(21) Stenseth, K., and Thyberg, J. (1989) Monensin and chloroquine inhibit transfer to lysosomes of endocytosed macromolecules in cultured mouse peritoneal macrophages. *Eur. J. Cell Biol. 49,* 326—333.

(22) Leamon, C. P., and Low, P. S. (1991) Delivery of macromolecules into living cells: A method that exploits folate receptor endocytosis. *Proc. Natl. Acad. Sci. U.S.A. 88,* 5572—5576.

(23) Wagner, E., Cotten, M., Foisner, R., and Birnstiel, M. L. (1991) Transferrin—polycation—DNA complexes: The effect of polycations on the structure of the complex and DNA delivery to cells. *Proc. Natl. Acad. Sci. U.S.A. 88,* 4255—4259.

BC9500610

ARTICLES

Recognition of Alternating Oligopurine/Oligopyrimidine Tracts of DNA by Oligonucleotides with Base-to-Base Linkages

Bei-Wen Zhou,[†] Christophe Marchand, Ulysse Asseline,[‡] Nguyen T. Thuong,[‡] Jian-Sheng Sun,[*] Thérèse Garestier, and Claude Hélène

Laboratoire de Biophysique, INSERM U201, CNRS URA481, Muséum National d'Histoire Naturelle, 43, rue Cuvier, 75231 Paris Cedex 05, France, and Centre de Biophysique Moléculaire, CNRS, 45071 Orléans Cedex 02, France. Received March 13, 1995[®]

A new concept is presented to design and synthesize modified oligonucleotides in order to extend the range of double-helical DNA sequences that can be recognized by oligonucleotides *via* triple helix formation. The DNA target is composed of adjacent oligopurine•oligopyrimidine domains where the oligopurine sequences alternate on the two DNA strands. Canonical (C,T)-motif triple helices are formed with each oligopurine•oligopyrimidine domain of the target sequence. The two third-strand oligonucleotides were joined together *via* an appropriate linker between the two terminal bases with either a 3′–3′ or a 5′–5′ polarity. Molecular modeling was used to predict the optimal length of the linker bridging two terminal bases. The interaction of DNA with such a modified oligonucleotide containing a $C^{3'}-^3'U$ linkage was studied by thermal dissociation, footprinting, and gel retardation experiments. They provide experimental evidence that the oligonucleotide does form a switched triple helix on this extended DNA target sequence. The binding of the so-called "switch oligonucleotide" is enhanced as compared to the two unlinked parental oligonucleotides which form triple helices with each oligopurine•oligopyrimidine domain of the target sequence.

INTRODUCTION

Interest in oligonucleotides that can form triple helices has been aroused since 1987 (*1, 2*), due to their potential biological and therapeutical applications for controling gene expression at both transcriptional (*3–7*) and replicational levels (*8*). During the last 5 years, several structural motifs of triple helices have been developed (reviewed in (*9*)). Some of these developments were devoted to overcoming the requirement for protonation at the N3 position of cytosine in one of the two canonical base triplets, C•G × C+, of a (C,T)-motif triple helix. As proposed earlier (*9*), the base triplets will be abbreviated as Y•R × Z where Y•R is the Watson–Crick base pair (Y is the pyrimidine and R the purine strand) and Z is the base in the third strand forming either Hoogsteen or reverse Hoogsteen hydrogen bonds with the purine (R) in the double helix. The isomorphism of base triplets has been highlighted as an important conformational requirement which should be taken into account in the design and synthesis of base triplets containing modified nucleotides (*9–12*).

Despite all these efforts, the so-called "antigene strategy" still suffers from an inherent restriction regarding DNA target sequences which should be relatively long stretches of oligopurine•oligopyrimidine double-helical sequences in order to ensure stable triple helix forma-

tion under physiological conditions. Substantial progress has been made to extend the range of double-helical DNA recognition *via* oligonucleotide-directed triple helix formation. There are mainly two classes of DNA target sequences that can form stable-enough triple helices which are different from canonical polypurine•polypyrimidine sequences: (i) the purine•pyrimidine sequence is interrupted by a single or a double base-pair inversion, and (ii) the target sequence is composed of adjacent and alternate fragments of shorter oligopurine•oligopyrimidine tracts.

In the first case, triple helices can still be formed by using an appropriate natural or modified nucleotide or an intercalating agent at the site of a single base-pair inversion. The rules for skipping over a single mismatch with a limited loss of affinity have been established (*13– 16*), mostly in the (C,T)-motif triple helix. However, the destabilization induced by a single mismatch is dependent on its nearest neighbors (*16*). A double base-pair inversion can be overcome by dimerization of two triple helix-forming oligonucleotides (*17*).

In the second case, several short triple helices can be formed in which the third-strand-oligonucleotides are hydrogen bonded to the oligopurine tracts, and all these short oligonucleotides are linked together as a single third-strand oligomer in order to take avantage of the additivity of the free energies of binding (*18–24*). This oligonucleotide binds to the target DNA composed of adjacent and alternate fragments of oligopurine• oligopyrimidine tracts and zigzags along the major groove, switching from one oligopurine strand to the next one at the 5′-purine–pyrimidine-3′, or 5′-pyrimidine– purine-3′ junctions (hereafter designated as 5′-RpY-3′ or 5′-YpR-3′ junction, respectively). This alternate strand triple helix is hereafter called "switched triple helix".
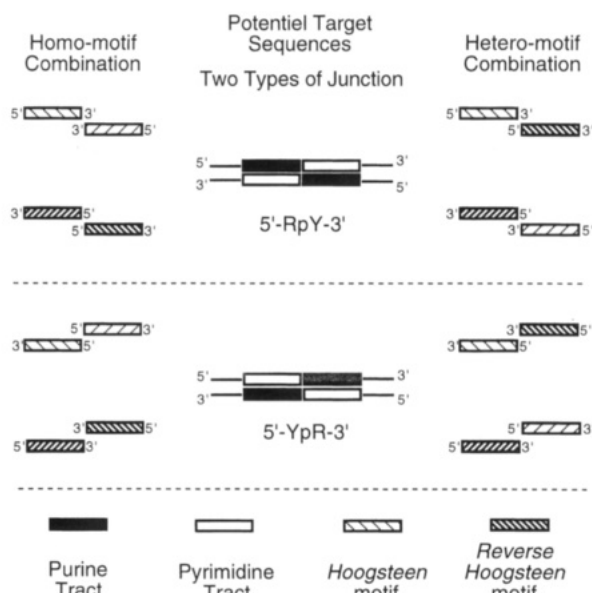
Figure 1. Schematic presentation of different approaches to extend the range of DNA sequences which can be recognized by switch oligonucleotides. The target sequences are made of adjacent and alternate oligopurine·oligopyrimidine tracts (center column). The first approach (left column) involves only one type of hydrogen-bonding scheme (Hoogsteen or reverse Hoogsteen motifs), while the second (right column) uses alternating Hoogsteen and reverse Hoogsteen motifs. The homomotif combination requires a linker at the junction, whereas the heteromotif combination may use a standard oligonucleotide (see text for details).

The different possibilities for "switched triple helix" formation are depicted in Figure 1, depending on the combination of triple-helix motifs. Triple-helix motifs involving hydrogen-bonding interactions in the Hoogsteen configuration adopt a parallel orientation of the third strand with respect to the purine second strand (e.g., (C,T)- and some (G,T)-motifs (11)), while the third strand runs antiparallel to the second strand in all motifs with reverse Hoogsteen configuration (i.e., (G,A)- and most (G,T)-motifs). They are hereafter referred to as Hoogsteen motifs or reverse Hoogsteen motifs, respectively.

When the hydrogen bonding pattern at the junctions changes from Hoogsteen to reverse Hoogsteen, or vice versa (hetero-motif combination), the two third-strand oligonucleotides run in the same direction along the major groove of the underlying double-helical DNA. Therefore, there is no need for a specific linker, provided that the number and the type of bases at the junction is properly chosen to remove any steric hindrance as well as to ensure simultaneous binding (18–21). Consequently, a standard oligonucleotide can be synthesized for switching over alternate purine strands at any junction.

In contrast, when binding of two oligonucleotides to adjacent but alternate oligopurine·oligopyrimidine sites involves the same hydrogen bonding scheme (Hoogsteen or reverse Hoogsteen), the two 3'- or 5'-ends face each other (homomotif combination). Therefore, a linker is required to tether the 3'- or the 5'-ends of the oligomers. Several linkers have been described in the (C,T)-motif switched triple helix to attach two oligonucleotides to each other through the 3'–3' or 5'–5' termini (22–24). Among these linkers, a 3'–3' linker made of a *p*-xylose dimer has been demonstrated to provide an appropriate length and a sufficient rigidity to span over the 5'-RpY-3' junctions and could afford a stable-enough binding of the switch oligonucleotide (24). Until now, there has been no satisfactory 5'–5' linker that has been shown to provide an effective cooperative binding at the 5'-YpR-3' junctions.

The present work is devoted to the development of a new approach for "switched triple helix" formation using the homomotif combination, particularly the (C,T)-motif triple helices. The two oligonucleotides are linked *via* their terminal bases at the junction between the two oligopurine·oligopyrimidine tracts. Molecular modeling using conformational energy minimization was used to determine the optimal linker for each type of junction. An experimental study dealing with an oligonucleotide forming a switched triple helix through a $C^{3'}-^{3'}U$ linkage illustrates the feasibility of this base–base linkage concept in an effort to extend DNA recognition sequences by switched triple helix formation.

MATERIALS AND METHODS

Oligonucleotides. Oligonucleotides were purchased from Genosys, Inc. (Cambridge, England). They were ethanol precipitated, and their concentration was measured from their absorbance at 260 nm using an extinction coefficient calculated according to a nearest-neighbor model (25, 26).

Chemical Synthesis of the 3'–3' Linked Oligonucleotides. The synthesis of the 3'–3' linked oligonucleotides was carried out according to the pathway presented in Figure 3. As previously described for the preparation of symmetrical base$^{3'}-^{3'}$base linked oligonucleotides (27), the key step was the synthesis of the bridged dimer **3** and its immobilization on a support. Preparation of the dimer **3** ($C^{3'}-^{3'}U$) required one additional step as compared with the synthesis of the symmetrical $C^{3'}-^{3'}C$ dimer. First, 5'-protected ^{5Br}dU was reacted with diaminopentane to give uracil substituted at the 5-position with the pentylamino linker **1**. Then the latter was reacted with the 5'–3' protected deoxyuridine activated at its 4-position by a triazolyl group **2** (28) to afford the protected dimer **3**. Attachment of dimer **3** to controlled-pore glass (CPG) and oligonucleotide synthesis were performed as previously reported (27) except that in this case only one nucleoside (dU) was bound to the support and there was no need for propylamine treatment. Chain elongation was carried out on the modified support **4** utilizing commercially available nucleoside 3'-*O*-(2-cyanoethyl)-*N*,*N*-diisopropylphosphoramidites on a Pharmacia Gene Assembler.

After removal of the protecting groups and cleavage from the support by concentrated ammonia treatment (3 h at room temperature) the modified oligonucleotide was purified by ion exchange chromatography. After purification and desalting, detritylation was performed by acetic acid treatment. The purity of the obtained compound was checked by liquid chromatography using ion exchange and reversed-phase analysis with detection at $\lambda = 260$ nm. Ion exchange analysis was performed on a DEAE 8HR column from Millipore using a linear gradient of NaCl (0.15–0.75 M in 20 min) in 0.025 M Tris/HCl buffer, pH 8, containing 10% CH_3CN, with a flow time of 1 mL/min. The oligonucleotide was eluted with a retention time of 15 min 36 s. Reversed-phase analysis was carried out on a Lichrospher 100 RP 18 (5 mm) column (125 × 4 mm) using a linear gradient of CH_3CN in 0.1 M aqueous triethylammonium acetate buffer, pH 7, with a flow rate of 1 mL/min (0% CH_3CN for 5 min, then 0–30% CH_3CN in 30 min). The retention time was 26 min 3 s. Nucleic base composition was ascertained by reversed-phase analysis after nuclease degradation with nuclease P1 from *Penicilium citrinum* and alkaline phosphatase. The nucleosides dC, dT, and a compound

identified as the product obtained after deprotection of the dimer were eluted on a Lichrospher 100 RP 18 column using the above-described conditions with the following retention times: 4 min 30 s, 11 min 11 s, and 22 min 24 s, respectively.

DNA Melting Experiments. Triple helix stability was measured by UV spectrophotometry. All DNA melting experiments were carried out on a Uvikon 940 spectrophotometer using quartz cuvettes of 1 cm optical pathlength. Uvikon 940 was interfaced to an IBM-AT computer for data collection and analysis. The cell holder was thermostated with a circulating liquid (80% water/ 20% ethyleneglycol) in a Haake D8 water bath. Temperature change of the water bath was monitored by a Haake PG20 thermoprogrammer, typically at a rate of 0.1 °C/min. The absorbance at 260 nm was recorded after each 1 °C increase in temperature (typically every 10 min). Temperature reading was achieved by using a thermocouple in a control cuvette. All samples were in 10 mM cacodylate buffer at pH 6.0 or 7.0, containing 0.1 M sodium chloride and 0.2 mM spermine. The melting curves of the same sample obtained upon cooling or heating were superimposable, indicating that the melting curve reflects equilibrium conditions (*29*). The melting temperature was evaluated as the temperature at which half-association (or dissociation) of the third strand from the double-helical target occurred.

Gel Retardation Assay. A nondenaturing 10% acrylamide gel (99:1 acrylamide/bis-acrylamide) containing 50 mM MES buffer, pH 6.0 and 5 mM MgCl$_2$ was prepared. One strand of the DNA template (CU1 or CU2, see Figure 2) was labeled at the 5'-end by T4 polynucleotide kinase using γ-^{32}P-ATP. One hundred nmol of different third strand oligonucleotides was added to 10 nmol of DNA template duplex. The mixture was incubated at 4 °C overnight in a 50 mM MES buffer, pH 6.0, 5 mM MgCl$_2$, and 10% sucrose. Electrophoresis was performed for 16 h (0.75 W) at 4 °C. Gels were dried, autoradiographed, and analyzed on a Molecular Dynamics Phosphorimager.

DNase I Assay. Footprinting experiments were carried out using DNase I as a cleaving agent. One strand of the 40 bp DNA template (CU1 or CU2, see Figure 2) was labeled at the 5'-end with T4 polynucleotide kinase using γ-^{32}P-ATP. Oligonucleotide concentrations in all experiments are referred to as strand concentrations. Experiments were performed as previously described (*30*), including the following modifications: the 40-bp fragment (20 nM) was usually incubated in 10 μL of buffer containing 10 mM sodium cacodalyte buffer at pH 6.5, 50 mM NaCl, 5 mM MgCl$_2$, 0.5 mM CaCl$_2$, 1 mM spermine, at the desired temperature overnight. Then DNase I was added (2 mg/mL final concentration). After 1 min 20 s, or 5 s for the DNase-I assays carried out at 4, 20, and 37 °C, respectively, the digestion was stopped by freezing in dry ice. After two lyophilizations, the digested samples were analyzed on a denaturing 20% acrylamide gel, autoradiographed, and analyzed on a Molecular Dynamics Phosphorimager.

Molecular Modeling. Molecular modeling by conformational energy minimization was carried out using the JUMNA program package (*31*). The current version of the JUMNA program (version 7.2) allows for the inclusion of any number of modified nucleotides into the calculation *via* the Nchem utility program, which is part of the JUMNA program package. The Nchem program was used both to calculate the partial charges and to evaluate the appropriate geometrical parameters for modified nucleotides, and prepare the file containing the information required by the JUMNA program. Nchem

utilizes a Huckel-Del Re procedure for calculation of the partial atomic charges (*32*). Neither water nor positively charged counterions were explicitly included in the energy minimization. However, their effects were simulated by a sigmoidal, distance-dependent, dielectric function (*33*) and by assignment of half of a negative charge to each phosphate group.

DNA coordinates were derived from the previously published B-triple helix (*34*) which is supported by NMR and vibrational spectroscopic data (*34–39*). All cytosines in the third strand are in the N3-protonated form. The calculation procedure using the JUMNA program consists of bridging together two terminal nucleotides at the junction in which cytosine and/or uracil are modified to a 4-(aminoalkyl)cytosine and/or a 5-alklyluracil, respectively. These two nucleotides were attached to each other at the end of each alkyl chain through a virtual bond with correct bond length and angular and torsional angles by applying appropriate constraints during energy minimization of the alternate strand triple-helical complex. Finally, an energy-minimized alkyl linker ranging in size from tetra- to hexamethylene between terminal nucleotides was introduced. Computations were carried out on a Silicon Graphics 4D/420GTXB workstation.

RESULTS

I. Molecular Modeling. Molecular modeling reveals that the conformational requirement for spanning over the 5'-RpY-3' junction is distinctly different from that of the 5'-YpR-3' junction. In the former case, the shortest distance separating two 3'-OH ends (about 12 Å) can be obtained by skipping two base pairs at the 5'-RpY-3' junction, whereas in the later case the shortest distance between two 5'-ends at the 5'-YpR-3' junction is almost the diameter of the cylinder of the triple helix (about 21 Å). It should be noted that the *p*-xylose dimer previously described (*24*) was well suited to link the 3'-ends of two oligonucleotides which were separated by two base pairs at the junction in the target sequence. By contrast, a long and flexible linker should be used in order to wrap around the triple helix to join the two 5'-ends at the 5'-YpR-3' junction, resulting in a substantial entropy loss.

On the basis of the above observations, it appeared that an alternative way to build a switched (C,T)-motif triple helix could be a linkage between the terminal bases at position 4 or 5 of pyrimidines. These positions are ideal linkage sites, because, first they are located near the bottom of the Watson–Hoogsteen groove [nomenclature suggested by Patel (*38, 39*)] in a (C,T)-motif triple helix, second, they would not disrupt the hydrogen bonding of base triplets, and third, they are prone to chemical modifications. The resulting advantage should be an entropically improved binding due to the very short linker (4–6 carbons), and the same strategy should be applicable to both 3'–3' and 5'–5' linkages since the interbase distance between terminal bases in the third strands is mainly defined by the neighboring base triplets regardless, to some extent, of their relative polarities.

As mentioned above, there are two families of junctions, i.e., 5'-RpY-3' and 5'-YpR-3' junctions. Within each family, there are only three distinct junctions. These are 5'-ApT-3', 5'-GpC-3', and 5'-GpT-3' (which is equivalent to 5'-ApC-3') for the 5'-RpY-3' junction and 5'-TpA-3', 5'-CpG-3', and 5'-TpG-3' (which is equivalent to 5'-CpA-3') for the 5'-YpR-3' junction. Therefore, a total number of six base–base dimers with tailor-made linkers joining the two terminal bases would be sufficient to cope with any junction.

Molecular modeling was performed for the six possible base–base dimers that could be used to link two oligo-

Table 1. Analysis of the Conformational Energies of the Energy-Minimized Triple Helices Containing Various Base–Base Dimers at All Six Junction Steps[a]

junction	dimer	linker	E_{WC}	E_{HG}	E_{III}	E_{TOT}
$5'$GpC$3'$	C$3'$ – $3'$C	$-(CH_2)_4-$	-578.1	-407.0	-47.3	$\underline{-1032.4}$
		$-(CH_2)_5-$	-564.1	-429.4	-21.2	-1014.7
$5'$GpT$3'$	C$3'$–$3'$U	$-(CH_2)_4-$	-554.4	-383.5	-84.2	-1022.1
		$-(CH_2)_5-$	-557.7	-373.3	-103.0	$\underline{-1034.0}$
		$-(CH_2)_6-$	-556.6	-386.6	-81.2	-1024.4
$5'$ApT$3'$	U$3'$–$3'$U	$-(CH_2)_4-$	-534.2	-360.0	-149.3	$\underline{-1043.5}$
		$-(CH_2)_5-$	-540.2	-350.4	-144.6	-1035.2
$5'$CpG$3'$	C$5'$–$5'$C	$-(CH_2)_4-$	-570.1	-436.9	-19.9	$\underline{-1026.9}$
		$-(CH_2)_5-$	-569.5	-448.2	21.2	-996.5
$5'$TpG$3'$	U$5'$–$5'$C	$-(CH_2)_4-$	-537.3	-394.2	-45.0	-976.5
		$-(CH_2)_5-$	-548.7	-395.9	-84.5	$\underline{-1029.1}$
		$-(CH_2)_6-$	-552.5	-414.3	-53.9	-1020.7
$5'$TpA$3'$	U$5'$–$5'$U	$-(CH_2)_5-$	-512.8	-386.1	-136.5	$\underline{-1035.4}$
		$-(CH_2)_6-$	-529.1	-370.2	-131.4	-1030.7

[a] The total conformational energy (E_{TOT}) was decomposed in terms of the intermolecular interaction energies involving Watson–Crick (E_{WC}) and Hoogsteen pairing (E_{HG}), as well as the intramolecular interaction energy within the switch oligonucleotide as third strand (E_{III}). Energy is given in kcal·mol^{-1}. The optimal linker for each junction is underlined.

nucleotides at the junctions described above. An inspection at the junction formed by two short (C,T)-motif triple helices in which the DNA target sequence is composed of alternate fragments of oligopurine•oligopyrimidine tracts reveals that the distance between the 4- and/or 5-position of the two terminal pyrimidines is about 5–6 Å at the $5'$-RpY-$3'$ junction, whereas it is in the range of 5–8 Å at the $5'$-YpR-$3'$ junction. A preliminary modeling study showed that a propylene linker was too short and that a linker longer than hexamethylene provided too much length and flexibility, resulting in unfavorable entropic loss which should be detrimental to the binding affinity of switch oligonucleotides. Therefore, a set of relatively short linkers ranging in size from tetra- to hexamethylene chains was investigated to join two bases together at the junction. Molecular modeling by conformational energy minimization was further carried out to evaluate the energy differences between these linkers for any given junction, thus leading to optimize the length of linker for each junction.

Table 1 summarizes the conformational energies for all junction steps. The total conformational energy (E_{TOT}) was decomposed in terms of intermolecular interactions involving Watson–Crick (E_{WC}) and Hoogsteen pairing (E_{HG}), as well as the intramolecular (van der Waals + electrostatic) interactions within the switch oligonucleotide in the third strand (E_{III}). For a given type of junction, among the linkers ranging from tetra- to hexamethylene, the best linker can be chosen on the basis of the total conformational energy (E_{TOT}). In all cases, the intramolecular interactions within the switch oligonucleotide in the third strand (E_{III}) make the difference, since the sum of the intermolecular interactions involving the Watson–Crick (E_{WC}) and Hoogsteen pairing (E_{HG}) remains nearly constant for a given junction. Furthermore, the terms E_{WC} and E_{HG} of the switched triple helix with the best linkers were quite identical to those found for the corresponding unlinked triple helices (results not shown), indicating that the global triple-helical structure was quite well preserved. In addition, conformational analysis showed that there were no marked changes in the triple-helical structure, and almost every sugar was in the C2′-endo conformation, except two cytosines near the junction which were in the O1′-endo conformation. A shorter or longer linker than the optimal linker induced a distortion at the junction due to either distance or

1) Target DNA sequence containing a $5'$-GpT-$3'$ ($5'$-ApC-$3'$) junction:

Box I

```
5'ATGTCGAC AAAAGAAAAGGG TCCTTTTCTTTT AGTACGCA3'  CU1
3'TACAGCTG TTTTCTTTTCCC AGGAAAAGAAAA TCATGCGT5'  CU2
```
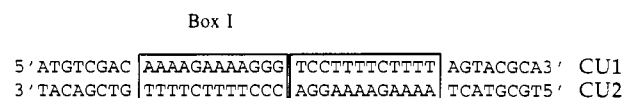
Box II

Oligonucleotides for triple helix formation :

5'TTTTCTTTTCCC3'   12TC

3'TCCTTTTCTTTT5'   12TCU

5'TTTTCTTTTCC<u>C–U</u>CCTTTTCTTTT5'   24SWT
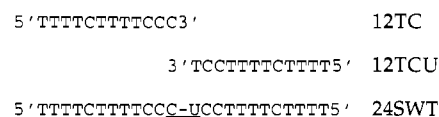
2) Control DNA sequence containing a 24-bp polypurine• polypyrimidine tract :

```
5'ATGTCGAC AAAAGAAAAGGGAGGAAAAGAAAA TCATGCGT3'  CTR
3'TACAGCTG TTTTCTTTTCCCTCCTTTTCTTTT AGTACGCA5'  CTY
```
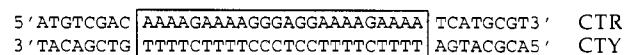
Oligonucleotide for triple helix formation :

5'TTTTCTTTTCCCTCCTTTTCTTTT3'   24TC
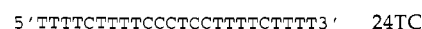
Figure 2. DNA target sequence and oligonucleotides used in the present study, where <u>C–U</u> indicates a C$3'$–$3'$U dimer (see Figure 3).

phasing problems which are detrimental to the stability of the switched triple helix.

In summary, what emerged from this modeling study is that there is an optimal length of linker for each of the six junctions with the assumptions made in the calculation procedures (see above). They are (i) a tetramethylene linker for the $5'$-GpC-$3'$, $5'$-ApT-$3'$, $5'$-CpG-$3'$ junctions and (ii) a pentamethylene linker for the $5'$-GpT-$3'$, $5'$-TpG-$3'$, $5'$-TpA-$3'$ junctions. It is worthy of note that the optimal length of linkers are the same for either the $5'$-GpC-$3'$ and $5'$-CpG-$3'$ junction or the $5'$-GpT-$3'$ and $5'$-TpG-$3'$ junction, whereas it requires one more methylene group for the $5'$-TpA-$3'$ junction as compared to the $5'$-ApT-$3'$ junction. This difference reflects nearly identical distances between the N4-position of cytosines at either $5'$-GpC-$3'$ and $5'$-CpG-$3'$ junction steps or between the N4-position of cytosine and the C5-position of uracil at either $5'$-GpT-$3'$ and $5'$-TpG-$3'$ junction steps. In contrast, the distance separating the C5-position of the two uracils is slightly different. They are about 6 Å at the $5'$-ApT-$3'$ junction and about 8 Å at the $5'$-TpA-$3'$ junction. A detailed energy analysis revealed that this difference originates from a better inter-third-strand base stacking interaction at the $5'$-ApT-$3'$ junction than that at the $5'$-TpA-$3'$ junction (data not shown).

II. Switching at a $5'$-GpT-$3'$ (or $5'$-ApC-$3'$) Junction by Using a C$3'$–$3'$U Dimer. Figure 2 shows the target DNA sequence composed of two oligopurine•oligopyrimidine tracts: each of them is 12 base pairs in length, and the purine strand of one tract is adjacent to the pyrimidine strand of the other one. Thus, the target sequence has a $5'$-GpT-$3'$ (or $5'$-ApC-$3'$) junction. The oligonucleotides 12TC and 12TCU can form triple helices with box I and box II, respectively.

According to the prediction of molecular modeling, a pentamethylene should be an optimal linker for joining the N4 position of the $3'$ terminal cytosine of the oligonucleotide 12TC to the C5 position of the $3'$ terminal uracil of the oligonucleotide 12TCU. Since all methylene groups prefer *trans, gauche+,* or *gauche−* conformations with respect to each other, the linker is spatially extended and matches the C$3'$–$3'$U distance without disrupting the terminal base triplets (Figure 4).
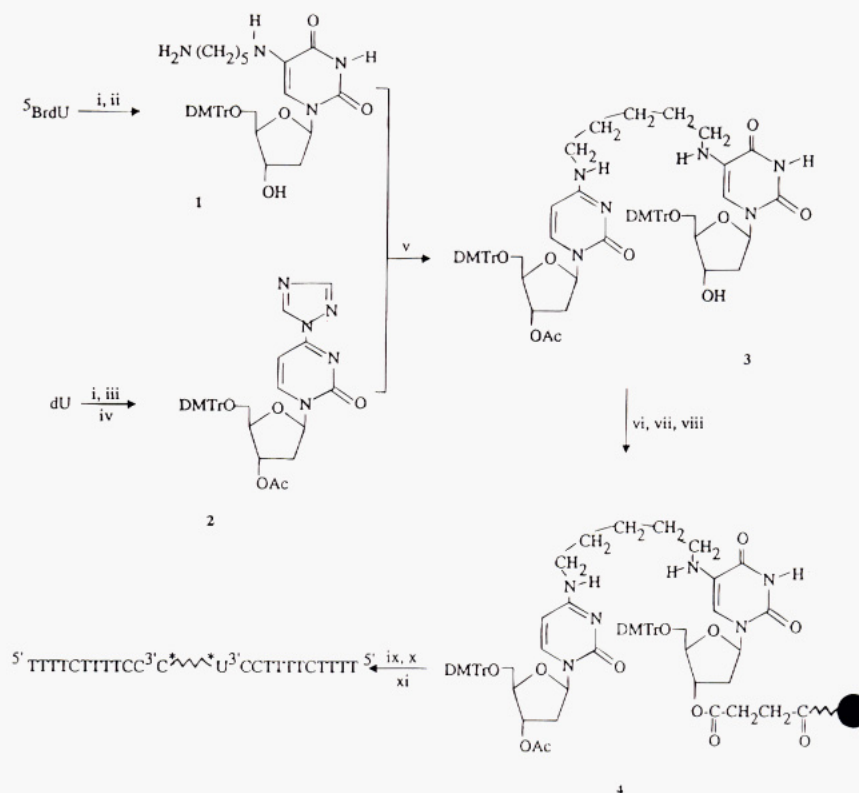
Figure 3. Pathway for the synthesis of the $C^{3'}-{}^{3'}U$-linked oligonucleotide. Reagents: DMTr = dimethoxytrityl; Ac = acetyl; ● = LCAA−CPG = long-chain alkylamine controlled-pore glass. Key: (i) DMTrCl, pyridine; (ii) 1,5 diaminopentane; (iii) CH₃COCl, pyridine; (iv) phosphorus oxychloride, triazole, CH₃CN; (v) CH₃CN; (vi) succinic anhydride, 4-(dimethylamino)pyridine, pyridine; (vii) *p*-nitrophenol, pyridine, dicyclohexylcarbodiimide, dioxane; (viii) LCAA−CPG, NEt₃, DMF; (ix) elongation of the oligodeoxyribonucleotide chain; (x) concentrated ammonia; (xi) H⁺.

UV Spectrophotometry. DNA melting experiments (Figure 5) showed that, at pH 7.0, the switch oligonucleotide 24SWT formed a triple helix which exhibited a higher melting temperature (28 °C) than each of the separated 12TC and 12TCU oligonucleotides (about 13 °C). These transitions could not be ascribed to self-association of oligonucleotides because the oligonucleotides did not exhibit any transition in the absence of target DNA (results not shown). Therefore, the observed transitions reflect triple helix dissociation, since the double-helical DNA fragment melted at 65 °C under the same conditions. In addition, there was no cooperative binding between oligonucleotides 12TC and 12TCU, since the melting curve obtained with the mixture of the two oligonucleotides 12TC + 12TCU with their DNA target was the superimposition of those with individual oligonucleotides. As a result of the requirement for cytosine protonation in the third strand, the stability of all triple helices was increased by 14 °C at pH 6.0 as compared with pH 7.0. A control experiment was carried out in which the oligopurine and oligopyrimidine sequences were reversed in box II, thus generating a 24-bp polypurine·polypyrimidine sequence. The thermal stability of a canonical (C,T)-motif triple helix formed by oligonucleotide 24TC with the 24-bp polypurine·polypyrimidine sequence was 10 °C higher than that of the switched triple helix formed by oligonucleotide 24SWT at the alternating target sequence (Table 2).

Gel Retardation Assay. The binding ability of different oligonucleotides was also assessed by gel retardation experiments at 4 °C (Figure 6). It can be seen that 100 nM of switch oligonucleotide 24SWT converts almost all duplex to triplex species, whereas the 12-mer oligonucleotides or their mixture (12TC and 12TCU) failed to convert a significant amount of duplex to triplex at
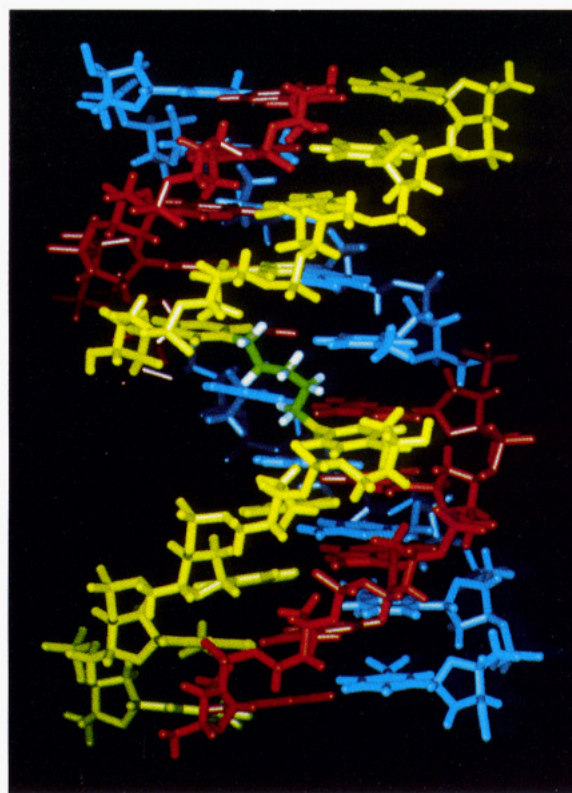
Figure 4. Molecular model of the energy-minimized switched triple helix at the $^{5'}$-GpT-$^{3'}$ (or $^{5'}$-ApC-$^{3'}$) junction by using a $C^{3'}-{}^{3'}U$ dimer in the switch oligonucleotide. The purines and purimidines in Watson−Crick duplex are colored in red and blue, respectively. The switch oligonucleotide is colored in yellow, except the pentamethylene linker which is colored in green and in white for carbon and hydrogen atoms, respectively.
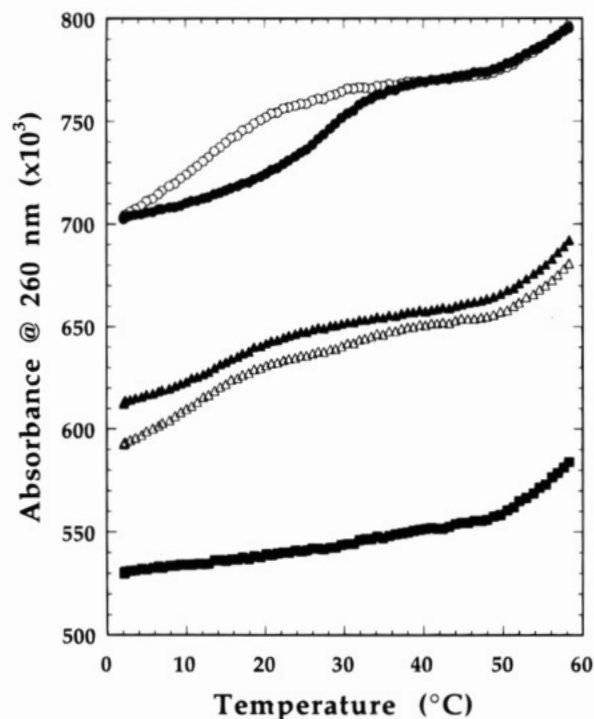
Figure 5. Thermal denaturation curves, at pH 7.0, of the mixtures of the 40-bp duplex CU1/CU2 (1.0 μM) with the switch oligonucleotide 24SWT (1.5 μM) (filled circles), a mixture of the two 12-mer oligonucleotides 12TC (1.5 μM) and 12TCU (1.5 μM) (open circles), the 12-mer oligonucleotide 12TC (or 12 TCU) (1.5 μM) (filled and open triangles). The melting curve of the duplex alone is indicated by filled squares. See Materials and Methods for conditions.

Table 2. T_m Values of Different Triple Helices at pH 6.0 and 7.0 (See Materials and Methods)[a]

duplex	oligonucleotides	T_m (± 1 °C)	
		pH 6.0	pH 7.0
CU1·CU2	12TC	26	12
	12TCU	27	14
	12TC+12TCU	27	13
	24SWT	42	28
CTR·CTY	24TC		38

[a] The concentrations of the duplex and the third-strand oligonucleotides were 1.0 and 1.5 μM, respectively.
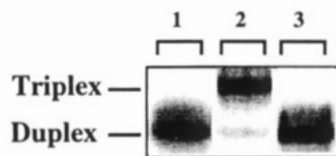
Figure 6. Gel retardation experiments at pH 6.0 and 4 °C in a MES buffer (see Materials and Methods), in the presence of the switch oligonucleotide 24SWT (lane 2) and the mixture of 12-mer oligonucleotides 12TC+12TCU (lane 3), at 100 nM concentration. The CU1 strand of 40-bp DNA fragment was radiolabelled at its 5′-end (lane 1).

the same strand concentrations. At higher concentrations (>1 μM) each of the 12mer oligonucleotides induced the formation of a triplex which migrated nearly halfway between the duplex and the triplex formed with the switch oligonucleotide 24SWT (results not shown).

Footprinting Experiments. The results of footprinting experiments performed at pH 6.5 using DNase I as DNA cleaving agent are shown in Figure 7. At 4 °C, the footprint of the switch oligonucleotide 24SWT at 1 μM was clearly visible at the expected target sequence, whereas the presence of both 12TC and 12TCU oligo-
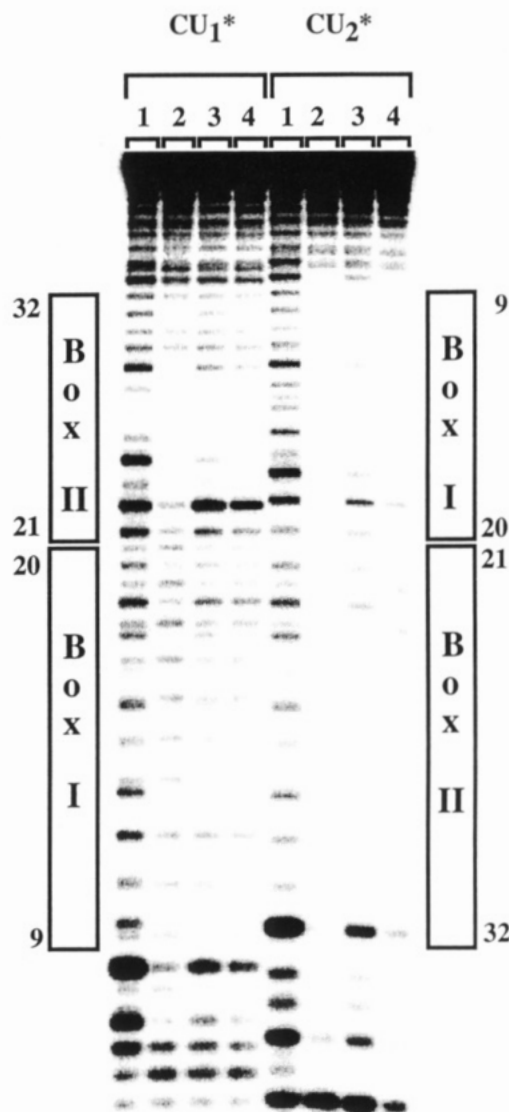
Figure 7. DNase-I footprinting experiment carried out at pH 6.5 at 4 °C (see Materials and Methods), in the presence of various oligonucleotides. The CU1 or CU2 strand of 40-bp DNA fragment was radiolabeled at its 5′-end. The locations of oligopurine·oligopyrimidine tracts are indicated by the boxes. Control expriment was performed in the presence of 1 μM nonspecific oligonucleotide (lane 1); Lane 2 was obtained in the presence of 1 μM of switch oligonucleotide 24SWT; and lanes 3 and 4 contained the mixture of 12-mer oligonucleotides 12TC + 12TCU, at 1 and 10 μM each, respectively.

nucleotides protected only weakly the target DNA fragment from DNase I cutting at the same concentration (1 μM each). A 10-fold increase in the concentration of both 12-mer oligonucleotides (10 μM each) provided an increased protection which became comparable to that observed at 1 μM concentration of the switched oligonucleotide. This difference was maintained at higher temperatures (result not shown) showing a stronger binding of the switch oligonucleotide as compared to both 12-mer oligonucleotides. These observations suggest that the binding affinity of the switch oligonucleotide to form a switched triple helix is at least 1 order of magnitude higher than that of the two separated oligonucleotides.

DISCUSSION

The experimental results obtained by different techniques support the concept of base−base linkage for designing oligonucleotides that can form switched triple

helices with enhanced binding affinity and thermal stability due to simultaneous binding of both portions of the oligomer. However, the thermal stability of this switched triple helix was still 10 °C lower than that observed for the full length 24-mer triple helix in which the purine·pyrimidine sequence in box II was reversed. Therefore, further efforts are required to improve the linkage at the junction by introducing a more rigid linker than the flexible alkyl chain used in the present experiments. The possibility of skipping over a base pair at the junction should also be considered in further evaluation of the base-to-base linkage approach.

The present work was aimed at demonstrating the feasibility of the concept of base–base linkage as a versatile way to extend the range of DNA sequences recognized by oligonucleotides forming switched triple helices. We have used a symmetric sequence to simplify the synthesis of the switch oligonucleotide. However, there is no major difficulty in synthesizing asymmetric sequences, provided two different protecting groups are incorporated into the base–base dimers. In this way, only six dimers, i.e., $C^{3'}-^{3'}C$, $C^{3'}-^{3'}U$, $U^{3'}-^{3'}U$, as well as $C^{5'}-^{5'}C$, $C^{5'}-^{5'}U$, $U^{5'}-^{5'}U$, are required in order to extend the range of recognition sequences by switch oligonucleotides which are able to form switched (C,T)-motif triple helices at any junction. The study of $5'-5'$ linkage is currently under way.

ACKNOWLEDGMENT

LITERATURE CITED

(1) Le Doan, T., Perrouault, L., Praseuth, D., Habhoub, N., Decout, J. L., Thuong, N. T., Lhomme, J., and Hélène, C. (1987) Sequence-specific recognition, photocrosslinking and cleavage of the DNA double helix by an oligo-[α]-thymidylate covalently linked to an azidoproflavine derivative. *Nucl. Acids Res. 15,* 7749–7760.

(2) Moser, H. E., and Dervan, P. B. (1987) Sequence-specific cleavage of double helical DNA by triple helix formation *Science 238,* 645–650.

(3) Cooney, M., Czernuszewicz, G., Postel, E. H., Flint, S. J., and Hogan, M. E. (1988) Site-specific oligonucleotide binding represses transcription of the human c-myc gene *in vitro. Science 241,* 456–459.

(4) Maher, L. J., III, Wold, B., and Dervan, P. B. (1989) Inhibition of DNA binding proteins by oligonucleotide-directed triple helix formation. *Science 245,* 725–730.

(5) Young, S. L., Krawczyk, S. H., Matteucci, M. D., and Toole, J. J. (1991) Triple helix formation inhibits transcription elongation *in vitro. Proc. Natl. Acad. Sci. U.S.A. 88,* 10023–10026.

(6) Duval-Valentin, G., Thuong, N. T., and Hélène, C. (1992) Specific inhibition of transcription by triple helix-forming oligonucleotides. *Proc. Natl. Acad. Sci. U.S.A. 89,* 504–508.

(7) François, J. C., Saison-Behmoaras, T., Thuong, N. T., and Hélène, C. (1989) Inhibition of restriction endonuclease cleavage via triple helix fomation by homopyrimidine oligonucleotides. *Biochemistry 28,* 9617–9619.

(8) Birg, F. Praseuth, D., Zerial, A., Thuong, N. T., Asseline, U., Le Doan, T., and Hélène C. (1990) Inhibition of simian virus 40 DNA replication in CV-1 cells by an oligonucleotide covalently linked to an intercalating agent. *Nucl. Acids Res. 18,* 2901–2908.

(9) Sun J. S., and Hélène C. (1993) Oligonucleotide-directed triple helix formation *Curr. Opin. Struct. Biol. 3,* 345–356.

(10) Hélène, C. (1991) The anti-gene strategy: control of gene expression by triple helix-forming oligonucleotides. *Anti-Cancer Drug Des. 6,* 569–584.

(11) Giovannangéli, C., Rougée, M., Montenay-Garestier, T., Thuong, N. T., and Hélène, C. (1992) Triple helix formation by oligonucleotides containing three bases T, C and G. *Proc. Natl. Acad. Sci. U.S.A.* 89, 8631–8635.

(12) Milligan, J. F., Krawczyk, S. H., Wadwani, S., and Matteucci, M. D. (1993) An antiparallel triple helix motif with oligodeoxynucleotides containing 2′-deoxyguanosine and 7-deaza-2′-deoxyxanthosine. *Nucl. Acids Res. 21,* 327–333.

(13) Griffin, L. C., and Dervan, P. B. (1989) Recognition of thymine·adenine base pairs by guanine in a pyrimidine triple helix motif. *Science 245,* 967–971.

(14) Mergny, J. L., Sun, J. S., Rougée, M., Montenay-Garestier, T., Barcelo, F., Chomilier, J., and Hélène, C. (1991) Sequence-specificity in triple helix formation: experimental and theoretical studies of the effect of mismatches on triple helix stability. *Biochemistry 30,* 9791–9798.

(15) Yoon, K., Hobbs, C. A., Koch, J., Sardaro, M., Kutny, R., and Weis, A. L. (1992) Elucidation of the sequence-specific third-strand recognition of four Watson–Crick base pairs in a pyrimidine triple-helix motif.*Proc. Natl. Acad. Sci. U.S.A. 89,* 3840–3844.

(16) Kiessling, L. L., Griffin, L. C., and Dervan, P. B. (1992) Flanking sequence effects within the pyrimidine triple helix motif characterized by affinity cleaving. *Biochemistry 31,* 2829–2834.

(17) Distefano, M. D., and Dervan, P. B. (1991) Cooperative binding of oligonucleotides to DNA triple-helix formation: dimerization via Watson–Crick hydrogen bonds. *J. Am. Chem. Soc. 113,* 5901–5902.

(18) Sun, J. S., De Bizemont, T., Duval-Valentin, G., Montenay-Garestier, T., and Hélène, C. (1991) Extension of the range of recognition sequence for triple helix formation by oligonucleotides containing guanines and thymines. *C. R. Acad. Sci. Paris, Série III 313,* 585–590.

(19) Beal, P. A., and Dervan, P. B. (1992) Recognition of double-helical DNA by alternate strand triple helix formation. *J. Am. Chem. Soc. 114,* 4976–4982.

(20) Jayasena, S. D., and Johnston, B. (1992) Oligonucleotide-directed triple-helix formation at adjacent oligopurine and oligopyrimidine DNA tracts by alternate strand recognition. *Nucl. Acids Res. 20,* 5279–5288.

(21) Sun, J. S. (1995) Rational design of switched triple helix-forming oligonucleotides: extension of sequences for triple helix formation. *Modelling of Biomolecular Structures and Mechanisms* (A. Pullman, B. Pullman, and J. Jortner, Eds.) pp 267–288, Kluwer Academic Publisher, London.

(22) Horne, D. A., and Dervan, P. B. (1990) Recognition of mixed-sequence duplex DNA by alternate-strand triple helix formation. *J. Am. Chem. Soc. 112,* 2435–2437.

(23) Ono, A., Chen, C. N., and Kan, L. S. (1991) DNA triplex formation of oligonucleotide analogues consisting of linker groups and octamer segments that have opposite sugar-phosphate backbone polarities. *Biochemistry 30,* 9914–9921

(24) Froehler, B. C., Terhorst, T., Shaw, J. P., and McCurdy, S. N. (1992) Triple helix formation and cooperative binding by oligonucleotides with a 3′–3′ internucleotide junction. *Biochemistry 31,* 1603–1609.

(25) Cantor, C. R., and Tinoco, I., Jr. (1965) Absorption and optical rotary dispersion of seven trinucleoside diphosphate. *J. Mol. Biol. 13,* 65–77.

(26) Cantor, C. R., Warshaw, M. M., and Shapiro, H. (1970) Oligonucleotide interactions. III. Circular dichroism studies of the conformation of deoxyoligonucleotides. *Biopolymers 9,* 1059–1077.

(27) Asseline, U., and Thuong, N. T. (1993) Oligonucleotides tethered *via* nucleic bases: A potential new set of compounds for alternate strand triple helix formation. *Tetrahedron Lett. 34,* 4173–4176.

(28) Sung, W. L. (1981) Synthesis of 4-triazolopyrimidine nucleotide and its application in synthesis of 5-methylcytosine-containing oligodeoxyribonucleotides. *Nucl. Acids Res. 9,* 6139–6151.

(29) Rougée, M., Faucon, B., Mergny, J. L., Barcelo, F., Giovannangeli, C., Garestier, T., and Hélène, C. (1992) Kinetics and thermodynamics of triple-helix formation: effects of ionic strength and mismatches. *Biochemistry 31,* 9269–9278.

(30) Duval-Valentin, G., and Ehrlich, R. (1988) Far upstream sequences of the *bla* promoter from TN3 are involved in complexation with E. coli RNA-polymerase. *Nucl. Acids Res.* *16*, 2031–2044.

(31) Lavery, R. (1988) In *Structure and Expression, Vol. 3, DNA Bending and Curvature* (W. K. Olson, R. H. Sarma, M. H. Sarma, and M. Sundaralingham, Eds.) pp 191–211, Adenine Press, New York.

(32) Lavery, R., Zakrewska, K., and Pullman, B. (1984) Optimized monopole expansions for the representation of the electrostatic properties of the nucleic acids. *J. Comput. Chem.* *5*, 363–373.

(33) Lavery, R., Sklenar, H., Zakrewska, K., and Pullman, B. (1986) The flexibility of the nucleic acids (II): the calculation of internal energy and applications to mononucleotide repeat DNA. *J. Biomol. Struct. Dyn. 3*, 989–1014.

(34) Ouali, M., Letellier, R., Adnet, F., Liquier, J. Sun, J. S., Lavery, R., and Taillandier, E. (1993) A possible family of B-like triple-helix structures: comparison with Arnott A-like triple-helix. *Biochemistry 32*, 2098–2103.

(35) Macaya, R. F., Schultze, P., and Feigon, J. (1992) Sugar conformations in intramolecular DNA triplexes determined by coupling constants obtained by automated simulation of P. COSY cross peaks. *J. Am. Chem. Soc. 114*, 781–783.

(36) Macaya, R. F., Wang, E., Schultze, P., Sklenai, V., and Feigon, J. (1992) Proton nuclear magnetic resonance assignments and structural characterization of an intramolecular DNA triplex. *J. Mol. Biol. 225*, 755–773.

(37) Radhakrishnan, I., and Patel, D. J. (1992) Solution conformation of a G. TA triple in an intramolecular pyrimidine·purine·pyrimidine DNA triplex. *J. Am. Chem. Soc. 114*, 6913–6915.

(38) Radhakrishnan, I. and Patel, D. J. (1993) Solution structure of a purine·purine·pyrimidine DNA triplex containing G·GC and T·AT triples. *Structure 1*, 135–152.

(39) Radhakrishnan, I. and Patel, D. J. (1994) Solution strucutre of a pyrimidine· purine·pyrimidine DNA triplex containing T·AT, C+·GC and G·TA triples. *Structure 2*, 17–32.

Molecular Imprinting Approach for the Recognition of Adenine in Aqueous Medium and Hydrolysis of Adenosine 5'-Triphosphate[†]

Jainamma Mathew* and Ole Buchardt

Center for Medical Biotechnology, Chemical Laboratory II, The H. C. Ørsted Institute, University of Copenhagen, Universitetsparken 5, DK-2100 Copenhagen, Denmark. Received October 12, 1994[⊗]

Polymers capable of recognizing adenine in aqueous medium were developed by the molecular imprinting technique using methacrylic acid and 4(5)-vinylimidazole as comonomers with ethylene glycol dimethacrylate as the cross-linking agent under different polymerization conditions. The affinity of these polymers for adenine and other nucleotide bases was compared. The association constant for the binding of adenine to the polymer is calculated to be 4.3×10^3 M^{-1}. Furthermore, binding of adenosine 5'-triphosphate (ATP) to the polymers was evaluated, and an enhanced binding compared to adenine was observed. The binding of ATP is pH dependent, with the maximum around pH 3. Results have been explained based on the hydrogen bonding and ionic interactions between ATP and the ligands on the polymer matrix. The catalytic effect of these polymers for the hydrolysis of ATP is briefly discussed.

INTRODUCTION

The recognition and subsequent complementary binding between a receptor and a target molecule is the first step in many vital supramolecular processes. The design of functional polymers that can selectively recognize molecules and catalyze reactions has become an active area of research in recent years (1–5). This technique, commonly referred to as molecular imprinting, is based on creating cavities which correspond to the shape of the target molecule in a highly cross-linked polymer matrix. Briefly, the method involves preorganization of the target molecule with functional monomers followed by polymerization in the presence of a large excess of the cross-linking agent. Removal of the target molecule by extraction leaves behind functional groups in a rigid polymer matrix at defined positions in a spatial arrangement that is complementary to the target molecule. Intermolecular interactions like hydrogen bonding, dipole–dipole interactions, and ionic interactions between the target molecule and the functional groups of the polymer matrix drive the molecular recognition phenomena.

The design of receptors that can selectively recognize nucleotide bases has gained importance from the theoretical as well as the application point of view. Adenine has been well studied in this regard, especially in organic solvents (6, 7). K. J. Shea et al., by the molecular imprinting method, have made polymers that can selectively recognize and bind adenine and related molecules in nonaqueous media (8). Recent interest has focused on adenine receptors in aqueous media (9).

The present study is aimed at developing receptor sites for adenine on a polymer matrix by the molecular imprinting technique, which in addition to recognizing adenine and adenine-containing molecules in aqueous medium is designed to have functional groups that can catalyze the ATP hydrolysis.

EXPERIMENTAL PROCEDURES

Ethylene glycol dimethacrylate and methacrylic acid are Aldrich products and were purified by distillation under reduced pressure. 2,2'-Azobis(isobutyronitrile) (AIBN) (Merck) was used as such. 4(5)-Vinylimidazole was obtained by heating urocanic acid (Aldrich) as reported (10). Thymidine 5'-triphosphate, sodium salt (TTP) (Sigma), cytidine 5'-triphosphate, disodium salt hydrate (CTP) (Aldrich), guanosine 5'-triphosphate, trisodium salt hydrate (GTP) (Aldrich), ATP (Aldrich), adenosine 5'-diphosphate, sodium salt hydrate (ADP) (Aldrich), and adenosine 5'-monophosphate monohydrate (AMP) (Aldrich) were used as received. All solvents used were of HPLC grade.

UV measurements were carried out on a Hewlett Packard 8452A diode array spectrophotometer. Fourier transform infrared (FTIR) spectra were recorded on a Perkin Elmer 1760 FT-IR spectrometer.

Preparation of the Polymers. The polymers P1, P2, P3, P4, and R0 were prepared using adenine as the template molecule. The following feed composition was used for P1–P3: methacrylic acid (2.3 mmol), vinylimidazole (1.7 mmol), adenine (0.2 mmol), and ethylene glycol dimethacrylate (10.6 mmol). The composition of P4 was the same except for a higher ethylene glycol dimethacrylate content (21.2 mmol). The reference polymer P0, without adenine, was prepared with the same monomer composition as P1–P3. Another reference polymer R0 was synthesized to study the role of imidazole groups in the polymer. The initial feed composition of R0 was methacrylic acid (2.3 mmol), adenine (0.2 mmol), and ethylene glycol dimethacrylate (10.6 mmol). The solvent employed was a mixture of methanol and water (95:5 v/v). AIBN (0.3 mol % of the total monomer) was used as initiator.

In a typical experiment, adenine (25 mg) was taken in a glass vessel and methacrylic acid (200 μL) was added followed by water (100 μL), which resulted in the gradual formation of a clear solution. After the addition of a solution of vinylimidazole (0.166 g in 1 mL of methanol), ethylene glycol dimethacrylate (2 mL), AIBN (6.6 mg), and methanol (2 mL), the clear homogeneous solution was deaerated and polymerized at 65 °C for 24 h.

The polymerization mixture was deaerated by bubbling nitrogen (P0, R0, P1, and P2) or by freeze–thawing thrice

Table 1. Binding of Various Nucleic Acid Bases to Polymers[a]

substrate (0.07 mM)	substrate bound in 10 min (μmol/g of polymer)					
	P0	R0	P1	P2	P3	P4
adenine	0.40 ± 0.25	2.30 ± 0.05	0.90 ± 0.05	1.20 ± 0.04	1.40 ± 0.03	1.20 ± 0.04
adenosine	0.36 ± 0.1	0.80 ± 0.1	0.45 ± 0.07	0.65	1.05 ± 0.05	1.03
cytosine	0.25	0.23	0.02	0.21	0.35	0.22 ± 0.01
thymine	0.15	0.23	0.05	0.13	0.22	0.12

[a] Temp = 22 °C, pH = 6.0, in aqueous medium.

(P3 and P4). P0, R0, P1, and P2 were polymerized in an atmosphere of nitrogen. During polymerization of P0, R0, and P2, nitrogen was continously bubbled through the reaction mixture, while for P1 the reaction vessel above the monomer mixture was deaerated by passing nitrogen. In the case of P3 and P4, the monomer mixture was taken in a glass tube, degassed by freeze–thawing, and sealed under vacuum. The polymers obtained were wet-ground and extracted (Soxhlet) with methanol (72 h) and water (24 h), resulting in 85–90% recovery of adenine. The polymers were then washed with methanol and dried under vacuum at room temperature. The dry polymer particles were separated according to their size.

Binding Studies. Binding studies were carried out by a continuous circulation (flow) method as well as by a batch procedure. In a typical flow system, 100 mg of the polymer particles were taken in a glass column connected to a peristaltic pump. A solution of the substrate in water (20 mL) was continuously circulated through the column at a constant flow rate. Depletion in concentration of the substrate was monitored by UV spectrophotometry. In a typical experiment, upon passing through P1 (100 mg) for 10 min, the absorbance of a 0.07 mM solution of adenine decreased from 0.99 to 0.92, leading to 0.9 μmol of adenine binding/g of the polymer. In the case of very low binding, the experiment was carried out with 500 mg of polymer. For the binding of cytosine on P1, the difference in absorbance was very low (absorbance decreased from 0.430 to 0.427) due to its poor binding on P1 (0.02 μmol/g of polymer).

Batch Binding. The polymer (20 mg) was incubated with 1 mL of an aqueous solution of adenine of known concentration in an Eppendorf tube at room temperature for 24 h with constant shaking. Subsequently, the solution was filtered and centrifuged and the concentration of adenine in solution determined by UV measurements at 260 nm. Experiments were carried out with P3 and P0 at various concentrations (0.1–0.5 mM) of adenine. Solutions of adenine (0.1–0.5 mM) without polymers were examined under identical conditions as blanks.

ATP Hydrolysis. Hydrolysis of ATP using the polymer was carried out at 22 °C. A solution of ATP in water (pH adjusted to 3 with dilute HCl) was circulated through the polymer in a glass column. After definite time intervals, a known volume of the solution was analyzed by HPLC. Concentrations of ADP and AMP formed were determined by integration of the peaks on HPLC (C_{18} column: reversed phase (VYDAC), eluent: water containing 0.2% heptafluorobutyric acid, isocratic, flow rate = 1 mL/min, detection wavelength λ = 258 nm). The adsorbed ATP or ADP/AMP could be desorbed from the polymer by increasing the pH of the solution to 11 (with dilute NaOH) and circulating it through the polymer. The products of the hydrolysis, viz., ADP and AMP, were quantitated using HPLC.

In an experiment to evaluate the selectivity of the polymers for the hydrolysis of ATP, a typical polymer (P3, 50 mg) was weighed into a conical flask containing 12 mL of an aqueous solution of ATP (0.6 mM, pH 2.8) and incubated at room temperature with constant shaking for 17 h. Thereafter, (a) 2 mL of the solution was centrifuged and concentrated to 200 μL and (b) the pH of the solution was adjusted to 11 by adding dilute NaOH, incubated for another 40 min. Samples (a) and (b) were analyzed by HPLC. A solution of ATP without polymer was used as a control. A similar procedure and identical conditions were employed for TTP, GTP, and CTP.

RESULTS AND DISCUSSION

The hydrogen bonding involved in host–guest interactions is most effective in aprotic organic solvents and is limited in aqueous medium. However, cooperative binding of several weak noncovalent forces governs the antigen–antibody and protein–nucleic acid interactions. In the protein–nucleic acid interactions, the most selective binding contacts were realized to involve at least two hydrogen bonds, which require the carboxylic acid group of aspartic or glutamic acid, the amide group of asparagine or glutamine, or the guanidinium group of arginine (7). Since the major interest concerned with organic host molecules is to imitate the biological molecular recognition, we have designed polymers that can recognize adenine and adenine-containing molecules and have investigated the binding of these molecules onto the polymer matrix in aqueous medium.

The template molecule, adenine, has been preorganized with the functional monomer methacrylic acid through electrostatic interactions or H-bonding. Multiple hydrogen bond formation between carboxylic acids and adenine has been reported (7, 8, 11). Zimmerman et al. have reported the effect of protic solvents on the complexation between a receptor having a carboxylic acid moiety and adenine in chloroform; addition of 10% and 50% CD_3OD has been found to reduce the stability of the complex by ca. 2.3 kcal mol^{-1} as compared to pure $CDCl_3$ (7). In our study, the nature of the complex methacrylic acid–adenine, whether it is formed via electrostatic interactions or H-bonding, is not clear. The complex is insoluble in water; however, it is soluble in methanol. Vinylimidazole is also expected to participate in the complex formation with adenine or with methacrylic acid. Polymerization of this organized assembly with an excess of a cross-linking agent results in a very rigid polymer matrix. Removal of the template adenine from the polymer by extraction leaves behind functional groups in a spatial arrangement that is complementary to adenine. Polymer particles of size 80–150 μm were employed for these studies.

Substrate Binding and Selectivity. Rebinding of adenine from an aqueous solution was carried out under flow conditions. Equilibrium binding was achieved in about 3 min. The amount of adenine bound per gram of polymer in 10 min for different polymers is summarized in Table 1. Binding to the reference polymer P0 was carried out to account for the nonspecific interactions. Both the reference as well as the imprinted polymers P1–P3 were made with the same feed composition of the monomers, under identical conditions. In the adenine-imprinted polymers some of the functional groups are

located in microcavities complementary to the shape of adenine while remaining groups are located on the surface of these polymer particles, the latter leading to nonspecific interactions. Thus, the imprinted polymers have both specific as well as nonspecific interactions. In the reference polymer where no template was used, all the functional groups are available for nonspecific interaction.

The reference polymer (P0) exhibits a lower degree of adenine binding compared to the imprinted polymers P1, P2, and P3. This indicates that, in addition to the hydrogen bonding or electrostatic interaction between the functional groups of the polymers and adenine, microcavities corresponding to the shape of adenine are also necessary for effective binding. Dunkin et al., in their investigation of imprinted polymers with 2,6-diamino-anthraquinone as the template molecule, have observed that the polymers in addition to recognizing 2,6-diamino-anthraquinone were also effective in recognizing anthracene, suggesting that the shape of the microcavity is a dominant factor (*12*). Within the experimental error, the binding capacity of P2 for adenine (1.2 μmol/g) is higher than that of P1 (0.9 μmol/g). During the preparation of P2, nitrogen was continously bubbled through the solution; the resulting polymer has an amorphous appearance and exhibits higher adenine uptake than P1, which has a glassy appearance. Even though P2 and P3 had the same initial monomer composition, the latter exhibits higher binding capacity compared to the former. The difference may be due to the different polymerization conditions employed and the consequent changes in the morphology of the polymers. P3 and P4 were prepared with different ratios of methacrylic acid to cross-linking agent (ethylene glycol dimethacrylate). The mol % of methacrylic acid in P3 is 16% while that in P4 is 9%. The former, having a lower cross-link density, exhibits a higher binding capacity for adenine (1.4 μmol/g) than P4 (1.2 μmol/g). A similar observation has been made earlier by Sellergren in studies on separation of D,L-PheNHPh using imprinted polymers having different methacrylic acid content (*13*). An increase in the concentration of methacrylic acid up to 50 mol % has been reported to increase the capacity factor and separation factor for D,L-PheNHPh. Binding of other substrates to these polymers was also carried out under identical conditions, and the results are shown in Table 1. The binding capacity of P1 and P2 for adenosine is about 50% of that for adenine, and it lies in the range 70–80% for P3 and P4. Reduced binding implies the absence of any favorable interaction between the polymer and hydroxyl groups of adenosine. Among the different nucleic acid bases, polymers P1–P4 exhibit 7–10 times enhanced binding of adenine compared to thymine and 4–6 times compared to cytosine. Binding of adenine to P0 is only about twice as high as that of cytosine and thymine. It can be suggested that, within the experimental error, the imprinted polymers exhibit selectivity toward adenine compared to other nucleotide bases.

Binding Capacity. Binding curves showing the amount of adenine bound in 24 h (in a batch method) as a function of concentration of adenine in solution for P0 and P3 are presented in Figure 1. The initial increase in binding is followed by a saturation/leveling off, indicating that the available receptor sites have been saturated with adenine. The association constant (K_{assoc}) for the binding of adenine to the polymer and the number of accessible sites (N) on the polymer have been calculated using the modified Scatchard equation (*13*):

$$1/K = C_f/N + (1/K_{assoc})N$$
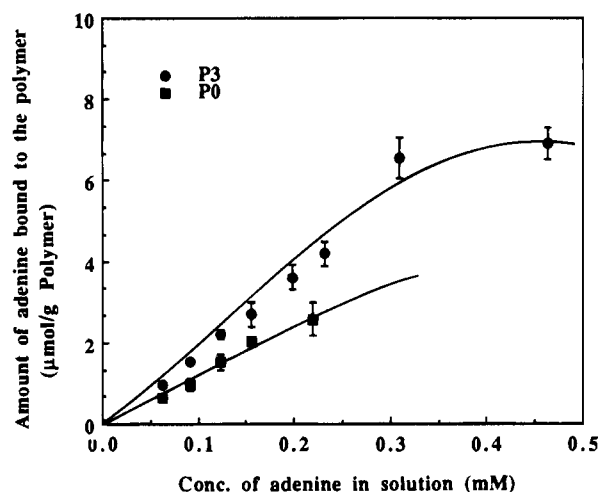
Figure 1. Concentration dependence of adenine binding in a batch process at 22 °C. Polymer (20 mg) was incubated with a solution of adenine (1 mL) for 24 h. Amount of adenine bound to the polymer was evaluated from the difference in absorbance of the solution before and after incubation. Each value is given as the average of 4 independent experiments.
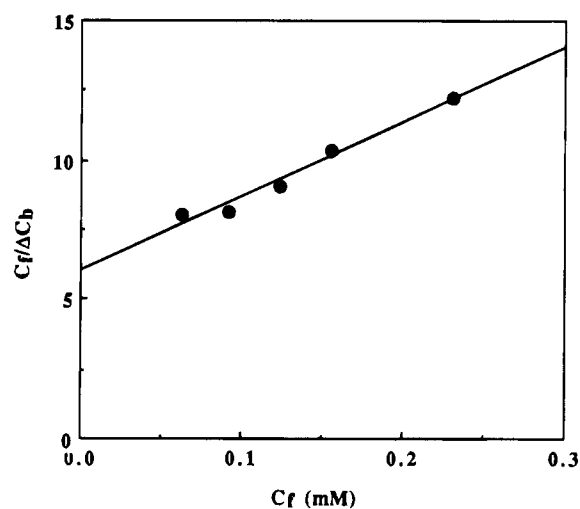
Figure 2. Modified Scatchard plot for the binding of adenine (data compiled from the values in Figure 1).

where K ($=C_b/C_f$) is the distribution constant for the solute between the polymer and solution, C_b is the concentration of solute bound to the polymer, and C_f is that of free solute in solution. In order to account for the nonspecific interactions, the amount of adenine bound to the reference polymer (P0) was subtracted from that bound to P3, and the resulting $1/K$ ($=C_f/\Delta C_b$) is plotted versus C_f. A linear plot is obtained with an intercept (Figure 2). The number of accessible sites has been calculated to be 1.86 μmol/g of polymer. The association constant K_{assoc} calculated from the slope and intercept is 4.3×10^3 M^{-1}. This value is significantly lower than that calculated by K. J. Shea et al., for a similar system in nonaqueous medium (*8*). However, considering the fact that these experiments have been carried out in aqueous medium where water effectively competes for the hydrogen bonding interactions, the observed association constant indicates an appreciable degree of receptor–ligand interaction. The binding strength calculated ($-\Delta G° = RT \ln K$) is about 4.9 kcal mol^{-1}. A recent study on the binding of adenosine derivatives to water-soluble adenine receptors has shown the association constants of 9-ethyl-adenine, adenosine, and 2',3'-cAMP to be 200, 150, and 660 M^{-1}, respectively (*9*). A relatively higher degree of binding in the present system may be attributed to
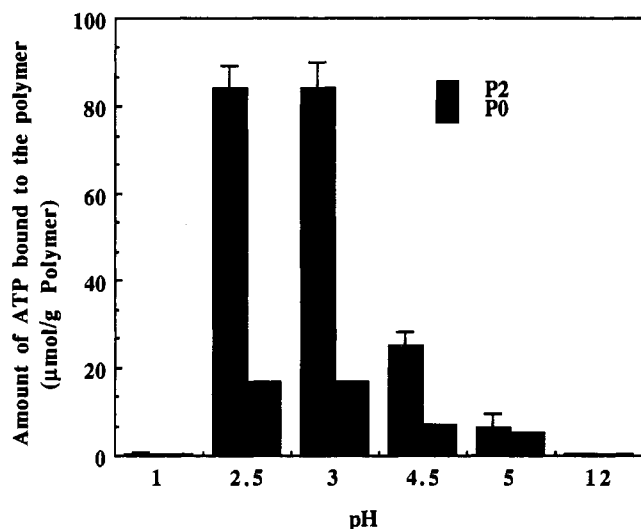
Figure 3. Variation in binding of ATP as a function of pH. A solution of ATP (20 mL, 0.5 mM), after adjusting the pH with dilute HCl, was circulated through a column containing 0.1 g of polymer for 30 min. The amount bound is calculated from the depletion in concentration of ATP in solution as measured from the difference in UV absorbance. Data are the average of 6 separate experiments.

Table 2. Influence of pH on the Binding of Nucleoside Triphosphates[a]

substrate (0.08 mM)	substrate binding (μmol/g of polymer)			
	P0		P1	
	pH x	pH 3	pH x	pH 3
ATP	0.8	9.4	1.7	18.2
GTP	0	9.6	0	10.1
CTP	0.8	3.5	1.7	6.2
TTP	0	13.7	0.2	10.7

[a] x is the pH of a solution of the substrate in water: ATP, x = 4.8; GTP, x = 5.6; CTP, x = 4.8; TTP, x = 6.2.

Table 3. pH-Dependent Variation in Binding of Adenine

time (min)	adenine uptake (μmol/g of polymer)					
	P0		P1		P3	
	pH 6	pH 3	pH 6	pH 3	pH 6	pH 3
1	0.42	0.52	0.29	0.43	1.50	0.52
3	0.81	0.12	0.90	0.50	1.40	1.08
5	0.75	0.04	0.95	0.13	1.33	0.80
10	0.73	0.01	0.90	0.08	1.39	0.16
15	0.78	0.01	0.98	0.06		
20	0.78	0.01	0.95	0.04		

[a] [Adenine] = 0.07 mM, temp = 22 °C, in aqueous medium.

simultaneous multiple interactions of adenine with the functional groups of the polymer. Unlike a homogeneous receptor or a small molecular nonhomogeneous receptor, a polymeric receptor offers additional stability to the receptor—ligand complex through its unique macromolecular properties and the cooperative functional group interactions.

ATP Binding and Hydrolysis. These polymers consisting of binding sites for adenine and nucleophilic catalytic groups (imidazole) can be visualized as enzyme mimicking polymers, as the imidazole group, similar to the histidine moieties in an enzyme, may participate in the catalytic reactions. Esterolytic activity of polymer-bound imidazoles toward activated esters such as *p*-nitrophenyl acetate, hexanoate, etc., has been reported (*14—16*). However, in the present study, the imidazole groups present in the polymer matrix did not exhibit any measurable hydrolysis of the diester of the polymer as evidenced by the virtually identical FT-IR spectra of the dry polymers before and after incubation with water at pH 2.5 for 48 h. This may be due to the relatively low imidazole content of the polymer. Even though the feed ratio of vinylimidazole to ethylene glycol dimethacrylate was 1:5, due to the lower reactivity of the former toward radical polymerization, the extent of incorporation in the polymer chain is very low compared to that of ethylene glycol dimethacrylate. Furthermore, control experiments carried out with a solution of ethylene glycol dimethacrylate and vinylimidazole in methanol—water (4:1 and 20:1 v/v) did not exhibit ester hydrolysis as followed by HPLC, excluding the possibility of any hydrolysis during polymerization. Here, we report on the catalytic effect of these polymers on the hydrolysis of ATP. Two of the phosphate bonds of ATP are extremely labile and on hydrolysis release about 7—9 kcal/mol (*17*). Binding of ATP to the polymer has been carried out under flow conditions. Compared to the reference polymer P0, the adenine-imprinted polymers show a higher ATP uptake. The binding of ATP by the polymer was pH dependent, with the maximim at about pH 3 (Figure 3). The ATP uptake at pH 2.5—3 is 8—10 times higher than that at pH 5 (pH of a 0.5 mM solution of ATP in water). A similar pH dependence has been observed for TTP, GTP, and CTP (Table 2). Consistently, the uptake at pH 3 is

about 10 times more for TTP, GTP, and CTP than that at the pH of each substrate in water. Such a pH-dependent variation in binding is indicative of ionic interactions between the polymer and the substrate (e.g., ATP). The functional groups of the polymer, viz., carboxyl and imidazole, may contribute to the ionic interaction. The influence of pH on the binding of adenine has also been studied by following adenine uptake as a function of time (continuous flow system) at pH 3 and 6; the results are presented in Table 3. In addition to relatively low maximum binding, the bound adenine desorbs at a faster rate at pH 3. This observation excludes any positive contribution of ionic interactions between the functional groups of the polymer and adenine to the enhanced ATP uptake at pH 3. Furthermore, other substrates such as TTP, GTP, and CTP also exhibit an enhanced binding at pH 3. Hence, the ionic interactions between phosphate groups and the carboxyl and/or imidazole groups of the polymer matrix may be the driving force. The role of imidazole in such interactions was investigated by following the pH-dependent binding of ATP to the reference polymer R0, which was made with only methacrylic acid as the comonomer and no vinylimidazole. As expected, no enhancement in binding occurred at low pH, suggesting that the ionic interactions between the imidazole groups of the polymer and phosphate groups are major contributing factors for the enhanced ATP uptake at pH 3. Even though a satisfactory explanation is difficult at this stage, it may be due to the pH-dependent protonation/deprotonation of ATP and its influence on the ionic interaction and hydrogen bonding. At around pH 3, the negative charges on phosphate groups are partially neutralized by protonation; in addition, the adenine ring is also protonated (*18*). Hence, at this pH, in addition to binding through specific recognition of adenine, there may be an enhanced complex formation via ionic interaction between the partially ionized phosphate groups of ATP and the imidazolium cation on the polymer. Further decrease in pH affects the ATP binding adversely. At low pH, all negative charges on phosphate groups are neutralized by protonation, decreasing the extent of ionic interactions (*18*). Y. Kato et al., in their studies on the interaction of cyclic AMP with water-soluble adenosine receptors, have observed significantly higher binding of cyclic AMP to
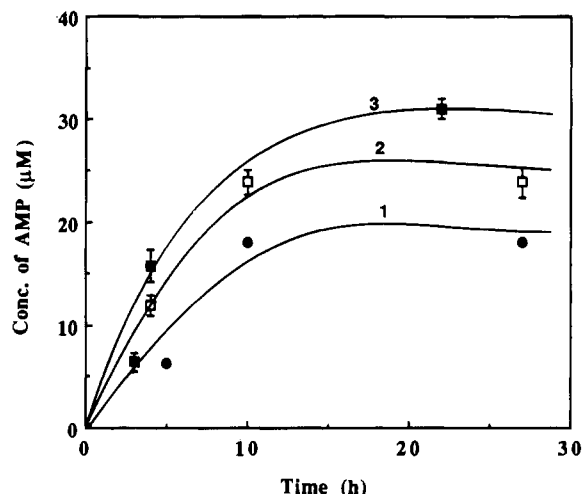
Figure 4. Concentration of AMP produced during the hydrolysis of ATP with P2 (0.1 g) as a function of time. (Initial concn of ATP: **1**, 45 μM; **2**, 90 μM; and **3**, 180 μM.) Initial pH of the solution = 3.0. Each value is the average of 3 experiments.

the receptor having a guanidinium moiety, which was attributed to the phosphate–guanidinium interaction resulting from both hydrogen bonding and electrostatic interactions (*9*). Under the present experimental conditions, during the initial 2 h of reaction, the product of hydrolysis was mainly ADP. Prolonged reaction resulted in formation of both ADP and AMP. (Separate experiments carried out under similar conditions have further shown that these polymers catalyzed the hydrolysis of ADP.) Hydrolysis has been carried out at different ATP concentrations, and the hydrolytic pattern is shown in Figure 4. In the HPLC analysis of the reaction mixture, peaks due to ATP and ADP were not well resolved. Hence, an accurate quantitation of the ADP content was difficult. The amount of AMP produced as a function of reaction time is shown in Figure 4. The extent of hydrolysis increased with an increase in the initial ATP concentration. Furthermore, increase in reaction time enhanced the degree of hydrolysis (AMP content) up to about 10 h, followed by the reaction reaching saturation, within experimental error. The reference polymer P0 exhibited hydrolysis only to a significantly lower extent (at [ATP] = 90 μM, the concentration of AMP obtained in 10 h was only 7 μM). R0, which was designed to have no imidazole groups, did not cause ATP hydrolysis. Selectivity toward ATP hydrolysis was determined in comparison with other triphosphates, viz., TTP, GTP, and CTP. Hydrolysis of TTP was less than 5%, and within experimental error, the hydrolysis of GTP and CTP was negligible. Procedures (a) and (b) employed for product analysis gave agreeable results. Suzuki et al. have investigated the mechanism of nonenzymatic hydrolysis of ATP by polyamines and polyimines (*17*). The maximum rate of hydrolysis was observed at around pH 3.0 and was attributed to the protonated imino nitrogens, forming a complex with ATP and favoring the hydrolysis of the latter. Similarly, the present study reflects that the imidazole groups of the polymer favor the hydrolysis of ATP either by a nucleophilic mechanism or by activating the attack by a water molecule. We have extended this approach to the recognition of deoxyoligonucleic acids containing adenine, and the results will be presented in due course.

ACKNOWLEDGMENT

LITERATURE CITED

(1) Wulff, G., and Schauhoff, S. (1991) Racemic resolution of free sugars with macroporous polymers prepared by molecular imprinting. Selectivity dependence on the arrangement of functional groups versus spatial requirements. *J. Org. Chem. 56*, 395–400.

(2) Vlatakis, G., Andersson, L. I., Müller, R., and Mosbach, K. (1993) Drug assay using antibody mimics made by molecular imprinting. *Nature 361*, 645–647.

(3) Robinson, D. K., and Mosbach, K. (1989) Molecular imprinting of a transition state analogue leads to a polymer exhibiting esterolytic activity. *J. Chem. Soc., Chem. Commun.*, 969–970.

(4) Beach, J. V., and Shea, K. J. (1994) Designed catalysts. A synthetic network polymer that catalyzes the dehydrofluorination of 4-fluoro-4-(p-nitrophenyl)butan-2-one. *J. Am. Chem. Soc. 116*, 379–380.

(5) Dhal, P. K., and Arnold, F. H. (1992) Metal-coordination interactions in the template-mediated synthesis of substrate-selective polymers: Recognition of bis(imidazole) substrates by copper(II) iminodiacetate containing polymers. *Macromolecules 25*, 7051–7059.

(6) Williams, K., Askew, B., Ballester, P., Buhr, C., Jeong, K. S., Jones, S., and Rebek, J., Jr. (1989) Molecular recognition with convergent functional groups. 7. Energetics of adenine binding with model receptors. *J. Am. Chem. Soc. 111*, 1090–1094.

(7) Zimmerman, S. C., Wu, W., and Zeng, Z. (1991) Complexation of nucleotide bases by molecular tweezers with active site carboxylic acids: Effects of microenvironment. *J. Am. Chem. Soc. 113*, 196–201 and references therein.

(8) Shea, K. J., Spivak, D. A., and Sellergren, B. (1993) Polymer complements to nucleotide bases. Selective binding of adenine derivatives to imprinted polymers. *J. Am. Chem. Soc. 115*, 3368–3369.

(9) Kato, Y., Conn, M. M., and Rebek, J., Jr. (1994) Water-soluble receptors for cyclic-AMP and their use for evaluating phosphate–guanidinium interactions. *J. Am. Chem. Soc. 116*, 3279–3284.

(10) Overberger, C. G., and Vorchheimer, N. (1963) Imidazole-containing polymers. Synthesis and polymerization of the monomer 4(5)-vinylimidazole. *J. Am. Chem. Soc. 85*, 951–955.

(11) Lancelot, G. (1977) Hydrogen bonding between nucleic acid bases and carboxylic acids. *J. Am. Chem. Soc. 99*, 7037–7042.

(12) Dunkin, I. R., Lenfeld, J., and Sherrington, D. C. (1993) Molecular imprinting of flat polycondensed aromatic molecules in macroporous polymers. *Polymer 34*, 77–84.

(13) Sellergren, B. (1989) Molecular imprinting by noncovalent interactions. Enantioselectivity and binding capacity of polymers prepared under conditions favoring the formation of template complexes. *Makromol. Chem. 190*, 2703–2711.

(14) Overberger, C. G., and Moritomo, M. (1971) Conformational effects and nonpolar interactions in poly[4(5)-vinylimidazole]-catalyzed solvolyses of neutral substrates. *J. Am. Chem. Soc. 93*, 3222–3228.

(15) Guthrie, J. P. (1972) Aggregation of p-nitrophenyl alkanoates in aqueous solution: A caution concerning their use in enzyme model studies. *J. Chem. Soc., Chem. Commun.*, 897–899.

(16) Leonhardt, A., and Mosbach, K. (1987) Enzyme-mimicking polymers exhibiting specific substrate binding and catalytic functions. *React. Polym. 6*, 285–290.

(17) Suzuki, S., Higashiyama, T., and Nakahara, A. (1973) Nonenzymatic hydrolysis reactions of adenosine 5'-triphosphate and its related compounds. 1. Hydrolysis reactions of ATP with some continous-chain polyamines. *Bioorg. Chem. 2*, 145–154.

(18) Saenger, W. (1984) *Principles of Nucleic Acid Structure* (Charles R. Cantor, Ed.) Springer Advanced Texts in Chemistry, Springer-Verlag.

Competitive Indirect ELISA for Ceftiofur Sodium and the Effect of Different Immunizing and Coating Antigen Conjugates

Beate G. Rose,* Carol Kamps-Holtzapple, and Larry H. Stanker

Food Animal Protection Research Laboratory, Agricultural Research Service, United States Department of Agriculture, 2881 F&B Road, College Station, Texas 77845. Received March 24, 1995⊗

Ceftiofur sodium is a broad spectrum, β-lactamase-resistant cephalosporin. Ceftiofur and desfuroyl-ceftiofur were used to develop competitive indirect enzyme-linked immunosorbent assays (CI-ELISA) for the determination of ceftiofur sodium. Hapten–protein conjugates were made using three different carrier proteins and three methods of conjugation. The first two methods use the free amine of ceftiofur as the site of conjugation, and coupling to bovine serum albumin and ovalbumin was achieved by using two different cross-linking reagents. The third conjugation procedure joins the hydrolyzed form of ceftiofur, desfuroylceftiofur, to the maleimide-activated carrier proteins, bovine serum albumin and keyhole limpet hemocyanin. A variety of immunization schedules is presented to show the effect of repeated immunizations on antibody maturation. Serum antibody levels were evaluated for each conjugation method using both homologous and heterologous conjugates as antigens. All of the immunogens resulted in the generation of anticeftiofur antibodies. The heterologous assay systems on average yielded more sensitive assays, but antisera obtained from all three immunogens were used successfully in developing enzyme-linked immunosorbent assays (ELISA's) for ceftiofur. Ceftiofur was detected in mouse sera in a concentration range of 3–500 ppb. The results illustrate that the method used to couple the hapten to a carrier protein as well as the site of coupling significantly influence the resulting enzyme-linked immunosorbent assays (ELISA's).

INTRODUCTION

Ceftiofur sodium (Figure 1) is a broad-spectrum, β-lactamase-resistant cephalosporin. Ceftiofur exhibits excellent antimicrobial activity by virtue of its 2-(2-aminothiazol-4-yl)-2-(methoxyimino)acetamide substituent at the C-7 position of the cephem nucleus (Labeeuw and Sahli, 1984; Yancey *et al.,* 1987). Ceftiofur has been approved by the FDA and is used for the treatment of respiratory diseases in cattle and horses (FDA, 1988, 1991).

Current detection methods for cephalosporins include HPLC procedures (Rouan, 1985) and biological assays (Wise *et al.,* 1980). Recent HPLC methods for ceftiofur can detect 0.5 ppm ceftiofur equivalents (Jaglan *et al.,* 1990; Gilbertson *et al.,* 1990). Other methods for the detection of ceftiofur include agar gel diffusion (Cervantes *et al.,* 1993; Owens *et al.,* 1990), Delvotest-P, which is a colorimetric bacterial inhibition test (Jaglan *et al.,* 1992; Owens *et al.,* 1990), the *Bacillus stearothermophilus* disk assay, the Charm test II, which is a receptor-binding assay (Jaglan *et al.,* 1992), and a cylinder-plate microbiological assay (Jaglan *et al.,* 1992; Gilbertson *et al.,* 1990). These tests require labor-intensive sample preparations, lengthy data acquisition times and in some cases costly and sophisticated equipment.

New simplified methods for detection of ceftiofur are desirable to speed analysis times, reduce expense, and decrease the use of organic solvents. Immunoassays meet these criteria. An increasing number of immunoassays that detect and quantify drugs and pesticides have been reported (Bekheit *et al.,* 1993a, 1993b; Goodrow *et al.,* 1990; Karu *et al.,* 1994; Krämer, *et al.,* 1994; Lucas *et al.,* 1993; Marco *et al.,* 1993; Schneider *et al.,* 1994; Vanderlaan *et al.,* 1991). In this paper we describe a CI-ELISA useful for detecting ceftiofur sodium. Antibodies were produced using ceftiofur and desfuroyl ceftiofur
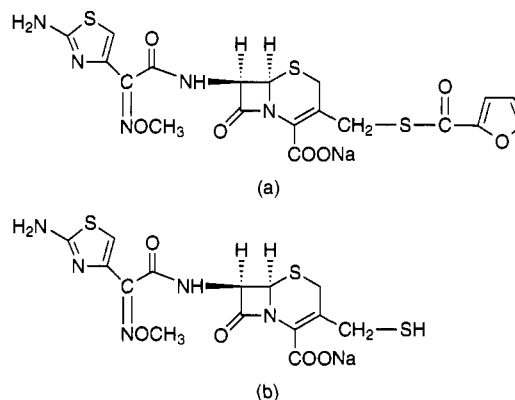
Figure 1. Structures of (a) ceftiofur sodium and (b) desfuroyl-ceftiofur sodium.

protein conjugates as immunogens, and these antibodies did not cross-react with similarly structured cephalosporins. The present paper describes the use of different linkage chemistries to conjugate ceftiofur to proteins. The quality of the resulting polyclonal antibodies is discussed in relation to the linkage chemistry used to produce the immunogen and the plate coating antigen.

MATERIALS AND METHODS

Reagents and Equipment. Ceftiofur sodium was kindly donated by The Upjohn Co. (Kalamazoo, MI). Cefteram sodium and ceftriaxone sodium were kindly donated by Hoffmann-La Roche, Inc. (Nutley, NJ). Cefuroxime sodium and ceftazidime pentahydrate were kindly donated by Glaxo Manufacturing Services Ltd. (Barnard Castle, County Durham, England). RIBI adjuvant was purchased from RIBI ImmunoChem Research, Inc. (Hamilton, MT). Bovine serum albumin (BSA), ovalbumin (OVA), goat anti-mouse immunoglobulin G conjugated to horseradish peroxidase, polyoxyethylene sorbitan monolaurate (Tween 20), and glacial

Table 1. Immunization and Bleeding Protocol

day of immunization or bleed	OVA–S–SMPB–Cef 0.1 mg/0.1 mL in Freund's adjuvant	OVA–S–GMBS–Cef 0.05 mg/0.1 mL in Freund's adjuvant	KLH–SMCC–desCef 0.1 mg/0.2 mL in Ribi adjuvant
1	0.05 mL/footpad	0.1 mL/footpad	0.2 mL ip
14			0.2 mL ip
23	0.1 mL ip	0.1 mL ip	
28			0.2 mL ip
37	0.1 mL ip	0.1 mL ip	
43			0.2 mL ip
50			bleed[a]
149	0.1 mL tail vein	0.1 mL tail vein	
156	bleed[a]	bleed[a]	
163			0.2 mL ip[b]
170			bleed[a]
260	0.1 mL ip[b]		
267	bleed[a]	0.1 mL ip[c]	
274		bleed[a]	

[a] Tail vein bleed. [b] Solution prepared in PBS-B.

acetic acid were purchased from Sigma Chemical Co. (St. Louis, MO). Sulfosuccinimidyl 4-(p-maleimidophenyl)-butyrate (s-SMPB), N-[(γ-maleimidobutyryl)oxy]sulfo-succinimide ester (s-GMBS), keyhole limpet hemocyanin (KLH), maleimide-activated BSA (BSA–SMCC), and maleimide-activated KLH (KLH–SMCC), were purchased from Pierce (Rockford, IL). Nunc-Immunoplates, Maxisorp F96, were purchased from PGC Scientifics (Gaithersburg, MD). K-Blue substrate was purchased from Elisa Technologies (Lexington, KY). Titan nondenaturing high-resolution agarose gels, cooling platform, gel box, running buffer (pH 8.8), and gel stain (Coomassie Blue) were obtained from Helena Laboratories (Beaumont, TX). Thin-layer chromatography was performed on precoated silica gel 60 F_{254} plates 0.2 mm from Riedel-de Häen (Gibbstown, NJ). Iscove's media, fetal bovine serum, penicillin/streptomycin solution, and complete Freund's adjuvant were obtained from GIBCO (Grand Island, NY). Balb/c mice were obtained from Harlan Sprague–Dawley (Houston, TX). A Bio-Rad Model 3550 microplate reader with software version 4.3 and reader-driver software 1.0 application program were obtained from Bio-Rad Laboratories (Hercules, CA).

Carrier Proteins. BSA and OVA were thiolated using 2-iminothiolane hydrochloride (Traut's reagent). Typically, 66 mg of BSA or 44 mg of OVA in 2.2 mL of dilute phosphate-buffered saline, PBS-A (0.05 M sodium phosphate, 0.075 M sodium chloride, 0.1 M EDTA in deionized water, pH 7.2), and a 3× molar excess of Traut's reagent dissolved in 20 μL of the same buffer were added together. The resulting mixtures were stirred overnight at ambient temperature. The thiolated BSA (BSA–SH) and thiolated OVA (OVA–SH) were dialyzed for several days against PBS-A. The maleimide-activated BSA and KLH were activated by the manufacturer using the cross-linking reagent sulfosuccinimidyl 4-(N-maleimidomethyl)cyclohexane-1-carboxylate (s-SMCC).

Hapten–Protein Conjugates. Ceftiofur was conjugated to BSA, OVA, BSA–SMCC, and KLH–SMCC by the following procedures.

Preparation of Ceftiofur–SMPB Conjugates. Ceftiofur sodium (82 mg) was dissolved in 500 μL of PBS-A, and 10 mg of s-SMPB in 20 μL of DMF was added. The resulting mixture was stirred for 10–15 min, added dropwise to 30 mg of BSA–SH (1.5 mL of a 20 mg/mL stock solution), stirred overnight at ambient temperature, and then dialyzed exhaustively against PBS-A. Similarly, 52 mg of ceftiofur sodium in PBS-A and 5 mg of s-SMPB in 20 μL of DMF were added dropwise to 20 mg of OVA-SH (1 mL of a 20 mg/mL stock solution), and the mixture was stirred overnight at ambient temperature

and dialyzed exhaustively against PBS-B (0.05-M sodium phosphate, 0.075-M sodium chloride in deionized water, pH 7.2). These conjugates were abbreviated as BSA–S–SMPB–Cef and OVA–S–SMPB–Cef, respectively.

Preparation of Ceftiofur–GMBS Conjugates. Ceftiofur–GMBS conjugates were prepared as described above except that s-SMPB was substituted for s-GMBS. These conjugates were abbreviated as BSA–S–GMBS–Cef and OVA–S–GMBS–Cef, respectively.

Preparation of Desfuroylceftiofur and Desfuroylceftiofur–SMCC Conjugates. The hydrolysis of ceftiofur was followed with slight modification according to the literature (Chapman and Owen, 1950). Potassium carbonate (30 mg) was dissolved in PBS-A (100 μL) and added to a solution of ceftiofur sodium (50 mg) in methanol (1 mL) and N,N-dimethylformamide (DMF, 40 μL). The reaction mixture was stirred overnight under an argon atmosphere to ensure complete hydrolysis of the furan ring (checked by TLC, $CHCl_3$–MeOH 1:1, developed in iodine). Evaporated solvents were replenished by addition of 500 μL of PBS-A. Following this, 1.5 N HCl was added to adjust the pH to 7. The solution containing the desfuroyl ceftiofur was then added dropwise to 1 mL of BSA–SMCC (5 mg/mL stock solution in deionized water) or 1 mL of KLH–SMCC (5 mg/mL stock solution in deionized water), stirred overnight in the cold and subsequently dialyzed against PBS-A and PBS-B, respectively. These conjugates were abbreviated as BSA–SMCC–desCef and KLH–SMCC–desCef, respectively.

All hapten–carrier protein conjugates were analyzed by nondenaturing gel electrophoresis (Kamps-Holtzapple et al., 1993).

Immunization and Bleeding Protocol. Female Balb/c mice were immunized with OVA conjugates of ceftiofur sodium, OVA–S–SMPB–Cef, OVA–S–GMBS–Cef, and the KLH conjugate of desfuroyl ceftiofur, KLH–SMCC–desCef, respectively, as outlined in Table 1. OVA–S–SMPB–Cef and OVA–S–GMBS–Cef were emulsified in complete Freund's adjuvant (1:1) and were injected into the hind footpads (50 μL, containing 50–100 μg of the conjugate). Subsequent injections were intraperitoneal (ip). Mice were immunized, boosted, and bled over a 274 day time period.

KLH–SMCC–desCef was suspended in Ribi adjuvant as recommended by the manufacturer and injected ip (50–100 μg). Subsequent injections were given ip using the same RIBI antigen preparation. Mice were immunized, boosted, and bled over a 170 day time period.

Mice were bled through the tail vein, and approximately 0.5 mL of blood was collected in 2 mL Eppendorf tubes, which were centrifuged in a microcentrifuge to

afford approximately 100 μL of blood serum. Blood sera were stored at 4 °C in 0.02% sodium azide.

Enzyme-Linked Immunosorbent Assay (ELISA). Ninety-six-well microtiter immunoplates were washed three times with a solution of 0.05% Tween 20 in deionized water and then coated with 100 ng/well (in 100 μL) of the coating antigens. The coating antigens used were BSA−S−SMPB−Cef (7 mg/mL stock solution), BSA−S−GMBS−Cef (18 mg/mL stock solution), and BSA−SMCC−desCef (5 mg/mL stock solution). They were diluted in deionized water and added to the wells, and the plates were dried overnight at 37 °C. The plates were subsequently washed three times with phosphate-buffered saline, PBS-9 (0.01-M sodium phosphate, 0.15 M sodium chloride in deionized water, pH 9), and the unbound active sites were blocked by addition of 200 μL/ well of 3% nonfat dry milk in PBS-9 for 30 min at 37 °C. The plates were then washed three times with PBS-9, 100 μL of dilute serum from the immunized mice was added, and the plates were incubated for 60 min at 37 °C. Unbound antibody was removed by washing five times with a solution of 0.05% Tween 20−water. Next, 50 μL of goat anti-mouse IgG−peroxidase conjugate (1: 500 dilution in assay buffer, AB, 0.1 M Tris, 0.15 M sodium chloride, 0.01% nonfat milk in deionized water, pH 7.75) was added followed by incubation of the plates at 37 °C for 60 min. Finally, the plates were washed five times with 0.05% Tween 20 solution, and 100 μL of K-Blue substrate was added to determine the bound-antibody−peroxidase conjugate. The plates were read at 655 nm using a 96-well plate reader, and data were collected on a Macintosh IIsi computer (Apple, Inc., Cupertino, CA).

Competitive Indirect Enzyme-Linked Immunosorbent Assay (CI-ELISA). Ninety-six-well microtiter immunoplates were coated with 100 μL of the coating antigens, BSA−S−SMPB−Cef, BSA−S−GMBS−Cef, or BSA−SMCC−desCef, as described above. Ceftiofur sodium, cefteram sodium, ceftriaxone sodium, cefuroxime sodium, and ceftazidime pentahydrate were used as competitors. Typically, the substance acting as competitor was dissolved in AB to give a solution corresponding to a final concentration of 100 ng/well in column 2 of the 96-well microtiter plates. The competitor was then serially diluted (1:2) across the plates. Columns 1, 11, and 12 were used as controls and therefore did not contain any competitor. The anti-ceftiofur serum (100 μL, diluted to a level representing approximately 50% maximum activity in a direct binding ELISA) was added to columns 2−12, and the plates were incubated for 60 min at 37 °C. Subsequent treatment of the plates and analysis of the data were done as described above.

RESULTS

Hapten Design. A wide variety of heterobifunctional cross-linking reagents are available to link small molecules (haptens) with various functional groups to carrier proteins. Ceftiofur was linked to carrier proteins through its free amine group *via* a heterobifunctional NHS−ester cross-linking reagent, s-SMPB, which is 14.5 Å in length. A covalent amide bond is formed when the NHS−ester reagent reacts with the primary amine group, subsequently releasing *N*-hydroxysuccinimide. Sulfhydryl groups react specifically with the maleimide portion of the heterobifunctional cross-linker at physiological pH. BSA and OVA were modified with Traut's reagent to convert all of the amine groups to free sulfhydryl groups for this purpose. A representative reaction scheme is shown in Figure 2. The furoic acid group in ceftiofur was hydrolyzed to afford a thiol, desfuroylceftiofur, thus

providing an alternate site for conjugation. The presence of the thiol group could easily be determined by TLC developed in iodine, a simple technique which shows thiols as bleached white spots and disulfides as brown spots (Brown and Edwards, 1968). Upon prolonged exposure to air, the bleached spots turn brown as the thiols oxidize. Once the presence of the desfuroylceftiofur was verified, the reaction mixture was neutralized and added to BSA−SMCC and KLH−SMCC (s-SMCC is 11.6 Å in length) at physiological pH (Figure 3). This is necessary since the reaction of amines with the maleimide ring predominates at higher pH values (Smyth *et al.*, 1964). In this case the free amine on ceftiofur would interfere with the desired conjugation. EDTA was included in the coupling buffer to prevent oxidation of the thiol group. In the case of the immunogen, EDTA was removed by exhaustive dialysis in phosphate buffer. Figure 4 shows the nondenaturing gel analysis of KLH (lane 1), SMCC-modified KLH (lane 2), and the immunogen, KLH−SMCC−desCef (lane 3). Conjugating desfuroylceftiofur to activated KLH introduces negative charges onto the protein at each site of conjugation due to addition of the negatively charged carboxylic acid group on desfuroylceftiofur. Thus, the desfuroylceftiofur−protein conjugate possesses a more negative net charge than KLH alone, and the conjugate migrates further in the gel toward the anode than does KLH or KLH treated with the cross-linker alone. All the conjugates were analyzed by this method to obtain qualitative evidence that the hapten had indeed been conjugated to the carrier proteins.

Immunization and Immune Response. Balb/c mice were immunized using immunogens prepared in RIBI and Freund's adjuvants, applying different immunization techniques in order to maximize the immune response to the injected immunogen. The immunization schedules are summarized in Table 1. Immunizations with OVA−S−SMPB−Cef prepared in RIBI according to the immunization schedule as suggested by the manufacturer did not result in production of the required antibodies to ceftiofur when serum was analyzed after the second immunization (data not shown). However, after a 5 month resting period two mice were boosted and rebled. Sera from these mice was used in a CI-ELISA and resulted in IC_{50} values of 0.1 and 0.16 ppm, respectively (data not shown). On the basis of these preliminary results, mice were immunized with OVA−S−SMPB−Cef and OVA−S−GMBS−Cef prepared in Freund's adjuvant on days 1, 23, and 37 (Table 1). The animals were rested for a period of approximately 5 months, after which they were boosted and bled. The activity of the antisera was evaluated in a titration ELISA using different plate-coating antigens. The dilution of the antisera which corresponded to 50% of the maximum activity in the titration ELISA was then chosen for the CI-ELISA. The resulting IC_{50} values from the competition against ceftiofur are outlined in Table 2. The immunogen of desfuroylceftiofur, KLH−SMCC−desCef, considered to be the more stable conjugate in animal tissue, was prepared in RIBI adjuvant, and antisera were tested on day 50 (Table 2) and subsequently on day 170 (Table 3).

Competitive Inhibition ELISA. When the OVA−S−SMPB−Cef immunogen was tested on a homologous plate system (BSA−S−SMPB−Cef antigen), IC_{50} values ranged from 50 to 150 ppb, whereas a more sensitive assay was obtained using a heterologous plate assay (BSA−S−GMBS−Cef antigen) with IC_{50} values ranging from 25−50 ppb. The sensitivity of the antisera obtained from OVA−S−GMBS−Cef immunized mice was greatly increased, from an IC_{50} of 400−700 ppb to an IC_{50} of 15−
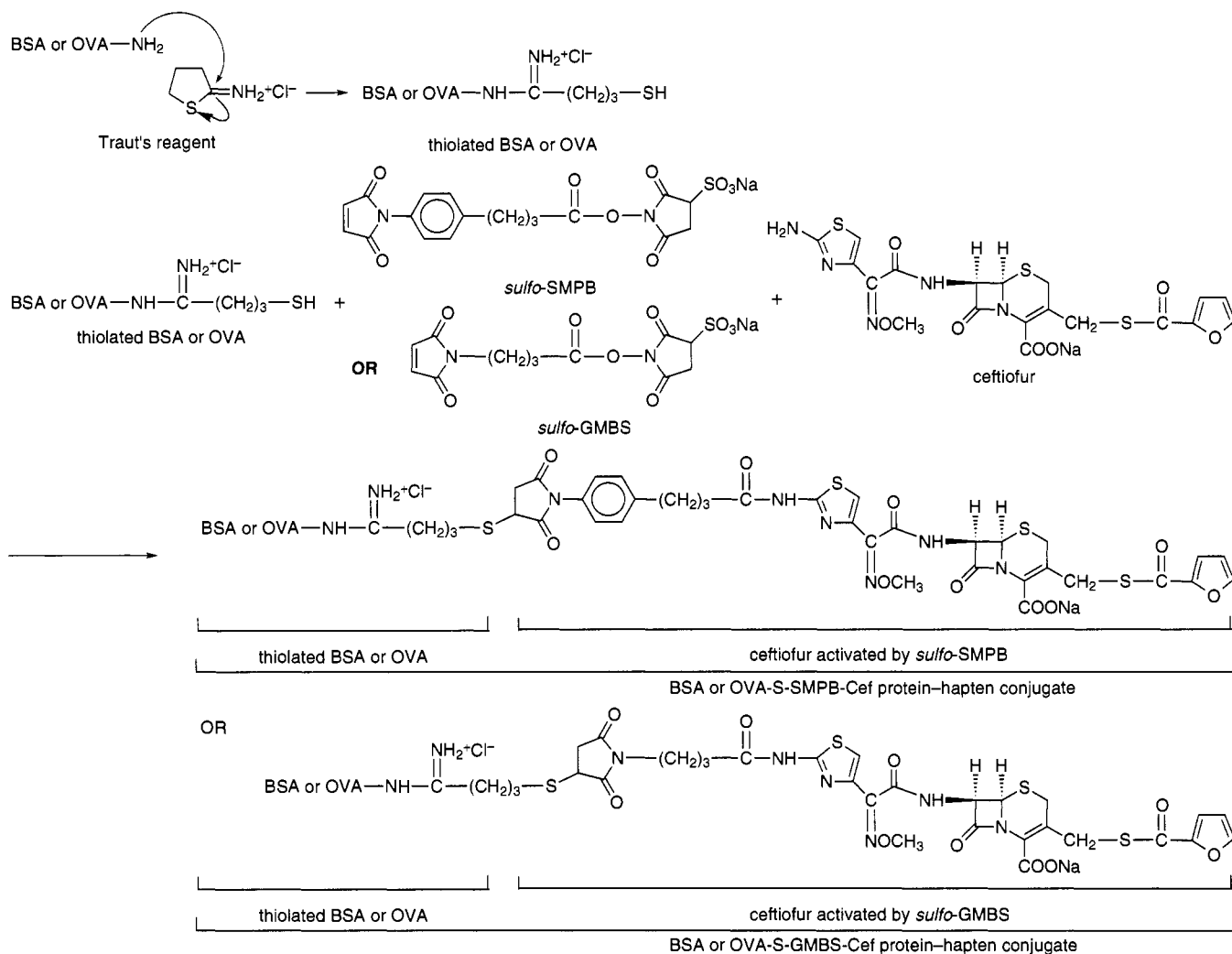
Figure 2. BSA or OVA activated with Traut's reagent to give thiolated BSA or OVA. The amine group on ceftiofur was activated with the heterobifunctional cross-linking reagents sulfo-SMPB and sulfo-GMBS. Thiolated BSA or OVA reacted with the maleimide portion of the cross-linking reagents to produce the BSA−S−SMPB−Cef and BSA−S−GMBS−Cef protein−hapten conjugates and the corresponding OVA−hapten conjugates.
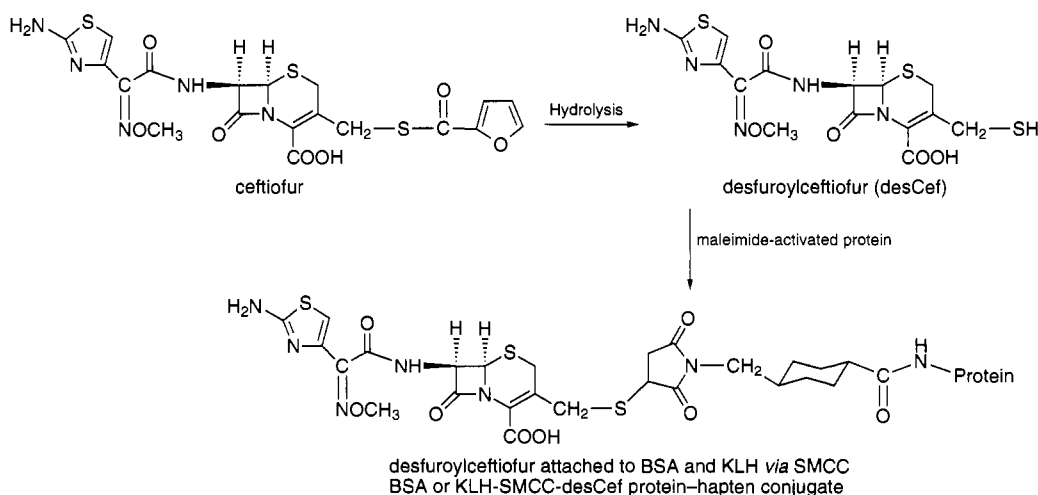
Figure 3. Hydrolysis of ceftiofur producing desfuroylceftiofur *in situ* and conjugation to maleimide-activated BSA (BSA−SMCC) and KLH (KLH−SMCC) to yield the BSA−SMCC−desCef and KLH−SMCC−desCef conjugates.

90 ppb when using BSA−S−SMPB−Cef as the plate-coating antigen. Antisera produced using the KLH−SMCC−desCef immunogen on average gave better results on BSA−S−GMBS−Cef coated plates than on BSA−S−SMPB−Cef plates with IC_{50} values ranging from 60 to 100 ppb compared to 200 to 500 ppb, respectively. As

the mice aged, the antisera for OVA−S−SMPB−Cef, OVA−S−GMBS−Cef, and KLH−SMCC−desCef appeared to deteriorate, and later bleeds gave less satisfying results (Table 3). However, improved sensitivity using a heterologous assay system was still observed for the OVA−S−SMPB−Cef and KLH−SMCC−desCef antisera.
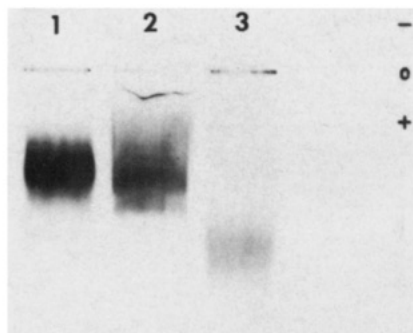
Figure 4. Nondenaturing gel analysis in running buffer, pH 8.8, of KLH, lane 1; KLH−SMCC, lane 2; KLH−SMCC−desCef conjugate, lane 3.

KLH−SMCC−desCef proved to be the best immunogen when the assay utilized BSA−S−GMBS−Cef-coated plates.

Competitive inhibition was examined with the following cephalosporins: cefteram sodium, ceftriaxone sodium, cefuroxime sodium, and ceftazidime pentahydrate. No cross-reactivity could be detected using polyclonal mouse sera.

DISCUSSION

Monitoring pesticide and drug residues in biological fluids and tissues can be greatly simplified by using immunoassay techniques rather than conventional analytical methods. However, target molecules need to be covalently linked to carrier proteins to elicit an immune response. The method of conjugation of the target molecule depends on the presence of suitable functional groups. The conjugated hapten should preserve the chemical and physical properties of the target compound and provide a handle which allows for coupling to carrier proteins (Harrison *et al.*, 1991a). Usually, higher affinity antibodies are obtained if the cross-linking reagent is spaced further away from the protein so that the antibody does not recognize the carrier protein as part of its epitope (Mattson *et al.*, 1993).

A suitable analysis for ceftiofur was based on the indirect ELISA method in which the ceftiofur−protein conjugate was immobilized on microtiter plates. Antisera were screened by this method using the homologous/heterologous approach. For the purpose of this discussion a homologous ELISA system refers to a system in which the hapten is the same for both the immunogen and the plate-coating antigen but the carrier proteins differ. A heterologous ELISA system refers to a system in which the immunogen and plate-coating antigens differ in carrier proteins, as well as haptens, or a heterologous hapten may consist of a slightly modified target molecule as in the case of ceftiofur and desfuroyl ceftiofur. The target molecule modified by the heterobifunctional cross-linking reagent is called the hapten. The hapten is subsequently conjugated to a carrier protein, thus forming the protein−hapten conjugate. Previously, heterologous assay systems have been shown to produce more sensitive assays than homologous assays (Harrison *et al.*, 1989, 1991a,b; Wie and Hammock, 1984; Schneider and Hammock, 1992).

Three conjugation procedures were adopted to study the effects of the attachment site of ceftiofur to the cross-linker and the cross-linker length on the production of antibody that is able to recognize free ceftiofur. Initial experiments with ceftiofur conjugated through the amino group *via s*-SMPB (14.5 Å in length) to BSA and OVA produced good antibody titers; however, these antisera did not bind free ceftiofur in a CI-ELISA. These results suggest that the OVA−S−SMPB−Cef conjugate possibly had produced antibodies which bound both the desired hapten and all or part of the linkage chemistry. The antibodies may not have bound the ceftiofur molecule itself or the antibodies may have formed low-affinity contacts with respect to ceftiofur.

Next, *s*-GMBS (10.2 Å in length), a similarly structured heterobifunctional cross-linking reagent, was employed to link ceftiofur to thiolated proteins, again *via* the amino group on ceftiofur. Sulfo-GMBS was chosen since it is known to be less immunogenic, thereby ensuring that the primary immune response to antigen−carrier protein conjugates is not influenced by a determinant on the cross-linker itself (Fujiwara *et al.*, 1988; Kitagawa *et al.*, 1983). As with the SMPB conjugate, only antibodies with weak relative affinities were observed with the GMBS conjugate, regardless of the antigen.

Some of the difficulties associated with the production of high affinity antibodies toward ceftiofur could stem from the fact that the furan ring in ceftiofur is cleaved off once it is in the animal tissue due to enzyme-catalyzed hydrolysis of the thioester bond. This results in the formation of desfuroyl ceftiofur, the hydrolyzed form of ceftiofur, and the furoic acid metabolite (Jaglan *et al.*, 1990). In other species such as rats and dogs, desfuroyl ceftiofur has been detected in the dimerized form. In this

Table 2. Percent Inhibition of Control (IC$_{50}$/ppb) Observed for Ceftiofur Sodium Antisera Tested against Different Plate Coating Antigens

				IC$_{50}$/ppb for plate coating antigens	
immunogen	day of bleed	serum	serum dilutions[a]	BSA−S−SMPB−Cef	BSA−S−GMBS−Cef
OVA−S−SMPB−Cef[b]	156	1	1:600	50	40
		2	1:600	80	50
		3	1:600	100	35
		4	1:600	100	25
		5	1:600	150	50
OVA−S−GMBS−Cef[b]	156	1	1:600	15	700
		2	1:600	25	400
		3	1:600	50	500
		4	1:600	90	600
		5	1:600	110	600
KLH−SMCC−desCef[c]	50	1	1:20 000	200	100
		2	1:20 000	500	60
		3	1:20 000	500	70
		4	1:20 000	200	60

[a] Serum dilutions representing approximately 50% maximum activity in a titration ELISA. These dilutions were used in the CI-ELISA experiments and tested on the corresponding plate coating antigens. [b] Immunogen prepared in Freund's adjuvant. [c] Immunogen prepared in Ribi adjuvant.

Table 3. Percent Inhibition of Control (IC₅₀/ppb) Observed for Antisera Collected at Later Times

immunogen	day of bleed	serum	serum dilutions[a] for plate coating antigens BSA–S–SMPB–Cef	BSA–S–GMBS–Cef	BSA–SMCC–desCef	IC₅₀/ppb for plate coating antigens BSA–S–SMPB–Cef	BSA–S–GMBS–Cef	BSA–SMCC–desCef
OVA–S–GMBS–Cef[b]	274	1	d	1:3200	1:200	d	e	e
		2	1:36	1:800	1:200	>1000	80	e
		3	1:40	1:1600	1:100	>1000	200	e
		4	1:20	1:600	1:100	e	e	e
		5	1:24	1:2500	1:100	e	200	e
OVA–S–SMPB–Cef[b]	267	1	1:800	1:400	1:400	e	e	300
		4	1:800	1:400	1:400	e	e	>1000
KLH–SMCC–desCef[c]	170	1	1:800	1:800	1:6400	>1000	3	e
		4	1:1600	1:1600	1:12 800	30	3	e

[a] Serum dilutions representing approximately 50% maximum activity in a titration ELISA. These dilutions were used in the CI-ELISA experiments and tested on the corresponding plate coating antigens. [b] Immunogen prepared in Freund's adjuvant. [c] Immunogen prepared in Ribi adjuvant. [d] Experiment not done, insufficient serum. [e] No competition observed.

case, desfuroyl ceftiofur is presumably bound to macromolecules *via* disulfide bonds (Jaglan *et al.*, 1989). Our strategy was to prepare desfuroyl ceftiofur *in situ* and conjugate the thiol group to maleimide-activated proteins, thus avoiding oxidation of the thiol to the disulfide and producing a more stable derivative. Our desire was to produce antibodies that would recognize the cephem nucleus, as well as the 2-(2-aminothiazoyl-4-yl)-2-methoxyaminoacetamide fragment. All three hapten protein conjugates delivered good antibody titers. However, evaluation by CI-ELISA showed that the KLH–SMCC–desCef conjugate possessed the antibody with the best relative affinity for ceftiofur.

The OVA–S–SMPB–Cef and OVA–S–GMBS–Cef immunogens prepared in adjuvants as suggested by the manufacturer and injected according to the recommended immunization schedule did not produce the required antibody response. The antibodies failed to recognize the free ceftiofur, suggesting either poor maturation of the antibody or recognition of the linkage chemistry by the antibody. Low-affinity contacts of the antibody with the functional groups associated with the linkage of the antigen thus result in the failure to detect the target molecule itself. This is not surprising since antibodies are produced by the B lymphocytes of the immune system, which are activated by exposure to the immunogens. Each individual B lymphocyte produces only one specific type of antibody; thus, only those clones are selected that have higher affinity binding sites at a certain level of the B cell population. This phenomenon of affinity maturation was first described by Siskind and Benacerraf (1969) and has subsequently been reported in more recent literature (Kamps-Holtzapple *et al.*, 1994; Zitron, 1994). After an extended immunization schedule, cross-reactivity with ceftiofur was observed which suggests that the affinity distribution is affected by the time interval between immunizations and resting periods. This can be explained by mutations that occur during the growth phase of the B cell response. During the resting period the concentration of the free immunogen is reduced and higher affinity clones can be selected (George *et al.*, 1993). The fact that the KLH–SMCC–desCef antibodies recognize free ceftiofur very well indicates that the furan ring probably plays a minor role in antibody binding. Because of site mutations, the nature of the antibody is known to change over time. Polyclonal antisera consist of a wide variety of antibody molecules of different specificity and affinity and each time an animal is bled, it yields a different "cocktail" of such antibodies as its immune response to the injected immunogen alters and memory B cell clones emerge and recede. The same animal can yield a highly specific antiserum directed against a chosen antigen in one bleed and a poor antiserum in another, thus resulting in inconsistent results.

CONCLUSION

In this study, a competitive indirect assay of antisera against ceftiofur is developed, and it is demonstrated that the sensitivity of the immunoassay varies with different plate-coating antigens, giving better results using heterologous assay systems. The experiments described here have created a basis for further work leading to valuable information concerning the choice of a protein–hapten conjugate which produces the best immune response and optimum experimental conditions for the production of monoclonal antibodies.

LITERATURE CITED

Bekheit, H. K. M., Lucas, A. D., Gee, S. J., Harrison, R. O., and Hammock, B. D. (1993a) Development of an enzyme-linked immunosorbent assay for the β-exotoxin of *Bacillus thuringiensis*. *J. Agric. Food Chem.* 41, 1553–1536.

Bekheit, H. K. M., Lucas, A. D., Szurdoki, F., Gee, S. J., and Hammock, B. D. (1993b) An enzyme immunoassay for the environmental monitoring of the herbicide bromacil. *J. Agric. Food Chem.* 41, 2220–2227.

Brown, P. R., and Edwards, J. O. (1968) A quick TLC test for detection of mercaptan groups in the presence of other types of sulfur functional groups. *J. Chromatogr.* 38, 543.

Cervantes, C., Brown, M. P., Gronwall, R., and Merritt, K. (1993) Pharmacokinetics and concentrations of ceftiofur sodium in body fluids and endometrium after repeated intramuscular injections in mares. *Am. J. Vet. Res.* 53, 573–575.

Chapman, J. H., and Owen, L. N. (1950) Dithiols part IV. The reaction of toluene-*p*-sulphonates and methane sulphonates with potassium thiolacetate: a new method for the preparation of thiols. *J. Chem. Soc. London* 579–585.

Food and Drug Administration. (1988) Animal drugs, feeds, and related products; ceftiofur sterile powder. *Fed. Regist.* 53, 5369–5370.

Food and Drug Administration. (1991) Implantation injectable dosage form animal drugs not subject to certification, ceftiofur sterile powder. *Fed. Regist.* 56, 119.

Fujiwara, K., Saita, T., and Kitagawa, T. (1988) The use of N-[β-(4-diazophenyl)ethyl] maleimide as a coupling agent in the preparation of enzyme-antibody conjugates. *J. Immunol. Methods 110*, 47–53.

George, J., Penner, S. J., Weber, J., Berry, J., and Claflin, J. L. (1993) Influence of membrane Ig receptor density and affinity on B cell signaling by antigen. *J. Immunol.* 151, 5955–5965.

Gilbertson, T. J., Hornish, R. E., Jaglan, P. S., Koshy, K. T., Nappier, J. L., Stahl, G., Cazers, A. R., Nappier, J. M., Kubicek, M. F., Hoffman, G. A., and Hamlow, P. J. (1990) Environmental fate of ceftiofur sodium, a cephalosporin antibiotic. Role of animal excreta in its decomposition. *J. Agric. Food Chem.* 38, 890–894.

Goodrow, M. H., Harrison, R. O., and Hammock, B. D. (1990) Hapten synthesis, antibody development, and competitive

inhibition enzyme immunoassay for *s*-triazine herbicides. *J. Agric. Food Chem. 38*, 990–996.

Harrison, R. O., Brimfield, A. A., and Nelson, J. O. (1989) Development of a monoclonal antibody based enzyme immunoassay of maleic hydrazide. *J. Agric. Food Chem. 37*, 958–964.

Harrison, R. O., Goodrow, M. H., and Hammock, B. D. (1991a) Competitive inhibition ELISA for *s*-triazine herbicides: assay optimization and antibody characterization. *J. Agric. Food Chem. 39*, 122–128.

Harrison, R. O., Goodrow, M. H., Gee, S. J., and Hammock, B. D. (1991b) Hapten synthesis and strategies for pesticide immunoassay development. In *Immunochemical methods for environmental analysis (M.* Vanderlaan, L. H. Stanker, B. E. Watkins, and D. W. Roberts, Eds.) ACS Symposium Series 451, pp 14–27, American Chemical Society, Washington, D.C..

Jaglan, P. S., Kubicek, M. F., Arnold, T. S., Cox, B. L., Robins, R. H., Johnson, D. D., and Gilbertson, T. J. (1989) Metabolism of ceftiofur. Nature of urinary and plasma metabolites in rats and cattle. *J. Agric. Food Chem. 37*, 1112–1118.

Jaglan, P. S., Cox, B. L., Arnold, T. S., Kubicek, M. F., Stuart, D. J., and Gilbertson, T. J. (1990) Liquid chromatographic determination of desfuroyl ceftiofur metabolite of ceftiofur as residue in cattle plasma. *J. Assoc. Off. Anal. Chem. 73*, 26–30.

Jaglan, P. S., Yein, F. S., Hornish, R. E., Cox, B. L., Arnold, T. S., Roof, R. D., and Gilbertson, T. J. (1992) Depletion of intramuscularly injected ceftiofur from the milk of dairy cattle. *J. Dairy Sci. 75*, 1870–1876.

Kamps-Holtzapple, C., Carlin, R. J., Sheffield, C., Kubena, L., Stanker, L. H., and DeLoach, J. R. (1993) Analysis of hapten-carrier protein conjugates by nondenaturing gel electrophoresis. *J. Immunol. Methods 164*, 245–253.

Kamps-Holtzapple, C., Stanker, L. H., and DeLoach, J. R. (1994) Development of a monoclonal antibody-based ELISA for the anthelminthic hygromycin B. *J. Agric. Food Chem. 42*, 822–827.

Karu, A. E., Goodrow, M. H., Schmidt, D. J., Hammock, B. D, and Bigelow, M. W. (1994) Synthesis of haptens and derivation of monoclonal antibodies for immunoassay of the phenylurea herbicide diuron. *J. Agric. Food Chem. 42*, 301–309.

Kitagawa, T., Fujiwara, K., Tomonoh, S., Takahashi, K., and Koida, M. (1983) Enzyme immunoassys of kanamycin group antibiotics with high sensitivities using anti-kanamycin as a common antiserum: reasoning and selection of a heterologous enzyme label. *J. Biochem. 94*, 1165–1172.

Krämer, P. M., Marco, M. P., and Hammock, B. D. (1994) Development of a selective enzyme-linked immunosorbent assay for 1-naphtol—the major metabolite of carbaryl (1-naphthyl-*N*-methylcarbamate). *J. Agric. Food Chem. 42*, 937–943.

Labeeuw, B., and Salhi, A. (1984) Cephalosporin derivatives, process for preparation thereof and drugs containing said derivatives usable as antibiotics. U.S. Pat. 4,464,367.

Lucas, A. D., Bekheit, H. K., Goodrow, M. H., Jones, A. D., Kullman, S., Matsumura, F., Woodrow, J. E., Seiber, J. N., and Hammock, B. D. (1993) Development of antibodies against hydroxyatrazine and hydroxysimazine: application to environmental samples. *J. Agric. Food Chem. 41*, 1523–1529.

Marco, M. P., Gee, S. J., Cheng, H. M., Liang, Z. Y., and Hammock, B. D. (1993) Development of an enzyme-linked immunosorbent assay for carbaryl. *J. Agric. Food Chem. 41*, 423–430.

Mattson, G., Conklin, E., Nielander, G., Savage, M. D., and Morgensen, S. (1993) A practical approach to cross-linking. *Mol. Biol. Rep. 17*, 167–183.

Owens, W. E., Xiang, Z. Y., Ray, C. H., and Nickerson, S. C. (1990) Detection of milk and mammary tissue concentrations of ceftiofur after intramammary and intramuscular therapy. *J. Dairy Sci. 73*, 3449–3456.

Rouan, M. C. (1985) Antibiotic monitoring in body fluids. *J. Chromatogr. 340*, 361–400.

Schneider, P., and Hammock, B. D. (1992) Influence of the ELISA format and the hapten-enzyme conjugate on the sensitivity of an immunoassay for *s*-triazine herbicides using monoclonal antibodies. *J. Agric. Food Chem. 40*, 525–530.

Schneider, P., Goodrow, M. H., Gee, S. J., and Hammock, B. D. (1994) A highly sensitive and rapid ELISA for the arylurea herbicides diuron, monuron, and linuron. *J. Agric. Food Chem. 42*, 413–422.

Siskind, G. W., and Benacerraf, B. (1969) Cell selection by antigen in the immune response. *Adv. Immunol. 10*, 1–50.

Smyth, D. G., Blumenfeld, O. O., and Konigsberg, W. (1964) Reaction of *N*, ethylmaleimide with peptides and amino acids. *Biochem. J. 91*, 589.

Vanderlaan, M., Stanker, L. H., Watkins, B. E., Roberts, D. W., Eds. (1991) Immunoassays for trace chemical analysis. Monitoring toxic chemicals in humans, food, and the environment. ACS Symposium Series 451, American Chemical Society, Washington, D.C.

Wie, S. I., and Hammock, B. D. (1984) Comparison of coating and immunizing antigen structure on the sensitivity and specificity of immunoassays for benzoylphenyl urea herbicides. *J. Agric. Food Chem. 32*, 1294–1301.

Wise, R., Wills, P. J., Andrews, J. M., and Bedford, K. A. (1980) Activity of cefotaxime (HR756) desacetyl metabolite compared with those of cefotaxime and other cephalosporins. *Antimicrob. Agents Chemother. 17*, 84–86.

Yancey, R. J., Jr., Kinney, M. L., Roberts, B. J., Goodenough, K. R., Hamel, J. C., and Ford, C. W. (1987) Ceftiofur sodium, a broad-spectrum cephalosporin: evaluation in vitro and in vivo in mice. *Am. J. Vet. Res. 48*, 1050–1053.

Zitron, I. M. (1994) Antibody molecules and the immune response. In *Antibody techniques* (V. S. Malik, E. P. Lillehoj, Eds.) pp 37–38, Academic Press, San Diego, CA.

BC950047N

Quantitative Analysis of 3′-Azido-3′-deoxythymidine Incorporation into DNA in Human Colon Tumor Cells

Minoti Sharma,* Rama Jain, Elizabeth Ionescu, and James W. Darnowski[†]

Department of Biophysics, Roswell Park Cancer Institute, Buffalo, New York 14263. Received March 14, 1995[®]

We have previously reported that 3′-azido-3′-deoxythymidine (AZT) can possess significant antineoplastic activity *in vitro* and *in vivo* when combined with agents which inhibit *de novo* thymidylate synthesis. Under these conditions cytotoxicity is closely associated with the degree to which AZT is incorporated into DNA. We now report a fluorescence postlabeling technique by which AZT incorporation into DNA can be quantitated without employing radiolabeled AZT. Cultured human colon tumor (HCT-8) cells were exposed to various concentrations of AZT alone and in combination with 5-fluorouracil (FUra). Control cells received the same amount of medium. DNA was isolated from harvested cell pellets (2×10^7). Enzymatic digestion of DNA to the mononucleotide level followed by HPLC analysis of the digest showed that the DNA preparation was free of RNA contamination. The DNA digest was conjugated with dansyl chloride *in situ* via the phosphoramidate derivative with ethylenediamine. HPLC analysis of the postlabeled nucleotides using fluorescence detection detected 105, 245, and 479 fmol of 5′-monophosphate of AZT (AZTMP) per μg of DNA from cells exposed to 20, 50, and 100 μM AZT, respectively. FUra (3 μM) doubled the AZT incorporation per μg of DNA in cells exposed to 50 and 100 μM AZT. These findings generally support our previously reported data which quantitated (^{3}H)AZT incorporation into cellular DNA and are discussed in light of the potential clinical utility of this technique in assessing the relationship between AZT incorporation into DNA and therapeutic action.

INTRODUCTION

We have reported, using a human colon tumor model, that AZT in combination with FUra or methotrexate (MTX) exert superior cytotoxic and antineoplastic effects compared to either drug alone (*1–3*). As a result, clinical analysis of AZT-based regimens for the treatment of cancer have been initiated, and presently phase II analysis of AZT + FU/LV is underway. Sommadossi *et al.* have reported that AZT-induced cytotoxicity in human bone marrow cells is related to AZT incorporation in DNA (*4*). Our group also has observed that AZT cytotoxicity correlated closely with the size of intracellular pools of di- and triphosphates of AZT and the amount of AZT incorporation into cellular DNA (*3*).

Thus far, all the reports correlating AZT incorporation in DNA and cytotoxicity have been based on studies utilizing radiolabeled AZT. As a result, clinical confirmation of the therapeutic relevance of AZT incorporation into DNA is not practical. Therefore, we now report a technique to analyze AZT incorporation into DNA using nonisotopic detection and demonstrate its capacity to quantitate the incorporation into cellular DNA. These results and the method are discussed in light of their potential utility in ongoing clinical trials.

MATERIALS AND METHODS

Chemicals and Reagents. The standard deoxynucleotides, 1-methylimidazole, 1-(3,3-bis(methylamino)-propyl)-3-ethylcarbodiimide hydrochloride (CDI), 5-(dimethylamino)naphthalene 1-sulfonylchloride (Dansyl chloride), protected mononucleotide phosphodiester, the enzyme nuclease P1, and FUra were purchased from Sigma

(St. Louis, MO). Ethylenediamine (EDA), triisopropylbenzenesulfonyl chloride (TPSCl), anhydrous pyridine, and 2-cyanoethyl phosphate (barium salt dihydrate) were obtained from Aldrich Chemical Co. AZT was the generous gift of the Burroughs Wellcome Co. (Research Triangle Park, NC), and RPMI 1640 medium and fetal bovine serum (FBS) were purchased from Gibco (Grand Island, NY). HPLC grade solvents, chemical, and disposable tissue culture supplies were obtained from Fisher Scientific (Medford, MA).

Cell Line. Continuous cultures of HCT-8 human colon adenocarcinoma cells, obtained from the American Type Culture Collection, were used in these studies. The biochemical and histological characterization of this cell line has been reported (*5*). Cells were cultured in sterile plastic tissue culture flasks as monolayers in RPMI 1640 medium supplemented with 10% fetal bovine serum (FBS) and passed twice weekly. Cell cultures were maintained in a humidified incubator at 37 °C in an atmosphere of 5% CO_2. Under these conditions their doubling time was 20 h and cells in logarithmic growth were used in all studies.

***In Vitro* Evaluation of Cytotoxicity.** HCT-8 cells (1×10^5) were added to 10 mL of RPMI 1640 media containing 10% FBS in 25 mL culture flasks. AZT and FUra previously dissolved in media were added at concentrations of 20, 50, and 100 μM AZT and 3 μM FUra either alone or in various noted combinations. Control cultures received the same amount of media without drug. After 5 days, cells were harvested and growth inhibition was determined as described previously (*1, 2*). Each experiment was performed in duplicate and repeated a minimum of four times.

For experiments to quantitate AZT incorporation into DNA and the effect of FUra on this parameter, approximately 3×10^6 HCT-8 cells were added to 150 mL flasks containing 50 mL of RPMI 1640 media, 10% FBS, and the various noted concentrations of either FUra and/

* To whom all correspondence should be addressed. Phone: (716) 845-8296. Fax: (716) 845-8899.
† Department of Medicine, Brown University and Roger Williams Hospital, Providence, Rhode Island 02908.
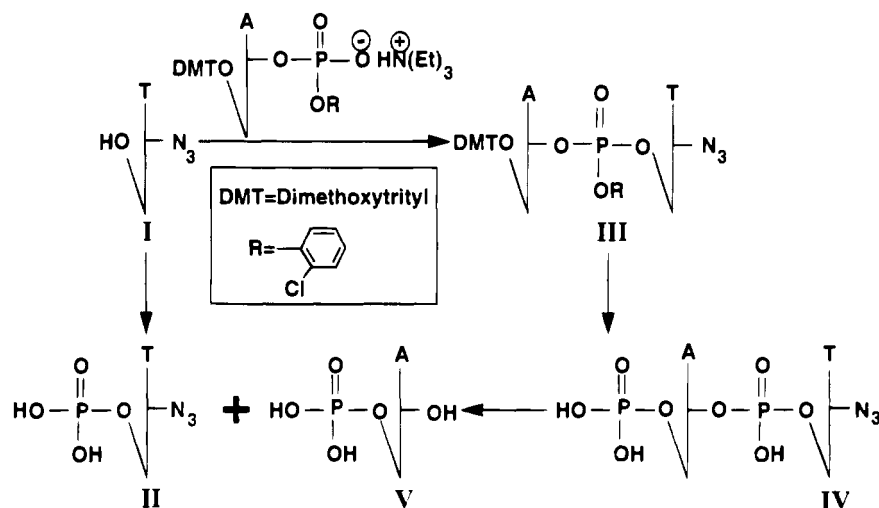
Figure 1. Scheme for the chemical synthesis of the 5'-monophosphate of AZT and its dinucleotide d(pApAZT).
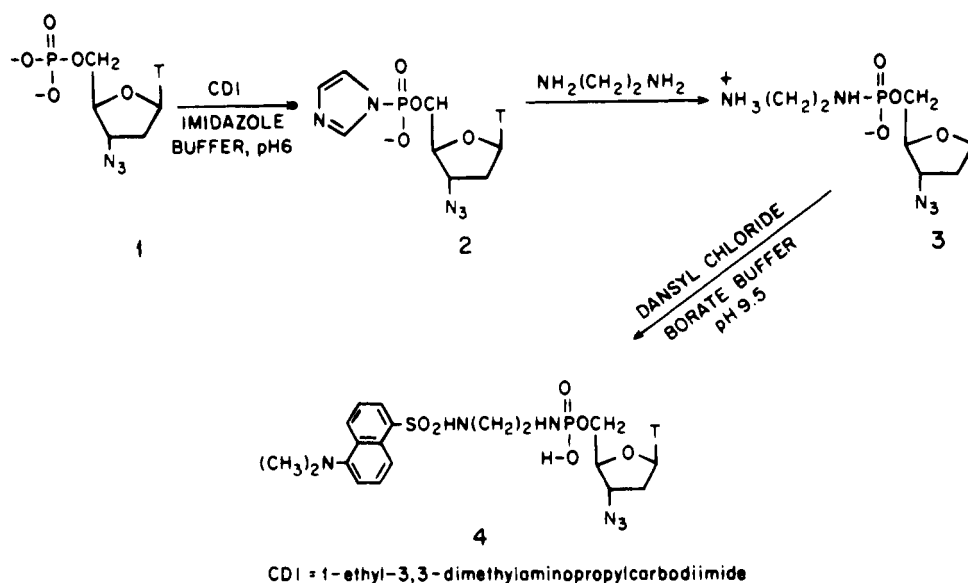
CDI = 1-ethyl-3,3-dimethylaminopropylcarbodiimide

Figure 2. Scheme for the synthesis of the fluorescence-labeled 5'-monophosphate of AZT.

or AZT. After 5 days the cells (approximately 2×10^7) were harvested following reported procedure (3).

Preparation of 5'-Monophosphate of AZT (AZTMP) and Its Dinucleotide d(pApAZT). The scheme for the synthesis of AZTMP and its dinucleotide d(pApAZT) is shown in Figure 1. AZT was phosphorylated with 2-cyanoethyl phosphate following a previously reported procedure (6). The fully protected dinucleoside monophosphate (III) was synthesized in the solution phase by a modified phosphotriester approach (7). The product was purified by column chromatography on silica using 0—5% methanol in dichloromethane. The pure product was phosphorylated with 2-cyanoethyl phosphate as in the case of AZT. After being deblocked with ammonia and pyridine (9:1 v/v), the product (IV) was isolated by C18 reversed phase chromatography (5 μm, 10 mm × 25 cm) using a 30 min linear gradient of 0—20% acetonitrile in 0.1 M ammonium acetate buffer and desalted on the same system using a linear gradient of 0—100% methanol in water. AZTMP (II) was also isolated by reversed phase HPLC under similar conditions. The chemical shifts in ppm with reference to TSP at 1.93 (d, 3H, CH₃), 2.49—2.52 (m, 2H, CH-2' and CH-2''), 4.06—4.23 (m, 3H, CH-5', CH-5'', CH-4'), 4.50—4.53 (m, 1H, CH-3'), 6.26—6.30 (t, 1H, CH-1'), and 7.7 (s, 1H, CH-6) were in agreement with the structure of AZTMP.

The downfield chemical shifts of the dinucleotide shown at 8.52 (s, 1H, AH-8), 8.27 (s, 1H, AH-2), 7.5 (s, 1H, AZT H-6), 6.46—6.49 (t, 1H, AH-1'), and 6.13—6.16 (t, 1H, AZT H-1') with respect to TSP supported the structure of d(pApAZT). Nuclease P1 digestion of IV afforded dAMP (V) and AZTMP (II) as shown in Figure 1. ¹H NMR measurements were done on a Bruker WP 200 spectrometer.

Figure 2 shows the scheme used for the synthesis of dansylated nucleotide. The phosphate group of AZTMP (1) reacts with water-soluble 1-(3,3-bis(methylamino)propyl)-3-ethylcarbodiimide (CDI) in 1-methylimidazole buffer at pH 6 to generate the phosphorimidazolidate 2 which when exposed to ethylenediamine (EDA) results in the formation of a stable 5'-phosphoramidate derivative 3. The free amino group of the phosphoramidate reacts readily with dansyl chloride in 50 mM borate buffer, pH 9.5, to yield the fluorescent-labeled nucleotide 4.

Fluorescence Postlabeling Assay of d(pApAZT). The dinucleotide (1 OD) was digested with nuclease P1 following reported procedure (8). The digest was filtered on an ultrafree microunit with 10 000 NMWL polysulfone membrane and labeled with dansyl chloride as described below. The filtrate was adjusted to pH 6 with 0.1 M NaOH and lyophilized. A cocktail (50 μL) prepared by

mixing 40 mg of CDI, 15 μL of EDA, and 8 μL of 1-methylimidazole in 1 mL of water, pH 6, was added to the lyophilized material. The reaction mixture was left at room temperature overnight to prepare the phosphoramidate derivative of the digested nucleotides. The pH of the reaction mixture was then adjusted to 9.5 with 0.2 M Na_2CO_3, and 50 μL of dansyl chloride (1 g/10 mL acetone) was added. After being stirred at room temperature in the dark for 1 h, the dansyl-labeled reaction mixture was filtered on a microcentrifuge to remove any particulate material, and the filtrate was frozen until ready for HPLC analysis. A sample of AZTMP (1 OD) was also dansylated following the same procedure.

Postlabeling and HPLC Analysis of Postlabeled DNA Digests. Typically, DNA was isolated from a pellet containing 2.5×10^7 cells. The pellet was lysed by a guanidinethiocyanate procedure (9). The protocol was modified by adding 0.75 vol of ethanol to the lysate. After 2 h at -22 °C, the mixture was centrifuged at 10000g for 20 min at 4 °C, and DNA was isolated from the supernatant by ethanol precipitation, proteinase K treatment of the precipitate, and organic extraction following the standard procedure. DNA was digested enzymatically to the nucleotide level, and the nucleotide profile of the digest was routinely monitored by HPLC to determine the purity of the preparation. Typically, 100 μg of DNA (2 OD) was digested with 2 μL of DNAse-1 (2000 KU/100 μL) and 2 μL of nuclease P1 (1 mg/mL) in 40 μL of Tris (10 mM), EDTA (0.1 mm), $MgCl_2$ (4 mM) buffer, pH 7.5 containing 2 μL of $ZnSO_4$ (10 mM) and 4 μL of NaOAc (38 mM, pH 5.0) at 37 °C overnight. The digest was derivatized with EDA cocktail following the procedure described for the DNA model study. However, in order to enrich the modified nucleotide from the normal nucleotides in the DNA digest, the phosphoramidate reaction mixture was fractionated by HPLC. A fraction corresponding to the retention time of phosphoramidate derivative of AZTMP was collected, lyophilized, and labeled by adding 25 μL of dansyl chloride in 100 μL of 0.1 M carbonate bicarbonate buffer, pH 9.5. An aliquot of the labeled, enriched fraction was analyzed by HPLC using fluorescence detection as shown in Figure 5. Alternatively, the EDA reaction mixture was reacted with dansyl chloride following the procedure described in the model study, and the postlabeled digest was fractionated by HPLC using fluorescence detection. A fraction corresponding to the retention time of dansylated AZTMP was collected isocratically with 23% acetonitrile in 0.1 M ammonium acetate. Reanalysis of an aliquot of the enriched fraction using the high-sensitive detector accessory under the same elution conditions detected the peak of interest.

HPLC Separation of Nucleotides of Normal and Modified Bases. Prior to labeling, the nucleotides were separated on a Radial-Pak LC cartridge 8MBC18 (10 μm, 8 mm × 10 cm) using a 30 min linear gradient of 0–20% acetonitrile in 0.1 M ammonium acetate, pH 7. The profiles were monitored at 254 nm using a Beckman variable wavelength detector with an Altex spectrophotometer cell. The postlabeled nucleotides were analyzed on a microsorb C18 column (5 μm, 4.6 mm × 25 cm) using a McPherson detector model 750B equipped with a highly sensitive detection accessory to monitor fluorescence. The elution conditions are described in the figure legends.

RESULTS AND DISCUSSION

In the present study the IC_{50} of AZT in HCT-8 cells after a 5-d exposure was approximately 67.5 μM. Under these conditions the IC_{50} of FUra was 2.3 μM. Analysis of combined effect of AZT and FUra revealed that these

Table 1. Analysis of the Combined Effect of FUra and AZT on IC_{50} of FUra or AZT in HCT-8 Cells[a]

incubation condition	IC_{50} (μM)	
	of FUra	of AZT
control	2.3 ± 0.2	67.5 ± 4.8
0.5 μM FUra		49.4 ± 6.2
1.5 μM FUra		32.0 ± 4.6
20 μM AZT	1.8 ± 0.3	
50 μM AZT	1.4 ± 0.4	

[a] Twenty-five mL tissue culture flasks containing 10 mL of RPMI 1640 media + 10% FBS, 1×10^5 cells and various concentrations of AZT alone, FUra alone, or their noted combinations, were incubated at 37 °C. After 5 days, the cells were harvested and the cell number was determined. Percent growth inhibition was quantitated using cells incubated without AZT or FUra as control. Each value represents the mean ± SE from four determinations.

agents exerted additive cytotoxic effects (Table 1). Upon closer examination, however, it was apparent that while FUra was able to increase the cytotoxic activity of AZT, AZT exerted less of an effect on the cytotoxicity of FUra. Previous results using radiolabeled AZT have suggested that, in this model, AZT-induced cytotoxicity was closely associated with the degree to which AZT was incorporated into DNA (1–3). Reflecting both the expense of these isotopic studies and their lack of utility in the clinical setting we have therefore attempted to develop a method to assess AZT incorporation into DNA by directly quantitating the AZT nucleotide content of DNA in cells exposed to this thymidine analogue.

To this end, the 5′-monophosphate of AZT and its dinucleotide derivative were synthesized and labeled as described in the methods (Figures 1 and 2). The labeling reactions, though shown in three steps in Figure 2, were carried out in a single pot. The overall yield was 90%. Thereafter, chromatographic conditions were devised to resolve the nucleotides of normal and modified bases both before and after labeling. Figure 3 shows the reversed phase HPLC profiles of (a) the dinucleotide d(pApAZT), (b) nuclease P1 digest of the dinucleotide, and (c) the normal nucleotides and AZTMP. It has been reported that nuclease P1 releases the normal nucleotides from modified DNA as 5′-monophosphate (pN) whereas the modified nucleotides, depending on the nature of modification, are excised as dinucleotide (pNpX, X = modified base) (10). A DNA model study shows that nuclease P1 excised AZT as 5′-monophosphate (pX). The retention times of the two peaks in profile b matched the retention times of authentic dAMP and AZTMP shown in profile c. This was further confirmed by cochromatography (results not shown). HPLC analysis of the postlabeled digest also supported such an observation (Figure 4b). Cochromatography (profile 4c) of the postlabeled digest of d(pApAZT) with the postlabeled dinucleotide demonstrated clearly that the peak at 21 min in the profile 4b is from labeled dAMP and not from the labeled dinucleotide. The labeled dinucleotide is eluted at 22.5 min as shown in the profile 4a. HPLC analysis of the postlabeled nucleotides of known concentrations also revealed that the labeling yields of AZTMP and its dinucleotide derivative were quantitative.

Figure 5 shows fluorescence postlabeling assay from control (profile c) and AZT exposed (profile b) HCT-8 cells. Unlike the DNA model study, enrichment of modified nucleotide is essential in order to detect the peak of interest in modified, cellular DNA by postlabeling technique from the huge background of normal nucleotides (10). As described in the methodology, the enrichment of the modified nucleotides from the normal nucleotides
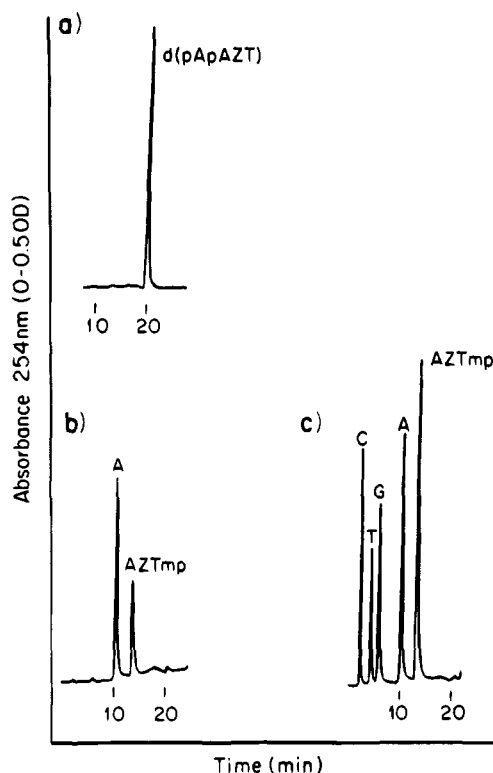
Figure 3. HPLC profiles of (a) d(pApAZT), (b) nuclease P1 digest of d(pApAZT), and (c) 5'-monophosphates of C, T, G, A, and AZT eluted with a 30 min linear gradient of 0–20% acetonitrile in 0.1 M ammonium acetate buffer, pH 7.

can be achieved by HPLC fractionation of the DNA digest both before and after labeling. The latter approach offers the advantage of enriching the modified nucleotide not only from the normal nucleotides but also from the excess labeling reagent. However, the successful application of this procedure depends on the chemical nature of the modified nucleotide. We observed that AZTMP can be resolved from the normal nucleotides both before and after labeling. The peak at 19 min in profile b of Figure 5 was identified as AZTMP by cochromatography of the postlabeled DNA digest with authentic, dansylated AZTMP (profile a). The percent digestion of DNA was calculated by HPLC, prior to labeling, from the integrated area of excised dAMP peak and the response factor of standard dAMP. The efficiency of digestion of modified DNA was 90% of control. The profiles in Figure 5 represent analysis of approximately 1 μg of DNA.

The results shown in Table 2 reveal the relationship between the media concentration of AZT and the degree of AZT incorporation into cellular DNA detected by fluorescence postlabeling technique. Each number in this table is an average of three independent measurements. Having demonstrated that the fluorescence postlabeling technique could be used to quantitate AZT incorporation into cellular DNA, we next assessed the effect of exposing cells to both FUra and AZT on the degree to which AZT was incorporated into cellular DNA in this model using nonisotopic detection. The results of these studies indicated that FUra (3 μM) coexposure doubled the incorporation of AZT into DNA from cells exposed to 50 μM (IC_{50}) and 100 μM (Table 2). Biochemical analysis of acid (PCA)-insoluble material from HCT-8 cells exposed to 5 μM FUra increased the incorporation of radiolabeled AZT into the nucleic acid fraction by 52% and also decreased the IC_{50} of AZT considerably. Furthermore, there appeared to be a FUra-related dose dependency to this
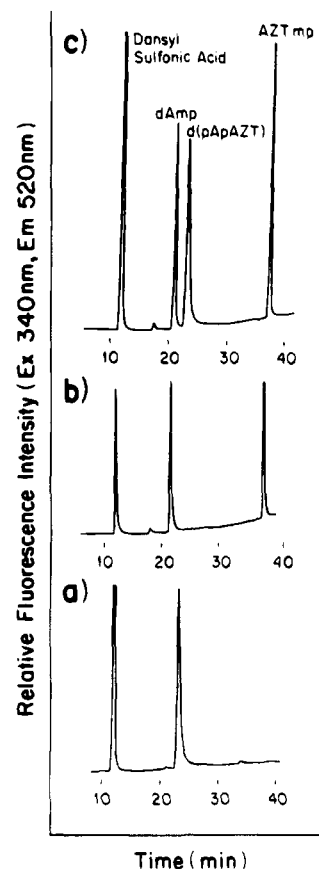
Figure 4. HPLC profiles of dansylated (a) d(pApAZT), (b) nuclease P1 digest of d(pApAZT), and (c) cochromatography of d(pApAZT) and its nuclease P1 digest eluted with a 30 min linear gradient of 18–30% acetonitrile in 0.1 M ammonium acetate buffer, pH 7.
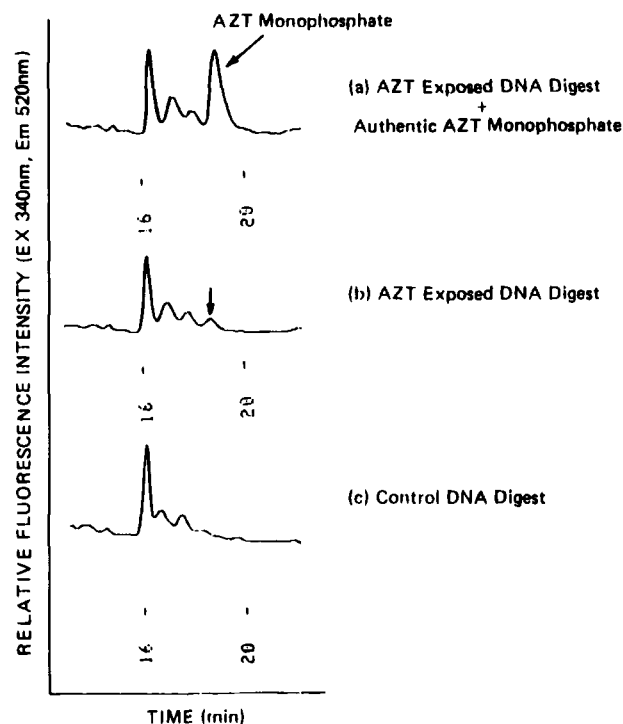
Figure 5. HPLC profiles of postlabeled DNA digests of HCT-8 cells (c) control, (b) AZT exposed, and (a) AZT exposed cochromatographed with dansylated AZTMP, eluted with 25% acetonitrile in 0.1 M ammonium acetate buffer, pH 7.

effect, perhaps reflecting more thymidylate synthatase inhibition at higher FUra concentration (*1*).

Table 2. Effect of Various Concentrations of AZT Alone and AZT plus FUra on AZT Incorporation into DNA of Exposed HCT-8 Cells

drug and concn	AZTMP (fmol/μg DNA)
none	
AZT, 20 μM	109 ± 5
AZT, 50 μM	245 ± 7
AZT, 100 μM	479 ± 11
AZT, 20 μM + FUra, 3 μM	114 ± 5
AZT, 50 μM + FUra, 3 μM	476 ± 9
AZT, 100 μM + FUra, 3 μM	980 ± 10

An AZT concentration-dependent relationship between AZT incorporation into cellular DNA and cytotoxicity has been reported by quantitating the tritium content of PCA insoluble material obtained from HCT-8 cells after exposure to (^{3}H)AZT (*1*). Fluorescence postlabeling assay of DNA in this model also shows a similar trend (Table 2) although the absolute amount of AZT incorporated into DNA as determined using radiolabeled AZT is 1 order of magnitude higher than those observed by nonisotopic detection. The labeling efficiency of AZTMP, as monitored by HPLC analysis of each reaction step shown in Figure 2, was 90−95%. It is unlikely that the procedural loss can account for the observed result reported by radiolabeling study (*1*). This difference may reflect, therefore, several differences between these methods. In the fluorescence postlabeling assay, prior to labeling, the nucleotide profile of DNA digest is routinely assessed by HPLC analysis to check the purity of DNA preparation. No such information was available for PCA insoluble material used to quantitate the radiolabeled AZT. In addition, it is difficult to make PCA insoluble material completely free of unwanted radiolabel, especially when material of relatively high specific activity is used.

AZT is presently used extensively in the treatment of AIDS and ARC, and significant research is directed toward identifying the mechanism(s) responsible for both its therapeutic activity and toxicity. In addition, several groups have reported that AZT can possess antineoplastic activity in combination with drugs which disrupt DNA synthesis and chemical evaluation of this potential is underway. Our present findings utilizing the fluorescence postlabeling technique to quantitate AZT incorporation into DNA suggest the important potential of this technique in studies to clinically monitor the fate of AZT without using radiolabeled drug. Clearly, further in vitro studies are essential in order to evaluate the therapeutic relevance of the two-drug regimen in cancer chemotherapy under clinical settings.

LITERATURE CITED

(1) Brunetti, I., Falcone, A., Calabresi, P., Goulette, F. A., and Darnowski, J. W. (1990) 5-Fluorouracil enhances azidothymidine cytotoxicity: In vitro, in vivo, and biochemical studies. *Cancer Res. 50*, 4026−4031.

(2) Tosi, P., Calabresi, P., Goulette, F. A., Renoud, C. A., and Darnowski, J. W. (1992) Azidothymidine-induced cytotoxicity and incorporation into DNA in the human colon tumor cell line HCT-8 is enhanced by methotrexate in vitro and in vivo. *Cancer Res. 52*, 4069−4073.

(3) Darnowski, J. W., and Goulette, F. A. (1994) 3′-Azido-3′-deoxythymidine cytotoxicity and metabolism in the human colon tumor cell line HCT-8. *Mol. Pharmacol. 48*, 1797−1805.

(4) Sommadossi, J. P., Carlisle, R., and Zhou, Z. (1989) Cellular pharmacology of 3′-azido-3′deoxythymidine with evidence of incorporation into DNA of human bone marrow cells. *Mol. Pharmacol. 36*, 9−14.

(5) Tompkins, W. A. F., Watrach, A. M., Schmale, J. D., Schultz, R. M., and Harris, J. A. (1974) Cultural and antigenic properties of newly established cell strains derived from adenocarcinoma of the human colon and rectum. *J. Natl. Cancer Inst. 52*, 1101−1110.

(6) Kelman, D. J., Lilga, K. L., and Sharma, M. (1988) Synthesis and application of fluorescent labeled nucleotides to assay DNA damage. *Chem.-Biol. Interact. 66*, 85−100.

(7) Sharma, M., and Box, H. C. (1985) Synthesis, modification with N-acetoxy-2-acetylaminofluorene and physicochemical studies of DNA model compound d(TACGTA). *Chem.-Biol. Interact. 56*, 73−88.

(8) Sharma, M., Jain, R., and Isac, T. V. (1991) A novel technique to assay adducts of DNA induced by anticancer agent cis-diamminedichloroplatinum (II). *Bioconjugate Chem. 2*, 403−406.

(9) Chirgwin, J. M., Przybyla, A. E., MacDonald, R. J., and Rutler, W. J. (1979) Isolation of biologically active ribonucleic acid from sources enriched in ribonuclease. *Biochemistry 18*, 5294−5299.

(10) Randerath, K., Randerath, E., Danna, T. F., Van Golen, K. L., and Putnam, K. L. (1989) A new sensitive ^{32}P-postlabeling assay based on the specific enzymatic conversion of bulky DNA lesions to radiolabeled dinucleotides and nucleoside monophosphates. *Carcinogenesis 10*, 1231−1239.

BC950042Q

High-Yield Affinity Alkylation of the Atrial Natriuretic Factor Receptor Binding Site

Xiaolan He,[†] Koji Nishio,[‡] and Kunio S. Misono*

Department of Molecular Cardiology, The Cleveland Clinic Foundation Research Institute, 9500 Euclid Avenue, Cleveland, Ohio 44195-5071. Received February 9, 1995[®]

To facilitate characterization of the atrial natriuretic factor (ANF) receptor, we have developed an affinity labeling procedure, stepwise affinity labeling, which allows specific labeling of ANF binding sites in adrenal plasma membranes at high yields. An iodoacetyl (IAc-), bromoacetyl (BrAc-), or maleimidobenzoyl group was attached to the amino-terminal α-amino group of the ANF(4−28) peptide, and the peptide derivatives were radioiodinated at Tyr-28 to obtain affinity reagents, $N^{4\alpha}$-IAc-[^{125}I]-ANF(4−28), $N^{4\alpha}$-BrAc-[^{125}I]ANF(4−28), and $N^{4\alpha}$-(maleimidobenzoyl)-[^{125}I]ANF(4−28). Receptor labeling was carried out in a stepwise fashion as follows: (1) Membranes were treated with p-chloromercuriobenzenesulfonic acid (PCMBS) or N-ethylmaleimide to block sulfhydryl groups; (2) the affinity reagent was allowed to bind to the receptor at 0 °C for 1 h; and (3) the membranes were washed to remove unbound reagent and were incubated at room temperature to effect alkylation reaction. Sodium dodecylsulfate (SDS)−polyacrylamide gel electrophoresis (PAGE) followed by autoradiography revealed specific labeling of a 130-kDa ANF receptor. On the basis of ^{125}I-radioactivity incorporated, the labeling yields were estimated to be 70%, 52%, and 21% for the reactions with IAc-[^{125}I]ANF(4−28), BrAc-[^{125}I]ANF(4−28), and (maleimidobenzoyl)-[^{125}I]ANF(4−28), respectively. The efficiency of receptor labeling by the stepwise procedure using IAc-[^{125}I]ANF(4−28) was 27-fold greater than that obtained by photoaffinity labeling using N₃Bz-[^{125}I]ANF(4−28) and 63-fold greater than that by direct cross-linking using disuccinimidylsuberate and [^{125}I]ANF(4−28) under comparable conditions. Digestion of the membrane protein labeled with IAc-[^{125}I]ANF(4−28) by BrCN, endoproteinase Glu-C, and endoproteinase Lys-C gave single radiolabeled bands with apparent masses of 40, 18, and 29 kDa, respectively. Reversed-phase HPLC separation of the digests also gave single major peaks. The confinement of the affinity label to one major fragment in each digest suggests that the cross-linking occurred at a single or a limited number of sites. The stepwise affinity labeling with the high cross-linking yield and specificity may be useful for analyzing the ANF receptor binding site structure.

Atrial natriuretic factor (ANF)[1] is a peptide hormone secreted by the heart atrium that has potent natriuretic (de Bold et al., 1981) and vasorelaxant activities (Currie et al., 1983; Grammer et al., 1983). The actions of ANF at its target organs, including the blood vessels, kidney, and adrenal gland, are mediated by cell membrane receptors that are directly coupled to guanylate cyclase (Cantin and Genest, 1985; Gerzer et al., 1987). The ANF receptor molecule consists of a single polypeptide chain with a molecular mass of about 130 kDa (Kuno et al., 1986; Takayanagi et al., 1987; Meloche et al., 1988), containing an extracellular ANF-binding domain, a single transmembrane sequence, and an intracellular region containing both protein kinase−homologous domain and guanylate cyclase domain (Chinkers et al., 1989). It has been suggested that, in the basal state, the kinase−homologous domain interacts with the guanylate cyclase domain, suppressing guanylate cyclase activity. Binding of ANF to the extracellular domain causes a conforma-

tional change that eliminates this suppression, thus elevating guanylate cyclase activity (Chinkers and Garbers, 1989). ATP, an allosteric effector, bound to the protein kinase−homologous domain, enhances ANF stimulation of guanylate cyclase. Although such a chain of events has been postulated, the actual structure of the receptor or the mechanism of interaction between ANF and the receptor remains largely unknown. This is in part because the binding site structure of the ANF receptor is not known.

Traditionally, chemical labeling of peptide receptor binding sites has been carried out either by photoaffinity labeling or by affinity cross-linking methods. However, both methods give low yields of labeled binding sites. In photoaffinity labeling, radicals are generated by photolysis. Photoradicals react indiscriminately at multiple sites on receptor polypeptides as well as with the surrounding solute and solvent molecules. Consequently, the net yield of cross-linking is small, and the reaction yields a complex mixture of unknown derivatives, making structural analysis extremely difficult (Ruoho et al., 1984). The bifunctional reagents used in affinity cross-linking are mostly electrophiles and have some level of chemical selectivity. However, in the major reaction path, cross-linker reagents simultaneously attack the potential acceptor residues on the receptor and ligand. This simultaneous attack leaves the other end of the cross-linker unable to cross-link and, hence, is unproductive in receptor labeling. For this reason, the net yield of the cross-linking generally does not exceed 5−10% (Pilch and Czech, 1984). Given the chemical complexity of the

[1] Abbreviations: ANF, atrial natriuretic factor; IAc, iodoacetyl; BrAc, bromoacetyl; N₃Bz−, azidobenzoyl; PCMBS, p-chloromercuriobenzenesulfonic acid; SDS, sodium dodecylsulfate; PAGE, polyacrylamide gel electrophoresis.

receptor protein and peptide ligand, the yield of one specific cross-linked structure is likely to be even lower.

To overcome these problems, we have developed a procedure, stepwise affinity labeling, for the ANF receptor. The method allowed highly specific labeling of the ANF receptor with labeling yields as high as 70% of receptor sites in adrenal membrane preparations. Radiochemical peptide mapping of the affinity-labeled membrane after BrCN, endoproteinase Glu-C, or endoproteinase Lys-C digestion showed that the labeling was confined to a single major peptide fragment, indicating that the labeling reaction was highly specific. The potential usefulness of this method for structural characterization of the peptide receptor binding site is discussed.

EXPERIMENTAL PROCEDURES

Materials. ANF(4−28) with the sequence Arg-Ser-Ser-Cys-Phe-Gly-Gly-Arg-Ile-Asp-Arg-Ile-Gly-Ala-Gln-Ser-Gly-Leu-Gly-Cys-Asn-Ser-Phe-Arg-Tyr (Misono et al., 1984a) was synthesized by the solid-phase method in an Applied Biosystems Model 431A peptide synthesizer (Foster City, CA). The initial loading of 9-fluorenyl-methyloxycarbonyl(Fmoc)amino acid on a (4-(hydroxy-methyl)phenoxy)methyl resin was effected by activating to its symmetric anhydride with dicyclohexylcarbodiimide in the presence of (dimethylamino)pyridine. Subsequent coupling of Fmoc-amino acid to the growing peptide chain was effected by *in situ* activation and coupling using 2-(1H-benzotriazol-1-yl)-1,1,3,3-tetramethyluronium hexa-fluorophosphate as an activating reagent in the presence of N-hydroxybenzotriazole. After synthesis, the peptide was cleaved from the resin and deprotected by treatment with a mixture of trifluoroacetic acid (10 mL), phenol (0.75 g), ethanedithiol (0.25 mL), thioanisole (0.5 mL), and dionized water (0.5 mL) at room temperature for 2 h. After filtration, the peptide was precipitated by methyl *tert*-butyl ether. The precipitate was washed several times with methyl *tert*-butyl ether, dissolved in water, and lyophilized. The disulfide bond between the Cys-7 and Cys-23 residues was closed by oxidation with dropwise addition of 10 mM K$_3$[Fe(CN)$_6$] into a dilute solution of the peptide (approximately 0.1 mM) at pH 7 with stirring at room temperature until a pale yellow color remained for 1 h (Sugiyama et al., 1984). The purification of the peptide was carried out by reversed-phase HPLC on a Vydac C-18 column (2.2 cm × 25 cm, The Separations Group, Hesperia, CA) using a linear CH$_3$CN gradient (from 2% to 60%) in 0.1% trifluoroacetic acid in water applied over a period of 60 min at a flow rate of 15 mL/min. Rat ANF(1−28) was prepared in a similar manner. ANF(1−28) was radioiodinated and used in receptor binding assay.

(Maleimidobenzoyl)-N-hydroxysulfosuccinimide and Iodogen (1,3,4,6-tetrachloro-3,6-diphenylglycoluril) were obtained from Pierce (Rockford, IL). BrAc-N-hydroxysuccinimide, IAc-N-hydroxysuccinimide, *p*-chloromercuriobenzenesulfonic acid (PCMBS), and diisopropylfluorophosphate were from Sigma (St. Louis, MO). [^{125}I]NaI (2.4 mCi/nA of iodine) was obtained from Amersham (Arlington Heights, IL). Endoproteinase Glu-C (*Staphylococcus aureus* protease V8; EC 3.4.21.19) was obtained from Worthington (Freehold, NJ) and endoproteinase Lys-C (EC 3.4.99.30) from Boehringer-Mannheim (Indianapolis, IN). All other chemicals were of reagent grade.

Analytical Procedures. Amino acid analysis was carried out after hydrolysis in 6 N HCl with 0.1% phenol at 110 °C for 20 h. Analysis was performed by reversed-phase HPLC after precolumn derivatization of primary

amino acids with *o*-phthalaldehyde in the presence of 3-mercaptopropionic acid and secondary amino acids with 9-fluorenylmethylchloroformate using the Amino-Quant HPLC System (Hewlett Packard, Wilmington, DE) according to the protocols provided by the manufacturer. Amino acid sequence analysis was carried out by Edman degradation in an Applied Biosystems Model 470A protein sequencer.

^{125}I radioactivity was measured in a Packard Auto-Gamma 500 γ counter (Meriden, CT) at a counting efficiency of 80%. To estimate the specific radioactivity of peptides, the amount of radioiodinated peptide was determined on the basis of the height of the UV absorption peak in the HPLC chromatogram. Corresponding iodinated but nonradioactive peptides were prepared, quantitated by amino acid analysis, and used as the standards in the HPLC. The molecular masses of peptides were determined by electro-spray ionization mass spectrometry carried out at the Protein and Carbohydrate Structure Facility at the University of Michigan.

Preparation of Bovine Adrenal Cortex Plasma Membranes. Bovine adrenal cortex plasma membranes were prepared by a modification of the method of Glossmann et al. (1974) as follows. Bovine adrenal glands were obtained from a local slaughterhouse. The outermost slices (1−2 mm thick) of the adrenal glands were collected using a Staddie-Riggs microtome. The slices were homogenized in four volumes of 10 mM NaHCO$_3$ in a blender for 20 s. Homogenization was repeated in a Polytron homogenizer (Brinkman, Westbury, NY) at the setting of 7 for 40 s. The homogenate was centrifuged at 1500g for 15 min at 4 °C. The supernatant was collected, and the centrifugation was repeated. The supernatant then was collected and centrifuged at 50000g for 2 h. The pellet was resuspended in 50 mM Tris−HCl buffer, pH 7.4, containing 0.15 M NaCl, 5 mM MgCl$_2$, 0.1% bovine serum albumin, and 0.05% bacitracin at a membrane protein concentration of approximately 1.5 mg/mL. The membrane suspension was divided into aliquots, quickly frozen in liquid nitrogen, and stored at −80 °C.

Preparation of $N$$^{4\alpha}$-IAc-ANF(4−28). To ANF(4−28) (10 nmol) in 50 μL of 50 mM HEPES buffer, pH 8.0, was added a 4-fold excess of IAc-N-hydroxysuccinimide in 10 μL of dimethylformamide. The reaction was allowed to proceed for 2 h at room temperature. The reaction mixture was acidified by adding an equal volume of 2 M acetic acid and was then chromatographed directly on a Vydac C-18 reversed-phase column (4.6 mm × 250 mm, Separations Group). Elution was carried out with a linear CH$_3$CN gradient from 0% to 60% over a period of 40 min in 0.1% trifluoroacetic acid in water at a flow rate of 1 mL/min. Elution was monitored by UV absorption at 214 nm. These conditions were used as standard conditions for all HPLC separations. $N$$^{4\alpha}$-IAc-ANF(4−28) was collected in a peak eluting at 24.0 min, while authentic ANF(4−28) was eluted at 23.0 min. Electrospray mass spectrometric analysis of this material gave a molecular mass of 2876.4 Da, which is consistent with the calculated mass value for $N$$^{4\alpha}$-IAc-ANF(4−28). Amino acid analysis gave a composition identical to that of ANF-(4−28). Edman degradation gave no phenylthiohydantoin amino acid, being consistent with iodoacetylation of the N-terminal α-amino group. The yield of $N$$^{4\alpha}$-IAc-ANF(4−28) ranged from 50% to 90%, depending on the preparation. Optimal yields were obtained with a 4- to 10-fold excess of the N-hydroxysuccinimide ester over the peptide. $N$$^{4\alpha}$-IAc-ANF(4−28) was aliquoted, dried in a Savant SpeedVac concentrator, and stored at −20 °C.

Preparation of $N^{4\alpha}$-BrAc-ANF(4−28). The synthesis and isolation of $N^{4\alpha}$-BrAc-ANF(4−28) was carried out in the same manner as above.

Preparation of $N^{4\alpha}$-(Maleimidobenzoyl)-ANF(4−28). (Maleimidobenzoyl)-*N*-hydroxysulfosuccinimide (40 nmol) in 5 μL of water was added to ANF(4−28) (10 nmol) in 50 μL of 50 mM HEPES buffer, pH 8.0. After 2 h, the reaction mixture was acidified by addition of an equal volume of 2 M acetic acid and chromatographed on a Vydac C-18 reversed-phase column as described above. Elution was monitored by UV absorption at 214 nm and at 340 nm. $N^{4\alpha}$-(Maleimidobenzoyl)-ANF(4−28) eluted at 2−3 min after the ANF(4−28) peak and showed absorption at both 214 and 340 nm. The absorption at 340 nm is caused by the maleimide moiety. The purified $N^{4\alpha}$-(maleimidobenzoyl)-ANF(4−28) was aliquoted, dried under a vacuum, and stored at −20 °C.

Radioiodination of Peptide Derivatives. $N^{4\alpha}$-IAc-ANF(4−28) (5−15 μg) in 60 μL of 0.2 M potassium phosphate buffer, pH 7.6, was placed in a glass tube (12 × 65 mm) coated with 50−100 μg of Iodogen. The reaction was initiated by adding 1 mCi of carrier-free [^{125}I]NaI (the specific activity at 2.4 mCi/nmol), unless otherwise specified. After 10 min, the mixture was acidified by adding an equal volume of 2 M acetic acid and chromatographed directly on a Vydac C-18 column as described above. Fractions were collected at 0.5 min intervals. Pass-through fractions were collected in tubes containing a solution of $Na_2S_2O_5$ in water to convert I_2 to nonvolatile iodide. ^{125}I radioactivity was monitored using a Beckman Model 120 Radioisotope detector (Beckman, Fullerton, CA). Monoiodo and diiodo derivatives of $N^{4\alpha}$-IAc-ANF(4−28) were eluted at about 1 and 2 min respectively, after the peak of uniodinated $N^{4\alpha}$-IAc-ANF-(4−28). The combined yield of the two radioiodinated derivatives was about 33% of the [^{125}I]NaI added to the reaction mixture. Similar results were obtained in radioiodination of $N^{4\alpha}$-BrAc-ANF(4−28) and $N^{4\alpha}$-(maleimidobenzoyl)-ANF(4−28). All affinity-labeling experiments were carried out using monoiodinated peptide derivatives.

For some experiments, [^{125}I]NaI (1 mCi) was diluted with 1.88 nmol of unlabeled NaI to a specific activity at 0.43 mCi/nmol before the iodination reaction. To estimate the specific activity of radioiodinated peptides, corresponding nonradioactive, mono- and diiodinated peptides were prepared, quantitated by amino acid analysis, and used as the standards in the HPLC separation. The amount of radioiodinated peptide was determined on the basis of the height of the UV absorption peak in the HPLC chromatogram. The specific radioactivities of the mono- and diiodo derivatives were estimated to be 0.40 mCi/nmol and 0.78 mCi/nmol, respectively, and were consistent with calculated values.

Preparation of N^ϵ-Acetyl-L-lysine Adducts from $N^{4\alpha}$-IAc-ANF(4−28), $N^{4\alpha}$-BrAc-ANF(4−28), and $N^{4\alpha}$-(Maleimidobenzoyl)-ANF(4−28). $N^{4\alpha}$-IAc-ANF(4−28) (8 μg) was reacted with 0.25 M N^ϵ-acetyl-L-lysine in 40 μL of 50 mM HEPES buffer, pH 8.5, at room temperature for 24 h. Reversed-phase HPLC of the reaction mixture under standard conditions gave a new discrete peak eluting at about 1 min after the peak of $N^{4\alpha}$-IAc-ANF-(4−28) (data not shown), which contained the N^ϵ-acetyllysine adduct of $N^{4\alpha}$-(methylenecarbonyl)-ANF(4−28) as determined by mass analysis. N^ϵ-Acetyllysine adducts were prepared from $N^{4\alpha}$-BrAc-ANF(4−28) and from $N^{4\alpha}$-(maleimidobenzoyl)-ANF(4−28) in a similar manner.

Receptor Binding Assay. A competitive binding assay with the bovine adrenal cortex membranes was carried out using [^{125}I]ANF(1−28) as a radioactive ligand (Misono et al., 1985). The assay mixture consisted of 50 mM Tris−HCl buffer, pH 7.4, 0.15 M NaCl, 1 mg/mL bovine serum albumin, 0.5 mg/mL bacitracin, [^{125}I]ANF-(1−28) (300000 cpm/incubation, the final concentration of [^{125}I]ANF(1−28) at approximately 0.14 nM), and varying concentrations of unlabeled ANF or its derivatives. Binding was initiated by adding bovine adrenal membranes (20 μg membrane protein) and continued for 1 h at 0 °C. The total volume was 0.5 mL. The bound [^{125}I]ANF(1−28) was separated from free [^{125}I]ANF(1−28) by filtration through a Whatman GF/C glass filter that was pretreated with 0.3% poly(ethyleneimine) for 10 min. Filters were washed eight times with 4 mL of 20 mM Tris−HCl buffer, pH 7.4, containing 0.15 M NaCl. The ^{125}I-radioactivity trapped on the filter was counted using the Packard Auto-Gamma 500 gamma counter.

Stepwise Affinity Labeling of ANF Receptor. The reaction was carried out on the bovine adrenal plasma membranes using $N^{4\alpha}$-IAc-[^{125}I]ANF(4−28), $N^{4\alpha}$-BrAc-[^{125}I]ANF(4−28), or $N^{4\alpha}$-(maleimidobenzoyl)-[^{125}I]ANF(4−28) as the affinity reagent. Prior to the reaction, the adrenal membranes were treated with PCMBS or *N*-ethylmaleimide to block sulfhydryl groups. This pretreatment step was essential for achieving specific labeling of the ANF receptors. The adrenal membranes (150 μg) were suspended in 90 μL of ice-cold 20 mM potassium phosphate buffer, pH 7.5, containing 2 mM EDTA and 0.15 M NaCl (buffer A). Ten μL of 50 mM PCMBS was then added to the membrane suspension and incubated at room temperature for 10 min, unless otherwise specified. In some experiments, the membranes were pretreated with 5 mM *N*-ethylmaleimide for typically 1 h. At the end of the incubation, the membrane suspension was diluted with 1 mL of buffer A containing 1 mM phenylmethanesulfonyl fluoride, 0.5 mM diisopropylfluorophosphate, and 2 mg/mL of carboxymethylated bovine serum albumin (Sigma). The membranes were collected by centrifugation and then resuspended in 90 μL of the same mixture. The affinity labeling experiment was carried out in a stepwise manner as follows.

Step 1. Binding of the Affinity Reagent to the Adrenal Membranes. $N^{4\alpha}$-IAc-[^{125}I]ANF(4−28), $N^{4\alpha}$-BrAc-[^{125}I]-ANF(4−28), or $N^{4\alpha}$-(maleimidobenzoyl)-[^{125}I]ANF(4−28) in 10 μL of water was added to the membrane suspension to a final concentration of 1 nM, unless otherwise specified. For the control experiment, unmodified ANF-(4−28) was added to a final concentration of 1 μM before the addition of the affinity reagent. The mixture was incubated at 0 °C in the dark for 60 min to allow binding. After the incubation, the membrane suspension was diluted with 1 mL of cold buffer A and centrifuged at 4 °C at 15000*g* for 5 min. The supernatant containing unbound reagent was removed.

Step 2. Alkylation Reaction. The membranes were resuspended in 100 μL of buffer A and incubated at room temperature for 4 h, unless otherwise specified, to effect alkylation reactions. After the reaction, the membranes were collected by centrifugation. To remove noncovalently bound affinity reagent, the membranes were resuspended in 1 mL of 20 mM sodium acetate buffer, pH 5.0, containing 0.15 M NaCl and 2 mM EDTA and incubated at room temperature for 30 min. The membranes were collected by centrifugation and were separated by SDS−PAGE. After the gel was dried, radiolabeled protein bands were detected by autoradiography.

Photoaffinity Labeling of ANF Receptor. Photoaffinity labeling was carried out using $N^{4\alpha}$-(azidobenzoyl)-ANF(4−28) [$N^{4\alpha}$-N$_3$Bz-ANF(4−28)] as a photoaffinity reagent as described previously (Misono et al.,

1985; Pandey et al., 1986). Bovine adrenal cortex membranes (150 μg) were incubated with $N^{4\alpha}$-N$_3$Bz-ANF(4–28) (300000 cpm/incubation, approximately 0.7 nM) in 100 μL of assay buffer at 0 °C for 1 h to allow binding. Membranes were collected by centrifugation and resuspended in the same buffer. Photolysis was performed using a 2.3-W Spectroline ultraviolet lamp (Westbury, NY) at 258 nm at a distance of 10 cm for 5 min.

Affinity Cross-Linking of ANF Receptor. Bovine adrenal membranes (150 μg) were incubated with [^{125}I]-ANF(4–28) (300000 cpm/incubation, 0.7 nM) in 100 μL of assay buffer at 0 °C for 1 h to allow binding. The membranes were collected by centrifugation and resuspended in 20 mM sodium phosphate buffer, pH 7.5 containing 0.15 M NaCl. Disuccinimidyl suberate in 10 μL of dimethyl sulfoxide, or bis(sulfosuccinimidyl)suberate in 10 μL of water, was added to a final concentration of 0.1, 0.5, or 1 mM. Cross-linking was allowed to proceed at room temperature for 1 h.

SDS–PAGE and Autoradiography. The labeled membranes were dissolved in sample buffer consisting of 50 mM Tris–HCl buffer, pH 6.8, 2% SDS, 10 mM dithiothreitol, and 7% glycerol, 0.001% bromophenol blue was added, and the mixture was boiled for 5 min. An aliquot of the mixture (10–20 μg membrane protein) was separated by SDS–PAGE in a 7.5% polyacrylamide gel. For the separation of protein digests, electrophoresis was carried out in a 4–20% polyacrylamide gradient gel. The gels were stained with Coomassie Blue G-250, destained, and dried. Autoradiography was carried out by exposing the dried gels to Kodak X-Omat AR film overnight at −80 °C.

Cyanogen Bromide Digestion of Affinity-Labeled ANF Receptor. Bovine adrenal membranes (200 μg) were affinity labeled with $N^{4\alpha}$-IAc-[^{125}I]ANF(4–28) by the stepwise affinity alkylation reaction described above. The labeled membranes were resuspended in 100 μL of buffer A. The membrane suspension was extracted with three volumes of a CHCl$_3$–CH$_3$OH mixture (2:1 v/v) with vigorous shaking followed by centrifugation. A white pellet formed at the interface of the aqueous and CHCl$_3$ layers and was collected. The pellet was resuspended in 100 μL of water, and the extraction with the CHCl$_3$–CH$_3$OH mixture was repeated. The pellet at the interface was collected and dried under vacuum.

The dried material was dissolved in 70% formic acid at a protein concentration of approximately 2 mg/mL. BrCN was added at a protein-to-reagent ratio of 1:1 (w/w), and the reaction was allowed to proceed at room temperature overnight under nitrogen in the dark. The digest was then diluted 20-fold with water and lyophilized. The dried material was resuspended in 100 μL of 10 mM NH$_4$HCO$_3$, and the lyophilization was repeated. The lyophilized material was separated by SDS–PAGE, and radioactive peptide fragments were detected by autoradiography.

Endoproteinase Digestion of Affinity-Labeled ANF Receptor. The bovine adrenal membranes (200 μg) were affinity labeled with $N^{4\alpha}$-IAc-[^{125}I]ANF(4–28) by the stepwise affinity alkylation. The membranes were then dissolved in 50 μL of 0.5% SDS and immediately heated at 100 °C for 10 min to inactivate endogenous proteases. After cooling, the mixture was diluted 5-fold with 0.1 M NH$_4$HCO$_3$, pH 8. Digestion with endoproteinase Glu-C was carried out at a protein-to-enzyme ratio of 10:1 at 23 °C overnight. Digestion with endoproteinase Lys-C was carried out in a similar manner except that the digestion was carried out in 0.1 M sodium phosphate buffer, pH 7.5, at 37 °C. The digestion was stopped by acidification with an equal volume of 2 M

acetic acid, and the mixture was lyophilized. The lyophilized material was separated by SDS–PAGE or reversed-phase HPLC, and the affinity-labeled fragments were detected by autoradiography or by counting ^{125}I-radioactivity.

RESULTS AND DISCUSSION

Affinity labeling of the ANF receptor was carried out with a procedure that we have termed stepwise affinity labeling. The procedure allowed specific labeling of the ANF receptor at yields substantially greater than those obtainable by the traditional photoaffinity labeling or affinity cross-linking methods. As the affinity reagent, we used the ANF(4–28) peptide in which a moderately reactive electrophilic moiety was incorporated synthetically. The higher labeling yield was achieved by carrying out the reaction in a stepwise fashion as follows: (1) ANF (428) with the attached electrophile was allowed to bind to the receptor in a plasma membrane suspension at 0 °C to suppress covalent reactions; (2) the membranes were collected by centrifugation, and the supernatant containing unbound ligand was removed; and (3) the membranes were resuspended, and the cross-linking reaction was effected by incubation at room temperature. The reaction combines the advantage of each of the photoaffinity labeling and the affinity cross-linking procedures to achieve a substantial improvement in the labeling yield.

ANF is a 28-residue peptide with the sequence Ser-Leu-Arg-Arg-Ser-Ser-Cys-Phe-Gly-Gly-Arg-Ile-Asp-Arg-Ile-Gly-Ala-Gln-Ser-Gly-Leu-Gly-Cys-Asn-Ser-Phe-Arg-Tyr, in which Cys-7 and Cys-23 are disulfide-linked (Misono et al., 1984a,b). The disulfide bond, the sequence in the ring structure, and the carboxyl-terminal sequence, Asn-24 through Arg-27, are critical for biological activity. On the other hand, the amino-terminal region, Ser-1 through Ser-6, and the carboxyl-terminal Tyr-28 residue are not essential for biological activity (for review, see Bovy (1990)). Certain substitutions can be introduced in these nonessential regions without significantly affecting the biological activity or the ability of the peptide to bind to the receptor. In the present study, the electrophilic reactive group was incorporated at the amino-terminal α-amino group of the ANF(4–28) peptide. The affinity reagents, $N^{4\alpha}$-IAc-ANF(4–28), $N^{4\alpha}$-BrAc-ANF(4–28), and $N^{4\alpha}$-(maleimidobenzoyl)-ANF(4–28), were prepared by reacting the ANF(4–28) peptide with IAc-N-hydroxysuccinimide, BrAc-N-hydroxysuccinimide, or (maleimidobenzoyl)-N-hydroxysuccinimide, respectively, at pH 8. Because ANF(4–28) contains no amino acid side chains that readily react with N-hydroxysuccinimide esters, only the amino-terminal α-amino group was expected to be derivatized. The reaction products were purified by reversed-phase HPLC and then radioiodinated at the Tyr-residue to obtain $N^{4\alpha}$-IAc-[^{125}I]ANF-(4–28), $N^{4\alpha}$-BrAc-[^{125}I]ANF(4–28), or $N^{4\alpha}$-(maleimidobenzoyl)-[^{125}I]ANF(4–28).

Because high affinity binding is the prerequisite for efficient receptor labeling, the effect of the amino-terminal modifications on the ANF binding was first tested as follows. $N^{4\alpha}$-IAc-ANF(4–28), $N^{4\alpha}$-BrAc-ANF-(4–28), and $N^{4\alpha}$-(maleimidobenzoyl)-ANF(4–28) were reacted with the α-amino group of N^ϵ-acetyl-L-lysine to obtain unreactive adducts, which in turn were used as competing ligands in competitive binding assays against [^{125}I]ANF(1–28) (Figure 1). The N^ϵ-acetyl-L-lysine adducts derived from $N^{4\alpha}$-IAc-ANF(4–28), $N^{4\alpha}$-BrAc-ANF-(4–28), and $N^{4\alpha}$-(maleimidobenzoyl)-ANF(4–28) were able to compete against [^{125}I]ANF(1–28) with efficiencies nearly equal to that of unmodified ANF(4–28). Scat-
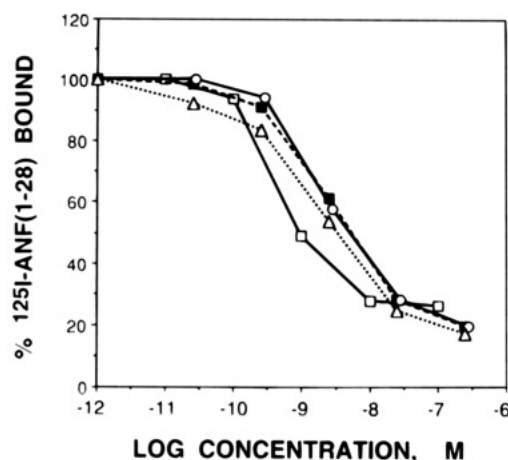
Figure 1. Competitive binding of amino-terminal-modified ANF derivatives against [^{125}I]ANF(1−28). Adrenal membranes (20 μg) were incubated with 0.14 nM [^{125}I]ANF(1−28) in the absence or the presence of varying concentrations of ANF(1−28) (□) or the N^{ϵ}-acetyllysine adduct prepared from $N^{4\alpha}$-(maleimidobenzoyl)-ANF(4−28) (○), $N^{4\alpha}$-BrAc-ANF(4−28) (■), or $N^{4\alpha}$-IAc-ANF(4−28) (△) at 0 °C for 1 h.

chard analysis gave K_d values of 1.8, 2.0, and 2.0 nM for the adducts obtained from $N^{4\alpha}$-IAc-ANF(4−28), $N^{4\alpha}$-BrAc-ANF(4−28), and $N^{4\alpha}$-(maleimidobenzoyl)-ANF(4−28), respectively. The same analysis yielded a K_d of 0.7 and 1.1 nM for ANF(1−28) and ANF(4−28), respectively. The calculated B_{max} values were unchanged at about 2 pmol/mg membrane protein. These results indicated that the amino-terminal modifications did not significantly affect the binding.

An initial application of the stepwise affinity labeling procedure to the adrenal membranes using $N^{4\alpha}$-(maleimidobenzoyl)-[^{125}I]ANF(4−28) (29 nM) as an affinity reagent produced a substantial amount of labeled 130-kDa ANF receptor band but also produced a large amount of background labeling (Figure 2 (top and bottom), lanes f and g). This result suggested that the reaction of the maleimidobenzoyl moiety was occurring much faster than the binding of the affinity reagent to the ANF receptor. The strongest nucleophile in protein side chains is the cystein sulfhydryl group. It seems likely that the large background labeling was the result of a rapid reaction between sulfhydryl groups of the membrane proteins and the maleimidobenzoyl moiety of the affinity reagent. Consistent with this speculation, the nonspecific labeling was nearly completely eliminated when sulfhydryl groups were blocked by pretreating the membranes with 5 mM PCMBS (Figure 2 (top), lanes a−e) or 5 mM N-ethylmaleimide (Figure 2 (bottom), lanes a−e). Moreover, the labeling of the 130-kDa ANF receptor was greater than the labeling obtained with untreated membranes, presumably because more of the reagent remained available to bind to the receptor. The labeling of the 130-kDa protein was completely abolished by inclusion of 1 μM ANF(4−28) (Figure 2 (top and bottom), lane e), demonstrating the labeling specificity. In the pretreatment of the adrenal membranes with PCMBS, a 10-min incubation was sufficient to obtain maximum specific labeling of the ANF receptor. With N-ethylmaleimide, the maximum effect was observed after a 60-min pretreatment. In either case, blocking the sulfhydryl group before addition of the affinity reagent effectively reduced nonspecific labeling reactions. Hence, all the subsequent affinity labeling experiments were carried out with membranes pretreated with 5 mM PCMBS for 10 min. These results also indicate that sulfhydryl groups are not involved in ANF binding to the receptor.
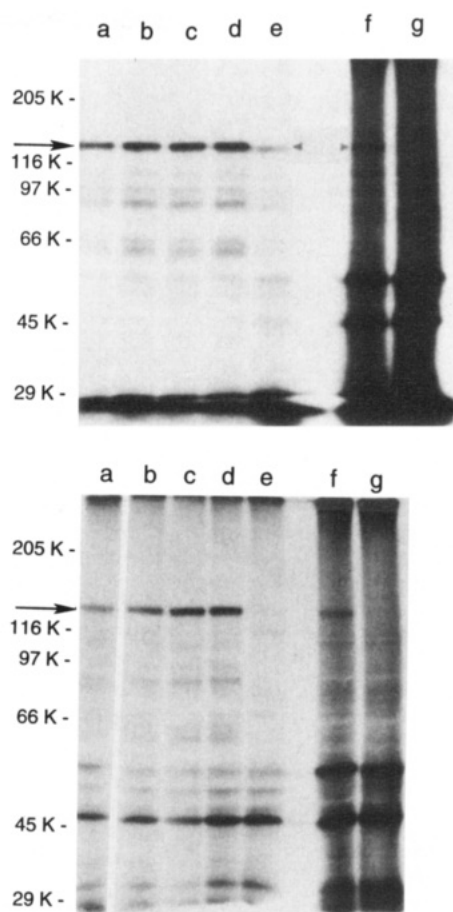
Figure 2. Effect of sulfhydryl group blockade with PCMBS or N-ethylmaleimide on the specificity of stepwise affinity labeling of the ANF receptor in bovine adrenal cortex plasma membranes by $N^{4\alpha}$-(maleimidobenzoyl)-[^{125}I]ANF(4−28). (Top) the adrenal membranes (150 μg) were incubated with 5 mM PCMBS for 0, 30, 60, or 90 min (lanes a, b, c, and d, respectively) before the initial binding step in the stepwise affinity labeling procedure. Lane e shows the control experiment where the labeling reaction was carried out in the presence of 1 μM ANF(4−28) with the membranes treated with 5 mM PCMBS for 90 min. Lanes f and g show results of the labeling reaction performed with untreated membranes in the absence (lane f) or the presence of 1 μM ANF-(4−28) (lane g). (Bottom) The same set of experiments as above were carried out except using N-ethylmaleimide.

The time course of the labeling reaction with $N^{4\alpha}$-BrAc-[^{125}I]ANF(4−28) (specific radioactivity at 0.43 mCi/nmol) is shown in Figure 3. As the first step, the adrenal membranes were incubated with $N^{4\alpha}$-BrAc-[^{125}I]ANF(4−28) at 0 °C for 1 h and then washed to remove unbound reagent. The covalent labeling reaction was initiated by raising the temperature of the membrane suspension to 23 °C. At time intervals, aliquots were taken, and the reaction was stopped by addition of 10 mM dithiothreitol. The incorporation of the ^{125}I-labeled ligand into the 130-kDa protein increased with time, reaching the maximal labeling in 2−3 h. The course of the reaction of $N^{4\alpha}$-IAc-[^{125}I]ANF(4−28) was similar to that of $N^{4\alpha}$-BrAc-[^{125}I]-ANF(4−28). The reaction of $N^{4\alpha}$-(maleimidobenzoyl)-[^{125}I]ANF(4−28) was slightly slower, reaching a maximum in 4−6 h (data not shown).

The first step of the incubation of the membranes with the affinity reagent at 0 °C for 1 h followed by washing to remove unbound reagent was essential in minimizing nonspecific labeling. Direct reactions with the affinity reagents at 23 °C resulted in increased levels of nonspecific labeling.

Figure 4 shows the results of labeling reactions carried out using different concentrations of $N^{4\alpha}$-IAc-[^{125}I]ANF-
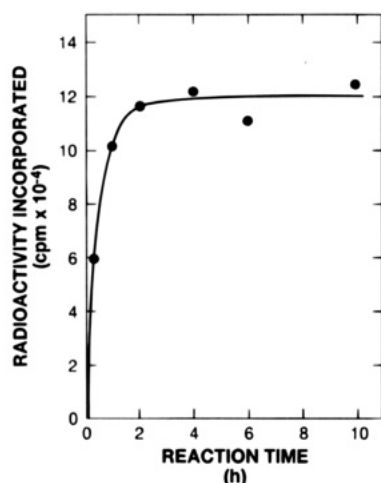
Figure 3. Time-course of ANF receptor labeling during the stepwise affinity labeling using $N^{4\alpha}$-BrAc-[^{125}I]ANF(4−28). Adrenal membranes (150 μg) pretreated with 5 mM PCMBS for 10 min were incubated with 28 nM $N^{4\alpha}$-BrAc-[^{125}I]ANF(4−28) at 0 °C for 1 h to allow binding. After unbound reagent was removed, the covalent labeling reaction was allowed to proceed at 23 °C. The ^{125}I-radioactivity incorporated into the 130-kDa band in SDS−PAGE was plotted against the incubation time.
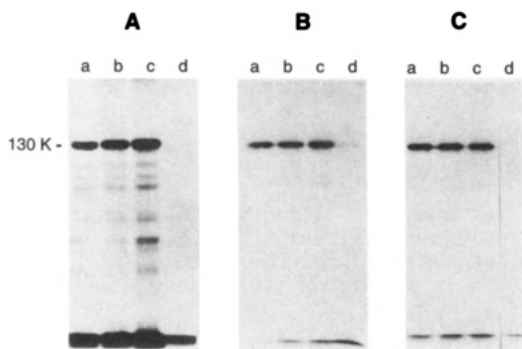
Figure 4. Stepwise affinity labeling of the ANF receptor in the bovine adrenal membranes using varying concentrations of $N^{4\alpha}$-IAc-[^{125}I]ANF(4−28), $N^{4\alpha}$-BrAc-[^{125}I]ANF(4−28), and $N^{4\alpha}$-(maleimidobenzoyl)-[^{125}I]ANF(4−28). Adrenal membranes (150 μg) pretreated with 5 mM PCMBS for 10 min were used. (A) The stepwise labeling reactions were carried out with 10, 30, 45 nM $N^{4\alpha}$-IAc-[^{125}I]ANF(4−28) (lanes a, b, and c, respectively). The control experiment (lane d) was carried out with 45 nM $N^{4\alpha}$-IAc-[^{125}I]ANF(4−28) in the presence of 1 μM ANF(4−28). (B) The labeling reactions with 10, 30, and 45 nM $N^{4\alpha}$-BrAc-[^{125}I]ANF(4−28) (lanes a, b and c, respectively). The control experiment (lane d) was carried out with 45 nM $N^{4\alpha}$-BrAc-[^{125}I]-ANF(4−28) in the presence of 1 μM ANF(4−28). (C) The labeling reactions with 10, 30, and 45 nM $N^{4\alpha}$-(maleimidobenzoyl)-[^{125}I]-ANF(4−28) (lanes a, b, and c, respectively). The control experiment (lane d) was carried out with 45 nM $N^{4\alpha}$-(maleimidobenzoyl)-[^{125}I]ANF(4−28) in the presence of 1 μM ANF(4−28).

(4−28), $N^{4\alpha}$-BrAc-[^{125}I]ANF(4−28), or $N^{4\alpha}$-(maleimidobenzoyl)-[^{125}I]ANF(4−28). The reagents with specific radioactivities at 0.43 mCi/nmol were used. The intensity of the labeled bands increased slightly with the concentrations of the reagents. The extent of labeling appears to depend mostly on the initial binding of the reagent to the receptor site at 0 °C. To estimate the yield of receptor labeling, sections of polyacrylamide gel containing the labeled 130-kDa band were excised, and the ^{125}I-radioactivity was counted. On the basis of the theoretical specific activity of the reagents (0.43 mCi/nmol at the reference time), the amounts of reagent incorporated into the 130-kDa receptor band were estimated to be 1.4, 1.04, and 0.42 fmol/μg of protein for the membranes that were labeled using 45 nM concentrations of $N^{4\alpha}$-IAc-[^{125}I]ANF(4−28), $N^{4\alpha}$-BrAc-[^{125}I]ANF(4−
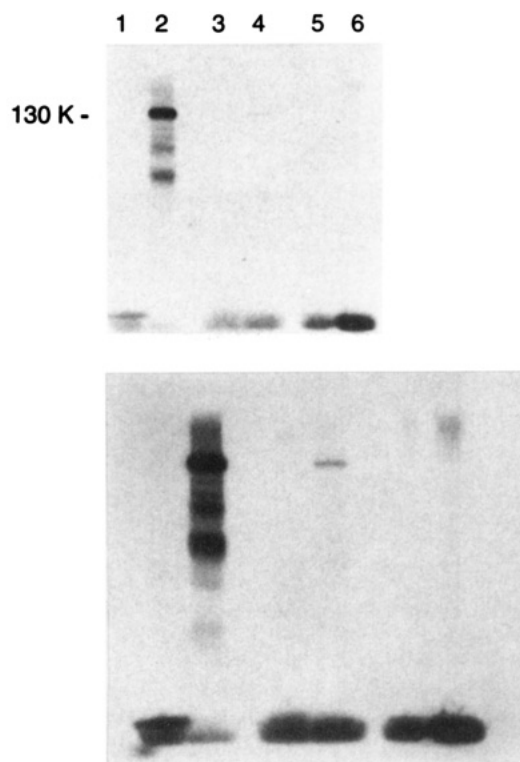
Figure 5. Comparison of the efficiency of ANF receptor labeling by the stepwise affinity labeling, photoaffinity labeling, and direct affinity cross-linking methods. Top: arenal membranes (150 μg) pretreated with 5 mM PCMBS for 10 min were affinity-labeled using the same concentrations (0.7 nM) of the affinity reagent, $N^{4\alpha}$-IAc-[^{125}I]ANF(4−28) (lanes 1 and 2), $N^{4\alpha}$-N$_3$Bz-[^{125}I]ANF(4−28) (lanes 3 and 4), and [^{125}I]ANF(4−28) (lanes 5 and 6) at 0 °C for 1 h in the presence (lanes 1, 3, and 5) or absence of 1 μM ANF(4−28) (lanes 2, 4, and 6). The reaction conditions are described in the text. Bottom: an autoradiogram of the same dried gel developed after longer period of exposure to an X-ray film.

28), and $N^{4\alpha}$-(maleimidobenzoyl)-[^{125}I]ANF(4−28), respectively. On the basis of the B_{max} of approximately 2 pmol/mg membrane protein as determined by the binding assay, the yields of receptor labeling were estimated to be 70%, 51%, and 22%, respectively. The yields may be improved further by using saturating concentrations of the affinity reagent during the initial binding step.

The efficiency of labeling by the stepwise method using $N^{4\alpha}$-IAc-[^{125}I]ANF(4−28) was compared against those efficiencies obtained by photoaffinity labeling using N$_3$-Bz-[^{125}I]ANF(4−28) and by direct affinity cross-linking using [^{125}I]ANF(4−28) and a cross-linker, disuccinimidyl suberate (Figure 5). To permit direct comparison, all the affinity ligands were radioiodinated using the same lot of carrier-free [^{125}I]NaI, and monoiodinated derivatives were used at the same concentrations (300000 cpm/incubation, at the final concentration of 0.7 nM) during the initial binding step. The stepwise affinity labeling gave a substantially greater labeling yield (lanes 1 and 2) than that obtained by photoaffinity labeling (lanes 3 and 4) or direct affinity cross-linking (lanes 5 and 6). On the basis of the amount of ^{125}I-radioactivity incorporated into the 130-kDa bands, the ratio of the labeling yields by the stepwise method, photoaffinity labeling, and direct cross-linking was 63:2.3:1.0. In the direct cross-linking reaction, varying the cross-linker concentration (0.1, 0.5, and 1.0 mM) or the use of a water-soluble cross-linker, bis(sulfosuccinimidyl)suberate, did not improve the extent of cross-linking.
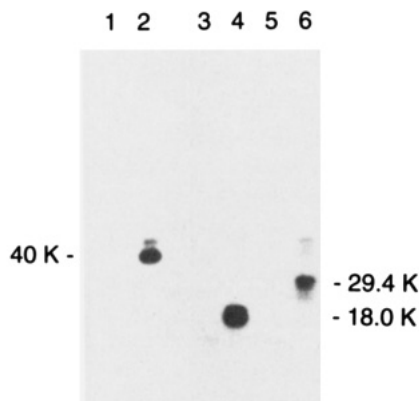
Figure 6. Separation of the affinity-labeled peptide fragment by SDS−PAGE using a 4−20% gradient gel. The bovine adrenal membranes were affinity-labeled using $N^{4\alpha}$-IAc-[^{125}I]ANF(4−28) in the presence (lanes 1, 3, and 5) or absence of 1 μM ANF-(4−28) (lanes 2, 4, and 6). The membrane protein was extracted and digested with BrCN (lanes 1 and 2), endoproteinase Glu-C (lanes 3 and 4), or endoproteinase Lys-C (lanes 5 and 6). The labeled peptides were detected by autoradiography.

To examine the chemical selectivity of the reaction for the amino acid side chains, the protein fraction extracted from the affinity-labeled adrenal membranes was analyzed by radiochemical peptide-mapping (Figure 6). The adrenal membranes were affinity labeled using $N^{4\alpha}$-IAc-[^{125}I]ANF(4−28) by the stepwise method. The protein extracted from the labeled membranes was digested with BrCN, endoproteinase Glu-C, or endoproteinase Lys-C and separated by SDS−PAGE, and peptide fragments labeled with ^{125}I were detected by autoradiography. BrCN-digestion of the labeled membrane protein yielded a single labeled fragment with an apparent molecular mass of 40 kDa (lane 2). This band was absent in the control experiment, in which the stepwise affinity labeling was carried out in the presence of 1 μM unmodified ANF(4−28) as a competing ligand (lane 1), demonstrating the specificity of labeling. The results also indicate that the linkage between the affinity label and the receptor polypeptide was stable under the conditions of the BrCN cleavage reaction.

The digestion with endoproteinase Glu-C was carried out in 0.1 M NH$_4$HCO$_3$, in which proteolysis is expected to occur only at glutamyl bonds (Houmard and Drapeau, 1972). Because ANF(4−28) does not contain the Glu residue, the digestion does not remove ^{125}I-label that is incorporated at Tyr-28 in the affinity reagent. SDS−PAGE of the digest gave a single labeled band with an apparent mass of 18 kDa (Figure 6, lane 4). This band was again absent in the control experiment (lane 3). Similarly, digestion with endoproteinase Lys-C gave a specific band with an apparent mass of 29 kDa (lanes 5 and 6).

Reversed-phase HPLC separation of the endoproteinase Lys-C digest also gave a single major ^{125}I-radioactivity peak (data not shown). This peak was eluted with a retention time (37 min) substantially longer than that of unreacted $N^{4\alpha}$-IAc-[^{125}I]ANF(4−28) (32 min), suggesting that the peak may contain a peptide fragment cross-linked with the affinity ligand. Similar results were obtained with the endoproteinase Glu-C digest, in which a single ^{125}I-radioactivity peak appeared at 38 min.

The generation of only one major labeled fragment in each digestion mixture suggests that the covalent labeling of the ANF receptor by the affinity reagent occurs at a single site or at a limited number of sites. These results clearly indicate considerable chemical selectivity in the reaction with the receptor side chains. Evidently, the

specific labeling of the ANF receptor depends on the specific binding of the ANF peptide to the receptor binding site. The reactive moiety attached to the ANF peptide would then react with the receptor protein residues that are within its geometric reach. Residues that may react with the haloacetyl and maleimide reagents include Cys, His, Met, Lys, Tyr, Ser, Thr, Asp, and Glu (Wilchek and Givol, 1977). Among these residues, the Cys-SH residue is the most reactive. The bifunctional reagents utilized in this study, IAc-*N*-hydroxysuccinimide, BrAc-*N*-hydroxysuccinimide, or (maleimidobenzoyl)-*N*-hydroxysuccinimide, have previously been used to cross-link proteins and peptides through a sulfhydryl group and an amino group (for a review, see Wong (1991)). The cross-linking reactions have been utilized, for example, to couple antigen peptides to carrier proteins (Kitagawa and Aikawa, 1976) or toxins to antibodies (Thorpe et al., 1984). However, because sulfhydryl groups react too rapidly with the IAc, BrAc, or maleimido group of the affinity reagents, it was necessary to block all accessible sulfhydryl groups in the membranes prior to the affinity labeling steps.

Among the side chain residues that are within the span of the reagent arm, a residue with the strongest nucleophilicity and with the optimal orientation would react most preferentially, thereby conferring a significant degree of chemical specificity to the reaction. The reaction of the electrophile, either the haloacetate or the maleimide, with any of those amino acid side chains is expected to yield a cross-linked structure of a form that has been well characterized. Identification of the affinity-labeled residue can also be facilitated by incorporation of a radioisotope, such as ^{14}C and ^{3}H, in the iodoacetyl or maleimide moiety. It is necessary to note that the α-hydrogen of the carboxylmethylene group is an acidic hydrogen and undergoes slow exchange with solvent proton.

Photoaffinity labeling of the ANF receptor using a *p*-benzoylphenylalanine-containing ANF peptide analog has been reported to provide a high yield of receptor labeling (McNicoll et al., 1992). However, the radical nature of the photoactivated reactant species may lead to cross-linking at multiple sites and yield a mixture of cross-linked structures that are of unknown forms (Dorman and Prestwich, 1994).

The increase in the yield of affinity labeling of the ANF receptor obtained here by the stepwise affinity labeling method represents a major improvement over the commonly used photoaffinity labeling and affinity cross-linking procedures. The high labeling yield, chemical selectivity of the reaction, and stability of the linkage are the essential requirements for a chemical probe that can be used to determine peptide receptor binding site structures. The stepwise procedure described here appears to satisfy all these requirements. Determination of the binding site sequence would be greatly facilitated by the availability of purified receptor protein. However, purification of cell membrane receptors, including the ANF receptor, generally requires a lengthy procedure and provides limited amounts of purified protein. Yet, certain membrane receptors cannot be solubilized in an active form and, hence, cannot be purified. These difficulties have often precluded structural characterization of the peptide receptor binding site. The present approach that provides high-yield specific labeling of the ANF receptor may allow a binding site sequence to be determined directly from a plasma membrane preparation after labeling and appropriate digestion of the membrane protein. Purification of an affinity-labeled binding site peptide from a complex mixture of protein digest may

be greatly facilitated by anti-ANF antibody affinity chromatography. The stepwise affinity labeling method for ANF receptors described in the present report may also be adaptable to certain other peptide hormone receptors.

ACKNOWLEDGMENT

Supporting Information Available: HPLC chromatograms showing preparation and purification of $N^{4\alpha}$-IAc-ANF(4–28), $N^{4\alpha}$-BrAc-ANF(4–28), $N^{4\alpha}$-(maleimidobenzoyl)-ANF(4–28), $N^{4\alpha}$-IAc-[^{125}I]ANF(4–28), $N^{4\alpha}$-BrAc-[^{125}I]ANF(4–28), and $N^{4\alpha}$-(maleimidobenzoyl)-[^{125}I]ANF(4–28) and HPLC peptide-mapping of the endoproteinase Lys-C digest of adrenal membranes that were affinity-labeled with IAc-[^{125}I]ANF(4–28) by the stepwise method (9 pages). Ordering information is given on any current masthead page.

LITERATURE CITED

Bovy, P. R. (1990) Structure Activity in the atrial natriuretic peptide family. *Med. Res. Rev. 10*, 115–142.

Cantin, M., and Genest, J. (1986) The heart as an endocrine organ. *Clin. Invest. Med. 9*, 319–327.

Chinkers M., and Garbers, D. L. (1989) The protein kinase domain of the ANP receptor is required for signaling. *Science 245*, 1392–1394.

Chinkers, M., Garbers, D. L., Chang, M. S., Lowe, D. G., Chin, H., Goeddel, D. V., and Schulz, S. (1989) A membrane form of guanylate cyclase is an atrial natriuretic peptide receptor. *Nature 338*, 78–83.

Currie, M. G, Geller, D. M., Cole, B. R., Boylan, J. G., Yu Sheng, W., Holmberg, S. W., and Needleman, P. (1983) Bioactive cardiac substances: Potent vasorelaxant activity in mammalian atria. *Science 221*, 71–73.

de Bold, A. J., Borenstein, H. B., Veress, A. T., and Sonnenberg, H. (1981) A rapid and potent natriuretic response to intravenous injection of atrial myocardial extract in rats. *Life Sci. 28*, 89–94.

Dorman, G., and Prestwich, G. D. (1994) Benzophenone photophores in biochemistry. *Biochemistry 33*, 5661–5673.

Gerzer, R, Heim, J.-M., Schutte, B., and Weil, J. (1987) Cellular mechanism of action of atrial natriuretic factor. *Klin. Wochenschr. 65*, 109–114.

Glossmann, H., Baukal, A. J., and Catt, K. J. (1974) Properties of angiotensin II receptors in the bovine and rat adrenal cortex. *J. Biol. Chem.* 825–834.

Grammer, R. T., Fukumi, H., Inagami, T., and Misono, K. S. (1983) Rat atrial natriuretic factor: purification and vasorelaxant activity. *Biochem. Biophys. Res. Commun. 116*, 696–703.

Houmard J., and Drapeau G. R. (1972) Staphylococcal protease: a proteolytic enzyme specific for glutamoyl bonds. *Proc. Nat. Acad. Sci. U.S.A. 69*, 3506–3509.

Kitagawa, T., and Aikawa, T. (1976) Enzyme coupled immunoassay of insulin using a novel coupling reagent. *J. Biochem. 79*, 233–236.

Kuno, T., Andresen, J. W., Kamisaki, Y., Waldmen, S. A., Chang, L. Y., Saheki, S., Leitman, D. C., Nakane, M., and Murad, F. (1986) Co-purification of an atrial natriuretic factor receptor and particulate guanylate cyclase from rat lung. *J. Biol. Chem. 261*, 5817–5823.

McNicoll, M., Escher, E., Wilkes, B. C., Schiller, P. W., Ong, H., and De Lean, A. (1992) Highly efficient photoaffinity labeling of the hormone binding domain of atrial natriuretic factor receptor. *Biochemistry 31*, 4487–4493.

Meloche, S., McNicoll, N., Liu, B., Ong, H., and De Lean, A. (1988) Atrial natriuretic factor R1 receptor from bovine adrenal zona glomerulosa: Purification characterization and modulation by amiloride. *Biochemistry 27*, 8151–8158.

Misono, K. S., Grammer, R. T., Fukumi, H., and Inagami, T. (1984a) Rat atrial natriuretic factor: Isolation, structure and biological activities of four major peptides. *Biochem. Biophys. Res. Commun. 123*, 444–451.

Misono, K. S., Fukumi, H., Grammer, R. T., and Inagami, T. (1984b) Rat atrial natriuretic factor: Complete amino acid sequence and disulfide linkage essential for biological activity. *Biochem. Biophys. Res. Commun. 119*, 524–529.

Misono, K. S., Grammer, R. T., Rigby, J. W., and Inagami, T. (1985) Photoaffinity labeling of atrial natriuretic factor receptor in bovine and rat adrenal cortical membranes. *Biochem. Biophys. Res. Commun. 130*, 994–1001.

Pandey, K. N. Inagami, T., and Misono, K. S. (1986) Atrial natriuretic factor receptor on cultured Leydig tumor cells: ligand binding and photoaffinity labeling. *Biochemistry 25*, 8467–8472.

Pilch P. F., and Czech M. P. (1983) Affinity cross-linking of peptide hormones and their receptors. *Recept. Biochem. Methodol. 1*, 161–175.

Ruoho, A. E., Rashidbaigi, A., and Roeder, P. E. (1983) Approaches to the identification of receptors utilizing photoaffinity labeling. *Recept. Biochem. Methodol. 1*, 119–160.

Sugiyama, M., Fukumi, H., Grammer, R. T., Misono, K. S., Yabe, Y., Morisawa, Y., and Inagami, T. (1984) Synthesis of atrial natriuretic peptides and studies of structural factors in tissue specificity. *Biochem. Biophys. Res. Commun. 123*, 338–344.

Takayanagi, R., Inagami, T., Snajdar, R. M., Imada, T., Tamura, M., and Misono, K. S. (1987) Two distinct forms of receptors for atrial natriuretic factor in bovine adrenocortical cells: purification ligand binding and peptide mapping. *J. Biol. Chem. 262*, 12104–12113.

Thorpe, P. E., Ross, W. C. J., Brown, A. N. F., Myers, C. D., Cumber, A. J., Foxwell, B.M. J., and Forrester, J. T. (1984) Blockade of the galactose-binding sites of ricin by its linkage to antibody specific cytotoxic effects of the conjugates. *Eur. J. Biochem. 140*, 63–67.

Wilchek M., and Givol D. (1977) Haloacetyl derivatives. *Methods Enzymol. 46*, 153–157.

Wong S. S. (1991) *Chemistry of protein conjugation and cross-linking*, CRC Press, Boca Raton, FL.

Synthesis, Binding Affinity, and Cross-Linking of Monodentate Photoactive Phenothiazines to Calmodulin

Miroslaw Golinski,[†] Paul J. DeLaLuz,[†] Rey Floresca,[†] Tavner J. Delcamp,[‡] Thomas C. Vanaman,*,[‡] and David S. Watt*,[†]

Department of Chemistry and Division of Medicinal Chemistry and Pharmaceutics, and Department of Biochemistry, University of Kentucky, Lexington, Kentucky 40506. Received May 2, 1995[⊗]

Various photoactive phenothiazines were synthesized that possessed a 2-azido, 3-azido, 2-benzoyl, or 1,3,4-trifluoro-2-azido functionality in combination with various modifications of the *N*-alkyl side chain. These phenothiazines were evaluated for their ability to inhibit the calmodulin-mediated activation of phosphodiesterase (PDE). All were active in inhibiting the action of calmodulin (CaM), but those possessing either a 3-azido and a 4-(4-methyl-1-piperazinyl)butyl side chain or a 2-benzoyl group and 3-(dimethylamino)propyl side chain proved to be most active ($I_{50} = 14 \pm 3$ μM and 7 ± 1 μM, respectively) when compared to the known inhibitor, chlorpromazine (CPZ, $I_{50} = 30$ μM). Calmodulin was photolabeled with *ca.* 35% efficiency in a light- and calcium-dependent fashion using a radiolabeled analog, 3-azido-10-(4-(4-[^{14}C]methyl-1-piperazinyl)butyl)phenothiazine, of one of these compounds. Competition studies using this radiolabeled analog and CPZ were consistent with binding to one or both of the hydrophobic binding pockets of CaM.

INTRODUCTION

Traditional heterobifunctional photoaffinity cross-linking reagents *(1)* provide a direct means for studying intra- and intermolecular interactions among proteins but suffer from several drawbacks. Principal among these problems is the promiscuous nature of the chemically reactive terminus of these reagents that typically reacts with a host of nucleophilic Lys or Cys residues within the protein under study *(2)*. To address this concern, we developed a new class of reagents described as "targeted, bidentate" cross-linking reagents *(3, 4)*. These reagents are distinguished from their predecessors in that they possess a ligand that guides the initial binding event of the reagent to one of the proteins under study and *two* photoactive groups that permit tethering of the reagent to different proteins by irradiation at different wavelengths.

Calmodulin (CaM)[1] plays an important regulatory role in its interactions with numerous other proteins *(5)* and represents an ideal system for the evaluation of new cross-linking reagents. Previous studies from these laboratories utilized a heterobifunctional cross-linking reagent possessing a photoactive aryl azide moiety and a chemically reactive succinimidyl (NHS) ester terminus *(2)*. Detailed investigations revealed a pattern of Lys reactivity that was dependent on the degree of calcium loading of CaM[1] and on the length of the linking arm connecting the salicylate terminus and the NHS[1] ester terminus. It appeared that modification of CaM with the salicylate-derived heterobifunctional reagents followed a time sequence in which initial noncovalent binding of the aromatic terminus of the reagent to one of the hydrophobic binding pockets was followed by modification of those Lys residues to which the exposed, chemically reactive NHS[1] ester could reach *(2)*.

A logical extension of this work involved the development of cross-linking reagents that would take advantage of the well-known binding of drugs like phenothiazines to the high-affinity and/or low-affinity hydrophobic binding pocket of CaM *(6–12)*. Direct photoaffinity labeling of CaM with a phenothiazine has been reported *(13)* as well as the preparation of phenothiazines with photoactive side chain substituents for use with dopamine receptor studies *(14)*. However, these reagents are not well suited for studies of the hydrophobic binding pockets of target proteins that bind the phenothiazine nucleus. As a first step in the development of "bidentate" cross-linking reagents with this capability, it was necessary to prepare various photoactive phenothiazines having 2-azido, 3-azido, 2-benzoyl, or 1,3,4-trifluoro-2-azido functionality in combination with various modifications of the *N*-alkyl side chain, to evaluate these phenothiazines for their ability to inhibit the calmodulin-mediated activation of phosphodiesterase (PDE), and to determine the cross-linking efficiency of one or more biologically active phenothiazines to CaM. It was also important to determine that a photoactive phenothiazine capable of inhibiting PDE[1] activation would also photolabel CaM with acceptable efficiency.

EXPERIMENTAL PROCEDURES

Calmodulin-Stimulated Phosphodiesterase Assays. Bovine brain activator deficient PDE, 5'-nucleotidase, and cAMP[1] were obtained from Sigma. Calmodulin was purified from bovine testes according to the proce-

* Corresponding authors. For chemical synthesis: David Watt, Department of Chemistry, University of Kentucky, Rose and Funkhouser Sts., Lexington, KY 40506. (Tel: (606) 257-5294. FAX: (606) 323-2800. E-mail: WATT@UKCC.UKY.EDU. For biochemistry: Thomas C. Vanaman, Department of Biochemistry, Chandler Medical Center, Rose St., Lexington, KY 40536 Tel: (606) 257-1347. FAX: (606) 257-7795. E-mail: VANAMAN@POP.UKY.EDU.

[†] Department of Chemistry and Division of Medicinal Chemistry and Pharmaceutics.

[‡] Department of Biochemistry.

[⊗] Abstract published in *Advance ACS Abstracts,* August 15, 1995.

[1] Abbreviations: CaM, calmodulin; cAMP, adenosine 3':5'-cyclic monophosphate; CPZ, chlorpromazine; DMF, *N,N*-dimethylformamide; DMSO, dimethyl sulfoxide; DTT, dithiothreitol; NHS, ester of *N*-hydroxysuccinimide; PDE, bovine brain activator deficient 3':5'-cyclic nucleotide phosphodiesterase; PPO, 2,5-diphenyloxazole; SDS–PAGE, sodium dodecylsulfate–polyacrylamide gel electrophoresis; TRIS; tris(hydroxymethyl)aminomethane.

Table 1. I_{50} Values from Calmodulin-Stimulated Phosphodiesterase Assays for Phenothiazine Analogs
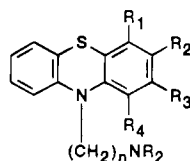
	R_1	R_2	R_3	R_4	n	NR_2	I_{50}, μM	I_{50}/I_{50} CPZ
1a[d]	H	N_3	H	H	3	NMe_2	43 ± 18	1.4
1b[c]	H	N_3	H	H	3	NMP^a	21 ± 8	0.7
1c[d]	H	N_3	H	H	4	NMe_2	23 ± 10	0.8
1d[c]	H	N_3	H	H	4	NMP^a	14 ± 3	0.5
2d[c]	H	H	N_3	H	4	NMP^a	21 ± 6	0.7
3a[d]	H	H	Bz^b	H	3	NMe_2	7 ± 1	0.3
3b[d]	H	H	Bz^b	H	3	NMP^a	3.5 ± 0.5	0.1
4d[c]	F	F	N_3	F	4	NMP^a	21 ± 3	0.7

a NMP = 4-methylpiperazinyl. *b* Bz = benzoyl. *c* Used as dimaleate salt. *d* Used as oxalate salt.

dure of Jamieson and Vanaman (15). Assay of PDE was performed according to the method of Wallace (16) with the following modification. Hydrolysis of the product of the reaction, adenosine 5'-monophosphate, was carried out with 5'-nucleotidase, and the subsequent release of inorganic phosphate was measured according to the method of Lanzetta (17). Each assay was performed at 30 °C in 0.2 mL of a buffer consisting of 50 mM TRIS,[1] 25 mM ammonium acetate, 3 mM magnesium acetate, 100 μM calcium chloride, and 5 mM DTT[1] at pH 8.0. Various concentrations of each inhibitor in triplicate were preincubated for 5 min with 500 ng/mL (30 nM) of calmodulin followed by the addition of 0.001 unit of PDE and a further preincubation of 5 min. The reaction was initiated by the addition of cAMP[1] to a final concentration of 1 mM. After 10 min, the reaction was stopped by incubating each sample at 90 °C for 2 min. After the addition of 0.2 unit of 5'-nucleotidase, each sample was incubated for an additional 15 min at 30 °C. An aliquot of 0.1 mL was transferred from each sample to 0.8 mL of Lanzetta reagent (17), and the mixture was incubated for at least 20 min before measuring the absorbance at 660 nm.

Data from triplicate runs was analyzed and plotted as the percent of the calmodulin-stimulated PDE activity at each inhibitor concentration with 100% representing the absorbance value of calmodulin-stimulated PDE in the absence of inhibitor minus the absorbance value of PDE assayed in the absence of calmodulin. For each inhibitor the effect on PDE activity in the absence of calmodulin was found to be <5% over the range of concentrations used. From each plot of percent activity versus inhibitor concentration an I_{50} value was determined which represents the concentration producing 50% inhibition of calmodulin-stimulated PDE activity. The I_{50} values reported in Table 1 represent the average of four separate experiments.

Photolysis Studies with 3-Azido-10-(4-(4-[^{14}C]-methyl-1-piperazinyl)butyl)phenothiazine ([^{14}C]-1d). Photolysis experiments were performed to demonstrate irradiation and Ca^{2-}-dependent incorporation of 3-azido-10-(4-(4-[^{14}C]methyl-1-piperazinyl)butyl)phenothiazine (1d) into CaM. Aliquots (0.5 mL) of stock solutions of CaM (5 mg/mL) in 10 mM NH_4HCO_3 were passed through a 1 × 3 cm column of Chelex-100 immediately prior to use in order to remove associated Ca^{2+}. Photolysis mixtures were then prepared containing 100 mM HEPES (pH 7.4), 50 μM CaM, 100 μM [^{14}C]-1d, and either 1 mM $CaCl_2$ or 5 mM EGTA. After preincubation

for 5 min at 25 °C, one half of each reaction mixture was transferred to a parafilm boat held on ice and irradiated with a hand-held ultraviolet light (Mineralite model UVGL-25) at a distance of 4 cm for 1 min. The reminder of the sample was treated identically except without irradiation. After treatment, samples were transferred to Eppendorf tubes, adjusted to a concentration of 10 mM in DTT[1] and 1% SDS, and analyzed by SDS–PAGE and autoradiography as described below.

Photolysis experiments were also used to demonstrate competition for binding between **1d** and CPZ[1]. Samples containing 20 μM CaM, 1 mM Ca^{2+}, and 80 μM [^{14}C]-1d with and without 2 mM CPZ were irradiated as described above with nonirradiated controls run in parallel to demonstrate specific reaction. Samples were prepared as described above following treatment and analyzed by SDS–PAGE and autoradiography as described below.

SDS–PAGE and Autoradiography. Samples containing 1% SDS and 10 mM DTT plus other constituents were treated at 100 °C for 2 min. Bromophenol blue tracking dye and glycerol were added and the samples applied to 15% polyacrylamide gels and electrophoresis performed in the presence of SDS as described by Laemmli (18). After tracking dye had migrated to within 1 cm of the bottom of the gel, the gels were removed from the apparatus and washed with H_2O. The protein bands were fixed by immersion of the gel in 10% formaldehyde for 15 min at 25 °C. The fixed gels were washed by soaking in deionized H_2O for 2 × 30 min, and were dehydrated by treatment in neat DMSO[1] for 30 min at 25 °C. Scintillant was introduced into the gel by soaking in a solution of 20% PPO[1] in DMSO for 20 min followed by washing with H_2O for 30 min which resulted in precipitation of the PPO. Gels were dried on Whatman 3MM under vacuum and exposed to Kodak X-Omat AR film backed with an intensifying screen. After overnight exposure, the resulting autoradiogram was developed with an X-ray film processor.

10-(3-Chloropropyl)-3-nitrophenothiazine (7). To a solution of 4.40 g (18 mmol) of 3-nitrophenothiazine (6) (19) in 36 mL of anhydrous DMSO at 18 °C under an Ar atmosphere was added in portions 1.44 g (36 mmol, 2 equiv) of 60% NaH in mineral oil. The mixture was stirred at 25 °C for 15 min. To this mixture was added 5.34 mL (8.50 g, 54 mmol, 3 equiv) of 1-bromo-3-chloropropane and the reaction temperature increased to 29 °C. The solution was stirred for 24 h. The reaction was quenched with 1.93 g (36 mmol, 2 equiv) of NH_4Cl that was added in small portions with cooling in order to destroy the excess of NaH. The quenched reaction mixture was stirred at 25 °C for 10 min. The mixture was poured into 200 mL of water and extracted with ether. The combined ether extracts were dried over anhydrous $MgSO_4$ and chromatographed twice on silica gel using EtOAc–hexane (gradient: 1:20 followed by 1:8) to give 2.67 g (46%) of a 92:8 mixture of **7** and 10-(3-bromopropyl)-3-nitrophenothiazine. The bromo compound could not be removed by recrystallization, although this was of no concern since either **7** or the bromo compound participated equally well in the next reaction. A pure sample of **7** was, however, prepared by treating 22 mg (68 μmol) of the mixture of chloro and bromo compounds in 600 μL of 1:6 water–DMF[1] with 1.73 μg (10.2 μmol, 0.15 equiv) of silver nitrate at 100 °C for 20 min. The product was purified by preparative layer silica gel chromatography to afford **7**: mp 94.5–95.5 °C (from hexane–EtOAc). Anal. ($C_{15}H_{13}ClN_2O_2S$) C, H. This reaction also furnished 1.78 g (35%) of a byproduct, 10-allyl-3-nitrophenothiazine: mp 96.5–97.5 °C (from hexane–EtOAc). Anal. ($C_{15}H_{12}N_2O_2S$) C, H.

10-(4-Chlorobutyl)-3-nitrophenothiazine (8). The procedure described for the preparation of **7** was repeated using 4.40 g (18 mmol) of 3-nitrophenothiazine (**6**) *(19)*, 6.22 mL (9.26 g, 54 mmol, 3 equiv) of 1-bromo-4-chlorobutane, and 1.44 g (36 mmol, 2 equiv) of 60% NaH in mineral oil to afford, after chromatography on silica gel using EtOAc−hexane (gradient: 1:20 followed by 1:8), 4.82 g (80%) of **8**: mp 87−88.5 °C (from EtOAc−hexane). Anal. (C$_{16}$H$_{15}$ClN$_2$O$_2$S) C, H.

3-Azido-10-(3-chloropropyl)phenothiazine (9). To a solution of 1.92 g (5.97 mmol) of **7** in 60 mL of thiophene-free benzene was added 102 mg (0.448 mmol, 0.075 equiv) of platinum oxide. The mixture was stirred at 25 °C for 20 h under a hydrogen atmosphere. A fresh portion (0.075 equiv) of the catalyst was added, and the mixture was stirred for an additional 2 h to reduce remaining small quantities (*ca.* 2−5%) of **7**. The catalyst was removed by filtration, and the filtrate was concentrated to afford 1.85 g of crude amine that was used directly in the next step. The amine was dissolved in 67 mL of DMSO and cooled to *ca.* 18 °C. To this solution was added 49 mL of 3 N HCl solution in portions, and the solution was cooled to 0 °C. A solution of 536 mg (7.76 mmol, 1.3 equiv) of sodium nitrite in 5 mL of water was added dropwise at such a rate that the temperature did not exceed 5 °C. At the end of the addition process, the mixture was stirred at 0 °C for an additional 15 min. A solution of 699 mg (10.8 mmol, 1.8 equiv) of sodium azide in 7 mL of water was added in portions at such a rate that the temperature did not exceed 5 °C. At the end of the addition process, the mixture was stirred at 0 °C for 1 h and at 25 °C for 1 h. The mixture was diluted with water, basified with an excess of saturated NaHCO$_3$ solution, and extracted with EtOAc. The combined extracts were dried over anhydrous MgSO$_4$ and concentrated. The residue was chromatographed on silica gel using EtOAc−hexane (gradient: 1:20 followed by 1:8) to afford 1.52 g (80%) of **9** as an oil which solidified at −5 °C: mp 40−43 °C. Anal. (C$_{15}$H$_{13}$ClN$_4$S) C, H.

3-Azido-10-(4-chlorobutyl)phenothiazine (10). The procedure described in the preparation of **9** was repeated with 4.47 g (13.4 mmol) of **8** to afford, after chromatography on silica gel using EtOAc−hexane (gradient: 1:20 followed by 1:8), 3.36 g (76%) of the azide **10** as an oil that solidified on standing at −5 °C: mp 27−29.5 °C. Anal. (C$_{16}$H$_{15}$ClN$_4$S) C, H.

3-Azido-10-(3-(dimethylamino)propyl)phenothiazine (1a). To a solution of 317 mg (1 mmol) of **9** in 5 mL of DMF at 0 °C in a pressure bottle was added 225 mg (1.5 mmol, 1.5 equiv) of NaI followed by 1.33 mL (902 mg, 20 mmol, 20 equiv) of cold dimethylamine. The flask was sealed with a valve attached to a pressure gauge, and the mixture was stirred at 70 °C for 4 h. The mixture was cooled to 0 °C, opened, and poured into 60 mL of water containing 5 mL of saturated NaHCO$_3$ solution. The solution was extracted with ether; the combined extracts were dried over anhydrous MgSO$_4$ and concentrated. The residue was chromatographed on silica gel using CHCl$_3$−MeOH (gradient: 20:1 followed by 8:1) to afford 241 mg (74%) of **1a** as an oil. Anal. (C$_{17}$H$_{19}$N$_5$S) C, H. The procedure described for the preparation of the oxalate salt of **1b** was repeated to afford the oxalate salt of **1a**: dp 161.5 °C (from CHCl$_3$). Anal. (C$_{19}$H$_{21}$N$_5$O$_4$S) C, H.

3-Azido-10-(4-(dimethylamino)butyl)phenothiazine (1b). The procedure described for the preparation of **1a** was repeated using 331 mg (1 mmol) of **10** to afford, after chromatography on silica gel using CHCl$_3$−MeOH (gradient: 20:1 followed by 8:1), 298 mg (88%) of **1b** as an oil. Anal. (C$_{18}$H$_{21}$N$_5$S) C, H. A solution of 26

mg (78 μmol) of **1b** in 1 mL of EtOAc was added to a stirred solution of 10 mg (78 μmol) of oxalic acid dihydrate in 0.5 mL of anhydrous EtOH followed by 2 mL of ether. The solid was collected by filtration, triturated with EtOAc and ether, and dried in vacuum to afford 23 mg (70%) of oxalate: dp 163 °C. Anal. (C$_{20}$H$_{23}$N$_5$O$_4$S) C, H.

3-Azido-10-(3-(4-methyl-1-piperazinyl)propyl)-phenothiazine (1c). The procedure described for **1a** was repeated using 300 mg (0.947 mmol) of **9** and 420 μL (3.79 mmol, 4 equiv) of 1-methylpiperazine. Unlike the procedure for **1a**, the reaction was conducted in a standard round-bottom flask instead of a pressure bottle, and the reagents were added at 25 °C instead of 0 °C to afford, after chromatography on silica gel using CHCl$_3$−MeOH (gradient: 20:1 followed by 8:1), 306 mg (85%) of **1c** as an oil. Anal. (C$_{20}$H$_{24}$N$_6$S) C, H. To a stirred solution of 21 mg (53.9 μmol) of **1c** in 1 mL of EtOAc was added a solution of 14 mg (119 μmol, 2.2 equiv) of maleic acid in 0.5 mL of anhydrous ether. The solid was collected by filtration, washed with EtOAc, and ether, and dried in vacuum to afford 28 mg (85%) of bismaleate: dp 167 °C (from MeOH). Anal. (C$_{28}$H$_{32}$N$_6$O$_8$S) C, H, N.

3-Azido-10-(4-(4-methyl-1-piperazinyl)butyl)-phenothiazine (1d). The procedure described for **1c** was repeated using 331 mg (1 mmol) of **10** and 444 μL (401 mg, 4 mmol, 4 equiv) of 1-methylpiperizine to afford, after chromatography on silica gel using CHCl$_3$−MeOH (gradient: 20:1 followed by 8:1), 329 mg (83%) of **1d** as an oil that solidified on standing at −5 °C: mp 44.5−47.5 °C. Anal. (C$_{21}$H$_{26}$N$_6$S) C, H. A similar procedure (different volumes of solvents) to that described for the preparation of the bismaleate salt of **1c** was repeated to afford the bismaleate salt of **1d**: dp 154 °C. Anal. (C$_{29}$H$_{34}$N$_6$O$_8$S) C, H.

10-(4-Chlorobutyl)-2-nitrophenothiazine (12). The procedure of Bossle *(20)* was modified as follows. To a solution of 2.25 g (9.21 mmol) of 2-nitrophenothiazine *(21, 22)* in 18.4 mL of anhydrous DMSO at 18 °C under an Ar atmosphere was added in portions 663 mg (16.6 mmol, 1.8 equiv) of 60% NaH in mineral oil. The mixture was stirred at 18 °C for 3 min, and 3.18 mL (4.74 g, 27.6 mmol, 3 equiv) of 1-bromo-4-chlorobutane was added. The mixture was initially stirred using an ice−water bath to keep the temperature below 28 °C. Following this initial 10−15 min period, the stirring was continued at 25 °C for 1.5 h. The ice−water bath was reapplied, and 985 mg (18.4 mmol, 2 equiv) of solid NH$_4$Cl was added in small portions in order to destroy the excess NaH. The mixture was stirred at 25 °C for 10 min and poured into 200 mL of water. The mixture was extracted with EtOAc. The combined EtOAc extracts were dried over anhydrous MgSO$_4$ and concentrated. The product was chromatographed on silica gel using 1:5 EtOAc−hexane to give 2.92 g (95%) of **12** as an oil. Anal. (C$_{16}$H$_{15}$ClN$_2$O$_2$S) C, H.

2-Azido-10-(4-chlorobutyl)phenothiazine (13). The procedure described for the preparation of **9** was repeated using 1.36 g (4.06 mmol) of **12** to afford, after chromatography on silica gel using hexane−EtOAc (gradient: 20:1 followed by 8:1), 613 mg (46%) of the azide **13** as an oil. Anal. (C$_{16}$H$_{15}$ClN$_4$S) C, H.

2-Azido-10-(4-(4-methyl-1-piperazinyl)butyl)-phenothiazine (2d). The procedure described for the preparation of **1c** was repeated using 282 mg (0.852 mmol) of **13** to afford, after 12 h of stirring and chromatography on silica gel using CHCl$_3$−MeOH (gradient: 20:1 followed by 8:1), 292 mg (87%) of **2d** as an oil. Anal. (C$_{21}$H$_{26}$N$_6$S) C, H. The procedure described for the preparation of the bismaleate salt of **1c** was repeated to

afford the bismaleate salt of **2d**: dp 155.5 °C (from MeOH). Anal. ($C_{29}H_{34}N_6O_8S$) C, H.

2-Benzoylphenothiazine (15). To 10 g (40.7 mmol) of 10-acetylphenothiazine (**14**) *(23, 24)* in 250 mL of anhydrous carbon disulfide was added 18.7 g (140 mmol) of $AlCl_3$ and 12.6 g (89.6 mmol) of benzoyl chloride. The mixture was refluxed under N_2 for 24 h. The solvent was evaporated under reduced pressure in a fume hood, and the residue was treated with ice. The slurry was acidified with concentrated HCl and diluted with 95% EtOH. The resulting mixture was refluxed for 5 h, concentrated, diluted with water, and extracted with EtOAc. The combined organic layers were washed with brine and dried over anhydrous Na_2SO_4. The crude product was chromatographed on silica gel using 1:5 EtOAc—hexane to give 9.2 g (75%) of **15**. No effort was made to isolate the 3-substitution product(s).

10-(3-Chloropropyl)-2-benzoylphenothiazine (16). To 4.6 g (14.9 mmol) of **15** in 60 mL of anhydrous DMSO was added 656 mg (16.4 mmol, 1.1 equiv) of NaH (washed with hexane to remove oil). The mixture was stirred under N_2 for 10 min at 25 °C. To this mixture was added 9.38 g (54.6 mmol) of 1-bromo-3-chloropropane. The mixture was stirred for 30 min and was quenched with 0.5 mL of MeOH. The mixture was diluted with 150 mL of water and extracted with EtOAc. The combined organic layers were washed with brine and dried over anhydrous Na_2SO_4. The crude product was chromatographed on silica gel using 1:8 EtOAc—hexane to give 5.5 g (97%) of **16** as a bright yellow oil.

2-Benzoyl-10-(3-(dimethylamino)propyl)phenothiazine (3a). The procedure of Schmelka and Zimmer *(25)* was repeated using 303 mg (1 mmol) of **15**, 83 mg (0.6 mmol) of anhydrous K_2CO_3, 44 mg (1.1 mmol) of powdered NaOH, 34 mg (0.1 mmol) of [(n-Bu)$_4$N]HSO$_4$, and 364 mg (3.0 mmol) of 3-chloro-1-(dimethylamino)-propane to afford, after chromatography on silica gel using 1:15 MeOH—CH_2Cl_2, 250 mg (65%) of **3a** as a bright yellow oil. Anal. ($C_{26}H_{26}N_2O_5S$) (oxalate salt, mp 97—98 °C) C, H.

2-Benzoyl-10-(3-(4-methyl-1-piperazinyl)propyl)-phenothiazine (3b). The procedure of Bossle *(20)* was repeated using 265 mg (0.7 mmol) of **16**, 105 mg (0.7 mmol) of sodium iodide, and 140 mg (1.4 mmol, 2 equiv) of 1-methylpiperazine in 2 mL of 2-butanone to afford, after chromatography on silica gel using 1:14 MeOH—CH_2Cl_2, 170 mg (55%) of **3b** as a bright yellow oil. Anal. ($C_{31}H_{33}N_3O_9S$) (bisoxalate salt, mp 128—129 °C) C, H.

2-Aminophenyl 2,3,5,6-Tetrafluoro-4-nitrophenyl Sulfide (18). To a suspension of 553 mg (4.0 mmol, 2 equiv) of anhydrous K_2CO_3 in 15 mL of anhydrous DMF under an Ar atmosphere was added 392 μL (416 mg, 2 mmol) of pentafluoronitrobenzene (**17**) followed by 214 μL (250 mg, 2 mmol) of 2-aminobenzenethiol. The mixture was stirred at 25 °C for 1 h, diluted with water, and extracted with ether. The combined ether extracts were dried over anhydrous $MgSO_4$ and concentrated. The product was chromatographed on silica gel using 1:8 EtOAc—hexane to afford 164 mg (26%) of **18** (mp 63.5—64.5 °C) in addition to 287 mg (45%) of slightly contaminated **18** (mp 60—62.5 °C). An analytical sample was obtained by recrystallization: mp 64.5—65 °C (from hexane-CHCl$_3$). Anal. ($C_{12}H_6F_4N_2O_2S$) C, H.

1,3,4-Trifluoro-2-nitrophenothiazine (19). A solution of 36 mg (114 μmol) of **18** and 20 μL (14.7 mg, 114 μmol) of *N,N*-diisopropyl-*N*-ethylamine in 114 μL of anhydrous DMF under an Ar atmosphere was stirred at 120 °C for 6 h. The mixture was cooled to 25 °C, diluted with water, and extracted with ether. The combined ether extracts were dried over anhydrous $MgSO_4$ and

concentrated. The product was chromatographed on silica gel preparative plate using 1:8 EtOAc—hexane (developed three times) to afford 31 mg (90%) of **19**: mp 172—173.5 °C (from hexane—EtOAc). Anal. ($C_{12}H_5F_3N_2O_2S$) C, H.

10-(4-Chlorobutyl)-1,3,4-trifluoro-2-nitropheno-thiazine (20). To a stirred solution of 1.27 g (4.26 mmol) of **19** and 4.90 mL (9.30 g, 42.6 mmol, 10 equiv) of 1-chloro-4-iodobutane in 8.5 mL of anhydrous DMSO at 18 °C under an Ar atmosphere was added in portions over a 1-min period 290 mg (7.24 mmol, 1.7 equiv) of 60% NaH in mineral oil. The mixture was stirred for 7 min. During addition of NaH and further stirring, the solution was not cooled, and the temperature rose to 37 °C. To this mixture was added 342 mg (6.39 mmol, 1.5 equiv) of solid NH_4Cl in small portions with ice—water bath cooling. The mixture was stirred for *ca.* 2 min at 15 °C and 5 min at 25 °C to destroy the excess NaH. The mixture was poured into 80 mL of water with 10 mL of saturated $NaHCO_3$ and was extracted with EtOAc. The combined EtOAc extracts were dried over anhydrous $MgSO_4$ and concentrated. The product was chromatographed on silica gel using hexane—EtOAc (gradient: 30:1 followed by 20:1) to afford 512 mg (31%) of **20**: mp 72.5—73.5 °C (*ca.* 1:50 EtOAc—hexane). Anal. ($C_{16}H_{12}$-ClF$_3$N$_2$O$_2$S) C, H.

2-Azido-10-(4-chlorobutyl)-1,3,4-trifluoropheno-thiazine (22). A solution of 429 mg (1.1 mmol) of **20** and 30 mg (0.11 mmol, 0.1 equiv) of platinum oxide in 7.2 mL of thiophene-free benzene was reduced under *ca.* 1—2 atm of H_2 at 25 °C for 4.5 h. A fresh portion (15 mg, 0.05 equiv) of the platinum oxide was added, and the mixture was stirred for an additional 1 h. The catalyst was removed by filtration, and the filtrate was concentrated to afford 407 mg of crude 2-amino-10-(4-chlorobutyl)-1,3,4-trifluorophenothiazine (**21**) that was used directly in the next step. The amine **21** was dissolved in 5 mL of DMSO and 5 mL of AcOH. The mixture was cooled to 0 °C. To this mixture was added 426 μL of concentrated H_2SO_4 followed by the dropwise addition of 270 μL (237 mg, 2.01 mmol, 1.82 equiv) of isoamyl nitrite *(26)* at such a rate that the temperature did not exceed 5 °C. The mixture was stirred at 0 °C for 10 min. To this mixture was added 53 mg (0.88 mmol, 0.8 equiv) of urea. The mixture was stirred for an additional 5 min. The mixture was diluted with 5 mL of cold water, and a solution of 197 mg (2.86 mmol, 2.6 equiv) of NaN_3 in 5 mL of cold water was added in portions. The temperature was not allowed to exceed 5 °C, and upon completion of the addition, the mixture was stirred at 0 °C for 1 h and at 25 °C for 1h. The mixture was diluted with water, diluted with saturated $NaHCO_3$ solution, and extracted with EtOAc. The combined extracts were dried over anhydrous $MgSO_4$ and concentrated. The residue was chromatographed on silica gel using hexane—EtOAc (gradient: 20:1 followed by 8:1) to afford 193 mg of impure **22** that was further purified by medium-pressure liquid chromatography using 1:4 CCl$_4$—hexane to afford 124 mg (29%) of **22** as an oil). Anal. ($C_{16}H_{12}$ClF$_3$N$_4$S) C, H.

2-Azido-10-(4-(4-methyl-1-piperazinyl)butyl)-1,3,4-trifluorophenothiazine (4d). The procedure described for the preparation of **1c** was repeated using 77 mg (20.1 μmol) of **22** and 67 μL (60.4 mg, 60.3 μmol, 3 equiv) of 1-methylpiperazine to afford, after 5 h of stirring and chromatography on preparative silica gel plate using 1:20 MeOH—CH_2Cl_2 (two developments) 74 mg (82%) of **4d** as an oil. Anal. ($C_{21}H_{23}F_3N_6S$) C, H. The procedure described for the preparation of the bismaleate salt of
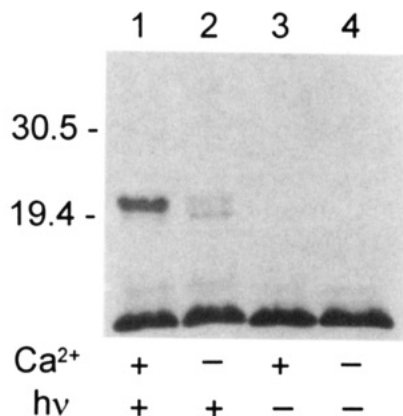
Figure 1. Photolabeling of CaM with phenothiazine [^{14}C]-**1d**. Reaction mixtures containing 50 μM CaM and 100 μM [^{14}C]-**1d** were photolyzed and subjected to SDS–PAGE[1] analysis and autoradiography as described in the Experimental Section. The position of standard molecular weight markers is shown to the left. As previously reported (2), CaM migrated much slower than its molecular weight should dictate. The heavy radiolabeled band at the bottom of the gel is present even in the absence of CaM and is assumed to be unincorporated [^{14}C]-**1d**. All lanes contained freshly prepared CaM exposed to chelex; +Ca^{2+} means that 1 mM CaCl$_2$ was present in the reaction; +$h\nu$ indicates that the reaction was irradiated.

2d was repeated to afford the bismaleate salt of **4d**: 83% yield, dp 159 °C (from MeOH).

3-Azido-10-(4-(4-[^{14}C]methyl-1-piperazinyl)butyl)-phenothiazine ([^{14}C]-1d). An ampule containing 1 mCi (17.2 μmol, 1 equiv) of [^{14}C]formaldehyde (58 mCi/mmol) in 0.05 mL of water was frozen using a dry ice–acetone bath. The ampule was opened, and a stirring bar was placed inside. The ampule was equipped with a septum and purged with N$_2$ gas in a fume hood. A solution of 6.5 mg (17.2 μmol) of **24** in 67 μL of MeOH containing 2.07 mg (34.4 μmol, 2 equiv) of acetic acid was added. The mixture was warmed to 25 °C. To the stirred mixture was added 6.9 μL (6.9 μmol, 0.4 equiv) of freshly prepared 1 M sodium cyanoborohydride solution in MeOH. The mixture was stirred at 25 °C for 1.5 h. The mixture was diluted with 0.75 mL of 1% NaOH and extracted with four 2 mL portions of Et$_2$O using a test tube and a pipette. The combined Et$_2$O extracts were dried over anhydrous Na$_2$SO$_4$ and concentrated. The residue was chromatographed on an analytical silica gel plate (10 × 20 cm) using 1:8 MeOH–CH$_2$Cl$_2$ as an eluent. The compound was washed from the silica gel using 1:5 MeOH–CH$_2$Cl$_2$, and the washings were concentrated. The residue was dissolved in 1:20 MeOH–CH$_2$Cl$_2$, filtered, and concentrated to give 3.3 mg (492 μCi, 49%) of [^{14}C]-**1d** (specific activity = 58 mCi/mmol) as an oil. To the oil in 1 mL of CH$_2$Cl$_2$ was added 125 μL (25.4 μmol, 3 equiv) of a 0.204 M solution of maleic acid in MeOH. The mixture was concentrated to afford the bis(maleate) salt of [^{14}C]-**1d** that was used for photolabeling studies without further purification.

RESULTS AND DISCUSSION

Synthesis of Photoactive Phenothiazines. Various photoactive phenothiazines **1–4** having either a 3-azido (27, 28), 2-azido (27, 29), or 2-benzoyl group (30) as well as a 1,3,4-trifluoro-2-azido functionality as shown in Figure 3 were selected for study. The alkylation (20) of 3-nitrophenothiazine (**6**) (19) with 1-bromo-3-chloropropane or 1-bromo-4-chlorobutane led to the desired N-(ω-chloroalkyl) nitrophenothiazines **7** and **8**, respectively, as shown in Figure 4. Reduction of these nitrophenothiazines without concomitant reduction of the
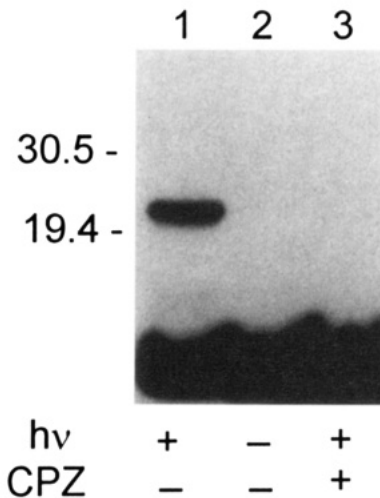
Figure 2. CPZ competition of phenothiazine [^{14}C]-**1d** in photolabeling of CaM. Reaction mixtures containing 20 μM CaM and 80 μM [^{14}C]-**1d** were photolyzed in the absence or presence of CPZ and subjected to SDS–PAGE analysis and autoradiography as described in the Experimental Section. The position of standard molecular weight markers is shown to the left. The migration pattern of CaM and the unincorporated radioactive band is as described in Figure 1. All lanes contained freshly prepared CaM exposed to chelex; +$h\nu$ indicates that the reaction was irradiated; and +CPZ indicates the presence of 2 mM CPZ.
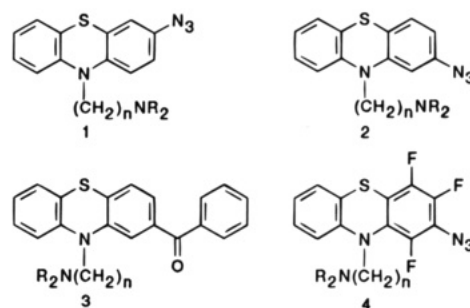
Figure 3. Key: **a**, $n = 3$, NR$_2$ = NMe$_2$; **b** $n = 3$, NR$_2$ = 4-methyl-1-piperazinyl; **c**, $n = 4$, NR$_2$ = NMe$_2$; **d**, $n = 4$, NR$_2$ = 4-methyl-1-piperazinyl.

chloride, diazotization, and azide substitution furnished the azidophenothiazines **9** and **10**, respectively. Attempts to develop a direct route to azidophenothiazines directly from phenothiazines were unsuccessful: the nitration of phenothiazine using ferric chloride in the presence of sodium nitrite was suggested to proceed *via* a phenazathionium ion to give 3-nitrophenothiazine, but this phenazathionium ion intermediate could not be trapped with sodium azide. Exposure of the azidophenothiazines **9** and **10** to either dimethylamine or 1-methylpiperazine in the presence of sodium iodide gave the desired phenothiazines **1a–d** that were conveniently stored as the oxalate or bismaleate salts. The same reaction sequence was applied to 2-nitrophenothiazine (**11**) (21, 22) to afford 2-azido-10-(4-(4-methyl-1-piperazinyl)butyl)phenothiazine (**2d**).

As shown in Figure 5, the Friedel–Crafts acylation (30) of 10-acetylphenothiazine (**14**) with benzoyl chloride furnished the 2-benzoylphenothiazine (**15**). The alkylation of **15** with 1-chloro-3-(dimethylamino)propane led to 2-benzoylpromazine (**3a**) directly. Alternatively, the alkylation of **15** with 1-bromo-3-chloropropane provided the N-(3-chloropropane) derivative **16**, and an S$_N$2 substitution with 1-methylpiperazine led to 2-benzoylperazine (**3b**).

Synthesis of the fluorinated phenothiazine analog, 2-azido-10-(4-(4-methyl-1-piperazinyl)butyl)-1,3,4-trifluo-
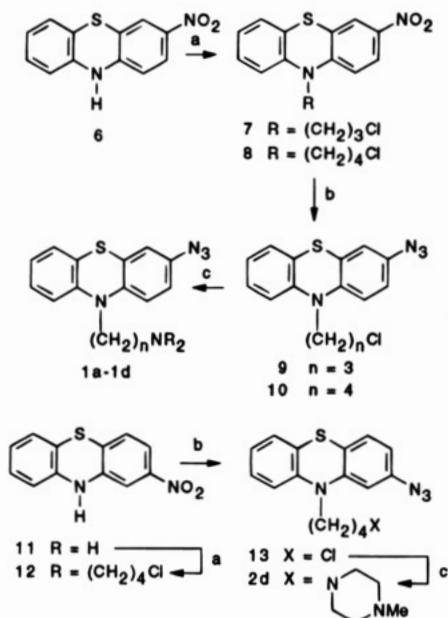
Figure 4. Reagents: (a) NaH, Cl(CH₂)ₙBr, DMSO, 25 °C; (b) H₂, PtO₂, benzene followed by NaNO₂, HCl, aqueous DMSO followed by NaN₃; (c) HNR₂, NaI, DMF, 70 °C.
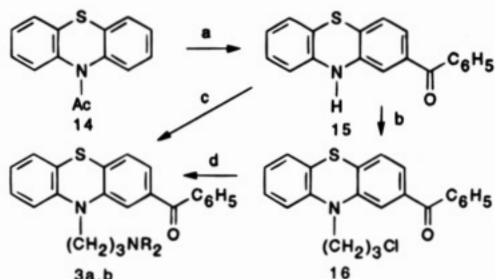
Figure 5. Reagents: (a) PhCOCl, AlCl₃ followed by HCl, 95% EtOH, reflux (75%); (b) NaH, Br(CH₂)₃Cl (97%); (c) K₂CO₃, [(n-Bu)₄N]HSO₄, NaOH, Cl(CH₂)₃NMe₂ (65%); (d) NaI, 1-methylpiperazine, 2-butanone (55%).

rophenothiazine (**4d**), involved an initial aromatic nucleophilic substitution reaction between pentafluoronitrobenzene (**17**) and 2-aminobenzenethiol to provide 2-aminophenyl 2,3,5,6-tetrafluoro-4-nitrophenyl sulfide (**18**), as shown in Figure 6. It was assumed, based on precedent *(31)*, that *para*-substitution predominated over *ortho*-substitution in this coupling reaction. Heating the sulfide **18** in the presence of *N,N*-diisopropyl-*N*-ethylamine in 0.1 M DMF led efficiently to a phenothiazine derivative. In the absence of base, the yield of the phenothiazine dropped dramatically. The ¹H and ¹³C NMR spectra were insufficient to distinguish between the desired 2-nitro-1,3,4-trifluorophenothiazine (**19**) and the isomeric 3-nitro-1,2,4-trifluorophenothiazine that might have arisen through a Smiles rearrangement *(32)*. An X-ray crystallographic study[2] (Figure 7) was necessary to confirm **19** as the structure of the product. The alkylation of **19** with 1-bromo-3-chloropropane, along the lines described earlier for nonfluorinated nitrophenothiazines, failed to produce 10-(4-chloropropyl)-1,3,4-trifluoro-2-nitrophenothiazine, but it was possible to intercept the anion of **19** with the more reactive alkylating agent, 1-chloro-4-iodobutane, in order to obtain the desired product, 10-(4-chlorobutyl)-1,3,4-trifluoro-2-nitrophenothiazine (**20**), in 31% yield.

---

[2] The details of the X-ray structure determination for 2-nitro-1,3,4-trifluorophenothiazine (**19**) will be reported in *Acta Crystallogr.*
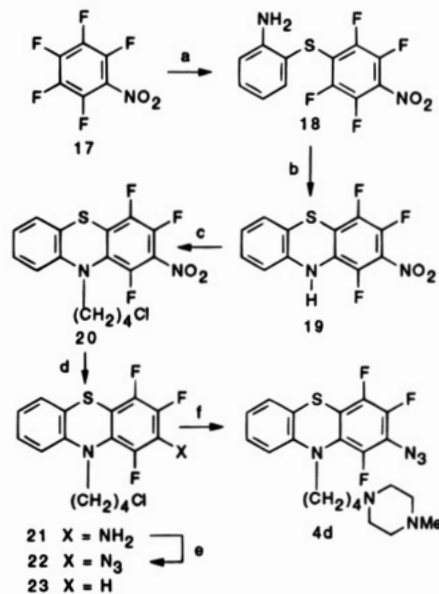
Figure 6. Reagents: (a) 2-aminobenzenethiol, (i-Pr)₂NEt, DMF, 25 °C (70%); (b) (i-Pr)₂NEt, DMF, 120 °C (90%); (c) NaH, Cl(CH₂)₄I, DMSO, 25 °C (31%); (d) H₂, PtO₂; (e) i-C₅H₁₁ONO, H₂SO₄, HOAc, DMSO followed by NaN₃ (29%); (f) 1-methylpiperazine, NaI, DMF, 70 °C (82%).
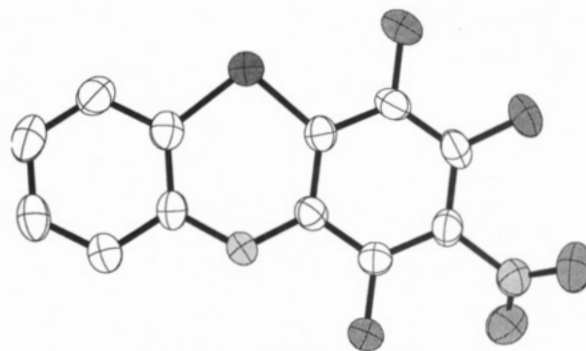
Figure 7. X-ray structure for 2-nitro-1,3,4-trifluorophenothiazine (**19**).

Reduction of 10-(4-chlorobutyl)-1,3,4-trifluoro-2-nitrophenothiazine (**20**) using hydrogen over platinum oxide proceeded uneventfully, but efforts to diazotize the intermediate amine **21** and introduce the azide using the usual conditions failed. Diazotization using isoamyl nitrite *(26)* in a mixture of acetic acid, dimethyl sulfoxide, and sulfuric acid followed by treatment with sodium azide led to the fluorinated 2-azidophenothiazine **22**. However, reduction of the intermediate diazonium salt to the phenothiazine **23** vied with the desired azide-substitution leading to **22**. Although the source of the hydride ion in this reduction was unclear, the electron deficient, fluorinated phenothiazine nucleus in **22** presumably promoted the formation of a diazine that decomposed to the reduced product **23**. Treatment of **22** with 1-methylpiperazine led to a preferential S_N2 substitution and furnished 2-azido-10-[4-(4-methyl-1-piperazinyl)butyl]-1,3,4-trifluorophenothiazine (**4d**).

Calmodulin-Stimulated Phosphodiesterase Assays. The I_{50} values for the inhibition of calmodulin stimulatation of phosphodiesterase (PDE) activity *(33–35)* are presented in Table 1 for each compound. With the exception of 3-azido-10-(3-(dimethylamino)propyl)-phenothiazine (**1a**), these compounds exhibited I_{50} values lower than that of CPZ ($I_{50} = 30$ µM) indicating higher potency than CPZ for inhibition of calmodulin-activation of PDE activity. The analogs **1b**, **1d**, and **2d** having a

C-2 or C-3 azide substituent on the phenothiazine ring and having a 4-methyl-1-piperazinyl moiety on the side chain gave better inhibition than analogs **1a** and **1c** having an *N*,*N*-dimethylamino moiety on the side chain. Slightly greater inhibition was observed in the C-3 azido series (*i.e.*, **1d** compared to **1b**) when an additional methylene unit was inserted in the 4-methyl-1-piperazinyl side chain in accord with the theoretical predictions by Gresh *(36)*.

The perfluorinated analog **4d** was comparable in activity to its nonfluorinated, 2-azido analog **2d**. The nonfluorinated, 2-azido analog **2d** and the fluorinated, 2-azido analog **4d** showed a 1.5-fold increase in I_{50} compared to the 3-azido analog **1d**. It was initially thought that there might be an advantage in utilizing **4d** for cross-linking studies that would identify those residues in the hydrophobic binding pockets of calmodulin that are in contact with the phenothiazine ring. Perfluorinated aryl azides have been shown to generate more reactive nitrene intermediates upon photolysis than the electrophilic dehydroazepines that are produced in the photolysis of nonfluorinated aryl azides *(37, 38)*. Previous studies *(2)* have demonstrated enhanced cross-linking into the plasma membrane (Ca^{2+}, Mg^{2+})-ATPase by CaM modified at a specific lysyl reside with a perfluorinated azide-containing compound.

In this study, the highest potency for inhibition of PDE activity was exhibited by phenothiazines **3a** and **3b** which have a photoactive benzoyl moiety at the C-2 position of the phenothiazine ring. These phenothiazines possess a benzophenone-like structure that may lend itself to efficient photoinsertion as described by Galardy and Craig *(39, 40)*. This outcome was not unexpected since these analogs have an additional hydrophobic moiety on the phenothiazine ring and also retain an *N*-alkyl side chain of at least three methylene units or more carrying a positive charge at neutral pH. These phenothiazines conform to the generalized amphipathic amine structure that Weiss *(41)* has proposed to be a requirement for potent inhibition of calmodulin action. The ability of these monodentate phenothiazine reagents to photoinsert into one or both hydrophobic pockets of calmodulin was next assessed as a first step in the development of the bidentate reagents for cross-linking with calmodulin to its multiple targets.

Although a number of photoactive phenothiazines were prepared, the 3-azidophenothiazine was readily synthesized and hence was the first photoactive derivative that was prepared in radiolabeled form. When subsequent studies revealed that the 3-azidophenothiazine photoinserted into CaM with excellent efficiency, efforts to investigate the cross-linking efficiency of other photoactive phenothiazines was abandoned. As will be described in the accompanying paper,[3] the efficiency of cross-linking using these 3-azidophenothiazines was a consequence of the proximity of nucleophilic methionine residues. Thioethers have been previously reported to intercept nitrene intermediates *(42)*.

Synthesis of a Radiolabeled Photoactive Phenothiazine. The potent activity of 3-azido-10-(4-(4-methyl-1-piperazinyl)butyl)phenothiazine (**1d**), isolated and utilized as the bismaleate salt, in the PDE assay (Table 1) suggested that a radiolabeled analog of **1d** would be a useful probe for testing the competitive binding of **1d** and other phenothiazine drugs to the hydrophobic pocket in
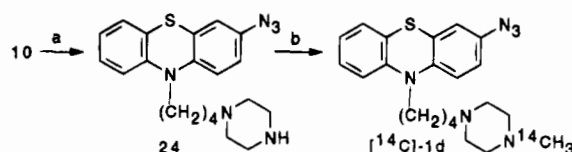
Figure 8. Reagents: (a) NaI, piperazine; (b) [^{14}C]-formaldehyde, NaBH$_4$.

CaM. As shown in Figure 8, the reductive methylation *(43)* of 10-(4-(1-piperazinyl)butyl)phenothiazine (**24**) using formaldehyde and sodium cyanoborohydride furnished **1d** in 67% yield despite the presence of the azido group. It was of interest that the reaction of **24** with methyl iodide in DMF led to a mixture of products from which **1d** was available in only low yield. Repetition of the reductive methylation with [^{14}C]-formaldehyde led to the desired [^{14}C]-**1d**, isolated as the bismaleate salt, with a specific activity of 58 mCi/mmol.

Photolabeling Studies. Figure 1 shows the results of photolabeling of CaM with the [^{14}C]-labeled **1d**, prepared as described in the previous section. The concentration of **1d** used, 100 μM, was approximately 10-fold the apparent K_i determined for inhibition of PDE activation by CaM in order to ensure reasonable saturation of the binding sites on CaM. The CaM concentration was fixed at 50 μM giving a molar ratio of [^{14}C]-**1d** to CaM of 2:1 that was necessary to enhance the probability of photolabeling both hydrophobic domains in CaM. Substantial incorporation of the [^{14}C]-**1d** into CaM was only observed on photolysis in the presence of Ca^{2+} (Figure 1, lane 1). No incorporation into CaM was observed in the presence of excess EGTA with or without irradiation (lanes 2 and 4), and no incorporation was observed on treatment in the presence of Ca^{2+} without light (lane 3).

Figure 2 shows the ability of CPZ to inhibit completely the incorporation of [^{14}C]-**1d** under similar conditions. Lane 1 in Figure 2 shows radioactivity incorporated on photolysis of 20 μM CaM with 80 μM [^{14}C]-**1d** in the presence of Ca^{2+} but without CPZ. As shown in lane 3, 2 mM CPZ completely abolished labeling, presumably as a result of simple competition for binding. Labeling under these conditions also required irradiation as shown in lane 2.

These studies show that, just as with phenothiazines bearing photoactive groups in the side chain, photoactivatable moieties incorporated directly into the phenothiazine nucleus can be used to modify CaM specifically in a calcium- and light-dependent manner. Studies presented in the accompanying paper[3] show that monodentate azidophenothiazine derivatives such as **1d** react with high efficiency after photoactivation and label sites in CaM consistent with phenothiazine-binding regions determined by physical studies.

It should be noted that CaM is used here primarily as a model system to test functional properties of the various phenothiazine compounds that we have prepared. Studies are in progress to examine other more physiological targets for binding including dopamine receptors and P-glycoprotein where these compounds may prove extremely useful in defining the nature of binding sites and targets for chemotherapy. This could lead to a new family of rationally designed therapeutic agents with greater selectivity of action.

ACKNOWLEDGMENT

---

[3] DeLaLuz, P. J., Golinski, M., Watt, D. S., and Vanaman, T. C. Synthesis and use of a biotinylated 3-azidophenothiazine to photolabel both amino- and carboxyl-terminal sites in calmodulin. *Bioconjugate Chem.* (in press).

Supporting Information Available: Spectral data for 10-(3-chloropropyl)-3-nitrophenothiazine (**7**), 10-allyl-3-nitrophenothiazine, 10-(4-chlorobutyl)-3-nitrophenothiazine (**8**), 3-amino-10-(3-chloropropyl)phenothiazine, 3-azido-10-(3-chloropropyl)phenothiazine (**9**), 3-azido-10-(4-chlorobutyl)phenothiazine (**10**), 3-azido-10-(3-(dimethylamino)propyl)phenothiazine (**1a**), 3-azido-10-(4-(dimethylamino)butyl)phenothiazine (**1b**), 3-azido-10-(3-(4-methyl-1-piperazinyl)propyl)phenothiazine (**1c**), 3-azido-10-(4-(4-methyl-1-piperazinyl)butyl)phenothiazine (**1d**), 10-(4-chlorobutyl)-2-nitrophenothiazine (**12**), 2-azido-10-(4-chlorobutyl)phenothiazine (**13**), 2-azido-10-(4-(4-methyl-1-piperazinyl)butyl)phenothiazine (**2d**), 2-benzoylphenothiazine (**15**), 10-(3-chloropropyl)-2-benzoylphenothiazine (**16**), 2-benzoyl-10-(3-(dimethylamino)propyl)phenothiazine (**3a**), 2-benzoyl-10-(3-(4-methyl-1-piperazinyl)propyl)phenothiazine (**3b**), 2-aminophenyl 2,3,5,6-tetrafluoro-4-nitrophenyl sulfide (**18**), 1,3,4-trifluoro-2-nitrophenothiazine (**19**), 10-(4-chlorobutyl)-1,3,4-trifluoro-2-nitrophenothiazine (**20**), 2-amino-10-(4-chlorobutyl)-1,3,4-trifluorophenothiazine, 2-azido-10-(4-chlorobutyl)-1,3,4-trifluorophenothiazine (**22**), and 2-azido-10-(4-(4-methyl-1-piperazinyl)butyl)-1,3,4-trifluorophenothiazine (**4d**) (6 pages). Ordering information is given on any current masthead page.

LITERATURE CITED

(1) Brunner, J. (1993) New photolabeling and crosslinking methods. *Annu. Rev. Biochem. 62,* 483–514.

(2) Crocker, P. J., Imai, N., Rajagopalan, K., Boggess, M. A., Kwiatkowski, S., Dwyer, L. D., Vanaman, T. C., and Watt, D. S. (1990) Heterobifunctional cross-linking agents incorporating perfluorinated azides. *Bioconjugate Chem. 2,* 419–424.

(3) Rajagopalan, K., Chavan, A. J., Haley, B. E., and Watt, D. S. (1993) Synthesis and application of bidentate photoaffinity cross-linking reagents: Nucleotide photoaffinity probes with two photoactive groups. *J. Biol. Chem. 268,* 14230–14238.

(4) Salvucci, M. E., Rajagopalan, K., Sievert, G., Haley, B. E., and Watt, D. S. (1993) Photoaffinity labeling of Rubisco Activase with ATP-benzophenone: Identification of the ATP γ-phosphate binding domain. *J. Biol. Chem. 268,* 14239–14244.

(5) Vanaman, T. C. (1983) Chemical approaches to the calmodulin system. *Methods Enzymol. 102,* 296–310.

(6) Levin, R. M., and Weiss, B. (1977) Binding of trifluoperazine to the calcium-dependent activator of cyclic nucleotide phosphodiesterase. *Mol. Pharmacol. 13,* 690–697.

(7) LaPorte, D. C., Wierman, B. M., and Storm, D. R. (1980) Calcium-induced exposure of a hydrophobic surface on calmodulin. *Biochemistry 19,* 3814–3819.

(8) Krebs, J., Buerkler, J., Guerini, D., Brunner, J., and Carafoli, E. (1984) 3-(Trifluoromethyl)-3-(m-[^{125}I]iodophenyl)-diazirine, a hydrophobic, photoreactive probe, labels calmodulin and calmodulin fragments in a Ca^{2+}-dependent way. *Biochemistry 23,* 400–403.

(9) Newton, D. L., Burke, T. R., Jr., Rice, K. C., and Klee, C. B. (1983) Calcium ion dependent covalent modification of calmodulin with norchlopromazine isothiocyanate. *Biochemistry 22,* 5472–5476.

(10) Newton, D. L., and Klee, C. B. (1984) CAPP-calmodulin: a potent competitve inhibitor of calmodulin actions. *FEBS Lett. 165,* 269–272.

(11) Newton, D. L., and Klee, C. B. (1989) Phenothiazine-binding and attachment sites of CAPP1-calmodulin. *Biochemistry 28,* 3750–3757.

(12) Jarrett, H. W. (1984) The synthesis and reaction of a specific affinity label for the hydrophobic drug-binding domains of calmodulin. *J. Biol. Chem. 259,* 10136–10144.

(13) Prozialeck, W. C., Cimino, M., and Weiss, B. (1981) Photoaffinity labeling of calmodulin by phenothiazine antipsychotics. *Mol. Pharmacol. 19,* 264–269.

(14) Soskic, V., and Maelicke, A. (1992) Synthesis and characterization of biotinylated and photoactivatable neuroleptics. Novel bifunctional probes for dopamine receptors. *Eur. J. Pharmacol. 226,* 109–120.

(15) Jamieson, G. A., and Vanaman, T. C. (1979) Calcium-dependent affinity chromatography of calmodulin on immobilized phenothiazine. *Biochem Biophys. Res. Commun. 90,* 1048–1055.

(16) Wallace, R. W., Tallant, E. A., and Cheung, W. Y. (1983) Assay of calmodulin by Ca2+-dependent phosphodiesterase. *Methods Enzymol. 102,* 39–47.

(17) Lanzetta, P. A., Alvarez, L. J., Reinach, P. S., and Candia, O. A. (1979) An improved assay for nanomole amounts of inorganic phosphate. *Anal. Biochem. 100,* 95–97.

(18) Laemmli, U. K. (1970) Cleavage of structural proteins during the assembly of the head of bacteriophage T4. *Nature (London) 227,* 680–685.

(19) Daneke, J., and Wanzlick, H.-W. (1970) Addition of nucleophilic compounds to phenazathionium cation generated *in situ. Liebigs Ann. Chem. 740,* 52–62.

(20) Bossle, P. C., Ferguson, C. P., Sultan, W. E., Lennox, W. J., Dudley, G. E., Rea, T. H., and Miller, J. I. (1976) Synthesis and biological activity of new 2-substituted analogs of fluphenazine. *J. Med. Chem. 19,* 370–373.

(21) Amoretti, L., Gardini, G. P., and Pappalardo, G. (1965) Synthesis of 2-nitrophenothiazine derivatives and acetylative reduction of the nitro group. *Ann. Chim. (Rome) 55,* 196–204; *Chem. Abstr.* **1965,** *63,* 2968c.

(22) Societe des Usines Chimiques Rhone-Poulenc, Belg. Pat. 611,116 (1962) Derivative of phenothiazine; *Chem. Abstr.* **1963,** *58,* 533bc.

(23) Michels, J. G., and Amstutz, E. D. (1950) Studies in the sulfone series. V. 2,8-Diaminophenothiazine-5-dioxide. *J. Am. Chem. Soc. 72,* 888–892.

(24) Baltzly, R., Harfenist, M., and Webb, E. J. (1946) Some phenothiazine derivatives. The course of the Friedel Crafts reaction. *J. Am. Chem. Soc. 68,* 2673–2678.

(25) Schmelka, S. J., and Zimmer, H. (1984) N-Dimethylaminopropylation in a solid-liquid two phase system: Synthesis of chlorpromazine, its analogs and related compounds. *Synthesis* 29–31.

(26) Smith, P. A. S., and Brown, B. B. (1951) The reaction of aryl azides with hydrogen halides. *J. Am. Chem. Soc. 73,* 2438–2441.

(27) Wildenauer, D. B., and Zeeb, B. (1982) The synthesis of phenothiazine derivatives with photoaffinity label and interactions with dopamine binding sites. *Adv. Biosci. 37,* 153–156.

(28) Wildenauer, D. B., and Zeeb-Wälde, B. Ch. (1983) Solubility of phenothiazines in red blood cell membranes as evidenced by photoaffinity labeling. *Biochem. Biophys. Res. Commun. 116,* 469–477.

(29) Lew, J. Y., Meller, E., and Goldstein, M. (1985) Photoaffinity labeling and purification of solubilized D_2 dopamine receptors. *Eur. J. Pharmacol. 113,* 145–146.

(30) Massie, S. P., Cooke, I., and Hills, W. A. (1956) Ring derivatives of phenothiazines. II. 2-Phenothiazinyl ketones and their derivatives. *J. Org. Chem. 21,* 1006–1008.

(31) Yakobson, G. G., Furin, G. G., Korbina, L. S., and Vorozhtsov, N. N., Jr. (1967) Aromatic nucleophilic substitution. X. Reaction of pentafluoronitrobenzene with pentafluorobenzenethiol. *J. Gen. Chem. USSR 37,* 1221–1224.

(32) Truce, W. E., Kreider, E. M., and Brand, W. W. (1970) The Smiles and related rearrangements of aromatic systems. *Org. React. 18,* 99–215.

(33) Leroy, M. J., Dumler, I., Lugnier, C., Shushakova, N. D., and Ferre, F. (1992) A new peptide (1150 Da) selectively activates the calcium-calmodulin sensitive isoform of cyclic nucleotide phosphodiesterase from human myometrium. *Biochem. Biophys. Res. Commun. 184,* 700–705.

(34) Tremblay, J., Chang, E., Kunes, J., and Hamet, P. (1991) Cyclic nucleotides and calmodulin-phosphodiesterase activator: potential biochemical markers of salt sensitivity. *Clin. Exp. Hypertens. A 13,* 735–743.

(35) Prozialeck, W. C., and Weiss, B. (1982) Inhibition of calmodulin by phenothiazines and related drugs: structure-activity relationships. *J. Pharmacol. Exp. Ther. 222,* 509–516.

(36) Gresh, N. (1987) Theoretical studies of the binding of trifluoperazine derivatives to site (82–93) of calmodulin: Effect of lenthenings of the methylene linker chain on the binding affinity. *Mol. Pharmacol. 31,* 617–622.

(37) Brunner, J. (1993) New photolabeling and crosslinking methods. *Ann. Rev. Biochem. 62,* 483–514.

(38) Schuster, G. B., and Platz, M. S. (1992) Photochemistry of phenyl azide. *Adv. Photochem. 17,* 69–143.

(39) Galardy, R. E., Craig, L. C., Jamieson, J. O., and Printz, M. P. (1974) Photoaffinity labeling of peptide hormone binding sites. *J. Biol. Chem. 249,* 3510–3518.

(40) Galardy, R. E., Craig, L. C., and Printz, M. P. (1973) Benzophenone triplet: a new photochemical probe of biological ligand-receptor interactions. *Nature New Biol. (London) 242,* 127–128.

(41) Weiss, B., Prozialeck, W. C., and Wallace, T. J. (1982) Interaction of drugs with calmodulin. Biochemical, pharmacological, and clinical implications. *Biochem. Pharmacol. 31,* 2217–2226.

(42) Poe, R., Schnapp, K., Young, M. J. T., Grayzar, J., and Platz, M. S. (1992) Chemistry and kinetics of singlet (pentafluorophenyl)nitrene. *J. Am. Chem. Soc. 114,* 5054–5067.

(43) Borch, R. F., Bernstein, M. D., and Durst, H. D. (1971) The cyanohydridoborate anion as a selective reducing agent. *J. Am. Chem. Soc. 93,* 2897–2904.

Synthesis and Use of a Biotinylated 3-Azidophenothiazine to Photolabel Both Amino- and Carboxyl-Terminal Sites in Calmodulin

Paul J. DeLaLuz,[†] Miroslaw Golinski,[†] David S. Watt,[*,†] and Thomas C. Vanaman[*,‡]

Department of Chemistry and Department of Biochemistry, University of Kentucky, Lexington, Kentucky 40536. Received May 2, 1995[®]

The biotinylated probe, 3-azido-10-(4-(4-biotinyl-1-piperazinyl)butyl)phenothiazine, was used to examine the phenothiazine binding domains in calmodulin (CaM) by photolabeling. This phenothiazine, synthesized from 3-azido-10-(4-(1-piperazinyl)butyl)phenothiazine and *d*-biotinyl tosylate, inhibited the CaM-mediated activation of phosphodiesterase (PDE) with an I_{50} of 12.5 ($\pm$2.8) μM. Photolabeling of CaM produced covalent adducts in excellent yield (32%) in a light- and Ca^{2+}-dependent manner. Studies performed over a range of drug concentrations suggested a 2:1 stoichiometry for the binding of the phenothiazine probe to CaM. Limited trypsin digestion and purification of the resulting fragments by either SDS–PAGE or HPLC provided two principal phenothiazine-containing peptides. Amino acid composition and sequence analyses performed on these two peptides established that both the N- and C-terminal domains in CaM, particularly the regions amino terminal to Ca^{2+}-binding loops 1 and 3, were modified by the photoactivated phenothiazine derivative. These data, particularly for the C-terminal domain, are in excellent agreement with the X-ray structure analysis of a 1:1 CaM–trifluoperazine complex.

INTRODUCTION

Phenothiazines were introduced as antipsychotic agents and rapidly gained wide acceptance for long term treatment of schizophrenia and other intractable behavioral disorders. Their success led to the development of other families of neuroleptics including thioxanthines, butyrophenones, dihydroindolones, and dibenzoxazepines. While these are effective agents, all possess a number of undesirable side-effects including tardive dyskinesia, drug-induced parkinsonism, neuroleptic malignant syndrome, and extrapyramidal disorders (akathisia, acute dystonias). Their action as antagonists at dopamine receptors led to one of the first attempts at *ab initio* rational drug design based on modeling of binding sites (*1*). Recent work demonstrating multiple isoforms of the dopamine receptor (*2*) offers the possibility of refining therapeutic specificities by designing isoform-specific agents. Better understanding of the molecular basis of side effects might also permit their elimination through rational design. It is now clear that calmodulin (CaM),[1] protein kinase C, and possibly other proteins can bind phenothiazines at concentrations higher than those required to block dopamine action, and these binding events may be responsible for at least some of these side effects. Indeed, recent work has shown that higher concentrations of these agents may actually improve efficacy of chemotherapy in some instances, particularly in the case of neoplasias which have acquired drug resistance through overexpression of the P-glycoprotein drug transporter product of the *MDR1* gene (*3*). The

latter effect has been hypothesized to result from the inhibition of CaM activation of the protein phosphatase, calcineurin (*4*). However, direct effects of phenothiazines on P-glycoprotein have not as yet been ruled out, and several photoreactive compounds label the P-glycoprotein itself (*5*, *6*).

It would be of substantial importance to have reagents that could be used both to identify and study different types of phenothiazine binding proteins in cell extracts and intact tissues and reagents that could also be used to examine the nature of the phenothiazine binding sites. While a number of chemically reactive and photactivatable reagents have been devised, their reactive moieties are invariably incorporated into the phenothiazine side chain that is not thought to be bound into target recognition sites as noted below. The accompanying paper (*7*) reports a systematic survey of a series of monodentate, azide-bearing phenothiazine derivatives using calmodulin as a model test system. The present paper extends this development to examination of the potential usefulness of a reagent that incorporates an azide group for efficient probing of binding pockets and a side chain biotinyl moiety for the detection and facile isolation of photolabeling products. These studies also provide a step toward the development of *bidentate* compounds incorporating two differentially photoreactive

---

* Corresponding authors. For chemical synthesis: David Watt, Department of Chemistry, University of Kentucky, Rose and Funkhouser Sts., Lexington, KY 40506. Tel: (606) 257-5294. FAX: (606) 323-2800. E-mail: WATT@UKCC.UKY.EDU. For biochemistry: Thomas C. Vanaman, Department of Biochemistry, Chandler Medical Center, Rose St., Lexington, KY 40536. Tel: (606) 257-1347. FAX: (606) 257-7795. E-mail: VANAMAN@POP.UKY.EDU.

† Department of Chemistry.

‡ Department of Biochemistry.

® Abstract published in *Advance ACS Abstracts,* August 15, 1995.

[1] Abbreviations: BCIP, 5-bromo-4-chloro-3-indolyl phosphate; BSA, bovine serum albumin; buffer A, 10 mM NaH_2PO_4 (pH 6.5), 2 mM EGTA; buffer B, 5 mM NaH_2PO_4 (pH 6.5), 2 mM EGTA, 50% acetonitrile; CaM, calmodulin; cAMP, adenosine 3': 5'-cyclic monophosphate; CPZ, chlorpromazine; DMF, *N,N*-dimethylformamide; DMSO, dimethyl sulfoxide; DTT, dithiothreitol; EGTA, ethylenebis((oxymethylene)nitrilo)tetraacetic acid; HEPES, 4-(2-hydroxyethyl)-1-piperazineethanesulfonic acid; HPLC, high-pressure liquid chromatography; NBT, nitro blue tetrazolium; NHS, ester of *N*-hydroxysuccinimide; PDE, bovine brain activator deficient 3':5'-cyclic nucleotide phosphodiesterase; PTH, phenylthiohydantoin; SDS–PAGE, sodium dodecylsulfate–polyacrylamide gel electrophoresis; TBS, 20 mM Tris–HCl pH 7.5, 500 mM NaCl; TFA, trifluoroacetic acid; TFP, trifluoperazine; TEMED, tetramethylethylenediamine.

functional groups for use in studies of protein−protein interaction involved in receptor signaling and drug action.

Previous studies of CaM using phenothiazines possessing a *chemically reactive* moiety incorporated in a side chain (8−10) yielded modification of Lys residues adjacent to the N- and/or C-terminal hydrophobic pockets. In each case, however, modification of CaM occurred outside the hydrophobic binding pockets and required detailed studies to determine the specific site of modification. Recent studies (11) with aryl azide-based reagents possessing an electrophilic NHS[1] ester highlight this problem. These studies demonstrated that the initial interaction of the aryl azide with one or both hydrophobic pockets of CaM and the "spacer" separating the aryl azide from the NHS ester defined the locus of neighboring lysines that subsequently reacted with the NHS ester. To avoid the chemically promiscuous nature of these reactive reagents, photochemically reactive phenothiazines were sought that could label directly the hydrophobic pocket to which they were bound. ^{1}H NMR studies indicated that both the N- and C-terminal hydrophobic pockets of CaM would bind phenothiazines through intercalation into the stacked aromatic side chains in a calcium-dependent manner (12).

Various photoactive phenothiazines with a 2-azido, 3-azido, 2-benzoyl, or 1,3,4-trifluoro-2-azido functionality in combination with a (4-methyl-1-piperazinyl)alkyl or a (dimethylamino)alkyl side chain possessed the ability to inhibit the calmodulin-mediated activation of phosphodiesterase (PDE) (7). The I_{50} values for these analogs and competition studies with chlorpromazine (CPZ), a drug reported to bind CaM, suggested that these photoactive phenothiazines interacted with one or both of these hydrophobic binding domains (7). A radiolabeled analog, 3-azido-10-(4-(4-[^{14}C]methyl-1-piperazinyl)butyl)phenothiazine (1), photolabeled CaM with excellent efficiency in a light- and calcium-dependent manner. The structure of the adducts produced in this photolysis of CaM and 1 are uncertain but presumably resulted from the chemical trapping of a nucleophilic amino acid residue by a dehydroazepine-like intermediate (13, 14). Unfortunately, these photoadducts were not amenable to HPLC[1] analysis in the low pH, TFA[1]-containing buffer commonly used for such separations.

At the same time that this radiolabeled phenothiazine 1 was under investigation, a second, biotinylated phenothiazine (3) was synthesized from d-biotin and 3-azido-10-(4-(1-piperazinyl)butyl)phenothiazine (2). Unfortunately, this phenothiazine 3 was inactive in the PDE[1] assay, but a corresponding phenothiazine 4, prepared from 2 and d-biotinol (15), proved active. It was anticipated that this biotinylated phenothiazine 4 would offer an advantage over the radiolabeled phenothiazine 1 in terms of the purification of photoadducts. We now report the efficient photolabeling of the C- and N-terminal hydrophobic domains in CaM using this new reagent, 3-azido-10-(4-(4-biotinyl-1-piperazinyl)butyl)phenothiazine (4).

EXPERIMENTAL PROCEDURES

Materials. Chelex cation exchange resin was purchased from Bio-Rad. Electrophoresis grade acrylamide, *N,N'*-methylenebis(acrylamide) and TEMED[1] were purchased from Fisher Scientific. HPLC grade acetonitrile was purchased from EM Science. Aqueous buffers were prepared with Milli-Q water and filtered through 0.22 μm Millipore filters before use. The Zorbax 300 SB-CN column (4.6 mm × 25 cm) was purchased from MAC-MOD Analytical, Inc. [^{125}I]Streptavidin (37 μCi/mg) was

purchased from Amersham. All other chemicals and enzymes were from Sigma.

Preparation of CaM. CaM was purified to homogeneity from bovine testes according to the procedure of Jamieson and Vanaman (16). Calcium-free CaM was prepared by passing a stock solution of the protein over a column of Chelex resin immediately prior to use.

CaM-Stimulated Phosphodiesterase Assays. Assay of cyclic 3':5'-nucleotide phosphodiesterase (PDE) was performed according to the method of Wallace (17) exactly as described in the accompanying paper (7).

Photolabeling of CaM with Phenothiazine 4. Photolabeling experiments were performed with a 2-fold molar excess of probe over CaM in a mixture containing 100 mM HEPES[1] (pH 7.4), 1 mM CaCl$_2$, and 50 μM CaM. This mixture was halved; each half was preincubated for 15 min at 25 °C and transferred to two Parafilm "boats" on ice. One sample was irradiated with a hand-held ultraviolet light (Mineralite Model UVGL-25) at a distance of 4 cm for 1 min at 254 nm, the other was held on ice but not irradiated. These treated samples were then transferred to Eppendorf tubes, diluted to final concentrations of 5 mM EGTA[1] and 10 mM DTT, and analyzed by SDS−PAGE.[1] A similar series of experiments were performed starting with a mixture containing 100 mM HEPES (pH 7.4), 5 mM EGTA, and 50 μM CaM.

Assessment of Photoinsertion. The solutions of CaM and phenothiazine 4 (Figure 1) treated in the presence and absence of light and Ca^{2+} were analyzed directly by 14% SDS−PAGE stained with Coomassie Blue (lanes 1−4, Figure 3). A similar set of gels were subjected to electroblot analysis (lanes 5−8, Figure 3) to detect the presence of biotin. Photolabeled CaM products formed in the presence of Ca^{2+} and light also were separated by reversed-phase HPLC techniques (Figure 4). The product mixture was applied to a Zorbax CN column (4.6 mm × 25 cm) and eluted at a flow rate of 1 mL/min with a 2 min isocratic wash of buffer A.[1] This was followed by a linear gradient of 0% to 20% buffer B[1] over an 8 min period and then a linear gradient of 20−70% buffer B over a 60 min period and an isocratic wash at 70% B for 20 min. The eluate was monitored simultaneously at 210 nm to detect protein and at 260 nm to detect the presence of the phenothiazine. Peak fractions that exhibited increased absorption at both wavelengths were collected and subjected to analysis by 14% SDS−PAGE.

Determination of Extent of Modification. In order to quantify the extent of photolabeling, the modified and native CaM were isolated, free of unincorporated probe and other reaction mixture constituents, and CaM content was quantified as follows. Samples were desalted by passage over Sephadex G-25 (15 × 50 mm) in 10 mM NH$_4$HCO$_3$, and the CaM-containing fractions were collected and concentrated by lyophilization. The modified CaM was separated from the native CaM by batch absorption on streptavidin−agarose to select for the presence of the biotin moiety. To this end, the dried, desalted fraction containing both modified and native CaM was dissolved in 100 mM HEPES (pH 7.4) to a final CaM concentration of 60 μM based on starting material. This buffer also contained 5 mM EGTA and 200 mM CPZ[1] to prevent simple binding of any adventitious biotinylated probe to unmodified CaM. Aliquots of the photolysis mixtures containing 10 μg of modified and native calmodulins were mixed with 40 mL of packed streptavidin−agarose (extensively prewashed with 100 mM NaH$_2$PO$_4$ at pH 7.0 followed by 100 mM HEPES at pH 7.4). Parallel analyses were performed on control samples containing 10 μg of untreated, native CaM in

order to correct for recovery and dilution during process-
ing. After incubation for 1 h at 25 °C with agitation on
a rotary shaker, the supernatant fractions containing
unbound CaM were harvested following centrifugation
in a microfuge (30 s). The CaM content of these pro-
cessed samples as well as initial reaction mixtures were
determined by SDS–PAGE (12.5%) and scanning den-
sitometry of the resulting Coomassie Blue-stained gel
(Figure 5).

**Modification of CaM as a Function of Probe
Concentration.** Photolysis as described above was
performed with Chelex-treated CaM in 100 mM HEPES
at pH 7.4 with 1 mM $CaCl_2$ and with increasing amounts
of probe (Figure 6). The samples were subjected to SDS–
PAGE (14%) and electroblotting analysis with identifica-
tion and quantification using [125I]streptavidin.

**Polyacrylamide Gel Electrophoresis and Elec-
troblot Analysis.** Samples were dissolved in a protein-
solubilizing mixture of 65 mM Tris–HCl, 2% SDS, 10%
glycerol, 5% β-mercaptoethanol, and 0.001% bromophenol
blue. These samples were heated to 100 °C for 4 min.
The resulting solutions were analyzed by 12.5%, 14%, or
17.5% SDS–PAGE (as noted) according to the procedures
of Laemmli (*18*). Gels were either stained with 0.25%
(w/v) Coomassie Brilliant Blue or transferred to Immo-
bilon-P membranes. The stained gels were scanned with
the AMBIS imaging system linked to a CCD video
camera module, and data were acquired and quantified
using AMBIS QuantProbe software. Transfer mem-
branes were blocked with a 1% solution of BSA in TBS
for 1 h at 25 °C and probed with either streptavidin–
alkaline phosphatase or [125I]streptavidin. The strepta-
vidin–alkaline phosphatase bound CaM was treated with
the BCIP/NBT color development system to generate a
colorimetric stain (*19*). Blots with [125I]streptavidin were
exposed to Kodak X-OMAT AR film back by an intensify-
ing screen at −70 °C, and the resulting autoradiogram
was developed with an X-ray film processor (*20*).

Identification of Modification Sites on CaM. Lim-
ited trypsin digestion of modified and native CaM was
performed in the presence of 1 mM $CaCl_2$ under condi-
tions described by Walsh (*21*). After digestion, proteoly-
sis was stopped by addition of soybean trypsin inhibitor.
The sample was analyzed by reversed-phase HPLC using
a 2-min isocratic wash of buffer A followed by a linear
gradient of 0–70% buffer B over a 38 min period at a
flow rate of 1 mL/min. Comparison of the elution
patterns (Figure 7) from typsinized, native CaM and
typsinized, modified CaM showed different retention
times for certain peaks. These peaks were collected and
used for amino acid composition and sequence analysis.
In addition, an analysis of the typsinized, native CaM
and typsinized, modified CaM using 17.5% SDS–PAGE
displayed two modified peptide bands in the latter (data
not shown), consistent with the results observed by HPLC
analysis.

**3-Azido-10-(4-(4-biotinoyl-1-piperazinyl)butyl)phe-
nothiazine (3).** The procedure of Hofmann (*22*) was
repeated with some modification using 64 mg (0.26 mmol,
1.3 equiv) of *d*-biotin (**5**), 42 mg (0.26 mmol, 1.3 equiv) of
1,1′-carbonyldiimidazole, and 76 mg (0.2 mmol, 1 equiv)
of 3-azido-10-(4-(1-piperazinyl)butyl)phenothiazine (**2**) (**7**)
in 1.8 mL of anhydrous DMF.[1] The mixture was stirred
at 25 °C for 20 h. The mixture was diluted with 20 mL
of 0.1 M K_2CO_3 solution and extracted with EtOAc. The
combined extracts were dried over anhydrous $MgSO_4$.
The residue was chromatographed on a preparative silica
gel plate using 1:15 $MeOH–CH_2Cl_2$ (two developments)
to give 100 mg (82%) of **3** as a foam. Anal. ($C_{30}H_{40}N_8O_3S_2$ ·
H_2O) C, H.

Figure 1. Key: (a) $LiAlH_4$, Et_2O, Py; (b) TsCl, Py; (c) **2**, DMSO,
75 °C; (d) 1,1′-carbonyldiimidazole, DMF, 80 °C; (e) **2**, DMF, 25
°C.

d-**Biotinol Tosylate (7).** A solution of 115 mg (0.5
mmol, 1 equiv) of *d*-biotinol (**6**) (*15*) in 2.5 mL of warm,
anhydrous pyridine under an Ar atmosphere was sus-
pended in an ice–water bath, and when the starting
material started to precipitate, 114 mg (0.6 mmol, 1.2
equiv) of tosyl chloride was added. The mixture was
stirred at 0 °C for 5 min and then at 25 °C for 3 h. The
mixture was poured into cold water and extracted with
CH_2Cl_2. The CH_2Cl_2 solutions were washed with 3.6 N
H_2SO_4 solution, and the aqueous wash solutions were
extracted with additional CH_2Cl_2. The combined CH_2-
Cl_2 solutions were washed with 10 mL of brine and dried
over anhydrous Na_2SO_4. The residue was chromato-
graphed on a preparative silica gel plate using 1:20
$MeOH–CH_2Cl_2$, redissolved in 1:30 $MeOH–CH_2Cl_2$, fil-
tered through a 0.5 cm bed of silica gel in order to remove
very polar decomposition products, and concentrated to
give 114 mg (59%) of **7**. A gram-scale repetition of this
experiment in which the crude product was induced to
crystallize by addition to water containing traces of
crystals obtained from the small scale experiment led to
product that was recrystallized twice from EtOAc: mp
142–143.5 °C. Anal. ($C_{17}H_{24}N_2O_4S_2$) C, H, N.

**3-Azido-10-(4-(4-biotinyl-1-piperazinyl)butyl)phe-
nothiazine (4).** A solution of 523 mg (1.38 mmol, 1.1
equiv) of 3-azido-10-(4-(1-piperazinyl)butyl)phenothiazine
(**2**) (**7**) and 481 mg (1.25 mmol) of *d*-biotinol tosylate (**7**)
in 5 mL of anhydrous DMSO[1] was stirred at 75 °C under
an Ar atmosphere for 5.5 h. The mixture was cooled to
25 °C and poured into a 1:4 mixture of 0.25 N NaOH
solution–brine. The solution was extracted with CH_2-
Cl_2. The combined extracts were dried over anhydrous
$NaSO_4$. The residue was chromatographed twice on silica
gel with 1:10:100 concentrated $NH_3–MeOH–CH_2Cl_2$ to
afford 302 mg (39%) of **4** as an oil.

The bismaleate salt of **4** was prepared in the usual
fashion. To a solution of 269 mg (0.45 mmol) of **4** in 10
mL of CH_2Cl_2 was added 116 mg (1 mmol, 2.2 equiv) of
maleic acid in 1.5 mL of MeOH. The product was
collected by filtration and washed with Et_2O to give 295
mg (79%; two crops) of salt. A small portion of the first
crop was recrystallized from MeOH to afford the analyti-
cal sample: dp 145 °C. Anal. ($C_{38}H_{48}N_8O_9S_2$) C, H, N.

RESULTS AND DISCUSSION

**Synthesis and Properties of Biotinylated Phe-
nothiazines.** As shown in Figure 1, the coupling of

Figure 2. Inhibition of 3':5'-cyclic nucleotide phosphodiesterase with phenothiazine **4**. The left axis represents the percentage of activity when maximal stimulation is achieved in the presence of CaM and absence of inhibitor. Phenothiazine **4** concentration is depicted by [μM]. Points were determined as the average of three separate analyses, and error bars show standard deviation.

Figure 3. Ca^{2+}-dependent cross-linking between CaM and the phenothiazine **4**. Lanes 1−4 show the Coomassie Blue-stained gel, and lanes 5−8 color developed in streptavidin-probed blot for samples prepared and run as described in the text. The position of molecular weight makers is shown to the left. All lanes contained freshly prepared CaM exposed to Chelex-100 prior to setting up photolysis mixtures. "Ca^{2+}" means that 1 mM CaCl$_2$ was added back to the reaction. Otherwise, the mixture contained 5 mM EGTA. "$h\nu$" indicates whether or not the reaction was irradiated.

3-azido-10-(4-(1-piperazinyl)butyl)phenothiazine (**2**) with an *N*-hydroxysuccinimide ester of *d*-biotin afforded a piperazine amide derivative of biotin, 3-azido-10-(4-(4-biotinoyl-1-piperazinyl)butyl)phenothiazine (**3**). The phenothiazine **3** was, however, inactive in the PDE assay. The inactivity of **3** was attributed to the conversion of one of the basic nitrogens of the piperazine ring to an uncharged amide. This suggested that an analog of **3** that retained both basic nitrogens of the piperazine ring might prove biologically active. With this supposition in mind, biotin was reduced to biotinol, activated as the tosylate **7**, and coupled to **2** to afford an *N*-alkylpiperazine derivative, 3-azido-10-(4-(4-biotinyl-1-piperazinyl)butyl)-phenothiazine (**4**) as shown in Figure 1. Phenothiazine **4** was soluble at a concentration of 1 mM in aqueous buffer solutions at *ca.* pH 7 and 25 °C. The UV absorption spectrum of **4** showed peaks at 310 nm and 260 nm that were characteristic of a 3-azidophenothiazine nucleus (data not shown). The 260 nm peak was reduced, but not eliminated, upon UV irradiation under the conditions set forth in the Experimental Procedures.

An essential feature of pharmacologically active phenothiazines is calcium-dependent binding to CaM that in turn inhibits activation of CaM-dependent enzymes. As shown in Figure 2, phenothiazine **4** gave dose dependent inhibition of CaM activation of 3':5'-cyclic nucleotide phosphodiesterase activity with an apparent $K_i = 12.5 \pm 2.8 \, \mu M$. This value compares favorably with that reported for the most active calmodulin antagonists, CPZ (30 μM) and trifluoperazine (17 μM) (*23*).

Photolabeling of CaM Using Phenothiazine 4. Samples of purified CaM were treated with the phenothiazine **4** in the presence and absence of light and Ca^{2+} in order to directly examine the specificity of binding. The photolabeled products were analyzed by two experimental methods: SDS−PAGE and HPLC. Labeled products were observed only in the presence of both light and Ca^{2+} as described in the Experimental Procedures. Of particular importance was the necessity of using freshly prepared CaM that had been treated with Chelex to remove any traces of Ca^{2+}. Without this Chelex treatment, sufficient residual Ca^{2+} was present to permit some binding of probe, presumably due to the exposure

of CaM hydrophobic binding pocket(s). This resulted in background photolabeling even in the presence of excess EGTA.

Lanes 1−4 in Figure 3 show a Coomassie Blue-stained SDS−PAGE gel for experiments conducted in the presence and absence of light and Ca^{2+}. Lanes 5−8 in that figure show the colorimetric stains obtained after treatment of an electroblot of an identical set of SDS−PAGE resolved products with streptavidin−alkaline phosphatase in order to detect the presence of biotin. The prominent band in lane 5 ran with a slightly slower mobility than the major, Coomassie Blue-stained band in lane 1, presumed to be unmodified CaM. This shift in mobility is expected. The mass of CaM (17.5 kDa) is increased approximately 5% by the addition of the biotinylated phenothiazine moiety (*ca.* 840 Da). In addition, the mobility of CaM is very sensitive to the presence of Ca^{2+} and hydrophobic pocket-directed ligands even under the denaturing conditions used for SDS−PAGE (*24*). These data demonstrate that the phenothiazine **4** with its biotin-containing side chain formed a covalent linkage to CaM in a light- and calcium-dependent reaction.

The photolysis mixture produced in the presence of Ca^{2+} was analyzed by reversed-phase HPLC as shown in Figure 4. The photolysis mixture, corresponding to the material shown in lanes 1 and 5 of Figure 3, showed an absorbance at 210 nm (solid line in Figure 4) that indicated the presence of protein and an absorbance at 260 nm (dashed line in Figure 4) that indicated the presence of the phenothiazine nucleus. The phenothiazine moiety has a large molar extinction coefficient at 260 nm relative to that of the six Phe residues of CaM. The asterisk in Figure 4 indicates the location of unmodified CaM as determined in a separate analysis.

The peaks indicated by arrows in Figure 4 also contained CaM but had a 20-fold higher ratio of absorbance at 260 nm to 210 nm than the material in the unmodified CaM peak. The large peak of 260 nm absorbing material eluting at *ca.* 63 min co-eluted with unreacted probe and was present in reaction mixtures lacking CaM. The peaks eluting at 55.7, 57.7, and 59.9 min were collected and analyzed to determine whether the UV-detected phenothiazine **4** was covalently attached or merely bound to CaM. The inset to Figure 4 shows
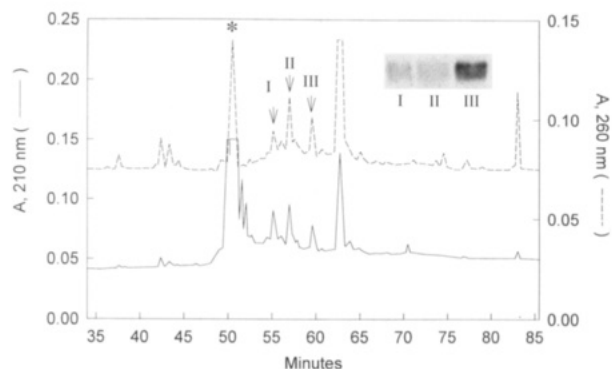
Figure 4. Separation of CaM and three CaM−phenothiazine 4 adducts using reversed-phase CN HPLC. The separation was achieved using a 2 min isocratic wash of buffer A, followed by a linear gradient of 0−20% buffer B over an 8 min period, and was completed by a linear gradient to 70% buffer B over 60 min period followed by an isocratic wash at 70% buffer B for 20 min. The asterisk denotes the elution of unmodified CaM. The arrows indicate putative CaM photoadducts (I−III). The left axis (solid line) is the UV absorbance scale at 210 nm, and the right axis (dashed line) is the UV absorbance scale at 260 nm. The inset is the SDS−PAGE purification and electroblot of the corresponding peaks collected. The blot was probed with streptavidin alkaline phosphatase and color developed with BCIP/NBT.

Figure 5. Coomassie Blue-stained gel of native and modified CaM exposed to streptavidin agarose. The position of molecular weight makers are shown to the left of the gel. Each lane contained CaM. The first two lanes represent 10 μg of unmodified CaM exposed (lane 2) or not exposed (lane 1) to streptavidin agarose. Correspondingly, the last two lanes represent 10 μg of modified CaM exposed (lane 4) or not exposed (lane 3) to streptavidin agarose.

the results of SDS−PAGE and electroblotting with streptavidin−alkaline phosphatase color development for aliquots of the three putative modified CaM peaks. Prominent stained bands migrating at the position of CaM were found in all three cases (I−III), demonstrating that these peaks represented CaM derivatives containing covalently attached biotinyl moieties. On the basis of the ratio of their 260 nm/210 nm absorbances (I = 0.63; II = 1.36; III = 1.88) and the relative intensities of streptavidin staining, peak III appeared to be labeled more heavily than either of the two earlier eluting peaks (*i.e.*, I and II). Data presented below suggest two distinct sites of labeling in CaM under these conditions. The presence of the peaks with these characteristics suggested the possibility that the components in peaks I and II represented two different mono-adducts and peak III represented the corresponding bis-adduct.

Efficiency of Photoincorporation. The cross-linking efficiency with the phenothiazine 4 was much higher than that observed using conventional unsubstituted aryl azides (*11*) but was consistent with the value reported for the ^{14}C-labeled congener 1 in the accompanying paper (*7*). The extent of covalent attachment of the biotinyl-containing phenothiazine 4 to CaM was measured by determining the amount of unmodified CaM remaining after first removing the biotinyl-containing photolabeled CaM from reaction mixtures by absorption with streptavidin−agarose. Mixtures containing 50 μM CaM and a 2-fold molar excess (100 μM) of phenothiazine 4 were irradiated in the presence of calcium as set forth in the Experimental Procedures. As a control, an identical sample of CaM and phenothiazine 4 was subjected to the same treatment but without irradiation. Photolysis generated a mixture of covalently modified CaM, unmodified CaM, and unattached, photoreduced phenothiazine that might be bound to CaM. The binding of unattached, photoreduced phenothiazine made the determination of the extent of modification of CaM difficult and required precautions to eliminate this latter possibility.

After photolysis, the bulk of the photolyzed but noncovalently attached phenothiazine was removed from the sample by passage through a small column of Sephadex G-50 in 10 mM ammonium bicarbonate. The excluded

fraction containing protein and minimal amounts of the photoreduced phenothiazine was collected and freeze-dried. It was important, however, to eliminate all traces of noncovalently attached, photoreduced phenothiazine since adventitious binding of this phenothiazine, containing the biotinyl group, to CaM would effect the outcome of the next streptavidin−agarose step. To this end, the freeze-dried, excluded fraction was redissolved in HEPES buffer containing 5 mM EGTA and 200 μM CPZ and then was subjected to batch absorption with streptavidin−agarose. The presence of EGTA served to chelate Ca^{2+}, unfold CaM, and thereby reduce the binding affinity of any photoreduced, noncovalently bound phenothiazine. Similarly, the presence of excess CPZ served to compete for any hydrophobic binding sites on any residual CaM and to eliminate binding of any photoreduced phenothiazine.

Aliquots of these solutions equivalent to 10 μg of CaM (based on starting material) were analyzed by SDS−PAGE before and after batch absorption with 40 μL of packed streptavidin−agarose as described in the Experimental Procedures. In Figure 5, lanes 1 and 2 represent controls in which 10 μg of CaM was exposed to phenothiazine 4 but *not* photolyzed. A comparison of lanes 1 and 2 shows the dilution caused by treating with streptavidin−agarose. Lanes 3 and 4 show an experiment in which 10 μg of CaM plus phenothiazine 4 was photolyzed and then treated. Substantially less CaM was detected by SDS−PAGE analysis from recovered samples of irradiated CaM (lane 4, Figure 4) after streptavidin−agarose absorption than from the unirradiated control (lane 2, Figure 4). The amounts of material present in these fractions prior to streptavidin treatment were comparable (lanes 1 and 3). The amounts of CaM detected in lanes 2 and 4 were determined by densitometry of the Coomassie Blue-stained bands. These values were then normalized to the amounts determined for the same bands in lanes 1 and 3, respectively, to correct for slight differences in the dilution of each sample. The difference between the normalized amounts detected in lanes 2 and 4 was used to estimate of the amount of covalently modified, biotin-containing CaM removed by specific absorption by streptavidin−agarose. Multiple analyses yielded a value of 68% (±2.6%) of unmodified CaM remaining in the sample in lane 4. By difference, 32% (±2.6%) of the original CaM in this
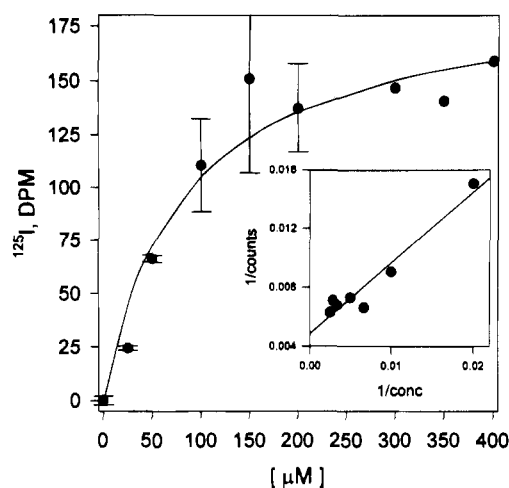
Figure 6. Modification of CaM as a function of probe concentration. Values were determined by excising bands of purified Western blots probed with [^{125}I]streptavidin and counting with a gamma detector. Phenothiazine **4** concentration is depicted by [μM]. Points were determined as the average of two separate analysis, and error bars show standard deviation.

sample was covalently modified by the biotin-containing phenothiazine **4**.

Figure 6 shows the results of photolabeling of CaM over a range of concentrations representing various molar ratios of added phenothiazine **4**. After irradiation in the presence of 1 mM Ca^{2+} under the conditions described in Experimental Procedures, the photolysis mixtures were subjected to SDS—PAGE and electroblotted on to Immobilon-P membranes. The resulting transfers were treated with [^{125}I]streptavidin after blocking with 1% BSA. The labeled CaM bands in each lane, located by autoradiography, were excised, and the amount of ^{125}I was determined by γ counting that was corrected for background counts in identical size strips excised from adjacent portions of the blot. The values shown in Figure 6 represent averages for two determinations with the range of values indicated by the error bars.

Since the concentration of CaM in the photolysis mixtures was 50 μM, the lowest concentration of probe which could be used effectively was 25 μM. This is twice the K_i for phenothiazine binding as determined by assays of inhibition of PDE activation. Therefore, these data represent a stoichiometric titration of phenothiazine-binding sites in the CaM molecule. As shown in Figure 6, photolabeling increased hyperbolically with the concentration of phenothiazine **4** up to a value of 100 μM, a concentration that represents a 2-fold molar excess of phenothiazine to CaM. This suggests that there are two distinct sites involved in photolabeling, within the limitations of this approach. A reciprocal plot of these data, shown as the inset to Figure 6, was linear, suggesting that these two sites have similar affinities for phenothiazine binding. Levin and Weiss (*25*) reported that CaM binds 2 mol of TFP^1/mole of protein with high affinity in the presence of Ca^{2+}. Massom (*26*) reported Ca^{2-}-dependent binding of up to 4 mol of TFP/ mole CaM at roughly equivalent affinities (*ca.* 6 μM). Only 2 mol of TFP, however, are competed by mellitin and appear to represent binding to the hydrophobic pockets. X-ray crystallographic analysis (*27*) has detected only one molecule of TFP bound per molecule of CaM in the C-terminal hydrophobic pocket as discussed below. Studies in the following section also show that two distinct sites in either half of the CaM molecule were labeled under these conditions.

Determination of Sites of Photolabeling in CaM.

Various attempts to isolate the biotinyl-containing products of photolabeling by chromatography under acidic conditions were unsuccessful owing to apparent instability of the linkage at low pH (*i.e.*, 1% TFA used in HPLC or pH 2.8 elution from anti-biotin IgG columns). As discussed by Vanaman (*28*), recovery of tryptic fragments from CaM on HPLC is enhanced at pH 6 and above owing to the high content of acidic residues in the molecule. The fact that digestion is limited in the presence of Ca^{2+} (*21*) provided for the isolation of larger fragments which simplified determination of the sites of modification.

Figure 7 shows the elution profiles obtained by reversed-phase HPLC separation on Zorbax CN (4.6 mm × 25 cm) of limited trypsin digests of a sample of CaM following maximal photolabeling (—) (*i.e.*, 100 μM **4** and 50 μM CaM) to yield *ca.* 32% modification as compared to the unmodified protein (- - -). The peaks labeled C_1 and C_2, indicated by the arrows in the figure, are tryptic peptides in unmodified CaM (- - -) that appear to be almost absent (20.2 min) or substantially diminished (30.2 min) in the profile from the modified protein (—). Conversely, the asterisks indicate the positions of two new peaks, B_1 (21 min) and B_2 (28 min), found only in the profile for the modified (—) protein, not the untreated CaM digest (- - -).

Peaks B_1 and B_2 were collected from the modified protein digest and subjected to amino acid composition and sequence analyses. The amino acid composition of B_1 contained tyrosine, histidine, and trimethyllysine which are only found in the C-terminal half of the molecule, as shown in Table 1. This assignment was further verified by automated sequence analysis of this isolated peak fraction which gave a single sequence in high yield commencing with Val 91 of the known CaM sequence. Degradation proceeded well through Asn 97 (cycle 7) after which a substantial drop in yield was obtained at Gly 98 as has previously been noted for this peptide from unmodified CaM (*28*). Degradation proceeded to yield unambiguous sequence for an additional 5 cycles through Ala 103. This clearly establishes that labeled fragment B_1 commences with residue 91, two residues before the start of the third calcium-binding loop. On the basis of the presence of a trimethyllysine and two arginines in the amino acid composition, it is likely that this product of limited trypsin digestion extends to at least Arg 126 in the CaM sequence, a position just before the fourth calcium-binding loop sequence, as indicated in Table 1.

The amino acid composition of fragment B_2 (Table 1) pool was best correlated with that expected for residues 1—30 of CaM. This is in agreement with the fact that repeated attempts to determine its amino terminal sequence by automated Edman degradation yielded no detectable Pth-amino acids as would be expected for a peptide commencing with the acetylated amino terminal alanyl residue of CaM (*29*). This sequence contains the first helical segment on the amino terminal side of calcium binding site 1 and extends through most of loop 1.

Newton (*30*) first reported the labeling of CaM with a CPZ derivative containing a side-chain isocyanate that, not surprisingly, was preferentially directed toward Ca^{2+}-dependent modification of Lys 75 (*31*) and, on more prolonged reaction, Lys 148 (*8*). Similarly, Faust (*10*) demonstrated that a side-chain NHS ester containing derivative of trifluoperazine was targeted for modification of Lys 148 and to a lesser extent, Lys 75 and 21. It is likely that the modification observed here also involves lysyl residues or possibly other nucleophiles including methionyl thioether moieties known to line the hydro-
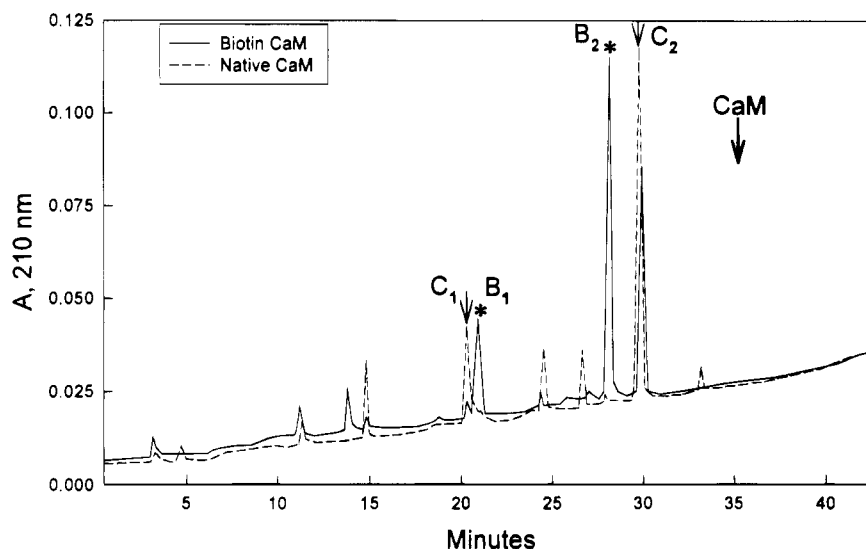
Figure 7. Separation of trypsinized fragments of native and modified CaM. The separation was achieved using a 2 min isocratic wash of buffer A, followed by a linear gradient of 0−70% buffer B over an 38 min period. The native CaM elution pattern is indicated by a dashed line, and the modified CaM elution pattern is indicated by a solid line. The arrow with CaM indicated the position of native, undigested CaM. The asterisks labeled with B_1 and B_2 indicate modified CaM peptides that have altered elutions compared to native CaM peptides. The arrows labeled with C_1 or C_2 are native CaM peptide peaks which appear to be diminished in the modified protein digest.

Table 1. Amino Acid Composition of Modified CaM Tryptic Fragments (Mol of Amino Acid/Mol of Peptide)

amino acid	HPLC B_1	residue 91−126[a]	HPLC B_2	residue 1−30[a]
Asx	4.3	6	6.0	4
Thr	1.7	2	3.2	5
Ser	3.6	1	0.8	1
Glx	5.2	5	8.0	7
Gly	8.1	3	5.0	3
Ala	4.2	2	3.0	3
Val	2.6	3	1.5	1
Met	0.0	2	0.7	1
Ile	1.8	2	2.0	2
Leu	3.0	3	2.4	3
Tyr	2.0	1	0.6	0
Phe	1.3	1	2.5	3
His	0.8	1	0.8	0
Lys	2.2[b]	2[b]	2.1	3
Arg	2.5	2	0.6	1

[a] Values taken from the amino acid sequence as determined by Watterson et al. (29). [b] These values include one residue of trimethyllysine, which under normal amino analysis conditions elutes together with lysine.

phobic pockets (32) and to be perturbed on phenothiazine binding (12). These residues also have been implicated as sites for photoattachment of benzoylphenylalanine containing synthetic peptide derivatives of the CaM binding domain of myosin light chain kinase (33).

It also should be noted that Krebs (34) demonstrated calcium-dependent photolabeling of CaM with the diazirine-based probe, TID or 3-(trifluoromethyl)-3-(m-[^{125}I]-iodophenyl)diazirine. On the basis of selective modifi-

cation of CaM fragments, they concluded that photolabeling occurred somewhere within residues 1−77, the amino-terminal half of the molecule, and between residues 78 and 106 in the C-terminal half, in agreement with our observations with the azidophenothiazine probe presented here.

Cook (27) has recently reported the three-dimensional X-ray crystal structure of a 1:1 TFP−CaM complex. Figure 8 shows a stylized version of that structure adapted directly from the atomic coordinates deposited in the Brookhaven Protein Data Base. The structure of the CaM backbone is depicted in standard ribbon format (N-terminal: magenta; C-terminal: mustard; connecting loop: blue) with the positions of bound calcium ions depicted as green van der Waals spheres. The original TFP molecule has been replaced in this picture with the biotinylated azidophenothiazine **4** by overlaying the phenothiazine nuclei and then making minor structural adjustments to eliminate unfavorable contacts in the biotin containing side chain by energy minimization programs (Quanta and CharmM). The phenothiazine **4** is displayed as van der Waals spheres in standard atomic colors as are the atoms of two methionine side chains (Met 109 on the left and below the blue azide group and Met 124 on the right and below the blue azide group) in the C-terminal hydrophobic pocket. These Met residues make intimate contact with the trifluoromethyl-bearing portion of the phenothiazine nucleus in the crystal structure of the TFP−CaM adduct. Most notably, the yellow sulfur atoms of these two residues sandwich the azido group (blue) within sufficient proximity to provide

Table 2. Sequence Analysis of Biotin-Modified CaM Peptides

sequence of HPLC B_1-labeled adduct:													
cycle no.	1	2	3	4	5	6	7	8	9	10	11	12	13
expected sequence (91−126)[a]	Val	Phe	Asp	Lys	Asp	Gly	Asn	Gly	Tyr	Ile	Ser	Ala	Ala
pmol of PTH[b] detected	39.5	28.5	43.3	32.7	33.0	19.5	16.8	5.5	5.1	4.6	0.8	1.8	2.7

sequence of HPLC B_2-labeled adduct:						
cycle no.	1	2	3	4	5	6
expected sequence (1−30)[a]	nd[c]	nd[c]	nd[c]	nd[c]	nd[c]	nd[c]
pmol of PTH[b] detected						

[a] Taken from the known sequence of CaM (29). [b] Picomoles of phenylthiohydantoin (PTH) derivative in each cycle was quantified using an Applied Biosystems Model 477 Automated Protein Sequencer. [c] Not detected.
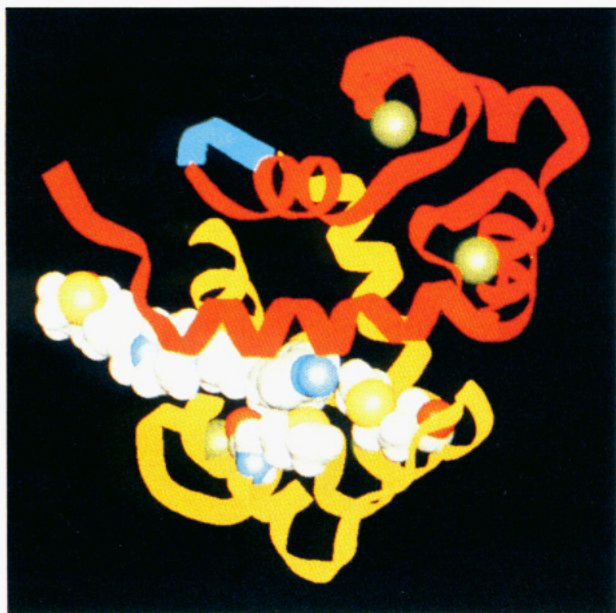
Figure 8. Model of phenothiazine **4** docked to the C-terminal pocket of calmodulin. The model shown is based on the structure of the 1:1 TFP–CaM complex (*27*). The coordinates for that structure were imported from the Brookhaven PBD into an Iris Silicon Graphics modeling computer using Quanta and CharmM. The phenothiazine **4** up to and including the piperazine ring was superimposed over the TFP molecule, and the biotin-containing side chain extension was fitted through energy minimization calculations. The CaM backbone is displayed in ribbon format with the amino terminal half of the molecule in magenta and the C-terminal half in mustard yellow. The short blue ribbon segment represents residues 75–80 of CaM that were not identified in the crystal structure analysis (*27*). For this region of the CaM molecule, the structure shown was modeled on the basis of the three-dimensional structure of the CaM–MLCK peptide complex as determined by Meador (*40*). Structures shown in van der Waals contact spheres are as follows: the four calcium ions (in green), the phenothiazine **4**, Met 109 (on the left and below the azide group in blue), and Met 124 (on the right and below the azide group in blue) in standard atomic color representations.

facile reaction with the photoactivated aryl azide. This is in excellent agreement with our chemical characterization of the C-terminal peptide adduct that showed no methione residues in the amino acid analysis, and this is also in agreement with the reported trapping of nitrene intermediates by thioethers (*35*).

The photolabeling of the N-terminal region of CaM documented here is not as readily correlated with the X-ray structure of the TFP–CaM complex. As noted above, Cook (*27*) found little evidence for binding of a second TFP molecule to the available N-terminal hydrophobic pocket in the reported crystal structure. Previous X-ray crystallographic analyses (*36, 37*) have indicated, however, the presence of up to four TFP molecules/CaM molecule in crystallized complexes. However, site occupancy for all but the single TFP bound in the C-terminal pocket were low as has also been observed by Cook and co-workers (W. Cook, personal communication). The most likely explanations for the observed photolabeling of the amino terminal region of CaM with phenothiazine **4** are as follows: (1) the N-terminal binding site has greater affinity for phenothiazine binding in solution than in the crystal; (2) photolabeling increases the apparent extent of phenothiazine binding to the N-terminal site by simple mass action; (3) the phenothiazine nucleus makes sufficient contact with the N-terminal region of CaM to permit labeling even when bound to the C-terminal pocket; and (4) covalent attachment of the phenothiazine to the C-terminal pocket alters

the conformation of the N-terminal pocket, increasing the latter's affinity for binding.

The concentration dependence of modification presented in Figure 6 and analysis of HPLC-purified CaM derivatives shown in Figure 4 indicated that CaM was photolabeled at two sites with equivalent reagent binding affinities. This would seem to mitigate against hypotheses 2 and 3. It should be noted that the bound TFP in the crystallized 1:1 complex interacts with portions of the N-terminal region of CaM, a finding that could otherwise lend support to proposal 3. However, that interaction does not involve the portions of the phenothiazine nucleus bearing the azide functionality in **4** (see Figure 8).

In attempting to assess hypotheses 1 and 4, we have previously demonstrated (*11*) that site accessibility in CaM is highly dependent on the saturation of all four sites with Ca^{2+}. It should be noted that the low pH (5.8) required for crystallization has been shown to impair Ca^{2+} binding (*38*) and might lead to less than full Ca^{2+} saturation. This could account for the differences between site occupancy in the crystal and our studies, particularly since the C-terminal pocket is exposed for aryl azide binding at lower Ca^{2+} concentrations than that at the N-terminus (*11*). The possibility that covalent modification could alter either Ca^{2+} or phenothiazine **4** affinities of the N-terminal pocket is also reasonable based on previous work demonstrating similar phenomena with fluorescent-labeled CaM derivatives (*39*).

Overall, the work presented here demonstrates that a bidentate azidophenothiazine containing a side-chain biotinyl moiety can be used effectively to study the nature of binding sites in target proteins. Studies are currently in progress to extend this approach to identify phenothiazine binding proteins in a variety of tissues, particularly those involved in *MDR1* function. These probes are also being used to study differential specificities and binding site structures in dopamine receptors.

Supporting Information Available: Spectral data for 3-azido-10-(4-(4-biotinoyl-1-piperazinyl)butyl)phenothiazine (**3**), *d*-biotinol tosylate (**7**), and 3-azido-10-(4-(4-biotinyl-1-piperazinyl)butyl)phenothiazine (**4**) (2 pages). Ordering information is given on any current masthead page.

LITERATURE CITED

(1) Marshall, G. R. (1987) Computer-aided molecular modeling of a D2-agonist dopamine pharmacophore. *J. Comput. Aided Mol. Des. 1*, 121–32.

(2) Civelli, O., Runzow., J. R., and Grandy, D. K. (1993) Molecular diversity of the dopamine receptors. *Ann. Rev. Pharmacol. Toxicol. 32*, 281–307.

(3) Lum, B. L., Gosland, M. P., Kaubisch, S., and Sikic, B. I. (1993) Molecular targets in oncology: Implications of the multidrug resistance gene. *Pharmacotherapy 13*, 88–109.

(4) Hait, W. N., and Aftab, D. T. (1992). Rational design and pre-clinical pharmacology of drugs for reversing multidrug resistance. *Biochem. Pharmacol. 43*, 103–107.

(5) Bruggenmann, E. P., Germann, U. A., Gottesman, M. M., and Pastan, I. (1989) Two different regions of phosphoglycoprotein are photoaffinity-labeled by azidopine. *J. Biol. Chem. 264*, 15483–15488.

(6) Greenberg, L. M., Yang, C.-P. H., Gindin, E., and Horwitz, S. B. (1990) Photoaffinity probes for the α_1-adrenergic receptor and the calcium channel bind to a common domain in P-glycoprotein. *J. Biol. Chem. 265*, 4394–4401.

(7) Golinski, M., DeLaLuz, P., Floresca, R., Delcamp, T. J., Vanaman, T. C., and Watt, D. S. (1995) Synthesis, binding affinity, and cross-linking of monodentate photoactive phenothiazines to calmodulin. *Bioconjugate Chem.* 6, 549–557.

(8) Newton, D. L., and Klee, C. B. (1989) Phenothiazine-binding and attachment sites of CAPP1-calmodulin. *Biochemistry 28,* 3750–3757.

(9) Jarrett, H. W. (1984) The synthesis and reaction of a specific affinity label for the hydrophobic drug-binding domains of calmodulin. *J. Biol. Chem. 259,* 10136–10144.

(10) Faust, F. M., Slisz, M., and Jarrett, H. W. (1987). Calmodulin is labeled at lysine 148 by a chemically reactive phenothiazine. *J. Biol. Chem. 262,* 1938–1941.

(11) Dwyer, L., Crocker, P. J., Watt, D. S., and Vanaman T. C. (1992) The effects of calcium site occupancy and reagent length on reactivity of calmodulin lysyl resdiues with heterbifunctional aryl azides. *J. Biol. Chem. 267,* 22606–22615.

(12) Klevit, R. E., Levine, B. A., and Williams, R. J. P. (1981) A study of calmodulin and it interaction with trifluoperazine by high resolution ¹H NMR spectroscopy. *FEBS Lett. 123,* 25–29.

(13) Brunner, J. (1993) New photolabeling and crosslinking methods. *Ann. Rev. Biochem. 62,* 483–514.

(14) Schuster, G. B., and Platz, M. S. (1992) Photochemistry of phenyl azide. *Adv. Photochem. 17,* 69–143.

(15) Flaster, H., and Kohn, H. (1981) Syntheses and spectral properties of 2-thiobiotin and biotin derivatives. *J. Heterocycl. Chem. 18,* 1425–1436.

(16) Jamieson, G. A., and Vanaman, T. C. (1979) Calcium-dependent affinity chromatography of calmodulin on immobilized phenothiazine. *Biochem. Biophys. Res. Commun. 90,* 1048–1055.

(17) Wallace, R. W., Tallant, E. A., and Cheung, W. Y. (1983) Assay of calmodulin by Ca²⁺-dependent phosphodiesterase. *Methods Enzymol. 102,* 39–47.

(18) Laemmli, U. K. (1970) Cleavage of structural proteins during the assembly of the head of bacteriophage T4. *Nature 227,* 680–685.

(19) Leary, J. J., Brigati, D. J., and Ward, D. C. (1983) Rapid and sensitive colorimetric method for visualizing biotin-labeled DNA probes hybridized to DNA or RNA immobilized on nitrocellulose. *Proc. Natl. Acad. Sci. U.S.A. 80,* 4045–4049.

(20) Brandt, P., Neve R. L., Kammesheidt, A., Rhoads, R. E., and Vanaman, T. C. (1992) Analysis of the tissue-specific distribution of m RNAs encoding of an alternately spliced form of PMCA4 at the cDNA and genomic levels. *J. Biol. Chem. 267,* 4376–4385.

(21) Walsh, M., and Stevens, F. C. (1977) Characterization of tryptic fragments obtained from bovine brain protein modulator of cyclic nucleotide phosphodiesterase. *J. Biol. Chem. 252,* 7440–7443.

(22) Hofmann, K., Finn, F. M., and Kiso, Y. (1978) Avidin-biotin affinity columns. General methods of attaching biotin to peptides and proteins. *J. Am. Chem. Soc. 100,* 3585–3590.

(23) Prozialeck, W. C., and Weiss, B. (1982) Inhibition of calmodulin by phenothiazines and related drugs: structure–activity relationships. *J. Pharmacol. Exp. Ther. 222,* 509–516.

(24) Klee, C. B., and Vanaman, T. C. (1982) Calmodulin. *Adv. Prot. Chem. 35,* 213–321.

(25) Levin, R. M., and Weiss, B. (1978) Specificity of the binding of trifluoperazine to calcium-dependent activator of phosphodiesterase and to a series of other calcium-binding proteins. *Biochim. Biophys. Acta 540,* 197–204.

(26) Massom, L., Lee, H., and Jarrett, H. W. (1990) Trifluoperazine binding to porcine brain calmodulin and skeletal muscle troponin C. *Biochemistry 29,* 671–681.

(27) Cook, W. J., Walter, L. J., and Walter, M. R. (1994) Drug binding by calmodulin: Crystal structure of a calmodulin–trifluoperazine complex. *Biochemistry 33,* 15259–15265.

(28) Vanaman, T. C. (1983) Chemical approaches to the calmodulin system. *Methods Enzymol. 102,* 296–310.

(29) Watterson, D. M., Sharief, F., and Vanaman, T. C. (1980) The complete amino acid sequence of the Ca²⁺-dependent modulator protein (calmodulin) of bovine brain. *J. Biol. Chem. 255,* 962–975.

(30) Newton, D. L., Burke, T. R., Jr., Rice, K. C., and Klee, C. B. (1983) Calcium ion dependent covalent modification of calmodulin with norchlopromazine isothiocyanate. *Biochemistry 22,* 5472–5476.

(31) Newton, D. L., and Klee, C. B. (1984) CAPP-calmodulin: a potent competitve inhibitor of calmodulin actions. *FEBS Lett.165,* 269–272.

(32) Babu, Y. S., Sack, J. A., Greenbough, T. J., Bugg, C. E., Means, A. R., and Cook, W. J. (1985) Three-dimensional structure of calmodulin. *Nature 315,* 37–40.

(33) O'Neil, K. T., Erickson-Viitanen, S., and Degrado, W. F. (1989) Photolabeling of calmodulin with basic, amphipathic alpha-helical peptides containing p-benzoylphenylalanine. *J. Biol. Chem. 264,* 14571–14578.

(34) Krebs, J., Buerkler, J., Guerini, D., Brunner, J., and Carafoli, E. (1984) 3-(Trifluoromethyl)-3-(m-[¹²⁵I]iodophenyl)-diazirine, a hydrophobic, photoreactive probe, labels calmodulin and calmodulin fragments in a Ca²⁺-dependent way. *Biochemistry 23,* 400–403.

(35) Poe, R., Schnapp, K., Young, M. J. T., Grayzar, J., and Platz, M. S. (1992) Chemistry and kinetics of singlet (pentafluorophenyl)nitrene. *J. Am. Chem. Soc. 114,* 5054–5067.

(36) Gehrig, L. M. B., Delbaere, L. J. T., and Hickie, R. A. (1984) Preliminary X-ray data for the calmodulin/trifluoperazine complex. *J. Mol. Biol. 177,* 559–561.

(37) Vandonselaar, M., Hickie, R. A., Quail, J. W., and Delbaere, L. J. T. (1994). Trifluoperazine-induced conformational change in Ca²⁺-calmodulin. *Nature Struct. Biol. 1,* 795–801.

(38) Haiech, J., Klee, C. B., and DeMaille, J. G. (1981) Effects of cations on the affinity of calmodulin for calcium: Ordered binding of calcium ions allows the specific activation of calmodulin-stimulated enzymes. *Biochemistry 20,* 3890–3897.

(39) Olwin, B. B., Edelman, A. M., Krebs, E. G., and Storm, D. R. (1984) Quantitation of the energy coupling between Ca²⁺, calmodulin, skeletal muscle myosin light chain kinase, and kinase substrates. *J. Biol. Chem. 259,* 10949–10955.

(40) Meador, W. E., Means, A. R., and Quiocho, F. A. (1992) Target enzyme recognition by calmodulin: 2.4 Angstroms structure of a calmodulin–peptide complex. *Science 257,* 1251–1255.

BC9500498

Synthesis and Binding Affinity of Bidentate Phenothiazines with Two Different Photoactive Groups

Miroslaw Golinski,[†] Paul J. DeLaLuz,[†] Tavner J. Delcamp,[‡] David S. Watt,[*,†] and
Thomas C. Vanaman[*,‡]

Department of Chemistry and Department of Biochemistry, University of Kentucky, Lexington, Kentucky 40506.
Received May 2, 1995[⊗]

The development of targeted, bidentate photoaffinity reagents for mapping the interacting domains
of calmodulin (CaM) with the enzymes that it regulates required the synthesis and evaluation of the
binding affinity of various phenothiazines. These photoaffinity reagents would possess a photoactive
3-azidophenothiazine group for cross-linking the hydrophobic binding domain of CaM, a second
photoactive benzophenone group that would be activated at a different wavelength than the
3-azidophenothiazine group, and a suitable radiolabel. Difficulties were encountered in identifying
those structural features that would be compatible with the introduction of a benzophenone group,
with the solubility of these benzophenone-substituted phenothiazines, and with the ability of these
phenothiazines to inhibit the calmodulin-mediated activation of phosphodiesterase. Solutions to this
problem involved the preparation of phenothiazines possessing a quaternary ammonium salt, a
zwitterionic amino acid, or a carbohydrate moiety. The phenothiazines that possessed photoactive
3-azido and benzophenone groups and in which one of the piperazine nitrogens in the side chain was
converted to a quaternary, *N*-methylammonium iodide inhibited the calmodulin-mediated activation
of phosphodiesterase at a level comparable to that of chlorpromazine.

INTRODUCTION

In the course of developing a new class of reagents described as "targeted, bidentate" cross-linking reagents for studying the interaction of calmodulin (CaM)[1] with the proteins that it regulates (1), photoactive phenothiazines were synthesized that could guide the initial binding event of the phenothiazine to CaM (2, 3). Phenothiazines that possessed a 2-azido, 3-azido, 2-benzoyl, or 1,3,4-trifluoro-2-azido functionality in combination with various modifications of the *N*-alkyl side chain were capable of inhibiting the CaM-mediated activation of phosphodiesterase (PDE) (2).

Calmodulin was photolabeled with excellent efficiency in a light- and calcium-dependent fashion using a radiolabeled analog, 3-azido-10-(4-(4-[¹⁴C]methyl-1-piperazinyl)butyl)phenothiazine ([¹⁴C]-**1**), shown in Figure 1 (2). Competition studies using this radiolabeled analog and chlorpromazine (CPZ) were consistent with binding with
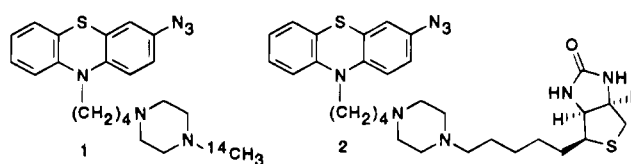
Figure 1. Photoactive phenothiazines with various "reporter" groups.

one or both of the hydrophobic binding pockets of CaM. The photolabeling of CaM using another analog, 3-azido-10-(4-(4-biotinyl-1-piperazinyl)butyl)phenothiazine (**2**) in Figure 1, followed by limited trypsin digestion and purification by either SDS–PAGE[1] or HPLC[1] provided two principal phenothiazine-containing peptides. Amino acid composition data and/or sequence data for these two peptides established that the photoactive phenothiazine had covalently modified both the C- and N-terminal hydrophobic binding pockets in CaM (3).

With these results in hand, we proceeded with plans to develop targeted, bidentate cross-linking reagents (4) in which a second photoactive benzophenone group (5, 6) would be incorporated into the 3-azidophenothiazine framework. The synthesis and application of a bidentate, nucleotide-based photoaffinity cross-linking reagent were recently reported (7–9). We describe the challenges of synthesizing bidentate reagents that possessed both photoactive groups and yet retained the ability to inhibit the CaM-mediated activation of PDE.[1]

EXPERIMENTAL PROCEDURES

Calmodulin-Stimulated Phosphodiesterase Assays. PDE and cAMP[1] were obtained from Sigma. Calmodulin was purified from bovine testes according to the procedure of Jamieson and Vanaman (10). Assay of PDE was performed according to the method of Wallace (11) with the following modification. Hydrolysis of the product of the reaction, adenosine 5'-monophosphate, was carried out with 5'-nucleotidase, and the subsequent release of inorganic phosphate was measured according

Table 1. I$_{50}$ Values from Calmodulin-Stimulated Phosphodiesterase Assays for Phenothiazine Analogs

phenothiazine reagent	I$_{50}$ μM	I$_{50}$/I$_{50}$ CPZ[a]
3	88 ± 13	ca. 3
4	>100	
5	>100	
6[b]	no inhibition	
7	>100	
8	>50	
9	>50	
10	12 ± 1	0.4
11	>100	
12	10 ± 3	0.3

[a] CPZ = chlorpromazine (I$_{50}$ = 30 μM). [b] Used as oxalate salt.

to the method of Lanzetta (*12*). Each assay was performed at 30 °C in a volume of 0.2 mL in a buffer consisting of 50 mM TRIS,[1] 25 mM ammonium acetate, 3 mM magnesium acetate, 100 μM calcium chloride, and 5 mM DTT[1] at pH 8.0. Various concentrations of each inhibitor in triplicate were preincubated for 5 min with 500 ng/mL (30 nM) of calmodulin followed by the addition of 0.001 unit of PDE and a further preincubation of 5 min. The reaction was initiated by the addition of cAMP to a final concentration of 1 mM. After 10 min, the reaction was stopped by incubating each sample at 90 °C for 2 min. The addition of 0.2 unit of 5'-nucleotidase was made to each sample followed by a 15 min incubation at 30 °C. An aliquot of 0.1 mL was transferred from each sample to 0.8 mL of Lanzetta reagent (*12*) and the mixture incubated for at least 20 min before measuring the absorbance at 660 nm. Data were plotted as the percent of the calmodulin-stimulated PDE activity at each inhibitor concentration with 100% representing the absorbance value of calmodulin-stimulated PDE in the absence of inhibitor minus the absorbance value of PDE assayed in the absence of calmodulin. For each inhibitor the effect on PDE activity in the absence of calmodulin was found to be <5% over the range of concentrations used. From each plot of percent activity versus inhibitor concentration an I$_{50}$ value was determined which represents the concentration producing 50% inhibition of calmodulin-stimulated PDE activity. The I$_{50}$ values reported in Table 1 represent the average of four separate experiments.

N'-(1-(4-(4'-(3''-Azido-10''-phenothiazinyl)butyl)piperazinyl)-N-(4'-benzoylphenylacetyl)-β-alanine Amide (3). The procedure of Hofmann (*13*) was modified as follows. To a solution of 93 mg (0.3 mmol) of N-(4-benzoylphenylacetyl)-β-alanine (see supporting information) in 0.5 mL of anhydrous DMF[1] under an Ar atmosphere was added 51 mg (0.315 mmol, 1.05 equiv) of 1,1'-carbonyldiimidazole. The mixture was protected from light and stirred at 80 °C for 20 min. The mixture containing N-(4-benzoylphenylacetyl)-β-alanine imidazolyl ester was cooled to 25 °C, and a solution of 114 mg (0.3 mmol) of 3-azido-10-(4-(1-piperazinyl)butyl)phenothiazine (see supporting information) in 1 mL of anhydrous DMF was added. The mixture was stirred at 25 °C for 14 h. The mixture was diluted with water and extracted with EtOAc. The combined extracts were dried over anhydrous MgSO$_4$ and concentrated. The residue was chromatographed on silica gel using CH$_2$Cl$_2$–MeOH (gradient 20:1, 10:1) and subsequently with EtOAc–MeOH (gradient 10:1, 6:1) to give 152 mg (75%) of **3** as a foam. Anal. (C$_{38}$H$_{39}$N$_7$O$_3$S·1/2H$_2$O) C, H.

N'-(1-(4-(4'-(3''-Azido-10''-phenothiazinyl)butylpiperazinyl)-N-(4'-benzoylphenylacetyl)methionine Amide (4). The procedure described for the preparation of **3** was repeated using 71 mg (0.192 mmol) of N-(4-

benzoylphenylacetyl)methionine (see supporting information) and 73 mg (0.192 mmol) of 3-azido-10-(4-(1-piperazinyl)butyl)phenothiazine (see supporting information) in 0.9 mL of DMF to afford, after chromatography with MeOH–CH$_2$Cl$_2$ (gradient 1:100, 1:75, 1:50, 1:40, 1:30), 116 mg (82%) of **4** as a foam.

N'-(1-(4-(4'-(3''-Azido-10''-phenothiazinyl)butyl)-piperazinyl))-N-(*tert*-butoxycarbonyl)-(S-4'-benzoylphenylacetyl)cysteine (5). To 546 mg (1.3 mmol) of N-(*tert*-butyloxycarbonyl)-S-(4-benzoylphenylmethyl)-cysteine (see supporting material) in 7 mL of anhydrous CH$_2$Cl$_2$ was added 151 mg (1.3 mmol) of N-hydroxysuccinimide and 298 mg (1.4 mmol, 1.1 equiv) of DCC. (Note: it was generally preferable to use the imidazolyl coupling procedure described for **3** in order to avoid the problem of separating the N,N-dicyclohexylurea byproduct encountered using this NHS procedure.) The solution was protected from light and stirred for 20 h at 25 °C under a N$_2$ atmosphere. The precipitate was removed by filtration. The filtrate was concentrated, redissolved in EtOAc, and again filtered. The filtrate was concentrated to give 675 mg (100%) of crude succinimidyl ester as a semisolid, a portion of which was used directly in the next reaction. To 50 mg (0.13 mmol) of 3-azido-10-(4-(1-piperazinyl)butyl)phenothiazine (see supporting information) in 2.5 mL of anhydrous DMSO was added 67 mg (0.13 mmol) of crude succinimidyl ester and 14 mg (0.14 mmol, 1.1 equiv) of anhydrous Et$_3$N. The solution was stirred at 25 °C for 24 h under a N$_2$ atmosphere and was protected from light. The mixture was diluted with EtOAc and washed with H$_2$O and brine. The combined organic layers were dried over anhydrous Na$_2$SO$_4$ and concentrated. The residue was chromatographed on silica gel using 1:20 MeOH–CH$_2$Cl$_2$ to give 87 mg (86%) of **5** as a semisolid. Anal. (C$_{42}$H$_{47}$N$_7$O$_4$S) C, H, N.

1-(N-(4-benzoylphenylacetyl)-β-alaninyl)-4-methylpiperazine (6). The procedure described for the preparation of **3** was repeated using 93 mg (0.3 mmol) of N-(4-benzoylphenylacetyl)-β-alanine (see supporting information), 54 mg (0.33 mmol, 1.1 equiv) of 1,1'-carbonyldiimidazole, and 40 μL (36.1 mg, 0.36 mmol, 1.2 equiv) of 1-methylpiperazine to afford, after column chromatography on silica gel with MeOH–CH$_2$Cl$_2$ (gradient: 1:20, 1:10) and subsequently with MeOH–EtOAc (gradient: 1:10, 1:6:, 1:4), 69 mg (58%) of **6**: mp 95–96 °C (recrystallized from hexane–EtOAc). Anal. (C$_{23}$H$_{27}$N$_3$O$_3$) C, H. The oxalate salt was prepared in the usual fashion: dp 159 °C. Efforts to secure a correct combustion analysis on the oxalate salt were hampered by the hygroscopic nature of the salt.

3-Azido-10-(4-(4-(4-(S-cysteinylmethyl)benzoyl)benzyl)-1-piperazinyl)butyl)phenothiazine (7). To 51 mg (0.42 mmol, 4 equiv) of L-cysteine in 1.2 mL of MeOH under an Ar atmosphere at 25 °C was added dropwise 0.28 mL (0.84 mmol, 8 equiv) of 3 N aqueous NaOH in order to obtain a clear solution. To the solution was added 66 mg (0.105 mmol) of 3-azido-10-(4-(4-(4-(chloromethyl)benzoyl)benzyl)-1-piperazinyl)butyl)phenothiazine (see supporting information) in 2.5 mL of MeOH and 2 mL of THF. The mixture was stirred for 40 min. The mixture was diluted with 30 mL of water and neutralized with of 1.5 g of NH$_4$Cl. The solution was extracted with three 25 mL portions of CH$_2$Cl$_2$. The combined extracts were dried over anhydrous Na$_2$SO$_4$ and concentrated. The crude product was dissolved in 3.5 mL of a mixture of 2:5 MeOH–CH$_2$Cl$_2$, precipitated by the dropwise addition of 2 mL of Et$_2$O, and filtered to give 46 mg (62%) of **7** as an amorphous solid: dp 153 °C.

3-Azido-10-(4-(4-(4-benzoylphenyl)methyl)-1-piperazinyl)butyl)phenothiazine (8). To a solution of

36 mg (95.7 μmol) of 3-azido-10-(4-(1-piperazinyl)butyl)-phenothiazine (see supporting information) in 287 μL of MeOH was added 12 μL (12.6 mg, 0.21 mmol, 2.2 equiv) of HOAc and 40 mg (0.191 mmol, 2 equiv) of 4-benzoyl-benzaldehyde (*14*). The solution was stirred for 2 min, and 43 μL (2.7 mg, 43 μmol, 0.45 equiv) of a freshly prepared 1 M solution of NaBH$_3$CN in MeOH was added. The solution was stirred for 3 h. To this solution was added an additional 4 μL (4.2 mg, 0.7 mmol, 0.73 equiv) of HOAc and 14.3 μL (0.90 mg, 14.3 μmol, 0.15 equiv) of 1 M NaBH$_3$CN solution. The solution was stirred for 0.5 h, and an additional 4 μL (0.25 mg, 4 μmol, 0.042 equiv) of 1 M NaBH$_3$CN solution was added. The mixture was stirred for 2 h, poured into 5 mL of 1% aqueous NaOH solution, and extracted with Et$_2$O. The combined extracts were dried over anhydrous MgSO$_4$ and concentrated. The residue was chromatographed on silica gel using a gradient of 1:100, 1:50, 1:30 MeOH–CH$_2$Cl$_2$ to give 42 mg (76%) of **8** as an oil. The bismaleate salt of **8** was prepared in the usual fashion. To a solution of 36 mg (0.0618 mmol) of **8** in 0.8 mL of CH$_2$Cl$_2$ was added a solution of 15 mg (0.127 mmol, 2.05 equiv) of maleic acid in 0.3 mL of MeOH. The solid was collected by filtration, washed with Et$_2$O, and dried in vacuum to afford 27 mg (55%) of bismaleate: dp 157 °C. Anal. (C$_{42}$H$_{42}$N$_6$O$_9$S) C, H, N.

***N*-1-(4-(4'-(3''-Azido-10''-phenothiazinyl)butyl))-*N'*-(1-(6-((4-benzoylbenzyl)oxy)-2,3,4,5-tetrahydroxy-hexyl))piperazine (9).** To a solution of 45 mg (0.099 mmol) of 6-*O*-((4-benzoylphenyl)methyl)-1,2:3,4-bis-*O*-isopropylidene α-D-galactopyranose (**25**) (see supporting information) in 3 mL of THF was added 2 mL of H$_2$O and 1 mL of concentrated HCl solution. The mixture was allowed to stand at 25 °C for 22 h. The stirred mixture was cooled with ice–water and neutralized with addition of solid NaHCO$_3$. The mixture was concentrated, and the residue was triturated with three 5 mL portions of 1:10 MeOH–CH$_2$Cl$_2$. The combined filtrates were chromatographed on an analytical silica gel plate (20 × 20 cm) with 1:10:100 H$_2$O–MeOH–CH$_2$Cl$_2$. The product was eluted from the collected silica gel band with 1:5 MeOH–CH$_2$Cl$_2$, redissolved in 1:20 MeOH–CH$_2$Cl$_2$ filtered, and concentrated to give 2 mg (5%) of one anomer and 12 mg (31%) of a more polar anomer as oils. As expected, reexamination of these fractions on TLC (silica gel) again showed two spots; no effort was made to assign the configuration of the anomeric center in these products. To a solution of 12 mg (31 μmol) of 3-azido-10-(4-(1-piperazinyl)butyl)phenothiazine (**14a**) (see supporting information) and of 12 mg (31 μmol) of the more polar anomer in a turbid mixture of 93 μL of MeOH and 93 μL of H$_2$O was added 3.6 μL (3.7 μg, 62 μmol, 2 equiv) of HOAc. The addition of HOAc produced a clear solution to which 12 μL (12.4 μmol, 0.4 equiv) of freshly prepared 1 M sodium cyanoborohydride solution in MeOH was added. After 40 min, the reaction was diluted with an additional 60 μL of MeOH, and the mixture was stirred at 25 °C for 16 h. The reaction was quenched by dilution with 2 mL of CH$_2$Cl$_2$ and the addition of an excess of solid anhydrous K$_2$CO$_3$. The solution was filtered, and the filter cake was washed with two 1 mL portions of 1:4 MeOH–CH$_2$Cl$_2$. The combined filtrates were chromatographed on an analytical silica gel plate (20 × 20 cm) with 1:10:100 H$_2$O–MeOH–CH$_2$Cl$_2$ (two developments). The product was eluted from the collected silica gel band using 1:5 MeOH–CH$_2$Cl$_2$ to give 10 mg of a residue that was dissolved in 1:20 MeOH–CH$_2$Cl$_2$, filtered, and concentrated to give 6 mg (26%) of **9** as an oil.
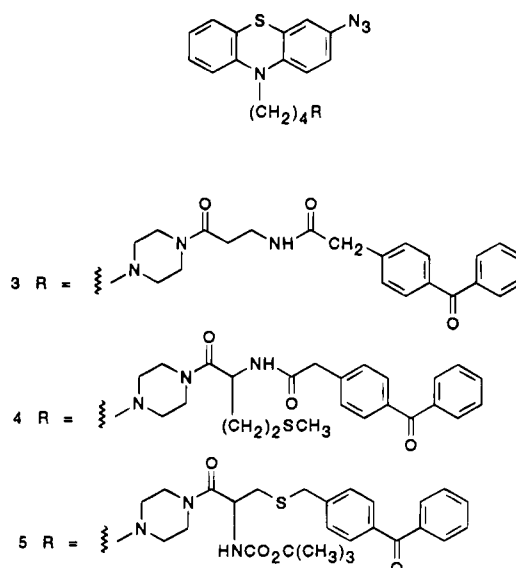
Figure 2. Photoactive phenothiazines with piperazinamide side chains.

Adduct 10 of Methyl Iodide and *N'*-(1-(4-(4'-(3''-Azido-10''-phenothiazinyl)butyl)piperazinyl))-*N*-(4'-benzoylphenylacetyl)-β-alanine Amide. A solution of 92 mg (137 μmol) of **3** and 171 μL (389 mg, 2.74 mmol, 20 equiv) of methyl iodide in 685 μL of CH$_2$Cl$_2$ was allowed to stand under an Ar atmosphere at 25 °C for 17 h. The mixture was concentrated, and the residue was chromatographed on silica gel using a gradient of 1:20, 1:10, and 1:5 MeOH–CH$_2$Cl$_2$ to give 97 mg (87%) of **10** as a foam.

Adduct 11 of Methyl Iodide and 3-Azido-10-(4-(4'-acetyl-1'-piperazinyl)butyl)phenothiazine. The procedure described for the preparation of **10** was repeated using 105 mg (248 μmol) of 3-azido-10-(4-(4'-acetyl-1'-piperazinyl)butyl)phenothiazine (see supporting information), 309 μL (704 mg, 4.96 mmol, 20 equiv) of methyl iodide, and 1.24 mL of CH$_2$Cl$_2$ to afford, after standing for 36 h and chromatography on alumina with a gradient of 1:50, 1:30, 1:20 and 1:10 MeOH–CH$_2$Cl$_2$, 128 mg (91%) of **11** as an oil. Trituration of an 18 mg sample with Et$_2$O afforded 10 mg of an amorphous solid that does not melt sharply (foams at 50 °C and decomposes at *ca.* 125 °C).

Adduct 12 of Methyl Iodide and *N'*-(1-(4-(4'-(3''-Azido-10''-phenothiazinyl)butyl)piperazinyl))-*N*-((4-benzoylphenyl)methyl)tartaric Acid Diamide. The procedure described for the preparation of **10** was repeated using 17 mg (24.1 μmol) of the amide of 3-azido-10-(4-(1-piperazinyl)butyl)phenothiazine and tartaric acid *N*-(4-benzoylphenyl)methyl amide, 30 μL (68 mg, 48.2 μmol, 20 equiv) of MeI, and 120 μL of CH$_2$Cl$_2$ at 25 °C for 42 h to afford, after chromatography on silica gel with MeOH–CH$_2$Cl$_2$ (gradient 1:10, 1:7, 1:5), 12 mg (60%) of **12** as an oil. The silica gel used in this purification was previously deactivated by loading on to a small column in MeOH and then passing 1:10 MeOH–CH$_2$Cl$_2$ through the column.

RESULTS AND DISCUSSION

The "bidentate" phenothiazines **3–5** in Figure 2 having a 3-azidophenothiazine at one terminus and a benzophenone group at the other terminus were synthesized in a straightforward fashion from 3-azido-10-(4-(1-piperazinyl)butyl)phenothiazine (*2*). The decision to incorporate a benzophenone group (*5*, *6*) was based upon the ability to activate this group at longer wavelengths than that
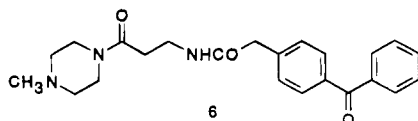
Figure 3. "Truncated" reagent: 1-(*N*-(4-benzoylphenylacetyl)-*β*-alaninyl)-4-methylpiperazine (**6**).

needed for the activation of the 3-azidophenothiazine. The selection of an amino acid "spacer" between these two photoactive groups was dictated by the need for a [³H]- or [³⁵S]-radiolabeled analog with high specific activity. The phenothiazines **3**–**5** were first synthesized in nonradiolabeled form in order to permit the evaluation of their binding affinity.

The phenothiazines **3**–**5** were assayed for their ability to inhibit the calmodulin-mediated activation of phosphodiesterase (PDE) relative to that of CPZ. These compounds were similar to monodentate phenothiazine reagents described previously that had promising activity in this assay (*3*). Phenothiazine **3** exhibited an I_{50} value (Table 1) approximately 3-fold greater than that of CPZ, an observation that indicated a lower potency than CPZ for inhibition of calmodulin-stimulated PDE activity. Phenothiazines **4** and **5** displayed such limited water solubility, presumably as a consequence of the increased size of the hydrophobic benzophenone terminus, as to preclude their evaluation in the assay (Table 1).

The diminished activity for the bidentate phenothiazines **3**–**5** relative to the monodentate analogs reported earlier (*2*) was attributed to the loss of one of the basic piperazine nitrogens characteristic of biologically active, piperazine-containing phenothiazines or to a competition between the benzophenone and the 3-azidophenothiazine moieties for the hydrophobic binding domain(s) of CaM (*15–21*). The latter possibility was excluded on the basis of the failure of the benzophenone **6** (Figure 3), which is a truncated form of the phenothiazine **3**, to inhibit the calmodulin-mediated activation of PDE relative to that of CPZ. Although some caution is needed in extrapolating from a single case, the loss of the basic piperazine nitrogen in the phenothiazines **3**–**5** seemed a more plausible explanation for their poor activity in the PDE assay than this latter type of competition. The piperazine moiety in biologically active phenothiazines is protonated at physiological pH and presumably interacts with a negatively charged, aspartate-rich region of CaM near the hydrophobic binding pockets. The poor activity displayed by the phenothiazines **3**–**5** suggested that alternative methods for linking the benzophenone to the phenothiazine were needed other than using a simple amide linkage to the piperazine.

Several phenothiazines were synthesized having a piperazine with two basic nitrogens. The synthesis of phenothiazine **7** (Figure 4) with a zwitterionic amino acid involved the sequential alkylation of 4,4′-bis(chloromethyl)benzophenone (*22*) with 3-azido-10-(4-(1-piperazinyl)butyl)phenothiazine and L-cysteine. In order to evaluate the influence of the terminal cysteine substituent in **7**, a reductive alkylation of 3-azido-10-(4-(1-piperazinyl)butyl)phenothiazine with 4-(benzoyl)benzaldehyde (*14*) was employed to acquire the phenothiazine **8** lacking the L-cysteine terminus. It was of chemical interest that it was possible to effect this reductive alkylation reaction in the presence of the 3-azidophenothiazine. Unfortunately, both of the phenothiazines **7** and **8** displayed little inhibition of calmodulin-stimulated PDE activity (Table 1) suggesting that the close proximity of the hydrophobic benzophenone group to the piperazine ring was not well tolerated.
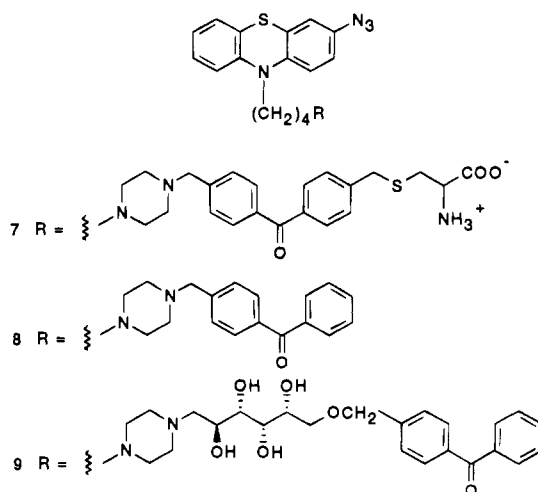
Figure 4. Photoactive phenothiazines with piperazine side chains.

The synthesis of the phenothiazine **9** (Figure 4) with a carbohydrate "spacer" between the phenothiazine and benzophenone termini employed a reductive alkylation of 3-azido-10-(4-(1-piperazinyl)butyl)phenothiazine (*2*) with 6-*O*-(4′-benzoylbenzyl)galactose. Unfortunately, this galactose-based phenothiazine **9** also displayed poor performance in the PDE assay (Table 1) for reasons that remain unclear. It is possible, although one case does not establish this point, that there is a delicate balance between providing a positively charged piperazinium ion at physiological pH and not providing other polar substituents in the immediate vicinity of the piperazine that could hydrogen bond to the aspartate-rich region of CaM.

The phenothiazines **10** and **11** possessing an ammonium salt were prepared in a straightforward alkylation of the PDE-inactive piperazines with methyl iodide. The locus of the newly introduced methyl group in these salts was assigned on the basis of ¹H and ¹³C NMR studies. The phenothiazine **10** exhibited good ability to inhibit calmodulin-stimulated PDE activity (Table 1) whereas the ammonium salt **11** exhibited only minimal activity in the PDE assay. The surprising level of activity displayed by the ammonium salt was again consistent with the beneficial effect of a positively charged piperazinium ring. Apparently, the adverse effect of removing one of the basic piperazine nitrogens in the piperazine-substituted phenothiazine **3** was overcome by the conversion to the *N*-methylpiperazinium-substituted phenothiazine **10**. The poor activity displayed by phenothiazine **11** underscores the interplay of the positively charged piperazinium ring with other side-chain structural factors in determining the overall activity.

The synthesis of the phenothiazine **12** (Figure 5) with a cleavable, tartrate "spacer" involved a standard coupling of 4-(aminomethyl)benzophenone (*7*) with sodium ethyl D-(+)-tartrate (*23*), nucleophilic substitution of the ester by 3-azido-10-(4-(1-piperazinyl)butyl)phenothiazine, and methylation. The subsequent synthesis of a radiolabeled version of **12** would make use of a [¹⁴C]-labeled tartrate spacer. Finally, the inclusion of an amide linkage between the piperazine and the tartrate as well as the introduction of polar hydroxyl groups augured poorly for the performance of this analog in the PDE assay based on comparisons with the phenothiazines **3**, **4**, **5**, and **9**, but the *N*-methylpiperazinium group offset these negative factors. In fact, the phenothiazine **12** displayed excellent activity in the PDE assay (Table 1).
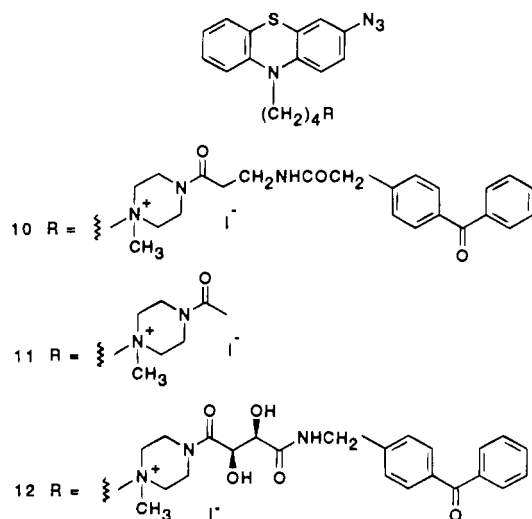
Figure 5. Photoactive phenothiazines with *N*-methylpiperazinium salt side chains.

In summary, the development of bidentate, targeted cross-linking reagents will require a sophisticated balance between photoactive phenothiazine and benzophenone ligands as well as well tailored side chains that are capable, as a minimum requirement, of providing a positively charged piperazinium group. Having demonstrated the viability of using 3-azidophenothiazines as a photoactive, *monodentate* agents for tethering the phenothiazine nucleus to the C-terminus of calmodulin (*2,3*), the subsequent development of *bidentate* reagents required the introduction of a second photoactive substituent, a benzophenone group. Although a variety of strategies were investigated for incorporating these benzophenones within an appropriate phenothiazine side chain, the *N*-methylpiperazinium salts proved most efficacious. The introduction of benzophenones with terminal zwitterionic amino acids and benzophenones with "internal" carbohydrates spacers proved unrewarding. In summary, these studies demonstrate the structural characteristics for *bidentate* phenothiazines capable of inhibiting the calmodulin-mediated activation of PDE relative to that of CPZ, and these studies set the stage for the application of bidentate phenothiazines as cross-linking reagents. These studies will be reported in due course.

ACKNOWLEDGMENT

Supporting Information Available: Experimental procedures for the preparation of 3-azido-10-(4-(1-piperazinyl)butyl)phenothiazine (**14a**), 3-azido-10-(4-(1-piperazinyl)butyl)phenothiazinium carbonate (**14b**), 3-azido-10-(4-(4'-acetyl-1'-piperazinyl)butyl)phenothiazine (**15**), 4-benzoylphenylacetic acid (**16**), succinimidyl 4-benzoylphenylacetate (**17**), *N*-(4-benzoylphenylacetyl)-*β*-alanine (**18**), *N*-(4-benzoylphenylacetyl)methionine methyl ester (**19**), *N*-(4-benzoylphenylacetyl)methionine (**20**), *N*-(*tert*-butoxycarbonyl)-*S*-(4-benzoylphenylmethyl)cysteine (**22**), 3-azido-10-(4-(4-(4-(4-(chloromethyl)benzoyl)-benzyl)-1-piperazinyl)butyl)phenothiazine (**23**), 6-*O*-((4-benzoylphenyl)methyl)-1,2:3,4-bis-*O*-isopropylidene-α-D-galactopyranose (**25**), tartaric acid ethyl ester *N*-(4-benzoylphenyl)methyl amide (**28**). Spectral data for *N*'-(1-(4-(4'-(3''-azido-10''-phenothiazinyl)butyl)piperazinyl))-*N*-(4'-benzoylphenylacetyl)-*β*-alanine amide (**3**), *N*'-(1-(4-(4'-(3''-azido-10''-phenothiazinyl)butyl)piperazinyl))-*N*-(4'-

benzoylphenylacetyl)methionine amide (**4**), *N*'-(1-(4-(4'-(3''-azido-10''-phenothiazinyl)butyl)piperazinyl))-*N*-(*tert*-butoxycarbonyl)-*S*-(4'-benzoyl)phenylacetyl)cysteine (**5**), 1-(*N*-(4-benzoylphenylacetyl)-*β*-alaninyl)-4-methylpiperazine (**6**), 3-azido-10-(4-(4-(4-(4-(*S*-cysteinylmethyl)benzoyl)benzyl)-1-piperazinyl)butyl)phenothiazine (**7**), 3-azido-10-(4-(4-((4-benzoylphenyl)methyl)-1-piperazinyl)butyl)phenothiazine (**8**), *N*-(1-(4-(4'-(3''-azido-10''-phenothiazinyl)butyl)))-*N*'-1-(6-((4-benzoylbenzyl)oxy)-2,3,4,5-tetrahydroxyhexyl)piperazine (**9**), adduct **10** of methyl iodide and *N*'-(1-(4-(4'-(3''-azido-10''-phenothiazinyl)butyl)piperazinyl))-*N*-(4'-benzoylphenylacetyl)-*β*-alanine amide, adduct **11** of methyl iodide and 3-azido-10-(4-(4'-acetyl-1'-piperazinyl)butyl)phenothiazine, amide of 3-azido-10-(4-(1-piperazinyl)butyl)phenothiazine and tartaric acid *N*-(4-benzoylphenyl)methyl amide, adduct **12** of methyl iodide and *N*'-(1-(4-(4'-(3''-azido-10''-phenothiazinyl)butyl)piperazinyl))-*N*-((4-benzoylphenyl)-methyl)tartaric acid diamide. Copies of ¹H NMR spectra for **3**, **4**, **5**, **7**, **8**, **9**, **10**, **11**, *N*'-(1-(4-(4'-(3''-azido-10''-phenothiazinyl)butyl)piperazinyl))-*N*-((4-benzoylphenyl)methyl)tartaric acid diamide (intermediate leading to **12**), **12**, **14a**, **14b**, 3-azido-10-(4-(1-(4-(carbomethoxy)-piperazinyl)butyl)phenothiazine, **15**, **20**, **22**, and **23** (40 pages). Ordering information is given on any current masthead page.

LITERATURE CITED

(1) Vanaman, T. C. (1983) Chemical approaches to the calmodulin system. *Methods Enzymol. 102*, 296–310.

(2) Golinski, M., DeLaLuz, P., Floresca, R., Delcamp, T. J., Vanaman, T. C., and Watt, D. S. (1995) Synthesis, binding affinity, and cross-linking of monodentate photoactive phenothiazines to calmodulin. *Bioconjugate Chem. 6*, 549–557.

(3) DeLaLuz, P., Golinski, M., Watt, D. S., and Vanaman, T. C. (1995) Synthesis and use of a biotinylated 3-azidophenothiazine to photolabel both amino- and carboxyl-terminal sites in calmodulin. *Bioconjugate Chem. 6*, 558–566.

(4) Brunner, J. (1993) New photolabeling and crosslinking methods. *Annu. Rev. Biochem. 62*, 483–514.

(5) Galardy, R. E., Craig, L. C., Jamieson, J. O., and Printz, M. P. (1974) Photoaffinity labeling of peptide hormone binding sites. *J. Biol. Chem. 249*, 3510–3518.

(6) Galardy, R. E., Craig, L. C., and Printz, M. P. (1973) Benzophenone triplet: a new photochemical probe of biological ligand-receptor interactions. *Nature New Biol. (London) 242*, 127–128.

(7) Rajagopalan, K., Chavan, A. J., Haley, B. E., and Watt, D. S. (1993) Synthesis and application of bidentate photoaffinity cross-linking reagents: Nucleotide photoaffinity probes with two photoactive groups. *J. Biol. Chem. 268*, 14230–14238.

(8) Salvucci, M. E., Rajagopalan, K., Sievert, G., Haley, B. E., and Watt, D. S. (1993) Photoaffinity labeling of Rubisco Activase with ATP-benzophenone: Identification of the ATP γ-phosphate binding domain. *J. Biol. Chem. 268*, 14239–14244.

(9) Maruta, S., Burke, M., and Ikebe, M. (1990) Cross-linking of the 25- and 20-kilodalton fragments of skeletal myosin subfragment 1 by a bifunctional ATP analogue. *Biochemistry 29*, 9910–9915.

(10) Jamieson, G. A., and Vanaman, T. C. (1979) Calcium-dependent affinity chromatography of calmodulin on immobilized phenothiazine. *Biochem.-Biophys. Res. Commun. 90*, 1048–1055.

(11) Wallace, R. W., Tallant, E. A., and Cheung, W. Y. (1983) Assay of calmodulin by Ca2+-dependent phosphodiesterase. *Methods Enzymol. 102*, 39–47.

(12) Lanzetta, P. A., Alvarez, L. J., Reinach, P. S., and Candia, O. A. (1979) An improved assay for nanomole amounts of inorganic phosphate. *Anal. Biochem. 100*, 95–97.

(13) Hofmann, K., Finn, F. M., and Kiso, Y. (1978) Avidin-biotin affinity columns. General methods for attaching biotin to peptides and proteins. *J. Am. Chem. Soc. 100*, 3585–3590.

(14) Zderic, J. A., Kubitschek, M. J., and Bonner, W. A. (1961) Synthesis of p-benzoylmandelic acid. *J. Org. Chem. 26,* 1635−1637.

(15) Levin, R. M., and Weiss, B. (1977) Binding of trifluoperazine to the calcium-dependent activator of cyclic nucleotide phosphodiesterase. *Mol. Pharmacol. 13,* 690−697.

(16) LaPorte, D. C., Wierman, B. M., and Storm, D. R. (1980) Calcium-induced exposure of a hydrophobic surface on calmodulin. *Biochemistry 19,* 3814−3819.

(17) Krebs, J., Buerkler, J., Guerini, D., Brunner, J., and Carafoli, E. (1984) 3-(Trifluoromethyl)-3-(m-[125I]iodophenyl)-diazirine, a hydrophobic, photoreactive probe, labels calmodulin and calmodulin fragments in a Ca^{2+}-dependent way. *Biochemistry 23,* 400−403.

(18) Newton, D. L., Burke, T. R., Jr., Rice, K. C., and Klee, C. B. (1983) Calcium ion dependent covalent modification of calmodulin with norchlopromazine isothiocyanate. *Biochemistry 22,* 5472−5476.

(19) Newton, D. L., and Klee, C. B. (1984) CAPP-calmodulin: a potent competitive inhibitor of calmodulin actions. *FEBS Lett. 165,* 269−272.

(20) Newton, D. L., and Klee, C. B. (1989) Phenothiazine-binding and attachment sites of CAPP1-calmodulin. *Biochemistry 28,* 3750−3757.

(21) Jarrett, H. W. (1984) The synthesis and reaction of a specific affinity label for the hydrophobic drug-binding domains of calmodulin. *J. Biol. Chem. 259,* 10136−10144.

(22) Golden, J. H. (1961) Poly-p-xylylene and related polymers. *J. Chem. Soc.* 1604−1610.

(23) Kalonia, D. S., and Simonelli, A. P. (1988) Development of an high performance liquid chromatographic method for the simultaneous analysis of the species involved in diethyl L-tartrate hydrolysis. *J. Chromatogr. 455,* 355−359.

Synthesis and Antiviral Activity of Peptide–Oligonucleotide Conjugates Prepared by Using N_α-(Bromoacetyl)peptides

Khalil Arar, Anne-Marie Aubertin,[†] Annie-Claude Roche, Michel Monsigny, and Roger Mayer*

Laboratoire de Biochimie des Glycoconjugués, Centre de Biophysique Moléculaire, CNRS, rue Charles-Sadron, F-45071 Orléans Cedex 02, France, and Institut de Virologie, INSERM U 74, 3 rue Koeberlé, F-67000 Strasbourg, France. Received January 10, 1995[⊛]

Antisense oligonucleotides represent an interesting tool for selective inhibition of gene expression. In order to direct oligonucleotides to specific compartments within the cell, we have investigated the possibility of coupling them to a signal peptide Lys-Asp-Glu-Leu (KDEL). This sequence should be able to convey oligonucleotides to the endoplasmic reticulum and from there to the cytosol and the nucleus where their targets are located. On this basis we prepared peptide–oligonucleotide conjugates by coupling, in a single step, a N_α-bromoacetyl peptide with an oligonucleotide bearing a thiol group, through a thioether bond. This paper deals with the definition of the optimal pH and temperature conditions leading to an efficient synthesis of peptide–oligonucleotide conjugates: the reaction was quantitative at pH 7.5 within few hours. This method was first set up using a 5′,3′-modified dodecanucleotide and a (bromoacetyl)pentapeptide as a conjugation model. Then a 5′,3′-modified pentacosanucleotide, complementary to the translation initiation region of the gag mRNA of HIV, was coupled to a (bromoacetyl)dodecapeptide containing a KDEL signal sequence. The anti-HIV activity of the pentacosanucleotide was compared with that of pentacosanucleotide–dodecapeptide conjugates linked through either a thioether bond or a disulfide bridge. The conjugate with a thioether bond has a higher antiviral activity than the peptide-free oligonucleotide and the conjugate linked via a disulfide bond.

INTRODUCTION

Antisense oligodeoxyribonucleotides are able to inhibit viral and cell gene expression in a sequence specific manner (*1*, *2*). Therefore, oligonucleotides are putative therapeutic agents. Their suspected site of action is either the cytosol or the nucleus. In any case, oligonucleotides have to cross a membrane as long as they are applied extracellularly. But since they are polyanions they are not able to cross a lipid bilayer. Free oligonucleotides enter cells by endocytosis and/or pinocytosis, and consequently, they are mainly found in endosomes (*3*). We hypothesized that oligonucleotides may cross the membrane from either the late endosome, the golgi apparatus, the endoplasmic reticulum–golgi intermediate compartment (ERGIC), or even the endoplasmic reticulum and proposed that oligonucleotides associated with a recognition signal specific for endoplasmic reticulum could increase the amount of oligonucleotide traveling toward these compartments. One such candidate is a peptide containing the segment Lys-Asp-Glu-Leu (KDEL) in a *C*-terminal position since KDEL is involved in the recycling of proteins from *cis*-golgi and ERGIC to endoplasmic reticulum (*4*).

On the bases of these data, we synthesized oligonucleotides substituted by a peptide containing a *C*-terminal KDEL sequence. The one-step synthesis of such hybrids, on solid-phase peptide or DNA synthesizers, has been reported (*5–7*). This method is, however, unsatisfactory due to the lack of "universal" protecting groups suitable for such a strategy and to side reactions during the coupling and the cleavage steps. Alternatively, such hybrids may be obtained by a postsynthesis conjugation

(*8–10*). Recently, we described a method where a N_α-maleimidopeptide was appended to an oligonucleotide substituted with a thiol group (*11*).

In this paper a postsynthesis conjugation is described by linking, through a thioether bond, in a single step, an oligonucleotide bearing a thiol group to a N_α-(bromoacetyl)-peptide containing a *C*-terminal KDEL sequence.

A dodecanucleotide, specific for Ha-*ras* around the point mutation in the 12th codon, was first coupled to a pentapeptide, as a short model. Then a pentacosanucleotide, complementary to the AUG initiation site of the HIV-1 gag mRNA, was coupled to a dodecapeptide. The antiviral activity of this peptide–oligonucleotide conjugate was assessed by monitoring its capacity to inhibit HIV-1 in infected human peripheral blood mononuclear cells.

MATERIAL AND METHODS

1,1′-Carbonyldiimidazole (CDI), 1,6-diaminohexane, *N,N′*-dicyclohexylcarbodiimide (DCC), and anisole were purchased from Merck (Darmstadt, Germany) ; tris(2-carboxyethyl)phosphine (TCEP)[1] from Molecular Probes (La Jolla, CA), bromoacetic acid from Aldrich (Strasbourg, France), *tert*-butyloxycarbonyl amino acids, Boc-Leu-PAM-resin, and *N*-hydroxybenzotriazole (HOBt) from Novabiochem (Laufelfingen, Switzerland), (benzotriazol-1yloxy)tris(dimethylamino)phosphonium hexafluorophosphate (BOP) from Richelieu Biotechnologies (Saint Hyacinthe, Canada), and fluorhydric acid (HF) from Setic-Labo (Magny-Les-Hameaux, France). Dimethylformamide was freshly distilled on (benzyloxycarbonyl)glycyl *p*-nitrophenyl ester. The 5′,3′-modified anti-gag pentacosa-

---

nucleotide phosphodiester 5'CTCTCGCACCCATCTCTC-TCCTTCT3' was purchased from Genosys Biotechnologies (Cambridge, England).

The peptides were synthesized on a Vega 250 peptide synthesizer (Du Pont, Wilmington, DE). The purity of synthetic peptides was assessed by analytical HPLC with a Waters 660E system controller and a Waters 991 photodiode array detector (Saint-Quentin en Yvelines, France) on a reversed-phase LiChrospher 100RP-18, 5 μm, 250 × 4 mm column (Merck) using a linear gradient from 5 to 90% CH$_3$CN in H$_2$O containing 0.1% TFA within 20 min. Amino acid analysis was performed on a Supelcosil LC-18-DB, 250 × 4.6 mm column (Supelco, Bellefonte, PA), upon hydrolysis by 5.6 N HCl at 105 °C for 24 h, using the phenyl isothiocyanate (PITC) derivatization method. The dodecanucleotide was synthesized on an Applied Biosystems DNA synthetizer Model 381A using fast oligonucleotide deprotection (FODs) and solid-phase phosphoroamidite chemistry. The purity of synthetic oligonucleotides and peptide—oligonucleotide conjugates was assessed by analytical HPLC on the column used to purify the peptide. The gradient used was linear from 5 to 30% CH$_3$CN in 0.1 M triethylammonium acetate (TEAAc), pH 7.0, within 30 min.

The ^{1}H (300 MHz) nuclear magnetic resonance spectra were recorded on a Bruker AM-300 spectrometer and are expressed as δ units (parts per million) relative to tetramethylsilane as internal reference in 99.95 DMSO-d_6 solution. Mass spectrometry analysis of the peptides and of the oligonucleotide derivatives was performed either on a Lasermat (Finnigan MAT, San Jose, CA) matrix-assisted laser desorption ionization time-of-flight mass spectrometer or a Fisons Bio-Q (Manchester, U.K.) mass spectrometer using an electrospray ionization technique (12).

Synthesis of Peptides Containing a KDEL Sequence. The peptide Br-CH$_2$-CO-Tyr-Lys-Asp-Glu-Leu-OH (3) was synthesized using a Boc-Leu-(phenylacetamido)methyl-substituted resin and a Boc/Bzl strategy according to Merrifield (13). The Boc protecting group was removed from the amino terminus with a solution of TFA 40% in CH$_2$Cl$_2$, followed by neutralization of the peptidyl resin with N,N-diisopropylethylamine. At the last step, bromoacetic anhydride reacted with the N$_\alpha$-amino terminal group to form the N-(bromoacetyl)-protected peptide-resin (14). The peptide was deprotected and released from the resin by treatment for 90 min at 0 °C with 10 mL of HF in the presence of 1 mL of anisole used as scavenger. The peptide was extracted with trifluoroacetic acid and precipitated in dry diethyl ether. The peptide purity was assessed by analytical HPLC on a reversed-phase LiChrospher 100RP-18, 5 μm, column using a linear gradient (from 5 to 90%) of CH$_3$-CN in H$_2$O containing 0.1% TFA in 20 min. The peptide was eluted at 18.9 min. The purified peptide was characterized by mass spectrometry [calcd 786.2 (monoisotopic), found 787.1]. Amino acid analysis: Tyr (0.90), Lys (0.96), Asp (1.10), Glu (1.04), Leu (1.00). ^{1}H NMR spectrum in DMSO-d_6: δ (ppm) 0.89 (dd, 6H, δCH$_3$ Leu), 1.30 (m, 2H, γCH$_2$ Lys), 1.50 (m, 1H, γCH Leu), 1.51 (m, 2H, βCH$_2$ Leu), 1.52 (m, 1H, β'CH Lys), 1.54 (m, 2H, δCH$_2$ Lys), 1.65 (m, 1H, βCH Lys), 1.73 (m, 1H, β'CH Glu), 1.9 (m, 1H, βCH Glu), 2.23 (m, 2H, γCH$_2$ Glu), 2.55 (m, 1H, βCH Tyr), 2.68 (m, 1H, β'CH Asp), 2.70 (m, 1H, β'CH Tyr), 2.74 (m, 2H, ϵCH$_2$ Lys), 2.92 (m, 1H, βCH Asp), 3.75 (s, 2H, CH$_2$ BrAc), 4.18 (m, 1H, αCH Leu), 4.27 (m, 1H, αCH Lys), 4.29 (m, 1H, αCH Glu), 4.45 (m, 1H, αCH Asp), 4.55 (m, 1H, αCH Tyr), 6.66 (d, 1H, 2–5 Tyr), 7.02 (d, 2H, 3-6 Tyr), 7.52 (m, 3H, ϵNH$_3$ Lys), 7.72 (d, 1H,

αNH Glu), 8.05 (d, 1H, αNH Leu), 8.21 (d, 1H, αNH Lys), 8.22 (d, 1H, αNH Tyr), 8.35 (d, 1H, αNH Asp).

Using the same strategy, we have prepared the peptide Br-CH$_2$-CO-Tyr-Gly-Glu-Glu-Asp-Thr-Ser-Glu-Lys-Asp-Glu-Leu-OH corresponding to the C-terminal sequence of the glucose regulated protein (GRP 78) resident in the lumen of the endoplasmic reticulum (15). This peptide, purified by HPLC, was eluted at 15.4 min using the same gradient system. The purified peptide was characterized by mass spectrometry [calcd 1533.5 (monoisotopic), found 1535.3].

Synthesis of 5'-Amino, 3'-Disulfide Bridge Oligonucleotide. (5' NH$_2$-R$_1$-oligonucleotide-R$_2$-S-S-R$_2$-OH). The oligonucleotide NH$_2$-R$_1$-d(5'ACACCGACGGCG3')-R$_2$-S-S-R$_3$ with R$_1$ = (CH$_2$)$_6$NHCO, R$_2$ = O(CH$_2$CH$_2$O)$_2$CH$_2$CH$_2$, and R$_3$ = (CH$_2$CH$_2$O)$_3$H, specific for Ha-*ras* around the point mutation in the 12th codon, was synthesized on a disulfide-derivatized solid support (10 μmol scale) as previously described (16). This oligonucleotide was purified on a reversed-phase LiChrospher 100RP-18 column using a linear gradient from 5 to 30% of CH$_3$CN in 0.1 M triethylamine acetate (TEAAc), pH 7.0, within 30 min. The oligonucleotide was eluted at 21.9 min. The protection of the oligonucleotide at both 5' and 3' ends prevents it from degradation by exonucleases. An amino group was added at the 5' end with the aim of introducing a fluorescent tag in order to study the intracellular traffic of the oligonucleotide and of the peptide—oligonucleotide conjugate.

Synthesis of the 5'-NH$_2$, 3'-Thiol Activated Group (S-S-Py) Dodecanucleotide (1). The disulfide bridge of 1 μmol of 5'-NH$_2$, 3'-disulfide bridge oligonucleotide was reduced with 1.1 μmol of tris(2-carboxyethyl)phosphine (TCEP) (17) in 1 mL of 0.1 M phosphate buffer, pH 7.0, at room temperature for 1 h to give quantitatively the 12 mer 3'-thiol activated group (S-S-Py) by reaction with 10 μmol 2,2'-dithiodipyridine. This oligonucleotide was eluted at 21.1 min upon HPLC using the above-described system.

Synthesis of Peptide—Oligonucleotide Conjugates through a Thioether Bond. According to Scheme 1, oligonucleotide-S-S-Py (1) (1 μmol), in 1 mL of 2 M NaCl, 0.1 M phosphate buffer pH 7.0, was reduced with 1.1 μmol of TCEP for 1 h at room temperature under nitrogen. Without extraction of the slight TCEP excess, 5 μmol of the peptide Br-CH$_2$-CO-Tyr-Lys-Asp-Glu-Leu-OH (3) was added directly into the solution of the oligonucleotide bearing a thiol function (2). The thiol function reacted with the N-(bromoacetyl)peptide within 5 h at room temperature, pH 7.0, giving a peptide—oligonucleotide conjugate in 100% yield based on the substitution of the oligonucleotide as shown on Figure 1.

The same strategy was used to prepare quantitatively a dodecapeptide—pentacosanucleotide conjugate by coupling the Py-S-S-R$_4$-d(5'CTCTCGCACCCATCTCTCTC-CTTCT3')-R$_5$-NH$_2$ oligonucleotide [with R$_4$ = (CH$_2$)$_6$PO$_2$– and R$_5$ = –OCH$_2$CH(CH$_2$OH)(CH$_2$)$_4$], with the Br-CH$_2$-CO-Tyr-Gly-Glu-Glu-Asp-Thr-Ser-Glu-Lys-Asp-Glu-Leu-OH peptide (Table 1).

Synthesis of a Dodecapeptide—Pentacosanucleotide Conjugate through a Disulfide Bond. The oligonucleotide Py-S-S-R$_4$-d(5'CTCTCGCACCCATCTCTCTCCTTCT3')-R$_5$-NH$_2$ (0.1 μmol in 1 mL of 0.1 M phosphate buffer, pH 7.0) was reduced with 0.11 μmol of TCEP at room temperature for 1 h to give the pentacosanucleotide 5'-thiol derivative. The conjugate was obtained by adding 2 μmol of the dodecapeptide C(Npys)GEEDTSEKDEL into a solution of the oligonucleotide bearing a thiol

function in 0.1 M phosphate buffer, pH 7.0, at room temperature under nitrogen (Table 1).

Characterization of the Conjugates. The progress of the ligation between the 3'-thiol dodecanucleotide and the (bromoacetyl)pentapeptide was followed by analytical HPLC on a reversed-phase LiChrospher 100RP-18 column (Figure 1). After purification, the peptide–oligonucleotide conjugate (compound 4) (t_R = 20.6 min) had the expected oligonucleotide spectral characteristics and the expected amino acid composition (Tyr(0.89), Lys-(1.15), Asp(0.95), Glu(1.11), Leu(1.00)); small amounts of glycine and other amino compounds deriving from oligonucleotide degradation during acidic hydrolysis were also detected. Electrospray mass spectrometry confirmed the molecular mass calculated for the peptide–oligonucleotide conjugate (*12*). These methods were used to purify and characterize all the conjugates.

Stability of the N_α-(Bromoacetyl)peptide at Different pH. To assess the stability of the (bromoacetyl)-peptide, Br-CH$_2$-CO-Tyr-Lys-Asp-Glu-Leu-OH was dissolved in 0.1 M sodium phosphate buffer (pH 7.0) or in 0.1 M sodium bicarbonate (pH 8.5). Solutions were kept at 25 °C, and aliquots were periodically withdrawn and subjected to HPLC analysis on a C18 column (data not shown). The (bromoacetyl)peptide incubated in a phosphate buffer, pH 7.0, or a bicarbonate buffer, pH 8.5, for 0, 1, 12, or 24 h was neither degraded nor polymerized. The bromoacetyl moiety did not react with the ε-amino group of lysine at any pH between 7.0 and 8.5.

Assay for HIV Inhibition. The assay procedure for measuring the anti-HIV activity of peptide–oligonucleotide conjugates in peripheral blood mononuclear (PBMC) cells was based on a quantitative detection of reverse transcriptase (RT) activity in the culture supernatant. PBMC from healthy donors (HIV seronegative), isolated by centrifugation, were propagated and infected with HIV-1 (IIIB) isolate as previously described (*18*). Thirty min after virus adsorption, cells were washed and then cultured at 4×10^5 cells/mL of culture medium in the presence of the oligonucleotide derivatives. On day 3, half of the medium was removed and replaced by a fresh medium containing the appropriate oligonucleotide derivative concentrations. Seven days later, the virus released from the cells was evaluated by the RT assay. The cytotoxicity of oligonucleotide derivatives was evaluated by the MTT method (*19*) in parallel with their antiviral activity. The MTT assay is based on the viability of infected cells and on the capacity of mitochondrial dehydrogenase of living cells to reduce 3-(4,5-dimethylthiazol-2-yl)-2,5-diphenyltetrazolium bromide into formazan. The quantity of formazan produced, measured at 540 nm, is in relation to the number of living cells.

RESULTS AND DISCUSSION

Synthesis Strategy. In an attempt at increasing their activity, antisense oligonucleotides were coupled to peptides containing in a *C*-terminal position a Lys-Asp-Glu-Leu (KDEL) sequence specifically recognized by a receptor allowing intracellular KDEL bearing proteins to recycle to the endoplasmic reticulum. Such peptide–oligonucleotide conjugates are expected to travel inside the cell to the endoplasmic reticulum and eventually to pass through a membrane to enter the cytosol and the nucleus where the antisense oligonucleotide targets are located.

The peptides Br-CH$_2$-CO-Tyr-Lys-Asp-Glu-Leu and Br-CH$_2$-CO-Tyr-Gly-Glu-Glu-Asp-Thr-Ser-Glu-Lys-Asp-Glu-Leu-OH were synthesized on a solid support according to the Merrifield strategy. Both contain an additional tyrosyl residue introduced as a radiolabelable tag. The

Scheme 1. Synthesis of a Peptide–Oligonucleotide Conjugate[a]

NH_2-R$_1$-ACACCGACGGCG-R$_2$-S-S-Py

(1)

↓ TCEP

NH_2-R$_1$-ACACCGACGGCG-R$_2$-SH   Br-CH$_2$-CO-Tyr-Lys-Asp-Glu-Leu-OH

(2)   (3)

|_____ pH 7.0 _____|

↓

5'NH_2-R$_1$-ACACCGACGGCG-R$_2$-S-CH$_2$-CO-Tyr-Lys-Asp-Glu-Leu-OH

(4)
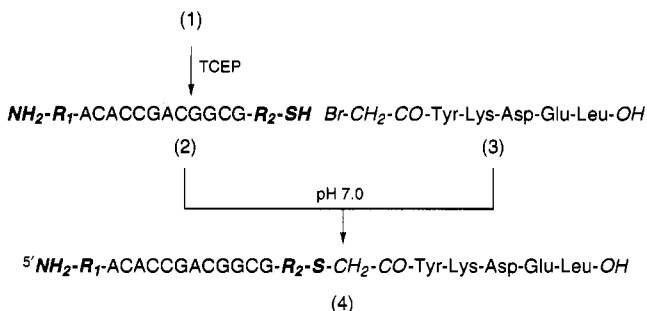
[a] Key: TCEP, tris(2-carboxyethyl)phosphine; Py, 2-pyridyl; R$_1$, (CH$_2$)$_6$NHCO; R$_2$, O(CH$_2$CH$_2$O)$_2$CH$_2$CH$_2$.
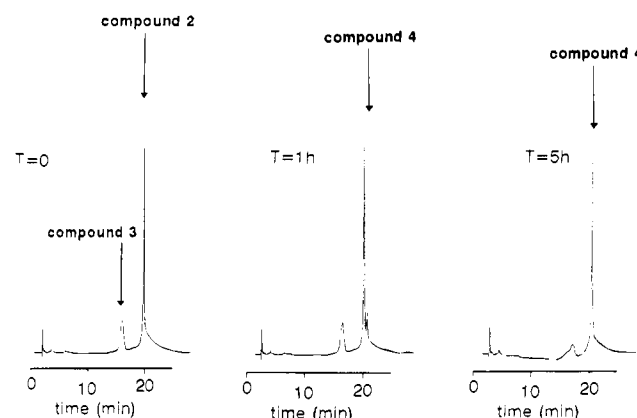
Figure 1. HPLC analysis of the formation of a pentapeptide–dodecanucleotide conjugate at pH 7.0, at 25 °C. Aliquots of the ligation reaction, taken at t = 0, t = 1, and t = 5 h, were immediately analyzed. The progress of the ligation was followed by reversed-phase HPLC on a Lichrospher 250 × 4 mm column. Mobile phase A was 0.1 M triethylamine acetate buffer (TEAAc), pH 7.0 + 5% acetonitrile, and mobile phase B was acetonitrile + 5% 0.1 M TEAAc. The gradient from 5% to 70% B was developed within 30 min. The flow rate was 1 mL/min. (Compounds 1–4 are those described in Scheme 1.)

synthesis of N_α-(bromoacetyl)peptides was achieved as follows: bromoacetic anhydride was prepared by condensation of 2 equiv of bromoacetic acid in the presence of 1 equiv of dicyclohexylcarbodiimide; the formation of the anhydride was assessed by the two characteristic IR bands at 1750 and 1830 cm^{-1}. Then the anhydride reacted with the α-amino group of the protected peptide on the resin. Finally, the peptide was deprotected and released from the resin using a standard HF deprotection.

A dodecanucleotide specific for Ha-*ras* around the 12th codon mutation point and bearing a thiol-activated group on its 3' end was synthesized by solid phase synthesis using a modified solid support according to Bonfils and Thuong (*16*). The protection of the 3' end of the oligonucleotide is requested in order to prevent exonuclease degradation.

Conjugates were formed by adding the (bromoacetyl)-peptide, as a solid, to the oligonucleotide bearing a thiol function either on its 3' or 5' end. Both the peptide and the oligonucleotide were readily soluble in the reaction buffer. The reaction steps for the conjugation are shown in Scheme 1. The thiol-substituted oligonucleotide reacted with the N_α-(bromoacetyl)peptide within 5 h at pH 7.0 as shown in Figure 1. The oligonucleotide–peptide ligation reaction was carried out at different pH (7.0, 7.5, 7.9, and 8.5). Figure 2 shows that the linkage efficiency
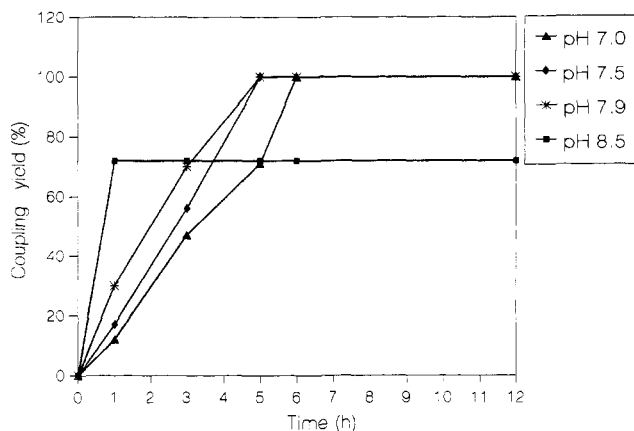
Figure 2. Synthesis of peptide–oligonucleotide conjugate at 25 °C, at various pH. The yield was calculated from the amount of conjugate determined upon HPLC analysis as described in Figure 1. Key: △, pH 7.0; ◆, pH 7.5; *, pH 7.9; ■, pH 8.5.
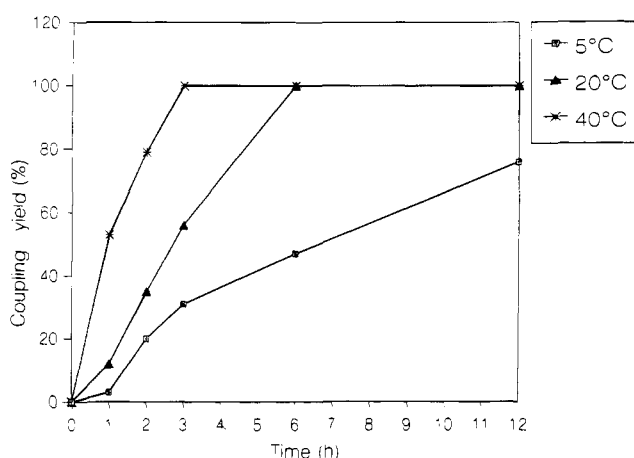
Figure 3. Synthesis of peptide–oligonucleotide conjugate at pH 7.0, at various temperatures. The yield was calculated from the amount of conjugate determined upon HPLC analysis as described in Figure 1. Key: □, 5 °C; △, 20 °C; *, 40 °C.

of the (bromoacetyl)peptide to the oligonucleotide-SH is pH-dependent. In 1 h, at pH 8.5, the yield of the peptide–oligonucleotide conjugate was 72%, but 28% of the oligonucleotide was evidenced as a dimer (t_R = 26.5 min). At optimal pH, ranging from 7.0 to 7.9, the yield was essentially quantitative with no trace of oligonucleotide monomer or dimer. Figure 3 shows that, at pH 7.0, the conjugation rate of the oligonucleotide with the peptide is also temperature dependent. At 40 °C, the reaction was completed in less than 3 h. From these data, its appears that the thioether bond was formed quantitatively when the reaction occurred at pH 7.5, at 40 °C. After purification, the conjugate had the spectral characteristics expected from both the oligonucleotide moiety and the amino acid moiety. Electrospray mass spectrometry confirmed the calculated molecular weight of the conjugate.

This procedure allowed the preparation, in quantitative yield, of conjugates containing a larger oligonucleotide
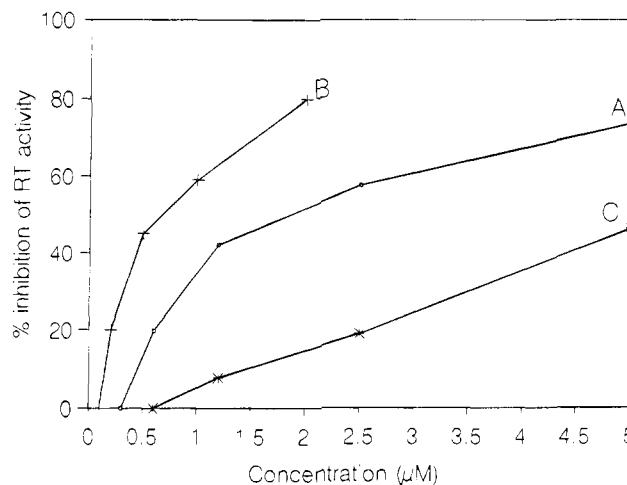
Figure 4. Anti-HIV-1 activity of peptide-free anti-gag pentacosanucleotide (A), of the anti-gag pentacosanucleotide substituted with the GEEDTSEKDEL peptide through a thioether bond (B), and through a disulfide bond (C). Infected cells were incubated with various oligonucleotide concentrations; after 3 days, half of the medium was replaced by fresh medium containing the oligonucleotide at the same concentration. The inhibition of reverse transcriptase (RT) activity was measured after 1 week of incubation in the presence of the oligonucleotide derivatives. All data represent the mean values of two independent experiments.

and a larger peptide. By this method, the peptide N_α-(bromoacetyl)Tyr-Gly-Glu-Glu-Asp-Thr-Ser-Glu-Lys-Asp-Glu-Leu-OH, corresponding to the *C*-terminal sequence of the glucose regulated protein (GRP 78), was conjugated with an antisense 5'-thiol-pentacosanucleotide specific for gag mRNA AUG site of HIV-1 (Table 1).

In order to study the influence of the nature of the bond between the peptide and the oligonucleotide, a conjugate, in which both moieties are linked through a disulfide bridge, was also prepared. This conjugate was obtained by coupling the thiol function carried by the anti-gag pentacosanucleotide to the dodecapeptide C(Npys)-GEEDTSEKDEL bearing a cysteine thiol activated group on its *N*-terminal end. The main characteristics of these compounds are reported in Table 1.

Antiviral Activity. The anti-HIV-1 activity of the conjugates was monitored, *in vitro*, by measuring the reverse transcriptase activity in the culture supernatant of infected human PBMC. After 7 days, the viruses released from the cells were assessed by using a reverse transcriptase (RT) assay. From Figure 4, it appears that the anti-gag pentacosanucleotide-S-CH_2-CO-YGEEDTSEKDEL conjugate (IC_{50} = 0.61 ± 0.03 μM; mean ± SD) was three times more efficient than the peptide-free anti-gag oligonucleotide (IC_{50} = 1.80 ± 0.14 μM) and 10 times more efficient than the anti-gag oligonucleotide-S-S-CGEEDTSEKDEL (IC_{50} > 5 μM), which contains a disulfide bridge instead of a thioether linkage. This result may be explained by the fact that the disulfide bridge is cleaved early (*20*) before reaching the cytosol or nucleus. In contrast, the 5',3' unmodified oligonucleotide was totally inactive at 10 μM, the highest concen-

Table 1. Molecular Mass and Retention Time of the Compounds Analyzed by HPLC As Described in Figure 1

compds	molecular mass		t_R (min)
	calcd	found	
anti-gag pentacosanucleotide Py-S-S-R$_4$-($^{5'}$CTCTCGCACCCATCTCTCTCCTTCT$^{3'}$)-R$_5$-NH$_2$	7887.9	7889	22.1
H-C(Npys)GEEDTSEKDEL-OH	1507.5	1508.9	23.9
anti-gag -S-S-CGEEDTSEKDEL-OH	9129.4	9132	21.8
Br-CH_2-CO-YGEEDTSEKDEL-OH	1533.5	1535.3	20.1
anti-gag-S-CH_2-CO-YGEEDTSEKDEL-OH	9232.5	9234	24.1

tration tested, supporting the protective effect of the 5′ and 3′ spacer arms against exonuclease degradation of the oligonucleotides. Even at the upper concentration used, the conjugates did not elicit any toxicity.

In conclusion, N_α-(bromoacetyl)peptides, which are easily prepared on a solid support, can be used for the efficient and reproducible preparation of peptide–oligonucleotide conjugates. At pH 7.5, the (bromoacetyl)-peptide reacts with a thiol group carried by an oligonucleotide leading, within 3 h at 40 °C, to a peptide–oligonucleotide conjugate, in a quantitative yield. Under these conditions, there was no evidence of reaction between the bromoacetyl group and either the phenol group of tyrosine or the ε-amino group of lysine residue of the peptide.

(Bromoacetyl)peptides have been used to prepare conformationally constrained cyclic or polymeric peptides and peptide–carrier conjugates (21, 22). The 1-(p-(bromoacetamido)benzyl)-EDTA was used for specific conjugation of BSA on its single free thiol group (23, 24). The reaction selectivity of the bromoacetyl group toward a sulfhydryl group at pH 7.5 is comparable to that of the iodoacetamido group and is significantly greater than that of maleimido or chloroacetyl groups (21). The use of TCEP as a reducing agent allows a one-pot preparation of a peptide–oligonucleotide conjugate; neither the extraction of the slight excess of TCEP nor the purification of the oligonucleotide mercaptan intermediate is required. In addition, oligonucleotide dimerization does not occur.

The addition of an endoplasmic reticulum retention KDEL signal peptide to the pentacosanucleotide significantly enhances its anti-HIV activity. Data concerning the comparison between the intracellular traffic of the conjugate and of the peptide-free oligonucleotide will be described elsewhere.

ACKNOWLEDGMENT

LITERATURE CITED

(1) Hélène, C., and Toulmé, J. J. (1990) Specific Regulation of Gene by Antisense, Sense and Antigene Nucleic Acids. *Biochim. Biophys. Acta 1049*, 99–125.

(2) Uhlmann, E., and Peyman, A. (1990) Antisense Oligonucleotides: A New Therapeutic Principle. *Chem. Rev. 90*, 544–584.

(3) Zhao, Q., Matson, S., Herrera, C. J., Fisher, E., Yu, H., and Krieg, A. M. (1993) Comparison of cellular binding and uptake of antisense phosphodiester, phosphorothioate and mixed phosphorothioate and methylphosphonate oligonucleotides. *Antisense Res. Develop. 3*, 53–66.

(4) Munro, S., and Pelham, H. R. B. (1987) A C-Terminal Signal Prevents Secretion of Luminal ER Proteins. *Cell 48*, 899–907.

(5) Juby, C. D., Richardson, C. D., and Brousseau, R. (1991)

(6) Haralambidis, J., Duncan, L., and Tregear, G. W. (1987) The Solid Phase Synthesis of Oligonucleotides Containing a 3′-Peptide Moiety. *Tetrahedron Lett. 28*, 5199–5202.

(7) Haralambidis, J., Duncan, L., Angus, K., and Treagear, G. W. (1990) The Synthesis of Polyamide–Oligonucleotide Conjugate Molecules. *Nucleic Acids Res. 18*, 493–499.

(8) Tung, C. H., Rudolph, M. J., and Stein, S. (1991) Preparation of Oligonucleotide–Peptide Conjugates. *Bioconjugate Chem. 2*, 464–465.

(9) Zhu, T., Wei, Z., Tung, C. H., Dickerhof, W. A., Breslauer, K. J., Georgopoulos, D. E., Leibowitz, M. J., and Stein, S. (1993) Oligonucleotide–Poly-L-Ornithine Conjugates: Binding to Complementary DNA and RNA. *Antisense Res. Develop. 3*, 265–275.

(10) Tong, G., Lawlor, J. M., Treagear, G. W., and Haralambidis, J. (1993) The Synthesis of Oligonucleotide-Polyamide Conjugates Molecules Suitable as PCR Primers. *J. Org. Chem. 58*, 2223–2231.

(11) Arar, K., Monsigny, M., and Mayer, R. (1993) Synthesis of Oligonucleotide–Peptide Conjugates Containing a KDEL Signal Sequence. *Tetrahedron Lett. 34*, 8087–8090.

(12) Potier, N., Van Dorsselaer, A., Cordier, Y., Roch, O., and Bischoff, R. (1994) Negative electrospray ionization mass spectrometry of synthetic and chemically modified oligonucleotides. *Nucleic Acids Res. 22*, 3895–3903.

(13) Merrifield, R. B. (1963) Solid Phase Peptide Synthesis. I. The Synthesis of a Tetrapeptide. *J. Am. Chem. Soc. 85*, 2149–2154.

(14) Robey, F. A., and Fields, R. L (1989) Automated Synthesis of N-Bromoacetyl-Modified Peptides for the Preparation of Synthetic Peptide Polymers, Peptide-Protein Conjugates, and Cyclic Peptides. *Anal. Biochem. 177*, 373–377.

(15) Sorger, P. K., and Pelham, H. R. B. (1987). The glucose-regulated protein grp94 is related to heat shock protein hsp90. *J. Mol. Biol. 194*, 341–344.

(16) Bonfils, E., and Thuong, N. T. (1991) Solid Phase Synthesis of 5′, 3′-Bifunctional Oligodeoxyribonucleotides Bearing a Masked Thiol Group at the 3′-End. *Tetrahedron Lett. 35*, 3053–3056.

(17) Burns, J. A., Bulter, J. C., Moran, J., and Whitesides, G. M. (1991) Selective reduction of disulfides by tris-(2-carboxyethyl)phosphine. *J. Org. Chem. 56*, 2648–2650.

(18) Schinazi, R. F., Mcmillan, A., Cannon, D., Mathis, R., Lloyd, R. M., Peck, A., Sommadossi, J. P., Clair, M. S., Wilson, J., Furman, P. A., Painter, G., Choi, W.-B., and Liotta, D. C. (1992) Selective Inhibition of Human Immunodeficiency Viruses by Racemates and Enantiomers of cis-5−Fluoro-1-[2-(Hydroxymethyl)-1,3-Oxathiolan-5-yl] Cytosine. *Antimicrob. Agents Chemother. 36*, 2423–2431.

(19) Pauwels, R., Balzarini, J., Baba, M., Snoeck, R., Schols, D., Herdewijn, P., Desmyter, J., and De Clercq, E. (1988) Rapid and Automated Tetrazolium-Based Colorimetric Assay for the Detection of Anti-HIV Compounds. *J. Virol. Methods 20*, 309–321.

(20) Feener, E. P., Shen, W., Ryser, H. J. (1990) Cleavage of Disulfide Bonds in Endocytosed Macromolecules. A Processing not Associated with Lysosomes or Endosomes. *J. Biol. Chem. 265*, 18780–18785.

(21) Bernatowicz, M. S., and Matsueda, G. R. (1986) Preparation of Peptide-Protein Immunogens Using N-Succinimidyl Bromoacetate as a Heterobifunctional Crosslinking Reagent. *Anal. Biochem. 155*, 95–102.

(22) Inman, J. K., Highet, P. F., Kolodny, N., and Robey, F. A. (1991) Synthesis of N^α-(tert-Butoxycarbonyl)-N^ϵ-[N-(Bromoacetyl)-β-Alanyl]-L-Lysine: Its Use in Peptide Synthesis for Placing a Bromoacetyl Cross-Linking Function at any Desired Sequence Position. *Bioconjugate Chem. 2*, 458–463.

(23) Rana, T. M., and Meares, C. F. (1990) Specific Cleavage of a Protein by an Attached Iron Chelate. *J. Am. Chem. Soc. 112*, 2457–2458.

(24) Rana, T. M., and Meares, C. F. (1991) Iron Chelate Mediated Proteolysis: Protein Structure Dependence. *J. Am. Chem. Soc. 113*, 1859–1861.

Facile Preparation of 3′ Oligonucleotide-Peptide Conjugates. *Tetrahedron Lett. 32*, 879–882.

Self-Complementary Oligodeoxyribonucleotides Containing 2'-O-(Anthraquinone-2-methyl)adenosine

Hemant M. Deshmukh, Seema P. Joglekar, and Arthur D. Broom*

Department of Medicinal Chemistry, College of Pharmacy, University of Utah, Salt Lake City, Utah 84112. Received May 15, 1995[⊗]

Incorporation of an intercalating agent into an oligodeoxynucleotide (ODN) has the potential to enhance binding affinity upon duplex formation, to increase ODN hydrophobicity, and to enhance resistance to nuclease hydrolysis. Site-specific intercalation has been achieved through the synthesis of 2'-O-(anthraquinone-2-methyl)adenosine(rA*) and its incorporation into the palindromic dodecanucleotide d(CGCrA*CATGTGCG). Melting temperature, CD spectra, 1D and 2D (DQF-COSY and NOESY) NMR spectra, and molecular models were obtained and compared with the unmodified dodecamer. The data clearly establish that intercalation of the anthraquinone ring into a predominantly B-type helix occurs between the A4–T9 and C5–G8 base pairs, significantly stabilizing the duplex and enhancing the hydrophobicity of the ODN.

INTRODUCTION

The chemistry, structural biology, and potential diagnostic and therapeutic applications of oligonucleotides are subjects of great current interest. The exquisite specificity of the genetic code and the relative ease of assembling sequences, which in principle, may inhibit the expression of a single gene in the entire human genome, have given great impetus to investigations intended to define the parameters required for the application of this technology to biologically relevant problems. A number of recent reviews document the rapid progress toward this goal (1–6).

Since the original demonstration by Zamecnik (7) of the feasibility of the antisense oligonucleotide concept in the inhibition of gene expression, much effort has gone into defining molecular modifications which may overcome the inherent limitations of oligodeoxynucleotides (ODN) as in vivo therapeutic agents. Thus, in order to take advantage of specificity intrinsic in the primary sequence, ODN must be able to penetrate membranes of target cells, be sufficiently stable to reach their targets without degradation in biological media, and have a high affinity for the target polynucleotide (8).

Attempts to achieve goals of increased lipophilicity and stability to nucleases have included modification of ODN with intercalating (9, 10), cleaving (11–13), alkylating (14, 15), or photocrosslinking (16) modifications at the 3'- and/or 5'-termini. Recently, considerable attention has been given to incorporation of 2'-O-alkyl- or aralkyl-substituted ribonucleosides into homooligomers or mixed (chimeric) deoxyribo/ribooligomers (17–19). Two recent publications described the attachment of an anthraquinone moiety to the 2'-hydroxyl of ribonucleosides, their incorporation into ODN, and assessment of the resulting stabilization of the duplex by melting experiments. In both cases, the stabilization was said to result from intercalation, although little direct evidence was presented in support of that hypothesis. In the first of these studies (20), the anthraquinone moiety was attached through a methylene group. In more recent work (21), the linker was six atoms in length. The methylene-linked

anthraquinone was said to cause significant global distortion of the duplex based on CD spectropolarimetry (20), but no further characterization of the presumed intercalation complex was provided.

A number of years ago we demonstrated that 2'-O-benzyladenosine in D_2O solution exists primarily in a conformation in which the purine and benzene rings are stacked, with the two rings overlapping and their planes nearly parallel (22). Such a conformation in the anthraquinone case would, indeed, favor intercalation in a duplex and would, by virtue of the constraints imposed by the methylene linker, permit intercalation only on the 3'-side of the nucleotide bearing the 2'-substituent.

The present report describes the synthesis of 2'-O-(anthraquinone-2-methyl)adenosine (Scheme 1), its incorporation into a self-complementary oligodeoxyribonucleotide, and characterization of the resulting duplex by NMR (1D, DQF-COSY, and NOESY), CD, UV, melting temperatures, and molecular modeling. In order to combine the properties of reasonable duplex stability, relative simplicity of NMR spectra, and a size compatible with NOESY experiments, self-complementary dodecanucleotide d(CGCACATGTGCG) and the modified oligo d(CGCrA*CATGTGCG) were synthesized; they will be referred to as "standard 12-mer" and "anthra 12-mer," respectively, where rA* is nucleoside 1 (Scheme 1).

EXPERIMENTAL PROCEDURES

General Methods. The ^1H-NMR spectra were recorded on either an IBM AF200 FT-NMR spectrometer at 200 MHz or a Varian Unity 500 MHz spectrometer. NMR samples of nucleosides were prepared using $(CD_3)_2$-SO or $CDCl_3$ with TMS or solvent peak as internal standard. The UV spectra and melting curves were recorded on a Hewlett-Packard diode array spectrophotometer. Low-resolution mass spectra were recorded on either a Finnegan MAT 95 or a VG 7050E mass spectrometer. Electrospray mass spectra were recorded on a Vestec 201 ionization instrument with a quadrupole mass analyzer. Thin-layer chromatography (TLC) was performed on Kieselgel 60F$_{254}$ aluminum-backed silica gel sheets. CD spectra were recorded on a JASCO J-720 spectropolarimeter. The oligomers were synthesized on an Applied Biosystems 380B instrument.

T_m **Determination.** All T_m values were determined on a Hewlett-Packard diode array spectrophotometer

---

equipped with an electronic temperature controlling device. Absorbance was measured at 1 °C intervals, and the cuvette was equilibrated at each temperature for 2 min. The oligomers were annealed by heating to approximately 70 °C in a water bath and then cooled slowly. Duplexes were kept in the refrigerator overnight before T_m measurements were carried out. Duplexes were formed at 1.58×10^{-4} M concentration in 0.1 M NaCl containing 10 mM phosphate buffer (pH 7). An aliquot of each solution was diluted 50-fold at 4 °C with the same buffer, and the T_m of the diluted solution was measured.

HPLC Purification and Analysis of Oligomers. All HPLC purification and analysis was performed on a Hitachi D-6200 HPLC system equipped with an L-3000 diode array spectrophotometer. DNA synthesized on a 1 μmol scale was purified on a preparative Whatman Partisil ODS reversed-phase column. Purified DNA was analyzed on a Rainin Microsorb C18 analytical column (25 mL × 4.4 mm). The solvents used for elution in both purification and analysis wereas follows.

Solvent A: 95% 50 mM ammonium bicarbonate buffer (pH 7):5% acetonitrile.

Solvent B: 80% 50 mM ammonium bicarbonate buffer (pH 7):20% acetonitrile.

The gradient used for purification was solvent A (0−4 min), linear gradient of A to B (4−15 min); solvent B (15−22 min), linear gradient B to A (22−32 min); solvent A (32−40); for analysis the gradient was solvent A (0−10 min); solvent A/solvent B, 1:1 (10−20 min); solvent A (20−30 min). The flow rate for purification was 2 mL/min, whereas that for analysis was 1 mL/min.

The oligomers synthesized on a 10 μmol scale were purified by size exclusion chromatography. A Sephadex G25 column (100 × 2.5 cm) was used to purify the standard 12-mer, whereas a G50 was used to purify the anthra 12-mer. Elution was performed with distilled water at a flow rate of 20 mL/h; fractions for the standard DNA were checked by HPLC on a BioRad SEC-125 gel filtration column; elution was performed by 50 mM phosphate buffer (pH 6.8) containing 0.1 M NaCl and 10 mM sodium azide. The fractions for the anthra 12-mer were checked by reversed-phase HPLC.

Nuclease Digestion and Analysis of Modified and Unmodified Oligomers. A mixture of oligonucleotide (0.5 OD units) with 50 mM Tris HCl (pH 8), 10 mM $MgCl_2$, snake venom phosphodiesterase (3 units), and bovine alkaline phosphatase (3 units) in 100 μL of distilled water was incubated at 37 °C for 12 h. Sodium acetate (0.05 M, pH 5, 15 μL) was added to the hydrolysis mixture followed by the addition of 230 μL of absolute ethanol. This mixture was chilled at −70 °C for 30 min and centrifuged at 30000*g* for 5 min. The supernatant was diluted with 1 mL of 95% ethanol, chilled, spun, decanted, and evaporated to dryness. The residue was redissolved in distilled water for HPLC analysis.

HPLC analysis for the hydrolysate of the unmodified oligomer was performed on a C18 column. A C8 column was used for analysis of the hydrolysate containing the more hydrophobic modified nucleoside. Elution was performed with a 50 mM potassium phosphate buffer (pH 4)/methanol gradient for the standard 12-mer hydrolysate; the anthra 12-mer hydrolysate was analyzed using 50 mM potassium phosphate buffer (pH 4) containing 30% acetonitrile.

NMR Experiments on Oligonucleotides. One- and two-dimensional proton data sets were collected on a Varian Unity 500 MHz spectrometer. One-dimensional temperature-dependent 500 MHz ^{1}H data sets were collected in 90% H_2O buffer/10% D_2O. For NOESY and DQF-COSY experiments, the oligomers were lyophilized

twice from 99.996% D_2O and then dissolved in 99.996% D_2O containing 100 mM NaCl and 20 mM phosphate buffer (pH 7) with (anthra 12-mer) or without (standard 12-mer) 10 mM $MgCl_2$. Two-dimensional phase-sensitive NOESY spectra of all the oligomers were collected using a 250 ms mixing time. All the data sets were acquired in the hypercomplex mode, with 256 increments in the t_1 dimensions, 32 or 64 scans per fid, and 2048 complex points in t_2. The t_2 dimension was processed with a Gaussian filter without line broadening. The t_1 increments were zero-filled to 2048 points and transformed with a Gaussian apodization function.

Two-dimensional proton phase-sensitive double quantum filtered COSY (DQF-COSY) data were collected using the standard pulse sequence with a 2 μs pulse repetition time and homospoil of 1 ms. The data sets were collected in the hypercomplex mode with 256 t_1 increments, 32 or 64 scans/fid, and 2048 complex points to t_2. The t_2 dimension was processed with a Gaussian filter. The t_1 increments were zero-filled to 2048 points and transformed with a Gaussian apodization function.

Molecular Modeling. The molecular modeling studies were performed on Silicon Graphics Iris or Indigo work stations. The molecules were visualized using Biosym (San Diego, CA) software. Minimizations and dynamics were performed using DISCOVER software. For simulation of nucleosides, CVFF potentials were used. All the nucleosides were first minimized by using the steepest gradient for 500 iterations and then by conjugate gradient for 2000 iterations. To obtain a global minimum, molecular dynamics simulations were used. All the dynamics were performed at 300 K for 50 ps including a 10 ps equilibration period. Lower energy conformers obtained in the molecular dynamics stimulation were further minimized to obtain a family of low energy conformers. The protocol used for initial minimization was used for these minimizations also.

Oligonucleotides were visualized using the biopolymer module of the Insight II software, and AMBER potentials were used during minimization of the oligonucleotides. The software was unable to assign a potential for C5 of adenosine when anthraquinone groups were attached on the 2'-hydroxyl. Potential "CB" was assigned to this carbon manually. The anthraquinone was manually intercalated inside the helix by torsioning the bonds between the anthraquinone ring and the 2'-hydroxyl. The torsions were removed, and the oligonucleotide was minimized first by 500 iterations of the steepest gradient minimizer and then by 2000 iterations of the conjugate gradient minimizer. Partial charges on the backbone phosphorus nuclei were reduced to 0.8, and those on the oxygen were reduced to −0.5 in some instances. All the hydrogen bonded atoms of the first three base pairs were fixed in space before minimizations.

2'-O-(Anthraquinone-2-methyl)adenosine (1). Synthesis of the title compound was performed generally according to the method of Yamana et al.*(20)* 2',3'-(Dibutylstannylene)adenosine (2.0 g, 4 mmol), 2-(bromomethyl)anthraquinone (2.40 g, 8 mmol), and cesium fluoride (1.20 g, 8 mmol) were mixed in 100 mL of anhydrous DMF. The reaction mixture turned black immediately but converted to a brown suspension after 1 h. The reaction was allowed to proceed for 48 h. The suspension was filtered, and the solvent was evaporated *in vacuo* to afford a residue which was dissolved in ethyl acetate (1 L). The ethyl acetate layer was washed with water, dried over sodium sulfate, and evaporated to dryness, and the compound was purified by silica gel chromatography using a gradient of methanol (0−2.5%) in chloroform: yield 1.9 g (19%); ^{1}H NMR [$(CD_3)_2SO$] δ

8.34 (s, 1H, H_8), 8.18 (m, 2H, Ar), 8.05 (s, H_2), 8.03 (m, 2H, Ar) 7.91 (m, 2H, Ar), 7.69 (d, 1H, Ar), 7.25 (broad s, 2H, NH_2), 6.10 (d, $J_{1',2'}$ = 6.0 Hz, 1H, 1'H), 5.45 (m, 2H, 5'-OH and 3'-OH), 4.88 (d, J_{gem} = 13.2 Hz, 1H, O-CH_2-Anth), 4.68 (m, 2H, OCH_2-Anth and 2'H), 4.42 (m, 1H, 3'H), 4.04 (m, 1H, 4'H), 3.65 (m, 2H, 5'H,5''H); MS m/z 488.154 725 (M + 1)$^+$ (calcd 488.157 008, diff = 2.3 mmu). The purity of the compound was checked by normal-phase HPLC.

N^6-Benzoyl-2'-O-(anthraquinone-2-methyl)adenosine (2). The title compound was synthesized according to the general procedure of Ti et al.(23). 2'-O-(Anthraquinone-2-methyl)adenosine (840 mg, 1.72 mmol) was dried by coevaporation (3×) with dry pyridine and dissolved in 25 mL of dry pyridine. Trimethylsilyl chloride (TMS chloride, 1.67 mL, 12.04 mmol) was added to the reaction. The mixture was stirred for about 1 h and 1 mL (8.6 mmol) of benzoyl chloride was added. After 5 min, 10 mL of 30% aqueous ammonia were added and the reaction was stirred for 45 min. The solvent was evaporated to dryness, and the residue was suspended in 25 mL of 1 N HCl. The suspension was extracted with ethyl acetate (3×). Solvent was evaporated to yield an oil. The oil was purified by silica gel chromatography using a gradient of methanol (0−2%) in chloroform: yield 62.8%; ^{1}H NMR [(CD_3)$_2$SO] δ 11.12 (s, 1H, NH), 8.68, 8.66 (2s, 2H, H_8 and H_2), 8.31−7.49 (complex multiplets, 12 H, Ar), 6.25 (d, $J_{1',2'}$ = 5.8 Hz, 1H, 1'H), 5.53 (d, 1H, 3'OH), 5.18 (t, 1H, 5'OH), 4.94 (d, J_{gem} = 13.3 Hz, 1H, OCH_2-Anth), 4.73 (m, 2H, OCH_2-Anth and 2'H), 4.45 (m, 1H, 3'H), 4.08 (m, 1H, 4'H), 3.34−3.28 (m, 2H, 5'H, 5''H); MS m/z 592.181 744 (M + 1)$^-$ (calcd 562.183 223, diff = 1.5 mmu). Purity of the compound was checked by normal-phase HPLC.

N^6-Benzoyl-5'-O-(dimethoxytrityl)-2'-O-(anthraquinone-2-methyl)adenosine (3). The title compound was synthesized according to the procedure given by Wu et al. (24). N^6-Benzoyl-2'-O-(anthraquinone-2-methyl)-adenosine (640 mg, 1.08 mmol) was dried by coevaporation with pyridine and was dissolved in 25 mL of pyridine. Dimethoxytrityl chloride (4.14 mg, 1.5 mmol) was added to the solution, and the reaction was allowed to stir for 12 h at 4 °C. Thin-layer chromatography indicated the presence of starting material; 100 mg of dimethoxytrityl chloride was added, and the reaction was continued for 12 more h. Methanol (5 mL) was added to quench the reaction. The solvent was evaporated under vacuum, and the residue was dissolved in ethyl acetate (50 mL). The ethyl acetate layer was washed with 5% $NaHCO_3$ (3×), water (75 mL), and brine and dried over sodium sulfate. The product was purified by silica gel chromatography with a gradient of hexane in chloroform (20% to 0%). Triethylamine (0.1%) was added to the solvent to prevent degradation of tritylated product: yield 51%; ^{1}H NMR [(CD_3)$_2$SO] δ 8.59 (2s, 2H, H_2 and H_8), 8.32−6.79 (complex multiplets, 25 H, Ar) 6.29 (d, $J_{1',2'}$ = 4.9 Hz, 1H, 1'H), 5.57 (d, 1H, 3'OH), 4.96 (d, 12.8 Hz, 1H, OCH_2-Anth), 4.85 (m, 2H, OCH_2-Anth and 2'H), 4.54 (m, 1H, 3'H), 4.20 (m, 1H, 4'H), 3.70 (s, 6H, −OCH_3), 3.32 (m, 6H, 5'H, 5''H and H_2O).

N^6-Benzoyl-5'-O-(dimethoxytrityl)-2'-O-(anthraquinone-2-methyl)adenosine 3'-O-(Cyanoethyl N,N-diisopropylphosphoramidite) (4). The title compound was synthesized according to the procedure given by Kierzek et al. (25). To β-cyanoethyl N,N,N',N'-tetraisopropylphosphorodiamidite (0.20 mL, 1.4 mmol) in acetonitrile (15 mL) was added 3 (490 mg, 0.548 mmol) and diisopropylammonium tetrazolide (467 mg, 0.27 mmol, dried in vacuo for 3 h). After 12 h, thin-layer chromatography indicated the presence of starting mate-

Scheme 1. Synthesis of 2'-O-(Anthraquinone-2-methyl)adenosine Nucleosides Using a 2',3'-Dibutylstannylene Derivative
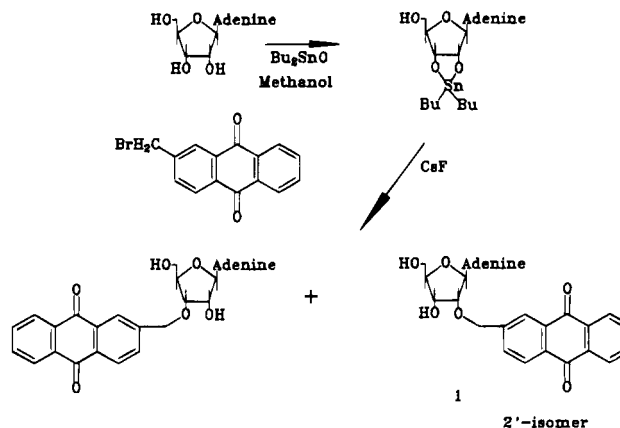
rial. More phosphorodiamidite (0.01 mL) was added, and the reaction was continued for 12 more h. The reaction was diluted with saturated sodium bicarbonate (50 mL) and extracted with dichloromethane (2×, 50 mL). Combined organic extracts were washed with brine (3×), dried over sodium sulfate, and concentrated in vacuo to obtain a dry foam. The foam was purified by silica gel chromatography using 20% hexane in chloroform containing 1% triethylamine: yield 500 mg (81.7%). ^{31}P-NMR gave the expected two signals (diastereoisomers) at 150.3 and 151.6 ppm relative to ortho phosphoric acid.

RESULTS

Chemistry. Synthesis of 2'-O-(anthraquinone-2-methyl)adenosine was attempted by the sodium hydride procedure of Ts'o and colleagues (26). However, this approach led to a complex mixture, probably due to miscellaneous reactions of the anthraquinone under strongly basic conditions. Consequently, 2'-O-(anthraquinone-2-methyl)adenosine was synthesized using 2',3'-(dibutylstannylene)adenosine as the starting material (20). The alkylation reaction proceeded very slowly even at high temperatures. The reaction rate was improved by adding cesium fluoride, which appears to act as a catalyst by forming a complex with the tin of 2',3'-(dibutylstannylene)adenosine; this complexation increases the nucleophilicity of the 2' and 3' hydroxyls. The yield of the reaction (Scheme 1) was approximately 19%.

Synthesis and Purification of Anthra 12-mer. The 2'-O-(anthraquinone-2-methyl)adenosine was protected by standard procedures and incorporated into the anthra 12-mer defined above on an automated DNA synthesizer. The coupling reaction using the modified nucleoside phosphoramidite was allowed to proceed for 10 min to ensure maximal coupling. The coupling yield was more than 90% for the modified nucleoside as judged by dimethoxytrityl release.

The anthra 12-mer was purified by size exclusion chromatography. Since the size separation range for G-25 is 1000−3500 and the molecular weight of the anthra DNA was slightly above this range, G-50 (molecular weight range 5000−10 000) was used for the purification. Adequate resolution was ensured by using a long column length (100 × 2.5 cm), slow elution rate (20 mL/h), and small fraction size. Initially, attempts were made to analyze the fractions by size exclusion HPLC. However, very broad peaks were obtained, suggesting the anthra 12-mer was equilibrating between two or more conformations at room temperature in the buffer used for elution. Consequently, reversed-phase HPLC was used to analyze the fractions.
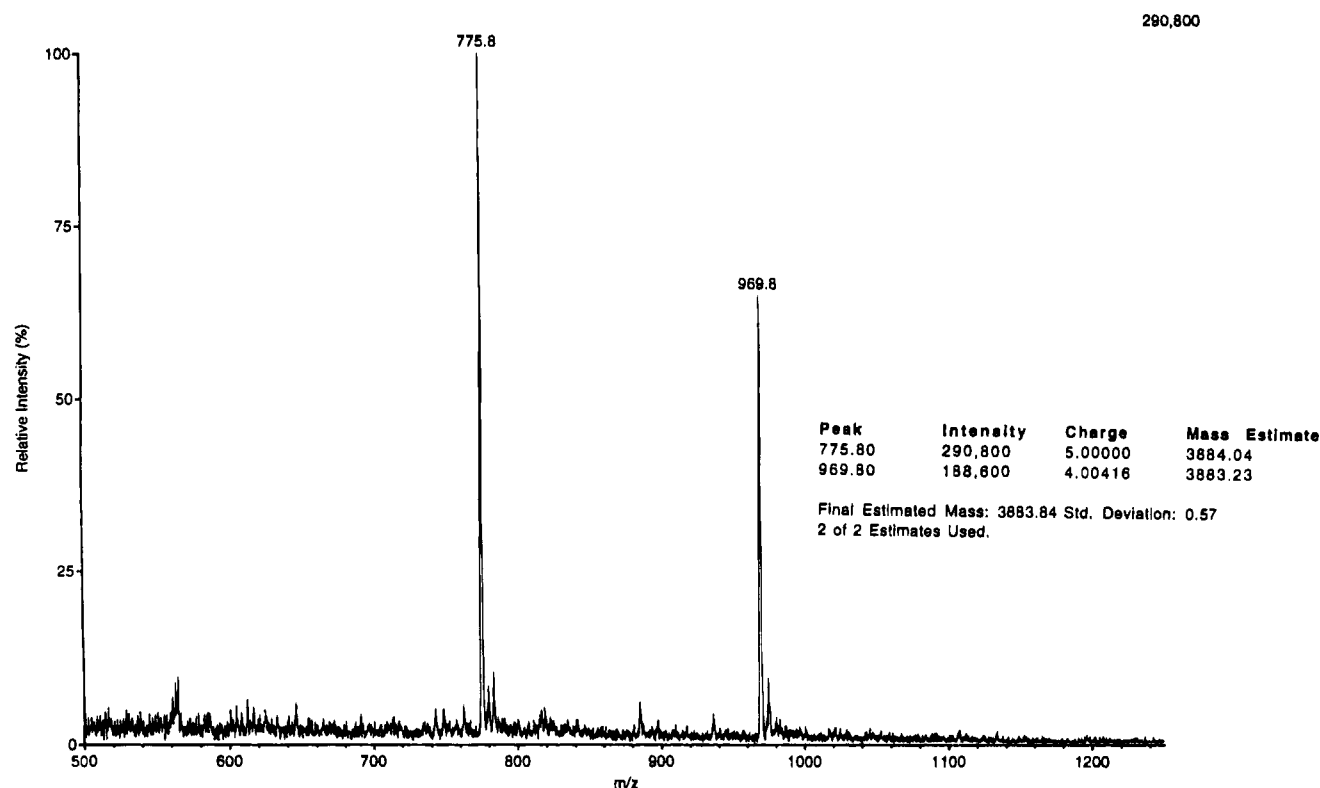
Figure 1. Electrospray mass spectrum for the anthra 12-mer.

The presence of 2'-O-(anthraquinone-2-methyl)adenosine was confirmed by hydrolyzing the oligonucleotide with snake venom phosphodiesterase and bacterial alkaline phosphatase. The nucleosides were freed from the enzyme and injected on the HPLC. 2'-O-(Anthraquinone-2-methyl)adenosine is very hydrophobic and is indefinitely retained on a C_{18} column. Consequently, a C_8 column was used to analyze the nucleosides. The nucleosides were eluted by 30% acetonitrile in potassium phosphate buffer (pH 4.0). The relatively high polarity of this system prohibited base-line separation of the normal nucleosides. The ratio of peak areas of 2'-O-(anthraquinone-2-methyl)adenosine peak to the normal nucleoside cluster was 10.3:1, very close to the expected 11:1.

The anthra 12-mer was subjected to electrospray mass spectral analysis to confirm the presence of all nucleotides. The electrospray mass spectrum shows multiple peaks for a single molecule since multiple charges are introduced in the ionization process. The mass spectrum for the anthra 12-mer is shown in Figure 1. The peak at 775.8 m/z has five negative charges; the mass derived from this spectrum is 3883.2, whereas the calculated mass equals 3882.3.

UV Melting Studies. Melting temperature curves (T_m) were taken in 0.1 M NaCl containing 10 mM phosphate buffer. The anthra 12-mer melted cooperatively at approximately 48 °C compared to 41.6 °C for the standard 12-mer. Thus, incorporation of each anthraquinone moiety stabilized the duplex by 3 to 3.5 °C. The melting curve consisted of a single smooth transition as would be expected for formation of a single duplex structure under these very dilute (3×10^{-6} M) conditions.

Circular Dichroism (CD) Studies. CD studies were performed by dissolving the anthra 12-mer in 0.1 M NaCl containing 10 mM phosphate buffer. Figure 2 shows the CD curves for the anthra 12-mer at various temperatures. The shape of the long wavelength maximum at lower temperatures (35−45 °C) seems to imply the presence of two peaks, one at 290 nm and the second at 280 nm, which are very poorly resolved. As temperature was increased, the first peak merged into the second. The CD spectrum at 45 °C (near the T_m) indicates the conformation of the anthra DNA is close to B-form. The presence of the unusual shape at low temperatures may indicate the presence of multiple conformations at low temperature, consistent with both the HPLC data noted above and the NMR studies described below. As the temperature is increased the peak shape becomes that of normal B-DNA, indicating melting of these conformations.

High Resolution NMR Studies. Alkylation of adenosine as described above gives rise to some 3'-O-aralkyl product as well as **1**. In order to establish unequivocally that **1** is indeed 2'-substituted, a combination of 1D NMR with 2D COSY and NOESY was used. The 5'- and (presumed) 3'-OH signals formed an overlapped multiplet centered at δ 5.45. COSY was used to establish the position of 2'-CH as δ 4.68 and 3'-CH as δ 4.42 by means of H1'−H2' and H2'−H3' cross-peaks. Both COSY and NOESY spectra reveal strong cross-peaks with the OH doublet signal at δ 5.45 and the δ 4.42 peak and no cross-peak with that at δ 4.68, establishing unequivocally that the aralkyl substituent must be at the C-2' oxygen. Oligonucleotides were dissolved in 0.1 M NaCl containing 20 mM phosphate buffer (pH 6.8) at a concentration of about 5 mM. The first experiment performed on the anthra 12-mer was observation of hydrogen-bonded imino protons. The 15 °C spectrum revealed more than the six hydrogen-bonded imino protons expected from the 2-fold symmetry of the duplex (data not shown), suggesting the presence of additional DNA conformers. As the temperature is increased to 25 °C, sharpening of the peaks is observed and some of the peaks disappear, consistent with melting of the less stable conformations.

It was reasoned that the addition of magnesium ion might stabilize one conformer and simplify the NMR spectrum. Hence, the anthra 12-mer was dialyzed to
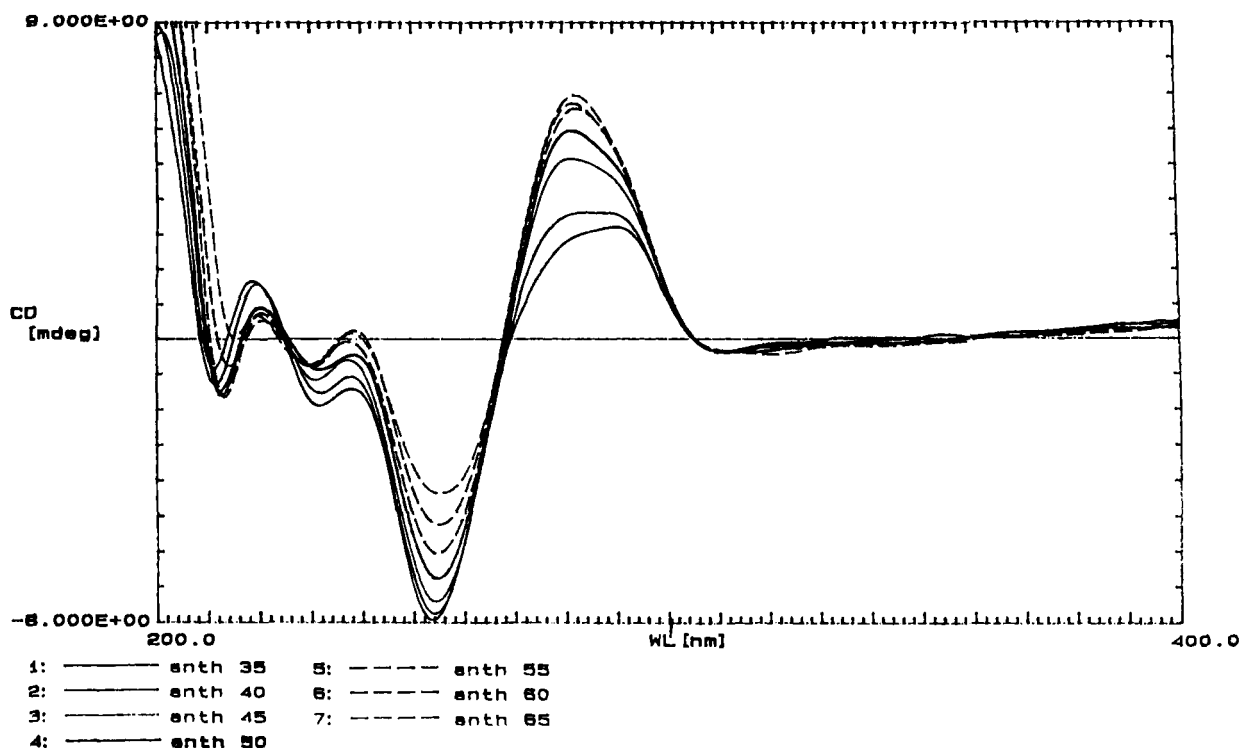
Figure 2. Circular dichroism (CD) spectra for the anthra 12-mer at various temperatures.

remove all the salts and then redissolved in 20 mM phosphate buffer (pH 7) containing 0.1 M NaCl and 0.01 M MgCl₂; all subsequent studies were carried out in this medium.

The anthra 12-mer was first subjected to imino proton analysis. Figure 3 shows imino proton spectra for the anthra DNA at various temperatures. The predominant conformation (35–55 °C) shows only five hydrogen-bonded imino protons instead of the six predicted for a palindromic duplex. It is likely this conformation is a duplex with the end base pair melted, which would explain the presence of only five imino protons. It is also plausible, albeit less likely, that the presence of an-thraquinone is causing some conformational change in the molecule which would result in breaking one of the interior hydrogen bonds or that a hairpin with a two base-pair loop was the predominant conformer. To resolve these speculations and to determine whether intercalation occurs, the anthra 12-mer was subjected to more extensive NMR analysis.

The one-dimensional spectrum of the anthra 12-mer was examined at various temperatures. These spectra also show considerable overlap at lower temperatures, confirming the presence of multiple conformations. The one-dimensional spectrum at 55 °C (Figure 4, aromatic region) is well-resolved, probably indicating the presence of a single conformation. Since the best resolution was observed at 55 °C, the two-dimensional analysis was performed at this temperature. The higher temperature required to melt unwanted conformers relative to the T_m observed by UV and CD results from the far greater oligonucleotide concentration required for NMR analysis.

Two-Dimensional NMR Spectroscopy. The un-modified d(CGCACATGTGCG) duplex was characterized by a combination of NOESY and DQF-COSY NMR according to the standard procedure developed by Hare et al. (*27*). As expected, the data were fully consistent with B-DNA geometry; chemical shift data for aromatic, methyl, and selected sugar protons are presented in Table
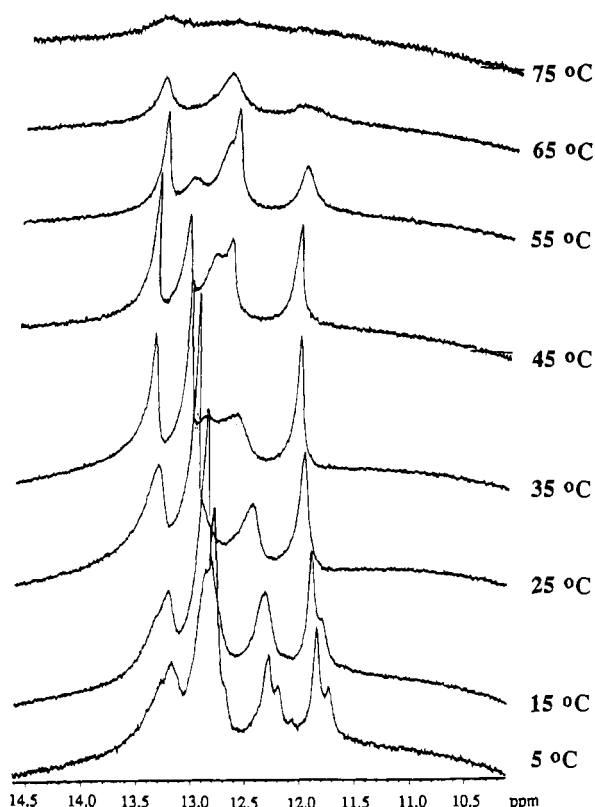
Figure 3. Imino proton spectra for the anthra 12-mer at various temperatures. These spectra were taken of the duplex (2.85 mM) in 99.996% D₂O, 100 mM NaCl, 20 mM phosphate buffer (pH 7), 10 mM MgCl₂.

1. The anthra 12-mer also was studied in detail by two-dimensional (NOESY and DQF-COSY) NMR spectros-copy. Figure 5 shows the expanded contour plot (aromatic-H1′ region) of the NOESY spectrum for the anthra 12-mer. Most of the peaks are well resolved and were used for the sequential assignments given in Table 2. How-
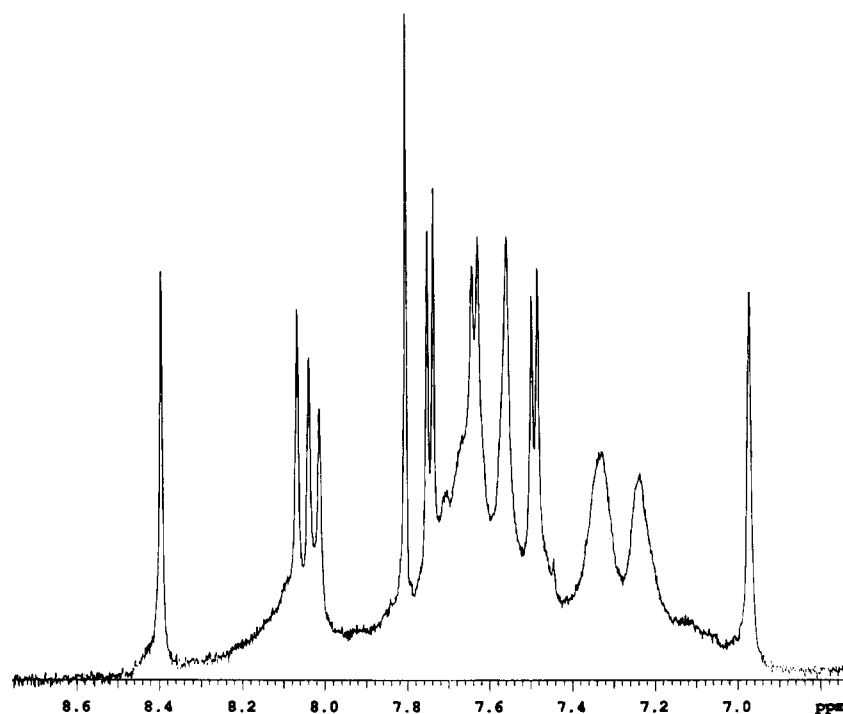
Figure 4. Aromatic region of the anthra 12-mer.
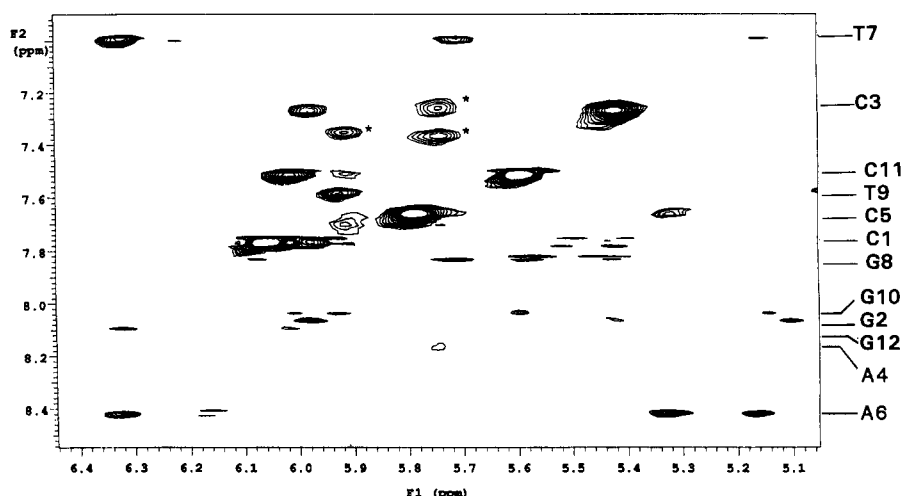
Figure 5. Expanded contour plot (aromatic-H_1 region) of the NOESY spectrum for the anthra 12-mer.

Table 1. Nonexchangeable ¹H Chemical Shifts (ppm) of d(CGCACATGTGCG)₂ in D₂O[a]

	H1'	H8/H6	H5/methyl	H2'/H2''
C1	5.43	7.34	5.57	2.11, 1.68
G2	5.59	7.67		2.42, 2.09
C3	5.27	7.09	5.14	2.09, 1.75
A4	5.91	7.98		2.62, 2.40
C5	5.23	7.00	5.01	2.10, 1.75
A6	5.89	7.92		2.63, 2.30
T7	5.48	6.84	1.05	2.16, 1.80
G8	5.61	7.48		2.44, 2.25
T9	5.51	6.88	1.00	2.16, 1.77
G10	5.53	7.60		2.36, 2.32b
C11	5.43	7.07	5.12	2.04, 1.62
G12	5.44	7.65		2.34, 2.05

[a] The solution was ?? M in ODN prepared in 99.996% D₂O containing 0.10 M NaCl and 0.02 M phosphate buffer (pH 7.0). [b] Values are estimates because of severe peak overlap.

ever, the intramolecular H8—H1' connectivity of A4 is very weak, and the H8—H1' connectivity of G8 is missing. These missing or weak connectivities are best explained on the basis of intercalation.

Table 2. Nonexchangeable ¹H Chemical Shifts (ppm) of d(CGCA*CATGTGCG)₂ where A* = 2'-O-(Anthraquinone-2-methyl)adenosine

	H1'	H8/H6	H5/methyl	H2'/H2''
C1	5.98	7.77	6.07	2.54, 2.07
G2	5.98	8.07		2.81, 2.77
C3	5.74	·7.27	5.43	2.43, 1.79
A4	5.75	8.17		4.81
C5	5.32	7.67	5.79	2.56, 2.40
A6	6.33	8.42		2.96, 2.82
T7	5.71	7.00	1.48	2.08, 1.53
G8	5.93	7.84		2.83, 2.69
T9	5.94	7.59	2.00	2.68, 2.35
G10	6.01	8.04		2.82, 2.72
C11	6.02	7.52	5.60	2.51, 2.06
G12	6.03	8.10		2.77, 2.57

Figure 6 shows the molecular stereo model for the intercalation of the anthraquinone ring. One can easily observe that the intercalation of the anthraquinone ring has expanded the space between A4 and C5 as well as between G8 and T9. The intercalation of the anthraquinone inside the helix forces the sugars of A4 and G8 to
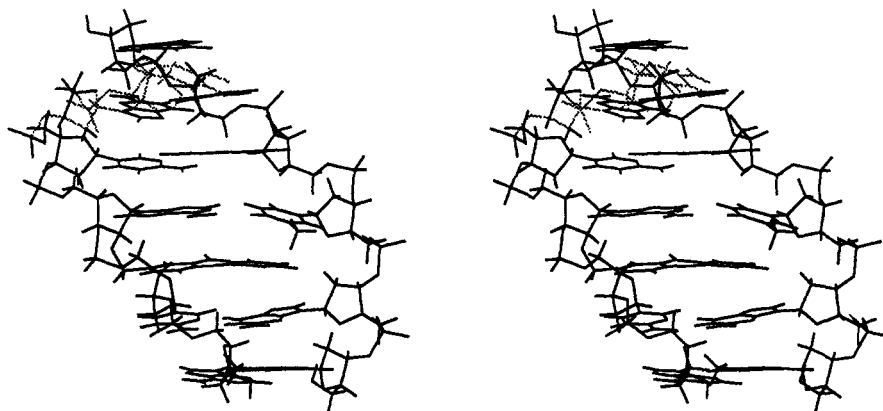
Figure 6. Stereo view of the anthra 12-mer. One-half the palindromic dodecamer is shown with the anthraquinone intercalated between the A4–T9 and C5-G8 base pairs.
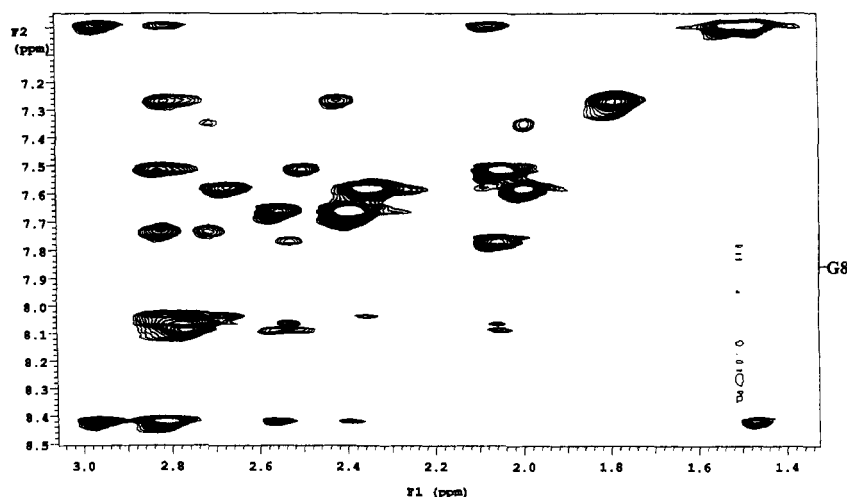
Figure 7. Expanded contour plot (aromatic H2′ region) of the NOESY spectrum for the anthra 12-mer.
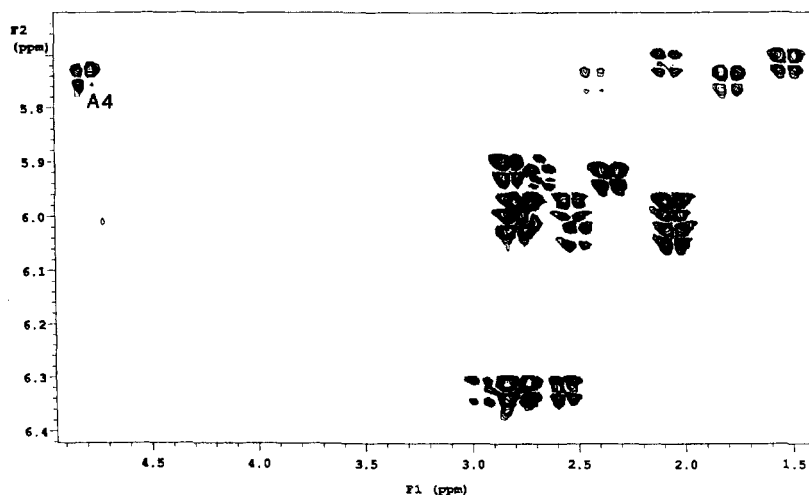
Figure 8. Expanded contour plot (H1′–H2′ region) of the DQF-COSY spectrum for the anthra 12-mer.

move away from the bases, accounting for the loss of connectivities between sugar and aromatic protons in the cases of A4 and G8. The aromatic-H1′ region provides more evidence for intercalation. The cross-peaks at 7.27 and 7.37 ppm (marked by asterisks in Figure 5) show connectivity between protons of the anthraquinone ring and H1′ of A4. A cross-peak observed at 7.36 ppm represents through-space connectivity between aromatic protons of anthraquinone and H1′ of T9, confirming that the anthraquinone ring stacks directly below the AT base pair.

Additional evidence for intercalation comes from the aromatic H2′ region of the NOESY spectrum (Figure 7). This region shows complete absence of cross-peaks between H2′ and H2″ of G8 with its own H8. It also shows aromatic methyl cross-peaks for thymidines. The aromatic methyl group normally shows connectivities with its own H6 and H8/H6 of the preceding base; these cross-peaks are clearly visible in the aromatic-methyl region of the standard 12-mer duplex (data not shown). The T7-methyl in the anthra oligo shows clear connectivity between its own H6 and H8 of A6. However, the

methyl group of T9 fails to show through-space connectivity with H8 of G8.

Two-dimensional NMR studies also provide important information about the sugar conformation of 2'-O-(anthraquinone-2-methyl)adenosine in the duplex. Figure 8 shows the expanded contour plot of the DQF-COSY spectrum for anthra DNA. The label indicates the cross-peak between H1' and H2' of A4. If the C3'-endo sugar conformation characteristic of ribonucleotides in RNA helices (28) or RNA—DNA hybrids (29) was found in A4, $J_{1',2'}$ would be undetectably small. Clearly, the observed cross-peak, albeit less intense than some of the deoxy-nucleotide signals, confirms a sugar conformational shift toward C2'-endo. This sugar conformation is required to enable intercalation of the anthraquinone ring below A4, as if it entered the helix through the major groove.

Molecular modeling studies are in agreement with this observation. The entry of the anthraquinone from the major groove explains the chemical shifts of anthraquinone. The proton at the 1 position on anthraquinone exhibited a chemical shift of δ 7.26, considerably upfield despite its proximity to the oxygen present in the center ring of the anthraquinone. This proton is completely within the shielding cone of adenine, whereas the other two (H_3 and H_4) are on the periphery.

DISCUSSION

The two-dimensional NMR studies described above conclusively prove intercalation of the anthraquinone ring. Thus, the stabilization provided by the anthraquinone is a result of intercalation and not hydrogen bonding between anthraquinone oxygen and amino group(s) in the minor groove. Intercalation forces the sugar conformation of 2'-O-(anthraquinone-2-methyl)adenosine toward C2'-endo. Although this is normally an unfavorable conformation for a ribonucleoside, the energy lost due to this conformational change must be significantly less than that gained by intercalation. These studies establish that even a methylene linker is adequate for inserting the intercalating agent inside the helix. They also show that the structure of the group conjugated at the 2'-hydroxyl plays a very important role in duplex stability.

These studies are in agreement with Yamana et al. (20) in observing stabilization of the DNA duplex. However, the stabilization is considerably less than that observed by Yamana et al. The shape of the CD curve observed by Yamana et al. is quite different than that exhibited by the standard B-form DNA. The shape of the CD spectrum depends upon the sequence of the oligonucleotide (30), which may explain the difference. We clearly demonstrate intercalation using two-dimensional NMR, whereas Yamana et al. based their conclusions on a narrow region of the CD curve (300—400 nm). The CD studies of Yamana et al. were interpreted as reflecting global changes in the geometry of the duplex. However, the CD, NMR and molecular modeling data presented here are consistent with a conformation altered only locally by intercalation of the planar anthraquinone system at temperatures high enough to eliminate nonspecific complex interactions while retaining a duplex structure. The presence of five exchangeable imino proton signals at 55 °C also strongly supports minimal disruption of B-DNA geometry, since the terminal G—C base pairs will certainly be frayed with loss of signal for that imino proton.

Thus, site-specific intercalation into a B-DNA duplex can be achieved by linking a planar hydrophobic functional group to the 2'-OH of an internally situated (or, presumably, 3' or 5'-terminal) ribonucleoside. Since the energetics of the system lead to a ribose sugar confor-mational change approaching a B-DNA-like sugar pucker, the overall B-DNA geometry is only minimally affected.

It will be of considerable interest to apply this approach to the study of DNA—RNA hybrids, which tend to assume a global conformation resembling A-type geometry. Those studies are in progress and will be reported elsewhere.

LITERATURE CITED

(1) Beaucage, S. L., and Iyer, R. P. (1993) The synthesis of modified oligonucleotides by the phosphoramidite approach and their applications. *Tetrahedron 49*, 6123—6194.

(2) Uhlmann, E., and Peyman, A. (1990) Antisense oligonucleotides: A new therapeutic principle. *Chem. Rev. 90*, 543—584.

(3) Beaucage, S. L., and Iyer, R. P. (1993) The synthesis of specific ribonucleotides and unrelated phosphorylated biomolecules by the phosphoramidite method. *Tetrahedron 49*, 10441—10488.

(4) Tonkinson, J. L., and Stein, C. A. (1993) Antisense nucleic acids—Prospects for antiviral intervention. *Antiviral Chem. Chemother. 4*, 193—200.

(5) Stein, C. A., and Cheng, Y.-C. (1993) Antisense oligonucleotides as therapeutic agents—Is the bullet really magical? *Science 261*, 1004—1012.

(6) Beaucage, S. L., and Iyer, R. P. (1992) Advances in the synthesis of oligonucleotides by the phosphoramidite approach. *Tetrahedron 48*, 2223—2311.

(7) Zamecnik, P., and Stephenson, M. (1978) Inhibition of Rous sarcoma virus replication and cell transformation by a specific oligodeoxynucleotide. *Proc. Natl. Acad. Sci. U.S.A. 75*, 280—284.

(8) Milligan, J. F., Matteucci, M. D., and Martin, J. C. (1993) Current concepts in antisense drug design. *J. Med. Chem. 36*, 1923—1937.

(9) Sun, J.-S., Francois, J.-C., Montenay-Garestier, T., Saison-Behmoaras, T., Roig, V., Thuong, N. T., and Hélène, C. (1989) Sequence-specific intercalating agents: Intercalation at specific sequences on duplex DNA via major groove recognition by oligonucleotide-intercalator conjugates. *Proc. Natl. Acad. Sci. U.S.A. 86*, 9198—9202.

(10) Mann, J. S., Shibata, Y., and Meehan, T. (1992) Synthesis and properties of an oligodeoxynucleotide modified with a pyrene derivative at the 5'-phosphate. *Bioconjugate Chem. 3*, 554—558.

(11) Iverson, B. L., and Dervan, P. B. (1987) Nonenzymatic sequence-specific cleavage of single-stranded DNA to nucleotide resolution. DNA methyl thioether probes. *J. Am. Chem. Soc. 109*, 1241—1243.

(12) Boidot-Forget, M., Chassignol, M., Takasugi, M., Thuong, N. T., Hélène, C. (1988) Site-specific cleavage of single-stranded and double-stranded DNA sequences by oligodeoxyribonucleotides covalently linked to an intercalating agent and an EDTA-Fe chelate. *Gene 72*, 361—371.

(13) Lin, S.-B., Blake, K. R., Miller, P. S., and Ts'o, P. O. P. (1989) Use of EDTA derivatization to characterized interactions between oligodeoxyribonucleoside methylphosphonates and nucleic acids. *Biochemistry 28*, 1054—1061.

(14) Vlassov, V. V., Gaidamakov, S. A., Zarytova, V. F., Knorre, D. G., Levina, A. S., Nikonova, A. A., Podust, L. M., and Fedorova, O. S. (1988) Sequence-specific chemical modification of double-stranded DNA with alkylating oligodeoxyribonucleotide derivatives. *Gene 72*, 313—322.

(15) Boutorin, A. S., Gus'kova, L. V., Imanova, E. M., Kobetz, N. D., Zarytova, V. F., Ryte, A. S., Yurchenko, L. V., and

Vlassov, V. V. (1989) Synthesis of alkylating oligonucleotide derivatives containing cholesterol or phenazinium residues at their 3′-terminus and their interaction with DNA within mammalian cells. *FEBS Lett. 254,* 129−132.

(16) Lee, B. L., Murakami, A., Blake, K. R., Lin, S.-B., and Miller, P. S. (1988) Interaction of psoralen-derivatized oligodeoxyribonucleoside methylphosphonates with single-stranded DNA. *Biochemistry 27,* 3197−3203.

(17) Lamond, A. I., and Sproat, B. S. (1993) Antisense oligonucleotides made of 2′-*O*-alkylRNA: Their properties and applications in RNA biochemistry. *FEBS Lett. 325,* 123−127.

(18) Lesnik, E. A., Guinosso, C. J., Kawasaki, A. M., Sasmor, H., Zounes, M., Cummins, L. L., Ecker, D. J., Cook, P. D., and Freier, S. M. (1993) Oligodeoxynucleotides containing 2′-*O*-modified adenosine: Synthesis and effects on stability of DNA:RNA duplexes. *Biochemistry 32,* 7832−7838.

(19) Morvan, F., Porumb, H., Degols, G., Lefebvre, I., Pompon, A., Sproat, B. S., Rayner, B., Malvy, C., LeBleu, B., and Imbach, J.-L. (1993) Comparative evaluation of seven oligonucleotide analogues as potential antisense agents. *J. Med. Chem. 36,* 280−287.

(20) Yamana, Kazushige, Nishijima, Y., Ikeda, T., Gokota, T., Ozaki, H., Nakano, H., Sangen, O., and Shimidzu, T. (1990) Synthesis and interactive properties of an oligonucleotide with anthraquinone at the sugar fragment. *Bioconjugate Chem. 1,* 319−324.

(21) Keller, T. H., and Häner, R. (1993) Synthesis and hybridization properties of oligonucleotides containing 2′-*O*-modified ribonucleotides. *Nucleic Acids Res. 21,* 4499−4505.

(22) Broom, A. D., and Christensen, L. F. (1974) A unique example of virtual proton−proton coupling in purine nucleosides. *J. Org. Chem. 39,* 2660−2662.

(23) Ti, G. S., Gaffney, B. L., and Jones, R. A. (1982) Transient protection: Efficient one-flask syntheses of protected deoxynucleosides. *J. Am. Chem. Soc. 104,* 1316−1319.

(24) Wu, T., Ogilvie, K. K., and Pon, R. T. (1989) Prevention of chain cleavage in the chemical synthesis of 2′-silylated oligoribonucleotides. *Nucleic Acids Res. 17,* 3501−3517.

(25) Kierzek, R., Caruthers, M. H., Longfellow, C. E., Swinton, D., Turner, D. H., and Freier, S. M. (1986) Polymer-supported RNA synthesis and its application to test the nearest-neighbor model for duplex stability. *Biochemistry 25,* 7840−7846.

(26) Yano, J., Kan, L. S., and Ts'o, P. O. P. (1980) A simple method of the preparation of 2′-*O*-methyladenosine. *Biochim. Biophys. Acta 629,* 178−183.

(27) Hare, C. R., Wemmer, D. E., Chou, S.-H., Drobny, G., and Reid, B. R. (1983) Assignment of the non-exchangeable proton resonances of d(C-G-C-G-A-A-T-T-C-G-C-G) using two-dimensional nuclear magnetic resonance methods. *J. Mol. Biol. 171,* 319−336.

(28) Chou, S.-H., Flynn, P., and Reid, B. (1989) Solid-phase synthesis and high-resolution NMR studies of two synthetic double-helical RNA dodecamers: r(CGCGAAUUCGCG) and r(CGCGUAUACGCG). *Biochemistry 28,* 2422−2435.

(29) Salazar, M., Fedoroff, O. Y., Miller, J. M., Ribeiro, N. S., and Reid, B. R. (1993) The DNA strand in DNA−RNA hybrid duplexes is neither B-form nor A-form in solution. *Biochemistry 32,* 4207−4215.

(30) Gray, D. M., Ratliff, R. L., and Vaughan, M. R. (1992) Circular dichroism spectroscopy of DNA. *Methods Enzymol. 211,* 389−405.

BC950044A

Cell-Specific Delivery of Bacteriophage-Encapsidated Ricin A Chain

Min Wu, William L. Brown, and Peter G. Stockley*

Department of Genetics, University of Leeds, Leeds LS2 9JT, U.K. Received March 8, 1995®

We have used covalent coupling of deglycosylated ricin A chain (RAC) to the assembly initiation/ translational repression RNA stem-loop (TR) of the bacteriophage MS2 to direct encapsidation of the toxin in bacteriophage capsids. Multiple copies of the TR–RAC conjugate can be incorporated into single capsid shells. The resultant particles can then be directed to specific cells by receptor-mediated endocytosis (RME) of complexes formed with anti-MS2 coat protein antibodies or by further covalent modification of the capsids by addition of human transferrin molecules. The results suggest that bacteriophage encapsidation and targeting is an efficient way to deliver toxins in a cell-specific fashion. The system may have widespread application in the field of targeted drug delivery, including antisense reagents.

INTRODUCTION

Viruses are natural vectors for the cell-specific delivery of macromolecules such as their own nucleic acids. RNA bacteriophages have long been used as paradigms of more complex viruses and as models in which to study the molecular details of viral infection, replication, assembly, etc. (Witherall *et al.*, 1991; Stockley *et al.*, 1993). The Group 1 phages, which include MS2, R17, and fr, are perhaps the best understood. Self-assembly of phage particles in these systems is triggered by a sequence-specific genomic RNA–coat protein interaction (Beckett and Uhlenbeck, 1988). Uhlenbeck and his colleagues have shown that for MS2/R17 the RNA sequence determinants for this interaction lie entirely within a 19 nucleotide (nt) operator fragment capable of forming a stem-loop (Figure 1a). The key features of this sequence for recognition have been probed by exhaustive sequence and functional group variation experiments (Witherall *et al.*, 1991; Talbot *et al.*, 1990; Stockley *et al.*, 1995).

In vivo coat protein binding accomplishes two distinct functions. Firstly, it prevents ribosome binding to initiate translation of the replicase cistron, the start codon for which ($A = +1$, see Figure 1a for numbering scheme) lies in the 3' base-paired leg of the stem. Thus, the stem-loop serves as a translational repression (TR) signal. Secondly, formation of the translational repression complex triggers assembly initiation, further coat protein subunits being added to the complex with no other apparent intermediates on the pathway to formation of a $T = 3$ quasiequivalent capsid. Capsid assembly does occur in the absence of RNA but only at higher protein concentrations. The TR fragment therefore acts as a catalyst, presumably by stabilizing a particular coat protein conformation (Stockley *et al.*, 1993, 1994).

Recently, we have determined the three-dimensional structure of the TR-coat protein complex by X-ray diffraction techniques by soaking chemically synthesized TR fragments into crystals of "empty" recombinant capsids (Valegård *et al.*, 1994). The structure of these operator capsids confirms that the identity elements which interact with the coat protein are largely restricted to the single-stranded residues, i.e., the bulged adenine at position A-10, the loop adenines at A-4 and A-7, and the

essential pyrimidine at −5. The residues at −10, −4, and −5 all make hydrogen bond interactions with residues on the coat protein subunits while A-7 is involved in an extended stacking interaction with the base-paired residues below the −5 pyrimidine, which is in turn stacked upon the side chain of Tyr85 in the protein. The importance of each of these individual intermolecular contacts for complex formation in solution has been confirmed by experiments using chemically synthesized variants of the TR (Stockley *et al.*, 1995). In the operator capsid the TR fragment has the form of a crescent in which the key interactions with coat protein occur at the narrow ends. Recently, the refined crystal structure of the operator capsid has become available (K. Valegård *et al.*, manuscript in preparation). This makes it clear that there are no RNA–protein contacts "below" the A - $13:U + 2$ base pair in the stem (Figure 1a).

The wild-type MS2 genome contains 3569nt of RNA (Furuse, 1987), whereas the operator capsid contains 90 copies of the TR fragment, one per coat protein dimer in the $T = 3$ shell (= 180 subunits). Thus, even at saturating ratios of TR:coat protein only just over 50% of the normal RNA packaging capacity of the phage shell is used. We speculated that covalent attachment of a ligand at one or other end of the TR fragment might allow encapsidation of that ligand in a shell of MS2 coat protein. Indeed, calculation of the internal volume of the capsids (Sansom, personal communication) suggest that multiple copies of such ligands could be encapsidated which might then be useful in drug delivery and targeting, especially of antisense reagents. This paper describes our initial results with this system using the glycoprotein toxin, ricin A chain (RAC) (Thorpe *et al.*, 1988), as the encapsidated ligand.

EXPERIMENTAL PROCEDURES

Materials. *N*-Succinimidyl *S*-acetylthioacetate (SATA), maleimide-activated horse radish peroxidase (HRP) kit, and sulfosuccinimidyl 4-(*N*-maleimidomethyl)cyclohexane-1-carboxylate (Sulfo-SMCC) were obtained from Pierce. Human apo-transferrin, rabbit anti-goat peroxidase-conjugated IgG, mouse anti-rabbit peroxidase-conjugated IgG, rabbit anti-ricin serum, *N*-succinimidyl 3-(2-pyridyldithio)propionate (SPDP), and DNase I were purchased from Sigma. Goat anti-ricin serum was purchased from Vector. Goat anti-human transferrin and rabbit anti-mouse fluorescein-conjugated IgGs were

* Author for correspondence. Phone: 44 (0) 1132-333-078. Fax: 44 (0) 1132-441-175.

from ICN. Mouse anti-transferrin receptor monoclonal antibody was from Becton Dickinson. NAP-25 and NAP-10 prepacked columns were obtained from Pharmacia. ECL Western blotting detection reagents were purchased from Amersham.

Purification of MS2 Wild-Type Empty Capsids. *E. coli* cells (TG1) were transformed to ampicillin resistance with an MS2 coat protein expression plasmid pTAC–ACP (Walton, 1993), which contains the MS2 coat protein gene downstream of the phage maturation (or A) gene as a 434 bp *Xba* I-*Xho* I fragment. Transformants were grown in 2TY medium (5 L) containing 100 μg/mL ampicillin to exponential phase, harvested, and subjected to sonication. After spinning at 17600g at 4 °C the supernatant was decanted, the DNA was removed by treatment with DNase I (10 μg/mL) in the presence of 6 mM magnesium acetate, and the proteins were precipitated with 33% saturated ammonium sulfate and finally dialysed against 0.01 M sodium phosphate, 0.14 M NaCl, pH 7.5 (PBS). The empty coat protein capsids were then purified by centrifugation through a 15%–45% (w/v) sucrose density gradient at 43500g for 18 h. Fractions containing the purified coat protein were identified by running aliquots on a Schägger SDS–PAGE gel (10%) (Schägger and von Jagow, 1987). The pooled fractions were then dialysed into 10 mM Hepes, 100 mM NaCl (pH 7.4) and stored at 4 °C for up to 3–4 weeks. However, for longer storage (up to 3 months) the samples were kept in sucrose buffer from the gradient centrifugation or in ammonium sulfate (8% w/v) at −20 °C.

Synthesis of Oligoribonucleotides. RNA oligonucleotides encompassing the TR sequence 5′ ACA-UGA-GGA-UUA-CCC-AUG-U-3′ were synthesized on an ABI DNA synthesizer 391 PCR-Mate as described previously (Murray *et al.*, 1994). TR derivatized with a thiol group at the 5′-end was synthesized using 5′-Thiol-Modifier C6 S-S (Cambio Ltd). The thiol-containing TR (TR–SH) also had a 5′ extension sequence of nine uridines to ensure that the encapsidated ligand did not interfere with TR–coat protein recognition. The synthesized oligonucleotides were deprotected with tetrabutyl ammonium fluoride (TBAF) and stored frozen in water at −20 °C. Dithiothreitol (DTT, 10 mM) was added to the TR–SH sample. The purity of the oligonucleotides was assessed by running them on a reverse-phase HPLC column (Murray *et al.*, 1994) and confirmed by electrophoresis on a denaturing polyacrylamide gel stained with ethidium bromide. The TR–SH samples were ≈ 90% pure by these criteria. TR or its derivatives were quantified spectrophotometrically using a value of 1 OD$_{260nm}$ ≈ 30 μg/mL of RNA.

Conjugation of the TR–SH to Ricin A Chain (RAC). A 0.75 mg portion of TR–SH was dialyzed into PBS and reacted with *N*-succinmidyl 3-(2-pyridyldithio)-propionate (SPDP, dissolved in absolute ethanol) at a molar ratio of 1:6 at room temperature for 1 h, before being dialyzed against PBS to remove excess reagent, and kept at 4 °C. One molecule of the modified TR–SH contained about one molecule of 2-pyridyl disulfide derived from SPDP as judged by the procedure of Carlsson *et al.* (1978). Briefly, an analytical aliquot of the modified TR–SH was diluted 1:100 with water and reduced by addition of 100 mM DTT. The extent of modification was calculated from the difference in absorbance at 343 nm before and after reduction. The pyridine 2-thione released has an extinction coefficient of ϵ_{343} = 8.08 × 10^3 M^{-1} cm^{-1}. A 0.65 mg portion of deglycosylated ricin A chain (RAC, Sigma) in 40% (v/v) glycerol, 10 mM galactose, 10 mM sodium phosphate, pH 6.0, was then reduced with 100 mM DTT at room temperature for 1 h and desalted into 10 mM sodium acetate, 0.14 M NaCl, pH 4.5 over a NAP-10 column before being mixed with the SPDP-modified TR–SH in an approximate molar ratio of 1:1, and the pH was adjusted to neutrality by addition of 10 × PBS. The solution was then flushed with nitrogen gas, kept at room temperature for 6 h, stored at 4 °C for 30 h. The conjugate appeared to be stable for up to 1 month.

There are a number of possible cross-linking pathways for the covalent attachment of SPDP-modified TR–SH to reduced RAC (see Scheme 2 of Carlsson *et al.*, 1978). However, they should all result in species containing a reversible disulfide linkage, which would be reduced inside target cells thus freeing the RAC from TR. To confirm this, the appropriate samples were analyzed by SDS–PAGE, stained with ethidium bromide. The extent of cross-linking was estimated either by densitometry of a photographic negative of the SDS–PAGE gel or by running analytical aliquots (≈24 μg) SPDP-modified TR–SH, RAC, or the conjugation mixture ± 100 mM DTT over a reverse-phase HPLC column. Chromatography was over a Dionex IonPac NS1-5 μm column at 55 °C at a flow rate of 1 mL/min. A linear gradient of acetonitrile in ammonium acetate was applied. Buffer A was 50 mM ammonium acetate, pH 6.5; buffer B was 50% (v/v) acetonitrile, 25 mM ammonium acetate, pH 6.5. Gradient was 0–100% B over 65 min. Profiles were recorded at 280 nm and the various species quantitated by tracing the profile, cutting out the peaks, and weighing the appropriate sections of the chromatogram.

Assembly of MS2–TR–RAC Particles. MS2 empty capsids were concentrated up to 10 mg/mL by centrifugation at 13000g for 4 h at 4 °C. A 1.4 mL portion of glacial acetic acid (17 M) was slowly added to 0.7 mL of the MS2 CP (10 mg/mL) and the solution kept on ice for 30 min before centrifugation at 6600g at 4 °C for 20 min. The supernatant was then desalted into 1 mM acetic acid by passage over a NAP-25 column, and the disassembled MS2 coat protein dimer fractions were pooled. Then 1/10th volume of 10 × TMK buffer (TMK, 100 mM Tris, 80 mM KCl, and 10 mM MgCl$_2$) was added to both the MS2 and TR–RAC and the solutions kept on ice for 5 min before being mixed to give a molar ratio for MS2 coat protein: TR–RAC of 10:1. The mixture was incubated at room temperature for 3 h and then stored at 4 °C for 33 h. The assembled MS2–TR–RAC particles were purified by size exclusion chromatography over a Sephadex G-150 column equilibrated and eluted with 10 mM sodium phosphate, 0.1 M NaCl, pH 7.5.

Covalent Modification of MS2–TR–RAC Particles. A 2 mg aliquot of *N*-Succinimidyl *S*-acetylthioacetate (SATA) was completely dissolved in 0.5 mL of dimethylformamide (DMF) by stirring, and 20 μL aliquots were stored at −20 °C. A 1 mL portion of MS2–TR–RAC (≈1 mg/mL) was modified by addition of a 70–fold molar excess relative to intact capsids (mol wt ≈ 2.5 MDa) of SATA solution in DMF (30 μL) at room temperature with gentle stirring for 30 min. The SATA-modified molecules were deacetylated by addition of 0.1 mL of freshly prepared hydroxylamine–HCl (Sigma) (25 mg in 0.5 mL water) and the reaction allowed to proceed at room temperature for 2 h. The modified MS2–TR–RAC particles containing free thiol groups were separated from the SATA reagent and its byproducts by desalting over a NAP-25 column equilibrated in 0.1 M sodium phosphate, 1 mM EDTA, pH 7.5, freshly prepared and filtered through a 0.22 μm disposable filter. At the same time, 1 mg of human apo-transferrin (Tfn, iron-free) dissolved in 1 mL of 0.1 M sodium phosphate, pH 7.5, freshly prepared and filtered, was reacted with 0.5 mg

of sulfosuccinimidyl 4-(N-maleimidomethyl)cyclohexane-1-carboxylate (Sulfo-SMCC, dissolved in 50 μL of the same buffer) at room temperature with constant stirring for 1 h to introduce maleimide groups. The solution was then centrifuged at 5600g at 4 °C for 15 min and the supernatant passed down a NAP-25 column equilibrated with 0.1 M sodium phosphate, pH 7.5 to remove the free reagent. Finally, the maleimide-activated Tfn was mixed with SATA-modified MS2−TR−RAC in a disposable 15 mL centrifuge tube, the solution immediately flushed with nitrogen gas, and the tube sealed with parafilm, kept at room temperature for 6 h, and then stored at 4 °C for at least 30 h.

The transferrin in the conjugated MS2−TR−RAC−Tfn particles was then converted to the ferric form by addition of iron citrate buffer (1 μL of 10 mM iron(III) citrate buffer, containing 200 mM citric acid with the pH adjusted to 7.8 by addition of sodium bicarbonate, per 0.2 mg of MS2−TR−RAC−Tfn) (Wagner *et al.*, 1991), and the particles were purified through a size exclusion Sephadex G-150 column equilibrated and eluted with PBS. The eluted fractions were analyzed spectrophotometrically and by EM and Western blotting to determine their protein content and state of aggregation.

Quantitation of Thiol Groups. The quantitation of free thiol groups on capsids or TR was carried out using Ellman's reagent, 5, 5′-dithiobis(2-nitrobenzoic acid) (DTNB) (Ellman, 1959). Briefly, 1 mL of the diluted sample (0.05 mg/mL) was mixed vigorously with 20 μL of Ellman's reagent solution (4 mg of DTNB in 1 mL of 0.1 M of Na$_2$ HPO$_4$, pH 8.0) and the absorbance at 412 nm recorded after standing for 15 min at room temperature. L-Cysteine was used as a standard.

Alternatively, thiols were also detected by radioactive assay using tritiated iodoacetic acid (^{3}H IAA). Samples in 0.1 M sodium phosphate, pH 8.0, were flushed with nitrogen gas for 2 h at room temperature. One μL of ^{3}H IAA (1 mCi/mL, NEN) was then added, and the samples were kept in the dark for 90 min at room temperature before being blotted onto Whatman paper (0.45 mm). The papers were washed with 10% (w/v) trichloroacetic acid (TCA) three times, dried, and counted in a liquid scintillation counter. The free thiol concentrations in the samples were determined by reference to a standard curve produced with L-cysteine.

Electron Microscopy. Transmission electron microscopy (TEM) was carried out using the negative staining procedure of Sugiyama *et al.* (1967). Briefly, the samples in PBS were fixed on colloidion carbon grids for 5 min and washed by soaking in deionized water for 10 s. The grids were then stained in 4% (w/v) uranyl acetate for 5 min and washed again in water (all the procedures at room temperature). Micrographs were produced on a JEOL Model JEM-100 at an accelerating voltage of 100 kV.

Western Blotting. Western botting was performed according to the protocol of Towbin *et al.* (1979) with the transfer buffer made according to Gershoni *et al.* (1982). Briefly, three Schägger SDS−PAGE minigels loaded with the same samples were run simultaneously and blotted onto 0.2 μm nitrocellulose sheets. After blocking of nonspecific sites with 1% (w/v) bovine serum albumin (BSA) 0.2% (v/v) Tween 20 in PBS at 4 °C overnight the sheets were reacted with three primary antibodies, rabbit anti-MS2 CP (Mastico *et al.*, 1993), anti-ricin, and anti-Tfn serum, respectively, at a titer of 1:1000 in the presence of 0.1% (v/v) Triton X 100. Visualization of the bands followed binding of HRP-linked secondary IgGs (1:1000) and development of the peroxidase activity using the Amersham ECL Western blotting detection system.

Protein Concentrations. For measurement of MS2 capsids, the absorbancies at 260 and 280 nm were determined and the content of the protein derived from the formula

protein concentration =
$$A_{280}\ 1.55 - A_{260}\ 0.76\ \text{(mg/mL) (Layne, 1957)}$$

The concentrations of Tfn or the derivatized particles were measured using the BCA assay kit from Pierce. The RAC concentrations were determined as follows. Derivatized particles or TR−RAC conjugates were loaded on an SDS−PAGE gel with a standard RAC parallel control. The gel was stained with Coomassie Blue R250, destained, and dried on a Model 583 Gel Dryer (Bio-Rad). The concentration was determined by densitometry on a Scanmaster densitometer using Sun Quantity 1 software. The RAC content was calculated by reference to a standard curve.

ELISA Assays. ELISA assays were carried out according to the procedure of Engvall and Perlmann, 1971 with some modification. The sandwich assay was used to measure the accessibility of the RAC associated with the MS2−TR−RAC particles. Anti-MS2 CP antibodies (50 μL of 100 μg/mL of stock solution in PBS) were dispensed into every well of a flat-bottomed 96-well polyvinyl chloride microtiter plate (Falcon) using a multichannel pipetter and the plate incubated overnight at 4 °C. Each well was then washed with PBS containing 0.1% (v/v) Tween-20 and aspirated using a multichannel washer/aspirator (Labsystems Autowash II). The wells were then treated with 3% (w/v) BSA for 1 h at 37 °C to block nonspecific binding. MS2−TR−RAC particles or control RAC were applied to wells in 50 μL aliquots in PBS containing successive 1:10 dilutions, the plate was incubated at 37 °C for 1 h and washed/aspirated as above, and then 50 μL of 1:1000 diluted goat anti-ricin antibody was added to each well and incubated at 37 °C for 1 h. The plate was washed/aspirated as above, and the secondary antibody, i.e., rabbit anti-goat Ig conjugated to HRP, loaded into each well (50 μL of 1:1000 dilution), and the plate incubated at 37 °C for 30 min. After aspiration as above, a 50 μL aliquot of developer solution (100 mM sodium citrate, 100 mM sodium acetate, pH 5.0, containing 0.04% (w/v) 3,3′-diaminobenzidine, and 0.003% (v/v) hydrogen peroxide) was added to each well and the plate incubated for 10 min at room temperature. The enzyme reaction was quenched by the addition of 25 μL of 2 M of sulfuric acid. The OD$_{495nm}$ values were measured using a Labsystems Multiscan Plus plate reader.

Cell Culture. The human leukemic cell line HL-60 has been described previously (Collins *et al.*, 1977). The cells were cultured in RPMI 1640 medium with 10% (v/v) fetal bovine serum (FBS) supplemented with 100 μg/mL of streptomycin and 100 IU/mL of penicillin. The transferrin receptor was expressing well on the proliferating HL-60 cells as judged by indirect immunofluorescence (Miyazama *et al.*, 1992). Anti-human transferrin receptor monoclonal antibody was reacted with the exponential HL-60 cells ($\approx$10[5] cells) and then washed out with PBS containing 2% (v/v) FBS followed by centrifugation at 65g for 5 min. The cells were then reacted with anti-mouse FITC-labeled Ig, washed out, and then mounted onto a glass slide after they were resuspended in 90% (v/v) glycerol in PBS. Expression of the Tfn receptor could be detected in HeLa cells cultured in DMEM medium with 10% (v/v) FBS and antibiotics. The Pu518 cells expressing Ig Fc receptor were cultured in RPMI 1640 medium.

The adherent cells (HeLa, Pu518) were soaked in 0.25% (w/v) trypsin (Gibco) for 10 min before passaging.

Cytotoxicity Assay of the MS2–TR–RAC Particle. A 90 µL aliquot of Pu518 cells ($\approx 4 \times 10^4$ cells in 90 µL medium) was added to each well of a flat-bottomed 96-well plate (Corning). Then 11 µL of rabbit anti-MS2 CP serum (1:100 dilution) was added to each well, and the plate cultured at 37 °C in a 5% (v/v) CO_2 incubator for 30 min. The reagents in PBS (e.g., MS2–TR–RAC, RAC, MS2, and TR-RAC at 1:10 or 1:2 successive dilutions) were added to each well. After 2 days culture, the percentage cell survival was determined using the crystal violet assay (Itoh et al., 1991; Kueng et al., 1989). Briefly, the cells were fixed with 6.5% (v/v) glutaraldehyde at room temperature for 20 min with shaking at 100 rpm on an orbital shaker (Griffin) and washed with PBS containing 0.1% (v/v) of Tween 20, and then the plate was air dried. A 70 µL aliquot of the crystal violet solution (Itoh et al., 1991) (0.75% (w/v) crystal violet, 0.25% (w/v) sodium chloride, 1.75% (w/v) formaldehyde in 50% (v/v) ethanol) was added to each well and the plate shaken at room temperature for 20 min. The plate was washed with deionized water containing 0.1% (v/v) of Tween 20 and air dried. Then 75 µL of 10% (v/v) acetic acid was added and shaken as above for 1 h. The plate was scanned for OD_{595nm} in a Labsystems Multiscan Plus reader. The percentage of cell survivals was calculated by comparing the reagent groups with their negative controls.

Cytotoxicity Assay of MS2–TR–RAC–Tfn. Ninety µL of HL-60 ($\approx 4 \times 10^4$ cells) was added to each well of a flat-bottomed 96-well plate, and the reagents (MS2–TR–RAC–Tfn, MS2, RAC, and TR-RAC at 1:10 or 1:2 successive dilutions) were applied to each well. Then the plate was cultured at 37 °C in a 5% (v/v) CO_2 incubator for 2 days. The surviving cells were counted using the Trypan Blue exclusion assay (Trypan Blue Solution, Sigma). The same procedures were used with HeLa cells as the target, but 50 µM desferrioxamine (Sigma) was added 18 h before the reagents and the numbers of surviving cells determined by the crystal violet assay.

Assay of Ricin A Chain Activity. *28S rRNA Depurination.* 28S rRNA depurination was performed as described by Wales et al (1993). HeLa cells were plated out at a density of 1×10^6 cells/well in 1 mL of Dulbecco's modified eagle medium (DMEM) containing 10% FBS, 4 mM glutamine, and 50 µM desferrioxamine and were incubated in 5% (v/v) CO_2 at 37 °C. After 24 h the medium was replaced by dilutions of the toxin in fresh medium, and the cells were incubated for a further 17 h. Then the medium was removed and retained on ice, and the cells were washed twice with ice-cold PBS, which was added to the retained medium. The cells were released from the wells by trypsin treatment and also added to the retained medium. The cells were pelleted by centrifugation at 180g for 5 min, and the supernatant was discarded. The cells were lysed by the addition of 150 µL of 0.15 M sodium acetate, 0.5% (w/v) SDS, pH 6.0. Three hundred µL of buffered phenol/chloroform was added to the lysate which was then transferred to 1.5 mL Eppendorff tubes, vortexed and centrifuged to separate the phases and the nucleic acids precipitated from the aqueous phase with ethanol. The pellet was resuspended in 100 µL of 50 mM MES–NaOH pH 7.0, 2 mM magnesium acetate and incubated with 15 units of RNase-free DNase (Boehringer Mannheim) at room temperature for 30 min. The mixture was then extracted with phenol/chloroform, and the RNA was precipitated with ethanol.

Primer Extension. Primer extension reactions were performed as described by Moazed et al (1985). Two µg of RNA was mixed in a final volume of 7.5 µL with 3 pmol of oligodeoxynucleotide primer (5'-CATAATCCCACA-GATGGTAGCTTCGCCCCATTGG-3' complimentary to bases 4369–4405 of 28S rRNA) in 50 mM K-Hepes pH 7.0, 5 mM potassium borate, 0.1 M potassium chloride. This hybridization mixture was heated to 90 °C for 1 min and then slowly cooled to 45 °C. One µL of the hybridization mixture was incubated in a final volume of 6 µL with 50 mM Tris·HCl (pH 8.5), 50 mM potassium chloride, 10 mM dithiothreitol, 10 mM magnesium chloride, 0.1 mM each dATP, dGTP, dTTP, 5 µCi of [α-^{32}P]-dCTP (Amersham), and 1 unit of M-MuLV reverse transcriptase (Boehringer Mannheim) at 37 °C for 30 min. The reaction was chased with 1 µL of a nucleotide mix containing 1 mM each dATP, dCTP, dGTP, and dTTP. After 15 min the reaction was halted and the transcripts were precipitated with 25 µL of 0.3 M sodium acetate and 75 µL of ethanol. The pellets were resuspended in 10 µL of 95% (v/v) formamide, 0.05% (w/v) bromophenol blue, 0.05% (w/v) xylene cyanol. Samples were denatured by heating to 90 °C before being loaded onto 0.5 mm $\times$ 38 cm 8% (w/v) polyacrylamide (1:20, bis: mono), 7 M urea, TBE gels and electrophoresed at approximately 1400 V for 1.5 h before being dried and autoradiographed.

RESULTS

Our goal was to encapsidate a drug molecule via covalent coupling to the MS2 assembly-initiation signal (Figure 1a,b). Deglycosylated ricin A chain was chosen as the test molecule because of the ease with which its biological action can be assayed. The loss of the B chain and its carbohydrate moieties makes the RAC much less toxic due to its limited ability to gain access to the cytoplasm of cells. These properties allow the effects of MS2-mediated delivery to be observed. Covalent coupling between the TR and RAC was achieved as follows. Solid-phase phosphoramidite chemistry (Talbot et al., 1990) was used to synthesize a 28nt fragment encompassing the TR sequence, having a 5' extension of nine uridines and a thiol modifier 5' residue. The uridines were added to ensure that covalent attachment of RAC would be unlikely to interfere with recognition of the TR by the coat protein. After synthesis, deprotection and purification the amount of free thiol groups on the reduced TR-SH available for coupling was determined by reaction with Ellman's reagent, DTNB, which suggested that $\approx 98\%$ of the RNA molecules contained reactive thiols.

TR–SH was then modified by reaction with the heterobifunctional cross-linking reagent SPDP, the extent of the reaction being monitored with DTNB. When the reaction was complete, SPDP-modified TR–SH was mixed with an approximately equimolar amount of reduced RAC. The nature of covalent cross-links between TR–SH and RAC was determined by electrophoresis of appropriate aliquots in a denaturing polyacrylamide gel stained with ethidium bromide. From Figure 2 (top) it can be seen that a species which migrates more slowly than RAC, but is inconsistent with RAC dimers, is produced by the cross-linking procedure, and this is lost upon reduction with DTT as expected for products containing a disulfide linkage. SPDP-modified TR–SH contains two species, the slowest of which may well represent the dimeric product TR–S–S–TR (Carlsson et al., 1978).

In order to quantitate the extent of cross-linking, aliquots of the various samples were analyzed by reverse-
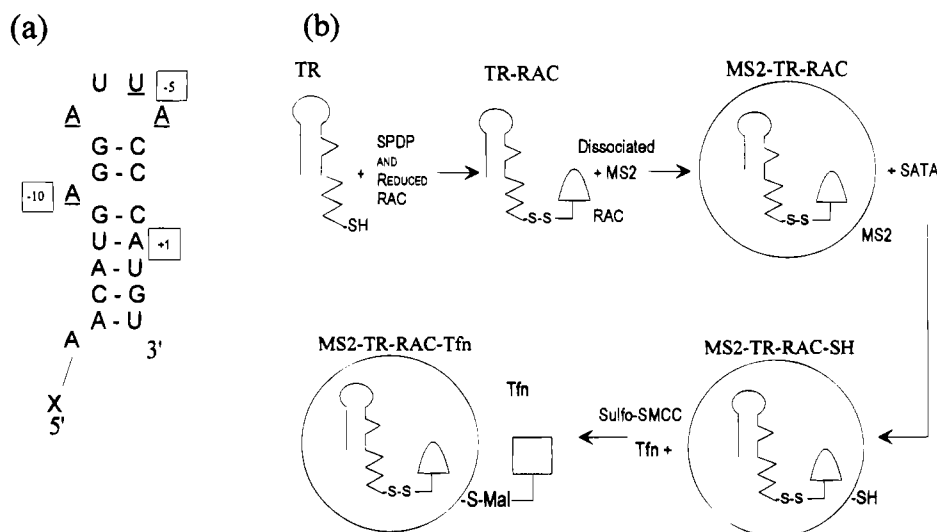
Figure 1. (a) Sequence and potential secondary structure of TR oligonucleotides used. Essential residues for recognition by the coat protein are underlined. X = 5′-fluorescein or 5′-HS-U$_9$. (b) Schematic showing the protocol for production of encapsidated ricin A chain and covalently modified capsids. Symbols are as follows: SATA, Sulfo-SMCC, and SPDP; cross-linking reagents (see Experimental Procedures); TR; MS2 assembly-initiation sequence with 5′-HS-U$_9$ extension; Tfn, human transferrin; S-Mal, thiomaleimide cross-link.

phase HPLC (Figure 2 (bottom)). Analysis of these chromatograms suggested that up to 27.6% of the original TR−SH molecules had become covalently attached to RAC. This figure agrees very well with the estimate of 31.6% based on densitometry of the SDS−PAGE (Figure 2 (top)). For the purpose of establishing MS2-mediated RAC delivery we chose not to purify the TR−RAC conjugate at this point using the mixture for the subsequent encapsidation steps. This makes determination of TR-RAC:capsid stoichiometry difficult since capsids could be produced containing no TR, TR-alone, TR−RAC, alone or mixtures thereof. We have therefore assumed for the subsequent experiments that TR molecules were modified to roughly 30% and were then evenly distributed in capsids formed.

We then determined whether TR−RAC conjugates would still trigger self-assembly of MS2 capsids. Wild-type coat protein subunits were disassembled from recombinant empty capsids (Mastico *et al.*, 1993) by treatment with glacial acetic acid and then mixed with the TR−RAC conjugation mixture at varying molar ratios in the standard TR−coat protein binding buffer, TMK. After equilibration, the mixture was passed through a gel filtration column and the material eluting in the excluded peak pooled and analyzed (Figure 3). TEM confirmed the presence of $T = 3$ capsids of the expected size. The particles had an A_{260}/A_{280} ratio of 1.17, consistent with the presence of an RNA−protein complex (A_{260}/A_{280} ratio for the empty capsids ≈ 0.63). Western blots of aliquots of these particles confirmed the presence of both MS2 coat protein and RAC.

It was then necessary to prove that the RAC was actually encapsidated rather than merely attached fortuitously to the outside of the particles. This was tested using anti-ricin antibodies in an ELISA sandwich assay (Figure 3 (bottom)). Anti-MS2 coat protein antibodies were used to coat a standard microtiter plate. Aliquots of the MS2−TR−RAC particles or control RAC were then added and any complexes formed probed with anti-ricin antibody. As Figure 3 (bottom) shows there was some slight retention of the control RAC at the higher concentrations. This could have been due to slight cross-reactivity of the anti-MS2 (see Figure 3 (second from bottom), lane 2) or anti-ricin antibodies or to non-specific retention in the wells. By contrast, there was hardly any

reactivity against the MS2−TR−RAC particles, which would have been expected to be tightly bound to the initial antibodies. Certainly, anti-ricin reactivity could only be detected at much higher concentrations than those required to observe RAC-mediated cell killing (see below). Although not necessarily definitive, these data are consistent with an internal location for the MS2-associated RAC. This result also suggested that there was relatively little cross-reactivity between the anti-MS2 and anti-ricin antibodies.

The differential recognition of MS2−TR−RAC particles by anti-MS2 CP and anti-ricin antibodies was then used to determine whether it was possible to direct cellular uptake of the particles via receptor-mediated endocytosis (RME) of the appropriate immune complex. The test cell line for these studies was Pu518, which expresses the immunoglobulin Fc receptor (Ralph and Nakoinz, 1977). The cytotoxicity results are shown in Figure 4 (left). Complexes of MS2−TR−RAC with anti-MS2 CP antibodies were considerably more toxic to the cells than MS2−TR−RAC complexed with anti-ricin antibodies (not shown), MS2−TR−RAC, TR−RAC, RAC alone (not shown), or MS2 empty capsids, although these other reagents did show some nonspecific toxicity. All of the reagents were nontoxic at similar concentrations when assayed against HeLa cells which do not carry the Fc receptor (data not shown). Control experiments using RAC and anti-ricin antibodies suggested that there was some protective effect of the antibodies (data not shown). It should be noted that the concentrations of RAC quoted for each of the reagents in Figure 4 (left) is necessarily less accurate than that for the TR−RAC conjugates (see earlier discussion of encapsidation stoichiometries). However, the use of immune complexes allows an exact comparison at identical concentrations of toxin. Subsequent larger scale experiments confirmed that cell death was due to RAC action by identifying the depurination of position 4324 in 28S rRNA (Figure 4 (right)).

In order to confirm that the MS2−TR−RAC particles could be targetted at a wide range of different cell types we then assessed the results of covalent addition to the outside of the particles of a ligand for RME. Human apo-transferrin (Tfn) was the ligand of choice since it has been used extensively in targetting studies of DNA−polylysine conjugates (Cotten *et al.*, 1990). Once again, thiol
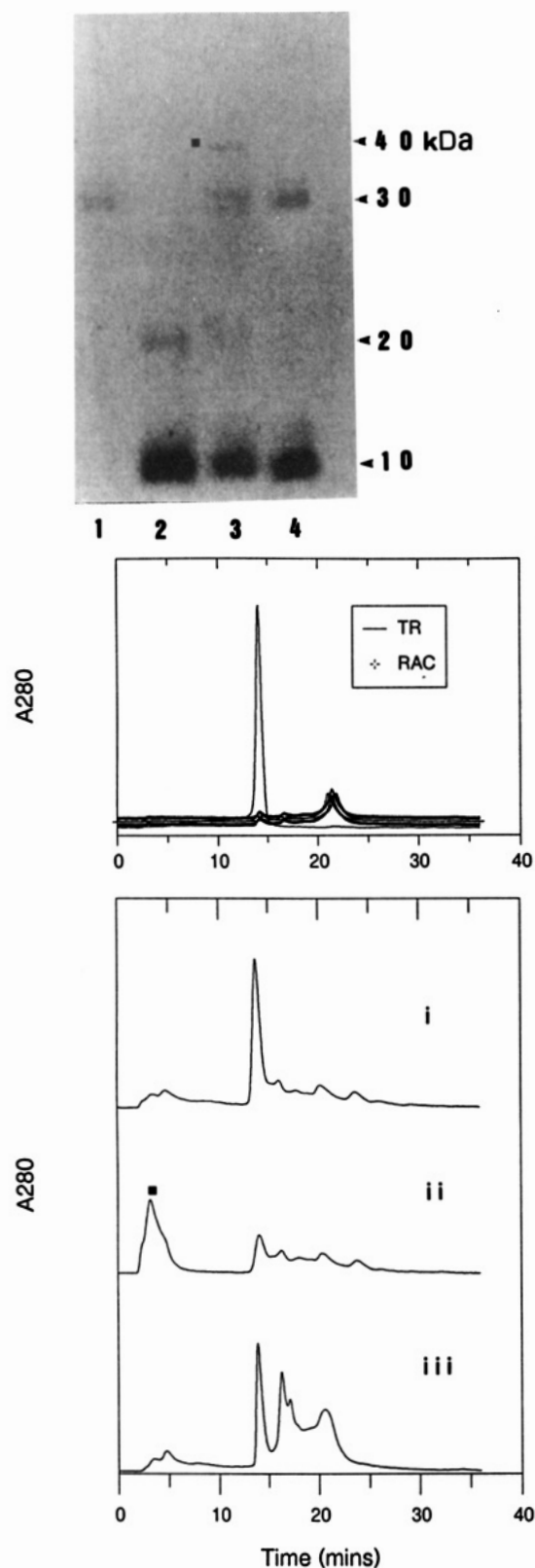
Figure 2. Covalent cross-linking of TR—SH to RAC. (Top) photograph of ethidium bromide stained 10% Schägger SDS—PAGE. Relative molecular masses were estimated from pre-stained markers (GibcoBRL): lane 1, RAC only; lane 2, SPDP-modified TR—SH, lane 3, TR—RAC conjugation mixture; lane 4, as in lane 3 but reduced by addition of 100 mM DTT. (Bottom) reverse-phase HPLC profiles of the TR—RAC conjugates. Top panel shows superimposed traces of unmodified TR (−) and RAC (+). Bottom panel shows (i) SPDP-modified TR—SH, (ii) TR—RAC conjugation mixture, and (iii) ii reduced by addition of 100 mM DTT. The position of the TR—RAC conjugate in both parts of the figure is highlighted with a ■.
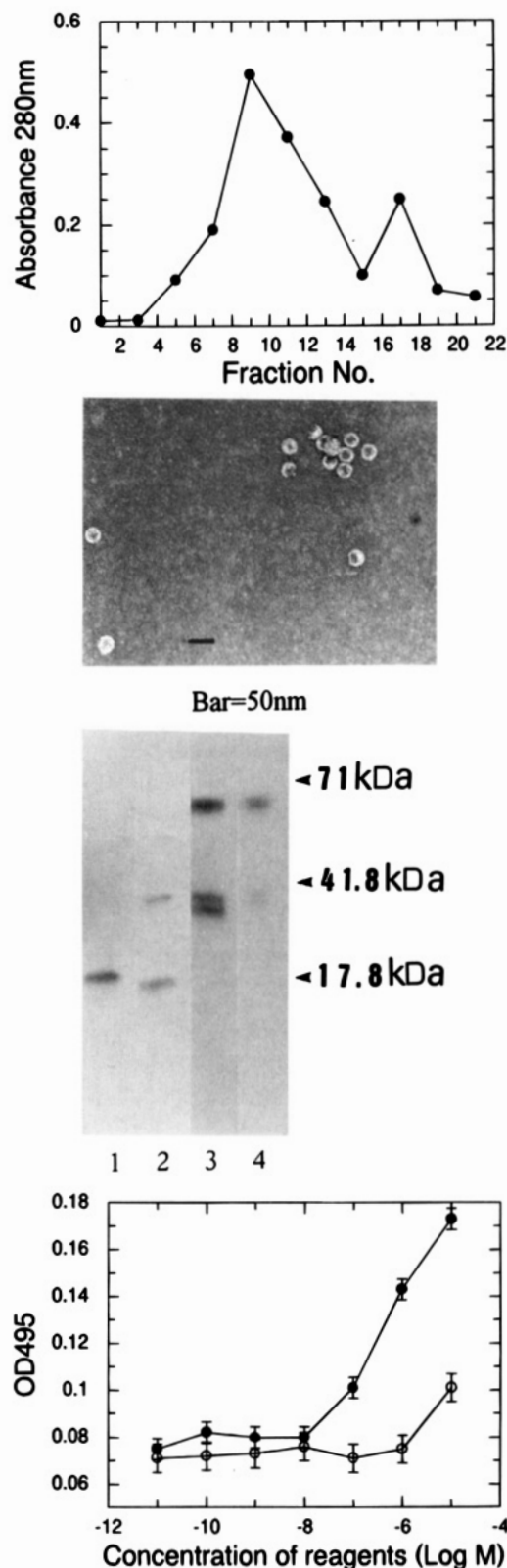
Figure 3. Analysis of MS2—TR—RAC particles. (Top) Absorbance elution profile of MS2—TR—RAC particles from the Sephadex G150 column; fractions were 1 mL. (Second from top) TEM of fraction 9 from the top panel. Bar = 50 nm. (Second from bottom) protein content of peak 9 (= MS2—TR—RAC) from the top panel determined by Western blotting. Lanes are as follows: 1, MS2 control; 2, MS2—TR—RAC; 3, RAC control; and 4, MS2—TR—RAC. Lanes 1, 2 and 3, 4 were probed with anti-MS2 coat protein antibodies and anti-ricin sera, respectively. Solid arrowheads indicate the approximate positions of molecular weight standards. (Bottom) results of ELISA titration with MS2—TR—RAC sandwich assay: ○, MS2—TR—RAC particles; or ●, RAC loaded, respectively.
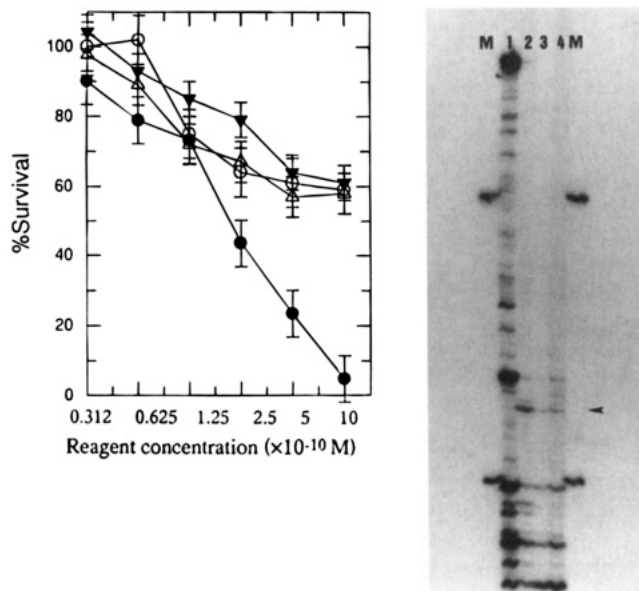
Figure 4. Cytotoxicity of MS2−TR−RAC particles in Pu518 cells in culture. (Left) graph of cell survival *vs* reagent concentration. Concentrations starting at 10^{-9} M and then with 2-fold dilution: ●, MS2−TR−RAC + anti-MS2 CP antibodies; ○, MS2−TR−RAC alone; △, TR−RAC; ▼, empty MS2 capsids. Data points represent averages of triplicate determinations. Reagent concentrations were determined as described in the Materials and Methods. (Right) primer extension analysis of RAC-treated HeLa cell 28S rRNA: Lane 1, untreated cells; lane 2, cells treated with 10^{-8}M RAC; lane 3, cells treated with 100 μL of MS2−TR−RAC−Tfn particles (≈10 μg total protein); lane 4, cells treated with 10 μL of MS2−TR−RAC−Tfn particles (≈1 μg total protein); M, φX174 RF DNA/*Hae* III restriction fragments as size markers. The arrowhead indicates the position of a termination site for reverse transcription corresponding to a transcript of 81 nt in length as expected for molecules undergoing RAC-mediated depurination at A4324 (Endo *et al.*, 1987).

chemistry was chosen for the conjugation. MS2−TR−RAC particles were modified using the reagent SATA. Deacylation of the modified products with hydroxylamine yielded capsids having the equivalent of one free thiol per coat protein subunit as judged by DTNB or IAA assays. These particles were then conjugated with Tfn which had been modified with the heterofunctional cross-linker Sulfo-SMCC to introduce maleimide groups. The resultant MS2−TR−RAC−Tfn particles were then treated with ferric ions to convert the Tfn to the active form (Wagner *et al.*, 1991) and the particles purified over a gel filtration column and characterized as before (Figure 5). Material eluting in the excluded volume contained $T = 3$ capsids as expected, and Western blotting confirmed the presence of MS2 coat protein, RAC, and Tfn in these fractions, consistent with the formation of the expected conjugates. Cytotoxicity studies with the MS2−TR−RAC−Tfn particles were then carried out using both HL-60 human leukemia cells and HeLa cells in culture. HL-60 cells express the transferrin receptor constitutively, whereas in HeLa cells the production of the receptor can be enhanced by treatment of the cells with desferrioxamine (Wagner *et al.*, 1991). The results are shown in Figure 6 and are consistent with the transferrin-mediated delivery of MS2-encapsidated RAC. The reagents were only mildly toxic to control Pu 518 cells over the same concentration range (data not shown).

DISCUSSION

Cell-specific drug delivery is a major goal for chemotherapeutic control of diseases. A large number of
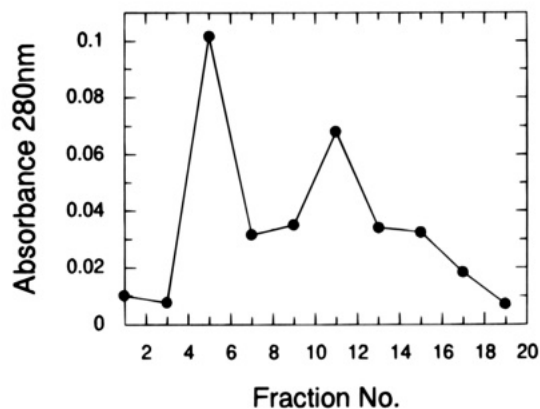
Bar=50nm

Figure 5. Analysis of MS2−TR−RAC−Tfn particles. (Top) absorbance elution profile of MS2−TR−RAC−Tfn particles from the Sephadex G150 column. Fractions were 1 mL. (Middle) TEM of fraction 5 from the top panel. Bar = 50 nm. (Right) protein content of fraction 5 from the top panel determined by Western blotting as in Figure 3c. Lanes are 1, MS2 control; 2, MS2−TR−RAC−Tfn; 3, RAC control; 4, MS2−TR−RAC−Tfn; 5, Tfn control; 6, MS2−TR−RAC−Tfn. Lanes 1 and 2, 3 and 4, and 5 and 6 were probed with anti-MS2, anti-ricin, and anti-Tfn antibodies and sera, respectively.

different approaches have been used in an attempt to achieve this goal. In general, all approaches consist of administration of a drug component coupled in some way to a targeting ligand. Such constructs can be artificial, such as a small molecular weight drug enclosed in liposomes which also contain specific antibodies to direct uptake of the construct, or based on natural vectors, such as viruses in which part of the viral genome has been replaced by a gene encoding, for example, a novel enzyme. The MS2 bacteriophage system offers a unique combination of these approaches to drug delivery which we term synthetic virion (SV) technology. Since the phage capsid assembly-initiation signal is well-characterized, easily synthesized, and coupled to potential drug molecules, it seemed an ideal way to produce encapsidated drug packages provided that modification of the TR fragment did not prevent assembly. Once encapsidated, the ligands
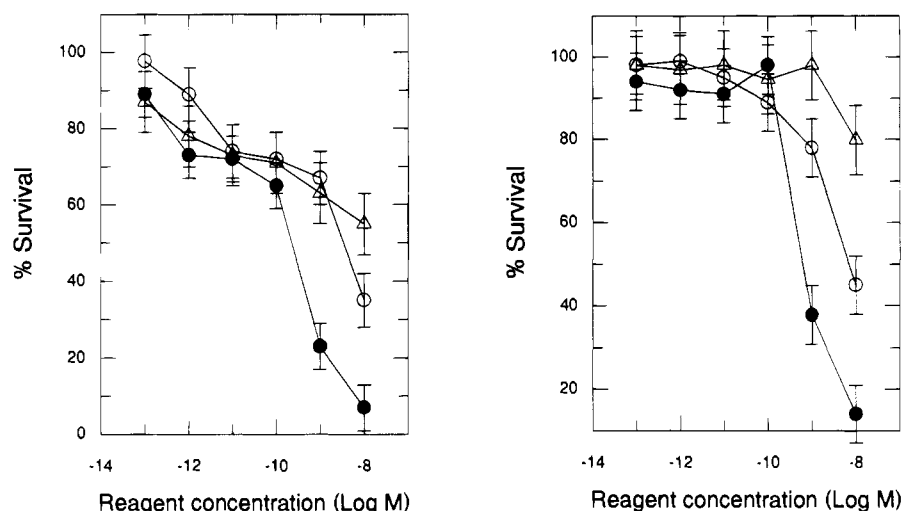
Figure 6. Cytotoxicity analysis of MS2−TR−RAC−Tfn: (left) HL60 cells and (right) HeLa cells after processing with 5 μM of desferrioxamine for 18 h; O, RAC alone; ●, MS2−TR−RAC−Tfn; △, MS2−TR−RAC plus uncrosslinked Tfn.

would be protected from degradation or recognition by the immune system. Coupling of a ligand for RME to the outside of the particle would then allow flexible targeting of the package to particular cell types, analogous to many natural viral component functions.

The data presented here demonstrate the feasibility of this approach. We have shown that the assembly-initiation signal can be covalently coupled to a large protein molecule (RAC) without significantly affecting the recognition of the TR or the self-assembly of the phage coat protein *in vitro*. Encapsidation of antisense reagents is even simpler and the extension to small molecular weight drugs straightforward (W. L. Brown, M. Wu, H. Rachael Hill, and P. G. Stockley, work in progress). Delivery of the RAC to cells in culture was then assayed using immune complexes formed with anti-MS2 coat protein antibodies. This has the advantage that it is not necessary to determine very accurate concentrations for the encapsidated ligand since the specificity is provided by the antibody used (Figure 4). The encapsidated, antibody-bound RAC is significantly more toxic than RAC alone with an LD_{50} in the nanomolar concentration range. The results suggest that once in the endosome the conjugated RAC is able to escape the capsid and penetrate to the cytoplasm. This is reasonable given the limited stability of MS2 capsids at endosomal pH and is consistent with the appearance of immuno-gold stained capsids in the endosomal compartment (J. Grimwood and P. G. Stockley, unpublished results). Cell-specific delivery was then demonstrated by covalent attachment of transferrin which has been used extensively in the past for targeted drug delivery studies (Wagner *et al.*, 1991, 1994). Once again, it appeared that the SVs containing RAC were successfully delivered to the endosomal compartment (Figure 6) and were effective in the nanomolar concentration range.

These results suggest the utility of MS2 as a drug delivery system. We have not as yet attempted to refine the system, for instance, by studying how the nature of the covalent attachments between the TR and RAC or the capsid and the transferrin affects toxicity, or the effects of altering the targetting ligand. Transferrin is unusual in that it remains bound to its receptor in the endosome and is rapidly recycled to the cell surface reducing the amount of time available for the SV to disassemble at the acidic pH. Other targeting ligands might result in accumulation of the SVs in the endosomal compartment, or it might be possible to increase cyto-

plasmic uptake by the addition of agents affecting the integrity of the lysosomal membrane (Wagner *et al.*, 1992, 1994). In the current experiments the efficiency of cross-linking between the TR and RAC was assumed to be relatively low ($\approx$30%), and particles were assembled with a mixture of derivatized and underivatized TRs. Increased toxicity might be expected if the TR−RAC conjugates were purified before encapsidation. SVs also have the advantages that they have a uniform size and defined mechanical properties, unlike liposomal systems, and the use of the TR sequence guarantees incorporation of the drug ligand of choice. Further work is in hand to compare the efficiency of ligand delivery by SVs to other more well-characterized delivery systems, such as poly-lysine conjugates, and also to examine the fate(s) of MS2 particles in mammals.

ACKNOWLEDGMENT

LITERATURE CITED

Beckett, D., and Uhlenbeck, O. C. (1988) Ribonucleo−protein complexes of R17 coat protein and a translational operator analog. *J. Mol. Biol. 204*, 927−938.

Carlsson, J., Drevin, D., and Axén, R. (1978) Protein thiolation and reversible protein-protein conjugation. N-succinimidyl 3-(2-pyridyldithio)propionate—a new heterobifunctional reagent. *Biochem. J. 173*, 727−737.

Collins, S. J., Gallo, R. C., and Gallagher, R. E. (1977) Continuous growth and differentiation of human myeloid leukemic cells in suspension culture. *Nature 270*, 347−349.

Cotten, M., Langle-Rouault, F., Kirlappos, H., Wagner, E., Mechtler, K., Zenke, M., Beug, H., and Birnstiel, M. L. (1990) Transferrin-polycation-mediated introduction of DNA into human leukemic cells: stimulation by agents that affect the survival of transfected DNA or modulate transferrin receptor levels. *Proc. Natl. Acad. Sci. U.S.A. 87*, 4033−4037.

Ellman, G. L. (1959) Tissue sulfhydryl groups. *Arch. Biochem. Biophys. 82*, 70−77.

Endo, Y., and Tsurugi, K. (1987) RNA N-glycosidase activity of ricin A chain. Mechanism of action of the toxic lectin ricin on eukaryotic ribosomes. *J. Biol. Chem. 262*, 8128–8130.

Engvall, E., and Perlmann, P. (1971) Enzyme-linked immunosorbant assay (ELISA) quantitative assay of immunoglobulin G. *Immunochemistry 8*, 871–879.

Furuse, K. (1987) Distribution of coliphages in the enviroment: general considerations. In *Phage Ecology* (S. M. Goyal, Ed.) pp 87–124, John Wiley and Sons, New York.

Gershoni, J. M., and Palade, G. E. (1982) Electrophoretic transfer of proteins from sodium dodecyl–polyacrylamide gels to a positively charged membrane filter. *Anal. Biochem. 124*, 396–405.

Itoh, N., Yonehara, S., Ishii, A., Yonehara, M., Mizushima, M., Hase, A., Seto, Y., and Nagata, S. (1991) The polypeptide encoded by the cDNA for human cell surface antigen Fas can mediate apoptosis. *Cell 66*, 233–243.

Kueng, W., Silber, S., and Eppenberger, U. (1989) Quantitation of cells cultured on 96-well plates. *Anal. Biochem. 182*, 16–19.

Layne, E. (1957) Spectrophotometric and turbidimetric methods for measuring proteins. *Methods Enzymol. 3*, 447–454.

Mastico, R. A., Talbot, S. J., and Stockley, P. G. (1993) Multiple presentation of foreign peptides on the surface of an RNA-free spherical bacteriophage capsid. *J. Gen. Virol. 74*, 541–548.

Miyazawa, M., Nishio, J., and Chesebro, B. (1992) Protein against Friend retrovirus-induced leukemia by recombinant vaccinia viruses expressing the *gag* gene. *J. Virol. 66*, 4409–4507.

Moazed, D., Stern, S., and Noller, H. F. (1986) Rapid chemical probing of conformation in 16 S ribosomal RNA and 30 S ribosomal subunits using primer extension. *J. Mol. Biol. 187*, 399–416.

Murray, J. B., Collier, A. K., and Arnold, J. R. P. (1994) A general purification procedure for chemically synthesized oligonucleotides. *Anal. Biochem. 218*, 177–184.

Ralph, P., and Nakoinz, I. (1977) Antibody-dependent killing of erythrocyte and tumor targets by macrophage-related cell lines: enhancement by PPD and LPS. *J. Immunol. 119*, 950–954.

Schägger, H., and von Jagow, G. (1987) Tricine-sodium dodecyl sulfate-polyacrylamide gel electrophoresis for the separation of proteins in the range from 1 to 100 kDa. *Anal. Biochem. 166*, 368–379.

Stockley, P. G., Stonehouse, N. J., Walton, C., Walters, D. A., Medina, G., Macedo, J. M. B., Hill, H. R., Goodman, S. T. S., Talbot, S. J., Tewary, H. K., Golmohammadi, R., Liljas, L., and Valegård, K. (1993) Molecular mechanism of RNA-phage morphogenesis. *Biochem. Soc. Trans. 21*, 627–633.

Stockley, P. G., Stonehouse, N. J., and Valegård, K. (1994) Molecular mechanism of RNA phage morphogenesis. *Int. J. Biochem. 26*, 1249–1260.

Stockley, P. G., Stonehouse, N. J., Murray, J. B., Goodman, S. T. S., Talbot, S. J., Adams, C. J., Liljas, L., and Valegård, K. (1995) Probing sequence-specific RNA recognition by the bacteriophage MS2 coat protein. *Nucleic Acids Res. 23*, 2512–2518.

Sugiyama, T., Herbert, T., and Hartman, R. A. (1967) Ribonucleo-protein complexes formed between bacteriophage MS2 RNA and MS2 protein *in vitro. J. Mol. Biol. 166*, 368–379.

Talbot, S. J., Goodman, S., Bates, S. R. E., Fishwick, C. W. G., and Stockley, P. G. (1990) Use of synthetic oligoribonucleotides to probe RNA–protein interaction in the MS2 translational operator complex. *Nucleic Acids Res. 18*, 3521–3528.

Talbot, S. J. (1991) Structural studies of RNA–protein interactions in the bacteriophage MS2. PhD thesis. University of Leeds.

Thorpe, P. E., Wallace, P. M., Knowles, P. P., Relf, M. G., Brown, A. N. F., Watson, G. J., Blakey, D. C., and Newell, D. R. (1988) Improved anti-tumor effects of immunotoxins prepared with deglycosylated ricin A chain and hindered disulfide linkages. *Cancer Res. 48*, 6396–6403.

Towbin, H., Staehelin, T., and Gordon, J. (1979) Electrophoretic transfer of proteins from polyacrylamide gels to nitrocellulose sheets: procedure and some applications. *Proc. Natl. Acad. Sci. U.S.A. 76*, 4350–4354.

Valegård, K., Murray, J. B., Stockley, P. G., Stonehouse, N. J., and Liljas, L. (1994) Crystal structure of an RNA bacteriophage coat protein operator complex. *Nature 371*, 623–626.

Wagner, E., Cotten, M., Mechtler, K., Kirlappos, H., and Birnstiel, M. L. (1991) DNA-binding transferrin conjugates as functional gene-delivery agents: synthesis by linkage of polylysine or ethidium homodimer to transferrin carbohydrate moiety. *Bioconjugate Chem. 2*, 226–231.

Wagner, E., Zatloukal, K., Cotten, M., Kirlappos, H., Mechtler, K., Curiel, D. T., and Birnstiel, M. L. (1992) Coupling of adenovirus to transferrin-polylysine/DNA complexes greatly enhances receptor-mediated gene delivery and expression of transfected genes. *Proc. Natl. Acad. Sci. U.S.A. 89*, 6099–6103.

Wagner, E., Curiel, D., and Cotten, M. (1994) Delivery of drugs, proteins, and genes into cells using transferrin as a ligand for receptor-mediated endocytosis. *Adv. Drug Delivery Rev. 14*, 113–135.

Wales, R., Roberts, L. M., and Lord, J. M. (1993) Addition of an endoplasmic reticulum retrieval sequence to ricin A chain significantly increases its cytotoxicity to mammalian cells. *J. Biol. Chem. 268*, 23968–23990.

Walton, C. (1993) Functional analysis of coat protein mutants in the RNA bacteriophage, MS2. PhD thesis, University of Leeds.

Witherell, G., Gott, J. M., and Uhlenbeck, O. C. (1991) Specific interaction between RNA phage coat proteins and RNA. *Proc. Nuc. Acid Res. Molec. Biol. 40*, 185–220.

BC950052R

Poly(ethylene glycol) Fluorescent Linkers

Annapurna Pendri, Anthony Martinez, Jing Xia, Robert G. L. Shorr, and Richard B. Greenwald*

Enzon, Inc., Piscataway, New Jersey 08854. Received May 31, 1995[⊗]

The first examples of PEG linkers containing the highly fluorescent dansyl group have been synthesized. Quantum yields of these PEG fluorescent linkers (PFL) were determined and utilized in calculating the PEG number of various protein conjugates. The method was also shown to be applicable to lower molecular weight drugs as exemplified by taxol.

A great number of polymeric substances have been used for chemical modification of proteins of therapeutic usefulness. Poly(ethylene glycol) (PEG) (*1*), a water soluble, nontoxic, and nonimmunogenic polymer, has been successfully used for this purpose. The functionalization of PEG and conditions for bioconjugation of its derivatives has been extensively reviewed (*2*). In the course of our work on PEG taxol (*3*) we had the need to prepare a fluorescent PEG linker. Although fluorescent derivatives of bioactive molecules are important tools for the quantitation and detection of cellular components, we were surprised to find no mention of these types of PEG compounds in the literature. A PEG chromophoric (UV) linker was recently used by Ladd (*4*) in order to quantitate the average number of PEG groups bound per mole of conjugated protein. Aromatic nucleophilic substitution of an *o*-nitro-substituted aryl fluoride by protein amino groups was utilized in the conjugation step of this approach.

We wish to report the facile synthesis of novel PEG linkers wherein the fluorescent probe is attached to the polymer via the aminoethanol intermediate 1. In the present study the dansyl group was chosen as the fluorescent probe and pendantly incorporated as a dansylsulfonamide into the PEG chain. The resulting derivatives are highly fluorescent, having large Stokes shifts, along with environmentally sensitive fluorescence quantum yields and emission maxima. The design of the key intermediate 2 provides a terminal hydroxy group that is utilized for further conversion to activated species. Illustratively, we have prepared succinimidyl carbonates and carboxylic acids, as well as carbazates, and conjugated these PEG fluorescent linkers (PFL) to the protein, bovine serum albumin (BSA), and lower molecular weight drugs exemplified by the anticancer agent taxol.

RESULTS

The synthetic approach taken is outlined in Scheme 1. Reaction of PEG chloride (*5*) with ethanolamine gave in high yield the PEG–ethanolamine derivative 1. Sulfonylation with dansyl chloride provided the key PEG intermediate 2, which was then converted to the desired succinimidyl carbonate linker 3. This was accomplished via the reactive chloroformate derivative which was generated in situ using triphosgene. Additional use was made of intermediate 2 by condensation with ethyl 3-isocyanatopropionate in the presence of tin catalyst. The resulting ester–carbamate 5a was hydrolyzed to the

Scheme 1[a]
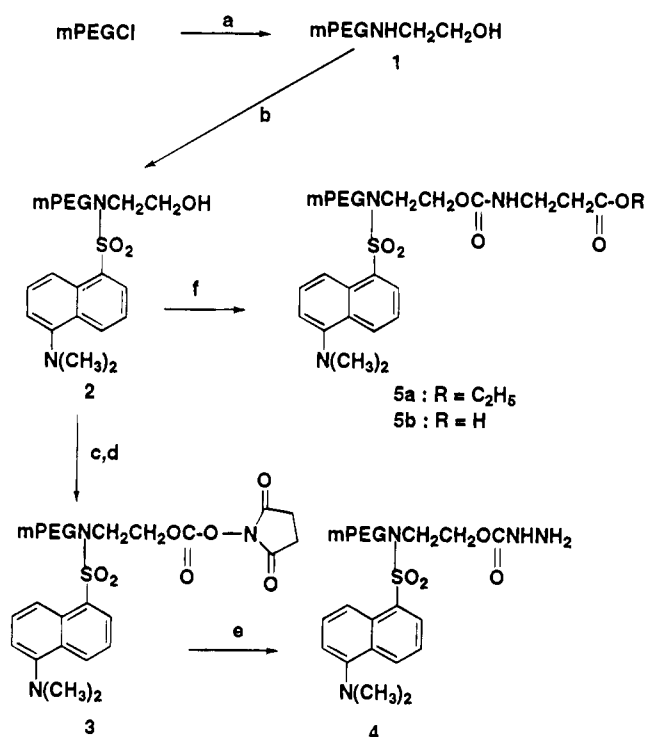
[a] Key: (a) $NH_2CH_2CH_2OH$, H_2O, 70 °C, 48 h; (b) dansyl chloride, diisopropylethylamine, toluene, 100 °C, 18 h; (c) triphosgene, toluene, diisopropylethylamine; (d) *N*-hydroxysuccinimide, 60 °C, 2 h; (e) NH_2NH_2, CH_2Cl_2; (f) $NCOCH_2CH_2CO_2Et$, dibutyltin dilaurate, toluene 50 °C.

acid **5b**. Linker **3** was also allowed to react with hydrazine to yield the carbazate **4**. Obviously, **5** can also be converted to active esters if so desired.

Conjugation of the two new PFL linkers **3** and **4** with BSA yielded PEG–protein conjugates **6** and **7** (Scheme 2) labeled at each site of the PEG attachment with the highly fluorophoric dansyl moiety. Quantitation of the dansylsulfonamide fluorescent intensities of **6** and **7**, at $\lambda_{em}536$ nm (Figure 1b), and comparison with the appropriate standard curves (Figure 1a) determines the protein concentration. Once the protein concentration is known, the number of PEG's per protein molecule can be calculated since the number of PEG groups is equivalent to the number of dansyl fluorophores in conjugates **6** and **7**. Similarly, coupling of PFL linker **5** with taxol according to the previously published procedures (*3*) gave the labeled PEG taxol derivative **8**. Compound **8** is potentially useful for determining the distribution of drug during in vivo pharmacokinetic studies (Figure 1c).

Scheme 2

3 H$_2$N-Protein → mPEGNCH$_2$CH$_2$OC-NHProtein
                                    | ||
                                   SO$_2$ O

N(CH$_3$)$_2$

6

4 HO$_2$CProtein → mPEGNCH$_2$CH$_2$O-C-NHNH-C-Protein
                                 | || ||
                                SO$_2$ O   O

N(CH$_3$)$_2$

7

5b HO-Drug → mPEGNCH$_2$CH$_2$O-C-NHCH$_2$CH$_2$C-O-Drug
                           | || ||
                          SO$_2$ O   O

N(CH$_3$)$_2$

8
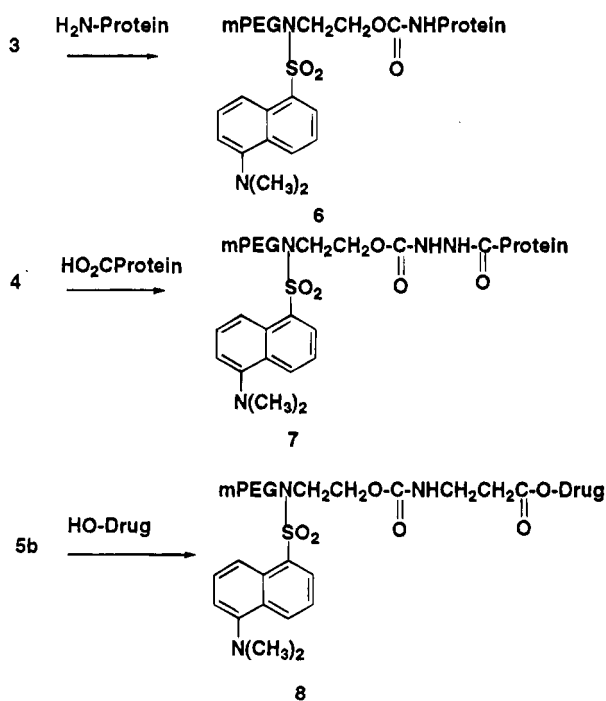
SUMMARY

We have synthesized the fluorescent dansyl containing PEG linkers **3** and **4** and demonstrated their utility by conjugating them with bioactive substances exemplified by BSA and using the fluorescent spectra to determine the PEG number of the conjugate. In addition, it can be appreciated that linker **5** can also be utilized for determining the pharmacokinetics of PEG drugs.

EXPERIMENTAL SECTION

General Methods. Unless stated otherwise, all reagents and solvents were used without further purification. NMR spectra were obtained using a 270 MHz spectrometer. Deuterated chloroform was used as the solvent unless otherwise specified. Fluorescence spectra were recorded on a Hitachi F-2000 fluorescence spectrophotometer. BSA and all buffer components were purchased from Sigma Chemical Co., and taxol was supplied by PhytoPharmaceuticals, Inc. All PEGs utilized had MW 5000 and were obtained from NOF America (New York). These polymers were dried under vacuum or by azeotropic distillation from toluene prior to use.

***N*-(2-Hydroxyethyl)PEGamine 1.** A solution of PEG chloride (*5*) (50 g, 0.01 mol) and ethanolamine (164 g, 2.7 mol) in water (100 mL) was placed in a sealed polypropylene bottle and heated at 70 °C for 48 h. Subsequent removal of the solvent from the reaction mixture followed by recrystallization of the residue from 2-propanol yielded 35.2 g (70%) of **1**. The product was characterized by ^{1}H and ^{13}C NMR.

***N*-Dansyl-*N*-(2-hydroxyethyl)PEGamine 2.** Dansyl chloride (2.4 g, 9 mmol)and diisopropylethylamine (1.6 g, 12 mmol) were added to a solution of **1** (15 g, 3 mmol) in toluene (150 mL). The reaction mixture was stirred at 100 °C for 18 h followed by removal of the solvent and recrystallization of the residue from 2-propanol to yield 13.9 g (88%) of **2** which was characterized by ^{1}H and ^{13}C NMR.

Succinimidyl Carbonate of *N*-Dansyl-*N*-(2-hydroxyethyl)PEGamine (3). Triphosgene (0.6 g, 2.0 mmol) and diisopropylethylamine (0.5 g, 4.0 mmol) were added to a solution of **2** (20.0 g, 4.0 mmol) in toluene (200 mL)

(a)

(5b) y = 0.22934 + 4.7058e-2x
      R^2 = 1.000

(4)   y = - 0.86223 + 4.5238e-2x
      R^2 = 0.999

Concentration of 4 & 5b(nM)

(b)

(6)   y = - 7.7790 + 3.3836x
      R^2 = 1.000

(7)   y = - 31.890 + 0.69317x
      R^2 = 0.998

Concentration of 6 & 7(nM)

(c)

y = - 4.4450 + 9.1800e-2x
R^2 = 0.999

Concentration of 8 (nM)
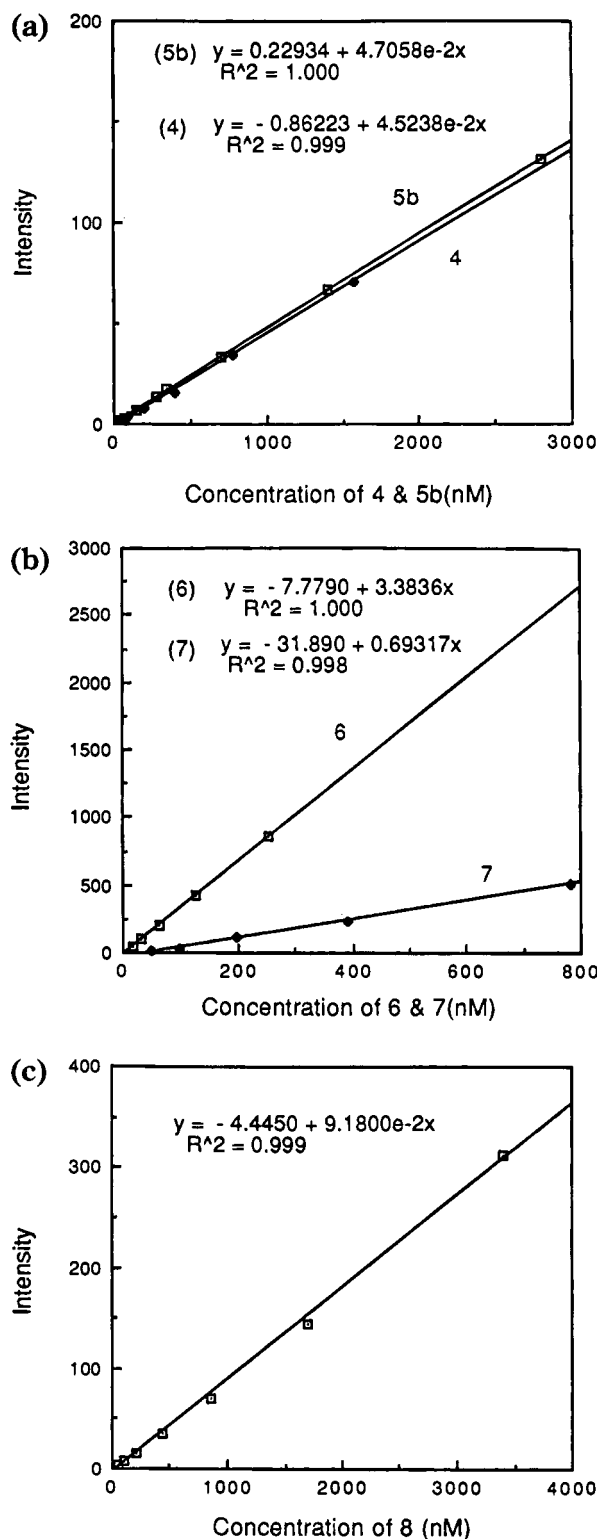
Figure 1. (a) Linear regression analysis of standard curves for PEG carbazate **4** (◆) and PEG acid **5b** (◇). Variation of fluorescence intensity with PEG linker (4 and 5b) concentration was measured. In the regression equation y = fluorescence intensity and x = PEG linker concentration (nM). (b) Linear regression analysis of PEG–BSA conjugate standard curves for compounds **6** (◇) and **7** (◆). Variation of fluorescence intensity with PEG conjugate (**6** and **7**) concentration was measured. In the regression equation *y* = fluorescence intensity and *x* = PEG conjugate concentration (nM). (c) Linear regression analysis of standard curve for PEG taxol **8**. Variation of fluorescence intensity with PEG linker **8** concentration was measured. In the regression equation *y* = fluorescence intensity and *x* = PEG taxol concentration (nM).

at 30 °C. The resulting mixture was stirred for 2 h at 50 °C, followed by the addition of *N*-hydroxysuccinimide (0.7 g, 6.0 mmol) and diisopropylethylamine (0.5 g, 4.0 mmol). The reaction mixture was stirred for 2 h at 60 °C and then overnight at room temperature, followed by removal of the solvent by distillation *in vacuo*. The residue was recrystallized from 2-propanol to yield 18.3 g of **3** (89%) which was characterized by ^{1}H and ^{13}C NMR.

PEG Carbazate 4. Anhydrous hydrazine was added to a stirred solution of **3** (1.0 g, 0.2 mmol) in dry dichloromethane (10 mL) (12 μL, 0.4 mmol). The reaction mixture was stirred overnight at room temperature followed by filtration through Celite and removal of the solvent by distillation *in vacuo*. Crystallization of the residue from 2-propanol yielded 0.7 g (75%) of **4** which was characterized by ^{1}H and ^{13}C NMR.

PEG Acid 5b. Ethyl 3-isocyanatopropionate (0.3 g, 2.3 mmol) and dibutyltin dilaurate (0.2 g, 0.4 mmol) were added to a solution of **2** (4.0 g, 0.8 mmol) in toluene (40 mL) at 40 °C. The resulting mixture was stirred overnight at 50 °C, followed by removal of the solvent *in vacuo*. Recrystallization of the residue from 2-propanol yielded 3.4 g (83%) of the ethyl ester **5a** which was characterized by ^{1}H and ^{13}C NMR.

A solution of **5a** (3.3 g, 0.6 mmol) and sodium hydroxide (0.2 g, 6.0 mmol) in water (25 mL) was stirred for 4 h at room temperature. The reaction mixture was acidified to pH 5 with 10% aqueous HCl and extracted with dichloromethane. Removal of the solvent from the dried extracts followed by recrystallization of the residue from 2-propanol yielded 2.6 g (81%) of **5b** which was characterized by ^{1}H and ^{13}C NMR.

Determination of Quantum Yield of 5b. PEG acid **5b** in water (0.76 mg/mL) was further diluted to give nine solutions with concentrations between 35 and 2.8 mmol. Fluorescence spectra of these solutions were acquired at $\lambda_{ex} = 332$ nm and $\lambda_{em} = 536$ nm. From the standard plot of fluorescence intensity vs concentration (Figure 1a), the quantum yield of **5b** was calculated to be 4.68×10^7 M^{-1} cm^{-1}.

Conjugation of PFL 3 to BSA, Compound 6. A 10 mg/mL solution of BSA protein was prepared by adding 1 mL of 0.05 M borate buffer, pH 9.0, to 10 mg of BSA. This solution was added to 20 mg (28 equiv) of **3** and heated at 30 °C for 30 min. The solution was purified by diafiltration against borate buffer and water in an Amicon Centricon-30 microconcentrator affording a yellow solution which was lyophilized to give **6** as a yellow powder.

Quantitation of PEG Number in 6. PEG conjugate **6** (4.8 mg) in 25 mL of water (0.192 mg/mL) was diluted 100-fold. Fluorescence intensity of **6** ($\lambda_{exc} = 332$ nm and $\lambda_{em} = 536$ nm) at this dilution was found to be 31.57 (Figure 1b). Using this value and employing the quantum yield 4.68×10^7 M^{-1} cm^{-1} obtained for **5b** produces the fluorophore concentration of 6.75×10^{-5}. Dividing the fluorophore concentration by the protein concentration (0.192 mg/mL = 2.82×10^{-6} M using a MW of 68 000 for BSA) gave the fluorophore to protein ratio which is equivalent to the number of fluorescent PEG's per mol of BSA. For product **6**, this number was found to be 24 PEG's per mol of BSA. (In BSA 60 lysine residues are available for conjugation.)

Determination of Quantum Yield of 4. PEG carbazate **4** in water (0.21 mg/mL) was further diluted to give six solutions with concentrations between 49 and 1.57 mmol. Fluorescence spectra of these solutions were acquired at $\lambda_{ex} = 332$ nm and $\lambda_{em} = 536$ nm. From the standard plot of fluorescence intensity vs concentration

(Figure 1a) the quantum yield of **4** was calculated to be 4.55×10^7 mol^{-1} cm^{-1}.

Conjugation of PFL 4 to BSA Compound 7. A 5 mg/mL solution of BSA protein was prepared by adding 2.5 mL of 0.1 M MES and 150 mM NaCl buffer, pH 5.0 to 13 mg of BSA. This solution was then added to **4** (28.7 mg, 28 equiv) and 1-(3-(dimethylamino)propyl)-3-ethylcarbodiimide (0.73 mg, 20 equiv). The solution was stirred at 25 °C for 17 h and purified by diafiltration against water in an Amicon Centricon-30 microconcentrator affording a yellow solution which was lyophilized to give **7** as yellow powder.

Quantitation of PEG Number in 7. PEG Conjugate **7** (6.9 mg) in 25 mL of water (0.276 mg/mL) was diluted 100-fold. The fluorescence intensity of **7** ($\lambda_{exc} = 332$ nm and $\lambda_{em} = 536$ nm) at this dilution was found to be 9.45 (Figure 1b). Using this value and employing the quantum yield of 4.55×10^7 M^{-1} cm^{-1} obtained for **4** produced a fluorophore concentration of 2.09×10^{-5}. Dividing the fluorophore concentration by the protein concentration (0.276 mg/mL = 4.10×10^{-6} M using a MW of 68 000 for BSA) gave the fluorophore to protein ratio which is equivalent to the number of fluorescent PEG's per mol of BSA. For product **7**, this number was found to be 5 PEG's per mol of BSA. (There are 59 glutamic and 40 aspartic acid residues available that can be modified with PEG).

Conjugation of PFL 5b to taxol, Compound 8. A solution of **5b** (1.0 g, 0.19 mmol), taxol (320 mg, 0.38 mmol), (dimethylamino)pyridine (46 mg, 0.38 mmol), and diisopropylcarbodiimide (59 μL, 0.38 mmol) in dry dichloromethane (5 mL) was stirred for 42 h at room temperature. Removal of the solvent *in vacuo* and recrystallization of the resultant residue from 2-propanol gave **8** (1.0 g, 83%), which was characterized by ^{1}H and ^{13}C NMR.

LITERATURE CITED

(1) All poly(ethylene glycol) derivatives discussed in this paper are terminated on one end of the polymer with a methyl group. The IUPAC nomenclature for the general polymer is α-hydroxy-ω-methylpoly(oxy-1,2-ethanediyl). We find it more convenient to refer to this material as PEG.

(2) For recent comprehensive reviews of the chemical and physical properties of poly(ethylene glycol)-modified compounds see: (a) Harris, J. M. (1992) In *Poly(Ethylene Glycol) Chemistry* (J. M. Harris, Ed.) Chapter 1, Plenum Press, New York. (b) Delgado, C., Francis, G. E., and Fisher, D. (1992) Crit. Rev. *Therap. Drug Carrier Systems* 9, 249−304. (c) Harris, J. M. (1985) *Macromol. J. Sci. Rev. Polymer Phys. Chem. C25*, 325−373. (d) Nucci, M. L., Shorr, R., and Abuchowski, A. (1991) *Adva. Drug Del. Rev. 6*, 133−151. (e) Katre, N. V. (1993) *Adv. Drug Del. Rev. 10*, 91−114. (f) Zalipsky, S. (1995) *Bioconjugate Chem. 6*(2), 150−165.

(3) Greenwald, R. B., Pendri, A., Bolikal, D., and Gilbert, C. W. (1995) *Bioorg. Med. Chem. Lett. 4*(20), 2465−70.

(4) Ladd, L. D., and Snow, A. R. (1993) *Anal. Biochem. 210*, 255−261.

(5) Greenwald, R. B., Pendri, A., and Bolikal, D. (1995) *J. Org. Chem. 60*(2), 331−336.

BC950051Z

Use of Phthaloyl Protecting Group for the Automated Synthesis of 3'-[(Hydroxypropyl)amino] and 3'-[(Hydroxypropyl)triglycyl] Oligonucleotide Conjugates

Huynh Vu,* Nancy Joyce, Michelle Rieger, David Walker, Ira Goldknopf, Theresa Schmaltz Hill, Krishna Jayaraman, and Dennis Mulvey

Triplex Pharmaceutical Corporation, 9391 Grogans Mill Road, The Woodlands, Texas 77380. Received February 21, 1995⊛

The chemical stability of oligonucleotides (ODNs) containing 3'-propanolamine was investigated. Invariably, all the ODNs synthesized from Fmoc-protected 3-aminopropane-1,2-diol–CPG support gave a mixture of three compounds at the end of automated synthesis as analyzed by denaturing PAGE and HPLC. On the basis of analytical procedures, these compounds were identified to be 3'-[N-acetyl-N-(hydroxypropyl)amino], 3'-[(hydroxypropyl)amino], and 3'-hydroxyl ODNs. The instability of the amino protecting group under the synthesis conditions was responsible for this observed heterogeneity. In order to evaluate the stability, a comparative study on the chemical stability of the ODN containing amino-protecting groups such as [(9-fluorenylmethyl)oxy]carbonyl (Fmoc), trifluoroacetyl (TFA), and phthaloyl was undertaken. The results indicate that the phthaloyl group provided the best stability for the synthesis of 3' amine-modified ODNs, and the protecting group is cleaved and deprotected in concentrated ammonium hydroxide:40% aqueous methylamine, 1:1, for 5–10 min, at 56 °C. The 3'-[(hydroxypropyl)triglycyl] ODN conjugates were also synthesized from Fmoc- and phthaloyl-protected (hydroxypropyl)triglycine–CPG supports.

INTRODUCTION

In the areas of antisense- and triple helix-based therapeutics, the stability of these compounds in the cellular environment is a critical issue. In cultured cells, unmodified ODNs appeared to be degraded primarily as a result of 3' exonuclease activity. Modification of the 3'-hydroxyl group with 3-aminopropane-1,2-diol was shown to enhance the nuclease stability significantly (*1, 2*). We and others (*3*) have observed that synthesis of oligonucleotides containing 3-aminopropane-1,2-diol using commercially available Fmoc-protected propanolamine–CPG support resulted in a heterogeneous mixture of at least three species. A systematic investigation of these mixtures revealed that the major component in them is the intact ODN with a 3'-[(hydroxypropyl)amino] (~85%), and the others are the ODN with 3'-[N-acetyl-N-(hydroxypropyl)amino] (~10%) and with 3'-hydroxyl (~5%). These ODNs were obtained probably as a result of the instability of the amino-protecting group of 3-aminopropane-1,2-diol under the synthesis conditions. Oligonucleotides that are intended for therapeutic applications should have a high level of purity. In addition, it is not desirable to have a mixture of three species during large scale synthesis. These two factors could dramatically limit the use of 3-aminopropane-1,2-diol in 3' modification in spite of their utility in enhancing the nuclease stability of ODNs.

The formation of 3'-[N-acetyl-N-(hydroxypropyl)amino] and 3'-hydroxyl species indicated that the loss of the amine protecting group or 3'-[(hydroxypropyl)amino] may be due to the instability of the amine protecting group under synthesis conditions. Nelson et al. (*4, 5*) used the Fmoc-protecting group on the amine during the preparation of supports containing 3-aminopropane-1,2-diol. We have investigated two other protecting groups, trifluoroacetyl (TFA) and phthaloyl, and compared them with

the Fmoc group. We also synthesized 3'-[(hydroxypropyl)triglycyl] conjugates using Fmoc- and phthaloyl-protected (hydroxypropyl)triglycine–CPG supports. In this paper, we present the synthesis, characterization, and chemical stability of the ODNs containing these 3' modifications.

MATERIALS AND METHODS

Materials. All reagents and anhydrous solvents using for chemical syntheses were purchased from Aldrich Chemical Co., Eastman Chemical Co., Fluka Chemical Corp., and TCI America. All nucleosidal phosphoramidites, and reagents for oligonucleotide syntheses were purchased from Applied Biosystem, Inc., and Millipore Corp. Aminopropyl-modified CPG (controlled pore glass) was from CPG Inc.

Instrumental. ¹H-NMR spectra were obtained on a Varian 400 MHz NMR spectrometer of Baylor College of Medicine NMR Center. Infrared (IR) spectra were obtained on a Perkin-Elmer Model 1420 infrared spectrophotometer. Elemental analyses were completed by Quantitative Technologies, Inc. (QTI) (Whitehouse, NJ). Oligonucleotides were synthesized on Applied Biosystems Models 380B or 392/4 and/or MilliGen Models Expedite 8909 and 8800. Preparative and analytical HPLC of oligonucleotides were performed on a Waters HPLC system by anion exchange chromatography on a suitable size of Q-Sepharose column for each synthesis scale.

Synthesis. (*1*) *Synthesis of 3-[N-[[(9-Fluorenylmethyl)oxy]carbonyl]amino]propane-1,2-diol* (*2*). 3-Aminopropane-1,2-diol (**1**, 20 g, 0.219 mol, Fluka) was dissolved in freshly distilled *N,N*-diisopropylethylamine (45.8 mL, 0.263 mol, Aldrich Chemical Co.) and anhydrous DMF (200 mL, Aldrich Chemical Co.). To the solution was added slowly 9-fluorenylmethyl chloroformate (51.2 g, 0.198 mmol, Eastman Chemical Co.). The solution was stirred at room temperature for 3 h. After stirring, the resulting mixture was concentrated to 100 mL, and the condensed solution was then poured slowly into a stirred ice-cooled saturated NaHCO₃ aqueous solution (2000 mL) with stirring. The white precipitate was filtered and

washed thoroughly with deionized water and dried under reduced pressure on a high vacuum pump to give product **2** (55.4 g, yield: 80.5%) as a white solid: mp 204−207 °C dec; IR λ_{max} (KBr) 1550, 1690, 3320 cm⁻¹; ¹H-NMR (DMSO-d_6) δ 3.20 and 3.32 (2 m, 2H, CCH_2NH), 3.51 (br, s, 2H, 2(COH)), 3.71 and 3.95 (2 br, s, 2H, CCH_2OH), 4.21 and 4.23 (2m, 2H, C₂CHOH and −CH−, Fmoc), 4.37, 4.39 (d, J = 6.88, 2H, −OCH_2−, Fmoc), 6.31 (b, s, 1H, CNHCO−), 7.29−7.777 (m, 8H, aromatic-H, Fmoc). Anal. Calcd for $C_{18}H_{19}NO_4$ (313.353): C, 68.99; H, 6.11; N, 4.47. Found: C, 68.84; H, 6.10; N, 4.43.

(2) Synthesis of 1-O-(4,4'-Dimethoxytrityl)-3-[N-[[(9-fluorenylmethyl)oxy]carbonyl]amino]propane-1,2-diol (3). 3-[N-[[(9-Fluorenylmethyl)oxy]carbonyl]amino]propane-1,2-diol (**2**, 16.23 g, 51.8 mmol) was dissolved in anhydrous pyridine (100 mL, Aldrich Chemical Co.). To the mixture was added dropwise a solution of 4,4'-dimethoxytrityl chloride (19.3 g, 56.9 mmol, TCI America) in anhydrous pyridine (60 mL). The solution was stirred at room temperature for 2 h, and then methanol (15 mL) was added and the resulting mixture stirred for 15 min to quench the reaction. The resulting mixture was concentrated to dryness to remove pyridine, and the residue was redissolved in dichloromethane (500 mL) which was washed with saturated $NaHCO_3$ aqueous solution (100 mL, twice) and then brine (100 mL, twice). The organic phase was dried over anhydrous Na_2SO_4 and concentrated to give a light yellow oil. The crude oil was purified by silica gel column chromatography using a gradient of n-hexane:ethyl acetate (2:1 and 1:1), ethyl acetate, and ethyl acetate:dichloromethane (1:1), as the eluents. The homogeneous fractions were combined and concentrated under reduced pressure to provide product **3** (22.2 g, yield: 80%) as a white solid foam: mp 78−83 °C; IR λ_{max} (KBr) 1510, 1720, 3420 cm⁻¹; ¹H-NMR (DMSO-d_6) δ 2.92 and 2.97 (2m, 2H, CCH_2N), 3.2 (m, 1H, C₂CHOH), 3.71 (s, 6H, (−OCH_3)₂), 3.72 (m, 1H, C₂CHC, Fmoc), 4.20 and 4.95 (m, d, 2H, CCH_2O), 4.25 (m, 2H, CCH_2O, Fmoc), 6.85−8.58 (m, aromatic-H, DMT, Fmoc). Anal. Calcd for $C_{39}H_{37}NO_6$ (615.726): C, 76.08; H, 6.06; N, 2.27. Found: C, 76.05; H, 6.47; N, 2.05.

(3) Synthesis of 1-O-(4,4'-Dimethoxytrityl)-2-O-(3-carboxypropionyl)-3-[N-[[(9-fluorenylmethyl)oxy]carbonyl]amino]propane-1,2-diol (4). 1-O-(4,4'-Dimethoxytrityl)-3-[N-[[(9-fluorenylmethyl)oxy]carbonyl]amino]propane-1,2-diol (**3**, 19.3 g, 31.3 mmol) was dissolved in anhydrous pyridine (120 mL). To the solution was added succinic anhydride (6.27 g, 62.7 mmol, Aldrich Chemical Co.) and 4-(dimethylamino)pyridine (0.77 g, 6.3 mmol, Aldrich Chemical Co.). The mixture was stirred for 2 h. The reaction mixture was concentrated to a heavy oil to remove pyridine. The oil was redissolved in dichloromethane (700 mL) and washed with water (150 mL, twice). The organic phase was dried over anhydrous Na_2SO_4. After concentration, the crude oil was purified by silica gel column chromatography using a gradient of n-hexane:ethyl acetate (1:1 and 1:2), ethyl acetate, and ethyl acetate:dichloromethane (1:1) as the eluents. The homogeneous fractions were combined and concentrated under reduced pressure to provide product **4** (12.3 g, yield: 55%) as a light yellow solid foam: mp 71−72 °C; IR λ_{max} (KBr) 1510, 1740 cm⁻¹; ¹H-NMR (DMSO-d_6) δ 2.63 (br, s, 4H, CO(CH_2)₂CO, succinyl), 3.31 and 3.36 (2m, 2H, CCH_2N), 3.50 (m, 1H, C₂CHOH), 3.75 (s, 6H, (−OCH_3)₂), 4.17 (m, 1H, C₂CHC, Fmoc), 4.32 and 5.15 (m, br, s, 2H, CCH_2O), 4.29 (m, 2H, CCH_2O, Fmoc), 6.09 (br, s, 1H, CNHCO−), 6.79−7.76 (m, aromatic-H, DMT, Fmoc). Anal. Calcd for $C_{43}H_{41}NO_9$ + H_2O (733.814): C, 70.38; H, 5.63; N, 1.90. Found: C, 70.52, H, 5.74, N, 2.06.

(4) Synthesis of Fmoc-Protected Propanolamine−CPG

Support 5 (6). 1-O-(4,4'-Dimethoxytrityl)-2-O-(3-carboxypropionyl)-3-[N-[[(9-fluorenylmethyl)oxy]carbonyl]amino]propane-1,2-diol (**4**, 4.2 g, 5.87 mmol) freshly synthesized and purified by silica gel column chromatography, O-benzotriazol-1-yl N,N,N',N'-tetramethyluroniumtetrafluoroborate (1.88 g, 5.87 mmol, Fluka Chemical Co.), 1-hydroxybenzotriazole hydrate (0.79 g, 5.87 mmol, Fluka Chemical Co.), and N-ethylmorpholine (0.75 mL, 5.87 mmol, Fluka Chemical Co.) were dissolved in anhydrous DMF (202.5 mL, 4.5 mL/g CPG). After 5 min of shaking, aminopropyl CPG (45 g, loading capacity: 81.5 μmol/g) was added to the mixture. The reaction mixture was swirled slowly for 4 h. After swirling, the support was filtered, washed thoroughly with DMF, dichloromethane, methanol, and ether, and dried under reduced pressure for 2 h. The unreacted free amino groups on the support were capped by acetic anhydride (34.63 mL, 0.367 mol, Aldrich Chemical Co.) and 1-methylimidazole (29.26 mL, 0.367 mol, Aldrich Chemical Co.) in THF (225 mL). After being swirled for 20 min, the resulting support was filtered and washed with acetonitrile, dichloromethane, methanol, and ether. The loading of the modified support **5** was estimated by (a) the measurement of trityl cation released by acidic treatment of synthesized support the estimation was 46.72 μmol/g) and (b) the measurement of N-(9-fluorenylmethyl)piperidine provided from the treatment of the support with piperidine (the estimation was 45.85 μmol/g) (7).

(5) Synthesis of Fmoc-Protected Propanolamine−TentaGel Support 6. Support **6** was synthesized using the synthesis procedure for support **5**. 1-O-(4,4'-Dimethoxytrityl)-2-O-(3-carboxypropionyl)-3-N-[[(9-fluorenylmethyl)oxy]carbonyl]aminopropane-1,2-diol (**4** , 3.2 g , 3.26 mmol), O-benzotriazole-1-yl-N,N,N',N'-tetramethyluroniumtetrafluoroborate (1.05 g, 3.26 mmol), 1-hydroxybenzotriazole hydrate (0.44 g, 3.26 mmol), N-ethyl morpholine (0.37 g, 3.26 mmol), anhydrous DMF (45 mL), and TentaGel-NH_2 (10 g, loading capacity: 220 μmol/g) were used. Capping and washing steps were also completed as described. The loading of compound **4** on TentaGel support was estimated to be 199 μmol/gram, by trityl measurement, and 166 μmol/gram, by N-(9-fluorenylmethyl)piperidine measurement (7).

(6) Synthesis of 4-(Phthalimidomethyl)-2,2-dimethyl-1,3-dioxolane (9). 4-(Chloromethyl)-2,2-dimethyl-1,3-dioxolane (**7**, 50.0 g, 0.33 mol, Eastman Chemical Co.) and potassium phthalimide (**8**, 74.2 g, 0.40 mol, Aldrich Chemical Co.) were suspended in anhydrous DMF (400 mL) and triethylamine (4.6 mL, 0.03 mol). The mixture was stirred at 110−120 °C overnight. After stirring, the mixture was cooled to room temperature and concentrated to a heavy oil to remove DMF. The residue was rediluted in 1 l of n-hexane:ethyl acetate (1:1), filtered through a silica gel bed (350 g), and washed with another liter of the same solvent system to remove the salt from the mixture. The combined filtrates was concentrated and the residue was recrystallized in ethyl acetate and n-hexane to provide a product **9** (65 g, yield: 75%) as a white solid; mp: 101−102 °C; IR λ_{max} (KBr) 1750, 1770, 2980 cm⁻¹. ¹H-NMR (DMSO-d_6) δ 1.22 and 1.31 (s, s, 3H, 3H, 2(−CH_3), ketal), 3.62, 3.65, 3.70, and 3.73 (4d, J = 6.0, 6.08, 6.58, and 6.51 Hz, H, H, OCH_2C), 3.77, 3.79, 4.0, and 4.03 (4d, J = 4.66, 4.58, 6.1, and 6.31 Hz, H, H, CCH_2N), 4.30 and 4.33 (2t, J = 5.98, 5.1 and 5.0, 6.1 Hz, H, CCHC), 7.87 (m, 4H, aromatic-H, phthaloyl). Anal. Calcd for $C_{14}H_{15}NO_4$ (261.277): C, 64.36; H, 5.79; N, 5.36. Found: C, 64.20; H, 5.65; N, 5.48.

(7) Synthesis of 3-Phthalimidopropane-1,2-diol (10). 4-(Phthalimidomethyl)-2,2-dimethyl-1,3-dioxolane (**9**, 26 g, 99.5 mmol) was dissolved in 200 mL of THF. To the

solution was added 200 mL of 1 N HCl in water. The solution was stirred for 2 h at room temperature. After stirring, the solution was concentrated to 150 mL, and saturated NaHCO$_3$ aqueous solution (150 mL) was added slowly to neutralize the acid. The aqueous solution was extracted three times with dichloromethane (250 mL each). The combined solvent extracts were washed with brine (twice) and dried on Na$_2$SO$_4$. The solvent was concentrated to a heavy oil, and the residue was recrystallized in *n*-hexane and ethyl acetate to yield a product **10** (30.6 g, yield: 69.5%) as a white solid: mp 112−113 °C; IR λ_{max} (KBr) 1720, 1770, 2930, 3300 cm^{-1}; ^{1}H-NMR (DMSO-d_6) δ 3.37 (m, 2H, OCH$_2$C), 3.58 and 3.60 (s, s, H, H, 2(COH)), 3.80 and 3.83 (2t, $J = 6.0$, 5.76 and 5.96, 5.6 Hz, H, H, C$_2$CHOH), 4.82 and 4.55 (t, d, $J = 5.68$, 5.76, and 5.08 Hz, H, H, CCH$_2$N), 7.84 (m, 4H, aromatic-*H*, phthaloyl). Anal. Calcd for C$_{11}$H$_{11}$NO$_4$ (221.212): C, 59.73; H, 5.01; N, 6.33. Found: C, 59.60; H, 4.91; N, 6.33.

(8) Synthesis of 1-O-(4,4'-Dimethoxytrityl)-3-(phthalimido)propane-1,2-diol (11). 3-Phthalimidopropane-1,2-diol (**10**, 10 g, 45.20 mmol) was dissolved in anhydrous pyridine (100 mL). To the solution was added slowly 4,4'-dimethoxytrityl chloride (18.5 g, 54.6 mmol) in pyridine (150 mL). The mixture was stirred at room temperature overnight. After stirring, the mixture was quenched with methanol (15 mL), and the resulting mixture was concentrated to a heavy oil to remove pyridine. The crude oil was then redissolved in dichloromethane (500 mL) which was washed with saturated NaHCO$_3$ aqueous solution (100 mL, twice) and brine (100 mL, twice). The organic phase was dried over anhydrous Na$_2$SO$_4$ and concentrated to give a light yellow oil. The crude product was purified by silica gel column chromatography using a gradient of *n*-hexane:ethyl acetate (2:1 and 1:1), and ethyl acetate as the eluents. The homogeneous fractions were combined and concentrated under reduced pressure to provide product **11** (22.2 g, yield: 84.5%) as a white solid foam: mp 70−72 °C; IR λ_{max} (KBr) 1710, 1770, 2920, 3450 cm^{-1}; ^{1}H-NMR (DMSO-d_6) δ 2.89, 2.91, 3.03, and 3.05 (4d, $J = 5.84$, 6.08, 4.64, and 5.04 Hz, H, H, OCH$_2$C), 3.64 (m, H, C$_2$CHOH), 3.67 and 4.0 (m, m, H, H, CCH$_2$N), 5.17 (d, $J = 5.44$ Hz, H, COH), 6.81−7.86 (m, 4H, and 13H, aromatic-*H*, phthaloyl and trityl). Anal. Calcd for C$_{32}$H$_{29}$NO$_6$ (523.585): C, 73.41; H, 5.58; N, 2.67. Found: C, 73.02; H, 5.63; N, 2.69.

(9) Synthesis of 1-O-(4,4'-Dimethoxytrityl)-2-O-(3-carboxypropionyl)-3-phthalimidopropane-1,2-diol (12). 1-O-(4,4'-Dimethoxytrityl)-3-phthalimidopropane-1,2-diol (**11**, 22 g, 42 mmol) was dissolved in anhydrous pyridine (200 mL). To the solution were added succinic anhydride (8.41 g, 84.0 mmol) and 4-(dimethylamino)pyridine (5.13 g, 42.0 mmol). The mixture was stirred at room temperature for 4 h. After stirring, the reaction mixture was concentrated to a heavy oil to remove pyridine. The oil was redissolved in dichloromethane (700 mL) and washed with water (150 mL, twice). The organic phase was dried over anhydrous Na$_2$SO$_4$. After concentration, the crude oil was purified by silica gel column chromatography using a gradient of *n*-hexane:ethyl acetate (1:1 and 1:2) and ethyl acetate as the eluents. The homogeneous fractions were combined and concentrated under reduced pressure to provide product **12** (22.4 g, yield: 85.5%) as a light yellow solid foam: mp 60−64 °C; IR λ_{max} (KBr) 1710, 1730, 1770, 2920 cm^{-1}; ^{1}H-NMR (DMSO-d_6) δ 2.38 and 2.49 (m, m, 4H, CH$_2$CH$_2$, 3-carboxypropionyl), 3.16 (m, 2H, OCH$_2$C), 3.82 (m, H, C$_2$CHO-(3-carboxypropionyl), 4.0 and 5.23 (m, m, 2H, CCH$_2$N), 6.81−7.86 (m, 4H and 13H, aromatic-*H*, phthaloyl and DMT). Anal. Calcd for C$_{36}$H$_{33}$NO$_9$ + H$_2$O (641.673): C, 67.38; H, 5.50; N, 2.18. Found: C, 67.26; H, 5.45; N, 2.08.

(10) Synthesis of Phthaloyl-Protected Propanolamine CPG Support (13). Support **13** was synthesized using the synthesis procedure for compound **5**. 1-O-(4,4'-dimethoxytrityl)-2-O-(3-carboxypropionyl)-3-phthalimidopropane-1,2-diol (**12**, 10.78 g, 17.29 mmol), O-benzotriazol-1-yl-*N,N,N',N'*-tetramethyluroniumtetrafluoroborate (5.55 g, 17.29 mmol), 1-hydroxybenzotriazole hydrate (2.34 g, 17.29 mmol), *N*-ethylmorpholine (2.19 mL, 17.29 mmol), anhydrous DMF (354 mL), and aminopropyl CPG (78.6 g, loading capacity: 110 μmol/g) were used. The unreacted free amino groups on the support were capped by acetic anhydride (81.15 mL, 0.86 mol) and 1-methylimidazole (68.56 mL, 0.86 mol) in THF (530 mL). The loading of support **13** (104.6 g) was estimated to be 97.2 μmol/g, by trityl measurement.

(11) Synthesis of 4-(Aminomethyl)-2,2-dimethyl-1,3-dioxolane (14). 4-(Phthalimidomethyl)-2,2-dimethyl-1,3-dioxolane (**9**, 31.04 g, 118.8 mmol) was dissolved in ethyl ether (500 mL). To the solution was added hydrazine hydrate (300 mL, Aldrich Chemical Co.). The mixture was stirred for 5 h. The aqueous phase was separated and mixed with 1 N NaOH aqueous solution (150 mL). The resulting aqueous solution was extracted with dichloromethane (three times, 250 mL each). The combined solvents was dried on Na$_2$SO$_4$ and concentrated to a light yellow oil which was distilled to provide product **14** (10.6 g, yield: 68%) as a colorless oil: bp 65−68 °C/0.4 mmHg; ^{1}H-NMR (DMSO-d_6) δ 1.25 and 1.30 (s, s, 3H, 3H, 2(−CH$_3$), ketal), 1.50 (br s, 2H, CNH$_2$), 2.60 (m, 2H, OCH$_2$C), 3.60, 3.62, and 3.97 (d, d, and t, $J = 6.12$, 6.08 and 5.96, 5.88 Hz, H, H, CCH$_2$N), 3.93 (t, $J = 6.32$, 7.64 Hz, H, CCHC).

(12) Synthesis of 4-[[N-(Trifluoroacetyl)amino]methyl]-2,2-dimethyl-1,3-dioxolane (15). 4-(Aminomethyl)-2,2-dimethyl-1,3-dioxolane (**14**, 10.6 g, 80.80 mmol) was dissolved in anhydrous pyridine (50 mL). The solution was cooled to 0 °C in an ice-cold water bath. To the mixture was added dropwise trifluoroacetic anhydride (11.24 mL, 80.80 mmol). The mixture was then stirred for 1 h at 0 °C and 1 h at room temperature. After stirring, the resulting mixture was diluted in dichloromethane (500 mL) and extracted twice with water (250 mL, three times). The solvent layer was dried on Na$_2$SO$_4$, concentrated, and distilled to give product **15** (16.09 g, yield: 87.6%) as a colorless oil: bp 82−85 °C/0.35 mmHg; ^{1}H-NMR (DMSO-d_6) δ 1.26 and 1.33 (s, s, 3H, 3H, 2(−CH$_3$), ketal), 3.31 (t, $J = 5.44$, 5.56 Hz, 2H, OCH$_2$C), 3.66 (m, H, CCHC), 3.98 and 4.16 (m, m, 2H, CCH$_2$N), 7.94 (m, 1H, NH).

(13) Synthesis of 1-O-(4,4'-Dimethoxytrityl)-3-[N-(trifluoroacetyl)amino]propane-1,2-diol (17). 4-[[N-(Trifluoroacetyl)amino]methyl]-2,2-dimethyl-1,3-dioxolane (**15**, 32 g, 141 mmol) was dissolved in THF (200 mL). To the solution was added 1 N HCl solution (200 mL). The mixture was stirred at room temperature for 2 h. After stirring, the solution was diluted with ethyl acetate (500 mL), the solvent layer was separated, and the aqueous layer was extracted with ethyl acetate (200 mL, twice). The combined solvents was dried on MgSO$_4$ and concentrated to give crude product (**16**, 29 g) as a yellow oil which was coevaporated with anhydrous pyridine (20 mL, three times) and tritylated with 4,4'-dimethoxytrityl chloride (71.7 g, 211.5 mmol) following the synthesis and purification procedures for compound **3** to yield product **17** (41.4 g, yield: 60%) as a white foam: ^{1}H-NMR (DMSO-d_6) δ 2.95, 2.97, 3.04, and 3.06 (d, d, d, d, $J = 5.68$, 5.72, 5.36, and 5.48 Hz, 2H, OCH$_2$C), 3.22 (quintet, $J = 7.16$, 6.12, 7.0, and 6.28 Hz, H, CCHC), 3.43 and 3.90 (t, t, and m, $J = 4.84$, 5.00 and 5.32, 4.88 Hz, 2H, CCH$_2$N), 3.74 (s, 6H, 2(OCH$_3$), methoxy), 5.10 (d,

$J = 5.52$ Hz, 1H, CO*H*), 6.88–7.46 (m, 13H, aromatic-*H*, DMT), 9.29 (br s, 1H, N*H*).

(14) Synthesis of 1-O-(4,4'-Dimethoxytrityl)-2-O-(3-carboxypropionyl)-3-[N-(trifluoroacetyl)amino]propane-1,2-diol (18). 1-O-(4,4'-Dimethoxytrityl)-3-[N-(trifluoroacetyl)-amino]propane-1,2-diol (**17**, 21.2 g, 43.31 mmol) was succinylated using the synthesis and purification procedures for compound **4** to give compound **18** (17.8 g, yield: 70%) as a white foam: ¹H-NMR (DMSO-d_6): δ 2.62 (br, s, 4H, CO(C*H*₂)₂CO, 3-carboxypropionyl), 3.12 (m, 2H, OC*H*₂C), 3.27 (H, CC*H*C), 3.40 and 3.45 (m, m, 2H, CC*H*₂N), 3.74 (s, 6H, 2(OC*H*₃), methoxy), 6.88–7.46 (m, 13H, aromatic-*H*, DMT), 9.34 (br,s, 1H, N-*H*).

(15) Synthesis of TFA-Protected Propanolamine CPG Support 19. Support **19** was synthesized using the synthesis procedure for compound **5**. 1-O-(4,4'-Dimethoxytrityl)-2-O-(3-carboxypropionyl)-3-[N-(trifluoroacetyl)amino]propane-1,2-diol (**18**, 8.4 g, 14.25 mmol), O-benzotriazol-1-yl-*N,N,N',N'*-tetramethyluroniumtetrafluoroborate (4.5 g, 14.25 mmol), 1-hydroxybenzotriazole hydrate (1.92 g, 14.25 mmol), 4-ethylmorpholine (1.8 mL, 14.25 mmol), anhydrous DMF (291 mL), and aminopropyl CPG (64.8 g, loading capacity: 110 μmol/g) were used. The unreacted free amino groups on the support were capped by acetic anhydride (67.18 mL, 0.71 mol) and 1-methylimidazole (56.6 mL, 0.71 mole) in THF (440 mL). The loading of support **19** (68.4 g) was estimated to be 81.5 μmol/g by trityl measurement.

(16) Synthesis of N-[[(9-Fluorenylmethyl)oxy]carbonyl]-glycylglycylglycine (21) (8). Glycylglycylglycine (**20**, 5 g, 26.43 mmol, TCI America) was suspended in bis(trimethylsilyl)acetamide (23.52 mL, 95.15 mmol, Aldrich Chemical Co.) and anhydrous DMF (90 mL). After being stirred at room temperature overnight, the mixture was cooled to −20 to −15 °C. To the stirred mixture were added 4-methylmorpholine (2.9 mL, 26.43 mmol, Fluka Chemical Co.) and 9-fluorenylmethyl chloroformate (6.84 g, 26.43 mmol). The mixture was stirred at this temperature for 2 h and at O °C for 30 min. The resulting mixture was concentrated under reduced pressure on a vacuum pump to a heavy oil and was precipitated in 2 N HCl aqueous solution (1 L). The light yellow precipitate was collected by filtration and washed thoroughly with water. The precipitate was resuspended in methanol: dichloromethane (1:1), and the mixture was concentrated to 200 mL to give a white precipitate which was filtered and washed with methanol. This precipitation was repeated three times to provide product **21** (8.29 g, yield: 76.2%) as a white solid; mp 220–222 °C dec; IR λ_{max} (KBr) 1555, 1745, 1760, 3040, 3300 cm⁻¹; ¹H-NMR (DMSO-d_6) δ 3.35 (br, s, 1H, O*H*), 3.67 (d, $J = 5.52$ Hz, 2H, −COC*H*₂NH−, linker), 3.75 (d, $J = 5.33$ Hz, 4H, 2(−COC*H*₂NH−), glycyl linker), 4.22 (t, $J = 6.61$ and 6.53 Hz, 1H, −CC*H*C₂, Fmoc), 4.29 (d, $J = 6.73$ Hz, 2H, −OC*H*₂CH-, Fmoc), 7.31–7.89 (m, 8H, aromatic-*H*, Fmoc), 7.51, 8.08, 8.10 (3 br s, 3H, 3(−CN*H*CO−), glycyl linker). Anal. Calcd for C₂₁H₂₁N₃O₆ (411.414): C, 61.31; H, 5.14; N, 10.21. Found: C, 61.67; H, 5.13; N, 9.93.

(17) Synthesis of 2-[N-[N-[[(9-Fluorenylmethyl)oxy]carbonyl]glycylglycylglycyl]amino]propane-1,3-diol (23). N-[[(9-Fluorenylmethyl)oxy]carbonyl]]glycylglycylglycine (**21**, 5 g, 12.15 mmol) and 2-aminopropane-1,3-diol (**22**, 1.33 g, 14.58 mmol) were dissolved in anhydrous pyridine (300 mL). To the solution were added 1-[3-(dimethylamino)propyl]-3-ethylcarbodiimide hydrochloride (EDC, 2.79 g, 14.58 mmol, Aldrich Chemical Co.) and 1-hydroxybenzotriazole (1.97 g, 14.58 mmol). The solution was stirred overnight. The reaction mixture was then concentrated to an oil, and the crude oil was redissolved in methanol : dichloromethane (1:1, 600 mL).

The solvent was concentrated to 100 mL to give a white precipitate which was separated by filtration and was washed thoroughly with methanol. This precipitation was repeated three times to provide product **23** (3.75 g, yield: 64.5%) as a white solid: mp 166–168 °C; IR λ_{max} (KBr) 1530, 1660, 1700, 3100, 3300, 3640 cm⁻¹; ¹H-NMR (DMSO-d_6) δ 3.43 (t, $J = 5.36$ and 5.45 Hz, 4H, 2(−C*H*₂-OH), linker), 3.68–3.76 (m, 7H, 3(−COC*H*₂NH−) and NHC*H*C₂, linker), 4.24 (t, $J = 7.17$ and 6.42 Hz, 1H, −CC*H*C₂, Fmoc), 4.30 (d, $J = 6.39$ Hz, 2H, −OC*H*₂CH−, Fmoc), 7.31–7.9 (m, 8H, aromatic-*H*, Fmoc and 2H, 2(-C-N*H*CO−), linker), 7.97, 8.07 (2 br s, 2H, 2(−C-N*H*CO−), linker). Anal. Calcd for C₂₄H₂₈N₄O₇ (484.509): C, 59.50; H, 5.82; N, 11.56. Found: C, 58.96; H, 5.89; N 11.53.

(18) Synthesis of 1-O-(4,4'-Dimethoxytrityl)-2-[N-[N-[[(9-fluorenylmethyl)oxy]carbonyl]glycylglycylglycyl]amino]-propane-1,3-diol (24). 2-[N-[N-[[(9-(Fluorenylmethyl)-oxy]carbonyl]glycylglycylglycyl]amino]propane-1,3-diol (**23**, 3.70 g, 7.64 mmol) was suspended in anhydrous pyridine (300 mL). To the mixture was added dropwise a solution of 4,4'-dimethoxytrityl chloride (3.88 g, 11.46 mmol, TCI America) in anhydrous pyridine (90 mL). The reaction mixture was stirred at room temperature overnight. Methanol (10 mL) was added to the reaction mixture to quench the reaction and after 15 min of stirring, the resultant solution was concentrated to an oil to remove pyridine, and the residue was redissolved in dichloromethane (200 mL) which was extracted with 10% citric acid aqueous solution (100 mL, twice). The solvent phase was dried over anhydrous Na₂SO₄, concentrated, and chromatographed on a silica gel column using a gradient of CH₂Cl₂:MeOH (19:1 and 9:1) as the eluents. The homogeneous fractions were combined and concentrated under reduced pressure to provide product **24** (2.1 g, yield: 35%) as a white solid: ¹H-NMR (DMSO-d_6) δ 2.98 (m, 2H, C*H*₂O-DMT), 3.51 (m, 2H, −C*H*₂OH, propanediol linker), 3.63 (br s, 2H, −COC*H*₂NH−, linker), 3.74 (s, 6H, 2(C*H*₃O−), methoxy), 3.74 (m, 4H, 2(−COC*H*₂NH−), linker), 4.0 (m, 1H, −CH₂C*H*NH−, linker), 4.28 (br, s, 1H, −CC*H*C₂, Fmoc), 4.59 (t, $J = 5.45$ and 5.48 Hz, 1H, -O*H*), 6.60–7.90 (m, 23H, aromatic-*H*, DMT, Fmoc and 2(−C-N*H*CO−), linker), 8.03 and 8.11 (2 br s, 2H, 2(N-*H*), linker). Anal. Calcd for C₄₅H₄₆N₄O₉ (786.882): C, 68.69; H, 5.89; N, 7.12. Found: C, 68.21; H, 6.10; N, 6.89.

(19) Synthesis of 1-O-(4,4'-Dimethoxytrityl)-2-[N-[N-[[(9-fluorenylmethyl)oxy]carbonyl]glycylglycylglycyl]amino]-3-O-(3-carboxypropionyl)propane-1,3-diol (25). 1-O-(4,4'-Dimethoxytrityl)-2-[N-[N-[[(9-fluorenylmethyl)oxy]carbonyl]glycylglycylglycyl]amino]propane-1,3-diol (**24**, 1.2 g, 1.52 mmol), succinic anhydride (0.76 g, 4.56 mmol, Aldrich Chemical Co.), and 4-ethylmorpholine (0.58 mL, 4.56 mmol) were dissolved in anhydrous DMF (20 mL). The solution was stirred at room temperature overnight. The resultant solution was concentrated to an oil to remove DMF and was chromatographed on a silica gel column using a gradient of CH₂Cl₂:MeOH (19:1 and 9:1), as the eluents. The homogeneous fractions were combined and concentrated under reduced pressure to provide product **25** (0.8 g, yield: 59%) as a white solid: ¹H-NMR (DMSO-d_6) δ 2.40 (br s, 4H, −C*H*₂C*H*₂−, 3-carboxypropionyl), 3.0 (m, 2H, C*H*₂O-DMT), 3.32 (br s, 2H, CC*H*₂O-(3-carboxypropionyl), 3.62 (m, 2H, −COC*H*₂NH−, linker), 3.73 (s, 6H, 2(C*H*₃O−)), 3.76 (m, 4H, 2(−COC*H*₂-NH−), linker), 4.08 (m, 1H, −CH₂C*H*CH₂−, propyl linker), 4.28 (br s, 1H, −CC*H*C₂, Fmoc), 6.88–7.90 (m, 23H, aromatic-*H*, DMT, Fmoc and 2(−CN*H*CO−), linker), 8.03 and 8.11 (2 br s, 2H, 2(N*H*), linker), 12.30 (br s, 1H,

COO*H*). Anal. Calcd for $C_{49}H_{50}N_4O_{12}$ + H_2O (904.970): C, 65.03; H, 5.79; N, 6.19. Found: C, 65.49; H, 6.25; N, 5.95.

(20) Synthesis of Fmoc-Protected (Hydroxypropyl)tri-glycine—CPG Support **26**. Support **26** was synthesized using the synthesis procedure for **5**. 1-*O*-(4,4'-Dimethoxy-trityl)-2-[*N*-[*N*-[[(9-fluorenylmethyl)oxy]carbonyl]gly-cylglycylglycyl]amino]-3-*O*-(3-carboxypropionyl)propane-1,3-diol (**25**, 0.8 g, 0.9 mmol), *O*-benzotriazol-1-yl-*N*,*N*, *N'*,*N'*-tetramethyluroniumtetrafluoroborate (0.29 g, 0.9 mmol), 1-hydroxybenzotriazole hydrate (0.12 g, 0.9 mmol), and 4-ethylmorpholine (0.12 mL, 0.9 mmol) were dissolved in anhydrous DMF (27 mL), and aminopropyl CPG (6.9 g, loading capacity : 87 μmol/g) was added. The unreacted free amino groups on the support were capped by acetic anhydride (4.0 mL, 45 mmol) and 1-methylimi-dazole (3.7 g, 45 mmol) in THF (20 mL). Triglycyl loading was estimated by both the measurement of trityl cation released by acidic treatment (26 μmol/g) and the mea-surement of the Fmoc group released by piperidine treatment (25.8 μmol/g) of the synthesized support.

(21) Synthesis of N-Phthaloylglycylglycylglycylglycine **(28)**. Phthalic anhydride (**27**, 6.0 g, 40.50 mmol, Aldrich Chemical) and glycylglycylglycine (**20**, 8.0 g, 42.28 mmol) were suspended in anhydrous DMF (200 mL). The mixture was refluxed at 195 °C for 3 h. The solution was allowed to cool to 45 °C, and concentrated to a heavy oil to remove DMF. The crude oil was precipitated in ice-cold methanol (500 mL) to provide product **28** (11.76 g, yield: 87%) as a white solid; mp 236—239 °C (dec); IR λ_{max} (KBr) 1565, 1645, 1720, 3100, 3290 cm^{-1}. ^{1}H-NMR (DMSO-d_6) δ 3.82 (d, J = 5.68 Hz, 4H, 2(−NHC*H*$_2$CO−), glycyl), 4.34 (s, 2H, −NC*H*$_2$CO−, glycyl), 7.91—7.97 (m, 4H, aromatic-*H*, phthaloyl), 8.28 and 8.61 (t, t, J = 5.80, 5.80 and 5.76, 5.72 Hz, 1H, 1H, 2(N*H*), glycyl), 12.65 (br s,1H,−COO*H*,glycyl). Anal. Calcd for $C_{14}H_{13}N_3O_6$ (319.273): C, 52.67; H, 4.10; N, 13.16. Found: C, 52.43; H, 4.09; N, 13.12.

(22) Synthesis of 2-[N-(N-Phthaloylglycylglycylglycyl)-amino]propane-1,3-diol **(29)**. *N*-Phthaloylglycylglycyl-glycine (**28**, 4.0 g, 12.53 mmol) and 2-aminopropane-1,3-diol (**22**, 1.37 g, 15.03 mmol) were dissolved in anhydrous pyridine (60 mL). To the solution was added 1-[3-(dimethylamino)propyl]-3-ethylcarbodiimide hydrochlo-ride (EDC, 2.88 g, 15.03 mmol) and 1-hydroxybenzotri-azole (HOBT, 2.03 g, 15.03 mmol). The solution was stirred at room temperature overnight. After stirring, the reaction mixture was concentrated to an oil and the crude oil was precipitated in methanol to provide product **29** (3.5 g, yield: 71.2%) as a white solid: mp 201—202 °C; IR λ_{max} (KBr) 1565, 1645, 1720, 3100, 3290 cm^{-1}. ^{1}H-NMR (DMSO-d_6) δ 3.38 (t, J = 5.40 and 5.56 Hz, 4H, 2 (CC*H*$_2$OH), propanediol), 3.69 (m, 1H, −CH$_2$C*H*CH$_2$−, propane), 3.73 and 3.77 (d, d, J = 5.64 and 5.56 Hz, 4H, 2(−NHC*H*$_2$CO−), glycyl), 4.28 (s, 2H, −NC*H*$_2$CO−, gly-cyl), 4.59 (t, J = 5.44 and 5.56 Hz, 2H, 2 (−CH$_2$O*H*), propanediol), 7.85—7.91 (m, 4H, aromatic-*H*, phthaloyl), 7.51, 8.12, and 8.58 (d, t, t, J = 8.04, 5.52 and 5.56, 5.48 and 5.52 Hz, 3H, 3(N-*H*), glycyl). Anal. Calcd for $C_{17}H_{20}N_4O_7$ (392.365): C, 52.04; H, 5.14; N, 14.28. Found: C, 51.74; H, 5.08; N, 14.18.

(23) Synthesis of 1-O-(4,4'-Dimethoxytrityl)-2-[N-(N-phthaloylglycylglycylglycyl)amino]-propane-1,3-diol **(30)**. 2-[*N*-(*N*-Phthaloylglycylglycylglycyl)amino]propane-1,3-diol (**29**, 10.89 g, 27.75 mmol) and 4-(dimethylamino)-pyridine (3.39 g, 27.75 mmol) were dissolved in anhy-drous pyridine (100 mL), anhydrous DMF (100 mL), and triethylamine (15.47 mL, 111 mmol). To the mixture was added dropwise 4,4'-dimethoxytrityl chloride (14.1 g, 41.62 mmol) in anhydrous pyridine (100 mL). The

solution was stirred at room temperature overnight. Methanol (50 mL) was added to quench the reaction, and after 15 min of stirring, the resultant solution was concentrated under reduced pressure on a high vacuum pump to a heavy oil. The crude oil was chromatographed on silica gel column using a gradient of CH_2Cl_2:MeOH (19:1 and 9:1) as the eluents. The homogeneous fractions were combined and concentrated under reduced pressure to provide product **30** (6.4 g, yield: 33.2%) as a white solid: mp 122—124 °C; IR λ_{max} (KBr) 1605, 1655, 1720, 3300 cm^{-1}; ^{1}H-NMR (DMSO-d_6) δ 2.93—2.99 (m, 2H, CC*H*$_2$ODMT, propanediol), 3.48 (t, J = 5.32 and 5.48 Hz, 2H, CC*H*$_2$OH, propanediol), 3.69—3.79 (m, 10H, 2(−NHC*H*$_2$CO−) and 2(−OC*H*$_3$), glycyl and methoxy), 3.98 (m, 1H, −CH$_2$C*H*CH$_2$−, propane), 4.28 (s, 2H, −NC*H*$_2$-CO−, glycyl), 4.62 (t, J = 5.20 and 5.36, 1H, −CH$_2$O*H*), propanediol), 6.87—7.38 (m, 13H, aromatic-*H*, trityl), 7.85—7.91 (m, 4H, aromatic-*H*, phthaloyl), 7.71, 8.11, and 8.55 (d, t, t, J = 8.48, 5.72 and 5.72, and 5.68 and 5.60 Hz, 3H, 3 (N*H*), glycyl). Anal. Calcd for $C_{38}H_{38}N_4O_9$ + 3/2H_2O (721.763): C, 63.23; H, 5.72; N, 7.76. Found: C, 63.25; H, 5.43; N, 7.71.

(24) Synthesis of 1-O-(4,4'-Dimethoxytrityl)-2-[N-(N-phthaloylglycylglycylglycyl)amino]-3-O-(3-carboxypropio-nyl)propane-1,3-diol **(31)**. 1-*O*-(4,4'-Dimethoxytrityl)-2-[*N*-(*N*-phthaloylglycylglycylglycyl)amino]propane-1,3-diol (**30**, 5.4 g, 7.77 mmol) was dissolved in anhydrous pyridine (100 mL). To the solution was added succinic anhydride (1.55 g, 15.54 mmol) and 4-(dimethylamino)-pyridine (0.95 g, 7.7 mmol). The mixture was stirred at room temperature for 4 h. After stirring, the reaction mixture was concentrated to a heavy oil to remove pyridine. The oil was redissolved in dichloromethane (500 mL) and washed with water (150 mL, twice). The organic phase was dried over anhydrous Na_2SO_4. After concentration, the crude oil was purified by silica gel column chromatography using a gradient of *n*-hexane: ethyl acetate (1:1 and 1:2) and ethyl acetate as the eluents. The homogeneous fractions were combined and concentrated under reduced pressure to provide product **31** (5.3 g, yield: 85.5%) as a light yellow solid foam: mp 52—54 °C; IR λ_{max} (KBr) 1605, 1655, 1720, 3300 cm^{-1}; ^{1}H-NMR (DMSO-d_6) δ 2.40 (br s, 4H, −COC*H*$_2$C*H*$_2$CO−, 3-carboxypropionyl), 2.98 (br s, 2H, CC*H*$_2$O-DMT), 3.32 (br s, 2H, CC*H*$_2$O-(carboxypropionyl), 3.73 (s, 6H, 2(−OC*H*$_3$), methoxy), 3.74 (m, 2H, −NC*H*$_2$CO−, glycyl), 4.08 (m, 1H, -CH$_2$-C*H*-CH$_2$−, propane), 4.16 (m, 2H, −NC*H*$_2$-CO−, glycyl), 4.27 (s, 2H, −NC*H*$_2$CO−, glycyl), 6.87—7.38 (m, 13H, aromatic-*H*, trityl), 7.85—7.93 (m, 4H, aromatic-*H*, phthaloyl), 7.85, 8.24, and 8.75 (3 br s, 3H, 3 (N*H*), glycyl), 12.25 (br s, 1H, COO*H*). Anal. Calcd for $C_{42}H_{42}N_4O_{12}$ + 4H_2O (866.874): C, 58.19; H, 5.81; N, 6.46. Found: C, 58.41; H, 5.37; N, 6.56.

(25) Synthesis of Phthaloyl-Protected Triglycine—CPG Support **(32)**. Triglycine—CPG support **32** was synthe-sized using the synthesis procedure for **5**. 1-*O*-(4,4'-dimethoxytrityl)-2-[*N*-(*N*-phthaloylglycylglycylglycyl)-amino]-3-*O*-(3-carboxypropionyl)propane-1,3-diol (**31**, 0.8 g, 0.9 mmol), *O*-benzotriazole-1-yl-*N*,*N*,*N'*,*N'*-tetramethyl-uronium tetrafluoroborate (0.29 g, 0.9 mmol), 1-hydroxy-benzotriazole hydrate (0.12 g, 0.9 mmol), 4-ethylmorpho-line (0.12 mL, 0.9 mmol), anhydrous DMF (27 mL), and aminopropyl CPG (6.9 g, loading capacity: 87 μmol/g) were used. The unreacted free amino groups on the support were capped by acetic anhydride (4.0 mL, 45 mmol) and 1-methylimidazole (3.7 g, 45 mmol) in THF (20 mL). Triglycyl loading was estimated by trityl cation released by acidic treatment (26 μmol/g).

Figure 1. Key: (i) **1**, DMF, diisopropylethylamine, Fmoc Cl; (ii) pyridine, 4,4'-dimethoxytrityl chloride; (iii) pyridine, succinic anhydride, DMAP; (iv) (a) TBTU, HOBT, DMF, N-ethylmorpholine, NH₂-modified support, (b) acetic anhydride, 1-methylimidazole; (v) **8**, Et₃N, 110 °C; (vi) 1 N HCl; (vii) **9**, hydrazine hydrate; (viii) trifluoroacetic anhydride; (ix) 1 N HCl; (x) (a) **20**, bis(trimethylsilyl)-acetamide, N-methylmorpholine, DMF, (b) −20 °C, Fmoc Cl; (xi) 2% HCl; (xii) EDC, pyridine; (xiii) **27**, DMF, 195 °C.

RESULTS AND DISCUSSION

The synthetic schemes of the preparations of protected 3-aminopropane-1,2-diol—CPG supports containing Fmoc **5** and **6**, phthaloyl **13**, and TFA **19**, for the synthesis of 3'-[(hydroxypropyl)amino] ODNs, and the preparation of protected 2-[N-(glycylglycylglycyl)amino]propane-1,3-diol—CPG supports containing Fmoc **26** and phthaloyl **32**, for the synthesis of 3'-[(hydroxypropyl)triglycyl] ODN conjugates, are shown in Figure 1. The Fmoc-protected propanolamine support was synthesized as described below. 3-Amino-1,2-propanediol (**1**) reacted with 9-fluorenylmethyl chloroformate under basic conditions to provide 3-N-[(9-fluorenylmethyl)oxy]carbonyl]aminopropane-1,2-diol (**2**, 80.5%), compound **2** was tritylated on the primary alcohol using 4,4'-dimethoxytrityl chloride to give 1-O-(4,4'-dimethoxytrityl)-3-N-[(9-fluorenylmethyloxy)carbonyl]aminopropane-1,2-diol (**3**, 80%) followed by succinylation to yield 1-O-(4,4'-dimethoxytrityl)-2-O-(3-carboxypropionyl)-3-N-[[(9-fluorenylmethyl)oxy]carbonyl]aminopropane-1,2-diol (**4**). Compound **4** was coupled

to amino-modified CPG (loading capacity: 81.5 μmol/gram) or TentaGel (loading capacity: 220 μmol/g) supports to give propanolamine supports **5** (46.72 μmol/g) and **6** (199 μmol/g) containing the Fmoc-protecting group. The preparation of the phthaloyl-protected 3-amino-1,2-propanediol support is described below. Phthaloyl-protected 3-aminopropane-1,2-diol **10** was synthesized by the treatment of 4-(chloromethyl)-2,2-dimethyl-1,3-dioxolane (**7**) with potassium phthalimide (**8**) followed by hydrolysis with 1 N HCl. Compounds **11**, **12**, and phthaloylpropanolamine—CPG **13** (97.2 μmol/g) were synthesized following the same procedures described above. The synthesis of TFA-protected 3-aminopropane-1,2-diol support is described below. 4-(Phthalimidomethyl)-2,2-dimethyl-1,3-dioxolane (**9**) was treated with hydrazine hydrate to give 4-(aminomethyl)-2,2-dimethyl-1,3-dioxolane (**14**). Compound **14** reacted with trifluoroacetic anhydride to yield 4-[[N-(trifluoroacetyl)amino]-methyl]-2,2-dimethyl-1,3-dioxolane (**15**). The hydrolysis of compound **15** using 1 N HCl gave TFA-protected

Figure 2. Gel electrophoresis analysis of the crude and HPLC-purified 3'-[(hydroxypropyl)amino] ODNs, oligo-1, synthesized from three modified supports, Fmoc- (**5**), TFA- (**19**) (using standard deprotection), and phthaloyl-protected (**13**) propanolamine—CPG (deprotected in 40% aqueous methylamine, overnight, at 56 °C). The gel shows that oligo-1 migrated one unit slower than the ODN containing 3'-N-acetyl. And 3'-hydroxyl ODN was observed between two ODNs, oligo-1 and n-1.

Figure 3. Gel electrophoresis analysis of the crude ODNs synthesized from N-acetylpropanolamine—CPG (lane 1), **13** (lane 2), T-CPG (lane 3), **32** (lane 4), and the mixture of the crude ODNs of lanes 1—4 (lane 5). The gel shows that 3' (N-acetylamino), 3'-amino (oligo-1), and 3'-OH ODNs separate clearly on PAGE gel, and 3'-(hydroxypropyl)triglycyl ODN (oligo-2) migrates about two units faster than 3' OH ODN.

3-aminopropane-1,2-diol **16**. Compounds **17**, **18**, and TFA-propanolamine—CPG **19** (81.5 µmol/g) were synthesized following the same synthesis procedures described above.

The Fmoc- and phthaloyl-protected 2-[N-(glycylglycyl-glycyl)amino]propane-1,3-diol—CPG supports (**26**, **32**) were synthesized as described below. Glycylglycylglycine (**20**) first reacted with 9-fluorenylmethyl chloroformate (**8**), followed by coupling with 2-aminopropane-1,3-diol (**22**), to give **23**. Compounds **24**, **25**, and Fmoc-propanol-triglycyl—CPG **26** (25.8 µmol/g) were prepared using the same procedures described above. Glycylglycylglycine (**20**) was condensed with phthalic anhydride (**27**) in DMF at 194 °C to yield N-phthaloylglycylglycylglycine (**28**). Compounds **29**, **30**, **31**, and phthaloyl-protected (hydroxypropyl)triglycine—CPG **32** (26.0 µmol/g) were synthesized using the same procedures described above.

Standard ODNs, N-acetylamino ODNs, and 3'-hydroxyl ODN were synthesized from N-acetyl-N-(hydroxypropyl)-amino CPG and N-acetyl-N-(hydroxypropyl)triglycyl—CPG supports which were simply prepared by deblocking the Fmoc-protected support **5** or **26** in 20% piperidine in DMF for 15 min, followed by capping with acetic anhydride and N-methylimidazole and commercially available T-CPG support . These ODNs were used as standards to identify the byproducts in the synthesis of 3'-modified ODN.

A stability study of Fmoc-protecting group to several basic conditions was initiated. Compounds 1-O-(4,4'-dimethoxytrityl)-3-[N-[[(9-fluorenylmethyl)oxy]carbonyl]-amino]propane-1,2-diol (**3**) and 1-O-(4,4'-dimethoxytrityl)-2-[N-[N-[[(9-fluorenylmethyl)oxy]carbonyl]glycyl-glycylglycyl]amino]propane-1,3-diol (**24**), the intermediates for the two Fmoc-protected supports **5** and **26**, were

treated with several basic solutions such as 4-(dimethyl-amino)pyridine (DMAP), triethylamine (TEA), N-meth-ylimidazole (NMI), and N-ethylmorpholine (NEM) in DMF from 3 to 30 min. The crude materials were analyzed by thin layer chromatography (TLC, dichloromethane:methanol 9:1, v/v). The product bands were isolated by preparative TLC and extracted by dichloromethane:methanol 1/1, v/v. The degraded compound, were characterized as 1-O-(4,4'-dimethoxytrityl)-3-aminopropane-1,2-diol and 1-O-(4,4'-dimethoxytrityl)-2-[(gly-cylglycylglycyl)amino]propane-1,3-diol by ^{1}H-NMR. The results showed that the Fmoc group of compounds **3** and **24** are unstable to DMAP, and TEA and stable to NMI and NEM. However, when these compounds were exposed in NMI for overnight at room temperature, 5—10% of unprotected compounds were detected by TLC. In the modified synthesis cycles at the 1 µmol scale having extended capping wait times using Fmoc-protected CPG **5**, the 3'-[N-acetyl-N-(hydroxypropanyl)amino] ODN was observed much more than the material synthesized using a standard cycle time. This result strongly showed that in the standard synthesis, a minor amount of N-acetyl-N-(hydroxypropyl)amino ODN may form by the loss of amine-protecting group under basic conditions of NMI, and the resulting unprotected amino group was subsequently acetylated by acetic anhydride, during the capping step in each synthesis cycle.

On the basis of these stability studies several 3' end propanolamine-modified ODNs were synthesized from 1 to 300 µmol scale using supports **5**, **6**, **13**, **19**, **26** and **32** on Applied Biosystems Models 380B and 392/4 and/or MilliGen Models Expedite 8909 and 8800 with a coupling efficiency of ≥97%. Two representative examples are
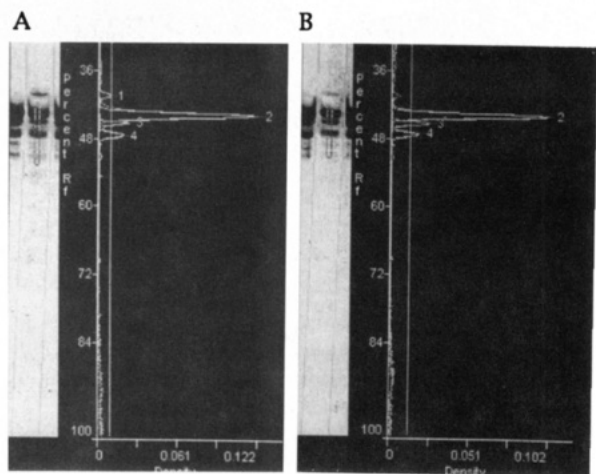
Figure 4. Gel densitometry analyses of the crude 3'-[(hydroxypropyl)amino]-modified ODNs, oligo-1, synthesized on Fmoc- (**5**, A) and TFA-protected (**19**, B) supports showed that the crude ODNs contained 3'-[(hydroxypropyl)amino] ODN (1−4.5% in A, 0−1% in B), oligo-1 (77 ± 3% in A, 75 ± 3% in B), 3'-hydroxyl ODN (7 ± 3% in A, 12 ± 3% in B), and n-1 ODN (10 ± 3% in A, 10 ± 3% in B).
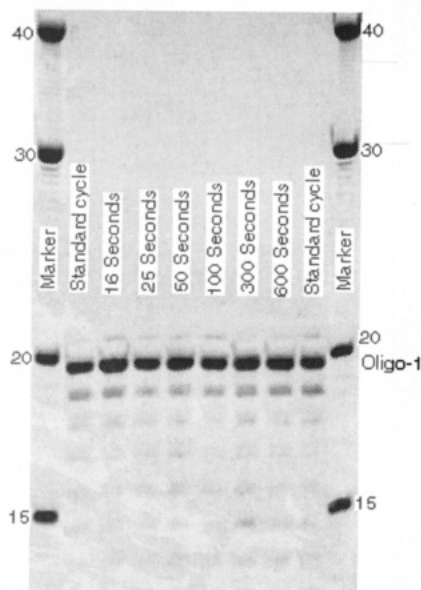
Figure 5. Gel electrophoresis analysis of the crude 3'-[(hydroxypropyl)amino] ODNs, oligo-1, synthesized at a 1μmol scale, on phthaloyl-protected propanolamine−CPG support **13** using modified cycles having extended capping wait times of 16, 25, 50, 100, 300, and 600 s and deprotected in 40% aqueous methylamine, overnight, at 56 °C. This result showed that the phthaloyl group was stable under basic conditions of the synthesis.

shown below:

oligo-1 5' GTGGTGGGTGGGTGGGT 3'-[(hydroxy-propyl)amino]

oligo-2 5' GTGGTGGGTGGGTGGGT 3'-[(hydroxy-propyl)triglycyl]

For the deprotection, a solution of concentrated ammonium hydroxide:40% aqueous methylamine, 1:1, was shown to be a fast cleavage/deprotection solution for ODN synthesis using phosphoramidites dA^{bz}, dG^{ibu}, dC^{ac}, and T. In this solution, oligonucleotide is cleaved from the support in 5 min at room temperature, and the protecting groups on nucleosides are removed in 5 min at 56 °C (9). Furthermore, Wolfe et al. showed that the phthaloyl protecting group can be removed from the amino group
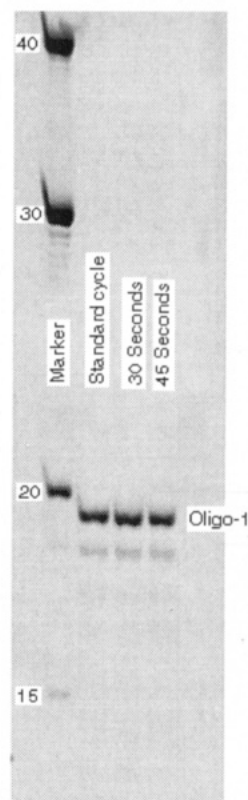
Figure 6. Gel electrophoresis analysis of the crude 3'-[(hydroxypropyl)amino] ODNs, oligo-1, synthesized at a 1 μmol scale, on phthaloyl-protected propanolamine−CPG support **13** using modified cycles having extended detritylation wait times of 30 and 45 s and deprotected in concentrated ammonium hydroxide: 40% aqueous methylamine, 1:1, for 5−10 min at 56 °C. This result showed that the phthaloyl group was stable to acidic conditions of the synthesis.

in 40% aqueous methylamine at room temperature (*10*). From these deprotection studies, cleavage/deprotection of ODNs containing three modifications were carried out under standard conditions using concentrated ammonium hydroxide, overnight, at 56 °C, or concentrated ammonium hydroxide: 40% aqueous methylamine, 1:1, for 5−10 min at 56 °C. We have found that the phthaloyl protecting group on ODN is also completely removed in concentrated ammonium hydroxide:40% aqueous methylamine, 1:1, for 5−10 min, at 56 °C. Crude ODNs were purified on a Waters HPLC system by anion exchange chromatography on a Q-Sepharose column (1.6 cm × 11 cm for 1 μmol, 2.2 cm × 11 cm for 10 μmol, and 9.0 cm × 11 cm for 100−300 μmol). The elution time of 3' amino-modified ODN, oligo-1, was about 60.7 min, and the elution time of 3'-[*N*-acetyl-*N*-(hydroxypropyl)amino]-modified ODN was about 62.1 and of 3'-hydroxyl ODN was about 59.2 min in the same buffer system (buffer A: 0.5 M NaCl; 10 mM, NaOH; buffer B: 1.5 M NaCl, 10 mM NaOH; flow rate: 2.5 mL/min, gradient 0−100 min, 90−40% A and 10−60% B).

Gel electrophoresis analysis using 1-ethyl-2-[3-(1-ethylnaphtho[1,2-*d*]-thiazolin-2-ylidene)-2-methylpropenyl]-naphtho[1,2-*d*]thiazolium bromide (Stains all, Sigma Chemical Co.) stained gel and analysis by densitometer of the crude 3' amino-modified ODNs synthesized from the above supports showed that in the crude ODNs synthesized from Fmoc- and TFA-protected propanolamine supports, 3'-[(hydroxypropyl)amino]-modified ODN, oligo-1 migrated one unit faster than the ODN containing 3'-*N*-acetyl-*N*-(hydroxypropyl)amino, and 3'-hydroxyl ODNs was observed between ODNs, containing 3'-propanolamine and *n*-1 (Figure 2). Both 3'-[*N*-acetyl-*N*-
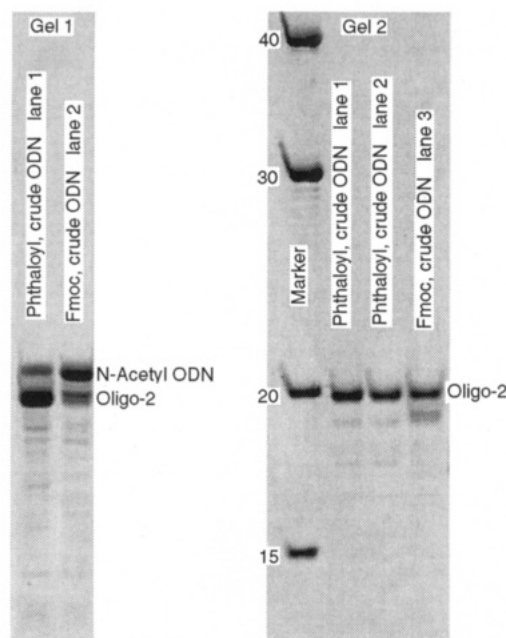
Figure 7. Gel electrophoresis analyses of the crude ODNs oligo-2 synthesized from Fmoc- (**26**, lane 2, gel 1; lane 3, gel 2) and phthaloyl-protected (**32**, lane 1, gel 1; lane 1 and 2, gel 2) (hydroxypropyl)triglycyline−CPG supports. The crude ODNs were deprotected in concentrated ammonium hydroxide:40% aqueous methylamine, 1:1, for 5−10 min, at 56 °C (lanes 1 and 3, gel 2), 40% aqueous methylamine, overnight, at 56 °C (lane 1, gel 1; lane 2, gel 2), and concentrated ammonium hydroxide, overnight, at 56 °C (lane 2, gel 1). These gels illustrate that the synthesis of oligo-2 using Fmoc-protected (hydroxypropyl)-triglycyl, **26**, and standard deprotection conditions gives 3′-[(*N*-acetyl-*N*-(hydroxypropyl)triglycyl] ODN as a major product.

(hydroxypropyl)amino] and 3′-hydroxyl ODNs were identified by comparison with standard ODNs on the same gel (Figure 3).

The ratio of 3′-*N*-acetyl ODN, oligo-1,3′-hydroxyl ODN, and *n*-1 ODN in the crude ODNs of the syntheses using Fmoc-protected CPG **5** and TFA-protected CPG **19**, revealed by densitometry analysis, that approximately 77 ± 3% and 73 ± 3% of the intact ODNs, oligo-1, with a 3′-[(hydroxypropyl)amino], were obtained in the above crude mixtures (Figure 4). Furthermore, in the synthesis using support **13**, neither 3′-*N*-acetyl nor 3′-hydroxyl ODNs were observed. In the synthesis cycle studies, when the capping step was extended to 16, 25, 50, 100, 300, and 600 s, as shown in Figure 5, and the detritylation step was extended to 30, 45 s, as shown in Figure 6, the syntheses of 3′-[(hydroxypropyl)amino] ODN, oligo-1 from phthaloyl-protected propanolamine support, using these modified cycles, still gave high quality full-length products. This result showed that the phthaloyl group is stable in basic and acidic conditions of ODN synthesis.

3′-[(Hydroxypropyl)tryglycyl] ODN conjugates, oligo-2 were also synthesized from Fmoc- (**26**) and phthaloyl-protected (**32**) (hydroxypropyl)triglycyl CPG supports. In the synthesis using support **26**, the concentration of the trityl of the first synthesis cycle was very low compared with the other trityls in the synthesis. The coupling efficiency of the synthesis was still ≥97%. However, the major component in the crude ODN which was deprotected under standard deprotection conditions (concentrated ammonium hydroxide, overnight, at 56 °C) was *N*-acetyl ODN (Figure 7, gel 1). The crude 3′-(hydroxypropyl)triglycyl] ODN conjugates, oligo-2 synthesized from supports **26** and **32** were deprotected under two deprotection conditions: concentrated ammonium hydroxide:40% aqueous methylamine, 1:1, for 5−10 min,

at 56 °C, and 40% aqueous methylamine, overnight, at 56 °C. The major component in these crude mixtures is oligo-2 (Figure 7, gel 2). A possible explanation could be that on the detritylation of the first cycle, the Fmoc group is cleaved and quenched with the trityl cation, and this intermediate is capped by acetic anhydride and NMI. The *N*-acetyl-linker bound support is stable after the first synthesis cycle in the deprotection step of ODN, and the acetyl group is removed under the fast deprotection conditions (concentrated ammonium hydroxide:40% aqueous methylamine, 1:1, for 5−10 min, at 56 °C), but not in standard deprotection condition.

CONCLUSIONS

The advantages of the phthaloyl-protecting group in the synthesis of 3′-amino terminal ODNs have been demontrated. Additionally, optional cleavage/deprotection conditions have been developed for this class of ODN's. Of interest is the observation that prolonged treatment of ODNs having 3′-amino termini to standard deprotection condition leads to the loss of the propanolamine side chain.

LITERATURE CITED

(1) Zendegui, J. G., Vasquez, K. M., Tinsley, J. H., Kessler, D. J., and Hogan, M. E. (1992) In vivo stability and kinetics of absorption and disposition of 3′ phosphopropyl amine oligonucleotides. *Nucleic Acids Res. 20*, 307−314.

(2) Asseline, U., and Thuong, N. T. (1990) New solid-phase for automated synthesis of oligonucleotides containing an aminoalkyl linker at their 3′ end. *Tetrahedron Lett. 31*, 81−84.

(3) Reed, M. W., Adam, A. D., Nelson, J. S., and Meyer, R. B. (1991) Acridine- and cholesterol-derivatized solid supports for improved synthesis of 3′ modified oligonucleotides. *Bioconjugate Chem. 2*, 217−225.

(4) Nelson, P. S. (1992) Multifunctional controlled pore glass reagent for solid phase oligonucleotide synthesis. U. S. Patent No. 5,141,813 (Aug 25, 1992).

(5) Nelson, P. S., Frye, R. A., and Liu, E. (1989) Bifunctional oligonucleotide probes synthesized using a novel CPG support are able to detect single base pair mutations. *Nucleic Acids Res. 17*, 7187−7194.

(6) Vu, H., Singh, P., Lewis, L., Zendegui, G. J., and Jayaraman, K. (1993) Synthesis of cholesteryl supports and phosphoramidite for automated DNA synthesis of Triple-helix forming oligonucleotides (TFOs). *Nucleosides Nucleotides 12*, 853−864.

(7) Melenhofer, J., Waki, M., Heimer, E. P., Lambros, T. J., Makofske, R. C., and Chang, C. (1979) Solid phase synthesis without repetitive acidolysis. Preparation of Leucyl-Alanyl-Glycyl-Valine using 9-fluorenylmethyloxycarbonylamino acids. *Int. J. Peptide Protein Res. 13*, 35−42, published by Munksgaard, Copenhagen.

(8) Vu, H., Hill, T. S., and Jayaraman, K. (1994) Synthesis and properties of cholesteryl-modified triple-helix forming oligonucleotides containing a triglycyl linker. *Bioconjugate Chem. 5*, 666−668.

(9) Reddy, M. P., Hanna, N. B., and Farooqui, F. (1994) Fast cleavage and deprotection of oligonucleotides. *Tetrahedron Lett. 35*, 4311−4314.

(10) Wolfe, S., and Hasan, S. K. (1970) Five-membered rings. II. Inter and intramolecular reactions of simple amines with *N*-substituted phthalimides. Methylamine as a reagent for removal of a phthaloyl group from nitrogen. *Can. J. Chem. 48*, 3572−3579.

Fatty Acid Acylated Peroxidase as a Model for the Study of Interactions of Hydrophobically-Modified Proteins with Mammalian Cells

Vladimir I. Slepnev,[†,‡] Laurent Phalente,[§] Hubert Labrousse,[§] Nikolai S. Melik-Nubarov,[†,⊥] Véronique Mayau,[§] Bruno Goud,[§] Gérard Buttin,[§] and Alexander V. Kabanov[*,†]

Laboratory of Biopolymer Chemistry, Russian Research Center of Molecular Diagnostics and Therapy (RCMDT), Simpheropolskii blvd. 8, Moscow 113149, Russia, and Unités de Génétique Somatique (URA CNRS 361) et d'Immunocytochimie (URA CNRS 359), Institut Pasteur, 25 rue du Dr. Roux, 75724 Paris Cédex 15, France. Received March 20, 1995[⊛]

Artificial fatty acylation of proteins has attracted significant attention during the last decade as a method for modification of protein specificity and efficacy of action on mammalian cells (A. V. Kabanov and V. Yu. Alakhov (1994) *J. Contr. Release 28*, 15–35). Horse radish peroxidase (HRP) is used in this work to study the interaction of a fatty acylated protein with various mammalian cells. The HRP is modified with the chloranhydride of the stearic acid in the reversed micelles of sodium bis-(2-ethylhexyl)sulfosuccinate (Aerosol OT) in octane, a convenient protocol allowing production of protein molecules with a controlled, low modification degree (A.V. Kabanov et al. (1987) *Ann. N. Y. Acad. Sci. 501*, 63–66). The influence of the hydrophobic group on the binding and internalization of HRP in MDCK, P3-X63-Ag8, CHO, and HepG2 cells is examined. The major results are as follows: (i) the fatty acylation of a protein significantly enhances its binding to all tested mammalian cell lines, with a line-specific efficiency; (ii) the binding efficiency can be modified by changing growth conditions in a defined medium; (iii) along with the enhancement of protein adsorption on the plasma membrane, fatty acylation increases internalization of the protein during incubations at 37 °C; (iv) internalized protein was observed in endocytic vesicles; no evidence was obtained for a cytoplasmic distribution. These results are discussed in connection with previously observed effects of the fatty acylated proteins on cell activity.

INTRODUCTION

Posttranslational modification of proteins with lipids, specifically fatty acid acylation, has been discovered over the past decade in yeast, plant, and animal cells and viruses (for reviews, see *1–5*). Numerous studies demonstrate that such modifications help proteins to insert into membranes and play an important role in the accomplishment of their physiological functions.

Recently, this natural way of protein hydrophobic modification has been used for enhancement of biopolymer interaction with lipid and cell membranes (for reviews, see *6–8*). Particularly, Peacock *et al.* used artificially fatty acylated antibodies for introduction of a

"surrogate receptor" into a cell membrane (*9, 10*) and to enhance cell-to-cell interactions (*11, 12*). Fatty acylated Fab-fragments of antibodies to neurospecific proteins have been used as effective vehicles for *in vivo* targeted delivery of a drug into the brain (*13*). Fatty acylation of bacterial and plant toxins has been shown to modulate their biological activity (*14, 15*). Fatty acylated antibodies directed against a virus protein were observed to reduce virus recovery when added to the virus-infected cells (*16–18*), suggesting that fatty acylated proteins penetrate into the cytoplasmic compartment of a mammalian cell (*19*). This modification also significantly enhances the therapeutic efficacy of the antiviral antibodies in the virus-infected animals (*20*). These works have demonstrated that artificial fatty acylation of proteins is a very useful tool for increasing biological activities of various proteins and design of drug delivery systems (*6, 8*). The phenomena described in refs 9–20 were observed with fatty acylated proteins with diverse functional activities (enzymes, toxins, antibodies, and their Fab-fragments), broad range of molecular masses (from 20 to 150 kDa), and various degrees of glycosylation. Furthermore, the end modification of the short complementary oligonucleotides with the long-chain alkyl groups has been reported to significantly enhance transport into cells and antisense activity of these oligonucleotides (*21–26*). The molecular mechanisms of these diverse phenomena has not been sufficiently understood. An improved knowledge of the influence of fatty acid groups on the capacity of biopolymers, particularly, proteins to bind with biological membranes and to facilitate transport into a cell is of both basic and applied interest. In order to explore this problem, appropriate model systems should be used that allow for easy

monitoring of the binding and intracellular distribution of the hydrophobically modified molecule. A convenient model to study the interaction of the fatty acylated proteins with mammalian cells is horseradish peroxidase (HRP). This enzyme has been previously used as a marker for endocytosis (27, 28). Furthermore, the accumulation of HRP into a cell and its intracellular localization can be assayed directly by measuring the enzyme catalytic activity. We have used the stearic acid acylated HRP to mimic the interaction of the fatty acylated proteins with various mammalian cell lines. Specifically, we examined the influence of the hydrophobic anchor on the binding and internalization of HRP to cells of different histotypes (MDCK, P3-X63-Ag8, CHO, and HepG2).

EXPERIMENTAL PROCEDURES

HRP Modification. HRP was purchased from Boehringer Manheim (EIA grade) and used without further purification. The protein *RZ* (absorbance ratio A_{403}/A_{280}) equaled 3.0. HRP was modified with stearoyl chloride in the reverse micelle system of Aerosol OT in octane using the method described (29, 30). Briefly, HRP solution (2.5—5.0 mg/mL) in 0.1 M Na—borate buffer (pH 9.5) was mixed with a 10-fold volume excess of 0.3 M Aerosol OT solution in octane. This mixture was shaken until it became optically transparent ($\simeq$5 min), and then a 10% solution of the stearoylchloride in octane was added and the reaction mixture was incubated for 2 h at room temperature. The protein was precipitated by adding a 5-fold volume excess of cold (−20 °C) acetone or cold (−40 °C) ethanol and separated by centrifugation at 2000 rpm. The precipitate was washed three times by repeated resuspension and precipitation in cold acetone or ethanol, dried, dissolved in 0.1 M Na—borate buffer (pH 8.0) containing 0.1% sodium deoxycholate, and purified by gel filtration on Sephadex G25 (or Biogel P4) using PBS (pH 7.4) as an eluent. The protein recovery from the reaction system was determined by measuring the protein concentration by the Lowry method (31) or spectrophotometrically at 280 and 403 nm. The HRP *RZ* and the catalytic activity in the reaction of *o*-phenylenediamine oxidation were determined. These activities were related to a HRP concentration in the samples obtained. The modification degree (number of fatty residues introduced in a protein molecule) of HRP was determined by titration of the free amino groups of the protein with TNBS using the method described (32). For the purpose of TNBS titration only, prior to HRP precipitation with acetone, the reversed micelle systems containing the protein were acidified with 5 μL of 0.2 M HCl (33). HCl was not added to the samples precipitated with ethanol. The TNBS titration was performed in 96-well plates. The optimal conditions for the titration were as follows: HRP concentration, 6 μM; TNBS concentration, 0.6 mM; 0.1 Na—borate buffer, pH 9.5. The 25 μL of the HRP aqueous solutions were introduced in the wells containing 250 μL of the buffer. The reaction was started by adding 25 μL of the TNBS solution. The blank wells contained the buffer solutions to which 25 μL of the distilled water (instead of the HRP samples) and 25 μL of the TNBS solution were added. The optical density at 403 nm was determined 2 h after the reaction was started. The degree of HRP modification (*N*), i.e., the number of stearic acid residues per protein molecule, was determined as follows

$$N = 4 \cdot [\Delta D_o - \Delta D_m]/\Delta D_o \qquad (1)$$

where ΔD_o is the change of the optical density in the wells

containing the unmodified HRP compared to the blank and ΔD_m is the change of the optical density in the wells containing the modified HRP compared to the blank; the total amount of the modifiable NH_2-groups in the HRP molecule equals 4.

Cell Lines and Culture Conditions. Cells were grown at 37 °C, in a 5% CO_2 atmosphere in media containing 10% fetal calf serum, penicillin, and streptomycin. The following lines were used: P3-X63-Ag8 (designated below: X63), a mouse myeloma line; CHO, a Chinese hamster ovary fibroblastic line; MDCK, the Mardin Derby canine kidney cell line; HepG2, a human hepatoma line. The X63 and CHO cells were grown in RPMI 1640 media (supplemented with 1 mM glutamine), MDCK cells were grown in 199 medium, and HepG2 cells were grown in RPMI medium supplemented with 10 mM Hepes (pH = 7.0). All lines were grown attached (MDCK, HepG2, CHO) or unattached (X63) in Petri dishes. The CHO cells were also grown in suspension (designated below as CHO*sus*). Attachment to plastic dishes (Corning) of repeatedly passaged CHO cells is weak and can be completely prevented by stirring in passages. CHO*sus* cells regain a division rate (1.5 div/24 h) that approximates the rate of attached cells within two to three passages. In the reported experiments, attached cells were trypsinized, centrifuged after serum addition, and grown in the spinner flasks for at least three passages, first from 10^5 to 5.10^5 and then from 10^4−5 × 10^4 to 10^5−5 × 10^5 cells.

HRP Binding. Cells (10^5 to 5 × 10^5), growing as monolayers in 24-well plates or distributed into such plates as samples from a suspension culture, were washed twice in serum-free medium (4 or 37 °C) and replaced with 0.2−1 mL of medium, with or without serum. The solution of unmodified or fatty acylated HRP in PBS (pH 7.2)—or PBS in the controls—was added to the cells. After incubation for various periods of time at 4 or 37 °C, the cells were washed at 4 °C (four times with serum free medium and then four times with PBS) and lyzed on ice in 10 mM Tris—HCl buffer (pH 7.6) containing 1% Triton X-100. HRP activity in the lysates was determined spectrophotometrically in 96-well plates. Aliquots of lysates (50 μL) were added to 200 μL of a fresh *o*-phenylenediamine solution (5 mg/mL) in 0.1 M citrate buffer (pH 5.0), containing 0.1% Triton X-100, 1 mg/mL BSA, and 0.02% H_2O_2. The reaction product was detected at 492 nm or at 450 nm after the reaction was stopped by addition of a 0.5% Na_2SO_3 solution in 2 N H_2SO_4 using a Multiskan photometer. Cell lysate components did not affect the determination of unmodified or fatty acylated HRP activity. HRP concentration in the lysates was determined by comparing HRP activity in the lysate to a standard curve of purified HRP. To avoid partial inactivation of the purified HRP at low protein concentrations the final dilution and incubation of the purified HRP were made in enzyme-free cell extract. To account for the possible effect of the cell lysate on the HRP activity the calibration curves for the unmodified and modified HRP were obtained in the presence of the enzyme-free cell lysates. Values for fatty acylated HRP were corrected to take in account the loss of activity of HRP during its modification.

HRP Internalization. When the amount of internalized HRP was determined, the cells were incubated with HRP, washed three times with cold serum free medium as described above, and incubated 30 or 60 min at 4 °C with proteinase K (5 mg/mL) in PBS. The medium was substituted for 10 min with fresh media containing aprotinine (10 U/mL), and the cells were washed three

Table 1. Characteristics of the HRP Modified with the Fatty Acid Residues

protein:reagent (molar ratio)	method of HRP extraction[a]	modificn degree[b]	enzyme activity after modificn[c] (%)
1:0	A	0	45
1:50	A	<0.1	80
1:100	A	0.6	50
1:200	A	1.0	50
1:300	E	1.1	nd
1:1000	E	3.2	nd

[a] HRP was precipitated from the reaction system by A, acetone, E, ethanol. [b] Number of fatty acid residues per protein molecule. [c] The activity of the modified HRP in the o-phenylenediamine oxidation reaction on the percentage basis of the activity of the native proteins.

times with cold medium and lysed with Triton X-100. HRP activity and protein concentration were determined as described above.

Intracellular Localization of HRP. For intracellular localization of HRP, cells grown on coverslips were incubated with unmodified or fatty acylated HRP without serum at 37 °C for 3 h and then washed and fixed with 4% paraformaldehyde in PBS for 20 min or in 1% glutaraldehyde in 0.1 M cacodylate (pH 7.4). HRP was then revealed using DAB and H_2O_2 as the substrates (34). Cells were visualized using a Zeiss photomicroscope.

RESULTS

HRP Modification with Fatty Acid Residues. The method of protein modification with water-insoluble reagents in the reversed micelles of Aerosol OT in octane (29) was used for coupling fatty acid residues to HRP. The product recovery after modification was 60–90% of the HRP taken into reaction. Some characteristics of the modified HRP are presented in Table 1. The solubility of modified HRP generated in these experiments lies in the range 0.3–1.0 mg/mL. The titration of the HRP free amino groups with TNBS revealed that the coupling of fatty acid residues with the protein molecules proceeds via amino group acylation. As shown earlier, proteins retain biological activity after modification in a reverse micelle system, although some inactivation may take place (7). The *RZ* values of HRP (35) after modification were 70–90% of the *RZ* of the unmodified HRP (data not shown). The catalytic activity of HRP after modification was at least 50% of the activity of the unmodified enzyme (Table 1). The decrease of the activity was apparently not a consequence of the introduction of fatty residues in the protein molecule but—presumably—of the treatment of the proteins with organic solvents during the modification procedure. The same loss of activity was observed for the HRP solubilized in the micellar system, incubated without adding the modifying reagent, and precipitated with acetone or ethanol. The degree of HRP modification depends on the molar ratio [fatty acid chloride]:[protein] in the reaction system. We have chosen for further experiments the HRP samples containing about 1 stearoyl group per protein molecule. The majority of studies on artificially modified proteins have been performed with a similar degree of modification (13–20). The naturally modified proteins commonly contain one to three fatty acid substituents (2).

Effect of Fatty Acylation on HRP Uptake. The effect of modification on HRP interaction with MDCK, X63, CHO, and HepG2 cells was studied. Specifically, we were evaluating the effect of this modification on the protein adsorption by the cell membrane and internalization into the cell. Below, we will use the term "uptake" to characterize the total binding of the protein with cells as a result of adsorption and endocytosis. The terms

Table 2. Uptake and Distribution of Unmodified HRP in MDCK Cells

HRP sample	cell-bound HRP[a] (mol × 10⁻³/cell)		
	total uptake	adsorption	internalization
unmodified	10	3	7
incubated in the reverse micelle system without modification and then precipitated	10	3.5	6.5

[a] HRP was incubated with cells for 1.5 h at 37 °C. HRP concentration: 20 μg/mL (0.5 μM). Internalized HRP was determined as the proteinase K-resistant fraction (see Materials and Methods); HRP adsorbed on the cell surface was calculated as the difference between total uptake and internalized protein.

"adsorption" and "internalization" refer to the protein binding on a cell surface and endocytosis into a cell, respectively. The experiments performed can be subdivided into the following four categories. First, the adsorption of HRP with cells was studied at 4 °C under the conditions where endocytosis is abolished or significantly diminished. Second, the uptake of HRP was studied at 37 °C. Third, to discriminate the adsorbed and internalized HRP the cells were treated with proteinase K after incubation with the protein; this treatment results in the removal of the protein from the external cell surface. Fourth, the intracellular localization of the internalized HRP was studied cytochemically. In the first three types of experiments the cells were incubated with the unmodified HRP for various periods of time and then washed and lyzed, and the amount of cell-bound HRP was determined by measuring the enzyme activity in the cell lysate (see Materials and Methods). The cytochemical study was performed on the fixed cells, incubated with HRP at 37 °C. The results obtained are presented in Figures 1–3 and Tables 1–6 and are summarized below.

(a) Unmodified HRP as a Control. During the modification procedure in the reversed micelle system HRP was exposed to various agents such as organic solvents and Aerosol OT. This treatment could possibly result in a change in the HRP properties, specifically, in alteration of its binding with the cells. To exclude this possibility the unmodified HRP was compared with HRP that was solubilized in the micellar system, incubated without adding the modifying reagent, and precipitated. Neither the uptake of HRP nor its adsorption and internalization were significantly affected as a result of this treatment (see, for example, Table 2). Thus, unless indicated otherwise, the unmodified HRP was used as a control in the experiments described below.

(b) Effect of Serum. As illustrated in Figure 1 for MDCK cells incubated for 3.5 h at 4 °C with unmodified or modified HRP, the binding of HRP is considerably enhanced by fatty acylation of the protein. The addition of 10% calf serum decreases the binding of modified HRP, while the binding of the unmodified protein is practically not affected. The inhibition of the binding of the modified protein appears to be due to the presence in serum of large amounts of protein with an affinity for fatty acids, such as albumin. However, even in the presence of serum the binding of the modified HRP is still substantially higher than binding of the unmodified protein (Figure 1). The experiments on HRP interaction with cells described below were carried out in serum-free medium unless indicated otherwise.

(c) HRP Adsorption on the Cell Surface at 4 °C. As shown in Table 3, some unmodified HRP was found associated with cells of every line after incubation at 4 °C. The attachment of a fatty acid group to HRP considerably (16–33 times) enhanced the recovery of the
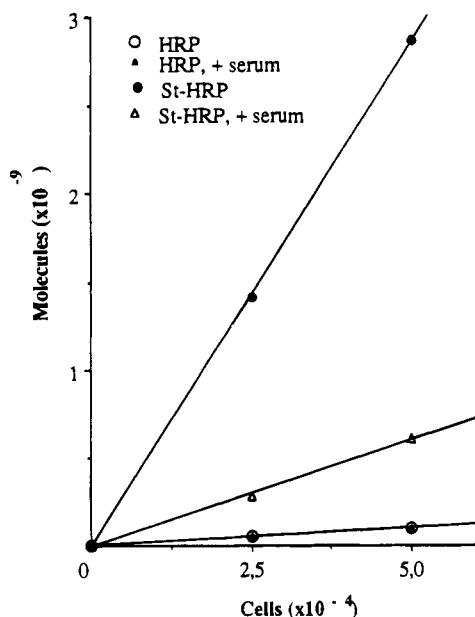
Figure 1. Effect of serum on the binding of native and modified HRP to MDCK cells at 4 °C. Cells incubated for 3.5 h with 10 μg/mL of unmodified HRP (HRP) or modified HRP (St-HRP; modification degree: 1.0); 10% fetal calf serum added to the incubation medium as indicated.

Table 3. Uptake of Native and Modified HRP by Cells of Different Lines after 3.5 h of Incubation at 4 and 37 °C

cell line	cell-bound HRP[a] (mol/cell × 10^{-3})				ratio of bound modified/native HRP molecules	
	4 °C		37 °C			
	native	modified[b]	native	modified[b]	4 °C	37 °C
MDCK	5.9	180	100	760	30	7.6
X63	13	430	40	800	33	20
CHO	26	430	220	770	16	3.5
HepG2	nd	nd	4.3	280		65

[a] HRP concentration: 20 μg/mL (0.5 μM); all incubations were for 3.5 h. [b] Modification degree: 1 stearic acid residue per protein molecule.

cell-associated protein. Treatment of the cells with proteinase K completely abolished the binding of the unmodified and modified HRP at 4 °C (data not shown). Therefore, under these conditions, both the unmodified and modified HRP are adsorbed on the external side of the plasma membrane. Generally, these results suggest that the fatty acid groups strongly increase the adsorption of HRP to the cell surface.

We examined the kinetics of uptake of modified HRP (Figure 2). The uptake at 4 °C in HepG2 cells was a saturable process; after 30 min incubation, the amount of cell-associated enzyme reaches the maximal value and then remains essentially constant during at least 3.5 h. This curve is likely to be the manifestation of the fast adsorption of the modified HRP on the external cell membrane.

(d) HRP Uptake at 37 °C. At 37 °C the uptake of unmodified HRP was increased by 3–17-fold compared to 4 °C uptake due to internalization of HRP into cells through the fluid phase endocytosis process (27). Modification further increased the amount of cell-associated HRP after incubation at 37 °C. The effect of lipid modification on HRP uptake varied from approximately 3 to approximately 60 times depending on the cell line studied (Table 3). As shown on Table 4 for MDCK and X63 cells, some interexperimental variation was observed in the number of HRP molecules bound by cells of the
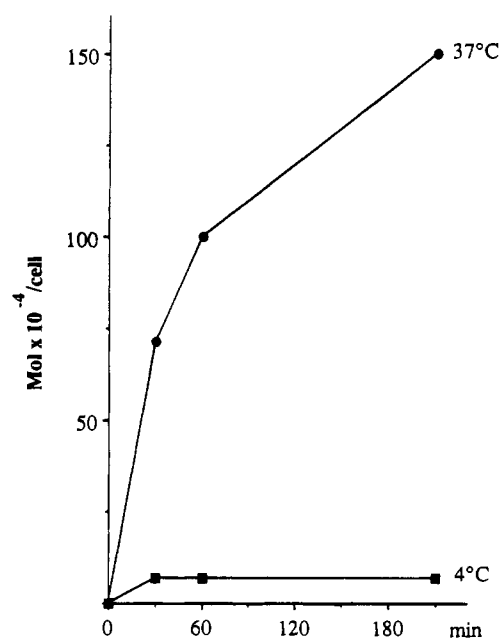
Figure 2. Kinetics of binding of modified HRP with HepG2 cells at 4 or 37 °C in serum-free medium. Concentration of modified HRP (modification degree: 1.0) equals 10 μg/mL.

same cell line (7.5 × 10^3 to 4.1 × 10^4 for MDCK; 6.2 × 10^3 to 4.0 × 10^4 for X63). However, the increase in HRP binding observed following modification of the protein was constant with the ratio of modified to unmodified being 9.3 (± 22.6%) for MDCK and 26 (± 45%) for X63. One observation made for all cell lines studied (except HepG2) is that the ratio of modified to unmodified HRP bound to the cells is markedly higher at 4 °C than at 37 °C (Table 3).

Direct evidence was obtained suggesting that a change in growth conditions can markedly modify the interactions between modified HRP and cells. As illustrated in Table 5, the binding of modified HRP to CHO cells grown in the same medium either attached to a support or in suspension (see Materials and Methods) was consistently higher when the cells were recovered from a suspension culture, although the medium components were identical and the two cell populations originated from the same culture a few passages earlier. It is possible that the 4-fold increase in uptake of modified HRP in the suspension culture compared to uptake in the cell monolayers is due to the increase of the cell surface area accessible for HRP binding. It is worth mentioning that the ratio of modified to unmodified HRP bound to the cells was notably greater in suspension culture compared to the cell monolayers. The possible reasons for that phenomenon are discussed below.

The kinetic analysis of uptake of modified HRP by HepG2 cells (Figure 2) was entirely consistent with the interpretation that the increased uptake measured at 37 °C is the consequence of a progressive internalization of the protein: in contrast to the saturation process characterizing the interaction of modified HRP with the cells at 4 °C, the amount of cell-bound enzyme continuously increased during 3.5 h.

(e) HRP Adsorption and Internalization at 37 °C. To evaluate internalization of the modified and unmodified HRP we determined the effect of proteinase K treatment on the amount of cell-bound proteins. The results of such experiments in CHO cells are shown in Table 6. All HRP (modified or unmodified) adsorbed at the cell surface at 4 °C was removed as a result of proteinase K treatment. In contrast, at 37 °C, only 30% of the modified protein is

Table 4. Uptake of Native and Modified HRP by Cells of Lines MDCK and X63 after 3.5 h Incubation at 37 °C

| cell line | experiments | cell-bound HRP[a] (mol × 10⁻³/cell) | | ratio modified/native |
		native	modified[b]	
MDCK	(1)	25	190	7.6
	(2)	19	220	11.6
	(3)	41	270	6.6
	(4)	12	130	10.8
	(5)	7.5	74	9.9
	av[c]	20.9 ± 13.1	177 ± 77	9.3 ± 2.1
X63	(1)	40	800	20
	(2)	6.2	200	32
	(3)	13	510	39
	(4)	27	330	13
	av[c]	21.5 ± 15.0	460 ± 260	26 ± 11.7

[a] HRP concentration: 20 μg/mL (0.5 μM). [b] Modification degree: 1 stearic acid residue per protein molecule. [c] Values are mean ±SEM.

Table 5. Uptake of Native or Modified HRP in CHO Cells Grown Attached (CHO) or in Suspension (CHO*sus*) after 2.5 h Incubation at 4 and 37 °C

| experiments | cells | temp (°C) | cell-bound HRP (mol × 10⁻²/cell) | | modified/ native |
			native	modified[a]	
(1)	CHO	4	7.9	95	12
	CHO*sus*	4	8.0	330	41
(2)	CHO	37	60	370	6
	CHO*sus*	37	100	2200	22

[a] Modification degree: stearic acid residue per protein molecule.

Table 6. Uptake and Distribution of Unmodified and Modified HRP Bound to CHO Cells at 4 and 37 °C

| | cell-bound HRP[a] (mol × 10⁻⁴/cell) | | | |
| | unmodified | | modified[b] | |
	4 °C	37 °C	4 °C	37 °C
total uptake	2.0	8.5	42	47
adsorbed protein[c]	2.0	<1.0	42	17
internalized protein[c]	<1	8.5	<1	30

[a] Incubation time was 3 h. HRP concentration: 20 μg/mL (0.5 μM). [b] Modification degree: 1 stearic acid residue per protein molecule. [c] Internalized HRP was determined as the proteinase K-resistant fraction (see Materials and Methods); HRP adsorbed on the cell surface was calculated as the difference between total and internalized protein.

accessible to protease. Figure 3 more precisely compares the kinetics of internalization versus total uptake of unmodified or modified HRP to MDCK cells at 37 °C. It shows that the fatty acylation of HRP results in the enhancement of both its adsorption and its internalization under the same conditions. In an independent experiment (not shown), all the unmodified or fatty acylated HRP adsorbed at 4 °C was again removed from these cells by proteinase K.

(f) HRP Intracellular Localization. The intracellular localization of unmodified and fatty acylated HRP at 37 °C was studied using the oxidation reaction of DAB by HRP (*34*). The brown insoluble product of this reaction is detected at the places where the enzyme is localized. Both the unmodified and modified HRP were found in intracellular vesicles of the cells (Figure 4). No diffuse staining which would have been characteristic of HRP distribution in the cytoplasm (*34*) was observed under our experimental conditions.

DISCUSSION

It is known that proteins modified with fatty acid residues can bind to natural and model lipid membranes.
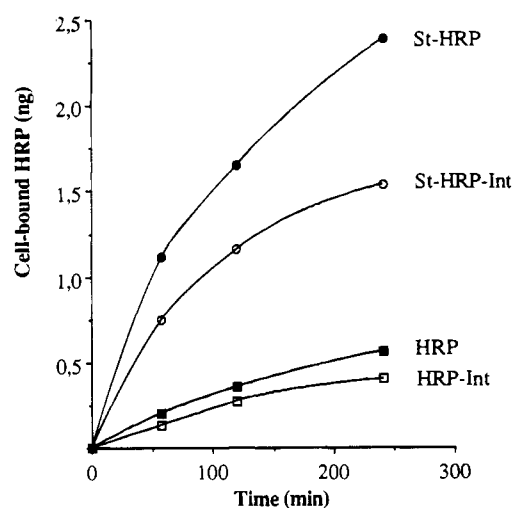
Figure 3. Kinetics of binding and internalization of unmodified and modified HRP by MDCK cells. Cells incubated at 37 °C (in serum-free medium) with 20 μg/mL of the proteins (HRP unmodified; St-HRP: modified (modification degree: 1)). The amount of internalized protein (HRP-Int, St-HRP-Int) was determined after proteinase K treatment (see Materials and Methods and Table 6).

In particular, artificial fatty acylation makes water-soluble proteins able to incorporate into liposomal membranes (*36–38*). Colsky and Peacock (*9–12*) reported that fatty acylated antibodies bind effectively to mammalian cells. The data reported here confirm and extend these observations and previous work from our laboratory (*13–21*).

Protein fatty acylation has been previously (*9–12, 36–38*) carried out with fatty acid chlorides or *N*-hydroxysuccinimide esters in aqueous sodium deoxycholate. Although the homogeneity of these preparations was not analyzed, the low solubility of the modified proteins indicates that they contain a significant fraction of molecules with a high degree of modification. For this reason, Colsky and Peacock (*9–12*) solubilized the modified proteins in deoxycholate solutions in their study on protein interactions with cells. But the anionic detergent possesses membranetropic properties and may significantly affect the plasma membrane state and the cell functional (e.g., endocytic) activity. Furthermore, in the experimental conditions used in refs *10* and *11* the high deoxycholate concentrations significantly reduced cell viability. In order to avoid these difficulties, we used in our previous studies (*13–21*) an essentially different method of protein modification with water insoluble reagents in reverse micelle system: it produces in high yields protein samples, homogeneous by their degree of
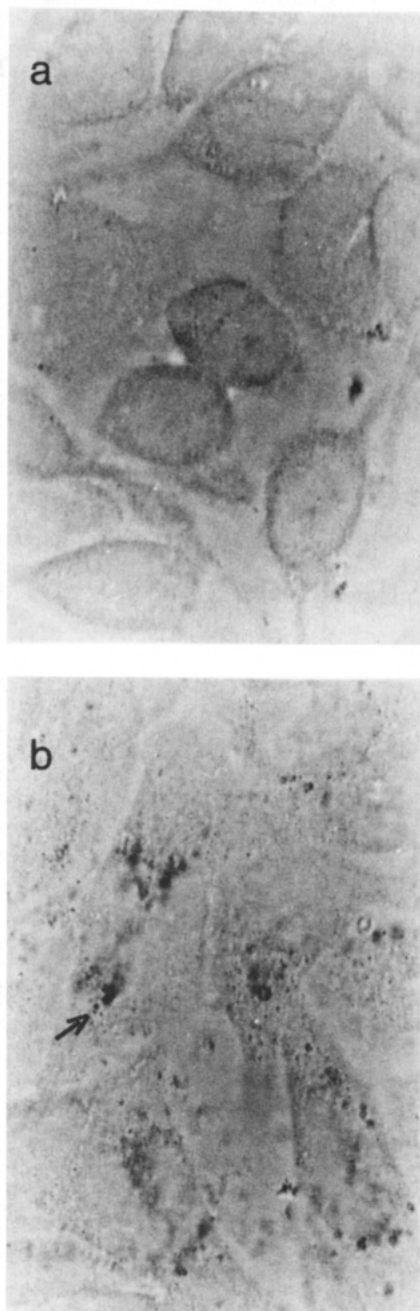
Figure 4. Intracellular localization of modified HRP in CHO cells: (A) untreated cells; (B) cells treated by modified HRP. Cells incubated at 37 °C (in serum-free medium) with 20 μg/mL of the modified HRP (modification degree: 1) for 3 h. Intracellular localization of modified HRP was assayed using DAB and H_2O_2 as the substrates' cells were visualized in a Zeiss photomicroscope.

modification and containing a controllable amount of fatty acid residues (7, 8).

The results obtained in this work clearly demonstrate that binding at 4 °C of HRP molecules to various cell types is considerably stimulated by fatty acylation. As previously reported for the binding of fatty acylated antibody (10-12), stimulation is inhibited in the presence of serum, presumably because serum proteins bind the fatty acid residues and thereby reduce their interaction with the cell membrane. At 4 °C, a temperature at which fluid phase endocytosis of HRP is greatly decreased (28), an increase in the amount of cell-associated HRP is expected to reflect enhanced adsorption of the modified protein to the cell membrane. Indeed, we observed saturation of HRP binding to HepG2 cells at 4 °C within

30 min; and all the protein adsorbed to the cells under such conditions remained accessible to external proteinase action. Taken together, the observations reported above show that the modification protocols employed in these experiments are adequate to generate fatty acylated proteins with an increased potential to bind membranes of a variety of mammalian cells.

The endocytosis of unmodified HRP at 37 °C has been well documented (27, 28). We studied the behavior of modified protein at this temperature. Under these conditions significant portions of modified HRP associated with cells were proteinase K-resistant which accounted for the protein internalization into cells. The adsorbed protein was measured as the proteinase K-sensitive fraction. Both the adsorption and internalization were significantly stimulated by HRP modification. The ratio of modified to unmodified HRP bound to a defined line at 37 °C was found to be remarkably constant in repeated experiments, despite variations in the absolute amount of bound proteins. Therefore, this ratio can be used to characterize the line-specific avidity of the mammalian cells for a fatty-acylated protein. Interestingly enough, in all our experiments a decrease in the modified to unmodified HRP ratio was observed for each cell line when the temperature was increased from 4 °C to 37 °C. This was due to increased endocytosis of the unmodified HRP compared to modified protein uptake at 37 °C. Furthermore, in the case of CHO cells the temperature increase leads to internalization of all surface-adsorbed unmodified HRP, while a significant amount of the modified protein remains bound to the surface of the cells at 37 °C. This result is consistent with the assumption that the unmodified HRP is mainly bound to the coated pits, while the modified protein binds both to the coated pit region as well as other sites on the membrane. As a result a substantial amount of the modified protein is not internalized through endocytosis and remains adsorbed at the cell surface at 37 °C. This hypothesis can also explain why the ratio of modified to unmodified HRP in CHOsus cells is greater than in CHO monolayers. The unmodified HRP binds on coated pits, which in the adherent cells are concentrated at the exposed portion of the cell membrane. Therefore, binding and internalization of the unmodified protein in CHO*sus* cells is comparable to that observed in confluent CHO monolayers. Contrarily, at both temperatures the binding of the modified HRP in the CHOsus is significantly greater relative to CHO monolayers, which reflects the increase in the surface area available for binding of the modified protein.

The model systems developed here should prove especially convenient to analyze some fundamental aspects of macromolecule transport governed by the recognition of defined fatty acid radicals. Structural differences in cell membranes may correspond to differences in the membrane state (lipid composition, microviscosity) or to the presence of more specific proteins (receptors) capable of binding the fatty acid residues.

It is worth mentioning that we have observed a significantly more pronounced effect of modification on HRP uptake in HepG2 cells compared to other cell lines. Our previous work on tissue distribution of fatty acylated proteins administered in the body indicates that modified antibody Fab fragments accumulate mostly in the liver (13). This accounts for the interaction of the fatty acylated protein with the hepatic plasma membrane fatty acid binding protein, known to play a role in hepatocellular fatty acid uptake (39). It will be of interest to determine if this receptor contributes to efficient inter-

nalization of the modified HRP into hepatic HepG2 cells observed in this work.

The cytochemical approach taken along this work to determine the fate of fatty acylated HRP molecules interacting with cultured mammalian cells shows that the modification stimulates attachment and internalization of the macromolecule but does not allow the recovery of a significant part of it as physiologically active cytosolic material (see also *8*). By the cytochemical method, we have not been able to detect in our experiments the presence of fatty acylated proteins in the cytoplasm.

Generally, the results obtained in this work demonstrate that HRP serves as a useful model for the study of interaction of the fatty acylated proteins with mammalian cells. However, one should be careful in applying the results from *in vitro* experiments to the *in vivo* situations. Besides serum effects there are other factors (degradation in liver, uptake in reticulo-endothelial system, etc.) that may significantly affect the fate of the fatty acylated proteins *in vivo*. As far as the serum is concerned, there will always be an equilibrium between modified proteins bound and unbound with serum proteins. Furthermore, cell surfaces (particularly, specific receptors on them) will compete with the serum proteins for binding with the modified proteins; with the "high affinity" surfaces or receptors being most successful in this competition. The rapid internalization of the modified proteins would additionally shift this equilibrium toward cell-bound forms and lead to accumulation of the modified protein in a certain tissue. The serum-free experiments described in the paper permit us to exclude the serum protein effects and to characterize the capacity of various cells to interact with the modified proteins. Another limitation of this model consists in the fact that HRP does not have a defined receptor providing for its specific binding on and internalization into cells (27). Therefore, while the approach proposed in this work is useful for elucidation of the effect of the fatty acid residue on the protein uptake, it cannot mimic the situation when the fatty acylated protein is also recognized by a cell in a protein-specific manner and internalized into a cell via the receptor-mediated endocytosis. The majority of the previous work on fatty acylated proteins (*13–21*) was conducted on the proteins that were capable of specific recognition of the receptors or antigens on the cell surface. These data indicate that specific binding with cell components can dramatically alter the fate of fatty acylated proteins during their interaction with cells *in vitro* or administration *in vivo*. Particularly, the modification of antibodies to virus antigens expressed on the external surface of the plasma membrane of virus-infected cells results in considerably stronger enhancement of antibodies binding with the infected cells, compared to the noninfected cells (*18*). The similar effect has been recently observed in our laboratory for a fatty acylated protein ligand (data in preparation). The specific binding of this protein and the receptor-mediated effect on cells are dramatically increased as a result of the modification. It is probable that similar mechanisms underlie the enhancement of the activity of some toxins observed earlier (*14, 15*). Furthermore, it has been reported that the fate of the fatty acylated Fab fragments of antibodies during their administration *in vivo* crucially depend on their tissue specificity (*13*). Unlike the fragments of the nonspecific antibodies that accumulate in the liver, the fragments of antibodies to the neurospecific antigens are delivered to the brain tissues. These specific phenomena observed with the fatty acylated proteins need subsequent study.

It will also be of interest to compare the behavior of artificially modified and naturally modified proteins that are bound on a membrane via a lipid anchor. It has been recently reported that phosphatidylinositol-anchored proteins are internalized through an unusual pathway that does not involve endocytosis through coated pits (*40*). Therefore, the localization at the specific regions of the plasma membrane and mechanism of internalization of the artificially modified proteins should be studied in detail to elucidate the possible effect of the chemical structure of the lipid anchor on the protein internalization pathways.

Further studies are also required to understand the intracellular fate of internalized fatty acylated proteins. Some of the questions to be addressed during these studies are listed below. Can the internalized fatty acylated protein be recycled to a cell surface? How does the fatty acylation affect the intracellular distribution and enzymatic degradation of a protein inside a cell? Are the internalization and intracellular distribution of fatty acylated proteins dependent on the chemical structure of a fatty acid anchor? The answers to these questions may help us to better understand the diverse phenomena observed with various fatty acylated proteins (*13–21*) and permit us to optimize their biological activity for subsequent biomedical applications.

ACKNOWLEDGMENT

LITERATURE CITED

(1) Low, M. G., and Saltiel, A. R. (1988) Structural and functional roles of glycosylphosphatidylinositol in membranes. *Science* 239, 268–275.

(2) Schultz, A. M., Henderson, L. E., and Oroszlan, S. (1988) Fatty acylation of proteins. *Ann. Rev. Cell. Biol.* 4, 611–647.

(3) Cross, G. (1990) Glycolipid anchoring of plasma membrane proteins. *Ann. Rev. Cell Biol.* 6, 1–39.

(4) Maltese, W.(1990) Post-translational modification of proteins by isoprenoids in mammalian cells. *FASEB J.* 4, 3319–3328.

(5) Chow, M., Der, C., and Buss, J. (1992) Structure and biological effects of lipid modifications on proteins. *Curr. Op. Cell Biol.* 4, 629–636.

(6) Torchilin, V. P.(1986) Liposomes as targetable drug carriers. *Crit. Rev. Ther. Drug Carrier Syst.* 2, 65–115.

(7) Kabanov, A. V., Alakhov, V. Yu., and Chekhonin, V. P. (1992) Enhancement of macromolecule penetration into cells and nontraditional drug delivery systems. In *Sov. Sci. Rev. D. Physicochem. Biol.* (V. P. Skulachev, Ed.) Vol. 11, Part 2, pp 1–77, Harwood Academic Publishers, Glasgow.

(8) Kabanov, A. V., and Alakhov, V. Yu. (1994) New approaches to targeting of bioactive compounds. *J. Contr. Release 28*, 15–35.

(9) Peacock, J. S., Londo, T. R., Roess, D. A., and Barisas, B. G. (1986) Biologic activity of antigen receptors artificially incorporated into lymphocytes. *J. Immunol.* 137, 1916–1923.

(10) Colsky, A. S., and Peacock, J. S. (1989) Palmitate-derivatized antibodies can function as surrogate receptors for mediating cell-cell interactions. *J. Immunol. Meth.* 124, 179–187.

(11) Colsky, A. S., and Peacock, J. S. (1991) Palmitate-derivatized antibodies can specifically "arm" macrophage effector cells for ADCC. *J. Leukocyte Biol.* 49, 1–7.

(12) Colsky, A. S., Mendez, L. E., and Peacock, J. S. (1991) FcR-independent antibody-mediated cellular cytotoxicity. *J. Leukocyte Biol. 49*, 548–555.

(13) Chekhonin, V. P., Kabanov, A. V., Zhirkov, Yu. A., and Morozov, G. V. (1991) Fatty acid acylated Fab-fragments of antibodies to neurospecific proteins as carriers for neuroleptic targeted delivery in brain. *FEBS Lett. 287*, 149–152.

(14) Alakhov, V. Yu., Kabanov, A. V., Kravtsova, T. N., Levashov, A. V., and Severin, E. S. (1989) The role of carbohydrate binding site of the Staphylococcus aureus enterotoxin A in its interaction with lymphoid cells and the effects of hydrophobic modification on the toxin biological activity. *Biologich. Membrany 6*, 582–586 (in Russian).

(15) Alakhov, V. Yu., Kabanov, A. V., Batrakova, E. V., Koromyslova, I. A., Levashov, A. V., and Severin, E. S. (1990) Increasing cytostatic effects of ricin A chain and Staphylococcus aureus enterotoxin A through in vitro hydrophobization with fatty acid residues. *Biotech. Appl. Biochem. 12*, 94–98.

(16) Kabanov, A. V., Ovcharenko, A. V., Melik-Nubarov, N. S., Bannikov, N. L., Alakhov, V. Yu., Kiselev, V. I., Sveshnikov, P. G., Kiselev, O. I., Levashov, A. V. and Severin, E. S. (1989) Fatty acid acylated antibodies against virus supress its reproduction in cells. *FEBS Lett. 250*, 238–240.

(17) Kabanov, A. V., Ovcharenko, A. V., Melik-Nubarov, N. S., Bannikov, N. L., Lisok, T. P., Klyushnenkova, E. V., Cherchenko, N. G., Alakhov, V. Yu., Kiselev, V. I., Sveshnikov, P. G., Levashov, A. V., Kiselev, O. I., and Severin, E. S. (1990) Effective inhibition of virus reproduction by hydrophobised antiviral antibodies. *Biomed. Sci. 1*, 63–67.

(18) Melik-Nubarov, N. S., Suzdaltseva, Y. G., Priss, E. L., Slepnev, V. I., Kabanov, A. V., Zhirnov, O. P., Sveshnikov, P. G., and Severin, E. S. (1993) Interaction of hydrophobized antiviral antibodies with influenza virus infected MDCK cells. *Biochem. Mol. Biol. Int. 29*, 939–947.

(19) Kabanov, A. V., Levashov, A. V., and Alakhov, V. Yu. (1989) Lipid modification of proteins and their membrane transport. *Protein Eng. 3*, 39–42.

(20) Kolomiets, A. G., Votyakov, V. I., Vladyko, G. V., Ovcharenko, A. V., Kabanov, A. V., Melik-Nubarov, N. S., Yaskovets, N. Yu., Malakhova, I. V., Eremin, V. F., Moroz, A. G., and Kolomiets, N. D. (1991) Antiviral activity and therapeutic efficiency of hydrophobized monoclonal antibodies to herpes simplex virus. *Dokl. Acad. Nauk SSSR, Ser. Biokhimiya 317*, 1487–1490, (in Russian).

(21) Kabanov, A. V., Vinogradov, S. V., Ovcharenko, A. V., Krivonos, A. V., Melik-Nubarov, N. S., Kiselev, V. I., and Severin, E. S. (1990) A new class of antivirals: antisense oligonucleotides combined with a hydrophobic substituent effectively inhibit influenza virus reproduction and synthesis of virus-specific proteins in MDCK cells. *FEBS Lett. 259*, 327-330.

(22) Vinogradov, S. V., Pheoktistov, V. S., and Kabanov, A. V. (1991) Fatty radical-modified antisense oligodeoxynucleotides as effective inhibitors of influenza virus reproduction. *Nucl. Acids. Symp. Ser. 24*, 281.

(23) Saison-Behmoaras, T., Tocque, B., Rey, I., Chassignol, M., Thuong, N. T. N. T., and Helene, C. (1991) Short modified antisense oligonucleotides directed against Ha-ras point mutation induce selective cleavage of the mRNA and inhibit T24 cells proliferation. *EMBO J. 10*, 111–1118.

(24) Cho-Chung, Y. S., Nesterova, M. V., Severin, E. S., and Vinogradov, S. V. (1991) Chemical modification enhances the inhibitory effect of regulatory subunit antisense oligodeoxynucleotide of cAMP-dependent protein kinase type I on cell proliferation. *Biochem. Int. 25*, 767–773.

(25) MacKellar, C., Graham, D., Will, D. W., Burgess, S., and Brown, T. (1994) Synthesis and physical properties of anti-HIV antisense oligonucleotides bearing terminal lipophilic groups. *Nucl. Acids Res. 20*, 3411–3417.

(26) Vinogradov, S. V., Suzdaltseva, Yu., Alakhov, V. Yu., and Kabanov, A. V. (1994) Inhibition of Herpes simplex virus 1 reproduction with hydrophobized antisense oligonucleotides. *Biochem. Biophys. Res. Commun. 203*, 959–966.

(27) Goud, B., Antoine, J.-C., Gonatas, N. K., Stieber, A., and Avrameas, S. (1981) A comparative study of fluid-phase and adsorptive endocytosis of horseradish peroxidase in lymphoid cells. *Exp. Cell. Res. 132*, 375–386.

(28) Steiman, R. M., Mellman, I. S., Muller, W. A., and Cohn, Z. A. (1983) Endocytosis and recycling of plasma membrane. *J. Cell Biol. 96*, 1–27.

(29) Kabanov, A. V., Levashov, A. V., and Martinek, K. (1987) Transformation of water-soluble enzymes into membrane active form by chemical modification. *Ann. N. Y. Acad. Sci. 501*, 63–66.

(30) Kabanov, A. V., Klibanov, A. L., Torchilin, V. P., Martinek, K., and Levashov, A. V. (1987) Efficiency of protein amino group acylation with fatty acid chlorides in reversed micelles of Aeorosol OT in octane. *Bioorganich. Khim. 13*, 1321–1324 (in Russian).

(31) Lowry, O. H., Rosenbrough, N. Y., Farr, A. L., and Randall, R. Y. (1951). Protein measurement with Folin phenol reagent. *J. Biol. Chem. 193*, 265–275.

(32) Friser, H. (1975) An improved 2,4,6-trinitrobenzenesulfonic acid method for the determination of amines. *Anal. Biochem. 64*, 284–288.

(33) Kabanov, A. V., Nametkin, S. N., Matveeva, E. G., Klyachko, N. L., Martinek, K., and Levashov, A. V. (1988) Relaxation phenomena in systems of protein-containing reverse micelles formed by surfactants in organic solvents. *Molek. Biol. 22*, 473–484 (in Russian) (Engl. ed., 382–391).

(34) Ternynck, T., and Avraméas, S. (1971) Peroxidase labeled antibody and Fab conjugates with enhanced intracellular penetration. *Immunocytochemistry 8*, 1175–1179.

(35) Zimmerlin, A., Wojtaszek, P., and Bolwell, G. P. (1994) Synthesis of dehydrogenation polymers of ferulic acid with high specificity by a purified cell wall peroxidase from french bean (Phaseolus vulgaris L.) *Biochem. J. 299*, 747–753.

(36) Huang, A., Tsao, Y. S., Kennel, S. J., and Huang, C. (1982) Characterization of antibody covalently coupled to liposomes. *Biochim. Biophys. Acta 716*, 140–149.

(37) Huang, A., Huang, L., and Kennel, S. J.(1980) Monoclonal antibody covalently coupled with fatty acid. *J. Biol. Chem. 255*, 8014–8018.

(38) Torchilin, V. P., Omelyanenko, V. G., Klibanov, A. L., Mikhailov, A. I., Goldanskii, V. I., and Smirnov, V. N. (1980) Incorporation of hydrophilic protein modified with hydrophobic agent into liposome membrane. *Biochim. Biophys. Acta 602*, 511–521.

(39) Berk, P. D., Wada, H., Horio, Y., Potter, B. I., Sorrentino, D., Zhon, S.-L., Isola, L. M., Stump, D., Kiano, C.-L., and Thung, S. (1990) Plasma membrane fatty acid-binding protein and mitochondrial glutamic-oxaloacetic transaminase of rat liver are related. *Proc. Natl. Acad. Sci. U.S.A. 87*, 3484–3488.

(40) Bamezai, A., Goldmacher, V. S., and Rock, K. L. (1992) Internalization of glycosyl-phosphatidylinositol (GPI)-anchored lymphocyte proteins. II. GPI-anchored and transmembrane molecules internalize through distinct pathways. *Eur. J. Immunol. 22*, 15–21.

Gadolinium(III) Di- and Tetrachelates Designed for *in Vivo* Noncovalent Complexation with Plasma Proteins: A Novel Molecular Design for Blood Pool MRI Contrast Enhancing Agents

Vladimir V. Martin, William H. Ralston,[†] Michael R. Hynes,[†] and John F. W. Keana*

Department of Chemistry, University of Oregon, Eugene, Oregon 97403, and Mallinckrodt Medical, Inc., 675 McDonnell Boulevard., P.O. Box 5840, St. Louis, Missouri 63134. Received February 17, 1995[⊗]

A new series of gadolinium chelates designed as blood pool contrast enhancing agents for magnetic resonance imaging applications is described. Complexes having four Gd(III) chelate units display a significant increase in molecular relaxivity per gadolinium ion in water ($9-13$ $L \cdot mmol^{-1} \cdot s^{-1}$) compared to Gd(III)–DTPA (5 $L \cdot mmol^{-1} \cdot s^{-1}$). A further jump in relaxivity (25 $L \cdot mmol^{-1} \cdot sec^{-1}$) in 4% BSA solution was observed in the case of a fatty acid-containing tetrachelate and is attributed to noncovalent binding of the tetrachelate to serum albumin. This agent was successfully used for imaging the rat circulatory system.

INTRODUCTION

Paramagnetic species enjoy wide use as contrast enhancing agents in biological and medical magnetic resonance imaging (MRI) applications owing to their ability to shorten the relaxation time of nearby water protons (*1*). Complexes of Gd(III) are particularly attractive owing to the presence of seven unpaired electrons in each Gd(III) ion and a long electron spin relaxation time (*2*). Compared to other paramagnetic transition ions or organic stable radicals, Gd(III) chelates provide maximum molar relaxivity.

Contrast agents designed to image the blood pool must remain in the vasculature for at least 30 min to allow for image acquisition. Filtration by the glomeruli in the kidney defines the molecular weight of blood pool agents to be >20 000 (*1, 3*). Several macromolecular contrast agents have been developed and tested for blood pool MRI applications. These reagents contain multiple Gd-chelated moieties in the form of complexes with diethylenetriaminepentaacetic acid (DTPA) residues covalently linked to a macromolecular carrier. Various natural and synthetic polymers have been employed as carriers including serum albumin (*3*), polylysine (PL) (*3*), polylysine–poly(ethylene glycol) conjugate (MPEG–PL) (*4*), and functionalized dextrans (*3, 5, 6*). Along with relatively long retention times in the vasculature (1–4 h, compared to 15–20 min for Gd–DTPA) (*3*) the macromolecular conjugates display a jump in molecular relaxivity up to 15 $L \cdot mmol^{-1} s^{-1}$ per Gd(III) ion compared to about 6 $L \cdot mmol^{-1} s^{-1}$ for the Gd–DTPA complex itself (*2, 3*). This so-called proton relaxivity enhancement effect (PRE) (*7*) is attributed to a lower, more optimal tumbling rate of the conjugated versus free paramagnetic unit (*3, 8*).

Recently, a new family of blood pool contrast agents based on Starburst dendrimer cascade polymers (*9*) was introduced by Wiener *et al.* (*10*). These compounds display the highest molecular relaxivity reported to date

(up to 34 $L \cdot mmol^{-1} \cdot s^{-1}$ per Gd ion) and excellent *in vivo* lifetimes and may not exhibit unwanted immune reactions observed with protein covalent conjugates (*11*).

Syntheses of macromolecular contrast reagents are typically accomplished by labeling of multiple accessible primary amino groups on the macromolecular carrier (protein, activated dextran, or synthetic dendrimer) with an excess of a functionalized precursor of the Gd–DTPA paramagnetic unit. DTPA anhydride (*3, 12*) and a phenyl isothiocyanate-substituted DTPA (*10, 13*) have been used for this purpose. The latter has the advantage of utilizing all five DTPA carboxyls for chelation of the metal, the result being a more stable complex compared to amide derivatives derived from DTPA anhydride (*14*). The resulting conjugate is subjected to complexation with Gd(III) ion followed by purification using size-exclusion chromatography, ultrafiltration, or dialysis. An alternative approach utilizes a preformed Gd–DTPA chemically reactive chelate unit as the labeling reagent (*6, 14*).

Any paramagnetic conjugate prepared by polymer labeling methodology possesses structural inhomogeneity derived from a variable degree of amino group involvement. Structural variability causes problems in synthetic reproducibility, purification, and in clinical use. Consequently, our research program has aimed at the preparation of structurally well-defined compounds. Recent results with Gd complexes (*15, 16*) and nitroxide radicals (*17, 18*) suggest that noncovalent binding of the contrast enhancer to a macromolecular carrier such as plasma proteins results in increases both in molecular relaxivity and intravascular retention. At the same time it is evident that MRI blood pool agents must contain more than one paramagnetic center to achieve sufficient contrast enhancement due to the limited number of binding sites on each protein molecule (*17*).

Earlier, we introduced the notion of molecular amplifiers (MAs) designed to deliver multiple copies of a pharmacologically active group to a targeted site (*6*). As part of the amplifier concept, the first members of a chemically well-defined series of MAs bearing several stable nitroxide free radical groups were synthesized for MRI applications (*19*). The amplifiers follow the structure motif shown diagrammatically as structure **1** and consist of a central core (CC) having one or more connection points substituted with branchers (B). Each of the branchers may provide one or more sites for the

covalent attachment of active groups. Another important structural feature of the MA is the presence of a targeting group (TG) that can be designed for a particular application. Depending on the nature of the targeting group, the MA might be used to modify accessible amino groups in proteins, to concentrate the MA in a particular environment such as a membrane bilayer, or to allow selective complexation with a nucleic acid or protein. Linker groups (L) are employed for connecting the targeting group to the central core.

1
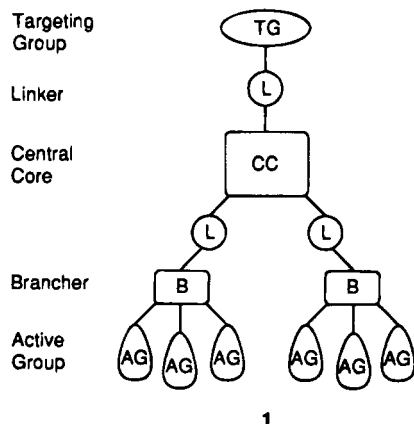
Herein, we report the synthesis of several MAs designed as contrast enhancing agents for the blood pool through complexation with plasma proteins. We also demonstrate the utility of these compounds for blood pool MRI applications in the rat.

EXPERIMENTAL PROCEDURES

General. Melting points were obtained in a Thomas-Hoover apparatus and are uncorrected. Infrared spectra were recorded in KBr pellets (concentration 0.2–0.5%) or in CCl_4 or $CHCl_3$ solutions (concentration 2–5%) on a Nicolet 5DX or a Nicolet Magna-IR 550 IR FT spectrometer. ^1H (300 MHz) and ^{13}C (75 MHz) NMR spectra were taken on a General Electric QE-300 FT spectrometer. Chemical shifts are reported in δ units referenced to solvent signals. The identity of the same compounds prepared by different methods was established by comparison of their IR and ^1H NMR spectra and/or TLC R_f or HPLC t_R values using coelution criteria. Analytical TLC was performed on Merck plastic-backed silica gel 60 F_{254} plates. Preparative TLC was done on Analtech Uniplate precoated silica gel glass-backed plates (20 × 20 cm × 1 mm) or on plates homemade from Merck silica gel 60 PF_{254} (40 × 30 cm × 3 mm). Analytical HPLC was performed on a Rainin Microsorb-MV C_{18} 0.46 × 25 cm column. Elution utilized gradients A (H_2O + 0.2% TFA) − B (MeCN + 0.2% TFA) with UV detection at 230 or 254 nm. Retention times and relative percent peak areas are reported. Preparative column chromatography utilized Baker silica gel (60–200 mesh). Flash chromatography utilized 200–425 mesh Davisil silica gel (Aldrich), grade 643. Size exclusion chromatography was performed on a Pharmacia-LKB Gradifrac system (UV detection at 280 nm) over Sephadex G-10 or Sephadex G-25 fine gels (bed 2.5 × 80 cm). Reagents were purchased from Aldrich Chemical Co. and used without purification unless noted. Solvents were purchased from Baker. Dry EtOAc and MeCN were prepared according to Perrin *et al.* (*20*). 1,5-Bis(phthalimido)-protected diethylenetriamine **10** was prepared by the procedure of

Sosnovsky *et al.* (*21*). The starting protected DTPA unit **14** was prepared according to Keana *et al.* (*14, 22*). All reactions were performed under a nitrogen atmosphere.

Relaxivity Studies. Relaxivities were determined using the longitudinal relaxation rate (*T1*) values measured on a 20 MHz Bruker Minispec. Compounds **2–7** and Gd–DTPA were prepared in deionized water and in a 4% bovine serum albumin (BSA) solution. The relaxivity (*R1*) value of each compound was calculated as a measure of the effective change in 1/*T* per unit of concentration. *R1* relaxivity values, in units of $L \cdot mmol^{-1} \cdot s^{-1}$, were determined using at least four concentrations of each compound.

Animal Imaging and Toxicity Studies. Vascular imaging was performed on a 250 g Sprague–Dawley rat. The animal was anesthetized with an intramuscular injection of ketamine (80 mg/kg) and xylazine (12 mg/kg) and a cannula placed into a lateral tail vein. Prior to imaging a 0.1 mL maintainance dose of pentobarbital (64 mg/mL) was administered through the cannula. The rat was placed in a Siemens Magnetom SP head coil and a three-dimensional time-of-flight preinjection scout MR angiogram was acquired using a gradient echo (FISP) sequence, TR 20 ms and TE 9 ms, in a 1.5 T Siemens Magnetom. Following acquisition of the scout image, the rat was injected via the cannula with a 20 mM solution of compound **4** in sterile water at 0.01 mmol of Gd/kg. Images were acquired at 15, 30, and 45 min post injection.

The preliminary acute iv toxicity was evaluated in one mouse per compound at an anticipated diagnostic dose. Conscious restrained mice, at one per compounds **2–4**, were injected at 0.01 mmol of Gd^{3+}/kg via a lateral tail vein and observed for 7 days. No histology was performed.

1,3-Bis(bromomethyl)-5-nitrobenzene (9). A mixture of 5-nitro-*m*-xylene (**8**) (3.02 g, 20 mmol), NBS (7.12 g, 40 mmol), and benzoyl peroxide (10 mg) in CCl_4 (50 mL) was refluxed for 16 h. The precipitated succinimide was filtered off and washed with CCl_4 (3 × 20 mL). The combined filtrate was evaporated, and the solid residue was crystallized from 3:1 hexane–EtOAc to yield 3.28 g (53%) of dibromide **9** as colorless crystals: mp 100–101 °C (from 1:10 hexane–EtOAc); IR (KBr) 1540, 1362, and 1215 cm^{-1}; ^1H NMR ($CDCl_3$) δ 4.52 (s, 4H), 7.75 (s, 1H), 8.19 (s, 2H); ^{13}C NMR ($CDCl_3$) δ 30.55, 123.66, 135.16, 140.40, 148.61; HRMS calcd for $C_8H_7NO_2{}^{79}Br_2$ 306.8844, found 306.8840.

1,3-Bis[[N,N-bis(2-N-phthalimidoethyl)amino]-methyl]-5-nitrobenzene (11). A mixture of dibromide **9** (1.98 g, 6.4 mmol), bis(phthalimide-protected) diethylenetriamine **10** (5.59 g, 15.4 mmol), and K_2CO_3 (3.45 g, 25 mmol) in MeCN (100 mL) was refluxed with vigorous stirring for 4 d. The inorganic material was filtered off and washed with MeCN (4 × 20 mL). The combined filtrate was evaporated, and the residue was chromatographed over silica gel (2.5 × 30 cm) to yield 2.34 g (42%) of protected hexaamine **11** as a white powder: mp 156–158 °C (from 1:5 hexane–EtOAc); IR (KBr) 1730, 1539, 1360, and 1211 cm^{-1}; ^1H NMR ($CDCl_3$) δ 2.78 (t, 8H, *J* = 5.5 Hz), 3.51 (s, 4H), 3.73 (t, 8H, *J* = 5.5 Hz), 7.28 (s, 1H), 7.64 (s, 2H), 7.68 (br s, 16H); ^{13}C NMR (DMSO-d_6) δ 35.80 (4C), 51.73 (4C), 56.82 (2C), 122.56 (1C), 123.39 (8C), 132.28 (8C), 134.83 (8C), 141.70 (1C), 147.98 (1C), 168.31 (8C); HRFAB MS calcd for ($C_{48}H_{40}N_7O_{10}$ + H) 847.2836, found 874.2823.

1,3-Bis[[N,N-bis(2-aminoethyl)amino]methyl]-5-nitrobenzene Hexahydrochloride (12). To a boiling suspension of hexaamine **11** (0.90 g, 1.03 mmol) in absolute EtOH (250 mL) was added hydrazine (2.5 mL,

77 mmol) with vigorous stirring. After about 10 min the mixture became a clear solution. After an additional 10 min reflux period it was cooled to room temperature and evaporated to dryness. The residue was evaporated twice with EtOH (30 mL) and evacuated to 0.1 Torr to remove the excess hydrazine. The solid was suspended in 2 N HCl (50 mL), stirred for 1 h, and filtered from insoluble phthalimidohydrazine. The filtrate was extracted with CHCl$_3$ (3 × 30 mL, discarded) and evaporated to dryness to leave a hygroscopic crude product. Crystallization from MeOH gave 0.39 g (66%) of hexaamine hexahydrochloride **12** as a yellow powder: mp 256–258 °C (MeOH); IR (KBr) 1539, 1360, and 1211 cm^{-1}; ^{1}H NMR (D$_2$O) δ 2.90 (t, 8H, J = 6.1 Hz), 3.18 (t, 8H, J = 6.1 Hz), 3.94 (s, 4H), 7.76 (s, 1H), 8.25 (s, 2H); ^{13}C NMR (D$_2$O) δ 36.41 (4C), 50.74 (4C), 57.65 (2C), 125.80 (2C), 137.50 (2C), 138.65 (1C), 149.50 (1C). Anal. Calcd for C$_{16}$H$_{31}$-N$_7$O$_2$•6HCl: C, 33.58; H, 6.52; N, 17.13. Found: C, 33.58; H, 6.84; N, 17.14.

1,3-Bis[[N,N-bis(2-isothiocyanatoethyl)amino]-methyl]-5-nitrobenzene (13). To a vigorously stirred mixture of NaHCO$_3$ (4.000 g, 40 mmol) and thiophosgene (1 N in CHCl$_3$, 2 mL, 2 mmol) in CHCl$_3$ (50 mL) was introduced a solution of hexaamine hexahydrochloride **12** (0.089 g, 0.16 mmol) in H$_2$O (1 mL) The mixture was stirred for 6 h and then MgSO$_4$ (10 g) was added to remove water. The inorganic material was filtered off and washed with CHCl$_3$ (5 × 10 mL). The combined filtrate was evaporated, and the oily residue was chromatographed on a silica gel TLC plate. Elution with CHCl$_3$ gave 0.045 g (56%) of tetraisothiocyanate **13** as a yellow solid: mp 62–64 °C (hexane); IR (KBr) 2212, 2129, 2063, 1528, 1440, and 1343 cm^{-1}; ^{1}H NMR (CDCl$_3$) δ 2.97 (t, 8H, J = 6.0 Hz), 3.62 (t, 8H, J = 6.0 Hz), 3.89 (s, 4H), 7.93 (s, 1H), 8.11 (s, 2H); ^{13}C NMR (CDCl$_3$) δ 44.31 (4C), 54.55 (4C), 58.69 (2C), 123.10 (1C), 133.16 (br s, 1C, C=S), 135.44 (1C), 141.75 (2C), 149.16 (1C). Anal. Calcd for C$_{20}$H$_{23}$N$_7$O$_2$S$_4$: C, 46.05; H, 4.44; N, 18.79; S, 24.58. Found: C, 45.85; H, 4.30; N, 18.47; S, 24.56.

Reaction of Tetraisocyanate 13 with Amine 14 To Give 15. A mixture of tetraisothiocyanate **13** (0.057 g, 0.11 mmol) and amine **14** (**22**) (0.270 g, 0.48 mmol) in CHCl$_3$ (3 mL) was stirred for 10 d at 50 °C and then evaporated and purified on a TLC plate (30 × 40 cm × 3 mm, eluent, 5% MeOH in CHCl$_3$) to give 0.201 g (65%) of nitro perester **15** as a yellow glassy solid: liquifies above 70 °C; IR (KBr) 1735, 1538, 1515, 1202, and 1028 cm^{-1}; ^{1}H NMR (DMSO-d_6 + 5% D$_2$O) δ 7.03 (d, 8H, J = 7 Hz), 7.29 (d, 8H, J = 7 Hz), 7.79 (s, 1H), 7.95 (s, 2H); ^{1}H NMR (CDCl$_3$ + 2% D$_2$O) δ 2.40–3.20 (gr, 40H), 3.30–3.80 (gr, 116H), 7.11–7.24 (br m, 8H), 7.27–7.40 (br m, 9H), 7.93 (s, 2H).

Reduction of Nitro Perester 15 To Give Amine 16. A solution of **15** (0.480 g, 0.17 mmol) and SnCl$_2$ (0.600 g, 3.16 mol) in MeOH (80 mL) was refluxed for 20 h, cooled to room temperature, and poured into EtOAc (250 mL). The mixture was washed with saturated NaHCO$_3$ (5 × 100 mL) and H$_2$O (2 × 50 mL), dried (MgSO$_4$) and evaporated. The residue was chromatographed on a preparative TLC plate (30 × 40 cm × 3 mm, eluent, 8% MeOH in CHCl$_3$) to give 0.358 g (76%) of amine **16** as a glassy solid: liquifies above 50 °C; IR (KBr) 3344, 2959, 1738, 1605, 1514, 1439, 1202 and 1021 cm^{-1}. ^{1}H NMR (DMSO-d_6) δ 2.40–2.95 (gr, 40H), 3.20–3.80 (gr, 116H), 6.35 (s, 1H), 6.45 (s, 2H), 7.09 (d, 8H, J = 8 Hz), 7.26 (d, 8H, J = 8 Hz), 7.55 (br, 4H, N-H), 9.65 (br, 4H, N-H).

Acylation of Amine 16 To Give 18. The acylating reagent N-hydroxysuccinimidyl methyl sebacate **17** was prepared as follows. A mixture of sebacic acid mono-methyl ester (0.216 g, 1 mmol), N-hydroxysuccinimide

(0.120 g, 1.04 mmol), and DCC (0.210 g, 1.02 mmol) in THF (30 mL) was stirred for 16 h and then filtered from DCU and poured into EtOAc (150 mL). The ethyl acetate solution was washed with saturated NaHCO$_3$ (5 × 20 mL) and H$_2$O (2 × 30 mL), dried, and evaporated to give 0.275 g (88%) of NHS ester **17** as colorless plates: mp 60–61 °C (hexane−EtOAc 1:1); IR (KBr) 1820, 1788, 1735, 1212, and 1072 cm^{-1}; ^{1}H NMR (CDCl$_3$) δ 1.31 (br, 8H), 1.61 (m, 2H), 1.73 (m, 2H), 2.29 (t, 2H, J = 7.6 Hz), 2.59 (t, 2H, J = 7.4 Hz), 2.82 (s, 4H), 3.66 (s, 3H); ^{13}C NMR (CDCl$_3$) δ 24.50, 24.85, 25.57 (2C), 28.64, 28.83, 28.91, 28.69, 30.90, 34.04, 51.41, 168.61, 169.13 (2C), 174.22. Anal. Calcd for C$_{15}$H$_{23}$O$_6$N: C, 57.50; H, 7.40; N, 4.47. Found: C, 57.58; H, 7.17; N, 4.46. A mixture of amine **16** (0.245 g, 0.09 mmol) and NHS ester **17** (0.157 g, 0.5 mmol) was stirred for 10 d at 50 °C and then cooled to room temperature and evaporated. The residual semi-solid was chromatographed on a preparative TLC plate (40 × 30 cm × 3 mm, eluent, 7% MeOH in CHCl$_3$) to give 0.137 g (53%) of amide **18** as a yellowish glassy solid: liquifies above 60 °C. Amide **18** was unstable and was immediately used in the next step.

Hydrolysis of Peresters 15, 16, and 18. In a 100 mL round-bottomed flask was stirred a mixture of the perester (0.060 mmol) and 1 N NaOH (4 mL, 4 mmol) in MeOH (15 mL) for 23 h at 45 °C, cooled to 25 °C, and evaporated to leave a solid residue. This crude product was suspended in MeOH (20 mL) and reprecipitated with acetone (75 mL). The product was filtered on a glass filter (F) and washed with acetone (5 × 20 mL) and ether (2 × 20 mL) to yield the corresponding sodium salt **19, 20, or 21** as a yellowish solid which was contaminated with some inorganic material, although no organic impurities were detected by NMR or HPLC.

Nitro derivative **19**: dec >250 °C; IR (KBr) 1598, 1541, 1411, 1332, and 1116 cm^{-1}; ^{1}H NMR (D$_2$O) δ 2.18 (m, 8H), 2.61 (m, 8H), 2.68 (m, 32H), 2.70–3.82 (gr, 48H), 7.08 (d, 8H, J = 6 Hz), 7.25 (d, 8H, J = 6 Hz), 7.72 (s, 1H), 8.14 (s, 2H); HPLC (gradient, 80% A, 20% B to 95% B over 20 min) 14.4 min (95%).

Amino derivative **20**: dec >250 °C; IR (KBr) 1593, 1411, 1332, and 1114 cm^{-1}; ^{1}H NMR (D$_2$O) δ 2.18 (br, 8H), 2.64–2.70 (br, 40H), 2.80–3.80 (gr, 48H), 7.09 (d, 8H, J = 8 Hz), 7.25 (d, 8H, J = 8 Hz); HPLC (gradient, 80% A, 20% B to 95%B over 20 min) 14.3 (98%).

Fatty acid derivative **21**: dec >250 °C; IR (KBr) 1592, 1411, 1331, and 1114 cm^{-1}; ^{1}H NMR (D$_2$O) δ 1.23 (m, 8H), 1.51 (m, 20H), 2.58 (br s, 36H), 2.65 (br s, 8H), 2.80–3.70 (gr, 40H), 6.66 (s, 2H), 6.70 (s, 1H), 7.09 (d, 8H, J = 7 Hz), 7.25 (d, 8H, J = 7 Hz); HPLC (gradient, 80% A, 20% B to 95% B over 20 min) 18.8 min (97%).

Complexation of 19–21 with Gd(III) ion. In a 20 mL three-neck flask equipped with a nitrogen inlet and pH-microelectrode was acidified a magnetically stirred solution of the sodium salt (0.08 mmol) in water (20 mL) with 0.2 N HCl to pH 6.5, and then GdCl$_3$•6H$_2$O (0.128 g, 0.45 mmol) in H$_2$O (1 mL) was added in one portion (pH dropped to 3). The mixture was stirred for 15 min and then the pH was gradually increased to 6 over 1 h and then to 9.5 over 4 h by dropwise addition of 0.1 N NaOH. The mixture was filtered through a double Metrigard prefilter (Gelman) and concentrated to 2 mL under vacuum. The concentrated solution was injected onto a size-exclusion chromatography column (Pharmacia 2.5 × 100 cm C-column packed with Sephadex G-25 Fine, bed volume 2.5 × 90 cm) and chromatographed with degassed water. The fractions containing product were ascertained by HPLC to be in the first group of peaks. Evaporation of the water gave the complexes as a yellow glassy powder.

Scheme 1

≡ R-4(L-GdNa₂)

2 R = NO₂
3 R = NH₂
4 R = NHCO(CH₂)₈COONa

≡ L-GdNa₂

L-GdLi₂   5

L-GdNa₂   6

7
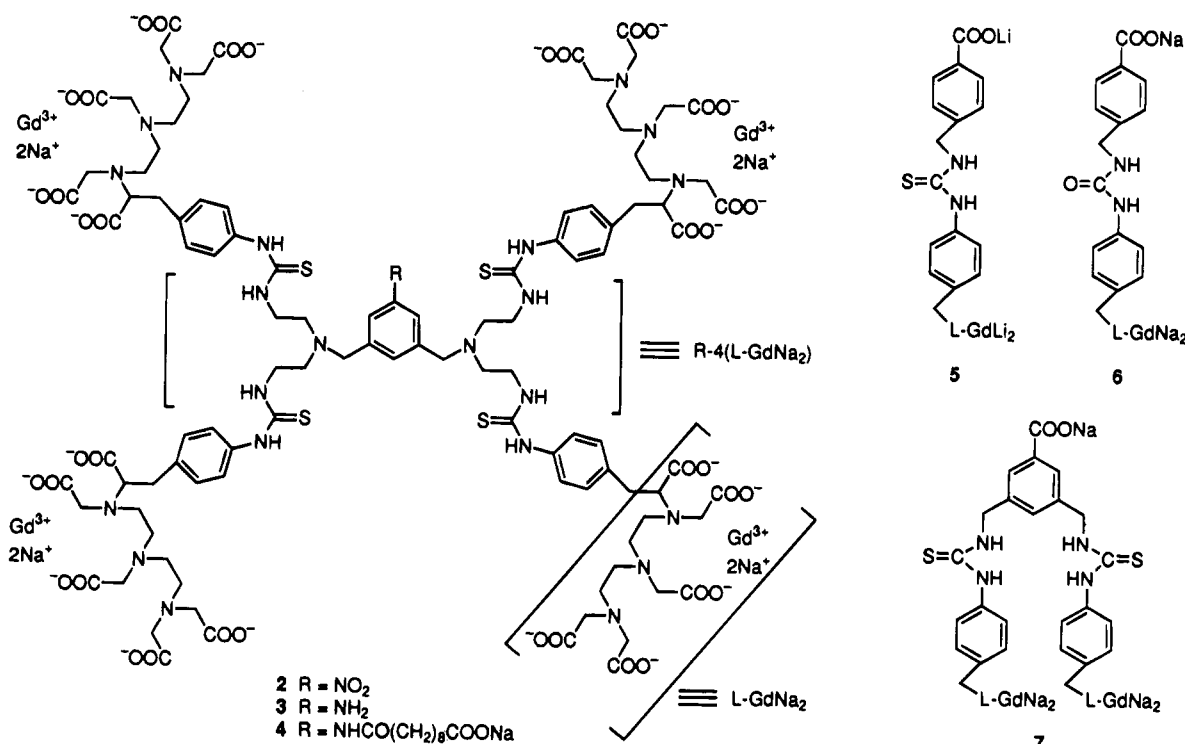
Nitro derivative **2**: yield, 44%; dec >250 °C; IR (KBr) 1598, 1404, 1321, and 1097 cm⁻¹; HPLC (gradient, 80% A, 20% B to 95%B over 20 min) 14.5 min (94%). Anal. Calcd for (C₁₀₉H₁₂₃N₂₃O₄₂S₄Gd₄Na₈·16H₂O): C, 34.73; H, 4.34; N, 8.96. Found: C, 34.75; H, 4.17; N, 8.86.

Amino derivative **3**: yield 62%; dec >250 °C; IR (KBr) 3429, 1602, 1403, 1323, and 1095 cm⁻¹; HPLC (gradient, 80% A, 20% B to 95%B over 15 min) 14.3 min (100%). Anal. Calcd for (C₁₀₄H₁₂₅N₂₃O₄₀S₄Gd₄Na₈·24H₂O): C, 33.66; H, 4.70; N, 8.68. Found: C, 33.69; H, 4.75; N, 8.74.

Fatty acid derivative **4**: yield 40%; dec >250 °C; IR (KBr) 1611, 1405, 1320, 1263, and 1095 cm⁻¹; HPLC (Microsorb C18, 20 to 95% B in 15 min) 19.0 min (96%). Anal. Calcd for (C₁₁₄H₁₄₀N₂₃O₄₃S₄Gd₄Na₉·28H₂O): C, 34.46; H, 4.97; N, 8.11. Found: C, 34.52; H, 4.88; N, 8.05.

Labeling of Human Serum Albumin. To a solution of amino tetragadolinium complex **3** (6.5 mg, 2 μmol) in HEPES buffer (0.5 mL; pH 8.2) was added 1 N CSCl₂ in CHCl₃ (20 μL, 20 μmol). The mixture was vigorously shaken for 7 min, and then it was extracted with CHCl₃ (3 × 1 mL) to remove the excess CSCl₂. To the aqueous phase containing isothiocyanate **22** was added a solution of HSA (13.8 mg, 0.2 mmol) in H₂O (0.5 mL), and the mixture was kept under nitrogen for 24 h and then loaded onto a Sephadex G-75 column (1.5 × 40 cm). The column was eluted with water (monitored by HPLC), and the major fraction was lyophilized to give 12.1 mg of paramagnetic (according to NMR) conjugate **23** as a white glassy solid.

RESULTS

Chemistry. Three new structurally related MAs **2**–**4** (Scheme 1) containing four Gd–DTPA units in the molecule were used in the present study along with mono Gd–DTPA complexes **5** and **6** and bis Gd–DTPA complex **7**. These latter three complexes were prepared in an earlier model study (*22*). The structural abbreviations L-GdNa₂ and R-4(L-GdNa₂) are defined in Scheme 1 for use below owing to the complexity of the structures.

Scheme 2

8

NBS / CCl₄

9

HN(CH₂CH₂NPht)₂ 10

MeCN, K₂CO₃

11

H₂N-NH₂ / EtOH

12 ·6HCl

Pht =

12

SCCl₂
NaHCO₃
H₂O/CHCl₃

13
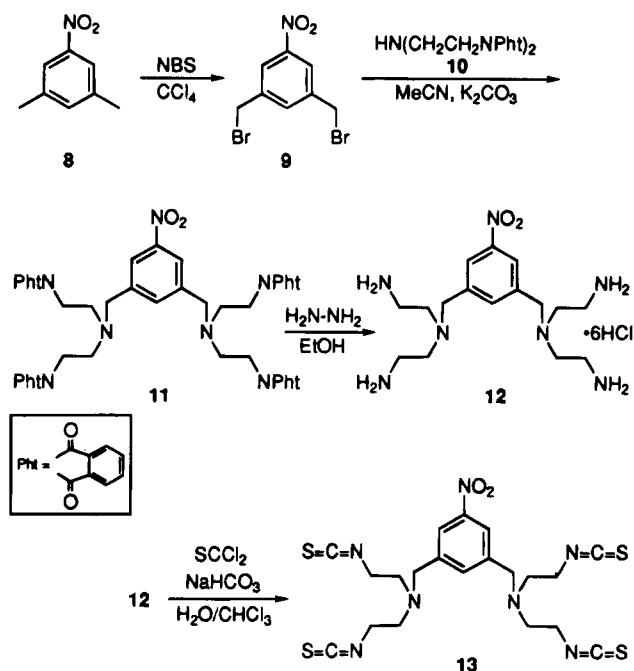
The synthesis of MAs **2**–**4** was accomplished as follows. 5-Nitro-*m*-xylene (**8**) (Scheme 2) was treated with NBS giving dibromide **9** which served as the central core of the MAs. The brancher units were derived from diethylenetriamine. Conversion into its bis-phthalimide derivative **10** and then reaction with **9** gave **11**. Treatment of **11** with hydrazine removed the phthalimide protecting groups, affording tetraamine **12** which consisted of the central core of the MAs and two attached brancher units. Activation of the four terminal amino groups in **12** was achieved by conversion of each amine into the corresponding reactive isothiocyanate moiety by reaction with excess thiophosgene giving tetraisothiocyanate **13**. Intermediate **13** incorporates four connection points for

Scheme 3

13 +

14

NO$_2$-4(L-Me$_5$) $\xrightarrow{\text{ii}}$ NH$_2$-4(L-Me$_5$) $\xrightarrow{\text{iii}}$ MeOOC(CH$_2$)$_8$CONH-4(L-Me$_5$)
15   16   18

↓iv   ↓iv   ↓iv

NO$_2$-4(L-Na$_5$)   NH$_2$-4(L-Na$_5$)   NaOOC(CH$_2$)$_8$CONH-4(L-Na$_5$)
19   20   21

↓v   ↓v   ↓v

NO$_2$-4(GdNa$_2$)   NH$_2$-4(L-GdNa$_2$)   NaOOC(CH$_2$)$_8$CONH-4(L-GdNa$_2$)
2   3   4

↓vi

S=C=N-4(L-GdNa$_2$) $\xrightarrow{\text{vi}}$ HSA-[NCSNH-4(L-GdNa$_2$)]$_n$
22   23
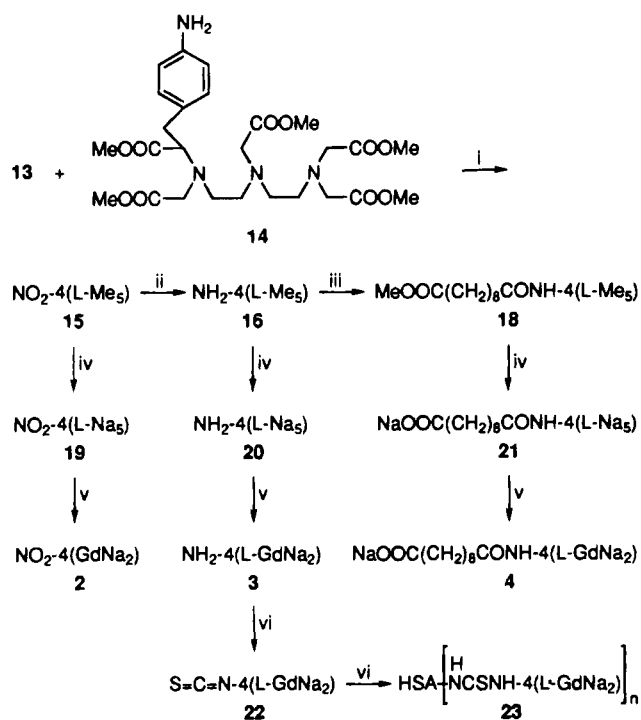
[a] Key: (i) CHCl$_3$, 50 °C; (ii) SnCl$_2$, MeOH; (iii) NHSOOC-(CH$_2$)$_8$COOMe (17), EtOAc; (iv) NaOH, MeOH; (v) GdCl$_3$, H$_2$O; (vi) SCCl$_2$; (vii) HSA.

Table 1. Relaxivity Values (L·mmol^{-1}·s^{-1})

compd	no. Gd/mol compd	R_1 in water per mol	R_1 in water per Gd(III)	R_1 in 4% BSA per mol	R_1 in 4% BSA per Gd(III)
Gd−DTPA	1	4.5	4.5	~5	~5
5	1	3.7	3.7	12.6	12.6
6	1	3.4	3.4	9.5	9.5
7	2	9.4	4.7	18.6	9.3
2	4	53.2	13.3	81.6	20.4
3	4	36.4	9.1	76.8	19.2
4	4	41.6	10.4	98.4	24.6
Gd−DTPA−EOB[a]	1	5.3	5.3	8.6[b]	8.6
(Gd−DTPA)−dextran[c]	15		10.5		NA[d]
(Gd−DTPA)−HSA[c]	30		14.5		NA[d]
(Gd−DTPA)−PL[c]	60		13.1		NA[d]
(Gd−DTPA)−PL−MPEG[e]	110		18		18
(Gd−DTPA)−PAMAM[f]	170		34		NA[d]

[a] Reference 16. [b] In plasma. [c] Reference 3. [d] NA: not available. The relaxivity in BSA is not expected to increase significantly over that in water. See text for rationale. [e] Reference 4. [f] Reference 10.

attaching active groups to the unit as well as an aromatic nitro group which can serve as an orthogonal site for attachment of the assembly to the target.

Connection of the four active (chelate) groups was achieved by the reaction of each terminal isothiocyanate with pentamethyl ester-protected amine **14** to give the nitro derivative **15** (Scheme 3). Amine **14** has been used previously in the synthesis of a bifunctional Gd−DTPA complex (14) as a convenient synthon for the introduction of the chelation units (22). The use of methyl ester-protected intermediates has proven to be more convenient than alternatives utilizing a preformed bifunctional Gd-chelate or its immediate Na-salt precursor since separation of the reaction mixtures and purification of the nonionic ester-protected intermediates can be easily achieved by conventional chromatography in organic solvents.

Permethyl ester **15** contains an aromatic nitro group which may be used for the attachment of potential targeting groups as the following series of reactions illustrates. Thus, ester **15** was reduced to the amino derivative **16** using SnCl$_2$ in methanol. Amine **16** was then acylated with the NHS ester of monomethyl sebacate **17** to give amide **18**. A sebacic acid derivative was chosen with the notion that the fatty acid chain might bind to the fatty acid binding site(s) on serum albumin (see below). Methyl ester-protected intermediates **15**, **16**, and especially **18** were found to undergo decomposition upon storage and were therefore used immediately after purification.

The deprotection of the carboxy groups was accomplished by basic hydrolysis. The resulting Na salts **19**−**21** were contaminated with inorganic salts; however, no organic impurities were detected by HPLC or NMR. Complexation with Gd(III) ion involved treatment of the Na salts with an excess of GdCl$_3$ followed by size-exclusion chromatography using deionized water and a column bed volume about 50 times larger than usually

recommended for desalting of samples of comparable volume (23). Separation of the chelates from free (non-chelated) Gd(III) ion was confirmed by detection of the diffuse zone of Gd(III) in collected eluant fractions with Arsenazo III (24). This zone appeared at a longer retention time than that observed for the chelates and did not overlap with the chelates. Compounds **2**−**4** were yellow glassy solids that were stable to storage and highly soluble in water. The HPLC peaks were slightly broadened owing to the presence of diastereomers.

Tetragadolinium amine **3** was activated for covalent conjugation to HSA by treatment with thiophosgene. Without isolation, the intermediate isothiocyanate **22** was allowed to react with HSA to yield the paramagnetic conjugate **23**.

Relaxivity. Molecular relaxivity values for Gd(III) chelates **2**−**7** obtained in deionized water and in 4% aqueous bovine serum albumin (BSA) are listed in Table 1. Values for Gd−DTPA and some covalent macromolecular conjugates have been included for purposes of comparison.

Animal Studies. A series of rat vascular system images were obtained at 15, 30, and 45 min after intraveneous administration of 0.01 mmol Gd(III)/kg of compound **4**. Images pictured in (Figure 1) display a good contrast enhancement lasting at least 45 min after administration. There were no observable signs of toxicity following iv injections of compounds **2**−**4** into mice.

DISCUSSION

The objective of the present study was to synthesize a family of molecular amplifiers capable of in vivo complexation with plasma proteins and to evaluate their utility as blood pool contrast enhancing agents. Reaction sequences used in this study are operationally simple and require conventional organic chemistry procedures for the preparation and purification of Gd(III) tetrachelates on a 0.1−0.3 g scale. Although the amino perester intermediates were not stable toward storage, the tetragadolinium MAs **2**−**4** were stable compounds with satisfactory analytical data. Infrared spectra of the MAs **2**−**4** were very similar to those of the diamagnetic immediate precursor sodium salts **19**−**21**. This indication of structural similarity is important since NMR spectra of the paramagnetic Gd(II) chelates **2**−**4** could not be obtained under conventional conditions whereas the structure of sodium salts **19**−**21** was well supported by NMR.

With regard to the relaxivity values shown in Table 1, two factors are noteworthy. First, there is a significant
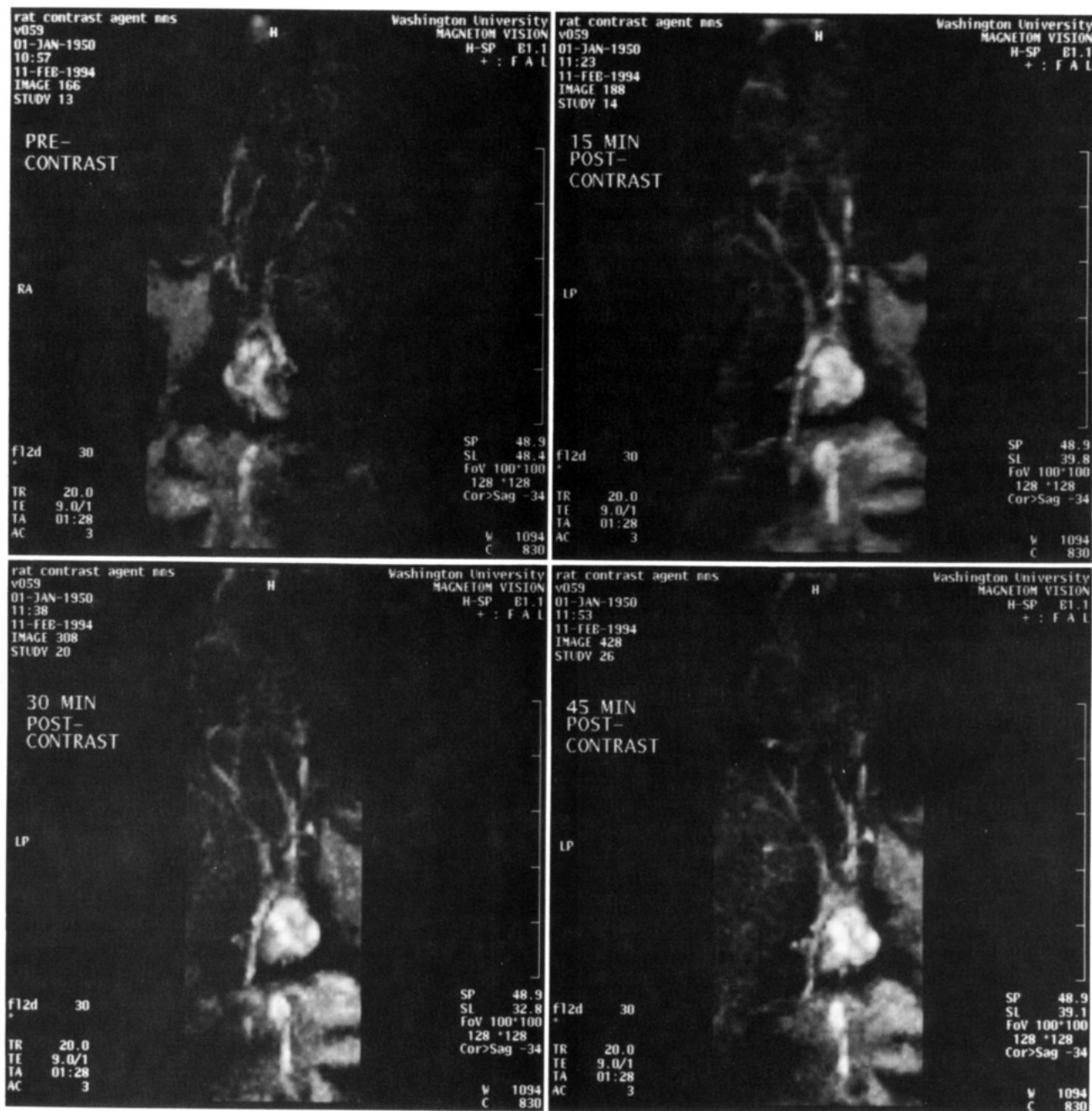
Figure 1. MR images: (A) obtained before administration of compound **4**; (B), (C), and (D) obtained in 15, 30, and 45 min, respectively, after administration of compound **4** (0.01 mmol/kg).

increase in relaxivity per Gd(III) ion for tetragadolinium MAs **2**–**4** in water compared to DTPA–Gd or digadolinium complex **7**. This may be due to the slower, more optimal tumbling rates of the larger complexes.

The other characteristic feature of compounds **2**–**4** is the further substantial jump in relaxivity per Gd(III) in BSA as compared to water. We attribute this effect to noncovalent complex formation with BSA. Complexation with a variety of small molecules is well-documented for serum albumins. Similar complexation was shown to cause PRE in the case of low-molecular weight paramagnetic species containing a single paramagnetic center (*15*–*18*). For example, ethoxybenzyl-DTPA–gadolinium (Gd–DTPA-EOB) shows a 62% increase in relaxivity in plasma as compared to water (Table 1) (*16*). Another indication of binding to BSA is the large increase in relaxivity observed for tetrachelate **4** which contains a fatty acid residue. Fatty acids are known to be among

the best serum albumin ligands (*25, 26*). A comparison of the relaxivities (Table 1) reported for (Gd–DTPA)-labeled dextran, HSA, PL, and MPEG–PL conjugates shows that these macromolecule-based conjugates do not provide further improvements over MAs **2**–**4**. Even the best (Gd–DTPA)–PAMAM Starburst derivative provides only a doubling of relaxivity on a per gadolinium basis in water. The relaxivity values for most of the macromolecular conjugates in albumin solutions have not been reported. However, we assume them to be close to the corresponding numbers in water as was observed in the case of (Gd–DTPA)–PL–MPEG (*4*) (Table 1) with little further PRE associated with noncovalent binding. This may be explained by noting that when low molecular weight particles are complexed with the albumin macromolecule, there is a large percent increase in apparent molecular weight of the assembly. Thus, the relaxivity improves dramatically owing to a slowing in tumbling

rates to more optimal values. On the other hand, when a macromolecular assembly of gadolinium complexes is further complexed with another macromolecule such as serum albumin then the percent increase in molecular weight is modest. This reasoning is consistent with other reports that further conjugation of macromolecular MRI contrast agents with plasma proteins does not lead to a significant increase in molar relaxivity (27).

Animal imaging studies show the potential of the fatty acid MA **4** as a blood pool contrast enhancement agent. There are three notable features. First, the dose necessary for contrast enhancement with **4** was less than one-half that used for vasculature enhancement with Gd—DTPA—polylysine having MWs ranging from 36 kD to 480 kD (28) and at least 10-fold less than a clinical dose of Gd—DTPA. Gd—DTPA is not an ideal MR angiography agent because it quickly leaves the vasculature [blood $t_{1/2}$ of 13 min (28)] and distributes to the extracellular spaces of the body. Second, the dynamics of the contrast enhancement obtained in a series of images over time point toward satisfactory intravascular retention for **4**. Third, preliminary animal studies would indicate no overt acute toxic effects of compounds **2**—**4** occurred in mice at anticipated diagnostic doses of 0.01 mmol Gd/kg.

The above experiments indicate that a fatty acid residue is a promising targeting group (structure **1**) for blood pool MAs. Our new chemically well-defined MAs may in principle be attached to other targeting groups in order to obtain selective contrast enhancement. A number of studies in other laboratories have been performed on labeling of antibodies with Gd—DTPA residues (1, 29). The number of sites on an antibody available for labeling are limited (27). Also, a high degree of modification of the antibody may compromise its ability to recognize its system. Thus, the use of MAs may be advantageous. With an eye toward the eventual labeling of antibodies with our MAs, a model reaction was performed in which the amino MA **3** was activated with thiophosgene. The resulting isothiocyanate **22** was used for the labeling of HSA. While the structure of the labeled HSA conjugate **23** has not been analyzed in detail, the conjugate displayed strong paramagnetic properties in preliminary NMR studies after purification by size-exclusion chromatography.

In conclusion, chemically well-defined MAs have been successfully employed in the design of a potential blood pool contrast agent. The design principles are flexible and can accommodate a variety of different targeting groups, core fragments, branchers, linkers, and active groups.

LITERATURE CITED

(1) Brasch, R. C. (1992) Contrast enhancement in MRI: Images of the future. *Adv. MRI Contrast.* **1**, 28–41.

(2) Weinmann, H. J., Brasch, R. C., Press, W.-R., and Wesbey, G. E. (1984) Characteristics of gadolinium—DTPA complex: a potential NMR contrast agent. *Am. J. Roentgenol.* **142**, 619–624.

(3) Brasch, R. C. (1991) Rationale and applications for macromolecular Gd-based contrast agents. *Magn. Reson. Med.* **22**, 282–287.

(4) Bogdanov, A. A., Weissleder, R., Frank, H. W., Bogdanova, A. V., Nossif, N., Schaffer, B. K., Tsai, E., Papisov, M., and Brady, T. J. (1993) A new macromolecule as a contrast agent for MR angiography: preparation, properties, and animal studies. *Radiology, 187*, 701–706.

(5) Bligh, S. W. A., Harding, C. T., Sadler, P. J., Bulman, R. A., Bydder, G. M., Pennock, J. M., Kelly, J. D., Latham, I. A., and Marriott, J. A. (1991) Use of paramagnetic chelated metal derivatives of polysaccharides and spin-labeled polysaccharides as contrast agents in magnetic resonance imaging. *Magn. Reson. Med.* **17**, 516–532.

(6) Mann, J. S., Huang, J. C., and Keana, J. F. W. (1992) Molecular amplifiers: synthesis and functionalization of a poly(aminopropyl)dextrane bearing a uniquely reactive terminus for univalent attachment to biomolecules. *Bioconjugate Chem. 3*, 154–159.

(7) Spanoghe, M., Lanens, D., Dommisse, R., Van der Linden, A., and Alder Weireldt, F. (1992) Proton relaxation enhancement by means of serum albumin and poly-l-lysine labeled with DTPA-gadolinium (3+): relaxivities as a function of molecular weight and conjugation efficiency. *Magn. Reson. Med. 10*, 913–917.

(8) Lauffer, R. B. (1990) Magnetic resonance contrast media: principles and progress. *Magn. Res. Q. 6*, 65–84.

(9) Tomalia, D. A., Baker, H., Dewald, J. R., Hall, M., Kallos, G., Martin, S., Roeck, J., Ryder, J., and Smith, P. (1985) A new class of polymers: Starburst®-dendric macromolecules. *Polymer J. (Tokyo) 17*, 117.

(10) Wiener, E. C., Brechbeil, M. W., Brothers, H., Magin, R. L., Gansow, O. A., Tomalia, D. A., and Lauterbur, P. C. (1994) Dendrimer-based metal chelates: a new class of magnetic resonance imaging contrast agents. *Magn. Reson. Med. 31*, 1–8.

(11) Baxter, A. B., Melnikoff, S., Stites, D. P., and Brasch R. C. (1991) Immunogenicity of gadolinium based contrast agents for magnetic resonance imaging: induction and characterisation of antibodies in animals. *Invest. Radiol. 26*, 1035–1040.

(12) Schmiedl, U., Ogan, M. D., Moseley, M. E., and Brasch, R. C. (1986) Comparison of the contrast-enhancing properties of albumin-(Gd—DTPA) and Gd—DTPA at 2.0 T: an experimental study in rats. *Am. J. Radiology 147*, 1263–1270.

(13) Brechbiel, M. W., and Gansow, O. A. (1991) Backbone-substituted DTPA ligands for ⁹⁰Y radioimmunotherapy. *Bioconjugate Chem. 2*, 187–194.

(14) Keana, J. F. W., and Mann J. S. (1990) Chelating ligands functionalized for facile attachment to biomolecules. A convenient route to 4-isothiocyanatobenzyl derivatives of diethylenetriaminopentaacetic acid and ethylenediaminetetraacetic acid. *J. Org. Chem. 55*, 2868–2871.

(15) Lauffer, R. B. (1989) Vivo enhancement of NMR relaxivity. U. S. Patent 4,880,008; (1990) *Chem. Abstr.* 112, 194602x.

(16) Schuhmann-Giampieri, G., Schmitt-Willich, H., Press, W.-R., Negishi, C., Weinmann, H.-J., and Speck, U. (1992) Preclinical evaluation of Gd—EOB—DTPA as a contrast agent in MR imaging of the hepatobiliary system. *Radiology 183*, 59–64.

(17) Bennett, H. F., Brown, R. D., Keana, J. F. W., Koenig, S. H., and Swartz, H. M. (1990) Interactions of nitroxides with plasma and blood: effect on 1/T1 of water protons. *Magn. Reson. Med. 14*, 40–55.

(18) Vallet, P., Van Haverbeke, Y., Bonnet, P. A., Subra, G., Chapat, J-P, and Muller, R. N. (1994) Relaxivity enhancement of low molecular weight nitroxide stable free radicals: Importance of structure and medium. *Magn. Reson. Med. 32*, 11–15.

(19) Keana, J. F. W., Lex, L., Mann, J. S., May, J. M., Park, J. H., Pou, S., Prabhu, V. S., Rosen, G. M., Sweetman, B. J., and Wu, Y. (1990) Novel nitroxides for spin-labelling, -trapping, and magnetic resonance imaging applications. *Pure Appl. Chem. 62*, 201–205.

(20) Perrin, D. D., Armarego, W. L. F., and Perrin, D. R. (1990) *Purification of Laboratory Chemicals*, 2nd Ed., Pergamon Press: New York.

(21) Sosnovsky, G., and Lukszo, J. (1986) In the search for new anticancer drugs, XVI. Selective protection and deprotection of primary amino groups in spermine, spermidine and other polyamines. *Z. Naturforsch. 41b*, 122–129.

(22) Martin, V. V., and Keana, J. F. W. (1995) 4-Aminobenzyl-substituted diethylenetriaminepentaacetic acid pentamethyl ester: a convenient intermediate for attachment of a DTPA

moiety to amine-containing target molecules. *Synth. Commun.* (in press).

(23) Anon. (1991) Gel Filtration. Theory and Practice. Pharmacia LKB biotechnology Bulletin, 5th ed., p 49, Uppsala, Sweden.

(24) Cheng, K. L., Ueno, K., and Imamura, T. (1982) *Handbook of Organic Analytical reagents*, pp 165–176, CRC Press, Boca Raton, FL.

(25) Peters, T. (1985) Serum albumine. *Adv. Protein Chem. 37*, 161–245.

(26) Aki, H., and Yamamoto, M. (1993) Biothermodynamic characterization of monocarboxylic and dicarboxylic aliphatic acids binding to human serum albumin: a flow microcalorimetric study. *Biophys. Chem. 46*, 91–99.

(27) Sieving, P. F., Watson, A. D., and Rocklage, S. M. (1990) Preparation and characterization of paramagnetic polychelates and their protein conjugates. *Bioconjugate Chem. 1*, 65–71.

(28) Vexler, V. S., Clement, O., Schmitt-Willich, H., and Brasch, R. C. (1994) Effect of varying the molecular weight of the MR contrast agent Gd–DTPA-polylysine on blood pharmacokinetics and enhancement patterns. *J. Magn. Reson. Imag. 4*, 381–388.

(29) Shreve, P., and Aisen, A. M. (1986) Monoclonal antibodies labeled with polymeric paramagnetic ion chelates. *Magn. Reson. Med. 3*, 336–340.

Generation of a Potent Chimeric Toxin by Replacement of Domain III of *Pseudomonas* Exotoxin with Ricin A Chain KDEL[†]

Carol Pitcher,[‡,§] Lynne Roberts,[‡] Stephen Fawell,[⊥] Alex G. Zdanovsky,[∥] David J. FitzGerald,[*,∥] and
J. Michael Lord[‡]

Department of Biological Sciences, University of Warwick, Coventry, CV4 7AL, U.K., Biogen Incorporated,
14 Cambridge Center, Cambridge, Massachusetts 02142, and Laboratory of Molecular Biology, DCBDC, National
Cancer Institute, National Institutes of Health, Building 37, Room 4B03, 37 Convent Drive MSC 4255,
Bethesda, Maryland 20892-4255. Received March 24, 1995[⊗]

Following cellular uptake, *Pseudomonas* exotoxin (PE) is cleaved by cellular protease which generates an enzymatically active C-terminal fragment (amino acids 280–613). This 37 kD fragment translocates to the cell cytosol where it ADP-ribosylates elongation factor 2 and inhibits protein synthesis. A recombinant hybrid toxin (designated PE–RTA) in which the ADP-ribosylation domain (domain III) was replaced by the RNA N-glycosidase domain of ricin (the A chain or RTA) has been produced in *E. coli*. The hybrid toxin effectively and specifically depurinated 28S ribosomal RNA, indicating that the ricin A moiety folded into its native conformation. The cytotoxicity of PE–RTA for L929 cells was approximately 100-fold less than either native PE or whole ricin. However, the addition of the tetrapeptide KDEL to the C-terminus of PE–RTA (producing PE–RTA KDEL) increased cytotoxicity to the level of the native toxins. By analogy to PE, both PE–RTA and PE–RTA KDEL would be proteolytically cleaved within PE domain II during cell entry. A single amino acid substitution, believed to disrupt an essential step in the transport of the catalytically active PE fragment to the cell cytosol (Trp281 to Ala: Zdanovsky, A.G., Chiron, M., Pastan, I., and FitzGerald, D. J. (1993) *J. Biol. Chem. 268*, 21791–21799), reduced the cytotoxicities of both PE and PE–RTA KDEL by approximately 100-fold. Taken together, these data show that the ricin A chain component of the hybrid toxin requires essential PE-derived sequences at both the N- and C-termini of the translocating fragment. Clearly, in the context of this fusion protein, ricin A chain cannot effect its own transfer to the cytosol.

INTRODUCTION

Pseudomonas exotoxin A (PE)[1] is a bacterial toxin that is potently cytotoxic to mammalian cells. The cytotoxic mechanism involves the binding of toxin to a receptor on the cell surface (*1, 2*), cell entry by receptor-mediated endocytosis (*3, 4*), traversal across an intracellular membrane to enter the cytosol (*5*), and finally inhibition of cellular protein synthesis by the catalytic ADP-ribosylation of elongation factor (EF)-2 (*6*). PE contains three distinct folding domains which are responsible for these functions (*7*). Domain Ia (residues 1–252) is responsible for receptor binding, domain II (residues 253–364) for membrane translocation, and domain III (residues 400–613) for ADP-ribosylation (*8*). Domain Ib (residues 365–399) has no known function and can be deleted without affecting cytotoxicity.

During endocytosis, PE is proteolytically cleaved within domain II (between Arg279 and Gly280) most likely by

¹ Abbreviations: PE, *Pseudomonas* exotoxin; RTA, ricin A chain; PEala281, mutant PE with tryptophan changed to alanine at residue 281; PE–RTA, fusion of domains Ia, II and Ib of PE with RTA; PE–RTA KDEL, fusion as above with the tetrapeptide LysAspGluLeu at the C-terminus.

the proprotein convertase furin to generate an N-terminal fragment of 28 kDa and a C-terminal fragment of 37 kDa, which remain covalently joined by a disulfide bond (*9–11*). The 37 kDa fragment (residues 280–613, designated PE37) ultimately crosses an intracellular membrane and enters the cytosol to reach and inactivate EF2 (*11*). The proteolytic processing step is essential for cytotoxicity since PE mutants that cannot be cleaved by furin are nontoxic, even though their cell binding and ADP-ribosylation activities are normal (*11, 12*). PE37 itself possess two additional requirements that are essential for cytotoxicity. The first is the sequence REDLK at the C-terminus of domain III (*13, 14*). In the holotoxin this sequence can be replaced only by KDEL or related sequences recognized by the KDEL receptor (*14*). This suggests that the interaction with the KDEL receptor facilitates the later stages of intracellular transport. Such an interaction could potentially deliver PE37 to the lumen of the ER from where translocation into the cytosol is believed to occur (*15*). The second additional requirement for cytotoxicity is for an intact N-terminus of PE37. Deletion of up to 7 residues from the N-terminus of PE37 or substitution of these residues significantly reduces cytotoxicity (*16, 17*). For example, replacement of Trp281 (the second residue of PE37) with Ala reduces toxicity to murine L929 cells by 100-fold (*17*). It has been proposed that the N-terminus of PE37 is important for initiating or mediating the translocation process (*16, 17*).

In the present study we have prepared a series of hybrid toxins in which domain III of PE was replaced by ricin A chain (RTA) (*18*). Following cellular uptake, proteolytic cleavage of such hybrids at the furin recognition site within domain II of PE would produce a 45 kDa fragment consisting of the PE translocation region followed by RTA. RTA is also believed to enter the cytosol

from the ER lumen by translocation across the ER membrane (*19*), possibly utilizing an existing ER membrane translocon in the reverse direction. Here we sought to determine whether the putative translocation function of RTA could effectively replace that of PE when the latter was mutationally impaired. The results we obtained clearly show that for these hybrid toxins the fragments generated by intracellular proteolysis still required functional PE sequences at both the N- and C-termini. This indicates that in this fusion context, PE sequences are essential for the effective intracellular transport and/or membrane translocation of a passenger protein normally thought capable of effecting its own transfer to the cytosol.

MATERIALS AND METHODS

Plasmids and Bacterial Strains. All the gene fusions were cloned into the pET3d expression vector (*20*) by standard techniques. The initial cloning steps and analysis of the plasmids was carried out in *E. coli* TG2 cells. For expression, the plasmids were transformed into *E. coli* BL21 (λDE3). This strain carries the T7 RNA polymerase gene under the control of an isopropyl 1-thio-β-D-galactopyranoside-inducible promoter. Plasmid pEX-2 (*21*) was used as the source of the native PE gene.

Tissue Culture. Murine L929 cells were obtained from the American Type Culture Collection and were maintained in Dulbecco's modified Eagle's medium supplemented with 5% fetal bovine serum, 50 units/mL penicillin, 50 μg/mL streptomycin, and 2 mM glutamine.

Construction of Expression Plasmids Encoding PE and PE–ricin A Chain Fusions. Figure 1 is a schematic illustration of the PE–RTA gene fusions constructed and the two PE clones that were constructed and expressed as controls.

Cloning of pET–PE. Plasmid pEX-2 was cut at unique Nco1 and EcoRI sites, and the 1798 bp fragment, which contained the bulk of the PE gene, was isolated and ligated, using two synthetic oligonucleotide pairs, to the large Xba1–EcoRI fragment derived from pET-3d. The oligonucleotides were designed to replace nucleotides 1–213 of the PE gene which were lost when the gene was excised from pEX-2. In addition, the synthetic oligonucleotides introduced a Bsa1 site to facilitate subsequent cloning of a fragment encoding the OmpA signal sequence. The vector product of the ligation described above was cut with Xba1–Bsa1, and the large fragment was purified. Cutting with restriction enzyme Bsa1 generates an EcoRI overhang, making it possible to ligate an 85 bp Xba1–EcoRI fragment encoding the OmpA signal sequence to the large Xba1–Bsa1 fragment. The fragment encoding the OmpA signal sequence was excised from the pINIII–OmpA1 vector (*22*). The resultant plasmid was designated pET–PE. The above cloning strategy which adds the OmpA signal sequence to the PE coding sequence also caused addition of three extra codons at the 5' end of the PE coding region. Thus, three additional amino acids (Ala-Asp-Leu) were present at the mature N-terminus of the secreted PE protein.

Cloning of PE–RTA and PE–RTA KDEL. The RTA coding sequence was ligated into unique SacII–BamH1 sites in pET-PE. PCR was used to engineer the appropriate restriction sites at the 5' and 3' ends of RTA and to add the KDEL coding sequence to the RTA C-terminus.

Cloning of pET-PE.281, pPEala281–RTA, and pPEala281–RTA KDEL. Construction of a mutant PE clone containing the codon mutation Trp281 to Ala281 in domain II has been described earlier (*17*). A Xba1–EcoRI fragment carrying the coding sequence of PE with

the OmpA signal sequence was cut from this clone and ligated to the Xba1–EcoRI fragment purified from pET-PE. The product of this ligation was designated pET–PE.281 and was used to construct the pPEala281–RTA and pPEala281–RTA KDEL clones, using identical steps to those used to clone pPE–RTA and pPE–RTA KDEL from pET–PE.

Expression and Analysis of Recombinant Proteins. The BL21 (λDE3) cells carrying the DNA of interest were grown in M9ZB containing 100 μg/mL of ampicillin, until the culture reached an OD_{600} of 0.6. Then the cells were induced by the addition of 0.4 mM isopropyl 1-thio-β-D-galactopyranoside. The cells were grown for a further 3 h before being harvested. Periplasmic fractions were isolated by osmotic shock. The pelleted cells were resuspended in 1/20 growth volume of 20% w/v sucrose, 30 mM Tris pH 7.4, and 1 mM EDTA. After incubation on ice for 10 min, the cells were centrifuged at 6000 rpm in Sorval 8 × 50 rotor at 4 °C for 10 min. The supernatant was discarded and the pellet resuspended in 1/20 growth volume of ice cold distilled water and kept on ice for 10 min. The cell fraction was pelleted by centrifugation at 8000 rpm in a Sorval 8 × 50 rotor at 4 °C for 10 min. The supernatant containing periplasmic proteins was recovered, and 1 M Tris pH 7.6 was added to a final concentration of 0.25 M. The periplasmic fractions were stored at −70 °C. Proteins were resolved by electrophoresis on 15% SDS–PAGE gels and visualized by silver staining or by Western blotting and subsequent incubation with rabbit anti-PE antibodies followed by anti-(rabbit IgG) alkaline phosphatase conjugate and color development.

***In Vitro* Activity of the PE–Ricin A Chain Fusion Proteins.** *(a) Estimation of the Amount of PE and PEala281 in the Periplasmic Fractions.* In vitro activity of PE was tested using the general method of Collier and Kandel (*23*). A 0.1–1.8 μg portion of PE was incubated with 40 mM Tris pH 8.0, 40 mM NH_4Cl, 20 mM DTT, 0.05 μCi ^{14}C-NAD, and 30 μL of enriched wheat germ in a total reaction volume of 50 μL. After 30 min at 37 °C, 0.5 mL of 12% TCA was added to each reaction, and the reactions were left on ice for 15 min before being centrifuged in a microfuge for 10 min at 4 °C. The pellets were washed with 6% TCA and repelleted as above, and the pellets were solubilized by addition of 100 mL of 0.5 M NaOH. After 1 h, the extracts were transferred to scintillation fluid, and the amount of ^{14}C-transferred to TCA precipitable material was measured. The activity of the PE in the extracts from *E. coli* was determined by comparison to the activity of known concentrations of PE (Sigma).

(b) Estimation of Amounts and in Vitro Activity of PE–RTA Proteins. The concentrations of the PE–RTA chain fusion proteins in the periplasmic fractions were quantified by SDS–PAGE and Western blotting. Known quantities of PE were run on SDS–polyacrylamide gels beside varying amounts of the periplasmic fractions. The gels were blotted and probed with rabbit PE antibodies. After incubation with anti-(rabbit IgG) alkaline phosphatase conjugate and color development, the blots were scanned on a Pharmacia LKB ultrascan enhanced laser densitometer.

To confirm that each of the fusion proteins had identical *in vitro* activities 0.1, 1, 2, and 5 ng of each of the PE-ricin A chain fusion proteins was incubated with 3 μg of purified reticulocyte ribosomes (*24*). The RNA was extracted, and 3 μg of each sample was treated with 20 μL of aniline/acetic acid pH 4.5 and incubated at 60 °C for 2 min. The RNA was analyzed on 1.2% agarose/50% formamide gels (*24*).
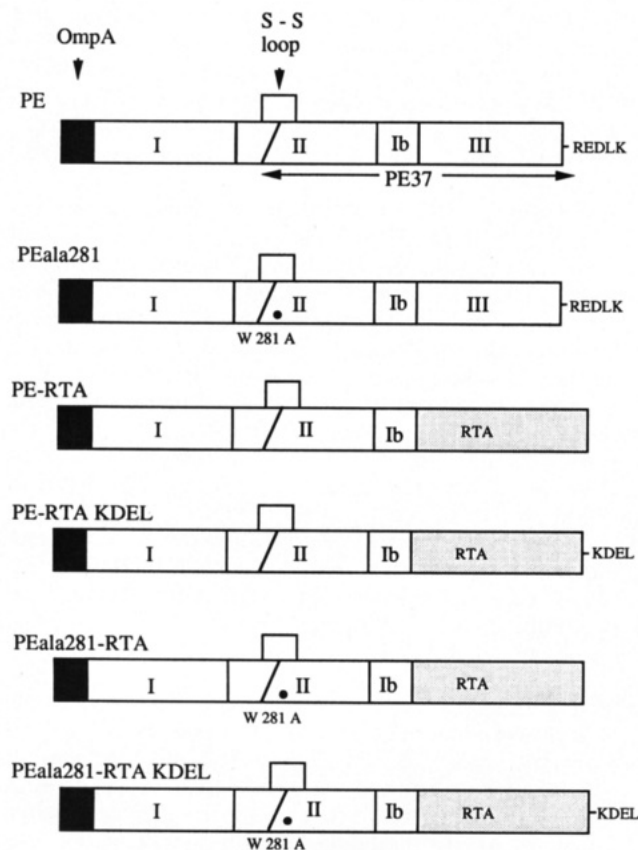
Figure 1. Schematic illustrations of the PE and PE−RTA fusions. The sloping line in the domain II disulfide loop indicates the proteolytic processing site between Arg279 and Gly280.

Figure 2. Expression of PE and PE−RTA fusion proteins in *E. coli*. The lane designated M shows molecular weight markers: lane 1, BL21 (λDE3) cells before induction; lane 2, BL21 (λDE3) cells after induction; lane 3, the supernatant from the sucrose wash; lane 4, the periplasmic fraction; lane 5, the cell pellet after osmotic shock, for A, PE; B, PEala281; C, PE−RTA; D, PEala281−RTA; E, PE−RTA KDEL; F, PEala281−RTA KDEL. The gel shown is a western blot of a reducing SDS-polyacrylamide gel where PE-containing proteins were visualized using rabbit anti-PE antibodies.

Cytotoxicity Assays. Protein synthesis inhibition assays were performed on murine L929 cells. Cells were plated out on 96 well plates at a density of 1.5×10^4 cells/well in 100 μL of medium the day before the assay. A range of concentrations of the test protein was added to the cells in 100 μL of complete medium and incubated overnight. Toxin was then removed, and the cells were incubated with 1 μCi of [^{35}S]methionine in 50 μL of PBS for a further 2 h. After 2 h the cells were washed three times with 5% TCA and then once with PBS. Cells were solubilized by the addition of 50 μL of 0.5 M NaOH per well, and the TCA-precipitable material was counted. Each toxin concentration was tested in quadruplicate, and the TCA precipitable counts were averaged. Protein synthesis was measured as a percentage of [^{35}S]methionine incorporation relative control cells treated with toxin-minus periplasm.

RESULTS

Construction of PE−RTA Gene Fusions. The fusions constructed are illustrated schematically in Figure 1. DNA encoding domain III of PE was replaced with DNA encoding RTA (to give PE−RTA) or RTA supplemented by addition of the ER retrieval sequence KDEL at its C-terminus (PE−RTA KDEL). PE−RTA is a chimeric toxin consisting of PE residues 1−412 (domains I, II, and Ib) followed by the 267 residues of RTA. Similar constructs were also prepared in which the Trp281 codon of PE domain II had been mutated to an Ala codon (to yield PEala281, PEala281−RTA, or PEala281−RTA KDEL, respectively). All toxin genes were preceded by DNA encoding the *E. coli* OmpA signal sequence to ensure targeting to the periplasm of *E. coli*.

Expression. Recombinant proteins were produced in *E. coli* strain BL21 (λDE3) (Figure 2). Induction by

Figure 3. Depurination of rabbit reticulocyte 28S ribosomal RNA by RTA or fusion proteins containing RTA. In A, ribosomes were incubated with 10 ng of RTA, RNA was extracted, treated with aniline (+) or not treated (−)- and separated by 1.2% denaturing agarose gel electrophoresis. The arrow indicates the ribonucleotide fragment released by aniline treatment of purinated RNA. Also shown are aniline-treated RNA samples from ribosomes incubated with periplasm containing B, PE−RTA; C, PE−RTA KDEL; D, PEala281−RTA; E, PEala281−RTA KDEL. Lane 1: 0.1 ng of recombinant protein. Lane 2: 1 ng. Lane 3: 2 ng. Lane 4, 5 ng.

isopropyl 1-thio-β-galactopyranoside resulted in the expression of recombinant proteins (Figure 2, lane 2) which were recovered in the periplasmic fraction (Figure 2, lane 4). Quantitation of toxin activity in periplasmic fractions was considered valid since control periplasm preparations that were spiked with either purified PE or RTA exhibited full activity.
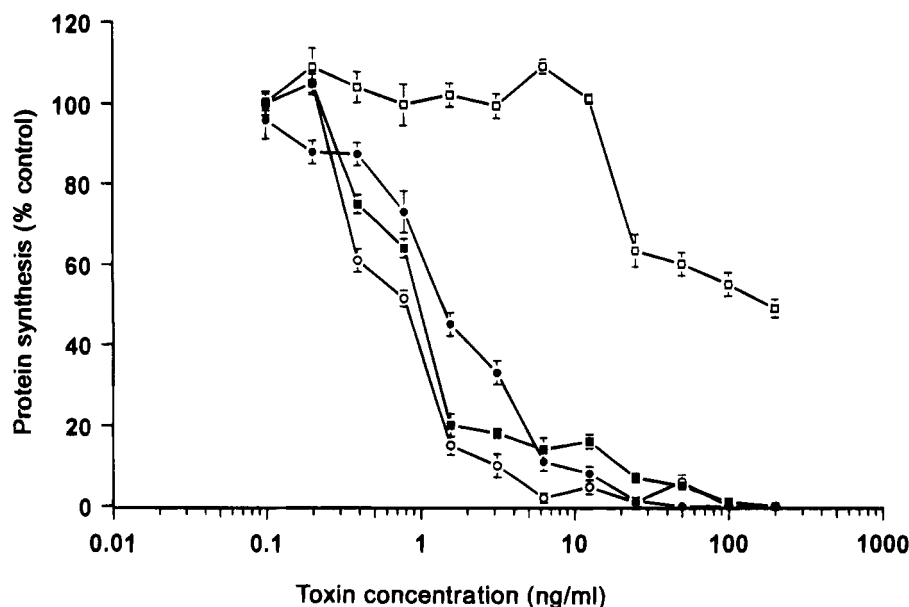
Figure 4. Inhibition of protein synthesis in L929 cells. Cells were incubated with various concentrations of purified PE (O), purified ricin (●), recombinant PE (■), or recombinant PEala281 (□), and [^{35}S]methionine incorporation into cellular protein was measured.

Table 1. Concentration of Toxin which Causes a 50% Inhibition of Protein Synthesis in L929 Cells

toxin	IC$_{50}$ (ng/mL)	toxin	IC$_{50}$ (ng/mL)
purified PE	0.8	PE–RTA	90.0
purified ricin	1.2	PEala281–RTA	≫200.0
PE	1.0	PE–RTA KDEL	1.3
PEala281	120.0	PEala281–RTA KDEL	130.0

Enzyme Activity. The RTA moiety present in the various PE–RTA fusion proteins was catalytically active since it rendered rabbit reticulocyte 28S ribosomal RNA susceptible to cleavage by aniline to yield the ~400 ribonucleotide RNA fragment diagnostic of ribosome depurination by RTA (*24*) (Figure 3, arrowed). Quantitation established that the RTA moieties in the various fusion proteins had very similar activities to each other and to native RTA (Figure 3).

Cytotoxicity. Cytotoxicity to murine L929 cells was determined by adding appropriately diluted periplasmic fractions containing the recombinant toxin directly to the cells. As such, the cytotoxicity of recombinant PE was essentially identical to that of purified PE and similar to that of purified ricin (Figure 4). In contrast, PE.281 was significantly less toxic than PE, with an IC$_{50}$ value over 100-fold higher than either purified or recombinant PE (Table 1) as described earlier (*17*). The cytotoxicity of PE–RTA was approximately 2 orders of magnitude less than PE or whole ricin (Table 1). The addition of the C-terminal tetrapeptide KDEL increased cytotoxicity to the level of whole ricin (Figure 5; Table 1). PEala281–RTA KDEL had reduced cytotoxicity (Figure 5), and when PE–RTA KDEL and PEala281–RTA KDEL are compared, this reduction is of the same order as that for PE and PEala281 (Table 1). PEala281–RTA was not cytotoxic at the highest concentration tested (Figure 5).

DISCUSSION

PE enters susceptible eukaryotic cells by receptor-mediated endocytosis and is cleaved by the cellular protease furin between Arg279 and Gly280 (*9*). The C-terminal 37 kD fragment (residues 280–613) resulting from cleavage then traverses an intracellular membrane to reach the cytosol where it rapidly brings protein synthesis to a halt. Recent evidence indicates that the residues important for the translocation of PE37 reside at its N-terminus (*17*). Changing Trp281, Leu284, or Tyr 289 to other residues did not adversely affect receptor binding, proteolytic cleavage by furin, or the ADP-ribosylation activity, but dramatically (up to 250-fold) reduced cytotoxic potency (*17*). To be fully cytotoxic, PE also requires the C-terminal sequence REDLK (residues 609–613) (*13*). This C-terminal region is believed to facilitate the later steps in intracellular transport and may retain the toxin in the ER prior to translocation. Thus, the N-terminus of PE37 is required for membrane translocation and the C-terminus for transport to a translocationally-competent compartment.

In contrast, ricin does not require proteolytic cleavage during cell entry because cleavage to separate the catalytically-active fragment (RTA) from the cell binding component (RTB) occurs during ricin biosynthesis in the *Ricinus* plant (*25*). In addition to its catalytic activity, RTA is also believed to have a translocation function and, in common with PE37, is thought to translocate into the cytosol from the ER lumen (*19*). However, RTA does not possess a C-terminal KDEL or KDEL-like sequence to facilitate transport to this organelle. Rather, it seems that the galactose-binding activity of RTB is required (*26*), perhaps permitting ricin to interact with a galactosylated cellular component undergoing retrograde transport from the TGN or Golgi to the ER (*19*). It has been shown that free RTA, in contrast to whole ricin, readily associates with and inserts into membranes (*27–29*). This implies that a normally buried hydrophobic pocket or domain within RTA becomes exposed upon dissociation of the subunits. The primary sequence (*30*) and three-dimensional structure (*31*) of ricin identifies a stretch of 12 hydrophobic amino acid residues (Val245–Val256) close to the C-terminus of RTA as the most likely candidate for a membrane interactive region. Thus, RTA may rely upon RTB for optimal routing in the cell and possesses a region at its C-terminus for membrane traversal or at least for the initial membrane insertion step prior to translocation. To further examine these proposed properties, we have produced a series of recombinant hybrid proteins in which PE domain III was replaced by RTA.
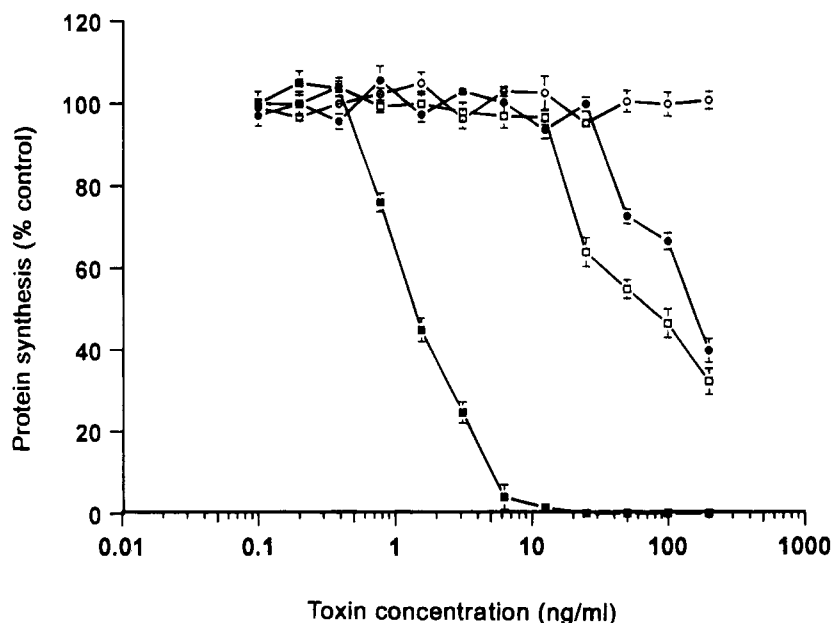
Figure 5. Inhibition of protein synthesis in L929 cells by recombinant fusion proteins. Cells were incubated with periplasmic fractions containing various concentrations of PE−RTA (●), PEala281-RTA (○), PE−RTA KDEL (■), or PEala281−RTA KDEL (□), and [^{35}S]-methionine incorporation into cellular protein was measured.

Replacing PE domain III with RTA (PE−RTA) produced a hybrid toxin whose toxicity to L929 cells was 80- to 100-fold lower than either native PE or ricin. This is consistent with the absence of an intracellular transport function since the addition of a C-terminal KDEL tetrapeptide to the RTA moiety of PE−RTA restored the level of cytotoxicity to that of whole ricin (PE−RTA KDEL IC_{50} 1.3 ng/mL) (Table 1).

The catalytically active fragment generated from PE−RTA KDEL by furin cleavage during intracellular transport should contain two putative translocation regions. The first 133 residues of this fragment would be identical to the PE37 counterpart (PE residues 280−412) and would therefore include the PE37 N-terminus and its translocation activity. The remainder of the fragment would comprise the 267 residues of RTA plus the C-terminal tetrapeptide, KDEL. This part of the molecule would presumably contain the proposed translocation region of RTA, possibly at the C-terminus. The addition of KDEL to the extreme C-terminus of RTA has already been shown to enhance activity (*32, 33*), indicating that its presence per se does not interfere with the translocation step.

In this study, we posed the following question: If the PE translocation function in PE−RTA KDEL is mutationally impaired, does the molecule remain potently toxic to L929 cells? A positive result would signify that efficient translocation of the RTA-containing fragment was being maintained by the proposed RTA translocation function. The answer was clearly no. We found that introducing the point mutation Trp281Ala into PE (to give PEala281) resulted in an over 100-fold loss in cytotoxicity in comparison to wild-type PE (Table 1), as reported previously (*17*). Significantly, introducing the W281A mutation into PE−RTA KDEL (to give PEala281−RTA KDEL) likewise resulted in a 100-fold loss in cytotoxicity in comparison with PE−RTA KDEL (Table 1). The putative RTA translocation function was clearly unable to compensate for the defective PE function caused by the W281A mutation. It therefore seems unlikely that RTA contains an independently acting C-terminal translocation domain. The hydrophobic stretch at the C-terminus of RTA may still be important for

membrane interaction, but the actual membrane penetration step may depend on a different region of RTA, for example, its N-terminus. If this were the case then the presence of 133 residues of PE at the N-terminus of the RTA-containing fragments generated here from PE−RTA KDEL must effectively mask and prevent expression of the RTA translocation function. RTA is assumed to be translocationally competent since RTA-containing immunotoxins can be as potently cytotoxic as whole ricin (*34*) and free RTA can reach the cytosol and depurinate ribosomes when added to cells at appropriate concentrations (*33*). The present study failed to provide any evidence for an RTA translocation function.

To investigate the functional properties of various toxin domains a number of different hybrid proteins have been generated. Domains I and II of PE were sufficient to transport barnase to the cell cytosol provided a C-terminal KDEL sequence was present (*35*). However, in a similar construction with DTA in place of domain III of PE, the need for a KDEL-like sequence was not apparent (*36*). In contrast, Leppla and colleagues have shown that the translocating activity of lethal factor from anthrax toxin was hindered by the presence of domain II sequences (*37, 38*). Thus, it is possible that translocating activities of one toxin can dominate another. In the structural context of a fusion with PE, it is clear that the RTA-containing moiety, which has a putative translocation function, still depends on both the PE C-terminus (KDEL) and the PE37 N-terminal region for effective transport and translocation to the cytosol.

ACKNOWLEDGMENT

LITERATURE CITED

(1) Kounnas, M. Z., Morris, R. E., Thompson, M. R., FitzGerald, D. J., Strickland, D. K., and Saelinger, C. B. (1992) The alpha 2-macroglobulin receptor/low density lipoprotein receptor-related protein binds and internalizes *Pseudomonas* exotoxin A. *J. Biol. Chem. 267*, 12420−12423.

(2) Thompson, M. R., Forristal, J., Kauffman, P., Madden, T., Kozak, K., Morris, R. E., and Saelinger, C. B. (1991) Isolation

and characterization of *Pseudomonas aeruginosa* exotoxin A binding glycoprotein from mouse LM cells. *J. Biol. Chem. 266*, 2390−2396.

(3) FitzGerald, D. J. P., Morris, R. E., and Saelinger, C. B. (1980) Receptor-mediated internalization of *Pseudomonas* toxin by mouse fibroblasts. *Cell 21*, 867−873.

(4) Saelinger, C. B., Morris, R. E., and Foertsch, G. (1985) Trafficking of *Pseudomonas* exotoxin A in mammalian cells. *Eur. J. Clin. Microbiol. 4*, 170-174.

(5) Ogata, M., Chaudhary, V. K., Pastan, I., and FitzGerald, D. J. (1990) Processing of *Pseudomonas* exotoxin by a cellular protease results in the generation of a 37,000-Da toxin fragment that is translocated to the cytosol. *J. Biol. Chem. 265*, 20678−20685.

(6) Iglewski, B. H., and Kabat, D. (1975) NAD-dependent inhibition of protein synthesis by *Pseudomonas aeruginosa* toxin. *Proc. Natl. Acad. Sci. U.S.A. 72*, 2284−2288.

(7) Allured, V. S., Collier, R. J., Carroll, S. F., and McKay, D. B. (1986) Structure of exotoxin A of *Pseudomonas aeruginosa* at 3.0 Angstrom. *Proc. Natl. Acad. Sci. U.S.A. 83*, 1320−1324.

(8) Hwang, J., FitzGerald, D. J., Adhya, S., and Pastan, I. (1987) Functional domains of *Pseudomonas* exotoxin identified by deletion analysis of the gene expressed in *E. coli*. *Cell 48*, 129−136.

(9) Chiron, M. F., Fryling, C. M., and FitzGerald, D. J. (1994) Cleavage of *Pseudomonas* exotoxin and diphtheria toxin by a furin-like protease prepared from beef liver. *J. Biol. Chem. 269*, 18167−18176.

(10) Ogata, M., Fryling, C. M., Pastan, I., and FitzGerald, D. J. (1992) Cell-mediated cleavage of *Pseudomonas* exotoxin between Arg279 and Gly280 generates the enzymatically active fragment which translocates to the cytosol. *J. Biol. Chem. 267*, 25396−25401.

(11) Ogata, M., Pastan, I., and FitzGerald, D. J. (1991) *Pseudomonas* exotoxin: analysis to toxin activation and conformational changes using monoclonal antibodies as probes. *Infect. Immun. 59*, 407−414.

(12) Jinno, Y., Ogata, M., Chaudhary, V. K., Willingham, M. C., Adhya, S., FitzGerald, D., and Pastan, I. (1989) Domain II mutants of *Pseudomonas* exotoxin deficient in translocation. *J. Biol. Chem. 264*, 15953−15959.

(13) Chaudhary, V. K., Jinno, Y., FitzGerald, D., and Pastan, I. (1990) *Pseudomonas* exotoxin contains a specific sequence at the carboxyl terminus that is required for cytotoxicity. *Proc. Natl. Acad. Sci. U.S.A. 87*, 308−312.

(14) Seetharam, S., Chaudhary, V. K., FitzGerald, D., and Pastan, I. (1991) Increased cytotoxic activity of *Pseudomonas* exotoxin and two chimeric toxins ending in KDEL. *J. Biol. Chem. 266*, 17376−17381.

(15) Pastan, I., and FitzGerald, D. (1991) Recombinant toxins for cancer treatment. *Science 254*, 1173−1177.

(16) Theuer, C. P., FitzGerald, D., and Pastan, I. (1992) A recombinant form of *Pseudomonas* exotoxin directed at the epidermal growth factor receptor that is cytotoxic without requiring proteolytic processing. *J. Biol. Chem. 267*, 16872−16877.

(17) Zdanovsky, A. G., Chiron, M. F., Pastan, I., and FitzGerald, D. J. (1993) Mechanism of action of *Pseudomonas* exotoxin: identification of a rate-limiting step. *J. Biol. Chem. 268*, 21791−21799.

(18) Lord, J. M., Roberts, L. M., and Robertus, J. D. (1994) Ricin: structure, model of action and some current applications. *FASEB J. 8*, 201−208.

(19) Pelham, H. R. B., Roberts, L. M., and Lord, J. M. (1992) Toxin entry: how reversible is the secretory pathway? *Trends Cell Biol. 2*, 183−185.

(20) Studier, F. W., Rosenberg, A. H., Dunn, J. J., and Dubendorff, J. W. (1990) Use of T7 RNA polymerase to direct expression of clone genes. *Methods Enzymol. 185*, 60−89.

(21) Winkler, G., Jakubowski, A., Turner, S., Liu, T,. Burrus,

B., McGray, P., Heanue, T., Rosa, M., Griffiths, B. A., Wali, A. et al. (1991) CD4-*Pseudomonas* exotoxin hybrid proteins: modulation of potency and therapeutic window through structural design and characterization of cell internalization. *Aids Res. Hum. Retroviruses 7*, 393−401.

(22) Ghrayeb, J., Kimura, H., Takahara, M., Hsiung, H., Masui, Y., and Inouye, M. (1984) Secretion cloning vectors in *Escherichia coli*. *EMBO J. 3*, 2437−2442.

(23) Collier, R. J., and Kandel, J. (1971) Structure and activity of diphtheria toxin. I. Thiol-dependent dissociation of a fraction of toxin into enzymatically active and inactive fragments. *J. Biol. Chem. 246*, 1496−1503.

(24) May, M. J., Hartley, M. R., Roberts, L. M., Krieg, P. A., Osborn, R. W., and Lord, J. M. (1989) Ribosome inactivation by ricin A chain: a sensitive method to assess the activity of wild type and mutant polypeptides. *EMBO J. 8*, 301−308.

(25) Lord, J. M. (1985) Precursors of ricin and *Ricinus communis* agglutinin. Glycosylation and processing during synthesis and intracellular transport. *Eur. J. Biochem. 146*, 411−416.

(26) Newton, D. L., Wales, R., Richardson, P. T., Walbridge, S., Sarena, S. K., Ackerman, E. J., Roberts, L. M., Lord, J. M., and Youle, R. J. (1992) Cell surface and intracellular functions for ricin galactose binding. *J. Biol. Chem. 267*, 11917−11922.

(27) Utsumi, T., Aizono, Y., and Funatsu, G. (1984) Interaction of ricin and its constituent polypeptides with dipalmitoylphosphatidylcholine vesicles. *Biochim. Biophys. Acta 772*, 202−208.

(28) Utsumi, T., Ide, A., and Funatsu, G. (1989) Ricin A chain induces fusion of small unilamellar vesicles at neutral pH. *FEBS Lett. 242*, 255−258.

(29) Ishida, B., Cawley, D. B., Reue, K., and Wisnieski, B. J. (1983) Lipid−protein interactions during ricin toxin insertion into membranes. Evidence for A and B chain penetration. *J. Biol. Chem. 258*, 5933−5937.

(30) Lamb, F. I., Roberts, L. M., and Lord, J. M. (1985) Nucleotide sequence of cloned cDNA coding for preproricin. *Eur. J. Biochem. 148*, 265−270.

(31) Montfort, W., Villafranca, J. E., Monzingo, A. F., Ernst, S. R., Katzin, B., Rutenber, E., Xuang, N. H., Hamlin, R., and Robertus, J. D. (1987) The three-dimensional structure of ricin at 2.8 Å. *J. Biol. Chem. 262*, 5398−5403.

(32) Wales, R., Chaddock, J. A., Roberts, L. M., and Lord, J. M. (1992) Addition of an ER retention signal to the ricin A chain increases the cytotoxicity of the holotoxin. *Exp. Cell Res. 203*, 1−4.

(33) Wales, R., Roberts, L. M., and Lord, J. M. (1993) Addition of an endoplasmic reticulum retrieval sequence to ricin A chain significantly increases its cytotoxicity to mammalian cells. *J. Biol. Chem. 268*, 23986−23990.

(34) Till, M., May, R. D., Uhr, J. W., Thorpe, P. E., and Vitetta, E. S. (1988) An assay that predicts the ability of monoclonal antibodies to form potent ricin A chain containing immunotoxins. *Cancer Res. 48*, 1119−1123.

(35) Prior, T., FitzGerald, D. J., and Pastan, I. (1991) Barnase toxin: a new chimeric toxin composed of *Pseudomonas* exotoxin A and barnase. *Cell 64*, 1017−1023.

(36) Guidi-Rontani, C. (1992) Cytotoxic activity of a recombinant chimeric protein between *Pseudomonas aeruginosa* exotoxin A and *Corynebacterium diphtheriae* diphtheria toxin. *Mol. Microbiol. 6*, 1281−1287.

(37) Arora, N., Klimpel, K. R., Singh, Y., and Leppla, S. H. (1992) Fusions of anthrax toxin lethal factor to the ADP-ribosylation domain of *Pseudomonas* exotoxin A are potent cytotoxins which are translocated to the cytosol of mammalian cells. *J. Biol. Chem. 267*, 15542−15548.

(38) Arora, N., and Leppla, S. H. (1993) Residues of 1−254 of anthrax toxin lethal factor are sufficient to cause cellular uptake of fuse polypeptides. *J. Biol. Chem. 268*, 3334−3341.

High Efficiency Photolabeling of Human Serum Albumin and Human γ-Globulin with [14C]Methyl 4-Azido-2,3,5,6-tetrafluorobenzoate

Raghoottama S. Pandurangi,[†] Srinivasa R. Karra,[†] Robert R. Kuntz,[*,†] and Wynn A. Volkert[‡]

Departments of Chemistry and Radiology and Research Service, H. S. Truman Memorial VA Hospital, University of Missouri, Columbia, Missouri 65211. Received March 28, 1995[⊗]

The efficiency of photolabeling of HSA and IgG with [14C]methyl 4-azido-2,3,5,6-tetrafluorobenzoate has been studied using size exclusion chromatography in conjunction with liquid scintillation counting. Labeling efficiencies of 78% for HSA and 82% for IgG have been determined. The extent of bond insertion into proteins exceeds the C−H insertion efficiency in cyclohexane with less wastage into anilinium and azo side products. These results suggest that the photoprobe accesses hydrophobic regions of both proteins prior to photolysis.

INTRODUCTION

A systematic study of the fundamental photochemistry of aryl azides by Keana et al. (1−3) and Platz et al. (4−7) has identified the perfluoroaromatic azides as potential photolabeling precursors. The photolabeling technique is an attractive alternative to chemical labeling techniques for the attachment of complexes of radionuclides (e.g., 109Pd, 99mTc, 186Re) to proteins and antibodies (8, 9). In the photolabeling approach, photoactivable moieties produce, upon excitation, highly reactive intermediates (e.g., nitrenes or carbenes) capable of efficient C−H or N−H bond insertion (10−14). In more rigid environments such as liquid crystals or matrix isolated systems at low temperatures, the probability of C−H bond insertion can be increased dramatically (15, 16). For this reason, it is expected that trapping of the photoactivable group in hydrogenic crevices of proteins might give very good efficiencies for covalent attachment of the photoprobe to the protein.

For applications in biochemistry and nuclear medicine where the attached probe/protein ratio must be kept near unity the efficiency of attachment is a very important consideration in photolabeling (17−20). At these low ratios, use of a radioactive probe greatly facilitates the identification, isolation, efficiency determination, and *in vivo* stability studies of the product. Modification of the perfluoroaryl ring can also alter the efficiency of insertion reactions. For example, Keana et al. (21) studied photolabeling efficiency on model solvents using a perfluoroaryl azide and iodinated analogues. In that study the C−H insertion yields for the iodinated derivatives were much lower than those observed with the parent perfluoroaryl azide. These yields were still higher than those obtained with the fully hydrogenated photoprobes.

Although the insertion reactions of the perfluoroaryl azides in model systems (e.g., cyclohexane, diethylamine, etc.) are well characterized, a systematic investigation of their conjugation with proteins is rarely attempted (22−24). In the development of photoprobes for protein

labeling, it is important to determine the relationship between the insertion characteristics of a photoprobe on model solvent/solute systems to the labeling of complex macromolecules containing a variety of functional groups and environments. For heterobifunctional chelating agents (25) carrying a photoactivable terminus for attachment to proteins, a direct determination of covalent attachment of the photoprobe to proteins and antibodies is essential. Recently, we demonstrated the utility of size exclusion chromatography (SEC-HPLC) to monitor the covalent modification of human serum albumin (HSA) using a long-wavelength photolabel (26). It was important to determine if the extent of labeling observed for HSA could be extended to antibodies in general. Also, it is of interest for predictive purposes to determine the relationship between the efficiency of covalent attachment to model solvents and to proteins when utilizing the same photoprobe. Here, we report the synthesis of a [14C]methyl analogue of 4-azido-2,3,5,6-tetrafluorobenzoate (ATFMB), its conjugation with HSA and human γ-globulin (IgG), and a comparison of insertion efficiency between the proteins and cyclohexane. IgG was chosen as a model for the labeling of monoclonal antibodies (MAbs) which have extensive applications in antibody targeting therapy (27). The unlabeled ATFMB is known to give efficient C−H insertion in cyclohexane (1) and should serve as an efficient photoprobe. Substitution of a [14C]methyl group on the ester permits monitoring of the photoconjugation by both spectroscopic and radiochemical means using SEC-HPLC.

EXPERIMENTAL PROCEDURES

All synthetic procedures were carried out in a dry nitrogen atmosphere and with prepurified solvents. Reactions involving the synthesis of azide derivatives were carried out in subdued light by wrapping the reaction vessels with aluminum foil. All reagents except for [14C]methanol were purchased from Aldrich. [14C]Methanol (48.2 mCi/mmol) was purchased from Sigma. HSA and IgG (Cohn Fractions II and III) were purchased from Sigma. Both proteins were used without further purification.

NMR spectra were taken in CDCl₃ with TMS as an internal standard for ¹H and in CFCl₃ for ¹⁹F spectra on a 300 MHz Bruker instrument. Thin layer chromtography (TLC) was performed on precoated glass−silica gel plates (E. M. Science, GF254) with 10% EtOAc−hexane as eluent. The R_f value of the azido ester was 0.6. UV spectra were recorded in cyclohexane on a Hewlett-

* Author to whom correspondence should be addressed: Department of Chemistry, 123 Chemistry Building, University of Missouri, Columbia, MO 65211. Tel: 314/882-2815.
† Department of Chemistry.
‡ Department of Radiology and Research Service, H. S. Truman V.A. Hospital.
⊗ Abstract published in *Advance ACS Abstracts*, September 1, 1995.
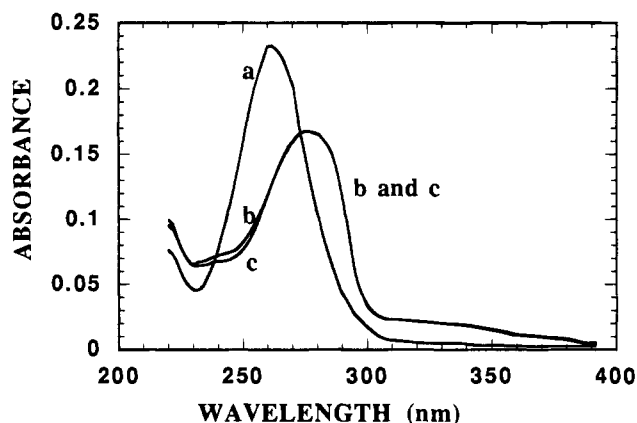
Figure 1. Absorption spectrum of 1.25×10^{-5} M [^{14}C]ATFMB in cyclohexane (a) before photolysis, (b) after 15 s exposure, and (c) after 2 min exposure to a 200 W super-pressure Hg lamp. Spectra b and c are nearly identical.
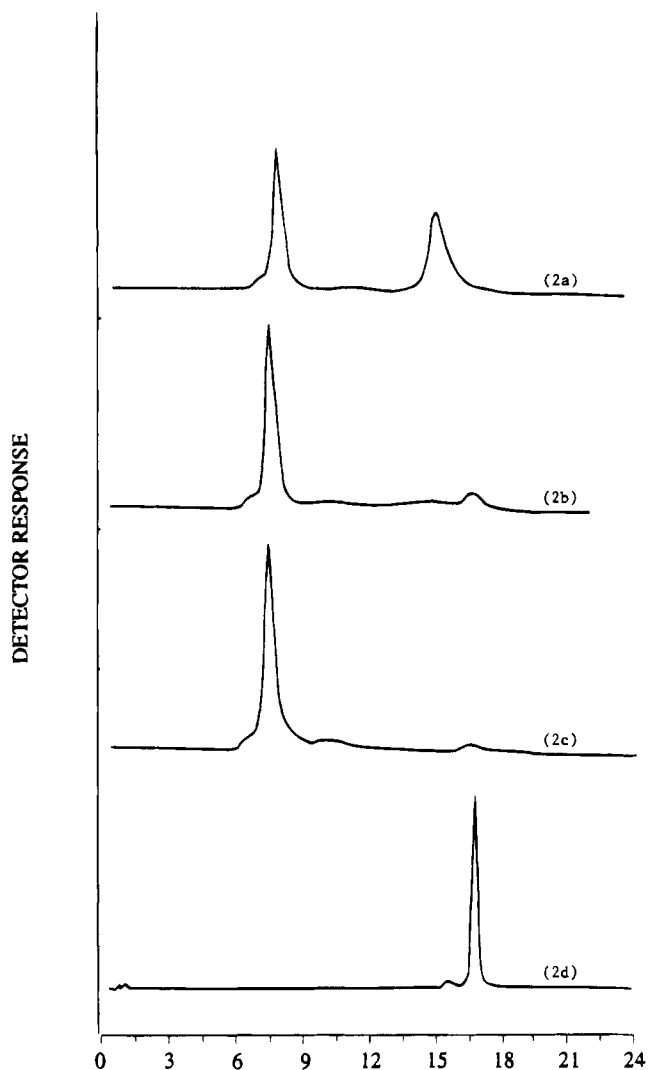
Figure 2. Size exclusion chromatogram (SEC-HPLC) of unlabeled ATFMB with and without HSA. Plots show relative 254 nm absorbance vs elution time (min) (a) before photolysis, (b) after 15 s exposure, (c) after 2 min exposure, and (d) after 2 min photolysis in buffer without HSA. Eluting solvent was a 0.02 M monobasic sodium phosphate buffer (adjusted to pH 6.8) containing 0.05 M sodium sulfate at a flow rate of 1 mL/min.

Packard (8452) diode array spectrometer with 1-cm pathlength cells. Protein-probe solutions were separated by HPLC using a BioRad Bio-Sil SEC 250 column. The eluent was a 0.02 M sodium phosphate (monobasic) buffer

containing 0.05 M sodium sulfate (pH = 6.8) at a flow rate of 1 mL/min. Absorption of the HSA-unlabeled probe solutions was monitored at 254 nm to characterize retention times and establish photolysis conditions. For the labeled probe, the detector was removed and 1 mL fractions were collected for liquid scintillation counting.

Photolysis. All photolysis experiments were conducted with a 200 W super pressure Hg lamp with or without a 320 nm cutoff filter. Solutions were purged with prepurified nitrogen for several minutes before photolysis.

Protein Conjugation. Protein labeling experiments were conducted by mixing 5 mL of 4×10^{-5} M solutions of the protein with 200 μL of a 10^{-3} M solution of either [^{12}C]-ATFMB or [^{14}C]-ATFMB in ethanol to give a 1:1 mol ratio. The photolysis time for probe destruction was predetermined with an equivalent concentration of unlabeled ATFMB in cyclohexane as monitored by C-18 reversed-phase HPLC as described earlier (*28*). These times were used for the protein-probe photolysis. Twenty μL samples of the [^{14}C]-ATFMB—protein mixtures were injected into the SEC-HPLC column before and after photolysis and the eluent collected in 1 mL fractions. Each fraction was combined with 10 mL of a scintillation cocktail (Optifluor-aqueous) and counted by liquid scintillation (Tracer Analytic Delta 300) with the energy window set for ^{14}C.

Synthesis of [^{14}C]Methyl 4-Azido-2,3,5,6-tetrafluorobenzoate. [^{14}C]Methanol (250 μCi) stored in a vacuum break seal vial was cooled in an ice-salt bath and the break seal ruptured under 2 mL of dry dichloromethane which filled the evacuated vial. The solution was transferred by syringe to a 25 mL flask as were 5×0.2 mL washings of the initial container. A solution of 13.2 mg of 4-azidotetrafluorobenzoyl chloride was dissolved in 10 mL of methylene chloride. Two mL of this stock (10.4 μmol) was mixed with 2 mL of a stock solution of triethylamine prepared by dissolving 5.2 mg of triethylamine in 10 mL of dry dichloromethane and the mixture added slowly via syringe to the [^{14}C]methanol solution. The mixture was stirred for 1 h during which time the reaction progress was monitored by TLC (detected by UV and AMBIS) for the ester at $R_f = 0.6$. After 1 h, the solution was concentrated to 0.1 mL by passing a stream of nitrogen over the solution. This material was deposited on a silica gel column and eluted with 6−8 mL of 3% ethylacetate/hexane and then with 10% ethyl acetate/hexane. The ester, eluting between 20 and 22 mL, was collected and evaporated by flushing N_2 gas through the solution. Radiochromatographic scanning indicated a single product with a radiochemical purity >95% by comparison with the sample's total activity. The ^{19}F NMR of this product showed the expected AA'XX' pattern reported for the unlabeled material (*1*).

Synthesis of Methyl 4-(Cyclohexylamino)2,3,5,6-tetrafluorobenzoate. A solution of methyl pentafluorobenzoate (4.52 g, 20 mmol) and cyclohexylamine (2.10 g, 21.2 mmol) in absolute ethanol containing 2 mL of triethylamine was refluxed overnight. The mixture was cooled, extracted with ether (3×50 mL), and dried over anhydrous $MgSO_4$. After filtration, ether was removed under vacuum to give light yellow crystals of the product. (2.11 g, 65% yield, mp 85 °C): ^{1}H NMR (CDCl$_3$) δ (ppm) 1.22 (m, 3H), 1.31 (m, 2H), 1.58 (m, 1H), 1.76 (m, 2H), 2.03 (m, 2H), 3.61 (m, 1H), 3.91 (s, 3H), 4.02 (m, 1H); ^{19}F NMR (CDCl$_3$) δ (ppm) -144.2 (m, 2F) and -161.2 (m, 2F); ^{13}C NMR (CD$_3$CN) δ (ppm) aromatic region 149 (m), 147 (m), 136 (m), 134 (m), 132 (s), aliphatic region 53.2 (t) (^4J(^{13}C$-^{19}$F) 4.3 Hz), 34.4 (s), 25.3 (s), and 24.6 (s).
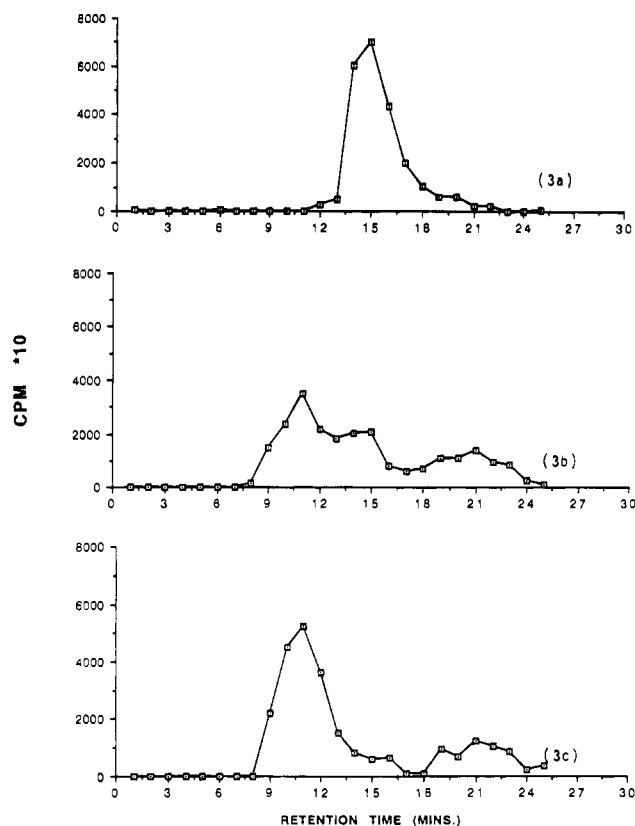
Figure 3. SEC-HPLC radiochromatogram of ^{14}C-labeled AT-FMB with HSA (a) before photolysis, (b) after 15 s exposure, and (c) after 2 min exposure. One mL fractions of the effluent (1 mL/min flow rate) were collected and counted by liquid scintillation. Buffer specifications are indicated in Figure 2.

HPLC analysis (CH_3CN/H_2O, 2/1) 1 mL/min, on a C-18 reversed-phase column gave a retention time which coincided with that for the adduct produced by photolysis of the photoprobe in cyclohexane.

RESULTS AND DISCUSSION

Photolysis in Cyclohexane. Photolysis of ATFMB in cyclohexane has been reported to give 57% of the C−H insertion product along with 21% of the aniline derivative and 11% of the azobenzene derivative (*1*). Photolysis of the ^{14}C ester in cyclohexane resulted in a red shift of the absorption maximum from 262 to 276 nm (Figure 1). The photoproduct spectrum coincides well with the absorption spectrum of the cyclohexane adduct synthesized independently from unlabeled methyl pentafluorobenzoate. Integration of the ^{19}F NMR of the photolyzed mixture (*28*) indicated 55% of the C−H inserted product which agrees with earlier reports (*1*).

Photolabeling of HSA. Equimolar solutions of HSA and unlabeled ATFMB were incubated for 1 h before injection into the SEC-HPLC column. In the unphotolyzed mixture, the photoprobe elutes at 15.3 min as compared to HSA at 8.2 min (Figure 2a). This control indicates a clean separation of the probe and protein before photolysis. Exposure of the mixture to the beam of an unfiltered 200 W Hg lamp results in 90% destruction of the probe after 2 min photolysis (Figure 2b,c). Use of the 320 nm cutoff filter to protect against protein photolysis increases the photolysis time to 15−20 min because light is only absorbed in the tail of the ATFMB absorption (λ_{max} = 268 nm). In the chromatogram, disappearance of the absorbance assigned to the photoprobe during photolysis is accompanied by an increase in the HSA absorbance. A new peak at 17.2 min appears
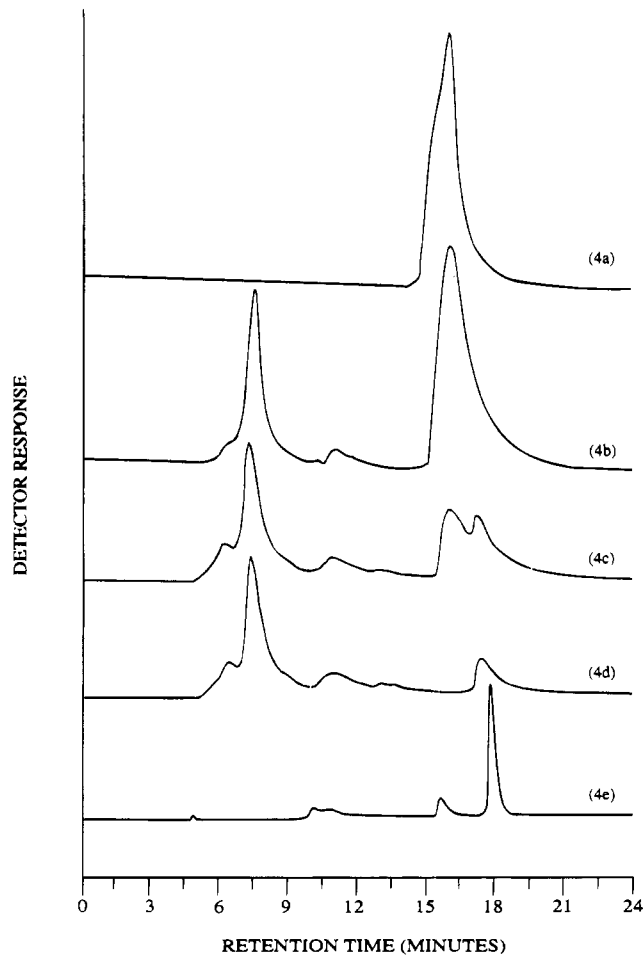
Figure 4. SEC-HPLC chromatogram of unlabeled ATFMB with and without IgG. Plots show relative 254 nm absorbance vs elution time (min): (a) unlabeled ATFMB, (b) mixture of ATFMB and IgG, (c) mixture after 15 s exposure, (d) mixture after 2 min exposure, (e) photolysis in the absence of IgG. Conditions identical to those indicated in Figure 2. Additional peaks in e can be assigned to unphotolyzed ATFMB and residual materials from prior IgG chromatograms.

in the chromatogram and persists even after >90% photoprobe destruction. This product is neither unphotolyzed probe nor attached probe and is possibly an anilinium-type product resulting from reactions of the triplet nitrene which is formed competitively with bond insertion of the singlet nitrene. Support for this assignment comes from photolysis of the photoprobe in a buffer solution without added protein (Figure 2d). The primary product from azide photolysis in hydroxylic solvents is the anilinium product (*1*) which appears here at 17.3 min consistent with the retention time of the minor product formed in the labeling studies.

Comparable experiments with the ^{14}C analogue were analyzed with a different pump-injection system, but employing the same HPLC column. The eluent was collected in 1 mL fractions and counted by liquid scintillation techniques. Peaks are shifted to somewhat longer times because a different injection system with longer dead time was employed. Figure 3a shows the radiochromatogram of the unphotolyzed mixture and indicates that the ^{14}C probe (fractions 14−17) is not associated with the protein fraction prior to photolysis. As photolysis progresses (Figure 3b,c), the activity shifts to the protein (fractions 9−14) and a new product (fractions 19−23). On the basis of relative activity, the protein fractions contains 78 ± 5% of the labeled probe which is believed to be covalently bound. The major part of the activity not
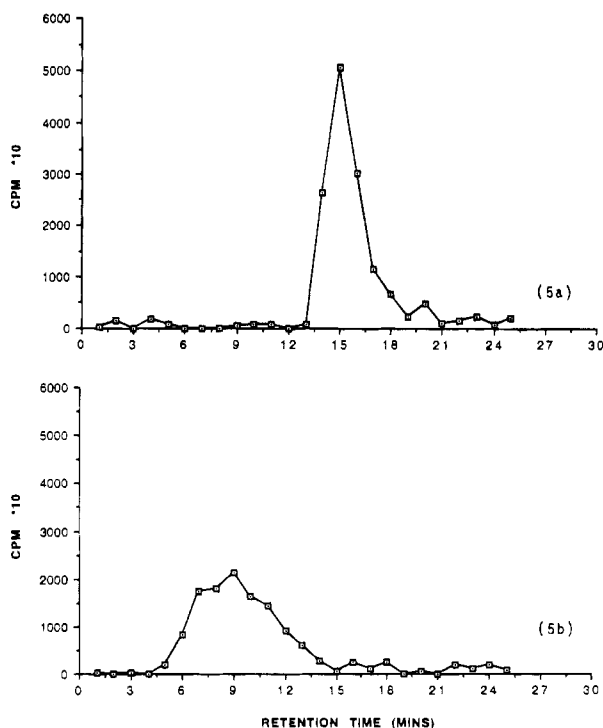
Figure 5. SEC-HPLC radiochromatogram of ^{14}C-labeled AT-FMB and IgG (a) before photolysis and (b) after 2 min photolysis. One mL fractions of the effluent (1 mL/min flow rate) were collected and counted by liquid scintillation. Buffer specifications are indicated in Figure 2.

associated with HSA is found in the region believed to be associated with the anilinium type products. We have shown previously that denaturing HSA with sodium dodecyl sulfate (SDS) does not result in a release of additional products, indicating the covalent nature of the binding (*26*).

Photolabeling of IgG. Photolabeling of IgG followed the same protocol established for HSA. The prephotolysis mixture of IgG and ATFMB (Figure 4b) shows two impurities which must be assigned to IgG since they do not appear in the ATFMB sample (Figure 4a). The higher molecular weight impurity (eluting before IgG) may be an aggregate, but the smaller species is not identified. Photolysis for 15 s (Figure 4c) and 2 min

(Figure 4d) shows a progressive depletion of the photoprobe and a lower molecular weight product similar to the one observed in HSA. Photolysis of the photoprobe in buffer without protein (Figure 4e) gives only the lower molecular weight material which we believe to be the anilinium product. Photolysis appears to enhance absorption by the aggregate impurity, but shows no effect on absorption of the unidentified impurity. The radiochromatogram (Figure 5) shows far less resolution because of the larger fractions collected for analysis. However, Figure 5a shows a clean separation of the probe from the protein region before photolysis. After photolysis, the radioactivity is found primarily in the protein elution region (6–12 min). Integration of the activity indicates that 82 ± 5% of the activity is bound to the protein. Unfortunately, the protein region of the radiochromatogram shows considerable broadness. Apparently, the peak assigned to the IgG aggregate is also labeled in this procedure. Currently, we are investigating this problem more carefully.

It is interesting to compare the efficiency of insertion efficiency in cyclohexane with the higher values observed for HSA and IgG (Scheme 1). Since singlet nitrene is known to deactivate in hydroxylic media, it appears that the hydrophobic probe becomes trapped in hydrophobic crevices of the protein prior to photolysis. This more rigid environment should favor insertion of the singlet nitrene over intersystem crossing to the triplet and also will tend to inhibit bimolecular reactions leading to azo products. It is not known whether the ~20% of unattached probe is due to intersystem crossing within the protein matrix or exposure of the singlet nitrene to the aqueous solvent during photolysis. However, the high degree of protein labeling (>78%) confirms the assumption that the insertion characteristics of 4-azidotetrafluoroaryl photoprobes in cyclohexane or cyclohexane/diethylamine are good indicators of ability to label proteins. In every case tried with this photoprobe, the protein labeling efficiency has surpassed the efficiency for insertion in model solvents.

CONCLUSIONS

The ^{14}C analogue of methyl 4-azido-2,3,5,6 tetrafluorobenzoate provides a convenient radiochemical probe for monitoring the extent of conjugation of the photoactivable probe with proteins using size exclusion chromatography. The short photolysis time required (2 min) for attachment

Scheme 1
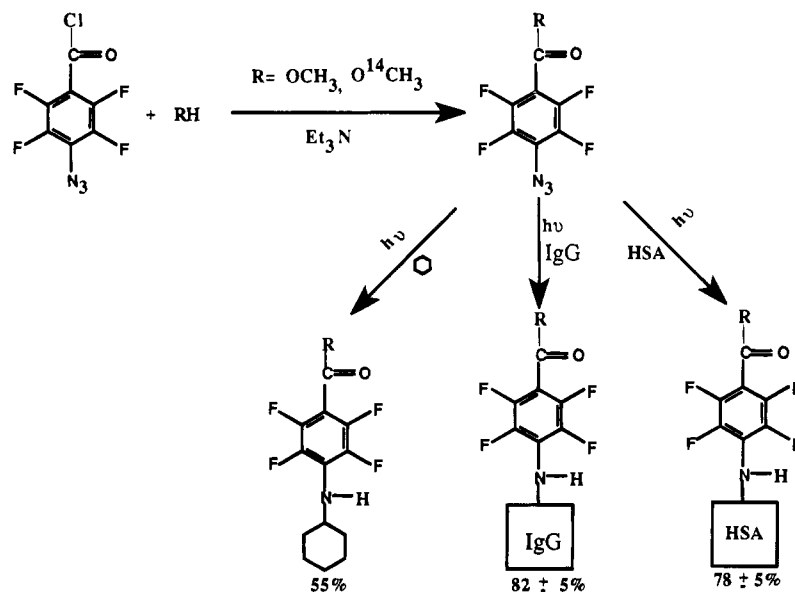
to the protein and the absence of external activating reagents necessary for conventional chemical labeling make this photolabeling technique attractive for use in biochemical labeling studies. Photolysis of the photoprobe in the absence of protein gives only the anilinium product which is cleanly separated from the protein by SEC-HPLC. The small yield of this side product in the presence of HSA or IgG suggests that the probe accesses hydrophobic regions of both proteins. This result, combined with earlier denaturation studies (26), strongly supports a covalent attachment between the probe and the protein. The high efficiency for covalent bond formation with both HSA and IgG suggests a general utility of the photochemical technique for antibody labeling. Investigation of the retention of immunoreactivity of labeled antibodies and their *in vivo* stability is currently under investigation, and results will be published elsewhere (29).

LITERATURE CITED

(1) Keana, J. F. W., and Cai, S. X. (1990) New Reagents for Photoaffinity Labeling: Synthesis and Photolysis of Functionalized Perfluorophenyl Azides. *J. Org. Chem. 55,* 3640.

(2) Keana, J. F. W., and Cai, S. X. (1989) Functionalized Perfluoroazides: New Reagents for Photoaffinity Labeling. *J. Fluorine Chem. 43,* 151.

(3) Cai, S. X., and Keana, J. F. W. (1989) 4-Azido-2-Iodo-3,5,6 Trifluorophenyl Carbonyl Derivatives. A New Class of Functionalized and Iodinated Perfluorophenyl Azide Photolabels. *Tetrahedron Lett. 30,* 5409.

(4) Poe, R., Grayzar, J., Young, M. J. T., Leyva, E., Schnap, K. A., and Platz, M. (1991) Remarkable catalysis of Intersystem Crossing of Singlet (Pentafluorophenyl) Nitrene *J. Am. Chem. Soc. 113,* 3209 and references cited therein.

(5) Poe, R., Grayzar, J., Young, M., Leyva, E., Schnapp, K. A., and Platz, M. S. (1993) Exploratory Photochemistry of Fluorinated Arylazides. Implications for the Design of Photoaffinity Labeling Agents. *Bioconjugate Chem. 4,* 172.

(6) Marcinek, A., Levya, E., Whitt, D., and Platz, M. S. (1993) Evidence for Stepwise Nitrogen Extrusion and Ring Expansion upon Photolysis of Phenyl Azide. *J. Am. Chem. Soc. 115,* 8609.

(7) Poe, R., Schnapp, K., Young, M. J. T., Grayzar, J., and Platz, M. S. (1992) Chemistry and Kinetics of Singlet (Pentafluorophenyl)nitrene. *J. Am. Chem. Soc. 114,* 5054.

(8) For reviews see: Brunner, J. (1993). New Photolabeling and Cross Linking Methods. *Ann. Rev. Biochem. 62,* 483.

(9) Bayley, H., and Staros, J. W. (1984) Photoaffinity Labeling and Related Techniques. In *Azides and Nitrenes, Reactivity and Techniques* (E. F. V. Scriver, Ed.) p 433, Academic Press, New York.

(10) Bayley, H. (1983) Reagents for Photoaffinity Labeling. *Photogenerated Reagents in Biochemistry and Molecular Biology* (T. S. Work and R. H. Burdon, Eds.) p 26, Elsevier, Amsterdam.

(11) Schurter, G. B., and Platz, M. S. (1992) Photochemistry of Phenyl Azide. *Advances in Photochemistry* (D. Volman, G. Hammond, and D. Neckers, Eds.) Vol. 17, p 69, Wiley/ Interscience, New York.

(12) Scriven, E. F. Y. (1982) Current Aspects of the Solution Chemistry of Aryl Nitrenes *Reactive Intermediates* (R. A. Abramovitch, Ed.) Vol. 2, p. 1, Plenum Press, New York.

(13) Iddon, B., Meth-Cohn, O., Schriven, E. F. Y., Suschitzky, H., and Gallagher, P. T. (1979) Developments in Arylnitrene Chemistry: Synthesis and Mechanisms. *Angew. Chem., Int. Ed. Engl. 18,* 900.

(14) Reiser, A., and Wagner, H. M. (1971) Photochemistry of the Azido Group. In *The Chemistry of the Azido Group* (S. Patai, Ed.) p 441, Wiley/Interscience, New York.

(15) Mahe, L., Izuoka, A., and Sugawara, T. (1992) How Crystalline Environment can Provide Outstanding Stability and Chemistry for Aryl Nitrenes. *J. Am. Chem. Soc. 114,* 7904.

(16) Leyva, E., Young, M. J. T., and Platz, M. S. (1986) High Yields of Formal C-H Insertion Products in the Reactions of Polyfluorinated Aromatic Nitrenes. *J. Am. Chem. Soc. 108,* 8307.

(17) For reviews see: Cavalla, D., and Neff, N. H. (1985) Chemical Mechanisms for Photoaffinity Labeling of Receptors. *Biochemical Pharm. 34,* 2821.

(18) Choudhry, V., and Westheimer, F. H. (1979) Photoaffinity Labeling of Biological Systems. *Annual Rev. Biochem. 48,* 293.

(19) Fedan, J. A., Hogaboom, G. K., and O'Donnell, J. P. (1984) Photoaffinity Labels as Pharmacological Tools. *Biochem. Pharm. 33,* 1167.

(20) Ji, J., and Ji, I. (1982) Macromolecular Photoaffinity Labeling With Radioactive Photoactivable Heterobifunctional Reagents. *Anal. Biochem. 121,* 286.

(21) Cai, S. X., Glenn, D. J., and Keana, J. F. W. (1992) Toward the Development of Radiolabeled Fluorophenyl Azide Based Photolabeling Reagents: Synthesis and Photolysis of Iodinated 4-Azido Perfluorobenzoates and 4-Azido-3,5,6-trifluorobenzoates. *J. Org. Chem. 57,* 1299.

(22) Pinney, K. G., Carlson, K. E., and Katzenellenbogen, J. A. (1990) [^{3}H] DU41165: A High Affinity Ligand and Novel Photoaffinity Labeling Reagent for the progesterone Receptor. *J. Steroid. Biochem. 35,* 179.

(23) Pinney, K. G., Carlson, K. E., Katzenellenbogen, B. S., and Katzenellenbogen, J. A. (1991) Efficient and Selective Photoaffinity Labeling of Estrogen Receptor Using Two Nonsteroidal Ligands That Embody Aryl Azide or Tetrafluoroaryl Azide Photoactive Functions. *Biochemistry 30,* 2421.

(24) Pinney, K. G., and Katzenellenbogen, J. A. (1991) Synthesis of Tetrafluoro-substituted Aryl Azide and It's Protio Analogue as Photoaffinity Labeling Reagents for the Estrogen Receptor. *J. Org. Chem. 56,* 3125.

(25) Pandurangi, R. S., Kuntz, R. R., Volkert, W. A., Barnes, C. L., and Katti, K. V. (1995) Phosphorus Hydrazides as Building Blocks for Potential Photoaffinity Labels. Synthesis and Coordination Chemistry of Perfluoroarylazide Conjugates of Phenylphosphonothioic Dihydrazide. *J. Chem. Soc., Dalton Trans.* 565.

(26) Pandurangi, R. S., Kuntz, R. R., and Volkert, W. A. (1995) Photolabeling of Human Serum Albumin by 4-Azido-(^{14}C-methylamino)trifluorobenzonitrile. A High Efficiency, Long Wavelength Photolabel. *Int. J. Appl. Radiat. Isotopes 46,* 233.

(27) Koppel, G. A. (1990) Recent Advances with The Monoclonal Antibody Drug Targeting for the Treatment of Human Cancer. *Bioconjugate Chem. 1,* 13.

(28) Pandurangi, R. S., Katti, K. V., Barnes, C. L., Volkert, W. A., and Kuntz, R. R. (1994) High Yields of Nitrene Insertion into Unactivated C-H Bonds. First Example of X-Ray-Crystallographic and ^{19}F NMR Analysis of the Photochemically Produced C-H Inserted Adduct. *J. Chem. Soc., Chem. Commun.* 1841.

(29) Pandurangi, R. S., Karra, S. R., Kuntz, R. R., and Volkert, W. A. (1995) Unpublished results.

BC9500570

TECHNICAL NOTES

[99mTc]Tricine: A Useful Precursor Complex for the Radiolabeling of Hydrazinonicotinate Protein Conjugates

Scott K. Larsen, Howard F. Solomon,[†] Gary Caldwell,[†] and Michael J. Abrams*

Johnson Matthey Pharmaceutical, 1401 King Road, West Chester, Pennsylvania 19380, and The R. W. Johnson Pharmaceutical Research Institute, Spring House, Pennsylvania 19477. Received May 4, 1995[⊗]

The stannous reduction of [99mTc]pertechnetate in the presence of tricine results in the formation of the new labeling precursor complex [99mTc]tricine. This complex has improved efficacy for the 99mTc labeling of hydrazinonicotinate-modified IgG compared to [99mTc]glucoheptonate. FAB mass spectral analysis of the product formed by the reaction of [TcOCl$_4$]$^{-1}$ with tricine indicates the formation of [TcO(tricine-2H)$_2$]$^{-1}$.

INTRODUCTION

Recently, we described the use of the hydrazinonicotinate group for the 99mTc labeling of proteins and peptides (1, 2). In this methodology, proteins are modified with the bifunctional reagent succinimidyl 6-hydrazinonicotinate hydrochloride (SHNH) and the resulting conjugate reacted with a 99mTc precursor complex (e.g., [99mTc]glucoheptonate) to yield 99mTc-labeled proteins in high radiochemical yield. Examples of the utility of this method include the labeling of polyclonal human IgG, monoclonal antibodies, fragment E1, and chemotactic peptides (2–5).

We now report the identification of a new precursor complex, [99mTc]tricine, that greatly enhances the efficiency of this protein-labeling technique.

EXPERIMENTAL PROCEDURES

Tricine and stannous chloride dihydrate were purchased from Aldrich and used as received. SHNH-modified IgG was prepared by a literature method (1). [Tc]Glucoscan kits were purchased from DuPont–Merck and [99mTc]glucoheptonate prepared according to the package insert. 99mTcO$_4$$^-$ was purchased as generator eluent from Mallinckrodt Medical. Na99TcO$_4$ was purchased from Oak Ridge National Laboratories, TN, and tetrabutylammonium oxotetrachlorotechnate(V) (TBA-[TcOCl$_4$]) was prepared by the method of Cotton and Davison et al. (6) **Caution:** 99Tc is a weak β-emitter. Precautions for the use of this material have been detailed elsewhere (7). Radiometric ITLC experiments were performed using a Bioscan System 200 Imaging Scanner. Freeze drying of samples was accomplished

using a Labconco Model 75034 freeze dryer. FAB mass spectra of samples dissolved in a 50:50 glycerol/3-nitrobenzyl alcohol matrix were recorded with a VG 7070 mass spectrometer equipped with an Ion Tech FAB gun and operated at an accelerating voltage of 8 kV. The FAB gun produced a beam of 6–8 keV argon neutrals.

Preparation of a Tricine/SnCl$_2$-Lyophilized Kit. Ninety-eight mL of chromatography grade (glass distilled and filtered) water which had been deoxygenated by boiling and cooling under argon was measured into an acid-washed, rinsed, and dried 150 mL Erlenmeyer flask containing 3.60 g of *N*-[tris(hydroxymethyl)methyl]glycine (tricine). The pH of the solution was adjusted to 7.1 using approximately 2.3 mL of 1 N NaOH solution. The flask was sealed with an airtight Septum and purged an additional 60 min with argon by cannula. A solution of SnCl$_2$·2H$_2$O, 50 mg/mL in deoxygenated 0.1 N HCl, was prepared under argon and 80 µL added to the tricine solution. One mL of the tricine/SnCl$_2$ solution was transferred by syringe to an argon-filled septum-capped vial, and the solution was frozen (−78 °C) and subsequently lyophilized. The lyophilized vials were capped and crimped under argon to render a final composition of 36 mg of tricine and 0.04 mg of SnCl$_2$ at pH 7.1. Alternatively, the tricine/SnCl$_2$ solution can be dispensed into vials, sealed, and frozen at −20 °C. These frozen vials are stable for at least several months.

Reconstitution of a Tricine/SnCl$_2$-Lyophilized Kit: Formation of [99mTc]Tricine. A septum-capped vial of lyophilized tricine/SnCl$_2$ was injected with 1 mL of 99mTcO$_4$$^-$ (20 mCi/mL) and immediately shaken vigorously until all the freeze-dried material was dissolved. Upon dissolution, the Tc–tricine sample was left for 15 to 30 minutes at room temperature before analysis. Analysis for formation of the Tc–tricine precursor complex was performed on ITLC–SG chromatography plates (Gelman Laboratories, Ann Arbor, MI). An 8 × 1 cm plate was used, and a 2.5 µL sample of the Tc–tricine

Bioscan:
ITLC-SG 1x8cm
saline
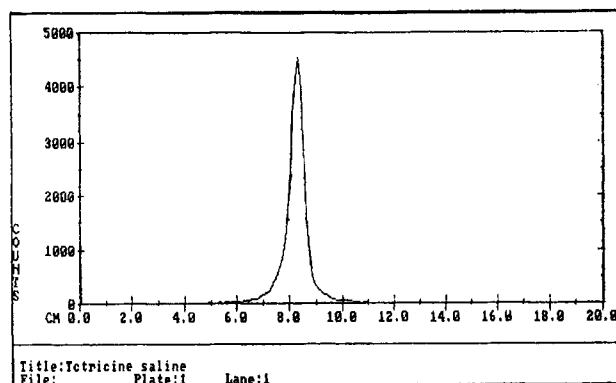
Bioscan:
ITLC-SG 1x8cm
MEK
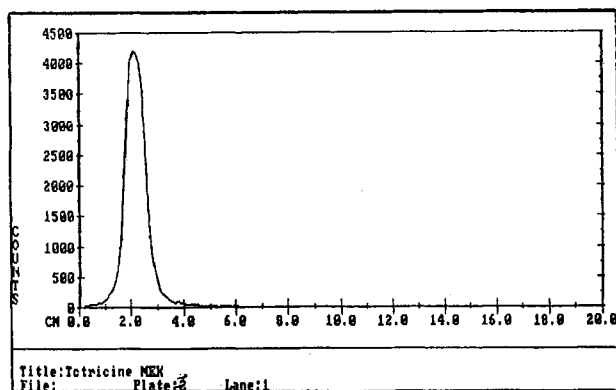
Figure 1. ITLC analysis of [⁹⁹ᵐTc]tricine.

solution was spotted at 1 cm and eluted with saline to yield <1% Tc—colloid at the origin and >99% Tc—tricine at the solvent front. When an 8 × 1 cm plate was used, a 2.5 μL sample of Tc—tricine solution was spotted at 1 cm and eluted with methyl ethyl ketone to yield >99% [⁹⁹ᵐTc]tricine at the origin and <1% TcO_4^- at the solvent front (see Figure 1).

Radiolabeling of SHNH-Modified IgG with [⁹⁹ᵐTc]Tricine vs [⁹⁹ᵐTc]Glucoheptonate. The rate of radiolabeling IgG modified with SHNH was measured with respect to the Tc—precursor complexes, Tc—tricine and Tc—gluheptonate. One hundred μL of the respective Tc-precursor at 15 mCi/mL was mixed with an equal volume of IgG—SHNH at 4.9 mg/mL and incubated for 1 h at room temperature. Each solution was sampled at 1, 10, 20, 30, 40, 50, and 60 min and analyzed by ITLC—SG chromatography using standard techniques: when an 8 × 1 cm plate was used a 2.5 μL sample of the protein solution was spotted at 1 cm and the plate eluted with 0.1 M sodium citrate (pH 5.5). Labeled IgG remains at the origin, and free [⁹⁹ᵐTc]tricine and TcO_4^- run to the solvent front. In addition, Tc—tricine was mixed with an equal volume of unmodified IgG to measure its non-specific radiolabeling to the protein.

The percent yield of radiolabeling IgG modified with SHNH was measured as a function of the specific activity
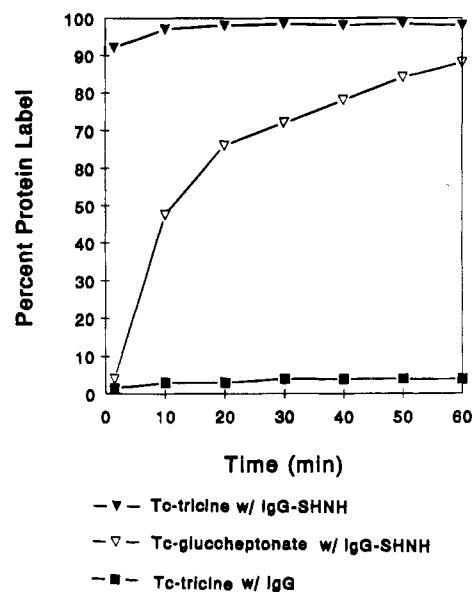
Figure 2. Comparison of the rate of radiolabeling of SHNH-modified IgG with [⁹⁹ᵐTc]tricine vs [⁹⁹ᵐTc]glucoheptonate.
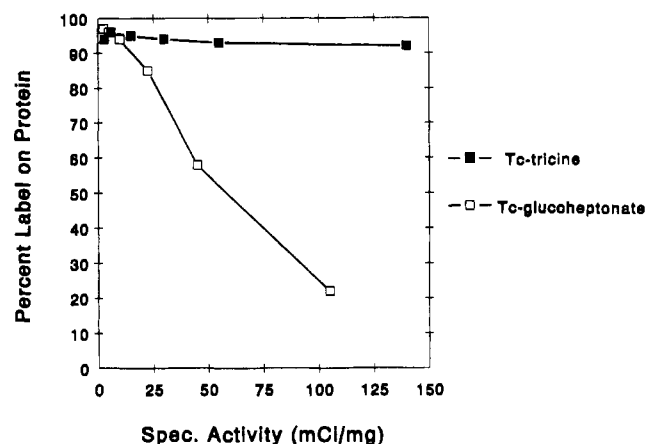
Figure 3. Comparison of radiolabeling of SHNH-modified IgG with [⁹⁹ᵐTc]tricine and [⁹⁹ᵐTc]glucoheptonate at varying levels of specific activity.

(mCi of ⁹⁹ᵐTc per mg of protein) of the solutions with respect to the two Tc—precursors: Tc—glucoheptonate and Tc—tricine. Two series of vials containing 100, 50, 20, 10, 5, and 2 μL of an IgG—SHNH solution (4.9 mg/mL in protein) were prepared. To each vial of one series was added 100 μL (14 mCi/mL) of the respective [Tc]—precursor, and the vials were incubated at room temperature for 1 h. The test solutions were analyzed by ITLC—SG chromatography.

Preparation of ⁹⁹Tc—Tricine. To a stirred solution of TBA[TcOCl₄] (0.025 g, 0.05 mmol) in methanol (10 mL) was added a methanolic solution of tetrabutylammonium tricine (prepared by dissolving 0.179 g tricine (1.0 mmol) in methanol (5 mL) containing 1.0 mmol of TBA[OH]). After 20 min solvent was removed from the amber reaction mixture by rotary evaporation and the residue subjected to mass spectroscopic analysis.

RESULTS AND DISCUSSION

[⁹⁹ᵐTc]tricine was prepared by the stannous reduction of ⁹⁹ᵐTcO₄⁻ in the presence of tricine at close to neutral pH. As is the case with most ⁹⁹ᵐTc radiopharmaceutical
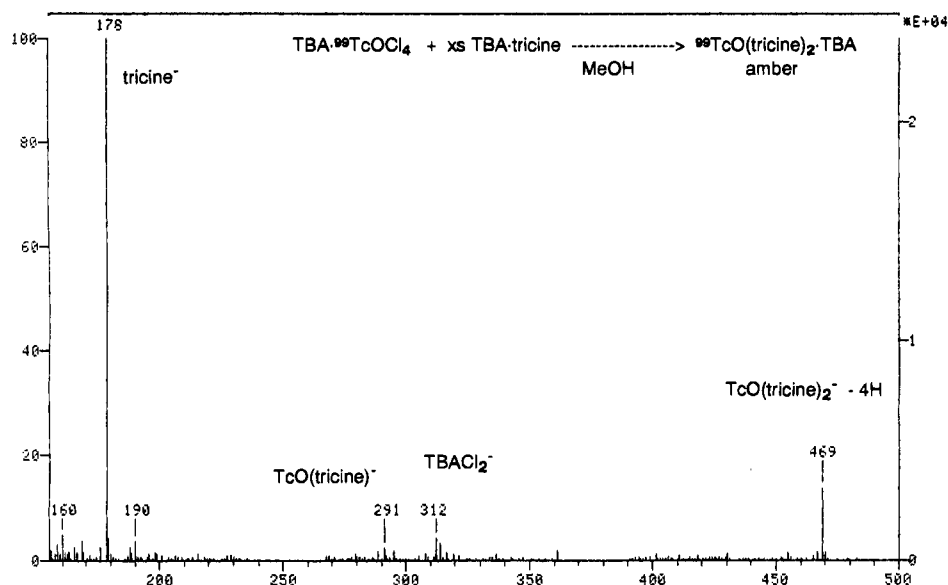
Figure 4. FAB mass spectrum of [^{99}Tc]tricine.

kits, the excess ligand serves to coordinate reduced technetium and to solubilize the stannous ion at neutral pH. The quality control test for the formation of [^{99m}Tc]-tricine is similar to that used for [^{99m}Tc]glucoheptonate, with the exception that methyl ethyl ketone is used instead of acetone for the determination of ^{99m}TcO$_4^-$ in the product.

In the labeling reactions with hydrazinonicotinate-modified IgG, [^{99m}Tc]tricine is markedly more reactive than [^{99m}Tc]glucoheptonate. As shown in Figure 2, at a specific activity of 1.5 mCi/mg IgG 90% radioincorporation is achieved by the time the first time point is measured (1 min). By 10 min >95% incorporation is reached. In contrast, the labeling reaction with [^{99m}Tc]-glucoheptonate is significantly slower, with ~90% radioincorporation achieved only after 60 min. This labeling reaction is specific to the hydrazinonicotinate function as shown by the minimal (4%) radioincorporation found in the reaction with [^{99m}Tc]tricine and unmodified IgG. Similar nonspecific labeling results were found with [^{99m}Tc]glucoheptonate.

With regard to specific activity, [^{99m}Tc]tricine is a far more effective precursor complex for the labeling of SHNH-modified IgG in comparison to [^{99m}Tc]glucohep-tonate. As shown in Figure 3, the labeling efficiency for [^{99m}Tc]glucoheptonate decreases dramatically at specific activity levels >25 mCi/mg whereas reactions of [^{99m}Tc]-tricine and IgG–SHNH achieve >90% radiolabeling of the protein for specific activities as high as 140 mCi/mg.

In an effort to characterize [Tc]tricine, the reaction of TBA[TcOCl$_4$] with tricine in methanol was investigated. The resulting amber complex was not stable in the absence of excess tricine. FAB mass spectra in negative ion mode showed a peak at m/z = 469 (see Figure 4) corresponding to [TcO(tricine-2H)$_2$]$^{-1}$.

A number of coordination complexes of tricine have been reported in recent years including complexes of Zn^{2+}, Cu^{2+}, Co^{2+}, Ni^{2+}, Cd^{2+}, and V^{5+} (*8, 9*). The mass spectroscopic results presented here indicate that Tc–tricine contains an oxo group, suggesting the +5 oxidation state for the technetium bound to two doubly deprotonated tricine molecules. The instability of the compound in the absence of excess ligand is consistent with its enhanced reactivity toward hydrazine groups.

There are suggestions in the literature that [Tc]gluco-heptonate is a Tc(V) complex coordinated to the ligand via diol groups (*10*). Crystallographic studies of Zn^{2+} and Ni^{2+} complexes of tricine indicate tridentate coordination of tricine including bound amine, carboxylate, and one hydroxyl oxygen (*8*). ^{13}C NMR studies of the interaction of tricine with V^{5+} gave similar results (*9*). Future work in our laboratory will focus on explaining the accelerated reactivity of [Tc]tricine toward organohydrazines compared to other precursor complexes.

LITERATURE CITED

(1) Abrams, M. J., Juweid, M., Tenkate, C. I., Schwartz, D. A., Hauser, M. M., Gaul, F. E., Fuccello, A. J., Rubin, R. H., Strauss, H. W., and Fischman, A. J. (1990) Technetium-99m human polyclonal IgG radiolabeled via the hydrazino nico-tinamide derivative for imaging focal sites of infection in rats. *J. Nucl. Med. 31*, 2022–2028.

(2) Schwartz, D. A., Abrams, M. J., Hauser, M. M., Gaul, F. E., Larsen, S. K., Rauh, D. and Zubieta, J. A. (1991) Preparation of hydrazino-modified proteins and their use for the synthesis of ^{99m}Tc-protein conjugates. *Bioconjugate Chem. 2*, 333–336.

(3) Hnatowich, D. J., Mardirossian, G., Rusckowski, M., For-garasi, M., Virzi, F., and Winnard, P. (1993) Directly and indirectly technetium-99m-labeled antibodies. A comparison of *in vitro* and animal *in vivo* properties. *J. Nucl. Med. 34*, 109–119.

(4) Knight, L. C., Abrams, M. J., Schwartz, D. A., Hauser, M. M., Kollman, M., Gaul, F. E., Rauh, D. A., and Maurer, A. H. (1992) Preparation and preliminary evaluation of technetium-99m-labeled fragment E$_1$ for thrombus imaging. *J. Nucl. Med. 33*, 710–715.

(5) Babich, J. W., Solomon, H., Pike, M. C., Kroon, D., Graham, W., Abrams, M. J., Tompkins, R. G., Rubin, R. H., and Fischman, A. J. (1993) Technetium-99m-labeled hydrazino nicotinamide derivatized chemotactic peptide analogs for imaging focal sites of bacterial infection. *J. Nucl. Med. 34*, 1964–1974.

(6) Cotton, F. A., Davison, A., Day, V. N., Gage, L. D., and Trop, H. S. (1979) Preparation and structural characterization of salts of oxotetrachlorotechnetate (V). *Inorg. Chem. 18*, 3024–3029.

(7) Davison, A., Orvig, C., Trop, H. S., Sehn, M., DePamphilis, B. V., and Jones, A. G. (1980) Preparation of oxobis(dithiolato) complexes of technetium (V) and rhenium (V). *Inorg. Chem. 19*, 1988–1992.

(8) Menabue, L., and Saladini, M. (1992) Transition metal (II) complexes of a biological buffer. Structural and spectroscopic study on Co(II), Ni(II), Cu(II), Zn(II), and Cd(II) complexes of N-[2-hydroxy-1,1-bis-(hydroxymethyl)ethyl]glycine. *J. Crystallogr. Spectrosc. Res. 22,* 713−719.

(9) Crans, D. C., and Shin, P. K. (1994) Characterization of vanadium (V) complexes in aqueous solutions: ethanolamine- and-glycine-derived complexes. *J. Am. Chem. Soc. 116,* 1305−1315.

(10) Hwang, L. L. Y., Ronca, N., Solomon, N. A., and Steigman, J. (1985) Complexes of technetium with polyhydridic ligands. *Int. J. Appl. Radiat. Isot. 36,* 475−480.

COMMUNICATIONS

Water-Soluble Block Polycations as Carriers for Oligonucleotide Delivery

Alexander V. Kabanov,*,† Sergey V. Vinogradov,‡ Yulia G. Suzdaltseva, and Valery Yu. Alakhov*,§

Moscow Institute of Biotechnology, Inc., and Department of Polymer Sciences, Faculty of Chemistry, Moscow State University, Vorobievy Gory, Moscow 119899, Russia. Received July 17, 1995[®]

Water-soluble, block copolymeric carriers consisting of polyoxyethylene (PEO) and polyspermine (PS) chains have been developed for the delivery of antisense oligonucleotides (oligo) into the target cells. These copolymers spontaneously form complexes with oligos in aqueous solutions. The PS block electrostatically binds to the oligo, and as a result, the stability of the oligo is increased. Similarly, the polar PEO block provides for the aqueous solubility of the complex. This paper (i) reports the synthesis of the diblock PEO–PS copolymer and (ii) evaluates the effects of the complexes formed between this copolymer and phosphodiester oligo, complementary to the splice junction of herpes simplex virus type 1 immediate early pre-mRNAs 4 and 5, on the reproduction of this virus in Vero cells. Infectious titer data 22 and 39 h post infection indicates that the copolymer-oligo complex inhibits the reproduction of the virus beyond the detection limit. Conversely, the free oligo inhibits the reproduction of the virus only 22 h postinfection, while 39 h postinfection significant virus titers are observed. The results of this study suggest that the copolymeric complex increases the sequence-specific inhibition effect of oligo on the virus reproduction.

During the past decade antisense oligonucleotides (oligos) have attracted significant attention as promising tools for the selective inhibition of gene expression and viral reproduction (*1–3*). However, the practical application of oligo for disease therapy has been hindered by the following major problems: (i) poor transport into cells; (ii) non-sequence-specific effects on cells; (iii) rapid degradation *in vitro* and *in vivo*; and (iv) rapid elimination from the body. One general approach to improve oligo performance *in vitro* and *in vivo* is to use a parenteral drug delivery system, the most comprehensively studied being cationic liposomes (*4*), lipopolyamines (*5*), and homopolycations (*6*). These carriers all spontaneously bind with the negatively charged oligo molecules to form complexes that have the following advantages for the oligo: (i) enhanced stability against nuclease degradation, (ii) enhanced uptake into the cells, and (iii) increased antisense activity *in vitro*. One problem with

* Corresponding authors.
† Present address: Department of Pharmaceutical Sciences, College of Pharmacy, University of Nebraska Medical Center, 600 South 42nd St, Omaha, NE 68198-6025. Tel.: (402) 559-9364. Fax: (402) 559-5060.
‡ Present address: Centre National de la Recherché Scientifique, Centre de Biophysique Moleculaire, 1A avenue de la Recherché Scientifique, 45071 Orleans, Cedex 2, France.
§ Present address: Supratek Pharma, Inc., and Immunology Research Center, Institute Armand-Frappier, University of Quebec, 513 boulevard des Prairies, Case Postale 100, Laval, Quebec H7N 4Z3, Canada.
[®] Abstract published in *Advance ACS Abstracts,* November 1, 1995.

Scheme 1. Synthesis of PS

2 H2N(CH2)3NH(CH2)3NH2 + Br(CH2)4Br

↓

H2N(CH2)3NH(CH2)3NH(CH2)4NH(CH2)3NH(CH2)3NH2

(*Intermediate 1*)

↓ 0.5 Br(CH2)4Br

H2N(CH2)3NH[(CH2)3NH(CH2)4NH(CH2)3NH]$_m$(CH2)3NH2

these carriers is that these complexes with oligos are often poorly water-soluble and tend to aggregate in aqueous solutions (*6*). To avoid this problem, we have developed another class of water-soluble block copolymeric carriers consisting of polyoxyethylene (PEO) and polyspermine (PS). The polycationic PS chains are structurally related to spermines that are naturally occurring DNA binding cations. Therefore, the PEO—PS copolymers spontaneously form polyelectrolyte complexes via electrostatic interactions with the negatively charged oligos in aqueous solutions. As a result of charge neutralization, the complexed sites are hydrophobic (*6*). However, the complex remains in aqueous solution due to the solubilizing effect of the PEO chains. The block polycationic complexes with oligos presumably represent amphiphilic block copolymeric compounds in which the water-soluble PEO chains are linked to hydrophobic blocks of the neutralized polycation and oligo. As a result, the complexes exhibit the ability to form micelles in aqueous solutions (*7*). Therefore, this approach is fundamentally related to the block copolymeric delivery systems that have recently been developed for parenteral administration of various drugs (*8—11*). This paper reports preliminary data on the synthesis of PEO-PS block polycations and evaluates the effects of oligos complexes with the copolymer on reproduction of herpes simplex virus type 1 (HSV-1) in Vero cells.

The synthesis of PEO—PS block polycations requires two stages. During the first stage (Scheme 1) the PS type polycations were synthesized by polycondensation of N-(3-aminopropyl)-1,3-propanediamine and 1,4-dibromobutane. A 6.55 g (50 mmol) portion of N-(3-aminopropyl)-1,3-propanediamine (Aldrich) was reacted with 5.4 g (25 mmol) of 1,4-dibromobutane (Fluka) in 100 mL of 1,4-dioxane for 16 h at 20 °C. The 1,4-dibromobutane was initially added dropwise to the reaction system during the first hour. The product of this reaction (intermediate 1) spontaneously precipitated from solution as the hydrobromide salt and was filtered and dried twice from a solution of 10% triethylamine in methanol using a rotary evaporator. This evaporation procedure was effective to remove the hydrogen bromide. The intermediate 1 was dissolved in 1,4-dioxane and reacted with 2.7 g (12.5 mmol) of 1,4-dibromobutane. Again, the reaction proceeded for 16 h at 20 °C, and the resulting products were recovered and dried as above. These products, which contained PS of varying degrees of polymerization as well as unreacted initial monomer, were neutralized with acetic acid to a pH of 7—8 and fractionated by gel

Scheme 2. Synthesis of the PEO—PS copolymer

H2N(CH2)3NH[(CH2)3NH(CH2)4NH(CH2)3NH]$_m$(CH2)3NH2

↓

HO[CH2CH2O]$_n$C(O)HN(CH2)3NH[(CH2)3NH(CH2)4NH(CH2)3NH]$_m$(CH2)3NH2

↓ + A, 1,1'-carbonyldiimidazole

HO[CH2CH2O]$_n$C(O)HN(CH2)3NH[(CH2)3NH(CH2)4NH(CH2)3NH]$_m$(CH2)3NH-A
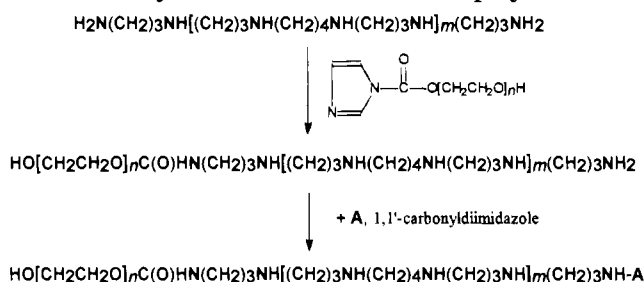
filtration on a column (3 × 50 cm) using Sephadex G-25 F equilibrated with 0.05 N acetic acid. The concentrations of PS in the fractions were determined gravimetrically. The concentrations of the free amino groups in PS molecules were determined by titrating the fractionated polymers with 2,4,6-trinitrobenzenesulfonic acid (*12*) and the number-average molecular masses of the PS (M_{PS}) calculated using the relationship: $M_{PS} = C_{PS}/2C_{NH2}$, where C_{PS} is the concentration of the PS (g/L), C_{NH2} is the concentration of amino groups (mol/L), and 2 is the coefficient accounting for two terminal amino groups in the PS molecules. Three PS fractions (I-III) were obtained, having average molecular masses of 980, 720, and 490 g/mol, respectively. The weight yields of these fractions were 19.5%, 20.4%, and 22.7%, respectively, while 27.2% accounted for the remaining initial monomers and intermediate 1. By comparing the experimental and calculated molecular masses of the polymers synthesized we concluded that the major PS components in the fractions II and III contain 12 and 9 N atoms, respectively, while fraction I consists of a mixture of PS with 15 and 18 N atoms (Table 1).

During the second stage (Scheme 2) the PS of fraction II was conjugated with PEO using the 1,1'-carbonyldiimidazole reaction. A 1.5 g (1 mmol) portion of PEO (MW 1500, from Fluka) was dissolved in 8 mL of 1,4-dioxane and reacted with 0.17 g (1 mmol) of 1,1'-carbonyldiimidazole (Aldrich) at 20 °C for 3 h. This reaction modifies one terminal hydroxyl group of PEO; however, the unmodified PEO and PEO modified by both ends are also produced. The reaction system was then supplemented with 1.44 g (2 mmol) of PS of fraction II in 8 mL of 1,4-dioxane and the mixture incubated at 20 °C for 16 h. This reaction formed conjugates of PEO with PS having various structures; in particular, triblock copolymers PEO—PS—PEO, and PS—PEO—PS, and the diblock copolymer PEO—PS. To separate these products their free amino groups were modified with 2'-deoxyadenosine (**A**). The reaction was initiated by supplementing the reaction system with 1 g of 2'-deoxyadenosine (Sigma) activated with 0.68 g of 1,1'-carbonylimidazole in 8 mL of 1,4-dioxane. (The excess of the reagents was used to ensure the modification of all free amino groups present). This reaction results in modification of the terminal amino groups of PS only, while the hydroxyl groups of PEO remain unmodified. The 2'-deoxyadenosine group was used as a chromophore to detect PS-containing products during further purification of the conjugate. The products were first purified by gel filtration on Sephadex G-25 F resin and then by reversed-phase HPLC on Silasorb

Table 1. Characteristics of PS in Fractions I–III and Theoretical Characteristics of the Major Components in These Fractions

fraction no.	content of NH2-groups, μmol per mg of PS	M_{PS}, g/moles	m estd for the major component	M_{PS} estimated for the major component, g/mol	no. of N atoms estd for the major component
I	2.04	985	4 and 5	871 and 1056	15 and 18
II	2.77	720	3	686	12
III	4.11	490	2	501	9

HSV-1 IE pre-mRNA 4,5 :   5' ...CUUCCCG<u>CAG|GAGGAACG</u>UC... 3'
AS5MAcr :   3' UGTC CTCCTTGC 5'
IE4,5SA :   3' GGCGTC CTCCTT 5'
S5MAcr :   3' UCGTTCCTGCCT 5'
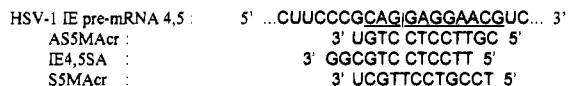
Figure 1. Nucleotide sequence of antisense oligos AS5Acr (15) and IE4,5SA (13), nonsense oligo S5MAcr (15), and the target intron-exon boundary of IE of mRNAs 4 and 5. The target sequence complementary to AS5Acr is underlined.

C_{16} column (9 × 240 mm, 10 μm, NPO "Chromatographia", Moscow, Russia) using the gradient of acetonitrile (5–40%) in 50 mM triethylammonium acetate buffer (pH 7.5). An independent experiment demonstrated that, under these conditions, the copolymers are well separated from both the unreacted PEO and unconjugated PS chains modified with 2'-deoxyadenosine. Several fractions of the block copolymers were obtained. We describe below only one, lower molecular mass fraction that contained the desired copolymer. The concentration of the 2'-deoxyadenosine groups in the copolymer of this fraction was 0.397 μmol per mg as determined spectrophotometrically by measuring absorbance of 2'-deoxyadenosine groups at 260 nm (2'-deoxyadenosine molar absorption coefficient at 260 nm equals 15 300 units). Since the spectra of this copolymer revealed the characteristic spectra of 2'-deoxyadenosine linked to the free amino groups of PS, it was unlikely that the polymer consisted of a triblock structure, PEO–PS–PEO, in which both terminal aminogroups of PS are linked to PEO chains. Furthermore, it was also unlikely that it had a triblock structure (A)PS–PEO–PS(A). The molecular mass of such a triblock copolymer would be 1260 g/mol, as determined from the content of 2'-deoxyadenosine groups in the copolymer assuming that two 2'-deoxyadenosine groups are linked to the two end amino groups in the (A)PS–PEO–PS(A) molecule. Further, since the molecular mass of two 2'-deoxyadenosine groups approximates 500 g/mol, this would result in PS–PEO–PS chains with a molecular mass of about 760 g/mole which is significantly lower than the molecular mass of the initial PEO. Therefore, we concluded that the copolymer obtained had a diblock structure PEO–PS(A). The molecular mass of this copolymer, as determined from the content of 2'-deoxyadenosine groups, approximates 2520 g/mol, which was consistent with the value calculated for the PEO–PS(A) diblock copolymer (= 2470 g/mol).

The effects of the PEO–PS(A) copolymer on the performance of antisense oligo was further evaluated using HSV-1 reproduction in Vero cells as a model. For these studies the 12-mer phosphodiester oligo AS5MAcr

having the polynucleotide structure **CGTTCCTCCTGU** HSV-1 was used. The target for this oligo was first identified by Kulka et al. (13, 14). These authors used methylphosphonate-based oligo IE4,5SA having sequence *TTCCTCCTGCGG*, complementary to the splice junction immediate early (IE) pre-mRNAs 4 and 5 of HSV-1 (italic types indicates methylphosphonate residues in IE4,5SA; the sequence common for IE4,5SA and AS5MAcr is underlined). The rationale for the choice of this sequence was based on the findings indicating that (i) IE genes play a regulatory role in HSV replication and (ii) RNA splicing may be involved in the control of gene expression (13). The AS5MAcr sequence is two nucleotides shorter at the 3' end compared to IE4,5SA (Figure 1). It also has U instead of C at the 3' end, which was necessary to introduce an acridine substituent (15). However, there are also two additional nucleotides at the 5' end of AS5MAcr compared to IE4,5SA, which are complementary to the target sequence (Figure 1). The 12-mer S5MAcr with randomized sequence **TCCGTCCTTGCU** identical in composition to antisense oligo was used as a "nonsense" oligo control. The unmodified antisense phosphodiester **CGTTCCTCCTGC** was previously reported to be inactive in inhibiting HSV-1 reproduction in concentrations up to 20 μM (15). Therefore, to evaluate the copolymer effects, both antisense and nonsense oligos AS5MAcr and S5MAcr were modified at the 5'-end with n-undecyl and at the 3'-end with acridine moieties (Figure 2). Such double-modified oligos reveal elevated activity and stability compared to unmodified phosphodiesters (15, 16). The n-undecyl modification (17) enhances oligo binding and uptake into cells. The acridine moiety intercalates into DNA and enhances binding of oligos with nucleic acid targets (18). In particular, the modified oligo AS5MAcr has previously been reported to effectively inhibit the HSV-1 reproduction in Vero cells in a sequence-specific manner in concentrations of 1–20 μM (15). The synthesis and effects of the AS5MAcr and S5MAcr in the absence of the copolymer are described elsewhere (15).

To prepare complexes between the oligos and PEO-PS-(A), 2 μmol of the copolymer in 0.5 mL of 0.1 M sodium acetate, pH 4.0 was mixed with 1 μmol of oligo in 0.5 mL of the same buffer, and then the system was diluted with RPMI-1640 media to obtain the desired concentration of the complex. The formation of the complexes between the PEO–PS(A) and oligo was confirmed by reversed-phase HPLC on a Silasorb C_{16} column. By using the fluorescence probe (perylene) technique (19), these com-
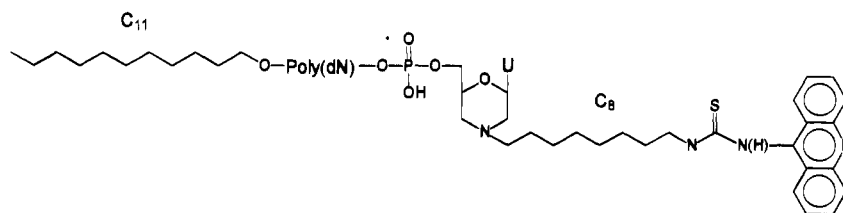
Figure 2. Structure of hydrophobically modified oligo derivative.

Table 2. Effect of 12-mer Oligos (II) and Their Complexes with PEO–PS(A) on the Reproduction of HSV-1 in Vero Cells

system studied	oligo concn, μM	copolymer concn, μM	infectious titer of HSV-1 (PFU/mL)	
			22 h	39 h
control	0	0	10^5	5×10^6
AS5MAcr	4	0	0	10^5
	2	0	6×10^3	10^6
complex of AS5MAcr and PEO–PS(A)	4	4	0	0
	2	2	10^3	2×10^5
complex of S5MAcr and PEO–PS(A)	4	4	10^5	5×10^6
PEO–PS(A)		4	10^5	not determined

plexes were shown to form micelles. The critical micelle concentration (cmc) for the complexes was in the order of several μM, which was in the cmc range of amphiphilic block copolymers (*19*). These results indicate that the binding of oligo to PS chains leads to formation of hydrophobic sites due to the charge neutralization (*6*), which leads to the complexes self-assembling into micelles.

The toxic effects of AS5MAcr and complexes formed between AS5MAcr and PEO–PS(**A**) were evaluated using HSV-1-infected Vero cells. In these experiments, the synthesis of cell and virus proteins was studied using a pulse–chase technique as previously described (*20*). The infected cells were incubated with 2, 7.5, and 20 μM of AS5MAcr or oligo–copolymer complex for 6 h after infection, which was at 0.1 PFU/cell multiplicity. (The uninfected or virus-infected cells which were not treated with oligos or complexes were used in the control experiments.) After incubation, the medium was replaced by fresh Hank's solution containing 20 μCi/mL of [^{14}C]-lactalbumin hydrolysate (Reakhim, Russia), and cells were incubated for 1 h at 37 °C and then washed and lysed with 0.1% sodium dodecylsulfate. The lysates were analyzed by polyacrylamide gel electrophoresis under Laemmli conditions (*21*), and autoradiographs were obtained using the R-film. All concentrations of oligo and complex studied inhibited the synthesis of virus-specific proteins beyond the detection limit. Significant inhibition of the synthesis of cell proteins was observed for 20 μM oligo and complex which was indicative of cytotoxic effect. Some inhibition of cell proteins was observed at 7.5 μM. Both at 20 and 7.5 mM concentration the inhibition was more pronounced in the case of free oligo compared to the complex, which suggests that the complex is less cytotoxic than free oligo. No cytotoxicity was observed both for the free oligo and complex at 2 μM.

The experiment on HSV-1 reproduction was performed as previously described (*15*). Briefly, monolayers of Vero cells were infected at 0.01 PFU/cell multiplicity with the virus. Oligos, PEO–PS(**A**), or their complexes were added to the cells at various concentrations 1 h prior to the infection. The complex formed between nonsense oligo and the copolymer was used in the control experiments to exclude nonspecific effects. After 8 h of incubation of the infected cells in the presence of oligonucleotides the medium was replaced with the fresh media containing fetal calf serum. The virus infectious titer (PFU/mL) was determined 22 and 39 h post infection on monolayers of Vero cells (*22*). All experiments were performed in triplicate. The variations in the infectious titers determined were less than 25%. The results of the experiment are presented in Table 2. The treatment with 4 μM AS5MAcr led to a decrease in the virus titer 22 h postinfection; however, substantial virus concentration was observed 39 h postinfection. When complexed with PEO–PS(**A**) this oligo inhibited virus reproduction beyond the detection limit after both 22 and 39 h postinfection. The copolymer also increased the inhibition effect of 2 μM AS5MAcr 22 and 39 h after infection. In the absence of oligo, the copolymer did not affect the infection. Furthermore, the effect of the copolymer on oligo activity was sequence specific, since no inhibition of the virus was observed with the complexes of nonsense oligo. Therefore, the PEO–PS(**A**) copolymer significantly prolonged the effect of antisense oligo. The enhanced activity of oligo delivered to the cell in the complexed form was probably due to one or both of the following reasons. Firstly, it may be due to the increase in uptake of the complexed oligos into cells that results in elevation of

intracellular oligo concentration. A similar correlation between the increased uptake and functional activity has been previously reported for the DNA–polycation complexes (*23*). Secondly, it may be due to stabilization of the complexed oligo against enzymatic degradation that increases the half-life of oligo in cells. The stabilization of nucleic acids incorporated into polyelectrolyte complexes against enzymatic digestion also has been reported (*24*). The studies on the mechanism of the observed effect of the PEO–PS(**A**) copolymer on oligo activity are currently in progress in our laboratories.

LITERATURE CITED

(1) Helene C. (1991) Rational design of sequence-specific oncogene inhibitors based on antisense and antigene oligonucleotides. *Eur. J. Cancer 27*, 1466–1471.

(2) Crooke R. M. (1991) In vitro toxicology and pharmacokinetics of antisense oligonucleotides. *Anti-Cancer Drug Design 6*, 609–646.

(3) Stein, C. A., and Cheng, Y.-C. (1993) Antisense oligonucleotides as therapeutic agents—is the bullet really magical? *Science (Washington DC) 261*, 1004–1012.

(4) Farhood, H., Gao, X, Son, K., Yang, Ya-Yun, Lazo, J. S., Huang, L., Barsoum, J., Bottega, R., and Epand, R. M. (1994) Cationic liposomes for direct gene transfer in therapy of cancer and other diseases. *Ann. N.Y. Acad. Sci. 716*, 23–35.

(5) Behr, J.-P. (1994) Gene transfer with synthetic cationic amphiphiles: prospects for gene therapy. *Bioconjugate Chem. 5*, 382–389.

(6) Kabanov, A. V., and Kabanov, V. A. (1995) DNA complexes with polycations for delivery of genetic material into cells. *Bioconjugate Chem. 6*, 7–20.

(7) Kabanov, A. V., Vinogradov, S. V., and Alakhov, V. Yu. (1995) New generation of polyelectrolyte complexes for targeting of antisense oligonucleotides. *Abstracts of Seventh International Symposium on Recent Advances in Drug Delivery Systems*, Salt Lake City, pp 213–215.

(8) Kabanov, A. V., Chekhonin, V. P., Alakhov, V. Yu., Batrakova, E. V., Lebedev, A. S., Melik-Nubarov, N. S., Arzhakov, S. A., Levashov, A. V., Morozov, G. V., Severin, E. S., and Kabanov, V. A. (1989) The neuroleptic activity of haloperidol increases after its solubilization in surfactant micelles. Micelles as microcontainers for drug targeting. *FEBS Lett. 258*, 343–345.

(9) Kabanov, A. V., Batrakova, E. V. Melik-Nubarov, N. S., Fedoseev, N. A., Dorodnich, T. Yu., Alakhov, V. Yu., Chekhonin, V. P., Nazarova, I. R., and Kabanov, V. A. (1992) A new class of drug carriers: micelles of poly(oxyethylene)-poly(oxypropylene) block copolymers as microcontainers for drug targeting from blood in brain. *J. Contr. Release 22*, 141–158.

(10) Yokoyama, M, Miaychi, M., Yamada, N., Okano, T., Sakurai, Y., Kataoka, K., and Inoue, S. (1990) Characterization and anticancer activity of the micelle-forming polymeric anticancer drug adriamycin-conjugated poly(ethylene glycol)–poly(aspartic acid) block copolymer. *Cancer Res. 50*, 1693–1700.

(11) Yokoyama, M, Okano, T., Sakurai, Y., Ekimoto, H., Shibazaki, C., and Kataoka, K. (1991) Toxicity and antitumor activity against solid tumors of micelle-forming polymeric anticancer drug and its extremely long circulation in blood. *Cancer Res. 51*, 3229–3236.

(12) Friser, H. (1975) An improved 2,4,6-trinitrobenzenesulfonic acid method for the determination of amines. *Anal. Biochem. 64*, 284–288.

(13) Kulka, M., Smith, C. C., Aurelian, L., Fishelevich, R., Meade, K., Miller, P., and Ts'o, P. O. P (1989) Site specificity of the inhibitory effects of oligo(nucleoside methylphosphonate)s complementary to the acceptor splice junction of herpes simplex virus type 1 immediate early mRNA 4. *Proc. Natl. Acad. Sci. U.S.A. 86*, 6868–6872.

(14) Kulka, M., Smith, C. C., Levis, J., Fishelevich, R., Hunter, J. C. R., Cushman, C. D., Miller, P. S., Ts'o, P. O. P., and Aurelian, L. (1994) Synergistic antiviral activities of oligonucleotide methylphosphonates complementary to herpes

simplex virus type 1 immediate-early mRNAs 4,5 and 1. *Antim. Agents Chemother. 38*, 675–680.

(15) Vinogradov, S. V., Suzdaltseva, Yu., Alakhov, V. Yu., and Kabanov, A. V. (1994) Inhibition of Herpes simplex virus 1 reproduction with hydrophobized antisense oligonucleotides. *Biochem. Biophys. Res. Commun. 203*, 959–966.

(16) Vinogradov, S. V., Pheoktistov, V. S., and Kabanov, A. V. (1991) Fatty radical-modified antisense oligodeoxynucleotides as effective inhibitors of influenza virus reproduction. *Nucl. Acids. Symp. Ser. 24*, 281.

(17) Kabanov, A. V., Vinogradov, S. V., Ovcharenko, A. V., Krivonos, A. V., Melik-Nubarov, N. S., Kiselev, V. I., and Severin, E. S. (1990) A new class of antivirals: antisense oligonucleotides combined with a hydrophobic substituent effectively inhibit influenza virus reproduction and synthesis of virus-specific proteins in MDCK cells. *FEBS Lett. 259*, 327–330.

(18) Helene, C. and Tolume, J.-J. (1989) Control of gene expression by oligodeoxynucleotides covalently linked to intercalating agents and nucleic acids cleaving reagents. In *Antisense Inhibitors of Gene Expression* (J. Cohen, Ed.) CRC Press, Boca Raton, FL.

(19) Kabanov, A. V., Nazarova, I. R., Astafieva, I. V., Batrakova, E. V., Alakhov, V.Yu., Yaroslavov, A. A., and Kabanov, V. A.

(1995) Micelle formation and solubilization of fluorescent probes in poly(oxyethylene-*b*-oxypropylene-*b*-oxyethylene) solutions. *Macromolecules 28*, 2303–2314.

(20) Melik-Nubarov, N. S., Suzdaltseva, Yu.G., Priss, E. I., Slepnev, V. I., Kabanov, A. V., Zhirnov, O. P., Sveshnikov, P. G., and Sevrin, E. S. (1993) Interaction of hydrophobized antiviral antibodies with influenza virus infected MDCK cells. *Biochem. Mol. Biol. Intern. 29*, 939–947.

(21) Laemmli, U. K. (1970) Cleavage of structural proteins during the assembly of the head of bacteriophage T4. *Nature 227*, 680–685.

(22) Freshney R. I. (1994) *Culture of Animal Cells*, 3rd ed., John Willey & Sons, Inc., New York.

(23) Kabanov, A. V., Astafieva I. V., Maksimova I. V., Lukanidin E. M., Georgiev G. P., and Kabanov V. A. (1993) Efficient transformation of mammalian cells using DNA interpolyelectrolyte complexes with carbon chain polycations. *Bioconjugate Chem. 4*, 448–454.

(24) Kabanov, A. V., Astafieva, I. V., Chikindas, M. L., Rosenblat, G. F., Kiselev, V. I., Severin, E. S., and Kabanov, V. A. (1991) DNA interpolyelectrolyte complexes as a tool for efficient cell transformation. *Biopolymers 31*, 1437–1443.

BC950076Y

TEACHING EDITORIAL

Bioanalytical Mass Spectrometry: Many Flavors to Choose

Joseph A. Loo

Parke-Davis Pharmaceutical Research, Division of Warner-Lambert Company, 2800 Plymouth Road, Ann Arbor, Michigan 48105. Received August 2, 1995

INTRODUCTION

Bioanalytical mass spectrometry (MS) is currently enjoying a surge in activity as the ionization methods matrix-assisted laser desorption/ionization (MALDI) (1, 2) and electrospray ionization (ESI) (3–5) enable mass spectrometers to measure molecular weights for biomolecules to greater than 100 kDa. As the capabilities for ionizing larger and larger molecules increase, applications of those capabilities have increased at a more substantial pace. Previously, volatilizing such large species without significant sample degradation had been a key limitation for gaseous ion methods such as mass spectrometry. Using the information these measurements provide is the next hurdle for the analyst; fortunately, a large number of problems exist in biochemistry and molecular biology which are amenable for study using these techniques.

In the "old days", perhaps 10 years ago, chemists and biochemists with a precious nanomole (or less) of peptide could take or send the sample to a mass spectrometry laboratory and obtain an accurate molecular weight, provided a fast atom bombardment (FAB) desorption/ionization (6) source was available on the mass spectrometer and provided the molecular mass was less than 5 kDa. In some cases, depending on the analyst, the instrumentation, and the sample itself, larger masses could be measured, but the methodology was neither routine nor commonplace. For biomolecules less than 3 kDa, sequence information from tandem mass spectrometry (MS/MS) experiments could be obtained, but, again, the results depended on the sample, the analyst, and the instrumentation. If the scientist was fortunate enough to have access to a lab with a Californium-252 plasma desorption (7) mass spectrometer, molecular weights in excess of 20–30 kDa could be measured, but the measurement was time-consuming.

Today, the situation for the biochemist has improved dramatically. That precious nanomole of peptide or protein can be submitted to a mass spectrometry lab for molecular weight analysis, but in addition to obtaining an accurate MW (to within ±0.05% or better), the scientist may receive perhaps 90% or more of the original sample back because of the sensitivity of electrospray ionization and matrix-assisted laser desorption/ionization MS. The remaining sample can be further chemically or proteolytically digested and resubmitted to the MS analyst for sequence information. Moreover, with the simplicity of many commercial mass spectrometry systems today, some biochemists can purchase a mass spectrometer for their laboratory or use an "open access" instrument (8), obtaining the necessary mass information in a timely manner.

This article will describe the basic reasons why mass spectrometry with ESI and MALDI has changed the nature in which many biochemistry laboratories perform research. There are an increasing number of options and MS experiments the scientist can choose. The principles of the desorption/ionization methods will be outlined, and several recent applications will be highlighted. There are several excellent reviews describing the field and applications of bioanalytical mass spectrometry (9–13) along with review articles on electrospray ionization (14, 15) and MALDI (2). It is hoped that readers unfamiliar with this growing field will accept this report as a basic guide and pointer to other reference sources and that it provides a spark to jump into the emerging world of mass spectrometry.

BASIC PRINCIPLES

A. Electrospray Ionization (ESI). *Ionization Mechanism, Multiple Charging, and Data Interpretation.* Electrospray ionization produces highly charged droplets by nebulizing liquids in a strong electrostatic field (Figure 1). The highly charged droplets, generally formed in a dry bath gas at atmospheric pressure, shrink by evaporation of neutral solvent until the charge repulsion overcomes the cohesive forces, leading to a "Coulombic explosion." The mechanism of ion formation itself is a volatile topic and has been treated in several reports (16–18). Whatever the ultimate process of ion formation, it is clear that ESI produces multiply charged molecules from solution under mild conditions. These ions generally arise by attachment of protons, alkali cations, or ammonium ions for positive ion formation, or with reversal of the polarity of the nebulizing electric field, negative ions are formed by proton abstraction.

Dole and colleagues originally described electrospray ionization in studies of ions from polymers of molecular weights in excess of 100 kDa (19–21). Dole conceived of the idea of using an electrospray process to produce intact large polymeric ions from learning about electrospraying automobile paint while working as a consultant to a paint company (22). Over a decade later, Dole's experiments were extended by John Fenn and co-workers (3, 23) and simultaneously by researchers in the former Soviet Union (24). These workers laid the foundation of ESI, demonstrating its ultimate utility for the analysis of macromolecules and as a potential interface for the combination of liquid chromatography with mass spectrometry. The production of molecules bearing multiple charges accesses higher molecular weights by extending the mass range for mass-to-charge (m/z) limited mass spectrometers. The multiple charging phenomenon has been demonstrated to apply to molecules of over 150 kDa, and it has permitted the measurement of relative mass with precision of better than 0.05%. [As a side note, Dole (22) writes that after presenting a talk on his ESI work at the annual American Society for Mass Spectrometry Conference in 1981, "I was quite surprised at quite a

* Phone: (313) 996-7515. Fax: (313) 998-2716. E-mail: Loo@AA.WL.COM.
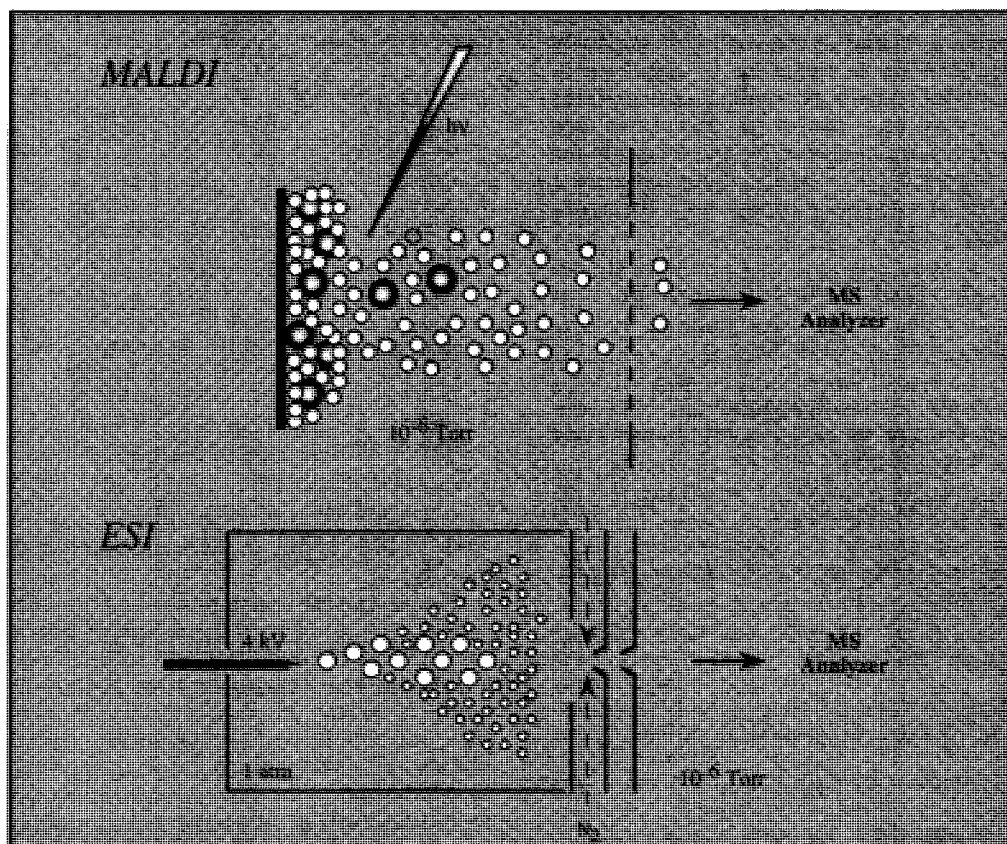
Figure 1. Schematic of ESI and MALDI processes.
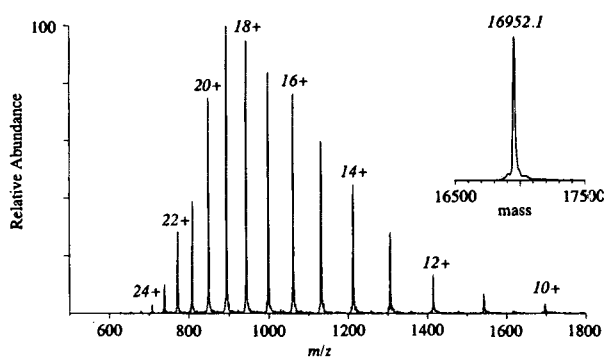
Figure 2. ESI mass spectrum of horse apomyoglobin. The deconvoluted spectrum (to the mass scale) is shown in the inset.

Figure 3. ESI mass spectrum of bovine albumin dimer (133 kDa).

large turnout of people to hear my talk." Although he only lived long enough to see the beginning of ESI-MS for biochemical applications, the modest Dole would have been truly astonished to see the size of an audience to hear him talk if he were alive today.]

Large biomolecules examined by ESI-MS typically show a distribution of multiply charged molecules and no evidence of fragmentation unless dissociation is induced during transport into the mass spectrometer by higher energy collisions. The ESI mass spectrum of horse skeletal muscle apomyoglobin (17 kDa) is shown in Figure 2. A distinctive bell-shaped distribution of charge states is typically observed in which adjacent peaks differ by one charge. For the apomyoglobin example illustrated, the most abundant multiply protonated ion is observed at m/z 893.12 for the 19^+ ion and the highest charge state observed is 25^+ (a small peak at m/z 679 in Figure 2). A feature of ESI mass spectra for most macromolecules is that the average charge state increases in an approximately linear fashion with molecular weight. This is further demonstrated in the ESI mass spectrum in Figure 3 for 133 kDa bovine albumin

dimer.

The net number of possible protonation sites in solution appears to be one of the principal factors affecting the maximum extent of multiple charging observed in positive ion ESI mass spectra. For most proteins so far examined (solution pH < 4), an approximate linear correlation is observed between the maximum number of charges and the number of basic amino acid residues (e.g., Arg, Lys, His, and the N-terminus) (*14, 15, 25*). Although there are a number of examples where this "rule" does not hold and it is not suggested that the charges are localized at these sites in the gas phase ion, one can use this relationship to provide a simple and quick estimate of the maximum number of expected charges. Again, increasing the multiple charging for a given molecule is especially important for mass spectrometers with a limited m/z range because it allows the instrument to detect molecular ions from large molecular species.

For positive ion ESI-MS, the determination of relative molecular mass (M_r) is simple, assuming that adjacent

peaks of a series differ by only one charge. The observed m/z ratios for each member of the suite of multiply protonated molecular ions are related by a series of simultaneous equations where M_r and charge are unknown variables. Any two peaks in the series are sufficient to determine M_r as shown by the example for apomyoglobin in Figure 2. The relationship between a multiply charged ion at mass-to-charge A with charge z_A and the M_r is described by

$$Az_A = M_r + M_c z_A$$

$$Az_A = M_r + 1.0079 z_A \qquad (1)$$

where, for this example, the charge carrying species (M_c) is a proton. The molecular weight of a second multiply protonated ion at m/z B is given by

$$Bz_B = M_r + 1.0079 z_B \qquad (2)$$

If $B > A$ and B is d peaks away from A ($d = 1$ for adjacent peaks), then

$$z_B = z_A - d \qquad (3)$$

Substituting (3) into (2) and then solving simultaneously with (1) for the charge of peak A yields

$$z_A = d(B - 1.0079)/(B - A) \qquad (4)$$

The charge for A is obtained by taking z_A as the nearest integer value, and thus the charge of each peak in the multiple charge distribution is assigned. Once charge is known, the molecular mass can be calculated from (1).

Thus, for the apomyoglobin example in Figure 2, if one considers the two adjacent peaks at m/z 848.67 (A) and 893.29 (B), the charge of peak A from eq 4 is 20 (an integer value) and the calculated MW from peak A is 16 953.2. If the calculated charge is not very close to an integer value, then either the peaks are not part of the same distribution (i.e., a mixture) or the relationship for the variable d in eq 3 is incorrect.

Calculation of M_r for each of the observed m/z values provides enhanced precision. Thus, for the data shown in Figure 2, a standard deviation of ±1.4 Da is observed for 15 m/z measurements from one spectrum (measured 16 952.1, sequence 16 951.5; see Table 1). Fenn and co-workers developed an algorithm that deconvolutes or converts the ESI m/z spectrum to a plot in the mass domain for calculation of mass and provides an easier to visualize graphical representation (26). Most commercial ESI-MS systems include some form of this deconvolution software package. Some also provide a program that uses maximum entropy methods for higher resolution deconvolution analysis (27). Relative molecular mass measurements for macromolecules of greater than 100 kDa have been demonstrated, and in favorable cases precision of measurement may be better than 0.05–0.01%. However, more accurate M_r measurements are required for larger molecules to differentiate mutations that produce 1 Da mass differences (i.e., for proteins, Asp and Asn, Leu/Ile and Asn, Glu and Gln). With higher resolution mass spectrometers such as magnetic sector (28, 29) and Fourier transform instruments (30–32), direct charge state assignment in even complex mass spectra is possible by measurement of the $^{12}C/^{13}C$ isotopic peak separation. This is demonstrated in Figure 4 for multiply charged molecules with up to 5^+ charges. The spacing between adjacent isotopic peaks is equal to (charge)$^{-1}$. The combination of high resolution and high

Table 1. Molecular Weight Calculation from ESI Mass Spectrum of Apomyoglobin[a]

m/z value	charge state	calcd MW	devn from mean
707.43	24^+	16954.13	+2.07
738.03	23^+	16951.51	−0.55
771.51	22^+	16951.05	−1.02
808.28	21^+	16952.71	+0.65
848.67	20^+	16953.24	+1.18
893.29	19^+	16953.36	+1.30
942.78	18^+	16951.90	−0.16
998.21	17^+	16952.44	+0.37
1060.48	16^+	16951.55	−0.51
1131.04	15^+	16950.48	−1.58
1211.89	14^+	16952.35	+0.29
1305.01	13^+	16952.03	−0.03
1413.82	12^+	16953.75	+1.68
1542.10	11^+	16952.01	−0.05
1695.85	10^+	16948.42	−3.64

av MW: 16952.06
standard devn: ±1.37
% standard devn: ±0.01
adduct ion mass: 1.0079
polarity: +
sequence MW: 16951.49

[a] ESI mass spectrum shown in Figure 2.
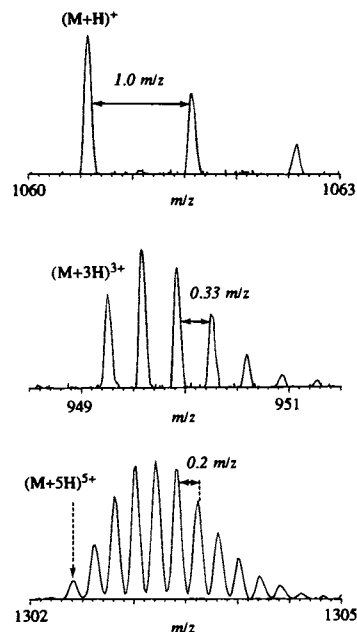
Figure 4. High resolution ESI mass spectra showing the (M + H)$^+$, (M + 3H)$^{3+}$, and the (M + 5H)$^{5+}$ ions for bradykinin (1060 Da), melittin (2845 Da), and bovine pancreatic trypsin inhibitor (6512 Da), respectively. The mass spectra were acquired on a magnetic sector instrument (46) with greater than 6000 resolving power (full width at half height).

accuracy may be crucial for unknown identification and complex mixture analysis.

Peptide and protein analyses by ESI-MS has generally been performed in the positive ionization mode. The more basic amino acid residues have sufficiently large pK_a values to ensure that proteins will be multiply protonated in acidic pH solutions. However, multiply deprotonated molecules can be produced by ESI in basic pH aqueous solution where basic residues are generally uncharged and acidic residues are deprotonated (33). Horse heart apomyoglobin in an aqueous 1% NH$_4$OH solution (pH ~ 11) yields an ESI mass spectrum with a bell-shaped multiple charge state distribution extending up to approximately the (M − 19H)$^{19-}$ charge state.
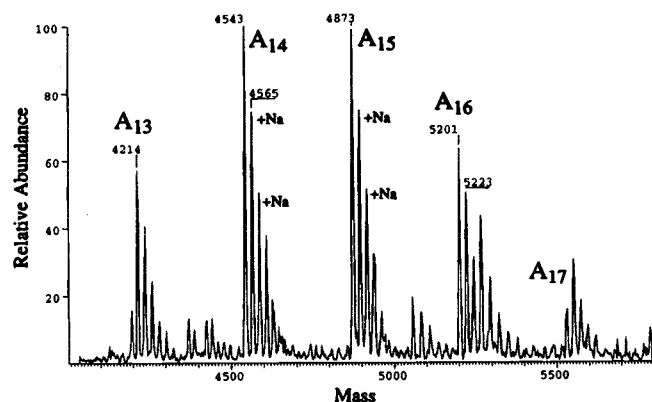
Figure 5. Negative ion ESI mass spectrum of a mixture of oligo(A)$_{12-18}$. The spectrum has been deconvoluted to the mass scale.

Horse myoglobin has 13 Glu and 7 Asp residues, corresponding closely to the maximum negative charge state observed.

The application of ESI-mass spectrometry to oligonucleotides has also been demonstrated (*14, 25*). Negative ion ESI mass spectra of small oligodeoxyribonucleotides are characterized by multiply charged molecular anions of the form $(M - nH)^{n-}$, with the charge presumably residing at the acidic bridging phosphodiester and/or terminal phosphate groups. Each nucleotide residue can potentially accommodate one negative charge. Small oligonucleotides ($m = 3-8$, where m is the number of nucleotide units) afford molecular ions to near the maximum possible charge state. As the mass increases, the extent of charging is approximately one-third of the number of residues. However, with increasing mass and with decreasing charge state for a given molecular anion, an increased contribution of species arising from the substitution of sodium for protons is observed. This substitution of Na^+ for H^+ among the increasing number of possible phosphate moieties reduces the measurable current for any given ion (by spreading out the signal over more channels) and thus the overall sensitivity of the analysis. With sufficient resolution, the separation of the members of these suites of molecular anions can be measured as shown in Figure 5 for a mixture of synthetic deoxyribonucleotides. In these circumstances the mass of the parent molecule may be determined with comparable precision and accuracy to that observed for polypeptides under positive ionization conditions. For larger synthetic deoxyribonucleotides, multiply charged molecular anions with broadened (unresolved) peaks due to alkali attachment are observed. In such cases, mass determinations can overestimate the M_r, with an error of the order of 1% for such measurements because each charge state contains a different (and unknown) average number of sodium counterions.

Experimental. The ESI "source" may be as simple as a small diameter metal capillary (*23*). A 1–20 μL/min flow of analyte solution, typically as water–methanol or water–acetonitrile mixtures with other additives such as acetic acid or formic acid, is infused to the capillary from syringes or liquid chromatographic columns. A typical source for ESI-MS is shown in Figure 1. A voltage of +4–6 kV is applied (for positive ion ESI) to the metal capillary. For experiments in which sample solution is directly infused to the ESI source, syringe pumps deliver controlled flows of analyte liquid. Stability of the ESI source depends critically on the stability of these flows. In the negative ion mode an electron scavenger, such as oxygen or sulfur hexafluoride (or air), is used to inhibit corona discharge at the capillary tip. Most recently, the

development of low solution flowrate ESI sources (for example, "micro electrospray") have dramatically improved the overall sensitivity of ESI-MS analyses to the femtomolar regime, even for MS/MS experiments (*34–36*).

The developers of ESI sources have always had chromatography or capillary electrophoresis interfaces in mind (*23*). The use of ESI-MS as an on-line detector for HPLC was demonstrated shortly after the development of ESI as an ionization source by Henion and co-workers (*37–40*). Higher resolution separations and higher sensitivity was achieved with capillary electrophoresis interfaced to ESI-MS by Smith's laboratory (*14, 41*). Today, one of the key features and reasons for the popularity of ESI-MS in biochemical facilities is the ability to easily interface to commercial chromatography and electrophoretic systems. In some cases, the additional use of a liquid sheath, or a layer of flowing liquid in conjunction with the chromatographic/electrophoretic effluent, augments the performance of the separation-ESI-MS combination (*42*). The high sensitivity (low picomole to femtomole) of the overall methodology together with tandem mass spectrometry for on-line structural information is an extremely powerful tool for the biochemical laboratory.

The most crucial feature of an ionization source operated at atmospheric pressure is the efficient sampling and transport of ions into the mass spectrometer vacuum. In many arrangements, charged droplets/ions produced at atmospheric pressure drift against a countercurrent flow of dry N_2 gas directed through an axial plenum toward the sampling aperture. This curtain of nitrogen serves as a drying agent, to exclude large droplets and particles, and to decluster the ions. As the ions pass through the orifice into the higher vacuum region, further declustering is accomplished by energetic collisions with background gas as the ions are accelerated into mass spectrometer. An alternative approach to droplet desolvation relies solely on heating during droplet transport through a heated metal or glass capillary (*43*) or lens housing (*44*). In these configurations, a countercurrent gas flow is not essential. An advantage of the heated capillary is the ease with which it can be adapted to a variety of MS configurations.

The most popular instruments with ESI-MS interfaces have been quadrupole mass spectrometers of modest m/z range and resolution, because of their relatively low cost and ease of operation. However, several examples of ESI interfaces to instruments with special advantages over quadrupole mass spectrometers are commercially available. The combination with magnetic sector instruments have been described by many researchers (*24, 28, 29, 45–48*). Capabilities for higher m/z resolution and higher energy collisionally activated dissociation (CAD) for tandem mass spectrometry experiments (e.g., peptide sequencing) are attractive features. ESI-MS data with ion trapping instruments such as the quadrupole ion trap (ITMS) (*49*) and the Fourier transform mass spectrometer (FTMS) (*30–32, 50*) are particularly encouraging. Significant advantages in MS/MS sensitivity, extended MS/MS (MS^n), and especially resolution are obtainable. McLafferty and co-workers (*30, 31*) have pioneered the combination of ESI with FTMS, demonstrating resolving powers > 10^6 and readily resolving up to the 18$^+$ charge state for equine myoglobin. More recently, results with time-of-flight instrumentation have been reported (*51–53*). The unlimited m/z range will be important for macromolecules and molecular complexes of relatively low charge. Standing's group has observed gas phase
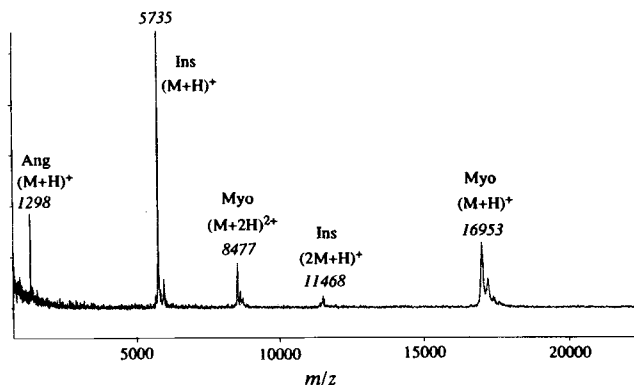
Figure 6. MALDI mass spectrum of a mixture of angiotensin I (Ang, 1296 Da), bovine insulin (Ins, 5734 Da), and horse apomyoglobin (Myo, 16952 Da).

protein multimers of greater than 10^6 Da with multiply charged ions extending beyond m/z 10 000 (*54*).

B. Matrix-Assisted Laser Desorption/Ionization (MALDI). *Ionization Mechanism and General Appearance of Spectra.* Laser desorption has been studied for many years as another method to volatilize large biomolecules for mass spectrometry. However, mass spectra for larger molecular weight compounds were frequently dominated by fragment ions with few if any intact molecular ions. At nearly the same time electrospray ionization was demonstrated, matrix-assisted laser desorption/ionization was developed as a method for analysis of proteins (*1, 2, 55–57*). The key to the MALDI process is the incorporation of the analyte into a matrix that absorbs radiation from the ultraviolet (or infrared) laser. Transfer of energy from the matrix to the sample leads to desorption of the solid to the gas phase for analysis by the mass spectrometer. Again, as with ESI, the mechanism of desorption and ion formation is complicated and unresolved. However, the formation of ions to nearly 10^6 Da and the high sensitivity of MALDI (subfemtomole) has lead to the explosive commercialization of MALDI–mass spectrometers and the incorporation of instruments in not only mass spectrometry laboratories but also biochemical facilities and laboratories where bench scientists are able to use the instrumentation.

The typical appearance of a MALDI mass spectrum is shown in Figure 6 for a mixture of angiotensin I (1296 Da), bovine insulin (5734 Da), and horse apomyoglobin (16 952 Da). The dominant feature of the spectrum is the appearance of an abundant singly charged molecular ion. In some cases, multiply charged ions of relatively low charge (2^+ to 5^+) are observed, depending on the sample matrix, the wavelength and power of the laser pulse, and the analyte. Also commonly observed are ions for gas phase aggregates (nonspecific), such as dimers, trimers, etc. This also depends on the choice of matrix and laser power. In comparison to ESI mass spectra, the appearance of only singly and lower charged ions generally allows for quicker and simpler interpretation of the data. MALDI mass spectra of complex mixtures of macromolecules are much easier to interpret that ESI spectra (without further computer support), where a suite of multiply charged ions representing each component is formed. The mass range of the MALDI–MS method is comparable to ESI–MS. A typical spectrum for a large protein is shown in Figure 7 for a monoclonal antibody, anti-β-galactosidase (150 kDa).

Experimental. The relative simplicity of a MALDI mass spectrum compared to an electrospray mass spectrum is mirrored by the simplicity of the experiment.
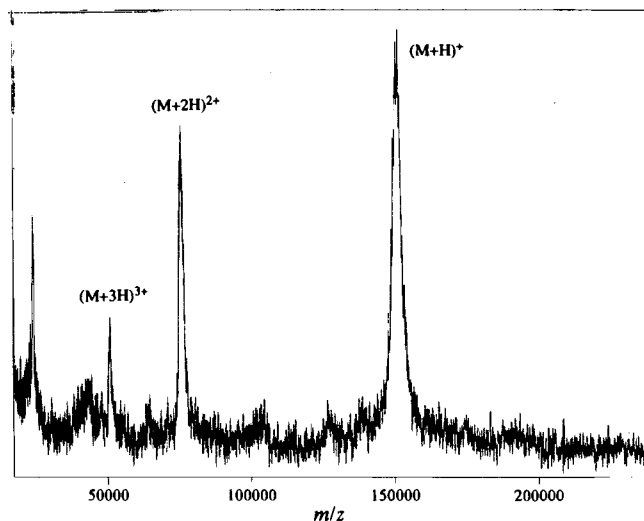
Figure 7. MALDI mass spectrum from 0.5 pmol of anti-β-galactosidase monoclonal antibody (150 kDa).

MALDI mass spectra are typically acquired on a time-of-flight mass spectrometer. The instrument consists of a laser source, a flight tube, and a detector. A simple analogy is a 100 m race. The contestants (ions) line up at the starting point (sample plate). When the gun (laser source) fires, the racers run in a straight line to the finish line (detector). The smaller, quicker runners reach the finish line before the larger, slower runners. Similarly, the smaller mass ions impact the detector surface before the larger mass ions. The instrument measures the flight time of each ion, which thus provides a measurement of mass.

In a typical experiment, biochemical samples are prepared by placing 1 μL of an aqueous solution of the analyte of interest [1–10 pmol/μL in 0.1% trifluoroacetic acid (TFA)] and 1 μL of an appropriate matrix solution (e.g., a saturated solution of the matrix in 1: 2 acetonitrile/0.1% TFA aq) on a sample target (~2 mm in diameter for each sample spot). The sample/matrix solution is then allowed to air dry at room temperature prior to insertion into the mass spectrometer.

The key idea of the method is to embed the analyte macromolecule in a suitable matrix of molecules having a strong absorption at the laser wavelength and present in high molar excess over the analyte. This induces an efficient transfer of the laser-pulse energy to the analyte and results in a soft desorption process, i.e., little or no fragmentation. The matrix may also play a role in the subsequent ionization of the analyte molecules. Popular MALDI matrices for peptide and protein analysis are α-cyano-4-hydroxycinnamic acid (4-HCCA), 1,5-dihydroxybenzoic acid (DHB), and 3,5-dimethoxy-4-hydroxycinnamic acid (sinapinic acid) (*58*) and for oligonucleotides, 3-hydroxypicolinic acid. Because of the low cost and small size of the nitrogen laser (N_2, 337 nm), it is by far the most common radiation source for the desorption process on commercial systems. In some cases, the UV region of the electromagnetic spectrum can be reached by more powerful lasers, such as Nd:YAG lasers [with the appropriate tripling (355 nm) or quadrupling (266 nm) of laser frequency]. The infrared region can be reached with a Er:YAG laser (2.3 μm). Although the power density of a nitrogen laser is more than adequate for most MALDI applications, the advantage of a YAG laser is the ability to access different wavelength regions. The use of the fundamental infrared frequency (1.06 μm) of a YAG laser has been shown to be advantageous for oligonucleotide analysis (*59*).

Time-of-flight (TOF) mass spectrometers are not typically considered high resolution instruments. However, several features can be added to improve resolution. An ion mirror (or reflectron) is incorporated into many commercial systems to correct for the initial ion energy spread of MALDI-produced ions that degrades resolution. Pulsed ion extraction (or delayed extraction) is a recent advance for MALDI-TOF mass spectrometers that can dramatically improve mass resolution for linear TOF instruments (*60*).

Although TOF mass spectrometers are the most popular MALDI detector, their limited (but rapidly improving) capabilities for high resolution and tandem MS experiments have encouraged the interface of MALDI to other types of mass spectrometers. MALDI has been interfaced to magnetic sector instruments, demonstrating much higher resolution than that obtainable on TOF systems and also MS/MS for structure information (*61, 62*). However, the somewhat limited m/z range of most magnetic sector instruments appears to limit its application to biomolecules of 25 kDa or less. Ion trap mass spectrometers (*63–65*), FT mass spectrometers (*66–68*), and the combination of an ion trap-TOF hybrid system (*69*) have also attracted much attention as a potentially powerful MALDI analyzer.

Given the situation in today's budget-conscious society, it may appear that a potentially economic option is a mass spectrometer system with both ESI and MALDI capabilities. A few commercial systems have such options available where the best of both worlds can be available on a single versatile instrument.

BIOCHEMICAL APPLICATIONS OF ESI-MS AND MALDI-MS

A. Biochemical Detection and Molecular Weight Determination. Determining the molecular weight of a biomolecule is a relatively quick and straightforward method to confirm the identity and integrity of a sample, and both ESI–MS and MALDI–MS are being used extensively for this purpose. Peptides and proteins have traditionally been analyzed by these mass spectrometric methods with high levels of success. Intact protein molecular weights in excess of 150 kDa have been measured by ESI–MS (*70, 71*) and MALDI–MS (*1, 72, 73*). Mass spectrometry is an important tool to differentiate between macromolecules of similar mass. For example, there are over 230 known variants of the β-chain human hemoglobin polypeptide, and a great majority involve a single amino acid substitution due to a single base substitution in the corresponding triplet codon of the DNA. Mass spectrometry, in particular ESI–MS, has been used to identify many of the hemoglobin variants (*74–77*).

A potential problem of ESI–MS of larger macromolecules is the requirement for resolution. Although multiple charging enables conventional mass spectrometers to measure molecular weights in excess of the mass-to-charge range, the individual peaks representing each charge state need to be adequately resolved to determine an accurate mass. The larger the molecule, the greater the maximum charge state (in general) and the smaller the spacing in m/z units between adjacent peaks. For example, for a 150 kDa molecule, the peak for the 150^+ charge state (at m/z 1001) is only 6.7 m/z units lower than the peak for the 149^+ charge. One method to circumvent this problem is to shift the charge state envelope to higher m/z or lower charge, either by adjusting the solution pH (to higher values for positive ions), by gas phase reactions with basic amines (proton transfer) to neutralize some of the charges (*78*), or by

collisional methods in the ESI interface (*79*). This increases the peak separation between adjacent charge states. For the 150 kDa mass example, the 50^+ charge state peak (at m/z 3001) is 61.2 m/z units lower than the 49^+ charge. Mass spectrometers with greater resolving power than conventional quadrupole analyzers, such as magnetic sector, ion trap, and especially Fourier transform instruments, should be able to measure masses for larger compounds and for complex mixtures.

MALDI coupled with time-of-flight instruments should not have this problem for analysis of large molecules because MALDI–MS does not depend on the formation of multiply charged ions for detection; i.e., the singly charged molecular ion carries a great deal of the ion current. Therefore, because of the unlimited mass-to-charge range of the time-of-flight mass spectrometer, detection of large ions has not been shown to be a problem. The analysis of a 500 kDa gramicidin S-synthase by Hillenkamp's group (*72*) and 939 kDa and 982 kDa human immunoglobulin IgM molecules by Nelson (*73*) support this hypothesis. However, again, higher resolution systems will be useful for mixtures and heterogeneous materials with closely spaced molecular weights.

An equally useful and important application of mass spectrometry is to detect and identify proteins that have been post-translationally modified. Cell regulation of protein function can be achieved through control of covalent modifications of the protein, such as glycosylation, phosphorylation, sulfation, and acylation. Mass spectrometry is a rapid and efficient method to detect these modifications. In the analysis by Roepstorff and co-workers (*80*) of a 45 kDa recombinant barley α-amylase, an enzyme important in malt production, at least three modifications were detected: C-terminal heterogeneous degradation, glutathionylation of a Cys residue, and O-glycosylation. ESI-MS was used to characterize legume plant lectins that commonly undergo C-terminal proteolytic processing to ragged ends, previously undetected by SDS–polyacrylamide gel electrophoresis (*81*).

The sensitivity of these mass spectrometric methods has opened many applications in biochemical research. Smith and co-workers have used ESI–MS and capillary electrophoresis to detect hemoglobin protein from a total of 10 red blood cells (*82*). Researchers have applied MALDI–MS to characterize peptide profiles directly from single neurons and nerve tissue (*83, 84*).

Other classes of biomolecules are amenable to analysis by mass spectrometry with ESI and MALDI. Oligonucleotides present a class very different from most peptides and proteins because of the nature of the molecule. In solution, nucleic acids are the most polar of the biomolecules. Because of the low pK_a of the phosphate backbone, every phosphate should be negatively charged in solution. The tenacity of oligonucleotides for sodium and magnesium binding is known to DNA/RNA scientists and to every mass spectrometrist who has handled these materials. This problem is illustrated in Figure 5 for an oligoadenylic acid sample analyzed by ESI–MS. However, once these features are factored in by the analyst, the measurement of molecular masses by ESI–MS and MALDI–MS can be nearly as straightforward as protein analyses.

Early reports of DNA and RNA analysis by electrospray mass spectrometry demonstrated that samples as large as 26 kDa 76-mer transfer RNAs can be measured (*14*). However, accurate mass measurement was problematic because of the heterogeneous nature of binding of salt, i.e., lower charge state ions showed more cation adduction than the higher charge states. Furthermore,

for the larger DNA and RNA samples, peaks due to sodium adduction were unresolved with quadrupole instruments. For these types of samples, mass accuracies of 0.1% or worse were typical. More recent reports have focused on methods to remove interferences from cation adduction, including extensive cold ethanol precipitation (*85*), addition of chelating agents such as CDTA, and addition of organic bases to the solution such as triethylamine and piperidine (*86, 87*). Removal of salts from the oligonucleotide samples has greatly improved the mass measurement accuracies to levels enjoyed by protein measurements, ±0.05−0.01%.

Matrix-assisted laser desorption ionization MS has also demonstrated enormous potential for oligonucleotide analysis. As with ESI, alkali salt adduct formation has also been problematic for MALDI, yielding poor resolution and low signal-to-noise. Methods to remove alkali salt interferences, including replacing sodium with the more volatile ammonium salt and a quick method involving the addition of a few beads of a polymeric cation-exchange resin in the NH_4^+ form to the analyte solution (*88*), have greatly improved the analysis of large oligonucleotides by MALDI−MS. In addition, using matrices optimized for oligonucleotide analysis, such as 3-hydroxy-picolinic acid for UV−MALDI−MS and succinic acid for IR−MALDI−MS, have improved detection limits and the molecular weight range. Nordhoff et al. published a spectrum of a 104-mer RNA sample (33 kDa) from 5 pmol loaded onto the sample probe (*59*). Lubman and co-workers used a Nafion substrate to detect ions for restriction enzyme digested double-stranded DNA plasmid up to a 267 base pair DNA sample (*89*). Mass spectra of DNA (*90*) and RNA (*91*) with molecular weights up to 150 kDa have been published. Stability of these large ions in the desorption/ionization process is still a problem. However, the significance of these results has not escaped researchers interested in developing high speed methods for sequencing DNA.

Another major class of biomolecules that has been analyzed by ESI and MALDI−MS are glycoproteins, carbohydrates, and complex oligosaccharides. The carbohydrate functionalities of glycoproteins are interesting because of their possible function. Characterization of the carbohydrate moiety of recombinant glycoproteins presents a significant challenge because the cDNA sequence provides little information regarding glycosylation and predicts only positions of potential sites of N-glycosylation. Moreover, although the molecular weight of most carbohydrates is relatively small compared to proteins (less than 10 kDa), the complexity from the numerous possible glycan linkages and branching patterns provides a considerable challenge for structure elucidation. Reinhold and co-workers (*92*) have recently published a thorough review of the application of ESI-MS for carbohydrate structure analysis, highlighting several of the many examples from their laboratory with an emphasis on glycolipids and glycoprotein glycans. ESI with MS/MS can provide information on sequence, linkage, and branching.

MALDI−MS has also been utilized for examining complex oligosaccharides. Hillenkamp's group (*93−95*) and others (*96*) demonstrated very early in the development of MALDI that carbohydrate analysis is viable. Mixtures of oligosaccharides from a variety of glycoproteins (e.g., ovalbumin, fetuin) were analyzed by Harvey et al. using MALDI and both time-of-flight and magnetic sector mass spectrometers (*62*). Martin and co-workers found that metastable decompositions result in ions representing the loss of hexose (Hex) and *N*-acetyl-

hexosamine (HexNAc) species could be used to provide structural information (*97*).

B. Structure Determination. An accurate molecular weight measurement provides some degree of confirmation for identity of the target molecule. However, a more complete indicator is to determine the sequence of the macromolecule. Although the speed and sensitivity of sequencing by conventional gas phase sequencers relying on Edman chemistry has been improving, tandem mass spectrometry (MS/MS) (*98, 99*) is also well established for peptide sequencing, especially for N-terminally blocked peptides, materials containing unnatural amino acids, and post-translationally-modified molecules. In combination with chemical and proteolytic digestion, protein sequencing by MS/MS can be a sensitive and powerful methodology (*100, 101*).

ESI−Tandem Mass Spectrometry and Peptide Mapping. Tandem mass spectrometry, as the phrase signifies, involves the coupled use of two stages of mass analysis. The first stage is used to select an ion (precursor ion) from which further structural information is to be obtained. The precursor ion is allowed to fragment by transfer of energy to the ion by a variety of means, including collisions with a background gas (e.g., argon, helium) or radiation from a laser (photodissociation). The second stage of mass analysis is used to detect and measure the mass of the resulting fragments or product ions.

The generation of multiply charged ions by electrospray ionization (ESI) has allowed the application of tandem mass spectrometry to larger biomolecules because of the higher collision cross sections and increased electrostatic forces. Collisionally activated dissociation (CAD) efficiency of *singly* charged molecules with molecular weight less than 2000 Da is generally higher for high energy (keV) collisions versus low energy (<500 eV) collisions. However, application of low energy CAD for *multiply* charged molecules can be used to generate sequence ions for larger polypeptides, as demonstrated by Loo et al. (*102*) and McLafferty and co-workers (*103*) in the CAD spectra of 66 kDa albumin proteins.

Figure 8a is a ESI tandem mass spectrum for the peptide bradykinin (1060 Da). In this experiment, the first mass spectrometry stage was used to select the (M + 2H)$^{2+}$ ion as the precursor ion for further dissociation. The doubly charged ion at m/z 531 then undergoes dissociation from collisions with a background gas. A second stage of mass spectrometry is used to measure the masses of the resulting fragments shown in Figure 8a. The nomenclature used to identify the peptide cleavage products has been described by Biemann (*101*). In short, fragment ions with the charge residing on the N-terminus of the peptide are denoted as a_n, b_n, and c_n product ions and fragments with the charge residing on the C-terminus are identified as x_n, y_n, and z_n ions, where n designates the residue number (counting from the N- or C-terminus, respectively). For example, the b_6 ion represents cleavage of the −CO−NH− bond between Ser-6 and Pro-7, with the positive charge retained on the N-terminus. A y_3 product ion is formed from cleavage of the same bond between Ser-6 and Pro-7 but the charge resides on the C-terminal fragment ion. Dissociation spectra of larger multiply charged molecules is similarly represented by the spectrum in Figure 8b for melittin, a 26 amino acid peptide (2845 Da). MS/MS of the (M + 3H)$^{3+}$ yields a series of 2+ y_n product ions, providing sequence information for a major portion of the molecule.

The application of tandem MS with electrospray ionization for protein sequencing has been demonstrated by many laboratories. The most effective method has been
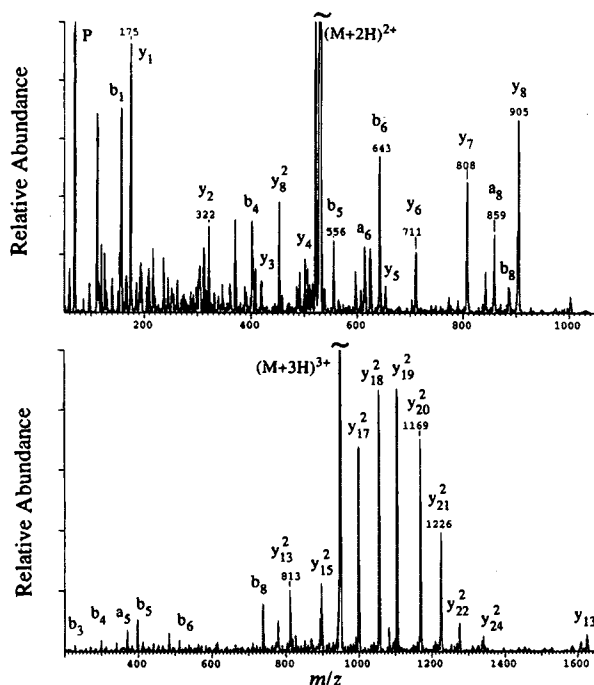
Figure 8. Electrospray ionization MS/MS spectra of the (M + 2H)$^{2+}$ ion of bradykinin (1060 Da) and the (M + 3H)$^{3+}$ ion of melittin (2845 Da). A magnetic sector-quadrupole hybrid mass spectrometer was used to acquire the data.

to combine chemical or proteolytic digestion with MS/MS. Tandem MS of tryptic peptides is very efficient because a basic residue (Arg or Lys) resides at the C-terminus and the amino-terminus is basic and unblocked, yielding a 2+ precursor ion. Dissociation of the 2+ ion produces easily interpretable singly charged fragments. Further combination with chromatographic separations (digestion → LC/ESI/MS/MS) provides a very powerful and rapid methodology for protein sequencing.

Identifying the sites of post-translational modifications is an important application of MS and tandem mass spectrometry (*104*). Methods to selectively detect phosphopeptides (*105*) or glycosylated peptides (*106*) using LC−ESI tandem mass spectrometry have been developed. Phosphopeptides containing phosphoserine, phosphothreonine, or phosphotyrosine yield fragment ions at m/z 63 (PO$_2^-$) and m/z 79 (PO$_3^-$). Glycosylated peptides are identified by a diagnostic m/z 204 (HexNAc$^+$) fragment ion. Selective monitoring of these diagnostic ions during an LC−MS/MS experiment of a digested protein mixture can be a sensitive and time-saving procedure for identification of sites of modifications. This combination of selective proteolysis, chromatography, and ESI−MS/MS has been used to locate the sites of phosphorylation of rhodopsin (*107, 108*).

Not long after the development of ESI−MS, there was considerable application of ESI−MS as a tool to investigate the mechanism of enzymes. Several research groups have used ESI−MS to detect covalent intermediates for a variety of enzymes. Covalent enzyme−inhibitor complexes for human leucocyte elastase (*109*) and β-lactamase (*110*) have been observed by electrospray MS. Furthermore, tandem mass spectrometry can then be used to locate the sites of enzyme modifications. The active sites of human glucocerebrosidease (*111*) and bacillus subtilis xylanase (*112*) were identified by using tandem mass spectrometry.

Peptide sequencing can be further improved by developing methods to minimize sample handling. Microscale reactors that have been interfaced to ESI sources have

been constructed. The direct incorporation of such on-line reactors with LC/ESI−MS and tandem MS has enormous potential for rapid protein sequencing. For example, Rosnack and Stroh (*113*) described a low-flow reactor for on-line ESI−MS monitoring of peptides digested with carboxypeptidase P for C-terminal sequence information. Up to the 30th residue (from the C-terminus) of myoglobin was determined by this method. Immobilized enzyme reactor columns have been described by a few reports. Davis et al. (*114*) reported the use of an immobilized trypsin column for the generation of tryptic peptides for cytochrome c and hemoglobin with subsequent ESI−MS analyses. By minimizing sample handling, subpicomole sensitivity for peptide sequencing by tandem mass spectrometry can be obtained. The microcapillary HPLC−ESI−MS/MS methods developed by Hunt and Shabanowitz have allowed their research group to sequence peptide antigens associated with class I and class II MHC molecules consuming less than 100 fmol of material (*115*).

The utility of ESI and tandem mass spectrometry for rapid sequencing of large oligonucleotides is demonstrated by the work of McLuckey (*116, 117*) and McLafferty (*118*). Although the tandem mass spectra appear to be relatively complicated, fundamental studies have established several common rules to guide interpretation. For example, oligonucleotide fragmentation is dominated by the stepwise loss of base followed by cleavage of the 3′ C−O bond of the relevant sugar (*117*). Extensive sequence information has been obtained for up to a 25-mer by ESI−MS/MS (*118*).

The future of tandem mass spectrometry may be represented by work from the Smith (*102, 119, 120*) and McLafferty (*31, 103, 121*) laboratories. Multiply charged ions for the intact protein can be subjected to collisionally activated dissociation to yield sequence informative product ions. Sequence information for proteins as large as 66 kDa serum albumin proteins from a variety of mammalian species have been obtained by direct MS/MS (*102, 103*). In a few cases, the sequence obtained from the N-terminus corrected errors in previously reported sequences. CAD mass spectra of multiply charged proteins have been compared between eight variants of the β-chain human hemoglobin polypeptide, whose modification covers various regions of the molecule (*77*). The application of high resolution MS with FTMS analysis greatly simplifies the enormous data interpretation challenge because product ion charge states can be directly identified by measuring the isotopic peak spacings. However, to date, a single MS/MS experiment for large peptides and proteins yields only a limited portion of the entire sequence. Also, the location of the fragmentation events is not predictable and is highly variable [although some common themes have been found, such as dissociation of bonds N-terminally located to a proline residue (*77, 120, 121*)]. In principle, instruments with MS^n capabilities such as FTMS and ion trap MS should be able to obtain greater amounts of sequence information through repetitive MS/MS stages.

Structure Determination by MALDI−MS. Prospects for using MALDI−MS to provide more structural details of macromolecules are encouraging. For example, Allison and co-workers (*122*) described a method that combines specific proteolysis, identification of the phosphopeptides after dephosphorylation by alkaline phosphatase, and determination of the phosphorylation sites by mass mapping with MALDI. Monitoring the products from enzymatic digestion by MALDI−MS is a simple and quick method to obtain structural information. Figure 9 shows the MALDI mass spectrum of a mixture of reaction

33mer (*M*r=10113) digest with Phosphodiesterase, type I

5'-GCCAGGGTTTCCCAGTCACGATGCAGAATTCA-3'
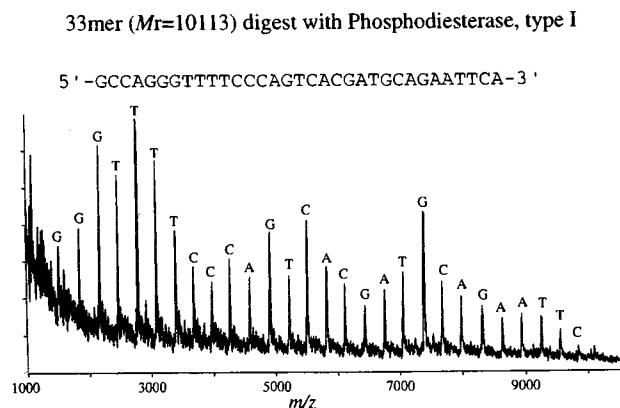
Figure 9. MALDI mass spectrum (with delayed extraction) of phosphodiesterase (type I) digestion of a 33-mer DNA sample (figure provided by Dr. Steve Martin, PerSeptive Biosystems, Framingham, MA).

PSD Spectrum of Renin Inhibitor
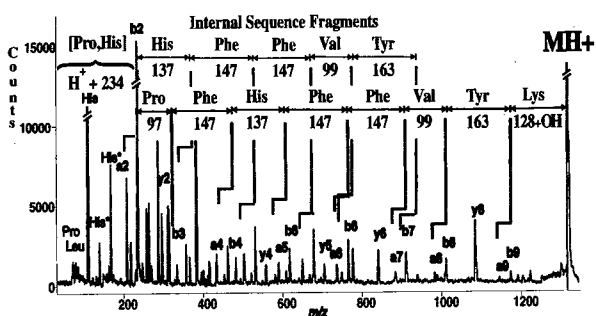
Figure 10. MALDI post-source decay fragmentation spectrum of renin inhibitor (PHPFHFFVYK, M_r 1318.5) (figure provided by Drs. Steve Martin and Wade Hines, PerSeptive Biosystems, Framingham, MA).

products resulting from exonuclease sequencing of a 33-mer DNA sample. The sequence for 28 out of 33 total residues can be easily read from a single mass spectrum.

However, gas phase fragmentation of MALDI-produced ions with subsequent mass analysis is also possible. Biomolecular ions may undergo fragmentation from multiple collisions with matrix and background molecules as they travel toward the detector in a TOF instrument. These product ions resulting from "post-source decay" (PSD) can be analyzed to provide a mass spectrum similar in appearance to a MS/MS spectrum (*123*). Figure 10 is a post-source decay MALDI mass spectrum of the decapeptide, renin inhibitor. Series of a_n, b_n, and y_n product ions from dissociation of the $(M + H)^+$ ion are produced.

A potentially rapid and sensitive method for sequencing peptides and proteins involves a modification of traditional gas phase Edman chemistry. The N-terminus of a peptide reacts with phenyl isothiocyanate (PITC) and in acidic solution and eventually forms the 3-phenyl-2-thiohydantoin (PTH) derivative and a peptide shortened by one amino acid. The PTH amino acid is extracted and identified by HPLC. Chait and co-workers (*124*) have described a novel twist to this automated procedure in which MALDI mass spectrometry is used to identify the resulting peptide which has been shortened. However, by introducing a small amount of a terminating reagent, such as phenyl isocyanate, into the reaction, a small amount of peptide is N-terminally blocked in each cycle and protected from further degradation. The cycle is repeated a defined number of times without analyzing for the resulting PTH amino acids. This procedure results in a nested set of peptides, or ladder sequence,
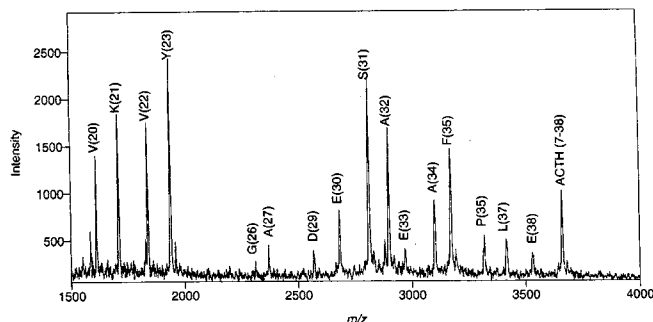
Figure 11. MALDI-MS peptide ladder sequencing of ACTH fragment 7–38 (M_r 3659) (figure provided by Dr. Steve Martin, PerSeptive Biosystems, Framingham, MA).

where adjacent mass peaks differ by one amino acid (*125*). To date, MALDI–MS sequencing of peptides and phosphopeptides less than 20 residues have been demonstrated by this method. However, in principle, much longer sequences should be amenable to this methodology in a more rapid fashion than conventional Edman sequencing (*124–126*), as demonstrated in the partial mass spectrum in Figure 11. Ladder sequencing of peptide ACTH fragment 7–38 results in the generation of peptide fragments whose mass defines the sequence of the parent peptide.

C. Separation Methods with Mass Spectrometry. *Liquid Chromatography and Capillary Electrophoresis with Mass Spectrometry.* Although the analysis of complex mixtures is a strength of the MS method (because individual m/z's are measured), it is often desirable to perform a high resolution separation prior to mass spectral analysis of biological materials to reduce the complexity of the experiment. Salts and buffers that can interfere with the MS analysis can be removed with an on-line separation step. The amount of sample may be limited and multiple purification stages are often precluded, necessitating an on-line measurement. Practical incentives exist to conduct biochemical research on the smallest scale possible. It is not surprising, therefore, that combined separations–MS analysis is of broad interest and that greater sensitivity is almost always desired. Any technique reducing the number of sample handling steps is almost universally advantageous.

Liquid chromatography is a mainstay of biochemical analysis. Microbore and microcapillary liquid chromatography are particularly well adapted to ESI because of their low flow rates (*39, 40, 127–132*). Larger column and larger flow rate chromatographic methods can also be amenable without the need for flow splitting with some of the advances in "megaflow" ESI sources (*133, 134*). The use of LC/ESI–MS for analysis of protein enzymatic digests and peptide mixtures has attracted great interest, particularly because sufficient sensitivity exists to allow on-line MS/MS of separated polypeptides (e.g., tryptic fragments). Many of the examples cited in previous sections of this review used LC/ESI–MS and MS/MS as the basis of their work. This hyphenated technique is now a common and accepted tool for biochemical research.

A less common separation methodology for on-line interfacing to mass spectrometry, but potentially more powerful is capillary electrophoresis (CE) in its various formats (zone electrophoresis, isotachophoresis, isoelectric focusing, polyacrylamide gel, micellar electrokinetic "chromatography") (*135*). CE allows for rapid high-resolution separations of very small sample volumes of complex mixtures. Combination with the inherent sensitivity and selectivity of mass spectrometry makes CE/MS a powerful bioanalytical technique (*136–138*). The

correspondence between CE and ESI flow rates and the fact that both are primarily used for ionic species in solution provide the basis for facile combination. Small peptides and proteins are easily amenable to capillary zone electrophoresis with ESI—MS analysis with good reproducibility (*50, 139*). Detection limits to the attomole regime (10^{-18} mol) have been reported with this combination (*140*).

While on-line separation methodologies can reduce overall analysis time and sample handling, off-line MS analysis of separation effluents offers an easy to implement technique, especially with MALDI—MS. For laboratories with only MALDI—MS capabilities, capturing LC fractions and applying a small aliquot to the MALDI target stage for mass analysis is a relatively quick and simple tool. Additional sample chemistry (e.g., digestion, reduction, alkylation, etc.) can be performed on the same sample spot to provide more structural information. MALDI—MS of CE effluents have also been demonstrated (*141–143*), with detection limits to the low picomole levels.

MS from Gel Electrophoresis Separations. Despite the superior mass accuracy of MALDI versus the 1–2% (occasionally much lower) accuracy common to sodium dodecyl sulfate—polyacrylamide gel electrophoresis (SDS—PAGE), electrophoresis of proteins will not be quickly supplanted by mass spectrometry alone. PAGE offers too much value and simplicity as an analytical and preparative technique. Two-dimensional gel electrophoresis, combining isoelectric focusing in one dimension with SDS—PAGE in the other dimension, is the premier technique for separating complex mixtures. Two thousand separate spots can be visualized from a 2-D gel, and it can be used to screen for proteins affected by disease states or perturbed in other ways. Two-dimensional gels become still more important as the genome project progresses and DNA sequences accumulate in databases. Gel spots must be mapped and identified to locate the products for which those gene sequences code. Traditional mapping methods, digests combined with Edman sequencing, are slow and require preparative amounts of material. Obtaining mass spectra from electrophoretic gels has become an important goal for mass spectrometrists.

Efforts to obtain mass spectra from gel-purified samples have mostly centered around examining the peptide products from enzymatic digests (*144–149*). In many studies, proteins were electroblotted to membranes such as PVDF or nitrocellulose, digests were performed on-membrane, and the peptides were extracted, purified by HPLC, and examined by MALDI or ESI (*150*). In other modifications, digests were performed in-gel (*147, 151*), or HPLC purification was omitted before MALDI analysis (*145–147, 149*). Proteins have been transferred by electroelution followed by solution digests (*148*). Finally, results have also been obtained by dispensing with the extraction and HPLC-cleanup steps, instead analyzing peptides directly off the membrane with MALDI (*144*). Databases can be searched for peptide masses allowing rapid identification of gel spots (*149–153*).

Mass analyses of intact proteins isolated from gels by either electroelution (*154, 155*), electroblotting (*156, 157*), or extraction (*158*) have also been explored by a few laboratories. A MALDI comparison using both infrared and ultraviolet lasers (*157*) found that infrared lasers performed better than UV lasers for desorption from electroblotted membranes, probably because of their larger penetration depth; it is thought that the proteins deeply penetrate the pores of the membrane during electroblotting. This superiority of infrared lasers is
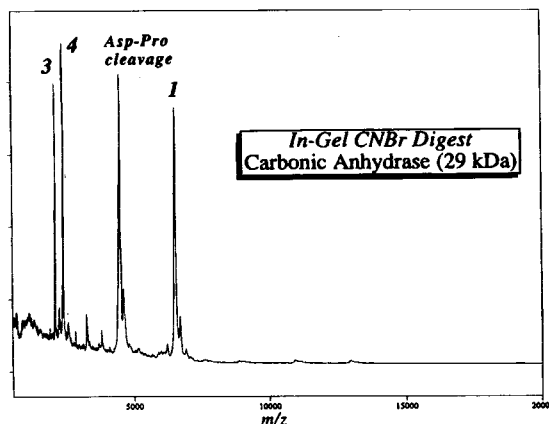
Figure 12. MALDI mass spectrum resulting from the in-gel cyanogen bromide digest of bovine carbonic anhydrase (29 kDa). Approximately 138 pmol of protein was loaded onto an IEF gel. The protein spot was digested with CNBr, and a mass spectrum was subsequently obtained directly from the spot.

unfortunate in that nearly all MALDI systems currently in use are equipped with UV lasers.

Recently, a streamlined approach to the mass spectrometric analysis of electrophoretically-isolated proteins has been developed (*159, 160*). By using thin layer gels, mass analysis of proteins directly from isoelectric focusing (IEF), native, or SDS gels, without electroblotting or electroelution, has been achieved. Digests may be performed in-gel with subsequent mass analysis, or membrane transfers can be accomplished by diffusive transfer. Transfer by passive diffusion allows alternative membranes such as polyethylene or Teflon to be employed. Figure 12 illustrates a spectrum obtained by this method from an in-gel CNBr digest of bovine carbonic anhydrase. Three of four predicted products are observed, as is the product of an acid-labile (Asp-Pro) bond cleavage.

D. Studying Molecular Interactions with Mass Spectrometry. *Noncovalent Interactions.* A more recent application of mass spectrometry is the study of biochemical interactions. Many types of protein—ligand binding are examples of intermolecular noncovalent interactions, including antibody—antigen, protein—cofactor, receptor—ligand, and enzyme—substrate pairings. Intermolecular noncovalent interactions are responsible for aggregation of folded polypeptide chains into multimers which determines a protein system's quaternary structure. Studying the nature of the interactions that maintain the quaternary structure of enzymes is essential for the understanding of cellular functions at the molecular level. Mass spectrometry experiments with protein oligomers can yield information on both the stoichiometry and molecular nature of subunit interactions.

When studying the physical interactions of a molecule or ion with a protein or other macromolecule, biochemists want to know, "How many? How tightly? Where? Why?" In order to answer these questions, one must determine whether the mass spectral data truly reflect the *solution* chemistry of the system or at least to what extent. Mass spectrometry is a powerful technique for analyzing *gas* phase molecules, but it also may eventually provide insight in the *solution* phase structure of biological molecules.

ESI is truly a gentle ionization method, yielding no molecular fragmentation (unless induced in the ESI atmosphere/vacuum interface) and allowing weakly bound complexes to be detected intact. There have been several examples of ESI—MS detection of noncovalently-bound complexes since the initial reports by Ganem and co-

Table 2. Noncovalent Biomolecular Complexes Observed by ESI−MS

molecular systems	comments and refs
peptide/protein complexes	
peptide multimers	*210, 211*
antisense peptide dimers	*212*
leucine zipper peptide dimer	*213*
ribonuclease *S*-protein/*S*-peptide	*165, 214*
Src SH2 domain−phosphopeptide inhibitors	*172, 215*
albumin−growth hormone releasing factor	*216*
polypeptide−metal ions	
angiotensin peptides−zinc	*217*
rubridoxin−iron	*218;* zinc (*190*)
ferredoxin−iron	*218*
metallothionein−transition metals	*189, 219*
histidine-rich glycoprotein−copper	*187*
estrogen receptor DNA-binding domain−copper/zinc	zinc finger protein (*185, 186, 188*)
nucleocapsid protein (NCp7)−zinc	zinc finger protein (*220, 221*)
cytochrome c oxidase subunit−copper	*222*
calmodulin−calcium	EF-hand protein (*191, 223*)
parvalbumin−calcium	EF-hand protein (*191, 223*)
stromelysin catalytic domain−zinc, calcium	*191*
glucocorticoid receptor DNA binding domain−zinc	zinc finger protein (*224*)
SPARC peptide−copper	extracellular matrix-binding protein (*225*)
lysozyme−copper, zinc	*226*
protein−small molecule	
peptide−antibiotics	vancomycin, ristocetin (*173*)
globin−heme	myoglobin (*46, 163, 218, 227−232*); hemoglobin (*46, 161, 229*)
FKBP−FK506, rapamycin	receptor−ligand (*161, 216, 231, 233, 234*)
albumin−FK506/FK520	*235*
lysozyme−*N*-acetylglucose hexasaccharide	enzyme-substrate/enzyme product (*162, 231, 234*)
avidin/streptavidin tetramer−biotin	*167, 168*
methionine synthase−cobalamine	*236*
catalytic antibody (single chain)−hapten	*237*
HIV-1 protease dimer−inhibitor	*238*
elastase−peptidic substrates/products	*239*
antithrombin III−heparin fragment	glycoprotein−pentasaccharide complex (*240*)
quaternary structure complexes	
HIV-1 protease	dimer (*238*)
avidin	tetramer (*167*)
streptavidin	tetramer (*168, 170*)
concanavalin A	tetramer (*46, 167, 169*)
hemoglobin	dimer/tetramer (*46, 167*)
alcohol dehydrogenase (ADH)	horse ADH, dimer; yeast ADH, tetramer (*171*)
pyruvate kinase	tetramer (*171*)
soybean agglutinin	tetramer (*53*)
gp45	dimer (*241*)
Transthyretin	tetramer (*242*)
nucleic acid complexes	
ribonuclease A−CMP	*243, 244*
aldose reductase−NADP+	*245*
ras−GDP	*246, 247*
adenylate kinase−AMP	*227*
Actinomycin D−ssDNA	*248*
DNA duplex	8-mer (*177, 231*); 20-mer (*174, 179*); 10-mer/20-mer (*178*)
DNA duplex−drug	12-mer/distamycin A (*175*)
DNA quadruplex	*176*
DNA−bis PNA	peptide nucleic acids (*249*)
gene V protein−DNA	protein dimer (*183, 184*)
others	
β-cyclodextrin inclusion complexes	piroxicam (antiinflamitory), terfenadine (antihistaminic) (*250*); Phe (*251*); Phe, Trp, bradykinin (*252*); amyloid protein (*253*); ephedrinium trifluoroacetate (*254, 255*); Phe and Trp methyl esters, propanolol (*256*)
calix[4]arenes−alkylammonium ions	host−guest (*257*)
commelinin	supramolecular pigment (*258*)
ferrichrome A analogue−iron	bacterial siderophore (*218*)
Le x glycosphingolipid and trisaccharide dimer−calcium	*259*
supramolecular assemblies	hydrogen bonded (*260, 261*)
capped polymetallic complex	*262*

workers (*161, 162*) on receptor−ligand and enzyme−substrate complexes and later by Chait's group (*163*) on the globin−heme interaction of myoglobin. Table 2 is a representative list of the many electrospray ionization MS studies of noncovalent complexes reported in the literature. Evidence is building that the observations

made by ESI−MS for these weakly-held systems reflects to some extent the nature of the interaction found in the solution phase. However, as Smith and Light-Wahl (*164*) point out, control experiments are necessary to rule out ubiquitous nonspecific interactions (i.e., nonspecific aggregation). For example, for a variety of ligands of

different binding strengths available for testing, the protein−ligand interaction found in the ESI−MS experiment should reflect the expected solution phase measurements. This was found for the ribonuclease *S*-protein/*S*-peptide system studied by Ogorzalek Loo et al. (*165*), where the protein−peptide complex with an *S*-peptide analog showed a weaker attraction as expected from solution phase binding experiments.

Multimeric proteins present an opportunity for ESI−MS to study very large molecular weight complexes. Many enzyme systems are composed of identical and nonidentical subunits that associate together to form the fully active species. "Quaternary ensembles of subunits provide a plan of macromolecular architecture with unique advantages in structure and in potential for flexibility in behavior and regulation." It is of general importance to obtain information regarding the self-assembly process of such systems such as subunit stoichiometry of the complete quaternary ensemble. Subunit interactions have been traditionally studied by techniques such as ultracentrifugation, gel permeation, size exclusion chromatography, X-ray crystallography, and nuclear magnetic resonance spectroscopy. Farmer and Caprioli have reported the utility of MALDI−MS for studying glutaraldehyde-crosslinked dimeric and tetrameric protein complexes (*166*).

Protein subunits are likely held together by intermolecular forces including hydrogen bonding and hydrophobic and ionic interactions. The gentleness of the electrospray ionization/desorption process enables weakly-bound complexes to remain intact upon transfer to the gas phase. Smith and co-workers (*164, 167−170*) and others (*46*) have presented ESI-MS results on tetrameric protein complexes such as avidin (64 kDa) and concanavalin A (102 kDa) (see Table 2). In these experiments, only monomer, dimer, and tetramer associations were observed. The absence of trimer and pentamer species suggests that the ESI-MS data reflect the specific solution phase interactions known to occur. Furthermore, Loo (*171*) reported results for alcohol dehydrogenase (ADH) proteins. The largest complex observed for horse liver ADH was the dimer (80 kDa), whereas the tetramer was observed for yeast ADH (147 kDa), again consistent with solution phase studies.

Evidence is mounting that suggests that under carefully controlled experimental conditions, the data from gas phase ESI−MS experiments on noncovalently-bound systems reflects the associations found in solution. Furthermore, ESI−MS can be used to determine the strength of these interactions. The binding of various peptide inhibitors to src SH2 (Src homology 2) domain protein (12.9 kDa) was examined by Loo and co-workers (*172*). SH2 motifs in proteins are critical in the signal transduction pathways of the tyrosine kinase growth factor receptors. SH2 domains bind to the phospho-tyrosine-containing growth factor receptors. Figure 13 shows the ESI mass spectrum of the src SH2 domain protein complex with the phosphopeptide, Ac-QpYEEIP-amide (*172*). From a mixture of several peptide inhibitors where the total peptide concentration is much greater than the protein concentration, the relative abundances of the src SH2 protein−phosphopeptide complexes observed in the ESI mass spectrum are consistent with their measured solution phase binding constants. Henion's group (*173*) recently demonstrated that data from ESI−MS experiments can be used to construct Scatchard plots for measuring the binding constants of vancomycin antibiotics with tripeptide ligands. Their gas phase results were in reasonable agreement with previously reported values.
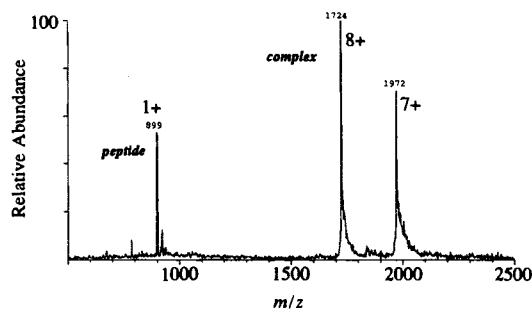
Figure 13. ESI mass spectrum of the 1:1 noncovalent complex between src SH2 domain protein (12.9 kDa) and the phosphopeptide Ac-QpYEEIP-NH$_2$ (*172*).

Nucleic acids and proteins are the principle polymeric components of biological systems. Their molecular structures have evolved in association with each other, and it is apparent that they are completely interdependent in a functional manner. The expression of the genetic information found in nucleic acids is dependent upon the specificity of their interaction with proteins. Thus, the development of techniques to study and understand the molecular details of protein−nucleic acid interactions has broad interest. ESI−MS of duplex DNA complexes was first demonstrated by the Smith group (Table 2) (*174, 175*). Only the complementary strands were found to form the complexes (after annealing) as expected. Later, the formation of specific quadruplex complexes in the presence of metals was studied (*176*). There have been several reports from other laboratories using ESI−MS to study DNA−DNA associations, as listed in Table 2 (*177−179*).

To characterize the noncovalent interactions between proteins and their nucleic acid substrates, both MALDI and ESI−MS have been applied. Although the MALDI process does not typically allow for survival of an intact noncovalently-bound complex, the use of crosslinking methods to form covalent bonds between interacting macromolecules is a viable method for MALDI−MS analysis. Barofsky and co-workers have reported on the MS characterization of UV-cross-linked protein−nucleic acid complexes (*180, 181*). Covalent bond formation between amino acids and nucleic acid residues in close proximity occurs upon UV irradiation (and sometimes in combination with a photoaffinity labeled substrate). Covalent protein−DNA complexes studied by the group include phage T4 gene 32 (gp32) single-stranded DNA-binding protein:(dT)$_{20}$ (*180*), transcription termination factor rho (single-stranded RNA-binding protein):4-thio-UDP (*180*), and DNA−repair enzyme uracil−DNA glycosylase (Ung):(dT)$_{20}$ (*181*). Stoichiometry of the interaction is readily assigned by the MALDI mass spectra. Furthermore, the sites of interaction for the Ung:DNA complex have been localized by proteolysis of the UV-cross-linked complex. Mass analysis of the proteolytic peptides still bound to DNA can define the DNA-binding domain of the native protein. A similar study was recently reported by Cohen et al. (*182*), in which the solution phase structure of the transcription factor DNA-binding protein, Max, was characterized. However, no covalent bond formation was used. Instead, the results from the limited proteolysis of the protein both in the absence and presence of DNA were evaluated to provide information about cleavage site accessibility. Protein regions that are buried or are involved in protein−protein or protein−DNA interactions should be protected from proteolysis.

The observation of a noncovalent protein−DNA complex by ESI−MS was recently reported (*183, 184*). Figure
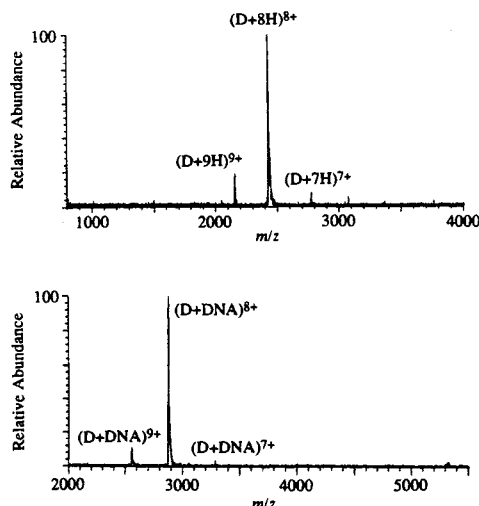
Figure 14. ESI mass spectra obtained with a Fourier transform mass spectrometer of gene V protein in 10 mM NH4OAc, showing multiply charged ions for the protein dimer (D) (top) and the gene V-oligonucleotide complex with 5'-AACGTTCT-GATC-3' (bottom) (*183, 184*) (figure kindly provided by Drs. Steven Hofstadler and Richard Smith, Pacific Northwest Laboratory, Richland, WA).

14 shows the ESI mass spectra of gene V single-stranded DNA binding protein (9.7 kDa). Gene V protein exists as a homodimer under physiological conditions; the protein dimer binds to DNA with a 1:1 stoichiometry for every eight bases of DNA. The top spectrum (Figure 14) shows the ESI mass spectrum of the protein dimer. Addition of a solution of a 12-mer DNA yields the exclusive formation of a protein dimer–DNA complex, consistent with NMR and gel-shift assays. Experiments with a larger 18-mer DNA sample produces the complex composed of a pair of protein dimers bound to 1 DNA molecule, again consistent with the known solution binding stoichiometry (*183, 184*).

Metal Binding Proteins. The interaction with metal ions, essential to catalytic function and structural stability, is an integral component of many enzymes (metalloenzymes). Techniques used to study the interaction between metal ions and biological materials include absorption spectroscopy, circular dichroism, and electron paramagnetic resonance spectroscopy and nuclear magnetic resonance (NMR) spectroscopy. A rapidly emerging method for investigating interactions between metal ions and biological molecules is mass spectrometry. To detect these interactions by mass spectrometry, a methodology is needed to transfer the interacting complex from an aqueous environment to the gas phase without disrupting or changing the *specificity* of the association in solution. At the very least, for the method to provide useful information to the protein scientist, the data from a mass spectrometry experiment should *correlate* well to the solution-phase interaction.

The potential of ESI–MS to determine peptide–metal ion stoichiometry in a rapid and sensitive fashion is promising. The ESI–MS results of Hutchens and co-workers (*185–188*) investigating the interactions of Cu^{2+} and Zn^{2+} to cysteine (sulfur)- and histidine-containing polypeptides suggest that ESI mass spectra reflect the *specific* association of the metal(s) to the peptide and can clearly be differentiated from nonspecific interactions due to clustering or adduct formation. Fenselau and coworkers (*189*) developed an ESI–MS strategy that provides analysis of metal ions in native and reconstituted metallothionein proteins. Acidic iron-binding proteins have also been investigated by ESI–MS (*190*). Intact

metal-loaded proteins were detected by negative ion ESI–MS. Hu et al. (*191*) described the application of ESI–MS to determine the calcium binding stoichiometry of Ca^{2+}-binding EF-hand proteins. Bovine calmodulin, bovine α-lactalbumin, and rabbit parvalbumin were found to bind specifically to four, one, and two Ca^{2+} ions, respectively, in agreement with previously reported results obtained by other physical methods. Many more examples are provided in Table 2.

Immunoaffinity Mass Spectrometry. The specificity of biochemical interactions has been exploited by physical methods such as affinity chromatography. The use of antibodies that are selective to an antigen is an important technique to separate and purify known substances from a complex mixture. Recently, the combination with MALDI–MS has proven to be a selective and sensitive detection method. There are several variations of the technique that have been reported. Hutchens and Yip modified the MALDI probe surface by attachment of the affinity-capture medium (*192*). A demonstration of their method called SEAC (surface-enhanced affinity capture) was provided by the selective detection of the 80 kDa glycoprotein lactoferrin from an infant urine sample by using a MALDI surface composed of porous agarose immobilized with single-stranded DNA as the affinity-capture medium. Tomer and co-workers have analyzed materials eluted from an immobilized metal ion affinity column and have also used MALDI–MS to directly analyze proteins bound to monoclonal antibody-bound stationary phases (*193*). Nelson et al. have refined the method and have pointed out another advantage with MALDI–MS detection: the capability to screen for multiple antigens in a single assay (*194*). Multiple antibodies can be used in a single experiment. The mass spectrometer can measure each individual antigen in a single spectrum at distinct *m/z* values. This was demonstrated in their example of selective detection of several venom proteins doped in a whole blood matrix (*194*).

Determining the antigenic site or epitope, the specific region of the protein in intimate contact with the antibody, has been the subject of recent reports. In a manner similar to that used to map out the protein sites in contact with an interacting DNA (see above), Tomer used MALDI–MS to map out the regions of gastrin-releasing peptide that are protected by the immobilized monoclonal antibody from proteolysis from trypsin, chymotrypsin, thermolysin, and aminopeptidase M (*195*). In a similar manner using multiple enzymes, Zhao and Chait mapped the epitope of melittin and glucagon-like peptide-1 (*196*). The peptide binding regions were identified by immunoprecipitation of the peptide fragments from the proteolytic mixture and MALDI-MS.

E. Studying Protein Conformation. Knowledge of a protein's three-dimensional structure is important for understanding and predicting its function in biological systems. The hydrogen exchange kinetics of a protein are sensitive to its structure in solution. Exchanging deuterium for labile hydrogens and monitoring the degree and rate of exchange is a well-established tool in protein structural studies. The hydrogen/deuterium (H/D) exchange rates for amide protons are influenced by the secondary and tertiary structure of a polypeptide. Hydrogen bonds of α-helices and β-sheets must break to allow exchange. Protection against exchange results from reduced exposure to solvent as well as from hydrogen bonding. Exchange rates of individual amide protons can be measured by nuclear magnetic resonance (NMR) spectroscopy to provide information regarding the dynamical processes of protein folding. Mass spectrometry can also provide important information regarding protein

conformation by monitoring the degree of deuterium exchange as a function of time. Internal hydrogens will less likely be exposed to the deuterated environment; therefore, no exchange will occur or exchange will occur at a much slower rate than for the more labile hydrogens on the surface of the structure. By measuring the mass shift caused by the incorporation of deuterium atoms (1 Da increase per hydrogen exchanged), the extent of H/D exchange can be determined.

Methods using electrospray ionization−mass spectrometry have demonstrated the potential to provide information regarding a protein's higher order structure. For example, influential work by Radford and co-workers have used ESI−MS H/D exchange experiments to study the folding rates of hen egg white lysozyme (*197*) and to study the molecular interactions of the folding-assistance protein, chaperonin GroEL (*198*). Chaperonin proteins are thought to assist proteins fold to their native-like states. By starting with a deuterated form of α-lactalbumin complexed to GroEL in solution, hydrogen exchange is initiated by introducing H_2O. The dissociated gas phase complex is monitored by mass spectrometry. In this fashion, the hydrogen exchange rate of α-lactalbumin complexed to GroEL can be measured as a function of incubation time in H_2O. This method was shown to provide new information about the conformational properties of the bound ligand. Studies by Anderegg and others have shown the application of electrospray ionization MS for determining the relative amounts of α-helices and β-sheets (*199, 200*).

Proteins can be denatured by a variety of methods, including the presence of high organic solvent content or a change in solvent pH. The resulting ESI mass spectra typically show an increase in average charge state for a denatured protein (*201*). As expected, data from ESI-MS H/D exchange experiments show a higher degree of deuterium incorporation for the protein in the denatured state (*202, 203*).

F. Combinatorial Libraries. Screening of large numbers of compounds has been the traditional method to identify novel lead compounds for drug discovery. The use of combinatorial chemistry to synthesize even greater numbers of compounds for screening is currently very popular with the pharmaceutical industry (*204*). The resulting vast mixture from these "libraries" are subjected to a target protein. The analytical characterization of these complex mixtures is a challenging task. Electrospray ionization MS is a useful method to identify potential problems in the synthesis of peptide libraries (*205*) and, in combination MS/MS, provides a rapid and reliable method to determine the composition (*206*). However, identification of the active compounds from these complex mixtures is a difficult task. Affinity column methods have been used to selectively isolate the active materials, which are then eluted off the column and identified by mass spectrometry. For example, an immobilized-src SH2 domain protein column coupled with HPLC-ESI mass spectrometry has been described by Kassel and co-workers to identify high affinity binding phosphopeptides (*207*).

Affinity capillary electrophoresis/MS (ACE/MS) is being developed as a method to identify candidate peptides from combinatorial libraries (*208*). The receptor is present in the capillary as part of the electrophoresis buffer. Ligands that interact tightly with the receptor will be retained as the unbound ligands travels through the column. Thus, the binding ligands will have slower electrophoretic mobilities relative to mobilities in the absence of the receptor. On-line ESI−MS is then used to identify the interacting ligand.

Youngquist et al. (*209*) described an elegant method that allows the identification and simultaneously, the sequence of an active peptide from resin-bound libraries. In a manner similar to the peptide ladder sequencing approach, a capping reagent is used to terminate the synthesis at each coupling step during the synthesis of the peptide library. The goal is to synthesize resin beads that carry not only the full length peptide, but also smaller amounts of the sequence specific termination products. The peptides from the active beads are chemically cleaved (by cyanogen bromide in this case) and analyzed by MALDI−MS. The mass spectrum contains an ion for the full-length active peptide, identifying the active compound, and ions for each shortened peptide. The mass difference between adjacent peaks provides the sequence of the active peptide.

CONCLUSIONS

The field of bioanalytical mass spectrometry is rapidly expanding in both applications and technology. While the complete field can not be covered in this article, there are a few generalizations about the current status of mass spectrometry. Classical biochemical methodologies can be enhanced with the incorporation of mass spectrometric experiments. The use of MS to monitor and identify proteolytic and chemical degradation products is a standard application. Using MS as an on-line detector for an immobilized enzyme column/HPLC experiment is an example of the symbiotic relationship between biochemistry and mass spectrometry. Another example of such a cooperative combination is the application of MS to gel electrophoresis. Proliferation of these types of new methodologies will increase in the next few years.

Electrospray ionization and MALDI are the two most popular desorption/ionization methods for biomolecule analyses. Over 50% of all presentations (out of over 1400) made at the most recent annual American Society for Mass Spectrometry (ASMS) conference used either ESI or MALDI or both techniques. It is difficult to predict whether another method will supplant these methods in the next decade or so. It is also difficult to choose which method to use for a biochemical analysis. In many respects, ESI and MALDI are complementary. Sometimes, for a particular sample, the ESI spectrum will indicate a different profile than the MALDI spectrum, depending on the sample conditions used, ionization efficiency for each analyte, etc. Of course, it is usually best to obtain a spectrum from both MS methods, if there is unlimited access to both methods. However, as found in human nature, people will have personal preferences for one method over another, but this will only serve to stimulate the further developments of ESI and MALDI. The developers of ESI−MS instrumentation will learn the reasons why the researchers using primarily MALDI−MS prefer "their" method, which will encourage the ESI camp to fix their "shortcomings", and vice versa.

It is increasingly difficult to keep up with all of the activity in the field. For those wishing to learn more about the new developments and applications of mass spectrometry, attending one the many scientific meetings and sessions devoted primarily to mass spectrometry is encouraged. The annual ASMS Conference is a week-long (and exhausting) meeting that presents the latest developments. Many academic and industrial institutions have either mass spectrometry facilities or biochemical core facilities with MS capabilities. The researchers in these facilities can be a useful source for information. "Cyberspace" is gaining popularity as a source for information regarding mass spectrometry.

There are several web-sites and news groups established by MS groups. Mass spectrometry vendors are also useful resources for learning more about what's hot in the field. The biochemical mass spectrometry community is a growing body that wishes to grow even larger. It can only do so by serving and listening to practicing biochemists for potential new applications.

ACKNOWLEDGMENT

LITERATURE CITED

(1) Karas, M., Bahr, U., Ingendoh, A., and Hillenkamp, F. (1989) Laser desorption/ionization mass spectrometry of proteins of mass 100 000 to 250 000 Dalton. *Angew. Chem., Int. Ed. Engl. 28*, 760–761.

(2) Hillenkamp, F., Karas, M., Beavis, R. C., and Chait, B. T. (1991) Matrix-assisted laser desorption/ionization mass spectrometry of biopolymers. *Anal. Chem. 63*, 1193A–1203A.

(3) Meng, C. K., Mann, M., and Fenn, J. B. (1988) Of protons or proteins. *Z. Phys. D: Atoms, Mol. Clusters 10*, 361–368.

(4) Fenn, J. B., Mann, M., Meng, C. K., Wong, S. F., and Whitehouse, C. M. (1990) Electrospray ionization-principles and practice. *Mass Spectrom. Rev. 9*, 37–70.

(5) Fenn, J. B., Mann, M., Meng, C. K., Wong, S. F., and Whitehouse, C. M. (1989) Electrospray ionization for mass spectrometry of large biomolecules. *Science 246*, 64–71.

(6) Barber, M., Bordoli, R. S., Elliott, G. J., Sedgwick, R. D., and Tyler, A. N. (1982) Fast atom bombardment mass spectrometry. *Anal. Chem. 54*, 645A–657A.

(7) Sundqvist, B., and Macfarlane, R. D. (1985) ^{252}Cf-plasma desorption mass spectrometry. *Mass Spectrom. Rev. 4*, 421–460.

(8) Taylor, L. C. E., Johnson, R. L., and Raso, R. (1995) Open access atmospheric pressure chemical ionization mass spectrometry for routine sample analysis. *J. Am. Soc. Mass Spectrom. 6*, 387–393.

(9) McCloskey, J. A., Ed. (1990) *Mass spectrometry*, Academic Press, San Diego, CA.

(10) Siuzdak, G. (1994) The emergence of mass spectrometry in biochemical research. *Proc. Natl. Acad. Sci. U.S.A. 91*, 11290–11297.

(11) Chait, B. T., and Kent, S. B. H. (1992) Weighing naked proteins: Practical, high-accuracy mass meassurement of peptides and proteins. *Science 257*, 1885–1894.

(12) Chait, B. T. (1994) Mass spectrometry—a useful tool for the protein x-ray crystallographer and NMR spectroscopist. *Structure 2*, 465–467.

(13) Senko, M. W., and McLafferty, F. W. (1994) Mass spectrometry of macromolecules: Has its time now come? *Annu. Rev. Biophys. Biomol. Struc. 23*, 763–785.

(14) Smith, R. D., Loo, J. A., Edmonds, C. G., Barinaga, C. J., and Udseth, H. R. (1990) New developments in biochemical mass spectrometry: Electrospray ionization. *Anal. Chem. 62*, 882–899.

(15) Smith, R. D., Loo, J. A., Ogorzalek Loo, R. R., Busman, M., and Udseth, H. R. (1991) Principles and practice of electrospray ionization—mass spectrometry for large polypeptides and proteins. *Mass Spectrom. Rev. 10*, 359–451.

(16) Blades, A. T., Ikonomou, M. G., and Kebarle, P. (1991) Mechanism of electrospray mass spectrometry. Electrospray as an electrolysis cell. *Anal. Chem. 63*, 2109–2114.

(17) Kebarle, P., and Tang, L. (1993) From ions in solution to ions in the gas phase—the mechanism of electrospray mass spectrometry. *Anal. Chem. 65*, A972–A986.

(18) Fenn, J. B. (1993) Ion formation from charged droplets: Roles of geometry, energy, and time. *J. Am. Soc. Mass Spectrom. 4*, 524–535.

(19) Dole, M., Mack, L. L., Hines, R. L., Mobley, R. C., Ferguson, L. D., and Alice, M. B. (1968) Molecular beams of macroions. *J. Chem. Phys. 49*, 2240–2249.

(20) Dole, M., Hines, R. L., Mack, L. L., Mobley, R. C., Ferguson, L. D., and Alice, M. B. (1968) Gas phase macroions. *Macromolecules 1*, 96–97.

(21) Mack, L. L., Kralik, P., Rheude, A., and Dole, M. (1970) Molecular beams of macroions. II. *J. Chem. Phys. 52*, 4977–4986.

(22) Dole, M. (1989) *My Life in the Golden Age of America*, Vantage Press, New York, NY.

(23) Whitehouse, C. M., Dreyer, R. N., Yamashita, M., and Fenn, J. B. (1985) Electrospray interface for liquid chromatographs and mass spectrometers. *Anal. Chem. 57*, 675–679.

(24) Aleksandrov, M. L., Gall', L. N., Krasnov, N. V., Nikolaev, V. I., and Shkurov, V. A. (1985) Mass spectrometric analysis of thermally unstable compounds of low volatility by the extraction of ions from solution at atmospheric pressure. *Zh. Anal. Khim. 40*, 1570–1580.

(25) Covey, T. R., Bonner, R. F., Shushan, B. I., and Henion, J. (1988) The determination of protein, oligonucleotide and peptide molecular weights by ion-spray mass spectrometry. *Rapid Commun. Mass Spectrom. 2*, 249–256.

(26) Mann, M., Meng, C. K., and Fenn, J. B. (1989) Interpreting mass spectra of multiply charged ions. *Anal. Chem. 61*, 1702–1708.

(27) Ferrige, A. G., Seddon, M. J., Green, B. N., Jarvis, S. A., and Skilling, J. (1992) Disentangling electrospray spectra with maximum entropy. *Rapid Commun. Mass Spectrom. 6*, 707–711.

(28) Cody, R. B., Tamura, J., and Musselman, B. D. (1992) Electrospray ionization/magnetic sector mass spectrometry: Calibration, resolution, and accurate mass measurements. *Anal. Chem. 64*, 1561–1570.

(29) Dobberstein, P., and Schroeder, E. (1993) Accurate mass determination of a high molecular weight protein using electrospray ionization with a magnetic sector instrument. *Rapid Commun. Mass Spectrom. 7*, 861–864.

(30) Beu, S. C., Senko, M. W., Quinn, J. P., Wampler, F. M., III, and McLafferty, F. W. (1993) Fourier-transform electrospray instrumentation for tandem high-resolution mass spectrometry of large molecules. *J. Am. Soc. Mass Spectrom. 4*, 557–565.

(31) McLafferty, F. W. (1994) High-resolution tandem FT mass spectrometry above 10 kDa. *Acc. Chem. Res. 27*, 379–386.

(32) Winger, B. E., Hofstadler, S. A., Bruce, J. E., Udseth, H. R., and Smith, R. D. (1993) High-resolution accurate mass measurements of biomolecules using a new electrospray ionization ion cyclotron resonance mass spectrometer. *J. Am. Soc. Mass Spectrom. 4*, 566–577.

(33) Loo, J. A., Ogorzalek Loo, R. R., Light, K. J., Edmonds, C. G., and Smith, R. D. (1992) Multiply charged negative ions by electrospray ionization from polypeptides and proteins. *Anal. Chem. 64*, 81–88.

(34) Wilm, M. S., and Mann, M. (1994) Electrospray and Taylor-cone theory, Dole's beam of macromolecules at last? *Int. J. Mass Spectrom. Ion Proc. 136*, 167–180.

(35) Andren, P. E., Emmett, M. R., and Caprioli, R. M. (1994) Micro-electrospray: Zeptomole/attomole per microliter sensitivity for peptides. *J. Am. Soc. Mass Spectrom. 5*, 867–869.

(36) Kriger, M. S., Cook, K. D., and Ramsey, R. S. (1995) Durable gold-coated fused silica capillaries for use in electrospray mass spectrometry. *Anal. Chem. 67*, 385–389.

(37) Bruins, A. P., Covey, T. R., and Henion, J. D. (1987) Ion spray interface for combined liquid chromatography/atmospheric pressure ionization mass spectrometry. *Anal. Chem. 59*, 2642–2646.

(38) Lee, E. D., Henion, J. D., and Covey, T. R. (1989) Microbore high performance liquid chromatography-ion spray mass spectrometry for the determination of peptides. *J. Microcolumn Sep. 1*, 14–18.

(39) Huang, E. C., and Henion, J. D. (1990) LC/MS and LC/MS/MS determination of protein tryptic digests. *J. Am. Soc. Mass Spectrom. 1*, 158–165.

(40) Huang, E. C., and Henion, J. D. (1991) Packed-capillary liquid chromatography/ion-spray tandem mass spectrometry determination of biomolecules. *Anal. Chem. 63*, 732–739.

(41) Smith, R. D., Olivares, J. A., Nguyen, N. T., and Udseth, H. R. (1988) Capillary zone electrophoresis-mass spectrometry using an electrospray ionization interface. *Anal. Chem. 60*, 436–441.

(42) Smith, R. D., Barinaga, C. J., and Udseth, H. R. (1988) Improved electrospray ionization interface for capillary zone electrophoresis-mass spectrometry. *Anal. Chem. 60*, 1948–1952.

(43) Chowdhury, S. K., Katta, V., and Chait, B. T. (1990) An electrospray-ionization mass spectrometer with new features. *Rapid Commun. Mass Spectrom. 4*, 81–87.

(44) Allen, M. H., and Vestal, M. L. (1992) Design and performance of a novel electrospray interface. *J. Am. Soc. Mass Spectrom. 3*, 18–26.

(45) Larsen, B. S., and McEwen, C. N. (1991) An electrospray ion source for magnetic sector mass spectrometers. *J. Am. Soc. Mass Spectrom. 2*, 205–211.

(46) Loo, J. A., Ogorzalek Loo, R. R., and Andrews, P. C. (1993) Primary to quaternary protein structure determination with electrospray ionization and magnetic sector mass spectrometry. *Org. Mass Spectrom. 28*, 1640–1649.

(47) Loo, J. A., and Pesch, R. (1994) Sensitive and selective determination of proteins with electrospray ionization magnetic sector mass spectrometry and array detection. *Anal. Chem. 66*, 3659–3663.

(48) Chapman, J. R., Gallagher, R. T., Barton, E. C., Curtis, J. M., and Derrick, P. J. (1992) Advantages of high-resolution and high-mass range magnetic-sector mass spectrometry for electrospray ionization. *Org. Mass Spectrom. 27*, 195–203.

(49) McLuckey, S. A., Van Berkel, G. J., Goeringer, D. E., and Glish, G. L. (1994) Ion trap mass spectrometry of externally generated ions. *Anal. Chem. 66*, A689–A696.

(50) Hofstadler, S. A., Wahl, J. H., Bruce, J. E., and Smith, R. D. (1993) On-line capillary electrophoresis with Fourier transform ion cyclotron resonance mass spectrometry. *J. Am. Chem. Soc. 115*, 6983–6984.

(51) Mirgorodskaya, O. A., Shevchenko, A. A., Chernushevich, I. V., Dodonov, A. F., and Miroshnikov, A. I. (1994) Electrospray ionization time-of-flight mass spectrometry in protein chemistry. *Anal. Chem. 66*, 99–107.

(52) Verentchikov, A. N., Ens, W., and Standing, K. G. (1994) Reflecting time-of-flight mass spectrometer with an electrospray ion source and orthogonal extraction. *Anal. Chem. 66*, 126–133.

(53) Tang, X.-J., Brewer, C. F., Saha, S., Chernushevich, I., Ens, W., and Standing, K. G. (1994) Investigation of protein–protein noncovalent interactions in soybean agglutinin by electrospray ionization time-of-flight mass spectrometry. *Rapid Commun. Mass Spectrom. 8*, 750–754.

(54) Chernushevich, I. V., Ens, W., and Standing, K. G. (1995) Studies of noncovalent interactions by time-of-flight mass spectrometry. *Proceedings of the 43rd ASMS Conference on Mass Spectrometry and Allied Topics*, Atlanta, GA, American Society for Mass Spectrometry, Santa Fe, NM (in press).

(55) Karas, M., and Hillenkamp, F. (1988) Laser desorption ionization of proteins with molecular masses exceeding 10 000 Daltons. *Anal. Chem. 60*, 2299–2301.

(56) Karas, M., Ingendoh, A., Bahr, U., and Hillenkamp, F. (1989) Ultraviolet-laser desorption/ionization mass spectrometry of femtomolar amounts of large proteins. *Biomed. Environ. Mass Spectrom. 18*, 841–843.

(57) Karas, M., Bahr, U., and Hillenkamp, F. (1989) UV laser matrix desorption/ionization mass spectrometry of proteins in the 100 000 Dalton range. *Int. J. Mass Spectrom. Ion Proc. 92*, 231–242.

(58) Beavis, R. C., and Chait, B. T. (1989) Factors affecting the ultraviolet laser desorption of proteins. *Rapid Commun. Mass Spectrom. 3*, 233–237.

(59) Nordhoff, E., Cramer, R., Karas, M., Hillenkamp, F., Kirpekar, F., Kristiansen, K., and Roepstorff, P. (1993) Ion stability of nucleic acids in infrared matrix-assisted laser desorption/ionization mass spectrometry. *Nucleic Acids Res. 21*, 3347–3357.

(60) Brown, R. S., and Lennon, J. J. (1995) Mass resolution improvement by incorporation of pulsed ion extraction in a matrix-assisted laser desorption/ionization linear time-of-flight mass spectrometer. *Anal. Chem. 67*, 1998–2003.

(61) Annan, R. S., Kochling, H. J., Hill, J. A., and Biemann, K. (1992) Matrix-assisted laser desorption using a fast-atom bombardment ion source and a magnetic mass spectrometer. *Rapid Commun. Mass Spectrom. 6*, 298–302.

(62) Harvey, D. J., Rudd, P. M., Bateman, R. H., Bordoli, R. S., Howes, K., Hoyes, J. B., and Vickers, R. G. (1994) Examination of complex oligosaccharides by matrix-assisted laser desorption/ionization mass spectrometry on time-of-flight and magnetic sector instruments. *Org. Mass Spectrom. 29*, 753–765.

(63) Jonscher, K., Currie, G., McCormack, A. L., and Yates, J. R., III. (1993) Matrix-assisted laser desorption of peptides and proteins on a quadrupole ion trap mass spectrometer. *Rapid Commun. Mass Spectrom. 7*, 20–26.

(64) Schwartz, J. C., and Bier, M. E. (1993) Matrix-assisted laser desorption of peptides and proteins using a quadrupole ion trap mass spectrometer. *Rapid Commun. Mass Spectrom. 7*, 27–32.

(65) Chambers, D. M., Goeringer, D. E., McLuckey, S. A., and Glish, G. L. (1993) Matrix-assisted laser desorption of biological molecules in the quadrupole ion trap mass spectrometer. *Anal. Chem. 65*, 14–20.

(66) Castoro, J. A., and Wilkins, C. L. (1993) Ultrahigh resolution matrix-assisted laser desorption ionization of small proteins by Fourier transform mass spectrometry. *Anal. Chem. 65*, 2621–2627.

(67) McIver, R. T., Li, Y. Z., and Hunter, R. L. (1994) High-resolution laser desorption mass spectrometry of peptides and small proteins. *Proc. Natl. Acad. Sci. U.S.A. 91*, 4801–4805.

(68) Sheng, L.-S., Covey, J. E., Shew, S. L., Winger, B. E., and Campana, J. E. (1994) Matrix-assisted laser desorption ionization Fourier-transform mass spectrometry. *Rapid Commun. Mass Spectrom. 8*, 498–500.

(69) Qian, M. G., and Lubman, D. M. (1995) A marriage made in MS. *Anal. Chem. 67*, A234.

(70) Feng, R., and Konishi, Y. (1992) Analysis of antibodies and other large glycoproteins in the mass range of 150 000–200 000 Da by electrospray ionization mass spectrometry. *Anal. Chem. 64*, 2090–2095.

(71) Siegel, M. M., Liu, D.-F., Tabei, K., Berkenkamp, S., and Hillenkamp, F. (1995) Characterization of filamentous hemagglutinin (FHA) (MW 230 kDa), lysyl-FHA and fragment A by ESI/MS and MALDI/MS. *Proceedings of the 43rd ASMS Conference on Mass Spectrometry and Allied Topics*, Atlanta, GA, American Society for Mass Spectrometry, Santa Fe, NM (in press).

(72) Hillenkamp, F., Karas, M., and Berkenkamp, S. (1995) MALDI-MS in the infrared: A critical evaluation. *Proceedings of the 43rd ASMS Conference on Mass Spectrometry and Allied Topics*, Atlanta, GA, American Society for Mass Spectrometry, Santa Fe, NM (in press).

(73) Nelson, R. W., Dogruel, D., and Williams, P. (1994) Mass determination of human immunoglobulin IgM using matrix-assisted laser desorption/ionization time-of-flight mass spectrometry. *Rapid Commun. Mass Spectrom. 8*, 627–631.

(74) Green, B. N., Oliver, R. W. A., Falick, A. M., Shackleton, C. H. L., Roitman, E., and Witkowska, H. E. (1990) Electrospray MS, LSIMS and MS/MS for the rapid detection and characterization of variant hemoglobins. *Biological Mass Spectrometry* (A. L. Burlingame, and J. A. McCloskey, Eds.) pp 129–146, Elsevier, Amsterdam.

(75) Shackleton, C. H. L., Falick, A. M., Green, B. N., and Witkowska, H. E. (1991) Electrospray mass spectrometry in the clinical diagnosis of variant hemoglobins. *J. Chromatogr. 562*, 175–190.

(76) Witkowska, H. E., Bitsch, F., and Shackleton, C. H. L. (1993) Expediting rare variant hemoglobin characterization by combined HPLC/electrospray mass spectrometry. *Hemoglobin 17*, 227–242.

(77) Light-Wahl, K. J., Loo, J. A., Edmonds, C. G., Smith, R. D., Witkowska, H. E., Shackleton, C. H. L., and Wu, C. S. C.

(1993) Collisionally activated dissociation and tandem mass spectrometry of intact hemoglobin β-chain variant proteins with electrospray ionization. *Biol. Mass Spectrom. 22*, 112–120.

(78) Ogorzalek Loo, R. R., Loo, J. A., Udseth, H. R., Fulton, J. L., and Smith, R. D. (1992) Protein structural effects in gas phase ion/molecule reactions with diethylamine. *Rapid Commun. Mass Spectrom. 6*, 159–165.

(79) Smith, R. D., Loo, J. A., Barinaga, C. J., Edmonds, C. G., and Udseth, H. R. (1990) Collisional activation and collision induced dissociation of multiply charged ions of large peptides and proteins produced by electrospray ionization. *J. Am. Soc. Mass Spectrom. 1*, 53–65.

(80) Sogaard, M., Andersen, J. S., Roepstorff, P., and Svensson, B. (1993) Electrospray mass spectrometry characterization of post-translational modifications of barley α-amylase-1 produced in yeast. *Biotechnology 11*, 1162–1165.

(81) Young, N. M., Watson, D. C., Yaguchi, M., Adar, R., Arango, R., Rodriguezarango, E., Sharon, N., Blay, P. K. S., and Thibault, P. (1995) C-Terminal post-translational proteolysis of plant lectins and their recombinant forms expressed in Escherichia coli—characterization of "ragged ends" by mass spectrometry. *J. Biol. Chem. 270*, 2563–2570.

(82) Hofstadler, S. A., Swanek, F. D., Gale, D. C., Ewing, A. G., and Smith, R. D. (1995) Capillary electrophoresis electrospray ionization Fourier transform ion cyclotron resonance mass spectrometry for direct analysis of cellular proteins. *Anal. Chem. 67*, 1477–1480.

(83) Li, K. W., Hoek, R. M., Smith, F., Jimenez, C. R., Vanderschors, R. C., Van Veelen, P. A., Chen, S., Van der greef, J., Parish, D. C., Benjamin, P., and Geraerts, W. P. M. (1994) Direct peptide profiling by mass spectrometry of single identified neurons reveals complex neuropeptide-processing pattern. *J. Biol. Chem. 269*, 30288–30292.

(84) Li, K. W., Vangolen, F. A., Vanminnen, J., Van Veelen, P. A., Van der greef, J., and Geraerts, W. P. M. (1994) Structural identification, neuronal synthesis, and role in male copulation of myomodulin-A of Lymnaea: A study involving direct peptide profiling of nervous tissue by mass spectrometry. *Mol. Brain Res. 25*, 355–358.

(85) Stults, J. T., and Marsters, J. C. (1991) Improved electrospray ionization of synthetic oligodeoxynucleotides. *Rapid Commun. Mass Spectrom. 5*, 359–363.

(86) Limbach, P. A., Crain, P. F., and McCloskey, J. A. (1995) Molecular mass measurement of intact ribonucleic acids via electrospray ionization quadrupole mass spectrometry. *J. Am. Soc. Mass Spectrom. 6*, 27–39.

(87) Greig, M., and Griffey, R. H. (1995) Utility of organic bases for improved electrospray mass spectrometry of oligonucleotides. *Rapid Commun. Mass Spectrom. 9*, 97–102.

(88) Wang, B. H., and Biemann, K. (1994) Matrix-assisted laser desorption/ionization time-of-flight mass spectrometry of chemically modified oligonucleotides. *Anal. Chem. 66*, 1918–1924.

(89) Bai, J., Liu, Y.-H., Lubman, D. M., and Siemieniak, D. (1994) Matrix-assisted laser desorption/ionization mass spectrometry of restriction enzyme-digested plasmid DNA using an active Nafion substrate. *Rapid Commun. Mass Spectrom. 8*, 687–691.

(90) Tang, K., Taranenko, N. I., Allman, S. L., Chang, L. Y., and Chen, C. H. (1994) Detection of 500-nucleotide DNA by laser desorption mass spectrometry. *Rapid Commun. Mass Spectrom. 8*, 727–730.

(91) Kirpekar, F., Nordhoff, E., Kristiansen, K., Roepstorff, P., Lezius, A., Hahner, S., Karas, M., and Hillenkamp, F. (1994) Matrix assisted laser desorption/ionization mass spectrometry of enzymatically synthesized RNA up to 150 kDa. *Nucleic Acids Res. 22*, 3866–3870.

(92) Reinhold, V. N., Reinhold, B. B., and Costello, C. E. (1995) Carbohydrate molecular weight profiling, sequence, linkage, and branching data: ES-MS and CID. *Anal. Chem. 67*, 1772–1784.

(93) Stahl, B., Steup, M., Karas, M., and Hillenkamp, F. (1991) Analysis of neutral oligosaccharides by matrix-assisted laser desorption/ionization mass spectrometry. *Anal. Chem. 63*, 1463–1466.

(94) Stahl, B., Klabunde, T., Witzel, H., Krebs, B., Steup, M., Karas, M., and Hillenkamp, F. (1994) The oligosaccharides of the Fe(III)-Zn(II) purple acid phosphatase of the red kidney bean—determination of the structure by a combination of matrix-assisted laser desorption ionization mass spectrometry and selective enzymic degradation. *Eur. J. Biochem. 220*, 321–330.

(95) Stahl, B., Thurl, S., Zeng, J. R., Karas, M., Hillenkamp, F., Steup, M., and Sawatzki, G. (1994) Oligosaccharides from human milk as revealed by matrix-assisted laser desorption/ionization mass spectrometry. *Anal. Biochem. 223*, 218–226.

(96) Mock, K. K., Davey, M., and Cottrell, J. S. (1991) The analysis of underivatised oligosaccharides by matrix-assisted laser desorption mass spectrometry. *Biochem. Biophys. Res. Commun. 177*, 644–651.

(97) Huberty, M. C., Vath, J. E., Yu, W., and Martin, S. A. (1993) Site-specific carbohydrate identification in recombinant proteins using MALD-TOFMS. *Anal. Chem. 65*, 2791–2800.

(98) McLafferty, F. W., Ed. (1983) *Tandem Mass Spectrometry*, Wiley-Interscience, New York.

(99) Busch, K. L., Glish, G. L., and McLuckey, S. A. (1988) *Mass Spectrometry/Mass Spectrometry. Techniques and Applications of Tandem Mass Spectrometry*, VCH, New York.

(100) Biemann, K., and Scoble, H. A. (1987) Characterization by tandem mass spectrometry of structural modifications in proteins. *Science 237*, 992–998.

(101) Biemann, K. (1988) Contributions of mass spectrometry to peptide and protein structure. *Biomed. Environ. Mass Spectrom. 16*, 99–111.

(102) Loo, J. A., Edmonds, C. G., and Smith, R. D. (1991) Tandem mass spectrometry of very large molecules: Serum albumin sequence information from multiply charged ions formed by electrospray ionization. *Anal. Chem. 63*, 2488–2499.

(103) Speir, J. P., Senko, M. W., Little, D. P., Loo, J. A., and McLafferty, F. W. (1995) High-resolution tandem mass spectra of 37–67 kDa proteins. *J. Mass Spectrom. 30*, 39–42.

(104) Rossomando, A. J., Wu, J., Michel, H., Shabanowitz, J., Hunt, D. F., Weber, M. J., and Sturgill, T. W. (1992) Identification of Tyr-185 as the site of tyrosine autophosphorylation of recombinant mitogen-activated protein kinase p42[mapk]. *Proc. Natl. Acad. Sci. U.S.A. 89*, 5779–5783.

(105) Huddleston, M. J., Annan, R. S., Bean, M. F., and Carr, S. A. (1993) Selective detection of phosphopeptides in complex mixtures by electrospray liquid chromatography/mass spectrometry. *J. Am. Soc. Mass Spectrom. 4*, 710–717.

(106) Carr, S. A., Huddleston, M. J., and Bean, M. F. (1993) Selective identification and differentiation of N-linked and O-linked oligosaccharides in glycoproteins by liquid chromatography-mass spectrometry. *Protein Sci. 2*, 183–196.

(107) Ohguro, H., Palczewski, K., Ericsson, L. H., Walsh, K. A., and Johnson, R. S. (1993) Sequential phosphorylation of rhodopsin at multiple sites. *Biochemistry 32*, 5718–5724.

(108) Papac, D. I., Oatis, J. E., Jr., Crouch, R. K., and Knapp, D. R. (1993) Mass spectrometric identification of phosphorylation sites in bleached bovine rhodopsin. *Biochemistry 32*, 5930–5934.

(109) Knight, W. B., Swiderek, K. M., Sakuma, T., Calaycay, J., Shively, J. E., Lee, T. D., Covey, T. R., Shushan, B., Green, B. G., Chabin, R., Shah, S., Mumford, R., Dickinson, T. A., and Griffin, P. R. (1993) Electrospray ionization mass spectrometry as a mechanistic tool—mass of human leucocyte elastase and a β-lactam-derived E-I complex. *Biochemistry 32*, 2031–2035.

(110) Aplin, R. T., Robinson, C. V., Schofield, C. J., and Waley, S. G. (1993) Use of electrospray mass spectrometry to investigate the inhibition of β-lactamases by 6-halogenopenicillanic acids. *J. Chem. Soc., Chem. Commun.* 121–123.

(111) Miao, S. C., McCarter, J. D., Grace, M. E., Grabowski, G. A., Aebersold, R., and Withers, S. G. (1994) Identification of Glu(340) as the active-site nucleophile in human glucocerebrosidase by use of electrospray tandem mass spectrometry. *J. Biol. Chem. 269*, 10975–10978.

(112) Miao, S. C., Ziser, L., Aebersold, R., and Withers, S. G. (1994) Identification of glutamic acid 78 as the active site

nucleophile in Bacillus subtilis xylanase using electrospray tandem mass spectrometry. *Biochemistry 33*, 7027–7032.

(113) Rosnack, K. J., and Stroh, J. G. (1992) C-Terminal sequencing of peptides using electrospray ionization mass spectrometry. *Rapid Commun. Mass Spectrom. 6*, 637–640.

(114) Davis, M. T., Lee, T. D., Ronk, M., and Hefta, S. A. (1995) Microscale immobilized protease reactor columns for peptide mapping by liquid chromatography/mass spectral analyses. *Anal. Biochem. 224*, 235–244.

(115) Hunt, D. F., Henderson, R. A., Shabanowitz, J., Sakaguchi, K., Michel, H., Sevilir, N., Cox, A. L., Appella, E., and Engelhard, V. H. (1992) Characterization of peptides bound to the class I MHC molecule HLA-A2.1 by mass spectrometry. *Science 255*, 1261–1263.

(116) McLuckey, S. A., Van Berkel, G. J., and Glish, G. L. (1992) Tandem mass spectrometry of small, multiply charged oligonucleotides. *J. Am. Soc. Mass Spectrom. 3*, 60–70.

(117) McLuckey, S. A., and Habibigoudarzi, S. (1993) Decompositions of multiply charged oligonucleotide anions. *J. Am. Chem. Soc. 115*, 12085–12095.

(118) Little, D. P., Chorush, R. A., Speir, J. P., Senko, M. W., Kelleher, N. L., and McLafferty, F. W. (1994) Rapid sequencing of oligonucleotides by high-resolution mass spectrometry. *J. Am. Chem. Soc. 116*, 4893–4897.

(119) Loo, J. A., Edmonds, C. G., and Smith, R. D. (1990) Primary sequence information from intact proteins by electrospray ionization tandem mass spectrometry. *Science 248*, 201–204.

(120) Loo, J. A., Edmonds, C. G., and Smith, R. D. (1993) Tandem mass spectrometry of very large molecules. 2. Dissociation of multiply charged proline-containing proteins from electrospray ionization. *Anal. Chem. 65*, 425–438.

(121) Senko, M. W., Beu, S. C., and McLafferty, F. W. (1994) High-resolution tandem mass spectrometry of carbonic anhydrase. *Anal. Chem. 66*, 415–417.

(122) Liao, P.-C., Leykam, J., Andrews, P. C., Gage, D. A., and Allison, J. (1994) An approach to locate phosphorylation sites in a phosphoprotein: mass mapping by combined specific enzymatic degradation with matrix-assisted laser desorption/ionization mass spectrometry. *Anal. Biochem. 219*, 9–20.

(123) Kaufmann, R., Kirsch, D., and Spengler, B. (1994) Sequencing of peptides in a time-of-flight mass spectrometer: Evaluation of postsource decay following matrix-assisted laser desorption ionization (MALDI). *Int. J. Mass Spectrom. Ion Proc. 131*, 355–385.

(124) Chait, B. T., Wang, R., Beavis, R. C., and Kent, S. B. H. (1993) Protein ladder sequencing. *Science 262*, 89–92.

(125) Metzger, J. W. (1994) Ladder sequencing of peptides and proteins - a combination of Edman degradation and mass spectrometry. *Angew. Chem., Int. Ed. Engl. 33*, 723–725.

(126) Bartlet-Jones, M., Jeffery, W. A., Hansen, H. F., and Pappin, D. J. C. (1994) Peptide ladder sequencing by mass spectrometry using a novel, volatile degradation reagent. *Rapid Commun. Mass Spectrom. 8*, 737–742.

(127) Huang, E. C., Wachs, T., Conboy, J. J., and Henion, J. D. (1990) Atmospheric pressure ionization mass spectrometry: detection for the separation sciences. *Anal. Chem. 62*, 713A–725A.

(128) Bruins, A. P. (1991) Liquid chromatography-mass spectrometry with ionspray and electrospray interfaces in phamaceutical and biomedical research. *J. Chromatogr. 554*, 39–46.

(129) Eshraghi, J., and Chowdhury, S. K. (1993) Factors affecting electrospray ionization of effluents containing trifluoroacetic acid for high-performance liquid chromatography/mass spectrometry. *Anal. Chem. 65*, 3528–3533.

(130) Wachs, T., Conboy, J. C., Garcia, F., and Henion, J. D. (1991) Liquid chromatography-mass spectrometry and related techniques via atmospheric pressure ionization. *J. Chromatog. Sci. 29*, 357–366.

(131) Niessen, W. M. A., and Tinke, A. P. (1995) Liquid chromatography mass spectrometry—general principles and instrumentation. *J. Chromatogr. A 703*, 37–57.

(132) Gelpi, E. (1995) Biomedical and biochemical applications of liquid chromatography mass spectrometry. *J. Chromatogr. A 703*, 59–80.

(133) Banks, J. F., Quinn, J. P., and Whitehouse, C. M. (1994) LC/ESI-MS determination of proteins using conventional liquid chromatography and ultrasonically assisted electrospray. *Anal. Chem. 66*, 3688–3695.

(134) Hopfgartner, G., Wachs, T., Bean, K., and Henion, J. (1993) High-flow ion spray liquid chromatography/mass spectrometry. *Anal. Chem. 65*, 439–446.

(135) Landers, J. P., Ed. (1994) *Handbook of Capillary Electrophoresis*, CRC Press, Boca Raton, FL.

(136) Smith, R. D., Wahl, J. H., Goodlett, D. R., and Hofstadler, S. A. (1993) Capillary electrophoresis/mass spectrometry. *Anal. Chem. 65*, A574–A584.

(137) Pleasance, S., and Thibault, P. (1993) Interfacing capillary electrophoresis with mass spectrometry. *Capillary Electrophoresis: Theory and Practice* (P. Camilleri, Ed.) pp 311–369, CRC Press, Boca Raton, FL.

(138) Cai, J. Y., and Henion, J. (1995) Capillary electrophoresis mass spectrometry. *J. Chromatogr. A 703*, 667–692.

(139) Thompson, T. J., Foret, F., Vouros, P., and Karger, B. L. (1993) Capillary electrophoresis electrospray ionization mass spectrometry—improvement of protein detection limits using on-column transient isotachophoretic sample preconcentration. *Anal. Chem. 65*, 900–906.

(140) Wahl, J. H., Goodlett, D. R., Udseth, H. R., and Smith, R. D. (1992) Attomole level capillary electrophoresis-mass spectrometric protein analysis using 5-μm-i.d. capillaries. *Anal. Chem. 64*, 3194–3196.

(141) Castoro, J. A., Chiu, R. W., Monnig, C. A., and Wilkins, C. L. (1992) Matrix-assited laser desorption/ionization of capillary electrophoresis effluents by Fourier transform mass spectrometry. *J. Am. Chem. Soc. 114*, 7571–7572.

(142) Van Veelen, P. A., Tjaden, U. R., Van der greef, J., Ingendoh, A., and Hillenkamp, F. (1993) Off-line coupling of capillary electrophoresis with matrix-assisted laser desorption mass spectrometry. *J. Chromatogr. 647*, 367–374.

(143) Weinmann, W., Parker, C. E., Deterding, L. J., Papac, D. I., Hoyes, J., Przybylski, M., and Tomer, K. B. (1994) Capillary electrophoresis-matrix-assisted laser-desorption ionization mass spectrometry of proteins. *J. Chromatogr. A 680*, 353–361.

(144) Vestling, M. M., and Fenselau, C. (1994) Poly(vinylidene difluoride) membranes as the interface between laser desorption mass spectrometry, gel electrophoresis, and *in situ* proteolysis. *Anal. Chem. 66*, 471–477.

(145) Patterson, S. D. (1994) From electrophoretically separated protein to identification: strategies for sequence and mass analysis. *Anal. Biochem. 221*, 1–15.

(146) Zhang, W. Z., Czernik, A. J., Yungwirth, T., Aebersold, R., and Chait, B. T. (1994) Matrix-assisted laser desorption mass spectrometric peptide mapping of proteins separated by two-dimensional gel electrophoresis—determination of phosphorylation in synapsin I. *Protein Sci. 3*, 677–686.

(147) Mortz, E., Vorm, O., Mann, M., and Roepstorff, P. (1994) Identification of proteins in polyacrylamide gels by mass spectrometric peptide mapping combined with database search. *Biol. Mass Spectrom. 23*, 249–261.

(148) Clauser, K. R., Hall, S. C., Smith, D. M., Webb, J. W., Andrews, L. E., Tran, H. M., Epstein, L. B., and Burlingame, A. L. (1995) Rapid mass spectrometric peptide sequencing and mass matching for characterization of human melanoma proteins isolated by two-dimensional PAGE. *Proc. Natl. Acad. Sci. U.S.A. 92*, 5072–5076.

(149) Henzel, W. J., Billeci, T. M., Stults, J. T., Wong, S. C., Grimley, C., and Watanabe, C. (1993) Identifying proteins from 2-dimensional gels by molecular mass searching of peptide fragments in protein sequence databases. *Proc. Natl. Acad. Sci. U.S.A. 90*, 5011–5015.

(150) Pappin, D. J. C., Hojrup, P., and Bleasby, A. J. (1993) Rapid identification of proteins by peptide-mass fingerprinting. *Curr. Biol. 3*, 327–332.

(151) James, P., Quadroni, M., Carafoli, E., and Gonnet, G. (1993) Protein identification by mass profile fingerprinting. *Biochem. Biophys. Res. Commun. 195*, 58–64.

(152) Mann, M., Hojrup, P., and Roepstorff, P. (1993) Use of mass spectrometric molecular weight information to identify proteins in sequence databases. *Biol. Mass Spectrom. 22*, 338–345.

(153) Yates, J. R., II, Speicher, S., Griffin, P. R., and Hunkapiller, T. (1993) Peptide mass maps: A highly informative approach to protein identification. *Anal. Biochem. 214*, 397–408.

(154) le Maire, M., Deschamps, S., Moller, J., Le Caer, J. P., and Rossier, J. (1993) Electrospray ionization mass spectrometry on hydrophobic peptides electroeluted from sodium dodecyl sulfate–polyacrylamide gel electrophoresis. Application to the topology of the sarcoplasmic reticulum Ca^{2+} ATPase. *Anal. Biochem. 214*, 50–57.

(155) Bonaventura, C., Bonaventura, J., Stevens, R., and Millington, D. (1994) Acrylamide in polyacrylamide gels can modify proteins during electrophoresis. *Anal. Biochem. 222*, 44–48.

(156) Eckerskorn, C., Strupat, K., Karas, M., Hillenkamp, F., and Lottspeich, F. (1992) Mass spectrometric analysis of blotted proteins after gel electrophoretic separation by matrix-assisted laser desorption/ionization. *Electrophoresis 13*, 664–665.

(157) Strupat, K., Karas, M., Hillenkamp, F., Eckerskorn, C., and Lottspeich, F. (1994) Matrix-assisted laser desorption ionization mass spectrometry of proteins electroblotted after polyacrylamide gel electrophoresis. *Anal. Chem. 66*, 464–470.

(158) Yanase, H., Cahill, S., Martin de Llano, J. J., Manning, L. R., Schneider, K., Chait, B. T., Vandegriff, K. D., Winslow, R. M., and Manning, J. M. (1994) Properties of a recombinant human hemoglobin with aspartic acid 99(β), an important intersubunit contact site, substituted by lysine. *Protein Sci. 3*, 1213–1223.

(159) Ogorzalek Loo, R. R., Stevenson, T. I., Mitchell, C., Loo, J. A., and Andrews, P. C. (1995) MALDI-MS of proteins directly from polyacrylamide gels. *Proceedings of the 43rd ASMS Conference on Mass Spectrometry and Allied Topics*, Atlanta, GA, American Society for Mass Spectrometry, Santa Fe, NM (in press).

(160) Ogorzalek Loo, R. R., Mitchell, C., Stevenson, T. I., Loo, J. A., and Andrews, P. C. (1995) Interfacing polyacrylamide gel electrophoresis with mass spectrometry. *Techniques in Protein Chemistry VII* (D. Marshak, Ed.), Academic Press, San Diego, CA (in press).

(161) Ganem, B., Li, Y.-T., and Henion, J. D. (1991) Detection of noncovalent receptor-ligand complexes by mass spectrometry. *J. Am. Chem. Soc. 113*, 6294–6296.

(162) Ganem, B., Li, Y.-T., and Henion, J. D. (1991) Observation of noncovalent enzyme-substrate and enzyme–product complexes by ion-spray mass spectrometry. *J. Am. Chem. Soc. 113*, 7818–7819.

(163) Katta, V., and Chait, B. T. (1991) Observation of the heme-globin complex in native myoglobin by electrospray-ionization mass spectrometry. *J. Am. Chem. Soc. 113*, 8534–8535.

(164) Smith, R. D., and Light-Wahl, K. J. (1993) Perspectives—the observation of non-covalent interactions in solution by electrospray ionization mass spectrometry—Promise, pitfalls and prognosis. *Biol. Mass Spectrom. 22*, 493–501.

(165) Ogorzalek Loo, R. R., Goodlett, D. R., Smith, R. D., and Loo, J. A. (1993) Observation of a noncovalent ribonuclease S-protein S-peptide complex by electrospray ionization mass spectrometry. *J. Am. Chem. Soc. 115*, 4391–4392.

(166) Farmer, T. B., and Caprioli, R. M. (1991) Assessing the multimeric states of proteins: Studies using laser desorption mass spectrometry. *Biol. Mass Spectrom. 20*, 796–800.

(167) Light-Wahl, K. J., Schwartz, B. L., and Smith, R. D. (1994) Observation of the noncovalent quaternary associations of proteins by electrospray ionization mass spectrometry. *J. Am. Chem. Soc. 116*, 5271–5278.

(168) Schwartz, B. L., Light-Wahl, K. J., and Smith, R. D. (1994) Observation of noncovalent complexes to the avidin tetramer by electrospray ionization mass spectrometry. *J. Am. Soc. Mass Spectrom. 5*, 201–204.

(169) Light-Wahl, K. J., Winger, B. E., and Smith, R. D. (1993) Observation of the multimeric forms of concanavalin-A by electrospray ionization mass spectrometry. *J. Am. Chem. Soc. 115*, 5869–5870.

(170) Schwartz, B. L., Bruce, J. E., Anderson, G. A., Hofstadler, S. A., Rockwood, A. L., Smith, R. D., Chilkoti, A., and Stayton, P. S. (1995) Dissociation of tetrameric ions of noncovalent streptavidin complexes formed by electrospray ionization. *J. Am. Soc. Mass Spectrom. 6*, 459–465.

(171) Loo, J. A. (1995) Observation of large subunit protein complexes by electrospray ionization mass spectrometry. *J. Mass Spectrom. 30*, 180–183.

(172) Loo, J. A., Hu, P., and Thanabal, V. (1995) Studying noncovalent protein–peptide interactions by ESI-MS. *Proceedings of the 43rd ASMS Conference on Mass Spectrometry and Allied Topics*, Atlanta, GA, American Society for Mass Spectrometry, Santa Fe, NM (in press).

(173) Lim, H.-K., Hsieh, Y. L., Ganem, B., and Henion, J. (1995) Recognition of cell-wall peptide ligands by vancomycin group antibiotics: Studies using ion spray mass spectrometry. *J. Mass Spectrom. 30*, 708–714.

(174) Light-Wahl, K. J., Springer, D. L., Winger, B. E., Edmonds, C. G., Camp, D. G., III, Thrall, B. D., and Smith, R. D. (1993) Observation of a small oligonucleotide duplex by electrospray ionization mass spectrometry. *J. Am. Chem. Soc. 115*, 803–804.

(175) Gale, D. C., Goodlett, D. R., Light-Wahl, K. J., and Smith, R. D. (1994) Observation of duplex DNA–drug noncovalent complexes by electrospray ionization mass spectrometry. *J. Am. Chem. Soc. 116*, 6027–6028.

(176) Goodlett, D. R., Camp, D. G., III, Hardin, C. C., Corregan, M., and Smith, R. D. (1993) Direct observation of a DNA quadruplex by electrospray ionization mass spectrometry. *Biol. Mass Spectrom. 22*, 181–183.

(177) Ganem, B., Li, Y. T., and Henion, J. D. (1993) Detection of oligonucleotide duplex forms by ion-spray mass spectrometry. *Tetrahedron Lett. 34*, 1445–1448.

(178) Doktycz, M. J., Habibigoudarzi, S., and McLuckey, S. A. (1994) Accumulation and storage of ionized duplex DNA molecules in a quadrupole ion trap. *Anal. Chem. 66*, 3416–3422.

(179) Bayer, E., Bauer, T., Schmeer, K., Bleicher, K., Maler, M., and Gaus, H. J. (1994) Analysis of double-stranded oligonucleotides by electrospray mass spectrometry. *Anal. Chem. 66*, 3858–3863.

(180) Jensen, O. N., Barofsky, D. F., Young, M. C., von Hippel, P. H., Swenson, S., and Seifried, S. E. (1993) Direct observation of UV-crosslinked protein-nucleic acid complexes by matrix-assisted laser desorption ionization mass spectrometry. *Rapid Commun. Mass Spectrom. 7*, 496–501.

(181) Jensen, O. N., Bennett, S. E., Mosbaugh, D. W., and Barofsky, D. F. (1994) Mass spectrometric characterization of UV-crosslinked protein-nucleic acid complexes. *Proceedings of the 42nd ASMS Conference on Mass Spectrometry and Allied Topics*, Chicago, IL, p 923, American Society for Mass Spectrometry, Santa Fe, NM.

(182) Cohen, S. L., Ferre-D'Amare, A. R., Burley, S. K., and Chait, B. T. (1995) Probing the solution structure of the DNA-binding protein Max by a combination of proteolysis and mass spectrometry. *Protein Sci. 4*, 1088–1099.

(183) Cheng, X., Harms, A. C., Smith, R. D., Morin, P. E., Goudreau, P. N., and Terwilliger, T. C. (1995) Characterization of protein-DNA complexes using ESI-MS. *Proceedings of the 43rd ASMS Conference on Mass Spectrometry and Allied Topics*, Atlanta, GA, American Society for Mass Spectrometry, Santa Fe, NM (in press).

(184) Cheng, X., Hofstadler, S. A., Bruce, J. E., Harms, A. C., Chen, R., Terwilliger, T. C., Goudreau, P. N., and Smith, R. D. (1995) Electrospray ionization with high performance Fourier transform ion cyclotron resonance mass spectrometry for the study of noncovalent biomolecular complexes. *Techniques in Protein Chemistry VII* (D. Marshak, Ed.), Academic Press, San Diego, CA (in press).

(185) Hutchens, T. W., and Allen, M. H. (1992) Differences in the conformational state of a zinc-finger DNA-binding protein domain occupied by zinc and copper revealed by electrospray ionization mass spectrometry. *Rapid Commun. Mass Spectrom. 6*, 469–473.

(186) Hutchens, T. W., Allen, M. H., Li, C. M., and Yip, T.-T. (1992) Occupancy of a C$_2$-C$_2$ type "zinc-finger" protein domain by copper. Direct observation by electrospray ionization mass spectrometry. *FEBS Lett. 309*, 170–174.

(187) Hutchens, T. W., Nelson, R. W., Allen, M. H., Li, C. M., and Yip, T.-T. (1992) Peptide-metal ion interactions in solution: Detection by laser desorption time-of-flight mass spectrometry and electrospray ionization mass spectrometry. *Biol. Mass Spectrom. 21*, 151–159.

(188) Allen, M. H., and Hutchens, T. W. (1992) Electrospray ionization mass spectrometry for the detection of discrete peptide/metal-ion complexes involving multiple cysteine (sulfur) ligands. *Rapid Commun. Mass Spectrom. 6*, 308–312.

(189) Yu, X. L., Wojciechowski, M., and Fenselau, C. (1993) Assessment of metals in reconstituted metallothioneins by electrospray mass spectrometry. *Anal. Chem. 65*, 1355–1359.

(190) Petillot, Y., Forest, E., Mathieu, I., Meyer, J., and Moulis, J. M. (1993) Analysis, by electrospray ionization mass spectrometry, of several forms of clostridium-pasteurianum rubredoxin. *Biochem. J. 296*, 657–661.

(191) Hu, P. F., Ye, Q.-Z., and Loo, J. A. (1994) Calcium stoichiometry determination for calcium binding proteins by electrospray ionization mass spectrometry. *Anal. Chem. 66*, 4190–4194.

(192) Hutchens, T. W., and Yip, T.-T. (1993) New desorption strategies for the mass spectrometric analysis of macromolecules. *Rapid Commun. Mass Spectrom. 7*, 576–580.

(193) Papac, D. I., Hoyes, J., and Tomer, K. B. (1994) Direct analysis of affinity-bound analytes by MALDI/TOFMS. *Anal. Chem. 66*, 2609–2613.

(194) Nelson, R. W., Krone, J. R., Bieber, A. L., and Williams, P. (1995) Mass spectrometric immunoassay. *Anal. Chem. 67*, 1153–1158.

(195) Papac, D. I., Hoyes, J., and Tomer, K. B. (1994) Epitope mapping of the gastrin-releasing peptide anti-bombesin monoclonal antibody complex by proteolysis followed by matrix-assisted laser desorption ionization mass spectrometry. *Protein Sci. 3*, 1485–1492.

(196) Zhao, Y. M., and Chait, B. T. (1994) Protein epitope mapping by mass spectrometry. *Anal. Chem. 66*, 3723–3726.

(197) Miranker, A., Robinson, C. V., Radford, S. E., Aplin, R. T., and Dobson, C. M. (1993) Detection of transient protein folding populations by mass spectrometry. *Science 262*, 896–900.

(198) Robinson, C. V., Gross, M., Eyles, S. J., Ewbank, J. J., Mayhew, M., Hartl, F. U., Dobson, C. M., and Radford, S. E. (1994) Conformation of GroEL-bound α-lactalbumin probed by mass spectrometry. *Nature 372*, 646–651.

(199) Wagner, D. S., and Anderegg, R. J. (1994) Conformation of cytochrome c studied by deuterium exchange electrospray ionization mass spectrometry. *Anal. Chem. 66*, 706–711.

(200) Wagner, D. S., Melton, L. G., Yan, Y. B., Erickson, B. W., and Anderegg, R. J. (1994) Deuterium exchange of α-helices and β-sheets as monitored by electrospray ionization mass spectrometry. *Protein Sci. 3*, 1305–1314.

(201) Loo, J. A., Ogorzalek Loo, R. R., Udseth, H. R., Edmonds, C. G., and Smith, R. D. (1991) Solvent-induced conformational changes of polypeptides probed by electrospray ionization-mass spectrometry. *Rapid Commun. Mass Spectrom. 5*, 101–105.

(202) Katta, V., and Chait, B. T. (1991) Conformational changes in proteins probed by hydrogen-exchange electrospray-ionization mass spectrometry. *Rapid Commun. Mass Spectrom. 5*, 214–217.

(203) Katta, V., and Chait, B. T. (1993) Hydrogen/deuterium exchange electrospray ionization mass spectrometry—a method for probing protein conformational changes in solution. *J. Am. Chem. Soc. 115*, 6317–6321.

(204) Gallop, M. A., Barrett, R. W., Dower, W. J., Fodor, S. P. A., and Gordon, E. M. (1994) Applications of combinatorial technologies to drug discovery. 1. Background and peptide combinatorial libraries. *J. Med. Chem. 37*, 1233–1251.

(205) Andrews, P. C., Boyd, J., Ogorzalek Loo, R., Zhao, R., Zhu, C.-Q., Grant, K., and Williams, S. (1994) Synthesis of uniform peptide libraries and methods for physico-chemical analysis. *Techniques in Protein Chemistry V* (J. W. Crabb, Ed.) pp 485–492, Academic Press, San Diego.

(206) Metzger, J. W., Stenanovic, S., Brunjes, J., Wiesmuller, K.-H., and Jung, G. (1994) Electrospray mass spectrometry and multiple sequence analysis of synthetic peptide libraries. *Methods (San Diego) 6*, 425–431.

(207) Kassel, D. B., Consler, T. G., Shalaby, M., Sekhri, P., Gordon, N., and Nadler, T. (1995) Direct coupling of an automated 2-dimensional microcolumn affinity chromatography-capillary HPLC system with mass spectrometry for biomolecule analysis. *Techniques in Protein Chemistry VI* (J. W. Crabb, Ed.) pp 39–46, Academic Press, San Diego, CA.

(208) Chu, Y.-H., Kirby, D. P., and Karger, B. L. (1995) Free solution identification of candidate peptides from combinatorial libraries by affinity capillary electrophoresis/mass spectrometry. *J. Am. Chem. Soc. 117*, 5419–5420.

(209) Youngquist, R. S., Fuentes, G. R., Lacey, M. P., and Keough, T. (1995) Generation and screening of combinatorial peptide libraries designed for rapid sequencing by mass spectrometry. *J. Am. Chem. Soc. 117*, 3900–3906.

(210) Busman, M., Knapp, D. R., and Schey, K. L. (1994) Observation of large multimers in the electrospray ionization mass spectrometry of peptides. *Rapid Commun. Mass Spectrom. 8*, 211–216.

(211) Smith, R. D., Light-Wahl, K. J., Winger, B. E., and Loo, J. A. (1992) Preservation of noncovalent associations in electrospray ionization-mass spectrometry: Multiply charged polypeptide and protein dimers. *Org. Mass Spectrom. 27*, 811–821.

(212) Loo, J. A., Holsworth, D. D., and Root-Bernstein, R. S. (1994) Use of electrospray ionization mass spectrometry to probe antisense peptide interactions. *Biol. Mass Spectrom. 23*, 6–12.

(213) Li, Y.-T., Hsieh, Y.-L., Henion, J. D., Senko, M. W., McLafferty, F. W., and Ganem, B. (1993) Mass spectrometric studies on noncovalent dimers of leucine zipper peptides. *J. Am. Chem. Soc. 115*, 8409–8413.

(214) Goodlett, D. R., Ogorzalek Loo, R. R., Loo, J. A., Wahl, J. H., Udseth, H. R., and Smith, R. D. (1994) A study of the thermal denaturation of ribonuclease S by electrospray ionization mass spectrometry. *J. Am. Soc. Mass Spectrom. 5*, 614–622.

(215) Anderegg, R. J., and Wagner, D. S. (1995) Mass spectrometric characterization of a protein ligand interaction. *J. Am. Chem. Soc. 117*, 1374–1377.

(216) Baczynskyj, L., Bronson, G. E., and Kubiak, T. M. (1994) Application of thermally assisted electrospray ionization mass spectrometry for detection of noncovalent complexes of bovine serum albumin with growth hormone releasing factor and other biologically active peptides. *Rapid Commun. Mass Spectrom. 8*, 280–286.

(217) Loo, J. A., Hu, P., and Smith, R. D. (1994) Interaction of angiotensin peptides and zinc metal ions probed by electrospray ionization mass spectrometry. *J. Am. Soc. Mass Spectrom. 5*, 959–965.

(218) Jaquinod, M., Leize, E., Potier, N., Albrecht, A. M., Shanzer, A., and Van Dorsselaer, A. (1993) Characterisation of non-covalent complexes by electrospray mass spectrometry. *Tetrahedron Lett. 34*, 2771–2774.

(219) Pleasance, S., Thibault, P., and Thompson, J. (1990) An evaluation of ion spray mass spectrometry for the analysis of metallothioneins. *Proceedings of the 38th ASMS Conference on Mass Spectrometry and Allied Topics*, Tucson, AZ, pp 720–721, American Society for Mass Spectrometry, East Lansing, MI.

(220) Surovoy, A., Waidelich, D., and Jung, G. (1992) Nucleocapsid protein of HIV-1 and its Zn^{2+} complex formation analysis with electrospray mass spectrometry. *FEBS Lett. 311*, 259–262.

(221) Fenselau, C., Yu, X., Bryant, D., Bowers, M. A., Sowder, R. C., II, and Henderson, L. E. (1994) Characterization of processed gag proteins from highly replicating HIV-1MN. *Mass Spectrometry for the Characterization of Microorganisms* (C. Fenselau, Ed.) ACS Symposium Series, pp 159–172, American Chemical Society, Washington, DC.

(222) Kelly, M., Lappalainen, P., Talbo, G., Haltia, T., Vanderoost, J., and Saraste, M. (1993) Two cysteines, two histidines, and one methionine are ligands of a binuclear purple copper center. *J. Biol. Chem. 268*, 16781–16787.

(223) Hu, P., and Loo, J. A. (1995) Determining calcium-binding stoichiometry and cooperativity of parvalbumin and calmodulin by mass spectrometry. *J. Mass Spectrom. 30*, 1076–1082.

(224) Witkowska, H. E., Shackleton, C. H. L., Dahlman-Wright, K., Kim, J. Y., and Gustafsson, J.-A. (1995) Mass spectrometric analysis of a native zinc-finger structure: the glucocorticoid receptor DNA binding domain. *J. Am. Chem. Soc.* 117, 3319–3324.

(225) Lane, T. F., Iruelaarispe, M. L., Johnson, R. S., and Sage, E. H. (1994) SPARC is a source of copper-binding peptides that stimulate angiogenesis. *J. Cell Biol. 125,* 929–943.

(226) Moreau, S., Awade, A. C., Molle, D., Le Graet, Y., and Brule, G. (1995) Hen egg white lysozyme-metal ion interactions: Investigation by electrospray ionization mass spectrometry. *J. Agric. Food Chem. 43,* 883–889.

(227) Loo, J. A., Ogorzalek Loo, R. R., Goodlett, D. R., Smith, R. D., Fuciarelli, A. F., Springer, D. L., Thrall, B. D., and Edmonds, C. G. (1993) Elucidation of covalent modifications and noncovalent associations in proteins by electrospray ionization mass spectrometry. *Techniques in Protein Chemistry IV* (R. H. Angeletti, Ed.) pp 23–31, Academic Press, San Diego, CA.

(228) Loo, J. A., Giordani, A. G., and Muenster, H. (1993) Observation of intact (heme-bound) myoglobin by electrospray ionization on a double-focusing mass spectrometer. *Rapid. Commun. Mass Spectrom. 7,* 186–189.

(229) Li, Y.-T., Hsieh, Y.-L., Henion, J. D., and Ganem, B. (1993) Studies on heme binding in myoglobin, hemoglobin, and cytochrome c by ion spray mass spectrometry. *J. Am. Soc. Mass Spectrom. 4,* 631–637.

(230) Konishi, Y., and Feng, R. (1994) Conformational stability of heme proteins *in vacuo. Biochemistry 33,* 9706–9711.

(231) Ganem, B., and Henion, J. D. (1993) Detecting noncovalent complexes of biological macromolecules: New applications of ion-spray mass spectrometry. *Chemtracts—Org. Chem. 6,* 1–22.

(232) McLuckey, S. A., and Ramsey, R. S. (1994) Gaseous myoglobin ions stored at greater than 300 K. *J. Am. Soc. Mass Spectrom. 5,* 324–327.

(233) Li, Y. T., Hsieh, Y. L., Henion, J. D., Ocain, T. D., Schiehser, G. A., and Ganem, B. (1994) Analysis of the energetics of gas-phase immunophilin ligand complexes by ion spray mass spectrometry. *J. Am. Chem. Soc. 116,* 7487–7493.

(234) Henion, J., Li, Y. T., Hsieh, Y. L., and Ganem, B. (1993) Mass spectrometric investigations of drug–receptor interactions. *Ther. Drug Monit. 15,* 563–569.

(235) Bakhtiar, R., and Stearns, R. A. (1995) Studies on noncovalent associations of immunosuppressive drugs with serum albumin using pneumatically assisted electrospray ionization mass spectrometry. *Rapid Commun. Mass Spectrom. 9,* 240–244.

(236) Drummond, J. T., Ogorzalek Loo, R. R., and Matthews, R. G. (1993) Electrospray mass spectrometric analysis of the domains of a large enzyme: observation of the occupied cobalamin-binding domain and redefinition of the carboxyl terminus of methionine synthase. *Biochemistry 32,* 9282–9289.

(237) Siuzdak, G., Krebs, J. F., Benkovic, S. J., and Dyson, H. J. (1994) Binding of hapten to a single-chain catalytic antibody demonstrated by electrospray mass spectrometry. *J. Am. Chem. Soc. 116,* 7937–7938.

(238) Baca, M., and Kent, S. B. H. (1992) Direct observation of a ternary complex between the dimeric enzyme HIV-1 protease and a substrate-based inhibitor. *J. Am. Chem. Soc. 114,* 3992–3993.

(239) Aplin, R. T., Robinson, C. V., Schofield, C. J., and Westwood, N. J. (1994) Does the observation of noncovalent complexes between biomolecules by electrospray ionisation mass spectrometry necessarily reflect specific solution interactions? *J. Chem. Soc., Chem. Commun.* 2415–2417.

(240) Tuong, A., Uzabiaga, F., Petitou, M., Lormeau, J. C., and Picard, C. (1994) Direct observation of the non-covalent complex between human antithrombin III and its heparin binding sequence by capillary electrophoresis and electrospray mass spectrometry. *Carbohydr. Lett. 1,* 55–60.

(241) Ganem, B., Li, Y. T., Hsieh, Y. L., Henion, J. D., Kaboord, B. F., Frey, M. W., and Benkovic, S. J. (1994) Analysis of the stoichiometry of the T4 gene 45 protein by ion spray mass spectrometry. *J. Am. Chem. Soc. 116,* 1352–1358.

(242) Green, B. N., and Oliver, R. W. A. (1995) ESI-MS analysis of the transthyretin tetramer and some non-covalent adducts. *Proceedings of the 43rd ASMS Conference on Mass Spectrometry and Allied Topics,* Atlanta, GA, American Society for Mass Spectrometry, Santa Fe, NM (in press).

(243) Camilleri, P., and Haskins, N. J. (1993) Investigating the noncovalent interaction of cytidylic acids with ribonuclease A by electrospray mass spectrometry. *Rapid Commun. Mass Spectrom. 7,* 603–604.

(244) Haskins, N. J., Ashcroft, A. E., Phillips, A., and Harrison, M. (1994) The evaluation of several electrospray systems and their use in non-covalent bonding systems. *Rapid Commun. Mass Spectrom. 8,* 120–125.

(245) Jaquinod, M., Potier, N., Klarskov, K., Reymann, J. M., Sorokine, O., Kieffer, S., Barth, P., Andriantomanga, V., Biellmann, J. F., and Van Dorsselaer, A. (1993) Sequence of pig lens aldose reductase and electrospray mass spectrometry of non-covalent and covalent complexes. *Eur. J. Biochem. 218,* 893–903.

(246) Ganguly, A. K., Pramanik, B. N., Tsarbopoulos, A., Covey, T. R., Huang, E., and Fuhrman, S. A. (1992) Mass spectrometric detection of the noncovalent GDP-bound conformational state of the human H-ras protein. *J. Am. Chem. Soc. 114,* 6559–6560.

(247) Ganguly, A. K., Pramanik, B. N., Huang, E. C., Tsarbopoulos, A., Girijavallabhan, V. M., and Liberles, S. (1993) Studies of the ras-GDP and ras-GTP noncovalent complexes by electrospray mass spectrometry. *Tetrahedron 49,* 7985–7996.

(248) Hsieh, Y. L., Li, Y. T., Henion, J. D., and Ganem, B. (1994) Studies of non-covalent interactions of actinomycin D with single-stranded oligodeoxynucleotides by ion spray mass spectrometry and tandem mass spectrometry. *Biol. Mass Spectrom. 23,* 272–276.

(249) Griffith, M. C., Risen, L. M., Greig, M. J., Lesnik, E. A., Sprankle, K. G., Griffey, R. H., Kiely, J. S., and Freier, S. M. (1995) Single and bis peptide nucleic acids as triplexing agents: Binding and stoichiometry. *J. Am. Chem. Soc. 117,* 831–832.

(250) Selva, A., Redenti, E., Zanol, M., Ventura, P., and Casetta, B. (1993) A study of β-cyclodextrin and its inclusion complexes with piroxicam and terfenadine by ionspray mass spectrometry. *Org. Mass Spectrom. 28,* 983–986.

(251) Sorokine, O., Letavernier, J. F., Leize, E., Ropenga, J., and Van Dorsselaer, A. (1992) Characterization of cyclodextrins and their inclusion compounds by mass spectrometry in electrospray mode. *Congr. Int. Technol. Pharm., 6th 5,* 423–430.

(252) Camilleri, P., Haskins, N. J., New, A. P., and Saunders, M. R. (1993) Analysing the complexation of amino acids and peptides with β-cyclodextrin using electrospray ionization mass spectrometry. *Rapid Commun. Mass Spectrom. 7,* 949–952.

(253) Camilleri, P., Haskins, N. J., and Howlett, D. R. (1994) β-Cyclodextrin interacts with the alzheimer amyloid β-A4 peptide. *FEBS Lett. 341,* 256–258.

(254) Bates, P. S., Parker, D., and Green, B. N. (1993) Characterisation of the complexation behaviour of lipophilic cyclodextrins by electrospray mass spectrometry. *J. Chem. Soc., Chem. Commun.* 693–696.

(255) Bates, P. S., Kataky, R., and Parker, D. (1994) Functionalized cyclodextrins as potentiometric sensors for onium ions. *Analyst 119,* 181–186.

(256) Haskins, N. J., Saunders, M., and Camilleri, P. (1994) The complxation and chiral selectivity of 2-hydroxypropyl-β-cyclodextrin with guest molecules as studied by electrospray mass spectrometry. *Rapid Commun. Mass Spectrom. 8,* 423–426.

(257) Lippmann, T., Wilde, H., Pink, M., Schafer, A., Hesse, M., and Mann, G. (1993) Host-guest complexes between calix[4]arenes derived from resorcinol and alkylammonium ions. *Angew. Chem., Int. Ed. Engl. 32,* 1195–1197.

(258) Kondo, T., Ueda, M., Yoshida, K., Titani, K., Isobe, M., and Goto, T. (1994) Direct observation of a small-molecule associated supramolecular pigment, commelinin, by electrospray ionization mass spectroscopy. *J. Am. Chem. Soc. 116,* 7457–7458.

(259) Siuzdak, G., Ichikawa, Y., Caulfield, T. J., Munoz, B., Wong, C. H., and Nicolaou, K. C. (1993) Evidence of Ca(2+)-dependent carbohydrate association through ion spray mass spectrometry. *J. Am. Chem. Soc. 115,* 2877−2881.

(260) Russell, K. C., Leize, E., Van Dorsselaer, A., and Lehn, J.-M. (1995) Investigation of self-assembled supramolecular species in solution by IL-ESMS, a new mass spectrometric technique. *Angew. Chem., Int. Ed. Engl. 34,* 209−213.

(261) Cheng, X., Gao, Q., Smith, R. D., Simanek, E. E., Mammen, M., and Whitesides, G. M. (1995) Detection of hydrogen-bonded supramolecular complexes using electrospray ionization from chloroform. *Rapid Commun. Mass Spectrom. 9,* 312−316.

(262) Leize, E., Van Dorsselaer, A., Kramer, R., and Lehn, J.-M. (1993) Electrospray mass spectrometry of the self-assembly of a capped polymetallic complex. *J. Chem. Soc., Chem. Commun.* 990−993.

ARTICLES

IL2–Ricin Fusion Toxin Is Selectively Cytotoxic *in Vitro* to IL2 Receptor-Bearing Tumor Cells

Arthur Frankel,*,[†] Edward Tagge,[‡] John Chandler,[‡] Chris Burbage,[†] Greg Hancock,[†] Joseph Vesely,[§] and Mark Willingham[§]

Departments of Medicine, Surgery, and Pathology, Medical University of South Carolina, Charleston, South Carolina 29425. Received April 12, 1995[⊛]

Fusion toxins consist of peptide ligands linked through amide bonds to polypeptide toxins. The ligand directs the molecule to the surface of target cells and the toxin enters the cytosol and induces cell death. Ricin toxin is an excellent candidate for use in fusion toxins because of its extreme potency, the extensive knowledge of its atomic structure, and the years of experience with RTA chemical conjugates in clinical trials. We synthesized a baculovirus transfer vector with the polyhedrin promoter followed sequentially from the 5′ end with DNA encoding the gp67A leader sequence, the tripeptide ADP, IL2, another ADP tripeptide, and RTB. Recombinant baculovirus was generated in Sf9 insect cells and used to infect Sf9 cells. Recombinant IL2-RTB protein was recovered at high yields from day 5 insect cell supernatants, partially purified by affinity chromatography, and characterized. The recombinant product was soluble and immunoreactive with antibodies to RTB and IL2, bound asialofetuin and lactose, and reassociated with RTA. In the presence of lactose to block galactose-binding sites on RTB, the IL2–RTB–RTA heterodimer was selectively cytotoxic to IL2 receptor, bearing cells. Specific cytotoxicity could be blocked with IL2. Thus, we report a novel targeted plant toxin fusion protein with full biological activity.

INTRODUCTION

Ricin toxin, the 65 kDa heterodimeric glycoprotein from castor bean seeds, consists of a lectin B chain (RTB)[1] disulfide linked to an enzymatic A chain (RTA) (*1*). Ricin intoxication of mammalian cells involves sequentially (a) RTB binding to β-galactosyl pyranoside groups on cell surface glycoproteins (*2*), (b) internalization by endocytosis (*3*), (c) transfer to the TR Golgi (*4*), (d) routing to a critical organelle, possibly the endoplasmic reticulum (*5*), (e) disulfide bond reduction with release of RTA (*6*), (f) translocation of RTA to the cytosol, and (g) catalytic inactivation of protein synthesis by hydrolysis and release of an adenine base from the elongation factor binding site of 26S rRNA in the 60S ribosomal subunit (*7*). A single molecule of ricin introduced into a cell can lead to cell death (*8*).

Because of this extreme potency, a number of groups have attached RTA or modified ricin molecules to new ligands to achieve selective cell killing *in vitro* and *in vivo* and then used these immunotoxins systemically in patients with refractory neoplasms. The Fab′ fragment of a murine monoclonal anti-CD22 antibody was coupled to chemically deglycosylated RTA and administered intravenously to patients with B-cell lymphomas (*9*).

While 50% of patients with antigen on the tumor cell surfaces showed a partial response, significant dose-limiting toxicity to vascular endothelium was observed. The small size (80 000 Mr) of the conjugate may have facilitated tumor penetration, but no studies of drug distribution were done. Mouse antibody to CD22 was coupled to chemically deglycosylated RTA and administered to lymphoma patients (*10*). Both partial and complete responses were observed, but again vascular leak syndrome was the dose-limiting toxicity. Higher peak concentration of immunotoxin in the serum, longer $T_{1/2}$, and larger AUC correlated with vascular injury. Murine monoclonal antibody to CD5 ws thiolated and coupled to RTA and administered to patients with chronic lymphocytic leukemia (*11*). At doses up to 16 mg/m², no immunotoxin could be demonstrated at extravascular sites. Mouse antibody to a 55 kDa epithelial cell surface glycoprotein was derivatized and conjugated to recombinant RTA and infused into patients with metastatic breast carcinoma (*12*). Four out of five patients developed anti-mouse Ig and anti-RTA antibodies. Ricin toxin was chemically blocked with an affinity ligand and cross-linked to an anti-CD19 monoclonal antibody (*13*). After administration to patients with lymphoma, different preparations of immunotoxin produced different degrees of hepatocyte damage. Further analysis revealed product heterogeneity with the more toxic species having one to two affinity ligands per ricin and the less toxic species with three affinity ligands per ricin. Thus, pharmacologic properties of drug heterogeneity, poor drug penetration, normal tissue toxicity, and immunogenicity have reduced the therapeutic index (ratio of dose producing toxicity/dose producing clinical efficacy) in clinical trials with RTA or blocked ricin immunotoxins. Methods have been

---

* Address correspondence to this author at the following address: Hollings Cancer Center Rm 306, MUSC, 171 Ashley Ave., Charleston, SC 29425. Tel: 803-792-1450. Fax: 803-792-3200.
† Department of Medicine.
‡ Department of Surgery.
§ Department of Pathology.

[1] Abbreviations: IL2, interleukin-2; RTB, ricin toxin B chain; RTA, ricin toxin A chain; IL2–RTB, fusion protein of interleukin-2 and ricin B chain.

sought to improve the pharmacologic properties of these protein therapeutics.

One approach has been to genetically engineer the toxin and ligand into a single well-defined molecule. Normal cell binding portions of diphtheria toxin and *Pseudomonas* exotoxin have been deleted and replaced with growth factors and single chain Fv's (*14, 15*). Clinical trials with TGFα-PE40 and DAB$_{389}$IL2 bacterial fusion toxins have shown excellent tolerance (minimal side effects or toxicities) and significant clinical activity (*16, 17*). A fusion protein consisting of basic fibroblast growth factor and the ribosome-inactivating protein saporin (FGF-SAP) has been expressed in *E. coli* (*18*). FGF-SAP demonstrated potent specific cell cytotoxicity (ID$_{50}$ = 5 × 10^{-11} M) and inhibited growth of B16 melanomas both in subcutaneous implants and lung metastases in mice. Surprisingly, few studies have been done directly comparing fusion toxins with chemical conjugates. Lappi reported no difference in vitro or in vivo between FGF-SAP linked by a cross-linker or by an amide bond (*18*). Kreitman compared anti-Tac-PE with the single chain fusion toxin anti-Tac(Fv)-PE40 (*19, 20*). In vitro and in vivo, the fusion toxin was approximately 1 log more active. An additional advantage of the fusion toxin was the reagent homogeneity.

Attempts have been undertaken to produce genetically engineered ricin or RTA fusion proteins, in part because of the extensive clinical experience with RTA and blocked ricin immunotoxins showing safety in patients (*9–13*) and, in part, due to the potential use of ricin fusion toxins in patients who have developed resistance to diphtheria toxin or *Pseudomonas* exotoxin fusion proteins. RTA inactivates protein synthesis by specifically depurinating a conserved adenosine in the 60S ribosomal subunit, while diphtheria toxin and *Pseudomonas* exotoxin act by ADP-ribosylating EF-2 (*7*). Thus, malignant cells are unlikely to show cross-resistance to both plant and bacterial toxins. Further, the amino acid sequence and three-dimensional structure of ricin is distinct (*21*) from the diphtheria toxin and *Pseudomonas* exotoxin, and thus, antibodies to one toxin do not react with the other toxins (unpublished observations). An RTA–diphtheria toxin loop–Staphylococcal protein A fusion protein was expressed in *E. coli*, enzymatically cleaved with trypsin, mixed with antibody, and exposed to antigen positive cells (*22*). Selective cytotoxicity was demonstrated. However, the fusion toxin antibody conjugate had unfavorable properties. The disulfide loop was exposed on the surface of the conjugate and readily reduced. The RTA–diphtheria toxin–protein A–immunoglobulin conjugate was very large (>200 000 Da). The conjugate was heterogeneous due to varying sites of protein A-immunoglobulin binding. Subsequently, tripartate fusion proteins were produced in *E. coli* with IL2–diphtheria toxin loop–RTA or IL2–factor Xa recognition sequence–RTA (*23*). Proteolytic cleavage with trypsin or factor Xa released the IL2 ligand and toxin without recovery of disulfide-linked product. Uncleaved chimeras showed no cytotoxicity to IL2 receptor-bearing cells. Finally, a factor Xa-specific site was introduced into the linker sequence of proricin and the modified proricin expressed in *Xenopus* oocytes (*24*). Although recombinant mutant proricin was produced, yields were in the nanogram range and protease sensitivity was low. Further, no fusion proteins with IL2 binding specificities were made.

We chose an alternative approach for genetic engineering of ricin. Previous studies document the need for an accessible disulfide bridge between ligand and RTA (*6, 22*). Consequently, we chose to produce recombinant RTB fusion proteins with novel ligands and reassociate

the molecule with RTA to recreate the natural disulfide bridge between RTA and RTB. The ligand was attached to the N-terminus of RTB based on our previous experience with an oligohistidine tag and the X-ray crystallographic structure of ricin (*21, 25*). In the present study, we synthesized DNA encoding the GP67A leader peptide, IL2, and RTB. Recombinant protein was expressed and secreted from insect cells. The fusion molecule was purified, reassociated with plant RTA, and tested for selective cytotoxicity to IL2 receptor positive cells in the presence of lactose.

EXPERIMENTAL PROCEDURES

Materials. Restriction endonucleases and T4 ligase were obtained from Promega (Madison, WI). [^{32}P]dCTP, [^{35}S]dATP, [^{3}H]leucine were obtained from Amersham (Arlington Heights, IL). Rabbit antiricin antibody, alkaline phosphatase conjugated goat anti-(rabbit IgG), alkaline phosphatase conjugated goat anti-(mouse IgG), asialofetuin, α-lactose, and other chemicals were from Sigma (St. Louis, MO). EX-CELL400 medium was obtained from JRH Scientific (Lexena, KS). Sf9 insect cells, TMNFH medium, BaculoGold DNA, and pAcGP67A transfer fector were from PharMingen (San Diego, CA). Prep-A-Gene DNA and plasmid purification matrices, low molecular weight prestained protein standardards, nitrocellulose paper, and other reagents for protein analysis were obtained from BioRad (Hercules, CA). The Sequenase kit for dideoxy sequencing was obtained from USB (Cleveland, OH). The Random Primer labeling kit was obtained from Stratagene (La Jolla, CA). Purified P2, P8, and P10 murine monoclonal antibodies to RTB and purified αBR12 murine monoclonal antibody to RTA were gifts of Dr. Walter Blattler, ImmunoGen (Cambridge, MA). RPMI1640 media, leucine-free RPMI1640, penicillin, streptomycin, Dulbecco's PBS, fetal bovine serum, and dialyzed fetal bovine serum were obtained from GIBCO BRL (Grand Island, NY). 3M Emphaze Biosupport medium AB1 azlactone functionality bis-acrylamide and lactosyl acrylamide were obtained from Pierce (Rockford, IL). The alkaline phosphatase Vectastain kit for Western blots was obtained from Vector Laboratories (Burlingame, CA). EIA plates and round-bottomed and flat-bottomed 96-well plates were from Costar (Cambridge, MA). Plant RTB, ricin, and RTA were obtained from Inland Laboratories (Austin, TX).

Construction of Plasmid. pDW27 plasmid containing DAB$_{389}$IL2 DNA was a gift of Dr. John Murphy (Boston University) (*27*). PCR was performed with pDW27 plasmid encoding DAB$_{389}$IL2 and the 5′ oligonucleotide 5′-GCAGCATCAGGATCCCGCACCTACTTC-TA-GCTCT-3′, which introduces a BamHI site followed by a CCC proline codon followed by DNA encoding the first six codons of IL2. The 3′ oligonucleotide was 5′-AGCTGCAGATGGAT-CGCGGTCAGGGTAGAGAT-GAT-3′, which contains the last six codons of IL2 followed by a GC and a BamHI site. The PCR product, which provided an IL2 DNA BamHI cassette maintaining the proper reading frame at both ends with the GP67A leader and RTB, was purified on a silica matrix (Prep-A-Gene, BioRad), digested with BamHI, and subcloned in BamHI restricted pAcGP67A-RTB plasmid (*24*). The final vector was double-stranded dideoxy sequenced by the Sanger method with Sequenase reagents (USB). One liter cultures of transformed *E. coli* were subjected to alkaline lysis, and the plasmid was purified by cesium chloride density gradient centrifugation.

Expression of Fusion Toxin. A 2 × 10^6 Sf9 sample of *S. frugiperda* ovarian cells maintained in TMNFH medium supplemented with 10% fetal calf serum was

cotransfected with pAcGP67A−IL2−RTB DNA (4 μg) and 0.5 μg of BaculoGold AcNPV DNA following the recommendations of the supplier (PharMingen). At 5 days post-transfection, medium was centrifuged and the supernatant tested in a limiting dilution assay with Sf9 cells and dot blots with random primer ^{32}P-dCTP labeled RTB DNA (Stratagene Prime-It kit) as previously described (*28*). Positive wells were identified and supernatants reassayed by limiting dilution until all wells up to 10^{-7} dilution were positive. Two rounds of selection were required. Recombinant virus in the supernatant was then amplified by infecting Sf9 cells at a multiplicity of infection (moi) of 0.1, followed by collection of day 7 supernatants. Recombinant baculovirus was then used to infect 2×10^8 Sf9 cells at an moi of 5 in 150 mL of EX-CELL400 medium (JRH Scientific) with 50 mM α-lactose in spinner flasks. Media supernatants containing IL2−RTB were collected day 6 postinfection.

Purification of IL2−RTB. Media supernatants were adjusted to 0.01% sodium azide and maintained through all purification steps at 4 °C. The supernatants were concentrated 15-fold by vacuum dialysis, centrifuged at 3000*g* for 10 min to remove precipitate, dialyzed against 50 mM NaCl, 25 mM Tris pH 8, 1 mM EDTA, 0.01% sodium azide, and 25 mM α-lactose (NTEAL), ultracentrifuged at 100000*g* for 1 h, and bound and eluted from a P2 monoclonal antibody−acrylamide matrix as previously described (*28*). P2 is an anti-RTB monoclonal antibody. The affinity matrix was prepared using Ultralink azalactone functionality bis-acrylamide following the recommendations of the manufacturer. Recombinant protein was adsorbed to the column in NTEAL, washed with 500 mM NaCl, 25 mM Tris pH 8, 1 mM EDTA, 0.1% Tween 20, 0.01% sodium azide, and 25 mM α-lactose, and eluted with 0.1 M triethylamine hydrochloride pH 11. The eluant was neutralized with 1/10 volume 1 M sodium phosphate pH 4.25 and stored at −20 °C until assayed. Four preparations were made.

Molecular Weight Determination. Aliquots of IL2-RTB, recombinant RTB, plant RTB (Inland Laboratories), and prestained low molecular weight standards (BioRad) were run on a reducing 15% SDS/PAGE, stained with Coomassie Blue R-250, dried between cellophane sheets, and scanned on a IBAS 2000 automatic image analysis system (Kontron, Germany).

Immunological Characterization. Aliquots of IL2-RTB, bacterial IL2 (Chiron), wild-type recombinant RTB, plant RTB, and prestained low molecular weight protein standards were run on a reducing 15% SDS−PAGE, transferred to nitrocellulose, blocked with 10% Carnations nonfat dry milk/0.1% BSA/0.1% Tween 20, washed with PBS plus 0.05% Tween 20, reacted with either 1:400 rabbit antibody to ricin (Sigma) or 1:100 mouse monoclonal antibody to IL2 (Genzyme), rewashed, incubated with alkaline phosphatase conjugated goat anti-(rabbit IgG) or anti-(mouse IgG) (Sigma), washed again, and developed with the Vectastain alkaline phosphatase kit (Vector Laboratories).

Costar EIA microtiter wells were coated with 100 μL of 5 μg/mL of monoclonal antibody P2, P8, or P10 reactive with RTB (gifts of Dr. Walter Blattler, ImmunoGen) or monoclonal antibody to IL2 (Genzyme), washed with PBS plus 0.1% Tween 20, blocked with 3% BSA, rewashed, and incubated with samples of IL-2-RTB or plant RTB, rewashed, reacted with 1:400 rabbit antibody to ricin, washed again, incubated with 1:5000 alkaline phosphatase conjugated goat anti-(rabbit IgG), rewashed, developed with 1 mg/mL of *p*-nitrophenyl phosphate in diethanolamine buffer pH 9.6, and read on a BioRad 450 Microplate reader at 405 nm.
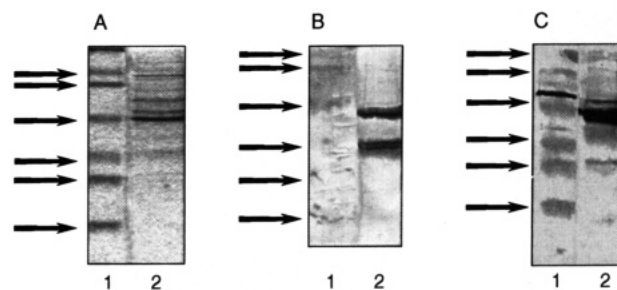
Figure 1. Fifteen percent reducing SDS−PAGE of IL2−RTB. (A) Coomassie stained. Lane 1: low molecular weight prestained BioRad protein standards as marked by arrows and are 20 000, 28 500, 34 400, 52 ,000, 86 000, and 112 000 daltons; lane 2: IL2−RTB. (B) Immunoblot using rabbit anti-ricin antibody. Lane 1: low molecular weight protein standards marked by arrows as above. Lane 2: IL2−RTB. (C) Immunoblot using mouse anti-IL2 antibody. Lane 1: low molecular weight standards. Lane 2: IL2−RTB.

Measurement of Lectin Activity. Asialofetuin (1 μg/mL) was bound to Costar EIA plate wells, and an ELISA was performed as previously detailed with samples of IL2−RTB and plant RTB (*28*). Samples of freshly reduced IL2−RTB were diluted in 50 mM NaCl/25 mM Tris pH 8/1 mM EDTA/0.01% sodium azide (NTEA), loaded on a lactosyl acrylamide matrix (Pierce), and washed with NTEA, and the lactose binding protein was eluted with NTEA plus 50 mM lactose. Fractions were assayed for RTB immunoreactive material using the P2 antibody ELISA described above.

Formation of Recombinant Heterodimer. Thirty μg of IL2−RTB was mixed with 90 μg of plant RTA in a total volume of 1 mL of PBS and then shaken overnight at room temperature. The reaction mixture was then analyzed by a ricin ELISA previously described (*25*). Reassociated mixtures were also analyzed by nonreducing SDS−PAGE followed by immunoblots with P10 anti-RTB monoclonal antibody and monoclonal antibody to IL2. Densitometric scanning with the automatic image analysis system was done to quantify the shift of immunoreactive material from 50 to 80 kDa.

Cytotoxicity to Mammalian Cells. Measurement of protein synthesis inhibition by ricin, IL2−RTB−RTA, and DAB$_{389}$IL2 (*14*) in cultured cells was done as previously described using HUT102 human T leukemia cells bearing the high affinity IL2 receptor, CEM human T leukemia cells bearing the intermediate affinity IL2 receptor, and OVCAR3 human ovarian carcinoma cells lacking the IL2 receptor. All three cell lines were obtained from the American Type Culture Collection (Rockville, MD). HUT102 cells intermittently release HTLV-1 and should be handled with care. All assays were performed in triplicate. In some experiments duplicate samples were incubated in the presence of 20 μg/mL of IL2 (Chiron). The ID$_{50}$ was the concentration of protein which inhibited protein synthesis by 50% compared with control.

A total of 1.5×10^4 HUT102 cells were placed in sterile Eppendorf tubes at 4 °C in 100 μL of leucine-poor RPMI1640 + 10% dialyzed fetal calf serum + 60 mM α-lactose with or without 20 μg/mL of IL2. Dilutions of IL2−ricin and ricin at varying concentrations were added in identical medium with or without IL2 and incubated at 4 °C for 30 min. Cells were pelleted at 2000*g* for 5 min, washed once with leucine-poor RPMI1640 + 10% dialyzed fetal calf serum + 60 mM α-lactose, resuspended in 150 μL of the same medium, and incubated at 37 °C in 5% CO_2 for 24 h. [^{3}H]leucine was added as above, and 4 h later cells were harvested with the PhD cell harvester
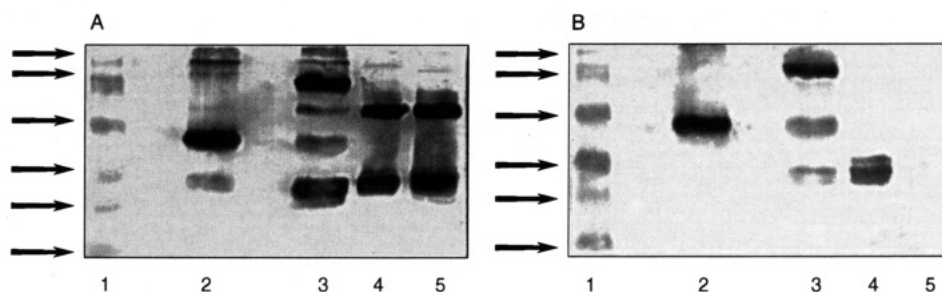
Figure 2. Fifteen percent nonreducing SDS–PAGE of IL2–RTB–RTA. (A) Immunoblot using mouse monoclonal antibody P10 to RTB. Lane 1: low molecular weight standards. Lane 2: IL2–RTB. Lane 3: IL2–RTB–RTA. Lane 4: RTA–plant RTB. Lane 5: RTA–recombinant RTB. (B) Immunoblot using mouse monoclonal antibody to IL2. Lane 1: low molecular weight standards. Lane 2: IL2–RTB. Lane 3: IL2–RTB–RTA. Lane 4: RTA–plant RTB. Lane 5: RTA–recombinant RTB. Densitometry of gel B confirmed 85% of the RTA immunoreactive material migrated at 80 kDa after reassociation.

and incorporated [^{3}H]leucine measured in a liquid scintillation counter. Blocking of selective cytotoxicity was estimated by comparing the ID$_{50}$ of toxins in the presence or absence of IL2 + lactose. There was no purification step after heterodimer reassociation. The free RTA concentration at the highest concentration of heterodimer in the assay (5×10^{-7} M) was 10^{-7} M. On all three cell lines, the ID$_{50}$ for free RTA was (2–3×10^{-6} M) (unpublished results). Thus, in the range of heterodimer ID$_{50}$'s (10^{-10}–10^{-12} M), the free RTA concentration (2×10^{-11} M to 2×10^{-13} M) should not produce cytotoxicity.

RESULTS

Yield and purity of IL2–RTB. Material post-affinity chromatography was subjected to SDS–PAGE and Coomassie staining (Figure 1A). Over 80% of the protein migrated as a single band at 50 kDa. On the basis of absorbance at 280 nm (1 mg/mL produced an OD$_{280}$ = 1.4) and densitometry, 1 mg/mL fusion protein was secreted per liter of insect cell culture. The major contaminants at 55, 60, and 90 kDa were not reactive with murine antibodies against RTA or IL2 and appeared in media of cells after lysis from wild-type AcNPV virus. They presumably represent insect cell derived proteins. Individual batches of IL2-RTB of about 150 μg were recovered from 150 mL of infected insect cell supernatants and were each adequate for all the studies undertaken.

Immunologic Cross-Reactivity. Immunoblots demonstrated reactivity with the same 52 kDa band using anti-RTB or anti-IL2 antibodies (Figure 1B,C). Interestingly, weaker bands of approximately 10–15% intensity relative to the 52 kDa band were observed at 35 kDa reactive with anti-RTB and 20 kDa reactive with anti-IL2 suggesting partial proteolysis occurred either intracellularly or in the medium. The site(s) of cleavage are unknown, but the size of the fragments and their specific reactivities with antibodies suggest the predominant site of cleavage is between the RTB and IL2 domain. This is not unusual for chimeras, as the secondary structure is likely to be least between domains.

Antibody ELISA's demonstrated similar reactivity of IL2–RTB and plant RTB with anti-RTB monoclonal antibodies. Relative to plant RTB, the monoclonal antibody P2 reacted 66% as well with IL2–RTB. P8 and P10 monoclonal antibodies reacted 100% as well with IL2-RTB molecules as with plant RTB. Anti-IL2 antibody reacted with at least 70% of the RTB immunocrossreactive molecules on a molar basis.

Lectin Activity. α-Lactose was coupled through the 6-hydroxyl groups of the glucosyl moiety to acrylamide, and binding of lectins was assessed. Plant RTB bound 100% to immobilized lactose, while 80% of recombinant wild-type RTB could be bound and eluted from lactosyl

Table 1. Cell Cytotoxicity of Toxins to Various Cell Lines

protein	ID$_{50}$ (M)		
	HUT102	CEM	OVCAR3
ricin	$(5 \pm 2) \times 10^{-10}$	$(2 \pm 1) \times 10^{-10}$	$(5 \pm 3) \times 10^{-10}$
IL2–RTB–RTA	$(4 \pm 1) \times 10^{-12}$	$(2 \pm 1) \times 10^{-10}$	$(6 \pm 2) \times 10^{-10}$
DAB$_{389}$IL2	$(2 \pm 1) \times 10^{-12}$	$(5 \pm 3) \times 10^{-9}$	$>10^{-8}$

[a] 2×10^4 cells in 150 μL of leucine-free RPMI1640 plus 60 mM α-lactose were combined with dilutions of toxins for 24 h at 37 °C/5% CO$_2$. 1 μCi/well ^{3}H leucine in 50 μL of the same media was added for 4 h at 37 °C/5% CO$_2$. Cells were harvested with a PhD cell harvestor on glass fiber mats, dried, and counted in Econofluor in a LKB liquid scintillation counter. ID$_{50}$ was the concentration of toxin reducing protein synthesis by 50%. Each assay perfomed three times. Standard deviations shown with mean.

acrylamide. Thirty percent of IL2–RTB attached to the matrix and eluted with 50 mM α-lactose.

Asialofetuin consists of the bovine serum protein fetuin from which the terminal sialic acids have been chemically removed, exposing galactosyl residues. Binding of IL2–RTB to asialofetuin adsorbed on microtiter wells provides an independent assay of galactose binding affinity. The asialofetuin ELISA demonstrated that IL2–RTB bound immobilized asialofetuin 59% as well as plant RTB and wild-type recombinant RTB. Both the lactose binding and asialofetuin binding assays suggest the fusion molecule retains much of the lectin activity of wild-type recombinant RTB. The slight reduction in binding affinity may be secondary to steric hindrance by IL2 or misfolding affecting one or more sugar-combining subdomains. This residual lectin property is not desirable for an *in vivo* therapeutic molecule.

Reassociation with RTA. IL2–RTB provides a ligand function and coupling function for the fusion toxin, but the polypeptide must be linked to RTA for cytotoxicity. RTB has numerous amino acid residues which interact with RTA and promote both stabilization of the toxic heterodimer and protection of the intersubunit disulfide bridge (*21*). Provided the IL2 amino acid residues do not lead to misfolding or steric hindrance of the interface sidechains, reassociation of IL2–RTB with RTA should occur spontaneously at concentrations of 10^{-6} M or higher of each component (*26*). Under the reaction conditions (10^{-6} M, PBS, room temperature, room air), 50% reassociation was achieved with plant RTA and either plant or recombinant RTB. Under identical conditions, 60% reassociation of IL2–RTB occurred based on ricin ELISA and immunoblots with anti-RTB antibody (Figure 2).

Cell cytotoxicity. Cytotoxicities of recombinant proteins and plant ricin for different cell lines are shown in Table 1. IL2–RTB alone was nontoxic (ID$_{50}$ > 10^{-8} M) for all the cell lines tested. Ricin and IL2–ricin showed some toxicity (ID$_{50}$ = 1–6×10^{-10} M) to IL2 receptor

negative cell lines in the presence of 60 mM α-lactose (Figure 3B,C). This residual toxicity is due to the presence of lectin binding sites on ricin and IL2−ricin that are incompletely blocked by 60 mM α-lactose. In contrast, IL2−ricin but not ricin was much more toxic to the IL2 receptor-positive HUT102 cells ($ID_{50} = 4 \times 10^{-12}$ M) in the presence of lactose (Figure 3A). The *in vitro* therapeutic window with lactose in the media was 125-fold. The control fusion toxin, $DAB_{389}IL2$, also showed selective toxicity to IL2 receptor-bearing cells. Since $DAB_{389}IL2$ lacks residual normal cell binding domains, the toxicity to nonreceptor bearing cells was considerably less (ID_{50}'s = $(5-15) \times 10^{-9}$ M).

If the increased sensitivity of HUT102 cells to IL2−ricin in the presence of lactose is due to receptor-specific binding, we should be able to block binding in the presence of excess IL2. HUT102 cells were exposed to IL2 (20 μg/mL) and 60 mM lactose or lactose alone with varying concentrations of IL2−ricin or ricin for 30 min at 4 °C. After cells were washed and then incubated overnight at 37 °C/5% CO_2, cellular protein synthesis was measured by incorporation of [³H]leucine. Each assay was repeated three times. The ID_{50} of ricin with standard deviation was $(3 \pm 2) \times 10^{-10}$ M in the presence of IL2 and $(6 \pm 3) \times 10^{-10}$ M in the absence of IL2. In contrast, the ID_{50} of IL2−ricin with standard deveiations was $(5 \pm 4) \times 10^{-12}$ M without IL2 and $(3 \pm 2) \times 10^{-10}$ M in the presence of excess IL2. The slightly lower specific toxicity of IL2−ricin under these conditions was due to the shortened exposure time.

DISCUSSION

We report the construction and expression of a novel ricin fusion protein in significant yields. The baculovirus expression system has been previously used to independently express human IL2 and ricin toxin B chain (*28, 29*). We now describe the expression of the hybrid protein, IL2−RTB. Other chimeric eukaryotic proteins have been successfully expressed in insect cells using recombinant baculovirus including a fusion of the F and HN glycoproteins of human parainfluenza virus type 3 and a single chain monoclonal antibody composed of the variable domain of the light chain connected through AGQGSSV to the variable domain of the heavy chain (*30, 31*). In each case, the fusion protein needed a signal sequence for segregation into the endoplasmic reticulum with subsequent proper folding, disulfide bond formation, and glycosylation. The folding of each portion of IL2−RTB was facilitated by attachment of IL2 to the N-terminus of RTB. The x-ray crystallographic three-dimensional structure of ricin shows the N-terminus of RTB participates to a small degree in folding of RTB and interaction with RTA (*21*). Our results extend our earlier observation that an oligohistidine tag attached to the N-terminus of RTB preserved folding for both the oligohistidine peptide and RTB (*25*). These observations provide the foundation for a general strategy of producing ricin fusion proteins by attachment of novel ligands to the RTB N-terminus.

Evidence in addition to secretion, solubility and yield that IL2-RTB had proper folding of both the IL2 and RTB domains was the similar immunological reactivity of soluble IL2−RTB, RTB, and IL2 with antibodies to IL2 and RTB. Anti-IL2 antibody bound IL2 and IL2−RTB comparably, and anti-RTB antibodies bound RTB and IL2−RTB approximately equally (see Results). TheELISA assay format permitted quantitative measurements of soluble proteins.

IL2−RTB retained most of the galactose-binding activity of plant and wild-type recombinant RTB. The X-ray
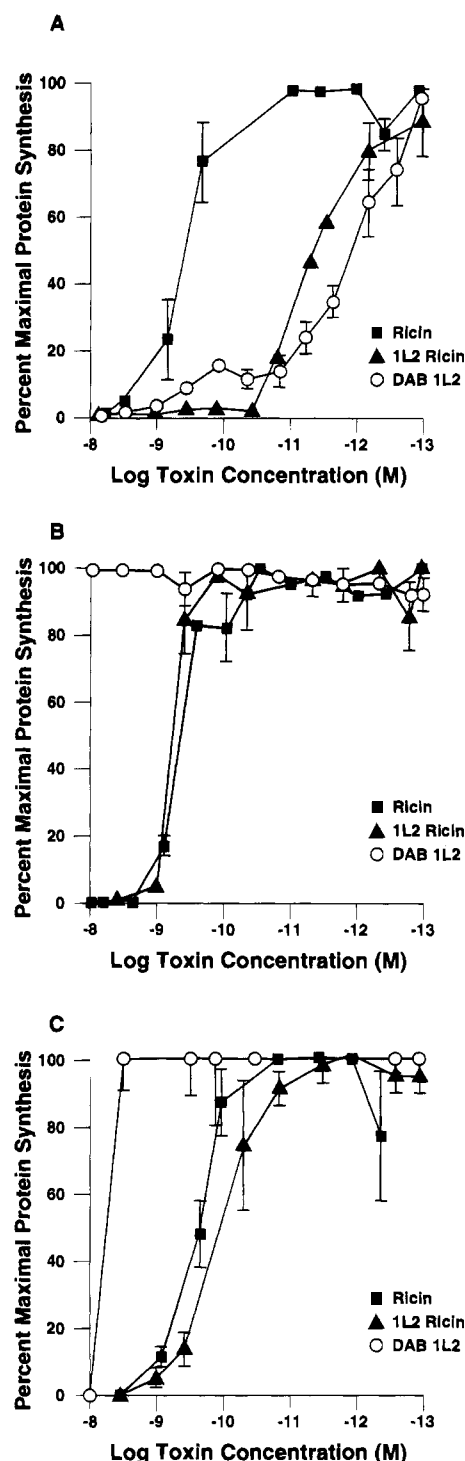
Figure 3. (A) HUT102 cell cytotoxicity measured by inhibition of protein synthesis using [³H]leucine incorporation. See text for details of assay. Key: ■, ricin in the presence of 60 mM lactose; ▲, IL2−RTB−RTA in the presence of 60 mM lactose; ○, $DAB_{389}IL2$ in the presence of 60 mM lactose. (B) Same as A except OVCAR3 cell cytotoxicity. (C) Same as A except CEM cell cytotoxicity. Standard deviations shown for single assay performed in triplicate. Standard deviation bars < 2% not shown. Each assay performed on three separate occasions, and standard deviations of ID_{50}'s shown in Table 1.

structure of ricin cocrystallized with lactose showed lectin sites in the 1α and 2γ subdomains remote from the N-terminus of RTB (*21*). Their independent behavior from the ligand will permit the systematic modification of sugar binding in recombinant ricin fusions. Previous work by Youle, Goldmacher, and Newton suggested some

residual lectin activity was critical for RTB enhancement of targeted ricin immunotoxin cytotoxicity (*4, 32, 33*).

Since the K_a of RTA–RTB association is 10^{-6} M^{-1} and our experiments employed concentrations of about 10^{-6} M, we expected 50% of IL2–RTB to reassociate with RTA (*26*). Our observation of 20% heterodimer formation suggests moderate efficiency of reassociation. Again, the X-ray structure shows the RTB amino acid residues interacting with RTA include RTB A1, D2, C4, F140, V141, F218, K219, N220, P260, and F262 (*22*). Thus, several residues are near the N-terminus and may affect reassociation, but the majority are distant from the surface N-terminal region. The recombinant heterodimers were stable at high dilutions, suggesting disulfide bond formation between RTA C259 and the free thiol of RTB C4 of IL2–RTB.

The IL2–RTB molecule alone was nontoxic to cells with or without the IL2 receptor and with or without lactose (see Results). Thus, no membrane lytic or other toxophore functions have been detected on the RTB moiety either alone or when targeted to cell surfaces with an alternate ligand. In contrast, IL2–RTB–RTA showed cytotoxicity in the absence of lactose indistinquishable from ricin. Thus, all the intoxication functions of ricin were present on the IL2–ricin fusion protein. In the presence of lactose, IL2–RTB–RTA showed selective and potent cytotoxicity to cells bearing the high affinity IL2 receptor (HUT102). The level of cytotoxicity to high affinity IL2 receptor containing cells was on the same order of magnitude as DAB$_{389}$IL2, a diphtheria toxin–IL2 fusion currently in clinical trials, and suggested the ricin-based genetically engineered immunotoxin was potent. Cells containing low levels of intermediate affinity receptor (CEM) or no receptor (OVCAR3) were no more sensitive to IL2–RTB–RTA than ricin alone in the presence of lactose. Future work will be focused on the partial removal of lectin function in the fusion toxin by site-specific mutagenesis. Such fusion toxins lacking significant normal tissue binding could then be studied in animal models of leukemia, lymphoma, or autoimmune diseases. We have prepared single-site and double-site RTB mutants. To date, significant residual cell binding and heterodimer cytotoxicity has been observed even with double-site mutants, suggesting three or more lectin sites on RTB (unpublished observations).

Competition experiments with excess ligand have been a frequently used method for confirming specificity of ligand–toxins (*14, 15*). Initial efforts to block our IL2–toxins with excess IL2 resulted in complete blockage of DAB$_{389}$IL2 cytotoxicity but minimal reductions in IL2–RTB–RTA killing. We reasoned that the residual lectin binding of the chimeric protein may have been strengthened after interaction with the cell surface and that the multivalent binding accelerated internalization at 37 °C. When we reduced the temperature to 4 °C to impair internalization and shortened exposure time to 30 min, we were able to block cytotoxicity with IL2 plus lactose. Thus, we were able to confirm the extreme rapidity of ricin fusion protein intoxication of cells and establish IL2 receptor specificity of the molecule.

This report describes successful production of a ricin toxin fusion protein with full biological potency. The reagent was produced in sufficient amounts and purity for studies of cell intoxication pathways. In the future, modified forms of this fusion protein (with reduced RTB lectin character) may be useful for *in vitro* and *in vivo* purging of IL2 receptor bearing cells.

LITERATURE CITED

(1) Olsnes, S., and Pihl, A. (1973) Different biological properties of the two constituent peptide chains of ricin, a toxic protein inhibiting protein synthesis. *Biochemistry 12*, 3121–3126.

(2) Baenziger, J., and Fiete, D. (1979) Structural determinants of Ricinus communis agglutinin and toxin specificity for oligosaccharides. *J. Biol. Chem. 254*, 9795–9799.

(3) Sandvig, K., and Olsnes, S. (1982) Entry of the toxic proteins abrin, modeccin, ricin and diphtheria toxin into cells. *J. Biol. Chem. 257*, 7504–7513.

(4) Youle, R., and Colombatti, M. (1987) Hybridoma cells containing intracellular anti-ricin antibodies show ricin meets secretory antibidy before entering the cytosol. *J. Biol. Chem. 262*, 4676–4682.

(5) Wales, R., Roberts, L., and Lord, J. (1993) Addition of an endoplasmic retrieval sequence to ricin A chain significantly increases its cytotoxicity to mammalian cells. *J. Biol. Chem. 268*, 23986–23990.

(6) Masuho, Y., Kishida, K., Saito, M., Umemoto, N., and Hara, T. (1982) Importance of the antigen-binding valency and the nature of the cross-linking bond in ricin A chain conjugates with antibody. *J. Biochem. 91*, 1583–1591.

(7) Endo, Y., and Tsurugi, K. (1987) RNA N-glycosidase activity of ricin A-chain. Mechanism of action of the toxic lectin ricin on eukaryotic ribosomes. *J. Biol. Chem. 262*, 8128–8130.

(8) Eiklid, K., Olsnes, S., and Pihl, A. (1980) Entry of lethal doses of abrin, ricin and modeccin into the cytosol of HeLa cells. *Exp. Cell Res. 126*, 321–326.

(9) Vitetta, E., Stone, M., Amlot, P., Fay, J., May, R., Till, M., Newman, J., Clark, P., Collins, R., Cunningham, D., Ghetie, V., Uhr, J., and Thorpe, P. (1991) Phase I immunotoxin trial in patients with B-cell lymphoma. *Cancer Res. 51*, 4052–4058.

(10) Amlot, P., Stone, M., Cunningham, D., Fay, J., Newman, J., Collins, R., May, R., McCarthy, M., Richardson, J., Ghetie, V., Ramilo, O., Thorpe. P., Uhr, J., and Vitetta, E. (1993) A phase I study of an anti-CD22-deglycosylated ricin A chain ummunotoxin in the treatment of B cell lymphomas resistant to conventional therapy. *Blood 82*, 2624–2633.

(11) Hertler, A., Schlossman, D., Borowitz, M., Blythman, H., Casellas, P., and Frankel, A. (1989) An anti-CD5 immuno-toxin for chronic lymphocytic leukemia: enhancement of cytotoxicity with human serum albumin-minensin. *Int. J. Cancer 43*, 215–219.

(12) Gould, B., Borowitz, M., Groves, E., Carter, P., Anthony, D., Weiner, L., and Frankel, A. (1989) Phase I study of an anti-breast cancer immunotoxin by continous infusion: report of a targeted toxic effect not predeicted by animal studies. *JNCI 81*,775–781.

(13) Grossbard, M., Lambert, J., Goldmacher, V., Blattler, W., and Nadler, L. (1992) Correlation between in vivo toxicity and preclinical in vitro parameters for the immunotoxin anti-B4 blocked ricin. *Cancer Res. 52*, 4200–4207.

(14) Bacha, P., Forte, S., McCarthy, D., Estis, L., Yamada, G., and Nichols, J. (1991) Impact of interleukin-2-receptor targeted cytotoxins on a unique model of murine interleukin-2-receptor-expressing malignancy. *Int. J. Cancer 49*, 96–101.

(15) Kreitman, R., and Pastan, I. (1994) Recombinant toxins. *Adv. Pharm. 28*, 193–219.

(16) Strom, T., Kelley, V., Murphy, J., Nichols, J., and Wood-worth, T. (1994) Interleukin-2-receptor-directed therapies: antibody-or cytokine-based targeting molecules. *Adv. Nephrology Necker Hosp. 23*, 347–356.

(17) Goldberg, M., Heimbrook, D., Russo, P., Sarosdy, M., Greenberg, R., Linehan, M., Fisher, H., Messing, E., Crawford, E., Oliff, A., and Pastan, I. (1995) Phase I clinical study of the recombinant oncotoxin TP40 in superficial bladder cancer. *Clin. Cancer Res. 1*, 57–61.

(18) Lappi, D., Ying, W., Barthelemy, I., Martineau, D., Prieto, I., Benatti, L., Soria, M., and Baird, A. (1994) Expression and

activities of a recombinant basic fibroblast growth factor-saporin fusion protien. *J. Biol. Chem. 269,* 12552−12558.

(19) Kreitman, R., Chaudhary, V., Waldmann, T., Willingham, M., FitzGerald, D., and Pastan, I. (1990) The recombinant immunotoxin anti-Tac(Fv)-Pseudomonas exotoxin 40 is cytotoxic toward peripheral blood malignant cells from patients with adult T-cell leukemia. *Proc. Natl. Acad. Sci. U.S.A. 87,* 8291−8295.

(20) Kreitman, R., Bailon, P., Chaudhary, V., FitzGerald, D., and Pastan, I. (1994) Recombinant immunotoxins containing anti-Tac(Fv) and derivatives of Pseudomonas exotoxin produce complete regressions in mice of an interleukin-2 receptor-expressing human carcinoma. *Blood 83,* 426−434.

(21) Rutenber, E., and Robertus, J. (1991) Structure of ricin B chain at 2.5 A resolution. *Proteins 10,* 260−269.

(22) O'Hare, M., Brown, A., Hussain, K., Gebhardt, A., Watson, G., Roberts, L., Vitetta, E., Thorpe, P., and Lord, J. (1990) Cytotoxicity of a recombinant ricin A Chain fusion protein containing a proteolytically-cleavable spacer sequence. *FEBS Lett. 273,* 200−204.

(23) Cook, J., Savage, P., Lord, J., and Roberts, L. (1993) Biologically active interleukin 2-ricin A chain fusion proteins may require intracellular proteolytic cleavage to exhibit a cytotoxic effect. *Bioconjugate Chem. 4,* 440−447.

(24) Westby, M., Argent, R., Petcher, C., Lord, J., Roberts, L. (1992) Preparation and characterization of recombinant proricin containing an alternative protease-sensitive linker sequence. *Bioconjugate Chem. 3,* 375−381.

(25) Afrin, L., Gulick, H., Vesely, J., Willingham, M., and Frankel. A. (1994) Expression of oligohistidine-tagged ricin B chain in Spodoptera frugiperda. *Bioconjugate Chem. 5,* 539−546.

(26) Lewis, M., and Youle, R. (1986) Ricin subunit association. Thermodynamics and the role of the disulfide bond in toxicity. *J. Biol. Chem. 261,* 11571−11577.

(27) Williams, D., Snider, C., Strom, T., and Murphy, J. (1990) Structure−function analysis of interleukin-2-toxin (DAB486-

IL-2) fragment B sequences required for the delivery of fragment A to the cytosol of target cells. *J. Biol. Chem. 265,* 11885−11889.

(28) Frankel, A., Roberts, H., Afrin, L., Vesely, J., and Willingham, M. (1994) Expression of ricin B chain in Spodoptera frugiperda. *Biochem. J. 303,* 787−794.

(29) Smith, G., Ju, G., Ericson, B., Moschera, J., Lahm, H., Chizzonite, R., and Summers, M. (1985) Modification and secretion of human interleukin-2 produced in insect cells by a baculovirus expression vector. *Proc. Natl. Acad. Sci. U.S.A. 82,* 8404−8408.

(30) Lehman, D., Roof, L., Brideau, R., Aeed, P., Thomsen, D., Elhammer, A., Wathen, M., and Homa, F. (1993) Comparison of soluble and secreted forms of human parainfluenza virus type 3 glycoproteins expressed from mammalian and insect cells as subunit vaccines. *J. Gen. Virol. 74,* 459−469.

(31) Laroche, Y., Demaeyer, M., Stassen, J., Gansemans, Y., Demarsin, E., Matthyssens, G., Collen, D., and Holvoet, P. (1991) Characterization of a recombinant single-chain molecule comprising the variable domains of a monoclonal antibody specific for human fibrin fragment D-dimer. *J. Biol. Chem. 266,* 16343−16349.

(32) Goldmacher, V., Lambert, J., and Blattler, W. (1992) The specific cytotoxicity of immunoconjugates containing blocked ricin is dependent on the residual binding capacity of blocked ricin: evidence that the membrane binding and A-chain translocation activities of ricin cannot be seperated. *Biochem. Biophys. Res. Commun. 183,* 758−766.

(33) Newton, D., Wales, R., Richardson, P., Walbridge, S., Saxena, S., Ackerman, E., Roberts, L., Lord, J., and Youle, R. (1992) Cell surface and intracellular functions for ricin galactose binding. *J. Biol. Chem. 267,* 11917−11922.

Fluorescent Labeling of Cysteine 39 on *Escherichia coli* Primase Places the Dye Near an Active Site[†]

Mark A. Griep* and Teresa N. Mesman

Department of Chemistry and the Center for Biotechnology, University of Nebraska, Lincoln, Nebraska 68588-0304. Received February 3, 1995[®]

Cysteine 39 of *Escherichia coli* primase is the most chemically reactive cysteine. Its high chemical reactivity is likely due to its proximity to primase's zinc, which is probably ligated to the adjacent residues 40–62. The zinc may stabilize the deprotonated form of cysteine 39 to make it chemically reactive. Primase is rapidly, site-specifically modified by fluorescein maleimide (FM) at this cysteine. Modification with FM at this residue does not lead to any activity loss in a coupled RNA/DNA synthesis assay, indicating that it is not a catalytically essential residue. In contrast, iodoacetamidefluorescein (IAF) modifies cysteine 39 more slowly and stoichiometrically inhibits activity. It was not clear why these two similar fluorescent dyes should have such different inhibitory effects when attached to the same cysteine. The IAF inhibition must be due to some property of the link between the fluorescein and the cysteine because that is how it differs from FM. The pK_a's of the fluoresceins from both FM- and IAF-modified primase are strongly shifted to lower values (approximately 5.4) compared to free fluorescein. These results strongly suggest that the deprotonated form of the fluoresceins are stabilized on primase by a strong interaction with the adjacent zinc in the zinc finger motif. The ability to place a noninhibitory FM at this site will be of great assistance in fluorescence energy transfer studies since the distances established to cysteine 39 will reflect the distance to the essential zinc finger motif.

Primase plays the central role at the replication fork during DNA synthesis (Kornberg and Baker, 1992; Marians, 1992). It interacts with DnaB helicase which unwinds the duplex DNA to create the single-stranded DNA (ssDNA[1]) template that is used by both primase and DNA polymerase III holoenzyme. Primase initiates primer synthesis once every approximately 1500 nucleotides on the lagging strand (Okazaki et al., 1968; Wu et al., 1992a,b; Zechner et al., 1992). Primase activity is limited to the replication fork by its strong interaction with DnaB helicase (McMacken et al., 1977) and its weak interaction with ssDNA (Swart and Griep, 1993). When the lagging strand DNA polymerase completes the previous Okazaki fragment, primase binds to the one of the next d(CTG) trinucleotides on the lagging strand ssDNA template and begins synthesizing an 11 ± 1 nucleotide RNA primer (Yoda et al., 1988; Yoda and Okazaki, 1991; Swart and Griep, 1993). The lagging strand DNA polymerase displaces primase from the RNA primer and elongates processively for about 1500 nucleotides from it to create the Okazaki fragment. Far from the replication fork, DNA polymerase I, RNase H, and DNA ligase

are all thought to be involved in removing the RNA primer and ligating the lagging strand into a high molecular weight DNA (Westergaard et al., 1973; Lehman, 1974; McMacken and Kornberg, 1978; Ogawa and Okazaki, 1980; Funnel et al., 1986).

To participate in lagging strand DNA synthesis, the proteins with which primase must minimally interact are DnaB helicase and DNA polymerase III holoenzyme. DnaB helicase is a hexamer of 52 300-Da protomers that migrates along the 3'→5' ssDNA strand (the lagging strand) in the direction of the replication fork (LeBowitz and McMacken, 1986). In the absence of duplex DNA to unwind, helicase is a single-stranded DNA-specific ATPase that is capable of enhancing the ability of primase to bind to the template. In the presence of ~36 nM hexameric DnaB helicase, 150 nM primase provides maximal primer synthesis (Arai and Kornberg, 1981), whereas, in the absence of DnaB helicase, much higher concentrations of primase are required for primer synthesis on single-stranded DNA (Swart and Griep, 1993). Thus, to initiate primer synthesis primase binds to helicase and then to the single-stranded DNA template. It is in this way that DnaB helicase acts as a "mobile promoter" for primer RNA synthesis (McMacken et al., 1977). Recent functional evidence indicates that helicase binds to the carboxyl-terminal 16-kDa portion of primase (Tougu et al., 1994). On the basis of sequence analysis (Ilyina et al., 1992), it can be predicted that it is the amino-terminal portion of DnaB helicase that binds to primase.

The evidence for a primase/DNA polymerase III holoenzyme interaction is considerable. The DNA yield and synthesis rates when starting from DNA polymerase initiation complexes (template/primer/DNA polymerase) are influenced by whether primase is allowed to synthesize a primer in the presence of the DNA polymerase (Griep and McHenry, 1989). When DNA polymerase binds to the primer while primase is synthesizing it, then the complex is more active than if primer synthesis is

[1] Abbreviations: DMSO, dimethyl sulfoxide; DTT, dithiothreitol; FM, 5-fluorescein maleimide; $FM_{1.0}$–primase, primase modified with a single FM (the maleimide moiety of the dye reacts by Michael addition with a primase sulfhydryl to create a succinimide linkage); IAF, 6-(iodoacetamido)fluorescein; $IAF_{0.48}$–primase, primase modified with 0.48 IAF/polypeptide (the iodide moiety of the dye is displaced upon reaction with primase to create acetamidefluoresceinylated primase); MALDI, matrix-assisted laser desorption ionization; PMPS, *p*-hydroxymercuriophenyl sulfonate.
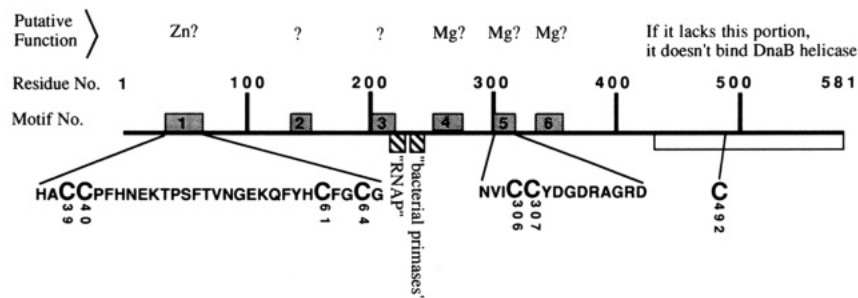
Figure 1. Seven cysteines of *E. coli* primase and their locations with respect to conserved sequences. Motifs 1–6 were established from amino acid sequence analysis and some of their possible functions taken from analogous motifs in other proteins (Ilyina et al., 1992). The "RNAP" and "bacterial primases" motifs were also identified by sequence analysis (Versalovic and Lupski, 1993). The location of the DnaB helicase binding domain was determined functionally by Tougu and co-workers (Tougu et al., 1994).

complete prior to adding the DNA polymerase. Thus, primer synthesis influences the ability of DNA polymerase to bind to the primer. Conversely, there is evidence that primer synthesis is highly controlled by DNA polymerase during rolling circle synthesis. A primer is not synthesized until the lagging strand DNA polymerase completes the elongation of the previous Okazaki fragment (Zechner et al., 1992; Wu et al., 1992b).

Together with single-stranded DNA binding protein, the helicase/primase/DNA polymerase complex represent the minimal proteins needed to replicate lagging strand DNA (Mok and Marians, 1987). The three enzymes form a complex, however transient, that is in excess of 1 MDa. Fluorescence resonance energy transfer is one of the few effective techniques that could establish the solution structure of such a large dynamic complex. To determine its overall structure and orientation at the replication fork will require establishing many different distances between protein and template sites. Likewise, specific reporter groups on each of the enzymes will be useful tools for establishing the static and dynamic effects that these enzymes have on one another. This paper describes the procedure for dye labeling primase at its active site to create a site-specific probe suitable for use in primase/helicase interaction studies.

The most chemically reactive groups on proteins are their amines and thiols. There are many fluorescent dyes of various chemistries that target these groups (Brinkley, 1992). The cysteine thiols are better targets for site-specific labeling than are the amines of the amino terminus and lysine side chain because there are usually fewer of them. For instance, primase from *E. coli* has seven cysteines and 22 lysines (Burton et al., 1983). Given the lower number of primase cysteines, these were first targeted by our laboratory as possible sites for specific fluorophore labeling. The number of cysteines in *E. coli* primase that can be expected to be chemically reactive is further limited because three of its cysteines (40, 61, and 64) are proposed to be involved in binding its one zinc atom (Ilyina et al., 1992; Stamford et al., 1992). This leaves cysteines 39, 306, 307, and 492 available for dye labeling.

The best reporter groups are near functional domains but do not interfere with their activity. Unfortunately for primase, its four available cysteines reside in three identified motifs (Figure 1). It is possible that labeling any one of them will inhibit some but not all activities of primase. Motif 1 is the putative zinc finger of primase, and cysteine 39 resides at its amino terminus (Ilyina et al., 1992). The role of the analogous zinc finger motif from bacteriophage T7 primase/helicase is to cause primer synthesis initiation to be template sequence-specific (Bernstein and Richardson, 1988). A fluorophore at this site may prevent primer synthesis because the

primase may not be able to specifically bind to ssDNA. However, it may not interfere with binding to DNA polymerase or to DnaB helicase. Cysteines 306 and 307 reside in conserved motif 5, a putative magnesium binding site (Ilyina et al., 1992). This domain shows some similarity to the catalytically active magnesium binding sites of DNA and RNA polymerases (Argos, 1988). Again, labeling at this site may inhibit primer synthesis activity but not binding to ssDNA, DNA polymerase, or DnaB helicase. Cysteine 492 resides within the helicase binding carboxyl terminus of primase (Tougu et al., 1994). A label at this site should not interfere with primer synthesis activity but may interfere with helicase binding.

This study shows that cysteine 39 of *E. coli* primase is the most chemically reactive cysteine. Labeling this residue with fluorescein maleimide is rapid (less than 10 min) and noninhibitory. In contrast, labeling this same residue with iodoacetamide fluorescein is slow (not complete in 4 h) and stoichiometrically inhibiting. This indicates that even though cysteine 39 is near an active site, it can be safely labeled by fluorescein maleimide. The ability to place a noninhibitory maleimide derivative in this location will provide a sensitive probe of the action at this site.

EXPERIMENTAL PROCEDURES

Proteins and Enzymes. Single-stranded DNA binding protein was isolated according to a published protocol (Lohman et al., 1986). DNA polymerase III holoenzyme and primase were isolated as described previously (Swart and Griep, 1993). Primase was isolated from a primase-overproducer that was manufactured by Dr. Roger McMacken's laboratory at of Johns Hopkins University. The concentration of native primase was determined using its extinction coefficient of 47 800 M^{-1} cm^{-1} at 280 nm. The activity of primase was measured by the standard assay in which primer synthesis is coupled to DNA synthesis. One unit of primase was defined as the amount needed to incorporate 1 pmol of (total) nucleotide/min into acid-precipitable DNA. The assay was performed at 30 °C for 5 min under conditions in which all other components were saturating. Primase from several preparations has had a specific activity of 2.1 units/ng (±0.3).

The activities of primase and the labeled primases were determined using the coupled primer synthesis/DNA synthesis assay (Bouché et al., 1975; Wickner, 1977; Johanson and McHenry, 1980; Griep and McHenry, 1989; Swart and Griep, 1993). In this assay, bacteriophage G4 single-stranded DNA complementary strand origin is primed once by primase at a known initiation sequence. The DNA polymerase III holoenzyme, also present in the assay, processively elongates a DNA polymer from the

RNA primer. The assay is quantitated according to the amount of tritiated thymidine incorporated into the nascent DNA strand. Primase could lose any of a number of activities and not be active in this assay. It could lose its ability to do the following: bind single-stranded DNA; specifically recognize its trinucleotide initiation sequence CTG; bind ribonucleotides; bind magnesium; bind DNA polymerase III holoenzyme. Thus, any step that precedes processive DNA synthesis by the DNA polymerase will lead to a loss of activity in this assay.

Fluorescent Labeling of Primase. 6-(Iodoacetamido)fluorescein (IAF) and 5-fluorescein maleimide (FM) were purchased from Molecular Probes (Eugene, OR) and prepared as 10-mM stock solutions in DMSO. In a typical 100 μL labeling reaction (Griep and McHenry, 1988), 50 μM primase and 600 μM dye were incubated in 50 mM HEPES, pH 7.5, 50 mM NaCl, 2.5% DMSO in the dark at room temperature for 15 min. The sample was then gel filtered on a S-200 column (0.9 × 18 cm) to remove unreacted dye from the primase and to establish the aggregation state of primase. Typical recoveries of both labeled and unlabeled primase from this column were in the range of 90 to 95%. Fractions containing greater than 30% of the peak fraction absorbance were pooled. The concentration of the IAF fluorescein was determined using ϵ_{495} of 75 000 M^{-1} cm^{-1} and the FM fluorescein using ϵ_{495} of 83 000 M^{-1} cm^{-1} (Molecular Probes, Eugene, OR); these represent the extinction coefficients for the fully unprotonated species (Martin and Lindqvist, 1975). As demonstrated in the Results, the pK_a's of the fluoresceins attached to primase were shifted to such low values that they were fully deprotonated at pH 7.5, allowing these extinction coefficients to be used. The primase concentration was determined by the Bradford assay (Bradford, 1976) using unlabeled primase as the standard. The concentration of the unlabeled primase was accurately determined using its extinction coefficient. Primase binds 2.03 times as much Coomassie Brilliant Blue as does immunoglobulin G, the usual Bradford assay standard.

The protein concentration within the labeled protein can be estimated using A_{280}', the corrected A_{280} of the labeled primase for the contribution from the dye (Brinkley, 1992), using the following equation:

$$A_{280'} = A_{280}(\text{labeled primase}) - \frac{A_{280}(\text{free dye})}{A_{495}(\text{free dye})(A_{495}(\text{labeled primase}))}$$

The A_{280}/A_{495} correction ratio as taken from the spectra of the free IAF is 0.326 and free FM is 0.254. Using these values gives protein concentrations that are in disagreement with Bradford assay determinations. Possible sources of error in the equation are that it assumes (1) that the dye does not perturb the UV-absorbing properties of the tyrosines and tryptophans of the protein and (2) that the protein does not perturb the UV- or visible-absorbing properties of the dye. The first assumption is reasonable for iodoacetamide and maleimide dyes since they do not react with the tyrosines or tryptophans. That there was no interference with the UV-absorbing properties of the protein was confirmed as indicated in the Results. Also, as indicated in the Results, the UV-absorbing properties of the dye are not altered when it is covalently attached to the protein. However, the visible absorption spectrum is significantly altered such that the dye's spectrum shifts by 4 nm to the red when covalently attached to the protein. The A_{280}/A_{495} correction ratio can be recalculated as ~0.43 for IAF and ~0.30

for FM when proper account is taken of the known concentrations of protein from the Bradford assay. Protein concentrations determined with these correction ratios were consistent (±10%) with the Bradford assay determinations.

Fluorescence Measurements. The fluorescence measurements were made using an Aminco-Bowman 2 spectrofluorometer controlled by an IBM running OS/2. The sample compartment was equipped with a stirring assembly and a temperature regulator; the compartment was maintained at 30.0 ± 0.1 °C. The excitation and emission band widths were each set at 4 nm except during the quantum yield measurements when the emission bandpass was set to 1 nm. All measurements have been corrected for background fluorescence and dilution effects.

Quantum yields were determined using the relationship $Q_x = (F_x A_{ref} Q_{ref})/(F_{ref} A_x)$, where Q was quantum yield, A was absorption at the excitation wavelength, F was area under the fluorescence emission curve, and the subscripts x and ref were the unknown and the reference samples (Parker and Rees, 1960). The concentrations of the unknown and reference were adjusted so that their absorbances were less than 0.05 to prevent any inner filter effects (Lakowicz, 1983). The reference quantum yield for disodium fluorescein in 100 mM NaOH was 0.92 (Weber and Teale, 1957).

The pH dependence studies were performed in APHTC buffer (Griep and McHenry, 1990) containing 10 mM of each of the following: acetic acid (pK 4.8 at 25 °C), PIPES (pK 6.8), HEPES (pK 7.6), Tris (pK 8.3), and CHES (pK 9.3). KOH was used to adjust the pH of the buffer combinations to create solutions of known pH. Aliquots of IAF—primase were added to these buffer solutions and absorbance and fluorescence emission spectra taken.

Tryptic Digestion, Fluorescent Peptide Isolation, and Peptide Identity. Tryptic digestion and fluorescent peptide isolation were performed essentially as described for the β subunit of DNA polymerase III holoenzyme (Griep and McHenry, 1990). Prior to tryptic digestion, fluorescently labeled primase (2 nmol, 130 μg) was dried to completion in a Savant SpeedVac and the residue dissolved in 50 μL of 7.0 M urea, 400 mM NH$_4$-HCO$_3$, pH 8.0, 5 mM DTT. This sample was incubated at 60 °C for 15 min to denature the protein and maintain the cysteines in a reduced state. After the mixture was cooled to room temperature, a final concentration of 10 mM iodoacetic acid was added to carboxymethylate the other cysteines to prevent them from forming mixed disulfides during subsequent steps. After this mixture was incubated for 5 min at ambient temperature, the volume was diluted 1:4 with water to lower the urea to 1.8 M. Trypsin was added at a 1:25 enzyme:substrate weight ratio and the mixture incubated for 20 h at 37 °C.

The tryptic peptides were resolved on an ISCO Spherisorb C18 column (100 × 4.6 mm). The modular HPLC setup consisted of a Milton Roy CM400 multiple solvent delivery system, a RheoDyne manual injector, a LDC analytical spectroMonitor 3100X for absorbance detection at 215 nm, a Shimadzu RF-535 for fluorescence detection by excitation at 440 nm and emission at 520 nm, and a Gilson FC-80 fraction collector set to collect 1 min of eluent per fraction. Half of the above described tryptic digestion sample was loaded into the injector loop and then the column. The peptides were eluted from the column using a 0.1% trifluoroacetate (pH 2.2) solution and the following acetonitrile gradient at a flow rate of 1 mL/min: 0—13% acetonitrile gradient over 5 min; 13—27% over 60 min; 27—90% over 5 min; maintain 90% over

5 min; 90−0% over 5 min. Fractions of 1 mL were collected. The fractions containing fluorescent substances were pooled, concentrated in a Speed-Vac, and rechromatographed on the C18 column with an even shallower central gradient. In the case of the main fluorescent peak, it was rechromatographed with a central gradient of 20−26% acetonitrile over a 60-min period.

A spreadsheet program was written to predict the percent acetonitrile required to elute each of the cysteine-containing peptides from the C18 column. The equation used in the prediction was based on the amino acid composition of the eluting peptides and the C18/0.1% trifluoroacetate partition coefficients for the amino acids in the peptide (Sasagawa et al., 1982). The equation for a linear 1% acetonitrile/min gradient was: % acetonitrile $= A \ln(1 + \Sigma_j D_j' n_j) + C$, where A was an empirically derived slope constant ($= 12.4$); D_j' was the nonweighted C18/0.1% trifluoroacetate partition coefficient for amino acid j (taken from Table II of Sasagawa et al. (1982)); n_j was the number of residues of amino acid j in the peptide; and C' was an empirically derived intercept constant ($= -30.3$). The partition coefficient for cysteine was available for both the carboxymethyl-modified or aminoethyl-modified forms but not for the fluoresceinylated form. In our calculations, the carboxymethylated cysteine partition coefficient was used for all cysteines.

Peptide amino acid sequence was determined by Edman degradation in an Applied Biosystems 420H by Laurey Steinke of the University of Nebraska Medical Center Protein Structural Core Facility. Mass spectral analysis was determined by MALDI in a Bruker Bench-TOF and by electrospray mass spectrometry by Ron Cerny of the University of Nebraska−Lincoln Midwest Center for Mass Spectrometry.

RESULTS

To monitor the interactions between the enzymes at a replication fork will require a way to monitor each of the enzymes independently of the others. One way to do this would be to attach different fluorescent probes to each of the participating enzymes. In this way, each enzyme could be monitored for the effects that the other enzymes have on it. The β subunit of DNA polymerase III holoenzyme has already been site-specifically labeled in such a way that it retains full activity (Griep and McHenry, 1988, 1990, 1992). As the next step for achieving the above goal, primase was targeted for fluorescent labeling.

Labeling Primase with Fluorescein Dyes. In the early trials, which were with IAF, primase was incubated with a 16-fold molar excess IAF dye for 15 min at pH 7.5. The same excess of dye was added to the solution three more times, each time incubating for 15 min. The solution was gel filtered on an S-200 column to remove unreacted dye and assess the Stokes' radius of the labeled primase. The fractions containing labeled primase were pooled and then quantitated for fluorescein using its extinciton coefficient of 75 000 M^{-1} cm^{-1} and for primase using the Bradford assay. Under the conditions described above, primase eluted as a monomer that was labeled with 0.48 IAF/primase and had a specific activity of 1.32 units/ng. This was about half of full activity (Figure 2). Unlabeled primase did not lose activity when incubated at room temperature for up to 2 days, indicating that it was the label that caused primase to lose activity. To modify primase to a greater extent with IAF requires incubations up to 4.5 h, although only involving three or four additions of excess IAF. The plot of specific activity versus modification demonstrated that primase
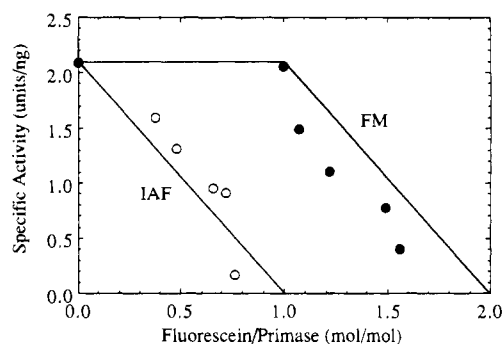
Figure 2. Activity plot of modified primase. Following modification of the primase with either IAF or FM, the protein was gel filtered on an S-200 column and then characterized for both the extent of modification and its specific activity in the coupled RNA/DNA synthesis assay. The line through the IAF modification data was drawn assuming that first site labeling caused proportional loss of activity. The lines through the FM modification data was drawn assuming that the first site labeled caused no loss of activity while the second site labeled caused proportional loss of activity.

was inhibited in direct proportion to modification. Therefore, the modified cysteine had either been an essential residue or the fluorescein was interfering with the function of an adjacent region.

FM reacted with primase much more rapidly than did IAF, especially the first residue modified. Within 5 s of adding a 16-fold molar excess of FM dye to a primase solution, the solution became orange rather than the yellow it would have been if added to buffer alone. After only 10 min of incubation, 1.0 cysteine was modified per primase, and it retained full activity (Figure 2). For FM, an extinction coefficient of 83 000 M^{-1} cm^{-1} was used. Merely 90 min was required to obtain the highest amount of FM modification presented (1.56 FM/primase and a specific activity of 0.36 units/ng). In contrast to IAF modification, the activity/modification plot of FM demonstrated that the first FM-modified residue did not inhibit primase activity (Figure 2), while the second FM-modified cysteine caused proportional inhibition.

The extinction coefficients for the fully unprotonated fluorescein were used in the above trials to quantitate the moles fluorescein. It will be shown below that the fluorescein pK's were low enough to justify this use with the pH 7.5 buffers used here. However, it should be noted that the IAF modification plot (Figure 2) would have a better proportional fit if an extinction coefficient of 92 000 M^{-1} cm^{-1} had been used and the FM modification data plotted would be better fit if an extinction coefficient of 75 000 M^{-1} cm^{-1} had been used.

Absorbance Spectra. A comparison of the FM$_{1.0}$−primase spectrum with that of the unreacted dye revealed that there was a 3.5-nm red shift from 492.5 to 496.0 nm of the fluorescein's absorption maximum when the dye was attached to primase (Figure 3). Similarly, the IAF$_{0.48}$−primase absorbance maximum red-shifted from 493.0 to 497.0 nm (data not shown). The visible difference spectrum between FM$_{1.0}$−primase and FM in pH 8.5 buffer also revealed the large spectral shift. Above 350 nm, the area above and below zero absorbance was nearly equal, indicating a simple environmental change rather than a change in the electronic structure of the moiety.

When the FM$_{1.0}$−primase/FM difference spectrum below 300 nm was compared to the absorption spectrum of unlabeled primase, they were found to be nearly superimposable (data not shown). Replacing the maleimide double bond with a thio−carbon bond in the labeled primase did not lead to a change in the dye's UV
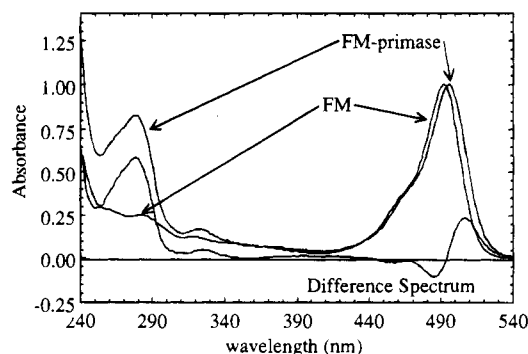
Figure 3. Normalized and difference spectra of $FM_{1.0}$–primase and unreacted FM. The absorbance spectra of $FM_{1.0}$–primase and unreacted FM (pH 8.5) were normalized to their absorbances at 497 and 493 nm, respectively. The difference spectrum was for labeled primase minus free dye.

absorbing properties. Below 300 nm, the UV difference spectrum between $FM_{1.0}$–primase and FM can be fully accounted for by the UV absorbing properties of primase alone. Thus, the dye did not alter the tyrosine and tryptophan spectral properties and none of the primase residues altered the dye's UV absorbing properties.

Quantum Yield and pK_a of Labeled Primase. The environment surrounding the reactive cysteine was further explored by determining the fluorescence properties of the labeled primases. The fluorescence emission maximum wavelength for $IAF_{0.48}$–primase in a moderate ionic strength pH 7.5 buffer was typical at 520 nm, and its quantum yield was 0.50. The emission maximum was also 520 nm for $FM_{1.0}$–primase but its quantum yield at pH 7.5 was 0.85. Fluorescein fluorescence is sensitive to its protonated state (Martin and Lindqvist, 1975) because deprotonation alters its electronic structure. As a result, both the extinction coefficient and the quantum yield are pH dependent.

Buffers of known pH were prepared, and the same amount of labeled primase was added to each solution. The same solution was used for both absorbance and fluorescence emission measurements. The fluorescence emission scans were collected while exciting, at 470 nm, the absorption isosbestic point to eliminate absorption differences from having an effect on the quantum yield determination. The quantum yield for $IAF_{0.48}$–primase was again determined to be 0.50 at pH 7.5. Hill plots of the A_{495} and quantum yield data (Figure 4) indicated that the pK_a for fluorescein on $IAF_{0.48}$–primase were 5.19 and 5.45, respectively (the data for $FM_{1.0}$–primase were similar and are summarized in Table 1). These were negatively shifted pK_a's for a fluoresceinylated compound. For $IAF_{0.48}$–primase, the Hill coefficients were 1.09 and 0.98, respectively, confirming that there was one protonatable group involved. Since the pK_a's were more than two pH units lower than pH 7.5, the fluoresceins will be more than 99% unprotonated at pH 7.5 and at their full quantum yields.

Determining the Cysteines to Which the FM and IAF Were Attached. There are seven cysteines in primase, and they reside on four tryptic peptides (Table 2). Three of the tryptic peptides have two cysteines. Even though this leads to a reduction in the number of possible peptides to which the fluorescein may be attached, it also leads to ambiguity as to which of the two cysteines were labeled on those tryptic peptides. Some evidence relating to this issue was obtained during Edman degradation.

$FM_{1.0}$–primase (and separately $IAF_{0.48}$–primase) was denatured, labeled with iodoacetate, and tryptically digested, and the tryptic peptides were resolved by a
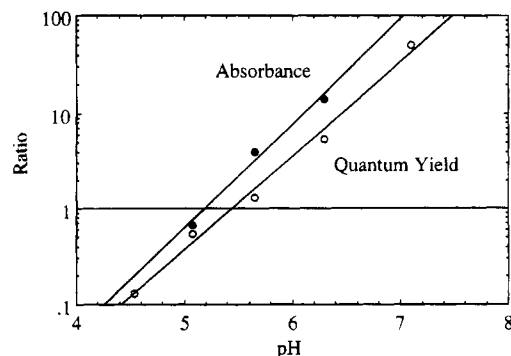
Figure 4. Hydrogen ion Hill plots of absorbance and quantum yields of $IAF_{0.48}$–primase. The absorbance and quantum yield were measured in the APHTC buffers described in the Experimental Procedures. The ratio was the $A_{495\ nm}$ or quantum yield at the indicated pH divided by the difference from the total signal change observed at the highest pH. Least-squares analysis to the absorbance data yielded the equation Ratio $= 10^{1.086(pH-5.19)}$ with $R^2 = 0.982$ and for the quantum yield data Ratio $= 10^{0.978(pH-5.44)}$ with $R^2 = 0.992$.

6-IAF labeled cysteine   5-FM labeled cysteine
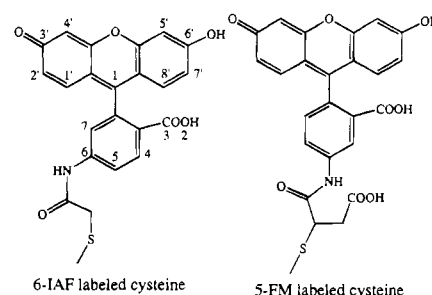
Figure 5. Structures of the fluorescein dyes attached to primase. The dyes were 6-(iodoacetamido)fluorescein and 5-fluorescein maleimide, and their structures as attached to primase are shown. The succinimide is shown in one of its two possible open ring forms. The numbering system is for the lactone form of the fluorescein rings, even though that was not the form studied here.

Table 1. Summary of Fluorescein-Labeled Primase

modified primase	$IAF_{0.48}$–primase[a]	$FM_{1.0}$–primase
labeling condns	four consecutive aliquots 15-fold dye excess for 15 min each	15-fold dye excess during less than 10 min
dye/primase	0.48	1.0
specific activity[b] (units/ng)	1.32 (~63%)	2.06 (~100%)
absorbance max (nm)	497	496
fluorescein pK_a	5.19	5.38
Hill coefficient	1.09	0.68
fluorescence emission max (nm)	520	520
quantum yield (%)	0.50	0.85
fluorescein pK_a	5.45	5.52
Hill coefficient	0.98	0.98

[a] The primase could be labeled with IAF to greater extents by incubating for longer periods of time. [b] Unlabeled primase from several preparations has a specific activity of 2.1 ± 0.3 units/ng.

shallow acetonitrile gradient on an analytical C18 column. The major fluorescent peak (80% of the total fluorescent species) eluted at about 25% acetonitrile and consisted of a primary peak with a trailing shoulder peak. There was a minor fluorescent peak (10% of the total) which eluted at about 13% acetonitrile. This peak was composed of several compounds with masses in the range of 400–500 amu as observed by MALDI and probably represents free fluorescein generated during workup. Another minor peak (10% of the total) eluted at the

Table 2. Predicted Cysteine-Containing Tryptic Peptides from Primase

amino acid sequence	residue nos.	no. of residues	% acetonitrile[a]	mass[b] +IAF+CM	mass[b] +FM+CM
NFHACCPFHNEK	35–46	12	24.6	1892.1	1932.1
QFYHCFGCGAHG NAIDFLMNYDK	57–79	23	33.9	3097.5	3137.5
ATNNVICCYDGDR	300–312	13	22.5	1889.0	1929.0
ELVNTCLSQPGLTT GQLLEHYR	487–508	22	32.0	2860.3	2900.3

[a] The predicted percent acetonitrile to elute the peptide from a C18 reversed-phase column was calculated as described in the Experimental Procedures. The prediction was for peptides containing all S-carboxymethylated cysteines. [b] Masses of the uncharged peptides were calculated as the sum of their residue masses. Acetamidofluorescein (IAF) will add 387.4 amu to the IAF–peptide, succinimido-fluorescein (FM) will add 427.4 amu to the FM–peptide, and S-carboxymethyl (CM) will add 58.0 amu to those peptides containing two cysteines.

location expected from full length primase. The major peak was pooled, concentrated, and rechromatographed on an even shallower gradient to remove closely eluting contaminants. Again, an early eluting species was observed (about 10% of the total fluorescent species) which had a mass in the range of 400–500 amu.

The first evidence as to the identity of the labeled peptide was the percent acetonitrile at which it eluted. The percent acetonitrile at which the four cysteine-containing peptides were predicted to elute was calculated using their amino acid compositions and the amino acid C18/0.1% trifluoroacetate partition coefficients (Sasagawa et al., 1982) (Table 2). The calculation assumed that the cysteines were labeled with iodoacetate, not fluorescein. Fluoresceinylated peptides would be expected to elute at slightly higher acetonitrile than the S-carboxymethylated peptides. Because the major peak eluted at about 25% acetonitrile, the calculations predicted that the labeled cysteine on either peptide 35–46 or peptide 300–312. Both of these peptides have two adjacent cysteines that could be labeled by a fluorophore.

The FM–peptide (estimated to be 220 pmol by fluorescence intensity comparison to FM–primase standards) was subjected to Edman degradation and a low yield of peptide (average 25 pmol) with the sequence NFHA?CPF-HN?K was obtained. This corresponded to peptide 35–46 in which the fifth residue should be a cysteine and the eleventh residue should be a glutamate (Burton et al., 1983). During cycle 6 but not 5, it was possible to establish that a cysteine was present by the appearance of a phenylthiohydantoin derivative of S-carboxymethylated cysteine which eluted near the position for a serine derivative. Only the zinc-ligated cysteine would have been free following denaturation and susceptible to iodoacetate labeling. Thus, by inference, cysteine 39 was the FM-labeled cysteine. No residue was positively identified during eleventh Edman degradation cycle due to a nonproteinaceous contaminant which eluted during every cycle where glutamate would. The nonproteinaceous material may have also reduced the Edman degradation yield. These data effectively ruled out peptide 300–312 as the site of fluorescent labeling.

The major fluorescent peak was characterized by electrospray mass spectrometry. Electrospray is precise to within about 0.01% (or 0.2 amu in 2000). The FM–peptide mass (M) was 1951.0 amu. This mass was 19 amu more than that predicted for a succinimide linkage to peptide 35–46 (Table 2). The less precise measurement by MALDI (about 1.0 amu in 2000) indicated that the mass (M) was 1947 which was 15 amu more than that predicted for a succinimide linkage (Table 2).

There were at least two possibilities to account for an increase in peptide mass of this magnitude. Ring opening of the succinimide to its succinamic acid form would increase the mass by 18 amu (due to H_2O). Succinimide ring opening has been reported by other workers (Wu et al., 1976; Lux and Gérard, 1981; Ishii and Lehrer, 1986).

It is interesting to note that the flexibility of the succinamic acid linkage of the FM–peptide would be similar to the acetamide linkage of IAF–peptide. Alternatively, sulfoxide formation at one of the thioethers would increase the mass by 16 amu (due to O). Oxidation could have occurred during peptide isolation.

$IAF_{0.48}$–primase was tryptically digested and chromatographed and its major fluorescent peptide collected (accounting for about 85% of the total fluorescent peptides). The IAF–peptide (estimated to be 430 pmol) was subjected to Edman degradation, and a low yield (average 23 pmol per residue) with the sequence NFHA?CPF-HN?K was obtained. This sequence corresponded to peptide 35–46. The M mass of the IAF-labeled peptide was 1890 amu according to MALDI. This was 2 amu less than that predicted for peptide 35–46 (Table 2). Since the MALDI instrument was precise to within about 0.05% (or 1.0 amu in 2000), this indicated close agreement.

The Effect of Magnesium, Nucleotides, Single-Stranded DNA and PMPS upon Fluorescence. At pH 7.5, the fluorescence intensity of $FM_{1.0}$–primase was not altered by the addition of up to 150 mM magnesium, up to 200 µM ATP or a mixture of nucleoside triphosphates, up to 100 µM nucleotides of M13Gori single-stranded DNA, or any combination thereof. This indicated that these components with which primase interacts either did not bind near cysteine 39 or their binding did not alter the fluorescein environment. The environment of fluorescein leads to changes in its fluorescence intensity changes only when the pK of its carboxyl is shifted higher or lower. The lack of fluorescence change when FM–primase binds to its substrates reflected a lack of pK shift to higher values for the fluorescein carboxylic acid.

The only way in which the fluorescein fluorescence was observed to change was in a PMPS titration (Figure 6). The FM–primase and IAF–primase fluorescence was quenched to the same extent when 3 equiv of PMPS had been added. Given that the fluorescein was attached to cysteine 39, it was located immediately adjacent to the "zinc finger" motif of primase (Figure 1) (Ilyina et al., 1992). Other studies in our laboratory have confirmed that the zinc in primase is ligated by three cysteines (Cook and M. A. Griep, unpublished results) such that PMPS can release the bound zinc from primase. PMPS is a cysteine-specific reagent used to characterize zinc-chelating cysteines (Boyer, 1954; Hunt et al., 1984; Giedroc et al., 1986; Wu et al., 1992c). The fluorescence quenching by PMPS could be due to either static quenching by the mercury atoms now in proximity to the fluoresceins or by a positive shift in the pK of the fluorescein carboxylate upon release of the zinc such that there was an apparent quenching at pH 7.5.

These two possibilities were tested by determining the pK of the fluorescein before and after the addition of 3 equiv of PMPS to FM–primase. The quantum yield of
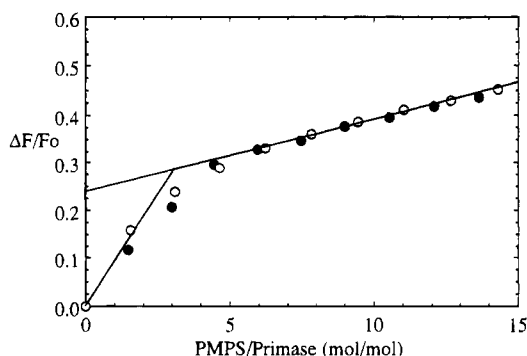
Figure 6. Fluorescence quenching of dye-labeled primase by PMPS. Dye-labeled primase (400 μL, 80 nM) was titrated with 1 μL aliquots of 50 μM PMPS in a buffer of 50 mM HEPES, pH 7.5, 50 mM KCl at 30 °C. The fluorescence intensity was monitored with excitation at 496 nm and emission at 520 nm. Fluorescence quenching was calculated after correction for background and dilution using the equation $(F_o - F)/F_o \ (= \Delta F/F_o)$, where F_o was the fluorescence intensity of the sample before adding PMPS and F was the fluorescence in the presence of PMPS.

fluorescein did not change, indicating that the PMPS had not caused static quenching. However, the fluorescein pK's for absorbance and quantum yield were shifted, respectively, to 6.1 and 6.4. These pK's after the addition of PMPS were in the middle of the range expected of a fluorescein. This result confirmed that the presence of zinc in primase had shifted the pK's to the observed low values (Table 1) and that zinc removal (by PMPS addition) had allowed them to return to less perturbed values.

DISCUSSION

It is possible to attach a noninhibiting fluorescent probe to a specific residue of primase that can be used in structural studies. Primase cysteine 39 is rapidly labeled by the fluorescent dye FM and retains full primer synthesis activity. The absorption and fluorescence properties of the FM are not significantly perturbed by its environment except that its pK_a is shifted to about 5.4. A probe at this site is even more useful since we also demonstrated that cysteine 39 is near an active site.

The iodoacetamide functional group of IAF reacts with cysteine 39 slower than does the maleimide of FM. This probably reflects the chemical reactivity of the dyes rather than the cysteine. The attached IAF inhibits primase activity completely in direct contrast to an attached FM. Since cysteine 39 can be labeled by FM without causing inhibition, it indicates that cysteine 39 is not an essential residue. The structural cause of the inhibition must lie in the linkage between the fluorescein moiety and the sulfur of cysteine 39. The attached IAF and FM may have different flexibilities due to their linkages. The different flexibilities may allow IAF to interfere with an adjacent region (or function) or prevent FM from doing so. The most obvious site to interfere with is the immediately adjacent zinc finger motif (Motif 1 in Figure 1) (Ilyina et al., 1992). Although it is also possible that the fluorophores interact with other sites within the tertiary structure. Differential inhibition by IAF and FM has been observed before with another protein (Griep and McHenry, 1988). What was not observed with this other protein was the large pK_a shift that is common to both types of fluorophores when attached to primase.

If the succinimide ring is hydrolyzed after attachment of FM to primase, then a carboxylate is created that is not present in the acetamide species (Figure 5). Perhaps the additional negative charge is beneficial to maintenance of activity? Succinimide ring opening has been

observed or postulated to occur in many other systems (Wu et al., 1976; Lux and Gérard, 1981; Farley et al., 1984; Ishii and Lehrer, 1986; Filoteo et al., 1987; Griep and McHenry, 1990).

The pK_a of either fluorescein attached to cysteine 39 is low at ~5.4 and possibly due to a strong interaction with the nearby zinc. The zinc would be expected to strongly stabilize the enolate form of fluorescein and thereby reduce its pK_a. Cysteine 39 may be the most chemically reactive cysteine among the seven of primase for the same reason. The zinc may lower the pK_a of cysteine 39's thiol to make it especially reactive to sulfhydryl-specific reagents. The pK_a shift indicates that the dye is strongly influenced by its environment, which includes the adjacent zinc-binding residues cysteine 40, 60, 64, and histidine 43. The pK_a for free or protein-bound fluorescein is typically near 6.2–6.9. Deprotonation of free fluorescein's xanthenone enol (the position 6' oxygen in Figure 5) to create dianionic fluorescein leads to the high absorbing ($\epsilon_{492 \ nm}$ = 88 000 M^{-1} cm^{-1}) and fluorescing (quantum yield = 0.92) species (Martin and Lindqvist, 1975). The monoanionic monoprotonated fluorescein absorbs ($\epsilon_{437 \ nm}$ = 30 000 M^{-1} cm^{-1} and $\epsilon_{475 \ nm}$ = 31 000 M^{-1} cm^{-1}) and fluoresces (quantum yield = 0.25–0.35) at lower wavelengths and with less intensity. The pK_a for the final deprotonation of fluoresceinylated biomolecules in moderate ionic strength buffers are typically only slightly shifted upward or downward relative to the free dye: the pK_a was 6.20 on ribonuclease A (Garel, 1976); the pK_a was 6.9 on dimeric and 6.6 on monomeric DNA polymerase III holoenzyme β subunit (Griep and McHenry, 1990); and the pK_a was from 6.5–7.2 on various transfer RNAs (Friedrich et al., 1988). A particularly illustrative example of a strongly downward shifted fluorescein pK_a is that which occurs when free fluorescein binds to anti-fluorescein antibody 4-4-20 (Omelyanenko et al., 1993). In this case, the crystal structure of the complex is known (Herron et al., 1989) and it is possible to establish that an adjacent arginine, L34, stabilized the enolate form of fluorescein which lowered the pK_a to 5.2. In contrast, antibody which was mutated to have a histidine at that position was hypothesized to stabilize the protonated form of fluorescein since the pK_a was slightly shifted upward by 0.4 pH units relative to free fluorescein.

A fluorescent probe at position 39 places it near two conserved motifs. The two motifs within the amino-terminal 70 residues of *E. coli* primase are a cationic cluster (Stamford et al., 1992) and a "zinc finger" motif (Ilyina et al., 1992). Residues 26–34 in bacterial primases consist of a cluster of five conserved lysines and arginines. This region is not present in bacteriophage primases. The importance of this region for function was demonstrated using *E. coli* primase. Mutant primase lacking the amino-terminal 27 residues is not functional in the coupled primer/DNA synthesis assay (Stamford et al., 1992). This demonstrates the importance of the first 27 amino acids for function. Even though position 27 truncation would delete only one of the residues within the cationic cluster, it may be a critical residue. Stamford and co-workers (Stamford et al., 1992) have hypothesized that this mutant lacks function because without the amino-terminal 27 residues the adjacent zinc finger motif cannot fold properly.

The motif that is even closer in the linear sequence to the fluorescent probe is the zinc finger motif. The zinc finger motif contains the highest percentage of conserved and identical residues among primases (Ilyina et al., 1992; Versalovic and Lupski, 1993). The sequence of this motif in bacterial primases is Cys-X$_2$-His-X$_{17}$-Cys-X$_2$-Cys

(CHCC class of zinc fingers) and in *E. coli* includes residues 40−64 (Figure 1). In fact, it has been determined that primase from *E. coli* has one zinc cofactor per polypeptide chain (Stamford et al., 1992) (Cook and M. A. Griep, unpublished results). Likewise, a peptide based on the *E. coli* zinc finger sequence is capable of binding zinc (M. A. Griep and Hromas, unpublished results), indicating that this portion of primase is responsible for the zinc binding.

In the present study, we found that three PMPS equivalents caused fluorescence quenching that was the result of a shift in the fluorescein pK. The simplest explanation is that PMPS was reacting with the three zinc-chelating cysteines, at residues 40, 61, and 64, to release the zinc. In the absence of zinc, the enolate form of the fluorescein would not be stabilized and the pK could return to more normal values. In fact, we have found that PMPS binds to the zinc-chelating cysteines of primase and releases its single zinc (Cook and M. A. Griep, unpublished results). The binding of PMPS to the remaining three cysteines of primase did not lead to additional fluorescein quenching. This was expected if the remaining three cysteines, residues 306, 307, and 492, were far removed from the modified cysteine 39.

The role of the zinc finger in primase has been determined for the primase from bacteriophage T7. Even though the bacterial and bacteriophage primases have considerable amino acid sequence differences, they do appear to share many conserved residues (Ilyina et al., 1992). Perhaps an example of a minor difference is that the zinc finger motif in bacteriophage differs from that in bacteria in that the putative ligating residues are all cysteine, Cys-X_2-Cys-X_{15-24}-Cys-X_2-Cys (CCCC class of zinc fingers). One important difference is that bacteriophage T7 and P4 primases are at the amino terminus of a polypeptide chain that also includes helicase (Ilyina et al., 1992; Ziegelin et al., 1993). In T7, it has been established that there is one zinc bound to the primase portion of the chain (Mendelman et al., 1994). It was established by site-directed mutagenesis that the above-indicated four cysteines play an important role with regard to protein function. A mutant primase/helicase in which the third cysteine was mutated to serine was found to bind less zinc than wild-type and did not catalyze template-dependent primer synthesis. On the basis of these observations, it is likely that all primases bind at least one zinc and that the zinc finger plays an important role in template-directed primer synthesis. However, the mechanism by which the zinc finger carries out its role in template-directed synthesis has not been proven.

To explain the role of the zinc finger in template-directed mutagenesis, Bernstein and co-workers (Bernstein and Richardson, 1988) hypothesized that the zinc finger domain of T7 primase/helicase was responsible for the specific trinucleotide recognition that is characteristic of most primases. For instance, *E. coli* primase initiates primer synthesis from d(CTG) and bacteriophage T7 from d(GTC) (Mendelman and Richardson, 1991). This hypothesis was made in analogy to the CCHH class of zinc fingers which are found in a particular class of eukaryotic transcription factors. The CCHH class of zinc fingers fold into a common type of secondary structure (Lee et al., 1992) which is coded for by its sequence. Two of these transcription factors bind specific sequences of duplex DNA via particular residues in their single α helix according to their crystal structures (Pavletich and Pabo, 1991, 1993). One major difference between the CCHH class and the primase class of zinc fingers is that the CCHH class specifically binds duplex DNA while pri-

mases specifically bind single-stranded DNA. It is also not clear whether all zinc fingers are capable of binding DNA or RNA with specificity. In addition, the secondary structure of CCHH zinc fingers may differ from the primase zinc fingers (Qian et al., 1993; Mendelman et al., 1994). However, this remains a very good hypothesis to explain the mechanism by which sequence-specific primer initiation is achieved using the zinc finger.

A possible related mechanism for the function of the primase zinc finger is selective binding of the initiating nucleotides ATP and GTP. This is taken in analogy to the studies of *E. coli* RNA polymerase. Besides the obvious functional similarities between transcription RNA polymerases and primase, there are underlying structural and functional similarities especially with regard to one of the zincs. The multisubunit *E. coli* RNA polymerase has two zinc prosthetic groups. The zinc from the β subunit of RNA polymerase (B-site Zn(II)) is removable by PMPS treatment (Giedroc and Coleman, 1986) as is the zinc from primase (Cook and M. A. Griep, unpublished results). Since the role of the removable RNA polymerase zinc is to bind the initiating nucleotide ATP (Chatterji and Wu, 1982; Chatterji et al., 1984), this may be the role that it plays in primase. To disrupt this function should disrupt ATP-directed initiation which can be interpreted as ssDNA sequence-specific initiation disruption since complementary base pair formation is also required for initiation.

Studies of the replication fork in action will require fluorescent probes for the various enzymes and proteins involved and once created can be used as sensitive probes of structure. For instance, the fluorescently labeled β-subunit of DNA polymerase III holoenzyme has already been shown to be sensitive to four different DNA-bound states of the polymerase (Griep and McHenry, 1992). To study the interactions between primase and the DNA polymerase during replication will require a site-specific label on primase that does not alter its ability to synthesize a primer or interfere with its ability to bind to the DNA polymerase. The present study has shown that IAF-labeled primase cannot be used for this purpose since it has reduced activity in the coupled RNA/DNA synthesis assay and must be deficient in one of those properties. However, an inhibitory label near the zinc finger domain may prove useful in some studies. The zinc finger domain is very far removed in primary sequence from the helicase-interacting carboxyl-terminal domain of primase and will probably not interfere with primase/helicase binding. A lack of primase/ssDNA binding may prove desirable when studying the primase−helicase interaction. Nevertheless, FM−primase is labeled at the same site, does not inhibit primer synthesis activity, and can certainly be used in further studies of the interaction of primase at a replication fork.

ACKNOWLEDGMENT

LITERATURE CITED

Arai, K.-i., and Kornberg, A. (1981) Mechanism of *dnaB* Protein Action. IV. General Priming of DNA Replication by *dnaB* Protein and Primase Compared with RNA Polymerase. *J. Biol. Chem. 256*, 5267−5272.

Argos, P. (1988) A Sequence Motif in Many Polymerases. *Nucleic Acids Res. 16*, 9909−9916.

Bernstein, J. A., and Richardson, C. C. (1988) A 7-kDa Region of the Bacteriophage T7 Gene 4 Protein Is Required for Primase but not for Helicase Activity. *Proc. Natl. Acad. Sci. U.S.A. 85*, 396–400.

Bouché, J.-P., Zechel, K., and Kornberg, A. (1975) *dnaG* Gene Product, a Rifampicin-resistant RNA Polymerase, Initiates the Conversion of a Single-stranded Coliphage DNA to Its Duplex Replicative Form. *J. Biol. Chem. 250*, 5995–6001.

Boyer, P. D. (1954) Spectrophotometric Study of the Reaction of Protein Sulfhydryl Groups with Organic Mercurials. *J. Am. Chem. Soc. 76*, 4331–4337.

Bradford, M. M. (1976) A Rapid and Sensitive Method for the Quantitation of Microgram Quantities of Protein Utilizing the Principle of Protein-Dye Binding. *Anal. Biochem. 72*, 248–254.

Brinkley, M. (1992) A Brief Survey of Methods for Preparing Protein Conjugates with Dyes, Haptens, and Cross-Linking Reagents. *Bioconjugate Chem. 3*, 2–13.

Burton, Z. F., Gross, C. A., Watanabe, K. K., and Burgess, R. R. (1983) The Operon that Encodes the Sigma Subunit of RNA Polymerase also Encodes Ribosomal Protein S21 and DNA Primase in *Escherichia coli* K12. *Cell 32*, 335–349.

Chatterji, D., and Wu, F. Y.-H. (1982) Direct Coordination of Nucleotide with the Intrinsic Metal in *Escherichia coli* RNA Polymerase: A Nuclear Magnetic Resonance Study with Cobalt-Substituted Enzyme. *Biochemistry 21*, 4657–4664.

Chatterji, D., Wu, C.-W., and Wu, F. Y.-H. (1984) Nuclear Magnetic Resonance Studies on the Role of Intrinsic Metals in *Escherichia coli* RNA Polymerase: Effect of DNA Template on the Nucleotide-Enzyme Interaction. *J. Biol. Chem. 259*, 284–289.

Farley, R. A., Tran, C. M., Carilli, C. T., Hawke, D., and Shively, J. E. (1984) The Amino Acid Sequence of a Fluorescein-Labeled Peptide from the Active Site of (Na,K)-ATPase. *J. Biol. Chem. 259*, 9532–9535.

Filoteo, A. G., Gorski, J. P., and Penniston, J. T. (1987) The ATP-Binding Site of the Erythrocyte Membrane Ca^{2+} Pump: Amino Acid Sequence of the Fluorescein Isothiocyanate-Reactive Region. *J. Biol. Chem. 262*, 6526–6530.

Friedrich, K., Woolley, P., and Steinhäuser, K. G. (1988) Electrostatic Potential of Macromolecules Measured by pK_a Shift of a Fluorophore. 2. Transfer RNA. *Eur. J. Biochem. 173*, 233–239.

Funnel, B. E., Baker, T. A., and Kornberg, A. (1986) Complete Enzymatic Replication of Plasmids Containing the Origin of the *Escherichia coli* Chromosome. *J. Biol. Chem. 261*, 5616–5624.

Garel, J.-R. (1976) pK Changes of Ionizable Reporter Groups as an Index of Conformational Changes in Proteins: A Study of Fluorescein-Labeled Ribonuclease A. *Eur. J. Biochem. 70*, 179–189.

Giedroc, D. P., and Coleman, J. E. (1986) Structural and Functional Differences between the Two Intrinsic Zinc Ions of *Escherichia coli* RNA Polymerase. *Biochemistry 25*, 4969–4978.

Giedroc, D. P., Keating, K. M., Williams, K. R., Konigsberg, W. H., and Coleman, J. E. (1986) Gene 32 Protein, the Single-Stranded DNA Binding Protein from Bacteriophage T4, Is a Zinc Metalloprotein. *Proc. Natl. Acad. Sci. U.S.A. 83*, 8452–8456.

Griep, M. A., and McHenry, C. S. (1988) The Dimer of the β Subunit of *Escherichia coli* DNA Polymerase III Holoenzyme Is Dissociated into Monomers upon Binding Magnesium(II). *Biochemistry 27*, 5210–5215.

Griep, M. A., and McHenry, C. S. (1989) Glutamate Overcomes the Salt Inhibition of DNA Polymerase III Holoenzyme. *J. Biol. Chem. 264*, 11294–11301.

Griep, M. A., and McHenry, C. S. (1990) Dissociation of the DNA Polymerase III Holoenzyme β_2 Subunits Is Accompanied by Conformational Change at Distal Cysteines333. *J. Biol. Chem. 265*, 20356–20363.

Griep, M. A., and McHenry, C. S. (1992) Fluorescence Energy Transfer Between the Primer and the β Subunit of *Escherichia coli* DNA Polymerase III Holoenzyme. *J. Biol. Chem. 267*, 3052–3059.

Herron, J. N., He, X.-m., Mason, M. L., Voss, E. W., Jr., and Edmundson, A. B. (1989) Three-Dimensional Structure of A Fluorescein-Fab Complex Crystallized in 2-Methyl-2,4-Pentanediol. *Proteins: Struct., Funct., Genet. 5*, 271–280.

Hunt, J. B., Neece, S. H., Schachman, H. K., and Ginsburg, A. (1984) Mercurial-promoted Zn^{2+} Release from *Escherichia coli* Aspartate Transcarbamoylase. *J. Biol. Chem. 259*, 14793–14803.

Ilyina, T. V., Gorbalenya, A. E., and Koonin, E. V. (1992) Organization and Evolution of Bacterial and Bacteriophage Primase-Helicase Systems. *J. Mol. Evolution 34*, 351–357.

Ishii, Y., and Lehrer, S. S. (1986) Effects of the State of the Succinimido-Ring on the Fluorescence and Structural Properties of Pyrene Maleimide-Labeled $\alpha\alpha$-Tropomyosin. *Biophys. J. 50*, 75–80.

Johanson, K. O., and McHenry, C. S. (1980) Purification and Characterization of the β Subunit of the DNA Polymerase III Holoenzyme of *Escherichia coli*. *J. Biol. Chem. 255*, 10984–10990.

Kornberg, A., and Baker, T. A. (1992) *DNA Replication*, W. H. Freeman and Company, New York.

Lakowicz, J. R. (1983) *Principles of Fluorescence Spectroscopy*, Plenum Press, New York.

LeBowitz, J. H., and McMacken, R. (1986) The *Escherichia coli* dnaB Replication Protein Is a DNA Helicase. *J. Biol. Chem. 261*, 4738–4748.

Lee, M. S., Mortishire-Smith, R. J., and Wright, P. E. (1992) The Zinc Finger Motif: Conservation of Chemical Shifts and Correlation with Structure. *FEBS Lett.309*, 29–32.

Lehman, I. R. (1974) DNA Ligase: Structure, Mechanism, and Function. *Science 186*, 790–797.

Lohman, T. M., Green, J. M., and Beyer, R. S. (1986) Large-Scale Overproduction and Rapid Purification of the *Escherichia coli* ssb Gene Product: Expression of the *ssb* Gene under λ P_L Control. *Biochemistry 25*, 21–25.

Lux, B., and Gérard, D. (1981) Reappraisal of the Binding Processes of *N*-(3-Pyrene)maleimide as a Fluorescent Probe of Proteins. *J. Biol. Chem. 256*, 1767–1771.

Marians, K. J. (1992) Prokaryotic DNA Replication. *Annu. Rev. Biochem. 61*, 673–719.

Martin, M. M., and Lindqvist, L. (1975) The pH Dependence of Fluorescein Fluorescence. *J. Lumin. 10*, 381–390.

McMacken, R., and Kornberg, A. (1978) A Multienzyme System for Priming the Replication of ϕX174 Viral DNA. *J. Biol. Chem. 253*, 3313–3319.

McMacken, R., Ueda, K., and Kornberg, A. (1977) Migration of *Escherichia coli* dnaB Protein on the Template DNA Strand as a Mechanism in Initiating DNA Replication. *Proc. Natl. Acad. Sci. U.S.A. 74*, 4190–4194.

Mendelman, L. V., and Richardson, C. C. (1991) Requirements for Primer Synthesis by Bacteriophage T7 63-kDa Gene 4 Protein: Roles of Template Sequence and T7 56-kDa Gene 4 Protein. *J. Biol. Chem. 266*, 23240–23250.

Mendelman, L. V., Beauchamp, B. B., and Richardson, C. C. (1994) Requirement for a Zinc Motif for Template Recognition by the Bacteriophage T7 Primase. *EMBO J. 13*, 3909–3916.

Mok, M., and Marians, K. J. (1987) Formation of Rolling-Circle Molecules during ϕX174 Complementary Strand DNA Synthesis. *J. Biol. Chem. 262*, 2304–2309.

Ogawa, T., and Okazaki, T. (1980) Discontinuous DNA Replication. *Annu. Rev. Biochem. 49*, 421–457.

Okazaki, R., Okazaki, T., Sakabe, K., Sugimoto, K., and Sugino, A. (1968) Mechanism of DNA Chain Growth: I. Possible Discontinuity and Unusual Secondary Structure of Newly Synthesized Chains. *Proc. Natl. Acad. Sci. U.S.A. 59*, 598–605.

Omelyanenko, V. G., Jiskoot, W., and Herron, J. N. (1993) Role of Electrostatic Interactions in the Binding of Fluorescein by Anti-Fluorescein Antibody 4-4-20. *Biochemistry 32*, 10423–10429.

Parker, C. A., and Rees, W. T. (1960) Correction of Fluorescence Spectra and Measurement of Fluorescence Quantum Efficiency. *Analyst 85*, 587–600.

Pavletich, N. P., and Pabo, C. O. (1991) Zinc Finger-DNA Recognition: Crystal Structure of a Zif268-DNA Complex at 2.1Å. *Science 252*, 809–817.

Pavletich, N. P., and Pabo, C. O. (1993) Crystal Structure of a Five-Finger GLI-DNA Complex: New Perspectives on Zinc Fingers. *Science 261,* 1701−1707.

Qian, X., Gozani, S. N., Yoon, H.-S., Jeon, C.-J., Agarwal, K., and Weiss, M. A. (1993) Novel Zinc Finger Motif in the Basal Transcriptional Machinery: Three-Dimensional NMR Studies of the Nucleic Acid Binding Domain of Transcriptional Elongation Factor TFIIS. *Biochemistry 32,* 9944−9959.

Sasagawa, T., Okuyama, T., and Teller, D. C. (1982) Prediction of Peptide Retention Times in Reversed-Phase High-Performance Liquid Chromatography During Linear Gradient Elution. *J. Chromatogr. 240,* 329−340.

Stamford, N. P. J., Lilley, P. E., and Dixon, N. E. (1992) Enriched Sources of *Escherichia coli* Replication Proteins: The dnaG Primase is a Zinc Metalloprotein. *Biochim. Biophys. Acta 1132,* 17−25.

Swart, J. R., and Griep, M. A. (1993) Primase from *Escherichia coli* Primes Single-Stranded Templates in the Absence of SSB or Other Auxiliary Proteins: Template Sequence Requirements Based on the Bacteriophage G4 Complementary Strand Origin and Okazaki Fragment Initiation Sites. *J. Biol. Chem. 268,* 12970−12976.

Tougu, K., Peng, H., and Marians, K. J. (1994) Identification of a Domain of *Escherichia coli* Primase Required for Functional Interaction with the DnaB Helicase at the Replication Fork. *J. Biol. Chem. 269,* 4675−4682.

Versalovic, J., and Lupski, J. R. (1993) The *Haemophilus influenzae dnaG* Sequence and Conserved Bacterial Primase Motifs. *Gene 136,* 281−286.

Weber, G., and Teale, F. W. J. (1957) Determination of the Absolute Quantum Yield of Fluorescent Solutions. *J. Chem. Soc.: Trans. Faraday Soc. 53,* 646−655.

Westergaard, O., Brutlag, D., and Kornberg, A. (1973) *J. Biol. Chem. 248,* 1361−1364.

Wickner, S. (1977) DNA or RNA Priming of Bacteriophage G4 DNA Synthesis by *Escherichia coli dnaG* Protein. *Proc. Natl. Acad. Sci. U.S.A. 74,* 2815−2819.

Wu, C.-W., Yarbrough, L. R., and Wu, F. Y.-H. (1976) *N*-(1-Pyrene)maleimide: A Fluorescent Cross-Linking Reagent. *Biochemistry 15,* 2863−2868.

Wu, C. A., Zechner, E. L., and Marians, K. J. (1992a) Coordinated Leading- and Lagging-Strand Synthesis at the *Escherichia coli* DNA Replication Fork. I. Multiple Effectors Act to Modulate Okazaki Fragment Size. *J. Biol. Chem. 267,* 4030−4044.

Wu, C. A., Zechner, E. L., Reems, J. A., McHenry, C. S., and Marians, K. J. (1992b) Coordinated Leading- and Lagging-Strand Synthesis at the *Escherichia coli* DNA Replication Fork. V. Primase Action Regulates the Cycle of Okazaki Fragment Synthesis. *J. Biol. Chem. 267,* 4074−4083.

Wu, F. Y.-H., Huang, W.-J., Sinclair, R. B., and Powers, L. (1992c) The Structure of the Zinc Sites of *Escherichia coli* DNA-dependent RNA Polymerase. *J. Biol. Chem. 267,* 25560−25567.

Yoda, K.-y., and Okazaki, T. (1991) Specificity of Recognition Sequence for *Escherichia coli* Primase. *Mol. Gen. Genet. 227,* 1−8.

Yoda, K.-y., Yasuda, H., Jiang, X.-W., and Okazaki, T. (1988) RNA-Primed Initiation Sites of DNA Replication in the Origin Region of Bacteriophage λ Genome. *Nucleic Acids Res. 16,* 6531−6546.

Zechner, E. L., Wu, C. A., and Marians, K. J. (1992) Coordinated Leading- and Lagging-Strand Synthesis at the *Escherichia coli* DNA Replication Fork. II. Frequency of Primer Synthesis and Efficiency of Primer Utilization Control Okazaki Fragment Size. *J. Biol. Chem. 267,* 4045−4053.

Ziegelin, G., Scherzinger, E., Lurz, R., and Lanka, E. (1993) Phage P4 α Protein Is Multifunctional with Origin Recognition, Helicase and Primase Activities. *EMBO J. 12,* 3703−3708.

A New Radioligand for the Epidermal Growth Factor Receptor: [111]In Labeled Human Epidermal Growth Factor Derivatized with a Bifunctional Metal-Chelating Peptide

Sandrine Rémy,[†] Raymond M. Reilly,[‡] Katherine Sheldon,[§] and Jean Gariépy*,[†]

Department of Medical Biophysics, University of Toronto, and The Ontario Cancer Institute, 610 University Avenue, Toronto, Ontario, Canada M5G 2C1. Received May 15, 1995[®]

More specific radiopharmaceuticals are currently being evaluated for the *in vivo* detection and therapy of breast cancer. The human epidermal growth factor (hEGF) represents a good radiopharmaceutical candidate in view of the reported overexpression of its receptor by breast cancer cells. To enhance the imaging potential of this peptide ligand, a synthetic strategy was developed to rapidly create small peptides containing a large number of metal-chelating groups that can be readily coupled to hEGF. A prototypic 15-amino acid branched peptide containing four EDTA-like chelator groups was assembled by solid phase peptide synthesis. The metal chelating peptide, abbreviated MCP-4-EDTA-SH, was selectively incorporated into hEGF(1–51) at its unique N-terminus amino group. The coupling of a single MCP-4-EDTA-SH into hEGF(1–51) was confirmed by SDS polyacrylamide gel electrophoresis, western blotting, and amino acid analysis. The protein conjugate was successfully labeled with [111]In. Its specific binding to EGF receptors present on MDA-MB-468 breast cancer cells confirmed that such a construct retains the properties of the natural ligand.

INTRODUCTION

Breast cancer represents a major cause of mortality in North American women with more than 40 000 deaths reported in 1994 alone (*1*). The epithelial cells of the breast are under the influence of a variety of hormones (estrogens, progestins, prolactin) and growth factors. An aberration in the hormonal milieu has been postulated to be one of the critical factors in the development of breast cancer (*2, 3*). Numerous studies have suggested that the level of expression of epidermal growth factor receptors (EGFRs) may represent a useful prognostic factor in breast cancer. The overexpression of EGFRs has been observed in many primary breast cancer tissues as well as in established breast tumor cell lines. It has been associated with a poor response to endocrine therapy with tamoxifen, a predilection to recurrent disease, and a decreased long-term survival (*4*). EGFR may thus be an attractive target for the design of imaging and therapeutic probes (*5, 6*). Radiolabeled monoclonal antibodies (MAbs) have been used to develop specific radiopharmaceuticals for imaging and for therapeutic strategies for breast cancer (*7*). However, the antigens targeted in past studies have not been agents that influence the progression of the disease. Radiolabeled MAbs against EGFR are presently being evaluated in terms of their ability to localize into solid tumors. ^{123}I-EGFR1 mAb and ^{125}I-anti-EGFR-425 have been used to image or treat brain gliomas in patients (*8, 9*), to image RT4 human bladder tumor xenografts in nude mice (*10*), while ^{111}In-mAb 225 is under investigation in phase I therapy and imaging trials in patients with squamous

cell lung carcinoma (*11*). The main problems with targeting approaches involving the use of monoclonal antibodies are associated with their low uptake by the tumor, slow elimination from the blood, and the production of human anti-mouse antibodies (HAMA) (*12*). The alternative approach of using the natural ligand, epidermal growth factor (EGF) itself, remains somewhat unexplored. One imaging study reported the use of ^{123}I-EGF in patients with advanced cervical cancer, with a high tumor/nontumor ratio, 6–8 h after injection (*13*). Another study demonstrated imaging of glioma tumors in rats following intracerebral injection of ^{99m}Tc-EGF (*14*). In terms of developing powerful radiolabeled imaging agents involving the use of protein-based targeting agents such as EGF, one is faced with the practical compromise of introducing a sufficient number of individual metal-chelating sites on such proteins to generate conjugates that are radiochemically useful without a complete loss of binding affinity of the modified targeting agent for its receptor (as a result of excessive labeling) (*15*). A simple strategy was thus developed based on the flexibility and rapidity of solid-phase techniques to design bifunctional branched peptides that incorporate a defined number of metal-chelating sites and possess a single reactive site that allows the peptide to be coupled unidirectionally to one designated site available on EGF.

We report the chemical and biological properties of a well-defined human EGF(1–51) construct that includes a branched peptide containing four metal-chelating sites, which can be radiolabeled with ^{111}In to a high specific activity and can bind to the EGFR-expressing breast tumor cell line, MDA-MB-468.

EXPERIMENTAL PROCEDURES

Chemicals. Human EGF(1–51) was a generous gift from Dr. Maratea (Creative BioMolecules, Hopkinton, MA). All Boc-protected amino acids were purchased from Nova Biochem (LaJolla, CA) and the MBHA resin from Applied Biosystems (Mississauga, Ontario, Canada). Trifluoroacetic acid (TFA, sequencing grade), α,β-diaminopropionic acid, and diisopropylethylamine (DIEA) were

* Author to whom correspondence should be addressed. Phone: (416) 946-2967. Fax: (416) 946-6529. E-mail: gariepy@ ocicl.oci.utoronto.ca.

† Department of Medical Biophysics, Ontario Cancer Institute.

‡ Division of Nuclear Medicine, The Toronto Hospital, and Faculty of Pharmacy, University of Toronto, Ontario, Canada.

§ Present address: Boston Biomedical Research Institute, 20 Stanisford St., Boston, MA 02114.

® Abstract published in *Advance ACS Abstracts,* September 15, 1995.

purchased from Schweizerhall, Inc. (South Plainfield, NJ). *tert*-Butyl bromoacetate was obtained from Aldrich Chemical Co. (Milwaukee, WI). Sodium thiophenoxide was prepared by addition of thiophenol to 1 molar equiv of sodium metal in diethyl ether. The suspension was vigorously shaken for 72 h at room temperature, and the resulting sodium thiophenoxide was recovered by filtration *(16)*. All reagent grade solvents and chemicals (acetonitrile, dichloromethane (DCM), dicyclohexylcarbodiimide (DCC), *N*-hydroxybenzotriazole (HOBt), β-mercaptoethanol, sodium borohydride, and 5,5'-dithiobis(2-nitrobenzoic acid) (Ellman's reagent (DTNB)) were purchased from BDH (Toronto, Ontario, Canada). $^{111}InCl_3$ (>50 mCi/mL) was obtained from Nordion (Kanata, Ontario, Canada). Na^{125}I (100 mCi/mL) was obtained from NEN/Dupont (Boston, MA) or Amersham (Oakville, Ontario, Canada).

Materials and Equipment. ^{1}H-NMR spectra were recorded at 500 MHz on a Brucker AM-500 spectrometer and resonance assignments reported in ppm downfield from the internal tetramethylsilane standard. Mass spectra (MS) were recorded on a VG Masslab 20−250 quadrapole spectrometer and UV spectra on a Beckman DU-30 spectrophotometer. Amino acid analyses were performed on a Beckman System Gold 166 analyzer after the samples had been hydrolyzed *in vacuo* for 24 h at 110 °C, in the presence of 6 N constant boiling HCl containing 0.1% (v/v) phenol. The branched peptide was synthesized on an Applied Biosystems Model 430 peptide synthesizer. Chromatography grade silica gel (200−425 mesh) was purchased from Fisher Scientific. Thin-layer chromatography (TLC) was performed using Whatman silica gel 60 Å fluorescent indicator plates. The extent of labeling of peptides with ^{111}In or ^{125}I was monitored by instant thin-layer chromatography on ITLC SG silica gel impregnated glass fiber sheets from Gelman Sciences (Ann Arbor, MI).

Cell Lines and Culture Conditions. The MDA-MB-468 breast cancer cell line *(17)* was obtained from Dr. Ron Buick (Ontario Cancer Institute, Toronto, Ontario) and routinely cultured in L-15 medium supplemented with 10% fetal calf serum (FCS) *(18)*.

EDTA-like Chelator Synthesis. The protected form of the chelator EDTA was prepared following a simple two-step procedure described by Arya and Gariépy *(19)*. Typically, α,β-diaminopropionic acid was refluxed for 20 h in redistilled acetonitrile in the presence of 10 molar equiv of DIEA and 7 molar equiv of *tert*-butyl bromoacetate. The reaction mixture was precipitated by adding toluene and filtered, and the filtrate was reduced to dryness. The resulting oily mixture was redissolved in toluene and extracted with 0.1 M phosphate buffer, pH 2.0. The organic phases were dried over MgSO$_4$, filtered, and evaporated. A flash chromatography step of the crude mixture loaded on a silica gel column provided the pure [(α,β,*N*,*N*-tetra-*tert*-butylcarboxy)methyl]diaminopropionic (*tert*-butylcarboxy)methyl ester in 60−80% yield. The eluent was 5% v/v acetone in chloroform: MS (FAB) MH$^+$ 675; ^{1}H-NMR (CDCl$_3$) 1.43−1.49 (m, 45 H, *t*-Bu), 3.14 (2 q, 2 H, NCH*CH*$_2$N, J_{Ha-Hb} = 6 Hz, $J_{Ha-Hb'}$ 8 Hz, $J_{Hb-Hb'}$ 13.9 Hz), 3.5−3.6 (2 s, 8 H, N*CH*$_2$COO*t*-Bu), 3.77 (q, 1 H, NC*H*CH$_2$N, J_{H1-H2} = 6 Hz, $J_{H1-H2'}$ = 8 Hz), 4.46−4.55 (2 d, 2 H, $J_{H-H'}$ 15.5 Hz, −O(O)C*CH*$_2$C-(O)O−).

The intermediate ester was converted to the protected form of the chelating agent that includes a single free carboxylic arm by reaction with 3−4 molar equiv of sodium thiophenoxide *(16)* in DMF at 100 °C for 2 h. The reaction mixture was precipitated by adding ethyl acetate and filtered, and the filtrate was reduced to dryness. The

resulting mixture, redissolved in ethyl acetate, was extracted with 0.1 M phosphate buffer, pH 2.0, and the organic phases were evaporated. The crude mixture was loaded on a silica gel column, and pure [(α,β,*N*,*N*-tetra-*tert*-butylcarboxy)methyl]diaminopropionic acid (*tert*-butyl protected EDTA-like groups) was recovered in 60% yield by flash chromatography. The eluent was 100% toluene to remove unreacted diaminopropionic *tert*-butyl ester followed by 2% v/v acetic acid in acetone: MS (FAB) MH$^+$ 561; ^{1}H-NMR (CDCl$_3$) 1.45−1.47 (m, 36 H, *t*-Bu), 3.12 (d, 2 H, NCHC*H*$_2$N, J_{Ha-Hb} = $J_{Ha-Hb'}$ = 7.5 Hz), 3.4−3.6 (m, 8 H, NC*H*$_2$COO*t*-Bu), 3.77 (t, 1 H, NC*H*CH$_2$N).

Peptide Synthesis. The metal-chelating peptide MCP-4-EDTA-SH (Figure 1) was prepared by solid-phase peptide synthesis using N-*tert*-butoxycarbonyl (Boc)-protected amino acids and MBHA resin support. The substitution on the resin support was 0.1 mmol/g of resin. The initial low substitution value on the resin ensures that crowding of the support with peptide chains will not occur as a result of two branching steps. Four branches were introduced in the peptide using two successive rounds of addition of (Nα, Nε) di-Boc-L-lysine. All couplings were carried out using symmetric anhydride derivatives of protected amino acids employing protocols established by the manufacturer (Applied Biosystems, Foster City, CA). Each coupling step was monitored by the quantitative determination of free amino group present on the resin (quantitative ninhydrin test). The efficiency of each coupling step was greater than 99% *(20)*. The *tert*-butyl-protected EDTA-like chelator (2 molar equiv in relation to the number of moles of free amino groups in the reaction vessel) was coupled to each of the four amino termini on the branched peptide, in the presence of 2 molar equiv of DCC and HOBt dissolved in 40% DMF/DCM. The slurry was mixed at room temperature for 16 h. The resin was then washed with DMF, and the coupling step was repeated. The completion of this step was monitored by quantitative ninhydrin and found to be greater than 99%. Any remaining free amino groups were acetylated for 15 min at room temperature with 10% (v/v) acetyl anhydride, 5% (v/v) DIEA prepared in DCM. The *tert*-butyl groups protecting the EDTA-like carboxylic groups were cleaved in 25% TFA/DCM for 2 h prior to chain detachment.

Cleavage, Recovery, and Analysis of MCP-4-EDTA-SH. The polymer was cleaved from the resin support with 10% (v/v) anisole, 10% (v/v) dimethyl sulfide, and 3% (v/v) thiocresol in anhydrous hydrogen fluoride at 0 °C for 90 min. The resin was extracted with several ether washes to remove scavengers and cleaved protecting groups. The branched peptide was then recovered by extracting the resin with 100% TFA. The resulting solution was reduced by rotary evaporation in a silanized flask to 2 mL and transferred to a polypropylene tube. The peptide was then precipitated by adding ice-cold ether (30 mL) to the tube and recovered by centrifugation. This cycle was repeated twice, and then the pellet was redissolved in water and lyophilized. The peptide was desalted on a BioGel P-2 column equilibrated with 50 mM ammonium bicarbonate. Fractions migrating with the column void volume were pooled and lyophilized. The composition of the branched peptide was confirmed by amino acid analysis performed on duplicate samples: Ala (1) found 1.2 ± 0.1; aminocaproic acid (5) found 4.6 ± 0.5; Gly (4) found 3.9 ± 0.1; Lys (3) found 2.7 ± 0.1; Tyr (1) found 1.3 ± 0.1. A peptide−resin sample was recovered and cleaved prior to the coupling of EDTA groups. The resulting peptide (lacking the EDTA groups) was analyzed by ion-spray mass spectrometry and shown to have the expected mass (MH$^+$, 1532). The presence
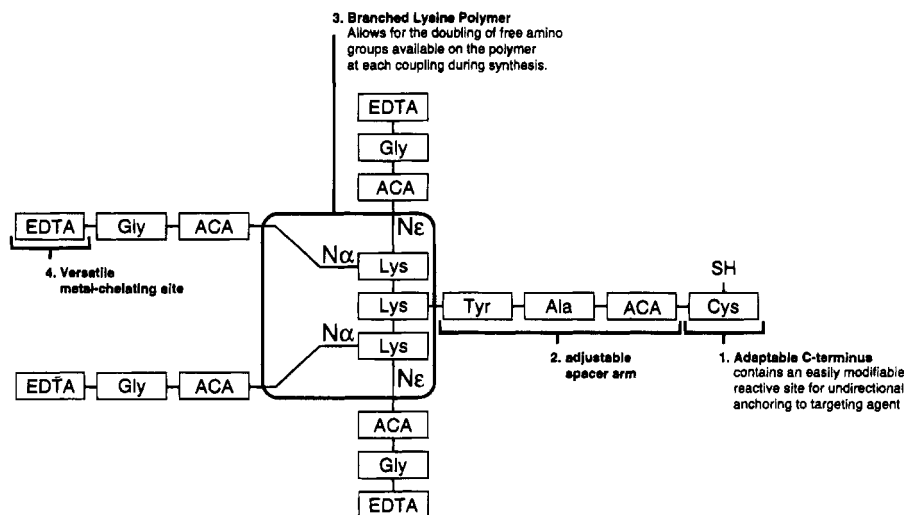
Figure 1. Structure of MCP-4-EDTA-SH, a heterobifunctional metal-chelating peptide that incorporates four EDTA groups and a single thiol moiety. Symbols: ACA, aminocaproic acid; Ala, alanine; Cys, cysteine; EDTA, EDTA-like chelator; Gly, glycine; Lys, lysine; Tyr, tyrosine.

of 4 EDTA (3.6 ± 0.2) groups was confirmed using the colorimetric procedure developed by Darbey (*21*).

Reduction of MCP-4-EDTA-SH. The presence of free sulfhydryl groups was quantified using a DTNB assay (*22*). The single thiol group on the peptide was reduced using sodium borohydride (*23*). Typically, 100 μL of a freshly prepared solution of sodium borohydride (0.1 M) in cold 0.1 M sodium borate buffer (pH 9.1) was dispensed into a tube containing 1 mg of the peptide MCP-4-EDTA-SH (0.36 μmol) dissolved in 1 mL of borate buffer. The reduction reaction was allowed to proceed on ice for 15 min. The solution was then acidified to pH 2.0 by dropwise addition of 6 N HCl in order to destroy the excess sodium borohydride. The pH of the reaction mixture was then adjusted to pH 6.0 with 4 N NaOH. The reduced peptide was then immediately mixed with the maleimide derivative of hEGF(1–51) to initiate the coupling reaction.

Maleimide Derivative of hEGF(1–51). The single amino group of hEGF(1–51) (N-terminus) was derivatized with the bifunctional crosslinking agent, (*m*-maleimidobenzoyl)-*N*-hydroxysulfosuccinimide ester (sulfo-MBS). Briefly, solid sulfo-MBS (2 mg; 4.6 μmol) was added to hEGF(1–51) (0.5 mg; 86.2 nmol) dissolved in 1 mL of PBS. The reaction was left to proceed at room temperature for 2 h with continuous agitation. The maleimide derivative abbreviated MB-hEGF(1–51) was desalted from excess unreacted sulfo-MBS by gel filtration on a BioGel P-6 column (1 cm × 10 cm) eluted with 0.1 M phosphate buffer pH 6.0.

Coupling of MCP-4-EDTA-SH to MB-hEGF(1–51). A freshly prepared solution of reduced MCP-4-EDTA-SH peptide (4-fold excess in relation to the number of moles of MB-hEGF(1–51)) was reacted with MB-hEGF(1–51) at 4 °C for 16 h. The conjugate was purified from unreacted MCP-4-EDTA-SH peptide by gel filtration on a BioGel P-30 column (1 × 10 cm) equilibrated with 0.1 M ammonium bicarbonate (pretreated on Chelex-100 resin). Fractions from the P-30 column were analyzed by ELISA as described above to detect the presence of hEGF(1–51) containing species. The conjugate eluted in the void volume peak, resolved from MB-hEGF(1–51), and the branched peptide (MCP-4-EDTA-SH). The coupling of a single MCP-4-EDTA-SH peptide to hEGF(1–51) was confirmed by comparing the ratio of amino acid present in the conjugate but **absent** in hEGF(1–51). Amino acid analyses were performed on triplicate
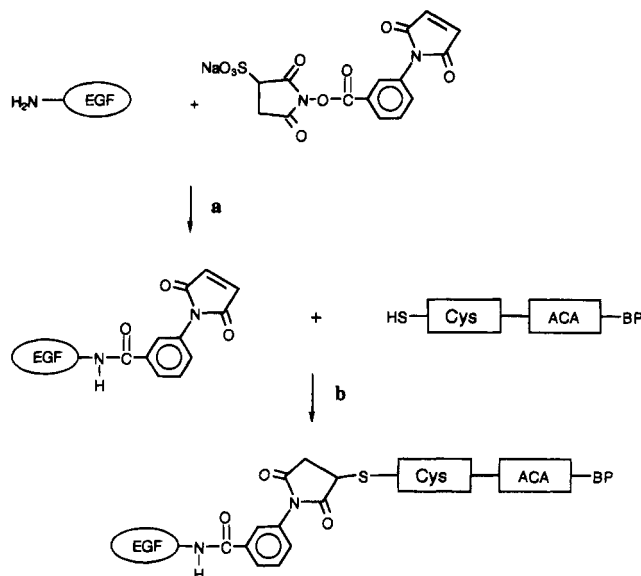
Figure 2. Conjugation scheme of MCP-4-EDTA-SH to hEGF-(1–51). Step a: reaction of N-terminus amino group of hEGF-(1–51) with sulfo-MBS. Step b: reaction of the maleimide group on MB-hEGF(1–51) with the free thiol group present on MCP-4-EDTA-SH. BP represents the branched peptide defined in Figure 1. Conjugation conditions are described in the Experimental Procedures.

samples: Ala (1) found 0.9 ± 0.2; aminocaproic acid (5) found 4.5 ± 0.2; Lys (3) found 2.5 ± 0.3. The chelating properties of MCP-4-EDTA-S-MB-hEGF(1–51) conjugate were confirmed by the binding of indium-111 (Figure 5).

Polyacrylamide Gel Electrophoresis. The conjugation of MCP-4-EDTA-SH to the protein MB-hEGF(1–51) was monitored by SDS polyacrylamide gel electrophoresis on 16% Tris–tricine gels following the method of Schagger and von Jagow (*24*) using a Mini-Protean II electrophoresis chamber (Bio-Rad; Hercules, CA). Each protein sample was diluted 1 in 4 with sample buffer containing 2% β-mercaptoethanol and 2% (w/v) Coomassie Blue G-250 and heated at 95 °C for 4 min before sample loading. The electrophoresis step was performed at 100 V (constant voltage), with a typical running time of 90 min. The gel was fixed with 10% acetic acid, 40% methanol in water for 0.5 h, stained with Coomassie Blue G-250 for 1 h, and finally destained in 10% acetic acid in water.
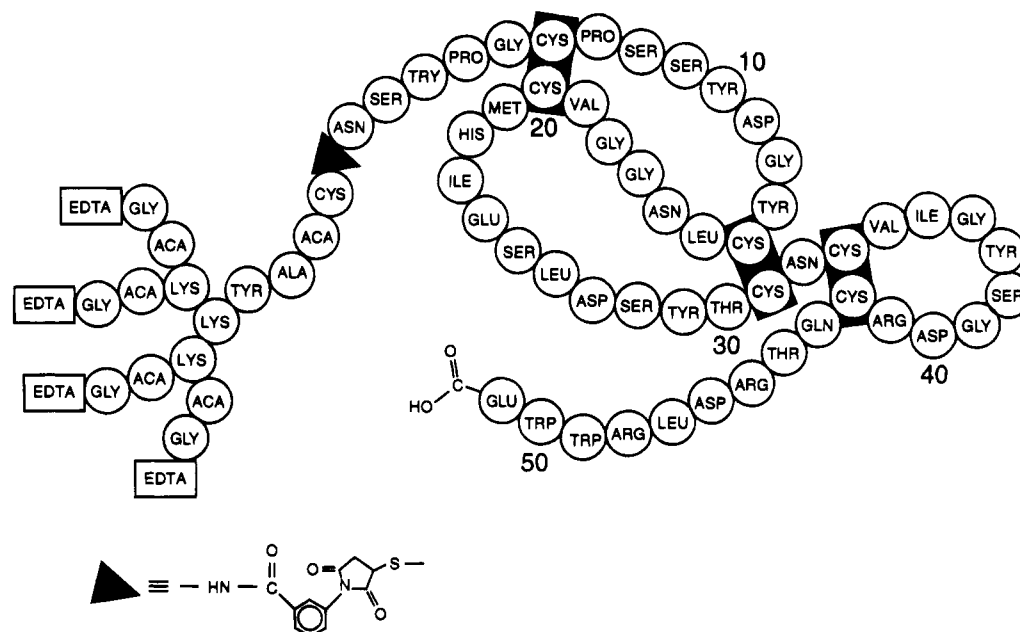
Figure 3. Primary structure of the MCP-4-EDTA-S-MB-hEGF(1–51) conjugate. Symbols: Δ, maleimidobenzoyl linker; ACA, amino caproic acid; EDTA, EDTA-like chelator. Three-letter codes were used for all amino acids.

Generation of Antisera against hEGF(1–51). New Zealand White female rabbits (2.5 kg) were immunized with four subcutaneous injections (0.25 mL/site) of a 1:1 mixture of hEGF(1–51) (250 μg) emulsified in sterile phosphate-buffered saline (PBS; 0.5 mL) and Freund's complete adjuvant (0.5 mL; Sigma Chemical Co., St. Louis, MO). The rabbits were boosted with four subcutaneous injections (0.25 mL/site) of a 1:1 mixture of hEGF(1–51) (250 μg) emulsified in 0.5 mL of PBS and 0.5 mL of Freund's incomplete adjuvant. Antisera titers toward hEGF(1–51) were tested by ELISA.

ELISA Assay. Purified hEGF(1–51) or hEGF(1–51) conjugate were used to coat microtiter wells (1 μg/well) for 2 h. After four washes with PBS, wells were incubated with 2% (w/v) bovine serum albumin (BSA) in PBS for 1 h. Unbound protein was removed by washing the wells with PBS. The antigen-coated wells were then incubated with dilutions of preimmune or postimmune serum (100 μL) for 1 h at room temperature. Wells were washed with PBS and incubated with peroxidase-conjugated goat anti-rabbit immunoglobulin antibody (1: 2000 in PBS) for 1 h. Following washes with PBS, the wells were incubated with 100 μL of 0.05% (w/v) 2,2′-azinobis(3-ethylbenzthiazoline-6-sulfonate) (ABTS) dissolved in 0.1 M sodium phosphate, 0.08 M citric acid, pH 4.0, and 0.003% (v/v) hydrogen peroxide. Absorbance readings at 405 nm were recorded with a Titretek Multiscan MCC/340 plate reader.

Western Immunoblot Analysis. Following SDS–PAGE, the protein bands were electrophoretically transferred to nitrocellulose membranes (Bio-Rad Lab., Hercules, CA) using a Polyblot transfer system (American Bionetics, Hayward, CA). Membranes were then treated for 1 h in 2% (w/v) Carnation powdered milk in TBS (100 mM Tris–HCl, 0.15 M NaCl, pH 7.4) followed by a 2 h incubation step with a 1:500 dilution of rabbit anti hEGF (1–51) antisera in TBS containing 0.2% (w/v) BSA or Carnation powdered milk. The membranes were washed and exposed to peroxidase-conjugated goat anti-rabbit immunoglobulin antibody (1:2000 in TBS) for 1 h. The presence of antibody complexes on membranes was detected using the method of Young (25). Briefly, washed membranes were incubated in a solution containing 10

mg of 4-chloro-1-naphthol and 30 mg of 3,3′-diaminobenzidine tetrahydrochloride dissolved in 5 mL of methanol and combined with 40 mL of PBS and 10 μL of 30% (v/v) hydrogen peroxide. Color development was stopped by washing the membranes with distilled water.

Radioiodination of hEGF(1–51). Human EGF(1–51) (2 μg) was labeled to a specific activity of 0.25 μCi/ng (1 mCi/nmol) with Na[125]I using Chloramine T as previously described (26).

Radioligand Binding Assays. MDA-MB-468 breast cancer cells (1.5 × 10^6 cells) were dispensed into 35 mm culture dishes and incubated for 1 h at 37 °C with 1 ng of ^{125}I-hEGF(1–51) in the presence of increasing amounts of unlabeled MCP-4-EDTA-S-MB-hEGF(1–51) or hEGF-(1–51) prepared in 0.2% (w/v) human serum albumin in PBS. The cells were then transferred to polystyrene tubes and centrifuged at 2000 rpm for 5 min to separate the cell pellet and the supernatant. The radioactivity associated with cell pellet and supernatant fractions were then measured in a γ scintillation counter. The percentage of ^{125}I-labeled hEGF(1–51) bound to breast cancer cells was plotted as a function of the total amount of MCP-4-EDTA-S-MB-hEGF(1–51) or hEGF(1–51) added (Figure 6).

[111]In Labeling of the hEGF(1–51) Conjugate. MCP-4-EDTA-S-MB-hEGF(1–51) (18 μg; 2.1 nmol) was dissolved in 0.1 M citrate buffer pH 6.5 and mixed with 3.6 × 10^-11 mol (1.8 mCi) of ^{111}In chloride, to a specific activity of ~50 mCi/mg. The labeling of the conjugate was followed using ITLC-SG plates developed in 0.1 M citrate buffer pH 4.5. In the presence of this mobile phase, the radiolabeled conjugate remained at the origin and the free ^{111}In migrated with the solvent front. The flexible chromatographic plate was then cut into 12 × 1 cm sections and the radioactivity associated with each segment was measured in a γ counter (Figure 5A). Unbound ^{111}In was removed by purification on a BioGel P-30 column (pasteur pipette) eluted with 0.1 M citrate buffer pH 4.5. Column fractions of 100 μL were collected (Figure 5B).
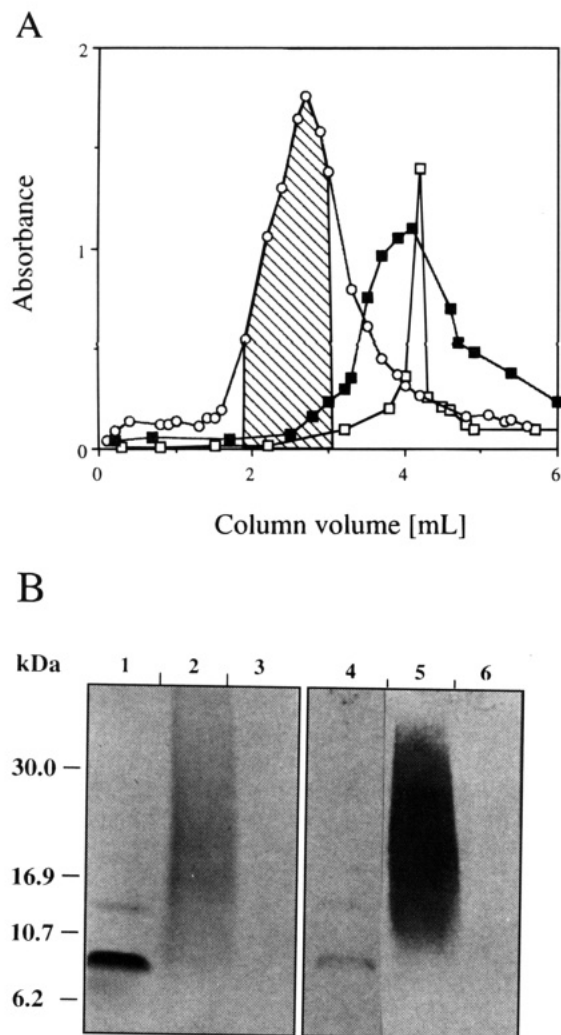
Figure 4. (A) Superimposed elution profiles of hEGF(1–51) (■), MCP-4-EDTA-S-MB-hEGF(1–51) conjugate (○), and of the MCP-4-EDTA-SH peptide (□) on a BioGel P-30 gel filtration column. Absorbance readings for hEGF(1–51) and its conjugate were recorded at 405 nm and represent ELISA assay measurements of hEGF(1–51) or its conjugate in column fractions. The presence of MCP-4-EDTA-SH in column fractions was detected at 280 nm. The hatched region highlighted in the elution profile of the conjugate indicates a typical pool of column fractions that would be recovered from this purification step. (B) Coomassie Blue stained Tris–tricine SDS–PAGE gel (lanes 1–3) and corresponding Western immunoblot (lanes 4–6): lane 1, 2 μg of hEGF(1–51); lane 2, 4 μg of MCP-4-EDTA-S-MB-hEGF(1–51) conjugate; lane 3, 10 μg of MCP-4-EDTA-SH peptide; lane 4, 2 μg of hEGF(1–51); lane 5, 4 μg of MCP-4-EDTA-S-MB-hEGF(1–51) conjugate; lane 6, 10 μg of MCP-4-EDTA-SH peptide. All methods are described in the Experimental Procedures.

RESULTS AND DISCUSSION

Overall Design of an EGF Construct that Incorporates a Metal-Chelating Peptide. The creation of heterobifunctional peptides that incorporate clusters of metal-chelating sites as well as chemically reactive groups represents a relatively unexplored strategy for producing new radiopharmaceutical agents. In particular, the coupling of such constructs to unique sites on targeting agents such as peptide hormones or antibodies would create well-defined, selective conjugates that could be labeled to potentially higher levels of specific activity. To design and facilitate the assembly of metal-chelating peptides (MCP), we combined the use of peptide branching strategies (27) and protected forms of metal chelators (19) into existing procedures in solid-phase peptide synthesis. In designing the prototypic metal-chelating
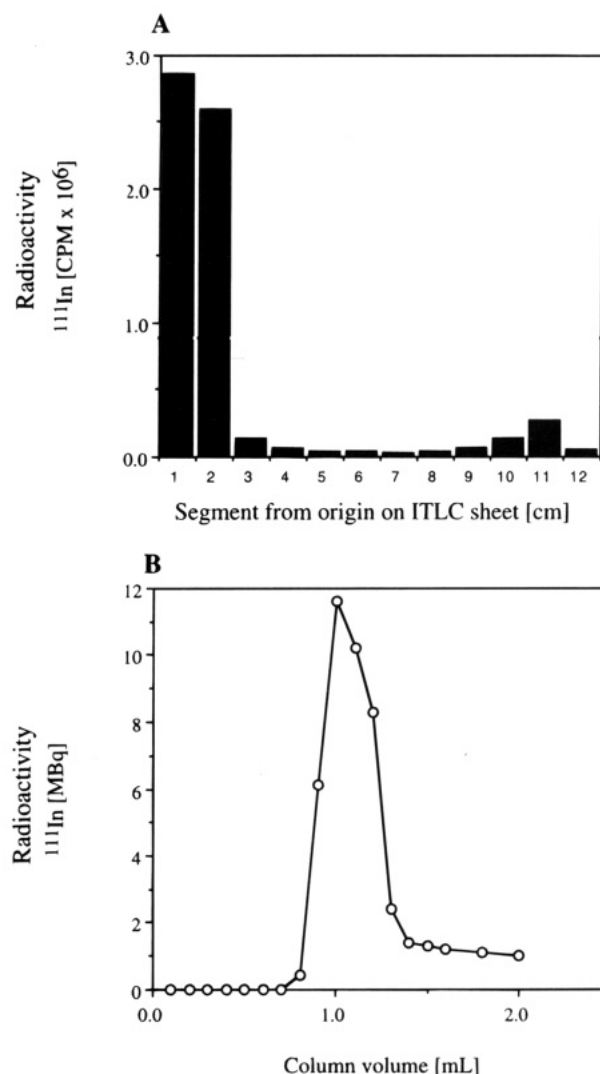
Figure 5. (A) Assessment of radiolabeling efficiency of the conjugate by thin-layer chromatography. An aliquot of the ^{111}In-MCP-4-EDTA-S-MB-hEGF(1–51) labeling mixture (4 μL) was spotted and developed on ITLC-SG plates. The radioactivity associated with each 1 cm segment on the plate was measured in a γ-counter. The labeled conjugate remained at the origin on the plate (segments 1–2) while unbound indium-111 migrated with the solvent front (segment 11). (B) Elution profile of the radiolabeled conjugate on a BioGel P-30 column. The ^{111}In-labeled conjugate eluted in the void volume of the column. The amount of residual free indium-111 (~15% of total counts) was estimated by counting the column itself following the elution of the radiolabeled conjugate. All methods are described in the Experimental Procedures.

peptide MCP-4-EDTA-SH (Figure 1), we introduced a unique thiol moiety at its C-terminus to couple this MCP to a targeting molecule. For several reasons, the human epidermal growth factor (hEGF) represented a useful and important peptide model for evaluating the impact of introducing MCP-4-EDTA-SH into a targeting agent. Firstly, hEGF is a small, single chain peptide of 53 amino acid (MW 6 kD) which is synthesized in lactating mammary glands, kidney, and submaxillary glands (28, 29). The overexpression of its receptor on the surface of breast tumor cells is associated with a poor prognosis in breast cancer patients (4). Secondly, the primary sequence of hEGF does not include lysine residues, and its single N-terminal amino group has been successfully derivatized in the past with fluorescein (30) or rhodamine (31) and ferritin (32) functionalities. Thus, only one MCP-4-EDTA-SH can be theoretically incorporated into this conjugate, eliminating an important source of structural

heterogeneity often observed in immunoconjugates. Thirdly, a fluoresceinated conjugate of hEGF exhibited similar binding affinities to native EGF (*30*), suggesting that the introduction of MCP-4-EDTA-SH at the N-terminus of hEGF would not drastically affect the complexation of the construct to the EGF receptor. Finally, the mass of hEGF in relation to MCP-4-EDTA-SH offered advantages over the use of antibodies, in terms of characterizing and purifying the final construct using standard electrophoretic and chromatographic techniques. Experimentally, a recombinant form of human EGF, abbreviated hEGF(1−51) (*33*), was used to construct our metal-chelating-hEGF conjugate. This EGF analogue lacks the final two non-essential C-terminus residues of hEGF (*34*).

Design and Synthesis of MCP-4-EDTA-SH. The bifunctional metal-chelating-peptide was termed MCP-4-EDTA-SH to reflect the presence of four EDTA groups able to bind with high affinity a large spectrum of multivalent cations and the incorporation of a single thiol group located at its C-terminus that permits its unidirectional coupling to other molecules. As illustrated in Figure 1, the first residue coupled to the solid support was cysteine. The protected thiol group on the side chain of the first residue served as the reactive site for incorporating the peptide construct into hEGF(1−51). The second residue introduced was aminocaproic acid. It acts as a molecular spacer between the peptide branches and the C-terminus reactive group. It also permits one to monitor the quality of the conjugation step with hEGF(1−51), since this residue is absent in proteins and can be quantified by amino acid analysis. Branching of the peptide was then initiated following the coupling of alanine and tyrosine. Briefly, (Nα-Boc, Nϵ-Boc)-lysine, an amino acid having its amino groups at the Cα and Cϵ positions protected with the same acid labile Boc protecting group, was introduced on the peptide resin. The approach of creating branched peptides using the two amino groups of lysine was popularized by Tam for the construction of immunogenic peptides (*27*). After the two Boc groups were cleaved with TFA, branching was initiated by coupling 2 equiv of (Nα,Nϵ-bis-Boc)lysine to the two available amino groups. After another round of acid deprotection, amino caproic acid (ACA) was coupled to the four free amino groups now available. Upon removal of Boc groups, four resulting amino groups were exposed to permit the coupling of glycine residues. Protected EDTA-like groups (*19*) were finally coupled to the exposed amino groups of glycine residues, and the polymer was detached from the resin support yielding MCP-4-EDTA-SH. The structure of the branched peptide was confirmed by amino acid analysis and mass spectroscopy (see Experimental Procedures).

The unidirectional incorporation of MCP-4-EDTA-SH into the maleimide-derivatized hEGF(1−51) results in conjugates that can be easily radiolabeled. Following pathway a outlined in Figure 2, the N-terminus of hEGF-(1−51) was reacted with the bifunctional crosslinking agent, (*m*-maleimidobenzoyl)-*N*-hydroxysulfosuccinimide ester (sulfo-MBS). The maleimide derivative, abbreviated MB-hEGF(1−51), was desalted on a BioGel P-6 column to remove excess unreacted cross-linker. MB-hEGF(1−51) selectively and rapidly reacted with the thiol group of the side chain of the cysteine present in MCP-4-EDTA-SH peptide. The thiol group on MCP-4-EDTA-SH was reduced with sodium borohydride (*26*) and monitored using a DTNB assay before the coupling step with MB-hEGF(1−51) was initiated (Figure 3). The resulting thiol-containing peptide was reacted immediately with MB-hEGF(1−51), and the conjugate was

desalted on a BioGel P-30 column. The conjugate eluted as a broad band in the volume of the column separated from unreacted MB-hEGF(1−51) and MCP-4-EDTA-SH (Figure 4A). The incorporation of a single branched peptide in the conjugate was confirmed by amino acid analysis (see Experimental Procedures) and SDS polyacrylamide gel electrophoresis. To further confirm that the broad band observed in SDS−PAGE represented the hEGF(1−51) conjugate, we performed western blot analyses on the conjugate using anti-hEGF(1−51) serum. The broad Coomassie Blue stained band observed on SDS−PAGE gel comigrated with a positive signal on western blots proving the presence of hEGF(1−51) in the conjugate (Figure 4B). In addition, results from both the Coomassie stained gel and the western blot clearly point out the lack of free hEGF(1−51) contamination in the resulting conjugate preparation. The broadness of the band observed for the conjugate reflects the nature of the peptide MCP-4-EDTA-SH itself. The presence of the branched peptide was not revealed by Coomassie Blue (Figure 4B, lane 3) or silver staining (result not shown). However, when the peptide alone was radioiodinated, autoradiograms of the SDS−PAGE gel show a broad band for the peptide (result not shown). The EDTA groups on the peptide contribute 16 carboxylic arms (with four different pKa's) to the conjugate. Consequently, up to 16 negative charges may be displayed on the branched peptide and its conjugates. Since migration on SDS−PAGE is dependent on a proper association of negatively charged SDS molecules with a protein, any heterogeneity in the charge to mass ratio of the conjugate due to the EDTA carboxylic arms would result in a broadening on the corresponding band on the gel.

EDTA-like chelators form "stable" chelate complexes with indium-111 (*35*). This radioisotope with its 3-day half-life and pure γ emission is suitable for radioimaging (*36*). In the labeling step, the hEGF(1−51) conjugate was concentrated and then dissolved in a minimum volume of citrate buffer pH 6.5 before adding "carrier free" ^{111}InCl$_3$. The yield of recovered radioactivity associated with the conjugate after gel filtration was typically >75% of the starting radioactivity. Analysis of the ^{111}In labeling reaction mixture by ITLC-SG plates showed the disappearance of the free isotope (indium citrate; R_f 1.0) after 30 min (Figure 5A). Most of the activity on the BioGel P-30 column was associated with the void volume peak containing the ^{111}In-labeled conjugate whereas the free radionuclide is included (Figure 5B). The specific activity of the labeled conjugate was typically between 50 and 60 μCi/μg protein.

The Conjugate Binds to Epidermal Growth Factor Receptors Expressed on the Breast Cancer Cell Line MDA-MB-468. The binding of hEGF(1−51) conjugate to the EGFRs on MDA-MB-468 breast cancer cells was assessed by measuring its ability to compete with ^{125}I-labeled hEGF(1−51) for the receptor sites. As shown in Figure 6, the MCP-4-EDTA-S-MB-hEGF(1−51) conjugate displaced, in a concentration-dependent manner, the binding of radioiodinated hEGF(1−51) to EGFRs with an affinity constant approximately 40-fold lower than hEGF(1−51). This partial loss in receptor affinity may reflect steric hindrance due to the addition of the branched peptide (2.8 kDa) to hEGF(1−51) (5.8 kDa).

In summary, we report the design and rapid synthesis of a metal-chelating peptide that incorporates four EDTA groups and one thiol group. The assembly of MCP-4-EDTA-SH was facile. The flexibility of the synthetic approach suggests that our initial design can be easily modified to alter the nature of the chelator, the number and composition of the branches, and the coupling
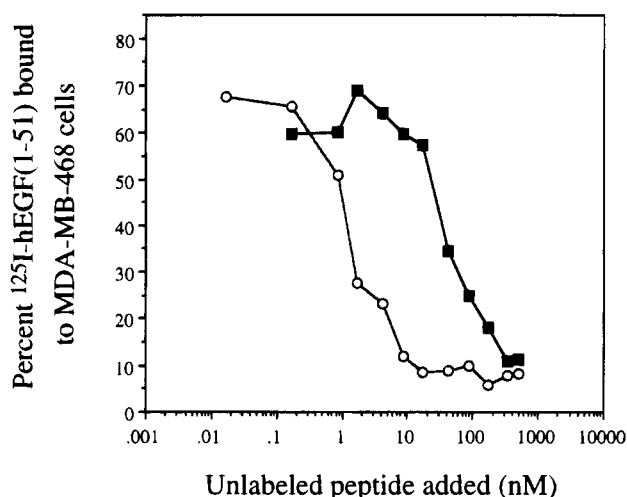
Figure 6. Displacement curves of ^{125}I-labeled hEGF(1–51) bound to its receptor on breast cancer cells by hEGF(1–51) and its conjugate. Displacement curves of ^{125}I-hEGF(1–51) binding to MDA-MB-468 cells were constructed using increasing concentrations of either hEGF(1–51) (O) or the MCP-4-EDTA-S-MB-hEGF(1–51) conjugate (■). All methods are described in the Experimental Procedures.

strategy to targeting agents. Human EGF(1–51) was successfully derivatized with a single MCP-4-EDTA-SH yielding a conjugate that binds specifically to its receptor on breast cancer cells. The conjugate labeled well with indium-111. Experiments are now in progress to assess the localization potential of this radiopharmaceutical agent in nude mice bearing MDA-MB-468 breast tumor xenografts.

ACKNOWLEDGMENT

LITERATURE CITED

(1) Boring, C. C., Squires, T. S., Tong, T., and Montgomery, S. (1994) Cancer statistics. 1994 *CA Cancer J. Clin. 44*, 7–26.

(2) Gullick, W. J. (1990) Growth factors and oncogenes in breast cancer. *Prog. Growth Factor Res. 2*, 1–13.

(3) Freiss, G., Prebois, C., and Vignon, F. (1993) Control of breast cancer cell growth by steroids and growth factors: interactions and mechanisms. *Breast Cancer Res. Treat. 27*, 57–68.

(4) Stainsbury, J. R. C., Farndon, J. R., Needham, G. K., Malcolm, A. J., and Harris, A. L. (1987) Epidermal growth factor receptor status as predictor of early recurrence of and death from breast cancer. *Lancet i*, 1398–1402.

(5) Baselga, J., and Mendelsohn, J., (1994) The epidermal growth factor receptor as a target for therapy in breast carcinoma. *Breast Cancer Res. Treat. 29*, 127–138.

(6) LeMaistre, F., Meneghetti, C., Howes, L., and Osborne C. K. (1994) Targeting the EGF receptor in breast cancer treatment. *Breast Cancer Res. Treat. 32*, 97–103.

(7) Merino, M. J., Monteagudo, C., and Neumann, R. D. (1991) Monoclonal antibodies for radioimmunoscintigraphy of breast cancer. *Nucl. Med. Biol. 18*, 437–443.

(8) Kalofonos, H. P., Pawlikowska, T. R., Hemingway, A., and Epenetos, A. A. (1989) Antibody-guided diagnosis and therapy of brain gliomas using radiolabeled monoclonal antibodies against epidermal growth factor and placental alkaline phosphatase. *J. Nucl. Med. 30*, 1636–1645.

(9) Brady, L. W., Markoe, A. M., and Woo, D. V. (1990) Iodine-125-labeled-anti-epidermal growth factor receptor-425 in the treatment of glioblastoma multiform. In *The present and future role of monoclonal antibodies in the management of cancer. Frontiers of Radiation Therapy and Oncology* (J. M. Vaeth and J. L. Meyer, Eds.) Vol. 24, pp 151–160, Karger: Basel.

(10) Harney, J. V., Liebert, M., Wedemeyer, G., Washington, R., Stein, J., Buchsbaum, D., Steplewski, Z., and Grossman H. B. (1991) The expression of epidermal growth factor receptor on human bladder cancer: potential use in radioimmunoscintigraphy. *J. Urol. 146*, 227–231.

(11) Divgi, C. R., Welt, S., Kris, M., et al. (1991) Phase I and imaging trial of indium-111–labeled anti-epidermal growth factor receptor monoclonal antibody 225 in patients with squamous cell lung carcinoma. *J. Natl. Cancer Inst. 83*, 97–104.

(12) Reilly, R. M., Sandhu, J., Alvarez-Diez, T. M., Gallinger, S., Kirsh, J., and Stern, H. (1995). Problems of delivery of monoclonal antibodies—pharmaceutical and pharmacokinetic solutions. *Clin. Pharmacokinet. 28*, 126–142.

(13) Schatten, C., Pateisky, N., Vavra, N., Ehrenbock, P., Angelberger, P., Sivolapenko, G., and Epenetos, A. (1991) Lymphoscintigraphy with ^{123}I-labeled epidermal growth factor. *Lancet 337*, 395–396.

(14) Capala, J., Barth, R. F., Bailey, M. Q., et al. (1994) Pharmacokinetics of intracerebrally administered epidermal growth factor (EGF) in normal and glioma bearing rats. *Proc. Am. Assoc. Can. Res.* 85th Annual Meeting, San Francisco, CA, p 380.

(15) Wang, T. S., Fawwaz, R. A., and Alderson, P. D. (1992) Reduced hepatic accumulation of radiolabeled monoclonal antibodies with indium-111-thioether-poly-L-lysine-DTPA-monoclonal antibody TP41.2 F(ab')$_2$. *J. Nucl. Med. 33*, 570–574.

(16) Sheehan, J. C., and Daves, G. D. (1964) Facile alkyl-oxygen ester cleavage. *J. Org. Chem. 29*, 2006–2008.

(17) Pollak, S., Siciliano, J. M., Cailleau, R., Wiseman, C. L., and Hsu, T. L. (1979) A human breast adenocarcinoma with chromosome and isoenzyme markers similar to those of the HeLa line. *J. Natl. Cancer Inst. 62*, 263–271.

(18) Filmus, J., Trent, J. M., Pollak, M. N., and Buick, R. N. (1992) Epidermal growth factor receptor gene-amplified MDA-468 breast cancer cell line and its nonamplified variants. *Molec. Cellular Biol. 7*, 251–257.

(19) Arya, R., and Gariépy, J. (1991) Rapid synthesis and introduction of a protected EDTA- like group during the solid-phase assembly of peptides. *Bioconjugate Chem. 2*, 323–326.

(20) Sarin, V. K., Kent, S. B. H., Tam, J. P., and Merrifield, R. B. (1981) Quantitative monitoring of Solid Phase Peptide Synthesis by ninhydrin reaction. *Anal. Biochem. 117*, 147–157.

(21) Darbey, A. (1952) Colorimetric determination of the sodium salts of ethylene diaminetetraacetic acid. *Anal. Chem. 24*, 373–378.

(22) Ellman, G. L. (1959) Tissue sulfhydryl groups *Arch. Biochem. Biophys. 82*, 70–77. Ishikawa, E., Imagawa, M., Hashido, S., Yoshitake, S., Hamaguchi, Y., and Veno, T. (1993) Enzyme labeling of antibodies and their fragments for immunoassay and immmunohistochemical staining. *J. Immunoassay 4*, 209–237.

(23) Rothbard, J. B., Fernandez, R., and Schoolnik, G. K. (1984) Strain-specific and common epitopes of gonococcal pili. *J. Exp. Med. 160*, 208–221.

(24) Schagger, H. and von Jagow, G. (1987) Tricine-SDS-polyacrylamide gel electrophoresis for the separation of proteins in the range from 1 to 100 kDa. *Anal. Biochem. 166*, 368–379.

(25) Young, P. R. (1989) Enhancement of immunoblot staining using a mixed chromogenic substrate. *J. Immunol. Methods 121*, 295–296.

(26) Carpenter, G., and Cohen, S. (1976) ^{125}I-Labeled human epidermal growth factor-binding, internalization, and degradation in human fibroblasts. *J. Cell Biol. 71*, 159–171.

(27) Tam, J. P. (1988) Synthetic peptide vaccine design: synthesis and properties of a high-density multiple antigenic peptide system. *Proc. Natl. Acad. Sci. U.S.A. 85*, 5409–5413.

(28) Cohen, S., and Carpenter, G. (1975) Human epidermal growth factor: isolation and chemical and biological properties. *Proc. Natl. Acad. Sci. U.S.A. 72,* 1317−1321.

(29) Starkey, R. H., Cohen, S., and Orth, D. N. (1975) Epidermal growth factor: identification of a new hormone in human urine. *Science 189,* 800−802.

(30) Haigler, H., Ash, J. F., Singer, S. J., and Cohen, S. (1978) Visualization by fluorescence of the binding and internalization of epidermal growth factor in human carcinoma cells A-431. *Proc. Natl. Acad. Sci. U.S.A. 75,* 3317−3321.

(31) Shechter, Y., Schlessinger, J., Jacobs, S., Chang, K.-J., and Cuatrecasas, P. (1978) Fluorescent labeling of hormone receptors in viable cells: preparation and properties of highly fluorescent derivatives of epidermal growth factor and insulin. *Proc. Natl. Acad. Sci. U.S.A. 75,* 2135−2139.

(32) Haigler, H. T., McKanna, J. A., and Cohen, S. (1979) Direct visualization of the binding and internalization of a ferritin conjugate of epidermal growth factor in human carcinoma cells A-431. *J. Cell Biol. 81,* 382−395.

(33) Mount, C. D., Lukas, T. F., and Orth, D. N. (1985) Purification and characterization of epidermal growth factor (β-urogastrone) and epidermal growth factor fragments from large volumes of human urine. *Arch. Biochem. Biophys. 240,* 33−42.

(34) Kuo, B.-S., Kusmik, W. F., Poole, J. C., Elsea, S. H., Chang, J., and Hwang, K.-K., (1992) Pharmacokinetic evaluation of two human epidermal growth factors (hEGF51 and hEGF53) in rats. *Drug Met. Disp. 20,* 23−30.

(35) Meares, C. F. (1986) Chelating agents for the binding of metal ions to antibodies. *Nucl. Med. Biol. 13,* 311−318.

(36) Wolf, W., and Shani, J. (1986) Criteria for the selection of the most desirable radionuclide for radiolabeling of monoclonal antibodies. *Nucl. Med. Biol. 13,* 319−324.

CORRECTIONS

Volume 6, Number 6, November/December 1995.

Sandrine Rémy, Raymond M. Reilly, Katherine Sheldon, and Jean Gariépy*

A NEW RADIOLIGAND FOR THE EPIDERMAL GROWTH FACTOR RECEPTOR: [111]IN LABELED HUMAN EPIDERMAL GROWTH FACTOR DERIVATIZED WITH A BIFUNCTIONAL METAL-CHELATING PEPTIDE

Page 686. The amino acid sequence of human EGF-(1−51) originally presented in Figure 3 was incorrect. The correct sequence of hEGF(1−51) and the three possible sites of attachment of the metal-chelating peptide MCP-4-EDTA to hEGF(1−51) are now presented in this revised version of Figure 3.
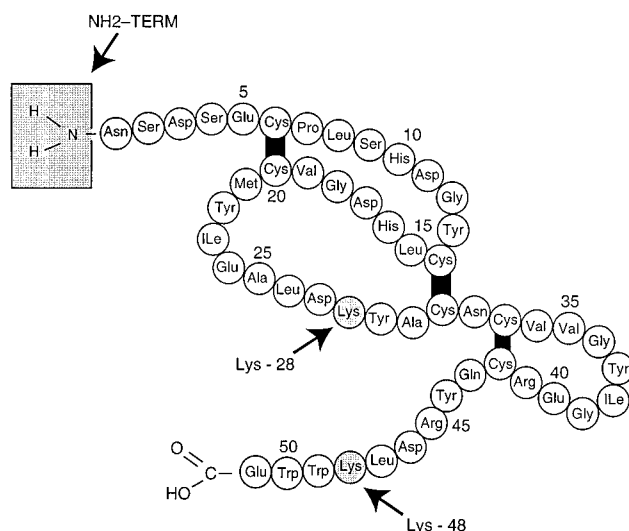
Figure 3. Primary sequence of human EGF(1−51). The amino terminus (gray box) and the ϵ-amino groups of lysine 28−48 (arrows) represent the three possible sites of attachment of the metal-chelating peptide MCP-4-EDTA to hEGF(1−51). The coupling reaction was performed at pH 7.4 to favor the addition of MCP-4-EDTA at the N terminus site of hEGF(1−51). The coupling of a single mole of MCP-4-EDTA per mole of hEGF-(1−51) was confirmed by amino acid analysis. Three-letter codes were used for all amino acids.

BC9601885

Synthesis of a Fluorescent Analog of Polychlorinated Biphenyls for Use in a Continuous Flow Immunosensor Assay

Paul T. Charles, David W. Conrad,† Megan S. Jacobs, John C. Bart,‡ and Anne W. Kusterbeck*

Center for Bio/Molecular Science and Engineering, Code 6900, Naval Research Laboratory, 4555 Overlook Avenue, S.W., Washington, DC 20375-5348. Received March 29, 1995⊗

A synthetic scheme has been developed for the preparation of a dye-labeled analog of polychlorinated biphenyls. The reaction of 2,3,5-trichlorophenol with 3-bromopropylamine hydrobromide under basic conditions was used to introduce a free primary amine group into the parent compound by formation of a stable ether linkage. Reaction of this amine with the succinimidyl ester of a sulfoindocyanine dye resulted in amide bond formation to produce a fluorescently-labeled product. The dye conjugate was used to charge a column containing immobilized antibodies against polychlorinated biphenyls. Upon application of samples containing various concentrations of polychlorinated biphenyls, the fluorescent analog was displaced from the column in amounts proportional to the concentration of analyte. Concentrations of polychlorinated biphenyl as low as 1 ppm were measurable using this system.

INTRODUCTION

Polychlorinated biphenyls (PCBs) are a class of some 209 compounds (called congeners) which are distinguished by their degree of chlorination (*1*). PCBs were used in the United States in a wide variety of industrial applications, such as transformer and capacitor dielectric fluids, printing inks, and pesticides (*2*), until the federal government began to regulate their manufacture and use in the mid-1970s (*3*). One of the more common forms of PCBs in industrial use is Monsanto's Aroclors, which are mixtures of many PCB congeners that contain a specific overall degree of chlorination (*e.g.*, Aroclor 1260 is a mixture of PCBs with an average percentage of chlorine by weight equal to 60%).

Given their known toxicity (*4–7*) and suspected carcinogenicity (*8*) in humans, PCBs have become one of the most important environmental pollutants targeted for analysis and remediation. The most frequently employed method for PCB analysis currently is gas chromatography (GC) with either electron capture detection (ECD) (*9*) or mass spectroscopic (MS) detection (*10*). Unfortunately, both GC–ECD and GC–MS, while being extremely sensitive and accurate, have several important drawbacks for widespread environmental analyses. These techniques require samples to be sent to off-site labs where highly-trained personnel usually take 1–2 weeks to complete the analysis. Additionally, these tests generally cost hundreds of dollars per sample, regardless of whether an environmental contaminant is present or not. Our device does not require the use of high-vacuum pumps necessary for GC–MS and is quite easily taken out into the field. Sample analysis at the site, along with the fact that each sample takes less than 5 min to analyze, cuts the turnaround time from weeks to minutes. Furthermore, negative samples can be run virtually cost-free, as only samples that contain the analyte in question deplete the column. Thus, one person with

minimal training can provide very cost-effective, on-site analysis compared with analytical labs. Other techniques have also been developed with the goal of providing less expensive, on-site analysis, including simple photometric tests (*11*) and immunoassays (*12–14*). Nevertheless, the present method is more cost effective in the end than handheld test kits and does not require reagent addition or timed incubations.

In this paper, we describe the synthesis of a dye-labeled analog of a PCB used in a fluorescence-based continuous flow immunosensor (*15*). This marks the first time that extremely hydrophobic analytes like PCBs have been analyzed in this fashion, as previous studies in this lab concentrated on more hydrophilic species (*16, 17*). Briefly, the continuous flow immunosensor is a semiautomated system in which the analyte-containing medium is allowed to flow through a column containing matrix-immobilized antibodies against the analyte. These antibodies are incubated with a fluorescent dye-labeled analog of the analyte before the analysis begins. As the analyte passes through the antibody matrix, some dye-labeled antigen is displaced from the antibody in favor of binding the analyte; the analog is then detected in a fluorometer located downstream from the column. We chose to use a derivative of 2,3,5-trichlorophenol as our PCB analog because the antibodies we employed in this work were produced using a trichlorophenyl hapten and not a polychlorinated biphenyl hapten. Cy5.29 was selected as the fluorescent dye because it has a large (>0.28) quantum yield, is water soluble due to the two sulfonate groups, and its emission maximum is far into the red (667 nm) where little interference is expected from naturally-fluorescent species in the water samples. In addition to a description of the synthesis of this dye-labeled antigen, preliminary results for the detection of various Aroclors will be presented.

EXPERIMENTAL PROCEDURES

The 2,3,5-trichlorophenol (Aldrich), 3-bromopropylamine hydrobromide (Aldrich), Cy5.29-OSu sulfoindocyanine dye (Biological Detection Systems, Inc., Pittsburgh, PA), polyclonal chicken anti-PCB IgY (*18*) antibodies (O.E.M. Concepts, Toms River, NJ), Aroclors 1248, 1254, and 1260 (ChemService, Westchester, PA), Aroclor 1242

† National Research Council (NRC) Postdoctoral Fellow.
‡ American Society for Engineering Education (ASEE) Postdoctoral Fellow.
* Author to whom correspondence should be addressed. Phone: (202) 404-6042. Fax: (202) 767-9594.
⊗ Abstract published in *Advance ACS Abstracts,* October 1, 1995.

(Ultra Scientific, North Kingstown, RI), activated column matrix (Emphaze chromatography beads, 3M), Triton X-405, reduced, (Aldrich), and phosphate-buffered saline (PBS) (NaCl 120 mM, KCl 2.7 mM, monobasic and dibasic phosphate buffer salts 10 mM, pH 7.4) (Sigma) were all used as received. TLC was performed using precoated silica gel 60 (EM Science) or C_{18} (Whatman) glass plates each of 0.25 mm thickness. Melting points were determined using a capillary melting point apparatus (MEL-TEMP II, Laboratory Devices) and are uncorrected. Chromatography was performed using an HPLC system consisting of two pumps (Model 510, Waters), an injector (Model U6K, Waters), and a photodiode array detector (Model 996, Waters). Reversed-phase columns (Nova-Pak C_8, or μBondapak C_{18}, Waters, Radial-Pak 8 × 100 mm) with linear gradients between water (0.2% acetic acid, pH 3.0) and methanol (0.2% acetic acid) were used in all experiments. Detection of the column effluent was achieved at 280 or 550 nm. Fluorescence detection of effluent from the immunosensor column was provided by a fluorometer with a 12 μL flow cell (JASCO, Model 821-FP). For a complete description of the flow immunosensor components see ref *17*. ^{1}H-NMR spectra were recorded using a 250 MHz spectrometer (IBM AM 250, Bruker). MS (high and low resolution) were performed by Shrader Analytical and Consulting Laboratories, Detroit, MI.

(2,3,5-Trichlorophenoxy)propylamine Hydrochloride (1). To 0.5 g (2.5 mmol) of 2,3,5-trichlorophenol in 9.0 mL of ethanol was added 0.55 g (2.5 mmol) of bromopropylamine hydrobromide. After the pH of the solution was adjusted to 12 by the dropwise addition of 4 M NaOH, the reaction mixture was allowed to reflux for 5 h. The solvent was removed under reduced pressure to give a crude yellow product. The residue was extracted with ether (3 × 20 mL), and the combined extracts were dried with anhydrous magnesium sulfate and filtered. Anhydrous HCl was bubbled through the solution for 1 min to yield the hydrochloride as a white precipitate. The product was purified by HPLC using a C_8 reversed-phase column and a linear solvent gradient between water/methanol (50/50) (containing 0.2% acetic acid) and methanol (containing 0.2% acetic acid) in 6.0 min at a flow rate of 2.0 mL/min. Detection at 280 nm showed the product to elute 1.92 min after the start of the gradient. Removal of the HPLC solvents under vacuum yielded 0.37 g (51%) of compound **1** (TLC, silica gel, methanol, R_f = 0.2, positive ninhydrin test): mp 118 °C; ^{1}H NMR (CD$_3$OD) δ 7.21 (d, 1H, arom, J = 2.2 Hz), 7.06 (d, 1H, arom, J = 2.2 Hz), 4.20 (t, 2H, OCH_2, J = 5.6 Hz), 3.25 (t, 2H, CH_2-NH$_2$, J = 6.7 Hz), 2.18 (quint, 2H, CH$_2$CH_2CH$_2$, J = 5.7 Hz); low-resolution mass spectrum (direct probe) calcd for $C_9H_{11}Cl_2NO$(free base - Cl + H) 220, found 220.

(2,3,5-Trichlorophenoxy)propyl−Cy5.29 (2). To a solution of 7.7 mg (26.5 mmol) of (2,3,5-trichlorophenoxy)-propylamine hydrochloride in 400 μL of sodium borate buffer (12.5 mM, pH 9.3) was added 5.1 mg (6.44 μmol) of Cy5.29-OSu. After the mixture was stirred for 2 h, 800 mL of water was added and the pH of the solution was adjusted to 6.0 with glacial acetic acid. Purification was by HPLC using a C_8 reversed-phase column and a linear solvent gradient between water/methanol (50/50) (containing 0.2% acetic acid) and methanol (containing 0.2% acetic acid) in 6.0 min at a flow rate of 2.0 mL/min. Detection at 550 nm showed the product to elute 7.96 min after the start of the gradient. Removal of the HPLC solvents under vacuum yielded 5.2 mg (87%) of compound **2** (TCPA−Cy5) (TLC, C_{18}, methanol/water (70:30), R_f = 0.7): ^{1}H NMR (CD3OD) δ 8.3 (t, 2H, J = 13 Hz, β, β' protons of bridge), 7.8−7.9 (s + m, 4H, 4-H, 4'-H, 6-H,

6'-H), 7.0−7.4 (m, 4H, 7-H, 7'-H and 4-H, 6-H of trichlorophenoxy moiety), 6.6 (t, 1H, J = 12 Hz, γ proton of bridge), 6.3 (dd, 2H, J = 14 Hz, α, α' protons of bridge), 4.1−4.3 (dt + m, 8H, α-, α'- CH$_2$ and NHCH_2, CH_2O), 3.2 (t, 2H, J = 6.8 Hz, CH_2C(O)), 2.1 (quint, 2H, J = 7.0 Hz, NHCH$_2$CH_2CH$_2$O), 1.1−2.0 (s + m, 21H, 5 CH$_2$ groups, with a s at 1.7 for 2 (CH$_3$)$_2$); low-resolution mass spectrum (positive ion, magic bullet) calcd for $C_{42}H_{47}Cl_{3}$-KN$_3$O$_8$S$_2$ 929, found 930 (M$^-$ + H), 914 (M$^+$ + H, Na substituted for K), 892 (M$^+$ + H, H substituted for K).

Coupling of Anti-PCB Antibody to Column Matrix. The support used for the immobilization of the anti-PCB antibody was Emphaze beads. These beads are about 60 μm in diameter and contain reactive azalactone groups that react with amines on the antibody to open the lactone ring and form a very stable amide bond between bead and antibody. Emphaze beads (0.24 g) were suspended in 4.0 mL of buffer (0.1 M sodium carbonate, 0.6 M sodium citrate, pH 8.5), mixed with a vortexer and sonicated for 5 min. The beads were centrifuged at 4000 rpm for 5 min, and the supernatant was removed. A 0.78 mL solution of polyclonal chicken anti-PCB antibodies (1.0 mg/mL) in the above buffer was added to the beads. The suspension was mixed for 1 h and centrifuged at 4000 rpm for 5.0 min with subsequent removal of supernatant. A 2.0 mL solution of Tris buffer (1.0 M, pH 8.0) was added to the antibody-coated support to deactivate all sites on the beads that did not react with the antibodies. The antibody-derivatized support was sequentially washed for 15 min with each of the following solutions: (1) phosphate-buffered saline (PBS), (pH 7.3, 2.0 mL), (2) 0.1 M NaCl (2.0 mL), and (3) PBS, (pH 7.3, 5 × 2.0 mL). The supernatant was assayed by measuring the absorbance at 280 nm in order to determine the amount of unbound antibody. From this measurement and the initial concentration of protein, the amount of antibody covalently linked to the beads was calculated.

Incubation of Antibody Binding Sites with (2,3,5-Trichlorophenoxy)propyl-Cy5.29 (2). Microcolumns (7.5 × 52 mm) were packed with 100 μL of the antibody-modified beads. After the column was rinsed with PBS (5 × 2.0 mL), the column support was incubated overnight at 4 °C in a solution of **2** (100 μL, 1.0−5.0 μM in PBS). Before measurements were taken using the column, it was rinsed with a degassed solution of PBS, pH = 7.4, containing 0.1% Triton X-405, reduced, and 15% ethanol (buffer A).

Detection of Aroclors. The Aroclor samples (in methanol) were dried by evaporation under a stream of nitrogen and then redissolved in buffer A. Serial dilution using buffer A was used to prepare concentrations of Aroclors ranging from 0.5 ppm to 20 ppm for testing in the flow immunosensor *(15)*. Triplicate samples of Aroclors (100 μL) were injected over the column starting with the lowest concentration and continuing to more concentrated samples.

RESULTS AND DISCUSSION

Synthetic Aspects. Scheme 1 outlines the synthesis of compound **1**. It is a Williamson ether synthesis in which the sodium salt of 2,3,5-trichlorophenol was reacted with 3-bromopropylamine hydrobromide to give 3-(2,3,5-trichlorophenoxy)propylamine. This species was then converted to the hydrochloride salt to afford compound **1** in 51% yield.

Compound **2** was prepared following the procedure outlined in Scheme 2. The sulfoindocyanine dye Cy5.29 is commercially available as the primary amine-reactive succinimidyl ester (Cy5.29-OSu). Formation of the amide

Scheme 1

1

Scheme 2

2

Figure 1. Dose−response curve for Aroclor 1254. The error bars represent 1 standard deviation, and each point on the curve is the average of three replicates.

Table 1. Limit of Detection for Aroclors

Aroclor	limit of detection (ppm)	Aroclor	limit of detection (ppm)
1242	10	1254	4
1248	5	1260	1

Table 2. Fluorescence Detector Response for Negative Controls

negative control	concn	response
2,4-dichlorophenol	20 ppm	small negative peak[a]
2,4,6-trichlorophenol	20 ppm	small negative peak[a]
2,4,5-trichloroaniline	20 ppm	none
2,4,5−trichlorophenoxyacetic acid	20 ppm	none
2,3,5,6-tetrachlorophenol	16 ppm	small negative peak[a]
2,3,4,5,6-pentachlorophenol	20 ppm	small negative peak[a]

[a] Fluorescence response signal below base line level.

bond was easily accomplished, and the product **2** was easily separated from the hydrolyzed Cy5.29 acid via HPLC using a reversed-phase C_8 column. The yield for this reaction was 87%.

Column Preparation. Immobilization of the anti-PCB antibody on a solid support by the outlined procedure yielded an 89% coupling efficiency, as determined by UV absorbance measurements at 280 nm. The antibody was then exposed to a solution of TCPA−Cy5 (1.0−5.0 μM in PBS) overnight in order to allow the dye-labeled antigen to bind to the antibody. Before the columns were used to detect PCBs, unbound and non-specifically bound dye conjugates were washed off the column by the initiation of buffer flow through the column. By monitoring the fluorescence (λ_{ex} = 635 nm and λ_{em} = 661 nm) of the eluant, a stable base line was determined to be achieved when the fluorescence change was less than 0.0002 AFU/min.

Aroclor Detection. Samples of buffer A spiked with

various concentrations of Aroclor 1242, 1248, 1254, and 1260 have been analyzed using the continuous flow immunosensor. Table 1 shows the detection limit for the various Aroclors using the TCPA−Cy5 conjugate described above. The detection limit is defined as the lowest concentration of analyte that could be reproducibly detected using our sensor. Parameters such as flow rate, identity and concentration of the organic cosolvent, identity and concentration of the surfactant, antibody affinity, and dye conjugate have not been fully optimized, and thus, additional experiments could quite possibly yield lower detection limits.

A typical dose response curve for Aroclor 1254 is shown in Figure 1. A linear relationship between the integrated peak area of the fluorescence response and the concentration of the Aroclor is observed in the 2−20 μg/mL (2−20 ppm) region. This leads to a detection limit of 4 ppm, which is already equal to the sensitivity demonstrated (*14*) by commercially-available immunoassay test kits. Table 2 contains the data for the negative control experiments, showing that the anti-PCB antibodies we used in these experiments have an excellent ability to discriminate between polychlorinated phenyl compounds and PCBs. In the case of each negative control, the concentration listed is merely the highest tested (chosen to be 10 times more concentrated than the Aroclors). Most likely, higher concentrations of these species will eventually lead to positive signals from the immunosensor, but we do not expect to encounter such large concentrations of chlorinated aromatics in aqueous samples.

Since polyclonal antibodies were used in this study, it is possible that a sample analyzed on a column calibrated with Aroclor 1260 would not analyze for the same quantity of PCB as the same sample assayed on a column standardized with Aroclor 1242. This is due to the possibility that only a few of the many congeners in an Aroclor may actually be recognized by the antibody and, thus, give rise to the measured signal. However, this problem is common to other antibody-based assays as well. Studies with the disposable immunoassay kits have shown that analyses of field samples can be reasonably accurate if care is taken to use the proper Aroclor as the standardizing agent (*14*). Immunoassays such as the continuous flow immunosensor or test kits are designed to process large quantities of samples on-site so that PCB-contaminated sites can be identified. Additional testing of the small subset of samples that test above the regulatory limit can then be done by laboratories employing traditional techniques in order to confirm the sites that need remediation.

CONCLUSIONS

A major obstacle in the development of fluorescence-based immunoassays for small molecules is the conjugation of the dye to the hapten in such a way that the binding affinity for the antibody is maintained. The synthesis of (2,3,5-trichlorophenoxy)propyl—Cy5.29 as a fluorescent analog of PCBs has allowed us to extend the continuous flow immunosensor technology into the realm of environmental detection of chlorinated organics. Although the sensor already has the necessary sensitivity to compete with the other portable immunoassays which are currently available, we plan to continue our investigation in this area in hopes of further optimizing the antibody—antigen binding interaction. New antibodies and other dye-labeled PCB analogs are currently being studied to this end, and future plans include the testing of sensor response towards specific PCB congeners and its effect on the overall analysis of Aroclors.

ACKNOWLEDGMENT

LITERATURE CITED

(1) Erickson, M. D. (1986) *Analytical Chemistry of PCBs*, Butterworth Publishers, Boston.

(2) Durfee, R. L., Contos, G., Whitmore, F. C., Barden, J. D., Hackman, E. E., and Westin, R. A. (1976) PCBs in the United States—Industrial Use and Environmental Distributions. Prepared for the U.S. Environmental Protection Agency, Office of Toxic Substances, Report No. EPA 560/6-76-005 (NTIS No. PB-252012).

(3) United States Congress, Toxic Substances Control Act, Public Law 94-469, Oct 11, 1976.

(4) McKinney, J. D. (1976) Toxicology of Selected Symmetric Hexachlorobiphenyl Isomers: Correlating Biological Effects with Chemical Structure. *Proceedings of the National Conference on Polychlorinated Biphenyls,* Nov 14–21, 1975, Chicago, IL, Environmental Protection Agency, Washington, DC.

(5) Biocca, M., Moore, J. A., Gupta, B. N., and McKinney, J. D. (1976) Toxicology of Selected Symmetrical Hexachlorobiphenyl Isomers. I. Biological Responses in Chicks and Mice. *Proceedings of the National Conference on Polychlorinated Biphenyls,* Nov 14–21, 1975, Chicago IL, Environmental Protection Agency, Washington, DC.

(6) Calandra, J. C. (1976) Summary of Toxicological Studies on Commercial PCB's. *Proceedings of the National Conference on Polychlorinated Biphenyls,* Nov 14–21, 1975, Chicago, IL, Environmental Protection Agency, Washington, DC.

(7) Safe, S. (1984) Polychlorinated Biphenyls (PCBs) and Polybrominated Biphenyls (PBBs): Biochemistry, Toxicology, and Mechanism of Action. *CRC Crit. Rev. Toxicol. 13,* 319–395.

(8) Kimbrough, R. D. (1980) Occupational Exposure. *Halogenated Biphenyls, Terphenyls, Napthalenes, Dibenzodioxins and Related Compounds* (R. D. Kimbrough, Ed.) pp 333–398, Elsevier/North-Holland Biomedical Press, New York.

(9) Environmental Protection Agency (1984) Organochlorine Pesticides and PCBs—Method 608. *Fed. Reg. 49*(209), 89–104.

(10) Longbottom, J. E., and Lichtenberg, J. J., Eds. (1982) Methods for Organic Chemical Analysis of Municipal and Industrial Wastewater. U.S. Environmental Protection Agency, Report No. EPA-600/4-82-057.

(11) Vo-Dinh, T., Pal, A., and Pal, T. (1994) Photoactivated Luminescence Method for Rapid Screening of Polychlorinated Biphenyls. *Anal. Chem. 66,* 1264–1268.

(12) Newsome, W. H., and Shields, J. B. (1981) Radioimmunoassay of PCBs in Milk and Blood. *Int. J. Environ. Anal. Chem. 10,* 295–304.

(13) Mattingly, P. G., and Brashear, R. J. (1992) Reagents and Method for Detecting Polychlorinated Biphenyls. U. S. Patent 5,145,790.

(14) Waters, L. C., Smith, R. R., Stewart, J. H., Jenkins, R. A., and Counts, R. W. (1994) Evaluation of Two Field Screening Test Kits for the Detection of PCBs in Soil by Immunoassay. *J. AOAC Int. 77,* 1664–1671.

(15) Kusterbeck, A. W., Wemhoff, G. A., Charles, P. T., Yeager, D., Bredehorst, R., Vogel, C.-W., and Ligler, F. S. (1990) A Continuous Flow Immunoassay for Rapid and Sensitive Detection of Small Molecules. *J. Immunol. Methods 135,* 191–197.

(16) Ogert, R. A., Kusterbeck, A. W., Wemhoff, G. A., Burke, R., and Ligler, F. S. (1992) Detection of Cocaine using the Flow Immunosensor. *Anal. Lett. 25,* 1999–2019.

(17) Whelan, J. P., Kusterbeck, A. W., Wemhoff, G. A., Bredehorst, R., and Ligler, F. S. (1993) Continuous-Flow Immunosensor for Detection of Explosives. *Anal. Chem. 65,* 3561–3565.

(18) The terminology of "IgY" for the antibody used in this study is the designation for a "IgG-like" protein that is found in both the chicken serum and egg yolk. This is the species which O.E.M. Concepts sells as its anti-PCB antibody.

BC950063K

Cell-Type Specific and Ligand Specific Enhancement of Cellular Uptake of Oligodeoxynucleoside Methylphosphonates Covalently Linked with a Neoglycopeptide, YEE(ah-GalNAc)₃

Jon J. Hangeland, Joel T. Levis, Yuan C. Lee,*,† and Paul O. P. Ts'o*

Department of Biochemistry, School of Hygiene and Public Health, The Johns Hopkins University, Baltimore, Maryland 21205, and Department of Biology, The Johns Hopkins University, Baltimore, Maryland 21218. Received May 17, 1995⊗

A novel, *structurally defined, and homogeneous* oligodeoxynucleoside methylphosphonate (oligo-MP) neoglycopeptide conjugate, [YEE(ah-GalNAc)₃]−SMCC−AET−pU^{m}pT̲₇, has been synthesized. The linkage between the carbohydrate ligand and the oligo-MP is a metabolically stable thioether. Experiments establish that uptake of this conjugate by human hepatocellular carcinoma (Hep G2) is cell-type specific when compared with its uptake by human fibrosarcoma (HT 1080) and human promyleocytic leukemia (HL-60). Uptake of the conjugate with Hep G2 cells can be totally inhibited by the addition of a 100-fold excess of free YEE(ah-GalNAc)₃ in the culture medium indicating the observed cell uptake is ligand specific. The conjugate is rapidly taken in by Hep G2 cells in a linear fashion reaching a saturation plateau of 26 pmol per 10⁶ cells after 24 h. Conjugation of oligo-MPs to ligands for hepatic carbohydrate receptors, such as YEE(ah-GalNAc)₃, represents an efficient and ligand-specific method for the intracellular delivery of oligo-MPs.

INTRODUCTION

The antisense (anticode) or antigene strategy for drug design is based on the sequence-specific inhibition of protein synthesis due to the binding and masking of the target mRNA or genomic DNA, respectively, by the synthetic oligodeoxynucleotide (oligo-dN)[1] and their analogs (*1*). Implicit in this strategy is the ability of oligo-dNs to cross the cellular membrane(s), thereby gaining access to the cellular compartments containing their intended target, and to do so in sufficient amounts for binding to its target to take place. Among the many oligo-dN analogs for application as antisense agents, nonionic oligonucleoside methylphosphonates (oligo-MPs) have been extensively studied (*2*). Oligo-MPs are totally resistant to nuclease degradation (*3*) and are effective antisense agents with demonstrative *in vitro* activity against herpes simplex virus type 1 (*4*), vesicular stomatitis virus (*5*), and human immunodeficiency virus (*6*) and are able to inhibit the expression of *ras* p21 (*7*). For oligo-MPs to exhibit antisense activity, however, they must be present in the extracellular medium in concentrations up to 100 μM (*4-7*).

* P.O.P.T.: Phone: (410) 955-3172. Fax (410) 955-4392. Y.C.L.: Phone: (410) 516-7041. Fax (410) 516-8716.
† Department of Biology.
[1] Abbreviations: AET, aminoethanethiol; ATCC, American Type Culture Collection, Rockville, MD; ATP, adenosine triphosphate; BAP, bacterial alkaline phosphatase; CPG, controlled pore glass support; DIPEA, diisopropylethylamine; D-MEM, Dulbecco's modified Eagle's medium; DMSO, dimethyl sulfoxide; dN, 2'-deoxynucleotide; D-PBS, Dulbecco's phosphate buffered saline; DTT, dithiothreitol; EDAC, 1-ethyl-3-[3-(dimethylamino)propyl]carbodiimide; EDTA, ethylenediaminetetraacetate; FCS, fetal calf serum; HBSS, Hank's balanced salt solution; HSA, human serum albumin; HSV-1, herpes simplex virus type 1; MEM, minimal essential medium with Earle's salts; MP, methylphosphonate; PAGE, polyacrylamide gel electrophoresis; PNK, bacteriophage T4 polynucleotide kinase; SMCC, N-hydroxysuccinimidyl 4-(N-methylmaleimido)cyclohexane-1-carboxylate; Tris, tris(hydroxylmethyl)amine.

Delivery of exogenous DNA into the intracellular medium is greatly enhanced by coupling its uptake to receptor-mediated endocytosis. Pioneering work by Wu and Wu (*8*) showed that foreign genes (*8a-c*) or oligo-dNs (*8d*), electrostatically complexed to poly-L-lysine linked to asialoorosomucoid, are efficiently and specifically taken into human hepatocellular carcinoma (Hep G2) cells through direct interaction with the asialoglycoprotein receptor. Since this initial study, other examples of receptor-mediated delivery of DNA have appeared including a tetra-antennary galactose neoglycopeide·oly-L-lysine conjugate (*9*), folate conjugates (*10*), an antibody conjugate (*11*), transferrin conjugate (*12*), and 6-phosphomannosylated human serum albumin (HSA) covalently linked to an antisense oligo-dNs via a disulfide bond (*13*). Recently, the triantennary *N*-acetylgalactosamine neoglycopeptide, YEE(ah-GalNAc)₃ (*14*), conjugated to human serum albumin which was in turn linked to poly-L-lysine, was shown to effectively deliver DNA into Hep G2 cells (*15*). In each instance, structurally *heterogeneous* conjugates were utilized to deliver DNA or oligo-dNs into cells. This strategy for the targeting and delivery of DNA can also be exploited for the targeting and delivery of oligo-MPs to specific cell types. In this paper, the synthesis, characterization, and cellular uptake profile of a *structurally defined and homogeneous* neoglycopeptide−oligo-MP conjugate, [YEE(ah-GalNAc)₃]−SMCC−AET−pU^{m}pT̲₇ (**6;** Figure 2), is described.[2]

EXPERIMENTAL PROCEDURES

Synthesis of [5'-³²P]-[YEE(ah-GalNAc)₃]−SMCC−AET−pU^{m}pT̲₇ (6). *General.* Methyl phosphonamidite synthons were a generous gift from JBL Scientific, Inc. All other reagents for the automated synthesis of **2** were purchased from Glen Research. HiTrap Q anion exchange columns were purchased from Pharmacia LKB

[2] U^{m}pT̲₇: U^m is 2'-O-methyluridine. The oligo-MP was constructed with a 5' terminal phosphodiester. T̲₇ denotes seven thymidine nucleosides linked by methylphosphonate diesters.

Biotechnology. Reversed phase high-performance liquid chromatography was carried out using a Microsorb C-18 column purchased from Rainin Instrument Co., Inc. Cystamine hydrochloride, 1-ethyl-3-[3-(dimethylamino)-propyl]carbodiimide (EDAC), 1-methylimidazole, anhyd dimethyl sulfoxide (DMSO), dithiothreitol (DTT), and Ellman's reagent were purchased from Aldrich and were used without further purification. Diisopropylethylamine (DIPEA) was purchased from Aldrich and was redistilled from calcium hydride prior to use. *N*-Hydroxysuccinimidyl 4-(*N*-methylmaleimido)cyclohexanecarboxylate (SM-CC) was purchased from Pierce. Waters SepPak C-18 cartridges were purchased from Millipore Corp. YEE-(ah-GalNAc)$_3$ was synthesized according to Lee et al. (*14a*) and was stored at 4 °C as an aqueous solution. Adenosine triphosphate (ATP) and [γ-^{32}P]-ATP were purchased from P—L Biochemicals, Inc., and Amersham, respectively. Polyacrylamide gel electrophoresis (PAGE) was carried out with 20 cm × 20 cm × 0.75 mm gels that contained 15% polyacrylamide, 0.089 M Tris, 0.089 M boric acid, 0.2 mM EDTA, pH 8.0 (1 × TBE), and 7 M urea. Samples were dissolved in loading buffer containing 90% formamide, 10% 1 × TBE, 0.2% bromophenol blue, and 0.2% xylene blue.

Synthesis of U^{m}pT$_7$ (2). The oligodeoxynucleoside methylphosphonate was synthesized on a controlled pore glass support (CPG) using 5′-*O*-(dimethoxytrityl)-3′-*O*-(methyl-*N,N*-diisopropylphosphonamido)thymidine and deprotected according to established methods (*16*). The final synthon incorporated into the oligomer at its 5′ end was 5′-*O*-(dimethoxytrityl)-2′-*O*-methyl-3′-(2-cyanoethyl-*N,N*-diisopropylphosphoramido)uridine. The final coupling step positioned a phosphodiester linkage between the terminal 5′-nucleoside and the adjacent nucleoside, which permitted phosphorylation of the 5′-terminal hydroxyl group with bacteriophage T4 polynucleotide kinase (PNK) and ensured the stability of the phosphodiester linkage toward endonuclease cleavage due to the presence of the 2′-*O*-methyl group (*17*). The crude oligo-MP was purified by HiTrap Q anion exchange chromatography (load with water containing <25% acetonitrile; elute with 0.1 M sodium phosphate, pH 5.8) and preparative reversed-phase chromatography (Microsorb C-18) using a linear gradient (solvent A: 50 mM sodium phosphate, pH 5.8, 2% acetonitrile; solvent B: 50 mM sodium phosphate, pH 5.8, 50% acetonitrile; gradient: 0—60% B in 30 min). The oligomer thus purified was ca. 97% pure by analytical HPLC contaminated by a small amount of the n-1 species.

Synthesis of [5′-^{32}P]-5′-O-[(N-(2-Mercaptoethyl)phosphoramidate]—U^{m}pT$_7$ (5). The purified oligomer (168 nmol), ATP (160 nmol), H$_2$O (75 μL), 10× PNK buffer (5 mM DTT, 50 mM Tris•HCl, 5 mM MgCl$_2$, pH 7.6; 10 μL), [γ-^{32}P]-ATP (1.1 × 10^{14} Bq/mmol, 3.7 × 10^6 Bq; 10 μL), and PNK (150 U in 5 μL) were combined and incubated at 37 °C for 16 h and evaporated to dryness. The residue was redissolved in 0.2 M 1-methylimidazole, pH 7.0 (100 μL), and 1.0 M cystamine hydrochloride, pH 7.2, containing 0.3 M EDAC (100 μL), and heated at 50 °C for 2 h (*18*). The excess reagents were removed by SepPak (loaded with 50 mM sodium phosphate, pH 5.8, 5% acetonitrile; washed with 5% acetonitrile in water; eluted with 50% acetonitrile in water). The solvent was evaporated *in vacuo* and crude cystamine adduct redissolved in 10 mM phosphate containing 50 mM DTT (200 μL) and heated to 37 °C for 1 h. The buffer salts and excess reductant were removed from the reaction mixture as before, and the crude product was dried *in vacuo*. The title compound 5, produced in 57% yield from 2, was used in the next step without further purification.

Synthesis of [5′-^{32}P]-[YEE(ah-GalNAc)$_3$]—SMCC—AET—pU^{m}pT$_7$ (6). The neoglycopeptide 1 (336 nmol) was dissolved in anhyd DMSO (40 μL) and treated with DIPEA (336 nmol) and SMCC (336 nmol). The reaction was allowed to stand at rt for 4 h and then added to the freshly prepared thiol 5. The reaction mixture was degassed and allowed to slowly concentrate under vacuum at rt. The crude 6 was dissolved in formamide loading buffer (100 μL), purified by PAGE (4 V/cm, 1.5 h), and recovered by the crush and soak method (50% acetonitrile in water). The overall yield of pure 6 was 25%. Upon treatment with 0.1 M HCl (37 °C, 1 h), 6 produced [5′-^{32}P]phosphorylated 2 due to hydrolysis of the P—N bond; however, 6 was unreactive toward DTT (50 mM, pH 8, 37 °C, 1 h), 3-maleimidopropionic acid (50 mM, pH 8, 37 °C, 1 h), Ellman's reagent (50 mM, pH 8, 37 °C, 1 h), and bacterial alkaline phosphatase (BAP; 70 U, 65 °C, 1 h). Sequential treatment of 6 with 0.1 N HCl and BAP resulted in complete loss of [^{32}P]-label as anticipated. Stoichiometric analysis of an unlabeled sample of 6 prepared identically showed it to contain 3 mol of *N*-acetylgalactosamine for each mole of conjugate,[3] consistent with the proposed structure, while pneumatically assisted electrospray mass spectrometry (Scripps Research Institute Mass Spectrometry Facility, La Jolla, CA) produced a single parent ion (negative ion mode) at *m/z* 4080 (calcd 4080.7), confirming the homogeneity of the sample.

Cellular Uptake Experiments. *General.* Minimal essential medium with Earle's salts supplemented with L-glutamine (MEM), Dulbecco's modified Eagle's medium (D-MEM), RMPI medium 1640 supplemented with L-glutamine (RMPI), Dulbecco's phosphate-buffered saline (D-PBS), fetal calf serum (FCS), sodium pyruvate (100 mM), nonessential amino acids (10 mM), aqueous sodium bicarbonate (7.5%), and trypsin (0.25%; prepared in HBSS with 1.0 mM EDTA) were purchased from GIBCO BRL. Human hepatocellular carcinoma (Hep G2), human fibrosarcoma (HT 1080), and human promyeleocytic leukemia (HL-60) cells were purchased from ATCC and were maintained in 1 × MEM supplemented with 10% FCS, 1 mM sodium pyruvate, and 0.1 mM nonessential amino acids (Hep G2), 1 × D-MEM supplemented with 10% FCS (HT-1080) or 1 × RMPI supplemented with 10% FCS (HL-60) in a Forma Scientific Model 3158 incubator maintained at 37 °C and 5% CO$_2$. Silicon oil was a generous gift from General Electric (product no. SF 1250). Cells were counted using a Coulter Cell Counter Model Z$_{BI}$.

Uptake Experiments with Hep G2 Cells or HT 1080. Cells were passaged into 2 cm wells and grown in the appropriate medium to a density of ca. 10^5 cells per well. The maintenance medium was aspirated, and the cells were incubated at 37 °C with 0.5 mL of medium that contained 2% FCS and was made 1 μM in [5′-^{32}P]-labeled 6. After the prescribed time had elapsed, a 5 μL aliquot of the medium was saved for scintillation counting and the remainder aspirated from the well. The cells were washed with D-PBS (2 × 0.5 mL), treated with 0.25% trypsin (37 °C, 2 min), and suspended in fresh growth medium containing 10% FCS. The suspended cells were layered over silicon oil (0.5 mL) in a 1.7 mL conical microcentrifuge tube and pelleted by centrifugation at 14 000 rpm (12 000*g*) for 30 s. The supernatent was

---

[3] The molar absorbance of U^{m}pT$_7$ was calculated to be 59 750 L/mol-cm by taking the sum of the molar absorbance values for each of the nucleosides contained in the structure. This value was in excellent agreement with the number of moles of GalNAc residues found to be contained in the conjugate.
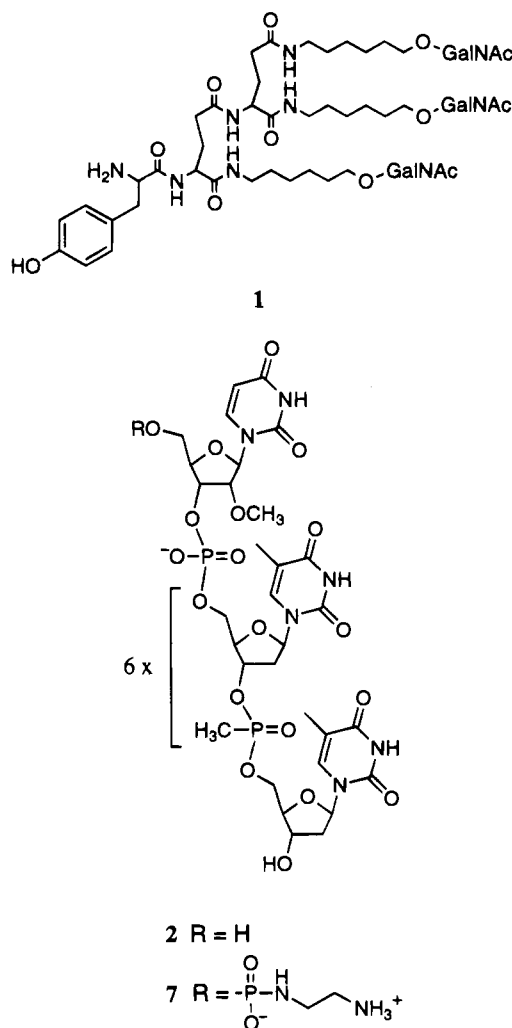
carefully decanted, and the cell pellet was lysed with 100 μL of a solution containing 0.5% NP 40, 100 mM sodium chloride, 14 mM Tris•Cl, and 30% acetonitrile. The quantity of [^{32}P]-labeled material and, by inference, the amount of **6** (or its breakdown products)[4] associated with the cell lysate, were determined by scintillation counting.

Uptake Experiments with HL-60 Cells. RMPI medium supplemented with 2% FCS and made 1 μM in [5'-^{32}P]-**6** was pre-treated with 7.5 × 10^6 HL 60 cells for 5 min at rt. The cells were removed by centrifugation (5 min). The medium (31 mL) was decanted and added to 7.5 × 10^6 fresh HL-60 cells. The cells were evenly suspended and the cell suspension divided into six 0.4 mL portions. The remainder was discarded. The cells were incubated in medium containing the conjugate **6** for the prescribed time and then collected by centrifugation (5 min), resuspended in 0.5 mL D-PBS, and layered onto silicon oil in a 1.7 mL conical microfuge tube. The cells were pelleted by centrifugation (12000*g*, 30 s) and lysed, and the amount of [^{32}P]-labeled material associated with the cells was determined by scintillation counting.

RESULTS AND DISCUSSION

Synthesis of [YEE(ah-GalNAc)₃]–SMCC–AET– pU^{m}pT₇ (6). Synthesis and purification of YEE(ah-GalNAc)₃ (**1**) (*14a*) and U^{m}pT₇ (**2**) (*16*) were carried out according to established procedures. In order to form a covalent link between **1** and **2**, we chose to modify the 5'-end of **2** using the method of Orgel (*18*). This introduced a disulfide into the oligo-MP, which in turn could be reduced with DTT to give a 5'-thiol. The neoglycopeptide **1** was modified in a complementary fashion using the heterobifunctional cross-linking reagent, SMCC, capable of combining specifically with the *N*-terminal amino group of **1**. Coupling of the maleimido group introduced by SMCC and the 5'-thiol of the modified oligo-MP resulted in linkage of the oligo-MP and neoglycopeptide via a metabolically stable thioether (Figure 2).

To begin the synthesis, **2** was phosphorylated using PNK and 0.95 equiv of [^{32}P]-ATP. Successful 5'-phosphorylation was confirmed by an increase in the electrophoretic mobility of the product compared to the parent oligo-MP owing to the increased negative charge from −1 to −3 upon addition of a 5'-phosphate and incorporation of ^{32}P into the structure (band A; Figure 3). Formulation of the end-labeling reaction in this way ensured that ca. 90% of the ATP was consumed, allowing efficient use of the [^{32}P]-ATP to radioactively label the conjugate. Modification of the 5'-phosphate was accomplished in two steps. The 5'-end-labeled oligo-MP was incubated at 50 °C with 0.5 M cystamine hydrochloride in a buffer containing 0.1 M 1-methylimidazole at pH 7.2 in the presence of 0.15 M EDAC to give the 5'-cystamine phosphoramidate in 65% yield. PAGE analysis of the reaction mixture showed the product to migrate significantly slower than the 5'-end-labeled oligo-MP. This observation is consistent with the change in charge from −3 to −1 due to the loss of a single oxyanion on the 5'-phosphate upon formation of the P—N bond and neutral-

[4] The exact structures of breakdown products of conjugate **6** have not been established. It is expected, however, that the neoglycopeptide will undergo significant biodegradation (glycolysis and proteolysis) upon endocytosis and partitioning to lysosomes. We report here the extent to which 5'-[^{32}P]-labeled **6** and the products of its biodegradation are associated with the cells. It is worth noting that the oligo-MP moiety of conjugate **6** is resistant toward endo- and exonuclease degradation (*3, 17*) and, therefore, is expected to remain unaltered inside the cell over the course of the experiment.

Figure 1. Structures of neoglycopeptide YEE(ah-GalNAc)₃ (**1**) and oligo-MP U^{m}pT₇ (**2**) and 5'-ethylenediamine capped U^{m}pT₇ (**7**).

ization of a second negative charge by the positively charged protonated primary amine present on the terminus of the cystamine group (compare bands A and B; Figure 3). Up to 35% of thymidine-modified oligo-MP was produced during this reaction (band C; Figure 3), and despite attempts to modify the reaction conditions (e.g., lowering the temperature and reducing the concentration of EDAC), its production could not be eliminated without concomitant reduction in yield of the desired cystamine adduct. This side product presumably arises due to reaction of EDAC with N-3 of thymidine to form a thymidine—EDAC adduct (*18, 19*). Reduction of the disulfide with 50 mM DTT at pH 8 was quantitative[5] and was accompanied by mobility shift to a faster migrating species due to the loss of the positively charged protonated primary amino group (compare bands B and C; Figure 3). In a separate reaction, **1** was combined with 1 equiv each of SMCC (**3**) and DIPEA in anhydrous DMSO and incubated at room temperature. Combination of this reaction mixture with thiol **5** could be carried out without complete consumption of SMCC by **1** since

[5] Although we chose to introduce a thiol onto the oligo-MP postsynthetically, in part to allow introduction of ^{32}P enzymatically at the 5'-terminus, the construction of the conjugate could as easily be carried out by introduction of a thiol linker during the solid phase synthesis of the oligo-MP using, for example, 6-(tritylthio)hexyl phosphoramidite (*19*) commercially available from Glen Research.
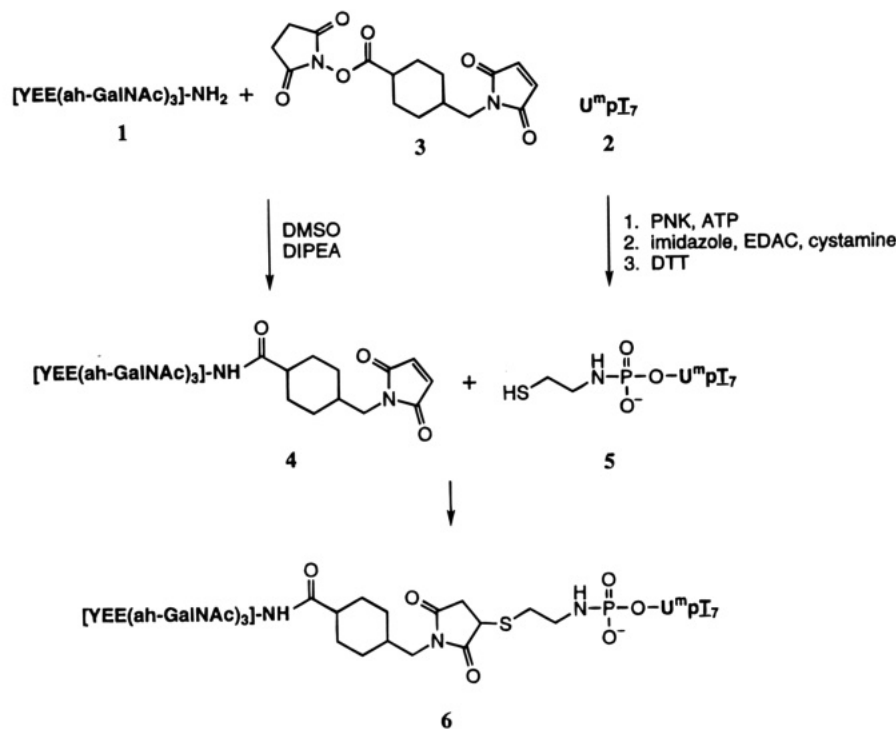
Figure 2. Reaction scheme for the synthesis of [YEE(ah-GalNAc)₃]–SMCC–AET–pU^{m}pT̲₇ (**6**).
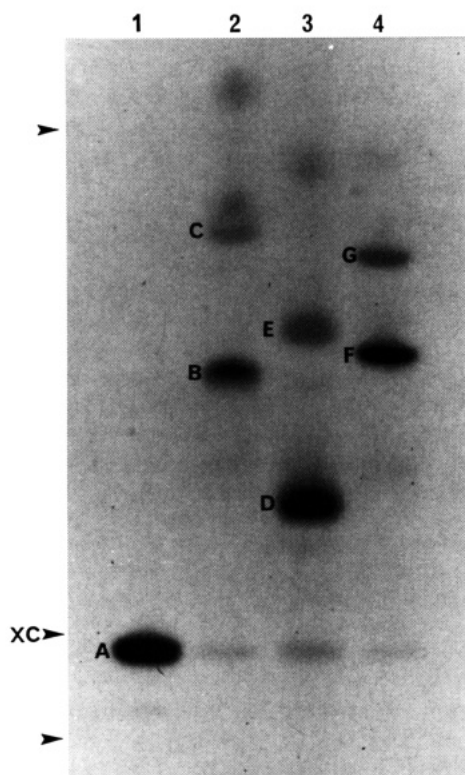
Figure 3. PAGE analysis (15% polyacrylamide, 4 V/cm, 2 h) of intermediates in the synthesis of conjugate **6**. Lane 1: [5′-^{32}P]-labeled **2** (band A). Lane 2: [5′-^{32}P]-cystamine adduct (band B) and corresponding thymidine–EDAC adducts (bands C). Lane 3: [5′-^{32}P]-thiol **5** (band D) and corresponding thymidine–EDAC adducts (bands E). Lane 4: [5′-^{32}P]conjugate **6** (band F) and corresponding thymidine–EDAC adducts (bands G).

the reactive groups present on **1**, **3**, and **5** combined regiospecifically, thereby yielding a *structurally defined and homogeneous* conjugate. As anticipated, the addition of the modified neoglycopeptide to the 5′-end of the activated oligo-MP was accompanied by a substantial slowing of its mobility by PAGE since the mass of the

conjugate **6** is significantly larger than that of the parent oligo-MP (band F; Figure 3). Following this scheme, **5** was completely converted to **6** when 2 equiv (based on starting oligo-MP **2**) of the neoglycopeptide **1** was used. The overall yield of the conjugate **6** was 24% (average of three syntheses) based on oligo-MP **2**. The homogeneity of **6** was confirmed by the detection of a single parent ion (negative ion mode) by electrospray mass spectrometry.

Cellular Uptake Experiments. We first investigated the cellular uptake of the conjugate **6**, both alone and in the presence of 100 equiv of free neoglycopeptide **1**, by Hep G2 cells to demonstrate that uptake by the cells was a result of binding of the neoglycopeptide moiety of **6** to the hepatic carbohydrate receptor. As a control, an oligo-MP modified at the 5′-end with ethylenediamine (**7**; Figure 1)[6] was also incubated with Hep G2 cells under identical conditions. In each instance, the modified oligo-MP was present at a concentration of 1 μM in medium containing 2% fetal calf serum (FCS) and incubations were carried out at 37 °C. The concentration of FCS was lowered from 10% to 2% in order to decrease the possibility of nonspecific binding of the oligo-MP conjugate with medium associated proteins. The uptake of conjugate **6** by the cells was rapid when incubated alone, loading the cells in a linear fashion to the extent of 7.8 pmol per 10^6 cells after only 2 h (Figure 4A).[4] In contrast, when a 100-fold excess of free **1** was present with 1 μM conjugate, association of **6** was only 0.42 pmol per 10^6 cells, a value essentially identical to that obtained with the control oligo-MP **7** (0.49 pmol per 10^6 cells). As an additional control, Hep G2 cells were incubated with **7** in the presence of a 10-fold excess of **1** to assess the

[6] Miller, P. S., and Levis, J. T. Unpublished results. Modification of the 5′-phosphate with ethylenediamine was accomplished by incubation of 5′-phosphorylated **2** with 0.1 M EDAC in a buffer containing 0.1 M imidazole at pH 7 at 37 °C for 2 h followed by overnight incubation with an aqueous solution 0.3 M ethylenediamine hydrochloride buffered to pH 7.0. This modification prevents removal of the 5′-phosphate by cellular phosphatase activity.
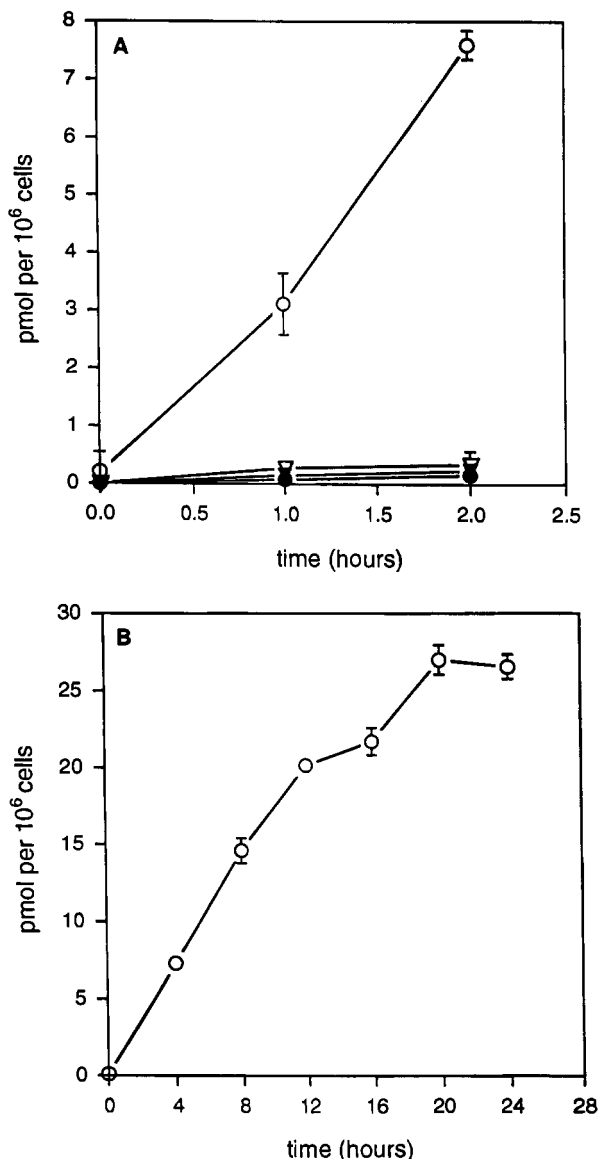
Figure 4. (A) Time course for the uptake by Hep G2 cells of 1 μM conjugate **6**, alone (O) and in the presence of 100 equiv of free **1** (●), and oligo-MP **7**, alone ($\triangledown$) and in the presence of 10 equiv of free **1** (▼). Cells were incubated at 37 °C for 0, 1, and 2 h, and samples were collected as described in the Experimental Procedures. Each data point represents the average of three trials ± one standard deviation. (B) 24 h time course for the uptake of conjugate **6** by Hep G2 cells. Cells were incubated at 37 °C and the cells collected as described in the Experimental Procedures. Each data point represents the average of three experiments ± one standard deviation.

Figure 5. Tissue specific uptake of conjugate **6** by Hep G2, HL-60, and HT 1080 cells. Cells were collected and the amount of [^{32}P] was determined at 3 and 24 h for each cell line. Experiments were done in triplicate and the data expressed as the average ± one standard deviation.

possibility that, despite the absence of a covalent link between **1** and **7**, **1** could cause enhanced uptake of **7** by the Hep G2 cells. Under these conditions, the amount of cell associated **7** following a 2-h incubation was only 0.60 pmol per 10^6 cells, significantly less than found with the conjugate **6**. In addition, we have examined the uptake of **6** by Hep G2 cells for longer times (1 μM conjugate, 37 °C) and found uptake of **6** to be linear up to ca. 24 h reaching a value of 26 pmol per 10^6 cells (Figure 4B). Over the course of the experiment, the cells continued to divide and increased in number by a factor of 1.5. The increase in cell number would, in part, contribute to the continued uptake of the conjugate by the cell mass. However, uptake of the conjugate **6** at 24 h is 3.7-fold greater than at 2 h, suggesting that all the cells, whether newly formed or not, are continuing to

actively take in the conjugate over the entire 24 h period and that the concentration of the conjugate within the cells had not yet reached a steady state. We conclude from the results of these experiments that (1) the observed enhanced uptake of conjugate **6** by Hep G2 cells occurs as a result of specific binding to the asialoglycoprotein receptor; (2) a covalent link between the oligo-MP and neoglycopeptide is essential for the observed enhancement of uptake; and (3) uptake of **6** by Hep G2 cells does not appear to reach a steady state up to ca. 24 h under the conditions used in this study.

The second issue to be addressed was that of cell-type specificity. It is well established that the asialoglycoprotein receptor is found on the surface of hepatocytes and represents an efficient means for selectively targeting this tissue for intracellular delivery of a variety of therapeutic agents (*21*). We examined tissue specificity by incubating three human cell lines, Hep G2, HL-60, and HT 1080, in medium containing 1 μM conjugate **6** and 2% FCS at 37 °C for 3 and 24 h. As was anticipated, the only cell line to exhibit signficant uptake of **6** was Hep G2. After incubation for 3 and 24 h, 8.5 and 26 pmol per 10^6 cells, respectively, was associated with the cells (Figure 5). In contrast, after 24 h only 0.10 and 0.53 pmol per 10^6 cells were associated with the HL-60 cells and HT 1080 cells, respectively. This result is consistent with previous findings, which showed the conjugate YEE(ah-GalNAc)$_3$−HSA−poly-L-lysine to deliver DNA primarily to the liver of mice (*15*).

CONCLUDING REMARKS

We have examined the cellular uptake and cell-type specificity of a novel, structurally defined and homogeneous oligo-MP−neoglycopeptide conjugate, [YEE(ah-GalNAc)$_3$]−SMCC−AET−pUmpT$_7$ (**6**), using three human cell lines. The cellular uptake of **6** by Hep G2 cells is remarkably efficient and appears to be linear up to 24 h, reaching maximum level of 26 pmol per 10^6 cells. Using an approximation that 10^6 cells represents a volume of 1 μL, then the *intracellular* concentration of this conjugate and its breakdown products can be as high

as 26 μM. In addition, little conjugate associates with HL-60 or HT 1080 cells, demonstrating that the neoglycopeptide **1** is capable of delivering the oligo-MP **2** in a highly selective manner to hepatocytes. Further work is being carried out to measure the rate of efflux from Hep G2 cells, to observe the interior distribution of the conjugate inside the cell, to identify the metabolites produced following uptake and efflux of the conjugate, and to assess fully the biological efficacy of antisense oligo-MP−neoglycopeptide bioconjugates in this cell uptake process. In collaboration with the immunology and virology laboratory of Dr. Laure Aurelian of the University of Maryland, we have recently obtained preliminary results from an *in vitro* biological assay that has shown another conjugate, [YEE(ah-GalNAc₃)]−SMCC−AET−pTpTCCTCCTGCGG, which contains an oligo-MP complementary to the splice acceptor site of immediate-early pre-mRNAs 4 and 5 of herpes simplex virus type 1 (HSV-1), was ca. 25-fold more effective at inhibiting infection of Hep G2 cells by HSV-1 than was its parent oligo-MP, pTpTCCTCCTGCGG (**4**). A complete description of this study will be disclosed in due course.

ACKNOWLEDGMENT

LITERATURE CITED

(1) Mirabelli, C. K., and Crooke, S. T. (1993) Antisense oligonucleosides in the context of modern molecular drug discovery and development. In *Antisense research and applications* (S. T. Crooke and B. LeBleu, Eds.) pp 7−35, CRC Press, Boca Raton.

(2) Ts'o, P. O. P., Aurelian, L., Chang, E., and Miller, P. S. (1992) Nonionic oligodeoxynucleotide analogs (Matagen as anticodic agents in duplex and triplex formation. *Ann. N.Y. Acad. Sci. 600*, 159−177.

(3) Miller, P. S., McParland, K. B., Javaraman, K., Ts'o, P. O. P. (1981) Biochemical and biological effects of nonionic nucleic acid methylphosphonates. *Biochemistry 20*, 1874−1880.

(4) (a) Smith, C. C., Aurelian, L., Reddy, M. P., Miller, P. S., and Ts'o, P. O. P. (1986) Antiviral effect of an oligo(nucleoside methylphosphonate) complementary to the splice junction of herpes simplex virus type 1 immediate early pre-mRNAs 4 and 5. *Proc. Natl. Acad. Sci. U.S.A. 83*, 2787−2791. (b) Kulka, M., Smith, C. C., Aurlian, L., Fishelevich, R., Meade, K., Miller, P., and Ts'o, P. O. P. (1989) Site specificity of the inhibitory effects of oligo(nucleoside methylphosphonate)s complementary to the acceptor splice junction of herpes simplex virus type 1 immediate early mRNA 4. *Proc. Natl. Acad. Sci. U.S.A. 86*, 6868−6872. (c) Kulka, M., Wachsman, M., Miura, S., Fishelevich, R., Miller, P. S., Ts'o, P. O. P., and Aurelian, L. (1993) Antiviral effect of oligo(nucleoside methylphosphonates) complementary to the herpes simplex virus type 1 immediate early mRNAs 4 and 5. *Antiviral Res. 20*, 115−120. (d) Kulka, M., Smith, C. C., Levis, J., Fishelevich, R., Hunter, J. C. R., Cushman, C. D., Miller, P. S., Ts'o, P. O. P., and Aurelian, L. (1994) Synergistic antiviral activities of oligonucleoside methylphosphonates complementary to herpes simplex virus type 1 immediate-early mRNAs 4, 5, and 1. *Antimicrob. Agents Chemother. 38*, 675−680.

(5) Agris, C. H., Blake, K. R., Miller, P. S., Reddy, M. P., and Ts'o, P. O. P. (1986) Inhibition of vesicular stomatitis virus protein synthesis and infection by sequence-specific oligodeoxyribonucleoside methyphosphonates. *Biochemistry 25*, 6268−6275.

(6) (a) Sarin, P. S., Agrawal, S., Civeira, M. P., Goodchild, J., Ikeuchi, T., and Zamecnik. (1988) Inhibition of aquired immunodeficiency syndrome virus by oligodeoxynucleoside methylphosphonates. *Proc. Natl. Acad. Sci. U.S.A. 85*, 7448−7451. (b) Zaia, J. A., Rossi, J. J., Murakawa, G. J., Spallone, P. A., Stephens, D. A., Kaplan, B. E., Eritja, R., Wallace, R. B., and Cantin, E. M. (1988) Inhibition of human immunodeficiency virus by using an oligonucleoside methylphosphonate targeted to the *tat*-3 gene. *J. Virol. 62*, 3914−3917. (c) Laurence, J., Sikder, S. K., Kulkosky, J., Miller, P., and Ts'o P. O. P. (1991) Induction of chronic human immunodeficiency virus infection is blocked by a methylphosphonate oligodeoxynucleoside targeted to a U3 enhancer element. *J. Virol. 65*, 213−219.

(7) (a) Brown, D., Zhipeng, Y., Miller, P., Blake, K., Wei, C., Kung, H.-F., Black, R. J., Ts'o, P. O. P., and Chang, E. H. (1989) Modulation fo *ras* expression by anti-sense, non-ionic deoxyoligonucleotide analogs. *Oncogene Res. 4*, 243−252. (b) Yu, Z., Chen, D., Black, R. J., Blake, K., Ts'o, P. O. P., Miller, P., and Chang, E. H. (1989) Sequence specific inhibition of in vitro translation of mutated or normal *ras* p21. *J. Exp. Pathol. N.Y. 4*, 97−107. (c).Chang, C. H., Miller, P. S., Cushman, C., Devadas, K., Pirollo, K. F., Ts'o, P. O. P., and Yu, Z. P. (1991) Antisense inhibition of *ras* p21 expression that is sensitive to a point mutation. *Biochemistry 30*, 8283−8286.

(8) (a) Wu, G. Y., and Wu, C. H. (1987) Receptor-mediated in vitro gene transformation by a soluble DNA carrier system. *J. Biol. Chem. 262*, 4429−4432. (b) Wu, G. Y., and Wu, C. H. (1988) Receptor-mediated gene delivery and expression in vivo. *J. Biol. Chem. 263*, 14621−14624. (c) Wu, G. Y., and Wu, C, H. (1988) Evidence for targeted gene delivery to Hep G2 hepatoma cells in vitro. *Biochemistry 27*, 887−892. (d) Wu, G. Y., and Wu, C. H. (1992) Specific inhibition of hepatitis B viral gene expression in vitro by targeted antisense oligonucleotides. *J. Biol. Chem. 267*, 12436−12439.

(9) Plank, C., Zatloukal, K., Cotten, M., Mechtler, K., and Wagner, E. (1992) Gene transfer into hepatocytes using asialoglycoprotein receptor mediated endocytosis of DNA complexed with an artificial tetra-antennary galactose ligand. *Bioconjugate Chem. 3*, 533−539.

(10) (a) Kamen, B. A., Wang, M.-T., Streckfuss, A. J., Peryea, X., and Anderson, R. G. W. (1988) Delivery of folates to the cytoplasm of MA104 cells is mediated by a surface membrane receptor that recycles. *J. Biol. Chem. 263*, 13602−13609. (b) Leamon, C. P., and Low, P. S. (1991) Delivery of macromolecules into living cells: a method that exploits folate receptor endocytosis. *Proc. Natl. Acad. Sci. U.S.A. 88*, 5572−5576. (c) Citro, G., Szczylik, C., Ginobbi, P., Zupi, G., and Calabretta, B. (1994) Inhibition of leukemia cell proliferation by folic acid−polylysine-mediated introduction of c-*myb* antisense oligodeoxynucleotides into HL-60 cells. *Br. J. Cancer 69*, 463−467.

(11) Trubetskoy, V., Torchilin, V. P., Kennel, S. J., and Huang, L. (1992) Use of N-Terminal modified poly(L-lysine)−antibody conjugate as a carrier for targeted gene delivery in mouse lung endothial cells. *Bioconjugate Chem. 3*, 323−327.

(12) (a) Wagner, E., Zenke, M., Cotten, M., Beug, H., and Birnstiel, M. L. (1990) Transferrin−polycation conjugates as carrier for DNA uptake into cells. *Proc. Natl. Acad. Sci. U.S.A. 87*, 3410−3414. (b) Wagner, E., Plank, C., Zatloukal, K., Cotten, M., and Birnstiel, M. L. (1992) Influenza virus hemagglutinin HA-2 N-terminal fusogenic peptides augment gene transfer by transferrin−polylysine−DNA complexes: Toward a synthetic virus-like gene-transfer vehicle. *Biochemistry 89*, 7934−7938.

(13) Bonfils, E., Dupierreux, C., Midoux, P., Thuong, N. T., Monsigny, M., and Roche, A. C. (1992) Drug targeting: synthesis and endocytosis of oligonucleotide-neoglycoprotein conjugates. *Nucleic Acids Res. 20*, 4621−4629.

(14) (a) Lee, R. T., and Lee, Y. C. (1987) Preparation of cluster glycosides and N-acetylgalactosamine that have sub-nanomolar binding constants toward mammalian hepatic Gal/GalNAc-specific receptors. *Glycoconjugate J. 4*, 317−328. (b) Oshumi, Y., Ichikawa, Y., and Lee, Y. C. (1990) Neoglycoproteins: Recent Progress and Future Outlook. *Cell Technol. 9* , 229−238.

(15) Merwin, J. R., Noell, G. S., Thomas, W. C., Chion, H. C., De Rome, M. E., McKee, T. D., Spitalny, G. L., and Findeis, M. A. (1994) Targeted delivery of DNA using YEE(ah-GalNAc)₃, a synthetic glycopeptide for the asialoglycoprotein receptor. *Bioconjugate Chem. 5*, 612−620.

(16) (a) Miller, P. S., Cushman, C. D., and Levis, J. T. (1991) Synthesis of oligo-2′-deoxyribonucleoside methylphosphonates. In *Oligonucleotides and analogues. A practical approach* (Eckstein, E., Ed.) pp 137−154, IRL Press, Oxford. (b) Hogrefe, R. I., Reynolds, M. A., Vaghefi, M. M., Yang, K. M., Riley, K. M., Klem, R. E., and Arnold, L. T., Jr. (1993) An improved method for the synthesis and deprotection of methylphosphonate oligodeoxynucleosides. In *Methods on Molecular Biology, vol 20: Protocols for Oligonucleotides and Analogs* (Agrawal, S., Ed.) pp 143−164, Humana Press, Inc.: Totown.

(17) Sproat, B. S., Lamond, A. T., Beijer, B., Neumer, P., and Ryder, U. (1989) Highly efficient chemical synthesis of 2′-O-methyloligoribonucleotides and tetrabiotinylated dervatives;

novel probes that are resistant to degradation by RNA or DNA specific nucleases. *Nucleic Acids Res. 17*, 3373−3386.

(18) (a) Chu, B. C. F., Wahl, G. M., and Orgel, L. E. (1983) Derivatization of unprotected polynucleotides. *Nucleic Acids Res. 11*, 6513−6529. (b) Chu, B. C. F., and Orgel, L. E. (1988) Ligation of oligonucleotides to nucleic acids or proteins via disulfide bonds. *Nucleic Acids Res. 16*, 3671−3691.

(19) Gilham, P. T. (1962) An addition reaction specific for uridine and guanosine nucleotides and its application to the modification of ribonuclease action. *J. Am. Chem. Soc. 84*, 687−688.

(20) Ede, N. J., Treagear, G. W., and Haralambridis, J. (1994) Routine Preparation of Thiol Oligonucleotides: Application to the Synthesis of Oligonucleotide−Peptide Hybrids. *Bioconjugate Chem. 5*, 373−378.

(21) Wu, G. Y., and Wu, C. H., Eds. (1991) Liver deseases, targeted diagnosis and therapy using specific receptors and lignds, Marcel Dekker, Inc., New York.

TECHNICAL NOTES

Primary Amino-Terminal Heterobifunctional Poly(ethylene oxide). Facile Synthesis of Poly(ethylene oxide) with a Primary Amino Group at One End and a Hydroxyl Group at the Other End

Yukio Nagasaki, Michihiro Iijima, Masao Kato, and Kazunori Kataoka*

Department of Materials Science and Technology, Science University of Tokyo, Noda 278, Japan.
Received June 16, 1995[®]

Well-defined poly(ethylene oxide) (PEO) with a cyano group at one end and a hydroxyl group at the other terminus was synthesized by the anionic ring opening polymerization of ethylene oxide (EO) initiated with (cyanomethyl)potassium (CMP) which was prepared by the metalation reaction of acetonitrile with potassium naphthalene in THF. Primary amino-terminal heterotelechelic PEO was obtained by the reduction of the cyano group at the end of the polymer chain by lithium aluminum hydride.

Recently, end-reactive PEOs have become more and more important in a variety of fields such as biology, biomedical science, and surface chemistry, due to their unique properties such as solubility and flexibility of the chains and basicity of the ether oxygens in the main chain (1, 2). For example, surface modifications by the end-reactive PEO prevent protein depositions to provide a biocompatible surfaces (3). Stabilization of proteins has been carried out extensively by a conjugation with the end-reactive PEOs, which induces several other benefits such as a decreased antigenicity and an increased solubility not only in water but also in organic solvents by maintaining their activities (4). Such PEO modification chemistries (sometimes called "PEGylation") have became a key area of interest in bioconjugate chemistry.

In general, PEO is synthesized by the ring opening polymerization of ethylene oxide (EO) initiated with an alkaline initiator such as potassium hydroxide (1). In this case, both chain ends should possess a hydroxyl group, and it is the so-called homotelechelic (5) PEO. PEO possessing a methoxy end group at one end and a hydroxyl group at the other end (semitelechelic PEO; methoxyPEO) can be obtained using potassium 2-methoxyethoxide as the initiator. In the first generation of PEGylation chemistry, the above two PEOs were utilized because of many kinds of commercially available samples with different molecular weights and controlled molecular weight distributions. Abuchowski et al. first reported (6) the activation method of a hydroxyl group using cyanuric chloride, followed by the modification of an enzyme. From this discovery, protein conjugation and also surface modification chemistries were extensively studied utilizing their procedure (2). However, the modifications by the cyanulate activated PEO have several problems since the primary amino groups must be derivatized. Some of the amino groups in the proteins are known to play an important role in its activity. The modification of such amino groups in the active center results in a significant decrease in the activity of the protein (7).

Harris and his co-workers (8) have comprehensively studied the synthesis of end-reactive PEOs possessing several kinds of functional groups such as primary amines, thiols, aldehydes, vinylsulfones, and activated esters. By utilizing such PEOs it has been revealed that a different modification method for the protein PEGylation resulted in activities (9, 10).

Most of the previously mentioned end-functionalized PEOs are semitelechelic or homotelechelic oligomers. To expand the utility of PEO's, a convenient synthesis of heterotelechelic (11) oligomers is needed. If such heterotelechelics can be synthesized easily, then these materials can be utilized as hetero-cross-linkers for different substances with defined spacer lengths and as surface modifiers with remaining reactive moieties at the free end. There are several reports on the synthesis of heterobifunctional PEOs using homotelechelic PEOs as the starting materials (12, 13). The synthetic methods, however, are complicated because they have to use several reaction steps to derivatize the PEO terminus. In addition, the efficiency of the derivatizations are not very high, meaning that the resulting PEO is a mixture of the starting homotelechelics and the resulting heterotelechelics to some extent.

Our strategy for heterotelechelic synthesis is to create a novel polymerization route of EO using new initiators containing defined functionalities. So far, we have synthesized heterotelechelics with a formyl group at one end and a hydroxyl group at the other end using an anionic ring opening polymerization of EO with potassium 3,3-diethoxypropoxide, followed by acid hydrolysis (14). Heterotelechelics with a primary-amino group at one end and a hydroxyl group at the other terminus were also synthesized using a silyl-protected potassium amide (15). In this case, the primary-amino group in N-methylethylenediamine was protected by 1,2-bis(dimethylchrolosilyl)ethane, and it was used as the initiator for polymerization of EO after the sec-amino group was converted to potassium amide. The silyl-amine at the end of the obtained polymer was easy to hydrolyze by acid to form the primary-amino terminated polymer. However, there were several disadvantages; for example, high skills are required for the synthesis of the silyl-

---
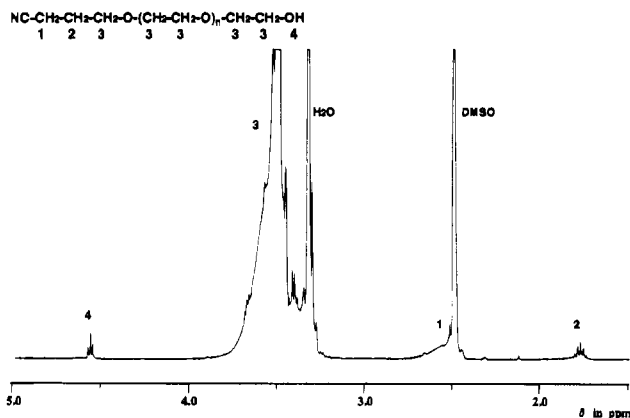
Figure 1. ^{1}H NMR spectrum of poly(ethylene oxide) initiated with (cyanomethyl)potassium in the presence of 18-crown-6 in THF.

Scheme 1
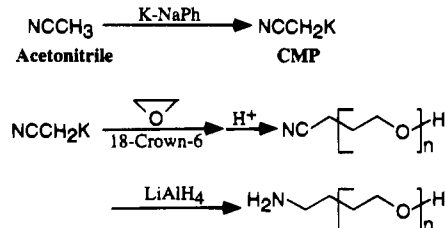
Table 1. ^{13}C NMR Chemical Shift Data of PEO Obtained with CMP as an Initiator (ppm)

$$N\overset{a}{C}\overset{b}{C}H_2\overset{c}{C}H_2\overset{d}{C}H_2(\overset{e}{O}\overset{f}{C}H_2\overset{f}{C}H_2)_n\overset{g}{O}\overset{h}{C}H_2\overset{h}{C}H_2OH$$

carbon	a	b	c	d	e	f	g	h
obsd	119.3	13.8	25.4	68.3	70.3	70.3	72.3	61.4
calcd	120.8	13.7	25.4	68.8	70.6	70.6	72.8	63.7

protected initiator and the resulting polymer possessed one tertiary amine at the α-end group. There are several reports on the EO polymerizations using amine-protected initiators (*16*, *17*). They had the same problems with the protections and the deprotections as our previous study. In this paper, we report the facile synthesis of primary amino-terminal heteroPEO initiated with CMP, which is easily synthesized using acetonitrile and potassium naphthalene, followed by a reduction of the cyano group with lithium aluminum hydride.

Since acetonitrile shows high acidity due to the electron-withdrawing effect of the cyano group ($pK_a = 25$ (*18*)), it is easy to metalate using an alkali metal alkyl such as butyllithium and potassium naphthalene (*19*). If the CMP can be utilized as the initiator for EO polymerization, the cyano-terminal heteroPEO can be formed. For the initiation of the anionic ring opening polymerization of EO, higher nucleophilicity than that of the alkoxylate anion must be provided (*20*). Since the acidity of the acetonitrile is lower than that of alcohol (pK_a (methanol) = 15 (*16*)), it is probable that the CMP has suitable reactivity to act as an initiator for EO polymerization.

To THF (30 mL) containing 18-crown-6 (3 mmol) in a 100 mL flask with a three-way stopcock under an argon atmosphere were added acetonitrile (4 mmol) and a THF solution of potassium naphthalene (*21*) (2 mmol) to form CMP. The 18-crown-6 was utilized to avoid possible side reactions such as a formation of dianion of acetonitrile. After liquid EO (240 mmol; −20 °C) was added via a cooled syringe (*22*), the mixture was allowed to react for 2 days at room temperature. As the reaction proceeded,
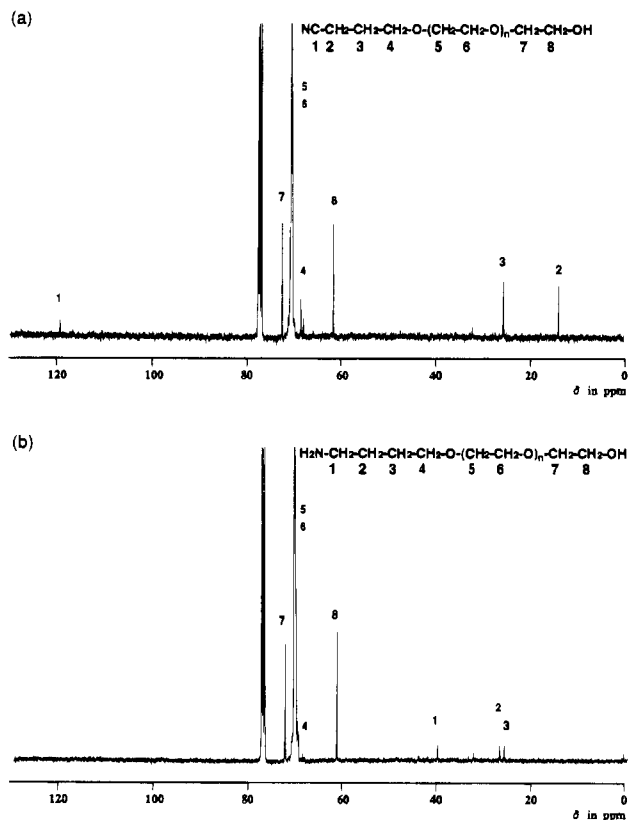
Figure 2. ^{13}C NMR spectra of poly(ethylene oxide) initiated with (cyanomethyl)potassium before (a) and after (b) the reduction by lithium auminum hydride in THF (the same sample as in Figure 1 was used).

the mixture became a viscous liquid. Polymers thus formed were purified by precipitation with an excess amount of ether and subjected to freeze-drying from benzene solution. A white powder was obtained in 77.5% yield.

From gel permeation chromatographic analysis (GPC), the number average molecular weight (M_n) of the polymer was determined to be 5200, with a molecular weight distribution (M_w/M_n (*23*)) of 1.17. The M_n of the polymer determined from GPC was slightly lower than that calculated using an initial monomer/initiator ratio (M_n = MW(EO)[EO]$_0$/[CMP]$_0$ + MW(acetonitrile) = 44 × 240/2 + 40 = 5320), suggesting that a small amount of water participated in the initiation of the polymerization. Figure 1 shows the ^{1}H NMR spectrum of the polymer after the purification by two fold reprecipitations in ether from THF solution, followed by freeze-drying with benzene. Triad signals appearing at 4.6 ppm are assignable to alcoholic protons ([4]H), while the triad signals appearing at 1.8 ppm are the methylene protons adjacent to cyanomethyl groups (^{2}H) as shown in Figure 1. The ratio of the area of these signals ([4]H/[2]H = 1.35/2) was again slightly higher than that expected from the calculated value for cyano-terminal heteroPEO (OH/CH$_2$CH$_2$CN = 1/2), indicating that a small amount of hydroxyl-terminal telechelic PEO (both OH end groups) was present as contamination due to the water impurity in the polymerization system. From the ^{1}H NMR and GPC analyses, it was concluded that ca. 10% of contaminating OH-telechelic PEO was present in the cyano-terminal heterobifunctional PEO (90%). In previous examples (where we have synthesized several types of heterobifunctional PEO (*14*, *15*, *24*, *25*)) using alkolate anion (O$^-$) and amido anion (N$^-$) as the initiators, no contaminating OH-telechelic PEO was present in the heterobifunctional

PEO formed. Carbanion as the initiator in the present polymerization system may affect the formation of OH-telechelic PEO, *viz.*, the carbanion may react with water, which is always presented the polymerization system. Such a side reaction produces a small amount of KOH which can react with EO to give OH-telechelic PEO. In a large scale polymerization with careful handling, however, the amount of water can be minimized.

Transformation of the terminal cyano group to a primary amino group was carried out by the addition of the THF solution (10 mL) of cyano-terminal-PEO (0.3 mmol) to a suspension of lithium aluminum hydride (6 mmol) in THF (10 mL) over 2 h. From the ^{13}C NMR spectrum (26) of the purified polymer shown in Figure 2, it was found that the signals derived from the cyano moiety completely disappeared and the four signals derived from the amino-methylene moiety appeared at 25.3, 26.9, 40.4, and 67.7 ppm, which are assignable to $-CH_2CH_2CH_2CH_2NH_2$, to $-CH_2CH_2CH_2CH_2NH_2$, to $-CH_2CH_2CH_2CH_2NH_2$, and to $-CH_2CH_2CH_2CH_2NH_2$ at the end of the polymer chain, respectively.

On the basis of the reported results, it is concluded that a heterobifunctional PEO with a primary amino group at one end and a hydroxyl group at the other end was synthesized, though ca. 10% of OH-terminated homotelechelic PEO was obtained due to the water impurities.

LITERATURE CITED

(1)) Bailey, F. E., Jr., and Koleske, J. V., Eds. (1991) *Alkylene Oxide and Their Polymers*, Vol. 35, Marcel Dekker: New York.

(2) Harris, J. M., Ed. (1993) *Poly(ethylene glycol) Chemistry, Biotechnical and Biomedical Applications*, Plenum Press: New York.

(3) For reviews see: (a) Merril, E. W. (1992) Poly(ethylene oxide) and Blood Contact: A Chronicle of One Laboratory. In *PEG Chemistry: Biotechnical and Biomedical Applications* (J. M. Harris, Ed.) pp 199–246, Plenum Press, New York. (b) Gölander, C.-G., Herron, J. N., Lim, K., Claesson, P., Stenius, P., and Andrade, J. D. (1992) Properties of Immobilized PEG Films and the Interaction with Proteins: Experiments and Modeling. In *PEG Chemistry: Biotechnical and Biomedical Applications* (J. M. Harris, Ed.) pp 221–246, Plenum Press, New York.

(4) For reviews see: (a) Yoshinaga, K., Ishida, H., Sagawa, T., and Ohkubo, K. (1992) PEG-Modified Protein Hybrid Catalyst. In *PEG Chemistry: Biotechnical and Biomedical Applications* (J. M. Harris, Ed.) pp 103–114, Plenum Press, New York. (b) Yomo, T., Urabe, I., and Okada, H. (1992) PEG-Coupled Semisynthetic Oxidases. In *PEG Chemistry: Biotechnical and Biomedical Applications* (J. M. Harris, Ed.) pp 115–126, Plenum Press, New York. (c) Veronese, F. M., Caliceti, P., Schiavon, O., and Sartore, L. (1992) Preparation and Properties of Monomethoxypoly(ethylene Glycol)-Modified Enzymes for Therapeutic Applications. In *PEG Chemistry: Biotechnical and Biomedical Applications* (J. M. Harris, Ed.) pp 127–138, Plenum Press, New York.

(5) The term telechelic oligomer was defined as an oligomer with reactive groups at the chain ends.

(6) Abuchowski, A., McCoy, J. R., Palczuk, N. C, van Es, T., and Davis, F. F. (1977) *J. Biol. Chem. 252*, 3582–3586.

(7) Yoshimoto, T., Nishimura, H., Saito, Y., Sakurai, K., Kamisaki, Y., Wada, H., Sako, M., Tsujino, G., and Inada, Y. (1986) *Jpn. J. Cancer Res. 77*, 1264–1272.

(8) Harris, J. M., Sedaghat-Herati, M. R., Sather, P. J., Brooks, D. E., and Fyles, T. M. (1992) Synthesis of New Poly(Ethylene Glycol) Derivatives. In *PEG Chemistry: Biotechnical and Biomedical Applications* (J. M. Harris, Ed.) pp 347–370, Plenum Press, New York.

(9) Chamow, S. M., Kogan, T. p., Venuti, M., Gadek, T., Harris, R. J., Peers, D. H., Mordenti, J., Shak, S., and Ashkennazi, A. (1994) *Bioconjugate Chem. 5*, 133–140.

(10) Takakura, Y., Kaneko, Y., Fujita, T., Hashida, M., Maeda, H., and Sezaki, H. (1989) *J. Pharm. Sci. 78*, 117–121.

(11) The term, heterotelechelics, was defined in our previous paper[24], which denotes a telechelic oligomer with a functional group at one end and another functional group at the other end.

(12) Means, G. E., Feeney R. E. (1990) *Bioconjugate Chem. 1*, 2.

(13) J. M. Harris, and M. Yalpani, Eds. (1985) *Polymer–Ligands Used in Affinity Partitioning and Their Synthesis*, Academic Press: New York.

(14) Nagasaki, Y., Kutsuna, T., Iijima, M., Kato, M., Kataoka, K., Kitano, S., and Kadoma, Y. (1995) *Bioconjugate Chem. 6*, 231.

(15) Kim, Y. J., Nagasaki, Y., Kataoka, K., Kato, M., Yokoyama, M., Okano, T., and Sakurai Y. (1994) *Polymer Bull. 33*, 1.

(16) (a) Furukawa, J., Saegusa, T., Matsushita, H., Kanbara, S., and Tanaka, H. Jpn. Pat. 7,016,468. (b) Huang, Y.-H., Li, Z.-M., and Morawetz, H. (1985) *J. Polym. Sci. 23*, 795.

(17) Sépulchre, M., Paulus, G., and Jérôme, R. (1983) *Makromol. Chem. 184*, 1849.

(18) March, J. (1992) *Advanced Organic Chemistry*, 4th ed., John Wiley & Sons, New York.

(19) Rappoport, Z., Ed. (1970) *The Chemistry of the Cyano Group*, John Wiley & Sons, New York.

(20) Tsuruta, T., and Kawakami, Y. (1988) Anionic Ring-Opening Polymerization: General Aspects and Initiation. In *Comprehensive Polymer Science: The Synthesis, Characterization, Reactions & Applications of Polymers* (G. C. Eastmond, A. Ledwith, S. Russo, and P. Sigwalt, Eds.) Vol. 3, Chain Polymerization I, pp 457–466, Pergamon Press, Oxford.

(21) Szwarc, M., Levy, M., and Milkovich, R. (1956) *J. Am. Chem. Soc. 78*, 2656.

(22) The syringe was cooled by liquid nitrogen for several minutes prior to use.

(23) M_w and M_n denote weight average and number average molecular weights, respectively.

(24) Yokoyama, M., Okano, T., Sakurai, Y., Kikuchi, A., Ohsako, N., Nagasaki, Y., and Kataoka, K. (1992) *Bioconjugate. Chem. 3*, 275.

(25) Cammas, S., Nagasaki, Y., and Kataoka, K. (1995) *Bioconjugate Chem. 6*, 223.

(26) The assignments of these signals were complete in reference to the literature on hydroxyl-terminated PEO[27] and are described in Figure 2.

(27) Kinugasa, S., Takatsu, A., Nakanishi, H., Nakahara, H., and Hattori, S. (1992) *Macromolecules 25*, 4848.

Peptide Attachment to Extremities of Liposomal Surface Grafted PEG Chains: Preparation of the Long-Circulating Form of Laminin Pentapeptide, YIGSR

Samuel Zalipsky,* Bhagya Puntambekar, Parthena Boulikas, Charles M. Engbers, and Martin C. Woodle†

SEQUUS Pharmaceuticals, Inc., 960 Hamilton Court, Menlo Park, California 94025. Received July 19, 1995®

Poly(ethylene glycol) (PEG)-grafted liposomes offer new opportunities as long-circulating platforms presenting biologically relevant ligands. In pursuit of this goal, liposomal conjugates of YIGSR were prepared by mild periodate oxidation of TYIGSR-NH₂ and incubation of the product with hydrazide–PEG–(distearoylphosphatidyl)ethanolamine-containing liposomes. The peptide-carrying liposomes, with up to 500 YIGSR residues per vesicle, despite exhibiting faster blood clearance rates than the parent liposomes in rats, remained in circulation for extended periods of time. Mean residence times for the parent liposomal formulation and conjugated preparations containing 200 and 500 YIGSR residues per vesicle were 28, 25, and 23 h, respectively. The results have important implications for systemic delivery of peptides and for their use as targeting moieties for PEG-grafted liposomes.

INTRODUCTION

During the last several decades a great many peptides with novel therapeutic potential have been synthesized. However, peptides as well as small proteins are often removed very rapidly from plasma circulation by glomerular filtration in the kidney followed by urinary excretion. This phenomena is viewed as a general obstacle to the efficient use of therapeutic peptides. As a result a search for the ways to increase systemic exposure of peptides is underway in a number of laboratories (1). For example, it was demonstrated that attachment of peptides (2) and proteins (3) to water-soluble polymers, which increases their molecular size, had measurable effect on lengthening their plasma residence time concomitant with an increase in bioavailability and in improved therapeutic index (4).

Until recently, classical liposomal formulations containing drugs loaded into their internal aqueous compartment proved effective for reaching mainly to mononuclear phagocyte system (MPS¹) tissues (5). The discovery of long-circulating (Stealth)² liposomes, prepared by inclusion of 3–7 mol % of methoxypoly(ethylene glycol)–distearoylphosphatidylethanolamine (mPEG–DSPE) in the vesicle-forming lipid mixture, allowed us to overcome limitations of classical liposomes, such as extensive hepatosplenic uptake and rapid clearance from circulation (6–9). Due to their persistence in bloodstream (half-lives in humans over 48 h), the PEG-grafted liposomes opened up possibilities for a whole set of new

applications (9). One of the new avenues suitable for exploration with the PEG-grafted liposomes is in their utilization as a long-circulating platform for the presentation of various biologically-relevant ligands. Peptides, for reasons indicated above, constitute an important group of such ligands with a potential to benefit from an increased systemic exposure. In particular, use of protein fragments containing specific receptor-binding domains can be expected to offer some advantages over similar use of antibodies, e.g., lower immunogenicity. In this paper, we report our initial results on attachment of peptides to extremities of PEG-grafted liposomes. These studies used a pentapeptide sequence, YIGSR, previously shown to be important in laminin receptor binding (10, 11). Our results demonstrate that a short peptide sequence can be linked efficiently to the polymer-grafted liposomes in a simple one-pot procedure. Most importantly, even the presence of a substantial amount of a cationic peptide, YIGSR, on the periphery of the liposome does not dramatically alter its circulating longevity and low hepatosplenic uptake.

EXPERIMENTAL PROCEDURES

General. Hz–PEG–DSPE was synthesized from PEG-2000 (Fluka) as described in detail elsewhere (12). TYIGSR-NH₂ was purchased from AnaSpec, Inc. (San Jose, CA). Sodium periodate, Nᵅ-acetylmethionine (NAM), cholesterol, and desferoxamine mesylate were purchased from Sigma (St. Louis, MO). Hydrogenated soy phosphatidylcholine (HSPC) was obtained from Natterman (Koln, Germany). Amino acid analysis was performed on hydrolyzed aliquots of peptide-conjugated liposomes at the Protein Structure Laboratory of the University of California, Davis.

Preparation of Liposomes. Liposomes composed of Hz–PEG–DSPE, HSPC, and cholesterol in a weight ratio of 1:3:1 (5.3:56.4:38.3 mol % ratio) with an average particle size of 100 ± 20 nm and 30–60 μmol of PL/mL were prepared by extrusion of multilamellar vesicles (MLV) using defined pore filters (Nuclepore) according to ref 8. Liposome particle size was determined by dynamic light scattering (Coulter N4MD, Hialeah, FL). Phospholipid concentrations were measured by phosphorus determination. Loading of [⁶⁷Ga]desferoxamine as

a liposomal radiolabel was achieved as previously described (*13*).

Preparation of YIGSR–Liposome Conjugates.
TYIGSR-NH$_2$ solution (0.2 mL, in HEPES buffer 25 mM, 0.9% saline, pH 7.2) was treated with freshly prepared stock solution of sodium periodate (20 μL) for 5 min in the dark (100 mM NaIO$_4$ stock solution was used for oxidation of 5 mM peptide solution and 200 mM periodate for 10 mM peptide). The excess of periodate was consumed by addition of NAM solution (20 μL, 1 M).[3] The stock solution of liposomes (2.2 mL, ≈ 50 μmol of PL/mL) in acetate buffer (0.1 M, pH 4.8) was mixed with the oxidized peptide solution and incubated overnight at ≈6 °C. The solution was extensively dialyzed against HEPES buffer (25 mM, 0.9% NaCl, pH 7.2) using Biodesign dialysis membrane MWCO 8000. Aliquots were sent for amino acid analysis and for phosphate analysis for determination of peptide to phospholipid (PL) ratio. The preparation obtained from 5 mM TYIGSR-NH$_2$ resulted in a peptide/PL mole ratio of 2.6×10^{-3}. Assuming 75 000 molecules of PL per 1000 Å liposome, this corresponds to ≈200 peptides per vesicle. Similarly, the preparation derived from 10 mM TYIGSR-NH$_2$ resulted in 7.3×10^{-3} mol of YIGSR/mol of PL, corresponding to ≈500 peptide residues per vesicle. Iodine-125-labeled peptide was prepared as follows. TYIGSR-NH$_2$ (0.2 mL of 4 mg/mL solution) in acetate buffer (0.1 M, pH 5.5) was pipetted into a test tube precoated with iodogen (prepared according to the procedure described in Pierce (Rockford, IL) catalog) and treated with Na^{125}I (2 μL, 1 mCi). After 45 min incubation at room temperature, the labeled peptide was purified on CM Sephadex (Pharmacia, 1 mL) column. The column preequilibrated with HEPES buffer (25 mM, pH 7.2) was loaded with the reaction solution and eluted with the same buffer to remove the free label. The peptide was eluted with NaCl (0.3 M in HEPES, pH 7.2). The oxidation and conjugation of T(^{125}I)YIGSR-NH$_2$ was performed as described above.

In Vivo Studies. Blood circulation and tissue distribution following intravenous administration were performed with male adult Sprague–Dawley rats (250–400 g) following standard procedures described elsewhere (*8*). Briefly, liposome samples prepared at 10 mM phospholipid in 10 mM desferoxamine mesylate in isotonic saline and radiolabeled with ^{67}Ga-oxine were administered intravenously at a dose of approximately 10–20 μmol of phospholipid/kg body weight. Blood levels at various times were determined by retro-orbital bleeding, while tissues were obtained surgically after 24 h. Tissue and blood levels of ^{67}Ga radioactivity were determined by γ counter. Pharmacokinetic analysis of concentration vs time data was performed using noncompartmental methods with the RSTRIP program (Micromath, Salt Lake City, UT). RSTRIP provides values for areas under the zero (AUC) and first moment (AUMC) concentration curves from which the derived parameters can be calculated. Mean residence time (MRT), the time it takes to eliminate 63.2% of the administered dose, was derived by the following formula: MRT = AUMC/AUC.

RESULTS AND DISCUSSION

Ligands of potential interest can be linked to polar head residues of specifically designed lipids coincorporated into liposomes. However, in the case of sterically

---

[3] Quick reduction in the amount of NAM commensurate with the amount of present periodate, presumably by conversion into methionine sulfoxide and sulfone derivatives, was confirmed by HPLC (Zalipsky, S. (unpublished results)).
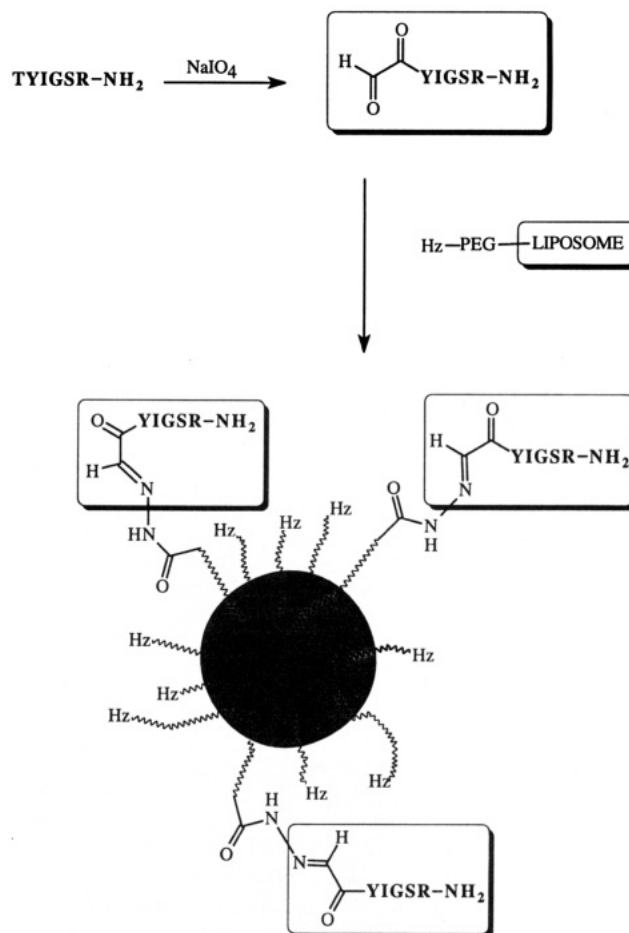
Figure 1. Schematic diagram of the coupling of periodate-oxidized TYIGSR-NH$_2$ to the terminal Hz groups of liposome-grafted PEG chains.

stabilized liposomes containing mPEG–DSPE the polymer chains interfere in both the conjugation reactions and interaction of the ligand with its biological target (*7, 14*). Therefore, it is preferable to covalently link the ligand molecules to distal ends of some of the PEG chains on the liposomal surface. This approach requires availability of end-group functionalized PEG–lipids (*15*). With this objective in mind, hydrazide–PEG–DSPE (Hz–PEG–DSPE) was recently introduced (*12*). This
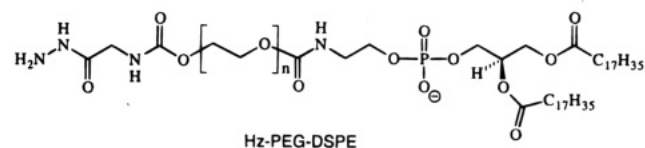
Hz-PEG-DSPE

derivative has been shown to incorporate readily into lecithin/cholesterol-containing lipid vesicles, having the same effect on liposomal pharmacokinetics and biodistribution as more commonly used mPEG–DSPE (*16, 17*). We utilized the reactivity of hydrazide groups positioned at the extremities of the grafted PEG chains for conjugation with YIGSR-NH$_2$. First, a reactive aldehyde group was generated on the N-terminal of the pentapeptide sequence by periodate oxidation of the hexapeptide TYIGSR-NH$_2$. The product, N^α-glyoxylyl-YIGSR-NH$_2$ was then coupled to Hz–PEG–DSPE-containing liposomes, as schematically depicted in Figure 1. Similar conjugation strategy relying on site-specific N-terminal modification of peptides (*18*) was recently described (*19, 20*). Both peptide oxidation and liposome attachment steps were carried out in a simple one-pot procedure. We

tissue	Hz−PEZ−liposome (control)	200 YIGSR/liposome	500 YIGSR/liposome
blood	33.4 (6.8)	24.5 (0.86)	18.4 (1.11)
liver	12.1 (1.20)	9.39 (1.37)	10.61 (1.16)
spleen	5.1 (0.47)	9.28 (3.02)	13.24 (1.69)
kidney	1.4 (0.22)	1.02 (0.17)	1.00 (0.17)
heart	0.36 (0.04)	0.21 (0.02)	0.31 (0.11)
lung	0.62 (0.23)	0.51 (0.05)	0.45 (0.08)
skin	0.09 (0.03)	0.10 (0.03)	0.12 (0.02)
muscle	0.08 (0.03)	0.04 (0.005)	0.04 (0.01)
bone	0.28 (0.09)	0.18 (0.01)	0.17 (0.03)

[a] Percentage of injection dose per organ. All values are mean of four animals (SD).
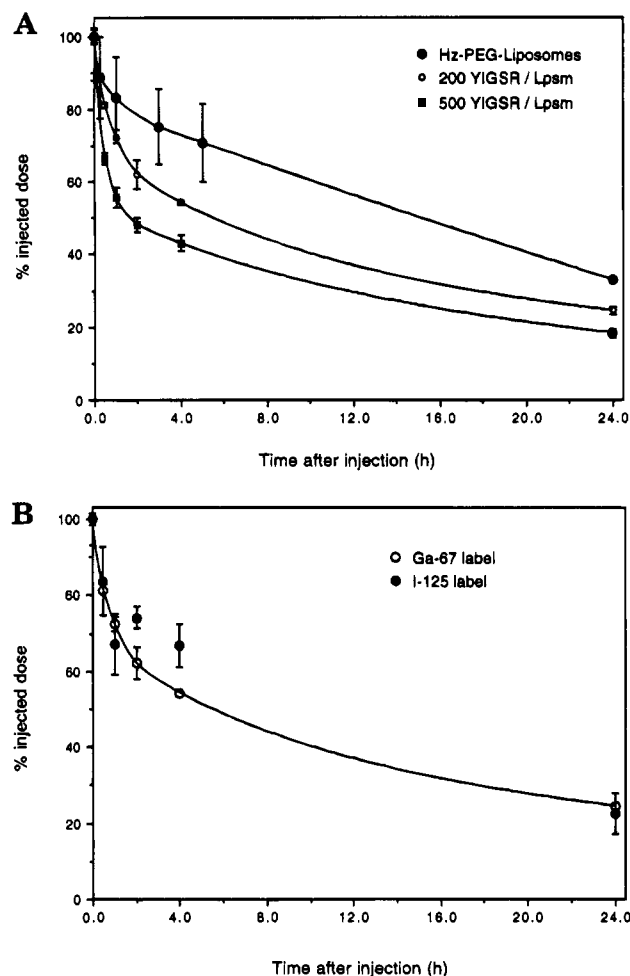
Figure 2. Blood lifetimes of liposomes prepared from HSPC, cholesterol, and Hz−PEG−DSPE (56.4:38.3:5.3 mol % ratio, 100 ± 20 nm diameter) and their conjugates with N^{α}-glyoxylyl-YIGSR-NH$_2$. Four rats per experiment. (A) Liposomes with [^{67}Ga]desferal-labeled aqueous compartment containing 200- and 500-linked YIGSR residues and the parent unconjugated liposomes. (B) Comparison of blood lifetimes of ^{67}Ga- and ^{125}I-labeled YIGSR−liposomes (200 residues per vesicle).

found this conjugation approach to be very convenient and reliable. The composition of peptide-linked liposomes was determined by phosphorus and amino acid analyses. The amounts of the linked peptide could be controlled by varying the conjugation parameters, excess of the peptide in the conjugation mixture, time of incubation. It was possible to achieve good conjugation yields (>50%) and high peptide to lipid ratios. There was no noticeable particle size alteration even after extensive peptide conjugation. After the conjugated and control liposomes were labeled with [^{67}Ga]desferal, we studied pharmacokinetics and biodistribution at 24 h postdose of YIGSR-containing liposome preparations containing 200 and 500 peptide residues per vesicle. The pharmacokinetic profiles of these formulations obtained in rats are shown in Figure 2A. It is evident that increasing the amount of bound peptide results in faster clearance from circulation. However, even heavily loaded preparation of 500 YIGSR residues per vesicle exhibited relatively long blood circulation. Mean residence times for 500 and 200 peptide per vesicle and the parent Hz−PEG−liposomes were 23, 25, and 28 h, respectively. The 24 h blood levels for these preparations were 18.4, 24.5, and 33.4% of the injected dose, respectively. The pharmacokinetics experiment repeated using ^{125}I-labeled peptide conjugate containing 200 YIGSR residues per vesicle produced essentially the

same clearance curve as in the case of aqueous compartment [^{67}Ga]labeled liposomes (Figure 2B). This indicates that the peptide and liposome components of the conjugate stay together in the time frame of the experiment. This indicates that the hydrazone attachments formed between peptide residues and the liposome-grafted PEG chains in the conjugates remain intact under *in vivo* conditions. This finding is consistent with the reported pH-dependent stability of N^{α}-glyoxylylpeptide-derived hydrazones (*19*).

Biodistribution results, summarized in Table 1, were similar to typical distributions of long-circulating, PEG-grafted liposomes (*8*). Increase in the amount of liposome-bound peptide was accompanied by a gradual increase in spleen accumulation. The percentages of the injected dose found in spleen were 5, 9, and 13%, respectively, for the parent Hz−PEG−liposomes and the 200 and 500 peptide residues per vesicle containing preparations.

Our results indicate that PEG-grafted liposomes can carry a substantial number of peptide residues per vesicle without sacrificing their beneficial biodistribution and pharmacokinetic properties to a great extent. Even the presence of positively charged residues, like YIGSR, did not significantly compromise the properties of PEG−liposomes (*21*). It is pertinent to note that similarly constructed immunoliposomes containing more than 35 conjugated residues per vesicle essentially lose their beneficial properties (*17, 22*). Since multivalency of ligand-carrying vesicles is expected to be important for efficient targeting to the intended sites, this might be an important advantage of peptide-carrying liposomes over analogous immunoglobulin-containing constructs.

The peptide chosen as a model sequence for this study, YIGSR, is of significant practical interest. It is the shortest sequence of basement membrane glycoprotein, laminin, retaining the ability to bind to laminin cell surface receptor (*11*). This binding activity plays an important role in metastasis (*10, 11*) and angiogenesis (*23*) processes. Recently published examination of pharmacokinetics and biodistribution of ^{99m}Tc-labeled YIGSR in rats and mice showed that over 97% of the injected peptide dose was cleared within 30 min without noticeable accumulation in any specific organ (*24*). Thus, in comparison, the extension of circulation lifetime of YIGSR, achieved by covalent fixation of the peptide residues to liposome-grafted PEG chains, described in this paper is truly remarkable.

Since most short peptide sequences can be readily prepared with Thr or Ser positioned at their N-terminals, they too can be utilized for preparation of long-circulating peptidoliposomes. While we are currently engaged in the biological evaluation of YIGSR-linked liposomes, we

would like to suggest the methodology described here as an approach for increase of systemic exposure of peptides.

CONCLUSIONS

Hydrazide—PEG—DSPE-containing liposomes are useful for covalent attachment of N^α-glyoxylyl-YIGSR-NH$_2$ residues, generated *in situ* from TYIGSR-NH$_2$, in a simple and reliable fashion. The hydrazone attachments formed in this conjugation process are stable under conditions existing in the bloodstream. The composition of the conjugated liposomes can be controlled by varying the reaction conditions, and it can be precisely determined by amino acid analysis. The covalent attachment of multiple YIGSR-NH$_2$ residues to the far end of PEG chains has only small effects on the pharmacokinetics and biodistribution of PEG—liposomes. Since most short peptide sequences can be readily obtained with Thr or Ser residues at the N-terminal, this methodology for preparation of peptide-linked liposomes should be of rather general scope. Our findings have important practical implications for systemic delivery of therapeutic peptides, most of which suffer from very rapid clearance from systemic circulation, as well as for the use of peptides as ligands for sterically stabilized liposomes.

LITERATURE CITED

(1) Lee, V. H. L., Ed. (1991) *Peptide and Protein delivery*, Marcel Dekker, New York.

(2) Braatz, J. A., Yasuda, Y., Olden, K., Yamada, K. M., and Heifetz, A. H. (1993) Functional peptide—polyurethane conjugates with extended circulation half-lives. *Bioconjugate Chem. 4,* 262—267.

(3) Knauf, M. J., Bell, D. P., Hirtzer, P., Luo, Z.-P., Young, J. D., and Katre, N. V. (1988) Relationship of effective molecular size to systemic clearance in rats of recombinant interlukin-2 chemically modified with water-soluble polymers. *J. Biol. Chem. 263,* 15064—15070.

(4) Katre, N. V. (1993) The conjugation of proteins with polyethylene glycol and other polymers: Altering properties of proteins to enhance their therapeutic potential. *Adv. Drug Delivery Rev. 10,* 91—114.

(5) Lasic, D. D. (1993) *Liposomes: From physics to applications*, Elsevier, Amsterdam.

(6) Woodle, M. C., and Lasic, D. D. (1992) Sterically stabilized liposomes. *Biochim. Biophys. Acta 1113,* 171—199.

(7) Klibanov, A. L., Maruyama, K., Beckerleg, A. M., Torchilin, V. P., and Huang, L. (1991) Activity of amphiphathic poly-(ethylene glycol) 5000 to prolong the circulation time of liposomes depends on the liposome size and is unfavorable for immunoliposome binding to target. *Biochim. Biophys. Acta 1062,* 142—148.

(8) Woodle, M. C., Matthay, K. K., Newman, M. S., Hidayat, J. E., Collins, L. R., Redemann, C., Martin, F. J., and Papahadjopoulos, D. (1992) Versatility in lipid compositions showing prolonged circulation with sterically stabilized liposomes. *Biochim. Biophys. Acta 1105,* 193—200.

(9) Lasic, D., and Martin, F., Ed. (1995) *Stealth Liposomes*, CRC Press, Boca Raton, FL.

(10) Kleinman, H., Graf, J., Iwamoto, Y., Sasaki, M., Schasteen, C., Yamada, Y., Martin, G. R., and Robey, F. A. (1989) Identification of a secondary active site in laminin for promotion of cell adhesion and migration and inhibition of in vivo melanoma lung colonization. *Arch. Biochem. Biophys. 272,* 39—45.

(11) Iwamoto, Y., Robey, F. A., Graf, J., Sasaki, M., Kleinman, H. K., Yamada, Y., and Martin, G. R. (1987) YIGSR, a synthetic laminin pentapeptide, inhibits experimental metastasis formation. *Science 238,* 1132—1134.

(12) Zalipsky, S. (1993) Synthesis of an end-group functionalized polyethylene glycol—lipid conjugate for preparation of polymer-grafted liposomes. *Bioconjugate Chem. 4,* 296—299.

(13) Woodle, M. C. (1993) Gallium-67-labeled liposomes with prolonged circulation: Preparation and potential as nuclear imaging agents. *Nucl. Med. Biol. 20,* 149—155.

(14) Zalipsky, S., Hansen, C. B., Lopes de Menezes, D., and Allen, T. M. (1995) Long-circulating PEG-grafted immunoliposomes. *J. Controlled Release* (in press).

(15) Zalipsky, S. (1995) Polyethylene glycol—lipid conjugates. In *Stealth Liposomes* (D. Lasic, and F. Martin, Eds.) pp 93—102, CRC Press, Boca Raton, FL.

(16) Zalipsky, S., Newman, M., Punatambekar, B., and Woodle, M. C. (1993) Model ligands linked to polymer chains on liposomal surfaces: Application of a new functionalized polyethylene glycol-lipid conjugate. *Polym. Materials: Sci. Eng. 67,* 519—520.

(17) Allen, T. M., Agrawal, A. K., Ahmad, I., Hansen, C. B., and Zalipsky, S. (1994) Antibody-mediated targeting of long-circulating (Stealth) liposomes. *J. Liposome Res. 4,* 1—25.

(18) Dixon, H. B. F. (1984) N-Terminal modification of proteins—a review. *J. Protein Chem. 3,* 99—108.

(19) Geoghegan, K. F., and Stroh, J. G. (1992) Site-directed conjugation of nonpeptide groups to peptides and proteins via periodate oxidation of 2-amino alcohol. Application to modification at N-terminal serine. *Bioconjugate Chem. 3,* 138—146.

(20) Gaertner, H. F., Rose, K., Cotton, R., Timms, D., Camble, R., and Offord, R. E. (1992) Construction of protein analogs by site-specific condensation of unprotected fragments. *Bioconjugate Chem. 3,* 262—268.

(21) Zalipsky, S., Brandeis, E., Newman, M. S., and Woodle, M. C. (1994) Long-circulating, cationic liposomes containing amino-PEG-phosphatidylethanolamine. *FEBS Lett. 353,* 71—74.

(22) Allen, T. M., Brandeis, E., Hansen, C. B., Kao, G. Y., and Zalipsky, S. (1995) A new strategy for attachment of antibodies to sterically stabilized liposomes resulting in efficient targeting to cancer cells. *Biochim. Biophys. Acta 1237,* 99—108.

(23) Sakamoto, N., Iwahana, M., Tanaka, N. G., and Osada, Y. (1991) Inhibition of angiogenesis and tumor growth by a synthetic laminin peptide, CDPGYIGSR-NH$_2$. *Cancer Res. 51,* 903—906.

(24) Zamora, P. O., Eshima, D., Graham, D., Shattuck, L., and Rhodes, B. A. (1993) Biological distribution of ^{99m}Tc-labeled YIGSR and IKVAV laminin peptides in rodents: ^{99m}Tc-IKVAV peptide localizes to the lung. *Biochim. Biophys. Acta 1182,* 197—204.